IDS'2018

21st International Drying Symposium

Proceedings

September 11-14, 2018
Universitat Politècnica de València

Valencia, Spain

I am delighted and truly honoured to welcome you to IDS2018. As you know this is a landmark event representing completion of four decades since the establishment of this biennial series in 1978 at McGill University, Montreal, Canada.

I am happy to note that IDS2018, like its predecessor events, has attracted significant academic and industry interest in drying research and development from around the world. Exchange of ideas and dissemination of knowledge about both fundamental aspects and industrial applications have been the prime motivations for holding IDS events around the globe. As an interdisciplinary and multidisciplinary field which combines complex multi-phase transport phenomena with material science, drying is also highly energy-intensive and has controlling influence on the dried product quality in diverse industrial sectors. I believe that IDS and sister conferences devoted to drying have had a very significant impact on enhancements in drying technologies and innovation in dryer design. Much remains to be done of course.

I am sure the participants in IDS2018 will find the proceedings and networking opportunities rewarding and their stay in the wonderful historic city of Valencia memorable.

Finally, on behalf of all the attendees may I take this opportunity to thank and congratulate the Program Chair and his hardworking Organizing Committee supported by authors, reviewers and of course all the volunteers assisting with the smooth running of this complex event.

Arun S. Mujumdar

IDS Honorary Chairman

In this 40th anniversary of IDS it is a real honour to host at the Universitat Politècnica de València the celebration of IDS2018.

This is an event that, like in all other its predecessors, has attracted worldwide attention. Over 300 researchers from over 40 countries will present more than 450 papers at this event. As we can see IDS2018 promises to be a highly successful event. We are confident the founder of the IDS series Arun S. Mujumdar, would be very proud of it.

On this occasion we wanted to bring the event inside the University campus in order to get the students more actively involved in the organization and to make them aware of the importance and the impact of drying on many industries and different aspects of our life. This is a down to earth field that many times has been underestimated by our students and it's value needs to be recognized. Drying involves many aspects that may attract the interest of our students, from sustainability to product quality and the diversity of products. Valencia and the Mediterranean area have a long tradition of addressing the drying process; just remember the importance of dried fish on the Roman times that you still it find in our markets.

The quality of the contributions is very high and the discussion during the event will enhance fruitful exchanges among the participants. We hope that the academic environment will help to attain the goal of a friendly and fruitful interaction in the beautiful city of Valencia. We believe this event will fulfil your expectations.

On behalf of the Organizing Committee

Antonio Mulet

Chairman IDS2018

Organizing committee

Co-Presidents:

Jose V. Garcia-Perez
Universitat Politècnica de València, Spain

Susana Simal
Universitat de les Illes Balears, Spain

Members

Juan A. Carcel
Universitat Politècnica de València, Spain

Jose Bon
Universitat Politècnica de València, Spain

Carmen Rosselló
Universitat de les Illes Balears, Spain

Jose Benedito
Universitat Politècnica de València, Spain

Ana Andrés
Universitat Politècnica de València, Spain

Gabriela Clemente
Universitat Politècnica de València, Spain

Neus Sanjuan
Universitat Politècnica de València, Spain

Antoni Femenia
Universitat de les Illes Balears, Spain

Valeria Eim
Universitat de les Illes Balears, Spain

Scientific committee

Co-presidents

Juan A. Carcel
Universitat Politècnica de València (Spain)

Carmen Rossello Matas
Universitat de les Illes Balears (Spain)

Members

Alejandra Salvador
Instituto Valenciano de Investigaciones Agrarias. IVIA (Spain)

Alex Martynenko
Dalhousie University (Canada)

Alicia Font
Universitat d'Alacant (Spain)

Amparo Quiles
Universitat Politècnica de València (Spain)

Amparo Salvador
Universidad de Castilla-La Mancha (Spain)

Ana Briones
Universidad de Castilla-La Mancha (Spain)

Antonia Montilla
Instituto de Investigación en Ciencias de la Alimentación-CIAL (Spain)

Antonio Martínez López
Instituto de Agroquímica y Tecnología de Alimentos (IATA-CSIC) (Spain)

Carme Garau
Institut de Recerca i Formació Agrària i Pesquera, Conselleria de Medi Ambient, Agricultura i Pesca, Illes Balears (Spain)

Christelle Turchiuli
AgroParisTech (France)

Chung-Lim Law
University of Nottingham (Malaysia)

Clara Talens
Azti-Tecnalia (Spain)

Cristina Arroyo
Food Safety Authority of Ireland (FSAI) (Ireland   )

Cristina Ratti
Université Laval (Canada)

Davide Fissore
Politècnico de Torino (Italy)

Diana Permuy
Suez Water Technologies and Solutions Spain (Spain)

Edith Corona Jimenez
Benemérita Universidad Autónoma de Puebla (Mexico)

Elena Fulladosa
Food Industries Area – IRTA (Spain)

Enrique Barrajón-Catalan
Universidad Miguel Hernández (Spain)

Enrique Riera
Instituto de Tecnologías Físicas (ITEFI)-CSIC (Spain)

Fabiano Fernandes
Unversidade Federal do Ceara (Brazil)

Fernando Antonio Cruz Peragón
Universidad de Jaén (Spain)

Francesco Marra
University of Salerno (Italy)

Francisco J. Barba
Universitat de València. Estudi General (Spain)

Gabriela Clemente
Universitat Politècnica de València (Spain)

Gail Bornhorst
University of California-Davis (USA)

Gemma Moraga
Universitat Politècnica de València (Spain)

Gianpaolo Ruocco
University of Basilicata (Italy)

Grzegorz Musielak
Poznan University of Technology (Poland)

Hao Feng
Unversity of Illinois at Urbana-Champaign (USA)

Henry Sabarez
CSIRO Agriculture and Food (Australia)

Henry Vaquiro
Universidad de Tolima (Colombia)

Hidefumi Yoshii
Kagawa University (Japan)

Hong-Wei Xiao
China Agricultural University (China)

Ignacio Lombraña
Universidad del Pais Vasco (Spain)

Irving I. Ruiz-Lopez
Benemérita Universidad Autónoma de Puebla, BUAP (Mexico)

Isabel Cambero
Universidad Complutense (Spain)

Isabel Hernando Hernando
Universitat Politència de València (Spain)

Jader Rodríguez-Cortina
Corporación Colombiana de Investigación Agropecuaria, Corpoica (Colombia)

James Lyng
University College of Dublin (Ireland)

Javier Telis-Romero
Universidade Estadual Paulista (Brazil)

Jefferson Corrêa
Unversidade Federal de Lavras (Brazil)

Jorge Moreno Cuevas
Unviersidad Bio Bio (Chile)

José García Reverter
ainia - Centro Tecnológico (spain)

José Luís Amorós
Universtat Jaume I (Spain)

Jose M. Barat
Universitat Politènica de València (Spain)

Josep Comaposada
Food Industries Area - IRTA (Spain)

Karim Allaf
Université de La Rochelle (France)

Lluis Torró
Biopartner S.L. (Spain)

Lyes Bennamoun
University of New Brunswick (Canada)

Mar Villamiel
Instituto de Investigación en Ciencias de la Alimentación (CIAL)-CSIC
(Spain)

Marco Dalla Rosa
Universita di Bologna (Italy)

Maria del Mar Camacho
Universitat Politècnica de València (Spain)

Martin Olazar
Universidad del País Vasco/Euskal Herriko Unibertsitatea (Spain)

Michael Bantle
SINTEF (Norway)

Miguel García Alvarado
Instituto Tecnológico de Veracruz (Mexico)

Min Zhang
Jiangnan University (China)

Mohamed Hemis
University Djilali Bounaama Khemis Miliana (Algeria)

Neus Sanjuán
Universitat Politècnica de València (Spain)

Nieves Corzo; , Spain (M)
Instituto de Investigación en Ciencias de la Alimentación-CIAL (Spain)

Nuria Martinez Navarrete
Universitat Politència de València (Spain)

Olga Martín Belloso
Universitat de Lleida (Spain)

Olvido Iglesias Huelga
Universidad de Oviedo (Spain)

Pepe Fernandez-Salguero
Universidad de Córdoba (Spain)

Per M. Walde
Norwegian University of Science and Technology-NTNU (Norway)

Pere Gou
Food Industries Area - IRTA (Spain)

Prabhat Nema
National Institute of Food Technology Entrepreneurship and Management (NIFTEM) (India)

Rafael Font
Universidad de Alicante (Spain)

Ramón Felipe Moreira Martínez
Universidad Santiago de Compostela (Spain)

Remedios González
Universitat de València (Spain)

Seddik Khalloufi
Agri-Food Canada (Canada)

Sihem Bellagha
Institut national agronomique de Tunisie, INAT (Tunisia)

Somkiat Prachayawarakorn
King Mongkut's University of Technology Thonburi (Thailand)

Sonia Ventanas
Universidad de Extremadura (Spain)

Stanislav Rudobashta
Russian State Agrarian University (Russia)

Stella M. Alzamora
Universidad de Buenos Aires (Argentina)

Sueli Rodrigues
Unversidade Federal do Ceara (Brazil)

Susana Simal
Universitat de les Illes Balears (Spain)

Valeria Eim
Universitat de les Illes Balears (Spain)

Vicente Micol
Universidad Miguel Hernández (Spain)

Volker Gaukel
Karlsruhe Institute of Technology (Germany)

Weibiao Zhou
National University of Singapore (Singapore)

IDS Advisory Panel

- **Mujumdar A. S.** (Canada), Honorary Chairman
- **Devahastin S.** (Thailand), Secretariat
- **Akinola A.** (Nigeria)
- **Alves - Filho O.** (Norway)
- **Andrieu J.** (France)
- **Barresi A**. (Italy)
- **Bruttini R.** (Italy)
- **Chen X. D.** (P. R. China)
- **Chen G.** (Hong Kong, P. R. China)
- **Emam - Djomeh Z.** (Iran)
- **Farkas I.** (Hungary)
- **Fortes M.** (Brazil)
- **Itaya Y.** (Japan)
- **Kechaou N.** (Tunisia)
- **Kemp I.** (UK)
- **Kowalski S.** (Poland)
- **Krokida M.** (Greece)
- **Kudra T.** (Canada)
- **Langrish T.** (Australia)
- **Law C. L.** (Malaysia)
- **Leonard A.** (Belgium)
- **Levy A.** (Israel)
- **Miao S.** (Ireland)
- **Mulet A.** (Spain)

- **Opara L.** (South Africa)
- **Pakowski Z.** (Poland)
- **Pang S.** (New Zealand)
- **Peczalski R.** (France)
- **Perré P.** (France)
- **Raghavan V.** (Canada)
- **Rodriguez - Ramirez** (Mexico)
- **Renstrom R.** (Sweden)
- **Rosello C.** (Spain)
- **Sarkar Md. S. H.** (Bangladesh)
- **Prachayawarakorn S.** (Thailand)
- **Schutyser M.** (Netherlands)
- **Taranto O.** (Brazil)
- **Thorat B.** (India)
- **Timofeev O.** (Finland)
- **Tsotsas E.** (Germany)
- **Yagoobi J.** (USA)
- **Zbicinski I.** (Poland)
- **Zhou W.** (Singapore)

INDEX

Key Notes

KEY NOTES

Drying of mangoes applying pulsed UV light as pretreatment

Braga, T.R.[a]; Silva, E.O.[b]; Rodrigues, S.[c]; Fernandes, F.A.N.[a]

[a] Universidade Federal do Ceara, Departamento de Engenharia Química, Fortaleza – CE, Brazil
[b] Embrapa Agroindústria Tropical, Fortaleza – CE, Brazil
[c] Universidade Federal do Ceara, Departamento de Engenharia de Alimentos, Fortaleza – CE, Brazil

*E-mail of the corresponding author: fabiano@ufc.br

Abstract

High intensity pulsed UV Light is a non-thermal treatment used in sanitization of fruits and vegetables. In this work, we have applied high intensity pulsed UV light as a pretreatment for convective air-drying evaluating the benefits of the pretreatment to the drying process and to the nutritional quality of the dried product. Mangoes were subjected to pulses of UV light. The pretreated samples were further dried in a convective oven-drier until 90% of the initial water content has been removed. Drying kinetics, water apparent diffusivity, vitamin B, vitamin C content and total carotenoids content were analyzed. Pulsed UV light showed to be an interesting pretreatment for mangoes given the higher nutritional content of the dried product.

Keywords: mango; drying; ultraviolet; vitamins; kinetics.

1. Introduction

New food product development should focus on retaining as much of the naturally occurring vitamin content as possible, on increasing the availability of vitamins, and on reducing the appearance of undesirable breakdown products. Factors that play a role in the degradation of vitamins during food processing include temperature, air, light, moisture content, water activity, pH and enzymes related to the food spoilage [1]. Air-drying reduces the moisture content of the product decreasing the effect of one of the primary factors, the water activity, that determines the rate of vitamin deterioration by several biochemical reactions [1]. However, air-drying may increase vitamin loss by increasing the food exposition to high temperature for a long period of time.

Pulsed ultraviolet (UV) light processing of foods is a nonthermal technology used to enhance the quality and safety of foods. Its uses range from sanitization of foods (primary use) to extension of shelf life of fruits and vegetables, and enhancement of phytochemical content in fruits [2,3]. UV treatment is currently in use by the industry especially in sanitization of fruit and vegetables. Several studies reported that UV light also contributed towards the enhancement of the nutritional quality of food products, enhancing vitamin content, total carotenoids content, antioxidant capacity and other phytochemical properties [3–5].

Despite the importance of quality parameters in dried foods, most published studies are limited to determining the drying rate and some diffusional aspects and only few studies have focused on evaluating the changes on product quality after drying. In this work, pulsed UV light was applied as a pretreatment prior to air-drying for the drying of mangoes. The influence of the pretreatment and the drying process on vitamins B1, B3, B5, B6 and C, total carotenoids as well as its influence on the effective water diffusivity were evaluated.

2. Materials and Methods

2.1 Preparation of samples

Mangoes (*Mangifera indica* L. var. Tommy Athikins) were bought from the local market (Fortaleza, Brazil). Only fruits with same maturity stage were used. Cubic samples (side 10 mm) were obtained using a household tool from the mango flesh. The moisture content was determined by oven drying at 110ºC until constant weight (24h).

2.2. Pulsed UV light pre-treatment

The pre-treatment was carried out in a pulsed UV light equipment (SteriBeam model Xe Matric A, Germany) equipped with a xenon flash lamp (19 cm). The samples (12 g ± 1 g) were placed inside the treatment chamber of the equipment (20 cm wide × 14 cm deep × 12 cm high) and subjected to UV light pulses. The samples were subjected to 10, 20, 30, 40 and 50 pulses of UV light. Each pulse corresponded to a fluence (energetic density) of 0.36 J/cm^2 and were delivered in 250 µs. All experiments were carried out in triplicate.

2.3 Air drying

Drying kinetics were carried out in a conventional convective oven-drier. Air-drying experiments with mango samples were carried out at 0.5 m/s (air velocity) and 60 °C (temperature). The drying experiments were conducted in triplicates and completed when the samples lost 90% of the initial weight. For each experiment, 25 ± 1 g cubes of mangoes were distributed over a custom sample holder inside the drying chamber.

The air-drying kinetics of mangoes was modeled assuming diffusion-controlled mass transfer. Only the falling-rate period (diffusion-controlled mass transfer period) was considered because the constant-rate period (heat transfer-controlled mass transfer period) was not observed. The model considered the solution of Fick's second law for cubic shaped samples (Equation 1) [6].

$$W(t) = W_{eq} + \left(W_{crit} - W_{eq}\right) \left[\sum_{n=0}^{\infty} \frac{8}{(2n+1)^2\pi^2} exp\left(-\frac{D(2n+1)^2\pi^2 t}{4a^2}\right)\right]^3 \quad (1)$$

2.4 Determination of vitamins

To determine the vitamins of the B complex, 1 g of fruit was homogenized with 6 mL of distilled water for 2 min using a cell homogenizer (Ultraturrax IKA model T25). The vitamins were extracted by adding sulfuric acid 0.25 M (1 mL) to the sample, which was heated for 30 min in a water bath (70 ºC). After cooling in an ice bath, the pH was adjusted to 4.5 using a 0.5 M sodium hydroxide solution. The sample was centrifuged at 8400× g for 10 min. The supernatant was collected and analyzed spectrophotometrically at 215 (Vitamin B5), 254 (Vitamin B1), 265 (Vitamin B3) and 716 (Vitamin B6) nm using water as blank. All analyses were carried out in triplicate and results were expressed as the vitamin gain/loss using the fresh fruit as reference.

2.5 Determination of total carotenoid content

The carotenoids were extracted milling 1 g of mango sample with 6 mL of distilled water in a cell homogenizer (Ultraturrax IKA model T25). Hexane (5 mL) was added and the mixture was vigorously stirred in a vortex for 1 min. The supernatant (hexane phase) containing the lipid fraction was collected and analyzed spectrophotometrically at 452 nm to determine the total carotenoids content, using hexane as blank. All analyses were carried out in triplicate.

3. Results and Discussion

3.1. Pulsed UV light pretreatment

Mangoes presented an initial moisture content of 84.2 ± 0.4 g water/100 g fresh fruit (wet basis). The moisture content of the samples decreased during the UV light pretreatment,

reducing the initial moisture content by 4.3 to 15.9%. Figure 1 presents the water loss observed as a function of the energetic density that was applied.
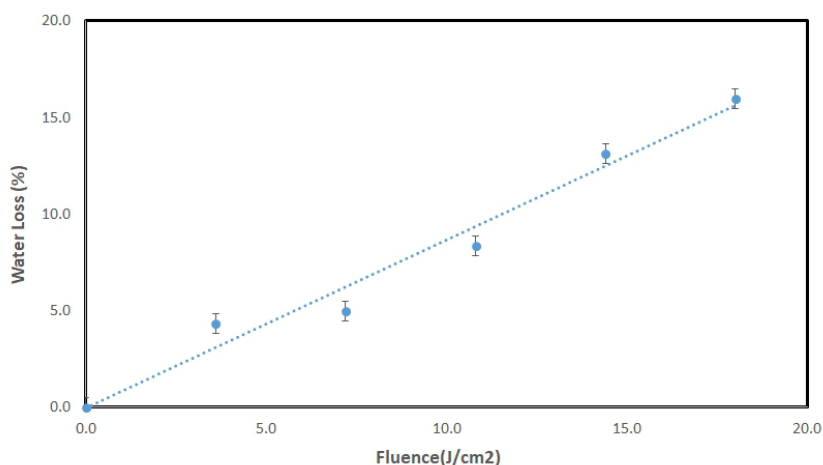
Fig. 1 Water loss during the pulsed UV light pretreatment as a function of the UV dosage applied to the samples.

Overall, pulsed UV light pretreatment contributed to an initial reduction of the moisture content of the samples.

3.2. Air-drying experiments

Figure 2 presents the experimental drying kinetics of mangoes obtained with and without application of pulsed UV light. Drying kinetics of mangoes presented the typical behavior observed for other fruits [7]. Only the falling rate period was observed during the drying process. Drying was carried out until 95% of the initial moisture was removed, corresponding to a final moisture content of 0.08 ± 0.01 g water/g dry matter.

The water apparent diffusivities in mangoes were calculated using Equation 1. The results are presented in Table 1. The diffusion model used in this work was adequate for describing the drying kinetics of mangoes cubes under the different experimental conditions, presenting R^2 values between 0.986 to 0.995.

Despite the initial reduction in moisture content attained during the pretreatment, the pulsed UV light pretreatment did not reduce the air-drying time. In fact, the samples took between 2 and 16% more time to dry than the untreated sample. It must be stated that the required air-drying time to reduce 80% of the initial moisture content was statistically similar among the sample not subject to pretreatment and the samples pretreated with a total energetic density above 10.8 J/cm^2.
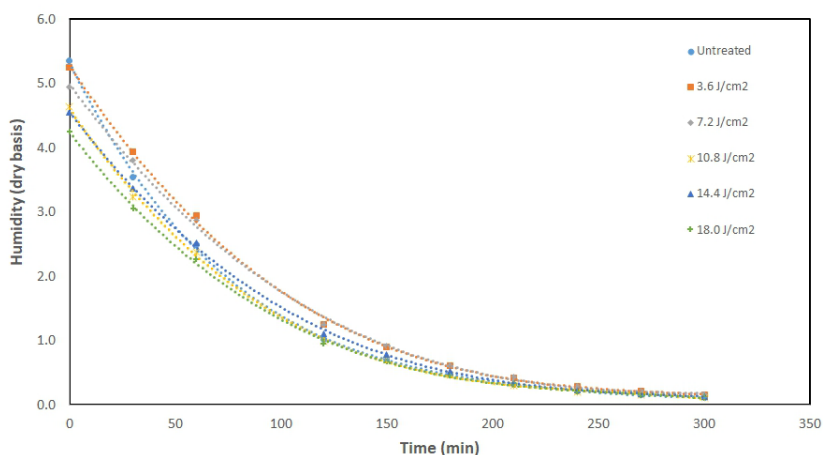
Figure 2. Moisture content (in dry basis) as a function of drying time for the samples with and without pulsed UV light pretreatment.

Table 1. Water apparent diffusivity of mangoes subjected to pulsed UV light pretreatment.

Total energetic density applied (J/cm^2)	Number of UV light pulses (#)	Apparent diffusivity (10^7 m^2/min)	R^2
0.0	0	4.37 ± 0.38 [a]	0.995
3.6	10	3.90 ± 0.03 [b]	0.986
7.2	20	3.76 ± 0.09 [b]	0.986
10.8	30	4.26 ± 0.12 [a]	0.987
14.4	40	3.92 ± 0.27 [a]	0.988
18.0	50	4.10 ± 0.01 [a]	0.991

As such, if the main objective of the pretreatment is to reduce the air-drying time, the pulsed UV light pretreatment would not be a proper technology to achieve this goal.

3.3. Vitamins and carotenoids content

The drying process decreased the content of vitamins and total carotenoids in mangoes. The retention of vitamins and total carotenoids depended on the vitamin, the use or not of pulsed UV light pretreatment and the intensity of the pretreatment.

Figure 3 presents the retention of vitamins and total carotenoids for non-pretreated mangoes subjected to air-drying. Total carotenoids content presented the lowest retention ratio (24.6

%), while vitamin B6 presented the highest retention ratio (97.7 %). The changes observed in Figure 3 represents the effect of heating in the vitamins and total carotenoid content.
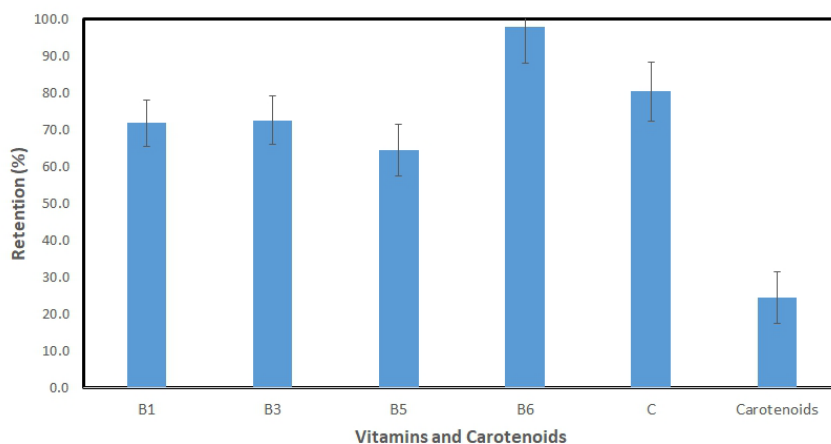
Figure 3. Retention of vitamins and carotenoids in mangoes after air-drying without UV pretreatment.

The pulsed UV light pretreatment showed a positive effect on vitamins B1, B3 and B5 when up to 7.2 J/cm2 where applied to the samples. Under such conditions, the dried product would present between 10.0 to 28.8 % more vitamins B1, B3 and B5 than the untreated dried product. Above the 7.2 J/cm2 level, the effect of the pretreatment is statistical non-significant (at a 95% confidence level), due to a probable degradation of these vitamins by UV light.

Vitamin B1 (thiamin) is the most thermolabile among the B vitamins, so degradation due to thermal effect was expected [8] and was confirmed by the experimental data. The effect of pulsed UV light seemed to be mainly positive and a trend of higher retention of vitamin was observed. The high energy of the pulsed light treatment may have broken the bound of the phosphorylated vitamin, changing it to its free and bioavailable form, thus resulting in a slightly higher content of this vitamin in the treated dried product.

The retention of vitamins B3 and B5 followed a similar trend. As with vitamin B1, the energy delivered by pulsed UV light might have broken the bound between the vitamin and its bounds, releasing an amount of vitamin that otherwise would be unavailable. This is plausible because vitamins, nucleotides and coenzymes absorbs UV energy and could use this energy to break the chemical bond between vitamins and nucleotides, and vitamins and coenzymes. The energy absorbed from pulsed UV light causes physical damages to membranes and other structures due to the release of chemical and physical bonds in these structures [9]. Thus, the same energy that is responsible for bond breaking damage in microorganisms can be responsible for the bond breaking reactions that release the bonded vitamins and transform it in free and bioavailable vitamins.

The pulsed UV light pretreatment had a significant negative effect on vitamin B6. The retention of vitamin B6 that was at 97.7 % for the dried untreated mango, dropped to retentions levels between 48 to 61 %. This vitamin is considered light-sensitive. As such, both UV light and visible light released by the pulses have degraded this vitamin resulting in a significant reduction in its content when the UV pretreatment was applied.

The UV pretreatment did not change significantly the amount of vitamin C in the dried product. The pretreatment was only statistically different (at a 95% level of confidence) when a fluence of 12 J/cm^2 was applied. Under this condition, the amount of vitamin C was 28.6 % higher than the untreated sample. Vitamin C is considered a light sensitive vitamin that present high UV light absorbance in the germicidal range (215 to 260 nm) but does not absorb significant light above 300 nm. The equipment used in our experiments releases light in a spectrum between 310 and 400 nm, thus it has not affected the vitamin C content of the mangoes samples.

The UV pretreatment increased the total carotenoids when a fluence up to 12 J/cm^2 was applied. Overexposure to high intensity UV light tended to degrade the carotenoids. The increase in the total carotenoid content can be attributed to an alteration of the carotenoid-binding protein with a consequent increase in availability of free carotenoids, which has been reported previously for mango juice subjected to UV light treatment [10].

4. Conclusions

Pulsed UV light decreased the initial moisture content of the mangoes samples but did not increase the effective water diffusion of mangoes nor reduced its drying time. The application of pulsed UV light increased the availability of vitamins B1, B3, and B5, vitamin C and carotenoids in the dried product. The light sensible vitamin B6 degraded significantly when compared to the untreated dried mango samples. Overexposure to pulsed UV light (dosages greater than 15 J/cm^2) degraded all vitamins and carotenoids, thus the UV dosage must be carefully optimized. Pulsed UV light can be a potential pretreatment for drying fruits given its simplicity, rapid application and because it confers better nutritional quality to dried mangoes.

Acknowledgements

References

[1] G.F.M. Ball, Vitamins in foods: analysis, bioavailability, and stability, CRC Press, Boca Raton, USA, 2006.

[2] T. Koutchma, I. Forney, C. Moraru, Ultraviolet light in food technology: principles and applications, CRS Press, Boca Raton, USA, 2009.

[3]   R. V. Tikekar, R.C. Anantheswaran, L.F. LaBorde, Ascorbic acid degradation in a model apple juice system and in apple juice during ultraviolet processing and storage, J. Food Sci. 76 (2011) 62–71.

[4]   T. Koutchma, UV light for processing foods, Ozone-Science Engeneering. 30 (2008) 93–98.

[5]   E. Cantos, C. Garcia-Viguera, S. Pascual-Teresa, F.A. Tomas-Barberan, Effect of postharvest ultraviolet radiation on resveratrol and other phenolics of cv. Napoleon table grapes, J. Agric. Food Chem. 48 (2000) 4606–4612.

[6]   J. Crank, The mathematics of diffusion, 2nd ed., Oxfort University Press, Glasgow, 1975.

[7]   F.A.N. Fernandes, S. Rodrigues, C.L. Law, A.S. Mujumdar, Drying of Exotic Tropical Fruits: A Comprehensive Review, Food Bioprocess Technol. 4 (2010) 163–185. doi:10.1007/s11947-010-0323-7.

[8]   K.T.H. Farrer, The thermal destruction of vitamin B1 in foods, Adv. Food Res. 6 (1955) 257–311.

[9]   K. Krishnamurthy, J.C. Tewari, J. Irudayaraj, A. Demirci, Microscopic and spectroscopic evaluation of inactivation of Staphylococcus aureus by pulsed UV light and infrared heating, Food Bioprocess Technol. 3 (2010) 93–104.

[10] V. Santhirasegaram, Z. Razali, D.S. George, C. Somasundram, Comparison of UV-C treatment and thermal pasteurization on quality of chokanan mango (Mangifera indica L.) juice, Food Bioprocess Technol. 94 (2015) 313–321.

Process intensification and process control in freeze-drying

Barresi, A. A.[*]; Pisano, R.

Department of Applied Science and Technology. Politecnico di Torino, Torino, Italy

*E-mail of the corresponding author: antonello.barresi@polito.it

Abstract

Widespread use of advanced process control allows reduction of costs, by reducing drying time and energy consumption. The "control of the freezing stage" (by forced nucleation) also appears to be beneficial to process intensification, as it can impact the product structure and modify the product resistance to mass transfer. An alternative way to increase the drying rate is the use of organic solvents as they can lead to larger solvent crystals, hence lower product resistance to vapor flow.

Atmospheric freeze-drying may be a good alternative to vacuum freeze-drying, as a way of increasing process efficiency. A further improvement can be obtained by combining atmospheric or vacuum freeze-drying with new technologies.

A further step towards process intensification is given by continuous plants, as this allows a dramatic increase in throughput and product quality uniformity.

Keywords: freeze-drying; process intensification; controlled nucleation; continuous process.

1. Introduction

The freeze-drying process is widely used in pharmaceuticals manufacturing, as well as for drying foodstuffs, as high-quality products can be obtained due to the low operating temperatures. Anyway it is quite an expensive process, and this fact limits applications in food and probiotic industry. Reduction of costs, by reducing drying time and energy consumption, and a better uniformity in end-product quality can be reached by means of process optimization and widespread use of advanced process control, but there is a big potential for process intensification by process modifications.

According to Stankiewicz and Moulijn [1], process intensification can be obtained by modifying equipment, to optimize critical parameters (e.g., heat transfer and mass transfer), or by process intensifying methods, changing the process or using alternative energy sources. Proposed control approaches, and in particular advanced process control, will be first discussed in this review. Other possibilities for process intensification will be then discussed, focusing in particular on controlled nucleation and process modifications in production of pharmaceuticals.

2. Process optimization and widespread use of advanced process control

Improvement of the process control has been recognized as a development need for the pharmaceutical industry over the last thirty years, but relatively few changes occurred at the production scale. It must be evidenced that today even the most advanced industrial freeze-dryers have no robust process control. An open-loop control approach is generally adopted, but rarely the cycle has been really optimized, and cycle transfer between different pieces of equipment or scale up is generally challenging [2-5].

Effective monitoring and control systems are required to manage the process in such a way that product quality is not jeopardized at the end of the process. Besides, as the duration of the freeze-drying process is an important concern, the control systems should be able to optimize in-line the operating conditions, namely the pressure in the drying chamber and the heating power, i.e. the temperature of the heating source. In the following different the methods proposed will be analyzed.

A first group of methods is based on the measurement of product temperature obtained through a thermocouple (or another temperature sensor); they optimize only the temperature of the heating element. In this case it is possible to use just the temperature measurement, with a fuzzy logic-based algorithm. Alternatively, a mathematical model can be coupled to the experimental measurements, thus obtaining a soft-sensor; this can be used

to calculate the optimal control actions using, for example, a PI algorithm, or calculating in line the design space of the process [6-8].

The second group of methods is based on the pressure rise test [9]; this is a technique for the in-line process identification that allows estimating both the state of the product (temperature and residual amount of ice) and the values of some model parameters. By this way a mathematical model can be used to optimize the process using, for example, a classic proportional algorithm, or an advanced Model Predictive Control algorithm [10,11]. Control logics based on measurement of heat or sublimation flux will be also discussed.

Control procedures are available also for the secondary drying step. The key feature of the method is the coupling of the measurement of the desorption rate, obtained by means of the PRT or other devices, with a mathematical model of the process [12].

3. Control of the freezing stage

Freezing plays a fundamental role in the freeze-drying process, as it determines product morphology and, therefore, drying performances and drug stability [13]. Therefore, it has become essential to increase the knowledge and control over this process. A brief overview of the tools which allow control of the impact of freezing on product morphology, and, consequently, on drying efficiency and product quality will be presented.

During freezing, the stochastic nature of nucleation is regarded as a demerit, because it is directly linked to vial-to-vial variability in terms of product morphology, drying behavior and, ultimately, product stability. Hence, lots of attention was given to the control of the temperature at which nucleation occurs, trying at least to make it as uniform as possible over a batch of vials. In fact, it is not actually possible to really "control the nucleation" even if this term is often used for simplicity; as said before, what is possible to do, is to force nucleation to take place at a given temperature and control the batch temperature holding it until nucleation is completed. The higher the nucleation temperature, the larger the ice crystal size, and thus the lower the cake resistance. In recent years, almost all the principal freeze-dryers manufacturers developed their proprietary technology to induce ice crystallization and to reduce the time span for completing the freezing in all the vials of the batch. Many patents were deposited, and different technical solutions were made commercially available, especially at the pilot-scale; even if many difficulties still limit somehow the application to large production scales of some methods, controlled ice nucleation starts moving also into manufacturing [14,15].

Ultrasound nucleation has been the object of an extensive research, but the passage from lab to commercial scale faced strong difficulties. The main problems were related to the difficulty to efficiently propagate the ultrasonic waves, and to scale the process, as the

optimum ultrasonic frequency depends on the set up. Actually commercially available equipment adopts either a variant of the ice fog, or the depressurization method, or the vacuum induced nucleation. The ice fog concept is probably the first method proposed to control nucleation (as it is known since 1990), but only recently the technical developments made it really suitable for practical applications.

The easiest and cheapest way to control nucleation is surely the vacuum induced surface freezing, VISF (also known as vacuum induced nucleation, VIN), as this technology requires no hardware, any equipment can be easily retrofitted, and there are limited sterility concerns (related to sterilization of large valves required for rapid depressurization) [16]. It is important to evidence that notwithstanding the concern for possible product denaturation, in particular with the depressurization and the VIN method (for the possible presence of small bubbles), all the discussed controlled nucleation technologies gave particularly good results; in fact, as a consequence of the larger ice crystals (and thus of their reduced solid surface), an improved stability even for very sensitive products was observed.

Thus the described methods are effective approaches to process intensification, but to guarantee the required final quality and uniformity of the batch, they must be coupled with methods that assure the temperature uniformity of all the vials. In all cases, the depressurization rate is the element that may limit the applicability to large units, as it poses constrains to the geometric characteristics of the apparatus and of the depressurization circuit.

4. Process modifications

The use of a strictly organic or organic/water system is beneficial to both product quality and process optimization. Potential advantages and disadvantages of use of organic solvents and cosolvents (mixed with water, that up to now has been the most common solvent used) in freeze-drying are widely discussed by Teagarden and Baker [17]. The main advantage in addition to the increase in solubility of the product, is the increase in rate of sublimation and hence decrease of drying time. However, before a specific solvent is used in the manufacture of a parenteral product, lyophilization professionals have to carefully weigh advantages and disadvantages.

The use of organic liquids, either as solvent or co-solvent, produces larger ice crystals and, thus, increases the average diameter of the pores created during ice sublimation. As a result, the product resistance to vapor flow decreases and, if product temperature does not change, the rate of sublimation increases, as said above. In addition to the reduction in product resistance, most of the cosolvents used in freeze-drying applications increase the rate of sublimation because they have a higher vapor pressure than water and, hence, they increase the driving force for mass transfer. In addition, a further reduction in energy consumption

results from the fact that the sublimation enthalpy of organic solvents is smaller than that of water ice. Unfortunately, organic solvents are rarely used in the manufacture of a lyophilized pharmaceutical product, mainly because of safety concerns. Specifically, attention has to be paid to how the organic solvents can be safely handled, e.g., preventing fires or explosions during their manipulation or avoiding contamination of the vacuum pump oil, which can decrease the pump efficiency and, hence, impede adequate control of pressure inside the equipment. Furthermore, in the case of mixture of solvents, monitoring the state of progress of drying might be very complex, because the various solvents can show significantly different rates of sublimation. Therefore, it is necessary to track the separation of the individual solvents, e.g., using sensors that are sensitive to only specific solvents and completely insensitive to others [18].

In food processing, vacuum freeze-drying produces dried products that retain almost all their original characteristics, e.g. color, flavor, and taste. The high specific surface area generally allows an easy and fast rehydratation. The drawback is represented by the cost of the operation: fixed costs can be high due to vacuum requirement, and the energy cost can be significantly higher with respect to other drying processes (the specific moisture extraction rate in a vacuum freeze-drying process is in the range of 0.4 kg of water per kWh). In order to reduce the cost and the energy consumption of the process, thus improving its sustainability, the atmospheric freeze-drying (drying with cold air or nitrogen at normal pressure) has been proposed [19,20]: in this case it is possible to achieve a specific moisture extraction rate ranging from 1.5 to 4.6 kg of water per kWh. For example it has been claimed that up to 35% of energy savings could be achieved when using atmospheric freeze-drying instead of vacuum freeze-drying for potato slices.

Most of the literature deals with atmospheric freeze-drying in fluidized bed dryers and in spray freeze-dryers. When the atmospheric freeze-drying is carried out in a fluidized bed it can take advantage of the high values of the heat and mass transfer coefficients; the product has to be frozen and granulated before drying. A drawback of the process is represented by the size reduction caused by mechanical cracking. As an alternative it is possible to carry out the process in a tunnel dryer, even if the heat and mass transfer is not so good.

A detailed comparison of vacuum and atmospheric freeze-drying has not been carried yet, and work is currently ongoing also in the labs at Politecnico di Torino. Surely drawbacks related to the limitation in process temperature, to avoid ice melting, and the necessity to recirculate and dry large volumes of gas at low temperature must be taken into account. In particular, atmospheric freeze-drying produces higher quality products (in comparison to traditional drying) but still entails long drying times. Energy consumption can be reduced by new technologies which use alternative forms and sources of energy for processing. These technologies can be applied to either enhance heat transfer between product and heat source, such as microwave, radiofrequency and infrared radiation, or simply intensify the rate of dehydration without increasing the amount of heat supplied to the product, e.g. by

using high intensity sonic and ultrasonic waves.

Spray freeze-drying seems to be a valuable alternative to produce a free-flowing powder, with high surface area, porous end product, and good instant characteristics, with enhanced solubility and a uniform and ultrafine particle size. Spray freeze-drying into liquids, gases (e.g. a refrigerated air stream), and into gases over a fluidized bed have been reported in the literature. This technology has also a good potential for continuous processes. Spray freeze-drying allows the massive production of pharmaceuticals for dry powder inhalation, and a more precise control of particle size compared to spray drying. Furthermore, the rapid cooling rates promote the formation of glassy water that is beneficial in preventing the aggregation of proteins during the cryo-concentration phase.

5. Continuous plants

Recently, many pharmaceutical manufacturers are trying to convert their processes in favor of continuous production. To achieve this objective, it is necessary to integrate those production steps, that are performed sequentially in a conventional batch configuration, in a continuous process, leading to more compact units with a higher degree of automation and fewer manual interventions. This is particularly true for the lyophilization of pharmaceuticals and biopharmaceuticals in unit-doses which, although it is a robust and well-established technology, still remains inefficient and expensive. For example, the drying behavior within a batch, as well as from batch to batch, is still a problem of deep concern, despite the elaborate equipment design and the sophisticated control systems recently introduced.

It must be noted that continuous freeze-drying find currently application mainly for soluble coffee production. Many patents have been deposited for food technology applications, but realizations are still very limited. In the pharmaceutical industry there are much more severe constrains, and just a relatively few patents have been deposited. In particular, so far, only two technologies have been proposed for the production of end-to-use lyophilized products in a continuous way [21,22]. In both technologies, processing time and equipment size is dramatically reduced, up to 10 times, and all manual interventions and breaks have been minimized reducing the risk of product contamination. Furthermore, in-line control can easily be implemented, and scale-up simply consists of adding parallel modules. Despite their numerous advantages, the application of these technologies to real cases in industry still requires time. The above proposed technologies are still in development, and their capability to work under GMP conditions, meeting all the stringent requirements of a pharmaceutical production, has not been completely demonstrated yet. Nevertheless, these solutions are concrete steps toward continuous manufacturing of lyophilized pharmaceuticals, similarly to what food industry did years ago.

6. Conclusions

Different approaches to process intensification, coupled with improved process control for freeze-drying have been discussed. In the last years, many progress have been carried out in process monitoring and control, including the control of the freezing step. Current research should favor the transition towards a more robust design of freeze-drying cycles, based on deep knowledge of phenomena involved rather than on empirical observations. This would be extremely beneficial, especially for the pharmaceutical industry, where particular emphasis is placed on product homogeneity and process control. Process modifications, like atmospheric freeze drying and spray-freeze drying are interesting alternatives whose real potentiality are currently under investigation. The most ambitious goal is certainly the realization of a continuous process at the industrial scale for pharmaceuticals.

The intensification of the process and the reduction of the processing costs, on the other way, may open new possibilities of wider application of freeze drying in processing of valuable foods and in particular of probiotics, for which the market is requiring higher qualitative standards.

7. References

[1] Stankiewicz, A.J.; Moulijn, J.A. Process intensification: Transforming chemical engineering. Chemical Engineering Progress 2000, 96, 22-34.

[2] Nail, S.; Gatlin, L.A. 1985. Advances in control of production freeze dryers. PDA Journal 1985, 39 (1), 16-27.

[3] Liapis, A. I., Pikal, M. J. Bruttini, R. Research and development needs and opportunities in freeze drying. Drying Technology 1996, 14 (6), 1265-1300.

[4] Sadikoglu, H.; Ozdemir, M.; Seker, M. Freeze-drying of pharmaceutical products: Research and development needs. Drying Technology 2006, 24, 849-861.

[5] Fissore, D.; Pisano, R.; Barresi, A.A. A model based framework to optimize pharmaceuticals freeze-drying. Drying Techno*logy* 2012, 30, 946-958.

[6] Fissore, D.; Pisano, R.; Barresi, A.A. On the use of temperature measurement to monitor a freeze-drying cycle for pharmaceuticals. In Proceedings of IEEE International Instrumentation and Measurements Technology Conference "I2MTC 2017", Torino, Italy, May 22-25, 2017; 1276-1281.

[7] Bosca, S.; Barresi, A.A; Fissore, D. On the use of model-based tools to optimize in-line a pharmaceuticals freeze-drying process. Drying Technology 2016, 34 (15), 1831-1842.

[8] Bosca, S.; Barresi, A.A.; Fissore, D. On the robustness of the soft-sensors used to monitor a vial freeze-drying process. Drying Technology 2017, 35 (9), 1085-1097.

[9]   Fissore, D.; Pisano, R.; Barresi, A.A. On the methods based on the Pressure Rise Test for monitoring a freeze-drying process. Drying Technology 2011, 29 (1), 73-90.

[10]   Pisano, R.; Fissore, D.; Barresi, A.A. Freeze-drying cycle optimization using Model Predictive Control techniques. Industrial &. Engineering Chemistry Research 2011, 50 (12), 7363-7379.

[11] Pisano, R.; Fissore, D.; Barresi A.A. In-line and off-line optimization of freeze-drying cycles for pharmaceutical products. Drying Technology 2013, 31 (8), 905-919.

[12]   Fissore, D.; Pisano R.; Barresi, A.A. Monitoring of the secondary drying in freeze-drying of pharmaceuticals. Journal of Pharmaceutical Science 2011, 100 (2), 732-742.

[13]   Kasper, J.C.; Friess, W.F. The freezing step in lyophilization: Physico-chemical fundamentals, freezing methods and consequences on process performance and quality attributes of biopharmaceuticals. European Journal of Pharmaceutics and Biopharmaceutics 2011, 78 (2), 248-263.

[14]   Thomas, P. Controlled ice nucleation moves into manufacturing. Pharmaceutical Manufacturing 2011, article 20.

[15]   Geidobler, R.; Winter, G. Controlled ice nucleation in the field of freeze-drying: Fundamentals and technology review. European Journal of Pharmaceutics and Biopharmaceutics 2013, 85 (2), 214-222.

[16]   Arsiccio, A.; Oddone, I.; Barresi, A.A.; Van Bockstal, P.-J.; De Beer, T. Vacuum Induced Surface Freezing as an effective method for improved inter- and intra-vial product homogeneity. European Journal of Pharmaceutics and Biopharmaceutics 2018 (in press). DOI: 10.1016/j.ejpb.2018.04.002

[17]   Teagarden, D. L.; Baker, D. S. Practical aspects of lyophilization using non-aqueous co-solvent systems. European Journal of Pharmaceutical Science 2002, 15 (2), 115-133.

[18]   Fissore, D.; Pisano, R.; Barresi, A.A. Process analytical technology for monitoring pharmaceuticals freeze-drying – A comprehensive review. Drying Technology 2018 (in press). DOI: 10.1080/07373937.2018.1440590

[19]   Claussen, I.C.; Ustad, T.S.; Strømmen, I.; Walde, P.M. Atmospheric freeze drying − A review. Drying Technology 2007, 25 (6), 957-967.

[20]   Fissore, D.; Coletto, M.; Barresi A.A. Atmospheric food freeze-drying: Challenges and opportunities. New Food 2013, 16 (5), 11-14.

[21]   Corver, J.A.W.M. Method and system for freeze-drying injectable compositions, in particular pharmaceutical compositions. US Patent 20140215845, 2012.

[22]   Pisano, R.; Capozzi, L.C.; Trout, B.L. Continuous freeze-drying and its relevance to the pharma/biotech industry. In Integrated Continuous Biomanufacturing III, Farid S. Alves P., Warikoo V. (eds.), ECI Symposium Series, 2017. http://dc.engconfintl.org/biomanufact_iii/70

Supercritical CO₂ drying of food matrices

Zambon, A.[a,b]; Vizzotto, T. M.[a]; Morbiato, G.[a]; Toffoletto, M.[b]; Poloniato, G.[c]; Dall'Acqua, S.[c]; De Bernard, M.[b]; Spilimbergo, S.[a*]

[a]Department of Industrial Engineering, University of Padova, via Marzolo 9, 35131 Padova, Italy
[b]Department of Biological Science, University of Padova, Via XXX, 35131 Padova, Italy
[c]Department of Pharmaceutical and Pharmacological Science, University of Padova, Via Marzolo 5, 35131 Padova, Italy

*E-mail of the corresponding author: sara.spilimbergo@unipd.it

Abstract

This work explore the use of supercritical CO2 drying as alternative technique for the obtainment of pasteurized and high quality dried product. Several tests were conducted on animal, vegetable and fruit matrixes in order to investigate the effectiveness of SC-CO2 drying process at different process conditions. Design of experiment was performed to find the optimal process conditions for vegetable and fruit matrices, using the final water activity of the products as key indicator for the drying efficiency. The inactivation of naturally present microorganisms and inoculated pathogens demonstrated the capability of SC-CO2 drying process to assure a safe product. Moreover, retention of nutrients was compared with conventional drying methods. Results suggest that supercritical drying is a promising alternative technology for food drying.

Keywords: supercritical drying; carbon dioxide; food drying; microbial inactivation

1. Introduction

Fresh food products, in particular ripped fruits and vegetables, are rich sources of nutrients with an important role in human health [1]. However, fresh products are seasonal and an optimal cold chain is needed to prolong their limited shelf life.

An alternative is represented by food dehydration, which is one of the oldest and widely used processes for the long-term maintenance of food products. By reducing the amount of moisture, the microbial and enzymatic activities are inhibited, promoting the extension of the product's shelf-life [2,3]. Conventional hot air-drying is one of the most commonly used dehydration process in food industry. Nevertheless the overall quality of the final product is often reduced by the combination of high temperatures and the presence of oxygen which promotes physical, structural, chemical and nutritional changes [4,5]. Higher retention of those compounds can be achieved using freeze-drying technology [6], however it is an expensive and very slow process, making it suitable only for high value foods [3,7].

Recently the use of carbon dioxide at supercritical conditions (Sc-CO_2) has been investigated as alternative drying food process, specifically for carrots [8], basil [9], mango and persimmon [10] and coriander [11], demonstrating to be a promising process for the retention of the original structure and the preservation of the most valuable compounds.

Within Sc-CO_2 drying the vapour-liquid interface can be avoided meaning that the water is removed as a liquid dissolved in the supercritical fluid. The result is a minor capillary stress for the product, which allows a better preservation of the original structure. Moreover, the critical point, and consequently the critical temperature (31.1°C), is low, which allows to operate at lower temperatures than conventional air drying, helping the prevention of the heat sensitive degradation's reactions and thus giving a final product with higher quality [8,9]. Sc-CO_2 have been largely investigated as alternative food pasteurization at low temperature [12] because it is able to inactivate microorganisms and enzymes.

The present work explore the use of Sc-CO_2 for drying and simultaneous pasteurization of foodstuff. The influence of process parameters (temperature, pressure, flow rate and treatment time) on the final water activity were studied within a Box Behnken Design method. Overall the results demonstate the possibility to obtain a high quality product microbiologically safe.

2. Materials and Methods

2.1 Sample preparation

Different types of food products were daily bought in the local market in Padua (Italy): red bell peppers (*Capsicum annuum, L.*), coriander (*Coriandrum sativum*), strawberry (*Fragaria ananassa*), apple (*Golden delicious*) and chicken breast fillet. The vegetables were cut into slices while coriander leaves were removed from the stem. The chicken breast fillet was cut into small cubes with a weigh of approximately 1g.

2.2 Sc-CO₂ drying apparatus and procedure

The high pressure carbon dioxide apparatus consists of a sapphire high pressure visualization cell (Separex S.A.S., Champigneulles, France) with an internal volume of 50 mL designed to withstand up to 400 bar and 100 °C. The plant includes a CO_2 tank, kept at room temperature, a chiller reservoir (M418-BC MPM Instruments, Milan, Italy), a HPLC pump (307 Gilson, Milan, Italy), and a thermostatic water bath (ME-Julabo, Seelbach, Germany) to keep the vessel at the desired temperature. Further details of the reactor and drying procedure are reported elsewhere [11,13]. Experiments were carried out between 40/60°C and 100/140 bar up to 16 hours of drying for red peppers, while 40°C and 100 bar were chosen for the other food products.

2.3 Experimental design

The Box Behnken Design was used to study the effect of supercritical CO_2 drying process parameters on the final water activity of treated red peppers. To quantify the relationship between the controlled input and the accomplished responses, a second order regression model was used. All the calculations were done using Minitab®.

2.4 Physical and chemical analysis

Water activity was measured (Hygropalm Rotronic, Bassersdorf, Switzerland) at the end of the process. Samples were weighted before (W_{start}) and after (W_{end}) the treatment and the weight loss in terms of percentage ΔW was calculated as (W_{start}-W_{end})/W_{start}. Chemical characterization was performed for flavonoids as previously described [11]. For all the HPLC analysis an Agilent 1260 system equipped with Diode array (126 series) and Ion trap Mass spectrometer (Varian/Agilent MS500) were used. For vitamin C 200 mg of grinded powder plant material were xtracted three times for 10 minutes in an ultrasound bath with 8 ml of solution composed of water with 1% (v/v) formic acid. Zorbax SB C3 4.6x 150mm (DTO Servizi, Spinea, Italy) was used for the stationary phase. Isocratic conditions of elution used two solutions: solution A was acetonitrile while solution B was water 1% formic acid. For the quantification, standard solutions of ascorbic acid (Sigma Aldrich, Milano, Italy) were used to build up a calibration curve in the range 3-120 ug/mL.

2.5 Microbial analysis

Mesophilic bacteria, mesophilic bacterial spores and yeasts and molds were counted before and after the treatments by means of the standard plate count technique, as previously described [11]. Breefly, mesophilic bacteria and spores were cultured using total plate count agar (Microbial Diagnostici, Catania, Italy) at 30°C within pour plate, while yeasts and molds were cultured with DRBC agar (Bitec S.r.l., Grosseto, Italy) supplemented with chloramphenicol at 22°C within spread plate. For the enumeration of mesophilic spores, the first dilution tubes were inserted in a thermostatic bath at 80°C for 10 min before plating. The incubation time for mesophilic bacteria and spores was 72 h, while 72-120 h for yeast and

molds. The enumeration was referred to the weight of initial fresh product and expressed in CFU/g. Reductions are expressed as $\log(N_0/N)$ where N_0 was the number of initial microorganisms in the untreated sample and N the number of viable microorganisms after the treatment, in CFU/g of fresh product. The limit of quantification was set to 200 CFU/g for the mesophilic bacteria and mesophilic bacterial spores, 2000 CFU/g for yeast and molds while the limit of detection was < 10 CFU/g < 100 CFU/g respectively. Experiments with inoculated pathogens (*E.coli, Salmonella* and *Listeria monocytogenes*) were performed on coriander, apple slices and strawberry slices following the protocol by Bordeaux et al [14]. Results were analyzed with one-way analysis of variance to compare effects of the different treatments with significance at $\alpha = 0.05$.

3. Results and Discussion

The drying kinetics, in terms of water activity and weight loss, were determined by increasing the drying time till a complete water removal. Figure 1 shows the water loss and water activity obtained during the drying of the red pepper. Similar behaviours were observed for the others food samples (data not shown).
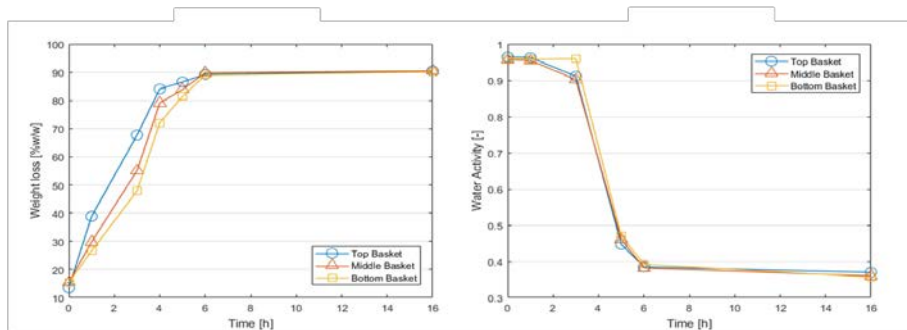
Fig. 1.

Water loss (left) amd water activity (right)at different drying times for red pepper. Data are reffered to three different hights of the reactors. Experiments were carried out at 40°C, 100bars and 150kg/h flow rate.

The response surface methodology was chosen to quantify the relationship between the controllable input parameters and the obtained response surfaces, in order to find the influence of the process conditions over the product quality. Fig 2 shows results obtained at 40°C and 16 hours drying that highlight the influence of pressure and pump frequency on the final water activity of the sample. Response surface analysis on strawberry demonstrated a similar behavior (data not shown). To demonstrate the capability of the technology to retain the active components of the fresh products, some chemical analyses were performed on the Sc-CO₂ dried product.

Zambon, A.; Vizzotto, T. M.; Morbiato, G.; Toffoletto, M.; Poloniato, G.; Dall'Acqua, S.; De Bernard, M.; Spilimbergo, S.
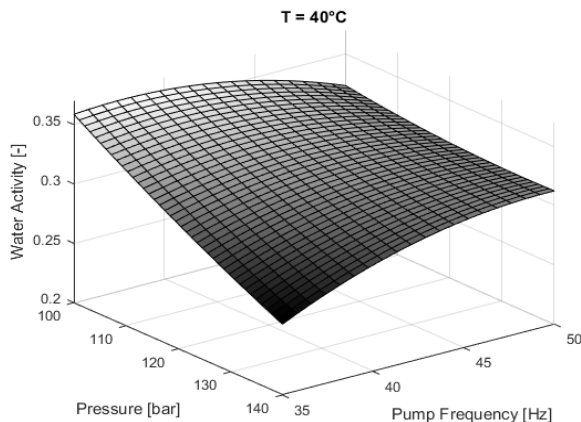
Fig. 2. Response surface for the water activity at 40°C and 16h drying as function of Pressure and Pump frequency.

For red pepper, the amount of flavonoids obtained was about 880 mg/100g of dried sample, reported in Table 1, are consistent with the literature; for instance Deepa et al. (2007) [1] reported phenolics in the range of 20–40 mg/100g of fresh product, which is similar to our results considering a loss of weight of 90% compared to the fresh product.

Table 1. Flavonoid and ascorbic acid content in dried red pepper (40°C. 100bar, 100kg/h flow rate)

Flavonoid [mg/100 g dry product]	Ascorbic acid [mg/100g dry product]
880.45 ± 2.4	1163.20 ± 5.3

The average content of ascorbic acid in fresh bell pepper is in the range of 64-220mg/100g of fresh product [1, 15]. As for flavonoids, we measured a higher content of ascorbic acid after Sc-CO_2 drying compared to the fresh product; the data can be explained with an apparent concentration of micronutrients caused by water removal during the process. Considering a water loss of about 90%, data of dried and fresh products are comparable and we can assert that SC-CO_2 drying technique is able to preserve the ascorbic acid content in the red pepper.

Microbiological inactivation was demonstrated on coriander, apple, strawberry and chiken breast fillet for the natural flora and specific pathogens (data not shown). Supercritical drying was able to complete inactivate yeasts and molds in all the samples considered; as regards bacteria, only the most sensitive mesophilia were inactivated on fruits, while a complete inactivation was possible on chicken. *E.coli, Salmonella* and *Lysteria monocytogen* were completely inactivate in all the food samples up to 8 log reduction.

4. Conclusions

Overall the results highlighted the potential of Sc-CO₂ drying technology to obtain a safe and dried products with unaltered nutritional value.

5. Acknowledgements

6. References

[1] Deepa, N., Kaur, C., George, B., Singh, B., Kapoor, H.C. (2007). Antioxidant constituents in some sweet pepper (Capiscum annum L.) genotypes during maturity, LWT-Food Science Technology, 40, 121-129.

[2] Di Scala, K., Crapiste, G. (2008). Drying kinetics and quality changes during drying of red pepper, LWT-Food Science Technology, 41, 789-795.

[3] Sagar, V.R., Suresj Kumar, P. (2010). Recent advances in drying and dehydration of fruits and vegetables: a review, Journal of Food Science and Technology, 47(1), 15-26.

[4] Vega-Gálvez, A., Di Scala, K., Rodríguez, K., Lemus-Mondaca, R., Miranda, M., López, J., Perez-Won, M. (2001). Effect of air-drying temperature on physico-chemical properties, antioxidant capacity, colour and total phenolic content of red pepper (Capsicum annuum, L. var. Hungarian), Food Chemistry, 81, 1580-1585.

[5] Wojdyło, A., Figiel, A., Lech, K., Nowicka, P., Oszmiański, J. (2014) Effect of Convective and Vacuum–Microwave Drying on the Bioactive Compounds, Color, and Antioxidant Capacity of Sour Cherries, Food and Bioprocess Technology, 7, 829-841.

[6] Barbosa, J., Borges, S., Amorim, M., Pereira, M.J., Oliveira, A., Pintado, M.E., Teixeira, P. (2015). Comparison of spray drying, freeze drying and convective hot air drying for the production of a probiotic orange powder, Journal of Functional Foods, 17, 340-351.

[7] Ratti, C. (2001). Hot air freeze-drying of high-value foods: a review, Journal of Food Engineering, 49, 311-319.

[8] Brown, Z.K., Fryer, P.J., Norton, I.T., Bakalis, S., Bridson, R.H. (2008). Drying of foods using supercritical carbon dioxide — Investigations with carrot, Innovative Food Science and Emerging Technologies, 9, 280-289.

[9] Bušić, A., Vojvodić, A., Komes, D., Akkermans, C., Belščak-Cvitanović, A., Stolk, M., Hofland, G. (2007). Comparative evaluation of CO2 drying as an alternative drying technique of basil (Ocimum basilicum L.) — The effect on bioactive and sensory properties, LWT-Food Science Technology, 40, 121-129.

[10] Braeuer, A.S., Schuster, J.J., Gebrekidan, M.T., Bahr, L., Michelino, F., Zambon, A., Spilimbergo, S. (2017). In Situ Raman Analysis of CO2—Assisted Drying of Fruit-Slices, Foods, 37(6), 1-11.

[11] Zambon, Alessandro, et al. "Microbial inactivation efficiency of supercritical CO2 drying process." Drying Technology (2018): 1-6.

[12] Spilimbergo, S., Matthews, M. A., & Zambon, A. (2018). Supercritical Fluid Pasteurization and Food Safety. In Alternatives to Conventional Food Processing (pp. 153-195).

[13] Zambon, A.; Vetralla, M.; Urbani, L.; Pantano, M.F.; Ferrentino, G.; Pozzobon, M.; Pugno, N.M; De Coppi, P., Elvassore, N.; Spilimbergo, S. Dry acellular oesophageal matrix prepared by supercritical carbon dioxide."The Journal of Supercritical Fluids, 2016, 115: 33-41.

[14] Bourdoux, Siméon, et al. "Inactivation of Salmonella, Listeria monocytogenes and Escherichia coli O157: H7 inoculated on coriander by freeze-drying and supercritical CO2 drying." Innovative Food Science & Emerging Technologies 47 (2018): 180-186.

[15] Chávez-Mendoza, C., Sánchez, E., Carvajal-Millán, E., Muñoz-Márquez, E., Guevara-Aguilar, A. (2013). Characterization of the Nutraceutical Quality and Antioxidant Activity in Bell Pepper in Response to Grafting, Molecules, 18, 15689-15703.

Ultrasound enhancement of osmotic dehydration and drying - Process kinetics and quality aspects

Musielak, G.

Institute of Technology and Chemical Engineering. Poznań University of Technology, Poznań, Poland

E-mail of the corresponding author: grzegorz.musielak@put.poznan.pl

Abstract

The aim of presented studies is to investigate of influence of ultrasonic assistance on both osmotic dehydration and convective drying. A wide range of different materials, as well as several osmotic agents were tested.

The obtained results show that the use of ultrasound always accelerates the investigated processes. The application of ultrasound may reduce the energy consumption of drying. Qualitative studies of dried materials do not give a definite answer about the effect of ultrasound on the quality of the products. Mathematical modelling of the ultrasound assisted drying indicates that so named "vibration effect" plays the biggest role in convective drying acceleration.

Keywords: osmotic dehydration; convective drying; ultrasound; process kinetics.

1. Introduction

Drying is one of the food preservation methods. The convective drying is the most commonly used technique. Unfortunately the method is slow and energy-consuming. Therefore, various methods to shorten the duration of the process and improve its energetical efficiency are investigated. One of the possibilities is the use of osmotic dehydratation as drying pretreatment. During the last two decades a great interest is directed to ultrasonic assistance of both osmotic dehydratation [1] and connective drying [1,2]. Also in the Department of Process Engineering, Poznan University of Technology, research in this area has been conducted for several years. The aim of this paper is to present a review of these research.

2. Materials and methods

2.1. Tested materials

A wide collection of various materials has been tested in the work of our team. Most of them are fruits and vegetables: apples [3-11], cherries [12], strawberries [9,13], raspberries [5,14], apricots [16] , carrots [9,17-21], green pepper [22], red pepper [11], potatoes [23], beetroot [24], onion [10]. In addition, kaolin was also tested [11,20].

2.2. Osmotic dehydratation – method

The simple osmotic dehydration and ultrasound assisted dehydratation (frequency 25 kHz) were tested to get the effect of ultrasound on the process kinetics and product quality. Aqueous solutions of glucose [12], fructose [6,17,19] and d-sorbitol [6] as working fluids were used. Kinetics and effectiveness of osmotic dehydratation were assessed on the basis of solid gain (*SG*), water loss (*WL*) and osmotic dehydratation rate (*ODR*):

$$\text{SG} = \frac{m_{st}-m_{si}}{m_i}, \quad WL = \frac{m_i-m_t}{m_i} + SG, \quad ODR = \frac{dm_t}{dt} \tag{1}$$

where m_{st}, m_{si} are masses of solid matter of osmotically dehydrated and fresh sample, respectively and m_i, m_t are the initial and actual mass of sample, respectively.

2.3. Drying – methods

Several different dryers were used in the research. The laboratory chamber dryer was used for simple convective drying after osmotic dehydration [12,17]. Hybrid drying (convective – microwave – radiative) after osmotic dehydratation was performed in prototype laboratory hybrid dryer [19]. All ultrasound assisted drying processes were carried out in one of two hybrid (convective – microwave – ultrasonic) laboratory dryers: cabinet dryer [3-5,7,8,10,11,13-16,18,20,22-24] and rotary dryer [6,9,21,24]. The influence of ultrasound assistance on convective drying [3-11,13-16,20-24] and on convective - microwave hybrid drying [11,13-16,18,19,21,22,24] was investigated. Continuous drying processes were studied in all papers, while in some works the intermitten drying was examined [2,11,12,15-17,20,24]. The samples mass and their temperature were measured continuously during

experiment. The moisture ratio $MR = (m_t - m_{eq})/(m_0 - m_{eq})$ as a function of drying time represents drying kinetics, where m_t, m_0 and m_{eq} are the instantaneous (for a given time of the process), initial and equilibrium sample mass, respectively.

Energy consumption was measured for the whole drying system with the electricity meter.

2.4. Quality assesment – methods

It is important to ensure the quality of the dried product. The basic parameters describing quality were: color change during drying (important from the consumer point of view) and water activity (responsible for durability of food).

The preservation of nutrients during the drying process is extremely important from the point of view of the food's value of the product. Retention of several nutrients were measured.

The dried product ability to irrigation was measured in rehydratation tests. Texture of dried apple was determined by compression tests with the acoustic emission measurement. Change of plant tissue microstructure (onion and apple) was observed.

3. Experimental results

3.1. Osmotic dehydratation

Osmotic dehydratation could be treated as predrying process. During simple osmotic dehydratation water loss (*WL*) ranged between 18% [12] to 51% [17] and solid gain (*SG*) ranged between 8% [17] to 12% [6,17]. The use of ultrasound to intensify the process caused *WL* increase by 14% [17] to 44% [19] and *SG* increase by 15% [17] to 45% [6]. It was also shown that osmotic dehydratation rate (*ODR*) increased [19].

After osmotic dehydratation, the samples were dried. Then the water activity and the color change of the samples were examined. The results of these tests indicate that the effect of ultrasound application on final water activity is negligible. The color change results are ambiguous. In works [12,17] a reduction in color change was obtained due to the use of ultrasound. On the other hand, the works [6,19] indicate an increase of this parameter

3.2. Drying

3.2.1. Drying kinetics and energetic effectiveness

Drying kinetics is described by drying curves (moisture ratio *MR* versus time) and temperature evolution. Figure 1 shows the results of convective drying (CV), convective-microwave drying (CVMV) and both methods ultrasound assisted (CVUS and CVUSMV, respectively). After the shortcut specifying the method (MV and US) the used power in watts was written. The use of ultrasounds during drying results in the process acceleration and in a slight increase in the temperature of the dried material. A clear acceleration in convective drying was obtained, while convective-microwave drying was only slightly accelerated.

Ultrasonic assistance of convective drying shortened the drying process from 11% [5] to 60% [15]. This shortening of drying time resulted in a reduction of total energy consumption from 9% [3] to 21% [14]. A slight acceleration of the convective-microwave drying process was associated with an increase in energy consumption.
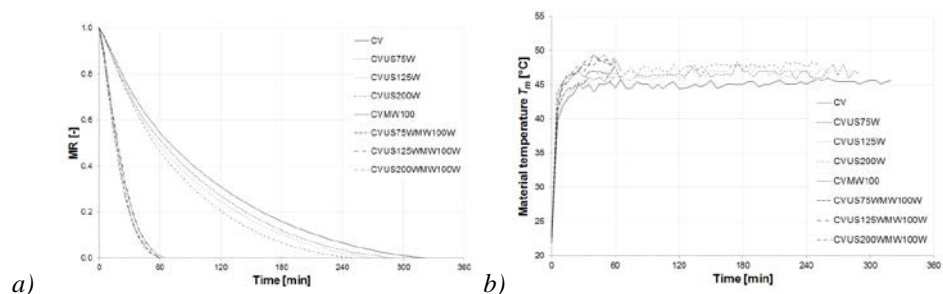
Fig. 1. Drying kinetics of carrots: a) drying curves; b) temperature of dried material [18]

3.2.2. Products quality

The use of ultrasound in each case resulted in a reduction in the color change. This reduction ranged between 12% [21,23] and 40% [13,18].

All studies indicate no impact of ultrasound on water activity. This parameter depends primarily on the final moisture content in the material, regardless of the drying method used.

Rehydratation ratio is defined as ratio of sample mass after rehydratation to initial sample mass (fresh material). Ultrasound application improved rehydratatin ratio from 14% [23] to 21% [16, 22]. This means that the use of ultrasound improves the internal structure.

The retention of vitamin C was improved due to ultrasound assistance (from 44% to 69% in green pepper [22] and from 68% to 70% in red pepper [11]). The obtained results regarding retention of phenolic compounds in carrot [18] are inconclusive. The use of ultrasound of low power caused a reduction in the phenolic compounds content while ultrasound of high power caused an increase in the content. The retention of carotenoids was improved due to ultrasound assistance (from 73,5% to 90% in carrot [18] and from 67% to 76% in red pepper [11]). The retention of betanin in red beetroot was improved from 27% to 33% [24]. The retention of anthocyanins in raspberries [11,15] was improved from 56% to 76%. Antioxidant activity of carrot [18] deteriorated due to the use of ultrasound. The activity decrease ranged between 13% to 33% (depending on US power) compared to simple convective drying.

Ultrasound assistance influenced changes in material texture [5]. Generally streght and Young modulus of material increased due to ultrasound application. Ultrasound dried crisps were more brittle although less crispy that convective dried ones.

The effect of ultrasound on the material structure was examined using an optical microscope [4, 10]. The application of ultrasound caused the increase of pore dimentions, the creation of microchannels and disruption of the tissue. These results were confirmed by SEM photographs of convective and ultrasound-convective dried apple [10].

4. Modeling of US assisted drying

4.1. Lumped capacities model

The lumped capacities model was proposed [3,25] to describe drying kinetics. The final system of coupled ordinary differential equations is as follows:

$$m_s \frac{dX}{dt} = -A_m h_m \ln \frac{\varphi|_{\partial B} p_{vs}(T_m)}{\varphi_a p_{vs}(T_a)} \tag{2}$$

$$m_s \frac{d}{dt}[(c_s + c_l X)T_m] = A_T h_T (T_a - T_m) - A_m l h_m \ln \frac{\varphi|_{\partial B} p_{vs}(T_m)}{\varphi_a p_{vs}(T_a)} + \Delta Q \tag{3}$$

where: A_m, A_T denote surfaces of mass and heat exchange, respectively; h_m, h_T – coefficients of mass and heat exchange, respectively; $\varphi_a, \varphi_{\partial B}$ – relative drying air humidity far and near dry material surface, respectively; p_{vs} – saturated vapor partial pressure (temperature dependent); c_s, c_l – specific heat of a solid and liquid, respectively; l – latent heat of evaporation; ΔQ – volumetric heat source describing ultrasound absorption.
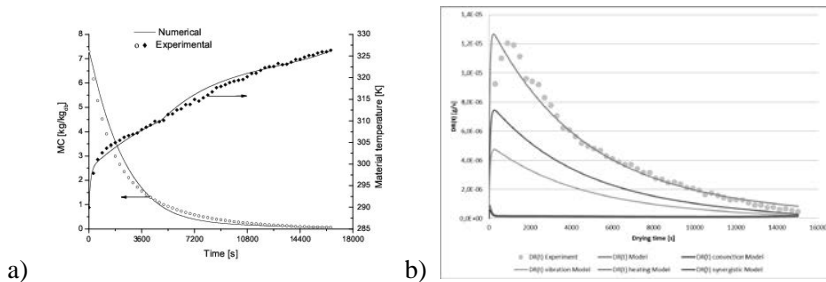
Fig. 2. Drying kinetics of carrots - experimental and numerical results: a) drying curves and temperature of dried material [12]; experimental and model drying rate and "vibration effect", "heating effect" and "synergistic effect" as a function of time

The model was applied to describe ultrasound assisted convective drying in [3,9,13,14,20,25]. The model shows very good compatibility with experimental data (Fig. 2a). The results of the process modeling make it possible to analyze the efficiency of ultrasound application. Additional parameters should be specified for this purpose. Drying rate DR expresses the rate of moisture decrease in the material during drying as a function of time and is determined as

$$DR(t) = -m_s \frac{dX}{dt} = A_m h_m \ln \frac{\varphi|_{\partial B} p_{vs}(T_m)}{\varphi_a p_{vs}(T_a)} \tag{4}$$

The ultrasound assistance improves the drying rate. This is due to three mechanisms associated with the use of ultrasound, namely "vibration effect", "heating effect" and "synergistic effect" [13,22]. The model separates these effects and allows to determine their share in the drying rate (Fig. 2b). The results indicate that the vibrating effect has the largest share in the acceleration of drying. The impact of the other two effects is much smaller.

4.2. Packed bed drying models and continuous model

Three models of ultrasound assisted bed drying were proposed [26-28]. All of these models assume lumped capacities of grains and continuous description of the whole bed. Models by Kowalski [26] and Kowalski, Rybicki [27] treat material as not shrinking. Model by Musielak [28] takes into account high shrinkage of grains. All these models describe drying kinetics as well as distributions of moisture content and temperature in the bed.

The continuous model, describing mass and heat transfer in a single body during ultrasound assisted drying is proposed in [7]. The model was developed basing on irreversible thermodynamics. The model allows to calculate and describe the drying kinetics, the distributions of moisture content and temperature in dried body and the shrinkage of the body.

5. Conclusions

The paper is a review of research, carried out in Department of Process Engineering, Poznan University of Technology, on the use of ultrasound to intensify osmotic dehydration and drying. In general, it can be concluded that the use of ultrasound significantly accelerates osmosis and convective drying. Thanks to this, energy efficiency of the processes increases. Ultrasonic assistance of microwave drying causes slight acceleration, therefore it is energy inefficient.

In most cases, the use of ultrasound has improved product quality. This is due to the shortening of the drying time and changes in the structure of the dried material.

Mathematical modeling allowed to describe the kinetics of the process. Thanks to this, the magnitude of the impact of individual phenomena on the intensification of drying could be determined.

6. Acknowledgements

7. References

[1] Siucińska, K.; Konopacka, D. Application of ultrasounds to modify and improve dried fruid and vegetable tissue: A review. Drying Technology 2014, 32, 1360-1368.

[2] Musielak, G.; Mierzwa, D.; Kroehnke, J.; Food drying enhancement by ultrasound - A review, Trends in Food Science & Technology 2016, 56, 126-141.

[3] Kowalski, S.J.; Pawłowski, A. Intensification of apple drying due to ultrasound enhancement, Journal of Food Engineering 2015, 156, 1-9.

[4] Kowalski, S.J.; Mierzwa, D. US-assisted convective drying of biological materials, Drying Technology 2015, 33(13), 1601-1613.

[5] Banaszak, J.; Pawłowski, A. Influence of ultrasound drying on properties of dried apple crisps. In Proceedings of the EuroDrying'2015, Budapest, Hungary, October 21-23.2015.

[6] Mierzwa, D.; Kowalski, S.J.; Ultrasound-assisted osmotic dehydration and convective drying of apples: Process kinetics and quality issues, Chemical and Process Engineering 2016, 37 (3), 383-391.

[7] Kowalski, S.J.; Rybicki, A. Ultrasound in wet biological materials subjected to drying, Journal of Food Engineering 2017, 212, 271-282.

[8] Kowalski, S.J.; Mierzwa, D.; Stasiak, M. Ultrasound-assisted convective drying of apples at different process conditions, Drying Technology 2017, 35(8), 939-947.

[9] Kowalski, S.J.; Mierzwa, D.; Szadzińska, J. Highly efficient vegetables drying technologies III: Ultrasound-assisted drying. In Handbook of Drying of Vegetables and Vegetable Products; Zhang, M., Bhandari, B., Fang, Z., Eds.; CRC Press, Taylor & Francis Group, Boca Raton: London, New York 2017, 81-116.

[10] Rajewska, K.; Mierzwa, D. Influence of ultrasound on structure of the plant tissue. Innovative Food Science and Emerging Technologies 2017, 43, 117-129.

[11] Musielak, G.; Mierzwa, D.; Pawłowski, A.; Rajewska, K.; Szadzińska, J. Hybrid and Non-Stationary Drying – Process Effectiveness and Products Quality. In Practical Aspect of Chemical Engineering; Ochowiak. M, Woziwodzki, S., Doligalski, M., Mitkowski, P.T., Eds.; Springer International Publishing AG: Cham, Switzerland, 2018; 319-338.

[12] Kowalski, S.J.; Szadzińska, J. Convective-intermittent drying of cherries preceded by ultrasonic assisted osmotic dehydration. Chemical Engineering and Processing, Process Intensification, 2014, 82, 65-70.

[13] Szadzińska, J.; Kowalski, S.J.; Stasiak, M. Microwave and ultrasound enhancement of convective drying of strawberries: Experimental and modeling efficiency, International Journal of Heat and Mass Transfer 2016, 103, 1065–1074.

[14] Kowalski, S.J.; Pawłowski, A.; Szadzińska, J.; Łechtańska, J.; Stasiak, M. High power airborne ultrasound assist in combined drying of raspberries. Innovative Food Science and Emerging Technologies 2016, 34, 225–233.

[15] Mierzwa, D.; Szadzińska, J. Non-stationary convective drying of raspberries assisted with microwaves and ultrasound, In Proceedings of EuroDrying'2017 – 6th European Drying Conference, Liege, Belgium, 19-21 June 2017.

[16] Szadzińska, J.; Łechtańska, J.; Kroehnke, J. Non-stationary convective drying assisted with microwaves and ultrasound. Inżynieria i Aparatura Chemiczna 2016, 55(5), 203-204.

[17] Kowalski, S.J.; Szadzińska, J.; Pawłowski, A. Ultrasonic-assisted osmotic dehydration of carrot followed by convective drying with continuous and intermitted heating. Drying Technology 2015, 33(13), 1570-1580.

[18] Kroehnke, J.; Radziejewska-Kubzdela, E.; Musielak, G.; Stasiak, M.; Biegańska-Marecik, R. Ultrasonic-assisted and microwave-assisted convective drying of carrot – drying kinetics and quality analysis. In Proceedings of the EuroDrying'2015, Budapest, Hungary, October 21-23.2015.

[19] Mierzwa, D.; Kowalski, S.J.; Kroehnke, J. Hybrid drying of carrot preliminary processed with ultrasonically assisted osmotic dehydration, Food Technology and Biotechnology 2017, 55(2), 197-205.

[20] Kowalski, S.J.; Szadzińska, J.; Pawłowski, A. influence of process parameters variation on hybrid nonstationary drying In Intermittent and Nonstationary Drying Technologies: Principles and Applications. Azharul Karim M., Chung-Lim Law, Eds.; CRC Press, Taylor & Francis Group, Boca Raton: London, New York 2017; 57-91.

[21] Mierzwa, D.; Musielak, G. Convective drying of carrot – influence of the microwave and ultrasound enhancement, In Proceedings of EuroDrying'2017 – 6th European Drying Conference, Liege, Belgium, 19-21 June 2017.

[22] Szadzińska, J.; Łechtańska, J.; Kowalski, S.J.; Stasiak, M. The effect of high power airborne ultrasound and microwaves on convective drying effectiveness and quality of green pepper, Ultrasonics Sonochemistry 2017, 34, 531–539.

[23] Kroehnke, J.; Musielak, G.; Boratyńska, A. Convective drying of potato assisted by ultrasound, PhD Interdisciplinary Journal 2014, 1, 57-65.

[24] Szadzińska, J. Hybrid-intermittent drying of red beetroot. In Proceedings of EuroDrying'2017 – 6th European Drying Conference, Liege, Belgium, 19-21 June 2017.

[25] Stasiak, M.; Musielak, G.; Kowalski, S.J. Optimization method of evaluation convective heat and mass transfer effective coefficients in drying process. In Proceedings of the EuroDrying'2015, Budapest, Hungary, October 21-23.2015.

[26] Kowalski, S.J. Packed bed drying enhanced with ultrasound. In Proceedings of the EuroDrying'2015, Budapest, Hungary, October 21-23.2015.

[27] Kowalski, S.J.; Rybicki, A. Ultrasonic assisted drying of packed bed. A modeling study. In Proceedings of the EuroDrying'2015, Budapest, Hungary, October 21-23.2015.

[28] Musielak, G. Modeling of heat and mass transfer during ultrasound-assisted drying of a packed bed consisting of highly shrinkable material. Chemical Engineering Research and Design 2018, 129, 25–33.

Using Life Cycle Assessment methodology to minimize the environmental impact of dryers

Léonard, A.[*]; Gerbinet, S.
PEPS group. Chemical Engineering, University of Liège, Belgium

*E-mail of the corresponding author: a.leonard@uliege.be

Abstract

Drying is known as a high energy consuming unit operation, representing between 12 to 25% of the global industrial energy consumption in developed countries. Consequently, drying contributes to several environmental impacts mainly associated to its heat or electricity requirements. One can cite global warming, emission of particles, acidification, photochemical ozone formation, …

Based on a literature review and some dedicated case studies, this work will illustrate how Life Cycle Assessment (LCA) can be used to evaluate the environmental impacts associated to a drying operation. The results will be presended in a way to indicate some eco-design strategies for dryers.

Keywords: drying; eco-design; Life cycle assessment; environmental impact.

1. Introduction

Drying is known as a high energy consuming unit operation, representing between 12 to 25% of the global industrial energy consumption in developed countries. Consequently, drying contributes several environmental impacts associated to heat or electricity production. One can think, among others, to global warming via greenhouse gas emissions, acidification or photochemical ozone formation via nitrogen oxides emissions, human toxicity via particule matter emissions, … Besides these impacts directly linked to energy consumption, industrial drying operations may also induce other environmental impacts, depending on the choice and the quantity of the materials it is made of, for example.

Life Cycle Assessment (LCA) is now considered as the most complete methodology to evaluate the potential environmental impacts associated with a process, product or service, following a cradle to grave approach. In addition to International Standards ISO 14040 [1] and 14044 [2], the European Joint Research Center developed guidance rules published in the International Reference Life Cycle Data System (ILCD) Handbook [3]. As mentioned in one guest editorial of A. Mumudar [4], LCA of competeting systems has to carried out before selecting the optimal one.

Based on a literature review and some dedicated case studies, this work will illustrate how this methodology can be used to assess the environmental impacts associated to a drying operation. The results will focus on the main process parameters influencing the environmental impacts in a way to indicate some eco-design strategies for dryers.

2. Materials and Methods

This section will summarize the principles of the LCA methodology allowing to understand the results that will be extracted from the literature and from our case studies.

Following ISO standards, LCA studies include 4 phases. The first step consists in defining the "goal and scope", namely determining the functional unit, to which all the results will be associated, the system boundaries, cut-off rules, time period, impact categories, etc. A typical functional unit could be 'the drying of one ton of product' with some specifications on final quality of the product (dryness, …). The system boundaries specifies the different so-called 'unit processes' included in the scope, for example, the supply chain, the feed preparation, the packaging, the maintenance, treatment of exhaust gases, …

The second step is called the Life Cycle Inventory (LCI). This phase involves data collection and modeling of the product system, as well as description and verification of data. The data must be related to the functional unit previously defined. Besides specific data, several databases can be used, as well as the scientific literature. The LCI provides information about inputs and outputs in form of elementary flows from and to environment for all the unit processes included in the system boundaries. In the context of drying, a part of the data can be obtained via process control sofwares or energy audit systems allowing the report of any consumption or emissions.
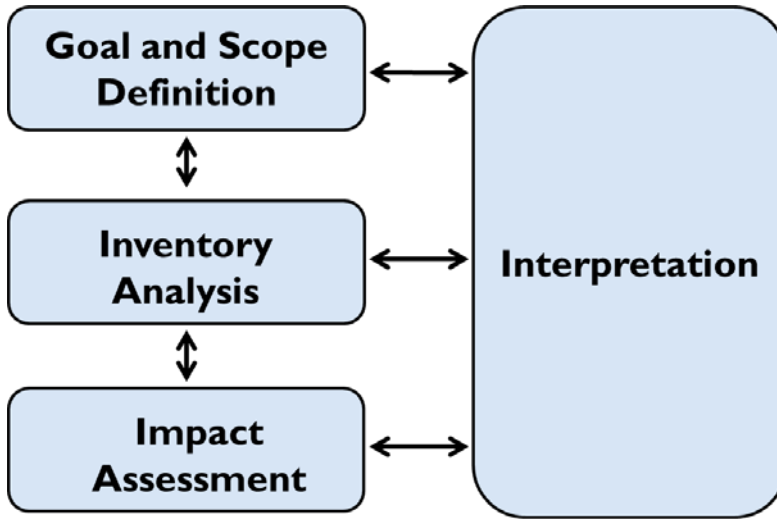
Fig. 1 The four steps of a Life Cycle Analysis.

The third step aims to convert the LCI results into environmental impacts, using several recommended methodologies (following the ISO Standards and the ILCD handbook). Depending on the methodology (ReCiPe, ILCD, Impact World, etc.), the contribution of the functional unit to impact categories such as global warming, eutrophication, acidification, inorganic respiratory effects, tropospheric ozone formation, etc. can be assessed. Fig. 2 illustrate 15 midpoint (problem oriented) impact categories and 3 areas of protection at endpoint. Characterization factors are used to calculate the contribution of each elementary flow of substances to the impacts they are known to be related.
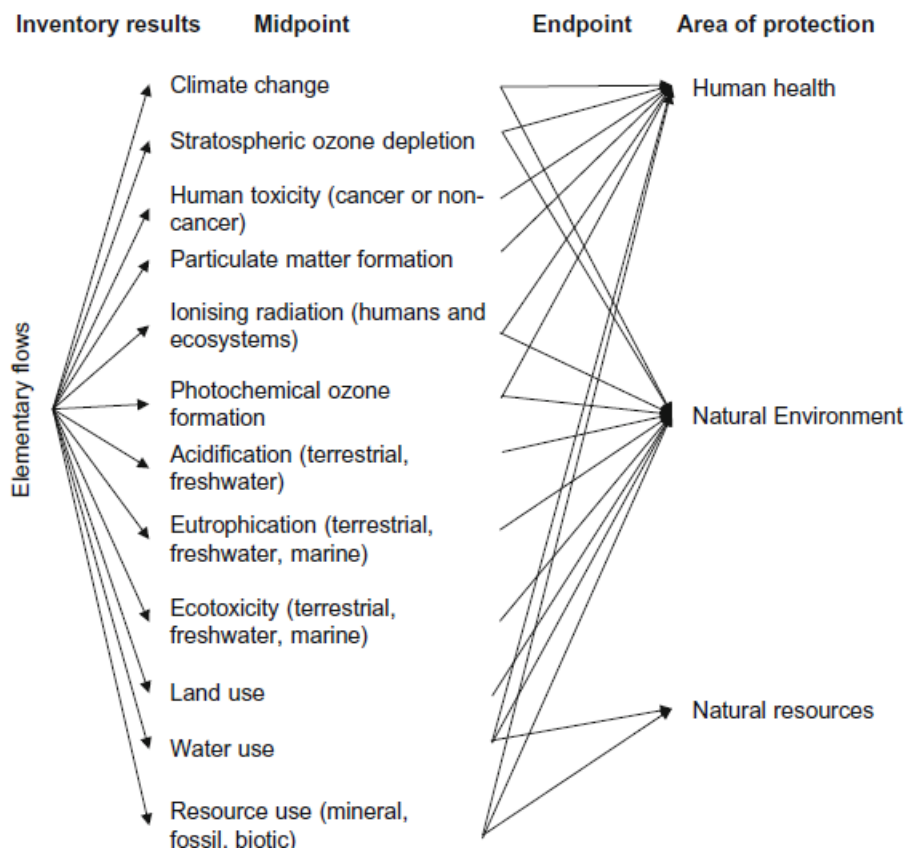
Fig. 2 Impact assessment according to the ILCD handbook.

The last step of a LCA is the interpretation of the results, with three significant steps: the identification of the significant issues, the evaluation of the quality of the study and the drawing of the conclusions, recommendations and reporting.

3. Literature review

Even through an increasing number of papers mention the importance of using an holistic approach to design drying in a sustainaible way, the number of studies really using LCA as an eco-design tool is still low.

Ciesielski and Zbicinski [5] compared two spray dryers, one at laboratory scale and one at industrial scale using LCA. They found that both units generated the greatest environmental load at the usage stage of the life cycle and have an effect mainly in the damage category of resources depletion.

De Marco et al. [6] studied the industrial production of apple powders. Both the drum drying and the storage are the steps that have high impacts (more than 35% each one) on

global warming potential and aquatic eutrophication; for the other midpoint categories, the main contribution (> 67 %) is due to drum drying.

Romdhana et al. [7] developed a general eco-design model of biomass drying. Their idea was to develop an assessment computer-aided process engineering tool that compares environmental impacts of different operating conditions and fuel types to support decision-makers for an improved compliance to environmental criterion. However their optimization only includes carbon footprint, which is not representative of the overall process performance.

Prosapio et al.[8] used LCA to optimize the production of strawberries by freeze-drying. They found that that agricultural steps, packaging and end of life only marginally influenced emissions, whereas processing steps are the main contributors. Their analysis revealed that the process was sensitive to vacuum drying time and rather insensitive to freezing time; They proposed an improved solution using osmotic pre-treatment allowing reduced process times and a decrease of 25% of emissions.

Van Oirschot et al.[9] used LCA to evaluate the system design of seaweed cultivation and drying. They found that the drying step (using light fuel oil in a industrial furnace) had the highest contribution on the environment.

4. Case study

In order to illustrate some information that can be used as decision support tool when designing dryers, a simplified LCA of a sludge dryer has been carried out, varying some parameters. The aim of the study is to compare the environmental impact associated to the evaporation of 1 ton of water, i.e. the functional unit, following the scenarios indicated in Table 1. Scenario 1 defines the base case.

Table 1. Modeling scenarios

Scenario	Thermal energy consumption kWh	Thermal energy production	Electricity consumption kWh	Electricity production
1	700	Gas boiler (EU-28)	80	EU-28 grid mix
2	700	Gas boiler (DE)	80	DE grid mix
3	700	Light Fuel Oil boiler (EU-28)	80	EU-28 grid mix
4	700	Biomass boiler (EU-28)	80	EU-28 grid mix
5	770	Gas boiler (EU-28)	80	EU-28 grid mix
6	700	Gas boiler (EU-28)	80	Wind power (EU-28)

The value of thermal and electrical energy consumptions correspond to the claimed performances of Innodry® 2E (Suez-Degrémont). Depending on the scenario, the thermal

energy is produced via gas, light fuel oil or biomass boiler, which technical characteristics corresponding to Germany (DE) or to the average situation found in EU-28. The electricity is taken from the grid, i.e. the German or average European one. All these scenario also include the transportation of the wet sludge (20% DS) on 100 km using a EURO 6 truck-trailer, up to 28 t gross weight. The dryer infrastructure in itsef has been neglected. GaBi 7 software and associated datasets have been used to carry out the LCA, with ReCiPe 2016 v1.1 Midpoint (H) as impact assessment method.

Fig. 3 shows the results at the characterization stage: for each of the selected impact category, the highest score is put at a value of 100% and other scores are represented using a relative scale. The absolute values are given in Table 2. In order to facilitate the interpretation of the results, only the most relevant impacts are given.
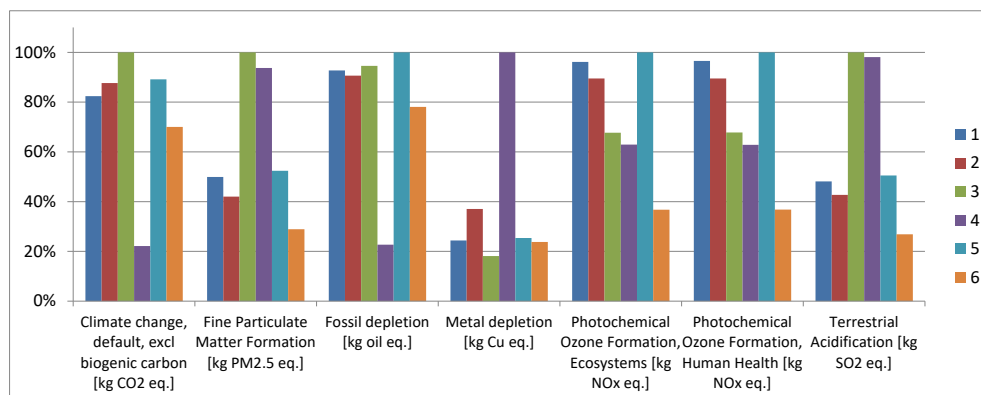
Fig. 3 Impact of the evaporation of 1 ton of water: characterization results.

Table 2. Characterization results

	1	2	3	4	5	6
Climate change, default, excl biogenic carbon [kg CO_2 eq.]	220	234	267	59	238	187
Fine Particulate Matter Formation [kg $PM_{2.5}$ eq.]	0,050	0,042	0,100	0,094	0,052	0,029
Fossil depletion [kg oil eq.]	86,6	84,6	88,3	21,2	93,4	72,9
Metal depletion [kg Cu eq.]	0,089	0,135	0,066	0,364	0,092	0,087
Photochemical Ozone Formation, Ecosystems [kg NOx eq.]	162	151	114	106	168	62
Photochemical Ozone Formation, Human Health [kg NOx eq.]	101	94	71	66	105	39
Terrestrial Acidification [kg SO_2 eq.]	0,153	0,136	0,318	0,312	0,161	0,085

The results show clearly the influence of the choice of the energy source, either thermal or electrical, on the environmental impact. The use of a biomass boiler (4) allows to reduce the climate change by 80% in comparison with light fuel oil (3). This biomass scenario also

gives the lowest impact regarding fossil depletion but the highest one for metal depletion. With respect to the base case, an increase of 10% of the thermal energy consumption (7) induces a similar relative increase in all categories. Bigger changes are obtained when replacing the electricity of the grid by wind power (6), especially for photochemical ozone formation and fine particle matter formation. The comparison between scenarios 1 and 2 also shows the impact of the localization of the drying plant on its environmental footprint.

As a sensitivity study, the transportation distance, initially fixed at 100 km, was set to 50 and 150 km, using energy consumptions of scenario 1. Fig. 4 shows that an increase of the transport distance influences almost all impact categories, except the ones related with photochemical ozone formation. Nevertheless, Table 3 indicates, for example, that an increase of 100 km leads to an increase of 15 kg CO_2 eq. This illustrates that the transportation step is not prevailing in this case study (less than 10%), in regards with a total climate change indicator of 220 for the base case. A more detailed analysis shows, in this case, that the most impacting step is the production of thermal energy, contributing to 78% of the climate change score.
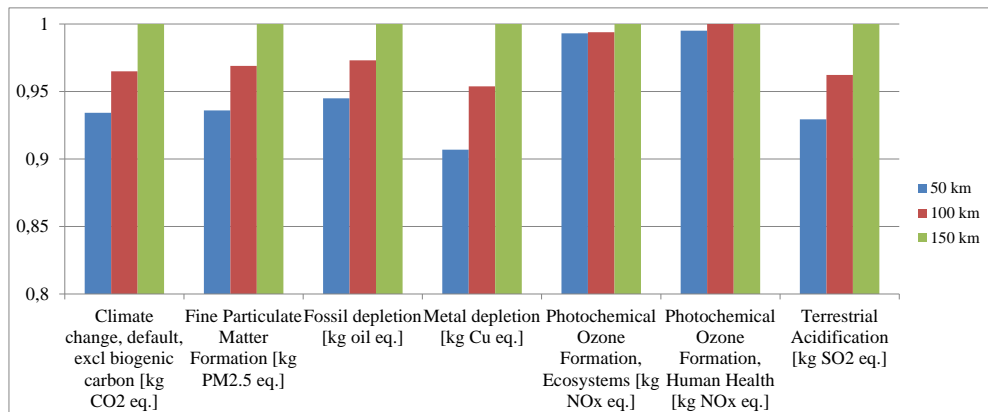
Fig. 4 Influence of the transportation distance on the impact associated to the evaporation of 1 ton of water: characterization results.

Table 3. Influence of transport distance - Characterization results

	50 km	100 km	150 km
Climate change, default, excl biogenic carbon [kg CO_2 eq.]	213	220	228
Fine Particulate Matter Formation [kg $PM_{2.5}$ eq.]	0,0482	0,0499	0,0515
Fossil depletion [kg oil eq.]	84,1	86,6	89
Metal depletion [kg Cu eq.]	0,084	0,089	0,093
Photochemical Ozone Formation, Ecosystems [kg NOx eq.]	162	162	163
Photochemical Ozone Formation, Human Health [kg NOx eq.]	100,4	101	101
Terrestrial Acidification [kg SO_2 eq.]	0,147	0,153	0,159

5. Conclusions

As already mentioned in 2011 by Haque [10] in his guest editorial, hopefully LCA will soon become one of the key tools that drying practitioners and R&D personnel will utilize on a regular basis. This very simple case study illustrates that LCA can be used to evaluate the influence on energy production source on the environmental impact. Besides logistical aspects, LCA could also includes the infrastructure (building material options, …), namely in the case where several configurations or technologies could be used. This tool could allow to predict whether energy intensification strategies are really worth and do not lead to impact shifting.

6. References

[1]   ISO, *ISO 14040, Environmental management - Life cycle assessment - Principles and framework. .* 2006.

[2]   ISO, *ISO 14044, Environmental management - Life cycle assessment - Requirements and guidelines. .* 2006.

[3]   Sustainability, E.C.-J.R.C.a.I.f.E.a., *International Reference Life Cycle Data System (ILCD) Handbook - General guide for Life Cycle Assessment - Detailed guidance.* 2010.

[4]   Mujumdar, A.S., *Editorial: Some Challenging Ideas for Future Drying R&D.* Drying Technology, 2012. **30**(3): p. 227-228.

[5]   Ciesielski, K. and I. Zbicinski, *Evaluation of environmental impact of the spray-drying process.* Drying Technology, 2010. **28**(9): p. 1091-1096.

[6]   De Marco, I., et al., *Life cycle assessment of apple powders produced by a drum drying process.* Chemical Engineering Transactions, 2015. **43**: p. 193-198.

[7]   Romdhana, H., C. Bonazzi, and M. Esteban-Decloux, *Computer-aided process engineering for environmental efficiency: Industrial drying of biomass.* Drying Technology, 2016. **34**(10): p. 1253-1269.

[8]   Prosapio, V., I. Norton, and I. De Marco, *Optimization of freeze-drying using a Life Cycle Assessment approach: Strawberries' case study.* Journal of Cleaner Production, 2017. **168**: p. 1171-1179.

[9]   van Oirschot, R., et al., *Explorative environmental life cycle assessment for system design of seaweed cultivation and drying.* Algal Research, 2017. **27**: p. 43-54.

[10] Haque, N., *Guest Editorial: Life cycle assessment of Dryers.* Drying Technology, 2011. **29**(15): p. 1760-1762.

Beyond freeze-drying of biologics: vacuum-foam drying and spray freeze-drying

Langford, A.[a]; Balthazor, B.[a]; Bhatnagar, B.[b]; Tchessalov, S.[b]; Hageman, M.J.[c]; Lukas, A.[d]; Plitzko, M.[d]; Luy, B[d]; Ohtake, S. [a]*

[a] Pfizer, Inc. BioTherapeutics Pharmaceutical Sciences, Chesterfield, MO, USA.

[b] Pfizer, Inc. BioTherapeutics Pharmaceutical Sciences, Andover, MA, USA.

[c] University of Kansas, Department of Pharmaceutical Chemistry, Lawrence, KS, USA.

[d] Meridion Technologies GmbH, Müllheim, Germany.

*E-mail of the corresponding author: Satoshi.ohtake@pfizer.com

Abstract

The complexity of biotherapeutics in development continues to increase as our capability in discovery and recombinant technology improves. While safety and efficacy remain the two critical aspects of all therapeutics, ensuring adequate stability is a challenge. Freeze-drying is a commonly-used processing technique to enhance the stability of biotherapeutic products, although the lengthy process time and low energy efficiency have led to the search for, and evaluation of, next-generation drying technologies, including spray freeze-drying and vaccum-foam drying. Both processes result in dosage forms that vary considerably from those produced by lyophilization and possess physical properties that may be deemed superior for their intended applications.

Keywords: vacuum-foam drying; spray freeze-drying; lyophilization; biotherapeutics; stabilization

1. Introduction

Most biological materials contain high water content (typically $\geq$ 80% w/w). Removal of water through drying provides numerous benefits, including ease of handling and storage, reduction in transportation costs, and improved stability, to name a few. Though all drying techniques share a common objective (i.e., dehydration), conceptually they are different and require modification/adaptation based on the properties of the compound.

Numerous commercially-approved products are manufactured by freeze-drying,[1] thus lyophilization represents the gold standard to which novel drying methods must be compared. Despite its prevalent use, novel technologies are continuously being evaluated, including vacuum foam-drying and spray freeze-drying, as will be described herein. Furthermore, there are a great number of drying technologies that are available, if not already in use, in the food, agriculuture, and textile industries.[2] As the sensitivity of pharmaceuticals is unique to the given compound, the selected drying technique may not be universally applicable. By understanding the drying mechanism and the stresses involved, the drying techniques can be tailored for effective use.

2. Materials and Methods

2.1. Vacuum-Foam Drying

2.1.1. T cell sample preparation

Primary human pan-T cells (STEMCELL Technologies Inc, Cambridge, MA) were expanded 3-4 fold and cryopreserved at -150°C. During formulation, frozen T cells were thawed at ambient temperature, centrifuged, supernatant removed, and resuspended in the appropriate formulation matrix.

2.1.2. Cell viability and count

Viability measurements were obtained using a NucleoCounter® 3000 (ChemoMetec A/S, Allerød, DK). Neat samples were diluted 4:1 in PBS and cell viability and count assay was performed using a Vai1-Cassette™. The procedure used membrane penetrating acridine orange (AO) and non-penetrating 4′,6-diamidino-2-phenylindole (DAPI) fluorescent dyes to assess cellular membrane integrity. Dried samples were allowed to recover for 3 hours following reconstitution and diluted in PBS prior to analysis.

2.1.3. Vacuum-Foam Drying and Freeze-Drying

Vacuum-foam drying and freeze-drying were performed using LyoStar lyophilizers (SP Scientific, Warminster, PA). Vacuum-foam drying cycles utilized pressures and shelf

temperatures ranging from 0.05 to 5 Torr and 5 - 30°C, respectively. The freeze-drying cycle utilized -30°C shelf temperature for primary drying at a pressure of 0.05 Torr.

2.2. Spray Freeze-Drying

Two process equipment types were utilized for spray freeze-drying. The first process step, spray freezing, was conducted at ambient pressure in a spray freezing chamber and the subsequent dynamic freeze drying of the frozen bulk was perfomed in a rotary bulk freeze dryer.

2.2.1. Spray Freezing

Spray Freezing in all scales was performed in a spray freezing chamber unit (SprayCon, Meridion, Germany) with frequency driven droplet formation nozzle(s) placed in the top lid. The droplet formation is achieved by controlled laminar jet break up. The cylindrical process chamber is double walled and cooled with gaseous and liquid nitrogen.

For all trials, the spray liquid is a 20% (w/w) sucrose solution, and a 300 µm orifice opening for the nozzle was used. For the freezing step, the main process parameters are: (i) for lab and pilot scale trials: - 150 °C gas temperature; spray rate: 19 g/min (1 nozzle); droplet size 550 ± 10 µm; (ii) for commercial scale trial: - 120 °C gas temperature; spray rate: 26 g/min / nozzle (3 nozzles), droplet size 550 ± 10µm

For lab and pilot scale trials, the process equipment used was a stand-alone equipment with intermediate frozen storage of material at -60°C. For commercial scale, the trial was conducted in a fully contained process line that integrates both the spray freezing equipment and the rotary freeze dryer; e.g., the freezing chamber continously discharges the frozen spheres into the precooled drum of the rotary freeze dryer.

2.2.2. Dynamic Freeze-Drying

Lyophilization of the frozen sucrose pellets was performed in three different scales of rotary freeze dryer (RFD) equipment (all by Meridion, Germany); RFD LyoMotion LAB (lab scale), LyoMotion 30 (pilot scale), and LyoMotion 200 (commercial scale). All scales used a rotating, double walled drum which was positionesd in a vacuum process chamber, to which a condenser was attached. The drum temperature was controlled in a range from – 55 °C up to +50 °C.

In all trials, sublimation energy was conveyed by contact heat, via the double wall of the rotating drum, and by infrared radiation emitted from one or more of the infrared sources that were positioned inside the drum above the moving bulk product surface. The pressure within the drying drum was maintained between 50 and 100 µbar at all three scales.

3. Results and Discussion

3.1. Vacuum-Foam Drying

Vacuum-foam drying (VFD) transforms a solution or suspension into a dried static foam through a vacuum-induced evaporation and boiling process. VFD enables removal of water at low temperatures, which is required for heat labile biotherapeutics, through the use of a strong vacuum (e.g., 1 -10 Torr). For pharmaceutical applications, VFD can be performed using a lyophilizer capable of pressure control at a higher range than a typical freeze-drying (FD) cycle. In VFD, the boiling process results in a final product that has an expanded foam structure. Fig. 1 demonstrates that increasing sucrose concentration from 15 to 40% (w/v), while maintaining a 1 mL fill, correlated with increasing foam volumes in the final product. The reproducibility and heterogeneity of a VFD product appearance is a challenge that should be considered during formulation and process development.

Fig 1 Vacuum-foam dried (VFD) preparations of 15%, 30%, and 40% sucrose (left to right).

Compared to other drying techniques, dry static foams have been reported to provide significant stabilization to biotherapeutics. For example, Abdul-Fattah and coauthors [3, 4] have demonstrated improved storage stability of a monoclonal antibody and live virus vaccine as a dried foam in comparison to those prepared by spray drying and freeze drying. Currently, the use of cryopreservation techniques are required to stabilize cell-based therapeutics since the health of cellular suspensions decreases over a short period of time. The ability to stabilize mammalian cells in the dried state may reduce the logistical challenges of a supply chain for therapeutics requiring extremely low storage temperatures.

The T cells used in this work are primary human pan-T cells that were stored at -150°C prior to preparation. T cell formulations evaluated include CryoStor® freeze media (with 0, 5 or 10% DMSO) and disaccharide-based formulations (20% sucrose/trehalose in PBS at pH 7.4) at 1E6 cells/mL with 1 mg/mL bovine serum albumin. CyroStor freeze media is a commercially available preservation medium utilized for cryopreservation of cells at multiple concentrations of DMSO. Disaccharide-based formulations have been reported to provide significant stabilization to mammalian cells though the drying process and in the dried state

[5, 6]. Viability of pre- and post-dried preparations were measured using a NucleoCounter® 3000 fluorescent cell counting and membrane integrity assay.

Prior to drying, viability of all formulations was measured and no significant difference was observed. The average viability of the liquid controls was $91 \pm 3\%$ (Fig. 2). All formulations were vacuum-foam dried using a fixed shelf temperature of 30 °C and the pressure was incrementally decreased from 5 to 0.05 Torr with a total drying time of 90 minutes. Drying was completed prior to an extended secondary drying step to minimize dehydration stress which could lead to additional viability loss. Fig. 2 presents the membrane integrity of T cell formulations following vacuum-foam drying and reconstitution with water. The viability of T cells after drying in CryoStor media was 65%, with the addition of 5 and 10% DMSO resulting in post-drying viability of 57 and 32%, respectively. The 20% sucrose and trehalose formulations resulted in post-drying viability of 63 and 65%, respectively. While greater than 60% T cell viability was retained after drying various DMSO-free formulations, the recovery could be improved further through optimization of formulation, drying process parameters, and residual water content.[2]
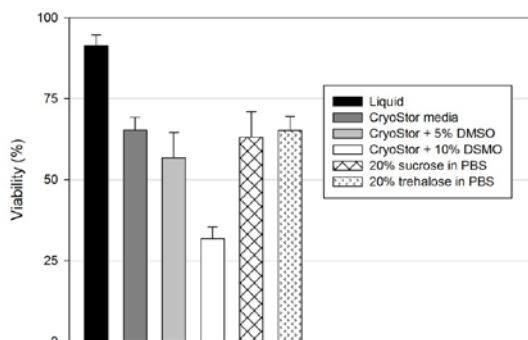
Fig. 2 Viability of human pan-T cell formulations after vacuum-foam drying compared to liquid controls. Data presented as average ± SD.

A follow-up evaluation compared the storage stability of 7E5 T cells/mL formulated in 30% trehalose and 3% BSA in PBS at pH 7.4 as liquid, freeze-dried and foam dried preparations at 5°C (Fig. 3). The freeze and vacuum-foam drying cycles were designed to target a residual water content of 9% (w.b.). There was a higher post-drying viability for the VFD preparation compared to FD, for which the process loss was 61 and 42% after FD and VFD, respectively. In order to decouple processing stress and storage stability, the viability results were normalized based on initial stability samples (post-drying). As shown in Fig. 3, the VFD preparation exhibited superior stability compared to liquid and FD preparations. At the same residual water content as a FD cake, these data provide evidence that T cells vitrified as a dried foam provides improved storage stability.
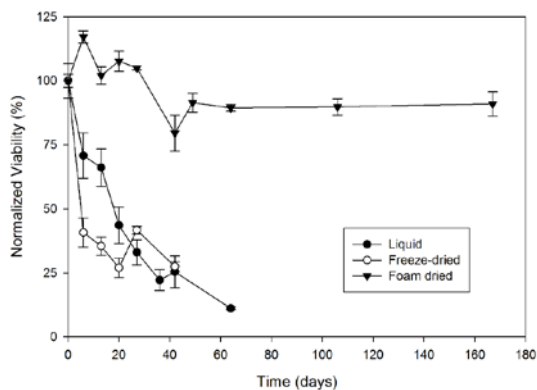
Fig. 3 Normalized viability of a liquid, freeze-dried, and foam dried preparations of T cells on stability at 5°C. Data presented as average ± 83% CI.

3.1. Spray Freeze-Drying

Spray freezing is often described as a process whereby the liquid droplets generated by spray nozzles (e.g., binary air nozzles or pressure nozzles) are directed into a cryogenic medium, often liquid nitrogen.[7] In such a case, the suspended frozen droplets are collected either by sieves or are collected after the cryogen has boiled off. For the spray freeze-drying technology presented herein, two unique processes have been developed and adapted for the use in the manufacture of parenteral pharmaceutical formulations.[8-10]

In the first process step, spray freezing, the frozen microspheres are generated as bulk by dispersing the substrate liquid into single droplets of homogeneous size,[11] utilizing a frequency nozzle, which fall through the cold gas (serving as cryogenic medium) and congeal to form frozen spheres. In contrast, the use of conventional spray nozzles results in a broader range of particle size with a significant amount of fines. The direct use of liquid nitrogen (LN_2) is avoided to minimize internal mechanical stress encountered during freezing, in particular for large particles. The freezing chamber is therefore designed as a cylindrical, double walled column. The process takes place under ambient pressure conditions. Droplet size depends on parameters such as flow rate, frequency, viscosity (based on formulation and temperature), and orifice diameter; for the current application, a (selectable) range for the droplets between 300 to 1000 µm was targeted. For scale-up, multiple nozzles were used, though the height of the freezing column remained unchanged.

The second process step is the freeze drying of the frozen bulk material. The dynamic lyophilization process conducted in a rotary freeze dryer provides process conditions that produce bulk product with high homogeneity (Fig. 4), while avoiding specific aspects of fluid bed processing.[12] Generally speaking, processing conditions such as pressure and temperature are quite comparable to parameters utilized in conventional freeze drying. There

are some differences to be noted, for example: the large surface of the frozen bulk increases heat and mass transfer, which generally allows for shorter drying times. Furthermore, the water vapor diffusion length is significantly reduced. A 10 mm lyo cake in a vial poses a maximum diffusion length of 10,000 µm; in a 1 mm microsphere, the maximum length is 500 µm. In conventional shelf freeze drying, the heat to a large portion is conveyed across the bottom of the glass vial; the drying front is moving from the top to the bottom, i.e. the heat transfer takes place across the frozen product. In dynamic freeze drying, the energy both from radiators and drum surface is transmitted to the surface of a particle, at which the drying front initiates.

Fig. 4 Spray Freeze-Dried microspheres generated for a 20% (w/w) sucrose solution.

The results for spray freeze-dried sucrose conducted at three scales are shown in Table 1. In all scales, residual water content less than 1% can be reached and that yield above 95% is possible in commercial scale. The lower yield in pilot scale is explained by the use of higher rpm of the drum in conjunctions with higher IR power. During drying, a pellet will loose 80-90 % of its weight. High water vapor flows would cause the pellets to get entrapped into the vapor flow, which would cause particles to leave the drum, reducing the yield. Additional factors need to be considered, such as solid content, as higher solid content reduces the loss in weight, and electrostatic phenomena, which may be significant if the particle size is too low. The level of residual water content achieved is comparable to that from conventional freeze drying.

Table 1. Results for 20% (w/w) sucrose solution processed at three scales

	Lab scale	Pilot scale	Commercial scale
Amount processed (kg)	1	6	107
Drying time (h)	5.5	16	29.25
Yield (%, w/w)	98.6	81.6	97.3
Residual water content (%)	≤ 1.0	≤ 1.0	≤ 0.6
Reconstitution time (min)	≤ 1.0	≤ 1.0	≤ 1.0

4. Conclusions

The complexity of biotherapeutics in development continues to increase as our capability in discovery and recombinant technology improves. While safety and efficacy remain the two critical aspects of all therapeutics, stability, both in terms of shelf-life and to stresses encountered during manufacturing, remains a challenge. Spray freeze-drying is a hybrid

processing technology comprising spray drying and bulk freeze-drying, while vacuum foam drying is a modified freeze-drying process that challenges the conventional processing conditions utilized in lyophilization. The former has matured to a level where the application of the technology even in commercial scale is in reach also for pharmaceutical applications, while the latter has provided enhanced stability to a complex biological beyond that provided by a conventional freeze-drying process. The development of *novel* drying technologies, such as the aforementioned processes, is a culmination of fundamental understanding gained in academia and leveraging the lessons learned through their utilization in orthogonal industries. For implementation, technical evaluation should include the scalability of the process, energy efficiency, as well as the capability to implement the technique in a GMP environment.

5.   Acknowledgements

6. References

[1] Costantino, H.R. Excipients for use in lyophilized pharmaceutical peptide, protein and other bioproducts. In *Lyophilization of Biopharmaceuticals*; Costantino, H.R., Pikal, M. J., Eds.; AAPS Press: Arlington, VA, 2004; pp 139-228.

[2] Walters, R. H.; Bhatnagar, B.; Tchessalov, S.; Izutsu, K. I.; Tsumoto, K.; Ohtake, S. Next generation drying technologies for pharmaceutical applications. *J. Pharm. Sci.* **2014**. 103 (9):2673-2695.

[3] Abdul‑Fattah, A. M.; Truong‑Le, V.; Yee, L.; Nguyen, L.; Kalonia, D. S.; Cicerone, M. T.; Pikal, M. J. Drying-Induced Variations in Physico-Chemical Properties of Amorphous Pharmaceuticals and Their Impact on Stability (I): Stability of a Monoclonal Antibody. *J. Pharm. Sci.* **2007**. 96 (8):1983-2008.

[4] Abdul-Fattah, A. M.; Truong-Le, V.; Yee, L.; Pan, E.; Ao, Y.; Kalonia, D. S.; Pikal, M. J. Drying-Induced Variations in Physico-Chemical Properties of Amorphous Pharmaceuticals and Their Impact on Stability II: Stability of a Vaccine. *Pharm. Res.* **2007**. 24 (4):715.

[5] Crowe, J. H.; Crowe, L. M.; Wolkers, W.; Tsvetkova, N. M.; Oliver, A.; Torok, Z.; Kheirolomoom, A.; Norris, J.; Satpathy, G.; Ma, X.; et al. Stabilization of Mammalian Cells in the Dry State. In *Advances in Biopreservation*; Baust, J. G., Baust, J. M., Eds.; CRC Press: Boca Raton, 2006; pp 383-411.

[6] Crowe, J. H.; Crowe, L. M.; Oliver, A. E.; Tsvetkova, N.; Wolkers, W.; Tablin, F. The trehalose myth revisited: introduction to a symposium on stabilization of cells in the dry state. *Cryobiology* **2001**. 43 (2):89-105.

[7] Yu, Z.; Garcia, A. S.; Johnston, K. P.; Williams III, R. O. Spray freezing into liquid nitrogen for highly stable protein nanostructured microparticles. *Eur. J. Pharm. Biopharm.* **2004**. 58 (3):529-537.

[8] Luy, B.; Plitzko, M.; Struschka, M. 2016. Process line for the production of freeze-dried particles. EP2764309.

[9] Struschka, M.; Plitzko, M.; Gebhard, T.; Luy, B. 2016. Rotary drum for use in a vacuum freeze-dryer.   EP2764310.

[10] Plitzko, M.; Struschka, M.; Gebhard, T.; Luy, B. 2015. A process line for the production of freeze-dried particles.   EP2764311.

[11] Mishra, M., ed. *Handbook of encapsulation and controlled release*. CRC Press: Boca Raton, 2015.

[12] Plitzko, M. 2006. "Freeze-drying in the fluidized bed: Possibilities and limits for use in pharmacy." Department of Pharmaceutical Sciences, University of Basel.

New technique of combined hot air and microwave drying to produce a new fiber ingredient from industrial by-products

Talens, C. [a]*; Castro-Giraldez, M.[b]; Fito, P.J.[b]

[a] AZTI—Food Research, Parque Tecnológico de Bizkaia, Astondo Bidea, Edificio 609, 48160 Derio, Bizkaia, Spain

[b] Instituto Universitario de Ingeniería de Alimentos para el Desarrollo, Universidad Politécnica de Valencia, Camino de Vera s/n, 46022 Valencia, Spain

*E-mail of the corresponding author: ctalens@azti.es

Abstract

The search for solutions to transform the by-products generated by the agri-food sector in high value-added ingredients is a priority. The aim of this research was to develop a microwave coupled with hot air drying technique allowing maximizing profits by reducing time and operational costs and to produce a dietary fiber ingredient with interesting technological properties for the development of healthy foods. The shrinkage-swelling phenomena occurred during drying changed the rehydration properties of the fibre ingredient obtained. An increase in particle size improved the fibre's swelling capacity when hydrated, allowing 50 % fat substitution in potato purees.

Keywords: hot air-microwave drying; orange peel; thermodynamics; GAB model; dietary fibre

1. Introduction

Sustainability is nowadays an investment for the future of any economic activity. The current situation of crisis has had an adverse impact in most industries, including the agri-food sector. However, this industry has been relatively the least affected when compared with other industrial sectors. This is mainly attributed to the fact that food products continue to be basic for consumers despite the economic downturn. Therefore, the agri-food sector is a key element in the European economy and can play a crucial role in the achievement of the objectives set in the EU's strategy for 2020: ensuring a sustainable framework of growth of a more competitive economy. The European agri-food industry has focused on energy efficiency and on reducing greenhouse gases emissions, along with better management of their resources as a way to improve its industrial competitiveness. In this sense, the search for solutions to transform the by-products generated in high value-added ingredients, is a priority. In this context, the juice industry, as fundamental sub-sector within the food sector, and large waste generator, must exploit the opportunity to transform their by-products into useful and profitable products for society. This transformation presents some difficulties which impede the profitability of the process. These difficulties are associated with the by-product, such as its compositional variability and its seasonality, and current techniques of transformation as the high energy cost in dehydration processes. This work represents an innovative and sustainable solution for overcoming the disadvantages associated with the high costs of stabilization, turning this by-products into high value-added ingredients, from both, nutritional and technological, points of view. The main aim was to develop a microwave coupled with hot air drying technique (HAD + MW) allowing maximizing profits by using the following strategy: reducing time and operational costs, producing a new ingredient rich in dietary fiber, with interesting technological properties for the development of healthy foods, studying the proposed comprehensive process and analyzing the new generated by-products.

The specific objectives were (i) to develop a thermodynamic model for understanding internal heating and water transport mechanisms occurring from the inside to the outside of orange peels during HAD + MW drying and to predict the chemical and structural transformations, (ii) to determine the sorption isotherms and the isosteric heat of sorption and to study its effect on the macrostructure and microstructure of the orange peel, (iii) to develop and to determine dielectric tools to predict the moisture and water activity by using dielectric spectroscopy and sorption isotherms, (iv) to compare the energy consumption of hot air drying (HAD) versus HAD + MW by analysing the physico-chemical and technological properties of the dietary fibre obtained and (v) to asses the technological and sensory properties of the new fiber obtained by using it as a fat replacer in potato pures.

2. Materials and Methods

Oranges (Citrus sinensis (L.) Osbeck var Washington Navel) were bought from a local supermarket in Valencia (Spain), and their peel was used for the experiments. Sixty orange peel cylinders (20 mm diameter and 3 mm thickness) were obtained using a core borer.

The size and shape of the samples were designed to resemble the small pieces of orange peel left after mechanical extraction of juice and the cuts made by a hammer crusher machine in the processing of orange peel. A diagram of the experimental procedure is shown in Fig. 1.
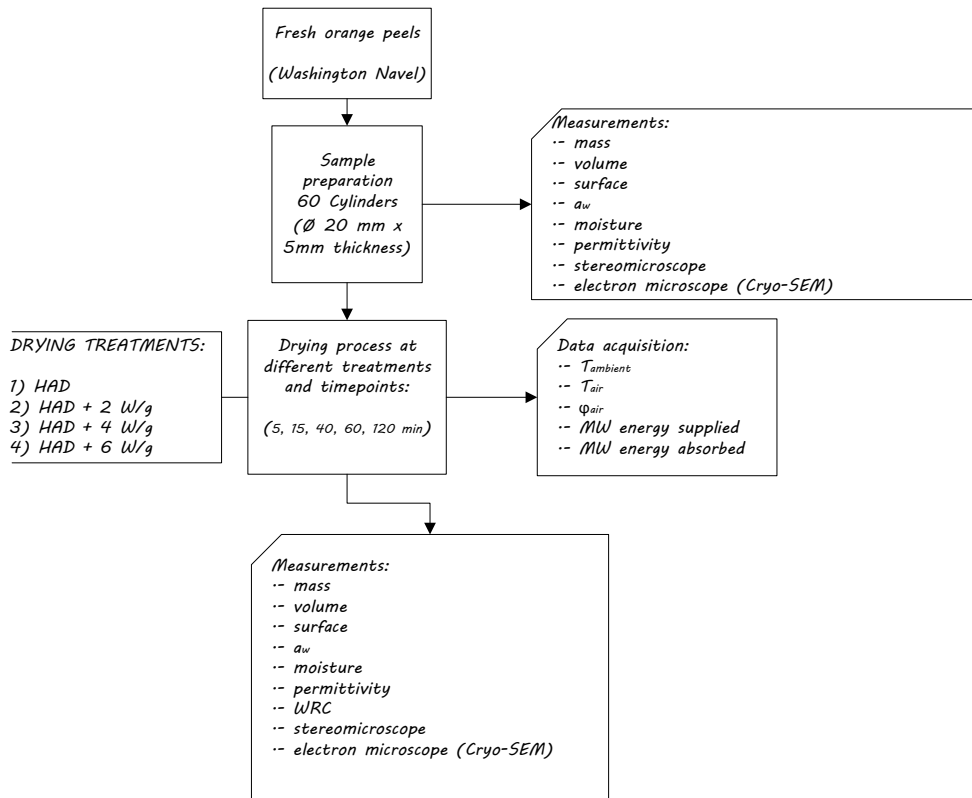
Fig. 1: Experimental procedure

Samples were subjected to HAD + MW, using a specially designed MW-air drying oven with a maximum output of 2000 W at 2450 MHz. For the experiments, the air velocity was 2.5 m/s, hot air temperature, 55 ºC, and the MW energy, 0, 2, 4 or 6 W/g. Four drying experiments were carried out (HAD, HAD + 2 W/g, HAD + 4 W/g and HAD + 6 W/g). Three orange peels samples (triplicate) were used for each drying time (5, 15, 40, 60 and

120 min) in each drying experiment. For fiber production, samples were milled after drying, using an ultracentrifuge mill (ZM 100, Retsch, Haan, Germany) with a sieve of 500 μm. At this stage, powder samples were sealed in plastic bags for further characterization.

2.1. Mass, volume, surface, a_w and moisture content

Samples were weighed using a precision balance Mettler Toledo AB304-S (precision: ± 0.001 g). Surface water activity was determined employing a dew point hygrometer Decagon Aqualab®, series 3 TE (precision: ± 0.003, dimensionless) (Decagon Devices Inc., Pullman, WA, USA). Measurements were performed using structured (not minced) samples; thus, the obtained a_w was considered the surface a_w. The water content of representative fresh orange peel sample and the samples dried for 120 min was determined. The samples were dried in a vacuum oven at 60 ℃ until constant weight was reached (AOAC method 934.06 2000). The moisture content of the samples at the intermediate stages was calculated from the weight loss during drying. Volume was determined by image analysis (Sony T90, Carl Zeiss optics), using Adobe Photoshop© software, obtaining the diameter and thickness of the samples in triplicate.

2.2. Microstructure

The microstructure of fresh and dried samples was analysed using Cryo-SEM. A CryoACryostage CT-1500C unit (Oxford Instruments, Witney, UK), coupled to a Jeol JSM-5410 scanning electron microscope (Jeol, Tokyo, Japan), was employed.

The samples were also examined under a Leica MZ APO™ stereomicroscope (Leica Microsystems, Wetzlar, Germany) with a magnification of 8× to 80×.

2.3. Permittivity

The permittivity was measured with an Agilent 85070E open-ended coaxial probe connected to an Agilent E8362B Vector Network Analyser. The system was calibrated by using three different types of loads: air, short-circuit and 25ºC Milli®-Q water. All determinations were made from 500 MHz to 20 GHz.

2.4. Water retention capacity and sweeling capacity

For the determination of WRC, approximately 0.5 g of each sample (precision ± 0.0001 g) was hydrated in 20 mL of distilled water in a 50 mL (adapted from Robertson et al. 2000). Swelling capacity, defined as the ratio of the volume occupied when the sample is immersed in excess of water after equilibration to the sample weight, was measured by the method of Raghavendra, Rastogi, Raghavarao and Tharanathan [39]. To 0.2 g of dry sample placed in a graduated test tube; around 10 mL of water was added to hydrate the sample for 18 h; then the final volume attained by fiber was measured and expressed as volume/g of original sample (dry weight).

2.5. Rheology

The rheological characterization of the samples was carried out using a controlled-stress AR 2000 rheometer (TA Instruments, Leatherhead, United Kingdom). Stainless steel parallel plate geometry of 40 mm diameter was used with a gap of 2 mm.

2.6. Sensory analysis

The sensory analysis of the purées was carried out by a panel formed by 7 trained tasters applying a quantitative descriptive analysis (QDA) according to the UNE-ISO 6658: 2008 and UNE 87025: 1996 standards. Unstructured scales of 10 points were used to analyze 6 sensorial attributes: 2 visually (homogeneity and viscosity) and 4 on the palate (granularity, fat character, creaminess and viscosity). Each taster evaluated 6 samples of potato puree in triplicate: HAD, HAD + 2 W/g, HAD + 4 W/g, commercial fiber, no fiber and the reference puree.

2.7. Statitcal analysis

To determine the statistical significance of the results, an analysis of variance (ANOVA) was carried out with confidence levels of 95 % ($p \leq 0.05$) and 99 % ($p \leq 0.01$) using the Statgraphics Plus 5.1 programme.

For the sensory analysis the statistical analysis was carried out through the R-project program (R version 3.0.1.) applying a one-way ANOVA to determine the significance of the differences between samples for the parameters analyzed. In addition, a contrast test (Tukey test) has been applied to establish among which samples these differences exist.

3. Results and discussion

A thermodynamic model was developed to explain the mechanisms involved in mass and energy transports throughout the combined drying by hot air and microwave. A continuous shrinkage in HAD samples was produced by the internal liquid water losses, and the samples treated by HAD+MW showed an internal swelling caused by the internal evaporation produced by the microwave energy. Depending on the predominant mechanisms (HAD shrinkage and MW swelling) samples suffer volumetric expansions or contractions (Fig. 2).
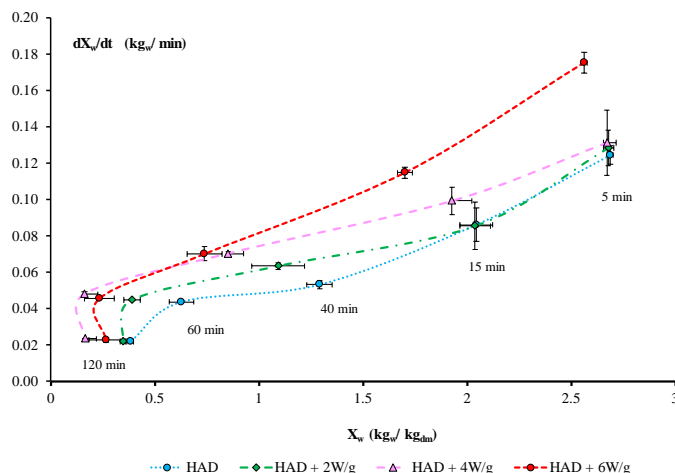
Fig. 2 Drying rate of orange peel samples dried by HAD and HAD + MW at different power intensities. Data represent means and standard deviation of experiments performed in triplicate.

The desorption isotherms of orange peel dried using different treatments (HAD + MW) were obtained and analysed. The results showed that the GAB model could be used to predict the moisture levels using the a_w measurements. The macrostructural and microstructural transformations were demonstrated and discussed in [1], taking into account the interactions of water with the tissue. The observed shrinkage/swelling phenomena clearly depended on the MW power and on the nature of the tissue.

It was possible to develop a dielectric isotherm technique (Fig. 3) by adapting the GAB model to predict the water activity in dried orange peel by using ε' (20 GHz). The physical meaning of the dielectric isotherm parameters (ε_0' and Cd) was studied and explained in [2]. The value of ε_0' at 20 GHz (γ-dispersion) represents the induction effect of the minimum quantity of adsorbed water or the monomolecular moisture layer. The parameter Cd is related with isosteric heat or the adsorption energy of the monomolecular moisture layer, as well as the C parameter of the GAB model. The application of MW power produced an increase of the isosteric heat or adsorption energy of the monomolecular layer, improving the surface tension of samples and thus the hygroscopicity, explaining the reduction of the ε_0' independently of the quantity of the water molecules adsorbed.

The chart shows ε' (20 GHz) on the y-axis (0 to 35) versus a_w on the x-axis (0 to 1), with the following embedded table:

TREATMENT	R² GAB* MODEL
HAD	0.8960
HAD + 2 W/g	0.9494
HAD + 4 W/g	0.8833
HAD + 6 W/g	0.9988
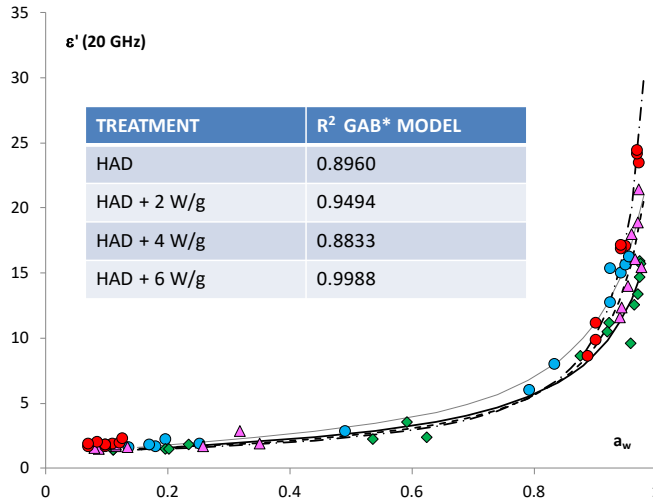
Fig. 3 Dielectric isotherm at 20 GHz of orange peel treated by different drying treatments. Color code same as Fig 2.

An important reduction in processing time (92 %) and energy consumption (77 %) was achieved compared to HAD. The drying treatment did not affect chemical composition or water retention capacities orange fibers. Total dietary fiber content was about 60 % with a ratio of soluble to insoluble fiber of 1:1. Although viscosity of both treatments showed similar values [3], the higher swelling capacity of HAD + MW treated fiber provoked a significant decrease in the viscoelasticity of the samples. An increase in particle size due to an increase in porosity during drying [4], improved fiber swelling capacity (Fig. 4).
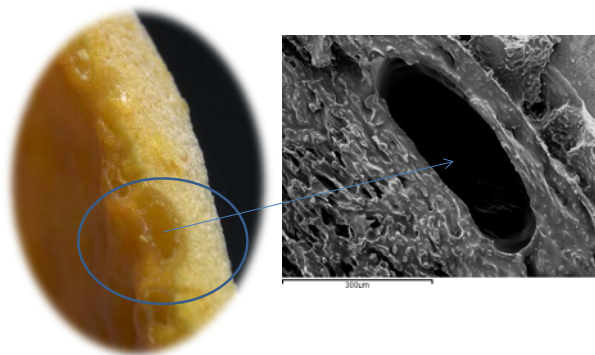
Fig. 4. Micrographs of orange peel samples dried by HAD + 2 W/g.

The fat content of processed potato purées with cream was reduced by 50% using different types of citrus fiber. All the fibers increased the visual viscosity and in mouth of the purées, as well as their behaviour viscoelastic The fibers obtained by air combined drying hot-microwave (4 W / g) presented a swelling capacity similar to commercial fiber. In addition, these fibers were perceived as more granular in the mouth which can be explained due to the greater volume increase when rehydrating.

4. Conclusions

This study has analyzed the microwave coupled with hot air process, developing tools that allow the adequate upscaling of the drying operation by adapting it to the best standards of quality of the final product. A monitoring system that ensures these standards has been designed. This model allows optimizing the traditional hot air drying, by coupling microwave, of orange peel waste as a novel process for citrus by-products valorization, reducing the process time and, therefore, process costs.

The quality and the energy consumption of the dietary fiber production process has been improved. The properties associated with its inclusion in food matrices have been optimized. Therefore, it can be concluded that combining the microwave treatment with hot air drying not only reduced the processing time but it also generated microstructural changes in the dried tissue that increase its water retention capacity. This improved the technological properties of this stabilised by-product, which will be of benefit during its further conversion into the dietary fibre.

5. References

[1] Talens, C.; Castro-Giraldez, M.; Fito, P. J., A thermodynamic model for hot air microwave drying of orange peel. Journal of Food Engineering. 2016 (175), 33-42.

[2] Talens, C.; Castro-Giraldez, M.; Fito, P. J., Study of the effect of microwave power coupled with hot air drying on orange peel by dielectric spectroscopy. LWT - Food Science and Technology 2016 (66), 622-628.

[3] Talens, C.; Arboleya, J. C.; Castro-Giraldez, M.; Fito, P. J., Effect of microwave power coupled with hot air drying on process efficiency and physico-chemical properties of a new dietary fibre ingredient obtained from orange peel. LWT - Food Science and Technology 2017 (77), 110-118.

[4] Talens, C.; Castro-Giraldez, M.; Fito, P. J., Effect of Microwave Power Coupled with Hot Air Drying on Sorption Isotherms and Microstructure of Orange Peel. Food and Bioprocess Technology 2018, 11 (4), 723-734.

Influence of drying on *in vitro* gastric digestion of beetroot: evaluation of the microstructure

Dalmau, M. E. [a]; Carcel, J. A.[b]; Eim, V.[a*]; Simal, S.[a]

[a] Department of Chemistry. University of the Balearic Islands, Palma, Spain.

[b] ASPA group. Department of Food Technology. Universitat Politècnica de València, Valencia, Spain

*E-mail of the corresponding author: valeria.eim@uib.es

Abstract

To better understand the influence of processing on the bioaccessibility of bioactive compounds during digestion, the microstructure of beetroot samples was observed prior to and after 180 min of in vitro digestion, by using scanning electron microscopy. Beetroot samples were subjected to convective drying at 60 ºC and 2 m/s and freeze-drying at -50 ºC and 30Pa. Dried beetroots were rehydrated prior to digestion by immersion in distilled water at 37 ºC during 90 min. To extract quantitative information related to cell size from the visual texture of beetroot, grey level granulometric methods from mathematical morphology were applied.

Keywords: freeze drying; convective drying; scanning electron microscopy; image analysis; image texture analysis.

1. Introduction

The nutritional values of plant foods are usually estimated according to their natural concentrations of nutrients, phytochemicals, and total antioxidant activity. These data are usually obtained by direct extraction with organic solvents.[1] However, these conditions are different from the physiological conditions that occur in the digestive tract. Furthermore, the biological properties of bioactive compounds found in vegetables depend on their bioaccessibility and bioavailability. [2] Bioaccessibility refers specifically to the quantity of nutrients which are released from the food matrix and presented to the intestinal brush border for transport into the cell.[3] Meanwhile, bioavailability refers to the quantity of nutrients which actually pass through the cell membrane and are available for use within the cell.[4] It is known that the influence of processing on food may be the result of cellular and structural changes. For example, freeze drying and convective drying have been shown to cause cellular changes in the food matrix. Huang et al.[5] found that freeze drying (-40 ºC, 100 Pa) in a microwave vacuum dryer (75-300 W, 5 kPa) resulted in cell wall shrinkage in apples (var. Red Fuji). Moreover, there is wide evidence that the physical state of the food matrix plays a key role in the release, mass transfer, accessibility, and biochemical stability of many food components.[6]

Microscopy is a useful tool for visualizing food structure at the tissular and cellular levels and for studying the influence of processing on *in vitro* digestion.[7,8] The characterization of samples by imaging techniques is completed by applying image analysis to quantify the structure observed. Techniques based on image texture analysis can be envisioned in order to quantify information on object size. There are four different types of image texture analysis: structural texture, statistical texture, model-based texture and transform-based texture. Among them, statistical texture is the most widely used in the food industry for its high accuracy and less computation time. Statistical texture, has been successfully applied to extract quantitive information related to cell size[9]. The methodology of statistical texture reflects changes in the intensity values of pixels. These may well contain information about the geometric structure of objects as this can be often reflected by such a change in intensity values. In food images, texture can, to some extent, reflect cellular structure of foodstuffs and thus can be used as an indicator of food quality. For example, texture can be used to reveal the tenderness of beef when colour and size features are not adequate. For this reason, among the large scale of applications of image analysis in the food industry, which is one of the top ten industries using computer vision, texture has been used regularly and its usage covers a variety of foods including baked products, cereal grains, fruits and vegetables.[10]

Thus, the objective of this study was to evaluate the effects of different drying methods and *in vitro* gastric digestion on the microstructure of beetroots (*Beta Vulgaris*) with image texture analysis using a statistical texture methodology.

2. Materials and Methods

2.1. Samples

Beetroot (*Beta vulgaris* var. conditiva) were purchased from a local supermarket (initial moisture content of 6.67±0.04 g water/g dm and total soluble solids of 10.8±0.4 ºBrix). The beetroot were stored at 4 °C for a maximum of one week. Cubes were cut (0.01 m edge) from the center regions of the beetroot tissue, not including the peel, and immediately processed.

2.2. Convective drying and freeze drying processes

Convective drying (CD) was carried out in a laboratory-scale hot air dryer previously described by Rodríguez et al.[11] operating at 60 ºC with an air velocity of 2 m/s. Samples were dried until a final moisture content of 0.17±0.03 g water/g dm. Freeze drying (FD) of beetroot cubes was carried out in a freeze-drier (Telstar LyoQuest, Spain) operating at −50 °C and a vacuum pressure of 30 Pa until a final moisture content of 0.07±0.01 g water/g dm. Before *in vitro* digestion, CD and FD samples were rehydrated by immersion in distilled water (25:100 (g beetroot/ml water)) at 37 °C until they reached final moisture content similar to raw samples (6.67 ± 0.04 g/ g dm) (aprox. 90 and 80 min, respectively).

2.3. *In vitro* digestion procedure

The beetroot samples were digested following the *in vitro* gastric digestion method reported by Bornhorst & Singh[12]. Beetroot cubes (ca. 200 g) were mixed with 80 ml of simulated saliva for 30 s, followed by immersion in 800 ml of simulated gastric juice previously heated to 37 ºC. The mixture was incubated in a shaking water bath (Unitronic 320 OR, Selecta, Spain) at 37 °C and 100 rpm for up to 3 h. Samples were taken initially (no digestion), and after 180 min of gastric digestion, microstructural analyses were made.

2.4. Microstructural analysis
2.4.1. *Scanning electron microscopy (SEM)*

Cell walls were observed by SEM of raw and drying samples before and after digestion. Beetroot cubes were soaked in liquid nitrogen in order to be fractured with a sharp razor blade, and freeze dried. Gold coating was performed using (E-5400, Polaron, UK) equipment (10-4 mbar, 20 mA, 80s). Samples were then observed in a S-3400N Hitachi SEM (Germany), accelerated at 15 kV and under a vacuum pressure of 40 Pa.

2.4.2. *Image texture analysis*

To quantify the effect of drying and gastric *in vitro* digestion on the beetroot structure, cell cavities of the raw and drying cubes before (CD and FD samples) and after (raw180, CD180 and FD180) 180 min of gastric *in vitro* digestion, were characterized in terms of their cell area and cell number per unit of area. Thus, scanning electron microscope photographs were analyzed by using an automatic image processing method which is based on the statistical

texture method and was performed using Image J 2.0.0. software. (Creative commons license). The real cell area value was correlated to a standard image whose dimensions were known. To establish a representative structural analysis, fifteen scanning electron microscope photographs of each sample were analyzed.[9]

Statistical analysis of the results was perfomed by using the "prctile" function of Matlab 2017b software (Mathworks Inc., USA). Thus, the percentile profile of cell number per unit of area of each sample was obtained. Analysis of variance (ANOVA) was applied to analyze the effects of processing in respect of the raw sample and the effects of *in vitro* digestion on microstructure parameters. Means were compared by Tukey's test at $p < 0.05$.

3. Results and discussion

3.1. Microstructural images (SEM)

The images of raw and processed samples before and after 180 min of *in vitro* gastric digestion are shown in Fig 1. Fig $1a_1$ shows the microstructure of raw samples prior to *in vitro* gastric digestion. The raw samples are composed of almost isodiametrical and polyhedral cells with few intercellular spaces, as was previously observed by Nayak et al.[7]. After 180 min of digestion (Fig $1a_2$) a significant cell lysis was observed, resulting in a smaller number of cells per unit area, along with increases in the intercellular space between remaining cells. Carnachan et al.[8] studied the microstructure of kiwi pulp after *in vitro* gastric digestion observed an increase in the intercellular space after *in vitro* digestion.

Cells exhibited shrinkage during the convective drying process, as can be observed in Fig $1b_1$, resulting in a greater disruption of the cellular structure than in raw samples. The effects of different convective drying conditions on the microstructure of apple have been previously evaluated. [13] These authors agreed that during drying, one of the most important phenomena is cell shrinkage, which leads to a major modification of the product structure and allows the release of water. Convective drying causes cells to rupture and dislocate which usually results in increased density with varying porosity.[14] It was also observed that cell shrinkage increased in CD samples after *in vitro* gastric digestion (Fig $1b_2$), completely eliminating the open pores on the surface of the structure and rupturing many of the interior cell walls.
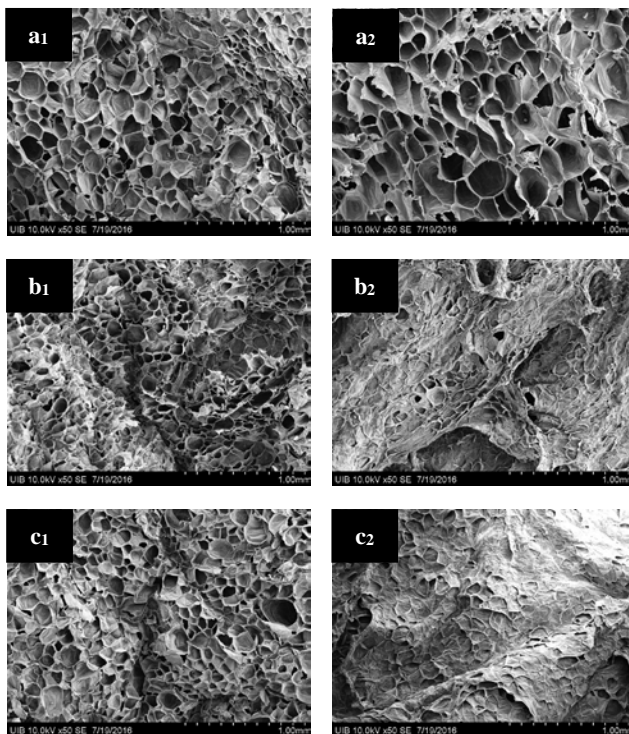
Fig. 1. SEM images of beetroot samples: a-Raw, b-CD and c-FD. 1- of initial beetroot samples (prior to in vitro digestion). 2-after 180 min of in vitro gastric digestion

Fig 1c_1 shows the microstructure of FD samples before *in vitro* digestion. A certain disruption of the cell structure was observed. This effect was also observed by Huang et al.[5] in freeze-dried Red Fuji apples, and in freeze-dried Idared apple by Lewicki & Pawlak. [15] An increase in the destruction of cell wall material can be observed as a result of the *in vitro* gastric digestion process (Fig 1c_2). These changes resulted in almost a complete elimination of the initial porous structure seen in undigested, raw beetroots. The same result was observed by Dalmau et al.[16] in freeze dried Granny Smith apples after 180 min of *in vitro* gastric digestion, when the changes during digestion eliminated most of the pore structure observed in undigested raw apples. Overall, microstructural changes were observed as a result of both drying process and *in vitro* gastric digestion compared to the undigested raw beetroot samples. Compared to the raw beetroots, CD beetroots exhibited the greatest changes, both before and after digestion.

3.2. Image texture analysis

Cell number per unit area of raw beetroot, drying beetroots (CD and FD samples) and beetroots after gastric *in vitro* digestion (raw180, CD180 and FD180) are presented in table 1. All beetroot drying samples present significantly higher cell number per unit of area

(p<0.05) than raw beetroots. Moreover, CD samples presented significantly higher cell number (p<0.05) than FD samples. The highest cell number per unit of area increase was observed in CD samples (47 ± 2 % compared to raw samples). This result may be due to the drying causing a collapse of the cell walls thus producing a volume shrinkage that results in a greater cell number per unit[8,21]. All samples after gastric *in vitro* digestion present significantly lower cell number per unit (p<0.05) than beetroot before *in vitro* digestion. No significant differences (p>0.05) were observed between the cell number per unit of raw samples and all drying beetroot samples. This result may be due to the fact that *in vitro* digestion causes a certain disruption of the cell structure which results in a lower cell number per unit. Different values of cell number per unit compared to raw sample (34-66% of reduction) after different treatments (inmmersion in boiling water, vacuum impregnation, freezing/thawing and compression) were also reported by Ramírez et al.[17].

Fig 2 represents the cell area percentile profiles of raw and drying samples before (raw, CD and FD samples) and after 180 min of gastric *in vitro* digestion (raw180, CD180 and FD180 samples). In this figure, the percentile represents the percentage of cell whose area is equal or smaller to one value. As can be seen in fig 2, different percentile profiles were obtained for each sample.

Table 1. Cell number per unit of area of the raw and drying (CD and FD) beetroot before and after 180 min of gastric in vitro digestion. Different lowercase letter indicate significant differences (p<0.05) for cell number per unit in a sample before and after in vitro digestion. Different capital letters indicate significant differences between the diferent method of processing (Tukey's test, p<0.05)

	Cell number/mm^2
Raw	289±4 aC
Raw 180	171±5 b
CD	425±1 aB
CD180	250±18 b
FD	370±40 aA
FD180	190±20 b

The percentile profiles of raw and drying samples (CD and FD samples) were coincident until ca 25. From there onwards, two groups of samples can be observed, one consisting of raw samples, and the second , of CD and FD samples, indicating that drying processes cause similar changes in cell structure. In raw samples the percentage of larger areas was higher; for example, 80% of areas were smaller than 0.067 mm^2 in raw samples and smaller than 0.016 mm^2 and 0.025 mm^2 in CD and FD samples, respectively. In all samples after *in vitro* digestion the percentage of larger areas was the lowest; for example, 80% of areas were smaller than 0.067 mm^2 and 0.310 mm^2 in raw samples before and after 180 min of gastric *in*

vitro digestion, 0.016 mm^2 and 0.116 mm^2 in CD samples before and after 180 min of gastric *in vitro* digestion, 0.025 mm^2 and 0.130 mm^2 in raw samples before and after 180 min of gastric *in vitro* digestion. The percentile profiles of raw and raw180 samples were coincident up to ca percentile 45. However the percentile profile of drying samples (CD and FD samples with CD180 and FD180 samples) were coincident ca percentile 25 and 50, respectively.
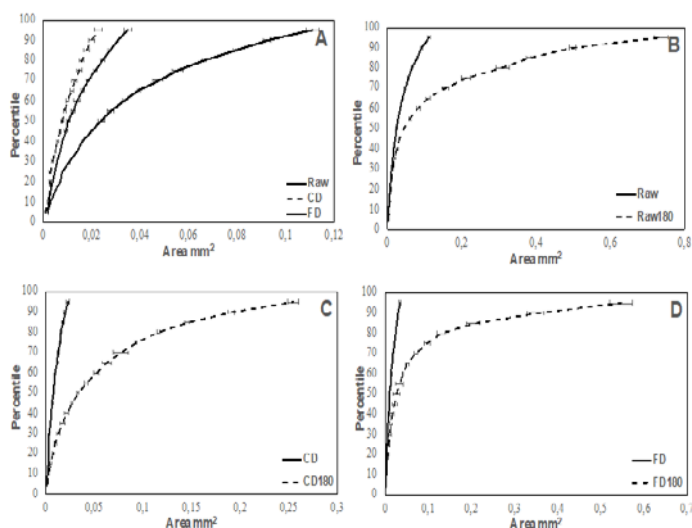
Fig. 2. Cell area percentile profiles of raw and drying samples before (A) and after (B, C and D) 180 min of gastric in vitro digestion.

4. Conclusions

Drying modified the microstructure of beetroots compared with that of raw beetroots. Microstructural analyses indicated significant cellular damage and changes as a result of drying and of *in vitro* gastric digestion. These structural modifications resulted in behavioral changes in beetroots during *in vitro* gastric digestion. The drying process caused cell wall collapses and gastric *in vitro* digestion caused a certain disruption of the cell structure Given the limited knowledge available on this subject at present, it would be interesting to investigate this area more deeply to better understand how processing and *in vitro* digestion can modify structural characteristics.

5. References

[1] Bouayed J, Hoffmann L, Bohn T. Total phenolics, flavonoids, anthocyanins and antioxidant activity following simulated gastro-intestinal digestion and dialysis of apple varieties: Bioaccessibility and potential uptake. Food Chem 2011;128(1):14–21.

[2] Saura-Calixto F. Dietary fiber as a carrier of dietary antioxidants: an essential physiological function. J Agric Food Chem 2011 59(1):43–9.

[3] Garrett DA, Failla ML, Sarama RJ. Development of an in vitro digestion method to assess carotenoid bioavailability from meals. J Agric Food Chem 47(10):4301–9.

[4] Wootton-Beard PC, Moran A, Ryan L. Stability of the total antioxidant capacity and total polyphenol content of 23 commercially available vegetable juices before and after in vitro digestion measured by FRAP, DPPH, ABTS and Folin–Ciocalteu methods. Food Res Int 2011;44:217–24.

[5] Huang LL, Zhang M, Wang LP, Mujumdar AS, Sun DF. Influence of combination drying methods on composition, texture, aroma and microstructure of apple slices. LWT - Food Sci Technol 2012;47(1):183–8.

[6] Aguilera JM. Why food microstructure? J Food Eng. 2005;67:3–11.

[7] Nayak CA, Suguna K, Narasimhamurthy K, Rastogi NK. Effect of gamma irradiation on histological and textural properties of carrot, potato and beetroot. J Food Eng 2007;79(3):765–70.

[8] Carnachan SM, Bootten TJ, Mishra S, Monro J a., Sims IM. Effects of simulated digestion in vitro on cell wall polysaccharides from kiwifruit (Actinidia spp.). Food Chem 2012;133(1):132–9.

[9] Devaux MF, Bouchet B, Legland D, Guillon F, Lahaye M. Macro-vision and grey level granulometry for quantification of tomato pericarp structure. Postharvest Biol Technol. 2008;47(2):199–209.

[10] Brosnan, T., & Sun, D.-W. Improving quality inspection of food products by computer vision - a review. Journal of Food Engineering, 2004; 61(1), 3-16.

[11] Rodríguez Ó, Ortuño C, Simal S, Benedito J, Femenia A, Rosselló C. Acoustically assisted supercritical CO2 extraction of cocoa butter: Effects on kinetics and quality. J Supercrit Fluids. 2014;94:30–7.

[12] Bornhorst GM, Singh RP. Kinetics of in Vitro Bread Bolus Digestion with Varying Oral and Gastric Digestion Parameters. Food Biophys. 2013;8(1):50–9.

[13] Rodríguez Ó, Santacatalina J V, Simal S, Garcia-Perez J V, Femenia A, Rosselló C. Influence of power ultrasound application on drying kinetics of apple and its antioxidant and microstructural properties. J Food Eng 2014;129:21–9.

[14] Smith BG, James BJ, Ho C a. L. Microstructural Characteristics of Dried Carrot Pieces and Real Time Observations during Their Exposure to Moisture. Int J Food Eng. 2007;3(4).

[15] Lewicki PP, Pawlak G. Effect of Drying on Microstructure of Plant Tissue. Dry Technol. 2003;21:657.

[16] Dalmau ME, Bornhorst GM, Eim V, Rosselló C, Simal S. Effects of Freezing, Freeze Drying and Convective Drying on In Vitro Gastric Digestion of Apples. Food Chem. 2017;215:7–16.

[17] Ramírez C, Troncoso E, Muñoz J, Aguilera JM. Microstructure analysis on pre-treated apple slices and its effect on water release during air drying. J Food Eng. 2011;106(3):253–61.

Simultaneous wetting and drying; fluid bed granulation and tablet film coating

Kemp, I.C. [a*]; van Millingen, A.[a]; Khaled, H.[a]; Iler, L.[b]

[a] GSK, David Jack Centre for R&D, Park Road, Ware, Hertfordshire, SG12 0DP, U.K.

[b] GSK, Global Pharma Manufacturing, Zebulon, North Carolina, U.S.A..

*E-mail of the corresponding author: ian.c.kemp@gsk.com

Abstract

Simultaneous wetting and drying occur in processes such as fluid bed (top spray) granulation, Wurster coating and tablet film coating. This gives control challenges, as the spraying and evaporation processes must be carefully balanced and the operating window is significantly narrower than for standalone drying processes. Significant recent advances in modelling have led to effective scale-up and operational strategies. Factors such as flow cessation during filter bag shaking can have a major effect. A design space can be predicted which is often non-orthogonal, and pharmaceutical regulatory authorities have accepted filing submissions using a design space justified by mechanistic modelling.

Keywords: pharmaceuticals; peak moisture content; bed temperature; conduction; design space.

1. Introduction

Most drying processes involve drying of a pre-wetted material, either a wet solid liquid or a liquid solution/suspension as in spray drying. However, a few processes involve simultaneous wetting and drying of the solids. This gives significant effects on the drying behavior, and additional challenges result in modelling, design and practical operation. This paper focuses on two processes of this type, both employed in the pharmaceutical industry: fluid bed (top spray) granulation and tablet film coating. Both have been previously described in texts such as Pandey and Bharadwaj [1] and Lyngberg et al. [2]. However, modelling of these processes has been relatively neglected compared to standalone drying processes, even though successful operation is only possible within a narrower operating range, particularly for fluid bed granulation, as shown below. Recent advances in modelling and process understanding have led to improved methods for design, scale-up and operation, and are described in this paper. Applications in the pharmaceutical industry are described, in particular the development of an appropriate Design Space and operational ranges.

2. Fluid bed granulation

In fluid bed granulation, binder solution is sprayed on to a fluidized bed of particles and evaporated off simultaneously. The initial mixture of powders is gradually transformed into granules held together by solid bridges. Normally, the bed moisture content (LOD, loss-on-drying) increases gradually during spraying and then falls during a final drying phase, as in Fig. 1. However, if the solution spray rate is too fast, uncontrolled agglomeration can result, with potential adverse effects both on product quality (dissolution or content uniformity) and operation (partial or complete defluidisation, and potential loss of the batch).
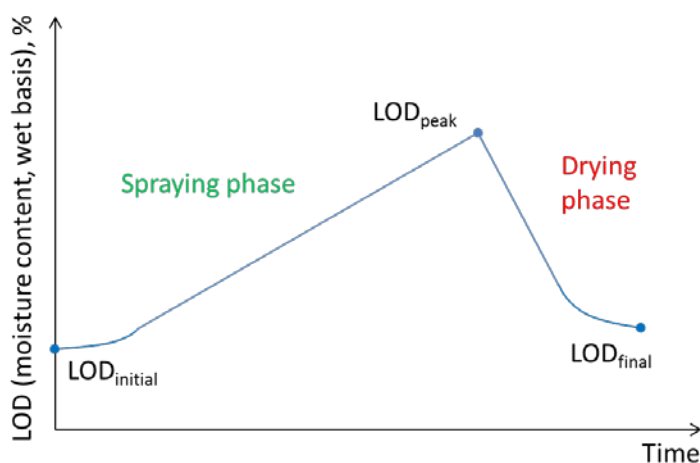
Fig. 1 Moisture content (LOD) during fluid bed granulation cycle.

2.1. Modelling - basic

The rate of moisture accumulation, and hence the peak LOD, can be calculated using a heat and mass balance. The fundamental approach was described by Gupta [3], and a similar model was presented by Lyngberg et al [2]. The water accumulation rate in the granules, m_{accu} (kg/h), is the difference between the water in the incoming spray and that removed by evaporation:

$$m_{accu} = m_{sol}(1 - x_b) - \left(\frac{Q_{air} - Q_{loss}}{h_{fg}}\right) \qquad (1)$$

Here, m_{sol} = solution spray rate (kg/h), x_b = binder concentration as mass fraction (kg/kg), h_{fg} = latent heat of evaporation (kJ/kg), Q_{loss} = heat loss rate (kJ/h), and Q_{air} (kJ/h) is the heat released from the air, defined in (2):

$$Q_{air} = m_{air}C_{p,air}(T_{in} - T_{out}) = F_{air}\rho_{air}C_{p,air}(T_{in} - T_{out}) \qquad (2)$$

Where ρ_{air} = air density (kg/m^3), $C_{p,air}$ = specific heat capacity of air (kJ/kgK).

Equations (1) and (2) show that four significant parameters affect the energy balance;

- Solution spray rate (m_{sol}, kg/h)
- Inlet air volumetric flow rate (F_{air}, m^3/h) or mass flow rate (m_{air}, kg/h)
- Inlet air temperature (T_{in}, ^{0}C)
- Outlet air temperature (T_{out}, ^{0}C).

In fluid bed drying or granulation, if the particle surfaces remain fully wetted, the outlet air is close to saturation conditions, and is approximately equal to the wet bulb temperature T_{wb} (^{0}C), which depends only on inlet air temperature and inlet air humidity Y_{in} (g/kg). Hence the four operating parameters which can affect heat input Q_{air} are $m_{sol,}$ F_{air}, T_{in} and Y_{in}.

The mass accumulated is summed over the spraying period and can be transformed into a peak value of the loss on drying, LOD, which is a wet-basis moisture content:

$$LOD_{peak} = \frac{M_{sol}}{M_{bed,final}}\left[(1 - x_b) + \frac{Q_{loss}}{h_{fg}m_{sol}} - \frac{Q_{air}}{h_{fg}m_{sol}}\right] + \frac{M_{W,initial}}{M_{bed,final}} \qquad (3)$$

Where $M_{bed,final}$ is the total mass of the bed at the end of granulation (including dry solids, binder and moisture) and $M_{W,initial}$ is the total mass of water in the bed before granulation.

2.2. Modelling - extended

The standard model allows for heat losses, but Kemp et al [4] pointed out that several other factors affect the heat balance:

i. Atomisation air flow from the two-fluid atomiser, normally at ambient temperature
ii. Additional heat from the initial preheated bed of solids
iii. Additional heat released when sprayed water becomes bound moisture
iv. Adjustments for periods when the spray or airflow are turned off or reduced, for example during filter bag shaking.

(i) can be handled by a small adjustment to Q_{air} and (ii) and (iii) by small adjustments to LOD_{peak}, which like heat losses are best obtained by back-calculation from experimental measurement, and are the cause of the initial flatter section in the moisture-time curve. However, (iv) can have a significant effect. Exhaust air filters may operate with either "simultaneous" or "consecutive" cleaning. In consecutive cleaning, only a proportion of the filter bags are shaken or reverse pulsed at any moment, and the air flow and spray both continue. However, in simultaneous cleaning, all the filter bags are shaken at the same time, and air flow and spray are usually stopped. Typically, the spray is stopped, the airflow is ramped down, the bag is shaken, the airflow is restarted and finally the spray is restarted. Hence the spray is off for a longer period than the airflow and the balance between heat input and evaporation is changed. We can define fractional times τ_{spray} and τ_{air} as the proportion of the cycle that the water and air are flowing. Equation (3) now becomes:

$$LOD_{peak} = \frac{M_{sol}}{M_{bed,final}} \left[\left(1 - x_b\right) + \frac{Q_{loss}}{m_{sol} h_{fg} \tau_{spray}} - \frac{Q_{air} \tau_{air}}{m_{sol} h_{fg} \tau_{spray}} \right] + \frac{M_{W,initial} - M_{corr}}{M_{bed,final}} \quad (4)$$

Where M_{corr} (kg) is a correction factor allowing for the preheating and binding effects.

For a given granulation formulation and equipment, most of the terms in equation (4) are fixed or nearly constant, and the only two which depend on operating parameters are Q_{air} and m_{sol}. Hence, peak LOD is predicted to vary with the ratio (Q_{air}/m_{sol}). From (1) and (4), high values of Q_{air}/m_{sol} will give less accumulation and low peak LOD; conversely, low Q_{air}/m_{sol} gives more accumulation and may give an excessive peak LOD.

Therefore, we can verify whether the mechanistic model fits well to a set of experimental data by plotting peak LOD against Q_{air}/m_{sol}. The expected slope and intercepts for peak LOD can be evaluated from equation (4).

2.3. Design space

Historically, operating conditions for pharmaceutical processes were often defined as a single set point, which was inconvenient and inflexible. The modern approach as defined in ICH Q8 [5] is to define a set of ranges for each key parameter, creating a "Design Space". The process can be operated anywhere within this envelope, but during development, it must be verified that the process can achieve key quality parameters under all possible operating conditions.

The analysis above shows that four operating parameters, m_{sol}, F_{air}, T_{in} and Y_{in}, can affect Q_{air}/m_{sol} and hence peak LOD. It is convenient to represent these as a two-dimensional design space by combining the first 3 parameters into Q_{air} (see Fig. 3 for an example). However, Q_{air}/m_{sol} plots as sloping lines on this diagram, and is a minimum at the bottom right-hand corner, giving a maximum value for the peak LOD. If this leads to overwetting and defluidisation, this region will not be acceptable for operation. However, if the maximum peak LOD for successful granulation is found by experiment, the corresponding value of Q_{air}/m_{sol} can be calculated and the available design space can be maximized by truncating the bottom right-hand corner. Likewise, if the top left-hand corner is too dry and gives poor granulation, this can also be truncated.

2.4. Application to a real pharmaceutical process

The model was applied to a real process for which experiments showed that stable granule size was obtained with a peak LOD of 12.2% or less [4]. Experimental data for peak LOD at both pilot-plant and commercial scale fitted well to a straight line when plotted against Q_{air}/m_{sol}, as shown in Figure 2. However, there was a substantial offset between the two sets of data. Using standard scaling rules based on the basic model in section 2.1, the LOD at commercial scale was significantly higher than predicted, and defluidisation was observed on a batch under "wet" conditions (high spray rate, low temperature, low airflow). The extended model in section 2.2 showed that the adjustments for atomization, moisture binding, bed preheating and heat losses were small, but that there was a substantial difference between the filter bag shaking regimes at pilot and commercial scale. The ratio τ_{air}/τ_{spray} was much greater at pilot scale, and when equation (4) was applied instead of (3), this correctly predicted the observed difference between pilot and commercial scale.
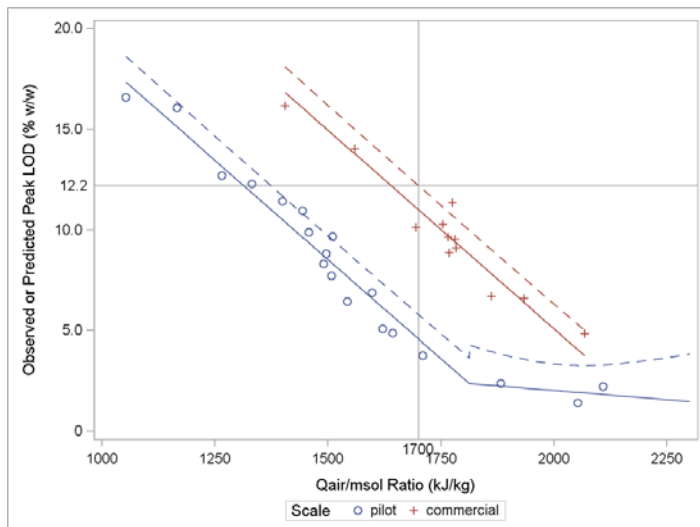
Fig. 2 Experimental results for peak LOD plotted against Q_{air}/m_{sol} ratio

The resulting commercial design space is shown in Figure 3. For operational simplicity, ranges can be defined for all the individual operating parameters, which plot as a rectangle which always falls within the design space. Moreover, the effect of changes in equipment can be anticipated, for example moving from a unit with simultaneous bag shaking (E1, broken lines) to consecutive shaking, where the air and liquid flows are continuous and $\tau_{spray} = \tau_{air} = 1$ (E2, solid lines). The value of Q_{air}/m_{sol} corresponding to the peak LOD is increased, the design space shrinks and the operating conditions need to be altered.
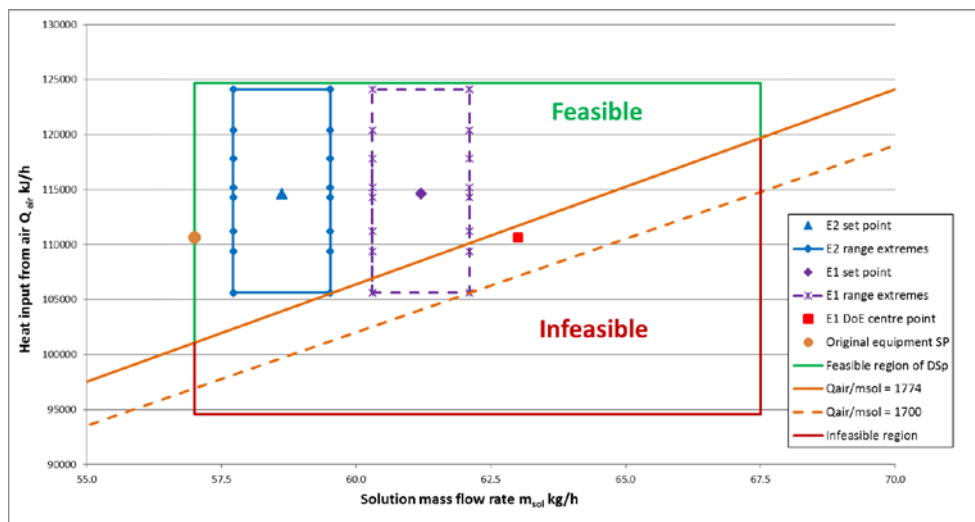
Fig. 3 Design and operating space at commercial scale with simultaneous bag shake and air cutoff (dotted lines) and consecutive bag shake with continuous flows (solid lines)

3. Tablet film coating

The most common type of pharmaceutical tablet coater is the perforated pan batch coater, in which coating solution is sprayed on to a region of the surface of a rolling bed of tablets. These tablets move back into the bulk bed within a few seconds and their surface must be sufficiently dry to avoid them sticking together, causing surface damage or "twinning".

Current models were reviewed by Kemp et al [6], and can include four main aspects:

1. Mass balance - relates spray rate, suspension concentration and solids throughput
2. Heat balance - relates air flow rate, inlet and exhaust temperature and spray rate
3. Drying kinetics - calculates heat transfer and evaporation rates at the tablet surface
4. Spray effects - relates spray rate, spray area, coating film thickness and coating time.

The first two categories are routinely used in operation [7] – van den Ban et al. However, little had previously been done to study tablet surface kinetics, although Ebey [8] noted that

heat and mass balances could not explain all observations and proposed an Environmental Equivalency (EE) factor to allow for this. Kemp et al [6] demonstrate that the locus of the boundary where overwetting and other adverse effects occur is dependent mainly on exhaust temperature and secondarily on spray rate. Again, this leads logically to the conclusion that if the size of the design space is to be maximized, it will have a sloping lower boundary. In practice, fixed operational ranges for exhaust temperature and spray rate will usually be more convenient, but the model also demonstrates that the key point where failure is most likely is the bottom right corner (low temperature, high spray rate). The modelling at tablet level also explains the long-standing observation that the bed temperature is significantly higher than the wet bulb temperature, unlike fluidised beds. At the tablet surface, the heat for evaporation is coming not primarily from the hot air, by convection, but by conduction from the warm tablet itself. The dry tablet bed is heated up by the air. For example, a coater with an air inlet temperature of 60^0C will typically have a bed temperature of 40-45^{0}C whereas the wet bulb temperature is 25^{0}C.

4. Comparison between the processes

Although fluid bed granulation and tablet film coating show many similar effects, there are some important conceptual differences. As noted above, in a fluidised bed of granules the heat of evaporation comes by convection from the hot air and the bed is normally at T_{wb}, whereas in a rolling bed of tablets the heat to evaporate the surface liquid film comes mainly by conduction from the tablet and the bed temperature is significantly above T_{wb}.

4.1. Modelling

Kemp [9] noted the distinction between models that can be "used once" (complex models to enhance process understanding) and "used regularly" (simple operational calculations). Both types of model are useful in these processes.

For fluid bed granulation, the full model can be "used once" for scale-up calculations and to establish the design space. A basic calculation of Q_{air}/m_{sol} can be used to ensure that the everyday operating conditions remain within the design space.

For tablet coating, the full model demonstrates the effects of surface drying kinetics, the design space shape and the number of coating passes. For normal operation, the heat and mass balance is sufficient, e.g. to give new coating times if the coating type is changed (Opadry® II can work at higher concentrations than Opadry® I), or required inlet temperature for a given exhaust temperature and spray rate when developing a DoE.

4.2. Design space

The analysis shows that both processes can have a trapezoidal design space with a sloping lower boundary regulated by overwetting effects [8]. However, the governing factors are

different. For fluid bed granulation the boundary line is given by the Q_{air}/m_{sol} value which is dependent on the macroscopic heat and mass balance. In contrast, for tablet film coating the boundary is regulated by kinetic effects, balancing the incoming spray rate with the evaporation rate at the tablet surface due to the local tablet temperature, and the slope is given by the variation of vapour pressure with temperature.

5. Conclusions

Processes involving simultaneous wetting and drying have significant differences from those involving only drying. Design, scale-up and control present specific challenges, and operating windows are often narrower. These effects can now be modelled successfully.

6. References

[1] Pandey, P. and Bharadwaj, R., eds. Predictive Modeling of Pharmaceutical Unit Operations", 1st Edition. Woodhead Publishing (Elsevier), 2016.

[2] Lyngberg, O., Bijnens, L., Geens, J., Marchut, A., Mehrman, S., Schafer, E. Applications of Modeling in Oral Solid Dosage Form Development and Manufacturing. In: Ierapetritou M., Ramachandran R. (eds) Process Simulation and Data Modeling in Solid Oral Drug Development and Manufacture, Methods in Pharmacology and Toxicology. Humana Press, New York, NY, USA, 2016.

[3] Gupta, R. Fluid bed granulation. Chapter 6 in Pandey & Bharadwaj, ref.[1].

[4] Kemp, I.C., van Millingen, A. and Khaled, H. Development and verification of a novel design space for fluid bed granulation using a mechanistic model. Paper submitted to Pharmaceutical Development and Technology, 2018.

[5] ICH Q8. ICH harmonised tripartite guideline: Pharmaceutical Development, Q8(R2), 2009. ICH (International Conference on Harmonisation of technical requirements for registration of pharmaceuticals for human use). Available online at www.fda.gov.

[6] Kemp, I.C., Iler, L., Waldron, M. and Turnbull, N. Modelling, experimental trials and design space determination for the GEA ConSigma™ coater. Paper accepted for Drying Technology, 2018. DOI: 10.1080/07373937.2018.1463244. Originally presented at Eurodrying 2017, Liege, Belgium.

[7] van den Ban, S.; Pitt, K.G.; Whiteman, M. Application of a tablet film coating model to define a process-imposed transition boundary for robust film coating. Pharmaceutical Development and Technology, 23:2 (2018), 176-182. DOI: 10.1080/10837450.2017.1384492..

[8] Ebey, G.C. A thermodynamic model for aqueous tablet film coating. Pharmaceutical Technology, **1987**; 11(4): 40-50.

[9] Kemp, I.C. Application of mechanistic drying models in pharmaceuticals and other industries. Paper submitted to Drying Technology, 2018.

Electrohydrodynamic (EHD) drying: fundamentals and applications

Martynenko, A.[*]; Kudra, T.

Department of Engineering, Faculty of Agriculture, Dalhousie University, Truro, NS, Canada

*E-mail of the corresponding author: alex.martynenko@dal.ca

Abstract

Following background to the phenomenon of electrohydrodynamics with concise review of basic features like shorter drying time, lower energy consumption and better product quality, the selected key factors affecting EHD drying are examined. These include the geometry of discharge electrodes, effects of air humidity on drying rate, depression of material temperature, and cooling effect of ionic wind.

Examples are given for: (i) prototype EHD dryers of multi-belt types, and (ii) pilot-scale multi-belt EHD dryer in vertical arrangement that can be aggregated into one unit of higher capacity, and vertical cylindrical EHD dryer with vibrated shelves.

Keywords: ionic wind; corona discharge; drying; energy; quality.

1. Introduction

Electrohydrodynamic (EHD) drying appears to be a viable technology alternative to conventional thermal drying for certain thermally-labile materials, such as high-value bioactive components of fruits and medicinal plants (polyphenols, flavonoids, dietary fiber, etc.), living cells (bacteria, yeasts and viruses), and non-living substances of biological origin (blood plasma, serum, hormones, antibiotics, probiotics, nutraceuticals, etc.).[1-4]

The benefits of EHD compared to hot air drying on food quality include lesser shrinkage [15, 16], higher rehydration ratio [15], preserved content of ascorbic acid (vitamin C) [17] and no discernible color degradation [16-20], though Li et al. [21] reported distinctive browning of okara cake just under the needle electrode. The quality-related benefits can be attributed to increased drying rate respectively by 1.5 to 4 times at high (5 ms^{-1}) and low (1 ms^{-1}) cross-flow air velocity, which translates into shorter drying time [22, 23] Although the sole ionic wind can favorably affect mass transfer, the combinations of EHD with low-temperature air drying[4-6], vacuum freeze drying[7] and auxiliary contact heating [8] have also been reported.

Energy consumption in EHD drying is much lower than that in hot air drying, likely because of targeted supply of energy for moisture evaporation and practically no heat lost with exhaust air. However, the favorable low energy consumption given in published papers is based on the "net" energy calculated from the applied voltage and current. Even though the real energy consumption by EHD and peripheral equipment ranges from 90 to 5000 kJkg^{-1} [2] it is still attractive for end used of EHD dryers. The energy-related issues in EHD drying have been reviewed by Kudra and Martynenko.[23]

Aside from purely experimental research on EHD drying of apples, carrot, potato, tomato, mushrooms, spinach, rapeseed, grapes blueberry, cranberry, etc., as well as model materials such as water, paper tissue, agar gel, wet sand and glass, theoretical studies on EHD drying are focused on determination of the ionic wind characteristics, such as space charge and corona current distributions [9, 10] or numerical solution of the mathematical model with experimental validation through drying experiments.[11-14]

Electrohydrodynamic (EHD) drying relies on the so-called corona (electric or ionic wind), originating from a sharp electroconductive needle or horizontal fine wire under high AC or DC voltage.[24] As a result, ions leaving discharge electrode impinge the surface of the drying material located on the metallic and electrically grounded plate-type electrode. The partially ionized gas molecules along with residual non-charged molecules create a jet-type gas flow between the discharge (needle or wire) electrode and the collecting (solid or perforated plate) electrode. Since some factors affecting EHD drying (e.g., voltage, current, temperature) are well presented in topical literature [25], this paper is focused on less elaborated factors, such as desirable geometry of electrodes and air humidity on EHD drying. Examples of large-scale dryers are also given.

2. Key factors in EHD drying

2.1. Geometry of discharge electrode

The fundamental studies on EHD drying were performed mostly with a single pin or wire, and only few of them used multi-pin electrodes, yet placed arbitrarily regarding geometrical arrangement (e.g., rectangular or triangular) and spacing between pins. However, because of conical form of the ionic wind [26], the impact surface of the wind from a single pin electrode on the plate electrode is circular unless disturbed by the air cross-flow, for example. Referring to multi-pin electrode it is intuitive to expect that the minimum distance between pins at a definite pin-to-material gap should result in a series of circular areas on the material surface which almost touch each other.[22]

It should be noted that the gaseous jet of ionic wind impinging the material under drying rebounds from the material surface along with the stream of evaporated moisture, which affects the aerodynamics of neighboring jets emitted from a multi-needle or multi-wire electrode. It means that the optimum spacing of pins is larger than theoretically predicted. This conclusion is supported by our own research [26] and literature data which indicate that single-pin electrode performs better that the multi-pin electrode.[27] The same effect is expected for multi-wire discharge electrode.

2.2. Effect of air humidity

Even though the air humidity plays significant role in the process of drying, its effect on the EHD performance has rarely been studied. Air humidity was measured in several studies by Lai[28] to calculate the Sherwood number but no explicit relationship for relative humidity was given. Bai et al.[29] presented results of vacuum freeze drying, which revealed better performance of EHD drying at ambient temperature 18ºC and relative humidity of 45% versus vacuum freeze drying (conditions were not specified, however).

To fill this gap in the knowledge we performed targeted research on EHD drying of sliced white champignons at various humidity levels controlled by dehumidifier.[30] The results show that high air humidity is detrimental for the performance of EHD drying. Decreasing air humidity from 70 to 30% significantly increased drying rate (drying rate constant increased more than threefold from 0.12-0.13 to 0.45-0.5 h^{-1}). These experiments confirmed that low air humidity is definitely desirable in EHD drying.

2.3. Depression of material temperature

Among various electrically-induced phenomena in EHD drying[2, 25] is a noticeable temperature drop in the boundary layer at the liquid-gas interface[31, 32], which was identified as large as 8 K per 100 micrometers.[33] Usually temperature depression of wet material is a result of water evaporation, which depends on the gradient of water vapor

pressure at the liquid-gas interface. The maximum value of temperature depression could be calculated through absolute air humidity Y (kg H$_2$O) (kg^{-1} dry air)

$$T_{DB} - T_{WB} = \frac{\Delta H_{WB}}{c_H}(Y_{sWBT} - Y) \qquad (1)$$

where T_{DB}, T_{WB} denote respectively the dry- and wet-bulb temperatures (K), ΔH_{WB} is the latent heat of evaporation at wet bulb temperature (kJ kg^{-1}), c_H quantifies the humid heat (kJ kg^{-1} K^{-1}), and Y_{sWBT} stands for the absolute air humidity at wet bulb temperature.[34] Our own research aimed at measuring temperature of the wet paper towel with thermal imaging camera revealed noticeably difference between air/material temperatures during EHD drying under controlled humidity of 11% and different air velocities.[35]
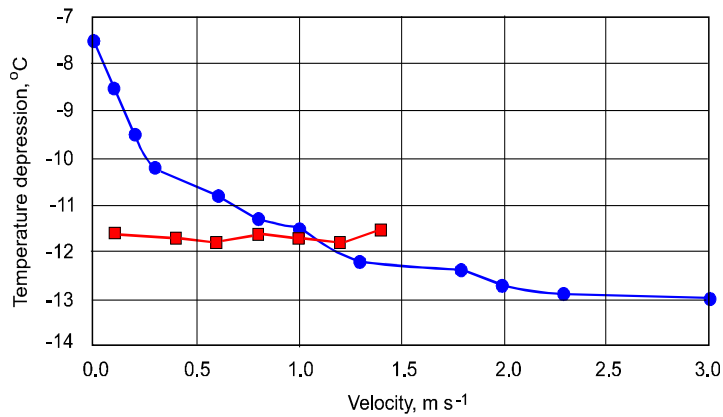
Fig. 1 Magnitude of temperature depression for paper towel exposed to forced air flow at 21.6ºC (blue points) and ionic wind (red points) generated at 9.5-15 kV.

It is evident that the temperature drop in humid air reflects typical psychrometric curve leveling off at high air velocity (above 6 ms^{-1}). Thus, the cooling effect of air flow is directly related to air velocity. In contrast, temperature drop due to ionic wind demonstrated completely different behavior. The range of ionic wind velocities below 1.0 ms^{-1} corresponded to electric field strength 3-4 kVcm^{-1} (9.5-12 kV), whereas ionic wind velocity above 1.0 ms^{-1} was induced by electric field above 4 kVcm^{-1} (13-15 kV). Interestingly, temperature drop due to ionic wind is larger than the effect of similar air flow at the range of low velocities, while is smaller for the velocity above 1.0 ms^{-1}. However, it should be noted that EHD-induced temperature of the material surface never attains the wet bulb temperature at convective air flow, which in this case is 13ºC at RH=11%. Interestingly, the cooling effect of EHD was found practically independent of ionic wind velocity up to 1.5 ms^{-1} above which the breakdown occurred because of excessively high electric field intensity.

2. Large-Scale EHD dryers

2.1. Prototype EHD dryers

It appears that the first prototype EHD dryer has been designed in Ukraine, in 1989 and tested for sliced apples.[36] The dryer has been built as a three-band conveyor unit fed with wet material at the upper band and discharged from the lower band. Although the dryer operates continuously with respect to material flow down from band-to-band the air in the dryer is basically stagnant. It means that moisture released from wet material builds-up air humidity and concentrations of volatile compounds and ionization products such as ozone. Therefore, after certain period the feeder is stopped and the empty dryer is blown with fresh ambient by a draft fan. The drying cycle is then repeated with the new batch of a drying material. The bands 0.8×0.3 m are driven at controlled velocity from 0.1 to 1 m/min. The needles in discharge electrodes with optimum packing density of 500 needles per 1 m^2 are made from molybdenum and powered with 10 to 30 kV AC at 50 Hz. The density of current about 0.01 A m^{-2} and power of 100 W m^{-2} results in apple temperature by 20 deg higher than the ambient temperature. Energy consumption for drying apple slices from 85 to 20% wb is on the order of 0.95-1.1 kWh per kg of evaporated water.

Another prototype of EHD continuous dryer is based on two belt conveyors 0.3 m wide and 3 m overall length with inter-stage mixing of the material.[37] Belts tilted at 11.5º are driven at fixed velocity of 0.33 ms^{-1}. Wire-type discharge electrode is made from stainless steel wire 0.5 mm in diameter with 5 cm spacing between neighboring wires. The wires arranged in parallel through a cable bus are connected to reversible polarity DC power supply with regulated voltage from 1 to 50 kV and current from 0 to 0.3 mA.

Tests with wet sand at 8-12 % wb in a 2-cm layer with 2.52 cm gap between discharge electrode and the material surface revealed drying enhancement by 1.35 at 12 kV and throughput of 3.1 kg of evaporated water per 1 hour. This dryer can be used for processing of granular materials in size up to 10 mm such as sand, gravel, preformed (extruded) pastes as well as sliced or diced fruits and vegetables.

2.2. Pilot-scale EHD dryers

As of year 2018 there is no information on commercially available EHD dryers. However, large EHD dryers of various designs have been custom-made in China for research purpose[38]. These dryers are basically of two types: (i) multi-band dryer in vertical arrangement (GXJ-2) that can be aggregated into one unit (GXJ-16), and (ii) vertical cylindrical dryer (GTJ-1.7) with vibrated shelves (Fig. 2).

The overall size is $1.6{\times}1.7{\times}\,2.4$ m (for GXJ-2) and $5.2{\times}3.5{\times}\,3.1$ m for GXJ-16 where numbers in the model signify drying area in m^2. Depending on the material, drying rate is over 3 kg of water per m^2h at corona power of 0.4 and 3.2 kW, respectively. The dryer is

equipped with dehumidifier with power 0.37 and 5.5 kW, respectively. The dryer GTJ-1.7 is 1.7 m in diameter with 5 shelves with drying area of 10 m^2 vibrated with amplitude 0-4 mm. Drying rate is over 5 kg of evaporated water per m^{2}h at corona power 2.2 kW. These dryers were used to dehydrate various whole and cut fruits and vegetables including specific plants used in Chinese medicine.
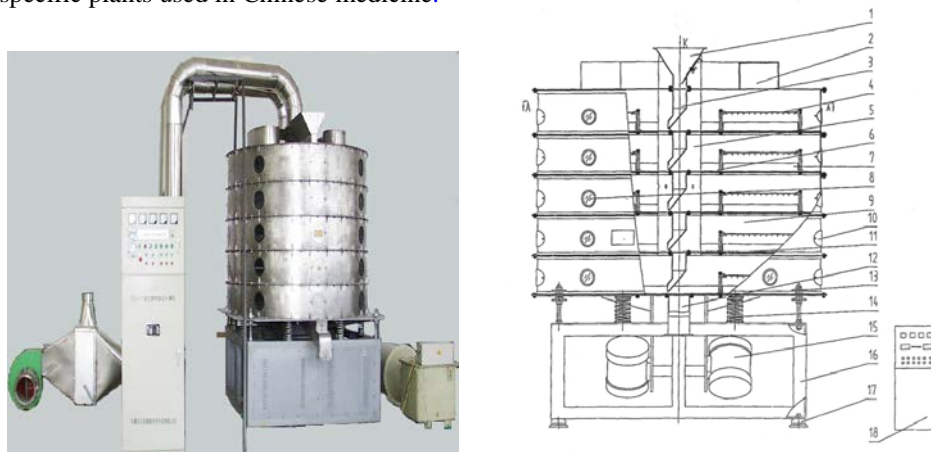
Fig. 2 The picture and schematics of the EHD dryer model GTJ-1.7. [38]

References

[1] Bajgai, T. R.; Raghavan, G. S. V.; Hashinaga, F.; Ngadi, M. O. Electrohydrodynamic drying – A concise overview. Drying Technology 2006, 7(7), 905 -910.

[2] Singh, A.; Orsat, V.; Raghavan, G. S. V. A comprehensive review on electrohydrodynamic drying and high-voltage electric field in the context of food and bioprocessing. Drying Technology 2012, 30(16), 1812-1820.

[3] Zhang, M.; Chen, H.; Mujumdar, A. S.; Zhong, Q.; Sun, J. Recent developments in high-quality drying with energy-saving characteristic for fresh foods. Drying Technology 2015, 33(13), 1590-1600.

[4] Alemrajabi, A. A.; Rezaee, F.; Mirhosseini, M.; Esehaghbeygi, A. Comparative evaluation of the effects of electrohydrodynamic, oven, and ambient air on carrot cylindrical slices during drying process. Drying Technology 2012, 30(1), 88-96.

[5] Dinani, S. T.; Hamdami, N.; Shahedi, M.; Havet, M. Mathematical modelling of hot air/electrohydrodynamic (EHD) drying kinetics of mushroom slices. Energy Conversion and Management 2014, 86, 70-80.

[6] Singh, A.; Vanga, S. K. K.; Nair, G. R.; Gariepy, Y.; Orsat, V.; Raghavan, G. S. V. Electrohydrodynamic drying of sand. Drying Technology 2017, 35(3), 312-322.

[7] Bai, Y.; Yang, Y.; Huang, Q. Combined electrohydrodynamic (EHD) and vacuum freeze drying of sea cucumber. Drying Technology 2012, 30(10), 1051-1055.

[8] Lai, F. C.; Wang, C. C. Drying of partially wetted materials with corona wind and auxiliary heat. In Proceedings of ESA Annual Meeting on Electrostatics, Minneapolis, USA, June 17-19, 2008; Paper B1.

[9] Zhao, L.; Adamiak, K. EHD flow in air produced by electric corona discharge in pin–plate configuration. Journal of Electrostatics 2005, 63 (3–4), 337-350.

[10] Ahmedou, S. A.; Rouaud, O.; Havet, M. Assessment of the electrohydrodynamic drying process. Food and Bioprocess Technology 2009, 2(3), 240-247.

[11] Chen, Y.; Barthakur, N. N.; Arnold, N. P. Electrohydrodynamic (EHD) drying of potato slabs. Journal of Food Engineering 1994, 23(1), 107-119.

[12] Huang, M.; Lai, F. C. Numerical study of EHD-enhanced water evaporation. Journal of Electrostatics 2010, 68(4), 364-370.

[13] Heidarinejad, G.; Babaei, R. Numerical investigation of electro hydrodynamics (EHD) enhanced water evaporation using Large Eddy Simulation turbulent model. Journal of Electrostatics 2015, 77, 76-87.

[14] Zhong, C.; Martynenko, A.; Wells, P.; Adamiak, K. Numerical investigation of the multi-pin electrohydrodynamic dryer: effect of cross-flow air stream. Journal of Food Engineering 2018 (submitted).

[15] Bajgai, T.R.; Hashinaga, F. High electric field drying of Japanese radish. Drying Technology 2001a, 19(9), 2291-2302.

[16] Alemrajabi, A. A.; Rezaee, F.; Mirhosseini, M.; Esehaghbeygi, A. Comparative evaluation of the effects of electrohydro dynamic, oven, and ambient air on carrot cylindrical slices during drying process. Drying Technology 2012, 30(1), 88-96.

[17] Bajgai, T.R.; Hashinaga, T. Drying of spinach with a high electric field. Drying Technology 2001b, 19(9), 2331-2341.

[18] Xue, X.; Barthakur, N.N.; Alli, I. Electrohydrodynamically-dried whey protein: an electrophoretic and differential calorimetric analysis. Drying Technology 1999, 17(3), 467-478.

[19] Hashinaga, F.; Bajgai, T. R.; Isobe, S.; Barthakur, N. N. Electrohydrodynamic (EHD) drying of apple slices. Drying Technology 1999, 17(3), 479–495.

[20] Esehaghbeygi, A.; Basiry, M. Electrohydrodynamic (EHD) drying of tomato slices (*Lycopersicon esculentum*). Journal of Food Engineering 2011, 104(4), 628-631.

[21] Li, F.D.; Li, L.T.; Sun, J.F.; Tatsumi, E. Effect of electrohydrodynamic (EHD) technique on drying process and appearance of okara cake. Journal of Food Engineering 2006, 77(2), 275-280.

[22] Kudra, T.; Martynenko, A. Design considerations for EHD drying. In Proceedings of 20th International Drying Symposium (IDS 2016), Gifu, Japan, 7-10 August, 2016.; Paper P-3-5

[23] Kudra, T.; Martynenko, A. Energy aspects in electrohydrodynamic drying. Drying Technology 2015, 33 (13), 1534-1540.

[24] Goldman, M.; Goldman, A.; Sigmond, R. S. The corona discharge, its properties and specific uses. Pure and Applied Chemistry 1985, 57 (9), 1353-1362.

[25] Martynenko, A.; Kudra, T. Electrically-induced transport phenomena in EHD drying - a review. Trends in Food Science and Technology 2016, 54, 63-73.

[26] Martynenko, A.; Kudra, T.; Yue, J. Multipin EHD dryer: Effect of electrode geometry on charge and mass transfer. Drying Technology 2017, 35 (16), 1970-1980.

[27] Lai, F. C.; Sharma, R. K. EHD - enhanced drying with multiple needle electrode, Journal of Electrostatics 2005, 63, 223-237.

[28] Alem-Rajabi, A.; Lai, F.C. EHD-enhanced drying of partially wetted glass beads. Drying Technology 2005, 23 (3), 597-609.

[29] Bai, Y.; Hu, Y.; Li, X. Influence of operating parameters on energy consumption of electrohydrodynamic drying. International Journal of Applied Electromagnetics and Mechanics 2011, 35, 57-65.

[30] Martynenko, A.; Kudra, T. Electrohydrodynamic drying of white champignons. In Proceedings of EuroDrying 2017 - 6th European Drying Conference, Liege, Belgium, June 19-21, 2017, 185-186. Poster 39.

[31] Barthakur, N.N. Electrohydrodynamic enhancement of evaporation from NaCl solutions. Desalination 1990, 78, 455-465.

[32] Hashinaga, F.; Kharel, G.P.; Shintani, R. Effect of ordinary frequency high electric fields on evaporation and drying. Food Science Technology International 1995, 1 (2), 77-81.

[33] Lindsay, A.; Anderson, C.; Slikboer, E.; Shannon, S.; Graves, D. Momentum, heat and neutral mass transport in convective atmospheric pressure plasma-liquid systems and implications for aqueous targets. Journal of Physics D: Applied Physics 2015, 48, 424007 (14 pp).

[34] Pakowski, Z.; Mujumdar, A.S. Basic Process Calculations and Simulations in Drying. In Handbook of Industrial Drying; Mujumdar, A.S., Ed.; CRC Press: Boca Raton, FL, 2015: 51-75.

[35] Martynenko, A.; Kudra, T. 2018 (unpublished results).

[36] Panchenko, M.S.; Panasyuk, A.L.; Mosievich, A.S.; Moroz, G.A. Application of threshold discharge to supply energy in drying of apple slices. Electronic Processing of Materials 1989, 3 (147), 61-64 (in Russian).

[37] Lai, F.C. A prototype of EHD-enhanced drying system. Journal of Electrostatics 2010, 68, 101-104.

[38] Liang, Y-Z.; Ding, C-J. High Voltage Electric Field Drying. In Modern Drying Technologies, 2nd Enhanced Edition; Pan, Y-K.; Wang, X-Z.; Liu, X-D. Eds.; Chemical Industry Press: Beijing, 2007; 840-858 (in Chinese).

FUNDAMENTALS, MODELING AND SIMULATION

Oral Presentations

Robust feedback control of continuously operated convective dryers for particulate materials

Seidel, C.ᵃ; Neugebauer, C.ᵃ; Dürr, R.ᵇ; Bück, Aᶜ*

ᵃ Automation/Modelling, Otto von Guericke University Magdeburg, Magdeburg, Germany
ᵇ KU Leuven, Leuven, Belgium
ᶜ Institute of Particle Technology, FAU Erlangen-Nuremberg, Erlangen, Germany

*E-mail of the corresponding author: andreas.bueck@fau.de

Abstract

Convective drying is a common process for the treatment of particulate solids also operated in continuous mode. Continuous operation is characterised by operation in steady-state with constant product throughput and constant product quality. Due to external influences, i.e. seasonal or local variations in the properties of the initial wet material, deviations in the product quality can result, for example over- or under-drying, or on-set of unwanted reaction. In this contribution a new feedback control concept is developed that is robust with respect to variations and uncertainties in the drying kinetics of the material and can reject and attenuate process disturbances.

Keywords: Process control; drying kinetics; robustness; fluidized bed; yeast.

1. Introduction

Drying, the removal of liquid from a solid material, is one of the major unit operations in solids processing, e.g. chemicals, pharmaceuticals, food and paper[1,2]. The liquid can be removed mechanically, e.g. draining, wringing, filtering, or thermally by induction of a phase change, e.g. by evaporation or sublimation of the liquid. Thermal drying is extensively used and is one of the most energy-intensive processes, taking up approximately 10-25% of a nation's energy output[1].

Considering convective drying of particulate solids, characteristic evaporation rates as a function of moisture content X, i.e. the mass of liquid per mass of dry solid, are shown in Fig. 1: For moisture contents $X > X_{cr}$, where X_{cr} is the material-specific critical moisture content, a constant evaporation rate is observed; for moisture contents $X_{hyg} < X < X_{cr}$ a material-dependent falling rate is observed. If the moisture content reaches X_{hyg}, thermodynamic (adsorption) equilibrium is attained and the evaporation rate vanishes.
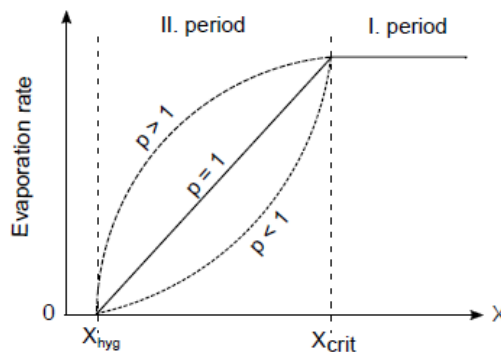
Fig. 1. Schematic overview of experimentally observed evaporation rates in drying of solids.

The first (constant) drying period refers to the surface-wet particle, i.e. direct heat and mass transfer between liquid and gas. In this period, the heat and mass transfer is gas-side controlled, i.e. the gas conditions, e.g. temperature and mass flow rate, directly determine the evaporation rate. In the second drying period, the falling rate period, moisture is mostly located in the (porous) interior -- heat and gas now have to penetrate the solid by conduction and diffusion first in order to evaporate the liquid; also the vapour has to be transported to the particle surface, e.g. by vapour diffusion or capillary pumping, before it can be taken up by the main gas flow. The farther inside the moisture is located, the longer diffusion and conduction processes take and thereby reduce the evaporation rate in the second drying period.

From this phenomenological description, two different aspects can be identified that influence the drying process: (1) gas-side conditions and (2) material properties. A variation of gas-side conditions only will yield different evaporation rates; the material-specific part, however, remains the same, i.e. the evaporation rates are qualitatively but not quantitatively similar.

An approachto model this effect is given by the concept of normalized drying curve ν (NDC), originally developed by van Meel[3]. Here, the second drying period rate is expressed in terms of the (known and constant) gas-side controlled first drying period rate. Main advantage of the NDC is that it can be obtained directly from considerably simpler measurements than effective diffusivity; main drawback is that it only allows describing the evolution of the average moisture content, X. However, as this value is of primary concern in many practical applications, the concept of normalised drying curve has found wide-spread use for dryer design, optimisation and troubleshooting.

The normalised drying curve is defined as:

$$\dot{\nu}(\eta) = \frac{\dot{m}_{evap,II}}{\dot{m}_{evap,I}}, \quad \eta = \frac{X - X_{hyg}}{X_{cr} - X_{hyg}},$$

(1)

where η denotes the normalised moisture content, with values $0 \leq \eta \leq 1$ denoting the second drying period. Given experimental data, the normalised drying curve can be fitted and used for process modelling and feedback controller design as will be shown in the following.

In this work, we present a general approach to robust feedback control of continuously operated convective dryers. In the following section, we present the dynamic drying model equations. Afterwards, the robust controller is designed and its main features are discussed. In the Results section, the performance of the controller, designed for a nominal operating point, is presented with respect to model uncertainties and different operating points. The work closes with Conclusions and Outlook on future work.

2. Process Modelling

For the purpose of this work, we pose the following assumptions: (i) The particulate phase in the apparatus can be (at least theoretically) considered as well-mixed. (ii) The gas-phase is also considered as well-mixed, i.e. no spatial gradients. (iii) The particulate phase is either mono-disperse or represented by a constant Sauter mean diameter d_{32}, i.e. a particle size distribution is not considered. Each particle dries as if it were a single particle. (iv) Drying is kinetically-controlled, i.e. drying gas is not close to saturation. (v) Drying takes place under approximately adiabatic conditions, i.e. sufficient insulation of apparatus provided to avoid significant heat loss to the environment. (vi) Particles enter the apparatus

with an average moisture content X_{in} at a dry mass flow rate m'$_{dry,in}$. (vii) Evaporation takes place from the total surface area of all particles. (viii) The average residence time of particles in the continuously operated dryer is τ, which can be regulated, e.g. by speed of conveyor, or hold-up mass control.

Then, starting from a mass balance of the wet solid $m_{wet} = X\, m_{dry}$, the following mass balances for the dry solid (hold-up) and the average moisture content can be derived:

$$\frac{dX}{dt} = \left(\dot{m}_{dry,in} X_{in} - \frac{m_{dry}}{\tau} X - \dot{m}_{evap} - X \frac{dm_{dry}}{dt} \right) / m_{dry},$$

$$\frac{dm_{dry}}{dt} = \dot{m}_{dry,in} - \frac{m_{dry}}{\tau}.$$

$$(2)$$

The evaporation rate is written as

$$\dot{m}_{evap} = \dot{m}_{evap,I}\, A\dot{\nu} = \varrho_g \beta (Y_{sat}(T_{in}) - Y_{in}) A\dot{\nu}$$

$$(3)$$

wherein A denotes the total particle surface area available for evaporation; and Y_{sat}-Y_{in} the maximum drying potential of the gas, which is determined by the inlet gas moisture content Y_{in} and the inlet gas temperature T_{in}. If significant heat losses occur (violation of assumption (v)), then Y_{sat}-Y_{in} decreases in value to Y_{out}-Y_{in}; the model structure, however, does not change.

The total surface area of particles can be determined from the hold-up mass $A = 6m_{dry}/(\rho\, d_{32})$. The mass transfer coefficient β is in general a function of the Sherwood, Reynolds, Prandtl and Schmidt number.

The normalised drying curve is denoted by $\nu(\eta)$; in order to use the normalised drying curve in process models, some functional form needs to be fitted. In this work, the following form is used:

$$\dot{\nu}(\eta) = \frac{p\eta}{1 + (p-1)\eta}$$

$$(4)$$

The virtue of this functional form is that one fitting parameter p suffices to describe the different curvatures. At p=1, corresponding to the linear relation $\nu(\eta) = \eta$, a change in curvature occurs that can be smoothly related to values $0 < p < 1$ and $p > 1$. It has to be noted that all material characteristics are lumped into the parameter p.

Under the stated restrictions, the presented model is able to calculate the dynamic and steady-state behaviour of a continuous convective dryer.

3. Robust Controller Design

The aim of the robust controller is to provide comparable performance of the uncertain drying process with respect to the nominal process conditions and parameters. Specifically, it should provide at different steady-states the required steady-state output (controlled output), provide not too slow process dynamics in doing so, avoid excessive control action, respecting known limits of the actuators and operating conditions, e.g. a maximum operating temperature.

These requirements can be met in (linear) controller design within the H_∞ framework[4]. Within this framework, a (linear) controller with transfer function $H_\infty(s)$ is determined such that a) the closed-loop process is asymptotically stable and b) the following functional is minimised:

$$\min_{H_\infty \ stabilizing} \left\| \begin{array}{l} S(s) \cdot W_1(s) \\ H_\infty(s)S(s) \cdot W_2(s) \\ T(s) \cdot W_3(s) \end{array} \right\|_\infty \tag{5}$$

Therein, s denotes the variable of the Laplace domain, S denotes the closed-loop sensitivity function, T* the closed-loop complementary sensitivity function, and W_i (i = 1, 2, 3) are weight functions.

To assess and quantify the process uncertainty, different models can be used. In this work, we restrict ourselves to the multiplicative uncertainty model: Given a linear open-loop stable nominal transfer function $G_{nom}(s)$, and a second, uncertain but open-loop stable transfer function G(s)\$, the multiplicative model uncertainty can be expressed as

$$\Delta_m(s) = (G(s) - G_{nom}(s))G_{nom}^{-1}(s) \tag{6}$$

A variation in parameters generates a family of transfer functions G(s) and a set of multiplicative uncertainty models $\Delta_m(s)$. Let the upper-bound of $\Delta_m(s)$ for a given set of variations be denoted by $\Lambda_m(s)$.

For design of performance, the weights W_i can be used: W_1 is used to design good disturbance rejection over a wide frequency region; W_2 directly influences the controller gain, thus limiting the control energy; and W_3 is used to achieve good reference tracking. For a multiplicative uncertainty model, $W_3(s) = \Lambda(s)$ is set.

Given the nominal model, the upper bound on model uncertainty and the weight functions, a robustly stabilising feedback controller can be readily computed by established control software, e.g. Matlab's Control System Toolbox.

4. Results

In the following, specific results of the design and performance of the controller are presented for fluidized bed drying of spherical baker's yeast pellets. Uncertain parameters are: p ranges in the interval [0.5, 2.5] with a nominal value of 1.5, and X_{crit}, the point of on-set of the second drying period which is known to slightly depend on drying temperature: X_{crit} in the interval [0.8, 1.2] with a nominal value of 0.98.

The manipulated variable is the gas inlet temperature $T_{gas,in}$, the controlled output is the average moisture content of the yeast pellets, X, i.e. a SISO control problem. Unmeasured disturbances are the solids and gas inlet moisture contents, X_{in} and Y_{in}, respectively. For reasons of comparison a standard SISO PI controller and a linear quadratic regulator (LQI) are also designed for the nominal case.

Both controllers are applied to the nonlinear model to assess their performance and robustness of the closed-loop. We start the presentation with the discussion of disturbance rejection. At the nominal steady state, a stepwise disturbance (X_{in} -15%) is applied at t= 30 minutes and ends after additional 10 minutes. At 50 minutes a second disturbance (Y_{in} + 115%) is applied for 10 minutes. The closed-loop response under both controllers is shown in Fig. 2. It can be seen that in the nominal scenario, both controllers have comparable performance, i.e. the settling times after a disturbance.

To investigate the impact of the (uncertain) parameter p, additional simulations were performed under otherwise nominal conditions. Figure 3 shows the results of a simulation with the maximum value p= 2.5. One can clearly observe that the performance of the H_∞-controller is constant in the parameter range, even at at a different set-point. Contrary, the PI-controller and LQI-controller lose performance at a non-nominal set point and the decrease in performance is higher with increasing value of p.

5. Conclusions

We presented an application of robust controller design to a wide range of continuously operated convective drying processes, where the main process uncertainty is in the parameters of the kinetics of the second drying period. We could show that these processes are asymptotically open-loop stable for practically relevant operating parameters. Suitable feedback controllers can be designed in the H_∞ framework given the knowledge of a nominal operating point and bounds on the parameters.

Future work will focus on the extension of this approach to MIMO problems, considering additional manipulated variables, e.g. the gas mass flow rate, and controlled outputs, e.g. product temperature or water activity.
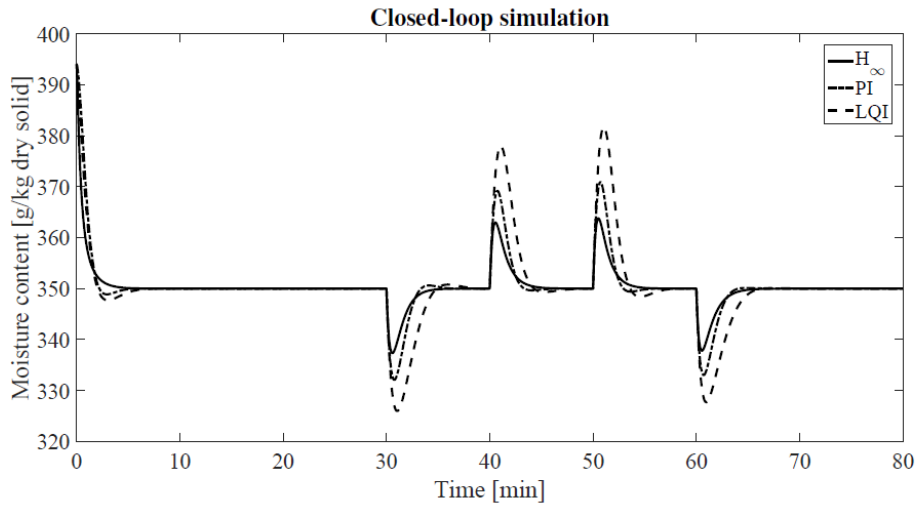
Fig. 2. Response of the controlled nominal system (H∞, PI and LQI controller) for the described disturbance scenario for the set points X = 350 (g water)/(kg dry solid).
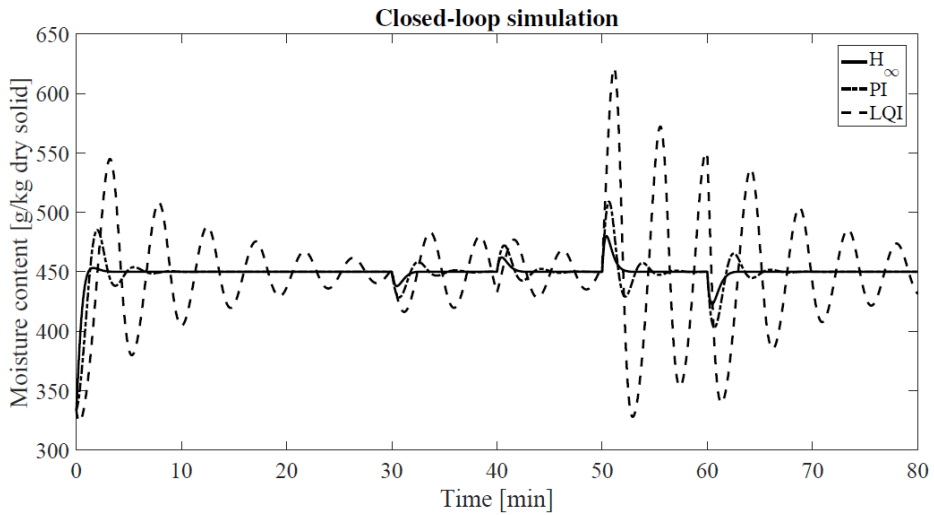
Fig. 3. Response of the controlled system (H∞, PI and LQI controller) for the described disturbance scenario for the non-nominal set-point X = 450 (g water)/(kg dry solid) and p= 2.5 (right).

6. Main Nomenclature

A		surface area	m^2
d		particle diameter	m
G,	S, T*	transfer functions	
m		mass	kg
p		parameter of NDC	
t		time	s
T		temperature	°C
X		solid moisture content (d.b.)	
Y		gas moisture content (d.b.)	

Greek letters

β	mass transfer coefficient	ms^{-1}
η	normalised moisture content	
ν	normalised drying rate	
ρ	mass density	kgm^{-3}
τ	mean residence time	s

Subscripts

crit	critical
in	inlet
hyg	hygroscopic
sat	saturation

7. References

[1] Kemp, I. Reducing dryer energy use by process integration and pinch analysis, Drying Technology 2005, 23 (5), 2089-2104.

[2] Tsotsas E. Influence of drying kinetics on partile formation: A personal perspective, Drying Technology 2012, 30 (11), 1167-1175.

[3] van Meel, D. Adiabatic convection batch drying with recirculation of air, Chemical Engineering Science 1958, 9, 36-44.

[4] Zhou, K.; Doyle, J. Essentials of robust control; Prentice Hall: Upper Saddle River, NJ, 1998.

Mathematical modeling of moisture evaporation in co-current foam spray drying

Jaskulski, M.[a]*; Lewandowski, A.[a]; Zbiciński, I.[a]

[a]Faculty of Process and Environmental Engineering, Lodz University of Technology, Wolczanska Str 213., 95-924 Lodz, Poland.

*E-mail of the corresponding author: maciej.jaskulski@p.lodz.pl

Abstract

Two models of foam drying are presented in the paper: single droplet drying and perfect mixing of phases spray drying models to describe mechanism of drying of droplet containing bubble.

Analysis of drying curves shows that in constant drying rate period and in the falling drying rate period, evaporation rate decreases due to particle shrinkage and increasing of resistance of moisture diffusion inside the solid crust. Increase of gas pressure in the bubble might cause particle breakage.

Slight differences between theoretical and experimental results caused by disregarding broken particles in the simulations proves accuracy of the developed model.

Keywords: spray drying, modeling, foamed materials, particle morphology

1. Introduction

Foaming of slurry in spray drying processes is a method to control rheological properties of feed like viscosity and density and morphology of powder. Powders obtained in foam spray drying process are characterized by lower bulk density, high porosity and particle sizes, enhanced solubility and wettability in relation to conventional spray drying. However, to control product quality, foam spray drying process must to be carried out in specific window of the process parameters selected individually for dried material.

In the literature there is lack of mathematical description of foamed spray drying process; existing models refer only to the constant drying rate period [1].

The aim of this work was to develop and validate mathematical model of foam spray drying process to determine morphological changes of particles and to estimate the quality of the product.

2. Foam spray drying model

Two models of foam drying were developed in the frame of the work: single droplet drying (SDD) model to check correctness of applied correlations and perfect phase mixing foam spray drying model to simulate drying process. All calculations were performed in Matlab and validated on a base of data obtained from the foam spray drying experiments performed at Lodz University of Technology [2].

2.1. Single droplet drying model

SDD model describes moisture evaporation of maltodextrin solution (DE12) from stationary droplet which contains a single saturated nitrogen bubble in constant ambient air temperature T_G, and humidity Y_G. In constant drying rate period, droplet shrinks due to water evaporation whereas in falling drying rate period, particle shrinkage stops because of crust solidification. In this period pressure in the gas bubble increases and might cause particle brakeage. The model allows to determine drying curves, particle density, porosity, crust thickness and pressure in the internal bubble.

2.1.1. Heat transfer

Moisture from the particle evaporates to surrounding air in temperature which, taking into account heat capacity of air and internal bubble, can be calculated from equation (1):

$$\frac{dT_p}{dt} = \frac{A_p \alpha_p (T_p - T_G) + h\left(\frac{dm_{p,a}}{dt} + \frac{dm_{p,b}}{dt}\right)}{m_p c_p + m_b c_b} \tag{1}$$

2.1.2. Mass transfer

Mass transfer model was based on the concept of characteristic drying curves [3]. Overall evaporation from the droplet/particle is a sum of moisture evaporation to the surrounding air and to the internal bubble, eq. (2):

$$\frac{dm_p}{dt} = \frac{dm_{p,a}}{dt} + \frac{dm_{p,b}}{dt} \tag{2}$$

Evaporation rate to drying air is calculated from the equation:

$$\frac{dm_{p,a}}{dt} = f M_w A_p \beta_p (C_s - C_G) \tag{3}$$

where heat and mass transfer coefficients (α_p and β_p) were calculated from McAdams correlations. Amount of water transferred to the bubble was determined from eq. (4):

$$\frac{dm_{p,b}}{dt} = m_N \frac{M_w}{M_N} \left(\frac{P_{st}}{P_a - P_{st}}\right) \frac{1}{dt} \tag{4}$$

To take into account decrease of drying rate (eq. (3)) in the falling drying rate period, coefficient f defined by relation (5) was used [5]. In constant drying rate period coefficient f is equal $f = 1$. After critical moisture content, due to increase in internal mass transfer resistance, f decreases to $f = 0$ at the equilibrium point. According to Woo et al. [4] coefficient f can be expressed as a function of moisture content:

$$f = \left(\frac{X - X_{eq}}{X_{cr} - X_{eq}}\right)^{3.22} \tag{5}$$

Critical moisture content for maltodextrin was determined experimentally in a frame of this work and calculated from eq.(5), (T_G in °C):

$$X_{cr} = 21555 \cdot T_G^{-2.106} \qquad\qquad R^2 = 0.976 \tag{6}$$

Equilibrium moisture content was calculated from GAB equation [5]:

$$X_{eq} = \frac{X_{mo} c k a_w}{(1 - k a_w)[1 + (c-1) k a_w]} \tag{7}$$

Where constants $c = 10.866$ and $k = 0.971$. Monolayer moisture content (X_{mo}) for maltodextrin is equal to 0.0518 kg/kg.

2.1.3. Particle morphology

Particle diameter was calculated from the sum of the volumes of liquid and internal gas bubble:

$$d_p = \sqrt[3]{\frac{6(V_L+V_b)}{\pi}} \tag{8}$$

In the constant drying rate period, change of liquid shell volume resulting from evaporation of moisture can be calculated from equation (9):

$$V_L = \frac{\rho_{L,0}(1+X_{cr})}{\rho_L(1+X_0)}\frac{\pi}{6}d_{p,0}^3 \tag{9}$$

In the falling drying rate period, particle can shrink due to thermal deformations of solidified crust. Particle shrinkage can be determined using modified equation proposed by Chen [6]:

$$V_L = \frac{\pi}{6}\left[d_{p,cr}\left(b+(1-b)\frac{X}{X_{cr}}\right)\right]^3 \tag{10}$$

Shrinkage coefficient *b* was calculated as a ratio of particle diameter when particle moisture content is equal to critical moisture content, to the final particle diameter measured experimentally. Equation (11) describes *b* as a function of drying air temperature (T_G in °C):

$$b = 0.41 + 0.0038T_G - 6.97\cdot10^{-6}T_G^2 \qquad R^2 = 0.971 \tag{11}$$

Volume of the internal bubble was calculated from the current bubble mass and density (12):

$$V_b = \frac{m_b}{\rho_b} \tag{12}$$

Density of the bubble depends also on the gas humidity and can be determined from equation (13):

$$\rho_b = \frac{P_b}{\frac{R}{M_N}T_p}(1+Y_b^*)\frac{1}{1+Y_b^*\frac{M_N}{M_W}} \tag{13}$$

Equation (12) can be transformed to equation (14) to calculate bubble diameter:

$$d_b = \sqrt[3]{\frac{6V_b}{\pi}} \tag{14}$$

Having diameter of particles (d_p) and bubbles (d_b), crust thickness (particle wall thickness) can be determined.

In constant drying rate period, pressure inside the particle was equal to the ambient pressure $P_b = P_a$. To calculate gas pressure inside the bubble in the falling drying rate period, we assumed proportional grow of pressure with particle temperature in isochoric process according to the equation (15):

$$P_b = P_a \frac{T_p}{T_{p,cr}} \tag{15}$$

Selected results of calculations are presented in Fig. 1. Fig. 1 shows grow of solid concentration and drying curve for the same initial bubble diameter and different initial droplet diameters.

Fig. 1 Solid concentration and evaporation rate from SDD model.

We may observe that as bigger droplet contains more liquid to be evaporated (initial bubble diameter is the same), particle solid concentration grows slower. Analysis of drying curves shows that in constant drying rate period evaporation rate slightly decreases due to particle shrinkage; in the falling drying rate period ($X < X_{cr} = 0.5$ kg/kg), drying rate falls down due to increasing of internal resistance of moisture diffusion inside the solid crust. Shape of drying curves is characteristic for evaporation from single droplets which confirms correctness of physical model of the process.

2.2. Co-current foam spray drying model

In co-current foam spray drying model air temperatures, particle velocities and air humidity were calculated from the heat, mass and momentum balance, equations (17) - (22) [7]. Foam spray drying calculations were carried out for perfect mixing of phases, axisymetrical flow of air and particles and monodispersed atomization. Momentum transfer between drying air and particles was determined from classical equations:

$$\frac{dv_{p,x}}{dt} = g\left(1 - \frac{\rho_G}{\rho_p}\right) - \frac{3}{4}C_D\frac{v_p(v_{p,x}-v_{G,x})\rho_G}{\rho_G d_p} \tag{17}$$

$$\frac{dv_{p,r}}{dt} = -\frac{3}{4} C_D \frac{v_p(v_{p,r} - v_{G,r})\rho_G}{\rho_G d_p} \tag{18}$$

$$\frac{dv_{p,z}}{dt} = -\frac{3}{4} C_D \frac{v_p(v_{p,z} - v_{G,z})\rho_G}{\rho_G d_p} \tag{19}$$

where v_p is relative particle velocity. Air humidity was calculated from mass balance:

$$\frac{dY_G}{dt} = \frac{-\dot{M}_L}{\dot{M}_G \rho_G} \left(\frac{\frac{dm_p}{dt}(1+X)}{m_{p,0} C_0 + m_{p,w}} \right) \tag{20}$$

Particle moisture content was determined from equation (21):

$$\frac{dX}{dt} = \frac{\frac{dm_p}{dt} + (Y_{eq} \cdot m_N - m_{G,W})(1+X)}{m_{p,0} C_0 + m_{p,w}} \tag{21}$$

Air temperature was determined from heat balance (22):

$$\frac{dT_G}{dt} = \frac{1}{\dot{M}_G c_G} \left(-\dot{M}_G(c_v T_G + h)\frac{dY_G}{dt} - \dot{M}_L(X c_w + c_s)\frac{dT_p}{dt} - \dot{M}_L c_w T_p \frac{dX}{dt} \right) \tag{22}$$

Selected results of calculations are shown in Fig.2. Figure 2 presents comparison of theoretically and experimentally determined wall thickness and particle density for different air temperatures and foaming gas rate. Final density of the material determined from the mathematical model decreased from 1300 kg/m^3 to 600 kg /m^3, which is in line with the experimental results. Differences in relation to the experiments are caused by disregarding broken particles in the simulations. Decrease in the wall thickness depends on the amount of gas introduced into the interior of the droplet. The higher degree of foaming, the larger gas bubble is trapped in the particle and the less material forms the particle.

Fig.2 Wall thickness and particle apparent density for a different air temperatures and different foaming gas rate.

3. Conclusions

Model of co-current foamed spray drying was developed to determine mechanism of droplet drying containing a single bubble.

Analysis of theoretical and experimental results shows that particle solid concentration grows slower for bigger droplet as it contains more liquid to be evaporated as initial bubble diameter is the same. In constant drying rate period evaporation rate slightly decreases due to particle shrinkage which typical for evaporation from droplets and confirms correctness of physical model of the process.

Density of the material determined from the mathematical model decreased twofold in relation to the initial which was in line with the experimental results. Decrease in the wall thickness is a function of the amount of gas introduced into the interior of the droplet. Particle wall thickness and particle density for different air temperatures and foaming gas rate are in line with the experimental results. Differences in relation to the experiments are caused by disregarding broken particles in the simulations.

4. Nomenclature

A	surface	m^3		T	temperature	°C
c	specific heat	$J\,kg^{-1}\,K^{-1}$		t	time	s
C	vapor concentration	$kg\,mol\,m^{-3}$		v	velocity	$m\,s^{-1}$
h	heat of evaporation	$J\,kg^{-1}$		V	volume	m^3
m	mass	kg		X	moisture content	$kg\,kg^{-1}$
M	molar weight	$kg\,mol^{-1}$		Y^*	saturated humidity	$kg\,kg^{-1}$
P	pressure	Pa		R	universal gas constant	$J\,mol^{-1}K^{-1}$

Greek letters

☐	heat transfer coefficient	$Wm^{-2}K^{-1}$
β	mass transfer coefficient	ms^{-1}
σ	stress	Pa

Subscripts

0	initial		L	liquid
a	ambient		N	nitrogen
b	bubble		p	particle

cr	critical	s	surface
eq	equilibrium	st	saturation
G	gas	w	water

5. References

[1] D. D. Frey and C. J. King, "Experimental and theoretical investigation of foam-spray drying. 1. Mathematical model for the drying of foams in the constant-rate period," *Ind. Eng. Chem. Fundam.*, vol. 25, no. 4, pp. 723–730, Nov. 1986.

[2] I. Zbicinski and J. Rabaeva, "Analysis of Gas Admixing Foam Spray–Drying Process," Dry. Technol., vol. 28, no. 1, pp. 103–110, Dec. 2009.

[3] R. B. Keey and M. Suzuki, "On the Characteristic Drying Curve," *Int. J. Heat Mass Transf.*, vol. 17, no. 12, pp. 1455–1464, 1974.

[4] M. W. Woo, W. R. W. Daud, A. S. Mujumdar, Z. Wu, M. Z. Meor Talib, and S. M. Tasirin, "CFD Evaluation of Droplet Drying Models in a Spray Dryer Fitted with a Rotary Atomizer," *Dry. Technol.*, vol. 26, no. 10, pp. 1180–1198, Sep. 2008.

[5] M. Jaskulski, P. Wawrzyniak, and I. Zbiciński, "CFD model of particle agglomeration in spray drying," *Dry. Technol.*, vol. 33, no. 15–16, 2015.

[6] X. Yang, J. Xiao, M.-W. Woo, and X. D. Chen, "Three-Dimensional Numerical Investigation of a Mono-Disperse Droplet Spray Dryer: Validation Aspects and Multi-Physics Exploration," *Dry. Technol.*, vol. 33, no. 6, pp. 742–756, Apr. 2015.

[7] T. A. G. Langrish, "Multi-scale mathematical modelling of spray dryers," *J. Food Eng.*, vol. 93, no. 2, pp. 218–228, Jul. 2009.

A mathematical model of spray drying granulation process in formulation

Kagami, H.

School of Medicine, Fujita Health University, Toyoake, Japan

*E-mail of the corresponding author: kagami@fujita-hu.ac.jp

Abstract

In this study, we apply the drying model of polymer solution coated on a flat substrate to the spray drying granulation process in formulation. In order to apply the former model to the drying of this spherical object, we consider this spherical object to be a stack of solution films applied on the spherical shell and discuss the drying process of each solution film. As a result, we see that the smaller the radius of curvature of the droplet, the more the fine particles tend to be unevenly distributed on the surface of the droplets during drying.

Keywords: model, numerical simulation, spray drying granulation, spherical, droplets

1. Introduction

Drying process of polymer solution coated on a substrate is very important in various industrial applications such as fabricating flat polymer thin films [1] and inkjet printing [2, 3]. Then we have proposed and modified a model of drying process of polymer solution coated on a flat substrate for flat polymer film fabrication [4 – 14]. Then we have proposed the method of thickness control of a thin film after drying [15 – 17]. And we have clarified dependence of distribution of polymer molecules on a flat substrate after drying on various parameters based on analysis of many numerical simulations of the model.

On the other hand, the demand that a flat polymer film should be formed not only on a flat substrate but also on a three-dimensional uneven substrate after drying a polymer liquid film coated on the substrate has been increasing with the advancement in microfabrication technology. Therefore, we expanded the above-mentioned model into the drying model of a polymer liquid film coated on three-dimensional structure. Then we analyzed dependence of distribution of polymer molecules on the three-dimensional structure on various parameters through many numerical simulations. The results were reported at IDS 2016 [18].

Then, in this study, we apply the drying model to the spray drying granulation process in formulation. Spray drying granulation is a type of wet granulation method in formulations. In the spray drying granulation, the slurry raw material is made into minute droplets and dried. Therefore, the object to be dried is spherical. In order to apply the former model to the drying of this spherical object, we consider this spherical object to be a stack of solution films applied on the spherical shell and discuss the drying process of each solution film. The difference in area between the upper surface and the lower surface in the minute volume of each solution film can be represented by the radius from the center of the spherical shell and is related to the difference in diffusion in the vertical direction.

As a result of numerical simulation of this modified model, it was found that the smaller the radius of curvature r of the droplet, the more the fine particles tend to be unevenly distributed on the surface of the droplets during drying.

2. Model

2.1. Theory and basic equations

As mentioned in previous papers, there are two dynamic models of the drying process of polymer solution coated on a flat substrate, namely, an evaporation model and a transport model for a non-equilibrium polymer solution (Kagami et al., 2002; Kagami, 2011; Kagami

and Kubota, 2011). The latter can be divided into two basic types of transport, that is, the following two diffusion paths (Kagami et al., 2002):

(1) Diffusion of solvent containing solutes (polymers) in the direction of evaporation of the solvent

(2) Change in concentration in a solution

Because details of theory and the basic equations have been reported in previous papers (Kagami et al., 2002; Kagami, 2011; Kagami and Kubota, 2011; Kagami, 2014a; Kagami, 2015), only the basic equations are shown here.

First, we consider the following evaporation model (Kagami et al., 2002).

$$G = \gamma(1 - \beta C) \tag{1}$$

Here, G is the evaporation rate, C is the concentration of the solution, and β is a constant. Furthermore,

$$\gamma = K\sqrt{\frac{M}{2\pi RT}} P_0 \tag{2}$$

is a correction factor, where P_0 is the vapor pressure, M is the molecular weight, R is the gas constant, T is temperature, and K is a correction factor for the theoretical evaporation rate (Hickman and Trevoy, 1952).

Then, the two diffusion models are formulated as follows. First, the diffusion equation for solvent containing solutes is written as

$$\frac{\partial V}{\partial t} = K_v \nabla^2 V \tag{3}$$

where V is the volume of solvent containing solutes included in a space and K_v is the diffusion coefficient of the solvent (Kagami, 2011). An evaporation term (Eq. (1)) is added to Eq. (3), which describes the interface between liquid and gas (vacuum), so Eq. (3) is modified to (Kagami, 2011)

$$\frac{\partial V}{\partial t} = K_v \nabla^2 V - \gamma(1 - \beta C) \tag{4}$$

Next, the diffusion equation governing the change in concentration in solution is written as (Kagami, 2014a; Kagami and Kubota, 2011)

$$\frac{\partial N}{\partial t} = K_C \nabla^2 N + \frac{N}{V}(K_V - K_C)\nabla^2 V - \frac{2K_C}{V}\nabla N \cdot \nabla V \tag{5}$$

where N denotes the number of solute molecules included in a space and K_C is the diffusion coefficient of the solution.

In this study, we consider a solution containing one type of solute and one type of solvent for simplicity. Therefore, we build our model mainly using Eqs. (1)–(5).

The diffusion coefficient, K_C, of the solution changes with time. As mentioned in previous studies, is written as (Kagami, 2011)

$$K_C = \frac{k_B T}{6\pi R \eta_0 \{[\eta]C + 1\}} \tag{6}$$

where k_B is the Boltzmann constant, η_0 is the viscosity of the solvent, and $[\eta]$ is the intrinsic viscosity.

2.2. Improvement of the avobe model in the case of spherical dry solution

Now consider the drying of spherical solution as in the case of sray drying granulation. In order to estimate the diffusion in each direction in the minute region in the spherical solution, consider the minute region S in the spherical solution between the distance r and $r + dr$ from the center O of the sphere.

For the sake of simplicity, let us consider a circle C of a cross section of this sphere cut by a plane passing through the center O of the sphere. Considering the cross section S_C of the micro region S cut off at the deviation angle θ in the circle C, it is as shown in Fig. 1, and the length in the circumferential direction and the length in the radial direction of the cross section S_C can be expressed as shown in Fig. 1.
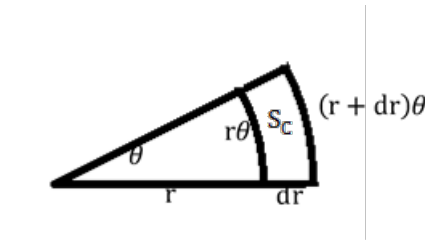
Fig. 1 The cross section S_C of the micro region S cut off at the deviation angle θ in the circle C

Now, if $r\theta = dq$, the length of the circular arc of radius r and the length of the circular arc of radius $r + dr$ in cross section S_C can be represented as dq and $dq\left(1 + \frac{dr}{r}\right)$, respectively. Assuming now that $dr = dq$, only the length of the arc of the radius $r + dr$ among the lengths in the circumferential direction and the radial direction of the cross section S_C is other $\left(1 + \frac{dr}{r}\right)$ times.

By replacing the deviation angle θ with the solid angle Θ and doing the similar consideration, only the area of the spherical surface with the radius $r + dr$ among the areas of each surface formed by cutting the minute region S at the solid angle Θ is other

$\left(1+\frac{dr}{r}\right)^2$ times. Namely, in diffusion in the spherical object, it is estimated that the ratio of

the diffusion coefficients of the upper surface and the lower surface is $\left(1+\frac{dr}{r}\right)^2$.

3. Results and Discussion

3.1. Condition of numerical simulation

In order to discuss the drying of the solution film of thickness dr coated on the surface of spherical body with curvature radius r, r is regarded as a parameter and $dr = 0.1[mm]$. Solvent vaporizes only on interface between liquid and gas (vacuum) and boiling is out of imagination. Volume of solvent V and the number of solute N in solution are homogeneous except for surface coming in contact with gas (vacuum). Concerning surface, 10% unevenness about N is given only to the upper surface of the solution film by homogeneous random number.

Simulation is ended when total volume of solvent become less than a fixed value, for it is thought that drying is completed, that is, solutes can move in solution no more then.

Initial values of parameters are set as follows; $K_C = 1.8750 \times 10^{-8}$[m²/s], $K_v = 1.2500 \times 10^{-8}$[m²/s], $\gamma = 5.7000 \times 10^{-14}$[m²/s].
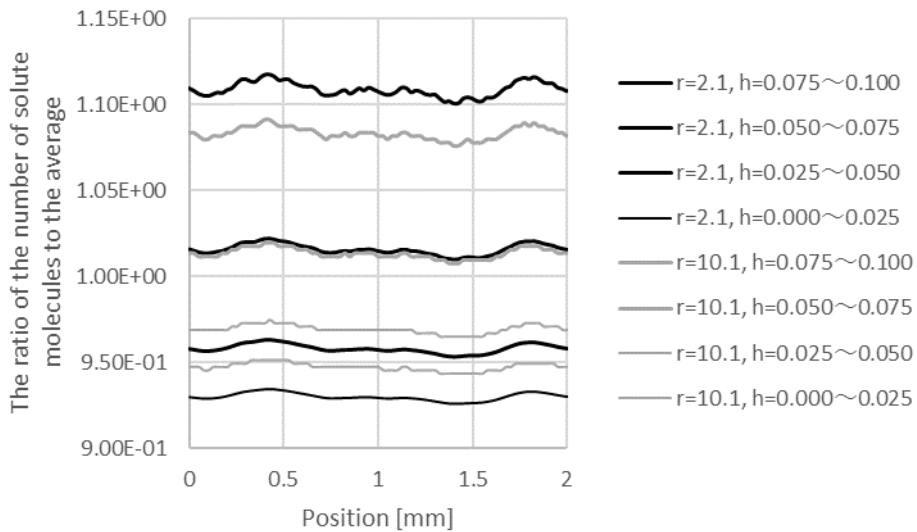
***Fig. 2 The r dependence of the amount of solute present in each layer of height
from the bottom of the solution film after drying***

3.2. Results of numerical simulation

Figure 2 shows the r dependence of the amount of solute present in each layer of height h from the bottom of the solution film after drying. From this result, it can be seen that as the radius of curvature r is smaller, the uneven distribution of the solute (or the fine particles) on the surface of the solution (or the slurry) film after drying becomes conspicuous.

4. Conclusions

In this study, we apply the drying model to the spray drying granulation process in formulation. In order to apply the former model to the drying of this spherical object, we consider this spherical object to be a stack of solution films applied on the spherical shell and discuss the drying process of each solution film.

As a result, we see that the smaller the radius of curvature   of the droplet, the more the fine particles tend to be unevenly distributed on the surface of the droplets during drying.

5. References

[1] Bornside, D. E., Macosko, C. W. and Scriven, L. E. Spin coating: One‐dimensional model. J. Appl. Phys., 1989, 66, 5185-5193.

[2] de Gans, B. J. and Schubert, U. S. Inkjet Printing of Well-Defined Polymer Dots and Arrays. Langmuir, 2004, 20, 7789-7793.

[3] Soltman, D. and Subramanian, V. Inkjet-Printed Line Morphologies and Temperature Control of the Coffee Ring Effect. Langmuir, 2008, 24, 2224-2231.

[4] Kagami, H., Miyagawa, R., Kawata, A., Nakashima, D., Kobayashi, S., Kitano, T., Takeshita, K., Kubota, H. and Ohmi, T. A model of coating and drying process for the flat polymer film fabrication. Proc. SPIE., 2002, 4754, 252-259.

[5] Kagami, H. A modified model of drying process of a polymer liquid film taking effects of latent heat and heat conductivity into account. Proc. SPIE., 2003, 5130, 220-227.

[6] Kagami, H. The influence of spatio-temporal variation of temperature distribution in a polymer solution on a flat substrate on formation of polymer film's thickness distribution during drying process - based on results of simulation of the modified model. Proc. SPIE., 2004, 5446, 135-142.

[7] Kagami, H. An additional modified model of drying process of a polymer liquid film – influence of an abrupt drop of vapor pressure peculiar to polymer solution –. The 9th Asia Pacific Physics Conference Proceedings, 2004, 10-10C.

[8] Kagami, H. Nonlinear dynamics that appears in the dynamical model of drying process of a polymer solution coated on a flat substrate. Proc. SPIE., 2007, 6417, 641704-1 - 8.

[9] Kagami, H. A modified dynamical model of drying process of polymer blend solution coated on a flat substrate. Proc. SPIE., 2008, 7028, 702825-1 - 9.

[10] Kagami, H. Characteristic three-dimensional structure of resist's distribution after drying a resist solution coated on a flat substrate : analysis using the extended dynamical model of the drying process. Proc. SPIE., 2009, 7273, 727335-1 - 8.

[11] Kagami, H. A modified dynamical model of drying process of a polymer solution having plural solvents coated on a flat substrate for a flat and homogeneous polymer film fabrication. Proc. SPIE., 2010, 7716, 771625-1 - 9.

[12] Kagami, H. and Kubota, H. Applying the dynamical model of drying process of a polymer solution coated on a flat substrate to effects of bumpy substrate. Proc. SPIE., 2010, 7764, 77640T-1 - 8.

[13] Kagami, H., Kubota, H. A dynamical model of drying process of a polymer solution having plural solvents and plural solutes (polymers) coated on a flat substrate for a flat and homogeneous polymer film fabrication. Physica Status Solidi, C 8, 2011, No. 2, 586-588.

[14] Kagami, H. Impact of the Marangoni effect on the thin film thickness profile after drying polymer solution coated on a flat substrate. JPS Conf. Proc., 2014, 1, 015087-1 - 5.

[15] Kagami, H. Thickness control of a thin film after drying through thermal and evaporative management in drying process of a polymer solution coated on a flat substrate: application of the dynamical model of the drying process. Proc. SPIE., 2011, 8068, 806813-1 - 6.

[16] Kagami, H. More minute thickness control of a thin film after drying through temperature, evaporation and concentration management in drying process of a polymer solution coated on a flat substrate. Proceedings of the 19th International Drying Symposium, Lyon, August 24-27, 2014, ISBN 978-2-7598-1631-6.

[17] Kagami, H. Control of the Marangoni Effect in the Drying Process of a Polymer Solution Coated on a Flat Substrate through Temperature, Evaporation and Solute Concentration Management. Athens Journal of Technology & Engineering, 2015, Volume 2, Issue 1, 45-53.

[18] Kagami, H. A model of drying process of a polymer liquid film coated on three-dimensional structure. In Proceedings of 20th International Drying Symposium, Gifu, Japan, August 8-10, 2016; A-1-4.

Mechanical and thermal segregation of milli-beads during contact heating in a rotary drum. DEM modeling and simulation.

Mesnier, A.ᵃ; Rouabah, M.ᵃ; Cogné, C.ᵃ; Peczalski, R.ᵃ*; Vessot-Crastes, S.ᵃ; Vacus, P.ᵇ; Andrieu, J.ᵃ

ᵃ Université de Lyon, Université Claude Bernard Lyon 1, Laboratoire d'Automatique et Génie des Procèdes (LAGEP), UMR CNRS 5007, Domaine de la Doua, Villeurbanne, 69616, France.
ᵇ Sanofi Pasteur, 1541 avenue Marcel Mérieux, Marcy l'Etoile, 69280, France.

*E-mail of the corresponding author: roman.peczalski@univ-lyon1.fr

Abstract

The flow mechanics and heat transfer phenomena within a bed of milli-metric size spherical beads rotated and heated by contact in a horizontal drum were simulated by means of commercial discrete element software EDEM. Mono-dispersed and bi-dispersed beds (two particle sizes or two particle densities) were considered. The mechanical segregation index (standard deviation of local bed compositions) and the thermal segregation index (standard deviation of beads temperatures) were calculated for the different types of bed and same operating conditions. The thermal segregation was found to be enhanced by mechanical segregation and was much stronger for bi-dispersed beds than for monodispersed one.

Keywords: rotating drum; particulate solid; segregation; contact heat transfer; DEM simulation.

1. Introduction

Modeling and simulation of processes involving stirred beds of particulate solids is a difficult task. The classical macroscopic and continuous medium approach gives a global scope of average trends but do not provide the local information which in some high added value processes like the pharmaceutical ones may be critical. In some cases even tiny processing discrepancies between individual particles must be avoided. During drying of granular beds, stirring is very often combined with contact heating and the powder flow mechanics is then coupled with heat transfer. For instance, vacuum contact heating is widely used in the pharmaceutical industry to dry granular products which are sensitive to oxygen and temperature. The vacuum contact drying of powder stirred bed has been firstly investigated in a macroscopic way ("penetration" model) by Schlünder and Mollekopf[1] for a mono-dispersed non sticky granular material. Kwapinska et al.[2] compared results obtained by the "penetration" analytical method with those obtained by numerical DEM.

More recently, several authors have independently investigated the effect of operating conditions on mixing and heating rates of rotated monodispersed granular material. Figueroa et al.[3] have studied various tumbler filling levels and cross-sectional shapes; Chaudhuri et al.[4] various revolution speeds, material types and baffles number and shapes; Gui et al.[5] and Komossa et al.[6] different revolutions speeds; Emady et al.[7] different revolution speeds and material thermal conductivities. However, to our best knowledge, no results were published to date concerning dispersed beds composed of particles of different sizes and materials. This is a major issue because real, industrial materials, even if carefully controlled before processing, are always slightly dispersed.

Rotating mixing of unperfectly monodispersed solid particulate beds unavoidably leads to mechanical segregation, i.e. to accumulation of smaller or/and denser particles in the core of the bed. In the previous study[8], radial and axial segregations were experimentally observed for a bi-dispersed bed with two particle sizes or two particle densities. The radial segregation index was measured for different drum filling ratios and for differnet baffles numbers and heights. The axial segregation index was found to be influenced by the friction coefficient on both drum front and rear walls.

It is thus expected that the bed spatial heterogeneities will lead to thermal heterogeneities because the beads temperature time evolutions depends on their trajectories and especially on their cumulated contact times with the heating wall. The aim of this paper was to investigate the impact of mechanical segregation on the thermal segregation in bi-dispersed beds as compared to a perfectly monodispersed (not mechanically segregated) bed. DEM was applied for modeling and simulation of spherical milli-beads flow and heat transfer in a rotating 'slice' type (nearly bidimensional) drum.

2. Materials and Methods

The simulations of the stirring and contact heating of milli-beads were realized with the commercial software EDEM 2017 (DEM Solutions, Edinburgh, UK). This software is based on the discrete elements method (DEM) which is a very powerfull modern tool to investigate and develop granular solid processes. In the DEM framework, each particle of the granular bed is considered to be distinct and has its own trajectory and speed. The particle-particle and particle-boundary interactions are checked at each time step and the resulting individual particle positions are updated. The main assumption of DEM modeling is that the particles are rigid (nondeformable) solid bodies but have the capability of small interpenetration during their contacts. The resulting decrease of the distance between the centers of two adjoining particles is called the penetration depth (δ) or overlap. The overlap is the fundamental variable which is directly related to the normal contact (interaction) force between the particles and the mechanical stiffness of the particles. This overlap is also the basis for evaluating the heat conductance between the particles as described in the next sections.

2.1 Mechanical DEM modeling

The determination of the position and speed of a given particle (identified by index i) is the time solution of the Newton second law for translational and rotational movement of a solid body. For translation, it writes :

$$m_i \frac{d^2 \vec{x}_i}{dt^2} = \sum_j F_{ij} + m_i g \tag{1}$$

where m_i is the particle mass, x_i its position vector and the right hand side of the equation is the resulting force, cumulating interactions with all adjoining (j) particles (and the wall of the vessel) and gravity. A similar equation can be written for the rotational movement.

For the purpose of this study, default modeling option in EDEM, the Hertz-Mindlin contact model[7] was used. In this model, the particle-particle mechanical interaction involves the normal impact force and the tangential friction force. The normal force is essentially elastic but both normal and tangential forces include damping components. The normal force is thus expressed by means of non linear visco-elastic behavior law :

$$F_{ij} = \alpha \delta_{ij}^{3/2} - \beta v_{ij} \tag{2}$$

where α is the elasticity coefficient depending on the material Young's modulus and particles radius, β is the damping coefficient depending on the kinetic energy restitution factor of the particles, δ_{ij} is the overlap between particle i and j and v_{ij} is the relative velocity of the two particles. The maximal tangential friction force is given by the *Coulomb* law which involves a material dependent friction coefficient.

2.2 Thermal DEM modeling

In tumbler systems, several heat-transfer phenomena coexist between neighboring particles and including walls : direct solid-solid heat conduction, conduction and convection through the insterstitial fluid and surface radiation. In this study, convection and radiation are neglected. The direct particle-particle conduction is expected to largely dominate due to the high ratio of conductivity of particles to the conductivity of interstitial gas and due to moderate surface temperatures.

In DEM framework, as already stated in the preceding section, two particles in contact interpenetrate each other at a depth depending on theirs dynamics and mechanical properties. For spherical particles, the contact radius R_c, which is the radius of the circle resulting from the two particles (spheres) overlapping, can be straightly derived from the penetration depth. Approximate analytical solutions of the *Fourier* conduction equation between two smooth, elastic particles with a finite small contact area have been proposed in the literature[5,6,7] and applied to evaluate the thermal conductance K_{ij} between the two particles centers :

$$K_{ij} = 2\lambda_{eff}R_c = 2\lambda_{ij}\sqrt{R_{ij}}\sqrt{\delta_{ij}} \tag{3}$$

where λ_{ij} is the harmonic mean of the thermal conductivities of the two materials, R_{ij} is the harmonic mean of the particles radii. The conductive heat flux between particle i and particle j writes simply :

$$\dot{Q}_{ij} = K_{ij}(T_j - T_i) \tag{4}$$

The total heat flux transferred to or from a given particle (i) is the sum of heat fluxes exchanged with all neighboring (j) particles and the thermal energy balance of a single particle writes :

$$m_i c_{pi} \frac{dT_i}{dt} = \sum_j \dot{Q}_{ij} \tag{5}$$

where c_{pi} is the particle specific heat capacity. The time integration of the above equation provides the thermal history of the considered particle.

2.3 Particulate bed global caracteristics

In order to caracterise globally and macroscopically the geometrical distribution (mechanical segregation) of each kind of beads and their temperature distribution (thermal segregation) within the bed, statistical indexes already introduced in the literature[3] were used. The mechanical segregation index was defined by :

$$MSI' = \sqrt{\frac{1}{N-1}\sum_{i=1}^{N}(C_i' - \langle C \rangle)^2} \tag{6}$$

where C_i' is the number fraction of one kind of beads (of the considered size or density) in a control volume i among N other control volumes, $<C>$ is the average number fraction of this kind of beads in the entire bed divided in N equal size control volumes. By analogy, the overall thermal segregation index was defined as :

$$TSI = \sqrt{\frac{1}{N-1}\sum_{i=1}^{N}(T_i - \langle T \rangle)^2} \qquad (7)$$

where T_i is the temperature of the bead i among all other beads, $<T>$ is the average temperature of all N beads of the bed. This index represents simply the standard deviation of beads temperatures. However, in case of bi-disperded beds, two beads populations coexist, according to their size or density. These two populations are mechanically separated (segregated) by the drum rotations and this will influence directly their thermal dispersion (segregation). In order to observe separately the thermal evolution of the two populations, a population (density or size) specific thermal segregation index was therefore defined :

$$TSI' = \sqrt{\frac{1}{M-1}\sum_{j=1}^{M}\left(T_j' - \langle T \rangle\right)^2} \qquad (8)$$

where T_j' is the temperature of bead j of a given kind among M other beads of the same kind.

2.4 Solver settings, material properties and process parameters

The simulations were realized on a DELL workstation (T7910) with two 10 cores processors (Intel Xeon E5-2660v3). The maximum processing time step was set at 40 % of the theoretical Rayleigh time step. This is the time taken for a shear wave to propagate through the particle which depends on the particle size and mechanical properties. The adjoining particles numerical search distance was set at 5 fold particle radius. The "Hertz-Mindlin with Heat Conduction model" was selected and a user defined routine called "Heat conduction for Geometry" was incorporated for implementing particles-wall direct heat conduction.

Table 1. Beads number for different bed types.

	Mono-dispersed	Bi-density	Bi-size
CA-2	-	-	27905
CA-3	16366	8183	8183
PP-3	-	8055	-

Polypropylene (PP) and cellulose acetate (CA) spherical beads of millimetric size (2 mm and 3 mm diameter) were used. The compositions of the three studied particulate beds are shown in Table 1. All materials mechanical and thermophysical properties needed for EDEM simulations are given in Table 2. The friction coefficients for pairs of materials were obtained by model identification (fitting experimental data) and are given in Table 3. The drum used in this study was a 'slice' type one with a large diameter to depth ratio. It had an internal diameter of 300 mm and an internal depth of 42 mm.

Table 2. Materials thermal and mechanical properties

BEADS	Property	Units	CA	PP
	Density [a]	[kg/m³]	1280	910
	Poisson's ratio [a]	[-]	0.4	0.42
	Elastic modulus [a]	[MPa]	1.0	1.0
	Shear modulus [a]	[MPa]	2.8	2.8
	Thermal conductivity [a]	[W/(m.K)]	0.36	0.22
	Specific heat capacity [b]	[J/(kg.K)]	1200	1700
	Coefficient of rolling friction [c]	[-]	0.01	0.01
	Coefficient of restitution [c]	[-]	0.3	0.3
DRUM			**Steel**	**Glass**
	Density [b]	[kg/m³]	7800	2500
	Poisson's ratio [b]	[-]	0.3	0.21
	Elastic modulus [b]	[GPa]	182	94.3
	Shear modulus [b]	[GPa]	70	39
	Thermal conductivity [b]	[W/(m.K)]	15	0.93
	Specific heat capacity [b]	[J/(kg.K)]	502	/
	Coefficient of rolling friction [c]	[-]	0	0.01
	Coefficient of restitution [c]	[-]	0.3	0.3

a - manufacturers data (M&L, CIPAM and other), b - web data (Azom, Engineers Edge)], c - data from this study

The front panel was made of glass, the rear one and the peripheral wall were made of stainless steel. The drum was equipped with 4 equidistant straight baffles with a height of 15 mm. All these dimensions corresponds to the set-up used in the previous experimental study[8]. The default revolution speed was 3 rpm which corresponds to very slow rotations often encountered for drying of pharmaceuticals. The initial beads temperature was 25 °C and the peripheral heating wall temperature was 50 °C.

Table 3. Solid-solid static friction coefficients

	Bead-Steel	Bead-Glass	Bead-Bead	
			CA	PP
CA	0.3	0.2	0.3	0.6
PP	0.3	0.2	0.6	0.6

3. Results and discussion

The simulations were realized for the 3 types of bed presented in Table 1. The mechanical segregation index (MSI) and the thermal segregation index (TSI), as defined in section 2.3, were calculated with MATLAB from EDEM data extracted for each simulation and were plotted as function of time on Figures 1 and 2.

According to Figure 1, except for a very short initial period, thermal segregation was the most important for the bi-density bed. Moreover, from the moment the bi-size bed MSI approached the bi-density MSI, the bi-size TSI fell below the mono-dispersed TSI. The bi-density bed TSI was significantly higher than the bi-size TSI, while the the MSI for both bi-

dispersed beds were rather close to each other near the simulation end. The correlation between MSI and TSI is thus not straightforward and must be further investigated.
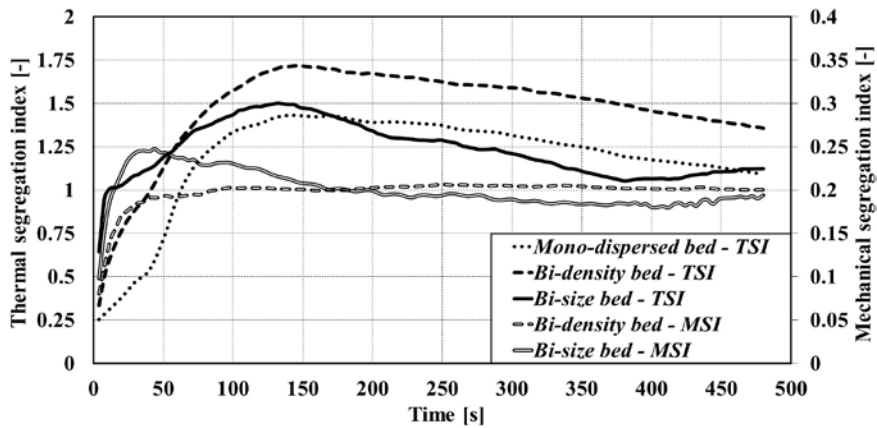
Fig. 1 Mechanical and thermal segregation indexes for different bed types.

As observed on Figure 2, the small beads specific TSI followed closely the overall TSI. The reason could be that the bi-size bed contained much more small than big beads (see bed compositions in Table 1). Therefore small beads thermal dispersion would have a much larger impact than the dispersion of big beads.
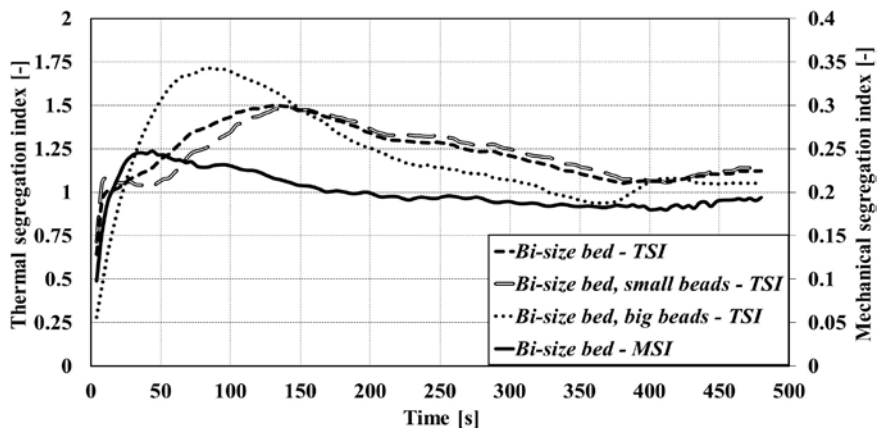
Fig. 2 Mechanical and thermal segregation indexes for the bi-size bed.

For the bi-density bed, the overall TSI was practically the average of the two specific TSIs (Figure not shown) because there was an equal number of light and heavy beads. As concerns average bed temperatures, plotted on Figure 3, the heating rate (curve slope) was stronger for the bi-size bed than for bi-density and mono-disperded beds and this deviation increased with time. This seemed rather odd because for the bi-size bed the small beads were in the core and the big ones at the periphery.

Mechanical and thermal segregation of milli-beads during contact heating in a rotary drum. DEM modeling and simulation.
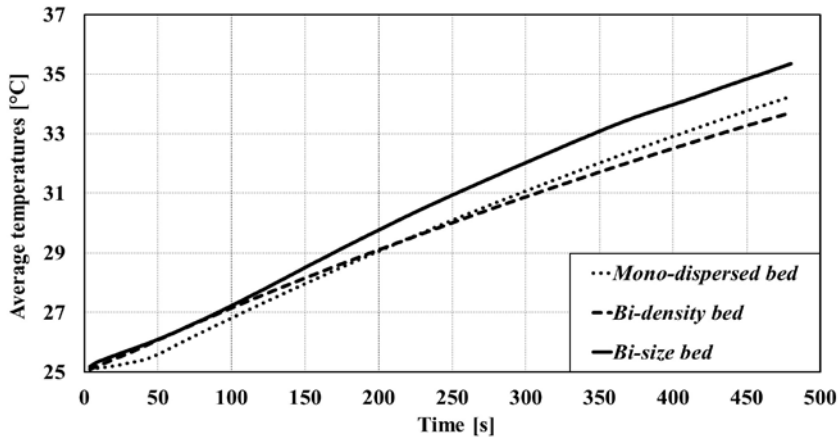
Fig. 3 Average temperatures for different bed types.

As there was much more small beads than big ones in the whole bed, one could expect that the average bed temperature would rather follow the temperature of the small ones which were colder and that the overall heating rate would be slower than for a bi-density bed. These results must be confirmed by carrying out the simulations for much longer times.

4. Conclusion

The mechanical segregation index (standard deviation of local bed compositions) and the thermal segregation index (standard deviation of beads temperatures) were calculated for mono-dispersed, bi-size and bi-density beds of spherical milli-beads submitted to same operating conditions. The thermal segregation was found to be enhanced by mechanical segregation and was much stronger for bi-dispersed beds than for monodispersed one. The bi-density bed exhibited unexpectedly stronger thermal segregation than the bi-size one.

5. References

[1] Schlünder, E.-U.; Mollekopf N. Vacuum contact drying of free flowing mechanically agitated particulate material. Chemical engineering and processing: Process Intensification 1984, 18(2), 93-111.

[2] Kwapinska, M.; Saage, G.; Tsotsas, E. Continuous versus discrete modelling of heat transfer to agitated beds. Powder Technology 2008, 181(3), 331–342.

[3] Figueroa, I.; Vargas, W.L.; McCarthy, J.J. Mixing and heat conduction in rotating tumblers. Chemical Engineering Science 2010, 65(2), 1045–1054.

[4] Chaudhuri, B.; Muzzio, F.J.; Tomassone, M.S. Experimentally validated computations of heat transfer in granular materials in rotary calciners. Powder Technology 2010, 198(1), 6–15.

[5] Gui, N.; Gao, J.; Ji, Z. Numerical study of mixing and thermal conduction of granular particles in rotating tumblers. AIChE Journal 2012, 59(6), 1906–1918.

[6] Komossa, H.; Wirtz, S.; Scherer, V.; Herz, F.; Specht, E. Heat transfer in indirect heated rotary drums filled with monodisperse spheres: Comparison of experiments with DEM simulations. Powder Technology 2015, 286, 722–731.

[7] Emady, H.N.; Anderson, K.V.; Borghard, W.G.; Muzzio, F.J.; Glasser, B.J.; Cuitino, A. Prediction of conductive heating time scales of particles in a rotary drum. Chem. Engineering Science 2016, 152, 45–54.

[8] Mesnier, A.; Peczaslki R.; Mollon, G.; Vessot-Crastes, S.; Vacus, P.; Andrieu, J. Segrégation des particules fines dans un tambour tournant. Expérimentation sur maquette et simulation DEM. In : Actes du 16ème Congrès de la SFGP, Récents progrès en génie des procédés, Vol. 110SFGP, Nancy, France, July 11-13, 2017.

The investigation of internal pressure development in convective drying of shrinking and non-shrinking materials using green and fired clay as an example

Adamska, A. [a*]; Pakowski, Z.[a]; Adamski, R.[a]

[a] Faculty of Process and Environmental Engineering, Lodz University of Technology, Lodz, Poland

*E-mail of the corresponding author: anna.adamska@dokt.p.lodz.pl

Abstract

The aim of present research was to measure and analyze the dynamic changes of internal pressure in shrinking vs. non-shrinking materials during convective drying for the use as a possible process control method.

Drying experiments were carried out on wet and fired clay at 50°C and 60°C. In addition, the shrinkage curve was investigated. Experimental measurements show the existence of 4 stages of the process. The comparison of the results for wet and fired clay shows differences in pressure trends.

During drying the internal pressure changes from underpressure to overpressure at the level of 3÷5kPa, what correlates well with transition from the first to the second drying period.

***Keywords:** ambient pressure drying; clay; shrinkage; pressure evolution*

1. Introduction

Ceramics is one of the oldest man-made materials and finds wide applications eg. in building sector (bricks, tiles), electric power industry (insulators), home and garden utensils (pottery) and advanced industries (ceramic filters, refractory materials etc.) [1].
Traditionally the cost of a product of the ceramic industry includes 30-40% of energy costs. The mass of which green ceramics is formed is based on clay, a natural aluminosilicate mineral, with necessary additives and water.
The removal of water from green ceramics consists of several stages, each of them requires properly selected drying process parameters in order to avoid deformation and cracking of the preformed elements [2]. Although the shrinkage of green ceramics in drying is small it is enough to cause these adverse effects if the evaporation rate is too high or uneven.

The losses caused by cracking in the production of ceramic tiles in the EU countries alone are estimated as 200 million euro per annum. Losses due to cracking and deformation are also inevitable in the production of decorative ceramics – stove tiles, ornaments or sculptures [3].

Literature survey and industrial experience indicate that this negative outcome of drying can be eliminated by slow or better intermittent drying. In intermittent drying the ceramics is dried in two repeating cycles: in hot air and in ambient air. During hot air drying the processs is fast, which causes shrinkage and resulting build-up of internal stresses, while in ambient air the process is slow and the stresses relax. The cycles are repeated and may be of equal or of variable duration. The time of each cycle is set on the basis of on-line measurement of drying kinetics and/or the exiting air temperature and humidity. The time of the cycle is calculated on the basis of an earlier developed drying model [4].

Drying related stresses in shrinking solids are important in drying many industrial products. Gradient of moisure content and related stresses lead to deformation and cracking [5].

From theoretical analysis it follows that internal pressure in the wet solid varies during the process of drying. So far the values of capillary and liquid pressure in the wet solid were predicted [6,7]. The direct measurement of this pressure was difficult. One of the first works published in 1996 used a complex experimental procedure to measure drying induced stresses in colloidal capillary-porous solids such as peat. To measure the internal pressure 4 to 5 mm rubber hollow spheres filled with water were placed in the sample during casting. They were connected by thin lines to external manometers. Stresses were measured with microtensometers. The distributions of capillary and internal pressure as a function of moisture content were presented [8]. Experimentally the internal capillary pressure was measured by Holt [9] in autogeneous shrinkage of concrete. Using a thin tube immersed in the middle of the block height and an external pressure transducer it was found

that the internal pressure is initially negative in the CRP and then turns positive in the FRP and at the end of the proces this pressure relaxes to the ambient value. In general, due to wide variety of wet solids an universal method of internal pressure measurement and interpretation is still being sought. Such measurement may provide valuable information on development of stresses in the material during drying [10].

The aim of this work is the analysis of transport of moisture in drying using the evolution of experimentally measured internal pressure in both wet green and fired clay. By using minature pressure transducers and telemetry such pressure can be messured in situ an the results transmitted to the required place. The obtained results may be used for control of the drying air parameters in response to the developing stresses in industrial scale, possibly also for many other shrinking materials.

2. Materials and Methods

2.1. Material specification

In the experiments performed in this work a clay material produced by Bolesławiec Refractory Materials Works, Bolesławiec, Poland was used. It is commonly used for manufacturing of artwork pieces, sculptured tiles etc. As plastifier 0.25 to 0.3% w.b. of water glass is added to mineral clay by the manufacturer.

The skeletal density of dry (non fired) clay measured by helium pycnometer is 2626.96 kg/m^3 and its porosity 0.3. The purchased press formed clay block of moisture content 0.3 kg/kg was directly used (in order to eliminate introduction of additional stresses) to cut cylindrical samples of 32.2 mm diameter and 27 mm tall.

2.2. Drying experiments

The convective drying experiments were preformed in a drying tunel described in detail elsewhere [11].

Two samples were used simultaneously in the experiment. One of them was placed on a rotating tray suspended under an electronic balance. This sample was armed with two thermocouples, one with its bead close to the periferal surface of the sample and the other placed axially. Both were connected to a transducer/transmitter situated on the tray and their signal transmitted to the computer. Both bases of the clay cylinder were covered tightly by perspex disks to eliminate heat and mass transfer to these surfaces.

The tray slowly rotated in order to equalize heat and mass transfer of the peripheral surface. The actual mass of the sample was continuously monitored by an electronic balance. The other sample was stationary and had a syringe needle with miniature pressure transducer inserted axially to measure axial pressure variations in time. Accurcy of measurements was: weight 10 mg, temperature ±1°C, pressure ±16 Pa.

Drying experiments were performed in temperatures of 50°C and 60°C with air velocity 1 m/s. Each experiment continued for ca. 10 hrs until equilibrium. The dried samples were then dried in an oven at 105°C to measure the remaining moisture. The difference of measured internal absolute pressure and actual atmospheric pressure was used for the analysis in Section 3.

3. Results and discussion

3.1. Shrinkage curve

The value of moisture content where shrinkage stops is on the level of critical moisture content ca. 0.19 kg/kg. All data points show a characteristic linear shrinkage behavior which is reported in literature for many other clays[13,14].
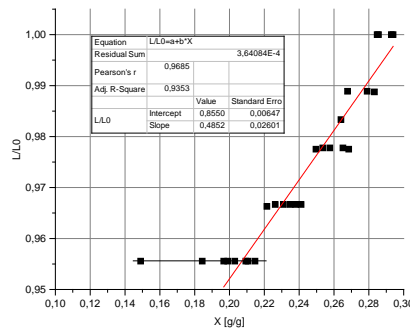
Fig. 1. Shrinkage curve

The dependence of sample dimension on its moisture content can be approximated with a straight line of the following form:

$$\frac{L}{L_0} = 0.855 + 0.4852X \tag{1}$$

By theory the linear shrinkage coefficient $\varepsilon_L = 0.4852$ which will be used in drying process simulation, is one third of the volumetric shrinkage coefficient ε_V. During drying the linear shrinkage is only ca. 5%, yet it is enough to create stresses above the strength of the solid.

3.2. Results of drying experiments

Fig. 4 presents the experimenal results (only data points –no curves fitted) for green clay at 50°C and 60°C. Fig. 4a and 4c contain the internal pressure (gray), moisture content (blue) and solid temperature in the axis of the sample (red) evolution. Fig. 4c and 4d show the external conditions in the tunnel. The air temperature was the only controlled parameter.

(a)

(c)

(b)

(d)
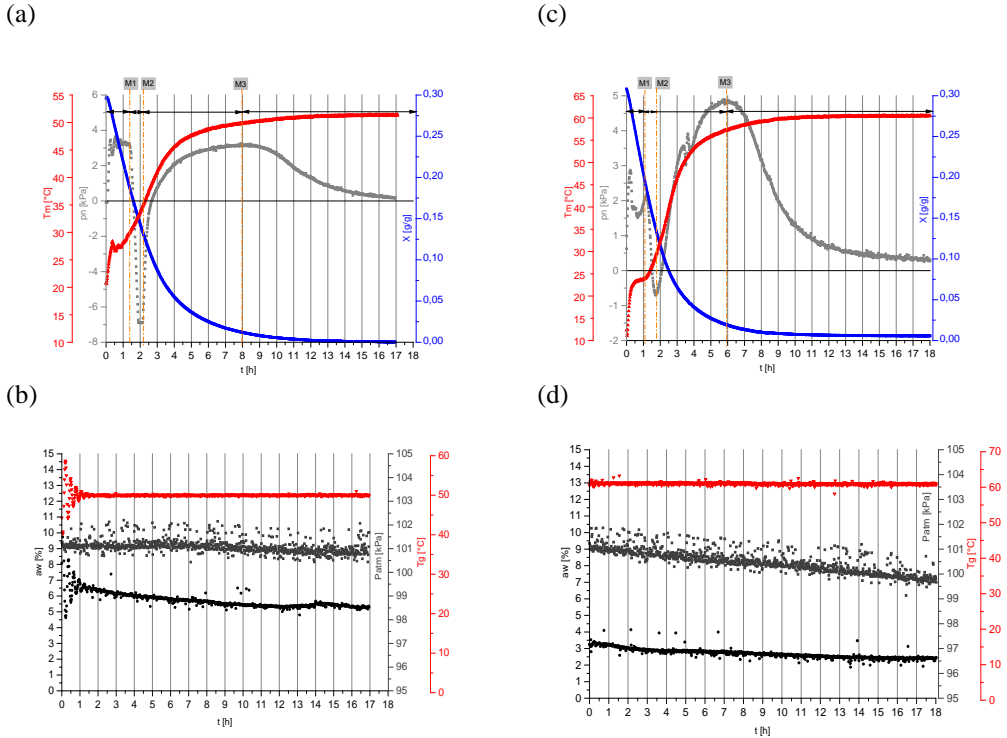
Fig. 4. The results for green clay drying at: (4a) 50°C (4c) 60°C where internal pressure (gray), moisture content (blue) temperature in the axis of the sample (red) and drying agent parameters for (4b) 50°C (4d) 60°C where atmospheric pressure (gray), water activity (black) gas temperature (red)

Four distinct stages can be identified in the process. First for 1.5 hr (from 0 to M1) an overpressure up to 2 kPa at 50°C and 3kPa at 60°C develops during the heating-up period when the sample reaches the wet-bulb temperature and during a short CRP. It is a result of sample heating and thermal expansion of water. Second stage begins at transition from CRP to FRP (X_{crit}=0.19 kg/kg) when a rapid fall of internal pressure is observed leading finally to underpressure (M1 to M2). Third stage (M2 to M3) starts after the shrinkage ceases i.e. after ca. 2 hrs and pressure begins to rise again simultaneously with solid temperatrure, which approaches the external temperature. The maximum of pressure is observed after 6-7 hrs and reaches 3 kPa at 50°C and 5kPa at 60°C. In the final stage pressure is relaxed to atmospheric pressure. For the fired clay wetted with distilled water, which shows no drying shrinkage, the results are shown in Fig.5. In this case three characteristic stages are observed. Here during heating stage (0 to W1) the internal pressure rises rapidly (there is no initial sustained overpressure as for green clay) and then falls to underpressure of -2kPa at 50°C and -0.8 kPa at 60°C which is less than for green clay. CRP begins after ca. 0.5 hr and lasts longer thn for green clay. At that stage the internal pressure begins to rise. When FRP

is reached (X_{crit}= 0.165 kg/kg)) rises to a maximum of 2.5 kPa at 50°C and 3 kPa at 60°C, however, at 60°C the maximum is reached at the final segment of this stage when the solid temperature approaches air temperature (W1 to W2).

So far the evolution of internnal pressure was only predicted by some advanced models. No experimental work, including [9], so far has presented the evolution of internal pressure in such detail as the present work.
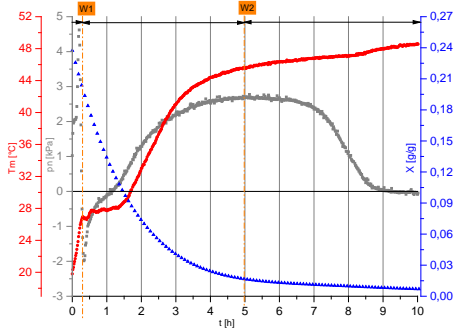
(a) (c)
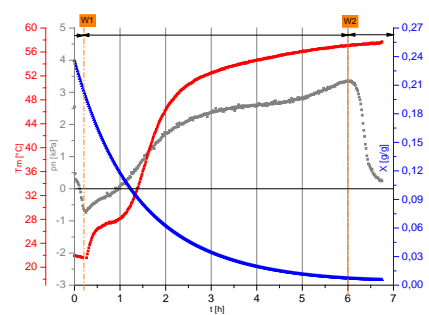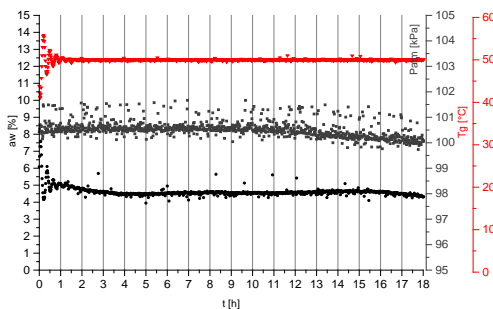
(b) (d)
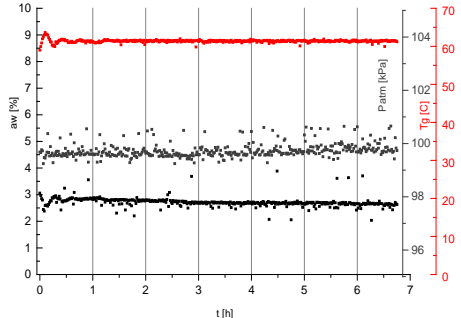
Fig. 5. The results for fired clay drying at : (4a) 50°C (4c) 60°C where internal pressure (gray), moisture content (blue) temperature in the axis of the sample (red) and drying agent parameters for (4b) 50°C (4d) 60°C where atmospheric pressure (gray), water activity (black) gas temperature (red)

4. Conclusions

Based on the presented results, it can be concluded that the internal pressure is more sensitive to changes occurring in the material than the temperature or mass changes are. The analysis of pressure changes inside the drying both in non-shrinking and shrinking material, enables more precise observation of phenomena of moisture transport and changes in the nature of stresses generated in the dried material (initially compression and then

stretching of the material). The obtained results will enable us to build a mathematical model to describe the convective drying process taking into account the internal pressure rate of change. Due to that, it will be possible to monitor the drying stresses generated in the material on a regular basis and control the process parameters so as to obtain the desired product without defects. Due to miniaturization of pressure sensors and the use of telemetric measurements, the method can be easily applied in an industrial scale to control the drying process.

5. Nomenclature

L	sample length	m
t	time	h
P	pressure	kPa
T	temperature	°C
X	moisture content	$kgkg_{d.b.}^{-1}$

Greek letters

ε	shrinkage coefficient	-

Subscripts

L	linear
V	volumetric
0	initial value

6. References

[1] Pereira da Silva W., Pereira da Silva e Silva C. M.D., Duarte da Silva L., de Oliveira Farias V.S.; Drying of clay slabs: Experimental determination and prediction by two-dimensional diffusion models. Ceramics International 2013, 39 (7), 7911-1919.

[2] Hubert J.; Léonard A.; Plougonven E.; Collin, F.; Boom clay drying behavior: experimental and numerical study. EuroDrying'2017 – 6th European Drying Conference, Liège, Belgium, 19-21 June 2017.

[3] Amoros J.L.; Sanchez, E.; Cantavella, V.; Jarque, J.C. Evolution of the mechanical strength of industrially dried ceramic tiles during storage. Journal of the European Ceramic Society 2003, 23, 1839–1845.

[4] Rybicki, A.; Sterowanie procesami suszenia materiałów wrażliwych na uszkodzenia skurczowe. Wydawnictwo Politechniki Poznańskiej 2012, 116 s.

[5] Augier, F.; Coumans, W.J.; Hugget, A.; Kaasschieter, E.F. On the risk of cracking in clay drying. Chemical Engineering Journal 2002, 86, 133–138.

[6] Chemkhi, S.; Khalfaoui, K.; Zagrouba, F. Modelling of saturated porous media

drying: Heat and mass transfer coupled with the material mechanical behavior. International Journal of Chemical Engineering and Applied Sciences 2013, 3 (1), 1-6.

[7] Cáceres, G.; , Bruneau, D.; Jomaa, W.; Two-Phase Shrinking Porous Media Drying: A Modeling Approach Including Liquid Pressure Gradients Effects. Drying Technology 2007, 25 (12), 1927 — 1934.

[8] Gamayunov, N.I.; Gamayunov, S.N. J. Change in the structure of colloidal capillary-porous bodies in the process of heat and mass transfer. Journal of Engineering Physics and Thermophysics 1996, 69, 721–725.

[9] Holt, E.E.; Early age autogenous shrinkage of concrete, Technical Research Centre of Finland, VTT Publications 2001.

[10] Hassanizadeh, S.M.; Handbook of Porous Media, Third Edition, Edited by Kambiz Vafai, CRC Press, Chapter 2, 2015, 47-62.

[11] Pakowski, Z.; Głębowski, M.; Adamski, R. Modeling of drying of highly shrinking materials using hydrogels as an example. Drying Technology 2006, 24, 1075–1081.

[12] Ketelaars, A.A.J.; Drying deformable media kinetics, shrinkage and stresses. Drying Technology 1994, 12 (4), 983-987.

[13] Chemkhi, S.; , Jomaa, W.; Zagrouba, F. Application of a Coupled Thermo-Hydro-Mechanical Model to Simulate the Drying of Nonsaturated Porous Media. Drying Technology 2009, 27 (7), 842 — 850.

[14] Hasatani, M.; ltaya, Y. Fundamental study on shrinkage of formed clay during drying-viscoelastic strain-stress and heat/moisture transfer. Drying Technology 1992, 10 (4), 1013-1036.

Multi-zone & multi-compartment model for dynamic simulation of horizontal fluidized bed granulator

Mielke, L.[a]*; Bück, A.[b]; Tsotsas, E.[a]

[a] Thermal Process Engineering, Otto von Guericke University Magdeburg, Germany.

[b] Institute of Particle Technology, FAU Erlangen-Nuremberg, Germany.

*E-mail of the corresponding author: lisa.mielke@ovgu.de

Abstract

Due to the ongoing development and implementation of process control and observation techniques in production processes of particulate products, the research on complexly designed process apparatuses has become of great interest. The work presented in this paper is focused on a model-based study on a multi-chamber horizontal fluidized bed apparatus for fluidized bed layering granulation. The model for the solid phase is extended by a new drying model. Because of the great variety of parameters that influence this complex system a preliminary model-based study on a simplified setup shall show which construction or process parameters influence the product quality.

Keywords: fluidized bed granulation; population balance modeling; surface moisture content; drying

1. Introduction

The demands on industrial processes in terms product quality are increasing due to continuing implementation of process control and observation techniques in production processes. In order to meet the quality requirements developed particulate products should consist not only of specified composition, but they should also have defined size distribution and structure. One process widely used for particle size enlargement and coating is the fluidized bed layering granulation process [1]. In earlier works on this issue a multi-zone and multi-compartment model for the dynamic simulation of a horizontal fluidized bed spray granulator has been derived and described [2,3]. In this paper the extension of this model by an additional drying model considering the wetted surface area is presented. The novel drying model is integrated in the existing dynamic multi-zone and multi-compartment layering granulation model.

2. Dynamic model and parameter study

The full model for the fluidized bed granulation plant includes the dynamic model for the time dependent particle and gas properties in the fluidized bed. The purpose of the fluidized bed model is to calculate quality features of the product, e.g. particle size distribution n, particle moisture content X_p and relative wetted surface area of the particles ψ_p, as well as the outlet gas properties such as temperature T_g and moisture content Y_g. A detailed description of the population balance model of the multi-zone and multi-compartment model for spray layering granulation used in this study can be found in [2,3].

Most dynamic drying models for fluidized bed drying and granulation contain mass and energy balances for the description of gas and particle phase. Greatest differences between these models can be found in the calculation of the evaporating mass flow rate or the assumed gas flow pattern. Established drying models for fluidized bed drying and layering granulation are presented in [5, 6, 7]. In this work a novel drying model is presented which takes the size of the initial spray droplets and the geometry of sessile droplets on the particles surface into account. In contrary to common models it allows a consideration of the wetted surface area as transfer area of the heat and mass flow due to evaporation.

In the following the main assumption and simplifications of the regarded model are stated. The particles of each compartment are considered to be ideally mixed. The gas phase in each chamber is also assumed to be ideally mixed. Heat losses to the environment are neglected. The spray droplets are distributed monodipersly. They will exclusively attach to the dry particle surface in a monolayer; overlay of sessile droplets is not considered. Also no percolation or diffusion of surface water into the core particle takes place. The impact area of single droplets on the particle surface as well as the contact area between gas and liquid remains constant during the drying process. Evaporation will only change the number of

droplets deposited on the particle surface and therefor the total wetted surface area. Sessile droplets have the shape of a ball scraper, therefore three parameter are sufficient to describe the geometry of the sessile droplet, the maximum height of the droplet h_{dr}, the contact angle θ_{dr} and the radius of the impact area a_{dr}.

Mass and energy balances for the solid phase, the liquid film and the gas phase for each chamber and compartment have been derived. Heat transfer coefficients between either the dry particle surface and the gas phase and the liquid film and the gas phase are calculated by standard Nusselt correlation for forced convection around a sphere under fluidized bed conditions. Whereas the heat transfer between the liquid film is assumed to be free convection around a sphere and the respective heat transfer coefficient is calculated with $Nu = 2$. The corresponding transfer areas are determined by the geometric specifications of the sessile droplets and water mass of the film.

To investigate the influence of the separation properties and the novel drying model on the product quality a parameter study is carried out. The model system consists of an apparatus divided in two chambers.
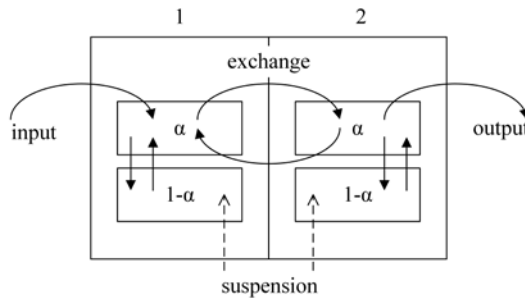
Fig. 1. Schematic representation of the apparatus used in parameter study.

Each chamber is divided into two compartments. The lower compartment is the spray zone, i.e. only particles contained in this compartment are directly in contact with the spray solution or suspension. In the upper compartment, the drying zone, particles are mixed and dried. In presently studied case the particle transport between the chambers can only take place between the upper compartments, the drying zones, of the chambers accounting for the use of overflow weirs.

In order to evaluate the influence of the shape factor of the separation function and the outlet probability on the product quality are studied. To show the dependencies of the drying model water mass flow rate of the spray, the initial droplet diameter, and contact angle of the sessile droplets are varied.

The following particle properties and process conditions at steady-state are observed within the scope of the parameter study. To represent the product particle size distribution particle

Sauter diameter and standard deviation are chosen. Furthermore the properties of the outlet flow, temperature and moisture content, as well as the product moisture content and the relative wetted surface area are recorded to show the main influence of the introduced drying model.

3. Results and Discussion

This section shows selected results of the 14 simulations that have been carried out. In this paper the results for the three influencing factors, k, $\dot{M}_{sus,w}$ and d_{dr}, are shown and discussed in the subsequent paragraphs.

The shape factor of the SF k has an effect on particle Sauter diameter and the particle diameter standard deviation. The model results for particle Sauter diameter and the corresponding standard deviation of particle inlet, chamber 1 and 2, as well as particle outlet for the three examined shape factors for the SF are presented in Figure 2 and 3. Particle processing leads to an increase of particle Sauter diameter and standard deviation of the particle diameter. During the process the particle Sauter increases in each subsequent chamber and reaches the highest value at the outlet. Due to the separation effect of the weirs between the chambers and at the outlet the standard deviation of the particle dimeter decreases on the particles' path through the plant. Increasing the shape factor k leads to more narrow separation functions and results in higher product Sauter diameters and decrease of the standard deviation particle diameter on the particles' path through the plant. The manipulation of the shape factor k shows no significant effect on gas outlet conditions, particle moisture content and wetted particle surface.
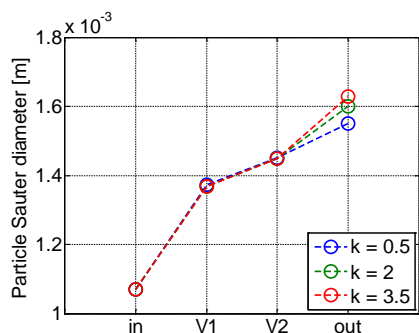
Fig. 2. Particle Sauter diameter for different shape factors of SF.
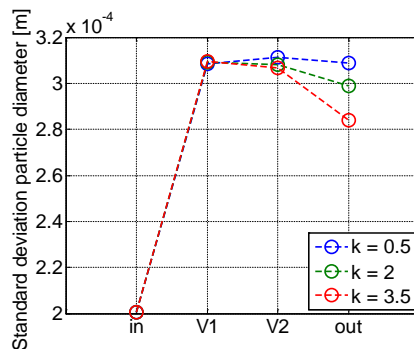
Fig. 3. Standard deviation of particle diameter for different shape factors of SF.

Figure 4 to Figure 7 show the simulation results for outlet gas temperature and outlet gas moisture content, product moisture content and wetted surface area depending on the mass flow rate of water contained in the spray. Increasing the mass flow rate of water in the spray

decreases the outlet gas temperature and increases the outlet gas moisture content due to the increased evaporation rate.
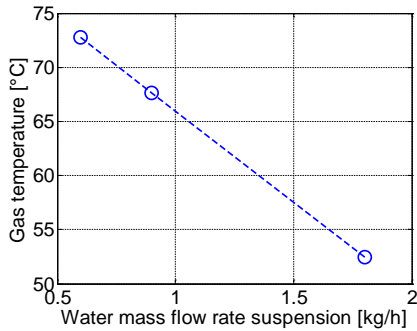
Fig. 4. Gas outlet temperature depending on water mass flow rate.
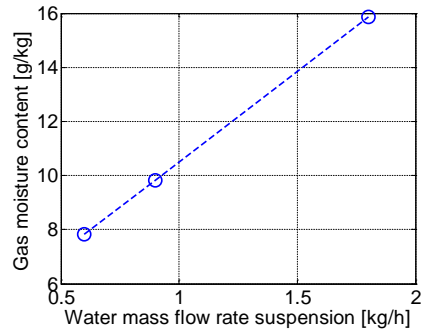
Fig. 5. Gas outlet moisture content depending on water mass flow rate.

Product moisture content and the corresponding wetted surface area are increasing with higher water mass flow rates of the spray. Due to the enhanced relative humidity of the process gas at higher water mass flow rates more water accumulates on the particle surface. Thus both product moisture content and wetted surface area are increasing.

The model results for product moisture and wetted surface area depending on the initial droplet diameter are presented respectively in Figure 8 and Figure 9. An increase of the initial droplet diameter leads to an increase of the product moisture content and wetted surface area. A reduction of the initial droplet diameter increases the contact area between the liquid film and the gas phase which leads to an enhancement of the evaporation rate and consequently to a reduction of particle moisture content and wetted surface area. An effect of the initial droplet diameter on gas outlet conditions cannot be observed.
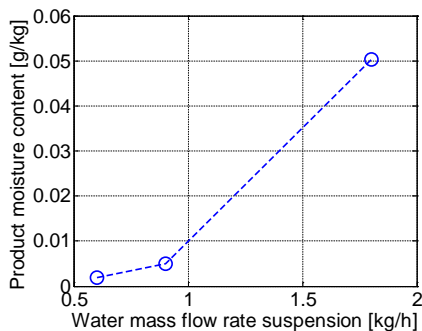
Fig. 6. Product moisture content depending on water mass flow rate.
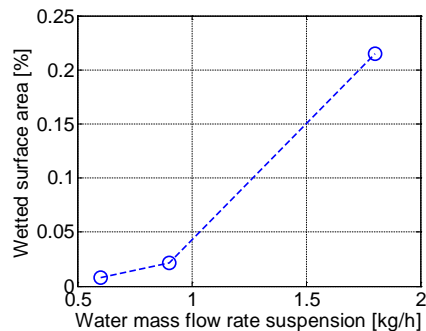
Fig. 7. Wetted surface area depending on water mass flow rate.
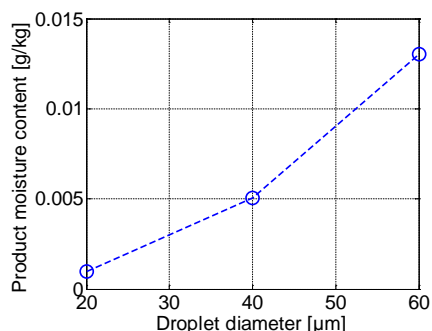
Fig. 8. Product moisture content depending on initial droplet diameter.
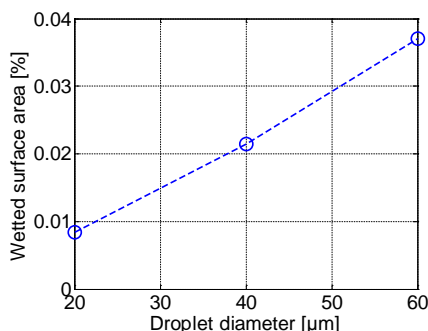
Fig. 9. Wetted surface area depending on initial droplet diameter.

4. Conclusions

The aim of the presented preliminary study was to identify what and how the chosen model parameters influence the most important product properties.

Manipulation of the parameters of the separation function only affects the particle growths and has no influence on thermal gas phase and particle properties, such as gas outlet conditions, product moisture content and wetted particle surface. However, a significant effect of the shape factor of the SF on the particle size distributions of the chambers and the product has been observed. Additionally a variation of the thermal process conditions in form of the water mass flow rate of the spray solution has been performed. The introduced water mass flow rate affects the outlet gas properties as well as the product moisture content and wetted surface area. Furthermore the influence of the initial droplet diameter on the product properties has been examined. Results show that the variation of the spray droplet features only influences product moisture content and wetted surface area and has no significant effect on the gas outlet conditions.

5. Nomenclature

a	Radius of impact area	m
d	Diameter	m
h, H	Height	m
k	Shape factor of separation function	-
l	length	m
M	Mass	kg
$\dot{M}$	Mass flow rate	kg s^{-1}

n	Number distribution	m⁻¹
$\dot{n}$	Number distribution rate	m⁻¹ s⁻¹
N	Number	-
p	Pressure	bar
P	Discharge probability	s⁻¹
T	Temperature	°C
T_{sep}	Separation function	-
w	Width	m

Greek letters

α	Relative size of drying zone	⁻¹
θ	Contact angle	°
ρ	Density	kg m⁻³
σ	Standard deviation	m
τ	residence time	s

Subscripts

0	Start
32	Sauter
bed	Fluidized bed
d	diameter
dr	droplet
g	Gas phase
in	inlet
out	outlet
p	particle
ref	reference
sep	separation
sh	shell
sus	suspension
w	water

6. Acknowledgements

7. References

[1] Mörl, L.; Heinrich, S.; Peglow, M. Chapter 2: Fluidized bed spray granulation. In Handbook of Powder Technology, Elsevier, 2007, 21-188.

[2] Meyer, K., Bück, A., Tsotsas, E. Dynamic multi-zone population balance model of particle formulation in fluidized beds. In Procedia Engineering World Congress on Particle Technology 2015, 102, 1456-1465.

[3] Meyer, K., Bück, A., Tsotsas, E. Dynamic modelling of particle formulation in horizontal fluidized beds. Computer Aided Chemical Engineering 2014, 33, 1765-1770

[4] Molerus, O.; Hoffmann, H. Darstellung von Windsichterkurven durch ein stochastisches Modell. Chemical Engineering Technology 1969, 45, 340-344.

[5] Groenewold, H.; Tsotsas, E. A new model for fluid bed drying. Drying Technology 1997, 15 (6-8), 1687–1698.

[6] Burgschweiger, J.; Tsotsas, E. Experimental investigation and modelling of continuous fluidized bed drying under steady-state and dynamic conditions. Chemical Engineering Science 2002, 57 (24), 5021–5038.

[7] Rieck, C.; Homann, T.; Bück, A.; Peglow, M.; Tsotsas, E. Influence of drying conditions on layer porosity in fluidized bed spray granulation. Powder Technology 2015,272, 120-131.

Measuring REA-based drying kinetics through temperature-moisture content relationship

Chen, X.D.[a]*; Putranto, A.[b]

[a] School of Chemical and Environmental Engineering, College of Chemistry, Chemical Engineering and Materials Science, Soochow University, Suzhou, Jiangsu Province, PR China

[b] School of Chemistry and Chemical Engineering, Queen's University Belfast, David Keir Building, Stranmilis Road, Belfast BT9 5AG, United Kingdom

*E-mail of the corresponding author: xdchen@mail.suda.edu.cn

Abstract

The reaction engineering approach (REA) has been proposed and implemented for modeling a number of challenging drying cases. While the modeling is simple and accurate, it is effective to generate the drying parameters. The relative activation energy is the fingerprint of the REA which describes the changes of internal behaviors inside the materials during drying. In this paper, a new method, based on combined heat and mass balance, is proposed and implemented to retrieve the relative activation energy of flat materials. The results indicate that the new approach can be used to retrieve well the activation energy of flat materials. The relative activation energy retrieved by the new approach is independent on the external drying conditions. This new approach can also potentially be used to evaluate the change of surface area of materials during drying

Keywords: reaction engineering approach (REA); modeling; relative activation energy; mass transfer;, heat transfer.

1. Introduction

The reaction engineering approach (REA) is a 'middle path' approach to model drying in which the changes of material structure during drying is encapsulated in the relative activation energy. It has been successfully applied to model a number of challenging drying cases including intermittent drying, infared-heating drying and microwave drying [1]. While the modeling is accurate, it has been found that the REA is effective in terms of generating the drying parameters. The relative activation energy calculated based on one accurate drying run can basically be used to project drying at other conditions since the relative activation energy is independent on the drying conditions. The relative activation energy of different drying conditions would collapse to the similar profiles [2]. In these studies, the activation energy is retrieved based on the mass balance where measurements of surface area, temperature and surface area of materials being drying are required.

In this study, for the first time, a new approach based on combined heat and mass balance is proposed and implemented for retrieving the activation energy of flat materials. The study is aimed to evaluate the applicability of the new approach to generate the relative activation energy as well as assess its applicability to mode drying kinetics of flat materials. Initially, the reaction engineering approach is reviewed briefly followed up by the proposal of new approach and applications of the new approach for generating the relative activation energy and modeling of drying of flat materials.

2. Materials and Methods

The reaction engineering approach (REA) was first proposed as a lumped parameter model where the drying rate (flux multiplied by surface area) of the moist materials can be expressed as the following:

$$m_s \frac{d\bar{X}}{dt} = -N_c A = -h_m A \left(\rho_{v,s} - \rho_{v,\infty} \right) \tag{1}$$

Equation (1) is basically correct for all cases where water leaves solid in vapor form. Even in the case of the lumped approach, there is no assumption of uniform moisture content in this REA approach. It was characterized with the mean moisture content.

The surface vapor concentration ($\rho_{v,s}$) can be correlated in terms of saturated vapor concentration of water ($\rho_{v,sat}$) by the surface relative humidity (RH_s) in the following equation [3]:

$$\rho_{v,s} = RH_s \cdot \rho_{v,sat}\left(T_s\right) = \exp\left(-\frac{\Delta E_v}{RT_s}\right) \rho_{v,sat}\left(T_s\right) \tag{2}$$

One can see that the surface *RH* is represented in an *Arrhenius* form. *ΔE_v* represents the increasing difficulty to remove moisture from materials as moisture content reduces (in

addition to the free water effect). Being a semi-empirical model, ΔE_v is ideally to be the mean moisture content ($\overline{X}$) dependent. T_s is the surface temperature of the material being dried (K). For a small temperature range say from 0ºC to just over 100°C, $\rho_{v,sat}$ (kg.m^{-3}) can in fact be approximated with the following equation [3]:

$$\rho_{v,sat}(T) = K_v \exp\left(-\frac{E_v}{RT}\right) \tag{3}$$

The approach of the activation process for moisture removal is thus claimed. On the other hand, condensation is a kind of precipitation process thus is not an activation process. The activation energy of the pure water evaporation reaction is equivalent to the value of the latent heat of water evaporation, which is also in line with the classical physical chemistry.

By using the REA, equation (1) can be expressed as:

$$m_s \frac{d\overline{X}}{dt} = -h_m A\left(\exp(\frac{-\Delta E_v}{RT})\rho_{v,sat}(T_s) - \rho_{v,\infty}\right) \tag{4}$$

Noting that the above equation has a parameter that is the surface temperature (T_s) for the moist porous material being dried, it can be troublesome to measure under certain circumstances.

It has been found, based on many previous practical experiences of using the REA approach, that drying experiments for generating the REA parameters need to be conducted where the air (or gas) humidity is very low in order to cover the widest possible range of ΔE_v versus $\overline{X}$.

The dependence of the additional activation energy on moisture content can then be normalized as:

$$\frac{\Delta E_v}{\Delta E_{v,\infty}} = \zeta(X - X_\infty) \tag{5}$$

where ζ is a function of moisture content difference (the current moisture content less the final equilibrium one), $\Delta E_{v,\infty}$ is the maximum when the moisture concentration of the sample approaches relative humidity and, for convective drying, the temperature of the drying air (gas):

$$\Delta E_{v,\infty} = -RT_\infty \ln(RH_\infty) \tag{6}$$

$X\infty$ is the equilibrium moisture content corresponding to $RH\infty$ and $T\infty$, which can be related to one another using the equilibrium isotherm. It is noted again that so far the experiments for gaining the relevant equation (7) has to be under the very dry condition so the final water content attained in experiments is usually fairy small.

For convective drying, the lumped energy balance can be represented as:

$$mC_p \frac{d\overline{T}}{dt} = hA\left(T_\infty - \overline{T}\right) + H_{drying}m_s \frac{d\overline{X}}{dt} \tag{7}$$

The relative activation energy is usually found by rearranging equation (4) into:

$$\Delta E_v = -R\overline{T}\ln\left[\frac{-\dfrac{m_s\dfrac{d\overline{X}}{dt}}{h_m A} + \rho_{v,\infty}}{\rho_{v,sat}\left(\overline{T}\right)} \right] \tag{8}$$

If the surface area A and the mass transfer coefficient h_m are known, or measured by separated experiments, one good run of drying experiment under the same drying air (gas) condition is sufficient for establishing equation (6), which is the core of the REA approach.

Here, now, we introduce *another kind* of approach based on the temperature-moisture content relationship. The lumped energy balance can be written as:

$$m_s\left(1+\overline{X}\right)\left(C_{pw}\frac{\overline{X}}{1+\overline{X}} + C_{p,s}\frac{1}{1+\overline{X}}\right)\frac{d\overline{T}}{dt} = hA\left(T_\infty - \overline{T}\right) + H_{drying}m_s\frac{d\overline{X}}{dt} \tag{9}$$

On both sides, we now divide them with the rate of drying, incorporating equation (9), we can obtain:

$$\left(C_{pw}\overline{X} + C_{p,s}\right)\frac{d\overline{T}}{d\overline{X}} = -\left(\frac{h}{h_m}\right)\frac{h\left(T_\infty - \overline{T}\right)}{\exp(\frac{-\Delta E_v}{R\overline{T}})\rho_{v,sat}\left(\overline{T}\right) - \rho_{v,\infty}} + H_{drying} \tag{10}$$

For flat sample geometry and parallel flow, one may have:

$$Nu = \frac{hL}{k_f} = C\mathrm{Re}^m\mathrm{Pr}^n \tag{11}$$

$$Sh = \frac{h_m L}{D_f} = C\mathrm{Re}^m Sc^n \tag{12}$$

Combining equations (10) and (12) results in the expression of relative activation energy retrieved by the new approach:

$$\Delta E_v = -RT ln \left[\frac{\frac{D_f}{k_f} \left(\frac{Pr}{Sc} \right)^n (T_b - T)}{\rho_{v,sat} (\Delta H_v - (X Cp_W + Cp_s) \frac{dT}{dX}} + \frac{\rho_{v,b}}{\rho_{v,sat}} \right] \qquad (14)$$

3. Results and discussion

The new method (based on equation (14)) is implemented to generate the relative activation energy of a mixture of polyvinyl alcohol (PVA) during drying at 35 and 55 ℃ [4-5]. The experimental details are presented previously [4-5] and reviewed briefly here in order to better understand the modeling framework. Materials used in this experiment were a mixture of equal proportion of partially hydrolyzed polyvinyl alcohol (80 wt%) and glycerol which has 88 wt% of water. 8 mL of the mixture was poured into a 90 mm diameter of Petri dish so that the initial thickness of sample was 1.3 mm. The velocity of the drying medium was set to 1 m.s⁻¹. The experiments were undertaken at drying air temperature of 35℃ and 55℃.

Figure 1 indicates the relative activation energy of polyvinyl alcohol (PVA) during drying at drying air temperature of 55 ℃. By using the new method (combined heat and mass balance, equation (14)), the relative activation energy of drying at drying air velocity of 1 and 2.8 m s⁻¹ collapses to the similar profiles. As expected, similar profiles are also produced based on the calculation using the mass balance only (equation (6)). Comparing the relative activation energy retrieved using the heat and mass balance with the mass balance only indicates that the profiles are very similar. The results suggest that the new method can produce well the relative activation energy of polyvinyl alcohol at drying air temperature of 55 ℃.

Figure 2 shows the relative activation energy of polyvinyl alcohol (PVA) during drying at drying air temperature of 35 ℃. The new method generates the very similar profiles of the relative activation energy for drying at drying air velocity of 1 and 2.8 m s⁻¹. In addition, the profiles of relative activation energy generated using the combined heat and mass balance collapse to those retrieved using the mass balance only.

The relative activation energy generated by the new method can be represented as:

$$\frac{\Delta E_v}{\Delta E_{v,b}} = \exp[-1.0794(X - X_b)^{1.6874}]$$

The similar expression is also shown for the relative activation energy retrieved by the mass balance only [6]. This is also supported by the profiles of relative activation energy generated by both methods as show in Figures 1 and 2. Therefore, the expression of the relative activation energy is independent on the retrieving method.
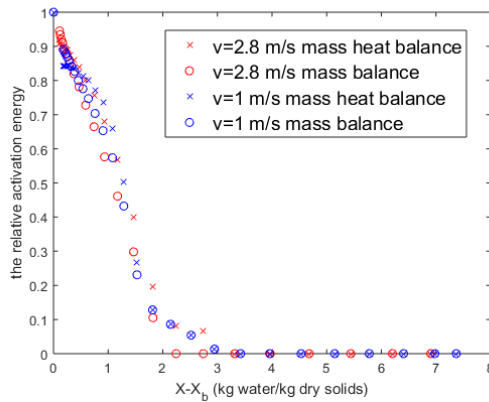
Figure 1. The relative activation energy of PVA mixture during drying at 55 ⁰C
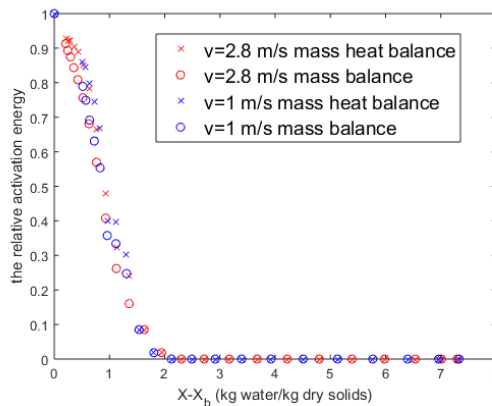
Figure 2. The relative activation energy of PVA mixture during drying at 35 ⁰C

Based on the generated relative activation energy, the new method can also be used to evaluate the change of surface area of materials during drying. Measurements of areas of materials (such as dairy droplets, fruits and leafy vegetables) can sometimes be difficult due to highly deformation during drying and irregularity of the materials. The accuracy of the measurements is needed in order to project the drying kinetics accurately. This new approach offers advantage of ability to measure the surface area during drying by combining the generated relative activation energy of specific materials with the mass balance or heat balance. Nevertheless, it is still uncertain whether the new approach can be implemented to generate the relative activation energy for spherical or cylindrical materials where the heat and mass transfer correlations are more complex.

4. Conclusions

In this study, the new approach to generate the relative activation energy of the reaction engineering approach (REA) is proposed and implemented. In the new approach, the heat

and mass balance is combined to yield the activation energy. Only a set of experimental data of moisture content and temperature during drying time is required to generate the relative activation energy. The results indicate that the new approach is applicable to retrieve the relative activation energy of flat materials. Different drying conditions result in the similar profiles of the relative activation energy. It is independent on external drying conditions which has also been highlighted for the relative activation energy retrieved using the mass balance only. The relative activation energy retrieved using combined both heat and mass balance gives the similar profiles of that evaluated based on mass balance only. Implemented in the REA, the relative activation energy evaluated by the new approach projects well the drying kinetics of flat materials.

5. Nomeclature

X	Moisture content on dry basis, kg.kg^{-1}
$\overline{X}$	Mean moisture content on dry basis, kg.kg^{-1}
N	Drying flux, kg.m^{-2}.s^{-1}
A	Surface area of single droplet or particle, m^2
Bi	*Biot* number (for heat transfer $Bi = hL/k$)
$Ch\text{-}Bi$	*Chen-Biot number*
D	Diffusivity, m^2.s^{-1}
D_v	Vapor diffusivity in air, m^2.s^{-1}
E	Activation energy, J.mol^{-1}
f	Relative drying rate function
g	Gravitational acceleration, m.s^{-2}
H_{drying}	Heat of drying/wetting, J.kg^{-1}
h	Heat transfer coefficient, W.m^{-2}K^{-1}
h_m	Mass transfer coefficient, m.s^{-1}
k	Thermal conductivity, W.m^{-1}.K^{-1}
M	Molecular weight, g.mol^{-1}
m_s	Mass of solids, kg
Nu	*Nusselt* number ($Nu = hL/k$)
Pr	*Prandtl* number
R	Ideal gas law constant
Re	*Reynolds* number ($Re = \rho uL / \mu$)
RH	Relative humidity
Sc	*Schmidt* number ($Sc = v/D$)
Sh	*Sherwood*
T	Temperature, K
t	Time, s
T_s	Surface temperature, K

T_{sat}	Adiabatic saturation temperature of drying air, K
u	Gas velocity, m.s^{-1}
X_∞	Equilibrium moisture content on dry basis, kg.kg^{-1}

Symbols

ρ	Density or concentration, kg.m^{-3}
μ	Dynamic viscosity, Pa.s
δ	Thickness, m
τ	Dimensionless time
ρ_v	Vapor concentration, kg.m^{-3}
Φ	Dimensionless water content
ς	Relative activation energy function
ξ	Relative rate of drying

6. References

[1] Chen, X.D., Putranto, A., 2015. Reaction engineering approach (REA) to modeling drying problems: recent development and implementations. *Drying Technology* 33, 1899-1910.

[2] Chen, X.D., Putranto, A., 2013. *Modeling Drying Processes: a Reaction Engineering Approach,* Cambridge: Cambridge University Press (ISBN: 9781107012103).

[3] X.D. Chen, G.Z. Xie, Fingerprints of the drying behavior of particulate or thin layer food materials established using a reaction engineering model, *Trans. IChemE Part C* 75 (1997) 213–222.

[4] N. Allanic, P. Salagnac, P., 2006. Glouannec, Convective and radiant drying of a polymer aqueous solution, *Heat Mass Transfer* 43, 1087–1095.

[5] N. Allanic, P. Salagnac, P. Glouannec, B. Guerrier, 2009. Estimation of an effective water diffusion coefficient during infrared-convective drying of a polymer solution, *AIChE J.* 55, 2345–2355.

[6] Putranto, A., Chen, X.D., Webley, P.A., 2010, Infrared and convective drying of thin layer of polyvinyl alcohol (PVA)/glycerol/water mixture - The reaction engineering approach (REA). *Chemical Engineering and Processing: Process Intensification* 49, 348-357.

Energy analysis and conservation opportunities in spray dryers

Patel, S. K.[a] ; Bade, M. H.[b*]

[a]Research Scholar, Sardar Vallabhbhai National Institute of Technology, Surat, Gujarat, India.
[b]Faculty, Department of Mechanical Engineering, Sardar Vallabhbhai National Institute of Technology, Surat, Gujarat, India.

*E-mail: bmh@med.svnit.ac.in, mukundbade@gmail.com

Abstract

Dryers are used for removal of moisture from an raw materials (such as effluent) to form a dried solids as per the requirements. For removal of the moisture, energy requirement is huge. Therefore, in this paper, methodology for heat recovery in one of the type of dryers as spray dryers is developed, which is simple and easy to apply. The proposed methodology is illustrated with the help of an example taken from literature. It is observed that the indirect heat recovery method could save energy maximum up to 82 % as compared to literature and 41 % higher than without heat recovery.

Keywords: Spray dryer, pinch analysis, heat recovery, effluent drying, energy saving.

1. Introduction

Spray dryer has been used for the removal of liquids by evaporation from concentrated solid solutions giving product out in the form of powder with various grain sizes. In recent years, it also become part of waste management treatment employed for removal of water part from effluent getting dried solid waste. Industrial effluents (dissolved liquid wastes) are produced as a waste from industrial and commercial activities from diversed field such as food, textile, oil, chemicals, pesticides etc. [1]. Effluents production in India will rise per capita rate of around 1 to 1.33 % annually from 2021 to 2031 [2]. In spray dryers, fluid atomized through the atomizer in the form of fine droplets, which instantly comes into contact with a flow of hot air, results in vaporization of liquid part of it. Spray dryers consume substantial thermal energy around 10 - 20 % of total industrial energy usage in most of the developed countries [3]. It is observed that a significant heat energy is wasted in the form of gases, exhaust from industrial effluent dryers. Many researchers have studied recovery of waste heat by different methods such as partial recirculation of exhaust gases as direct heat recovery, heating inlet fresh air by exhaust gases as indirect heat recovery, etc. Kilkovsky et al. [4] studied indirect heat recovery from flue gases of waste and biomass incinerator plant. Ogulata [5] investigated the potential of heat recovery in textile drying by using heat exchangers such as recuperators, regenerators and heat pumps. The methodology proposed for the determination of Performance characterstics and efficiency of heat exchanger, heat pump and combined system (heat exchanger and heat pump) are described in details [6]. Johnson et al. [7] discussed various techniques of thermal system analysis to optimize drying process for spray dryer of air and superheated steam types and illustrated with case study of milk powder plant. Golman and Julklang [8] reported exhaust gas heat recovery through partial recirculation of exhaust air in spray dryer of alumina slurry plant. In this plant, alumina slurry is atomized and dried in spray dryer, recovering value added product from it. Bade and Bandyopadhyay [9] proposed methodology for targeting the thermal oil required for process heating using pinch analysis and extended it for integration of other thermal systems. There is a paucity of information in literature for heat recovery and energy analysis of industrial effluents spray dryer. The purpose of the current work is to develop mathematical model of spray dryer based on mass and energy balance equations and to propose simple methodology for indirect heat recovery of spray dryers depends on pinch analysis.

Feed supplied to dryer contents moisture in range of 30-40 % reduced from as high as 99 % [1] present in effluent by concentration in mechanical vapour recompression (MVR) and/or thermal vapour recompression (TVR). To analyze the energy performance of the dryers and to have simplicity for individual mass balance of solids in waste feed and dried powder as well as water in waste feed and moisture in exhaust and fresh air, each stream is shown

with mass of individual constituent content in it as shown in Fig. 1. Further, complete spray dryer is considered as control volume boundary with inlet and outlet streams and energy interaction with surrounding systems. The mathematical model is formulated on the basis of overall mass and energy balance equations applied to control volumes of dryer.
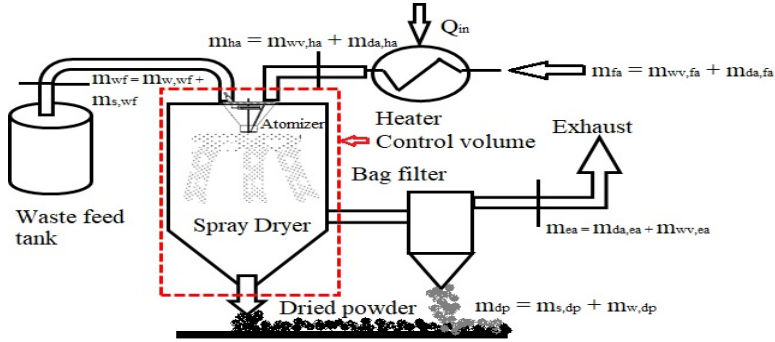
Fig. 1 Illustrative diagram of spray dryer.

2. Model of spray dryer without heat recovery

One of the approach to improve energy efficiecy of spray dryers is by recovering waste heat in exhaust either by indirectly or directly and recirculation of this thermal energy in to dryer. This energy recovery will be best analysed by developing the model of spray dryers. Model developed here is simple based on mass and energy balance equations. Overall mass and energy balance equations for the spray dryer is denoted as:

$$\left(m_{w,wf} + m_{s,wf}\right) + \left(m_{wv,ha} + m_{da,ha}\right) = \left(m_{wv,ea} + m_{da,ea}\right) + \left(m_{s,dp} + m_{w,dp}\right) \tag{1}$$

$$Q_{in} = m_{da,ha} * Cp_{da,ha} * \left(T_{da,ha} - T_{ref}\right) + m_{wv,ha} * Cp_{wv,ha} * \left(T_{wv,ha} - T_{ref}\right) \tag{2}$$

Energy content in various streams of total control volume of spray dryer and energy transfer for spray drying system are summarized as follows:

Heat input; $\qquad Q_{in} = Q_{s,wf} + Q_{w,wf} + Q_{da,ha} + Q_{wv,ha}$ $\qquad\qquad$ (3)

Heat Output; $\qquad Q_{out} = Q_{da,ea} + Q_{wv,ea} + Q_{s,dp} + Q_{w,dp}$ $\qquad\qquad$ (4)

Where,

$$Q_{s,wf} = m_{s,wf} * Cp_{s,wf} * \left(T_{s,wf} - T_{ref.}\right); \tag{3a}$$

$$Q_{w,wf} = m_{w,wf} * Cp_{w,wf} * \left(T_{w,wf} - T_{ref.}\right) \tag{3b}$$

$$Q_{da,ha} = m_{da,ha} * Cp_{da,ha} * \left(T_{da,ha} - T_{ref.}\right); \tag{3c}$$

$$Q_{wv,ha} = m_{wv,h} * Cp_{wv,ha} * \left(T_{wv,ha} - T_{sat@dpt}\right) + m_{wv,ha} * L_{vap@dpt} + m_{wv,ha} * Cp_{wl} * \left(T_{dpt} - T_{ref.}\right) \tag{3d}$$

$$Q_{da,ea} = m_{da,ea} * Cp_{da,ea} * \left(T_{da,ea} - T_{ref.}\right) \tag{4a}$$

$$Q_{wv,ea} = m_{wv,ea} * Cp_{wv,ea} * \left(T_{wv,ea} - T_{sat@dpt}\right) + m_{wv,ea} * L_{vap@dpt} + m_{wv,ea} * Cp_{wl} * \left(T_{dpt} - T_{ref.}\right) \tag{4b}$$

$$Q_{s,dp} = m_{s,dp} * Cp_{s,dp} * \left(T_{s,dp} - T_{ref.}\right) \tag{4c}$$

$$Q_{w,dp} = m_{w,dp} * Cp_{s,dp} * \left(T_{s,dp} - T_{ref.}\right) \tag{4d}$$

The difference between the quantity of water in the waste feed and water in the dry product is termed as water evaporated from the dryer. Mass of dry air is constant at inlet and outlet shown in Eq. (6a), only mass of water vapour are changing in air stream. Relations of humidity and dry air at various locations in the dryer are given by Equations (6b, c) and (7).

$$m_{da,ha} = m_{da,ea} \qquad (6a) \qquad m_{wv,ha} = \omega_{ha} * m_{da,ha} \qquad (6b) \qquad m_{wv,ea} = m_{wevap.} + \omega_{ha} * m_{da,ha} \qquad (6c)$$

The humidity ratio at exhaust is given as: $\quad \omega_{ea} = \left(m_{wevap.} + m_{wv,ha}\right)/m_{da,ha}$ $\qquad\qquad (7)$

However, the minimum mass flow rate of dry hot air at inlet to drying chamber can be determined by simplifying mass and energy balance equations as:

$$m_{da,ha} = \frac{\left(\begin{array}{c}\left(m_{wevap.} * Cp_{wv,ea} * \left(T_{da,ea} - T_{sat@dpt}\right)\right) + m_{wevap.} * \left(L_{vap@dpt}\right)_{ea} + m_{wevap.} * C_{pwl} * \left(T_{dpt} - T_{ref}\right)_{ea} + m_{s,dp}\right) \\ * C_{ps,dp}\left(T_{s,dp} - T_{ref}\right) + m_{w,dp} * C_{pw,dp}\left(T_{s,dp} - T_{ref}\right) - \left(m_{swf} - C_{ps,wf}\left(T_{swf} - T_{ref}\right) - \left(m_{w,wf} * C_{pw,wf}\left(T_{s,wf} - T_{ref}\right)\right)\right)\end{array}\right)}{\left(\begin{array}{c}C_{pda,ha}\left(T_{swf} - T_{ref}\right) + \omega_{ha} * C_{pwv,ha}\left(T_{da,ha} - T_{sat@dpt}\right) + \omega_{ha} * L_{vap@dpt,ha} + \omega_{ha} * C_{pwl}\left(T_{dpt} - T_{ref}\right)_{ha} - \left(C_{pda,ea} * \left(T_{da,ea} - T_{ref}\right)\right) \\ - \left(\omega_{ha} * C_{pwv,ea} * \left(T_{da,ea} - T_{sat@dpt}\right)\right) - \omega_{ha} * \left(L_{vap@dpt}\right)_{ea} - \omega_{ha} * C_{pwl} * \left(T_{dpt} - T_{ref}\right)_{ea}\end{array}\right)} \qquad (8)$$

The proposed methodology for evaluating the mass flow rate of hot air (m_{ha}) and humidity ratio at exhaust air (ω_{ea}) are summarized in the form of flowchart in Fig. 2. This methodology is validated by illustrative example 1 [8] for without heat recovery (base case) taken from literature in following sub-section 2.1.

2.1. Illustrative example 1: Without heat recovery [8]

An illustrative example 1 taken from literature [8] to explain and validate proposed methodology. Process parameters in Table 1 are reproduced from [8]. Problem is to determine minimum mass flow rate of drying air keeping moisture removal constant. In this calculation, the exhaust gas temperature is assumed to be constant.

As hot air inlet temperature increases, the mass flow rate of hot air and total heat supplied to the dryer reduces resulting in increasing efficiency of drying process as shown in Fig. 3.
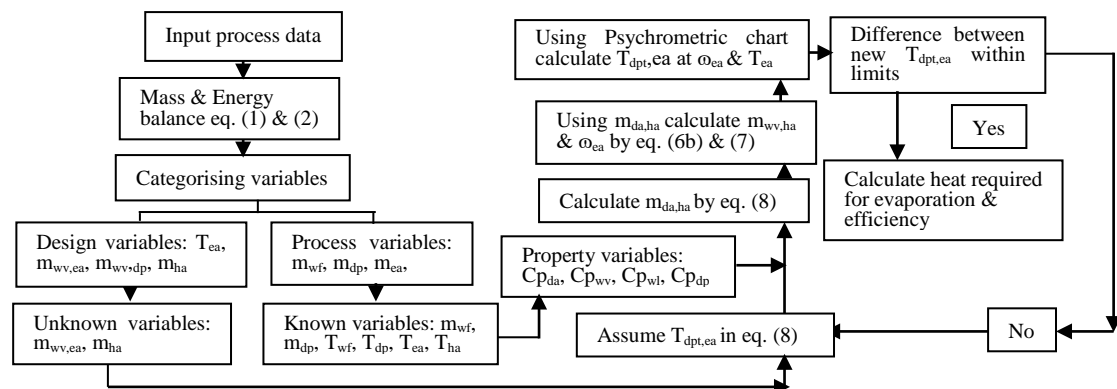
Fig. 2 Flow chart of spray drying computation.

Table 1. Process parameters [8]**.**

Parameters	Data	Parameters	Data
Drying air temperature	230 °C	Temperature of slurry	20 °C
Slurry feed rate	50 kg/h	Reference temperature	20 °C
Slurry water content	40 %	Relative humidity	70 %
Ambient temperature	30 °C	Moisture content in dried prod.	3 %
Vol. flow rate of drying air	3200 m³/h		
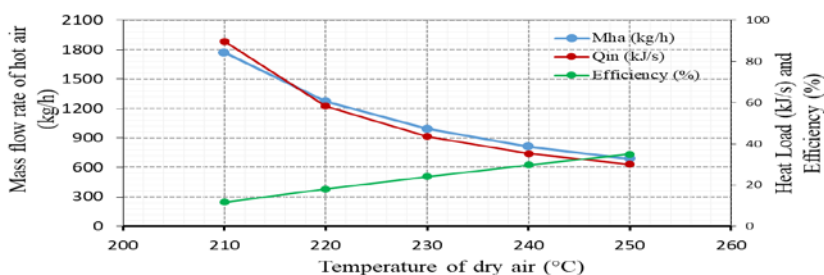
Fig. 3 Effect of temperature on mass flow rate of hot air, heat load and efficiency of the dryer.

3. Model of spray dryer with indirect heat recovery

Indirect heat recovery (IHR) is applicable when mixing of exhaust air is not permitated with feed or direct mixing of exhaust air is not possible. Heat exchager is assumed as counter flow with suitable minimum approach temperature between exhaust air and inlet fresh air. The schematic diagram of IHR is shown in Fig. 4. Heat energy is transferred from hot fluid to cold fluid. Subsequently, temperature of preheated air is raised up to required by heater. In this case, heat is recovered from entire exhaust air with minimum approach temperature. The main drawback of IHR is deposition of agglomerates on the surface of the tubes, which is high mainly when the mass flow rate and moisture content of exhaust air is higher causing increased operating and maintenance cost of the heat exchanger.

3.1. Methodology for indirect heat recovery

The proposed methodology for determination of total heat supplied by heater and drying efficiency are summarized in Fig. 5. In this methodology, to determine maximum possible heat recovery from exhaust air, pinch analysis a well known heat recovery tool is applied [10]. Property data such as specific heat of water vapour and dry air is taken from property table, which is used to calculate enthalpy change for water vapours and dry air as:

$$\Delta H = \omega \left[m_{wv,ea} * Cp_{wv,ea} * (T_{wv,ea} - T_{sat.}) + m_{wv,ea} * L_{vap@dpt} + m_{wv,ea} * Cp_{wl} * (T_{dpt} - T_{ref}) \right] \tag{9}$$

$$\Delta H = m_{da,ea} * Cp_{da,ea} * (T_{da,ea} - T_{ref}) \tag{10}$$

With the help of Illustrative example 1 applicability of proposed methodology given in Section 3.1 is demonstrate as following section.
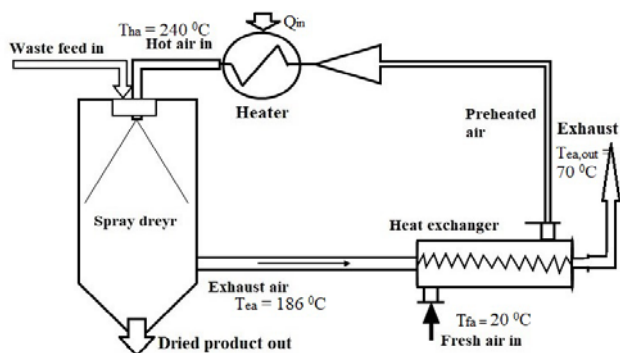
Fig. 4 Schematic diagram of indirect heat recovery through heat exchanger.
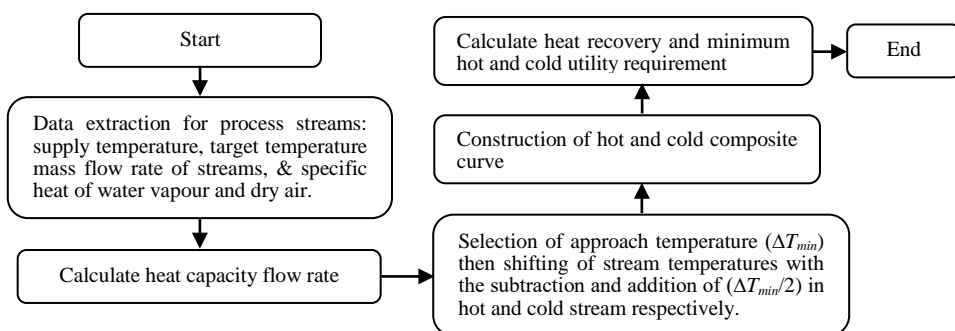
Fig. 5 Flowchart for indirect heat recovery through pinch analysis.

3.2. Illustrative example 1 revisited: Indirect heat recovery [8]

Input process data is same as given in Section 2.1. As outlet temperature of exhaust gas is higher than the dew point temperature, only sensible heat will be recovered from exhaust. Using pinch analysis hot composite curve (HCC) and cold composite curve (CCC) are plotted [3] as shown Fig. 6. After matching of the HCC and CCC for minimum approach temperature of 50 °C, the overlapping between the composite curves represents the maximum heat recovery 27.372 kJ/s between hot exhaust air and incoming fresh air and the uncovered upper section of the cold composite curve shows external heating requirement of 10.38 kJ/s for the fresh air. It is observed that the indirect heat recovery method could save energy maximum up to 82 % as compared to literature (for same without heat recovery configuration) and 41 % as compared to without heat recovery (base case) as shown in Table 3 for spray dryer with inlet hot air temperature of 240 °C.

Table 2. Illustrative example 1 revisited for indirect heat recovery.

Streams	Actual temp. (°C)		Shifted temp. (°C)		Mass flow rate (kg/s)	Humidity ratio (kg/kg dry air)
	T_s	T_t	T_s	T_t		
Exhaust air, dry	186	70	161	45	0.2225	0.037
Water vap.,ea	186	70	161	45	0.00834	
Fresh air, dry	20	180	45	205	0.2225	0.019
Water vap.,fa	20	180	45	205	0.00422	

Table 3. Comparative results for drying air temperature of 240 °C

S.N.	Methods ⟶ Parameters ↓	Without heat recovery (Literature)	Without heat recovery (Base case)	Indirect heat recovery (pinch analysis)
1	Heat load (kJ/s)	60	35.29	10.38
2	Mass flow rate of hot air at inlet (kg/h)	2100	813	813
3	Energy saving (%)	--	41	82
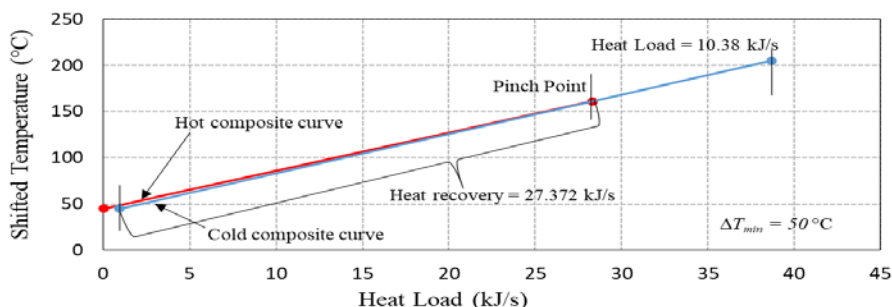
Fig. 6 Hot and cold composite curve for illustrative example 1 revisited.

4. Conclusions

In the present work, fundamental approach of mass and energy balance equations is applied to develop the mathematical model of spray dryer. Proposed methodology for indirect heat recovery of spray dryers is based on pinch analysis. Each process stream is divided into separate stream for constituents content in, which is helpful to apply pinch analysis and to consider variation in heat capacities mainly of moisture and dry air. It is observed that heat recovery could reach up to maximum of 82 % as compared to literature results for same case. Additonally, this approach helps to reduce the operating cost of dryers by reducing the flow rate of air and the capital cost by reducing heat transfer area. Further, compared to base case (without heat recovery), 41 % energy saving is possible with reduction in mass flow rate of hot air.

5. Nomenclature

m	mass	kg/h or kg/s	T	Temperature		°C
Q	Heat load	kJ/s	H	Enthalpy		kJ/kg
Cp	Specific heat	kJ/kgK °C	L	Latent heat of vaporization		kJ/kg
CP	Heat capacity flow rate	kJ/K °C				

Greek letters

ϖ Humidity ratio   kg water/kg dry air

Subscripts

da	dry air		in	input	vap	vaporization
dp	dry product		min	minimum	w	water
dpt	dew point temperature		out	outlet	wf	waste feed
ea	exhaust air		ref	reference	wv	water vapour
evap	evaporation		s	solid		
ha	hot air		sat	saturation		

6. References

[1] Mujumdar, A.S., Handbook of industrial drying, Fourth ed., CRC Press : Taylor & Francis, Boca Raton; London; New York 2015.

[2] Dieter Mutz, Common Effluent Treatment Plants: Overview, Technologies and Case Examples, New Delhi, India 2015.

[3] Kemp, I.C., Fundamentals of Energy Analysis of Dryers. *Modern Drying Technology* 2014, *4–4*, 1–45.

[4] Kilkovsky, B.; Stehlik, P.; Jegla, Z.; Tovazhnyansky, L.L.; et al., Heat exchangers for energy recovery in waste and biomass to energy technologies - Energy recovery from flue gas. *Applied Thermal Engineering* 2014, *64*, 213–223.

[5] Ogulata, R.T., Utilization of waste-heat recovery in textile drying. *Applied Energy* 2004, *79*, 41–49.

[6] Krokida, M.K.; Bisharat, G.I., Heat Recovery from Dryer Exhaust Air. *Drying Technology* 2004, *22*, 1661–1674.

[7] Johnson, P.W.; Langrish, T.A.G.; Johnson, P.W.; Langrish, T.A.G., Inversion Temperature and Pinch Analysis , Ways to Thermally Optimize Drying Processes. *Drying Technology* 2011, *29*, 488–507.

[8] Golman, B.; Julklang, W., Analysis of heat recovery from a spray dryer by recirculation of exhaust air. *Energy Conversion and Management* 2014, *88*, 641–9.

[9] Bade, H.M.; Bandyopadhyay, S., Thermal integration of heat transfer fluid systems. *Asia-Pacific Journal of Chemical Engineering* 2013, *9*, 1–15.

[10] Kemp, I.C., Reducing dryer energy use by process integration and pinch analysis. *Drying Technology* 2005, *23*, 2089–2104.

The construction of thermodynamic expressions needed in the physicochemical mathematical model required for the rational physical and quantitative evaluation of the freeze drying process of pharmaceutical solutions employing tertiary butyl alcohol as a co-solvent

Wang, J. C.[a]; Bruttini, R.[b]; Liapis, A. I.[a*]

[a] Department of Chemical and Biochemical Engineering, Missouri University of Science and Technology, 110 Bertelsmeyer Hall, 1101 North State Street, Rolla, Missouri 65409-1230, USA

[b] Criofarma – Freeze Drying Equipment, Strada del Francese 97/2L, 10156 Turin, Italy.

*E-mail of the corresponding author: ail@mst.edu

Abstract

A thermodynamic model employing the UNIFAC (Dortmund) method was developed to determine the currently unavailable partial vapor pressures of the binary gas mixture of water and tert-butyl alcohol (TBA) in equilibrium with their frozen solid mixtures. The results agree satisfactorily with the experimental data and indicate that TBA has higher vapor pressures which lead to higher total pressures at the moving interface that could result in larger total pressure gradients and convective mass transfer rates in the dried layer during primary drying. But the higher total pressures reduce the magnitude of the bulk diffusivity of the gas mixture and combined with the smaller Knudsen diffusivity of TBA could significantly impact the competing mass transfer mechanisms during freeze drying.

Keywords: Freeze drying; Water and tert-butyl alcohol (TBA); UNIFAC (Dortmund); Partial vapor pressures; Convective flow and bulk and Knudsen diffusion

1. Introduction

The presence of organic solvents as co-solvents with water in pharmaceutical and biological solutions could reduce the degradation rate of the pharmaceutical/biological product in water and/or increase its solubility. It has been shown experimentally [1] to affect the freezing characteristics of the solution during the freezing stage as well as during the primary and secondary stages of the freeze drying process. In the production of a number of anti-cancer drugs, the tertiary butyl alcohol (TBA, or 2-methyl-2-propanol) represents the organic co-solvent in the water solutions with varying concentrations dependent on the biotechnology method of production and the nature of the anti-cancer drug. Currently due to strict quality and toxicity standards required by the Food and Drug Administration (FDA), most of TBA is removed prior to the freeze drying of the drug solution. In order to ascertain if this is the only or best strategy, it is of paramount importance to acquire both physical and quantitative knowledge of the unsteady state variations and their interactions that occur during the freeze drying process in the (i) temperature and heat transfer rates in the frozen and porous dried layers of the product, (ii) mass transfer mechanisms and rates in the porous dried layer, (iii) relative residual amounts of frozen water and TBA in the frozen solid layer which affect the partial pressures of the vapors of water and TBA at the moving interface separating the frozen and porous dried layers during the primary drying stage, and (iv) the amounts of sorbed (bound) water and TBA on the surface of the pores of the dried layer during the primary and secondary drying stages. Because these data cannot be measured experimentally during the freeze drying process, it becomes necessary to construct and solve an unsteady-state and multi-dimensional in space mathematical model of the freeze drying process in order to determine, evaluate, and analyze the dynamic behavior of items (i) – (iv) for ascertaining whether or not the presence of TBA in the drug solution could reduce the drying times of the primary and secondary drying stages of the freeze drying process and, furthermore, whether the presence and distribution of the residual TBA in the three-dimensional space of the product being freeze dried could result in the violation of the strict quality and toxicity standards required by the FDA for the freeze drying of pharmaceuticals.

The mathematical model required to be constructed and solved for the freeze drying process of frozen solutions of pharmaceuticals involving water and an organic co-solvent like TBA has now to consider the vapor pressures and mass transfer rates of a ternary gas mixture (inert gas, water, and TBA) in the porous dried layer of the product, which is more complex than the models [2-6] for a binary mixture (inert gas and water) system. The off-diagonal terms of the diffusivity tensor for the three species will require careful examination of the relative concentrations of water and TBA vapors in the pore structure of the dried layer at different temperatures, in order to ascertain whether or not these off-diagonal terms and their effects on the heat and mass transfer processes need to be included in the structure of the mathematical model. The construction and solution of this new class of freeze drying models and the achievement of its aforementioned purposes require the following two pieces of fundamental physical information: (a) the thermodynamic model whose expressions provide the partial pressures of water and TBA vapors in equilibrium with the binary frozen mixtures of water and TBA as a function of temperature and of the mole

fractions of water and TBA in the frozen solid phase, and this necessary information also provides the important partial pressures of the vapors of water and TBA at the moving interface separating the frozen and dried layers of the product being freeze dried during the primary drying stage of the freeze drying process, and (b) the equilibrium adsorption/desorption isotherms of the sorbed (bound) binary mixtures of water and TBA on the surface of the pores of the dried layer which provide the concentrations of water and TBA in the binary sorbed (bound) mixture as a function of the temperature and of the partial vapor pressures of water and TBA in the gas phase in the pores of the dried layer, and this provides in the mathematical model the quantitative expressions needed to represent binary competitive adsorption/desorption through which the residual amounts of sorbed water and TBA as well as their distributions in the three-dimensional space of the dried layer of the product at any given time and especially at the end of the secondary drying of the freeze drying process could be calculated, so that we can determine whether the strict quality and toxicity criteria of the FDA are properly satisfied.

In this work the UNIFAC method coupled with the Dortmund parameter values for the subgroups of the binary mixture comprised of the species of water and TBA is employed and a thermodynamic equilibrium model is constructed. This model can provide the partial pressures of the vapors of water and TBA in equilibrium with the frozen solid phase of the binary mixture of frozen water and TBA, as a function of the temperature and of the mole fractions of water and TBA in the binary mixture of the frozen solid phase. The results obtained from the thermodynamic equilibrium model constructed and solved in this work are compared with the experimental results of Kasraian and DeLuca [7] and the agreement between the theoretical and the experimental results is found to be good. Therefore, this work considered the necessary and very important research problem stated in item (a) above and provides a satisfactory solution to this important research problem.

2. Thermodynamic Models and Methods

The thermodynamic equilibrium of a species between its pure liquid phase and its frozen mixture can be represented by

$$\ln\left(x_i\gamma_i\right) \approx \frac{\Delta H_{tri}^{fus}}{RT_{tri}}\left(1 - \frac{T_{tri}}{T}\right) - \frac{\Delta C_P^{sl*}}{R}\left[1 - \frac{T_{tri}}{T} + \mathbf{ln}\left(\frac{T_{tri}}{T}\right)\right] \quad , \tag{1}$$

where x_i and γ_i are the mole fraction and activity coefficient of species i, respectively, and l^* represents its subcooled liquid state at a temperature below its triple point (T_{tri}). Equation (1) has also been used as a means to predict solid-liquid equilibrium for mixture systems. For the binary frozen mixture of water and TBA, its experimental solid-liquid equilibrium phase diagram as demonstrated by Kasraian and DeLuca [7] is quite complex and has two eutectic points. The water-rich region forming pure solid ice and the TBA-rich region forming pure solid TBA were first read from the phase diagram [7] to estimate γ_i based on Eq. (1) and compared with those estimated by the modified UNIFAC (Dortmund) group contribution method [8]. For this purpose, the needed triple point and molar heat of fusion at T_{tri} (ΔH_{tri}) are 273.16 K and 6004 J/mol for water and 298.96 K and 6700 J/mol for TBA (National Institute of Standards and Technology, NIST WebBook), respectively. Within the

temperature ranges, the heat capacity difference, $\Delta C_P^{sl*} = C_P^{l*} - C_P^s$, for water is correlated into $\left(\dfrac{234.784}{T - 229.760} + 69.924 \right) - \left(0.1051T + 8.323 \right)$ J/mol-K, T in K, while for TBA it is based on $C_P^{l*} = C_{tri}^l = 2125.37$ J/mol-K (NIST WebBook) and C_P^s interpolated from the reported experimental data [9]. The activity coefficients are shown in Fig. 1 where the levels of agreement could be considered practically satisfactory, especially for the water-rich region, when there is a lack of both experimental data and an alternative theoretical approach.

Despite their importance to the freeze drying operation as well as to the intended mathematical modeling, the partial pressures of the water and TBA vapors above their frozen binary mixtures appear not to have been measured experimentally or reported in the literature. Instead, only the total pressures of the eutectic mixtures at 90 wt% TBA (x_{TBA} = 0.6863) have been measured and correlated [10]. In order to further verify the practical usefulness of the thermodynamic methods and models employed and presented in this work, the UNIFAC (Dortmund) method was applied in the following approach to estimate the total eutectic pressures,

$$P_{tot} = P_W + P_{TBA} = \gamma_W x_W P_W^{l*} + \gamma_{TBA} \left(1 - x_W \right) P_{TBA}^{l*} \quad . \tag{2a}$$

$$P_W^{l*} \left(\mathrm{Pa} \right) = 612 \exp \left[-\frac{45054}{R} \left(\frac{1}{T} - \frac{1}{273.16} \right) \right] \quad , \quad T \text{ in K} \quad . \tag{2b}$$

$$P_{TBA}^{l*} \left(\mathrm{Pa} \right) = \exp \left(-\frac{5583.5}{T} + 27.925 \right) \quad , \quad T \text{ in K} \quad . \tag{2c}$$

It is clear from the results presented in Fig. 2 that the thermodynamic approach presented here is able to produce the eutectic pressures satisfactorily within the ranges measured by experiments. The approach presented here could thus be considered a useful and reasonable one, especially in the absence of experimental thermodynamic data as currently is the case, for estimating the partial pressures of water and TBA vapors at other compositions in equilibrium with their binary frozen solid mixtures.
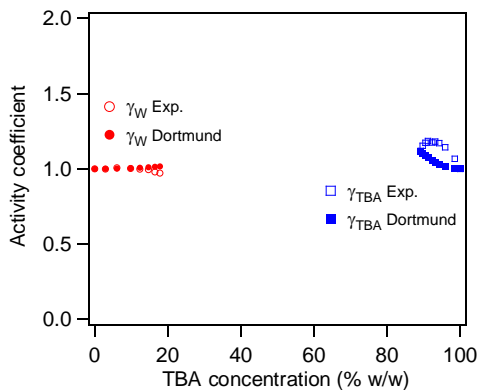
Fig. 1 Activity coefficient as a function of the TBA concentration
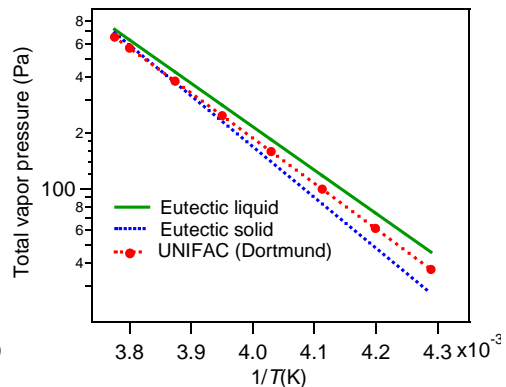
Fig. 2 Total pressure of eutectic mixtures at $x_{TBA} = 0.6863$

The partial pressures of water and TBA vapors resulting from the approach presented here at different temperatures and water mole fractions in the binary frozen solid phase are plotted in Fig. 3, while the total pressure resulting from adding the two partial pressures together is plotted in Fig. 4. It should be noted that the highest temperature selected to be considered here is -8.3 °C because this is the lower eutectic temperature below which the binary mixtures are frozen solids over the entire compositional range [7,10]. To incorporate the results of the partial vapor pressures into a future mathematical modeling study of the freeze drying process, well-correlated analytical expressions are much more desirable. For this purpose, only the activity coefficients, as indicated by Eqs. (2a)-(2c), need to be correlated. The functional form of the Non-Random Two-Liquid (NRTL) activity model was found to provide excellent correlations for the partial pressures with the following temperature-dependent parameters where R is the ideal gas constant and T is in K,

$$\ln \gamma_{\mathrm{W}} = \ln\left(\frac{P_{\mathrm{W}}}{x_{\mathrm{W}}}\right) = x_{\mathrm{TBA}}^2\left[\frac{b_{21}}{RT}\left(\frac{G_{21}}{x_{\mathrm{W}}+x_{\mathrm{TBA}}G_{21}}\right)^2 + \frac{G_{12}b_{12}/RT}{\left(x_{\mathrm{TBA}}+x_{\mathrm{W}}G_{12}\right)^2}\right] \quad , \tag{3a}$$

$$\ln \gamma_{\mathrm{TBA}} = \ln\left(\frac{P_{\mathrm{TBA}}}{1-x_{\mathrm{W}}}\right) = x_{\mathrm{W}}^2\left[\frac{b_{12}}{RT}\left(\frac{G_{12}}{x_{\mathrm{TBA}}+x_{\mathrm{W}}G_{12}}\right)^2 + \frac{G_{21}b_{21}/RT}{\left(x_{\mathrm{W}}+x_{\mathrm{TBA}}G_{21}\right)^2}\right] \quad , \tag{3b}$$

$$\begin{cases} G_{12} = \exp\left(-\alpha\dfrac{b_{12}}{RT}\right) \\ G_{21} = \exp\left(-\alpha\dfrac{b_{21}}{RT}\right) \end{cases} ; \quad \begin{cases} \alpha = 1.628 - 0.00992T + 1.860\times10^{-5}T^2 \\ b_{12}\,(\mathrm{J/mol\text{-}K}) = -11874.652 + 101.182T - 0.120T^2 \\ b_{21}\,(\mathrm{J/mol\text{-}K}) = -7429.529 + 58.534T - 0.108T^2 \end{cases} \cdot \tag{3c}$$

It is worth noting here that, as pure species or as components with the same mole fractions in the frozen solid mixtures, water has noticeably lower sublimation partial pressures (see Fig. 3) than those of TBA vapor and the resulting total pressure in the porous dried layer of
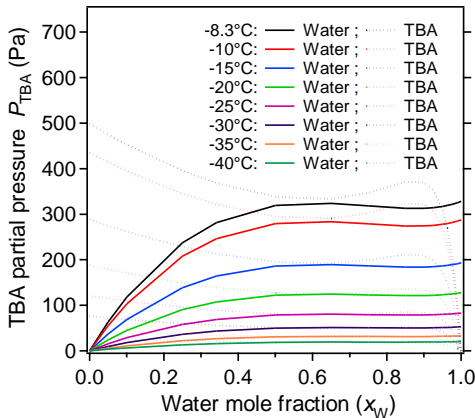
Fig. 3 Partial vapor pressure as a function of temperature and water mole fraction in the binary frozen solid mixture
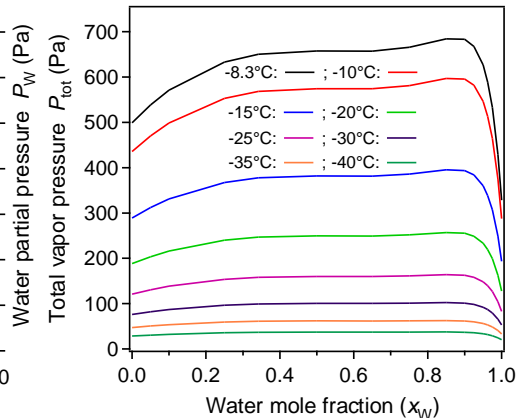
Fig. 4 Total vapor pressure as a function of temperature and water mole fraction in the binary frozen solid mixture

the product being freeze dried is significantly higher than in the case where water was the only solvent and, thus, the resulting total pressure gradient between the moving interface and the drying chamber pressure could be larger and provide an increase in the total convective mass transfer rate of the water and TBA gas mixture due to the presence of TBA. Therefore, TBA could sublime faster during primary drying and facilitate the mass transfer of water vapor from the frozen product and possibly reduce the primary drying time. But there are additionally two diffusion mass transfer mechanisms occurring simultaneously with convective mass transfer in the porous dried layer of the product, namely Knudsen and bulk diffusion. The Knudsen diffusivity is independent of total pressure, but it has dependencies on temperature and molecular mass. Taking a representative pore radius of 1000 Å, the Knudsen diffusivities [11] of water and TBA vapors in the porous dried layer were calculated and plotted in Fig. 5. As expected, water being lighter than TBA by a factor of approximately 4, has a Knudsen diffivisity about two times larger than that of TBA. The binary bulk diffusivity [11] is affected by both temperature and total pressure, which are both varying during freeze drying. Given the low total pressure condition (see Fig. 4) and considering the effective collision diameters of water and TBA being 2.64 Å [12] and 5.40 Å [13], respectively, the binary bulk diffusivities were calculated [11] and are represented by solid curves in Fig. 6 where the total vapor pressures are also included (dashed curves) for reference. Even the lowest bulk diffusivity in the range occurng at -8.3 °C and $x_{TBA} \approx 0.85$ is still 50-100 times greater than the Knudsen diffusivities of water and TBA vapors.

Enthalpically, water and TBA have very similar heats of sublimation, both around 51 kJ/mol [10,14], so their frozen binary mixtures also require a similar heat of sublimation [10]. This fact likely reduces the number of variables to control when devising an optimal heating strategy for the freeze drying process. In this respect, the system temperature cannot exceed -8.3 °C as it is the lowest melting temperature of the frozen water-TBA mixtures over the entire compositional range, which is also an eutectic point [7] occurring at 17.8 wt%
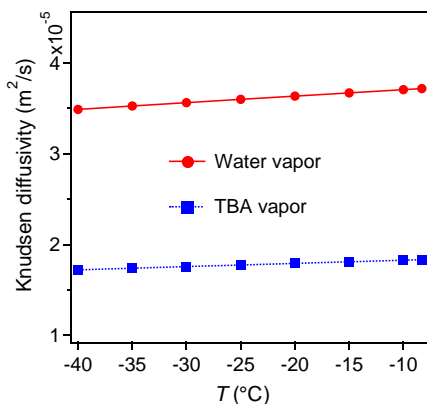
Fig. 5 Knudsen diffusivity of water and TBA as a function of temperature
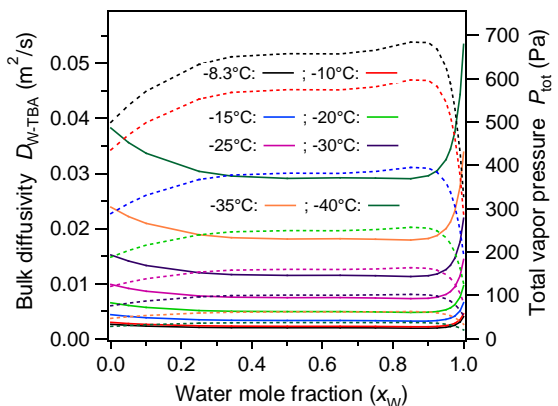
Fig. 6 Binary bulk diffusivity and total vapor pressure as a function of temperature and water mole fraction in the binary frozen solid mixture

TBA (x_{TBA} = 0.05). Similar heats of sublimation also attest, from the viewpoint of the Clausius–Clapeyron equation, the constantly higher pressures of TBA vapor over those of water vapor, and hence faster removal of TBA than water could occur during the primary drying stage of the freeze drying process. But the above data still point to water being a major process controlling species with respect to system constraints that have to be satisfied in the freeze drying process of pharmaceutical water solutions with TBA as a co-solvent.

3. Conclusions

Due to the limitations of current experimental techniques, a new class of physicochemical mathematical models is needed in order to enable rational physical and quantitative evaluation of the freeze drying process of pharmaceutical water solutions involing tertiary butyl alcohol (TBA) as a co-solvent. The construction and solution of such models require knowledge of the vapor pressures of water and TBA in equilibrium with their binary frozen solid mixtures, but these pressure data were not available to date. A thermodynamic approach based on the UNIFAC method coupled with the Dortmund parameters was developed to provide the needed pressure data as a function of temperature and of the mole fraction of the binary frozen solid mixture of water and TBA. The results have further been correlated into analytical expressions using a NRTL type model function. The results indicate the TBA vapor pressues to be constantly higher than those of water vapor and this leads to higher total pressure gradients in the porous dried layer of the product that could increase the convective mass transfer rates and support the experimental observation that TBA is removed relatively faster than water during the primary drying stage. When the bulk and Knudsen diffusion coefficients were evaluated under the temperatures and total vapor pressures that could be encountered in freeze drying, the former was found to be at least 50-100 times higher in magnitude than the latter. But the higher in magnitude total pressures of the binary gas mixtures of water and TBA which are due to the significantly larger vapor pressures of TBA, reduce the magnitude of the bulk diffusion coefficient. Furthermore, the Knudsen diffusion coefficient of TBA vapor is significantly smaller than that of water vapor. These effects on the magnitudes of the diffusivities could affect the mass transfer rates due to bulk and Knudsen diffusion during the primary and secondary drying stages. To ascertain the relative importance of the competing mass transport mechanisms of convection and bulk and Knudsen diffusion on the drying rates, one has to construct and solve an unsteady-state and spatially multi-dimensional freeze drying model that accounts for the effects of TBA presented here, while the thermodynamic expressions developed and presented in this work are a necessary component of the mathematical physics structure of such a model.

4. References

[1] Rey, M.; May, J.C. Freeze Drying/Lyophilization of Pharmaceutical and Biological Products; Marcel Dekker: New York, 2004.

[2] Millman, M.J.; Liapis, A.I.; Marchello. J.M. An analysis of the lyophilization process using a sorption – sublimation model and various operational policies. AIChE Journal 1985, 31 (10), 1594-1604.

[3] Sadikoglu, H.; Liapis, A.I. Mathematical modelling of the primary and secondary

drying stages of bulk solution freeze drying in trays: Parameter estimation and model discrimination by comparison of theoretical results with experimental data. Drying Technology 1997 (3-4), 15, 791-810.

[4] Liapis, A.I.; Bruttini, R. Exergy analysis of the freeze drying of pharmaceuticals in vials and trays. International Journal of Heat and Mass Transfer 2008, 51, 3854-3868.

[5] Liapis, A.I.; Bruttini, R. A mathematical model for the spray freeze drying process: The drying of frozen particles in trays and in vials on trays. International Journal of Heat and Mass Transfer 2009, 52, 100-111.

[6] Bruttini, R; Liapis, A.I. The drying rates of spray freeze drying systems increase through the use of stratified packed bed structures. International Journal of Heat and Mass Transfer 2015, 90, 515-522.

[7] Kasraian, K.; DeLuca, P.P. Thermal analysis of the teriary butyl alcohol–water system and its implications on freeze drying. Pharmaceutical Research 1995, 12 (4), 484-490.

[8] Gmehling, J.; Li, J.; Schiller, M. A modified UNIFAC model. 2. Present parameter matrix and results for different thermodynamic properties. Industrial & Engineering Chemistry Research 1993, 32 (1), 178-193.

[9] Oettin, F.L. The heat capacity and entropy of 2-methyl-2-propanol from 15 to 330 K. Journal of Physical Chemistry 1963, 67 (12), 2757–2761.

[10] Bogdani, E.; Daoussi, R.; Vessot, S.; Jose, J.; Andrieu, J. Implementation and validation of the thermogravimetric method for the determination of equilibrium vapour pressure values and sublimation enthalpies of frozen organic formulations used in drug freeze–drying processes. Chemical Engineering Research and Design, 2011, 89 (12), 2606–2612.

[11] Geankoplis, C.H. Transport Processes and Separation Process Principles; Prentice Hall: Upper Saddle River, New Jersey, 2003.

[12] Hirschfelder, J.O.; Curtiss, C.F.; Bird, R.B. Molecular Theory of Gases and Liquids; Wiley: New York, 1954.

[13] Westgate, P.J.; Ladisch, M.R. Sorption of organics and water on starch. Industrial & Engineering Chemistry Research 1993, 32 (8), 1676-1680.

[14] Murphy, D.M.; Koop, T. Review of the vapour pressures of ice and supercooled water for atmospheric applications, Quarterly Journal of the Royal Meteorological Society 2005, 131 (608), 1539-1565.

Implementation of P-Controller in Computational Fluid Dynamics (CFD) Simulation of a Pilot Scale Outlet Temperature Controlled Spray Dryer

Afshar, S.[a]*; Jubaer, H.[a]; Metzger, L.[b]; Patel, H.[c]; Selomulya, C. [a]; Woo, M.W. [a]

[a]Department of Chemical Engineering, Monash University, Clayton Campus, Victoria 3800, Australia

[b]Department of Dairy Science, South Dakota State University, Brookings, SD 57007, USA

[c]Dairy Foods Research and Development, Land O'Lakes Inc, USA

*E-mail of the corresponding author: sepideh.afshar@monash.edu

Abstract

Most of the CFD simulations of spray dryers reported in the literature utilizes a fixed air inlet temperature numerical framework. In this paper, a numerical framework was introduced to model spray drying as an outlet air temperature controlled process. A P-controller numerical framework was introduced which allows the inlet temperature to be automatically adjusted based on the required outlet temperature set point. This numerical framework was evaluated with a simulation of a two-stage pilot scale spray drying system at the Davis Dairy Plant (South Dakota State University) which is used for commercial contract spray drying operation.

Keywords: CFD simulation; Multi-Stage Spray Drying; P-Controller

1. Introduction

Spray drying is a popular unit operation in drying industry in which dry powder can be produced by removing moisture from a liquid material using a hot gas. This is a preferred method where heat sensitive material are used in food and dairy industries. The spray drying involves multiphase flow with heat, mass and momentum transfer between drying gas flow and the discrete phase. Therefore, controlling and designing spray dryers is time-consuming and complicated task particularly where the intent is large-scale production volume [1].

The use of CFD simulations for the design and analysis of spray dryers have been widely reported in the literature [2-5]. A survey of the simulation reported so far revealed that all the simulations employed a fixed inlet conditions (temperature) from which the outlet conditions (temperature) will be predicted. In actual commercial operations, the spray dryer is mainly outlet temperature controlled where the inlet temperature is adjusted (by the control system or sometimes manually), accounting for the evaporation within the chamber, to meet the desired outlet temperature. Such backward computation of the inlet temperature is not trivial in a CFD simulation. Therefore, there is a need for the development of a numerical framework to capture the outlet controlled operation of spray dryers.

In this work, to address this gap in knowledge, a numerical P-Controller was developed for implementation in a CFD simulation of a spray drying system. An industrial scale two-stage spray drying system at Davis Dairy Plant located at South Dakota State University (SDSU) with an external vibrating fluidized bed was modelled where the operation was outlet temperature controlled. In the operation of the SDSU dryer, spraying micellar casein concentrate, the desired temperature of side outlet was set at 82.2°C. Numerical challenges in the development of the P-Controller framework will be further discussed in this paper.

2. Description of the SDSU spray dryer system

Fig. 1 shows the dimensions of the spray drying unit modelled in this paper. The bottom outlet from the chamber leads to the external vibrating fluidized bed as the second stage dryer. The actual mass flow rate of the drying air entering the chamber was not measured or monitored as part of the control system. From the manufacturer's blower performance curve and the measured average pressure at the chamber inlet, the air mass flow rate was determined to be 1.1 kg/s.

The combined operation of the inlet air blower and the main outlet suction blower was used to maintain a negative pressure of approximately 677 Pa (gauge) within the chamber. This negative pressure was measured at approximately the middle elevation of the top conical region of the drying chamber. The bottom outlet pressure was unknown. Simulation of

airflow and particles trajectories ratios between two outlets revealed that the -250 Pa pressure would be a reliable prediction for the bottom outlet [6].

In the startup of the spray dryer, the dryer is firstly heated up with the inlet hot air without spray. At this stage, the automatic system will be manually overridden and a higher temperature, typically at around 161.1-214.4°C to achieve an outlet temperature of 82.2°C, will be used depending on the intended spray rate. Once the dryer reaches the desired outlet temperature, feed spray will be initiated and the automated inlet temperature control will be activated. By intuition, evaporation would have provided cooling to the hot air stream and this would have led to the need for a higher temperature to compensate in maintaining the outlet air temperature. The automatic control system will then increase the inlet air temperature to maintain the outlet temperature at the set point.

3. Modelling approach

The 3D simulations (Fig. 1) of spray dryer with a mesh size of 275764 elements were undertaken using ANSYS Fluent V17.1. [7]. The details of mesh dependency is described in [6]. Boundary condition for air inlet was mass flow inlet that was entered according to the manufacturer's blower air flow specifications (mass flow rate=1.1 kg/s). The walls of the chamber were specified as non-slip insulated wall boundaries. The side outlet (-677 Pa) and the bottom outlet (-250 Pa) were specified as pressure outlets. This approach allowed numerical capturing of the negative pressure within the drying chamber. The pseudo tracer analysis and how to predict the bottom outlet pressure is explained in [6]. Convergence criteria was 1×10^{-3} for all scaled residuals.

Transient simulations were undertaken. The Reynolds-time averaged Navier–Stokes conservation equations were used to describe the airflow field. The turbulence in the air was modelled using the standard k–ε model. It has been demonstrated that k–ε model performs much better in transient simulations than steady-state simulations particularly in spray drying systems [8]. For pressure–velocity coupling, the coupled algorithm was used. The transport, turbulence and species equations were discretized using a second-order upwind scheme. Pressure equation was discretized using the PRESTO scheme. A time step size of 0.05s with 10 iterations per time step was sufficient to capture the transient self-sustained central jet flapping behavior of the flow field. This time step size was also adopted by past reports simulating industrial scale spray dryers with inlet air flow of the same magnitude in velocity [9,10]. Particle injection time step sizes were set 0.05s. The "escaping wall" boundary condition was employed at the dryer walls, which assumes that all the particles deposit at the wall upon collision with the wall.
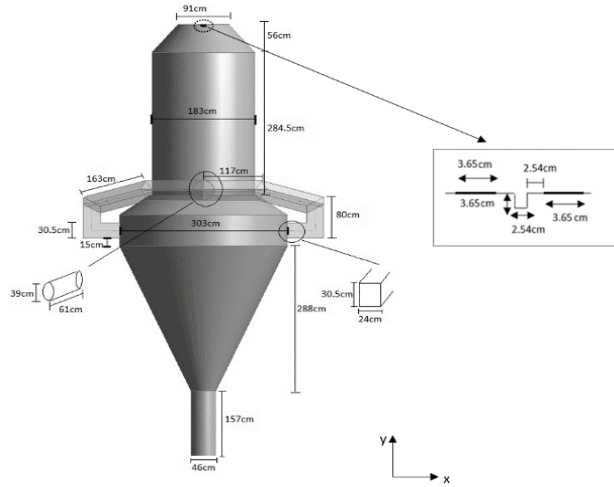
Fig. 1 Dimensions of spray drying chamber

3.1. Equations

Continuity equation is described in Equation (1):

$$\frac{\partial(\alpha_q \rho_q)}{\partial t} + \nabla.\left(\alpha_q \rho_q \vec{v}_q\right) = 0 \tag{1}$$

where q is either gas or solid.

Gas phase-momentum is described in Equation (2):

$$\frac{\partial}{\partial t}(\alpha_g \rho_g \vec{v}_g) + \nabla.\left(\alpha_g \rho_g \vec{v}_g \vec{v}_g\right) = \nabla.\bar{\bar{\tau}}_g - \alpha_g \nabla P + \alpha_g \rho_g \vec{g} + \beta(\vec{v}_s - \vec{v}_g) \tag{2}$$

Droplet trajectories were captured by the Lagrangian framework. This formulation (Equations (3) to (5)) tracks each discrete droplet individually within the air flow by integrating the motion equations governed by Newton's second law and including the influence of the relevant drag force interaction with the air.

$$\frac{dv_s}{dt} = C_D \frac{18\mu}{\rho_s d} \times \frac{Re}{24}(v_g - v_s) + g\left(\frac{\rho_s - \rho_g}{\rho_s}\right) \tag{3}$$

$$C_D = \frac{24}{Re}[1 + 0.15(Re)^{0.687}] \tag{4}$$

where

$$Re = \frac{\rho_g d\left(v_g - v_s\right)}{\mu_g} \tag{5}$$

The heat transfer model is explained in Equation (6):

$$mC_p \frac{dT_s}{dt} = hA(T_g - T_s) - \nabla.H_{evap} m_s \frac{dT_s}{dt} \tag{6}$$

The heat transfer coefficient was calculated using Ranz-Marshall equation:

$$Nu = 2 + 0.6Re^{0.5}Pr^{0.33} \tag{7}$$

The distribution of droplet diameters in the spray is assumed to obey the Rosin–Rammler distribution function [11]. The Rosin-Rammler model is given by Equations 8-9:

Authors: Afshar, S.; Jubaer, H.; Metzger L.; Patel, H.; Selomulya, C.; Woo, M.W.;

$$Y_s = e^{-(d/\bar{d})^n} \tag{8}$$
$$n = \frac{ln(-lnY_s)}{\ln(d/\bar{d})} \tag{9}$$

where Y_s is retained mass fraction of particle, d is the particle diameter, $\bar{d}$ is the mean particle diameter and is $394\times10^{-7}\mu$m, n is the size distribution parameter and is 2.4. The corresponding maximum and minimum droplet size are taken as $200\times10^{-8}\mu$m and $672\times 10^{-8}\mu$m. User-defined functions (UDFs) in Fluent were developed to describe the shrinkage behavior of particles and Reaction Engineering Approach (REA) models. The particle mixture density was modified using linear shrinkage model [12, 13] (see Equation 10):

$$\frac{d}{d_0} = b + (1+b)\frac{X}{X_0} \tag{10}$$

where d_0 is the initial diameter of the particle/droplet, X_0 is the particle/droplet initial moisture (kg kg^{-1}) on dry basis, and for MCC particles, b is 0.59 [14]. The Reaction Engineering Approach (REA) [15] model for 20 wt% solid content MCC is presented in Equation (11):

$$\frac{\Delta E_v}{\Delta E_{v,e}} = 0.012(X-X_e)^6 - 0.142(X-X_e)^5 + 0.6142(X-X_e)^4 - 1.2944(X-X_e)^3 + 1.483((X-X_e)^2 - 1.0771(X-X_e) + 1.0023 \tag{11}$$

This equation was determined from single droplet measurements in SDSU. The equilibrium moisture content (X_e) for MCC was calculated using Guggenheim-Anderson-de Boer (GAB) model. The constants were taken from [16], and described in Equation 12:

$$X_e = \frac{(0.564 \times RH)}{1 + 6.01RH - 5RH^2} \tag{12}$$

4. Results and Discussion

4.1. Development of the P-Controller numerical scheme

As mentioned in Section 2, the essence of the P-Controller is the continuous adjustment of the inlet temperature based on the outlet temperature relative to the desired outlet temperature set point. In this study, the desired outlet temperature was 82.2°C. In the Fluent framework, the UDF is implemented (hooked) to provide input to the air inlet temperature. The first key aspect of the numerical implementation is that there is a proportional gain parameter embedded into the code which subsequently translates to the step adjustment to the inlet temperature. From trial and error, there was a need to implement an arbitrary maximum possible change to the inlet temperature to ensure stable numerical computation. This limiter to certain extent will be affect by how the simulation is initialized prior to the activation of the P-controller (in case the initial outlet temperature difference relative to the set point is large). The second key aspect to the

numerical implementation is that a response time of the controller was embedded into the framework.

A 'counter' approach was used in the current code corresponding to the enforced number of flow field iterations per time step in the simulation. Both parameters, proportional gain (and the arbitrary limiter) and the response time will affect the simulation time required to achieve a stable air flow outlet temperature. In this work, only the response time was evaluated while keeping the proportional gain parameter constant.

4.2. Evaluation on the effect of different controller response time

Preliminary transient simulations with a fix inlet temperature (without P-controller) showed that characteristic response time of the simulation was approximately 10 seconds. In other words, it takes 10 seconds until the outlet temperature reaches 82.2°C. Therefore the number of time steps to receive a feedback from P-Controller, between the initial inlet temperature and the calculated outlet temperature was 200, as each time step size was set 0.05 second. The time-step response of 10 seconds was taken as the base study, and the 25s and 35s time-step responses were also investigated. For the brevity, the 25s time-step results were not presented here. Fig. 3 (a-d) shows the inlet and side outlet temperature profiles where time responses are 10s and 35s respectively.
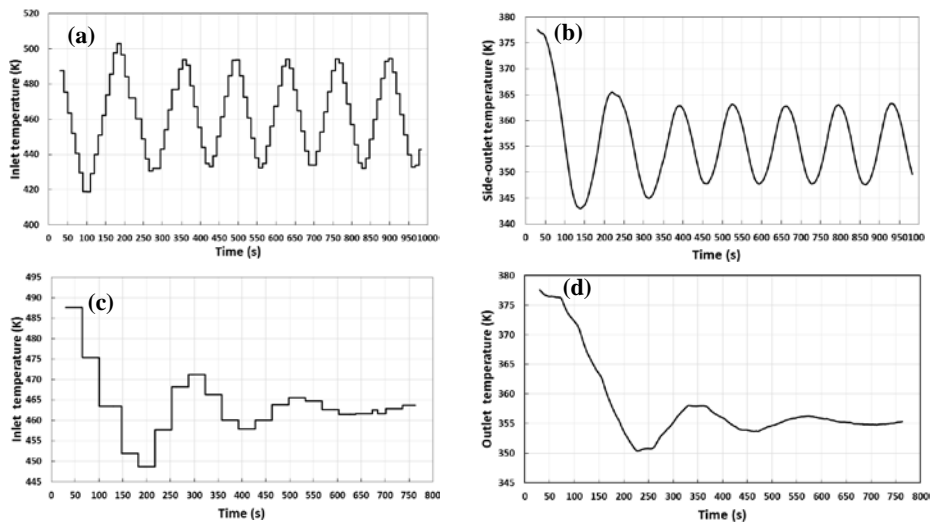
Fig. 3 Temperature profiles (a) inlet temperature: 10s time-step response (b) side-outlet temperature: 10s time-step response (c) inlet temperature: 35s time-step response (d) side outlet temperature: 35s time-step response

As can be seen from Fig. 3(a,b), the temperature profiles kept fluctuating where the time-step response is 10s and the final inlet tempeture is not predictable. However, at 35s time-step responses (Fig.3(c,d)) the temperature profiles were stabilized after approximately

750seconds. The temperature profiles were stabilized after 970 seconds where time-step responses were 25s (For the brevity the figures are not shown here). The measured experimental inlet temperature was 447K, and the predicted CFD inlet temperature was 463K

(Fig. 3(c)). The corresponding error is 3.5%, and it could be due to the uncertainties in other parameters of the simulation such as the atomization parameters or the estimation of the bottom outlet pressure. Nevertheless, this is the first reported attempt in the implementation of the P-Controller for a CFD simulation of spray dryers.

3. Conclusions

CFD simulations of two-stage spray dryer were performed where the inlet temperature was estimated using a P-Controller. The crucial step to estimate the inlet temperature was to predict the proper time-step responses between the inlet and the side-outlet. Comparison of three different time-step responses showed that the longer the time-step responses are the shorter the time required to achieve stabilized temperature profiles. It was found that the time-step response of 35s is adequate to achieve the stabilized temperature profiles. It was proved that the presented P-Controller approach was reasonably able to predict the inlet temperature, however the corresponding error can be due to the uncertainties in obtaining operating parameters from the semi-commercial plant. Future applications of this approach, for faster computation, may require an initial overall black-box mass and energy balance to provide the initial inputs to the dryer from which the P-Controller can then be used for further refinement to the CFD analysis.

Nomenclature

A	Area, [m^2]
b	constant value in Eq. 10
C_D	drag coefficient, [-]
C_p	specific heat capacity, [$J.kg^{-1}.K^{-1}$]
d	diameter, [m]
$\bar{d}$	mean diameter, [m]
ΔE_v	apparent activation energy, [$J.mol^{-1}$]
g	acceleration due to gravity, 9.81 [ms^{-2}]
h	heat transfer coefficient, [Wm^2K^{-1}]
H_{evap}	Heat of evaporation [$J.kg^{-1}$]
m	mass, [kg]
Nu	Nusselt number, [-]
Pr	Prandtl number [-]

P	pressure, [Pa]
Re	Reynolds number, [-]
RH	relative humidity
t	time, [s]
T	Temperature, [K]
v	velocity, [$m\ s^{-1}$]

Greek symbols

α	volume fraction, [-]
μ	dynamic viscosity, [Pas]
ρ	density, [kgm^{-3}]
$\bar{\bar{\tau}}$	stress tensor, [Pa]

Subscripts

e	equilibrium
g	gas phase
s	particle phase

4. References

[1] Mujumdar, A.S.; Handbook of Industrial Drying; Taylor & Francis; Philadelphia, 2007.

[2] Langrish, T.A.G.; Fletcher, D.F. Spray drying of food ingredients and applications of CFD in spray drying. Chemical Engineering and Processing 2001, 40(4), 345-354.

[3] Salem, A.; Ahmadlouiedarab M.; Ghasemzadeh K. CFD approach for the moisture prediction in spray chamber for drying of salt solution. Journal of Industrial and Engineering Chemistry 2011, 17(3), 527-532.

[4] Kieviet, F.G.; Van Raaij, J.; De Moor, P.P.E.A.; Kerkhof, P.J.A.M. Measurement and modelling of the air flow pattern in a pilot-plant spray dryer. Institution of Chemical Engineers 1997, 75, 321-328.

[5] Gabites, J.R.; Abrahamson, J.; Winchester, J.A. Air flow patterns in an industrial milk powder spray dryer. Chemical Engineering Research and Design 2010, 88(7), 899-910.

[6] Afshar, S.; Metzger, L.; Patel, H.; Selomulya, C.; Woo, M.W.; A practical approach to estimate outlet boundary conditions for CFD modelling of industrial multistage spray dryers. International Journal of Drying Technology 2018 (submitted).

[7] ANSYS, Inc. ANSYS®Fluent, in Help system, ANSYS FLUENT Users Guide, Release 17.1; ANSYS, Inc.: U.S.A., 2016.

[8] Harvie, DJE.; Langrish, TAG.; Fletcher, DF. Numerical simulations of gas flow patterns within a tall-form spray dryer. Transations of the Institution of Chemical Engineers 2001, 79 (3), 235–248.

[9] Gabites, JR.; Abrahamson, J.; Winchester, JA. Air flow patterns in an industrial milk powder spray dryer. Chemical Engineering Research and Design 2010, 88 (7) 899-910.

[10] Jin, Y.; Chen, XD. Entropy production during the drying process of milk droplets in an industrial spray dryer. International Journal of Thermal Sciences 2011, 50 (4) 615-625.

[11] P. Rosin, E. Rammler, Journal of the Institute of Fuel, 7 (1933) 29-36.

[12] Lin, S.X.Q.; Chen, X.D. Changes in milk droplet diameter during drying under constant drying conditions investigated using the glass-filament method. Food and Bioproducts Processing 2004, 82(3), 213-218.

[13] Fu, N.; Wai Woo, M.; Selomulya, C.; Chen, X.D. Shrinkage behaviour of skim milk droplets during air drying. Journal of Food Engineering 2013, 116(1), 37-44.

[14] Yang, X.; Xiao, J.; Woo, M.W.; Chen, X.D. Three-Dimensional Numerical Investigation of a Mono-Disperse Droplet Spray Dryer: Validation Aspects and Multi-Physics Exploration. Drying Technology 2015, 33(6), 742-756.

[15] Chen, X.D.; Xie, G.Z. Fingerprints of the drying behaviour of particulate or thin layer materials established using a reaction engineering model. Transactions of the Institution of Chemical Engineers 1997, 77 (A), 21-38.

[16] Foster, K.D.; Bronlund, J.E.; Paterson, A.H.J. The prediction of moisture sorption isotherms for dairy powders. International Dairy Journal 2005, 15(4), 411-418.

Application of Multivariate Image Analysis to Thermal Images for on-line Monitoring of the Freeze-Drying Process

Colucci, D.[a,b*], Prats-Montalbán, J. M.[a], Fissore, D.[b]; Ferrer, A.[a]

[a]Multivariate Statistical Engineering Group, Department of Applied Statistics, Operations Research and Quality. Universitat Politècnica de València. Camino Vera s/n, 46022. València, Spain.

[b]Dipartimento di Scienza Applicata e Tecnologia, Politecnico di Torino, Corso Duca degli Abruzzi 24, 10129 Torino, Italy.

*E-mail of the corresponding author: domenico.colucci@polito.it

Abstract

A new Process Analytical Technology (PAT) has been developed and tested for on-line process monitoring of a vacuum freeze-drying process. The sensor uses an infrared camera to obtain thermal images of the ongoing process and multivariate image analysis (MIA) to extract the information after automatic detection and segmentation of the region corresponding to the product in every vial. A reference model was built, using the information of six batches, and different kind of anomalous events, involving either single vials in the batch or the whole batch, were simulated to test the capacity of the MIA-based monitoring system to promptly identify them.

Keywords: freeze-drying; process monitoring; infrared image; multivariate image analysis.

1. Introduction

Vacuum freeze drying (VFD) is a highly attractive process for the water removal in thermal sensitive products, mainly pharmaceutical ones, since water is removed at low temperature by sublimation. Monitoring of critical quality attributes of the product, e.g. its temperature, is required to guarantee that the desired characteristics are obtained in the final product. Besides, it is required that the monitoring system does not interfere with product dynamics.

In the past, many approaches to this problem, based on the measurement of product temperature, sublimation rate, heat flux to the product, among the others, were proposed and tested [1], in particular at lab-scale. The measurement of the temperature of the product, possibly in a well-defined position (e.g. the bottom of the vial), was studied in detail and successfully applied for process monitoring and control [2]. The main drawback, up to this moment, of this approach is that the temperature measurement has to be performed using a thermocouple stuck into the product and this does not guarantee neither the sterility requirements nor that the sensor is not interfering with the ongoing process.

In this work we used an infrared camera, instead of a thermocouple, for temperature measurement. Differently from the system proposed in the literature, we placed the camera inside the chamber, thus being able to monitor the vials in several positions, and not only on the top shelf of the freeze-dryer [3], thus extending the monitoring capacity of the system. Unfortunately, thermal images include a lot of useless (i.e. everything that is outside the vial) information and also the one directly related with the process is highly noisy, redundant and correlated. The first problem is a matter of gray-scale image segmentation, and traditional image analysis, as well as computer vision, supply a lot of tools for working out this kind of matters; the second is a frequent problem when dealing with real industrial data, and latent based multivariate statistical techniques can easily deal with this kind of problems.

The idea underlying the development of a latent variable multivariate monitoring system is that only a few underlying events are driving the process, and all the measurements we obtain are just a different sight on this underlying driving force. Multivariate statistical methods allow us to obtain a model of the process by projecting the information into a low dimensional space defined by latent variables and, in this reduced space, we can build control charts able to detect any deviation from the normal operating conditions [4]. Principal component analysis (PCA) has been widely studied and applied for this purpose being also able to successfully deal with the highly auto-correlated and cross-correlated data typical of batch processes [5] such as VFD intrinsically is. Multivariate control charts for batch process monitoring have been proposed by Nomikos and MacGregor [6].

2. Materials and Methods

2.1. Experimental

Drying experiments were carried out using a lab scale equipment LyoBeta 25™ freeze-dryer (Telstar, Spain). In all tests ten vials (ISO 8362-1 8R) were placed at 30 cm from the camera, and a new image was acquired every five minutes. Each vial in the batches has been assigned with a number referring to the position in the shelf as Figure 1 shows.

The normal operating conditions (NOC) set was obtained processing a solution of 10% b.w. sucrose (Sigma Aldrich, 99.5%), 5 ml per vial, at -20°C and 20 Pa. Six batches were processed in the same operating conditions, thus obtaining 60 observations, corresponding to the 10 vials monitored in the 6 tests. The detection ability of the system was evaluated in four additional batches (i.e. observations from 61 to 100). In batch 7, after 5 hours of drying, chamber pressure was raised to 50 Pa; in batch 8 the shelf temperature was set to -10°C while in batch 10 a solution 5% b.w. of sucrose was used. Batch 9 aimed to prove the ability of the model to detect faults affecting the single vials and, while shelf temperature and chamber pressure were set to the NOC values, only four vials (corresponding to observations 81, 88, 89 and 90) were filled with the 10% solution. A piece of glass was inserted into two vials, one was filled with pure water, one with the same 5% b.w. solution used for batch 10 and the remaining two with respectively 2.5 and 7.5 ml of solution.

Due to the vibrations of the equipment, during batch three, vial 7 felt down and was considered as a fault, while the remaining nine vials were considered successfully dried.

2.2. Image segmentation and data acquisition

The thermal images are 256x320 pixels. The camera is equipped with a 63°x50° lens which leads to a slight optical distortion, known as barrel effect. This second order deviation from the ideal rectilinear projection can be compensated remapping the pixels according to the following equation:

$$r_{new} = r_{old} + f \cdot r_{old}^2 \tag{1}$$

where *r* is the distance from the center of the image of a generical pixel and *f* a correction factor (negative in this kind of optical aberration) depending on the distance between the camera and the object [7]. In all our tests the same distance was used this factor is approximately constant and equal to -1.5.

After optical correction, the Hough transform [8] was used to detect the position of the vials in the images, as shown in Figure 1. Being known the diameter of the vials bottom and the length of the line detected by the Hough transform we were able to infer the width of a single pixel and thus, as we know also the height of the vial, the height of the mask.

The whole portion of the image corresponding to the product into every vial was segmented and, to study the evolution over time of the temperature distribution, mean, standard deviation (std), skewness and kurtosis of the temperature in this region were measured. The results were collected into a three-dimensional data structure $\underline{\mathbf{X}}$ *(I × J × K)* where *I* is the number of observation, being each vial intended as a single observation, *J* is the number of variables measured, and *K* is the number of time instants.

2.3. Batch process monitoring

The data structure was batch-wise unfolded obtaining a matrix $\mathbf{X}$(*I×JK*) [5]. After mean centering and scaling **X**, a PCA model with *A* principal component was built using the available observations, obtained in batch 1 to 6.

$$X = T \cdot P' + E \tag{2}$$

where **T** is the *I×A score* matrix, **P** is the *A×JK loading* matrix and **E** is the *I×JK* residual matrix. The number of principal components that maximizes the classification skills of the model was determined as that who maximizes the following function:

$$f_A = (1 - \alpha) \cdot (1 - \beta) \tag{3}$$

where *α* is the overall type I error rate (i.e. false positive rate) and *β* is the overall type II error rate (i.e. false negative rate). Once the latent variable sub-space is known, unusual behaviors can be detected using two multivariate control charts: Hotelling T^2 (T^2) and the squared prediction error (*SPE*) defined by equations 4 and 5 for each observation:

$$T^2 = \sum_{a=1}^{A} \frac{t_a^2}{\lambda_a} \quad (4) \qquad\qquad SPE = \sum_{c=1}^{KJ} e_c^2 \quad (5)$$

where t_a is the *a*-th score and e_c is the error obtained after predicting the measurement of variable *c* for a certain observation. Upper control limits (UCL) for these charts were computed both empirically, that is taking the percentile of the actual values measured for the same NOC observations, and using their theoretical statistical distributions [6]. Once the number of principal components has been fixed, the possible outliers that would contribute to raise the control limits have been detected and purged. Due to the reduced number of batches available, a *one-batch-out cross-validation* approach was used: each batch is in turn removed from the NOC data set used to build the PCA, all the observations are projected, and those observations that prove to be outliers are removed.

The main issue when dealing with on-line multivariate SPC is the imputation of the missing information [6], a good approach being regression on the available NOC data used to build the PCA model [9]. In this work the *Trimmed Score Regression* (*TSR*) method has been used [10]. In on-line monitoring the *SPE* is computed only on the information measured at instant *k*, and for this reason is called *instant SPE* (*SPEI*):

$$SPEI_c = \sum_{c=1+(k-1)J}^{KJ} e_c^2 \qquad (6)$$

Nomikos and MacGregor proposed to use the errors on a moving window of five instant measurements to compute the UCL limits for this statistic [6]. The percentage of time instants that *SPEI* overtake the UCL in in-control batches, also called Overall type I (OTI) risk, should be lower than the imposed significance level (ISL = 0.5%) and for this reason the UCL have been manually tuned [11]. *Nf* is the number of instantaneous faults for the overall trial set.

$$OTI = 100 \cdot \frac{Nf}{I \cdot K} \% \qquad (7)$$

3. Results

Figure 2 reports an example of the 10 trajectories, one for each vial, described by the four variables measured during the drying process in one of the reference batch. Average temperature shows an asymptotic behavior up to the thermal equilibrium. The standard deviation (std), after a sudden decrease, grows up until a maximum is reached at almost 9 h; then, it slowly decreases again until reaching an almost constant value at 36 h. Both skewness and kurtosis show a maximum, followed by a local minimum around 9 hours. An almost constant value is kept from 36 h to the end. The local maxima (or minima) seems to correspond to the first slope change of the Pirani/Baratron pressure ratio. The constant values at the end indicates that the thermal equilibrium has been reached and the primary drying is over. Significant differences in these thermal trajectories may reveal an abnormal heat transfer, that is an anomalous drying kinetic and a lower product quality.

From the analysis of the scree plot and the cumulative variances plot (not reported) we decided to evaluate f_A for a number of components going from 5 to 13, that is from 83.9% to 95.4% of the whole variance. Figure 3 shows that f_A clearly shows a maximum when 10 PC are used (93.6% variance explained). Observation 21 appeared as the only outlier during the one-batch-out cross-validation step, and for this reason has been removed from the final data set. The UCL for T^2, depending only on the number of PC extracted and the number of observations, are constant but there is a remarkable difference between the theoretical and the empirical value; being the former (20.9) always lower than the latter (36.3). On the other hand, the UCL for *SPEI* computed with the theoretical distribution and the one obtained taking the percentile of 99.5% are always very similar. After tuning the control limits, the obtained OTIs were 0.496% for *SPEI* and zero for T^2.

The classification performance of this monitoring system has been evaluated by projecting all the batches (one hundred vials/observations) on the obtained model. Tuned empirical limits performed slightly better than the theoretical ones and have been used. Figure 4 shows an example of the resulting control chart for three observations: number 5, a vial of the NOC set, always below the UCL; number 21 that was removed as an outlier and has been detected as a fault by the *SPEI* control chart only; and number 75 dried at a higher shelf temperature

and lies over the control limits of both statistics almost all the time. The control charts for *SPEI* detected 10 false positives observations in the trial set (6, 9, 10, 15, 16, 19, 25, 31, 40, 50). Observations 21 and 27 (the one that felt down in batch 3) have been detected as faults as well as all the observations of the anomalous batches 7, 8 and 10. In batch 9 six vials were tampered and all of them have been correctly discriminated, while all the remaining good vials resulted into false positives. The T^2 control chart reported thirteen false negatives. Only two of the four vials of batch 9 dried with the original 10% sucrose solution (observations 81 and 90) have been correctly found to be successful drying tests. Observations 88 and 89 have been highlighted as faults.

Looking at the observations that appeared as false positives in *SPEI* (they are 6, 9, 10, 15, 16, 19, 25, 31, 40, 50) we can notice a certain periodicity in the results. Position 1 and 10 in every batch corresponds to the external vials, directly radiated by the chamber walls. Observation 21, as well as 81 and 90, appear to support this hypothesis. In the first three batches a thermocouple was located inside the vials in position 5 and 6, see Figure 2. This slight difference into the data structure of observation 6, 15, 16 and 25 might be due to the influence of the thermocouple on the drying kinetics.

These observations overtake the control limits on a limited number of time instants. If we accept these spurious errors as part of the unavoidable statistical error rate, that is, we consider the phenomena responsible for these instantaneous faults cannot jeopardize the quality of the resulting product, the fault detection performance could be further optimized. This new relaxation of the control limits was achieved by considering faults only the observations that cross the control limits in more than 5% of the time instants. In this way all the false positives in *SPEI* where properly classified as successful tests except observations 81 and 90. No further improvement was possible for Hotelling T^2 control charts since lowering the UCL to include the false negatives raises new false positives. This lower detection ability of T^2 control charts, when dealing with data from batch processes, has already been reported in the literature and is basically due to the strong auto-correlation in the data [11].
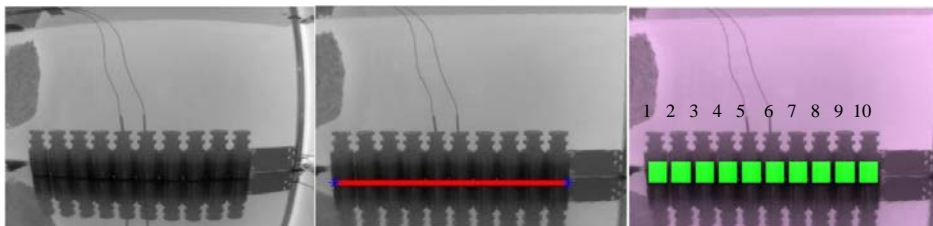
Fig. 1: Image preprocessing and segmentation.
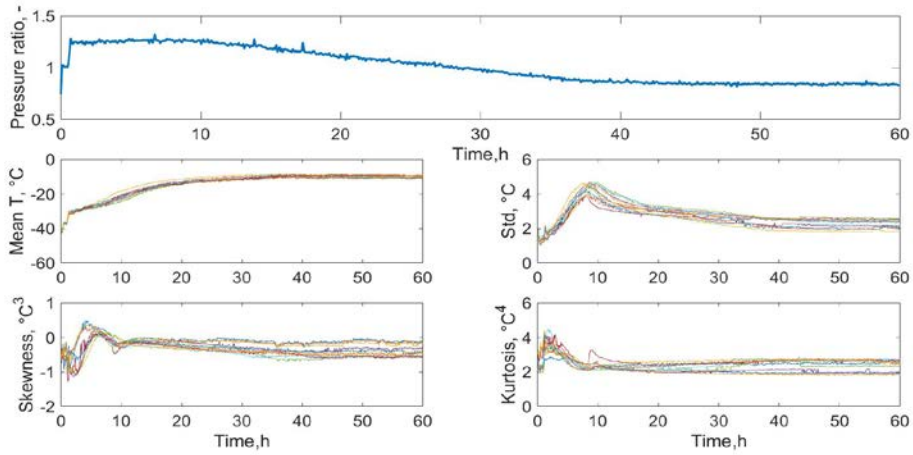
Fig. 2: Pirani Baratron ratio and temperature trajectories
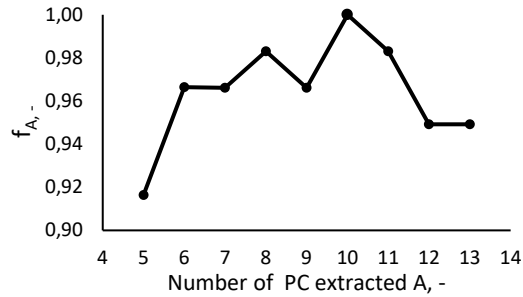
Fig. 3: Optimal number of Principal Components
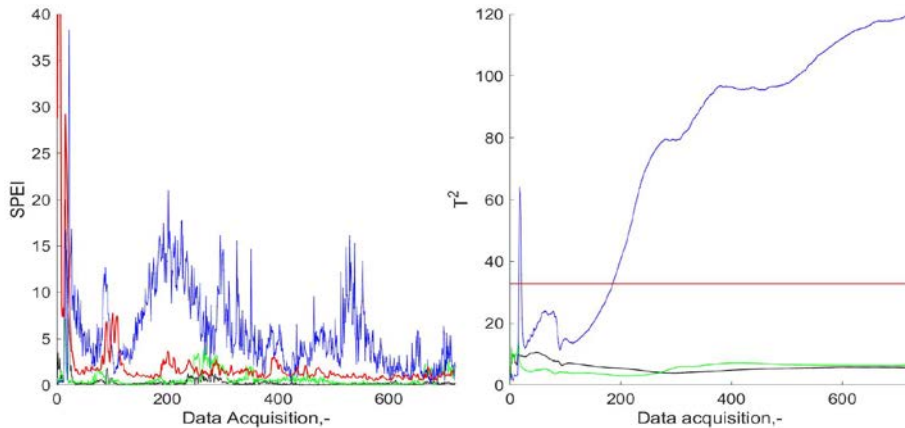
Fig. 4: Control charts for observation 5 (black line) and 21(signaling only in SPEI, green line) and 75 (signaling in SPEI an T^2, blue line). Red line tuned empirical UCLs.

4. Conclusions

In this work MIA techniques have been applied to thermal images of the VFD process and a PAT for real time monitoring have been developed and successfully tested. The sensor, using an infrared camera, is completely non-invasive and have no side-effects on the process kinetics. This technology proved to be quite sensitive being able to discriminate the slight effect on the product of either a thermocouple inserted into some vials or chamber walls radiation. Future works will aim to prove the possibility to use this PAT and the infrared imaging technology for process control and optimization purposes.

5. References

[1] Fissore, D.; Pisano, R.; Barresi, A.A. Process analytical technology for monitoring pharmaceuticals freeze-drying – A comprehensive review. Drying Technology, In press (DOI: 10.1080/07373937.2018.1440590).

[2] Fissore, D.; Pisano, R.; Barresi, A.A. On the use of temperature measurement to monitor a freeze-drying process for pharmaceuticals. In Proceedings of I2MTC – 2017 IEEE International Instrumentation and Measurement Technology Conference, May 22-25, Torino, Italy. 1276-1281

[3] Emteborg, H.; Zeleny, R.; Charoud-Got, J.; Martos, G.; Luddeke, J.; Schellin, H.; Teipel, K. Infrared thermography for monitoring of Freeze-Drying processes: instrumental developments and preliminary results. Journal of Pharmaceutical Sciences 2014, 103, 2088-2097.

[4] Kourti, T; MacGregor, J.M. Multivariate SPC methods for process and product monitoring. Journal of Quality Technology 1996, 28(4), 409-428.

[5] Kourti, T. Multivariate dynamic data modeling for analysis and statistical process control of batch processes, start-ups and grade transitions. Journal of Chemometrics 2003, 17, 93-109.

[6] Nomikos, P.; MacGregor, J.M. Multivariate SPC charts for monitoring batch processes. Technometrics 1995, 37, 41-59.

[7] De Villiers, J.P.; Leuschner, F.W.; Geldenhuys, R. Centi-pixel accurate real-time inverse distortion correction. In Proceedings of SPIE, 2008, 7266, 11-1-11-8.

[8] Gonzalez, R.C.; Woods, R.E.; Eddins, S.L. Digital image processing using Matlab. Pearson education, Inc.: Upper Saddle River, New Jersey, 2004.

[9] Arteaga, F.; Ferrer, A. Framework for regression-based missing data imputation methods in on-line MSPC. Journal of Chemometrics 2005, 19, 439-447.

[10] Arteaga, F.; Ferrer, A. Dealing with missing data in MSPC: several methods, different interpretations, some examples. Journal of Chemometrics 2002, 16, 408-418.

[11] Camacho, J.; Picó, J.; Ferrer, A. Multi-phase analysis framework for handling batch process data. Journal of Chemometrics 2008, 22, 632-643.

Feasibility of Vis/NIR spectroscopy and image analysis as basis of the development of smart-drying technologies

Sturm, B. [a*]; Moscetti, R. [b]; Crichton, S.O.J.[a]; Raut, S. [a]; Bantle, M, [c]; Massantini, R.[b]

[a] Process and Systems Engineering in Agriculture Group, Department of Agricultural and Biosystems Engineering University of Kassel, Witzenhausen, Germany

[b] Department for Innovation in Biological, Agro-food and Forest system (DIBAF),
Tuscia University, Viterbo, Italy

[c] Department of Energy Processes, SINTEF Energy Research, Trondheim, Norway

*E-mail of the corresponding author: barbarasturm@daad-alumni.de

Abstract

Drying is a complex, dynamic, unsteady and nonlinear process that, when not optimized on a system level, may be responsible for (1) significant quality degradation and (2) energy wastage. Consequently, new drying technologies must be designed combining non-invasive at-/on-/in-line advanced measurement and control systems with models cross-linking all relevant aspects of product quality changes and heat and mass transfer phenomena.

This paper presents preliminary results on the use of RGB imaging, NIR spectroscopy and Vis-NIR hyperspectral imaging for real-time monitoring of physicochemical changes of apples and carrots during drying.

Keywords: *chemometrics, artificial intelligence, deep learning*

1. Introduction

Commercial drying of apple and carrot produce is generally conducted according to drying strategies developed decades ago. These strategies operate to a large degree based on strict control of the characteristics of raw material at the input stage. This strict sorting, however, results in a significant proportion of produce being wasted prior to any processing. This coarse sorting at the input stage, however, does not guarantee that, after the set drying process, the entire produce will be of the same quality or will even fulfill the minimum quality required by consumers. In recent years, the organic sector has put significant efforts into the development of clear definitions for gentle and quality oriented ways of processing plant based foodstuffs to supplement existing regulations and guarantee premium quality of the product whilst reducing resource depletion [1].

The use of non-invasive measurement and control systems have shown a great potential for improvement of the product quality [2]. Simple solutions can readily be implemented into existing processes (e.g. dynamic control of product temperature [3]), while integration of advanced solutions is not possible nor financially viable in practice. Thus, there is a need for smart processing systems which allow for simultaneous multi-factor control (i.e. air temperature, velocity, humidity) to guarantee high-value end products, while enhancing energy demand and resource efficiency, by implementing innovative and reliable microcontrollers, sensors, resources, tools and practices at low cost and embracing various R&D areas (e.g. computer vision, hyper-/multispectral imaging, deep learning, etc.) [4].

Aim of this study was, therefore, the development of non-invasive measurement systems based on RGB imaging, Vis/NIR Hyperspectral imaging and NIR spectroscopy in combination with analysis algorithms to determine colour development, water content and chemical components throughout the drying process. These technologies and techniques are essential to provide inputs for the development of product quality driven adaptive control systems for drying. Eventually, these systems are intended to be transferred to simpler solutions and integrated into smart control systems for product quality oriented drying.

2. Materials and Methods

2.1 RGB imaging study on apples

Organic apples var. Red Delicious with the origine Italy were sourced from a local supplier (Trondheim, Norway) and stored at 8°C until processing. For the trials slices of 5 mm were cut. Core and skin were not removed.

Drying experiments were conducted at 20 and 40 °C with relative air humidities of 25, 40 and 60 % using an experimental drying chamber built at SINTEF. The chamber was equipped with a camera system, including an LED barlight for illumination. Details on the experimental set-up and conduction of trials are presented by Bantle [5].

Analysis of optical alterations was conducted using the OpenCV libraries for image processing, using images taken every 5 minutes during the drying tests. RGB values were transformed into CIE-XYZ color space according to the ISO Standrad 13655 and then further processed to receive the CIE-L*a*b values. A detailed procedure is given by Bantle et al. [5].

2.2 Vis/NIR Hyperspectral imaging study on apples

Apples var. Golden Delicious were sourced from a local retailer (Witzenhausen) and stored at room temperature until use. The apples were de-cored and sliced to 5mm thickness and cut to a uniform outer diameter of 65mm. Drying was conducted in a hot air convection oven at 50°C.

Drying tests were conducted using a convective air cabinet dryer (HT-Mini, Innotech Ingenieurgesellschaft mbH, Altdorf, Germany) at 50 and 70°C. Measurement protocols followed those described by Crichton et al. [6].

Samples were imaged using a Specim V10E PFD hyperspectral camera (Schneider Optics Xenoplan 1.9/35) in conjunction with a linear translation stage (Specim Spectral Imaging Ltd., Finland). Three 60W halogen GU10 bulbs were used for illumination. A detailed description of the image processing moisture content prediction protocols followed is given by Crichton et al. [6].

2.3 Near infrared spectroscopy study on carrots and apples

Organic carrots (*Daucus carota L.,* var. Romance) and apples (*Malus domestica* B. var. Gala) were purchased and immediately stored at 4 ± 1 °C until processing. Carrot slices and apple wedges were prepared by washing and cutting samples using a sharp ceramic knife. The slices and wedges were subjected to 8-h hot-air drying and batch sampling was performed at every hour of drying. The dehydration process was conducted at 40°C (carrot) and 60°C (apple). Samples were divided into two groups, one of which was subjected to a blanching pre-treatment before hot-air drying and one that was dried without pre-treatment (i.e. hot-water blanching at 95°C for 1.45 min for carrots and microwave blanching at 850W for 45 sec for apples). Each batch was subjected to both NIR spectral data acquisition and determination of CIELab colour, moisture content (wet basis), water activity (a_w), soluble solids content and total carotenoid content (carrot only).

Absorbance spectra were acquired using a spectrophotometer mod. Luminar 5030 (Brimrose Corp., Baltimore, USA) (range 1100-2300 nm, 2-nm resolution). Each sample was measured in duplicate on two opposite sides of each slice/wedge (i.e. 4 spectra per sample).

Chemometric analysis was performed following spectral pre-treatments including Standard Normal Variate, Multiplicative Scatter Correction, Savitzky-Golay first and second

derivatives with a second or third order polynomial fitted over a window of five, seven, nine or eleven features, as well as Mean Centering [7, 8].

Regression models were computed using the partial least squares (PLS) regression through the SIMPLS algorithm [9]. The samples were randomly split as calibration set (C) and the prediction set (P). The venetian blinds cross-validation with 10 data splits was performed. Root Mean Square Error (RMSE), BIAS and coefficient of determination (R^2) were employed as model performance metrics [10]. PLS models were computed to predict changes in chemical and physicochemical attributes during 8-h dehydration process.

3. Results

3.1 RGB imaging-based analysis of color changes in apples

The employed camera system and associated developed codes allowed for the reliable real-time measurement of changes in product quality at the set measurement intervals. Fig. 1 shows the impact of drying conditions on the resulting changes in the a* and b* values. It is evident that all settings led to an increase of both a* and b* values, signifying the change of visual appearance of the samples. The most beneficial drying conditions for maintenance of the appearance were at 20 °C (T) and 25 % RH.

The developed real-time monitoring system for color (and shape) changes will make it possible to include information of the current color changes in the control consideration of a smart drying system. This is of particular importance as consumers tend to judge a product's quality by its visual appearance.
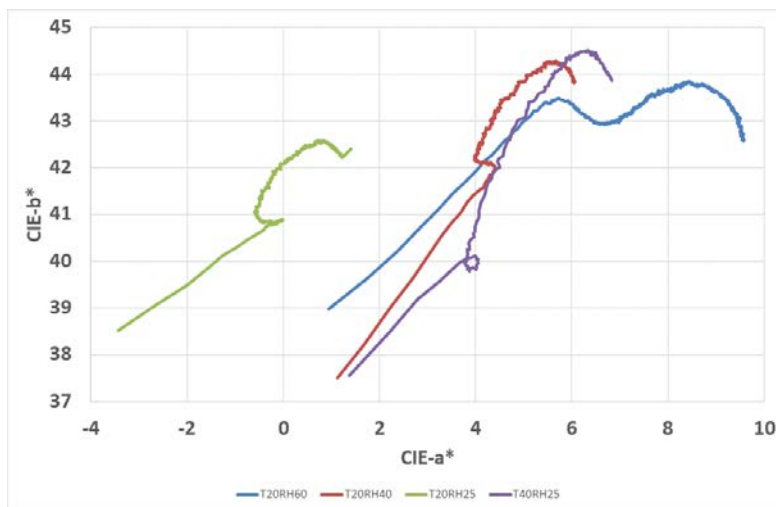
Fig 1: Development of CIE-a* as a function of CIE-b* for different drying conditions, tempertures are given as T and relative humidity as RH in the graph

Vis/NIR hyperspectral water content determination in apples

PLSR analyses with the full reflectance spectra were carried out across the complete data set. For both conditions PLSR was performed for models varying from 1-20 components with 10-fold creation and testing. The 3-component [540 nm, 817 nm, 977 nm] PLSR model satisfied the minimal RMSE criterion. Table 1 gives an overview of the results for full and reduced spectra.

Table 1: Performance of moisture content PLSR models

	Full Spectrum				Reduced (3-wavelength set)			
Setting (°C)	Calibration		Test		Calibration		Test	
	r^2	RMSE (g/g) *[M.C. %]*	r^2	RMSE (g/g) *[M.C. %]*	r^2	RMSE (g/g) *[M.C. %]*	r^2	RMSE (g/g) *[M.C. %]*
50	1.00	0.01 *[0.12]*	1.00	0.11 *[1.32]*	0.99	0.18 *[2.16]*	1.00	0.09 *[1.08]*
70	1.00	0.03 *[0.36]*	1.00	0.07 *[0.84]*	1.00	0.18 *[2.16]*	0.98	0.05 *[0.60]*

For the deeper understanding of the drying behavior of foodstuffs in terms of heat and mass transfer, and the performance analysis of the applied drying devices, a spatial and temporal evaluation of moisture content development during the drying process is intrinsic. Thus, the spatial variation of reflectance spectra at different times of the drying process was used to visualize the development of moisture content throughout the drying process as well as the spatial difference of said moisture content (Fig. 2).
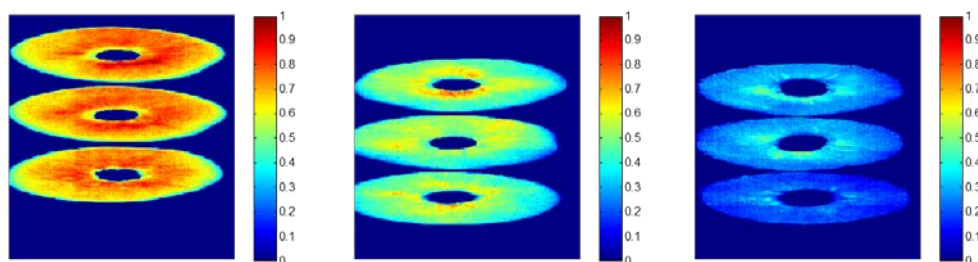
Fig 2: Normalised moisture distribution for apple slices before (left), during (middle) and at the end of the drying process.

Further studies using hyperspectral imaging on apples [11], meat [12] and potatoes [13, 14] show similarly promising results. A reduction of the wavelengths needed for detection of product features will allow for the transfer to simpler systems, e.g. colour or black and white cameras in combination with either selective lighting or band pass filters. This could then also be combined with full color detection described above, as well as physical feature detection, as described by Bantle et al. [5] if sequential feature detection is implemented. This method will in turn open new possibilities for deeper analyisis of the drying process and consequentlythe integration of feature analysis into smart drying process control.

3.2 Near infrared spectroscopy study on carrots and apples

3.2.1   Regression models (carrots)

Poor results ($R^2 < 0.70$) were obtained for the prediction of soluble solids content for the unblanched treatment. Conversely, regression models with good ($R^2 \geq 0.80$), very good ($R^2 \geq 0.90$) or excellent ($R^2 \geq 0.95$) predictability were obtained to monitor changes in soluble solids content (only for blanched carrots), a_w (Fig. 3a), moisture content (Fig. 3b), total carotenoids content (Fig. 3c) and color changes (Fig. 3d) of carrot slices during drying, regardless of thermal treatment. Except for the calibration model for color changes, the coefficient of determination (R^2) was higher than 0.90 for the parameters. Thus, for the test set validation with one quarter of the data (randomly selected) RMSEPs ranging from 0.03-0.04 for a_w, 0.03-0.04 for moisture content and 22.62-29.51 for total carotenoids content were obtained.
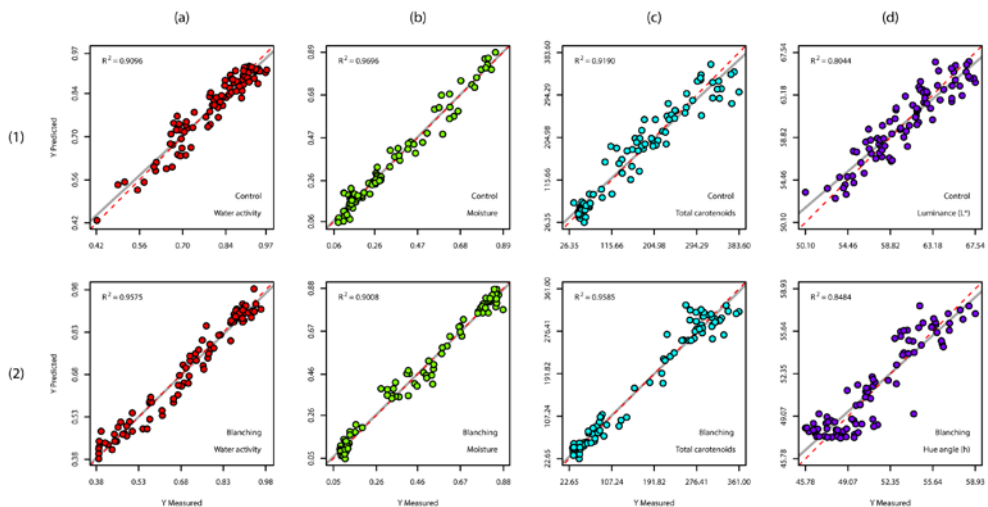
Fig 3: PLS regression plots of Y-measured (reference) and Y-predicted (NIR) values for water activity (column a), moisture (column b), total carotenoids content (column c) and colour changes (column d) monitored during 8-h drying in both unblanched (row 1) and blanched (row 2) carrots. PLS regression plots refer to models based obtained from the full spectrum.

3.2.2   Regression models (apples)

PLS regression models with good or excellent predictability were obtained to monitor changes in a_w (Fig. 4a), moisture content (Fig. 4b), chroma (Fig. 4c) and SSC (Fig. 4d) of apples wedges during drying, regardless of type of thermal treatment. Except for the calibration model for chroma, the coefficient of determination (R^2) was higher than 0.96 for all the aforementioned quality parameters. Thus, for the test set validation with one quarter of the data (randomly selected) RMSEPs ranging from 0.03-0.04 for a_w, 0.04-0.05 for moisture content and 4.54-4.99 for SSC were obtained. The latter performance parameter was comparable with both calibration and cross-validation results.
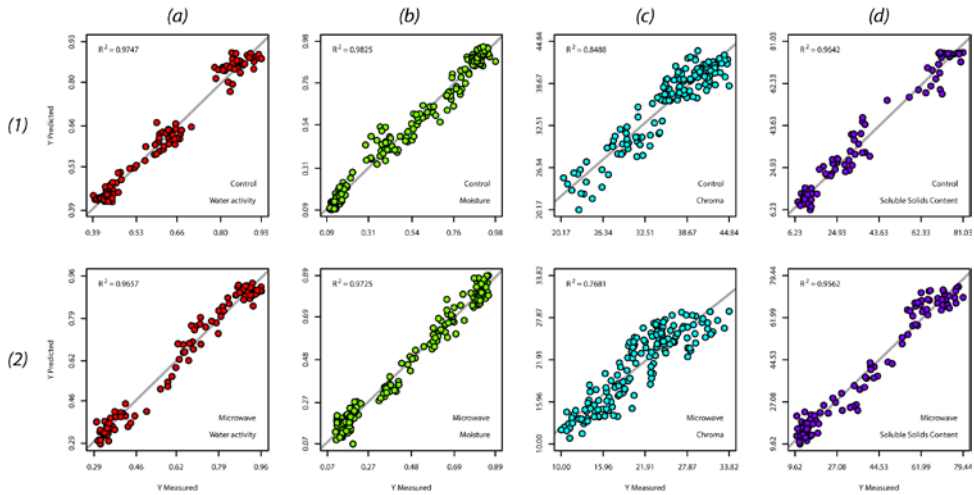
Fig 4: PLS regression plots of Y-measured (reference) and Y-predicted (NIR) values for water activity (column a), moisture (column b), chroma (column c) soluble solids content (column d) monitored during 8-h drying in both control (row 1) and microwave (row 2) treated apples. PLS regression plots refer to models based obtained from the full spectrum.

4   Conclusions

In this study, the potential of single-point NIR spectroscopy, Vis/NIR hyperspectral imaging and RGB imaging was evaluated to proactively and non-destructively detect and monitor changes in quality parameters (i.e. water activity, moisture content, total carotenoids content, colours and SSC) of both apples and carrots. For this purpose, regression and classification models were successfully developed obtaining either very good or excellent results in terms of R2 and RMSE. These promising results encourage additional research to develop low-cost dynamic multi factorial process control strategies (based on a Quality by Design approach) using machine learning architectures to produce quality dried products while reducing the environmental impact of the drying processes. Future research should include features not covered by the instrumentation used for this study, increasing the light-beam intensity, and/or combining other chemometric methods, as these could improve the performance of the measurement systems and, thus, the robustness of the smart-drying system under development.

5   Acknowledgements

6 References

[1] EC. Reg (EC) 889/2008 http://cerescert.com/portal/fileadmin/externdocs/889_2008_compressed.pdf

[2] Wu, D; Sun, D-W. Advanced applications of hyperspectral imaging technology for food quality and safety analysis and assessment: A review — Part I: Fundamentals. Innovative Food Science & Emerging Technologies. 2013; 19, 1–14.

[3] Sturm, B.; Nunez Vega, A.M.; Hofacker, W. Influence of process control on drying kinetics, colour and shrinkage of air dried apples, Applied Thermal Engineering 2014, 62 (2), 456-460

[4] Sarah, Y. Project Jupyter gets $6M to expand collaborative data-science software, http://news.berkeley.edu/2015/07/07/jupyter-project/.

[5] Bantle, M.; Kopp, C., Claussen, I.C.; Tolstorebrov, I. Influence oft he low temperature drying process on optical alternations of organic apple slices. In Proceedings of the 21st International Drying Symposium, Valencia, Spain, September 11-14, 2018

[6] Crichton, S.O.J.; Shrestha, L.; Hurlbert, A.; Sturm, B. Prediction of moisture content and chromaticity of raw and pre-treated apple slices during convection drying using hyperspectral imaging, Drying Technology 2018, doi: 10.1080/07373937.2017.1356847

[7] Savitzky, A.; Golay, M. J. E. Smoothing and Differentiation of Data by Simplified Least Squares Procedures. Analytical Chemistry 1964, 36(8), 1627–1639.

[8] Boysworth, M. K.; Booksh, K. S. Aspects of multivariate calibration applied to near-infrared spectroscopy; Burns, D. A.; Ciurczak, E. W. Eds.; Handbook of Near-Infrared Analysis, CRC Press: New York, 2008; 207–229.

[9] de Jong, S. SIMPLS: An alternative approach to partial least squares regression. Chemometrics and Intelligent Laboratory Systems 1993, 18 (3), 251–263.

[10] Moscetti, R.; Saeys, W.; Keresztes, J. C.; Goodarzi, M.; Cecchini, M.; Danilo, M.; Massantini, R. Hazelnut Quality Sorting Using High Dynamic Range Short-Wave Infrared Hyperspectral Imaging. Food and Bioprocess Technology 2015, 8 (7), 1593–1604.

[11] Shrestha, L., Moscetti, R., Crichton, S.O.J., Hensel, O., Sturm, B. Organic apples (cv. Elstar) quality evaluation during hot-air drying using Vis/NIR hyperspectral imaging. In Proceedings of the 21st International Drying Symposium, Valencia, Spain, September 11-14, 2018

[12] Gersdorff, G.; Porley, V.; Retz, S.; Hensel, O.; Crichton, S.O.J.; Sturm, B. (2017). Drying kinetics and quality parameters of dried beef (biltong) subjected to different pre-treatments, Drying Technology, 36 (1), 21-31.

[13] Amjad, W.; Crichton, S.O.J; Munir, A.; Hensel, O.; Sturm, B. Hyperspectral imaging for the determination of potato slice moisture content and chromaticity during the convective hot air drying process, Biosystems Engineering 2018, 166, 170-183.

[14] Moscetti, R.; Sturm, B.; Crichton S.; Massantini, R. Monitoring of organic potato (cv. Anuschka) during hot-air drying using Vis/NIR hyperspectral imaging, Science of Food and Agriculture 2017, doi: 10.1002/jsfa.8737

Modeling of atmospheric freeze-drying for sliced fruits

Horie, A.[a]; Kobayashi, T.[a]; Nakagawa, K.[a*]

[a] Division of Food Science and Biotechnology, Graduate School of Agriculture, Kyoto University, Sakyo-ku Kitashirakawa Oiwakecho, Kyoto 606-8502, Japan

*E-mail of the corresponding author: kyuya@kais.kyoto-u.ac.jp

Abstract

A mathematical model that simulates atmospheric freeze-drying for apple slices was developed based on the classical mass and heat balance equations. When operated above the glass transition temperature, product shrinkage and micro-collapse due to the glass-rubber transition occurred. So, instead of assuming formation of dried and frozen zones, a glassy matrix with particular vapor pressure was assumed. Apparent vapor pressure of apple slices in the glassy state was experimentally measured and summarized in a diagram, and the values in this diagram were employed for the simulation. This approach well predicted drying kinetics with reasonable accuracy with simplified equations.

Keywords: atmospheric freeze-drying; food; mathematical model; glassy state

1. Introduction

Freeze-drying is known as one of the best drying methods in terms of preservation of product qualities. Vacuum freeze-drying (VFD) process is widely implemented in food and pharmaceutical industries, and variations of products are commercialized. Atmospheric freeze-drying (AFD) is basically equivalent to vacuum freeze-drying, where the ice sublimation is the major dehydration mechanism. The water vapor pressure difference between the frozen zone and the ambient gas is the driving force of the mass transfer. In order to operate drying at below sub-zero temperature, the air humidity must be low at appropriate level. A heat-pump system is commonly used to make low humidity air. The condenser temperature of the heat-pump unit is necessarily set lower than the product temperature during drying, and the dehumidified air must properly be heated up to realize appropriate drying rate. Numbers of studies on AFD process were motivated to optimize this heat-pump drying system in terms of the energy consumption and drying rate.[1-4]

Drying temperature (air temperature) applied for AFD is usually at around –10 to 0ºC. So, the product temperature during drying, that could be several degrees lower than the drying temperature depending on the drying rate, is much higher than the case of VFD. When drying agricultural products, a typical AFD run places the products above their glass transition temperatures ($T^{\flat}_g$). For example, the $T^{\flat}_g$ value of strawberry ranges from –33 to –41ºC, that of apple is at around –42ºC, and peach at around –36ºC.[5] Considering that the drying rate is not rapid as the case of a hot air drying, product temperature could be several degree below the air temperature that is far above the glass transition temperature. At this temperature, the product deformation such as shrinkage and/or micro-collapse occur as a consequence of the glass-rubber/ glass-liquid transitions. In such cases, the dried cake layer, that commonly forms during a typical freeze-drying run, does not clearly separate from the frozen zone. In order to simulate this drying system, it is necessary to develop a model that is different from commonly employed two zone models consisted with frozen and dry zones.

In this study, mathematical model that simulates atmospheric freeze-drying for apple slices was developed. This study was targeted for an atmospheric freeze-drying process operated far over the glass transition temperature of the products, where we must admit the product deformation such as shrinkage and micro-collapse due to glass-rubber transition.

2. Mathematical Model

A product placed in the atmospheric freeze-dryer is dried by convective air. A product (i.e. a slice of apple) has porous structures derived from cellular microstructures. The external and some parts of the inner pore surfaces contact to the external air flow. Whereas, the other parts of the surfaces contribute to the convection with the internal air flow (Fig. 1). The surface that contributes to the internal convection is written with the total product surface, namely:

$$A_{\text{in}} = \gamma A_{\text{total}} \tag{1}$$

Here, γ is the coefficient that gives the surface that is not influenced by the convective air. The surface that effectively contributes to the external convection can be written as:

$$A_{\text{eff}} = (1 - \gamma)A_{\text{total}} \tag{2}$$

The mass transfer equation of the vaporized water vapor can be written with the mass transfer coefficients of the external and internal boundary layers, namely:

$$\frac{dm}{dt} = \frac{P_i/T_i - P_{\text{air}}/T_{\text{air}}}{1/(1-\gamma)A_{\text{total}}k_{\text{gex}} + 1/\gamma A_{\text{total}}k_{\text{gin}}} \frac{M}{R} \tag{3}$$

The heat transfer equation can be written with the heat transfer coefficients of the external and internal boundary layers:

$$Q = \frac{T_i - T_{\text{air}}}{1/(1-\gamma)A_{\text{total}}h_{\text{ex}} + 1/\gamma A_{\text{total}}h_{\text{in}}} \tag{4}$$

Assuming that the system is at a quasi-steady state, the heat flow is balanced with the mass flow.

$$Q/\Delta H = \frac{dm}{dt} = \frac{P_i/T_i - P_{\text{air}}/T_{\text{air}}}{1/(1-\gamma)A_{\text{total}}k_{\text{gex}} + 1/\gamma A_{\text{total}}k_{\text{gin}}} \frac{M}{R} = \frac{T_i - T_{\text{air}}}{1/(1-\gamma)A_{\text{total}}h_{\text{ex}} + 1/\gamma A_{\text{total}}h_{\text{in}}} \frac{1}{\Delta H} \tag{5}$$

The solution of this equation provides the value of T_i. The calculation was performed with spreadsheet software (Microsoft Excel®) by non-linear regression using solver add-in. It should be noted that the water vapor pressure P_i at the temperature T_i was given as a function of the moisture content of product as the detail explained in the later section.
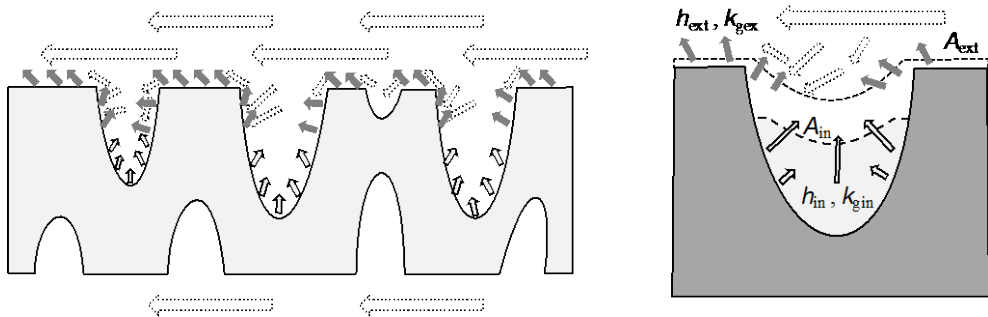
Fig. 1 Schematic illustration of AFD model.

3. Materials and Methods

3.1. Atmospheric freeze-drying

The atmospheric freeze-dryer that composed with a condenser and heating devise was set-up as schematized in Fig. 2. The condenser temperature was set at around –30ºC, and the out-gas temperature could be controlled by the heating devise in the range of –20 to 5ºC. The air flow rate in the drying room was controlled by an electric fan in the range of 0.1 to 0.5 m/s. Four slices of apple (15×15×5 mm) were set in a plastic tray and suspended from a load-cell (A&D, Japan). The weight loss during drying was monitored with the load-cell. Apple slices were first frozen with the convective air at –30ºC, and then the air temperature was increased at a selected heating rate from –10 to 5ºC and the weight loss was recorded with data logging system.
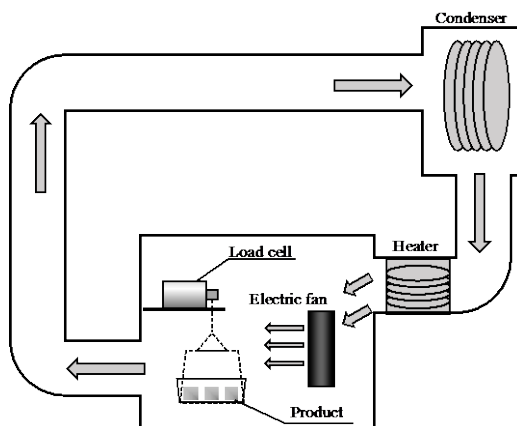
Fig. 2 Drying apparatus.

3.2. Ice sublimation test

The ice sublimation test was conducted in order to determine mass and heat transfer coefficients. Distilled water was filled in a plastic tray and frozen in the devise. Weight losses were monitored at selected temperature and air velocity settings. The temperature of the sublimating ice (T_p) and the sublimation rate (dm/dt) were collected with the selected operating conditions. The obtained values were applied to Equation 5 to estimate k_{gex} and h_{ex} values by applying $A_{in}=0$, $A_{ex}=A_{total}$.

3.3. Measurement of apparent water vapor pressure of apple slice

The use of apparent water vapor pressure as a function of the temperature and moisture content was a key part of this study. The relationship among these parameters were determined by the pressure rise test with a specially designed experimental set as illustrated

in Fig. 3. An apple slice was first vacuum freeze-dried, and then placed in a desiccator with a solution saturated with various salts (LiCl, $MgCl_2$, KNO_3 and $Mg(NO_3)_2$) in order to humidify the dried product. The moisture content of the humidified sample was measured by a moisture meter (A&D, Japan), and the other portion was set in the sample room and the measurement devise was immersed in a cooling bath of which temperature was set at a selected temperature in the range of –30 to 0ºC. The external room that was separated with a bellows valves was first evacuated with a rotary type vacuum pump. After stabilizing the temperature and pressure, the bellows valve was rapidly opened for 2–3 seconds and immediately closed. The pressure rise due to the vaporization was monitored for 1 hour with a pirani gauge that was set in the sample room.
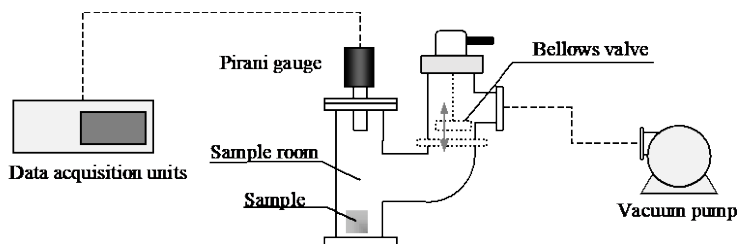
Fig. 3 Pressure rise measurement set-up.

4. Results and Discussions

4.1. Apparent water vapor pressure of apple slices

Some selected results of the pressure rise test were shown in Fig. 4. One can clearly see that the pressure rose just after opening the bellows and stabilized at a certain pressure level. Fig. 4A shows the dependency of the vapor pressure on the temperature; the pressure, as expected, was higher at higher temperature. However, the absolute values of the pressure were significantly lower than the equilibrium vapor pressure value of pure water. It means that several hours was not enough for the system to reach at an equilibrium state. Fig. 4B suggested that the time required for reaching at an equilibrium state was greatly affected by the moisture content of the apple slice; the apparent vapor pressure was higher for the sample with higher moisture content. The effective vapor pressure that a product shows during drying could be the pressure that was measured by the pressure rise test. We thus employed the value of the pressure from the pressure rise test at the point of 1 hour, and the values were plotted as a function of temperature and solid content (converted from the moisture content value). As summarized in a diagram in Fig. 5, this is a key characteristic of the present apple that is distinguished from the other products showing different drying kinetics. The solid line in the diagram correspond to the glass transition line; the closer the glass transition line, the apparent vapor pressure significantly decreases.
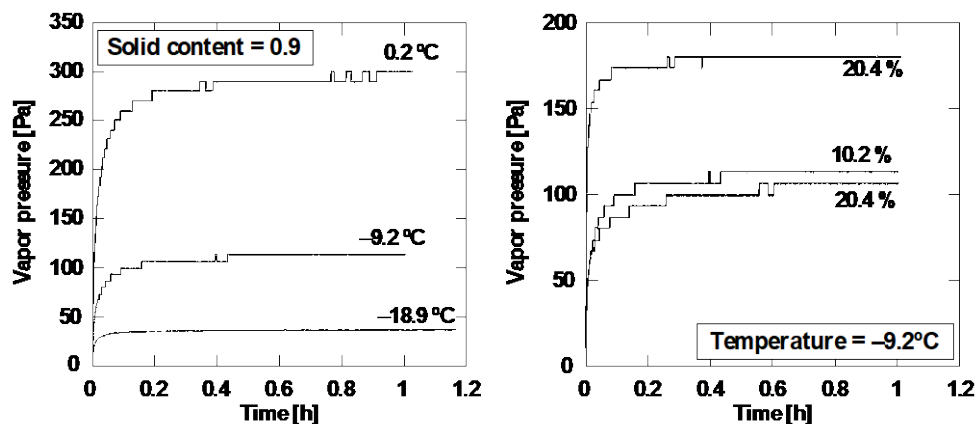
Fig. 4 Pressure rise of apple slice under sub-zero temperature.
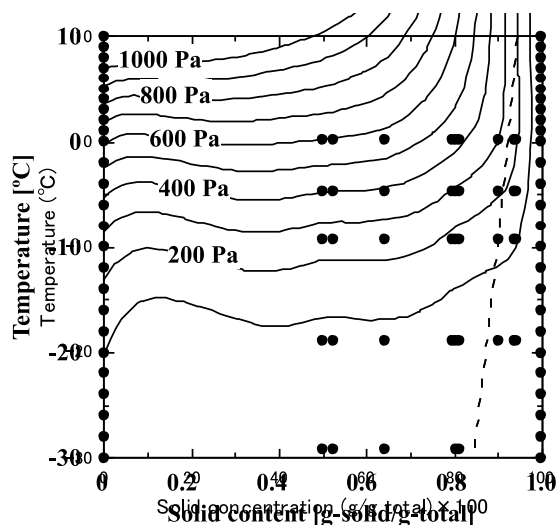
Fig. 5 Apparent water vapor pressure contour lines as a function of temperature and solid content.

4.2. Freeze-drying run

A result of the atmospheric freeze-drying run is shown in Fig. 6. The air flow temperature was operated as shown in this figure by the present drying apparatus, and the consequence of the weight loss was plotted in the same figure. Air temperature was programmed to increase as the progress of drying in order to reduce total drying time. A simulation was carried out based on the mathematical model by applying the experimentally obtained air flow temperature. The water vapor pressure value, that is dependent on the temperature and

moisture content, was estimated from the surface plots shown in Fig. 5 by applying a simulated product temperature and moisture content values. The parameters applied for the simulation were listed in Table 1. The simulated drying curve is compared in Fig. 6 with the experimental curve. It was obvious that the simulation well predicts the experimental drying kinetics. The present simulation is based on a mechanistic mathematical model, so it simultaneously gives the other important values such as product temperature, mass and heat flow rates, etc. The simulated product temperature during drying plotted in Fig. 6 suggested that the drying progressed far above the glass transition temperature of apple, so some phenomena that may occur in a rubbery system (e.g. shrinkage, micro-collapse) are not avoidable in this drying system. The simulation could thus be more accurate by introducing a variable drying surface area instead of mean total surface area (A_{total}) and mass transfer coefficient values (k_{gin}). The air temperature was well programed to realize the driving force for heat transfer until the final stage of the drying. This simulation approach would be useful to design favorable drying protocol.
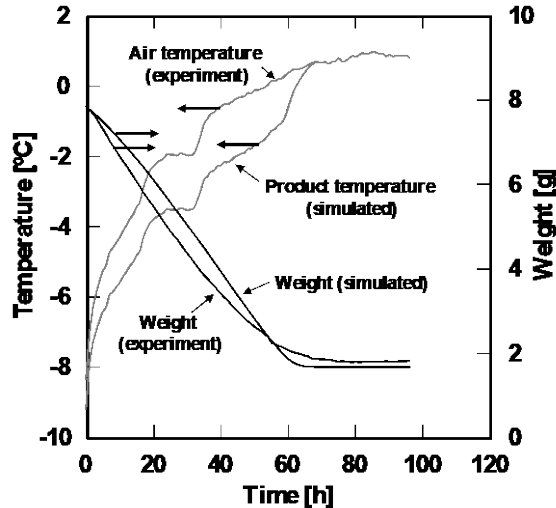
Fig. 6 Drying curves; comparison between experimental and simulated curves

Table 1. Parameters for simulation

Parameter	Value	Parameter	Value
A_{total} [m²]	9.7×10^{-2}	h_{gex} [Wm⁻²K⁻¹]	49.2
γ [-]	0.99	h_{gin} [Wm⁻²K⁻¹]	13.7
k_{gex} [ms⁻¹]	1.01×10^{-2}	P_{air} [Pa]	104.9
k_{gin} [ms⁻¹]	1.47×10^{-2}	R [J mol⁻¹K⁻¹]	8.314
ΔH [J kg⁻¹]	2.4×10^{6}	T_{air} [K]	253
M [kg mol⁻¹]	1.8×10^{-2}		

5. Conclusions

A mathematical model that simulates atmospheric freeze-drying for sliced fruits was developed and applied to apple slice drying. Apparent vapor pressure of the apple slice was measured by the pressure rise test and the obtained values were summarized in a diagram. The pressure values were dependent on the temperature and moisture content; the closer the glass transition line, the apparent vapor pressure significantly decrease. Simulations carried out with this diagram well predict drying kinetics with reasonable accuracy with simplified equations.

6. Nomenclature

A_{total}	total surface area	m^2
γ [-]	inner surface ratio	-
k_{gex}	mass transfer coefficient	ms^{-1}
k_{gin}	mass transfer coefficient	ms^{-1}
ΔH	latent heat of vaporization	$J\,kg^{-1}$
h_{gex}	heat transfer coefficient	$Wm^{-2}K^{-1}$
h_{gin}	heat transfer coefficient	$Wm^{-2}K^{-1}$
M	molar mass of water	$kg\,mol^{-1}$
m	mass of product	kg
P_{air}	water vapor pressure in the air flow	Pa
P_i	water vapor pressure at the drying interface	Pa
Q	heat flow	$J\,s^{-1}$
R	ideal gas constant	$J\,mol^{-1}K^{-1}$
T_{air}	temperature of the air flow	K
T_i	temperature at the drying interface	K
t	time	s

7. References

[1] Alves-Filho, O. Combined Innovative Heat Pump Drying Technologies and New Cold Extrusion Techniques for Production of Instant Foods. Drying Technology 2002, 20, 1541-1557.

[2] Claussen, I.C.; Andresen, T.; Eikevik, T.M.; Str∅mmen, I. Atmospheric Freeze Drying—Modeling and Simulation of a Tunnel Dryer. Drying Technology 2007, 25, 1959-1965.

[3] Wolff, E.; Gibert, H. Atmospheric freeze-drying part 1: Design, experimental investigation and energy-saving advantages. Drying Technology 1990, 8, 385-404.

[4] Claussen, I.C.; Ustad, T.S.; Str∅mmen, I.; Walde, P.M. Atmospheric Freeze Drying—A Review. Drying Technology 2007, 25, 947-957.

[5] Slade, L.; Levine, H.; Reid, D.S. Beyond water activity: Recent advances based on an alternative approach to the assessment of food quality and safety. Critical Reviews in Food Science and Nutrition 1991, 30, 115-360.

Thermodynamic model of freeze-drying of poultry breast using infrared thermography

Tomas-Egea, J.A.[a]; Castro-Giraldez, M.[a]; Fito, P.J.[a*]

[a] Instituto Universitario de Ingeniería de Alimentos para el Desarrollo. Universitat Politècnica de València, Valencia, Spain

*pedfisu@tal.upv.es

Abstract

Food dehydration is one of a main process to preserve meal. In order to optimaze a freeze-drying operation a physic model is needed to well describe the thermodynamic behaviors involved in this process. In this work, a thermographic camera and different physico-chemical determinations are used to monitor many phenomena that occur during the lyophilization of poultry breast. Finally, a non-continuous irreversible thermodynamic model, based on thermal infrared measures and in shrinkage/swelling mechanism, has been developed, wich explains the behaviours produced throughout the meat freeze-drying process.

Keywords: freeze-drying, thermodynamic model, infrared thermography, poultry.

1. Introduction

Lyophilization is a drying process that consists in sublimate ice into vapour, producing water desorption, and one possibility can be to bring the product below the triple point (273.16 K and 611.73 Pa) of the water state diagram. This process gets very low water activities and does not heat the product, which is an advantage when thermolabile compounds are present[1,2,3]. Once the product has frozen below its eutectic point and generated vacuum, the product begins the elimination of water in two consecutive phases: sublimation and evaporation. When the frozen product reaches the vapor pressure, the freezing water fraction of the product is sublimated starting from the surface, creating a sublimation front that advances towards the center. With the advance of the front, there is a zone that has sublimated the freezing water, but still has water adsorbed as liquid phase[4,5]. The steam, coming from the front, causes a mechanical drag of the adsorbed water, which removes it and causes its desorption by evaporation.

Considering the importance of dehydration processes to conserve food, it is necessary to study them closely. For this, the process can be modeled with equations such as the Gibbs free energy, which can describe the thermodynamic behavior of the food throughout the process. These equations have been used previously in orange peel[6] and pork meat[7]. The water transport its also modeled in pork meat[8] and tomato[9]. Also, another freeze-dried products has been modeled like Strawberries[10] or black currant juice[11] as well as generic mathematical models[12].

Infrared thermography is a technique that allows to predict the temperature along a surface by receiving the flow of photons emitted by a body. Therefore, the possibility of monitoring the process with this technology gives us the ability to develop kinetic models of drying, thanks to the possibility of follow the temperature distribution over a surface, over a period of time[13].

The aim of this research is the development of a thermodynamic model of freezedrying process of poultry meat using infrared thermography.

2. Materials and Methods

2.1. Experimental procedure

For the experimental phase, poultry breast samples (*Pectoralis major*) were used. Cylinders of 2 cm in diameter and 2 cm in height were obtained by a punch. The cutting of the cylinders was perpendicular to the fibers. Two cylinders were used for each lyophilization and this operation was carried out in triplicate. The samples were frozen at -40 °C and introduced into the dry chamber of the lyophilizer, at a distance of 1.5 cm between them. During the

lyophilization, the temperature of the surface in one of the two chicken cylinders, as well as the reference material and the environment was controlled by type K thermocouples. In addition, the thermographic camera was introduced inside the lyophilizer for a continuous recording of the process.

In order to characterize the samples, this determinations were made before and after the lyophilization: mass, water activity, humidity and volume. In addition, the density of frozen and lyophilized product was determined.

2.2. Physico-chemical measurements

The mass of the samples was determined with a Mettler Toledo AB304-S balance, with an accuracy of $\pm$ 0.001 g. The humidity of the sample was obtained following the ISO 1442 (1997) standard for meat products, drying the samples at 110 ℃ and atmospheric pressure for 48 hours until reach a constant mass. The water activity was determined with a dew point hygrometer Aqualab®, series 3 TE, with an accuracy of $\pm$ 0.003. The volume was determined by image analysis, using Adobe © Photoshop © CS6 software. The density of frozen and lyophilized sample was determined by the pyknometer method. All measurements were made in triplicate.

2.3. Freeze drying operation

The thermographic camera was placed at 15 cm from the samples, with an angle of 0° and focusing the flat surface of the cylindrical samples. A reference material of known emissivity ($\varepsilon = 0.95$) (Optris GmbH, Berlin, Germany) was placed between both samples.

The control of the temperature during the lyophilization, the inside, the reference material and the sample, was carried out with three K-type thermocouples, all of them connected to an Agilent 34901A multiplexer (Agilent Technologies, Malaysia); for the automatic recording of the measurements, the Agilent data acquisition equipment 34972A (Agilent Technologies, Malaysia) was used. The internal pressure control was carried out with the lyophilizer's own pressure sensor.

The lyophilizer used for the experimental was the Lioalfa-6 from Telstar, Germany. With a working pressure of 35 to 50 Pa and a cooling circuit at -45 ℃. All the cables and sensors necessary for the data collection were introduced in the dry chamber replacing the original stopper of the lyophilizer with one of rubber, and filled in with silicone to achieve the necessary vacuum.

2.4. Medida de infrarrojos

The thermal images were acquired using the Optris PI 160 termographic camera (Optris GmbH, Berlin, Germany). It uses a two-dimensional focal plane array with 160x120 pixels, a spectral range of 7.5 to 13 µm, a resolution of 0.05 °C and an accuracy of $\pm$ 2 %. The camera

covers a temperature range of -20 to 900 °C. It has a field of vision of 23°x17° with a minimum distance of 2 cm. The camera uses Optris PI Connect software (Optris GmbH, Berlin, Germany).

3. Results and discussion

The temperature values obtained from the thermographic camera are not real, therefore, the correction developed by Traffano-Schiffo et al., 2014[7] was applied.

When the sublimation front advances, it alters the composition of the sample. The areas that have already been sublimated reduce their heat transmission because a loss of water, which causes a change in trend in the evolution of temperature with respect to time. Figure 1 shows this change in trend. So, the sublimation temperature and the process time can be extracted for each point of the sample's profile.
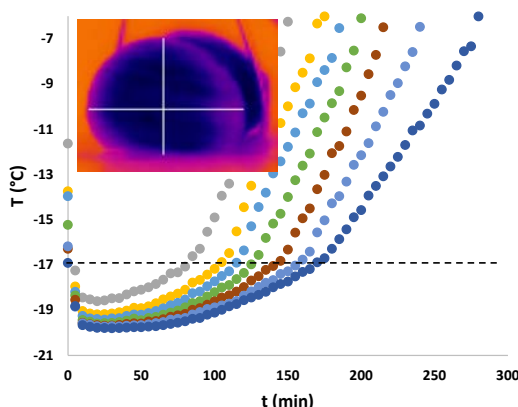
Fig. 1 Evolution of the temperature for different points of the profile over time.

With the sublimation temperature it is possible to calculate the water activity (a_w) using the Fontan and Chirife equation (1981) (Eq. 1).

$$-\ln(a_w) = 9.6934 \cdot 10^{-3} \cdot \Delta T_f + 4.761 \cdot 10^{-6} \cdot \Delta T_f^2 \tag{1}$$

Where: ΔT_f = difference between the initial freezing temperature and the the sample (K).

From this a_w and the poultry sorption isotherm at low temperatures, it is possible to obtain the non-freezeable water fraction (x_w^{NF}) of the product at the sublimation time. The isotherm parameters modeled by GAB are $x_{w0} = 11.009 - 0.4589T + 0.0116T^2$; $C = -3423.2 + 1144T - 77.248T^2 + 1.4357T^3$; $K = 0.9419 - 0.0034T + 0.0006T^2 - 0.00001T^3$. Substracting to the overal water fraction, the non-freezeable water, it is possible to obtain the ice fraction.

Once the lyophilization process has begun, sample can be divided in two volumetric areas: the sublimated zone (partially dehydrated) and frozen zone, separated by the sublimation front (Fig. 2). When the frozen water sublimates, appears a vapour flux from the sublimation front to the surface, crossing the sublimated zone and evaporating a part of adsorved water by mechanical dragging. Mass of each zone throughout the process has been estimated using the volume difference between cylinders and the density of freeze-dried and frozen product.
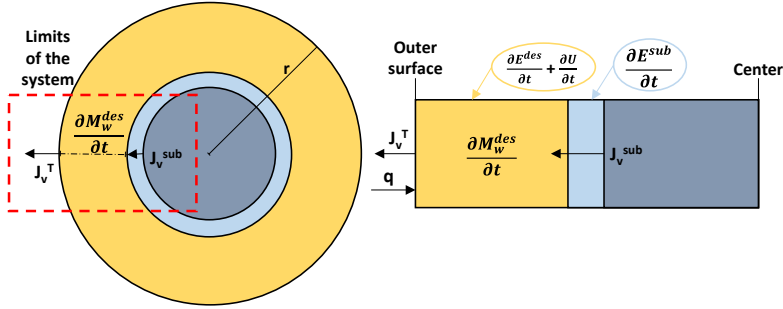
Fig. 2 Diagram of the different zones and phenomena. ☐ *Sublimated area;* ☐ *Sublimation front;* ☐ *Frozen zone. The limits of the system are highlighted in red, enlarged to the right with the molar and energy balances.*

In order to obtain the different mechanism involved in the freezedry process, it is necessary to estimate the water flux, using a molar water balance in the sublimated zone (Eq. 2).

$$J_v^T \cdot S_{ext} = J_v^{sub} \cdot S_{sub} + \frac{\partial M_w^{des}}{\partial t \cdot M_{rw}} \tag{2}$$

When the vapor flux comes from the sublimation can be calculated as follows (Eq. 3):

$$J_v^{sub} = \frac{x_w^f \cdot \rho_{wf} \cdot \Delta r}{\Delta t \cdot M_{rw}} \tag{3}$$

Where: J_v^T = overall vapour flux leaving the system (mol·s^{-1}·m^{-2}); S_{ext} = external surface of the cylinder (m^2); J_v^{sub} = sublimated vapour flux (mol·s^{-1}·m^{-2}); S_{sub} = surface of the sublimation front (m^2); M_w^{des} = evaporated water mass (kg); t = process time (s); x_{wf} = freezed water mass fraction (kg·kg^{-1}); ρ_{wf} = density of frozen water (kg·m^{-3}); M_{rw} = Molecular water mass (18 g·mol^{-1}). The last term of mass balance represents the negative accumulation of adsorved water molecules induced by mechanical drag of these molecules by the strong vapour streams produced in the sublimation front.

In order to continue determine the mechanism of water dehydration, the equation 4 that describes the free energy variation was applied[14].

$$dG = -SdT + VdP + Fdl + \psi de + \sum_i \mu_i \, dn_i \tag{4}$$

Where: SdT = entropic term related to heat flux; VdP = mechanical energies related to the variation of pressure; Fdl = mechanical energies related to the elongation force (resistance of the tissue to expand); ψde = effect of the electric field induced by ions; $\sum_i \mu_i \, dn_i$ = sumatory of the chemical potentials of the species "i", with the rest of the variables state are constant.

When the variation of free energy is represented per mole of water, the extended water chemical potential is obtained (Eq. 5).

$$\Delta \mu_w = \frac{\Delta G}{\Delta n_w} \tag{5}$$

Where: $\Delta \mu_w$ = water chemical potential (J·mol^{-1}); ΔG = Gibbs free energy variation (J); Δn_w = water moles (mol).

Combining the equations 4 and 5, the equation 6 is obtained, which describes the water chemical potential in the system described in figure 2 (sublimated zone) . In this equation, the last term is not included, because the desorption caused by the difference between water activities in the sample is negligible compared with the entropic term and those of mechanical energies. Moreover, ψde term also is negligible since the sample only presents native ions.

$$\Delta \mu_w^{des} = s_w \Delta T + v_w \Delta P + F_w dl \tag{6}$$

Where: s_w = partial water molar entropy (J·K^{-1}·mol^{-1}); ΔT = gradient of temperature between surface and sublimation front (K); v_w = partial water molar volume (m^3·mol^{-1}); ΔP = pressure variation (Pa); $F_w dl$ = elongation force (J). It is possible to estimate the entropic and the pressure term by using the sublimation temperature and its corresponded sublimation pressure obtained from Fig. 2.

Applying the Onsager relations[14], the water molar flux is related to the water chemical potential, working as a driving force for water transport, through the phenomenological coefficient (Eq. 7).

$$J_w^T = L_w \cdot \Delta \mu_w \tag{7}$$

Where: J_w = water molar flux (mol·s^{-1}·m^{-2}); L_w = phenomenological coefficient (mol^2·J^{-1}·s^{-1}·m^{-2}); $\Delta \mu_w$ = water chemical potential (J·mol^{-1}).

From the equation 7 it is possible to calculate the phenomenological coefficient after 200 min, where value remains constant because the sublimation front is reaching the center and the swelling resistance of the tissue is negligible ($L_w = 1.14 \cdot 10^{-5}$ mol^{2}J^{-1}s^{-1}m^{-2}). Therefore, applying this value along the treatment it is possible to estimate the elongation term (Fig 3a). Using the expansion of the sublimated area, and estimating the ice space loosed in the sublimation it is possible to calculate the increment of the porosity ($\Delta \varepsilon$). Fig. 3b shows the relation between the elongation term and the increment of the porosity, where it is possible to observe that the swelling process of tissue is proportional to the reduction of the elongation

term, reducing the swelling resistance of the tissue reaching its maximum expansion in its minimum resistance.
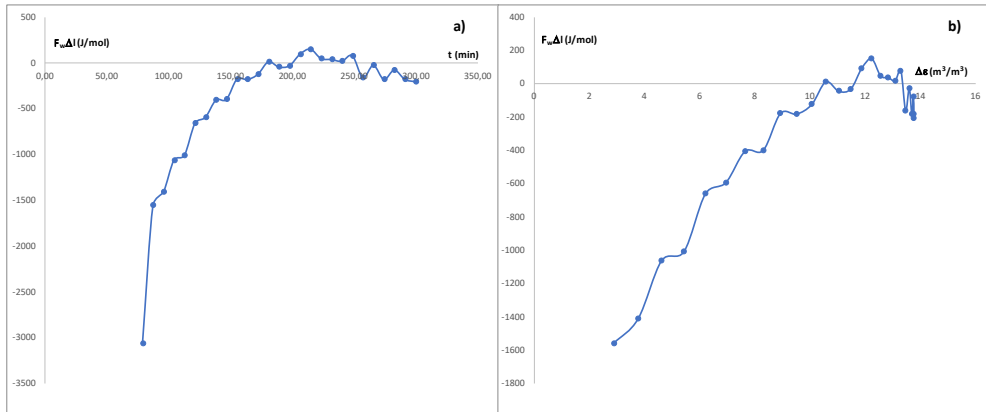
Fig. 3a Elongation term vs process time; 3b Elongation term vs increment of the porosity.

4. Conclusions

Has been developed a non-continuous irreversible thermodynamic model based in thermal infrared measures and in shrinkage/swelling mechanism that explains the behaviours produced throughout the meat freeze-drying process.

Acknowledgements

References

[1] Freire, F.B.; Vieira, G.N.; Freire, J.T.; Mujumdar, A.S. Trends in modeling and sensing approaches for drying control. Drying Technology 2014, 32(13), 1524–1532.

[2] Moses, J.A.; Norton, T.; Alagusundaram, K.; Tiwari, B.K. Novel drying techniques for the food industry. Food Engineering Reviews 2014, 6(3), 43–55.

[3] Ratti, C.; Hot air and freeze-drying of high-value foods: a review. Journal of Food Engineering 2001, 49, 311-319.

[4] Ramšak, M.; Ravnik, J.; Zadravec, M.; Hriberšek, M.; Iljaž, J. Freeze-drying modeling of vial using BEM. Engineering Analysis with Boundary Elements 2017, 77, 145-156.

[5] Duan, X.; Yang, X.; Ren, G.; Pang, Y.; Liu, L.; Liu, Y. Technical aspects in freeze-drying of foods. Drying Technology 2016, 34:11, 1271-1285.

[6] Talens, C.; Castro-Giraldez, M.; Fito, P.J. A thermodynamic model for hot air microwave drying of orange peel. Journal of Food Engineering 2016, 175, 33-42.

[7] Traffano-Schiffo, M.V.; Castro-Giraldez, M.; Fito P.J.; Balaguer, N. Thermodynamic model of meat drying by infrarred thermography. Journal of Food Engineering 2014, 128(0), 103-110.

[8] Clemente, G., Bon, J., Sanjuán, N., Mulet, A. Drying modelling of defrosted pork meat under forced convection conditions. Meat science 2011, 88(3), 374-378.

[9] Akanbi, C.T.; Adeyemi, R.S.; Ojo, A. Drying characteristics and sorption isotherm of tomato slices. Journal of food engineering 2006, 73(2), 157-163.

[10] Hammami, C.; Rene, F. Determination of freeze-drying process variables for Strawberries. Journal of Food Engineering 1997, 32, 133-154.

[11] Irzyniec, Z.; Klimczak, J.; Michalowski, S. Freeze-Drying of the black currant juice. Drying Technology 2007, 13:1-2, 417-424

[12] Nakagawa, K.; Ochiai, T. A mathematical model of multi-dimensional freeze-drying for food products. Journal of Food Engineering 2015, 161, 55-67.

[13] Vadivambal, R.; Jayas, D.S. Applications of thermal imaging in agriculture and food industry-a review. Food and Bioprocess Technology 2011, 4(2), 186-199.

[14] Castro-Giraldez, M.; Fito, P.J.; Fito P. Non-equilibrium thermodynamic approach to analyze the pork meat (Longissimus dorsi) salting process. Journal of Food Engineering 2010, 99(1), 24-30.

Rotary Wheel Atomizer Study Using Computational Fluid Dynamics and Full-Scale Testing

Joensen, T.[a]; Kuhnhenn, M.[b]; Vinther, F.[a*]; Reck, M.[a]; Tropea, C.[b].

[a] GEA Process Engineering A/S. Soeborg, Denmark

[b] Institute of Fluid Mechanics and Aerodynamics. Technische Universität Darmstadt, Darmstadt, Germany.

*E-mail of the corresponding author: frank.vinther@gea.com

Abstract

This study models the internal fluid flow from the center to the edge of a rotary atomizer wheel, the flow out of the atomizer, including the film, rivulet and ligament formation, as well as the subsequent atomization process associated with the atomizer outflow using computational fluid dynamics with a volume of fluid approach.

The model shows how fluid exits through the overflow and not through the bushing at high inlet fluxes and can reproduce experimental results of power consumption. Furthermore, the drop-size distribution at a given distance from the bushing exit is in good agreement with experimental results.

Keywords: Spray drying; Rotary Atomizer; CFD; Droplet size; Volume of Fluid.

1. Introduction

Feed atomization is one of the most important process steps in spray drying. In the chemical industry, rotary atomizers are often used because they are flexible, can handle abrasive materials and operate at very large capacities. Although development of atomizer wheels is usually based on a trial and error approach current designs are very advanced. New tools, like tailored computer simulations, are therefore needed to design a new and significantly improved generation of atomization wheels. These wheels will reduce atomizer power consumption, suffer less wear and can operate at higher capacity while avoiding overflow as described below. All this while improving the droplet size distribution which is the most important output from the atomizer. The size distribution influences every downstream aspect of the powder production process, ranging from drying chamber depositions to cyclone and bag filter efficiency and further on to packing, and of course, final powder characteristics and properties [1,2].

The fluid flows into the rotary wheel nearly at the center, from here the fluid enters narrow channels or bushings. From the entrance into the bushings to the exit of the atomizer the fluid and the air is accelerated towards the exit due to the centrifugal force and is at the same subject to a substantial Coriolis force. In addition, there are internal forces within the fluids e.g., surface tension and viscous forces. The combination of these forces and the complex geometry makes understanding of the fluid flow within a rotary atomizer extremely difficult.

Computational Fluid Dynamics (CFD) as a numerical method for solving the equations of motion gives an opportunity to directly simulate the flow under various operating conditions and various geometries. This will be the focus of this paper and will be thoroughly elaborated in the next section. Previous studies where CFD is used to model various aspects of spray drying includes [3,4,5,6].

The results obtained from this study is then compared to existing in-house atomization experiments where the power usage and droplet size distribution are measured. Furthermore, it should be noted that this study is a continuation of previous studies [7,8,9,10]. Here information about the method used in the experiments, that are referred to in this study, can be found.

2. Materials and Methods

Albeit, several different wheels have been modelled, and results will be presented accordingly. We will, in this paper, only present the CFD-model for one geometry. We will, however, present results for other geometries since these have been simulated in a similar way. The differences in geometry for the rotary atomizer wheels presented in this paper consists of different diameters of the rotary wheel, different number of bushings in the rotary wheel, as well as slight deviations in the geometry of the cavity of the wheel.

One of the wheels modelled consists of eight bushings equally distributed over the circumference of the wheel. Hence, symmetry considerations allow us to model a subdomain of the wheel, i.e., $\theta \in [-\pi/8: \pi/8]$ with a bushing at the center of the domain, i.e., $\theta=0$, where θ represents an angle (rad).
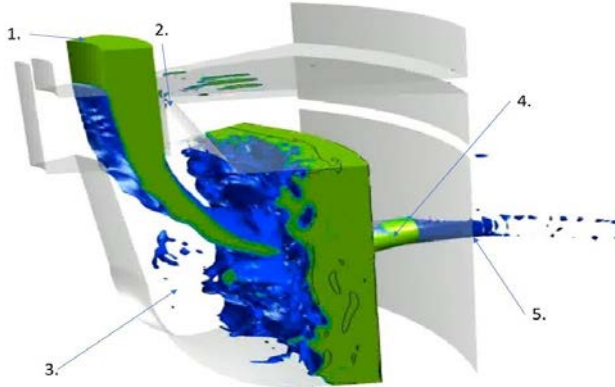
Fig. 1 Illustration of the geometry of the simulated part of a wheel. Indicated by numbers and arrows are 1) inlet, 2) overflow, 3) cavity, 4) bushing 5) exit. Notice, how water enters through the inlet and exits through the overflow and the bushing.

In Fig. 1 the geometry of the modelled domain is shown. The modelled domain consists of the inlet, the wheels cavity of the wheel, the bushing, the 'overflow area' and the outside of the bushing, i.e., the drying chamber.

To give realistic flow distributions to the inlet, the flow in the liquid distributor prior to the inlet has, although not shown in this paper, been modelled for different feed rates. The solution to these prior investigations have been used as boundary conditions for the inlet flow.

Under normal operating conditions the fluid will move from the inlet through the cavity of the wheel, through the bushing and out into the drying chamber. Under abnormal operating conditions, i.e., very high values of the feed rate, part of the fluid will exit the wheel through the overflow. In the small part of the drying chamber included in this model, the breakup of the exiting jet and thin film annulus is modelled. Here the resulting drops are accounted for and the size distribution a size distribution is calculated.

All simulations presented in this study have been performed using ANSYS Fluent with a volume of fluid (VOF) approach.

2.1 Governing equations

The governing equations for fluid and the air are the Navier-Stokes equation and continuity equation of fluid and air where subscript j represents one of the fluid phases air (a) or water

(w) and ε, is the fraction of component j. Note that there are only two phases – hence, $\varepsilon_a + \varepsilon_w = 1$.

$$\frac{\partial}{\partial t}\left(\varepsilon_j \rho_j\right) + \nabla \cdot \left(\varepsilon_j \rho_j \boldsymbol{u}\right) = 0 \tag{1}$$

$$\frac{\partial}{\partial t}\left(\varepsilon_j \rho_j \boldsymbol{u}\right) + \nabla \cdot \left(\varepsilon_j \rho_j \boldsymbol{u}\boldsymbol{u}\right) = -\varepsilon_j \nabla p + \nabla \cdot \left(\varepsilon_j \boldsymbol{\tau}_j\right) + \varepsilon_j \rho_j \boldsymbol{g} + \boldsymbol{f}. \tag{2}$$

Here, $\boldsymbol{u}$, is the velocity field (m/s), ρ, is the density (kg/m^3), ε, is the volume, p is the pressure (Pa) and $\boldsymbol{g}$, is the gravitational acceleration (m/s^2) and $\boldsymbol{f}$ (N/m^3) represents forces per unit volume, not accounted for by the motion of the fluid, i.e., centrifugal force, surface tension and the Coriolis force. Here, the stress tensor, $\boldsymbol{\tau}_j$, is given by

$$\boldsymbol{\tau}_j = \mu_j \left([\nabla \boldsymbol{u} + \nabla \boldsymbol{u}^T] - \frac{2}{3}(\nabla \cdot \boldsymbol{u})\boldsymbol{I}\right), \tag{3}$$

where, μ, is the viscosity (Pa·s) and $\boldsymbol{I}$ represents the unit matrix. Note that the water is modelled as incompressible whereas the air is compressible. Turbulence is modelled with a RANS (k, ω) model.

2.2 Boundary conditions

2.2.1 Walls

On the walls we impose a no flux condition in direction of the normal vector and a no-slip condition in tangential direction. I.e., there is no transport of fluid through solid walls and the relative velocity between the fluid and a solid wall is zero.

2.2.2 Outlet

At the surface of the domain where the fluid exits into the drying chamber a zero gauge pressure boundary condition is imposed.

2.2.3 Periodic boundary conditions

At all boundaries normal in the direction of the rotation has a periodic boundary, i.e., what exits on one side enters on the other. Hence,

$$\alpha\left(r, -\frac{\theta}{8}, z\right) = \alpha\left(r, \frac{\theta}{8}, z\right). \tag{4}$$

Here α represents conserved properties, i.e., velocity field, $\boldsymbol{u}$, the pressure, p, the volume of fluid fractions, ε_f, as well as the turbulence parameters k and ω.

2.2.4 Inlet

As mentioned the velocity field at the inlet for different volumetric inlet fluxes, $\dot{V}$ (m³/s) and different geometries, Ω, has been determined in a previous study. The velocity field, $\boldsymbol{v}$ (m/s) at the inlet for different feed flows are used as a boundary condition at the inlet. Hence,

$$\boldsymbol{u}_i = \boldsymbol{v}_i(\dot{V}, \Omega). \tag{5}$$

2.3 Mesh

The mesh used is a swept mesh with the special ability of adapting size according to the gradient of volume of fluid, i.e., the mesh has small elements in the interface between fluid and air. This adaptive mesh ensures that the resolution of the air-water interface improved without compromising the simulation time. An illustration of the mesh and the size adaption is shown in Fig. 2.
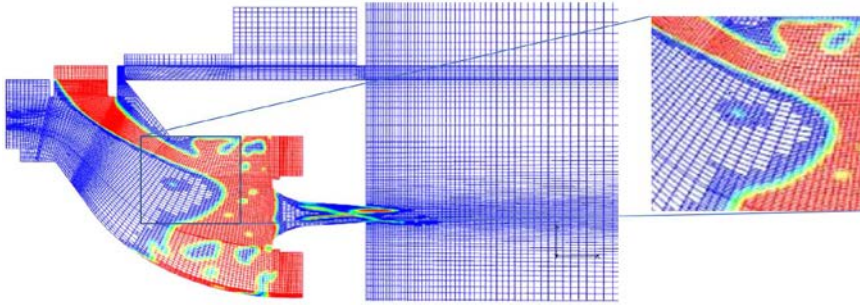
Fig. 2 Illustration of the mesh as well as how the mesh is refined depending on the VOF-gradient. The red part of the figure represents water and the blue is air.

2.4 Drop size calculations

To estimate the drop size in the simulations, a virtual surface is included at a given distance from the bushing exit. The volume of fluid droplets that passes through this virtual surface is then directly related to the volume of a sphere and the radius is calculated accordingly. The observation of droplets passing through the virtual surface is collected for enough time to give a reasonable size distribution.

3. Results and discussions

As mentioned in the introduction the results from the CFD-simulations are compared to experimental results. Firstly, we shall relate the findings from the simulations to experimental power consumptions. Secondly, we shall relate the droplet size distribution from the simulations to experimental results.

3.1 Power consumption and wheel capacity

The equation governing the power consumption is given by,

$$P = \dot{m}_b(\omega R_b)^2 = (\dot{m}_f - \dot{m}_o)(\omega R_b)^2. \tag{6}$$

Here, P is the power (W), $\dot{m}_b$, is the liquid mass-flux (kg/s) through the bushing, ω is the angular velocity (rad/s), R_b (m) is the radius at the bushing exit, $\dot{m}_f$ is the mass-flux of feed (kg/s) and, $\dot{m}_o$ is the mass-flux of liquid through the overflow (kg/s). Hence, a linear dependency of power versus inlet flux is expected if no fluid passes through the overflow, i.e., $\dot{m}_o = 0$. Furthermore, a larger power consumption is needed for larger angular velocities of the rotary atomizer. Trivially, the linear dependence between power and feed flow ceases to exist when fluid passes through the overflow – which will happen at a sufficiently high inlet-fluxes.

It is, however, not trivial that simulations from CFD and experiments performed on the wheels simulated are able to produce overflow for the same values of the influx.

The power distribution is a function of inlet flux, both experimental and from simulations, are presented in Fig. 3 for three different angular velocities. As seen there is a good agreement between experiment and simulations. For small values of the inlet flux there is a linear tendency between power consumption and inlet flux. Increasing the inlet flux even further causes a higher fraction of the fluid to pass through the 'overflow' inducing a larger deviation from the straight line.
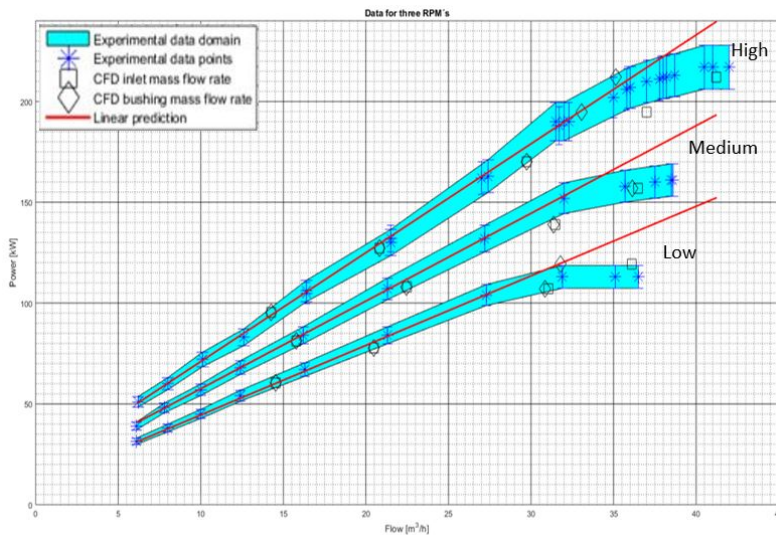
Fig. 3 Power consumption as a function of feed-rate for CFD simulations and experimental data for three different RPM – increasing from bottom to top.

It can also be seen from Fig. 3 that the critical inlet flux is increasing for increasing angular velocity of the wheel. This is expected due to the larger acceleration of the fluid in radial direction due to an increase in centrifugal force. As seen from the figure there is an excellent agreement between the CFD simulations and experiments made on the wheel simulated at

corresponding angular velocities. In figure Fig. 1 it is illustrated how fluid passes through the overflow during simulations.

3.2 Prediction of atomization and droplet size distribution

Experimental results of the drop-size distribution as well as measured drop-size distribution from the simulations are shown in Fig. 4. As seen there is a good qualitative agreement between the two. The droplet-size depends among other things on the exiting jet from the bushing. The exiting jet and breakup from a simulation and experiment are shown in Fig. 5.
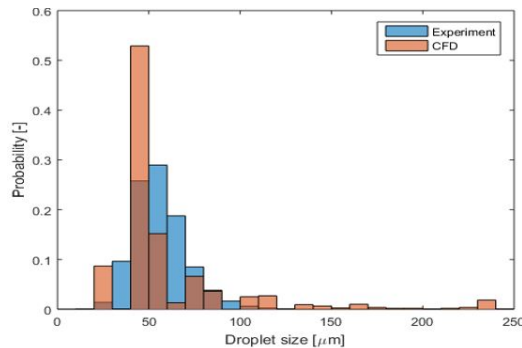
Fig. 4 Droplet size distribution from CFD simulations and experimental results measured at 110 mm from the bushing exit at an angular velocity of 29000 RPM.
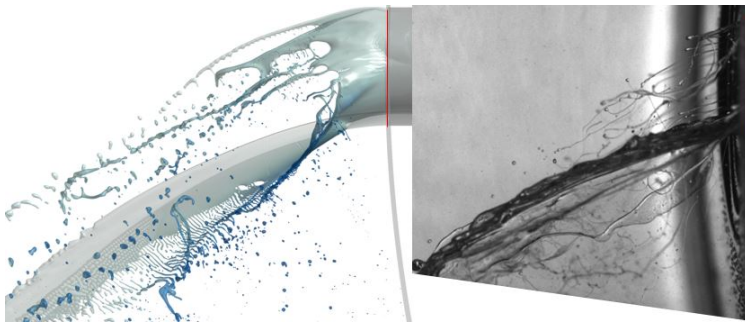
Fig. 5 Snapshot from the CFD-simulations (left) and experiment (right) of the breakup of the thin film and exiting jet into droplets.

The ability to reproduce experimental results serves as a validation of the model. This validation is a first step for future research, where extraction of valuable information, e.g., total wall shear stress, mixing, rivulet height, film thickness for different fluids and different operating conditions. This in return allows for topology optimization, power consumption and essentially optimized conditions for drying and end-product.

The inclusion of CFD in our production line allow us to design new geometries for rotary wheels, and operate them at optimal feed rates and angular velocities in terms of power

consumption. Furthermore, the ability to estimate the droplet size distribution for any given fluid makes it possible to give optimal conditions for the final product. Hence, enables us to produce tailor made solutions for a given product and increasing value for industry.

4. Conclusions

The CFD model presented in this study gives valuable insight in the fluid flow and interaction between fluid and air in a rotary atomizer. The model can reproduce experimental results for power consumption and droplet size-distribution.

5. References

[1] Lefebvre, A.H. Atomization and Sprays; Combustion: An International Series. Hemisphere Publishing Corporation, 1989.

[2] Masters, K. Spray Drying Handbook; Longman Scientific & Technical, Essex, England, 1991.

[3] Ullum, T.; Sloth, J.; Brask, A. Predicting Spray Dryer Deposits by CFD and an Empirical Drying Model. Drying Technology 2010, 28(5), 723-729.

[4] Huang, L.X.; Kumar, K.; Mujumdar, A.S. A comparative study of a spray dryer with rotary disc atomizer and pressure nozzle using computational fluid dynamic simulations. Chemical Engineering and Processing: Process Intensification 2006, 45(6), 461-470.

[5] Woo, M.W.; Daud, W.R.W.; Mujumdar, A.S.; Wu, Z.; Talib, M.Z.M.; Tasirin, S.M. CFD Evaluation of Droplet Drying Models in a Spray Dryer Fitted with a Rotary Atomizer. Drying Technology 2008, 26(10), 1180-1198.

[6] Gianfrancesco, A.; Turchiuli, C.; Flick, D.; Dumoulin, E. CFD Modeling and Simulation of Maltodextrin Solutions Spray Drying Control Stickiness. Food and Bioprocess Technology 2010, 3(6), 946-955.

[7] Kuhnhenn, K.; Oberthür, A.; Roisman, I.V.; Joensen, T.V.; Tropea, C. Droplet Size Determination on a Rotary Atomizer Wheel with Time-Shift Technique in Comparison to Analytical Theory. ILASS – Europe 2016, 27'th Annual Conference on Liquid Atomization and Spray Systems, 4-7 September 2016, Brighton, UK.

[8] Kuhnhenn, K.; Luh, M.; Joensen, T.V.; Roisman, I.V.; Tropea, C. Experimental Characterization of Spray generated by a Rotary Atomizer Wheel. ILASS – Europe 2017, 28'th Annual Conference on Liquid Atomization and Spray Systems, 6-8 September 2017, Valencia, Spain.

[9] Kuhnhenn, K.; Roisman, I.V.; Tropea, C.; Joensen, T.V. Study of the internal flow in a rotary atomizer and its influence on the resulting spray. 9th World Conference on Experimental Heat Transfer, Fluid Mechanics and Thermodynamics, 12-15 June 2017, Iguazu Falls Brazil.

[10] Kuhnhenn, K.; Joensen, T.V.; Reck, M.; Roisman, I.V.; Tropea, C. Study of the internal flow in a rotary atomizer and its influence on the properties of the resulting spray. International Journal of Multiphase Flow 2018, 100, 30–40.

FUNDAMENTALS, MODELING AND SIMULATION

Poster Presentations

Modeling of Particle Behavior in a Wurster Fluidized Bed: Coupling CFD-DEM with Monte Carlo

Jiang, Z.[a,b*]; Rieck, C.[a]; Bück, A.[a,b]; Tsotsas, E.[a]

[a] Thermal Process Engineering. Otto von Guericke University Magdeburg, Magdeburg, Germany

[b] Institute of Particle Technology. FAU Erlangen-Nuremberg, Erlangen, Germany.

*E-mail of the corresponding author: zhaochen.jiang@fau.de

Abstract

CFD-DEM approach is applied to investigate circulation motion of particles in a mono-disperse system under both dry and wetting conditions. Good agreement between simulation results and measurement data is observed, in terms of cycle time and residence time in dry condition. The deposition of droplets on the particle surface is modeled by a Monte Carlo approach. The influence of cohesion forces on the macroscopic particle circulation is discussed. In addition, information about coating coverage, the layer thickness and particle size distribution can be predicted by this integrating approach.

Keywords: CFD-DEM; Wurster coater; Monte Carlo; cohesion force; residence time.

1. Introduction

Particle coating is widely applied in pharmaceutical, food and fertilizer industry. The Wurster coater can be used as a batch or a continuous fluidized bed to precisely control the quality of the coated product [1]. The entire coating process is considerably complex, caused by a large number of sub-processes, including wetting, drying and film formation; and by the presence of different zones with different controlling parameters (such as gas velocity, gas temperature, and spray rate), as shown in Fig. 1. The enhanced understanding of particle dynamics in different zones is significant to optimize drying kinetics that governs particle formation in coating.
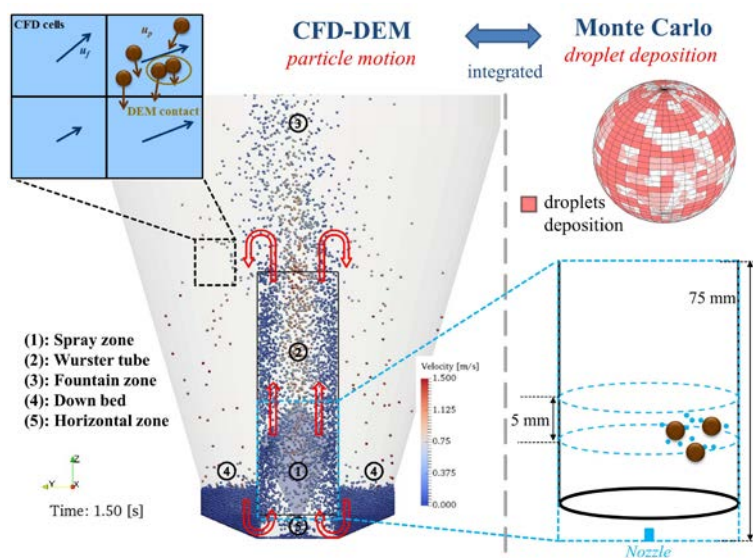
Fig. 1 Modeling of particle behavior by CFD-DEM for particle motion integrating Monte Carlo for droplet deposition (The Wurster coater is divided into 5 process zones; and the droplet deposition takes place in the region marked by the light blue rectangle).

The circulation motion of particles under dry conditions has been investigated in experiments and simulations [2, 3]. However, published studies of the influence of cohesion forces existing in spray zone on the circulation motion are very limited. In this study, computational fluid dynamics-discrete element method (CFD-DEM) was used to investigate the particle motion in the Wurster coater, under both dry and wetting conditions. The influence of cohesion forces, relating to wetting properties and process parameters, on the residence time and the cycle time are discussed based on the analysis of all individual particle trajectories. For the prediction of particle size, a two-zone population balance modeling is usually used to predict the growth of particles during the coating process. In this work, the event of droplet deposition modeled by a Monte Carlo approach [4] was integrated with the particle motion predicted by the CFD-DEM approach, which creates a relatively cost-effective multiscale

numerical method to predict particle size distribution and coating coverage during the coating process. The effect of cohesion forces in the Wurster tube on particle size distributions for different process times is discussed.

2. Methodology

2.1 CFD-DEM approach

The CFD-DEM approach has been widely applied to investigate the complex granular flow in chemical applications. The CFD-DEM approach can capture the macroscopic particle dynamics in the multiphase flow, simultaneously providing an insight into behavior of individual particle scale including particle-particle interactions, as shown in Fig. 1. The open source code OpenFoam+LiGGGHTS (CFDEM®project) was used for this study. The detailed governing equations of solid and gas phase, Gidaspow drag model, Hertz soft sphere contact model and rolling model can be found in our previous works [3, 5].
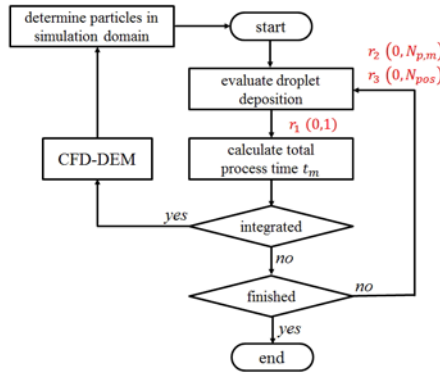
Fig. 2 Flow chart of the Monte Carlo integrated with CFD-DEM including required random numbers ($N_{p,m}$ is the number of particles in the Monte Carlo domain).

2.2 Cohesion model

The capillary force and viscosity force have been implemented into the DEM code [6]. The equation for calculating the capillary force F_c (N) of a specific particle-pair geometry was obtained by fitting the set of discrete solutions of the Laplace equation, expressed as:

$$F_c = \pi\sigma\sqrt{R_i R_j}\left[C + exp\left(A\frac{d_{inter}}{\max(R_i, R_j)} + B\right)\right], \tag{1}$$

where R_i and R_j are radii of two particles (m), d_{inter} is the inter-particle distance (m), and σ is the surface tension of lqiud (N/m). The coefficients A, B and C are functions of liquid volume V_l (m³), contact angle θ (radians) and larger particle radius $R_{max} = max(R_i, R_j)$ [6]. The liquid volume between two particles is assumed to be evenly distributed when the inter-particle distance is larger than the rupture distance $D_r = (1 + 0.5\theta) \cdot V_l^{1/3}$ (m).

The viscosity force F_v (N) can be calculated as:

$$F_{v,n} = 6\pi\mu R^* v_n \frac{R^*}{d_{inter}}, \qquad F_{v,t} = 6\pi\mu R^* v_t \left[\frac{8}{15} ln \frac{R^*}{d_{inter}} + 0.9588\right], \qquad (2)$$

where μ is the fluid dynamic viscosity (Pa·s), $R^* = R_i R_j/(R_i + R_j)$ is the equivalent radius; and v_n and v_t are relative velocity of two particles in normal and tangential directions (m/s), respectively. The capillary force and viscosity force are included into Newton's law of motion for individual particle. Note that these two forces only exist in the Wurster tube and wall boundaries are assumed in dry condition.

2.3 Monte Carlo approach

According to the geometry of spray zone, the simulation domain for Monte Carlo is the cylinder with the height of 75 mm and the radius of the Wurster tube, and the bottom of the domain is aligned with the tip of the spray nozzle, as shown in Fig. 1. The particles in the Monte Carlo domain were determined by the CFD-DEM data. The overview of the Monte Carlo integrated with CFD-DEM is given in Fig. 2. In each Monte Carlo time step Δt_m, one droplet deposition event is guaranteed to happen in the Monte Carlo domain. The time step can be calculated from the number flow rate of droplets injecting into the system, expressed as:

$$\Delta t_m = -(\frac{6\dot{M}}{\pi\rho_d d_d^3})^{-1} \ln r_1, \qquad (3)$$

where $\dot{M}$ is the mass flow rate of solution and r_1 is a uniformly distributed random number for the interval (0,1). The droplet diameter is constant. Once the total Monte Carlo process time t_m exceeds 0.01 s, CFD-DEM simulation was advanced for 0.01 s and number of particles in the Monte Carlo domain $N_{p,m}$ was updated based on new CFD-DEM data.

To evaluate the individual droplet deposition, two more random numbers are required: r_2 to pick up the particle from the domain and r_3 to choose deposition position on the single particle surface. In current work, each particle in the domain has the same possibility to receive the droplets. Based on the work of Rieck et al. [4], the number of positions (with same size) per particle N_{pos} is calculated by $N_{pos} = d_p^2/d_{contact}^2$. The diameter d_{contat} is the diameter of contact area, which depends on the contact angle and droplet volume. N_{pos} was rounded to an integer value in the code. Each position can have four statuses labeled by four numbers in the model: 1) no droplet (initial), 2) with wetting droplet, 3) with dry droplet and 4) no droplet (new). In cases of label 1, 3 and 4, the droplet deposition event can occur. If a wetted position (2) is selected, a new random number r_3 is generated until the requirement of deposition is satisfied.

The criterion for determining dry or wet position is related to the drying process of the deposited droplet, expressed as:

Table 1. Summary of the setup for CFD-DEM integrating with Monte Carlo

Parameters	Value	Unit
Particle phase (DEM)		
Particle diameter $d_{p,0}$	1.75	mm
Particle density ρ_d	1420	kg/m^3
Particle number	50 000	-
Gas phase (CFD)		
Gas density ρ_g	1.2	kg/m^3
Dynamic viscosity	1.84×10^{-5}	Pa·s
Gas flow rate (fluidization $\dot{V}_g$/atomization)	80.3/3.5	m^3/h
Gas temperature	50	^{o}C
Moisture content of fluidization gas Y_{inlet}	1	g/kg
Liquid phase (Monte Carlo)		
Droplet diameter d_d	50	μm
Droplet density ρ_d	1000	kg/m^3
Solid density of coating solution ρ_s	1000	kg/m^3
Mass flow rate $\dot{M}$	0.25	kg/h
Solid mass fraction ϵ_s	0.3	-
Porosity of coating layer φ_s	0.5	-
Liquid content α_l	0.001	-
Surface tension σ	0.072	N/m
Contact angle θ	30	^{o}
Liquid viscosity μ	10^{-4}	Pa·s
CFD-DEM simulation parameters		
CFD time step	5×10^{-5}	s
CFD cell number (structured hexahedral)	81600	-
DEM time step	10^{-5}	s
Integrate time Monte Carlo and CFD-DEM	0.01	s
Simulation time	20	min

$$t_m \geq t_{deposition} + \Delta t_{drying}, \tag{4}$$

where $t_{deposition}$ is the moment the droplet deposition happens, and Δt_{drying} is the drying time of the deposited droplet. Considering the first drying period only, the Δt_{drying} can be calculated by [4]:

$$\Delta t_{drying} = \frac{\left(\frac{1}{6}\pi d_d^3\right) \cdot \rho_d \cdot (1 - \epsilon_s)}{\beta_m A_{dep} \rho_g (Y_{sat} - Y)}, \tag{5}$$

where β is the mass transfer coefficient (m/s), Y_{sat} is the adiabatic saturation moisture content of fluidization gas (g liquid/kg dry gas), and $Y = Y_{inlet} + \dot{M} \cdot (1 - \epsilon_s)/(\dot{V}_g \cdot \rho_g)$ is the moisture content of bulk gas. A_{dep} is the curved area of deposit droplet in contact with the gas (m^2), which can be calculated by:

$$A_{dep} = \frac{1}{2}\frac{\pi \cdot d_{contact}^2}{1 + \cos\theta}. \tag{6}$$

The thickness of solid layer in single position on particle surface h_i can be calculated as:

$$h_i = \left(\frac{d_{core}^3}{8} + \frac{3}{4}\frac{N_{pos}\cdot\left(\frac{1}{6}\pi d_d^3\right)\cdot\frac{\rho_d\cdot\epsilon_s}{\rho_s\cdot\varphi_s}}{\pi}\right)^{1/3} - d_{core}, \tag{7}$$

where d_{core} is the diameter of core particle. The coating coverage Ψ can be evaluated by:

$$\Psi = \frac{N_{pos,tot} - N_{pos,free}}{N_{pos,tot}}, \tag{8}$$

where $N_{pos.tot}$ and $N_{pos.free}$ are total number of positions and number of positions without droplet, respectively. With the average coating thickness h_m, the particle diameter can be expressed as: $d_p = d_{core} + 2h_m$.

2.4 Simulation setups

The mesh of Wurster coater was built by O-grid method [3], according to the configuration used in PEPT experiments [2]. The initial particle diameter $d_{p,0}$ is 1.75 mm. All important simulation parameters in the sub-models of CFD-DEM integrating with Monte Carlo are summarized in Table 1. The coupling interval between DEM and CFD is 100 time steps of DEM; and the integrating interval with Monte Carlo is 0.01 s, which is approximately $2d_{p,0}/v_m$ (mean particle velocity in the Wurster tube).

3. Results and discussion

3.1 Particle circulation motion

As shown in Fig. 3, the global circulation of particle from simulation with cohesion forces (0.1 %) is very similar to that in dry condition; however, the particles tend to be clustered in the Wurster tube. The detailed value of mean cycle time and mean residence time are listed in Table 2. The ideal cycle time and residence time in the Wurster tube were found to be in good agreement with PEPT measurement data in dry condition. However, the non-ideal cycle was underestimated in the simulation. With the effect of cohesion forces, the ideal cycle time and the fractions of ideal cycle are decreased, resulting in the increase of total cycle time. The decrease of the fractions of ideal cycle may cause by upwards and downwards motion of particle clustering in the Wurster zone.

3.2 Particle coating

Figure 4 left) shows the coating coverage of a sample particle after 70 s and the spherical particle was mapped into 2D space based on number of deposition positions. The gray level

dry condition $\qquad\qquad\qquad\qquad\qquad$ $\alpha_l = 0.1\ \%$
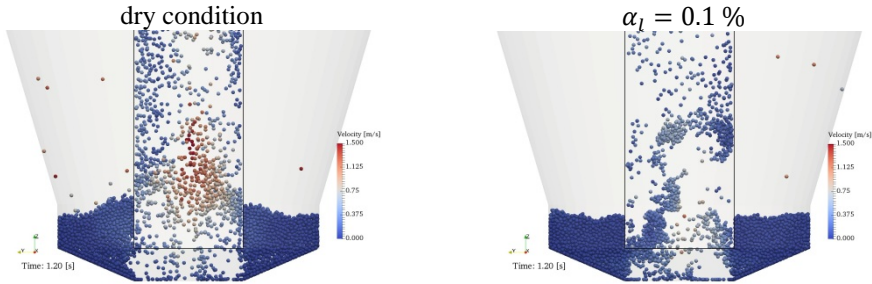
Fig. 3 Influence of cohesion forces on particle motion in the Wurster coater.

Table 2. Comparison of ideal cycle time, overall cycle time, residence time

Variable	CFD-DEM simulation		Measurement [2]
	dry	$\alpha_l = 0.1\%$	*dry*
$\bar{t}_{ic}$ [s]	4.98 (52.8)	4.25 (33.5)	4.84 (99.0)
$\bar{t}_c$ [s]	5.82 (61.5)	6.42 (73.3)	6.14 (89.8)
r_n [%]	78.3	60.2	55.3
$\bar{t}_{r,t}$ [s]	0.96 (33.7)	0.90 (44.6)	1.00 (-)
$\bar{t}_{r,s}$ [s]	0.15 (22.1)	0.14(28.3)	-

$* \bar{t}_{ic}$ is mean ideal cycle time, $\bar{t}_{ic}$ is mean total cycle time, r_n is number ratio of ideal cycle, $\bar{t}_{r,t}$ and $\bar{t}_{r,t}$ are mean residence times in Wurster tube and spray zone; the coefficient of variation (CV) is in the brackets.
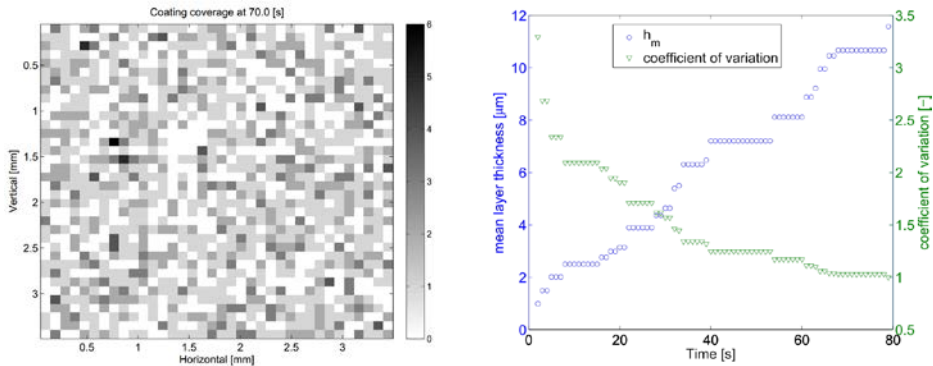
Fig. 4 Coating coverage and layer thickness of sample particle from wetting simulation: left) droplet deposition on single particle, right) layer thickness and CV with respect to time.

represents the number of deposition droplets in each pixel. According to Eq. (8), the coating coverage at this moment is 67 %. However, the coating coverage cannot roundly measure the uniformity of coating layer. The coefficient of variation (the ratio of standard deviation to mean) of the layer thickness is 1.05 at this moment. Figure 4 right) shows that the mean layer thickness increases and the coefficient of variation decreases. The variation only happens when the particle passes through the Wurster tube. Figure 5 show the size distributions under dry and wetting conditions. There are wider distributions of particle diameter d_p for simulations with cohesion forces for different process times.
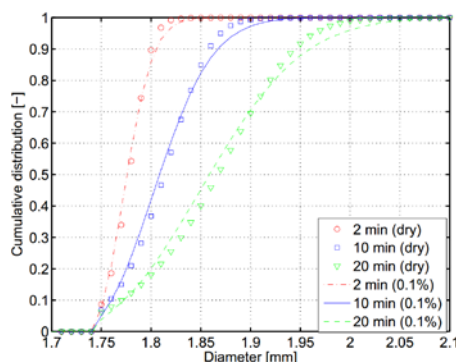
Fig. 5 Particle size distributions of 50000 particles in different process time (both dry and wetting).

4. Conclusion

Cohesion forces scatter distributions of cycle time, residence time and particle size. It is important to provide enough drying capacity in fluidization gas to prevent the appearance of particle agglomeration and achieve high product quality in the Wurster coating process.

5. Acknowledgements

6. References

[1] Tsotsas, E. Multiscale approaches to processes that combine drying with particle formation. Drying Technology 2015, 33, 1859–1871.

[2] Li, L.; Rasmuson, A.; Ingram, A.; Johansson, M.; Remmelgas, J.; von Corswant, C.; Folestad, S. PEPT study of particle cycle and residence time distributions in a Wurster fluid bed. AIChE 2015, 61, 756–768.

[3] Jiang, Z.; Bueck, A.; Tsotsas, E. CFD–DEM study of residence time, droplet deposition, and collision velocity for a binary particle mixture in a Wurster fluidized bed coater. Drying Technology 2018, 36(6), 638–650.

[4] Rieck, C.; Bück, A.; Tsotsas, E. Monte Carlo modeling of fluidized bed coating and layering processes. AIChE J 2016, 62, 2670–2680.

[5] Jiang, Z.; Hagemeier, T.; Bueck, A.; Tsotsas, E. Color-PTV measurement and CFD-DEM simulation of the dynamics of poly-disperse particle systems in a pseudo-2D fluidized bed. Chemical Engineering Science 2018, 179, 115–132.

[6] Soulié, F.; Cherblanc, F.; El Youssoufi, M.; Saix, C. Influence of liquid bridges on the mechanical behaviour of polydisperse granular materials. International Journal for Numerical and Analytical Methods in Geomechanics. 2006, 30, 213–228.

CFD model-supported design of monodisperse co-current spray dryers

Jaskulski, M.[a]*; Tran, T.T.H.[b]; Tsotsas, E.[c]

[a] Faculty of Process and Environmental Engineering, Lodz University of Technology, Wolczanska Str 213., 95-924 Lodz, Poland.

[b] School of heat engineering and refrigeration, Hanoi University of Science and Technology, 1st Dai Co Viet, Hanoi, Vietnam.

[c] Thermal Process Engineering, Otto von Guericke University Universitaetplatz 2, 39106 Magdeburg, Germany.

E-mail of the corresponding author: maciej.jaskulski@p.lodz.pl

Abstract

In this study the operation of spray drying chambers fitted by the multi-stream monodisperse atomizer was simulated by the previously developed CFD model of skim milk spray drying. A series of CFD simulations of skim milk monodisperse spray drying were performed. The influence of different nozzle positions, initial droplet diameters (180 μm and 167 μm) and the way of air introduction (vertical or swirling with 30° or 60° angle) on the drying process were checked. Parameters like drying air and particle residence time, wall deposition, inter-particle collisions, protein thermal deactivation, air velocity and temperature profiles were compared for each case.

Keywords: CFD, spray drying, skim milk, monodisperse atomizers, optimization.

1. Introduction

Spray drying process for powder production and dehydration is widely used in many sectors of industry. Low content of solids in the liquid feed sprayed inside the drying chamber results in a large amount of energy required for particle solidification and evaporation of moisture. Therefore, the spray drying process consumes much energy used for preparation of the drying agent. Continuous growth in the demand for spray dried products makes improvements in the spray drying process necessary, not only in regard of energy and substrates consumption but also of product quality.

Modern technologies of computational simulation allow to design or optimize the production process of powders with properties directly specified by the customers. Spray drying process optimization performed by CFD techniques can also be used to solve production problems in certain regions of the drying chamber. An example has been given by a series of CFD simulations of a detergent counter current spray drying tower performed by Wawrzyniak [1]. In this work a theoretical solution of problems related to powder baking near the hot air inlet area was proposed. Particle deposition on the wall and its effect on spray drying tower operation has been widely studied in the literature [2]. Especially, the effects of flow hydrodynamics and air flow direction on the trajectories of particles, residence time and deposition inside of the drying chamber has been studied [3]. In CFD studies of air hydrodynamics in spray drying towers mostly the effect of different ways of air introduction on flow stability inside of the chamber has been checked [4]. Simulations with swirl air distribution were verified on the basis of experimental investigations [5]. Not only airflow and drying efficiency can be simulated by the CFD models. More advanced studies on particle morphology allow to include into the CFD simulations models of agglomeration, particle formation or material degradation during the spray drying.

Particle agglomeration occurs mostly in counter current and mixed flow spray dryers, having significant influence on particle size distribution in the final product. In some production processes full control of the size of particles in the dried powder is required. For this reason CFD simulations are used to identify theoretically regions where agglomeration can take place [6] or to predict final particle size distribution in the product [7]. In food industry, like skimmed milk powder production, it is also necessary to take into account influence of process parameters on product quality. CFD simulations of the influence of drying parameters on lysine loss were performed for example by Schmitz-Schug [8].

In the presented article the influence of drying conditions, swirl flow, monodisperse multi-stream atomizer configurations and droplet diameter on the drying efficiency, product quality, agglomeration probability and wall deposition will be predicted by the developed CFD skimmed milk spray drying model. All simulation results are compared to show the impact of each parameter on the drying process and to show which configuration and

parameters can give optimal results in spray drying of skimmed milk when using novel monodisperse multi-stream atomizers.

2. Materials and Methods

The presented manuscript is a summary of the European project ENTHALPY whose task is to optimize skim milk powder production via spray drying. Design of new spray dryer can be supported by the CFD simulations and for this reason mathematical model of skim milk drying and thermal inactivation of the proteins need to be developed.

2.1. CFD model of skim milk spray drying

Development of the CFD model of skim milk spray drying process starts with the series of single droplet drying (SDD) experiments performed for milk and milk components in wide range of operating conditions [10]. Based on obtained data advanced model of single droplet drying was developed. This model takes into account internal circulation of liquid in droplet, spatial gradient of solid concentration, temperature and moisture distribution and calculation of inflation and deflection of particle in elevated temperatures [11]. Next developed model was simplified and implemented into the CFD solver. To verify correctness of performed simulations calculation results were compared with experimentally obtained data from the test spray drying installation constructed on Otto von Guericke University in Magdeburg [12]. The test installation will later colled OVGU dryer. Additionally, evaporation model was combined with the protein inactivation model to calculate degradation of the skim milk powder during the spray drying process [13]. A full mathematical description of the models and details of the dryer geometry and settings of the CFD solver can be found in the quoted articles. Here only brief description of CFD simulations is presented.

2.2. Geometry and nozzle configurations

Tested spray drying tower is a co-current installation with narrow drying chamber: total height is 6.5 m with 0.4 m inner diameter [12]. Instead of a standard two-fluid spray nozzle the newly designed monodisperse multi-stream droplet atomizer was used [14]. It was assumed that dryer will be fed by four monodisperse atomizers. Each printing head has a base plate with 150 outlets placed in one line. Each outlet generates a single stream of droplets with constant initial diameter which depends on the size of the outlet and on the frequency of the piezo element inside the printing head. In CFD simulations special arrangements of the heads, which lead to a variation in the shape and dimensions of their supporting plates, were tested. Each configuration of the printing heads has a different denotation which will be used further in the description of results:

- **CI_1** – four printing heads arranged one next to the other. Heads are mounted on the round base (diameter 214 mm) plate used in the OVGU dryer.

- **SQ_2** – four printing heads arranged one beside the other. Heads are mounted on the rectangular (188 mm x 188 mm) base plate.
- **RI_3** – four printing heads arranged on a ring support plate (internal diameter = 150 mm, external diameter = 290 mm, distance of printing head from the axis = 80 mm)
- **CR_4** – four printing heads mounted on an equal-armed cross with arms of length 133 mm and breadth 42 mm.

To distinguish different air inlet directions additional markings were added to the name of the geometry:

- **Ax** – axial flow of air (example Cl_Ax).
- **30** – airflow with 30° swirl (example Cl_30).
- **60** – airflow with 60° swirl (example Cl_60).

ANSYS Meshing software was used for grid generation. Near the wall area, where the highest gradients of velocity are predicted, a five-step boundary layer was generated. Finally, a fine mesh with 385k tetrahedral elements was generated. For every case, with different printing head configurations, a new mesh was generated with different computational elements on the atomizer support plate and air inlet surface. Those differences change the mesh structure near the air inlet area. However, all mesh quality parameters and number of mesh element were kept constant.

2.3. Operating parameters

Skimmed milk with initial solid mass fraction equal to 45% was used as the feed in the simulations. Initial diameter of the droplets injected into the drying chamber depends on the frequency of the piezo element inside of the printing head. In this report two frequencies were tested, 12 kHz and 15 kHz which generate droplets with diameters of 180 microns and 167 microns respectively. The mass flow rate of skimmed milk solution was equal to 0.018 kg/s, with an inlet temperature of 55°C. Initial velocity of the droplets was 18.7 m/s.

Air inlet on top of the dryer was set up as mass flow inlet boundary condition. In every simulated case the mass flow rate of air was constant and equal to 0.1 kg/s. Air was assumed as dry ideal gas with initial temperature of 200°C. In simulations with vertical airflow direction, inlet air vectors were set as normal to the boundary. In simulations with swirl airflow, air direction vectors were inclined to the inlet surface by an angle of 30° or 60°. Centre of rotation was the tower axis.

To calculate the number of inter-particle collisions it was necessary to perform all calculations in transient state. The number of time steps maintained for every simulation was 400 with time step size of 0.1 s. In simulations with axial flow of air the realizable *k-ε* turbulence model was used. However, in simulations with rotary movement of air the turbulence model was changed to the RNG *k-ε* turbulence model with switched on option of swirl dominated flow, which is recommended for calculations with rotary airflow.

2.4. Simulations results

Simulations results were summarized in Table 1. Swirling air distribution has a significant impact on particle flow trajectories. Particles rotation increases their residence time inside the drying chamber.

Table 1. Summary of the CFD simulations results

Case study	Particle residence time, s		Outlet air temperature, °C		H_2O removed, %	
	180 μm	167 μm	180 μm	167 μm	180 μm	167 μm
CI_Ax	3.08	3.23	62.61	63.01	92.32	91.93
CI_30	3.95	4.24	64.96	63.39	95.15	98.65
CI_60	5.46	4.83	70.09	68.11	87.91	89.06
SQ_Ax	2.92	3.21	62.65	63.04	93.08	98.47
SQ_30	3.97	4.30	62.86	63.12	98.69	98.66
SQ_60	6.80	4.55	68.58	67.48	95.98	96.57
RI_Ax	3.87	4.17	63.48	63.52	98.77	98.89
RI_30	4.23	4.23	74.06	72.91	86.97	88.06
RI_60	4.76	4.51	72.8	72.27	95.56	96.17
CR_Ax	4.24	4.24	63.57	64.15	96.25	96.69
CR_30	6.12	5.75	66.11	65.95	97.72	98.02
CR_60	6.39	6.55	72.62	71.29	86.03	85.88
Case study	Probability of collision, %		Wall deposition, %		Protein activity level, %	
	180 μm	167 μm	180 μm	167 μm	180 μm	167 μm
CI_Ax	5.27	5.13	0.47	0.42	96.05	95.83
CI_30	2.85	1.98	0.84	0.89	94.21	94.67
CI_60	7.78	8.33	2.15	2.06	95.54	97.14
SQ_Ax	5.77	4.91	0.60	0.44	91.62	95.26
SQ_30	1.77	1.76	0.82	0.85	94.97	94.66
SQ_60	8.65	8.72	2.07	2.11	96.07	97.21
RI_Ax	5.32	5.66	0.41	0.48	90.76	94.68
RI_30	9.07	9.05	1.76	1.75	96.03	96.15
RI_60	9.47	9.26	3.30	3.41	95.00	96.02
CR_Ax	5.88	6.56	0.44	0.45	93.51	94.56
CR_30	3.38	3.16	1.17	1.13	96.81	96.45
CR_60	7.93	8.76	3.27	3.39	94.31	94.67

Based on the evaporation model, temperature distribution inside the spray dryer was obtained. The temperature of the continuous phase decreases along the tower because the

heat is transferred to the discrete phase for moisture evaporation. Swirling flow of the air and particles shows an interesting relationship with the temperature drop due to moisture evaporation. Comparison of time average outlet air temperature shows that in cases with higher swirl air movement the final air temperature is higher. This phenomenon can be explained as follows: In cases of axial flow of air particles are falling in the whole volume of the dryer, which results in a low temperature region near to the tower axis. With increasing swirl angle particles are moving to the dryer wall and the low temperature region is also moved from the dryer centre near to the dryer wall. For 60° swirl angle all particles are flowing near the wall where due to evaporation and heat loses to the environment air temperature is lowest. Due to this, in cases with swirl movement of air the evaporation rate of particle moisture is lower and the overall consumption of energy decreases. From the analysis of changes in evaporation rate of particles following conclusions can be drown:

For vertical flow in cases Cl_1 and SQ_2 where particle injections are concentrated near to the tower axis, the highest concentration of water source terms can be observed in the middle of the drying tower. In RI _3 and CR_4 nozzle configurations particles are better distributed in the volume of the dryer.

Swirling introduction of air significantly changes the pattern of evaporation regions inside the dryer. With axial air flow evaporation takes place in the middle of the dryer. With an increase in the angle of air rotation the centrifugal force that pushes the particle toward the walls of the dryer also increases. Near to the wall evaporation rate is lower due to lower air temperature. However the drying process is much longer, due to longer residence time of particles inside the drying chamber. Analysis of drying efficiency shows that 30° swirl increases the residence time and this improves drying efficiency. However too strong rotation pushes particles into the low temperature region and decreases drying efficiency.

From the CFD simulations we determined regions, in which inter-particle collisions can take place. With axial air flow particle collision regions are distributed in the whole volume of the drying chamber. With increasing angle of air rotation collision regions are moved to the dryer wall. With small swirl angles (30°) when particles are not reaching the dryer wall, rotary movement decreases the inter-particle collision probability.

Powder deposition on the dryer walls is an undesirable process during spray drying. This phenomenon can reduce the product quality or, in extreme case, stop the drying process by clogging the drying chamber. Analysis of contours where powder can be deposited and overall percentage of feed storage on the dryer wall shows that in such a narrow spray dryer swirling movement of air is not recommended and strongly increases powder deposition on the dryer walls. According to the deactivation model, the two parameters that control the activity of the protein in skimmed milk are moisture content and temperature of particles. From the point of view of protein deactivation analysis, strong swirling movement of air decreases deactivation rate despite the longer residence time of particles inside the drying

chamber. Near to the wall particles are dried slower in low temperature region which results in lower protein deactivation.

3. Conclusions

Series of CFD skimmed milk drying simulations of the co-current spray dryer fitted by multi-stream monodisperse atomizer were performed. Comparison of obtained simulations results shows:

- The use of monodisperse atomizer allows to obtain a more orderly flow of particles inside the drying chamber than in the simulations with standard polidisperse nozzle.
- Greater spacing between atomizer heads (like in the suggested ring or cross configuration) increases drying efficiency.
- In co-current spray towers with narrow diameter of chamber swirling air flow is not recommended due to:
  - o Creating centrifugal forces which increase wall deposition and particle collision rate.
  - o Much energy from the air is not used for the evaporation process. Dryer has lower efficiency.
  - o Less uniform radial distribution of air velocities and temperatures.
- Dryers with axial movement of air fitted by monodisperse atomizer have lower probability of powder agglomeration and wall deposition than dryer with standard two-fluid spray nozzles.
- Powders obtained from dryers with monodisperse atomizers have higher protein activity level than products obtained from standard production.
- Produced powder will have uniform particle size.

Simulation of OVGU dryer shows that for the new monodisperse atomizer the best construction is a high and narrow co-current spray dryer. Axial air flow without recirculation prevents agglomeration, wall deposition and overheating of particles. Co-current spray drying allows for better control by changing flow the rate and temperature of the drying agent. The optimal diameter of the tower depends on the number of installed printing heads. However it is recommended that each printing head should be separated by an air inlet to increase drying efficiency and prevent collisions between the particle streams.
CFD simulations of skimmed milk spray drying feed by monodisperse atomizer show big advantages over other drying processes performed by standard nozzles. Produced powder is expected to have high quality and uniform particle size which can be of crucial in pharmaceutical, cosmetic and food powders production.

4. Acknowledgements

5. References

[1]   P. Wawrzyniak, M. Podyma, and I. Zbicinski, "Industrial Spray Tower Hot Air Inlets Area Temperature Control," *J. Chem. Eng. Japan*, vol. 50, no. 10, pp. 768–774, 2017.

[2]   V. Francia, L. Martin, A. E. Bayly, and M. J. H. Simmons, "Influence of wall friction on flow regimes and scale-up of counter-current swirl spray dryers," *Chem. Eng. Sci.*, vol. 134, pp. 399–413, Sep. 2015.

[3]   V. Francia, L. Martin, A. E. Bayly, and M. J. H. Simmons, "An experimental investigation of the swirling flow in a tall-form counter current spray dryer," *Exp. Therm. Fluid Sci.*, vol. 65, pp. 52–64, 2015.

[4]   C. Lebarbier, T. K. Kockel, D. F. Fletcher, and T. A. G. Langrish, "Experimental Measurement and Numerical Simulation of the Effect of Swirl on Flow Stability in Spray Dryers," *Chem. Eng. Res. Des.*, vol. 79, no. 3, pp. 260–268, Apr. 2001.

[5]   D. B. Southwell and T. A. G. Langrish, "The Effect of Swirl on Flow Stability in Spray Dryers," *Chem. Eng. Res. Des.*, vol. 79, no. 3, pp. 222–234, Apr. 2001.

[6]   L. Malafronte, L. Ahrné, F. Innings, A. Jongsma, and A. Rasmuson, "Prediction of regions of coalescence and agglomeration along a spray dryer—Application to skim milk powder," *Chem. Eng. Res. Des.*, vol. 104, pp. 703–712, Dec. 2015.

[7]   M. Jaskulski, P. Wawrzyniak, and I. Zbiciński, "CFD Model of Particle Agglomeration in Spray Drying," *Dry. Technol.*, vol. 33, no. 15–16, pp. 1971–1980, 2015.

[8]   I. Schmitz-Schug, U. Kulozik, and P. Foerst, "Modeling spray drying of dairy products – Impact of drying kinetics, reaction kinetics and spray drying conditions on lysine loss," *Chem. Eng. Sci.*, vol. 141, pp. 315–329, Feb. 2016.

[9]   P. Wawrzyniak, A. Polańczyk, I. Zbicinski, M. Jaskulski, M. Podyma, and J. Rabaeva, "Modeling of Dust Explosion in the Industrial Spray Dryer," *Dry. Technol.*, vol. 30, no. 15, pp. 1720–1729, Dec. 2012.

[10]   T. T. H. Tran, J. G. Avila-Acevedo, and E. Tsotsas, "Enhanced methods for experimental investigation of single droplet drying kinetics and application to lactose/water," *Dry. Technol.*, vol. 34, no. 10, pp. 1185–1195, Jul. 2016.

[11]   T. T. H. Tran, M. Jaskulski, J. G. Avila-Acevedo, and E. Tsotsas, "Model parameters for single-droplet drying of skim milk and its constituents at moderate and elevated temperatures," *Dry. Technol.*, vol. 35, no. 4, pp. 444–464, Mar. 2017.

[12]   T. T. H. Tran, M. Jaskulski, and E. Tsotsas, "Reduction of a model for single droplet drying and application to CFD of skim milk spray drying.," *Dry. Technol.*, vol. in press., 2017.

[13]   M. Jaskulski, J. C. Atuonwu, T. T. H. Tran, A. G. F. Stapley, and E. Tsotsas, "Predictive CFD modeling of whey protein denaturation in skim milk spray drying powder production," *Adv. Powder Technol.*, 2017.

[14]   H. van Deventer, R. Houben, and R. Koldeweij, "New Atomization Nozzle for Spray Drying," *Dry. Technol.*, vol. 31, no. 8, pp. 891–897, Jun. 2013.

Pore network model of primary freeze drying

Vorhauer, N.[a]*; Först, P.[b]; Schuchmann, H.[c]; Tsotsas, E.[a]

[a] Otto-von-Guericke University Magdeburg, Universitätsplatz 2, 39106 Magdeburg, Germany

[b] TU München, Gregor-Mendel-Straße 4, 85354 Freising, Germany

[c] Wilhelm Büchner Hochschule, Ostendstraße 3, 64319 Pfungstadt bei Darmstadt, Germany

*E-mail of the corresponding author: nicole.vorhauer@ovgu.de

Abstract

The pore scale progression of the sublimation front during primary freeze drying depends on the local vapor transport and the local heat transfer as well. If the pore space is size distributed, vapor and heat transfer may spatially vary. Beyond that, the pore size distribution can substantially affect the physics of the transport mechanisms if they occur in a transitional regime. Exemplarily, if the critical mean free path is locally exceeded, the vapor transport regime passes from viscous flow to Knudsen diffusion. At the same time, the heat transfer is affected by the local ratio of pore space to the solid skeleton. The impact of the pore size distribution on the transitional vapor and heat transfer can be studied by pore scale models such as the pore network model. As a first approach, we present a pore network model with vapor transport in the transitional regime between Knudsen diffusion and viscous flow at constant temperature in the dry region. We demonstrate the impact of pore size distribution, temperature and pressure on the vapor transport regimes. Then we study on the example of a 2D square lattice, how the presence of micro and macro pores affects the macroscopic progression of the sublimation front.

Keywords: pore size distribution; transitional vapor transport; pore network model; fractured sublimation front.

1. Introduction

Primary lyphilization, or freeze drying, is a coupled process of heat and mass transfer through frozen matter, which is usually a block of a frozen solution or a packing of frozen particles, e.g. [1]. The heat of sublimation is usually provided by contact of the frozen material to a shelf with higher temperature and by radiation. The heat transfer from the shelf to the sublimation front, at lower temperature (usually saturation temperature is anticipated at the sublimation front), occurs mainly by heat conduction through the ice phase, if the thermal condutivity of the solid is assumed to be low (usually $\lambda_{ice} \, \square \, \lambda_{solid}$). It is thus plausible that the local distribution of solid and ice phase significantly affects the transport of heat. Especially in case of a strongly heterogeneous distribution of solid and ice, the heat transfer rate can vary locally and affect the structure of the sublimation front. Similarly, vapor transport from the sublimation front to the surface of the frozen material is affected by the distribution of solid and pores, which emerge from sublimation of the ice phase. It is basically expected that more vapor can be transported through larger pores while the occurrence of smaller pores results in the deceleration of drying, e.g. [2]. From this it can be concluded that the drying process might be optimized in terms of drying time and capacity of the dryer based on the control of the distribution of ice crystal sizes (in regard of heat transfer through the ice saturated region of the frozen material) and the distribution of pore sizes (in regard of vapor transfer through already dry regions). For this reason, frozen solutions are foamed to obtain a heterogeneous distribution of pores [3]. Foamed frozen matter is characterized by smaller pores which are saturated with ice at the start of drying and larger unsaturated pores which result from the admixion of gas to the liquid solution before and during the first stage of freezing. As shown in [3] by experiments with a frozen aqueous solution of mannitol stabilized by a mixture of skim milk and sodium carboxymethylcellulose, drying can be much faster using this method, because the transport of vapor is positively affected in presence of the large pores.

It will be discussed in this paper that the simulation of vapor transport through a heterogeneous porous medium of interconnecting and interpenetrating large and small pores, such as in the experiment of [3], represents a special situation in which traditional model approaches or empirical models might rather be substituted by pore network models. The motivation behind that, is the assumption of a transitional vapor transport regime between Knudsen diffusion (in smaller pores) and viscous flow (in larger pores), which cannot be captured by the traditional continuous models or empirical approaches, which essentially blur the different transport properties into effective parameters. Basically, different flow regimes, i.e. either based on a gradient in total pressure (viscous flow) [4] or based on a gradient in vapor pressure (Knudsen diffusion) [5-9] underly the classical models of freeze drying. The distinction between the different flow regimes is generally based on the Knudsen-number,

$$Kn = \frac{\Lambda}{d} \, ,\tag{1}$$

with pore diameter d and the mean free path of the diffusing molecules

$$\Lambda = \frac{\mu}{P}\sqrt{\frac{\pi \tilde{R} T}{2}} \, .\tag{2}$$

In Eq. (2) μ denotes the dynamic vapor viscosity in Pa s^{-1}, P the pressure in Pa, $\tilde{R}$ the ideal gas constant in J kmol^{-1} K^{-1} and T the temperature in K.

Continuum flow (i.e. Darcy flow with no-slip conditions) is expected for $Kn < 0.001$, while slip flow is expected for $0.001 < Kn < 0.1$. Molecular (Knudsen) flow, based on a concentration gradient of the diffusing substance, occurs for $Kn > 10$, e.g. [10]. In the transitional range between $Kn > 0.1$ and $Kn < 10$, neither the Darcy equation of viscous flow ($\dot{m}_v = -(\rho k / \mu) \nabla P$) nor the molecular flow equation ($\dot{m}_v = -D_{Kn}(\tilde{M}/\tilde{R}T)\nabla P_v$) can provide an exact approach. However, in many situations this range is relevant for freeze drying because of the occurrence of very low pressures, i.e. highly diluted gases. In this range, the approach e.g. presented in [10] can be applied. This is further elaborated in the following section in conjunction with the pore network model.

2. Pore network model

The pore network model is based on the concepts e.g. given in [11]. In the simplest case, the porous medium can be represented by a square lattice of pores and throats of varying width and length. Here, we present the results from drying of a pore network with 50x51 pores (4949 throats) of length $L = 100$ µm and with the pore size distribution given in Fig. 1. Note the bimodal distribution of pore sizes, i.e. the presence of pores with smaller radius (peak in Fig. 1) and the tailing of the curve to throats with greater radius (similar as in experiments discussed in [2]). The pores are arranged in a way, that the radii of vertical throats and the pores in every fifth vertical column (i.e. columns [1, 6 11, 16, 21, 26, 31, 36, 41, 46, 51] as indicated by the inlet of the figure) are three times larger than the remaining throats and pores.
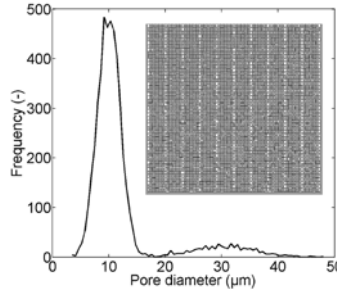
Fig.1 Pore size distribution of the investigated 2D pore network. Note the tailing of the curve towards greater radii (i.e bimdodal pore size distribution).

The simulation is realized with constant temperature $T^* = T = $ -38°C and pressure inside the drying chamber $P_v^\infty = P = $ 10 Pa. The parameters of water are $\tilde{M}_v = $ 18.02 kg kmol^{-1} (molar mass), ice density $\rho_{ice} = $ 918 kg m^{-3} and dynamic viscosity of the vapor phase $\mu_v = $ 2.5 · 10^{-6} Pa s^{-1}. The equilibrium vapor pressure is computed from

$$log_{10} P_v^* (mbar) = a \cdot (T_0 / T(K) - 1) + b \cdot log_{10} (T_0 / T(K)) + c \cdot (1 - T_0 / T(K))$$
$$+ log_{10} (P_{v,0}^*) \quad , \quad (3)$$

with $T_0 = $ 273.15 K, $P_{v,0}^* = $ 6.1071 mbar and $a = $ -9.09718, $b = $ -3.56654, $c = $ 0.876793. [12]. It is $P_v^* (T^* = -38°C) = $ 16.0580 Pa.

Computation of vapor transport through the dry zone of the pore network (white throats and pores in Fig. 3 below) follows the semi-empirical approach proposed e.g. in [10] based on the works of Knudsen. The mass flow rate is given by

$$\dot{M}_v (kg \ s^{-1}) = -KA \frac{\tilde{M}_v}{\tilde{R}T} \frac{\Delta P}{L} , \quad (4)$$

with cross sectional area A in m^2, pressure gradient between two neighbor pores ΔP in Pa and throat length L in m. The transport coefficient K is computed from

$$K (m^2 s^{-1}) = \frac{d^2 P}{32 \mu} (1 + 8.88 Kn + 4.96 Kn^2) \quad (5)$$

[10] and Kn from Eq. (1). Each term in Eq. (5) can be related to the contribution of the different flow regimes: the first term of Eq. (5) represents the contribution of Poisseuille flow, the second term of slip flow and the third term of Knudsen flow. Note that the

calculation of K is an iterative problem if it is assumed that $P = P_v$, i.e. the total pressure gradient is equal to the vapor pressure gradient. Then pressure varies with position x (also refer to Fig. 3) and K varies accordingly (Eq. (5)).

Figure 2 shows the dependency of K on pore sizes in the range between $r = 1$ µm and $r = 1$ mm with pressure and temperature as in the pore network simulation (Fig. 2a) and for constant pore radii $r = 10$ µm and varying ratio T/P (Fig. 2b). As can be seen, Knudsen flow dominates as long as pore radii are smaller than approximately 10 µm; however for radii $r > 10$ µm slip flow and Poisseuille flow become increasingly important (Fig. 2a). In the range between $r = 1$ µm and $r = 25$ µm (Fig. 1), K increases almost linearly by about 32 %. A similar picture is drawn for constant radius, $r = 10$ µm: In the range $0.01 < T/P < 100$ K Pa^{-1} transitional flow occurs if pressure varies between ~ 2 Pa and ~235 hPa, leading to a global minimum at $T/P \cong 0.48$ K Pa^{-1} (given $T = -38°C$).

a)   b)
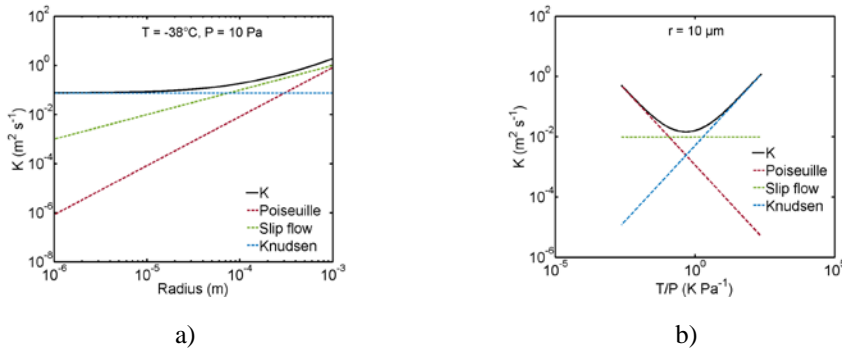
Fig. 2 Contribution of flow regimes to vapor transport a) for constant temperature and pressure and b) for constant radius.

The pore network simulation is started from an initially fully saturated network. The vapor pressure field is computed from the boundary conditions of each pore [11] and the vapor flow rate between two pores is computed from Eq. (4). The sublimation rate from ice saturated pores and throats at the sublimation front is then calculated from

$$\dot{M}_{sub} = -\dot{M}_v. \qquad (6)$$

The vapor pressure field as well as the transport parameters (essentially K) are updated after the complete emptying of either a throat or a pore.

3. Simulation Results

Figure 3 shows the distribution of ice phase and dry solid phase resulting from a pore network simulation realized with the parameters specified above. Most striking is the structure of the sublimation front evolving in the pore network with bimodal pore size distribution (Fig. 1). Obviously, in the transitional regime vapor flow through larger pores (in every 5th column) is accelerated compared to the flow through smaller pores (in the neighbourhood). This leads to the erosion of the sublimation front and faster progression of the gas phase in pores with greater diameter.
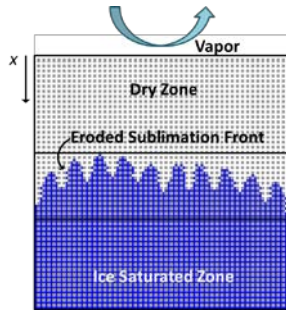
Fig. 3 Freeze drying of a 2D pore network. The ice phase appears in blue, empty pores in white and the solid in gray. Vapor escapes from the top edge.

Figure 4a shows the least advanced position of the sublimation front (measured from the open side of the pore network) as a function of the total ice saturation, i.e. the sublimation front velocity. As can be seen, the macroscopic velocity of the sublimation front is approximately constant in this representation. However, the saturation profiles in Fig. 4b indicate that the front is significantly broadening with progressive invasion of the pore network. This is a result of the assumption of transitional flow in a pore network with bimodal pore structure (Fig. 1) and the higher vapor transport rates in pores with greater radius which allow for higher sublimation rates according to Eq. (6). This is in agreement with experimental results reported in [2]. Furthermore, as indicated by the dashed lines in Fig. 4b, the slice averaged relative humidity, $\varphi = P_v / P_v^* \left(T^* \right)$, is approximately $\varphi = 1$ in the region of the fractured front and decreases only slightly towards the network surface due to the low spread of vapor pressures ($\Delta P = P_v^* - P_v^\infty$). This shall further be elucidated in future research related to collapse phenomena, e.g. [13].

a)   b)
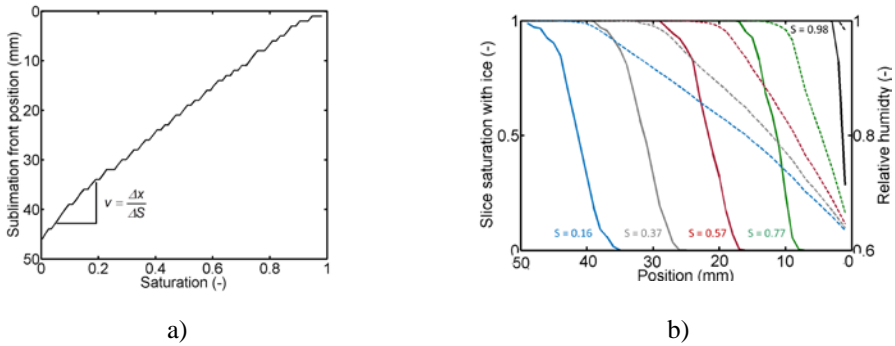
Fig. 4 Analysis of drying kinetics and sublimation front structure: a) sublimation front velocity in terms of $\Delta x/\Delta S$, b) slice average saturation profiles (solid lines) and relative humidity (dashed lines) for different overall network saturations S with ice phase.

4. Summary and outlook

We have presented the results of a pore network simulation of freeze drying applying a bimodal structure of the pore space. It could be shown that in the transitional regime between molecular diffusion and viscous flow, drying can be accelerated due to the presence of macro pores. The interpretation of this outcome is twofold: on the one hand, drying performance can be positively affected by pore design (i.e. in terms of drying time and capacity), on the other hand, higher demands are imposed on process control if the occurance of material collapse is associated with the local drying rate or rather the spatial variation of the velocity of the sublimation front. We thus aim to study in more detail in a future work freeze drying in the transitional regime by 2D and 3D pore network models with different structures of the pore space.

5. References

[1] Liapis, A.I.; Bruttini, R. A mathematical model for the spray freeze drying process: The drying of frozen particles in trays and in vials on trays. International Journal of Heat and Mass Transfer 2009, 52, 100–111.

[2] Foerst, P.; Lechner, M.; Vorhauer, N.; Schuchmann, H.; Tsotsas, E. Experimental investigation on pore size distribution and drying kinetics druing lyophilization of sugar solutions. In Proceedings of 21st International Drying Symposium, Valencia, Spain, September 11–14, 2018.

[3] Wang, W.; Hu, D.; Pan, Y.; Zhao, Y.; Chen, G. Freeze-drying of aqueous solution frozen with prebuilt pores. AIChE Journal 2015, 61 (6), 2048-2057.

[4] Liapis, A.I.; Bruttini, R. Freeze Drying. In: Handbook of Industrial Drying, Mujumdar, A.S., Ed.; CRC Press, Taylor and Francis Group, Boca Raton, 2015, 259-282.

[5] Hottot, A.; Vessot, S.; Andrieu, J. A direct characterization method of the ice morphology. Relationship between mean crystals size and primary drying times of freeze drying processes. Drying Technology 2004, 22 (8), 2009-2021.

[6] Rasetto, V.; Marchisio, D.L.; Fissore, D.; Barresi, A.A. On the use of a dual-scale model to improve understanding of a pharmaceutical freeze-drying process. Journal of Pharmaceutical Sciences 2010, 99 (10), 4337-4350.

[7] Raman, P.; Rielly, C.D.; Stapley, A.G.F. Freeze drying microscopy as a tool to study the sublimation kinetics of a freeze drying process. In: In Proceedings of 19th International Drying Symposium, Lyon, France, August 24–27, 2014.

[8] Chitu, T.; Vessot, S.; Peczalsky, R.; Andrieu, J.; Woinet, B.; Francon, A. Influence of operating conditions on the freeze-drying of frozen particles in a fixed bed and modeling data. Drying Technology 2015, 3, 1892-1898.

[9] Trelea, I.C.; Passot, S.; Marin, M.; Fonseca, F. Model for heat and mass transfer in freeze drying of pellets. Journal of Biomechanical Engineering 2009, 131, 074501-1.

[10] Zarekar, S.; Bück, A.; Jacob, M.; Tsotsas, E. Reconsideration of the hydrodynamic behavior of fluidized beds operated under reduced pressure. Powder Technology 2016, 287, 169-176.

[11] Metzger, T.; Tsotsas, E.; Prat, M. Pore-network models: A powerful tool to study drying at the pore level and understand the influence of structure on drying kinetics. In: Modern Drying Technology, Vol. 1: Computational Tools at Different Scales; Tsotsas, E., Mujumdar A.S., Eds.; Wiley-VCH: Weinheim, 2007, 57–102.

[12] Goff, J.A.; Gratch, S. Low-pressure properties of water from -160° to 212°F. Trans. Amer. Soc. Heat Vent. Eng. 1946, 52, 95-121.

[13] Meister, E.; Gieseler, H. Freeze-dry microscopy of protein/sugar mixtures: Drying behavior, interpretation of collapse temperatures and a comparison to corresponding glass transition data. J. Pharm. Sci. 2008, 98, 3072-3087.

Moisture diffusion coefficient estimation in peas drying by means of a modified Hawlader and Uddin method

Martínez-Vera, C.*; Vizcarra-Mendoza, M. G.

Departamento de Ingeniería de Procesos e Hidráulica, Universidad Autónoma Metropolitana-Iztapalapa. Apartado Postal 55-534, México D.F., 09340, México.

*E-mail of the corresponding author: cmv@xanum.uam.mx

Abstract

The aim of the present work is to determine the moisture diffusion coefficient in peas applying, in a first step, a methodology previously published in the literature by Uddin et al.[1] for determining constant diffusion coefficients taking in account the volume reduction associated to the drying process. Then, in a second step, refine it by means of an optimization step. The optimization step is justified because the methodology of Uddin et al. is based in a solution of the diffusion equation that is not mathematically valid for the drying-shrinking problem.

Keywords: : moisture diffusivity; drying-shrinking; peas drying.

1. Introduction

Usually bio-products such as fruits and vegetables have high initial moisture content and present appreciable volume shrinkage during the drying process. Shrinkage of biological materials takes place simultaneously with moisture diffusion during drying and thus may affect the drying rate. It is important to take into account the shrinking phenomena when determining the moisture diffusion coefficients. When this phenomenon is not negligible there are not analytical solutions available for the equations describing this moisture diffusion process. In these cases changes in radius should be taken into consideration when predicting moisture profiles and, also when estimating diffusion coefficients. Not taking into account volume shrinkage leads to over-estimated diffusion coefficients (Xianxi et al.[2]; Guohong et al.[3]).

A simple method for determining diffusion coefficients taking into account the variation in radius was proposed by Uddin et al.[1]. It is based on a modification to the one term truncated infinity series solution that takes into account the reduction in radius. Examples of its application to drying can be found in Hawlader et al.[4], Giovanelli et al.[5], García et al.[6], Martínez et al.[7, 8].

The aim of the present work is to determine the moisture diffusion coefficient in peas applying, in a first step, the methodology previously published in the literature by Uddin et al.[1] for determining constant diffusion coefficients taking into account the volume reduction associated to the drying process. Then, in a second step, the diffusivity values are adjusted in order to satisfy a more rigorous model of the drying-shrinking problema by means of an optimization procedure. The optimization step is justified because the methodology of Uddin et al. is based on a solution of the diffusion equation that is not valid for drying-shrinking problems. Finally, in a third step, by means of another optimization step, the model of the shrinking phenomena is improved.

2. Materials and Methods

2.1. Uddin methodology

Mass transfer processes are commonly described by the second Fick's law, the phenomenological parameter in this equation is the mass diffusion coefficient. Analytical solutions to the diffusion equation for mass transfer in solids are available for some cases under certain assumptions among which could be mentioned constant volume and constant diffusivity. In particular, for unidirectional mass transfer in slabs or spheres with a symmetry boundary condition at the centre and a Dirichlet boundary condition at the external border, with uniform initial diffusant content, these solutions are given in the form of infinite Fourier series and are the departing point for the determination of constant moisture diffusion coefficients at a constant temperature from the truncated to just one term or at most to a few terms of the series when volume shrinkage is not relevant. A method presented in the literature for determining diffusion coefficients taking into account the radius variation was proposed by Uddin et al.[1]. It is based on a modification of the one term truncated infinity series solution to take into account the reduction in radius.

In the Uddin et al. methodology the moving boundary condition is introduced a posteriori in the solution for the fixed boundary condition. As signalled properly by Hawlader et al.[4] this approach is a simplified one and the diffusivity coefficient determined by his method can be considered an effective diffusivity. However, the methodology provides an effective diffusion coefficient of the specimen under given drying conditions which is valid for the assumed model.

The Uddin et al. approach departs from an approximated solution to the moisture transfer in the solid when the shrinkage is neglected. The analogous equations for spherical coordinates analogus to those presented by Uddin et al. for a slab are :

$$Ln\left(\frac{c}{c_0}\right) = Ln\left(\frac{6}{\pi^2}\right) - \frac{\pi^2\,D\,t}{R^2} \tag{1}$$

Where c indicates de volumetric moisture concentration (kg/m^3), c_{eq} the equilibrium moisture content, c_0 the initial moisture content, R the particle radius (m) Then D, the moisture diffusion coefficient, could be obtained from the slope of a plot of $Ln(\omega/\omega_0)$ versus t or t/R^2 for those cases in which the shrinkage is negligible. For those cases for which this condition is not sustainable the proposed methodology proceeds as follows. The reduced radius R' at time t was related to the moisture content at each time instant by the following equation:

$$\frac{R'}{R} = \left(\frac{\omega_t}{\omega_0}\right)^n \tag{2}$$

Where R_0 is the radius at the initial time, R' is the reduced radius, ω_0 is the initial moisture content (kg water/kg dry mass) and ω_t is the moisture content at time t. n is an exponent to be found which makes that the plot of $Ln(\omega/\omega_0)$ versus t/R'^2 results in almost a straight line. A value of n equal 0 means there is not shrinkage and a value of $n=1$ would indicate that the reduction in volume is equal to the volume of the water transferred to the air.

In the present work we start with the diffusion coefficients obtained with the Uddin et al. approach. In the second step the drying process is posed, as a direct moving boundary problem in which the diffusion coefficient is assumed as known and with experimental radius-time data. The model (given below) is numerically solved, the average moisture concentration at each integration time step is obtained and the average moisture content profile is compared with the experimental results. If the difference between the experimental and the predicted profile is beyond certain tolerance according to a predefined norm the diffusion coefficient is improved through an optimization algorithm until the desired tolerance is satisfied. The model is implemented in the software Berkeley Madonna discretizing the spatial variable of the distributed parameter model by finite differences and integrating the set of ordinary differential equation with one of the integration methods available in the software. The optimization step is carried on by means of the optimization algorithm with which Berkeley Madonna is provided with experimental radius-time data. The optimization procedure is carried on taking as objective function the minimization of the difference between the predicted moisture content and the experimental one at the time for which this difference is higher. After finding the optimal diffusion with experimental radius-time data, in the third step, by means of another optimization procedure, the model of the shrinking phenomena is improved taking as objective function the minimization of

the difference between the predicted radius and the experimental one at the time for which this difference is higher.

2.2. Model of the drying process considering shrinkage

Assuming that the drying process is described by the diffusion equation, considering that the concentration is a function of volume and time, that the volume is as well a function of time and, after transforming the moving boundary problem into a fixed boundary problem by means of a change of variable ($z=r/R$) in order to have variations of the dimensionless spatial variable between 0 and 1 (Crank[10]), the following equation is obtained:

$$\frac{dc}{dt} = \frac{1}{(z \cdot R)^2} \frac{\partial}{\partial z}\left(z^2 \cdot D \frac{\partial c}{\partial z}\right) + \frac{1}{R}\frac{\partial c}{\partial z} z \frac{dR}{dt} \qquad 0 \leq z < 1,\ t > 0 \tag{3a}$$

where r denotes the radial distance from the centre of the sphere (m).The consideration of a spherical particle leads to a symmetry condition at the centre of it:

$$\frac{\partial c}{\partial z} = 0 \quad z = 0, \forall\, t \tag{3b}$$

An equilibrium condition is assumed at the solid-gas interface:

$$c = c_{eq} \quad z = 1, \forall\, t \tag{3c}$$

A uniform moisture content profile inside the solid is assumed at the initial time:

$$c = c_0 \quad 0 \leq z < 1,\ t = 0 \tag{3d}$$

Assuming that the solid´s volume reduction is proportional to the volume of water lost by it (Aguerre et al.[11]), the following equation gives the shrinking rate

$$\frac{dR}{dt} = -\frac{\beta\, D}{\rho_w R}\left[\frac{\partial c}{\partial z}\right]_{z=1} \tag{3e}$$

Where β is a proportionality constant introduced in order to fit the model predictions with the experimental data to be found. The initial condition for this equation is:

$$R = R_0\,, \quad t = 0 \tag{3f}$$

The average volumetric moisture concentration $\bar{c}(t)$ is given by

$$\bar{c}(t) = \frac{1}{V_p}\int_0^{V_p} c(r,t)\,dv \tag{4}$$

In order to solve the above equations when the diffusion coefficient is assumed to be known, the spatial variable is discretized by finite differences leading to a set of ordinary differential equations which are integrated with a proper method for stiff equations.

3. Results and discussion

This work departs from experimental data obtained in a small scale batch fluidized bed drier for drying of peas (Gómez et al.[12]). Peas were dried at three different temperature levels of the air fed to the drier: 50, 60 and 70 °C. The moisture content and the diameter of the peas were recorded along the drying time. These data were fitted by analytical expressions in order to have available the moisture content and the diameter at each time instant during the drying process.

Table 1. *Diffusion coefficient and adjusted exponent in eq. (2) obtained with the* **Uddin** *method.*

T [°C]	n	D_{ef} x10^8 [m^2s^{-1}]
40	0.75	3.04
50	0.55	4.053
60	0.55	3.04
70	0.45	1.013

The effective moisture diffusion coefficients of peas dried at each one of the temperature levels at which the experiments were carried on were determined applying the methodology proposed by Uddin et al. described above. The values obtained are presented in Table 1 (Martínez et al.[8]). Posteriorly, the constant values obtained were tested in the more rigorous model of the drying process represented by equations (3a-3d and 4). These equations were solved discretizing the spatial variable (radius) by finite differences and the set of ordinary differential equations were integrated together with the boundary conditions by means of an integration method proper for stiff equations. In these simulations the experimental radius values corresponding to each integration time step were provided by the corresponding fitted expression to the radius-time experimental values. These values ofthe diffusion coefficients, as expected, led to poor predictions of the moisture evolution as shown by the dashed lines in Figs. 1, 2 and 3 which can be compared with the solid ones which represent the experimental values. The diffusion coefficients obtained are between $1x10^{-8}$ and $4x10^{-8}$ m^2s^{-1}.
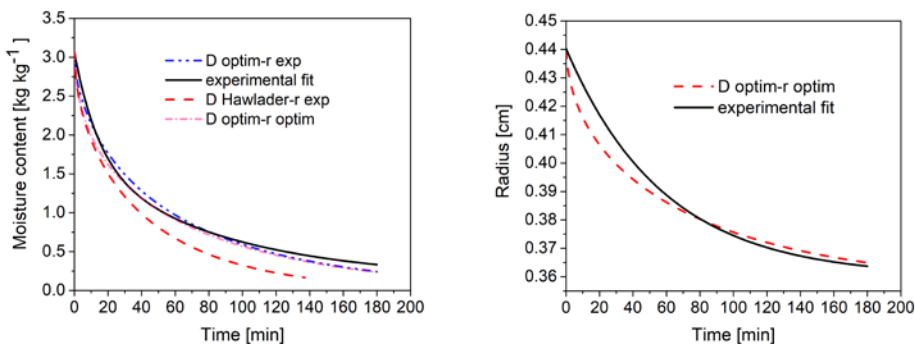
Fig. 1. Moisture content profiles and experimental and predicted radius profiles at inlet air temperature of 50° C.

In a second step the diffusion coefficients were improved in order to give a better agreement with the experimental moisture content profiles when the model given by equations (3a-3d and 4) was employed. This was done by an optimization procedure utilizing the optimization tool included in the software Berkeley Madonna. In this optimization step the experimental radius values given by the radius-time fitted expression were employed. The objective function to be minimized was the absolute value of the difference between the moisture content experimental value and the predicted one at each integration time step. The variable to be optimized was the effective diffusion coefficient. The profiles obtained with the optimized values in the rigorous model but still with the experimental radius values are shown in figures 1, 2 and 3 by the dash-dot-dot-dash lines. The improvement in the agreement between the experimental moisture content profile and the predicted by the simulations can easily be appreciated.
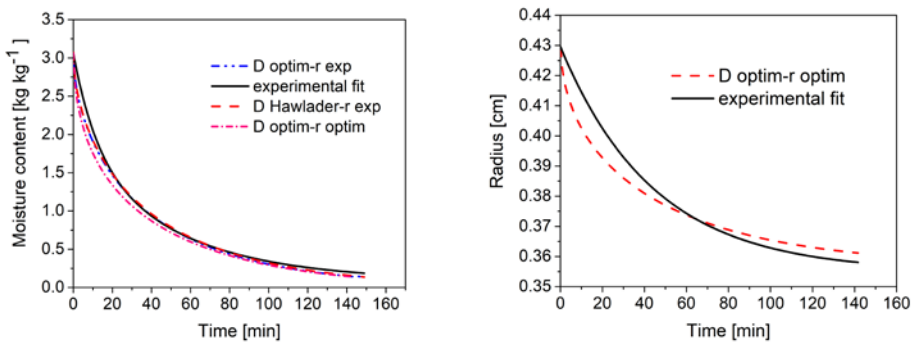
Fig. 2 Moisture content profiles and experimental and predicted radius profiles at inlet air temperature of 60 °C.

However, even though the moisture content predictions were quite acceptable, the radius evolution predictions given by equations (3e-3f) were quite poor. Therefore, a third step was carried on in order to improve the particle size predictions. This was done through a second optimization step with the optimization algorithm included in the software Berkeley Madonna in which the variable to be optimized was the parameter β introduced in equation (3e). The objective function to be minimized was the absolut value of the difference between the experimental radius and the predicted one at the time in which this difference was bigger before the optimization. The results in the moisture content are shown in figures 1, 3 and 5 by the short dash-dot-short dash lines. It can be appreciated that the predictions of the moisture content profiles employing the experimental radius values and those obtained with radius values given by the model does not differ appreciably. The radius profiles obtained with equations (3a-3f and 4) and the experimental ones are shown, for each temperature level considered in this work, in figures 1, 2 and 3. It can be seen that, even though, the particle size predictions are not as good as the moisture content predictions, they are acceptable.
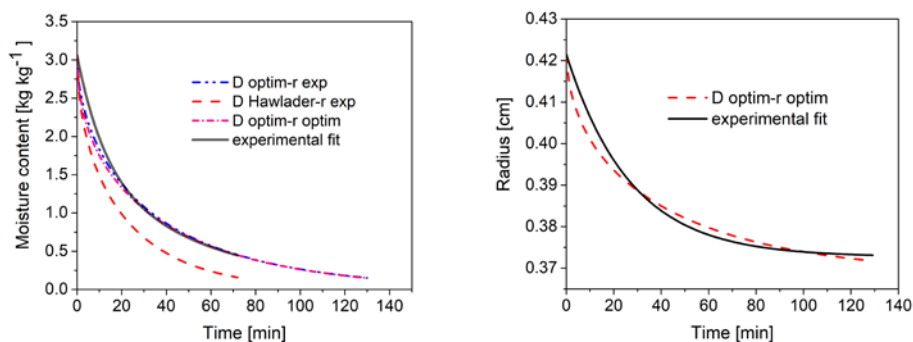
Fig. 5 Moisture content profiles and experimental and predicted radius profiles at inlet air temperature of 70° C.

4. Conclusions

A methodology proposed by Udin and Hawlader for the determination of moisture diffusion coefficients taking into account the shrinkage of the stuff being dried that is easily applied provides diffusivity values that are taken as first guesses of an optimization procedure under a more rigorous model. Having obtained the optimal moisture diffusion coefficients employing the experimental radius evolution data a second optimization step is carried on in order to obtain an acceptable prediction of the radius evolution. The results obtained shows a very good agreement with the experimental moisture content evolution at the three temperature levels analysed and an acceptable agreement with the experimental radius evolution.

References

[1] Uddin M. S.; Hawlader M. N. A.; Rahman S. Evaluation of Drying Characteristics of Pineapple in the production of pineapple powder. Journal of Food Processing and Preservation 1990, 14, 375–391.

[2] Xianxi Liu; Junruo Chen; Meihong Liu; Ziliang Li; Yifei Tao; Daigen Zhu. (2010), The Effect of Biological Material's Tissue Shrinking on Moisture Diffusivity during Hot-air-drying. In Proceedings of the World Automation Congress, Kobe, Japan, 2010; 255-260.

[3] Guohong Liu; Junruo Chen; Meihong Liu; Xinxin Wan. Shrinkage, porosity and density behavior during convective drying of bio-porous material. Procedia Engineering 2012, 31, 634-640.

[4] Hawlader M. N. A.; Uddin M. S.; Ho J. C.; Teng A. B. W. Drying Characteristics of Tomatoes. Journal of Food Engineering 1991, 14, 259-268.

[5] Giovanelli G.; Zanoni B.; Lavelli V.; Nani R. Water Sorption, drying and antioxidant properties of dried tomato products. Journal of Food Engineering 2002, 52, 135-141.

[6]   García-Hernández A., M. Vizcarra-Mendoza, C. Martínez-Vera, H. Vázquez-Torres. Thin Layer Drying of Tomato Cubes in a Dryer Tunnel. In Proceedings of the Sixth Nordic Drying Conference, Copenhague, Denmark, June 5-7, 2013.

[7]   Martínez Vera, C.; Anaya Sosa, I.; Vizcarra Mendoza, M. G. Diffusion Coefficient Estimation in Shrinking Solids. A Case Study: Tomato. American Journal of Food Science and Technology 2015, 5 (3), 132-136.

[8]   Martínez Vera C.; Vizcarra Mendoza, M.G.; Samperio Domínguez, L. A. ; Gómez Rojas, H. M. Concentration dependent diffusion coefficient estimation in peas and cranberries drying considering shrinkage: an observer approach. In Proceedings of the Second Nordic Baltic Drying Conference. Hamburg, Germany, June 7-9, 2017.

[9]   Crank, J. The Mathematics of Diffusion (2nd ed.); Oxford University Press: 1975.

[10]   Aguerre R. J.; Tolaba M.; Suárez C. Modeling volume changes in food drying and hydration, Latin American Applied Research 2008, 38, 345-349.

[11]   Gómez Rojas, H. M.; Arredondo Bote, G. M.; Mar Antonio, S. I. , México, 2016.Desarrollo de un proceso para producir chicharos secos para su comercialización y conservación. B.Ch.E. Thesis. Universidad Autónoma Metropolitana.

New model for the rehydration characteristics of white yam at different temperatures

Akinola, A. A.[*]; Ezeorah, S. N.; Nwoko, E. P.

[a] Department of Chemical and Petroleum Engineering, University of Lagos, Lagos, Nigeria.

*E-mail of the corresponding author: akinjideakinola@gmail.com

Abstract

A new model describing the variation in the rehydration ratio with rehydration time for yam slices is presented here. Also presented, is a new model for the rehydration kinetics of yam slices. Mass and moisture content rehydration data were collected while rehydrating 3.0 mm thick dehydrated yam slices. Regression analysis established that the mass rehydration data better fitted a two-term exponential equation rather than a second-order polynomial equation. Also, for the rehydration kinetics, the moisture content rehydration data was better fitted to a new empirical model rather than the Weibull, Peleg, and Exponential models.

Keywords: Rehydration Ratio Models; Rehydration kinetic models; Yam; Weibull, Peleg, and Exponential models.

1. Introduction

White yams *(Dioscorea rotundata)* are very nutritious and are an excellent source of energy and dietary fiber [1,2,3,4,5,6]. Yams are eaten routinely and they constitute a dominant portion of the standard diet for many people. They are used, worldwide, in many different recipes. For this reason, there is a need for these commodities to be transported to the many locations where they are consumed. However, they are heavy, constituting of at least 70% water. Dehydrating yams like most foods and agricultural products are becoming an essential method of processing before being shipped to where they will be consumed. Dehydration is also performed for preservation purposes.

The dependence of many dehydrated food and agricultural commodities in the present marketplace is increasing as this is a means of extending the length of time that the products may be stored without becoming unfit for future use. Rehydration operations, therefore, are gaining importance as these dried products will need to be rehydrated before use. There is, therefore, need to understand the issues relating rehydration operations concerning the design and the operations of these processes.

Mathematical modeling has been useful in the study, design, optimization, and operations of these rehydration processes [7, 8]. This study involves investigating the rehydration kinetics and estimating other rehydration characteristics of the dehydrated products.

The models that have been used to study the rehydration characteristics of foods are the Peleg model [9], the Weibull distribution model [10, 11, 12] and the exponential model [9, 13]. However, for accurate use of these models, more knowledge, in addition to the rehydration data and knowledge of some physical parameter(s) of the product being studied, is required. For the Peleg, [14], Weibull distribution and Exponential models knowledge of the initial moisture content before rehydration is required. For the Exponential model, the equilibrium moisture content also, needs to be known; and for the Weibull model, knowledge of scale and shape parameters of the samples are required [15]. Presented in this study is a new rehydration model for yam that requires only the moisture content rehydration data, and a comparison of all the four (4) rehydration models are performed.

2. Materials and Methods

2.1 Sample Preparation

White yam tubers acquired from the local market were washed, peeled, cut into 3 mm thick slices. The slices were dried in a Refractance Window™ dryer until the moisture content was about 0.03g-water/g-solid. The dehydrated samples were kept in air-tight polyethylene bags and stored in a refrigerator until further use in the rehydration experiments.

2.2 Rehydration experiments

The dried samples were brought to room temperature before starting the rehydration experiments. Rehydration of the samples was done in 250-mL beakers filled with distilled water. The beakers were immesed in a thermostatically controlled water bath, and each set of experiments was performed at 27 ºC, 40 ºC, 60 ºC and 80ºC ($\pm$0.5ºC). Approximately 3.75 $\pm$ 0.25g was immersed in 100 ml of distilled water for periods of 10, 20, 30, 40, 50,

60, 80, 100, 120, 150, 180, 210 and 240 minutes. The temperature of the water inside the beakers was determimed with a thermocouple. A perforated plexiglass cup was used to cover the samples to ensure they were entirely immersed in the water in the beakers during rehydration. After rehydration, the water was drained from the flask, and excess water on the samples was removed using tissue paper. The samples were then weighed. The moisture content of the samples was determined using an OHAUS moisture analyser [16]. Every experiment was done in triplicate.

2.3 Modelling The rehydration ratio

The rehydration ratio (RR) was calculated according to equation 1.

$$RR = W_t/W_o \qquad\qquad 1$$

where W_t is the mass of rehydrated sample at time t and W_o is the initial mass of sample to be rehydrated.

The rehydration ratios and rehydration times were correlated first according to the two term exponential equation of the form given in equation 2 and then with the second order polynomial equation of the form given in equation 3 [17].

$$RR = = p_1*exp(p_2*t) + p_3*exp(p_4*t) \qquad\qquad 2$$

where p_1, p_2, p_3, and p_4, are constants observed from regression analysis and t is the rehydration time in minutes.

$$RR = p_5*t^2 + p_6*t + p_7 \qquad\qquad 3$$

where p_5, p_6, and p_7, are constants observed from regression analysis and t is the rehydration time in minutes.

2.4 Modelling The rehydration data

The experimental rehydration kinetics data were fitted to the equations 4, 5, 6 and 7 to determine the model that best describes the rehydration kinetics of the yam slices.

Peleg $\qquad\qquad M_t = M_o + (t/(a+bt)) \qquad\qquad 4$

Weibull $\qquad\qquad M_t = M_o [1 - exp(-(t/\alpha)^\beta)] \qquad\qquad 5$

Exponential $\qquad\qquad \boldsymbol{M_t = (M_0 - M_e)\exp(ct^d) + M_e} \qquad\qquad 6$

New Model $\qquad\qquad M_t = g\ exp(h\ t) + j\ exp(q\ t) \qquad\qquad 7$

where M_t is the moisture contents at time t, M_o is the initial moisture content, M_e is the equilibrium moisture content, and α, β, a, b, c, d, g ,h, j, and q are constants observed from regression analysis

For quality fit, the coefficient of determination (R^2), should be closest to unity while the sum of square-error (SSE), and the root-mean-square-error (RMSE) should closest to zero. The methods of estimating R^2, SSE and RMSE are discussed extensively in the literature [18, 19]. In this work, the software package from Matrix Laboratory (MATLAB) was used to perform the statistical analysis.

3. RESULTS AND DISCUSSIONS

3.1 Evaluation of the Rehydration Ratio models

Four sets of rehydration experiments were performed at rehydration water temperatures of 27, 40, 60, and 80ºC. The rehydration ratio at each rehydration time was calculated according to equation 1 using the weight data obtained during the rehydration experiments. Table 1 presents the statistical parameters when the rehydration ratios were correlated with rehydration time according to equations of the form given in equation 2 and 3. Table 1 clearly indicates that the two-term exponential model fits the rehydration ratio vs. time data better than the polynomial model. For the two-term exponential equation form, the R^2 values were closer to unity and the SSE and RMSE values were closer to zero than the polynomial equation form. Table 2 shows the constants obtained with a 95% confidence bound, by fitting the rehydration ratio data to the exponential equation form presented in equation 2.

Table 1 Statistical Parameters for Yam when correlating Rehydration Ratios with Rehydration Time at different temperature

		Exponential Equation Form			Polynomial Equation Form		
S/N	Water Temp.	R2	RMSE	SSE	R2	RMSE	SSE
1	27ºC	0.9966	0.0180	0.0032	0.9245	0.0808	0.0719
2	40ºC	0.9860	0.0311	0.0097	0.9447	0.0591	0.0384
3	60ºC	0.903	0.0214	0.0046	0.9420	0.0501	0.0276
4	80ºC	0.9864	0.0317	0.0100	0.9803	0.0364	0.0146

Table 2 Constants For The Models Obtained By Fitting Rehydration Data The Exponential Equations and Polynomial Model For Yam Slices

S/N	Temp.	Exponential Model Constants	Polynomial Model Constants
1	27ºC	$p_1 = 1.921 \pm 0.052$ $p_2 = 0.000752 \pm 0.00015315$ $p_3 = -0.8875 \pm 0.09005$ $p_4 = -0.04318 \pm 0.00888$	$p_5 = -2.041e\text{-}05 \pm 1.07E\text{-}05$ $p_6 = 0.00813 \pm 0.002628$ $p_7 = 1.45 \pm 0.1255$
2	40ºC	$p_1 = 2.077 \pm 0.114$ $p_2 = 0.0006457 \pm 0.0002971$ $p_3 = -0.6219 \pm 0.13385$ $p_4 = -0.03468 \pm 0.017725$	$p_5 = -1.543e\text{-}05 \pm 7.80E\text{-}06$ $p_6 = 0.006547 \pm 0.00192$ $p_7 = 1.691 \pm 0.092$
3	60ºC	$p_1 = 2.116 \pm 0.04$ $p_2 = 0.0008455 \pm 0.00011835$ $p_3 = -0.4871 \pm 0.23$ $p_4 = -0.0761 \pm 0.044295$	$p_5 = -5.903e\text{-}06 \pm 5.90E\text{-}06$ $p_6 = 0.003884 \pm 0.0016265$ $p_7 = 1.975 \pm 0.078$
4	80ºC	$p_1 = 2.152 \pm 0.1395$ $p_2 = 0.0009701 \pm 0.00033105$ $p_3 = -0.3082 \pm 0.1325$ $p_4 = -0.0285 \pm 0.0284985$	$p_5 = -7.178e\text{-}06 \pm 4.815E\text{-}06$ $p_6 = 0.004868 \pm 0.0011835$ $p_7 = 1.936 \pm 1.993$

Fig. 1 shows a plot of the variation in the experimental and the predicted (Exponential) rehydration ratio with drying time at different temperatures for white yam. The plots of the experimental and predicted rehydration ratios vs. time are observed as expected to be a good fit as expected from the regression analysis shown in Table 1.

3.2 Evaluation of the Rehydration kinetics models

The moisture content data obtained from the rehydration experiments were fitted to the New Model, the Weibull model, the Peleg model, and the Exponential model presented in equations 4, 5, 6 and 7. Table 3 presents the statistical results of correlating the moisture content rehydration data using the Peleg, Weibull, and Exponential and New models. For quality fit, the model chosen to best fit the rehydration kinetics of the yam slices is the one that meets the following three criteria: R^2 is closest to unity, and SSE and RMSE are closest to zero. While most of the models fitted the moisture content experimental data with a coefficient of variance values exceeding 0.9600, the R^2 for the New model was the one closest to unity for all the temperatures. For the experiments performed at 27ºC, 40ºC, 60ºC, and 80ºC, R^2 exceeded 0.995 for the New model.
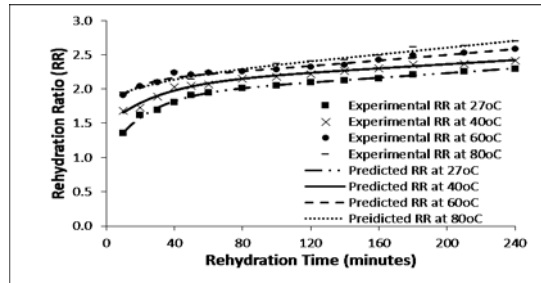
Fig. 1 Variation in Rehydration Ratio with Drying Time at Different Temperatures for white yam

Table 3 Regression constants correlating the moisture content rehydration data using Different Models

S/N	Temp	Models	R^2	RMSE	SSE	S/N	Temp	R^2	RMSE	SSE
1	27ºC	New	0.997	1.511	15.00	3	60ºC	0.996	1.596	25.46
		Peleg	0.995	2.772	92.19			0.952	4.866	284.15
		Weibull	0.977	6.089	444.92			0.976	3.454	143.19
		Exponential	0.976	6.234	466.40			0.976	3.473	144.73
2	40ºC	New	0.996	1.842	33.91	4	80ºC	0.993	2.248	50.53
		Peleg	0.988	3.050	111.59			0.881	8.195	805.82
		Weibull	0.966	5.174	321.28			0.982	3.171	120.63
		Exponential	0.965	5.224	327.42			0.982	3.152	119.22

Also, for the temperatures considered, the SSE, and RMSE, values were the least for the New model. The implications are that the New model best fits the rehydration data among the models examined. However, the SSE, and RMSE values are large. This implies that the model should only be used in the range of process conditions studied and should not be used for predictions outside that range. The coefficients obtained by fitting rehydration moisture content data to the new model for the yam slices is presented in Table 4.

Table 4 Coefficients Obtained By Fitting Rehydration Moisture content Data to the New Model For Yam Slices

S/N	Temp	27ºC	40ºC	60ºC	80ºC
1	α	99.76	46.11	24.63	17.3
2	β	0.5035	0.335	0.2729	0.3065
3	a	0.1588	0.06158	0.0321	0.03559
4	b	5.133e-3	5.282e-3	05.215e-3	4.904e-3
5	c	-0.0935	-0.2692	-0.408	-0.4084
6	d	0.5118	0.339	0.2757	0.3096
7	g	136.1	154.6	164.2	176.1
8	h	1.177e-3	8.899e-4	7.985e-4	8.05e-4
9	J	-128.4	-116.8	-85.58	-59.72
10	q	-0.03772	-0.06141	-0.06353	-0.03705

To further validate that the new rehydration model best fits the moisture content rehydration data, a simple linear regression analysis was performed between the experimental and predicted rehydration values. The relationship between the experimental and predicted rehydration moisture content values is also presented in Table 5.

Table 5 Relationship Between the Experimental and Predicted Rehydration Moisture Content Values

S/N	Temp.	Equation	R^2
1	27	$PMC = 0.9991 EMC$	0.9945
2	40	$PMC = 0.9997 EMC$	0.9962
3	60	$PMC = 1.0018 EMC$	0.9977
4	80	$PMC = 0.9998 EMC$	0.9925

where *PMC* is the predicted moisture content and *EMC* is the experimental moisture content

Fig 2 shows the variation in moisture content of the yam samples with time rehydrated at different temperatures.

Fig 2 Variation in Moisture contents of yam with rehydration time at 27,40, 60, and 80ºC

The plots show that for any given time, the moisture content of the yam sample is higher as temperature increases. The plots show that as the rehydration temperature increases the extent of rehydration increases. In the first ten minutes, the moisture content of the yam slices for rehydration temperatures of 27, 40, 60 and 80ºC are 46.69, 91.53, 120.41, and 137.87 g-water/g-solid respectively. There is a 3-fold magnitude in the moisture content of the samples rehydrated with a water temperature of 80ºC over the moisture content of sample rehydrated at 27ºC. However, after about 240 minutes, the difference in the magnitude of the moisture contents decreases; the moisture content ranged from 179.02 - 212.60 g-water/g-solid for rehydration done in the temperature range of 27 -80 ºC.

4 Conclusions

White yam (*Dioscorea rotundata*) slices, 3.0 mm thick, were dehydrated in a Refractance Window™ dryer. The dehydrated yam slices were rehydrated at 27, 40, 60 and 80ºC. Mass and moisture content variation data with time were collected. By fitting the mass

rehydration data to rehydration ratio models and the moisture content rehydration data to rehydration kinetics data, the following are the conclusions,.

The two-term exponential equation fits the rehydration ratio variation data better than the second order polynomial equation proposed by Singh and Pandey[17]. For the rehydration temperatures considered, the R^2 values for the two-term exponential equation were closest to unity in all cases. For the samples rehydrated at 27, 40, 60 and 80ºC, R^2, for the two-term exponential equations was 0.9966, 0.9860, 0.9903, and 0.9864 respectively as opposed to 0.9245, 0.9447, 0.9420 and 0.9803 for the second-order polynomial equation. Also, for the samples rehydrated at 27, 40, 60 and 80ºC, the root-mean-square-error (RMSE) were 0.0180, 0.0311, 0.0214 and 0.0317 respectively and the sum-of-squared-error (SSE) were 0.0032, 0.0097, 0.0046 and 0.0100 respectively. All the RMSE and SSE values are close to zero.

When rehydrating the slices, the mass (Fig. 1) and moisture content (Fig. 2) values reached higher values for the same rehydration time as the temperature increased. The rehydration ratio and moisture content for the slices rehydrated at 80ºC were about 50% higher for samples rehydrated at 27ºC after ten minutes.

For the moisture rehydration data, the new model better fits the rehydration kinetics than the Peleg, Weibull and Exponential rehydration models for the process temperatures studied. Among the models investigated, the R^2 value for the new models was closest to unity for all the process temperatures studied.

5. References

[1] United States Department of Agriculture (USDA), (2017a), Agricultural Research Service USDA Food Composition Databases, Retrieved August 30, 2017 from https://ndb.nal.usda.gov/ndb/foods/show/3266?man=&lfacet=&count=&max=&qlookup=&offset=&sort=&format=Abridged&reportfmt=other&rptfrm=&ndbno=&nutrient1=&nutrient2=&nutrient3=&subset=&totCount=&measureby=&Qv=1&Q6170=1&Qv=21&Q6170=1

[2] United States Department of Agriculture (USDA), (2017b), Agricultural Research Service USDA Food Composition Databases, Retrieved August 30, 2017 from https://ndb.nal.usda.gov/ndb/foods/show/3207?fg=&manu=&lfacet=&format=&count=&max=50&offset=&sort=default&order=asc&qlookup=potato%2C+raw&ds=&qt=&qp=&qa=&qn=&q=&ing=

[3] Hackett, A. F., Rugg-Gunn, A. J., Appleton, D. R. and Coombs, A., (1986), Dietary sources of energy, protein, fat and fibre in 375 English adolescents, Human Nutrition. *Applied Nutrition* [01 Jun 1986, 40(3):176-184]

[4] Subar, A. F., Krebs-Smith, S. M., Cook, A. and Kahle, L. L., (1998a), Dietary sources of nutrients among US children, 1989–1991, Pediatrics, Volume 102 No. 4 October 1998

[5] Subar, A. F., Krebs-Smith, S. M., Cook, A. and Kahle, L. L., (1998b), Dietary sources of nutrients among US adults, 1989 to 1991, Journal of the American Dietetic Association, Volume 98, Issue 5, May 1998, Pages 537-547.

[6] Reedy, J. and Krebs-Smith, S. M., (2010), Dietary Sources of Energy, Solid Fats, and Added Sugars Among Children and Adolescents in the United States, J Am Diet Assoc. 2010 October; 110(10): 1477–1484. doi:10.1016/j.jada.2010.07.010.

[7] Marinos-Kouris, D., Maroulis, Z. B., and Kiranoudis, C. T., (1996), Computer Simulation of Industrial Dryers, Drying Technology: An International Journal, 14:5, 971-1010, DOI: 10.1080/07373939608917137

[8] Vagenas, G. K. and Marinos-Kouris, D., (1991), The Design and Optimization of an Industrial Dryer for Sultana Raisins, Drying Technology: An International Journal, 9:2, 439-461, DOI: 10.1080/07373939108916675

[9] Gowen, A., Abu-Ghannam, N., Frias, J., & Oliveira, J. (2007). Influence of pre-blanching on the water absorption kinetics of soybeans. Journal of Food Engineering, 78(3), 965-971.

[10] García-Pascual, P., Sanjuán, N., Melis, R., & Mulet, A. (2006). Morchella esculenta (morel) rehydration process modelling. Journal of Food Engineering, 72(4), 346-353.

[11] Machado, M. F., Oliveira, F. A., & Cunha, L. M. (1999). Effect of milk fat and total solids concentration on the kinetics of moisture uptake by ready-to-eat breakfast cereal. International journal of food science & technology, 34(1), 47-57.

[12] Marabi, A., Livings, S., Jacobson, M., & Saguy, I. S. (2003). Normalized Weibull distribution for modeling rehydration of food particulates. European Food Research and Technology, 217(4), 311-318.

[13] Kashaninejad, M., Maghsoudlou, Y., Rafiee, S., & Khomeiri, M. (2007). Study of hydration kinetics and density changes of rice (Tarom Mahali) during hydrothermal processing. Journal of Food Engineering, 79(4), 1383-1390.

[14] Misra, M. K., & Brooker, D. B. (1980). Thin-layer drying and rewetting equations for shelled yellow corn. Transactions of the ASAE, 23, 1254–1260.

[15] Saguy, I. S., Marabi, A., & Wallach, R. (2005). New approach to model rehydration of dry food particulates utilizing principles of liquid transport in porous media. Trends in Food Science & Technology, 16(11), 495-506.

[16] OHAUS Corporation, (2011), Instruction Manual MB45 Moisture Analyzer, OHAUS Corporation, 7 Campus Drive, Suite 310, Parsippany, NJ 07054 USA.

[17] Singh, N. J., Pandey, R. K., (2011), Rehydration characteristics and structural changes of sweet potato cubes after dehydration, American. Journal of Food Technology 6 (8): 709-716

[18] Ogunnaike, B. A., (2011). Random Phenomena: Fundamentals of Probability and Statistics for Engineers. CRC Press.

[19] Johnson, R. A., (2017), Miller and Freund's Probability and Statistics for Engineers. Pearson Education © 2017. ISBN 10: 1-292-17601-6, ISBN 13: 978-1-292-17601-7.

A pore-scale study on the drying kinetics and mechanical behavior of particle aggregates

Pham, T. S.ª; Chareyre, B.b,c; Tsotsas, E.ª; Kharaghani, A.ª*

ª Department of Thermal Process Engineering, Otto von Guericke University, Magdeburg, Germany

b 3SR, University Grenoble-Alpes, Grenoble, France

c 3SR, CNRS, Grenoble, France

*E-mail of the corresponding author: abdolreza.kharaghani@ovgu.de

Abstract

A discrete thermo-mechanical drying model is developed to investigate the interaction between the porous structure and the drying characteristics of dense particle aggregates. The solid phase consists of polydisperse spherical particles in the micrometer range and the void space is constructed by a complementary network of tetrahedral pores. A modified version of the classical invasion percolation algorithm is set up to describe the preferential evaporation of the confined liquid in the pores. Thus, the evolution of the liquid distribution throughout the complex disordered medium can be simulated. In a one-way coupling scheme, capillary forces caused by both fluid pressure and surface tension are computed over time from the filling state of pores and they are applied as loads on each primary particle in the discrete element method. Based on this robust approach the drying kinetics and the mechanical behavior of several different aggregates with various fractions of small and large particles are simulated and quantified.

Keywords: Pore network model; discrete element method; Solid-fluid interaction; capillary force, Convective drying.

1. Introduction

Drying in porous media has been subjected to a wide range of scientific investigation, from soil layers [1] to a porous wick in loop heat pipe [2] or a membrane in a fuel cell [3]. This process consists of various complex events, such as two-phase flow together with phase change, or the interaction between fluid and solid phases, which may cause some undesired mechanical effects. These effects mainly depend upon moisture distribution, which is affected by drying conditions and the porous media skeleton. Substantial efforts have been made to numerically investigate the drying problem at the pore scale. After the pioneered work by Prat [4], many other studies have been conducted to take into account many physical effects, e.g. liquid viscosity [5], gravity [6] or liquid film [7].

In addition, the pore network modeling method has been combined with discrete element method (DEM) to account for the solid phase geometry explicitly [8]. Therefore, local effects on a solid phase (such as cracks or shrinkage) has been described for the case of *monosized* aggregates having regular [9] or irregular [10] pore structure. Such effects are caused by capillary forces, which depend on the evolution of the liquid-gas interface as well as surface tension during the drying process. The solid phase is defined as a particle aggregate and based on this a pore network is generated using the Voronoi tessellation that can approximate the void phase [11]. However, this Voronoi graph has a shortcoming when applied for a polydisperse aggregate, which is a packing composed of primary particles with different sizes. In this case, regular Delaunay triangulation generates the graph to weighted points, which are the radii of particles [12]. This regular Delaunay triangulation method has been used in a pore assembly approach developed by Bruno et al. [13] in order to study the fluid flow problems in granular porous media. The fluid flow model has been coupled with DEM to calculate the capillary force exerting on each particle of the aggregate. This approach has been further improved and applied for several applications. Based on this approach, Catalano et al. [14] investigated the fluid-solid interaction for the case of oedometer test; Chao Yuan et al. [15] studied the hydromechanical response (shrinkage and swelling) during drainage; Sweijen et al. [16] simulated swelling of super absorbent polymers.

The goal of this work is to develop a versatile discrete model that can simulate the mechanical behavior of particle aggregates during convective drying. In this meso-scale model, the solid phase is explicitly described as an assembly of spherical primary particles. The fluid flow within the void space structure is modeled using the pore assembly method while the geometrical representation and the mechanical behavior of the solid skeleton are simulated by DEM. The coupling between these two parts is achieved by handling the interfacial interaction between the fluid and the solids phase. Impact of the internal structure of the porous media on the drying kinetics, for the case of 3D particle aggregates with various fractions of coarse and fine primary particles, has been presented.

2. Materials and Methods

2.1. Aggregate generation - solid phase representation

The solid phase is represented by a packing of particles. This particle aggregate is generated by using YADE [17], which is an open-source software based on the discrete element method. A set of very loose particles with a uniform size distribution is enclosed in a parallelepiped. The resulting packing conforms in a gas-like state with no contacts between particles. Mechanical loading is subsequently applied to confer a solid-like nature to the packing.
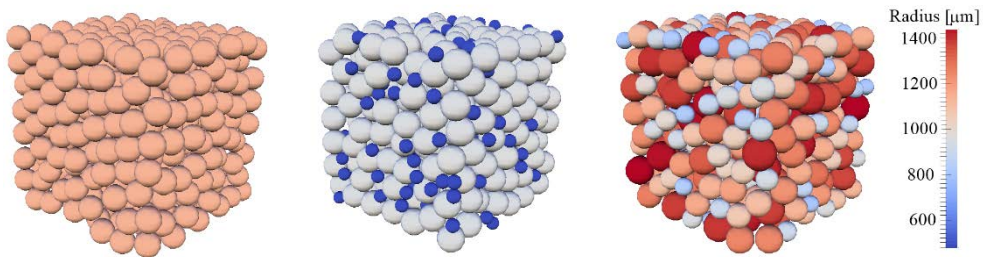
Fig. 1 Representation of monodisperse (left), bidisperse (middle), and polydisperse (right) particle aggregates.

2.2. Pore network generation - void space representation

The void space between primary particles is represented by a network of pore bodies and pore throats (see Figs. 2 and 3). This pore network is defined by a weighted Delaunay tessellation of the granular assembly. The pore body is subtracted from the finite volumes of the corresponding tetrahedral cell, which has its vertices locating at centers of associated particles (Fig. 2a), by the part of the solid volume of these associated particles locating within the domain of the tetrahedral cell. Each pair of pore bodies is connected to each other through one common facet (pore throat) between them (Fig. 2b). This pore throat has no volume and serves as the capillary threshold between the two corresponding pore bodies. Therefore, at a given time, the geometry of the packing defines an open network of connected voids.
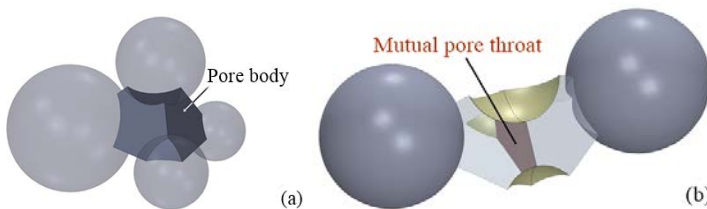
Fig. 2 Representation of a pore body and associated neighboring particles (a) and of two neighboring pore bodies sharing one mutual pore throat (b).
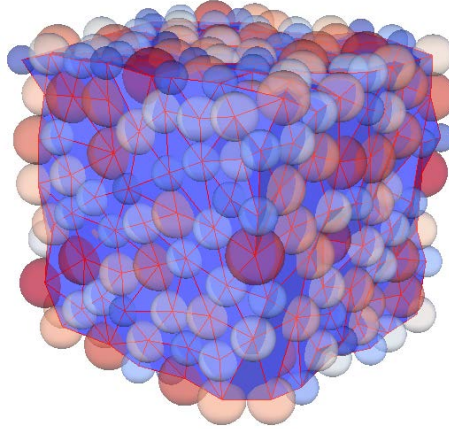
Fig. 3 Pore network triangulated based on the particle aggregate.

2.3. Drying algorithm

The isothermal discrete drying algorithm used in this work was based on the work of Metzger et al. [18]. The drying phenomenon is interpreted as an invasion percolation driven by evaporation of liquid into vapor. Vapor diffusion in gas-filled pore bodies is governed by diffusion with Stefan correction. The boundary conditions are applied here for the vapor pressure as saturation value at liquid-gas interface and value of bulk air at top of boundary layer. Besides, the pore size is big enough (more than 100 µm) so that the Kelvin effect, i.e. the reduction of equilibrium vapor pressure over a curved liquid-vapor interfaces may be neglected [18]. The movement of this menisci is not tracked continuously since the time is discretized based on each complete emptying of one single pore in each simulation step. This is due to the assumption that the movement of the liquid-vapor interface, which can be referred to as a Haines jump [19], is much faster than the duration of the evaporation occurring at that meniscus. During each calculation step, vapor flow rates are assumed as constant without accounting for local accumulation of vapor in the gas phase. Additionally, in the gas-filled section of the partially saturated pore bodies, it is assumed that the gas is saturated with vapor (local equilibrium), hence neglecting any vapor resistance in this section. Then, the following mass balances are applied for all gas-filled pore bodies of unknown vapor pressure pv:

$$\sum_{j=1}^{4} \dot{M}_{v,i} = \sum_{j=1}^{4} A_{ij} \frac{\delta}{L_{ij}} \frac{p\tilde{M}_v}{\tilde{R}T} \ln\left(\frac{p - p_{v,i}}{p - p_{v,j}} \right) = 0 \qquad (1)$$

Due to the random spatial distribution of the pore size, the liquid phase in the liquid-filled region of the network tends to be gradually separated into numerous isolated liquid clusters [6]. In the absence of viscous and gravity forces, liquid flow within these isolated clusters is totally controlled by capillary pressure, which is the pressure difference at the liquid-gas interface in each pore body locating at the boundary of each liquid cluster. If it is assumed that the gas pressure is the same everywhere within the gas-filled section of the void space,

then due to capillary pumping effect there is only one pore body in each liquid cluster, whose saturation changes in each calculation step. This pore body is the one having the highest liquid pressure, i.e. lowest capillary pressure, and it will hereafter be referred as entry pore. For every moment of the simulation, each liquid cluster has one entry pore and different entry pores can have different pore volume, pore saturation and evaporation rate. Consequently, the time required to totally invade these entry pores will be different. Therefore, the time step of the drying simulation is determined based on the liquid cluster which has its entry pore empty totally first.

2.4. Capillary force calculation

The capillary force exerting on each particle consists of two contributions. The first contribution is induced by the fluid pressure in pore bodies. It is calculated based on the gas and liquid pressure and the surface area of the solid particle being in contact with each corresponding fluids. The second capillary force contribution is the result of interfacial tension acting on the three phase (solid-liquid-gas) contact line. The method used for calculating this capillary force follows the work in [16].

3. Simulation results

We consider here a three-dimensional pore network initially saturated with single-component liquid (pure water). In this network the effects of gravity and liquid viscosity are neglected. The water vapor can only elude from the network through the boundary layer locating at the top surface of the sample while a zero-flux condition is applied at other surfaces. It is also assumed that the bulk air is totally dry, i.e. vapor pressure is equal to zero. The temperature of the entire network is uniform at 20 °C. We also neglect the liquid film effect – which can be significant for pores with square or polygonal cross section [21].
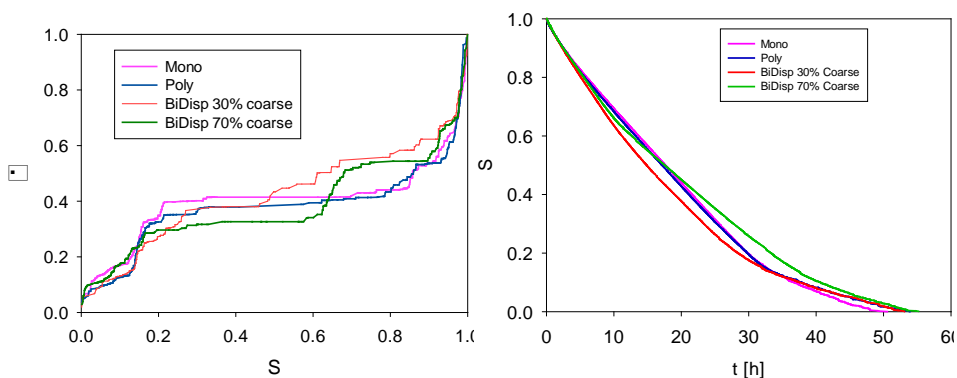
Fig. 4 Normalized drying curves of mono, poly and bidisperse particle aggregates.

The drying curves obtained for four different particle size distributions, i.e. mono, poly and two bidisperse aggregates with different volume fractions of coarse and fine particles, are presented in Figure 4. These curves show similar drying characteristics: a sharp drop at the beginning followed by a semi-constant evaporation rate period and ended with the falling rate period. These observation is in agreement with previous works [20]. Besides, the total time required to dry the aggregates are also presented. Although these four aggregates have approximately equal porosity and the same physical size of the whole domain, they still have differences in the spatial distribution of the fluid channel within the network. The liquid distribution obtained from the fluid flow calculation in each invasion step is the input for the calculation of capillary force in DEM module. Dynamic simulations are run to visualize the evolution of capillary forces during the drying process of the polydisperse aggregate (Fig. 5). Such capillary forces will subsequently be loaded to primary particles as external loads, and thus the particle motion shall be computed using DEM. We conjecture that different local distributions of fluid can lead to different mechanical responses. Detailed and systematical analysis will be addressed in the near future.
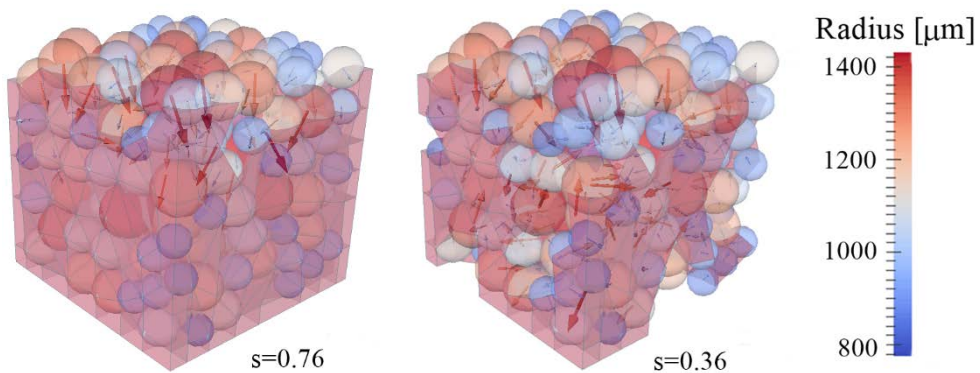
Fig. 5 Evolution of capillary force field (shown by arrows) in a polydisperse particle aggregate during drying.

4. Conclusion

A new discrete pore network model has been developed to investigate the fluid flow problem in dense particle aggregates consisting of spherical particles. The proposed approach integrates the pore assembly method with DEM. The aggregate was first generated using DEM based on given micro-scale properties, i.e. porosity, geometrical dimension and particle size distribution. Then, a numerical algorithm is developed to solve the fluid flow problem for the case of convective drying. It was shown that the developed model is capable of capturing the typical characteristic of this classical drying problem, i.e. constant rate period, falling rate period. Moreover, the obtained liquid distribution is then used as an input for calculating the capillary force field exerting on each particle of the aggregate. This is the first

step to couple the fluid flow model with DEM in order to simulate the thermo-mechanical behavior of *polydisperse* particle aggregates during drying.

5. Nomenclature

$\dot{M}$	Mass flow rate	kgs^{-1}
A	Area of cross section	m^2
L	Distance between the center of two adjacent pore bodies	m
p	Atmospheric pressure	Pa
$\tilde{M}$	Molar mass	kgkmol^{-1}
$\tilde{R}$	Ideal gas constant	Jkmol^{-1}K^{-1}
T	Temperature	K

Greek letters

δ	Vapor diffusivity	m^{2}s^{-1}
γ	Surface tension	Nm^{-1}

Subscripts

v	vapor

6. References

[1] Or, D.; Lehmann, P.; Shahraeeni, E.; Shokri, N. Advances in Soil Evaporation Physics—A Review. *Vadose Zone Journal* 2013, 12(4).

[2] Le, K.H.; Kharaghani, A.; Kirsch, C.; Tsotsas, E. Pore Network Simulations of Heat and Mass Transfer inside an Unsaturated Capillary Porous Wick in the Dry-out Regime. *Transport in porous media* 2016, 114(3), 623–648.

[3] Straubhaar, B.; Pauchet, J.; Prat, M. Pore network modelling of condensation in gas diffusion layers of proton exchange membrane fuel cells. *International Journal of Heat and Mass Transfer* 2016, 102, 891–901.

[4] Prat, M. Percolation model of drying under isothermal conditions in porous media. *International Journal of Multiphase Flow* 1993, 19(4), 691–704.

[5] Nowicki, S.C.; Davis, H.T.; Scriven, L.E. Microscopic determination of transport parameters in drying porous media. *Drying Technology* 1992, 10(4), 925–946.

[6] Laurindo, J.B.; Prat, M. Numerical and experimental network study of evaporation in capillary porous media. Phase distributions. *Chemical Engineering Science* 1996, 51(23), 5171–5185.

[7] Yiotis, A.G.; Boudouvis, A.G.; Stubos, A.K.; Tsimpanogiannis, I.N.; Yortsos, Y.C. Effect of liquid films on the drying of porous media. *AIChE Journal* 2004, 50(11), 2721–2737.

[8] Kharaghani, A. Irregular Pore Networks and Mechanical Effects During Drying of Porous Media. PhD thesis: Magdeburg, 2010.

[9] Kharaghani, A.; Metzger, T.; Tsotsas, E. A proposal for discrete modeling of mechanical effects during drying, combining pore networks with DEM. *AIChE Journal* 2011, 57(4), 872–885.

[10] Kharaghani, A.; Metzger, T.; Tsotsas, E. An irregular pore network model for convective drying and resulting damage of particle aggregates. *Chemical Engineering Science* 2012, 75, 267–278.

[11] Aurenhammer, F. Voronoi diagrams---a survey of a fundamental geometric data structure. *ACM Computing Surveys* 1991, 23(3), 345–405.

[12] Edelsbrunner, H.; Shah, N.R. Incremental topological flipping works for regular triangulations. *Algorithmica* 1996, 15(3), 223–241.

[13] Chareyre, B.; Cortis, A.; Catalano, E.; Barthélemy, E. Pore-Scale Modeling of Viscous Flow and Induced Forces in Dense Sphere Packings. *Transport in porous media* 2012, 92(2), 473–493.

[14] Catalano, E.; Chareyre, B.; Barthélémy, E. Pore-scale modeling of fluid-particles interaction and emerging poromechanical effects. *International Journal for Numerical and Analytical Methods in Geomechanics* 2014, 38(1), 51–71.

[15] Yuan, C.; Chareyre, B.; Darve, F. Deformation and stresses upon drainage of an idealized granular material. *Acta Geotechnica* 2017, 40(3), 405.

[16] Sweijen, T.; Nikooee, E.; Hassanizadeh, S.M.; Chareyre, B. The Effects of Swelling and Porosity Change on Capillarity. *Transport in porous media* 2016, 113, 207–226.

[17] Smilauer, V.; Catalano, E.; Chareyre, B.; Dorofeenko, S.; Duriez, J.; Dyck, N.; Elias, J.; Er, B.; Eulitz, A.; Gladky, A.*; et al.* Reference Manual; Zenodo, 2015.

[18] Metzger, T.; Tsotsas, E.; Prat, M. Pore-Network Models: A Powerful Tool to Study Drying at the Pore Level and Understand the Influence of Structure on Drying Kinetics: in "Modern Drying Technology: Computational Tools at Different Scales, Vol. 1. Edited by A.Mujjumdar and E.Tsotsas, 2007.

[19] Armstrong, R.T.; Berg, S. Interfacial velocities and capillary pressure gradients during Haines jumps. *Physical review. E, Statistical, nonlinear, and soft matter physics* 2013, 88(4), 43010.

[20] Yiotis, A.G.; Tsimpanogiannis, I.N.; Stubos, A.K.; Yortsos, Y.C. Pore-network study of the characteristic periods in the drying of porous materials. *Journal of colloid and interface science* 2006, 297(2), 738–748.

Investigation of 3D particle flow in a flighted rotating drum

Zhang, L.Y. [a,b*]; Weigler, F. [a]; Jiang, Z.C. [b]; Idakiev, V. [b]; Mörl, L. [b]; Mellmann, J. [a]; Tsotsas, E. [b];

[a] Department of Postharvest Technology. Leibniz Institute for Agricultural Engineering and Bioeconomy, Potsdam, Germany.
[b] Faculty of Process & Systems Engineering. Otto-von-Guericke University Magdeburg, Magdeburg, Germany.

*E-mail of the corresponding author: lzhang@atb-potsdam.de

Abstract

To validate the particle motion in flighted rotating drum (FRD), a laboratory FRD was built and operated at 15% filling degree and 10 rpm rotation speed using plastic balls as bed material. The particle tracking velocimetry (PTV) and magnetic particle tracking (MPT) techniques were applied to investigate the particle flow behavior. The 3D particle flow was modeled by Discrete Element Method (DEM) with LIGGGHTS. The height of the barycenter for overall particles and particle instantaneous velocity were calculated from PTV and DEM data. The 3D time-averaged particle velocity distribution obtained from MPT experiment and DEM simulation was compared.

Keywords: flighted rotating drum; particle motion; particle tracking velocimetry; magnetic particle tracking; DEM simulation.

1. Introduction

Flighted rotary drum (FRD) has been widely used in food and mineral industries for drying or cooling processes, as flights lift up particles and give them a higher chance to contact with gas. In last decades, much work has been carried out on FRD including particle mixing behavior, residence time distribution and discharge characteristics of flights [1]. However, few papers reported on particle movement, which is closely related to drying or cooling performance of drum. This is perhaps due to the limitation of experimental conditions and the complicated particle motion.

In order to investigate the characteristics of particle movement in FRD, particle tracking velocimetry (PTV) technique was utilized in current work to provide detail information of particle distribution and instantaneous velocities. Moreover, the magnetic tracking technique (MPT) was applied to evaluate particle velocity distribution in 3D. To simulate the particle motion, a 3D DEM model was developed, and the results obtained were compared with experimental data.

2. Materials and Methods

2.1. Experimental setup

The experimental setup consisted of a laboratory FRD, a high-speed camera system, and a magnetic tracking system as Fig. 1 schematically depicts.
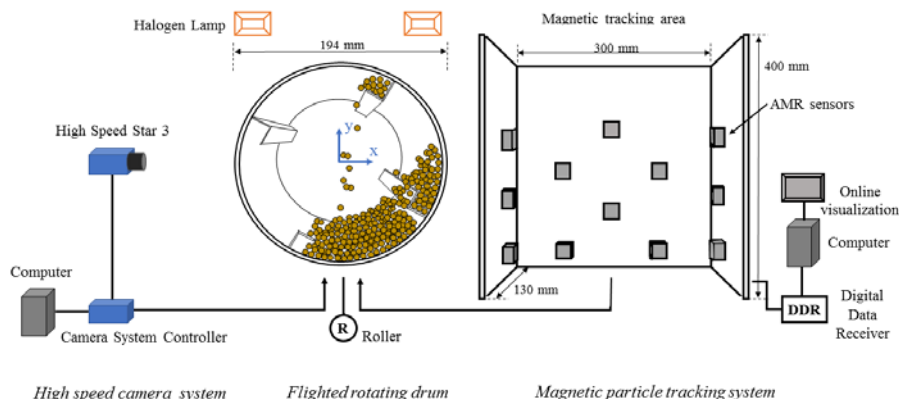
***Fig. 1 Sketch of experimental setup, including a flighted rotating drum (middle),
a high-speed camera system (left) and a magnetic particle tracking system (right).***

2.1.1. Flighted rotating drum (FRD)

Figure 1 shows the horizontally placed drum with inner diameter of 194 mm and length of 150 mm. Four rectangular flights were installed with a flight-length-ratio of 1.0. Fine sand (0.1 - 0.3 mm) was glued on inner wall to prevent particle slippage; but end walls were kept

smooth and transparent. The drum was made of acrylic glass, flights were made of aluminum. Spherical plastic balls were used as bed material with a diameter of d_p=6 mm and a bulk density of ρ_b = 596 kg/m^3. The experiments were conducted at 15% filling degree (volume based) and 10 rpm of drum rotating speed.

2.1.2. High-speed camera system

A high-speed camera system including a Photron high-speed camera (LaVision, CMOS chip) and a DaVis image acquisition software (LaVision) were used. Detailed parameters of the image system are listed in Table. 1. Two continuous illuminating 400 W halogen lamps

Table 1. Parameters of the image system.

Parameters	Value	Unit
Display resolution	1024 ×1024	pixel
Frame rate	500	fps
Exposure time	1/11,000	s
Dynamic range	10	bit
Local length	60	mm
f-number	2.8	-

were utilized to provide sufficient light, as shown in Fig. 1. The camera was positioned in front of the drum and adjusted to get a full view field of drum with 200 × 200 mm^2. With this setting, an approximate spatial resolution scale factor S_f of 5.17 pixel/mm was obtained from the standard geometry calibration process in the DaVis software. The experiment lasted 19.2 s with a number of 9600 images, which was sufficient to represent the periodicity of particle flow in the FRD. The experiments were repeated three times.

2.1.3. Magnetic tracking system

In the magnetic tracking system, 12 Anisotropic Magneto Resistive (AMR) sensors were installed on three acrylic glass plates, which provided a closed tracking volume of 300 mm × 400 mm × 130 mm as shown in Fig. 1. The sensors were arranged and calibrated to provide an optimal measurement of the magnetic field strength. All sensors were connected to a data acquisition device, which recorded data and sent them to a lab computer via USB interface. Online visualization and data evaluation were achieved by associated software 'MagDat' and 'MagCal', respectively.

2.2. Measurement techniques

2.2.1. Particle tracking velocimetry

The particle tracking velocimetry (PTV) is a non-intrusive, image-based measurement technique to acquire particle velocities. By combining particle segmentation and tracking algorithms, a large number of particles could be tracked simultaneously.

The particle-mask correlation method was applied to identify and determine the positions (coordinates x and y) of individual particles [2, 3]. A template particle matrix (m × m pixels), a key parameter in this process, was defined with the size of $d_p \cdot S_f$ pixels (rounding down to the nearest even number). The value of template matrix was averaged from 20 template particles that were selected manually. Then, a tracking algorithm named probability relaxation method was utilized to establish particle trajectories by tracking particle positions in consecutive image frames [3, 4]. During this process, three radiuses - the maximum displacement radius, neighboring radius and the quasi-rigidity radius - were defined as $1.2 \cdot U_{max} \cdot S_f \cdot \Delta t$, $1.0 \cdot U_{max} \cdot S_f \cdot \Delta t$ and $0.1\,2 \cdot U_{max} \cdot S_f \cdot \Delta t$ pixels, to search candidate particles and neighboring particles in the 1st or 2nd frame. The U_{max} was calculated based on the particle velocity during free fall in gas.

2.2.2. *Magnetic tracking technique*

The magnetic monitoring is based on continuous tracking of the magnetic marker. The evaluation of the measured data provides accurate information about the movement of tracer and, thus, enables investigating particle motion in a dense granular bed [5]. In this work, a 5 mm long cylindrical neodymium-iron boron with diameter of 3 mm was used as the magnet. By embedding it into a plastic ball, the tracer kept the same shape and size with other particles. With a measuring frequency of 250 Hz, the MPT system could record the Cartesian coordinates x, y, z of tracer every 6 ms. One experiment lasted 6 minutes and was repeated three times.

2.3. Discrete element method (DEM) simulation

In the current work, the open source software LIGGGHTS was adopted for the DEM simulation. The motion of each particle in the Lagrangian framework was calculated by the Newton's second law with ignoring the particle-fluid interaction due to the big density difference between particle and gas phase. Based on a filling degree of 15% in the experiment, 3474 particles were inserted into the simulation chamber as shown in Fig. 2.
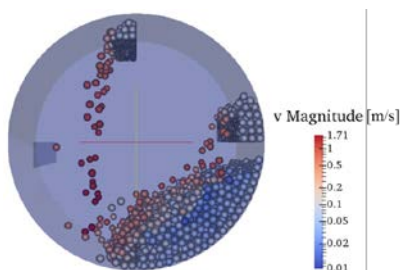
Fig. 2 Snapshot of particle distribution in the DEM simulation.

The particle interactions were calculated by the Hertzian contact model with tangential history tracking [6]. In this soft-sphere contact model, the effect of spring and dash-pot

appear through stiffness κ and damping coefficient η, which were determined by the physical material properties of Poisson ratio σ, Young's modulus E and the coefficient of restitution e. The detailed material properties of particles are listed in Table. 2. DEM simulation was run for 120 s in total, but only from the last 30 s data was extracted at 0.002 s intervals for further analysis.

Table 2. Material properties and model parameters for DEM simulation.

Parameters	Value	Unit
Young's modulus E [7]	10^7	Pa
Poisson ratio σ	0.3	-
Rolling coefficient κ_r [8]	0.01	-
Coefficient of restitution e [9]	0.68	-
Friction coefficient μ_f [10]	0.2	-
Time step Δt_{DEM}	5×10^{-6}	s
Simulation time t_{sim}	120	s

2.4. Post-processing of experimental and simulation data

2.4.1. Barycenter calculation

To describe the location of the overall particles in the FRD, the barycenter r_c was used as calculated from Equation (1a). The r represents the particle coordinates value x, y or z. The m_i denotes the mass of particle i and n the particle number. Considering that the plastic balls are regular spheres with uniform density, the equation is simplified as Equation (1b).

$$r_c = \frac{\sum_{i=1}^{n} m_i \cdot r_i}{\sum_{i=1}^{n} m_i} \quad \text{(a)}; \qquad r_c = \frac{\sum_{i=1}^{n} r_i}{n} \quad \text{(b)}; \qquad (1)$$

2.4.2. Particles velocity calculation

The particle instantaneous velocity was calculated from the particle coordinates $r(t_2)$ and $r(t_1)$ for the case $t_2 \rightarrow t_1$ by Equation (2). With the spatial velocity components v_x, v_y and v_z, the total particle velocity can be determined by Equation (3) in 3D.

$$v(t_1) = \lim_{t_x \rightarrow t_1} \frac{r(t_2) - r(t_1)}{t_2 - t_1} \tag{2}$$

$$v_{3D}(t) = \sqrt{v_x(t)^2 + v_y(t)^2 + v_z(t)^2} \tag{3}$$

3. Results and Discussion

3.1. Barycenter migration

Due to the pushing force of the flights, the position of the overall particles was raised increasing the particle-gas contact and, thus, heat transfer. Figure 3 represents the

normalized Y coordinate of the barycenter for overall particles over time for two drum rotations (12 s duration) as obtained from the PTV measurement and DEM simulation. As the figure illustrates, the barycenter rotated every 1.5 s corresponding to a quarter of one rotation of the flights. Furthermore, the DEM data agreed well with the PTV measurement.
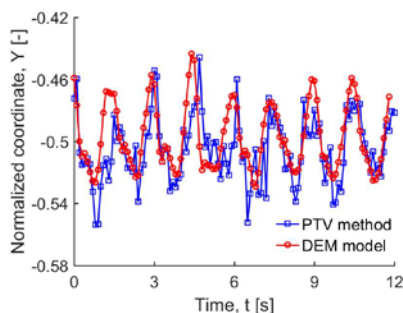
Fig. 3 Normalized Y coordinate value of particles barycenter in 12 s duration time (two rotating circles) by PTV method and DEM model.

3.2. Particle instantaneous velocity

Figure 4 shows the particle instantaneous velocity fields from PTV measurement and DEM simulation for the flight positions of $0°$, $30°$, $60°$ to the horizontal, respectively.
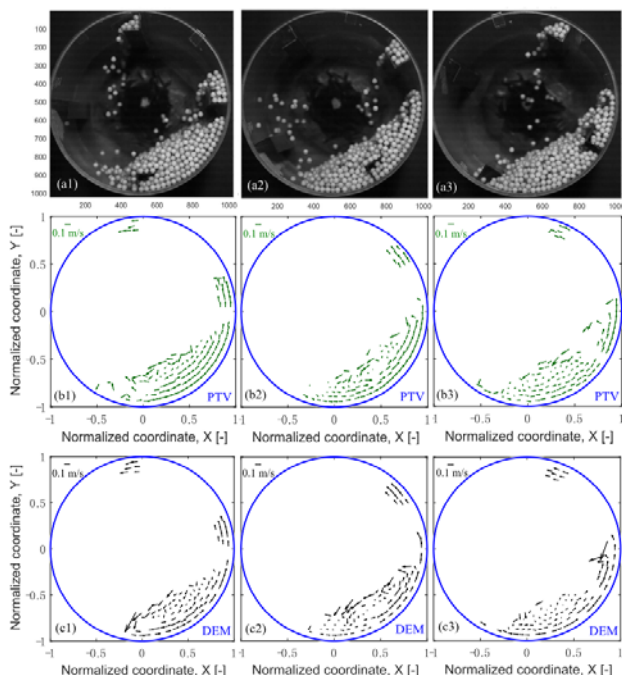
Fig. 4 Instantaneous particle distribution (a1-a3) and velocity vectors from PTV measurement (b1-b3) and DEM model (c1-c3) at the time of 0 s (a1, b1, c1), 0.5 s (a2, b2, c2) and 1.0 s (a3, b3, c3).

Since the PTV is limited to 2D studies, the particles located in the fist layer behind the front plate were chosen in DEM simulation to generate the particle velocity fields. The figures a1-a3 show the images of instantaneous particle distributions. The vortex in the dense phase at the bottom is clearly visible in Fig. 4 b1-b3 and c1-c3. The passive phase on flights presented a relatively homogeneous velocity distribution as they moved synchronous with the rotating wall. It is important to notice that, with different location of the flights, not only the position of vortex center dynamically changes but also the thicknesses of active and passive layers. This effect greatly accelerates the mixing of dense phase and, thereby, the heat transfer. The DEM data are in good agreement with PTV data.

3.3. Particle velocity distribution

Considering that PTV is limited to 2D, the 3D time-averaged and normalised velocity distributions were compared between MPT and DEM data in Fig. 5 to further validate particle motion in the FRD.
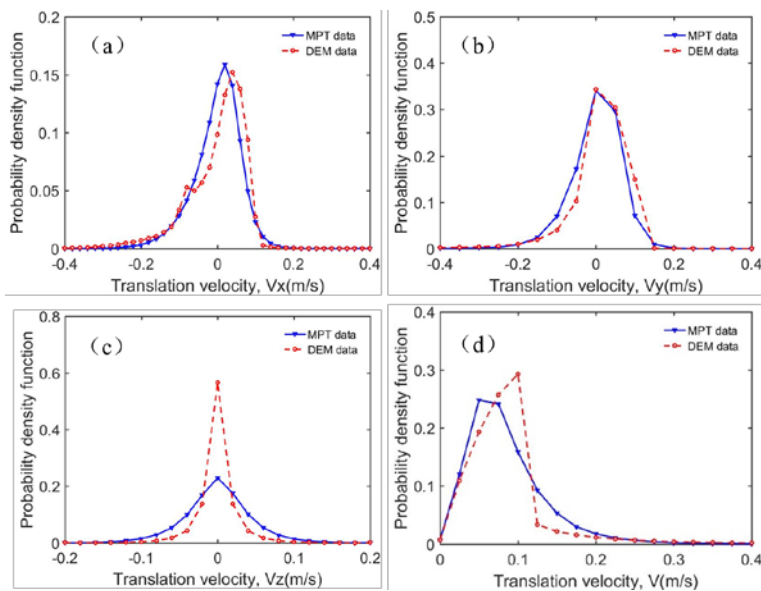
Fig. 5 Probability density distribution of particle translational velocity components by MPT measurement and DEM simulation: (a) Vx; (b) Vy; (c)Vz; (d) total velocity V.

It should be noted that the MPT data was obtained from 18 mins (three repeated experiments) to ensure a high accuracy of data distribution. While, due to computational limitations, the data from all particles (3,474 in total) were chosen from the last 30 s (5 rotating circles) of the DEM simulation for comparison. For radial velocity Vx and Vy, very similar distributions were obtained from MPT and DEM data, see Fig. 5a, b. The curves are asymmetric in shape which may be due to the influence of flights. Whereas, the axial velocity distribution Vz shows symmetry (Fig. 5c). Furthermore, the DEM data display a narrower distribution and a sharper peak. Potential reason for this difference could be attributed to the collision model selected in DEM. The total velocity distribution of the

MPT and DEM data show a comparable trend in lower velocity region, but apparent differences in higher velocity region, as shown in Fig. 5d. In general, there is reasonable agreement in the velocity distribution between MPT experiment and DEM model.

4. Conclusion

To investigate the particle motion in the FRD, two experiment techniques, PTV and MPT, were applied. The particle motion was modeled by using the DEM. A periodically upward movement of particles was confirmed. Moreover, the position of the vortex generated in dense phase varied over time, and the particle transient velocity distributions displayed asymmetric profiles. All these effects are caused by the flights. In addition, the DEM results agreed well with the PTV and MPT measurements.

5. References

[1] Delele, MA; Weigler, F.; Mellmann, J. Advances in the application of a rotary dryer for agricultural products: A review. Drying Technology 2015, 33 (5), 541-558.

[2] Takehara, K.; Etoh, T. A study on particle identification in PTV particle mask correlation method. Journal of Visualization 1998, 1 (3), 313-323.

[3] Jiang, Z.; Hagemeier, T.; Bueck, A.; Tsotsas, E. Experimental measurements of particle collision dynamics in a pseudo-2D gas-solid fluidized bed. Chemical Engineering Science 2017, 167, 297-316.

[4] Brevis, W.; Niño, Y.; Jirka, G. H. Integrating cross-correlation and relaxation algorithms for particle tracking velocimetry. Experiments in Fluids 2011, 50(1), 135-147.

[5] Idakiev, V.; Mörl, L. How to measure the particle translation and rotation in a spouted and fluidized bed. Journal of Chemical Technology and Metallurgy 2013, 48(5), 445-450.

[6] Tsuji, Y.; Tanaka; T., Ishida, T. Lagrangian numerical simulation of plug flow of cohesionless particles in a horizontal pipe. Powder Technology 1992, 71, 239–250.

[7] Chen, H.; Xiao, YG.; Liu, YL.; Shi, YS. Effect of Young's modulus on DEM results regarding transverse mixing of particles in a rotating drum. Powder Technology 2017, 318, 507-517.

[8] Goniva, C. C.; Kloss, N. G.; Deen, J. A.; Kuipers, M.; S. Pirker, Influence of rolling friction on single spout fluidized bed simulation, Particuology 2012, 10(5), 582–591.

[9] Jiang, Z.; Rieck, C.; Bueck, A.; Tsotsas, E. Estimation of coefficient of restitution of irregularly shaped particles on horizontal substrates, 8th International Granulation Workshop, Sheffield, UK, June 28-30, 2017.

[10] Santos, D. A.; Barrozo, M. A.; Duarte, C. R.; Weigler, F.; Mellmann, J. Investigation of particle dynamics in a rotary drum by means of experiments and numerical simulations using DEM. Advanced Powder Technology 2016, 27(2), 692-703.

Thermo-economic analysis of an efficient lignite-fired power system integrated with flue gas fan mill pre-drying

Han, X.[a]; Wang, J.[a]; Liu, M.[a]; Karellas, S.[b]; Yan, J.[a]

[a] State Key Laboratory of Multiphase Flow in Power Engineering, Xi'an Jiaotong University, Xi'an 710049, China

[b] Laboratory of Steam Boilers and Thermal Plants, National Technical University of Athens, 9, Heroon Polytechniou Street, Zografou 15780, Greece

*E-mail of the corresponding author: yanjj@mail.xjtu.edu.cn

Abstract

Lignite is a domestic strategic reserve of low rank coals in many countries for its abundant resource and competitive price. Combustion for power generation is still an important approach to its utilization. However, the high moisture content always results in low efficiencies of lignite-direct-fired power plants. Lignite pre-drying is thus proposed as an effective method to improve the energy efficiency. The present work focuses on the flue gas pre-dried lignite-fired power system (FPLPS), which is integrated with fan mill pulverizing system and waste heat recovery. The thermo-economic analysis model was developed to predict its energy saving potential at design conditions. The pre-drying upgrade factor was defined to express the coupling of pre-drying system with boiler system and the efficiency improvement effect. The energy saving potential of the FPLPS, when applied in a 600 MW supercritical power unit, was determined to be 1.48 %-pts. It was concluded that the improvement of boiler efficiency mainly resulted from the lowered boiler exhaust temperature after firing pre-dried low moisture content lignite and the lowered dryer exhaust gas temperature after pre-heating the boiler air supply.

Keywords: lignite; pre-drying; thermodynamic analysis; thermo-economics.

1. Introduction

Lignite is still considered as a domestic and abundant energy source for many countries. [1] Power generation is an important approach to utilization of lignite resources. However, the high moisture content always results in low efficiencies of lignite-direct-fired power plants. Pre-drying is an effective method to improve the energy efficiency because it removes the redundant moisture and increases the heating value of the lignite entering the furnace. [2,3]

Many works have been performed concerning the performance analysis of the pre-dried lignite-fired power systems (PLPSs) based on energy and exergy criteria and/or economic and environmental indicators. In China, Liu et al. [4] conducted process modeling of the steam pre-drying power system using Aspen Plus, and investigated the exergy destruction distributions of a 600 MW unit under nominal and partial loads. Moreover, biomass pre-drying [5] and solar pre-drying [6] were studied, respectively, to further demonstrate the energy saving potential of pre-drying. Zhu et al. [7] carried out an energy analysis of a lignite steam pre-drying power system with an efficient waste heat recovery system. Xu et al. [8] modeled a lignite power system integrated with boiler exhaust gas pre-drying, and analyzed the energy saving potentials with different lignite types and pre-drying degrees. Recently, different configurations of solar pre-drying were proposed by Xu et al. [9] The selection of drying heat source is gradually extended to renewable energy sources, which aims to further improve the energy efficiency of low rank coals. In Greece, Atsonios et al. [10] examined various scenarios of lignite drying and utilization depending on power load variation of the plant during certain periods of the day, in order to simultaneously increase the plant efficiency and reduce the electricity cost. Rakopoulos et al. [11] assessed different lignite-fired plant configurations for combined heat and power production for use in district heating networks, in terms of environmental, technical, and economic criteria. Avagianos et al. [12] presented a thermodynamic methodology for the prediction of lignite fired boilers at low power loads; even below the current technical minimum, when pre-dried lignite is employed. Drosatos et al. [13] conducted numerical simulation of a lignite-fired boiler using pre-dried lignite as supporting fuel for flexible operation. As summarized by Agraniotis et al. [14], state-of-the-art lignite pre-drying technologies can not only improve the energy efficiency but also operation flexibility. Energy saving of lignite pre-drying also attracts other researchers worldwide lately. For example, Fushimi et al. [15] developed drying process based on self-heat recuperation technology and evaluated the thermal efficiency penalty and costs. Kambara et al. [16] compared the thermal efficiencies for an existing 316 MWe power plant with and without steam tube dryers (STDs), and found that the improvement can be up to 4.2 %-pts. Giuffrida et al. [17] presented a detailed analyses based on mass and energy balances of lignite-fired air-blown gasification-based combined cycles with CO_2 pre-combustion capture. Akkoyunlu et al. [18] carried out an economic assessment of drying prior to grinding mill process in lignite-fired thermal power plants. It was indicated that the growth in the boiler efficiency ranged between 3.9-12.6% when there

was a 10% decrease in moisture content. Moon et al [19] developed a combination of low rank coal drying with power generation, and investigated the influences of steam extraction point and amount of drying coal on the thermal efficiency. In brief, an agreement has reached that pre-drying can improve the efficiency of lignite power generation, but system optimization still requires specifications and methodologies.

The authors have reported earlier predicted energetic performance of the FPLPS at off-design conditions [20] and suggested possible performance improvement through the energy matching in the drying process [21]. It is necessary to provide a comprehensive idea of technical and economic feasibility of lignite pre-dying. The major objective of this study is thereby to be a demonstration of a detailed thermo-economic analysis of flue gas mill pre-drying concept. It is continuation of works associated with lignite pre-drying power systems.

2. Materials and Methods

2.1. System Layouts

A conceptual schematic of the FPLPS system is depicted in Fig. 1. The common features of the FPLPS include the use of flue gas as drying agent in the drying tubes and fan mills, the integration of an open pulverizing system with the boiler, the concentration of water vapor in the dryer exhaust gas, and the air pre-heating by the dryer exhaust gas. More specifically, the flue gas dryer exhaust gas, containing a large amount of water vapor, is not recycled to the furnace but led to the heat recovery system, in which the waste heat is utilized to pre-heat the air supply of the boiler.
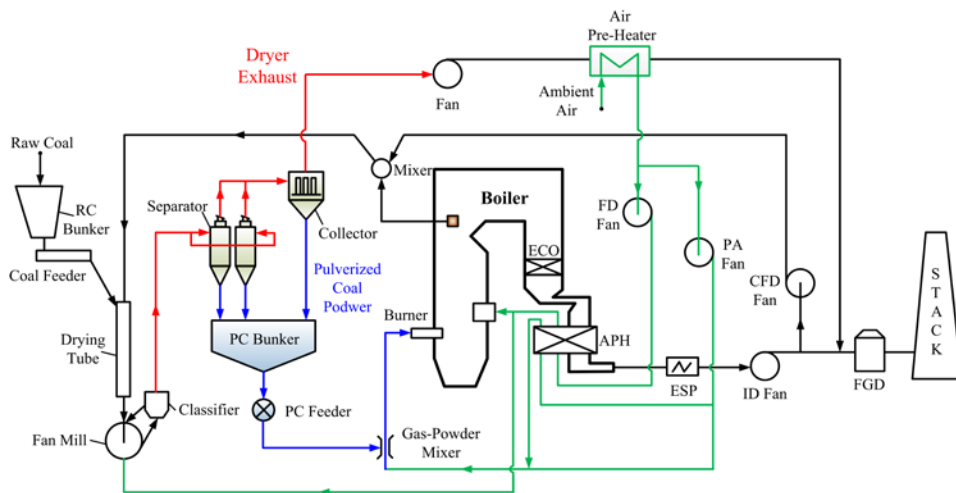
Fig. 1. System layout of the FPLPS.

2.2. Thermo-economic analysis model

Raw lignite is fed into the dryer, in which a part of the moisture content is removed and the heat supply is basically conserved with the latent heat of moisture evaporation $\Delta M \cdot h_v$. Accordingly, the LHV of the pre-dried lignite is derived as:

$$\text{LHV}_{pc} = (\text{LHV}_{ar} + \Delta M \cdot h_v)/(1 - \Delta M) \qquad (1)$$

where ΔM is the mass of evaporated moisture per kg raw lignite (kg·kg^{-1}), also defined as **pre-drying degree**, and h_v is the water latent heat of vaporization.

$$\Delta M = (M_{ar} - M_{pc})/(100 - M_{pc}) \qquad (2)$$

where M_{ar} and M_{pc} are the moisture contents in the raw and pre-dried lignite, respectively. The moisture content of pre-dried lignite can be calculated as:

$$M_{pc} = 0.048 \cdot M_{ar} \cdot R_{90} \cdot t_{de}^{-0.46} \qquad (3)$$

In the present work, a dimensionless **pre-drying upgrade factor** is defiend as:

$$k_{pd} = 1 + \Delta M \cdot h_v/\text{LHV}_{ar} \qquad (4)$$

In this way, boiler efficiencies on different basis can be derived as:

$$\eta_{b,t_{ref}=t_0} = k_{pd} \cdot \eta_{b,t_{ref}=t_{ap}} \qquad (5)$$

The plant thermal efficiency, η_{tot}, can be calculated by the combined product of the efficiencies of the main components, and is expressed as follows:

$$\eta_{tot} = \eta_b \eta_p \eta_{sc} \eta_m \eta_g \qquad (6)$$

where η_b is the boiler efficiency (t_0 basis), η_p the heat supply pipe efficiency, η_{sc} the steam cycle efficiency, η_m the mechanical efficiency, and η_g the electric generator efficiency. The plant thermal efficiency improvement, $\Delta\eta_{tot}$, is calculated as:

$$\Delta\eta_{tot} = \eta_{tot,FPLPS} - \eta_{tot,CLPS} \qquad (7)$$

3. Results and Discussion

3.1. Case Study

3.1.1. Benchmark parameters

To evaluate the energy saving potential of the FPLPS comprehensively, simulation calculations on a 600 MW water-cooled supercritical unit were carried out based on the simulation algorithm introduced above. Detailed specifications in simulation and calculation, such as the thermal parameters of the heat regenerative system, can be found in Ref.[21]. The properties of the Chinese Yimin lignite, with 39.5% moisture content are given in Table 1.

Table 1. Properties of Chinese Yimin lignite

M_{ar}, %	A_{ar}, %	C_{ar}, %	H_{ar}, %	O_{ar}, %	N_{ar}, %	S_{ar}, %	LHV, MJ·kg^{-1}
39.50	12.09	34.59	2.03	11.30	0.35	0.14	11.79

To conduct thermodynamic analysis, it is firstly necessary to determine the moisture content of pre-dried lignite with given parameters. According to the empirical correlation (Eq.1), the moisture content after grinding and milling can be obtained, as a function of pre-drying degree and R_{90} (Fig. 2). M_{pc} is calculated as 9.82% when t_{de} equals 110 °C. The heating value can also be calculated, as shown in Fig. 3. The HHV and LHV are elevated by 49.1% and 59.5%, respectively. Obviously, with higher pre-drying degree, the rank of

the lignite is improved. The plant efficiency benefit is expected. As summarized in Table 2, compared with conventional lignite-fired power system (CLPS), the plant thermal efficiency can be improved by 1.48 %-pts.
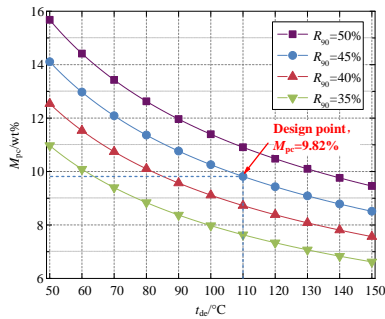
Fig. 2. M_{pc} in terms of R_{90} and t_{de}.
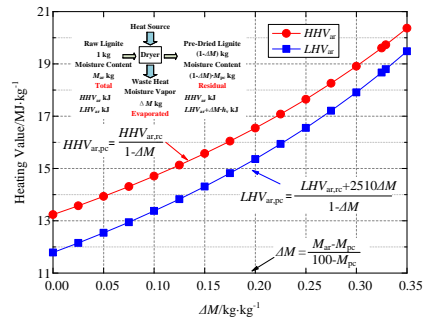
Fig. 3. Heating value in terms of ΔM.

Table 2. Comparison of the parameters and thermo-economics of the CLPS and FPLPS

Items	Unit	CLPS	FPLPS
Boiler exhaust temperature, t_{be}	°C	144	110
Air pre-heating temperature, t_{ap}	°C	-	55
Dryer exhaust temperature, t_{de}	°C	150	110
Boiler efficiency on t_{ap} basis, $\eta_{b,t_{ref}=t_{ap}}$	%	-	89.49
Pre-drying upgrade factor, k_{pd}	-	-	1.07
Boiler efficiency on t_0 basis, $\eta_{b,t_{ref}=t_0}$	%	92.59	95.76
Steam cycle efficiency, η_i	%	47.67	47.67
Plant thermal efficiency, η_{tot}	%	43.26	44.74

3.1.2. Thermodynamic analysis

The joint influences of boiler exhaust temperature (t_{be}), dryer exhaust temperature (t_{de}), air pre-heating temperature (t_{ap}) on the energy efficiency improvements are depicted in Fig. 4. It can be seen in Fig. 5 that the plant efficiency improvement varies with t_{be}, t_{de}, and t_{ap} linearly. The $\Delta\eta_{tot}$ increases by 0.09 %-pts when t_{de} decreases by 10 °C, 0.18 %-pts when t_{be} decreases by 10 °C, and 0.16 %-pts when t_{ap} increases by 10 °C. To sum up, the decrease of t_{de}, t_{be} and increase in t_{ap} contribute to the total $\Delta\eta_{tot}$ by 0.38 %-pts, 0.62 %-pts, and 0.48 %-pts, respectively.

The pre-drying upgrade factor (k_{pd}) is defined in the present work to demonstrate the energy saving mechanism of pre-drying from energy analysis perspective. It is shown in Fig. 6 that the k_{pd} increases linearly with the pre-drying degree (ΔM) with given lignite properties. It is calculated as 1.07 for Yimin lignite, which means that the boiler efficiency is increased by 7%. The k_{pd} increases by 0.02 with 0.1 kg·kg^{-1} increase in ΔM. As a result, the boiler efficiency increases with the pre-drying degree (Fig. 7).
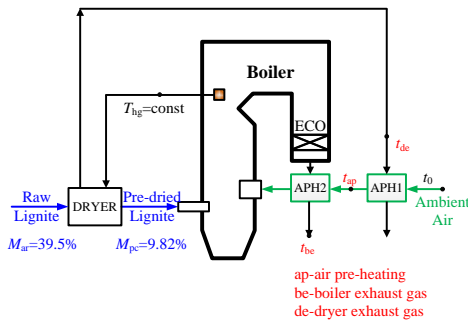
Fig. 4. Schematic of the key temperatures in FPLPS.

Fig. 5. Influence of t_{be}, t_{de}, and t_{ap} on $\Delta\eta_{tot}$

Fig. 6. k_{pd} as a function of ΔM.
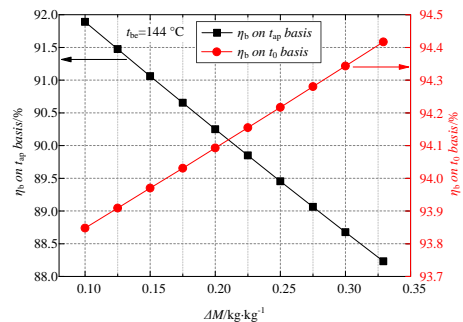
Fig. 7. Boiler efficiencies in terms of ΔM.

3.2. Parametric analysis

Apart from the key temperatures above, the plant efficiency improvement also depends on drying process parameters. Pre-drying degree and dryer efficiency are the parameters, from the perspectives of moisture removal and thermal conversion, respectively. The uncertainty in the calculation of the moisture content should be taken into consideration, as well as the dryer efficiency. Therefore, it is necessary to investigate the variations of the improvement.

3.2.1. Influence of pre-drying degrees

It is shown in Fig. 8 that the $\Delta\eta_{tot}$ increases ΔM linearly. Moreover, the slope increases with t_{be}. It means that for lignite-fired boilers with high exhaust temperature, the energy saving potential is remarkable. For example, when t_{be} is equal to 144 °C and 110 °C, respectively, the $\Delta\eta_{tot}$ increases by 0.12 %-pts and 0.05 %-pts, with 0.1 kg·kg^{-1} increase in ΔM.

3.2.2. Influence of dryer efficiency

The dryer efficiency influences the energy saving potential significantly, as shown in Fig. 9. When the dryer efficiency drops below the design value, the $\Delta\eta_{tot}$ decreases sharply. Especially, there exit critical dryer efficiencies with given boiler exhaust temperature. For example, when t_{be} is equal to 144 °C, the $\eta_{d,cri}$ is approximately 80%. When the dryer efficiency gets lower than that, the FPLPS does not save coal any more. It can be attributed to the fact that although kpd does not change with dryer efficiency, the heat load of the dryer increases with decreasing dryer efficiency and the boiler efficiency drops.

Fig. 8. Δη$_{tot}$ as a function of ΔM.

Fig. 9. Δη$_{tot}$ as a function of η$_d$.

4. Conclusions

A theoretical framework of modeling and thermo-economics on lignite pre-drying is presented in the present work, which offers a comprehensive idea of economic feasibility of lignite utilization integrated with flue gas fan mill pre-drying. The main conclusions are:

1) A pre-drying upgrade factor was defined to decouple the drying and boiler systems. When the moisture content decreased from 39.5% to 9.82%, the pre-drying degree was 0.33 kg·kg^{-1}, and pre-drying upgrade factor was calculated to be 1.07. As a result, the plant thermal efficiency improvement of the FPLPS compared with CLPS can be up to 1.48 %-pts, when the boiler exhaust gas temperature, the dryer exhaust gas temperature and the air pre-heating temperature were set as 110 °C, 110 °C, and 55 °C, respectively.

2) Through parametric analyses, the contributions of key design temperatures and pre-drying conditions to the energy saving potential of the FPLPS were analyzed. Results showed that the plant efficiency improvement resulted from pre-drying and air supply pre-heating increased by 0.09 %-pts, 0.16 %-pts, and 0.18 %-pts with 10 °C increase in the dryer exhaust temperature, 10 °C decrease in the air pre-heating temperature, and 10 °C decrease in the boiler exhaust temperature, respectively.

5. Acknowledgments

6. References

[1] Pusat, S.; Akkoyunlu, M.T.; Erdem, H.H. Evaporative drying of low-rank coal. In Sustainable Drying Technologies; Olvera, J.d.R.; Intech, 2016; 59-78.

[2] Nikolopoulos, N.; Violidakis, I.; Karampinis, E.; et al. Report on comparison among current industrial scale lignite drying technologies (A critical review of current technologies). Fuel 2015, 155: 86-114.

[3] Zhu, Q. Update on lignite firing. Available: https://www.usea.org/sites/default/files/062 012_Update%20on%20lignite%20firing_ccc201.pdf; 2012 [accessed 03.28.2018].

[4] Liu, M.; Li, G.; Han, X.Q.; et al. Energy and exergy analyses of a lignite-fired power plant integrated with a steam dryer at rated and partial loads. Dry Technol 2017, 35(2): 203-217.

[5] Liu, M.; Zhang, X.W.; Han, X.Q.; et al. Using pre-drying technology to improve the exergetic efficiency of bioenergy utilization process with Combustion: A case study of a power plant. Appl Therm Eng 2017, 127: 1416-1426.

[6] Liu, M.; Wang, C.Y.; Han, X.Q.; et al. Lignite drying with solar energy: Thermodynamic analysis and case study. Dry Technol 2017, 35(9): 1117-1129.

[7] Zhu, X.; Wang, C,A.; Tang, C.L.; et al. Energy analysis of a lignite predrying power generation system with an efficient waste heat recovery system. Dry Technol 2016, 34(4): 420-427.

[8] Xu, C.; Xu, G.; Zhao, S.F.; et al. A theoretical investigation of energy efficiency improvement by coal pre-drying in coal fired power plants. Energy Convers Manag 2016, 122: 580-588.

[9] Xu, C.; Bai, P.; Xin, T.T.; et al. A novel solar energy integrated low-rank coal fired power generation using coal pre-drying and an absorption heat pump. Appl Energy 2017, 200, 170-179.

[10] Atsonios, K.; Violidakis, I.; Sfetsioris, K.; et al. Pre-dried lignite technology implementati-on in partial load/low demand cases for flexibility enhancement. Energy 2016, 96: 427-436.

[11] Rakopoulos, D.; Agraniotis, M.; Grammelis, P.; et al. Efficient CHP-plant configuration for district heating systems utilizing low-rank coals. J Energy Eng 2016, 04016066.

[12] Avagianos, I.; Atsonios, K.; Nikolopoulos, N.; et al. Predictive method for low load off-design operation of a lignite fired power plant. Fuel 2017, 209: 685-693.

[13] Drosatos, P.; Nikolopoulos, N.; Nikolopoulos, A.; et al. Numerical examination of an operationally flexible lignite-fired boiler including its convective section as supporting fuel pre-dried lignite. Fuel Process Technol 2017, 166: 237-257.

[14] Agraniotis, M.; Bergins, C.; Stein-Cichoszewska, M.; et al. High-efficiency pulverized coal power generation using low-rank coals. Low-Rank Coals for Power Generation, Fuel and Chemical Production; Luo, Z.Y.; Agraniotis, M. Woodhead Publishing, 2017; 95-124.

[15] Fushimi, C.; Dewi, W.N. Energy efficiency and capital cost estimation of superheated steam drying processes combined with integrated coal gasification combined cycle. J Chem Eng J 2015, 48(10): 872-880.

[16] Kambara, S.; Noguchi, T.; Watanabe, K.; et al. Improvement of thermal efficiency for a low rank coal fired power plant. J JPN Inst Energy 2016, 95: 144-151 (in Japanese).

[17] Giuffrida, A.; Moioli, S.; Romano, M.C.; et al. Lignite-fired air-blown IGCC systems with pre-combustion CO_2 capture. Int J Energy Res 2016, 40: 831-845.

[18] Akkoyunlu, M.T.; Erdem, H.H.; Pusat, S. Determination of economic upper limit of drying processes in coal-fired power plants. Dry Technol 2016, 34(4): 420-427.

[19] Moon, S.W.; Kim, J.H.; Kim, T.S. Performance analysis of a coal fired power plant combined with low rank coal drying technology. The KSFM J Fluid Machinery 2017, 20(5): 21-26 (in Korean).

[20] Han X,Q.; Liu, M.; Zhai, M.X.; et al. Investigation on the off-design performances of flue gas pre-dried lignite-fired power system integrated with waste heat recovery at variable external working conditions. Energy 2015, 90(2): 1743-1758.

[21] Han, X.Q.; Liu, M.; Wu, K.L.; et al. Exergy analysis of the flue gas pre-dried lignite-fired power system based on the boiler with open pulverizing system. Energy 2016, 106: 285-300.

Drying behavior, diffusion modeling of *cuminum cyminum L.* undergoing microwave-assisted fluidized bed drying

Babaki, A.; Askari, G.[*]; Emamdjomeh, Z.

Transport Phenomena Laboratory (TPL), Departmatn of Food Science and Technology, College of Agriculture and Natural Resources, University of Tehran, Karaj, Iran

*E-mail of the corresponding author: iraskari@ut.ac.ir

Abstract

In order to conserve cuminum cyminum L. during long storage periods, the drying kinetics of this seed undergoing microwave-assisted fluidized bed dryer at various microwave output power (300, 600 and 900w), air velocity (10, 15 and 20 m/s) and air temperatures (45, 55 and 65°c) were studied. The main aim of this research is developing a mathematical model of mass transfer to investigate the microwave-assisted fluidized bed drying of cuminum cyminum L. seed. In this paper, we tried to discover a good model to evaluate moisture effective diffusivity (D_{eff}).

Keywords: cuminum cyminum L, microwave-assisted drying, mathematical modeling,

1. Introduction

Cumin *(cuminum cyminum)* is one of the functional and valuable spices in food preparations. It is popular for its strong, sweet aroma and slightly bitter taste. In addition to its seasoning application, its pharmaceutical properties are influential. Cumin name originally derived from the Greek word "kyminon".Several functional benefits of cumin consumption are: hypolipidemic, digestion stimulating, antispasmodic, wound-healing, anti-microbial, anti-oxidant, carminative and anti-inflammatory agent. Ground cumin is commonly used in Iranian culinary and confectionary, meaty Moroccan foods and classic German foods [1-4]. Iran was among the countries that devote themselves to the large surface area of the land was cultivated cumin, and its production in this area was about 12,000 tons per year [5].

Drying is frequently used in agricultural and food processing. Essential oils are important part in herbs, due to thir importance and thermal sensitivity they have to dried at moderate thermal condition and short time [6]. Fluidized bed drier has high thermal efficiency in solid drying. Direct intact between samples and heating medium leads to simultaneous as well as rapid heat, and mass transfer. However conductive heat transfer from surface to the inside of materials is still slow. This may be solved by using microwave assisted fluidized bed drier. This article focuses on mathematical modeling of cumin as an assumed cylindrical shaped seed, dried undergoing various treatment in order to assess water loss procedure.

2. Materials and Methods

2.1. Dying procedure

Cumin seeds were purchased from local grocery in Karaj city (north of Iran) in October. At first they were cleaned manually then got uniformed by a sieve having 20 meshes. Predetermined amount of water added to a certain quantity of samples obtain determained moisture content. A pilot-scale microwave- assisted fluidized bed dryer was applied for dehydration experiments. For each test, 50 g cumin seeds slightly poured into drying dish to make them uniform. The drying tests were conducted at three levels of power (300, 600, 900w), air temperature (45, 55, 65ºC) and air velocity (5, 7.5, 10 m/s) to reach a specific moisture content (5.66% d.b). V=4.5 m/s is experimentally determined as the minimum fluidization velocity. Moisture ratio was calculated based on following equation [7]:

$$MR = \frac{M - M_e}{M_0 - M_e} \qquad (1)$$

<div align="center">Table.1 independent variables</div>

Factor	Name	Units	Minimum	Maximum	Mean
A=X_1	temperature	ºc	45	65	55
B=X_2	Microwave power	w	300	900	600
C=X_3	Air velocity	m/s	10	20	15

2.2. Mathematical modelling and Moisture diffusivity determination

In order to facilitate the calculation of the effective diffusion coefficient, a new method was designed and developed. In this case, the oval shaped cumin seed was considered as a cylinder with the surface are a similar to the elliptical cumin seed. So firstly, side surface area of elliptical cumin particles were calculated by circulating equation (2) around horizontal "a" axis (fig 1) [8].
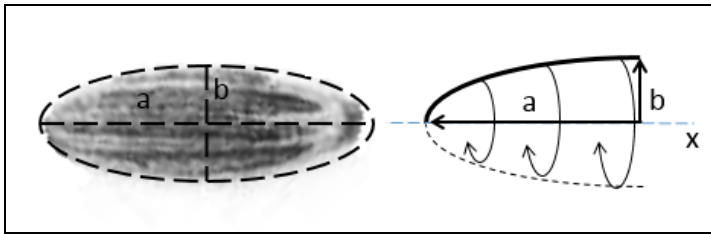
<div align="center">Figure 1. Cumin seed scheme for the model geometry</div>

$$s = 2\pi \int_0^a y\sqrt{1 + y'^2} \, dx \tag{2}$$

For an entire ellipsoid:

$$s = 4\pi \int_0^a y\sqrt{1 + y'^2} \, dx \tag{3}$$

Then via equating ellipsoid surface area with cylinder surface area, the radius (r_c) was calculated from following equation:

$$2\pi r_c(2a) + 2\pi r_c^2 = 2\pi ab\left[\frac{Arcsin\sqrt{a^2 - b^2}}{\frac{\sqrt{a^2 - b^2}}{a}} + \frac{b}{a}\right] \tag{4}$$

Large radius of 20 seeds were measured by digital caliper with an accuracy of 0.01 mm (Mitutoyo, Japan) and their average value was considered as' a' factor in above equation.

Water loss process during solid dehydration consists of several complex mechanisms. With regard to this fact, Fick's second low effective diffusivity have been considered as a combination of mentioned mechanisms [6, 9].

$$\frac{\partial M}{\partial t} = Div[D_{eff}(gradM)] \tag{5}$$

Initial and boundary conditions of eq (9) with ignoring shrinkage are defined as follow:

$$t = 0, \qquad M = M_0$$

$$t > 0, \qquad r = 0, \qquad \frac{\partial M}{\partial r} = 0$$

$$t > 0, \quad r = r_c \qquad and \quad z = L, \qquad M = M_e$$

Fickian equation solution could be simplified to infinite slab and cylinder and finite cylinder by assuming the first part in series expansion of their equation respectively [9, 10]:

$$MR_{is} = \frac{M - M_e}{M_0 - M_e} = \frac{8}{\pi^2}\exp(-B_{is}t) \tag{6}$$

$$MR_{ic} = \frac{M - M_e}{M_0 - M_e} = \frac{4}{\beta_1^2}\exp(-B_{ic}t) \tag{7}$$

$$MR_{fc} = \frac{M - M_e}{M_0 - M_e} = \frac{32}{\pi^2\beta_1^2}\exp(-B_{fc}t) \tag{8}$$

Wherein:

$$B_{is} = \pi^2 D_{slab} / L^2 \tag{9}$$

$$B_{ic} = \beta_1^2 D_{cyl}/r_c^2 \tag{10}$$

$$B_{fc} = \frac{\pi^2 D_{slab}}{L^2} + \frac{\beta_1^2 D_{cyl}}{r_c^2} \tag{11}$$

Where D_{slab} and D_{cyl} are the moisture diffusivities that were assumed equal. L and r_c are the real length of cumin seed and the computed radius of the cylinder in eq (4) in the order given and $\beta_1=2.4048$ was obtained from the tables of the first kind of zero order Bessel function ($J_o(a\alpha_n)=0$) [10]. The constant B can be determined by plotting ln(MR) against drying time (s) for any experiment.

3. Results and discussion

3.1. Drying kinetic

The Cumin samples (M_0 =35.44% (d.b)) were dried to M=5.66% (d.b). Central composite design (CCRD) with three indepenfdent variables includes microwave output power, air temperature, air velocity, on three levels, at the central point plan was applied. As expected, moisture content kept decreasing by increasing drying time, temperature and microwave power, (fig.2 a and b). In table.2 drying rate values based on different test conditions, are provided. During microwave heating, water components due to their higher dielectric loss factor, absorb a greater amount of microwave energy and reach the boiling temperature, consequently the pressure in the interior of the material develops, this causes the moisture to move from the inside to the surface [11, 12]. At first, internal heating caused by microwave, moves liquid water towards surface of samples (Darcy's law). With the progress of the drying procedure, internal moisture supply is not able to provide the surface evaporation process. Thus, after this stage, dehydration is driven by vapor diffusion and Darcy's flow [13]. As can be seen in fig.2c, air flow rate increase to more than minimum fluidization velocity (15 m/s) has no effect on drying rate and drying time, because increasing air velocity, increases bed pressure drop.

Fig.2 effect of microwave power (a: v=15m/s, T=55ᵒC) air temperature (b: p=600w, v=15m/s) and air velocity (c: p=600w, T=55ᵒC) on drying rate.

From a certain speed onwards, the amount of pressure drop has been stabilized and there isn't much change in it. Constant pressure drop is due to change in the nature of the bed particles from fixed state to fluid state, so from this point on, pressure drop will be same as liquid static pressure drop and depend on height of bed [14].

3.2. Effective moisture diffusivity and activation energy

Effective moisture diffusivity: Radius value obtained from eq (8) is 0.373 mm. by using slope of fig.3 graphs and putting them in eq (15), effective moisture diffusivity under various test conditions was determined. The measured D_{eff} values for cumin seeds are presented in table.2.

As shown, D_{eff} values were ranged from 3.820×10^{-11} to 2.746×10^{-10} m²/s. This result is in accordance with results obtained from most food stuffs (10^{-12} -10^{-8} m²/s) [15, 16]. It is observed that the highest amount of D_{eff} is related to P=900w and T=65°C and the lowest amount of D_{eff} is related to P=300w and T=45°C. It was observed that increasing the temperature of drying air and microwave power, increased the effective moisture diffusivity.
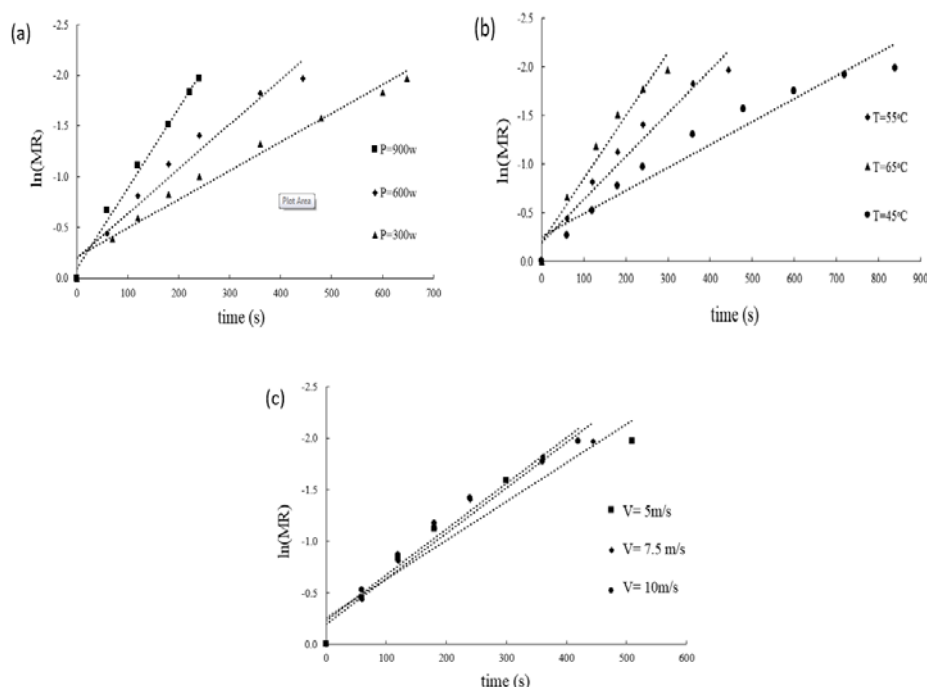
Fig.2 effect of microwave power (a: v=15m/s, T=55°C) air temperature (b: p=600w, v=15m/s) and air velocity (c: p=600w, T=55°C) on drying rate.

These results are in agreement with the results of microwave drying of pandanus leaves [17] and hot-air and microwave drying of pineapple [15] and fluidized bed drying of canola [16]. There is no significant effect of various velocity of drying air on slope of fig.3c and consequently on D_{eff} was observed. As mentioned earlier, this action is due to the mechanism of pressure drop during drying procedure.

Table. 2 Amounts of DR, RMSE, SSE and D_{eff} of cumin seed undergoing different drying condition

Microwave power (w)	Air temperature (^{o}C)	Air velocity (m/s)	Drying rate (1/s)	D_{eff} (m^2/s) $\times 10^{-10}$	R^2
300.00	65.00	10.00	0.004	0.883	0.9813
900.00	45.00	10.00	0.005	1.074	0.8936
300.00	65.00	20.00	0.004	0.955	0.891
300.00	45.00	10.00	0.002	0.382	0.9661
600.00	55.00	20.00	0.005	1.051	0.9587
900.00	65.00	20.00	0.011	2.746	0.9694
900.00	55.00	15.00	0.009	1.886	0.9918
300.00	45.00	20.00	0.002	0.405	0.9581
900.00	65.00	10.00	0.01	2.459	0.9997
600.00	65.00	15.00	0.006	1.552	0.9572
300.00	55.00	15.00	0.0035	0.668	0.9745
900.00	45.00	20.00	0.005	1.218	0.9342
600.00	55.00	15.00	0.005	1.062	0.9601
600.00	55.00	10.00	0.004	0.883	0.924
600.00	45.00	15.00	0.002	0.573	0.9429

4. Conclusion

Drying specifications of cumin seeds were assessed during microwave-assisted fluidized bed drying at various levels of air temperature, microwave power and air velocity. The entire dehydration process occurred in the falling rate period. Applying higher values of microwave output power, air temperature and air velocity enhanced drying rate and D_{eff}. Although increased to more than the minimum fluidization velocity of air flow rate, did not show a significant impact on drying rate. Simulation elliptical cumin seed to cylinder, to obtain D_{eff} and E_a offered good results with high amount of R^2. Usage of RSM ensured that the selected factors had significant effect on responses and on each other as well. Increment in air temperature and air velocity used in this study, caused decrement in E_C value but microwave power affected on E_C in increasing manner. And finally optimum condition obtained by RSM offered that operating minimum fluidization velocity, maximum value of microwave power and air temperature, maximize drying rate value and minimize energy consumption value.

5. References

[1] Aliakbarlu, J., S.K; Sadaghiani; S. Mohammadi, *Comparative evaluation of antioxidant and anti food-borne bacterial activities of essential oils from some spices commonly consumed in Iran.* Food Science and Biotechnology, 2013. 22(6): p. 1487-1493.

[2] Amin, G.; *Cumin*. Vol. 111. 2012, Tehran: Tehran University of Medical Sciences Press.

[3] Zomorodian, A; M. Moradi, *Mathematical modeling of forced convection thin layer solar drying for Cuminum cyminum.* Journal of Agricultural Science and Technology, 2010. 12: p. 401-408.

[4] Rai, N., et al., *A Monographic Profile on Quality Specifications for a Herbal Drug and Spice of Commerce-Cuminum cyminum L.* International Journal of Advanced Herbal Science and Technology, 2012. 1(1): p. pp. 1-12.

[5] Al-Snafi, A.E.; *The pharmacological activities of Cuminum cyminum-A review.* IOSR Journal of Pharmacy, 2016. 6(6): p. 46-65.

[6] Torki-Harchegani, M., et al., *Dehydration behaviour, mathematical modelling, energy efficiency and essential oil yield of peppermint leaves undergoing microwave and hot air treatments.* Renewable and Sustainable Energy Reviews, 2016. 58: p. 407-418.

[7] Askari, G.; Z. Emam-Djomeh.; S. Mousavi.; *Heat and mass transfer in apple cubes in a microwave-assisted fluidized bed drier.* Food and Bioproducts Processing, 2013. 91(3): p. 207-215.

[8] Piskunov, N.S., *Differential and integral calculus*. Vol. 2. 1974: Mir.

[9] Souraki, B.A.; D. Mowla, *Axial and radial moisture diffusivity in cylindrical fresh green beans in a fluidized bed dryer with energy carrier: Modeling with and without shrinkage.* Journal of Food Engineering, 2008. 88(1): p. 9-19.

[10] Crank, J., *The mathematics of diffusion*. 1979: Oxford university press.

[11] Mahendran, R.; G. Jayashree.; K. Alagusundaram. *Application of computer vision technique on sorting and grading of fruits and vegetables.* J Food Process Technol, 2012. 10: p. 2157-7110.

[12] Rattanadecho, P.; N. Makul, *Microwave-assisted drying: A review of the state-of-the-art.* Drying Technology, 2016. 34(1): p. 1-38.

[13] Qi, L.-L., et al., *Comparison of drying characteristics and quality of shiitake mushrooms (Lentinus edodes) using different drying methods.* Drying technology, 2014. **32**(15): p. 1751-1761.

[14] Goksu, E.I.; G. Sumnu.; A. Esin, *Effect of microwave on fluidized bed drying of macaroni beads.* Journal of Food Engineering, 2005. **66**(4): p. 463-468.

[15] Ghasemi, H.; H. Amini; M. Khayat, *An experimental study of fluidization of solids particles in a bubbling fluidized bed.* Modares Mechanical Engineering, 2015. 14(16).

[16] Gazor, H.R.; A. Mohsenimanesh, *Modelling the drying kinetics of canola in fluidised bed dryer.* Czech Journal of Food Sciences, 2010. **28**(6): p. 531-537.

[17] Rayaguru, K.; W. Routray, *Microwave drying kinetics and quality characteristics of aromatic Pandanus amaryllifolius leaves.* International Food Research Journal, 2011. 18(3).

Model of the solutes transfer during osmotic dehydration of vegetal matrices: a proposal

Muñiz, S.[a*]; Méndez, L.[a]; Rodríguez, J.[a]; Sandoval, S.[a]

[a]. Instituto Politécnico Nacional, Centro Interdisciplinario de Investigación para el Desarrollo Integral Regional Unidad Oaxaca, Calle Hornos 1003, Santa Cruz Xoxocotlán Oaxaca, CP 71230, México.

*E-mail of the corresponding author: sahylin85@gmail.com

Abstract

Osmotic dehydration of apple was modeled considering the mechanisms involved in the solutes transfer within the plant matrix: impregnation and diffusion. The model mathematical writing includes the impregnation layer thickness, the diffusion thickness, a water bulk flow and the convective resistance. Apple cylinders were dehydrated at 30, 50 ° C and 30, 50 ° Brix and a motion of 0.15 m/s. The Reynolds number was of 250 for 30°C-30°Bx and 500 for 50°C-50°Bx. Schmidt numbers was of 4000 for 30 ° C-30 ° Bx and 4200 for 50 ° C-50 ° Bx.

Keywords: transfer; solute; impregnation; osmotic dehydration.

1. Introduction

The understanding of the mechanisms involved in the solutes transfer within the food is fundamental to develop a predictive model of the osmotic dehydration operation. The mechanisms present in the solute transport of the osmotic solution within the plant tissue have not been elucidated. The solute transfer models developed so far, describe the osmotic solution migration by calculating a global transfer coefficient that considers a gradient of solute concentration uniform inside the food, limiting the identification of the mechanisms involved: diffusion or impregnation (Muñiz and others, 2017).

These models apply Crank's solutions to Fick's law to determine the transfer coefficient and they suppose some simplifications that contradict experimental findings that show the presence of solutes concentrated layers on the material surface, particularly when saccharides and sweeteners are used as osmotic solutions, which are evidence of an unequal distribution of osmotic solution within the plant matrix (Assis and others, 2015; Seguí and others, 2012).

Unlike the models available in the literature that consider a global solute transfer coefficient, this work proposes a model that describes the mechanisms involved in the transfer of the solute within the plant matrix: impregnation and diffusion and assumes boundary conditions that they take in counts the effect of external and internal resistances in the fruit-osmotic solution interface.

2. Materials and Methods

2.1. Boundary conditions for the modeling of solute transfer in osmotic dehydration.

Apples samples were considered as slab and solute transported was assumed to occur in one direction. For boundary conditions the overall solute transfer process depend of the relationship of internal and external resistances in the osmotic solution-apple interface, determined by Reynolds and Schmidt numbers.

2.2. Movement velocity and dimensionless numbers.

Apple samples were moved in a vertical in a vertical direction at frequencie of 100 cycles/minutes about 0.15 m/s.

Solution movement was affected significantly by solute movement, therefore the interface resistance was not negligible. Thus at the solution-apple interface the boundary conditions is:

$$K(C_\infty - C_s) = -D_s \left(\frac{\partial C}{\partial x} \right)_s$$

(1)

K-mass transfer coefficient (m/s), C_∞- solution concentration far from the interface (kg/m^3) and C_S-solution concentration at the interface apple-osmotic solution (kg/m^3).

The velocity was determined by the equation (2):

$$U = \frac{2\pi R w}{\cos(2\pi w t_m)}$$

(2)

U-verticalvelocity (m/s), ω-frequency (cycles/minutes),R- radius (0.015 m) and t_m-time of the movement (s).

The relative velocity of apple sample and solution was supposed to be the average velocity of apple. This velocity was used for calculation of Reynolds (Re) and Schmidt (Sc) numbers.

$$Re = \frac{LU\rho_s}{\mu}$$

(3)

$$Sc = \frac{\mu}{\rho_s D}$$

(4)

L-diameter of apple sample (m), ρ_s-solution density (kg/m^3), μ-viscosity of the sucrose solution (kg/ms), D-binary diffusivity (m^2/s). Sucrose solution viscosity and density were estimated from the literature.

2.3. Penetration depth of the solute or active zone.

The penetration depth of the solute (z_p) was determined experimentally using the scanning electron microscopy (SEM) technique. The apple sample was analyzed in cross section from the surface to the center. The thickness of the area where structural changes are observed was determined and used to estimate the penetration depth of the solute or active zone. In addition, the tissue area beyond the zone of structural change was observed to check if it remained as at the beginning of the treatment.

Prior to SEM examination, the materials were osmotically dehydrated by applying a factorial experimental design at two levels for temperature (30, 50°C), a sucrose osmotic solution concentration (30, 50 °Bx) and a motion level of 0.15 m/s. Three replicates for each treatment were conducted. High-quality stereo images and surface parameters were recorded from samples osmotically dehydrated and cut in cross section. For the study by SEM, the cross section of the apple sample was analyzed dividing it into 5 areas from the

outermost layer to the center. Area 1 corresponds to the outermost surface of the sample and area 5 to the material center.

2.4. Modelling of transport mechanisms during osmotic dehydration of fruit in sucrose solution.

Modifying the mathematical writing of the equations that describe the solutes transport in OD requires an analysis of the mechanisms involved: impregnation and diffusion. For this it is necessary to take into account the following considerations: water bulk flow acts as a resistance that opposes the transfer of the solute and limits it to migrate mostly in the superficial layers of the food; the water flow from food is greater than the flow of solutes entering the plant matrix; water flow is the sum of: water in the pores (free water) + water in the extracellular volume + water in the intracellular volume (bound water); water that leaves the plant matrix is transferred mainly by capillary diffusion; solute flow is the sum of: solute in the pores + solute in the extracellular volume concentration of the osmotic solution inside the food changes; the highest concentration of the solute is impregnated on the surface of the plant matrix when solutions of saccharides and natural sweeteners are used; hydrodynamic boundary layer influences the initial concentration of the impregnation layer C_i; thickness of the impregnation layer δ_{imp} changes with the time of the process. Based on the above assumptions, the following equations are proposed to determine the transfer of solutes in OD:

$$\frac{\partial C}{\partial t} = solute\ flow\ potential - water\ flow\ potential \tag{5}$$

$$\frac{\partial C}{\partial t} = \nabla^2 Cs - \nabla^2 Cw \tag{6}$$

$$\frac{\partial C}{\partial t} = \gamma(Diffusion) - \gamma(Capillary\ diffusion) \tag{7}$$

$\nabla^2 Cs$ -solute flow potential; $\nabla^2 Cw$-water flow potential; C-concentration (kmol/m^3), t-time (s), γ-coefficient.

3. Results and discussions

Reynolds number (Table 1) for the experiment was found to be approximately 205 and 500 for 30°C-30°Bx and 50°C-50°Bx respectively with 0.15 m/s of motion level. The flow regime for both experience were thus laminar flow. The calculation of dimensioanles

numbers showed the average Reynolds number of all the experiments was small (<600) and very high Schmidt numbers (4000 for 30 ° C-30 ° Bx and 4200 for 50 ° C-50 ° Bx).

Table 1. Properties of the osmotic solution to determine the Reynolds number

Temperature (•C)	Concentration (•Bx)	Diameter (m)	Velocity (m/s)	Re	Sc
30	30	0.015	0.10	250	4000
50	50	0.015	0.10	500	4200

During osmotic fruit dehydration, sucrose or synthetic osmotic solutions are generally used, in a mass fraction of 60% w / w or more. These solutions have high viscosity and have low diffusion. These operating conditions imply high Sc numbers and low Re numbers, generally in laminar flow regime (Bui and others, 2009).

From the thickness of the zone where the structural change was observed, the value of the penetration depth of the solute z_p was estimated. Scanning electron microscopy turned out to be an efficient technique (Figures 1 and 2) for the detection of structural changes areas in the osmotically dehydrated apple tissue.
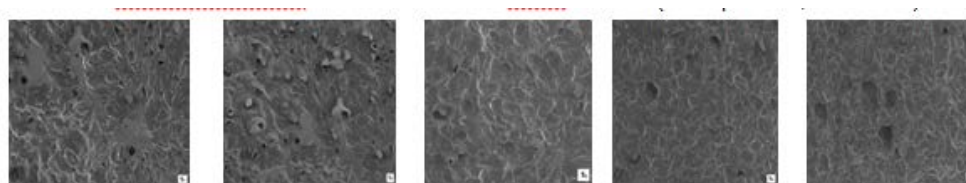
Fig. 1. Micrograph of dehydrated apple in sucrose 50 • C-50 • Bx. Increase 50x (S1-surface; S5-center).
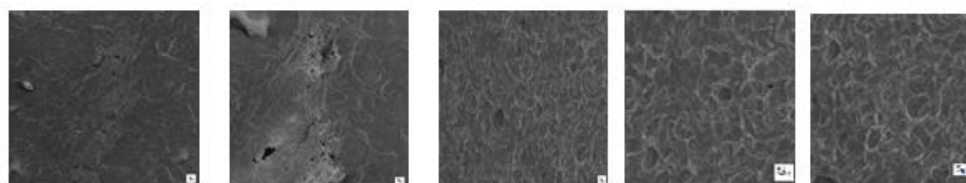
Fig. 2. Micrograph of dehydrated apple in sucrose 30 • C-30 • Bx. Increase 50x (S1-surface; S5-center).

In 1 and 2 areas the greatest structural changes are observed, these being the closest to the external surface of the material. In these areas, we observed certain zones where the structure of the tissue is collapsed with the presence of solids that clog the pores and the intercellular spaces disappear. In areas 3, 4 and 5 closest to the center of the sample, small and irregularly shaped intercellular spaces are observed, very similar to those presented in

the microscopy of the fresh apple. The values of the solute penetration depth estimated were 3.03 and 3.68 mm for the conditions of 30 °C-30 °Bx and 50 °C-50 °Bx.

4. Conclusions

This model can be useful for the design and optimization of the industrial osmotic dehydration process since it will be able to successfully predict the area where the superficial impregnation of the sucrose occurs and the area where the solute diffuses.

5. References

[1]   Muñiz, S.; Méndez, L.; Rodríguez, J. Solute transfer in osmotic dehydration of vegetable food: a review. Journal of food science 2017, 82(10):2251-2259.

[2]   Assis, F., Morais, R., Morais, A. Mass transfer in osmotic dehydration of food products: comparison between mathematical models. Food Engineering Reviews 2015, 8(2):116-133.

[3]   Seguí, L.; Fito, P.; Fito, P. Understanding osmotic dehydration of tissue structured foods by means of a cellular approach. Journal of Food Engineering 2012, 110(2).

[4]   Bui, H.; Makhlouf, J.; Ratti, C. Osmotic dehydration of tomato in sucrose solutions: Fick´s law classical modeling. Journal of food Science 2009, 74(5).

Three-dimensional measurement of internal structure in frozen food materials by cryogenic microtome imaging system

Do, G. [a]*; Sase, S. [a]; Bae, Y. [b]; Maeda, T. [c]; Ueno, S. [d] and Araki, T. [e]

[a] College of Bioresource Science, Nihon University, Kanagawa, Japan

[b] College of Life Science and Natural Resources, Sunchon National University, Jeollanam-do, Korea

[c] Nisshin Foods INC., Tokyo, Japan

[d] Faculty of Education, Saitama University, Saitama, Japan

[e] Graduate School of Agricultural and Life Sciences, The University of Tokyo, Tokyo, Japan

*E-mail of the corresponding author: dogabsoo@nihon-u.ac.jp

Abstract

The objective of this work was to establish a three-dimensional measuring method for the size, morphology and distribution of internal structure such as ice crystals, bubbles and solids content within an ice cream sample by using a cryogenic microtome spectral imaging system (CMtSIS). The 3-D images of ice crystals, bubbles and milk solids were recognized by reconstructing the circles in 2-D images into 3-D spheres; and the Overrun by Volume (ORV) was obtained by incorporating the area of bubbles on integrated image and the volume of bubbles in the 3-D image.

Keywords: Ice crystal, Bubble, Internal structure, Spectral imaging, Micro- to macro-scale, Freeze-Drying

1. Introduction

Most food materials are composed of limited structural elements such as a solid content, bubble and ice crystal. The internal structure in frozen food materials undergoes metamorphic changes due to recrystallization process which increases the size of ice crystals during frozen storage. The size and shape of internal structure formed in a frozen material strongly influence the final quality as well as the freezing rate or heat flux and the direction of heat flow within the material during freezing. For a proper understanding of the behavior of heat or mass transfer in frozen food materials and the behavior of freeze-drying, knowledge of the internal structure of frozen food materials is required. Ice cream is considered as a complex multiphase system consisting of bubbles, ice crystals and milk solids, and the final quality of which is influenced by the correlation between the size, morphology and distribution of the multiphase formed during the manufacturing process. Attempts have been made to observe bubbles and ice crystals on the cross sections of ice cream by using an optical microscope [1] or by indirect methods using SEM [2] or Cryo-SEM [3]. The SEM and Cryo-SEM allow the identification of morphological difference between bubbles and ice crystals by the micro asperity of a sublimated sample surface, but it is difficult to determine whether a sublimated seam is caused by an ice crystal or by a bubble. Furthermore, the measurement of bubble size by traditional methods would result in misleading numbers due to limitations in observing the entire volume of a bubble. Different cross sections would provide different diameters for the same bubble. And the values of the diameters reported by traditional methods might not correlate well with the final quality of ice cream since the measurements on bubbles, ice crystals and milk solids were taken from separate samples. X-ray micro-computed tomography (X-ray μCT) has been applied to three-dimensional (3-D) structural elements of frozen food materials [4, 5]. It is based on the contrast in X-ray images generated by differences in X-ray attenuation arising from differences in the density of material within a sample. Also, frozen food materials that contain water are freeze-dried to clarify density contrast. The objective of this work was to establish a 3-D measuring method for the size, morphology and distribution of internal structure such as ice crystals, bubbles and solids content within ice cream samples prepared at three different overrun levels.

2. Experimental Equipment and Materials

2.1. Cryogenic microtome spectral imaging system

The CMtSIS [6] consists of a microtome unit, an automatic high-precision XY stage, an image acquisition unit (visible, fluorescence and spectroscopic), and a 3-D image processor (Fig. 1). The CMtSIS allows consecutive image acquisition of the cross sections of a frozen sample exposed by multi-slicing with a minimum thickness of 0.25 μm. The temperature of the heat exchanger is controlled from room temperature to –160°C by regulating the flow

rate of liquid nitrogen and the power to an electric heater installed in the heat exchanger. Microscale and macroscale images can be obtained with a high-power objective lens of a microscope installed on the automatic high-precision XY stage (ALD-106-H1P, Chuo Precision Industrial Co., Ltd., Japan) that can be mechanically adjusted with a resolution of 6 µm within a maximum area of 60×60 mm^2. The image of each cross section is captured with a highly sensitive CCD and an NIR camera, and is recorded by the 3-D image processor. A 3D image is reconstructed from a series of consecutively acquired 2-D images.
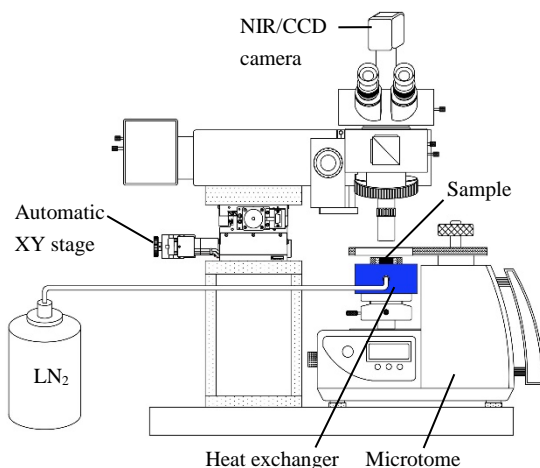
Fig. 1 Schematic diagram of cryogenic microtome spectral imaging system (CMtSIS).

2.2 Materials and methods

A lump of vanilla ice cream mix (from ZAO, Yamada milk Co., Ltd. Miyagi, Japan) with a formulation of 8% milk fat, 10% milk solids-not-fat, sugar, honey, stabilizer and an emulsifier was taken from a commercially available soft ice cream. Ice cream samples at three different overrun levels (low, medium, and high) were produced by an automatic batch preezer (191 P/SP/N, Carpigiani group, bologna, Italy). Ice cream agglomerate shaped into a cylindrical sample with a diameter of 10 mm and a height of 10 mm was shock frozen in liquid nitrogen. The sample was embedded in an optimal cutting temperature (OCT) compound and a ring of dry ice. The sample, OCT compound, and the ring of dry ice fixed on the heat exchanger were sliced together, and cross-sectional images were then captured by the CCD camera through a microscope. Bubbles, ice crystals and milk solids in the ice cream sample were identified from the CMtSIS iamges by the microscale to macroscale measurement method previously reported by Do et al. [6].

3. Results and Disussion

3.1. Overrun by weight

Overrun is the industrial term for the amount of air added to frozen dessert products, and the percent overrun of ice cream by weight can be calculated by the following equation [7]:

$$\% \text{ Overrun by weight (OR)} = \frac{Wt.\,of\,mix - Wt.\,of\,same\,vol.\,of\,ice\,cream}{Wt.\,of\,same\,vol.\,of\,ice\,cream} \times 100 \qquad (1)$$

The overrun of commercial ice cream can range from 24% (super-premium) to 94% (light and fluffy). Percent overrrum by weight was measured for the ice cream samples prepared at three overrun levels and the mean values were 11.5%, 44.0% and 73.8% for low, medium, and high overrun levels, respectively (Table 1).

Table 1.   Precent overrun by weight

Statistics		Overrun levels		
		Low	**Medium**	**High**
OR	Maximun	12.7	46.7	75.7
	Minimun	10.3	40.9	72.0
	Mean	11.5	44.0	73.8
	SD	1.0	1.4	1.9

3.2. Measurement of bubble

A total of 36 image frames was obtained from a sliced surface by using the CCD camera, the ×50 magnification lens, and the automatic high-precision XY stage. Each frame covered an area of 194×154 µm^2. The 36 frames were integrated into a single image by a 3-D image processor. Fig. 2 shows an integrated raw image and a binary image representing the boundaries of identified bubbles covering a measurement area of 1164×924 µm^2 with a total of 7800×6180 pixels. Fig. 3 shows the distribution of equivalent circle diameters of the bubbles in the sample of 11.5% OR (low overrun). A total of 480 bubbles was recognized from the integrated image: the equivalent circle diameters ranged from 1.1 to 101.9 µm with a mean of 24.8 µm, and the measured areas ranged from 0.9 to 8144.9 µm^2 with a mean of 637.8 µm^2. Fig. 4 shows the distribution of equivalent circle diameters of the bubbles found in the sample of 44.0% OR (medium overrun). A total of 1988 bubbles was recognized from

a) Raw iamge   b) Boundaries of bubbles
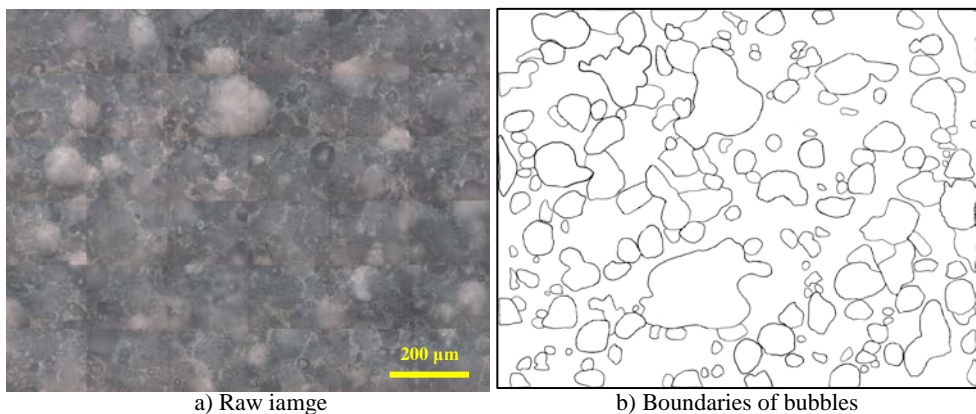
Fig. 2 Binarization of an integrated image to identify the bubbles in an ice cream sample.
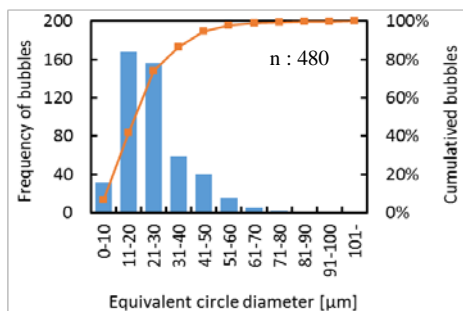
Fig. 3 Equivalent circle diameter of bubbles in the sample of 11.6% OR.
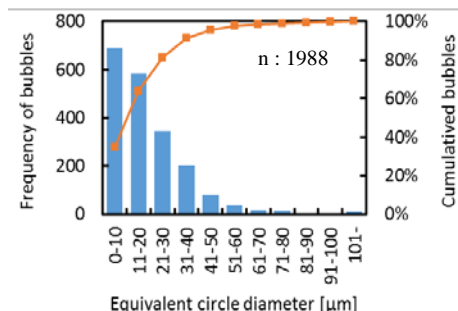
Fig. 4 Equivalent circle diameter of bubbles in the sample of 44.0% OR.

the integrated image: the equivalent circle diameters ranged from 1.1 to 140.4 μm with a mean of 25.8 μm, and the areas ranged from 0.9 to 15479.8 μm^2 with a mean of 749.0 μm^2. Fig. 5 shows the distribution of the equivalent circle diameters of the bubbles in the high overrun sample (73.8% OR). A total of 692 bubbles was recognized from the integrated image: the equivalent circle diameters ranged from 1.1 to 248.2 μm with a mean of 40.3 μm, and the areas ranged from

Fig. 5 Equivalent circle diameter of bubbles in the sample of 73.8% OR.

0.9 to 48362.0 μm^2 with a mean of 2035.9 μm^2. The actual size of the integrated images was 1164×924 μm^2 and from these images the range of the areas of the recognized bubbles was determined to be from microscale of 0.9 to macroscale of 48362.0 μm^2.

3.3. Overrun by volume

The CMtSIS has functions to capture the cross-sections exposed by multi-slicing of a frozen sample with a minimum thickness of 1 μm and to reconstruct a 3-D image utilizing a series of consecutively acquired 2-D images. The volume rendering method was employed as the optimum one for the system to measure internal structures. Using this method the volume can be determined from the surface areas of quantitative 2-D information. Overrun can be determined as the percentage increase in volume or area of the mix that occurs as a result of air addition, and can also be calculated by the following equation [7]:

$$\% \text{ Overrun by volume (ORV)} = \frac{Vol. of\ ice\ cream\ -\ Vol. of\ mix\ used}{Vol. of\ mix\ used} \times 100 \quad (2)$$

Fig. 6 compares the OR values calculated from the weight measurements and the ORV values obtained from the area of bubbles on integrated image analysis using the CMtSIS for the ice cream samples prepared at three overrun levels. The means of obtained ORV values were 10.5%, 42.8%, and 77.7% for low, medium, and high overrun levels, respectively; whereas the corresponding OR measurements were 11.5%, 44.0%, and 73.8%. Thus, the measurement accuracy of the CMtSIS was verified in estimating the percent overrun by volume for frozen ice cream samples.
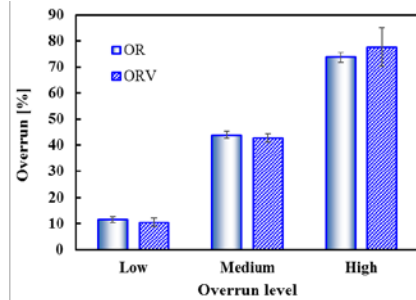
Fig. 6 OR and ORV for different overrun levels.

3.4. Three-dimensional measurement of the internal structure of ice cream

An ice cream sample of 12.7% OR was prepared to measure the 3-D internal structure. Although the bubbles, ice crystals and milk solids could be recognized from an original 2-D image (Fig. 7) by visual evaluation, it was difficult to obtain a binary image of these only by applying automatic thresholding techniques. Therefore, the boundaries of individual bubbles, ice crystals and milk solid were traced manually on a digitizing board (Cintiq 21UXTZ-2100, WACOM Ltd, Japan) as shown in the upper row of Fig. 7. After extracting the pixels within the traced boundaries and obtaining binary images, the volumes of each bubble and ice crystal were calculated to represent the morphology. The 3-D images of bubbles, ice crystals and milk solids were reconstructed using 100 cross-sectional images (slicing thickness: 4 μm). The 3-D images of bubbles, ice crystals and milk solids (the lower row of Fig. 7) were reconstructed based on the binary images. The dimension of each 3-D image was 260 μm in length, 206 μm in width and 400 μm in height. By using an image processing software (TRI/3D VOL, Ratoc Ltd, Japan), the volumes of each bubble and ice crystal were calculated from the 3-D images. A total of 1178 bubbles was recognized by reconstructing the circles in the 2-D images into 3-D spheres and their volumes ranged from 0.125 mm^3 to 490.421 mm^3 with a mean of 2.342 μm^3 as shown in Fig. 8. Furthermore, an ORV of 14.8% was obtained by incorporationg the volume of bubbles in the 3-D image for the ice cream sample of 12.7% OR. A total of 186 ice crystals were recognized by reconstructing the circles in the 2-D images into 3-D spheres and their volumes ranged from 0.125 mm^3 to 5493.684 mm^3 with a mean of 34.483 mm^3 as shown in Fig. 9. By observing the 3-D images (Fig. 7-b, c), it is recognized that the bubbles are evenly distributed in the ice cream sample, but the ice crystals are less evenly distributed. Milk solids are observed in the form of a retinal structure circumscribing bubbles and ice crystals as shown in Fig. 7-a.d. The bubbles are observed within ice crystals and milk solids.

Measurement of bubbles is difficult when using SEM or Cryo-SEM because of sublimation at the sample surface. Ice crystals and bubbles within a sample can be resolved by the vacant spaces left after freeze-drying. Since all vacant spaces are treated as ice crystals and bubbles in the analysis of a freeze-drying process, some questions may be raised to the identification of ice crystals and bubbles. Therefore, a 3-D measuring method for the size, morphology and distribution of internal structure such as ice crystals, bubbles and solids content within an ice cream sample was established in this research by using the CMtSIS.

| a) Ice cream | b) Bubble | c) Ice crystal | d) Milk solid |
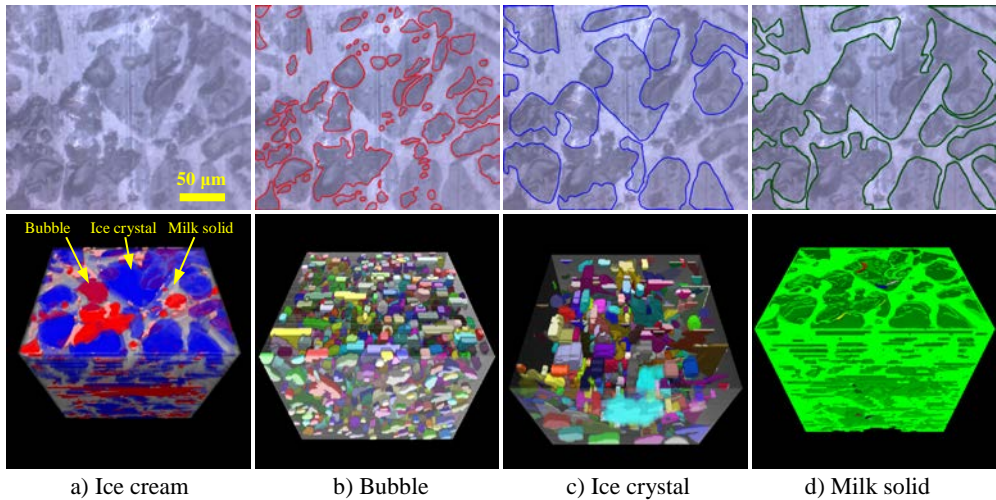
Fig. 7 Morphology and distribution of internal structure of ice cream.
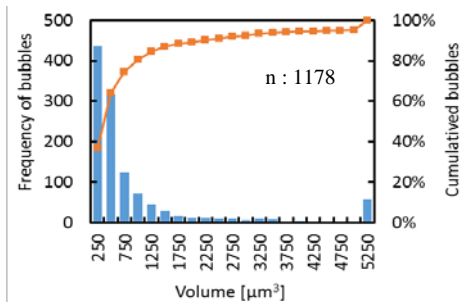
Fig. 8 Distribution of volume of bubbles.
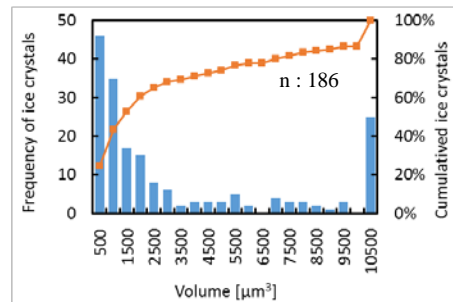
Fig. 9 Distribution of volume of ice crystals.

4. Conclusions

A novel technique was developed for the detection of 3-D internal structure of ice cream samples produced at different overrun levels and its high accuracy was verified by using the CMtSIS. The following conclusions were reached:

1. The actual size of the integrated images was 1164×924 µm² and from these images the range of the areas of the recognized bubbles was determined to be from microscale of 0.9 to macroscale of 48362.0 µm².

2. The means of obtained ORVs were 10.5%, 42.8%, and 77.7%, whereas the means of the measured ORs were 11.5%, 44.0% and 73.8% for the ice cream samples produced at three overrun levels (low, medium, and high, respectively).

3. The estimated volumes of bubbles ranged from 0.125 mm³ to 490.421 mm³ with a mean of 2.342 µm³, and those for ice crystals ranged from 0.125 mm³ to 5493.684 mm³ with a mean of 34.483 mm³ in the 3-D image for the ice cream sample of 12.7% OR.

4. The ORV of 14.8% was obtained by incorporating the volume of bubbles in the 3-D image in the case of the ice cream sample of 12.7% OR.

5. Acknowledgment

6. References

[1] Chang Y., Hartel R.W. (2002), Development of air cells in a batch ice cream freezer, Journal of Food Engineering, 55, pp71-78

[2] Eisner M. D., Wildmoser H., Windhab E. J. (2005), Air cell micro structuring in a high viscous ice cream matrix, Colloids and Surfaces A: Physicochem. Eng. Aspects, 263, pp390-399.

[3] Goff H.D. Verespej E., Smith A.K. (1999), A study of fat and air structures in ice cream, International Dairy Journal, 9, pp817-829.

[4] Zhao, Y.; Takhar, P. S. Micro X-ray computed tomography and image analysis of frozen potatoes subjected to freeze-thaw cycles, LWT - Food Science and Technology, 2017, 79, 278-286.

[5] Jin, J.; Yurkow, E. J.; Adler, D.; Lee, T. Improved freeze drying efficiency by ice nucleation proteins with ice morphology modification, Food Research International, 2018, 106, 90-97.

[6] Do, G.; Sase, S.; Bae, Y.; Maeda, T.; Ueno, S.; Araki, T. Microscale to Macroscale Measurement of Bubbles in Frozen Materials with Cryogenic Microtome Spectral Imaging System, Japan Journal of Food Engineering, 2017, 18(3), 125-132.

[7] Goff, H. D.; Hartel, R.W. Ice cream, seventh edition; Springer: New York, 2013; 184-191.

Dynamic optimization of the transmission efficiency between the solid state microwave sources and the microwave applicator

Zuber, S.[a]*; Joss, M.[a]; Tresch, S.[b]; Kleingries, M.[b]

[a] Institute for electrical engineering. Lucerne University of Applied Sciences and Arts, Lucerne, Switzerland

[b] Institute for mechanical engineering and energy technology. Lucerne University of Applied Sciences and Arts, Lucerne, Switzerland

*E-mail of the corresponding author: simon.zuber.01@hslu.ch

Abstract

Microwaves are a fast way to dry moist goods through volumetric heating. During the drying process, materials change their electrical properties. As a result, the impedances at the feed port of the applicator will change and the microwave source is not matched anymore. The amount of reflected power increases and the process efficiency reduces. New semiconductor high power sources can perform a dynamic impedance matching. A lab scaled functional model with two sources was designed and realized. For measuring the scattering parameters during the process run, an embedded two-port vector network analyzer was added. Measurement results confirm the feasibility of the concept.

Keywords: Microwave drying, dynamic efficiency optimization, multichannel feed, solid state based microwave source

1. Introduction

Microwaves (mw) allows a volumetric heating method used to dry moist goods. The volumetric heating is faster than conventional drying as soon as the surface of the good becomes dry and the core is still wet [1]. The most common method for an mw source in industrial applications today is the magnetron. It builds on proven technology, is cost-effective and can also produce power in the kW range. But it also has some disadvantages such as the need of a high tension power supply and an output signal at a fix frequency. For optimum power transfer, the source is impedance matched to the load. However, during the drying process, materials change their electrical properties. And this will change the wave distribution inside the microwave applicator too. As a result, the impedance at the feed port of the applicator will change and the source is not matched anymore. The amount of reflected power increases and the process efficiency reduces. Figure 1 shows the measured reflected power in percentage in relation to the moisture content in a drying process. Underneath a certain moisture content, the reflected power increases. This is led by means of a circulator to an artificial load and converted into heat.
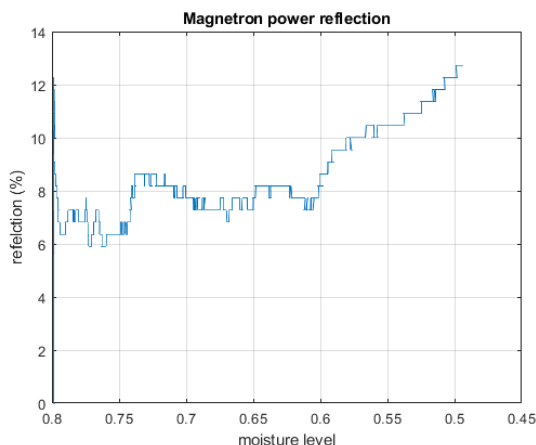
Fig. 1 increasing power reflection of a magnetron heating system due to load change

Frequency synthesizers and semiconductor power amplifiers for the 2.45 GHz ISM band are becoming available for industrial applications. An mw source based on these components is able to change the frequency and phase of the created signal. This enables dynamic impedance matching, based on a search for the best frequency and phase condition.

Three dimensional finite element electromagnetic field simulations of several microwave chambers and drying goods have shown, that two feed ports are especially a benefit in a drying process [2]. This comes from the fact that a two port applicator allows a smoother electromagnetic field distribution, even if the volume of the good is shrinking over the drying process. In addition, during the drying process the impedance matching of two ports must be adapted continuously. Simulation results presented in previous papers showed that the optimum frequency and the optimal phase shift between two feeds can be estimated by means

of complex scattering parameters [3] [4]. The objectives of our work were to verify the various simulation results by means of a lab scaled functional model of a two port applicator. In addition, we show the feasibility of a tunable mw source based on semiconductor components. Such a source is a prerequisite for searching the optimum operating point in the drying process.

Chapter two lists the applied methods and materials we used in our work. Chapter three describes the measurement and optimization algorithm. In the following chapter four, the system architecture of the two port mw source is explained. In chapter five measurement results are explained and discussed. The final chapter six contains the conclusion and hints for further work.

2. Materials and Methods

For the functional model of a semiconductor based two port mw source with frequency synthesizer, phase adaptation and embedded vector network functionality for measuring the scattering parameters (s-parameter), a suitable printed circuit board based microwave circuit was designed and produced. Although the available microwave output power was limited to 250 mW the measurement principles and the verification of the optimization algorithm could be done.

The two port mw source was connected to the applicator by means of WR340 waveguides. The applicator is made of aluminum and has a box type shape with the size of 0.61*0.69*0.51 m. It works as a multimode oven [1]. The test good is placed on a weighing system in the center of the applicator, which allows to continuously weight the good during the drying process. In order to avoid the condensation of water vapor on the walls of the applicator, a ventilation system was installed.

In order to check the quality of the measured s-parameters with the built-in measuring device, all parameters were additionally measured with a Rhode & Schwarz commercial network analyzer.

The used test good was a mixture of flour and water.

3. Algorithm for efficiency calculation

The overall efficiency η_{tot} of a microwave heating system depends on various efficiency factors of the subsystems.

$$\eta_{tot} = \eta_{gen}\,\eta_{feed}\,\eta_{trans}\,\eta_{appl} \quad (1)$$

The efficiency of the microwave source η_{gen} is mainly determined by the efficiency of the solid state power amplifier. The factor of feeder network efficiency η_{feed} covers the losses of coupling elements, waveguides, power combiner and feeder antennas. The efficiency

factor of transmission η_{trans} is a figure of how good the impedance matching works. The efficiency factor η_{appl} from the applicator describes the losses due to heating up the metal walls by means of electrical induction.

The focus of our work is the optimization of η_{trans}. This factor strongly dependents on the impedance matching between the feeder and the applicator with its drying good. For optimizing the transmission efficiency, we define two ways how to measure and calculate it. Both methods are applicable for a microwave applicator with two feeds.

The first method is suitable if both sources are simultaneously active and the electromagnetic fields are overlapped. The efficiency is calculated from the ratios between the reflected waves $b_{1,2}$ and the input waves $a_{1,2}$ at the individual feeder ports of the microwave applicator. The indices gives the individual port number. Because these waves represent voltage waves, the square of them are proportional to the power which leads directly to the needed power efficiency figure. The wave b_1 is a superposition of the reflected wave at port one and the through connection part from port two. In the same way the wave b_2 consists of the reflected wave at port two and the part which is transferred from port one. η_{trans} will be maximized if the individual wave reflection at the ports can be minimized and the feed trough parts can be minimized. To find the optimal operation point the measurement and calculation for η_{trans} must be done separately for every frequency and phase difference between the two sources.

$$\eta_{trans} = 1 - \frac{1}{2}\left|\frac{b_1}{a_1}\right|^2 - \frac{1}{2}\left|\frac{b_2}{a_2}\right|^2 \quad (2)$$

The second method is based on the s-parameters and thus only on source must be active during the measurement process. This method is more complex but needs less measurements [4]. This is possible because the phase information for the superposition of the two sources is included in the s-parameter. The s-parameter is defined as a ratio between an input wave a and a reflected wave b. The index gives the individual port number. The first index of an s-parameters gives the number of the destination port and the second index the number of the source port. The s-parameters are complex numbers.

$$s_{11} = \frac{b_1}{a_1} \, , with \, a_2 = 0 \quad (3)$$

$$s_{12} = \frac{b_1}{a_2} \, , with \, a_1 = 0 \quad (4)$$

$$s_{21} = \frac{b_2}{a_1} \, , with \, a_2 = 0 \quad (5)$$

$$s_{22} = \frac{b_2}{a_2} \, , with \, a_1 = 0 \quad (6)$$

The transmission efficiency for a desired phase difference $\Delta\varphi$ can now be calculated by

$$\eta_{trans} = 1 - \frac{1}{2}\left|s_{11} + s_{12}e^{j\Delta\varphi}\right|^2 - \frac{1}{2}\left|s_{22} + s_{21}e^{-j\Delta\varphi}\right|^2 \quad (7)$$

For finding the optimal operating point with the highest η_{trans}, measurements must be done over all frequencies and calculations over all phases and frequencies.

4. Architecture of the system

To proof the concept that a microwave heating system based on semiconductor components allows a high transmission efficiency for several goods and moisture levels, a test hardware was built. The architecture of the system is shown in figure 2.
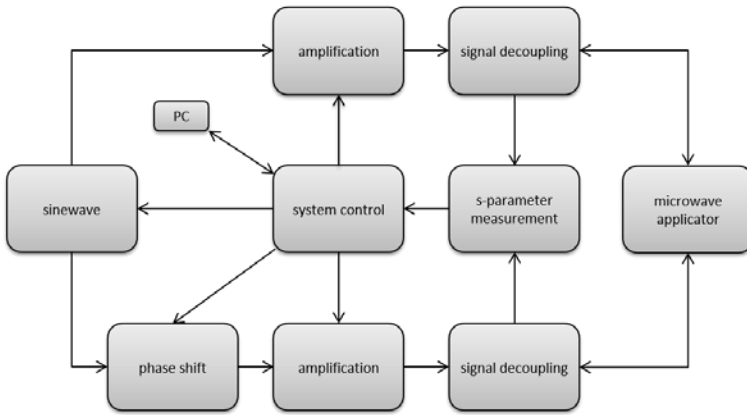
Fig. 2 block diagram of the functional prototype

The two sinewave signals are created with high performance, wideband rf synthesizers LMX2582 from Texas Instruments. This synthesizers are able to adjust both the output frequency and phase with a 32-bit resolution.

As for proofing the concept a high power is not needed, the two sinewave signals are only amplified with a driver amplifier MGA-30489 from Avago. The amplifier delivers 250 mW of microwave power.

For executing the s-parameter measurement the forward and the reflected signal wave must be separated first. A high power integrated directional coupler X3C26P1 from Xinger is used for this task. Only -30 dB of the individual signal waves are decoupled for the measurement.

The s-parameter measurement is done with an rf gain and phase detector AD8302 from Analog Devices. In the system control part a microcontroller is used for calculating the efficiency parameter. It also calibrates the measured values [5] and controls the other sub-systems such as sinewave generation, phase shifting and amplification.

5. Results and Discussion

To validate the concept and the prototype hardware several measurements with various material mixtures as indicated in table 1 have been done.

Table 1. Material mixtures

Moisture level:	Water:	Flour:
80% water	400 g	100 g
50% water	100 g	100 g
20% water	25 g	100 g

For the different measurement campaigns the frequency range from 2.4 GHz till 2.5 GHz with a step size of 1 MHz was swept through. For each frequency point the s-parameters where measured. With these set of s-parameters the efficiency for all frequencies and phase differences with a resolution of one degree where calculated with (7). Subsequently the highest efficiency η_{trans} over all phase differences is searched for each frequency. This maximum efficiency for all frequencies of the three moisture levels are depicted in figure 3.
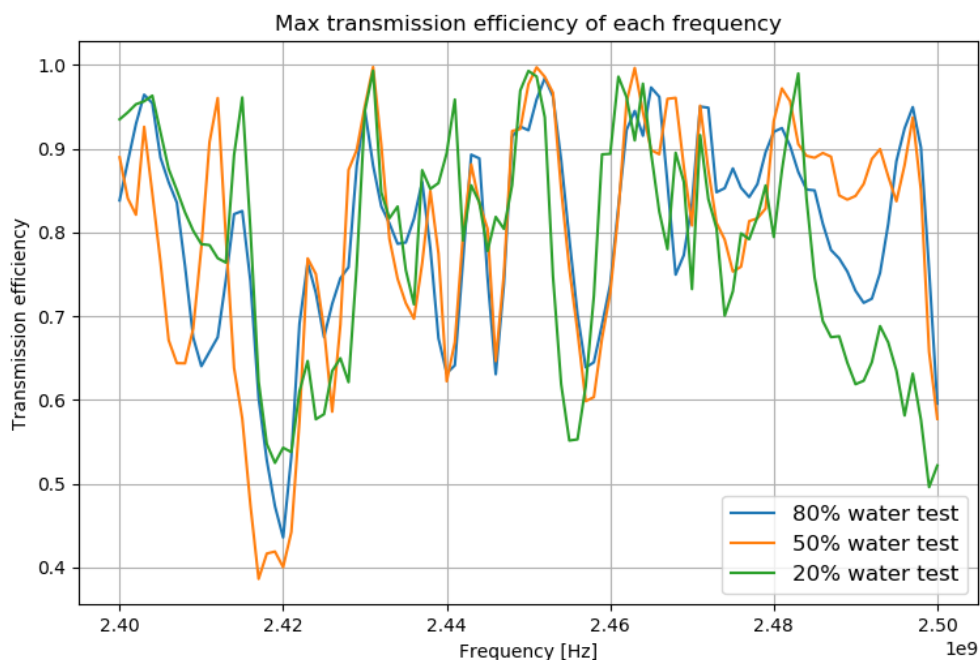
Fig. 3 calculated transmission efficiencies based on s-parameter measurements

The optimal frequency and phase difference changes during the drying process. Table 2 shows the best values found for the three moisture levels. The efficiency value remains almost on the same high level over all three measurement series.

Table 2. Ideal parameters

moisture level:	best efficiency:	frequency:	phase difference:
80% water	0.984	2.452 GHz	190°
50% water	0.997	2.451 GHz	202°
20% water	0.993	2.450 GHz	201°

For validating the measurement accuracy of the prototype hardware, a comparison of the calculated efficiency values have been done. The results are illustrated in figure 4. The blue color curve shows the calculated values with (7) based on s-parameter measurements done with the vector network analyzer ZVL6 from Rhode&Schwarz. The yellow curve shows the results calculated with (7) based on s-parameter measurements of the prototype hardware. And the green curve are the results based on the calculation method of (2). All three methods are very close to each other if the reflected power is small. However, the calculated efficiency values differ with increasing reflections.
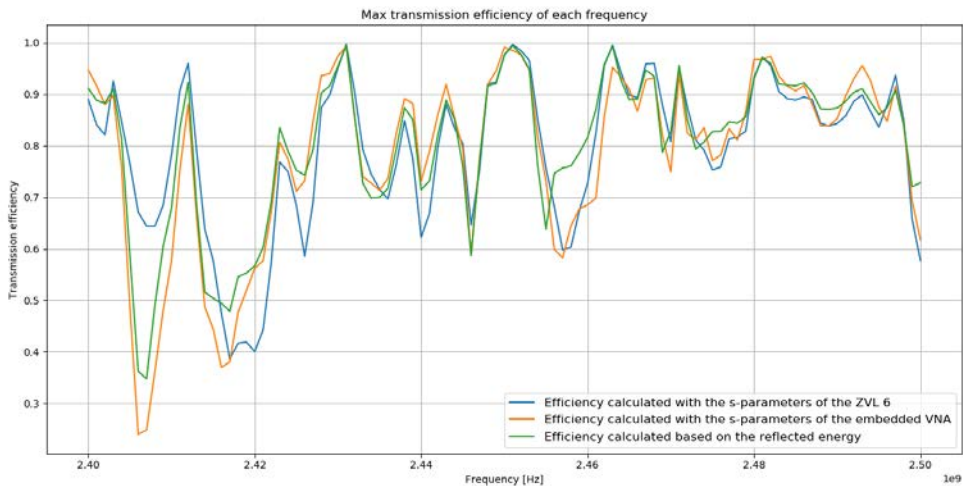
*Fig. 4 comparison of measurement methods (**mixture with 50% moisture level**)*

6. Conclusions

A microwave heating system is a fast and efficient way to dry goods. The classical solution based on a magnetron as microwave source gets problems to put the energy into the dry good if electrical properties changes at low moisture levels. A heating system based on a semiconductor solution as microwave source shows promising results. Such a system allows the adaptation of operation frequency and phase and offers an impedance tuning function during the running process. With an s-parameter measurement the optimal frequency point and phase difference can be determined and allows a maximization of the transmission efficiency. For a proof of concept, a lab scaled functional model was developed. An embedded system with two frequency synthesizers generates the two feeder signals. The power, frequency and phase of the signals can be controlled by means of a microcontroller system. For measuring the s-parameters during the process, an embedded two-port vector network analyzer was added. The obtained measurement results fulfill the expectations.

7. References

[1] R. Meredith, Engineers' Handbook of Industrial Microwave Heating, The Institution of Engineering and Technology, 2007, pp. 54-63.

[2] S. Zuber and M. Joss, "Multichannel Microwave Applicator," Lucerne, Switzerland, 2017.

[3] P. Korpas, A. Więckowski and M. Krysicki, "Effects of applying a frequency and phase-shift efficiency optimisation algorithm to a solid-state microwave oven," Institute of Radioelectronics, Warsaw University of Technology, 2016.

[4] A. Wieckowskia, P. Korpas, M. Krysickia, F. Dughiero, M. Bullo, F. Bressan and C. Fager, "Efficiency optimization for phase controlled multi-source microwave oven," Institute of Radioelectronics, Warsaw University of Technology, Warsaw, Poland, 2014.

[5] T. Valeria, A. Ferrero and M. Sayed, Modern RF and Microwave Measurement Techniques, Cambridge University Press, 2013.

Discrete modeling of ion transport and crystallization in layered porous media during drying

Rahimi, A.[a]*; Metzger, T.[b]; Kharaghani, A. [a]; Tsotsas, E. [a]

[a] Chair of Thermal Process Engineering, Otto von Guericke University of Magdeburg, Germany.
[b] Chemical and Process Engineering, BASF SE, Ludwigshafen, Germany.

*E-mail of the corresponding author: arman.rahimi@ovgu.de

Abstract

In this work, an isothermal pore network model has been utilized to investigate ion transport and crystallization in layerd porous media during drying. Said network consists of two distinct layers each with a different pore size distribution. One-dimensional approximation at the throat level describes transport phenomena for liquid, vapor, and dissolved salt. An explicit time stepping scheme has been used to obtain fluid pressure fields and ion concentration. Various simulations are carried out which indicate the effect of mean pore size disparity in the top and bottom layer, as well as the effect of drying rate on final crystal distribution.

Keywords: pore network modeling, composite material, drying porous media, crystallization, ion transport.

1. Introduction

Layered materials are among the most essential products influencing our lives ranging from everyday use to construction and industrial processes. Painted surfaces, interior wallpapers, composite materials, and fuel cell membrane-electrode combination are among many examples of layered materials. Depending on the application these layered materials may be exposed to a solution (or suspension) at one or several stages of their lifetime. Additionally in the majority of cases said exposure is accompanied by drying that has varying effects which also depends on production and applications of these materials. To this goal, it is paramount to study and identify factors affecting each scenario. In order to provide more context as to which parameters influence precipitation pattern several studies will be looked into in this section.

Preservation of masonry and cultural heritage is an important area where undesired crystallization within porous material is to be avoided. In this framework Pel et al.[1] studied one-sided drying of fire-clayed bricks contaminated by salt solution. In that work, nuclear magnetic resonance technique was used to measure moisture and NaCl content within the material. In the end it has been concluded that in historical objects generally the formation of efflorescence cannot be avoided. In a similar study the effect of crystallization inhibitors, whose function is to allow a higher degree of supersaturation before nucleation, on drying of fired-clay bricks and Granada limestone is studied by Gupta et al.[2]. Satisfactory results were achieved as the mass percentage of the nondestructive efflorescence has been dramatically elevated in the presence of inhibitors. Norouzi Rad et al.[3] studied the pattern of efflorescence formation depending on the spatial distribution pores sized at the surface of a packing of sand grains. Observations indicate that salt crystals are more inclined to form at the small pores as they stay wet for a longer time during drying as pores are sufficiently large to avoid blockage. That study points to the importance of porous media heterogeneity in crystal formation.

With sufficient context on drying induced crystallization in porous media, several studies on crystallization in layered porous structures will be reviewed here. One-sided drying of plaster/substrate systems, where evaporation happens always at the plaster surface, was studied through various experiments by Petković et al.[4]. Small pores are at the evaporating side when plaster is paired with Bentheimer sandstone. This leads to the majority of salt crystals to form at the surface or within the plaster layer. On the other hand, in a plaster/calcium-silicate brick system (smaller pores located in the substrate) although some salt crystallized in the plaster layer, a significant amount of crystals was found within the brick. The aforementioned nuclear magnetic resonance technique is used to study the effect of paints on drying behavior of plaster/substrate systems and stone specimens by Diaz Gonçalves et al.[5]. It is concluded that crystallization pattern varies depending on many variables such as the pore size of the interior region, hydrophobicity of the paint, and the

salt itself. This indicates that for such systems any kind of predictive statement should be limited to the specific framework and conclusions should be drawn very cautiously.

In this work, a 3D pore network represents the void space of the porous material. The bi-layered structure is modeled by two networks stacked on top of each other leading to a so-called "near surface" (top) and "interior" (bottom) region. Each region has its distinct pore size distribution which is sampled from a normal distribution. The entire network is initially filled with salt solution and evaporation takes place from the top. Simulations are carried out for various combinations of pore size distribution in the bottom and top layer as well as various drying rates. For the sake of comparison the top layer is kept identical among all simulations. Results are presented as solid deposit mass as well as saturation profiles.

2. Model description

The selected pore network model consists of two different types of pore geometry. The volume of the liquid in the network is located in the cylindrical pore-throats which are positioned perpendicular to one another. The connection between the throats is established via pore-nodes with no volumes. The nodes provide the computational gird required for vapor and liquid pressure calculation.

2.1. Pore network drying model

Drying is considered only from the top, therefore the vapor flow out of the network is modeled in a diffusive boundary layer above the network. The liquid and vapor flow in the entire network are considered quasi-stationary within the network time-steps. It is important to mention that all colligative properties of the salt solution is neglected or in other words the liquid is considered as pure water for liquid flow calculations. This leads to variation of several physical properties, in the course of drying, to be neglected. Said physical parameters include: liquid-gas surface tension, vapor pressure, liquid viscosity, etc.

Vapor diffusion within each throat in the gas-side network is calculated using Stefan correction coupled with the isothermal conditions. The equation can be written as follows:

$$\dot{M}_{v,ij} = A_{ij} \frac{\delta}{L} \frac{P\widetilde{M}_v}{\widetilde{R}T} \ln\left(\frac{P-p_{v,i}}{P-p_{v,j}}\right), \qquad (1)$$

where δ is the binary diffusion coefficient between water vapor and air (m^2/s), A_{ij} and L_{ij} the throat cross-sectional area and length (m^2 and m) respectively, P the gas pressure (Pa), T the air temperature (K), $\widetilde{M}_v$ molar mass of water (kg/kmol), $\widetilde{R}$ universal gas constant (J/kmolK), and p_v partial pressure of water in the gas phase.

The vapor pressure field is calculated by using Equation (1) in mass conservation law for every gas pore with unknown vapor pressure coupled with pores at P_v^* and $P_{v,\infty}$ as boundary conditions, which leads to a system of algebraic equation.

Liquid flow rate in the network is governed by the Hagen-Poisueille equation which is written for a throat as follows:

$$\dot{M}_{w,ij} = \frac{\pi r_{ij}^4}{8\mu_w L}\left(P_{w,i} - P_{w,j}\right),\qquad(2)$$

where r_{ij} represents the throat radius (m), μ_w the dynamic viscosity of water (Pa·s), and P_w the liquid pressure at the nodes. Similar calculation procedure as for the vapor pressure is considered here for liquid pressure field. The boundary conditions are defined as pressure level for moving menisci and liquid flow rate for stationary menisci. More detailed discussion on the basic drying model can be obtained in Metzger et al.[4].

2.2. Ion migration model

Salt concentration in liquid throats in the network is modeled by a 1D advection-diffusion equation. Advection term is assumed to follow a plug flow and Fick's law governs diffusion in the throats. Discretizing said equation over the space in the throat-node geometry leads to the following:

$$\frac{dC_{ij}}{dt} = U\left(\frac{C_i - C_{ij}}{L_{ij}}\right) + 2D\,\frac{C_i - 2C_{ij} + C_j}{L_{ij}^2},\qquad(3)$$

where C is the concentration of salt in the solution (kg/m³), U the superficial velocity of liquid in the element (m/s), and D the binary diffusion coefficient between solute and solvent (m²/s). Indices i and j refer to nodes on either side of the throat ij with liquid flow from node i to node j.

2.3. Crystallization

During drying, enrichment of salt takes place due to evaporation of solvent. In this model, salt concentration is tracked over time steps and rises as time goes by. At the end of every time step all liquid throats in the network are scanned and throats that exceed a certain degree of supersaturation (C^{*+}) are subject to crystallization. In that case the excess amount of salt is precipitated until salt concentration falls below the saturation concentration (C^{*-}). Therefore, said amount of precipitated salt is calculated as follows:

$$M_{s,ij} = V_{ij}(C_i - C^{*+}).\qquad(4)$$

It is assumed that the time scale for crystallization is significantly shorter than that of the ion migration which leads to an instant crystallization model in this case.

3. Simulation results

Pore network simulations are carried out with a 3D cubic pore network comprised of 15 (lateral)×15 (lateral)×19(vertical) nodes. This network is constructed as two distinct layers stacked on top of each other with each layer containing 9 counts of slices in the vertical direction. Throats throughout the network have a uniform length of 6 μm whereas their radii are sampled from a different normal distribution function for each layer. The top layer is kept identical across all simulations with a mean throat radius of 1000 nm whereas the bottom layer has 2 different variations presented in Table 1.

Table 1. Throat radii distribution of the bottom layer

network	1	2
mean radius (nm)	100	1500
standard deviation (nm)	20	150

The physical parameters used in the simulations are shown in Table 2.

Table 2. Physical parameters.

μ_w (Pa.s)	ρ_l (kg/m^3)	σ_l (N/m)	δ (m^2/s)	D (m^2/s)	C* (kg/m^3)
1×10^{-3}	1.27×10^3	7.2×10^{-2}	2.5×10^{-5}	1×10^{-9}	1×10^2

3.1. Network 1

Network 1 is comprised of two layers with monomodal pore size distributions. In this case the bottom layer has smaller throats compared to the top layer. Final crystal mass profile obtained by slice averaging is presented in Fig. 1 for 3 different drying rates. These various drying rates are simulated by adjusting the value of saturation vapor pressure (P_v^*) until the desired drying times, as shown in Table 3, are achieved.

Table 3. Drying rate date

drying rate	slow	moderate	fast
P_v^* (Pa)	160	1600	7384
drying time (s)	1200	120	24

Low initial salt concentration of 10 kg/m^3 is considered for the first set of simulations which provides enough room for ion diffusion in the liquid before saturation concentration is reached. It is observed that the profile for the case of slow drying (Fig. 1 (a)) is far more homogeneous and the gradient increases as drying rate speeds up. Moreover, looking directly at the first slice (at the surface) it can be seen that almost double the amount of crystals are found at the surface for the case of fast drying (Fig. 1 (c)) compared to slow drying. Another important factor that can play an important role depending on the

application is the amount of solid deposit found at the interface between the two layers. This value seems to remain unchanged between these sets of simulation yet it is quantified as a moderately low amount.

Fig. 1. Final crystal mass profile of network 1 with initial salt concentration of 10 kg/m³ for (a)

slow drying, (b) moderate drying, and (c) fast drying.
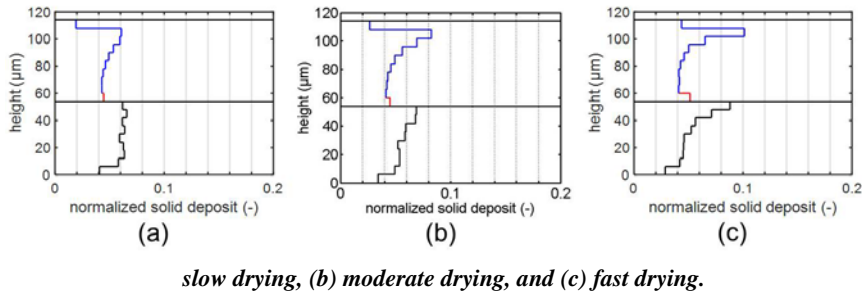
Elevating the initial salt concentration to 90 kg/m³ (very close to saturation) drastically alters the final solid distribution in the system. It can be seen that such high initial concentration eliminates final gradient in crystal distribution except for the top and interfacial slices (Fig. 2).
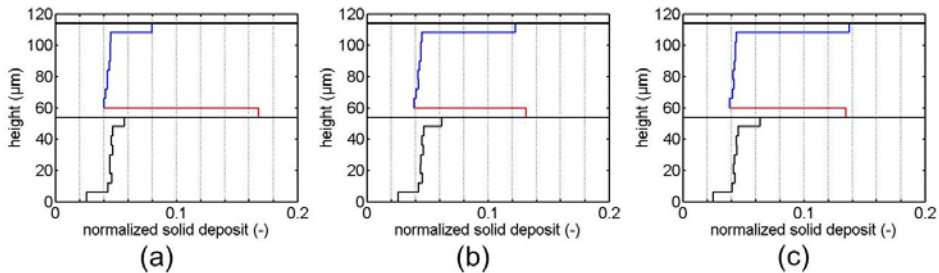
Fig. 2. Final crystal mass profile of network 1 with initial salt concentration of 90 kg/m³ for (a) slow drying, (b) moderate drying, and (c) fast drying.
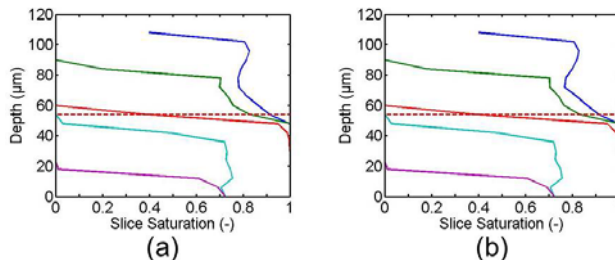
Fig. 3. Saturation proflies in the course of drying for network one obtained from simulations with (a) slow drying and (b) fast drying.

Additionally the profiles look much more alike for the three different drying rates. These effects are attributed to the lack of ion diffusion caused by high initial concentration. This significant similarity also hints at lack of change in the liquid transport regime between for the various drying rates. This has been confirmed by comparing saturation proflies for the cases of slow and fast drying which look close to identical (Fig. 3).

3.2. Network 2

The final set of simulations are carried out with network 2 where the bottom layer has considerable larger throats and the top layer. In this case the trend of crystal mass profile for varying drying rate is very similar to that of the network 1 as no viscous stabilization of the drying front is achieved. Therefore a comparison of network 1 and 2 is presented here which is more fruitful.
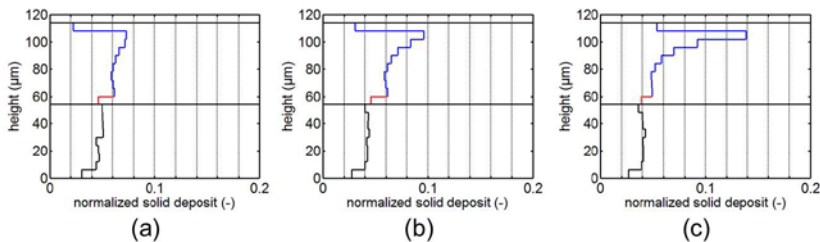
Fig. 4. Final crystal mass profile of network 2 with initial salt concentration of 10 kg/m³ for (a) slow drying, (b) moderate drying, and (c) fast drying.

The important characteristic of the network 2 is that once breakthrough to the bottom layer takes place in the absence of viscous stabilization the majority of the evaporated liquid is supplied by large throats in the bottom layer due to high capillary pressure. This continues until the connection between the liquid in the top and bottom layer is lost and capillary pumping is not possible. This behavior is completely opposite to that of the network 1 (Fig. 1) where almost no capillary pumping from the bottom layer to the top layer is possible. This explains the significantly lower amount of solid deposit in the bottom layer and the elevated amount in the top layer for network 2 (Fig. 4). The fact that liquid connection is almost entirely lost at the early stages of drying explains lack of crystal mass gradient in the bottom layer as ion back diffusion from evaporation site to the this region is not possible.

The results for increased concentration demonstrate significant accumulation of crystals at the top slice (Fig. 5) which was also observed for network 1 (Fig. 2). However it is the clear difference between the two networks is observed at the interface of the two layers. Almost no accumulation of crystals at the interface is observed for network 2 (Fig 5). The accumulation that is observed at the interface for network 1 is due to the fact that the bottom is almost fully saturated as the top layer dries out (a result of small pores with low capillary pressure). This means that as the drying front arrives at the interface, the bottom

layer starts to dry in a similar fashion as to the top layer. In case of network 2 at the moment that drying front reaches the interface the liquid connection in the bottom layer has already been lost (due to capillary pumping to the surface). Consequently recession of drying front continues without a halt to the end of drying.
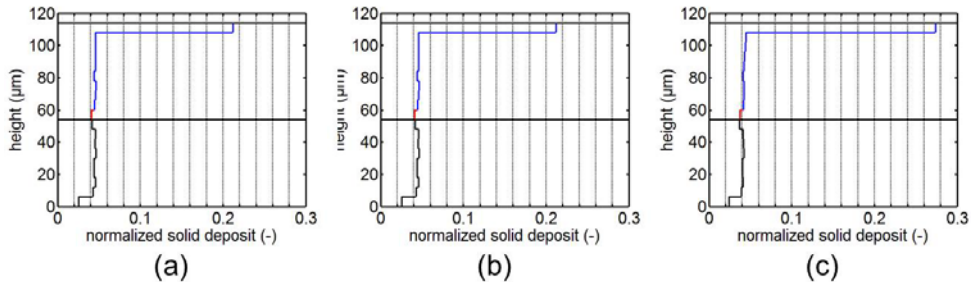
Fig. 5. Final crystal mass profile of network 2 with initial salt concentration of 90 kg/m³ for (a) slow drying, (b) moderate drying, and (c) fast drying.

4. Conclusions

In this work, a 3D pore network model has been utilized to run simulations for drying of layered porous materials in the presence of dissolved components. The majority of salt crystals are accumulated in the top layer for network with large pores in the bottom. For low concentration similar amount of crystals is obtained in both layers for network with smaller pores in the bottom. Moreover, enrichment at the interface between two layers is achieved only with high initial concentration and network with smaller pores in the bottom layer.

5. References

[1] Pel, L; Huinink, H.; Kopinga, K. Ion transport and crystallization in inorganic building materials as studied by nuclear magnetic resonance. Applied Physics Letters 2002, 81(15), DOI 10.1063/1.1512326.

[2] Petković, J.; Huinink, H.; Pel, L.; Kopinga, K.; van Hees, R. P. J. Salt transport in plaster/substrate layers. Materials and Structures 2007, 40, 475–495.

[3] Gupta, S.; Terheiden, K.; Pel, L.; Sawdy, A. Influence of ferrocyanide inhibitors on the transport and crystallization processes of sodium chloride in porous building materials. Crystal Growth & Design 2012, 12(8), 3888–3898.

[4] Gonçalves, T. D.; Pel, L.; Rodrigues, J. D. Influence of paitns on drying and salt distribution processes in porous building materials. Construction and Building Materials 2009, 23(5), 1751–1759, Compatibility of Plasters and Renders on Salt Loaded Substrates.

[5] Metzger, T.; Irawan, A.; Tsotsas, E. Isothermal Drying of Pore Networks: Influence of Friction for Different Pore Structures. Drying Technology 2007, 25, 49–57.

[6] Norouzi Rad, M.; Shokri, N.; Sahimi, M. Pore-scale dynamics of salt precipitation in drying porous media. Physical Review E, 2013, 88:032404.

Dependency of continuum model parameters on the spatially correlated pore structure studied by pore-network drying simulations

Lu, X.; Kharaghani, A.[*]; Tsotsas, E.

Thermal Process Engineering, Otto von Guericke University Magdeburg, Magdeburg, Germany

*E-mail of the corresponding author: abdolreza.kharaghani@ovgu.de

Abstract

Pore-network simulations are carried out for monomodal and bimodal pore structures with spatially correlated pore-size distributions. The internal and surface relationships between the partial vapor pressure and saturation as well as the moisture transport coefficient for these model porous structures are identified from the post-processing of the corresponding pore-network model solutions. The simulation results show that the deviation of the partial vapor pressure from the saturation vapor pressure in the presence of liquid – which is referred to as non-local equilibrium effect – in the bimodal pore structures is less pronounced than in the monomodal pore structures. For the monomodal pore structures the moisture transport coefficient profile is not unique over the entire drying process, whereas this profile depends marginally on the drying history of the bimodal pore structures. Finally the ability of the continuum model to predict the results of the pore-network simulations for multiple realizations of the pore space is assessed.

Keywords: *Scale transition, Moisture transport coefficient, Pore structure, Discrete model, Continuum model*

1. Introduction

The drying characteristics of porous media can essentially be described via modeling on two different length scales: at the effective-medium scale, continuum models (CM) based on volume averaging have been developed, in which the underlying transport phenomena are described by gradients in spatially averaged quantities and controlled by nonlinear effective parameters [1]. While the CMs are readily competent on the application side, they require macroscopic parameters and suffer from major shortcomings in theoretical aspects. The alternative approach operates at the pore scale and is referred to as discrete pore-network modeling. Discrete network models with different representations of the pore space have been developed, which can be divided into two categories: In the work of Yiotis et al. [2] the entire pore space is represented by pore bodies, leaving the throats as conductors and capillary barriers. This representation is suitable for the large pore volume. It may however fail to represent properly the structures with small pores. Prat et al. [3] and Metzger et. al. [4] approximated the void space with hydraulic pore throats and numerical pore nodes. This model is referred to as throat-node-model (TNM) in this work.

Metzger et al. [4] investigated how important is the role of pore structure (with monomodal pore size distribution (PSD) and bimodal PSD) on the intraparticle heat and mass transfer and thus drying kinetics. Vey recently, Moghaddam et al. [5] assessed the classical continuum model by the help of pore network simulations. In these simulations pore networks were generated with a throat radius distribution of 250±25 µm, resulting in a network porosity of 0.594. In these networks the pore space volume is overestimated due to the throat overlaps at nodes. This void space overestimation is avoided in throat-pore-model (TPM), which is developed in this work. Moghaddam et al. [5] calculated the continuum model parameters from TNM simulations. The results indicated that the moisture transport coefficient and the vapor pressure-saturation relationship are not unique over the entire drying process.

The relationships between the pore structure and the CM parameters are unknown. The aim of this work is to study the dependence of the parameter functions – the internal and surface relationships between the partial vapor pressure and saturation as well as the moisture transport coefficient – on the spatially correlated structures by means of the TPM. The ability of the continuum model to predict the results of the TPM simulations for multiple realizations of the pore space is also assessed.

2. Model descriptions

2.1 The continuum model

Assuming isothermal condition and constant gas pressure during the entire drying process, the mass transport is dominated in the direction perpendicular to the medium surface which

provides the evaporation demand. According to the total conservation of moisture (liquid and vapor phases), the continuum model is thus expressed by:

$$\varepsilon \frac{\partial S}{\partial t} = \frac{\partial}{\partial z}(D(S)\frac{\partial S}{\partial z}) \, , \tag{1}$$

with the boundary condition of no accumulation at the interface:

$$\dot{m}_v = -\frac{D_{va}\tilde{M}_v}{\tilde{R}T\delta}\ln(\frac{P - P_{v\infty}}{P - \varphi P_v^*}) \, , \tag{2}$$

where ε, S, and t (s) denote the porosity, the *local* saturation ($0 < S \le 1$) and the time, respectively; $P_{v\infty}$ (Pa) the vapor pressure in the bulk air, P (Pa) the atmosphere pressure, δ (m) the thickness of the diffusive mass boundary layer, which is located between the network open surface and the bulk air. The time-dependent moisture transport coefficient D (m²/s) as well as the boundary conditions need to be known in order to solve Eq. 1. Two parameters D and φ, which is called the vapor pressure-saturation, are estimated from pore network simulations.

2.2 Pore network drying model

The pore network model is defined on a three-dimensional regular lattice of pores and throats. The pores are spherical space and throats are cylindrical tubes (Figure 1a). The throat and pore radii are randomly set from normal distributions with corresponding means and standard deviations. The pore radii are chosen such that the pore radius is larger or equal with the largest radius of neighboring throats. Initially all throats and pores are saturated with liquid existing as free water. Periodical boundary conditions are applied on the lateral faces of the network. The extended boundary layer is considered in this model, which is a playground for the external mass transfer of vapor.

(a)   (b)
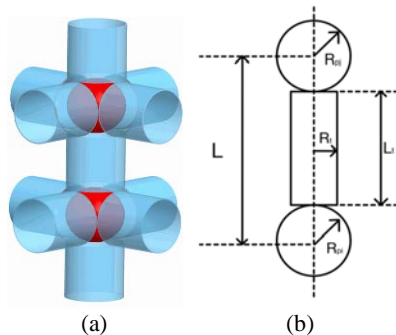
Figure 1 Schematics of throat-pore-model (TPM) in 3D (a) and in 2D (b).

Three kinds of pores and three kinds of throats are classified in the algorithm: empty pores and throats; full pores and throats; and partially filled pores and throats. The pores contain variables of interests, namely the liquid pressure and the vapor partial pressure. Transport phenomena are described at the discrete level of pores and throats in one spatial dimension. In this model, the center distance between two pores (i and j in Figure 1b) are fixed (L=1000 µm). The radii of pores (R_p) and throats (R_t) are drawn randomly from normal distributions. The throat length (L_t) depends on the radii of two pores located at throat ends.

The Stefan law is used to describe the vapor transport in the gas-filled region of the network and the boundary layer. The quasi-steady vapor diffusion between two pores is described by:

$$\sum_j \dot{M}_{v,ij} = \sum_j g_{v,ij} P \ln\left(\frac{P - P_v^j}{P - P_v^i}\right), \quad g_{v,ij} = \frac{D_{va}\tilde{M}_v}{\tilde{R}T\left(\dfrac{R_{pi}}{A_{pi}} + \dfrac{L_t}{A_t} + \dfrac{R_{pj}}{A_{pj}}\right)}, \tag{3}$$

where A_p, and A_t (m²) denote the cross section area of pore (i.e. πR_p^2) and of throat (i.e. πR_t^2), D_{va} (m²/s) the diffusion coefficient of vapor in air, $\tilde{R}$ (J/kmol K) the universal gas constant, $\tilde{M}_v$ (kg/kmol) the molar mass of vapor and T (K) the temperature. P_v is the vapor pressure at pores.

The Poiseuille's law is used to describe the liquid viscous flow as:

$$\sum_j \dot{M}_{w,ij} = \sum_j g_{w,ij}(P_w^i - P_w^j), \quad g_{w,ij} = \frac{\pi\rho_1}{8\mu} \frac{1}{\left(\dfrac{R_{pi}}{R_{pi}^4} + \dfrac{L_t}{R_t^4} + \dfrac{R_{pj}}{R_{pj}^4}\right)}, \tag{4}$$

where ρ_l (kg/m³) denotes the liquid mass density, and μ (m²/s) the liquid viscosity. Considering the viscous and capillary forces at the same time, stationary and moving menisci are determined in an iterative manner. The evaporation drives the drying process leading to drainage of moving menisci. The reimbibition can locally occur depending on the local liquid pressure. The time steps forward when one meniscus empties or (re)fills at every moment during drying. In the next steps the mass balance for vapor and liquid phases are solved again. Details on the algorithm can be found in Metzger et al. [4].

In this paper, we generated two pore network structures with monomodal PSD and bimodal PSD. The TPM was applied to generate these two structures. In the network with monomodal PSD, throat and pore radii are drawn randomly from a normal distribution with the given values of standard deviation and mean radius. The network with bimodal PSD is constructed with micro- and macro-channels. The macro-channels are placed vertically in the network.

2.3 Parameter functions

The PN simulations yield the vapor and liquid pressure fields as well as the liquid distribution over time. This information is used to determine both the internal and surface relationships between vapor pressure and saturation φ as well as the moisture transport coefficient D. The finite volume method is applied to determine these parameter functions. A three-dimensional network is virtually divided into horizontal slices with constant thickness Δz at distinct times during the drying process. Details of this method is explained in Moghaddam et al. [5].

3. Simulation results

The continuum model parameters are determined from the simulations conducted for monomodal and bimodal pore structures with spatially correlated pore-size distributions. In order to reduce the level of uncertainty on parameter estimates, 10 realizations of pore network were considered. The structural characteristics of PN are given in Table 1.

Table 1 Structural characteristics of pore networks.

Structural property	Monomodal PSD	Bimodal PSD
Network size (pore)	$25 \times 25 \times 51$	$25 \times 25 \times 51$
Boundary layer size (node)	$25 \times 25 \times 10$	$25 \times 25 \times 10$
Mean radius (µm)	250	micro-channel: 200 macro-channel: 350
Standard deviation (µm)	25	25
Center distance between two pores (mm)	1	1
Network porosity	0.35	0.337

Figure 2 shows the calculated moisture transport coefficient for the two pore structures. As can be seen, the D-S curves depend strongly on the drying history in the networks with monomodal PSD. This dependency is however less pronounced in the networks with bimodal PSD. Similar moisture transport coefficient profiles are identified by Moghaddam et al. [5], but only for the pore structures with monomodal PSD. As can also be seen, the value of moisture transport coefficient increases when altering the pore structure from monomodal PSD to bimodal PSD, especially in the period during which moisture transport occurs mainly through the liquid phase (S_{net} = 1.0-0.7). In the network with bimodal PSD the local saturation varies rather uniformly and confines within a small range of S = 1.0-0.65 due to the presence of macro-channels. However, in the network with monomodal PSD the dry region develops rather early due to the presence of strong viscous effect.

Hence the saturation profiles vary with a broad range of S = 1.0-0.2 during the first drying period (S_{net} = 1.0-0.7). In the work of Moghaddam et al. [5], conducted with the pore structures of monosized PSD, the range of local saturation variation is wider S =1.0-0 during the first drying period. One reason for this wide variation could be due to the overestimation of the throat volume in the TNM.
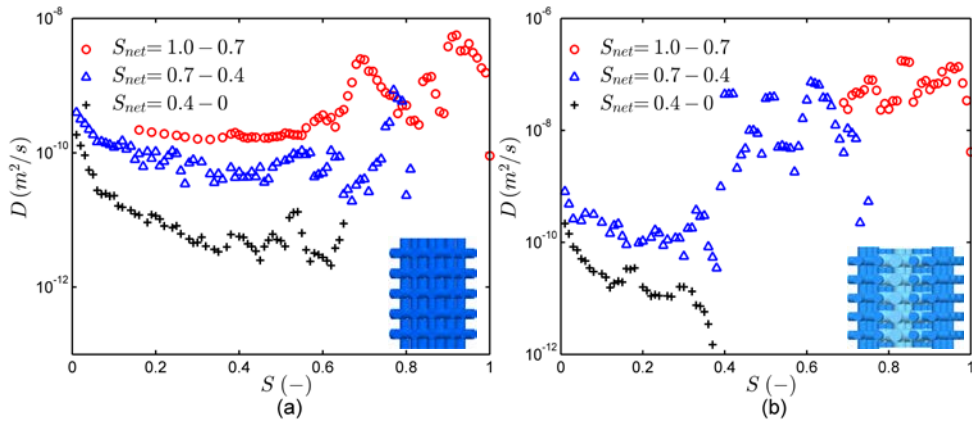
Figure 2** **Simulated moisture transport coefficients D for the pore structures with (a) monomodal PSD and (b) bimodal PSD. The values are averaged over 10 realizations for local saturation S intervals.

The coefficient profiles are similar for the both pore structures when moisture transport occurs mainly through the vapor phase. This is so because the moisture transport in the vapor phase is driven by the vapor pressure difference, which is related to the liquid structure (or interfacial area).

The behavior of moisture transport coefficient in the vapor phase can be better understood from the vapor pressure-saturation relationship (φ). Moghaddam et al. [5] observed a none-local equilibrium (NLE) effect, i.e. the deviation of the vapor pressure from the saturation vapor pressure in two-phase zone, in the pore network simulations. This effect is also observed in the both pore structures (Figure 5). The NLE is strong in the network with monomodal PSD. The liquid controlled range is enlarged in the networks with bimodal PSD due to an efficient capillary pumping. Figure 5 indicates that the vapor pressure deviates significantly from the saturation pressure at low saturation in the both pore structures. The NLE effect appears at early time of the drying process (S_{net} = 1.0-0.65) in the networks with monomodal PSD. This is so because of the drying front stabilization by viscous force. However, this effect appears later (S_{net} = 0.55-0.45) in the networks with bimodal PSD.

The two parameter functions calculated from the PN simulations are plugged into the continuum model (Eq. 1). The results obtained from the solution of the CM and from the

PN simulations are shown together in Figure 6. For the network with monomodal PSD, the CM predicts fairly the saturation profiles, except those profiles at high network saturation where the moisture transport coefficient values are scattered. This discrepancy may nonetheless be reduced when the parameters are determined for more realizations of larger pore networks.

A fairly good agreement between the CM predictions and the discrete simulations of the pore structures with bimodal PSD is observed (see Fig. 6b). The fact that at high saturation the variation of the moisture transport coefficient value is limited to a small range has led to this good match.
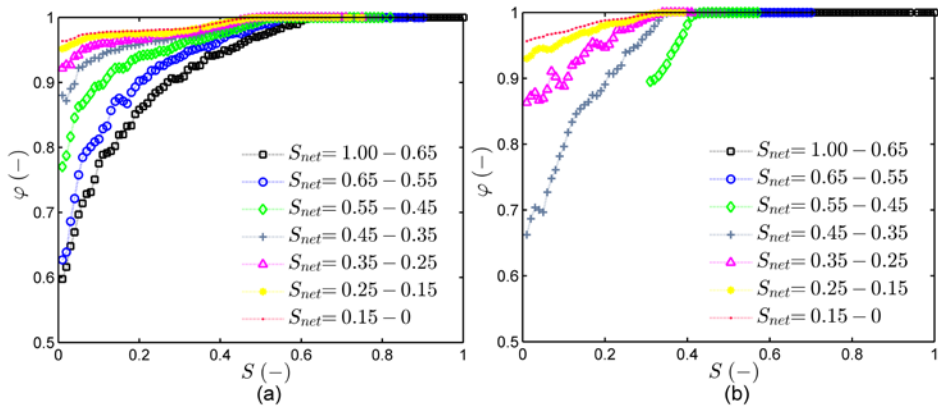
Figure 5 The vapor pressure-saturation relationships for the pore structures with (a) monomodal PSD and (b) bimodal PSD. The values are averaged over 10 realizations.
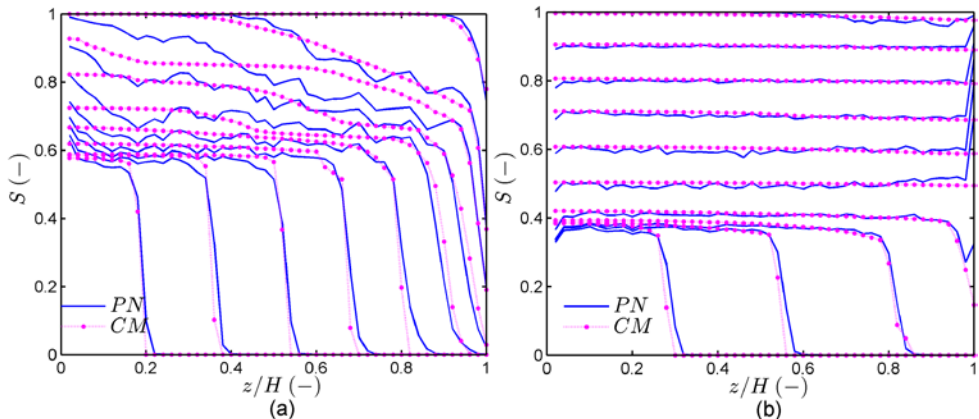
Figure 6 The continuum model predictions and the pore network simulations: (a) monomodal PSD and (b) bimodal PSD. The saturation profiles of PN are averaged over 10 realizations. From top the profiles belong to network saturation of 0.99, 0.9, 0.8, 0.7, 0.6, 0.5, 0.4, 0.3, 0.2, and 0.1, respectively.

4. Conclusions

In this paper, two different pore network structures (with monomodal and bimodal PSDs) are constructed. The values of moisture transport coefficient in the networks with bimodal PSD are large and confined into a narrow range of saturation in the first drying period. During the receding period of drying, the viscous drag forces dominate the capillary forces in both models. In this period, moisture transport mainly occurs in the vapor phase. Therefore, the moisture transport coefficient profiles are similar in the both pore structures during this drying period. The internal resistance for moisture transport is induced by the formation of liquid clusters and single menisci. The non-local equilibrium effect is observed for the both pore structures and it is more pronounced in the networks with monomodal PSD.

The continuum model is solved and assessed for the both pore structures. It has been seen that the one-equation CM is able to predict the saturation profiles obtained from the pore networks with monomodal PSD, except those profiles at high local saturation. This is because a small scatter of the moisture transport coefficient value can significantly impact the solution of the CM. The possible reasons for the scattered values could be due to both small network size and averaging method. Nevertheless, the agreement between the CM solutions and the PN simulations is improved when the networks with bimodal PSD are used.

5. Acknowledgments

6. References

[1] S. Whitaker, Simultaneous heat, mass, and momentum transfer in porous media: A theory of drying, in: J.P. Hartnett, T.F. Irvine (Eds.), Advances in Heat Transfer, Elsevier1977, pp. 119-203.
[2] A.G. Yiotis, A.K. Stubos, A.G. Boudouvis, Y.C. Yortsos, A 2-D pore-network model of the drying of single-component liquids in porous media, Advances in Water Resources 24 (2001) 439-460.
[3] M. Prat, Recent advances in pore-scale models for drying of porous media, Chemical Engineering Journal 86 (2002) 153-164.
[4] T. Metzger, A. Irawan, E. Tsotsas, Isothermal drying of pore networks: Influence of friction for different pore structures, Drying Technology 25 (2007) 49-57.
[5] A.A. Moghaddam, M. Prat, E. Tsotsas, A. Kharaghani, Evaporation in capillary porous media at the perfect piston-like invasion limit: Evidence of nonlocal equilibrium effects, Water Resources Research 53 (2017) 10433-10449.

Use of a multi-vial mathematical model to design freeze-drying cycles for pharmaceuticals at known risk of failure

Scutellà, B.[a]*; Trelea, I. C.[b]; Bourlès, E.[a]; Fonseca, F.[b]; Passot, S.[b]

[a] GSK Vaccines, Rixensart, Belgium

[b] UMR GMPA, AgroParisTech, INRA, Université Paris Saclay, 78 850 Thiverval-Grignon, France

*E-mail of the corresponding author: bernadette.z.scutella@gsk.com

Abstract

Freeze-drying is a dehydration method suitable for the stabilization of heat-labile pharmaceutical products, such as vaccines. Due to the vial-to-vial variability of heat and mass transfer during the process, the value of the critical process parameters (e.g., product temperature, sublimation rate) may be different between vials and batches often present significant product quality heterogeneity. The aim of this work was the development of a dynamic, multi-vial mathematical model making it possible to predict risk of failure of the process, defined as the percentage of vials potentially rejected by quality inspection. This tool could assist the design of freeze-drying cycle.

Keywords: *lyophilization; vaccines; heat and mass transfer; mathematical modeling; design space*

1. Introduction

Freeze-drying is a discontinuous process used to dry heat sensitive products by means of sublimation of the previously frozen product (primary drying), followed by desorption of the unfrozen water (secondary drying). Due to the use of low temperature, freeze-drying process is often the only solution to produce pharmaceutical and biological products (e.g., vaccines) with acceptable characteristics of stability, shelf-life, and potency. During the process design, two main constraints need to be taken into account in order to guarantee acceptable quality attributes of the final product, such as the visual aspect of the freeze-dried cake and the moisture content. Firstly, the product temperature has to be maintained below a critical value (namely collapse temperature) during the sublimation and desorption steps, to avoid the loss of the porous product structure. Furthermore, the desorption step should be carried out long enough to reach the target value of residual moisture content in the final product. However, due to the vial-to-vial variability of heat and mass transfer, the value of the critical process parameters (e.g., product temperature, sublimation rate and desorption rate) may be different between vials and the process can often result in vial batches presenting a significant heterogeneity in the product quality. Several mathematical models [1-5] were developed for the design of the primary drying and secondary drying steps. Most of these models were based on average values of the model parameters (e.g., product resistance, vial heat transfer coefficient, characteristic desorption time) over the vial batch and only few of them took into account the variability of the model parameters [2, 3] due to differences in heat and mass mechanisms between vials processed in the same or different batches. The understanding and quantification of the mechanisms responsible for product quality variability can lead to a better prediction of the process parameters distribution and consequently of the risk of failure associated to the process.

Our goal in the present study was to develop a multi-vial dynamic mathematical model for freeze-drying for the process design, taking into account sources responsible for heat and mass transfer variability among vials. The developed model was then used to propose a new quality risk-based approach for the design of the primary and secondary drying steps of the freeze-drying process, which includes the evaluation of the percentage of vials potentially rejected for specific combinations of operating variables.

2. Theory

2.1. Mathematical model

The heat flux received during the process by the vial is assumed to mainly serve for the ice sublimation during primary drying and for the water desorption in secondary drying, the difference being responsible for temperature variation of product and vial in transient regimes. The evolution of product temperature T_p (assumed to be the same as the vial) during primary and secondary drying can be determined as:

$$C_p \frac{dT_p}{dt} = \dot{Q}_{SV} - \Delta H_{sub} \dot{m}_{sub} - \Delta H_{des} \dot{m}_{des} \tag{1}$$

Heat transfer during primary drying

The heat transfer between the shelf and the vial $\dot{Q}_{SV}$ depends on the temperature difference between the shelf (T_S) and the product (T_p), and can be expressed in term of vial heat transfer coefficient K_V:

$$\dot{Q}_{SV} = \left(\frac{1}{K_V} + \frac{l_I(t)}{\lambda_{ice}} \right)^{-1} A_{BV} (T_S - T_p) \tag{2}$$

The term K_V depends on the vial bottom dimensions (vial–shelf contact area A_c and depth of bottom curvature l_{BV}) and the chamber pressure P_C and can be defined as:[6]

$$K_V = C_1 A_c + K_r + \frac{C_2 P_C}{1 + C_2 \frac{l_{BV}}{\lambda_v} P_C} \tag{3}$$

K_r being the radiation contribution of the top and bottom shelf.[6]

Mass transfer during primary drying

During primary drying the sublimation flux can be defined by the difference between the equilibrium pressure at the ice-vapour interface P_{v_i} and the partial vapour pressure in the chamber P_{v_C}:

$$\dot{m}_{sub} = \frac{A_i}{R_p} (P_{v_i} - P_{v_C}) \tag{4}$$

where R_p is the the mass transfer resistance of the dried layer, which depends linearly on the dried layer thickness for the considered product:[7]

$$R_p = R_{p_0} + l_d R_{p_1} \tag{5}$$

P_{v_i} can be calculated from the Clausius Clapeyron equation from the sublimation interface temperature,[6] and P_{v_C} is defined as in Trelea et al.[8] assuming ideal gas law for water vapour in the drying chamber:

$$\frac{dP_{v_C}}{dt} = \frac{R_g T_C}{V_C M_W} \left(\sum_1^{N_V} (\dot{m}_{sub} + \dot{m}_{des}) - \dot{m}_{CN} \right) \tag{6}$$

Finally, the fraction of ice f contained in the product evolves with time as a function of the sublimation rate $\dot{m}_{sub}$ as:

$$m_0 \frac{df}{dt} = -\dot{m}_{sub} \tag{7}$$

Mass transfer during secondary drying

The multilayer model developed by Trelea et al.[9] was used to describe the desorption kinetics in secondary drying.

2.2. Heat and mass transfer variability in freeze-drying

Four sources of inter-vial product quality variability were considered in this study:

➢ *Vial geometry*: K_V is influenced by the shelf-vial contact area A_c and the depth of bottom curvature l_{BV} (Equation 3). Thus, differences in these dimensions among the vials can results in variability of the heat transfer among the vials on the shelf. In the present study, the distributions of K_V at different chamber pressures over the vial batch were calculated based on the normal distributions of A_c and l_{BV}, as previously proposed by Scutellà et al.[6]

➢ *Edge vial effect*: It is well known that vials located at the periphery of the shelf receive an additional heat transfer by radiation from the wall and the rail and conduction through the gas between the chamber wall, the rail and the side wall of the vials. This phenomenon is known as edge vial effect. In the present study, the additional radiation heat flow rates from the wall and rail to the edge vials were calculated for edge vials using the Stefan-Boltzmann equation, as proposed in the 3D simplified radiation model developed by Scutellà et al. [10]

➢ *Mass transfer resistance*: The product resistance variability in a large batch of vials was previously quantified as normal distributions of R_{p_0} and R_{p_1} in Scutellà et al.[7]

➢ *Desorption kinetics*: The variability of the desorption kinetics was previously quantified as normal distributions of characteristics desorption times in Scutellà et al. [11]

2.3. Prediction of the risk of vial rejection

The developed mathematical model was used to propose a quality risk-based approach for the design of the primary and secondary drying steps of the freeze-drying process. The risk of failure of the primary drying step was calculated in terms of vials potentially rejected by considering two main constraints: (i) the product temperature had to be maintained at any time below a critical value (i.e., the glass transition temperature for amorphous products); (ii) the sublimation had to be completed at the end of primary drying (i.e., $f = 0$). For the design of the secondary drying step, the constraints were: (i) the final moisture content had to be equal or lower than the target moisture content (1.5 %) and (ii) the temperature at any moment had to be lower than the glass transition temperature of the dry product. The range of acceptable combinations of operating variables (i.e., T_s, P_C, operating time) was then identified based on the target level of risk. The capability of the pilot freeze-dryer was considered to be not limiting regardless of the operating conditions.

2.4. Numerical solution

The developed model was solved using Matlab R2014b software provided of the Statistics Toolbox (The MathWorks, Inc., Natick, MA). The analysis of the effect of the heat and mass

transfer variability on the critical process parameters during freeze-drying was performed using the Monte Carlo method. This method consisted in simulation of batches of 100 representative vials with random normal distributions of the considered model parameters (A_C, l_{BV}, R_{p_0}, R_{p_1}, τ_{ref_1} and τ_{ref_2}). Due to computer limitations, the number of simulated vials (100) was significantly smaller than the actual number of vials in the freeze-dryer (2310).

3. Simulated system

In the present work, the model was used to simulate freeze-drying process performed in the pilot freeze-dryer REVO (Millrock Technology, Kingston, United States). The equipment was composed of a drying chamber equipped with three shelves and a condenser running at temperature of -75 °C. A total of 770 glass tubing vials (Müller + Müller, Holzminden, Germany) were supposed to be loaded on each shelf. The vials had a total volume of 3 mL and were all filled with 1.8 mL of 5 % aqueous sucrose solution. Furthermore, the vial array was surrounded by a metallic rail (shielding 70 % of the lateral wall of the vials). The shelf was considered to be at a temperature of -50 °C at the beginning of primary drying.

4. Results

The developed model was used to predict the risk of failure of the process in terms of percentage of vials potentially rejected. Potential vial rejection of the primary and secondary drying steps were predicted for different combinations of operating variables (shelf temperature, chamber pressure, operating time) to select the best cycle at the maximum allowed risk (1 %). Figure 1A presents the percentage of vial rejection due to a product temperature higher than T'_g observed performing a primary drying of 84 hours in function of the chamber pressure and shelf temperature. Typical ranges of chamber pressure and shelf temperature used in the pharmaceutical industry were explored, respectively between 4 and 10 Pa, and -40 °C and -10 °C. The results shows that, if a value of shelf temperature higher than -27 °C is applied during primary drying, the percentage of vial rejection become higher than 1 % for most of the pressures tested. Furthermore, Figure 1B presents the percentage of vial rejection due to the sublimation not completed at the end of primary drying observed performing a primary drying step of 84 hours in function of the shelf temperature and chamber pressure. A shelf temperature higher than -30 °C has to be considered to avoid the presence of ice at the end of the primary drying time. Thus, the use of a shelf temperature of -27 °C and a chamber pressure between 4 and 9.3 Pa during primary drying step of 84 h results in a percentage of vial rejection lower than the maximum allowed one (1 %). Figure 2A presents the risk of vial rejection associated to the secondary drying step due to a product temperature higher than T_g. A range of shelf temperatures between 0 °C and 40 °C was explored, and the pressure was maintained constant at 6 Pa. The product temperature remains below the critical value regardless of the shelf temperature applied during the secondary

drying step, because the product dries enough during the shelf temperature ramp (1°C min^{-1}). Figure 2B presents the risk of vial rejection of associated to the secondary drying step due to a final moisture content in the product higher than the target value of 1.5 %. A shelf temperature higher than 4 °C will lead to no vial rejection if secondary drying is carried for at least 45 h. As product temperature remains below the critical value regardless the shelf temperature value used, the optimal operating conditions for secondary drying will be a shelf temperature of 40 °C and an operating time of 4 h, which leads to a vials rejection lower than 1 %.
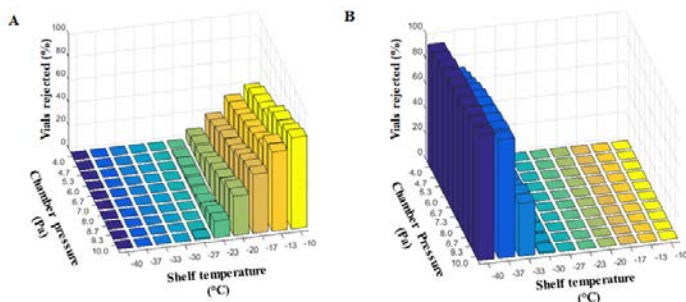
Fig. 1 Potential vial rejection (%) in primary drying performed at different chamber pressures and shelf temperatures due to (A) a product temperature higher than the critical value (T$'_g$) and (B) sublimation not completed after 84 h of primary drying.
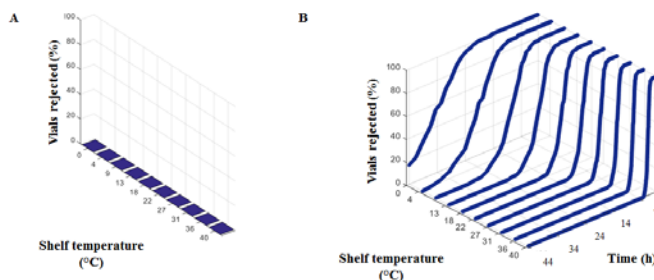
Fig. 2 Potential vial rejection (%) in secondary drying due to (A) a product temperature higher than the critical value (T$_g$) during the whole duration of the secondary drying step and (B) product moisture content higher than the target value (1.5 %) for different shelf temperatures and operating times.

5. Conclusions and perspectives

In this work, a multi-vial, dynamic mathematical model of the primary and secondary drying steps of the freeze-drying process was developed, including the heterogeneity of parameters such as the vial dimensions, the vial position on the shelf and the random nucleation process. The model was used to calculate the risk of failure of the primary and secondary drying steps for a 5 % sucrose solution processed in a pilot freeze-dryer, expressed in terms of percentage of vials potentially rejected. In the future, the proposed model will be experimentally

validated and used to calculate the design spaces of primary and secondary drying for the cycle transfer and scale-up of the process.

Nomenclature

A	Cross sectional area (m^2)
C_1, C_2	Parameters of Equation 3 $(W\ m^{-4}K^{-1}), (W\ m^{-2}K^{-1}\ Pa^{-1})$
C_p	Heat capacity $(J\ K^{-1})$
ΔH	Latent heat $(J\ kg^{-1})$
f	Mass fraction of ice in the product
K	Heat transfer coefficient $(W\ m^{-2}K^{-1})$
l	Layer thickness (m)
$\dot{m}$	Water vapour flow rate $(kg\ s^{-1})$
m	Mass (kg)
M_W	Molecular mass of water $(g\ mol^{-1})$
N	Number of vials
P	Pressure (Pa)
$\dot{Q}$	Heat flow rate (W)
R_g	Ideal gas constant $(J\ K^{-1}kmol^{-1})$
R_p	Product resistance $(Pa\ m^2\ s\ kg^{-1})$
R_{p_0}, R_{p_1}	Parameter of Equation 5 $(Pa\ m^2 s\ kg^{-1}), (Pa\ m\ s\ kg^{-1})$
t	Time (s)
T	Temperature (K)
V	Volume (m^3)

Greek

β	Mass transfer parameter $(s\ kg^{-1}\ K^{-1})$
λ	Thermal conductivity $(W\ m^{-1}\ K^{-1})$
τ_{ref}	Characteristic desorption time at reference temperature (s)

Subscripts and Superscript

0	Initial
B	Bottom
C, c	Chamber and contact, respectively
CN	Condenser
d	Dried
des	Desorption
f	Frozen
i	Interface
ice	Ice
P	Product
r	Radiation
S, s	Shelf and solids, respectively

sub	Sublimation
T	Top
V, v	Vial and vapour, respectively
w	Water

References

[1] Pikal, M.J. Use of Laboratory Data in Freeze Drying Process Design: Heat and Mass Transfer Coefficients and the Computer Simulation of Freeze Drying. PDA Journal of Pharmaceutical Science and Technology 1985, 39, 115-139.

[2] Mortier, S.; Van Bockstal, P.J.; Corver, J.; Nopens, I.; Gernaey, K.V.; De Beer, T. Uncertainty analysis as essential step in the establishment of the dynamic Design Space of primary drying during freeze-drying. Eur J Pharm Biopharm 2016, 103, 71-83.

[3] Pisano, R.; Fissore, D.; Barresi, A.A.; Brayard, P.; Chouvenc, P.; Woinet, B. Quality by design: optimization of a freeze-drying cycle via design space in case of heterogeneous drying behavior and influence of the freezing protocol. Pharm Dev Technol 2013, 18(1), 280-295.

[4] Velardi, S.A.; Barresi A.A. Development of simplified models for the freeze-drying process and investigation of the optimal operating conditions. Chem Eng Res Des 2008, 86(1), 9-22.

[5] Gan, K.H.; Bruttini R.; Crosser O.K.; Liapis A.I. Freeze-drying of pharmaceuticals in vials on trays: effects of drying chamber wall temperature and tray side on lyophilization performance. Int J Heat Mass Transfer 2005, 48, 1675-1687.

[6] Scutella B.; Passot S.; Bourles E.; Fonseca F.; Trelea I.C. How Vial Geometry Variability Influences Heat Transfer and Product Temperature During Freeze-Drying. J Pharm Sci 2017, 106(3), 770-778.

[7] Scutellà B.; Trelea I.C.; Bourlés, E.; Fonseca, F.; Passot, S. Determination of the product resistance variability and its influence on the product temperature in pharmaceutical freeze-drying. Eur J Pharm Biopharm. Submitted.

[8] Trelea, I.C.; Fonseca, F.; Passot, S.; Flick D. A Binary Gas Transport Model Improves the Prediction of Mass Transfer in Freeze Drying. Drying Technology 2015, 33(15-16), 1849-1858.

[9] Trelea, I.C.; Fonseca, F.; Passot, S. Dynamic modeling of the secondary drying stage of freeze drying reveals distinct desorption kinetics for bound water. Drying Technology 2015, 34(3), 335-345.

[10] Scutellà B.; Plana-Fattori A.; Passot S.; Bourlès E.; Fonseca F.; Flick D.; Trelea, I.C. 3D mathematical modelling to understand atypical heat transfer observed in vial freeze-drying. Appl Therm Eng 2017, 126, 226-236.

[11] Scutellà, B.; Bourlès, E.; Tordjman, C.; Fonseca, F.; Mayeresse, Y.; Trelea, I. C.; Passot, S. Can the desorption kinetics explain the residual moisture content heterogeneity observed in pharmaceuticals freeze-drying process? In proceedins of 6th European Drying Conference, Liegi, Belgium, July 19-21, 2017.

Comparison between the finite differences, finite volume and finite element methods for the modelling of convective drying of fruit slices

Castro, A.M [a]; Mayorga, E.Y[b]; Moreno,F.L[c*]

[a] Biosciences Doctorate Program, Universidad de la Sabana, Chía, Cundinamarca, Colombia
[b] Mathematics Department, Engineering Faculty, Universidad de la Sabana, Chía, Cundinamarca, Colombia
[c*] Agroindustrial Process Department, Engineering Faculty, Universidad de la Sabana, Chía, Cundinamarca, Colombia

*E-mail corresponding author: : leonardo.moreno@unisabana.edu.co

Abstract

Three numerical methods, finite differences, finite volume and finite element, were compared to know their convenience in the simulation of convective drying of fruit slices. The mathematical treatment, the stability, the convergence and the sensibility were analysed for each method. The data of the simulations were compared with the data of feijoa dried at 60°C, 5 mm of thickness and air velocity of 0.5ms^{-1}. The error was 7%, 13% and 17% for finite element, finite volume and finite differences respectively. The method selection depends on the software, the required data precision and the use of the model.

Keywords: mathematical model; convective drying; numerical methods

1. Introduction

Feijoa fruit (*Acca Sellowiana* Berg) is a crop adapted from Brazil and North Uruguay to the Colombian Andes [1] [2]. In Colombia, there are 1000 ha planted. Drying is an alternative to extend the shelf life of the fruit and to preserve the functional characteristics of the fruit. The convective drying of fruits is the most used drying technique to remove the moisture of the fruits because of its simplicity and low cost [3, 4]. The mathematical modelling is a useful tool to predict and understand the mass, heat and momentum transfer during drying. The theoretical models are based on the fundamental physics of drying. The use of the theoretical models is increasing thanks to the availability of the advanced numerical computation and to its relevance for the fruit drying understanding.

Choosing the numerical method to solve the PDEs system is a key step in the modelling of convective drying. Three common numerical methods applied are finite differences, finite volume and finite elements, also known as gridbased methods [5]. The finite differences method use the decomposition of the differential terms of PDE in discrete representations through the domain discretization in a rectangular grid. This method generates time evolution chains linked to initial conditions. The finite volume method also discretizes the domain generating several polyhedral volumes. Those volumes are controlled by numercal methods related to differential and integral approximations [6]. The finite elements method uses the same type of domain decomposition as finite volume, but the approximation is different. The weak formulation of the model is necessary for the generation of the algorithm. The aim of the present study is the comparison between the finite differences, finite volume and finite element methods for the modelling of convective drying of feijoa slices.

2. Materials and Methods

2.1 Mathematical modelling

Three numerical methods to simulate the convective drying of fruit slices were compared. The model was formulated with the following assumptions:(i) the geometry is a slab ; (ii) the model is in 2D; (iii) mass transfer inside the fruit is performed by diffusion and the heat transfer by conduction; (iv) the evaporation occurs only at the surface; (iv) thermophysical properties of fruit dependent of composition and temperature; (v) effective diffusion is constant and (v) shrinkage is accounted. Eqs (1) and (2) represent the heat and mass transfer equations [7, 8].

$$\frac{\partial T}{\partial t} = \alpha \left(\frac{\partial^2 T}{\partial x^2} + \frac{\partial^2 T}{\partial y^2} \right) \qquad (1) \qquad \frac{\partial X}{\partial t} = D_{eff} \left(\frac{\partial^2 X}{\partial x^2} + \frac{\partial^2 X}{\partial y^2} \right) \qquad (2)$$

At initial time (t=0), the moisture content and the temperature of the slice correspond to its initial values. X_o= 5.53 Kg water/Kg dry solids. T_o= 305K. The boundary conditions for moisture transport are represented by Eqs 3 and 4.

$$\left.\frac{\partial X}{\partial z}\right|_{z=0} = -\frac{h_m}{\rho_s D_{eff}}(C_0 - C_{air}) \quad (3) \qquad \left.\frac{\partial X}{\partial z}\right|_{z=L} = \frac{h_m}{\rho_s D_{eff}}(C_0 - C_{air}) \quad (4)$$

The signs depend on the position of the boundary. In an analogous way, boundary conditions for heat transfer were considered. The concentration of water vapor in the air and in the fruit surface (C_{air},C_o) were determined with the equations reported for the ASHRAE. [9]. The shrinkage was included with the approximations used by [8,10,11] .

2.2 Numerical methods
The finite difference method was applied with two approaches, the explicit, where the derivative of the temperature and moisture with respect to the position was based on the information of the previous time. Through central finite differences an equation with an only unknown variable was obtained, which is easy to solve. The second approach was the implicit method where the Crank- Nicholson method was applied to the second term of Eqs. 1 and 2. Here, the derivative was performed in the next level of time. Algebraic equations expressed through tridiagonal matrices were obtained and thus solving the system. This is repeated until complete the time of simulation. This method was implemented through an in house code programmed in Matlab 8.3.

The volume finite method started with the prediction of the moisture and temperature at the boundaries. For this purpose, a triangular and regular mesh through the domain was established. Then, a recursion algorithm that uses the information of the previous time was employed. Then the moisture and temperature distribution inside the domain was calculated by the Green theorem application. This theorem solves the right side of Eqs 1 and 2. With this approach a volume integral is converted in a line integral. The PDEs system in 2D passes to 1D facilitating the implementation of the numerical method. The moisture content and temperature at the center of each triangle of the mesh was determined. Then, the moisture and temperature values were determined at the vertices and so on until complete all the triangles of the mesh. This process was repeated for each time step during the simulation time. This approach uses linear equations system that lead to the creation of tridiagonal matrices. This method was implemented through an in house code programmed in Matlab 8.3.

The finite element method was implemented in the software FreeFem++ 3.46. For the implementation the weak formulation of the mass and heat transfer problem was required. The software uses an algorithm based on the Gauss theorem which is applied to the right side of Eqs. 1 and 2. This theorem is a generalization of integration by parts. It allows to

rewrite a line integral which is related with the boundary conditions of the PDE. This approach allowed the equations solution with algebraic methods.

The simulation data was compared with moisture content curves of feijoa slices of 5mm, dried at 60°C, air velocity of 0.5ms^{-1} and parallel to the samples. The convective dryer (EDIBON) was used. The goodness of fit was evaluated through the mean relative deviation modulus.

3. Results and discussion

The averaged experimental and predicted moisture content by the three numerical methods are presented in Fig.1. The relevance of the numerical solution method for accurate simulations was observed. First, the moisture content curve obtained by the finite difference method was lower than the experimental values at the beginning of the process. Then, in the middle of the drying, the predicted data were higher than the experimental data. The error fot the finite diference method was 17%. Second, the volume finite method showed a curve over the experimental data, but closer than the finite differences. The error of finite volume method was 13%. Finally, the simulated curve by the finite elements method was slightly over the experimental values. Then, as the drying time progresses, the simulated and experimental values are closer. The error was of 7%. The simulations behavior can be explained through the numerical approximation employed by each solution method. Also, by the assumptions and parameters of the mathematical model.

The explicit finite difference method is easy to apply. However, this method was unstable in time intervals partitions of space because the derivative is based on the information of the previous time. On the other hand, the implicit method establishes that the derivative of the temperature or moisture with respect to the position is not performed in the previous time [13]. The derivative is performed in the next level of time. This numerical approximation is more stable against time jumps, partitions of space and variable parameters of the model such as physicochemical and transport properties. Also this method allows to couple the mass and heat transfer with acceptable accuracy. A disadvantage is the rectangular grid structure. This does not allow better data accuracy. Also it is not suggested for irregular geometries. This is important because the kwnoledge of the simulation conditions are related with the existence of a solution to the PDEs system and good convergence of the model[14].

The application of the volume finite method allowed a better simulated data than finite differences. This indicates that the numerical approaches used by this method and the model parameters allowed good data accuracy. With the use of an in house code and accessible software an initial moisture transfer analysis can be done. However, the coupling between mass and heat transfer was more difficult with the use of an in house code. To overcome this problem the finite elements method is suggested.
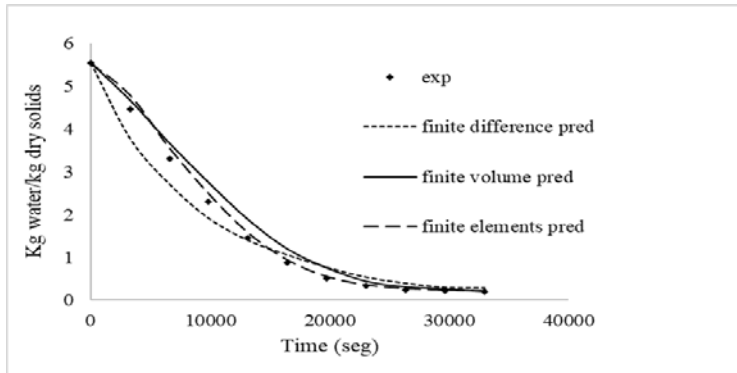
Fig 1. Averaged moisture content predicted by the three numerical methods compared to the experimental data.

The simulated curve obtained by the finite element method had a good agreement with the experimental data. Also, the use of the method and the software allowed the consideration of more real drying parameters for the model such as variable physicochemical, transport properties and shrinkage. Also, it was possible to optimize the convective transfer coefficients obtaining better results that the programation of the finite volume which constant transport properties were considered.

The Fig. 2 represents the evolution of moisture content in function of the slice thickness during drying time. This figure was determined through the finite differences method. As exécted, the boundaries are first dried and finally the center of the product.
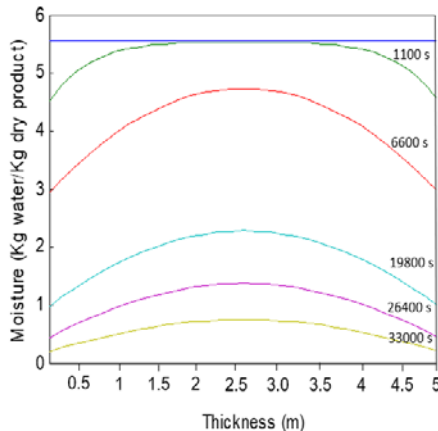
Fig 2. Moisture content evolution in fruit slice during drying by finite difference method

The Fig. 3 also shows evolution of moisture content in function of the slice thickness during drying time. This figure was obtained with the volume finite method in 2D. It is

observed a representative drying behavior which corresponds to the initial loss of moisture in the boundaries followed by the inner of the product.
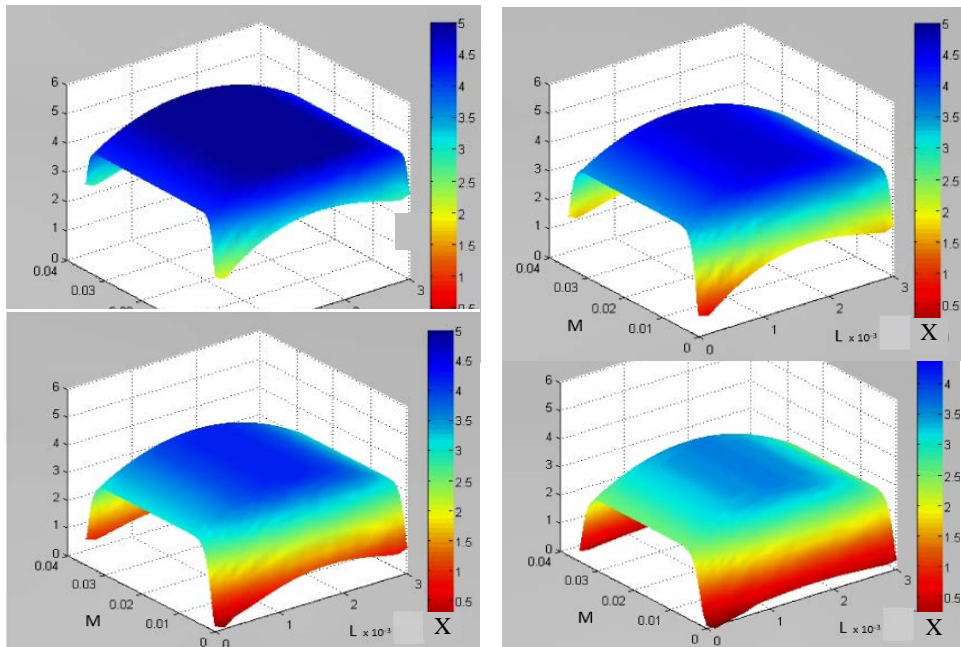
Fig 3. Moisture content evolution in fruit slice during drying by volume finite method

Simultaneous heat nad mass transfer was predicted by the finte elemtents method. The Fig. 4 shows the temperature distribution inside the slice during drying by the finite elements method. The heat transfer from the surface of the product to its interior was observed. This corresponds to the sensible heat transferred by convection from the air to the product and its transport inside the product by conduction. Then, the temperature increases close to the air temperature.
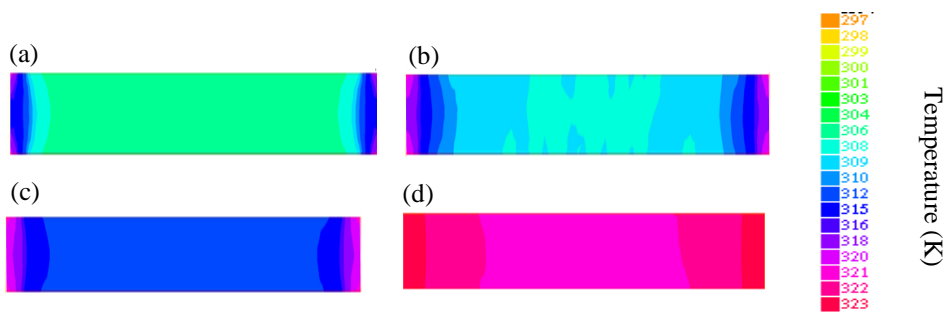
Fig 4. Temperature distribution inside the slice during drying simulation by the finite elements method. (a) 3000 s. (b) 6000 s. (c) 12000 s. (d) 15000 s.

4. Conclusions

The method of finite differences allowed to coupled the heat and mass transfer but with stability and convergence problems. However it is recomendable for apply the approaches of the numerical solutions at initial stages of drying studies.

The coupling of the system with an in-house code was more difficult for the finite volume method. The finite volume method was suitable to predict moisture diffusion as a first step in drying modelling.

The finite element method was the most suitable method. The model can be improved and the parameters of the model can be optimized with this method.

The finite volume and finite elements methods require strong mathematical treatment which increases the computational costs. However, these methods present less convergence and stability problems than finite differences. Also, they are recommended for multi-scale studies.

The three methods have disadvantages for modelling irregular geometries, deformable boundaries and large deformations due to the 'grid' nature of those methods.

The understanding of the numerical method allowed to know the numerical approximations to solve the PDEs and therefore to know the benefits and challenges of the method.

5. Nomenclature

C	concentration of water vapor	kg m^{-3}	x,y, z	cartesian oordinates	m
C_o	concentration of water vapor on the product surface	kg m^{-3}	X	moisture content	kg water kg^{-1} dry product
D_{eff}	effective moisture diffusivity	m^{2}s^{-1}	Greek letters		
h_m	mass transfer coefficient	m s^{-1}	α	thermal diffusivity	m^{2}s^{-1}
L	product thickness	m	ρ_s	density of solid product=dry mass/total volume	kg m^{-3}
M	lenght of the product	m	Subscripts		
t	drying time	s	air	air	
T	absolute temperature	K	in	initial	

References

[1]   Parra-Coronado, A; Fischer,G and Camacho-Tamayo,J. Development and quality of pineapple guava fruit in two locations with different altitudes. Bragantia Campinas. 2015, 74 (3), 359–366.

[2]   Weston,R.J. Bioactive products from fruit of the feijoa (Feijoa sellowiana, Myrtaceae): A review. Food Chem. 2010. 121 (4), 923–926.

[3]   Wojdyło, A; Figiel, P; Legua, K; Lech, Á; Carbonell-Barrachina, and Hernández, F. Chemical composition, antioxidant capacity, and sensory quality of dried jujube fruits as affected by cultivar and drying method. Food Chemistry.2016.207, 170–179.

[4]   Castro, A.M; Mayorga, E.Y and Moreno F.L. Mathematical modelling of convective drying of fruits: A review. J. Food Eng. 2018. 223,152–167.

[5]   Rathnayaka C.M; Karunasena, H.C; Gu, Y.T; Guan, L and W. Senadeera. Novel trends in numerical modelling of plant food tissues and their morphological changes during drying – A review. J. Food Eng. 2017. 194, 24–39.

[6]   Moukalled, F; Mangani, L and Darwish, M. The finite volumen method in computational fluid dynamics, 1st ed. Springer International Publishing, 2015.

[7]   Esfahani, J.A; Majdi, H and Barati, E. Analytical two-dimensional analysis of the transport phenomena occurring during convective drying: Apple slices. J. Food Eng. 2014. 123, 87–93.

[8]   Tzempelikos, D.A; Mitrakos, D; Vouros, A.P; Bardakas, A.V; Filios, A.E and Margaris, D.P. Numerical modeling of heat and mass transfer during convective drying of cylindrical quince slices. J. Food Eng. 2015. 156, 10–21.

[9]   ASHRAE. Handbook-Fundamentals. American Society of Heating, Refrigeration and Air-Conditioning Engineers Inc. Atlanta, 2009.

[10]   Ben Mabrouk, S; Benali, E and Oueslati, H. Experimental study and numerical modelling of drying characteristics of apple slices. Food Bioprod. Process.2012, 90 (4), 719–728.

[11]   Guiné, R.P. Pear drying: Experimental validation of a mathematical prediction model. Food Bioprod. Process.2008, 86 (4), 248–253.

[12]   Lomauro, C.J; Bakshi, A.S and Labuza, T.P. Evaluation of food moisture sorption isotherm equations. Part I: Fruit, vegetable and meat products. Leb. und-Technologie. 1985,18 (2), 111–117.

[13]   Kulkarni, N and Rastogi, K. Comparison of Explicit Finite Difference Model and Galerkin Finite Element Model for Simulation of Groundwater Flow. Int. J. Innov. Res. Adv. Eng. 2014,1 (2), 23–30.

[14]   Mayorga, E and Giniatoulline, A. On the Existence , Uniqueness, Stabilization and Limit Amplitude for Non- Homogeneous System Modelling Internal Non-Stationary Waves in Stratified Flows. Pacific J. Appli Math. 2011, 3 (4),45–62.

The role of boundary conditions on the dynamics of green coffee beans in a rotated dryer

Machado, M.V.C.; Resende, I.A.; Lima, R.M.; Brandão, R.J.; Pivello, M.R.; Nascimento, S.M.; Duarte, C.R., Barrozo, M.A.S.[a]*

[a] Federal University of Uberlândia, Chemical Engineering School, Uberlândia/MG, Brazil.

*E-mail of the corresponding author: masbarrozo@ufu.br

Abstract

Coffee drying and roasting are usually performed in rotated dryers; therefore, the study of particle dynamics in this equipment is of great relevance to improve their efficiency and hence the quality of the final product. Thus, this work aimed to investigate experimentally and numerically the dynamics of coffee beans in a rotary dryer. The Euler-Euler model was employed to reproduce the particle velocity profile in the rolling regime under different boundary conditions. The results shown that the lower specularity coefficient (0.01), which characterizes the smooth wall and free slip condition, reproduced the bed behavior that most resembled the experimental one. On the other hand, the other coefficients (0.1 and 1.0) showed an increasing deformation in the bed surface, different from the observed experimental behavior. It was also verified that, as the filling degree increases, the bed surface deformation becomes more pronounced.

Keywords: coffee; rotated dryer; simulation; specularity coefficient.

1. Introduction

During the processing of coffee beans, roasting and drying can be performed in rotary drums. These equipment also have a wide range of applications in the industry, such as mixing, drying, granulation, milling and coating. Rotary drums can process many types of raw materials, with large size distributions and different physical properties.

The efficiency of rotatory drums, depending on the process in question, is highly dependent on the granular movement in the interior, which in turn is related to the energy, mass and momentum transfer rates [1]. Therefore, to improve the efficiency of these equipment requires detailed information about the movement of the particles inside.

Rotating drums can show seven different flow regimes (sliding, surging, slumping, rolling, cascading, cataracting and centrifuging), which depend on the rotational speed, filling degree, physical properties of granular materials and drum geometry[2]. Each one with its own specific flow behavior, which increase the complexity in its study.

Cristo *et al*. [3] recommend the rolling regime for coffee roasting, in order to ensure a uniform heat transfer within the equipment. This regime, which is studied in the present work, is characterized by two different regions: a passive region, found near the drum wall, where particles move as a solid body, and an active region, found near the bed material surface, where the particles avalanche and cascade downward. The physical mechanisms such as, mixing and segregation, heat and mass transfer, and so on, mainly occur in the active region.

Parallel to experimental studies, the numerical simulations arise as a complementary tool in the granular flows investigation. In the present paper, the granular flow was simulated using the Euler-Euler approach along with the kinetic theory of granular flow. In this kind of simulation both phases are treated as interpenetrating continua and the Eulerian approach solves a set of moment and continuity equations for each phase. However, the simulated results are very sensitive to the selected boundary conditions. So, the proper choice of these boundary condition on the wall is of crucial importance to represent the experimental behavior.

In the context of the multiphase granular model, the specularity coefficient appears as one of the boundary conditions to be used. The specularity coefficient is a representation of the fraction of collisions between the particle and wall (contour), which transfer lateral momentum to the wall [4]. This coefficient is closely related to the flow conditions and the properties of the wall and there are no experimental determination about it reported in the literature. The value of the specularity coefficient (φ) depends on the sliding condition of the wall and its roughness. Thus, it can range from 0, for perfectly specular collisions, with a smooth wall condition and free slip, and 1, for perfectly diffuse collisions with rough wall and zero slip [5].

Despite the relevance of the boundary conditions for Eulerian simulations, there are few studies about the influence of interactions between particles and the wall on the behavior of the solid phase in rotary dryers. Therefore, the present paper aims to investigate the effect of the boundary conditions on the simulation results of the movement of coffee particles during the rolling regime in a rotating dryer, comparing the simulation with the experimental behavior.

2. Materials and Methods

2.1. Experimental Setup

Green coffee beans were the particulate material used in this study, with the following specifications: average diameter 5.24 mm, density 1368.3 kg/m³, sphericity 0.88, moisture (dry base) equal to 12.15 and angle of repose of 38.4°. The experimental tests were conducted in a stainless steel rotating dryer, with the following dimensions: diameter 21.5 cm and length 50 cm. The front and back walls of the cylinder are made of transparent glass that allows the visualization of the coffee beans movement inside the drum. The inner wall of the dryer was coated with a P80 sandpaper.

The particle velocity profiles were obtained by the image analysis technique using a high speed camera (up to 2000 frames/s). The videos were recorded for the following filling degrees:10, 20, 30, 40 and 50% and at a rotational speed of 12.5 rpm, which characterizes the rolling regime. Using ImageJ® and Meazure™ softwares, it was possible to trace the particles individually in different picture frames. Thus, the velocity of each particle was determined by subtracting the positions of the same particle in two distinct frames. That is, immediately after x2 and y2 (see Figure 1); and before x1 and y1 of the reference line, and then dividing this result by the time interval between the respective frames (t2-t1). Figure 1 shows the positioning of the reference line over the bed radius (r), along which the velocity were measured. From these profiles, it is possible to find the location of the interface between the active and passive layers along the reference line, determined by the point of inversion of the direction of displacement of the particles. In other words, the point where the particles velocity is nearly zero and delimits the transition between the two regions of rolling regime (active and passive) [8].

$$v_{px} = \frac{x_2 - x_1}{t_2 - t_1}$$

$$v_{py} = \frac{y_2 - y_1}{t_2 - t_1}$$
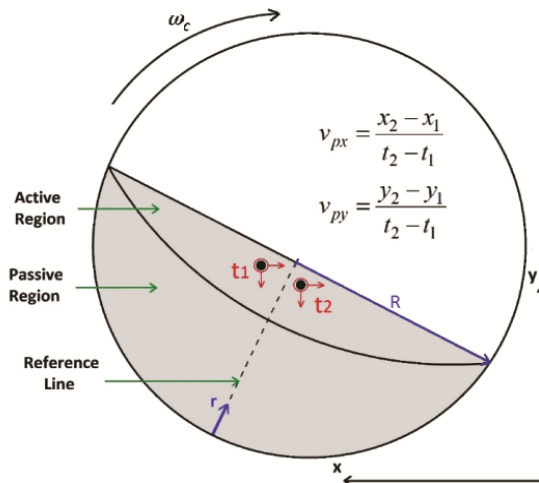
Fig. 1: Methodology for particle velocity measurement during the rolling regime.

2.2. Numerical Methodology

All simulations were performed in Fluent® 14.0 software, using the Eulerian methodology and the Eulerian Granular Multiphase Model to characterize the fluid and the granular phase behavior inside the rotating dryer. To describe the interactions between the solid phases (particle-particle and particle-wall), it was used the Granular Kinetic Theory. For the granular viscosity, the model of Syamlal *et al.* [6] was used. For the bulk granular viscosity, the solids pressure and the radial distribution function, the models of Lun *et al.* [7] were used.

The no-slip condition was used to describe the boundary conditions in the wall relative to the fluid phase. Meanwhile, for the solid phase, it was used the boundary conditions given by the specularity coefficient [5]. Equation 1 expresses the tangential velocity of the solid phase at the wall $\left(u_{sw} \right)$ in terms of specularity coefficient $\left(\varphi \right)$.

$$u_{sw} = \frac{-6\alpha_{S,\max}\mu_S}{\sqrt{3}\sqrt{\theta_S}\,\pi\varphi\rho_S\alpha_S g_{0,ss}}\frac{\partial u_{sw}}{\partial n} \tag{1}$$

Where α_S and ρ_S are the volume fraction and the solid phase density, respectively. θ_S and μ_S are the granular temperature and solid viscosity, $g_{0,ss}$ is the radial distribution function.

3. Results and Discussion

3.1. Analysis of the wall boundary conditions: specularity coefficient

For the purpose to verify the effect of the wall boundary conditions, different values of specularity coefficient (φ) were analyzed in the Eulerian simulation of the coffee beans in a rotary dryer. Hereafter, it is presented a qualitative analysis of the experimental and numerical results, the latter being obtained for the specularity coefficients equal to 1.0; 0.1 and 0.01. Figures 3, 4, 5, 6 and 7 show the distribution of the solid phase in the front wall of the dryer and also in the transverse plane located in half the length, for filling degrees of 10, 20, 30, 40 and 50 %, respectively.

From the Figures 2, 3, 4, 5 and 6, it is possible to note that the simultions with the lowest specularity coefficient value, which characterizes the smooth wall and free-slip condition, better reproduced the experimental behavior, for all filling degrees values evaluated. Concerning to the other specularity coefficients values (0.1 and 1.0), it also can be observe an increasing in bed surface deformation, presenting a divergence from the observed experimental behavior. This is due to the fact that the highest specularity coefficient (1.0) characterizes the rough wall condition, resulting in a high friction between the wall and the particles, and carrying the particles at higher heights. Also, it can be verified that as the filling degree increases, this bed surface deformation becomes more pronounced.

Comparing the solid fraction distributions in the front wall and in the plane at the half length of the dryer, it can be observed a difference in the bed behavior only for the specularity coefficient equal to 1.0. For low values of this parameter, this wall effect is not perceived, since the solid distribution in the wall and in the plane in the middle are practically coincident.
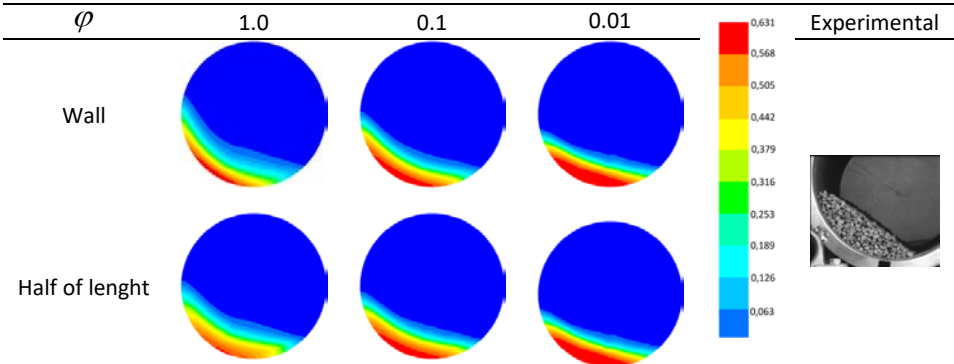
Fig. 2: Solids volume fraction for different values of specularity coefficient at $f = 10\%$
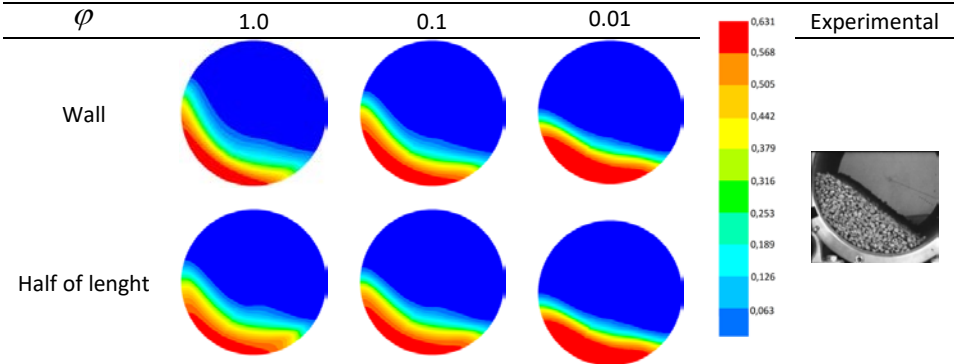
Fig. 3: Solids volume fraction for different values of specularity coefficient at $f = 20\%$
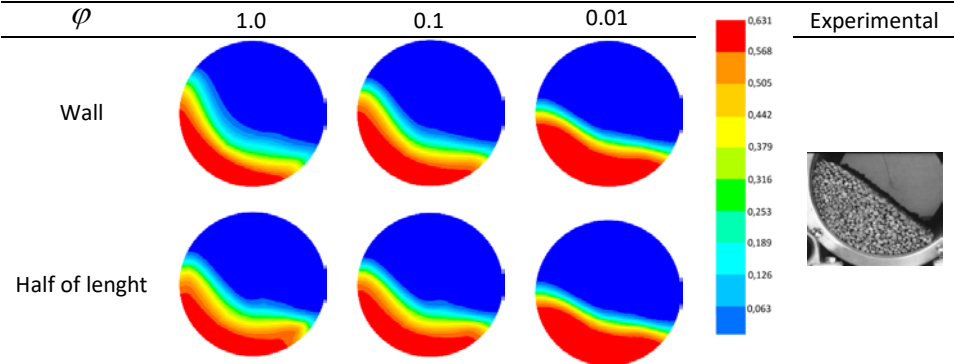
Fig. 4: Solids volume fraction for different values of specularity coefficient at $f = 30\%$
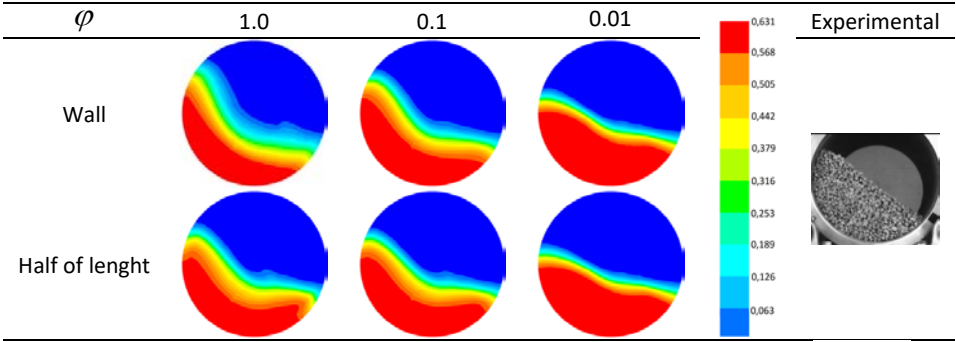
Fig. 5: Solids volume fraction for different values of specularity coefficient at $f = 40\%$
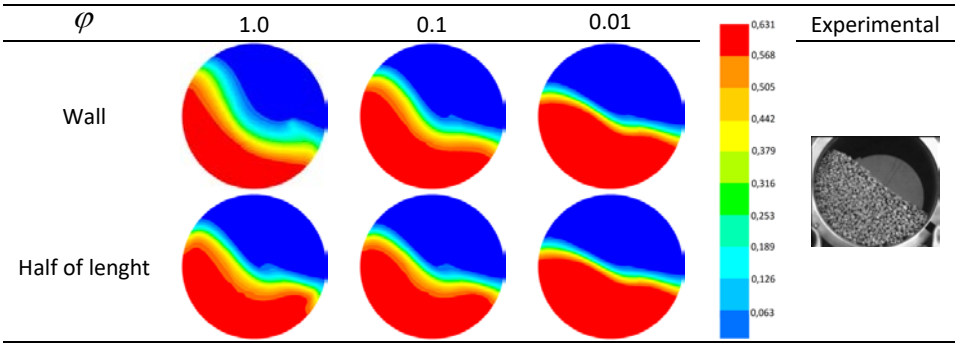
Fig. 6: Solids volume fraction for different values of specularity coefficient at $f = 50\%$

3.2. Particle velocity profiles

In addition to the qualitative analysis, it was also present a quantitative analysis of the particle velocity obtained by the simulation using different values of specularity coefficients. Figure 7 (a), (b), (c), (d) and (e) show the experimental and simulated results of the velocity profile of coffee beans, for filling degrees of 10, 20, 30, 40 and 50%, respectively.

Figure 7 results show that, for all filling degrees, the transition from the passive to the active layer obtained by simulation occurs at radial positions smaller than those obtained experimentally. Thus, the point of inversion of the direction of displacement of the particles is underestimated by the numerical model. This evidence is more pronounced for the lower specularity coefficient (0.01), which is justified by the greater slippage in the wall, characterized by this condition.

Moreover, it is noted that for the greater filling degrees, the behavior of the simulations performed with the higher specularity coefficients values (0.1 and 1.0), becomes more similar in the passive region. Such similarity is also observed for the active region in all evaluated filling degree values. Although there is a large difference between these two specularity coefficients values, the results presented by them are quite similar, suggesting that simulations performed within this range of values (0.1 - 1.0) would not result in different information.
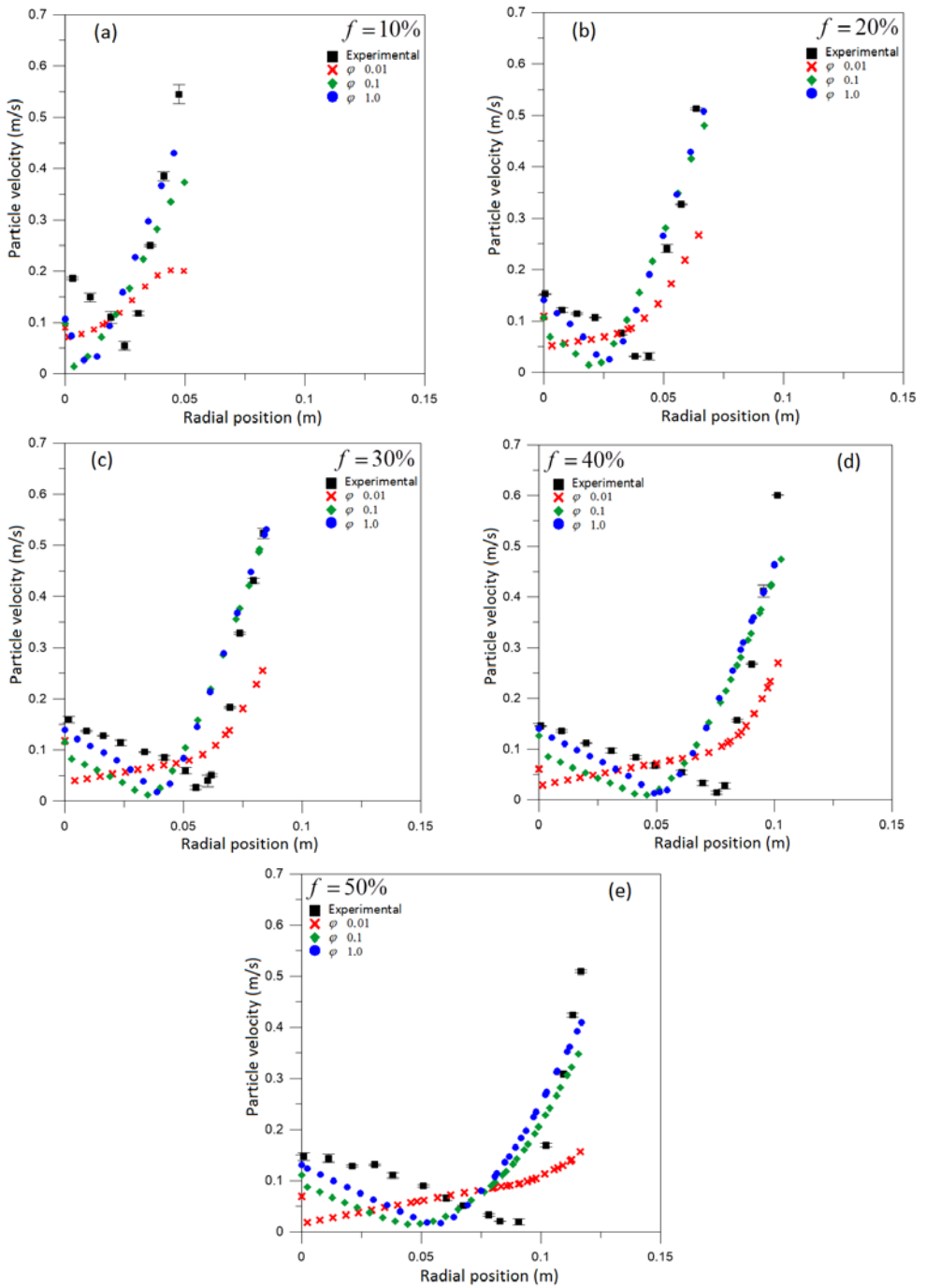
Fig. 7: Experimental and numerical particle velocity profiles for different filling degrees.

4. Conclusions

This work assessed the boundary conditions effects on the coffee beans dynamics inside a rotating dryer by comparing numerical results with experimental data. It was observed that the lower specularity coefficient (0.01), which characterizes the smooth wall and free slip condition, reproduced the qualitative bed behavior that most resembled the experimental one. On the other hand, the other coefficients (0.1 and 1.0) showed an increasing deformation in the bed surface, different from the observed experimental behavior. It was also verified that, as the filling degree increases, the bed surface deformation becomes more pronounced. However, the particle velocities profiles obtained by simulation with this lower specularity coefficient lead to a transition from the passive to the active layer at radial positions smaller than those obtained experimentally.

5. Acknowledgments

6. References

[1] SANTOS, D.A., PETRI, I.J., DUARTE, C.R., BARROZO, M.A.S. Experimental and CFD study of the hydrodynamic behavior in a rotating drum. Powder Technology 2013, 250, 52-62.

[2] MELLMANN, J. The transverse motion of solids in rotating cylinders – forms of motion and transition behavior. Powder Technology. 2001, 118, 251-270.

[3] CRISTO, H.P., MARTINS, M.A., OLIVEIRA, L.S., FRANCA, A.S, Transverse flow of coffee beans in rotating roasters, Journal of Food Engineering 2006, 75, 142-148.

[4] LI, T.; BENYAHIA, S., Revisiting Johnson and Jackson Boundary Conditions for Granular Flows, American Insitute of Chemical Engineers (AIChE) 2011,58 (7), 2058–2068.

[5] JOHNSON, P.C., e JACKSON, R., Frictional-Colisional Constitutive Relations for Granular Materials with Application to Plane Shearing, J. Fluid Mech. 1987, 176, 67-93.

[6] SYAMLAL, M., ROGERS, W., O'BRIEN, T.J, MFIX documentation: Theory Guide, National Technical Information Service, vol. 1, U.S. Department of Energy, Springfiled, USA, 1983.

[7] LUN, C.K.K., SAVAGE, S.B., JEFFREY, D.J., CHEPURNIY, N. Kinetic theories for granular flow: inelastic particles in coquette flow and singly inelastic particles in a general flow fiel, J. Fluid Mech, 1984, 140, 233-256.

[8] MACHADO, M.V.C., NASCIMENTO, S.M., DUARTE, C.R., BARROZO, M.A.S., Boundary conditions effects on the particle dynamic flow in a rotary drum with a single flight, Powder Technology 2017, 317, 341-349.

Lattice Boltzmann modeling and simulation of isothermal drying of capillary porous media

Zachariah, G. T.ª; Panda, D.ª; Surasani, V. J.ª*

ª Department of Chemical Engineering, Birla Institute of Technology and Science, Pilani-Hyderabad Campus, Hyderabad, India, 500078

*E-mail of the corresponding author: surasani@hyderabad.bits-pilani.ac.in

Abstract

Modeling of dring of capillary porous media is difficult due to the complex and coupled heat and mass transfer that occur at dynamic liquid-gas-sold interface. Thus far, drying was simulated using either continuum models or pore-network models, both of which have limitations. In this work, the Lattice Boltzmann Method (LBM) is used to simulate the drying in porous media. The LBM is ideal for such simulations as it can incorporate complex effects in a simple way to exhibit realistic fluid-gas interface during drying of capillary porous media.

Keywords: Lattice Boltzmann Method; Capillary Porous media; Drying, Pore Network.

1. Introduction

Drying of porous media is one of the most energy intensive operations in numerous industries such as textile, food, agriculture and etc. Experimental methods have been established to understand the macroscopic drying kinetics, whereas experimentation for the detailed micro scale transport behavior such as phase and temperature distributions and the corresponding micro-macro interactions still need significant scientific development. Modeling and simulation provides an efficient method for investigating such microscopic behavior. Simulation of the drying of porous media is a challenging task as it involves mass, momentum and heat transfer in a three-phase system (solid, liquid and gas) [1]. Various modeling techniques have been used in the past to simulate such complex processes including classical continuum methods [2], discrete Pore Network Models (PNM) [1] and more recently, the Lattice Boltzmann Method (LBM) [3]. Classical continuum models simulate the complex behavior of the fluid in the porous media macroscopically. These models are derived from either homogenization [2] or volume averaging techniques [4]. The continuum assumption in these models imposes an additional length scale constraint on its application. Moreover, models based on Darcy's law ignore non-equilibrium and inertial effects as the flow is at low Reynolds numbers.

A more promising alternative is the discrete pore network model, which is derived from statistical physics concepts like percolation theory, fractal concepts and scaling theory[1]. These involve representing the void space in a porous medium as a pore network and solving the governing equations on this network. Discrete pore network models are especially useful when the effects of pore space or long-range correlations are strong. Despite its various advantages, the pore network models have numerous shortcomings that need to be addressed. For one, the actual porous media has to be converted into a pore network before simulating which is a complex and time-consuming process, especially for more complicated and broad pore size distribution. Further, such models have always assumed either the pore or the throats to be of zero volume which is unrealistic [1]. The fluid-air interface develops dynamically with time and depends on the capillary pressures and the pore and throat geometry. The inclusion of these effects is necessary to improve the accuracy of the pore network model. The Lattice Boltzmann Method provides an alternative by accommodating the actual geometry of porous media.

The LBM is a relatively new mesoscopic method [3] which has repeatedly proven its ability to simulate transport in porous media. It involves solving the discrete Boltzmann equation to reproduce the Navier-Stokes equation in the continuum limit. This can be shown by conducting a Chapman Enskog expansion of the Boltzmann equation [5]. It is simple and accurate to incorporation of complex geometries. And LBM is efficient with parallelization capabilities which make it ideal for simulations in porous media. Further, due to its roots in

statistical physics, it can easily simulate multi-physics processes including multiphase and multi-component flow, cavitation etc. without explicitly tracking the interface as is done in continuum and pore-network models.H. El. Abrach, et. al.[6] investigated the drying of deformable porous media using LBM, macroscopically. Sukop et.al. [7] demonstrated the applicability of the Lattice Boltzmann method in simulating several micro-scale porous phenomenon such as adsorption, wetting, liquid retention and capillary condensation. The present work explains on how LBM can simulate the intricate microscopic interactions between such phenomenon, leading to complex fluid behaviour, such as capillary pumping and haines jumps [8], in non-deformable porous media.

2. Lattice Boltzmann Method (LBM)

In LBM, the motion of fluid is described by a set of particle distribution functions (PDF), which helps quantify the number of particles with a particular velocity at a certain location in space. The evolution of this PDF with time is described by the lattice Boltzmann equation (LBE) with, in this case, the Bhatnagar-Gross-Krook (BGK) collision operator [9]. The LBE is written as

$$\frac{\partial f_k}{\partial t} + c_k \frac{\partial f_k}{\partial x_i} = \Omega_k(f) + F_k \tag{1}$$

Where, f_k is the particle distribution function in the kth direction, c_k is the velocity in the kth direction, F_k is the forcing term and Ω_k is the collision operator given by

$$\Omega_k(f) = -\frac{1}{\tau}(f_k - f_k^{eq}) \tag{2}$$

Where, τ is the relaxation time and is the equilibrium distribution function given by the Maxwell Boltzmann Distribution, which can be approximated into the following simple form:

$$f_k^{eq}(r,t) = \rho w_k \left(1 + 3e_k u + \frac{9}{2}(e_k u)^2 - \frac{3}{2}u^2\right) \tag{3}$$

The LBE is solved by discretizing the space, time and the velocity. Various different velocity discretization schemes have been developed. In this study, we use the two-dimensional nine velocity model (D2Q9).

For this scheme, the discrete velocities, and are given by:

$$e_k = \begin{cases} (0,0) & k=0 \\ (\pm 1,0)c, (0,\pm 1)c, & k=1,2,3,4 \\ (\pm 1,\pm 1)c, & k=1,2,3,4 \end{cases} \qquad w_k = \begin{cases} 4/9 & k=0 \\ 1/9, & k=1,2,3,4 \\ 1/36, & k=1,2,3,4 \end{cases} \qquad (4)$$

The macroscopic properties we require, such as the density and velocity are derived from the PDF as

$$\rho = \sum_{n=1}^{n} f_k \qquad\qquad \rho u = \sum_{n=1}^{n} e_k f_k \qquad (5)$$

2.1. Incorporating Phase Change Models

In LBM, phase separation is achieved by incorporating a force on the particles at a node based on the particle density in the adjacent nodes, i.e., fluid in one node will experience a force in the direction with the higher neighboring density. In this study, the interaction force is incorporated into the model by shifting the velocity in the equilibrium distribution as given below:

$$u^{eq} = u + \frac{\tau F_{\text{int}}}{\rho(x)} \qquad\qquad \text{`} \qquad (6)$$

It is also possible to incorporate the interaction force via direct body forcing, where an additional term is added after the collision process [10]. The most commonly used method is the one proposed by Shan and Chen for Multiphase simulation[11]The inter-particle force is then taken as:

$$F_{\text{int}}(x) = -G\psi(x)\sum_{k=1} w_k \psi_k(x+e_k)e_k \qquad (7)$$

Where, G is an interaction strength constant and is either negative or positive for attraction and repulsion respectively, w_k is the weight function given in equation 4 and ψ is the effective mass, a function of density. This formulation results in an equation of state given by:

$$P = c_s^2 \rho + \frac{c_0}{2} g[\psi(\rho)]^2 \qquad (8)$$

Where, cs is the velocity of sound, c_0 is a parameter determined by the chosen lattice structure and   is a parameter that controls the magnitude of the inter-particle forces.

The formulation of ψ can be designed to incorporate a more accurate Equation of State if required[12]. Equation 8 can be rearranged to give:

$$\psi(\rho) = \sqrt{\frac{2(p_{EOS} - c_s^2 \rho)}{c_0 g}} \qquad (9)$$

Here, P_{EOS} is the equation of state used, which, in this case, is the Carnahan Starling equation of state, given by:

$$p_{EOS} = \rho RT \frac{1 + b\rho/2 + (b\rho/4)^2 - (b\rho/4)^3}{(1 - b\rho/4)^3} - a\rho^2 \qquad (10)$$

Applying to equation 7 and combining the numerical approximations of the gradient [13], we get:

$$F_{int}(x) = c_0 \beta G \nabla \psi(x) - (1 - \beta)c_0 G \Delta \nabla \psi^2(x)/2 \qquad (11)$$

Where G is taken as -1 to ensure a positive value under the root and   is a weighting factor that can be tuned for each equation of state. For the CS equation of state β is taken as 1.16.

Here, wall interaction is incorporated in a similar way, by assuming the walls to have density equal to the liquid density. Therefore, $\rho_{wall} = \rho_{liquid}$. This gives the formulation:

$$F_{ads}(x) = -G_{ads}\psi(x)\sum_{k=1}^{n} w_k \psi_{wall}(x + e_k)e_k \qquad (12)$$

3.   Simulation Results and Discussion

In this study, we simulated the drying of two types of porous media: structured and irregular. The structured porous medium consisted of equally spaced horizontal and vertical throats intersecting in circular pores, while the irregular porous media did not exhibit any observable pattern. Figure 1 shows the simulated results obtained using Lattice Boltzmann method. In the porous medium as shown in Figure 1A, the radius of the pores are much higher than that of the throats. This implies that there is a sudden and large increase in radius of the meniscus, thereby making it unstable/instabilities during drying. Therefore, the interface moves rapidly to the next stable orientation. This causes the surrounding liquid to be pumped outward and thus causing smaller pores and throats to be filled. This phenomenon can be observed in Figure 1A. The emptying of the pore circled in red leads to the refilling of the vertical throat circled in blue. Such effects are more prominent and discernable near the edges of the porous media where the pumping is only possible in limited directions. This phenomena of Haines jump events can significantly change the liquid orientation in the porous media as well as cause fluctuations in drying rate. Predicting such phenomenon is therefore essential to creating accurate models of drying.
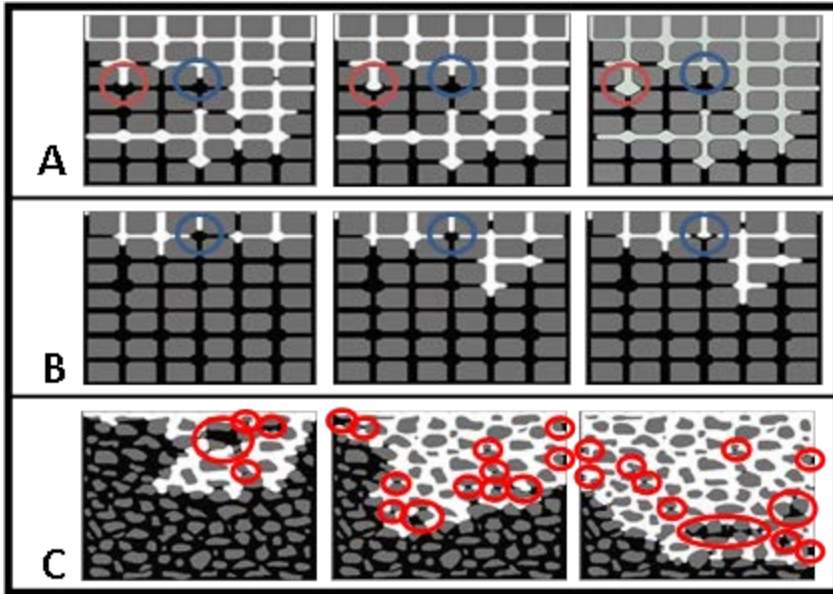
Figure 1: A) Occurance of Haines jump (red) leads ot refilling of vertical throat (blue). B) Effect of surface tension impedes the emptying of pore (blue). C) Large extend of sluster formation.

Apart from the geometry of the porous media, the properties of the wetting fluid also plays a crucial part in the drying. One such property, the surface tension, can prevent the invasion of a pore even though its adjoining throats are empty, as shown in Figure 1B. It can be seen that the pore (circled in blue) does not invade for a considerable amount of time even though two of its adjacent throats are empty. As explained, emptying of pores creates unstable intermediate interfaces. This unstability is due to the high surface energy present at the interface. Therefore, to invade a pore, the surface energy of the interface has to become equal to or larger than the intermediate interfacial energy. This is usually achieved due to reduction in pressure above the interface, and so, increase in surface tension and energy. Hence, pores are not invaded until the surface energy of the pore reaches a threshold value.

The structured porous media shown above is merely an approximation of the actual porous media, which vary widely in shape and size of both pores and throats. Figure 1C shows a more random type of porous media where the drying phenomena is simulated. Here, the wide range of sizes and shapes lead to clusters formation (red). These clusters may be very small and local to single throats, or large and spanning several pores. These clusters of liquid are bounded by interfaces of high capillarity. This implies that such clusters remain idle until and unless the surrounding pressure reduces sufficiently. It is therefore possible for clusters to exist even after the drying completes. Such bounded liquid can lead to significant problems in drying efficiency and quality of products and so, have to be accounted for.

4. Conclusions

Modelling of drying of porous media has been done in the past using various techniques such as Pore Network Models and Continuum models and have met with some success. Here, we used a Carnahan Starling equation of state based high density ration Lattice Boltzmann Method to model the same under realistic operating conditions. The following key observations were made from this study:

1. Haines jumps cause significant changes in liquid orientation and can lead to unexpected variations in drying rate.

2. Surface energy of the interface plays an important role in deciding which pore to invade and when.

3. Highly randomized and realistic porous media exhibit high levels of liquid entrapment and cluster formation

It can be concluded that the Lattice Boltzmann Method provides an accurate and plausible alternative to continuum and pore network models when it comes to modeling in porous media.

5. References

[1] Surasani, V.K., T. Metzger, and E. Tsotsas, *Influence of heating mode on drying behavior of capillary porous media: Pore scale modeling.* Chemical Engineering Science, 2008. **63**(21): p. 5218-5228.

[2] Sánchez-Palencia, E., *Non-homogeneous media and vibration theory*. Lecture notes in physics. 1980: Springer-Verlag.

[3] Benzi, R., S. Succi, and M. Vergassola, *The lattice Boltzmann equation: theory and applications.* Physics Reports, 1992. **222**(3): p. 145-197.

[4] Quintard, M. and S. Whitaker, *Transport in ordered and disordered porous media: volume-averaged equations, closure problems, and comparison with experiment.* Chemical Engineering Science, 1993. **48**(14): p. 2537-2564.

[5] Nourgaliev, R.R., et al., *The lattice Boltzmann equation method: theoretical interpretation, numerics and implications.* International Journal of Multiphase Flow, 2003. **29**(1): p. 117-169.

[6] El Abrach, H., H. Dhahri, and A. Mhimid, *Lattice Boltzmann method for modeling heat and mass transfers during drying of deformable porous medium.* AIP Conference Proceedings, 2011. **1453**(1): p. 211-216.

[7] Sukop, M.C. and D. Or, *Lattice Boltzmann method for modeling liquid-vapor interface configurations in porous media.* Water Resources Research, 2004. **40**(1): p. W015091-W0150911.

[8] Armstrong, R.T. and S. Berg, *Interfacial velocities and capillary pressure gradients during Haines jumps.* Physical Review E - Statistical, Nonlinear, and Soft Matter Physics, 2013. **88**(4).

[9] Bhatnagar, P.L., E.P. Gross, and M. Krook, *A model for collision processes in gases. I. Small amplitude processes in charged and neutral one-component systems.* Physical Review, 1954. **94**(3): p. 511-525.

[10] Martys, N.S. and H. Chen, *Simulation of multicomponent fluids in complex three-dimensional geometries by the lattice Boltzmann method.* Physical Review E - Statistical Physics, Plasmas, Fluids, and Related Interdisciplinary Topics, 1996. **53**(1): p. 743-750.

[11] Shan, X. and H. Chen, *Lattice Boltzmann model for simulating flows with multiple phases and components.* Physical Review E, 1993. **47**(3): p. 1815-1819.

[12] Yuan, P. and L. Schaefer, *Equations of state in a lattice Boltzmann model.* Physics of Fluids, 2006. **18**(4).

[13] Kupershtokh, A.L., et al., *Stochastic models of partial discharge activity in solid and liquid dielectrics.* IET Science, Measurement & Technology, 2007. **1**(6): p. 303-311.

Drying kinetics of cellulose nanofibers suspensions

Al Zaitone, B.

Department of Chemical and Materials Engineering, King Adulaziz University, Jeddah, Kingdom of Saudi Arabia

*E-mail of the corresponding author: balzaitone@kau.edu.sa

Abstract

Cellulose nanofibers (CNF) is used in various pharmaceutical applications due to its unique characteristics i.e., biodegradability, mechanical and biological properties. CNF is often produced by spray drying process, knowledge of the drying kinetics in terms of mass and heat transfer on the scale of single droplet is important for process development and model validation.

Acoustic levitator was used to study drying process of CNF suspension at different air temperatures and initial CNF concentrations. The unique property of acoustic levitation to hold single droplet contactless in the air, enables to study particle morphology during drying process, calculate evaporation rate and estimate particle porosity. Results show that packed particles result at lower initial concentration and temperature has a moderate influence on mean porosity of CNF dried particles.

Keywords: acoustic levitation; droplet; drying kinetics; Cellulose Nanofibers.

1. Introduction

Cellulose nanofibers (CNF), is a promising biopolymer. The high surface area of CNF makes it suitable as a nanofiller to enhance the mechanical properties of composite materials [1]. The rheological and physio-chemical properties, allow CNFs to stabilize emulsions of different types and improve the drug delivery of active materials in poor soluble aqueous solutions [2]. The strength with low weight and high surface area make CNF a good candidate for capsule reinforcement [3], on the other hand CNF can play a significant role in producing sustained drug release formulation, the CNFs form a fiber network that hinder the diffusion of drug [3].

Cellulose nanofibers are mainly produced form cellulosic botanical sources such as wood, cotton, hemp or flax. The isolation of Cellulose nanofiber is achieved via mechanical or chemical processes, which result in gel-like liquid suspension that held cellulose nanostructures. CNFs are extracted from the aqueous medium via evaporation of the solution through lyophilization [4], supercritical drying and spray drying [5].

Spray drying is widely used in many industries, e.g. chemical, food and pharmaceutical processing. In spray drying, droplets generation is followed by solvent/liquid evaporation leading to a final powder product. The short retention time in spray drying, makes it ideal for heat sensitive materials. Controlling the drying kinetics is decisive to minimize the liquid amount in the particles and enhance good mechanical properties. Physico-chemical properties of the solution together with operating parameters, greatly influence drying kinetics.

Since experiments on real sprays are difficult to interpret and only integral information about an ensemble of droplets can be obtained, simple and idealized configurations considering single droplets are often preferred for investigation of such spray drying situations.

The experimental work presented in this paper deals with the drying process of individual CNF suspension droplets. The focus of drying experiment was to determine the drying kinetics at various process parameters i.e., gas drying temperature, CNF loading. The acoustic levitation has been used, exhibiting an almost steady positioning of the sample; hence providing a unique opportunity to observe a droplet throughout the entire drying period. The imaging technique allows for accurate measurement of temporal change of droplet diameter and vertical size, that were used to calculate drying rate and mass of the droplet during the drying process and estimation of dried particle porosity.

The paper is organized as follows: in the next section, materials and methods i.e. acoustic levitation are described and the influence of the acoustic streaming on liquid evaporation is discussed, thereafter, the experimental and theoretical results are presented. The paper ends with the conclusions.

2. Materials and Methods

2.1. Materials

The CNF used for the microparticles production was obtained from Process Development Center University of Maine (Orono, USA) in form of 3.0% aqueous gel. The nominal fiber diameter is 50 nm and fiber length up to few hundred micrometers. Deionized distilled water was used to prepare CNF suspension.

2.2. Methods

2.2.1. Preparation of CNF suspension for single droplet drying

The CNF aqueous gel solid content was proofed by drying 10 different samples of CNF aqueous gel in an oven at 60 °C for 10 hours, the mass fraction of dry fibers was estimated to be 3.5%±0.13. The desired suspensions were prepared by diluting CNF aqueous gel using deionized distilled water. CNF suspension was homogenized using magnetic stirrer for 30 mins to assure homogeneity of the cellulose fibers suspensions. The desired concentrations of CNF suspension were 2,4 and 6 mg(CNF)/ml (water).

2.2.2. Single droplet drying apparatus

The ultrasonic levitator was used for the drying experiments; the main setup is sketched in *Fig. 1*, it consists of an acoustic levitator which operates at 58 kHz sound frequency. The emitted ultrasonic waves leave the transducer and propagate throught the gas mesdium to hit the concave reflector and then bounce to the transducer forming the so-called standing wave. The acoustic force generated by this standing wave is capable of stable positioning of the liquid or solid samples. The levitatator is equiped with heating chamber, and drying temperature up to 120 °C of the gas can be achieved. The imaging system consists of a CMOS camera connected to a macro lens, it allows for monitoring the droplets. The droplet is illuminated via LED back light, the shadow image captured by the camera is anaylzed online to calculate droplet equivalent diameter, vertical position and aspect ratio. A microliter syringe with long needle is used to insert axially the droplet into the acoustic field.

Influence of the acoustic field

The interaction between the acoustic field and CNF droplets suspended by the acoustic force generates streaming flow around the droplet. Several authors [6, 7] studied the induced flow and quantify its effect on the evaporation of the liquid. The acoustic streaming were first defined Schlichting [8], these streaming are divided into two categories; the inner acoustic streaming which drives the mass and heat transfer between the droplet surface and the surrounding gas medium [6, 9].
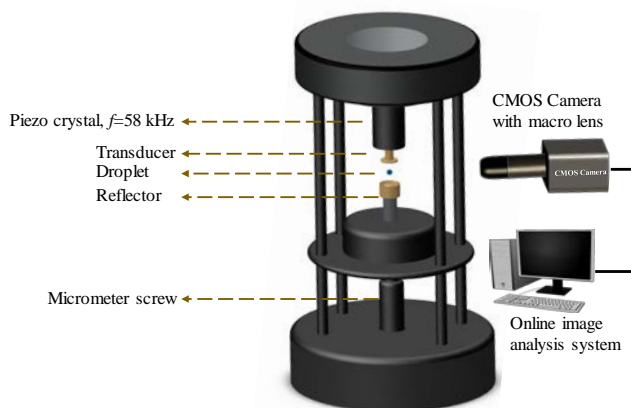
Fig. 1 Schematic picture of the acoustic levitator.

The second streaming flow is called outer acoustic streaming which represent toroidal vortices, these vortices trap the evaporated liquid from the droplet. Therefore, the vapor is accumulated around the droplet and alter the far-field vapor concentration. As more vapor is trapped by the outer acoustic streaming, the evaporation rate is reduced and comparison with model become rather difficult. A depletion of the accumulated vapor from such vortices becomes mandatory to have reproducible results and enable model validation. An air flow of 0.85 l/min is inserted surrounding the droplet to destroy the outer acoustic streaming and remove the vapor accumulated around the droplet [10].

3. Results and Discussion

3.1. NFC Microparticle production

CNF has strong affinity to water, at very small CNF concentration ca. 3.5% wt., a slurry is formed, in order to generate small droplets using the microliter syringe, suspension at very low CNF loading were prepared, namely 2,4, and 6 mg CNF per ml of water.

The drying temperature was varied in the range (20-80 °C), droplets of 1.0-2.0 µl of the suspension was introduced into the acoustic field, once the drying experiment finished the particle was collected to study its morphology and surface structure under scanning electron microscopy. As shown in *Fig. 2*, the drying of CNF suspensions droplet results in water evaporation and an agglomerate of fibrous structure is formed. The initial droplet size was 1.5 mm. at the end of drying course in the acoustic levitator, the dried particle size is reduced to ca.~200-300 µm diameter and an agglomerate of the nanofibers was obtained. It can be seen that particles are not spherical, *Fig. 2*a shows the surface morphology of the particle where the nanofiber consolidated together, *Fig. 2*c depicts the internal structure of the particle after it has been broken, the porous structure and the random alignment of the fibers can be

easily noticed, despite the length of the cellulose nanofibers, they have been folded inside the droplet due to high surface tension of the water comparing to the soft cellulose nanofibers structure.

a)   b)   c)
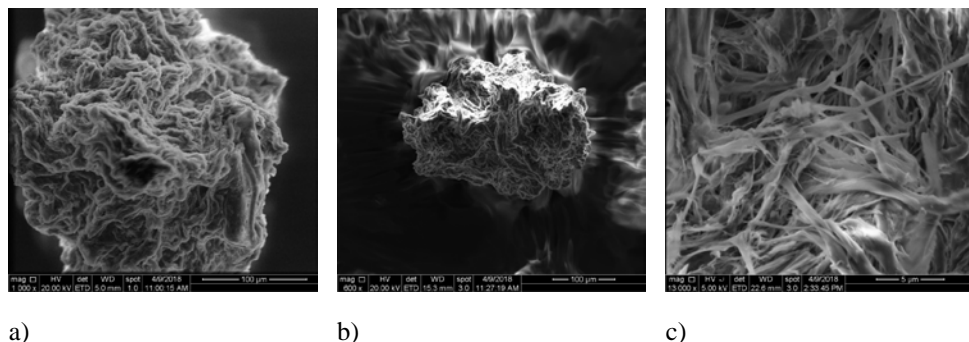
Fig. 2 Scanning Electron Microscopy images of dried cellulose nanofibers suspensions a) 6mg/ml at 80°C b) 6mg/ml at 60 °C and c) internal structure of broken particle.

3.2. Evaporation rate and porosity estimation

The drying rate and the mean porosity of dried particle is disued in this section. Four different temperatures were investigated, the surface decay of the droplets is shown in ***Fig. 3***, the higher the temperature is, the droplet drying rate becomes faster. The experiments in ***Fig. 3*** were conducted with the same initial volume namely 2µl and different loading of CNF was used. The drying curves in terms of normalized surface area decay can be divided into two stages, the first one, where the loading of CNF is very low, mass fraction of CNF is less than 0.05% wt., the evaporation rate here follows the well-known d^2-law. Actually, for small CNF loading, the drying curve is similar to the evaporation of pure water, once the loading of CNF increases, it starts competing with the available sites for water evaporation, as more of the solids accumulated on the surface, the evaporation of the liquid becomes slower i.e., second stage begins. Finally, the droplet forms an agglomerate of cellulose nanofibers, the size of the particle remains constant.

The evaporation rate was calculated from the slope of the temporal evolution of the surface decay curves and represented by a solid line in ***Fig. 3***.

The porosity of the dried particle is an important parameter for modelling drying kinetics, the water passes through particle voids to reach the surface. On the other hand CNF can play a significant role in producing sustained drug release formulation, the CNFs form a fiber network that hinder the diffusion of drug [3]. At lower particle porosity, the drug diffusion become slower, porosity is calculated using the equation:

$$\varepsilon = 1 - \frac{m_s}{\rho_s V_p} \tag{1}$$

Where, ε is the porosity, m_s, ρ_s is the mass and density of solids respectively, V_p is the volume of the particle in m^3. As depicted in *Fig. 3*, higher porosity is obtained for lower initial CNF concentration, while temperature has a moderate influence on mean particle porosity.
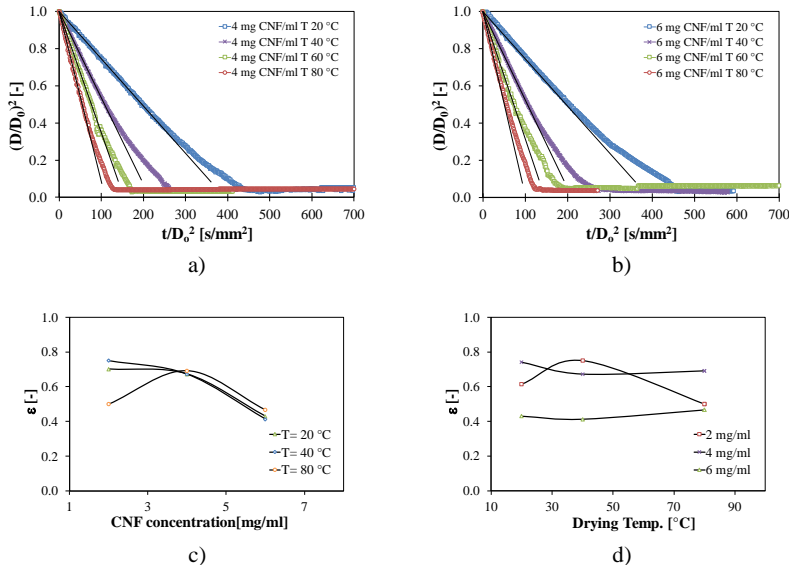
Fig. 3 Temporal evolution of surface area decay of CNF suspension droplet for a) 4mg CNF/ml, b) 6mg CNF/ml at 20,40,60 and 80 °C, the initial droplet volume is 2.0 µl. c) & d) calculated mean porosity of dried CNF particle as a function of CNF loading and drying temperature, respectively.

3.3. Constant and falling rate periods

Suspension of CNF droplet exhibit upon course of drying changes in physical properties, i.e., density of the droplet increases as more liquid is evaporated, the shape of the droplet changes until the final morphology evolves at the end of the drying. In case of mass transfer rate, droplet drying shows in general two regimes, the first one is called constant rate period and the second one is falling rate period [11, 12].

In constant rate period the evaporation of the liquid occurs from a wet particle surface. As depicted in *Fig. 4*, evaporation of the liquid is accompanied by size reduction i.e., droplet normalized surface area decreases with time. The shrinkage of droplet continues, and the concentration of CNF increases until a small particle or grain of CNF is formed. During the constant rate period the evaporation rate occurred occurs at constant wet bulb temperature, the evaporation rate is calculated form the volume change of the droplet of the liquid:

$$\frac{dm_{d,c}}{dt}\bigg|_{const} = -\rho_d \frac{\Delta V}{\Delta t} \tag{2}$$

Where V is the volume of the droplet in m^3 and ρ_d is droplet density in kg/m^3.

As the liquid evaporates, the droplet alters its vertical position in the acoustic field. The vertical position is function of droplet's volume and weight [6], it rises in the acoustic field towards pressure node as shown in *Fig. 4*.

Once the volume and aspect ratio of the droplet/particle seized, the *constant rate period* comes to its end and the *falling rate period* starts, this is marked by constant surface area in *Fig. 4*, here, the shadow image technique is not able any more to deliver information about the mass transfer rate because the particle/grain has now a constant volume that is calculated from its meridional section.

The evaporation of the liquid continues and by monitoring the vertical position of the grain in the acoustic field, further information about the mass transfer can be found. The acoustic force acts against gravity force and once the droplet volume is constant, any decrease in particle weight due to liquid evaporation force the droplet to move upwards to the adjacent pressure node.

The mass of the particle can be easily found by interpolation of the vertical position in the falling rate period, knowing that the rise of the particle in the acoustic field is now only function of the density.

$$m_{d,f}(t) = \frac{\Delta m_{f,max}}{\Delta y_{f,max}} \cdot \left(vert.pos(t) - vert.pos(t_{f0}) \right) + m_{d,c} \qquad (3)$$

Where, $m_{d,f}$ is the mass of droplet in the falling in kg, $\Delta m_{f,max}$ and $\Delta y_{f,max}$ are maximum difference of particle mass and particle vertical distance respectively and calculated between the beginning and the end of the falling rate period. $m_{d,c}$ is the mass of droplet at the end of constant rate period. The mass of the liquid at the end of falling rate period is approximately zero, t_{f0} is the time in seconds when falling rate period begins.
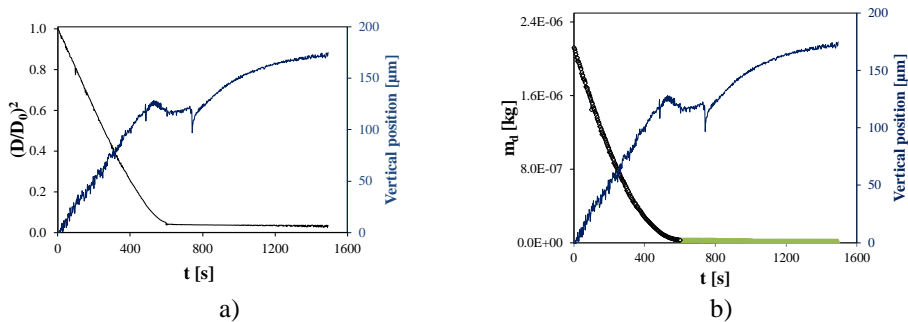
***Fig. 4** Vertical position of the droplet (CNF 6 mg/ml TE 40 °C) during the course of drying, the first stage of drying is designated by volume reduction of the droplet and the second stage of drying is designated by rise in the acoustic field at constant volume.*

The above results show the importance of the acoustic levitator to measure the drying kinetics of CNF suspension droplets, and its ability to measure particle's drying rate in both constant and falling rate periods. The estimated porosity of dried particle which is an important product property and was obtained for different drying temperatures and CNF loadings.

4. Conclusions

The drying kinetics and porosity of CNF dried particle has been investigated, a series of experiments were conducted in the acoustic levitator to mimic the spray drying process occurred in spray dryer. Drying rates and the evolution of particle morphology were monitored using the shadow imaging technique. Particle shape and inner structure of cellulose nanofibers were analysed by SEM technique. The drying rate of droplet increases at high temperatures. The porosity of the dried particles shows an increase for higher CNF initial concentrations and drying temperature has a moderate influence on particle porosity.

5. References

[1] Santos, F., Iulianelli, G. C. V., Inês, M., and Tavares, B. The Use of Cellulose Nanofillers in Obtaining Polymer Nanocomposites: Properties, Processing, and Applications. *Materials Sciences and Applications* 2016, 7 (5), 257-294.

[2] Löbmann, K., and Svagan, A. J. Cellulose nanofibers as excipient for the delivery of poorly soluble drugs. *International Journal of Pharmaceutics* 2017, 533 (1), 285-297.

[3] Kolakovic, R., Laaksonen, T., Peltonen, L., Laukkanen, A., and Hirvonen, J. Spray-dried nanofibrillar cellulose microparticles for sustained drug release. *International Journal of Pharmaceutics* 2012, 430 (1-2), 47-55.

[4] Han, J., Zhou, C., Wu, Y., Liu, F., and Wu, Q. Self-assembling behavior of cellulose nanoparticles during freeze-drying: Effect of suspension concentration, particle size, crystal structure, and surface charge. *Biomacromolecules* 2013, 14 (5), 1529-1540.

[5] Peng Y, Y. H. G. J. D. Spray-drying cellulose nanofibrils: effect of drying process parameters on particle morphology and size distribution. *Wood and Fiber Science* 2012, 44 (4), 1-14.

[6] Yarin, A. l., Brenn, G., Kastner, O., Rensink, D., and Tropea, C. Evaporation of acoustically levitated droplets. *Fluid Mech.* 1999, 399, 151-204.

[7] Trinh, E. H., and Robey, J. L. Experimental study of streaming flows associated with ultrasonic levitators. *Phys. Fluids* 1994, 6 (11), 3567-3579.

[8] Schlichting, H. *Boundary Layer Theory*, McGraw-Hill, Inc., 1978.

[9] Gopinath, A., and Mills, A. F. Convective Heat Transfer From a Sphere Due to Acoustic Streaming. *Journal of Heat Transfer* 1993, 115 (2), 332-341.

[10] Al Zaitone, B. A., and Tropea, C. Evaporation of pure liquid droplets: Comparison of droplet evaporation in an acoustic field versus glass-filament. *Chemical Engineering Science* 2011, 66 (17), 3914-3921.

[11] Nesic, S., and Vodnik, J. Kinetics of droplet evaporation. *Chemical Engineering Science* 1991, 46 (2), 527-537.

[12] Mujumdar, A. S. *Handbook of Industrial Drying*, Marcel Dekker, New York, 2006.

Convective air drying of brown seaweed *Bifurcaria bifurcata* in thin layer configuration

Arufe, S.; Sineiro, J.; Chenlo, F.; Moreira, R.

Department of Chemical Engineering, Universidade de Santiago de Compostela, Rúa Lope Gómez de Marzoa, Santiago de Compostela, E-15782, Spain.

*E-mail of the corresponding author: ramon.moreira@usc.es

Abstract

Air drying kinetics of Bifurcaria bifurcata brown seaweed at 35, 50, 60 and 75°C were determined. Experimental drying data were modelled using two-parameter Page model (n, k). Page parameter n was constant (1.28) at tested temperatures, but k increased significantly with drying temperature from 35 to 60ºC and was invariant at higher temperatures (up to 75ºC). Drying experiments allowed the determination of the critical moisture content of seaweed (1.6 ± 0.2 kg water (kg d.b.)⁻¹). Mass transfer coefficients during constant drying rate period and effective coefficients of water diffusion during falling drying rate period were evaluated, assuming cyclindrical geometry and considering volumetric shrinkage.

Keywords: algae, diffusivity, drying kinetics, modelling, shrinkage

1. Introduction

Bifurcaria bifurcata is a brown seaweed geographically distributed in the Western Europe and Sahara coasts. The main use is the extraction of compounds (alginates and other products) used by pharmaceutical, cosmetics and food industries [1]. Although the human consumption of this seaweed is not as extended as other seaweeds such as *Laminaria spp.*, *Undaria pinnatifida*, its high content of polysaccharides, proteins and minerals [2] and antioxidants [3] makes attractive the use of this seaweed as food product. In fact, the direct human consumption worldwide in recent years is increasing.

Drying is a very employed operation in order to obtain stable food products whose storage as fresh product can be difficult. In the case of seaweeds, traditionally the water removal is carried out by solar drying, but the increasing demand of more homogenous and better quality dried products must be satisfied by means of the use of other industrial methods like convective hot air drying. In this sense, the experimental determination of the more adequate drying conditions is necessary to obtain a final dried product with acceptable characteristics. A scarce number of studies on mathematical modelling of drying kinetics of seaweeds can be found in literature. In example, Lemus et al. [4] studied the drying kinetics of the red seaweed *Gracilaria chilensis* and Vega-Gálvez et al., [5] the drying of brown seaweed *Macrocystis pyrifera*. However, no studies on drying kinetics of fresh *Bifurcaria bifurcata* were found. The aim of this work was to determine the drying kinetics of *Bifurcaria bifurcata* at different temperatures and the corresponding modelling of the drying periods.

2. Materials and Methods

Fresh brown *Bifurcaria bifurcata* seaweeds (4.59 ± 0.28 kg water·(kg dry solid)$^{-1}$, d.b.) selected with similar sizes (100-150 mm length and 1.5-2.0 mm diameter) were dried in a hot air convective dryer (Angelantoni, Challenge 250, Italy), at four air temperatures (35, 50, 60 and 75ºC). Relative humidity (30%) and air velocity (2 m·s^{-1}) remained constant. Seaweeds were placed on a metallic mesh (45x45 cm^2) allowing the transversal air flow during drying. A thin layer configuration involving the use minimum amount of seaweeds to cover initially the drier tray (load density of 2.04 ± 0.02 kg·m^{-2}) was employed.

Samples were weighed using a balance (Cobos D-6000-CS, ± 0.1 g, Spain), during drying until achieve a constant weight. All experiments were performed, at least, in triplicate.

Drying kinetics were modelled by Page model [6], Eq. (1):

$$MR = e^{-kt^n} \tag{1}$$

where k (min^{-n}) and n (-) are the model parameters. The dimensionless moisture content or moisture ratio, MR (-), was calculated by Eq. (2):

$$MR = \frac{X_t - X_{eq}}{X_0 - X_{eq}} \tag{2}$$

where X_t is the moisture content (d.b.) at any drying time, X_0 is the initial moisture content (d.b.) and X_{eq} is the equilibrium moisture content of the sample (d.b.).

2.1. Sample surface area and shrinkage determination

Sample surface area and shrinkage of seaweeds were estimated following the same procedure. Samples (0.5-1.5 g) dried at several times were immersed into n-heptane at 21ºC. The initial volume (V_0, m³) of the samples and the volume at different drying times (V), were measured applying Archimedes' principle. A volume shrinkage with moisture content (V/V_0 vs X) relationship was obtained. External surface area of the monolayer was estimated assuming cylindrical geometry of the seaweed and the tray surface is fully covered initially. The initial radius of seaweed branches was determined ($2.3 \pm 0.3 \ 10^{-3}$ m). Volume shrinkage was mainly governed by radius decrease ($L/r_0 > 100$) and Eq. (3) was obtained:

$$\frac{V}{V_0} = \frac{\pi r_x^2 L}{\pi r_0^2 L} \rightarrow r_x = \sqrt{\frac{V r_0^2}{V_0}} \tag{3}$$

where L (m) is the length, r_0 and r_X (m) the initial and the radius of sample at different moisture content. The surface area ratio of monolayer can be calculated by Eq. (4):

$$\frac{S_X}{S_0} = \frac{2\pi r_X L N_S}{2\pi r_0 L N_S} = \frac{r_X}{r_0} \tag{4}$$

where S_X (m²) is the surface area of seaweed monolayer at each moisture content, S_0 the initial surface area of the monolayer and N_s is the number of seaweed samples that can be placed in the monolayer ($L/(2 \ r_0)$). Employing the Eq. (3), the relationship between surface area of seaweed monolayer and volumetric seaweed shrinkage resulted on Eq. (5):

$$\frac{S_X}{S_0} = \sqrt{\frac{V}{V_0}} \tag{5}$$

The determination of surface area of seaweeds monolayers allowed the specific drying rate, w_s (kg water kg dry solid⁻¹ m⁻² min⁻¹), evaluation by means of Eq. (6):

$$w_s = \frac{1}{S_X} \frac{X_{t_{n-1}} - X_{t_n}}{t_n - t_{n-1}} \tag{6}$$

The w_s vs X curve was used for the critical moisture content (X_c, d.b.) evaluation at tested temperatures and the end of the constant drying rate period.

2.1.1. Constant drying rate period modelling

During the constant drying rate period the coefficients of mass transfer (K_t, m s⁻¹) and the convective heat transfer (h_t, W·m²·K⁻¹), were determined by Eqs. (7) and (8):

$$w = \frac{X_{t_{n-1}} - X_{t_n}}{t_n - t_{n-1}} = \frac{K_t \rho_{air} a}{\rho_s}(Y_i - Y_{air}) \tag{8}$$

$$w = \frac{h_t a}{\Delta H_v \rho_s}(T_i - T) \tag{9}$$

where w (kg water·kg dry solid^{-1}·s^{-1}) is the mass flow of evaporated water, Y_i and Y_{air} (kg water (kg dry air^{-1})) are the interphase and bulk absolute moisture content of air, respectively, ρ_{air} (kg·m^3) is the air density at drying temperature, ρ_s (kg dry solid·m^{-3}) is the apparent density of seaweed layer, a (m^2·m^{-3}) is the total interfacial surface (assuming water transfer by both sides of the layer) per unit of layer volume, T_i and T (ºC) are the interphase and dry temperature of air, respectively and ΔH_v (J·kg^{-1}) is the latent heat of vaporization of water at the interphase temperature. The interphase properties (Y_i and T_i), during pre-critical drying period, were considered as the wet-bulb properties of the air employed for drying.

2.1.2. Falling drying rate period modelling

The falling drying rate period of drying was modelled employing the analytical solutions to Fick's diffusion equation to determine the effective coefficients of water diffusion through the sample under some assumptions [6]. Briefly, the distribution of the moisture within the product is uniform; at t > 0 surface reaches equilibrium moisture and all resistances to water removal are inside the material (the external resistances are negligible). Moreover, the shrinking effect on the characteristic dimension (r_x) of seaweeds was taken into account. The fitting of the experimental data of the falling drying rate period was carried out employing the following ratio, Eq. (10):

$$\frac{M_t}{M_\infty} = \frac{X - X_e}{X_c - X_e} \tag{10}$$

where M_t (g) is the amount of water removed at time t (min), M_∞ (g) is the total amount of water removed until the equilibrium is reached. The analytical solutions associated to the cylindrical geometry for short Eq. (11) and long Eq. (12) times are:

$$\frac{M_t}{M_\infty} = \frac{4}{\pi^{1/2}}\left(\frac{D_{eff}\cdot t}{r_x^2}\right)^{1/2} - \frac{D_{eff}\cdot t}{r_x^2} - \frac{1}{3\cdot\pi^{\frac{1}{2}}}\left(\frac{D_{eff}\cdot t}{r_x^2}\right)^{3/2} \quad \text{when} \quad 0 < M_t/M_\infty < 0.6 \tag{11}$$

$$\frac{M_t}{M_\infty} = 1 - \sum_{n=1}^{\infty}\frac{4}{\alpha_n^2}e^{-D_{eff}\cdot\alpha_n^2\cdot t/r_x^2} \quad \text{when} \quad 0.4 < M_t/M_\infty < 1 \tag{12}$$

where α_n (-) are the roots of the first order Bessel function for each term *n*. In this case, three terms (α_1, α_2 and α_3 are 2.405, 5.520 and 8.654) of the Eq. (12) were considered enough to fit the experimental data. Water diffusivity values for short and long times were obtained using Microsoft Excel (Solver add-on) by means of nonlinear programming in which the root mean square error, E_{RMS}, between experimental and calculated data is minimized. The final values of water diffusivity for the whole falling rate period were calculated by the weighted

arithmetic mean (as function of the number of data for each time) of the water diffusivity obtained with the corresponding models for short and long times.

3. Results and Discussion

Figure 1 (left) shows the drying kinetics of *Bifurcaria bifurcata* at different temperatures. As it can be seen, a temperature increase from 35ºC to 60ºC decreased the drying time. The necessary drying time to achieve a MR of 0.03 was shortened from 100 to 60 min with no differences between drying at 60ºC or 75ºC.
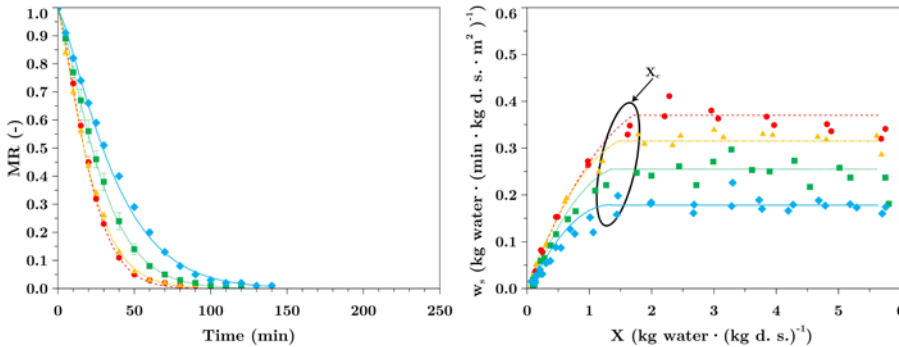
Fig. 1 Experimental drying (left) and specific drying rate curves (right) for Bifurcaria bifurcata at 35ºC (♦), 50ºC (■), 60ºC(▲) and 75ºC (●). Lines correspond to Eq. (13) (right) and to diffusional model (postcritical period) and Eq.(8) (precritical period) for cylindrical geometry (right).

Drying kinetics experimental data were satisfactorily ($R^2 \geq 0.999$) fitted employing Page model, Table 1. No significant differences existed between drying at 60ºC and 75ºC which means that regarding drying time, the drying at 60ºC is more adequate. Moreover, *n* parameter of Page model was constant for all drying temperatures. This fact, allowed the establishment of a unified model able to fit drying kinetics throughout the range of temperatures tested (35-60ºC):

$$MR = e^{-(-1.36 \cdot 10^{-3} - 2.90 \cdot 10^{-4}T)t^{1.28}} \tag{13}$$

Table 1. Values of the Page model parameters (k, n), Eq. (2) and statistical coefficients (R^2, E_{RMS}) for drying curves of Bifurcaria bifurcata.♣

T (ºC)	$k \cdot 10^3$ (min⁻ⁿ)	n (-)	E_{RMS} (-)	R^2
35	8.7±0.08[c]		0.01	0.999
50	12.8±1.15[b]	1.28	0.01	0.999
60	17.8±0.65[a]		0.01	0.999
75	18.6±0.77[a]		0.01	0.999

♣. Data value of each parameter with different superscript letters in columns are significantly different (P≤0.05).

Comparing with other brown seaweeds dried in similar conditions it can be said that *Bifurcaria bifurcata* has a similar behavior with drying temperature of the one observed for *Fucus vesiculosus* (FV) [7]. However, this behaviour was different of the one observed for other brown seaweed such as *Ascophyllum nodosum* and *Undaria pinnatifida* where temperatures higher than 60ºC significantly decreased drying time [8].

3.1. Sample surface area and shrinkage during drying determination

The specific drying rate in thin layer configuration was evaluated using Eq. (6) considering that S_x varied with seaweed moisture content according to a empirical non-linear relationship:

$$\frac{S_x}{S_0} = \sqrt{-1.0 + 1.06e^{-0.11X}} \tag{14}$$

The shrinkage of samples during drying significantly reduced the characteristic dimension (*r*) of seaweeds. *r* from $1.2\pm0.1\cdot10^{-3}$ to $5.8\pm0.3\cdot10^{-4}$ m at X_c. No significant differences on shrinkage behavior of seaweeds with temperature were observed indicating that these properties are more related to moisture content than to air drying rate. Experimental shrinkage data in terms of variation of characteristic dimension with time were correlated with moisture content as follows:

$$r_x = \sqrt{-1.0 + 1.06e^{-0.11MR} \cdot (1.2 \cdot 10^{-3})^2} \tag{15}$$

where MR is evaluated by Page model, Eq. (1).

The specific drying rate *vs* moisture content for all tested temperatures is shown in Figure 1 (right). It can be clearly observed the common drying periods. Namely, at high moisture content the constant drying rate period and below X_c begins the falling rate period. No noticeable variations were observed on X_c with temperature (1.6±0.2 d.b.).

3.2. Constant drying rate period: mass and heat transfer coefficients

The modelling of constant drying rate period employing Eqs. (8) and (9) showed that no significant differences were found in the convective mass (K_t) and heat (h_t) transfer coefficients with temperature.

In the case of K_t ($(21.8 \pm 2.0)\cdot10^{-3}$ m·s⁻¹) the values are higher than those observed by da Silva et al. [9] who reported values of K_t from 0.8 ± 10^{-3} to 1.9 ± 10^{-3} m·s⁻¹ for pear drying in a forced air oven at higher temperatures (between 68 and 92ºC).

The corresponding values of h_t (19.9±0.9 W·m⁻²·K⁻¹) are in the range reported by Bird et al. [10] who indicated that a typical magnitude of convective heat transfer coefficient varies from 3 to 20 W·m⁻²·K⁻¹.

3.3. Falling drying rate period: effective coefficient of water diffusion through the seaweed

During the falling-rate period the shrinking effect on the characteristic dimension was taken into account in order to obtain the water diffusion coefficient through the seaweed. Diffusional modelling of drying during post-critical period was satisfactorily performed ($R^2 > 0.986$ and $E_{RMS} < 0.03$) by diffusional model for cylindrical geometry (Eqs. (11) and (12)), Table 2.

Table 2. Effective coefficients of diffusion of water (D_{eff}) and statistical coefficients (R^2, E_{RMS}) for Bifurcaria bifurcata seaweed drying at different temperatures.[♣]

T (ºC)	$D_{eff}\cdot 10^{12}$ (m²·s⁻¹)	E_{RMS} (-)	R^2
35	12.43 ± 0.64^c	0.02	0.988
50	18.14 ± 0.92^b	0.03	0.998
60	21.97 ± 0.27^a	0.03	0.986
75	20.35 ± 1.31^a	0.03	0.989

[♣]Data value of each parameter with different superscript letters in columns are significantly different ($P\leq0.05$).

Water diffusion coefficient (D_{eff}) significantly increased with drying temperature below 60ºC, but no differences were observed between drying at 60ºC and 75ºC. This trend of D_{eff} with temperature could be related to seaweed biopolymers could be washed away by the water flow and placed in the cell walls. This fact could make diffusion of water more difficult when drying above > 60ºC takes place and consequently the typical increase of water diffusion with drying temperature is lost.

Compared with other works employing the same geometry, the obtained values were lower than those reported by Vega-Gálvez et al. [5] (2.8 to 22.4·10^{-9} m²·s⁻¹) for drying temperatures from 30 to 70ºC for *Gracilaria chilensis* seaweed. Despite of this difference, it can be said that the values are in the range of the typical values for food stuff (10^{-9} to 10^{-11} m²·s⁻¹ [11]).

4. Conclusions

Bifurcaria bifurcata drying experiments in thin layer configuration (from 35ºC up 75ºC) indicate that drying temperature increase up to 60ºC significantly decrease drying time in order to achieve the same moisture content, but no differences exist between drying at 60ºC 75ºC. There are no significant differences on mass transfer coefficient with drying temperature increase during the constant drying rate period. However, the water diffusion coefficient during falling drying rate period shows a significant increase from 35 to 60ºC, with no differences between drying at 60ºC and 75ºC which may be related to seaweed biopolymers washed away by the water flow and placed in the cell walls when drying above > 60ºC takes place.

5. Acknowledgements

6. References

[1] Mabeau, S.; Fleurence, J. Seaweed in food products: biochemical and nutritional aspects. Trends in Food Science & Technology 1993, 4, 103–107.

[2] Gómez-Ordóñez, E.; Jiménez-Escrig, A.; Rupérez, P. Dietary fibre and physicochemical properties of several edible seaweeds from the northwestern spanish coast. Food Research International 2010, 43, 2289–2294.

[3] Nagai, T.; Yukimoto, T. Preparation and functional properties of beverages made from sea algae. Food Chemistry 2003, 81, 327–332.

[4] Lemus, R.A.; Pérez, M.; Andrés, A.; Roco, T.; Tello, C.M.; Vega-Gálvez, A. Kinetic study of dehydration and desorption isotherms of red alga *Gracilaria*. LWT-Food Science and Technology, 2008, 41, 1592–1599.

[5] Vega-Gálvez, A.; Tello-Ireland, C.; Lemus, R. Mathematical simulation of drying process of chilean gracilaria (*Gracilaria chilensis*). Ingeniare. Revista chilena de ingeniería 2007, 15, 55–64.

[6] Page, G. E. Factors influencing the maximum rates of air drying shelled corn in thin layers. Ph.D. thesis, Purdue University, 1949.

[7] Moreira, R.; Chenlo, F.; Sineiro, J.; Arufe, S.; Sexto, S. Journal of Food Processing and Preservation 2017, 41: e12997.

[8] Chenlo, F.; Arufe, S.; Díaz, D.; Torres, M.D.; Sineiro, J.; Moreira, R. Journal of Applied Phycology 2018, (in press) DOI 10.1007/s10811-017-1300-6.

[9] da Silva, A. N.; Coimbra, J. S.; Botelho, F. M.; de Moraes, M. N.; de Faria, J. T.; Bezerra, M.; Martins, M. A.; Siqueira, A. M. Pear drying: Thermodynamics studies and coefficients of convective heat and mass transfer. International Journal of Food Engineering 2013, 9, 365–374.

[10] Bird, R. B.; Stewart, W. E.; Lightfoot, E. N. Transport phenomena. John Wiley & Sons Inc., 2nd ed. New York, 2002.

[11] Rizvi, S. Engineering properties of food, chap. Thermodynamics of foods in dehydration. Marcel Dekker: New York, 1986, 133–214.

Hybrid solar-gas-electric dryer optimization with genetic algorithms

El Ferouali, H.[a]; Gharafi, M.[b]; Zoukit, A.[a]; Doubabi, S.[a]; Abdenouri, N.[a]*
[a] LSET, Cadi Ayyad University, Marrakech, Morocco.
[b] Department of Mathematics, Laboratory of Applied Mathematics and Computer Science, Cadi Ayyad University, Marrakech, Morocco.

*E-mail of the corresponding author: n.abdenouri@uca.ma

Abstract

To promote the hybrid solar dryers for use even under unfavorable weather and to overcome the intermittance state issue, the energy consumption should be optimized and the response time should be reduced. This work concerns a drying chamber connected to a solar absorber where the air can be heated also by combustion of gas and by electric resistance. To optimize the control parameters, an evolutionary optimization algorithm simulating natural selection was used. It was combined with a predictive model based on the artificial neural networks (ANN) technique and used as a fitness function for the genetic algorithm (GA). The ANN is a learning algorithm that needs training through a large dataset, which was collected using CFD simulation and experimental data. Then a GA was executed in order to optimize two objectives: The energy consumption and the t95% response time in which the drying chamber temperature reaches its set point (60°C). After optimization, a 30% decrease of the t95% response time, and 20% decrease of the energy consumption were obtained.

Keywords: hybrid solar dryer; artificial neural network; temperature regulation; energy consumption; genetic algorithm.

1. Introduction

The solar drying process offers a promising alternative way of preservation foods and crops at a favorable energy cost unlike conventional energy sources. However, at night and in the cloudy time, the dehydration process slows extending the drying time. Even more, multiple rehydration of products harms their quality. Hybrid version of solar dryers can offer a wide respond to a wider demand. It reduces energy costs and the drying process is ensured in spite of the alternation of the climatic conditions. The hybrid dryer can ensure a continuous and controlled drying process by using a secondary energy sources [2].

The electric heating resistance was combined to solar air heater in previous works where a prototype was designed in a favorable conditions for optimized power consumption [3]. Unfortunately, this dryer is efficient just for the low air flow rates. In fact, the energy contribution by using the auxiliary heater increased from 74.92% to 86.78% by increasing the air flow rate from 1m/s to 2m/s.

The auxiliary heating system based on gas combustion has been studied in many cases. It was employed in a tunnel dryer by using a heat exchanger connected the gas burners and placed inside the drying chamber [4]. In addition, López-Vidaña et al. [5] suggested putting the burner inside the drying chamber. However, in most cases, the flue gases released by combustion affect the dried products.

In this work, a heat exchanger placed inside the solar collector with a separated exhaust of flue gases was considered. This new configuration seems to be practical, safe and easy to handle.

Modeling of the dryer is one of the most important aspects of drying technology. Most of these models were established by using several techniques such as: computational fluid dynamics (CFD), artificial neural network, Fuzzy, thermal modeling and energy balance mathematical modeling [6]. Computational Fluid Dynamics CFD is usually used to model and predict the temperature and velocity fields in the studied area.

The aim of this work is to optimize the control parameters in order to reduce the cost and the response time of drying. This case requires multi-objective optimization of a relatively complex system. Genetic algorithms are best suited for such application, since they allow the approximation of global optimums while avoiding local ones[7]. The flip side of a genetic algorithm is that it need a large number of design points for an accurate estimate output parameters. The design points were noted by using CFD tools as a predictive method of the dryer [8].

2. Materials and Methods

2.1. The hybrid solar-gas-electric dryer

The hybrid solar-gas dryer consists of a solar-gas collector where the air is heated by solar radiation and by 9 gas burners fitted in the collector (Fig.1). Geometric and thermophysical specifications of the solar-gas collector are given in [9]. The electric heating consists of two electric resistances of 2000W each one, positioned inside the drying chamber (Fig. 2). The drying chamber's volume is 1m^3, and its walls are insulated by 5cm of mineral fiber.
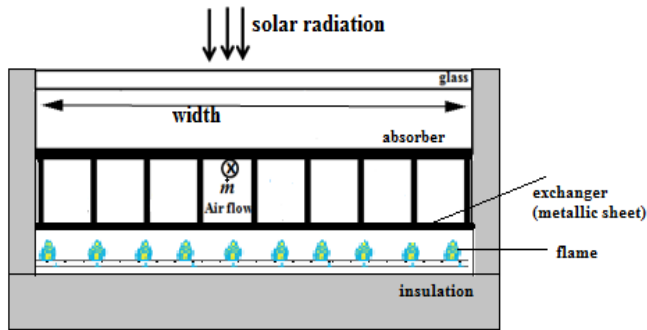
Fig. 1 Solar-gas collector.
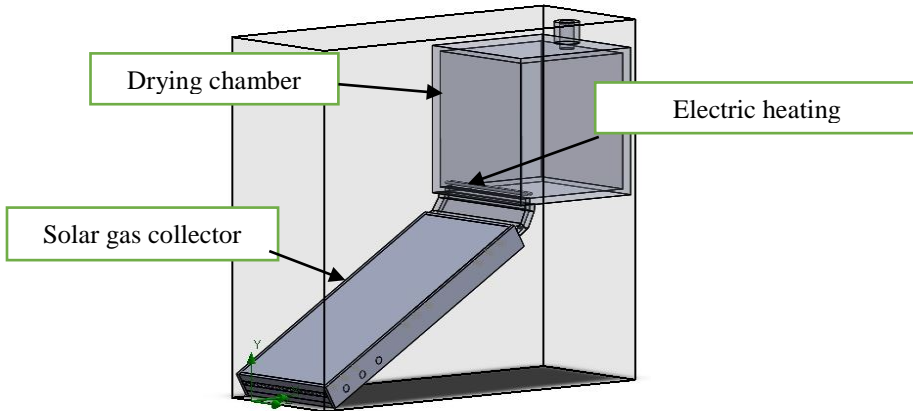
Fig. 2 Design and simulation of the hybrid solar-gas-electric dryer.

2.2. CFD modeling

3D simulations were done on SolidWorks Flow Simulation. The software solves Navier-Stokes equations with the Finite Volume Method (FVM). The κ–ε model was used in this calculation. Solar radiation is modeled to be perpendicular to the glass of the solar-gas collector. Whereas, the flames of the burners are modeled as volume heat sources located under a metallic sheet (exchanger). The electric auxiliary heater is modeled by two volume

heat sources of 2KW each as maximum value. Simulations were performed in forced convection at an air flow rate of 0.025kg/s in transient state for 90 min. The input parameters are solar radiation [0-900W/m²], gas power [0-5000W], and electric power [0-4000W]. The mean drying chamber temperature was controlled at 60°C. Hence, the electric and gas heaters are not always activated during the time dependent simulation. Their activation is dependent on the mean drying chamber air temperature that represents the goal value. They were turned on until the goal value is bit greater than the specified control value (60°C). The value of the dead band is considered as equal to 3°C, Thus, the volume heat sources is turned off until the control value became lower than 57°C.

The following specifications were used in the CFD modeling:
The solar-gas collector is oriented southward under an angle of 30° versus the horizontal.
- The model uses the discrete ordinates (DO) radiation model.
- The wind velocity is equal to 5m/s and its direction is 40°. Ambient temperature is equal to 25°C.
- Local refinement of the mesh is used in this model in order to take into account the peculiarities of the model's geometry; the mesh is composed from 304179 cells.

2.3. Predictive modeling and optimization

A genetic algorithm (GA) was used to optimize the control parameters. This method starts by creating a population of random members of the same species as the optimized object. Then, the performance of each member of the population was evaluated according to fitness function. Upon the evaluation phase members with higher scores proceed to the crossover operation, where their control parameters can be transferred to next generation. To monitor the (GA) optimization process, the overall score of the population were tracked, and its distribution along with the best fit score. This case corresponds to a multiobjective optimization: quality (q), response time (t) and the cost (c). Many variants of the (GA) were used in order to get the best results, the Table 1 shows the used options in each variant:

Table 1. Genetic algorithms configurations.

(GA) ID	Fitness function	Population size	Mutation rate	Best fit criterion
1	Min(q, t, c)*	2000	0.3	Lowest score
2	RMS(Q,T,C)*	2000	0.4	Lowest score
3	Centroid of 3 objectives*	500	0.2	Lowest score
4	Sum of the objectives scores	500	0.2	Lowest score

*q, t, c: output of the dryer's performance, the normalized to the worst possible output.

*Q, T, C: the raw output of the dryer's performance.

*The centroid method is based on a geometric tool which is the CENTROID of equilateral triangle, where its summits are the objectives. Each summit is weighted by the performance of the dryer in the objective. The fitness function is evaluated by calculating the distance of

a performance output centroid and the geometrical center. Loweer the distance is, better the members fits the solution. The fit is evaluated as follows:

Let *q*, *t* and *c* be the quality ratio, the time response ratio and the cost ratio respectively:

$$q = 1 - \frac{Absolute\ error}{Maximum\ Absolute\ error} \qquad (1)$$

$$t = 1 - \frac{Response\ time}{Drying\ time} \qquad (2)$$

$$c = 1 - \frac{Energy\ invested}{Energy\ of\ full\ power\ functionning} \qquad (3)$$

The Euclidian distance of the generated point to the geometrical center of the triangle can be written as:

$$d = \frac{1}{q+t+c} \sqrt{\frac{1}{4}(c-t)^2 + 3\left(\frac{q}{3} - \frac{t+c}{6}\right)^2} \qquad (4)$$

The implementation of the genetic algorithm was done on MatLab, using the "GA" built in function. However, this method requires the evaluation of the output of a large number of control points. Since a CFD simulation response time is inadmissible big, the Artificial Neural Networks (ANN) method developed here is more suitable to predict the solar dryer response for each input parameters. A neuron is fundamentally a node that accepts weights inputs and fires an output from 0 to 1 depending on whether the weighted sum of the inputs exceeds a threshold or not. The threshold is called the bias of the neuron. The neural networks method is a learning algorithm, it consists of changing the weights of each neuron proportionally to their contribution to the error and with smoothing ratio, called learning rate. It can be used for both regression and classification, but according to our modeling problem, it performs well in classification. To do so, an encoding method was established to transform a floating value into one hot binary string. Which is a string of zeros and one in one spot, this spot indicate the class of the value.

For instance, assuming that a temperature variable is within a range of 10 to 50°C, the value of 25°C can be represented as: 0 1 0 0 , with a bin of 10°C. To define a deep neural net, the following arguments are required: The number of layers, the number of nodes per layer, the learning rate, the feed forward batch size, the number of epochs, the cost function and the optimizer.

In our case, a neural network of two terminal layers (input and output) was used. In addition to that we defined 3 hidden layers. The numbers of nodes per layer are respectively

3, 350, 400, 350, 30. The dataset size is 27 000 record. 10% of this data is used for testing. The number of runned epochs in a training session is 100 000 epoch. AdamOptimizer was used to change the weights of the nodes with a learning rate of 0.001. In order to avoid the overfitting problem, the data was shuffled every epoch. The implementation of the neural network model was done with tensorflow running on a CPU. The algorithm was written in Python. The average training time was about 72 hours on a machine of the following specifications: 8Gb of memory, Intel i7 Quad Core processor of a processing frequency of 3.40GHz.

3. Results and discussion

The proposed method consists of generating data using CFD simulation along with experimental results to train a neural network model. The generated data was validated against the experimental data, the reached accuracy level was about 95%. The size of the dataset collected is 27000, with 7 columns: solar radiation, electric power, gas power, absolute error on the temperature inside the dryer, the t95% response time, and the electric and gas energy invested.

The generated data is then transformed in order to train a classification model based on the neural networks method, the method allowed us to predict the performance output data in any control point in a few hundred milliseconds with an accuracy of 95%. The generated data is then transformed in order to train a classification model based on the neural networks method, the method allowed us to predict the performance output data in any control point in a few hundred milliseconds with an accuracy of 95%. Fig 3 shows the evolution of the accuracy during the training session. The accuracy in the beginning of the training is very low, but as the steps increase the accuracy increases but at a decelerating rate.

The predictive model was exported and served to the genetic algorithm written in MatLab to execute the optimization code, the Table 2 shows the results for 4 cases using the sum of the objectives as fitness function which yielded the best results.

The average gain on the cases studied is about 20%. it is calculated assuming that the electric energy cost approximately twice as the gas energy. The following formula is used to evaluate the gain on the cost after optimization:

$$G_{cost} = 0.6 \times \frac{E_{Opt,Elec}}{E_{Elec}} + 0.3 \times \frac{E_{Opt,gas}}{E_{gas}} \tag{5}$$
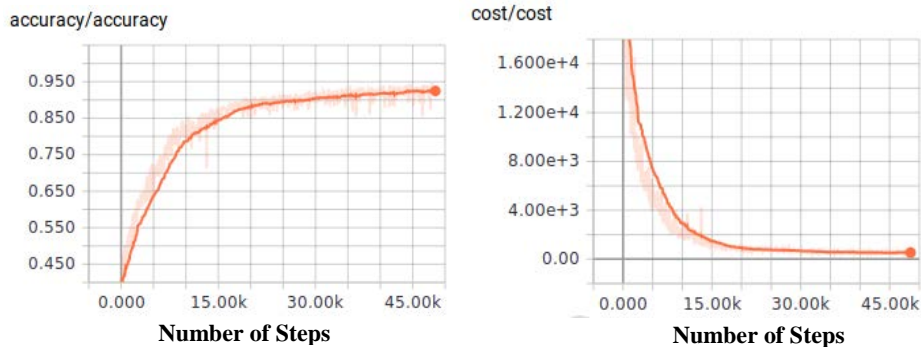
Fig. 3 cost and accuracy of the predictive model during a training session.

Table 2. results of the optimization

Solar radiation	Electric Power (W)	Gas power (W)	Absolute Error (°C)	Response Time (min)	Electric energy (Wh)	Gas Energy (Wh)
900	2543.0	5000.0	0.5	2.0	607.5	1803.75
500	3982.0	5000.0	0.5	2.3	948.0	1470.0
200	4000.0	4152.0	2.0	4.0	3199.0	2963.0
0	2411.0	5000.0	1.2	6.0	2015.0	3946.0

4. Conclusions

In this paper an optimization method of a solar dryer performance is proposed. A predictive model was built with artificial neural networks technique. In order to generate the training dataset for the learning session of the model, several CFD simulations were conducted to determine the gas and electric consumptions, and the 95% response time of the dryer while its drying chamber temperature is controlled at 60°C. After the training session, the predictive model reached an admissible level of accuracy about 95%, in about 50000 epochs. Then a genetic algorithm was performed in order to optimize two main goals that were defined as follow: The energy consumption and the t95% response time in which the drying chamber temperature reaches its set point (60°C). The size of the population is 500, with a mutation chance of 2%. ANN model was used to calculate the fitness function. After 150 generations, we obtained a 30% decrease of the t95% response time, and 20% decrease of the energy consumption.

5. Nomenclature

q	Quality ratio
t	Reponse time ratio
c	Energy cost ratio
G_{cost}	Gain on the energy cost after optimization

$E_{Opt,Elec}$	Consumed electric energy after optimization	(Wh)
E_{Elec}	Consumed electric energy before optimization	(Wh)
$E_{Opt,Gas}$	Consumed gas energy after optimization	(Wh)
E_{Gas}	Consumed gas energy before optimization	(Wh)

6. Acknowledgements

7. References

[1] Basunia, M.A.; Abe, T. Thin-layer solar drying characteristics of rough rice under natural convection. Journal of food engineering 2001, 47(4), 295-301.

[2] Reyes, A.; Mahn, A.; Vásquez, F. Mushrooms dehydration in a hybrid-solar dryer, using a phase change material. Energy Conversion and Management 2014, 83, 241-248.

[3] Boughali, S.; Benmoussa, H.; Bouchekima, B.; Mennouche, D. ; Bouguettaia, H.; & Bechki, D. Crop drying by indirect active hybrid solar–Electrical dryer in the eastern Algerian Septentrional Sahara. Solar Energy 2009, 83(12), 2223-2232.

[4] Oueslati, H.; Mabrouk, S. B.; Marni, A. Design and installation of a solar-gas tunnel dryer: Comparative experimental study of two scenarios of drying. In Proceedings of the 5th International Renewable Energy Congress (IREC) 2014, 1-6.

[5] López-Vidaña, E. C.; Méndez-Lagunas, L. L.; Rodríguez-Ramírez, J. Efficiency of a hybrid solar-gas dryer. Solar Energy 2013, 93, 23-31.

[6] Prakash, O.; Laguri, V.; Pandey, A.; Kumar, A.; Kumar, A. Review on various modelling techniques for the solar dryers. Renewable and Sustainable Energy Reviews 2016, 62, 396-417.

[7] Ahmadi, M.H.; Ahmadi, M.A.; Feidt, M. Performance optimization of a solar-driven multi-step irreversible brayton cycle based on a multi-objective genetic algorithm. Oil & Gas Science and Technology–Revue d'IFP Energies nouvelles 2016, 71 (1), 16.

[8] Wang, T.;Gao, H.; Qiu, J. A combined adaptive neural network and nonlinear model predictive control for multirate networked industrial process control. IEEE Transactions on Neural Networks and Learning Systems 2016, 27 (2), 416–425.

[9] El Ferouali, H.; Zoukit, A.; Salhi, I.; Doubabi, S.; Abdenouri, N.; & El Kilali, T. Heat transfer in a solar-gas-electric hybrid dryer for the control of its operation and for energy management and storage. In Electrical Sciences and Technologies in Maghreb (CISTEM) IEEE, 1-6.

Multivariable modeling of an innovative hybrid solar-gas dryer

Zoukit, A.; Elferouali, H.; Salhi, I.; Doubabi, S.; Abdenouri, N[*].
LSET, Cadi AYYAD University, Marrakech 4000 Morocco

*E-mail of the corresponding author: n.abdenouri@uca.ac.ma

Abstract

The main goal of this paper, is to propose a multivariable control model (MM) issued from CFD study of an innovative hybrid solar-gas dryer to simulate the drying chamber temperature in three modes of operation: Solar mode, Gas mode and hybrid mode. There is an indirect heating of drying air instead of direct heating inside the drying chamber. The air temperature obtained by CFD is still closed to one obtained by multivariable model (MM) with an RMSE under 2.31. the proposed multivariable model leads to a quick output parameters estimation related to each cilmate conditions and so, to an easy control of a hybrid solar dryer.

Keywords: Hybrid dryer; Multivariable model; solar dryer simulation; solar dryer control; Least square methods.

1. Introduction

Currently, solar energy is an important alternative source of energy. It is free, abundant, inexhaustible and non-polluant in comparison with higher price and shortage of fossil fuels [1]. Solar drying of agriculture products is one of the most important potential applications in the countries in development [2]. Actually, framers and citizens dry crops such as (date, grapes, tea, menth and tomato) by spreading them in thin layers, on mats, paved ground or in the field, exposing them directly to the sun radiation. The drying by his archaic way affect strongly the quality of dried product and leads to a large post-harvest deterioration [3]. Indirect solar dryer can easily overcome these issues while using solar radiation as energy source for drying process [4].

In the other hand, the solar dryers are still limited by the intermittent fact and it could not be effective without the presence of another source. However, to enhance the quality of dried products and to optimize energy consumption, many works were carried out to design a dryer where the hot air is produced regularly and where the drying parameters (temperature, humidity and airflow) are under control.

In contrast, hybrid solar-gas dryers are widly used for drying a variety of products. They operate with solar energy in addition to an other energy source which is gas power. According to the literature survey, many works used an external boiler where the gas is burned and the hot air is produced and conducted to the drying chamber [5]. This technique requires a huge operational space and regular maintenance which make the drying system more complex. In other works [6,7], conceived a hybrid solar-gas dryer using a gas burner inside the drying chamber where the dried product adsorb many gaseous species resulting from the combustion of the gas.

Some reaserchers have already employed CFD to simulate the temperature, air velocity and relative humidity at various locations inside the drying chamber [8,9,10]. However, due to the complexity in the drying chamber, obtaining accurate results by CFD study requires a high level of grid density so a performing computational ressources [11].

This paper is proposed to design and simulate a hybrid indirect solar-gas dryer to best controlling drying process. The indirect heating of air inside the drying chamber guarantees the safety and improves the quality of the dried product. CFD modeling of the hybrid dryer is established in order to investigate its thermal performances in term of the threshold of drying temperature. A multivariable model issued from CFD simulation was developed based on non linear least square methods. The developed model leads to predict the drying temperature inside the drying chamber with a huge reduction in simulation time and leads also to easily synthesize a control system of the drying temperature.

2. Materials and Methods

The hybrid solar-gas dryer was designed and simulated using Solidworks Flow simulation developed by Dassault systems Solidworks crops. The dryer consists of a cubic drying chamber of (1m * 1m * 1m), fitted with perforated plate trays of stainless steel. The drying chamber is combined with a solar-gas collector used to generate regularely the hot air. The solar part of the collector is a finned plate solar air heater, the absorber's length is L= 2m and its width is W = 0.95m and it is made from aluminium. The top side of the absorber is painted with matt black glycerpphtalic lacquer. The absorber containes 24 fins made from 1 mm thick aluminium. The top side of the absorber is covered by 3mm glass with a separation of 0.05m with the absorber. The solar collector is fitted with a heat exchanger (metallic sheet) placed under the absorber. The back up heating system is a set of 9 burners located under the exchanger and monitored by a valve. The drying air passes through the flat plate collector between the absorber and the exchanger. The synoptic of the hybrid dryer is presented in Fig. 1.
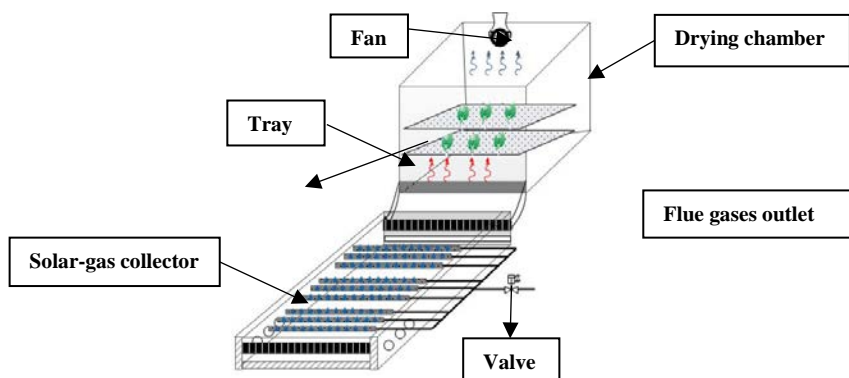
Fig. 1 Synoptic of the hybrid solar-gas dryer

3. Simulation appraoch

CFD is used for air temperature and airflow distribution inside the drying chamber accomplished by 3-dimentional governing equation (mass, momentum and energy equation) along with initial and boundary conditions under transient and turbulent flow assumptions. Since the small temperature variations, the hot air is considered as incomprehensible flow.

3.1 Simulation model

Fig. 2 demonstrates the 3-D solar-gas hybrid dryer simulation model. This model used single component model with assumptions of incompressible and unsteady-state flow. Simulations were conducted using a grid density of (1,906,000).
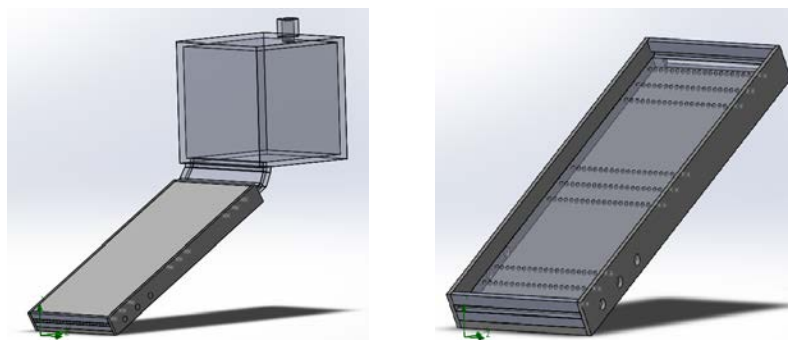
Fig. 2 CFD conception of the hybrid dryer

3.2   Initial and boundry conditions.

The initial temperatures of chamber walls, surface of tubular burners and inside air were taken equal to 25°C. The inlet air velocity was 0.025kg s^{-1} calculated from the flow rate of the ventilating fan while the inlet temperature and the relative humidity were assumed to be at 25°C and 50% respectively. These values are typical average ambient ones in Marrakesh at Morocco. The flames of the burners are modeled as volume heat sources located under a metallic sheet. The flames' diameter is 1cm and their number is 216 (24 flames for each burner). Hence, the power of each flame is Pg/216, with Pg is the total gas power (W). The solar-gas collector is fitted with apertures in the both sides and in the outlet allowing the natural circulation of the necessary air for total combustion.

4.   Multivariable model of the hybrid solar-gas dryer

In this paper, a hybrid solar-gas dryer designed in SolidWorks is consedred as a non linear multivariable system. Solar radiation (G), gas power (Pg) and airflow ($\dot{m}$) are considered as the main inputs of the dryer and the drying chamber temperature (Tch) is considered as output parameter.

4.1   Static characteristics

The static characteristics of the dryer are necessary for a description of the behavior of the system. It consists on measuring the output on the basis of inputs in steady state. Statics characteristics of the dryer lead to easily identify the linear zones and operating points which help for shapping the input signals for modeling the system.

The average drying temperature (Tch) was measured on the basis of solar radiation, gas power and airflow. The measurements were carried out in the steady state.

The static characteristic of (Tch) on basis of (G) was built varying the solar radiation in a range of 0-1200W m^{-2} while considering gas power and airflow constant ($Pg = 2$kW and $\dot{m} = 0.025$kg s^{-1}). wherease, the static characteristic of (Tch) on basis of (Pg) was built varying

the gas power in a range of (0-5 kW) while considering solar radiation and airflow constant ($G = 700$ W m^{-2} and $\dot{m}= 0.025$kg s^{-1}). The static characteristic of (*Tch*) on basis of ($\dot{m}$) was built varying the airflow in a range of (0.005-0.07 kg s^{-1}) while considering solar radiation and gas power constant ($G = 700$ W m^{-2} and $Pg = 3$kW) (Fig. 3).
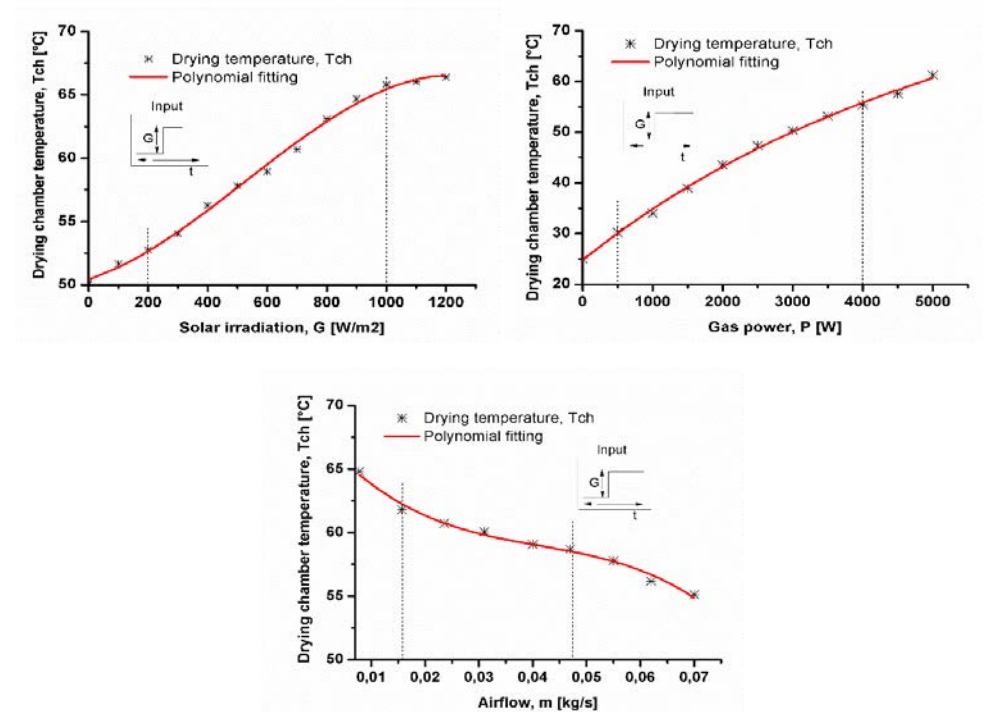
Fig. 3 Static characteristics of the hybrid dryer

4.2. Generation of input signals

The used input test signals for modeling the dryer are Pseudo Random Binary Sequences (PRBS). The PRBS is a two state signal varying between the maximum and the minimum points of each linear zone. In addition, at least one of the PRSB pulses should be greater than the system rise time [12].

The measurements were conducted in transitory state. The time simulation was set to 20 hours of operation.

The obtained input/output were loaded into the system identification Toolbox of Matlab environment using (Ident) in order to identify the linear model of the hybrid dryer. The system identification provided using Matlab allows building mathematical models of a dynamic system based on non-linear least squares estimation method.

The simulation result of the identified linear multivariable model fitted the CFD simulation with 90% of accuracy. for control purpose, this is an accurate model.

The hybrid dryer state space multivariable model is represented by:

$$A = \begin{bmatrix} -0.0030 & -0.0202 \\ -0.0141 & -0.1701 \end{bmatrix}; B \begin{bmatrix} -0.00046 & 6.87e^{-6} & 4.959e^{-6} \\ -0.00180 & 2.66e^{-5} & -0.00039 \end{bmatrix}; C = [238.4 - 0.56]$$

To verify the validity and the effectiveness of the proposed multivariable model. The temperature profile inside the drying chamber obtained by CFD simulation is compared with the temperature predicted by multivariable model. The CFD average drying chamber temperature at three operating modes of the solar dryer (solar mode (900W m^{-2}), gas mode (3kW) and hybrid mode (600W m^{-2}; 2kW)) was considered for comparison with the multivariable model simulation. CFD and Multivariable model simulation results were plotted against clock time as shown in Figs. (4a-4b-4c). The temperature profile of CFD simulation was almost similar to that of Multivariable model. The root main square error RMSE remains under 2.31.

(a)

(b)

(c)
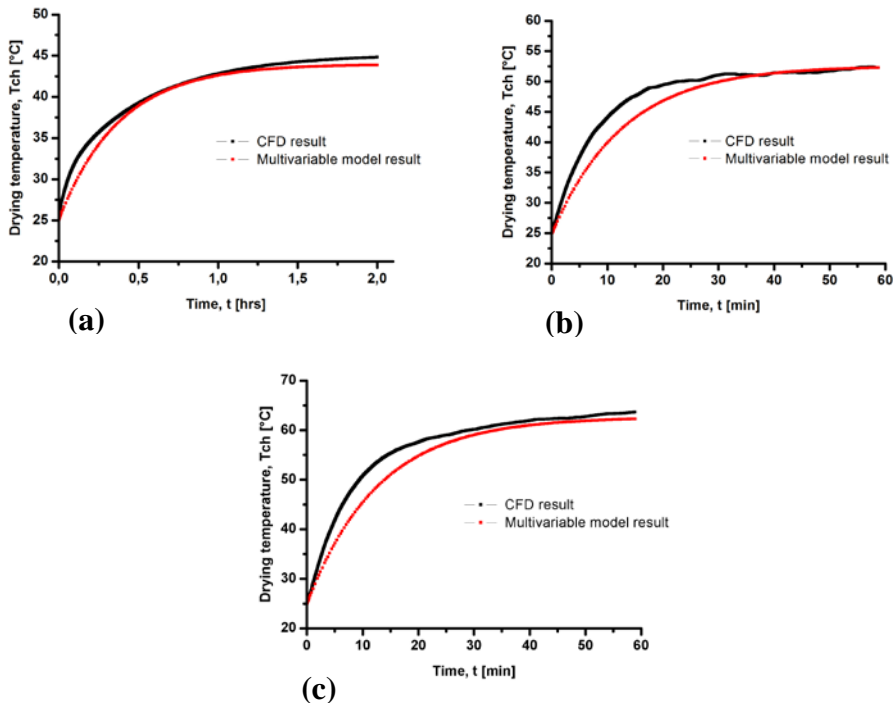
Fig. 4 Comparison between the simulated CFD and MM output; a. solar mode; b. hybrid mode; c. gas mode

5. Conclusion

A multivariable model of the hybrid dryer for predicting the drying temperature was developed based on nonlinear least square methods taking into account solar radiation, gas power and airflow as the main input parameters. The predicted temperatures by multivariable model were compared with the CFD ones based on mean root square error (RMSE). From the values of RMSE (0.91-2.38), it is inferred that the predicted values by multivariable model are in harmony with the observed values by CFD. The multivariable model leads to predict the temperature with a remarkable reduction in simulation time. The threshold of drying temperature has been investigated in three operating modes of the dryer: solar mode, gas mode and hybrid mode. The range of the reached temperature (45.2°C, 53.4°C and 62.4°C) is suitable for drying a wide variety of products. The developed multivariable model will be useful to synthesize a temperature controller in order to control the drying temperature in a suitable range for the product to be dried and improves their quality.

6. Aknoledgement

7. References

[1] Basunia, M.A.; Abe, T. Thin layer solar drying characteristics of rough rice under natural convection. Journal of Food Engineering 2001. 47(4), 295–301.

[2] Boughali, S.; Benmoussa, H.; Bouchekima, B.; Mennouche, D.; Bouguettaia, H.; Bechki, D. Crop drying by indirect active hybrid solar - Electrical dryer in the eastern Algerian Septentrional Sahara. Sol. Energy 2009. 83, 2223–2232.

[3] Bala, B.K.; Mondol, M.R.A.; Biswas, B.K.; Das Chowdury, B.L.; Janjai, S. Solar drying of pineapple using solar tunnel drier. Renewable Energy 2003. 28, 183–190.

[4] Madhlopa, A.; Ngwalo, G. Solar dryer with thermal storage and biomass back-up heater. Solar Energy 2007. 81, 449–462.

[5] Tadahmum Yassen A.; Hussain Al-Kayiem H. Experimental investigation and evaluation of hybrid solar/thermal dryer combined with supplementary recovery dryer. Solar Energy 2016. (134), 284–293.

[6] Oueslati H.; Benmbrouk S.; Mami A. Design and Installation of a Solar-Gas Tunnel dryer. The fifth International Renewable Energy Congress IREC 2014. 1–6.

[7] López-Vidaña E.; Méndez-Lagunas L.; Rodriguez-Ramirez J. Efficiency of a hybrid solar-gas dryer. Solar Energy 2013. (93), 23–31.

[8] Junchangpood A.; Chanvattana V.A. simulation of temperatures and velocities distribution of a hot-air stream of a rubber smoke sheet drying room using CFD. Conf. Mech. Eng. Netw. Thail 2007. 24, 1041-1047.

[9] Tekasakul P.; Dejchanchaiwong R.; Tirawanichakul Y.; Tirawanichakul S. Three-dimensional numerical modeling of heat and moisture transfer in natural rubber sheet drying process. Drying Technology 2015. 33, 1124-1137.

[10] Promtong M.; Tekasakul P. CFD study of flow in natural rubber smoking room: I. validation with the present smoking-room. Appl. Therm. Eng 2007. 27, 2113-2121.

[11] Sonthikun S.; Chairat P.; Fardsin K.; Kirirat P.; Kumar A.; Tekasakul P. Computational fluid dynamic analysis of innovative design of solar-biomass hybrid dryer: An experimental validation. Renewable Energy 2016. 92, 185–191.

[12] Ioan Dore L. System identification and control. HERMES Edition.; Paris, 1993.

Identification of moisture transport mechanism in gypsum during convective drying

Adamski, R.; Adamska, A.; Pakowski, Z.

Faculty of Process and Environmental Engineering Lodz Technical University, Lodz, Poland

*E-mail of the corresponding author: robert.adamski@p.lodz.pl

Abstract

Gypsum is a popular building material. Drying and rewetting of gypsum is a process of practical importance. This work presents the experimental results of kinetic of drying, heating and internal pressure development in rewetted gypsum cylinders. Analysis of the observed changes is presented. Additionally sorption isotherms, permeability and dependence of Young's modulus on moisture content were measured. These data will be used in the model of the process under development.

Keywords: internal pressure, permeability, Young's modulus

1. Introduction

Gypsum is commonly used as a building material in the form of gypsum blocks, plasterboards, fillers and renders. It is also used by other industries e.g. ceramic industry for making molds. In buildings moisture in gypsum materials is present both during setting and normal use due to its hygroscopicity. It influences energy consumption, air quality in houses and durability of the material. It is therefore important to know more about the mechanism of heat and moisture exchange with surroundings and their transfer in the gypsum materials. Literature of the subject is abundant in models which serve for prediction of spatial and temporal variations of temperature and moisture content in building materials. The models usually require performing experimental determination of model parameters like specific heat, heat conductivity, moisture diffusivity [1,2] and permeability [3,4]. The knowledge of microstructural changes and interactions of water and the material of crystalline structure like gypsum, especially in heat and mass transfer processes is one of key issues influencing mechanical properties of the gypsum products. Gypsum materials change their mechanical properties depending on their wetness and the reason are week bonds of crystalline adhesions. Repeating cycles of humidification-dehumidification may lead to shrinkage, deformations and cracks as described in numerous publications [5]. Several works concentrate on heat and mass transfer during drying of building materials like plasterboard, and wood [6], brick and render including determination of moisture content profiles [7], analysis of external parameters as pressure [8], wind speed [9] and analysis of the determination of the influence of drying kinetics [10] on distribution of stresses in the material.

The aim of this work is to experimentally analyses the drying process of gypsum by measuring its kinetics of mass, temperature and internal pressure in drying and measure necessary parameters i.e. sorption/desorption isotherms, Darcy permeability and Young's modulus of wet gypsum. These observations will be used in the model of drying including stress development in the solid (under construction).

2. Materials and Methods

Commercial gypsum powder of building grade produced by Piotrowice company under a brand name Alpol. It is destined for using as building material and filler as well as for casting of prefabricates. The powder was mixed with recommended water/gypsum ratio equal to 0.65. Cast gypsum is a material that doesn't shrink during drying.

2.1 Sorptional equilibrium

Desorption isotherms at low temperature were measured by a standard method of saturated salt solutions at 20°C and 50°C and atmospheric pressure. Additionally experiments were

made in superheated steam in the range of temperatures of 120°C to 200°C in a separate set-up also at atmospheric pressure

2.1 Drying kinetics

Drying experiments were performed in a drying tunnel described elsewhere [18]. Cylindrical samples 28 mm in diameter and 54 mm high were used. Drying was performed at 50°C and air velocity of 1 m/s. Air humidity was not controlled.

2.1 Permeability

Permeability was measured by hydraulic method described elsewhere [12] using compressed air permeation. Gypsum disks 13 mm in diameter and 2 mm thick were used. Experiments were made on dry gypsum which was then soaked . Measurements were made in duplicate.

2.1 Mechanical properties

For modeling of drying stresses the dependence of Young's modulus on moisture content is required. The dependence was measured using seasoned gypsum samples of given moisture content and standard Instron testing machine. The experiments were made in duplicate.

3. Results

3.1 Sorptional equilibrium

The results are shown in Fig. 1 in the form of 3D dependence of moisture content X on water activity a_w and temperature T. Two isotherms for 20°C and 50°C and an isobar in the range 120°C-200°C are shown. It is visible that equilibrium moisture content rapidly increases with water activity and slowly decreases with temperature. This indicates that gypsum is only slightly hygroscopic.

The data points were fitted with Chen and Clayton equation (1) with coefficients available in Table 1. The fit is of satisfactory quality.

$$a_w = \exp\left(a_1 T^{a_2} \exp\left(a_3 T^{a_4} X\right)\right) \tag{1}$$

Table 1. Coefficients of equation (1)

	Coeff.	value	Confidence interval		R²
Chen&Clayton	a_1	-14,107	-26,516	-1,698	
	a_2	-0,344	-0,575	-0,112	0.963
	a_3	-1.283e6	-2.221e6	-3.461e5	
	a_4	-2,515	-2,732	-2,298	
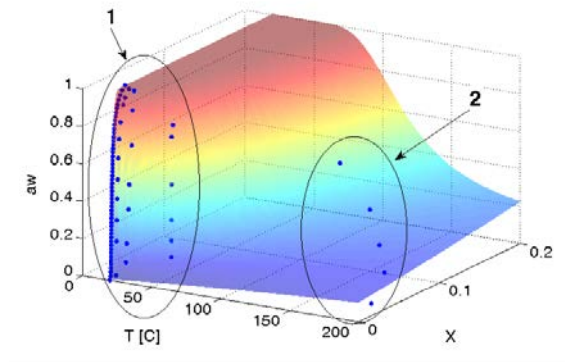
Fig. 1 Dependence of equilibrium moisture content on water activity and temperature
1-isotherms 20•C and 50•C, 2-isobar.

4.1 Drying kinetics

An exemplary test run results are shown in Fig. 2. Fig. 2a shows how air parameters: atmospheric pressure, temperature and water activity vary during the process.

a)   b)   .
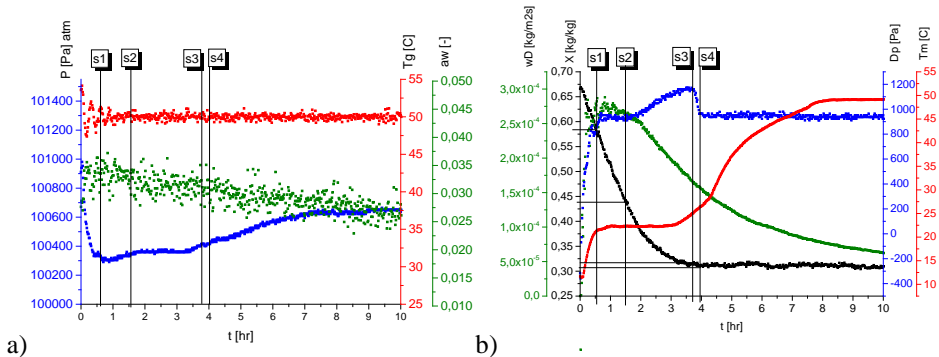
Fig.2. a) Air parameters, b) Drying kinetics at 50•C

A sample of initial MC=0.67 kgkg$^{-1}_{dm}$ and temperature 12^{0}C is dried with air of temperature 50^{0}C and RH=3.5%. In the time range from 0 to S1 the solid heats up to the wet-bulb temperature. During that time MC decreases to 0.57 kgkg$^{-1}_{dm+}$ and internal pressure rapidly decreases to -400 Pa and then rises to +900 Pa. The initial pressure drop may be a result of fast evaporation at still initial axial temperature. The mass flux "drags" water from the inside creating underpressure. When the axial temperature increases thermal expansion of liquid causes pressure to rise. At the end of this time drying rate reaches 2.75e-4 kgm^{-2}s^{-1}.

In this phase of the process the solid is saturated and the dominating mechanism is Darcy flow. It is worth noticing that while the axial pressure is negative, the inner part of the

sample is compressed and when positive it is stretched. If the resulting stress should exceed material strength the solid would crack.

The time range from S1 to S2 corresponds to CRP where MC decreases from initial value 0.57 kgkg^{-1}$_{dm}$ down to 0.47 kgkg^{-1}$_{dm}$, The dominating mechanism is Darcy flow in liquid phase. From S2 to S3 we have the FRP - drying rate decreases, the temperature increases to 25^{0}C and internal pressure increases to +1200 Pa, reaching maximum. In this range mass transport takes place in liquid phase, vapor phase and gas phase of water vapor and air, and a penetration of the evaporation front is observed. As proposed in [11] the transport fluxes are: water in liquid phase where the driving force is pressure gradient in liquid phase, flux in vapor-gas phase driven by pressure gradient, diffusional flux in gas phase driven by vapor concentration gradient and finally flux of bound water with MC as the driving force. The last two fluxes govern the range from S3 to S4 where MC decreases to the equilibrium value, pressure decreases to +900 Pa and temperature increases. In the remaining time all parameters remain constant except temperature which increase further reaching the external air temperature.

5.1 Permeability

Permeability was measured according to the Polish National Standard PN-EN 993-4. The governing Darcy equation has the form:

$$k_g = Q\eta_G \frac{h}{A} \frac{1}{(p_1 - p_2)} \frac{2p_1}{(p_1 + p_2)} k \tag{2}$$
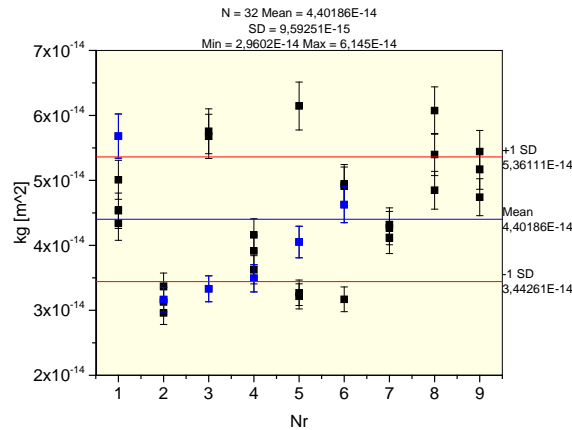
Fig.3. Permeability of samples (black - dry, blue - wet)

In this work actual pressure varies in time while in PN-EN 993-4 is steady. Another difference is that the quoted standard requires samples of cylindrical shape 50x50 mm

while in our experiments samples were much smaller. Experimental error was estimated as less than 6 %. The results are shown in Fig. 3 both for dry and wet samples of MC=0.65 kg/kg. The straight blue line is the mean value of $4.40 \cdot 10^{-14}$ m^2 and the red lines are at 1 standard deviation off this value. The entire range of results for wet sample was $3 \cdot 10^{-14}$m^2 to $6 \cdot 10^{-14}$m^2. Similar values were obtained in [13] by the method of PN-EN 993-4 [3,14]. The values for wet samples were in the range $3 \cdot 10^{-14}$m^2 to $5 \cdot 10^{-14}$m^2.

6.1 Mechanical properties

Strength of plaster is a results of bonds between the forms of gypsum (anhydrite, semihydrate and dihydrate), sulfur compounds, water and residuals [15]. Typically compression and bending strength are measured, rarely the Young's modulus [16]. Mechanical characteristics of plaster depend mainly on porosity, placement and structure of gypsum crystals formed during hydration of calcined gypsum [17]. On the other hand they also depend on the actual condition of plaster resulting from ambient conditions like temperature and humidity. Although gypsum sets in ca 25 min after mixing with water it reaches full mechanical strength after 28 days according to ASTM C215, 1991. Only then the mechanical tests can be performed. The results of this work are shown in Fig. 4.
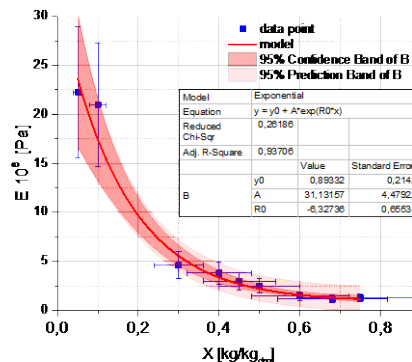
Fig.4. Young's modulus dependence on moisture content of rewetted gypsum

The approximating equation has the form:

$$E = \left[0.89332 + 31.13157 \left(\exp\left(-6.32736 X \right) \right) \right] \cdot 10^8 \tag{3}$$

3.   Conclusions

Results of this work indicate that hardened gypsum is slightly hygroscopic as sorption isotherms indicate and bound water range at room temperature is below MC of ca. 0.03 kg/kg. It also shows negligible shrinkage in drying. Yet MC significantly influences the Young's modulus, which exponentially decreases with increasing MC.

During convective drying gypsum exhibits the initial drying period (IDP), constant-rate period (CRP) and falling drying period (FRP). However the internal pressure is only partly related to these periods. In the IDP pressure first rapidly decreases to ca. -400 Pa and then increases to +900 Pa. Ic CRP the pressure first stabilizes and at the final stage of CRP begins to increase. It continues to increase in FRP reaching the maximum of +1200 Pa and at the end of the FRP it falls again to +900 Pa. These variations cause changes in internal stresses. The observed changes of pressure shed some light on moisture transport in the solid which only can be explained with a suitable model. The work on the model is in progress.

Nomenclature

A	area	m^2
E	Young's modulus	Pa
Q	flow rate	m^3s^{-1}
T	temperature	°C
X	moisture content	$kgkg^{-1}$
h	flow path length	m
k	correction coefficient	
p	pressure	Pa

Greek letters

η_G	Viscosity of air	Pa s

Subscripts

1	in
2	out

4. References

[1] Adan, O. C. G., Determination of moisture diffusivities in gypsum renders. HERON-ENGLISH EDITION-,1995 40, 201-216.

[2] Bennamoun, L., Kahlerras, L., Michel, F., Courard, L., Salmon, T., Fraikin, L., Léonard, A., Determination of moisture diffusivity during drying of mortar cement: experimental and modeling study. International Journal of Energy Engineering, 2013, 3(1), 1-6.

[3] Milsch H., Priegnitz M., Blöcher G., Permeability of gypsum samples dehydrated in air, Geophysical Research Letters, 2011, 38, s.2-6.

[4] Lee, C. Y., Water desorption characteristic of red gypsum, 2015

[5]   Beyea S.D., Balcom B.J., Bremner T.W., Prado P.J., Cross A.R., Armstrong R.L., Grattan-Bellew P.E., The influence of shrinkage-cracking on the drying behaviour of White Portland cement using single-point imagining (SPI), Solie State Nuclear Magnetic Resonance, 1998, vol. 13, pp. 93-100

[6]   Pasanen A.L., Kasanen J.P., Rautiala S., Ikäheimo M., Rantamäki J., Kääriäinen H., Kalliokoski P., Fungal growth and survival in building materials under fluctuating moisture and temperature conditions, International Biodeterioration and biodegradation, 2000, vol. 46, pp. 117-127

[7]   Karoglou M., Moropoulou A., Krokida M.K., Maroulis Z.B., A powerful simulation for moisture transfer in buildings, Building and Environment, 2007, vol. 42, pp. 902-912

[8]   Yoo J.H., Lee H.S., Ismail M.A., An analytical study on the water penetration and diffusion into concrete under water pressure", Construction and Building Materials, 2011, vol. 25, pp. 99-108

[9]   Jacobsen S., Aarseth L.I., Effect of wind on drying from wet porous building materials surfaces – A simple model in steady state, Materials and Structures, 1999, vol. 32, pp. 38-44

[10] Moropoulou A., Karoglou M., Giakoumaki A., Krokida M.K., Maroulis Z.B., Saravacos G.D., Drying kinetics of some building materials, Brazilian Journal of Chemical Engineering, 2005, vol. 22, pp. 203-208

[11] Whitaker S., Simultaneous Heat, Mass, and Momentum Transfer in Porous Media: A Theory of Drying, Advances in heat transfer, 1977, vol. 13

[12] Pakowski Z., Adamski R., Kokocińska M., Cross-fiber dry wood Darcy permeability of energetic willow Salix viminalis v.Orm, Drying Technology, 27: 1379–1383, 2009

[13] Pawlak M., The influence of composition of gypsum plaster on its technological properties, Archives of Foundry Engineering, 2010, vol.10, 4, 55-60

[14] Wang Q., Liu H., The Experimental Research on the Water Vapour Permeability of Construction Gypsum Plaster Materials, Materials for Renewable Energy & Environment, 2011, s.850-854.

[15] Singh, M., Role of Phosphorgypsum Impurities on Strength and Microstructure of Selenite Plaster. Construction and Building Materials, 2005, Vol. 19pp. 480-486.

[16] Verbeek, C.J.R., du Plessis, B.J.G.W., Density and Flexural Strength of Phosphorgypsum-polymer Composites, Construction and Building Materials, 2005, 19, pp. 265-274.

[17] Singh, M., Garg, M., Relationship between Mechanical Properties and Porosity of Waterresistant Gypsum Binder. Cement and Concrete Research, 2, 1996, pp. 449-456

[18] Pakowski Z, Adamski R., Formation of underpressure in an apple cylinder during convective drying, Drying Technology,, 30: 1238–1246, 2012

Modeling of kinetics of drying process of polycaproamide granules considering its sorption properties

Kosheleva M.K.[a*]; Dornyak O.R.[b]; Maklusova M.S.[a]

[a] Russian state University after A. N. Kosygin (Technology. Design. Art), Moscow, Russia.
[b] Voronezh State University of Forestry and Technologies after F.G. Morozov, Voronezh, Russia.

*E-mail of the corresponding author: *oxtpaxt@yandex.ru*

Abstract

The results of experimental and theoretical research of heat and mass transfer in polycaproamide granules during convective drying are presented.

Keywords: *convective drying, mathematical modeling, polycaproamide.*

1. Introduction

Drying process of polycaproamide granules is one of the stages of technological chain during production of polyamide fiber caprone. Rather high level of dehydration of granules during drying process should be provide to obtain high quality fiber. Average final moisture content of the material should be not more than 0.1%. We know that at low values of moisture content drying process of polycaproamide is sharply slows down and the distribution of moisture content is substantially nonuniform. In this case calculation of kinetics of granules dehydration should be provide using local coefficient values of mass transfer (diffusion of moisture). Results of calculations which illustrate features of heat and mass transfer processes during convective drying of cylindrical granules are presented. Two local parameters of mass transfer are using for calculation – coefficient of moisture diffusion in polycaproamide (in the form of a liquid) a_m and criteria of phase transfer ε. These parametres are depends on material moisture content and temperature in given point of material at certain point in time.

2. Materials and Methods

The object of drying is polycaproamide. Average degree of polymerization is 130-200, average molecular weight is 15000-23000. The structure of samples was research by three independent methods. Method of mercury porosimetry, electron microscopy and sorption method were used.

The predominant pore radius is 1000 Å. Such pores are filled only at direct contact with liquid phase but not during sorption process and its presence in polycaproamide associated probably with mechanical impact during preparation of a substance but not with supramolecular structures. Photos of fracture of polycaproamide crumb obtained using an electron microscope confirm the presence of large pores in the material.

The specific volume of pores is 0.022 cm^3/g. Isotherm of sorption of moisture vapor by polycaproamide was obtain using vacuum sorption installation with weights of Mac-Ben-Bakr. Maximum hygroscopic humidity at 22ºC is about 8%. The existence of a loop of sorption hysteresis the appearance of which indirectly indicates partial swelling of polycaproamide in water is established.

Drying kinetics curves for samples of polycaproamide received in convective dryer equipped with devices for monitoring and controlling the parameters of the drying agent The radius of the granule was $R_{gr}=1.375 \cdot 10^{-3}$ m, length - $L_{gr}=4 \cdot 10^{-2}$ m. The relative humidity of the environment was maintained equal to $\varphi_c \sim 3\%$. The speed of drying agent was 25 m/s. Kinetic curves at different temperatures in the range from 90 to 150ºC are rpesented on Fig.

1. The set air temperature was maintained with accuracy 0,1°C. The weighing accuracy was 10^{-6} kg/m^3.

Character of experimental kinetics curves allow to draw a conclusion about essential nonlinearity of effective coeficient moisture conductivity in the granule of polycaproamide which is associated with the specific nature of phase transitions in macromolecular systems. The intensity of vaporization here depends not only on the amount of heat supplied but also on the rate of arrival of the volatile component to the evaporation surface (the outer surface of the granule and the interphase boundary of liquid-vapor in microcracks and pores). Diffusion transfer in polymer systems at low solvent contents is limiting for interfacial mass transfer [1].

3. Mathematical model

Nonstationary nonlinear axisymmetric 2D model similar [2] which generalizes the well-known mathematical model of the diffusion-filtration heat and moisture transfer of A.V. Lykov [3] using for description of heat and mass transfer processes during drying. It is constructed as the limiting case of models based on the mechanics of multiphase systems [4-5]. The mathematical model includes transfer equations averaged over the microvolume of the material:

- liquid phase transfer equation

$$\frac{\partial u}{\partial t} = \frac{1}{r}\frac{\partial}{\partial r}\left[r a_m\left(u,T\right)\frac{\partial u}{\partial r}\right] + \frac{\partial}{\partial z}\left[a_m\left(u,T\right)\frac{\partial u}{\partial z}\right] - \frac{s_{12}j}{\alpha_3\rho_3^0}; \tag{1}$$

- heat transfer equation

$$c\rho\frac{\partial T}{\partial t} = \frac{1}{r}\frac{\partial}{\partial r}\left[r\lambda\left(u,T\right)\frac{\partial T}{\partial r}\right] + \frac{\partial}{\partial z}\left[\lambda\left(u,T\right)\frac{\partial T}{\partial z}\right] - L_{12}\varepsilon\rho\frac{\partial u}{\partial t}; \tag{2}$$

$$\lambda = \alpha_1\lambda_1 + \alpha_2\lambda_2 + \alpha_3\lambda_3; \ c\rho = \alpha_1 c_{p1}\rho_1 + \alpha_2 c_{p2}\rho_2 + \alpha_3 c_{p3}\rho_3;$$

- equation for vapor-gas phase pressure

$$c\rho\frac{\partial p_1}{\partial t} = p_1\frac{K_{13}}{\mu_1}\left[\frac{1}{r}\frac{\partial}{\partial r}\left(r\frac{\partial p_1}{\partial r}\right) + \frac{\partial^2 p_1}{\partial z^2}\right] + \frac{p_1}{c\rho T}\frac{\partial T}{\partial t} + \frac{p_1 L_{12}\varepsilon}{cT}\frac{\partial u}{\partial t} +$$

$$+ \frac{p_1}{B_1}\frac{\partial B_1}{\partial t} - \frac{p_1}{\alpha_1}\frac{\partial \alpha_1}{\partial t} + \frac{s_{12}jTB_1}{\alpha_1} - \frac{p_1 L_{12}\varepsilon}{cT}\cdot\frac{s_{12}j}{\alpha_3\rho_3}; \tag{3}$$

- equation for the concentration of the vapor component.

$$\frac{\partial\left(\alpha_1\rho_1\left(1-\chi\right)\right)}{\partial t} = \frac{1}{r}\frac{\partial}{\partial r}\left[r\left(\alpha_1\rho_1\left(1-\chi\right)\right)\left(v_1^r + w_{1g}^r\right)\right] +$$

$$+\frac{\partial}{\partial z}\left[\alpha_1\rho_1\left(1-\chi\right)\right)\left(v_1^z + w_{1g}^z\right)\right] = 0\,;\ \chi = \frac{\rho_{1v}}{\rho_1}\,;\ 1-\chi = \frac{\rho_{1g}}{\rho_1}\,. \tag{4}$$

Where: a_m - water diffusion coefficient, m²/s; B - individual gas constant, J/(kg·K); c - thermal capacity, J/(kg·K); j - rate of evaporation, kg/(m²·s); K_{ij} - coefficient of i-phase penetrability in j- phase m²; L_{12} - latent heat of evaporating water, J/kg; t – time, s; p – pressure, Pa; T – temperature, K; r - radial coordinate, m; R - universal gas constant, J/(mol·K); s_{12} - specific surface area of the section of phases, m⁻¹; u - moisture content, kg/kg; v – velocity, m/s; w - diffusive velocity, m/s; z - axial coordinate, m; α - volumetric content, m³/m³; ε – criterion of phase transitions; φ - relative humidity; λ - thermal conductivity, W/(m²·K); ρ - density, kg/m³; χ - concentration of steam in a gas mixture, kg/kg. Subscripts: 1 - gas vapour mixture; 2 - fluid phase; 3 - solid phase; g – gas; v – vapor; 0 - initial state. Superscripts: r, z - components of vectors.

The transfer equations (1-4) are supplemented by the equation of the sorption polytherm, the equations of state for the vapor and gas components, the Fick diffusion law, the Darcy filtration law, the Dalton law for calculating the intensity of phase transitions, the Antoine formula for determining the saturated vapor pressure at a defined temperature:

$$u = f\left(T,\varphi\right)\,;\ p_1 = \rho_1 TB_1\,;\ p_{1g} = \rho_{1g} TB_{1g}\ ;\ p_{1v} = \rho_{1v} TB_{1v}\,;\ \rho_1 = \rho_{1v} + \rho_{1g}\,;$$

$$B_1 = B_{1v} + \left(1-\chi\right)B_{1g}\,;\ w_{1g}^r = \frac{\rho_1}{\rho_{1g}}D\frac{\partial\chi}{\partial r}\,;\ w_{1g}^z = \frac{\rho_1}{\rho_{1g}}D\frac{\partial\chi}{\partial z}\,;\ v_1^r = -\frac{K_{13}}{\mu_1}\frac{\partial p_1}{\partial r}\,;$$

$$v_1^z = -\frac{K_{13}}{\mu_1}\frac{\partial p_1}{\partial z}\,;\ j = \kappa_2\frac{p_{sat}\left(T\right) - p_{1v}\left(T\right)}{p_{atm}}\,;\ p_{sat} = \exp\left(A_s - \frac{B_s}{T+C_s}\right)\,; \tag{5}$$

where: D - diffusion coefficient m²/s ; μ - dynamic viscosity, Pa·s; $\overline{v}$ - fluid molar volume, m³/mol; A_s, B_s, C_s – empirical coefficients. Subscripts: atm – atmospheric; sat – saturation.

The initial and boundary conditions have the form:

$$T\left(0,r,z\right) = T_0\,;\ u\left(0,r,z\right) = u_0\ ;\ p_1\left(0,r,z\right) = p_{10}\,;\ \chi\left(0,r,z\right) = \chi_0\,; \tag{6}$$

$$-\lambda\frac{\partial T}{\partial n}\bigg|_\Gamma = \alpha^h\left(T\big|_\Gamma - T_c\right)\,;\ u\big|_\Gamma = u_{eq}\,;\ \chi_\Gamma = \chi_c\ ;\ p_1\big|_\Gamma = p_c\,. \tag{7}$$

Subscripts: eq – equilibrium; 0 - initial state; c - surrounding medium; Γ - external boundary of a granule; n – normal. Parameter α^h - coefficient of heat transfer, W/(m·K).

Important elements of the model are the original computational formulas for calculating the time-varying local diffusion coefficients of liquid a_m and the values of the phase transition criterion ε. These formulas were obtained by analyzing a more general mathematical model of heat and mass transport of transport constructed on the basis of the mechanics of multiphase systems [4-5]:

$$a_m = -\frac{K_{23}}{\mu_2}\frac{RTu}{\overline{v}}\frac{1}{\varphi}\frac{\partial\varphi}{\partial u} \; ; \; \varepsilon = \frac{c_{v1}}{L_{12}}\frac{T-T_{sat}}{1+u} \; . \tag{8}$$

The nonstationary nonlinear mathematical model (1-8) has been researched numerically. The equations are solved by an implicit method of finite differences using the control volume approach as described by [6].

4. Results of experiments and numerical analysis

Calculations were carried out at the values of the thermophysical parameters of water, water vapor, air according to [7]. For other parameters, the values are: ρ_3=1150 ; K_{13}=1.0·10^{-16} m^2; K_{23}=1.5·10^{-23} m^2; κ_2=1.7·10^{-12} kg/(m^2·s); s_{12}=6.6·10^6 m^{-1}; λ_3=0.25 W/(m^2·K); c_{p3}=2100 J/(kg·K). The heat transfer coefficient α^h was determined taking into account the drying agent's speed according to known empirical relationships. The polytherm of sorption of polycaproamide was obtained on the basis of experimental data:

$$u = u_{max}(T)\varphi^{a_0 k^\varphi} \; ; \; u_{max}(T) = u(T_0) - \alpha_T(T-T_0) \; .$$

The values of the parameters of the sorption polytherm are determined as follows: a_0=0.9567; k=4.796; T_0=295 K; $u(T_0)$=0.08891; α_T=0.0002517 K^{-1}.

The results of numerical calculations of drying kinetics of the polycaproamide granule satisfactorily coincide with the experimental curves of high-temperature drying (Fig. 1). By increasing the temperature of the air in the drying chamber, the duration of the process of dehydrating granules of polycaproamide can be significantly reduced. The drying of the granules at the temperature of the drying agent T_c=423 K is approximately 4 times faster than at T_c=383 K. The influence of the ratio R_{gr}/L_{gr} on the dewatering intensity of the granule is shown in Fig. 2. It should be noted that the main contribution to slowing down the drying process with increasing R_{gr}/L_{gr} is not the shape of the granule (tablet or elongated cylinder), but its volume, which also increases.
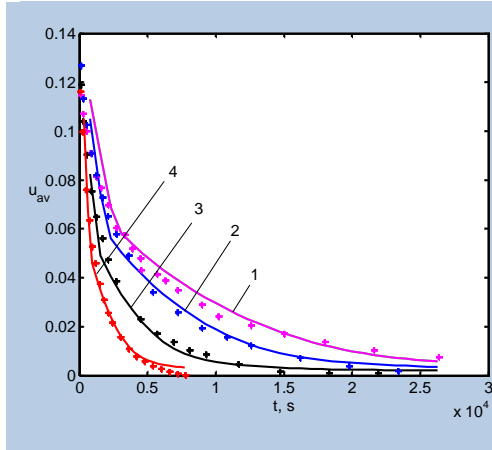
Fig. 1. The change in time with the average volume of moisture content of the polycaproamide granule with $R_{gr} = 1.375 \cdot 10^{-3}$ m, $L_{gr} = 0.04$ m at $\varphi_c=0.03$ for $T_c=373$ K – 1, 383 – 2, 403 – 3, 423 – 4.
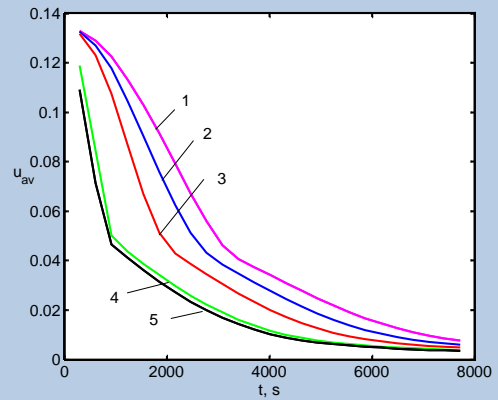
Fig. 2. The change in time with the average volume of moisture content of the polycaproamide granule at $T_c=423$ K, $\varphi_c=0.03$, $L_{gr} = 0.04$ m for $R_{gr}/L_{gr}=5 – 1$, $1 – 2$, $0.5 – 3$, $0.1 – 4$, $0.005 – 5$.
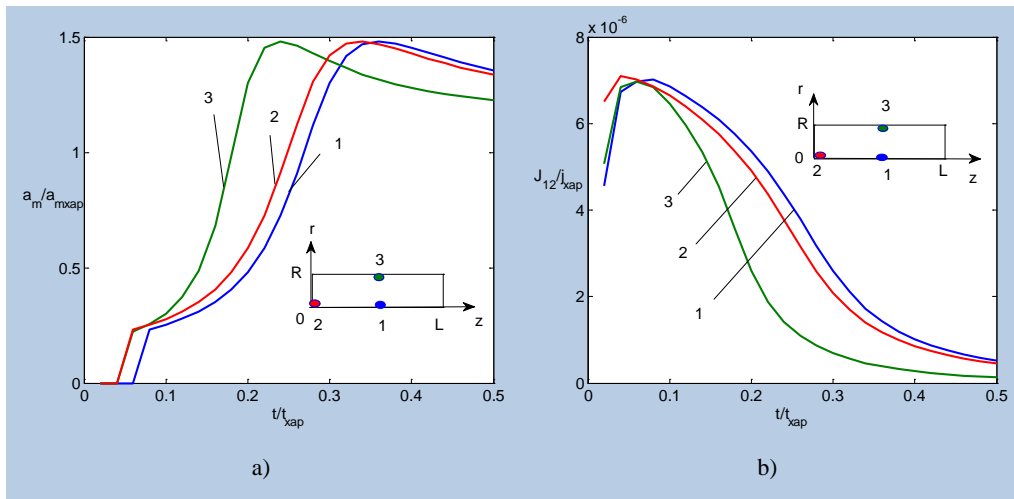
Fig. 3. The change with time of the local values of the diffusion coefficient (a) and the intensity of vaporization (b) in the cross section of the polycaproamide at $T_c=423$ K, $\varphi_c=0.03\%$ for $R_{gr}/L_{gr}=0.1$, $t_{xap}= 15456$ s, $a_{m \, xap} =1.63 \cdot 10^{-11}$ m²/s, $j_{xap} =3.06 \cdot 10^{-6}$ kg/(m²·s).

The moisture transfer in this process is carried out as a transfer of the liquid phase due to the gradient of the disjoining pressure in the boundary layers of water, if the moisture content of the material is below the maximum hygroscopic humidity, and also as the transfer of the vapor component, the production of which occurs throughout the volume of

the granule. Fig. 3 illustrates how the contribution of different moisture transfer mechanisms at individual points of the cross section of the granule varies with time. The motion of the liquid phase, characterized by the value $a_m > 0$, begins after the stage of material heating and intensive removal of moisture in the form of vapor. After a decrease in the value of u below the maximum hygroscopic moisture content, a flow of liquid from the region with a higher saturation to a region of lower saturation begins at this temperature, with the diffusion coefficient a_m increasing, reaching a maximum (Fig. 3a). The intensity of vaporization decreases (Fig.3b), which is associated with a decrease in saturated vapor pressure above the interphase surface and a decrease in its activity.

a)

b)

c)

d)
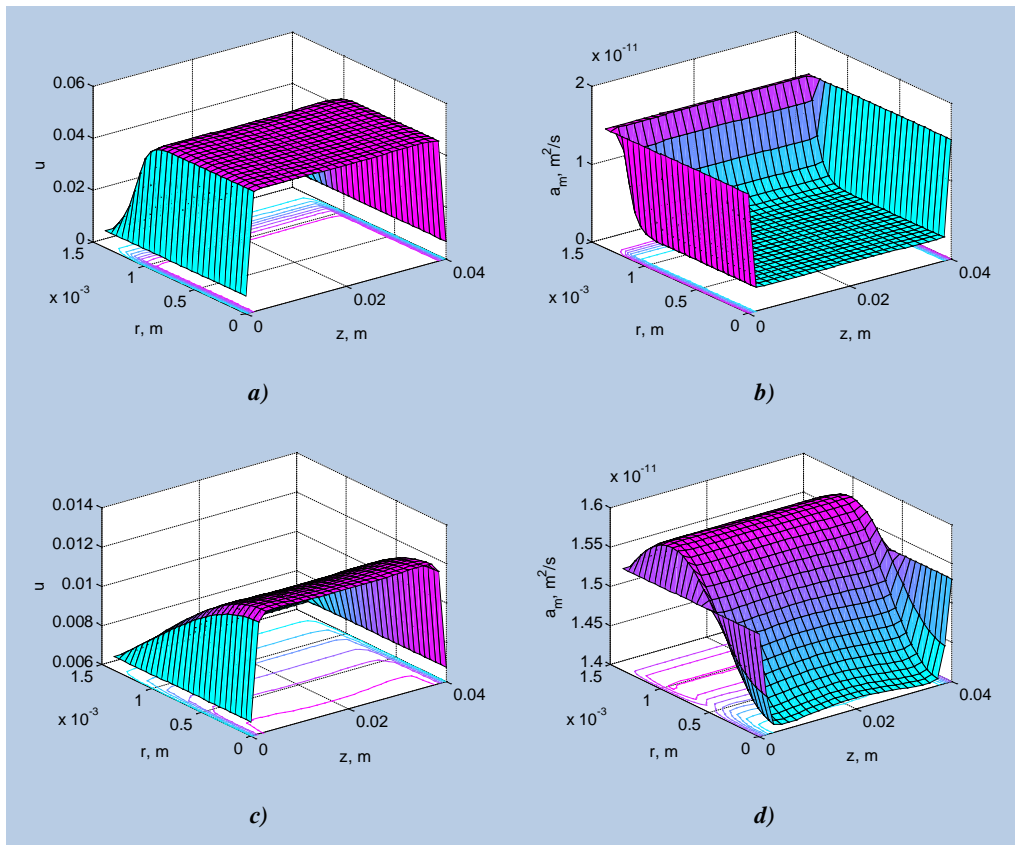
Fig. 4. The distribution in the plane r-z moisture content (a,c) and local diffusion coefficient of liquid phase (b,d) at the instants t = 13138 s – (a,b), 19722 – (c,d) during drying the granules with $R_{gr} = 1.375 \cdot 10^{-3}$ m, $L_{gr} = 0.04$ m at $T_c = 383$ K, $\varphi_c = 0.15$, $T_0 = 295$ K, $u_0 = 0.013$.

The distribution of the water diffusion coefficient over the granule cross-section and the corresponding moisture content distribution during drying are shown in Fig. 4 for different

instants of time. In the early stages of dehydration in the central zone of the granule, the moisture content exceeds the maximum hygroscopic humidity. Mass transfer occurs here due to evaporation, the coefficient of diffusion transfer of water is practically zero (Fig. 4a). Over time, this area is reduced (Fig. 4c), and at the end of the process it disappears. The distribution of the water diffusion coefficient across the cross-section of the granule a_m transforms with time (Fig. 4b, d) and gradually equalizes at low moisture content.

5. Conclusions

Comparison of the results of mathematical modeling of heat and mass transfer in the granule and data from the laboratory experiment on the kinetics of drying granules of polycaproamide showed good agreement between the calculated and experimental data. The constructed mathematical model allows to form energy-efficient regimes of granule polycaproamide drying.

6. References

[1]   Levitsky, S.P.; Shulman, Z.P. Bubbles in Polymeric Liquids. Dynamics and Heat-Mass Transfer; Technomic Publishing Co.: Lancaster, 1995.

[2]   Kosheleva, M.K.; Dornyak, O.R.; Apalkova, M.S. Mathematical modeling of heat and mass transfer during drying of granules carrier for nickel catalyst. In Proceedings of Second Nordic Baltic Drying Conference, Hamburg, Germany, June 7-9, 2017; 70.

[3]   Luikov, A.V. Heat and Mass Transfer in Capillary-Porous Bodies; Pergamon Press: Oxford, 1966.

[4]   Nigmatulin, R.I. Dynamics of multiphase media; Hemisphere: Washington, 1991.

[5]   Whitaker, S. Simultaneous Heat, Mass and Momentum Transfers in Porous Media: A Theory of Drying. Advances of Heat Transfer 1977, 13, 119 – 203.

[6]   Patankar, S. V. Numerical heat transfer and fluid flow; Hemisphere: Washington, 1980.

[7]   Vargaftik, N.B. Handbook of thermophysical properties of gases and liquids; Science: Moscow, 1972.

Computational fluid dynamics simulation of spray dryers: transient or steady state simulation?

Afshar, S.[a]; Jubaer, H.[a]; Chen, B.[c]; Xiao, J.[b]; Chen, X.D.[b]; Woo, M.W.[a,*]

[a]Department of Chemical Engineering, Monash University, Clayton Campus, Victoria 3800, Australia
[b] Chemical and Environmental Engineering, College of Chemistry, Chemical Engineering and Material Sciences, Soochow University, Suzhou, Jiangsu, China
[c]Department of Mechanical Engineering, Monash University, Clayton Campus, Victoria 3800, Australia

*E-mail of the corresponding author: meng.woo@monash.edu

Abstract

Self-sustained fluctuating airflow behaviour in spray drying chambers is in essence an unsteady phenomenon requiring the transient CFD simulation framework. There is currently, however, a mixture of steady state and transient CFD simulations of spray dryers practised and reported in the literature. The choice between steady state and transient approach significantly affects the computation time of the simulation and subsequently the adoption of this approach by industry. This paper firstly examines in detail the bottleneck in computation time of the transient simulation approach. Based on past reports, this review paper then presents a discussion and provides several recommendations on the use of steady state and transient simulation approach for spray dryers.

Keywords: CFD simulation, spray drying, transient, steady state, fluctuations

1. Introduction

The start-up of an industrial spray drying operation typically involves an initial heating of the chamber with hot air, followed by the spray of water to mimic the evaporation rate of the intended product feed. Once the outlet air conditions are approximately achieved, the product feed spray is introduced. This is then followed by a short period of operation, during which the product is diverted and operation adjustments are made, until stable outlet air and product conditions are achieved. These stable conditions are called the steady state operating condition. Examining the overall spray drying process from such a macro plant-wide view, beyond the initial start-up phase, the a spray drying process is typically operated indeed in a steady state mode.

There are experimental evidences to suggest that even if the overall operation is steady state, the airflow pattern within the spray drying chamber may exhibit significant transient fluctuations [1][2]. Such transient air flow behaviour manifests in form of a self-sustained flapping from side to side. Such self-sustained transient behaviour was experimentally observed even for spray dryers fitted with nozzle and rotating disc atomizers (the latter would have significant swirl in the airflow pattern) and in large scale dryers with an internal static fluidized bed [3]. It is noteworthy that the self-sustained fluctuations were observed on relatively long time scales and were spatially coherent fluctuations; incontrast to small time scale and small length scale turbulent fluctuations.

Against the backdrop of a steady state spray drying operation, one may naturally raise the following question: Is it important for us to account for the self-sustained transient airflow behaviour in the analysis of spray dryers? Answering this question with a straightforward "yes" or "no" would naturally instigate a long debate and legitimate dispute, since it always boils down to the purpose of the simulation. However, if the interest is on the overall process i.e. mass and energy balance of the process, the answer is most likely "no". On the other hand, for specific studies such as those on detailed drying behaviour, wall deposition, agglomeration etc. particularly with the development in the application of the Computational Fluid Dynamics (CFD) technique for spray drying analysis, which currently allows detailed analysis of the flow field within the chamber to be performed, accounting for the self-sustained transient behaviour may become crucial. Reports available in the literature, however, are not conclusive on whether or not this phenomenon should be accounted for. The former, in essence, is unable to capture the self-sustained behaviour. This review paper provides a discussion and analysis based on these reports with the aim of providing a guideline for future works in selecting a suitable approach for CFD modelling of spray dryers.

2. Steady versus transient CFD analysis and its implications

It is important to firstly define the structure of a steady and a transient CFD analysis of spray dryer, so that the subsequent discussion can be made on the same benchmark. This review

paper centres around the Euler-Lagrangian framework. Within this framework, the hot dehydrating air is computed in the Eulerian framework as a continuous medium while the particles are numerically injected into the simulated flow field as discrete Lagrangian phase. In this review, the term 'particles' refers to droplet or solid particles interchangeably. Two-way coupling is normally used in the simulation framework where the air imparts momentum, mass (moisture content) and energy change to the particles and vice versa; the latter two parameters are due to the drying process that the droplets are subjected to. Details on this aspects of a CFD simulation of spray dryers can be found in other publications [4].

Adopting the Euler-Lagrangian framework, Figure 1 shows two different numerical approaches in which a steady and a transient spray dryer simulation can be undertaken. Solutions with the transient framework will certainly involve higher computational requirements and longer computation time. From the authors' experience, however, given the computing power available nowadays, such differences may not be the significant factor affecting the potential selection between the steady and the transient framework. As a comparison, a steady state flow field simulation may take several hours while a transient flow field simulation may take a few days. The key difference lies in how the particles are injected into the flow field and in the way the two-way coupling is incorporated in both frameworks.

In the steady state framework, each particle is introduced into the flow field and tracked throughout the flow field until it leaves the simulation domain. This is then repeated depending on the number of particles specified to be injected to capture the stochastic behaviour of the particle movement and the particle size distribution of the spray. In essence, even though the source terms determined from the tracking of particles are accumulated for the subsequent incorporation into the steady state solution, there is only one particle numerically present in the simulation at any point. Therefore, the number of numerical loops required to achieve a converged solutions (Figure 1) is only dependent on the number of particle injection specified (which is fixed) and the 'numerical' speed at which the source terms are incorporated into the flow field solution. This 'numerical' speed is certainly dependent on the two-way coupling algorithm used and it is not the intention of this review paper to focus on any particular scheme.

Conversely, in the transient framework, particles are injected continuously at each discrete time step. During this time step, the particles injected into the simulation domain are only tracked and moved by one spatial step size. As opposed to steady state simulations, they are not tracked throughout the domain until those leave the chamber. Hence, as the simulation progresses in time, denoted by the loop in Figure 1, the number of particles within the chamber progressively increases leading to a further increase in the computational requirements at each time step. A fully developed flow field in this case, needs to account for not only the development of the temperature, momentum and humidity profile within the chamber, but also the development of the number of particles within the chamber. A well developed flow filed should have a relatively stable number of particles indicating that the system has 'truly' entered the steady state operation behaviour. The simulation time required to achieve such fully developed simulation is, therefore. significantly determined by the physical characteristics and the size of the spray dryer (larger drying chamber will expect to have more particle accumulation and vice versa) and not merely by the coupling algorithm, as in the steady state simulations. From the authors' experience, this takes significantly longer

time, in the order of weeks for large scale industrial dryers, when compared to the steady state simulations.

The transient simulation framework also warrants significantly different approach to the post-processing analysis of the particle drying history, which is one of the primary results from the CFD simulations. In the steady state approach, as each particle is tracked throughout the simulation domain until it leaves the domain, it is straightforward and easy to track and monitor the drying history of each particle. Determination of the particle conditions at the outlet of the dryer will only require collating the conditions of all the injected particle (those that leave the domain via the outlet) tracked one-by-one in the simulation. On the other hand, similar tracking and monitoring of the particle history in the transient framework will require large and simultaneous storage of all the particles within the simulation domain. For comparison, in a steady state simulation, an injection of hundreds or thousands of particles will normally be sufficient to account for the size distribution of the feed spray [5]. In a transient simulation, depending on the size of the dryer, the number of accumulated particles may be in the range of tens of thousands or hundreds of thousands of particles [6][7]. Determination of the particle conditions at the outlet will then require further time averaged sampling of particles leaving the system [6][7]. Even though the implemented parcel tracking method in the Eulerian-Lagrangian framework, which allows a parcel representing a group of identical particles having the same fate to be tracked in lieu of tracking each individual particle, eases the conundrum of tracking and storing information about so many particles, the remaining computational and postprocessing effort required still is far from negligible.

In order to overcome these limitations in transient simulation post-processing, a pseudo-steady analysis method was developed in which the flow field is developed with fully transient airflow computation accompanied by transient particle tracking for a low velocity spray dryer. Particle history is then analysed and obtained by adopting an instantaneous snapshot of the developed flow field and undertaking steady state particle tracking through the flow field [8][9]. The premise of this post-processing approach assumes that, in view of the self sustained fluctuating behaviour, a snap shot at any particular flow time is representative of the overall flow behaviour in the system. Comparison on using snapshots at different flow time provided compelling evidence to support this assumption. Further comparison is, however, required with full transient analysis and with dryers of different configurations to better validate this technique. Even if this could be fully resolved or verified, the transient simulation framework would still need long computation time to fully develop the flow field incorporating transient simulation tracking (Figure 1). An earlier report can also be found adopting this approach excluding the two-way coupling [10] i.e. no build-up of humidity or reduction of the air temperature due to droplet evaporation could be predicted and fed back to the solution.

Steady state framework

Initialization of the flow

↓

Steady state solution of the flow field

↓

Steady state injection of particles into the flow field (each particle is tracked until it leaves the chamber via the boundary)

↓

Steady state solution of the flow field to incorporate the momentum, mass and energy sources from the particles

↓

Converged and developed flow field

↓

Particle post-processing: Steady state injection of particles

Transient framework

Initialization of the flow

↓

Pseudo-steady state solution of the flow field

↓

Transient solution of the flow field until developed self-sustained behaviour

↓

Injection of particles into the flow + tracking of the movement of particles for one time step

↓

Transient solution of the flow field for one time step incorporation the momentum, mass and energy source from the particles

↓

Developed flow field and particle number within the chamber

↓

Particle post-processing: Time sampling of particles or pseudo-steady analysis

Fig. 1 Numerical approaches to undertaking steady or transient CFD simulations of spray dryers

Based on the comparison presented above, it can be concluded that it is obviously more attractive to adopt the steady state simulation approach. This will then allow the CFD simulation technique to be used in a more routine-manner, which will be particularly important for the adoption of this technique by industry. Nevertheless, the same question still prevails: How accurately do steady state simulations capture the reality of a potentially fluctuating flow field in spray dryers? At any rate, the ensuing question will be: in what situation can we employ a steady state simulation? In an attempt to answer these important questions, detailed comparison were undertaken based on past reports in the literature. However, this part of the review was not included here due to page limitation.

3. Understanding the numerical source of self-sustained fluctuation

The fact that self-sustained fluctuations discussed in this review may occur even in symmetrical geometries suggests that it must be initiated from some 'imbalance' in the system. There is a series of numerically based reports elucidating the self-sustained fluctuation behaviour based on the sudden flow expansion theory. The premise of this theory is that a certain flow regime characterized by the Reynolds or Swirl number and the expansion ratio will have the propensity to exhibit self-sustained flow behavior [11][12][13][14]. The jet feedback mechanism was proposed later on, expanding on the theory of expansion to elucidate the potential unbalanced pressure within the chamber, leading to the self-sustained fluctuation behavior [15].

In a real physical system, there are many factors which may contribute to such imbalance such as slight asymmetry in the drying chamber or in the inlet flow of air (no perfect system in reality). These imbalances are then sustained or propagated and consequently reflected by the inherent propensity of the system for self-sustained fluctuations, as discussed in the preceding section. For a numerical system, however, where the geometry and the input parameters for a CFD simulation can be perfectly symmetrical, such asymmetric physical seed for the initiation of self-sustained fluctuation will not be available. One may argue that even though the geometry and the inputs are symmetrical, the meshing of the system, particularly if tetrahedral meshes are used, may lead to numerically asymmetric solution to the flow field. However, it must be noted that self-sustained fluctuations were predicted even when very structured symmetrical hexahedral meshes were used [14]. Basing our discussion on the solution of the turbulent flow field with the Reynolds Averaged Navier Stokes (RANS) equations and its subsequent closure models, there is no stochastic element in the mathematical framework. Hence, if the mesh used is symmetrical, the RANS framework should theoretically provide a symmetrical solution. What is then the source of asymmetry, which provides the seed for the occurrence of self-sustained fluctuation behaviour in a numerical model?

Eliminating the possible influence of the physical geometry, meshing and mathematical model as discussed, the seed for or the instigation of 'numerical' self-sustained fluctuation

must then be attributed to numerical imbalance during the solution of the flow field. Such numerical imbalance may propagate into imbalances predicted in the physical flow field, building up the potential for self-sustained fluctuations. If this argument is to be further extended, it can be noted that perhaps, the numerical coupling with particles introduced into the simulation may also contribute to such instability, as was reported by Jubaer et al. [16]. Whether or not such imbalances propagate into self-sustained flow behaviour will certainly depend on the propensity of the spray drying chamber for 'dampening' such physical or numerical imbalances. The understanding on the numerical source of self-sustained fluctuation is important in guiding the numerical approach employed in the CFD simulation of spray dryers. Perhaps, as a 'robust' approach to encompass all the possibilities to capturing the self-sustained fluctuation, there may be a need for an element of numerical imbalance in the simulation domain; a system which inherently is not self-sustained in fluctuation would damp the imbalance anyway and vice versa.

5. Conclusions

A key numerical bottleneck in transient CFD simulation of self-sustained fluctuating flows in spray dryers is the long computation time required for two-way coupling during flow development. There is a strong need for future numerical development to overcome this limitation so that the CFD technique can be used in a more routine manner. From the reports available in the literature, there is currently no clear guidelines on the use of steady or transient simulation approach when analysing pilot or industrial scale spray dryers. This paper recommends to ascertain the significance of the fluctuating behaviour with the transient simulation framework, on a case-by-case basis. This is particularly important if an asymmetric flow field was predicted for a symmetrical simulation domain. A few numerical guidelines are proposed. It was further reasoned that numerical imbalance may be the seed for self-sustained fluctuations observed in CFD simulations of spray dryers. Whether or not this numerical imbalance propagates into physical imbalances leading to flow fluctuation behaviours, depends on the characteristics of the spray drying geometry relative to its operating conditions, which may or may not contribute to dampening these imbalances.

6. References

[1]   Southwell, D.B.; Langrish, T.A.G. The effect of swirl on flow stability in spray dryers. Chemical Engineering Research and Design 2001, 79: 222-234.

[2]   Langrish, T.A.G.; Oakley, D.E.; Keey, R.B.; Bahu, R.E.; Hutchinson, C.A. Time-dependent flow patterns in spray dryers. Chemical Engineering Research and Design 1993, 71: 355-360.

[3] Gabites, J.R.; Abrahamson, J.; Winchester, J.A. Air flow patterns in an industrial milk powder spray dryer. Chemical Engineering Research and Design 2010, 88: 899-910.

[4] Woo, M.W. Computational Fluid Dynamic Simulation of Spray Dyers – An Engineer's Guide. 2016. CRC Press. US, Florida.

[5] Woo, M.W.; Daud, W.R.W.; Mujumdar, A.S.; Wu, Z.H.; Talib, M.Z.M.; Tasirin, S.M. CFD evaluation of droplet drying models in a spray dryer fitted with a rotary atomizer. Drying Technology 2008, 26(10), 1180-1198.

[6] Jin, Y.; Chen, X.D. A three-dimensional numerical study of the gas/particle interactions in an industrial-scale spray dryer for milk powder production, Drying Technology 2009, 27(10), 1018–1027

[7] Jin, Y.; Chen, X.D. Numerical study of the drying process of different sized particles in an industrial scale spray dryer. Drying Technology 2009, 27(3), 371-381.

[8] Woo, M.W.; Rogers, S.; Lin, S.X.Q.; Selomulya, C.; Chen, X.D. Numerical probing of a low velocity concurrent pilot scale spray drying tower for mono-disperse particle production – unusual characteristics and possible improvements. Chemical Engineering and Processing 2011, 50(4), 417-427.

[9] Woo, M.W.; Rogers, S.; Selomulya, C.; Chen, X.D. Particle drying and crystallization characteristics in a low velocity concurrent pilot scale spray drying tower. Powder Technology 2011, 223, 39-45.

[10] Kota, K.; Langrish, T.A.G. Prediction of Deposition Patterns in a Pilot-Scale Spray Dryer Using Computational Fluid Dynamics (CFD) Simulations. Chemical Product and Process Modeling 2007, 2(3): Article 26.

[11] Fletcher D.F.; Guo B.; Harvie D.J.E.; Langrish T.A.G.; Nijdam J.J.; Williams J. What is important in the simulation of spray dryer performance and how do current CFD models perform? Applied Mathematical Modelling 2006, 30, 1281-1292.

[12] Guo, B.; Langrish, T.A.G.; Fletcher, D.F. CFD simulation of precession in sudden pipe expansion flows with low inlet swirl. Applied Mathematical Modelling 2002, 26: 1-15.

[13] Guo, B.; Langrish, T.A.G.; Fletcher, D.F. Simulation of gas flow instability in a spray dryer. Chemical Engineering Research and Design 2003, 81(A): 631-638.

[14] Guo, B.; Langrish, T.A.G.; Fletcher, D.F. Simulation of turbulent swirl flow in an axisymetric sudden expansion, AIAA Journal 2001, 39(1): 96-102.

[15] Woo, M.W.; Daud, W.R.W.; Mujumdar, A.S.; Talib, M.Z.M.; Wu, Z.H.; Tasirin, S.M. Non-swirling steady and transient flow simulations in short-form spray dryers. Chemical Product and Process Modelling 2009, 4(1), 20.

[16] Jubaer, H.; Afshar, S.; Xiao, J.; Chen, X.D.; Selomulya, C.; Woo, M.W. On the Importance of Droplet Shrinkage in CFD-Modelling of Spray Drying. Drying Technology 2017 (doi: 10.1080/07373937.2017.1349791)

Semi empirical models for drying of agricultural products by used structured artificial neural networks

Bessenyei, K.; Kurják, Z.; Beke, J.
Institute for Process Engineering. Szent István University, Gödöllő, Hungary

*E-mail of the corresponding author: bessenyei.kornel@gek.szie.hu

Abstract

We compared a semi empirical and an empirical model. The empirical model is a multilayer ANN. The semi empirical model is a custom multilayer ANN. It is a structured model, and we define the structure by hand before the training of the network. The influence of the neuron numbers on the accuracy of the models was also investigated by statistical approach.

We found that the custom multilayer ANNs developed like this, are suitable for modelling the drying process of agricultural materials. They also provide the ability to improve the applicability of the empirical models. Furthermore, the semi empirical model has a higher sensitivity on neuron number applied.

Keywords: drying; energetics; artificial neural network; semi-empirical model.

1. Introduction

The complexity of the water removal process, and the inhomogenities of the process variables both in time and space make the modelling of the drying process of agricultural products difficult. The usability of theoretical models is limited due to the stochastic material properties. [4] In these cases, the application of empirical models is essential. [5] However, in the most cases we have theoretical information about the process. Applying this information to the model it will became semi-empirical and possibly improve the usability compared to the pure empirical. [3]

Artificial intelligence techniques are also found in drying. [6] They are used for process variable prediction [10][12][15], process control [9][11][13] or for soft sensors[14]. Artificial neural networks (ANN) are sucsefully applied on all these fiels on their own, or combined with other AI or conventional techniques. [8] The use of ANN requires attention and awareness as the structure, the training and data preparation have significant effect on usability of the model. [7]

Earlier we found that artificial neural networks (ANN) are suitable to model the drying of agricultural products. [1] They are empirical models, but can be turned into semi-empirical when we use the combination of smaller ANNs in a suitable structure instead of one unstructured model. [2]

It can happen that we have a priori information about the structure of the system (to be modelled), but don't have the data to train the subsequent ANNs that make up the semi-empirical model as a combination of smaller individually trained networks. In this case a single, but structured ANN can be created. The ANN can be defined by hand. It is called a custom artificial neural network. It can have a structure like the combination of smaller ANNs have, but the model can be trained without having any data for the internal connection.

The statistical approach that we used earlier [1] can help us to find the optimal structure of the network. The models' performance can be highly influenced by the applied number of the layers, and the number of the neurons in the layers. There are structures and neuron numbers that will never ever provide us an accurate model. On the other hand, there are structures what provide us accurate model with a high probability.

This paper is about the semi-empirical ANN models made from structured analytical neural networks and it is looking for answers to the following questions: Is it possible to construct such a model? Is it possible to find an optimal model? Is it better than the pure empirical?

2. Materials and Methods

The measurement data is taken from an experimental drying of tomato pomace in a laboratory dryer. The drying apparatus is a convective batch dryer. The dried material is placed into the drying chamber on perforated sheet metal trays in three layers. The psychrometric properties of the drying air are measured before and after each layer, the flow rate is measured with an orifice at the duct inlet. The water removal is measured with gravimetric method. For data acquisition five-minute sampling rate was used.
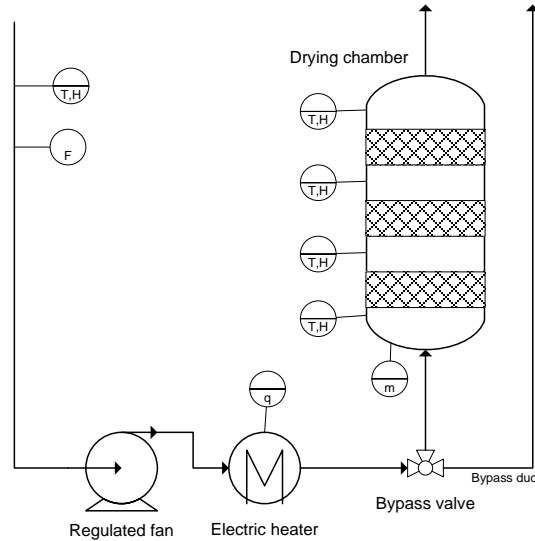
Fig. 1. Schematic of the dryer. (T-temperature, H-humidity, F-flow rate, m-mass, q-heat flow)

The wet-base moister content of the raw material was about 80% at the begining and 6% at the end of the drying experiment. The flowrate of the drying air was 370m^3/h and the temperature was set according to table 1. 2 kg tomato pomes was put on each tray in a 40 mm thick layer.

Table 1. Temperature of the drying air

experiment	temperature [°C]
1	40
3	110
5	75
6	55

From the preliminary data analysis four data sets have been chosen for the models: experiment 1, 3, 5 and 6. From these data sets experiment 1 has systematic error, and not

used for training the models but for test. It is required that the model shall approximate experiment 1 with a significantly higher error.

The first model constructed is purely empirical. According to the earlier works on this topic [1], a two-layer ANN has been chosen. Two such models were defined and we use the simpler one as it can be found on figure 2 below. The simplified model does not deal with the layers; it is like a one-layer dryer.
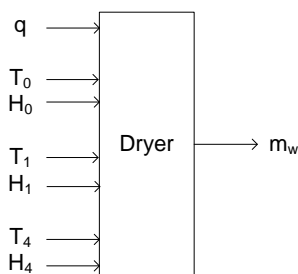
Fig. 2. Empirical model of deep bed dryer. (m_w-water removal rate, T_0-ambient air temperature, T_1-air temperature at drying chamber inlet, T_4-air temperature at drying chamber outlet, H_0-ambient air humidity, H_1-humidity at drying chamber inlet, H_4-air humidity at drying chamber outlet)

The semi-empirical model is considering that the dryer consists of a burner and a drying chamber. The connection of the two components is the flow rate of the drying media.
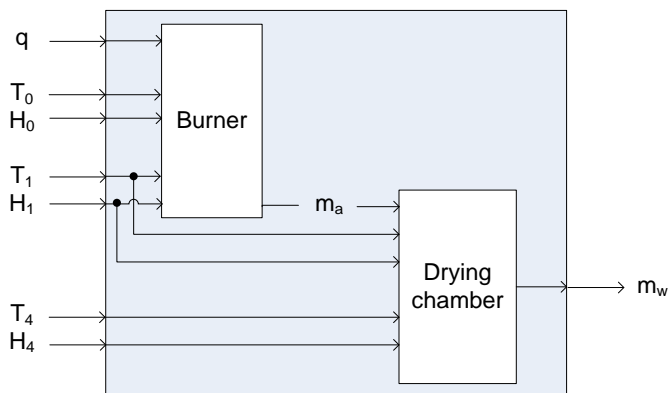
Fig. 3. Semi-empirical model of the deep bed dryer. (m_a-flow rate of the drying air)

For the burner a one-layer ANN was used. For the drying chamber and the simplified empirical model, a two-layer structure was used. For the determination of the optimal neuron numbers in each layer the statistical approach was used. [1] We compared several networks with different neuron numbers in each. Table 2 contains the neuron numbers we used.

After the training of the ANN models, we tested them. All the experiment data was given to the model inputs and the model output was compared to the measured data. For each simulation the cumulated squared error was calculated as the measure of model performance.

$$Cumulated\_squared\_error = \sum(measured - simulated)^2 \qquad (1)$$

Table 2. Neuron numbers per layer

model	layer	neurons
empirical	1st	1-15
	2nd	1-15
semi empirical	burner	1-10
	drying chamber 1st	1-15
	drying chamber 2nd	1-15

We also checked the correlation of the model output with the measured data. Figure 4 shows the algorithm of the whole process. Each structure was trained and tested 5 times. At the end, the results were shown in diagrams and the optimal model structure was chosen. The optimal model is the model with the smallest expected value and little standard deviation of cumulated squared error. The optimal models output should also have a good correlation with the measurement data.
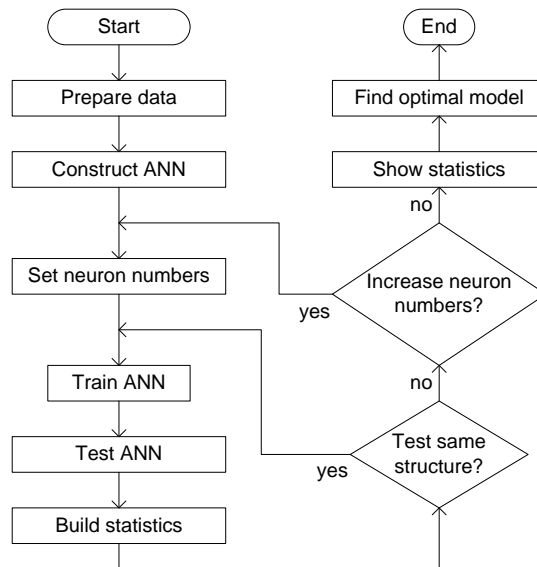
Fig. 4. Workflow of finding the optimal model

3. Results and Discussion

The empirical model has 2 hidden layers. We used the method on Figure 4 to construct empirical models with different neuron numbers according to Table 2. The results can be observed on Figure 5. The structure of the optimal empirical model and its performance is shown in Table 3.

Table 3. Optimal models

model	layer	neurons	error
empirical	1st	7	0.862
	2nd	9	
semi empirical	burner	1	2.6
	drying chamber 1st	13	
	drying chamber 2nd	11	
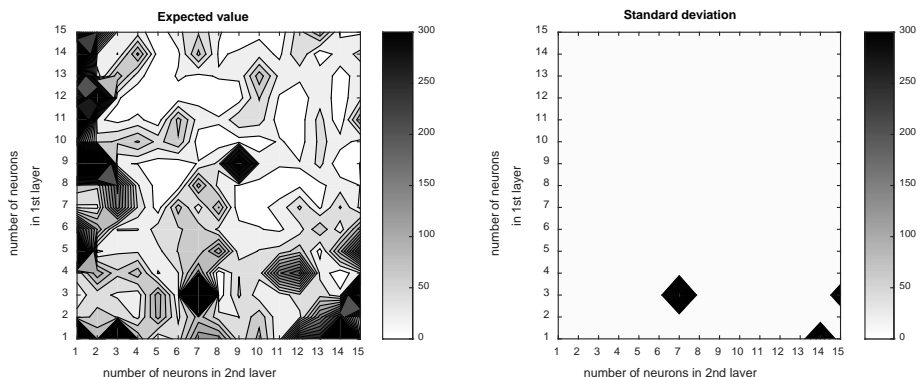
Fig. 5. Performance of the empirical model with different neuron numbers.

The semi empirical model always has 3 hidden layers: one for the burner and two for the drying chamber. We used the same method as for the empirical model thus on Figure 4. The results cannot be shown on one diagram as the 3 layers of neurons span a 3-dimensional space rather than a 2-dimensional. But it is possible to show on several diagrams. We need as many diagrams, as many neurons we have in a chosen layer. We choose the burner layer, because it has less possible number of neurons than the others. This way we got the smallest number of diagrams. Figure 6 contains the optimal structure. The structure of the optimal semi empirical model and its performance can be found in Table 3.
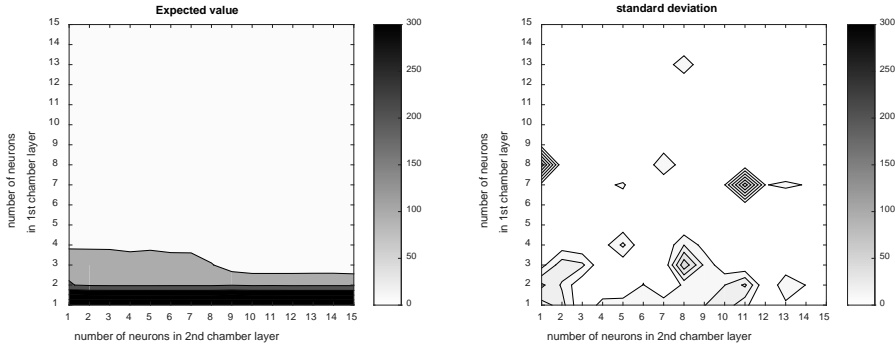
Fig. 6. Performance of the semi empirical model with a single neuron in the burner layer.

There are several near optimal structures on figure 6. On the other hand there are structures with significantly higher error what probably make the model unusable. If the burner has one neuron the 1st chamber layer should have at least 3 or 4 neurons. The diagrams with higher neuron numbers for the burner show significantly higher error. Because of the limited space we did not include in this paper all the diagrams but they are very similar to Figure 7 in the aspect that the model with all those neuron numbers has significantly higher error.
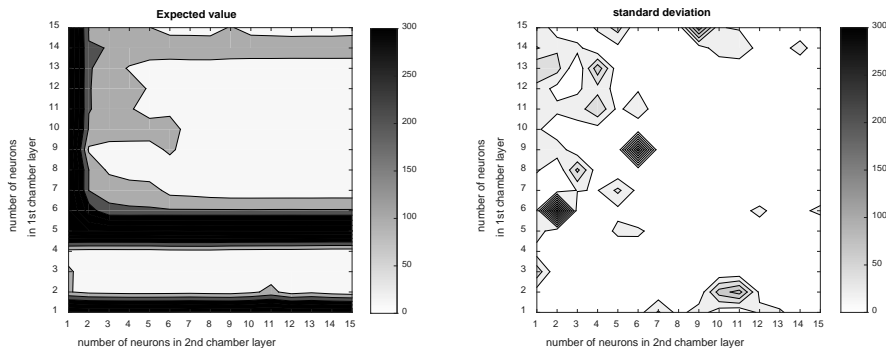
Fig. 7. Performance of the semi empirical model with 2 neuron in the burner layer.

4. Conclusions

Empirical and semi empirical models both approximated the measurement data with acceptable error.

It was possible to construct a semi empirical model with a custom ANN that is suitable for modelling the drying process of tomato pomace.

There are significant differences in model performance depending on the model structure and the number of neurons used in its layers.

The statistical method we used can highlight the unusable and potentially usable structures.

With the statistical method we used it was possible to find the optimal model structure.

5. References

[1] Bessenyei, K.; Kurják Z.; Deákvári, J.; Beke J. Modelling of tomato pomace drying process with artificial neural network. In Proceedings of 5th European Drying Conference, Paris, France, October 2-5, 2013.

[2] Bessenyei, K.; Kurják Z.; Beke J. Semi empirical models with artificial neural network. In Proceedings of 6th European Drying Conference, Budapest, Hungary, October 21-23, 2015.

[3] Cubillos, F. A.; Wyhmeister, E.; Acuna, G.; Alvarez, P. I. Rotary dryer control using a gre-box neural model scheme. Drying Technology 2011, 29, 1820–1827.

[4] Ghaderi, A.; Abbasi, S.; Motevali, A.; Minaei, S. Comparison of mathematical models and artificial neural networks for prediction of drying kinetics of mushroom in microwave-vacuum drier. Chemical Industry & Chemical Engineering Quarterly 2012, 18 (2), 283−293.

[5] Tohidi, M.; Sadeghi, M.; Mousavi, S. R.; Mireei, S. A. Artificial neural network modeling of process and product indices in deep bed drying of rough rice. Turkish journal of agriculture and forestry 2012, 36(6), 738-748.

[6] Martynenko, A. Artificial intelligence: Is it a good fit for drying? Drying Technology 2018, 36(8), 891-892.

[7] Farkas, I. Use of Artificial Intelligence for the Modelling of Drying Processes. Drying Technology 2013, 31, 848–855.

[8] Aghbashlo, M.; Hosseinpour, S.; Mujumdar, A. S. Application of Artificial Neural Networks (ANNs) in 175 Drying Technology: A Comprehensive Review. Drying Technology 2015, 33, 1397–1462.

[9] Nakamura, G.; Bentes, F.; Freire, J. Control of the Moisture Content of Milk Powder Produced in a Spouted Bed Dryer Using a Grey-Box Inferential Controller. Drying Technology 2015, 33(15-16), 1920-1928.

[10] Martínez-Martínez, V.; Gomez-Gil, J.; Stombaugh, T. S.; Montross, M. D.; Aguiar, J. M. Moisture Content Prediction in the Switchgrass (Panicum virgatum) Drying Process Using Artificial Neural Networks, Drying Technology 2015, 33:14, 1708-1719.

[11] Jianshuo Li; Qingyu Xiong; Kai Wang; Xin Shi; Shan Liang; Min Gao. Temperature control during microwave heating process by sliding mode neural network. Drying Technology 2016, 34(14), 1708-1719.

[12] Prerna Khawas; Kshirod Kumar Dash; Arup Jyoti Das; Sankar Chandra Deka. Modeling and optimization of the process parameters in vacuum drying of culinary banana (Musa ABB) slices by application of artificial neural network and genetic algorithm. Drying Technology 2016, 34(4), 491-503.

[13] Jianshuo Li; Qingyu Xiong; Kai Wang; Xin Shi; Shan Liang. A recurrent self-evolving fuzzy neural network predictive control for microwave drying process. Drying Technology 2016, 34(12), 1434-1444.

[14] Mansoureh Mozaffari; Asghar Mahmoudi; Kaveh Mollazade; Bahareh Jamshidi. Low-cost optical approach for noncontact predicting moisture content of apple slices during hot air drying. Drying Technology 2017, 35(12), 1530-1542.

[15] Ergün, A.; Ceylan, I.; Acar, B.; Erkaymaz, H. Energy–exergy–ANN analyses of solar-assisted fluidized bed dryer. Drying Technology 2017, 35(14), 1711-1720.

Image Segmentation and 3D reconstruction for improved prediction of the sublimation rate during freeze drying

Capozzi, L. C.ª; Arsiccio, A.ª; Sparavigna, A. C.ª; Pisano, R.ª; Barresi, A. A.ª*

ª Department of Applied Science and Technology, Politecnico di Torino, Torino, Italy

*E-mail of the corresponding author: antonello.barresi@polito.it

Abstract

In a freeze drying process, the freezing step determines the pore size distribution within the product, which, in turn, affects the sublimation rate. Traditionally, pore analysis is carried out on SEM images by means of a manual, time-consuming approach. Here, an image segmentation technique was used to automatize this process and improve its reliability. A 3D structure of the cake was then reconstructed from the distribution of the super-pixels. We show that the approach herein proposed can remarkably improve prediction of the sublimation rate with respect to traditional methods.

Keywords: Freezing; Freeze-Drying; Image Segmentation; 3D Reconstruction

1. Introduction

During freeze drying, water is removed by sublimation and desorption from a previously frozen product. When designing a freeze drying process, it is well-known that the freezing step is extremely relevant for both process performance and product quality [1]. In fact, different freezing protocols result in different pore size distributions within the product, affecting both sublimation and desorption rates. More specifically, the nucleation event, and, in particular, the temperature at which the first ice crystal nuclei are formed, is of major importance in the freezing process, as it determines the pore size distribution which will then be formed in the dried sample. In particular, a low nucleation temperature will result in the formation of small pores. These small pores will then offer a large resistance to water vapor flow during primary drying, thus decreasing the sublimation rate. From this viewpoint, a problem with the traditional freezing approaches, such as shelf ramped freezing, is that they do not allow control of the nucleation temperature, which will therefore be stochastically distributed. However, some techniques have been developed to overcome this problem [1,2]. Among them, vacuum induced surface freezing (VISF) was demonstrated to be beneficial for both product homogeneity and process performance [3,4]. In fact, VISF can be used to induce nucleation at a higher temperature in all the vials being processed. This higher nucleation temperature results in the formation of larger pores within the dried samples, boosting the sublimation rate. For instance, in Figure 1 two Scanning Electron Microscopy (SEM) images are shown, representing a 5% w/w mannitol sample after freeze drying. In the case of Figure 1a, VISF was used, while the sample in Figure 1b was processed using the conventional shelf-ramped freezing protocol.
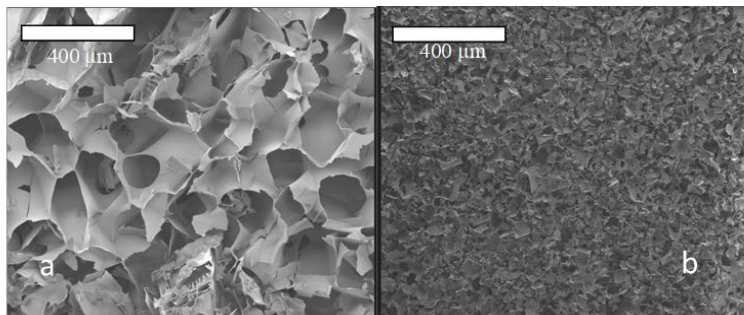
Fig. 1 SEM images of 5% w/w mannitol samples obtained using VISF (a) or shelf ramped freezing (b).

The huge difference in sample morphology which can be observed translates into remarkably different cycle performance; it is therefore clear that the information on the pore size distribution is crucial for the proper design of a freeze-drying process. Although many other

approaches have been proposed in the past, such as X-ray tomography [5], the most common technique remains off-line SEM analysis. This is generally achieved by means of a manual analysis of the resulting images. The manual approach is, however, highly time consuming, and the results obtained are subjective and, therefore, poorly reliable. Therefore, we recently proposed a method based on the segmentation of SEM images to automatically determine the pore size distribution [6]. In the above-mentioned work, we showed that image segmentation could quickly and reliably allow resolution of the porous structure of the sample under investigation. Here we propose a further improvement of this technique, which combines the analysis of the levels of grey-tones to the detection of edges between different domains. Moreover, we will show that, from the super-pixels distribution obtained as a result of segmentation, a 3D structure of the cake may be reconstructed by means of a stochastic approach. We will prove that the reconstruction obtained can fairly well represent the main features of the real dried cake. This result is important, since the generated structure may then be used within a computational fluid dynamics (CFD) simulation, to estimate the tortuosity of the sample [7]. Since both the pore size distribution and the tortuosity factor enter into the definition of the mass transfer resistance to vapor flow, the approach herein proposed could remarkably improve prediction of the sublimation rate, which is at the basis of any model for the freeze-drying process.

2. Materials and Methods

2.1 Freeze drying cycles and SEM analysis

The formulation investigated in this work was a 5% w/w mannitol solution, prepared from distilled water and mannitol powder (Sigma Aldrich). The vials employed (type 1, 10R, 45x24 mm, Schott AG, Germany), where filled in with 3 ml of sample solution, and loaded onto the shelves of a freeze-dryer LyoBeta 25 (Telstar, Terrassa, Spain). For the conventional (shelf ramped) freezing tests, the refrigerating fluid temperature was decreased to -45°C at 0.7 °C/min.

As regards VISF, the product was first equilibrated at −5°C for 45 min and, then, the chamber pressure was reduced to 130 Pa until nucleation was observed. The pressure was then quickly released to the atmospheric value, and the product was equilibrated at −10°C for 1 h. To complete the freezing of the product, the refrigerating fluid temperature was subsequently decreased to −45°C at 0.7°C/min and held for 1 h. Finally, drying was performed at 10 Pa, and -10°C. The internal structure of the resulting cake was analyzed by means of a Scanning Electron Microscope (SEM, FEI type, Quanta Inspect 200, Eindhoven, the Netherlands).

2.2 Image Segmentation for the processing of SEM images

In [6], we described a segmentation approach, based on the analysis of the levels of grey-tones, for the determination of the pore size distribution in freeze dried samples. Here, we propose an improved version of this technique, in which the detection of the edges between the pores and the surrounding scaffold is included in the analysis. First, the SEM image is processed to enhance the edges in it, that is processed to detect the regions where we have a large gradient in the topography. Among the methods for edge detection, the Retinex filter, which is available in GIMP (the GNU Image Manipulation Program [8]), was chosen. Then, this information is merged to that concerning the topography itself and the image converted into a binary black and white map (Figures 2a and 2b). From the resulting map, the pores are automatically selected, as described in [6], and as shown in Figures 2c and 2d.
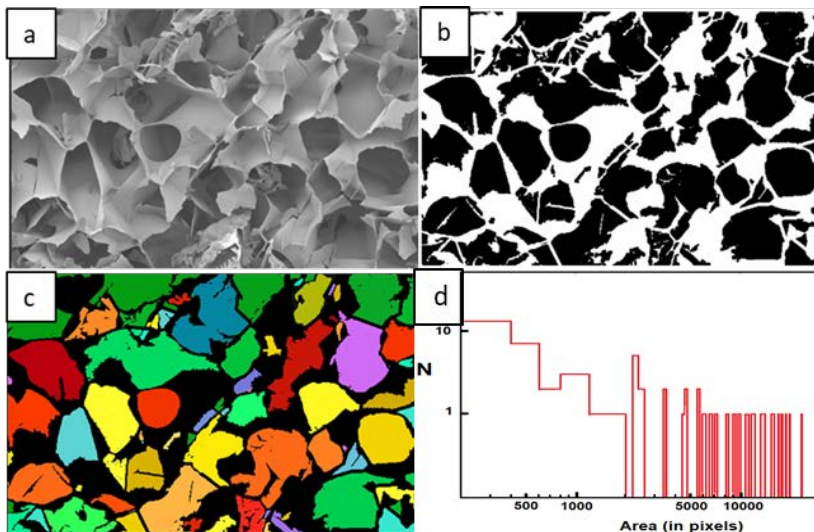
Fig. 2 (a) SEM and (b) binary images corresponding to mannitol 5% w/w, freeze dried using VISF. (c) Segmentation of the original SEM image, where the domains are represented by different colors. (d) Distribution of the super-pixels (in logarithmic scales), obtained by counting them according to their area (in pixels).

2.3 Prediction of the resistance to mass transfer

The resistance to mass transfer, R_p, was calculated from the average pore dimension D_p, as calculated using either the manual approach, or the image segmentation technique, by means of the following equation,

$$R_p = \frac{3}{2}\frac{\tau^2}{\varepsilon}\frac{L_d}{D_p}\sqrt{\frac{\pi R T}{2 M_w}}$$

(1)

where R and M_w are the universal gas constant and water molecular weight, respectively. As can be seen, R_p is a function of the dried layer thickness L_d, and depends on the product temperature T, and on the dried product tortuosity factor τ and porosity ε, as well.

2.4 Stochastic reconstruction of 3D structures

Using the information obtained from image analysis, a 3D structure of the dried cake was then reconstructed, for the case of the product obtained by VISF (Figure 1a). To do this, spherical pores were stochastically built into an 800 x 800 x 800 µm original bulky cube. The dimension of the spheres was chosen so as to reproduce the pore size distribution obtained from image segmentation (Figure 2d). As shown in Figure 3 this procedure was iterated until the desired value of porosity was reached. No constraints were imposed on the position of the sphere centers, so that interpenetration of the pores was possible, as illustrated in Figure 3. This was done in order to better reproduce the real structure of a freeze-dried product, where the porous structure is, generally, highly interconnected.
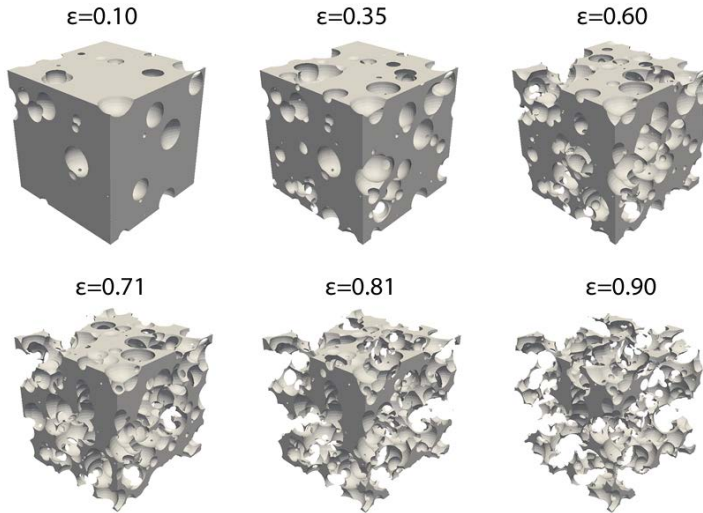
Fig. 3 Reconstruction of a lyophilized cake with different void fraction.

3. Results and Discussion

The image segmentation technique described in section 2.2 was applied to the SEM images shown in Figure 1. As illustrated in a previous work [6], this technique allows calculation of the super-pixels distribution within the SEM image, from which an average pore size can be extracted. For instance, using segmentation, average pore dimensions of 140±30 μm and 36±6 μm were obtained for VISF (Figure 1a) and shelf ramped freezing (Figure 1b), respectively. By contrast, using the traditional approach, that is, manually selecting and measuring a sufficiently large number of pores, the conventional freezing protocol and VISF resulted in an average diameter of 20±8 μm and 120±36 μm, respectively. As can be seen, both techniques measured a larger average pore size in the case of VISF, which was expected, because of the higher nucleation temperature in the case of controlled nucleation. However, the pore dimension is not sufficient for an accurate estimation of the resistance to mass transfer R_p, since another required parameter is the tortuosity factor τ, whose value is generally only roughly hypothesized. Typically used values span between 1.2 and 3.8 [9], and this range translates into a large uncertainty in the value of R_p, as shown in Figure 4.
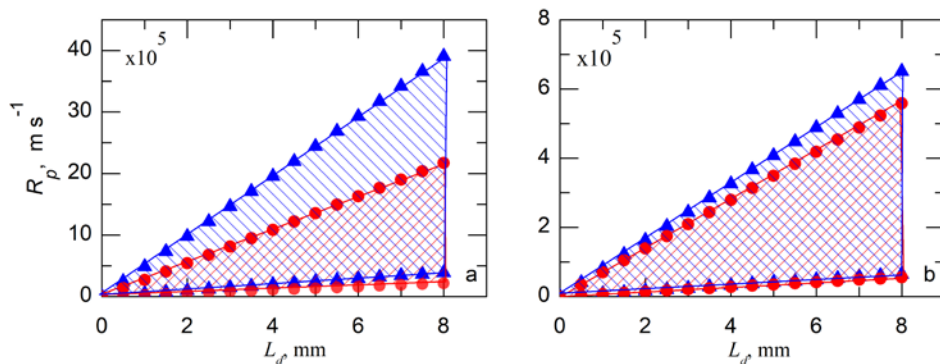
Fig. 4 Uncertainty in the value of R_p as function of the dried layer thickness L_d, due to the uncertainty on τ. The range 1.2–3.8 was considered for τ. (a) conventional freezing, and (b) VISF. ●: Values calculated using Eq. 1, in which the pore dimension D_p was obtained by the image segmentation approach; ▲: Values calculated using Eq. 1, in which the pore dimension D_p was obtained by the traditional manual approach.

A possible solution to this problem can be found combining image analysis and CFD simulations. In fact, as described in section 2.4, a 3D structure of the dried cake might be reconstructed using the super-pixels distribution obtained from image segmentation. An example of reconstructed structure, for varying values of porosity, is shown in Figure 3. The stochastic approach used for the 3D reconstruction was validated against the original SEM image, as outlined in Figure 5. A 800 x 800 x 400 μm slice was isolated from the reconstructed cube, and a 2D section (Figure 5b) was obtained from this slice, using a grey-

tone scale ranging from white to black to represent perspective. This was done in order to simulate the same type of representation obtained in a typical SEM analysis. As can be seen comparing Figures 5a and 5b, there was a striking similarity between the original SEM image and the 2D section obtained from the 3D reconstruction. To further confirm this similarity, Figure 5b was analyzed using image segmentation, and the super-pixels distribution was calculated (Figure 5c). Remarkably, the resulting distribution compares fairly well with that obtained for the original SEM image (Figure 2d). This means that the 3D reconstruction preserves most of the features of the original sample, and could therefore allow an easier analysis of the properties which influence the sublimation rate; for instance, by a CFD simulation of water vapor flow through the reconstructed 3D structure.
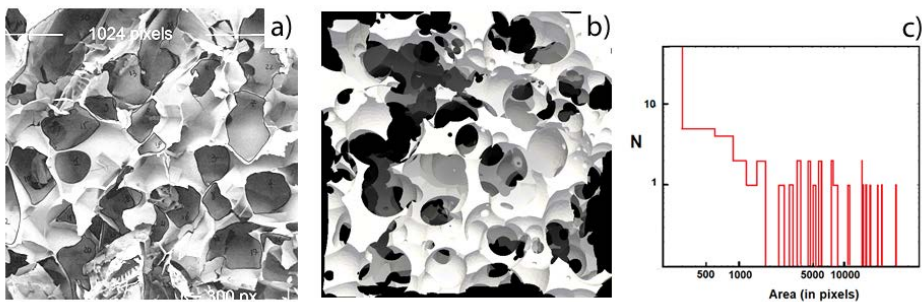
Fig. 5 Validation of the 3D reconstruction approach: a) SEM image, b) upper view of a slice of the 3D structure and c) super-pixels distribution in Fig. 5b.

4. Conclusions

In the present work, a new approach has been proposed for the estimation of both the pore size distribution and the tortuosity factor within a freeze dried sample. Work is in progress to simulate the fluid dynamics in the 3D reconstructed matrix. Subsequently, analysis of the velocity vectors for the water vapor during the simulation would make it possible to estimate the tortuosity of the sample, and, thus, to calculate a more accurate value for the mass transfer resistance; the same procedure discussed in [7] for granular beds obtained by spray-freezing can be adopted. The described method may allow a significantly improved fitting of experimental data with respect to other traditional modeling techniques. We are therefore convinced that the approach herein outlined could be extremely beneficial, paving the way for a more robust design of the freeze drying process.

5. Acknowledgements

6. References

[1] Kasper, J.C.; Friess, W.F. The freezing step in lyophilization: Physico-chemical fundamentals, freezing methods and consequences on process performance and quality attributes of biopharmaceuticals. European Journal of Pharmaceutics and Biopharmaceutics 2011, 78 (2), 248-263.

[2] Pisano, R.; Arsiccio, A.; Nakagawa, K.; Barresi, A.A. Control, measurement and prediction of the impact of freezing on product morphology: A step towards improved design of freeze-drying cycles. Drying Technology 2018, accepted.

[3] Oddone, I.; Pisano, R.; Bullich, R.; Stewart, P. Vacuum-induced nucleation as a method for freeze-drying cycle optimization. Industrial and Engineering Chemistry Research 2014, 53 (47), 18236-18244.

[4] Oddone, I.; Van Bockstal, P.-J.; De Beer, T.; Pisano, R. Impact of vacuum-induced surface freezing on inter- and intra-vial heterogeneity. European Journal of Pharmaceutics and Biopharmaceutics 2016, 103 (1), 167-178.

[5] Pisano, R.; Barresi, A.A.; Capozzi, L.C.; Novajra, G.; Oddone, I.; Vitale-Brovarone, C. Characterization of the mass transfer of lyophilized products based on X-ray micro-computed tomography images. Drying Technology 2017, 35 (8), 933-938.

[6] Arsiccio, A.; Sparavigna, A.C.; Pisano, R.; Barresi, A.A. Measuring and predicting pore size distribution of freeze-dried solutions. Drying Technology 2018, in press. DOI: 10.1080/07373937.2018.1430042

[7] Capozzi, L.C.; Boccardo, G.; Barresi, A.A.; Pisano, R. Computer-aided property estimation of micro-particles in packed-beds for freeze-drying applications. In Proceedings of 20th International Drying Symposium, Gifu, Japan, August 7-10, 2016; paper A-4-3.

[8] Finlayson, G.D.; Hordley, S.D.; Drew, M.S. Removing shadows from images using retinex. In Proceedings of 10th Color and Imaging Conference, Scottsdale, Arizona, January 2002; 73-79.

[9] Goshima, H.; Do, G.; Nakagawa, K. Impact of ice morphology on design space of pharmaceutical freeze-drying. Journal of Pharmaceutical Sciences 2016, 105 (6), 1920-1933.

Mathematical relationship between glass transition temperature and water activity of cellular and non-cellular food systems

Nguyen, T. K.[a,c]; Khalloufi, S.[b,*]; Ratti, C.[a,b]

[a] Institute of Nutrition and Functional Foods (INAF), Université Laval, QC, Canada, G1V 0A6

[b] Soils and Agri-Food Engineering Department, Université Laval, QC, Canada, G1V 0A6

[c] Food Science Department, Université Laval, QC, Canada, G1V 0A6

*E-mail of the corresponding author: seddik.khalloufi@ulaval.ca

Abstract

Cellular and non-cellular-solid food systems were used to obtain experimental data of a_w and Tg as a function of moisture content during drying. GAB, Gordon-Taylor, and Khalloufi-Ratti models were used to obtain the state diagrams of the four food systems investigated. The results suggest that the GAB and Khalloufi-Ratti models can successfully be used to capture the experimental data. In terms of plasticizing effect, it seems that cellular and non-cellular systems have comparable values. Although the number of food samples explored in this study was limited, it is suggested that the chemical composition could have more impact on Tg and stability than the presence of cell structures.

Keywords: Isotherms; Glass Transition; Cellular and Non-Cellular Food Systems; Modeling.

1. Introduction

Several mathematical models are available for describing sorption isotherms. The widely used model for food matrices is Guggenheim-Anderson-de Boer (GAB) [1]. This model is based on the monolayer moisture concept, and may be used to provide estimative values of critical moisture content and relative humidity for safe storage of dried foods [2]. With repect to bio-material, the Flory-Huggins model has been also able to properly describe sorption isotherms [3, 4].

The concept of glass transition has been widely applied to food, polymer, material and pharmaceutical sciences to relate physical, chemical and structural changes to the physical state of the material [2]. In general, the *Tg* value depends on the thermal history of the material, the molecular weight of the polymer chains, the presence of a plasticizer, the degree of crystallinity and sample composition [5]. Water, with low molecular weight and low *Tg* (-135ºC) [6], is the most important plasticizing agent in foodstuffs, increasing the flexibility of matrix and decreasing *Tg*. Water plasticization effect may be well represented in foods by the Gordon-Taylor (G-T) equation [7] and, for polymer blends, by the Couchman and Karasz (C-K) equation [8]. Khalloufi et al. (2000) developed an equation to represent glass transition temperature of fruit powders as a function of water activity, which proposes a sigmoid rather than linear representation of *Tg* in the whole range of water activity [9].

Both water activity and glass transition have been used extensively in the literature to evaluate storage stability [10, 11]. The combination of these two parameters can be used to obtain the state diagram. [12] which can help to select packaging material and optimizing ingredient in food formulation. Furthermore, the state diagram can be used to design and optimize drying equipment, as well as to model and control processing, i.e. determination of the end-point of drying or assessing the energy requirement by choosing optimum temperature and moisture content to avoid undesirable effects [13]. So far, the state diagrams for various foodstuffs have been reported in literature [2, 14, 15, 16]. However, none of this data compared cellular to non cellular systems. In addition, state diagams for maltodextrins, carrots and potatoes are rare in the open littertaure [17].

The objective of the current study was to develop the state diagrams for potato, carrot and two agar-maltodextrin model systems (AM DE19 and AM DE36), by measuring the glass transition temperature and water sorption isotherms. The GAB and Flory-Huggins equations were used to describe the sorption isotherms, while the G-T equation, for the glass transition temperature. The relationship between *Tg* and a_w was established from Khalloufi-Ratti model [9]. State diagrams for the four products were built from mathematical representations for *Tg*, a_w and moisture content and compared with experimental data.

2. Materials and Methods

2.1. Material and processing

Maltodextrin was provided by Laboratory Mat (Quebec city, Canada). Agar was delivered by Becton Dickinson and Company (Sparks, MD 21152 USA). White potatoes (W1386 variety) were provided by Gosselin G2 Inc. (Quebec City, Canada). Carrots were purchased directly from a local market in Quebec, Canada (ATV farms, Quebec). Two cellular systems (potato and carrot) and two non-cellular systems (water-agar-maltodextrin: AM DE19 and AM DE36) were used in this study. The non-cellular models were prepared in a mass proportion of water/agar/maltodextrin of 1/0.015/0.15. Cylindrical samples were made and cut from random positions within the sample with a hollow punch in 1cm-diameter by 4cm-long cylinders. Samples were dried by convection in an Armfield tunnel dryer (Model UOP8-G, Hampshire, UK) with air at 55ºC and air speed of 1.6m/s, until constant weight.

2.2. Sorption Isotherms

Materials with various moisture contents and water activities were obtained by re-humidification of powdered air-dried samples at various relative humidity levels over saturated salt solutions in desiccators at 25°C. Relative humidity of the saturated solutions was checked by measuring their water activity with an Aqualab (model series 3, Decagon Devices Inc, USA).

2.3. Glass transition temperature (Tg)

The glass transition temperature of equilibrated samples was measured with a Differential Scanning Calorimeter DSC Pyris 1 (Perkin Elmer, Shelton, CT, USA).

2.4. Mathematical modeling

The mathematical relationships used in this contribution are presented in Table 1.

Table 1. Mathematical relationships between moisture content (X) , water activity (a_w), and/or glass transition temperature (Tg)

Model & Refernce	Mathematical expression	Eq.
GAB [1]	$X = \dfrac{(X_m\, Y\, K\, a_w)}{(1 - K\, a_w)(1 - K\, a_w + Y\, K\, a_w)}$	(1)
Flory-Huggins [3]	$\ln a_w = \ln(1 - \phi_p) + \phi_p - \dfrac{\phi_p}{N} + \chi \phi_p^2$	(2)
Gordon-Taylor [7]	$Tg = \dfrac{(1 - w)\, Tg_s + k\, w\, Tg_w}{(1 - w) + k\, w}$	(3)
Khalloufi-Ratti [9]	$Tg = \dfrac{A\, a_w{}^2 + B\, a_w + C}{D\, a_w{}^2 + E\, a_w + 1}$	(4)

3. Results and discussion

Figure 1 shows the results obtained by using the Flory-Huggins model to describe water activity as a function of volume fraction. The Flory-Huggins model was satisfactory for carrot, but not for other food systems investegated in this contribution (e.g. AM DE19, AM DE36 and potato). According to Kocherbitov (2016), the Flory-Huggins equation is not able to describe the glassy part of water sorption isotherms of some polymers [4]. As the Flory-Huggins model was not suitable for all the four food systems, the GAB model model will be used for the next steps of this study (Figure 2 and Table2).
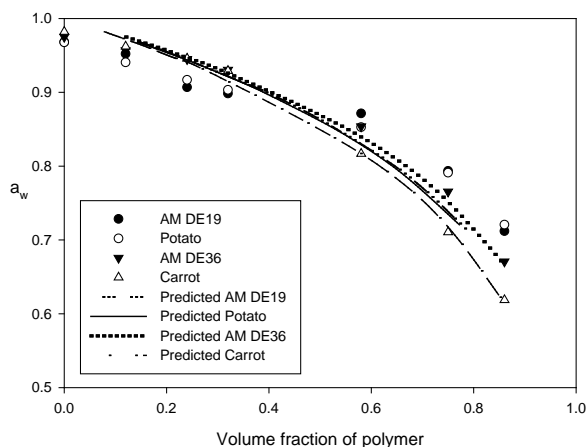
Figure 1. Comparison between experimental data and predictions of Flory-Huggins model

The *Tg* values for carrots and potatoes, obtained in this investigation, are close to those reported by Karmas et al. (1992). Georget et al. (1999) detected two glass transition temperatures for carrot material associated with two phases: a sugar-rich phase and a cell wall-rich phase. The *Tg* value found in the current study is considered to be in agreement with those of the sugar-rich phase but lower than those of the cell wall rich phase [17]. Three main saccharides occurring commonly in carrot roots are glucose, fructose and sucrose [18], thus the glass transition temperature in carrots are related to *Tg* for those three types of sugars. The *Tg* value of carrots is also similar to the one of rich glucose-fructose fruit such as raspberry ($Tg_s = 42.62$°C) [2]. In the case of potato, the *Tg* value in both native or non-native potato starch reported in literature (120°C) is much higher than the experimental data found in the present study (49.8 ±12.3°C) for dry potato [5, 19]. Significant differences between *Tg*

values of dried potato tuber and potato starch was also observed by Chirife et al. (1996). According to Biliaderis et al. (1986), the absence of a clearly detectible glass transition in native starch is due to the amorphous chains locked by crystalline domains, the decrease of mobility of the amorphous chain by physical crosslinks and the presence of inter-crystalline phases that do not follow normal thermal behavior. The constants Tg_s and k of the Gordon-Taylor model (Eq. 3) were estimated by non-linear regression for the four types of sample materials, which results are shown in Table 2. The k values of the four products studied in the present work were in the range reported for fruits and vegetables such as onion (k = 4.3), raspberry (k = 4.7), strawberry (k = 4.3), mango (k = 4.5), kiwifruit (k = 4.9), gooseberry (k = 5.7) and banana (k = 6.1) [2, 14, 15, 16, 20, 21]. The k value is an estimate of the plasticization effect of water, which means the strength of interaction between water and the food solids. Higher values indicate a greater plasticizing effect of water on solids [12]. From Table 2, it can be observed that water has a greater plasticizing effect on potato than on carrot. For carrot, this plasticizing effect of water was the lowest among the four products.

Table 2. Parameters involved in the Gordon-Taylor model (Eq. 3, Table 1)

	Tg (°C)	k	r^2
AM DE19	108.4	4.9	0.97
AM DE36	81.9	5.2	0,99
Potato	76.2	6.8	0.99
Carrot	35.2	4.3	0.96

State diagrams (Figure 2) was built by using experimental data and the predictions obtained from the mathematical model of GAB expression (for water sorption) and from Khalloufi-Ratti model (for glass transition temperature). As it can be seen, the predictions obtained by both models are in agreement with the experimental data. The monolayer water content (X_m) obtained from the *GAB* equation is an important parameter for stability of foods, which depends on chemical composition and temperature of the material. A product is most stable below X_m where rates of deteriorative reactions are minimal [22]. At temperature of 25°C, the estimated values of the parameter X_m is 0.049 kg/kg (db) for *AM DE19*, 0.065 kg/kg (db) for *AM DE36*, 0.056 kg/kg (db) for potato. These values were found to be lower than the one

for carrot, which was 0.195 kg/kg (db). These results are close to those reported by Kiranoudis et al. (1993) which found that the X_m value of potato was 0.087 and that of carrot was 0.21 kg/kg (db).
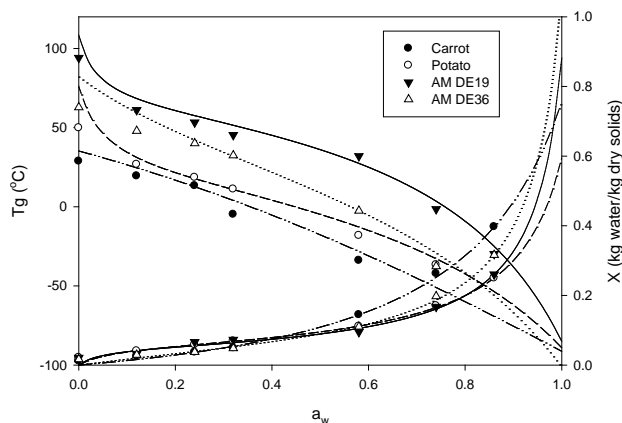
Figure 2. State diagram of cellular and non-cellular food materials. Lines are predicted data obtained by using GAB and Khalloufi-Ratti models

The relationship between a_w and Tg has been reported to be sigmoid [11]. The Khalloufi-Ratti model [9] allows capturing this sigmoidal profile for all the food sytems investigated in this study (Figure 2). This model is a combination of paramters obtained previously from *Gordon-Taylor* and *GAB* models (Table 1).

Table 2 shows the critical water content and critical water activity of four products at 4°C and 25°C obtained from state diagram (Figure 2). The critical water content (CWC) and critical water activity (CWA) are the value at which the glass transition occurs, at a determined storage temperature of the product. These value are helpful to show the dependence of Tg of product on moisture content or water activity. For example, if the AM DE19 is conserved at 25°C, the CWC and CWA at which the glassy system AMDE19 transformed to a rubbery state is 0.096kg/kg dm and 0.536, respectively. According to the water activity concept, foods are most stable at their monolayer moisture content. While the glass transition concept propose that amorphous matrix are more stable at or below the corresponding Tg [10, 13].

Table 3. Critical water activity (aw_c) and Critical water content (X_c)

	4ºC		25ºC	
	a_{wc}	X_c	a_{wc}	X_c
AM DE19	0.6765	0.1336	0.5389	0.0966
AM DE36	0.4883	0.0865	0.3439	0,0567
Potato	0.3416	0.0711	0.1453	0.0450
Carrot	0.3303	0.0493	0.1105	0.0145

4. Conclusions

Water activity (a_w) and glass transition temperature (Tg) are relevant concepts to predict the stability of food products. The Flory-Huggins model was able to describe the sorption isotherm of carrot but not for other food systems investigated in this study. GAB and Khalloufi-Ratti models were succusfuly able to capture the experimental profile of cellular and non cellular food systems. These two mathemetaical models can be used to construct the state diagrams which describes the physical states as a function of water activity and water content of foods. This state diagram can be used as a significant tool to help food scientists, food engineers and food-packaging researchers to develop processing protocols and selecting storage conditions. In terms of plasticizing effect of water, it seems that cellular and non-cellular systems have comparable values. Although the number of food samples used in this study was limited, this contribution suggests that the chemical composition of food systems could have more impact on their Tg and stability than the presence of cell structures. Further investigations with diverse food systems are required to confirm this preliminary finding.

5. References

[1] Al-Muhtaseb, A.H.; McMinn, W.A.M.; Magee, T.R.A. Moisture Sorption Isotherm Characteristics of Food Products: A Review. Food and Bioproducts Processing. 2002, 80, 118-128.1

[2] Syamaladevi, R.M.; Sablani, S.S.; Tang, J.; Powers, J.; Swanson, B.G. State diagram and water adsorption isotherm of raspberry (Rubus idaeus). Journal of Food Engineering. 2009, 91, 460-467.2

[3] Hancock, B.; Zografi, G. The Use of Solution Theories for Predicting Water Vapor Absorption by Amorphous Pharmaceutical Solids: A Test of the Flory–Huggins and Vrentas Models. Pharmaceutical Research. 1993, 10, 1262-1267.3

[4] Kocherbitov, V. The nature of nonfreezing water in carbohydrate polymers. Carbohydr Polym. 2016, 150, 353-8.4

[5] Thiewes, H.J.; Steeneken, P.A.M. The glass transition and the sub- T g endotherm of amorphous and native potato starch at low moisture content. Carbohydrate Polymers. 1997, 32, 123-130.30

[6] Johari, G.P.; Andreas, H.; Erwin, M. The glass–liquid transition of hyperquenched

water. Nature. 1987, 330, 552.31

[7]   Gordon, M.; Taylor, J.S. Ideal copolymers and the second-order transitions of synthetic rubbers. i. non-crystalline copolymers. Journal of Applied Chemistry. 1952, 2, 493-500.32

[8]   Couchman, P.R.; Karasz, F.E. A Classical Thermodynamic Discussion of the Effect of Composition on Glass-Transition Temperatures. Macromolecules. 1978, 11, 117-119.33

[9]   Khalloufi, S.; El-Maslouhi, Y.; Ratti, C. Mathematical Model for Prediction of Glass Transition Temperature of Fruit Powders. Journal of Food Science. 2000, 65, 842-848.34

[10]   Chirife, J.; del Pilar Buera, M.; Labuza, T.P. Water activity, water glass dynamics, and the control of microbiological growth in foods. Critical Reviews in Food Science and Nutrition. 1996, 36, 465-513.3

[11]   Roos, Y.; Karel, M. Applying state diagrams to food processing and development. Food technology. 1991, 45, 66, 68.35

[12]   Sablani, S.S.; Syamaladevi, R.M.; Swanson, B.G. A Review of Methods, Data and Applications of State Diagrams of Food Systems. Food Engineering Reviews. 2010, 2, 168-203.29

[13]   Sablani, S.S.; Kasapis, S.; Rahman, M.S. Evaluating water activity and glass transition concepts for food stability. Journal of Food Engineering. 2007, 78, 266-271.38

[14]   Moraga, G.; Martínez-Navarrete, N.; Chiralt, A. Water sorption isotherms and phase transitions in kiwifruit. Journal of Food Engineering. 2006, 72, 147-156.40

[15]   Sá, M.M.; Sereno, A.M. Glass transitions and state diagrams for typical natural fruits and vegetables. Thermochimica Acta. 1994, 246, 285-297.42

[16]   Zhao, J.-H.; Liu, F.; Wen, X.; Xiao, H.-W.; Ni, Y.-Y. State diagram for freeze-dried mango: Freezing curve, glass transition line and maximal-freeze-concentration condition. Journal of Food Engineering. 2015, 157, 49-56.43

[17]   Georget, D.M.R.; Smith, A.C.; Waldron, K.W. Thermal transitions in freeze-dried carrot and its cell wall components. Thermochimica Acta. 1999, 332, 203-210.47

[18]   Baranski, R.; Allender, C.; Klimek-Chodacka, M. Towards better tasting and more nutritious carrots: Carotenoid and sugar content variation in carrot genetic resources. Food Research International. 2012, 47, 182-187.55

[19]   Farahnaky, A.; Farhat, I.A.; Mitchell, J.R.; Hill, S.E. The effect of sodium chloride on the glass transition of potato and cassava starches at low moisture contents. Food Hydrocolloids. 2009, 23, 1483-1487.56

[20]   Wang, H.; Zhang, S.; Chen, G. Glass transition and state diagram for fresh and freeze-dried Chinese gooseberry. Journal of Food Engineering. 2008, 84, 307-312.

[21]   Moraga, G.; Talens, P.; Moraga, M.J.; Martínez-Navarrete, N. Implication of water activity and glass transition on the mechanical and optical properties of freeze-dried apple and banana slices. Journal of Food Engineering. 2011, 106, 212-219.

[22]   Rahman, M.S. State diagram of foods: Its potential use in food processing and product stability. Trends in Food Science & Technology. 2006, 17, 129-141.12

Modeling sorption isotherms and isosteric heat of sorption of roasted coffee beans

Collazos-Escobar, G.A.[a*]; Gutiérrez-Guzmán, N.[a]; Váquiro-Herrera, H.A.[b]; Cortes-Macias, E.T.[a]

[a] *Facultad de Ingeniería. Centro Surcolombiano de Investigación en Café CESURCAFÉ. Universidad Surcolombiana. Neiva-Huila-Colombia.*
[b] *Facultad de Ingeniería Agronómica,, Universidad del Tolima, Ibagué-Tolima-Colombia*

E-mail of the corresponding author: gentlcollazosescobar09@gmail.com

Abstract

The aim of this work was determine the sorption isotherms in roasted beans of specialty coffee at temperatures of 25, 30 and 40 °C and water activities between 0.1 and 0.8 using the dynamic dew point method. The experimental sorption data were modeled using 12 different equations to represent the dependence of equilibrium moisture content with a_w and temperature. The net isosteric heat of sorption was determined from the experimental sorption data using the Clausius-Clapeyron equation. The Weibull model satisfactorily modeled the effect of the temperature on the hygroscopic equilibrium in roasted coffee beans (R^2_{adj} =0.902 and RMSE = 0.00550 kg·kg^{-1}d.b.). The net isosteric heat of sorption increase with increased moisture content.

Keywords: *water activity; sorption properties; equilibrium moisture content; hygroscopicity.*

1. Introduction

Coffee beans are a highly hygroscopic matrix and could readily take up moisture when exposed to the environment during storage [8], this condition may affect the coffee bean freshness. For proper handling of roasted coffee beans it is necessary to know, among other properties, the water sorption isotherms, which describe the relationship between the equilibrium moisture content and the water activity at constant temperature and pressure [2]. There are many sorption models proposed in literature to represent the water sorption in foods [16], some models are empirical or semi-empirical equations. Due to the complex in the food matrices, there are not a unique model to describe entirely of the agri-food products [3]; therefore is necessary to validate from experimental data the best model for both the material and the air conditions.

The objective of this work was to determine and model the moisture isotherms of roasted coffee beans at temperatures of 25, 30 and 40 °C and water activities between 0.1 and 0.8 using the dynamic dew point method.

2. Materials and Methods

2.1 Coffee samples

Nine samples of wet processed coffee (*Coffea arabica* L.) from Huila region (Colombia) were sensory analyzed to SCAA (Specialty Coffee Association of America) methodology in the South Colombian Coffee Research Center (CESURCAFÉ) by four experts panelists [12]. The coffee beans were roasted in a laboratory equipment (TC-150R,Quantik, Colombia).

2.2. Experimental determination of the sorption isotherms

Sorption isotherms were determined at water activities between 0.1 and 0.8 and temperatures of 25, 30 and 40 °C by the dynamic dew point method (DDI). The measurements were carried out in a Vapor Sorption Analizer (VSA Aqualab Decagon Device, Inc. Pullman, WA) at water-activity intervals of 0.01 and 0.05 for adsorption and desorption, respectively, and a flow rate of 100 ml/min.

2.3 Modeling sorption isotherms

The sorption isotherms of roasted coffee beans were represented mathematically using the 12 models shown in Table 1, where X is the equilibrium moisture content (kg·kg^{-1}, dry basis), a_w is the water activity, K, C, C_0 and K_0 are GAB model parameters, H_m is the monolayer sorption heat (kJ·mol^{-1}), H_n is the multilayer sorption heat (kJ·mol^{-1}), λ is the evaporation enthalpy of water (kJ·mol^{-1}), T is the absolute temperature (K), R is the universal gas constant (kJ·mol^{-1}·K^{-1}) and b_i are empirical model parameters.

Table 1. Mathematical model to define roasted coffee beans isotherms

Model	Reference	Mathematical expression	Equation
GAB	[6, 10]	$X = \dfrac{X_m C K a_w}{[(1 - K a_w)(1 - K a_w + C K a_w)]}$	(1)
		$C = C_0 \exp\left(\dfrac{H_m - H_n}{RT}\right)$	(2)
		$K = K_0 \exp\left(\dfrac{\lambda - H_n}{RT}\right)$	(3)
Oswin	[1]	$X = b_1 \left(\dfrac{a_w}{1 - a_w}\right)^{b_2}$	(4)
Smith	[13]	$X = b_1 + b_2 \ln(1 - a_w)$	(5)
Chung-Pfost	[11]	$X = b_1 + b_2 \ln(-\ln a_w)$	(6)
Kunh	[15]	$X = \left(\dfrac{b_1}{\ln a_w}\right) + b_2$	(7)
Caurie	[9]	$X = \mathrm{Exp}(b_1 + b_2 a_w)$	(8)
Iglesias and Chirife	[5]	$X = b_1 + b_2 \left(\dfrac{a_w}{1 - a_w}\right)$	(9)
White and Eiring	[15]	$X = \dfrac{1}{(b_1 + b_2 a_w)}$	(10)
Peleg	[14]	$X = b_0 a_w^{b_1} + b_2 a_w^{b_3}$	(11)
DLP	[14]	$X = b_0 + b_1 x + b_2 x^2 + b_3 x^3$ $x = \ln(-\ln a_w)$	(12)
Polynomial	[11]	$X = b_0 + b_1 a_w + b_2 a_w^2 + b_3 a_w^3$	(13)
Weibull	[17]	$X = b_1 + \mathrm{Exp}^{b_2(1 - a_w^{b_3})}$	(14)

*It has been considered that the parameters of the empirical equations have a linear dependence with the temperature ($b_i T_{abs} + b_{i.1}$).

2.3.1 Parameter estimation and statistical analysis

The tool Curve Fitting of Matlab® R2017b (The MathWorks Inc., Natick, MA, USA) was used to identify the model parameters and calculate the 95% confidence intervals of parameters. The adjusted determination coefficient (R^2_{adj}) and the root mean square error (*RMSE*) were used as goodness-of-fit statistics.

2.4 Determination of the net isosteric heat of sorption

Sorption heats were calculated through the direct use of moisture sorption isotherms by applying the Clausius–Clapeyron equation (15). Estimations of net isosteric heat of sorption have been found in literature integrating Equation (15) between two temperatures (Eq.(16)). It is reported in literature that Riedel equation (17) adequately describes the influence of temperature on water activity. By combining Equations (16) and (17), another expression to estimate net isosteric heat of sorption may be considered (Eq. (18)) [7].

$$q_{sn} = -R\left[\frac{\partial(\ln a_w)}{\partial\left(\frac{1}{T}\right)}\right]_x \tag{15}$$

$$q_{sn} = R\left[\frac{T_1 T_2}{T_2 - T_1}\ln\frac{a_{w_2}}{a_{w_1}}\right] \tag{16}$$

$$\ln\left(\frac{a_{w_2}}{a_{w_1}}\right) = A_r \exp(-B_r W)\left(\frac{1}{T_1} - \frac{1}{T_2}\right) \tag{17}$$

$$q_{sn} = C_r \exp(-B_r W) \tag{18}$$

When A_r, B_r are constants of the riedel equation and C_r being *Ar·R*.

3. Results and Discussion

The Table 2 presents the four mathematical models with the best fit of the experimental data, considering the effect of temperature; the Weibull model could be considered the which best represent experimental data, since reached high value of the R^2_{ajs} coefficient 0.9021 and *RMSE* lower than 0.01 kg·kg^{-1} d.b; the others eigh mathematical models (Smith, Chung pfost, WhiteAndEiring, Caurie, IglesiasAndChirife, Kunh, Oswin y Peleg) they resulted with values of the r²adj coefficient below 0.8 and RMSE higher than 0.1 kg·kg^{-1} d.b.

The Figure 1. Presents the experimentals isotherms and the values obtained with the Weibull model at 25, 30 and 40 °C. The resulting isotherms are of the type III form, accord with classification of Brunauer [4]. The type III Isotherms obtained for roasted coffee beans, could be due to Maillard reactions in the roasting coffee process.

Table 2. Estimated model parameters and statist

Models	Parameters	Confidence Intervals 95%	R^2_{adj}	RMSE
Polynomial	$b_3 = 0.6772$	[0.5966, 0.7578]	0.8814	0,0060
	$b_{2.1} = 7.201 \times 10^{-3}$ K^{-1}	[4.972$\times10^{-3}$, 9.43$\times10^{-3}$]		
	$b_2 = -0.9754$	[-1.11, -0.8407]		
	$b_{1.1} = -4.753 \times 10^{-3}$ K^{-1}	[-6.883$\times10^{-3}$, -2.622$\times10^{-3}$]		
	$b_1 = 0.3964$	[0.3135, 0.4794]		
	$b_{0.1} = 9.488 \times 10^{-4}$ K^{-1}	[4.761$\times10^{-4}$, 1.421$\times10^{-3}$]		
	$b_0 = -0.0283$	[-0.0442, -0.0123]		
DLP	$b_3 = -0.0161$	[-0.0181, -0.0141]	0,8956	0,0056
	$b_{2.1} = -0.2968$	[-0.3238, -0.2699]		
	$b_2 = 9.784 \times 10^{-4}$ K^{-1}	[8.903$\times10^{-4}$, 1.066$\times10^{-3}$]		
	$b_1 = 5.263 \times 10^{-3}$	[3.739$\times10^{-3}$, 6.787$\times10^{-3}$]		
	$b_0 = 8.071 \times 10^{-5}$ K^{-1}	[7.718$\times10^{-5}$, 8.425$\times10^{-5}$]		
Weibull	$b_{3.1} = 4.071$	[1.731, 6.41]	0,9021	0,0055
	$b_3 = -9.532 \times 10^{-3}$ K^{-1}	[-0.01712, -1.941$\times10^{-3}$]		
	$b_{2.1} = -162.1$	[-230.3, -93.84]		
	$b_2 = 0.4704$	[0.2509, 0.69]		
	$b_{1.1} = -0.0746$	[-0.1066, -0.0426]		
	$b_1 = 3.25 \times 10^{-4}$ K^{-1}	[2.198$\times10^{-4}$, 4.301$\times10^{-4}$]		
GAB	$H_m = 3.24 \times 10^4$ kJ·mol^{-1}	[-1.849$\times10^5$, 2.498$\times10^5$]	0,661	0,0096
	$H_n = 4.50 \times 10^4$ kJ·mol^{-1}	[3.696$\times10^4$, 5.305$\times10^4$]		
	$C_0 = 1.983 \times 10^4$ K^{-1}	[-1.649$\times10^6$, 1.689$\times10^6$]		
	$K_0 = 1.032$ K^{-1}	[-2.372, 4.436]		
	$X_m = 0.01916$ (d.b)	[0.01597, 0.02235]		

Tabla 3. Estimation of the net isosteric heat of sorption with the Riedel equation

Model	Parameters	Confidence Intervals 95%	R^2_{adj}	RMSE
Riedel(x) = A_r*exp(-B_r*x)*0.00016066	$A_r = -7.578 \times 10^4$	[-2.261$\times10^{-5}$, 7.458$\times10^{-4}$]	0.629	0.071
	$B_r = 120.3$	[58.03, 182.5]		
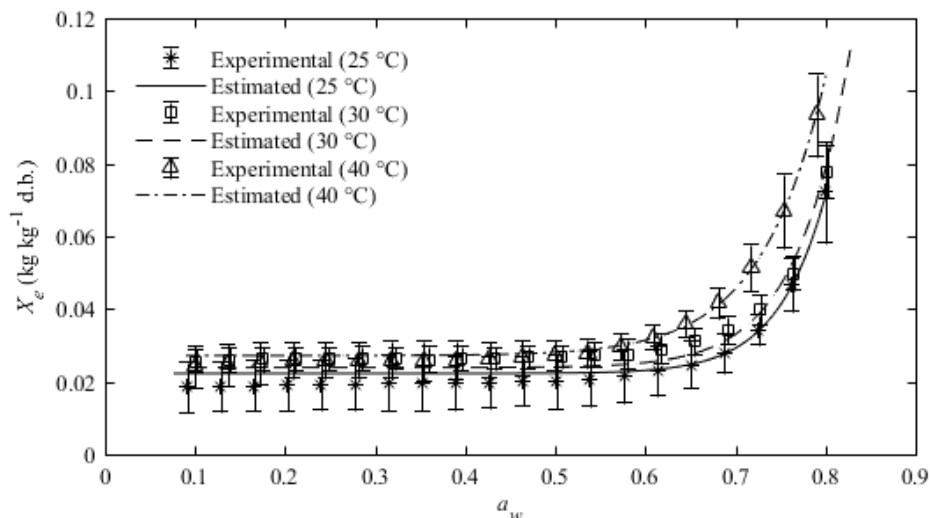
Fig 1. Experimentals Sorptiom Isotherms in roasted coffee beans at 25•C, 30•C y 40•

3.1. Net isosteric heat of sorption (q_{st})

The Table 3 presents the parameters and the fit coefficients for Riedel equation in the net isosteric heat of sorption estimated for roasted coffee beans. The results showed that the Reidel model not provide a good fit; besides this, in the Figure 2 showed just a similar trend but not a good fit.
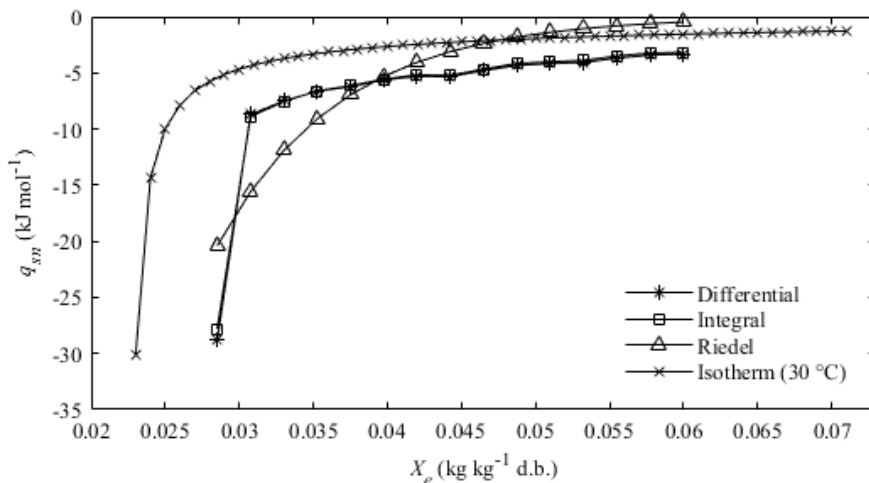
Fig 2. Variation of net isosteric heat of sorptiom diferecnial and integrated in roasted coffee beans

4. Conclusions

The equilibrium moisture content increases when temperature increases at constant water activity. The Weibull model was considered the best equation for describing sorption isotherms of roasted coffee beans. The isotherms behaved in a way typical of food rich in soluble components. The net isosteric heat of sorption increases with increments of equilibrium moisture content, indicating a strong bond energy. The trends of the sorption isotherms was similar to those reported for roasted coffee beans of others cultivars.

5. References

[1] Aguirre-Laredo, R. Y., Rodriguez-Hernandez, A. I., Velazquez, G., 2016. Modelling the effect of temperature on the water sorption isotherms of chitosan films. Food Science and Technology. DOI: http://dx.doi.org/10.1590/1678-457X.09416

[2] Bastıoğlu, A. Z., Koç, M., Ertekin, F. G., 2017. Moisture sorption isotherm of microencapsulated extra virgin olive oil by spray drying. Food Measure DOI 10.1007/s11694-017-9507-4

[3] Bon, J., Vaquiro, H. A., Mulet, A., 2012. Modeling sorption isotherms and isosteric heat of sorption of mango pulp CV. Tommy atkins. Biotecnología en el Sector Agropecuario y Agroindustrial. Vol 10 No. 2 (34 - 43). Consultado el 10 de septiembre de 2017. http://www.scielo.org.co/scielo.php?script=sci_arttext&pid=S1692-35612012000200005

[4] Brunauer, S., Deming, S. L., Deming, E. W., Teller, E., 1940. On a Theory of the van der Waals Adsorption of Gases. J. Am. Chem. Soc.. DOI: 10.1021/ja01864a025

[5] Caballero-Cerón, C., Serment-Moreno, V., Velazquez, G., Torres, J. A. Welti-Chanes, J., 2017. Hygroscopic properties and glass transition of dehydrated mango, apple and banana. J Food Sci Technol https://doi.org/10.1007/s13197-017-2963-3

[6] Ferreira de souza, J. S.; Vaquiro, H. A; Villa-Velez, A. H.; Polachini, C. T.; Telis-Romero, J.; International Journal of Food Engineering. 2014. DOI: 10.1515/ijfe-2014-0138

[7] García-Pérez, J. V., Cárcel, J. A., Clemente, G., Mulet, A., 2008. Water sorption isotherms for lemon peel at different temperatures and isosteric heats. Swiss Society of Food Science and Technology. Published by Elsevier Ltd. All rights reserved. doi:10.1016/j.lwt.2007.02.010

[8] Iaccheri, E., Laghi, L., Cevoli, C., Berardinelli, A., Ragni, L., Romani, S., Rocculi, P., Different analytical approaches for the study of water features in green and roasted coffee beans. Journal of Food Engineering. https://doi.org/10.1016/j.jfoodeng.2014.08.016

[9] Khawas, P., Chandra, D. S., 2016. Moisture sorption isotherm of underutilized culinary banana flour and its antioxidant stability during storage. Journal of Food Processing and Preservation ISSN 1745-4549. doi:10.1111/jfpp.13087

[10] Machado, B. F., Corrêa, P. C., Horta de Oliveira, Cecon, P. R., Ferreira, S. F., 2017. Kinetic modeling of water sorption by roasted and ground coffee. Acta Scientiarum

[11] Mousa, W., Mohamad, F., Jinap, S. G., Mohd, H., Radu, S., 2012. Sorption isotherms and isosteric heats of sorption of Malaysian paddy. J Food Sci Technol DOI 10.1007/s13197-012-0799-4

[12] SCAA - Specialty Coffee Association of America. 2015. SCAA Protocols cupping specialty coffee.Consultado el 5 de enero de 2018. http://scaa.org/?page=resources&d=cupping-protocols

[13] Shigehisa, T., Inoue, T., Kumagai, H., 2015. Matematical model of water sorption isotherms of UBC. Fuel Processing Technology. DOI http://dx.doi.org/10.1016/j.fuproc.2014.11.023

[14] Shittu, T. A., Idowu-Adebayo, F., Adedokun, I. I., Alade, O., 2015. Water vapor adsorption characteristics of starch-albumen powder and rheological behavior of its paste. Nigerian Food Journal. DOI: http://dx.doi.org/10.1016/j.nifoj.2015.04.014

[15] Sormoli, M. E., Langrish, T. A.G., 2015. Moisture sorption isotherms and net isosteric heat of sorption for spray-dried pure orange juice poder. LWT - Food Science and Technology. http://dx.doi.org/10.1016/j.lwt.2014.09.064

[16] Staudt, P. B., Kechinski, C. P., Tessaro. I. C., Marczak, L. D. F., Soares, R de P., Cardozo, N. S. M., 2013. A new method for predicting sorption isotherms at different temperatures using the BET model. Journal of Food Engineering. DOI http://dx.doi.org/10.1016/j.jfoodeng.2012.07.016

[17] Uribe, L., Vega-Gálvez, A., Di Scala, K., Oyanadel, R., Torrico, S. J., Miranda, M., 2011. Characteristics of Convective Drying of Pepino Fruit *(Solanum muricatum* Ait.): Application of Weibull Distribution. Food Bioprocess Technol. DOI 10.1007/s11947-009-0230-y

Modeling the Water Sorption Isotherms of *Warionia Saharae* and determination of sorption heats and drying kinetics

Fedol, A. [a*]; Cheriti, A.[a]

[a]* Faculty of Medicine, Facmed-univ-oran1,Oran ,31000,Algeria

[a]* Department of Chemistry, Kasdi Merbah University , Ouargla, 30000, Algeria

[a] Phytochemistry & Organic Synthesis Laboratory, Faculty of Medicine, UTMB, Bechar, 08000, Algeria.

*E-mail of the corresponding author: amelfedol@yahoo.fr

Abstract

The hygroscopic equilibrium of Warionia saharae was studied, which allowed getting an idea of the equilibrium water content relative to a given humidity. The results of this study made it possible to have the sorption curves. The results of this study made it possible to obtain the sorption curves necessary for know the storage conditions of the plant and the study of its drying kinetics. The static gravimetric method was used to determine sorption isotherms of Warionia saharae leaves at 30and 40 ∘C and in the range of water activity varying from 0.063 to 0.898. The Gab, Peleg models was found to be the most suitable for describing the sorption curves. The isosteric heat calculated by applying the Clausius–Clapeyron equation .The desorption isosteric heat was higher than the isosteric heat of adsorption and both decreased continuously with increasing of the equilibrium moisture content. The experimental results obtained allowed us to determine the temporal evolution of the drying kinetics as a function of the moisture content. The curve of the evolution of the water content as a function of time shows the absence of the phases product temperature and constant drying rate

Keywords: *Sorption isotherm, isosteric heats, modelling, kinetics, Warionia saharae.*

1. Introduction

The Warionia saharae, which belongs to the important composite's family, is an endemic species of North Africa, characterized by a discerning odour [1]. The leaves of Warionia saharae are used in traditional medicine to treat inflammatory diseases, gastrointestinal disorders and against epileptic crisis [2,3]. Crude extracts of this plant showed anti-inflammatory and cytotoxic activities against a cancer cell line (KB cells) [4,5]. The methanolic soluble fraction of the dichloromethane extract of Warionia saharae afforded cytotoxic and anti-inflammatory sesquiterpene lactones [3-6], while hexanoic extract showed the presence of several hydrocar bon acid derivatives [7].Like many other herbs, is highly seasonal in nature. In order to preserve this seasonal and highly perishable plant and make them available to consumers all year round at low prices, it is subjected to post harvest technological treatments [8].Several process technologies have been employed on an industrial scale to preserve food products; the major ones are canning, freezing, and dehydration. Among these, drying is especially suited for developing countries with poorly established low-temperature and thermal processing facilities. It offers a highly effective and practical means of preservation to reduce postharvest losses and offset the shortages in supply. Drying is a simple process of moisture removal from a product in order to reach the desired moisture content and is an energy intensive operation. The prime objective of drying apart from extended storage life can also be quality enhancement, ease of handling, further processing and sanitation and is probably the oldest method of food preservation practiced by humankind [9].In the literature several methods are mentioned to analyze the drying of hygroscopic products (theoretical, empirical and semiempirical).The empirical models of drying show a direct relationship between average moisture content and drying time.

2. Materials and Methods

The leaves of *Warionia saharae*, used for the drying experiments were collected from the region of southwest Algeria (Jebel Anter, wilaya of Bechar). In the period of May 2012.The moisture content was measured and the equilibrium moisture contents of *Warionia* were determined at temperatures of 30 and 40 ◦C over a water activity range of 0.063–0.89 using the static gravimetric method. For prevent destroy plant chemical components like essential oils, the leaves of *Warionia saharae*, were drying in shade.

2.1. Equilibrium moisture content determination

The desorption equilibrium moisture contents of Warionia saharae leaves were determined at temperatures of 30 and 40 ◦C over using the static gravimetric method. This method

involves the use of saturated salt solutions to maintain constant relative humidity (aw) in enclosed still moist air at a certain temperature to obtain the complete sorption isotherms. The mass transfer between the product and the ambient atmosphere was assured by natural diffusion of the water vapor and the water activity of the product equals the relative humidity of the atmosphere at equilibrium conditions. Seven saturated salt solutions (KOH, KF, K2CO3, NaNO3, NaCl, KCl and BaCl2).

3. Modeling of the drying curves

Four models were used to describe the sorption isotherms (table.1). The goodness of fit for each model can be evaluated based on the relative percent error (P), which compares the absolute difference between the predicted moisture contents with the experimental moisture contents. Relative percent errors values lower than 10 % indicate a good fit [11].

Table 1 .Mathematical models applied to drying curve

Model name	Formula
Peleg	$Xeq = A(aw)^C + B(aw)^D$
Gab	$Xeq = \dfrac{ABC\, a_w}{(1 - Ca_w)(1 - Ca_w + CBa_w)}$
Caurie	$Xeq = \exp(a + b * x)$
Bet modifie	$Xeq = \dfrac{(A + B.T)Ca_w}{(1 - a_w)(1 - a_w + Ca_w)}$

Xeq, moisture content, % (kg/kg d.b.); aw, water activity (decimal); t, absolute temperature a,b,c and d constants specific to individual equations [12].

4. Result and discussion

4.1. Sorption isotherms

In this study, models were used in predicting the sorption isotherms of *Warionia leaves*. Based on the statistical analysis, average relative error and standard error estimation were used to select the best model describing the shade drying curves of *Warionia saharae* leaves. Peleg and Gab models has a correlation coefficient value of 0.998, which is higher than Bet and Caurie. This means that Peleg and Gab models are the most suitable models for describing the relation between equilibrium moisture content and water activity. It was observed also that the moisture content decreases with time and drying rate increases with increasing temperature.

Table 2. Modeling parameters of Warionia Saharea

Parameters	T °C	Table 2.a. Estimated parameters of the different models fitted to the desorption data				Table2.b.Estimated parameters of the different models fitted to the adsorption			
		Peleg	Gab	Caurie	Bet modifie	Peleg	Gab	Caurie	Bet modifie
A	30	1.880	0.085	-5.119	-0.015	0.122	0.085	-4.940	-1.50E+2
	40	1.666	0.070	-6.003	-0.015	0.833	0.063	-4.663	-1.55E+2
B	30	0,101	0.0143	5.510	0.498	0.205	19.59	-5.133	0.498
	40	8.073	2.5E+001	6.453	0.498	6.186	31.74	4.425	0.4.984
C	30	0.2706	1.004	-	8.115	1.325	0.986	-	4.10E+1
	40	0.144	1.024	-	3.402	0.104	0.982	-	7.81E+1
D	30	0.5380	-	-	-	6.650	-	-	-
	40	0.3669	-	-	-	0.243	-	-	-
r	30	0.996	0.998	0.968	0.998	0,988	0,992	0.979	0,989
	40	0.998	0.997	0.983	0.994	0.987	0.980	0.966	0.978
P(%)	30	8.605	3,622	38.085	3.616	17,220	13,945	44,728	14,922
	40	3.044	8.204	36.856	19.731	10,227	10,620	31.183	12.362
SEE	30	0,005	0,002	0,037	0,001	0,030	0,034	0,006	0,047
	40	0.001	0.001	0.032	0.005	0,001	0.001	0.019	0.002

P is average relative error (Eq. 1); *SEE*: is standard error estimation (Eq. 2); *r* is correlation coefficient; *A, B, C, D*are parameters of the equations; *T* is temperature (°C).

$$P = \frac{100}{N} \sum_{i=1}^{N} \frac{Xe_{i,exp} - Xe_{i,pre}}{Xe_{i,exp}} \quad (1)$$

$$SEE = \sqrt{\sum_{i=1}^{N} \frac{(Xe_{i,exp} - Xe_{i,pre})^2}{N - n_p}} \quad (2)$$

4.2.Net isosteric heat of sorption

The isosteric heat of sorption, were calculated from the equilibrium data at different temperatures using The Clausius –Clapyron equation .The curve shows that the heat of desorption decreased with increase in moisture content. The decrease in the isosteric heat with the increase in sorbed water content may be attributed to the fact that sorption initially occurs on the most active sites such as hydrophilic polar groups giving rise to the greatest interaction energy. With increase in the moisture content, as these sites become occupied, sorption occurs on the less active sites viz., peptide bonds or hydrophobic hydration sites resulting in lower heats of sorption [13,14].The heat of desorption is greater than that of

adsorption at low moisture contents for all the samples studied. This indicates that energy required in the desorption process is greater than that in the adsorption process [15]. The isosteric heats of desorption and adsorption of water in Warionia saharae leaves can be expressed mathematically as a power function of moisture content(3and 4):

$$Q_{st(adsorption)} = 137.48 - 17.839X_{eq} + 78.138X_{eq}^2 - 0.111X_{eq}^3 \qquad (3)$$

$$Q_{st(desorption)} = 236.98 - 29.312X_{eq} + 1.226X_{eq}^2 - 0.016X_{eq}^3 \qquad (4)$$
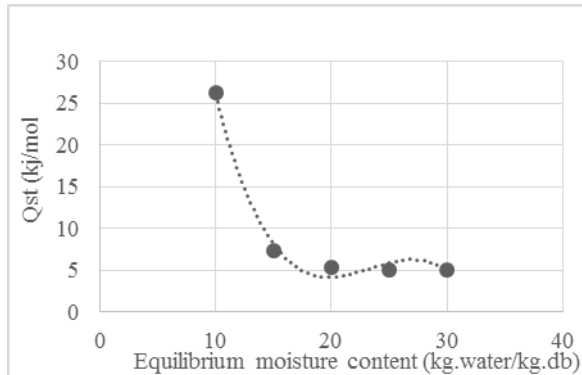
Fig.1 Adsorption isosteric heat
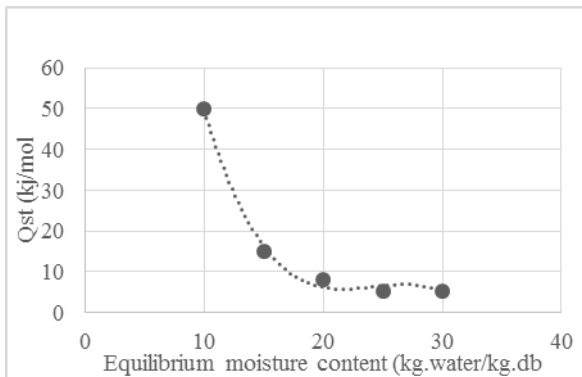
Fig .2 Desorption isosteric heat

4.3. Drying rate:

As seen in figure 5 the drying rate decrease rapidly in the first period of drying and slowly as drying progresses .The constant rate period is absent in the drying curves of *Warionia saharae*. Similar results were obtained for all agricultures and medicinal products [16]. These results can be explained by diffusion phenomena in the solid. This is a complex mechanism involving water in both liquid and vapour states, which is very often characterised by a so-called "effective diffusivity" [17].
The dimensionless drying rate was determined by the relation (3) :

$$f = \frac{-\left(\frac{dX}{dt}\right)_t}{\left(\frac{dX}{dt}\right)_0} \qquad (3)$$

Where , $\left(\frac{dX}{dt}\right)_0$,the initial drying rate .

The figure 3and 4 illustrate de variation of moisture ratio as a function of drying time. It is clear from these figures that the moisture content has an exponential decrease; it decreases continuously with the drying time.To determine the ratios of moisture during drying we used the following expression (4):

$$X^* = \frac{X(t)-Xeq}{Xi-Xeq} \qquad (4)$$

Where
X*: moisture ratio; X(t) : water content of product (% d.b.); X_i: initial water content of the product (% d.b.); X_{eq} : equilibrium water content of the product (%d.b.).
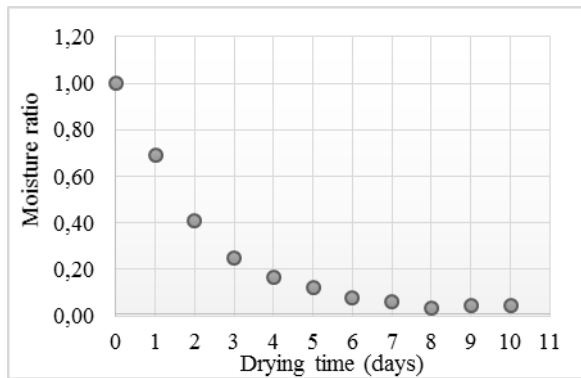
Fig.3 moisture ratio as a function of drying time
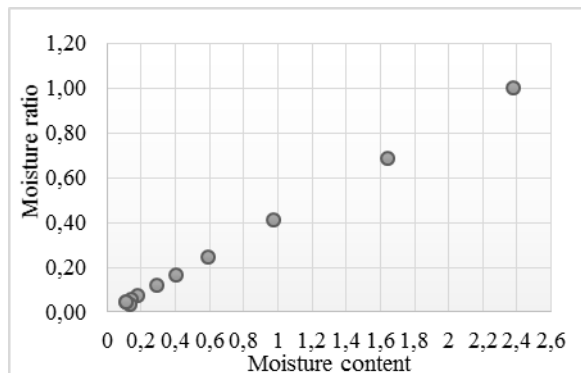
Fig .4 moisture ratio as a function of moisture content
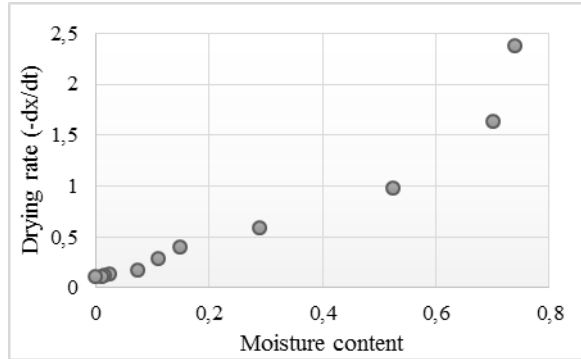
Fig.5 Drying rate as a function of drying time
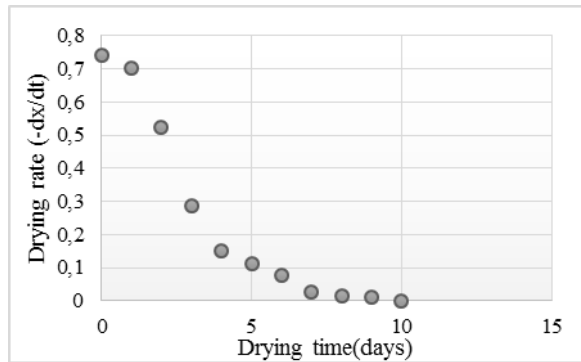
Fig.6 Drying rate as a function of moisture content

5. Conclusions

The sorption isotherms of Warionia saharae leaves were determined with the static gravimetric method .Peleg and Gab models were found the most suitable to describe the relationship between equilibrium moisture content and water activity .the isosteric heat of sorption were using the Clausius–Clapeyron equation. The heats of sorption increased with decreasing moisture content. The drying rate was characterized by the absence of the period (0) and (1) which corresponds to the period of drying at increasing rate and at a constant rate respectively and the presence of the single period of the decreasing rate. That have been observed in the drying of different fruits and vegetables. The modelling of kinetics curves will be established in our next paper.

6. References

[1] Bonnet and Maurry, P. Etude sur le *Warionia Saharae* . Benth & coss.Assoc. Fr. Avanc. Sc. Congrès de Paris 1889.

[2] Bellakhdar,J. La pharmacopée marocaine traditionnelle médecine arabe ancienne et savoir populaire. ibis press 1997,208.

[3] Bellakhdar , J.; Baayaoui ,A.; Kazdari ,A ; Marechal , J. Al Biruniya 1986, 3, 7-50.

[4] Hilmi ,F.; Sticher ,O .; Heilmann . Nat Prod 2002 , 65, 523-526.

[5] Hilmi ,F.; Sticher, O .; Heilmann .Planta Med 2003, 69 , 462-464.

[6] Hilmi, F.; Gertsch, J.;Bremner ,P.;Valovic ,S.;Heinrich ,M.; Sticher ,O .; Heilmann.Bioorg Med Chem 2003, 11, 3659-3663.

[7] Essaqui , A. ; Elamrani, A. ;Benaissa ,M. ; Rodrigues ,A.I. ;Yoongho, L. Essent Oil-Bearing Plants 2004 , 7(3), 250-254.

[8] Yurtsever , S .Mathematical modeling and evaluation of microwave drying kinetics of mint(*menthe spicata L*). Applied science 2005, 5(7),1266-1274.

[9] Mujumdar, A.S.2.Handbook of Industrial drying, Taylor and Francis group, U.K.2007

[10] Paulo , C. C.; Evandro d. C. M.; Rocinely, P. d. .Mathematical modeling of the drying kinetics of the leaves of lemon grass (Cymbopogon citratus Stapf) and its effects on quality. IDESIA 2014 ,32,(4) 43-56 .

[11] Mc Laughlin, C. P.; MAGEE, T. R. A. The determination of sorption isotherm and the isosteric heats of sorption for potatoes. Food Engineering, v 1998. 35(3), 267-280.

[12] Yu, L., Mazza ; Jayas ,D.S. Moisture sorption of characteristics of freeze-dried, osmo-dried and osmo-air dried cherries. Transactions of the ASAE 1999, 42(1): 141–147.

[13] Delgado, A. E.; Sun, D.-W. Desorption isotherms for cooked and cured beef and pork .Food Engineering 2002B, 51, 163–170.

[14] Jayendra Kumar, A.; Singh, R.R.B.; Patil, G.R.; Patel, A.A. Effect of temperature on moisture desorption isotherms of kheer 2005, LWT, 38, 303–310.

[15] Wang, N.; Brennan, J. G. Moisture sorption isotherm characteristics of potatoes at four temperatures. Food Engineering 1991, 14, 269–282.

[16] Kouhila, M. Etude expérimentale et théorique de cinétiques des séchages convectifs partiellement solaires des plantes médicinales et aromatiques (Menthe, Verveine, Sauge et Eucalyptus) de la région de Marrakech (PhD Thesis) Universite Cadi Ayyad de Marrakech, Morocco 2001, 170.

[17] Al Hodali, R. Numerical simulation of an agricultural foodstuffs drying unit using solar energy and adsorption process (PhD Thesis). Université Libre de Bruxelles. Belgium 1997.

Hybrid cylinder dryer for the drying of sheet-form materials with hot air

Kim, S.I.[a*]; Oh, S.H.[a]; Chun, W.P.[a]; Park, K.H.[a]; Yu, B.H[a,b]

[a] Energy Saving Technologies lab. Department of Energy Efficiency and Materials. Korea Institute of Energy Research, Daejeon, Republic of Korea (ROK)

[b] Energy Conversion System lab. Department of Mechanical Engineering. Chungnam National University, Daejeon, Republic of Korea (ROK)

*E-mail of the corresponding author: praygod@kier.re.kr

Abstract

In this paper, we introduce a novel energy-efficient dryer that uses hot air as a combined heating method of heat conduction and convection heat transfer. The dryer consisting of rotary cylinders and arched jackets is structurally different from conventional dryers. We designed and built a hybrid 4-cylinder dryer for sheet-form materials. The energy consumption to evaporate unit water is about 930 kcal/kg moisture from the experimental results of a hybrid 4-cylinder dryer. The hybrid 4-cylinders dryer has a compact structure with about 1/3 of the size of a conventional dryer for the drying of sheet-form materials.

Keywords: Dryer; Hot Air; Sheet-form; Energy Efficiency; Hybrid

1. Introduction

Research and development (R&D) in industrial drying systems has been focused primarily on technological advances that improve drying efficiency and lower energy costs. According to the survey, the annual energy consumption of domestic industrial dryers is about 7% of the total industrial energy consumption. Since the energy consumed in the drying process for textile/paper is about 30% to 50% of the total energy consumption, it is urgent to increase the energy efficiency of dryers for textile/paper. Domestic fabrication technology for dryers is at the level of advanced countries, but the domestic core technologies such as system design, control technology, and post-processing are about 70% compared to advanced countries and still depend on advanced technology. It is expected that the development of high energy efficiency and commercialization technology in the domestic drying field have a significant effect from the viewpoint of energy saving.

This study proposes a new type of a dryer with high energy efficiency using hot air. The dryer consisting of rotary cylinders and arched jackets is structurally different from conventional textile/paper dryers. The rotary cylinder in contact with the sheet-form materials is thermally optimized through numerical methods. The arched jacket allows the hot air coming from the rotary cylinder to come into contact with the sheet-form materials. The energy consumption to evaporate unit moisture for the proposed dryer is about 930 kcal/kg water from the experimental results of a hybrid 4-cylinder dryer.

2. Drying wet materials and numerical analysis

2.1. Drying wet materials

The drying characteristics of drying wet materials may be determined by a drying curve. Figure 1 shows the drying curves of various textile samples. As shown in Fig. 1, the change in the moisture content of the textile is apparent, but the first and second falling drying-rate period are not clearly distinguished. The feature of the drying curves of the textiles in which the falling drying-rate period is not clearly shown is important in the design of a dryer.

2.2. Thermal design of a rotary cylinder

A rotary cylinder in this study uses hot air differently from a conventional cylinder using steam and has fins on the cylinder inner surface for the purpose of improving the heat transfer. Heat flowing into the center of the cylinder is conducted to the cylinder outer surface, and the heat is transferred to the drying wet material in contact with the cylinder outer surface. In this study, numerical analysis is used to calculate the heat transfer

according to the number and shape of fins. For the shape design of fins, case studies are carried out under the same conditions as Table 1. The optimal shape of the cylinder selected in this study is shown in Fig. 3. The cross-sectional area of the cylinder decreases along the direction of hot air flow and the fin is wavy shape.
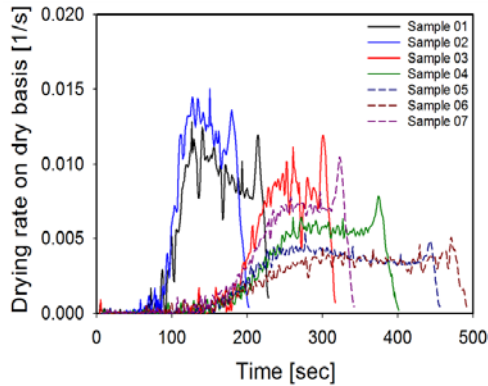
Fig. 1 Drying curves of textile samples.
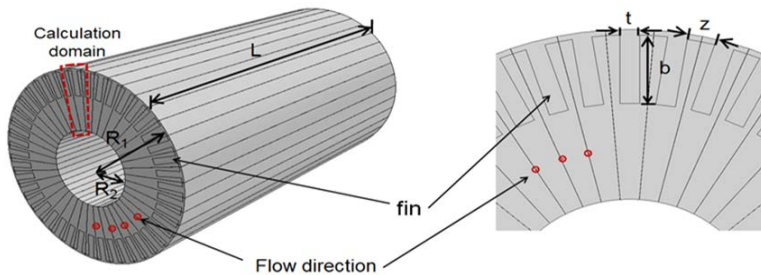
Fig. 2 Rotary cylinder and simulation domain.

Table 1. Constraints for simulation of a rotary cylinder

Inlet temperature of hot air	180 ℃
Outer radius of cylinder	0.25 m
Inner radius of cylinder	0.125 m
Length of cylinder	2.0 m
Hot air velocity	4.5 m/s
Fin material	Aluminium 6063-T5
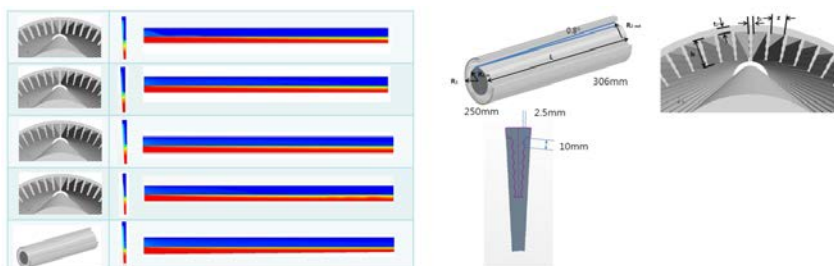
Fig. 3 Temperature variation according to the flow direction of hot air in single fin.

2.3. Arched jacket

The hot air exhausted through the cylinder is brought into contact with the drying wet material in the arched jacket. When designing an arched jacket, it is important to have uniform velocity distribution in the direction perpendicular to the flow in terms of drying quality. The numerical analysis approach is used to design the arched jacket. Figure 4 (a) shows that the flow tends to lean toward one side of the jacket in the original design. In order to make the flow of hot air uniform, numerical analysis is conducted to introduce guide vanes and flow analysis according to the change of guide vane shape. The numerical results are shown in Fig. 4 (b).

(a)   *(b)*
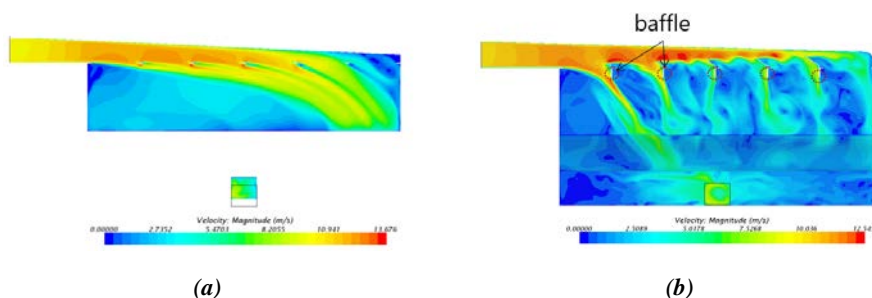
Fig. 4 Velocity distribution in the arched jacket.

3. Results and discussion

3.1. Dryer with 4-cylinders

Based on the results from numerical analysis, the dryer with 4-cylinders is fabricated as shown in Fig 5. The dryer has four rotary cylinders, a burner, blowers and other elements. In addition, the dryer is configured to facilitate the management of the apparatus. The hot

air flow was controlled for the purpose of minimizing the moisture content deviation of drying products in the horizontal direction after drying, and the active control tensioner was installed to reduce the tension acting on the drying wet materials due to the cylinders.

Fig. 5 Dryer with 4-cylinders

3.2. Temperautre deviation of the drying system

In this study, the deviation of hot air temperature means the difference between the values of the measured temperature over a certain period of time. The temperature deviation is to confirm the temperature uniformity of the hot air supplied to the drying system and the basic system stability such as the energy efficiency evaluation of the dryer and the temperature stability of the system. The test is performed by measuring the temperature at the inlet of the cylinder for 1 hour, and checking whether the temperature deviation between the maximum temperature and the minimum temperature is within $\pm 5\,^\circ$ C. In the test results, since the temperature deviation is $\pm 2.9\,^\circ$ C, it can be judged that the temperature stability of the system is excellent.

3.3. Drying efficiency

Drying efficiency is used to evaluate the energy savings of a dryer. The energy saving of the dryer is compared with the energy consumption of a conventional dryer and the developed dryer. a conventional dryer is a through-flow drying method in which hot air hits onto the surface of textiles. Table 2 shows experimental conditions and drying efficiency. The initial moisture content of the textiles is about 55 w.t% and the drying capacity is 200 kg/hr. Energy consumption is measured using an integrating wattmeter and a gas meter. The drying efficiency is defined as Eq. (1).

Table 2. Comparison of drying efficiency

	Existing dryer	Novel dryer
Initial M.C	55 w.t%(w.b)	
Final M.C	3 w.t%(w.b)	
Hot air temp.	180 ℃	
Drying capacity	200 kg/hr	
Drying efficiency	30.4 %	58.1 %

$$\varepsilon = \frac{Latent\ heat\ of\ evaporated\ moisture}{Total\ energy\ of\ heat\ and\ electricity} \times 100\ [\%] \tag{1}$$

As shown in Table 2, the drying efficiency of the developed dryer compared to the conventional dryer shows a great difference. It can be seen that the developed dryer in this study has a drying efficiency twice as high as that of the conventional dryer. The energy consumption to evaporate unit moisture is about 930 kcal/kg water from the experimental results of the hybrid dryer. The dryer has a compact structure with about 1/3 of the size of the conventional hot air dryer.

4.   Conclusions

The purpose of this study is to develop a dryer for sheet-form materials with high energy efficiency. The novel dryer is a cylinder type using hot air. While a conventional dryer using only direct heating or indirect heating, the proposed dryer adopts a multiple heating system. The developed dryer dramatically increased the drying efficiency and is a unique device that differentiates from the conventional dryer in the usage of the heat source. In order to utilize a combined heating method of direct heating and indirect heating, precise analysis and complicated design should be performed. We have successfully developed the 200kg/hr dryer with 4-cylinders through R&D. The energy consumption to evaporate unit water is about 930 kcal/kg water from the experimental results of a hybrid dryer.

5.   Acknowledgements

Thermodynamic properties and moisture sorption isotherms of two pharmaceutical compounds

Zammouri, A.[a]*; Ben Zid, M.[b]; Kechaou, N.[c]; Boudhrioua Mihoubi, N.[b]

[a] Laboratoire de Biotechnologie et Valorisation des Bio-Géo Ressources, LR11ES31. Institut Supérieur de Biotechnologie de Sidi Thabet, Univ. Manouba, BP-66, 2020 Ariana-Tunis, Tunisie, Tel: +21671537040; Fax: +21671537044.

[b] Laboratoire de Physiopathologies, Alimentation et Biomolécules, LR17ES03. Institut Supérieur de Biotechnologie de Sidi Thabet, Univ. Manouba, BP-66, 2020 Ariana-Tunis, Tunisie, Tel: +21671537040; Fax: +21671537044.

[c] Groupe de Recherche en Génie des Procédés Agroalimentaires, Ecole Nationale d'Ingénieurs de Sfax, Université de Sfax, BP 1173 3038, Sfax, Tunisie.

* E-mail of the corresponding author：amel.zammouri@gmail.com

Abstract

This investigation examines and compares the water sorption isotherms and the thermodynamic properties of two pharmaceutical preparations (Hypril and Azix) intended to be manufactured with the same process plant and equipment. The moisture equilibrium isotherms were determined at 50, 60 and 70 °C using a gravimetric technique. Five isotherm models were explored for their fitting to the experimental data. Azix showed sigmoid type II isotherms while Hypril showed type III isotherms according to the BET classification. All investigated models fitted well the water sorption isotherms of Hypril. By contrast, only GAB and Adam and Shove equations gave appropriate fit to the experimental data of Azix. For both formulations, the isosteric heat and the differential entropy decreased sharply with the increase of equilibrium moisture content to minimum values and thereafter remain constant. In the case of Azix, the integral enthalpy decreased with equilibrium moisture content while the integral entropy increased until reaching a constant value. Contrariwise, Hypril showed decreasing of the integral enthalpy and entropy with the equilibrium moisture content.

Keywords: sorption isotherm, enthalpy, entropy, spreading pressure, pharmaceutical formulations

1. Introduction

Tablets are the most popular advantageous drug dosage form used today. They ensure best protection to the drug against temperature, humidity, oxygen, light and stress during transportation. They present also the best-combined properties of chemical, mechanical and microbiological stability of all the oral form. The manufacture of tablets involved several steps: mixing of therapeutic agents with exipients, granulation of the mixed powders, mixing the obtained granules with other excipients such as lubricants and finally compression into tablets. Wet granulation is a widely applied process in the pharmaceutical industry used to improve powder flow characteristics thereby enhancing the compressibility of the drug. In a typical wet granulation, the water is initially added to the mixed powders to form large agglomerates which will be dehydrated in order to remove water. The drying operation is a crucial step, usually accomplished in fluid-bed dryers, whereby a warmed and low humidity air passed through the agglomerates via a gill plate. Water interacts with pharmaceutical solids not only at this level but also at all stages of manufacture. Therefore, water–powder interaction is a major factor in the formulation, processing, and performance of solid dosage forms. Determination of sorption isotherms of pharmaceutical preparations and deduced thermodynamic properties allows the control of corresponding drying process and modeling of their drying kinetics.

1. Material and Methods

Azix (Azithromycine- 500 mg, Anhydrous Dibasic Calcium Phosphate, Pregelatinised starch, Sodium starch glycolate, Magnesium stearate) and Hypril (Enalapril maleate-20 mg, Hydrochlorothiazid -12, 5 mg , Sodium bicarbonate, Lactose Monohydrate, Maize starch, Microcrystalline cellulose, Sodium starch glycolate, Magnesium stearate) preparations are provided from Pharmaghreb® company (Tunisia).

2.1. Determination of sorption isotherms

The experimental sorption isotherms of Azix and Hypril preparations were established using the static gravimetric method. The experimental setup consisted of 11 air-sealed glass jars provided with perforated supports in which triplicate samples weighing 0.1 g ($\pm$ 0.0001g) were exposed to the humid atmospheres. Sulfuric acid solutions of known concentration were used to reach 0.06 to 0.95 water activity values. The prepared glass jars were then placed in temperature controlled cabinets maintained at 50, 60 and 70 °C $\pm$ 1 C. Each sample was weighed at the beginning of experiment and at intervals of 24 h until constant mass was reached. The equilibrium moisture content was determined according to the AOAC official method [1].

2.2. Sorption models and statistical analyses

The equilibrium moisture data were fitted with five mathematical models shown in Table 1. The nonlinear regression analysis (MATLAB®) was used to estimate the constants of the models from the experimental results. To evaluate the goodness of fit of each equation, the coefficient of determination R^2 , the adjusted R^2, the roots mean squared error (RMSE) and the sum of squares due to error (SSE) were determined by using the following equations [2] (Eqs 1 to 6):

The coefficient of determination R^2 measures the model adequacy , $(0 \leq R^2 \leq 1)$:

$$R^2 = \frac{explained\ variation\ of\ y}{total\ variation\ of\ y} = \frac{SSR}{SST} \quad (1)$$

SSR is the regression sum of squares which reflects the amount of variation in y explained by the model:

$$SSR = \sum_{i=1}^{n}(\hat{y}_i - \bar{y})^2 \quad (2)$$

SST is the total sum of squares:
$$SST = \sum_{i=1}^{n}(y_i - \bar{y})^2 \quad (3)$$

Where y_i is the equilibrium moisture content at observation i, $\bar{y}$ is the mean value of y_i of the n observations and $\hat{y}_i$ is the value of y estimated from the regression model for observation i.

The corrected or adjusted $\bar{R}^2$:

$$\bar{R}^2 = 1 - (1 - R^2)\frac{(n-1)}{(n-k)} \quad (4)$$

Where n is the total number of observations and k is the number of model parameters.
$$RMSE = \left(\frac{SSE}{n-k}\right)^{1/2} \quad (5)$$

Where SSE is the error sum of squares or sum of the residuals which reflects the variation about the regression line:
$$SSE = \sum_{i=1}^{n}(y_i - \hat{y}_i)^2 \quad (6)$$

2.3. Calculation of thermodynamic properties

The net isosteric heat (net enthalpy) of sorption (q_{st}) was obtained from the moisture sorption data using the Clausius-Clapeyron equation [3] :

$$\frac{d(ln a_w)}{d\left(\frac{1}{T}\right)} = -\left(\frac{q_{st}}{R}\right) \quad (7)$$

In which $q_{st} = Q_s - \Delta H_{vap}$ where a_w is the water activity, q_{st} is the net isosteric heat of sorption (kJ mol^{-1}), Q_{st} is the isosteric heat of sorption (kJ mol^{-1}), ΔH_{vap} is the heat of

vaporisation (kJ mol^{-1} water), R is the universal gas constant (8.314 J mol^{-1} K^{-1}) and T is the absolute temperature (K). The value of q_{st} was calculated from the slope of the plot between values of $\ln(a_w)$ and 1/T at constant moisture content. The differential entropy (S_d) of sorption can be calculated from Gibbs–Helmholtz equation as follows:

$$S_d = \frac{q_{st} - G}{T} \qquad (8)$$

Where G is the Free Gibbs energy calculated as:

$$G = RT\ln(a_w) \qquad (9)$$

Substituting Eq. (9) into Eq. (8), and after rearranging, the final form is :

$$-\ln(a_w)|_W = \frac{-q_{st}}{RT} + \frac{S_d}{R} \qquad (10)$$

By plotting $\ln(a_w)$ versus 1/T, for a constant moisture content (W), the S_d can be determined from the intercept (S_d/R). The S_d values at different moisture contents are found from the determination of the relation between S_d and moisture content. The net integral enthalpy, q_{eq} is an integral molar quantity and is calculated in a similar manner to the isosteric heat of sorption but at constant spreading pressure instead of constant moisture content .

$$q_{eq} = -R\left[\frac{d(\ln a_w)}{d(1/T)}\right]_\phi \qquad (11)$$

$\ln(aw)$ was plotted against 1/T at constant spreading pressure. The net integral enthalpy was determined from the slope of the straight line and plotted against moisture content. The net integral entropy of sorbed water, ΔS_{eq}, is given as:

$$\Delta S_{eq} = -q_{eq}/T - R\ln(a_w)^* \qquad (12)$$

$(a_w)^*$ is the geometric mean water activity obtained at different temperatures and at constant spreading pressures.

3. Results and Discussion

3.1. Water sorption isotherms

The moisture sorption isotherms of Azix and Hypril at different temperatures are displayed in Fig. 1.
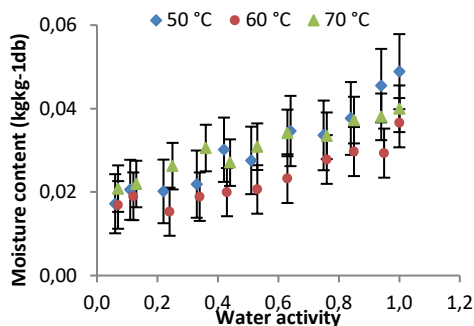
Fig. 1a Experimental moisture sorption isotherms of Azix at 50 °C, 60 °C ,70 °C
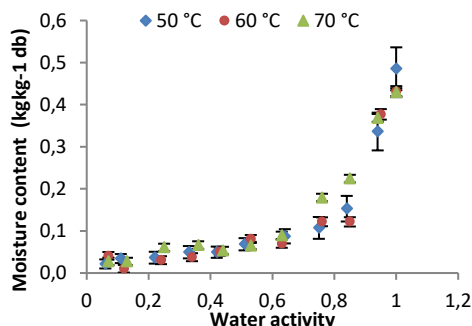
Fig. 1b Experimental moisture sorption isotherms of Hypril at 50 °C, 60 °C ,70 °C

The moisture sorption isotherms of Azix showed moisture levels from 1.5% to approximately 5% over water activity range from 0.06 to 0.95 at the examined temperatures (Fig 1.a). These findings are in line with those of [4] who reported the same trend for spray- dried pure azithromycin, the active ingredient of Azix preparation. Indeed, the moisture behavior of pure azithromycin determined using a dynamic vapour sorption system showed 6 % of water absorbed at relative humidity of 90%. Hypril exhibited the same moisture levels as Azix over water activity range from 0.06 to 0.44. Thereafter, the level of adsorbed water increased sharply from 7% to approximately 50% (Fig1.b) . This behavior could be ascribed to the degradation of Enalapril maleate in the presence of lactose and magnesium stearate at very high humidities and temperatures. Enalapril maleate powder is stable under moderate heat and humidity (40°C - 75% RH) [5]. However, when it is prepared in tablet formulations by wet granulation with lactose, starch and magnesium stearate enalapril maleate would degrade to form a diketopiperazine by dehydration and the diacid by hydrolysis. These degradates increase with temperature.

Inspection of Fig. 1a and Fig. 1b indicates that there is no significant effect of temperature on the sorption isotherms of Azix and Hypril formulations. The same behavior was observed on the moisture isotherms of crystalline, amorphous and predominantly crystalline lactose powders established at 12, 20, 30 and 40 °C [6].

3.2. Mathematical modelling

The results of nonlinear fitting of sorption models are shown in Table 1. All the examined models provided a good description of the isotherms of Hypril, the optimal one is the Oswin model which presented the most suitable fitting. As to Azix formulation, only GAB and Adam and Shove models gave appropriate fit between the experimental and the predicted data.

Table 1. Estimated parameters of the different models fitted to the sorption data for Azix and Hypril

Models	Constants	Azix			Hypril		
		50	60	70	50	60	70
GAB (Berg and Bruin 1981) $w = A + Ba_w + Ca_w^2 + Da_w^3$	C	136.10	5778.0	122.40	9.5030	2.0670	1.0010
	K	0.5872	0.5540	0.3592	0.9173	0.8944	0.7963
	w_m	0.0201	0.0153	0.0258	0.0413	0.0504	0.1133
	SSE	4.25e-5	3.12e-5	1.87e-5	2.88e-3	0.0106	0.0044
	R^2	0.9615	0.9282	0.9541	0.9868	0.9481	0.9773
	RMSE	2.30e-3	1.97e-3	1.53e-3	0.0189	0.0364	0.0236
Peleg (Peleg, 1993) $w = A(a_w)^B + C(a_w)^D$	A	-2.0400	-246.6	-11.09	0.08489	3.4720	0.4728
	B	0.8992	1.1900	0.8758	0.4787	3.6130	3.0790
	C	2.0840	246.60	11.130	0.4059	-3.0510	-0.0481
	D	0.8883	1.1900	0.8727	8.5820	3.5340	3.1430
	SSE	2.39e-4	3.00e-3	1.39e-4	7.42e-4	0.0183	8.80e-3
	R^2	0.7837	-5.903	0.6594	0.9966	0.9102	0.9554
	RMSE	5.84e-3	0.0207	4.46e-3	0.0103	0.0512	0.0354
Adam and Shove (Chirife and Iglesias 1978) $w = A + Ba_w + Ca_w^2 + Da_w^3$	A	0.0151	0.0181	0.0177	-0.0367	-0.0316	-0.0023
	B	0.03983	0.0114	0.0432	0.8998	0.7664	0.4558
	C	-0.04789	0.0369	-0.0484	-2.5500	-2.1730	-1.2620
	D	0.04141	0.0093	0.0273	2.1510	1.8690	1.2490
	SSE	4.234e-5	2.63e-5	1.75e-5	0.0045	0.0110	1.46e-3
	R^2	0.9617	0.9395	0.9571	0.9792	0.9460	0.9926
	RMSE	2.45e-3	1.94e-3	1.58e-3	0.0254	0.0397	0.0144
Modified Henderson (Thompson et al. 1968) $w = \left(-\dfrac{\ln(1 - a_w)}{A(T + B)} \right)^{1/c}$	A	465.20	3141.0	3621.0	0.0298	0.0239	0.0312
	B	231.80	2820.0	3289.0	-90.94	-80.630	-120.5
	C	3.6430	4.3260	4.7900	0.7836	0.6787	0.8895
	SSE	5.08e-5	5.22e-5	2.95e-5	4.26e-3	7.94e-3	3.32e-3
	R^2	0.9315	0.7856	0.9076	0.9461	0.9216	0.9692
	RMSE	2.69e-3	0.0027	0.0020	0.02469	0.03368	0.0218
Oswin (Oswin 1946) $w = \left(-\dfrac{\ln(1 - a_w)}{A(T + B)} \right)^{1/c}$	A	0.0282	0.0216	0.0296	0.0611	0.0521	0.0813
	B	5.6320	8.0180	8.9340	1.6370	1.5120	1.8020
	SSE	4.083e-5	4.12e-5	3.17e-5	1.05e-3	3.77e-3	2.38e-3
	R^2	0.9450	0.8307	0.9006	0.9867	0.9628	0.9780
	RMSE	2.26e-3	0.0022	1.99e-3	1.14e-2	0.0217	0.0172

3.3. Isosteric heat of sorption and sorption entropy

The results in Fig. 2 illustrate a progressive decrease in the net isosteric heat of sorption (net enthalpy) with increasing moisture content for both formulations. The values of net isosteric heat of sorption are high for equilibrium moisture content < 0.10 kg/kg and then decreased rapidly until equilibrium moisture contents reach respective values of 0.15 and   2 kg/kg d.b for Azix and Hypril, and then they decreased smoothly with increasing moisture content. Azix showed higher values of net isosteric heat than Hypril. This suggests that the energy to be supplied to dehydrate Azix would be higher than the energy needed to dehydrate Hypril. The differential entropy as a function of moisture content, illustrated by Fig. 3, shows the same tendency as the net isosteric heat. The sorption entropy of Azix exhibited higher magnitude than that of Hypril.
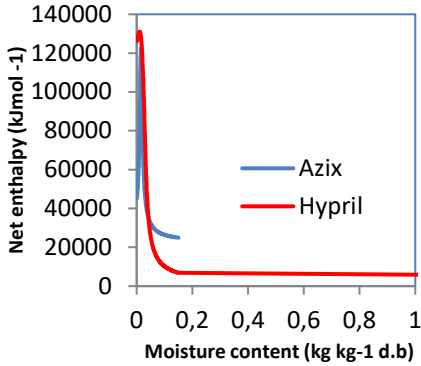
Fig. 2a Net isosteric heat of Azix and Hypril formulations
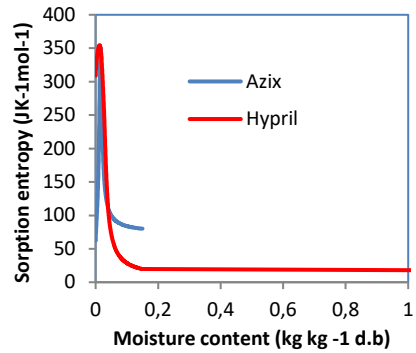
Fig. 2b Sorption entropy of Azix and Hypril formulations

3.4. Integral enthalpy and entropy

The variations in net integral enthalpy with the moisture content for Azix and Hypril are shown in Fig. 3**.** On the whole range of equilibrium moisture content, the integral enthalpy of both products decreases as a function of equilibrium moisture content until reaching minimum values then they remains constant.
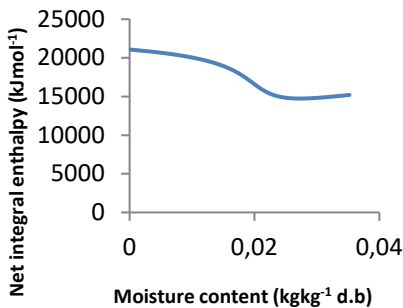
Fig. 3a Net integral enthalpy of Azix formulation
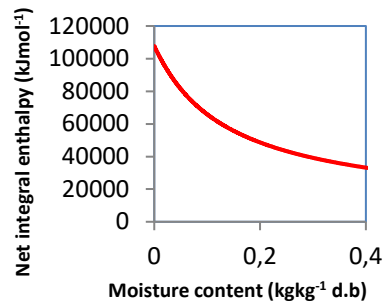
Fig. 3b Net integral enthalpy of Hypril Formulation

Variations of the net integral entropy (Fig.4) of Azix and Hypril showed different trends. Values decreased with equilibruim moisture content for Hypril and increased for Azix. The better conditions to assure stability to the powders during storage [7] are those corresponding to lower entropy values.
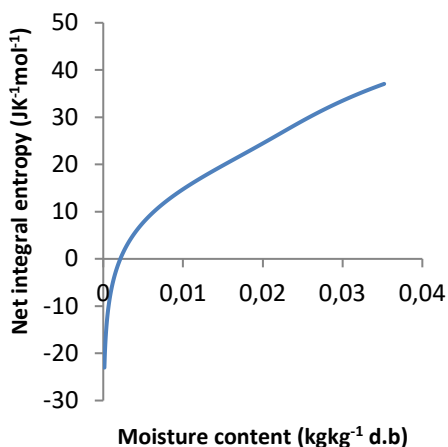
Fig. 4a *Net integral entropy of Azix formulation*
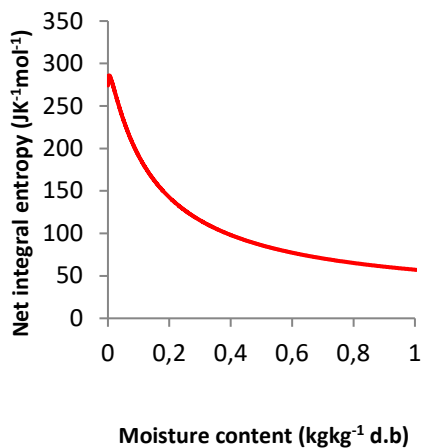
Fig. 4b *Net integral entropy of Hypril formulation*

4. Conclusions

This study affords an understanding of the sorption isotherms and the thermodynamic properties of two powders with different compositions. The obtained results suggest that the two products could be dehydrated at lower temperature (50°C) since the isotherms of sorption are independent of temperature. Azix preparation seems to be less hygroscopic and more stable than Hypril preparation which requires less energy to be dehydrated.

5. References

[1] AOAC AOAC Official method, 1990.

[2] Reddy, T. A. Applied Data Analysis and Modeling for Energy Engineers and Scientists: Springer US, 2011.

[3] Kechaou N. Thesis 'Etude théorique et expérimentale du processus de séchage de produits agroalimentaires', Faculté des Sciences de Tunis, 2000.

[4] Zhou, Q.; Loh, Z. H.,;Yu, J.; Sun, S.-p.; Gengenbach, T., Denman, J. A. How Much Surface Coating of Hydrophobic Azithromycin Is Sufficient to Prevent Moisture-Induced Decrease in Aerosolisation of Hygroscopic Amorphous Colistin Powder. The AAPS Journal. 2016 , 18(5), 1213-1224, doi:10.1208/s12248-016-9934-x.

[5] Al-Omari, M. M.,; Abdelah, M. K.; Badwan, A. A.; Jaber, A. M. Y. Effect of the drug-matrix on the stability of enalapril maleate in tablet formulations. Journal of Pharmaceutical and Biomedical Analysis. 2001, 25(5), 893-902, doi:https://doi.org/10.1016/S0731-7085(01)00399-5.

[6] Bronlund, J.; Paterson, T. Moisture sorption isotherms for crystalline, amorphous and predominantly crystalline lactose powders. International Dairy Journa l 2004, 14(3), 247-254, doi:https://doi.org/10.1016/S0958-6946(03)00176-6.

[7] Cano-Higuita, D. M.; Villa-Vélez, H. A.; Telis-Romero, J.; Váquiro, H. A.; Telis, V. R. N. Influence of alternative drying aids on water sorption of spray dried mango mix powders: A thermodynamic   approach. Food and Bioproducts Processing 2015, 93, 19-28, doi:https://doi.org/10.1016/j.fbp.2013.10.005.

Comparison between bubbling and turbulent regime for the simulation of batch pharmaceutical powders fluidized bed drying

Zammouri, A.[a*]; Boudhrioua Mihoubi, N.[b]; Kechaou, N.[c]

[a] Laboratoire de Biotechnologie et Valorisation des Bio-Géo Ressources, LR11ES31. Institut Supérieur de Biotechnologie de Sidi Thabet, Univ. Manouba, BP-66, 2020 Ariana-Tunis, Tunisie,.

[b] Laboratoire de Physiopathologies, Alimentation et Biomolécules, LR17ES03. Institut Supérieur de Biotechnologie de Sidi Thabet, Univ. Manouba, BP-66, 2020 Ariana-Tunis, Tunisie,

[c] Groupe de Recherche en Génie des Procédés Agroalimentaires, Ecole Nationale d'Ingénieurs de Sfax, Université de Sfax, BP 1173 3038, Sfax, Tunisie.

* E-mail of the corresponding author : amel.zammouri@gmail.com

Abstract

The two-phase theory has been frequently used to model fluidised bed drying. At high air velocities, a transition from the bubbling regime to the turbulent regime may occur. In this work, we compare a bubbling model and a turbulent model for the simulation of a two pharmaceutical powders drying in a pilot plant and an industrial plant fluidised bed. The bubbling model was based on a discrete variable bubble size. Heat and mass transfer coefficients were based on the Kunii and Levenspiel correlation [1]. Flow regime was supposed to be completely mixed for the emulsion phase. For the turbulent model, the bubble size is not anymore discrete but continuous and bubble phase is less distinguishable than in the bubbling regime. Heat and mass transfer were those proposed by Foka[2]. In addition, the freeboard section was considered since high entrainment is specific of this regime. Gas backmixing was taken into account by considering a plug flow with axial dispersion for the interstitial gas flow. The bubble phase being dilute, was modeled by a plug flow. A plug flow was also considered for the freeboard gas. The solid phase was supposed to be completely mixed. The bubbling regime simulation gave good agreement with experiment in the case of the pilot plant experiment, while the turbulent model better simulated the industrial scale experiment.

Key words: batch fluidized bed, pharmaceutical powder, drying, modeling, bubbling, turbulent

1. Introduction

Drying of pharmaceutical products is frequently carried in batch fluidized bed dryers. Fluidisation offers the advantage of high heat and mass transfer rates due to the elevated specific surface area created. Generally, the drying end is determined by analyzing the moisture content at different times. Several works [3-4] proved that more rigorous control could be obtained by mathematical modeling. Models proposed considered either bubbling regime or turbulent regime fluidisation. The transition between these two regimes, at high air velocities, should be better experimentally determined. Correlations proposed to determine the transition velocity depend generally on experimental system used. In this work, a bubbling regime model based on the two phase theory is compared to a turbulent regime model for the simulation of the drying kinetics of an A type particles and a B type particles pharmaceutical powders. Sorption isotherms determined experimentally were used to describe the falling drying rate period.

2. Experimental study

2.1. Material properties

The drying experiments were carried with two pharmaceutical products supplied by Pharmaghreb industry (Tunisia), an A type particles (Hypril) and a B type particles (Azix).

2.2. Equilibrium sorption study

Sorption isotherms of the two products were determined by contacting the solid samples with air at a variety of relative humidity at a fixed temperature. Equilibrium water sorption was measured, at different temperatures, by static gravimetric method with sulfuric acid solutions at different concentrations.

2.3. Drying kinetic study

Fluidized bed-drying experiments for group A type particles were carried in a Diosna MinilabXP (Germany). conical laboratory scale bed. Drying kinetics for group B type particles were obtained from a Glatt WSD-CD-30(USA) conical industrial scale fluidized bed . Experimental conditions are listed in table 1. Air heated at the desired temperature was supplied at the bottom of the conical chamber. The bed temperature was on line measured. The solid moisture content was determined by a moisture analyser (Mettler Toledo, Switzerland).

At the beginning of the fluidized bed experiments, the A type powder was initially very cohesive showing a Geldart C powder characteristics. The entire bed mass rose as plug when hot air was blown into the bed. After a short time of drying, the moisture content decreased, the Geldart C type cohesive powder shifts to a Geldart A powder. The plug was broken manually and a fluidization state was attained. The same trend was obtained for B type particles.

Zammouri, A.[a]; Boudhrioua Mihoubi, N.[b]; Kechaou, N.[c]*

Table 1. Experimental conditions and physical materiel properties

Geldart group	A	B
Mean diameter(µm)	48.8	384.72
Density(kg/m^3)	649.35	702
Superficial air velocity (m/s)	0.97	2.26
Inlet air temperature (°C)	47	50
Initial air temperature (°C)	24	18.4
Relative humidity(%)	60	60
Initial solid moisture (dry basis,%)	29.55	19.74
Critical moisture (dry basis,%)	13,00	4.00
Solid mass (wet basis, kg)	1	36.9
Column diameter(m)	0.16	0.5
Column height (m)	0.5	2.0

3. Mathematical modeling

3.1. Bubbling regime model

The behaviour of the fluidized bed dryer is based on the two-phase theory: a bubble phase and an emulsion phase [1, 3]. The emulsion phase is at minimum fluidisation conditions and consists of interstitial gas and solid phase. Due to the buoyancy force, all the gas in excess of minimum fluidisation by passes the particles and rises through the bed as bubbles containing very small amount of solids. The governing equations are the equations of mass and heat conservation for bubble phase, interstitial gas and solid emulsion phase. These equations are detailed in [3,4]. The bubble diameter is a key parameter in the modeling of a bubbling fluidised bed and have a great importance on its performance. Several correlations were proposed to calculate the bubble diameter. For B type particles, the Darton's [5] correlation is largely used, it takes account of bubbles coalescing as they rise in the bed.

For A type particles, the correlation proposed by Horio and Nonaka [6] is selected. The authors proved that, for fine particles, a stable equilibrium bubble size could be obtained due to their successive coalescence and splitting.

3.2. Turbulent regime model

The turbulent regime is characterised by a breakup of coalesced bubbles to smaller ones. The large bubble renewal frequency caused by coalescing and splitting leads to a better interchange between bubbles and interstitial gas. The bubble size decrease reduces the short cut leading so to less gas back mixing and an increase in the gas solid contact. At the same time, the solids back mixing is also violent in turbulent fluidization. Experimental evidence [7] proved that gas flow is intermediate between an ideal plug flow and ideal agitated flow. As the bubbles erupt at the bed surface, they burst and particles splash into freeboard above the bed. At high velocities, high entrainment is produced. The particles are carried over in the freeboard. Two regions coexist in the bed:

- A bottom dense bed region with a high solid concentration and overall voidage ε
- An upper dilute freeboard region with an axial variable voidage ε_z

3.2.1. Dense bed balance equations

The equations for the bubbling regime can be extended to the turbulent fluidization with no distinct bubble phase, but rather low and high-density phases with a different bubble phase voidage.

Dense phase interstitial gas mass balance

The dense phase is no longer at the minimum fluidisation conditions and voidage ε_d is greater than ε_{mf} because of solid entrainment. Axial dispersion is considered and mass and heat transfer coefficients between the low and high density phases are different than those used for discrete bubbles.

$$\rho_G u_d \frac{\partial x_e}{\partial z} + D_{ax}\rho_G \varepsilon_d (1-\delta_b)\frac{\partial^2 x_e}{\partial z^2} - K_{be}\rho_G \delta_b (x_e - x_b) \tag{1}$$
$$+ (1-\varepsilon_d)(1-\delta_b)\frac{6}{d_p}\sigma(x_p^* - x_e) = \varepsilon_d(1-\delta_b)\rho_G \frac{\partial x_e}{\partial t}$$

Where x_e is the moisture content of the dense phase interstitial gas on dry basis (kg/kg) and x^*_p is the moisture content of drying gas on particle surface. σ is evaporation coefficient (kg m^{-2} s^{-1}). ε_d is the dense phase voidage and δ_b is the lean phase voidage. D_{ax} is the axial dispersion coefficient (m^2/s).

At the bed entrance and exit the Danckwerts Boundary conditions were used for the axial dispersed low.

Zammouri, A.[a*]; Boudhrioua Mihoubi, N.[b]; Kechaou, N.[c]

Dense phase interstitial gas energy balance

$$-\rho_G u_d (c_G + x_o c_v) \frac{\partial T_e}{\partial z} + k_g \varepsilon_d (1 - \delta_b) \frac{\partial^2 T_e}{\partial z^2} - H_{be} \rho_G \delta_b (T_e - T_b) \tag{2}$$
$$- (1 - \varepsilon_d)(1 - \delta_b) \frac{6}{d_p} (T_e - T_p) [c_v \sigma (x_p^* - x_e)$$
$$+ h_p] - \frac{1}{A_c dz} h_w S_w (T_e - T_w) = \varepsilon_d (1 - \delta_b) \rho_G (c_G + x_e c_v) \frac{\partial T_e}{\partial t}$$

The interphase mass transfer coefficient (s^{-1}) is given by a correlation proposed by [2]

$$K_{be} = 1.631 \, S_c^{0.37} u_o \tag{3}$$

The heat transfer coefficient H_{be} ($w/m^3.K$) determined by the Chilton-Colburn analogy.

The dense bed voidage and Peclet number are correlated as proposed by [7]:

Dense phase solid mass balance

The axial dispersion in the turbulent regime increases largely with the gas velocity giving up an homogeneous solid phase in the bed. The following equations describe mass and heat transfer between solid and interstitial gas.

$$-\frac{\rho_s}{1 + \frac{\rho_s}{\rho_w} x_c} \frac{\partial x_p}{\partial t} = \frac{6}{d_p} \sigma (x_p^* - x_e) + \frac{\rho_s}{1 + \frac{\rho_s}{\rho_w} x_c} D_s \frac{\partial^2 x_p}{\partial z^2} \tag{4}$$

$$\frac{6}{d_p} h_p (T_e - T_p) - \frac{6}{d_p} \sigma (x_p^* - x_e) [\gamma_o + c_v (T_e - T_{ref}) - c_w (T_e - T_{ref})] + k_s \frac{\partial^2 T_p}{\partial z^2} \tag{5}$$
$$= \frac{\rho_s}{1 + \frac{\rho_s}{\rho_w} x_c} (c_p + x_p c_w) \frac{\partial T_p}{\partial t}$$

3.2.2. Freeboard balance equations

The plug flow model is used to describe the drying upper dilute region or freeboard. The mass and heat balance for the gas phase are:

$$-\rho_G u_o \frac{\partial x_f}{\partial z} + +(1 - \varepsilon_z) \frac{6}{d_p} \sigma (x_p^* - x_f) = \varepsilon_z \rho_G \frac{\partial x_f}{\partial t} \tag{6}$$

$$-\rho_G u_o (c_G + x_o c_v) - (1 - \varepsilon_z) \frac{6}{d_p} (T_f - T_p) [c_v \sigma (x_p^* - x_f) + h_p] \tag{7}$$

$$- \frac{1}{A_c dz} h_w S_w (T_f - T_w) = \varepsilon_z \rho_G (c_G + x_e c_v) \frac{\partial T_f}{\partial t}$$

Several correlations were proposed to determine solid decay in the freeboard, but they give predictions that differs each from others. However, it is largely accepted that concentration in the freeboard decreases exponentially with height.

$$\frac{\varepsilon^* - \varepsilon_z}{\varepsilon^* - \varepsilon} = \exp(-a_z * (z - h_i)) \tag{8}$$

ε is the de dense bed voidage. ε_z is the freeboard voidage at z. ε^* is the asymptotic voidage at $z \to \infty$ in the dilute region.

$$\varepsilon_z = \varepsilon^* - (\varepsilon^* - \varepsilon)\exp(-a_z * (z - h_i)) \tag{9}$$

The position of the point of inflexion h_i separating the dilute and dense bed regions can be calculated in a trial manner using the solids inventory in the dryer.

4. Results and discussion

The set of ordinary derivatives thus obtained was solved with Matlab solver(MALAB R2012b). For the group A type particles and B type particles, the moisture sorption isotherms obtained experimentally were fitted by the modified-Hendersen correlation:

$$RH_A = \frac{P_v}{P_w} = 1 - \exp(-0.0298 * (T_p - 90.94)X_p^{0.78}) \tag{10}$$

$$RH_B = \frac{P_v}{P_w} = 1 - \exp(-465.2 * (T_p + 231.8)X_p^{3.64}) \tag{11}$$

RH is the relative humidity, T_p is the particle temperature and X_p is solid moisture content on dry basis (kg/kg).

The comparison between solid moisture content simulations as function of time for bubbling and turbulent regime models to experimental results is illustrated in **Fig.1 and Fig.2**. For A type particles, bubbling regime gives better fitting of experimental results than turbulent one. The latter regime overestimates the drying rate. The completely mixed flow is more realistic than the axially dispersed flow. For B type particles, the bubble diameter was calculated by Darton correlation. [1] suggested that a constant bubble diameter value of 0.05 m could be convenient for the simulations. [4] obtained good predictions with a constant bubble diameter of 0.06m and an air superficial velocity of 2.4m/s. The equivalent bubble diameter value obtained with (2) for A type particles was also 0.06m. A simulation with this diameter was so tried. It is noted that Darton correlation largely underestimated the drying rate. This is due to the growth of bubble size by coalescence as they rise in the bed which causes mass and heat transfer decrease. At high superficial velocities, splitting of bubbles occur and constant equivalent bubble diameter is more realistic. However the turbulent regime is more

Zammouri, A.[a*]; Boudhrioua Mihoubi, N.[b]; Kechaou, N.[c]

convenient for this powder and gives the better prediction of experimental data. This regime is characterised by considerable solid entrainment in the freeboard zone.
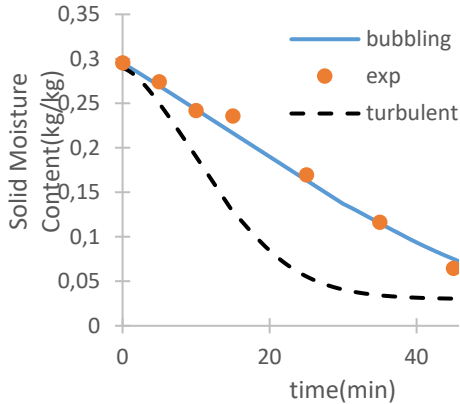
Fig.1 Simulated and experimental solid moisture as function of time (A type particles)
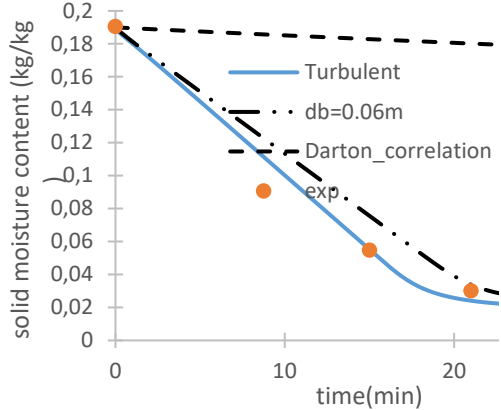
Fig.2 Simulated and experimental solid moisture content as function of time(B type particles)

While the solid concentration in this section is very dilute relatively to the dense region (**Fig. 3**), drying continues in the freeboard region. From **Fig.4,** it can be noted that air moisture content in the dense bed is higher than that in the freeboard zone. Moisture is driven more efficiently to air in the dense bed but freeboard contributes also to performing drying kinetics. Freeboard contribution becomes more important as the product is dried in the falling rate period where there is no more surface water. The same trend was found by [8].

To ensure homogenous solid moisture content in the bed, axial dispersion was added to solid mass and heat balances. To test the influence of axial solid dispersion coefficient, four values were assigned to Ds: 10, 1, 0.1 and 0.01 m^2/s. The simulations results of solid moisture content variation with time and with axial coordinates are presented in **Fig.5 and Fig.6.** Closer inspection of these figures shows that for Ds values, 0.1,1 and 10 m^2/ s solid particles are perfectly mixed and there is no influence of Ds value on solid moisture content as function of time. This is in well agreement with the results of [9] where Ds values were stated to be in the range 0.5-10m^2/s. In this work a Ds value of 1m^2/s was used for all simulation as suggested by [2]. For the lowest Ds value 0.01 m^2/s, an axial solid moisture content dispersion appears and a little deviation from experimental data is obtained.

5. Conclusions

A comparison between bubbling regime and turbulent regime batch-fluidized bed drying of an A and a B pharmaceutical powders has been made. Simulation results show that the experimental drying kinetic is better predicted by the bubbling regime in the case of the A type particles while for the B type particles turbulent regime model is more convenient
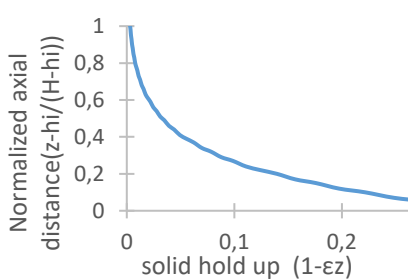
Fig.3 Solid hold up profile in the freeboard for B type particles
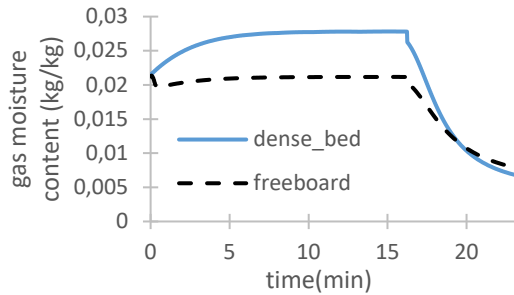
Fig.4 Simulated gas moisture content in dense phase and freeboard as function of time (B particle)
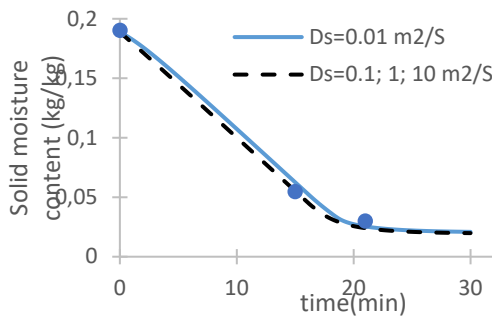
Fig.5: Simulated solid moisture content as function of time at different Ds
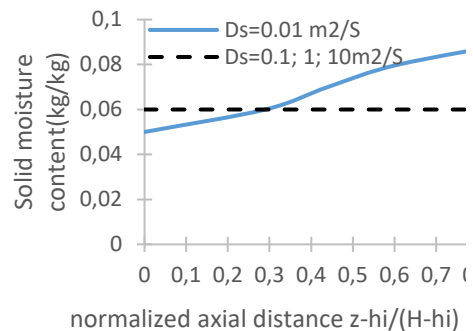
Fig.6: Simulated solid moisture content as function of axial distance at different Ds

6. References

[1] Kunii, D.; Levenspiel, O. Fluidization Engineering. Wiely: New York, 1969

[2] Foka, M.; Chaouki, J., Guy C., Klvana, D. Gas phase hydrodynamics of a gas solid turbulent fluidized bed reactor. Chem. Eng. Sci 1996, 557, 13-723

[3] Wang, H. G.; Dyakowski, T.; Senior, P.;Raghavan, R. S. ;Yang, W. Q. Modelling of batch fluidized bed drying of pharmaceutical granules. Chem. Eng. Sci 2007a, 62, 1524–1535

[4] Villegas, J.A.; Li, M.; Duncan, S.R. ; Wang, H.G. ;Yang, W.Q. Modeling and control of moisture content in a batch fluidized bed dryer using tomographic sensor. Proceedings of the American Control Conference 2008, 3350-3355

[5] Darton, R.C.; Lanauze, R.D.;Davidson, J.F.; Harrison, D. Bubble growth due to coalescence in fluidized beds. Trans. Inst. Chem. Eng 1977, 55, 274-280

[6] Horio, M.; Nonaka, A. A Generalized Bubble Diameter Correlation for Gas-Solid Fluidized Beds. AIChEJ 1987, 33, 1865-1872

[7] Bi, H.T.; Ellis, N.; Abba, I.A.; Grace, J.R. A state-of-the-art review of gas-solid turbulent fluidization, Chem. Eng. Sci 2000, 55, 4789-4825

[8] Briens, L.; Bojarra, M. Monitoring fluidized bed drying of pharmaceutical granules. AAPS Pharm. Sci. Tech 2010, 11, 1612–1618

[9] Breault, R.W. A review of gas–solid dispersion and mass transfer coefficient correlations in circulating fluidized beds. Powder Technol 2006,163, 9–17

Modeling and simulation of intermittent drying of high moisture foods

Filippin, A.P.[a]; Tada, E.F.R.[a]; Thomeo, J.C.[a]; Mauro, M.A.[a*]

[a] UNESP - São Paulo State University, Institute of Biosciences, Humanities and Exact Sciences (IBILCE), São José do Rio Preto, SP, Brazil

*Corresponding author: cidam@ibilce.unesp.br

Abstract

This study aimed at the modeling and simulation of intermittent drying to be applied to highly deformable moist foods such as apples. Mass transport modeling considered two stages: the first at 95, 85 and 75ºC air temperatures, and the second at 60ºC. The shrinkage was correlated with the sample moisture and included in the model that was solved by the finite differences method. The first stage temperatures affected the water diffusivity in the second stage. This model was suitable for simulating the water profiles during the two-stage intermittent drying, showing an efficient fitting to the experimental data.

Keywords: *thermal intermittence; coefficient diffusion effective; shrinkage; apple drying.*

1. Introduction

Drying is an antique unit operation widely used by the food industry and it is based on moving of water from high to low moisture zones until reach a frontier and to be removed in the form of vapor. This operation favors the stability of the foods because it increases their shelf life due to the considerable decrease in the water activity of the material [1-3]. However, the energy demand of the drying operation is very high and besides that, can promote undesirable nutritional and organoleptic losses.

The recent literature has reported the intermittent drying processes as an alternative to decrease these negative impacts and to minimize energetic costs [4,5]. Intermittent drying consists in changing of the operational conditions during drying. In the case of the temperature variation during the process, referred as thermal intermittence, a high temperature is used in the beginning of the process favoring the evaporation. During this period the surface of the product is saturated and the water evaporation ensures its low temperature [6]. When instauration zones begin to appear on the surface, the drying air temperature is reduced.

The knowledge and control of the heat and mass transfer phenomena during drying is fundamental to establish process conditions that promote improvement in the quality of the product. In the case of variable process conditions, such as in the intermittent drying, the recent literature [4] has reported the necessity of intense investigation and understanding of the moisture and temperature evolution during the whole process. Mathematical models can be used to estimate physical and transport parameters, and to predict spatial and temporal moisture and temperature profiles. However, it is necessary that appropriate conditions be considered. In this sense, this study proposes modeling and simulation of temporal and spatial profiles of the water content in apple slices during intermittent drying in two stages.

2. Materials and Methods

2.1. Sample preparation: The Fuji cv. apples (*Malus domestica*) were sanitized with water and then sliced (5 mm thick) using a slicer (ECO, Brazil). The slices were placed between two metallic screens to avoid deformation during the drying.

2.2. Convective dryer: The drying experiments were carried out using two identical tray dryer with forced convection as described by Filippin et al. (2018) [5]. The air flowed parallel to the samples. Dryer 1 was kept at 75, 85 or 95 ºC and dryer 2, at 60 ºC.

2.3. Drying tests: During the first stage of intermittent dryings, the trays were placed in dryer 1. After 45 minutes, they were removed from the dryer 1 and immediately inserted into the dryer 2, where remained until the samples reached constant weight. In both dryers the drying air velocity was 2 m·s^{-1}. The samples were weighed successively during the drying using a semi-analytical balance (Gehaka, BK 4000, Brazil).

2.4. Experimental determination of sample shrinkage: The shrinkage was described as a linear function of the moisture content on dry basis. The thickness was measured at each trial at the beginning and end of drying by using a micrometer screw (Mitutoyo, MDC-25SB, Japan).

2.5. Analytical methods: The total solids content of fresh and dried apple slices were gravimetrically determined in triplicate by drying in a vacuum oven at 60 ºC and 10 kPa to constant weight. The water activity of the samples was measured in triplicate at 25 ºC in a hygrometer (Aw sprint; Novasina, Switzerland).

2.6. Mathematical modeling: Considering that drying can be described by the falling-rate period and that liquid diffusion is the principal mass transfer mechanism, the drying kinetics were evaluated based on Fick's second law [7] presented in Eq. 1 in its modified form, in terms of the mass fractions (dry basis, d.b.). It was assumed a constant solids concentration. The slice was considered as a flat plate with mass flow along the thickness of the apple (z-axis).

$$\frac{\partial X}{\partial t} = D_{eff} \frac{\partial^2 X}{\partial z^2} \tag{1}$$

where X is the mass fraction of water on a dry weight basis ($kg \cdot kg^{-1}$) D_{eff} represents the effective diffusivity ($m^2 \cdot s^{-1}$), z is the thickness and t is the time (s).

Initial conditions for the first and second stage of the intermittent drying are presented in Eq. 2 and 3, respectively.

$$t = 0 \quad \left| \begin{array}{ll} X_1 = \overline{X}^0 & \tag{2} \\ X_2 = X_2^0(z) & \tag{3} \end{array} \right.$$

where the sub index 1 and 2 represent the first and the second stage, respectively, and the super index 0 represents the initial condition. At the second stage, the initial water mass fraction is a function of de distance z, because there is a spatial distribution profile of water content in the sample at the end of the first stage.

Eqs. 4 and 5 represent the spatial conditions.

$$z = \pm L/2 \qquad X = X^{eq} \tag{4}$$

$$z = 0 \qquad \frac{\partial X}{\partial z} = 0 \qquad\qquad (5)$$

where L is the initial thickness of the apple slice and $z = 0$ refers to the central position on the z-axis (symmetry condition) and X^{eq} is the water mass fraction in equilibrium. Eq. 4 and 5 were employed in both drying stages.

In this study, the thickness shrinkage was described by a linear equation as a function of moisture and, therefore, included in the Eq. 1

The parabolic partial differential equations were solved by finite differences method using MATLAB software (MathWorks Inc., Natick, Massachusetts, USA). The moisture profile generated in the first stage was the initial condition of the second stage. The effective diffusion coefficients (D_{eff}) were determined by minimizing the (relative) deviations between predicted and observed average water contents in the slices. For this, the predicted water profiles were integrated and compared with the observed values.

The estimated parameter D_{eff} was evaluated based on the best fit using statistical indicators as such as the coefficient of determination of the fit (R^2), the mean relative error (P%) and on the root mean square error (RMSE).

$$P(\%) = \frac{100}{N} \sum_{1}^{n} \frac{|X^{exp} - X^{cal}|}{X^{exp}} \qquad\qquad (6)$$

$$RMSE = \left[\frac{1}{N} \sum_{1}^{n} \left(MR^{cal} - MR^{exp} \right)^2 \right]^{\frac{1}{2}} \qquad\qquad (7)$$

where X^{calc} represents the water content on a dry basis, X^{exp} is the experimental value, MR^{exp} is the experimental moisture ratio, MR^{calc} the calculated moisture ratio and N represents the number of observations or residuals.

3. Results and Discussion

The moisture and water activity of the samples for the treatments are shown in Table 1.

Table 1. Moisture and water activity of the fresh and dried samples

Treat.	Moisture			a_w
	Fresh sample	Dried Sample	Equilibrium	Dried sample
T1	0.869 ± 0.002	0.047 ± 0.001	0.033 ± 0.001	0.275 ± 0.016
T2	0.860 ± 0.002	0.043 ± 0.001	0.032 ± 0.001	0.237 ± 0.013
T3	0.863 ± 0.002	0.050 ± 0.001	0.032 ± 0.002	0.248 ± 0.016

The experimental curves of the intermittent drying are shown in Fig.1.
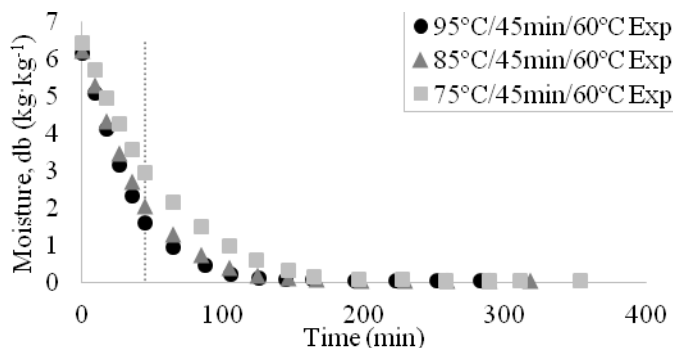
Fig 1. Experimental curves of the intermittent drying

It was observed that the intermittent drying curves exhibit a discontinuity between the first and second stages, indicated by the vertical dashed line. The relation between the drying rate and the air temperature is evidenced by the difference between the curves in the first stages, in which higher drying air temperature promoted a more pronounced slope of the curve. In addition, after 45 min at 75°C, the sample average moisture reached 75% on wet basis (or 2.97, d.b.), while at 95°C the average moisture was 62% (1.63, d.b.).

Table 2 shows the effective diffusivity obtained at each stage of the intermittent drying treatments and the statistical parameters evaluated.

Table 2. Diffusion coefficients (D_{eff}) R^2, *P(%) and RMSE*

Treatment	T (°C)	$D_{eff} \times 10^{10}$ (m²·s^{-1})	R^2	P(%)	RMSE
T1	95	7.00	0.990	3.1	0.032
	60	3.40	0.999	28.7	0.005
T2	85	5.90	0.992	2.3	0.027
	60	3.10	0.999	25.0	0.004
T3	75	4.50	0.985	2.8	0.034
	60	2.75	0.999	22.4	0.011

The P(%) values obtained in the second stage were higher than those obtained in the first stage and they were above 10%, which is considered as a reference value [8]. However, since the P(%) value is calculated as a relative residual, the error value is amplified as the moisture content decreases through the second stage of drying. The values of RMSE, a non-relative parameter, were satisfactory for both stages as well as the coefficient of determination (R^2), indicating that the proposed model presented a good fit to the experimental data.

Experimental and simulated curves are shown in Fig. 2.
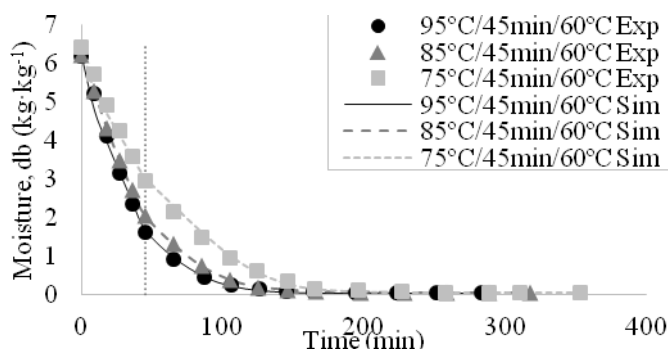
Fig. 2. Experimental (Exp) e simulated (Sim) drying curves

It is important to highlight that drive forces are not only related to mass concentration gradients, although this is the main driving force of the phenomenon [7]. Temperature gradients, which are more significant in the beginning of the process, will also influence the water transport [6]. However, in the case of a single-parameter model, D_{eff} encompasses all possible parameters that effectively influence the mass transport.

The effective diffusion coefficients of the first stage (Table 2) showed exponential temperature dependence, which was empirically represented by an Arrhenius type equation, as described in Eq. 8. This equation has been reported in the literature to describe the D_{eff} as a function of the air-drying temperature [9,10]. For the first stage, the activation energy was 23.59 kJ·mol^{-1} ($R^2 = 0.987$), as follows:

$$D_{eff} = 1.57 \times 10^{-6} \exp^{-23.59/RT} \tag{8}$$

in which D_{eff} assumes the value of 1.57×10^{-6} m^2·s^{-1} when the temperature (T) tends to infinite and R is the universal gas constant in kJ·mol^{-1}·K^{-1}.

Although the air-drying temperatures of the second stages were the same (60ºC), the D_{eff} values were different. Therefore, a dependence on the first stage air-drying temperature was found. The increase of 10°C in the first stage temperature led to an increase of about 11% in the D_{eff} of the second stage. This result indicates that the first stage temperature contributed to the second stage efficiency, probably because of modifying the vegetable structure that would make the water exit easier in the later stage.

The drying has been represented in the literature through empirical models such as the Peleg, Page, Handerson and Pabis and Lewis and fundamental mathematical models [4,11]. Regarding the intermittent drying, some authors model the initial condition of subsequent stages by considering a homogeneous spatial distribution of the water [9,12]. This

consideration is reasonable when tempering times are used between the stages, since this procedure provides redistribution of the water content in the solid during the holding time. Therefore, a moisture profile of the initial stage could be used to calculate the ideal tempering time required for the moisture to become homogeneous [13].
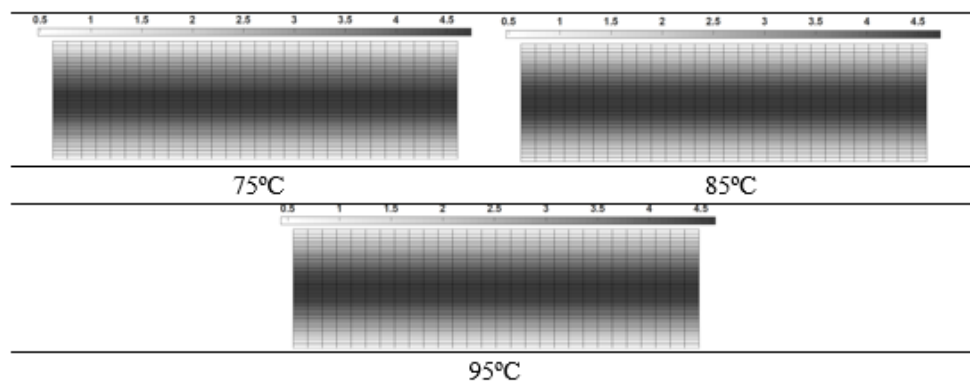
Fig. 3. Spatial distribution of water in the apple slice at the end of the first stage at 75, 85 and 95ºC.

In the case of the thermal intermittence applied in this study, at the end of the first stage the profile of spatial water distribution was evident, as shown in Fig. 3. At the end of the first stage at 95ºC, the water content was about 9 times larger at the centre of the sample than at the surface, which highlights the need to consider the moisture profile in the initial condition of the second stage. Thus, the approximation of moisture profile to experimental mean moisture would be a misconception that could underestimate the D_{eff} values.

Consideration of the shrinkage in the model also contributed to the good fit of the model. In this study, it was assumed that only the thickness dimension varied. In fact, as variation of the radial dimension of the slices was small, the mass transfer area could be neglected without considerably affecting the accuracy of the model fitting.

4. Conclusions

The proposed diffusive model was appropriated to simulate water profiles during two-stage intermittent drying of deformable foods, since it presented a good fit to the experimental data. The effective diffusion coefficients found in the second stage depended on the first stage temperature.

5. Acknowledgements

6. References

[1] Mayor L, Sereno AM. Modelling shrinkage during convective drying of food materials: a review**.** J Food Eng 2004, 61, 373-386.

[2] Mujumdar AS, Law CL. Drying Technology: Trends and Applications in Postharvest Processing. Food and Bioprocess Technology 2010 3,843–852.

[3] Demarchi SM, Ruiz NAQ, Concellón A, Giner SA. Effect of temperature on hot-air drying rate and on retention of antioxidant capacity in apple leathers. Food Bioproducts Processing, 2013, 91, 310-18.

[4] Kumar, C.; Karin, M. A.; Joardder, M. Intermittent Drying of Food Products: A Critical Review. Journal of Food Engineering, 2014, 121, 48–57.

[5] Filippin, A.P.; Molina Filho, L.; Fadel, V.; Mauro M.A. Thermal intermittent drying of apples and its effects on energy consumption. Drying Technology 2018. https://doi.org/10.1080/07373937.2017.1421549

[6] Treybal, R. E. Mass Transfer Operations; McGraw-Hill Book Co: Singapore, 1980.

[7] Crank, J. The Mathematics of Diffusion; Claredon Press:Oxford, 1975.

[8] Lomauro, C. J.; Bakshi, A. S.; Labuza, T. P. Evaluation of Food Moisture Sorption Isotherm Equations. Part I: Fruit, Vegetables and Meat Product. Food Science and Technology (LWT), 1985, 18(2), 111–117.

[9] Vaquiro, H. A.; Clemente, G.; Garcia-Perez, J. V.;Mulet, A., Bon, J. Enthalpy-Driven Optimization of Intermittent Drying of Mangifera indica L. Chemical Engineering Research and Design, 2009, 87(7), 885–898.

[10] Iguaz, A.; San Martín, M. B.; Maté, J. I.; Fernández, T.; Vírseda, P. "Modelling effective moisture diffusivity of rough rice (*Lido* cultivar) at low drying temperatures", Journal of Food Engineering 2003, 59(2), 253-258.

[11] Cihan, A.; Kahveci, K.; Hacihafizoğlu, O. Modelling of Intermittent Drying of Thin Layer Rough Rice. Journal of Food Engineering, 2007, 79(1), 293–298.

[12] Silva, V.; Figueiredo, A. R.; Costa, J. J.; Guiné, R. P. F. Experimental and Mathematical Study of the Discontinuous Drying Kinetics of Pears. J. Food Eng. 2014,134, 30–36.

[13] Carmo, J.E.F.; Lima, A.G.B.; Silva, C.J. "Continuous and Intermittent Drying (Tempering) of Oblate Spheroidal Bodies: Modeling and Simulation." International Journal of Food Engineering 2012, 8(3), 1556-3758.

The aggregation rate constant of the discrete population balance model in hot melt fluidized bed coating process

Xin, W. [a]; Yan, Y.[b]; Qing, X. [a,b*]; Long W [a,b]

[a] International Joint Research Center of Low-Carbon Green Process Equipment; College of Mechanical Engineering, Tianjin University of Science &Technology, Tianjin 300222, China
[b] Tianjin Key Laboratory of Integrated Design and On-line Monitoring for Light Industry & Food Machinery and Equipment, Tianjin 300222, China.

*E-mail of the corresponding author: xuqing@tust.edu.cn

Abstract

During hot melt fluidized bed coating, particle agglomeration leads to non-uniform particle size. In this study, Population Balance Model (PBM) is used to establish the conservation of the size of particles in the system. In order to solve the population balance model, it is discretized. The aggregation kernel of the particles can be described by the Equi-partition of Kinetic Energy (EKE) kernel based on the gas dynamics theory. The EKE kernel is incorporated into a discrete population balance (DPB) model, and the effective aggregation rate constant is obtained by fitting with the experimental data.

***Key words**: Hot melt fluidized bed, PBM, DPB, EKE kernel, Aggregation rate constant.*

1. Introduction

Hot melt fluidized bed coating is an advanced technology for the preparation of microcapsules and it is commonly used in the food, pharmaceutical, and chemical industries. The coating process involves the agglomeration and breakage of the particles. In most studies of the model, the agglomeration model is used to describe the coating process. Tan et al (2004c) [1] showed that the agglomeration rate of the particles was much greater than the breakage rate in the melt granulation experiments. For the coating process of particle groups, particles of different sizes are transformed into each other through nucleation, growth, and breakage. Through the introduction of the particle population balance model (PBM), a conservation relationship is established between particles of various sizes in the system. Anette et al[2] established a theoretical model to quantitatively explain the agglomeration growth rate, which was in good agreement with the experiment; C.F.W. Sanders et al[3] predicting high shearing granulation behavior in the granulation process based on discrete population balance (DPB) model; Tan et al[4,5] deduced the EKE kernel based on particle growth kinetics theory to describe the net growth rate of hot melt spray fluid bed coating. In these models, the growth process of the particles is reflected from different aspects. However, the study on the constant of aggregation rate in the process of hot melt fluidized bed coating is rare.

This study only considers the agglomeration process in the coating process of hot melt fluidized bed. The main purpose is to incorporate the EKE kernel into a discrete population balance (DPB) model and use MATLAB for numerical simulation. The experimental data is fitted to a discrete population balance model to obtain an effective constant for aggregation rate.

2. Simulation Methods

2.1 Establishment of a population balance model (PBM)

In the process of hot melt fluidized bed coating, the agglomeration and breakage of particles resulted in non-uniform particle size. A population balance model (PBM) is introduced to establish a conservation relationship for each size particle in the system, describe the change of particle size distribution with time or space during the coating process, and reflect the process of particle growth and extinction. PBM is expressed by describing the rate of change of the particle size distribution density function. The model equation is:

$$\frac{\partial n(t,v)}{\partial t} = B^0(t,v) - \frac{\partial}{\partial v}[G(t,v)n(t,v)]$$

$$+ \frac{1}{2}\int_0^v \beta(t,v-\varepsilon,\varepsilon)n(t,v-\varepsilon)d\varepsilon - n(t,v)\int_0^\infty \beta(t,v\varepsilon)n(t,\varepsilon)d\varepsilon \qquad (1)$$

$$+ \int_0^\infty S(t,\varepsilon)b(v,\varepsilon)n(t,\varepsilon)d\varepsilon - S(t,v)n(t,v)$$

$$- O(t,v)n(t,v)$$

where $n(t,v)$ is a number density function, v and ε are the mass of particles or granules, B is the nucleation rate, G is the growth rate, β is an aggregation kernel, S is a selection function, b is a breakage function.

The aggregation kernel uses the EKE kernel described by Hounslow (1998) [6] based on the theory of gas dynamics. Expressed as:

$$\beta_{i,j} = \beta_0(t)(l_i + l_j)^2 \sqrt{\frac{1}{l_i^3} + \frac{1}{l_j^3}} \qquad (2)$$

where β_0 is the second-order rate constant, and l_i and l_j represent particles of size i and j. This model uses the particle flow dynamics theory described by Goldschmidt et al[7] to provide a theoretical basis for the particle collision frequency in a fluidized bed. β_0 can be expressed as:

$$\beta_0(t) = \psi g_{ij}\sqrt{\frac{3\theta_s}{\rho}} \qquad (3)$$

where ψ is defined as the ratio of the aggregation rate to the collision rate, g_{ij} is the particle radial distribution function, ρ is the particle density, θ_s is the particle temperature. Based on this work, it is considered that β_0 should be a constant for any set of experimental conditions, so in all the work here, β_0 can be described by the value of a single time-independent parameter.

2.2 Solution to the population balance equation

In order to solve the equation of population balance model, this study uses the method of discretization[8].It ensures correct prediction of particles number and volume for the aggregation terms. In the discretization scheme used, the length domain is divided into

geometric intervals where the ratio of the upper and lower limits of each size interval is $r = \sqrt[3]{2}$. By assuming that the system is well-mixed, the discrete equation that gives the rate of change of the number of particles in the i th interval is:

$$\frac{dN_i}{dt} = N_{i-1} \sum_{j=1}^{i-2} 2^{j-i+1} \beta_{i-1,j} N_j + \frac{1}{2} \beta_{i-1,j-1} N^2{}_{i-1}$$
$$- N_i \sum_{j=1}^{i-1} 2^{j-1} \beta_{i,j} N_j - N_i \sum_{j=1}^{n_{eq}} \beta_{i,j} N_j \tag{4}$$

N is the number of particles in a particular size class. Use MATLAB to solve the discretized numerical model.

2.3 Calculation of the aggregation rate constant β_0

The rate extraction problem is treated as a simple chi-square minimization process in the manner of Press et al[9]. In considering only the aggregation model, assuming that the aggregation rate is independent of time, the equation (2), (4) is simultaneously fitted with the mass-based experimental data to obtain the aggregated rate constant β_0 for the entire experiment. Using the integral fitting technique to minimize the chi-square method χ^2:

$$\chi^2(p) = \sum_i \sum_k \{ [\hat{W}_i(t_k) - \tilde{W}_i(t_k, p)]^2 \} \tag{5}$$

Where P is the fitting parameter vector, $\hat{W}_i$ is the mass-weighted particle size distribution of the experiment, and $\tilde{W}_i$ is the predicted particle size distribution.

3. Experimental

Using the method of spray cooling granulation, the citric acid is subjected to granulation experiments using a fluidized spray granulation device. Experimental device flow chart shown in fig 3-1:
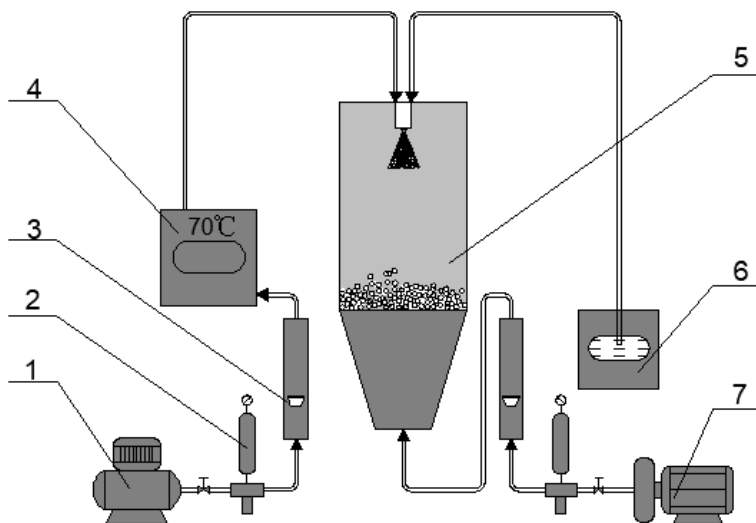
Fig 3-1 Citric acid experiment flow chart. 1, Air compressor; 2, Water separator; 3, Air flow meter; 4, Constant temperature water bath; 5, Spray fluidized bed; 6, Lipid; 7, Fan.

The experimental materials selected citric acid particles and lipid (butter), citric acid particles as the core material, and lipid as the wall material. 150 g of citric acid particles are weighed and frozen in a freezer at -30°C for 24 hours. The lipid is heated and melted and sent to the nozzle, mixed with air in the nozzle, and then atomized into droplets. The citric acid particles are placed in a spray fluidized bed and the fluidized citric acid particles collide with the atomized droplets to wet, coat, and granulate.

The absolute pressure of atomization during the experiment is 0.6 MPa. The flow rate of citric acid particles is 0.5m/s. The experiments are divided into 4 groups. The fluidization time is 0.5min, 1.0min, 1.5min and 2.0min respectively. Each set of experiments is repeated 3 times. At the end of the experiment, the fan is turned off and the nozzle spray is stopped. The experimental sample is taken out and sieved. The percentage of mass is used as an important criterion for evaluating granulation, and the particle size distribution of each set of experimental samples is determined.

4. Results and discussion

The particle size distribution of each experimental sample is shown in fig 4-1:

(a)t=0min   (b)t=0.5min

(c)t=1.0min   (d)t=1.5min

(e)t=2.0min   (f)Mean Size
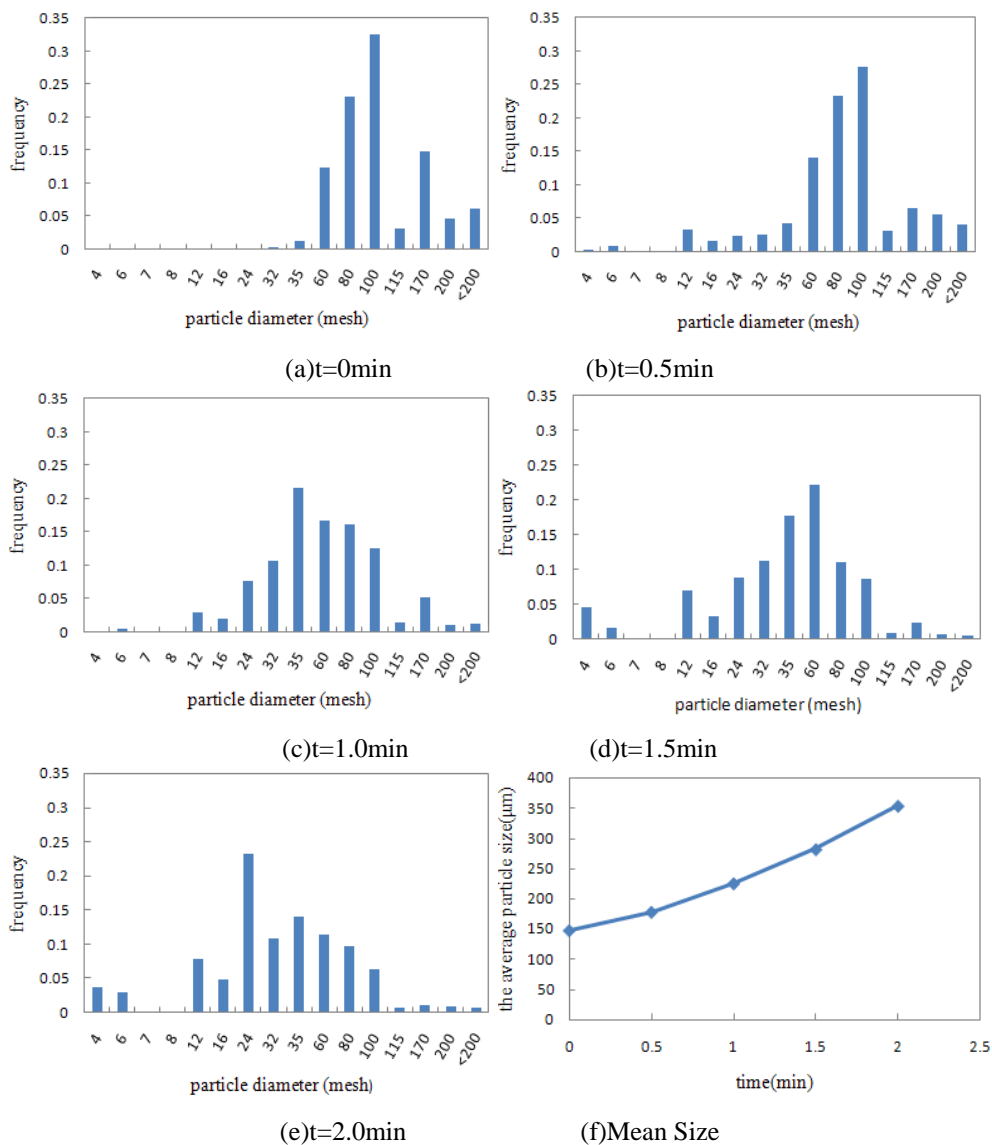
Fig 4-1 Particle size distribution based on mass at different time.The last figure shows the change mean size.

As shown in fig. 4-1, at t = 0min, that is, the citric acid particles are not embedding with lipid at the initial time. The distribution of particles is observed to be concentrated between 60 mesh and 200 mesh, with a particle size of 100 mesh particles having the highest mass percentage, accounting for 23%.

As shown in fig (b), the lipid is atomized and coated on citric acid particles. After spraying for 0.5 min, the experiment is ended and the particle size distribution is analyzed. Compared with fig (a), the particle size distribution range is larger, mainly distributed between 12 and 200 mesh, with the largest distribution of citric acid particles between 60 mesh and 100 mesh. However, the percentage of particles with a particle size of 100 mesh is still the largest, accounting for 28%. This is because the lipid is applied atomically to the fluidized citric acid particles so that the particles are coated and the diameter of the particles increases. However, when the coating is applied for 0.5 min, the percentage of the particles between 4 and 6 mesh was almost zero.

In fig (c), the experiment is performed for 1.0 min. It can be observed from the figure that the particle size distribution is mainly concentrated between 12 mesh and 100 mesh, among which the citric acid particles distributed between 24 mesh and 100 mesh are the most, and the citric acid particles with particle size 35 mesh are the most distributed, accounting for 21%, Compared to fig (b), the percentage of particles in each particle size range increased. Particles between 115 mesh and 200 mesh gradually decreased with increasing experimental time. This is due to the fact that as the experimental time increases, more lipid and citric acid particles contact and collide, so that the particles are sufficiently agglomerated, the particles in a small size range are reduced, and the particle size is increased. Relative to fig (b), the particle size distribution of fig (c) is relatively uniform, showing a normal distribution as a whole.

Fig (d) shows that the entire experiment is 1.5 minutes. Compared to (c), large granules of citric acid are present, with an increase in granule size of 4 mesh citric acid particles, and few particles between 115 mesh and 200 mesh. The particle size range of the particles is also concentrated between 12 mesh and 100 mesh. At this point, the particle size distribution is 60 mesh with the largest percentage of particles, accounting for 22%.

The particle size distribution in fig (e) is similar to that of fig (d). The particle size distribution range is basically the same and is mainly concentrated between 12 mesh and 100 mesh. However, the particle size distribution of 24 mesh particles is the largest, accounting for 23%.

With the increase of the experimental time, citric acid is embedded in lipid, and the average particle diameter increases. This is because the lipid is sprayed onto the fluidized particles after atomization and the particles are coated.When the experiment time increases, the quality of the atomized wall material increases, while the quality of the core material does not change. Then, the mass-based particle size distribution of citric acid particles at different times is fitted to a discrete population balance model. Solve using MATLAB to get β_0 =7.5*10$^{(-6)}$ kg m$^{-1/2}$ s^{-1}.

5. Conclusion

A hot melt fluidized bed coating experiment using lipid-citric acid as the research object. The agglomeration of particles leads to non-uniform particle size, The particle size distribution range is larger, mainly concentrated between 12 mesh and 100 mesh, and the mass-based particle size distribution as a whole shows a normal distribution.

The experimental data is fitted to a discrete population balance model, and the aggregation rate constant $\beta_0 = 7.5 * 10^{(-6)}$ kg m$^{-1/2}$ s^{-1}.

6. References

[1] Tan H.S.; Salman A.D.; Hounslow M.J. Kinetics of fluidised bed melt granulation IV: Selecting the breakage model. Powder Technology 2004, 143–144, 65–83.

[2] Anette P.; Klaus K., Bernhard C.L. Preparation of sustained release matrix pellets by melt agglomeration in the fluidized bed: Influence of formulation variables and modeling of agglomerate growth. European Journal of Pharmaceutics and Biopharmaceutics 2010, 74, 503–512.

[3] Sanders C.F.W.; Willemse A.W.; Salman A.D.; Hounslow W.J. Development of a predictive high-shear granulation model. Powder Technology 2003, 138, 18-24.

[4] Tan H.S.; Salman A.D.; Hounslow M.J. Kinetics of fluidized bed melt granulation—II: Modelling the net rate of growth. Chemical Engineering Science 2006, 61, 3930–3941.

[5] Tan H.S.; Salman A.D.; Hounslow M.J. Kinetics of fluidised bed melt granulation V: Simultaneous modelling of aggregation and breakage. Chemical Engineering Science 2005, 60, 3847 – 3866.

[6] Hounslow, M.J. The population balance as a tool for understanding particle rate processes. Kona Powder & Particle Journal 2014, 16, 179–193.

[7] Goldschmidt, M.J.V. Hydrodynamic modelling of fluidised bed granulation. Ph.D. Thesis, Process Technology Institute of Twente, Twente University, Enschede, 2001.

[8] Hounslow, M.J.; Ryall, R.L.; Marshall, V.R. A discrete population balance model for nucleation, growth and aggregation. A.I.Ch.E. Journal 1988, 11(34), 1821–1832.

[9] Press,W.H.; Teukolsky, S.A.; Vetterling,W.T.; Flannery, B.P. Numerical Recipes in FORTRAN: The Art of Scientific Computing. seconded. Cambridge University Press, Cambridge, 1992.

Study of the hot air drying process of chicken breast by non-invasive techniques

Tomas-Egea, J.A.[a]; Castro-Giraldez, M.[a*]; Colom, R.J.[b]; Fito, P.J.[a]

[a] Instituto Universitario de Ingeniería de Alimentos para el Desarrollo. Universitat Politècnica de València, Valencia, Spain

[b] Instituto de Instrumentación para Imagen Molecular, Universitat Politècnica de Valencia, Valencia, Spain.

*marcasgi@upv.es

Abstract

Food drying is one of the main unit operations for food preservation and it is based on the difference of chemical potential between the product and a fluid with lower chemical potential. The objective of this work was the development of a thermodynamic model of chicken meat drying process using infrared thermography; also the viability of using dielectric spectroscopy as a monitoring system was analyzed. A thermodynamic model has been developed to predict the expansion/contraction phenomena of poultry meat throughout the drying process. Moreover, it was demonstrated that permittivity is a non-destructive method to monitor the evolution of drying process.

Keywords: *Poultry meat, hot air drying, permittivity, infrared, drying kinetics.*

1. Introduction

Food drying is one of the main unit operations to preserve food[1]. The process is carried out by the difference of chemical potential between the product and a fluid (hot air) with lower chemical potential. Drying is based on three stages: induction period, period of constant drying speed and period of decreasing drying speed. During the first stage, the water transport occurs due to the difference of chemical potential between the food and the hot air, increasing the temperature of the surface. In the second stage, all the heat is used to evaporate the water, which comes from the inside faster than it evaporates from the surface, therefore, its temperature does not change. After this, the product is dried until the speed with which the water reaches the surface is less than the rate of evaporation and the heat received is used to evaporate the water as well as to heat the product.

Given the importance and extended use of hot air drying in the food industry, to model the behavior of the sample that occurs during dehydration is very useful to optimize the industrial process. A similar thermodynamic model was already reported for hot air drying process of pork meat[2]. Several authors have modeled the water transport of other products like red pepper[3], salty pork meat[4,5], apple[6] and sweet potato[7].

The permittivity (ε*) is the physical property that describes the interaction between a flux of photons and the medium through which photons circulate. Thus, the analysis of the electrical properties of a flux of photons when it passes through a biological system allow determining the quantity and state of the chemical species of the system. Infrared thermography is a technique that provides information about the heat transfer in meat tissues[8] and consists in the measurement of the infrared radiation emitted by a body surface getting an image of its thermal distribution. Thus, infrared thermography and the permittivity analysis, offer the possibility to analyze the process by a non-destructive way.

The objective of this work is the development of a thermodynamic model of the chicken meat drying process using infrared thermography; also the viability of using dielectric spectroscopy as a monitoring system is analyzed.

2. Materials and Methods

2.1. Raw Material

The experiments were carried out using boneless broiler breasts (Pectoralis major) obtained from a local supermarket. Cylinders of poultry breast were used for each analysis (2 cm of diameter and 1 cm of height); the cylinders were cut in perpendicular direction to the fibers.

2.2. Experimental procedure

Two samples were placed inside the hot air dryer. The drying operation was carried out, for a period of 67 hours, at a temperature of 40 °C and an air velocity of 1.5 m·s^{-1}. One of the

samples was hung from a Mettler Toledo PG503-S balance (precision of ± 0.01 g) in order to register the mass throughout the drying process. The other sample was placed on the right side of the dryer on a grid. This sample allow controlling continuously the surface temperature. Moreover, two needle electrodes sensor was placed on this sample to measure the permittivity by continuous radiofrequency spectrophotometry. The flat face of both cylindrical samples was located in perpendicular to the drying air. A reference material of known emissivity (ε = 0.95 - Optris GmbH) was placed next to the samples. Also, the temperature of the drying air, sample, reference material and environment were measured with K-thermocouples connected to an Agilent multiplexer 34901A (Agilent Technologies, Malaysia) and registered by an Agilent Data Acquisition equipment 34972A (Agilent Technologies, Malaysia). After the drying treatment, the samples were kept in aqualab® disposable sample cups, sealed with parafilm® for further analysis.

Water activity, moisture and volume were measured in fresh samples and also in dried samples. Mass, permittivity and thermal images were registered continuously as was explained above.

2.3. Infrared measurements

The infrared analysis was carried out following the method decribed by Traffano-Schiffo et al. (2014)[9], using an infrared camera (Optris PI® 160 thermal imager, Optris GmbH, Berlin, Germany) installed in front of the sample, at an angle of 0º relative to the plane in which the samples were placed. The camera uses a two-dimensional Focal Plane array with 160x120 pixels, a spectral range of 7.5-13 μm, resolution of 0.05 °C and an accuracy of ± 2%. The camera covers at a temperature range of -20 to 900 ° C. It has a field of vision of 23 ° x17 ° with a minimum distance of 2 cm. The camera uses Optris PI Connect software (Optris GmbH, Berlin, Germany).

2.4. Radiofrequency measurements

The sensor used was developed by the Dielectric Properties Laboratory (Instituto Universitario de Ingenieria de Alimenos para el Desarrollo IuIAD) and the Instituto de Instrumentación para Imagen Molecular (I3M) both belonging to the Universitat Politècnica de València (UPV), Valencia, Spain. It consists of two needle electrodes located on both sides of the cylindrical face of the sample. The sensor is connected to an Agilent 4294A impedance analyzer. The measuring frequency range is from 40 Hz to 1 MHz and the calibration is performed in open and short-circuit.

2.5. Physico-chemical measurements

Water activity was determined with a dew point hygrometer Aqualab®, series 3 TE, with an accuracy of ± 0.003. The mass of the samples was determined with a Mettler Toledo AB304-S balance, with an accuracy of ± 0.001 g. The volume was determined with Adobe ©

Photoshop © CS6 software by image analysis. Moisture was obtained with the ISO 1442 (1997) standard for meat products, drying the samples at 110 ºC and atmospheric pressure until reaching a constant mass.

3. Results and discussion

The monitoring of the process with the termographic camera need a correction in the temperature values, that made Traffano Schiffo et al., 2014[9].

With the evolution of the real temperature obtained by the camera and the physicochemical determinations, it is possible to apply irreversible thermodynamics to model the drying process, in order to analyze the influence of the structure in the water transport during drying. For this purpose, the Gibbs free energy variation (Eq. 1)[10] was applied in the system interface described in figure 1.

$$dG = -SdT + VdP + Fdl + \psi de + \sum_i \mu_i \, dn_i \qquad (1)$$

Where: SdT represents the entropic term related to heat fluxes; VdP represents the mechanical energies related to the variation of pressure; Fdl represents the mechanical energies related to the elongation force; and ψde represents the effect of the electric field induced by solved ions. The term $\sum_i \mu_i \, dn_i$ corresponds to the activity term and is the addition of the chemical potentials of the "i" component, being constant the rest of state variables.
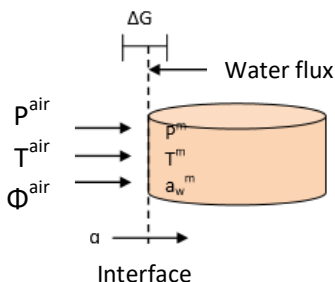
Fig. 1 Diagram of the interface of the chicken sample during drying.

Considering the variation of free energy per mole of water, it is possible to define the extended chemical potential of water according to the equation 2.

$$\Delta \mu_w = \frac{\Delta G}{\Delta n_w} \qquad (2)$$

Where: $\Delta \mu_w$ = chemical potential of water (J·mol^{-1}); ΔG = variation of Gibbs free energy (J); Δn_w = moles of water (mol).

Combining the last two equations, the equation 3 is obtained. The terms Fdl and ψde of the equation 1 could be neglected, since the muscle tissue is elastic and the meat only has native ions.

$$\Delta\mu_w = -s_w \left(T^{air} - T^m\right) + v_w \left(P^{air} - P^m\right) + RT^m \ln \frac{a_w^m}{\varphi^{air}} \qquad (3)$$

Where: s_w = partial molar entropy of the water (J·K^{-1}·mol^{-1}); T = temperature (K); v_w = partial molar volume of water (m^3·mol^{-1}); P = pressure (Pa); R = constant of ideal gases (8.314472 J·K^{-1}·mol^{-1}); a_w = water activity of sample; φ = relative ambient humidity. Being the superindexes: m = sample; air = air.

With the temperatures obtained by means of infrared thermography and the evolution of the moisture of the sample, estimated with the variation of mass during the process and the initial moisture, the entropic term can be calculated. For the activities term, a sorption isotherm of poultry was obtained and modeled by GAB (x^0_w = 0.077, C = 420, K = 0.98) (Fig. 2). Finally, the term of mechanical energies of the equation 3 (second term) can not be calculated, since the pressure variation of the sample can not be measured.
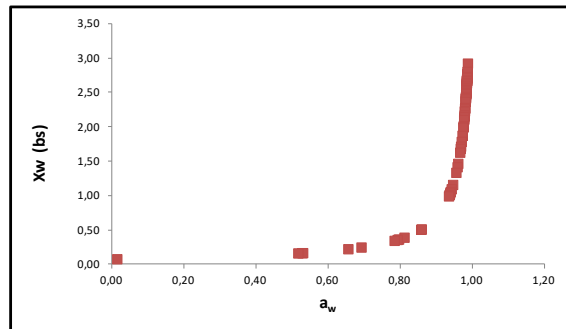
Fig. 2 Poultry sorption isotherm.

According to Onsager's relations[10], the molar water flux is related to its chemical potential, which acts as a driving force for water transport, by means of the phenomenological coefficient (Eq. 4). The phenomenological coefficient is constant in reversible processes, but if the storage of mechanical energy produces irreversible breaks in the medium, the phenomenological coefficient will evolve as a function of the transformation suffered by the tissue.

$$J_w = L_w \cdot \Delta\mu_w \qquad (4)$$

Where: J_w = molar flow of water (mol·s^{-1}·m^{-2}); L_w = phenomenological coefficient (mol^2·J^{-1}·s^{-1}·m^{-2}); $\Delta\mu_w$ = chemical potential of water (J·mol^{-1}).

In order to obtain the phenomenological coefficient, water flux was estimated as follows (Eq. 5):

$$J_w = \frac{\Delta M_w^m \cdot M_0^m}{\Delta t \cdot S^m \; Mr_w} \tag{5}$$

Where: J_w = water flux (mol·s^{-1}·m^{-2}); ΔM_w^m = variation of water mass of the sample (kg); M_0^m = initial mass of the sample (kg); Δt = time of the process (s), S^m = surface of the sample (m^2); Mr_w = molecular mass of water (18 g·mol^{-1}).

As was explained above, it is not possible to calculate the mechanical term of the chemical potential, therefore the chemical potential of water was determined without considering the mechanical terms ($\Delta\mu_w^*$). With the water flux and the chemical potential of water was determined without considering the mechanical terms, the phenomenological coefficient was estimated (Eq. 6).

$$L_w^* = \frac{J_w}{\Delta\mu_w^*} \tag{6}$$

In figure 3 it can be apreciated that there is a linear relation between L_w^* and J_w after 15 minutes of drying. Therefore, following that linear prediction of the phenomenological coefficient it is possible to estimate the mechanical terms with the equation 7 (Fig. 4).

$$v_w \, \Delta P = \Delta\mu_w - \Delta\mu_w^* \tag{7}$$
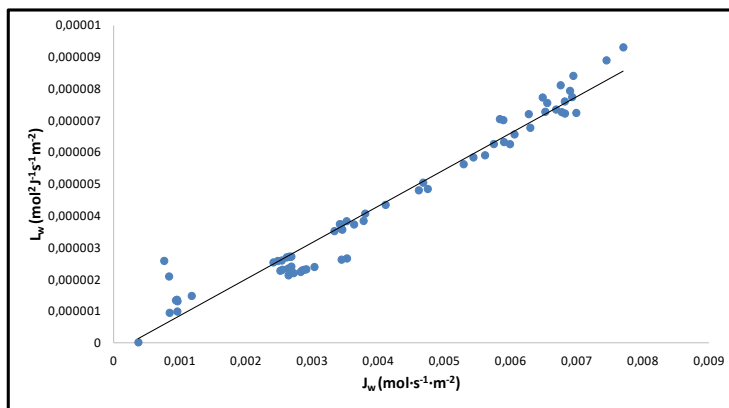
Fig. 3 Relation between the phenomenological coefficient, without considering the mechanical terms, and the water flux from 15 minutes of drying until the end of the treatment.

The evolution of the mechanical energy indicates that there is an expansion of the tissue during the first 400 minutes, followed by a contraction associated with the remaining functioning of the muscle from that time (Fig. 4).
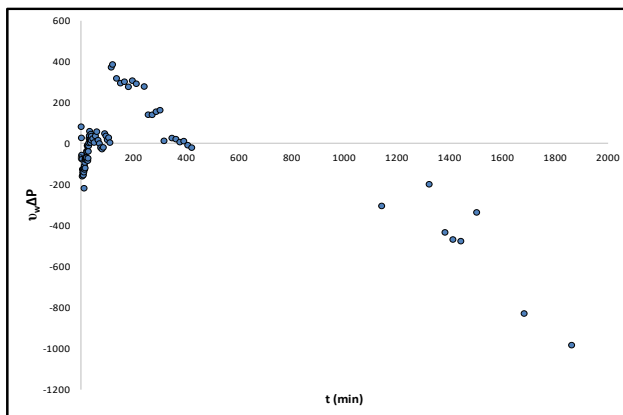
Fig. 4 Evolution of mechanical energy, developed from the thermodynamic model, throughout the drying treatment.

The permittivity in radiofrequency was measured throughout the drying treatment. It was found a linear relation between the dielectric constant in α-dispersion (40 Hz) and the number of water molecules when the sample still presents liquid phase, since this dispersion is fundamentally related to the mobility of the ions dissolved in meat liquid phase. With the drying time, the content of the liquid phase begins to decrease (samples with adsorbed water only) and also the mobility of the ions. The value of the dielectric constant in this dispersion becomes practically null.

4. Conclusions

It has been demonstrated that infrared thermography is a good technique to monitor the process of drying in poultry meat, providing information of heat transfer in biological tissues, being possible to obtain the evolution of the emissivity of the meat. Thus, with this technique, it is possible to non-invasively obtain the surface temperature of the sample during the treatment.

A thermodynamic model has been developed to predict the expansion/contraction phenomena of poultry meat throughout the drying process, as well as to evaluate the driving forces of the drying process.

Finally, a direct relation between the permittivity in α-dispersion with regard to the number of water molecules has been demonstrated. It can be concluded that the permittivity is a non-destructive and rapid method to monitor the evolution of the drying process.

Acknowledgements

References

[1] Ratti, C.; Hot air and freeze-drying of high-value foods: a review. Journal of Food Engineering 2001, 49, 311-319.

[2] Doymaz, I.; Pala, M. Hot-air drying characteristics of red pepper. Journal of Food Engineering 2002, 55(4), 331-335.

[3] Gou, P.; Comaposada, J.; Arnau, J. Meat pH and meat fibre direction effects on moisture diffusivity in salted ham muscles dried at 5 ºC. Meat science 2002, 61(1), 25-31.

[4] Clemente, G.; Bon, J.; Sanjuán, N.; Mulet, A. Drying modelling of defrosted pork meat under forced convection conditions. Meat science 2011, 88(3), 374-378.

[5] Wang, Z.; Sun, J.; Liao, X.; Chen, F.; Zhao, G.; Wu, J.; Hu, X. Mathematical modeling on hot air drying of thin layer apple pomace. Food research international 2007, 40, 39-46.

[6] Diamante, L.M.; Munro, P.A. Mathematical modelling of hot air drying of sweet potato slices. Food science and technology 1991, 26, 99-109.

[7] Traffano-Schiffo, M.V.; Castro-Giraldez, M.; Fito P.J.; Balaguer, N. Thermodynamic model of meat drying by infrarred thermography. Journal of Food Engineering 2014, 128(0), 103-110.

[8] Workmaster B. A.; Palta, J. P.; Wisniewski, M. Ice nucleation and propagation in cranberry uprights and fruit using infrared video thermography. Journal of the American Society for Horticultural Science 1999, 124, 619.

[9] Traffano-Schiffo, M. V.; Castro-Giráldez, M.; Fito, P. J.; Balaguer, N. Thermodynamic model of meat drying by infrarred thermography. Journal of Food Engineering 2014, 128, 103-110.

[10] Castro-Giráldez, M.; Fito, P.J.; Fito P. Non-equilibrium thermodynamic approach to analyze the pork meat (Longissimus dorsi) salting process. Journal of Food Engineering 2010, 99(1), 24-30.

Flat plate solar air heater with helical integrated fins for drying processes

Al-Neama, M. A.[a] ; Farkas, I.[b]*

[a] Mechanical Engineering Doctoral School. Szent István University, Gödöllő, Hungary
[b] Department of Physics and Process Control. Szent István University, Gödöllő,Hungary

*E-mail of the corresponding author: Farkas.Istvan@gek.szie.hu

Abstract

In this study, an experimental investigation was carried out on solar system consists of many main components; solar air collector, drying chamber and air blower. Manufacturing and an analysis of two active double-pass solar air collector integrated with unfinned and helical finned absorbers have been carried out. The helical fins increased the standers solar collector (unfinned) efficiency by about 6%. In five hours for 2 kg of apple slices drying, the final weight of the dried product is 1.237 kg using an unfinned solar collector, while 1.039 kg using helical finned solar collector.

Keywords: solar drying, air heater, thermal performance, helical fins.

1. Introduction

Drying is a complicated process including the transient transfer of mass and heat with several rate processes, such as physical or chemical transformations, which, in turn, may cause changes in product quality as well as the mechanisms of heat and mass transfer [1].

Air heater is the essential equipment through which solar energy is converted into heat energy. However, how to increase the thermal efficiency of solar air heaters becomes a significant challenge. In this paper, the design of different solar air heater with different absorber plate is discussed. Many parameters are affecting significantly on thermal performance of the solar collector, such as area of absorber, shape of absorber, speed of air, number of flow passes, number of glasses, material of absorber,…, etc. The major parameters which discussed in this paper is the absorber shape and absorber area. Solar air collectors are classified basically into two types: bare plate and cover plate solar air heaters.

The bare plate solar air heaters consist simply of an air duct, the upper surface of which operates as the solar-energy absorber plate and the back surface insulated. For covered-plate solar air-heating collectors, to reduce upward heat losses from solar air heaters transparent cover materials above and usually parallel to the absorber plate are used of one or more [2]. The performance of solar collectors under low-temperature conditions measured and simulated. The experimental results showed that for temperatures below ambient and for cases without irradiance, unglazed collectors performed better than glazed ones, with considerable heat gains from condensation and frost. The glazed collectors are not suitable to operate at temperatures below the dew point as condensation and frost conditions might lead to deterioration of materials, compromising the reliability and durability of this type of collector [3].

The performance of a double pass solar air heater tested in the previous studies, and the results showed that the thermal efficiency of double pass solar air collector with the porous material is 20–25% and 30–35% higher than that of double-pass solar collector without porous material and single pass collector respectively [4]. The effect of the cross-sectional configurations on the thermal performance of the plastic solar air heater is examined. The results indicated that the highest efficiency was achieved for the circular shape about 80% at a flow rate of 0.18 kg/s and average solar radiation of 925 W/m^2 [5]. The solar radiation incident on solar collector has little effect on the efficiency of the collector, although it has a significant impact on the ambient air temperature around the collector. The outlet air temperature in flow channel increases almost linearly with insolation [6].

According to the above brief review for past literature, in the recent paper, manufacturing, and analysis of active double-pass solar air collector integrated with helical shaped finned absorber is done to be carried out.

2. Materials and Methods

In this study, an experimental investigation was carried out on solar system consists of many principal components to achieve study goals. The solar system includes mainly of solar air heater, drying cabin and inline air blower. Insulated air ducts have connected the elements. The system designed, manufactured and tested in the laboratory of the Department of Physics and Process Control, Szent István University, Gödöllő, Hungary.

2.1. Solar air collector

A simple double air-pass solar air collector had been manufactured with 120×50×15 cm length, width and thickness (external dimensions) respectively. The outer case of solar air collector is made from wood sheets and bars with different thicknesses with dimensions. For study purpose, two absorbing surfaces are made from copper sheet with 1.5 mm thickness and thermal conductivity 385 W/mK (see Fig. 1). A black matt paint used to enhance these surfaces properties (selective surface). A polystyrene material with thermal conductivity 0.038 W/mK is used as back insulation. Back insulation thickness is 2 cm, and dimensions are 120×50 cm length and width respectively. The sides of the body were well insulated to prevent heat loss by using self-adhesive rubber foam tape with a thickness of 3 mm. A transparent cover fixed on the top edges of the collector wood case and thermal insulation at the bottom base side of the wooden case. A 4 mm thick plastic glass sheet used to cover solar collector.
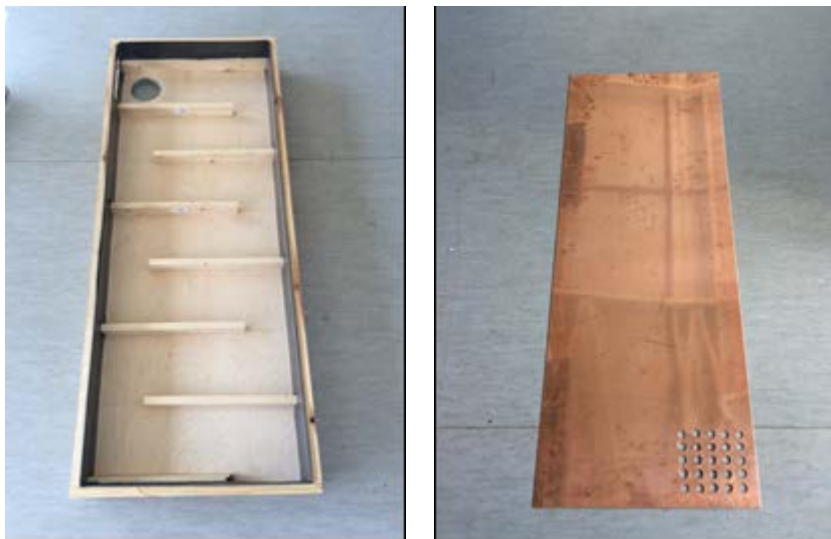
Fig. 1. Wooden case and absorbing surface of solar air heater

The first absorber is flat absorber (un-finned) with dimensions 46.2×121.8 cm, while the second absorber had made with the same aspects of the first surface with helical Aluminum fins to increase its area of surface. The dimensions of attached fins are shown in Fig. 2. Fins function is expanding air streams length with the absorber surface to improve the useful heat transfer to the air. The space between every two buffers is 17 m. Areas of air heater inlet, exit and second channel entrance are the same, to avoid pressure reduction through the solar collector.

4 cm

66.2 cm
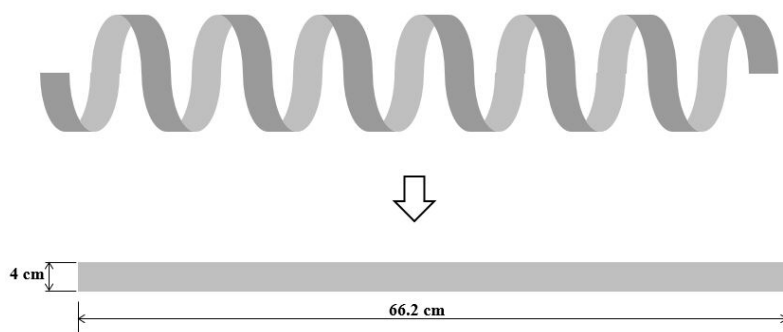
Fig. 2. Helical extended surfaces dimensions

The air recirculated from first to second air channel through 25 holes, which made on the absorber. Second air channel designed using many wood buffers which fixed on the back surface of a solar collector as shown in Fig. 1. Air circulates through the solar collector, inline air blower in air duct between solar heaters and surrounding has been used. According to Duffie and Beckman, flat-plate solar collector tilted in a way that it receives maximum solar radiation during the day and to be perpendicular to solar radiation rays at noon. The best stationary orientation is due South in the northern hemisphere and due North in the southern hemisphere. Therefore, the two solar air heaters in this work are oriented facing South line and tilted at 45o to the horizontal according to the solar chart for Budapest region (Budapest 47.5o N, 19.05o E) [7].

2.2. Drying cabin

The drying chamber is made with five trays where the different products items are placed. The external chamber dimensions are 50×50×100 cm length, width, and height respectively, as shown in Fig. 3. Dryer walls have been made from polystyrene with 5 cm thickness and thermal conductivity 73 W/mK, except the front wall of chamber made from

4 mm plastic glass sheet for observing. The five trays made from plastic nets and fixed with 10 cm distance between each. The chamber integrated with the solar air heater by a small duct (indirect drying) with 10 cm diameter.

All air leakages from drying space closed totally as possible. The product sample which used through this study is apple. Apple selected as a sample because of its high initial moisture content and its high maximum allowable temperature. The initial moisture content and maximum allowable temperature for an apple during drying process are 80% (wet base) and 70 °C respectively [8].
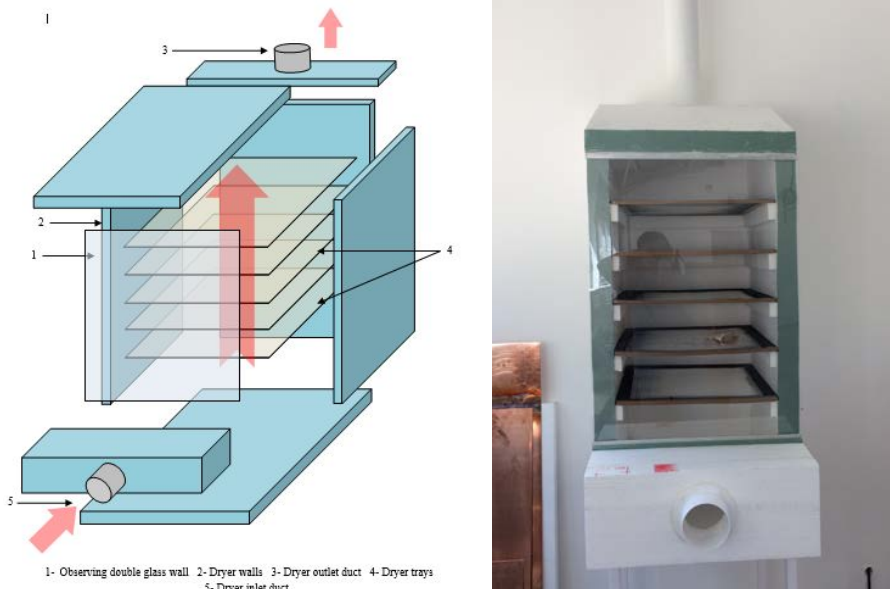
Fig. 3. Layout of drying chamber

3. Results

Two sets of results are collected, the first set shows the experimental results of the double air pass unfinned solar heater test, the second set shows the experimental results of double air pass helical finned solar heater test. Airspeed for these tests is 2.3 m/s with air duct cross-section area 0.00635 m². Properties of air which considered for performance calculations are 1.2 kg/m³ and 1000 J/kgK density and air specific heat at constant pressure respectively. The tests carried out on 2nd and 9th of October 2017. The daily efficiency for unfinned solar collector was 54.8%. The helical fins increased the standers solar collector

efficiency by about 6%. Fig. 4 and Fig 5 showed the relative humidity and temperature stratification in drying chamber by using unfinned solar air collector. Fig. 6 and Fig 7 showed the relative humidity and temperature stratification in drying chamber by using helical finned solar air collector.
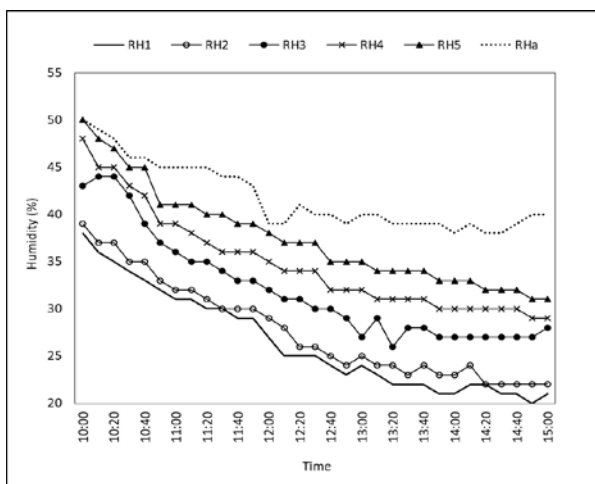
Fig. 4. Relative humidity distribution in drying chamber by using unfinned collector
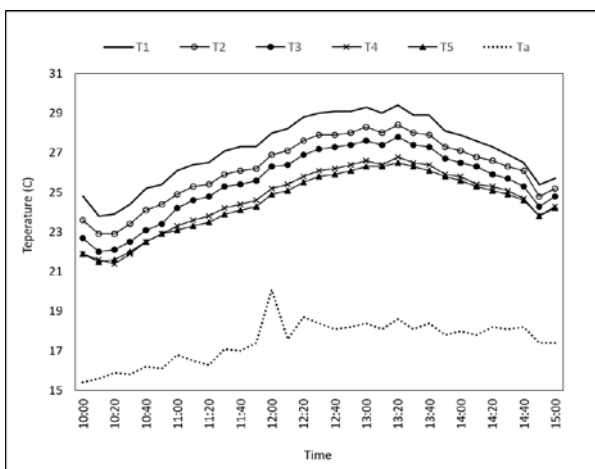
Fig. 5. Temperature distribution in drying chamber by using unfinned collector

It is clear that the product loses of its moisture in a short time at the beginning of the process, and much time is needed for the remaining water content to be lost. Humidity stratification is more obvious with using unfinned collector. In five hours for 2 kg of apple slices drying, the final weight of the dried product is 1.237 kg using an unfinned solar collector, while 1.039 kg using helical finned solar collector.
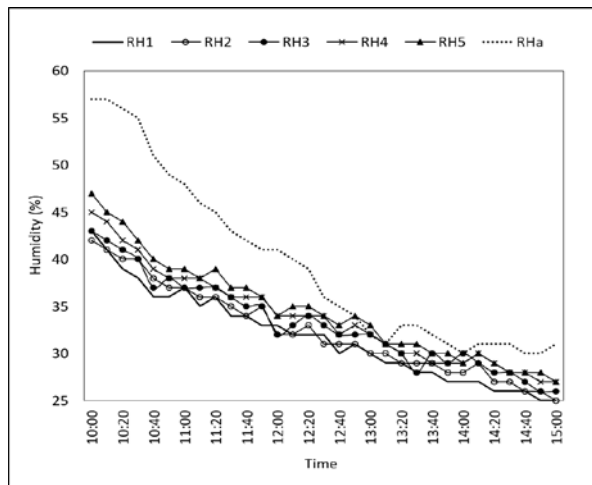
Fig. 6. Relative humidity distribution in drying chamber by using helical finned collector
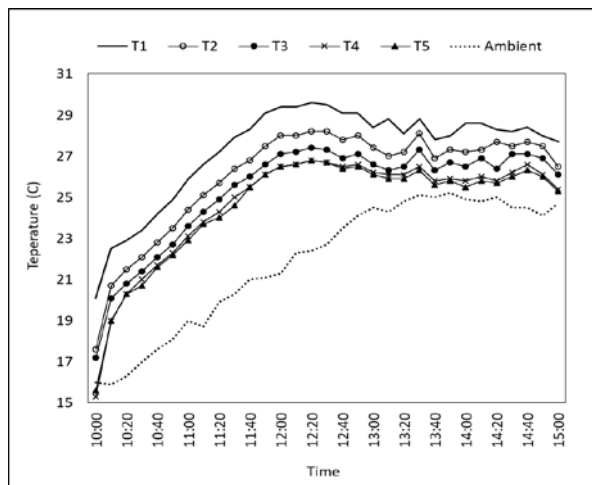
Fig. 7. Temperature distribution in drying chamber by using helical finned collector

4. Conclusions

1. The daily efficiency for unfinned solar collector was 54.8%.

2. The helical fins increased the standers solar collector efficiency by about 6%.

3. In five hours for 2 kg of apple slices drying, the final weight of the dried product is 1.237 kg using an unfinned solar collector, while 1.039 kg using helical finned solar collector.

4. The costs of designing and manufacturing process of solar drying system are low compared with other drying methods.

5. The maintenaces costs are uncomplicated and cheap.

6. Clean process with low electricity consumption.

5. References

[1] Neményi, M.; Farkas, I.; Czaba, I.; Kovács, A. Drying characteristics of maize hybrids' components. Hungarian Agricultural Engineering 1994, 7, 40-41.

[2] Ekechukwu, O.; Norton, B. Review of solar-energy drying Systems II: an overview solar drying technology. Energy Conversion and Management Journal 1999, 40, 615-655.

[3] Bunea, M.; Eicher, S.; Hildbrand, C.; Bony, J.; Perers, B.; Citherlet, S. Performance of solar collectors under low temperature conditions: Measurements and simulations results. Paper presented at Eurosun, 2012, Rijeka, Croatia.

[4] Ramani, B.M.; Gupta, A.; Kumar, R. Performance of a double pass solar air collector. Solar Energy 2010, 84, 1929–1937.

[5] Abdullah, A.S.; El-Samadony, Y.A.F; Omara, Z.M. Performance evaluation of plastic solar air heater with different cross sectional configuration. Applied Thermal Engineering 2017, 121, 218-223.

[6] Rai, S.; Chand, P.; Sharma, S.P. An analytical investigations on thermal and thermohydraulic performance of offset finned absorber solar air heater. Solar energy 2017, 153, 25-40.

[7] Duffie, J.; Beckman, W. Solar Engineering of Thermal Processes. Fourth edition, John Wiley & Sons, New Jersey. USA, 2013.

[8] Sharma, A.; Chen, C.R.; Lan, N.V. Solar-energy drying systems: A review, Renewable and Sustainable Energy Reviews Journal 2009, 13, 1185-1210.

Drying of sugarcane bagasse in a partially filled horizontal drum

Tada, É. F. R. [a]*; Bück, A.[b]; Casciatori, F. P.[c]; Thoméo, J. C.[a]

[a] Department of Food Engineering and Technology. Institue of Biosciences, Humanities and Exact Sciencies. São Paulo State University, São José do Rio Preto, Brazil

[b] Institute of Particle Technology. Friedrich-Alexander University Erlangen-Nuremberg, Erlangen, Germany.

[c] Chemical Engineering Department, Center of Exacts Sciences and Technology. São Carlos Federal University, São Carlos, Brazil.

*E-mail of the corresponding author: erikartada@gmail.com

Abstract

One-phase model have been reported to describing the simultaneous heat and mass transfer in a horizontal drum partially filled by sugarcane bagasse with attention to the loss of water promoted by the increase of temperature. Mass and energy balances were written in MatLab language and solved by finite difference method. Predicted temporal and spatial profiles of moisture content and temperature are shown. Experimental tests were carried out in a horizontal drum and the temporal profiles were obtained. Great adjustments between experimental and predicted data were observed, indicating that the model is able to describe the transport phenomena in this system.

Keywords: horizontal drum; heat and mass balances; sugarcane bagasse; solid-state fermentation process.

1. Introduction

Rotary drums are widely employed in several industrial processes involving particulate systems. Specifically in solid-state fermentation processes, the use of rotary drum bioreactors have been investigated because these equipments offer more mechanisms to control of operational conditions during the fermentation process [1].

Solid-state fermentation (SSF) is a prodigious technology that it enables the obtention of high-value compounds from solid cultive of microorganisms in wet agro-industrial residues [2], as such the fibers of sugarcane bagasse [3]. Promissors results have been reported by literature in laboratorial scale on the yield of compounds through FES [4]. However, the industrial scale yet is not available to use due to difficulties related to scale-up of bioreactors for FES, such as the undesirable increases of temperature during the process. Considering the use of rotation in intermittent regime as a mechanism of heat removal, the particles bed keeps static during long periods and then are periodically moved. This allows tha analysis of this process from a static bed in a horizontal drum.

The increase in the temperature observed during SSF process can promote other phenomena that deserve attention, such as the loss of water in heated regions of the bed. The recent literature has reported that the moisture content of the organic particles is directly related to bed properties as porosity and efficient thermal conductivity [5,6]. Fundamental studies have been reported about the no-reactional particulate systems in geometries similar to bioreactors and are important to understand some aspects about transport phenomena in these systems [7,8]. In this context, this work aims the proposition of heat and mass balances to descrive the temperature and water profiles in a partially filled horizontal drum by a sugarcane bagasse bed, in attention to possible water remotion due to increases on the temperature.

2. Materials and Methods

2.1. Phsysical situation

The physical situation in this case study is presented in Fig. 1. The horizontal drum was built in stainless stell and has 10 cm of inner dimeater and 20 cm of length. The inner wall of the drum was kept at constant temperature (45 ºC or 65 ºC) and the bed was initially at 25 ºC. The bed was continually heated by heat penetration through of the wall and the water removal occurried simultaneously as a response to increases in the temperature. The fibers of sugarcane bagasse were employed at 3 kg-water/kg-dried solid, which is corresponding to the operational condition for a solid-state fermentation process [3,9].
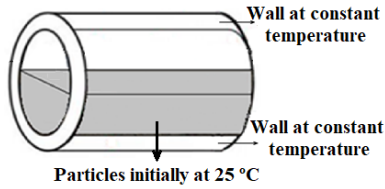
Fig. 1. Physical situation to verify the water removal in a partially filled horizontal drum due to increase in the temperature.

2.2. Mathematical model

A one-dimensional and one-phase model was proposed to describing the temporal and spatial temperature and water profiles in a partially filled horizontal drum. The water balance is shown in Eq. (1). In this equation, the first therm of left hand represent the temporal variation of water in the bed, the first therm of the right hand represent the spatial variation of water in the radial direction and the last term represent the water removal due to increase in the temperature. In this term, it was assumed that the moisture of the particles was carried by the air amidst the porous bed. The air was continuously heated and it described radial flow thorugh of the bed with velocity V_r.

$$\frac{\partial X}{\partial t} = D_{eff}\left[\frac{1}{r}\frac{\partial X}{\partial r} + \frac{\partial^2 X}{\partial r^2}\right] + \frac{\rho_a}{\rho_s}V_r f\frac{dT}{dr} \tag{1}$$

The energy balance is shown in Eq. (2).

$$\rho_b Cp_b\frac{\partial T}{\partial t} = K\left[\frac{1}{r}\frac{\partial T}{\partial r} + \frac{\partial^2 T}{\partial r^2}\right] + \left[(Cp_a - \lambda f)\rho_a V_r\frac{\partial T}{\partial r}\right] \tag{2}$$

The initial and boundary conditions are shown in Eqs. (3) to (8).

$$t = 0,\quad \left|\begin{array}{l} T = T_0 \\[2mm] X = X_0 \end{array}\right. \tag{3}\tag{4}$$

$$r = r_{i(\theta)},\quad \left|\begin{array}{l} K\dfrac{\partial T}{\partial r} = -\alpha\,(T - T_\infty) \\[3mm] D_{eff}\dfrac{\partial X}{\partial r} = -\beta\,(X - X_{eq}) \end{array}\right. \tag{5}\tag{6}$$

$$r = R, \qquad \begin{cases} T = T_w & (7) \\[2em] D_{eff} \dfrac{\partial X}{\partial r} = 0 & (8) \end{cases}$$

in which $r = r_{i(\theta)}$ is the superfitial position and $r = R$ represents the wall of the drum.

For the solution, the spatial variation were discretized by finite difference method. The resultant equations were written in MatLab® language and solved by *ode15s* for a geometry of a partially filled cincunference, as described by [8].

2.2.1. Parameters of the model

The effective diffusivity of the water through the bed have been experimentally determined by [10] as a function of the temperature. The effective thermal conductivity of sugarcane bagasse bed as a function of moisture content of the fibers was extracted from [5].

The coefficients α and β were teorically estimed using correlations available in the literature for the parallel flow of a fluid above the surface of a rugous flat plate. The velocity V_r was estimed using correlations for free convection through a packed-bed constituted by spherical particles.

2.2.2. Simulations and verification of the model

Simulations were carried considering the temperature of the wall (T_w) at 45 or 65 ℃ and the temporal predicted profiles were compared with experimental profiles. The experimental tests were carried out in a jacketed horizontal drum (inner diameter: 10 cm, length: 20 cm). The inner wall of the drum was kept at 45 or 65 ℃ and the fibers of sugarcane bagasse were insered in the drum at 25 ℃ and about 3 kg-water/kg-dried solid in filling degree 0.5. Samples of the bed were collected to determination of moisture content in a drying oven at 105 ℃ until constant weight. The quality of adjustment was evaluated thorugh statistical indicators such as the coefficient of determination (R^2) and the root mean square error (RMSE).

3. Results and Discussion

The temporal mean temperature profiles for T_w at 45 and 65 ℃ are shown in Fig. 2.
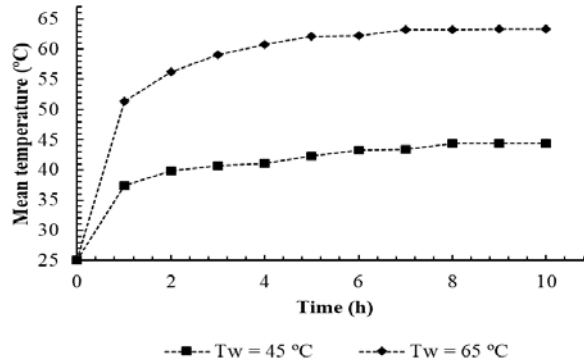
Fig. 2. Temporal mean temperature profiles of a sugarcane bagasse bed in a horizontal drum with temperature of the wall drum at 45 and 65 ºC.

The temperature increases subtly in the first hour as reported by [11] for a bed composed by dried fibers of sugarcane bagasse in this same horizontal drum. Discrete increase on the temperature were observed for the interval from 1 to 4 hours and the thermal equilibrium was obtained around t = 4 h of process for all conditions. It indicates that the initial no-isothermal problem becomes an isothermal problem along the time and it could be approximated and solved just through a mass balance for the equilibrium temperature in the interval from t = 4 h to t = 10 h. The spatial moisture content profiles for T_w at 45 and 65 ºC for t = 1 hour (on left hand) and 10 hours (on right hand) are shown in Fig. 3.
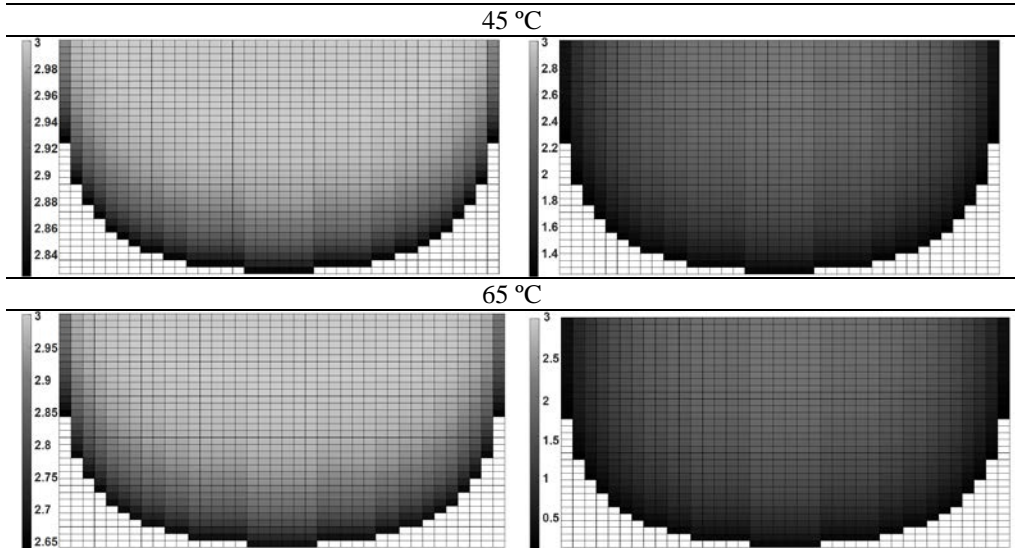
Fig. 3. Spatial moisture profiles (kg/kg-ds) of a sugarcane bagasse bed in a horizontal drum with temperature of the wall drum at 45 and 65 ºC.

The mass flux was observed in the radial direction from the wall to the surface of the bed. The presence of the air in the headspace promoted discrete variation on the moisture content in the surface of the bed because the air was partially satured on water vapor and its capacity to carry water was reduced. After 10 hours of process, the simulated profiles show that the system is near to the mass equilibrium.

The verification of the model is shown in Fig. 4 and 5 for the temperature and moisture profiles, respectively, for T_w at 45 and 65 ºC. Good agreements were observed between experimental and predicted profiles and them were supported by statistical indicators ($R^2 >$ 0,95 and RMSE < 0,62).

    (a) 45 ºC; $R^2 = 0.96$; RMS = 0.21   (b) 65 ºC; $R^2 = 0.95$; RMSE = 0.62
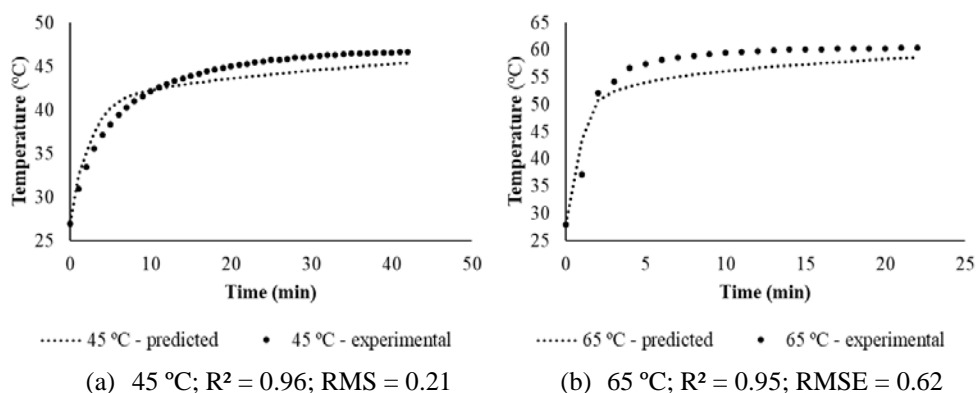
Fig. 4. Predicted and experimental temperature profiles in a horizontal drum partially filled by fibers of sugarcane bagasse (Tw = 45 ºC (a) or 65 ºC (b); T0 = 25 ºC).

    (a) 45 ºC; $R^2 = 0.99$; RMS = 0.06   (b) 65 ºC; $R^2 = 0.97$; RMSE = 0.06
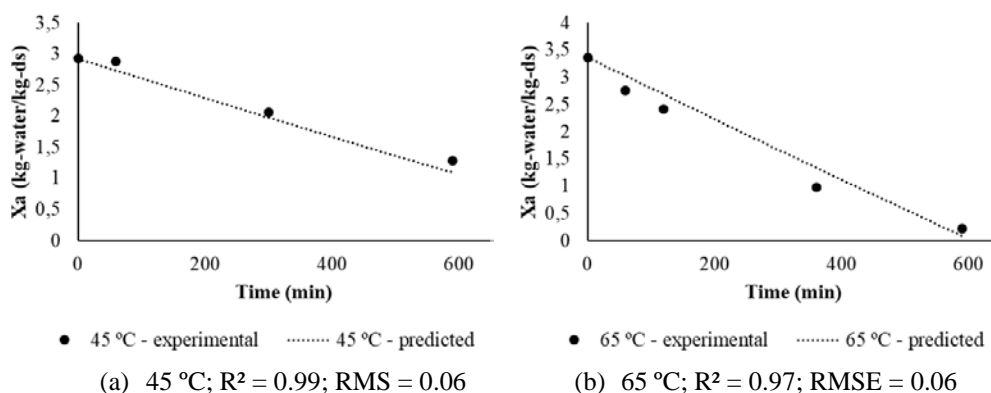
Fig. 5. Predicted and experimental moisture profiles in a horizontal drum partially filled by fibers of sugarcane bagasse (Tw = 45 ºC (a) or 65 ºC (b); T0 = 25 ºC).

4. Conclusions

The proposed model to describing the simultaneous heat and mass transfer in a sugarcane bagasse bed in a horizontal drum presented great adjustment with the experimental data ($R^2 \geq 0.95$ and RMSE ≤ 0.62) for temperatures of the drum wall at 45 and 65 ºC. The temporal temperature profiles shown that the thermal equilibrium is reached and the problem could be solved just through a isotherm mass balance. The loss of water in the regions near to the drum wall was visible in the spatial moisture profiles, indicating that the mass balance is sensible to increase in the temperature.

5. Nomenclature

Cp	specific heat	J Kg^{-1} K^{-1}
D$_{eff}$	effective diffusivity	m² s^{-1}
f	air capacity to carrier water	Kg Kg-air^{-1}
K	effective thermal conductivity	W m^{-1} K^{-1}
r	radial coordinate	m
t	time	s, min or h
T	temperature	ºC
V	velocity	m s^{-1}
X	moisture content in dried basis	Kg Kg-ds^{-1}

Greek letters

α	convective heat transfer coefficient	W m^{-2} K^{-1}
β	convective mass transfer coefficient	m s^{-1}
ρ	density	Kg m^{-3}
λ	latent heat of evaporation of water	J Kg^{-1}

Subscripts

0	initial	i(θ)	surface
∞	headspace	s	solid
a	air	r	radial direction

| b | bed | | w | wall |
| eq | equilibrium | | | |

6. References

[1] Durand, A. Bioreactor design for solid state fermentation bioreactors. Biochemical Engineering Journal 2003, 13, 113–125.

[2] Pandey, A. Solid-state fermentation. Biochemical Engineering Journal 2003, 13, 81-84.

[3] Zanelato, A. I.; Shiota, V. M.; Gomes, E.; da Silva, R.; Thoméo, J. C. Endoglucanase production with the newly isolated Myceliophtora sp. I-1d3b in a packed bed solid state fermentor. Brazilian Journal of Microbiology 2012, 43, 1536-1544.

[4] Bhargav S.; Panda, B. P.; Ali, M.; Javed, S. Solid-state Fermentation: An Overview. Chemical and Biochemical Engineering 2008, 22(1), 49-70.

[5] Casciatori, F. P.; Laurentino, C. L.; Lopes, K. C. M.; Souza, G. A.; Thoméo, J. C. Stagnant effective thermal conductivity of agro-industrial residues for solid-state fermentation. International Journal of Food Properties 2013, 16(7), 1578-1593.

[6] Casciatori, F. P.; Laurentino, C. L.; Toboga, S. R.; Casciatori, P. A.; Thoméo, J. C. Structural properties of beds packed with agro-industrial solid by-products applicable for solid-state fermentation: Experimental data and effects on process performance. Chemical Engineering Journal 2014, 255, 214-224.

[7] Herz, F.; Mitov, I.; Specht, E.; Stanev, R. Experimental study of the contact heat transfer coefficient between the covered wall and solid bed in rotary drums. Chemical Engineering Science 2012, 82, 312-318.

[8] Tada, É. F. R.; Bück, A.; Casciatori, F. P.; Tsotsas, E.; Thoméo, J. C. Investigation of heat transfer in partially filled horizontal drums. Chemical Engineering Journal 2017, 316, 988-1003.

[9] Casciatori, F. P.; Bück, A.; Thoméo, J. C.; Tsotsas, E. Two-phase and two-dimensional model describing heat and water transfer during solid-state fermentation within a packed-bed bioreactor. Chemical Engineering Journal 2016, 287, 103-116.

[10] Tada, É. F. R. Produção de celulases fúngicas por fermentação em estado sólido em tambor horizontal parcialmente preenchido: modelagem, simulação e experimentação. 2018. 100 f. Qualificação de Doutorado. Instituto de Biociências, Letras e Ciências Exatas, Universidade Estadual Paulista, São José do Rio Preto. In Portuguese.

[11] Bertucci, V. F.; Tada, É. F. R.; Thoméo, J. C. Modelagem e simulação de transferência de calor em tambor horizontal parcialmente preenchido com partículas orgânicas. In: Anais do XII Congresso Brasileiro de Engenharia Química em Iniciação Científica. São Paulo: Blucher, 2017. In Portugese.

Moisture content modeling and effective moisture diffusivity determination during convective solar drying of blackberry (*rubus spp*) and basil (*Ocimum basilicum L.*)

López-Ortiz, A.[a,b]*; Gallardo-Brígido, J.C.[a]; Silva-Norman, A.[c]; Pilatowsky-Figueroa, I.[a]; García-Valladares, O.[a]; Rodríguez-Ramírez, J.[d]

[a] Laboratorio de Secado Solar, Coordinación de Refrigeración y Bombas de Calor, Instituto de Energías Renovables, Universidad Nacional Autónoma de México. Temixco, Morelos. México.
[b] Catedrática CONACyT. Consejo Nacional de Ciencia y Tecnología. Ciudad de México.
[c] Posgrado en Ciencias de la Sostenibilidad. Universidad Nacional Autónoma de México.
[d] Instituto Politécnico Nacional, Centro Interdisciplinario de Investigación para el Desarrollo Integral Regional (CIIDIR) Unidad Oaxaca, Santa Cruz Xoxocotlán Oaxaca, México.

*E-mail of the corresponding author: alo@ier.unam.mx

Abstract

The goal of reducing energy consumption (EC), losses and waste (FL) in the food processing is a challenges in the worldwide. The use of active solar greenhouse dryers (GHD) for EC and FL reductions has increased due to its capacity, and low operating costs. In this work the effective diffusivity (Deff) and the moisture content modeling were analized for basil (Ocimum basilicum) and blackberry pulp (Rubus rosoideae) dried in a conventional stove (CD) and an GHD coupled to an additional air solar heating system (SCH$_a$). The loss of water and the drying rate in food materials dehydrated in the GHD is consistent with the increment or decrement of temperature during the solar day. The D$_{eff}$ values for basil and blackberry pulp was ranged between -1.1044x10^{-7} and -3.9167x10^{-9}. The solar energy obtained in the GHD supplied the heating requirements. In general, the Page's model was the best fit for the drying kinetics for basil and blackberry pulp.

Keywords: Solar Collector for air heating, solar energy, variable conditions.

1. Introduction

In the world, 1.3 billion tons of food loss and waste are generated each year [1]. Therefore, it is necessary to implement food conservation methods. These technologies could also allow the reduction of energy consumption.

The energy consumption for food preservation in Mexico is not fully quantified. According to SENER of Mexico, (2016), 28.9% of the energy is used by the industrial sector in this country. The major energy consumption of the food industry is 43% and it is used for processing and distribution. Processing, drying, and curing are the most energy-intensive farm operations, due to the high costs of heating and the removal of moisture from the saturated air and the food matrix[2].

Drying is a unitary operation, that allows the water reduction from food, to extend its shelf life. Different solar drying systems have been used for food preservation, and they are classified as follows: direct, indirect, and mixed solar drying technologies[3]. Solar greenhouse dryers are classified as direct solar drying systems. They have been used for the drying of grains, fruits, and vegetables[3,4,5,6]. However, drying times are long and the product quality is poor[7,8].

Solar greenhouse dryers can also be connected to an air solar heating system (SCHa). The air heating concept or preheating system was recently introduced[9]. This system was used for drying of pepper, where different air mass flows rates and the drying kinetics were analyzed. The maximum temperature inside the greenhouse dryer was 45°C.

Moreover, there are drying predictive models, and, they derived from Fick's second law and Newton's law of cooling[7,8,9,10]. But, the study of effective diffusivity is necessary in this novel system. Therefore, the main objective of this work was to evaluate the moisture diffusivity of basil (*Ocimum basilicum*) and blackberry (*Rubus rosoideae*), which were dehydrated in a solar greenhouse dryer coupled with an additional air solar heating system.

2. Modeling

The mass transfer phenomenon in drying has been simplified when considering the liquid mass transportation according to Fick's second law, where the driving force is a concentration gradient.

$$\frac{dX_a}{dt} = -D_{Ax} \frac{d\rho X_a}{dx^2} \tag{1}$$

Considering that the water movement is unidirectional, in a case of a flat plate with a constant diffusivity, the equation (1) can be expressed according to Crank & Park[11] in the following form,

$$W = \frac{X_{(t)}-X_e}{X_0-X_e} = \frac{8}{\pi^2}\sum_{i=0}^{\infty}\frac{1}{(2n+1)^2}e^{-\frac{\pi^2}{4\cdot l^2}(2n+1)^2 D_{Ax}\cdot t} \tag{2}$$

Where W is the normalized moisture content. Simplifying the equation (2), the Fick's second law solution is expressed as:

$$W = \frac{X_{(i)}-X_e}{X_0-X_e} = \frac{8}{\pi^2}e^{-\frac{\pi^2}{4\cdot l_o^2}{}^2 D_{Ax}\cdot t} \tag{3}$$

Where the diffusive coefficient (D_{Ax}) can be evaluated considering an effective mass transference (D_{eff}).

2.1. Empirical and semi-empirical modeling

Semi-empirical models are calculated for specific conditions of relative moisture, temperature, and air-drying speed. In solar drying, empirical and semi-empirical models have been used on thin plane plates to describe the behavior of W during the process (Table 1). The adjustable parameters must be calculated for each food type and drying condition. Some models are derived from the solution of Newton's law of cooling equation and others from Fick's second law (Equation 1).

Table 1. Predictive models for W

Semi-empirical models	Model	Equation	Reference
Models Resulting from Newton's Law of Cooling	Newton	$W = \exp(-kt)$	[12]
	Page	$W = \exp(-kt^n)$	[13]
	Modified Page	$W = \exp(-(kt)^n)$	[7]
Models Resulting from Fick's Second Law of Diffusion	Henderson and Pabis	$W = a\exp(-kt)$	[14]
	Logarithmic	$W = a\exp(-kt) + c$	[15]
	Two-term	$W = a\exp(-kt) + b\exp(-k_1 t)$	[16]
	Two-term exponential	$W = a\exp(-kt) + (1-a)\exp(-k_1 t)$	[17]
	Midilli and Kucuk	$W = a\exp(-kt^n) + bt$	[18]
Empirical models	Wang and Singh	$W = 1 + at + bt2$	[19]

Where W can be adjusted to the shown models in Table 1. In this work, adjustments were made to the Newton's, Page's, and Wang and Singh's equations.

2.2. Statistical analysis

The square root means deviation (RMSD) between the predicted and experimental data were evaluated with the following equation,

$$RMSD = \sqrt{\frac{\sum_{i=1}^{i=n}(W_{Exp,i}-W_{Th,i})^2}{n-1}} \tag{4}$$

The main deviation between the experimental data and the results produced by the model were evaluated with relative error:

$$Error(\%) = \frac{100}{n} * \sum_{i=1}^{i=n} \frac{(W_{Exp,i} - W_{Th,i})^2}{W_{Exp,i}} \tag{5}$$

The reduced chi-square value of (χ^2) was calculated as follows,

$$\chi^2 = \frac{\sum_{i=1}^{i=n}(W_{Exp,i} - W_{Th,i})^2}{n - N} \tag{6}$$

where $W_{Exp,i}$ represents the experimental moisture ratio, $W_{Th,i}$ is the humidity ratio predicted by the mathematical model, n is the number of observations and N is the number of constants.

3. Materials

Basil (Ocimum basilicum) was obtained from a local farmer in Tequesquitengo, Morelos, Mexico, and blackberry (Rubus rosoideae) from Los Reyes, Michoacán, Mexico was used. In the basil drying case, only leaves were used. The samples were put over a perforated plastic mesh, covering a total surface of 16 m^2. The blackberry was liquefied and the seeds separated. A thin layer of about 5 ± 1 mm of strawberry pulp was spread over 40.4 x 26.5 cm trays. In this case, a drying surface of 8 m^2 was used for the drying process. The results were compared with samples dried in an electric oven at 60°C with forced convection at 1 m/s. The weight loss was measured during the drying process.

3.2. Description of the drying equipment

A solar greenhouse dryer (Figs 1 and 2) was used (GHD), it was connected to an air solar heating system (SCH$_a$). The air solar heating system was constituted by three air heating flat plate solar collectors that consist in a box with insulation, an absorber, and a glass cover. The collector dimensions are 2.10 m in length, 1.20 m in width and 0.093 m in thickness. The cover was made of texturized corrugated tempered glass with a thickness of 4 mm. The SCH$_a$ was oriented to the south and inclined at an angle of 22° to the horizontal plane to maximize the absorption of solar radiation during the test. For the air inlet to the GHD a radial fan (Air Technology, CFD-7-3, Mexico) was connected to the SCH$_a$. Therefore, the system can be operating with natural or forced convection (Figure 1). Two air-diffusers with honeycomb structure for air distribution in the GHD was connected in the south wall. For air moisture and air flow removal from the GHD, two air fans (SilentVent, HAE 150) was connected in the north wall. The temperature was measured using Type T thermocouples (uncertainty of ± 1°C). The solar irradiation (W/m^2) outside and inside of the GHD was measured using two pyranometers (Kipp & Zonen, CMP6, Netherlands). The air humidity (HR%) was measured using sensors (AOSONG, DHT22, uncertainty of ± 2%). The inlet and outlet air velocity was measured using an anemometer (Extech Instruments, SDL 350).

The tests were carry out in Temixco, Morelos, Mexico (18.85° latitute North and -99.2333° longitude East and an altitude of 1219 m above sea level). The experiments were done in the months of March, May, and June 2017. In the tests with forced convection, an air velocity of 0.58 m/s ± 0.12 m/s was used and a maximum irradiance of 806 W/m^2 was recorded.
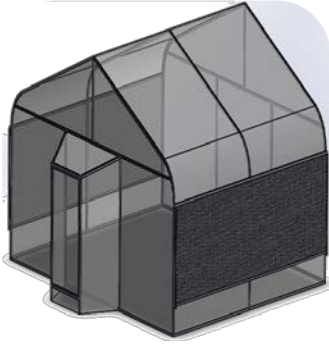
Fig. 1 Solar greenhouse dryer (GHD). Outside view. view without the plastic cover and with air heaters.
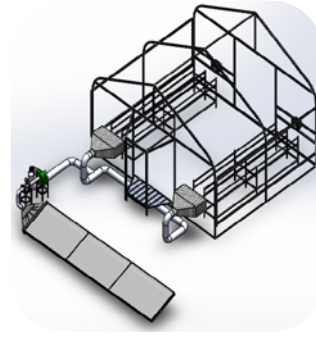
Fig. 2 Solar greenhouse dryer (GHD),

A software for data acquisition was used during the test. The data collecting was done every 30 s.

3. Results

The maximal average drying temperature into the greenhouse was 44.02 ± 1.90 °C with a maximal average solar irradiance of 806.34 ± 6.12 W/m^2 and inlet average air velocity of 0.58 ± 0.12 m/s of the greenhouse. In figure 2, the drying kinetics of dehydrated basil and blackberry are observed. In the greenhouse (GHD) and electrical stove (CD), the drying kinetics are according to the typical behaviour of drying processes. The initial moisture content of basil was 7.021 ± 0.001 kg$_w$/kg$_{ds}$ and for the blackberry was 9.470 ± 0.422 kg$_w$/kg$_{ds}$. For the basil (Figure 2a.), the drying time in the GHD was 330 minutes and in the CD was 123.8 minutes. Figure 2b shows the blackberry pulp drying kinetics, in the stove the drying time was 480 minutes. But in the GHD, the dehydration was prolonged until a second day (960 minutes).

The ln(W) (figure 3) was used to get the linearization of equation 3[20], considering the decreasing drying rate interval. With CD, the slope is less than with GHD, due to the mean temperature of each system (60 and 43.52°C for CD and GHD respectively).

The D$_{eff}$ results with the slopes of the lines in fig. 3 shows a difference in the values obtained (Table 2). It can be observed that the D$_{eff}$ values for blackberry pulp are greater than the basil; therefore, the mass transference is major in the blackberry pulp. Furthermore, the D$_{eff}$ values

for CD indicate that a higher mass flux can be obtained. Nevertheless, the energy-saving with GHD is greater than with CD, and a good dried product was obtained in both technologies.

| (a) | (b) |
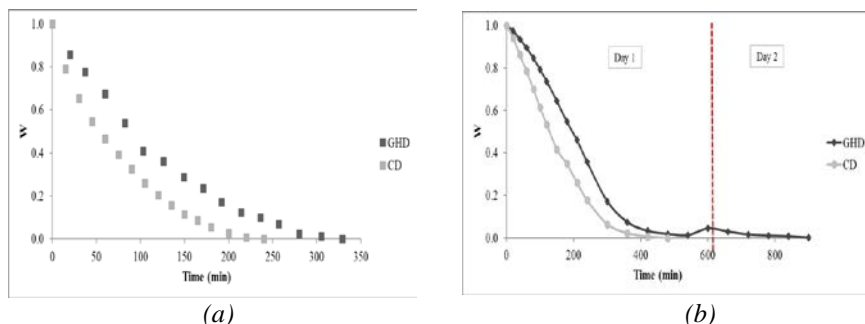
Fig. 2 Basil (a) and blackberry (b) drying kinetics, using greenhouse dehydrated (GHD) and electrical stove (CD).

| (a) | (b) |
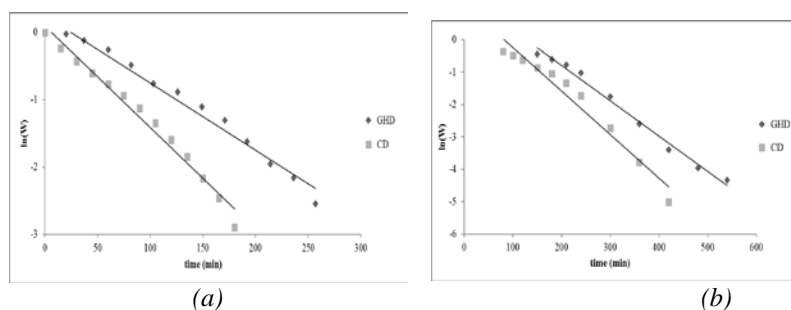
Fig. 3 ln (W) vs drying times for (a) basil, and (b) blackberry pulp.

Table 2. Effective diffusivity values

	R^2	D_{eff} (m^2/s)
CD, Blackberry	0.961	-1.3577E-07
GHD, Blackberry	0.989	-1.1044E-07
CD, Basil	0.981	-3.9167E-09
GHD, Basil	0.977	-2.5938E-09

Table 3 shows adjustable parameters and the values for Newton's, Page's, and Wang and Singh's models for the blackberry and basil experiments. In the basil-GHD, the best adjustment with Wang and Singh's equation was found, followed for Page's model. In the basil-CD, blackberry-GHD and blackberry-CD the best was with Page's, it was due to a minor value of %error, χ^2 and RMSD and major value of R^2.

Table 3 Adjustable parameters for different mathematical models

	Parameters	Newton	Page	Wang and Singh
Basil GHD	n	0.0000	1.2331	-0.0063
	k	0.0086	0.0027	0.0000
	R^2	0.9831	0.9954	0.9966
	RMSD	0.6551	0.3410	0.2957
	X^2	0.0018	0.0005	0.0004
	%error	3.1998	0.7705	0.1517
Basil CD	N	0.0000	1.0439	-0.0096
	K	-0.0136	0.0112	0.0000
	R^2	0.9926	0.9932	0.9820
	RMSD	0.4033	0.3858	1.5941
	X^2	0.0007	0.0007	0.0113
	%error	1.8917	1.4044	30.1498
Blackberry GHD	N	0.0000	1.7241	-0.0030
	K	-0.0042	0.0001	0.0000
	R^2	0.9476	0.9971	0.9724
	RMSD	2.0173	0.1802	18.1547
	X^2	0.0080	0.0001	0.6824
	%error	13.334	0.8703	10509
Blackberry CD	N	0.0000	1.4323	-0.0046
	K	-0.0060	0.0007	0.0000
	R^2	0.9657	0.9982	0.9959
	RMSD	0.9548	0.2213	6.4654
	X^2	0.0043	0.0003	0.2144
	%error	9.0764	0.4720	811.31

4. Conclusions

The loss of water and the drying rate in food materials dehydrated in the greenhouse dryer (GHD) is consistent with the increment or decrement of temperature during the solar day. The D_{eff} values for basil and blackberry pulp was ranged between 1.1044×10^{-7} and -3.9167×10^{-9}. The D_{eff} values for CD was higher than for GHD, and in both technologies, a good dried product was obtained. In GHD the sun supplied the heating requirements for free. In general, the Page's model was the best fit for the drying kinetics for basil and blackberry pulp.

5. Nomenclature

D_{Ax}	Moisture diffusivity	s/m^2
D_{eff}	Effective moisture diffusivity	s/m^2
l	sample thickness	M
N	Number of constants	
n	Number of observations	
t	Time	min
T	Temperature	°C
X	Moisture content	kg of water/kg dried solid
W	Dimensionless moisture content	

Greek letters

ρ	density	kg/m^3
π	pi constant	

Subscripts

e	equilibrium
exp	experimental
o	initial
Th	theoretical

6. References

[1] Gustavsson, J. Global Food Losses and Food Waste. Rome : FAO, 2011.

[2] Initiatives by Member States and international organizations are being undertaken to create an enabling environment at all levels for the . s.l. : FAO, 2011.

[3] Prakash, O. y Kumar, A. Solar green house drying: A review. Renewable and Sustainable Energy Reviews, 2014, 29, 905–910.

[4] Sethi, V.P. y Arora, S. Improvement in green house solar drying using inclined north wall reflection.. SolarEnergy, 2009, 83, 1472-1484.

[5] Rathore, N.S. y Panwar, N.L. Experimental studies on hemi cylindrical walk-in type solar tunnel dryer for grape drying. Applied Energy, 2010, 87 (8), 2764-2767.

[6] Janjai, S., y otros. A large-scale solar greenhouse dryer using polycarbonate cover: Modeling and testing in a tropical environment of Lao People's Democratic Republic. Renewable Energy, 2011, 36, 1053-1062.

[7] Diamante, L.M. y Munro, P.A. Mathematical modelling of the thin layer solar drying of sweet potato slices. Solar Energy, 1993, 51 (4), 271–276.

[8] Sonmete, M.H., y otros. Mathematical modeling of thin layer drying of carrot slices by forced convection. Food Measurement and Characterization, 2017, 11, 629.

[9] Azaizia, Z., y otros. Investigation of a new solar greenhouse drying system for peppers. International Journal of hydrogen energy, 2017, 42, 8818-8826.

[10] Gulcimen, F., Karakaya, H. y Durmus, A. Drying of sweet basil with solar air collectors. Renewable Energy, 2016, 93, 77-86.

[11] Crank, J. y Park, G.S. Diffusion in Polymers. New York : Academic Press, 1968.

[12] Mujumdar, A.S. Handbook of Industrial Drying. New York : Marcel Dekker, 1987.

[13] Page, G.P. Factors Influencing the Maximum Rates of Air Drying Shelled Corn in Thin Layers. Lafayette, IN, : (Unpublished masterthesis), Purdue University, USA, 1949.

[14] Henderson, S. y Pabis, S. Grain drying theory: temperature effects on drying coefficient., J. Agric. Eng. Res., 1961, 6, 169-174.

[15] Singh, S, y otros. Drying and rehydration characteristics of water chestnut (Trapa natans) as a function of drying air temperature. Journal of Food Engineering, 2008, 87, 213-221.

[16] Madamba, P.S., Driscoll, R.H. y Buckle, K.A. The thin layer drying characteristics of garlic slices. J. Food Eng., 1996, 29, 75–97.

[17] Henderson, S. M. Progress in developing the thin layer drying equation. Transactions of American Society of Agricultural Engineers, 1974, 17, 1167-1172.

[18] Midilli, A., Kucuk, H. y Yapar, Z. A new model for single layer drying. Dry. Technol., 2002, 20, 1503-1513.

[19] Wang, C.Y. y Singh, R.P. A Single Layer Drying Equation for Rough Rice. American Society of Agricultural Engineers, ASAE Paper. St. Joseph. MI: American Society. Agri. Eng. 1978, 78, 3001.

[20] Tütüncü, M.A.; Labuza, T. P. Effect of Geometry on the Effective Moisture Transfer Diffusion Coefficient. J. Food Engineering, 1996, 30, 433-447.

Drying characteristics and mathematical modelling of the drying kinetics of oyster mushroom (*Pleurotus ostreatus*)

Satimehin, A. A. [a]*; Oluwamukomi, M. O. [b]; Enujiugha, V. N. [b]; Bello, M.[b]

[a] Department of Agricultural and Bioresources Engineering, Federal University Oye-Ekiti, Nigeria
[b] Department of Food Science and Technology, Federal University of Technology, Akure, Nigeria

*E-mail of the corresponding author: adesola.satimehin@fuoye.edu.ng

Abstract

This study was conducted to determine the drying characteristics of oyster mushroom (Pleurotus ostreatus) at 50, 60 and 70 °C. Pleurotus ostreatus were cleaned and dried in a laboratory cabinet dryer. The drying data were fitted to six model equations namely Newton, Pabis and Henderson, Logarithmic, Two-term diffusion, Wang and Singh, as well as Modified Henderson and Pabis equations. The goodness of fit of the models were evaluated by means of the coefficient of determination (R^2), root mean square error (RMSE) and reduced chi-square (χ^2). The Logarithmic model best describes the drying data and could be used to predict its drying behaviour.

Keywords: oyster mushroom; thin-layer drying; characteristics; modelling

Drying characteristics and mathematical modelling of the drying kinetics of oyster mushroom (Pleurotus ostreatus).

1. Introduction

Drying is the removal of moisture from food material, to make it stable and thus promote its shelf life. Mushrooms are highly perishable and lose their qualities during storage. Due to the high moisture content, there is the problem of seasonal availability and wastage. The shelf life of mushrooms is only due to 2 to 5 days after harvest depending on the variety, hence there is a need for adequate preservation to ensure proper shelf stability and all year round availability without quality compromise [1]. Drying is seen as the removal of undesired moisture from a product. Many agricultural products are dried for various purposes like safe storage, easy handling, value addition, further processing and quality improvement [2]. Therefore, the drying process offers an alternative way for food material consumption and especially, the seasonal and perishable ones. The renewed interest in high quality fast-dried foods [3] and the upward swing in the demand for convenient foods including ready to eat and instant products, which are desired to contain the minimum quantities of additives and preservatives [4] is increasing the interest in drying operations. The drying process can be carried out using the sun (solar drying), though it is cheap however this method of drying is time consuming, it is climate dependent, time consuming and produces products of low quality especially in terms of colour and microbial infestation. Hence the conventional means of drying is a better alternative because they were able to overcome this short comings even thou, they may be more expensive and out of all the different mechanical means of drying such as drum dryer, freeze dryer, fluidized bed dryer, the hot air oven drying (cabinet dryer) is the most commonly used because they are generally acceptable and they are cheaper. Drying kinetics is generally evaluated experimentally by measuring the weight of a drying sample as a function of time. Drying process can be described completely using an appropriate drying model, which is made up by differential equations of heat and mass transfer in the interior of the product and at its interphase with the drying agent. The drying behaviour of biological materials can be predicted using many thinlayer drying mathematical models which have been classified into three groups namely; theoretical (Fick's second law of diffusion), semi-theoretical (Lewis, Page, modified Page, Henderson-Pabis, logarithmic, Two-term, Two-term exponential, approximation of diffusion, Verma, etc.), and empirical (Wang-Singh). These models have been found to be drying time and constants, dependent while influence of all other factors is negligible [5]. The objectives of this study therefore were to: (i) to study the drying kinetics of oyster mushroom specie (*Pleurotus ostreatus)* in a cabinet dryer, (ii) to evaluate a suitable thin layer drying model, and (iii) the optimum temperature of drying at which best quality product is obtainable.

2. Materials and Methods

2.1. Material

Freshly harvested samples of oyster mushrooms (*Pleurotus ostreatus)* were cleaned and used for the drying study. Before the commenement of a drying test, the initial moisture content of the mushrooms was determined.

2.2. Experimental procedure

Drying experiments were performed in a laboratory cabinet dryer designed in the Department of Food Science and Technology, Federal University of Technology, Akure, Nigeria. The dryer consists of a centrifugal fan to supply the air flow, an electric heater, and an electronic proportional controller. The temperature and relative humidity in the drying chamber were measured by temperature sensor (accuracy $\pm 1\%$) and relative humidity sensor (accuracy $\pm 2\%$), respectively. The air velocity in the drying chamber was measured with a Tri-Sense hot wire probe anemometer (accuracy$\pm 2\%$). Air flow was perpendicular to the drying surfaces of the samples and the hot air used in the drying process was circulated in the cabinet. The dryer was started about one hour before each drying run to achieve steady-state conditions. After the dryer had reached this condition, 100 g samples of the mushroom were uniformly spread in a single layer on a sample tray and were dried. The drying experiments were performed at 50, 60 and 70 °C air temperatures. The air velocity was kept constant at 0.6 m/s in all drying experiments. Relative humidity of the ambient air changed between 21% and 23%. During drying, the samples were removed at intervals and weighed. Removing, weighing, and replacing the mushrooms took about 1 min. The weight loss of the samples was recorded using an electronic balance (Midfield, MF-1000, Göttingen, Germany) in a range of 0–1100 ($\pm$0.01g) at hourly intervals until no measurable weight loss was observed. At the end of each drying experiment, the final moisture content of the sample was determined. Moisture contents were reported on wet basis. The amount of dry matter was calculated by using the mean final moisture content and the weight of the dried mushrooms [6]. All the experiments were replicated three times at each air temperature and the average values were used. Calculations of the moisture ratio, correlation coefficient, mean bias error, random square error and fitting the values generated into six drying models were carried out [6].

2.2.1. *Moisture ratio*

The moisture ratio (MR) of oyster mushrooms during the single layer drying experiments was calculated using equation (1).

$$MR = \frac{M_t - M_e}{M_0 - M_e} \qquad (1)$$

Some investigators [7]; [6]; [8] observed continuous fluctuations in the instantaneous moisture content during the drying processes, and therefore reduced equation (1) to:

$$MR = \frac{M_t}{M_0} \qquad (2)$$

where MR indicates the moisture ratio (dimensionless quantity), M_0 the initial moisture content (kg water/ kg dry matter, M_t the instantaneous moisture content at time t > 0 (kg water/kg dry matter), and M_e the equilibrium moisture content (kg water/ kg dry matter).

2.2.2.   *Drying rate*

The drying rates of the samples were calculated using equation (3)

$$\frac{dM}{dt} = \frac{M_{(t+\Delta t)} - M_t}{\Delta t} \qquad (3)$$

where $\frac{dM}{dt}$ denotes the drying rate and Δt is elemetal time increment (hr).

2.3. Mathematical modelling of the drying curve

The drying curves obtained were evaluated to find the most suitable model for describing the drying process of the selected mushroom species. Drying curves data were fitted into six (6) thin-layer drying equations at three temperatures 50, 60 and 70 °C. The drying curves obtained were processed for drying rates to find the most convenient model among the six different expressions (Table 1). A nonlinear regression analysis was performed using the SigmaPlot and Microsoft Excel 2010 Statistical software to evaluate model parameters and determine the predicted moisture ratio for each model equation. The correlation coefficient (R^2) is generally considered one of the primary criteria for evaluating the goodness of fit of a drying model. It was therefore used for comparing the predictive ability of the models in this study. Other criteria used for model evaluation and comparison are reduced chi-square (χ^2) and root mean square error (RMSE). The model with the highest R^2 and lowest χ^2 and RMSE was condidered to best fit the drying data [9], [10]. Both χ^2 and RMSE were calculated, respectively, from the following equations.

$$\chi^2 = \frac{1}{(N-n)} \sum_{i=1}^{N} \left(MR_{o,i} - MR_{p,i} \right)^2 \qquad (4)$$

$$RMSE = \sqrt{\frac{1}{N} \sum_{i=1}^{N} \left(\frac{MR_{o,i} - MR_{p,i}}{MR_{o,i}} \right)^2} \qquad (5)$$

Where MR and $\overline{MR}$ are the instantaneous and average moisture ratio values, while the subscripts o,i and p,i denote the ith observed (i.e. experimental) and predicted moisture ratio, respectively. N is the number of observations, and *n* is the number of constants in the drying model.

3. Results and Discussion

The changes in the moisture content during drying of the three species of oyster mushrooms are presented in Fig. 1 at different temperatures of 50, 60 and 70 °C. The drying behaviour of the samples exhibited the characteristic moisture desorption behaviour. High rate of moisture removal was observed, followed by the slower moisture removal in the later stages. This characteristic behaviour can be attributed to the various forms in which water is present in the food products. In the progression of drying process, the moisture ratio was observed to decrease non-linearly with respective to drying time for all the samples. Various reporters such as Doymaz [11] and Kingsley *et al.* [12] also observed that it is a general trend adopted by other food products such as sweet potatoes and mulberry. The drying rate for the *Pleurotus ostreatus* decreased with time and decreasing moisture contents and drying occur in the falling rate period. There was no constant rate-drying period in the entire drying process from the curves shown in Figure 1, all the drying process occurred in falling drying period, rather there was an increasing drying rate as drying progressed, which shows that drying is govern by the intense internal water and vapour flow and the drying processes were mainly controlled by diffusion mechanisms. The time taken for drying of mushroom samples varied with drying temperature, the drying time decreases with increase in drying temperature, the drying time was higher at 50ºC and lowest at 70 °C for all the samples. This trend agrees with the observation of several authors on the drying of various food materials [13], [14], [15].

3.1 Mathematical Modelling of Drying Curves

Table 1 shows the result of the statistical analysis for the six models namely; Newton, Pabis and Henderson, Logarithmic, Two-term, Wang and Sighn and Modified Henderson and Pabis. Drying constants a, b, c, d, g and h for the thinlayer drying obtained from drying data (moisture ratio against drying time) for the *Pleurotus ostreatus* mushrooms at varied temperatures 50, 60 and 70 °C at fixed air velocity 1 m/s respectively. The regression results presented in Tables 2 shows that Logarithmic model gave the lowest RMSE and $\varkappa^2$ when compared with the other five models. It also gave the highest R^2. Hence it is the model that best fits the drying of *Pleurotus ostreatus* mushrooms. This agrees with Doymaz [16] who reported that the Logarithmic model equation as the best fit model. However, this is at variance with Tulek [17] who reported that the model of Midilli et. al. [8] is the best fit model to predict the drying characteristics of mushrooms.
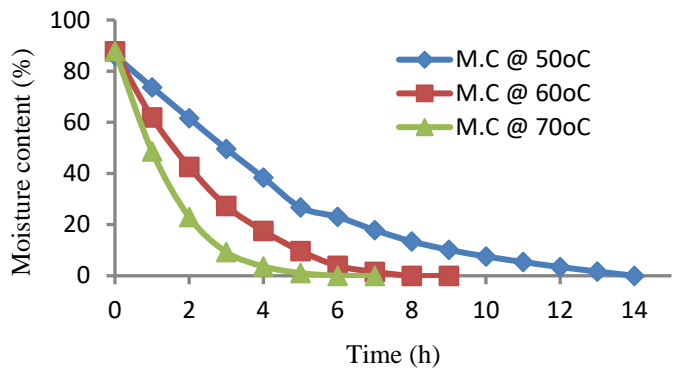
Fig. 1 Moisture content curves of *Pleurotus ostreatus* at different temperatures (ºC)

Table 1. Result from linear progression analysis for dried Pleurotus ostreatus

Model name	T °C	R^2	$\chi 2$	RMSE
Newton	50	0.9871	0.0010	0.0299
	60	0.9909	0.0013	0.0328
	70	0.9953	0.0007	0.0223
Pabis and Henderson	50	0.9907	0.0013	0.0352
	60	0.9919	0.0007	0.0255
	70	0.9956	0.0006	0.0230
Logarithmic	50	0.9978	0.0003	0.0147
	60	0.9985	0.0028	0.0439
	70	0.9978	0.0004	0.0157
Two-term	50	0.9907	0.0012	0.0276
	60	0.9919	0.0026	0.0398
	70	0.9956	0.0010	0.0223
Wang and Singh	50	0.995	0.0005	0.0208
	60	0.9934	0.0018	0.0152
	70	0.9715	0.0043	0.0016
Modified Pabis and Henderson	50	0.9907	0.0085	0.0714
	60	0.9919	0.0153	0.0610
	70	0.9956	0.2069	0.2275
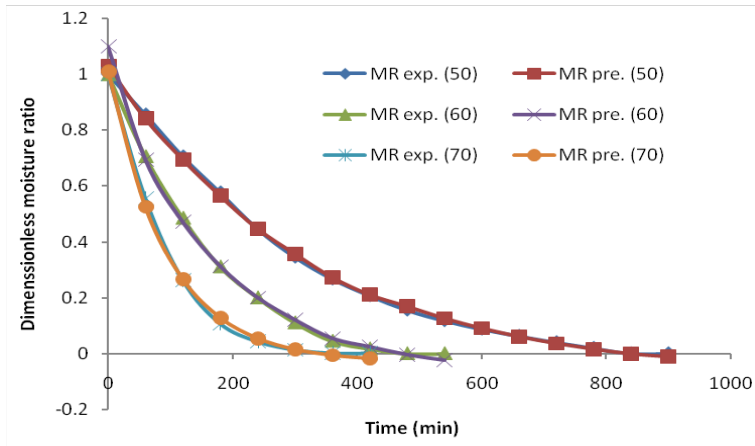
Fig. 2 Comparison between experimental and predicted moisture ratio for Pleurotus ostreatus using the logarithmic model

3. Conclusions

The drying behaviour of oyster mushroom (*Pleurotus ostreatus*) exhibited the characteristic moisture desorption behaviour. High rate of moisture removal was observed at the beginning, followed by a slower rate moisture removal at the later stages. The drying rate for the *Pleurotus ostreatus* decreased with decreasing moisture contents and drying occur in the falling rate period, with internal diffusion in the mushroom. An increase in the drying temperature reduced the drying time and increased the drying rate. Drying air temperature of 60 °C was found to be better as it gave dried product with lower shrinkage, better colour and better crispness. Logarithmic model gave the best fit to the drying data, and thus considered to best predict drying characteristics of *Pleurotus ostreatus*.

5. References

[1] Omojiba, G.O.; Idah, P. Effects of Temperature and Drying Time on the moisture content, colour and texture of dried Tomatoes. Proceeding 3rd Annual conference of School of Engineering and Engineering Technology. Federal University of Technology, Minna. (2001), Pp 33-37.

[2] Demir, V.; Gunhan, T.; Yagcioglu, A. K. Mathematical modelling of convection drying of green table olives. *Biosystems Engineering*. 2007, 98: 47-53.

[3] Maskan, A.; Kaya, S.; Maskan, M. Hot air and sun drying of grape leather (pestil). *Journal of Food Engineering*. 2002, 54; 81-84.

[4] Shi, Q.; Xue, C.; Zhao, Y.; Li, Z.; Wang, X. Drying characteristics of horse mackerel (Trachurus japonicus) dried in a heat pump dehumidifier. *Journal of Food Engineering*. 2008, 84: 12-20.

[5] Hashemi G, Mowla D, Kazemeini M. Moisture diffusivity and shrinkage of broad beans during bulk drying in an inert medium fluidized bed dryer assisted by dielectric heating. *Journal of Food Engineering*. 2009, 92:331–338.

[6] Togrul, I. T. and Pehlivan, D. Mathematical Modelling of Solar Drying of Apricots in Thin Layers. *Journal of Food Engineering*. 2002, 55: 209-216.

[7] Yaldiz, O.; Ertekin, C.; Uzun, H. I. Mathematical Modelling of Thin Layer Solar Drying of Sultana Grapes. *Energy*. 2001, 26 : 457–465.

[8] Midilli, A.; Kucuk, H. Mathematical modelling of thin layer drying of pistachio by using solar energy. *Energy Conversion and Management*. 2003, 44(7), 1111-1122.

[9] Goyal, R. K.,; Kingsley, A. R. P.; Manikantan, M. R.; Ilyas, S. M.. Thin layer drying kinetics of raw mango slices. *Biosystems Engineering*. 2006, 95(1): 43-49.

[10] Babalis, S. J.; Papanicolaou, E.; KyriaKis, N.; Belessiotis, V. G. Evaluation of thin layer drying models for describing drying kinetics of figs. (*Ficuscaica*). *Journal of Food Engineering*. 2006, 75, 205-214.

[11] Doymaz, I. Convective drying kinetics of strawberry. *Journal of Chemical Engineering and Processing*. 2008, 79:243-248.

[12] Kingsley, R. P.; Goyal, R.K.; Manikantan, M.R.; Ilyas, S. M. Effects of pre-treatment and drying air temperature on drying behaviour of peach slice. *International Journal of Food Science and Technology*. 2007, 4: 65-69.

[13] Akanbi, C. T.; Adeyemi, R. S.; Ojo, A. Drying characteristics and sorption isotherm of tomato slices. *Journal of Food Engineering*. 2006, 73(2): 157-163.

[14] Sacilik, K. The thin layer Modelling of Tomato Drying Process. *Journal of Food Engineering*. 2007, 79: 23-30.

[15] Famurewa, J. A. V.; Olumofin, K. M. Drying kinetics and influence on the chemical characteristics of dehydrated okra (*Abelmoschusesculentusi*) using cabinet dryer. *European Journal of Engineering and Technology*. 2015, 3(2): 7-19.

[16] Doymaz, I. Effect of pre-treatment using potassium metabisulphite and alkaline ethyl oleate on the drying kinetics of apricots. *Biosystems Engineering*. 2004, 89, 281-287.

[17] Tulek, Y. Drying kinetics of oyster mushroom (*Pleurotus ostreatus*) in a convective hot air dryer. Journal of Agricultural Science and Technology. 2011, 13: 655-664.

Thermodynamic model of Ca(II)-alginate beads drying by spectrophotometry

Santagapita, P.R.[a,b]; Castro-Giraldez, M.[c]; Traffano-Schiffo, M.V.[c]; Fito, P.J.[c*]

[a] Universidad de Buenos Aires. Facultad de Ciencias Exactas y Naturales. Departamentos de Industrias y Química Orgánica. Buenos Aires, Argentina

[b] CONICET-Universidad de Buenos Aires. Instituto de Tecnología de Alimentos y Procesos Químicos (ITAPROQ). Buenos Aires, Argentina.

[c] Instituto Universitario de Ingeniería de Alimentos para el Desarrollo, Universitat Politècnica de València, Camino de Vera s/n, 46022 Valencia, Spain.

*E-mail of the corresponding author: pedfisu@tal.upv.es

Abstract

The purpose of this work was to study the drying process of Ca(II)-alginate beads with/without sucrose, monitored by infrared thermography (IRT), in order to describe the critical points and the transformations suffered by the systems. Beads were obtained by the drop method and the drying process was performed at 40 ºC and 1.5 m/s. IRT was measured by a thermal imager Optris PI® 160. Mass, a_w, x_w and volume were also obtained. It was demonstrated that IRT is a good monitoring tool, able to analyzed heat transfer in colloidal systems. A thermodynamic model able to predict the mechanical phenomena of the beads throughout drying process has been developed.

Keywords: encapsulation; thermodynamic; spectrophotometry; drying; beads.

1. Introduction

Over the years, crosslinked hydrogels have been widely studied as suitable matrices for the stabilization and controlled release of biomolecules, both in the food, chemical and pharmaceutical industries [1]. Ca(II)-alginate is one of the anionic polyelectrolyte most used for the encapsulation of bioactive compounds due to its low-cost, its non-toxic character, eco-friendly and biocompatibility [2,3]. Nevertheless, Ca(II)-alginate shows some disadvantages such as high biomolecule leakage, low mechanical strength and large pore size [4]. Moreover, their high water activity also make them susceptible of microorganism deterioration [5]. Therefore, the coupled application of conservation treatments, such as hot air drying and the addition of protective disaccharides (as sucrose) can improve the stability of the hydrogels.

Drying operation is one of the most widely used unit operations to preserve products over time, and it involves a lot of mechanisms coupled together [6,7]. According to the traditional kinetic theory, it is divided into three main stages: induction period, constant drying velocity period and falling drying rate period [8]. An innovative technique used to control this process is the infrared thermography (IRT). IRT is an excellent method, used for studying heat transfer, which converts the radiation emitted by a body surface into temperature data without establishing contact with the object [9]. Taking into account that drying process involves a lot of mechanisms coupled together, where heat and mass transfers and mechanical effects take place simultaneously [10], the combined used of irreversible thermodynamics and infrared thermography represents a good and promising tool.

The aim of this research is to determine the real critical points in the transformation of Ca(II)-alginate beads with/without sucrose during the drying process, by means of an irreversible thermodynamic model which considers gradients of activity, temperature and mechanical energies.

2. Materials and Methods

2.1. Materials

Sodium alginate (Algogel 5540) from Cargill S.A. (San Isidro, Buenos Aires, Argentina), molecular weight of $1.97 \cdot 10^5$ g/mol and mannuronate/guluronate ratio of 0.6; D-sucrose (Scharlab S.L., Barcelona, Spain), molecular weight of 342.2 g/mol. 0.05 M sodium acetate buffer pH 3.8 was prepared from acetic acid and sodium acetate (Scharlab S.L., Barcelona, Spain) [11].

2.2. Hydrogel beads preparation

Two different formulations were used: alginate (A) and alginate-sucrose (AS). All the solutions were prepared in 0.05 M sodium acetate buffer pH 3.8. For A beads preparation, 25 mL of 1% (w/v) sodium alginate solution was dropped into 250 mL of 2.5% (w/v) CaCl2 (Scharlab S.L., Barcelona, Spain) solution. For AS preparation, a 1% (w/v) alginate with 20%

(w/v) sucrose was dropped into the 2.5% (w/v) $CaCl_2$ solution supplemented with 20% (w/v) sucrose using the same procedure previously described. A peristaltic pump (Damova S.L., Barcelona, Spain, model CPM-045B) was used to Ca(II)-alginate bead production according to the drop method described by Traffano-Schiffo et al., (2017), with a pump speed at 20 ± 0 rpm, regulated by an inverter Panasonic DV-700 (Oasaka, Japan) [12]. The $CaCl_2$ solution (with or without sucrose) was maintained in a cold bath with constant stirring by using a vortex IKA® MS3 basic (IKA, Staufen, Germany). A needle with 0.25 mm diameter and 6 mm length (Novofine 32 G, Novo Nordisk A/S, Bagsvaerd, Denmark) was used for the dropping. The distance between the needle and the $CaCl_2$ solution was 6.0 cm. After beads generation, they were maintained for 15 min in $CaCl_2$ solution (with constant stirring), and then they were washed 5 times with bidistilled cold water (5±1 °C) in order to remove free Ca^{2+}. Then, they were maintained at 4 ℃ until the drying treatment and further characterization.

2.3. Drying process

Ca(II)-alginate beads were placed into the interior of a conventional air dryer. Considering previous results, the temperature and the optimal air velocity values were determined at 40 ℃ and 1.5 m/s, during a total drying time previously optimized at 22 and 24 min for A and AS, respectively. The drying air flow was kept turbulent to prevent the boundary layer from preventing inhomogeneous drying of the samples. The mass of the beads was measured continuously by a balance Mettler Toledo AB304-S (Greifensee, Switzerland) with a precision of ±0.001. The infrared analysis was carried out following the method decribed by Traffano-Schiffo et al. (2014) [13], using an infrared camera (Optris PI® 160 thermal imager, Optris GmbH, Berlin, Germany) installed in front of the sample, at an angle of 45º relative to the plane in which the samples were placed. The camera uses a two-dimensional Focal Plane array with 160x120 pixels, a spectral range of 7.5-13 μm, resolution of 0.05 °C and an accuracy of ± 2%. A reference material of known emissivity (ε = 0.95 - Optris GmbH) was placed next to the samples and recorded with the infrared camera with the aim to correct the emissivity of the sample. Also, the temperature of the drying air, beads, reference material and environment were measured with K-thermocouples connected to an Agilent multiplexer 34901A (Agilent Technologies, Malaysia) and registered by an Agilent Data Acquisition equipment 34972A (Agilent Technologies, Malaysia). Thermal images were analyzed by the software Optris PI Connect (Optris GmbH). After the drying treatment, the samples were kept in aqualab® disposable sample cups, sealed with parafilm® for further analysis. Mass, water activity, moisture, size and shape were measured in wet samples, immediately after drying (non-equilibrated samples) and also after 24 h at 4 °C in order to allow them to reach the equilibrium (equilibrated samples).

2.4. Hydrogel beads characterization

Water content (x_w) was obtained gravimetrically by the weight difference of the beads. The drying conditions were preosusly described by Santagapita et al. (2008). Water activity (a_w) of beads was determined by a dew point Hygrometer Decagon (Aqualab®, series 3 TE, Decagon Devices, Pullman, WA, USA), using a special sample holder. A calibration curve was performed with saturated salt solutions of known a_w. Measurements were made in duplicate. The size and shape were analyzed through digital images captured by a digital camera and analyzed by the free license software ImageJ (http://rsbweb.nih.gov/ij/), as was described by Aguirre Calvo & Santagapita (2016) [14]. At least 30 wet or dried beads of each system were analyzed.

3. Results and discussion

In order to obtain the surface (interfacial) temperature during beads drying, an infrared model has been developed. There are two phenomena involved in the transformation of the energy that reaches the pyrosensor of the infrared camera at the real surface temperature of the sample. Firstly, the fluid located between the pyrosensor and the emitter sample (in this case is air) could be not totally transmitter, inducing a default error to the energy received. Secondly, the energy of the environment produces an overestimation of the energy emitted by the surface of the sample, adding an error in excess for the measured temperature. Therefore, it is necessary to include these phenomena as was previously developed by Traffano-Schiffo et al. (2014) [13].

In order to calculate the real temperature that is emitted by the surface of the sample obtained by the infrared camera, it is necessary to know the emissivity of the sample. Thus, comparing the temperature of the reference surface obtained by the thermocouple and the infrared camera (corrected with its known emissivity $\varepsilon_{ref} = 0.95$), it is possible to calculate the energy being overestimated by reflection of the environment (Eq. 1). Once this energy is known, with the temperature data obtained with the thermocouple and the camera, it is possible to calculate the emissivity of the sample.

$$E_T^{ref} = \varepsilon_{ref} \cdot \sigma \cdot T_{ref}^4 + E_{surr} \tag{1}$$

Where E_T^{ref} is the energy flux of the reference material (W/m^2) and T_{ref} is the temperature registered by the K-thermocouple (K) and E_{surr}, the energy flux emitted by the surroundings (W/m^2).

Figure 1 shows the surface temperature of the sample and the emissivity calculated for A samples. It is possible to observe that until 15 min the drying temperature is not reached (remaining at wet temperature), indicating that the mobility of the water inside the Ca(II)-alginate matrix is so high because the water transport is controlled by the superficial evaporation, from this minute, the internal mechanisms regulate the dehydration process.
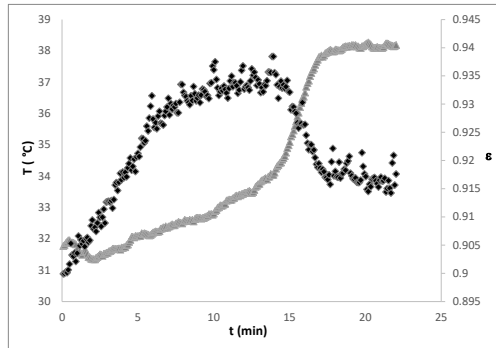
Fig. 1. Surface temperature variation (♦) and emissivity evolution (▲) of alginate beads.
In order to model the transport, it has been necessary to characterize the mean water activity of the beads with regard to their moisture. Figure 2 shows the sorption isotherms obtained by the dynamic technique [8], for each sample.

Bead System		X_{m0} (kg$_w$/kg$_s$)	C	K	Q_L (J/mol)
A	TREATED	0.354	15.64	1.023	7155
	EQUILIBRATED	0.288	11.98	1.025	6462
AS	TREATED	0.229	12.88	1.012	6650
	EQUILIBRATED	0.127	8.02	1.028	5418
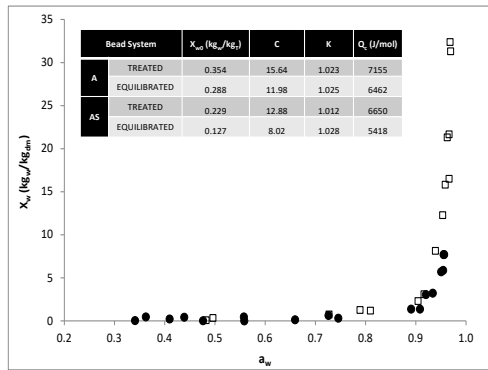
Fig. 2. Desorption isotherm (equilibrated samples), where (□) corresponds to alginate and (●) alginate-sucrose beads.The table shows the GAB parameters obtained.

With the aim to describe the different behaviors involved in the drying process, a thermodynamic approach has been developed. Gibbs free energy variation can be explained by the following equation [15]:

$$dG = -SdT + VdP + Fdl + \psi de + \sum_i \mu_i \, dn_i \qquad (2)$$

Where SdT corresponds to the thermic term and it is directly related to heat fluxes, VdP and Fdl are the mechanical energies related to the structural changes; corresponding to the pressure variation and to the elongation force, respectively; and ψde represents the effect of the electric field induced by solved ions. The term $\sum_i \mu_i \, dn_i$ corresponds to the activity term and is the addition of the chemical potentials of the "i" component, being constant the rest of state variables.

If the variation of free energy per mole of water is considered, it is possible to define the extended water chemical potential ($\Delta\mu_w$) (J/mol) as the quotient between the variation of the Gibbs free energy (J) and the variation of moles of water (mol). From the extended water chemical potential and Eq. 2 it is possible to obtain Eq. 3. It should be note that the terms Fdl and ψde can be neglected because Ca(II)-alginate beads are an elastic system and there is no ions effect in the medium, respectively.

$$\Delta\mu_w = -s_w \left(T^{air} - T^{samp}\right) + v_w \left(P^{air} - P^{samp}\right) + RT^{samp} \ln \frac{a_w^{samp}}{\varphi^{air}} \qquad (3)$$

Where s_w corresponds to the partial molar entropy of water (J/K mol); v_w, the partial molar volume of water (m^3/mol); P, the pressure (Pa); R, the ideal gases constant (8.314472 J/K mol) and φ, the relative moisture. The superscripts *samp* and *air* refer to the sample and the air surrounding it, respectively.

Once the entropic and the activities terms are obtained, it is possible to calculate the water chemical potential without considering the mechanical terms $\Delta\mu_w^*$ (Fig. 3). In the Figure, it is possible to observe how, for AS beads, the gradient decreases much earlier than A beads. This is due to the effect of higher water activity values in alginate samples, which allows them to maintain a higher value of water activity for longer.
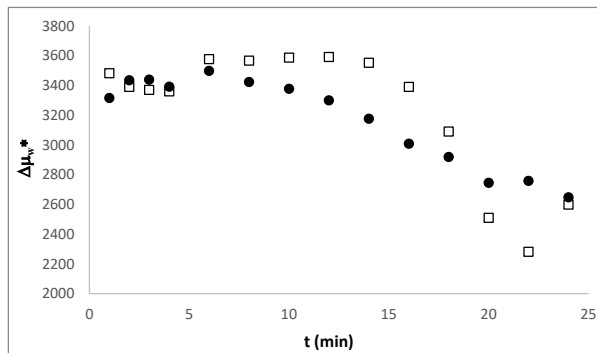
Fig. 3. Water chemical potential evolution without considering the mechanical terms, where (□) corresponds to alginate and (●) alginate-sucrose beads.

Applying the first relation of Onsager [13], the water molar flux (J_w) (mol/s m^2) is related to the water chemical potential, as a driving force of the water transport, by the phenomenological coefficient (L_w) (mol^2/J s m^2) (Equation 4).

$$J_w = L_w \cdot \Delta\mu_w \qquad (4)$$

Applying Eq. 4 with data of chemical potential without considering the mechanical terms and the water fluxes, it is possible to obtain the phenomenological coefficient without considering the mechanical term (L_w^*). Figure 4 shows the evolution of the phenomenological coefficient, calculated without mechanical terms during drying. It is possible to observe how the coefficient increases from minute 15 to compensate the imbalance between the water flux and the chemical potential obtained from the terms of activity and entropy, when it would be expected to follow a proportionality between both extensive variables as the relation of Onsager shows.

There is a linear relationship between the phenomenological coefficient without considering the mechanical terms and the water flux during the entire drying process in both systems. Therefore, following this linear prediction of the phenomenological coefficient and extending

it for the entire drying treatment, the mechanical terms could be estimated from the following equation:

$$v_w \, \Delta P = \, \Delta \mu_w - \, \Delta \mu_w^*$$ (5)
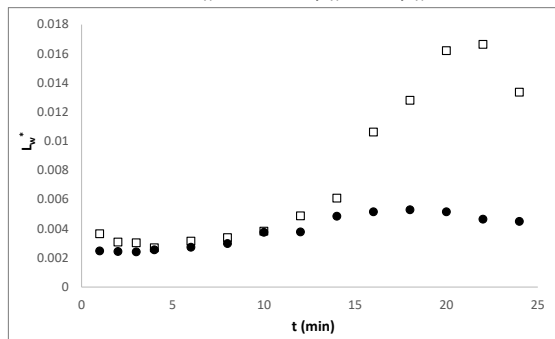
Fig. 4. Phenomenological coefficient evolution during drying, where (□) corresponds to alginate and (●) alginate-sucrose beads.

Figure 5 shows the evolution of the pressure term during drying process for both systems. As can be observed in this figure, the alginate samples suffer strong over atmospheric pressures from the minute 15 of the process caused by a great contraction of the system, which greatly accelerates the dehydration process. However, alginate-sucrose samples suffer the contraction process from minute 10, generating minor overpressures. This indicates that the addition of sucrose to the Ca(II)-alginate structure weakens the mechanical resistance to the shrinkage of the matrix, reducing its capacity to store liquid phase.
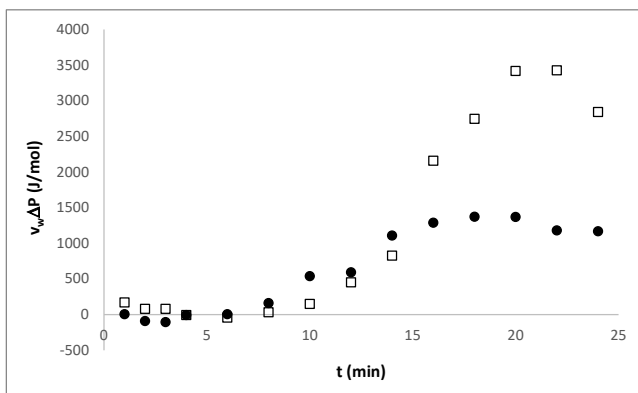
Fig. 5. Evolution of the pressure term during drying process, where (□) corresponds to alginate and (●) alginate-sucrose beads.

4. Conclusions

It has been demonstrated that IRT is a good tool to control the drying process of Ca(II)-alginate beads, providing valuable information about the heat transfer in colloidal systems, being possible to obtain the evolution of the beads emissivity during drying.

It has been developed a thermodynamic model based in Gibbs free energy. The desorption isotherm was also obtained.

5. Acknowledgements

6. References

[1] Santagapita, P. R., Mazzobre, M. F., & Buera, M. P. (2012). Invertase stability in alginate beads: Effect of trehalose and chitosan inclusion and of drying methods. Food Research International, 47(2), 321-330.

[2] Aguirre Calvo, T. R., Busch, V. M., & Santagapita, P. R. (2017). Stability and release of an encapsulated solvent-free lycopene extract in alginate-based beads. LWT-Food Science and Technology, 77, 406-412.

[3] Traffano-Schiffo, M. V., Castro-Giraldez, M., Fito, P. J., & Santagapita, P. R. (2017a). Encapsulation of lactase in Ca (II)-alginate beads: Effect of stabilizers and drying methods. Food Research International, 100, 296-303.

[4] Traffano-Schiffo, M. V., Aguirre Calvo, T. R., Castro-Giraldez, M., Fito, P. J., & Santagapita, P. R. (2017b). Alginate beads containing lactase: stability and microstructure. Biomacromolecules, 18, 1785-1792.

[5] Rahman, M. S., & Labuza, T. P. (1999). Water activity and food preservation. In M. S. Rahman (Ed.), Handbook of food preservation. New York: Marcel Dekker, pp. 448–471.

[6] Clemente, G., Sanjuán, N., Cárcel, J. A., & Mulet, A. (2014). Influence of temperature, air velocity, and ultrasound application on drying kinetics of grape seeds. Drying technology, 32(1), 68-76.

[7] Kumar, C., Karim, M. A., & Joardder, M. U. (2014). Intermittent drying of food products: A critical review. Journal of Food Engineering, 121, 48-57.

[8] Traffano-Schiffo, M. V., Castro-Giraldez, M., Colom, R. J., & Fito, P. J. (2015). Study of the application of dielectric spectroscopy to predict the water activity of meat during drying process. Journal of Food Engineering, 166, 285-290.

[9] Vadivambal, R., & Jayas, D. S. (2011). Applications of thermal imaging in Agriculture and Food Industry—A Review. Food and Bioprocess Technology, 4, 186–199.

[10] Clemente, G., Bon, J., Sanjuán, N., Mulet, A. (2011). Drying modelling of defrosted pork meat under forced convection conditions. Meat Science, 88 (3), 374–378.

[11] Smidsrød, O., Larsen, B., Painter, T., & Haug, A. (1969). The role of intramolecular autocatalysis in the acid hydrolysis of polysaccharides containing 1,4-linked hexuronic acid. Acta Chemica Scandinavica, 23(5), 1573-1580.

[12] Traffano-Schiffo, M. V., Castro-Giraldez, M., Fito, P. J., Perullini, M., & Santagapita, P. R. (2018). Gums induced microstructure stability in Ca (II)-alginate beads containing lactase analyzed by SAXS. Carbohydrate Polymers, 179, 402-407.

[13] Traffano-Schiffo, M. V., Castro-Giráldez, M., Fito, P. J., & Balaguer, N. (2014). Thermodynamic model of meat drying by infrared thermography. Journal of Food Engineering, 128, 103-110.

[14] Aguirre Calvo, T., & Santagapita, P. (2016). Physicochemical characterization of alginate beads containing sugars and biopolymers. Journal of Quality and Reliability Engineering, 2016, 1-7.

[15] Castro-Giraldez, M., Fito, P. J., & Fito, P. (2010). Non-equilibrium thermodynamic approach to analyze the pork meat (Longissimus dorsi) salting process. Journal of Food Engineering, 99(1), 24-30.

Development and use of three-dimensional image analysis algorithms to evaluate puffing of banana slices undergone combined hot air and microwave drying

Satienkijumpai, A.[a*]; Jinorose, M.[a*]; Devahastin, S.[b]

[a] Department of Food Engineering. Faculty of Engineering. King Mongkut's Institute of Technology Ladkrabang, 1 Soi Chalongkrung 1, Ladkrabang, Bangkok, 10520, Thailand.

[b] Department of Food Engineering. King Mongkut's University of Technology Thonburi, 126 Pracha u-tid Road, Tungkru, Bangkok, 10140, Thailand.

*E-mail of the corresponding author: maturada.ji@kmitl.ac.th

Abstract

Puffing is an attractive alternative for the production of healthy crisp snacks without frying. Although image analysis has been used in some prior studies to evaluate puffing, such an evaluation was made only in one or two dimensions, which is inadequate when a sample deforms in three dimensions. In this study, use of combined hot-air and microwave drying to dry and puff banana slices was first evaluated. Algorithms were then developed to characterize the changes in the appearance of puffed banana slices. Various image-based parameters, both in two and three dimensions were assessed and used to monitor the puffing.

Keywords: Deformation; Puffing; Imge analysis; Physical properties; Surface texture

1. Introduction

Snacks, especially those made from fruits and vegetables, have recently received increasing attention and are widely consumed by health-conscious consumers. Such an increased consumption is due to the fact that modern consumers are paying more attention to their health and trying to switch from traditional to non-sugary and low-fat or even fat-free snacks. Low-fat or fat-free snacks, which are produced by hot air drying, however, suffer important drawbacks; these snacks generally exhibit inferior texture to those obtained via the process of frying. An alternative drying technology is clearly needed to alleviate the drawbacks. Combined hot-air and microwave drying has indeed been suggested and applied to produce dried fruit snacks with more desirable texture.[1] The superior texture is due to puffing, which occurs due to rapid expansion of the fruit microstructure as a result of rapid internal evaporation of water into vapor that cannot escape from such a microstructure at an adequate rate.

Puffing is generally evaluated and reported in terms of volumetric deformation, which is calculated as the ratio of the volume of a sample after drying to that before drying.[2] However, volumetric deformation cannot be used to describe non-uniform or irregular puffing, which normally takes place and can significantly affect the appearance and hence the consumer's acceptance of a final product.[3] It has in fact been reported that two pieces of a material may exhibit similar volumetric shrinkage (or deformation) despite the fact that they had gone through different methods of drying and clearly possess different forms (shape and size) of deformation.[4]

Although image analysis has been used in some earlier studies to evaluate deformation during drying, attempts were usually made only to evaluate deformation in one or two dimensions, which is not adequate when a sample deforms non-uniformly[3] or exhibits irregularly rugged surface in three dimensions such as in the case of puffing. This is simply because one and two dimensional imagings are much easier than three-dimensional imaging, eventhough they cannot accurately well represent deformation.[3] In addition, despite some recent attempts to describe deformation using indicators derived from image-based information, most studies only focused on uniform deformation of simple shapes, e.g., spherical, cylindrical and cubical shape.[3] The ability to precisely identify the shape and its changes of an irregularly shaped materials remains a challenge.

In this study, the use of combined hot-air and microwave drying to dry and puff banana slices was first evaluated. Algorithms and software were developed to characterize the changes in the appearance of puffed banana slices. Various image-based parameters, both in two dimensions (i.e., projected area, major and minor axes, equivalent diameter, perimeter, fractal dimension, extents, form factor and aspect ratio) and three dimensions

(i.e., image-based volume, surface area, sphericities, Wadell's roundness, radius ratio and Hoffmann shape entropy), were assessed and used to monitor the puffing.

2. Materials and Methods

2.1. Banana slices preparation

Banana of the Namwa variety (*Musa sapientum* L. (ABB group)) was used in this study. Banana was purchased from a local supermarket and kept at room temperature (28° ± 3° C) until its total soluble solids (TSS) reached 28.5° ± 0.5º Brix. Banana was peeled and sliced to the dimensions of 5 ± 0.5 mm in thickness and 30.0 ± 2.0 mm in diameter; the dimensions were measured by a Vernier caliper (Winston, Japan).

2.2. Drying and puffing experiments

Drying experiments were conducted in a convective hot-air dryer (Memmert, UF30, Germany) at 70° ± 5° C until the banana moisture content reached either 10, 20, 30 or 40% dry basis (d.b.). Puffing was then conducted in a domestic microwave oven (Samsung, MS23K3513AW, Malaysia) at an input powder of 800 W for either 0, 20, 40 or 60 s.

2.3. Image acquisition

Two-dimensional images of banana slices were first taken via the use of a scanner (Epson, V30, Indonesia) at 300 dpi with black background to reduce the shadow. Three-dimensional images were produced from the two-dimensional images as per the procedures developed by Jinorose et al.[3] Two-dimensional images were preprocessed by MeshLab (ISTO-CNR, Visual computing Laboratory) to reduce unwanted objects and then reconstructed using Autodesk Recap 360 software (Autodesk Inc., San Rafael, CA) into three-dimensional images.

2.4. Image analysis

Each 2D image was preprocessed and analyzed using MATLAB® (version R2015b, MathWorks Inc., MA). Image segmentation was conducted by converting RGB image into binary image using Otsu's thresholding method. Edge detection and holes filling were performed to segment the area of interest (AOI). All the basic image parameters including projected area, major axis length, minor axis length, equivalent diameter, perimeter and extent were calculated using the functions of MATLAB® image processing tools box. Other parameters were also calculated as per the following equations.[5]

$$\text{Extent 2} = \frac{A}{D_{\text{fmax}}D_{\text{fmin}}} \tag{1}$$

$$\text{Form factor} = \frac{4\pi A}{P^2} \tag{2}$$

$$\text{Aspect ratio} = \frac{D_{\text{fmax}}}{D_{\text{fmin}}} \tag{3}$$

In the case of 3D analysis, after a 3D image was reconstructed, the image was converted into an STL file and imported into COMSOL Multiphysics® version 3.5 (COMSOL, Inc., Sweden) to calculate the image-based volume, surface area, sphericity, Wadell's sphericity, Wadell's roundness, radius ratio and Hoffmann shape entropy.[5,6] 'fine mesh' setting was adopted when assigning meshes to the object prior to the calculation.

$$\text{Sphericity} = \frac{(36\pi)^{\frac{1}{6}} V^{\frac{1}{3}}}{SA^{\frac{1}{2}}} \tag{4}$$

$$\text{Wadell's sphericity} = \frac{SA_{\text{v}}}{SA} \tag{5}$$

$$\text{Wadell's roundness} = \frac{4A}{\pi D_{\text{fmax}}^{2}} \tag{6}$$

$$\text{Radius Ratio} = \frac{R_{\text{min}}}{R_{\text{max}}} \tag{7}$$

$$\text{Hoffmann shape entropy} = \frac{1}{\ln(\frac{1}{3})} \sum_{i=1}^{3} p_i \ln p_i \tag{8}$$

2.5. Moisture content determination

The moisture content of a sample was determined as per AOAC method 984.25 (2000).

2.6. Volume determination

The volume of a sample was determined as per the methods of Yan et al.[7] The sample was suspended in 125 mL of 95% *n*-heptane, which was filled in a 250-mL beaker placed on a 3-digit balance (Want, WT3203N, China).

All experiments were performed in triplicate and the results, where appropriate, are reported as mean values and standard deviations.

3. Results and discussion

3.1. Drying of banana slices

Preliminary experiments revealed that banana slices suffered phase transition and stuck to the tray when drying was conducted at 90° C. Drying was therefore conducted at 50 and 70° C; the degrees of puffing (or deformation) and visual appearance were noted to be almost the same at the same moisture content either when drying was conducted at 50 or

70° C. As a result, drying at 70° C was finally selected in the interest of time and energy conservation.

3.2. Puffing of banana slices

After drying to the predetermined moisture content, puffing was conducted. Selected images of the samples at different puffing time are shown in Fig. 1. Deformation occurred rather uniformly until about 40 s, after which the sample started to deformed non-uniformly. This visually observed critical point corresponded to the moisture ratio of around 0.4-0.5 (Fig. 2a).
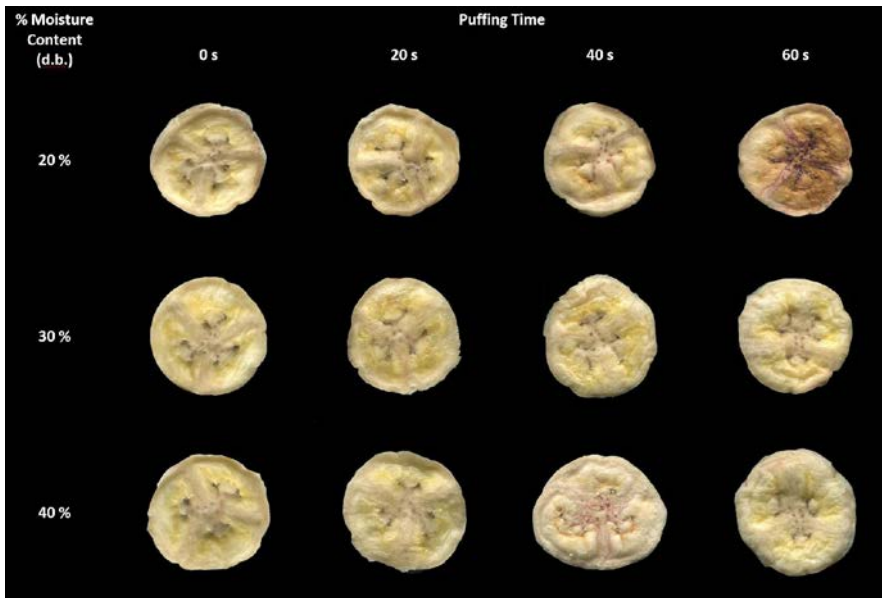
Fig. 1 2D images of banana slices during puffing.

The evolution of the degree of puffing (volumetric deformation) as a function of the moisture ratio with moisture content prior to puffing as a parameter is shown in Fig. 2b. Degree of puffing increased linearly even when the moisture ratio reached around 0.2 (or the puffing time of around 60 s as seen in Fig. 2a). It is important to note that the degree of puffing, which was obtained from liquid displacement measurement, could not identify the start of the non-uniform deformation period, which took place at around 40 s as mentioned earlier.

(a) (b)
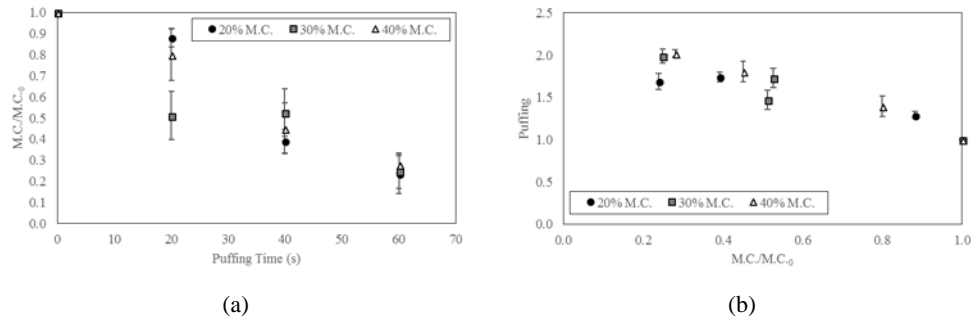
Fig. 2 (a) Moisture ratio as a function of puffing time of banana slices.
(b) Degree of puffing of banana slices as a function of moisture ratio.

3.3. Image-based information

Fig. 3a shows the evolutions of the 2D image-based parameters as a function of the moisture ratio of banana slices undergoing puffing. When considering which parameters could be used to describe the non-uniform deformation (or, in other words, change of shape), only the aspect ratio and extent 2 could be used. It is seen that while other parameters stayed unchanged, these two parameters started to vary significantly when the moisture ratio was around 0.5, beyond which their values started to increase. This corresponded to the critical point where non-uniform deformation was observed to start (see Fig. 1). Nevertheless, these two parameters could only identify the onset of the non-uniform deformation but not the deformation itself. These 2D parameters could also not be used to monitor the volume change of the samples, as expected. Since puffing naturally involves the change of volume, inability to monitor such a change is clearly inadequate.

(a) 2D image-based parameters (b) 3D image-based parameters
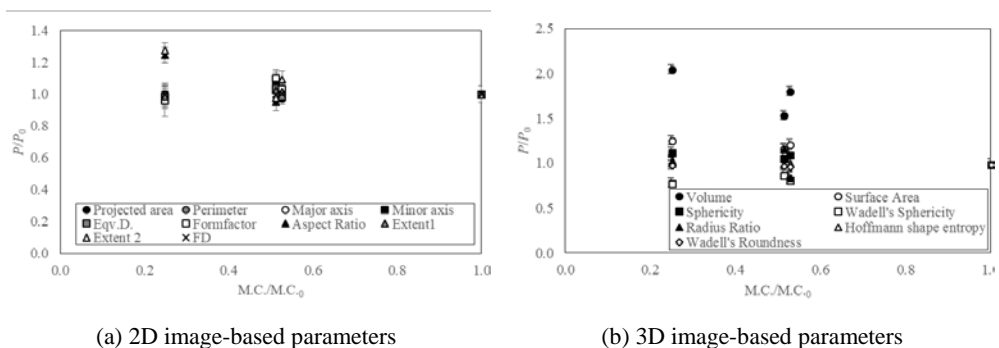
Fig. 3 (a) Evolutions of image-based parameters as a function of moisture ratio of banana slices
undergoing puffing. P = parameter of interest; 0 = initial value.

Interestingly, form factor and fractal dimension, which are widely used to indicate circularity and shape changes, remained unchanged over the whole puffing period. This incorrectly implies that banana slices retained their shape throughout the process, which contradicted to the visual observation results. This is most probably because 2D top-view images are not adequate for the evaluation of a sample with rugged surface (as in our case of puffed banana slices). For this reason, choosing appropriate parameters is very important if non-uniform deformation is to be monitored; widely used parameters cannot always be used for such a purpose.

Fig. 3b shows the evolutions of the 3D image-based parameters as a function of the moisture ratio of banana slices undergoing puffing. The volume and surface area values were those of the reconstructed 3D images; the values increased with decreasing moisture ratio. Only the Wadell's sphericity exhibited a similar trend to the aspect ratio and extent 2 (started to decrease after the moisture ratio was lower than 0.5) and might be able to be used to monitor the non-uniform deformation.

Based on the aforementioned observations, volume and surface area along with the Wadell's sphericity should be used to monitor the puffing of banana slices. Fig. 4 indeed illustrates that the volume as obtained from image analysis agreed well with the values obtained from the liquid displacement experiments.
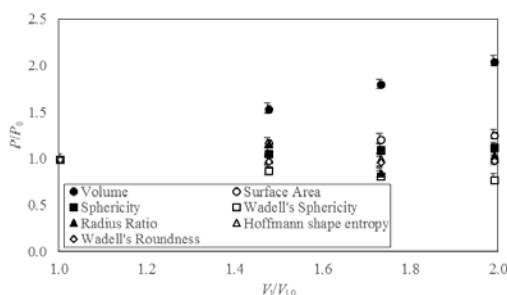
Fig. 4 Evolutions of 3D image-based parameters as a function of volume ratio of banana slices undergoing puffing. P = Parameter of interest; 0 = initial value.

4. Conclusions

Image analysis algorithms were developed to characterize puffing, which is a non-uniform deformation phenomenon, of banana slices in three dimensions. Various image-based parameters, both in 2D and 3D, were calculated and tested for their suitability to monitor such a deformation. As for the 2D-based parameters, aspect ratio and extent 2 could be used to indicate the start of the non-uniform deformation period; Wadell's sphericity represented the 3D-based parameters that could be used to perform the similar task. These parameters, however, could not be used to monitor the volume change of the samples. 3D-based volume

and surface area along with the Wadell's sphericity should instead be used to monitor the puffing of banana slices.

5. Acknowledgements

6. Nomenclature

A	Projected area	cm^2
D_{fmax} , D_{fmin}	Maximum and minimum ferret diameter	m
Major, Minor	Major and minor axis length	cm
P	Perimeter	cm
p_i	Ratio between length of each dimension to sum of length of all dimension in 3D image	
$R_{\max}$	Radius of the smallest circumscribe in 3D image	voxel
$R_{\min}$	Radius of the biggest inscribe sphere in 3D image	
SA	Surface area of sample from 3D image	cm^2
SA_v	Surface area of sphere that have same volume from 3D image	cm^2
V	Volume of sample from 3D image	cm^3

7. References

[1] Paengkanya, S.; Soponronnarit, S.; Nathakaranakule, A. Application of microwaves for drying of durian chips. Food and Bioproducts Processing 2015, 96, 1-11.

[2] Tabtiang, S.; Prachayawarakon S.; Soponronnarit, S. Effects of osmotic treatment and superheated steam puffing temperature on drying characteristics and texture properties of banana slices. Drying Technology 2012, 30(1), 20-28.

[3] Jinorose, M.; Stienkijumpai, A.; Devahastin, S. Use of digital image analysis as a monitoring tool for non-uniform deformation of shrinkable materials during drying. Journal of Chemical Engineering of Japan 2017, 50(1), 785-791.

[4] Devahastin, S.; Niamnuy, C. Modelling quality changes of fruits and vegetables during drying: a review. International Journal of Food Science and Technology 2010, 45, 1755-1767.

[5] Neal, F.B.; Russ, C.J. Measuring Shapes; CRC Press: Boca Raton, 2012; 231-290.

[6] Bullard, J.W.; Garboczi, E.J. Defining shape measures for 3D star-shaped particles: sphericity, roundness, and dimensions. Powder Technology 2013, 249, 241-252.

[7] Yan, Z.; Sousa-Gallagher, M.J.; Oliveira, F.A.R. Shrinkage and porosity of banana, pineapple and mango slices during. Journal of Food Engineering 2008, 84(3), 430-440.

On the importance of heat and mass transfer coupling for the characterization of hygroscopic insulation materials

Perré, P.[a,b]; Challansonnex, A.[a]

[a] LGPM, CentraleSupélec, Université Paris-Saclay, 91 190 Gif-sur-Yvette, France
[b] LGPM, CentraleSupélec, Centre Européen de Biotechnologie et de Bioéconomie (CEBB), 51 110 Pomacle, France.

*E-mail of the corresponding author: patrick.perre@centralesupelec.fr

Abstract

The present work is focused on mass transfer characterization of hygroscopic materials used for insulation, such as Low Density Fibreboards. Due to their particular morphology, these panels present a very high mass diffusivity in the connected gaseous phase and a very low thermal conductivity. This combination of properties exacerbates the coupling between heat and mass transfer in transient state.

Based on experimental data obtained with an original set-up and relevant simulations performed using a comprehensive physical formulation, a throughout vision of this question is proposed in the present study. In particular, we emphasize on:

- The impressive change in core temperature in terms of magnitude and duration,
- The great impact of the internal temperature gradient, which slows down mass diffusion,
- The dramatic error on mass diffusivity value if the coupling is ignored.

Keywords: *experiment; identification; modelling; RH at back-face; transient state.*

On the importance of heat and mass transfer coupling for the characterization of hygroscopic insulation materials.

1. Introduction

The thermal performances of constructions are getting more and more challenging and designers need to model physical phenomena with great accuracy [1-3]. Among them, the strong influence of coupled heat and mass transfer on energy consumption is well established. This is especially true for renewable materials, which generally have a high moisture buffering effect. Consequently, Building Energy Simulations (BES) models must account for coupled heat and mass transfer, which gave rise to a strong demand for mass transfer characterization: mass diffusivity and sorption isotherms. In addition, due to side effects such as molecular relaxation and dual-scale effects, these materials must be characterized in transient state as these materials are always in transient-state in buildings.

However, the characterisation of hygroscopic materials is not simple as, due to the latent heat of vaporization, no mass transfer can occur without heat transfer. Consequently, the temperature field is not uniform in the sample, which induces gradients of saturated water vapour, well known to affect mass diffusion. The present work is focused on a particular family of building materials: LDF or other hygroscopic insulation materials. Due to their particular morphology, these materials present a very high mass diffusivity in the connected gaseous phase and a very low thermal conductivity. Together with the hygroscopicity, this combination of properties exacerbates the coupling between heat and mass transfer in transient state. This fact is carefully analysed in the present work, using a unique combination of experiments and simulations.

2. Materials and Methods

2.1. Experimental set-up
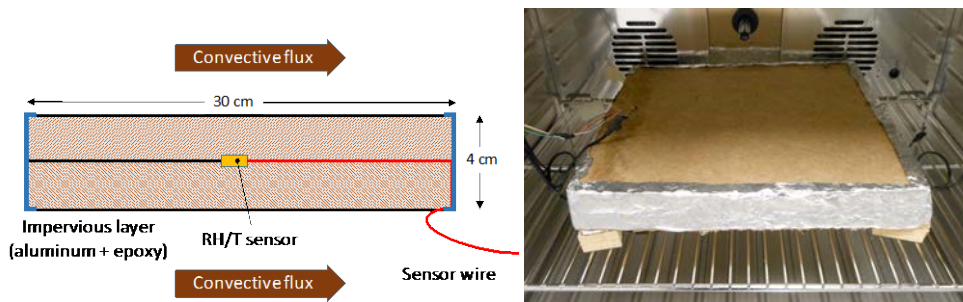
Fig. 1 - Schematic cross-sectional view of the double plate (left) and photograph of the sample placed inside the climatic chamber (right).

The material used in the present work is LDF (160 kg.m^{-3} low-density fiberboard produced by Steico, Therm). The experiment consists in submitting a sample face to a sudden variation of RH and to record the evolution of RH on the other face [4]. To rigorously assess the coupling between heat and mass transfer in this case of insulation material, a specific design was imagined to avoid any thermal perturbation and obtain 1-D transfer without any

heat and mass flux at the back face of the sample (Fig. 1). For that purpose, a temperature/RH sensor (Sensirion SHT25, HDI Electronics, Perois, France) was placed between two 20-mm thick plates of LDF. Side effects were avoided by choosing large dimensions (30 cm x 30 cm), which is more than 7 times the diffusion thickness. Finally, to avoid lateral water vapor leakages, the two superimposed LDF plates were coated with an aluminium foil glued to the lateral faces by epoxy resin. This double sample is placed inside a climatic chamber (HPP110, Memmert, Schwabach, Germany) to control external conditions. Three RH/T sensors are placed inside the chamber to record the actual conditions applied to the sample.

2.2. Results

Fig. 2 presents a typical example of experimental data. This test was performed for a double layer of LDF panel (ρ = 160 kg.m^{-3}, thickness = 2 x 20 mm) for a stepwise change of RH from 20% to 40% at 35°C. Low RH values were intentionally chosen to reduce the effect of molecular relaxation on the dynamic of sorption equilibrium [5]. The RH collected at the back-face of the sample needs about 10 hours to reach the new external RH. This information is the basic information used to identify the dimensionless mass diffusivity of the panel in the method proposed in [4].

What is new in figure 2 is the temperature collected at the back-face of the sample. This value is relevant thanks to the symmetrical configuration: as the back-face of the sample is the value in the centre of two large plates, the assumption of 1-D transfer is valid and not artefact of heat transfer is likely to perturb the temperature value. As a result, we can observe an impressive temperature peak due to condensation: this peak is large in magnitude (more than 4°C above the ambiance) and in duration (more than 10 hours, the same duration as for mass transfer). Simulation performed using a comprehensive formulation of coupled heat and mass transfer will be used to analyse this impressive coupling and its effect on material characterisation.

3. The physical formulation

A comprehensive physical formulation was used in the present work. More detailed information regarding this set of equations can be found in published works [6]. For the sake of simplification, all liquid water contributions have been discarded, as the sample stays inside the hygroscopic domain. The simplified transport equations read as follows:

Water conservation

$$\rho_s \frac{\partial X}{\partial t} + \nabla \cdot \left(\rho_v \bar{v}_g \right) = \nabla \cdot \left(\rho_g \, f \, \boldsymbol{D}_v \cdot \nabla \omega_v + \rho_b \boldsymbol{D}_b \nabla X \right) \tag{1}$$

On the importance of heat and mass transfer coupling for the characterization of hygroscopic insulation materials.

Energy conservation

$$\frac{\partial}{\partial t}\left(\varepsilon_g(\rho_v h_v + \rho_a h_a) + \overline{\rho}_b \overline{h}_b + \varepsilon_s \rho_s h_s\right) + \nabla\cdot\left((\rho_v h_v + \rho_a h_a)\overline{\boldsymbol{v}}_g\right)$$
$$= \nabla\cdot\left(\lambda_{eff}\nabla T + \rho_g \boldsymbol{f}\,\boldsymbol{D}_v(h_v\nabla\omega_v + h_a\nabla\omega_a) + h_b\rho_b\boldsymbol{D}_b\nabla X\right) \tag{2}$$

Air conservation

$$\frac{\partial\left(\varepsilon_g\rho_a\right)}{\partial t} + \nabla\cdot\left(\rho_a\overline{\boldsymbol{v}}_g\right) = \nabla\cdot\left(\rho_g \boldsymbol{f}\,\boldsymbol{D}_v\nabla\omega_a\right) \tag{3}$$
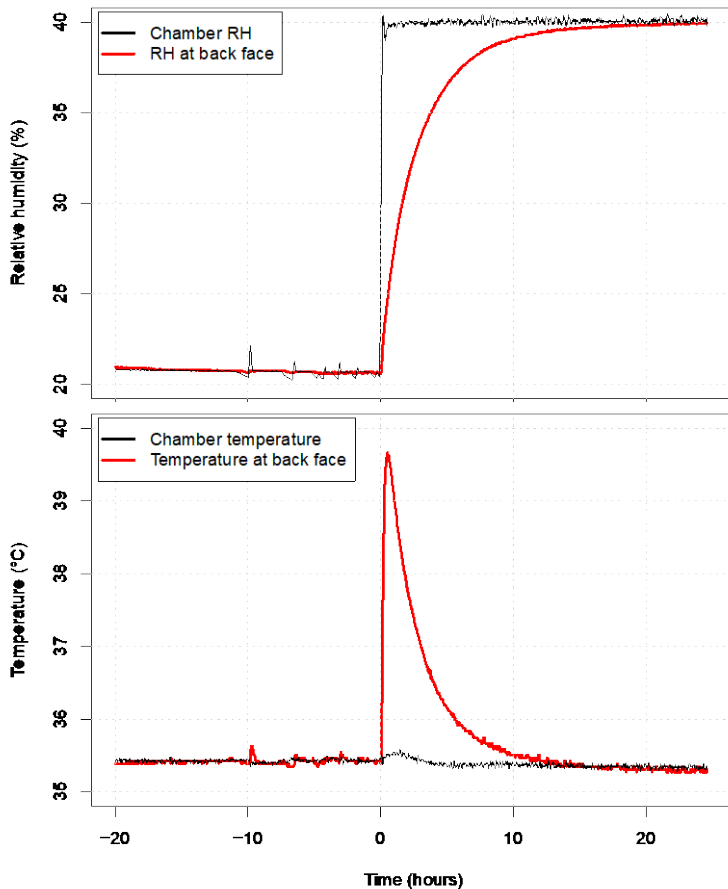
Fig.2 - *Experimental results for a double plate (2 x 20 mm) of LDF (160 kg.m^-3): time evolution of RH (top) and temperature (bottom) at the back-face of the sample.*

Boundary conditions

At the external faces of the sample, the boundary conditions were assumed to be of the following form:

$$\mathbf{J}_v\big|_{x=0} \cdot \mathbf{n} = h_m\, c\, M_v \ln\left(\frac{1 - x_{v,\infty}}{1 - x_v\big|_{x=0}}\right)$$

$$\mathbf{J}_q\big|_{x=0^+} \cdot \mathbf{n} = h\left(T\big|_{x=0} - T_\infty\right)$$

$$P_g\big|_{x=0^+} = P_{atm}$$

(4)

where $\mathbf{J}_v$ and $\mathbf{J}_q$ represent the fluxes of water vapour and the heat at the boundary, respectively, while x denotes the distance from the boundary along the external unit normal.

In the previous equations, the barycentric gaseous velocity comes from the generalized Darcy's law:

$$\overline{v}_g = -\frac{K\,k_g}{\mu_g}\nabla p_g$$

(5)

In the hygroscopic domain, the total flux of mass should be expressed as the sum of two parallel fluxes (bound water and water vapour). However, as this work is solely devoted to Low Density Fibreboards, the contribution of bound water diffusion to the macroscopic flux can be neglected. In equations (1-3), $\mathbf{D}_v$ is the water vapour diffusivity, f the dimensionless diffusivity, ρ_g the bulk density of gas, ρ_s the bulk density of the lingo-cellulosic part, X the moisture content (dry basis) and ω_v the mass fraction of water vapour.

The reduced diffusivity f characterizes the porous medium: f ranges from 0 (sample impervious to any moisture transfer) to 1 (open sample having the same behaviour of an air layer at rest). This set of equations was solved by the very fast 1-D version of *TransPore* with actual boundary conditions used as input data. A full simulation requires about one second of CPU time on a personal computer, even when using thousands of experimental times t_i to unroll the boundary conditions. The time step of *TransPore* was adjusted throughout the simulation, not only to secure convergence, but also to obtain the simulated results at the exact experimental times.

4. Results and discussion

Fig. 3 depicts simulation results for our reference test ($f = 0.5$ and $\lambda = 0.05$ W.m^{-1}.K^{-1}). The f value allows the experimental RH value at the back-face to match the experimental data. The value of thermal conductivity is determined by a classical mixture law using the gaseous and solid volume fractions and their conductivities. After the sudden increase in RH, water vapour condensates on the front face of the sample. By releasing the latent heat of vaporization, this moisture flux heats up the surface. Because of this temperature

increase, the vapour pressure at the surface increases as well, as it is the product of water activity by the saturated vapour pressure, which increases rapidly with temperature. The primary effect of this change in surface vapour pressure is to reduce the external driving force, which slows down the process [7]. This temperature increase eventually affects the whole sample, by a tricky coupling of heat and mass transfer: the temperature increase at one point increases the mass fraction of vapour, which gives rise to a vapour flux that condensates in neighbouring parts. In turn, condensation increases the temperature further inside the medium, which allows the process to continue inwards. This produces a "heat wave" propagating towards the back-face, clearly visible on the temperature profiles. Once this wave reaches the back-face of the sample, a temperature gradient establishes towards the external face, to drive outwards the heat supplied in the medium via the latent heat of vaporization. In figure 3, the effect of this temperature gradient on the mass fraction of vapour is obvious, namely for the profiles at 10 and 30 minutes: although the internal value of moisture content (MC) is still close to the initial value, the mass fraction of vapour already increased significantly due to the temperature rise.
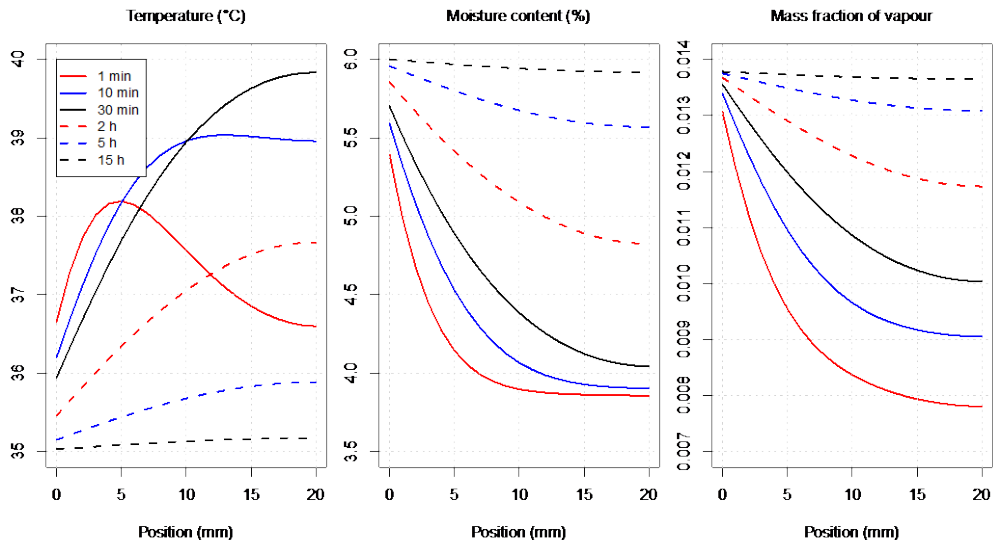
Fig. 3 – Profiles computed at selected times for the reference test (f = 0.5 and λ = 0.05 W.m^{-1}.K^{-1}).

The model is also able to compute the time evolution of the two variables measured during the experiment: temperature and RH at the back face of the sample. The reference test is in perfect agreement with the experiment, which confirms the relevance of the chosen thermal conductivity value. In addition several virtual configurations were computed:

Modified thermal conductivity (x 2 and x 0.5): these simulations exhibit the crucial effect of thermal conductivity, not only on the temperature overshoot (peak at respectively 38.6°C and 41.2°C instead of 39.8°C) but also on the dynamic of RH evolution,

No heat and mass coupling: the coupling is easily cancelled by setting the latent heat of vaporization, Lv, to zero. Consistently, the temperature remains at the external temperature. As a consequence of the absence of coupling, the dynamic of RH evolution is much faster (2.5 hours instead of 4.3 hours for the reference test to attain 35% of RH). This confirms the importance of the heat and mass coupling on the global behaviour.

No internal heat transfer: setting the conductivity λ to zero cancels the heat flux inside the sample. Consequently, the latent heat of vaporization released by condensation cannot be driven towards the exchange face. A balance between water intake and temperature rise takes place: the amount of water condensed in the solid phase raises the temperature until the mass fraction of vapour equals the external value. The steady-state is obtained with an MC increase of 0.5% (against ca. 2% for the reference test) and an temperature of 43.4°C. In this extreme, virtual, configuration, the coupling completely stops mass transfer !
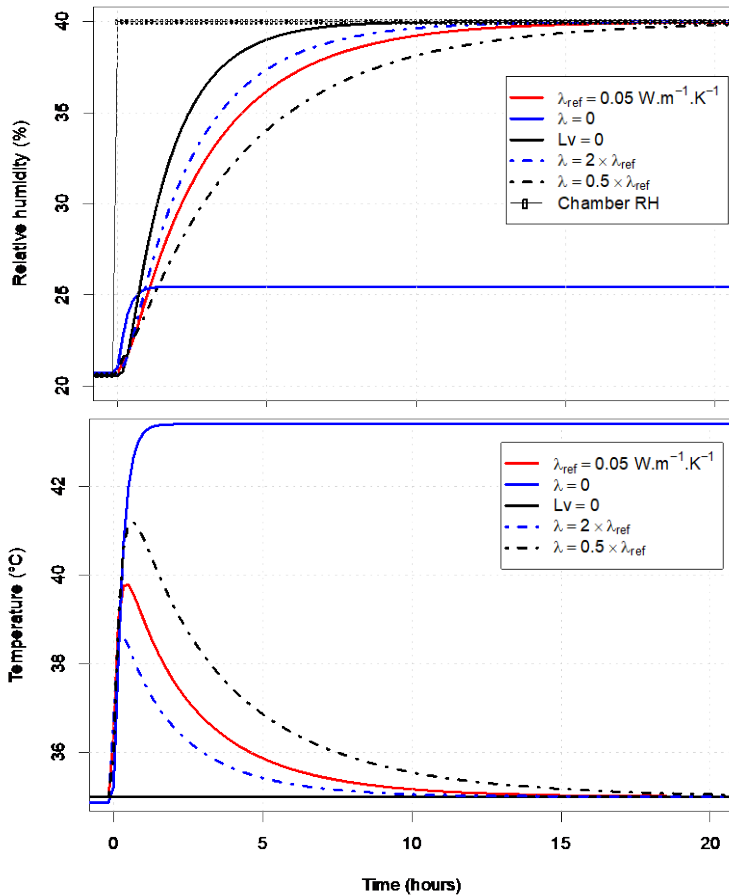
Fig. 4 - Simulation results for LDF (160 kg.m⁻³): RH (top) and temperature (bottom) at the back-face versus time. The various virtual configurations tested are defined in the legend.

5. Conclusions and prospects

Based on experimental data obtained using an original set-up and relevant simulations performed using a comprehensive physical formulation, a throughout vision of the heat mass transfer in Low Density Fiberboards is proposed in the present study. In particular, we emphasize on:

- The impressive change in core temperature in terms of magnitude and duration,
- The great impact of the internal temperature gradient, which slows down mass diffusion,
- The dramatic error on mass diffusivity value if the coupling is ignored.

Further works are in progress in our team to go even further in the analysis of coupled transfers in hygroscopic materials used for building insulation. Besides the heat and mass transfer coupling, sorption hysteresis, dual-scale effects and molecular relaxation have also to be taken into account. However, the strong coupling between these phenomena forces us to be very careful when determining the unknown parameters by inverse analysis. To gain in robustness, several physical parameters will have to be measured during experiments in transient state. By this way, additional parameter values, such as thermal conductivity, could be determined by inverse method.

6. References

[1] Delgado, J., Ramos, N. M., Barreira, E., De Freitas, V., 2010. A critical review of hygrothermal models used in porous building materials. Journal of Porous Media 13, 221–234.

[2] Crawley D.B., Lawrie L.K., Winkelmann F.C., Buhl W., Huang Y., Pedersen C. O., Strand R.K., Liesen R.J., Fisher D.E., Witte M.J., Glazer J., 2001 - EnergyPlus : creating a new-generation building energy simulation program, Energy and Buildings, 33 (4): 319–331.

[3] Piot A., Woloszyn M., Brau J., Abele C., 2011 - Experimental wooden frame house for the validation of whole building heat and moisture transfer numerical models, Energy and Buildings, 43 (6): 1322-1328.

[4] Perré P., Pierre F., Casalinho J., Ayouz M., 2015 - Determination of the mass diffusion coefficient based on the relative humidity measured at the back face of the sample during unsteady regimes, Drying Technology, 33: 1068-1075.

[5] Olek W., Perré P. and Weres J., 2011 - Implementation of a relaxation equilibrium term in the convective boundary condition for a better representation of the transient bound water diffusion in wood, Wood Sci. Technol., 45: 677-691.

[6] Perré P., Turner I., 1999 - A 3-D version of TransPore: a comprehensive heat and mass transfer computational model for simulating the drying of porous media, Int. J. Heat Mass Transfer, 42: 4501–4521.

[7] Perré P., 2015 - The proper use of mass diffusion equations in drying modeling: introducing the drying intensity number, Drying Technology, 33: 1949-1962.

A physical interpretation of the use of fractional operators for modelling the drying process

Perré, P.[a,b]; Turner, I.[c]

[a] LGPM, CentraleSupélec, Université Paris-Saclay, 91 190 Gif-sur-Yvette, France

[b] LGPM, CentraleSupélec, Centre Européen de Biotechnologie et de Bioéconomie (CEBB), 51 110 Pomacle, France.

[c]School of Mathematical Sciences and ARC Centre of Excellence for Mathematical and Statistical Frontiers, Queensland University of Technology, Brisbane, Australia

*E-mail of the corresponding author: patrick.perre@centralesupelec.fr

Abstract

Fractional order derivatives provide useful alternatives to their integer order counterparts due to their ability to model memory and other properties of the porous medium, such as nonlocal behaviour. These phenomena are driven by the constrained interactions within the complex and non-homogeneous microstructures evident at the pore scale.

In this work, we investigate the suitability of time and space fractional operators for modelling drying processes and provide a physical interpretation of these operators. At first, the concept and the general formulation in the case of a 1-D finite domain is summarised. Then a selection of simulations allowed us to analyse the physical effects of these operators on the solution. In particular, we elucidate:(I)the ability of these operators to break the fundamental relationship between mean square displacement and time in the simple example of diffusion in an open space, (ii) the caution to be taken with the formulation of boundary conditions and source terms to obtain consistent balance equations, (iii) the effect of fractional in space diffusion as a way to alter the MC profiles compared to standard diffusion, therefore potentially avoiding the dependence of the diffusivity on the variable

Keywords: *Fractional Calculus; Transport in Porous Media; Finite Volume Method; Matrix Transfer Technique; Matrix Functions.*

1. Introduction

Modelling the transport of moisture through heterogeneous porous media finds application across a number of important environmental problems, such as drying [1] and groundwater flow in freshwater coastal aquifers [2-4]. Experimental work performed by Perré et al. [5] highlighted that the traditional diffusion equation did not adequately describe the absorption of water in the cell wall of beech wood. An unrealistically small diffusion coefficient was required to best fit the experimental data, which was clearly impractical. The observed experimental phenomenon exhibited a large deviation from the stochastic process of Brownian motion, which is a typical case of anomalous, or non-Fickian, diffusion. The bound water migration through the cell walls was thought to be anomalous because the water molecules that are bound to the macromolecules via their hydrogen bonds move by successive jumps within the complex structure of these macromolecules. This finding motivated us to explore alternate modelling approaches for this process.

Based on this assumption, Turner et al. [1] derived a coupled anomalous transport model, which introduced a moisture potential linked to the moisture content field via a non-local fractional-in-space operator involving the Laplacian raised to a negative fractional index. The simulation results highlighted that this model accurately described the absorption of water in the cell wall and provided a good overall mass balance error. Most importantly however, good agreement with experimental data for a suitable range of diffusivity values was achieved only for a fractional index of $\alpha = 0.76$ ($\alpha = 2$ is standard Fickian diffusion).

Both Turner et al. [1] and Fomin et al. [6,7] proposed a fractional-in-space model of the form:

$$\frac{\partial X}{\partial t} = -D_\alpha D_b (-\Delta)^{\frac{\alpha}{2}} X$$

(1)

for the so-called *super-diffusion* of moisture in the porous matrix. In Fomin et al. [6,7] the Caputo definition is adopted for the fractional-in-space operator, whereas in Turner et al. [1] the fractional Laplacian is defined in terms of its spectral decomposition together with homogeneous boundary conditions (BCs). One notes, however, that it can be shown using Laplace transforms that the two definitions are equivalent on semi-infinite domains.

The solution of (1) with standard (Dirichlet, Neumann or Robin) inhomogeneous BCs has been explored previously by the authors [8-10]. In deriving equation (1) the following expression for the moisture flux was used:

$$j = -\rho_0 D_b \nabla \mathcal{X}$$

(2)

where c was defined as the moisture potential.

Using this expression for the moisture flux leads to the BCs at the exposed surface $\partial \Omega$ of the domain Ω being defined for a given function $\boldsymbol{f}$ as

$$\boldsymbol{j} \cdot \boldsymbol{n} = f(X) \text{ on } \partial \Omega$$

(3)

Clearly BC (3) is nonlinear and very challenging even for the standard problem $\alpha = 2$. One of the aims of this research is to provide an analysis of such problems. Another important contribution of this work is the extension of the model (1-3) to include both fractional in time and space operators in the mass conservation balance law, as well as a nonlinear source term $\boldsymbol{g(u)}$. The derivation of analytical and numerical solutions is quite complex and will therefore not be presented here. We focus primarily on the following:

- The best fractional modelling framework to ensure mass conservation is achieved.
- Whether fractional in space diffusion can be used as a way to avoid the dependence of the diffusivity on the variable.
- The effect of the material thickness on the global behaviour for fractional in space or fractional in time formulations.

We also pay careful attention to the caution that must be taken with the formulation of boundary conditions and source terms to obtain consistent balance equations.

2. Fractional Transport Model

Before commencing the model derivation, we provide some preliminary background information on the various definitions of the fractional in time and space operators used throughout the paper.

Definition 1. Caputo fractional derivatives on a finite interval [11]

Let $[\boldsymbol{a},\boldsymbol{b}]$ be a finite interval of the real axis, $\alpha > 0, n - 1 < \alpha < n$, $n \in \mathbb{N}$, then the left sided Caputo fractional derivatives with order α is given by

$$^{C}D_{a-}^{\alpha} f(t) = \frac{1}{\Gamma(n-\alpha)} \int_{a}^{t} \frac{f^{(n)}(\xi)d\xi}{(t-\xi)^{\alpha-n+1}}$$

(4)

where the gamma function is defined as $\Gamma(t) = \int_{0}^{\infty} t^{z-1} e^{-t} \, dt, \Re(z) > 0$ with $t^{z-1} = e^{(z-1)\log t}$ and $\log t \in \mathbb{R}$.

Definition 2. Riemann-Liouville fractional derivatives [11]

Let $[\boldsymbol{a},\boldsymbol{b}]$ $(-\infty < a < b < \infty)$ be a finite interval of the real axis, $f(t) \in AC^{n-1}([a,b])$ and $n - 1 < \alpha < n, n \in \mathbb{N}$, then the left-sided Riemann-Liouville fractional derivative of order α is given as

$$^{RL}D_{a+}^{\alpha}f(t) \;=\; \frac{1}{\Gamma(n-\alpha)}\frac{d^{n}}{dt^{n}}\int_{a}^{t}\frac{f(\xi)\,d\xi}{(t-\xi)^{\alpha-n+1}}$$

(5)

Definition 3. (Fractional Laplacian) [8, 9, 10]

Let $\{\varphi_n\}$ be a complete set of orthonormal eigenfunctions corresponding to eigenvalues λ_n^2 of the operator $(-\frac{d^2}{dx^2})$ on a bounded domain $-L < x < L$, with homogeneous boundary conditions $\mathcal{B}(\varphi)=0$ defined at $x=-L$ and $x=L$. Let $\mathcal{F}_\gamma = \{f \in C(\Omega) | \sum_{n=1}^{\infty} |\lambda_n^\gamma|\,|c_n|^2 < \infty, c_n = \langle f, \varphi_n \rangle, \gamma = \max(2\alpha,0)\}$. Then, for any $f \in \mathcal{F}_\gamma$ we define $(-\frac{\partial^2}{\partial x^2})^{\alpha/2} f = \sum_{n=1}^{\infty} \lambda_n^\alpha c_n \varphi_n$.

2.1. Fractional Modelling Framework

Assuming the solid matrix is rigidly fixed, we can express the mass $m = \rho_0 X$ where X is the moisture content. The flux of mass is taken as either standard (Fickian) diffusion ($\alpha = 2$) with $j = -\rho_0 D_b \nabla X$, or anomalous (non-Fickian) diffusion ($0 < \alpha < 2$) with $\overline{j} = -\rho_0 D_b \nabla \mathcal{X}$ and the moisture potential defined as $\mathcal{X} = D_\alpha(-\Delta)^{\frac{\alpha-1}{2}} X$. The constant D_b has the usual dimensions of diffusivity ($m^2 s^{-1}$), whereas the constant D_α is introduced, if for no other reason, to recover the correct units for the flux, i.e. $D_\alpha = 1 \; m^{\alpha-2}$.

To complete the formulation, one needs an initial condition and boundary conditions, which are usually given in terms of a mass flux that is typically a nonlinear function of X. A one-dimensional framework for these fractional models provides the perfect mechanism by which to test these important hypotheses and to study the evolution of the solution behaviour. In order to achieve these objectives, we discuss the following generalised one-dimensional model that must be solved for X:

2.2. General formulation - Fractional in Time and Space:

$$\frac{\partial X}{\partial t} = {}^{RL}D_{0+}^{1-\gamma}\left[D_b\frac{\partial^2 \mathcal{X}}{\partial x^2}\right] + g(X), \;\; -L < x < L, t > 0, \; 0 < \alpha \le 2$$

$${}^{RL}D_{0+}^{1-\gamma}\left[-D_b\frac{\partial \mathcal{X}}{\partial x}(-L,t) + \sigma_L \mathcal{X}\right] = f_1(X), \; x=-L, t>0$$

$${}^{RL}D_{0+}^{1-\gamma}\left[D_b\frac{\partial \mathcal{X}}{\partial x}(L,t) + \sigma_R \mathcal{X}\right] = f_2(X), \; x=L, t>0$$

$$X(x,0) = X_0(x), \text{ with } 0 < \gamma < 1, \; 0 < \alpha \le 2$$

In this formulation, σ_L, σ_R are regularisation parameters with the choice $\sigma = 0$ giving Neumann boundary conditions (suitable when only time fractional operators are employed); $\sigma \to \infty$ gives Dirichlet conditions and otherwise mixed or Robyn type conditions prevail. We explore finite values of σ ($\sigma \ll 1$) to ensure non-singularity of the fractional potential operator $(-\Delta)^{\alpha/2-1}$ at the smallest eigenvalue. The functions $f_1(X), f_2(X), g(X)$ and $X_0(x)$ are assumed smooth and defined in the context of the problem. We also use the relationship between the Caputo and Riemann-Liouville fractional derivatives given in [11].

A key point in our investigations will be the way in which the fractional operators are applied to the boundary fluxes and source terms to ensure consistent physical behaviour is observed and that an overall mass conservation is achieved.
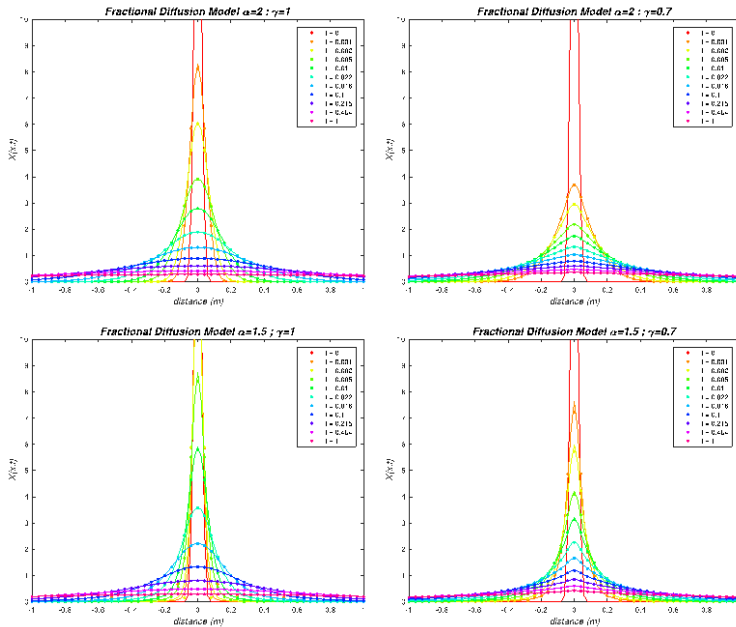
Fig. 1 Plots of moisture content profiles for test problem 1 at various times for (a) standard diffusion ($\alpha = 2, \gamma = 1$); (b) fractional in time ($\alpha = 2, \gamma = 0.7$); (c) fractional in space ($\alpha = 1.5, \gamma = 1$); (d) Fractional in time and space ($\alpha = 1.5, \gamma = 0.7$).

3. Results and discussion

The first problem presented here concerns the time-evolution of an initial field in an infinite domain. Therefore, neither BCs, nor source terms are involved in the model formulation. To come back to the basic definition of diffusion, the initial profile is chosen as a narrow Gaussian curve, likely to be close to the diffusion of a Dirac function (Fig. 1). Consistently,

the mean square displacement (MSD) is proportional to time for normal diffusion (Fig. 2a). This slope equals the fractional value γ for the fractional in time diffusion (Fig. 2b).

In this case, the total mass is conserved, however the allocation of this mass over time is very different from standard diffusion: the center value decreases rapidly at short times but is much slower at longer times compared to normal diffusion. The fractional in space diffusion produces a MSD quasi-proportional to time, which is similar to normal diffusion. However, this MSD is obtained with different spatial fields: the center peak is higher than for normal diffusion at similar times, but this is compensated by a slight moisture increase over long distances, even at short times. The fractional in time and space diffusion accumulates these trends (Fig. 1d).
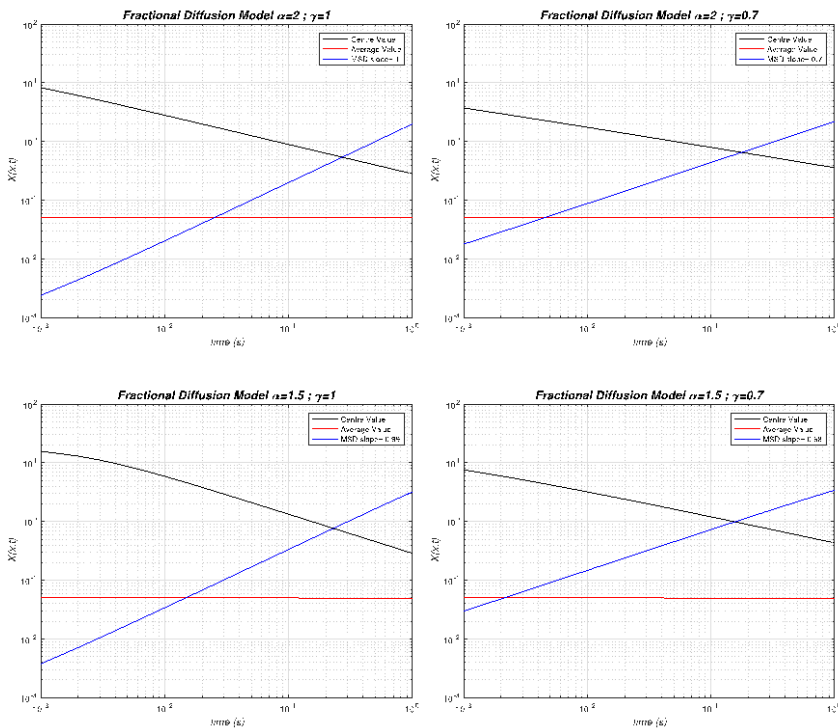
Fig. 2 Plots of means square displacement (MSD), average and centre value for test problem 1 (a) standard diffusion; (b) fractional in time ($\alpha = 2, \gamma = 0.7$); (c) fractional in space ($\alpha = 1.5, \gamma = 1$); (d) Fractional in time and space ($\alpha = 1.5, \gamma = 0.7$).

The solution of the general problem when BCs and/or source terms are involved is more challenging. In particular, great care should be taken in the way the fractional operator has to be applied to the source term and boundary fluxes for the mass balance to be respected. Due to space restrictions, these developments cannot be presented here.

As a final example, we show in Fig. 3 simulation results for different assumptions in the absence of a source term and with Newman boundary conditions (obtained in the general formulation with $\sigma = 0.001$). The standard diffusion exhibits a classical behavior as a result of the flux imposed at the boundaries. The profiles first establish and maintain the same shape which is just regularly shifted towards lower values along time to respect the mass balance. In Fig. 3a, the distance between two successive profiles is exactly the same, as the profiles are plotted with constant time intervals. At first sight, the fractional in time solution (Fig. 3b) is similar to standard diffusion. Note however that the profiles evolve in shape, becoming steeper and steeper as time advances. This effect is more spectacular for the fractional in space solution (Fig. 3c). In this case, the profiles are very steep near the exchange faces. In this case, the spatial rather than the temporal effects modify the local ability of the flux to establish as a function of the moisture gradient.
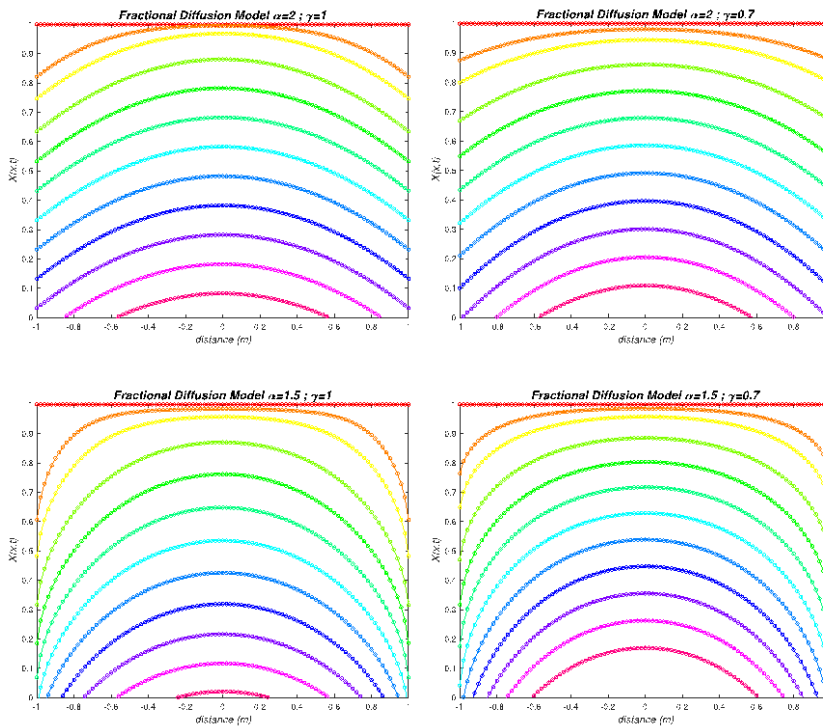
Fig. 3 Plots of moisture content profiles for Newman BC at various times for (a) standard diffusion; (b) fractional in time ($\alpha = 2, \gamma = 0.7$); (c) fractional in space ($\alpha = 1.5, \gamma = 1$); (d) Fractional in time and space ($\alpha = 1.5, \gamma = 0.7$).

The fractional in time and in space solution (Fig. 3d) combines these two effects: again, the fractional in time operator acts more particularly at longer times, for which the profiles are steep both at the boundaries due the fractional in space operator and inside the slab due to

the fractional in time operator. One can easily imagine that when combined, these two behaviors may address different kinds of experimental observation.

4. Conclusion

In this work, we investigated the suitability of fractional operators for simulating drying processes and we also provided a physical interpretation of these operators. At first, a general formulation in the case of a 1-D finite domain was summarised. Then a selection of simulations allowed us to identify the physical effects of these operators on the solution behaviour. In particular, we highlighted:

- The ability of these operators to break the fundamental relationship between mean square displacement and time in the simple example of diffusion in an open space,
- The caution to be taken with the formulation of boundary conditions and source terms to obtain consistent balance equations (not detailed here because of the space restrictions),
- The effect of space fractional diffusion to change the MC profiles compared to standard diffusion, therefore potentially avoiding the dependence of the diffusivity on the variable.

5. References

[1] I. Turner, M. Ilic and P. Perré, Drying Technology, 2011, 29, 1932 - 1940.

[2] R. Chittaranjan, T.R. Ellsworth, A.J. Valocchi and C.W. Boast, J. Hydrology, 1997, 193, 270-292.

[3] Y. Zhang, D.A. Benson, D.M. Reeves, Advances in Water Resources, 2009, 32:561-581.

[4] D. A. Benson, S.W. Wheatcraft and M.M. Meerschaert, Water Resources Res., 2000, 36, 1413–1423.

[5] P. Perré, A.C. Houngan and P. Jacquin, Drying Technology, 2007, 25:1341-1347.

[6] S. Fomin, V. Chugunov, T. Hashida, Proc. R. Soc. A, 2005, 461, 2923-2939.

[7] S. Fomin, V. Chugunov, T. Hashida, Transp. Porous Med., 2010, 81,187-205.

[8] M. Ilić, F. Liu, I. Turner, and V. Anh, Fract. Calc. Appl. Anal., 2005, 8, 323-341.

[9] M. Ilić, F. Liu, I. Turner, and V. Anh, Fract. Calc. Appl. Anal., 2006, 9, 333–349.

[10] M. Ilić, I. Turner, and V. Anh, Journal of Applied Mathematics and Stochastic Analysis, 2008, Article ID 104525.

[11] F. Liu, P. Zhuang and Q. Liu, Science Press, China, November 2015, ISBN 978-7-03-046335-7.

Theoretical and experimental investigation of temperature and moisture distributions and changes in nutritional quality during Intermittent Microwave Convective Drying

Khan, M.I.H.[a, b]; Pham, N.D.[a]; Karim, M.A.[a*]

[a] Science & Engineering Faculty, Queensland University of Technology,
 2 George St, Brisbane, QLD 4000, Australia
[b]Department of Mechanical Engineering, Dhaka University of Engineering & Technology
Gazipur-1700, Bangladesh.

*E-mail of the corresponding author: azharul.karim@qut.edu.au

Abstract

Intermittent microwave convective drying (IMCD) is an advanced drying system where a unique volumetric heating mode is facilitated. However, the physical phenomena of IMCD system and its effect on nutritional quality are not well understood yet. The aim of this research is to develop a coupled IMCD and quality prediction model and experimentaslly validate it. A coupled 3D mathematical model considering Maxwell's equation for electromagnetic heating, and reaction kinetics for predicting quality was developed and validated. COMSOL Multiphysics, engineering software was used to solve the developed model. It is found that IMCD significantly affect the nutritional quality during drying of apple tissue.

Keywords: Food material; Microwave; heat and mass transfer; Quality; 3D modelling

1. Introduction

Drying, like any other food processing methods, is a very energy intensive operation that accounts for up to 15% all industrial energy usage [1]. Understanding the coupled heat and mass transfer during drying are the dominant factor for optimising the energy and quality [2-3]. The physics-based mathematical models can provide realistic understanding of drying process.

A conventional drying or hot air drying is the easiest way of drying [4-5]. However, longer time consumption, formation of crust at the surface due to an elevated temperature, lower energy efficiency and poor quality attributes are associated with convective drying [6]. To overcome these problems, microwave drying is introduced. Microwave drying is getting popularity because it heats the sample quickly, is energy efficient, and easy to control [7]. However, the drying process using microwaves is known to yield low-quality product if not appropriately applied [8]. Hence, microwave drying has usually been combined with other drying techniques including convective hot air, vacuum and freeze-drying to achieve more uniform, fast and effective drying without significant quality loss [9]. Microwave-aided convective hot-air drying has been successfully used for some agricultural products such as grapes [10], carrot [11], apple and mushroom [12], potato[13]. However, continuous supply of microwave and convective heat may cause uneven heating or overheat or create hot spots iin the product. Heat and mass transfer should be carefully balanced to avoid such overheating and to use applied energy more efficiently [14]. Also, the quality degradation has been frequently reported during drying of foods with the continuous application of microwave energy due to uneven temperature and moisture distribution [15]. This problem can be eliminated by the application of microwave energy in a pulsed or intermittent manner that is defended as intermittent microwave convective drying (IMCD).

Intermittent microwave convective drying has proved itself an alternative method to avoid uneven heating, and to improve product quality and energy enhancement by allowing redistribution of temperature and moisture profiles within the product during off times, due to thermal diffusion [16]. Considering the benefits of IMCD drying, many researchers investigated the drying kinetics for different food samples [8, 16, 17] experimentally or empirically. However, only experimental work cannot provide the physics for the heat and mass transfer involved in the process. Physics based mathematical modelling can provide a physical understanding of heat and mass transfer during IMWC. Malafronte, et al. [18] used multiphysics approach to model microwave-assisted convective drying. They considered heat and mass transfer and variable dielectric properties in their model. A comprehensive model for heating in microwave oven of mashed potato was developed by Chen, et al. [19]. However, these models did not consider intermittency of microwave power; thus, the temperature redistribution by means of intermittency of microwave heat source was not investigated. On the other hand, there are some single-phase models which consider the intermittency of microwave heat source [20] but these are only for microwave heating without considering mass transfer. Kumar, et al. [21] developed IMCD model using Lambert's law and observed that the predicted temperature is higher than the experimental value at the end of drying. Moreover, they pointed out that according to Lambert's law the sample surface always absorbed maximum power irrespective of moisture content, which is obviously not correct. Therefore, in this case,

Maxwell model is the more accurate options to predict the microwave field distribution during IMCD.

In addition to this, the quality degradation is the main problem for conventional drying system. In this case, IMCD could be the best solution as it heated the sample intermittently in a periodic cycle [21]. However, the theoretical studies that deals about the effect of intermittency on quality degradation during IMCD are very rare. Therefore, the main aim of the present work is to develop a coupled 3D IMCD and quality prediction model considering the Maxwell equation for the volumetric heat generation, and reacktion kinetics for predicting the quality degradation during IMCD.

2. Model Development

2.1 Governing Equations

2.1.1 *Energy equation*

The energy balance is considered using Fourier's Law of heat transfer, as given below.

$$\rho c_p \frac{\partial T}{\partial t} = \underline{\nabla}.(k_{eff} \underline{\nabla} T) + Q_m \tag{1}$$

Where T is the temperature (°C) at time t, is the density of the sample (kg/m³), is the specific heat of the material (J/kg/K), is the thermal conductivity of the material (W/m/K), Q_m is the volumetric heat source.

2.1.2 *Mass transfer equation*

Mass balance equation is developed based on Fick's law of diffusion that is given by,

$$\frac{\partial c}{\partial t} + \underline{\nabla}.\left(-D_{eff} \underline{\nabla} c\right) = 0 \tag{2}$$

where *c* is the instantaneous moisture concentration (mol/m³), t is time (s) and D_{eff} is the effective moisture diffusivity (m²/s).

2.1.3 *Maxwell's equation for electromagnetics and heat generation*

Maxwell's equations provide the electromagnetic field at any point in the computational domain. In frequency domain time harmonic Maxwell's equations can be written as [22].

$$\nabla \times \left(\frac{1}{\mu} \nabla \times E\right) - \frac{\omega^2}{c}(\varepsilon' - i\varepsilon'')E = 0 \tag{3}$$

Where, *E* is the electric field strength, ω is the angular frequency of the microwave oven, c is the speed of light, ε', ε'', μ are the dielectric constant, dielectric loss factor, and electromagnetic permeability of the material, respectively.

The total electromagnetics heat sources represent electromagnetic losses, Q_m, given by, [23]

$$Q_m = Q_{rh} + Q_{ml} \tag{4}$$

Where, Q_{rh} is the resistive loss and Q_{ml} is the magnetic loss. For food products, the magnetic losses are negligible, i.e. $Q_{ml} = 0$.

The resistive loss can be calculated as

$$Q_{rh} = 0.5 \cdot \vec{J} \cdot \vec{E}^* \qquad\qquad (5)$$

Where, $\vec{E}^*$ is the conjugate of E and the electric current density $\vec{J}$ is given by

$$\vec{J} = \sigma \cdot E = 2\pi f \varepsilon_0 \varepsilon'' \cdot E \qquad\qquad (6)$$

Where f is the frequency of microwave, σ is the electrical conductivity, ε'' is the dielectric loss factor and ε_0 is permittivity in free space.

2.1.4   Quality prediction model

The equation for a degradation reaction:

$-dC/dt = k.C$ (7)

Integration lead to

$C = Co \; exp[-ko.exp(-(\Delta Ea)/(Qe \times Pr + T))]$ (8)

where *Co* is the initial concentration of nutrient, *Pr* is the power ratio, and *ko* is the pre-exponential factor.

3. Material and Method

3.1 Drying Experiment

A new IMCD drying system has been developed to conduct the experiment, as shown in Figure 1. The IMCD system consisted of three main parts: an axial flow fan, a 3-phase 6kW heater, and a modified NN-SD691S Panasonic inverter microwave oven (2450 MHz, maximum 1100W power capacity). Moisture loss was recorded automatically by the load cell connected to a computer. The internal temperature evolution of the sample was monitored by 4 fibre optic thermal sensors which were connected to Fiber Optical 4-Channel Thermometer (OPTO con AG, Germany). The power ratio was programmed to trigger the microwave heating at the controlled condition. IMCD operations were performed at microwave power 100W, power ratio (on/off) of 1/4, and convective temperature of 60 °C, respectively. On the completion of drying, the samples were cooled for 30 min in desiccators, wrapped with aluminium foil and store in a laboratory freezer at -18ºC for further analysis.
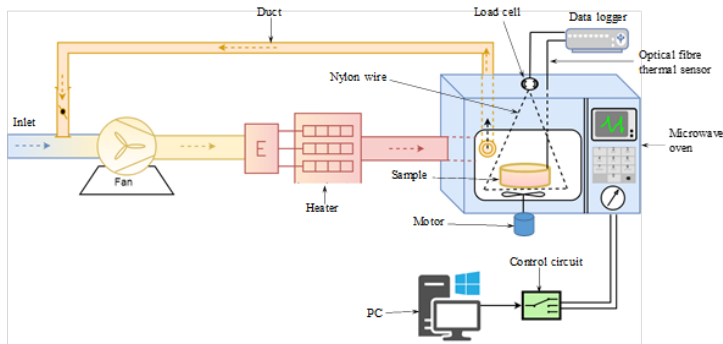
Fig. 1: Schematic diagram of the IMCD experimental setu

3.2 Analytical Determinations

3.2.1 Total phenolic extraction and content measurement

The amount of total polyphenol in the samples were determined by the Folin-Ciocalteau method [24] with some modification. The sample was extracted in extraction solvent (methanol / distilled water (50:50 v/v)) in amber vial at laboratory condition before homogenized in 20 mL of extraction solvent at maximum speed in Waring mini container blender in1 minute. Extracts were centrifuged at 15,000 g for 15 minutes at 20 ºC. The supernatant was filtered through a Whatman no. 3 analytical filter paper. Then 0.5ml of the diluted extract solution was mixed with 2.5 ml Folin– Ciocalteau reagent (10%) and allowed 5 minutes to react, then added 0.5ml of 7.5% Na2CO3 solution. After 30 minutes of incubation in a water bath at 37^0C, the absorbance was measured against water at 765 nm by Cary 50 UV Spectrophotometer.

3.2.2 HPLC analysis of ascorbic acid (Vitamin C)

The sample was extracted in extraction solvent (3 % metaphosphoric acid, 1 mM Na2EDTA). Extracts were centrifuged at 15,000 g for 15 minutes. The supernatant was filtered through a Whatman no. 3 filter paper. Extraction processes were repeated three times.Vitamin C contents were determined based on Asami et al's [25] HPLC method with some modifications. The analysis was carried out using an Dionex UHPLC RS3000 system. The reverse-phase separation was obtained using a Waters Symmetry C18 column (4.6 x 250 mm, 5 µm). The isocratic mobile phase was HPLC graded water with 1mM EDTA and 25mM sodium acetate buffer acidified to pH 4.25 with o-phosphoric acid.

3. Results and Discussion

4.1 Drying Kinetics

Average moisture content of the sample throughout the whole drying time was calculated and validated with the extensive experimental results, as shown in Figure 4. It is found that the simulated moisture content is consistent with the experimental data. To find the accuracy of the predicted data, the goodness of Fit (R^2) was calculated and found that the value of R^2 is 0.975. This precise R2 value indicates the developed model is quite accurate and able to predict the moisture distribution of plant-based food material during IMCD. For better interpretation about the moisture level throughout the IMCD process, 2D moisture concentration profile were drawn, as shown in Figure 5. It can be seen that the initial moisture concentration for a fresh apple tissue is uniformly distributed in the whole sample (Figure 5a). The moisture concentration decreases while drying is in progress (Figure 5 b-e). Interestingly, it can be observed that the moisture concentration is higher at the left side of the sample as compared to the right side. This is mainly due to the non-uniform microwave energy although the temperature distribution remain almost uniform, as shown in Figure 6.

Figure 6 shows the average temperature distribution during IMCD drying. It can be seen the experimental results are closely matched with the simulated results. The dispersion pattern (fluctuation) of this figure indicates the tempering and heating period during IMCD drying. The different peak points indicate the heating time (microwave on time) and the various nadir points mean tempering time. During the IMCD, microwave heats the sample rapidly for few seconds (20s) and then it was stopped automatically for a period (e.g 60s) for completing on cycle (80s).
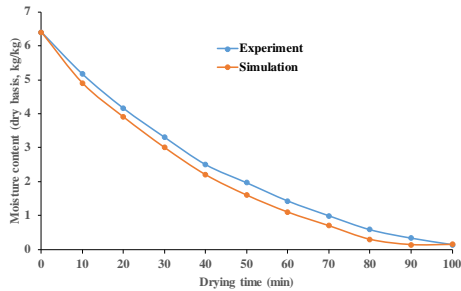
Fig. 4 The average moisture content during IMCD drying
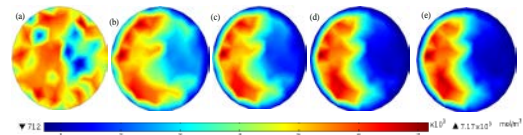
Fig 5: The concentration distribution at different stages of IMCD (a) at 0 min (b) at 20 min (c) at 40 min (d) at 80 min, and (e) at 100 min

The frequent microwave stop allows a time to redistribute the heat energy within the sample properly, prevents the material from overheating and therefore the better quality of the product (discussed in section4.2) can be maintained. The trend of the temperature distribution remains almost similar throughout the whole drying processes although a little attenuation can be observed at the final stages of drying. This temperature distribution mainly depends on the moisture concentration at different stages of drying (Figure 5) because microwave mainly heat firstly where it gets more moisture. At the final stages of drying, most of the water has been transported by continuous evaporation due the IMCD process progress simultaneously. As a result, most of the sample become dry, and hence the microwave cannot generate more heat. Due to this reason, the temperature decreases at the final stages of drying.
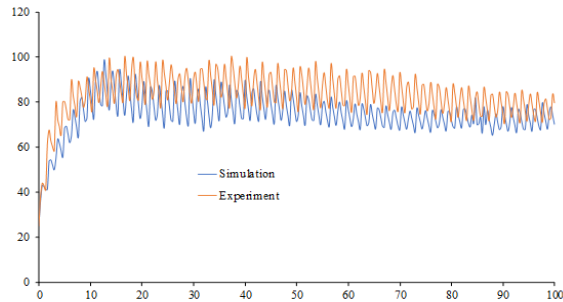
Fig. 6: The average temperature distribution during IMCD drying

4.2 Reaction Kinetics

Understanding of IMCD process on important quality parameters such as ascorbic acid (AA) and total polyphenol content (TPC) is an important issue due to their thermos labile sensitivities and should be taken into account in the drying process. Initial values of AA and TPC were found to be 4.842 (mg/100g fresh weight) and 70.74 (mg/100g fresh weight), respectively in a fresh granny smith apple. Figures 7 and 8 represent the degradation kinetics of AA and TPC in the Granny Smith apple slice. It can be seen that the retention remaining AA, and TPC values were reduced with drying time, and the degradation rate accelerated with increasing temperature and microwave

power density, meaning that the loss of bioactive compounds increased. This study found that, at the beginning of the process, the effect of moisture content on the reaction rate of AA degradation seems to be predominant, while the temperature effect becomes major as the process proceeds. The degradation rate of AA was low at the beginning of the IMCD process (Figure 7) with the reduction of moisture content from 86% to 60% (Figure 4). When moisture content reached 55–60%, the rate of this reaction reached a maximum value and at moisture contents below 55%, the rate decreased significantly (Figure 7) with moisture reduction. This rapid degradation phenomenon can be attributed to the destruction of cell structure under microwave heating as it can lead to ascorbic acid release and contribute to the rapid oxidation of ascorbic acid.

Considering the evolution of ascorbic acid retention during the drying process in the present paper (Figure 7), experimental data were fitted to a first-order kinetic model. The natural logarithmic ratio of nutrient retention (ln C/C0) versus drying time representation revealed linear correlations with the degradation rate constant (k) and coefficients of determination (R) higher than 0.98 (Figure 8), suggesting that the model was suitable in describing the degradation of ascorbic acid during IMCD drying of granny smith apples.
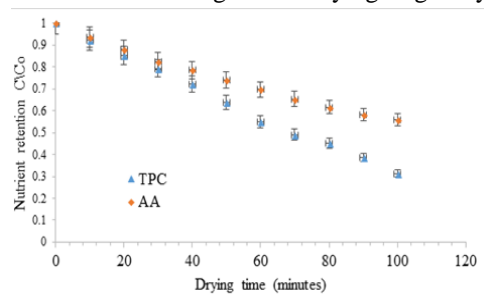
Fig. 7 Kinetics of ascorbic acid and total polyphenol alteration of Granny Smith apple during IMCD
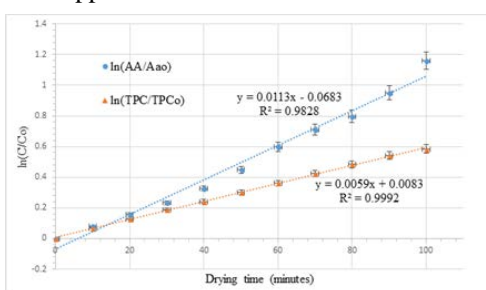
Fig 8: Predicted first-order kinetics of retention of nutrient during IMCD drying Granny Smith apple

In addition, apple is a good source of total polyphenol, which can be affected by temperature, oxygen, pH, metal, the release of polyphenol oxidase (PPO) and other parameters. It can be seen from Figure 7, the TPC degrads highly at the first 40 minutes of IMCD, and extends even beyond the first drying period corresponded to the activation of PPO enzyme and rapid linear decrease of free moisture during IMCD drying. Then TPC gradually decreases over the vast majority of the time to reach the final stage where degradation is found to be marginal. Finally, between the two key nutrients in apple tissue, the degradation rate of ascorbic acid is higher than total polyphenol. This is may be due to higher thermal sensitivity of ascorbic acid as compared to TPC.

4. Conclusion

In this research, an IMCD model for food drying has been developed to predict the moisture and temperature distribution and its effect on quality of apple tissue. A 3D model has been developed considering Maxwell equations to generate volumetric heating and reaction kinetics to predic the quality degradation during IMCD drying. The developed model was then validated with the experimental results. It has been found that the predicted moisture and temperature distribution results is fully consistent with the experimental results. The precise goodness of fit (R^2) value

indicates the developed model is quite accurate and able to predict the moisture distribution of plant-based food material during IMCD. It is also found that the IMCD significantly alter two different key nutrient qualities: ascorbic acid and total polyphenol content of apple tissue. Between these two nutrients, ascorbic acid has the highest tendency to alter its character during IMCD as compared to total polyphenol content.

5. References

[1] Beedie, M., Energy saving-a question of quality. Dairy Industries International 1995, 60 (12), 27.

[2] Khan, M. I. H.; Kumar, C.; Joardder, M. U. H.; Karim, M. A., Determination of appropriate effective diffusivity for different food materials. Drying Technology 2017a, 35 (3), 335-346.

[3] Khan, M. I. H., Joardder, M. U. H., Kumar, C., & Karim, M. A. (2018). Multiphase porous media modelling: A novel approach to predicting food processing performance. Critical reviews in food science and nutrition, 58(4), 528-546.

[4] Joardder, M. U., Brown, R. J., Kumar, C., & Karim, M. A., Effect of cell wall properties on porosity and shrinkage of dried apple. International Journal of Food Properties, 2015, 18(10), 2327-2337.

[5] Joardder, M. U., Kumar, C., Brown, R. J., & Karim, M. A., A micro-level investigation of the solid displacement method for porosity determination of dried food. Journal of Food Engineering, 2015, 166, 156-164.

[6] Chou, S. K. C., K. J., New hybrid drying technologies for heat sensitive foodstuffs. Trends in Food Science & Technology 2001, 12 (10), 359-369.

[7] Datta, A. K.; Ni, H., Infrared and hot-air-assisted microwave heating of foods for control of surface moisture. Journal of Food Engineering 2002, 51 (4), 355-364.

[8] Soysal, Y.; Ayhan, Z.; Eştürk, O.; Arıkan, M. F., Intermittent microwave–convective drying of red pepper: Drying kinetics, physical (colour and texture) and sensory quality. Biosystems Engineering 2009, 103 (4), 455-463.

[9] Wang, J.; Xiong, Y.-S.; Yu, Y., Microwave drying characteristics of potato and the effect of different microwave powers on the dried quality of potato. Eur Food Res Technol 2004, 219 (5), 500-506.

[10] Tulasidas, T. N.; Raghavan, G.S.V.; Norris, E.R., Microwave and convective drying of grapes. Transactions of the ASAE 1993, 361861–1865.

[11] Prabhanjan, D. G.; Ramaswamy, H. S.; Raghavan, G. S. V., Microwave-assisted convective air drying of thin layer carrots. Journal of Food Engineering 1995, 25 (2), 283-293.

[12] Funebo, T.; Ohlsson, T., Microwave-assisted air dehydration of apple and mushroom. Journal of Food Engineering 1998, 38 (3), 353-367.

[13] Khraisheh, M. A. M.; McMinn, W. A. M.; Magee, T. R. A., A multiple regression approach to the combined microwave and air drying process. Journal of Food Engineering 2000, 43 (4), 243-250.

[14] Gunasekaran, S., Pulsed microwave-vacuum drying of food materials. Drying Technology 1999, 17 (3), 395-412.

[15] Yongsawatdigul, J.; Gunasekaran, S., Microwave-vacuum drying of cranberries: part ii. quality evaluation. Journal of Food Processing and Preservation 1996, 20 (2), 145-156.

[16] Gunasekaran, S., Pulsed microwave–vacuum drying of food materials. Drying Technology 1999, 17, 395-412.

[17] Beaudry, C.; Raghavan, G. S. V.; Rennie, T. J., Microwave Finish Drying of Osmotically Dehydrated Cranberries. Drying Technology 2003, 21 (9), 1797-1810.

[18] Malafronte, L.; Lamberti, G.; Barba, A. A.; Raaholt, B.; Holtz, E.; Ahrné, L., Combined convective and microwave assisted drying: Experiments and modeling. Journal of Food Engineering 2012, 112 (4), 304-312.

[19] Chen, J.; Pitchai, K.; Birla, S.; Negahban, M.; Jones, D.; Subbiah, J., Heat and mass transport during microwave heating of mashed potato in domestic oven--model development, validation, and sensitivity analysis. J Food Sci 2014, 79 (10), E1991-2004.

[20] Gunasekaran, S.; Yang, H.-W., Optimization of pulsed microwave heating. Journal of Food Engineering 2007, 78 (4), 1457-1462.

[21] Kumar, C.; Joardder, M. U. H.; Farrell, T. W.; Millar, G. J.; Karim, M. A., Mathematical model for intermittent microwave convective drying of food materials. Drying Technology 2016, 34 (8), 962-973.

[22] Chen, J.; Pitchai, K.; Birla, S.; Negahban, M.; Jones, D.; Subbiah, J., Heat and Mass Transport during Microwave Heating of Mashed Potato in Domestic Oven—Model Development, Validation, and Sensitivity Analysis. Journal of Food Science 2014, 79 (10), E1991-E2004.

[23] Wentworth, S. M., Fundamentals of Electromagnetics with Engineering Applications. John Wiley: 2004.

[24] Socha, R.; Juszczak, L.; Pietrzyk, S.; Fortuna, T., Antioxidant activity and phenolic composition of herbhoneys. Food Chemistry 2009, 113 (2), 568-574.

[25] Asami, D. K.; Hong, Y.-J.; Barrett, D. M.; Mitchell, A. E., Comparison of the Total Phenolic and Ascorbic Acid Content of Freeze-Dried and Air-Dried Marionberry, Strawberry, and Corn Grown Using Conventional, Organic, and Sustainable Agricultural Practices. Journal of Agricultural and Food Chemistry 2003, 51 (5), 1237-1241.

DRYING PRODUCTS

Oral Presentations

Effects of different drying conditions on curcumin concentration in turmeric

Li, Q.; Driscoll, R.; Srzednicki, G. *

School of Chemical Engineering, The University of New South Wales, Sydney 2052, Australia

*E-mail of the corresponding author: georgesrz@yahoo.com

Abstract

Turmeric (Curcuma longa), belongs to Zingiberaceae family. The rhizomes contain bioactive compounds of the curcuminoids group (natural phenols). They are used in food and pharmaceutical industry. The aim of this research was to acquire dried turmeric with high total curcumin content. In this study, optimum turmeric drying conditions and new extraction techniques were explored. Fresh turmeric samples were subjected to constant vs changing drying air temperatures and pre-treatment (blanching). Changing drying air temperature and use of non-blanched turmeric slices resulted in the highest concentration of curcumin. Ultrasonic extraction instead of soxhlet extraction improved the extraction efficiency and decreased extraction time.

Keywords: Turmeric, Curcumin; Drying; Blanching; Extraction

1. Introduction

Turmeric, known as *Curcuma longa*, belongs to the Zingiberaceae family like ginger and cardamom. It is an erect perennial herb which has a short stem with large oblong leaves and produces ovate, pyriform or oblong rhizomes. The rhizomes may have many branches and are of brownish-yellow colour. The aroma of turmeric is musky, pepper-like and the flavour is slightly aromatic, bitter. The colour of dried turmeric varies from orange brown to pale yellow or reddish yellow. The main compounds responsible for these properties are curcuminoids that include curcumin, demethoxycurcumin and bis-demethoxycurcumin. They are mainly extracted from dried turmeric. Curcuminoids are natural phenols and produce a pronounced yellow colour. They are popular as pigments in food industry that uses turmeric oleoresin as the starting material. The rhizome of turmeric is an important raw material to extract curcumin that contains 3.1%~10%. The dried rhizome contains 45%~50% starch, 40%~50% cellulose[1].They are also well known for their pharmaceutical and nutritional properties, particularly as anti-oxidants. The pharmaceutical properties include anticancer, antibacterial, anti-infective and insecticidal effect.

In turmeric powder manufacturing, dehydration is an important process step since the water activity can be reduced by drying so that the growth and reproduction of food spoilage microbial can be inhibited by passivating the food enzymes which would cause adverse chemical reactions[2]. Thereby it helps extend the shelf life of food and reach the preservation goals. However, different drying conditions may affect the amount of curcumin content in turmeric powder. Thus, the curcumin should be extracted after drying and the concentration of curcumin can be detected by using HPLC measuring method at 425 nm wavelength. There are several extraction methods for curcumin including soxhlet.

The aim of this research was to acquire dried turmeric with high total curcumin content. In this study, optimum turmeric drying conditions and new extraction techniques have been explored before quantitating the curcumin in dried rhizomes by HPLC.

2. Materials and Methods

2.1. Turmeric Samples

2.1.1. Sample Procurement

Matured, healthy and fresh turmeric rhizomes were supplied by Earthcare Enterprises located in Maleny on Queensland's Sunshine Coast Hinterland. They were refrigerated and transported in a thermally insulated container to the University of NSW laboratory in Sydney. Once in the laboratory, they were placed in zip bags made from polyethylene film and kept in a freezer at -20 °C until needed for experiments.

2.1.2. Sample preparation

The frozen turmeric samples were removed from the freezer and left overnight in a refrigerator at + 4 °C. after procurement.

For each drying run, around 70 g of rhizomes were weighed and peeled to obtain around 50 g of peeled rhizomes that were either quartered or sliced (slices 5 mm thick).

2.1.3. Blanching

Some of the quartered samples were blanched in 70 °C water bath for different times (5, 15 and 30 minutes). After blanching, the samples were dipped into ice cold water directly for 1 minute and then left for 10 minutes to allow the water to drip off

2.1.4. Moisture content determination

The moisture content in the fresh and also in the dried slices was determined following the AOAC Official Method 934.06[3]. Triplicate samples of of turmeric (5 g) were dried in a convection oven at 110 °C for 6 hours.

2.2. Drying experiments

2.2.1. Dryer

The drying experiments were carried out in a cabinet dryer designed in the workshop of the School of Chemical Engineering of the University of New South Wales. The cabinet dryer (see Fig. 1) has an electric heater (15 kW) fitted with a PID controller and a fan (0.75 kW). The airflow is parallel to the tray on which the drying samples are placed in a thin layer. The temperature and relative humidity were monitored and recorded with a datalogger. The weight loss was recorded with an electronic balance placed under the samples holding tray.
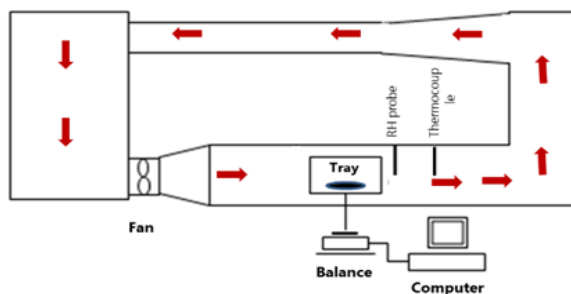
Fig. 1 Cabinet dryer.

2.2.2. *Drying conditions*

The drying conditions were defined either by a constant temperature or a changing temperatue (see Table 1). The reason for choosing the drying temperatures in the range 40-60 ºC was that this corresponds to temperatures used by the industry including solar drying. Including changing conditions within this temperature range in addition to constant conditions was aiming at exploring the possibility of increasing the curcumin recovery.

Table 1. Drying conditions for experiments

Run	Temperature (ºC)	RH (%)	Shape	Blanching (min)
1	40	20	quartered	0
2	40	20	sliced	0
3	50	10	quartered	0
4	50	10	sliced	0
5	50	20	quartered	0
6	55	12	quartered	0
7	55	12	sliced	0
8	60	10	quartered	0
9	60	10	sliced	0
10	60	20	quartered	0
11	60	20	sliced	0
12	60	10	quartered	5
13	60	10	quartered	15
14	60	10	quartered	30
15	60 – 50	20	sliced	0
16	50 – 60	20	sliced	0
17	60 – 40	20	sliced	0
18	40 – 60	20	sliced	0
19	50 – 40	20	sliced	0
20	40 – 50	20	sliced	0

2.3. Curcumin determination

2.3.1. *Extraction*

A sample of dried turmeric (5 g) was ground for 1 min in the Single-phase Resis Tanlestart Grinder (Shanghai Rihui Electrical Machinery Co). Each ground sample was passed through a sieve (250 μm size).

The powder sample (1.00 g) from each drying treatment was placed in a centrifuge tube (medical grade polypropylene) tube. An aliquot of 15 mL 100% ethanol (HPLC grade) was added into each tube and mixed. Then the tubes were closed with a cap and sonicated for 1

hour at 55 °C. After sonication, the tubes should be covered with an aluminium foil and vortexed for 1 h at room temperature. Then, all samples should be diluted by mixing 750 µL of extraction solution with 750 µL of 100% ethanol (HPLC grade) and then filtered.

2.3.2.   Quantitation by HPLC

The solvents used in the quantitation work were as follows: 100% ethanol (HPLC grade) manufactured by Merck Pty Ltd; acetic acid (HPLC grade) manufactured by VWR; acetonitrile (HPLC grade) manufactured by VWR; Milli-Q Water (HPLC grade).

The curcumin analytical standard was obtained from Fluka.

HPLC detection was performed by applying a Shimadzu-LC system (Shimadzu, Japan) including an LC-20AD liquid chromatograph, a SIL-20A HT auto sampler (auto-injector), a CBM-20A communications bus module (UV-VIS detector), LC Solution software and the Xterra C18 Column (MS 3.5 µm; length: 150 mm; diameter: 2.1 mm, Waters, Ireland).

The HPLC assay was implemented in a reverse-phase by using an isocratic elution with a total flow rate of 0.1500 mL/min, a column oven temperature of 30 °C; a mobile phase of 2% acetic acid and 100% acetonitrile (60:40); a detection wavelength of 425 nm for curcumin. The injection volume was 20 µL. All solutions were filtered by using the glass vacuum filtration apparatus and accessories with filter membrane (hydrophilic PTFE with 0.45 µm pore size) under the fume cupboard prior to HPLC injection. The total time for testing was 10 min for each sample.

Standard solutions of curcumin in pure ethanol were prepared separately from the stock solution with the concentration of 1000 µg/mL that was diluted with 100% ethanol to obtain concentrations of 20 µg/mL, 30 µg/mL, 40 µg/mL, 5 0µg/mL, 60 µg/mL, 70 µg/mL of standard solutions. A calibration curve was produced on the basis of the values obtained.

3. Results and discussion

3.1. Moisture content

The samples were dried until a constant weight of the sample was obtained, i. e. had to remain unchanged during at least three consecutive readings. This corresponded to the equilibrium moisture content for a given set of drying conditions (temperature and RH).

The drying runs 1-4 and 6-11 were set up to compare different effects of the sample shape (sliced vs. quartered) on the equilibrium moisture content of dried samples. It appears that at drying air temperatures of 40, 50 and 55 °C at any of the three RH values (10, 12 or 20%), the quartered samples had a higher mosture content. However, at 60 °C there was no difference in the final moisture content between the different shapes of cut turmeric

rhizomes. As for runs 12-14 it appears that there was no effect of blanching time on the final moisture content. Finally, the runs 15-20 are showing the effects of drying conditions on the final mosture content. It appears that in all six runs the procedure of starting with the higher drying temperature and then changing it to lower one (60 °C to 40 °C vs 40 °C to 60 °C) resulted in a higher final moisture content.

Table 2. Average equilibrium moisture content for each run

Run Number	Run conditions	Equilibrium Moisture Content (% db)	Drying time (min)
1	40 ºC 20%RH (quartered)	7.50	220
2	40 ºC 20%RH (sliced)	7.29	196
3	50 ºC 10%RH (quartered)	4.40	243
4	50 ºC 10%RH (sliced)	4.32	147
5	50 ºC 20%RH (quartered)	5.65	204
6	55 ºC 12%RH (quartered)	3.69	188
7	55 ºC 12%RH (sliced)	3.44	145
8	60 ºC 10%RH (quartered)	2.49	247
9	60 ºC 10%RH (sliced)	2.51	157
10	60 ºC 20%RH (quartered)	4.59	202
11	60 ºC 20%RH (sliced)	4.58	187
12	60 ºC 10%RH (quartered, blanched 5 min)	2.48	272
13	60 ºC 10%RH (quartered, blanched 15 min)	2.52	272
14	60 ºC 10%RH (quartered, blanched 30 min)	2.51	280
15	60 ºC 20%RH to 50 ºC 20%RH (sliced)	5.54	176
16	50 ºC 20%RH to 60 ºC 20%RH (sliced)	4.81	192
17	60 ºC 20%RH to 40 ºC 20%RH (sliced)	6.76	186
18	40 ºC 20%RH to 60 ºC 20%RH (sliced)	5.28	177
19	50 ºC 20%RH to 40 ºC 20%RH (sliced)	7.21	299
20	40 ºC 20%RH to 50 ºC 20%RH (sliced)	5.95	264

3.2. Curcumin content

With regard to the effect of RH during drying of sliced non-blanched rhizomes at 60 °C it was found that sample from run 11 exposed to 20% RH had a 23% higher curcumin concentration (3.53 mg/g dry matter) than sample from run 9 (2.86 mg/g dry matter).

As for the effect of of the drying temperature at the same RH (20%), during drying of sliced non-blanched rhizomes, it is found that sample from run 2 had a 13% higher concentration of curcumin (3.99 mg/g dry matter) than sample 11 (3.53 mg/g dry matter). The drying

temperature of samples 2 and 11 was 40 °C and 60 °C, respectively. The same phenomenon was observed when comparing the effects of drying air temperature on the curcumin content in quartered rhizome samples, see samples 1 (3.86 mg/g dry matter) vs. sample 10 (2.86 mg/g dry matter) and sample 5 (2.81 mg/g dry matter) dried at 40 °C, 60 °C and 50 °C, respectively. Hence, it can be considered that a lower drying temperature leads to a higher curcumin content.

Table 3. Curcumin content in dried samples

Run number	Weight of curcumin extracted from dried samples (μg) [a]	Curcumin concentration on dry matter basis (mg/g dry matter)
1	1.24	3.86
2	1.97	3.99
3	1.08	2.70
4	1.67	3.33
5	1.39	2.81
6	1.57	3.82
7	n.a.[b]	n.a.
8	1.27	2.49
9	1.69	2.86
10	1.25	2.88
11	1.88	3.53
12	1.30	2.37
13	1.42	3.27
14	1.68	3.72
15	1.26	3.04
16	1.39	3.32
17	1.09	6.95
18	1.22	3.70
19	1.80	4.01
20	1.52	4.96

[a]) Total weight of curcumin extracted from entire dried sample; [b]) n.a. = data not available

With regard to the difference between quartered and sliced samples, the comparison of results from runs 1 vs 2, 3 v 4 and 10 vs 11 shows clearly that the dried quartered samples had a lower curcumin content.

Finally, with regard to the effects of changing conditions on the curcumin content, they resulted generally in a higher concentration than constant conditions.

In this experiment, ultrasonic extraction was used in extraction instead of traditional soxhlet extraction. The time of ultrasonic extraction was 1 h. It was determined after comparing the

sonication at 55 °C for 15 min, 30 min and 1 hour. It is found that there was no peak at 425 nm wavelength times of less than 1 hour. This extraction method is reported to strength extraction efficiency and decrease extraction time [4]. The use of sonication had a significant advantage over the conventional soxhlet extraction taking several hours.

4. Conclusions

This study compares the concentration of curcumin in samples of dried turmeric rhizomes subjected to different drying treatments. It has been found that the changing conditons and use of of non-blanched sliced turmeric rhizome dried at 40 °C and 20%RH yielded 3.99 mg curcumin/g dry matter which was higher than in any other sample dried under constant conditions. In comparison, the changing conditions resulted in higher curcumin content. Moreover, blanching would generally lead to a higher concentration of curcumin in the dried samples. Finally, 20% RH led to a higher concentration of curcumin than 10% RH.

5. Nomenclature

RH   relative humidity   %

6. References

[1] Burnham T.H. 'Review of natural products'. St. Louis: Facts and Comparisons. 1993, 38(22): pp. 23-26

[2] Adhami S, Rahimi A, Hatamipour MS,. 'Freeze drying of quince (*Cydonia oblonga*): Modelling of drying kinetics and characteristics'. Korean Journal of Chemical Engineering 2013, 30(6), 1201–1206.

[3] AOAC. Official methods of analysis (Vol. 534). W. Horwitz (Ed.). Association of Official Analytical Chemists, Washington, DC, 2006.

[4] Dhanalakshmi N. P, Nagarajan R,. World Academy of Science, Engineering and Technology 2011, 5: pp.11–29.

Electrically enhanced drying of white champignons

Bashkir, I.; Kudra, T.; Martynenko, A.[*]

Department of Engineering, Faculty of Agriculture, Dalhousie University, Truro, NS B2N, Canada

*E-mail of the corresponding author: alex.martynenko@dal.ca

Abstract

Electrohydrodynamic (EHD) drying is a novel non-thermal dewatering technology using electric discharge in air to enhance dehydration of heat-sensitive biomaterials. Low energy consumption and high product quality make it attractive for industry. In this study, the mushrooms slices have been dried under sole EHD with 12, 14, and 16 kV DC, and EHD in combination with air cross-flow at 1 m s^{-1} and different relative humidity (RH) from 30 to 70 %. It was found that drying kinetics was exponential over initial moisture contents from 3.3 to 14.1 g·g^{-1} (db). The equilibrium moisture content ranged from 0.15 to 0.1 g g^{-1} depending on RH. Decrease of RH or air cross-flow significantly improved efficiency of EHD drying.

Keywords: mushrooms; electrohydrodynamic; ionic wind; air humidity; equilibrium moisture content.

1. Introduction

Electrohydrodynamic (EHD) drying is regarded as a non-thermal dewatering technology, suitable for drying of heat-sensitive materials because of high product quality and low energy consumption.[1] Hence, it is excellent alternative as compared to hot-air convective drying of mushrooms with extremely short shelf life, which should be consumed or processed within hours after harvest.[2]

Commonly accepted hypothesis is that EHD drying occurs due to ionic wind. The effect of ionic wind on shiitake mushrooms drying was first investigated by Xue et al.[3] under 6, 8, 10, 12 kV AC (electric field strength from 3 to 6 kV cm^{-1}), concurrent airflow at 45ºC and 40% RH. The results showed that electro-convective drying for 10-14 hours was faster by 1.1 to 1.6 times compared to control. The effect of ionic wind increased with increasing voltage and decreased with increasing airflow rate. However, slight browning of the dried shiitake gills under the effect of ionic wind was noticed. Dutta et al.[4] showed that pre-treatment of mushroom slices with AC electric field 4.3 kV cm^{-1} accelerated subsequent convective or freeze drying. They also reported that the EHD pre-treatment improved quality of dry mushrooms, in particular lesser shrinkage, higher rehydration ratio and enhanced color as compared to control. Dinani et al.[5, 6] investigated the effect of EHD in combination with hot air drying at 60ºC and 10% RH for voltages 17, 19 and 21 kV DC, and gaps between electrodes 5, 6 and 7 cm. Electric field accelerated drying rate by 1.38, 1.41, and 1.43 times for voltages, and by 1.52, 1.36, and 1.33 times for gaps, so one can conclude that increasing of electric field strength significantly increased water diffusion in mushrooms. These experiments were done under conditions of natural convection. Similar experiments with EHD in combination with hot-air drying at 45ºC under conditions of forced convection [7-9] showed significant effect of air velocity. The enhancement of the drying rate due to EHD was as high as 1.40, 1.56, and 1.78 times at 0.4 m s^{-1}, while at 2.2 m s^{-1} these were 1.08, 1.03, and 0.97 times (no significant effect of EHD). These results confirmed previous conclusions of Xue et al.[3] that EHD is efficient only under low air velocities, while increase of air velocity above certain threshold results in purely convective drying. Unfortunately, all these experiments with mushrooms were conducted for combination of EHD with hot air drying with temperature as the dominant drying factor. These settings hindered the role of EHD in drying, making difficult interpretation of sole EHD effect on drying kinetics and product quality.

Promising experiments on EHD mushroom drying confirmed the importance of industrial scaling of the EHD technology. This research was initiated on the request of industry partner Jantex Ltd (Poland) to improve efficiency and quality of white champignons drying because of high sensitivity of product color to drying temperature. The main objective of this paper is to present preliminary results of EHD drying of sliced white champignons, including the effects of relative humidity, air cross-flow, initial moisture content, electric

field strength and configuration of discharge electrode, which are instrumental for industrial scaling of EHD technology.

2. Materials and methods

White champignons (Highline, Leamington, Canada) purchased from a local grocery were cut perpendicularly to the head into 5-mm slices and then spread uniformly in a single layer on the collecting electrode. Initial mass of sliced champignons varied from 30 to 34 g. Initial moisture content was in the range 3.3 to 14.1 kg kg^{-1} (db).

Experimental apparatus is shown in Figure 1. The drying chamber (1) was made of Plexiglas (40×20×20 cm) with two openings 10 cm in diameter. Discharge electrode (2) was built from 143 needles arranged into 11×13 rows giving 1×1 cm needles packing density or 42 needles arranged into 6×7 rows giving 2×2 cm needles packing density. Discharge electrode was connected to the positive pole of a DC high voltage source, while aluminum plate (3) with the size (20×10 cm) was used as a grounded electrode. Both electrodes were placed in the drying chamber. The room air humidity was maintained at 20% by the air conditioning system. Airflow velocity was maintained at 1.0 m s^{-1} by a 1.5 W fan (5) and measured with the hot wire anemometer HD300 (Extech Instruments, USA). High voltage (6) was supplied by DC power supply BAL-32-5 (Voltronics, USA). Voltage and current were recorded continuously using the LabView2012 (National Instruments, USA) data acquisition system with USB-6120 interface and desktop computer (7). The weight of mushrooms was determined with a digital scale (4) (model HCB 1002, Adam Equipment, Oxford, CT, USA).
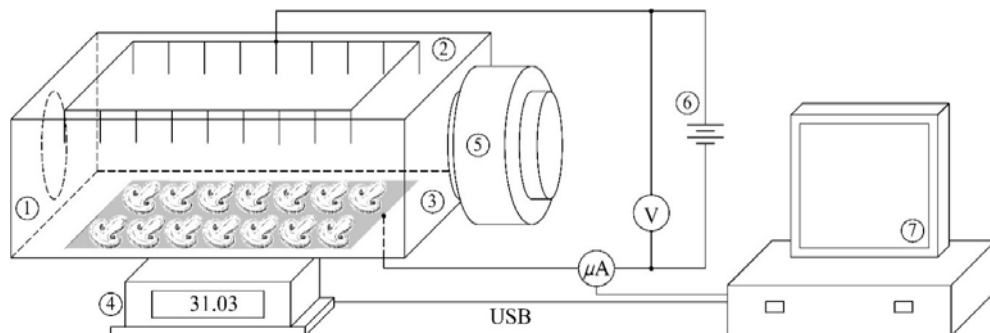
Fig. 1 EHD experimental setup.

Experiments for determination of equilibrium moisture content were carried out for sole EHD at 12, 14, and 16 kV with a gap 3.0 cm between electrodes, or EHD combined with air cross flow of 1.0 m s^{-1}. The effect of initial moisture content on EHD drying rate was measured for fresh slices and for slices after storage in the cooler from one to three days. The effects of EHD (1) and EHD + air cross-flow (2) were compared with sole air cross-

flow (control 1) or natural convection (control 2) for the same batch of slices. Drying rate for each treatment was calculated for 30 min using four-steps drying protocol. For these experiments the RH was kept constant at 20±2% and room temperature of 20±0.5ºC.

3. Results and discussions

The effect of discharge electrode geometry and air humidity on drying kinetics is shown in Figure 2. The effect of 1×1 and 2×2 cm needle packing density was studied at 15 kV, 3.5 cm gap, RH 70-80% and air cross-flow 0.4 m s^{-1} (Fig. 2A). Drying kinetics showed the difference between effects of two electrodes. In particular, 1×1 electrode initiated linear drying kinetics (constant drying rate), which indicates convection-limited conditions. In contrast, 2×2 electrode initiated exponential drying kinetics (falling drying rate), which indicates diffusion-limited drying. Both cases have been reported in literature,[5,10] however the reason for the difference in drying behaviour has not been discussed.

Better results of EHD drying, obtained with 2×2 electrode, determined preferable use of such electrode in further experiments. The effect of 30, 50, and 70% relative humidity on the drying kinetics was studied with 2×2 electrode at 22 kV, 3.5 cm gap (electric field 6.3 kV cm^{-1}) and superficial velocity of air cross-flow 1.0 m s^{-1} (Fig. 2B).
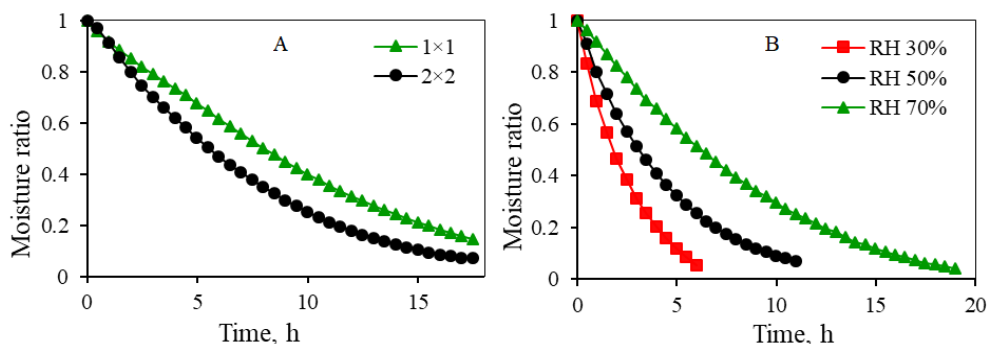
Fig. 2 Moisture kinetics for different discharge electrodes (A) and relative humidity (B).

Drying time was in the range from 7 to 20 hours, depending on relative humidity. The equilibrium moisture content at the end of drying was in the range from 0.1 to 0.15 g g^{-1}. This moisture content for white champignons corresponds to the range of water activities a_w from 0.3 to 0.35[11], which is considered as safe for shelf-life stability.[12] These data demonstrate how important is to maintain low air relative humidity in the EHD drying.

Effect of sole EHD and EHD combined with convective air cross-flow on drying kinetics is presented in Figure 3. It follows that drying rate increases with voltage, which corresponds to results reported earlier.[8, 9] Drying time to reach 0.2 g g^{-1} of moisture content (dashed line) significantly decreased from 25 h at 4.0 kV cm^{-1} to 12 h at 5.3 kV cm^{-1}. Effect of combined air cross-flow and ionic wind was significant at 12 and 14 kV, however at 16 kV

the drying effect of sole ionic wind was higher. This result is difficult to explain within existing theories of EHD drying. Therefore, the phenomenon of interaction between ionic wind and air cross-flow requires additional research.
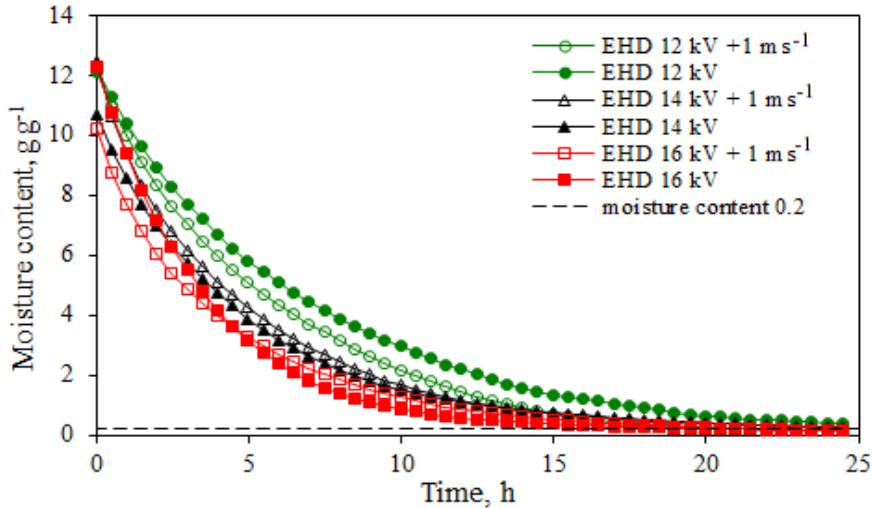
Fig. 3 Effect of EHD drying and combined EHD with convective cross-flow drying (1.0 ms^{-1}) under different voltages on drying time (3 cm gap, 20% RH).

The effective moisture diffusivity (D_{eff}) can be calculated from the following equation:

$$D_{eff} = \ln\left(\frac{\pi^2}{8}MR\right)\cdot\left(\frac{4L^2}{\pi^2 t}\right) = (-0.0851 - 0.4053\ln MR)\cdot\frac{L^2}{t} \qquad (1)$$

Based on equation (1) it is possible to estimate instantaneous diffusion coefficient from experimentally determined parameter k:

$$D_{eff} = (-0.0851\cdot\frac{1}{t} + 0.4053k)\cdot L^2 \qquad (2)$$

Results of experimental evaluation of k for different modes of EHD drying are presented in Figure 4. Parameter k was stable over drying period from 0 to 14 hours in the wide range of voltages with/without forced convection, which indicates a suitability of the exponential model for approximation of drying kinetics in EHD drying. Based on the average value of parameter k, the effective moisture diffusivity coefficient has been calculated (Table 1):

Table 1. Effective moisture diffusivity coefficient, $D_{eff}\cdot 10^{-10}\ m^2\,s^{-1}$

Drying	12 kV	14 kV	16 kV
EHD	3.29 ± 0.31	4.84 ± 0.11	6.42 ± 0.30
EHD + 1.0 m s^{-1}	3.78 ± 0.23	5.09 ± 0.14	5.39 ± 0.20
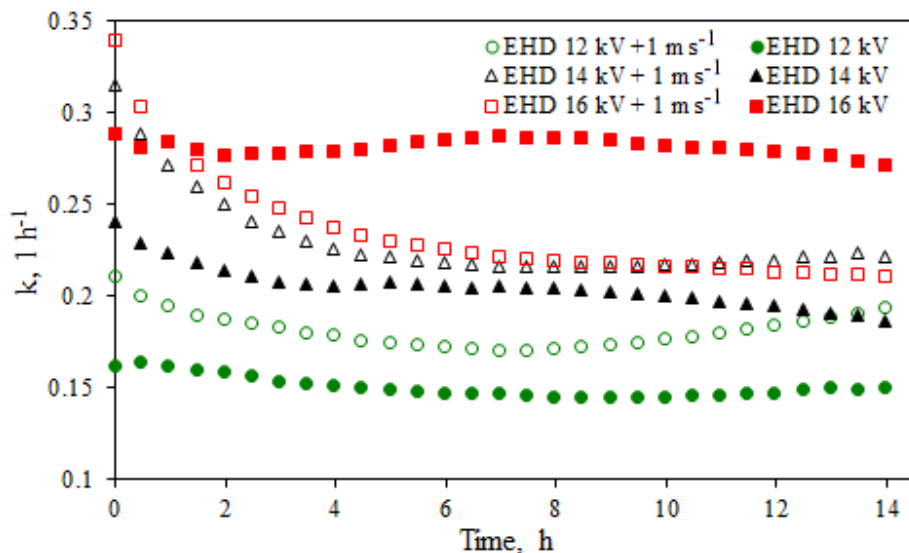
Fig. 4 Velocity of EHD drying and EHD + convective cross-flow drying (1.0 m s⁻¹) under different voltages on drying time.
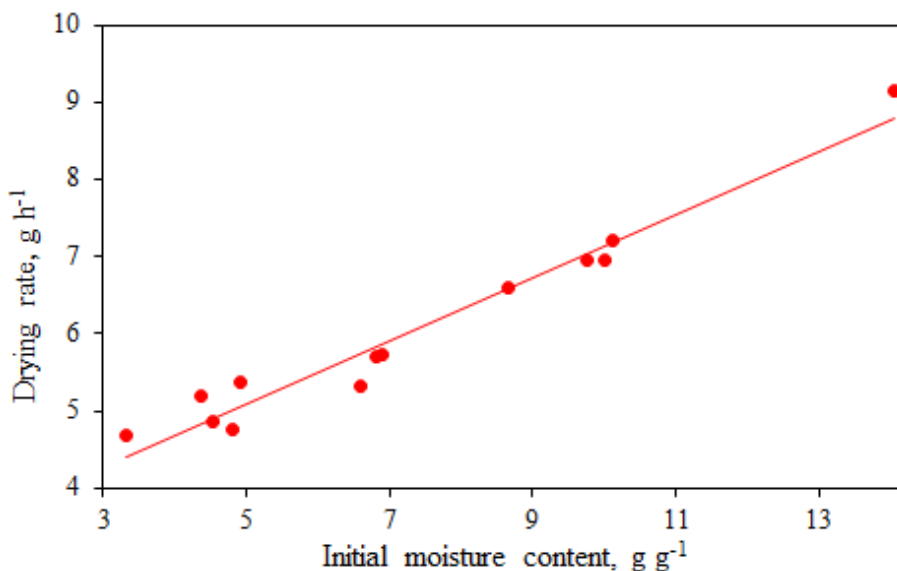
Fig. 5 Dependence of drying rate (DR) on initial moisture content (X_o) at EHD 14 kV and RH 20% (fitted linear regression DR = 3.056 + 0.4087 X_o with R^2 = 0.962)

From these results it is clear that drying rate is proportional to moisture content, which validates initial assumption, underlying simplified diffusion model. To study interactions between forced air cross-flow and electro-convection, the four-step experimental protocol

was designed, exploring three cases in various combinations: (1) Sole EHD, (2) air cross-flow, and (3) EHD with simultaneous air cross-flow (Fig. 6).
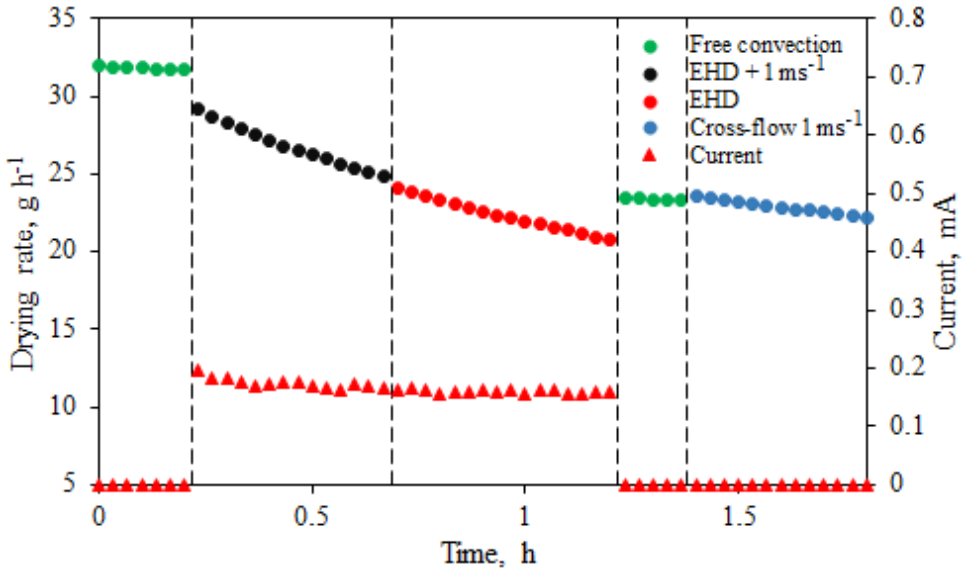
Fig. 6 An interactions between forced air cross-flow (1 m s⁻¹) and electro-convection (18 kV) at 3.5 cm gap, 20±2% RH.

The case # 3 was found to be the most efficient. The enhancement ratio was: EHD/Free convection = 6.66/1.4 = 4.757, EHD/Cross-flow = 6.66/3.36 = 1.982, EHD+Cross-flow/Free convection = 10.04/1.4 = 7.171, EHD+Cross-flow/Cross-flow = 10.04/3.36 = 2.988. It follows that EHD effect was always positive, resulting in enhancement of drying rate in the range from 1.98 to 7.17 times.

4. Conclusions

1. EHD drying kinetics typically followed the exponential curve, hence it is diffusion-limited and could be described by Fick's equation.
2. Drying rate of white champignons is proportional to initial moisture content, increases with electric field strength and with decrease of relative humidity.
3. The effect of needle packing density on drying rate of white champignons was significant.
4. The effect of 1.0 m s⁻¹ cross-flow air on EHD drying was found significant at 12 and 14 kV, while at 16 kV the drying rate was higher than EHD without air cross-flow.
5. Effect of electric field on effective moisture diffusion was much more pronounced in the case of sole EHD: from $3.38 \cdot 10^{-10}$ m^2 s^{-1} (12 kV) to $7.22 \cdot 10^{-10}$ m^2 s^{-1} (16 kV).

5. References

[1]   Kudra, T.; Martynenko, A. Energy aspects in electrohydrodynamic drying. Drying Technology 2015, 33, 1534–1540.

[2]   Giri, S.K.; Prasad, S. Drying kinetics and rehydration characteristics of microwave-vacuum and convective hot-air dried mushrooms. Journal of Food Engineering 2007, 78 (2), 512–521.

[3]   Xue, G.R.; Limoto, M.; Uchino T. Drying of shiitake mushrooms using ionic wind generated by corona discharge. Journal of the Japan Society of Agricultural Machinery 1996, 58 (4), 53–60.

[4]   Dutta, B.; Raghavan, G.S.V.; Dev, S.R.S.; Liplap, P.; Murugesan, R.; Anekella K.; Kaushal, T.A. Comparative study on the effects of microwave and high electric field pretreatments on drying kinetics and quality of mushrooms. Drying Technology 2012, 30 (8), 891–897.

[5]   Dinani, S.T.; Havet, M.; Hamdami, N.; Shahedi, M. Drying of mushroom slices using hot air combined with an electrohydrodynamic (EHD) drying system. Drying Technology 2014a, 32 (5), 597–605.

[6]   Dinani, S.T.; Hamdami, N.; Shahedi, M.; Havet, M. Mathematical modeling of hot air/electrohydrodynamic (EHD) drying kinetics of mushroom slices. Energy Conversion and Management 2014b, 86, 70–80.

[7]   Dinani, S.T.; Havet, M. Drying kinetics and energy consumption of combined convective-electrohydrodynamic (EHD) drying of mushroom slices. In 19-th International Drying Symposium. Lyon, France. August 24–27, 2014c.

[8]   Dinani, S.T.; Havet, M. The influence of voltage and air flow velocity of combined convective-electrohydrodynamic drying system on the kinetics and energy consumption of mushroom slices. Journal of Cleaner Production 2015a, 95, 203–211.

[9]   Dinani, S.T.; Hamdami, N.; Shahedi, M.; Havet, M.; Queveau, D. Influence of the electrohydrodynamic process on the properties of dried button mushroom slices: A differential scanning calorimetry (DSC) study. Food and Bioproducts Processing 2015b, 95, 83–95.

[10]   Singh, A.; Vanga S.K.K.; Nair, G.R.; Gariepy Y.; Orsat, V., Raghavan, V. Electrohydrodynamic drying of sand. Drying Technology 2017, 35 (3), 312–322.

[11]   Argyropoulos, D.; Rainer, A.; Mueller, J. Establishing moisture sorption isotherms of wild mushroom varieties using a dynamic vapor sorption method. XVII-th World Congress of the International Commission of Agricultural and Biosystems Engineering (CIGR). Québec City, Canada June 13-17, 2010.

[12]   Labuza, T.P.; McNally, L.; Gallagher, D.; Hawkes, J.; Hurtado, F. Stability of intermediate moisture foods. 1. Lipid Oxidation. Journal of Food Science 1979, 37, 154–159.

Influence of drying conditions on process properties and parameter identification for continuous fluidized bed spray agglomeration

Strenzke, G.[a]*; Golovin, I.[b]; Wegner, M.[b] ; Palis, S.[b,e] ; Bück, A.[d] ; Kienle, A.[b,c]; Tsotsas, E.[a]

[a] Chair of Thermal Process Engineering, Institute of Process Engineering, Otto von Guericke University, Magdeburg, Germany.

[b] Institute of Automation Engineering, Otto von Guericke University, Magdeburg, Germany.

[c] Max-Planck-Institute for Dynamics of Complex Technical Systems, Magdeburg, Germany.

[d] Institute of Particle Technology, Friedrich-Alexander University Erlangen-Nuremberg, Erlangen, Germany.

[e] National Research University "Moscow Power Engineering Institute", Moscow, Russia.

*corresponding author, Tel.: +49 391 67 18320, E-Mail: gerd.strenzke@ovgu.de

Abstract

Agglomeration is a particle formulation process in which at least two primary particles are combined to form a new one. The growth of agglomerates depends on interactions of particles covered with wet spots that generated by depositions of binder droplets. This work experimentally compares the influence of external feed rate and sprayed binder content on product properties and process stability with internal separation at different drying conditions. Due to the identification of parameters a populations balance model (PBM) is developed. The PBM includes the agglomeration kernel function, which characterizes the kinetics, i.e. the rate at which primary particles build agglomerates.

Keywords: spray fluidized bed agglomeration; drying; continuous process; internal separation; population balances

1. Introduction

Agglomeration is a particle formulation process in which at least two primary particles are combined to form a new one. The principle of fluidized bed spray agglomeration is especially used in chemical, food and pharmaceutical industry[1]. The advantages are good mixing and uniform high heat and mass transfer rates between particle, liquid and gas phase. Compared to previous batch processes the additional benefits of continuous processing are a constant product quality and higher throughputs. In case of fluidized bed spray agglomeration, a solid-contained liquid, called binder, is sprayed on the particles. The binder can be a solution, suspension or melt. The present work experimentally compares the influence of external feed rate and sprayed binder content on product properties and process stability with internal separation at different drying conditions. Product properties like particle size distribution or structure of agglomerates depend on these conditions and due to this, there are changes in product qualities, e.g. solubility, flowability or creation of dust free atmospheres. The growth of agglomerates depends on interactions of particles covered with wet spots that generated by depositions of binder droplets. Due to evaporation of water from the binder, wet connections between primary particles are transformed to solid bridges[2]. Therefore, the drying rate associated with gas temperature and moisture content finally determines the rate and quality of agglomeration.

2. Materials and Method

The starting materials for the fluidized bed and continuous feeding during the process are glass beads with distributed shapes, shown in Fig. 1. The Sauter diameter is 200 µm, measured optical by Camsizer, Retsch Technologies GmbH, Germany.
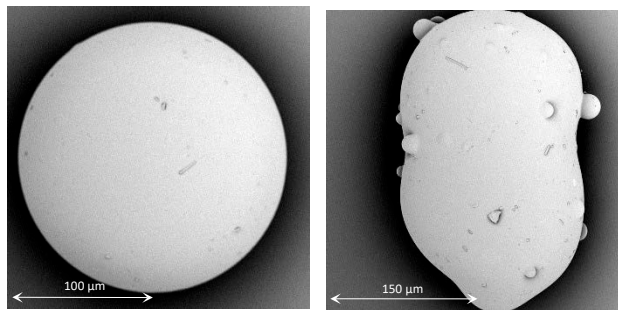
Fig. 1: different shapes of glass beads as primary particles

The operating binder is a solution of water and hydroxylpropylmethylcellulose (HPMC). HPMC is a biological binder also known as Pharmacoat and is used in food and pharmaceutical industries. In the present work it is used as a solution with water and a mass concentration of 4 %. To carry out the experiments a cylindrical fluidized bed is used, illustrated in Fig. 2. The fluidized bed is in a pilot plant scale.
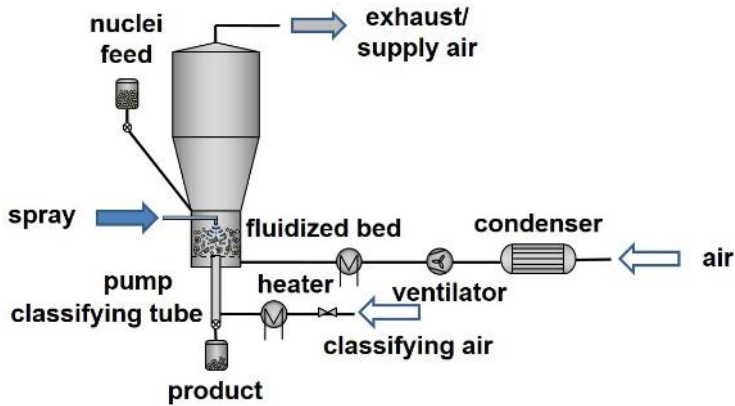
Fig. 2: Scheme of the fluidized bed

The particles are fluidized by heated ambient air air, which enters the fluidized bed chamber from the bottom throught a distributor plate. The Chamber of the fluidized bed has a diameter of 300 mm. The spray nozzle, which atomized and sprayed the solution in top-spray configuration, is installed at a distance of 420 mm above the distributor plate of the fluidized bed. An external pump supply the feeding of the solution. Particles having the target size are continuously discharged by internal classification through a tube, which is centrally installed at the bottom of the fluidized bed. The important parameters (inlet temperature – T_{inlet}, air mass flow – $\dot{M}_{inlet}$, feed rate – $\dot{M}_{Feed}$, HPMC content – w and binder spray rate – $\dot{M}_{Spray}$) are shown in Table 1, all experiments started with a bed mass of 8 kg.

Table 1: Experimental parameter

Experiment	T_{inlet}, [°C]	$\dot{M}_{inlet}$, [kg/h]	$\dot{M}_{Feed}$, [g/min]	w, [% HPMC]	$\dot{M}_{Spray}$, [g/min]
T1F150	80	275	150	4	55.5
T1F250	80	275	250	4	55.5
T1F350	80	275	350	4	55.5
T2F150	100	275	150	4	55.5
T2F250	100	275	250	4	55.5
T2F350	100	275	350	4	55.5

3. Results and Discussion

The Comparisons of the results of the 4 Experiments, shown in Fig. 3 and Fig. 4, are indicate that the product size of the experiments at 100 °C are smaller and the product size increase with decreasing feed rate. A break takes place during the experiment at 80 °C, for a feed rate of 150 g/min (at 35 min).
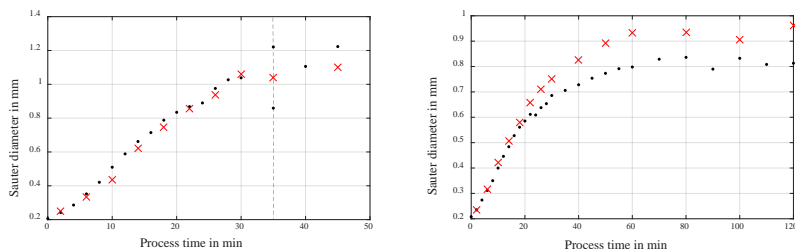
Fig. 3: Sauter diameter of bed (·) and product (x) samples for 150 g/ min at 80 °C (left) and 100 °C (right)
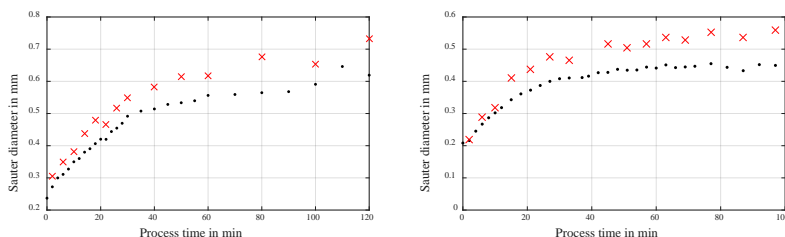
Fig. 4: Sauter diameter of bed (·) and product (x) samples for 350 g/ min at 80 °C (left) and 100 °C (right)

The reason is the lower evaporation rate of the water content from the solid bridges between the glass beads at lower temperature. Due to this, the residence time of with binder wetted surface get longer. It is more time to collide and connect with other wetted surfaces. The influence of the feed rate is also clear visuable, especially for the experiments at 100 °C. Here at low feed rate the product particles reached a size of 0.9 mm. With increasing the feed rate the size is getting smaller. The structure analysis of the agglomerates with the Scatter electrone microscope (SEM) prove the study, that at lower temperatures more binder is on the particles. The structure analysis of the agglomerates are shown in Fig. 5 and Fig. 6. For both temperatures the lowest feed rate indicates a partial coating. This means a part up to the whole particle surface is covered with the binder. With increasing the feed rate, more particles enter the spray zone and the binder solution is more distributed over the bed particles. The particles in figure 6 are indicates optically a more compact structure as in figure 5, which is proved by Camsizer measurements, shown in Table 2. This indicates that the dense of the agglomerates increase by the inlet temperature, which is confirmed by Dadkhah[3].

Table 2: Density of agglomerates at experimental parameters

Temperature [°C]	F150	F250	F350
80	>1.2	1.44	1.6
100	1.47	1.7	1.7
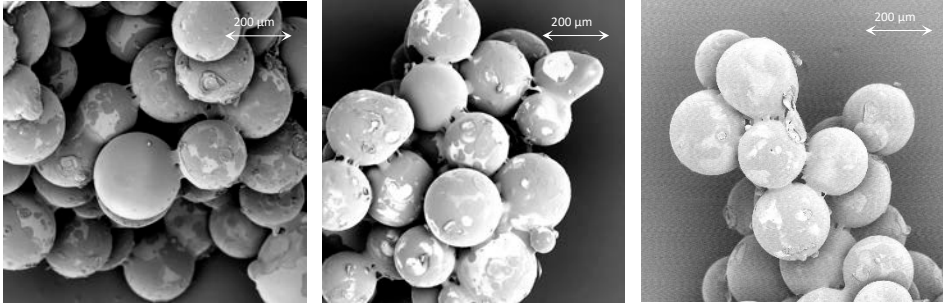
Fig. 5: SEM pictures of product particles at 80 °C with 150 g/min (left), 250 g/min (middle) and 350 g/min (right)
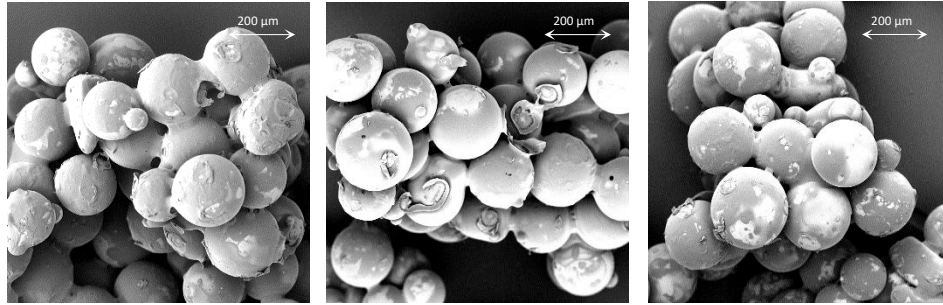
Fig. 6: SEM pictures of product particles at 100 °C with 150 g/min (left), 250 g/min (middle) and 350 g/min (right)

In order to describe the dynamic behaviour of continuous fluidized bed spray agglomeration, the following population balance model can be used:

$$\frac{\partial n(t,v)}{\partial t} = \dot{n}_{feed}(t,v) - \dot{n}_{prod}(t,v) + \dot{n}_{agg}(t,v), \qquad (1)$$

where n symbolizes the number density distribution, v denotes the particle volume, $\dot{n}_{feed}(t,v)$, $\dot{n}_{prod}(t,v)$ and $\dot{n}_{agg}(t,v)$ represent particle fluxes due to the external particles feed, the reflux of the product particles and agglomeration process respectively. The formation and growth of agglomerates including initial condition can be described by:

$$\dot{n}_{agg}(t,v) = \frac{1}{2}\int_0^v \beta(t,u,v-u)\, n(t,u)n(t,v-u)du - \int_0^\infty \beta(t,u,v)n(t,v)n(t,u)\, du, (2)$$

$$n(t=0,v) = n_0(v), \qquad (3)$$

where $\beta(t,u,v)$ is an agglomeration function (kernel) characterizing the kinetics of the agglomeration process. This kernel can be represented as a product of a coalescence kernel

$\beta(u, v)$, which depends only on the volume of the agglomerating particles and an agglomeration efficiency $\beta_0(t)$, which is a positive possibly time-dependent function:

$$\beta(t, u, v) = \beta_0(t)\beta(u, v). \qquad (4)$$
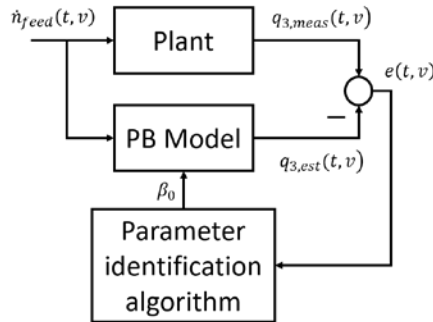
Fig. 7: Scheme of parameter identification

The Estimation of kinetics for an agglomeration is particularly challenging due to its highly nonlinear process dynamics. The coalescence kernel $\beta(u, v)$, being a nonnegative symmetric function of two variables, describes an impact of particle sizes on the probability of its effective collision. In order to understand the formation of agglomerates in a first step the mechanical kernel based on Brownian motion[7] can be applied for simulation model:

$$\beta(u, v) = \beta_0 \left(v^{\frac{1}{3}} + u^{\frac{1}{3}} \right) \left(v^{-\frac{1}{3}} + u^{-\frac{1}{3}} \right). \qquad (5)$$

Assuming that time dependency of the agglomeration efficiency β_0 can be neglected, this scalar parameter can be estimated from the experimental particle size distributions using a parallel model approach Fig. 7 [4]. Substituting this mechanical kernel into the population balance model a linear regression problem can be formulated:

$$\min_{\beta_0} \int_0^T \left\| q_{3,meas}(t) - q_{3,est}(t, \beta_0) \right\|_2^2 \, dt . \qquad (6)$$

In order to compute the given population balance model the method of lines can be applied, where the spatial coordinate is discretized using the cell-average method [8] on a logarithmic grid. The experimental and simulation results with Brownian motion kernel are depicted in Fig. 8. In Fig. 9 is shown a comparison of the initial and steady state distribution. It can be seen that using this theoretical kernel for continuous fluidized bed spray agglomeration

process yields a qualitatively good approximation of the process particularly for steady-state region.
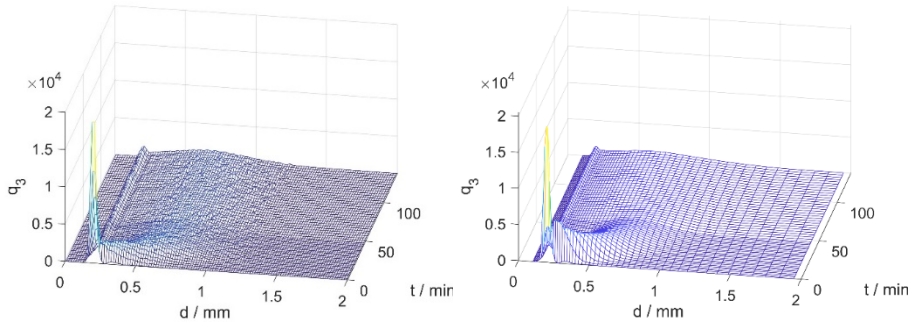
Fig. 8: Experimental (left) and simulated (right) particle size distribution q_3
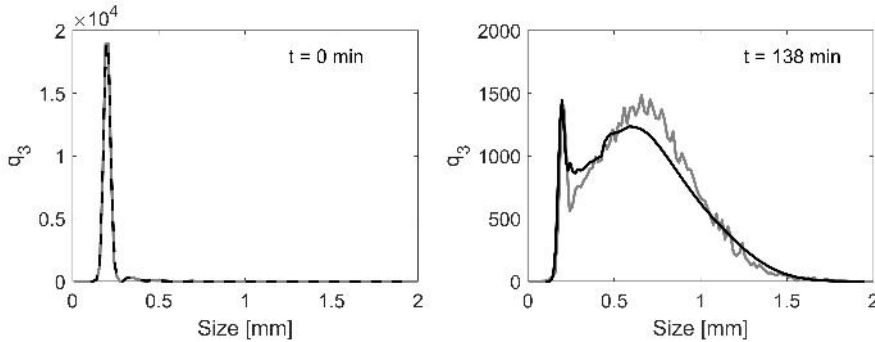
Fig. 9: Experimental (grey) and simulated (black) particle size distribution q_3 for the initial (left) and steady state (right) distribution

4. Conclusions

The Influence of the temperature and feed rate on the particle were investigated. The results of the experiments show that a lower temperature lead to bigger agglomerates. The increasing of the feed rate indicates smaller particles. A high temperature and high feed rate should be result in smaller product particles. The results of the structure investigations does not indicate a preferd shape, like sphericals or sticks, at different temperatures or feed rates.

The developed PBM model was qualitatively good approximation of the process particularly for steady-state region. In order to get more precise process approximation another kernel functions of more degrees of freedom, e.g. Laurent polynomials of two variables[6], bilinear basis functions[5], or time dependency of the agglomeration efficiency $\beta_0(t)$ can be taken into account.

5. Acknowledgement

6. References

[1] Bück, A., Tsotsas, E., 2016. Encyclopedia of Food and Health. Vol.1. Oxford: Academic Press, Ch. Agglomeration, pp. 73 – 81.

[2] Terrazas-Velarde, K., Peglow, M., Tsotsas, E., 2011, Kinetics of fluidized bed spray agglomeration for compact and porous particles, Chemical Engineering Science 66, pp. 1866-1878

[3] Dadkhah, M., Tsotsas, E., 2014. Influence of process variables on internal particle structure in spray fluidized bed agglomeration

[4] Palis, S., Kienle, A., 2013. "Online parameter identification for continuous fluidized bed spray granulation", 5th International Conference on Population Balance Modelling - PBM (Bangalore).

[5] Chakraborty, J., Kumar, J., Singh, M., Mahoney, A., Ramkrishna, D., 2015. Inverse problems in population balances. Determination of aggregation kernel by weighted residuals. Ind. Eng. Chem. Res. 54, pp. 10530–10538.

[6] Eisenschmidt, H., Soumaya, M., Bajcina, N., Le Borne, S., & Sundmacher, K., 2017. Estimation of aggregation kernels based on Laurent polynomial approximation. Computers & Chemical Engineering 103, pp. 210-217.

[7] Schwabl, F., 2006. Statistische Mechanik. Springer-Verlag Berlin Heidelberg.

[8] Kumar, J., 2006. Improved accuracy and convergence of Discretized Population Balance for Aggregation: The cell average technique. Chemical Engineering Science, 61, pp. 3327–3342.

Encapsulation of krill oil by spray drying

Takashige, S.[a]; Hermawan Dwi, A.[a];Sultana, A.[a]; Shiga, H.[b]; Adachi, S.[b]; Yoshii, H.[a*]

[a] Department of Applied Biological Science, Faculty of Agriculture, Kagawa University,
 2393, Ikenobe, Miki-cho, Kita-gun, Kagawa 761-0795, Japan

[b] Department of Agriculture and Food Technology, Faculty of Bio-environmental Science, Kyoto
 Gakuen University, 1-1 Nanjo Ohtani, Sokabe-cho, Kameoka, Kyoto 621-8555, Japan.

*E-mail of the corresponding author: foodeng.yoshii@ag.kagawa-u.ac.jp

Abstract

An oil from Pacific krill (Euphausia pacifica) has a high content of PUFAs and phospholipids. The sediment was formed with homogenization of krill oil and maltodextrin (MD; dextrose equivalent (DE) = 19) solution using sodium caseinate, gum arabic, hydrolyzed whey protein or modified starch as a surfactant. Quillaja saponin could form the emulsion without the sediment. MD (28.5 wt%) was solubilized with distiller water (50 wt%) and mixed with krill oil (20wt%) and Quillaja saponin (1.5 wt%). The homogenized solution was spray-dried using Okawara-L8 spray dryer with a centrifugal atomizer. Spray-dried powder was evaluated in the oil-droplet size and surface-oil content.

Keywords: krill oil, emulsion, Quillaja saponin, spray drying, PUFAs

1. Introduction

Krill oil (KO) is a rich souce of long chain n-3 polyunsaturated fatty acids (PUFAs) such as eicosapentaenic acid (EPA) and docosahexaenoic acid (DHA) [1], which have phospholipids, and has been suggested to have the higher bioavailability compared with fish oil. KO contains astaxanthin as antioxidant. Encapsulated KO has been used as a dietary supplement. PUFAs are inherently unstable and prone to oxidation. Gomez-Estaca et al. [2] investigated the encapsulation of an astaxanthin-containing lipid extract from shrimp waste by complex coacervation using a novel gelatin-cashew gum complex. Haidor et al. [3] investigated the encapsulation of KO using chitosan nanoparticle with emulsification and the electrostatic interaction to triphosphate. Sanguansri et al. [4] investigated the encapsulation of KO using the mixture of protein and carbohydrates by spray drying and showed the protein enhanced the oxidative stability of KO during storage. Yamada et al. [5] showed 8-hydroxyeicosapentaenoicacid (8-HEPE) acts as a peroxisome proliferator-activated receptor ligand and had higher activity than EPA. KO from the Pacific Ocean near Sanriku contained 8-HEPE.

The encapsulation efficiency of fish oil by spray drying is affected by several parameters such as oil-droplet diameter, solid and oil contents, and processing conditions. The surface-oil ratio is the most important parameter that estimates the shelf life of fish oil in spray-dried powders. Ghani et al. [7] investigated effects of oil-droplet diameter and DE of MD on the surface-oil ratio of microencapsulated fish oil and showed the surface-oil ratio was remarkably increased when the ratio of the average reconstituted oil-droplet diameter to the average particle diameter was higher than 0.01. Ghani et al. [8] investigated also the effect of DE of MD on oxidation stability in encapsulated of fish oil with MD by spray drying. They indicated that the fish oil in spray-dried powder encapsulated fish oil prepared using MD of DE = 25 and 19 had lower peroxidative values (PVs) than those prepared with MD of DE = 11. The difference in PV can be ascribed to the difference in the surface-oil ratio of the spray-dried microcapsules.

In this study, the formation of emulsified KO was investigated with various emulsifier and the stability of encapsulated KO using MD (DE=19) and saponin emulsifier was examined at 50ºC.

2. Materials and Methods

2.1. Materials

KO was purchased from Koyo Chemical Co., Ltd. (Osaka, Japan). In the formation of KO emulsion, sodium caseinate, hydrolyzed whey protein, gum arabic, modified starch or saponin emulsifier were used. Sodium casienate and rosemary extract oil (RO) was gifted

from Mitsubishi-Chemical Foods Corporation (Tokyo, Japan). Hydrolyzed whey protein, Emulup® was purchased from Morinaga Milk Industry Co. Ltd. (Tokyo, Japan) and gum arabic was from Wako Pure Chemical Industries, Ltd. (Osaka, Japan). Saponin emulsifier was Quillayanin S-100 from Maruzen Pharmaceuticals Co., Ltd. (Hiroshima, Japan) MD (DE=19) was gifted from Matsutani Chemical Industry Co., Ltd. (Itami, Japan). Other chemical reagents used were analytical grade chemicals from Wako Pure Chemical Industries, Ltd.

2.2. Method

2.2.1. Formation of KO emulsion

MD solution was prepared by dissolving MD in distilled water at 80 °C and cooling to room temperature. KO was blended with the solution to give 50 wt% solid content. The composition of the solution was 20 wt% KO, 1.5 wt% emulsifier, 28.5 wt% MD, and 50 wt% distilled water. The solution was mixed using a rotor-stator type homogenizer (Polytron, PT-6100; Kinematica, Littau, Switzerland) at 7,500 rpm for 3 min with a 30 s interval after 1 min and 2 min. This solution was further homogenized using a high-pressure homogenizer (Star Burst Mini; Sugino Machine Limited, Uozu, Japan) at 100 MPa for two passes.

2.2.2. Spray drying

The feed emulsions were spray dried using a pilot scale spray dryer (Ohkawara-L8; Ohkawara Kakouki Co., Ltd., Yokohama, Japan) equipped with a centrifugal atomizer. The feed rate was 25 mL/min, the atomizer speed was 10,000 rpm, and the air flow rate was set at 110 kg/h. In the drying process, the temperatures of inlet and outlet air were 140 °C and 70 to 95 °C, respaectively
. After being cooled to room temperature, the collected powders were stored in closed glass containers at −80 °C until use.

2.2.3. Analysis of oil-droplet and powder-particle diameters

The size distributions of the oil droplets in the feed and reconstituted emulsion and the spray-dried powder particles were measured with a laser diffraction particle size analyzer (SALD-7100; Shimadzu Corporation, Kyoto, Japan) equipped with a batch sample cell. The reconstituted emulsion were obtained by dissolving the spray-dried powders in distilled water. The feed and reconstituted emulsion were pipetted directly into the cell containing distilled water for respective measurements. Meanwhile, the particle size distributions of the spray-dried powders were analyzed by dispersing the powders in 2-methyl-1-propanol. The volume-based diameter (D_{43}) was considered to be the mean diameter for all measurements.

2.2.4. *Scanning electronic microscopy (SEM)*

Surface and cross-cut images of encapsulated fish oil powders were observed by a JSM 6060 SEM (JEOL, Tokyo, Japan). The samples were placed onto the SEM sample holder using double-sided tape and coated with Pt-Pd using an MSP-IS Magnetron Sputter (Vacuum Device, Inc., Tokyo, Japan). The cross-cut structures were prepared using procedure as described by Soottitantawat et al. [8].

2.2.5. *Measurement of DHA and EPA contents in KO*

Approximately 0.2 g of oil or 0.5 g of powders was weighed in the test tube. Two ml of *N, N*-dimethylformamide (DMF) was added to solubilize KO in the tube. Then, 2 mL
 of hexane was added to extract KO from DMF and was stirred with a vortex mixer (Vortex-GENIE 2 Mixer, G-560 type, M&S Instrument Inc., Osaka, Japan). Hexane was sampled and 0.5 mL of KO was used to be methyl esterified with Fatty Acid Methylation Kit and Fatty Acid Methyl Ester Purification Kit (Nacalai Tesque, Inc., Kyoto, Japan). One µL of methyl esterified oil was injected to gas chromatography-mass spectrometry (GC-MS, Shimazu Corp., Kyoto, Japan) with a fused silica capillary column (30 m x 0.25mm x 0.25 µm; DB-1, Agilent Technologies Japan Ltd., Tokyo, Japan).

3. Results and Discussions

3.1. Formation of KO emulsion

KO emulsion was formed with quillayanin, sodium casienate, hydrolyzed whey protein, or arabia gum as 3 wt% emulsifier in the solid powder by the mechanical homogenization (8,000 rpm for 3 min). The KO emulsions using sodium casienate, hydrolyzed whey protein, and arabia gum separated into two phase solution. No phase-separation occurred for the KO emulsion using quillayanin as emulsifier. Oil-droplet diameters for KO emulsions were measured with a laser diffraction particle size analyzer at 3 h after the emulsification. Except KO emulsion using quillayanin, the lower phase solution was used to measure oil-droplet diameter. Figure 1 shows the distributions of oil-droplet diameter for four KO emulsions. KO emulsions using sodium casienate and arabia gum formed aggregates and had larger oil-droplet diameter above 10 µm. KO contains about 18wt% phospholipids. Genelally phospholipid make aggragtion with proteins. These results show that protein emulsifier could not be used to emulsify KO. Saponin emulsifier, quillayanin was suitable emulsifier to form stable emulsion.
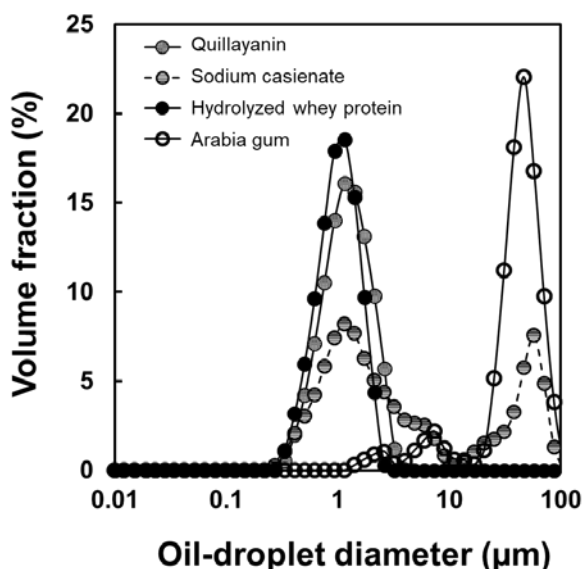
Fig. 1. ***Distribution of oil-droplet diameter for KO emulsion using emulsifier, quillayanin, sodium casinate, hydrolyzed whey protein or arabia gum.***

3.2 Formation of spray-dried KO powder

By using quillayanin as an emuslifer, spray-dried KO powders were produced by two homogenization conditions, the mechanical homogenization and high-pressure homogenization. The spray-dried powder was also formed for the case where rosmary extract as an antioxidant was added to KO at mechanical homogenization. Table 1 shows physical properties of three spray-dried powders. Average oil-droplt diamters for three spray-dried powders were about 1.1-1.4 μm. Moisture contents were about 2 wt% for the mechanical homogenization and 3.6wt% for high-pressure homogenization. Reconstituted oil-droplet and powder diameters were about 1.4 μm and 58 μm for the mechanical homogemization and 1.1 μm and 70 μm, respectively. Figure 2 shows SEM images of surface structures and cross-cut sructures of spray-dried powders. SEM images of cross-section structures for KO encapsylated spray-dried KO powders show clear oil-droplet distribution in spray-dried powder.

Table 1. Physical properties od spray-dried powders.

	KO emulsion		Spray-dried powder		
	Oil-droplet diameter (μm)	Viscosity (mPa·s)	Moisture content (%)	Reconstituted oil-droplet diameter (μm)	Powder diameter (μm)
Mechanical homogenization (7500rpm)	1.31±0.04	6.89±0.44	2.00±0.20	1.41±0.03	58.3±6.10
High-pressure homogenization (100MPa)	0.81±0.005	7.54±0.12	3.58±0.36	1.13±0.004	70.2±1.11
Mechanical Homogenization +rosemary extract	1.31±0.02	18.17±0.46	2.33±0.15	1.40±0.003	57.1±2.33
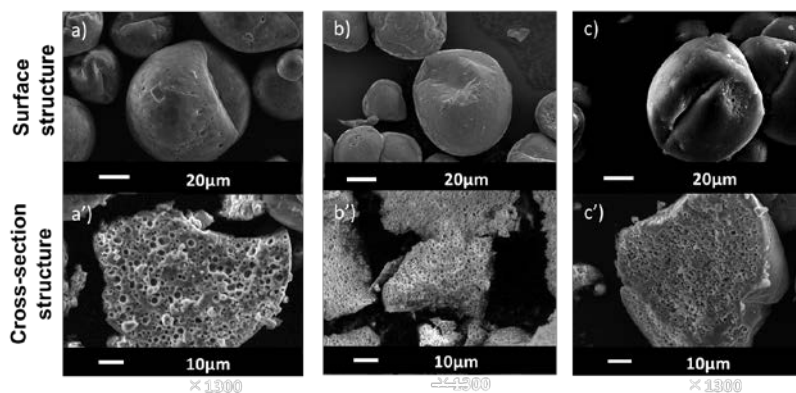
Fig. 2. SEM images of spray-dried KO powder by the mechanical homogenization (a, b and a', b') and high-pressure homogenization. KO in spray-dried powder for b and b' contained rosemary extract oil.

3.2. Stabilty of EPA and DHA in spray-dried KO powder

Stabilities of EPA and DHA were investigated in spray-dried KO powders at 50ºC for one- and two-week storages. Figure 3 indicates the retentions of EPA and DHA to the intial content of EPA and DHA in KO, KO plus 5wt% RO in KO, spray-dried KO powder by the

high-pressure homogenization (HP), KO encapsulated spray-dried powder by the mechanical homogenization (MH), and KO, which contined with 5wt% RO, encapsulated spray-dried powder with MH. The retentions of EPA about 0.4 in KO and KO contained 5wt% RO were higher than these of DHA about 0.1. The addition of RO to KO did not affect the retentions of EPA and DHA. The retentions of EPA and DHA for spray-dried KO powder by MH were higher than those of KO wncapsulated spray-dried powder with HP. These results sugest the force during homogenization affected the stability of EPA and DHA. In spray-dried powder, RO addition improved the retention of DHA siginificantly in spray-dried powder. After two-weeks storage at 50ºC, the retentions of EPA and DHA were obtained about 0.8 in spray-dried KO (+5wt% RO) powder. The encapsulation of KO could improve the stability of EPA and DHA. However, suitable homogenization condition and antixodant concentration should be investigated to obtain the more stable KO encapsulated spray-dried KO powder.
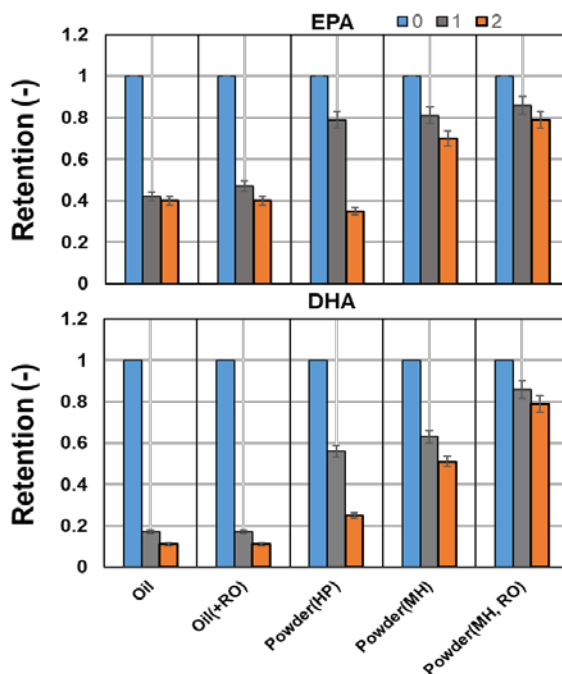
Fig. 3. Stability of EPA and DHA at 50ºC for on- and two-week storage

4. Conclusions

Spray-dried KO powder was formed by emulsification and spray drying. KO contained 5wt% RO could be encapsulated with MD (DE=19) using quillaja saponin as an emulsifier. After two-weeks storage at 50ºC, the retentions of EPA and DHA were about 0.8 in encapsulated

5. Acknowledgement

6. References

[1] Grandois, JL.; Marchioni, E.; Zhao, M.; Giuffrida, F.; Ennahar, S.; Bindler, F. Investigation of natural phosphatidylcholine sources: separation and identification by liquid chromatography−electrospray ionization−tandem mass spectrometry (LC−ESI−MS2) of Molecular Species. Journal of Agricaltural Food and Chemistry, 2009, 57 (14), 6014–6020.

[2] Gomez-Estaca, J.; Comunian、T.A.;.Montero, P.; Ferro-Furtado, R.; Favaro-Tirindade, C.S. Encapsulation of an astaxanthin-containing lipid extract from shrimp waste by complex coacervation using a novel gelatin–cashew gum complex. Food Hydrocolloids, 2016, 61, 155-162.

[3] Haider, J.; Majeed, H.; Williams, P.A.; Safdar, W.; Zhong, F. Formation of chitosan nanoparticles to encapsulate krill oil (*Euphausia superba*) for application as a dietary supplement. Food Hydrocolloids, 2017, 63, 27-34.

[4] Sanguansri,L.; Shen, Z.; Bhail, S.; Cheng, LJ.; Ying, DY.; Augustin, MA. Novel formulations and process for development of microencapsulated krill oil. http://aocs.files.cms-plus.com/Meetings/Affliated/LSanguansri_Novelformulations.pdf

[5] Yamada, H.; Kikuchi, S.; Hakozaki, M.; Motodate, K.;Nagahora, N.; Hirose, M. 8-hydroxyeicosapentaenoic acid decreases plasma and hepatic triglycerides via activation of peroxisome proliferator-activated receptor alpha in high-fat diet-induced obese mice. Journal of Lipids, 2016, Article ID 7498508, 9 pages.

[7] Ghani, AA.; Adachi, S.; Sato, K.; Shiga, H.; Iwamoto, S.; Neoh, TL.; Adachi, S.; Yoshii, H. Effects of oil-droplet diameter and dextrose equivalent of maltodextrin on the surface-oil ratio of microencapsulated fish oil. Journal of Chemical Engineering of Japan. 2017, 50, 799-806,

[8] Ghani, AA.; Adachi, S.; Shiga, H.: Neoh TL.; Adachi, S.; Yoshii, H. Effect of different dextrose equivalents of maltodextrin on oxidation stability in encapsulated fish oil by spray drying. Bioscience, Biotechnology, and Biochemistry, 2017, 81, 705-711.

[9] Soottitantawat, A.; Yoshii, H.; Furuta, T.; Ohgawara, M.; Linko,P. Microencapsulation by spray drying: Influence of emulsion size on the retention of volatile compounds. Journal of Food Science, 2003, 68, 2256-2262.

Thin layer drying behaviour of fermented cocoa (*Theobroma cacao* L.) beans

Mujaffar, S.[a*]; Ramroop, A.[a]; Sukha, D.[c]

[a] Food Science and Technology Unit, Department of Chemical Engineering, The University of the West Indies, St. Augustine, Trinidad and Tobago, West Indies. Tel.:+1 868 662 2002 Extension 82190.

[b] Cocoa Research Centre, The University of the West Indies, St. Augustine, Trinidad and Tobago, West Indies.

*E-mail of the corresponding author: saheeda.mujaffar@sta.uwi.edu

Abstract

To assess the impact of a rest interval and bean turning on the thin-layer drying behavior of fermented cocoa beans, beans of mixed Trinitario varieties were dried in a cabinet oven at three temperatures (40, 50, 60°C) using three drying regimes, namely; continuous drying, intermittent drying (drying for 8h with a rest period of 16h), and intermittent drying with turning of beans. Moisture content, water activity, pH and colour attributes were measured and sensory evaluation of the cocoa liquor carried out on selected samples. Drying curves were constructed and drying rate constants (k) and effective diffusivity (D_{eff}) values determined.

Keywords: *Oven-drying; Fick's Law; Rate constant; Diffusion coefficient*

1. Introduction

Drying of fermented beans is an important step in the primary processing of cocoa (*Theobroma cacao* L.) beans, which are dried to reduce the moisture content from about 60% to 6-7% for safe storage and transportation. During drying, oxidative chemical reactions that occur during fermentation to reduce the astringency and bitterness of the bean continue[1]. The rate of drying and the final moisture content of dried beans have a direct impact on bean quality and value-added products such as cocoa liquors and chocolates. Too rapid drying can result in the formation of a physical barrier to moisture and volatile acid movement, resulting in brittle beans with high acidity. Too slow drying can favour mould growth during storage and handling.

Sun-drying of cocoa beans is the most widely practiced method of drying due to the simplicity and use of natural energy. Sun-drying is, however, weather dependent, requires large areas of floor space and is labour intensive as the beans must be frequently mixed during drying. Artificial drying systems are used to shorten drying time and increase the rate of moisture removal from the beans[2,3,4,5,6,7]. The negative effects of rapid drying are thought to be alleviated during traditional sun-drying due to the low drying temperatures experienced, the regular turning of beans to ensure uniform drying, and through a 'resting' period which takes place during the evening and night-time. The tempering or rest period is reported to assist with moisture redistribution in the beans before the next drying phase commences[10]. For artificially dried beans, the risk of high bean acidity is exacerbated due to the typically high drying temperatures used[8,9,10].

The objective of this study was to investigate the oven-drying of Trinitario (fine or flavor cocoa) beans at three temperatures (40, 50 and 60°C), with the specific objective of comparing the drying behaviour and selected quality attributes of beans dried continuously with that of beans handled in a manner which simulates the traditional sun-drying practice, namely, a rest period with and without the turning of beans.

2. Materials and Methods

Fermented cocoa beans of mixed Trinitario varieties were obtained from the Cocoa Research Centre (CRC) cocoa processing facility and dried in a Unitemp Drying Cabinet (LTE Scientific Ltd., Greenfield, Oldham). Beans were dried at 40, 50 and 60°C. The relative humidity of the drying air at each of the three oven temperatures averaged 60, 40 and 25%, respectively and the air velocity was less than 0.5 m/s. Beans were weighed (0.01±0.005g) using an Ohaus Explorer Pro Balance, Model EP2102C (Ohaus Corporation, NJ, USA) and drying was continued until there was virtually no change in weight. For Continuous drying (CD), beans were placed into the oven and dried until constant weight

was achieved. For Intermittent drying (ID), beans were allowed to dry at the respective temperatures for 8 hours, packaged and stored in a cool room (24°C) for 16 hours and re-loaded onto the trays the next morning. Beans were handled similarly for the last method; Intermittent with turning of beans (ID+Turn), with the additional turning (mixing) of beans at each weighing time. Bean moisture content, water activity (a_w), pH and colour was assessed as previously described[11] and *Hue angle (°)* and *Chroma* were calculated as given in Equations 1 and 2[12].

$$Hue = Arc \tan\left(\frac{b^*}{a^*}\right) \tag{1}$$

$$Chroma = \sqrt{(a^{*2} + b^{*2})} \tag{2}$$

Drying rates and Moisture Ratio (*MR*) values were calculated as described by Mujaffar et al.[11] and liqour samples produced from selected dried beans were assessed based on thirteen flavour attributes[13].

3. Results and Discussion

The initial moisture content and water activity values of fermented bean samples ranged from 0.78 to 1.02 g H_2O/g DM (44 - 51% wb) and 0.954 to 0.966, respectively. Drying curves showing the change in moisture content with total drying time for each drying method for the range of temperatures are given in Figs. 1 (a) through (c).
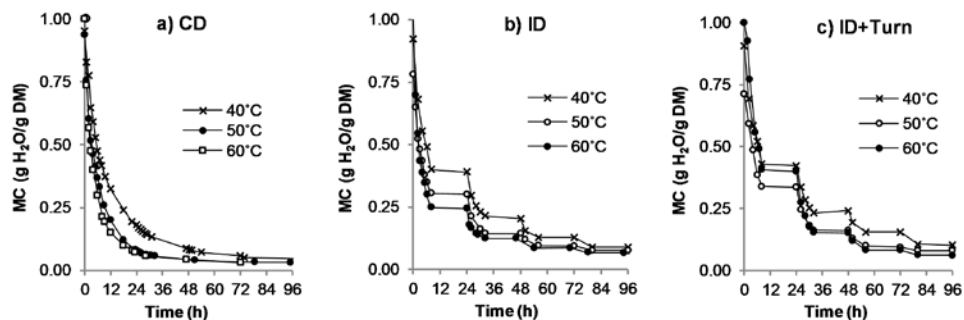
Figure 1. Drying curves for cocoa beans dried as a function of total drying time.
CD-Continuous ID-Intermittent ID+Turn (Intermittent with Turning)

Moisture content during drying was significantly affected by total drying time, drying temperature, drying treatment and time-temperature, time-treatment and temperature

treatment interactions ($p \leq 0.05$). As also expected, the intermittent drying of beans (Figs. 1b and c) resulted in a step-wise decrease in moisture values due to the rest period during which there was no drying. For continuously dried beans (Fig. 1a), the effect of increasing temperature on the decline in moisture was most evident during the first 24h of drying, with higher temperatures effecting a greater decline in moisture. Bean moisture content, water activity values and the time taken to reach equilibrium moisture content are given in Table 1. Given that the moisture content of 6-8% (wb) is the industry standard as the maximum safe storage limit for cocoa beans, the time taken for beans to attain a 7% moisture value is also given in Table 1.

Table 1. Moisture content, water activity values, time taken to reach equilibrium and 7% (wb) moisture content in dried cocoa beans.

Temperature (°C)	Treatment	MC (g H$_2$O/g DM)	a$_w$	Time to Equilibrium (h)		Time to 7% MC (h)	
				Total	Actual	Total	Actual
40	CD	0.040[d]	0.569[b]	147[e]	147[a]	48[d]	48[a]
	ID	0.046[bc]	0.518[d]	224[a]	80[c]	102[a]	38[b]
	ID+Turn	0.050[ab]	0.530[d]	224[a]	80[c]	119[a]	45[a]
50	CD	0.032[e]	0.594[a]	95[f]	95[b]	24[e]	24[d]
	ID	0.051[a]	0.487[e]	200[b]	72[e]	80[b]	32[c]
	ID+Turn	0.048[ac]	0.525[d]	200[b]	72[e]	79[bc]	31[c]
60	CD	0.030[e]	0.551[c]	72[g]	72[d]	13[e]	13[e]
	ID	0.050[c]	0.521[d]	174[d]	64[f]	62[cd]	27[cd]
	ID+Turn	0.030[e]	0.465[f]	176[c]	56[g]	80[b]	30[c]

CD-Continuous ID-Intermittent ID+Turn (Intermittent with Turning)
Means in a column without a common superscript letter differ ($p < 0.05$)

Total drying time (time to attain equilibrium moisture content) for beans dried continuously at 60°C was half that of beans dried at 40°C. As expected, the drying of beans using intermittent drying (with and without turning) increased the total drying time approximately 1.5-fold at 40°C, 2.0-fold at 50°C and 2.5-fold at 60°C. Drying is enhanced at the higher temperatures, which favours increased moisture movement and increased drying potential of the air. The initial rapid decline in moisture content has been attributed to the higher moisture content of bean testa, due residual wet mucilage coating. As the testa dries and hardens, diffusion of moisture from the cotyledon to the outer surface of the bean is gradually restricted[14]. Compared with beans dried continuously, equilibrium moisture values were generally higher in intermittently dried beans (Table 1). For beans dried at 40°C, there was a slightly greater decline in moisture content in the beans dried

intermittently (ID) and with turning (ID+Turn), demonstrating that the rest period impacted positively on the decline in moisture at this temperature. No discernible drying treatment effect was observed for beans dried at 50 and 60°C. Hii et al.[7] also noted that the tempering period has little effect on the moisture reduction in beans dried at higher temperatures. The drying potential of the air at 40°C would be expected to be lower than at the higher temperatures, therefore, moisture redistribution to the surface of the bean during the rest period may have assisted the drying process. It is therefore likely that the rest interval improves moisture movement during traditional sun-drying due to the low temperatures (below 50°C) experienced during sun-drying, as well as a deeper depth of beans, typically 0.05m, compared with the single layer of beans used in this study.

The drying rate constants (k) were determined from the initial straight line portions of plots of ln free moisture (ln MR) as a function of actual drying time (t). As given in Table 2, k-values increased as drying temperature increased ($p \leq 0.05$) and there was a temperature-treatment interaction effect ($p \leq 0.05$). Generally, as temperature increased the k-value increased. Drying treatment (CD, ID, ID+Turn) did not appear to have a discernible impact on the k-value, which was expected as the k-values apply to the initial stages of the drying process. The temperature dependence of the D_{eff} values and the activation energy for beans dried continuously was estimated from a plot of ln D_{eff} versus $1/T$ with the E_a value of 24.28 KJ/mol ($R^2 = 0.9984$) obtained for continuously dried beans (CD), 36.0 KJ/mol ($R^2 = 0.9316$), and 18.8 KJ/mol for intermittently dried beans with mixing (ID+Turn) ($R^2 = 0.9369$).

Table 2. *Drying rate constants (k) and diffusion coefficients (D_{eff}) for dried cocoa beans.*

Temperature (°C)	Treatment	K (1/min)	D_{eff} (m^2/s)
40	*CD*	0.1260[bd]	3.55 x 10^{-10}
	ID	0.1120[cd]	3.17 x 10^{-10}
	ID+Turn	0.0945[d]	2.66 x 10^{-10}
50	*CD*	0.1650[b]	4.65 x 10^{-10}
	ID	0.1420[bc]	4.01 x 10^{-10}
	ID+Turn	0.1070[cd]	3.02 x 10^{-10}
60	*CD*	0.2210[a]	6.22 x 10^{-10}
	ID	0.2590[a]	7.30 x 10^{-10}
	ID+Turn	0.1460[bc]	4.11 x 10^{-10}

CD-Continuous ID-Intermittent ID+Turn (Intermittent with Turning)

Means in a column without a common superscript letter differ ($p < 0.05$)

*D$_{eff}$ = k (4L^2/π^2) where L = half thickness 0.005m

At the end of drying of beans to equilibrium moisture content, there were no major visible differences in colour or appearance, although beans dried at 40°C generally appeared to be lighter in colour compared with beans dried at 50°C, and beans dried at 60°C looked slightly shrivelled. For all the drying treatments, pH values (of both testa and cotyledon) were generally higher in beans dried continuously at 50°C and lowest at 60°C (Fig.2). High acidity of beans dried continuously at 60°C was reduced through intermittent drying (with or without turning), as evidenced by a significant ($p \leq 0.05$) increase in pH values. It has been recommended that drying of beans be performed at bean temperatures not exceeding 60°C to avoid retention of excessive acids[15].
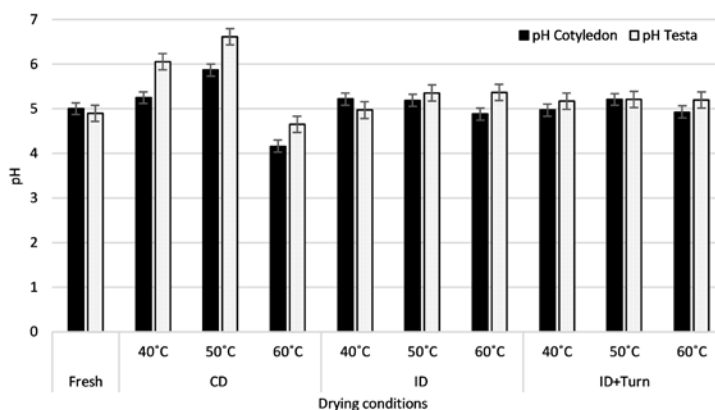
Fig. 2. pH values of bean testa and cotyledon
CD-Continuous ID-Intermittent ID+Turn (Intermittent with Turning)

While trends in L^*, a^*, *Hue* and *Chroma* values were not apparent, it was noted that colour attribute values were lower in all beans dried at 40°C. For beans dried at 50°C, no significant differences were seen amongst key flavour attributes such as Cocoa flavour, Bitterness, Total Fruity and Total Floral notes. Astringency scores ranged from 7.4 in beans dried continuously to 7.0 and 6.9 in beans dried intermittently, without and with turning. Total acidity scores were low, ranging from 2.4 to 3.6.

Conclusions

Drying temperature had a significant impact on the drying rate and pH of beans dried continuously. Drying rates were optimized at 50°C, with these beans being least acidic. Increasing the drying temperature to 60°C resulted in shrivelled beans which were most acidic. With the exception of beans dried at 40°C, the introduction of a rest interval and turning of beans did not improve moisture loss. It is possible that improved moisture movement due to a rest interval during traditional sun-drying may be due to the low

temperatures (below 50°C) experienced during sun-drying, as well as the depth of bean layer during drying.

Nomenclature

A - drying constant
a_w - water activity
D_{eff} - diffusion coefficient (m^2/s)
DM - dry matter (g)
E_a - activation energy (J/mol)
FW - fresh weight (g)
k - drying rate constant (1/min)
L - half-thickness of sample (m)
L^*, a^*, b^* - colour attributes
M - moisture content (g H_2O/g DM)
MR - moisture Ratio ($M-M_e/M_o-M_e$)
R^2 - coefficient of determination
e - equilibrium
o - initial

Acknowledgement

References

[1] Hii, C.L. Modelling of the cocoa drying kinetics. Malaysian Cocoa Journal 2008, 4, 51-59.

[2] Faborode, M.O.; Favier, J.F.; Ajayi, O.A. On the effects of forced air drying on cocoa quality. Journal of Food Engineering 1995, 25(4), 455-472.

[3] Ndukwu, M.C. Effect of drying temperature and drying air velocity on the drying rate and drying constant of cocoa bean. Agricultural Engineering International: CIGR Journal 2009, XI (1091), 1-7.

[4] Chineye, N.M.; Ogunlowo, A.S.; Olukunle, O.J. Cocoa bean (*Theobroma cacao* L.) drying kinetics. Chilean Journal of Agricultural Research 2010, 70(4): 633-639.

[5] Musa, N.A. Drying characteristics of cocoa beans using an artificial dryer. Journal of Engineering and Applied Sciences 2012, 7(2), 194-197.

[6] Hii, C. L.; Law, C.L.; Cloke, M.; Suzannah, S. Thin layer drying kinetics of cocoa and product quality. Biosystems Engineering 2009, 102, 153-161.

[7] Hii, C. L.; Law, C.L.; Cloke, M. Modeling using a new thin layer drying model and product quality of cocoa. Journal of Food Engineering 2009, 90, 191–198.

[8] Zahouli, G.I.B.; Tagro Guehi, S.; Monké Fae, A.; Ban-Koffi, L.; Gnopo Nemlin, J. Effect of Drying Methods on the Chemical Quality Traits of Cocoa Raw Material. Advance Journal of Food Science and Technology 2010, 2(4), 184-190.

[9] Rodriguez-Campos, J.; Escalona-Buendía, H.B.; Contreras-Ramos, S.M.; Orozco-Avila, I.; Jaramillo-Flores, E.; Lugo-Cervantes, E. Effect of fermentation time and drying temperature on volatile compounds in cocoa. Food Chemistry 2012, 132(1), 277-288.

[10] Guehi, T.S.; Zahouli, I.B.; Ban-Koffi, L.; Fae, M.A.; Nemlin, J.G. Performance of different drying methods and their effects on the chemical quality attributes of raw cocoa material. International Journal of Food Science and Technology 2010, 45(8), 1564-1571.

[11] Mujaffar, S.; Sukha, D.; Ramroop, A. Comparison of the drying behavior of fermented cocoa (*Theobroma cacao* L.) beans dried in a cocoa house, greenhouse and mechanical oven. In Proceedings of the International Symposium on Cocoa Research, Lima, Peru, November 13-17, 2017; 1-7.

[12] Konica Minolta Sensing Incorporated. Precise Color Communication; Konica Minolta Sensing Incorporated: Osaka, Japan, 2003.

[13] Sukha, D.A.; Butler, D.R.; Umaharan, P.; Boult, E. The use of an optimized organoleptic assessment protocol to describe and quantify different flavour attributes of cocoa liquors made from Ghana and Trinitario beans. European Food Research and Technology 2008, 226(3), 405-413.

[14] Hii, C. L.; Law, C.L.; Suzannah, S. Drying kinetics of the individual layer of cocoa beans during heat pump drying. Journal of Food Engineering 2012, 108, 276–282.

[15] Jinap, S.; Thien, J.; Yap, T.N. Effect of drying on acidity and volatile fatty acids content of cocoa beans, Journal of the Science of Food and Agriculture 1994, 65(1), 67-75.

Microencapsulation of pumpkin seed oil by spray dryer under various process conditions and determination of the optimal point by RSM

Geranpour, M. [a*]; Emam-Djomeh, Z.[b]; Asadi, G.[a]

a Department of Food Science and Technology, Science and Research Branch, Islamic Azad University, Tehran, Iran.
b Transfer Phenomena Laboratory (TPL), Department of Food Science, Technology and Engineering, University of Tehran, Iran.

*E-mail of the corresponding author: m.geranpour@yahoo.com

Abstract

The objective of this research was to microencapsulating the pumpkin seed oil (PSO) by the spray dryer and also investigating the effects of some process conditions on physicochemical properties of PSO microparticles. Inlet drying air temperature (140-180°C), aspirator rate (55-75%), and peristaltic pump rate (5-15%) effects were studied. Moisture content (%W.b.), Microencapsulation Efficiency (MEE, %) and Peroxide value (POV, meq/kg sample) considered as model responses. Consequently, the ideal drying state for microencapsulation of PSO as a result of optimizing by Response Surface Methodology (RSM) determined with the aim of minimizing the Moisture content and POV and maximizing the MEE.

Keywords: Microencapsulation; spray dryer; pumpkin seed oil; optimization; RSM.

1. Introduction

pumpkin (Cucurbita pepo.) seed oil is a functional food and comprises various bioactive components such as vitamins[1], poly and monounsaturated fatty acids, proteins and minerals[2,3]. The major part of fatty acids of pumpkin seed oil (PSO) is linoleic acids (Omega-6 fatty acids) which is one of the most beneficial substances for human health[2]. Moreover, it has positive effects such as having anti-inflammatory and diuretic properties[4], decreasing total and LDL cholesterol levels, improving treatment of benign prostate hyperplasia[4], relieving diabetes by improving hypoglycemic activity[5], etc. In addition, utilization of PSO from pumpkin seeds as agro-industrial wastes, reduce the growth of environmental problems[6]. Microencapsulation is considered as an approach, which protects bioactive compounds, improves their stability and even can mask the unpleasant feelings during eating[7]. This process incorporates food ingredients in small capsules that may range from micrometer to millimeter in size and may have different shapes[8]. Among the numerous developed microencapsulation techniques, spray drying is the oldest and most widely used procedure in food industrial sector due to providing high-quality products[9]. Therefore the aim of this study was to investigate the process conditions as independent variables on dependent variables and suggest the optimal point for producing the PSO microencapsulated powder.

2. Materials and Methods

2.1. Materials

Pure PSO (Cucurbita pepo species, Styarica variety) was purchased after cold pressed process from Zardband Co.(Tehran, Iran). The used wall materials were gum Arabic (GA), maltodextrin DE-6 (MD), and whey protein concentrate (WPC) with 80% protein supplied by Merck Co.(Darmstadt, Germany), Roquette Co.(Lestrem, France), and Hilmar Ingredients Co.(California, USA), respectively.

2.2. Emulsion preparation

The ratio of 10% core material, 20% wall material, and 70% water was used to prepare the emulsion[10]. Utilizing the formulation of 17% GA, 17% WPC, and 66% MD, wall materials were dissolved in distilled water one day before emulsification to access complete hydration. PSO was gradually added to the barricade material solution and homogenized at 1000 rpm for 5 min using a rotor-stator homogenizer (Ultraturrax Ika T25, Deutschland, Germany) at ambient temperature[11].

2.3. Drying apparatus and Microencapsulation of PSO

laboratory scale dryer (BÜCHI Mini spray dryer B-191, Flawil, Switzerland) equipped with a two-fluid internal mixing nozzle atomizer with 0.7 mm diameter used. Before each

experiment, the dryer run with distilled water about 15 minutes to achieve the steady-state condition. The spray drying conditions examined in this study were inlet drying air temperature (140-180 C), aspirator rate (55-75%), and peristaltic pump rate (5-15%).

2.4. Analysis of microparticles

2.4.2. Moisture content

Moisture content was determined by drying 2 grams of powders at 70 C to constant weight (24 hours) in the oven according to AOAC method (1984) and reported as %W.b[12].

2.4.3. Microencapsulation efficiency

Microencapsulation efficiency (MEE) was measured based on the method described by Bae and Lee[13]. Surface oil was measured by extraction with hexane. According to preliminary tests, PSO is not volatile oil. Thus, total oil weight was assumed to be equal to the initial oil. Consequently, MEE was calculated using the following equation:

$$\text{MEE} = \frac{\text{Total oil} \_ \text{Surface oil}}{\text{Total oil}} \times 100 \qquad (1)$$

2.4.4. Peroxide value

The POV was denoted after 3 months according to ISO 3976/IDF standard 74:2006 method[14], which is based on the co-oxidation of Fe (II) to Fe (III) and formation of the reddish Fe (III)-thiocyanate complex. The absorbance of the samples was read at 500 nm by a spectrophotometer against the blank solution [15]. Finally, the following equations were used to calculate the POV[14]:

$$\text{POV} = \frac{0.5\text{mc}}{55.84\text{m}} \qquad (2)$$

$$\text{mc} = \frac{\text{E}}{\text{b}} \qquad (3)$$

where m is the fat weight expressed as g, 55.84 is the atomic weight of Fe3+, E is the absorbance of the sample determined using a spectrophotometer, and b is the slope of the Fe (III) calibration curve obtained as 0.0276 from its standard plot.

2.4.5. Experimental design

The response surface methodology (RSM) was utilized to investigate the effects of process conditions on dependent variables, and also optimization. For this purpose, the Design-Expert software (State Ease Inc., Minneapolis, USA), version 11 was used and 17 random

runs in 5 central points were designed by Box-Behnken experimental design (BBD) in a full factorial plan. All data in this study were reported as averages of triplicate experiments.

3. Results and Discussion

The results of ANOVA and regression coefficients for the model by eradicating the non-significant terms of responses are listed in Table 1.

Table 1. ANOVA results and regression coefficients for responses surface quadratic model.

Source	DF	Moisture content (%W.b.)			MEE (%)			POV in month 3 (meq.pov/1kg sample)		
		COEF F	SS	P-Value	COEF F	SS	P-Value	COEFF	SS	P-Value
Model		3.18	7.96	0.0177*	78.54	267.74	0.0219*	16.98	90.55	0.0002*
linear										
b_1	1	-0.23	0.44	0.1441	0.029	0.0066	0.9742	0.25	0.51	0.3008
b_2	1	-0.18	0.25	0.2549	2.82	63.51	0.0133*	-1.37	14.99	0.0005*
b_3	1	0.41	1.33	0.024*	2.18	38.15	0.0382*	1.72	23.77	0.0001*
quadratic										
b_{11}	1	-0.25	0.27	0.2397	-1.54	9.96	0.2341	-0.6	1.52	0.095
b_{22}	1	-0.49	0.99	0.0427*	3.07	39.8	0.0353*	-0.26	0.29	0.4255
b_{33}	1	-0.78	2.54	0.0054*	4.2	74.34	0.0093*	1.03	4.49	0.0128*
interaction										
b_{12}	1	0.44	0.78	0.0636	-0.24	0.23	0.8502	2.6	27.03	< 0.0001*
b_{13}	1	-0.5	1.02	0.0401*	0.34	0.45	0.7902	1.11	4.91	0.0104*
b_{23}	1	0.075	0.023	0.7201	-3.15	39.75	0.0354*	-1.83	13.34	0.0007*
Residual	7		1.13			41.12			2.85	
Pure error	4		0.0029			7.98			0.0019	
R^2		0.87			0.86			0.96		
Adj-R^2		0.71			0.69			0.93		
CV (%)		16.36			2.98			3.74		
Adequate precision		6.63			6.78			22.01		

*: significant effect at level p<0.05

The significance of all terms was expressed at a probability (P) level of 0.05. The results showed that the suggested model was quadratic for the whole responses.The following mathematical equation was fitted to data:

$$y = \beta_0 + \beta_1 X_1 + \beta_2 X_2 + \beta_3 X_3 + \beta_{11} X_1^2 + \beta_{22} X_2^2 + \beta_{33} X_3^2 + \beta_{12} X_1 X_2 + \beta_{13} X_1 X_3 + \beta_{23} X_2 X_3 + \varepsilon$$

where βn are constant regression coefficients, y is the predicted response (Moisture content, MEE and POV), and $X_1, X_2,$ and X_3 are the coded independent variables.

3.1. Moisture content

Moisture content varied between 1.19% and 3.35% wet basis. Peristaltic pump rate had the most significant effect (P < 0.05) on the MEE (Fig. 1a). As the inlet air temperature increased, the drying chamber temperature increased, which caused a decrease in the

moisture content. By raising aspirator rate, the supplied energy in the drying chamber increased and the moisture of droplets in the chamber evaporated more easily. At high peristaltic pump rates and subsequently high atomized emulsion in the drying chamber, the contact time of droplets with the hot drying air reduced; hence, their interior evaporation retarded. This procedure resulted in the generation of microcapsules with high moisture content at high feed flow rates. Similar results were reported by Goula et al.[16], Aghbashlo et al.[10], and Muzaffar and Kumar[17] about the effect of inlet air temperature, aspirator rate and peristaltic pump rate on spray drying, respectively. Fig. 1b shows the levels of inlet air temperature and peristaltic pump rate on moisture content.
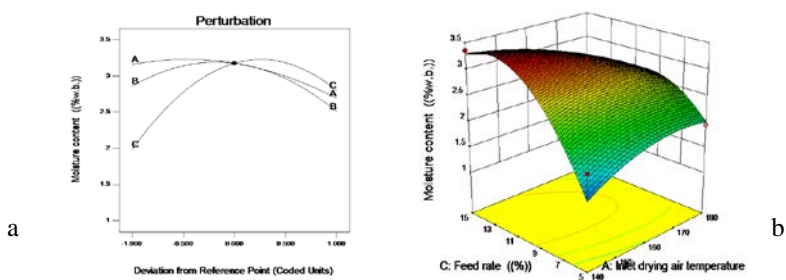
Fig.1. Effect of variables on moisture content(a), 3D response surface plot for moisture content (b).

3.2. Microencapsulation efficiency

The MEE varied from a minimum value of 75.36% to a maximum value of 90.95%. As demonstrated in Fig. 2a, increasing both aspirator rate and peristaltic pump rate directly affected and increased MEE. Fig. 2b shows the 3D surface response for MEE.
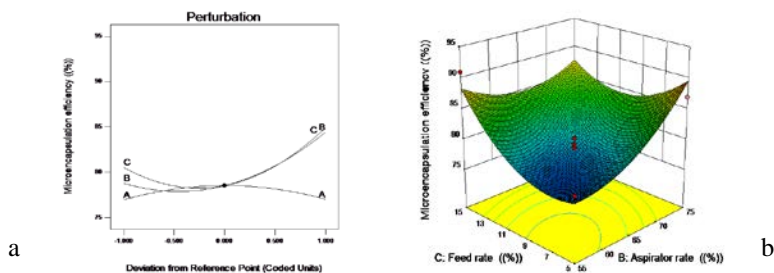
Fig. 2. **Effect of independent variables on MEE (a), 3D response surface plot for MEE (b).**

The fast formation of crust at early stages as a result of enhancing aspirator rate plays a vital role in generating particles with high MEE[18]. This acceleration in crust formation diminished diffusion of oil to the surface of microcapsules and consequently increased MEE. This was similar to the explanation of Aghbashlo et al in 2012[10]. The higher velocity of feed flow rate resulted in producing smaller particles during the drying process.

Break of the particles as the result of their collision with each other in the drying chamber was the main reason for this phenomenon[19], which hastened the crust layer formation. Moreover, it reduced the amount of surface oil and correspondingly enhanced MEE.

3.3. Peroxide value

After 3 months, the POV of the produced PSO microcapsules was found to be between 12.11 and 23.08 meq/kg. Inlet air temperature was an ineffective parameter in altering the POV ($p > 0.05$; Fig. 3a). The 3D response surfaces for powder POV are illustrated in Fig. 3b, 3c, and 3d. As discussed earlier, increased aspirator rate increased the MEE (Fig. 2a) and led to high oil protection against oxidation and resulted in the reduction of POV (Fig. 3a). The presence of produced particles with high POV at high ranges of feed flow rate probably might be attributed to the chemical and physical changes taking place in the formation of the capsule walls. The higher the accumulated droplets in the drying chamber as a result of increasing the feed flow rate, the lower was the time spent for drying, which led to the appearance of the crust with insufficient solidity on the outer layer of particles. Aghbashlo et al.[10] reported similar results for POV, which was influenced by feed flow rate.
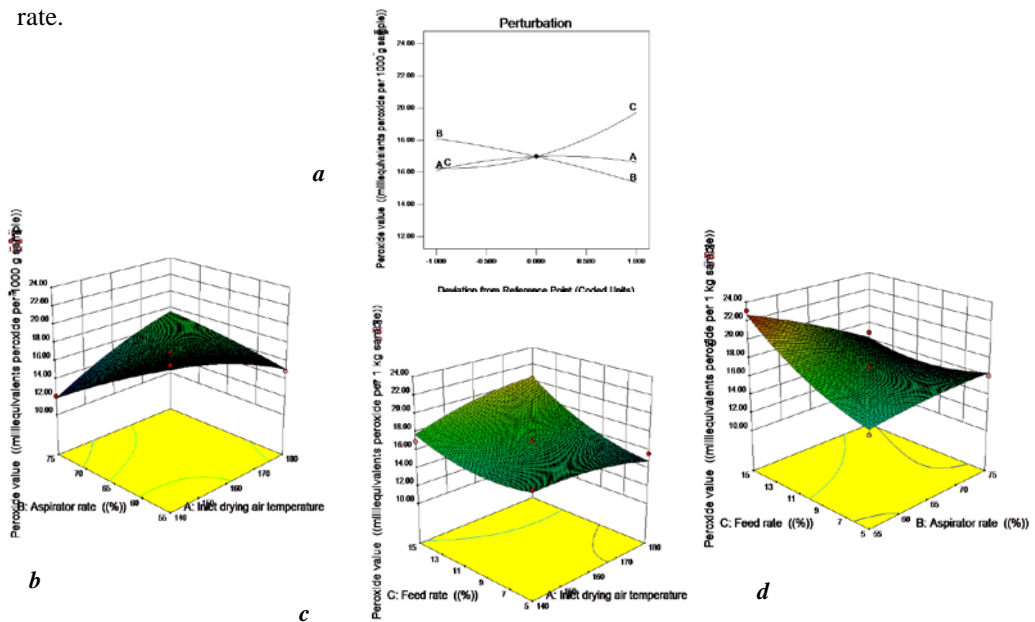
Fig. 3. Effect of independent variables on POV(a), 3D response surface plots for POV (b,c, and d.).

The maximum and the minimum determined POV after 3 months was 23.08 meq/kg and 12.11 meq/kg, respectively. The microencapsulated powder was produced again under process conditions which the mentioned POV was determined, and the POV measured immediately were 9.03 and 6.93 meq/kg, respectively. Comparing these amounts of POV before and after the passage of the time represented that microencapsulation by a spray

dryer, could protect the PSO against the huge amount of lipid oxidation, which might occur for the un-encapsulated oil after three months.

3.4. Optimization

In order to achieve the best conditions for a process, optimization which is an essential tool to obtain acceptable results from various processes, used. As the higher amounts of MEE and lower amounts of POV lead to lower deterioration of pumpkin seed oil by oxygen and lengthened storage time of the product[10], optimization performed to minimizing the Moisture content as a characteristic of the drying process, maximizing the MEE and minimizing the POV. Consequently, the ideal drying state for microencapsulation of PSO was suggested by RSM to be inlet air temperature of 140 °C, aspirator rate of 75 %, and peristaltic pump rate of 5% to offer moisture content of 0.27 (%W.b.), microencapsulation efficiency of 88.60%, and peroxide value of 13.97 meq/kg sample with the total desirability of 89%.

4. Conclusion

The research indicates that spray drying is the suitable method to obtain the high amount of MEE in microencapsulating of PSO under the studied process conditions. Spray drying conditions such as aspirator rate and peristaltic pump rate significantly affected the characteristics of PSO microcapsules. Inlet air temperature had no significant effect on alteration of output responses, which could be related to its low range of variation (140–180 °C).Microencapsulation by a spray dryer could protect the PSO against the high amount of lipid oxidation according to POV analysis.

5. References

[1] Stevenson, D. G., Eller, F. J., Wang, L., Jane, J. L., Wang, T. and Inglett, G. E. Oil and tocopherol content and composition of pumpkin seed oil in 12 cultivars. Journal of Agricultural and Food Chemistry. 2007, 55(10), 4005-4013.

[2] Xanthopoulou, M.N., Nomikos,T., Fragopoulou,E., Antonopoulou, S. Antioxidant and lipoxygenase inhibitory activities of pumpkin seed extracts. Food research international. 2009, 42, 641-646.

[3] Gohari Ardabili, A., Farhoosh, R., and Haddad Khodaparast, M. H. Chemical composition and physicochemical properties of pumpkin seeds (Cucurbita pepo Subsp. pepo Var. Styriaka) Grown in Iran. Journal of Agricultural Science and Technology. 2011, 13, 1053-1063.

[4] Fruhwirth, G. O., & Hermetter, A. Seeds and oil of the Styrian oil pumpkin: Components and biological activities. European Journal of Lipid Science and Technology. 2007, 109(11), 1128-1140.

[5] Fu, C., Shi, H., Li, Q. A review on pharmacological activities and utilization technologies of pumpkin. Plant Foods for Human Nutrition. 2006, 61(2), 73-80.

[6] Da silva, A. C. and Jorge, N. Bioactive compounds of the lipid fractions of agro-industrial waste. Food Research International. 2014, 66(1), 493- 500.

[7] Nedovic, V., Kalusevic, A., Manojlovic, V., Levic, S., & Bugarski, B. An overview of encapsulation technologies for food applications. procedia Food Science. 2011, 1 (1), 1806-1815.

[8] Aberkane, L., Roudaut, G., Saurel, R. Encapsulation and oxidative stability of PUFA - rich oil microencapsulated by spray drying using pea protein and pectin. Food and Bioprocess Technology. 2014, 7(5), 1505-1517.

[9] Tonon R. V., Grosso, C. R. F., Hubinger, M. D. Influence of emulsion composition and inlet air temperature on the microencapsulation of flaxseed oil by spray drying. Food Research International. 2011, 44(1), 282-289.

[10] Aghbashlo, M., Mobli, H., Madadlou, A. & Rafiee, S. The correlation of wall material composition with flow characteristics and encapsulation behavior of fish oil emulsion. Food Research International. 2012, 49(1), 379-388.

[11] Gallardo, G., Guida, L., Martinez, V., Lopez, M. C., Bernhardt, D., Blasco, R., Pedroza-Islas , R., & Hermida, L. G. Microencapsulation of linseed oil by spray drying for functional food application. Food Research International. 2013, 52(2), 473-482.

[12] AOAC International, Official analytical methods of AOAC International. MD, USA: Gaithersburg. 1984.

[13] Bae, E. K., & Lee, S. J. Microencapsulation of avocado oil by spray drying using whey protein and maltodextrin. Journal of Microencapsulation. 2008, 25(8), 549-560.

[14] ISO 3976/IDF 74. Milk fat - Determination of peroxide value. (second edition). 2006.

[15] Partanen, R., Raula, J., Seppänen, R., Buchert, J., Kauppinen, E. and Forssell, P. Effect of relative humidity on oxidation of flaxseed oil in spray dried whey protein emulsions. Journal of Agricultural and Food Chemistry. 2008, 56(14), 5717-5722.

[16] Goula, A. M., Adamopoulos, K. G. & Kazakis, N. A. Influence of spray drying conditions on tomato powder properties. Drying Technology. 2004, 22, 1129-1151.

[17] Muzaffar, K., Kumar, P. Parameter optimization for spray drying of tamarind pulp using response surface methodology, Powder technology. 2015, 279, 179-184.

[18] Bhandari, B. R., Dumoulin, E. D., Richard, H. M. J., Noleau, I., Lebert, A. M. Flavor encapsulation by spray drying – application to citral and linalyl acetate. Journal of Food Science, 1992, 57(1), 217-221.

[19] Seddighi pashaki, A., Emam-djomeh, Z., Askari, G. Evaluation of spray drying parameters on physicochemical properties of seedless black Barberry (Berberis Vulgaris L.) juice. 20th International Drying Symposium. 2016, Japan.

Nano spray drying of pharmaceuticals

Arpagaus, C.

NTB University of Applied Sciences of Technology Buchs, Institute for Energy Systems, Werdenbergstrasse 4, 9471 Buchs, Switzerland, +41 81 755 34 94

E-mail of the corresponding author: cordin.arpagaus@ntb.ch

Abstract

Spray drying plays a crucial role in the processing of pharmaceutical products such as pills, capsules, and tablets as it is used to convert drug containing liquids into dried powdered forms. Nano spray drying is in particular used to improve drug formulation by encapsulating active ingredients in polymeric wall materials for protection and delivering the drugs to the right place and time in the body. The nano spray dryer developed in the recent years extends the spectrum of produced powder particles to the submicron- and nanoscale with very narrow size distributions and sample quantities in the milligram scale at high product yields. This enables the economical use of expensive active pharmaceutical ingredients and pure drugs. The present paper explains the concept of nano spray drying and discusses the influence of the main process parameters on the final powder properties like particle size, morphology, encapsulation efficiency, and drug loading. Application results of nano spray drying for the formulation and encapsulation of different drugs are reviewed.

Keywords: nano spray drying; pharmaceuticals; drug encapsulation; particle size; powder

1. Introduction

Spray drying is a simple, fast, and scalable drying technology that is well established in the pharmaceutical industry. Many pharmaceutical products such as pills, capsules, and tablets are processed in dried powdered form. In the course of the rapid progress of nanocapsulation techniques, nano spray drying technology has developed to improve the formulation and administration of drugs with solid colloidal particles in the submicron size range. It enables the encapsulation of active ingredients in polymeric wall materials providing enhanced environmental protection (e.g. against oxidation, light, and temperature), stability, handling, storage, and controlled drug release properties. The nanonization and structual change improves the particle solubility and redispersibility of the final drug product in aqueous solutions. This study explains the concept of nano spray drying, the influence of the main process parameters on the powder properties (e.g. particle size, morphology, encapsulation efficiency, drug loading), and discusses different pharmaceutical applications. More detailed information on the formation of nanocapsules by nano spray drying can be found in several review studies [1–12], in particular in a recently published book chapter by Arpagaus et al. [1].

2. Process Parameters of a Nano Spray Dryer

Figure 1 shows the functional principle of a nano spray dryer and the adjustable process parameters and formulation variables. The droplet generation is based on vibrating mesh technology ejecting precisely sized droplets into the drying chamber.
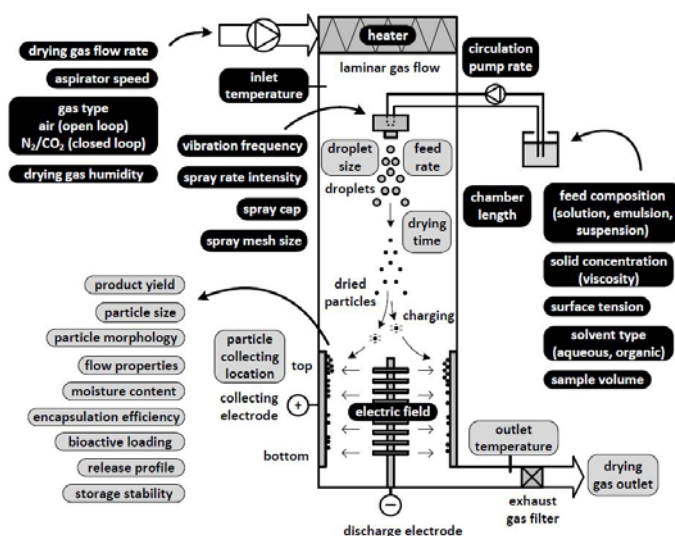
Figure 1 Process parameters and formulation variables for a nano spray dryer [1].

21ST INTERNATIONAL DRYING SYMPOSIUM
EDITORIAL UNIVERSITAT POLITÈCNICA DE VALÈNCIA

With a 4.0 µm spray mesh approximately 3 to 8 µm water droplets are produced [1,8]. The dried particles are captured in an electrostatic particle collector providing high particle collection efficiency. The cooling effect of the evaporating solvent keeps the droplet temperature low, so that heat sensitive products can be dried with negligible degradation. Table 1 povides an overview of the main process parameters and their influence on the final powder product. The thickness of each arrow illustrates the strength of the relationship. The key parameters controlling the final particle size are the spray mesh size and the solid concentration. The submicron size is typically reached when a 4.0 µm spray mesh and diluted solutions of 0.1 to 1% (w/v) are used.

Table 1 Influence of the main process parameters in nano spray drying (⬆/⬇ strong, ↑/↓ weak increasing/decreasing influence, – minimal or no influence) [1].

Process parameter	Outlet temperature	Droplet size	Particle size	Feed rate	Moisture content	Yield	Stability
Drying gas flow rate ↑	⬆	–	–	–	⬇	–	–
Drying gas humidity ↑	↑	–	–	–	⬆	↓	–
Inlet temperature ↑	⬆	–	↑	–	↓	↑	⬇
Spray mesh size ↑	↓	⬆	⬆	⬆	–	–	↑
Spray rate intensity ↑	⬇	↑	↑	⬆	↑	–	⬇
Circulation pump rate ↑	–	↑	↑	↑	–	–	↑
Solid concentration ↑	↑	–	⬆	⬇	↓	↑	–
Surfactant / stabilizer ↑	–	↓	↓	↑	–	↑	⬆
Solvent instead of water	⬆	↓	↓	↑	⬇	↑	–

Depending on the application, an optimized set of process parameters can be found, e.g. by design of experiment studies [1]. Organic solvents like dichloromethane, acetone, ethanol, methanol, acetonitrile, ethylacetate, and mixtures thereof with water are typically used in nano spray drying of pharmaceuticals. The selection is based on the drug solubilization and the encapsulating wall materials, as well as on the required drying temperatures. For acqueous applications, the outlet temperatures range between 28 and 59 °C [2]. The optimal drying temperatures of for example poly(lactic-co-glycolic acid) (PLGA) dissolved in dichloromethane lies in a range of 29 to 32 °C [12].

Numerous excipients, dispering agents, binders and stabilizers are applied in drug formulation studies, including water-soluble saccharides (e.g. arabic gum, alginate, chitosan, cyclodextrin, cellulose derivatives, modified starch, maltodextrin, pectin, mannitol, lactose trehalose), proteins (i.e. gelatin, serum albumin, whey protein, sodium caseinate, silk fibroin, leucine), water-soluble synthetic polymers (e.g. poly(vinyl alcohol), poly(ethylene glycol) or poly(acrylic acid) (Carbopol)), hydrophobic synthetic polymers (e.g. PLGA, poly(ε-caprolactone), poly(vinyl pyrrolidone) (Kollidon), Eudragit), and fats (e.g. stearic acid and glyceryl behenate (Compritol)).

The morphology of particles prepared by nano spray drying depends on the drying conditions and the feed properties. Dense, hollow, porous, composites, and encapsulated structures (i.e. single-core, multi-core, irregular, or multi-walled) with spherical, wrinkled, shriveled, or even doughnut-like shapes can be obtained [1]. Figure 2 illustrates some examples of nano spray dried particles including salbutamol, albuterol in mannitol, cyclosporine in PLGA, trehalose, β-galactosidase in trehalose, and bovine serum albumin.
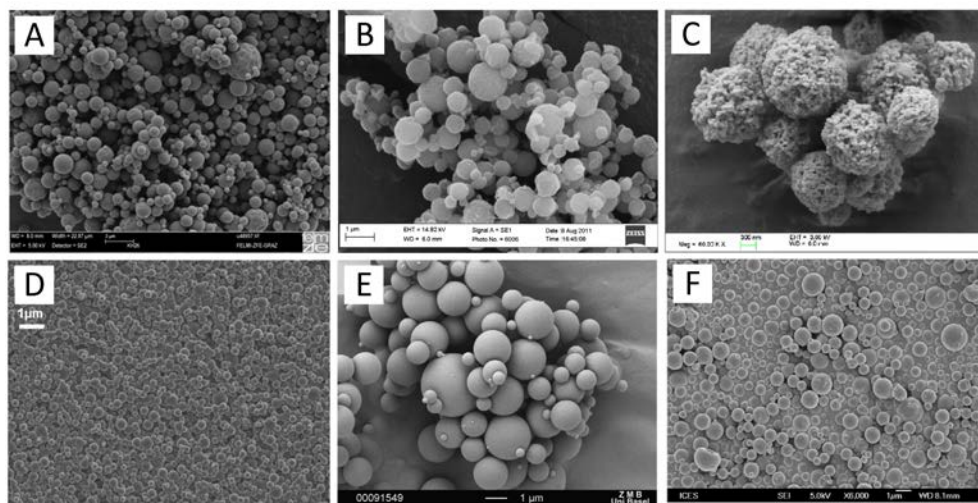
Figure 2 Examples of nano spray dried particles: A: Salbutamol sulfate (1% solid concentration, nano spray dried at 100 °C) [13]; B: Albuterol sulfate in mannitol, L-leucine and poloxamer 188 (30:48:20:2 mixing ratio, 0.5% in water-ethanol solution (80:20), 70 °C) [14]; C: Cyclosporin in PLGA (50:50, 15 kDa, dissolved in DCM, 29°C) [12]; D: Trehalose with addition of 0.005% polysorbate 20 (0.1%, 120 °C) [8]; E: β-galactosidase in trehalose (1:2 mixing ratio, 5%, 80°C) [11]; F: Bovine serum albumin with 0.05% Tween 80 (0.5%, 120 °C) [6].

In general, slow drying leads to more compact particles, while fast and high temperature drying favours the formation of hollow particles with thin shells. Surfactants balance the surface-to-viscous forces inside of the drying droplet and enable the formation of a smooth spherical surface. Composite particles prepared from suspensions and nano spray drying provide a high specific surface area. Most nano spray dried drugs tend to be amorphous due to the too short drying time to form crystalline structures. To prevent recrystallization, the dried powders are stored under dry and controlled conditions.

3. Applications of Nano Spray Dried Pharmaceuticals

The number of publications on nano spray dried pharmaceuticals has risen sharply after the market launch of the Nano Spray Dryer B-90 in 2009 [1]. The formulations contain drugs and excipients for the treatment of various diseases, including

- *asthma* (e.g. salbutamol, terbutaline, or fluticasone),

- *inflammation* (e.g. dexamethasone and azithromycin, or pain and fever reducer indomethacin and nimesulide),

- *cystic fibrosis* (e.g. antibacterial dexketoprofen in Kollidon and Eudragit nanoparticles, or azithromycin in leucine),

- *diabetes* (e.g. sitagliptin, vildagliptin, and metformin in mucoadhesive Carbopol and gelatin),

- *pulmonary arterial hypertension* (e.g. resveratrol in poly(caprolactone), or sildenafil in PLGA),

- *tuberculosis* (e.g. capreomycin or pyrazinamide in L-leucine, or ethambutol mixed with chitosan carrier particles),

- *Alzheimer's and Parkinson's diseases* (e.g. nanocrystals of calpain inhibitor steroids),

- *breast cancer* (e.g. simvastatin loaded PLGA particles), or *lung cancer* (e.g. methotrexate, carboplatin in gelatine, or paclitaxel),

- *bacterial infections* (e.g. amoxicillin, ciprofloxacin, gatifloxacin, clarithromycin, or levofloxacin),

- *fungal infections* (e.g. antifungal griseovulfin)

- *ophthalmic disorders* (e.g. calpain inhibitor nanocrystals or dirithromycin incorporated in Kollidon),

- *high blood pressure* (e.g. nimodipine in PLGA or pure nicergoline nanoparticles),

- *congestive heart failure* and *edema* (e.g. diuretic furosemide).

The drug-loaded nano spray dried particles are administered in various ways underlining the versatility of the applications, such as mainly *pulmonary* (e.g. optimized respirable particles of 1 to 5 µm size) and *oral*, but also *intravenous* (e.g. simvastatin in PLGA as cancer chemotherapeutics, antipsychotic clozapine and risperidone in PLGA, or small interfering RNAs loaded in human serum albumin particles to treat genetic disorders), *topically* as creams to the skin (e.g. anti-inflammatory dexamethasone, antibacterial gentamicin in

gelatin-pectine, amoxicillin loaded chitosan, antifungal econazole in cyclodextrin, soy isoflavones for skin cancer treatment or as anti-ageing agent), or as nanoparticulate powder (e.g. as a wound dressing during surgery), *ophthalmic* (e.g. anti-inflammatory steroids in eye drop solutions, or dirithromycin to treat ocular bacterial infections), *intraperitoneal* (e.g. encapsulated paclitaxel as cytostatic in anticancer therapy), *intravesical* (e.g. as drug delivery system to treat local bladder diseases), and even *cerebral* (e.g. with nimodipine in PLGA regulating the dilatation of blood vessels).

Typical experimental process parameters for nano spray drying are listed in Table 2 and can be used as first guess values for applying identical or similar substances. The main organic solvents used to dissolve poorly water soluble drugs are ethanol, acetone, and DCM. With highly diluted solutions containing 0.1 to 1% (w/v) solids concentrations, finest solid particles down to 100 nm can be obtained by nano spray drying.

Table 2 Typical experimental process parameters for nano spray drying of pharmaceuticals.

Solvent	Inlet drying temperature [°C]	Outlet drying temperature [°C]	Drying gas type	Drying gas flow rate [L/min]	Solid concentration [% w/v]	Spray mesh size [μm]	Feed Rate [mL/h]
Water	60 to 120	30 to 60	Air	100 to 140		4.0	5 to 25
Ethanol	50 to 110	30 to 50	Air	100 to 120	0.1 to 10	5.5	20 to 65
Acetone	40 to 70	25 to 40	Inert gas	90 to 120		7.0	30 to 160
DCM	30 to 50	20 to 35	(N_2/CO_2)	80 to 120			

Pure drug particles in the nanosize dimensions and the amorphous state offer higher absorption rates and bioavailability, and encourage future developments in this research area. Nanocapsules, with their reduced size and large specific surface area, provide pronounced improvement in controlled drug release and bioavailabilty. This enables the generation of target drug delivery systems. Under optimized conditions uniquely high product yields of about 76 to 96% can be achieved to process small sample amounts of substances in the range of 10 mg to 2.5 g.

Variations in the yield may occur due to particle depositions around the spray cap and the chamber walls, nozzle blockage, or due to losses during the manual collection of the powder with a rubber spatula.

However, the ability to process small sample amounts makes a nano spray dryer very suitable for testing valuable biological materials such as for example monoclonal antibodies, recombinant proteins, or siRNA-based therapeutics. Moreover, nano spray drying enables the encapsulation of drugs in polymers with high efficiency of over 95% and adjustable drug loading.

4. Conclusions

Nano spray drying has been successfully applied for a wide range of pharmaceutical applications, such as increasing the bioavailability of poorly soluble drugs by nanoisation and structural modification, as well as the encapsulation of nanoparticles, nanoemulsions and nanosuspensions in biocompatible polymeric wall materials for sustained drug release. Encapsulation efficiencies of over 95% are achieved by adjustable drug loadings. Smallest sample amounts ranging from 10 mg to 2.5 g with uniquely high yields of over 95% can be processed, which enables the economical use of valuable active pharmaceutical ingredients.

Compared to conventional spray drying processes, nano spray drying relies on vibrating mesh technology to produce an ultrafine spray. A highly efficient electrostatic powder collector to extend the size spectrum of separable particles to the nanoscale.

The most important adjustable process parameters are the drying gas temperature, the drying gas flow rate, the spray mesh size, the solvent type, the solids concentration in the feed, and the selection of the corresponding exipients, stabilizers and surfactants. Depending on the application, an optimized set of parameters can be found. Submicron spray dried particles can be formed down to a size of only 100 nm with diluted solutions of 0.1 to 1% (w/v) solids concentration. Different particle morphologies can be created, including dense, hollow and porous particles with spherical, wrinkled, or donut shapes.

The drying process is gentle and contributes to maintaining the stability and activity of heat-sensitive materials, such as peptides, proteins, hormones and amino acids. The prepared drug loaded particles are administered in various ways, including pulmonary, oral, intravenous, topically, ophthalmic, intraperitoneal, intravesical, or even cerebral, which underlines the versatility of the nano spray drying technology.

To further explore the potentials of nano spray drying future research should focus on the further commercialization of this technology to an industrial scale. There is an increasing need for scale-up.

The main application trends are in the areas of pulmonary drug delivery, nanotherapeutics, the encapsulation of nanoemulsions with poorly water-soluble active ingredients and the formulation of nanocrystals for a higher bioavailability.

5. References

[1]   Arpagaus, C.; John, P.; Collenberg, A. and Rütti, D. Chapter 10: Nanocapsules formation by nano spray drying, in *Nanoencapsulation technologies for the food and nutraceutical industries*, S.M. Jafari, ed., Elsevier Inc., 2017, 346–401.

[2]   Arpagaus, C. A Novel Laboratory-Scale Spray Dryer to Produce Nanoparticles, Drying Technology 2012, 30, 1113–1121.

[3]   Arpagaus, C. Nano Spray Dryer B-90: Literature review and applications, best@buchi Information Bulletin, Number 63/2011, 2011, .

[4]   Arpagaus, C.; Rütti, D. and Meuri, M. Chapter 18: Enhanced Solubility of Poorly Soluble Drugs Via Spray Drying, in *Drug Delivery Strategies for Poorly Water-Soluble Drugs*, D. Douroumis and A. Fahr, eds., John Wiley & Sons, Ltd., 2013, 551–585.

[5]   Wong, T.W. and John, P. Advances in Spray Drying Technology for Nanoparticle Formation, in *Handbook of Nanoparticles*, M. Aliofkhazraei, ed., Springer International Publishing, 2015, 1–16.

[6]   Lee, S.H.; Heng, D.; Ng, W.K.; Chan, H.-K. and Tan, R.B.H. Nano spray drying: A novel method for preparing protein nanoparticles for protein therapy, International Journal of Pharmaceutics 2011, 403, 192–200.

[7]   Li, X.; Anton, N.; Arpagaus, C.; Belleteix, F. and Vandamme, T.F. Nanoparticles by spray drying using innovative new technology: The Büchi Nano Spray Dryer B-90, Journal of Controlled Release 2010, 147, 304–310.

[8]   Schmid, K.; Arpagaus, C. and Friess, W. Evaluation of the Nano Spray Dryer B-90 for pharmaceutical applications, Pharmaceutical Development and Technology 2011, 16, 287–294.

[9]   Schmid, K.; Arpagaus, C. and Friess, W. Evaluation of a Vibrating Mesh Spray Dryer for Preparation of Submicron Particles, Respiratory Drug Delivery 2009, 323–326.

[10]   Arpagaus, C. Spray Drying R&D Solutions – BÜCHI's Nano Spray Dryer: A world novelty in laboratory scale, ONdrugDelivery, March 2010, page 30, available on www.ondrugdelivery.com, 2010, , pp. 40–41.

[11]   Bürki, K.; Jeon, I.; Arpagaus, C. and Betz, G. New insights into respirable protein powder preparation using a nano spray dryer, International Journal of Pharmaceutics 2011, 408, 248–256.

[12]   Schafroth, N.; Arpagaus, C.; Jadhav, U.Y.; Makne, S. and Douroumis, D. Nano and microparticle engineering of water insoluble drugs using a novel spray-drying process, Colloids and Surfaces B: Biointerfaces 2012, 90, 8–15.

[13]   Littringer, E.M.; Zellnitz, S.; Hammernik, K.; Adamer, V.; Friedl, H. and Urbanetz, N. a. Spray Drying of Aqueous Salbutamol Sulfate Solutions Using the Nano Spray Dryer B-90 - The Impact of Process Parameters on Particle Size, Drying Technology 2013, 31, 1346–1353.

[14]   Son, Y.-J.; Longest, P.W.; Tian, G. and Hindle, M. Evaluation and modification of commercial dry powder inhalers for the aerosolization of a submicrometer excipient enhanced growth (EEG) formulation, European Journal of Pharmaceutical Sciences 2013, 49, 390–399.

21ST INTERNATIONAL DRYING SYMPOSIUM
EDITORIAL UNIVERSITAT POLITÈCNICA DE VALÈNCIA

Evolution of "Chili" Tunisian landrace durum wheat sprouts properties after drying

Jribi, S.[a*]**; Gliguem, H.**[a]**; Nagy, A.**[b]**; Zsolt, N.G.**[b]**; Szalóki-Dorkó, L.**[b]**; Naàr, Z.**[b]**; Bata-Vidàcs, I.**[c]**; Marzougui, S.**[d]**; Cserhalmi, Z.**[b]**; Debbabi, H.**[a]

[a] National Institute of Agronomy of Tunisia (INAT), Research Unit UR17AGR01 "Innovation & Tradition", University of Carthage, 43 Avenue Charles Nicolle, 1082 Tunis, Tunisia.
[b] Food Science Research Institute, National Agricultural Research and Innovation Centre, Herman Otto utca 15, H-1022 Budapest, Hungary
[c] Agro-Environmental Research Institute, National Agricultural Research and Innovation Centre, Herman Otto utca 15, H-1022 Budapest, Hungary
[d] National Institute of Cereal Crops (INGC), 8170 Bou Salem, Tunisia.

*E-mail of the corresponding author: Sarra.jribi@gmail.com

Abstract

Sprouting is a green technology contributing in improving cereals and pulses nutritional properties. However sprouts have a high water content limiting their shelf-life. This research focused on the impact of drying technology on physico-chemical, functional and nutritional properties of Tunisian landrace durum wheat (Triticum durum)"Chili" sprouts for their use as a functional ingredient. Three technologies were evaluated: lyophilisation, micro-wave vacuum drying and oven drying at 50°C. Sprouted seeds flour properties were significantly (p<0.05) affected by the drying methods used. Lyophilisation led to the highest preservation of bioactive compounds followed by micro-wave vacuum drying. The way of evolution of physico-chemical and functional properties depended on drying method used.

Keywords: Sprouts; drying; functional properties; bioactive compounds.

1. Introduction

Consumers perception of eating has changed: food products are not only needed for satisfying hunger. They are also considered as a key factor in improving health and wellbeing [1]. To satisfy this need, food manufacturers are more and more interested in developing products with added nutritional value. Sprouting is an old practice used to enhance naturally seeds' nutrients and bioactive compounds [2]. Sprouting process increases also seeds moisture content. Thus sprouts couldn't have a long shelf life.

Drying is the simplest and the oldest method used for food preservation [3]. Several methods could be used to dry agricultural products, from home drying (oven, sun) to developed technologies. Depending on the used method, drying may lead to quality degradation [3]. Modifications affecting products' components (proteins, carbohydrates, lipids…) occurring during drying contribute in a modification of dried products functional properties [4]. For food manufacturers, these properties are an important parameter to take into account in food formulation. Particularly, for functional foods development, added to functional properties nutritional ones have a high interest.

The aim of this study is to evaluate the effect of different drying methods (convective hot air, lyophilisation and microwave vacuum drying) on physico-chemical, functional and nutritional properties of "Chili" Tunisian landrace durum wheat sprouts for its further use as a functional ingredient.

2. Materials and Methods

2.1. Plant material

"Chili" Tunisian cultivar of durum wheat (*Triticum durum*) was used in this study. It was introduced from France, and the pure line was registered in 1953 [5]. Samples (Harvested in 2015) were kindly provided by the National Gene Bank of Tunisia (BNG, Tunisia).

2.2. In vitro sprouting

Durum wheat seeds (*Triticum durum*) were germinated for 48h after their disinfection with 1 % (V/V) hypochlorite sodium solution.

2.3. Drying

Three drying methods were tested: convective hot air drying (L-MIM 320, Hungary) at 50°C, lyophilisation (Christ freeze dryer alpha 1-4 LCS,Germany) after freezing at -80°C and intermittent microwave vacuum drying (MVD) (60s on/off power at 850Wand a vaccum pressure of 1kPa) using custom-designed MVD dryer.

Authors : Jribi, S.; Gliguem, H. Nagy, A.; Zsolt, N.G.; Szalóki-Dorkó, L.; Naàr, Z.; Bata-Vidàcs, I.; Marzougui, S.; Cserhalmi, Z.; Debbabi, H.

All drying experiments were performed in triplicate until reaching at least 15% water content. After drying, all samples were milled (Retsch Grindomix GM 200, Germany) and stored at 4°C until analysis.

2.4. Physico-chemical properties

Moisture content of all samples was analyzed using the AOAC oven method [6]. Novasina LabMaster a_w (Switzerland) was used for water activity determination at 25°C. Color was measured with a Konica Minolta Croma Meter CR 400 (Japan). The color parameters L*, a* and b* were evaluated. Bulk density was determined according to the procedure previously described [7].

2.5. Bioactive compounds

Folin-Ciocalteu method was used for total phenol content assessement [8]. Total carotenoid pigments were determined [9]. DPPH (1,1-diphenyl-2-picrylhydrazyl) radical scavenging activity (DPPH RSA) was measured according to the suggested previously [8] with slight modification during extraction: Extraction was made with 80% (v/v) aqueous methanol solution, for 2 h at 37 °C. Samples were afterwards centrifuged at 6,000 rpm for 30min. The supernatant was used for the determination of antioxidant capacity.

Antioxidant activity was calculated according to the following formula:

$$\%\text{DPPH RSA}= (1- A_{Sample/t=30}/A_{Control/t=0})*100$$

2.6. Functional properties

Water absorbance capacity (WAC) and Oil absorbance capacity (OAC) were determined [10]. Swelling power was evaluated following the described procedure [7].

2.7. Statistical analysis

Statistical analysis was carried out using the Minitab software (Minitab 17). All experiments were carried out in triplicate and the average values were reported together with standard deviations. Analysis of variance (ANOVA) was performed using the Fisher test. Significance was defined at $p < 0.05$.

3. Results

3.1. Physico-chemical properties

As shown in table 1, drying, regardless the method used, contributed to a significant decrease in water content and water activity. Results obtained show that shelf life may be extended as bacterial growth induced by sprouting could be stopped at the obtained levels of water activity.

Drying induced changes in color parameters: a decrease in lightness was observed after oven and micro-wave vacuum drying unlike lyophilisation. For redness and yellow index, sprouted micro-wave vacuum dried samples showed a significant increase while a significant decrease was observed after oven drying and lyophilisation.

Table 1. Evolution of physico-chemical parameters of Chili's sprouted wheat flour (n=3)

Treatement	Water content (%)	Water activity (a_w)	Lightness index (L^*)	Redness index (a^*)	Yellow index (b^*)
Raw	10.13±0.07[d]	0.488±0.00[c]	74.99±0.06[b]	2.87±0.02[b]	18.94±0.03[a]
Sprouted	59.81±0.09[a]	0.991±0.00[a]	--	--	--
Oven drying	10.78±0.09[c]	0.533±0.00[b]	74.76±0.03[b]	2.01±0.01[c]	17.12±0.10[b]
Lyophilisation	8.01±0.16[e]	0.330±0.00[e]	78.35±0.00[a]	1.47±0.01[d]	16.15±0.01[c]
Micro-wave vacuum drying	13.83±0.04[b]	0.478±0.00[d]	67.48±0.40[c]	3.68±0.08[a]	19.34±0.40[a]

Means in same column that do not share same letters are significantly different, according to Fisher' s test.
--: Not determined

3.2 Functional properties

Results describing evolution of functional properties after sprouting and drying are summarized in table 2. Functional properties are a key factor in food conception. These properties are related to flour characteristics (composition, structure, cristallinity, polar groups…) [11]. Sprouting is a physiological event marked by degradation of macro-molecules such as protein and starch [12, 13]. As shown in table 2, functional properties of Chili's sprouted wheat flour were affected not only by sprouting, but also by the drying method: a significant decrease ($p<0.05$), depending on the drying method used, was observed in bulk density and swelling power as found previously [7]. The decrease in swelling power could be linked to the degradation of starch molecules during sprouting [14]. A decrease in water absorbance capacity was observed after drying except for micro-wave vacuum dried samples. For oil absorbance capacity, both sprouting and drying, the method used, induced a significant increase if compared to raw seeds. These findings are in agreement with a previous study dealing with sprouted cereals [15].

Authors : Jribi, S.; Gliguem, H. Nagy, A.; Zsolt, N.G.; Szalóki-Dorkó, L.; Naàr, Z.; Bata-Vidàcs, I.; Marzougui, S.; Cserhalmi, Z.; Debbabi, H.

Table 2. Evolution of functional properties of Chili's sprouted wheat flour after drying (n=3)

Treatment	Bulk density (g/ml)	Water absorbance capacity (WAC)(g/g)	Oil absorbance capacity (OAC)(g/g)	Swelling power (g/g)
Raw	0.77±0.01[a]	0.92±0.00[b]	1.02±0.00[d]	6.11±0.05[a]
Oven drying	0.74±0.00[b]	0.90±0.01[b]	1.05±0.02[c]	3.74±0.08[c]
Lyophilisation	0.74±0.00[b]	0.84±0.00[c]	1.28±0.01[b]	3.71±0.05[c]
Micro-wave vacuum drying	0.62±0.00[c]	1.57±0.04[a]	1.35±0.02[a]	4.53±0.07[b]

Means in same column that do not share same letters are significantly different, according to Fisher' s test.

3.3 Nutritional properties

Comparing raw seeds flours to sprouted freeze dried ones shows a significant increase in bioactive compounds (+18.7% for carotenoids, +118.7% for total phenol content) and consequently in antioxidant activity (+31.6%). In fact, lyophilisation process is known by preserving products nutritional and sensory properties [16]. Our results about the role of sprouting in enhancing bioactive compounds are in agreement with previous studies [2]. Despite nutritional improvement induced by sprouting, micro-wave vacuum and convective drying decreased carotenoids and total phenol amounts significantly. Highest losses were obtained after oven drying, probably due to drying process duration if compared to micro-wave vacuum drying one.

Table 3. Effect of drying method on bioactive compounds and anti-oxydant activity of Chili's sprouted wheat flour

Treatment	Carotenoids (mg β carotene/kg dm)	Total phenol content (mg GAE/g dm)	DPPH RSA %
Raw	18.53±0.23[b]	19.93±0.49[b]	32.50±0.82[b]
Oven drying	8.50±0.24[c]	7.28±0.07[d]	18.54±0.87[d]
Lyophilisation	21.99±0.42[a]	43.59±0.34[a]	42.78±0.39[a]
Micro-waves vacuum drying	18.06±0.18[b]	13.00±0.06[c]	24.99±0.45[c]

Means in same column that do not share same letters are significantly different, according to Fisher' s test

GAE: Gallic Acid Equivalent, dm: dry matter bases, DPPH RSA: (1,1-diphenyl-2-picrylhydrazyl) radical scavenging activity

4. Conclusion

Results of this study showed that drying amplified modifications induced by sprouting Chili's durum wheat seeds. All tested drying methods led to a decrease in moisture content and water activity which may increase sprouts shelf life and promote their use in cereal products. However, only lyophilisation allowed preservation of nutritional improvement obtained by sprouting. Evolution of functional properties depends on drying process adapted.

5. References

[1] Küster-Boluda, I ; Vidal-Capilla, I. Consumer attitudes in the election of functional foods. Spanish Journal of Marketing - ESIC 2017, 21, 65-79.

[2] Plaza, L.; De Ancos, B. ; Cano, M. P. Nutritional and health-related compounds in sprouts and seeds of soybean (Glycine max), wheat (Triticum aestivum.L) and alfalfa (Medicago sativa) treated by a new drying method. European Food Research and Technology 2003, 216, 138–144.

[3] Maskan M. Microwave/air and microwave finish drying of banana. Journal of Food Engineering 2000, 48, 71-78.

[4] Dehnad, D. ; Jafari, S.M. ; Afrasiabi, M. Influence of drying on functional properties of food biopolymers: From traditional to novel dehydration techniques. Trends in Food Science & Technology 2016, 57, 116-131

[5] Ammar, K.; Gharbi, M. S. ; Deghaies M. Wheat in Tunisia. In Banjean, A. P., Angus W. J., Van Ginkel, M. The world wheat book: a history of wheat breeding Lavoisier, Londres-Paris-New York.2011.

[6] AOAC, 2000. Official Methods of Analysis, 17th ed. Association of Official Analytical Chemists.

[7] Singh, A.; Sharma, S.; Singh, B. Effect of germination time and temperature on the functionality and protein solubility of sorghum flour. Journal of Cereal Science 2017, 76, 131-139.

[8] Aprodu, L.; Banu, L. Antioxidant properties of wheat mill streams. Journal of Cereal Science 2012, 56, 189-195.

[9] Pasqualone, A.; Laddomada, B.; Centomani, I.; Paradiso, V. M.; Minervini, D.; Caponi, F.; Summo, C. Bread making aptitude of mixtures of re-milled semolina and selected durum wheat milling by-products. LWT - Food Science and Technology 2017, 78, 151-159.

[10] Kaushal, P.; Kumar, V.; Sharma, H.K. Comparative study of physicochemical, functional, antinutritional and pasting properties of taro (Colocasia esculenta), rice

Authors : Jribi, S.; Gliguem, H. Nagy, A.; Zsolt, N.G.; Szalóki-Dorkó, L.; Naàr, Z.; Bata-Vidàcs, I.;
Marzougui, S.; Cserhalmi, Z.; Debbabi, H.

(Oryza sativa) flour, pigeonpea (Cajanus cajan) flour and their blends. LWT - Food Science and Technology 2012, 48, 59-68.

[11] Gouw, V.P. ; Jung, J. ; Zhao, Y. Functional properties, bioactive compounds, and in vitro gastrointestinal digestion study of dried fruit pomace powders as functional food ingredients. LWT - Food Science and Technology 2017, 80, 136-144.

[12] Fardet, A. New hypotheses for the health-protective mechanisms of whole-grain cereals: what is beyond fibre? Nutrition Research Reviews 2010,23, 65–134.

[13] Koehler, P.; Hartmann, G.; Wieser, H.; Rychlik, M.Changes of Folates, Dietary Fiber, and Proteins in Wheat as affected by germination. Journal of Agriculture and Food Chemistry 2007, 55,4678-4683.

[14] Hung, P. V.; Maeda, T.; Yamamoto, S.; Morita, N. Effects of germination on nutritional composition of waxy wheat. Journal of the science of food and agriculture 2011,92,667-672.

[15] Elkhalifa, A. E.; Bernhardt, R. Influence of grain germination on functional properties of sorghum flour. Food Chemistry 2010, 121, 387-392.

[16] Wojdyło, A.; Figiel, A.; Legua, P.; Lech, K.; Carbonell-Barrachina, A.A.; Hernández, V. Chemical composition, antioxidant capacity, and sensory quality of dried jujube fruits as affected by cultivar and drying method. Food Chemistry 2016, 207, 170–179.

Cellulosic fibre drying: fundamental understanding and process modeling

Mondal, S.[*]; Agarwala, P.; Dutta, S.; Nimbalkar, V.; Pande, P.; Dhumal, S.

Aditya Birla Science & Technology Company Private Limited, Navi Mumbai, India.
*E-mail of the corresponding author: sabyasachi.mondal@adityabirla.com

Abstract

Process modeling of conveyer dryer for cellulosic fibre drying demands many fundamental insights. Present study highlights detailed cellulosic fibre drying aspects like mass transfer correlation relating mass transfer rate with process conditions, normalized drying curve and critical moisture content. Cellulosic fibre drying follows falling rate period, where rate of mass transfer decreases with moisture content. Conveyer dryer process model for commercial cellulosic fibre drying was developed and validated successfully. Moderate drying strategy derived based on developed process model and drying fundamentals was deployed at commercial scale which helped in reducing the moisture variability.

Keywords: Cellulosic fibre, Conveyor dryer, Process Model, Sherwood number, Moderate drying.

1. Introduction

Cellulosic fibres provide key attributes of comfort and softness to the final textile fabrics [1]. The widely used cellulosic fibres are cotton and man-made cellulosic fibres (viscose, lyocell, modal, etc.). Commercially all man-made cellulosic fibres are prepared by dissolving specific grades of pulp in a solvent, extruding into fibres followed by regeneration in a spin bath, cutting into specific lengths, web formation by steam/air sparging, treatment/washing and subsequently drying. The drying process is preceded by squeezing of fibre mat to remove excess water and opening the fibres in a mat opener. The drying process in case of cellulosic fibres, are pre dominantly carried out in hot air conveyer dryers to achieve desired moisture content in the final product [2]. Standard size (250 kg) bales are made out of dried fibres with a fibre meeting quality specs of 10.5- 11.5 wt. % (dry basis) moisture content.

Low moisture variability and low levels of wet and over-dried fibres are key drivers to get good processibility and yarn quality in the downstream industry of converting fibres to yarn [3]. Major factors imparting variability are dryer inlet moisture variation and methodology adopted during drying operation. Precise control over dryer inlet moisture variability in cellulosic fibre was very difficult to achieve whereas effective control over dryer operation was the most practically feasible option. Improvement in fibre opening, mat uniformity, over drying followed by conditioning and control of air flow distribution inside the dryer by modifying the internal dryer design have been attempted historically [4]. These improvements alone have a limitation to reduce the variability, if not coupled effectively with control of operational parameters like air temperature, humidity and air distribution over fibre web. Mathematical modeling supported by specific product drying fundamentals, understanding of heat, mass and momentum aspects have also helped in getting effective control over moisture and its variability [5, 6, 7]. Efforts towards understanding the cellulosic fibre drying fundamentals and its use in commercial scale conveyer dryer process modeling to control the fibre quality forms the basis of this study as it was not reported in the literature.

A process model for commercial scale cellulosic fibre dryer was developed in Aspen, supported with data from understanding of cellulosic fibre drying fundamentals like drying rate curve, fibre critical moisture content and mass transfer correlation relating process parameters. Main goal of this study was to reduce moisture variability of cellulosic fibre at commercial scale with precise control in a narrow range (10.5-11.5 wt. % on dry basis) and lower energy consumption during drying operation.

2. Materials and methods

Cellulosic fibre, in the form of viscose staple grey fibre, was used in this study from a leading man-made fibre manufacturer in India i.e. GRASIM industries. Commercial samples with

standard fibre length (38 mm) and diameter (45 μm) were chosen for the experimental studies to avoid raw material variability factor.

2.1. Experimentation for fundamental understanding of drying

Two separate experimental set-ups were developed to gather information for viscose fibre drying. First set-up was used to find out the drying kinetics and the second set-up to develop the correlation between mass transfer co-efficient and diffusivity. Developed fundamental understanding about drying kinetics and mass transfer correlation was used in Aspen model.

2.1.1.   Drying kinetics experiments

Experiments were performed at different air temperatures (80°C, 100°C, 120°C and 140°C) to find out the critical moisture content and drying rate curve of viscose staple fibre. Fully dried commercial viscose fibre samples were soaked in known water quantity for experimental purpose. Initial moisture of viscose fibre was at 300% and maximum overall sample weight in individual experiment was chosen to be around 2g based on analyzer limitations. Moisture analyzer continuously recorded moisture percentage and sample weight in every 30 seconds based on the thermo-gravimetric principle. Each experiment was repeated three times to check the repeatability.

2.1.2.   Mass transfer correlation experiments

Drying kinetics is mainly driven by rate of mass and heat transfer coupled with momentum. A decreasing linear period with decreasing drying rate is generally happen after a critical point where drying rate is depended on drying conditions [8] similar to constant rate period. Therefore, mass transfer correlation was developed (Equation 1) using Sherwood number with air temperature (T_G,°C), air absolute humidity (Y, kg moisture/kg dry air) and inlet fibre moisture content (X_{in}, kg moisture/kg dry fibre).

$$Sh = f(T_G, Y, X_{in}) \tag{1}$$

A separate set-up was developed where air of desired humidity (from air handling unit) was heated with the help of electric coils to raise the air temperature and wet viscose fibre sample was positioned at the bottom of the drying unit with cross-flow of hot air through fibre web/mat. Temperature and humidity sensors were placed in desired location of the setup to monitor the air quality. During experiments, air velocity was maintained at 0.6 m/s, similar to commercial dryer operation. Experiments were designed with three different air temperatures (60, 80 and 100^{0}C), four different moisture content of fibre sample (20, 40, 70 and 100 wt. %) and three different absolute humidity conditions (0.022, 0.065 and 0.12 kg/kg dry air). A total of forty-five set of experiments were planned for developing the mass transfer correlation, which was validated with five more random experiments.

2.2. Development of process model

Fundamental understanding generated through experimental insights gave an idea about the preferable operational procedure. However, an optimum solution was essential to adopt in commercial plant operation. Aspen process simulation tool was used to predict the optimized solution with the help of experimentally generated basic data on viscose fibre drying.

Complete conveyor dryer (Fig. 1) was modeled with counter-current flow of air and viscose fibre, where each dryer zone was represented as a single dryer unit. Commercial conveyer dryer was divided into two sectional dryers, i.e. Dryer-A and Dryer-B, with further sub divisions of each sectional dryer. Fibre (solid) moved in axial (horizontal) direction with plug flow in each dryer, which operated at adiabatic saturation. NRTL (non-random two liquid) thermodynamic method was selected as a base method and STEAM-TA was opted for free water method as high pressure steam was used for air heating. A two stage heater-condenser arrangement was used to highlight the indirect air heating phenomena in Aspen.

→Fibre Flow;→Ambient Air;→Hot Air;⊸Exhaust Air; - →Steam;→Condensate;⤳Heat Flow;□Drying Zone
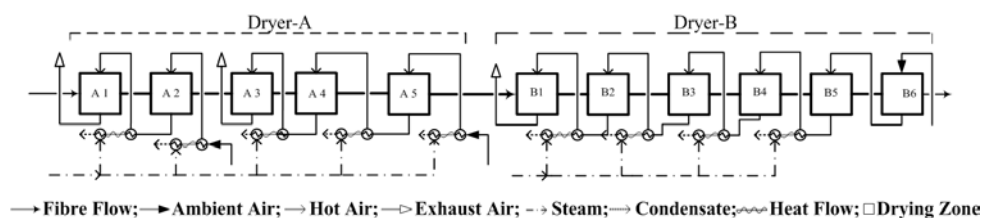
Fig. 1: Schematic representation of developed Aspen model: Multistage conveyor dryer

Mass and energy balance equations for both gas (air) and solid (fibre) phases were used in the background, which are inbuilt in Aspen [9]. Experimentally generated fundamentals, like mass transfer correlation, critical and equilibrium moisture content [10] and normalized drying rate with shape factor of viscose fibre were incorporated as input to Aspen model.

3. Results and discussion

3.1. Drying curve: Viscose cellulosic fibre

Drying rate curves were generated based on moisture data, as shown in Figure 2 (a), for viscose fibre at four different temperatures as per the procedure explained in section 2.1. Increase in drying temperature shows increase in drying rate, which diminishes towards end of drying i.e. at an equilibrium moisture content. Equilibrium moisture content of viscose staple fibre was around 8-12 % for 30-60 % RH at 25°C [10].

Slope change of drying rate versus moisture content highlighted distinct periods like preheat zone, constant rate and falling rate period. Drying rate was observed to be very high at the preheat zone. Constant drying rate period typically follows preheat zone, due to continuous moisture availability at fibre surface where drying rate is controlled by heat transfer rate. Unavailability of moisture at the viscose fibre surface was observed in falling rate period where rate of moisture evaporation decreases with reduction in fibre moisture content. Transition from constant drying rate period to falling rate happens at a particular moisture content known as critical moisture content (Fig. 2a) which is ~ 130 % for viscose fibre. Whereas in commercial/ plant scale fibre dryer inlet moisture ~100% ($< X_C$) which depicts drying occurs in falling rate period.
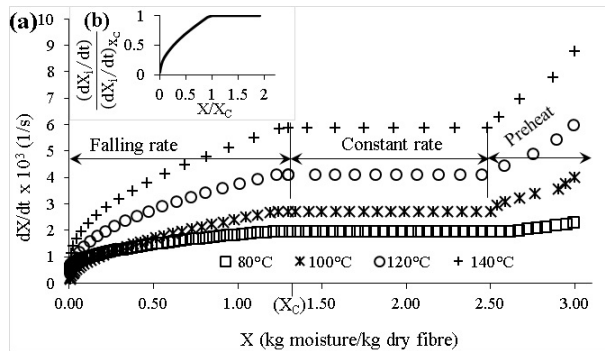
Fig. 2: Viscose staple fibre: (a) drying rate curve at different temperatures (Critical moisture content, X_C = 130 %) and (b) normalize drying rate verses normalize moisture content

Drying rate specification in Aspen is typically provided in the form of normalized average drying rate curve where individual drying rate was normalized with constant drying rate (Equation 2) and the individual moisture content was normalized with critical moisture content. Figure 2 (b) showed average normalized drying rate for viscose staple fibre, which was temperature independent. Drying rate shape factor (F) [9], Equation 2, was found to be around 'one' for viscose fibre.

$$\vartheta(n) = \left(\frac{dX_i}{dt}\right) \Big/ \left(\frac{dX_i}{dt}\right)_{i=X_C} = 2. F.\left(\frac{X}{X_C}\right) - (2. F - 1)\left(\frac{X}{X_C}\right)^2 \qquad (2)$$

3.2. Mass transfer correlation with process parameters

An attempt has been made here to understand the mass transfer rate aspects in commercial cellulosic fibre dryer. The rate of evaporation is proportional to moisture concentration gradient from fibre surface to air where proportionality constant is convective mass transfer coefficient where local mass transfer coefficient is proportional to Sherwood number

Mostly, Sherwood number used to explain convective mass transfer. In case of porous material drying, two scenarios have observed in commercial dryer, one side moisture removal from fibre surface to air through convective mass transfer and in other side transportation of moisture from materials capillary to the surface through diffusion mass transfer which may lead to decreasing wetted surface drying [8]. A single stage convective drying unit model was used in Aspen to calculate the Sherwood number for each experiment to match the extent of drying rate for different input process parameters. A simplified predictive mass transfer correlation:

$$Sh = a(T_G{}^b)(e^{g.Y})(e^{h.X_{in}}) \tag{3}$$

Statistical tool was used to estimate the constants with regression coefficient, R^2 value of 74%. Equation 4 shows a final version of mass transfer correlation using Sherwood number which was used in process model to estimate the local mass transfer coefficient of cellulosic (viscose) fibre and enhance the model robustness during optimization of drying.

$$Sh = \exp(-3.33).T_G{}^{(-0.095)}.\exp(0.9.X_{in}).\exp(-(9.5.Y)) \tag{4}$$

Correlation clearly highlights proportional dependence on inlet fibre moisture content whereas air absolute humidity and temperature shows inverse with Sherwood number.

3.3. Model validation

Data from commercial production unit for outlet fibre moisture, steam/fibre ratio, exhaust air humidity, temperature, were used to validate the developed process model. Comparison of plant data and model predictions show maximum error of 7% whereas majority error numbers were <5 %. In addition, it has been shown that the process model predicts the plant operational drying curve (Fig. 3), and also increases confidence in developed cellulosic fibre drying process model. Multiple model validation strongly confirms that the developed model is capable of predicting temperature profile with other operational parameters to get the desired moisture quality.

3.4. Drying rate optimization for commercial conveyor dryer

Cellulosic fibre mat thickness, of around 200 mm, formed on the conveyer belt of the dryer significantly affects the moisture variation, as there exists no surface renewal mechanism in conveyor dryer except the effect induced by intermediate opener placed between Dryer-A and Dryer-B. Hot air flows in a cross flow manner through the moving fibre mat. Humidity starts occurring gain as air passes through the fibre mat with reduction in temperature and driving force for moisture removal. This phenomenon creates moisture variation within the mat and it continues till dryer end. Overall, drying rate has a potential to induce moisture variability at commercial scale and there is a scope for optimization of the same to reduce such variability. Commercially, first sectional dryer (Dryer-A) was operated at higher

temperature to remove approximately 75% moisture with fast drying rate (Figure 3), whereas second sectional dryer (Dryer-B) removes around 15- 20% of moisture at lower zone temperature. Mass transfer rate of moisture to the fibre surface along with available moisture carrying capacity of the hot air controls the overall drying operation.
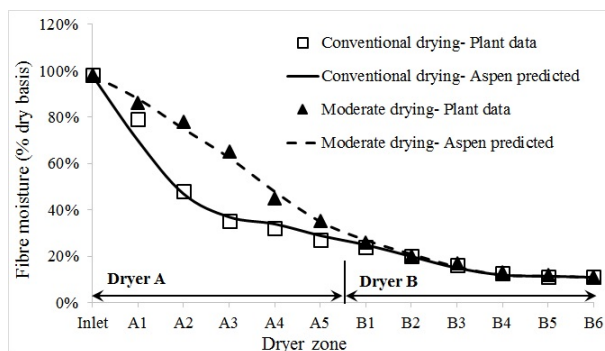
Fig. 3: Drying curve: Plant and Aspen predictions for conventional and moderate drying strategy

In a few initial zones, due to high moisture content, convective mass transfer rates are high due to sufficient moisture present at the fibre surface and air temperature creates enough driving force to remove the moisture. This phenomenon observed typically at early stage of falling rate period. After few zones, transportation of moisture from capillary to fibre surface is dominated by diffusion where moisture evaporation happens at decreasing rate. Drying rate decreases with decrease of moisture content. Also, correlation (Equation 4) clearly shows higher Sherwood number at initial stage due to the impact of convective mass transfer and lower value of Sherwood number after few initial zones was due to lower convection mass transfer where impact of diffusion on drying process is high. Facilitation of the diffusion process to overcome capillary forces demands raising the fibre surface temperature. Overall fundamental insights along with multipoint validation provided confidence to deploy process model predictions of optimum parametric combination known as moderate drying strategy for targeting moisture variability reduction.

Figure 3 shows the comparison between drying curve of conventional (fast) and moderate drying strategy along with model predicted. In the moderate drying strategy, drying curve is shifted upwards compared to conventional due to lower temperatures adopted at the initial zones. Disappearance of this shift occurs at the start of Dryer-B due to higher temperatures adopted during start of Dryer-B which increases the fibre surface temperatures by ~ 10^0C higher than conventional. Developed moderate drying strategy is adopted in commercial

plant and improved in-spec bales by 18 % (from 63 % to 81 %) within narrow range (10.5-11.5 %) by reduction in moisture variability along with 9% reduction in steam consumption.

4. Conclusion

A fundamental understanding of cellulosic fibre (viscose) drying was obtained in terms of critical moisture content, normalized drying curve and mass transfer correlation. Commercial viscose fibre drying operation falls under falling rate period where convective mass transfer along with diffusion limits the moisture removal. Conveyer dryer process model for commercial viscose fibre drying was developed and validated successfully. Model suggested optimum process parameter combination maintained during drying operation at commercial scale reduced moisture variability by 18 % along with steam consumption reduction of 9 %.

5. Acknowledgement

6. References

[1] Ahmat, C. Modelling of the Drying Behaviour of Regenerated Cellulosic Fabrics. Tekstil ve Konfeksiyon 2017, 27 (4), 373–381.

[2] Lisyakova, G.V.; Serkov, A.T.; Tsyganov, K.I. Drying and Conditioning of Viscose Staple Fibre. Khlmicheskle Volokna 1986, 6, 28–32.

[3] Uyanik, S.; Baykal, P.D. Effects of Fibre Types and Fibre Blends Ratio on Vortex Yarn Properties. The Journal of the Textile Institute 2017, 108.

[4] Jamaleddine, T. J; Ray, M. Application of Computational Fluid Dynamics for Simulation of Drying Processes: A Review. Drying Technology 2010, 28, 120–154.

[5] Pang, S. Mathematical Modelling of MDF Fibre Drying: Drying Optimization. Drying Technology 2000, 18 (7), 1433–1448.

[6] Fritzell, E.; Melander, O.; Rasmuson, A. The Drying Kinetics and Equilibrium Moisture Content. Drying Technology 2009, 27, 993–998.

[7] Mujumdar, A.S.; Fundamental Aspects. In Handbook of Industrial Drying. 3, Lodz, Poland; Taylor & Fransis Group, LLC, 2014; 4–31.

[8] Belhamri, A.; Characterization of the First Falling Rate Period During Drying of Porous Material. Drying Technology 2003, 21(7), 1235–1252.

[9] Levine, J.; Lakshmanan, A.; Peers, Z. Jump Start: Modeling Convective Dryers in Aspen Plus V8.0, Aspen Technology, 2013.

[10] Sousa, L.H.C.D.; Pereira, N.C.; Motta Lima, O.C.; Fonseca, E.V. Equilibrium Moisture Isotherms of Textiles Materials. Maringá 2001, 23(6), 1363–1368.

Study and optimization of freeze-drying cycles of a model probiotic strain

Verlhac, P.[a*] ; Vessot-Crastes, S.[a] ; Degobert, G.[a] ; Cogne, C.[a] ; Andrieu, J.[a] ; Beney, L.[b] ; Gervais, P.[b]

[a] Université de Lyon, Université Claude Bernard Lyon 1, Laboratoire d'Automatique et Génie des Procédés (LAGEP), UMR CNRS 5007, Domaine de la Doua, 69100, Villeurbanne, France
[b] Univ. Bourgogne Franche-Comté, AgroSup Dijon, PAM UMR A 02.102. F-21000, Dijon, France

*E-mail of the corresponding author: pierre.verlhac@univ-lyon1.fr

Abstract

This work is based on the experimental study of the freeze-drying process to understand the impact of numerous factors on the survival rates of a model probiotic strain of Lactobacillus casei type. With the aim to find out if cell density in the matrix and survival rates are linked, we have studied the location of the cells after freeze drying inside a porous matrix composed of a lactose basis with a polymer, the polyvinylpyrrolidone (PVP) in various amounts. The best survival rate were obtained at slow freezing rate for a formulation containing 5% (m/V) of lactose and 5% (m/V) of PVP.

Keywords: Freeze-Drying; Freezing; Probiotics; L. Casei ATCC 393.

1. **Introduction**

According to Food and Agriculture Organization of the United Nations and World Health Organization, probiotics are defined as "live micro-organisms which, when administered in adequate amounts, confer a health benefit on the host"[1]. Probiotics are generally temperature sensitive bacteria (with different degrees of sensitivity depending on the numerous strains), which loss a part of their viability and their favorable health properties during their dehydration processes and, next, during the storage and transport steps before their consumption. Many factors such as temperature, oxygen level, osmotic pressure and pH stresses have an important impact on their viability and, on their health promoting effect. Two types of methods are mainly used to stabilize and to maintain a long term activity level, namely the freezing and more or less soft drying techniques such as spray-drying, fluidized bed drying and freeze-drying. The freeze-drying is known as the method that usually leads to the best results in term of many quality factors of the freeze dried cake (viability rate, rehydration rate, etc.) despite various damaging effects generated by the freezing and sublimation/desorption phenomena (crystal growth; cryoconcentration, etc.)[2]. Nevertheless, this method has the major inconvenient to lead to the highest operating costs due to the very severe operating conditions of this discontinuous process which has to be carried out at very low levels of temperature and total gas pressure. During this long and complex soft dehydration process, three phase changes are taking place so that the living bacteria have to endure numerous stresses more or less interdependent and deeply understood (thermal, osmotic, pH, sub-cooling, intracellular crystallization…). Moreover, important differences exist between the different probiotic's species, sub-species and strains, particularly in terms of resistance to the severe process conditions generally encountered[3]. This is why the main objective of our work was to establish a rational protocol of optimization of freeze-drying cycles with a model probiotic strain, easily adaptable to other bacteria. This protocol is based on the reduction of stress effects in order to obtain the highest survival rates. Firstly we studied the cell immobilization by adsorption or inclusion inside a porous matrix. We have chosen to investigate on a formulation constituted of lactose (a popular effective cryoprotectant known for not influencing the cells content) and polyvinylepyrrolidone (PVP) which is a polymer widely used in the pharmaceutical industry due to its interesting properties of stabilization[4]. Indeed, PVP has been already used as cryoprotectants and has a higher glassy transition (Tg') than most of the saccharides so that it can reduce the drying time by increasing the sublimation and desorption limit temperatures.The freezing protocol - especially the freezing rate -which could prove to be the key damaging step of the whole freeze-drying process, was investigated. Indeed, this step appeared to be the most lethal period for micro-organisms mainly because of osmotic phenomena occuring at the cell level. Then, we have investigated the influence of the total amount of each component in the formulation on the location of the bacteria in the solid matrix and on the survival rate.

2. Materials and Methods

2.1 Bacteria and growth conditions

The strain Lactobacillus Casei ATCC® 393™ (Alliance Bio Expertise, Guipry, France) was rehydrated from the Kwik-Stik® -containing the original dried strain- and then isolated on a MRS agar petri dish and finally incubated for 48h at 37°C. A single colony was collected from the plate and inoculated in 100mL MRS broth and finally incubated for 24h at 37°C under orbital shaking (150 rpm). Next a 1% diluted solution was prepared in 150 mL MRS broth and incubated under orbital shaking (150 rpm) during 30h.

2.2 Formulation composition

Once the stationary phase was obtained, the bacterial suspension was centrifuged at 7000 g during 10min at ambient temperature and next washed twice with saline buffer solution (0,85%NaCl (m/V)). Then the pellet was suspended again before processing. Various solutions were prepared with a Kollidon®30 (PVP) and monohydrate lactose basis in the range of concentration from 1% to 10% (m/V) or only with the saline buffer (Table 1).

Table 1. Index of the formulation composition

Nomenclature	Weight Lactose composition (m/V)	Weight Kollidon®30 composition (m/V)
K5	0%	5%
L5	5%	0%
KL10-5	5%	10%
KL1-1	1%	1%
KL5-5	5%	5%
KL10-10	10%	10%

2.3 Freezing and thawing protocol

Immediately after formulation, the solutions were poured into 6mL glass vials and next frozen from ambient temperature up to -45°C at different freezing rates, namely: 0.5; 1; 2; 5°C/min and a very fast rate by immersing directly the vials into liquid nitrogen. We investigated the effect of cold thermal stresses at the slowest rates by introducing, before the freezing step, a temperature plateau at 5°C during ½h. Then, the temperature was maintained during 2h before the thawing step which was performed by immersing the vials into distilled water at 37°C and next, immediately diluted for the enumeration.

2.4 Freeze-Drying process

A slow freezing rate was chosen, namely at 0.5°C/min with a temperature plateau at 5°C. The sublimation step (primary drying period) was performed slowly under vacuum at 150

Pa and around -40°C. Next, the desorption step (secondary drying period) was achieved during 24h at 20°C under 50 Pa. All the vials were closed immediately inside the freeze-dryer chamber, hermetically sealed and finally stored at 4°C. Lyophilisates were rehydrated quickly at 20°C by addition of an adequate amount of saline buffer solution for enumeration of viable bacteria.

2.5 Enumeration and residual moisture

The rehydrated powder and the thawed solution were decimally diluted and next incubated at 37°C during 72h to enumerate the colony forming unit (CFU). Every enumeration was conducted in triplicate. The moisture contents in the freeze-dried vials were determined by the classical the Karl-Fisher method (860 KF Thermoprep - Metrohm). Samples of the freeze-dried cake (between 10 and 20 mg) were introduced into the Karl-Fisher oven at 150°C.

3. Results and Discussion

3.1 Effect of the addition of PVP and lactose on the bacterial viability
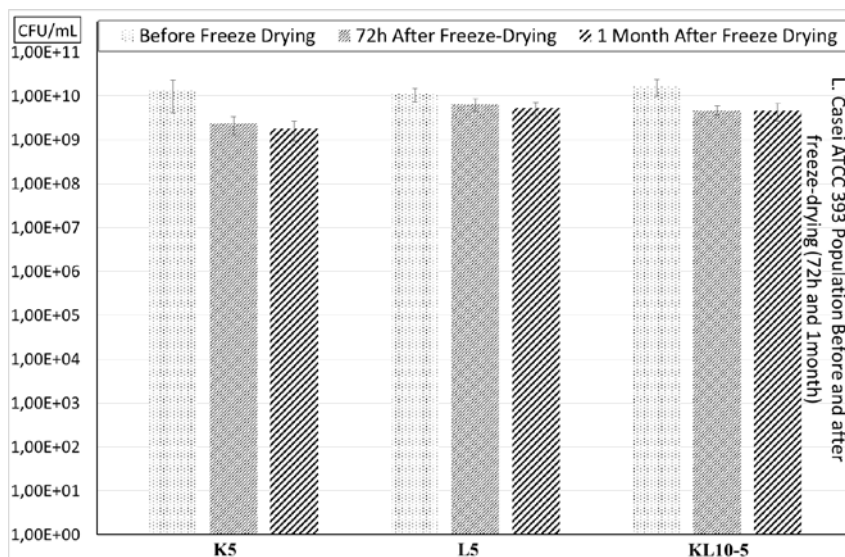
Fig. 1 Effect of polymer PVP and lactose on the viability of Lactobacillus Casei after freeze drying.

Bacterial suspensions were mixed with pure lactose (Ref. **L5**) or pure polymeric solution (Ref. **K5**) or a mixture of different concentration of these two components (**KL10-5** Cf Table 1). No significant differences on bacterial viability were observed between these formulations after freeze-thawing. These results show that the presence of this polymer had not detrimental effects on the survival of bacteria, so that we concluded that it could be used as protectant of our formulation. After freeze-drying, survival rates exhibited light

differences between the different formulations of protectants (Fig.1). Just after process the concentration of viable bacteria decreases more when the polymer was the only protectant (**K5**). With the lactose formulation (**L5**), the survival of bacteria appeared to reach the highest values, even after one month of storage. However, the solution **KL10-5** seemed to present the highest stability after one month of storage even if the survival ratio right after the end of the whole freeze-drying process was slightly affected. This means that a formulation that combined lactose and PVP components could offer a high stabilizing effect for the storage. This favorable effect could be explained by the matrix vitrification phenomenon which could entrap and protect the cells during the process, by reducing the mechanical stresses induced by ice crystal growing, but also during the storage, by increasing the stability due to the high glassy transition values of the PVP[5].

KL10-5 (3000x)   20μm   L5 (3000x)   20μm

KL10-5 (12 000x)   5μm   L5 (12 000x)   5μm
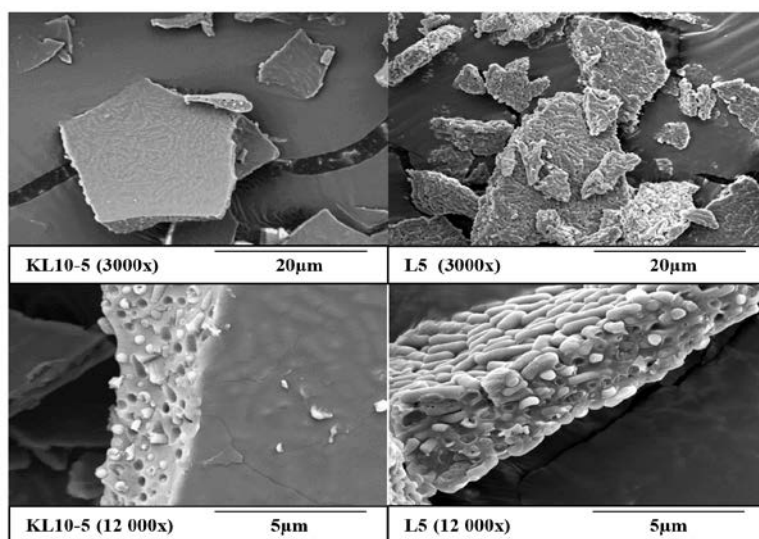
Fig. 2 SEM photography of the repartition of dried L. Caseï ATCC 393 in the porous matrix based on lactose and Kollidon® 30 or only lactose.

Next, SEM photographs (Fig.2) allowed to observe the position of the bacteria located in the freeze-dried solid matrix. In the case of formulation **KL10-5**, the bacteria did not appeared at the pore's surface and seemed included inside the solid part of the freeze-dried matrix. On the contrary, for the **L5** formulation, as the relative amount of dry matter of lactose was smaller, the bacteria covered the pore's surface of the matrix. This behaviour could explain why the survival rate was lower with the **KL10-5** formulation than with the **L5** one. When the matrix was fixed during the freezing step, the bacteria may have suffered high local pressure levels due to Ostwald ripening phenomena during and just after the crystallization step. However, on a long time scale, the morphology and the structure of the solid matrix of the mixture could allow a higher survival ratio due to the formation of a

thick solid layer which can prevent the diffusion of water and oxygen up to the cells[6].Experiments were carried out to find out the less damaging freezing kinetics. It appeared that a slow freezing rate around 0.5°C/min with a stabilization temperature step between 0.5 and 1h before the starting of the freezing at 5°C led to the best survival rate, with no significant reduction of viable bacteria. This could be related to a cold stress response from the bacteria, because, in reaction to the stress, the cells may produce Cold Shock Proteins allowing them to prevent damages[7]. Other hypothesis has been proposed on the dehydration rate of the cells, due to slow osmotic pressure variations preventing intracellular water crystallization due to cell water exit[8]. These results have to be compared with experimental data showing the influence of nucleation temperature.
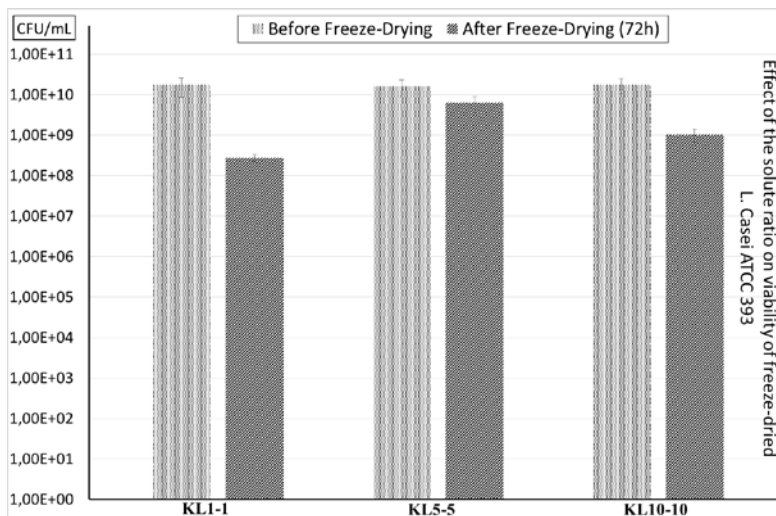
Fig. 3 Effect of the amount of solute on the viability of L. Caseï ATCC 393

3.2 Influence of the amount of solute protectants on the bacteria location and viability

After observing the differences in the repartition of bacteria and morphology of the solid matrix with SEM pictures (as mentioned above), we characterized the influence of the amount of dry matter on the final viability of bacteria. We have chosen to investigate, at the same weight ratio, two extreme compositions and one central composition of the scale (Table 1). Some of the freeze-dried cakes were observed by SEM and the others were rehydrated for plate counting. For the lyophilisate that contained the lower solute concentration (**KL1-1**), we obtained approximately a 2-log reduction of the viable bacteria after freeze-drying while less than 0.5-log reduction for the **KL5-5** and around 1.2-log reduction for the **KL10-10** (Fig.3). The SEM photograph of Fig. 4 showed that the freeze-dried matrix network formed by **KL1-1** formulation was very thin with a high density of bacteria.
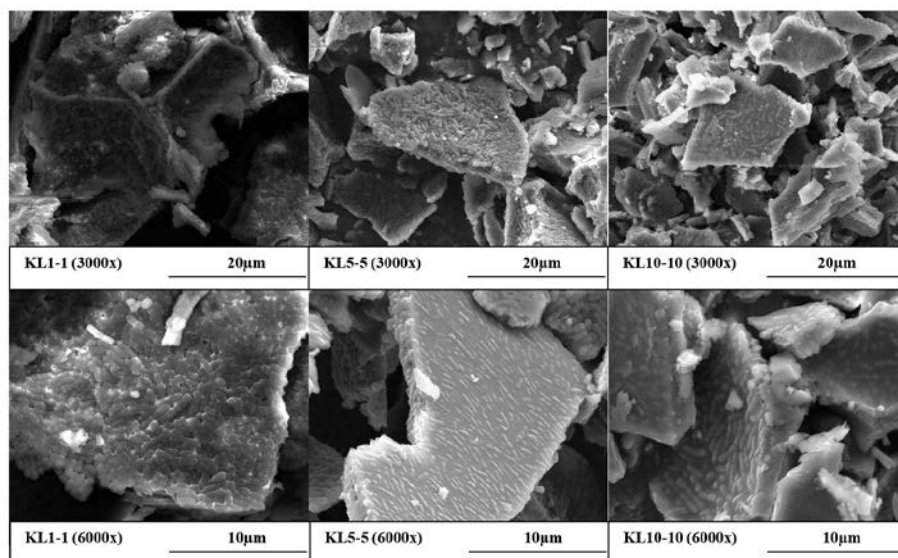
Fig. 4 SEM photography of the repartition of dried L. Caseï ATCC 393 in the porous matrix based on extreme lactose and Kollidon®30 content.

The physical aspect with **KL1-1** at macroscopic scale was not enough consistent and the freeze-dried cake was difficult to analyze due to its fragility. Other experiments and photographs carried out with only buffered solutions and with only bacteria led to very low survival rates. The differences in bacterial location and on matrix structure for **KL5-5** and **KL10-10** formulation were more difficult to find out. In both cases we could observe a thick structure recovering the cells. Nevertheless, differences in the viability seemed to be linked to the mass ratio between dried excipients (lactose and PVP) and dried bacteria. In the case of low amounts of excipients, the bacteria were directly exposed to water during the rehydration process. Indeed, the rehydration rate had probably a great influence on the final viability ratio of the cells and the amount of solute exerted probably an important buffer effect on the mechanisms of water transfer to the cells. In another hand, a too important content of excipients could unbalance the osmotic equilibrium of bacteria with their surrounding solution during the formulation and freezing steps and, by the way, could generate too important water flows crossing the cells walls which resulted to important cell death ratios or viability losses[8]. That's why a balance should be established between too low content of protectant resulting in a loss of efficiency and a too high content, providing high stresses to the cells. Nevertheless, the **KL5** formulation presented the highest survival ratios with this soft freeze-drying protocol. Then, our forecoming work will focus on this formulation with the aim of parameters optimization and design space set up.

4. Conclusion

This study presents the effect of composition and of freezing parameters of a PVP Kollidon®30 and lactose based formulation on the viability of a L. Casei strain during a standard freeze-drying cycle. The polymer and cells were considered as compatible since no significant reduction was observed on the viability of the probiotic strain, even after one month of storage. The SEM photographs showed that the type and the concentration of solute in the cells preparation have an important impact on the cells location inside the freeze-dried matrix and, consequently, on the survival ratio. The KL5-5 formulation led to the best bacteria survival ratio with less than 0.5 log reduction after a standard freeze-drying cycle. Nevertheless, it is still difficult to conclude on the mechanisms explaining the best observed viability at this composition. These results indicated that the PVP can be used with this probiotic strain, and, moreover, it may preserve the viability of bacteria for long time storage in the freeze-dried form. Our next study will focus on the process optimization parameters and the design space set up allowing a viable and stable freeze-dried product.

5. References

[1] Food and Agriculture Organization of the United Nations and World Health Organization, Eds., Probiotics in food: health and nutritional properties and guidelines for evaluation. Rome 2006.

[2] J. Barbosa *et al.*, "Comparison of spray drying, freeze drying and convective hot air drying for the production of a probiotic orange powder," *Journal of Functional Foods*, vol. 17, pp. 340–351, août 2015.

[3] O. F. Celik and D. J. O'Sullivan, "Factors influencing the stability of freeze-dried stress-resilient and stress-sensitive strains of bifidobacteria," *Journal of Dairy Science*, vol. 96, no. 6, pp. 3506–3516, juin 2013.

[4] Y. Furushima, K. Ishikiriyama, Y. Ueno, and H. Sugaya, "Analysis of the state of water in polyvinylpyrrolidone aqueous solutions using DSC method," *Thermochimica acta*, 2012.

[5] J. H. Crowe, S. B. Leslie, and L. M. Crowe, "Is vitrification sufficient to preserve liposomes during freeze-drying?," *Cryobiology*, vol. 31, no. 4, pp. 355–366, Aug. 1994.

[6] G. Lemetais, S. Dupont, L. Beney, and P. Gervais, "Air-drying kinetics affect yeast membrane organization and survival," *Appl Microbiol Biotechnol*, vol. 96, no. 2, pp. 471–480, Oct. 2012.

[7] J. R. Broadbent and C. Lin, "Effect of Heat Shock or Cold Shock Treatment on the Resistance of Lactococcus lactis to Freezing and Lyophilization," *Cryobiology*, vol. 39, no. 1, pp. 88–102, août 1999.

[8] P. Gervais, P. A. Marechal, and P. Molin, "Effects of the kinetics of osmotic pressure variation on yeast viability," *Biotechnol. Bioeng.*, vol. 40, no. 11, pp. 1435–1439, décembre 1992.

Enhancing antioxidant property of instant coffee by microencapsulation via spray drying

Sakawulan, D. [a]; Archer, R.[b]; Borompichaichartkul, C.[a]*

[a] Department of Food Technology, Faculty of Science, Chulalongkorn University, Phayathai Road, Patumwan, Bangkok 10330, Thailand.

[b] Massey Institute of Food Science and Technology, Massey University, Palmerston North 4442, New Zealand.

*E-mail of the corresponding author: chaleedab@hotmail.com, chaleeda.b@chula.ac.th

Abstract

This study is aimed to improve the antioxidant property of instant coffee by using microencapsulation technique and spray drying. Concentrated coffee extract was mixed with Konjac glucomannan hydrolysate (KGMH) and Maltodextrin (MD). The mixture of coating material and coffee extract was then spray dried at 160 - 180 °C inlet air temperature and at 85-90 °C outlet air temperature. KGMH can preserve retention of phenolic compounds, DPPH scavenging activity and antioxidant activity of FRAP (p<0.05 of instrant coffee better than other treatment.

Keywords: Hydrolysed Konjac Glucomannan; Spray Drying; Microencapsulation; Instant Coffee, Antioxidant

1. Introduction

Coffee brews as one of the most popular beverages in the world has extensively studied for health concern. Moreover, many people choose coffee as their daily drink due to its effect to body health. Coffee brews are accepted as a rich source of compounds possessing antioxidant and radical scavenging activities. Coffee is high in phenolic compounds, especially chlorogenic acids and their degradation products such as caffeic, ferulic and coumaric acids, polyphenols, trigonelline and alkaloids including caffeine and also high amount of melanoidins which exhibit significant antioxidant activities [1, 2].

Comparing antioxidant capacity in one cup from different form of coffees, instant coffee accounted for the highest amount of essential substances which expressed antioxidant capacity that 3-4 times higher than ground coffee. During the manufacturing of instant coffee, antioxidant and other essential compounds are concentrated which resulted in enhancing of antioxidant capacity compare to roasted bean powder [3].

More advantages of instant coffee stimulate the research more deeply in its production. The conventional processes of instant coffee are spray drying and freeze drying, both techniques have some limitations regarding energy consumption and final product qualities. Freeze drying produces the best product quality in term of aroma recovery, but it uses high energy and time that affected the production cost. While, spray drying leads the high production capacity at low investment, but engender higher thermal impact and resulted in decreasing of essential compounds such as natural antioxidants. In fact, that spray drying is the most applicable process in instant coffee industry yet gives lower antioxidant and flavor compounds than other processing, thereupon considering other techniques to lowering thermal impact is proposed.

Microencapsulation offered as a solution to reduce the core reactivity from essential compounds with the environmental factor. Konjac glucomannan (KGM) is neutral polysaccharides with mannose residues as predominant monomer and glucose as secondary sugar. The deep exploitation of KGM and its derivatives has been paid considerable attention in recent year. What is more, KGM in form of flour and hydrolysate can be conveniently used to wider application in some fields such as food science, pharmaceutical science, chemistry and biotechnology [4]. One of the latest experiments that has been deeply studied is investigation of hydrolyzed KGM on spray drying microencapsulation. Previous study have shown that hydrolyzed KGM (KGMH) worked as wall material by spray drying technique in antimicrobial powder, flavor encapsulated powder and nutraceutical powder [5, 6, 7]. Therefore, the aims of this study were to investigate the utilization of hydrolyzed KGM on encapsulation efficiency and to obtain the suitable spray drying condition in the production of high antioxidant instant coffee microencapsulation.

2. Materials and Methods

2.1 Materials

Medium dark/roast of Arabica roasted was provided by. Mannanase 50,000,000 IU per gram enzyme, food grade (Bosar Biotechnology, China) was used. Maltodextrin (MD) DE 10-15 (Food grade) was purchased from Chemipan (Bangkok, Thailand).

2.2 Methods

2.2.1 Coffee extract and coffee solution preparation for spray drying

Fine ground Arabica coffee (Green Net SE Co., Ltd, Bangkok, Thailand) (24 g) and 115 ml hot water are used in coffee extraction by using Moka Pot 22.5 x 10 cm (YAMI® YM-6007, China). Then coffee extract was evaporated by vacuum rotary evaporator (BÜCHI R-114, BÜCHI Labortechnik AG, Flawil, Switzerland) to get 10 °Brix of total solid. After that KGM hydrolysis is prepared by using Mannanase with 125 units per gram KGM is used for hydrolysis reaction. Modification method from previous study [6] was used to conduct KGM hydrolysis. All KGM hydrolysis was conducted under a controlled condition at 40±1 °C and 200 rpm of an overhead stirrer for 1 hour. Then KGMH solution was added by MD powder to adjust wall material concentration at 20% (w/w). For instance, 5% MD was added to 15% KGMH solution. Moreover, 20% KGMH was not added by MD, while 20 % MD solution (w/w) was used as control. Arabica coffee extract and wall material at ratio 2.2:1 (w/w) was mixed to obtain total solid mixture at 15% (w/w). Mixing process was done by magnetic stirrer for 5 minutes of stirring.

2.2.2 Spray drying

Drying experiment was done in a co-current Mini Spray Dryer (BÜCHI B-290, BÜCHI Labortechnik AG, Flawil, Switzerland). with inlet temperature at 160-180 °C and outlet temperature at 85-90 °C by adjusting flow rate.

2.2.3 Antioxidant properties analysis

Total phenolic compounds (TPC) was performed by Folin-Ciocalteu and calculated using gallic acid equivalent (CGA) [2]. Antioxidant activity was examined by DPPH scavenging ability method at 515 nm of spectrophotometric analysis [3]. Moreover, Ferric Reducing Antioxidant Power (FRAP) also used to examined antioxidant activity [2]. The FRAP measurement was done by spectrophotometry at 595 nm. Amount of chlorogenic acid was observed by using HPLC (Varian Prostar, USA) and the spectra were detected by Prostar 335 Photodiode Array Detector at 278 nm.

3. RESULTS AND DISCUSSION

3.1 Antioxidant Property

Fig. 1 presented antioxidant activity and amount of phenolic compounds and chlorogenic acid based on coffee solid in coffee extract and instant coffee powder. The results have shown that spray drying microencapsulation process, especially when using KGMH as wall material, was able to shield phenolic and antioxidant compounds.
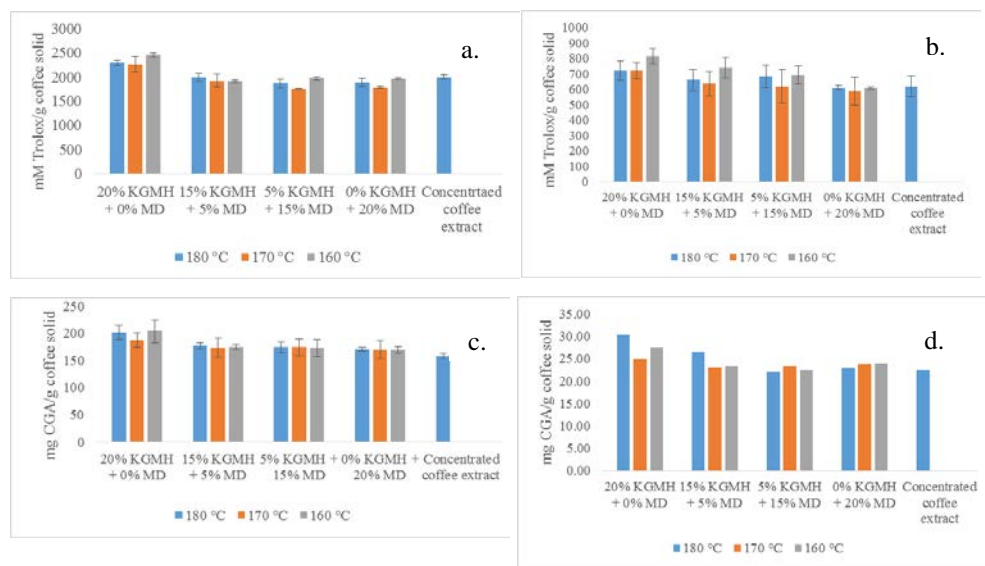
Fig. 1 Antioxidant activity of instant coffee measured by (a) DPPH (b) FRAP (c) total phenolic content (d) chlorogenic acid

In TPC measurement (Fig. 1c), the highest phenolic content in instant coffee powder was the formulation of 20% (w/w) KGMH at 160 °C with 204.04±20.98 mg CGA/g coffee solid

(p<0.05), while the coffee extract presented 157.87±4.95 mg CGA/g coffee solid. To confirm TPC result, a specific phenolic compound which is chlorogenic acid (Fig. 1d) was observed by HPLC. In the current study, amount of chlorogenic acid in concentrated coffee extract had 22.49±1.35 mg/g coffee solid, while instant coffee powder contained 22-30.60 mg/g coffee solid. Among the treated instant coffee powders, 20% (w/w) KGMH instant coffee powder produced at 180 °C presented the highest content. In general, increasing KGMH concentration and inlet temperature lead to the higher chlorogenic acid content. On the other hands, DPPH scavenging ability results (Fig. 1b) have shown a similar pattern with TPC experiment where the highest value was exhibited by 160 °C spray dried of 20% (w/w) KGMH instant coffee powder (813.30±100.89 mM Trolox/g coffee solid) (p<0.05), while the extract presented 619.21±130.91 mM Trolox/g coffee solid. During spray drying, high temperature might trigger some reactions such as phenolic degradation and Maillard reaction which can create new compounds that possess higher antioxidant capacity. It is noted that in coffee mixture, antioxidant activity is contributed by phenolic compounds and melanoidins (non-phenolic). Since DPPH method has a wide range of mechanism, the new compounds created during drying could possibly be detected and express antioxidant capacity. Furthermore, in FRAP method (Fig. 1a), the similar formulation in TPC and DPPH methods was noted to have the highest value which accounted for 2,453.23±122.50 mM Trolox/g coffee solid (p<0.05).

3.2 Physical properties

The effects of spray drying conditions and wall material solutions on physical properties of microencapsulated instant coffee were observed including moisture content, water activity, water solubility index (WSI), water absorption index (WAI) and surface morphology shown in Table 1. The results pointed out that increasing KGMH concentration while decreasing MD concentration was tending to produce a lower yield. The increasing of inlet temperature was contributed to better production yield but it was inconsistent. The highest yield was produced by wall material of 20% (w/w) MD at 160 and 180 °C of inlet temperature (p<0.05) which accounted for 65.27%±4.67 and 64.00%±8.03. In all inlet temperature, 20% (w/w) KGMH alone was exhibited comparable results with the mixture of KGMH and MD as wall materials. This result was in line with Tolun *et al.* (2016) [8] which have a similar wall material design with current study and concluded that MD (DE 17-20) alone produced the highest yield at 52.77%, while when MD was mixed with gum Arabic the results had a contrary influence on the yield. During spray drying, instant coffee with KGMH was had more loses because of KGMH properties. KGMH solution is stickier than MD solution, therefore, the amount of adhered sample in drying chamber after drying was found higher in KGMH instant coffee sample.

Table 1. Product yield, moisture content, and water activity of instant coffee

Inlet temperature (°C)	Wall material	Product yield (%)	Moisture content (% w.b.)[ns]	Water activity[ns]
160	20% (w/w) KGMH	53.66±4.81[a]	3.73±0.52	0.24±0.02
	15% (w/w) KGMH + 5% (w/w) MD	52.54±1.88[a]	3.42±0.34	0.22±0.05
	5% (w/w) KGMH + 15% (w/w) MD	61.39±2.65[bcd]	3.75±0.09	0.23±0.00
	20% (w/w) MD	65.27±4.67[d]	3.64±0.53	0.23±0.02
170	20% (w/w) KGMH	54.30±0.15[ab]	3.52±0.36	0.21±0.01
	15% (w/w) KGMH + 5% (w/w) MD	53.07±1.77[a]	3.66±0.22	0.23±0.01
	5% (w/w) KGMH + 15% (w/w) MD	58.31±3.10[abcd]	3.72±0.04	0.23±0.02
	20% (w/w) MD	62.26±6.31[cd]	3.58±0.28	0.22±0.03
180	20% (w/w) KGMH	55.27±2.37[abc]	3.37±0.29	0.25±0.03
	15% (w/w) KGMH + 5% (w/w) MD	53.24±2.91[a]	3.68±0.30	0.25±0.03
	5% (w/w) KGMH + 15% (w/w) MD	61.39±2.65[bcd]	3.40±0.23	0.24±0.01
	20% (w/w) MD	64.00±8.03[d]	3.54±0.10	0.24±0.01

Values in a column followed by different letters are significantly different ($p<0.05$)

ns: non-significant

WSI is an important property to repeal powder behavior in aqueous and its reconstitution ability**.** Table 2. presented the WSI of microencapsulated instant coffee powder from different spray drying condition and formulation. In general, the value of WSI was in contrary to the amount of KGMH used but correlated with increasing of inlet temperature. The most solubilize powder was come from instant coffee produced from 20% (w/w) MD at 180 °C (98.98±0.87%) while the lowest WSI was 20% (w/w) KGMH powder at inlet temperature 170 and 160 °C (89.03±3.68 and 88.95±5.16%) ($p<0.05$). Similar finding from Jafari *et al.* (2017) [9] who found that juice powder with 25-45% (w/w) MD as drying aids

have WSI above 90%, while Adamiec *et al.* (2012) [5] noted that by using combination KGMH and gum Arabic at wall material concentration at 9% (w/w) presented WSI at 67-69%. Even though KGMH instant coffee exhibited the lowest WSI, the value of WSI was still above 88% which mean that all instant coffee powder still have a good solubility.

Table 2. Water solubility index (WSI) and water absorption index (WAI) of instant coffee

Inlet temperature °C	Wall material	WSI (%)	WAI (%)
160	20% (w/w) KGMH	88.95±5.16[a]	8.94±1.51[c]
	15% (w/w) KGMH	91.89±4.10[abc]	3.07±0.76[a]
	5% (w/w) KGMH	96.54±0.88[cd]	3.13±1.36[a]
	20% (w/w) MD	94.08±3.57[cd]	3.20±0.72[a]
170	20% (w/w) KGMH	89.03±3.68[a]	9.01±1.54[c]
	15% (w/w) KGMH	91.90±3.06[abc]	4.59±1.49[ab]
	5% (w/w) KGMH	96.00±0.79[bcd]	3.83±1.60[ab]
	20% (w/w) MD	96.80±2.34[cd]	3.27±1.33[a]
180	20% (w/w) KGMH	89.38±3.61[a]	8.80±1.89[c]
	15% (w/w) KGMH	90.35±3.54[abc]	5.91±1.19[b]
	5% (w/w) KGMH	92.47±5.78[abcd]	5.41±0.64[ab]
	20% (w/w) MD	98.98±0.87[d]	3.58±0.73[ab]

Values in a column followed by different letters are significantly different ($p<0.05$)

4. CONCLUSIONS

Antioxidant property of instant coffee can be enhanced by microencapsulation using KGMH as an appropriate natural wall material. KGMH concentration affected antioxidant and other physicochemical properties. Increasing KGMH concentration leads to the better antioxidant properties including TPC, antioxidant capacity by DPPH and FRAP and chlorogenic acid content. The wall material was able to shield almost all antioxidant component and resulted in the excessive retention percentage. The application of KGMH alone as wall material exhibited the best retention percentage compare to microcapsule made from KGMH-MD in all ratio and MD alone. The inlet temperature of spray drying was showing an important role in antioxidant properties. The increasing of inlet

temperature was correlated with lower retention of antioxidant properties except for chlorogenic acid that was increased. In general, the lowest inlet temperature (160 °C) produced better overall antioxidant properties than spray drying at 170 and 180 °C. The best condition of producing instant coffee from this study is 20% (w/w) KGMH as wall material at 160 °C inlet temperature of spray drying.

5. REFERENCES

[1] Brezová, V.; Šlebodová, A.; Staško, A. Coffee as a source of antioxidants: An EPR study. Food Chemistry 2009, 114, 859-868.

[2] Vignoli, J. A.; Bassoli, D. G.; Benassi, M. T. Antioxidant activity, polyphenols, caffeine and melanoidins in soluble coffee: The influence of processing conditions and raw material. Food Chemistry 2011, 124, 863-868.

[3] Pérez-hernández, L. M., Chávez-Quiroz, K., Medina-Juárez, L. A.;; Meza, N. G. Phenolic characterization, melanoidins, and antioxidant activity of some commercial coffees from Coffea arabica and Coffea canephora. J. Mex. Chem. Soc 2012, 56(4), 430-435.

[4] Zhang, Y.-Q.; Xie, B.-J.; Gan, X. Advance in the applications of konjac glucomannan and its derivatives. Carbohydrate Polymers 2005, 60, 27-31.

[5] Adamiec, J.; Borompichaichartkul, C.; Srzednicki, G.; Panket, W.; Piriyapunsakul, S.; Zhao, J. Microencapsulation of kaffir lime oil and its functional properties. Drying technology 2012, 30, 914-920.

[6] Wattanaprasert, S.; Borompichaichartkul, C.; Vaithanomsat, P.; Srzednicki, G. Konjac glucomannan hydrolysate: A potential natural coating material for bioactive compounds in spray drying encapsulation. Engineering in Life Sciences 2017, 17, 145-152.

[7] Yang, J.; Xiao, J.-X.; Ding, L.-Z. An investigation into the application of konjac glucomannan as a flavor encapsulant. European Food Research and Technology 2009, 229, 467-474.

[8] Tolun, A.; Altintas, Z.; Artik, N. Microencapsulation of grape polyphenols using maltodextrin and gum arabic as two alternative coating materials: Development and characterization. Journal of biotechnology 2016, 239, 23-33.

[9] Jafari, S. M.; Ghalegi Ghalenoei, M.; Dehnad, D. Influence of spray drying on water solubility index, apparent density, and anthocyanin content of pomegranate juice powder. Powder Technology 2017, 311, 59-65

Ambient temperature drying of therapeutic protein solution with use of microwave

Tsuruta, T. [a*]; Ogawa, T.[b]; Abe, R. [b]; Tanigawa, H.[a]

[a] Faculty. Department of Mechanical Engineering. Kyushu Institute of Technology, Fukuoka, Japan.
[b] Graduate School of Mechanical Engineering. Kyushu Institute of Technology, Fukuoka, Japan.

*E-mail of the corresponding author: tsuruta.takaharu393@mail.kyutech.jp

Abstract

High quality drying of therapeutic protein-solution is important in medical and pharmaceutical processing. Freeze-drying is mostly used, but it takes a long drying-time and causes damages of protein structures. In order to improve the drying quality, we propose a microwave vacuum drying performed at ambient temperatures under low-pressure conditions. We are focusing on the Parma-Zyme method for the evaporative drying of protein solutions such as egg white or lysozyme with vitrification. Circular dichroism (CD) spectroscopy is used to detect protein conformation changes due to the drying, and it is found that the ambient temperature drying can preserve the protein conformation.

Keywords: *Microwave vacuum drying; Freeze-drying; Therapeutic protein; Egg white; Lysozyme*

1. Introduction

In recent years, with the progress of biotechnology, the development of pharmaceutical products using biopolymers such as proteins has been rapidly developed. However, it is difficult to stably stored in solution state, many proteins preparations are preserved by freeze-drying (FD). Generally, FD takes a long time (about 1 to 3 days) due to drying accompanied by sublimation of ice, and requires large energy. In addition, changes in the hydration state due to freezing and concentration may result in deactivation and aggregation of proteins. Therefore, studies are under way to prevent denaturation by adding compounds and additives to protein formulations [1]. Considering the situation, we propose a method using a microwave vacuum drying (MVD) as a new method instead of FD. MVD promotes evaporation of water under reduced pressure condition and supplies only latent heat of vaporization by microwave, resulting in the drying at room temperature. It is possible not only to prevent protein damage but also to drastically shorten the dering time. We are focusing on the Perma-Zyme method for the evaporative drying with vitrification, because it has a possibility to increase the vitrification temperature up to the room temperature [2]. Figure 1 shows a solid/liquid state diagram of sucrose water system [3]. In the method of FD, the long process (A-B-C-D) must be followed to get the glassy state for the vital preservation. On the other hand, if the direct phase transition from liquid to solid (glass) at room temperature (A-D), it would have great advantages in the bioindustries. In this study, drying experiments of egg whites and lysozyme protein solutions were carried out using three drying methods of FD, MVD, and a combination of FD and MVD. After the drying, preservation of protein structure/activity, drying time, and solubility were evaluated.
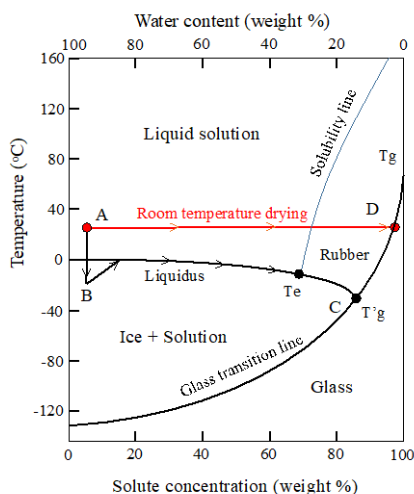
Fig.1 Solid/liquid state diagram of the sucrose water system.

2. Experimental Apparatus and Methods

2.1. Drying methods

The experimental apparatus for the microwave vacuum drying is shown in Fig. 2. The drying system consists of the vacuum drying container, vacuum pump, and microwave irradiation equipment [4, 5]. The drying chamber is a cylinder made from stainless steel, which has an inner diameter of 590 mm and a height of 345 mm. The microwave is introduced into the chamber from the side. The microwave generator has a magnetron with a 3 kW irradiation power at 2.45 GHz. We can select some intermittent irradiation patterns with a different power as well as a continuous irradiation. In order to irradiate the sample uniformly, a turntable is set at the bottom of the chamber. During the experiment, the samples on the table are rotated at a rate of 3rpm.

As experimental samples, 5 g of egg whites (albumin) and 5 g of lysozyme aqueous solution (0.5 g of lysozyme + 4.5 g of purified water) were used as a model of protein solution. The sample is placed in a PFA Petri dish of 50mm in inner diameter. In MVD, four set of samples were placed in a vacuum container, and drying was performed with a microwave output of 50 to 100 W at a pressure of 20 kPa. In FD, the sample was frozen in a freezer at -25 ° C for more than 12 hours, then the frozen sample was set in a vacuum container and dried at a temperature of 5 °C under a pressure of 200 Pa.
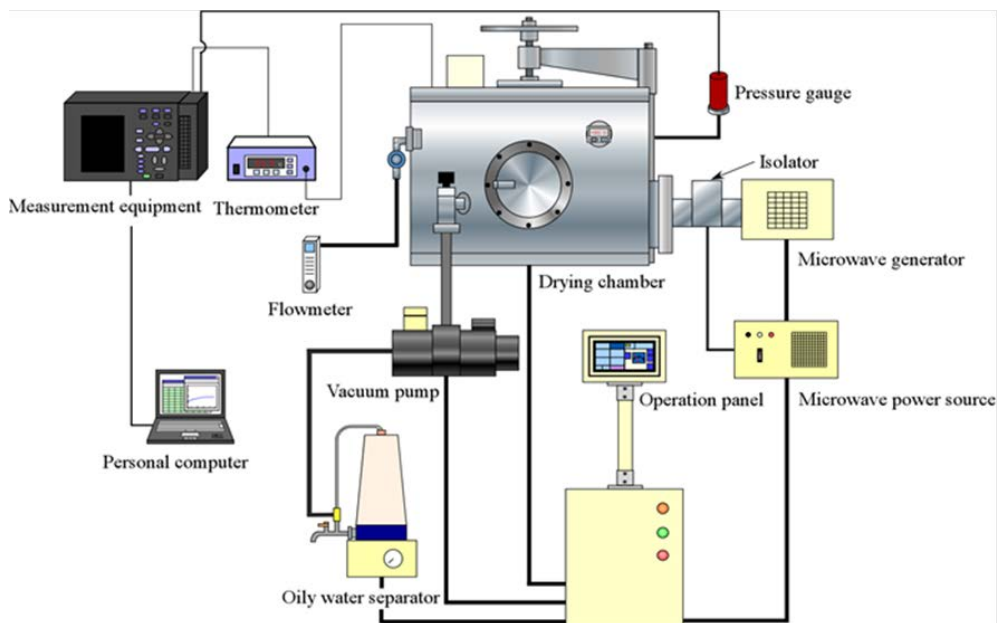
Fig.2 Microwave vacuum drying system.

2.2. Evaluation method of protein conformation changes

Molecular structure analysis was performed using a circular dichroism spectrometer (CD; JASCO Corporation J-820) in order to confirm the denaturation of proteins by drying. Three kinds of dried egg white by MVD, FD and their combination were subjected to the tests. As a reference sample showing thermal damage, the egg white heated at 98 °C for 10 minutes was examined as well as the raw egg white. Ultraviolet visible spectrophotometer (Hitachi High-Tech Science U-3310) was used to adjust to the same concentration, and ultra pure water was used as a solvent.

2.3. Measurement of the residual activity of protein

It is most important to confirm the residual activity of the protein. Therefore, the degradation activity of lysozyme was measured using the UV spectrophotometer. Micrococcus luteus was added to 50 mM phosphate buffer solution so that the absorbance at a wavelength of 600 nm was 1.0 Abs in a 1 cm glass cell to prepare a substrate solution. The aqueous solution of lysozyme of 20 µl was dropped into 2980 µl of the substrate solution, and the time change in absorbance at 600 nm due to substrate degradation of lysozyme was measured. The activity of lysozyme was evaluated assuming that the absorbance immediately after the dropping was 100% and the absorbance after the decomposition was 0%.

2.4. Solubility test

Solubility is important factor for a practical use in medical area. In this study, 0.05 g of dried egg white was dissolved in 5 ml of water and time change of concentration of albumin was measured.

3. Results and Discussions

3.1. Drying of egg white

Figure 3 shows appearances of egg white before and after the drying. The raw egg white is transparent as in (a), it is seen in (b) that dried egg white is a transparent film even after the MVD drying. On the other hand, in the FD of (c) and 1h-MVD+FD of (d), it became a porous state like a sponge cake. In the FD, since ice crystals are dried by sublimation, the ice crystal parts become voids and porous. In 1h-MVD+FD, it is considered that ice crystals became smaller by first 1-hour drying by the MVD, and the porosity decreased. Also, we can see many large cracks in (d).

(a)   (b)   (c)   (d)
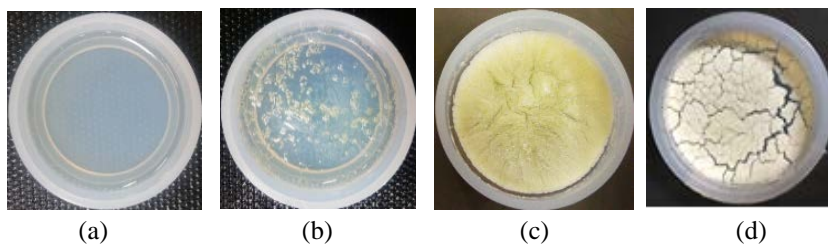
Fig.3 Photographs of egg white before and after drying.
(a) Raw white egg, (b) MVD, (c) FD, (d) 1h-MVD+FD
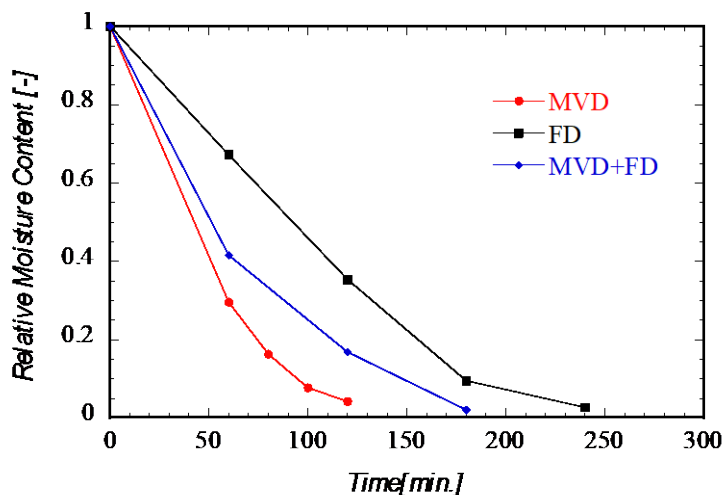
Fig.4 Time transients of moisture content ratio.

Figure 4 shows the time transient of the relative moisture content in each drying process. Drying was carried out until water contents became 0.05 or less. In MVD, the drying temperature was kept bellow 25 °C. Compared to FD, MVD was able to reduce drying time by about 50% and MVD+FD by about 20%.

3.2. Molecular structure analysis of egg white (albumin)

The results of structural analysis on dried egg albumin by CD are shown in Fig.5. It is known that the albumin has two negative peaks at 210 nm and 218 nm in the CD signal. The present results for FD, MVD and MVD+FD indicate two negative peaks similar to the raw egg albumin [6]. However, the CD intensity of the 98 °C-heated sample decreased in wide ranges, and the negative peaks shifted to shorter wavelengths of 207 nm and 217 nm, which indicates that alpha-helix structure of albumin has changed due to heating. It is

confirmed from the results that the room temperature dryings can preserve the albumin without any structural damages.
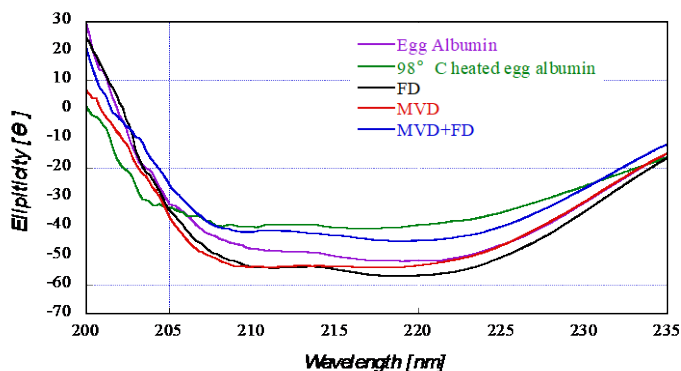
Fig.5 CD spectral analysis of albumin aqueous solution.

3.3. Residual activity of lysozyme

Figure 6 shows the residual activity of lysozyme measured using UV, where the absorbance at 600 nm of wave length was measured by dropping lysozyme into the substrate solution at 150 s. It can be seen that the absorbance of lysozyme heated at 98 °C has not changed. This is because lysozyme was inactivated and could not decompose micrococcus luthus. In contrast, lysozyme processed by FD, MVD, MVD+FD has decreased absorbance after 150s, indicating that the activity of degrading micrococcus leutus can be preserved. The results of calculating the decomposition rate are shown in Table 1. There is no clear difference in the drying method compared to lysozyme.
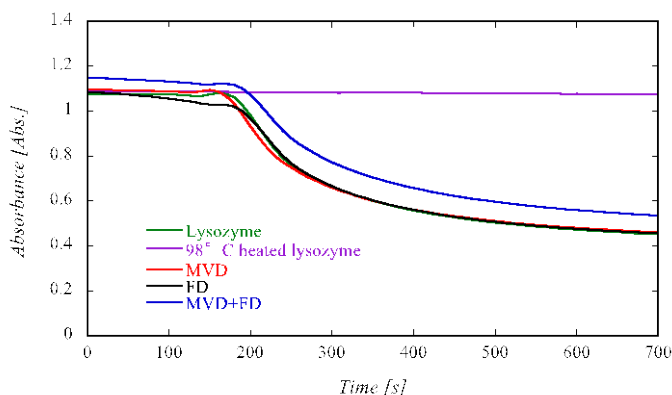
Fig.6 Remaining activity measurement of lysozyme aqueous solution.

Table 1. Decomposition rate

	Lysozyme	MVD	FD	MVD+ FD
Decomposition rate (Abs/s)	0.003791	0.003924	0.003517	0.003192

3.4. Comparison of solubility

Figure 7 compares the time transient of concentration when 0.05 g of dried egg white is dissolved in 5 ml of ultrapure water. It can be seen that the sample by FD treatment dissolved in approximately 10 minutes, while the sample by MVD took about 40 minutes. About 80% or more of sample by MVD + FD has dissolved in the first 20 minutes and it can be said that it is more soluble than MVD. This indicates that ice crystal formation during the freezing contributes the faster solubility.
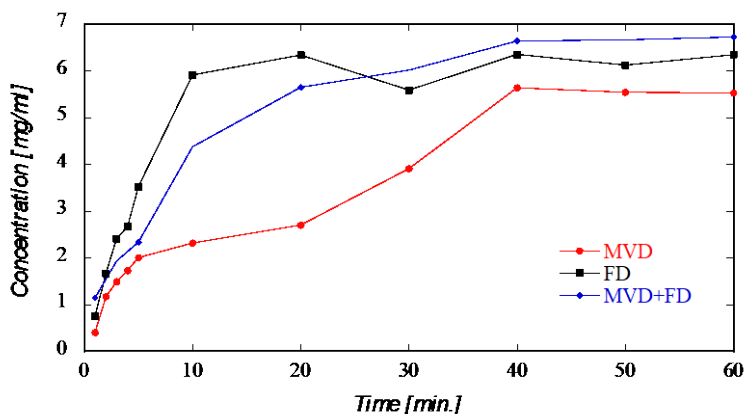
Fig.7 Comparison of solubility of MVD, FD and MVD+FD.

4. Conclusions

The protein aqueous solutions, egg white (albumin) and lysozyme, were dried using three kinds of drying methods, i.e. the freeze-drying (FD) and the microwave vacuum drying (MVD) and their combination, and the conformation change and the activity of preserved protein were examined. Circular dichroism (CD) spectrometer is used to detect protein conformation changes in the drying of albumin, which indicates that the MVD at room temperature can preserve the protein conformation. Also, the UV measurement of the residual activity of lysozyme with use of the micrococcus luteus shows that the room temperature drying shows good performance for the residual activity. It is concluded that the MVD at room temperature enables a less damages and a rapid drying compared to the

FD. It should be noted that MVD is inferior in solubility compared with the FD. The combination of MVD and FD has a possibility for better performances in solubility and drying time.

5. Acknowledgements

6. References

[1] Vázquez-Rey, M.; Lang, D.A. Review; Aggregates in monoclonal antibody manufacturing processes. Biotechnology and Bioengineering 2011, 108 (7), 1494–1508.

[2] Mathias, S.F.; Franks, F.; Hatley, R.H.; The stabilization of proteins by freeze-drying and by alternative methods. In polypeptide and protein drugs: production, characterization and formulation; Hider, R.C, Barlow, D., Eds.; Ellis Horwood Limited.: West Sussex, 1991; 120-131.

[3] Franks, F. Improved freeze-drying: from empiricism to predictability. Cryo-Letters 1990, 11, 93-110.

[4] Tsuruta, T.; Hayashi, T. Enhancement of microwave drying under reduced pressure condition by irradiation control and external air supply. In Proceedings of the Third Nordic Drying Conference NDC2005, Karlstad, Sweden, June 15–17, 2005.

[5] Tsuruta, T.; Tanigawa, H.; Sashi, H. Study on shrinkage deformation of food in microwave-vacuum drying. Drying Technology 2015, 33(5), 1830-1836.

[6] Townend, R.; Kumosinski, T.F.; Timasheff, S.N.; Fasman, G.D.; Davidson, B. The circular dichroism of the β structure of poly-l-lysine 1966 23(2), 163-169.

Immobilization of *Candida rugosa* lipase on eco-friendly supports by spouted-bed technology: Use in the synthesis of isoamyl caprylate

[*]**Costa-Silva, T.A.;[a] Carvalho, A.K.F.;[b] Souza, C.R.F.;[a] Freitas, L.;[b] De Castro, H.F.;[b] Oliveira, W.P.[a]**

[a] Faculty of Pharmaceutical Sciences of Ribeirão Preto, University of São Paulo, Brazil
[b] Engineering School of Lorena, University of São Paulo, Brazil

[*]E-mail of the corresponding author: costa.silva@usp.br

Abstract

Candida rugosa lipase (LCR) was immobilized on low-cost supports (by-products) and dried using a spouted-bed system. The yields of immobilized derivatives were in the range 61.5–78.7%. Lipase immobilized on rice husk showed the best results, presenting 94.1% of the original activity, followed by sugarcane bagasse (90.3%) and green coconut fiber (87.3%). Moisture content in the obtained powders varied between 4.7 and 5.6% and the water activities were in the range 0.21–0.35. Among all the tested biocatalysts for aroma production the lipase immobilized on rice husk showed the highest activity towards the formation of isoamyl caprylate (62.40 g.L^{-1}).

Keywords: Spouted bed dryer; Enzyme dehydration; Enzyme immobilization; Enzyme stabilization; Aroma production.

1. Introduction

Lipases (triacylglycerol acylhydrolase - EC 3.1.1.3) are serine hydrolases formerly characterized by the ability to reacting with a wide range of substrate with a high enantio and regio selectivity.[1] However, the commercialization of enzymes with potential industrial applications, including lipases, depends on their stability during enzymatic reaction and/or storage period.[2] In fact, the water presence in enzyme formulations is the mainly drawbacks for protein stabilization and consequently, for enzyme application.[3] Drying technologies can be utilized to obtain dehydrated and stable thermosensitive products like microbial enzymes.[4] On the other hand, enzyme immobilization are other mechanisms used to improve enzymes properties (like stability, activity, inhibition by reaction products and selectivity toward non-natural substrates), and allows recovery and reuse of the biocatalyst.[2] In this work, we associated the benefits of drying and immobilizing processes and performed them in a single step employing a spouted bed system. Furthermore, we used eco-friendly supports like coconut fibers, rice husk and sugarcane bagasse to prevent emergence of environment ethical issues and cut down the production costs of immobilization processes. Additional information on the catalytic activity was obtained by testing the immobilized derivatives obtained in synthetic applications, that is, in the esterification reaction of isoamyl alcohol with caprylic acid.

2. Materials and Methods

2.1 Enzymatic activity of the free and immobilized lipase

Candida rugosa lipase from Sigma-Aldrich was used in the immobilization assays. Lipase activity assay was performed using ρ-nitrophenyl palmitate (p-NPP) as substrate according to Mayordomo et al. (2000).[5] The mixture was incubated at 40°C for 30 min and then 0.5 mL of 2% trizma base was added.[6] The optical density was measured at 410 nm. Enzymatic activity is given as μmol of *p*-NPP produced per minute per mg of enzyme (IU).

2.2 Lipase Immobilization on agricultural byproducts

"In natura" Agricultural byproducts supplied by local farmers, were oven dried, ground and sieved to obtain particles with sizes between 50 and 150 mesh - Figura 1.
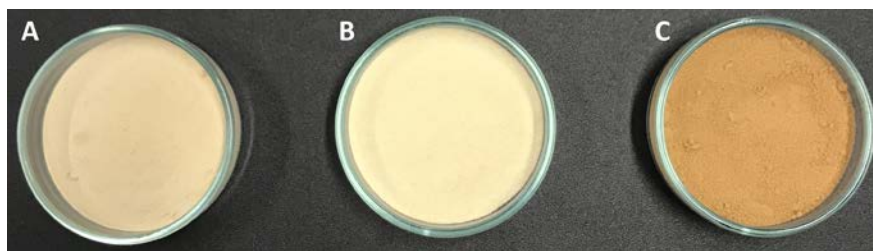
Fig. 1. Agricultural by-products used as support for lipase immobilization: (A) rice husk, (B) sugarcane bagasse, (C) green coconut fiber.

The supports were activated using glutaraldehyde prior to the covalent immobilization method. *Candida rugosa* lipase was immobilized in the by-products previously activated by covalent binding in the presence of polyethylene glycol as a stabilizing agent.[8]

2.3 Spouted Bed Drying of Immobilized Lipase

Immobilized *C. rugosa* lipase was dried using a homemade conical–cylindrical spouted bed, with an internal angle of the conical base of 40° and inlet orifice diameter of 15 mm. A cylindrical column with a diameter of 85mm and height of 300mm was connected to the conical base. Concave cylindrical Teflon particles with a mean diameter of 5.45mm and density of 2,160 kg/m^3 were used as inert material. Table 1 shows the operating parameters of the spouted bed dryer.

Table 1. Spouted bed parameters set for drying of enzyme-support system.

Spouted bed drying parameters	
Inlet gas temperature (T_{gi}), °C	100.0
Drying gas flow rate (Q), m^3/min	0.660
Feed system position	top spray
Mass feed flow rate (Ws), g/min	5.5
Static bed height (H_0), cm	5.5
Mass of inert material (M_i), g	255.0

2.4 Dryer Performance and Product Properties

The spouted bed drying performance and physicochemical product properties were assessed by the following assays: **A. Enzymatic activity:** The lipase activity assay was performed using *p*-NPP as the substrate according to Mayordomo et al.[5] using an immobilized derivative (10 mg) in 50mM of phosphate buffer, pH 6.5. **B. Product stability:** The stability of the immobilized derivatives was assessed by determination of the enzyme activity of dried powder during 3 months of storage at 5 °C. **C. Reuse cycles:** Residual enzymatic activity determination for immobilized lipase after each batch of reaction was determined. The immobilized derivative was recovered by centrifugation and washed with buffer (sodium phosphate buffer 50mM, pH 6.5) for the next reaction test. **D. Product moisture content (Xp):** The moisture content of the spouted bed–dried product was determined by the oven drying method at 105 °C up to a constant weight and was calculated from triplicate analyses. **E. Water activity (aw):** Water activity was determined using an AQUALAB 4TEV-Decagon according to the method of Norenã et al.[9] **F. Efficiency of powder production:** The product recovery (R_E) was defined as the ratio between the total mass of the product recovered to the mass of immoblilized enzyme composition fed to the system (dry basis).

2.5 Synthesis of Isoamyl Caprylate using the immobilized *Candida rugosa* lipase

Reaction systems consisted of isooctane (20 mL), isoamyl alcohol (0.30 mol/L), caprylic acid
(0.30 mol/L) and immobilized lipase derivatives (30 units activity/mL of substrate). The
mixture was incubated at 40 °C for 48 h with continuous shaking at 150 rpm. The consumed
isoamyl alcohol and the formed product were determined by gas chromatography using a 5%
DEGS CHR-WHP 80-100 mesh 6 ft 2.0 mm ID and 1/8" OD column (Restek, Frankel
Commerce of Analytic Instruments Ltd, SP, Brazil) and octanol as an internal standard.[10]
Caprylic acid concentrations were titrated with 0.02 mol.L^{-1} potassium hydroxide solution
using phenolphthalein as an indicator. The alcohol molar conversion (X, %), the productivity
(P, g.L^{-1} isoamyl caprylate h^{-1}) and initial reaction rates (A, μM isoamyl caprylate min^{-1}.g^{-1}
catalyst) were calculated based on Perez et al. (2007).[11]

3. Results and Discussion

Table 2 shows the effect of different supports and glutaraldehyde concentration on outlet
drying gas temperature (T_{go}), temperature inside the spouted bed dryer (T_{in}), process yield
(R_E), and residual enzyme activity (R_{EA}) of the product.

*Table 2. Effect of support and glutaraldehyde concentration on outlet drying gas temperature, bed
temperature, process yield and residual lipase activity.*

Support	GLU (%)	T_{go} (°C)	T_{in} (°C)	R_E (%)	R_{EA} (%)
Rice husk	0.5	81.5±0.6	59.1±0.6	61.5	48.5±0.7
	1.5	78.1±0.4	58.5±1.1	76.2	94.1±0.4
	2.5	79.9±1.2	60.1±0.2	73.0	71.9±1.2
Sugarcane bagasse	0.5	80.8±0.5	59.4±1.3	66.4	53.6±1.1
	1.5	79.3±0.9	58.1±0.9	78.7	90.3±1.4
	2.5	81.8±0.3	60.8±0.2	73.5	62.0±0.9
Green coconut fiber	0.5	82.1±0.5	61.4±1.3	65.1	44.9±1.3
	1.5	79.3±0.9	59.1±0.9	74.6	87.3±0.9
	2.5	81.8±0.3	60.8±0.2	70.8	51.0±1.2

The residual enzymatic activity of all drying formulations used in this study was in the range
44.9-94.1%. Among all preparations evaluated, those containing 1.5% of glutaraldehyde
showed the best result because they exhibited the highest retention of enzyme activity after
spouted bed drying in all assays. *Candida rugoda* lipase immobilized in rice husk actived
with 1.5% of glutaraldehyde showed the best result maintaining 94.1 % of intitial enzyme
activity. The inlet gas temperature used during the drying process was 100 °C, a temperature

that theoretically could provoke enzyme denaturation. However, the spouted bed dryer mechanism and the cooling effect caused by water evaporation prevents the loss of enzymatic activity. Indeed, the average temperature inside the spouted bed (Tin) was 59.7 °C, a condition more appropriate for termosensitive biomaterials comparatively to the inlet temperature applied. The immobilized devivatives recovery rate was compatible with the expected production when a home-made spouted bed is used. Efficiency of powder productions were in the range 61.5–78.7%, depending on the support used. Table 2 shows the moisture content, water activity and residual lipase activity after storage period and five reuse cycles for the lipase immobilized on byproducts actived with 1.5 % of glutaraldehyde. The moisture content in the obtained powders ranged from 2.3 to 5.7% while the water activities of the immobilized derivatives were in the range 0.18–0.33. These values are considered safe to avoid microorganisms growth.[12] Stability tests were performed for all spouted bed dried samples which were stored at 5°C for up to 3 months. The immobilized derivatives obtained had decreased enzyme activity with an average of only 12.4%, whereas the free enzyme form lost 51.7% of its initial activity in the same period. It can be observed that the biocatalysts prepared retained an average of 67.3% of the initial activity after five reuse cycles. Lipase immobilized in rice husk showed the best result maintaining 71.4% of initial enzyme activity. The enzyme activity retention after reuse cycles is very important parameter related to the feasibility of applying on industrial scale.

Table 2. Moisture content, water activity and residual lipase activity after storage period and five reuse cycles for the lipase immobilized on byproducts actived with 1.5 % of glutaraldehyde.

Support	Xp (%, d.b.)	A_w (-)	Storage R_{EA} (%)	Reuse R_{EA} (%)
Sugarcane bagasse	5.0 ± 0.93	0.25 ± 0.09	88.5 ± 1.13	68.6 ± 1.12
Green coconut fiber	5.6 ± 1.20	0.35 ± 0.05	82.4 ± 0.79	62.1 ± 0.93
Rice husk	4.7 ± 0.85	0.21 ± 0.03	91.7 ± 0.58	71.4± 1.03

To verify the behavior of the biocatalysts in non-aqueous media, additional information on the catalytic activity was obtained by testing the immobilized derivatives in synthetic applications, that is, in the esterification reaction of isoamyl alcohol with caprylic acid. This reaction has been suscesfully used to screen the best source of lipase to mediate the synthesis of aroma ester using fusel oil and caprylic acid, being the *Candida rugosa* selected as the most suitable lipase. The results for the tested immobilized lipases are shown regarding consumption of the starting materials and ester formation as a function of time (Figure 2), being the results summarized on Table 3. For all tested lipase immobilized derivatives, the reaction was driven towards to completion (molar conversion higher than 80%) at 48 h. For all runs, no reverse reaction was observed and both starting material were simultaneously consumed with the correspondent ester formation. Under these conditions, productivities

(1.12 - 1.30 g.L^{-1} isoamyl caprylate h^{-1}) were similar for all immobilized derivatives though different initial reaction rates were found (192 to 617 μM min^{-1}.g^{-1}) depending on the support used to immobilize the *Candida rugosa* lipase (LCR). The highest intial rate was found for the LCR immobilized on rice husk and the lowest for LCR immobilized on green coconut fiber.
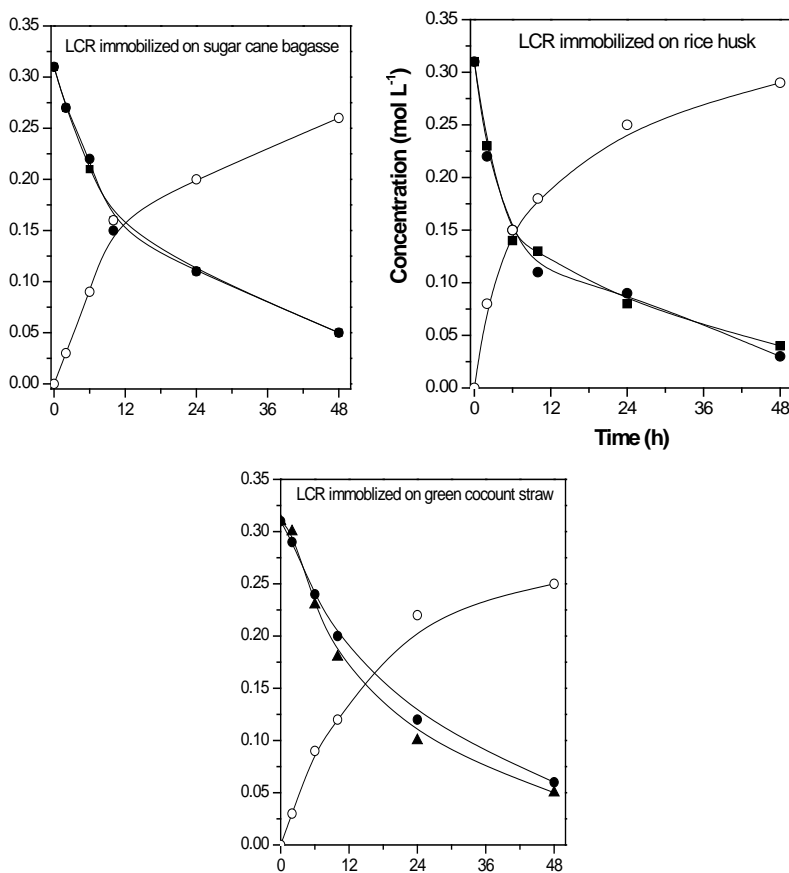
Fig. 2. Performance of Candida rugosa lipase immobilized on different matrixes in the synthesis of isoamyl caprilate (○) from isoamyl alcohol (●) and caprylic acid (▲) at equimolar ratio (40°C, 150 rpm, 0.30 mol.L^{-1} of each starting material in the presence of isooctane as solvent).

Among all the tested biocatalysts the LCR immobilized on rice rusk showed the highest activity towards the formation of isoamyl caprylate (62.40 g.L^{-1}). This is an expected behavior compared with published data, since rice husk is considered among several matrixes derived from lignocellulosic materials the most suitable support for immobilizing lipases due to its high silica contents.[8]

Table 3. Values for initial reaction rate, productivity (P) and molar conversion in the synthesis of isoamyl caprylate by C. rugosa lipase immobilized on different matrixes at 40 ˚C.

Immobilized Lipase	Reaction rate ($\mu M.min^{-1}g^{-1}$)	P[a] ($g\,L^{-1}\,h^{-1}$)	Molar conversion[a] (%)
Sugar cane bagasse	263	1.16	83.87 ± 0.56
Rice husk	617	1.30	88.71 ± 2.20
Green coconut straw	192	1.12	82.25 ± 2.28

[a] Calculated at 48 h reaction

4. Conclusions

The high values of enzyme activity retention and low water content of immobilized derivatives obtained showed that the use of agricultural by-products (eco-friendly supports) combined with the spouted-bed system is a promising technology to be applied for immobilization and stabilization of enzymes of commercial appeal. The tested immobilized lipases showed potential to catalyze the esterification reactions although at different rates. The highest performance was attained by the LCR immobilized on rice husk.

5. Nomenclature

A_w	Water activity	(-)
H_0	Static bed height	(cm)
M_i,	Mass of inert material	(g)
P	Productivity	($g\,L^{-1}\,h^{-1}$)
RE	Process yield	(%)
R_{EA}	Residual enzyme activity	(%)
Tgi	Inlet gas temperature	(°C)
Tgo	Outlet gas temperature	(°C)
Tin	Temperature inside the spouted bed	(°C)
Q	Volumetric flowrate of the spouting gas	(m^3/min)
Ws	Enzyme composition feed flowrate	(g/min)
Xp	Product moisture content	(%, db)
GLU	Glutaraldehyde	-

6. Acknowledgements

7. References

[1] Costa-Silva, T.A.; Nogueira, M.A.; Souza, C.R.F.; Oliveira, W.P.; Said, S. Lipase production by endophytic fungus *Cercospora Kikuchii*: Stability of enzymatic activity after spray drying in the presence of carbohydrates. Drying Technology 2011, 29, 1112–1119.

[2] Mateo, C.; Palomo, J.M.; Fernandez-Lorente, G.; Fernandez-Lafuente, R. Improvement of enzyme activity, stability and selectivity via immobilization techniques. Enzyme and Microbial Technology 2007, 40, 1451–1463.

[3] Adlercreutz, P. Immobilisation and application of lipases in organic media. Chemical Society Reviews 2013, 42, 6406−6436.

[4] Costa-Silva, T.A.; Souza, C.R.F.; Oliveira, W.P.; Said, S. Characterization and spray drying of lipase produced by the endophytic fungus *Cercospora kikuchii*. Brazilian Journal Chemical Engineering 2014, 31, 849-858.

[5] Mayordomo, I.; Randez-Gil, F.; Pietro, J.A. Isolation, purification, and characterization of a cold-active lipase from *Aspergillus nidulans*. Journal of Agricultural and Food Chemistry 2000, 48, 105–109.

[6] Costa-Silva, T.A.; Souza, C.R.F.; Said, S.; Oliveira, W.P. Drying of enzyme immobilized on eco-friendly supports. African Journal of Biotechnology 2015, 14, 3019-3026.

[7] Andrade, G.S.S.; Carvalho, A.K.F.; Romero, C.M.; Oliveira, P.C.; De Castro, H.F. Mucor circinelloides whole-cells as a biocatalyst for the production of ethyl esters based on babassu oil. Bioprocess and Biosystems Engineering 2014, 37, 2539−2548.

[8] Costa-Silva, T. A.; Cognette, R. C.; Souza, C. R. F.; Said, S.; Oliveira, W. P. Spouted bed drying as a method for enzyme immobilization. Drying Technology 2013, 31, 1756−1763.

[9] Norenã, C.Z.; Hubinger, M.D.; Menegalli, F.C. Técnicas básicas de determinação de atividade de água: Uma revisão. Boletim da Sociedade Brasileira de Ciência e Tecnologia de Alimentos 1996, 30, 91–96.

[10] Vilas Bôas, R.N.; Biaggio, F.C.; Giordani, D.S.; De Castro, H.F. Enzymatic synthesis of isopentyl caprylate using fusel oil as feedstock. Quimica Nova 2017, 40, 541-547.

[11] Perez, V.H.; Silva, G.S.; Gomes, F.M.; De Castro, H.F. Influence of the functional activating agent on the biochemical and kinetic properties of *Candida rugosa* lipase immobilized on chemically modified cellulignin. Biochemical Engineering Journal 2007, 34, 13–19.

[12] Beauchat, L.R. Microbial stability as affected by water activity. Cereal Food World 1981, 26, 345–349.

Recent developments in functional bakery products and the impact of baking on active ingredients

Zhang, L. [a,b]; Boom, R.M. [a]; Chen, X.D. [b]; Schutyser, M.A.I. [a]

[a] Laboratory of Food Process Engineering, Wageningen University, Wageningen, the Netherlands.
[b] School of Chemical and Environmental Engineering, Soochow University, Suzhou, China.

*E-mail of the corresponding author: maarten.schutyser@wur.nl

Abstract (100 words)

Active ingredients can be supplemented into a bakery product to produce functional food. However, the preservation of the functionality of these active ingredients during baking remains a challenge for food industry. A deeper understanding of the underlying interactions between functionality and baking is highly desired for developing innovative functional bakery products with significant health benefits and high product quality. In this work, recent advances in the development of functional bakery products are reviewed. The interactions between the baking process and the functionality of the supplemented active ingredients are discussed and the perspective of future research is addressed.

Keywords: baking; active ingredients; probiotics; inactivation kinetics; functional food

1. Introduction

A functional food can be defined as a modified food or food ingredient that may provide a health benefit to the consumer beyond its basic nutrients. Bakery products can be fortified with health-promoting active ingredients to produce non-dairy-based functional food. The viability of the active ingredients such as probiotics in the final products should be sufficient to confer beneficial influence on consumer health. However, for baking process it is a challenge to maintain the functionality of these heat-sensitive active ingredients as high temperatures are involved.

This review aims to illustrate recent advances and challenges in the development of functional bakery products. The interactions between the baking process and the funcationality of the active ingredients are discussed, as well as new technologies such as microencapsulation to preserve the active ingredients during baking. Manufacturing of functional bakery products of good quality and sufficient health-promoting properties leads to interesting research questions and the perspective of future research is addressed.

2. Recent advances in the development of fuctional bakery products

The father of modern medicine Hippocrates declared 2500 years ago that food intake may be beneficial to health: "*Let food be thy medicine and medicine be thy food.*" In modern food industry, a new food category called "functional foods" emerged as a result of the increasing awareness of the link between personal health & well-being and diet. To date, there is no unitary accepted definition for functional foods, nevertheless three main concepts are involved in most of the proposed definitions in literature, i.e., health benefits, nutritional functions and technological processes [1]. Among these concepts, 'technological processes' refer to i) the development of functional foods by optimizing traditional food processing technologies, e.g. fortification of foods with dietary fibre; ii) technologies designed to prevent the deterioration of active ingredients, e.g. microencapsulation; iii) technologies aimed to design personalized functional foods, e.g. application of nutrigenomics; 3D food printing. To simplify, functional foods can be defined as modified food or food ingredients that can provide health benefits to the consumers beyond its basic nutrients.

Functional foods introduced into the market include for example beverages, dairy products, confectionery products, bakery products and breakfast cereals [2]. The category of functional bakery products is newer and received increasing attention in scientific studies. Bakery products are not only nutritious plant-based foods containing macronutrients (e.g. starch and dietary fibre) and micronutrients (e.g. antioxidants and minerals), the transportation and storage of bakery products is also less demanding compared to liquid-form products such as yoghurt. In addition, the worldwide consumption of baked goods on a daily basis makes

these products interesting to serve as potential vehicles to deliver health-promoting ingredients to the human diet.

Table 1 lists some recent studies of functional bakery products with a special focus on bread which is one of the most-consumed staple foods. The main active ingredients supplemented to bakery goods include probiotics and prebiotics (dietary fibres), antioxidants and phenolic compounds [3]. Other functional ingredients are oils and lipids, minerals and salts, and vitamins [2]. Among these ingredients, probiotics and prebiotics are important in human nutrition because of their influences on the gastrointestinal (GI) microbiota. Probiotics are defined as 'live microorganisms which confer a health benefit on the host when administered in adequate amounts' [4]. Prebiotics are short chain carbohydrates which are non-digestible by digestive enzymes in the upper GI tract of humans, but are 'consumed' selectively by some types of bacteria (typically bifidobacteria and/or lactobacilli). Prebiotics can therefore enhance the activity of those beneficial bacteria [5]. The alleged health-promoting benefits of the aforementioned functional bakery products are diverse, e.g. reducing serum cholesterol and blood pressure, reducing the risk of coronary heart diseases, lowering the glycaemic response after food consumption, treating human intestinal barrier dysfunctions [6–10].

Table 1. *An overview of scientific studies focusing on functional bakery products.*

Ingredient	Product	Incorporation strategy	Baking condition	Functionality
Probiotics				
Lactobacillus rhamnosus R011 [11]	biscuit	mix microentrapped cells in whey protein isolate into dough	baked at 280 °C for 5 min	4.5×10^5 CFU/g (initial viability 1.3×10^7 CFU/g)
Lactobacillus acidophilus [12]	bread	apply edible coating layers onto the surface of part-baked bread	baked off at 180 °C for 16 min	~7 log CFU/70 g bread
Lactobacillus reuteri DSM 17938 [13]	chocolate Soufflé	supplement cells microcapsules into dough	70 g dough; frozen at -18 °C; 2 h; baked at 180 °C; 10 min	~3-6 log CFU/g sample from core
Bifidobacterium lactis Bb12 [14]	bread	mix cell suspension into dough	60 g dough; baked at 165, 185 or 205 °C for 12 min	~2-3 log CFU/g (initial viable counts in dough 2.1×10^6 CFU/g)
Lactobacillus rhamnosus GG [15]	bread	apply probiotic containing film solution on the surface	air dry the prebaked bread at 60 °C; 10 min or	7.6-9.0 log CFU/30-40 g bread slice

		of prebaked pan bread	180 °C; 2 min	
(Continued)				
Bacillus coagulans MTCC 5856 [16]	muffin	mix spray-dried bacteria powder into batter	baked at 205 °C for 20-25 min	7.14 log CFU/g (initial viable counts in batter 6.99 log CFU/g)
Prebiotics				
carob fibre/inulin/pea fibre [17]	bread	add 3% fibre to dough	100 g dough; baked at 190 °C for 20 min	total dietary fibre in bread: carob fibre 5.06 %; inulin 5.14 %; pea fibre 5.38 %;
β-glucans & arabinoxylans [18]	flat bread	substitute wheat flour with 20 % barley fibre-rich-fractions	diameter of circular dough sheet 20 cm; baked at 540 °C for 70 s	total β-glucans 3.0 g, arabinoxylans 4.2 g per flat bread
hemicellulose B [19]	bread	add hemicellulose B to dough	baked at 200 °C, baking time N/A	3.87 % dm dietary fibre in baked bread
bacterial nanocellulose (BNC) [20]	bread	disperse BNC gel in water and mix with other ingredients	70 g dough; baked at 195 °C for 23 min	N/A
Others				
tea catechins [21]	bread	mix green tea extract into dough	baked at 215 °C for 11 min	tea catechins content: 0.53 mg/g bread
phenolic antioxidants [22]	bread	substitute wheat flour with fruit phenolic extracts	baked at 155 °C for 60 min	the phenolic recovery ranged from 9 % to 39 %; total antioxidant activity increased
anthocyanin [23]	bread	mix anthocyanin-rich black rice extract powder into dough	50 g dough; baked at 200 °C for 8 min	79 % of cyanidin-3-glucoside was retained in bread crumb after baking

3. Bread baking process

Bread is one of the most-consumed staple foods worldwide. Bread making is a complex process involving dough mixing, proofing (i.e., fermentation), baking and cooling. Among these steps, baking is of great importance because heat and mass transfer occurs simultaneously and interdependently inside the dough during baking, along with a series of physical and chemical changes, e.g. water evaporation, gas cell expansion, starch gelatinization, protein coagulation, dough-crumb transition and crust formation [24]. These changes are dominated by heat and mass transfer mechanisms inside the oven chamber as well as in the product, and interact in a complex manner, which significantly influence the

product quality. A deeper understanding of the bread baking process is necessary to better control the quality of the final products.

During baking, the heat transport in the dough is dominated by the classic 'evaporation-condensation' mechanism [25]. Hence, the temperature in the crumb reaches a plateau of 100 °C while the moisture content remains similar to that of the dough (40 w/w%); the temperature in the crust keeps increasing to the oven temperature (if the baking time is long enough) and the moisture content reduces more significantly (to 20 w/w%) compared to the crumb [26]. These distinct temperature and moisture content histories in the inner part and the outer layer of the dough result in bread with unique macroscopic features, i.e., soft and porous crumb and crispy and dense crust. In addition, the brown colour of the crust and the flavour/aroma of the bread are formed during baking due to the Maillard reactions.

4. Factors influence the functionality of active ingredients

The development of functional bread is challenging for the food industry because active ingredients may fully or partly lose their bioactivity or bioavailability during manufacturing due to either the high baking temperature or their interaction with other ingredients, e.g. decreased bioavailability of water-extractable arabinoxylan in bread due to ferulic acid-protein cross-links [27]. Therefore, it is important to investigate the interactions between the bread making process and the addition of active ingredients.

On the one hand, the baking process can influence the bioactivity of heat-sensitive ingredients supplemented to bread e.g. probiotics [14]. Although certain probiotic strains (i.e., *Bacillus coagulans*) may show high heat resistance due to their ability to form spores (see Table 1) [16], several strategies have been investigated to preserve other probiotic strains (i.e., lactic acid bacteria) under stressful conditions, e.g. micro-entrapment or encapsulation, edible film, coatings, and micro-beads [28–30]. However, application of these technologies may alter quality-attributes of bread. For example, starch based coatings containing probiotics changed the crispness of the bread crust [12]. Nevertheless, data available for the wide application of microencapsulation of active compounds in thermal-processed foods are still rare [31]. Furthermore, a recent study on the inactivation kinetics of *Lactobacillus plantarum* showed that the moisture content of the bread matrix influenced the survial of the embedded bacteria [26]. The survival of this bacterium after baking appeared higher in the crust compared to the crumb for certain balking conditions, which was attributed to the lower moisture content and denser matrix structure in the crust. New strategies to enhance survival of probiotics during baking could therefore benefit by lowering moisture content of the close environment in which the cells are embedded, e.g. via encapsulation or embedded in a thin dried film at the surface of the bread.

On the other hand, incorporation of active ingredients into bread can influence the product quality in either a positive or a negative manner. For example, sourdough fermentation can produce bread with increased specific volume and softer crumb, and some of the added lactic acid bacteria (LAB) produce metabolites with antimicrobial activity, which prolong the shelf-life of bread [32–34]. However, supplementation of some other active ingredients can compromise the organoleptic properties of the products, therefore the modern food industry is seeking for techniques to resolve this problem [35]. For example, encapsulation technology is employed to reduce off-flavours caused by the incorporation of omega-3 fatty acids [36]. Another example is that the substitution of wheat flour with fibre-rich-fractions negatively influences the aesthetic properties of the bread (e.g. dark discolouration, harder crumb with lower loaf volume) [37], which consequently lowers the acceptance of the fortified bread by consumers [38]. In this context, enzymatic pre-treatment of the fibre-rich-fractions might be done to modify their baking properties [39].

5. Conclusion and future perspectives

To develop functional bread that contains sufficient active ingredients without compromising product quality, systematic study on the interactions between the functional ingredients and the baking process is of great importance. Several questions for furture research are identified: i) develop kinetic models for the inactivation of active ingredients during baking based on experimental data, which can be coupled to heat & mass transfer models of baking. The combined model may be used to optimize the baking process to better retain the functionality of active ingredients; ii) further explore the encapsulation of the active ingredients to enhance their resistance against moist-heat during baking; iii) investigate the functionality of the active ingredients during digestion, and the health-promoting properties of those ingredients in clinical trials.

5. References

[1]   Bigliardi B, Galati F. Innovation trends in the food industry : The case of functional foods. Trends in Food Science and Technology. 2013;31(2):118-129.

[2]   Pinto D, Castro I, Vicente A, Bourbon AI, Cerqueira MA. Chapter 25: Functional Bakery Products: An Overview and Future Perspectives. In: Zhou W, Hui YH, De Leyn I, et al., eds. Bakery Products Science and Technology: Second Edition.; 2014:431-452.

[3]   Dziki D. Current trends in the enhancement of antioxidant activity of wheat bread by the addition of plant materials rich in phenolic compounds. Trends in Food Science and Technology. 2014;40:48-61.

[4]   FAO/WHO. Guidelines for the Evaluation of Probiotics in Food. Food and Agricultural Organization of the United Nations and World Health Organization Working Group Report. London Ontario, Canada; 2002.

[5]   Al-Sheraji SH, Ismail A, Yazid M, Mustafa S, Yusof RM, Hassan FA. Prebiotics as functional foods : A review. Journal of Function Foods 2013;5(4):1542-1553.

[6]   Korem T, Zeevi D, Zmora N, et al. Bread affects clinical parameters and induces gut

microbiome-associated personal glycemic responses. Cell Metabolism. 2017;25(6):1243-1253.

[7]   Aleixandre A, Miguel M. Dietary fiber and blood pressure control. Food & Function 2016;7(7):1864.

[8]   Quirós-Sauceda AE, Palafox-Carlos H, Sáyago-Ayerdi SG, et al. Dietary fiber and phenolic compounds as functional ingredients: interaction and possible effect after ingestion. Food & Function. 2014;5(6):1063.

[9]   Brownlee IA, Chater PI, Pearson JP, Wilcox MD. Dietary fibre and weight loss: Where are we now? Food Hydrocolloids. 2016:(In press).

[10] Zubillaga M, Weill R, Postaire E, Goldman C, Caro R, Boccio J. Effect of probiotics and functional foods and their use in different diseases. Nutrition Research. 2001;21(3):569-579.

[11] Reid AA, Champagne CP, Gardner N, Fustier P, Vuillemard JC. Survival in food systems of Lactobacillus rhamnosus R011 microentrapped in whey protein gel particles. Journal of Food Science. 2007;72(1):31-37.

[12] Altamirano-Fortoul R, Moreno-Terrazas R, Quezada-Gallo A, Rosell CM. Viability of some probiotic coatings in bread and its effect on the crust mechanical properties. Food Hydrocolloids. 2012;29(1):166-174.

[13] Malmo C, La Storia A, Mauriello G. Microencapsulation of Lactobacillus reuteri DSM 17938 Cells Coated in Alginate Beads with Chitosan by Spray Drying to Use as a Probiotic Cell in a Chocolate Soufflé. Food Bioprocess Technology. 2013;6(3):795-805.

[14] Zhang L, Huang S, Ananingsih VK, Zhou W, Chen XD. A study on Bifidobacterium lactis Bb12 viability in bread during baking. Journal of Food Engineering. 2014;122(1):33-37.

[15] Soukoulis C, Yonekura L, Gan HH, Behboudi-Jobbehdar S, Parmenter C, Fisk I. Probiotic edible films as a new strategy for developing functional bakery products: The case of pan bread. Food Hydrocolloids. 2014;39:231-242.

[16] Majeed M, Majeed S, Nagabhushanam K, Natarajan S, Sivakumar A, Ali F. Evaluation of the stability of Bacillus coagulans MTCC 5856 during processing and storage of functional foods. International Journal of Food Science and Technology. 2016;51:894-901.

[17] Wang J, Rosell CM, Barber CB de. Effect of the addition of different fibres on wheat dough performance and bread quality. Food Chemistry. 2002;79(2):221-226.

[18] Izydorczyk MS, Chornick TL, Paulley FG, Edwards NM, Dexter JE. Physicochemical properties of hull-less barley fibre-rich fractions varying in particle size and their potential as functional ingredients in two-layer flat bread. Food Chemistry. 2008;108(2):561-570.

[19] Hu G, Huang S, Cao S, Ma Z. Effect of enrichment with hemicellulose from rice bran on chemical and functional properties of bread. Food Chemistry. 2009;115(3):839-842.

[20] Corral ML, Cerrutti P, Vázquez A, Califano A. Bacterial nanocellulose as a potential additive for wheat bread. Food Hydrocolloids. 2017.

[21] Wang R, Zhou W. Stability of tea catechins in the breadmaking process. Journal of Agricultual & Food Chemistry. 2004;52(26):8224-8229.

[22] Sivam AS, Sun-Waterhouse D, Waterhouse GIN, Quek S, Perera CO. Physicochemical properties of bread dough and finished bread with added pectin fiber and phenolic antioxidants. Journal of Food Science. 2011;76(3):97-107.

[23] Sui X, Zhang Y, Zhou W. Bread fortified with anthocyanin-rich extract from black rice as nutraceutical sources: Its quality attributes and in vitro digestibility. Food Chemistry. 2016;196:910-916.

[24] Lucas T. Chapter 19: Baking. In: Zhou W, Hui YH, Leyn I De, M. A. Pagani, C. M. Rosell, J. D. Selman NT, eds. Bakery Products Science and Technology: Second Edition. John Wiley & Sons, Ltd.; 2014:335-354.

[25] De Vries U, Sluimer P, Bloksma AH. A quantitative model for heat transport in dough and crumb during baking. Cereal Sci. Technol. Sweden, Proc. an Int. Symp. 1989:174-188.

[26] Zhang L, Taal MA, Boom RM, Chen XD, Schutyser MAI. Effect of baking conditions and storage on the viability of Lactobacillus plantarum supplemented to bread. LWT - Food Science & Technology. 2018;87:318-325.

[27] Hartmann G, Piber M, Koehler P. Isolation and chemical characterisation of water-extractable arabinoxylans from wheat and rye during breadmaking. European Food Research & Technology. 2005;221:487-492.

[28] Champagne CP, Gardner NJ, Roy D. Challenges in the addition of probiotic cultures to foods. Critical Review of Food Science and Nutrition. 2005;45(1):61-84.

[29] Lakkis JM. Chapter 8: Encapsulation and controlled release in bakery applications. In: Lakkis J, ed. Encapsulation and Controlled Release Technologies in Food Systems, Second Edition. John Wiley & Sons, Ltd.; 2016:204-235.

[30] Vos P de, Faas MM, Spasojevic M, Sikkema J. Encapsulation for preservation of functionality and targeted delivery of bioactive food components. International Dairy Journal. 2010;20:292-302.

[31] Pitigraisorn P, Srichaisupakit K, Wongpadungkiat N, Wongsasulak S. Encapsulation of Lactobacillus acidophilus in moist-heat-resistant multilayered microcapsules. Journal of Food Engineering. 2017;192:11-18.

[32] Cizeikiene D, Juodeikiene G, Paskevicius A, Bartkiene E. Antimicrobial activity of lactic acid bacteria against pathogenic and spoilage microorganism isolated from food and their control in wheat bread. Food Control 2013;31(2):539-545.

[33] Black BA, Zannini E, Curtis JM, Gänzle MG. Antifungal Hydroxy Fatty Acids Produced during Sourdough Fermentation : Microbial and Enzymatic Pathways , and Antifungal Activity in Bread. Applied Environmental Microbiology. 2013;79(6):1866-1873.

[34] Moore MM, Bello FD, Arendt EK. Sourdough fermented by Lactobacillus plantarum FST 1.7 improves the quality and shelf life of gluten-free bread. European Food Research & Technololgy. 2007;226(6):1309-1316.

[35] Patel AR, Velikov KP. Colloidal delivery systems in foods : A general comparison with oral drug delivery. LWT - Food Science & Technology. 2011;44(9):1958-1964.

[36] Gökmen V, Ataç B, Barone R, Fogliano V, Kaplun Z. Development of functional bread containing nanoencapsulated omega-3 fatty acids. Journal of Food Engineering. 2011;105(4):585-591.

[37] Curti E, Carini E, Bonacini G, Tribuzio G, Vittadini E. Effect of the addition of bran fractions on bread properties. Journal of Cereal Science. 2013;57(3):325-332.

[38] Izydorczyk MS, Dexter JE. Barley β-glucans and arabinoxylans: Molecular structure, physicochemical properties, and uses in food products-a Review. Food Research International. 2008;41(9):850-868.

[39] Messia MC, Reale A, Maiuro L, Candigliota T, Sorrentino E, Marconi E. Effects of pre-fermented wheat bran on dough and bread characteristics. Journal of Cereal Science. 2016;69:138-144.

The effect of drying on the mechanical properties and structure of biodegradable films

Rosa, G. S.[a, b*]; Vanga, S. K.[b]; Gariepy, Y.[b]; Raghavan, V.-[b]

[a]Chemical Engineering, Federal University of Pampa, Bagé, Rio Grande do Sul, Brazil
[b]Department of Bioresource Engineering, McGill University, Ste-Anne-de-Bellevue, Quebec, Canada

*E-mail of the corresponding author: gabrielarosa@unipampa.edu.br

Abstract

The aim of this study was to investigate the effect of convective and vacuum drying on properties of biodegradable films. The film-forming solutions were prepared with bovine gelatin and carrageenan. The films solutions were dried in convective and vacuum dryers at temperatures of 40, 50 and 60 ºC. The results of convective drying kinetics of biofilms showed a constant drying rate period followed by a falling drying rate period. The results of thickness showed dependence with moisture content present in films.Carrageenan films showed promising results, with high values of tensile strength and elongation for convective drying at 60 ºC.

Keywords: gelatin; carrageenan; drying; biofilm

1. Introduction

The resulting environmental impact of the high consumption of plastic materials in the food industry has encouraged packaging industry to develop biodegradable packaging materials

that can be used as substitutes for the current synthetic polymers [1]. The biopolymer based packaging films offers several advantages due to their good biodegradability, biocompatibility, environmentally-friendliness, and even edibility [2]. Biopolymer films have been generally classified according to the source of the original polymer utilized. Among the main raw materials, the polysaccharide-based or protein-based materials are the most widely used [3].

Gelatin is an animal protein extracted from skins, bones and connective tissue of animals by controlled hydrolysis of the fibrous insoluble collagen [4;5]. It is well known that gelatin has been widely used in food industries due to its film-forming ability and its use as an outer film to protect food from drying and exposure to light and oxygen [6]. Carrageenans are natural and water soluble sulfated polysaccharides extracted from red seaweeds [7]. The differences in the chemical structure of carrageenans are essential for their physicochemical properties and the helical structure formation leading to varied applications [8]. Park (1996) [9] reported that Kappa-carrageenan is able to produce a clear film with excellent mechanical and structural properties with high tensile strength.

In order to produce efficient packaging films, the properties of films must be optimized for commercial applications. The formation of polymeric films occurs during solvent evaporation and includes complex heat and mass transfer phenomena and polymeric chain reorganization [10]. Several researchers reported on the influence of drying conditions on the mechanical and barrier properties of alginate, whey protein, chitosan, gelatin biofilms [11; 12; 13; 14]. However, the literature does not show results of impact of drying on carrageenan films. The aim of this study was to investigate the effect of convective and vacuum drying on properties of biodegradable films produced from bovine gelatin and carrageenan.

2. Materials and Methods

2.1 Materials

Gelatin from bovine skin and kappa-carrageenan were used as biopolymeric matrix while glycerol (analytical grade) was used as a plasticizer. All reagents were obtained from Sigma-Aldrich (USA); distilled water was available in the laboratory for preparation of all solutions.

2.2 Biofilm formation and Drying

Gelatin and carrageenan films were produced by the casting method, using the methodology proposed by Martiny [15]. The convective drying of films was performed in a custom made laboratory convective hot-air dryer. The perpendicular air flow coming from the blower was heated by an electrical heater. The inlet and outlet air temperatures were measured outside the shielded cavity using type-T thermocouples. The convective drying conditions were 40, 50 and 60 ºC at an air velocity of one m/s. The drying curves ($(M\text{-}M_e)/(M_0\text{-}M_e)$ as a function of time) were obtained. The equilibrium moisture content was assumed as the final moisture

content, when the drying rate was practically null, at each drying condition. The drying rates were determined using Equation 1.

$$R = -\frac{L_s}{A} \cdot \frac{dM}{dt} \qquad (1)$$

where, R is the drying rate (kg.h^{-1}.m^{-2}), L_s is dried solids mass (kg), A is drying area (m²), M is the moisture content (kg.kg^{-1}, d.b.) and t is time (h).

The vaccum drying of films was performed in a vaccum oven (StableTemp, Cole-Parmer, USA) with controlled temperature connected with vaccum line (25" Hg) for 48 h. The same temperatures studied in convective dryer (40, 50 and 60 ºC) were applied for vaccum drying.

2.4 Biofilm characterization

The biofilm thickness was measured using a electronic digital micrometer (Marathon Co, CO030025, Canada) with 0.001 mm of resolution. Mean thickness was calculated from ten measurements taken at different locations on biofilm samples, according to Ferreira et al. [16]. Water vapor permeability (WVP) of biofilms was determined gravimetrically using the ASTM standard method E96/E96M-05 [17]. Tensile strength (TS) and elongation percentage (E) at break point were measured uniaxially by stretching the specimen in one direction using a Universal Testing Machine (50 N load cell - Instron 4502, USA) according to the ASTM standard method D-882-02 [18] . Scanning electron micrographs (SEM) of the film samples submitted to different drying temperatures and methods were obtained using a scanning electron microscope (Hitachi, TM 3000, Japan). Experimental data were analyzed by Statistica 7.1 software. Mean comparasions were carried out by Tukey test (p < 0.05 was considered as significant).

3. Results and Discussion

Typical drying curves obtained are illustrated in Figure 1. Overall drying kinetic curves obtained for biofilms samples under different drying conditions showed the same behavior. In all experiments, the drying kinetics of biofilms showed a constant drying rate period followed by a falling drying rate period. The drying of high moisture materials typically presents a constant drying rate period and one or two falling rate periods [19].The moisture contents of the samples at the end of the drying process were in the range of 0.2 to 1.8 g.g^{-1} (d.b.) and the time taken to reach the final moisture content (M_e) increased from 234 min to 360 min.
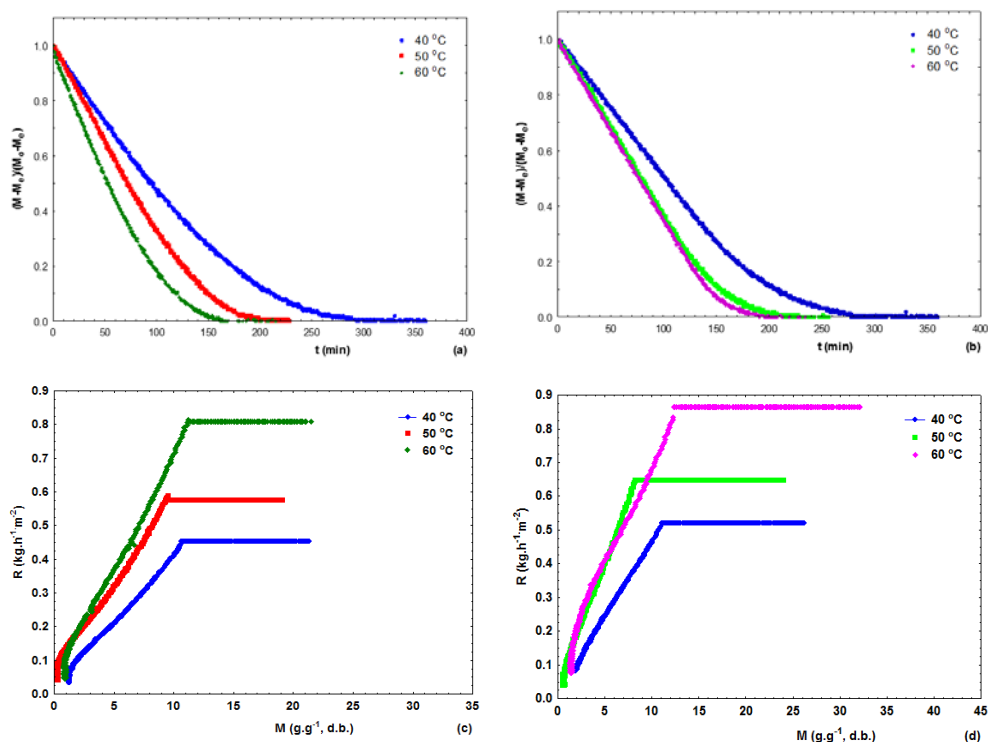
Fig. 1 Drying curves of biofilms at diferent operation conditions:
(a) and (c) gelatin films; (b) and (d) carrageenan films.

As the moisture content of the samples was very high during the initial phase of the drying, higher drying rates were observed. As the drying progressed, the moisture loss (solvent-water) from the product resulted in the fall of drying rate. Various studies also reported that drying curves of polymers dispersed in solvents showed an initial period of constant drying rate before the falling rate period [19; 20; 21]. During the falling rate period, water movement may occur in the films via liquid diffusion, which is driven by moisture gradients, and vapor diffusion. This is enhanced by the vapor partial pressure gradients induced by the temperature gradients. Because pores were not observed in the SEM micrographs of film (Figure 2), liquid movement via capillarity is less probable [22; 19].

Table 1 shows the values obtained for thickness, water vapor permeability (WVP), tensile strength (TS) and elongation (E) of the gelatin and carrageenan biofilms.

Table 1. Physical and mechanical properties of gelatin and carrageenan films.

	Thickness (mm)	WVP (g.m^{-1}.s^{-1}.Pa^{-1})	TS (MPa)	E (%)
G-Conv 40 ºC	0,122 ±0,007[bc]	1,99.10^{-10}±3,80.10^{-12} [c]	24,50±3,58[ab]	80,76±8,92[ab]
G-Conv 50 ºC	0,100±0,007[ab]	1,47.10^{-10}±4,91.10^{-12} [ab]	30,19±2,11[b]	128,56±21,12[b]
G-Conv 60 ºC	0,128±0,016[c]	1,91.10^{-10}±5,76.10^{-12} [bc]	21,10±5,61[ab]	115,84±28,96[b]
G-Vacc 40 ºC	0,106±0,003[abc]	1,47.10^{-10}±1,83.10^{-11} [ab]	28,17±7,84[b]	68,10±2,80[ab]
G-Vacc 50 ºC	0,090±0,008[a]	1,38.10^{-10}±4,35.10^{-12} [a]	13,86±3,75[a]	19,16±3,08[a]
G-Vacc 60 ºC	0,080±0,008[a]	1,32.10^{-10}±1,35.10^{-12} [a]	12,19±2,04[a]	25,57±6,53[a]
C-Conv 40 ºC	0,081±0,002[bc]	1,32.10^{-10}±2,34.10^{-12} [ab]	41,48±0,85[ab]	64,49±5,06[ab]
C-Conv 50 ºC	0,089±0,004[a]	1,38.10^{-10}± 1,65.10^{-12} [a]	37,73±4,99[a]	80,66±8,11[b]
C-Conv 60 ºC	0,087±0,004[ab]	1,421.10^{-10}±4,05.10^{-12} [a]	42,63±5,64[ab]	68,69±13,62[ab]
C-Vacc 40 ºC	0,089±0,003[a]	1,35.10^{-10}±4,94.10^{-13} [a]	48,26±3,46[ab]	69,82±4,25[ab]
C-Vacc 50 ºC	0,074±0,007[c]	1,20.10^{-10}±2,10.10^{-12} [b]	54,44±3,16[b]	62,42±1,14[a]
C-Vacc 60 ºC	0,087±0,004[ab]	1,42.10^{-10}±2,03.10^{-12} [a]	44,78±3,31[ab]	56,89±3,59[ab]

Average±deviation (n=10 for thickness, n=2 for WVP, n=3 for mechanical properties)
Different letters in the same column (separated gelatin (G-) and carrageenan (C-) films) indicate significant differences between samples ($p < 0.05$)

The film thicknesses were in the range of 0.074 to 0.128 mm and showed significant difference ($p>0.05$) regarding films obtained from diferents drying methods and temperatures. Ahmad et al. [23] reported that the thickness depends on the components and the water content in film structure. Gelatin biofilms obtained showed properties similar to those published by other authors. Nishihora [24] reported a thickness of 0.086 mm and WVP of 1.82.10^{-10} g.m^{-1}.s^{-1}.Pa^{-1}; Albertos et al. [25] reported WVP of 2.10^{-10} g. m^{-1}.s^{-1}.Pa^{-1}; Bertan [26] showed thickness values between 0.075 and 0.128 mm; Musso et al. [27] reported a WVP from 6.5.10^{-10} to 7.9.10^{-10} g.m^{-1}.s^{-1}.Pa^{-1}, tensile strength from 3.4 to 4.6 MPa and elongation between 159 to 206 %.

Martins et al. [28] produced carrageenan films and obtained thickness of 0.052 mm, 16.18 % elongation and 19.95 MPa for tensile strength. Several studies with carrageenan films have shown WVP from $5.8.10^{-11}$ to $2.18.10^{-8}$ g. $m^{-1}.s^{-1}.Pa^{-1}$ [28; 29; 30; 31; 32; 33], tensile strength from 11.64 to 26.29 MPa and elongation from 2.54 to 45 % [28; 31; 33; 34].

The data reported in the literature for tensile strength and elongation are smaller than those obtained in this work. This was attributed to the differences in the preparation, composition and proportions of the film-forming solutions. Results for carrageenan films looked promising. Normally, a high tensile strength in the formulated film is common, however the flexibility of the film, indicated by the elongation is a very important parameter. This enables better applicability of this film in packaging [35].

There were no significant difference (p<0.05) between the WVP, tensile strength and elongation of carrageenan biofilms obtained from convective drying. Also, gelatin biofilms obtained from convective drying did not show significant difference for tensile strength and elongation. This is a desirable since the convective drying can be faster when the temperature is 60 ºC.

SEM images of gelatin and carrageenan films are shown in Figure 2. Among the films, the gelatin films were more homogeneous and transparent, while the carrageenan film had the highest density of clusters and the highest opacity. These images show smooth and homogeneous surfaces for gelatin films. Despite the carrageenan films showing a heterogeneous surface, it was not possible to see defects and cracks. The non-uniformity of carrageenan films was attributed to the early gelation during casting [31].

| (a) | (b) | (c) | (d) |
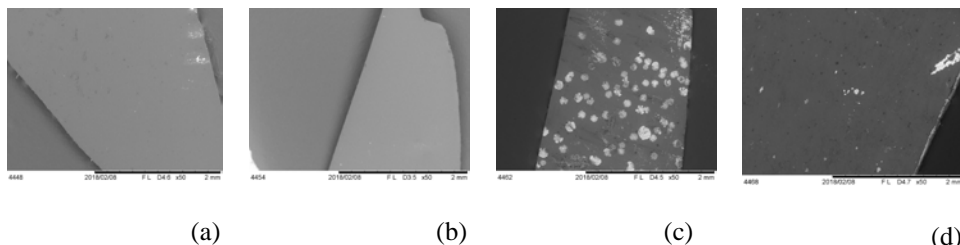
Fig. 2 SEM micrographs of surface of films obtained from (a) gelatin-convective drying at 50 ºC, (b) gelatin-vaccum drying at 50 ºC, (c) carrageenan-convective drying at 50 ºC, (d) carrageenan-vaccum drying at 50 ºC.

4. Conclusions

The development of this research allowed to investigate the effect of convective and vacuum drying on properties of gelatin and carrageenan films. The convective drying kinetics showed a constant drying rate period followed by a falling drying rate period, wich is typical of materials with high moisture content. The results of thickness showed dependence with

moisture content present in films. Carrageenan films showed promising results, with high values of tensile strength and elongation even for those made in the convective dryer at 60 ºC.

5. Acknowledgements

6. References

[1] Rhim, J.W. Mechanical and water barrier properties of biopolyester films prepared by thermo-compression. Food Science and Biotechnology 2007, 16 (1), 62–66.

[2] Salmieri. S.: Lacroix. L. Phvsicochemical Properties of Alginate/Polycaprolactone-Based Films Containing Essential Oils. J. Agric. Food Chem. 2006, 56, 10205-10214.

[3] Park, H.; Byun, Y.; Kim, Y.; Whiteside, W.; Bae, H. Innovations in food packaging (2nd ed.). Processes and applications for edible coating and film materials from agropolymers. Academic Press, 2014.

[4] Karim, A.A.; Bhat, R. Gelatin alternatives for the food industry: Recent development challenges and prospects. Trends in Food Science & Tehcnology 2008, 19, 644-656.

[5] Patil, R.D.; Mark, J.E.; Apostolov, A.; Vassileva, E.; Fakirov, S. Crystallization of water in some crosslinked gelatins. European Polymer Journal 2000, 36 (5), 1055-1061.

[6] Arvanitoyannis, I.S. Formation and properties of collagen and gelatine films and coating. In A. Gennadios (Ed.), Protein-based films and coating. Boca Raton: Florida, 2002, 275-302.

[7] Campo, V.L.; Kawano, D.F.; Silva, D.B.; Carvalho, I. Carrageenans: Biological properties, chemical modifications and structural analysise A review. Carbohydrate Polymers 2009, 77, 167-180.

[8] De Ruiter, G.A.; Rudolph, B. Carrageenan biotechnology. Trends in Food Science & Technology 1997, 8, 389-395.

[9] Park, H. Gas and mechanical barrier properties of carrageenan-basedbiopolymer films. Food Science and Industry 1996, 29, 47-53.

[10] Putranto, A.; Chen, X.D.; Webley, P.A. Infrared and convective drying of thin layer of polyvinyl alcohol (PVA)/glycerol/water mixturedThe reaction engineering approach (REA). Chemical Engineering and Processing 2010, 49, 348-357.

[11] Da Silva,M.A.; Bierhalz, A.C.K.; Kieckbush, T.G. Influence of drying conditions on physical properties of alginate films. Drying Technology 2012, 30, 72-79.

[12] Denavi, G.; Tapia-Blácido, D.R.; Añón, M.C.; Sobral, P.J.A.; Mauri, A.N.; Menegalli, F.C. Effects of drying conditions on some physical properties of soy protein films. Journal of Food Engineering 2009, 90, 341-349

[13] Fernández-Pan, I.; Ziani, K.; Pedroza-Islas, R.; Maté, J.I. Effect of drying conditions on the mechanical and barrier properties of films based on chitosan. Drying Technology 2010, 28, 1350-1358.

[14] Menegalli, F.C.; Sobral, P.J.A.; Roques, M.A.; Laurent, S. Characteristics of gelatin biofilms in relation to drying process conditions near melting. Drying Technology 1999, 17, 1697-1706

[15] Martiny, T.R. Development of biodegradable films based on gelatine and carrageenans of the red algae gigartina skottsbergii incorporated with fluid extract of olive leaves. 137 p. MSc.(Master in Engineering), Federal University of Pampa , 2017

[16] Ferreira, C.O.; Nunes, C.A.; Delgadillo, I.; Silva, J.L. Characterization of chitosan whey-protein films at acid pH, Food Res. Int. 2009, 42, 807-813.

[17] ASTM. Standard methods of water vapor transmission of materials. Method: E96/E96M05. Philadelphia: American Society for Testing Materials, 2005.

[18] ASTM. Standard test methods for tensile properties on thin plastic sheeting. Method: D 882. Philadelphia: American Society for Testing Materials, 2002.

[19] Moraes, J.O; Scheibe, A.S.; Carciofi, B.A.M.; Laurindo, J.B.; Conductive drying of starch-fiber films prepared by tape casting: Drying rates and film properties, LWT - Food Science and Technology 2015, 64, 356-366.

[20] Stupa, M.V.; Platonov, E.K.; Milkhailov, V.T. Mathematical model of drying of granulated anid. Fibre Chemistry, 2003, 35, 233-236.

[21] Karapantsios, T.D. Conductive drying kinetics of pregelatinized starch thin films. Journal of Food Engineering 2006, 76(4), 477-489.

[22] Kerr, W.L. Food drying and evaporation processing operations. Handbook of Farm Dairy, and Food Machinery 2007, 303-340

[23] Ahmad, M.; Hani, N.M.; Nirmal, N.P.; Fazial, F.F.; Mohtar, N.F.; Romli, S.R. Progress Org. Coating 2015, 84, 115-127.

[24] Nishihora, R.K. Properties of crosslinked gelatin films by enzymatic and physical route. 96 p. MSc. (Master in Chemical Engineering), Federal University of Santa Catarina, 2015.

[25] Albertos, I.; Avena-Bustillos, R.J.; Martín-Diana, A.B.; Dub, W.X.; Rico, D.; McHugh, T.H. Antimicrobial Olive Leaf Gelatin films for enhancing the quality of coldsmoked Salmon Food Packaging and Shelf Life 2017, 13, 49-55

[26] Bertan, L.C. Development and characterization of biofilms based on polymers from renewable sources and its application in the packaging of bread of form. 188 p. PhD (Teshis in Food Technology), State University of Campinas, 2008.

[27] Musso, Y.S.; Salgado, P.R.; Mauri, A.N. Smart edible films based on gelatin and curcumin Food Hydrocolloids 2017, 66 8-15.

[28] Martins, J.T.; Cerqueira, M.A.; Bourbon, A.I.; Pinheiro, A.C.; Souza, B.W.S.; Vicente, A.A. Synergistic effects between k-carrageenan and locust bean gum on physicochemical properties of edible films made thereof. Elsevier, Food Hydrocolloids, v. 29, p. 280-289, 2012.

[29] Karbowiak, T.; Debeaufort, F.; Champion, D.; Voilley, A. Effect of Plasticizers (Water and Glycerol) on the Diffusion of a Small Molecule in Iota-Carrageenan Biopolymer Films for Edible Coating Application. Biomacromolecules 2006, 7, 2011-2019.

[30] Larotonda, F.D.S. Biodegradable films and coatings obtained from carrageenan from *Mastocarpus stellatus* and starch from Quercussuber. Faculty of Engineering of the University of Porto. Ph.D thesis, 2007..

[31] Paula, G.A.; Benevides, N.M.B.; Cunha, A.P.; Oliveira, A.V.; Pinto, A.M.B.; Morais, J.P.S.; Azeredo, H.M.C. Development and characterization of edible films from mixtures of κ-carrageenan, ι-carrageenan and alginate. Elsevier, Food Hydrocolloids 2015, 47, 140-145.

[32] Rhim, J.W. Physical-Mechanical Properties of Agar/κ-Carrageenan Blend Film and Derived Clay Nanocomposite Film. Journal of Food Science 2012,. 77 (12), 66-73.

[33] Shojaee-Aliabadi, S.; Hosseini, H.; Mohammadifar, M.A.; Mohammadi, A.; Ghasemlou, M.; Hosseini, S.M.; Khaksar, R.Characterization of k-carrageenan films incorporated plant essential oils with improved antimicrobial activity. Carbohydrate Polymers 2014, 101, 582-591.

[34] Cha, D.S.; Choi, J.H.; Chinnan, M.S.; Park, H.J.Antimicrobial Films Based on Na-alginate and k-carrageenan. Lebensmittel-Wissenschaft and Technologie (LWT) 2002, 35, 715-719.

[35] Kim, Y.T; Min, B.; Kim, K.W. General Characteristics of Packaging Materials for Food System. Innovations in Food Packaging: Second Edition. Elsevier, 2013.

Investigation of influence of pre-treatment and low-temperature on drying kinetics, sorption properties, shrinkage and color of brown seaweeds (Saccharina Latissima)

Tolstorebrov, I.ᵃ*; Eikevik, T.M.ᵃ; Petrova, I.ᵃ; Shokina, Y.ᵇ; Bantle, M.ᶜ

a Department of Energy and Process Engineering, Norwegian University of Science and Technology, NO-7049 Trondheim, Norway

Tel.: +47 73593742,

b Department of Food Production Technology, Murmansk State Technical University, Murmansk Russian Federation

c Sintef Energy Research, Trondheim Norway

*E-mail of the corresponding author: ignat.tolstorebrov@ntnu.no

Abstract

Drying kinetics of Saccharina latissima (raw and blanched) at low temperatures (10.0, 25.0 and 38.0 °C) was studied. The effective moisture diffusivity coefficient varied due to temperature alterations in the range between 1.4 and 4.5 10^{-10} m^2/s for raw and 0.91 and 2.56 10^{-10} m^2/s for blanched seaweeds. Significant changes in structural properties and chemical composition resulted in a much longer drying time of blanched seaweeds, when compared with raw. Drying temperature of 38.0 °C resulted in more brown color, when compared with other samples. Sorption characteristics of dried raw seaweeds depended on salt content and showed high accumulation of moisture at relative humidity of air of 80.0 %. The blanched seaweeds showed linear accumulation of moisture within increasing of relative humidity of drying air from 20.0 to 80.0 %, but high level of hysteresis was determined between sorption and desorption isotherms. The shrinkage development within dewatering of blanched and raw samples was also studied.

Keywords: brown seaweeds, drying kinetics, sorption isotherms, color

1.   Introduction

As much as 36 % (30 million tons of total harvest) of seaweed is used as a direct food source[1]. The main representatives of the food-grade seaweeds are: Laminaria japonica (Kombu) and Saccharina latissima (Royal Kombu) [2], which are mostly produced and consumed inAsia. At the same time the key advantage (and the main potential) of the seaweed industry in Europe is its independence from three main resources, that limit conventional agriculture: land, water and fertilizers [3]. The brown seaweeds Saccharina Latissima are cultivated now in Norway with the aim to produce food-grade products. However, the harvesting season is short and raw material has a very low stability. Thus, the effective stabilization method is required.

Drying is the common way to preserve food products like seaweed and most of the seaweeds are sold in a dried form [4]. Solar and natural drying of seaweeds is a cost-effective method. At the same time climate conditions can result in a high final moisture content in dried porduct[5] due to high moisture absorption ability [6], aslo, the process 5 or 7 days [7] and this is not a feasible and safe to apply the method for food graded seaweeds for European market. The demand for traceability and safety appears, when the drying process is used for food production. Drying of seaweeds for long time and/or at high temperature influences negatively on their carbohydrates, amino acid composition and vitamin content [8]. The resent study of Saccharina Latissima revealed that decreasing of the drying temperatures results in the increasing of quality[9]

The task of this study was the determination of the main process dependencies for the low temperature drying of Saccharina Latissima after frozen storage with the aim of implementation this knowledge into the sustainable drying process.

2.   Materials and Methods

2.1 Characterization of raw material

The brown algae *Saccharina latissima*, which is commonly referred as kelp (Sugar kelp or kombu) was used for the experiments. The seaweeds was cultivated for one year in an aquaculture farm, which is situated in Sør-Trøndelag (Norway). Harvesting season was 3 days in May 2016 to maintain the best quality of the seaweeds and avoid high amount of biofouling. The seaweed was harvested into nets (75-150 kg). The nets were buffered in the seawater at the farm for up to 1 weeks before processing. Then the seaweeds were sorted to remove seaweed of a bad quality. Afterwards, the seaweed was weighed out and packed inside vacuum bags with high barrier properties (2.0 kg each). Freezing was at –46 °C for 20-25 min until the temperature inside the bag reached -18.0 °C. The bags were packed in cardboard boxes, put on pallets and placed in freeze storage at -18 °C. The freezing process was applied to stabilize the product, because harvesting season is short (few days) and high

amount of biomass is difficult to process before deterioration will start. Chemical composition of the aquaculture seaweeds is given in the Table 1.

Table 1. Chemical composition of Saccharina latissima at harvesting season (analysis performed by accredited analytical laboratory Kystlab preBIO, Frøya, Norway).

Chemical composition	%, d.b.	Minerals , mg/kg d.b.	
Proteins	11.2	Potassium	84000
Fats	2.9	Sodium	52000
Carbohydrates	55.3	Calcium	10000
Incl. Dietary fiber	46.6	Magnesium	7500
Ash	37.9	Sulfur	7300
Incl. Salt (NaCl)	14.6	Iodine	3670
Water	900.0	Phosphrus	1700

2.2 Experiment description

The frozen seaweeds were divided into two groups: one was blanched seaweeds another group was raw seaweeds without any processing. Frozen seaweeds were defrosted at +5.0 °C in refrigeration cabin to avoid significant degradation of tissues. The blanching took place in a boiling water (100.0 ºC) for 1.0 min. The balnched seaweeds were immediately cooled in water (5.0 °C). The drying took place on shelves in drying chamber with a closed loop air circulation. The following parameters were varied during drying experiments: air temperature: 10, 25 and 38 ºC; amount of seaweed's layers: 1 layer, 2 and 3. The seaweeds were placed in a drying chamber on shelves parallel to the air flow. Relative humidity of drying air for all cases was 16.0 ±4.0 %. Drying air velocity 1.5±0.5 m/s. The drying process was stopped when the moisture content was in the range between 20.0 and 10.0% d.b.

2.3 Determination of drying kinetics

The drying behaviors were modelled using Newton model. The drying behavior itself was characericed via determination of the effective moisture diffusivity. This material property was derived from the drying kinetics via analytical solution of the Fick's second law of diffusion (infinite slab).

2.4 Determination of sorption and desorption properties at different temperatures

Sorption isotherms were determined for dried balnched and dried raw seaweeds at 10.0, 25.0 and 38.0 °C. Desorption properties were determined by drying of raw seaweeds at 25.0 °C 20.0 % RH.

2.5 Determination of color

Color was analyzed with the assistance of ColorFlex EZ Spectrophotometer (HunterLab, USA) using CIE L*C*h* scale. The lightness L* varies from black (L*=0) to perfect white (L*=100). The chromaticity C* reflects the colorfulness; when C*=0, the object is considered to be colorless. Hue is an attribute of a visual sensation, according to which an area appears be similar to one of the perceived colours or to a combination of two of them. It is measured in degrees from 0 to 360°, rose (h*=0°), yellow (h*=90°), green-blue (h*=180°), and blue-violet (h*=270°).

2.6 Statistical analysis

The analysis of variance (ANOVA: single test and two-factor test with replication) was applied to analyze the obtained data. The difference was considered significant at $p<0.05$. All the experimental points were done in six parallels, except of desorption isotherm determination, where each point represents a single experiment. A regression analysis was done with a software DataFit 8.1 program (Oakdale Engineering).

3.   Results and Discussion

3.1. Influence of pretreatment and drying modes on color of seaweeds

The blanching process alternated the lightness (L*), chrominance (C), and hue (h) of the seaweeds ($p<0.05$). The typical brown-olive color (by human eye perception) of the seaweeds visually changed to green, this was reflected by increasing of hue by 12⁰ and alteration of chrominance by 71.0 %, Table 2. The lightness of dried raw samples were significantly higher when compared with dried blanched ($p<0.05$). This might be possible due to deposits of salts and other water soluble compounds (for example, mannitol) on the surface of the dried blades of Saccharina latissima, which created a layer on surface with high reflective properties. Chrominance of dried raw seaweeds was also higher ($p<0.05$). Some interesting observations were found regarding the influence of temperature on the hue-value of the dried seaweeds. The drying temperature of 38.0 °C resulted in a slight decreasing of the hue-value, so the color became more "orange (brown)" (in terms of L*C*h* color space), while the seaweeds dried at 10.0 °C showed more "yellow-green" color. This was valid both for raw and blanched seaweeds. One of the possible explanation may be a higher oxidation rate of the pigments by oxygen at a higher temperatures [10].

Table 2. Color parameters of raw and blanched seaweeds before and after drying

Type of seaweeds	Before drying (Color parameters)								
	L*, (-)		C, (-)		h,º		a*, (-)		b*, (-)
Raw seaweeds	9.78 (0.96)		8.08 (1.97)		80.23 (1.45)		1.39 (0.43)		7.96 (1.94)
Blanched seaweeds	11.54 (1.29)		13.84 (1.63)		92.00 (4.04)		-0.13 (1.25)		14.74 (1.39)
	After drying (Color parameters)								
	L*, (-)			C, (-)			H,º		
	Temperature, °C								
	38.0	25.0	10.0	38.0	25.0	10.0	38.0	25.0	10.0
Blanched seaweeds	23.1[a]	23.7[a]	23.83[a]	6.4[c]	5.76[c]	6.59[c]	81.39[e]	82.85[e]	86.86[f]
	(1.54)	(2.19)	(1.23)	(2.84)	(1.89)	(1.32)	(5.66)	(4.57)	(3.3)
Raw seaweeds	25.86[b]	27.25[b]	27.91	8.71[d]	8.39[d]	8.42[d]	83.39[e]	86.00[f]	86.73[f]
	(1.12)	(2.78)	(2.46)	(1.33)	(1.02)	(1.09)	(3.07)	(2.53)	(3.03)

3.2 Sorption-desorption characteristics of Saccharina latissima

The dried raw and blanched seaweeds behave differently during absorption of moisture from the ambient air (Fig. 1). Dried blanched seaweeds showed higher accumulation of moisture at low relative humidity of air (from 20.0 to 40.0 % RH) for all the investigated samples, when compared with raw seaweeds ($p < 0.05$). While, the trend was changed at 60.0 % RH. Further increasing of the relative humidity in the climate chamber to 80.0 % resulted in a sharp alteration of moisture content in dried raw seaweeds for all the investigated temperatures ($p < 0.05$), while dried blanched seaweeds showed almost linear trend of moisture increasing in the range of RH between 20.0 and 80.0 %. The temperature variation between 10.0 and 38.0 °C did not influence on the sorption characteristic of the blanched seaweeds.

The similar behavior was observed by Sappati et al., [11] studied the sorption isotherms of Saccharina latissima at 20.0 °C. The sharp increasing of the equilibrium moisture content of raw seaweeds at 80.0 % and relatively low water absorbance at RH below 60.0 % can be explained by hygroscopic point of salts, which occupy the significant share among other compounds. For example, hygroscopic point of NaCl appears at 75.5 % RH at 25.0 °C, KCl at 82.0 % RH. The salt concentration in raw seaweeds was determined at 14.4 % d.b., while blanched seaweeds were almost salt-free (below 0.5 % d.b). Desorption isotherms were determined at 25.0 °C and compared with sorption profiles at the same temperature. It is interesting to note, that hysteresis phenomena was relatively small for raw seaweeds, while blanched seaweeds showed a significant change in structural properties during drying. It may happens due to freezing and blanching process when the cell membranes were broken and water soluble compounds were easily washed out and replaced by a free water. Thus, significant irreversible shrinkage appears during drying process of blanched seaweeds.
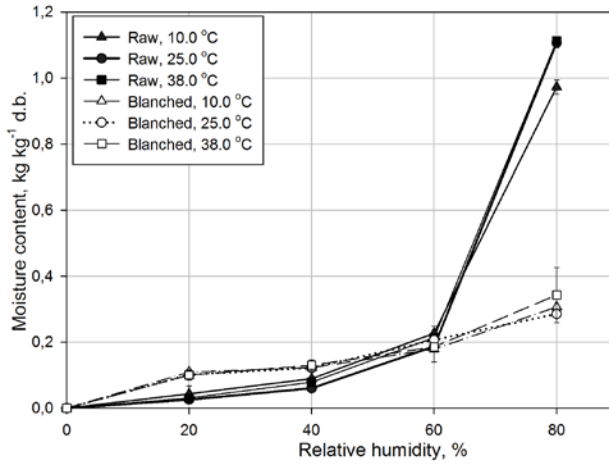
Figure 1. Sorption characteristics of Saccharina Latissima

3.3 Shrinkage of raw and blanched seaweeds during dewatering
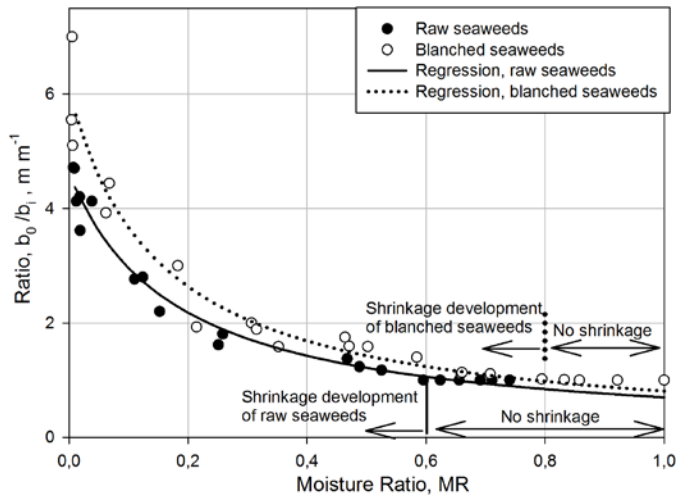
Figure 2. Shrinkage of raw and blanched seaweeds during drying

The drying processes resulted in a significant reduction of blade thickness for raw and blanched seaweeds, Fig. 2, while surface area reduced only by 20.0..25.0 %.

The thickness reductions was much more developed for blanched blades, when compared with raw samples ($p < 0.05$). Also, raw seaweeds retained their thickness much longer during

dewatering when compared with blanched. The first traces of the thickness decreasing were detected at MR of 0.6 and 0.8 at 25.0 °C for raw and blanched seaweeds respectively.

3.4 Drying kinetics of seaweeds

The drying kinetics was investigated for raw and blanched seaweeds. The raw seaweeds showed initial moisture content at 900.0 (50.0) % d.b. Tthe moisture content of the blanched seaweeds was found at 2079.0 (100.0) % d.b. Dehydration of raw seaweeds was much faster, when compared with blanched. This can be explained by the higher moisture content of blanched seaweeds and also may be linked with the changes of their structure after blanching. The increasing of temperature accelerated the dewatering of the seaweeds both raw and blanched, and the highest dewatering rate was observed for 38.0 °C.

Newton model was implemented to obtain the regression equations for all the drying temperatures ($R^2>0.98$; Prob(F)<0.000014; F(Ratio) >700). The empirical drying coefficient k was found in the range between 0.008 and 0.22 1/min due to the influence of temperature and variation of thickness of the sample.

Table 3. Coefficients for Newton equation and effective moisture diffusivity

Type of seaweeds	Drying temp., °C	Drying coefficient, 1/min		
		1 layer	2 layers	3 layers
Raw seaweeds	10.0	0.07(0.01)	0.015(0.01)	0.016(0.001)
	25.0	0.13 (0.01)	0.033(0.01)	0.021(0.001)
	38.0	0.22 (0.01)	0.055(0.01)	0.036(0.001
Blanched	10.0	0.035 (0.001)	0.017(0.002)	0.008(0.002)
	25.0	0.051 (0.001)	0.025(0.003)	0.013(0.002)
	38.0	0.060 (0.001)	0.031(0.004)	0.015(0.001)
		Effective diffusivity, D m²/s*10¹⁰		Average
		1 layer	2 layers	3 layers	
Raw seaweeds	10.0	1.50	1.20	1.50	**1.4 (0.17)**
	25.0	2.80	2.60	2.60	**2.7 (0.11)**
	38.0	4.50	4.00	5.00	**4.50 (0.5)**
Blanched seaweeds	10.0	0.95	0.90	0.90	**0.91 (0.03)**
	25.0	1.10	1.50	1.10	**1.2 (0.23)**
	38.0	2.50	2.60	2.60	**2.56 (0.05)**

The average values of effective moisture diffusivity (Table 3) increased with increasing of the drying temperature and reached the highest value of $3.5*10^{-10}$ m²/s at 38.0 °C. The effective moisture diffusivities of blanched seaweeds were relatively lower, when compared with raw seaweeds. The results of this study were in agreement with the resent study on Saccharina latissima [11], when the effective moisture diffusivity was determined at $2.95*10^{-10}$ m²/s at 40.0 °C and 25.0% RH.

4. Conclusions

Drying kinetics of Saccharina latissima (raw and blanched) at low temperatures (10.0, 25.0 and 38.0 °C) was studied. The effective moisture diffusivity coefficient varied due to temperature alterations in the range between 1.4 and 4.5 10^{-10} m²/s for raw and 0.91 and 2.56 10^{-10} m²/s for blanched seaweeds. Significant changes in structural properties and chemical composition resulted in a much longer drying time of blanched seaweeds, when compared with raw. Drying temperature of 38.0 °C resulted in more brown color, when compared with other samples. Sorption characteristics of dried raw seaweeds depended on salt content and showed high accumulation of moisture at relative humidity of air of 80.0 %. The blanched seaweeds showed linear accumulation of moisture within increasing of relative humidity of drying air from 20.0 to 80.0 %, but high level of hysteresis was determined between sorption and desorption isotherms. The shrinkage development within dewatering of blanched and raw samples was also studied.

5. Asknowledgement

6. References

[1] FAO The state of world fisheries and aquaculture: opportunities and challenges. 2014, Rome: FAO.

[2] Chopin, T. Seaweed aquaculture provides diversified products, key ecosystem functions Part II. Recent evolution of seaweed industry. Kye acosyst. Func. 2012, 14, p. 24-27.

[3] Radulovich, R. Massive freshwater gains from producing food at sea. Water Policy 2011, 13(4), p. 547.

[4] Forster, J.; Radulovich, R. Chapter 11 - Seaweed and food security A2 - Tiwari, Brijesh K, in Seaweed Sustainability; D.J. Troy, Editor; Academic Press: San Diego, 2015

[5] Phang, H.-K.; Chu, C.-M.; Kumaresan, S.; Rahman, M.M.; Yasir, S.M. Preliminary study of seaweed drying under a shade and in a natural draft solar dryer. International Journal of Science and Engineering 2015, 8(1), p. 10-14.

[6] Lemus, R.A.; Pérez, M.; Andrés, A.; Roco, T.; Tello, C.M.; Vega, A. Kinetic study of dehydration and desorption isotherms of red alga Gracilaria. LWT - Food Science and Technology 2008, 41(9), p. 1592-1599.

[7] Fudholi, A.; Othman, M.Y.; Ruslan, M.H.; Yahya, M.; Zaharim, A.; Sopian, K. Design and testing of solar dryer for drying kinetics of seaweed in Malaysia, in Proceedings of the 4th WSEAS international conference on Energy and development - environment - biomedicine. 2011, World Scientific and Engineering Academy and Society (WSEAS): Corfu Island, Greece. p. 119-124.

[8] Chan, J.C.C.; Cheung, P.C.K.; Ang, P.O. Comparative Studies on the Effect of Three Drying Methods on the Nutritional Composition of Seaweed Sargassum hemiphyllum (Turn.) C. Ag. Journal of Agricultural and Food Chemistry 1997, 45(8), p. 3056-3059.

[9] Stévant, P.; Indergård, E.; Ólafsdóttir, A.; Marfaing, H.; Larssen, W.E.; Fleurence, J.; Roleda, M.Y.; Rustad, T.; Slizyte, R.; Nordtvedt, T.S. Effects of drying on the nutrient content and physico-chemical and sensory characteristics of the edible kelp Saccharina latissima. Journal of Applied Phycology 2018.

[10] Mise, T.; Ueda, M.; Yasumoto, T. Production of fucoxanthin-rich powder from Cladosiphon Okamuranus. Advance Journal of Food Science and Technology 2011, 3(1), p. 73-76.

[11] Sappati, P.K.; Nayak, B.; van Walsum, G.P. Effect of glass transition on the shrinkage of sugar kelp (Saccharina latissima) during hot air convective drying. Journal of Food Engineering 2017, 210, p. 50-61.

Stabilization of encapsulated probiotics from the bacterium *Lactobacillus casei* by different drying techniques

Acosta-Piantini, E. M.[a]*; Villarán, M. C.[b]; Lombraña, J. I.[c]

a, c Dept. of Chemical Engineering. F. of Science and Technology UPV/EHU. P.O. Box 644. 48080 Bilbao (Spain)

b Tecnalia foundation, Alava Technology Park, Spain

*E-mail of the corresponding author: eacosta004@ikasle.ehu.eus

Abstract

The main objective of this work is to encapsulate and dry the bacterium probiotic Lactobacillus casei applying three different drying techniques (lyophilization, fluidized bed and flash freeze drying) as well as to evaluate their viability during storage in the dark at 20ºC and 34% relative humidity for 28 days. In addition, to compare viability of the bacterium processed with flash freeze drying with cryoprotectant (skim milk) and without cryoprotectant.

In the case of flash freeze drying, the final level of viability shows the potential of this drying technique with much less operating costs than lyophilization.

Keywords: Encapsulated, probiotics, lactobacillus, casei, drying

1. Introduction

Encapsulation and drying techniques are alternatives which trying to protect probiotics microorganisms of the effect of environmental agents that may affect their viability, during processing, storage and consumption and their passage through the gastrointestinal tract by allowing them to maintain their viability and functionality over time [1, 2] by reducing cell damage to retain cells within encapsulation materials that generate their isolation [3, 4].

Probiotic bacteria are live microorganisms which when administered in adequate amounts confer health benefits to the host, beyond their inherent nutritional contribution [5, 6]. The bacteria are encapsulated, dried and converted into powder for use in food and pharmaceutical applications, as the powder is easy to handle, transport and store. Different drying techniques can be used for the encapsulation of probiotics.

In this project we evaluated flash freeze drying, lyophilization and fluidized bed.

Flash freeze drying (FFD process is developed by the freezing of the product through the application of vacuum. Then, a considerable fraction of water is removed by vaporization during freezing and once frozen the rest by sublimation, obtaining in this way a dry paste which favours the preservation of the product [7]. This technology enables the encapsulation of biological materials to reduce the rate of chemical reactions and degradation by heat [8].

Many factors responsible for microbial survival have been reported during and after the freeze-dried, among them, the bacterial species, the physiological state, cell density, effect of protectors [9], freezing rates and other process parameters, as well as rehydration [10].

Lyophilisation is a technique which also is developed by the freezing of the product and after the application of vacuum, the water is removed only by sublimation while Fluidized Bed Drying is a process in which heated gas is, usually conditioned air with controlled velocity, is passed through a bed of suspending solid particles, dragging the removed water.

The main objective of this work is to encapsulate and dry the bacterium probiotic *Lactobacillus casei* applying different drying techniques as well as to evaluate their viability during storage. In addition, to compare the viability of the bacterium L casei, processed with Flash Freeze Drying with cryoprotectant (skim milk) and without cryoprotectant.

2. Materials and Methods

Lactobacillus casei 431 biomass was produced using Man Rogosa Sharpe (MRS) culture medium. The final probiotic required an encapsulation treatment with alginate and chitosan in a Jet-cutter equipment, and then dried by three different treatments: Flash freeze drying (FFD), lyophilization and fluidized bed.

Probiotics were packaged in vacuum, stored in the dark at 20ºC and 34% relative humidity for 28 days. Measurements of water activity and microbiological analysis were performed on the 7th, 14th, 21st and 28th days of storage.

2.1. Obtaining of microbial biomass

Strains of L. casei 431 were supplied by Christian Hansen & Cia and kept in their original packaging at temperature of - 80°C. They were activated in MRS broth and incubated at 37 °C for 24 hours under aerobic conditions with moderate stirring (200 rpm). Biomass recovered by centrifugation (4000 rpm at 15°C). The centrifuged fraction presented a concentration of cells around of 10^9 units forming colonies (CFU) per gram and the supernatant was discarded. Finally, the cells were washed with sterile water, and preserved in refrigeration (6±2°C) until used.

2.2. Encapsulation

For encapsulation process, we suspended the bacteria in alginate and received it in a bath of Chitosan using a Jett Cutter at following operations conditions: flow 25 g/s, 170 nozzle, pressure 1.5 bar and motor 4,000 rpm. Then, the mass of microcapsules were divided in three groups: a) fluidized bed drying b) lyophilization and c) flash freeze drying. In addition, we divided flash freeze drying in two groups: c.1) with cryoprotectant (skim milk sterile) and c.2) without cryoprotectant.

2.3. Drying techniques

Fluidized bed drying (FBD) was made in a Glatt GmbH dryer, model Uni-Glatt, with the following conditions: temperature in air 30°C, temperature out air 24°C and temperature product 12°C. The process drying was carried out until to obtain the required water activity in the product.

Lyophilization was carried out in a Telstar Lyo beta 25 equipment, with fluid temperature of 5.1 °C, condenser temperature - 76.3 °C and heating temperature of 23.1°C, with full cycle of 48 hours, beginning at a freezing temperature of - 40°C to 0.1 mbar during 4 hours, followed by a 24 hour primary dried at 40°C and 4 hours of secondary drying at 20°C and at 0.05 mbar, 10 hours more.

For Flash Freeze Drying (FFD), we used a Telstar Lyo Quest equipment in which pressure was reduced from atmospheric to 0.02 mbar in 30 min with the heating device at 30 ºC during sublimation.

Dried material was packed in polyethylene bags and stored in controlled temperature (20±2 ° C) store and moisture relativity of 60 %.

2.4. Study of bacteria survived and stability

To determine the effect of the agent cryoprotectant (sterile skim milk) on viability of encapsulated microorganisms, the number of viable cells was determined before and after freeze-drying and drying, every 7 days during storage at 20±2°C for 28 days. We used as criteria of stability: the viability during storage (CFU/g) and water activity. These parameters were determined every seven days by triplicate.
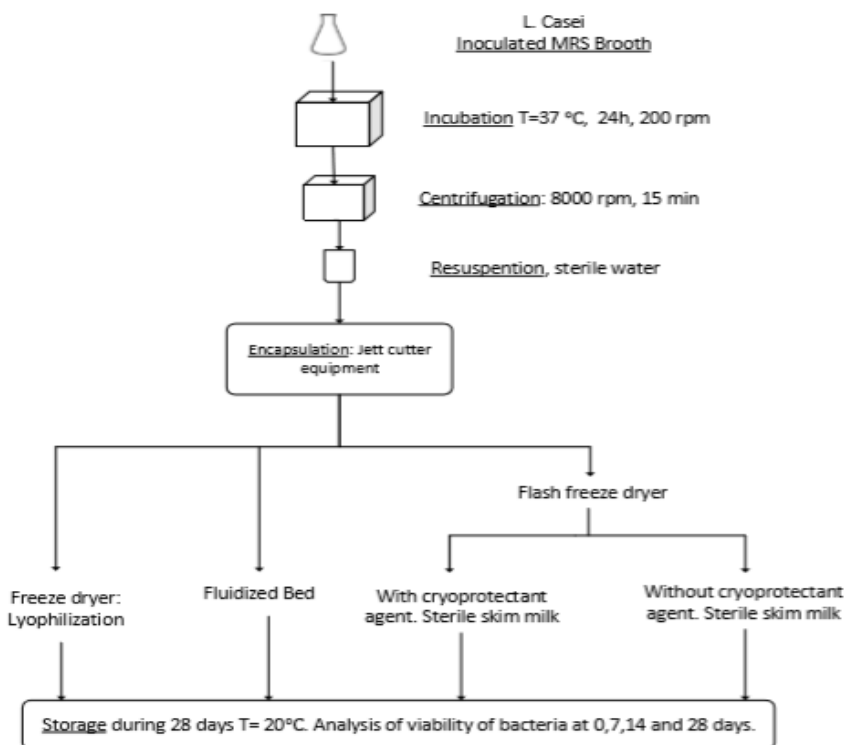
Figure 1. Flowchart with the methodology used for encapsulation and drying L. casei

2.5. Viability

Analysis of viability was made taken a gram of encapsulated material, soaked in 10 ml of buffered 0.1 sterile water, homogenized with vortex. A volume of 100 µL of dilution it was sown surface on MRS medium and incubated under aerobic conditions at 37°C for 48 hours. Counts were performed in duplicate and expressed as cfu g-1 (dry basis), for each experimental condition [11]. The figure 1 show flowchart with the methodology used for encapsulation and drying of *L. casei.*

2.6. Physicochemical characterization

Water activity (a_w) was determined in a hygrometer Novasina, Bab master aw, Switzerland.

2.7. Experimental design and statistical analysis

An experimental design was applied with a factor (storage time) with repeated measurements where the experimental units were followed over time. The results correspond to the average of three replicates and are presented as mean ± standard deviation. An analysis of variance (ANOVA) and Tukey test with a level of significance to $p < 0.05$ was applied to the data analysis.

3. Results and discussion

3.1. Drying techniques effect

The results show significant differences between the results of feasibility among the three treatments, presenting the Fluidized Bed Drying (FBD) the lower viability. Besides, there were significant differences between the water activity of capsules treated in three treatments, showing freeze-dried capsules the lower water activity.

After FFD, see Table 1, the bacterium presented a viability level of 5.3 x 10^{10} CFU/g, which is equivalent to 84.49% survival, only a little less than by lyophilization, in which the viability test gave 7.9 x 10^{10} CFU/g or an 86.19% survival.

In the case of FFD, although a certain decrease in viability during storage was observed, from 5.1 x 10^{10} CFU/g (7th day) to 4.7 x 10^9 CFU/g (28th day), or a survival variation from 99.8 to 90.3%, the final level of viability is important because shows the potential of this technical drying.

Table 1. Cell survival after drying and during storage for the three drying techniques. The values of a_w (20 ºC) correspond to the end of drying

Drying technique	Cell viability* - Drying		Water activity (a_w)	Cell viability** - Storage	
	Before	**After**		**7th day**	**28th day**
Lyophilization	4.4 E12	7.9E10 (86.19)	0.0993	7.2E10(99.6)	6.2 E9 (90.19)
FBD	5.1 E12	7.1E8	0.3075	8.1E7	0
FFD	4.92 E12	5.3E10 (84.49)	0.0775	5.1E10(99.8)	4.7 E9 (90.3)

* Cell viability values are expressed in CFU/g, numbers between brackets are the survival percent respect to the cell content before drying.

** In the case of storage, numbers between brackets are the survival percent respect to the cell content after drying.

3.2. Storage

Respect to the dried stored samples the results show that the L. Casei lyophilized presented at the end of the 28th day of storage a viability level of 5.3 x 10^{10} CFU/g, which is equivalent to 84.49% survival, only a little less than by lyophilization, in which the viability test gave 7.9 x 10^{10} CFU/g or an 86.19% survival.

In the case of FFD, see Table 1, although a certain decrease in viability during storage was observed, from 5.1 x 10^{10} CFU/g (7th day) to 4.7 x 10^9 CFU/g (28th day), or a survival variation from 99.8 to 90.3%, the final level of viability is important because shows the potential of this drying technique with much less operating costs than lyophilization. [12]

3.3. Physicochemical properties

Water activity values are considered critical parameters for the survival of micro-organisms and on the stability of microcapsules during storage. Measurements were made at the beginning and end of storage, and they are reported in the Table 1.

Some authors claim that the adverse effect or not, of the drying techniques is related to aspects as the bacterial species, the addition of protective substances, initial cell concentration, physiological state of microorganisms, rate of freezing by the generation of osmotic stress, temperature and conditions of rehydration, among others [13]. In this study FBD presents the lowest water activity, which encourages the preservation of probiotic material.

4. Conclusions

Flash Freeze Drying (FFD) is set to become a promising drying technique with similar results to lyophilization but with much less process time and operating costs.

The use of milk as a protectant showed advantages on the results of feasibility, so its use is recommended.

The importance of these results reveal that, under adequate drying treatment, it is possible to stabilize probiotic material with Flash Freeze Drying (FFD) process in viable conditions for extending its shelf life.

5. Nomenclature

g/s	grams per second
mbar	milibar
ml	millilitre
µL	microlitre
ºC	Celsius degrees
rpm	revolutions per minute
CFU/g	colony forming units per gram
a_w	Water activity

6. Acknowledgements

7. References

[1] Semyonov, D.; Ramon, O.; Levin-Brener, L.; Gurevich N. S. E. Microencapsulation of Lactobacillus paracasei by spray freeze drying. Food Res Int, 2010, 43, 193-202.

[2] González, R. E. J.; Mendoza, L.; Morón, B. Efecto de la Microencapsulación sobre la Viabilidad de Lactobacillus delbrueckii sometido a Jugos Gástricos Simulados. Inf Tecnol, 2015, 26 (5), 11-16.

[3] Ranadheera, R. D.; Baines, S. K; Adams, M. C. Importance of food in probiotic efficacy. Food Res Int, 2010, 43 (1), 1-7.

[4] Ray, S., Raychaudhuri, U.; Chakraborty, R. An overview of encapsulation of active compounds used in food products by drying technology. Food Biosci, 2016, 13, 76-83.

[5] Guarner, F.; Shaafsma, G. Probiotics. International Journal Microbiology. 1998, 39, 237-238.

[6] Shah, N.P. From Bulgariam milks to probiotics fermented milks.

In IDF World Dairy Summit, Parma Italy, October 15 – 19, 2011.

[7]   Fritzen-Freire, C. B.; Prudencio, E. S.; Amboni, R. D.; Pinto, S. S. Microencapsulation of bifidobacteria by spray drying in the presence of prebiotics, Food Res Int, 2012, 45 (1), 306-312.

[8]   Strasser, S.; Neureiter, M.; Geppl, R.;   Braun, R.; Danner, H.   Influence of lyophilization, fluidized bed drying, addition of protectants, and storage on the viability of lactic acid bacteria. J App Microbiol. 2009, 107, 167-177.

[9]   Shamekhi, F. M.; Shuhaimi, A.;   Ariff, B;   Yazid, A. M. Optimization of a cryoprotective medium for infant formula probiotic applications using response surface methodology. Ann Microbiol, 2012, 62, 911–921.

[10] Kearney, X. C., Stanton, C.; Kelly, J.; Fitsgerald. G. F.; Ross, R. P. Development of a spray dried probiotic yogurt containing Lactobacillus paracasei NFBC 338. Int. Dairy J, 2009, 19, 684-689.

[11] Champagne, C. P.; Ross, R. P.; Saarela, M.; Hanen, K. F.; Charalampopoulos, D. Recomendations for the viability asessment of probiotics as concentrated cultures in a food matrices, Int J Food Microbiol, 2011, 149, 185-193.

[12] Martin, J.M.; Lara-Villoslada, F.; Ruiz, M.A.; Morales, M.E. Microencapsulation of bacteria: A review of different technologies and their impact on the probiotic effects. Innovative Food Science and Emerging Technologies 2015, 27, 15-20.

[13] Zhao, G.; Zhang. Effect of protective agents, freezing temperature, rehydration media on viability of malolactic bacteria subjected to freeze-drying. J App Microbiol, 2005, 99, 333-338.

Coupling of microwave to convective drying for improving fruit quality

Bahloul, N.[a*]; Balti, M. A.[a]; Guellouze, M. S.[b]; Kechaou, N.[a]

[a] Groupe de Recherche en Génie des Procédés Agro-alimentaires, Laboratoire de Mécanique des Fluides Appliquée, Génie des Procédés et Environnement, Ecole Nationale d'Ingénieurs de Sfax, Université de Sfax, BP 1173, 3038, Sfax, Tunisia.

[b] Laboratoire d'Etudes des Systèmes Thermiques et Energétique, Ecole Nationale d'Ingénieurs de Monastir, Université de Monastir, Tunisia.

*E-mail of the corresponding author: neilabahloul@yahoo.com

Abstract

The present study aims to find the best drying method to minimize the duration of the operation while respecting the nutritional value of the product. Experiments of convective drying and microwave radiation were respectively carried out with a convective dryer (heat temperature: 65 °C and air velocity: 1.3 m/s) and a microwave oven (power level: 100 W and frequency: 2450 MHz). Six coupling tests between the convective drying and microwave radiation were conducted. The only variable condition is the time output of tomatoes from the convective dryer or the microwave oven corresponding to an intermediate mass ratio (IMR) 0.5, 0.4 and 0.3. The microwave drying removes the bound water faster than convective drying. This explains the observed time savings due to convection-microwave and microwave-convection combined drying. The combination of convection drying and microwave drying to an IMR 0.5 preserved better the red color and the antioxidants of the tomato. Thus, the convection–microwave combined drying (IMR 0.5) proved most suitable for preserving the quality of tomatoes.

Keywords: convective drying; microwave; coupled drying; color.

1. Introduction

Tunisia is ranked among the top ten countries in the world in terms of tomato processing, with a local production of 1.2 million tons of tomatoes in 2013, fifty thousand tons of which are destined for processing [1]. Furthermore, the export of dried tomatoes has shown remarkable growth in recent years. Tomato is an herbaceous climacteric fruit, which belongs to the order of Solanale, the family of Solanaceae and the genus of Lycopersicon. It is native to the northwestern South of America and it is grown in warm and temperate countries around the world. According to some studies, regular consumption of tomatoes or tomato products can reduce the risk of cancer, as well as cardiovascular diseases, diabetes and osteoporosis [2],[3]. Indeed, Tomato is a fruit which is rich in antioxidant compounds, and more particularly, in polyphenols and vitamin C. The transformation processes involve one or more heat treatments which can affect the levels of antioxidants and thus the nutritional quality of the products. In fact, these micro-constituents can be partially degraded under the effect of heat and light. In this context, our study aims to find the best mode for drying tomatoes by combining convective drying and microwaves in order to minimize the duration of the operation while respecting the nutritional value of tomatoes.

2. Materials and Methods

2.1. Raw material

The tomato samples used for drying are "round" varieties grown under a greenhouse and supplied from the "AGRIFOOD" Tunisian company.

2.2. Determination of drying kinetics

2.2.1. *Convective drying experiments*

The drying kinetics of the tomatoes were performed using the convective drying loop of the research group GP2A (ENIS). After setting the air flow, the controller starts to heat up to the set temperature. Once the experimental conditions are stable, the samples to be dried are washed and cut into quarters. Then, the samples are placed on a suitable support; this support is suspended in the horizontal test vein by a hook located below a precision balance. The drying kinetics are determined through the measurements of the mass variation of the samples over time by means of a digital precision electronic scale. This balance is linked to a computer and equipped with a data output enabling the acquisition of the mass over time by means of a suitable software. The experimental conditions carried out with the convective drying loop are fixed at a temperature of 65 ° C., an air velocity of 1.3 m / s and a final mass ratio of 0.2, imposed by the manufacturer.

2.2.2. *Microwave drying experiments*

The drying experiments were carried out in a domestic microwave oven at a frequency of 2450 MHz and three power levels (100, 300 and 600 W) for a cycle of 15 seconds. The

drying end criterion is also the final mass ratio of 0.2. Preliminary tests at different power levels were carried out and led to the choice of the lowest power (100 W) for subsequent experiments based on the visual appearance of tomatoes during drying.

2.2.3. Experimental protocol of convective and microwave coupled drying

Six coupling tests were carried out under the same drying conditions as: a temperature of 65 ° C., an air velocity of 1.3 m / s, a power of 100 W and a final mass ratio of 0, 2. The only variable condition is the intermediate output time from the convective dryer or the microwave oven corresponding to an intermediate mass ratio (IMR) of 0.5; 0.4 and 0.3. This ratio corresponds to the breaking point and the change from one drying mode to another:

- 3 assays of coupling convective drying (Co) to microwave radiation (Mo) at 3 IMR: 0.5; 0.4 and 0.3.

- 3 other coupling tests by switching from microwave drying (Mo) to convective drying (Co) at 3 IMR: 0.5; 0.4 and 0.3.

2.3. Physicochemical analysis

2.3.1. Preparation of extracts

The extraction is carried out using an ultrasonic bath. One gram of crushed tomatoes is mixed with 50 ml of pure ethanol for 2 hours. The solvent was evaporated on a rotary evaporator. Dry extracts stored at 4 ° C are obtained until use.

2.3.2. Water content

The water content, X (kg of water / kg M.S.) is calculated using the following equation:

$$X = \frac{m - ms}{ms} \qquad (1)$$

with: m: mass of the wet sample (kg), ms: mass of the dry sample (kg).

2.3.3. Ascorbic acid analysis

The ascorbic acid content is measured by the 2,6-dichloroindophenol titration method [4].

2.3.4. Color analysis

The color is measured using a colorimeter (Konica Minolta CR 300) with CIE Lab system (L *, a*, b*). Statistical analysis was performed using SPSS software (version 13, Inc. SPSS, Chicago, USA) at a confidence interval of 95%.

3. Results and discussion

3.1. Kinetics of convective and microwave drying

Figure 1 shows the evolution of the reduced water content as a function of the drying time for the convective (65 ° C. and 1.3 m / s) (FIG. 1 a) and for microwaves drying (at 100 W) (FIG. 1b). The drying time needed to obtain a final mass ratio of 0.2 (i.e. a final water content of 0.25 kg water / kg DM) is 5 hours and 21 minutes. The water content decreases rapidly at the first time and then more and more slowly at the end of the drying. Indeed, at the beginning of drying, the mechanism of water displacement through the pores walls of the solid towards the surface is carried out in an accelerated manner. At the end of the drying process, increasing the temperature in the center of the product and decreasing its water content result in a new state of equilibrium in the product. Thus, water is increasingly hard to migrate into the product and the internal transfer of matter becomes a limiting phenomenon [5].
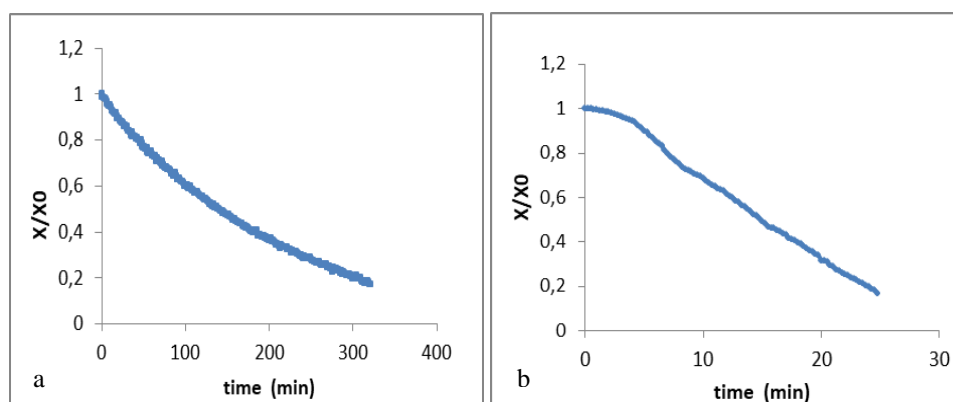
Figure 1: Evolution of the reduced water content as a function of the drying time by: (a) forced convection drying at 65 ° C and 1.3 m / s (X0 = 24.263 kg water / kg M.S); and (b) microwaves radiation at 100 W (X0 = 24.258 kg water / kg M.S)

Microwave drying at a relatively low power (100 W) allows to achieve the same mass ratio of 0.2 (i.e. a final water content of 0.25 kg of water / kg DM) in 25 minutes; that means a gain of 4 hours and 56 minutes compared to convective drying. Despite the short duration of microwave treatment and the visual aspect, the sample had a softer texture and showed intense yellowing of the skin that we did not notice for convection dried samples; hence, the idea of combining convective drying with microwaves seems to be interesting.

3.2. Coupled drying

Figure 2 shows the evolution of the reduced water content as a function of time for the various alternating convection / microwave and microwave / convection drying modes. In the early stages of drying, the kinetic rates obtained by convection-microwave coupled drying at different IMR are similar to that of convective drying. After that, the water content decreases rapidly under the effect of microwave radiation compared to the convective drying applied alone.
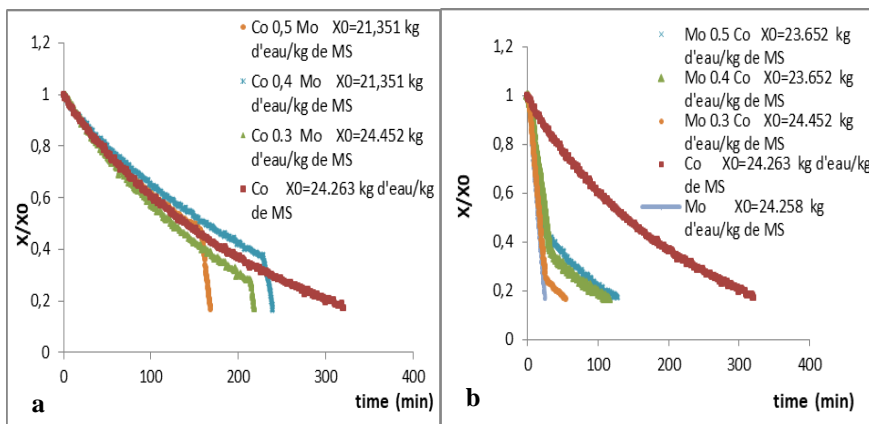
Figure 2: Evolution of the reduced water content as a function of the drying time obtained by (a) convection-microwave coupled drying, (b) microwave–convection coupled drying.

Thus, microwave drying allows removing the weak bonded water more rapidly than convection drying. In the beginning, the kinetic rates obtained by microwave-convection coupled drying at different IMR are similar to that of microwave drying; while at the end of drying, they are comparable to that of convective drying. Microwave radiations permit to reduce the water content of the product more quickly than convective drying. This fact results in a remarkable reduction of the drying time compared to that of convection drying and convection-microwave coupled drying.

3.2.1. Drying for an intermediate mass ratio of 0.5

The evolution of the reduced water content as a function of drying time is shown in Figure 3 for different convection / microwave and microwave / convection coupled drying and at each IMR. It is noted that microwave radiations followed by convective drying (Mo 0.5 Co) reduce the drying time by 3 hours and 13 minutes compared to convective drying (Co). While convective drying followed by microwave radiation (Co 0.5 Mo) allows decreasing the duration by 2 hours and 33 minutes.
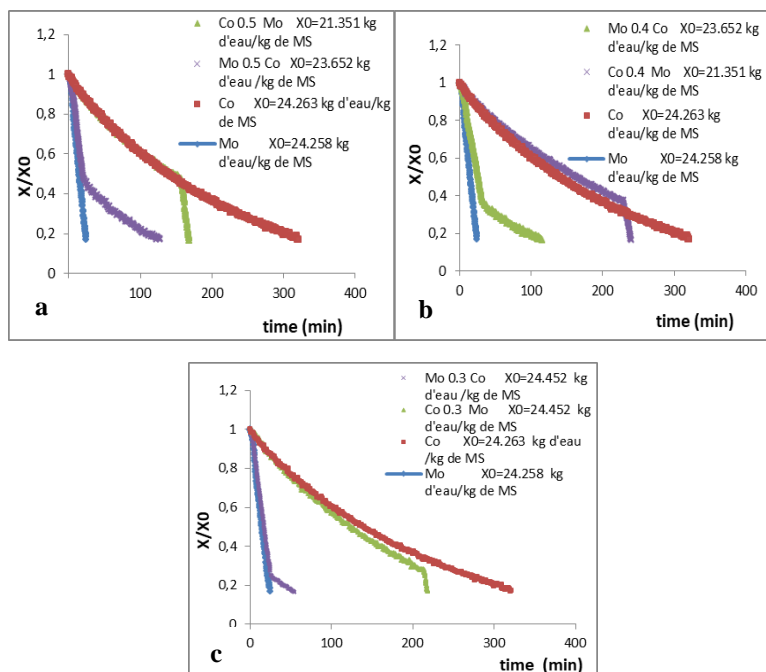
Figure 3: Evolution of the reduced water content as a function of time for the convection / microwave and microwave / convection dryings at: (a) IMR of 0.5; (b) IMR of 0.4 and

(c) IMR of 0.3

3.2.2. Drying for an intermediate mass ratio of 0.4

The coupled drying which starts with microwave radiation (Mo 0.4 Co) lasts 1 hour and 55 minutes, ie a gain of 2 hours and 4 minutes compared to the convective-microwave drying (Co 0.4 Mo) and 3 hours and 25 minutes compared to convective drying applied alone. The convection-microwave coupled drying lasts 3 hours and 59 minutes, thus reducing the drying time of 1 hour and 21 minutes compared to the convective drying.

3.2.3. Drying for an intermediate mass ratio of 0.3

The drying duration obtained by microwave-convection drying (Mo 0.3 Co) is 54 min, giving a gain of 4 h 26 min with respect to the convective drying. The convection-microwave drying (Co 0.3 Mo) allows a gain of 1 h 42 min compared to the convective drying (drying time is equal to 3h 38 min). Based on the drying time criterion, which is the most important for the manufacturer, we can opt for microwave-convection drying at this stage. However, the visual appearance of dried tomatoes by convection- microwave mode seems to be better. Therfore, biochemical analyzes were carried out on dried tomatoes.

3.3. Determination of quality parameters

3.3.1. Color analysis

Measurement of color by referring to the CIE Lab coordinates (L *, a * and b *) shows that luminance (L *) of dried tomatoes is lower than that of fresh tomato (Figure 4). This fact can be explained by the non-enzymatic browning during drying. The values corresponding to the convection-microwave drying with a transition mass ratio of 0.5 and 0.4 are close to that of fresh tomato. Regarding the (a *) index, it is noted that the values obtained after convective-radiative drying of tomatoes at transition ratios of 0.5 and 0.4 are significantly greater than those obtained for fresh tomato. The (b *) values obtained after microwave, microwave-convective drying and convective drying of tomatoes increase significantly with respect to that of fresh tomato.
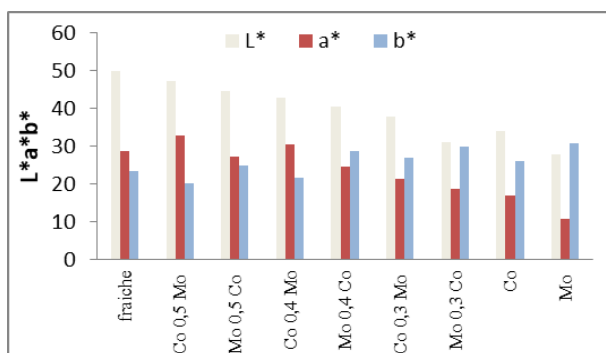
Figure 4: Effect of drying on the color of tomatoes

3.3.2. Ascorbic acid

The ascorbic acid contents of the dehydrated tomatoes are summarized in Table 1. As a result of the heat treatments undergone by the tomato, the vitamin C content is reduced in comparison with that of fresh product. The convective-microwave dryings, for IMR of 0.5; 0.4 and 0.3, lead to vitamin C loss due to tomato exposure to heated air (65 ° C). After microwave-convection drying, vitamin C loss was greater in dried tomatoes than in other samples. Thus, convective-microwave (Co 0.5 Mb) drying better preserves ascorbic acid in tomatoes.

4. Conclusions

Microwave drying eliminates weak bonded water faster than convection drying. This explains the saving in time observed after convection-microwave and microwave-convection drying. Based on the nutritional quality attributes of the tomato, the convection–

microwave combined drying (IMR 0.5) proved most suitable for preserving the quality of tomatoes.

Table 1: Ascorbic acid contents of tomatoes (mg / 100g DM)

Drying conditions	Ascorbic acid content
Fresh	384.441 ±0.175
Co 0.5 Mo	234.375 ±0.022
Mo 0.5 Co	111.877 ±0.023
Co 0.4 Mo	136.491 ±0.021
Mo 0.4 Co	102.387 ±0.011
Co 0.3 Mo	130.293 ±0,011
Mo 0.3 Co	97.286 ± 0.000
Co	109.905 ±0.011
Mo	81.394 ±0.023

5. Acknowledgments

6. References

[1] FAO, 2013, Faostat.fao.org

[2] Davies, J.N. ; Hobson, G.E. The constituents of tomato fruit-the influence of environment. nutrition. and genotype. CRC Critical Reviews in Food Science and Nutrition 1981, 15, 205-280.

[3] Rao, A.V. Lycopene Content of Tomato Products: Its Stability, Bioavailability and In Vivo Antioxidant Properties. Food and nutrition research 2006, 10, 1016-1043.

[4] AOAC, Officials Methods of Analysis. Vitamin C (ascorbic acid) in vitamin preparations and juices: 2, 6 dichloroindophénol titrimetric method final action. 43.064 and 43.065, 1984

[5] Bahloul, N.; Boudhrioua, N.; Kouhila, M.; Kechaou N. Drying characteristics of convective solar drying of olive leaves. Journal of Food Process Engineering 2009, 34 (4), 1338-1362.

Ohmic heating/vacuum impregnation treatments on osmodehydrated apples enriched in polyphenols from concentrated pomegranate juice

Moreno, J.[*]; Zuñiga, P.; Guerra, M.E.; Mella, K.

TECBAL group. Department of Food Engineering, Universidad del Bio-Bio, Chillán, Chile.

*E-mail of the corresponding author: jomoreno@ubiobio.cl

Abstract

The aim of this work was to study the combination of osmodehydration (OD), coupled with Ohmic Heating (OH) and Pulsed Vacuum (PV) and to introduce natural compounds from a cryoconcentrated pomegranate juice (47°Brix) at 30, 40 and 50 °C into apple matrix, during 180 min. PV was performed at 50 mbar for 5 min at the beginning of the process and OH generates an electric field of 6.6 V/cm. The results indicated that treatments reduced water content and increase polyphenol content of apples, evidencing that the osmotic treatment improve mass transfer, especially when they are applied together at higher temperatures.

Keywords: Ohmic heating; pulsed vacuum; cryoconcentration; enriched; pomegranate.

1. Introduction

As consequences in a change of lifestyle and eating habits diseases such as obesity, cardiovascular problems, diabetes type II, hypertension, cancer among others have increased (1). These adverse effects have developed the interest in healthy food and the consumption food functional food (2). Functional foods include bioactive compounds (BAC), which have health benefits as well as their nutritional value. Vitamins, polyphenols, and minerals are found in BAC (2).

Pomegranate (Punica granatum L.) has gain interest in the past few years for its nutritional and antioxidant activities (3). Pomegranate juice is a potential source of anthocyanins, flavonoids, organic acids, ellagic acid (4). Therefore, its health benefits are associated with those chemical characteristics. Therefore, its health benefits are associated with those chemical characteristics.

Freeze concentration (also called cryoconcentration) as mention before, is an emerging technology, which consists on entirely or partially freezing the liquid food solution for later separation of the ice fraction from the liquid. Vitamins as polyphenols are thermolabile compounds, by using FC the high nutritional value and organoleptic characteristics can be protected (5).

The ohmic heating (OH) is a thermal process, in which energy is generated by the passage of an alternating electrical current that diffuses through the food (2). The PV has been widely used to obtain a rapid penetration of compounds in vegetable tissues and enriches fruits and vegetables with antioxidants, vitamins, minerals, among others (6).

Osmotic dehydration (OD) is the process in which water is partially removed from the cellular material when it is exposed to a concentrated solution of solutes. The type of osmotic agent used and its molecular weight or ionic behavior affects the kinetics of water elimination and the gain of solids (7), during the OD mass transfer occurs through semipermeable cell membrane making substantial changes in the tissue structure (8).

The aim of this work was to study the combination of osmodehydration (OD), Pulsed Vacuum (PV), Ohmic Heating (OH) and to introduce natural compounds from a concentrated pomegranate juice at 30, 40 and 50 °C into an apple matrix, during 180 minutes.

2. Materials and Methods

2.1. Sample preparation

Pomegranate (cv. Wonderful) and apples (cv. Granny Smith) were acquired in the local market (Chillán, Chile) and stored under refrigeration (5 °C) until processing. The

pomegranates were cut in half and removed the seeds manually for juice extraction and filtered to eliminate any residue.

2.2. Osmotic agent

To obtain the osmotic agent, freeze concentrated pomegranate juice, block freeze concentrated as described by (9) with modifications. Samples were frozen -20 °C for 12 h and place in a refrigerated centrifuge (Eppendorf 5430R) operated at 15 °C for 15 min for the first cycle and 10 min for the second and third cycle at a speed of 1878 RCF.

2.3. Osmodehydration treatments assisted by pulsed vacuum and ohmic heating.

Osmodehydration (OD) at atmospheric pressure and pulsed vacuum (PVOD) with conventional and ohmic heating (OH) at 30, 40, 50 °C, using a thermoregulated bath as described by (10). The freeze concentrated pomegranate juice was exposed to an alternating current at 60 Hz and 50 V, generating an electric field E of 6.66 V/cm.

2.4. Total phenolic content (TPC)

The total phenolic content was determined through a colorimetric method by Folin-Ciocalteu (FC) reagent (11) using gallic acid as standard. Treated samples extracts (100 µL) were mixed with 7900 µL distilled water, 500 µL FC reagent and 1500 µL sodium carbonate. The sample was incubated 120 min before measurement at 760 nm in a spectrophotometer (Shimadzu Scientific 1600 UV/VIS, USA). Results were expressed mg of gallic acid equivalents in 100 g of dry matter (mg GAE/ 100 g d.m.). 2.5. Compositional analysis

Soluble solids and moisture content were determined the effect of osmodehydration time over water loss, mass loss, solid gain and water activity (aw). Moisture content was determined according to the method defined by the AOAC, 2000 (12). The solute gain was determined as described by Moreno et al., (2016), the solid content was measured using a digital refractometer (Leica Mark II, Buffalo, NY, USA). The Xss and Xw content were determined for both fresh and treated, the compositional changes were calculated through the following equations. Samples water activity (aw) was determined using a dew point hygrometer (Aqua Lab Model 4TE, Pullman, USA). Measurements were executed in triplicate and the mean values are informed.

2.6. Physical properties

The firmness of the samples was evaluated with a Texture Analyzer TA-XT (Stable Microsystems, Haslemere, UK), using a slice shear blade the mechanical parameter was considered as maximum peak force and reported as N. Apple slices color, fresh and treated, was measured with a spectrocolorimeter (Konica Minolta CM-500). The CIE L* a* b*

coordinates used a D_{65} illuminant and 10° observer as a system reference. The color was measured in triplicate.

3. Results and Discussion

3.1 Total phenolic content (TPC)

The phenolic content of the treated apple samples is expressed in mg gallic acid equivalent (GAE) in 100 g of dry matter. As Fig. 1 shows the apples treated with PVOD/OH at 30 °C had higher retention of TPC throughout the processing time (180 min), followed by PVOD/OH 50 °C; the samples with the lowest phenolic retention were the PVOD 40 °C OD/OH 50 °C.
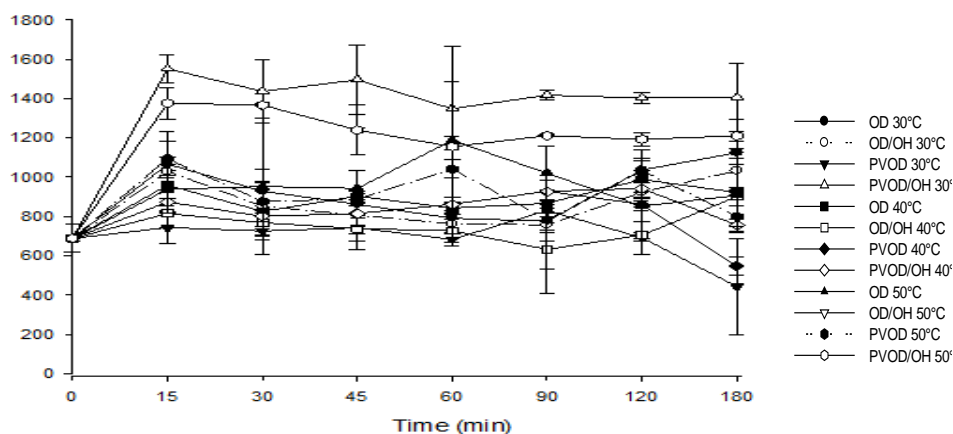
Fig. 1 Total phenolic content (TPC) kinetics of osmodehydrated apple using cryoconcentrated pomegranate juice for 180 min. OD: osmotic dehydration at atmospheric pressure, PVOD: osmotic dehydration with vacuum pulsed vacuum, OH: ohmic heating (OD/OH and PVOD/OH) at 6.66 V/cm

Furthermore, the total phenolic content decreases for all treated samples after 30 min of the process except PVOD/OH 30 °C; this may be due to the kind of treatment, temperature and time. Also after de processing time most of the treatments retained at least the same amount of TPC as in time 0, except PVOD 40 °C, such finding differs with (10); in which the fresh sample had a significant difference in the TPC compare to the treated.

3.2 Compositional changes and water activity

Table 1 shows the compositional changes between the fresh and different treatments of osmodehydration after 180 min of processing. According to previous findings, osmotic dehydration with concentrated juice is more significant compared to osmotic dehydration with sucrose (13). The combination of PVOD/OH 40 and 50 °C, and PVOD 30 °C had the highest solute gain had more significant water loss and solid gain, due to the diffusion and convection forces, both which facilitate the mass transfer process. Application of pulsed vacuum eases the osmotic agent into the matrix pores and facilitates the water loss and has a beneficial effect on the kinetics, reaching equilibrium easily (10). Also, the combination of OD/OH encouraged more substantial concentration levels in samples than OD.

Table 1. Composition parameters of fresh and processed samples (processing time: 180 min) water mass fraction (X_w), soluble solids mass fraction (X_{ss}), water loss ($\Delta M^w{}_t$), solid gain ($\Delta M^{ss}{}_t$) and water activity (a_w).

Treatments	X_w	X_{ss}	$\Delta M^w{}_t$	$\Delta M^{ss}{}_t$	a_w
Fresh	0.85 ± 0.01^g	0.22 ± 0.02^a	-	-	$0.98 \pm 0.09^{\ g}$
OD 30°C	0.58 ± 0.01^f	0.33 ± 0.02^b	-0.32 ± 0.04^c	0.63 ± 0.12^d	$0.91 \pm 0.01^{d,e}$
OD/OH 30°C	$0.56 \pm 0.01^{d,e,f}$	0.77 ± 0.02^d	-0.85 ± 0.03^c	2.14 ± 0.15^a	$0.91 \pm 0.01^{e,f}$
PVOD 30°C	$0.56 \pm 0.01^{d,e,f}$	0.90 ± 0.12^e	-0.27 ± 0.01^a	$0.45 \pm 0.08^{d,e}$	$0.91 \pm 0.01^{c,d}$
PVOD/OH30°C	$0.55 \pm 0.05^{d,e,f}$	0.72 ± 0.03^d	-0.27 ± 0.01^a	$1.88 \pm 0.08^{a,b}$	0.92 ± 0.01^f
OD 40°C	$0.57 \pm 0.01^{e,f}$	0.47 ± 0.23^c	-0.66 ± 0.08^b	$1.50 \pm 0.06^{b,c}$	$0.91 \pm 0.01^{e,f}$
OD/OH 40°C	$0.52 \pm 0.01^{d,c,d}$	0.79 ± 0.04^d	-0.66 ± 0.05^b	1.35 ± 0.81^c	$0.90 \pm 0.01^{\ c,d}$
PVOD 40°C	$0.54 \pm 0.01^{b,c,d}$	$0.82 \pm 0.03^{d,e}$	-0.36 ± 0.16^a	$0.51 \pm 0.03^{d,e}$	$0.91 \pm 0.01^{d,e,f}$
PVOD/OH 40°C	$0.51 \pm 0.03^{a,b,c}$	0.78 ± 0.01^d	-0.31 ± 0.24^a	$1.27 \pm 0.22^{d,e}$	$0.90 \pm 0.01^{b,c}$
OD 50°C	$0.57 \pm 0.01^{e,f}$	0.76 ± 0.02^d	-1.15 ± 0.01^d	$2.08 \pm 0.45^{a,b}$	0.92 ± 0.01^f
OD/OH 50°C	$0.47 \pm 0.02^{a,b}$	$0.80 \pm 0.06^{d,e}$	-0.33 ± 0.09^a	$0.51 \pm 0.07^{d,e}$	0.89 ± 0.01^b
PVOD 50°C	$0.52 \pm 0.01^{c,d,e}$	$0.79 \pm 0.02^{d,e}$	-0.28 ± 0.07^a	0.52 ± 0.10^d	$0.92 \pm 0.01^{e,f}$
PVOD/OH 50°C	$0.49 \pm 0.01^{a,b}$	$0.81 \pm 0.01^{d,e}$	-0.35 ± 0.01^a	0.65 ± 0.03^d	0.87 ± 0.00^a

Different letters ([a, b, c,...g]) in each column indicate significant differences at $p \leq 0.05$, according to a LSD test.

In this case, the mass transfer in PVOD and PVOD/OH in comparison to the OD is due to the unsteadiness of particles in the juice. Likewise, inadequate dissemination of the components may occur when gradients pressure in the vegetable tissue provoke the irregular flow of the osmotic agent through the structure and consequently accumulate bioactive components in some areas (14); making the mass transfer harder in OD.The most significant water activity reduction was in PVOD/OH 50 °C, followed by OD/OH 50 °C in contrast to the fresh sample. This difference is attributed to temperature, pH, and

electroporation which promote the gain of freeze concentrated pomegranate juice and water loss (15).

3.4 Changes in physical properties

Table 2 shows the values obtained for the fresh and treated apple, the hue angle (h*ab), chrome (C*ab) and change in color (ΔE). Previous studies have demonstrated L increases with the osmotic treatments (15). However, samples with the combination of PVOD and PVOD/OH have reduced L, due to the concentration of anthocyanins from the pomegranate juice, this same effect reported by (9) treated sample had lower L than the fresh one. The ΔE was higher in the same treatments as the L, this due to the content of anthocyanin pigments present in the cryoconcentrated pomegranate juice. The firmness values acquired from the mechanical test (Table 2). A sample of PVOD 30 °C had the firmness highest value which indicates a higher resistance. Fresh sample differs significantly from the samples treated at 50 °C. Although, values from treatments at 40 °C had no difference with the fresh sample, as well as OD/OH and PVOD at 30 °C.

Table 2. Firmness and color determination in fresh and treated apples with three temperatures (30 C, 40 C, 50 °C).

Treatments	Firmness (N)	Color			
		L*	C*ab	h*ab	ΔE
Fresh	12.75 ± 3.53[c]	64.38 ± 5.53[c]	16.80 ± 3.16[d]	96.48 ± 3.06[a]	---
OD 30°C	26.34 ± 3.83[d,e]	29.27 ± 2.12[b]	30.63 ± 2.14[f]	199.88 ± 0.69[g]	45.14 ± 2.97[d]
OD/OH 30°C	15.99 ± 1.05[c]	26.43 ± 1.79[b]	23.96 ± 5.48[e]	198.31 ± 2.10[f,g]	45.80 ± 3.54[d]
PVOD 30°C	29.35 ± 4.19[e]	22.25 ± 3.19[a,b]	15.58 ± 7.28[c,d]	194.91 ± 3.38[e,f]	39.85 ± 1.43[b,c]
PVOD/OH30°C	10.87 ± 2.88[b,c]	20.57 ± 1.18[a,b]	3.84 ± 0.49[a]	178.17 ± 2.80[b]	48.91 ± 4.78[e,f]
OD 40°C	14.61 ± 2.70[b,c]	29.27 ± 2.12[a,b]	30.63 ± 2.14[f]	199.88 ± 0.69[g]	47.89 ± 0.60[d,e]
OD/OH 40°C	9.34 ± 0.61[b,c]	24.70 ± 1.81[a,b]	17.47 ± 3.30[d]	197.50 ± 1.09[f,g]	42.03 ± 2.63[c]
PVOD 40°C	17.34 ± 2.97[c,d]	21.63 ± 1.53[a,b]	9.75 ± 3.12[b]	191.83 ± 0.31[d]	45.72 ± 0.76[d]
PVOD/OH 40°C	8.57 ± 1.88[b,c]	20.62 ± 0.51[a]	3.45 ± 0.63[a]	183.74 ± 1.49[c]	51.82 ± 1.97[f,g]
OD 50°C	2.88 ± 1.57[a]	23.06 ± 1.14[a]	13.97 ± 3.68[b,c,]	197.59 ± 1.53[f,g]	50.65 ± 1.91[e,f]
OD/OH 50°C	2.70 ± 0.17[a]	22.96 ± 2.03[a]	10.99 ± 1.19[b,c]	196.69 ± 0.15[f,g]	38.25 ± 2.00[b]
PVOD 50°C	5.34 ± 1.75[b]	21.01 ± 0.16[a]	3.92 ± 1.08[a]	188.74 ± 2.81[d]	51.69 ± 1.99[f]
PVOD/OH 50°C	6.27 ± 0.87[b]	20.67 ± 0.72[a]	3.06 ± 0.96[a]	189.30 ± 2.62[d]	54.73 ± 2.47[f]

Different letters ([a..g]) in each column indicate significant differences at $p \leq 0.05$, according to a LSD test.

4. Conclusion

The combination of pulsed vacuum and ohmic heating in the osmodehydration of apple slices at 30 °C affected the retention of total phenolic content positively during processing time (180 min). Osmotic dehydration combined with pulsed vacuum and ohmic heating at 50 and 40 °C intensifies the solid gain and water loss due to the diffusion and convection forces which accelerated the mass transfer process. PVOD/OH and OD/OH 50 °C had the most significant water activity mainly cause by the electroporation and temperature. The changes in color were significant in C*ab (chrome) in L* (lightness), and values in treated apple slices with PVOD and PVOD/OH due to retention of anthocyanins from the freeze concentrated pomegranate juice. The highest firmness was observed in a sample of PVOD 30 °C. Therefore, our results suggest that PVOD/OH process at 50 °C by 180 min is the optimal treatment for osmodehydrated apples with freeze concentrated pomegranate juice.

5. Acknowledgements

6. References

[1] Stelzer, I., Zelzer, S., Raggam, R. B., Prüller, F., Truschnig-Wilders, M., Meinitzer, A. & Reeves, G.. Link between leptin and interleukin-6 levels in the initial phase of obesity-related inflammation. Translational Research, 2012, 159(2), 118-124.

[2] Moreno, J., Zúñiga, P., Jara, E., Gianelli, M., Mella, K., & Petzold, G. (2017). Ohmic Heating and Bioactive Compounds. In J. Moreno, Innovative Processing Technologies for Foods with Bioactive Compounds. Boca Raton, FL., United States of America: CRC Press, 2017, págs. 31-60.

[3] Mirdehghan, S. H., & Rahemi, M.. Seasonal changes of mineral nutrients and phenolics in pomegranate (Punica granatum L.) fruit. Scientia Horticulturae, 2007, 111(2), 120-127.

[4] Fuster-Muñoz, E., Roche, E., Funes, L., Martínez-Peinado, P., Sempere, J. M., & Vicente-Salar, N. Effects of pomegranate juice in circulating parameters, cytokines, and oxidative stress markers in endurance-based athletes: A randomized controlled trial. Nutrition, 2016, 32(5), 539-545.

[5] Petzold, G., Orellana, P., Moreno, J., Junod, J., & Bugeño, G. (2017). Freeze concentration as a technique to protect valuable heat-labile components of foods. In J. Moreno, Innovative Processing Technologies for Foods with Bioactive Compounds Boca Raton, FL., United States of America: CRC Press, 2017, págs. 31-60.

[6] Neri, L., Di Biase, L., Sacchetti, G., Di Mattia, C., Santarelli, V., Mastrocola, D., & Pittia, P. Use of vacuum impregnation for the production of high quality fresh-like apple products. Journal of Food Engineering, 2016, 179, 98-108.

[7] Moreira, P., & Xidieh, M. (2004). Mass transfer kinetics of osmotic dehydration of cherry tomato. Journal of Food Engineering, 2004, 61, 291-295.

[8] Quiles, A., Hernando, I., Pérez-Munuera, I., Llorca, E., Larrea, V., & Ángeles Lluch, M. The effect of calcium and cellular permeabilization on the structure of the parenchyma of osmotic dehydrated 'Granny Smith apple. Journal of the Science of Food and Agriculture, 2004, 84(13), 1765-1770.

[9] Petzold, G., Orellana, P., Moreno, J., Cerda, E., & Parra, P. Vacuum-assisted block freeze concentration applied to wine. Innovative Food Science & Emerging Technologies, 2016, 36, 330-335.

[10] Moreno, J., Gonzales, M., Zúniga, P., Petzold, G., Mella, K., & Munoz, O. Ohmic heating and pulsed vacuum effect on dehydration processes and polyphenol component retention of osmodehydrated blueberries (cv. Tifblue). Innovative Food Science & Emerging Technologies, 2016, 36, 112-119.

[11] Waterhouse, A. L. Determination of total phenolics. Current protocols in food analytical chemistry, 2002, I1.1.1-I1.1.8.

[12] [AOAC] Association of Official Analytical Chemist. Moisture in fruits. An adaptation of method 934.06. Official methods of analysis of Association of Official Analytical Chemist International 16th ed., Gaithersburg, Maryland, USA, 2000.

[13] Chambi, H. N. M., Lima, W. C. V., & Schmidt, F. L. (2016). Osmotic dehydration of yellow melon using red grape juice concentrate. Food Science and Technology (Campinas), 2016, 36(3), 468-475.

[14] Betoret, E., Sentandreu, E., Betoret, N., Codoñer-Franch, P., Valls-Bellés, V., & Fito, P. Technological development and functional properties of an apple snack rich in flavonoid from mandarin juice. Innovative Food Science & Emerging Technologies, 2012, 16, 298-304.

[15] Moreno, J., Simpson, R., Sayas, M., Segura, I., Aldana, O., & Almonacid, S. Influence of ohmic heating and vacuum impregnation on the osmotic dehydration kinetics and microstructure of pears (cv. Packham's Triumph). Journal of Food Engineering, 2011, 104(4), 621-627.

Valorization of the tomato to obtain a powder rich in antioxidant constituents

Mennouche, D. [a,b,*]; Boubekri, A. [a,c]; Bouchekima, B. [a,d] ; Boughali, S. [a,f] ; Moumeni, R. [a,b] ; Boutadjine, D. [a]

[a] Université Kasdi Merbah Ouargla, Laboratoire de Développement des Energies Nouvelles et Renouvelables dans les Zones Arides et Sahariennes Ouargla 30000, Algeria.
[b] Département de Génie des Procédés, Université Kasdi Merbah Ouargla 30000, Algeria
[c] Département des Energies Renouvelables, Université Kasdi Merbah Ouargla 30000, Algeria
[e] Département de Génie Mécanique, Université Kasdi Merbah Ouargla 30000, Algeria.
[f] Département de Physique, Université Kasdi Merbah Ouargla 30000, Algeria.

*E-mail of the corresponding author: mennouche@gmail.com; mennouche.dj@univ-ouargla.dz

Abstract

The tomato (Lycopersicon esculentum), widely consumed fresh fruit but also in processed form, is recognized for its nutritional qualities, rich in micro components, such as carotenoids (lycopene in particular), phenolic compounds and vitamin C.

The goal of this work is to valorize the tomato; in the form of paste, seeds, peel and mixture of seeds-peel; in order to obtain a powder rich in antioxidant constituents. Convective drying of the various tomato by-products (paste, seeds, peel and mixture) is an essential process in the valorization of the studies products. The results obtained, showed that our analysed samples are rich in phenolic compounds. The mixture seeds-peel has slightly higher total polyphenol content (190.65 mg EAG / ml), peel (157.36 mg EAG / ml), seeds (140.56 mg EAG / ml) and the paste (120 mg EAG / ml).

The evolution of the color of dried by-products (method L, a, b), shows that the mixture (seeds-peel) has a better result of parameter "a" (indicates the red color and signifies the presence of Lycopene).

Keywords: tomato, drying, antioxidant, polyphenols.

1. Introduction

Tomatoes are a major source of lycopene, which helps in the prevention of many chronic diseases such as cancer and heart diseases [1]. They also contain various nutritional (Vitamin A, C, and E), non nutritional (beta-carotene, carotenoid, flavonoids, flavone and total phenolic), minerals, and dietary fiber [2-3].

The very high water content of tomato (approximately 90%) favors its degradation in the fresh state and its physical-chemical's and microbiological deterioration.

According to the Food and Agricultural Organization (FAO), the global production of tomato, in 2016, exceeds 177 million tons of which 1280570 tons were produced in Algeria.

The aim of this work is to valorize the tomato; in the form of paste, seeds, peel and mixture of seeds-peel; in order to obtain a powder rich in antioxidant constituents.

2. Materials and methods

2.1. Drying experiments

Drying experiments were performed on tunnel dryer (Fig.1) installed in the mechanical engineering laboratory, Ouargla University, Algeria. The dryer is a forced convection dryer intended for the drying of food products. Four removable stainless steel plates that can be placed in a channel (drying chamber) of dimension (250 cm x 50 cm x 50c m). The drying chamber is thermally insulated with polystyrene (thickness = 3cm), the outer part of which is covered by four galvanized sheets. The drying of the different samples of tomatoes is carried out on a tray (surface of 620 cm^2) and exposed to air flow, serves on the one hand to heat the product to be dried, and on the other hand, to evacuate the quantity of releasing moisture. The mass loss of product is controlled by a digital scale. The temperature and relative humidity of the air are detected by a combined temperature and humidity sensor. An additional sensor serves to measure the velocity of the air flow.

The air coming from the external environment is preheated by an electrical resistance. Under the effect of a fan with adjustable speed, drying air circulates in the drying chamber, passes through the product at a constant drying temperature and comes out at a lower temperature and high humidity.

2.2. Sample preparation

Fresh local tomatoes were bought from local market in Ouargla, Algeria. They were separated using a visual criterion like color, size, absence of physical damage and uniform maturation degree. The samples of different by-products were prepared according to the following steps : Fresh tomatoes were washed with water to eliminate dust, bacteria, dirt and insect larvae. Tomatoes were crushed using a Star Mix blender. The by-products: paste,

seeds, peel and mixtures of seeds and peel were separated using a sieve (2 mm thickness) and dropped in a permeable bag for a few hours.

1. drying channel, 2. drying racks, 3. door, 4. process schematic,
5. air velocity sensor, 6. measuring point for humidity and temperature, 7. digital balance, 8. bracket for drying plates,
9. measuring point with humidity and temperature sensor,
10. switch cabinet with digital displays, 11. fan
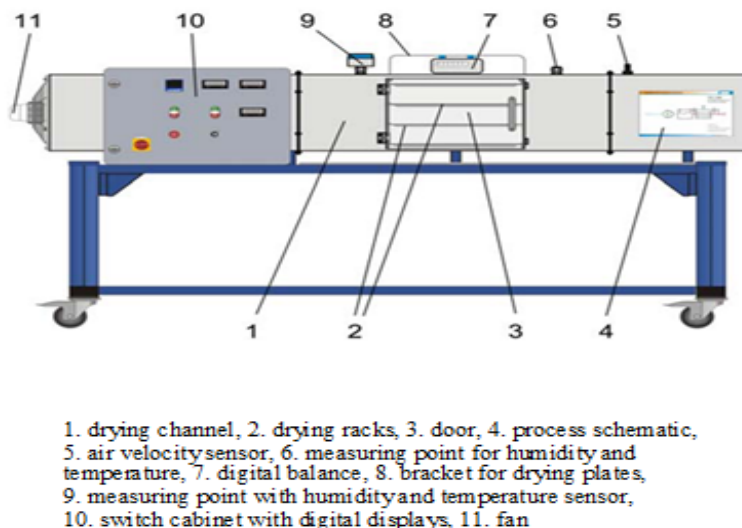
Fig. 1. Drying system

2.3. Moisture measurements

Water content of different samples was determined using a moisture Analyzer (Sartorius MA 45, accuracy ± 0.01), operating in the following conditions:

Sample weight (3g); temperature analysis (105 °C). The device stops automatically once the weight of the sample becomes constant. Moisture content is expressed on a dry basis, kg water/kg dry matter.

2.4. Total polyphenols analyses

Total phenolic content of the samples was measured by the spectrophotometric method [4]. 5 g of the powder of each by-product is macerated in 100 ml of a hydroalcoholic mixture MeOH (methanol-water) (80/20 : v/v) for 48 hours at room temperature, after the methanol is evaporated by rotavapor at 65 °C and the mixture is filtered by wattman paper to obtain a crude hydroalcoholic extract, finally the phenolic extract is kept at 6 °C until it is used. For the determination of total polyphenol, we introduce in a test tube 0.2 ml of extract of each by-product of tomato (prepared in distilled water with suitable dilutions), 1 ml of Folin-

Cicalteu reagent (10 times diluted) and 0.8 ml of the solution Na_2Co_3 at 7.5 % (7.5 g in 100 ml). The mixture is incubated at ambient temperature for two hours. The reading is performed against a blank without extract using a spectrophotometer at 765 Nanometer (nm).

2.5. Antioxidant activity

The evaluation of the antioxidant activity is based on the reduction reaction of (Fe^{+3}) present in the potassium ferrocyanide complex in (Fe^{+2}), the reaction is revealed by the yellow-colored transfer of ferric iron (Fe^{+3}) in green blue color of ferrous iron (Fe^{+2}), the intensity of this coloration is measured by spectrophotometer at 700 nm. The experimental protocol [5] used is that of 0.5 ml of sample of our extract at different concentrations is mixed with 1.25 ml of a 0.2M phosphate buffer solution (pH 6.6) and 1.25 ml of a solution of potassium ferricyannide $K_3Fe (CN)_6$ at 1% (1 g of $K_3Fe (CN)_6$ in 100 ml of distilled water). Incubation of the prepared mixture in a water bath at 50 ° C for 20 minutes then the mixture is cooled. 2.5 ml of 10 % trichloroacetic acid is added to stop the reaction. 1.25 ml of the supernatant is added to 1.25 ml of distilled water and 0.25 ml of a freshly prepared solution of 0.1% ferric chloride. The reading is against a white at 700 nm.

2.6. Color measurements

The color of fresh and dried by-products was measured using a Minolta CR-400 colorimeter [6] allowing the acquisition of the Hunter *L, a, b* color scale values. *L* is lightness/darkness parameter, *a* the redness/greenness one and *b* the yellowness/blueness one.
Where L_0, a_0 and b_0 refer to the color values for the fresh by-producs of tomato.

3. Results and discussion

Fig. 2 illustrates the amount of total phenolics (TP) in various by-products of tomato. Our results showed that all the by-products of tomato are a good source of TP compounds.

The peel powder contained the highest level of TP compared to the powders of seeds and paste. The amounts of TP in peel powder increase 16,8 % and 20,56 % respectively to the seeds and paste powders. These results of this study are in accordance with Ramandeep et al. [7], who reported that the highest levels of total phenolics were detected in the peel of three tomato cultivars (Excell, Tradiro and Flavourine). In addition, this study has also identified the by-product of peel tomato as an important reservoir of TP compounds.

Fig. 2 shows also that the mixture (consisting of peel and seeds of tomatoes) powder contained the highest levels of TP compared to those of peel, seeds, and paste, powders.

This result shows that the mixture powder (peel and seed) is an important contributor to the major antioxidants of tomatoes. Therefore, removal of tomato peel and seeds during their fresh consumption or home cooking present a significant loss of the antioxidants. Similarly,

the discard of tomato slurry (consisting of peel and seeds of tomatoes) during tomato processing industry   means a loss of antioxidants.
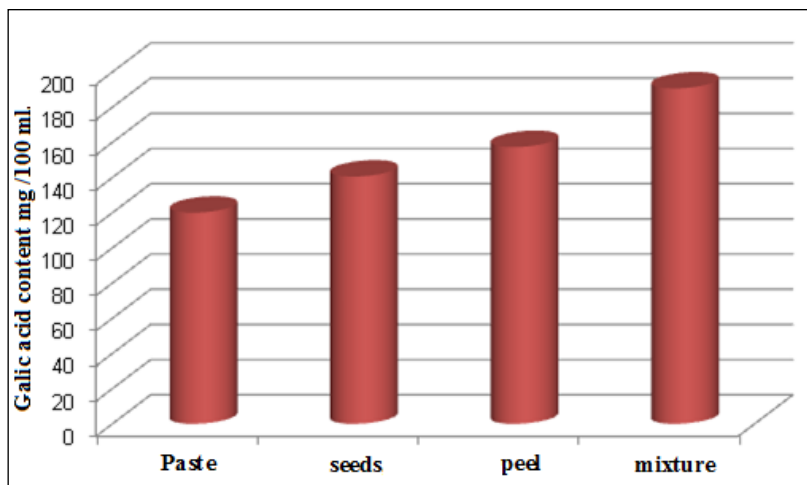
Fig. 2. Total polyphenol content of different by-products of tomato

The presence of the reductants in the extracts causes the reduction of iron Fe^{3+} ferricyanide complex to the ferrous form. Therefore, Fe^{2+} can be evaluated by measuring and monitoring the increase in green, blue colour density in the reaction medium at 700 NM. In other words, the $FeCl_3$ / K_3Fe $(CN)_6$ system confers on the method, the sensitivity for the determination of the polyphenol concentrations, which participate in the redox reaction [8]. According to the ascorbic acid curve, the reducing power of the four extracts is measured according to their absorbance.

The values presented in Figure 3 show the reducing power of the four extracts at different concentrations. From our results of the four extracts tested, an increase in iron reduction (increase in absorbance) is proportional to the concentrations used.

All our extracts have significantly lower antioxidant activity than that of the reference (ascorbic acid), for the latter the reduction is almost total from a concentration of 0.5 mg / ml. The extracts of the mixture powder (seeds and peel) is more active compared to the powders of the peel, the seeds, and the paste. The reducing power of the four extracts is due to the presence of lycopene and hydroxyl group in the phenolic compounds that can serve as electron donors. Therefore, antioxidants can be considered as reducing and inactivating oxidants.
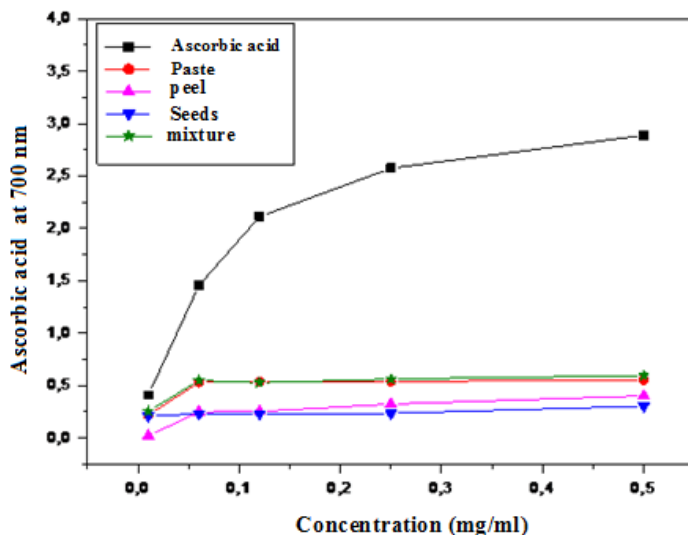
Fig. 3. Reducing power of the four extracts and ascorbic acid.

Figure 4 demonstrates the evolution of the coordinates (L, a, b) for the four by-products. It should be noted that the mean value of the a parameter ; indicates the red color and signifies the presence of Lycopene; in the mixture (S-P) was 40. Rosa et al [9]. reported that the increase of a parameter is directly associated with lycopene synthesis and a significant correlation was observed between lycopene and a. Marcos et al. [10] also, have found highly significant and exponential correlations between lycopene and a parameter. Based on the literature previously cited, it should be conclude that the lycopene content in the mixture (S-P) presents a better result compared to the other by-products.
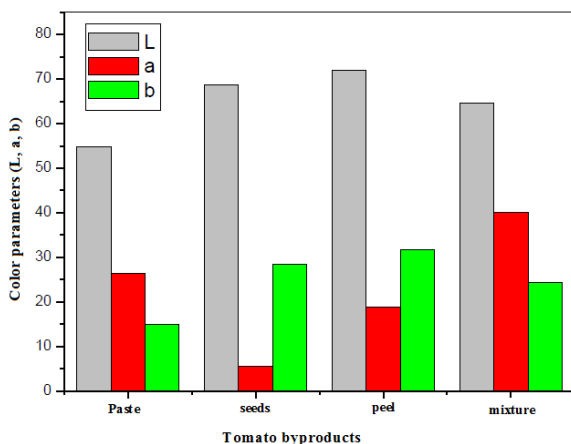
Fig. 4. Evolution of coordinates (L, a, b) for the four by-products

4. Conclusion

The valorization of the tomato; in the form of paste, seeds, peel and mixture of seeds and peel; to obtaining a powder rich in antioxidant constituents have been studied.

The convective drying of the various tomato by-products presents an indispensable step for the valorization of the tomato in powder form.

The results obtained showed that our analyzed samples are rich in phenolic compounds, whose mixture of seeds and peel has a slightly higher total polyphenol content (190.65 mg EAG / 100ml) compared to that of peel, seeds and paste which have 157.36, 140.56 and 120 mg EAG / 100ml respectively. This result confirms their high antioxidant potency which was proportional to different concentrations. This result has been confirmed by the color analyzes and the antioxidant

5. References

[1] C. Chawla, D. Kaur, D.P.S.Oberoi, D.S. Sogi. Drying caracterisics, sorption isotherms, and lycopene retention of tomato pulp. *Drying Technology* 26, 1257,1264, 2008.

[2] P. Rajkumar, S. Kulanthaisami, G.S.V. Raghavan, Y.Gariépy, V. Orsat. Drying kinetics of tomato slices in vacuum assisted solar and open sun drying methods. *Drying Technology* 25, 1349-1357, 2007.

[3] J. N. Davies, G. E. Hobson. The constituents of tomato fruit. The influence of environment, nutrition, and genotype. CRC Crit. Rev. in Food Sci. *Nutri* 15, 205-280, 1981. [4] Spanos, G. A., and Wrolstad, R. E. "Influence of processing and storage on the phenolic composition of Thompson seedless grape juice." J. Agric. Food Chem. 38, 1565-1571. 1990.

[5] Ching-Hui Chang a,b, Hsing-Yu Lin b , Chi-Yue Chang b , Yung-Chuan Liu a. Comparisons on the antioxidant properties of fresh, freeze-dried and hot-air-dried tomatoes. Journal of Food Engineering 77, 478–485, 2006.

[6] Arslan, D., Ozcan, M. M., & Menges, H. O.. Evaluation of drying €methods with respect to drying parameters, some nutritional and colour characteristics of peppermint (Mentha xpiperita L.). Energy Conversion and Management, 51, 2769–2775, 2010.

[7] Ramandeep K. Toor, Geoffrey P. Savage. Antioxidant activity in different fractions of tomatoes. Food Research International 38, 487–49, 2005.

[8] Amarowicz R, Estrella I, Hernandez T, Robredo S, Troszynska A, Kosinska A, Pegg R. Free radicals-scavenging capacity: antioxidant activity and phenolic composition of green lentil (*Lens culinaris*); Food Chemistry 121.705-711, 2010.

[9] Rosa Arias, Tung-Ching Lee, Logan Logendra, and Harry Janes. Correlation of Lycopene Measured by HPLC with the L*, a*, b* Color Readings of a Hydroponic Tomato and the Relationship of Maturity with Color and Lycopene Conten. J. Agric. Food Chem., 48, 1697−1702 ; 2000.

[10] Marcos Hernández, Elena Rodríguez, and Carlos Díaz. Free Hydroxycinnamic Acids, Lycopene, and Color Parameters in Tomato Cultivars. J. Agric. Food Chem., 55, 8604–8615. 2007.

Effect of solar radiation on cooking/drying process of grapes using solar oven.

Bailey, J.[b]; Castro-Giráldez, M.[a]; Esteves, A.[b]; Fito, P. J.[a*]

[a] Instituto Universitario de Ingeniería de Alimentos para el Desarrollo, Universitat Politècnica de València, Camino de Vera s/n, 46022 Valencia, Spain.

[b] Instituto de Ambiente, Hábitat y Energía (INAHE) - Consejo Nacional de Investigaciones Científicas y Técnicas (CONICET) - CCT-Mendoza, Av. Ruiz Leal s/n - Parque Gral. San Martín (5500), Mendoza, Argentina

*E-mail of the corresponding author: pedfisu@tal.upv.es

Abstract

Solar ovens have become a very popular technology for cooking, specially, in underdeveloped countries where access to firewood is scarce, time consuming and expensive. The benefits of solar cooking are multiple, such as saving money, as this device requires no fuel, as well as having an important impact in the environment, decreasing carbon dioxide emissions and decreasing deforestation.

One challenge for food industry is to get to know the behaviour of food cooked with solar technology. The aim of this study was to model the drying process of white and red grape in solar oven using thermodynamics and spectrophotometry measurements, controlling the irradiation effect blocking the Ultraviolet radiation using a polarized vinyl film

Keywords: sun radiation; thermodynamics; solar oven; drying.

1. Introduction

Grape is the second most widely cultivated fruit in the world after the orange and it is of great commercial interest [1]. It contains large amounts of phytochemicals including phenolics, flavonoids, anthocyanins and resveratrol, which offer health benefits. Antioxidant compounds include vitamins, phenols, carotenoids, and flavonoids. Among the last group, flavones, isoflavones, flavanones, flavonols, anthocyanins and catechins are the most important, and exhibit substantial antioxidant activity [2]. The high content of grapes in phenolics, flavonoids, and anthocyanins have been suggested to be responsible for their health benefits [3] and these benefits have been well described [4].

Other benefits, as described by Meng et al (2017) [5] such as Melatonin, which was recently reported to be present in wine in 2008, as well as resveratrol and hydroxytyrosol, are regarded as bioactive compounds in grapes and wines and have positive effects for human health.

Regarding the drying of this fruit, it is a slow and energy intensive process because the waxy peel has low permeability to moisture [6]. Nevertheless, Peinado et al. (2013) [7] reported that Pedro Ximenez grapes, exposed to sunlight, presented a higher antioxidant capacity than fresh grapes. Thus it is reasonable to infer that both UV radiation and temperature bring about changes in the phenolic profile when fresh grapes are processed into raisins by sun drying.

Drying is one of the most commonly followed methods of preservation for fruits, vegetables and fruit products [8]. Natural sun drying of fruits is still practiced largely unchanged from ancient times in many tropical and subtropical countries. This method is the cheapest and is successfully employed in grapes producing countries. In many of these countries, more than 80% of food is being produced by small farmers in developing countries. These farmers dry food products by natural sun drying, an advantage being that solar energy is available free of cost, but there are several disadvantages which are responsible for degradation and poor quality of the end product [9].

In many rural locations in Africa and most developing countries, grid-connected electricity and supplies of other non-renewable sources of energy are either unavailable, unreliable or, for many farmers, too expensive. Thus, in such areas, crop drying systems that employ motorised fans and/or electrical heating are inappropriate. The large initial and running costs of fossil fuel powered dryers present such barriers that they are rarely adopted by small scale farmers. The traditional open sun drying utilised widely by rural farmers has inherent limitations: high crop losses ensue from inadequate drying, fungal attacks, insects, birds and rodents encroachment, unexpected down pour of rain and other weathering effects. In such conditions, solar-energy crop dryers appear increasingly to be attractive as commercial propositions [10].

In pursuit of achieving the Sustainable Development Goals (SDGs) – and previously the Millennium Development Goals – introducing clean cooking technologies remains a popular option for development actors. One such technology is the solar cooker (SC), a device that makes direct use of sunlight to cook food or pasteurize drinks. While there are multiple designs, the general principle is that these devices channel and concentrate sunlight through mirrors, which is then converted to heat and used for cooking [11].

Thermodynamically, multiple studies were carried out by this research group regarding structural changes of meat as consequence of drying process. The infrared thermography (IRT) has shown to be a valuable tool to carry out studies regarding the infrared spectrum, as it is a non-contact and non-destructive method that provides temperature information of the whole body and not only one point [12, 13, 14].

The aim of this study was to model the drying process of white and red grape in solar oven using thermodynamics and spectrophotometry measurements, controlling the irradiation effect by blocking the Ultraviolet radiation using a polarized vinyl film.

2. Materials and Methods

1.1. Materials

Experiments were carried out using two different types of grapes (*Vitis vinífera*): red table grape "Red Globe" and white table grape "Regal". Both types of grapes were bought at local commerce in Valencia, Spain, and selected according to their homogeneity in size and color. They were stored at 8ºC until usage in sample cups, sealed with Parafilm® in order to avoid water losses.

2.2. Physicochemical Determinations

Mass was determined by using a Mettler Toledo Balance (±0.0001) (Mettler-Toledo, Inc., USA).

The water activity (a_w) was determined by a dew point Hygrometer Decagon (Aqualab®, series 3 TE, Decagon Devices, Pullman, WA, USA), with precision $\pm0,003$. Moisture was determined by drying in a vacuum oven at 60 ºC until constant weight was reached (AOAC Method 934.06, 2000). Soluble solids content of the pulp liquid phase was determined by the refractometetric index (ºBrix) with a refractometer calibrated with distilled water at 25 ºC (ABBE, ATAGO Model 3-T, Japan).

2.3 Drying process

A solar oven (model Suntaste Compact, SunOK, Portugal) of 52x43x32 cm was used for the drying. Samples were placed in the described order in the middle of the oven, close to the door, in order to favor its drying. The door of the oven was not fully closed, leaving a 10 cm space at the upper surface to enable drying and images from an infrared camera Optris PI®

160 thermal imager (Optris GmbH, Berlin, Germany). This setup was located approximately at 20 cm of the sample surface and at an angle of 45º relative to the plane in which the samples were placed. The camera was connected to a computer to record. A certified emissivity label of 25 mm diameter ($\varepsilon = 0.95$) (Optris GmbH, berlin, Germany) was used as a reference emitter to calculate the reflected energy received by the infrared camera.

Temperatures during drying were controlled by 5 K-thermocouples and 2 radiofrequency sensors connected to an Agilent multiplexer 34972A data acquisition system (Agilent Technologies, Malaysia) and registered by Agilent.

At the same time as the drying started and the registering of temperatures, radiofrequency and infrared images were recorded, manual analysis were carried out every fifteen minutes: the air velocity was measured inside the oven and outside with a digital anemometer (Proster® RoHS, Model PST-TL090 series, wind accuracy ±5% China). Air humidity was also registered in and out with a humidity meter (TRACKlife, RoHS, Model HM01, accuracy ±3% RH at 25 ºC, 20%-80% RH, ±3.5% RH at other ranges, China) and thirdly, day light intensity and in the solar oven was registered with a digital luxometer (D-LUXmeter, RoHS, accuracy ±4%, resolution 0.1 lx, range 0,1-200,000 lx, resolution 0,1 lx, China).

Procedure difference was that on one of the days, a window vinyl film with control heat and 96% UV rays blockage was placed over the solar oven´s glass (Rabbitgoo®, A023-45B, China) and on the other day the oven´s glass had no vinyl. The vinyl is PVC electrostatic film plus a back with PET release film.

2.4 Solar Oven

The solar oven (SunTaste, SunOk©, Portugal) is made out of cork agglomerate with water based varnish to diminish UV effects. It also contains aluminium and an ultra-clear glass cover of 4mm thickness with a UV transmittance (T_{uv}) of 84.5%.

A solar box cooker basically consists of an insulated box with a transparent glass cover and reflective surfaces to direct sunlight into the box. The inner part of the box is painted black in order to maximize the sunlight absorption.

2.5 Infrared measurements

Thermal images were acquired using the Optris PI® 160 thermal imager (Optris GmbH, Berlin, Germany). It uses a two-dimensional Focal Plane array with 160 x 120 pixels, a spectral range of 7.5-13 μm, resolution of 0.05 ºC and an accuracy of ± 2%. The camera covers a temperature range of -20 to 100 ºC. It has a field view of 23º x 17º with a minimal focus distance of 0.02 m. The camera is supported by the software Optris PI Connect (Optris GmbH, Berlin, Germany).

3. Results and discussion

The heating process of the red and white grape surface was produced by a combined effect of absorption of photon energy in the solar spectrum and by convection heat transmission with the air inside the solar oven. Figure 1 shows a sequence of treatment monitored by IRT, where it is possible to observe how the samples are heated by IRT (thermal infrared).
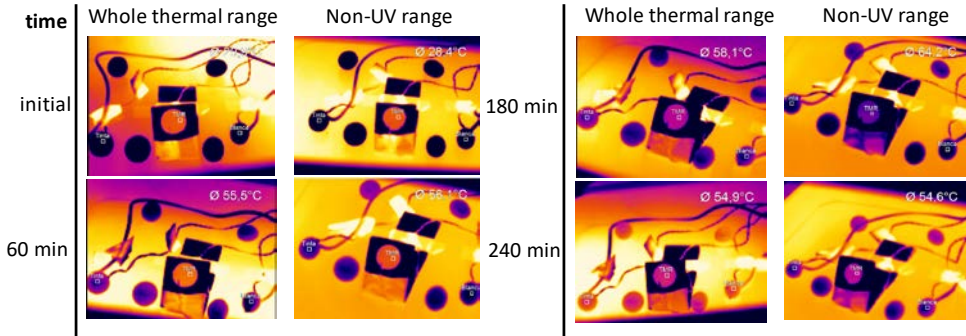
Figure 1. Sequence of grapes heating analized by IRT, for treatment with whole thermal infrared and for same range without the ultraviolet range.

Figure 2a and b show the surface temperature of the samples and of the air temperature with respect to the treatment time, where it is possible to observe how the temperature of the samples is always above that of the air. This behaviour occurs in both treatments, with ultraviolet spectrum and without this section of the spectrum. However, analyzing the internal and external measurements of light intensity in figure 2c and d, it is possible to observe how the effect of the solar oven mirrors cause an increase of the internal intensity in the treatment that include the ultraviolet range but this does not occur in the other treatment, when the ultraviolet spectrum is blocked.

Applying an energy balance on the surface of the samples, it is possible to calculate the amount of thermal energy accumulated as the addition of the heats received by radiation and by convection, see equation 1.

$$\frac{dE}{dt} = q_{rad} + q_{conv} \qquad \text{(eq. 1)}$$

Only the internal energy will accumulate because most of the sun spectrum that receives the surface is the thermal spectrum (IR, VIS and UV), with small radiation at lower frequencies (RF and MW) and nil at higher frequencies. Therefore, it is possible to estimate the temperature increasement by time measured by TIR, mass of sample and specific heat estimated by Chen model.

$$\frac{dE}{dt} = \frac{dU}{dt} = MC_P \frac{dT}{dt} \qquad \text{(eq. 2)}$$

For a natural convection (measuring the air velocity and relative humidity) it is possible to calculate the individual heat coefficient, and with the temperature difference between the surface and the air it is possible to estimate the heat loss to the environment.

$$q_{conv} = h \, (T_s - T_{amb}) \tag{eq. 3}$$
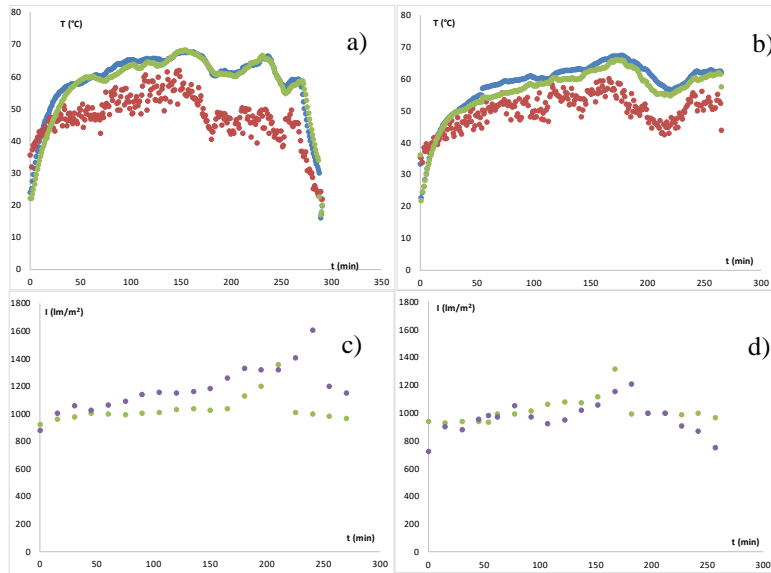
Figure 2. a) and b) represents the air temperature (●), red grape surface temperature (●) and white grape surface temperature (●), and c) and d) the light intensity express in lm/m2 for external (●) to the solar oven and internal (●). Where a) and c) represents treatment with whole thermal range radiation and b) and d) for same range radiation without the ultraviolet spectra.

Figure 3 shows the accumulation energy in the samples, the heat losses to the air and the heat gain by radiation, where it is possible to observe how the infrared and visible range are the most important for the warming because differences are not appreciated between both treatments.

Finally, the results of the drying process are shown in table 1, where it is possible to observe how dehydration occurs in the high moisture isotherm section, where small variations of water activity (in this case not significant) represent high variations in moisture (in this case very significant) producing a 20% of weight loss in all samples. However, there are no differences between treatments with or without ultraviolet spectrum.
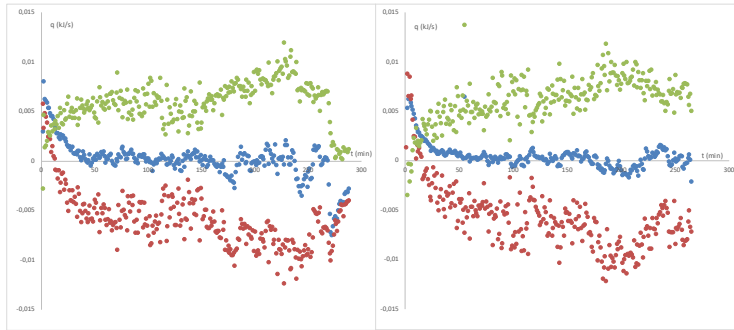
Figure 3. represents the energies (kJ/s) explained on equation 1 applied in white grape; where (●), represents the convection heat (eq. 3); (●) represents the accumulated internal energy (eq. 2) and (●) represents the radiation heat. a) represents treatment with whole thermal range radiation and b) for same range radiation without the ultraviolet spectra.

Table 1. Initial and final physical and compositional values of samples in both treatments.

		initial			final			
		xw (kg_w/kg_T)	zs (ºBrix)	a_w	xw (kg_w/kg_T)	zs (ºBrix)	a_w	ΔM (kg/kg)
thermal range	Red grape	0,870 ± 0,002	9,70 ± 0,14	0,984 ± 0,002	0,83 ± 0,05	11,7 ± 1,1	0,980 ± 0,005	-0,20 ± 0,08
	White grape	0,807 ± 0,002	16,80 ± 0,15	0,977 ± 0,003	0,76 ± 0,02	21 ± 2	0,971 ± 0,004	-0,20 ± 0,08
non-UV range	Red grape	0,870 ± 0,002	9,70 ± 0,14	0,984 ± 0,002	0,85 ± 0,02	11,9 ± 0,7	0,9849 ± 0,0010	-0,21 ± 0,05
	White grape	0,807 ± 0,002	16,8 ± 0,15	0,977 ± 0,003	0,785 ± 0,009	20,4 ± 0,8	0,9741 ± 0,0006	-0,20 ± 0,03

4. Conclusions

It has been shown that it is possible to remove the irradiating solar spectrum or ultraviolet range, which generates food oxidation, with no decrease of the heating capacity or dehydration of a solar oven.

5. Acknowledgements

6. References

[1] Azzouz, S.; Hermassi, I.; Toujani, M.; Belghith, A. (2016). Effect of drying temperature on the rheological characteristics of dried seedless grapes. Food and Bioproducts Processing, 100 (A), 246-254.

[2] Wang, H.; Cao, G.; Prior, R.L. (1997). Oxygen radical absorbing capacity of anthocyanins. J.Agric. Food Chemistry, 45, 304-309.

[3] Yang, J.; Martinson, T.E.; Liu, R.H. (2009). Phytochemical profiles and antioxidant activities of wine grapes. Food Chemistry, 116 (1), 332-339.

[4] Fabani, M.P.; Baroni, M.V.; Luna, L.; Lingua, M.S.; Monferran, M.V.; Paños, H.; Tapia, A.; Wunderlin, D.A.; Egly Feresin, G. (2017). Changes in the phenolic profile of Argentinean fresh grapes during production of sun-dried raisins. Journal of Food Composition and Analysis, 58, 23-32.

[5] Meng, J.-F.; Shi, T.-C.; Song, S.; Zhang, Z.-W.; Fang, Y.-L. (2017). Melatonin in grapes and grape-related foodstuffs: A review. Food Chemistry, 231, 185-191.

[6] Adiletta, G.; Russo, P.; Senadeera, W.; Di Matteo, M. (2016). Drying characteristics and quality of grape under physical pretreatment. Journal of Food Engineering, 172, 9-18.

[7] Peinado, J.; López de Lerma, N.; Peralbo-Molina, A.; Priego-Capote, F.; de Castro, C.; McDonagh, B. (2013). Sunlight exposure increases the phenolic content in postharvested white grapes. An evaluation of their antioxidant activity in Saccharomyces cerevisiae. Journal of Functional Foods. 5 (4), 1566-1575.

[8] Prakash, O.; Kumar, A. (2017). Solar Drying Technology: Concept, design, testing, modeling, economics and environment. Green energy and technology, 1, 3-38.

[9] Jairaj, K.S.; Singh, S.P.; Srikant, K. (2009). A review of solar dryers developed for grape drying. Solar Energy, 83 (9), 1698-1712.

[10] Ekechukwu, O.V.; Norton, B. (1999). Review of solar-energy drying systems II: an overview of solar drying technology. Energy Conversion and Management, 40 (6), 615-655.

[11] Iessa, L.; De Vries, Y.A.; Swinkels C.E.; Smits, M.; Butijn, C.A.A. (2017). What's cooking? Unverified assumptions, overlooking of local needs and pro-solution biases in the solar cooking literature. Energy Research & Social Science, (28), 98-108.

[12] Traffano-Schiffo, M.V., Castro-Giraldez, M., Colom, R.J., Fito, P.F. (2015). Study of the application of dielectric spectroscopy to predict the water activity of meat during drying process. Journal of Food Engineering, 166, 285-290.

[13] Traffano-Schiffo, M.V., Castro-Giráldez, M., Fito, P.J., Balaguer, N. (2014). Thermodynamic model of meat drying by infrared thermography. Journal of Food Engineering, 128, 103-110.

[14] Cuibus, L., Castro-Giráldez, M., Fito, P.J., Fabbri, A. (2014). Application of infrared thermography and dielectric spectroscopy for controlling freezing process of raw potato. Innovative Food Science & Emerging Technologies, 24, 80-87.

Microstructural characterization of apple tissue during drying using X-Ray microtomography

Rahman M. M. [a], Billah, M. M. [b], Khan, M.I.H.[a], Karim, M.A [a*]

[a] School of Chemistry Physic and Mechanical Engineering, Science and Engineering Faculty, Queensland University of Technology, Australia

[b] Department of Arts and Sciences, Ahsanullah University of Science and Technology, Dhaka-1208, Bangladesh

*E-mail of the corresponding author: *azharul.karim@qut.edu.au*

Abstract

This study aims to investigate the complex microstructural changes in plant-based food materials during drying by using X-ray micro-computed tomography (X-ray µCT) along with the image analysis. The apple samples were dried at 60 °C and tested using X-ray µCT at different stages of drying. The porosity, cell and pore size distribution were determined from the micro-CT data set. It was observed that significant changes in porosity, cell and pore size distribution take place at different drying times and moisture contents. X-ray µCT can serve as a very promising tool to elucidate the evolution of the food microstructure during the drying process.

Keywords: Food drying, characteristics, X-ray microtomography, nondestructive evaluation.

1. Introduction

Drying of fruits and vegetables is a complex process as their structures are heterogeneous and changes in microstructures significantly affect the drying process [1-3]. Plant-based food material consists of cells and intercellular spaces. The major component of plant-based food materials is the water which is distributed in the cells and intercellular spaces [4-5]. Therefore, it is crucial to understand the evolution of microstructural characteristics to make an accurate prediction of energy requirement and the physical quality during drying of plant-based food material.

There are several methods such as Scanning electron microscope, light microscope, X-ray microtomography reported in the literature for the investigation of cellular structure in the fresh food sample [6-7]. However, very limited research has been conducted to investigate the evolution of the microstructural characteristics during drying of food material. The researchers have anticipated the cell breakdown under certain drying condition [8-9]. Cell collapse depends on internal thermal stress that first develops near the surface and gradually penetrates to the center of the sample during convective drying [8]. In other words, entire food sample does not reach breakdown temperature at a time. Therefore, it is critical to investigate the evolution of the cellular level structure during the drying process.

The proper microstructural information regarding the changes of cellular structure and porosity of the plant-based food is required to improve the physical quality of the dried food [10]. Most of the microstructural investigation techniques used by the researchers are destructive and invasive [11-13]. Therefore, these methods are not suitable for the structural characterization of the plant-based food material during drying [14-15]. The limitations of the destructive and the invasive methods justify the importance of high resolution non-destructive and non-invasive methods. There is a major gap in the literature regarding the application of the non-invasive method to investigate the micro level structural changes during drying of food material [14]. Hence, the evolution of microstructural characteristics during the drying process is still not clear to the food engineers. To address this research gap, X-ray μCT can be a very useful technique to elucidate the cellular level structural changes during food drying [16]. Therefore, the main aim of this work is to experimentally investigate the change in microstructural characteristics (Cells and pore size distributions) during drying of apple tissue.

2. Materials and Methods

2.1 Sample preparation and the drying experiment

Drying was carried out in a laboratory-scale temperature-controlled convective dryer. Granny Smith apple was taken as a sample for this experiment. The fresh apples were collected from the local market and stored in a refrigerator at 4°C to keep them fresh before the drying

experiment. Prior to the drying test, the samples were taken out from the refrigerator and kept at the room temperature for an hour for achieving thermal stability of the sample. The samples were then washed and cut into cylindrical slices of 10 mm thickness and 20 mm diameter. The dryer was started 30 min before of the experiment for allowing the system reaches the steady state condition. The drying experiments were performed at 60°C temperature. For each drying experiment; six samples were taken. During each experiment, air velocity of 0.7 m/s and the relative humidity range between 60-65% were maintained. The moisture content of the sample at the different stage of drying was measured using X-ray microtomographic images. The details of the moisture content measuring technique can be found in author's previous work [14].

2.2 X-ray microtomography

In this study, X-ray µCT was used to investigate the micro level structural changes. X-ray µCT is able to scan the entire sample to obtain micro-level information such as cell and pore size distribution without the need for serial cuts or chemical treatment. Therefore, the same sample can be used at the next stages of the drying process. To observe the micro level morphological changes, the samples were taken out from the dryer tray after every 30 min during drying. Before placing into the X-ray µCT, the samples were kept in a desiccator to avoid the natural rehydration to the ambient condition of the laboratory. The apple samples were scanned using a Scanco-40 µCT high-resolution desktop µ-CT system which consists of a resolution of 6 µm. The scanning was operated at 55KV, and the images were taken through 0°-180° of rotation. The process is controlled by a built-in a software package which uses the back-projection algorithm. After the scanning, the samples were placed back into the dryer, and the scanning images were collected for the further investigations.

2.3 Image processing and data analysis

The grayscale images obtained from the X-ray µCT was transferred to MATLAB image processing environment for further processing. The image processing involved the noise elimination and segmentation. The noise elimination was performed by the intensity thresholding and the filtering process. Segmentation was performed after the noise elimination process to characterize solid materials in the microscopic images. For this purpose, Watershed algorithm was used. The area of the cells and intercellular spaces are obtained from the pixel of the X-ray tomographic images of the food material. At the different stages of drying the images were collected and the area was calculated. The change of shrinkage was estimated from the area ratio (AR) by the following relationship

$$AR = \frac{A_x}{A_0} \tag{1}$$

where, A_x is the area of the cell/intercellular space at a different stage of drying, A_0 is the area of cell/intercellular space of fresh sample.

The porosity of the samples at different stages of drying was determined from the X-ray μCT data. The porosity was calculated by the following relationship [17]:

$$Porosity = \frac{V_{Int}}{V_T} \tag{2}$$

where, V_{Int} is the total volume of the intercellular space and V_T is the total volume of the sample.

The area distribution of cell and intercellular space in tissue was estimated by probability density function as given below [18]

$$\Pr(a \leq x \leq b) = \int_a^b f(x)dx \tag{3}$$

where, x is the variable denotes the area of the cell or intercellular spaces.

3. Result and discussion

The structural change of food material is the result of collapse and shrinkage of the cells and cell walls during the drying period when significant loss of water takes place [19-20]. There is a significant difference between collapse and shrinkage. Collapse takes place when cellular or tissue level structure breaks down irreversibly; whereas shrinkage refers to a reversible reduction in the size of food material. The shrinkage of the apple tissue was measured from the tomographic image analysis. The tomographic image of the fresh apple and dried apple is presented in Figure 1. In this figure, the high-intensity region of the image represents the cellular area while the low-intensity region of the image represents the intercellular space area. The fresh tissue the cells are intact and filled with water. In the dried tissue, the cellular area shrinks due to the moisture loss. It is interesting to observe that the overall shrinkage of the sample is arbitrary. This kind of shrinkage is known as anisotropic shrinkage.

The apple tissue has the amorphous structure, and during the drying process, it shows the anisotropic shrinkage. Therefore, it is ideal to estimate the shrinkage of apple tissue in terms of area ratio. The evolution of the areal shrinkage as a function of moisture content at 60°C is presented in Figure 2. It is clear from the figure that the apple tissue experiences 35% shrinkage during the drying process. This kind of shrinkage phenomena is commonly known as large deformation. Several factors are responsible for the shrinkage phenomena including the structural heterogeneity and the drying temperature.
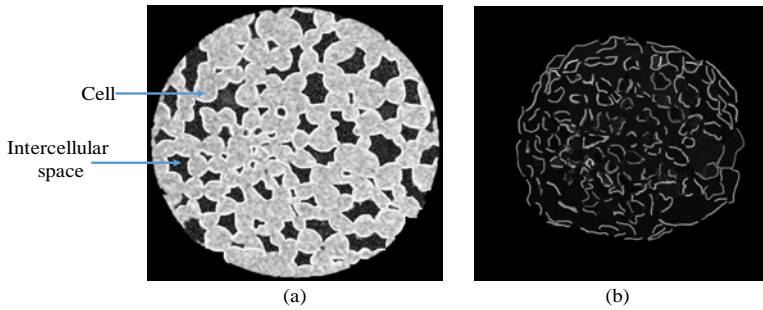
Figure 1. X-ray tomographic image of (a) fresh apple tissue and (b) dried at 60°C temperature
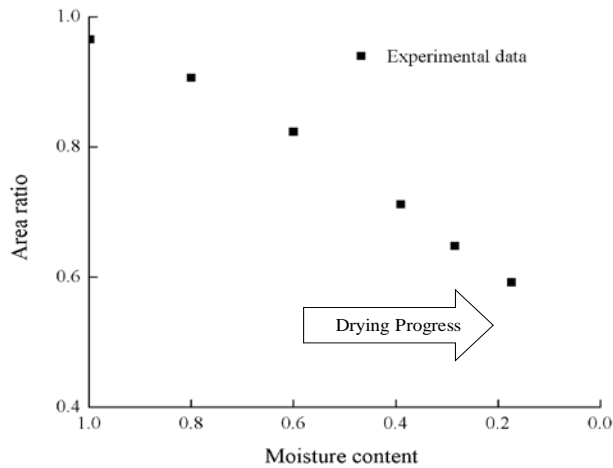
Figure 2. Evolution of areal shrinkage of apple as a function of moisture content during drying at 60°C.

The size of cells and intercellular spaces were obtained from the tomographic image analysis. The size distribution of cells and the intercellular spaces in fresh apple tissue is presented in Figure 3. It can be seen that in fresh sample, the cellular area is distributed in a wide range. It was also observed that the cell size is bigger than the intercellular spaces.

Figure 4 represents the evolution of the area of cells and intercellular spaces during the drying process. After 60 min drying the size of the cellular area is reduced slowly while the area of the intercellular space changes rapidly (Figure 4a). This is because a negative pressure is created inside the cells due to the removal of water during the drying process. The water migration process in this stage is mainly the free water removal. Owing to ongoing moisture migration, the collapse of cells and intercellular spaces is increased at the later stages of drying. After 350 min drying time, it was found that the pore size distribution is greater than the cell size distributions (Figure 4b).
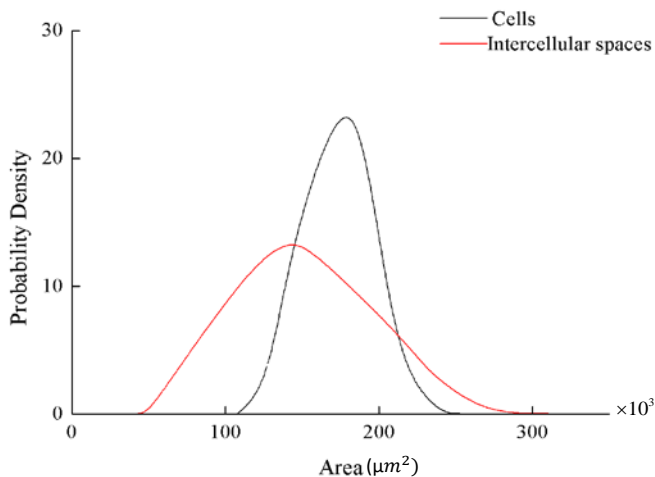
Figure 3. Areal distribution of cell and intercellular space in fresh apple tissue

The porosity of the samples was calculated from the images using equation (2). The porosity of the plant-based food materials also shows an interesting relationship with moisture content. Figure 5 shows the changes in porosity of apple sample at 60°C drying temperature against the moisture content. It can be seen that a decreasing trend of porosity has been found just before an inversion starts at moisture ration of 0.7 (Dry basis). This may be due to the shrinkage of initial porosity of apple at the early stage of drying [11]. After that, porosity keeps increasing steadily with moisture content until the end of the drying.
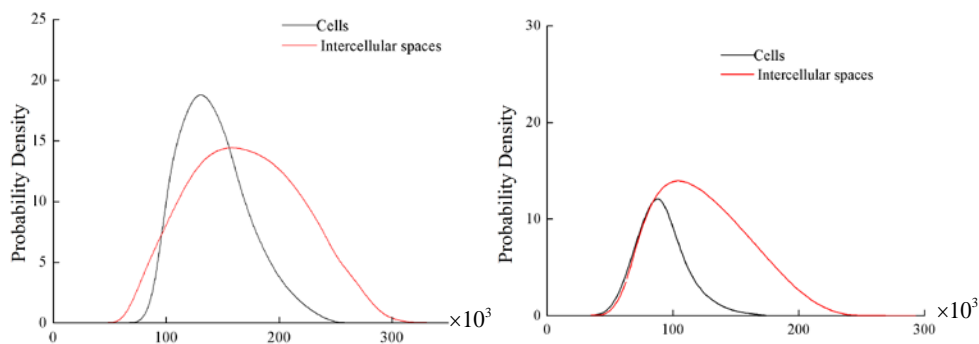
Figure 4. Areal distribution of cell and intercellular space after (a)60 min, (b) 350 min of drying
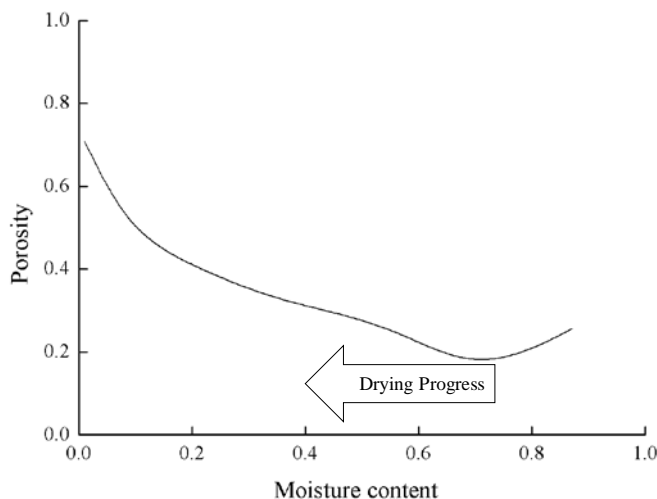
Figure 5. Evolution of porosity of apple during drying at 60°C

4. Conclusion

This paper investigates the evolution of microstructural characteristics of apple samples as a function of moisture content during drying. The applicability of X-ray microtomography along with the image processing technique in the analysis of cell and intercellular space size distribution in fruits and vegetable during drying is established in this study. This technique is nondestructive and requires minimum effort in sample preparation. It has been found that the cell and the pore size distribution of the food material change significantly over the drying period. The cellular area is larger than the intercellular area in the fresh apple tissue. Nevertheless, towards the end of the drying process, a larger amount of intercellular spaces was observed, which is directly related to the porosity of the apple tissue. The quantitive information of this study will facilitate the future researchers to understand the relationship between the moisture content and the evolution of microstructure during the drying process. The findings of this investigation will help the food engineers to develop and validate accurate food drying model which will lead to the design of an efficient food drying process.

5. Acknowledgment

6. References

[1] Joardder, M. U.; Kumar, C.; Karim, M., Food structure: its formation and relationships with other properties. *Critical reviews in food science and nutrition* **2017,** *57* (6), 1190-1205.

[2] Rahman, M.; Mekhilef, S.; Saidur, R.; Mustayen Billah, A.; Rahman, S., Mathematical modelling and experimental validation of solar drying of mushrooms. *International Journal of Green Energy* **2016,** *13* (4), 344-351.

[3] Karim, M. A.; Rahman, M. M.; Pham, N. D.; Fawzia, S., Food Microstructure as affected by processing and its effect on quality and stability. In *Food Microstructure and Its Relationship with Quality and Stability*, Elsevier: 2017; pp 43-57.

[4] Khan, M. I. H.; Wellard, R. M.; Nagy, S. A.; Joardder, M.; Karim, M., Investigation of bound and free water in plant-based food material using NMR T 2 relaxometry. *Innovative Food Science & Emerging Technologies* **2016,** *38*, 252-261.

[5] Kumar, C.; Joardder, M. U. H.; Farrell, T. W.; Millar, G. J.; Karim, M. A., Mathematical model for intermittent microwave convective drying of food materials. *Drying Technology* **2016,** *34* (8), 962-973.

[6] Khan, M. I. H.; Karim, M., Cellular water distribution, transport, and its investigation methods for plant-based food material. *Food Research International* **2017**.

[7] Joardder, M. U. H.; Brown, R. J.; Kumar, C.; Karim, M. A., Effect of Cell Wall Properties on Porosity and Shrinkage of Dried Apple. *International Journal of Food Properties* **2015,** *18* (10), 2327-2337.

[8] Khan, M. I. H.; Wellard, R. M.; Nagy, S. A.; Joardder, M.; Karim, M., Experimental investigation of bound and free water transport process during drying of hygroscopic food material. *International Journal of Thermal Sciences* **2017,** *117*, 266-273.

[9] Rizzolo, A.; Vanoli, M.; Cortellino, G.; Spinelli, L.; Contini, D.; Herremans, E.; Bongaers, E.; Nemeth, A.; Leitner, M.; Verboven, P., Characterizing the tissue of apple air-dried and osmo-air-dried rings by X-CT and OCT and relationship with ring crispness and fruit maturity at harvest measured by TRS. *Innovative Food Science & Emerging Technologies* **2014,** *24*, 121-130.

[10] Kumar, C.; Joardder, M. U. H.; Farrell, T. W.; Karim, M. A., Investigation of intermittent microwave convective drying (IMCD) of food materials by a coupled 3D electromagnetics and multiphase model. *Drying Technology* **2018,** *36* (6), 736-750.

[11] Joardder, M. U.; Kumar, C.; Brown, R. J.; Karim, M., A micro-level investigation of the solid displacement method for porosity determination of dried food. *Journal of Food Engineering* **2015,** *166*, 156-164.

[12] Joardder, M. U.; Kumar, C.; Karim, M., Prediction of porosity of food materials during drying: Current challenges and future directions. *Critical Reviews in Food Science and Nutrition* **2017,** (just-accepted).

[13] Rahman, M. M.; Joardder, M. U. H.; Khan, M. I. H.; Pham, N. D.; Karim, M. A., Multi-scale model of food drying: Current status and challenges. *Critical Reviews in Food Science and Nutrition* **2018,** *58* (5), 858-876.

[14] Rahman, M. M.; Joardder, M. U. H.; Karim, A., Non-destructive investigation of cellular level moisture distribution and morphological changes during drying of a plant-based food material. *Biosystems Engineering* **2018,** *169*, 126-138.

[15] Khan, M. I. H.; Nagy, S. A.; Karim, M. A., Transport of cellular water during drying: An understanding of cell rupturing mechanism in apple tissue. *Food Research International* **2018,** *105*, 772-781.

[16] Rahman, M. M.; Kumar, C.; Joardder, M. U. H.; Karim, M. A., A micro-level transport model for plant-based food materials during drying. *Chemical Engineering Science* **2018,** *187*, 1-15.

[17] Joardder, M. U.; Karim, A.; Kumar, C.; Brown, R. J., *Porosity: Establishing the Relationship Between Drying Parameters and Dried Food Quality*. Springer: 2015.

[18] Rahman, M. M.; Gu, Y. T.; Karim, M. A., Development of realistic food microstructure considering the structural heterogeneity of cells and intercellular space. *Food Structure* **2018,** *15*, 9-16.

[19] Ramos, I. N.; Branda˜o, T. R. S.; Silva, C. L. M., Structural Changes During Air Drying of Fruits and Vegetables. *Food Science Technology International* **2003,** *9* (3), 201–6.

[20] Devahastin, S.; Niamnuy, C., Modelling quality changes of fruits and vegetables during drying: a review. *International Journal of Food Science and Technology* **2010,** *45* (9), 1755-1767.

DRYING PRODUCTS

Poster Presentations

Solar drying of strawberry coated with nopal mucilage: It's effect on phenolic compounds

León, M.J.ª; López-Ortiz, A.ª,ᵇ; Pilatowsky, F.I.ª; Méndez, L.L.L.ᶜ

ª Sistemas energéticos. Universidad Nacional Autónoma de México-Instituto de Energias Renovables.
ᵇ Consejo Nacional de Ciencia y Tecnología.
ᶜ Instituto Politécnico Nacional, CIIDIR Oaxaca.

*E-mail of the corresponding author: marijoseleon95@gmail.com

Abstract

The objective of this study was to evaluate the effect of indirect solar drying (ISD) and conventional (CD) (40, 50, 60 °C) on the concentration of phenolic compounds of strawberry slices, coated with opuntia mucilage (Opuntia ficus indica), and measured with the spectrophotometric method. The indirect solar dryer uses solar-thermal and photovoltaic technology with temperatures between 40 and 60 °C. The concentration of anthocyanins was higher in the ISD than in CD. The strawberry coated with the nopal mucilage has a preservation of phenolic compounds in CD and IDS.

Keywords: strawberry, solar drying, phenolic compounds.

1. Introduction

The nutraceutical compounds are active biological substances that can be found in foods as natural compounds, they may provide nutritional and health benefits (Amarante et al, 2001), as well as, the prevention of diseases and improvement of the physiological functions of the organism (Garzon, 2008). Strawberry contains nutraceutical compounds as flavonoids, phenolic compounds, and anthocyanins (Giampieri, Tulipani, Alvarez-Suarez, & Quiles, 2012). The study of conditions and pre-treatments for hot-air drying are necessary to minimize the physical and chemical changes during the process. New quality products, attractive to the consumer due to the nutritional value, can be obtained (Adiletta et al 2016).

A pre-treatment as mucilage coatings lead to increased raw strawberry shelf life and improve effects on color, texture, and sensory quality of the fruit (Del Valle et al, 2003). Opuntia genus is widely known for its mucilage production (Saenz et al, 2004). Mucilage, a natural polymer with a great capacity to absorb water, is considered as a potential source of industrial hydrocolloid (León et al, 2010). Mucilage contains L-arabinose, D-galactose, L-rhamnose and D-xylose and galacturonic acid (Sepúlveda et al, 2007).

Drying is the most expensive unit operation due to the energy requirements in the drying chamber, as, heating by gas, electricity, or biomass. However, the price of fuel is the main economic factor that affects drying operations; also; the pollution and the environmental consequences of this process (Babu et al, 2018).

Solar energy is harnessed to improve solar heating systems in drying, using equipment for controlling the air flow and the greenhouse effect (Kamruzzaman et al 2017). Solar dying equipment improves the protection of the product against environmental contaminants (Abhay et al 20017). It also improves the protection of the product against environmental contaminants (Sharma et al, 2009).

The solar dryers can be the direct, indirect and mixed type, with or without forced convection (Ramana, 2009). In the indirect solar dryers, the solar collector for air heating and the drying chamber are separated (Mahesh et al 2016). The air is heated in the collector and solar radiation does not affect the food placed into the drying chamber. The drying is faster compared to open sun drying due to their shape and dimensions (Lingayat et al, 2017). Solar dryers design generally needs air ventilation system guarantees adequate moisture removing from inside them, environmentally friendly concept, seeking energy efficiency and using easily accessible materials (Visavale, 2012).

2. Materials and Methods

The strawberry was obtained from the local market in Morelos, México. The fresh strawberries were washed and disinfected with a colloidal silver solution in the concentration indicated by the supplier. They were subsequently rinsed to remove any

remaining residue. The samples were selected manually, and the sepal and wick eliminating.

2.1 Color

The color of raw strawberry was measured during drying according to L * a * b * values. The parameters a * and b * were used to calculate the Hue angle according to the following equation:

$$Hue = \text{Tan}^{-1}\left(\frac{b^*}{a^*}\right)$$

[1]

2.2 Moisture

The determination of moisture content of raw strawberry coated with opuntia mucilage (*Opuntia ficus indica*) was measured during drying using the AOAC 972, 1990 method.

2.3 Coating (Opuntia ficus indica)

The opuntia mucilage extraction was carried out from cladodes of 6 months, harvested in the month of January. A cladode: water (1:2) ratio was used. Cladodes were cut into slices of 1 x 1 cm. The slices were weighed and placed in a stainless-steel container with distilled water. The heat treatment was carried out for 3 minutes at 80 ° C with constant stirring. The mucilage was separated by decantation method and refrigerated (Lopez-Ortiz et al, 2016).

The coating method used for the present project was by immersing and emerging the strawberry in the nopal mucilage for its subsequent placement in the dryer trays.

2.3 Conventional drying

Three temperatures (40, 50 and 60 ° C) were tested with an air velocity of 1 m/s.

2.4 Indirect solar drying (ISD)

The experimental indirect solar dryer system (ISD) was previously described in (Castillo-Téllez, Pilatowsky-Figueroa, López-Vidaña, Sarracino-Martínez, & Hernández-Galvez, 2017). The indirect solar dryer consists of a horizontal tunnel of rectangular shape with a constant section of flow with forced convection. Five flat plates solar collector for water heating was used. A radiator type heat exchanger was used for air-water heat transfer. Food samples were placed into the indirect solar dryer. For the air flow was an impulse by a fan connected to five photovoltaic solar panels. Temperature and air velocity were registered using a data acquisition system. The air velocity into the dryer was according to the solar irradiance (Gama, 2007).

Fresh strawberry coated with opuntia mucilage were placed in plastic meshes and introduced in the drying chamber. Fresh strawberry coated with cactus mucilage were placed in plastic meshes and introduced in the drying chamber. The air velocity in this dryer was according to the solar irradiance.
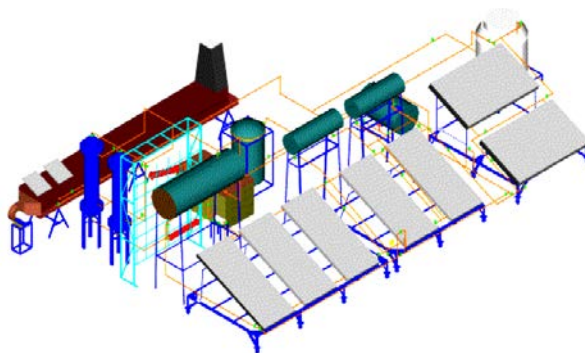
Fig. 1 Indirect solar dryer type tunnel

2.5 Data acquisition

The solar irradiance was obtained from the meteorological and calorimetric station of the UNAM. The geographical location of the Instituto de Energías Renovables - UNAM, in Temixco, Morelos, (18.85° latitude North and -99.2333° longitude East and an altitude of 1219 m above sea level). The solar dryer was instrumented with thermocouple T type temperature sensors, in different points: entrance and exit of solar collectors for water heating, entrance, and exit of the heat exchanger and along to the interior of the tunnel type-drying chamber. Temperature reading time intervals every 30 s. The water flow for heat exchanger was controlled at 10 L/s. The air velocity was measured and recorded with an anemometer at the entrance of the drying chamber.

2.6 Determination of anthocyanin

The pH-differential method was used to determine the total anthocyanin content (AC) according to the methodology reported by Giusti and Wroldstad (1996), using two buffer systems: potassium chloride buffer (0.025 M, pH = 1.0) and sodium acetate buffer (0.04 M, pH = 4). The content of anthocyanins was calculated as equivalents of Pelargonidin-3-glucoside (molecular weight (MW) = 449.2 g/mol, molar extinction coefficient (ε) = 26,900 L/mol/cm), the dilution factor (FD) of 0, was taken as the value of $A_{vismax515}$ and A_{700nm} for the sample of the two pH. Quartz cells of 1 cm light passage.

$$A= (A_{vismax} - A_{700nm})pH1 - (A_{vismax} - A_{700nm})pH4.5 \qquad [1]$$

$$AC\ (mg/L) = (A \times MW \times FD \times 1000) / (\varepsilon \times 1) \qquad [2]$$

3 Results and discussion

3.1 Color

The strawberry dried at 60 °C showed a change in color (darkening). The changes in strawberry coloring are due to different enzymes or chemicals, the degradation of the precursor's compound of the red pigmentation in the strawberry is labile to the prolonged

exposure of temperatures. During drying chemical reactions are slowed down as water activity decreases.
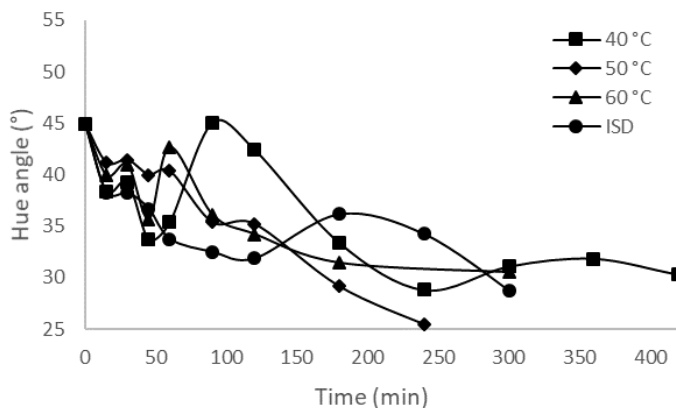
Fig. 2 Kinetics of color
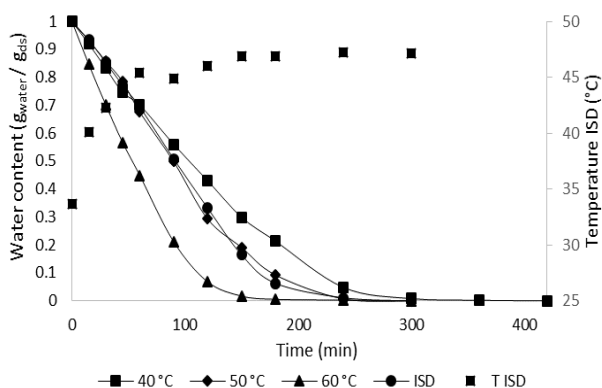
Fig. 3 Kinetic of moisture

3.2 Kinetic of drying

Drying time for 50, 60 °C and ISD were 5 hours, while at 40° C drying time was 7 hours. The coating does not affect the moisture transfer during the drying process (Lopez-Ortiz et al, 2016). During the first 180 minutes, it had major mass transfer during drying which includes the water transfer from inside of the strawberry to the surface and the water removal from the surface to the environment. Figure 3 shows two drying periods; in the first period, the conditions of the surface of the food reaches an equilibrium with the hot air conditions. The drying kinetics at 60 ° C shows a greater decrease in moisture content in the food reaching values of 9.8% wet bases after 300 minutes. Also, in the drying kinetics of the ISD can be observed that the moisture losses were low during the first 120 min due

to the initial drying temperature (30 °C). After 120 min, the drying kinetic was similar to 50°C in the convective dryer. This behavior was due to the increment in the temperature during the solar day. The second period is when the food already loses most of the water there is a decrease in the rate of drying, which makes it difficult to moisture movement as noted from the 180 minutes until reaching 300 minutes, which represents the end of the dehydrated.

3.3 Measurements of solar drying

During the ISD process, the water inlet temperature, the inlet temperature of the tunnel-type solar dryer and the outlet temperature were measured, having a maximum of 62.47 ° C water inlet and after the water leakage 58.46 ° C, having a loss in water temperature due the heat transfer to the air, the maximum temperature difference was 15 °C ± 0.05 obtained at 13:30 hrs.
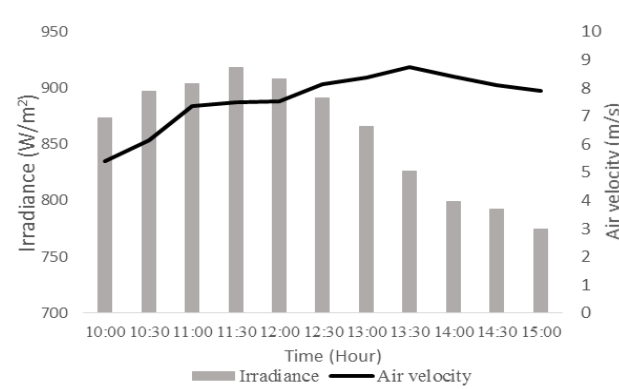
Fig. 4 Irradiance and air velocity during the solar drying process
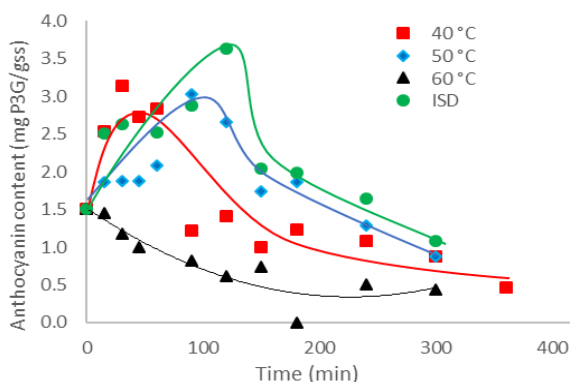
Fig. 5 Kinects of anthocyanin content

The initial direct irradiance measured during drying in the solar tunnel-type was 873 W/m^2 at 10:00 am and a final irradiation at the end of the drying of 774.2 W/m^2 at 15:00 pm. The maximum solar irradiance was 918 W/m^2 at 11:30 am, and the average was 858.96 W/m^2.

3.4 Phenolic compound: Anthocyanin

The anthocyanins were measured by the differential pH method in a double-beam spectrophotometer, of which 1 g of sample was used from its beginning until 60 minutes, after which the amount of sample for analysis had to be reduced to 0.1 g.

The samples were analyzed according to the dehydrated temperature having an initial concentration of 1.5 ± .3 gP3G/g$_{ds}$. For drying at 40 °C, 50 °C and ISD, the concentration of anthocyanin had an increment in until the 120 minutes, after this it had a diminution in its content. The diminution was due the compounds are sensitive to prolonged exposure to temperature, being affected after 150 minutes in the different two temperatures in conventional drier and indirect tunnel-type solar drier. The concentration of anthocyanin was mostly preserved in the tunnel-type solar dryer, considering a final content of 1.07 gP3G/g$_{ds}$, reducing 28.61 % of the initial concentration, unlike the different convection dryer dehydration temperatures (40 -68.92%, 50-42.2%, and 60 ° C-71.32%).

4. Conclusions

The coating does not affect the moisture transfer during the drying process. The drying kinetics at 50 °C was similar to drying kinetics in the ISD, besides of the nonconstant conditions in air velocity and temperature. The color in the dehydration at 40 °C in a conventional dryer had a minor darkening of the red color. The drying at 60 °C had a mayor darkening. The concentration of anthocyanin was greater preserved in the tunnel-type solar dryer, considering a final content of 1.07 g gP3G/g of Pelargonidin 3-Glucoside, preserving the compound in 34.70% in relation to the initial concentration.

5. Acknowledgment

6. References

[1] Adiletta, G., Russo, P., Senadeera, W., Di Matteo, M. (2016). Drying characteristics and quality of grape under physical pretreatment. Journal of Food Engineering. Vol. 172. Pp. 9-18. https://doi.org/10.1016/j.jfoodeng.2015.06.031.

[2] Amarante, C., Banks, N.H., 2001. Post harvest physiology and quality of coated fruits and vegetables. Hort. Rev. 26, 161-238.

[3] Babu, A.K., Kumaresan, G., Antony Aroul Raj, V., Velraj. R. (2018). Review of leaf drying: Mechanism and influencing parameters, drying methods, nutrient preservation, and mathematical models. Renewable and Sustainable Energy Reviews. Vol. 90. Pp. 536-556. https://doi.org/10.1016/j.rser.2018.04.002.

[4] Castillo-Téllez, M., Pilatowsky-Figueroa, I., López-Vidaña, E.C., Sarracino-Martínez, O., Hernández-Galvez, G. (2017) Dehydration of the red chilli (Capsicum annuum L., costeño) using an indirect-type forced convection solar dryer. Applied Thermal Engineering. Vol.

[5] 114. Pp. 1137-1144.

[6] Del-Valle A.V., Hernandez-Muñoz, A.P., Guarda, M.J. (2004) Development of a cactus-mucilage edible coating (Opuntia ficus indica) and its application to extend strawberry (Fragaria ananassa) shelf-life. Food Chemistry 91, 751–756.

[7] Gama P., Jose D. 2007. Análisis teórico experimental de un deshidratador solar combinado (térmico – fotovoltaico) para el tratamiento de arroz. Tesis Instituto de Energías Renovables - UNAM.

[8] Garzon G., 2008. Antocianinas como colorantes naturales y compuestos bioactivos. Universidad Nacional de Colombia.

[9] Giampieri, F., Tulipani, S., Alvarez-Suarez, J.M., Quiles, J.V., Mezzetti, B., Battino, M. (2012) The strawberry: Composition, nutritional quality, and impact on human health. Nutrition, Vol. 28 - 1, 9-19, ISSN 0899-9007, https://doi.org/10.1016/j.nut.2011.08.009.

[10] Giusti, M.M., Wrolstad, R.E. (1996) Characterization of Red Radish Anthocyanins. Journal of Food Science, 61, 322-326. http://dx.doi.org/10.1111/j.1365-2621.1996.tb14186.x

[11] Kamruzzaman, M.D., Uyeh, D.D., Jang, I.J., Woo, S.M., Ha, Y.S. (2017). Drying characteristics and milling quality of parboiled Japonica rice under various drying conditions. Engineering in Agriculture, Environment and Food. Vol. 4- 4. Pp 292-297. https://doi.org/10.1016/j.eaef.2017.08.001.

[12] Kumar, M., Sansaniwal, K.S., Khatak, P. (2016). Progress in solar dryers for drying various commodities. Renewable and Sustainable Energy Reviews. Vol. 55. Pp. 346-360. https://doi.org/10.1016/j.rser.2015.10.158.

[13] León-Martínez, F. M., Méndez-Lagunas, L. L., Rodríguez-Ramírez, J. (2010) Spray drying of nopal mucilage (Opuntia ficus-indica): Effects on powder properties and characterization. Carbohydrate Polymers. Vol. 81. PP. 867-870.

[14] Lingayat, A., Chandramohan, V.P., Raju, V.R.K. (2017). Design, Development and Performance of Indirect Type Solar Dryer for Banana Drying. Energy Procedia. Vol. 109. Pp. 409 - 416. https://doi.org/10.1016/j.egypro.2017.03.041.

[15] López-Ortiz, A., Torres F., Morales, M., Rodríguez, R., Lilia M., Sadoth S., Isaac P. (2016). Japan. Effect of edible natural polymer coating on strawberry slices dried by convection. The 20th International Drying Symposium.

[16] Marthy, M.V.R. (2009) A review of new technologies, models and experimental investigations of solar driers. Renewable and Sustainable Energy Reviews. Vol. 13. Pp 835 – 844.

[17] Saenz, C., Sepúlveda, E., Matsuhiro, B. (2004). Opuntia spp. mucilage's: A Functional Component with Industrial Perspectives. Journal of Arid Environments. 57. 275-290. 10.1016/S0140-1963(03)00106-X.

[18] Sharma, A., Chen, C. R., Vu Lan, N (2009) Solar-energy drying systems: A review. Renewable and Sustainable Energy Reviews. Vol. 13. PP. 1185-1210.

[19] Sepúlveda, E., Sáenz, C., Aliaga, E., Aceituno, C. (2007) Extraction and characterization of mucilage in Opuntia spp. Journal of Arid Environments 68, 534–545.

[20] Visavale G.L. (2012). "Principles, Classification and Selection of Solar Dryers". In Solar drying: Fundamentals, Applications and Innovations. Singapore.

Optimization of the spray drying process for the obtaining of coconut powder (*Cocos nucifera* L.) fortified with functionally active compounds

Lucas-Aguirre, J.C [a, b*]; Giraldo, G.[b]; Cortes, R.M. [a]

[a] Universidad Nacional de Colombia - Sede Medellín. Calle 59 A N 63-20, Medellín, Colombia.
[b] Universidad del Quindío. Carrera 15 Calle 12 Norte, Armenia – Colombia.

*E-mail of the corresponding author: jclucas@uniquindio.edu.co

Abstract

The objective of this work is to contribute to the generation of a significant advance of the coconut agroindustry in Colombia, for which the process of spray drying was optimized to obtain coconut powder added with functionally active components (CP+PAC) (calcium and vitamins C, D_3 and E), food that is framed in the context of functional foods. Initially, the behavior of the physicochemical properties of the coconut during storage at a temperature of 25ºC was evaluated. Then the base emulsion was designed, determining the influence of the composition of emulsions based on coconut milk, on its physicochemical stability, the answer surface methodology was used with a central composite design, considering the independent variables: water/coconut ratio; xantan gum; coconut fiber; terbutilhidroquinona. Subsequently, it was experimentally optimized according to the operating characteristics of the dryer and the product, using a response surface design based on five independent variables: Maltodextrin, air inlet temperature, air outlet temperature, atomizer disk speed and vacuum pressure in the drying chamber. Finally, the stability of the PC+PAC properties was evaluated, using a factorial design based on the independent variables: storage temperature, storage time and packaging.

Keywords: coconut, colloidal system, deposit formation, yield, vitamins.

1. Introduction

The coconut is a crop of great importance both economically and subsistence, directly dependent on more than 80 million people in more than 90 countries, in addition to the importance for its nutritional and medicinal values [1]. One of the most used techniques for the production of powders from liquid solutions and suspensions of fruit juices and pulp is spray drying (SD), with powdered food being valuable matrixs in terms of transport, packaging, storage and life useful [2], it is also one of the most effective techniques, which protects, stabilizes, releases the compounds and at the same time allows its solubility in an aqueous medium [3].

The coconut chain is identified as one of the most interesting for the Pacific and Atlantic coasts of Colombia, due to the impact it has on the population, seen from the families that depend on primary production to its commercialization and consumption. For which it is intended to provide the agroindustrial sector, the technological basis for obtaining a variety of dehydrated powders based on coconut and excellent quality attributes, which would represent new alternatives for diversification, in addition to contributing to the reduction of nutritional deficiencies in the population. In this context, this research aims to contribute in the medium to long term to increase the consumption of coconut drinks after reconstitution and to encourage the production of powdered coconut milk (CM) as a raw material for multidominios of the sector of the food industry and national and international markets

The objective of this work is to contribute to the generation of a significant advance of the Colombian agroindustry from the research, which allows the optimization of the process of spray drying (SD) for obtaining coconut powder added with physiologically active components (calcium and vitamins C, D_3 and E) (CP+PAC), food that is part of the context of functional foods.

2. Materials and Methods

Cocos (*Cocos nucifera* L.) variety Malayan Dwarf (manila) or Alto Pacifico (typical) from the Colombian Pacific region were used, with a flowering age at harvest of approximately 12 months and a post-harvest time between 15 and 36 days, time in which through preliminary studies was shown to have acceptable quality to be used as raw material for processing. The whole coconuts to be used were initially washed with water and disinfected with a 200 ppm sodium hypochlorite solution, then the coconut water (CW) was removed and blanched for 20 min in boiling water at T≈ 96°C (local barometric pressure≈ 640 mmHg), subsequently the shell of the coconut pulp (CP) was removed. The selected CP was again subjected to a water washing process and disinfection with hypochlorite, cutting into pieces and grinding (mill TM32 INOX BRAHER 3HP - 16801002).

The characterization of the PC+PAC properties were carried out according to the following methodologies: humidity (%) (X_w): official method AOAC 930.15 [4]; Water activity (a_w): determined with a dew point hygrometer at 25ºC (Aqualab 3TE series, Decagon, Devices,

Pullman, WA, USA) [5]; Solubility (S): method used by Cano-Chauca et al., (2005) modified [6]; Peroxide Index (PI): was performed on the extracted oil, obtained according to the method of Bae and Lee (2008) modified [7], where 4 g of powder was taken. The PI was determined by the spectrophotometric method based on the ability of peroxides to oxidize ferrous ions to ferric ions, which react with various reagents that produce colored complexes [8].

The quantification of vitamins E and D_3 was performed by high performance liquid chromatography (HPLC) (Shimatzu Prominence 20A), using a reverse phase column (C18 - 5 μm 4.6 mm x 250 mm), diode array, mobile phase: acetonitrile/methanol/water (45.3/51.2/3.5), flow: 1 mL/min, oven temperature 40°C and wavelengths of 325 and 265 nm, respectively. The quantification of vitamin C was also performed by HPLC, using a column in reverse phase (C18 RP-5 μm 4.6 mm x 250 mm), diode array, mobile phase: KH_2PO_4 0.02 M pH= 3.00 (Ortho-Phosphoric Acid 85%), flow: 1 mL/min, furnace temperature of 35°C, wavelength of 244 nm and an injection volume of 5 μL. The extraction of vitamin C was carried out according to the methodology adapted by Peña-Correa et al., (2013) [9]; while the extraction of vitamins D_3 and E was carried out according to the methodology proposed by Cortés (2004) modified [10] by inclusion by ultrasound treatment for 20 min to the samples treated with hexane. Calcium quantification was performed by the spectrophotometry method by flame atomic absorption, according to NTC 4807 (2000), supported by ISO 5151 (2003). The CP+PAC fortification criteria were set within the framework of the declaration of nutritional properties established in Resolution 333 of 2011 (Ministry of Social Protection Colombia), for the purpose of declaring the descriptor "Rich in" or "Excellent source of " CFA in a 100 g serving.

The particle sizes were determined as percentiles D_{10}, D_{50} and D_{90}, using the Mastersizer 3000 (Malvern Instrument Ltd., Worcestershire, UK), after dispersing the samples in 500 mL of distilled water until obtaining a darkening value of 10±1%, considering the size distribution from the theory of Mie and using the refractive index of 1.52 [11]. The color was determined by means of the CIE-La*b* coordinates, using an X-Rite spectrophotometer model SP62, illuminant D65, observer of 10° as reference [5]. Additionally, micrographs of the CP+PAC were made using a scanning electron microscope (Jeol 5910LV) at 15 Kv [6], where the samples were deposited on a copper conductive tape and on a sample holder, then they were coated with gold in a vacuum evaporator (Dentom Vacumm, 30 mA, 5 kV, 100 millitorr).

Preparation of the feed emulsion to the dryer: Batches of 3000 g of dryer feed emulsion (DFE) were prepared, initially a mixture of CP, CW and drinking water with a ratio ((CW+ H_2O)/CP) was homogenized in an Osterizer 600 Watts blender (position III) for 5 min, then the mixture was filtered on a 500 μm mesh screen, separating the fiber from the LC. The fiber was subjected to a drying process at 40°C for 48 hours and then to a dry milling (IKA MF 10.1 mill, USA). The CM was homogenized again in a Silverson series L5

homogenizer using the emulsifying head at 10000 rpm for 10 min, adding the native milled fiber (5-15% w/w) and the rest of the ingredients: milk whey (Instant WPC 80) as surfactant (0.5%), NaCl (9 mMol/L), xanthan gum (0.5-1.0% w/w), terbutilhydroquinone (TBHQ) (100-200 mg/kg) and CFA in the chemical forms of Calcium Citrate powder (6.0 g) (BELL CHEM), Vitamin C (1.0 g) (Ascorbic acid): 99.5% powder, BELL CHEM), Vitamin D_3 (0.5 g) (Colecalciferol): 512900 IU/g powder, BELL CHEM), Vitamin E (1.0 g) (DL-α-Tocopherol Acetate): 50% USP GRADE powder, BELL CHEM). A cooling bath was used during the preparation to control that the temperature of the DFE will not exceed 35°C

Spray drying process: A co-current flow pilot spray dryer was used (Vibrasec, model PASLAB 1.5). The evaluation of the spray drying process was carried out using the response surface methodology with a central composite design, considering the independent variables: Maltodextrin (MD) (5-15%), air entry temperature (AET) (150-170°C), air outlet temperature (AOT) (80-90°C), atomizer disk speed (ADS) (24000-28000 rpm) and vacuum pressure in the chamber (VPC) (1.0-1.88 "H_2O) and the dependent variables: Process performance (R*) kg solids of the powder obtained/kg solids of the DFE; Deposit formation (DF) kg adhered material/kg DFE; Xw; a_w; solubility (S); Retention of the PAC (%); Particle size (D_{10}, D_{50}, D_{90}); PI, color (L*, a*, b*).

Process for assessing the stability of coconut powder during storage: The product was packed in multicoated bags made by Alico SA, laminated film thickness (PET): 12 μm, aluminum foil: 8 μm polyethylene sealant layer: 100 μm, weight of 136.54 g/m², with water vapor barrier <1 cc/m_2 x 24h x atm) and O_2 <1 cc/m² x 24h x atm). The samples were stored in climatic chambers conditioned at a relative humidity of 65%, with the treatments applied: 15-N_2, 15-Amb, 25-N_2, 25-Amb, 35-N_2 and 35-Amb, at storage times (tA): 0, 30, 60, 90, 120, 150 and 180 days. The dependent variables evaluated were: Xw, a_w, S, color (L*, a*, b*), PI, %R-VC, %R-VD_3, %R-VE, %R-ABTS, %R-DPPH, %R-FT, %R-Ca, particle size (D_{10}, D_{50}, D_{90}) and microstructural analysis.

For both the process of optimization of the emulsion and the drying process, the effect of the independent variables was determined using the multiple regression method for the prediction of the linear, quadratic coefficients and the interaction of the independent variables in the surface models In response, a polynomial model of order 2 (equation 1) was used:

$$Y = \beta_0 + \beta_A A + \beta_B B + \beta_C C + \beta_D D + \beta_A{}^2 A^2 + \beta_B{}^2 B^2 + \beta_C{}^2 C^2 + \beta_D{}^2 D^2 + \beta_{AB} AB + \beta_{AC} AC + \beta_{AD} AD + \beta_{BC} BC + \beta_{BD} BD + \beta_{CD} CD \quad (1)$$

Where β_o is a constant, β_A, β_B, β_C y β_D is the linear coefficient of each factor; $\beta_A{}^2$, $\beta_B{}^2$, $\beta_C{}^2$ y $\beta_D{}^2$ is the quadratic coefficient of each factor; β_{AB}, β_{AC}, β_{AD}, β_{BC}, β_{BD} y β_{CD} is the product coefficient of the interactions of the factors. The adequacy of the models was carried out using the lack of fit test and the regression coefficient (R^2); In addition, the analysis of

variance (ANOVA) was performed with a confidence level of 95%. The matrix of the experimental design, the analysis of the results and the optimization procedure were carried out using the software Statgraphics Centurión XVI.I. From the conditions of optimal operation, three additional experiments were carried out to verify the accuracy of the model with respect to the real response variables, in order to verify the regression models and for stability in the storage a design was applied. with a factorial arrangement of the order 6*7 with two independent variables: treatment and time, where the treatment is defined as the combinations (temperature-packaging) and packaging was carried out in N_2 atmosphere and under environmental conditions.

3. Results and discussion

In the 1st phase of physicochemical characterization of the raw material (coconut) to identify the ideal conditions and determine the adequate time for its transformation as a raw material, the results showed a general deterioration of the CP and CW after 36 days of storage, mainly due to the increase in acidity, fermented odor, moisture loss (X_w), lipid oxidation, softening and discoloration of the CP, among others.

In the 2nd phase of design and optimization of the base emulsion, the optimal conditions were: water/coconut ratio ((CW+H_2O)/CP): 2.0; xanthan gum: 0.5%; Coconut fiber (CF): 5.0%; antioxidant (TBHQ): 200 mg/kg, reaching a potential-ζ: -45.6±2.5 mV; viscosity: 741.7±25.5 cP; color (L*: 67.5±0.7, a*: 3.2±0.2 and b*: 8.6±0.5); Peroxide value (PI): 0.14±0.04 meqH_2O_2/kg; particle size (D_{10}: 4.3±0.8 μm, D_{50}: 323.7±43.6 μm and D_{90}: 743.0±65.1 μm) and total solids (TS): 20.0±0.3%.

The numerical experimental optimization was carried out in order to obtain optimal values for independent variables, thus determining the desirable response parameters that allow obtaining a final product with the appropriate quality attributes. For this case and according to the statistical results found, the criteria were the following: approximate viscosity of 1000 cP (condition of maximum viscosity allowed by the dryer), higher percentage of TS, higher L*, less enzymatic browning and oxidation of the lipids (<IP and <potential ζ). These response variables were significantly influenced by the xanthan gum and %FC, being the variables that tend for a better emulsion behavior, and where the antioxidant becomes a supporting factor that tends to the good performance of the xanthan gum interaction and %FC [12, 13, 14].

In the 3rd phase of optimization of the SD process according to the operational characteristics of the dryer and the product, where the results obtained from the dependent variables and the ANOVA performed, were planned taking into account the most important variables of the process, maximizing S, L*, R*, D_{90} and PAC; minimizing H, Hu, PI and DF, it was also set at an average value of X_w and a_w, since its fluctuations were not very large, where the optimal conditions were: air inlet temperature (AIT): 170°C; Air outlet

temperature (AOT): 85.8°C; Atomizer disk speed (ADS): 26.676 rpm; Vacuum pressure in the chamber (VPC): 1.6 "H2O; percentage of maltodextrin (%MD): 7.0.

Under these process conditions, the experimental values of the response variables were as follows: humidity: 1.7±0.4%; a_w: 0.170±0.020; solubility (S): 58.4±2.1%; hygroscopicity (H): 8.4±0.6%; L*: 79.5±0.9; a*: 1.5 ± 0.1; b*: 9.5 ± 0.5; % vitamin C retention (%R-VC): 32.4±6.2; %R-VE: 6.1±1.9; %R-VD$_3$: 7.8±1.8; %R-Ca: 41.7±2.9; Wettability (Hu): 263.0±19.8 s; peroxide index (PI): 2.4±1.3 meqH$_2$O$_2$/kg fat; Deposit formation (DF): 32.4±2.3%; yield (*R): 44.0±1.0%, and particle size distribution D$_{10}$: 1.7±0.1 μm; D$_{50}$: 8.5±2.1 μm; D$_{90}$: 78.2±24.3 μm; obtaining a product with good quality attributes; Additionally, the proximal composition of PC+PAC was: fat: 30.5±0.9%, protein: 4.1±0.5%, total dietary fiber: 23.9±1.6%, ashes: 2.3±0.0%, highlighting the dietary fiber, which confers benefits on consumer health, in addition to its PAC present [15, 16, 17].

And in the 4th phase, it was determined that the best treatment for PC+PAC storage, with respect to all the response variables, was 15°C-N$_2$, where the humidity gain and the increase in aw were low for this type of products and the percentages of retention of vitamins and antioxidants were the highest, reaching values at 180 days of: X$_w$: 2.97±0.09%; a$_w$: 0.342±0.009; color: (L*: 77.96±0.04, a*: 1.44±0.06 and b*: 8.59±0.13); S: 51.48±2.30%; IP: 0.225±0.19 meqH$_2$O$_2$/kg fat; %R-VC: 62.56±5.70; %R-VD3: 51.00±0.99; %R-VE: 57.18±3.23; %R-FT: 50.89±4.78; %R-DPPH: 91.88±1.79; %R-ABTS: 42.14±2.18; D$_{10}$: 2.44±0.12 μm; D$_{50}$: 51.49±1.48 μm; D$_{90}$: 153.80±14.0 μm [18, 19] (see figure 1).
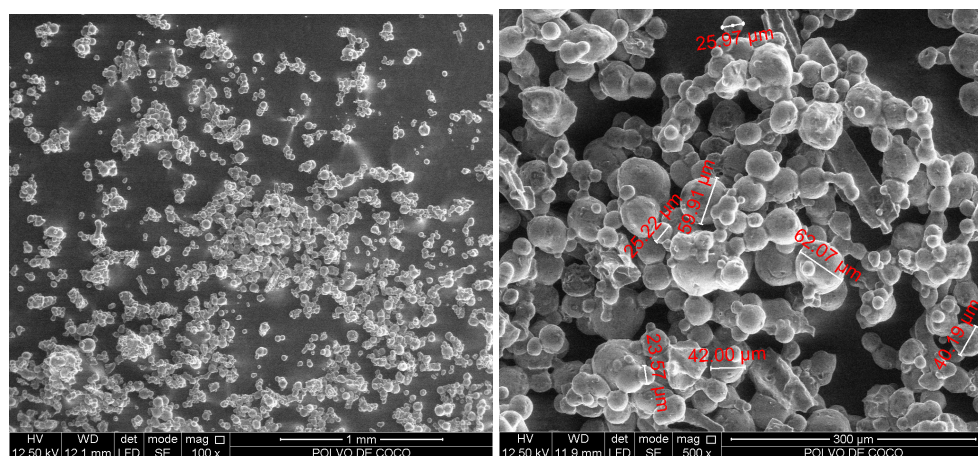
Fig. 1. Micrographs of PC+PAC obtained by SA at 100X and 500X.

4. Conclusions

In general, the intermediate levels of the hydrocolloid and fiber added are those that tend for a better emulsion behavior, the ratio ((CW+H$_2$O)/CP) although it influences in some

specific cases, it is not very determinant, while the antioxidant becomes in a support factor that tends to the good performance of the hydrocolloid and fiber interaction.

The experimental optimization carried out using statistical tools represents an effective way to define the most appropriate conditions of the SD process, and at the same time represents a significant advance for its subsequent industrial scaling and its potential generation of added value to the coconut agro chain.

According to the behavior of the PC+PAC during the storage this is a hygroscopic product, potentially sensitive to oxidative processes during storage, which could lead to changes in color, flavors or strange odors, so it will require a packing with low permeability to water vapor and O_2, to minimize these changes.

5. References

[1] Siriphanich, J.; Saradhuldhat, P.; Romphophak, T.; Krisanapook, K., Pathaveerat, S.; Tongchitpakdee, S. Coconut (*Cocos nucifera* L.). In: Yahia, E. (Ed.). Postharvest-Biology and Technology of Tropical and Subtropical Fruits. Vol 3: Cocona to Mango. Woodhead Publishing in Food Science Technology and Nutrition, Cambridge, UK. 2011; 8-33.

[2] Muzaffar, K.; & Kumar, P. Effect of soya protein isolate as a complementary drying aid of maltodextrin on spray drying of tamarind pulp. Drying Technology 2015; 34, 142-148.

[3] Kha, T.C.; Nguyen, M.H.; Roach, P.D.; Stathopoulos, C.E. A storage study of encapsulated gac (*Momordica cochinchinensis*) oil powder and its fortification into foods. Food and Bioproducts Processing 2015; 96, 113–125.

[4] AOAC. Official methods of analysis of the Association of Official Analytical Chemists 1990; 2 vols. 15th ed. Washington, DC.

[5] Cortés-Rodríguez, M.; Guardiola, L. F.; Pacheco, R. Aplicación de la ingeniería de matrices en la fortificación de mango (var. Tommy Atkins) con calcio. Revista Dyna 2007, 74 (153), 19-26.

[6] Cano-Chauca, M.; Stringheta, P.C.; Ramos, A.M.; Cal-Vidal, J. Effect of the carriers on the microstructure of mango powder obtained by spray drying and its functional characterization. Innov. Food. Sci. Emerg. 2005, 6, 420-428.

[7] Bae, E.K.; & Lee, S.J. Microencapsulation of avocado oil by spray drying using whey protein and maltodextrin. Journal of Microencapsulation 2008, 25 (8), 549–560.

[8] Hornero-Méndez, D.; Pérez-Gálvez, A.; Mínguez-Mosquera, M.I. A Rapid Spectrophotometric Method for the Determination of Peroxide Value in Food Lipids with High Carotenoid Content. J. Am. Oil Chem. Soc. 2001, 78 (11), 1151–1155.

[9] Peña-Correa, R.F.; Cortés-Rodríguez, M.; y Gil-González, J.H. Estabilidad Fisicoquímica y Funcional de Uchuva (*Physalis peruviana* L.) Impregnada a Vacío con Calcio y Vitaminas B_9, D y E, Durante el Almacenamiento Refrigerado. Rev.Fac.Nal.Agr. Medellín 2013, 66 (1), 6629-6638.

[10] Cortés, M. 2004. Desarrollo de productos de manzana deshidratados enriquecidos con vitamina E. Tesis Doctoral en Ingeniería de Alimentos. Universidad Politécnica de Valencia 2004, Valencia, España. 254 p.

[11] Mirhosseini, H.; Ping Tan, C.; Hamid, N.S.A.; Yusof, S. Effect of Arabic gum, xanthan gum and orange oil contents on ζ-potential, conductivity, stability, size index and pH of orange beverage emulsion. Colloids and Surfaces A: Physicochem. Eng. Aspects 2008, 315, 47–56.

[12] Thaiphanit, S.; Schleining, G.; Pranee, A. Effects of coconut (*Cocos nucifera L.*) protein hydrolysates obtained from enzymatic hydrolysis on the stability and rheological properties of oil-in-water emulsions. Food Hydrocolloids 2016, 60, 252-264.

[13] Piorkowski, D.T.; McClements, D.J. Review. Beverage emulsions: Recent developments in formulation, production, and applications. Food Hydrocolloids 2014, 42, 5-41.

[14] Niu, F., Zhang, Y., Chang, C., Pan, W., Sun, W., Su, Y. Influence of the preparation method on the structure formed by ovalbumin/gum arabic to observe the stability of oil-in-water emulsion. Food Hydrocolloids 2017, 63, 602-610.

[15] Cortés-Rojas, D.F.; Fernandes-Souza, C.R.; Pereira-Oliveira., W. Optimization of spray drying conditions for production of *Bidens pilosa L.* dried extract. Chemical Engineering Research and Design 2015, 93, 366–376.

[16] Tontul, I.; Topuz, A. Review. Spray-drying of fruit and vegetable juices: Effect of drying conditions on the product yield and physical properties. Trends in Food Science & Technology 2017, 63, 91-102.

[17] Zotarelli, M.F.; Martins-da Silva, V.; Durigon, A.; Dupas-Hubinger, M.; Borges-Laurindo, J. Production of mango powder by spray drying and cast-tape drying. Powder Technology 2017, 305, 447–454.

[18] Islam-Shishir, M.R.; Taip, F.S.; Saifullah, Md.; Aziz, N.Ab.; Talib, R.A. Effect of packaging materials and storage temperature on the retention of physicochemical properties of vacuum packed pink guava powder. Food Packaging and Shelf Life 2017, 12, 83–90.

[19] Jafari, S.M.; Ghalenoei, M.G.; Dehnad, D. Influence of spray drying on water solubility index, apparent density, and anthocyanin content of pomegranate juice powder. Powder Technology 2016, 311, 59–65.

Effect of phospholipid composition on the structure and physicochemical stability of proliposomes incorporating curcumin and cholecalciferol

Chaves, M.A. [a]; Pinho, S.C.[a*]

[a] Department of Food Engineering, School of Animal Science and Food Engineering, University of São Paulo, Av Duque de Caxias Norte 225, Pirassununga, SP, Brazil

*E-mail of the corresponding author: samantha@usp.br

Abstract

Proliposomes are dry phospholipid-based particles in which bioactives can be entrapped, and that can produce liposomal suspensions if adequately hydrated. In our study, curcumin and cholecalciferol were incorporated in proliposomes obtained by coating of micronized sucrose. Different mass ratios of Lipoid S40 and Phospholipon 90H were used to produce the proliposomes. The powders were structurally characterized and bioactives content were analyzed over 60 days of storage. Curcumin and cholecalciferol amounts in F100CV formulation were 100 and 98.7% of their initial amount, respectively. Strucutral characterization showed bioactives were successfully incorporated in concentrations compatible with recommended daily dosages.

Keywords: *proliposomes, curcuminoid, vitamin D_3, Raman spectroscopy, powder characterization*

1. Introduction

Proliposomes are defined as dry, free-flowing powders composed mainly of phospholipids and that can instantly form liposome dispersions upon addition of an aqueous solution under appropriate conditions [1]. Advantages attributed to proliposomes as the convenience for transportation, distribution, and dosing, including the production of capsules/tablets, easier to be industrialized [2].

Curcumin is the major yellow hydrophobic pigment of the rhizomes of *Curcuma longa*. Nowadays, despite its use as food spicy, curcumin has been studied by pharmaceutical and medical researchers because of its antioxidant, anti-inflammatory and anti-carcinogenic actions [3]. However, the main limitation for the application of curcumin in food is its low water solubility and its poor bioavailability [4]. Cholecalciferol (vitamin D_3) is the naturally occurring form of vitamin D. It plays an important role in regulation of calcium homeostasis and mineralization of bones [5]. Unfortunately, vitamin D_3 carency affects almost 50% of worldwide population due, mostly, to lifestyle habits and environment factors that reduce the exposition to sunlight [6]. Thus, its supplementation is highly necessary as few enriched food are commercially available. However, as curcumin, vitamin D_3 is extremely sensitive to higher temperatures and exposure to light [7]. Hence, encapsulation in lipid delivery system could increase their stability and bioacessibility [8,9].

In this study, curcumin and cholecalciferol were incorporated in proliposomes obtained by coating of micronized sucrose. The powders were characterized by Raman spectroscopy (RS) and Fourier-transform infrared spectroscopy (FTIR). In addition, proliposomes were analyzed in terms of their morphology, hygroscopicity, solubility, and amount of bioactives retained. Data revealed by this research will help to show the feasibility to produce proliposomes containing both bioactives in concentrations compatible with their recommended daily dosage for further application in food formulations.

2. Materials and Methods

2.1. Production of proliposomes by coating of micronized sucrose

Proliposomes production was based in the methodology described by Silva et al. (2017) [10]. Different mass percentages of phospholipids were tested: 50% Lipoid S40 + 50% Phospholipon 90H (F50), 70% Lipoid S40 + 30% Phospholipon 90H (F70), and 100% Lipoid S40 (F100).

2.2. Spectroscopical characterizaton of the proliposomes

The spectra in the infrared regions were obtained in the 4000-400 cm^{-1} region by using a Perkin Elmer FT-IR Spectrometer (Waltham, MA, USA). Raman spectroscopy analyses

were performed with a RAMII (Billerica, MA, USA) in the 4000-400 cm^{-1} region with Ge detector and a 1064 nm laser.

2.3. Morphololgy of proliposomes by scanning electron microscopy (SEM)

Morphology was studied using a scanning electron microscope (model 3000 TM; Hitachi, Japan) equipped with TM3000 software.

2.4. Hygroscopicity and solubility

The proliposomes were characterised in terms of hygroscopicity according to the procedure described by Cai and Corke (2000) [11]. The solubility of the proliposomes was determined according to the method of Eastman & Moore (1984) [12].

2.5. Quantification of bioactives in proliposomes

Curcumin quantification was carried out according to Silva et al. (2017) [10]. Concentrations were obtained by absorbance readings at 425 nm in a spectrophotometer (Libra S22; Biochrom, Cambridge, UK). Regarding cholecalciferol retained in proliposomes, these values were obtained by high-performance liquid chromatography (Shmadzu; Kyoto, Japan) according to Staffas and Nyman (2003) [13].

3. Results and Discussion

3.1. Visual aspect and morphology of proliposomes

The visual aspect of blank and curcumin-cholecalciferol-loaded proliposomes are shown in Figure 1. The powders containing curcumin presented an intense and characteristic yellow color. The formulation prepared with only Lipoid S40 (F100) seemed to be more agglomerated than the produced with Phospholipon 90H. This may be due because Lipoid S40 is a non-hydrogenated phospholipid, with a strong tendency to absorve moisture from the environment.
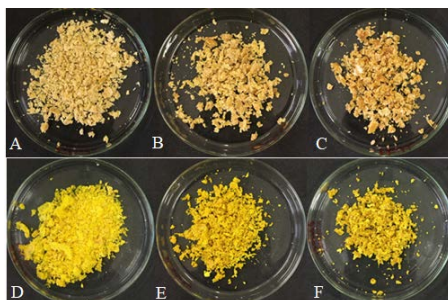
Figure 1. Visual aspects of blank (superior line) and curcumin-cholecalciferol-entrapped (inferior line) proliposomes produced with (A, D) 50% Lipoid S40; (B, E) 70% Lipoid S40; (C, F) 100% Lipoid S40

The coating of micronized sucrose by phospholipids produced flake powders whose morphological characteristics are shown in the scanning electron micrographies illustrated in Fig. 2. In the SEM micrographs, it is possible to distinguish a layer of phospholipid coating the micronized sucrose granules. The coated material presented very irregular and different shapes, with many agglomerates in the visual fields.
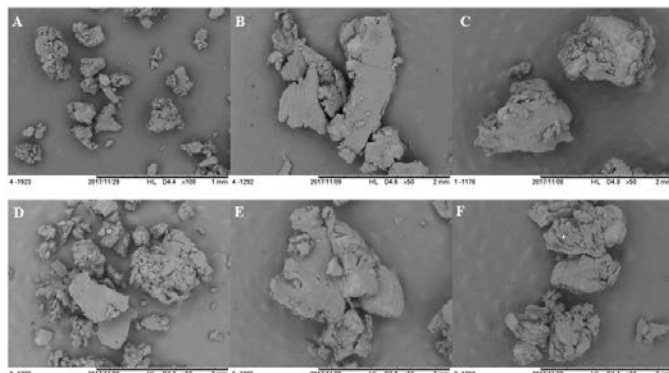
Figure 2. Micrographies obtained by scanning electronic spectroscopy for the blank (superior line) and curcumin-cholecalciferol-entrapped (inferior line) proliposomes produced with (A, D) 50% Lipoid S40; (B, E) 70% Lipoid S40; (C, F) 100% Lipoid S40. Scale: 2nm. Magnitude: 50x

3.2. Fourier-transform infrared spectroscopy (FTIR)

The characteristic absorption peaks for blank and loaded proliposomes obtained by FTIR are shown in Figure 3. No major changes were detected in the spectra of empty and loaded proliposomes. Intense vibration peaks were observed at 2854 and 2920 cm^{-1} in all spectra. These peaks are related to $_s\upsilon(CH_2)$, and the higher their intensity, the more ordered are the acyl chains of the phospholipids. Therefore, as shown in Figs. 3E and 3F, higher amounts of Lipoid S40 in the proliposomes led to a reduction in the peak intensities. Such reduction was mainly due to the high content of unsaturated phospholipids in Lipoid S40, which helps to decrease the acyl chains ordering [10]. On the other hand, assymetrical stretching mode of a P=O group is identified by a peak in the range 1200-160 cm^{-1} according to Lewis and McElhaney (1996) [14]. In this case, proliposomes showed this peak as the located in the wavenumber near 1043 cm^{-1}. Popova and Hincha (2003) [15] stated this peak increased its position with hydrogen bonding. Regarding these peaks in Figs 3E and 3F, it can be verified a slight decrease, an indication that part of sucrose interacted with the polar heads of phospholipids, in a behavior that resembles that in which sucrose is used as cryoprotector during the production of lyophilized liposomes [16]. These interactions caused also a decrease in C=O stretching, which was located at 1741 cm^{-1}. Summarily, it can be stated that part of sucrose interacted with some polar heads of the phospholipids presented in Lipoid S40, hindering the coating process [10].
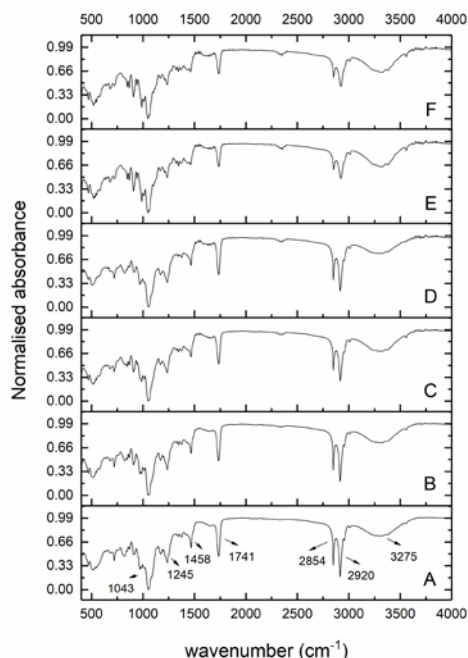
Figure 3. FTIR spectra obtained for formulations F50 (A); F50CV (B); F70 (C); F70CV (D); F100 (E) and F100CV (F).

3.3. Raman spectroscopy

Figure 4 shows the FT-Raman spectra obtained for blank and loaded proliposomes. The bands at 1596 and 1632 cm^{-1}, are attributed to v(C=C) motions of the inter-ring chain of curcumin and to v(C=O)/v(C=C) vibrations in the side aromatic rings of both curcumin and cholecalciferol. As can be seen, these peaks appeared only on formulations F50CV and F70CV. Therefore, it can be stated that in formulation F100CV both bioactives remained entrapped in the phospholipid matrix in their amorphous form. Changes in the broadening of the 1596 and 1632 cm^{-1} bands seen between F50CV and F70CV are due to conformational modifications on the side aromatic rings that can cause a variation of the electronic conjugation degree along the entire molecule [17]. Other Raman peak assignments for curcumin were obtained by Mohan et al. (2012) [18] and appeared in F50CV and F70CV spectras, as it follows: 1125 cm^{-1} (δ(CCH) of aromatic rings and δ(C–OH) of the enolic group coupled to δ(C=CH) in the inter-ring chain), 1241 cm^{-1} (δ(CH) of the aromatic rings, combined to v(C–O) of the ether groups linked to these rings), 1295 cm^{-1} (δ(CCH) of the inter-ring chain (C^{10} and C^{11}), and 1439 cm^{-1} (δ(CCC), δ(CCH) and δ(C–OH) of aromatic rings). Cholecalciferol peak at 1650 cm^{-1} was possibly covered by peak at 1655 cm^{-1} commonly found in polyunsaturated lipids [19]. In addition, the low

concentration of cholecalciferol added in proliposomes may have remained within the surrounding matrix, which explained the absence of its related peak.
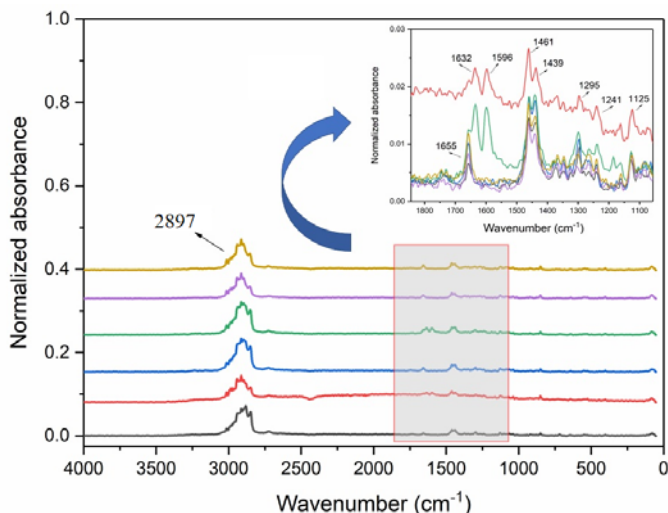
Figure 4. FT-Raman spectra obtained for formulations F50 (black); F50CV (red); F70 (blue); F70CV (green); F100 (purple) and F100CV (orange).

3.4. Hygroscopicity, solubility and amount of bioactives retained

Physicochemical parameters obtained for proliposomes over 60 days of storage are in Table 1. Higher hygroscopicities were obtained for proliposomes with higher contents of Lipoid S40. These values can be considered low, which is a highly desirable characteristic for powders. The incorporation of the hydrophobic actives in proliposomes did not lead to a decrease in solubility values. This result corroborates what was mentioned before, that both molecules remained entrapped in phospholipid matrix. However, the values obtained were quite lower than those obtained by Silva et al. (2017) [10] which also produced proliposomes containing curcumin by coating of micronized method. Additionally, it is important to mention that Silva et al. (2017) [10] produced proliposomes using only Phospholipon 90H, which contains a higher number of hydrogenated phospholipids, which are easier to be dispersed in aqueous medium.

The amount of bioactives retained in proliposomes after 60 days of storage are presented in Table 1. Considering that curcumin and cholecalciferol are highly sensitive to degradation, the results obtained can be considered promising, as 100% of curcumin and more than 85% of the cholecalciferol initially present in the powder were preserved.

Table 1. Physicochemical parameters obtained for blank and loaded proliposomes

	Solubility (%)	Hygroscopicity (%)	Preserved bioactives (after 60 days) (%)	
			Curcumin	Cholecalciferol
F50	$36.4^C \pm 2.02$	$7.24^B \pm 0.23$	-	-
F50CV	$42.4^B \pm 0.64$	$5.90^C \pm 0.23$	100 ± 1.18	92.3 ± 3.50
F70	$44.5^A \pm 0.93$	$6.49^C \pm 0.31$	-	-
F70CV	$44.8^A \pm 1.38$	$7.50^{BC} \pm 1.47$	100 ± 0.91	85.1 ± 0.10
F100	$37.9^C \pm 1.36$	$11.1^A \pm 2.66$	-	-
F100CV	$42.5^{AB} \pm 1.49$	$8.62^{AB} \pm 1.54$	100 ± 1.04	98.7 ± 0.37

4. Conclusions

The experimental data indicate it is possible to produce proliposomes containing curcumin and cholecalciferol by coating of micronized sucrose. The process of coating with phospholipid was effective as illustrated by SEM images. Proliposomes presented low hygroscopicity and moderate solubility, which not hinders the production of liposome dispersions, as mechanical energy can be applied during their preparation. The amount of cholecalciferol added to the formulations was low, which hindered its determination by spectroscopies. The results showed the feasibility of producing proliposomes incorporating both bioactives in concentrations compatible with their recommended daily dosage for further application in food formulations.

5. References

[1] Payne, N.I.; Browning, I.; Hynes, C.A. Characterization of Proliposomes. Journal of Pharmaceutical Sciences 1986, 75 (4), 330–333.

[2] Patel, G.M.; Shelat, P.K.; Lalwani, A.N. QbD based development of proliposome of lopinavir for improved oral bioavailability. European Journal of Pharmaceutical Sciences 2017, 108, 50-61.

[3] Cuomo, F.; Cofelice, M.; Venditti, F.; Ceglie, A.; Miguel, M.; Lindman, B.; Lopez, F. In-vitro digestion of curcumin loaded chitosan-coated liposomes. Colloids and Surfaces B: Biointerfaces 2017. In Press.

[4] Zou, L.; Zheng, B.; Liu, W.; Liu, C.; Xiao, H.; McClements, D.J. Enhancing nutraceutical bioavailability using excipient emulsions: Influence of lipid droplet size on solubility and bioaccessibility of powdered curcumin. Journal of Functional Foods 2015, 15, 72-83.

[5] Picciano, M.F.; Dwyer, J.T.; Radimer, K.L. Dietary supplement use among infants, children and adolescents in the United States, 1999-2002. Archives of Pediatrics and Adolescent Medicine 2007, 161 (10), 978-985.

[6] Holick, M.F. Vitamin D deficiency. The New England Journal of Medicine 2007, 357 (3), 266-281.

[7] Luo, Y.; Teng, Z.; Wang, Q. Development of zein nanoparticles coated with carboxymethyl chitosan for encapsulation and controlled release of vitamin D3. Journal of Agricultural and Food Chemistry 2012, 60 (3), 836-843.

[8] Park, S.J.; Garcia, C.V.; Shin, G.H.; Kim, J.T. Development of nanostructured lipid carriers for the encapsulation and controlled release of vitamin D3. Food Chemistry 2017, 225, 213-219.

[9] Jin, H-H.; Lu, Q.; Jiang, J-G. Curcumin liposomes prepared with milk fat globule membrane phospholipids and soybean lecithin. Journal of Dairy Science 2016, 99 (3), 1780-1790.

[10] Silva, G.G.; Jange, C.G.; Rocha, J.S.S.; Chaves, M.A.; Pinho, S.C. Characterisation of curcumin-loaded proliposomes produced by coating of micronised sucrose and hydration of phospholipid powders to obtain multilamellar liposomes. International Journal of Food Science and Technology 2017, 52 (3), 772-780.

[11] Cai, Y.Z.; Corke, H. Production and properties of spray-dried Amaranthus betacyanin pigments. Journal of Food Science 2000, 65 (7), 1248-1252.

[12] Eastman, J.E.; Moore, C.O. Cold Water Soluble Granular Starch for Gelled Food Composition. U.S. Patent 4465702, 14 ago. 1984.

[13] Staffas, N.; Nyman, A. Determination of cholecalciferol (vitamin D3) in selected foods by liquid chromatography: NMKL collaborative study. Journal of AOAC International 2003, 86 (2), 400-406.

[14] Lewis, R.N.; McElhaney, R.N. Fourier transform infrared spectroscopy in the study of hydrated lipids and lipid bilayer membranes. In Infrared Spectroscopy of Biomolecules (Mantsch, H.H. & Chapman, D., editors), Wiley, Chichester, 159–202.

[15] Popova, A.V.; Hincha, D.K. Intermolecular Interactions in Dry and Rehydrated Pure and Mixed Bilayers of Phosphatidylcholine and Digalactosyldiacylglycerol: A Fourier Transform Infrared Spectroscopy Study. Biophysical Journal 2003, 85 (3), 1682-1690.

[16] Doxastakis, M.; Sum, A.K.; Pablo, J.J. Modulating Membrane Properties: The Effect of Trehalose and Cholesterol on a Phospholipid Bilayer 2005, 109 (50), 24173-24181.

[17] Castillo, M.L.R.; López-Tobar, E.; Sanchez-Cortes, S.; Flores, G.; Blanch, G.P. Stabilization of curcumin against photodegradation by encapsulation in gamma-cyclodextrin: A study based on chromatographic and spectroscopic (Raman and UV–visible) data. Vibrational Spectroscopy 2015, 81, 106-111.

[18] Mohan, P.R.K.; Sreelakshmi, G.; Muraleedharan, C.V.; Joseph, R. Water soluble complexes of curcumin with cyclodextrins: Characterization by FT-Raman spectroscopy. Vibrational Spectroscopy 2012, 62, 77-84.

[19] Schultz, Z.D. Raman Spectroscopy and Imaging of Biomolecules using Targeted Nanoparticles. Biophysical Journal 2012, 102 (3), 201a.

Physical properties of commercial infant milk formula products

Murphy, E.G[a]; Regost, N.E[b]; Roos Y.H[c]; Fenelon M.A[a]*

[a]Teagasc Food Research Centre, Moorepark, Fermoy, Co. Cork, Ireland
[b]Manager, Infant Formula Technologies, H&H Group, Paris, France
[c]School of Food and Nutritional Sciences, University College Cork, Cork, Ireland
*E-mail of the corresponding author: mark.fenelon@teagasc.ie

Abstract

The physical properties of 12 commercially available infant milk formula (IMF) and follow-on (FO) powders were assessed. Polarised light micrographs of powders revealed that two types of powders existed: Type I - homogenous mixtures of milk powder particles and Type II – heterogeneous mixtures of milk powder particles and tomahawk-shaped α-lactose monohydrate crystals. Conventionally employed correlations between particle size, flowability and compressibility were found to be highly dependent on the presence of crystalline lactose in powders. Overall, results showed the importance of micro-structural evaluation during analysis of physical properties of dairy powders and, in particular, IMF/FO powders.

Keywords: max. Infant formula; microstructure; physical properties.

1. Introduction

Infant milk formula (IMF) powders are dehydrated emulsions consisting of the protein, fat carbohydrate, vitamins and minerals necessary to nourish infants in the absence of breast milk. Composition of powders changes as infants grow and IMF is classified into "stages" based on the age of the infants i.e. from birth, 6 months +, 1 year, follow on (FO), etc.. The U.S. Food and Drug Administration (2003) classify IMF manufacturing processes into three categories: 1) wet processing, 2) dry processing or 3) a combination of wet and dry-blending. In wet processing, ingredients are hydrated in water to the desired composition and are subsequently spray dried [1]. Dry processing involves mixing of dried ingredients and is often employed in combination with spray dried base powder [2].

The manufacturing process has a large effect on the physical quality of dairy powders [1, 3-6]. Powder particle size can be controlled by viscosity of feed concentrate and agglomeration during spray drying [7, 8]. Large powder particle sizes generally increase flowability due to a reduction in the area of contact between particles during flow [9]. However, other factors can affect flowability, which in some cases can lead to a weak relationship between particle size and flowability. The surface composition of powder particles is especially important in dehydrated emulsions and high quantities of non-emulsified fat at the powder surface can reduce flowability [10]. Shape of particles can also affect flowability of powders with more spherical powders having greater flowability [11]. α-lactose monohydrate crystals are generally pyramidal or tomahawk shaped [12] and thus may reduce spherocity, and possibly, flowability of powders if present.

In recent years there has been an increase in the publications dealing with IMF manufacture [1, 5, 6, 13, 14]. Hanley et al. [13] provided some information regarding the physical properties of a limited number of commercial IMF samples, whereas the others did not equate data obtained to standard commercial products. This aim of this study were to determine differences in physical quality of commercial IMF related to composition of powders, microstructure and/or processes employed by manufacturers.

2. Materials and Methods

2.1 Commercial infant milk formula

A total of 12 IMF and FO powders were studied. 9 samples were purchased from an Irish supermarket and 3 samples of non-Irish IMF powders were donated by Biostime Inc. (Guangzhou, P.R. China). Crystalline structure of the powders was determined using polarised light microscopy (Olympus Corporation, Tokyo, Japan) and powders were subdivided into two categories; I – a homogenous mix of milk powder particles (n=6) and II – a heterogeneous mix of milk powder particles and crystalline particles (n=6).

2.2 Powder properties

Particle size distribution was measured by a Mastersizer 3000 (Malvern Instruments Ltd., UK) as described elsewhere [14]. Sauter mean diameter, D[3,2], which gives the diameter of a sphere with the same volume to surface area ratio of the whole distribution was used as a measure of particle size. D(v,0.1), which gives the diameter below which 10 % of the distribution (by volume) lies, was used to quantify the amount of fine particles in the distribution.

Particle shape was measured by Morphologi G3 (Malvern Instruments Ltd., UK). Powders were dispersed on to a microscope plate, using pressurised air. The air pressure used was 4 bar, which was applied to the sample dispersion for 10 milliseconds; a settling time of 1 minute was then allowed for powder particles to disperse on the microscope plate.

Bulk density and surface free fats were determined as per GEA Niro Standard [15]. The difference between poured and tapped (100 times) bulk densities gave the compressibility of the powder. Particle densities were measured by a helium gas pyconometer, AccuPyc II 1340 (Micromeritics, GA, USA).

2.3 Flowability

Flowability was measured by two methods: 1 – the time taken for a defined volume of powder to leave a rotating drum [15] and 2 – flow function measured using a Powder Flow Tester (Brookfield Engineering Laboratories Inc., MA, USA). For the drum flowability method it was noticed some powder would always adhere to the walls of the drum and would not exit. Therefore, the flowability from this method was defined as a flow-rate given by: $F_d = (g_{p1} - g_{p2})$/time, where F_d is the drum flowability (g/s); g_{p1} and g_{p2} represent the amount of powder (g) in the drum at the start and finish of the test, respectively. Flow function was determined as described by Crowley et al. [16]. Five uniaxial normal stresses (0.3 to 2.4 kPa) were applied to each powder, in combination with three over-consolidation stresses at each normal stress. The Jenike flow index (i), was used to characterise the flow of the powders (Table 1; [11]).

Table 1. Jenike flow index (i) classification

Flowability	Hardened	Very cohesive	Cohesive	Easy-flow	Free-flowing
i	<1	<2	<4	<10	>10

2.4 Statistical analysis

A t-test was used to compare Type I and II powders.. Pearson's r was used to determine the degree of correlation between the two sample sets. This was calculated using the CORREL function of Microft Excel

3. Results and Discussion

3.1 Powder properties

Polarised light microscopy revealed that standard IMF powders (made from intact bovine proteins) could be classified into two groups; I – homogenous powders and, II – heterogeneous mixtures of non-crystalline particles and distinct crystalline particles (Figure 1). Type I powders showed small degrees of crystallinity indicated by bright areas within particles. This may be a result of partial lactose crystallisation which could occur, for example, if powder is not cooled sufficiently after spray drying or absorbs moisture locally during storage. The crystalline particles observed in Type II powders were very likely α-lactose monohydrate due to their pyramidal or tomahawk shape [12]. The presence of crystalline lactose in Type II powders could indicate a manufacturing process where a base powder containing protein and fat ingredients was manufactured by spray drying, after which α-lactose monohydrate crystals were added by dry-blending [2].
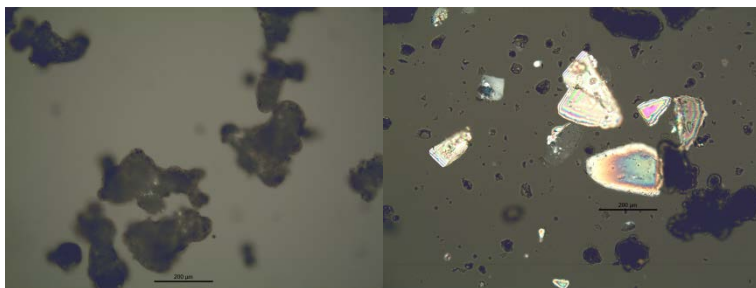
Figure 1. Polarised light images of Type I (powder 1) and II (powder 10) powders. Scale bar is 200 μm.

There were significant ($P < 0.05$) differences in powder particle size and shape between Type I and II powders (Table 2). Type I powders had less fine particles (D(v,0.1)), and as a result Sauter Mean Diameter, D[3,2], was significantly larger ($P < 0.05$). D[3,2] gives the diameter of a sphere with the same volume to surface area ratio as the whole powder distribution [5]. The significantly larger D[3,2] of Type I powders, compared to Type II powders, indicated that the specific surface area of Type I powders was lower. Type I powders were less elongated than Type II; measured elongation means were 0.18 ± 0.02 and 0.25 ± 0.03, respectively. The presence of crystalline lactose tomahawks/pyramids in Type II powders (Figure 1) likely contributed to the greater elongation observed. Surface free fat content did not vary significantly ($P > 0.05$) between Type I (0.96 ± 0.30 g free fat 100 g $^{-1}$ powder) and Type II (0.81 ± 0.22 g free fat 100 g $^{-1}$ powder) powders.

Table 2. Powder particle size and surface free fat for individual powders (mean of two replicates). Average values presented below were calculated based on powder type ± standard deviation

Powder Type	Powder No.	D [3,2] (μm)	D(v,0.1) (μm)	Span of particles	Surface free fat (% w/w of powder)
I	1	183.0 ± 6.0	103.3 ± 1.5	1.5	1.5 ± 0.0
I	2	139.0 ± 0.1	77.4 ± 0.1	1.5	0.6 ± 0.0
I	3	166.2 ± 0.1	90.8 ± 0.3	1.6	1.1 ± 0.0
I	4	181.4 ± 7.1	129.0 ± 3.8	1.1	0.8 ± 0.0
I	5	170.0 ± 0.1	112.0 ± 0.6	1.3	1.0 ± 0.0
I	6	220.1 ± 10.1	140.5 ± 6.93	1.2	0.8 ± 0.0
Average I		**176.5 ± 26.5**	**108.8 ± 23.5**	**1.4 ± 0.2**	**1.0 ± 0.3**
II	7	160.0 ± 7.5	92.4 ± 4.1	1.6	0.9 ± 0.0
II	8	162.0 ± 1.7	100.9 ± 2.1	1.5	0.9 ± 0.0
II	9	117.0 ± 0.1	62.1 ± 0.1	1.8	0.4 ± 0.0
II	10	149.3 ± 1.5	87.6 ± 0.7	1.6	1.1 ± 0.0
II	11	143.0 ± 1.4	82.3 ± 0.1	1.6	0.8 ± 0.0
II	12	126.1 ± 1.7	68 ± 0.8	1.8	0.7 ± 0.0
Average II		**142.9 ± 18.2**	**82.2 ± 14.8**	**1.7 ± 0.1**	**0.8 ± 0.2**

3.2 Flowability

Flowability of powders was measured by two means; a – Jenike flow index and b – the rate at which powder exited from a rotating drum. Table 3 summarises the flowability data. All powders measured had a flow index (i) of greater than 4 and, thus, were deemed to be easy flowing powders over the range of consolidating stresses applied [9]. There was no significant difference in flow index or drum flowability behaviour between Type I and II powders. Flow index and drum flowability were highly correlated for Type I powders (r = 0.95) and somewhat correlated for Type II powders (r = 0.69).

Type II powders had lower particle size (P < 0.05), were less spherical (P < 0.05) and were more elongated (P < 0.05) compared to Type I powders. Taking this into account, it is perhaps surprising that average flowability of Type I and II powders was not significantly different (Table 3; P >> 0.05 for both flow index and drum flowability). Large particle size is generally desirable for good powder flowability [17]. Large powder particles reduce specific surface compared to smaller particles which reduces cohesive inter-particular interactions. In addition, increased spherocity of particles has been found to positively affect flowability [11]. However, particle size can often be weakly correlated with flowability [9] possibly due to the effect of surface composition, which also plays an important role in flowability [10]. Presence of crystalline lactose in Type II powders likely resulted in different overall surface composition compared to Type I powders. This difference could explain the good flow behaviour of Type II powders. Similarly,

Yazdanpanah and Langrish [18] found that skim milk powder particles with crystalline surfaces and amorphous cores had better flowability than fully amorphous particles.

Table 3. Flowability of powders (mean of two replicates ± standard deviation). Average values presented below were calculated based on powder type ± standard deviation

Powder Type	Powder No.	Flow index (i)	Drum flow (g min^{-1})
I	1	6.5 ± 0.3	32.9 ± 1.0
I	2	4.6 ± 0.3	11.2 ± 0.2
I	3	4.7 ± 0.2	17.4 ± 1.7
I	4	7.7 ± 0.8	38.5 ± 1.2
I	5	7.7 ± 0.1	38.5 ± 1.5
I	6	8.7 ± 0.5	38.2 ± 1.2
Average I		**6.6 ± 1.6**	**29.4 ± 11.6**
II	7	8.7 ± 3.4	39.0 ± 0.3
II	8	8.3 ± 0.1	29.0 ± 1.3
II	9	4.4 ± 0.3	24.8 ± 0.1
II	10	6.9 ± 0.3	35.1 ± 0.1
II	11	5.6 ± 0.4	34.6 ± 1.0
II	12	4.7 ± 0.2	20.2 ± 0.4
Average II		**6.4 ± 2.1**	**30.5 ± 6.8**

3.3 Compressibility

Compressibility was measured by two means a – difference in powder volume before and after tapping 100 times b – difference in volume before and after flow index analysis. No significant ($P < 0.05$) difference in compressibility was observed between Type I and II powders. Compressibility measured during flow index testing was always higher than compressibility measured by tapping, indicating higher compressive force in the former measurement. Correlation between the two tests was high for Type I powders ($r = 0.99$) but for Type II powders no correlation was observed ($r = 0.16$). The exact reason why there was strong correlation for Type I powders and no correlation for Type II powders is unclear, but may be related to the presence of lactose crystals in Type II powders.

High compressibility of powders is often reported to be related to poor flowability [11, 16, 19]. Table 4 shows correlations, for Type I and II powders, between all flowability and compressibility measurements. For Type I powders, compressibility was well correlated with flowability; r was between -0.9 and -1 in each case. The negative sign of r indicated that as compressibility increased, flowability decreased. For Type II powders, compressibility obtained by tapping was not correlated to flowability. Correlation of compressibility to flowability in Type II powders was higher when compressibility obtained from flow index was used. It is possible that, at the lower compression associated with the tapping test, lactose crystals present in Type II powders may have affected the established relationship between compressibility and flowability. It is clear from Table 5 that different methods which supposedly measure the same parameter i.e. compressibility, can be

influenced by powder structure. Researchers must take into account powder structure when drawing conclusions from compressibility and flowability data.

Table 4. Correlation (Pearson's r) between compressibility and flowability measurements for Type I and II powders (n = 6 for each correlation)

	Type I		Type II	
	Drum flowability	Flow index	Drum flowability	Flow index
Compressibility by tapping	-0.94	-0.90	0.35	0.33
Compressibility by flow index	-0.98	-0.93	-0.88	-0.75

4. Conclusions

Quick structural analysis of IMF powders using polarised light microscopy gave an indication of the process used for powder manufacture. The presence of large lactose tomahawk crystals in some IMF powders indicated a manufacturing process where at least some degree of dry blending of lactose was utilised. The presence of lactose crystals resulted in markedly different powder behaviour compared to similar powders containing no crystalline lactose. This highlights the importance of powder microstructural analysis to compliment more commonly used measurements of particle size, compressibility and flowability during analysis of powder behaviour.

References

[1] McCarthy, N.A.;Gee, V.L.;Hickey, D.K.;Kelly, A.L.;O'Mahony, J.A.;Fenelon, M.A., Effect of protein content on the physical stability and microstructure of a model infant formula. International Dairy Journal, 2013. 29,53-59.

[2] Mullane, N.R.;Whyte, P.;Wall, P.G.;Quinn, T.;Fanning, S., Application of pulsed-field gel electrophoresis to characterise and trace the prevalence of Enterobacter sakazakii in an infant formula processing facility. International Journal of Food Microbiology, 2007. 116,73-81.

[3] De Vilder, J.;Martens, R.;Naudts, M., Influence of process variables on some whole milk powder characterisitcs. Milchwissenschaft, 1976. 31(7),396-400.

[4] De Vilder, J.;Martens, R.;Naudts, M., The influence of dry matter content, the homogenisation and the heating of concentrate on the physical characteristics of whole milk powder. Milchwissenschaft, 1979. 34(2),78-84.

[5] McCarthy, N.A.;Kelly, A.L.;O'Mahony, J.A.;Hickey, D.K.;Chaurin, V.;Fenelon, M.A., Effect of protein content on emulsion stability of a model infant formula. International Dairy Journal, 2012. 25,80-86.

[6] Murphy, E.G.;Tobin, J.T.;Roos, Y.H.;Fenelon, M.A., A high-solids steam injection process for the manufacture of powdered infant milk formula. Dairy Science and Technology, 2013. 93,463-475.

[7] Masters, K., Atomization, in Spray Drying In Practice. 2002, SprayDryConsult International ApS: Charlottenlund, Denmark. p. 129-179.

[8] Masters, K., Spray-air contact, particle formation and drying, in Spray Drying In Practice. 2002, SprayDryConsult International ApS: Charlottenlund, Denmark. p. 180-215.

[9] Fitzpatrick, J.J.;Barringer, S.A.;Iqbal, T., Flow property measurement of food powders and sensitivity of Jenike's hopper design methodology to the measured values. Journal of Food Engineering, 2004. 61,399-405.

[10] Kim, E.H.J.;Chen, X.D.;Pearce, D., Effect of surface composition on the flowability of industrial spray-dried dairy powders. Colloids and Surfaces B: Biointerfaces, 2005. 46(3),182-187.

[11] Fu, X.;Huck, D.;Makein, L.;Armstrong, B.;Willen, U.;Freeman, T., Effect of particle shape and size on flow properties of lactose powders. Particuology, 2012. 10(2),203-208.

[12] Shaffer, K.;Paterson, A.H.J.;Davies, C.E.;Hebbink, G., Stokes shape factor for lactose crystals. Advanced Powder Technology, 2011. 22(4),454-457.

[13] Hanley, K.J.;Cronin, K.;O'Sullivan, C.;Fenelon, M.A.;O'Mahony, J.A.;Byrne, E.P., Effect of composition on the mechanical response of agglomerates of infant formulae. Journal of Food Engineering, 2011. 107,71-79.

[14] Murphy, E.G.;Tobin, J.T.;Roos, Y.H.;Fenelon, M.A., The effect of high velocity steam injection on the colloidal stability of concentrated emulsions for the manufacture of infant formulations. Procedia Food Science, 2011. 1,1309 - 1315.

[15] GEA-Niro. Analytical methods for dry milk products. 2012 28 Sept 2012]; Available from: www.niro.com/methods

[16] Crowley, S.V.;Gazi, I.;Kelly, A.L.;Huppertz, T.;O'Mahony, J.A., Influence of protein concentration on the physical characteristics and flow properties of milk protein concentrate powders. Journal of Food Engineering, 2014. 135,31-38.

[17] Schuck, P.;Dolivet, A.;Jeantet, R., Dehydration processes and powder properties, in Analytical Methods for Food and Dairy Powders. 2012, Wiley-Blackwell: West Sussex, UK. p. 1-43.

[18] Yazdanpanah, N.;Langrish, T.A.G., Egg-shell like structure in dried milk powders. Food Research International, 2011. 44(1),39-45.

[19] Schuck, P.;Dolivet, A.;Jeantet, R., Determination of flowability anf floodability indices, in Analytical Methods For Food and Dairy Powders. 2012, Wiley-Blackwell. p. 129-143.

Relaxation of ceramic tile stresses generated by fast drying: a kinetic model

Amorós, J.L. [a, b]; Cantavella, V.[c]; Blasco, E. [a*]

[a] Instituto de Tecnología Cerámica – Asociación de Investigación de las Industrias Cerámicas.

[b] Department of Chemical Engineering. Universitat Jaume I, Campus Universitario Riu Sec, 12006 Castellon, Spain.

[c] Esmalglass-Itaca Grupo, 12191 La Pobla Tornesa, Castellón, Spain.

*E-mail of the corresponding author: encarna.blasco@itc.uji.es

Abstract

Unfired tile mechanical properties are very important in the ceramic tile manufacturing process. Inadequate mechanical properties lead to rejects (both in unfired and fired tiles). Unfired tile mechanical strength changes significantly after the tiles exit the industrial dryer. This behaviour can be explained by assuming that the fast-drying process generates stresses in the tile, which subsequently relax. A kinetic model has been derived, based on Maxwell's viscoelastic elements, which explains the development of dried tile mechanical strength. This increases asymptotically when the dried tiles are stored in dry conditions. However, if tiles adsorb humidity (upon exiting the dryer), tile mechanical strength rises and then decreases. This is the result of two opposing phenomena: stress relaxation raises mechanical strength while the concurrent rise in moisture content lowers mechanical strength. The developed model successfully describes this joint mechanical behaviour.

Keywords: ceramic tiles, fast drying, stress relaxation, kinetic model.

1. Introduction

Simultaneous heat and mass transport during fast drying (20min) of ceramic tiles produces temperature and, in particular, moisture content gradients in the tiles [1]. Such differential drying would also lead to differential drying shrinkage of the layers if they were not joined together. However, as each individual layer cannot shrink freely, mechanical stresses develop among the layers. Indeed, faster drying of the tile faces generates a moisture content gradient inside the tile, causing the tile faces to be subjected to tensile stresses while the inner tile is under compression. These stresses are not eliminated immediately, so that tile mechanical strength will vary after the tile has been dried and has exited the dryer, as the residual stresses generated during fast drying relax.

This study was undertaken to develop a kinetic model that describes the development of unfired tile mechanical strength after tile drying, both during tile storage in a completely dry and in a humid environment (70% relative humidity).

2. Materials and Methods

Floor tiles measuring 31x31x1cm, made by industrial pressing of a standard spray-dried powder, were used. Fast drying (20min) was performed in a horizontal industrial dryer. Moisture content and mechanical strength were determined in all test pieces. Mechanical strength was determined by three-point bend testing [2]. Ten tiles were used for each test condition.

3. Results and discussion

3.1 Stress relaxation in dried tiles placed in bags to keep the tiles dry

Unfired tile mechanical strength, σ_B, rises considerably during dried tile storage time in bags owing to relaxation of the stresses generated in the tile during drying (Fig. 1). The proposed model that describes these results is based on the following assumptions:

i) The unfired tile is assumed to consist of a series of uniform layers of infinitesimal thickness, each of which is subject to different uniform residual stress.

ii) The viscoelastic behaviour of each layer can be described by a Maxwell element [3].

iii) Total strain is independent of time and position.
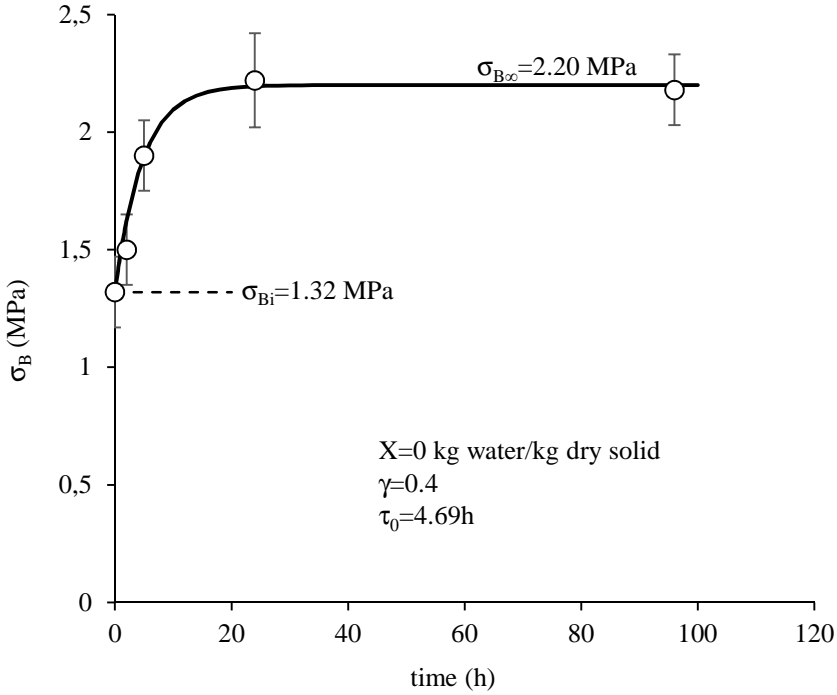
Fig. 1. Variation of the mechanical strength, σ_B, of dried tiles placed in bags with storage time. Fit of the experimental data to the developed model, Eq. 3.

These assumptions yield the Maxwell model stress relaxation, which describes the evolution of the residual stress, σ, for a layer:

$$\sigma = \sigma_i \exp\left(-\frac{t}{\tau_0}\right) \qquad \text{Eq. 1}$$

where σ_i is the initial residual stress (at the dryer exit) (MPa) and τ_0 is the relaxation time of the dried material (h).

iv) In a bending test, tile mechanical strength, σ_B (MPa), is the maximum tensile strength that the bottom layer can withstand. Consequently, during the relaxation process, σ_B is the difference between the mechanical strength of the already relaxed layer, $\sigma_{B\infty}$ (MPa), and the residual stress, σ, acting upon this layer:

$$\sigma_B = \sigma_{B\infty} - \sigma \qquad \text{Eq. 2}$$

Introducing Eq. 1 in Eq. 2 yields:

$$\sigma_B = \sigma_{B\infty}\left[1 - \gamma exp\left(-\frac{t}{\tau_0}\right)\right]$$

Eq. 3

where:

$$\gamma = \frac{\sigma_{B\infty} - \sigma_{Bi}}{\sigma_{B\infty}}$$

Eq. 4

where σ_{Bi} is dried tile mechanical strength at the dryer exit.

This equation describes de evolution, with relaxation time, of the mechanical strength of dried tiles stored in bags to keep the tiles dry (tile moisture content: X=0 kg water/dry solid).

The solid line in Fig. 1 is the plot of Eq. 3. Excellent fit was found.

3.2 Relationship of relaxed unfired tile mechanical strength, σ_{BR}, to moisture content, X

Fig. 2 shows the mechanical strength of stress-free (relaxed) unfired tiles, σ_{BR}, versus moisture content, X, for different experiment series: by moisture adsorption in dried tiles and on drying as-pressed tiles to different moisture contents.

The following equation relates σ_{BR} to moisture content, X, [4] [5]:

$$\sigma_{BR} = \sigma_{BR0}exp(-\beta X)$$

Eq. 5

where σ_{BR0} is the mechanical strength of stress-free dry tiles (MPa) and β is a fit parameter.

The solid line in Fig. 2 is the plot of Eq. 5. Excellent fit was found.
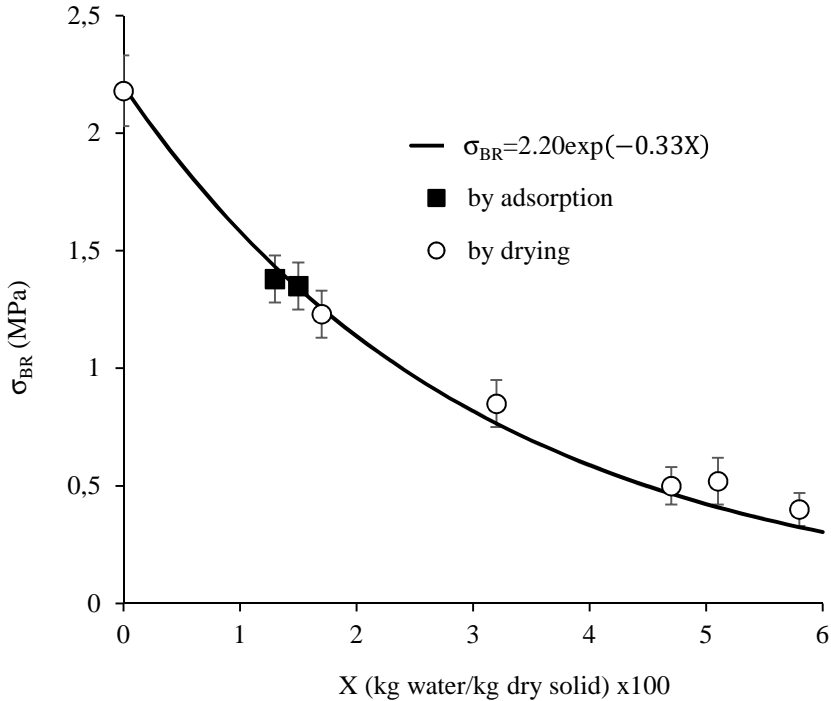
Fig. 2. Effect of moisture content, X, on stress-free unfired tile mechanical strength, σ_{BR}. Fit of the experimental data to Eq. 5.

3.3 Development of dried tile mechanical strength on storage in ambient air

When a tile emerging from the dryer is stored in ambient air (T=20ºC and relative humidity=70%), it will simultaneously be subject to moisture adsorption and stress relaxation. The sum of the opposing effects that each of these phenomena has on unfired tile mechanical strength causes the variation of this property with time to exhibit a maximum value (Fig. 3).
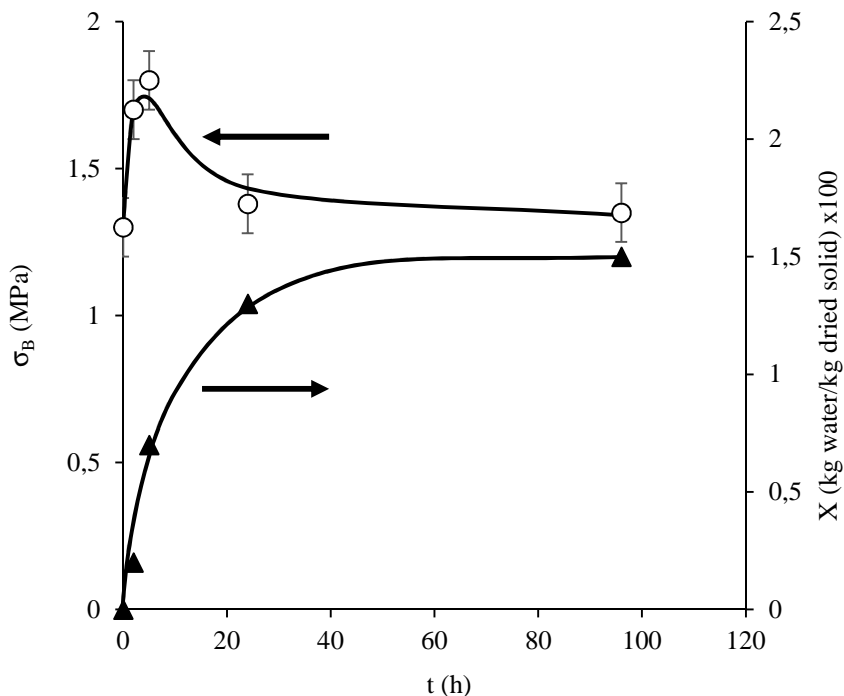
Fig. 3. Variation of dried tile mechanical strength, σ_B, and moisture content, X, with storage time in ambient air (T=20ºC and relative humidity=70%).

To derive the model the following modifications must be performed in Eq. 3:

i) As moisture content increases, stress relaxation becomes faster, so that τ decreases according to the following expression:

$$\tau^{-1}=\tau_0^{-1}+\alpha X \qquad \text{Eq. 6}$$

where α is a fit parameter. Consequently, in Eq. 3, τ_0 must be replaced with Eq. 6.

ii) $\sigma_{B\infty}$ must be replaced with Eq. 5.

iii) γ does not depend on moisture content, X. This parameter is the same as the γ calculated in the previous fit to Eq. 3.

Taking into account the aforementioned assumptions, the final equation becomes:

$$\sigma_B=\sigma_{BR0}\exp(-\beta X)\left[1-\gamma\exp\left(-\left(\frac{1}{\tau_0}+\alpha X\right)t\right)\right] \qquad \text{Eq. 7}$$

For this particular case, substituting the fit parameter values into Eq. 7 yields:

$$\sigma_{B=}2.20\exp(-0.33X)\left[1\text{-}0.4\exp\left(-\left(\frac{1}{4.69}+100X\right)t\right)\right] \qquad \text{Eq. 8}$$

The agreement between Eq. 8 and the experimental data is good (Fig. 3). The equation reproduces the peak strength attained after a certain time.

4. Conclusions

Unfired ceramic tile mechanical strength changes significantly after the tiles exit the industrial dryer. Dried tile mechanical strength increases asymptotically when the tiles are stored in dry conditions. When these tiles adsorb humidity, tile mechanical strength exhibits a peak.

A model has been developed, based on Maxwell's viscoelastic element, which successfully describes this mechanical behaviour.

The relationship between the mechanical strength of stress-free unfired tiles and tile moisture content was found to be independent of whether the process involved modifying tile moisture content by drying or by moisture adsorption.

5. References

[1] Mallol, G.; Cantavella, V.; Llorens, D.; Feliu, C., "Study of ceramic tile drying under non-isothermal conditions and its industrial applications," in *Proceedings of the 7th Conference and Exhibition of the European Ceramic Society*, Uetikon-Zuerich, 2002.

[2] Amorós, J. L.; Cantavella, V.; Jarque, J. C.; Feliu, C., "Green strength testing of pressed compacts: an analysis of different methods," *Journal of the European Ceramic Society,* no. 28, p. 701–710, 2008.

[3] Moreno, R., Reología de suspensiones cerámicas, Madrid: Consejo Superior de Investigaciones Científicas (CSIC), 2005.

[4] Amorós, J. L., Pastas cerámicas para pavimentos de monococción. Influencia de las variables de prensado sobre las propiedades de la pieza en crudo y sobre su comportamiento durante el prensado y la cocción, Burjasot: PhD Thesis. Universidad de Valencia, 1987.

[5] Jarque, J. C., Estudio del comportamiento mecánico de soportes cerámicos crudos: mejora de sus propiedades mecánicas, Castellón: PhD thesis. Universitat Jaume I, 2001.

Fixed-bed drying of grains: analysis of the structural properties of packed-beds of non-spherical particles

Altino, H.O.N.ª; Ferreira, M.C.ª*

ª Chemical Engineering Department, Federal University of São Carlos, São Carlos, São Paulo, Brazil.

* E-mail of the corresponding author: mariaf@ufscar.br

Abstract

Structural properties of packed-beds of non-spherical biological materials were investigated. The particles tested were oats, lentil, barley and soy, with sphericity ranging from 0.4 to 0.8. Porous alumina particles with sphericity of 0.98 were also included. The particles dimensions and sphericity were measured under moisture content ranging from the equilibrium up to 24% (dry basis). Mean voidage, bulk density, permeability and tortuosity of the packed-beds were obtained in the whole moisture range. The data were used as input into a correlation to predict Sherwood numbers under constant air velocity and the results were compared to evaluate the influence of packing characteristics on convective mass transfer.

Keywords: Sphericity; Permeability, Tortuosity, Fixed-Bed Dryers.

1. Introduction

It is well-known that variables such as particle shape, size, surface roughness, among others, influence the gas-particle interaction in fixed-bed drying because the packed bed permeability, tortuosity, interparticle contact and residence time are greatly affected by them. For particles of irregular shape and wide size distribution, a great number of packing arrangements can be achieved, leading to changes in the local porosity and contact area that affect the heat and mass transfer rates. Drying is a preservation method widely used for grains, a class of materials that exhibits a widespread variety of shape and sizes. Besides, the dimensions and shape of grains often change throughout drying due to the shrinkage, making the design of drying equipment a challenging task [1]. The influence of the particle properties on fixed-bed drying is useful information for a fundamental analysis of drying processes of grains and seeds.

As a preliminary stage of a study aimed at investigating how the packed-bed characteristics may affect convective fixed-bed drying, a characterization of the packed-bed's structural properties was performed for different biological materials. Particles' characteristic dimensions, volume, equivalent diameter, surface area, sphericity and density were obtained as a function of the moisture content. The bulk density, mean voidage, permeability and tortuosity were obtained for the different packed-beds. The experimental data were used as input to an empirical correlation based on the packed-bed properties to evaluate the mass transfer coefficients and compare the mass transfer potential of each bed.

2. Materials and Methods

2.1. Particulate materials

The biological materials were selected to cover a wide range of characteristics: soy (*Glycine max* L.), green lentils (*Lens culinaris*), barley (*Hordeum vulgare* L.) and oats (*Avena sativa*). Nearly spherical porous alumina particles with a diameter of 2.5 mm were included to serve as a standard material for comparison. The dehydrated materials were purchased from a local market and either humidified or dried to reach specified moisture content (X) (% d.b.), which were set to 24%, 16%, 9% and the equilibrium moisture (X_{eq}). Humidification was done by placing 150 g samples in polyethylene plastic packages, adding the necessary amount of deionized water and storing the sealed packages at 4°C for 48 h. The drying was performed in a hot-air drying oven (TE-394/1, Tecnal®) at 50°C.

2.2. Physicochemical characterization

Particles were assumed to have a triaxial spheroid shape. The length (L_p), width (W_p) and mean diameter (D_m) of 60 particles were measured by the image analysis technique using the software Image-Pro Plus® 6.0. The thickness (T_p) was measured using a digital caliper. The volume (V_s) and sphericity (φ) were calculated according to [2]. The packed-beds' bulk density (ρ_b) was obtained by measuring the weight and volume of the samples, using a digital scale (AS 1000, Marte®) and a glass measuring cylinder with diameter of 5.0×10^{-2} m. Small portions of particles were discharged from a constant height through a funnel into a graduated glass vessel. The vessel was tapped over a flat surface until a constant volume. The apparent density (ρ_a) was estimated by liquid pycnometry with toluene (99.5%, Dinâmica®). The mean voidage (ε_b) was evaluated from the values of ρ_a and ρ_b [2]. The measurements were performed in triplicate.

2.3. Determination of the permeability and tortuosity

The packed-bed static pressure drops were measured in a cylindrical vessel with diameter (D) of 5.0×10^{-2} m and height of 29.5×10^{-2} m (the ratio D/D_m varied from 7.0-16.0). The pressure taps were distributed along the vessel height at each 5 cm. The particles were randomly packed according to the same procedure described in section 2.2. The pressures (P) were measured under different air flow rates and at a constant air temperature (27°C). The air velocity (U) ranged between 0.05-0.58 m.s^{-1}. The permeability (κ) was obtained from a linear regression of Eq. (1), with experimental values of ΔP and U. The tortuosity (τ) was estimated based on the capillary model, using Eq. (2) [3].

$$\frac{\Delta P}{Uz} = \frac{\mu}{\kappa} + \frac{c}{\sqrt{\kappa}}\rho U \tag{1}$$

$$\tau = \frac{\varepsilon_b^3 D_m^2 \varphi^2}{72\kappa(1-\varepsilon_b)^2} \tag{2}$$

2.4. Mass transfer coefficients

To evaluate how the packed-bed structure affect the mass transfer in a hypothetical drying limited by the external resistance, the mass transfer coefficients were estimated from a generalized semi-empirical correlation developed for porous media. As described in [4], the equation assumes that packed-bed structure can be described by a capillary geometry and defines a wall energetic criterion (Xe_w). The correlation is given by:

$$Sh = 3.66 + 0.101\left[1 + \frac{\pi}{4}\frac{1-\varepsilon_b}{\varepsilon_b}(\tau-1)\left(1 + \frac{\varepsilon_b}{\tau^2}Sc^{\frac{1}{3}}e^{-\frac{11-\varepsilon_b}{3}\frac{\sqrt{\tau Y}Xe_w^{\frac{1}{8}}}{\varepsilon_b}}\right)\right]Xe_w^{\frac{11}{48}}Sc^{\frac{1}{3}} \tag{3}$$

The dimensionless groups Xe_w, Sh, Re and Sc were estimated according to [4]. The diffusivity of moisture in the air (D_A) was obtained from [5]. Air physical properties and D_A were estimated at ambient temperature (30°C). The aspect ratio (Y) was obtained from the ratio of particle thickness over particle width, T_p/W_p [4].

3. Results and Discussion

3.1. Particles characteristics

The particles' linear dimensions, (L_p, W_p, T_p), mean diameter (D_m), volume (V_s) and sphericity (φ) are shown in Figs. 1(a) to 1(f).
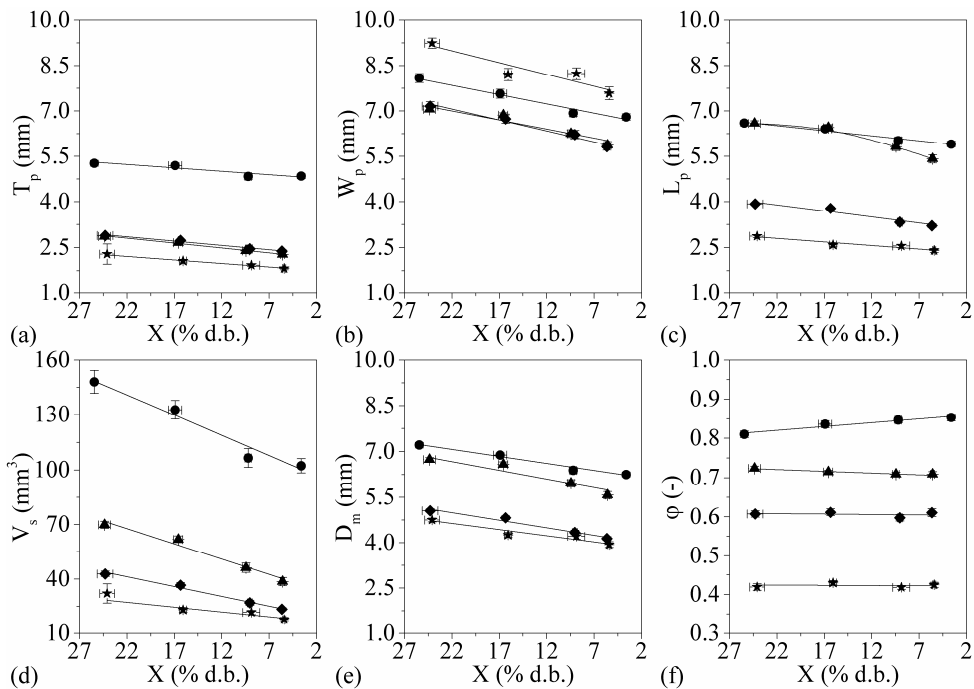
Fig. 1 Particles' dimensions and sphericity as a function of the moisture content; T_p (a), W_p (b), L_p (c), V_s (d), D_m (e) and φ (f). Legend: soy (●), lentil (▲), barley (◆) and oats (★).

A reduction in X resulted in a linear decrease in the particles' dimensions, owing to the shrinkage phenomenon that appears as a result from an unbalance between the material's inner pressure and the external pressure [6]. Shrinkage is usually observed in food materials with a solid matrix in the rubbery state [6,7]. The particles characteristics of alumina are not shown because its dimensions do not change with moisture variation. The results and

qualitative behavior of variables in Fig. 1 are consistent with those reported in the literature [8-11]. Although the linear dimensions change, φ is not significantly affected by the moisture reduction, as can be observed in Fig. 1(f).

3.2. Packed-beds structural properties

The particles' sphericity are, in a decreasing order, 0.98 (alumina), 0.8 (soy), 0.7 (green lentils), 0.6 (barley) and 0.4 (oats). It is worth noting that the particles differ also in size, shape, apparent density and surface roughness. All these variables may affect the packing structure, however the differences cannot be avoided when working with biological particles. The variation of ρ_b and ε_b as a function of φ are shown in Fig. 2 for X equal to 24% and for dry particles (equilibrium moisture). The results obtained at 16% and 9% stayed between the upper and lower limits and for the sake of concision are not shown in the graphs.
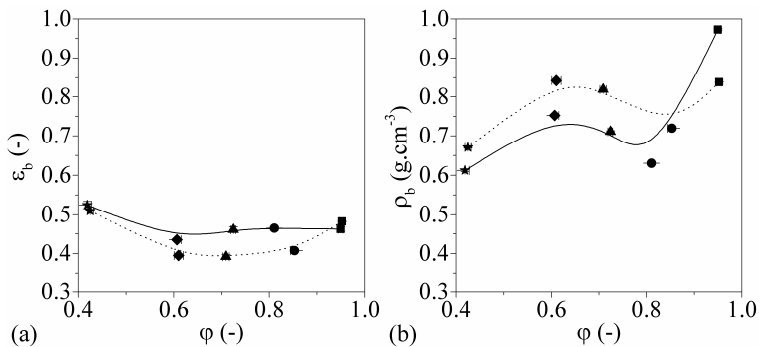
Fig. 2 Bulk properties as a function of φ:** ε_b **(a) and ρ_b **(b) for alumina (■), soy (●), lentil (▲), barley (◆) and oats (★). Legend: moistures contents of 24% (——) and X_{eq} (⋯⋯).

Fig. 2 (a) shows that at a constant X, ε_b did not vary significantly as φ was reduced from 0.98 to 0.60. Only at φ=0.40 a slight increase was observed, suggesting that packed-beds of oats tend to produce large pores. However, it is not clear why ε_b was not affected by the moisture content in this particular case. The variation of ρ_b with φ is complex and does not show a clear trend, as can be seen in Fig. 2(b). At a constant X, ε_b and ρ_b depend not only on φ, but also on additional factors, such as the particles' dimensions and ρ_a. Additionally, the variation of D_m and ρ_a with moisture content is different for each particle. Even the particles' surface roughness can be affected by moisture and it is quite difficult identifying the different contributions of each variable in the packed-bed structure. The apparent density of alumina, for instance, decreases as X is reduced, as its volume does not change. On the other hand, the grains shrink and an opposite behavior is observed. Therefore,

several combined effects are responsible for the patterns observed in Figs. 2(a) and 2(b). The qualitative dependence of ρ_b and ε_b on X were similar to those reported by [8-11] for lentil, barley, soy and oats, respectively. A reduction of X caused an increase in ρ_b (Fig. 2 (b)) and a decrease in ε_b (Fig. 2 (a)), which is probably associated to the decrease in D_m observed as the moisture content is reduced (Fig. 1(e)). For random packing of non-spherical particles, smaller values of D_m generate smaller intraparticle void spaces, thus increasing ρ_b and decreasing ε_b [12]. Alumina presented an atypical behavior, because D_m does not change with X for this particle.

The influence of X on κ and τ is displayed in Fig. 3 as a function of φ. A decrease in X resulted in lower values of κ and higher values of τ. This can be attributed again to the reduction of D_m with X due to the shrinkage of grains, and is consistent with the patterns described in Figure 2.
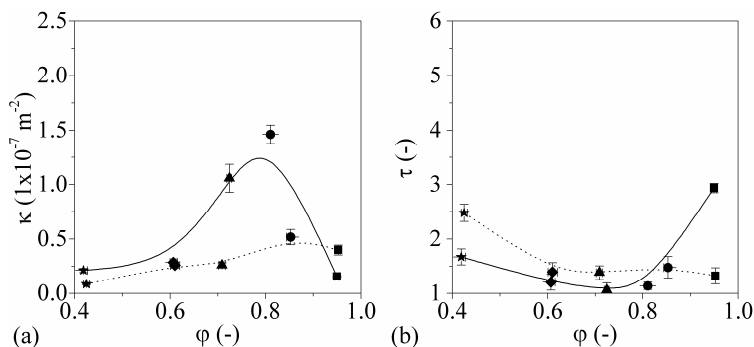
Fig. 3 Packed-bed parameters as a function of φ for alumina (■), soy (●), lentil (▲), barley (◆) and oats (★); κ (a) and τ (b). Legend: moistures contents of 24% (———) and X_{eq} (·······).

It is also observed in Fig. 3 that, at a constant X, κ tends to decrease with the decrease in φ and τ tends to increase. According to the literature [5], deviations from the spherical shape may contribute to reducing the pore diameter. However, for the particles considered here, not only the particle shape but other variables, such as the size and apparent density can affect the packed-beds' structural properties. It can also be observed that the influece of φ on κ and τ is much more evident at a high X, which is probably related to the dependence of the grains' dimensions on X. Once more, an atypical behavior is observed for alumina for the aforementioned reasons.

3.3. Mass transfer coefficients

The values of *Re* and *Sh* were estimated for the different packed-beds at U=0.58 m.s^{-1} and are shown in Fig. 4 as a function of φ, for values of X equal to 24%, 16%, 9% and X_{eq}. *Re* was calculated based on the estimated capillary diameters.

At X=24%, it can be observed in Fig.4(a) that *Re* is practically constant for the packed-beds of different particles, regardless of the value of φ. Only for alumina a significant increase in *Re* was observed, which is attributed to the smaller size of this particle. At a low moisture content (X=9%), a slight decrease in *Re* is observed as φ increases from 0.4 to 0.7 and it increases again as φ is further increased. The variation in this case is much lower than observed at X=24%. These quite different patterns are justified by the influence of the moisture content on the particles' dimensions. The dependence of *Sh* on φ in Fig. 4(b) shows quite similar patterns to those observed in Fig. 4(a), as the convective mass transfer is directly correlated to *Re*. High values of *Re* favor fluid turbulence, flow eddies and mixing and contribute to increasing mass transfer, as the boundary layer thickness and mass transfer resistance are reduced [13]. Therefore, higher values of *Sh* are observed under higher values of *Re*. Among the biological particles tested, and at a constant X, higher *Sh* were observed in the packed-beds of oats, which is the particle of lower sphericity.
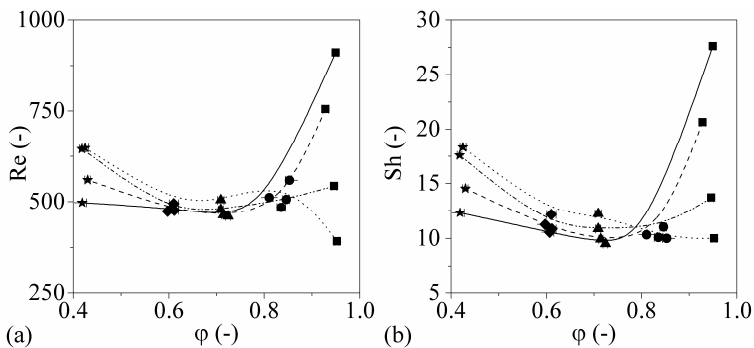
Fig. 4. Estimated values of Re (a) and Sh (b) as a function of φ for alumina (■), soy (●), lentil (▲), barley (♦) and oats (★) at 0.58 m.s^{-1}. Legend: moisture of 24% (——), 16% (- - - -), 9% (-·····-) and X_{eq} (·······).

4. Conclusions

Based on the experimental data, it was verified that the permeability and tortuosity of packed-beds of soy, oat, lentil and barley were significantly affected by the particles shape and size and by the moisture content. The results suggest that the packed-bed structure may change significantly throughout drying depending on the particle characteristics, as the particles dimensions vary with their moisture content, while their shape practically do not

change. Because each particle was differently affected by the moisture content and have distinct shape and sizes, no consistent correlation between the structural properties such as mean voidage, bulk density, permeability and tortuosity to the particle characteristics could be identified.

5. References

[1] D.B. Brooker, F.W. Bakker-Arkema, W. Hall, Drying and storage of grains and oilseeds, Van Nostrand Reinhold, New York (1992) 450.

[2] N. Mohsenin, Physical properties of plant and animal materials, Gordon and Breach, New York, 1970.

[3] D. Lasseux, F. J. Valdés-Parada. On the developments of Darcy's law to include inertial and slip effects. C. R. Mec. 345 (2017) 660–669

[4] J. Comiti, E. Mauret, M. Renaud, Mass transfer in fixed beds: proposition of a generalized correlation based on an energetic criterion, Chem. Eng. Sci. 55 (2000) 5545-5554.

[5] T.R. Marrero, E.A. Mason, Gaseous diffusion coefficients, J. Phys. Chem. Ref. Data. 1 (1972) 3-118.

[6] L. Mayor, A.M. Sereno, Modelling shrinkage during convective drying of food materials: A review, J. Food Eng. 61 (2004) 373-386.

[7] B.R. Bhandari, T. Howes, Implication of glass transition for the drying and stability of dried foods, J. Food Eng. 40 (1999) 71-79.

[8] S.D. Deshpande, S. Bal, T.P. Ojha, Physical Properties of Soybean, J. Agric. Eng. Res. 56 (1993) 89-98.

[9] E. Isik, Moisture dependent physical and mechanical properties of green laird lentil (Lens culinaris) grains, Pakistan J. Biol. Sci. 10 (2007) 474-480.

[10] C.A. Sologubik, L.A. Campañone, A.M. Pagano, M.C. Gely, Effect of moisture content on some physical properties of barley, Ind. Crops Prod. 43 (2013) 762-767.

[11] A. Shah, F.A. Masoodi, A. Gani, B.A. Ashwar, Geometrical, functional, thermal, and structural properties of oat varieties from temperate region of India, J. Food Sci. Technol. 53 (2016) 1856-1866.

[12] R.M. German, Particle Paking Characteristics, Metal Powder Industries Federation, Princeton, 1989.

[13] J. Comiti, M. Renaud, Liquid-solid mass transfer in packed beds of parallelepipedal particles: energetic correlation, Chem. Eng. Sci. 46 (1991) 143-154.

Effects of ozone pretreatment on drying kinetics and quality of Granny Smith Apple dried in a fluidized bed dryer

Fonteles, T. V.[a]; Nascimento, R. B. R.[a]; Rodrigues, S.[a*]; Fernandes, F. A. N.[b]

[a] Department of Food Engineering. Federal University of Ceará, Ceará, Brazil

[b] Department of Chemical Engineering. Federal University of Ceará, Ceará, Brazil

*E-mail of the corresponding author: sueli@ufc.com

Abstract

This study aimed to evaluate the effects of ozone pretreatment on drying of green apple carried out in a fluidized bed dryer to determine drying kinetics and identify operating parameters for improved product quality. Results reveal that drying temperature in different levels affected water diffusivity and retention of bioactive compounds. The ozone pretreatment showed unexpected results since the pretreatment reduced the water difusivity and promoted an increase in the enzyme activity. The treatment time strongly afftected the final polyphenoloxidase and peroxidase activities. On the other hand, the ozone treatment resulted in lower color changes compared to non-ozone treated dried apples.

Keywords: diffusivity; polyphenoloxidase; enzymatic browning; ozone.

1. Introduction

Foods with high moisture like fruits and vegetables are dried to increase shelf storage and to reduce the storage and transportation costs. However, the drying methods used for food should be not only efficient and economical but also produce high quality, tasty and nutritious products with good uniformity, appearance, and texture. The main challenge in drying food is to maintain the quality of the product[1,2].

The drying process is related to the simultaneous application of heat and removal of food moisture. The main parameters that control the drying rate of fruits are the air temperature, relative air humidity and air velocity as processing conditions variables. These parameters are chosen based on the nature of the food and the particular design of the dryer[3,4]. Fluidized bed drying is a method for controlled and mild drying of wet solids. A proper bed flow control provides a homogeneous drying, with greater drying efficiency without the application of excessive heat and mass transfer when compared to other conventional drying systems. However, the efficiency of a conventional fluidized bed system is usually low. It is, therefore, desirable to improve the efficiency of the drying process.

Pretreatment with ozone in fruits and vegetables is usually carried out to prolong its shelf life. One of the applications of ozone as a preservative treatment in fresh fruits and vegetables is due to the effective increase of the antioxidant defense system by increasing the activity of superoxidase dismutase (SOD), peroxidase (POD) and catalase (CAT)[5].

Polyphenoloxidases are enzymes responsible for the enzymatic browning in fruits and vegetables. These enzymes also cause degradation of polyphenols, leading to discoloration and loss of antioxidant activity[2].

Thus, this study aimed to evaluate the application of ozone pretreatment before drying of green apple carried out in a mini vibrated fluidized bed dryer to determine drying kinetics and identify the main operating parameters for improved product quality.

2. Materials and Methods

2.1 Preliminary drying tests

The apples (Granny Smith variety) were cut in cubes (0.5 cm) and dried at 40, 45 or 50 ° C in a mini fluidized bed dryer and evaluated in different temperature and air flow parameters (Table 1). The final moisture obtained was 10 % (dry base), and the processing effects on color parameters, phenolic compounds, antioxidant capacity (DPPH)[6] and the polyphenol oxidase (PPO) and peroxidase (POD) activities[2] were evaluated. The optimum drying temperature was selected based on the effective water diffusivity of apple cubes calculated using Fick's law.

Table 1. Drying parameters

Temperature (°C)	Airflow (m³/min)	Final Airflow (m³/min)	Drying time (h)
40	75	40	2
45	75	40	2
50	75	40	2

2.2 Ozone pretreatment

To evaluate the blanching effects of ozone pretreatment on dried apples, the cubes were inserted into a glass column reactor with a sintered glass porous plate (4.5 cm in diameter and 30 cm hight), coupled to a Model O & L1.5 Portable Ozone Generator, (OzoneLife, São José Dos Campos, São Paulo, Brazil).

For ozone pretreatment, samples with 65 g of green apple cubes were exposed to different processing times: 10, 20 or 30 minutes. The oxygen flow was 250 mL/min and the ozone production was 40.9 mg / L.

For drying, 55 g of ozone pretreated green apple cubes were dried in a fluidized bed dryer (Labmaq do Brasil, Ribeirão Preto, São Paulo, Brazil). The ozone pretreated apples were dried at 50 ºC because this temperature resulted in the highest diffusivity of drying.

2.3 Quality parameters of the dried apples

The sample's moisture was determined using a moisture balance (Marconi, Piracicaba-Brazil). The water activity was determined at 25°C with a water activity meter (AquaLab, Decagon CX-2, Pullman, Washington, USA). The drying kinetics the thermal diffusivity apples were calculated according to the Fick´s law.

The instrumental color was determined using a Minolta CR300 colorimeter (Tokyo, Japan) and the color parameters were expressed as L* (whiteness/darkness), a* (redness/greenness), b* (yellowness/blueness), C* (saturation index) and °*h* (hue angle). The readings were done in quintuplicate and the total color difference (ΔE), was calculated according to the following equation:

$$\Delta E = \sqrt{(\Delta L)^2 + (\Delta a)^2 + (\Delta b)^2} \tag{1}$$

Total phenolic compounds were determined by the Folin-Ciocaulteu method[2].

3. Results and Discussion

3.1 Effects of fluidized bed drying on bioactive compounds and drying kinetics

According to the results presented in Table 2, fluidized bed drying has influenced the activity of the spoiling enzymes reaching almost 80% of inactivation for PPO and POD at 50°C after 2 hours of drying. Yemenicioglu et al. (1997)[6] reported that the time required for 50% reduction of initial PPO activity of Granny Smith apples at 68°C and 78°C was 35 and 3 min, respectively, showing the effect of temperature on PPO. Antioxidant capacity (DPPH) also decreased due to the drying processes. However, at 40°C it was observed an increase of 200% for total phenolic compounds (TPC), which agrees to the highest antioxidant value found at 40 ºC. Possibly, drying promoted the release of insoluble phenolics increasing both the phenolic content and the antioxidant activity. Water activity reached values below 0.4, after 2 h (50°C), 2.4h (45°C) or 3h (40°C) of drying, which is appropriate to prevent bacterial and fungi growth. The results suggest that fluidized drying is a viable technology for drying apples.

Table 2. Residual concentrations of total phenolic compounds, polyphenol oxidase (PPO), peroxidase (POD) and total antioxidant activity (DPPH) of fluidized bed dried green apple

Temp.	Residual Concentrations (%)				Diffusivity $(10^9 \text{ m}^2/\text{min})$
	TPC	PPO	POD	DPPH	
40°C	301.47±22.78	30.46±1.07	31.61±0.89	101.44±0.32	8.50 ± 1.02
45°C	88.11±2.92	31.42±1.00	39.53±1.51	36.82±2.78	11.50 ± 0.85
50°C	78.25±1.14	21.36±2.54	15.30±0.43	27.82±0.79	16.50 ± 3.20

3.2 Ozone pretreatment

The ozone pretreatment reduced the water diffusivity as showed in Table 3, which leads to a reduced drying efficiency. The negative effect on the water diffusivity was proportional to the ozone application time. After 30 min of ozone pretreatment, the diffusivity was reduced by 43%. This might be occurred probably due to structural changes after increasing time exposure to ozone.

Table 3. Diffusivity values of ozone pretreated apples at 50 $^\bullet$ C

Time (min)	Diffusivity $(10^9 \text{ m}^2/\text{min})$
0	16.50 ± 3.20
10	15.80
20	12.90
30	9.39

The results of the color analysis are presented in Table 4. The color difference (ΔE) was calculated against the control sample (non-dried apple). For all pretreated samples, the drying process increased the total color difference, but this variation was lower when the drying was combined with the ozone pretreatment. Thus, it is possible to state that the application of ozone before drying reduced the color changes during drying. The mechanism involved are object of future studies.

Table 4. Colors values of fluidized bed dried green apple

	L*	C*	h	a*	b*	ΔE
Control-OZ 10	76.03	24.51	99.42	-4.01	24.18	-
OZ 10	68.53	9.74	100.65	-1.80	9.57	16.56
OZ 10 + FB	62.19	14.80	91.63	-0.47	14.80	17.09
Control-OZ 20	72.34	24.21	114.97	-10.22	21.95	-
OZ 20	69.17	13.39	100.58	-2.46	13.16	12.14
OZ 20 + FB	63.08	15.09	92.43	-0.64	15.08	14.99
Control-OZ 30	72.02	14.21	101.07	-2.73	13.94	-
OZ 30	63.30	22.15	87.28	1.05	22.12	11.06
OZ 30 + FB	76.03	24.51	99.42	-4.01	24.18	13.85
Control	86.53	22.05	107.80	-6.73	20.99	-
FB 50°C	68.73	17.09	76.08	4.11	16.59	21.3

Control: non-processed apple; OZ – sample submitted to ozone treatment; OZ+FB – sample submitted to ozone treatment followed by fluidized bed drying.

Table 5 shows the residual activity of PPO and POD after ozone pretreatment and fluidized bed drying.

Table 5. Residual activities (%) of ozone pre-treated and fluidized bed dried green apple

	POD	PPO
OZ 10	442.96 ± 5.90	162.28 ± 13.94
OZ 10 + FB	243.80 ± 13.22	30.54 ± 13.25
OZ 20	85.71 ± 2.96	102.42 ± 4.84
OZ 20 + FB	182.56 ± 8.84	48.68 ± 8.50
OZ 30	76.24 ± 0.0	121.10 ± 3.06
OZ 30 + FB	54.92 ± 3.06	49.55 ± 6.04

The maximum reduction (23.76%) was achieved after 30 minutes of ozone exposure. An inhibitory effect of ozone on POD occurred probably due to the high oxidation potential of ozone[7]. For PPO the activity increased up to 62% after short time ozone processing (10 min) and then it was reduced. After drying, PPO activity decreased probably due to the temperature effect (Table 2). The highest enzymes inactivation was achieved in the samples treated with ozone by 30 minutes. However, the POD and PPO residual activity were higher than the found in the samples dried without the ozone pretreatment.

Conclusions

Our results suggest that fluidized bed drying is a viable technology for drying apples. The ozone pretreatment resulted in unexpected results since the pretreatment reduced the water difusivity and promoted an increase in the enzyme activity. The treatment time strongly afftected the final PPO and POD activity. On the other hand, the ozone treatment resulted in lower color changes when compared to non-ozone treated dried apples.

To our knowledge this the first study applying ozone as pretreatment for fruit drying. The results strongly suggest a behavior similar to the ultrasound pre-treatment where some parameters can increase or decrease depending on the intensity and processing time. Thus, more studies on the effect of ozone as pretreatment for drying fruits are necessary to understand the mechanism of the effects reported in the present study.

References

[1]   Zhang, M.; Chen, H.; Mujumdar, A. S.; Tang, J.; Miao, S.; Wang, Y. Recent Developments in High-Quality Drying of Vegetables, Fruits, and Aquatic Products. *Crit. Rev. Food Sci. Nutr.* 2017, *57* (6), 1239–1255.

[2]   Fonteles, T. V.; Costa, M. G. M.; de Jesus, A. L. T.; de Miranda, M. R. A.; Fernandes, F. A. N.; Rodrigues, S. Power Ultrasound Processing of Cantaloupe Melon Juice: Effects on Quality Parameters. *Food Res. Int.* 2012, *48* (1), 41–48.

[3]   Sharada, S. Studies on Effect of Various Operating Parameters & Foaming Agents-Drying of Fruits and Vegetables. *Int. J. Mod. Eng. Res.* 2013, *3* (3), 1512–1519.

[4]   Sivakumar, R.; Saravanan, R.; Elaya Perumal, A.; Iniyan, S. Fluidized Bed Drying of Some Agro Products - A Review. *Renew. Sustain. Energy Rev.* 2016, *61*, 280–301.

[5]   Chen, J.; Hu, Y.; Wang, J.; Hu, H.; Cui, H. Combined Effect of Ozone Treatment and Modified Atmosphere Packaging on Antioxidant Defense System of Fresh-Cut Green Peppers. *J. Food Process. Preserv.* 2016, *40* (5), 1145–1150.

[6]   Yemenicioğlu, A.; Özkan, M.; Cemeroğlu, B. Heat Inactivation Kinetics of Apple Polyphenoloxidase and Activation of Its Latent Form. *J. Food Sci.* 1997, *62* (3), 508–510.

[7]   Miller, F. A.; Silva, C. L. M.; Brandão, T. R. S. A Review on Ozone-Based Treatments for Fruit and Vegetables Preservation. *Food Eng. Rev.* 2013, *5* (2), 77–106.

Effects of Assistance of High Frequency Dielectric and Infrared Heating on Vacuum Freeze Drying Characteristics of Food Model

Hashimoto, A.ᵃ*; Suehara, K.ᵃ; Kameoka, T.ᵃ; Kawamura, K.ᵇ

[a] Graduate School of Bioresources, Mie University, Tsu, Mie, Japan.

[b] Energy Applications Research & Development Center, Chubu Electric Power Co., Inc., Nagoya, Japan.

*E-mail of the corresponding author: hasimoto@bio.mie-u.ac.jp

Abstract

By combining vacuum freeze drying combined with high-frequency dielectric and/or infrared heating, the drying time for frozen gels containing 1% agar with sucrose or sodium chloride was successfully shorten, and the drying time was influenced by the heating methods and by the additive component to the sample. Additionally, it was experimentally confirmed that the power consumption for freeze drying combined with electromagnetic wave heating could be reduced because of the shortened drying time. Consequently, this study could be a very important step for designing a vacuum freeze drying process optimally combining electromagnetic wave heating for each sample component.

Keywords: freeze drying, electromagnetic wave heating, food model, sucrose, sodium chloride

1. Introduction

Vacuum freeze drying (FD) is less physical and with less chemical changes in the sample qualities; in recent years the application fields have been expanded. Vacuum FD is commonly and widely utilized for high quality preservative foods [1]. However, the drying time for conventional FD is very long (for example; several tens of hours). Therefore, freeze drying is actively studied for the purpose of shortening the drying time. Wang et al. performed FD of sliced potatoes by combining microwave heating, and established the drying time could be shortened by 37% [2, 3]. Microwave, combined FD is not enough uniform heating under the high vacuum. Additionally, Pan et al. tried to shorten the FD process of sliced bananas in consideration of the influence of infrared irradiation [4]. Furthermore, Schössler et al. studied an ultrasound assisted freeze drying of red bell pepper pieces cut into 1-cm squares, but noted only a minimal effect [5].

We then focused our attention on high-frequency dielectric (HF) heating to directly heat frozen foods for the purpose of the reduction of the time of the vacuum FD. The combined vacuum FD and HF heating has the potential of a multi-stage operation without a heating medium, and a large number of samples could be vacuum freeze-dried at one time. As the results, drying time could be shortened by using HF heating [6]. However, on the first half of the drying, the combination effect was very slight. This study aims to further shortening the drying time by combining vacuum FD combined with HF and/or infrared (IR) heating since infrared rays could be significantly absorbed by all phases of water. As the food model, a cylindrical frozen agar gel was selected because of easy formability and adjustments to its components. We then study the effects of the assistance of HF and/or IR heating on the FD characteristics and the influences of the additive of sucrose or sodium chloride (NaCl) to the food model on them.

2. Materials and Methods

2.1. Materials

Frozen agar gels containing 1 wt% agar were used as the food model samples. We also made the frozen agars including sucrose of 20 wt% or NaCl of 7.5 wt% as the drying samples. The outline of the sample preparation procedure is shown in Figure 1. The agar, sucrose and NaCl were of special grade and obtained from Wako Pure Chemical Industries (Osaka, Japan). The initial water content of the agar was preciously controlled by

suppressing the moisture evaporation. The formed sample was stored in a freezer which was set to 253 K.
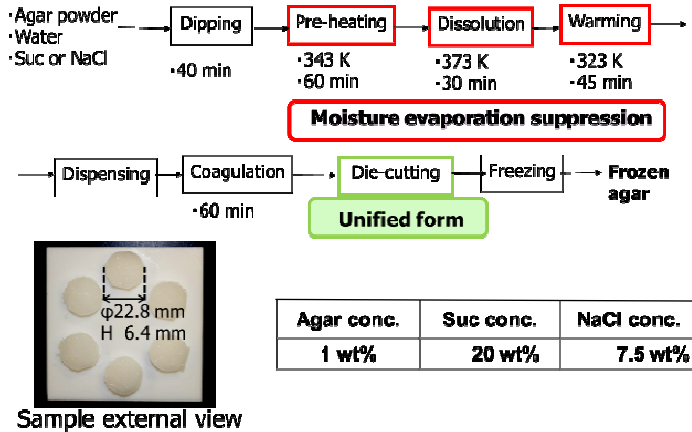
Fig. 1 Outline of sample preparation procedure.

2.2. Experimental apparatus

Drying experiments were performed in a Lab-scale vacuum chamber (Espec Co., Ltd., Osaka, Japan) equipped with the high frequency dielectric and infrared radiative heating

① Vacuum chamber   ② HF introduction part   ③ Optical fiber temperature and humidity sensors   ④ Thermometer   ⑤ Drying sample   ⑥ Thermal and electrical insulator   ⑦ Upper electrode   ⑧ Lower electrode   ⑨ Matching box   ⑩ Vacuum exhaust valve   ⑪ Piping leak valve   ⑫ HF power source (13.56 MHz)   ⑬ Oil-sealed rotary vacuum pump   ⑭ Oil-water separator   ⑮ Data logger (pressure, HF power recorder)   ⑯ P C   ⑰ Teflon® plate   ⑱ Teflon® O-ring   ⑲ Optical fiber type temperature sensor   ⑳ Infrared heaters

Fig. 2 Schematic diagram of high frequency dielectric heating with freeze-dryer.

systems. A scheme of the drying equipment is presented in Figure 2. The output power of the high frequency dielectric heating is automatically adjusted to a set point by the matching box ⑨ during freeze-drying. The upper electrode ⑦ has the holes on the circumference for transmitting the infrared rays from the infrared heaters ⑳ equipped on the top plate inside the vacuum chamber ①. The infrared radiative power is controlled by adjusting the energization time to the infrared heaters. A vacuum pump was used for maintaining the vacuum in the chamber. The data of the pressure, high frequency traveling wave power and high frequency reflection wave power are recorded using the data logger ⑮.

2.3. Drying experiments

Six frozen agar samples are put on the Teflon® plate (82× 82× 10.5 mm) and are kept in a freezer set at 253 K overnight. The samples and the plate were put on the lower electrode. To avoid the heat transfer from the lower electrode to the sample, a Teflon® O-ring (φ3, 60 mm inside diameter) ⑱ was put on the lower electrode ⑧, and the samples ⑤ on the plate ⑰ were put on the O-ring. The distance from the sample to the upper electrode (GND) was set at 15 mm based on the preparatory experiment results.

In case of the assistance of HF heating, after the pressure in the vacuum chamber reached around 100 Pa, HF power was supplied to the frozen samples and the drying experiment was started. During drying, the sample temperature and the pressure in the chamber were continuously monitored. At the specified drying time, one agar was sampled from the chamber after the inner pressure was returned to atmospheric pressure. Drying of the remaining agar samples were then started again. To determine the moisture content of the sample, the sample after vacuum freeze drying was dried in an oven set at 378 K for 24-72 hours. The dry weight of the sample was gravimetrically measured.

3. Results and Discussion

3.1. Drying characteristics

The influences of the HF power on the combined vacuum freeze drying characteristics of the frozen agar gel were experimentally studied, and Figure 3 shows the influences on the time courses of the normalized water content (ω/ω_0) relative to the initial one (ω_0) for the frozen agar gel (no additive) and of the sample temperatures. As shown in Figure 3, the drying rate was accolated by combining electromagnetic wave heating. The drying time was shortest when HF and IR heating were simultaneously used (HF+IR). However, the

sample temperature rose and the part became burned. We then performed the other combination of HF and IR heating with FD (HF+IR→HF). Drying with HF+IR was carried out in the initial stage, and infrared irradiation was cut off when the sample temperature began to rise. As the result, the temperature rise of the sample was suppressed, and it was possible to shorten the drying time almost the same as HF+IR drying.

Drying of frozen agar supplemented with sucrose or NaCl was performed by combining electromagnetic wave heating, and Figure 4 shows the relationship between the drying time t_d and the final temperature of the samples. We then performed the preliminary approach to quantitatively confirm the differences of the drying characteristics of each sample. For the additive free sample under the FD process without the assistance of HF and/or IR heating, the time course of the normalized water content was fitted using the following simple
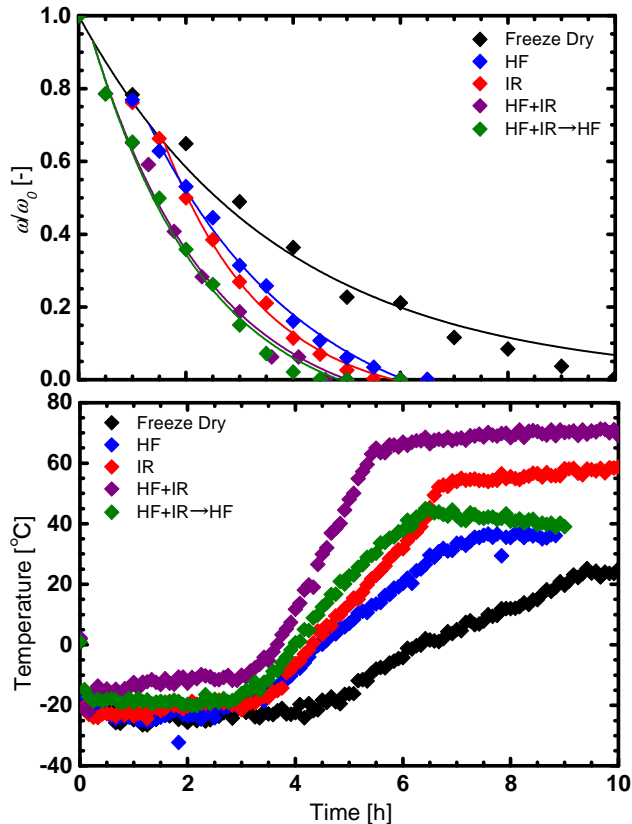
Fig. 3 Time courses of normalized water contents and temperatures of frozen agar gel (no additive).

exponential equation.

$$\omega/\omega_0 = \exp(-kt)$$ (1)

Here, t and k are the drying time and the drying rate constant, respectively.

For the other samples, the curve fitting for the time courses of the normalized water content was carried out using the following equation which modified Eq. (1) from the middle of the drying process [6].

$$\omega/\omega_0 = \left\{ (\omega/\omega_0)_s - 1 \right\} + \exp\{ -k_1(t - t_s) \}$$ (2)

Here, t_s and $(\omega/\omega_0)_s$ are the start point of the exponential curves for parallel translation of Eq. (1). An intersection of both curves expressed by Eq. (1) and (2) means the critical point of the drying characteristic. k_1 is the drying rate constant for the latter exponential curve. We could then calculate the drying time t_d based on Eq.(2).

As indicated in Figure 4, for the samples added sucrose as an organic substance, the effect of shortening the drying time was more pronounced for IR heating assistance than for HF heating assistance. In addition, for the samples added NaCl as an electrolyte substance, no significant difference was observed in the time reduction effect by HF and IR heating assistance, but the dry sample temperature was lower for HF heating assistance than in for IR heating assistance.
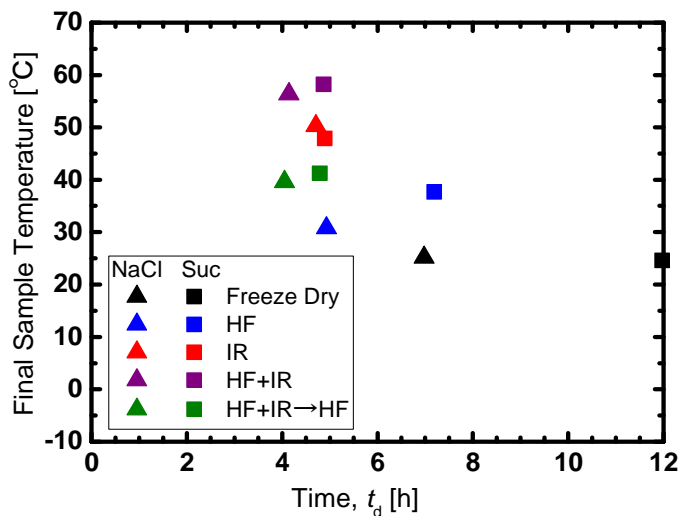
Fig. 4 Relationship between dried sample temperature and drying time.

3.2. Electric power consumption during drying process

We also measured the electric power consumption during each drying process. Figure 5 illustrates the relationship between the electric power consumption and the drying time. It was confirmed that the power consumption could be reduced by shortening the drying time with the assistance of electromagnetic wave heating. In addition, based on the near-infrared spectroscopic imaging results of the dried samples (data not shown), it was experimentally confirmed that the component changes of the dried samples except for those dried under the HF+IR drying conditions could be negligible. Consequently, from the experimental results indicated in Figure 3, 4 and 5, the effectiveness of the assistance of electromagnetic heating to vacuum FD of the food model was experimentally found.
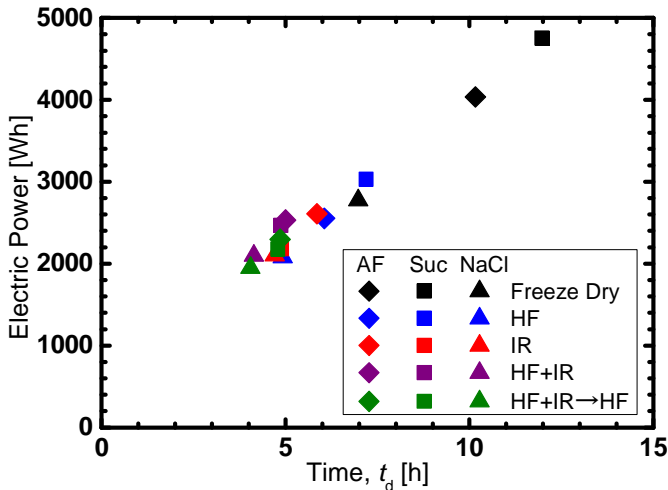
Fig. 5 Relationship between electric power consumption and drying time.

4. Conclusions

By controlling the combined use conditions of HF and/or IR heating for each sample component, drying time could be shortened. Additionally, a vacuum freeze drying process could be optimally designed by combining electromagnetic wave heating with the reduction of electric power consumption and without the quality change of the dried sample.

5. Nomenclature

k	drying rate constant	h^{-1}
t	drying time	h

Greek letters

ω	water content	kg-water kg^{-1}-dry material

Subscripts

0	initial state
1	state after critical point
s	start point defined by Eq. (2)

6. References

[1] Duan, X.; Yang, X; Ren, G; Pang, Y.; Liu, L; Liu, Y. Technical aspects in freeze-drying of foods. Drying Technology 2016, 34, 1271-1285.

[2] Wang, R.; Zhang, M.; Mujumdar, A.S. Effect of food ingredient on microwave freeze drying of instant vegetable soup. LWT-Food Science and Technology 2010, 43, 1144-1150.

[3] Wang, R.; Zhang, M.; Mujumdar, A.S. Effects of vacuum and microwave freeze drying on microstructure and quality of potato slices, Journal of Food Engineering 2010, 101, 131-139.

[4] Pan, Z.; Shih, C.; McHugh, T.H.; Hirschberg, E. Study of banana dehydration using sequential infrared radiation heating and freeze-drying, LWT – Food Science and Technology 2008, 41 1944-1951.

[5] Schössler, K.; Jäger, H.; Knorr, D. Novel contact ultrasound system for the accelerated freeze-drying of vegetables, Innovative Food Science and Emerging Technologies 2012, 16, 113-120.

[6] Kawamura, K; Suehara, K.; Kameoka, T.; Hashimoto, A. Characteristics of combined vacuum freeze drying and high frequency dielectric heating of a food model. In Proceedings of 20th International Drying Symposium, Gifu, Japan, August 7-10, 2016, C-4-5.

Estimation of the apparent glass transition temperature of spray-dried emulsified powders and yeast powders by their flavor release behavior under temperature ramping conditions

Sultana, A.[a,b,c]; Zhu, J. L.[a]; Yoshii, H.[a,b]*

[a] Department of Applied Biological Science, Kagawa University, Japan

[b] Department of Applied Bioresource Science, Ehime University, Japan

[c] Department of Food Processing and Engineering, Chittagong Veterinary and Animal Sciences University, Bangladesh

*E-mail of the corresponding author: foodeng.yoshii@ag.kagawa-u.ac.jp

Abstract

Flavor release from powders depends on the glass transition temperature (T_g) and water absorption. This study reports a simple method to estimate the apparent T_g by aroma sensing upon flavor release from spray-dried powders. Four different wall materials (maltodextrin (MD), MD blends with fructose at 20 and 40wt%, and yeast cells) were used to encapsulate flavors by spray-drying. The apparent T_g values of MD and MD with 20 and 40wt% fructose were determined as 130, 110, and 75 °C, respectively, similar to those calculated by the Gordon–Taylor equation. The slow flavor release from dried-yeast powder afforded the highest T_g.

Keywords: yeast; flavor; encapsulation; spray drying; aroma sensor.

Estimation of the apparent glass transition temperature of spray-dried emulsified powders and yeast powders by their flavor release behavior under temperature ramping conditions

1. Introduction

Spray drying is a unique technique to encapsulate active compounds. The rapid drying rate, availability of the instrumentation, and continuous operation processing make spray drying a widely useable technique in the encapsulation field. Additionally, good quality powders and high flavor-retention powders can be obtained by spray drying. Encapsulation is the entrapment of an active material inside a wall material. The encapsulation of flavors in solid powders has great benefits as it can reduce the volatility losses, protect from adverse environments, and increase their shelf-life and stability. The encapsulation efficiency differs vastly among different wall and core materials. The glass transition temperature (T_g) is a key property that affects the release of flavors from encapsulated powders.[1] Chirife and Karel[2] and Roos and Karel[3] have described how flavor retention or release from amorphous matrices may be due to the transformation of said amorphous matrices from a glassy to a rubbery phase. They highlighted two causes for this transition: an increase in the moisture content and an elevated temperature. At the T_g, the molecular movement in the powder increases and the amorphous material changes from a glassy to a rubbery state, with consequences of stickiness and collapse of the powder.[4] Furthermore, the stickiness of the powder observed at the T_g results in poor quality and low yields during drying, and handling and storage problems.[5] Therefore, the determination of the T_g of wall materials is very important for application in encapsulating powders. Usually, the glass transition temperature is measured by differential scanning calorimetry (DSC). However, the determination of T_g values by DSC is very difficult due to the small changes in the heat capacity near the T_g.

In this study, a method for the measurement of the T_g of flavor-encapsulated spray-dried emulsified powders and yeast powders is proposed using a simple instrument named aroma sensor. The rapid increment in flavor release from the encapsulating powders was monitored using a ramping method (linear programmed temperature gradient).

2. Materials and Methods

2.1. Materials

Drum-dried yeast cells, *Saccharomyces cerevisiae* cells (partially β-glucan extracted), were obtained from Fuji Foods Corp. (Yokohama, Japan). Maltodextrin (MD, DE = 19) and fructose (Fr) were kindly donated by Matsutani Chemical Industries, Ltd. (Itami, Japan). Sodium caseinate, the emulsifier, was received from Mitsubishi-Chemical Foods Corp. (Tokyo, Japan). The flavors, i.e., the core materials, hexanol, *d*-limonene, and ethyl hexanoate were purchased from Wako Pure Chemical Industries, Ltd. (Osaka, Japan). All

other chemicals were of analytical grade and obtained from Wako Pure Chemical Industries, Ltd. (Osaka, Japan).

2.2. Methods

2.2.1. Preparation of d-limonene and ethyl hexanoate-encapsulated yeast powders

d-Limonene and ethyl hexanoate were encapsulated in yeast cells following the method described by Sultana et al.[6]

2.2.2. Preparation of hexanol-encapsulated emulsified powders

Three different powders were prepared by changing the MD-to-Fr ratio in the feed solution. Powders of MD (100%) and blends of MD and Fr at ratios of 4:1 and 3:2 were prepared using a pilot spray dryer Ohkawara-L8 (Ohkawara Kakouki Co., Ltd., Yokohama, Japan) equipped with a centrifugal atomizer. Feed solutions were prepared by dissolution of MD or its blends with Fr (38.5 wt%) together with sodium caseinate (1.5 wt%) and hexanol in medium chain triglyceride (MCT) oil (10 wt%) in distilled water (50 wt%). The solid content was maintained at 50 wt%. Hexanol was diluted in MCT oil at a ratio of 1:4 (%wt). The mixture was homogenized using a mechanical homogenizer, a polytron homogenizer (PT-10, Kinematica GA, Littau, Switzerland), at 8000 rpm for 3 min. Finally, the carrier solution was spray-dried at an inlet air temperature of 160 °C, atomizer speed of 10,000 rpm, and feed flow of 20 mL/min. The outlet temperature was monitored at 83–106 °C.

2.2.3. Analysis of the d-*limonene and ethyl hexanoate extracted from yeast powder*

The encapsulated *d*-limonene and ethyl hexanoate were extracted from yeast cells and analyzed by gas chromatography following the procedure described by Sultana et al.[7]

2.2.4. Analysis of hexanol from flavor-encapsulated powders

The flavor-encapsulated powder (0.1 g) was completely dissolved in 5 mL of distilled water in a glass bottle. Diethyl ether with cyclohexanone (5 mL of 1000 ppm) was added as the internal standard and the mixture was vortexed for 20 min at 20 °C in a high speed shaker (CM-1000, Tokyo Rikakikai Co., Ltd., Tokyo, Japan). After centrifugation, a small amount of anhydrous sodium sulfate was added to the upper phase and 1 µL was injected in a gas chromatograph-mass spectrometer (GC-MS, Shimadzu Corp., Kyoto, Japan). The GC-MS

was equipped with a fused silica capillary column (30 m × 0.25 mm × 0.25 µm; DB-1, Agilent Technologies Japan Ltd., Tokyo, Japan). The column temperature was programmed from 80 to 260 °C at a rate of 3 °C/min and from 260 to 300 °C at 20 °C/min, where the temperature was maintained constant for 28 min.

2.2.5. *Measurement of the apparent T_g of flavor-encapsulated powders with aroma sensor*

The flavor-encapsulated powder (1 g) was placed in a glass vessel ($24^d \times 45^h$ mm) and covered with a rubber cap. The cap of the glass vessel had holes for two needles, one for nitrogen supply and the other one for air sampling. The air sampling port was connected to a handheld odor meter (KANOMAX, OMX-SRM model, Kobe, Japan) through a polyurethane tube (PISCO, Okayama, Japan). The released flavors were detected by the aroma sensor. A nitrogen flow rate of 30–50 mL/min was maintained depending on the aroma strength of the sample. To determine the aroma strength of the encapsulated yeast powder, a Tee connector was connected to the tube from the sampling vessel to the sensor to dilute the flavor concentration. The vessel was placed in an aluminum block on a digital plate heater, which was used to control the temperature of the powder at two different ramp rates (0.5 and 1°C/min). The powder temperature was recorded with a data logger. The data filing software OMX-SRM was installed in the computer to collect the released flavor data during the whole process. The apparent T_g was the intercept temperature of the tangent line in the flavor release plot.

3. Results and Discussion

3.1. Measurement of the apparent T_g of emulsified flavor powders

The moisture content of the emulsified flavor powders was below 2%, whereas the retention of encapsulated hexanol in the MD (DE = 19) and MD with 20 or 40 wt% Fr samples was about 100%, 70%, and 65%, respectively. Figure 1 shows the hexanol release behavior of the emulsified powders with the increasing temperature at rates of 1 and 0.5 °C/min. The flavor strength gradually increased with the temperature, even though the flavor strength was very low near 20 °C. However, the strength of the flavor sharply increased at a certain temperature, indicating the glass transition temperature of the wall material. The apparent glass transition temperature is the intercept point of the tangent line for the hexanol release rate (flavor strength detected by the aroma sensor). The apparent glass transition temperature of the MD (DE = 19) and MD with 20 and 40 wt% Fr containing powders were determined to be around 130, 110, and 75°C, respectively.
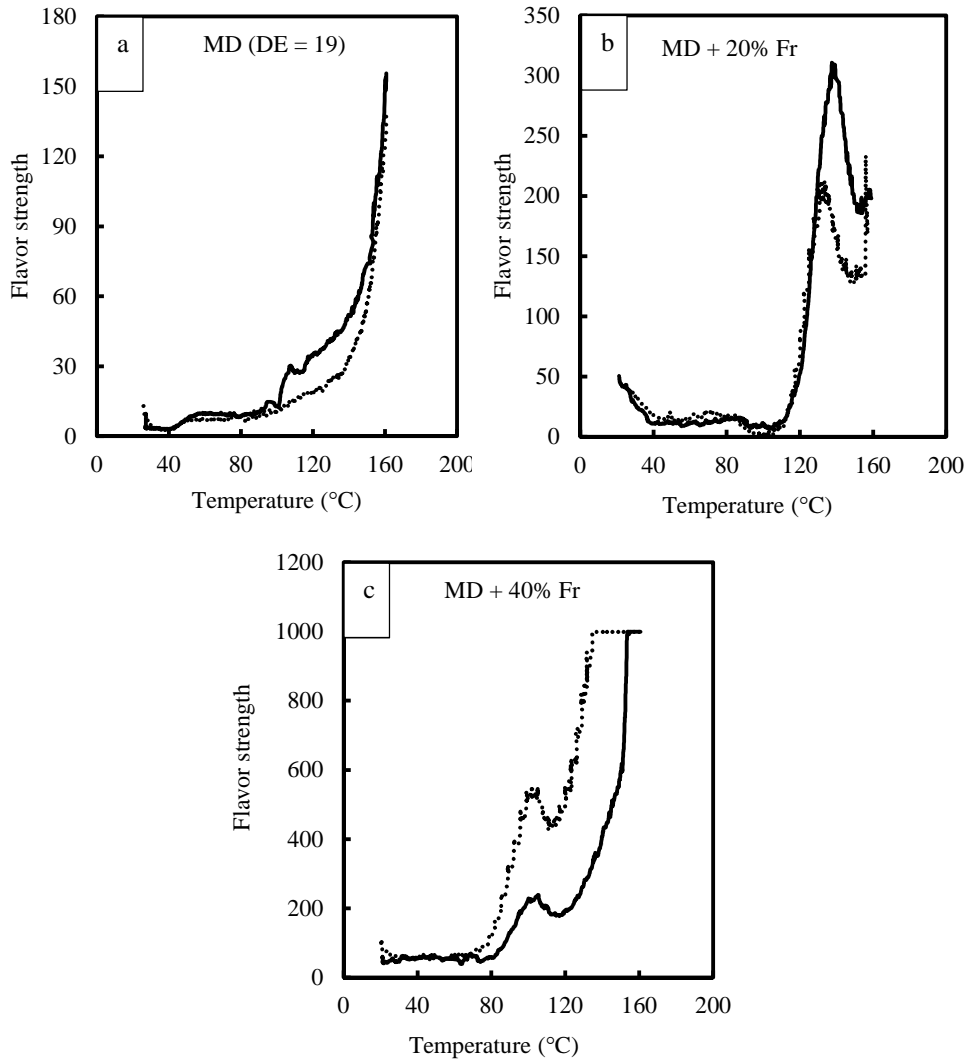
Fig. 1 Hexanol release behavior of emulsified powders: (a) maltodextrin (DE = 19), (b) MD with 20 wt% Fr, and (c) MD with 40 wt% Fr (solid lines: 1 °C/min; dotted lines: 0.5 °C/min).

It can be seen that the addition of Fr to MD reduces its glass transition temperature. The low T_g of pure Fr, which was reported by Roos[8] to be 5 °C, reduces the apparent T_g of the wall material. It must be noted that the T_g values for the above mentioned powders calculated using the Gordon–Taylor equation are very similar to the experimental values shown in the graphs.

3.2. Measurement of the apparent T_g of flavor-encapsulated yeast powders
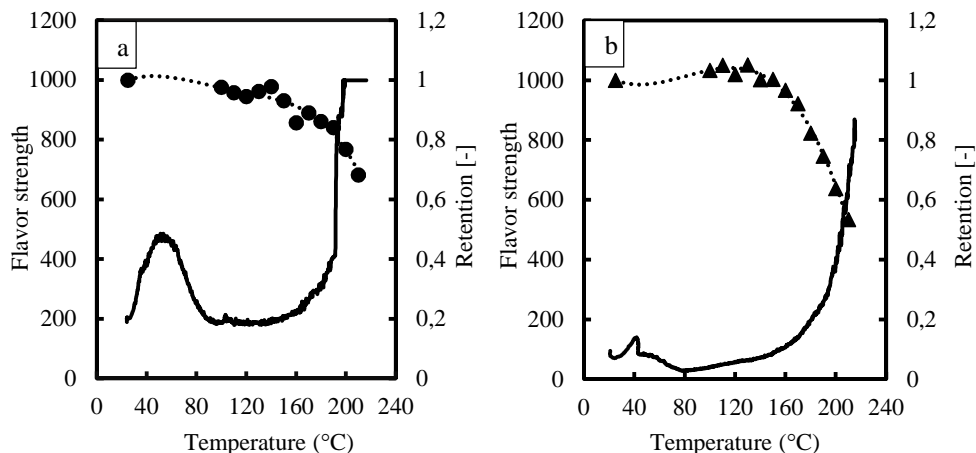
Fig. 2 Release behavior of (a) ethyl hexanoate and (b) d-limonene from yeast powders (solid lines: flavor strength; dotted lines: retention of flavor).

Figure 2 illustrates the release behavior of ethyl hexanoate and *d*-limonene from yeast cells with the increasing temperature at 1 °C/min. The initial high flavor strength possibly corresponds to the surface flavor of the yeast powder. After that, the flavor strength decreases to finally increase again at very high temperatures (180–190 °C). The complex structure of yeast, i.e., the presence of different sugars, proteins, and others species, hampers the accurate monitoring of the flavor release. To confirm the apparent T_g of the flavor-encapsulated yeast powders, *d*-limonene and ethyl hexanoate were extracted from yeast cells under ramping temperature conditions (at 1 °C/min) and analyzed by GC-FID. The retention of the encapsulated flavor was calculated following the method by Sultana et al.[6] The obtained intercept point was very similar to the apparent T_g value found using the aroma sensor. The presence of trehalose, sucrose, and other sugars in yeast cells may be the reason behind the high apparent T_g of yeast cells.

4. Conclusions

The apparent glass transition temperatures of flavor encapsulated spray-dried powders were successfully determined using an aroma sensor. The apparent T_g of powders composed of MD (DE = 19) and MD with 20 and 40 wt% Fr were approximately 130, 110, and 75 °C, respectively. The increasing temperature rate did not significantly affect the T_g of the encapsulating powders. In contrast, yeast cells exhibited a slower release of flavors and higher T_g value.

5. Acknowledgement

6. References

[1] Carolina, B.C.; Carolina, S.; Zamora, M.C.; Jorge, C. Glass transition temperatures and some physical and sensory changes in stored spray-dried encapsulated flavors. LWT - Food Science and Technology 2007, 40, 1792–1797.

[2] Chirife, J.; Karel, M. Effect of structure disrupting treatments on volatile release from freeze-dried maltose. Journal of Food Technology 1974, 9, 13–20.

[3] Roos, Y.; Karel, M. Plasticizing effect of water on thermal behavior and crystallization of amorphous food models. Journal of Food Science 1991, 56, 38–43.

[4] Levine, H.; Slade, L. A polymer physico-chemical approach to the study of commercial starch hydrolysis products (SHPs). Carbohydrate Polymers 1986, 6, 213–244.

[5] Shrestha, A.K.; Howes, T.; Adhikari, B.P.; Wood, B.J.; Bhandari, B.R. Effect of protein concentration on the surface composition, water sorption and glass transition temperature of spray-dried skim milk powders. Food Chemistry 2007, 104, 1436–1444.

[6] Sultana, A.; Tanaka, Y.; Fushimi, Y.; Yoshii, H. Stability and release behavior of encapsulated flavor from spray-dried *Saccharomyces cerevisiae* and maltodextrin powder. Food Research International 2018, 106, 809–816.

[7] Sultana. A.; Miyamoto, A.; Hy, Q.L.; Tanaka, Y.; Fushimi, Y.; Yoshii, H. Microencapsulation of flavors by spray drying using *Saccharomyces cerevisiae*. Journal of Food Engineering 2017, 199, 36–41.

[8] Roos, Y. Characterization of food polymers using state diagrams. Journal of Food Engineering 1995, 24, 339–360.

Hot air drying combined vacuum-filling nitrogen drying of apple slices: Drying characteristics and nutrients

Huang, X.L.[a]*; Li, T.[a]; Li, S.N.[a]; Wu, Z.H.[b]; Xue, J.[a]

[a] College of Food Engineering and Nutritional Science, Shaanxi Normal University, Xi'an, 710119, China

[b] College of Mechanical Engineering, Tianjin University of Science and Technology, Tianjin, 300222, China

*E-mail of the corresponding author: cauxlhuang@hotmail.com

Abstract

In this paper, hot air drying (HAD) was applied when moisture content of apple slices range from 50% to 86%, and then vacuum-filling nitrogen drying (VFND) was used till moisture content reaching 7%. Results showed that, the drying rate of apple slice during VFND period increased with temperature increment and decreased with increment of slice thickness; compared to freezing dried samples, samples dried in this research were owned lower Vc and higher flavonoid; when HAD (70℃,3.0m/s)+VFND(relative pressure 0.08MPa, 50℃) and thickness of 6.0mm, nutrients reached better levels: retentions of Vc, total phenolics and flavonoid were 1.63mg/100g, 4.07mg/100g and 2.10mg/100g, respectively.

Keywords: apple slices, hot air drying, vacuum-filling nitrogen drying, drying rate, nutrients

1. Introduction

Apple is a main fruit in many countries. As the results from Wang and others, till 2013, the annual production of fresh apple fruit in China is about 39.7 million t, accounting for 49% of the global production[1]. Fresh apple fruits are usually graded for higher economic benefit. Fresh apples with the better quality would just be fresh consumed while the apples with the poor quality are generally used to produce juice, jam, and dried products for examples apple chips or nature apple powder and so on. Drying process of apple is a better way to prolong storage. And the main drying techniques used to dehydrate apple slices include FD, HAD, VD, HAD combined VD, and so on. HAD apple slices is the conventional technology studied widely in the past two decades[2-4], however, browning and oxidation even hardening happened during HAD[5-7], which induced undesirable quality. Freeze drying can produce perfect quality dried fruits and vegetables[8,9], but it also high energy consumption. So, various combine drying methods applied to dry fruit and vegetable appear in recent years. Hazervazifeh et al. studied combined microwave-hot air and other drying methods dehydration of apple slices and found that, microwave power 2000W at 70°C with the air velocity of 2.0m/s can induce the minimum drying time[10]. However, fruit and vegetable dried by microwave combined hot air does not always maintain the better quality, for example low rehydration[11]. Huang and others investigated effects of combined drying methods on composition, aroma, eating quality of apple slices[12]; in their studies, freeze-drying, freeze-drying + microwave vacuum drying and microwave vacuum drying + freeze-drying were used to dry apple slices; and the results showed that, microwave had significant effects on aroma, total phenols and pectin, and longer drying time high temperature at desorption drying stage and short time higher temperature at microwave vacuum drying period during freeze-drying + microwave vacuum drying induced lower retention of both aroma and reducing sugar. It was proved that vacuum drying can afford a low oxygen environment and the retention of various nutrients in vegetables and fruits could be better. Nitrogen is an inert gas and if it was filled with vacuum drying circumstance, it may be induce dried products with better quality.

The aim of this work is to study the drying characteristics of HAD + VFND dried apple slices and the quality of apples slice including retention of vitamin C, total phenolics and flavonoid. For this purpose, experiments of apple slices dried after HAD and then dried in VFND under different conditions were conducted and nutrients were also determined.

2. Materials and methods

2.1. Samples preparation

Fresh apples malus pumila mill were obtained from local market and stored at 3-4°C in a refrigerator and were used within 14 days. The initial moisture contents of fresh apples were within 85 to 87% (wet basis), which were determined by hot air oven method at 103-105°C until the constant mass. Samples were sliced to the thicknesses of 2.0-8.0mm after peeling and then immersed into 0.2% ascorbic acid solution for 2minites to restrain browning.

2.2. Hot air drying

Apple slices were dried with hot air at 70°C with the velocity of 3.0m/s after immersed into 0.2% ascorbic acid solution for 2 minutes and the moisture contents were declined from about 86% to 50%w.b. During hot air drying, the weights of samples were obtained by electronic balance with an accuracy of 0.001g every 10 minutes.

2.3. Vacuum-filling nitrogen drying

The half dried apple slice samples were dried in vacuum-filling nitrogen drying oven until the moisture contents were about 7% w.b. In vacuum-filling nitrogen drying method, materials were put into vacuum oven, and then vacuuming(10kPa)→filling with nitrogen (near 0.1MPa)→vacuuming(10kPa)→filling with nitrogen (near 0.1MPa)→vacuuming (10kPa). Temperatures were range from 50 to 80°C during VFND. While during vacuum-filling nitrogen drying, the weights of samples were obtained every 20 minutes.

2.4. Nutrients assay

Dried apple slices were crushed by a pulverizer, and nutrients in nature apple powder were determined.

In this research, vitamin C was determined by Philin's reagent colorimetry according to the methods of Benassi & Antunes[13]and Marfil, Santos &Telis[14] with some modifications. Apples powder of 0.500g was homogenized with the extraction solution (2 g oxalic acid/100g solution) and diluted to 50ml with the extraction solution in a volumetric flask, and then vacuum filtered after 30 minutes' standing. Filtrate of 10ml was taken for titration with 2,6-dichlorophenolindophenol solution (50mg 2,6-dichlorophenolindophenol/250ml pure water). When the pink color of filtrate did not disappear in 15s, the titration end point was determined. All analyses were performed in triplicate.

The flavonoid content of apple powder was analyzed according the method described by Jia etal[15] with slight amendments. 1.000g apple powder was homogenized with 50ml of ethamol (7:10) for 60 minutes and then vacuum filtrated. 1.0ml of the filtrate was placed in a 25ml volumetric flask, 10ml of ethamol (7:10) and 1ml of $NaNO_2$(1:20) were added and shaken well, 10ml of 1 mole per litre NaOH was added after 6 minutes, and the total volume was made up to 25ml with ethamol (7:10). After 15 minutes' standing, this sample was placed in colorimetric tube and the absorbance was measured at 510nm.

Total phenolics content of natural apple powder were determined by the Folin-Ciocalteau method[16]. Apple powder of 1.000 grams were added to the ethanol solution with the content of 75% and diluted to 50ml. 5ml of sample was taken into volumetric flask，50ml of pure water and 4ml of Folin-Ciocalteu reagent were also added. After 3-4minutes' standing, 8ml of 10% sodium carbonate was put into the volumetric flask. And the final volume was made up to 100ml with pure water. After 120 minutes of reaction at 25℃, absorbance at 765nm was measured and used to calculate the phenolic contents using a standard curve prepared with gallic acid. All measurements were conducted in triplicate.

3. Results and discussion

3.1. Hot air drying characteristic of apple slice

In this paper, drying rate was expressed as follow:

$$DR = \frac{MC_{t-\Delta t} - MC_t}{\Delta t} \qquad (1)$$

Where $MC_{t-\Delta t}$ and MC_t represented moisture content at the time of $t-\Delta t$ and t, separately, dry basis, %; t was drying time, min; and Δt was time interval, min.

During HAD apple slices, there existed significant falling rate period, and the constant rate period was obvious for apple slices with the thickness of 2.0mm, while it was not evident for the apple slices with the thicknesses of 4.0-8.0mm, such as figure 1. Because, there exists longer path and greater resistance in the thicker slices for water molecules migrating. Moisture content of apple slices declined more slowly as the increase of the slice thickness.
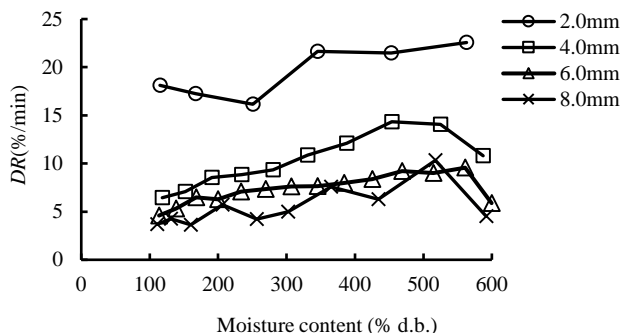
Fig. 1 Curves of dehydration rate of apple slices with different thicknesses during HAD(70 ℃, 3.0m/s)

3.2. Vacuum-filling nitrogen drying characteristics of apple slice

After HAD, apple slices were dried with VFND until the moisture content lower than 7.0%w.b. And there is only falling rate period for apple slices during VFND, showed in figures 2 and 3, owning to bound water in apple slices in this period.

During VFND, dehydration rate of apple slices declined as the decrease of temperatures and the increase of the slices thickness. As the analyzed above, there are the longer path and greater resistance for moisture to transfer to surface in the thicker apples slices. And when the thickness was 2.0mm, the greatest dehydration rate appeared which is approximate twice of that with the thicknesses of 6.0, 8.0mm. The higher temperature, the greater drying rate is for apple slices dried in vacuum-filling nitrogen condition, and it was the same as the results from apple slices vacuum drying[17].
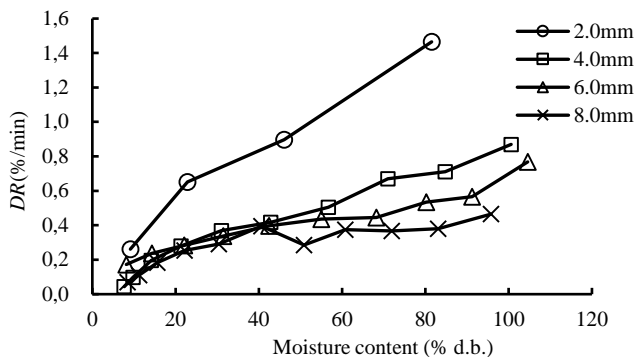
Fig. 2 Drying rate curves of apple slices during VFND with different thicknesses (60°C)
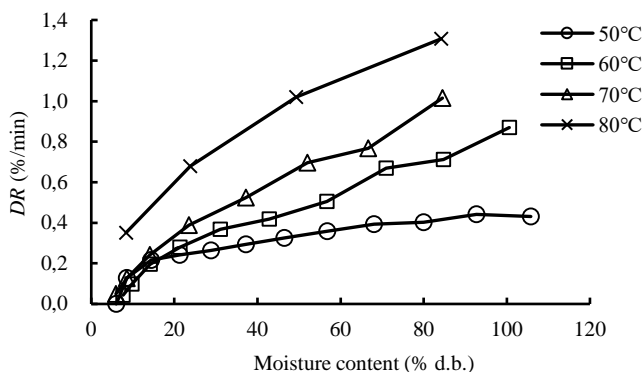
Fig. 3 Drying rate curves of apple slices during VFND at different temperatures (4.0mm)

3.3. Nutrients of apple slice dried with combined drying methods

Nature apple powder was made by the dried apple slices dried with different drying methods. And the nutrients of Vc, total phenolics, flavonoid in apple powder were expressed as mg/100g of initial fresh samples, showed in table 1. From table 1, it was found that, retentions of Vc in samples dried with HAD+VFND were lower than that of samples dried with FD, while the retentions of total phenolics of both samples dried with HAD+VFND and FD were at the same levels, and flavonoid retentions of samples dried with combined drying were almost higher to that of FD. Results reviewed that the combined method of HAD+VFND could be an available method for maintain flavonoid and total phenolics of apples; although vitamin C in samples dried with HAD+VFND was lose seriously, just only about 30% to 52% of that in fresh apples. And when HAD at 70℃, 3.0m/s combined with VFND at temperature 50℃, relative pressure -0.08MPa and slice thickness of 6.0mm, nutrients in dried sample were better: the vitamin C content of 1.63mg/100g, total phenolics content of 4.07mg/100g and the flavonoid content of 2.12mg/100g. In generally, it is available for HAD combined VFND to dehydrate apple slice.

Table 1. Contents of nutrients in nature apple powder produced by various drying methods

Thickness (mm)	Temperature (℃)	Vc (mg/100g)	total phenolics (mg/100g)	flavonoid (mg/100g)
2.0	50	1.38±0.03	3.57±0.14	2.10±0.06
2.0	60	1.50±0.03	3.61±0.05	1.71±0.03
2.0	70	1.29±0.03	4.03±0.06	1.55±0.04
2.0	80	1.04±0.05	3.52±0.06	1.39±0.03
4.0	50	1.81±0.03	3.43±0.06	1.20±0.02
4.0	60	1.32±0.09	3.29±0.09	1.21±0.04
4.0	70	1.26±0.06	3.19±0.05	1.03±0.04
4.0	80	1.66±0.06	3.35±0.04	1.08±0.02
6.0	50	1.63±0.09	4.07±0.00	2.12±0.07
6.0	60	1.49±0.02	2.83±0.02	1.55±0.01
6.0	70	1.58±0.02	3.61±0.07	1.77±0.09
6.0	80	1.58±0.02	3.36±0.06	1.83±0.08
8.0	50	1.74±0.05	3.01±0.01	1.46±0.04
8.0	60	1.55±0.08	3.33±0.03	1.58±0.04
8.0	70	1.38±0.03	3.41±0.00	1.67±0.09
8.0	80	1.23±0.09	3.57±0.04	1.80±0.05
2.0mm , FD		2.81±0.06	3.72±0.02	1.49±0.04
fresh sample		3.51±0.21	19.52±0.11	6.39±0.22

Effects of temperatures during VFND period on vitamin C retention of apple slices dried with HAD+VFND showed in table1. It was clearly found that, when the temperature was set 50 ℃ during VFND period, vitamin C content of samples dried with combined method was higher than others. Because, vitamin C is heat sensitive material and is decomposed seriously as the increase of the drying temperature[18]. However, the difference of vitamin C among all samples was not obvious when apples were sliced with different thicknesses.

Total phenolics in apple slice slightly declined with the increase of slice thickness. As thickness of apple slice became greater, drying time was longer that mean samples were exposed to high temperature condition for longer time, and it would induce lower retention of total phenolics.

Retention of flavonoid in samples was decreased firstly and then increased with the increase of slice thickness, showed in table1. When slice thickness was 2.0mm, flavonoid retention in

apples slice was decreased with the increase of temperature, while the result was on the contrary when slice thickness was 8.0mm. The main reasons were that, it took short drying time to reach moisture content safe level when slice thickness was 2.0mm at different drying temperatures during VFND period, and lower temperature can keep flavonoid at better level; however, the drying time became longer when slice thickness was 8.0mm at all temperatures, especially at lower temperature, that means samples were exposed in the high temperature condition for long time.

4. Conclusion

In combined drying method of HAD+VFND, the drying rate of apples slice in VFND period was significantly affected by thickness and temperature. Retention of total phenolics and flavonoid in both samples dried with HAD+VFND and FD were at same levels although vitamin c was lower in samples dried with combined method. VFND might be an available drying technique for resisting oxidation reaction during drying process of fruits and vegetables.

Acknowledgements

5. References

[1] Wang, N.; Wolf, J.; Zhang, F.S. Towards sustainable intensification of apple production in China—Yield gaps and nutrient use efficiency in apple farming systems. Journal of Integrative Agriculture 2016,15(4),716-725.

[2] Zlatanović, I.; Komatina, M.; Antonijević, D. Low-temperature convective drying of apple cubes. Applied Thermal Engineering 2013,53(1),114-123.

[3] Velić, D.; Planinić, M.; Tomas, S.; Bilić, M. Ingfluence of airflow velocity on kinetics of convection apple drying. Journal of Food Engineering 2004,64(1),97-102.

[4] Nieto, A.; Salvatori, D.; Castro, M.A.; Alzamora, S.M. Air drying behavior of apples as affected by blanching and glucose impregnation. Journal of Food Engineering 1998,36(1),63-79.

[5] Martynenko,A.; Janaszek, M.A. Texture changes during drying of apple slices. Drying Technology 2014,32(5),567-577.

[6] Gong, Z.; Zhang, M.; Sun, J. Physico-chemical properties of cabbage powder as affected by drying methods. Drying Technology 2007, 25(5),913-916.

[7] Rajkumar, G.; Shanmugam, S.; Galvâo, M. S.; Sandes, R.D.D.; Neta, M.T.S.L.; Narain, N.; Mujumdar, A.S. Comparative evaluation of physical properties and volatiles profile of cabbages subjected to hot air and freeze drying. LWT-Food Science and Technology 2017, 80(7),501-509.

[8] Reyes, A.; Mahn, A.; Huenulaf, P. Drying of apple slices in atmospheric and vacuum freeze dryer. Drying Technology 2011,29(9),1076-1089.

[9] Marques, L.G.; Freire, J.T. Analysis of freeze-drying of tropical fruits. Drying Technology 2005,23(9),2169-2184.

[10] Hazervazifeh, A.; Nikbakht, A.M.; Moghaddam, P.A. Novel hybridized drying methods for processing of apple fruit: energy conservation approach. Energy 2016, 103(1),679-687.

[11] Seremet (Ceclu), L.; Botez, E.; Nistor, O.V.; Andronoiu, D.G.; Mocanu, G.D. Effect of different drying methods on moisture ratio and rehydration of pumpkin slices. Food Chemistry 2016, 195(1),104-109.

[12] Huang, L.L.; Zhang, M.; Wang, L.P.; Mujumdar, A.S.; Sun, D.F. Influence of combination drying methods on composition, texture, aroma and microstructure of apple slices. LWT-Food Science and Technology 2012, 47(1),183-188.

[13] Benassi, M.T.; Antunes, A.J. A comparison of meta-phosphoric and oxalic acids as extractant solutions for the determination of vitamin C in selected vegetables. Arquivos de Biologia e Tecnologia 1988, 31(4),507-513.

[14] Marfil, P.H.M.; Santos, E.M.; Telis, V.R.N. Ascorbic acid degradation kinetics in tomatoes at different drying condition. LWT-Food Science and Technology 2008,41(9),1642-1647.

[15] Jia, Z.S.; Tang, M.C.; Wu, J.M. The determination of flavonoid contents in mulberry and their scavenging effects on superoxide radicals. Food Chemistry 1999,64(4),555-559.

[16] Yu, L.L.; Zhou, K.K.; Parry, J. Antioxidant properties of cold-pressed black caraway, carrot, cranberry, and hemp seed oils. Food Chemistry 2005, 91(4), 723-729.

[17] Vacuum drying of apples (cv. Goldon Delicious): drying characteristics, thermodynamic properties, and mass transfer parameters. Heat and Mass Transfer 2018, online first.

[18] Timoumi,S.; Mihoubi, D.; Zagrouba, F. Shrinkage, vitamin C degradation and aroma losses during infra-red drying of apple slices. LWT-Food Science and Technology 2007,40 (9),1648-1654.

Bioavailability of freeze-dried and spray-dried grapefruit juice vitamin C

Camacho, M.M.[a]; Igual, M.[a]; Martínez-Lahuerta, J.J.[b]; Martínez-Navarrete, N [a*]

[a] CUINA group. Department of Food Technology. Universitat Politècnica de València, Valencia, Spain

[b] Centre Auxiliar Juan Llorens, Valencia (Spain).

*E-mail of the corresponding author: nmartin@tal.upv.es

Abstract

An alternative as to offer higher stable and easy handling than fresh fruit is in powdered form, as long as the process used to obtain it ensures a high quality product. The objective of this study was to compare the bioavailability of the vitamin C of a juice prepared from powdered grapefruit obtained by freeze-drying and by spray-drying. A trial was conducted with 11 healthy volunteers. A relative increase of 1,4 – 25,8 % of blood serum vitamin C concentration was quantified after juices intake, with no significant differences (p>0.05) due to the process used to obtain the powder.

Keywords: vitamin C; bioavailability in humans; grapefruit powder; freeze-drying; spray-drying.

1. Introduction

Consumer attention is currently focused on healthy eating habits. Fruit juices can be clearly included in a healthy diet as they contain different health-promoting bioactive compounds, mainly vitamin C and phenolic. Nevertheless, consumer also looks for high quality, stable and ease to handle foods. In this sense, fruit powder may be an interesting alternative to offer a juice after being rehydrated. Different techniques can be used to obtain food powder, freeze-drying and spray-drying being the most commonly used as they offer very high quality products. A lot of studies, too much to be cited in the context of this manuscript, have been carried out to evaluate the impact of different food processes on the product quality. In fact, many processes have been optimized taking into account these quality aspects. Nevertheless, the studied quality attributes are related to the composition, physical, chemical or biochemical properties or sensory aspects, among others. Nonetheless, we have not found any study investigating the impact of the processes on the bioavailability of the bioactive compounds potentially responsible for the functional value of foods.

The biological functions of vitamin C depend upon its ability to act as an electron donor. Among these it acts as cofactor for a variety of enzymes with critical functions throughout the body, functions as a highly effective water-soluble antioxidant and it is suggested that is involved in the regeneration of vitamin E in vivo[1,2]. Reported beneficial effects of this vitamin include increased baroreflex sensitivity, improved endothelial vascular function, augmented inotropic and thermogenic response to beta-adrenergic stimulation, decreased systemic inflammation and reduced fluid requirements during recovery from thermal injury, improved fatigue resistance, increased iron bioavailabilty and decreased risk of cardiovascular diseases[3,4,5]. Severe vitamin C deficiency produces scurvy. Despite humans are unable to synthesize their own vitamin C, it must be easily obtained from the diet, principally through a adequate fruit and vegetable consumption[1].

The research on which this study is part, started with the comparison of freeze drying (FD) and spray drying (SD) as two drying technologies with which to obtain grapefruit powder with the lowest water content, hygroscopicity, luminosity, color change and the highest content of total phenolic, total carotenoids, vitamin C and antioxidant capacity, despite the highest powder yield [6]. In that study, response surface methodology (RSM) was used to evaluate the effect of three process variables on the different mentioned properties. The considered process variables were the amount of gum Arabic and bamboo fiber added to prevent the powder stickiness, also as the feed inlet water content or the inlet air temperature in the case of FD and SD processes, respectively. The conclusion of that study was that FD might be proposed as a better technology than SD with which to obtain grapefruit powder with a higher vitamin C and total carotenoids content. Taking these

results into account, the aim of the present study was to investigate if there was a different impact of the previously optimized FD and SD processes on the bioavailability of the vitamin C.

2. Materials and Methods

2.1 Tested grapefruit products

The volunteers who participated in the trial consumed two grapefruit juices. They were obtained by rehydration of the grapefruit powder obtained by freeze-drying (FDJ) and by spray-drying (SDJ) of a previously formulated grapefruit mix. The same grapefruit (*Citrus paradise* var. Star Ruby) batch, purchased in a local supermarket (Valencia, Spain), was used to obtain both powdered products which were processed taking into account the optimum conditions proposed in the previously mentioned study[6]. Briefly, peeled and grounded grapefruit was mixed with 4.2 g GA + 0.6 g BF/100 grapefruit pulp to obtain FDJ or with 4.3 g GA + 2.1 g BF/100 liquidized grapefruit to obtain SDJ. No shelf temperature was applied during FD and inlet air temperature for SD was 120 ºC. FD cake was crushed to obtain a powder which was vacuum packed and freezing stored until used. SD powder was stored in the same conditions. The vitamin C content of the grapefruit batch used in the study, analyzed as described below, was 41.8 mg /100g pulp.

Each powder was rehydrated in the day of the trial, two hours before being given to the participants. The amount of water to be added to the powder was calculated in order to ensure a juice which offers the same amount of grapefruit own's solutes present in the grapefruit batch used for the study. The corresponding mass balance was applied to this end, taking into account the water mass fraction of the grapefruit, the amount of GA and BF added to the prepared mix and the water mass fraction of the obtained powders.

2.2 Research participants

Ethical approval for the trial was obtained from the Ethics Committee of the Universitat Politècnica de València (Valencia, Spain). The trial was conducted with a total of 11 healthy volunteers from different countries of South America and Europe, who met the inclusion and exclusion criteria established for the study. Inclusion criteria included age within the range of 18–40 years, with a normal body mass index (BMI between 19 and 29 kg/m^2). Exclusion criteria included smokers and people with special dietary habits (vegetarians, vegans, macrobiotics, etc.), allergic to any food, pregnant or with intention to be in the trial period, medicated (includes dietary supplements: vitamin, protein, etc.),

suffering infectious diseases by blood (positive serology for hepatitis B virus and C or human immunodeficiency virus), presenting some picture of intestinal malabsorption, suffering metabolic diseases (diabetes, dyslipidemia, thyroid disorders, etc.) and suffering cardiovascular or kidney diseases (high blood pressure, renal insufficiency, etc.). All the 11 selected participants signed the corresponding informed consent after being explained about the nature, purpose and risks of the study.

2.3 Experimental design and blood sample collection

A crossover design was considered for the clinical trial. With this design, each research participant consumed both juices, obtained from FD and SD rehydrated powders, in different time periods separated by 15 days. One of the advantages of crossover designs in contrast to parallel ones is that the former could yield the same level of statistical power or precision with a lower sample size, as each subject serves as his/her own matched control, thus blocking the variability due to the subjects.

All the participants in the study were cited on two different days, one for FDJ consumption and another one for SDJ. Each day, each subject underwent a first overnight fasting blood test and another one 4 h after having drunk 400 g of the corresponding juice which was given with no meal. They were not allowed to eat anything in the 4 h between extractions. Two blood samples from each participant were collected into BDVacutainer SSTII Advance Tubes (REF 367953), that were allowed to coagulate for 30 min and after centrifuged at 20 ºC and 1500 x *g* for 10 min to separate the serum which was analyzed in its vitamin C content. Serum concentration of ascorbic and dehydroascorbic acids, as related to grapefruit juice vitamin C bioavailability, was analyzed by means of HPLC as described below. The mean value (and standard deviation) of the two tubes of each subject was considered as the corresponding result.

2.4 Vitamin C analysis

The total vitamin C content of the grapefruit batch used for the study was analyzed as described by Igual et al.[7] and Xu et al.[8]. The same methodology slightly modified was used to quantify the total vitamin C content present in serum. Briefly 0.5 mL serum was mixed with 1 mL of a 20 g/L DL-dithiothreitol solution for 2 h at room temperature and in darkness. Afterwards, 1 mL of this mixture was extracted with 2.25 mL 0.1% oxalic acid for 3 min and immediately filtered through a 0.45 mm membrane filter before injection. The HPLC conditions were: Ultrabase-C18, 5 mm (4.6 x 250 mm) column (Análisis Vínicos, Spain); mobile phase 0.1 % oxalic acid, volume injection 20 mL, flow rate 1 mL/min, detection at 243 nm and at 25 ºC. A standard solution (Panreac, Spain) was prepared.

2.5 Statistical analysis

The difference in serum vitamin C concentration before and after the juices intake was considered as the response variable, taken as a measurement of the juice vitamin C bioavailabity. A multifactor analysis of variance was performed for this response variable taking into account the factors individual and juice, with a total of 11 individuals and 2 juices tested. Statgraphics Centurion XVI.II for Windows was used for the statisticall analysis.

3. Results and discussion

Figure 1 shows the vitamin C concentration found in blood serum. The fasting serum vitamin C values of the paticipants in the trial varied between 10.1 and 13.6 mg/L. As expected from the country of habitual residence of the participants, all of them were above the adequate level of plasma vitamin C (i.e. 50 µmol/L[1] = 8.80 mg/L), with any hypovitaminosis case detected.
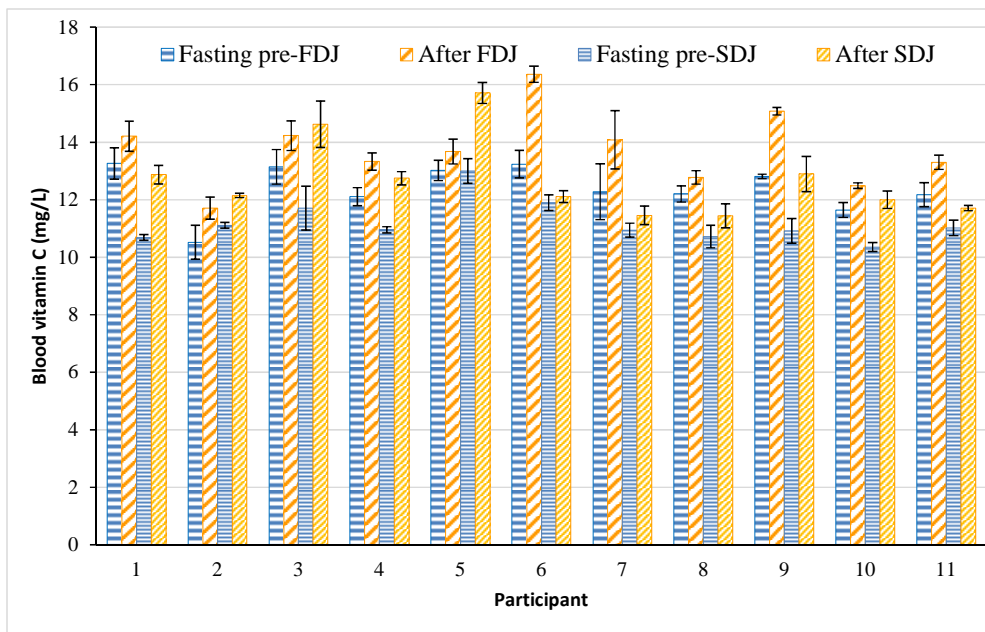
Fig. 1. Mean value and standard deviation of serum blood vitamin C concentration analyzed in the participants the days of consuming reconstituted freeze-dried (FDJ) and spray-dried (SDJ) juices, both fasting and 4 h after the intake of each juice.

The level of vitamin C in the blood serum of all the participants in the trial increased after the ingestion of each juice, the level reached varing between 11.1 and 16.6 mg/L (Fig. 1). This increase, compared to the basal fasting level, evidenced the absorption of vitamin C from juices. When comparing the circulating concentration of vitamin C fasting with the one 4 h following the ingestion of the juices, an increase between 0.17 and 3.27 mg/L was observed. The increase related to the fasting level, for each participant, is shown in Figure 2, this relative increase being in the range 1.4 – 25.8 %.
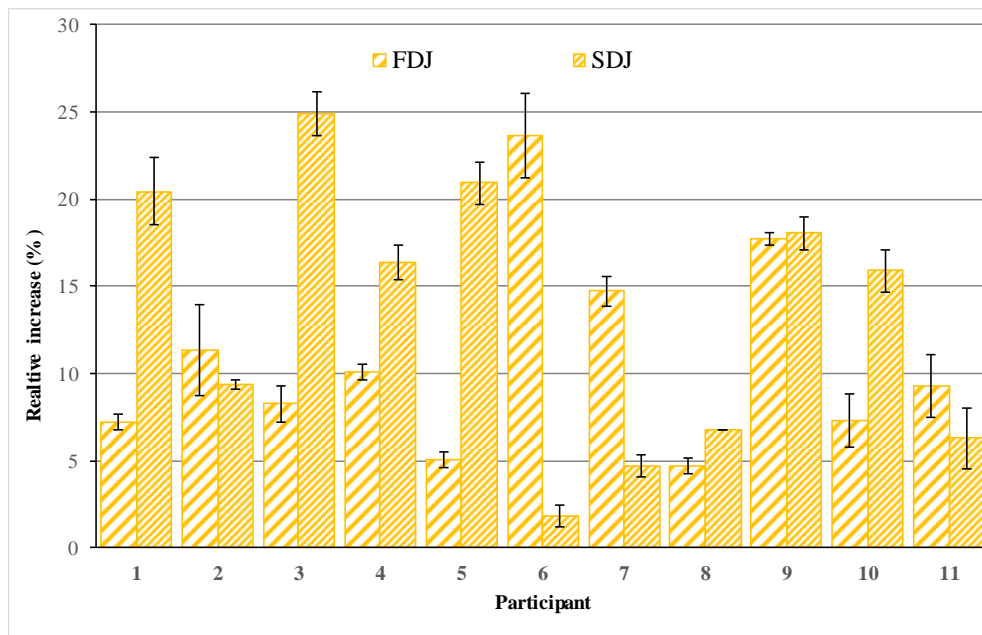
Fig. 2. Mean value and standard deviation of the relative increase of serum blood vitamin C concentration suffered by the participants due the intake of reconstituted freeze-dried (FDJ) and spray-dried (SDJ) juices.

Taking into account the average values of the 22 relative increase values considered, for each of the 11 people on the day of the intake of each of the juices, only three times the relative increase in the concentration of vitamin C in blood compared to fasting baseline was below 5%. In eight cases this increase was between 5 and 10%, in three between 10 and 15%, in four between 15 and 20% and in four between 20 and 25%. In order to compare the blood vitamin C increase caused in each participant by FDJ and SDJ ingestion, an ANOVA was carried out with the factors juice and individual. No significant differences ($p > 0.05$) were observed in any case. In this way, the mean 10.85 % relative increase of blood circulating vitamin C in the participants in the trial caused by FDJ ingestion was not

significant different (p>0.05) to the mean 13.23 % detected after SDJ ingestion (standard error 2.5). As far as the individuals is concerned, the mean relative increase caused by the two juices tested was not significant different (p>0.05) in any of them, the lowest relative incrase being 5.7 % and the highest 17.9 % (standard error 0.06). In this way a relative increase of vitamin C in blood due to juices intake of 12% can be assumed as a grand mean of the 22 average values considered.

4. Conclusions

Vitamin C present in juices prepared by rehydration of grapefruit powder obtained by freeze-drying and by spray-drying is absorbed by the human body, without differences in its bioavailability due to the different process applied to obtain the powder.

5. Acknowledgements

6. References

[1] Pearson, J.F.; Pullar, J.M.; Wilson, R.; Spittlehouse, J.K.; Vissers, M.C.M.; Skidmore, P.M.L.; Willis, J.; Cameron, V.A.; Carr, A.C. Vitamin C Status Correlates with Markers of Metabolic and Cognitive Health in 50-Year-Olds: Findings of the CHALICE Cohort Study. Nutrients, 2017, 9, 831.

[2] Bruno, R.S.; Leonard, S.W.; Atkinson, J.; Montined, T.J.; Ramakrishnane, R.; Bray, T.M.; Trabera, M.G. Faster plasma vitamin E disappearance in smokers is normalized by vitamin C supplementation. Free Radical Biology and Medicine, 2006, 40(4), 689-697.

[3] Davis, J.L.; Paris, H.L.; Beals, J.W.; Binns, S.E.; Giordano, G.R.; Scalzo, R.L.; Schweder, M.M.; Blair, E.; Bell, C. Liposomal-encapsulated Ascorbic Acid: Influence on Vitamin C Bioavailability and Capacity to Protect Against Ischemia–Reperfusion Injury. Nutrition and Metabolic Insights, 2016, 9, 25–30.

[4] Monahan, K.D.; Eskurza, I.; Seals, D.R. Ascorbic acid increases cardiovagal baroreflex sensitivity in healthy older men.American Journal of Physiology-Heart and Circulatory Physiology, 2004, 286(6), H2113-7.

[5] Ye, Z.; Song, H. Antioxidant vitamins intake and the risk of coronary heart disease: meta-analysis of cohort studies. European Journal of Preventive Cardiology, 2008,15(1),26-34.

[6] Agudelo C., Igual M., Camacho M.M.; Martínez-Navarrete N. Effect of process technology on the nutritional, functional, and physical quality of grapefruit powder. Food Science Technology International, 2017, 23(1), 61-74.

[7] Igual, M.; Ramires, S.; Mosquera, L.H.; Martínez-Navarrete, N. Optimization of spray drying conditions for lulo (*Solanum quitoense* L.) pulp. Powder Technology, 2014, 256, 233–23.

[8] Xu, G.; Liu, D.; Chen, J.; Ye, X.; Maa, Y.; Shi, J. Juice components and antioxidant capacity of citrus varieties cultivated in China. Food Chemistry, 2008, 106, 545–551.

Economic feasibility of freeze-drying to obtain powdered fruit

Camacho, M.M.[a]; Casanova, M.A.[a]; Fenollosa, L.[b]; Ribal, J.[b]; Martínez-Lahuerta, J.J.[c]; Martínez-Navarrete, N.[a*]

[a]CUINA group. Department of Food Technology. Universitat Politècnica de València, Valencia, Spain
[b]Dpto. de Economía y Ciencias Sociales. Universitat Politècnica de València, Valencia, Spain
[c]Centre Auxiliar Juan Llorens, Valencia, Spain

* E-mail of the corresponding author: nmartin@tal.upv.es

Abstract

Fruit is a highly valuable food whose consumption should be encouraged. In addition, it would be desirable to design processes and products to channel the surplus and take advantage of the post-harvest losses that limit its fresh marketing. Freeze-drying is a known industrial process that permits the obtaining of high quality products, despite having always been labeled as very expensive. In this study, the economic feasibility of freeze-drying to obtain powdered fruit has been proven, as it yields a product more than twice as cheap as when obtained by spray-drying, recognized for its low cost.

Keywords: freeze-drying; spray-drying; economic profitability; production costs

1. Introduction

The influence of climatic conditions on fruit production makes seasonal surpluses an inherent characteristic of the sector. In addition, they are highly perishable foods that in the phases of post-harvest, storage and transport lose a part of their properties, which limits their fresh consumption. Last but not least, a great deal of fruit is lost both in wholesale and household waste. In this sense, preventing the waste of fruit becomes a challenge for society. For this reason, it seems appropriate to propose viable new processed fruit products, so that their surpluses are used and the consumption of this food is promoted. Freeze-drying is a dehydration technique that allows high quality products to be obtained, ones which are highly stable and very easy to handle, in terms of their greater ease of transport and storage. However, this process has always been labeled as a very expensive one. Spray-drying also allows high quality powder to be obtained from food. An important difference between the two processes is that freeze-drying may take advantage of all the edible part of the fruit in the form of a puree, whereas the liquidized fruit is required for the spray-drying, with the consequent generation of a greater quantity of by-products. In both cases, the obtained powdered product will be of great microbiological, chemical and biochemical stability. However, it could present important physical problems related to the glass transition of its amorphous matrix. In the rubbery state, the structural collapse of the amorphous matrix occurs. In the case of powdered products this leads to phenomena such as stickiness development[1]. To avoid this problem, the incorporation of high molecular weight biopolymers as stabilizers is suggested[2]. In this context, the research team involved in this study has worked towards obtaining powdered fruit by freeze-drying and spray-drying. In this sense, the amount of biopolymers to be added has been optimized in order to obtain a powdered grapefruit with a high product yield and also of high physical, nutritional and functional quality[3]. The obtained results allow freeze-drying to be put forward the propose as a better technique than spray-drying for the purposes of obtaining high quality fruit products. However, from the perspective of the commercial viability of new products, it is essential to consider the final consumer cost, dependent on both the initial investment and the cost associated with its production. Thus, it seems necessary to perform an economic analysis by comparing both processes, which was the objective of the present study.

2. Materials and Methods

The industrial processes considered in this study were freeze-drying and spray-drying. The raw material needed to carry out both of them were grapefruit (*Citrus paradisi,* var. Star Ruby), gum Arabic (GA, Scharlab) and bamboo fiber (BF, Vitacel® BAF 200). Water was also needed in the case of spray-drying.

Camacho, M.M.; Casanova, M.A.; Fenollosa, L.; Ribal, J.; Martínez-Lahuerta, J.J.; Martínez-Navarrete, N.

2.1. Quantification of the initial investment

To quantify the initial investment, the machinery necessary to implement both processes was considered. To select the different equipment needed in each case, the estimated product production volume was considered, as were its technical characteristics and price. In order to propose the necessary amount of powder product, it was assumed that its final use was to be rehydrated for the purposes of obtaining a fruit juice. In order to fix the fruit juice to be obtained, the average annual production of refrigerated juice by a company located in the Valencian Community between 2009 and 2014, 87 t, was selected as a reference value. The amount of raw material to be processed by each process was calculated taking into account the amount of powdered product needed to obtain the 87 t of rehydrated juices[4]. The most appropriate and economical machinery was selected from what was proposed by the different manufacturing companies and consequently dimensioned.

2.2. Production cost analysis

Variable and fixed production costs were calculated. Variable costs depend on the quantity of product produced and include raw material, personnel costs, electrical costs and the management of by-products (grapefruit peel, pulp and water removed from fruit). The fixed costs are independent of the quantity produced and include maintenance and amortization, calculated according to the straight-line method, which consists of dividing the machinery acquisition value by the useful life according to the technical information.

2.3. Investment analysis

To calculate the minimum cost of the product, a static analysis was carried out, comparing income and expenses and equalling the profit to zero. On the other hand, to calculate the price that provides a minimum profitability, a dynamic analysis was carried out. A discount rate calculated as the sum of a risk-free rate plus a risk premium was used. As a risk-free rate, the average of the 10-year bond yield on the primary market, issued by the Spanish government in 2016, was taken, this being 1.6%. As a risk premium, 5.5% was considered. These data were obtained from a study carried out in 2015 on 41 countries [5]. Therefore, the assumed discount rate was 7.1%.

3. Results and discussion

3.1. Selected machinery

To prepare the sample for freeze-drying, an industrial automatic-feeding knife peeler (1000 - 1100 grapefruit/h). was selected. The selected crusher was a hammer mill with vertical axis (1500 kg/h). The grinding process does not generate waste because the hammers of the mill disintegrate the particles until they reach the right size. For the sample to be spray-dried, a high-performance centrifugal liquidizer was chosen. This machine guarantees a quick process so that product oxidation is minimized. In this case, obtaining the liquidized product generates a by-product in the form of grapefruit pulp. According to the technical characteristics of the selected equipment, for each kilo of fruit that enters the liquidizer, 0.383 k of pulp and 0.617 k of liquidized fruit are obtained. The obtained by-product has been supposed to be commercialized. For both processes, a horizontal shaft vane mixer was selected to incorporate the biopolymers and the water into the puree or the liquidized fruit, thus achieving a better product homogenization.

Due to the characteristics of the sample and the estimated production volume, two freeze-dryers based on conduction heat transfer and a centrifugal spray-dryer were chosen. In the case of freeze-drying, this process was estimated to require 24 hours of operation to sublimate the water correctly[3]. For this reason, two freeze-dryers have been considered working in parallel so that they can operate continuously every day. In the case of the spray-dryer, as the one that most suited the required volume of powder production actually has a higher production capacity, the corresponding operational costs were refitted to the latter in order not to discriminate by oversizing it.

For the packaging of the obtained powdered products, an opaque material of very low water vapour permeability was selected, so as to prevent the humidification and destruction of photosensitive compounds, such as vitamin C. The selected packaging machine allows different formats to be used. A mono-dose (44.5 g of powder) and another one for the HORECA channel (379 g of powder) were chosen. These quantities respond to the powder needed to obtain a glass of juice of 125 cm^3 and 1100 cm^3, respectively.

3.2. Production costs

To obtain the 87 t of juice assumed as the reference value, 26,551 kg of powder obtained either by freeze-drying or by spray-drying need to be rehydrated. The corresponding raw material required (grapefruit, GA, FB and water) and its cost was calculated by taking into account the yield of each selected machine and our own preliminary experiences[4] (Table

1). Assuming the price of the raw materials, according to commercial data (0.73 €/kg grapefruit, 78.9 €/kg GA, 2.5 €/kg FB and 0.0025 €/kg water), the total annual costs were 771,309.27 and 2,704,407.92 € for freeze-drying and spray-drying, respectively. As can be observed in Table 1, the total cost of the raw material needed for the spray-drying process is 3.5 times higher than for freeze-drying. The former has a much lower powder yield than the latter, especially due to the powder loss that occurs in the spray-dryer itself. A significant part of the powder remains adhered to the walls and nozzle of the equipment. For this reason, the fruit cost of spray-drying is 6 times that of freeze-drying.

Table 1. Daily needs (Dn) and annual cost (Ac) of raw materials for freeze-drying (FD) and spray-drying (SD) processes

	Grapefruit	**GA**	**BF**	**Water**
Dn FD (kg/day)	654,1	20,60	2,94	147
Dn SD (kg/day)	3885	57,03	28,52	1425,8
Ac FD (€)	174.281,76	593.207,37	2.685,85	134,29
Ac SD (€)	1.035.088,26	1.641.998,13	26.020,51	1.301,03

The total cost in machinery for each technology is presented in Table 2. The initial investment in machinery is 1.4 times higher for the spray-drying than for the freeze-drying process, even though a freezer is used for freeze-drying and two freeze-dryers are required working in parallel. The spray-dryer and the 2 freeze-dryers account for 96% and 94% of the total machinery investment in each process.

Table 2. Variable and fixed production costs and product price in monodose and HORECA format

	Freeze-drying	**Spray-drying**
Electric costs (€)	354.861,65	41.955,41
Raw material costs (€)	770.309,27	2.704.407,92
By-products costs (€)	-658,98	-17.777,56
Personnel expenses (€)	150.970,26	368.494,39
Amortization (€)	55.266,67	73.355,56
Maintenance (€)	97.500,00	130.800,00
Investment in machinery (€)	955.000	1.288.000
Total cost (€)	1.428.248,86	3.301.235,72
Static price mono dose (€/ud)	2,39	5,53
Static price HORECA (€/ud)	17,94	41,47

The electrical cost is usually one of the highest in this type of industry. To calculate the total electrical cost, it is necessary to calculate the energy cost due to electricity

consumption and the contracted power cost that is necessary for the machines to operate. To calculate the electrical cost, the consumption of each selected machine, the number of machines needed in each stage, the working hours per machine and the power were considered (Table 2). For these calculations, an electricity tariff was selected which considers different prices of the kWh depending on whether it is a weekday or weekend and also on the operating hours of the day. When comparing the electrical costs of both processes, it can be affirmed that freeze-drying has an annual consumption that is 8.5 times higher than spray-drying.

Amortization is an economic term referring to the distribution over time of a durable value, with a maximum linear coefficient, or a maximum percentage regulated in the accounting that is allowed to amortize annually, of 12%. The annual amortization has been calculated based on the quotient between the price of the machinery and its useful life. The useful life was considered to be what was specified in the technical characteristics of each machine, except in the case of the freeze-dryer and the spray-dryer. As there were no data available for these equipment, the accounting useful life was considered, this being 18 years according to the provisions of Law 27/2014, of November 27. The amortization of the spray-dryer was 1.3 times higher than that of the freeze-dryer (Table 2). This is due to the fact that the machinery used in the spray-drying technique has a higher cost than what was used for freeze-drying. Again, the freeze-dryer and the spray-dryer are the machines with the highest cost in amortization, due to the much higher acquisition cost of these equipment.

As regards by-products, there are two that could be exploited by other companies: the grapefruit peel after both processes and the pulp that is separated when liquidizing in the case of spray-drying. In these cases, it has been considered that the peel and pulp can be sold at 0.015 and 0.025 €/kg, respectively, according to the average price provided by various companies in the sector. Taking into account the volume of the generated by-products, their sale would provide the income that is observed in Table 2. Thus, the only thing that would cause a real cost would be the discharge of water. Therefore, there is really no a net cost in the management of by-products, but an income that, in the case of spray-drying, is 26 times higher than the income obtained from the management of by-products generated with the freeze-drying.

3.3. Minimum price of the product: static analysis

The total annual cost of the spray-drying technique is 2.3 times higher than that of freeze-drying (Table 2). Figure 1 shows the percentage represented by each item over the total cost. The maintenance and amortization expenses in the case of spray-drying are 1.34 and 1.32 times, respectively, those of freeze-drying. This is because of the greater initial

investment in machinery. In adition, the personnel cost needed to obtain the spray-dried powder is 2.4 times that of the freeze-dried, while the electrical cost for the spray-drying process is 8.5 times lower than for freeze-drying. Such a great difference is due to the need for a vacuum in the case of freeze-drying and the operating time per kg of the fresh product. The highest cost in both processes is that of the raw material, which is 54% and 82% for freeze-drying and spray-drying, respectively. This difference is due to the low yield of the latter when working with fruit.

The static price, or the final product cost, in the case of the spray-dried powder is 2.31 times higher than that of the freeze-dried (Table 2). It was calculated for the two formats with which the powder product was considered to be packaged.
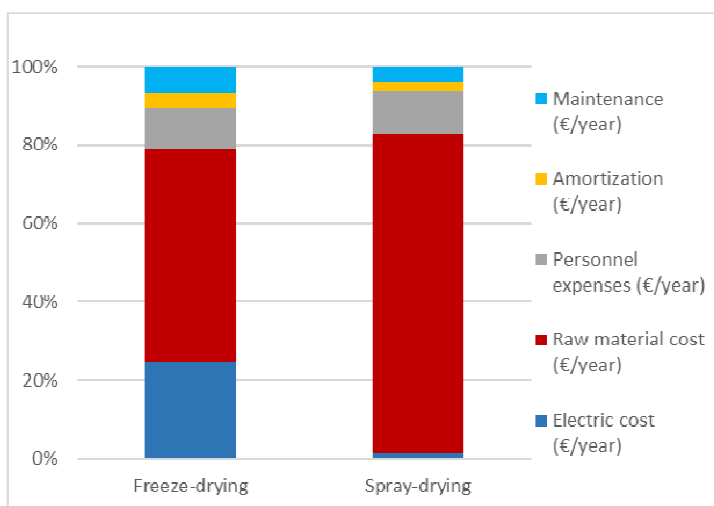
Fig. 1 Percentage of the cost represented by each of the items considered, calculated as related to the total cost of the freeze-drying and spray-drying processes.

3.4. Price of the product that provides a minimum profitability: dynamic analysis

To calculate this price, the internal rate of return (IRR) and the net present value (NPV) were calculated for both the freeze-drying and spray-drying processes. To this end, it is necessary to know the different cash flows that are calculated, in turn, from the extraordinary payments (renovations in machinery originally planned and that are taken as 5% of the value of the machine when new) and ordinary charges (capital inflows from the sale of the product). In this case, we have considered the NPV null hypothesis in order to calculate the price that will result in IRR being 7, which is the same as looking for the price that will obtain a 7% profitability. Thus, for freeze-dried powder, the price is 2.84 and

21.25€ per unit in the mono-dose and HORECA formats, respectively. The corresponding prices for the spray-dried powder is 6.13€ and 45.95€ per unit.

4. Conclusions

This economic study shows that the application of freeze-drying to obtain powdered fruit provides a product at a cost that is less than half that of spray-drying, a process known for its low cost. The lower cost of freeze-drying is mainly due to the poor yield of spray-drying in the case of fruit processing. Thus, although the electrical costs are 8.5 times higher in the case of freeze-drying, both the cost in raw material and the initial investment in machinery, personnel costs, maintenance and amortization are higher in the case of spray-drying. So much so that the estimated price for a dose of grapefruit powder equivalent to a piece of fruit, for example, would be 2.84 versus 6.13 euros depending on whether it was obtained by freeze-drying or by spray-drying, respectively.

5. Acknowledgements

6. References

[1] Roos, Y. Characterization of Food Polymers Using State Diagrams. Journal of Food Engineering 1995, 24(3), 339-360.

[2] Telis, N.V.; Martínez-Navarrete, N. Biopolymers used as drying aids in spray drying and freeze drying of fruit juices and pulps. In: Biopolymer Engineering in Food Processing. V. Telis (Ed.). CRC Press. Taylor & Francis Group, Boca Raton, FL. 2012, 279-326.

[3] Agudelo, C.; Igual, M.; Camacho, M.M.; Martínez-Navarrete, N. Effect of process technology on the nutritional, functional and physical quality of grapefruit powder. Food Science and Technology International, 2017, 23(1), 61-74.

[4] Casanova, M.A. Estudio de viabilidad para la comercialización de fruta en polvo. Trabajo Final de Grado E.T.S.I.A.M.N; Universitat Politècnica de Valencia. Spain, 2014.

[5] Fernandez, P.; Ortiz, A.; Acin, I. F.. Discount Rate (Risk-Free Rate and Market Risk Premium) used for 41 countries in 2015: a survey. IESE Business School, 2015, 1, 3-20.

Influence of freeze-drying conditions on orange powder flowability

Uscanga, M[ab].; Silva, A[a].; Egas, L.[a]; Camacho, M.M.[b]; Martínez-Navarrete, N[b]
[a] Universitat Politècnica de València, Valencia, Spain
[b] Instituto Tecnológico de Veracruz, Veracruz, México.

*E-mail of the corresponding author: mdmcamvi@tal.upv.es

Abstract

Freeze-drying may be a good alternative to get less perishable fruit products. The objective of the present study was to evaluate the impact of freeze-drying conditions of an orange puree on some flow related and rehydration properties of the obtained powders. The results showed that the application of heat during freeze-drying does not affect the parameters studied. However, the partial dehydration of the initial sample results in a lesser porosity and wettability values.

Keywords: *freeze-drying; porosity; wettability; angle of repose; particle size distribution.*

1. Introduction

Fruits are basic foods and of great interest in human nutrition. The benefit of fruit consumption in health seems to be related to the presence of various compounds that belong to the group of phytochemical or bioactive substances. The daily consumption of fruits, in sufficient quantity and in a well-balanced diet, helps to avoid serious diseases, such as heart disease, cardiovascular accidents, diabetes and cancer, as well as deficiencies of important micronutrients and vitamins[1]. However, the consumption of fruit has declined gradually in recent years, since they have changed the eating habits of society. Despite the great benefits of fruit consumption, two major problems limit its availability, its seasonality and its short shelf life.

The orange is the fruit of the sweet orange tree that belongs to the genus Citrus of the Rosacea's family. Its nutritional composition highlights its low energy value, thanks to its high water content and its high content of vitamin C, folic acid and minerals such as potassium, magnesium and calcium. It contains appreciable amounts of beta-carotene, responsible for its typical color and known for its antioxidant properties, in addition to malic, oxalic, tartaric and citric acids, which enhance the action of vitamin C. The amount of fiber is appreciable and this is found mainly in the white part between the pulp and the bark, so that its consumption favors the intestinal transit. The orange has been selected as the object of this study because it is one of the most typical products of the country. Due to the great production that exists, Spain has become one of the largest producers of orange in the world and an asset for export. For this reason the orange represents a product of great importance in the economy of the country.

Currently, new alternatives for the development of less perishable products are being proposed. Powdered products represent a good option as healthy foods, lengthening the useful life of the product and facilitating its transport. Freeze-drying is a technology that consists of dehydrating the freeze product at low pressure. The process does not require the application of high temperatures, however its high cost has limited its use in the food industry. Therefore, the main interest is to find alternatives to minimize energy consumption, in order to decrease the process cost preserving the quality of the product. In this study, two options are proposed for this purpose, as they are the partial dehydration of the feed food and the application of heat during the process. However, this may affect the characteristics of the obtained powder in terms of the size and density of the particles, their porosity and surface properties, among others. In turn, these characteristics will determine the characteristic flow and / or rehydration behavior of a powder. Taking into account all of the above, the objective of this work was to know the impact of a pre-dehydration treatment and of the application of shelf temperature while the freeze-drying of a formulated orange puree on the properties of the obtained powder.

2. Materials and Methods

2.1. Raw material and formulation

Orange (*Citrus x sinensis* var. Navelina) always acquired in the same chain of supermarkets in Valencia was used for the study. To obtain the orange puree, the fruit was washed, peeled, cut and crushed in a food processor (Thermomix TM 21, Vorwek, Spain). Gum Arabic and bamboo fiber (5 and 1 g, Shaurlau-Vitacel, respectively) were added to 100 g puree and homogenized with the same food processor. The ºBrix of the mixture were measured (Refractometer Mettler Toledo 30Px), this being 17 ºB. A part of this orange formulation, named O, was reserved. The rest of the sample was partially dehydrated (Moulinex Ultimys Duocombi, 600W) by heating in short period times until the sample reached 22 ºB. This partially dehydrated orange formulation was named OD.

2.2. Freeze-drying

Each formulation was placed in aluminium plates, 1 cm thickness, and freeze in a LIEBHERR MEDLINE equipment at -45 ° C for 48 hours. The freeze-drying step was carried out in a Telstar Lyo Quest 55 equipment operating at -50 ºC in the condenser and at 0.063 mbar, for 48 hours. Samples O and OD were freeze-dried with the shelfs at room temperature and sample O was also freeze-dried at 40 °C in the shelf (sample O40).

2.3. Obtaining powder

The cakes obtained from the freeze dryer were crushed in a food processor (Thermomix TM 21, Vorwek, Spain), at speed 5 for 20 s to obtain a powder. Batches of about 40 g of the powder were sieved through 800 μm mesh, with the corresponding top and bottom placed, to select the particles lower than this size which were characterized in the properties described below. A vibrating drum (AMP0.40, CISA, Barcelona, Spain), 50 Hz, for 5 minutes was used to this end.

2.4. Particle size distribution

A batch of about 40 g of the obtained powder lower than 800 μm was again sieved in the same vibrating drum and conditions. The mesh of the sieves used in this case were 500, 300, 200, 150 and 100 μm, with a top and a botton placed in the column of sieves.The powder collected in each sieve and in the bottom was weighed.

2.5. Angle of repose

This is the angle formed between the slope of the product when dropped down from 5 cm height from the horizontal surface. The test consists of pouring 15 g of powdered product in a funnel (top diameter= 80 mm, stem = 11 mm diameter, 29 mm length; Overall height = 85

mm) and measuring the diameter and height of the formed product cone, applying equation (1).

$$\alpha° = \arctan * \left(\frac{2h}{d}\right)$$ (1)

where h = height from the top of the formed product cone (cm); d = maximum cone product diameter (cm), taken as an average of at least 6 values.

2.6. Wettability

A modified UNE[2] standard method for milk powder was used. Briefly 10 g of powder were weighed and dropped progressively (in 25 s) into 250 g of water, measuring the time (s) from when the powder falls until all the particles in the sample have been wetted.

2.7. Bulk flow properties

The porosity (ε) was calculated from the true and bulk densities by using equation (2). The true density (ρ) of the sample was calculated from its individual components. In this case, water and carbohydrates, both own and added, were considered to be the main components of the samples (equation 3). The apparent density (ρ_a) was calculated by dropping the sample in a graduated tube until approximately 10 mL, with the help of a funnel; the weight and volume of the exact sample was recorded. Finally the previous sample was compacted using a vortex (1200 rpm, t = 10 s) and the volume of the sample was recorded again to calculate the value of bulk density (ρ_b). Based on these data it was possible to calculate the Hausner Index and the Carr Index by using equations (4) and (5).

$$\varepsilon = \frac{\rho - \rho_b}{\rho}$$ (2)

$$\frac{1}{\rho} = \frac{x_w}{\rho_w} + \frac{x_{CH}}{\rho_{CH}}$$ (3)

$$I_H = \frac{\rho_b}{\rho_a}$$ (4)

$$I_C = \frac{\rho_b - \rho_a}{\rho_b}$$ (5)

where ε is the porosity; ρ, ρ_b and ρ_a (g/cc) are the true, bulk and apparent densities of the powder, respectively; x (w/w), ρ_w (g/cc) and ρ_{CH} (g/cc) are the mass fraction and density (20 °C) of water (0.9976 g/cc[3]) and carbohydrates (1.4246 g/cc[3]), respectively.

3. Results and Discussion

The particle size distribution is represented in figure 1. All the samples had the greater proportion of particles with a size lesser than 100 µm. In these range, OD sample stands out above the other two samples.
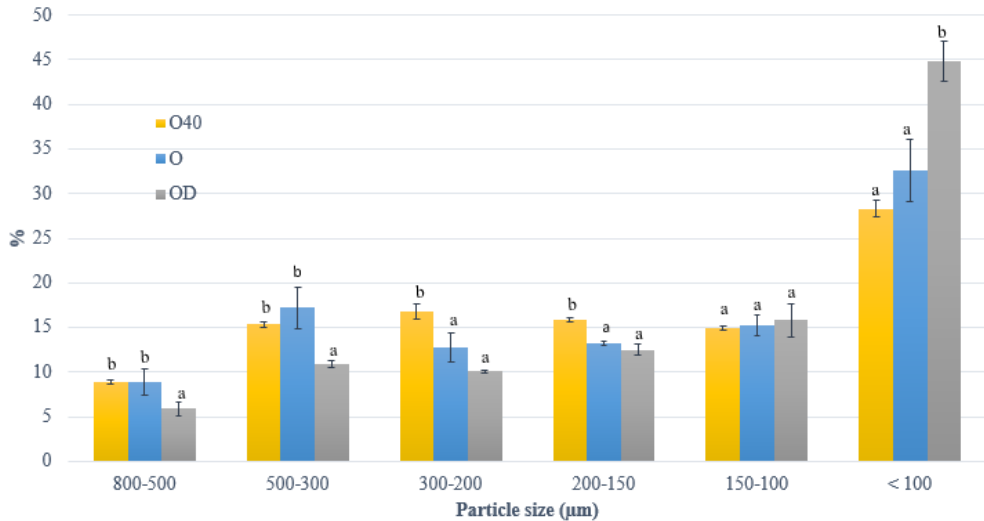
Figure 1. Relative powder particle size distribution (µm) obtained from the formulated puree orange freeze-dried at room temperature (O), formulated and pre-dehydrated puree orange freeze-dried at room temperature (OD) and formulated puree orange freeze-dried at 40 ºC (O40).

The pondered average size particle of each sample was calculated from powder particle size distribution (table 1). Significant differences ($p < 0.05$) were observed among all the samples, sample OD40 being the one with the greatest average particle size and sample OD the one with the smallest average particle size. Particle size may be related with the fracture resistance of the cake when crushed, the greater the resistance the greater the particle size. The increase in the solutes concentration of the microwave pre-dehydrated sample will lead to a decrease in the freezing rate. In this case, greater ice crystals are expected to be formed. This will suppose to obtain a cake with greater porous size and more fragile. On the other hand, when 40 ºC shelf temperature is applied during freeze-drying, the drying of the sample is accelerated. In this case, smaller pores size are formed and a more resistant cake is obtained (data not publicated).

Measured properties related to powders flowability are presented in table 1. Samples doesn´t show sifnificant differences ($p > 0.05$) regarding the angle of repose. The values ranged from 40,35º to 42,51º, which are included among acceptable flow properties[4].

Table 1. Mean values (± standard deviation) of the properties measured to the powder obtained from the formulated puree orange freeze-dried at room temperature (O), formulated and pre-dehydrated puree orange freeze-dried at room temperature (OD) and formulated puree orange freeze-dried at 40 ºC (O40).

Property	Sample		
	O40	O	OD
Average size particle (mm)	0.210[a] ± 0.008	0.1703[b] ± 0.0006	0.117[c] ± 0.004
Angle of repose (º)	43[a] ± 2	40.3[a] ± 0.5	41.7[a] ± 0.5
Wettabillity (s)	571[b] ± 54	467[b] ± 18	1924[a] ± 400
Porosity (%)	77.1[a] ± 0.6	80.1[a] ± 1.4	69[b] ± 3
Hausner index	1.124[a] ± 0.018	1.11[a] ± 0.06	1.20[a] ± 0.08
Carr index (%)	11.0[a] ± 1.4	10[a] ± 5	17[a] ± 6

The same lowercase letter within rows indicates homogeneous groups established by ANOVA (p<0.05).

The wetting time is inversed related to wettability, the higher the wetting time the worse the wettability. In this way, the microwave pre-dehydrated sample before freeze-drying (OD, table 1) showed the worst degree of wetting. This probably may be related with the smaller average particle size of this sample[5]. The lesser particle size induces the particles aggregation and the lump formation.

It is well recognized that dehydrated products obtained from freeze-drying are highly porous[6]. However, it is observed that OD sample, which was microwave pre-dehydrated before freeze-drying, shows a value of porosity much lower than the other two samples (table 1). This may also be related to the smaller average particle size of this sample. It has been observed that porosity decreased with decreasing the particle size, because of the decrease in the inter-particle voids with smaller sized particles[6].

Hausner and Carr indexes indicate the level of interaction between particles and therefore the flow properties. There was no significant differences (p<0.05) between the values of both indexes for the samples. According the classification of Farmacopea[4], all the samples show an excellent to acceptable flowability.

4. Conclusions

The different freeze-drying conditions used in this study doesn´t affect the flowability of the freeze-dried orange powder. Nevertheless, pre-dehydration of the formulated orange puree decreases the mechanical resistance of the obtained cake so that a powder with a smaller average particle size may be obtained. This affects the rehydration capacity of the freeze-dried powder, with increased wetting time. In this sense, 40 ºC shelf temperature during

freeze-drying may be recommended in order to short the process time and to get a product with both a good flow behavior and good wettability.

5. Acknowledgements

6. References

[1] Martínez-Navarrete, N.; Camacho, M.M.; Martínez-Lahuerta, J.J. Los compuestos bioactivos de las frutas y sus efectos sobre la salud, 2008, Actividad Dietética, 12(2), 64-68.

[2] UNE 34849, Instant dried milk. Determination of dispersibility and wettability, 1986.

[3] Choi, Y.; Okos, M.R. Thermal properties of liquid foods. Review. In: Physical and Chemical properties of food, M.R. Okos (Ed.), American Society of Agricultural Engineers, Michigan, USA, 1986, pp. 35-77.

[4] Real Farmacopea Española. Ministerio de Sanidad, Servicios Sociales e Igualdad. Agencia Española de Medicamentos y Productos Sanitarios. fifth ed. Madrid, 2015.

[5] Ferrari, C.C.; Marconi, S.P.; Dutra, I.; Zaratini, F.; de Aguirre, J.M. Influence of carrier agents on the physicochemical properties of blackberry powder produced by spray drying. International Journal of Food Science and Technology, 2012, 47(6), 1237-1245.

[6] Caparino, O. A.; Tang, J.; Nindo, C.I.; Sablani, S.S.; Powers, J.R.; Fellman, J.K. Effect of drying methods on the physical properties and microstructures of mango (Philippine "Carabao" var.) powder. Journal of Food Engineering, 2012, 111(1), 135-148.

Impact of shelf temperature on freeze-drying process and porosity development

Egas-Astudillo, L. A.; Silva, A.; Uscanga, M.; Martínez-Navarrete, N.; Camacho, M. M.ᵃ*.

ᵃ CUINA group. Department of Food Technology. Universitat Politècnica de València, Spain.

*E-mail of the corresponding author: mdmcamvi@tal.upv.es

Abstract

The freeze-drying kinetics and the superficial porosity development of grapefruit puree. The impact of biopolymers addition (gum Arabic and bamboo fiber) and to apply (40 ºC) or not shelf temperature (room temperature) was considered. To increase the shelves temperature during freeze-drying allowed to an important drying time reduction and doesn't supposed a lower porosity related to the collapse development of the structure. Biopolymers do not affect the drying kinetics. From this results, biopolymers addition and to heat at least up to 40 ºC during grapefruit freeze-drying should be recommended.

Keywords: freeze-drying; shelf temperature; drying kinetics; image analysis; pore size distribution.

1. Introduction

The growing consumer demand for expanding the diversity of food products has resulted in a rapid development of the food ingredients market. Most of these food products are supplied in powdered form and the technologies involved in their production are increasingly important, since their quality and functionality strictly correspond to the efficiency of the production processes [1,2]. Today, the growing awareness of consumer health is forcing food producers to add natural ingredients to food products. Fruit ingredients in powdered form can be applied in many food and pharmaceutical products to improve their color and taste and, at the same time, to provide the human body with an additional constituent for health promoting[1]. The quality of a fruit powder depends to a large extent on the drying / grinding conditions, as well as on the composition and physical properties[2,3]. Within this context, freeze-drying emerges as a gentle dehydration technique that represents the ideal process for the production of high value dry products. This technique is known for its ability to maintain the quality of the product (color, shape, aroma and nutritional value) greater than many other drying methods, due both to its low processing temperature as to the virtual absence of oxygen during processing, which minimizes degradation reactions[4]. Other prominent factors include the structural rigidity exhibited by the previous freezing of the food, as well as the limited mobility of frozen water, that prevents collapses and contractions of the solid matrix when drying[5,6]. The freeze-drying process consists mainly of two stages in which the product is frozen first and then a controlled amount of heat is applied under vacuum (vacuum freeze drying) or at atmospheric pressure (atmospheric freeze drying) to promote an initial stage where the sublimation of ice crystals occurs and a secondary stage where the desorption of the remaining non-frozen water occurs[2,4-6,]. To improve the control of any dehydration process giving high quality dried products, it is important to have models to simulate drying curves in different conditions[7]. It is important to note that the composition of the fruit (for example, pectin, dietary fiber, oligosaccharides, polyphenols) influences the degree to which the fruit can be transformed into a powder. In this sense it is necessary to point for the low glass transition temperature (Tg) exhibited by the dried fruit products[8]. To exceed the Tg involves the change of the amorphous matrix from a highly stable glassy state to a more unstable rubbery one. In the glassy state structural collapse of powdered products occurs. As in the case of powdered fruit the Tg is in the range of the room temperature, to add high molecular weight biopolymers is suggested[8]. High quality freeze-dried materials are characterized by a low bulk density and high porosity in addition to a minimal shrinkage and negligible collapse. However, it is important to mention that the fraction of the food collapsed during freeze-drying can increase with the heating temperature of the shelf. In fact, many authors have related the most intense contraction exhibited when freeze-drying is carried out at higher temperatures[9] and the greater porosity of freeze-dried materials with the lower freeze-drying temperatures[2]. The aim of this study was to determine the impact of both to

add gum Arabic and bamboo fiber and to increase the shelf temperature to 40 ºC during the freeze-drying of grapefruit puree. The effect on the drying kinetics and the porosity of the obtained product have been studied.

2. Materials and Methods

The citrus grapefruit (*Citrus paradise* var. Star Ruby) was purchased in a local market (Valencia, Spain). The fruits were selected according to their size, firmness and absence of physical damage. Biopolymers used to stabilize the powdered product: gum Arabic (GA) Scharlab and Bamboo Fiber (FB) Vitacel® BAF 200.

2.1. Sample preparation and process conditions

The peel, albedo and central axis were detached manually from the grapefruit before being crushed (Thermomix Vorwerk TM-21). The obtained product was characterized in its water and soluble solid content (vacuum oven JP Selecta, 60 ± 1ºC and pressure <100 mm Hg; Mettler Toledo 30PX refractometer). Two samples of grapefruit puree were prepared, one without the addition of biopolymers (G) and another one with the addition of 4.2% GA and 0.58% FB (GB) (Thermomix Vorwerk TM-21 working at speed 2 for 300 s)[10]. Both samples were also characterized in the water and soluble solid content. Samples G and GB were placed in aluminum trays (1 cm thickness, $\cong$27 g), a pair per sample and after they were frozen (Liebherr LGT 2325) at -45 ºC for 6h. The frozen samples were freeze-dried for different times from 1.5 to 21 h in a Telstar Lyo Quest-55 freeze-dryer. The pressure of the chamber (0.09 mbar) was maintained and the temperature of the shelves was varied: without applying heat to the shelves (samples RT, room temperature) and applying 40 °C to the shelves (samples 40). In this way, four samples were processed: G(RT), G(40), GB(RT) and GB (40). Each freeze-drying process was carried out twice. Samples obtained at the different freeze-drying times were weighed (accuracy 0.0001 g). Two images by sample were taken using a Canon EOS 350D digital camera placed in a Kaiser RS2XA, at 23 cm from the sample, and illuminated with a standard white light (6500K). The images were acquired with a focal aperture of 55 mm (Lens EFS 18-55) and in automatic mode.

2.2. Modeling of drying kinetics

The drying kinetics was studied on the basis of the mass loss by the samples. The residual water content present in the obtained samples was calculated based on Eq. (1) and used to obtain the moisture ratio (MR) evolution (Eq. 2).

$$X_{wt} = \frac{m_o * X_{wo} - (m_o - m_t)}{m_o * (1 - X_{wo})} \qquad (1)$$

$$MR = \frac{X_{wt} - X_{we}}{X_{wo} - X_{we}} \approx \frac{X_{wt}}{X_{wo}} \qquad (2)$$

Where X_{wt}, m_t, X_{wo}, m_o and X_{we} indicate the water content (g water / g sample, db) and the mass (g) of the freeze-dried sample at time t, of the sample that enters to the freeze-drier, and of the sample freeze-dried at equilibrium, respectively. The equilibrium water content values are usually very low, and the Eq. 2 is often simplified assuming Xwe=0 without a significant change in the MR value [11].

Preliminary tests conducted in this study proved that the best fit to our data was obtained with the modified Page model (Eq. 3) [1, 11]. The Matlab R2015b software was used to fit the drying model. For each sample, the MR (Eq. 2) calculated for each freeze-drying experiment was fitted to the model and the mean value of the model constants was considered as the corresponding result.

$$MR = a * e^{-k*t^n} \qquad (3)$$

Where *k*, *n* and *a* are the constants of the model and *t* the freeze-drying time (h).

2.3. Number and pore size distribution

The pore size distribution was based on the area of the superficial pores formed in the samples. The area of the pores at each freeze-drying time in every sample was analyzed from the images (section 2.1) analyzed by means of the software image J, 1.51g [12,13]. The frequency or number of pores formed of each size was stablished based on a geometric distribution of the areas containing the minimum and the maximum values found in the image analysis and considering 30 area range. From this data, the mean area of the pores ($\overline{A}$ mm^2) at each freeze-drying time was also calculated (Eq. 4).

$$\overline{A} = \frac{\sum_i (A_i * F_i)}{\sum_i F_i} \qquad (4)$$

Where *i* is each area range, A is the greatest range area (mm^2), F is the pore frequency.

3. Results and Discussions

3.1 Drying kinetics

The water and soluble solute content of the grapefruit puree used in the study were 0.876 ± 0.004 g water / g sample and 11.47 ± 0.12 ºBrix. They changed to 0.830 ± 0.001 g water / g of sample and 15.23 ± 0.06 ºBrix after biopolymers addition. For each sample, these water contents were those considered as the corresponding (X_{w0}). The change of MR during the

freeze-drying of the different processed samples is presented in Figure 1. As it can be observed, the drying time was greatly reduced when 40 ℃ shelf temperature was applied.
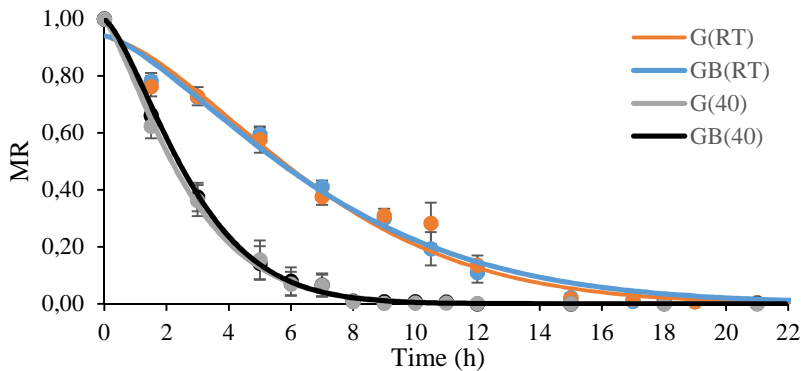
Fig.1 Experimental and predicted (modified Page's model) moisture ratio evolution throughout the freeze-drying of grapefruit samples with (samples GB) and without (samples G) biopolymers added and applying (samples 40) or not (samples RT) heat to the shelves.

Kinetic data were fitted to the modified Page model (Table 1). The *k* and a parameters were lower (p<0.05) when the freeze-drier shelfs were not heated, with no significant differences (p>0.05) between the samples with and without biopolymers added. This behavior is related with the enhanced heat transfer promoted when heating the shelfs, which is linked to an increased drying rate of the process and a decreased drying time [14,15]. Table 1 shows the drying time needed to achieve a target water content of 0.04 g water/g dry sample (db), this assumed as a normal water content for this kind of products. To heat the shelves just to 40 ℃ during the freeze-drying considerably reduces the process time up to 52 - 60 %.

Table 1. Mean values and standard deviation in brackets of the constants of the modified Page's model (k, n and a). Time needed to reach 0.04 g water/g sample (db): $t^{0.04}$. Freeze-dried samples: grapefruit with (samples GB) and without (samples G) biopolymers added and applying (samples 40) or not (samples RT) heat to the shelves.

Sample	k	n	a	R^2	RSME	$t^{0.04}$ (h)
G(RT)	0.041±0.009a	1.57±0.11b	0.934±0.009a	0.978	0.040	21.8±1.6b
GB(RT)	0.056±0.011a	1.41±0.08ab	0.941±0.009a	0.964	0.046	23.6±1.0b
G(40)	0.25±0.04b	1.31±0.10a	0.993±0.003b	0.993	0.018	10.4±1.6a
GB(40)	0.20±0.01b	1.42±0.10ab	0.996±0.002b	0.994	0.016	9.5±1.5a

(*)Adjusted regression coefficient (R^2), root mean square error (RMSE; Different (a, b) letters in columns indicate non-homogeneous groups established by the ANOVA (p<0.05).

3.2   Number and pore size distribution

Figure 2 shows, as an example, the number of pores of each areas range considered that was formed in samples G(RT) and GB(RT) freeze-dried for 22 h and in samples G(40) and GB(40) freeze-dried for 10 h. These were approximately the times needed to reach a sample with 0.04 g water/ g sample (db) (Table 1). A similar pore number distribution was observed at each studied freeze-drying time (data not shown) which was used to calculate the pore mean area (Fig. 4). As it can be observed in Fig. 3, at each temperature, more pores were formed in samples without biopolymers added. This could be related with a certain cryoprotector effect of the biopolymers, these decreasing the amount of ice formed [8]. On the other hand, in samples G or GB, the higher the temperature, the greater the pore number related to the faster drying rate. Taking into account what it was observed visually in freeze-dried samples, the number of pores formed may be related with the firmness of the structure. In this sense the interaction of the added biopolymers with the own's fruit solutes seems to promote a more compact and firmer structure and a higher drying rate to a weaker one.

For each sample and freeze-drying time, a mean pore size was calculated (Figure 3). As it can be observed, the samples freeze-dried at room temperature showed a greater mean pore size than when heated at 40 ºC and, at each temperature, it was greater when no biopolymers were added. In this case, both the biopolymers presence and to increase the drying temperature contribute to decrease the pore size.
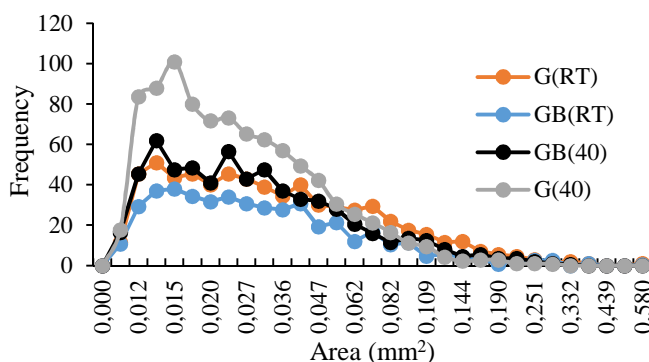
Fig. 2. Distribution of the number of pores (frequency) formed of each area range. Samples: grapefruit with (samples GB) and without (samples G) biopolymers added and heating (samples 40) or not (samples RT) the shelves.
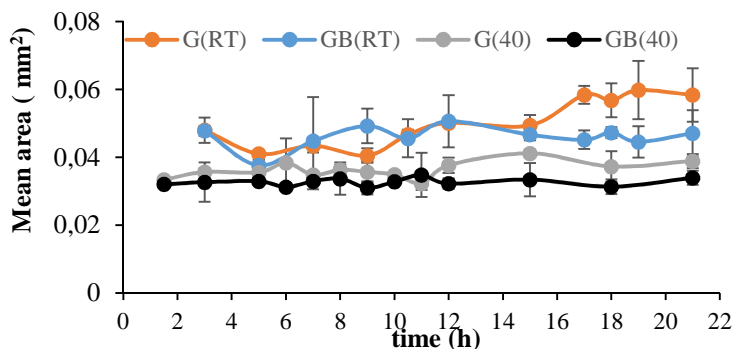
Fig. 3 Mean area of the pores formed throughout the freeze-drying time. Samples: GB and G: grapefruit with (samples) and without (samples G) biopolymers added and heating (samples 40) or not (samples RT) the shelves.

4. Conclusions

To increase the shelves temperature to 40 ℃ during freeze-drying decreases in more than 50 % the drying time and allows to obtain a sample with more pores formed although these being smallest. The gum Arabic and bamboo fiber added to stabilize the dried product doesn't affect the drying rate although it shows less and smallest pores. As no collapse of any of the obtained samples was observed, to add the biopolymers to grapefruit puree and to heat the shelfs to 40 ℃ during freeze-drying should be recommended.

5. Acknowledgements

6. References

[1] Michalska, A.; Wojdylo, A.; Lech, K.; Lysiak, G. P.; Figiel, A. Physicochemical properties of whole fruit plum powders obtained using different drying technologies. Food Chemestry 2016, 207, 223–232.

[2] Karam, M. C.; Petit, J.; Zimmer, D.; Baudelaire-Djantou, E.; Scher, J. Effects of drying and grinding in production of fruit and vegetable powders: A review. J. Food Engineering 2016, 188, 32–49.

[3] Hua, T.C.; Liu, B.L.; Zhang, H.; Freezing-Drying of Food. In Freeze-Drying of Pharmaceutical and Food Products; CRC Press., Eds.; Woodhead Publishing Limited.: New York, 2010; 141-182.

[4] Hammami, C.; René, F. Determination of freeze-drying process variables for strawberries. J. Food Engineering 1997, 32(2),133–154.

[5] Nireesha, G.; Divya, L.; Sowmya, C.; Venkateshan, N.; Niranjan-Babu, M.; Lavakumar, V. Lyophilization/Freeze Drying: A Review. Ijntps 2013, 3(4), 87–98.

[6] Kasper, J. C.; Friess, W. The freezing step in lyophilization: Physico-chemical fundamentals, freezing methods and consequences on process performance and quality attributes of biopharmaceuticals. European Journal of Pharmaceutics and Biopharmaceutics 2011, 78 (2), 248–263.

[7] Simal, S.; Femenia, A.; Garau, M. C.; Rosselló, C. Use of exponential, Page's and diffusional models to simulate the drying kinetics of kiwi fruit. J. Food Engineering 2005, 66(3), 323–328.

[8] Telis, N.V.; Martínez-Navarrete, N.; Biopolymers used as drying aids in spray drying and freeze drying of fruit juices and pulps. In Biopolymer Engineering in Food Processing; CRC Press.,Eds.; Taylor & Francis Group.: Boca Raton, 2012; 279-326.

[9] Bronfenbrener, L.; Rabeea, M. A. Kinetic approach to modeling the freezing porous media: Application to the food freezing. Chemestry Engineering Process 2015, 87, 110–123.

[10] Agudelo, C.; Barros, L.; Santos-Buelga, C.; Martínez-Navarrete, N.; Ferreira, I.C.F.R. Phytochemical content and antioxidant activity of grapefruit (Star Ruby): A comparison between fresh freeze-dried fruits and different powder formulations. LWT - Ciencia y Tecnología de Alimentos 2017, 80, 106-112.

[11] Calín-Sánchez, Á.; Kharaghani, A.; Lech, K.; Figiel, A.; Carbonell-Barrachina, Á.A.; Tsotsas, E. Drying Kinetics and Microstructural and Sensory Properties of Black Chokeberry (Aronia melanocarpa) as Affected by Drying Method. Food Bioprocess Technology 2014, 8(1), 63–74.

[12] Russ, J. C.;Measuring features. In Image analysis of food microstructure; CRC Press., Eds.; Woodhead Publishing Limited.:Washington, 2005; 300-312.

[13] Broeke, J.; Pérez Mateos, J. M.; Pascau, J.; Image segmentation and feature extraction with ImageJ. In Image Processing with ImageJ; Livery Place., Eds.; Publishing Packt.:Birmingham, 2015; 49-99.

[14] Azzouz, S.; Guizani, A.; Jomaa, W.; Belghith, A. Moisture diffusivity and drying kinetic equation of convective drying of grapes. J. Food Engineering 2002, 55(4), 323–330.

[15] Benlloch-Tinoco, M.; Moraga, G.; Camacho, M.M.; Martínez-Navarrete, N. Combined Drying Technologies for High-Quality Kiwifruit Powder Production. Food Bioprocess Technology 2013, 6, 3544–3553.

Effect of saccharide additives on dehydration–drying kinetics and quality properties of dried kiwi fruit products

Ueno, S.[a]*; Iijima, R.[a]; Harada, M.[a]; Liu, H.[b]; Shimada, R.[a]; Fukami, K.[c]

[a] Faculty of Education, Saitama University, Saitama, Japan.

[b] Graduate School of Agricultural and Life Sciences, The University of Tokyo, Tokyo, Japan.

[c] San-ei Sucrochemical Co., Ltd. Aichi, Japan.

*E-mail of the corresponding author: shigeakiu@mail.saitama-u.ac.jp

Abstract

The effects of saccharide additives on the dehydration and drying properties as well as the quality properties of dried kiwi fruit products were investigated. Sliced kiwi fruits were soaked and dehydrated in citric acid, glucose, sucrose and the pH-adjusted sugar solutions, individually. Osmotic dehydration and drying kinetic parameters were calculated using exponential models. Drying rate constants and water activities of dried kiwi fruits with osmotic dehydration were superior to those without osmotic dehydration. Soaking solutions with a lower pH led to a decrease in lightness. However, soaking sokution pH had no significant effect on the water activity or drying kinetics.

Keywords: drying; kinetics; kiwi fruit; osmotic dehydration

1. Introduction

Kiwi fruit (*Actinidia deliciosa*) is a popular fruit due to its taste, cost, cooking affinity, nutrition and functional properties. Kiwi fruit is low in fat and sodium, and it is high in organic acids, vitamin C, vitamin E, folic acid, dietary fibre, potassium and polyphenols. Vitamin C, vitamin E and polyphenols show strong antioxidant activities. Additionally, many components in kiwi fruit have a positive effect on human health. Therefore, the consumption of kiwi fruit in Japan has approximately doubled in the last 10 years.

Dried fruit is known to have a long shelf life and has specific texture, taste and functional properties [1-3]. The manufacturing process of dried fruits requires a certain amount of sugar; however, consumers pay attention to their health, and dried fruits with less sugar or without sugar are more desirable. Thus, food companies in Japan have been developing new dried fruit products, such as those with lower calories.

The manufacturing process of dried fruit products involves two main procedures, osmotic dehydration and a drying process. Osmotic dehydration draws water from the fruit and adds a sweet taste by soaking the fruit in a sugar solution [4]. Osmotic dehydration also prevents colour degradation and hardening. Sugar-soaked fruits are then dried in a hot air drying oven or by sun drying. While osmotic dehydration and drying characteristics of fruits are well established [1-4], the addition of pH-adjusted saccharides has rarely been reported in osmotic dehydration and drying processes.

The objectives of this study were to investigate the effect of pH in osmotic dehydration solutions on dehydration and drying properties and to investigate the quality properties of dried kiwi fruit products.

2. Materials and Methods

2.1. Osmotic dehydration of fresh kiwi fruit

Saccharides, such as glucose, sucrose, maltose, citric acid (Wako Pure Chemical Industry, Osaka, Japan), sorbitol, erythritol (B Food Science Co., Ltd., Tokyo, Japan) and trehalose (Hayashibara, Okayama, Japan), glucose and sucrose adjusted to pH 2.0 were selected as soaking solutions for osmotic dehydration.

Fresh kiwi fruits (Zespri, New Zealand) were purchased from a local supermarket. Kiwi fruits were cut into 10-mm-wide slices and weighed. Sliced kiwi fruits were soaked in 60% (w/w) soaking solutions at 60°C for 80 min at 50 rpm in a shaking water bath (Taitec, Saitama, Japan). During soaking, kiwi fruit slices were weighed every 5 min. The kiwi fruit slices were gently wiped with paper towel after soaking.

2.2. Drying of osmotic-dehydrated kiwi fruit and kinetic analysis

After osmotic dehydration, the kiwi fruit slices were transferred to a drying oven (WFO-410W, Nakayama Rika, Saitama, Japan) and dried at 80°C for 6 h. During drying, kiwi fruits were weighed every 30 min. Based on the weight changes during drying, moisture content was calculated as the time course of the sample weight and equilibrium dry weight. Drying characteristics were evaluated by several mathematical models. The dimensionless relative moisture content against drying time was plotted as a drying curve. Utilising the drying curves of samples with different osmotic dehydration solutions, kinetic parameters of the most simplified model, known as the exponential model [4], were calculated as follows:

$$MR = (M - M_e) / (M_0 - M_e) \tag{1}$$

$$MR = \exp(-kt) \tag{2}$$

Where MR and M indicates the dimensionless relative moisture content and the certain moisture content, M_0 indicates the initial moisture content, M_e indicates the equivalent moisture content, k indicates the drying rate constant (min^{-1}) and t indicates the drying time (min). Usually, this model does not provide an accurate simulation of the drying curve for many foods, particularly by underestimating the beginning of the drying curve and overestimating the later stages [5]. Therefore, another exponential model called the Page model was also applied [5,6].

$$MR = \exp(-kt^n) \tag{3}$$

Where n indicates the empirical constant. Equations (2) and (3) were applied to the dimensionless relative moisture content during drying, and the drying rate constant k was calculated using Kaleida Graph 4.0 J (Hulinks, Tokyo, Japan).

2.3. Quality analyses of dried kiwi fruit

Several quality factors are important for both consumers and food suppliers; consumers mainly determine product quality based on the colour of dried fruit in a supermarket, while the most important factor for suppliers is the shelf life. We determined the quality of dried kiwi fruits by surface colour and water activity in this study. Colour parameter L*a*b* (L; lightness, a; green-red, b; blue-yellow) of quarter-cut dried kiwi fruits was measured using a colour metre (ZE2000, Nippon Denshoku Industry. Co. Ltd., Tokyo, Japan). Two-thirds of the cut dried kiwi fruits were fixed in a plastic pan for water activity measurements using

a water activity metre (LabMaster aw, Novasina, Switzerland). All experiments were performed in quintuple, and results are presented as means ± standard deviations.

3. Results and Discussion

3.1. Colour

The colour of fresh kiwi fruit and dried kiwi fruit with or without (dried control) selected osmotic dehydration was measured (Table 1). Fresh kiwi fruit showed the lowest a* value, and fresh and dried control kiwi fruits showed higher L* values. Dried samples in which the pH was adjusted to 2.0 showed slightly lower L* and b* values compared with non-pH-adjusted samples (sucrose, pH 6.0, and glucose, pH 3.8). Dried fruits soaked in citric acid solutions showed the lowest L* and b* values and the highest a* values. Combinations of osmotic dehydration and drying processes led to a decrease in lightness. These results suggest that kiwi fruit's green pigments, such as chlorophyll a and b, melt into the soaking solution during osmotic dehydration and change during the thermal drying process, resulting in a change in the colour of dried kiwi fruits. However, colour changes in dried kiwi fruit soaked in sucrose and glucose solutions were limited, and these products would be more acceptable to consumers.

Table 1. Colour parameters of dried kiwi fruit with saccharide and pH-adjusted sugar solutions

Sample	L*	a*	b*
Fresh	48.9 ± 1.6	−6.9 ± 1.0	28.4 ± 1.5
Dried control (no sugar)	49.2 ± 2.9	1.5 ± 0.7	30.1 ± 2.0
60% sucrose, pH 6.0	47.0 ± 2.9	1.4 ± 1.0	32.1 ± 1.8
60% sucrose, pH 2.0	45.5 ± 2.8	1.6 ± 0.8	29.5 ± 1.5
60% glucose, pH 3.8	45.6 ± 3.9	1.8 ± 1.0	30.3 ± 2.7
60% glucose, pH 2.0	43.9 ± 3.0	1.6 ± 1.2	29.7 ± 1.8
6% citric acid	37.2 ± 2.5	3.8 ± 0.9	23.9 ± 2.0
60% citric acid	35.0 ± 2.6	7.9 ± 1.1	21.3 ± 2.2

3.2. Water activity

The water activity in food products is a well-known index of storability. While the water activity of dried kiwi fruit without osmotic dehydration was 0.61, those of osmotic-dehydrated samples ranged from 0.43 to 0.49 (Table 2). The shelf life of a food product at a given water activity may vary depending on the structure and composition of the food material, and spoilage is a concern. Microbial activity, enzyme reaction, browning reaction and lipid oxidation are strongly dependent on water activity. In this study, the microbial activities, such as those of bacteria, yeast and mould, and enzyme reactions were limited

when the water activity ranged from 0.43 to 0.49. These results indicate that osmotic dehydration with sugar (including pH-adjusted samples) improves the shelf life.

Table 2. Water activity of dried kiwi fruit

Sample	Water activity
Dried control (no sugar)	0.61 ± 0.08
60% sucrose, pH 6.0	0.49 ± 0.02
60% sucrose, pH 2.0	0.48 ± 0.01
60% glucose, pH 3.8	0.48 ± 0.01
60% glucose, pH 2.0	0.47 ± 0.01
6% citric acid	0.47 ± 0.03
60% citric acid	0.43 ± 0.04

3.3. Kinetic analysis of drying

Based on the weight changes during drying, the moisture content was calculated as the time course of the sample weight and equilibrium weight. Then, the dimensionless relative moisture content against drying time was plotted as a drying curve. The most simplified model was applied to the drying curves. The lowest drying rate constant of dried kiwi fruit was observed in the control (Table 3). In contrast, osmotic-dehydrated samples showed higher values than the dried control (Table 3). The pH-adjusted dried samples had values similar to those of non-pH-adjusted samples. Moreover, dried samples with a citric acid solution showed lower values than those with sucrose or glucose.

Osmotic dehydration with saccharide solutions enhanced drying. However, the soaking solution pH did not have any apparent effect on the drying characteristics. A lower soaking solution pH would destroy the internal structures of kiwi fruit, such as membranes, and once membranes are destroyed during osmotic dehydration and drying processes, the internal structure of kiwi fruit will easily shrink. Therefore, the drying rate constants of lower pH samples did not increase compared with those without a pH adjustment.

Table 3. Drying rate constants of dried kiwi fruit

Sample	Drying rate constants (min^{-1})
Dried control (no sugar)	0.0045 ± 0.0001
60% sucrose, pH 6.0	0.0059 ± 0.0001
60% sucrose, pH 2.0	0.0062 ± 0.0005
60% glucose, pH 3.8	0.0062 ± 0.0005
60% glucose, pH 2.0	0.0063 ± 0.0001
6% citric acid	0.0055 ± 0.0001
60% citric acid	0.0058 ± 0.0007

3. Conclusions

We investigated the effects of saccharide additives on dehydration–drying kinetics and the quality properties of dried kiwi fruit. Drying rate constants and water activities of dried kiwi fruits with osmotic dehydration were superior to those without osmotic dehydration. Soaking solutions with a lower pH led to a decrease in lightness. However, soaking sokution pH had no significant effect on the water activity or drying kinetics. The combination of sugar and citric acid for a single soaking solution would enable to investigate a novel physicochemical and taste parameters. Further analysis of taste characteristics are essential for the dried fruit industry.

4. References

[1] Pan, Y.K.; Zhao, L.J.; Zhang, Y.; Chen, G.; Mujumdar, A.S.; Osmotic dehydration pretreatment in drying of fruits and vegetables. Drying Technology 2003, 21, 1101-1114.

[2] Sablamni, S.; Drying of fruits and vegetables: retention of nutritional/functional quality. Drying Technology 2006, 24, 123-125.

[3] Nijhuis, H.H.; TorringaH.M.; Muresan, S.; Yuksel, D.; Leguijt, C.; Kloek, W. Approaches to improving the quality of dried fruit and vegetables. Trends in Food Sci. Technol. 1998, 9, 13-20.

[4] Talens, P.; Escriche, I.; Martinez-Navarrete, N.; Ciralt, A. Influence of osmotic dehydration and freezing on the volatile profile of kiwi fruit. Food Res. Int. 2003, 36, 635-643.

[5] Simal, S.; Femenia, A.; Garau, M.C.; Rossello, C. Use of exponential, Page's and diffusional models to simulate the drying kinetics of kiwi fruit. J. Food Eng. 2005, 66, 323-328.

[6] Ueno, S.; Shigematsu, T.; Karo, M.; Hayashi, M.; Fujii, T. Effects of high hydrostatic pressure on water absorption of adzuki beans. Foods 2015, 4, 148-158.

Drying of wastes of almond shells in conical spouted beds

San José, M.J.; Alvarez, S.; López, R.

Departamento de Ingeniería Química. Universidad del País Vasco UPV/EHU, Bilbao, Spain

*E-mail of the corresponding author: mariajose.sanjose@.ehu.es

Abstract

The goal of this study was to prove the feasibility of a conical spouted bed dryer for the drying of wastes of almond tree fruit. The drying operating regimes ranges in sspouted beds contactors were determined. The drying tests were conducted in the spouted bed regime under determined experimental conditions. Beds consisting of almond shells were dried at drying air temperatures ranging from room temperature to 140 ºC. The drying behaviour was assessed based on the decrease in moisture content of almond shells with the time and the effect of drying air temperature on the drying process was analyzed.

Keywords: Almond shells wastes; conical spouted beds; biomass wastes; drying

1. Introduction

World energy consumption has increased by 28% in 2017 and renewable fuels are the world's fastest-growing energy source, predicting an increase of 2.3%/year between 2015 and 2040 [1]. Biomass is a key renewable resource, which supplies 14% of the world's energy consumption. Since biomass wastes usually have high moisture content, in order to increase the yield of thermal valorization of these wastes, it is advisable to reduce the moisture content previously.

Almond nut production annually generates more than 4,800 dry tons of by-products per 1,000 acres of harvested almond trees [2]. This biomass wastes including shells, hulls, and pruning, composed mainly by cellulose, lignin and hemicelluloses are suitable for energy production. The most common treatments for these wastes are landfills, compostage, recycling and direct burning [3]. However, there is little research of energy uses for waste from almond processing including gasification, pyrolysis, and combustion or co-firing [2]. World production of almonds was estimated about 3.2 million tonnes in 2016, being the United States the largest producer with 2 million tonnes. Spain is the second world's almond producer, with a yearly production around 200 thousand tonnes [4]. Almond shell is the hard layer between the hull and the almond nut, which protects the almond from insects while on the almond tree (*Prunus dulcis*).

Spouted beds technology can be an appropriate alternative for energy exploitation of renewable biomass wastes, with a previous reduction of moisture content of biomass wastes by drying, due to the high mass and energy transfer. Conical spouted beds have been applied for drying biomass wastes such as agricultural wastes [5-6], vineyard pruning wastes [7] sludge wastes [8-11], of yeast [12].

2. Materials and Methods

The experimental unit used, Fig. 1, comprises a conical dryer, a blower, two high efficiency cyclones, an electrical preheater and thermocouples. The conical dryer (Fig. 1) made of AISI-310S stainless steel is externally insulated to reduce heat loss, has an angle of 36º, base diameter of 0.03 m and inlet gas diameter to inlet dryer diameter ratio, D_o/D_i, 1/2, 2/3 and 1. The geometric factors of this dryer are listed in Table 1.

The drying air velocity was determined by the air flow rate measured by mass flowmeter, installed at the inlet pipe, and controlled by a computer to an accuracy of ±0.5%.
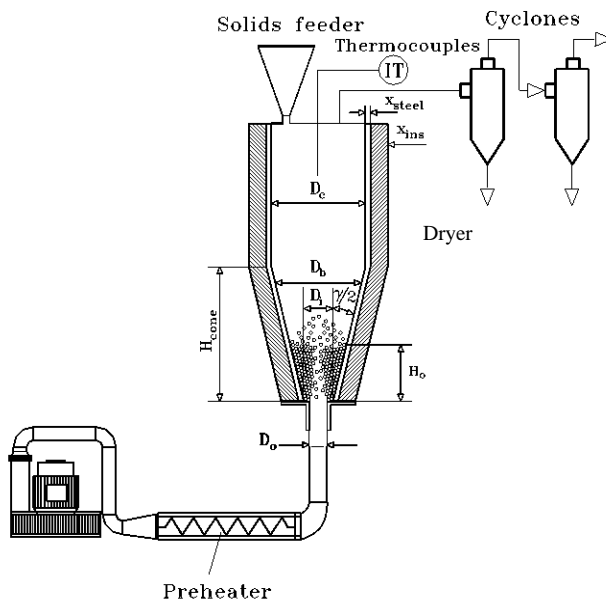
Fig. 1 Schematics of the experimental plant and of the conical spouted bed dryer with an outline of solid particles movement in the spouted bed regime.

Table 1. Geometric factors of the conical spouted bed dryer

Conical spouted bed dryer		
Diameter of the cylindrical section	D_c (m)	0.23
Cone angle	γ (deg)	36
Gas inlet diameter	D_o (m)	0.015, 0.02 and 0.03
Diameter of the cone bottom	D_i (m)	0.03
Upper diameter of the stagnant bed	D_b (m)	$D_i + 2 H_o \tan (\gamma/2)$
Height of the conical section	H_{cone} (m)	0.31
Stagnant bed height	H_o (m)	between 0.03 and 0.20
Thickness of the dryer wall	X_{steel} (mm)	2
Thickness of the insulation	X_{ins} (mm)	14

During the drying process, solids were sampled by a suction pump, and the solids moisture content was measured by Mettler Toledo HB43-S Halogen hygrometer. Room temperature, the relative air humidity and air humidity at the inlet and the outlet were measured using Ahlborn MT8636-HR6 thermal conductivity detectors (accuracy ± 2% relative humidity). The drying air temperature was measured by a K-type thermocouple (relative error: the greater ± 0.75% or ± 2.2°C) located at the inlet to the dryer.

Biomass wastes studied, Fig. 2, were almonds shells. In the industry almonds are washed before peeling. Almonds shells have a density of 1220 kg/m³, particle sizes 5-8 mm and moisture content 25-30 wt%. Bed masses of almond shells used are 100-400 g. Solids moisture content is measured by Mettler Toledo HB43-S Halogen hygrometer (accuracy ± 0.01 %).

(a)   *(b)*
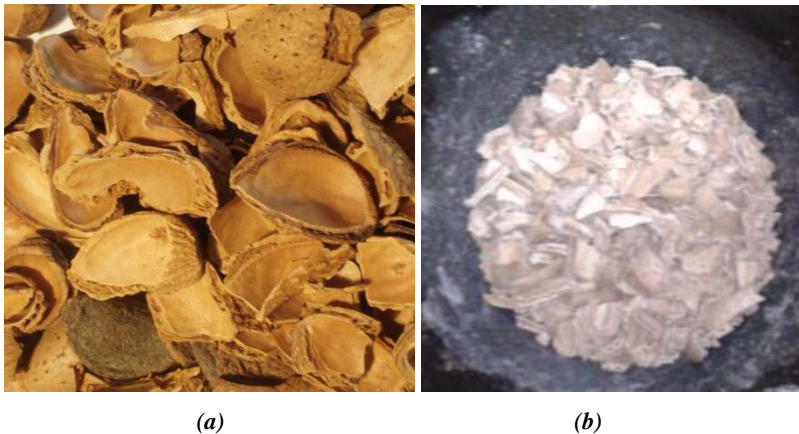
Fig. 2 (a) Grinded wet almond shells wastes inside the feeder. (b) Grinded dry almond shells wastes inside the conical spouted bed dryer.

3. Results and discussion

The performance of conical spouted beds for drying of beds formed from almond shells and operation conditions at inlet gas temperature at room temperature and at 105 °C have been established in this paper. Likewise, the evolution of solids moisture content has been measured with the time, and effect of operating conditions on drying time has been analyzed.

In order to prove the feasibility of the conical spouted bed dryer for thermal exploitation of almonds shells, the range of the stable operating regimes of homogeneous beds formed from wastes of almond shells was determined. The minimum air flow rate necessary to achieve the spouted bed regime was characterized by pressure drop fluctuations with a standard deviation less than 10 Pa [13]. The experimental values of minimum air velocity corresponding to the spouted bed regime are shown in Fig. 3 for beds consisting of wastes of almond shells with stagnant bed height (H_o) in the range of 0.02-0.14 m along with an outline of solid particles in the stagnant bed and in the spouted bed regime for a system taken as example. Starting in the stagnant bed, increasing stagnant bed height, the air velocity necessary to reach the spouted bed regime increases, therefore the velocity operating range over the minimum spouting flow is narrower. The spouted bed regime is

reached in all studied systems, characterized by the vigorous cyclic movement as is shown inside the conical dryer, Fig. 1.

With the aim of determining the drying behaviour of the conical spouted bed dryer, beds consisting of the almond shells waste were dried under different experimental conditions.
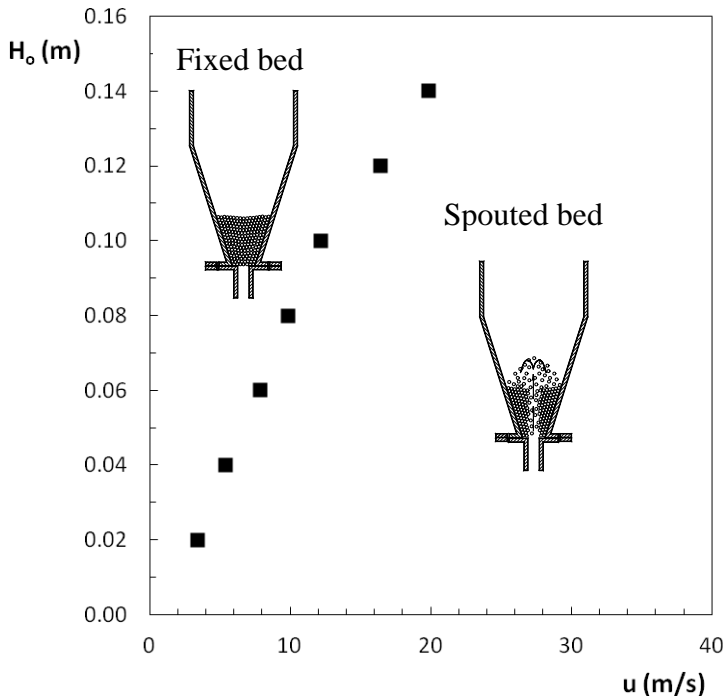
Fig. 3 Operating map of stagnant bed height versus the gas velocity. Experimental system: γ= 36° D_o= 0.03 m, almond shells of d_s= 5.6 mm.

The experimental results for the time evolution of the moisture content of almonds shells, X, from the initial moisture content of 40 wt % (d.b.) to the equilibrium moisture content are plotted in Fig 4 for a bed consisting of 400 g of wet almond shells with drying air temperatures of 25 and 105 ºC. The air flow rate, was high enough, so that the outlet air humidity was lower than saturation humidity, resulting in a driving humidity gradient. The drying process was assumed concluded when the difference between two consecutive measurements of solids moisture content did not exceed ±0.05 wt%.

At the beginning of the process the decrease in the moisture content is more pronounced, almost proportional, controlled by evaporation of free moisture. At the end of the drying process, variation of almond shells moisture content is asymptotic until the moisture content reaches its equilibrium value.
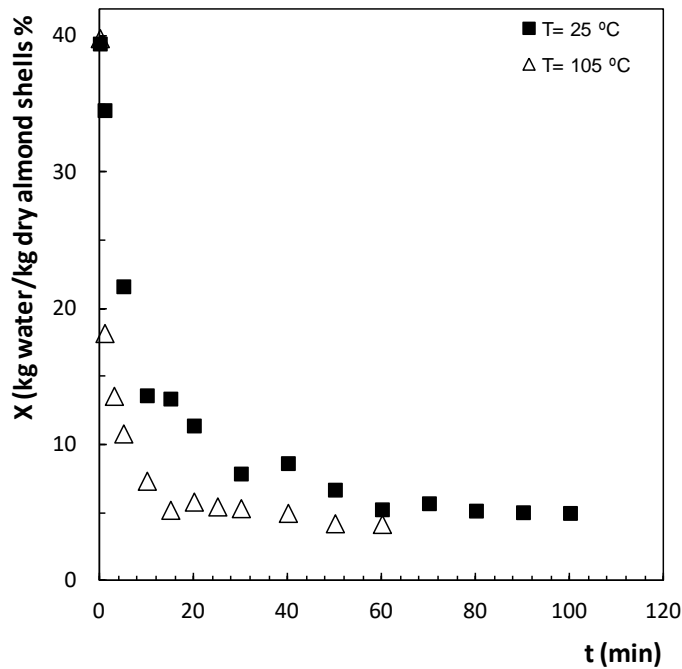
Fig. 4 Time evolution of the moisture content of a bed of almond shells. Experimental system: γ= 36º; D_o= 0.03 m, M= 400 g, d_S = 5.6 mm, initial moisture content 33 wt % (d.b.), u= 1.10 u_{ms}; T= 25 and 105 ºC.

As the inlet air temperature is increased, the solids moisture content decreases faster, with shorter drying time to reach the moisture equilibrium content, which depends on the inlet air temperature and the relative humidity. In drying of almonds shells, as inlet air temperature is increased 80 ºC, from 25 to 105 ºC, drying time is decreased by around 75% from 60 to 15 minutes.

4. Conclusions

The feasibility of a conical spouted bed equipment for thermal exploitation of almond shells wastes by drying in the spouted bed regime has been proven at low air temperatures. The range of operating regimes beds consisting of almond shells has been determined under different experimental conditions.

The moisture content of almond shells decreases almost proportionally with time from the initial moisture content to equilibrium moisture content, and this disminishing is more noticeable at the beginning of the drying process, at high moisture content. The drying time

to reach the equilibrium moisture content decreases with increasing drying air temperature around 75% with a temperature increase of 80 ℃.

Acknowledgements

5. Nomenclature

D_b	upper diameter of the stagnant bed, $D_b = D_i + 2 H_o \tan (\gamma/2)$	m
D, D_i, D_o	diameter of the cylindrical section, of the dryer base, and of the gas inlet	m
d_S	mean Sauter diameter	m
H, H_c, H_o	height of the cylindrical section of the dryer, of the conical section and of the stagnant bed	m
t	time	min
T	temperature	℃
M	solids mass	kg
X	solids moisture content (dry basis),	kg water/kg dried sludge, %
X^*	equilibrium solids moisture content (dry basis),	kg water/kg dried sludge, wt %
X_{steel}, X_{ins}	thickness of the dryer wall and of the insulation	m
u, u_{ms}	velocity of the air and air minimum spouting velocity	m/s

Greek letters

γ	angle of the conical section of the dryer	deg
ρ_s	density of solids	kg /m^3

Subscripts

        d   drying

        ms   minimum spouting

6. References

[1] U.S. Energy Information Administration, 2017. International Energy Outlook 2017.

[2] Chen, P.; Cheng, Y.; Deng, S.; Lin, X.; Huang, G.; Ruan, R. Utilization of almond residues, International Journal of Agricultural and Biological Engineering 2010, 3 (4), 1-18.

[3] García, A.N.; Esperanza, M.M.; Font. R. Comparison between product yields in the pyrolysis and combustion of different refuse. Journal of Analytical and Applied Pyrolysis 2003, 68-69, 577-598.

[4] FAO Data. http://www.fao.org/faostat/en/#data/QC/visualize

[5] San José, M.J.; Alvarez, S.; López, L.B.; García, I. Drying of mixtures of agricultural wastes in a conical spouted bed contactor. Chemical Engineering Transactions 2011, 24, 673-678.

[6] San José, M.J., Alvarez, S., López, R. Modelling of drying of biomass wastes in a conical spouted bed dryer. Computer Aided Chemical Engineering 2017, 40, 517-522.

[7] San José, M.J.; Alvarez, S.; García, I; Peñas, F.J. A novel conical combustor for thermal exploitation of vineyard pruning wastes. Fuel 2013,110, 178–184.

[8] San José, M.J.; Alvarez, S.; Ortiz de Salazar, A.; Morales, A.; Bilbao, J. Shallow spouted beds for drying of sludge from the paper industry. Chemical Engineering Transactions 2010, 21, 145-150.

[9] San José, M.J.; Alvarez, S.; López, L.B.; Olazar, M.; Bilbao, J. Conical spouted beds contactors for drying of sludge from the Paper industry. In Drying 2010 (Vol B); Barleben-Magdeburg: Docupoint GmbH, 2010, 1242-1248.

[10] San José, M.J.; Alvarez, S.; Peñas, F.J.; García, I. Cycle time in draft tube conical spouted bed dryer for sludge from paper industry. Chemical Engineering Science 2013, 100, 413-420.

[11] San José, M.J.; Alvarez, S.; García, I.; Peñas, F.J. Conical spouted bed combustor in clean valorization of sludge wastes from Paper industry for obtaining energy. Chemical Engineering Research and Design 2014, 92, 672–678.

[12] Spreutels, L.; Haut, B.; Chaouki, J.; Bertrand, F.; Legros, R. Conical spouted bed drying of baker's yeast: Experimentation and multi-modeling. Food Research International 2014, 62, 137-150.

[13] San José, M.J.; Alvarez, S. Bed pressure drop in conical spouted beds with a draft tube in thermal treatment of wastes of different particle diameter, density and shape. Chemical Engineering Technology 2015, 38(4), 709-714.

Effect of air drying temperature on phytochemical properties of brown seaweed *Bifurcaria bifurcata*

Arufe, S. V.; Sineiro, J.; Chenlo, F.; Moreira, R.[*].

Department of Chemical Engineering, Universidade de Santiago de Compostela, Rúa Lope Gómez de Marzoa, Santiago de Compostela, E-15782, Spain.

*E-mail of the corresponding author: ramon.moreira@usc.es

Abstract

The purpose of this study was to determine the effects of convective air-drying at different temperatures (35, 50, 60 and 75°C) on the color of Bifurcaria bifurcata (BB) seaweed powders obtained after milling, the antioxidant activity and polyphenolic and carbohydrate content of the aqueous extracts obtained by ultrasound-assisted extraction. BB seaweed powders exhibited significant color differences between powders obtained from BB dried at 35ºC (yellowish-green) and 50–75 °C (brown). High air drying temperature (above 60ºC) significantly reduced the total polyphenolic, carbohydrate content and scavenging activity of aqueous extracts of BB.

Keywords: *Phaeophyceae Antioxidant activity Carbohydrates Color Polyphenols*

1. Introduction

The safety and toxicity issues related with synthetic antioxidants [1] can explain the increasing interest in natural antioxidants to replace synthetic additives in foods or nutraceuticals. Natural antioxidants are effective in protecting the body against damage caused by Reactive Oxygen Species (ROS) and extending the storage time of food. They have the capability not only to improve oxidative stability but also to provide a wide variety of additional health benefits [2]. They inhibit or prevent the oxidation of a substrate and evolve to protect biological systems against damage induced by ROS.

It has been demonstrated that antioxidant compounds from seaweeds have health benefits such as antimutagenic, anti-viral, amelioration of diabetic complication, bactericides, etc. Some types of polyphenols and tannins (*i.e.* phlorotannins) have strong antioxidant activities, and they are abundant in brown macroalgae [2]. Regarding the potential uses of brown seaweeds, due to their interesting antioxidant properties, it is necessary to study how the processing (including operations such as collection, preservation (drying) and storage, among others) affects the biological activity of certain compounds. Traditionally, seaweeds are sundried for long periods and the final properties can be altered. The current increase of marine algae production rates requires the application of faster and controlled industrial methods. In this sense, in order to overcome the long periods of natural sun drying (days), several alternatives can be useful such as freeze-drying or convective hot air drying, which is the most widely employed method for preserving biological materials, where the air conditions (temperature, relative humidity and velocity) are controlled [3].

Several authors studied the effect of different drying techniques on the antioxidant properties of extracts of different seaweeds such as *Sargassum sp.*, *Kappaphycus alvarezii*, *Gracilaria chilensis*, among others [4,5]. However, no studies assessing the effect of drying conditions on phytochemical properties of *Bifurcaria bifurcata* were found in the literature. Consequently, the main objective of this work is to determine the effect of the air drying temperature on color and phytochemical properties of brown seaweed *Bifurcaria bifurcata*.

2. Materials and Methods

Bifurcaria bifurcata seaweeds previously dried at 35, 50, 60, and 75ºC in a hot convective air dryer were milled in order to obtain seaweed powders. Milling was carried out using a centrifugal mill (ZM 200, Retsch GMBH, Germany). The rotor speed was adjusted to 8000 rpm and a standard sieve (500 μm) was employed. The milled systems obtained at different drying temperatures (BB35P, BB50P, BB60P, and BB75P) were stored at 5ºC in polyethylene plastic bags under vacuum with a vacuum-packer (Sammic V201, Spain) for further utilization.

Color of obtained powders and their different particle size fractions obtained after sieving (sieves from 40 up to 500 µm) was determined using a colorimeter (Chroma Meter CR-400, Konika Minolta, Japan). Color was measured by means of CIELab coordinates: L* (whiteness (L* = 0) or brightness (L* = 100)), a* (redness (a* > 0) or greenness (a* < 0) and b* (yellowness (b* > 0) or blueness (b* < 0)). Moreover, total color difference parameter (ΔE^*, Eq. (1)) for each size fractions (i) was estimated and classified according to [6] using as reference (r) the color coordinates of the seaweed powder prior to sieving (whole).

$$\Delta E^* = \sqrt{(L_i^* - L_r^*)^2 + (a_i^* - a_r^*)^2 + (b_i^* - b_r^*)^2} \tag{1}$$

Seaweed aqueous extracts were obtained from the different dried seaweed powders in order to determine the effect of air drying in total polyphenols and carbohydrate content and the antioxidant activity of seaweeds. Samples of powdered seaweed, were processed with an ultrasound sonicator (Hielscher, UIP-1000 hdT, Germany) to enhance the extraction of polyphenols and carbohydrates. All experiments were carried out in batch. The procedure starting with a rehydration step (15 min) before extraction. Then extraction operation took place using a 200 mL beaker at controlled temperature (< 35ºC) employing a cold water bath to avoid that high temperatures could affect the antioxidant activity. All extractions were performed using water as solvent. The equipment operated with a frequency of 20 kHz and the irradiation power (< 1000 W) was regulated in the ultrasound generator at 80% amplitude. The conditions were 4 min of contact time and 30 $w \cdot w^{-1}$ of liquid-solid ratio. Finally, obtained extracts were centrifuged at 12400 rpm for 15 min using a high speed laboratory centrifuge (2-15, Sigma, UK), and the supernatant obtained was then filtered by pressure using syringe filters with a pore size of 0.25 µm and used for characterization analysis. All seaweed aqueous extracts were analyzed by means of DPPH scavenging activity, total solids, polyphenols and carbohydrate content.

The quantitative determination of total polyphenols content (TP) was measured as phloroglucinol (PHL) equivalents following a colorimetric method [7]. TP was evaluated in reference to raw seaweed powder sample (mg PHL·(100 g dry powder)$^{-1}$, TP_w) and also to total solids content in the extract (mg PHL·(100 g dry solids)$^{-1}$, TP_s).

Carbohydrates content of the extracts was determined following a method previously reported [8]. Carbohydrates content was expressed as glucose equivalents (GL) referred to raw seaweed powder sample (mg GL·(100 g dry powder)$^{-1}$, CHO_w) and also to total solids content in the extract (mg GL·(100 g dry solids)$^{-1}$, CHO_s).

The DPPH scavenging activity assay measures the capacity of a system to react with a free radical agent (2, 2-diphenyl-1-picrylhydrazyl, DPPH). It was employed the method proposed by Brand-Williams [9]. In its radical form, DPPH· shows an absorption peak at

515 nm, but upon reduction by an antioxidant (AH) or a radical species (R·) the absorption disappears. As the reaction takes time to fully develop, for the determination of the DPPH scavenging activity absorbance is measured every 5 min until it reaches the stationary state. Scavenging activity, SA, is evaluated by means of Eq. (2):

$$SA(\%) = \frac{A_0 - A_f}{A_0} \cdot 100$$

(2)

where A_0 (-) is the absorbance at time 0 and A_f is the absorbance after one hour.

3. Results and Discussion

3.1. Color characterization

The trends for color parameters values of powders from seaweeds dried at 35, 50, 60 and 75ºC with the corresponding particle size fractions are displayed in Figure 1.
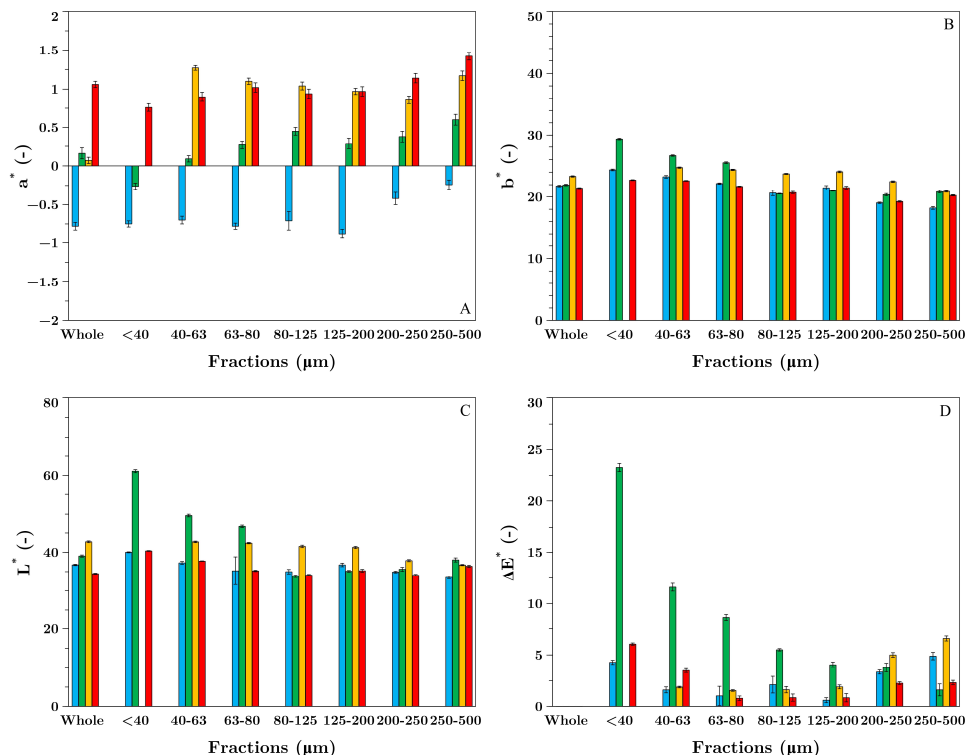
***Fig. 1** a* (A), b* (B), L* (C) and ΔE* (D) color parameters of Bifurcaria bifurcata seaweed powders obtained after drying at different temperatures 35ºC (■), 50ºC (■), 60ºC (■) and 75ºC (■).*

Specifically, a* parameter values increased with increasing drying temperature. It is noticiable that the trend of a* changes from green to red with drying temperatures above 35ºC. Regarding particle size effect, a* increased in general for all assessed seaweed powders.

The effect of drying temperature did not cause relevant changes in b* values. All seaweed powders have a yellowness predominance (b* > 0). Regarding color properties of size fractions, b* slightly decreased for all systems as mean size increased. Both trends might be related to the presence of still structurally undamaged parts of the seaweed in the biggest particles.

It can be seen that L* parameter significantly decreased with increasing particle size up to 200-250 µm for all drying temperatures. Nevertheless, regarding drying temperature effect, no clear trends were observed.

The evaluation of total color difference (ΔE*) trend showed minimum values at intermediate particle sizes (from 80 to 200 µm). Particularly, the found color difference can be classified as small ΔE*= 0.60, 1.60, 1.54, and 0.79 for BB35P, BB50P, BB60P, and BB75P, respectively, according to [6].

Summarizing, drying temperature effect on color properties of *Bifurcaria bifurcata* seaweed powders modifies from greenness to redness predominance at drying temperatures above 35ºC.

3.2. Seaweeds extracts

3.2.1. Total polyphenols content

Total polyphenols content values (TP) of aqueous extracts from *Bifurcaria bifurcata* dried at different temperatures are shown in Figure 2.
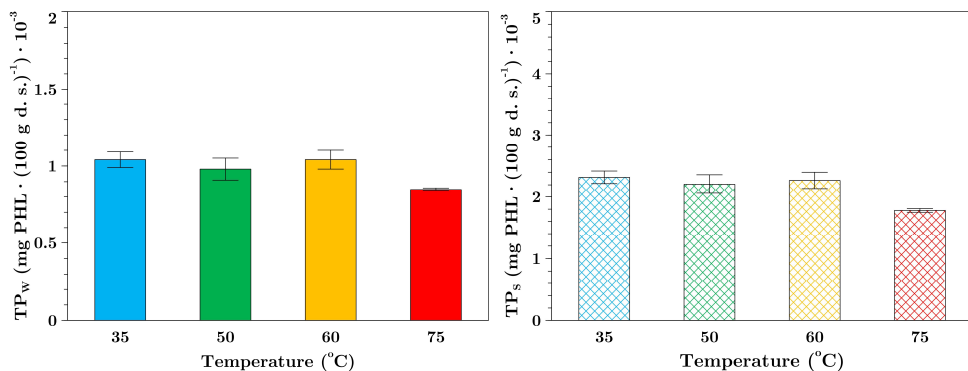
Fig. 2 Total Polyphenols (TP) of aqueous extracts of Bifurcaria bifurcata powders formerly dried at different temperatures (35ºC (■), 50ºC (■), 60ºC (■) and 75ºC (■)): referred to raw powder (mg

PHL·(100 g dry powder)⁻¹, TP_w (left) and total solids content in the extract (mg PHL·(100 g dry solids)⁻¹, TP_s (right).

It can be observed that TP_w content of *Bifurcaria bifurcata* extracts did not significantly change when drying with air-drying temperatures lower than 60ºC. TP_s in the extracts showed the same trend. The fact that both parameters, one referred to raw powder (TP_w) and the other to total solids content in the extract (TP_s) indicates that the significant differences in TP can be attributed to the different temperatures employed during drying and not to differences in the extraction yields.

Extracts obtained from seaweeds dried at 75ºC rendered the lowest TP values indicating that air-drying temperature clearly influences TP content of the extracts. The use of a hot air-drying technique can lead to thermally-promoted physical and chemical processes *i.e.* structural collapse of cells during drying, textural modifications, migrations of chemical compounds, accumulation of substances in cell membranes and several chemical reactions) during this step, which make difficult the subsequent extraction of phenolic compounds.

3.2.2. Carbohydrate content

The effect of drying temperature on carbohydrate content (CHO) of extracts can be observed in Figure 3.
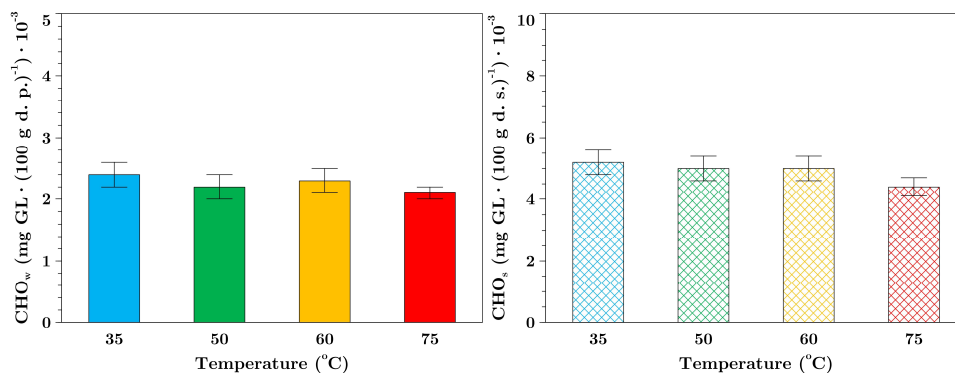
Fig. 3 Carbohydrate content (CHO) of aqueous extracts of Bifurcaria bifurcata powders formerly dried at different temperatures (35ºC (■), 50ºC (■), 60ºC (■) and 75ºC (■)): referred to raw powder (mg GL·(100 g dry powder)⁻¹, CHO_w (left) and total solids content in the extract (mg GL·(100 g dry solids)⁻¹, CHO_s (right).

As in the case of TP content, air-drying temperatures higher than 60ºC significantly decreased CHO content. The extracts obtained from BB75 showed the minimum values of CHO_w and CHO_s (2103 ± 143 mg eq. GL/100 g dry powder and 4426 ± 301 mg eq. GL/100 g dry solid, respectively) and the maximum value of CHO content was observed for BB35 (2394 ± 167 mg eq. GL/100 g dry powder and 521 ± 363 mg eq. GL/100 g dry solid, respectively). These results might be related to the physical and chemical processes that

may difficult the extraction of carbohydrates, in the same mode than the phenolic compounds. Similarly, to the TP content results, CHO obtained results indicated that their differences should be attributed to the effect of drying conditions (temperature) and not to the differences in the extraction yields, because trends of CHO_w and CHO_s values with temperature were similar.

3.2.3. Antioxidant activity

The antioxidant activity of aqueous seaweed extracts was evaluated by means of total DPPH radical scavenging activity (SA), Table 1.

Table 1. Radical scavenging activity (SA) of extracts from *Bifurcaria bifurcata* seaweeds dried at different temperatures.

Drying Temperature (ºC)	SA (%)
35	58.3±2.3[a]
50	54.7±7.2[a]
60	55.4±0.7[a]
75	45.3±2.5[b]

♣Data are presented as means±standar deviation. Data value of each parameter with different superscript letters in columns are significantly different (P≤0.05).

The effect of air drying temperature was very similar to the previously described for TP and CHO. Air drying temperatures higher than 60ºC significantly decreased the SA of *Bifurcaria bifurcata* aqueous extracts. The reduction in TP content and SA at high drying temperatures may be due to several factors: release of phenolic compounds bound to cell wall during drying; thermal degradation by oxidative enzymes; phenolic compounds may rapidly degrade at drying temperatures above 40ºC; binding of polyphenols to other substances (proteins) or alterations in their chemical structure [5,10,11].

The observed trend of SA and TP was previously reported in literature by other authors. Tello-Ireland et al. [5] reported a loss of antioxidant activity when drying *Gracilaria chilensis* at high temperatures (70ºC) and Gupta et al. [10] a 30% decrease in TP of *Himanthalia elongata* when dried at 40ºC in comparison with fresh seaweed.

4. Conclusions

Air drying temperature has a clear effect on phytochemical properties of brown seaweed *Bifurcaria bifurcata.* Regarding color properties, temperatures of drying higher than 35ºC enhance a change from greenness to redness predominance on the color of the seaweeds powders. In the case of total polyphenolic and carbohydrate contents and scavenging activity of the aqueous extracts, all parameters are significantly reduced when drying at temperatures higher than 60ºC. These results clearly define the drying conditions to be employed for this brown seaweed when specific properties of the final powders or extracts are required.

5. Acknowledgements

6. References

[1] Khairy, H.M.; El-Sheikh, M.A. Antioxidant activity and mineral composition of three mediterranean common seaweeds from Abu-qir bay, Egypt. Saudi Journal of Biological Sciences, 2015, 22, 623–630.

[2] Cornish, M.L.; Garbary, D.J. Antioxidants from macroalgae: potential applications in human health and nutrition. ALGAE, 2004, 25, 155–171.

[3] Santchurn S.J.; Arnaud E.; Zakhia-Rozis N.; Collignan, A. Drying: principles and applications. In: Huy YH (ed) Handb. Meat meat process, 2nd edn. CRC Press, Boca Raton 2012; 506.

[4] Ling, A.L.M.; Yasir, S.; Matanjun, P.; Abu Bakar, M.F. Effect of different drying techniques on the phytochemical content and antioxidant activity of *Kappaphycus alvarezii*. Journal of Applied Phycology, 2015, 27, 1717–1723.

[5] Tello-Ireland, C.; Lemus-Mondaca, R.; Vega-Gálvez, A.; López, J.; Di Scala, J. Influence of hot-air temperature on drying kinetics, functional properties, color, phycobiliproteins, antioxidant capacity, texture and agar yield of alga *Gracilaria chilensis*. LWT - Food Science and Technology, 2011, 44, 2112–2118.

[6] Adekunte, A.O.; Tiwari, B.K.; Cullen, P.J.; Scannell, A.G.M.; O'Donnell, C.P. Effect of sonication on color, ascorbic acid and yeast inactivation in tomato juice. Food Chemistry, 2010, 122, 500–507.

[7] Singleton, V.L.; Rossi, J.A. Colorimetry of total phenolics with phosphomolybdic-phosphotungstic acid reagents. American Journal of Enology and Viticulture, 1965, 16, 144–158.

[8] DuBois, M.; Gilles, K.A.; Hamilton, J.K., Rebers, P.A.; Smith, F. Colorimetric method for determination of sugars and related substances. Analytical Chemistry, 1956, 28, 350–356.

[9] Brand-Williams, W.; Cuvelier, M.; Berset, C. Use of a free radical method to evaluate antioxidant activity. LWT - Food Science and Technology, 1995, 28, 25–30.

[10] Gupta, S.; Cox, S.; Abu-Ghannam, N. Effect of different drying temperatures on the moisture and phytochemical constituents of edible irish brown seaweed. LWT - Food Science and Technology, 2011, 44, 1266–1272.

[11] Le Lann, K.; Jégou, C.; Stiger-Pouvreau, V. Effect of different conditioning treatments on total phenolic content and antioxidant activities in two *Sargassacean* species: Comparison of the frondose *Sargassum muticum* (yendo) fensholt and the cylindrical *Bifurcaria bifurcata* r. ross. Phycological Research, 2008, 56, 238–245.

Effect of spray drying conditions on antioxidants activity, flavonoids and total phenolic compounds of stevia rebaudiana

Chaparro-Hernández, I.[a]; Rodríguez-Ramírez, J.[a*], Méndez-Lagunas, L.[a], Barriada-Bernal, L.G. [a,b]

[a] Instituto Politécnico Nacional CIIDIR Oaxaca, Hornos 1003 Sta. Cruz Xoxocotlán, Oaxaca 71230, México.

[b] Consejo Nacional de Ciencia y Tecnología, Hornos 1003 Sta. Cruz Xoxocotlán, Oaxaca 71230, México

*E-mail of the corresponding author: jrodrigr@ipn.mx

Abstract

In this work the spray drying of the fresh stevia leaves aqueous extract without encapsulating agents was carried out. The effect of the inlet air temperature (160-200 ºC) and the feed flow rate (2-3 kg/h) on the total phenolic content, the total flavonoid content and the antioxidant capacity were evaluated using Folin-Ciocalteau, aluminum chloride and DPPH methods respectively. The inlet air temperature had a significant effect on all parameters evaluated that showed a decrease when increasing the inlet air temperature, the feed flow rate had a significant effect on total flavonoids content and the antioxidant capacity, by increasing the feed flow rate the inhibition of the DPPH radical decreased and the total flavonoid content increased. The treatment at 160 ºC and 3 kg/h retained highest total flavonoid content and the antioxidant capacity.

Keywords: *Phenolic compounds, stevia, spray drying, antioxidant capacity*

1. Introduction

Several families of compounds with nutraceutical y functional properties have been described in the stevia polyphenolic family. These compounds include phenolic compounds[1], flavonoids[2] and tannins[3].

Spray drying is a continuous operation technology commonly used to obtain high concentrations of soluble compounds[4]. For plant extracts, spray drying has been used to obtain products with high physical, chemical and microbiological stability, low storage costs and long shelf life[5].

This research aimed to evaluate the effect of the inlet air temperature and the feed flow (FF) rate of the spray drying of fresh stevia leaves aqueous extracts on the total phenolic compounds (TPC) and the antioxidant capacity (AA).

2. Materials and Methods

2.1 Raw material

Fresh leaves of S. *rebaudiana* variety Morita II were collected from an organic crop in Oaxaca, Mexico (Fig.1).

Fig. 1 Fresh stevia leaves.

2.2 Aqueous extract

Distilled water at 80 ºC was added to the fresh leaves in 5:1 v/w ratio, followed by ultrasonic extraction at 25 ºC. Afterward, it was left at 25 ºC for 48 h in the dark. The extract was filtered using a mesh sieve (pore size 0.149 mm).

2.3 Spray drying

A Mobile Minor concurrent flow spray dryer (Niro Copenhagen, Denmark), equipped with a pneumatic pulse rotary atomizer (TS-Minor, M02/B), was used. The atomization rate was set at 23,000 rpm, and the drying air flow was 84 ± 2 kg/h.

2.4 Moisture content and total solids

Moisture contents was determined according to the AOAC[6] method 934.01. The total solids of the extract, expressed as gram of dry matter per liter (g_{dm}/L), was determined according the AOAC[6] 990.19 method.

2.5 Determination of total phenolic content

Phenolic compounds were extracted with methanol acidified with hydrochloric acid at 1% (v/v).The total phenolic content was analyzed by the Folin-Ciocalteu method, as described by Periche et al [7].

2.5 Determination of antioxidant capacity

An 80% methanol solution was used for extraction of antioxidant compounds. The antioxidant capacity (%) was measured with the DPPH method according to Shukla et al [8].

2.7 Determination of total flavonoid content

An 80% methanol solution was used for extraction of flavonoids.The aluminum chloride colorimetric method was used, according to Kumazawa et al[9]. The absorbance was read at 510 nm. Standard de quercetin was used as references. Flavonoids were expressed as quercetin equivalent per litre (mg QE/mL).

2.8 Conversion of concentration units

In order to compare the effect of the drying conditions on the content of total phenolic compounds, the total flavonoid content and the antioxidant activity, the measurement units were expressed on a dry basis, using Eqs. (1) and (2):

$$C_T = \frac{C_C \times V_{ex}}{W_{dl}} \tag{1}$$

W_{dl} was calculated using Eq. (2):

$$W_{dl} = w_{fl}\left(1 - X_{wb}^{f}\right) \tag{2}$$

2.9 Statistical analysis

All the analysis were performed on triplicates. A 2^2 factorial design, with three central points, was applied to evaluate the effect of inlet air temperature (T_{in}) (160 and 200 ºC) and FF rate (2 and 3 kg/h) on the total phenolic content, antioxidant activity and total flavonoids content. Data analysis was done using ANOVA, and a response was performed with Statistica software Ver. 7.

3. Results and discussion

The concentration of phenolic compounds in the fresh leaves was 77.00 ± 0.59 GAE/g_{dl}, which was higher than that reported in other works. Periche et al[7] reported an average content of 44.40 ± 1.04 GAE/g_{dl} while Lemus-Mondaca et al [11] obtained 0.29 ± 0.02 GAE/g_{dl}.

The drying process significantly influenced ($p<0.05$) the phenolic compounds content. In all drying treatment (Table 1) the phenolic compound content decreased when the drying temperature was raised. The powders showed an average phenolic compounds loss of 57%. The FF rate did not have a significant effect on TPC ($p>0.05$). The results obtained in this work contrast with those obtained by Periche et al[7]. (2015), who dried stevia extracts by convection and lyophilized reporting an increased total phenolic content as temperature increases. This inconsistency could be due to direct exposure of the extract of ground fresh stevia leaves to the spray drying conditions. Therefore, the phenolic compounds were more exposed during the spray drying as opposed to when the whole leaf is dried, in which the phenolic compounds are protected in the vacuoles[12].

Table 1. Total phenolic, flavonoids and antioxidant capacity content.

Temperature °C	Feed flow rate kg/h	Phenolic compounds mg GAE/g_{dl}	Flavonoids mg QE/g_{dl}	Antioxidant capacity %
Fresh leaves		77 ± 0.59	170.45 ± 0.61	93.66 ± 0.55
200	2	40.90 ± 0.57	110.47 ± 0.48	88.68 ± 0.64
200	3	41.48 ± 0.78	117.26 ± 1.08	76.93 ± 0.30
160	2	49.93 ± 0.91	117.10 ± 0.24	86.36 ± 0.68
160	3	47.21 ± 0.11	124.68 ± 0.58	90.13 ± 0.78

The flavonoid concentration in the fresh leaves was 170.45 ± 0.61 mg QE/g_{dl}. In all drying treatments the flavonoid concentration decreased (Table 1).

For instance, Lemus-Mondaca et al [12] reported, in fresh samples, an lower amount of 0.89 ± 0.02 mg QE/g_{dl}. The flavonoids concentration was affected by the drying process ($p<0.05$), showing a decrease with the increase in temperature and an increased when FF decrement. This results could be because flavonoids are sensitive to oxidation and thermal degradation during spray drying[5].

The inlet air temperature and the FF rate significantly impacted ($p<0.05$) on the antioxidant capacity. The highest antioxidant capacity was observed at the lowest temperature (160 °C)

and the highest FF (3 kg/h). This results were similar to Georgetti et al[13] and Krishnaiah et al[14] who reported similar behavior for spray-dried soybean extract and *Morinda citrifolia*.

4. Conclusions

Spray drying is an efficient technology for the preservation of the antioxidant compounds of the fresh stevia leaves aqueous extract, even without the use of encapsulating agents. The antioxidant capacity of the final product ranged from 76 to 90%. The treatment at 160 ℃ and 3 kg/h retained highest total flavonoid content and the antioxidant capacity Therefore, the aqueous stevia leaves extract could be considered as a natural source of antioxidants, with prospects to be considered as a food complement.

5. Nomenclature

C	Total phenolic content, total flavonoid content or antioxidant activity concentration	mg/g_{dl}
FF	Feed flow rate	kg/h
V	Water volume	mL
W	Weight of the leaves	g_{dl}
X	Moisture content	g_w/g

Subscripts

C	Concentration obtained from the calibration curve	
dl	Anhidra leaves	
ex	Used for extraction	
fl	Fresh leaves	
in	Inlet	
dm	Dry matter	
T	Total	
wb	Water basis	

Superscripts

f	Fresh leaves

6. References

[1] Shukla, S.; Mehta, A., Mehta, P.; Bajpai, V. K.. Antioxidant ability and total phenolic content of aqueous leaf extract of Stevia rebaudiana Bert. Experimental and Toxicologic Pathology 2012, 64(7–8),807–811.

[2] Abou-Arab, A. E.; Abou-Arab, A. A.,; Abu-Salem, M. F. Physico-chemical assessment of natural sweeteners steviosides produced from Stevia rebaudiana bertoni plant. African Journal of Food Science 2010, 4(5), 269–281.

[3] Gasmalla, M.; Yang, R.; Amadou, I.; Hua, X. Nutritional Composition of Stevia rebaudiana Bertoni leaf: effect of drying method. Tropical Journal of Pharmaceutical Research 2014, 13(1), 61

[4] Taylor, P.; Souza, C. R. F.; Oliveira, W. P., Souza, C. R. F.; Oliveira, W. P. Powder Properties and system behavior during spray drying of *Bauhinia forficata* link extract. Drying Technology 2007, 6(24),37–41.

[5] Anandharamakrishnan, C.; Ishwarya, S. P. Spray Drying Technique for Food Ingredient Encapsulation; Wiley Blackwell, 2015

[6] A.O.A.C. Official Methods of Analysis of the Association of Official Analytical Chemists. Arlingtong, Virginia. 1984

[7] Periche, A.; Castelló, M. L.; Heredia, A.; Escriche, I. Influence of drying method on steviol glycosides and antioxidants in *Stevia rebaudiana* leaves. Food Chemistry 2015, 172, 1–6.

[8] Shukla, S.; Mehta, A., Mehta, P.; Bajpai, V. K. Antioxidant ability and total phenolic content of aqueous leaf extract of Stevia rebaudiana Bert. Experimental and Toxicologic Pathology 2012, 64(7–8), 807–811.

[9] Kumazawa, S.; Hamasaka, T.; Nakayama, T. Antioxidant activity of propolis of various geographic origins. Food Chemistry 2004, 84, 329-339.

[10] Méndez-Lagunas L.L.; Rodríguez-Ramírez J.; Cruz-Gracida M.; Sandoval-Torres S.; Barriada-Bernal G. Convective drying kinetics of strawberry (Fragaria ananassa): effect on antioxidant activity, anthocyanins and total phenolic content, Food Chemistry 2017, 230, 174–181,2017

[11] Lemus-Mondaca, R.; Ah-Hen, K.; Vega-Gálvez, A.; Honores, C.; O. Moraga, N. *Stevia rebaudiana* leaves: effect of drying process temperature on bioactive components, antioxidant capacity and natural sweeteners. Plant Foods for Human Nutrition 2016, 71(1), 49–56.

[12] Bruneton, J. Farmacognosia, Fitoquímica, Plantas Medicinales (Vol. 1); Acribia: España, 2001

[13] Georgetti, S. R.; Casagrande, R.; Souza, C. R. F.; Oliveira, W. P.; Fonseca, M. J. V. Spray drying of the soybean extract: Effects on chemical properties and antioxidant activity. LWT - Food Science and Technology 2008, 41(8), 1521–1527

[14] Krishnaiah, D.; Sarbatly R.; Nithyanandam R. Microencapsulation of *Morinda citrifolia* L. extract by spray-drying. Chemical Engineering Research and Design 2012, 90(5), 26-36

Effects of drying conditions on the content of glycosides and antioxidants of packed bed of stevia leaves

Rodríguez-Ramírez J.ª*, Noyola-Altamirano, B.ª, Barriada-Bernal, L.G.ª,ᵇ, Méndez-Lagunas L.L. ª

ª Instituto Politécnico Nacional CIIDIR Oaxaca, Hornos 1003 Sta. Cruz Xoxocotlán, Oaxaca 71230, México.
ᵇ Consejo Nacional de Ciencia y Tecnología, Hornos 1003 Sta. Cruz Xoxocotlán, Oaxaca 71230, México.

*E-mail of the corresponding author: jrodrigr@ipn.mx

Abstract

The commercial value of stevia dehydrated leaves is related to the content of glycocides and their appearance. The present work approaches the effect of packed bed drying conditions (temperature, flow rate and solid loading) on glycosides and antioxidants activity of stevia leaves of Morita II variety. Diffusion coefficient was calculated. The drying times ranged between 34 and 160 minutes, the temperature was the most significant factor followed by solid loading and flow rate. Drying increases the concentration of antioxidants, stevioside and reduces rebaudioside A.

Keywords: drying, packed bed, stevia rebaudiana, glycosides, antioxidants

Effects of drying conditions on the content of glycosides and antioxidants of packed bed of Stevia leaves

1. Introduction

Stevia leaves are a source of bioactive compounds, among which are steviol glycosides that confer a high sweetening capacity and antioxidant compounds such as phenols and flavonoids, which has a therapeutic value[1]. The commercial value of stevia dehydrated leaves is related to the content of glycosides and their appearance. Some drying methods has been applied on stevia leaves, among shade drying, convective drying with longitudinal-flow at low (30 and 80°C) and high temperatura(100 and 180°C) and liophylization[2, 3, 4]. In the traditional process, fresh leaves are spread on a mesh or perforated plate in thin or thick layer and warm air is forced through the layer leaves to remove the moisture. The drying time could be reduced by fluidizing the leaves, but the quality of the final product may decrease. This research aimed to evaluate the effect of the drying conditions (temperature, flow rate and solid loading) of packed bed (PB) of stevia leaves Morita II variety on glycosides and antioxidants content.

2. Materials and Methods

2.1. Raw material

Fresh leaves of S. *rebaudiana* variety Morita II were collected from an organic crop in Oaxaca, Mexico (latitude: 16º19', longitude: 98º23'). Fresh leaves with no mechanical damage, no apparent evidence of fungi or bacteria harm and uniform color were selected.

The dimensions, density, and moisture content of the fresh leaves were measured. The void fraction of the bed was calculated by dividing the density of the bed between the density of the leaves. The thickness was measured with a micrometer. The area of the leaves was measured with image analysis using the ImageJ® version 1.50i program. The density of the leaves was determined using the buoyant force method (YDK 01S kit, Denver Instrument).

The moisture content was determined by the method 934.01 of the AOAC. [5].

2.2. Fixed Bed Drying

The samples were dehydrated in a lab scale fluidized bed dryer with a glass fluidization tube with a height of 50 cm, a diameter of 10 cm and a thick of 0.2 cm. The packed bed drying process was carried out introducing the load of leaves in a perforated plastic basket. The dried air is heated with an electric resistance of 1 kW and the temperature is regulated by a PID controller (Love control, 32DZ). The air flow is regulated with an adjustable AC drive controller using a asynchronous motors (Altivar™ 16 Telemecanique). The drying kinetics were obtained by weighing the fluidization tube and the loading of the stevia leaves in a precision balance (Sartorius ED4202S-CW), considering time intervals determined by the drying conditions (2, 3 or 5 min). The drying was finished when the weight does not change in three consecutive measurements. The effective diffusion coefficient was calculated using

the analytical solution of the Fick equation considering only the first term of the serie and employing experimental data (Ln(X-X_f/Xo-X_f) vs time), with lineal tendence and a coefficient correlation >0.995.

2.3. Antioxidant compounds.

The measurement of antioxidant capacity (**C_A**), total phenolic content (**F_T**) and total flavonoid content (**F_L**), were determined using the 2,2-diphenyl-1-picrylhydrazyl free radical scavenging activity, the Folin-Ciocalteu method and the aluminum chloride colorimetric method respectively, as detailed by Méndez-Lagunas *et al.* [6]. All the chemical products were purchased in Sigma–Aldrich.

2.4. Steviol glycosides compounds.

2.4.1. Chemicals and reagents

Acetonitrile and water (HPLC grade, Sigma Aldrich, USA) were used for the mobile phase preparation. Standard of stevioside and rebaudioside A were purchase in Sigma Aldrich.

2.4.2. Sample preparation

Fresh (0.4 g) or dry (0.1 g) ground leaves were mixed 5 mL de agua. The mixture was sonicated at 44 KHz for 20 minutes at room temperature and centrifuged at 2080 rpm for 5 min. The supernatant was separated from the precipitate. Two consecutive extractions were made to the precipitate. The accumulated volume of the supernatant was measured and stored in amber vials. An aliquot (20 µl) of the accumulated of the three supernadant consecutives extractions was used for the quantification of stevioside (E_V) and rebaudioside A (R_A).

2.4.3. HPLC analysis

An isocratic HPLC method was performed for the determination of steviol glycosides using an ODS Hypersil C18 column (250×4.6 mm, particle size 5 µm) and a UV detector set at 210 nm. The mobile phase consisted of acetonitrile-water (35:65, v/v) at a flow rate of 1 ml/min. Data analysis was carried out using Chromera software. Calibration curves of stevioside and rebaudioside A were constructed over the range 0.03-0.9 mg/ml. In order to compare the effect of the drying conditions on the R_A and E_V concentrations, the units of measure were expressed on the basis of dry matter (mg/g_{dm}).

2.5. Experimental design and statistical analysis

The drying tests were carried out following a 3x2x2 complete factorial experimental design with 3 replicas. The factors studied were temperature, T (40, 50 and 60 °C), air flow, ū, (2 and 3.5 m/s) and area solid loading, ρ_A (1.5 and 3 kg/m^2).

All the chemical analysis was performed on triplicates. The analysis of variance (ANOVA) was used to evaluate the effect of operating conditions on the drying time, the concentration of antioxidants (antioxidant capacity, total phenols and flavonoids) and the concentration of glycosides (stevioside and rebaudioside A). The software NCSS version 9 was used to perform the statistical analysis.

3. Results and Discussions

3.1. Physical characteristics. Fresh stevia leaves had a moisture content (Xo) of 0.75 ± 0.03 kg_w/kg_{wm}, a thickness of 2.08 ± 0.1 mm, a maximum equivalent diameter of 6.53 cm and a minimum of 2.53 cm. The density of the leaves was 0.95 ± 0.031 g/cm^3. The packed bed of 1.5 kg/m^2 solid loading had a bed height of 3.2 cm, a bulk density of 60 kg/m^3 and a void fraction of 0.93, while the bed of 3.0 kg/m^2 had a height of 5.2 cm, a bulk density of 80 kg/m^3 and a void fraction of 0.92.

3.2. Drying kinetics. Figures 1 show drying curves of packed bed of stevia leaves. The curves are grouped depending on the drying temperature, the air flow and the packing. The drying rate increases with the increase in temperature and air velocity, as well as with the decrease of solid loading. At low air flow the packaging has a greater effect on the drying rate. The drying rate curves have a second-order polynomial tendency.
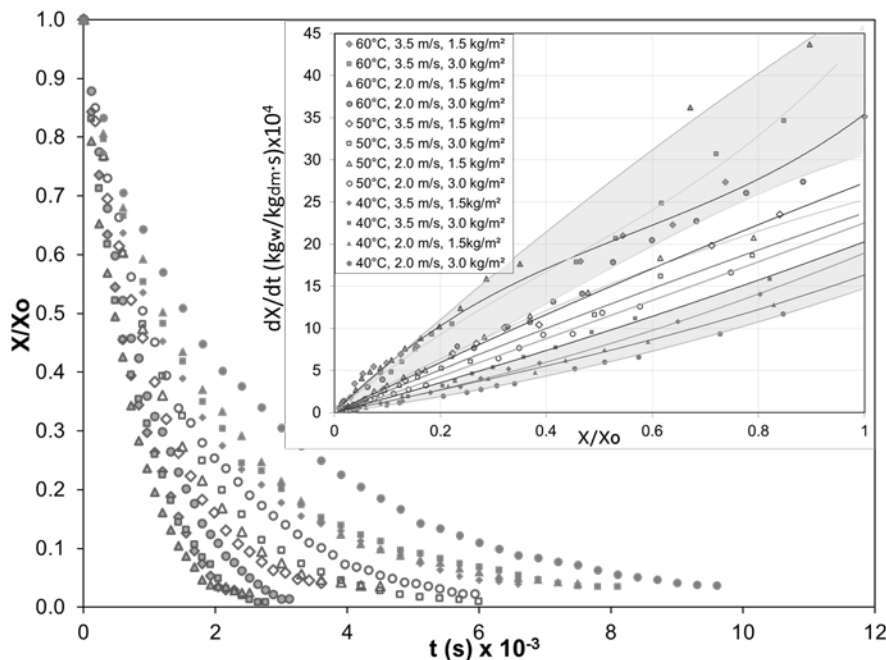
Fig. 1 Drying curves of leaves of stevia in packed bed.

Table 1. Effective diffusivity in stevia leaves and drying time of packed bed of leaves.

T (°C)	ū (m/s)	ρ_A (kg/m^2)	t (min)	D_{eff} *10^{10} (m^2/s)
40	2.0	3.0	160	6.73
40	2.0	1.5	130	9.31
40	3.5	3.0	135	9.74
40	3.5	1.5	124	10.65
50	2.0	3.0	87	11.61
50	2.0	1.5	75	16.18
50	3.5	3.0	70	13.26
50	3.5	1.5	60	15.80
60	2.0	3.0	40	18.17
60	2.0	1.5	36	21.74
60	3.5	3.0	36	21.27
60	3.5	1.5	34	21.27

Table 1 shows the diffusivity of water and the drying time to reach a moisture content of 0.10 kg$_w$/ kg$_{dm}$. Drying temperature followed by the solid loading and the air flow and the air temperature-solid loading interaction are statistically significant (p <0.05) on drying time. The drying time in trays with longitudinal flow,[3] is three times less than with flow through in packed bed. The air temperature is significant (p <0.05) on effective diffusivity. The air flow and the solid loading affect the diffusivity value, however, its effects are less than the temperature.

3.3. Antioxidant compounds. The content of phenolic compounds, flavonoids and antioxidant capacity are shown in table 2. The antioxidant capacity of dryed stevia leaves is similar with the fresh leaves. The content of phenols and flavonoids is higher in dry leaves than in fresh stevia leaves, however, the drying conditions studied did not have a significant effect. The solid loading could give a difference in antioxidant compound. The increase in polyphenols may be due to the breakdown of cellular constituents of the material, associated with the availability of precursors of phenolic molecules that are derived from the non-enzymatic interconversion between its.[3, 7]

3.4. Steviosides compounds. The content of rebaudioside A (R$_A$) decreases and the content of stevioside (E$_V$) is increased in dehydrated leaves relative to fresh leaves (Table 3). The degradation of steviol glycosides by hydrolysis has been proposed to explain this behavior [8]. A decrease in rebaudioside A may be related to the increase in the content of stevioside. The three variables, temperature, air velocity and charge density, as well as their interactions,

have a significant effect (p <0.05) on the content of E_V and R_A. Lower flow rate and higher solid loading give a higher content of R_A.

Table 2. Total phenolic compounds, flavonoids and antioxidant capacity of stevia leaves.

T	ū	ρ_A	F_T	F_L	C_A
°C	m/s	kg/m²	mgGAE/g_{dm}	mgQE/g_{dm}	%Inh
	Fresh		71.50±1.74	161.46±1.0	92.79±0.13
40	2.0	1.5	91.33±0.39	135.14±3.75	91.55±1.63
40	2.0	3.0	114.60±1.01	275.90±1.35	92.58±0.95
40	3.5	1.5	95.82±2.92	126.45±3.33	92.00±0.12
40	3.5	3.0	118.04±0.11	373.86±3.97	93.80±0.34
50	2.0	1.5	115.27±1.25	342.88±5.71	91.72±2.90
50	2.0	3.0	118.19±0.07	319.96±9.60	93.66±0.33
50	3.5	1.5	81.85±1.86	100.19±3.99	92.40±1.75
50	3.5	3.0	102.08±1.29	264.89±3.47	92.93±0.52
60	2.0	1.5	91.35±1.67	259.49±6.67	93.16±0.57
60	2.0	3.0	94.43±0.07	308.48±5.70	92.80±0.29
60	3.5	1.5	83.85±0.89	276.59±3.29	92.65±0.40
60	3.5	3.0	114.45±4.72	402.68±1.42	93.31±0.18

Table 3. Rebaudioside A and stevioside content of stevia deshydrated leaves.

T	ū	ρ_A	R_A	E_V
°C	m/s	kg/m²	mg/g_{dm}	mg/g_{dm}
	Fresh		154.69±0.13	22.54±0.08
40	2.0	1.5	79.57±7.96	38.27±15.01
40	2.0	3.0	87.14±1.82	45.21±14.08
40	3.5	1.5	87.97±1.84	41.45±0.19
40	3.5	3.0	86.15±4.72	40.33±3.79
50	2.0	1.5	92.94±4.43	35.25±13.02
50	2.0	3.0	85.95±1.12	51.85±2.28
50	3.5	1.5	77.42±11.51	36.13±9.34
50	3.5	3.0	86.72±5.75	40.78±1.39
60	2.0	1.5	81.81±0.32	30.67±10.84
60	2.0	3.0	88.91±0.87	43.07±19.67
60	3.5	1.5	82.80±4.64	38.94±10.70
60	3.5	3.0	83.68±5.46	44.02±6.02

4. Conclusions

The three variables evaluated (temperature, air flow and solid loading) had a significant effect on the drying time. The order of importance was the temperature, the solid loading and the flow rate.

The drying in packed bed increases the content of phenols and flavonoids of stevia leaves, none of the variables studied was significant in the content of antioxidants, however, the solid loading is a factor that must be taken into consideration; the higher the solid loading, the higher the antioxidant content.

The drying in packed bed reduce the content of rebaudioside A (R_A) and increases the content of stevioside (EV) of stevia leaves. The load of solids was a significant factor, the higher solid loading, the higher content of steviosides.

The proposed drying conditions for the conservation of the physicochemical properties in packed bed of the stevia leaves are 50°C, 2 m/s and 1.5 kg/m^2

5. References

[1] Wölwer-Rieck, U. The leaves of Stevia rebaudiana (Bertoni), their constituents and the analyses thereof: A review. Journal of Agricultural and Food Chemistry 2012, 60(4), 886–895.

[2] Periche, A.; Castelló, M. L.; Heredia, A.; Escriche, I. (2015). Influence of drying method on steviol glycosides and antioxidants in Stevia rebaudiana leaves. Food Chemistry 2015, 172, 1–6.

[3] Lemus-Mondaca, R.; Ah-Hen, K.; Vega-Gálvez, A.; Honores, C.; Moraga, N. Stevia rebaudiana Leaves: Effect of Drying Process Temperature on Bioactive Components, Antioxidant Capacity and Natural Sweeteners. Plant Foods for Human Nutrition 2016, 71(1), 49–56.

[4] Gasmalla, M.; Yang, R.; Amadou, I.; Hua, X. Nutritional Composition of Stevia rebaudiana Bertoni leaf: effect of drying method. Tropical Journal of Pharmaceutical Research 2014, 13(1), 61.

[5] AOAC Official Methods of Analysis of the association of official analytical chemists. Arlingtong, Virginia, 1984.

[6] Méndez-Lagunas L.L.; Rodríguez-Ramírez J.; Cruz-Gracida M.; Sandoval-Torres S.; Barriada-Bernal G. Convective drying kinetics of strawberry (*Fragaria ananassa*): effect on antioxidant activity, anthocyanins and total phenolic content. Food Chemistry 2017, 230, 174–181.

[7] Shukla, S.; Mehta, A.; Mehta, P.; Bajpai, V.K. Antioxidant ability and total phenolic content of aqueous leaf extract of Stevia rebaudiana Bert. Experimental and Toxicologic Pathology 2012, 64(7–8), 807–811.

[8] Jooken, E.; Amery, R.; Struyf, T.; Duquenne, B.; Geuns, J.; Meesschaert, B. Stability of Steviol Glycosides in Several Food Matrices. Journal of Agricultural and Food Chemistry 2012 60 (42), 10606-10612.

Effect of ultrasound on drying kinetics of El Henna leaves (Lawsonia inermis)

Bennaceur, S.[a]*; Bennamoun, L.[b]; Mulet, A. [c]; Draoui, B. [a]; Carcel, J. A.[c]

[a] Laboratoire d'Energétique en Zones Arides, Université Tahri Mohamed de Béchar, Algeria.

[b] Department of Mechanical Engineering, University of New Brunswick, NB,Canada.

[c] ASPA group, Department of Food Technology, Universitat Politècnica de València, Valencia, Spain.

*E-mail of the corresponding author: bssaide@yahoo,fr

Abstract

In this work the influence of some process variable on drying rate of henna leaves was studied. For this reason, henna leaves were dried (1 m/s) with and without ultrasound application at three temperatures, 40, 50 and 60 °C. As can be expected, the higher the temperature the faster the drying process. Ultrasound application increase drying rate at every temperature tested. Drying kinetics were modeled by using different experimental models. Weibull model provided the best fit for henna leaves drying kinetics.

Keywords:Ultrasonic; Weibull model; henna leave;, temperature.

1. Introduction

Henna *(Lawsonia inermis)* leaves (Fig. 1) is an important product consumed widely in Algerian society. This plant is found mainly in the southern region of Algeria and it is available eight months a year. Its height can reach 2-3 m at the end of its life. The dark green oval leaves (2-4 cm long) present hih interest not only for cosmetic but also for medicinal issues [1].

Among the methods used to conserve medicinal plants, drying is one of the most extended. The reduction of the moisture content prevents the degradation of this material [2] making possible its use for different applications [1]. The traditional drying of henna by exposition to the sun is being substituting by convective hot air drying. This permits to standardize the production and avoid problems such as contamination with particles (dust) or insects. However, drying can highly affect the quality attributes of henna leaves. Therefore drying kinetics studies can contribute to the better understanding of the process and select the best drying conditions that permits to obtain a high quality product.

Fig. 1 The fresh leaves of El henna (Lawsonia inermis).

High intensity ultrasound has been used to intensify drying process. This could permit the use of milder drying conditions that can improve the product quality. Thus, the aim of this work was to determine the drying kinetics of henna leaves at different temperatures and quantify the influence of the application of ultrasound during the process.

2. Materials and Methods

2.1. Experimental drying

2.1.1. Sample preparation

The henna leaves studied were cultivated and neatly transported by air from the wilaya of Béchar, in the south west of Algeria, to the laboratory of the Analysis and Simulation of Agro-food Process (ASPA) research group, Food Technology Department, Universitat Politècnica de València, Spain. There, they were stored in a refrigerator at 5±1 °C until drying experiments. The moisture content was measured by placing the samples in a vacuum oven at 70 °C and 200 mmHg until constant weight, following standard method n°934.06 [3].

2.1.2. Experimental drying kinetics

Drying kinetics were carried out in an ultrasonically-assisted convective dryer previously described [4,5]. This equipment is a laboratory scale dryer modified to apply power ultrasound, with automatic control of the air temperature and velocity and provided with an automatic sample weighing system.

01	Fan
02	Heating unit
03	Anemometer
04	Three-way valve
05	Thermo-couple
06	Sample loading chamber
07	Coupling material
08	Pneumatic moving arms
09	Ultrasonic transducer
10	Vibrating cylinder
11	Sample holder
12	Balance
13	Impedance matching unit
14	Wattmeter
15	High-power ultrasonic generator
16	PC
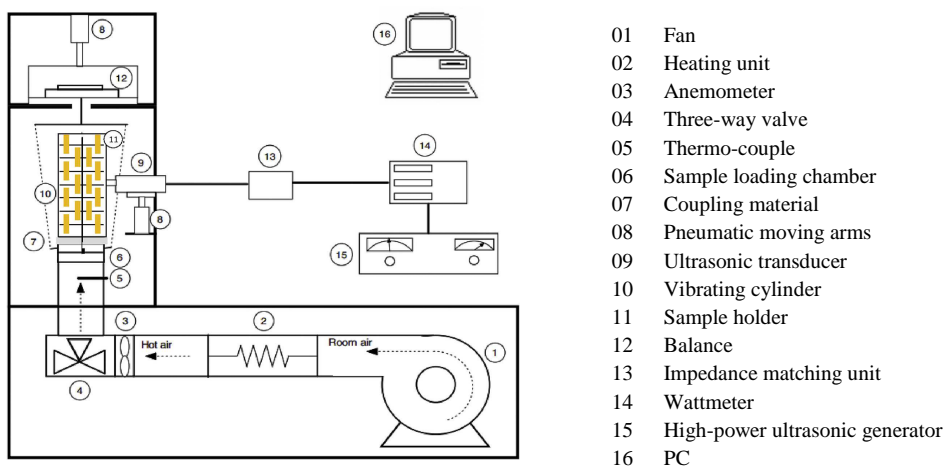
Fig. 2 Scheme of ultrasonicallyassisted convective drier[6].

The drying experiments were carried out in triplicate at three different air temperatures (40, 50 and 60 °C) without (Air) and with ultrasound application (Air+US; 21.7 kHz, 20.5 kW/m^3). In every case, an air velocity of 1 m/s was used. The dehydration process was stopped when samples lost 75% of their initial weight.

2.2. Drying kinetics

The evolution of moisture content of samples during drying was determined by weighting the henna leaves after different drying times and the initial moisture content [7]. The equilibrium moisture content of the henna leaves was experimentally obtained by placing the henna samples at the drying conditions for a very long time. This time was enough to have no difference in sample weight for two hour. Then the moisture content of samples was expressed in non-dimensional way by using Eq. 1 [8].

$$MR = \frac{X(t) - X_{eq}}{X_0 - X_{eq}} \tag{1}$$

Where MR is the non-dimesional moisture content or moisture ratio, $X(t)$ is the moisture content after a drying time (kg water/kg dry matter, d.m.), X_0 is the initial moisture content of samples (kg water/kg d.m.) and X_{eq} (kg water/kg d.m.) is the equilibrium moisture content.

2.3. Mathematical modeling

Given the complexity of the phenomena involved in the drying of a product, it has been proposed mathematical models of different complexity including theoretical and empirical models. Thus, theroretical models can provide parameters, such as diffusivity, than can help to better understand the drying process. On the other hand, empirical or semi-empirical relationships permit to describe the drying curves and quantify the influence of drying conditions on drying rate. [8] Thus, in the case of this work eight different empirical models were used to describe the drying kinetics (Table 1).

Table 1. Mathematical models applied to the experimental drying kinetics

Name of model	Model
Newton	$MR = \exp(-kt)$
Page	$MR = \exp(-kt^n)$
Henderson and Pabis	$MR = a \times \exp(-kt)$
Logarithmique	$MR = a \times \exp(-kt) + c$
Tow term	$MR = a \times \exp(-k_0 t) + b \times \exp(-k_1 t)$
Weibull	$MR = \exp(-t/k)^n$
Diffusion approach	$MR = a \times \exp(-kt) + (1-a) \times \exp(-kbt)$
Wang and Singh	$MR = 1 + a.t + b.t^2$

The parameters of each equation were identified by using the non-linear optimization method of Marquardt-Levenberg (CurveExpert and Origin 6.1 sotware). To assess the goodness of the fit, the correlation coefficient (r) (Eq. 2) and standard error (EST) (Eq. 3) were calculated.

$$r = \sqrt{1 - \frac{\sum_{i=1}^{n_{exp.data}} \left(MR_{\exp i} - MR_{cali} \right)^2}{\sum_{i=1}^{n_{exp.data}} \left(\overline{MR}_{\exp} - MR_{\exp i} \right)^2}} \tag{2}$$

$$EST = \sqrt{\frac{\sum_{i=1}^{n_{exp.data}} \left(MR_{\exp i} - MR_{cali} \right)^2}{n_{exp.data} - n_{param}}} \tag{3}$$

Where MRcali is the calculated value of the non-dimesional moisture content by using the tested model, MRexpi is the experimental value of equilibrium moisture content, nparam is the number of parameters of the particular model and nexp.data is the number of experimental points. The mean value of the non-dimesional moisture content ($\overline{MR}$) was calculated as follows:

$$\overline{MR} = \frac{1}{n_{exp.data}} \sum_{i=1}^{n_{exp.data}} MR_{\exp i} \tag{5}$$

3. Results and discussion

3.1. Experimental drying kinetics

The initial moisture content of henna leaves was 2.33 kg water/kg d.m. Temperature affects the experimental drying kinetics; the higher the temperature the faster the process (Fig. 3). Thus, the time needed to achieve a moisture content of 1 kg water/kg d.m. was 2.64 h at 40 ºC, 1.94 h at 50 ºC and 1.25 h at 60 ºC.

Ultrasound application significantly accelareted drying of Henna leaves (Fig. 4). In this sense, at 40 ºC, drying time in experiments carried out with ultrasound was 50 % lower than the needed in experiments carried out without ultrasound application. The influence of ultrasound in drying rate was quite similar at the different temperatures tested.
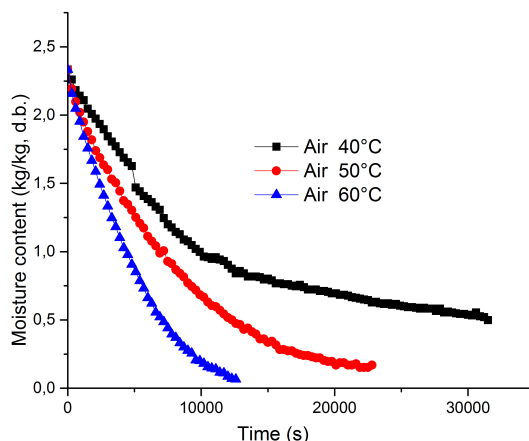
Fig. 3 Experimental drying kinetics of the Henna leaves without ultrasound application .

3.2. Modelling

Among the different models tested, the Weibull model gave the best fit, that is, the highest value of *r* parameter and the lowes of *EST*. The model parameters identified are shown in Table 2. The studied process variables, temperature and ultrasound application, did not significantly affect ($p<0.05$) the *n* parameter. This parameter is related with the product considered.

On the contrary, *k* parameter, which is inversely proportional to the drying rate, was affected by both, temperatue and ultrasound application. Thus, the higher the temperature, the lower the *k* value, which indicates a faster drying.

The application of ultrasound also reduced the identified k figures, meaning a lower time of drying becoming this influence more important at moderate drying temperature. Thus, at ºC, the *k* identified in *Air+us* experiments was 27% lower than the idientified in *Air* experiments. This difference was 16 % at 50 ºC and only 7% at 60 ºC.

Table 2. Weibull model parameters identified by fitting to the experimental drying kinetics of henna leaves at different temperature and without (Air) and with (Air+us) ultrasound application. Correlation coefficient (r)and standar error (EST)

Type of experiment	Temperature (ºC)	n	K	r	EST
Air	40	0.900	14434.7	0.9948	0.0208
Air+us	40	1.062	10523.7	0.9985	0.0136
Air	50	1.088	7495.6	0.9979	0.0173
Air+us	50	0.993	6286.0	0.9962	0.0207
Air	60	1.114	4705.3	0.9939	0.0271
Air+us	60	1.171	4391.8	0.9900	0.0322

Henna leaves dried at 40 ºC, with or without ultrasound application, kept their green color while samples dried at higher temperature showed a brown color. This fact indicates the limited deterioration of the active product at the lowest temperature tested compared with the highest ones. Therefore, ultrasound application represent an alternative to intensify drying rate during drying at milder tempertures and preserving product quality.
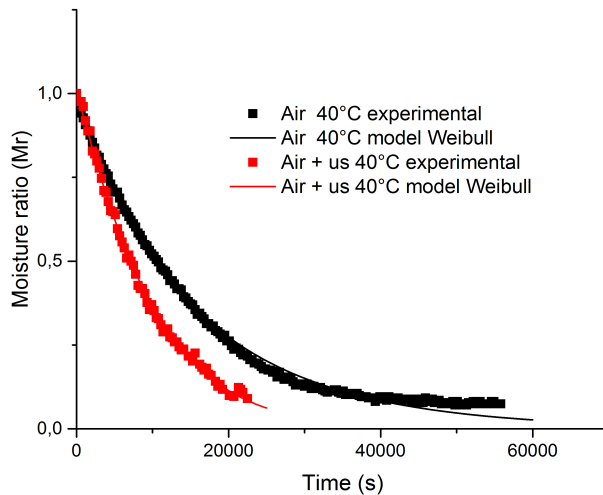
Fig. 4 The experimental moisture ratio described by the Weibull model of the Henna leaves without and with ultrasound.

4. Conclusions

The drying kinetics of henna leaves was affected by both temperature and ultrasound application. The higher the temperature the faster the process. However, the green color of samples, which is a measurement of the quality of final product, was maintained only at the lowest temperature tested, 40ºC. The ultrasound application accelerate the drying. Its application at low temperature was an interesting alternative to accelerate the drying maintain the quality.

5. Acknowledgements

6. References

[1] Fortin, D.L.O.M. ; Maynart, G. Plantes médicinales du Sahel; Enda-Editions : Dakar, 2000.

[2] Tiris, C.; Tiris, M.; Dincer, I. Energy efficiency of a solar drying system. International Journal of Energy Research 1996, 20, ,767–770,

[3] AOAC . Official method of analysis of the Association of Official Analytical Chemists International. 16th edition, 3rd revision, March, 1997.

[4] Carcel, J.A.; García-Perez, J.V.; Riera, E.; Mulet, A. Influence of high intensity ultrasound on drying kinetics of persimmon. Drying Technology 2007, 25, 185-193.

[5] Riera, E.; García-Perez, J.V.; Carcel, J.A.; Acosta, V.; Gallego-Juarez, J.A. Computational study of ultrasound-assisted drying of food materials. In Innovative Food Processing Technologies: Advances in Multiphysics Simulation. Knoerzer, K., Juliano, P., Roupas, P., Versteeg, C. Eds.; John Wiley & Sons Ltd, 2011, 265-301.

[6] Do Nascimento, E.M.G.C; Mulet, A.; Ramírez-Ascherí, J.L.; Piler De Carvalho, C.W.; Cárcel, J.A.. Effects of high-intensity ultrasound on drying kinetics and antioxidant properties of passion fruit peel. Journal of Food Engineering 2016, 170, 108-118.

[7] Lahsasni, S.; Kouhila, M.; Mahrouz, M.; Idlimam, A.; Jamali, A. Thin layer convective solar drying and mathematical modeling of prickly pear peel (Opuntia ficus indica). Energy 2004, 29(2), 211-224.

[8] Belghit, A.; Kouhila, M.; Boutaleb, B.C. Experimental Study of Drying Kinetics by Forced Convection of Aromatic Plants. Energy Conversion and Management 2000, 41(12), 1303–1321.

[9] Santacatalina, J.V.; Rodríguez, O.; Simal, S.; Cárcel, J.A.; Mulet, A.; García-Pérez, J.V. Ultrasonically enhanced low-temperature drying of apple: Influence on drying kinetics and antioxidant potential. Journal of Food Engineering 2014, 138, 35-44.

Spray drying of lipid nanosystems (SLN and NLC) loaded with *Syzygium aromaticum* essential oil

Rosa, D.M.; Oliveira, W.P.[*]

University of São Paulo, Faculty of Pharmaceutical Sciences of Ribeirão Preto, Ribeirão Preto, Brazil

*E-mail of the corresponding author: wpoliv@fcfrp.usp.br

Abstract

A quality by design approach was used to investigate the influence of formulation composition and spray drying conditions on physicochemical properties of redispersable lipid based nanosystems loaded with Syzygium aromaticum essential oil. Four critical independent variables were studied: presence or absence of the liquid lipid oleic acid (0% - 1%), of the cationic surfactant CTAB (0% and 1%), inlet drying temperature (60 ºC -80 ºC), and ratio of the drying aids (ADJ) regarded to total formulation constituents weight (1:1 and 2:1). Resuls showed the production of spray dried redispersable lipid systems loaded with essential is feasible under very restrict conditions.

Keywords: Encapsulation; lipid systems; essential oil; spray drying; redispersable.

1. Introduction

Currently, significant attention has been addressed towards the use of essential oils (EOs) in food, pharmaceutical and cosmeceutical sectors, mainly due to their broad spectrum of proven biological activities, particularly antifungic, antibacterial insecticide, antiviral, antioxidant, among others.[1] EOs are hydrophobic, volatile and odoriferous liquids, produced by the plant secondary metabolism, and consist of complex mixtures of chemicals.[2] Several limitations exhibited by the EOs such as the high volatility, insolubility in aqueous systems and propensity to degraded due to environmental factors, would deter they use in more elaborated products. Encapsulation processes can modulate and improve the EO physicochemical properties, thus expanding its potential of use in a high variety of products. In this way, the incorporation of essential oils in lipid systems such as solid lipid nanoparticles (SLNs) and nanostructured lipid carriers (NLCs) can be a promising strategy to modify its physicochemical properties; which might positively alter its stability, volatility, water solubility, bioavailability and biological activity.[3] Since the SLNs and NLCs are generally presented in liquid forms; the drying of these systems can furnish a redispersible powdered product with higher shelf-life; which can be reconstituted when exposed to aqueous solution or be used in more refined applications.[4-6] The drying process as well as the constituents of the encapsulating composition affects directly the physicochemical product properties, such as product granulometry, microstructure, redispersability capability, retention of bioactive compound, and so on. These characteristics affect strongly the product functionality, stability and other technological and biopharmaceutical properties. Several drying technologies can be used to dehydrated these systems, including freeze drying and spray drying.[7] Although spray drying is one of the most used method for drying and encapsulation of thermosensitive materials, its use for drying of emulsions and other lipid systems are barely reported in the current literature.[8,9] Most of the lipids and surfactants used to develop these systems (and the EOs as well), are liquid at ambient temperature or present low melting temperatures, turning their dehydration process challenging. On the other hand, *Syzygium aromaticum*, popularly knowed as clove, is an important aromatic plant rich in phenolic antioxidants, and has been used for centuries as a food preservative and pain reliever.[10] Clove buds contains an essential oil rich in eugenol, substance usually linked to its biological properties, such as antioxidant, antimicrobial, larvicide, and anti-inflammatory. So, clove EO is a promising active phytopharmaceutical ingredient. Therefore, the aim of this work was to investigate the spray drying of lipid based nanosystems (SLNs and NLCs) loaded with *Syzygium aromaticum* EO, evaluating the effects of formulation composition and spray drying temperature on physicochemical properties of the dried product.

2. Materials and Methods

Syzygium aromaticum EO (from a clove essential oil producer located in Valença, BA, Brazil), solid lipid Precirol® ATO 5 (glyceryl palmitostearate - Gattefossé, France – Melting point ~56 °C), liquid lipid oleic acid (cis-9-octadecanoic acid - LabSynth, Brazil), anionic surfactant Kolliphor P 188 (Poloxamer® 188 - BASF, Brazil), cationic surfactant CTAB (cetyl trimethylammonium bromide - Sigma-Aldrich, Germany - Melting point 237-243 °C), and reverse osmose water were the materials used for the development of primary SLNs and NLCs. Arabic gum (AG - Nexira, Brazil), Aerosil® 200 (SiO_2 - Evonik Degussa, Germany), Maltodextrin DE-10 (MD - Ingredion, Brazil), were used as spray drying aid (ADJ). Eugenol and eugenyl acetate with purity of 99.0 % and 98.0 % respectively (Sigma-Aldrich, Germany), HPLC grade solvents (Sigma-Aldrich, Germany), and milliQ® water were used in the quantification of Eugenol (EU) and Eugenyl acetate (ACT) by high performance liquid chromatography with diode array detection (HPLC-DAD).

2.1 Preparation of SLNs and NLCs formulations

The preparation of the SLNs and NLCs loaded with *Sygyzium aromaticum* EO was conducted by the phase inversion method. Solid lipids were melted at 10 ºC above their melting temperature, and mixed with 1 % of the liquid lipid oleic acid (only for NLCs). EO at concentration of 3 % (wet basis) was added to this lipid phase and maintained at same temperature. 3% of Poloxamer 188 and 1% of CTAB (when used) were solubilized in the reverse osmose water and kept at the same temperature of the lipid phase. Then, the aqueous phase was slowly dispersed in the lipid phase under magnetic stirring, and then submitted to a ultraturrax (UltraTurrax T-18 IKA WORKS, Inc., Wilmington, NC, EUA) at 21.500 rpm during 3 minutes.[10] To reduce the particle size of the NLCs, the lipid system was submitted to ultrasonic processing (US), using a VCX-750 (SONICS Vibracell, Newtown, EUA) with a 13 mm probe at amplitute of 45%, during 30 minutes at cycles of 5 minutes on and 2 minutes off.[11] The total amount of solid lipid, plus liquid lipid and CTAB were set constant at 10% (wet basis). Hence, the ADJ (SiO_2:GU:MD - 1:3:6), hydrated overnight, were added to the primary lipid compositions at 1:1 or 2:1 ratio regarded to the total amount of formulation components (dry basis). After a stabilization period of 24 hours, the SLNs and NLCs formed were characterized, to determine the effects of composition constituents on selected physicochemical properties. Differential scanning calorimetry of the formulations prepared (freeze-dried) were conducted in a PerkinElmer calorimeter (mod. Jade-DSC), running from 20 to 250 °C, heating rate at10 °C/min, and N_2 atmosphere (3.0 kgf/cm^2) to estimate their melting and crystallization temperatures.

2.2 Spray drying of the SLNs and NLCs loaded with *Sygyzium aromaticum* EO

The drying runs were performed in a SD05 spray dryer (Lab-Plant UK Ltd, Huddersfield, UK), operating in a concurrent flow regime. First, the system was fed with distilled water to

stabilize the SD temperature and humidity profiles. The outlet gas temperature was measured each 5 minutes to detect the instant when the process attains steady state, after which the feed of encapsulating composition began. Operating conditions were: feed rate 4 g/min, diameter of the atomizer nozzle 1 mm, drying gas flow rate 60 m^3/h, pressure and flowrate of atomizing air of 3 bar and 17 L/min, respectively; and inlet drying temperatures (Tgi) of 60 and 80 °C. Solids concentration (Cs) was set at 26%. Samples of the spray dried powders were reserved, and their physicochemical properties determined.

2.2.1 Experimental planning

A 2^{4-1} fractional factorial design with addition of a central point[12] was used to study the effect of following variables: presence or absence of the liquid lipid oleic acid (OA - 0% - 1%), of the cationic surfactant CTAB (0% and 1%), inlet spray drying temperature (60 ºC and 80 ºC), and ratio of ADJ regarded to total formulation constituents (1:1 and 2:1 – dry basis). The set of experiments conducted are presented in Table 1 (coded variables). Regression analysis were performed to evaluate the significance of the effects of processing variables on product properties and drying performance.

Table 1. Processing conditions used according to the 2^{4-1}experimental design.

Run	T_{gi} (-)	CTAB (-)	OA (-)	ADJ (-)
F1	-1	-1	-1	-1
F2	1	-1	1	-1
F3	-1	-1	1	1
F4	1	-1	-1	1
F5	-1	1	1	-1
F6	1	1	-1	-1
F7	-1	1	-1	1
F8	1	1	1	1
F9	0	0	0	0

2.2.2 Determination of SD product properties and drying performance

The moisture content, water activity, content and retention of marker compounds were measured for the SD powders. The moisture content was determined by Karl Fischer titration, using a Karl Fischer 870 Titrino Plus (Methrom, Switzerland). The water activity was determined in an Aqua Lab 4Tev® water activity meter (Decagon devices, USA) using the capacitance electrode. Results were expressed as mean and deviation of triplicate mesurements. The concentrations of eugenol (EU) and eugenyl acetate (ACT) in liquid and spray dried samples were determined by a validated high performance liquid chromatography method (HPLC).[9] Retention of EU (R_{EU}), and ACT (R_{ACT}) were defined as the percentual ratio of the amount of marker compounds in the SD product related to the values in original liquid formulation (dry basis). Particle sizes (dp) and the polydispersity index (PDI) of the liquid and redispersed SD samples were determined by dynamic light scattering (DLS) using

a Zetasizer Nano ZS90 (Malvern, UK). Zeta potential (Z) was measured in the same equipment, using the specific measurement cell. The SD samples were redispersed with reverse osmose water at the original concentration and stirred for 30 minutes. Then, the original and redispersed samples were diluted to 1:200 (v/v) before the measurements (triplicate assays). Microphotographs of selected SD samples were acquired by scanning electronic microscopy (S.E.M. - Zeiss mod. EVO 50). Product recovery (R_{EC}), defined as the percentual ratio of the mass of SD product collected by the cyclone by the total mass fed (dry basis), was used as a measure of spray drying performance. The outlet spray drying gas temperatures were monitored during the drying.

3. Results and discussion

Nine distinct lipid compositions were produced according to the experimental planning (Table 1). After 24 hours, the compositions were characterized through determination of dp, PDI, Z, and the contents of eugenol (EU) and eugenyl acetate (ACT). The pH and electrical conductivity of compositions ranged from 4.23 to 4.93 and from 359.0 to 1,068.2 (µS/cm), respectively (data not shown). The amount of marker compounds in the liquid compositions are linked to the ADJ ratio; decreasing conversively with this composition variable.

3.1 Effects of processing variables on product properties and drying performance

The moisture content of the SD product varied slightly with processing variables, reaching a mean value of 5.3 ± 0.4 (% w/w d.b). The water activity (a_w) of the SD powders ranged from 0.357 to 0.578. Values of water activity lower than 0.5 are desired to avoid microbial spoilage of dried powders, resulting in longer shelf-life.[13] Most of SD powders reach water activity bellow this value, except compositions F4 and F6 that show a_w of 0.578 ± 0.003 and 0.568 ± 0.003, respectively, although none of the variables studied showed statistical significant effect on a_w. The physicochemical properties (EU, ACT, R_{EU}, R_{ACT}, dp, PDI and Z) of the SD product and of the redispersed samples were submitted to a regression analysis (Table 2). Table 2 shows similar effects of processing variables on the responses EU, ACT, R_{EU}, R_{ACT}, with $R^2 \geq 0.95$. The increase in T_{gi} leads to a decrease in these responses ($\alpha \leq 0.05$), perhaps due to the increase of drying energy available, which can contribute to the increase of volatilization of EO constituents. The effect of ADJ on EU and ACT are expected (dilution effect), but its effects on R_{EU} and R_{ACT} were in an opposite direction to the normal reasoning, seemingly due to the interactions between ADJ and the main lipid formulation constituents (CTAB, OA, poloxamer 188, and precirol). The addition of OA in the lipid systems increased EU, ACT, R_{EU}, R_{ACT}, as expected for NLCs, compared to SLN, but this effect only show statistical significance for ACT ($\alpha \leq 0.05$). Surfaces responses of EU as a function of CTAB and ADJ for SLNs and NLS are presented in Fig. 1 ($T_{gi} = 60°C$). Spray dried products with 7% of EU were formed at selected processing conditions.

***Table 2*. Regression coefficients and their statistical significance for selected process responses.**

FACTORS	PROCESS RESPONSES							
	EU (mg/g)	ACT (mg/g)	R_{EU} (-)	R_{ACT} (-)	dp (nm)	PDI (-)	Z (mW)	R_{EC} (%)
Mean	35.836*	2.910*	34.96*	44.88*	1680.7* *	0.54*	-29.33*	46.67*
T_{gi}	-8.309*	-0.448*	-8.14*	-6.70**	66.6	0.05**	1.567	-3.45
ADJ	-11.334*	-0.790*	-3.86**	-4.86**	-77.1	0.00	-0.367	-2.48
CTAB	8.586*	0.388*	9.61*	7.56*	-43.2	-0.06**	3.892**	3.32
OA	1.516	0.160**	1.37	2.56	-313.1	0.05**	-1.642	1.48
R^2	0.956	0.959	0.984	0.973	0.258	0.918	0.725	0.715

* Effect significant at $\alpha \leq 0.01$ - ** Effect significant at $\alpha \leq 0.05$

Fig. 2 shows graphs comparing data of dp, PDI and zeta potential of the original lipid systems with the corresponding values for redispersed SD samples. It can be seen that nanosized liquid SLNs and NLCs were engineered (F1 to F4), with small polydispersity index (PDI) and adequate |Z|. Significant increase of the droplets size for formulations containing CTAB were observed, perhaps due to interaction between the negatively charged[14] Arabic gum with the cationic lipid CTAB. This interactions were strong enough to invert the zeta potential of the CTAB primary lipid systems (without ADJ),[11] from highly positive values (+32.97 to +44.03 mW) to negative (from -30.8 ± 0.1 to -21.0 ± 1.0), linked to ADJ amount and OA addition. Therefore, a previous scrutiny of the charges of the composition constituents is highly recommended to reduce the likelihood of occurrence of unwanted interactions. The graphs also show good redispersion properties of SD powders; although some compositions exhibit dp slightly higher than the initial value, except for F6 to F8 products (containing CTAB). The redispersed SD powders with CTAB (F5 to F9) showed a reduction of PDI comparatively to initial composition. Similar values of [Z] were observed for the redispersed SD product and the original liquid lipid systems. These results give robust evidences that our initial goal, the production of redispersible SLNs and NLCs loaded with *Sygyzium aromaticum* OE, is feasible. Fig. 3 shows S.E.M. micrographs of selected spray dried SLNs and NLCs; showing predominance of spherical somewhat wrinkled particles. The addition of OA caused a slight decrease in dp (Figs. **c** and **d**). Strutural changes in the SLNs and NLCs are linked to their thermal and crystalline properties. DSC analysis show small differences in temperatures and enthalpies of fusion and crystallization, linked to systems composition (data not shown).

Fig. 4 shows the experimental results of R_{EC} as a function of the outlet SD temperature. The solid line shows linear fit of the experimental data, indicating a tendency of decrease of R_{EC} conversely with T_{gs}. Traced lines shows the mean values of melting and crystallization

temperatures of lipid compositions. Drying at temperatures at left side of these lines show positive effects on R_{EC}.
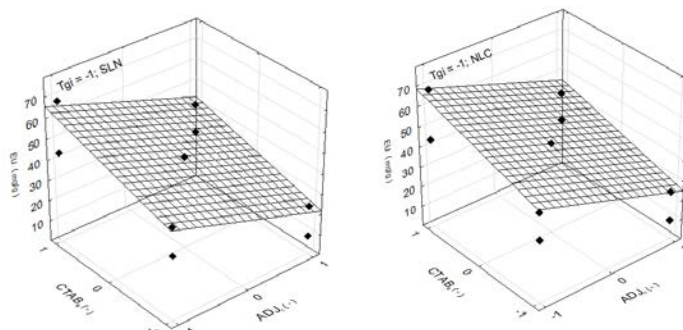
Fig. 1 Effects of CTAB and ADJ on Eugenol content in spray dried SLN and NLC ($T_{gi} = 60$ °C).
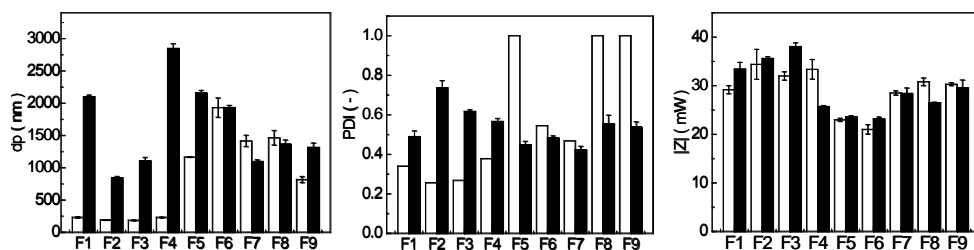
Fig. 2. Comparison of particle size (dp), Polidispersity index (PDI) and zeta potential (|Z|) of the original liquid lipid system and of the redispersed SD product (respectively, open and solid columns).
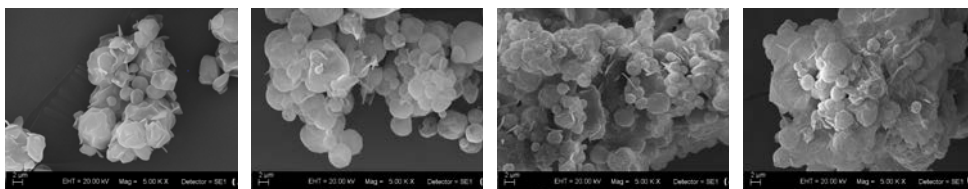
Fig. 3. S.E.M. images of the SD powder. a: SLN ($T_{gi} = 60$ °C, ADJ = 1:1; CTAB = 0%); b: SLN ($T_{gi} = 80$ °C, ADJ = 1:1; CTAB = 1%); c: NLC ($T_{gi} = 80$ °C, ADJ = 1:1; CTAB = 0%); d: NLC ($T_{gi} = 60$ °C, ADJ = 1:1; CTAB = 1%).
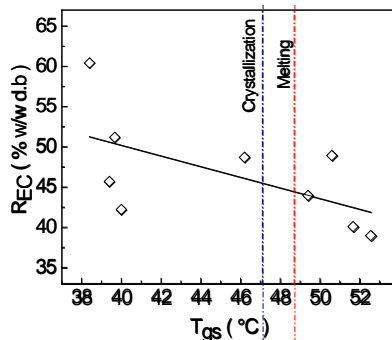
Fig. 4. R_{EC} as a function of T_{gs}

4. Conclusions

The properties of the nanosized lipid systems loaded with EO are affected by processing conditions. EU and ACT in SD products depend on drying temperature and formulation constituents. R_{EU} was higher (~50-60%) for systems with CTAB and OA, at lower SD temperature. Dried SLNs and NLCs are easily redispersed, indicating the potential of this technology.

5. Acknowledgements

6. References

[1] Sherry, M.; Charcosset, C.; Fessi, H. ; Greige-Gerges, H. Essential oils encapsulated in liposomes: A review. J. Liposome Res. 2013, 23(4), 268-75.

[2] Matos, F.J.A.; Oliveira, F. *Lippia sidoides* Cham.- farmacognosia, química e farmacologia. Revista Brasileira Farmácia. 1998, 70(3/4), 84-87.

[3] Bilia, A.R.; Guccione, C.; Isacchi, B.; Righeschi, C.; Firenzuoli, F.; Bergonzi, M.C. Essential oils loaded in nanosystems: A developing strategy for a successful therapeutic approach. Evid. Based Complement. Alternat. Med., 2014, Article ID 651593,14 pages.

[4] Christensen, K.L.; Pedersen, G.P.; Kristensen, H.G. Preparation of redispersible dry emulsions by spray drying. Int. J. Pharm. 2001, 212, 187-194.

[5] Gallarate, M.; Mittone, E.; Carlotti, M.E.; Trotta, M. Formulation of dry emulsion for topical applications. J. Dispersion Science and Technology 2009, 30(6), 823–833.

[6] Zhao, Y.; Chang, Y.X.; Hu, X.; Liu, C.Y.; Quan, L.H.; Liao, Y.H. Solid lipid nanoparticles for sustained pulmonary delivery of Yuxingcao essential oil: Preparation, characterization and in vivo evaluation. Int. J. Pharm. 2017, 516(1-2), 364-371.

[7] Tan, A., Rao, S., Prestidge, C.A. Transforming lipid-based oral drug delivery systems into solid dosage forms: an overview of solid carriers, physicochemical properties, and biopharmaceutical performance. Pharm. Research 2013,30(12), 2993-3017.

[8] Freitas, C.; Müller, R.H. Spray drying of solid lipid nanoparticles (SLN^{TM}). European J. Pharm. Biopharm 1998, 46(2), 145-151.

[9] Cortés-Rojas, D.F.; Souza, C.R.F.; Oliveira, W.P. Encapsulation of eugenol rich clove extract in solid lipid carriers. J. Food Engineering 2014, 127, 34-42.

[10] Pérez-Jiménez, J.; Neveu, V.; Vos, F., Scalbert, A. Identification of the 100 richest dietary sources of polyphenols: an application of the Phenol-Explorer database. Eur. J. Clin. Nutrition 2010, 64(Suppl 3), S112-20.

[11] Rosa, D.M.; Oliveira, W.P. *Syzygium aromaticum* essential oil loaded in nanosystems: Effect of system composition (Po5). Proc. 3rd Latin-American Symposium on Microencapsulation 2017, 82-83.

[12] Montegomery, D.C. Design and analysis of experiments, 8th Ed., John Wiley and Soons: USA, 2012.

[13] Labuza, T.P.; Altunakar, L. Water activity in foods: fundamentals and applications. Blackwell Publishing Ltd: Oxford, UK, 2007.

[14] Klein, M.; Aserin, A.; Ishai, P.B.; Garti, N. Interactions between whey protein isolate and gum Arabic. Colloids Surf. B Biointerfaces. 2010, 79(2), 377-83.

Effect of rehydration on texture properties of Mexican plum (*Spondias purpurea* L.) dehydrated by tray drying and freeze drying

Guillén-Velázquez, P. [a]*; Muñoz-López, C. [a]; Cantú-Lozano, D. [a]; Luna-Solano, G.[a]

[a]*Departamento de Estudios de Posgrado e Investigación, Instituto Tecnológico de Orizaba. Orizaba, Veracruz, México*

*E-mail of the corresponding author: paulina.guillen@hotmail.com

Abstract

Mexican plum (Spondias purpurea L.) is a fruit with high nutritional content. Freeze and tray drying increases its shelf life, however non-reversible changes may ocurr. Properties as rehydration capacity and texture are considered as a measure of the injury to the material caused by drying. In this sense, the objective of this research was to evaluate the texture profile of dehydrated plum during rehydration and compare it with properties of raw plum. Freeze drying provided a product with less tissue damage reflected in the high rehydration capacity and texture characteristics very close to original unlike those dehydrated by hot air.

Keywords: Mexican plum; rehydration; texture profile analysis.

Effect of rehydration on texture properties of Mexican plum (Spondias purpurea L.) dehydrated by tray drying and freeze drying

1. Introduction

Mexican plum (*Spondias purpurea* L.) is a fruit with qualities and potential for many different applications in the food industry. Nevertheless, the plums are mainly commercialized in local markets and have an incipient postharvest management with few methods for postharvest conservation currently in place [6]. Drying techniques, as freeze drying and tray drying, can be an excellent alternative to make their shelf-life longer and commercialization easier. It allows conversion of perishable materials into stabilized products by lowering water activity to appropriate levels, thus preventing microbial spoilage and quality deterioration [7].

Freeze drying prevents undesirable shrinkage and produces materials with high porosity, good nutritional quality, superior texture, aroma, flavor and color retention [10]. In contrast, tray drying is the most widely employed method for preserving food materials because of its simplicity and low cost that demands small investments for industries. It is commonly used for drying fruits and vegetables using hot air as a carrier of heat [12].

Despite advantages of preserving foodstuffs, drying methods may cause many non-reversible physical and chemical changes in the material such as color, nutritional value, shrinkage, texture etc. [3] Thus, rehydration can be considered as a measure of the injury to the material caused by drying and treatments preceding dehydration [5]. According to Farahnaky and Kamali the ultimate objective of rehydration process is to obtain a product with textural properties similar or close to original [4].

Textural properties of a food are that group of physical characteristics that arise from the structural elements of the food, are sensed primarily by the feeling of touch, are related to the deformation, disintegration, and flow of the food under a force, and are measured objectively by functions of mass, time, and distance [2]. It is known that the sensations experienced as the food material deforms and fractures during the initial stages of biting/chewing govern our acceptance or rejection of the product [1]. In this way, textural parameters can be considered as an attribute to assess acceptability and quality of products.

There are few studies of textural properties of dried and rehydrated foodstuffs, in special Mexican plums. Thus, the purpose of this work was to study the evolution of texture properties during rehydration process of plum slices dehydrated by tray drying and freeze drying.

2. Materials and Methods

2.1 Raw material

Mexican plums ("beetroot" ecotype) were obtained from Orizaba and Coscomatepec, Veracruz, Mexico and selected according to the ripening degree (30 % green, 70 % red).

The plums were washed and cut into slices of 3 cm of diameter and 0.2 cm of thickness for tray drying (TD) and 1.4 cm of diameter and 0.2 cm of thickness for freeze drying (FD). For freeze drying, the plum slices were frozen at -20 °C during 2 hours.

2.2 Drying process

Hot air drying was performed in a pilot scale vertical tray dryer (MOD-SEM-2 Polinox, MX) at air temperature of 53 °C during 4.5 h. The freeze drying was conducted in a laboratory scale dryer (Mod-742004 Labconco, USA) at 0.1 mbar vacuum pressure during 4.3 h [10].

2.3 Texture Profile Analysis

The texture profile analysis (TPA) was performed on fresh, dehydrated and rehydrated slices of plum using a Texture Analyzer (CT3-100, USA). TPA involved properties as hardness, cohesiveness, springiness and adhesion and was carried out by two compression cycles and operating conditions of the equipment were selected according to the drying method applied in order to reach a right compression of the product. Cylindrical probes were used to perform TPA tests (25.4 mm diameter, 35 mm length for TD; 12.7 mm diameter, 35 mm length for FD). Table 1 shows operating conditions used for each size of slice, with its respective drying method.

Table 1. Operating TPA conditions

Operating conditions	Tray drying		Freeze drying	
	Fresh/ Rehydrated	Dehydrated	Fresh/ Rehydrated	Dehydrated
Trigger (N)	0.01471	0.01471	0.01471	0.01471
Deformation (mm)	1	1	2	1
Speed (mm/s)	1.2	1	1.5	1

Rehydration of plum slices was performed in water and milk at 10, 20 and 30 °C. For TPA test an amount of 7 slices were added to the immersion media. Every 5, 10, 15, 20, 25, 30 and 35 min a different slice was taken out, drained in absorbent paper and set in the texture analyzer to measure the texture parameters during rehydration. Every experiment was made by triplicate.

3. Results and discussion

3.1 Texture analysis of rehydrated freeze dried plums

Differences on texture properties during rehydration (Fig. 1 and 2) can be attributed to the swelling and the leaching of solubles also these results can be explained based on the fact that at short times of rehydration, samples are not still equilibrated with the presence of

great gradients of moisture content from surface to centre [9] and in consequence, affecting to the measure of texture profile.

Graphics (Fig. 1 and 2) show texture properties of freeze dried plum during rehydration and its variation with respect time. Analysis of variance (ANOVA) and the test of mean comparison (Dunnett) were conducted with a level of significance of 0.05. Texture properties of fresh plum were selected as the control. Final value of hardness (water, 10 °C) had no significant differences compared with fresh plum. In contrast there were significant differences at higher rehydration temperatures.

With respect to rehydration in milk, final values of hardness remained unchanged at the end of rehydration process with every temperature. Cohesiveness at 10 and 30 °C of plum rehydrated in water showed similar values than non-dried plum. On the other hand, rehydration in milk allowed to reached final cohesiveness values with no significant difference for all the temperatures used.
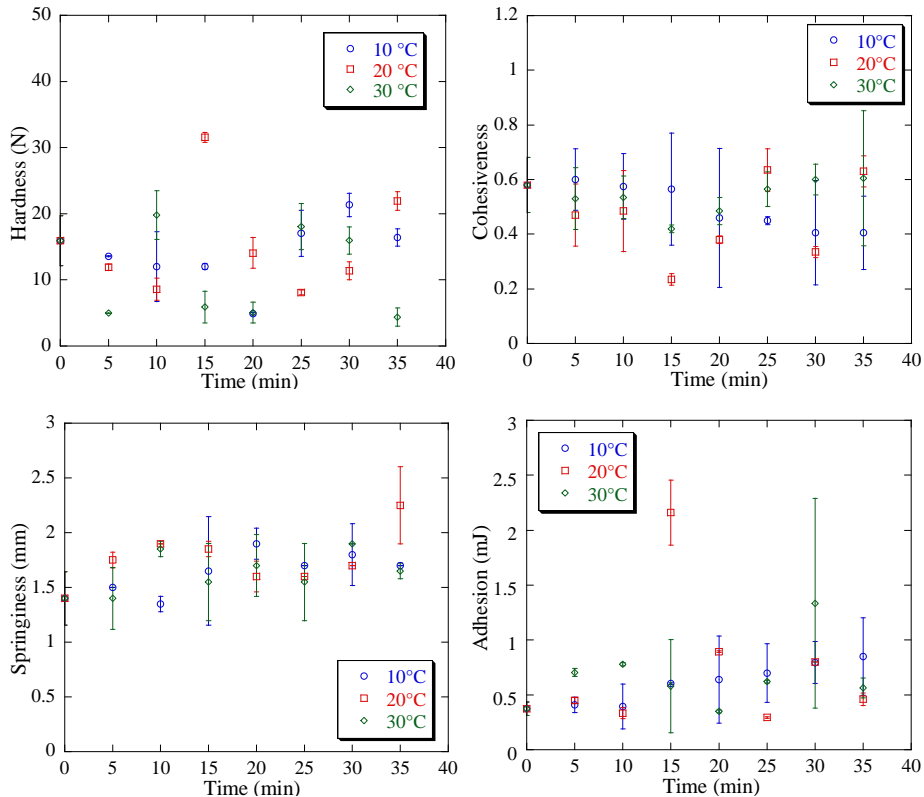
Fig. 1 Textural properties during rehydration of freeze dried plum immersed in water.
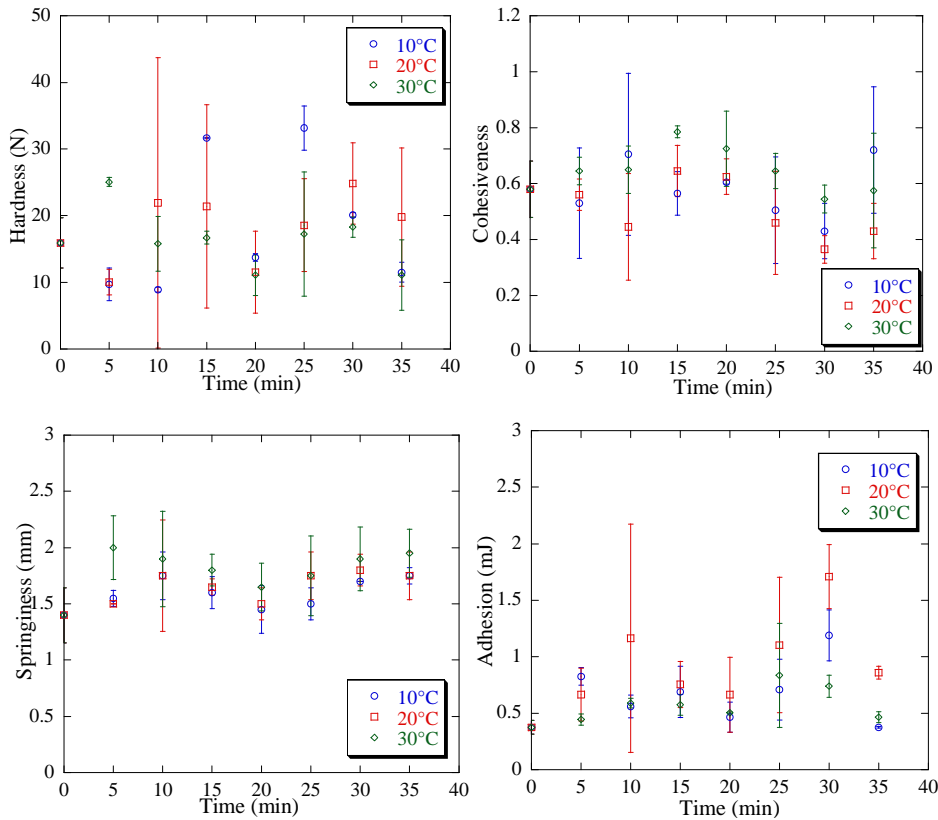
Fig.2 Textural properties during rehydration of freeze dried plum immersed in milk.

Springiness characteristics only showed significative differences at the ending of the rehydration in water at 20 °C, increasing from 1.5 to 2.25 mm. Slices of plum rehydrated in milk kept similar springiness than fresh ones. Adhesion characteristics had no significant differences in final values for both rehydration medias and rehydration temperatures.

3.2 Texture analysis of rehydrated hot air dried plums

Textural properties of hot air dried slices of plum during rehydration and its variation with respect time are presented in Fig. 3 and 4. Statistical analysis indicated that hardness of plum rehydrated in water (10 and 30 °C) had no changes compared to fresh product. Milk immersion allowed to reach similar values at 10 and 20 °C. Cohesiveness final values presented no significant differences for water rehydration of plum. Milk immersion presented only significative differences at 20 °C. With respect to springiness, final values after immersion in water showed differences at 30 °C. In contrast, milk rehydration at the three temperatures used, presented higher values that were significantly different from fresh

plum. Finally, adhesion for plum rehydrated in water was similar to fresh one at 10 °C; milk immersion reached the same characteristics at 10 and 20 °C.

As can be seen, there were variations of texture properties during and at the ending of rehydration process, it can be attributed to the drying method used. According to Meda and Ratti [8], hot-air drying usually destroys the food thus, the final air dried products have a compact structure and a reduced volume, which can explain a non-uniform restoration of its original form, and as a consequence, variations during texture evaluation.

Assesment of texture profile of rehydrated plum slices allowed to see a clear influence of the drying methods. Freeze dried slices of plum presented less differences when compared to the fresh fruit. In contrast plums dehydrated by hot air, showed more variations on texture properties during rehydration. These differences were attributed to the tissue collapse and cell damage produced by higher air temperatures [11].
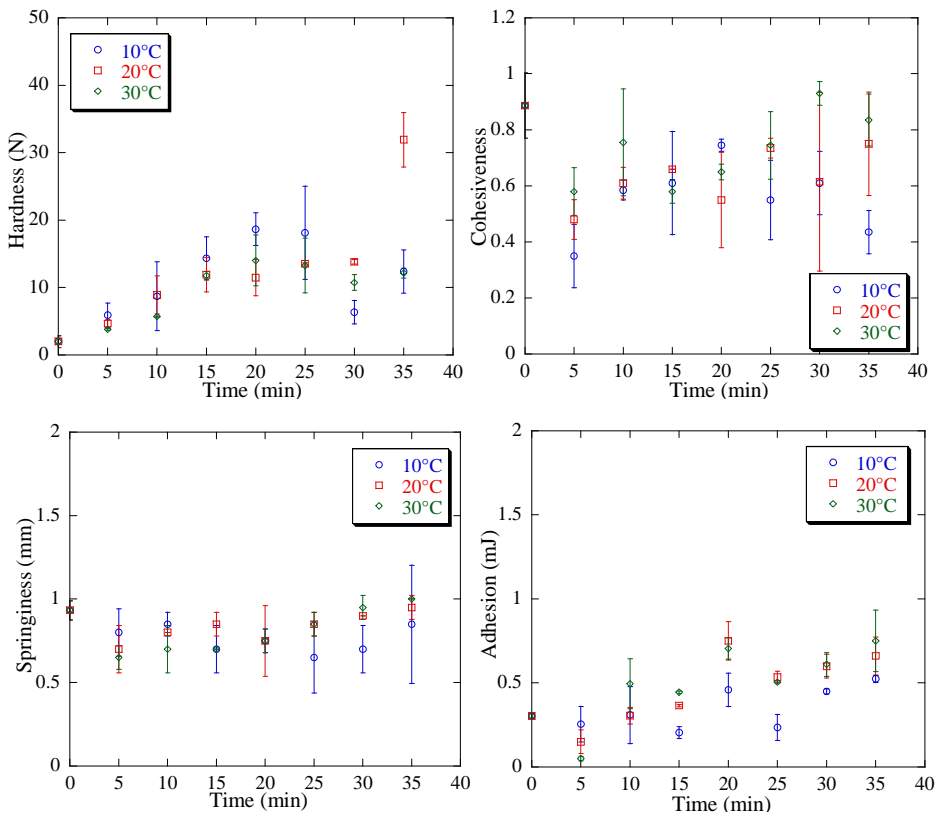
Fig.3 Textural properties during rehydration of hot air dried plums immersed in water.
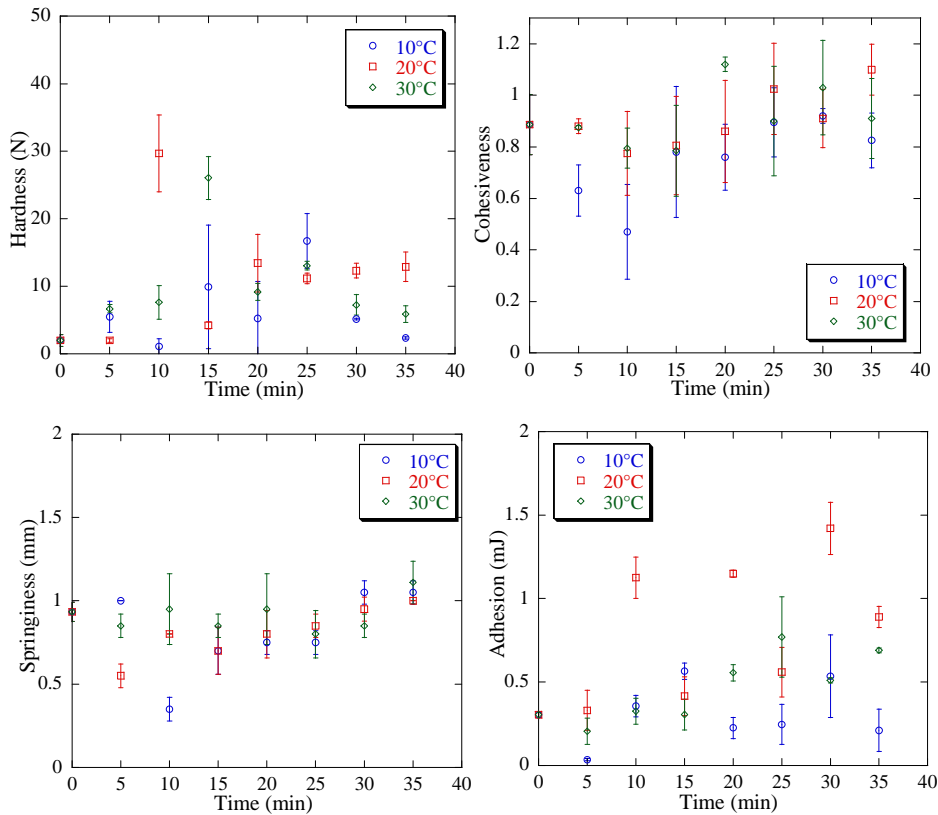
Fig.4 Textural properties during rehydration of hot air dried plums immersed in milk.

4. Conclusions

The texture studies were carried out on fresh, dehydrated and rehydrated plum slices, determining the parameters of hardness, cohesiveness, springiness and adhesion. Plum slices dehydrated by hot air presented more significative differences with respect to fresh plum that were attributed to the high temperatures during drying producing more structural damage as a consequence. On the other hand freeze drying allowed to reach texture characteristics close to fresh plum at the end of the most rehydration experiments. Finally it was possible to conclude that TPA provides valuable information not only after dehydration but also rehydration and application in freeze dried and hot air dried products, as plums, assures to the consumers a product with high quality and similar texture as fresh one, increasing its potential as snacks and cereal-based products.

5. References

[1] Alvarez, M.D., Saunders, D.E.J., Vincent, J.F.V., Jeronimidis, G. An engineering method to evaluate the crisp texture of fruit and vegetables. Journal of Texture Studies 2000, 31, 457-473.

[2] Bourne, M.C. Food texture and viscosity: concept and measurement. Academic press. USA, 2002.

[3] Ergün, K., Çalışkan, G., Dirim, S.N. Determination of the drying and rehydration kinetics of freeze dried kiwi (Actinidia deliciosa) slices. Heat Mass Transfer 2016, 52(12), 2697–270.

[4] Farahnaky, A., Kamali, E. Texture hysteresis of pistachio kernels on drying and rehydration. Journal of Food Engineering 2015, 166, 335–341

[5] Krokida, M., Maroulis, Z. Structural properties of dehydrated products during rehydration. International Journal of Food Science and Technology 2001, 36, 529-538.

[6] Maldonado-Astudillo, Y.I., Alia-Tejacal, I., Núñez-Colín, C.A., Jiménez-Hernández, J., Pelayo-Zaldívar. Postharvest physiology and technology of *Spondias purpurea* L. and S. mombin L. Scientia Horticulturae 2014, 174, 193–206.

[7] Marques, L.G., Prado, M.M., Freire, J.T. Rehydration characteristics of freeze-dried tropical fruits. LWT - Food Science and Technology 2009, 42, 1232–1237.

[8] Meda, L., Ratti, C. Rehydration of freeze-dried strawberries at varying temperatures. Journal of Food Process Engineering 2005, 28, 233–246.

[9] Moreira, R., Chenlo, F., Chaguri, L., Fernandes, C. Water absorption, texture, and color kinetics of air-dried chestnuts during rehydration. Journal of Food Engineering 2008, 86, 584–594.

[10] Muñoz-López, C., Urrea-Garcia, G. R., Jiménez-Fernandez, M., Rodríguez-Jiménes G., Luna-Solano, G. Effect of drying methods on the physicochemical and thermal properties of Mexican plum (*Spondias purpurea* L.). CyTA - Journal of Food 20017, 16:1, 127-134.

[11] Vega-Galvez, A., Lemus-Mondaca, R., Bilbao-Sainz, C., Fito, P., Andres, A. Effect of air drying temperature on the quality of rehydrated dried red bell pepper (var. Lamuyo). Journal of Food Engineering 2008, 85, 42–50.

[12] Villegas-Santiago, J., Calderón-Santoyo, M., Ragazzo-Sánchez, A., Salgado-Cervantes, M.A., Luna-Solano, G. Fluidized bed and tray drying of thinly sliced mango (*Mangifera indica*) pretreated with ascorbic and citric acid. International Journal of Food Science and Technology 2011, 46, 296–1302.

Evaluation of the physicochemical properties of dehydrated artisanal cheese during storage

Calis-Pérez C. J. [a]*; Dominguez-Niño, A.[a]; Urrea-Gacía, G. R.[a]; Luna-Solano, G. [a]

[a] Departamento de estudios de posgrado e investigación: Instituto Tecnológico de Orizaba

*E-mail of the corresponding author: carlosjaircalisperez@hotmail.com

Abstract

Artisanal fresh cheese is a type of cheese from Hispanic origin and one of the most consumed; however, its shelf life is short due to of its pH is close to neutrality, high a_w and low salt content. The fluidized bed drying was employed as an efficient alternative to fresh cheese; however, in order to achieve the desired shelf life in a product, it is necessary to study different packaging and storage conditions that will depend on the specific characteristics of the product. A design of factorial experiments 2^3 was adopted, the storage study was carried out for 90 days, studying two qualitative variables: type of packaging and type of atmosphere in the packaging, and one quantitative variable: drying temperature.

Keywords: Dehydrated cheese; storage; water activity; type of packing.

1. Introduction

Artisanal cheese is the most recognized cheese of Latin American origin and the most consumed internationally. Fresh cheeses have short shelf life because of their pH (near to neutrality), the high water activity and the low salt content. Usually, the shelf life of fresh cheese under refrigeration is seven days[3,5]. For this reason, fluidized bed drying was employed as an efficient alternative to preserve perishable food[4]. However, the need for proper packaging for traditional products has pushed to design packaging conditions according to the characteristics of each food[2]. Shelf life is an important feature of all foods and it may be define as the period that the food retains an acceptable level of eating quality from a safety and organoleptic point of view[10]. It is well known that vacuum packaging not only reduces the incidence of oxidative damage and inhibits aerobic bacteria, but also preserves sensory quality in foods, because under vacuum conditions, oxygen in the package headspace is reduced to <1%, maintaining stable moisture and water activity[6]. For this reason, vacuum packaging is an interesting alternative to storage in dehydrated samples as cheese.

2. Materials and Methods

2.1 Drying process

The artisanal cheese was obtained from a cheese making group located in the city of Tlalixcoyan, Veracruz, México. A fluidized bed dryer (Model Restch TG-200) was employed for the drying process. Drying conditions for this study were selected according to results reported by Domínguez-Niño *et al*.[4] (air temperature of 50 and 60 °C, drying time of 60 min and particle size of 2 cm).

2.2 Packaging of dehydrated cheese

The dehydrated cheese samples (12.1 g), were packaged in two types of packing (13.2 x 9.5 cm) made out of polyethylene and metalized with 30 µ thickness. The samples were sealed by means of a vacuum packing machine (Food saver model sealing system FSFSSL3880) under atmospheric conditions: air and vacuum (VP).

2.3 Physicochemical characterization

Moisture content: The moisture content was determined using an infrared moisture balance (MA35 SARTORIUS, Germany), at 65°C and 1 g of cheese.

Water activity (a_w): the dehydrated cheese samples were analized at 25 °C using Aqualab water activity meter (model SERIES 3 TE, DECAGON, Washington).

Color difference: the sample color was measured by colorimeter of HunterLab (model MiniSccan XE plus, Associates Laboratory, Retson, VA, USA). The equipment was calibrated with white and black standards tiles. The experimental color was determined by reflectance mode and expressed by *L*, *a* and *b* parameters. The color difference (Δ*E*) was calculated using the following equation reported by Lozano-Acevedo et al.[8].

$$\Delta E = \sqrt{(\Delta L)^2 + (\Delta a)^2 + (\Delta b)^2} \qquad (1)$$

Where ΔL = L of dried sample at storage time-L of initial dried sample, Δa= a of dried sample at storage time -a of initial dried sample and Δb= b of dried sample at storage time-b of initial dried sample.

Protein, sodium chloride and fat content: the protein content of the stored cheese was determined by a standard Kjeldahl method, using a nitrogen conversion factor of 6.38 for dairy products. Sodium chloride was assessed following the method described by James[7] and fat content was quantified by extraction method using Soxhlet equipment.

2.4 Experimental design

A mixed experimental design 23 was used. In this design two qualitative variables were analyzed type of packing (polyethylene and metalized) and atmosphere type (air and vacuum), and, as a quantitative variable, drying temperature of 50 and 60°C, thus making a total number of eight experimental storage condition (Table 1).

Table 1. Experimental storage conditions of dehydrated cheese

Experiment	Drying temperature (°C)	Packing type	Atmosphere
1	50	Polyethylene	Air
2	50	Polyethylene	Vacuum
3	50	Metalized	Air
4	50	Metalized	Vacuum
5	60	Polyethylene	Air
6	60	Polyethylene	Vacuum
7	60	Metalized	Air
8	60	Metalized	Vacuum

3. Results and discussion

3.1 Moisture content

Figure 1 shows the evolution of moisture of dehydrated cheese under different storage conditions (Table 1). The statistical analysis using the Dunnett test (α=0.05) shows less

significant differences in the samples that were dehydrated at 60°C. The increase in moisture
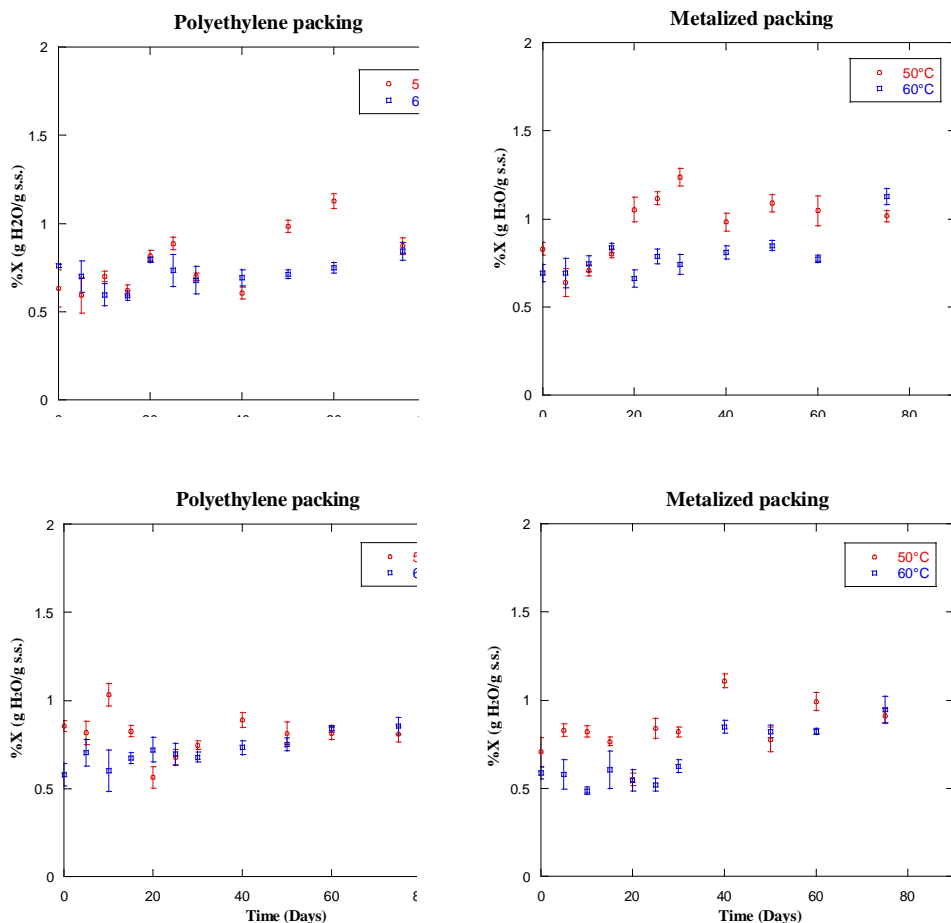
Figure 1. Evolution of moisture content in dehydrated cheese stored under different conditions: a) air and b) vacuum.

3.2 Water activity

Figure 2 shows the results obtained from the evolution of water activity of dehydrated cheese during storage at different conditions. The statistical analysis using the Dunnett test ($\alpha = 0.05$) showed the existence of significant differences in the stored cheese with respect to the initial samples. The dehydrated samples at 60°C and stored under vacuum conditions were maintained below 0.6 units during the 90 days of storage, which can assure that the cheese is free of microbial growth and enzymatic deterioration.

Similar results were found by Akarca et al.[1] who reported that vacuum packaging prolongs the microbiological quality of mozzarella cheese for a considerably longer period of time.
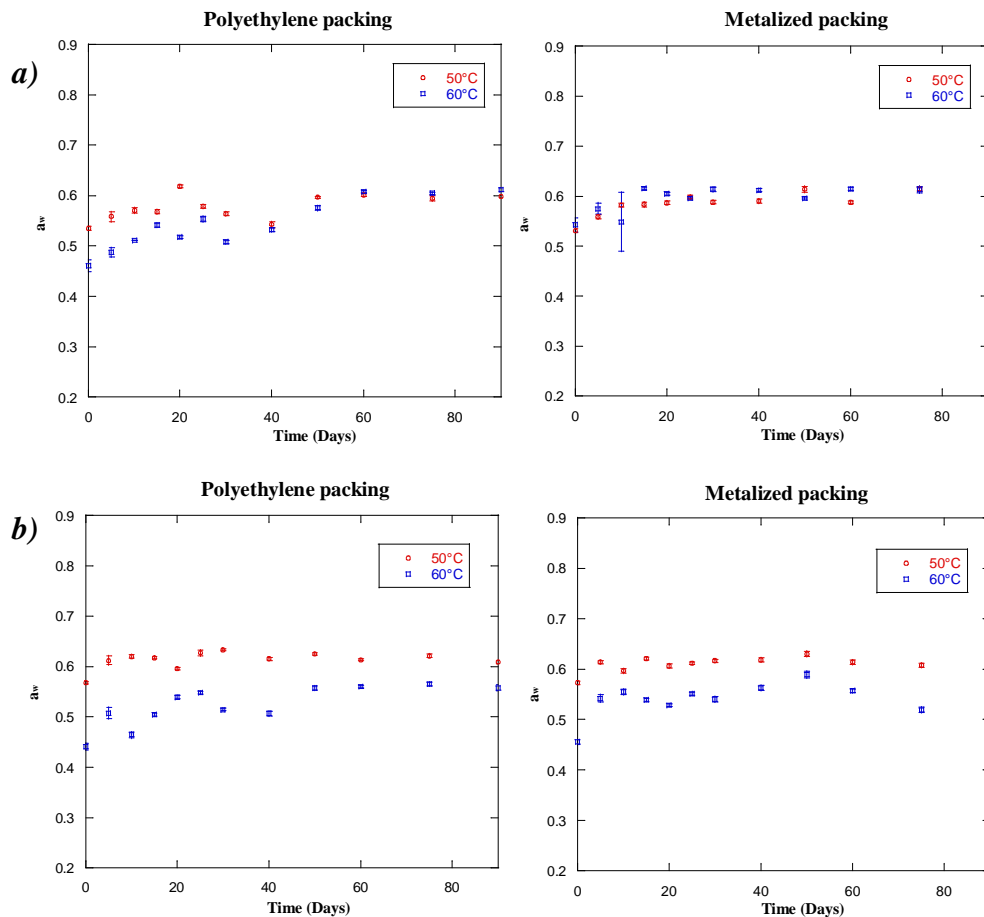
Figure 2. Evolution of water activity in dehydrated cheese stored under different conditions: a) air and b) vacuum

3.3 Color difference

Figure 3 shows the results obtained for the color difference during storage at different conditions. The statistical analysis using the Dunnett test (α=0.05) indicated significant changes among the different storage conditions.

During storage, a slight increase in *a* values and a clear increase in *b* values were observed. Therefore, a tendency towards yellowing occurred. According to the literature, dehydrated

foods lose color due to the oxidation of highly unsaturated molecules once exposed to light, air and chemical changes[9].
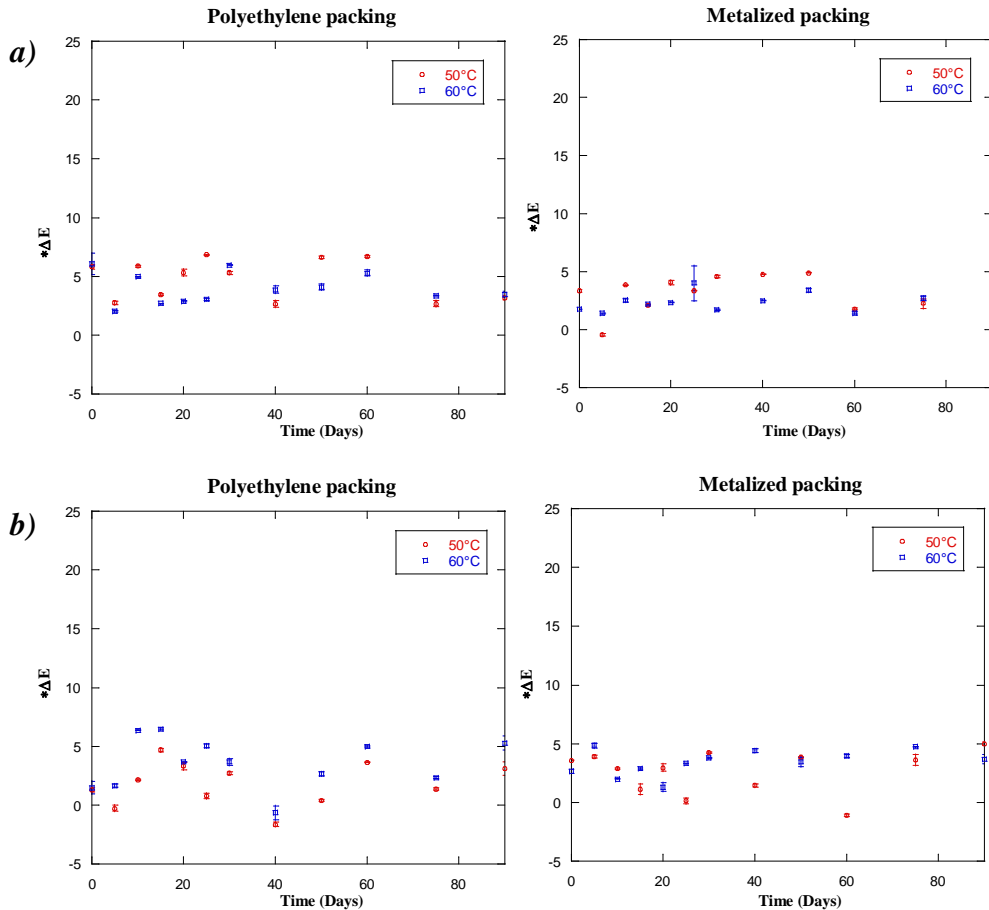
Figure 3. Evolution of color difference in dehydrated cheese stored under different conditions: a) polyethylene and b) metalized.

3.4 Protein, fat and sodium chloride content

During the drying process the concentration of proteins, fat and NaCl in the cheese samples increased considerably due to the elimination of water in the product. The cheese samples showed a decrease in the content of proteins, fat and NaCl after storage with respect to the sample analyzed at time zero, 40.4477, 35.8573 y 3.2901% (Table 2). The analysis of variance (α=0.05) showed that the drying temperature had influence on the protein and fat content at the end of storage, this can be attributed to the gain of moisture during storage.

The results may indicate that the conditions of use of the storage reduce the oxidation reactions in the dehydrated cheese. The use of vacuum packaging has shown to maintain stability in parameters such as color and fat and protein content, maintaining its physicochemical quality.

Table 2. The experimental results of protein, sodium chloride, fat content of dehydrated cheese at the end of storage period.

Experiment	Protein content (%)	Fat content (%)	NaCl content (%)
01	37.9848	41.1643	3.0947
02	38.0924	38.2357	3.1295
03	38.4578	41.2845	3.2236
04	38.0628	39.4582	3.0568
05	40.1912	38.7047	3.6326
06	39.5431	40.4399	3.4123
07	40.2083	41.1547	3.4072
08	40.1238	37.6055	3.469

4. Conclusions

According to the results obtained in this study, samples packed in vacuum and dehydrated at 60 ° C were found to be adequate for storage for 3 months, because they obtained the lowest moisture gain and maintained water activity below 0.6 units allowing to guarantee the stability of the product. The content of proteins, fat and NaCl was maintained during the storage period, ensuring the physico-chemical quality of the dehydrated cheese. Finally, dehydrated cheese can be used as a snack or as an ingredient in traditional food because it has similar characteristics to the fresh cheese.

5. References

[1] Akarca, G.; Tomar, O.; Gök, V. Effect of different packaging methods on the quality of stuffed and sliced mozzarella cheese during storage. Food Processing and Preservation 2015, 39 (6), 2912-2918.

[2] Costa C.; Lucera A.; Lacivita V.; Saccotelli M.A.; Conte A.; Del Nobile M.A. Packaging optimization for portioned Canestrato di Moliterno cheese. Society of dairy technology 2016, 69 (3), 401-409.

[3] Del Caro, A.; Sanguinetti, A.M.; Fadda, C.; Murittu, G.; Santoru, A.;Piga, A. Extending the shelf life of fresh ewe's cheese by modified atmosphere packaging. International Journal of Dairy Technology 2012, 65 (4), 548-554.

[4] Domínguez-Niño A.; Buendia-González A.N.; Cantu-Lozano D.; Andrade-González I.; Luna-Solano G. Efecto del secado por lecho fluidizado sobre las propiedades fisicoquimicas y microbiologicas del queso fresco mexicano. Revista mexicana de ingeniería química 2016, 15(3), 869-881.

[5] Faccia, M.; Mastromatteo, M.; Conte, A.; Del Nobile M.A. Influence of the diferent sodium chloride concentrations on microbiological and physicochemical characteristics of Mozzarella cheese. Journal of Dairy Research 2012, 79 (4), 390-396.

[6] Garabal, J.I.; Alonso, P.R.; Franco, D.; Centeno, J.A. Chemical and biochemical study of industrially produced San Simón da Costa smoked semi-hard cow´s milk cheeses: effects of storage under vacuum and different modified atmospheres. Journal of Dairy Science 2010, 93 (5), 1868-1881.

[7] James C.S. Analytical chemistry of foods. Editorial Chapman & Hall, Londres 1995.

[8] Lozano-Acevedo, A., Fernández, M.J., Sánchez, A.R., García, G.R. y Solano G.L. Fluidized bed drying of thinly sliced potato (Solanum tuberosum). Potato Research 2011, 88 (4), 360-366

[9] Koca, N.; Burdurlu, H.S.; Karadeniz, F. Kinetics of colour changes in dehydrated carrots. International Journal of Food Engineering 2007, 78 (2), 449-455.

[10] Ucherek, M. An integrated approach to factors affecting the shelf life of products in modified atmosphere packaging (MAP). Food Reviews International 2004, 20 (3), 297-307.

The infrared radiation and vacuum assisted drying kinetics of flue-cured tobacco leaf and its drying quality analysis

Zhu, W.[*]; Guo, G.; Liu, C.; Cheng, L.; Wang, L.

Zhengzhou Tobacco Research Institute of CNTC, Zhengzhou, Henan, China

*E-mail of the corresponding author: wkzhu79@163.com

Abstract

Dehydration is widely involved in tobacco processing such as tobacco leaf curing, tobacco trip redrying and cut tobacco drying, which plays a key role due to its effect on the physical and chemical quality of tobacco. The current drying methods in tobacco processing mainly use heat conduction, heat convection or their combination to dehydrate tobacco materials. However, radiation heat transfer as one of basic heat transferways has not been investigated in the tobacco drying. In the present work, infrared radiation dryer was designed to explore the tobacco infrared radiation drying characteristics. The effect of radiation heat transfer conditions and vacuum on the drying kinetics and temperature of tobacco leaves was investigated. Diffusion coefficient of middle tobacco leaves C2F is between 0.848×10^{-10} ~ 1.597×10^{-10} m²/s. At the same time, the pore structure andpetroleum ether tobacco extracts in dried tobacco were also analyzed in order to explore the different effects of infrared radiation drying and traditional drying technology on tobacco quality.

Keywords: Flue-cured tobacco; Infrared radiation; Vacuum; Dryingkinetics; Tobacco quality

1. Introduction

In tobacco primary processing, drying plays a key role due to its effect on the physical and chemical quality of tobacco[1]. Therefore, to explore new drying method is always the focus of tobacco processing technology. In terms of heat transfer ways, the current drying methods in tobacco processing mainly use heat conduction, heat convection or their combination to dehydrate tobacco materials. However, radiation heat transfer as one of basic heat transfer ways has not been investigated in the literatures involving tobacco drying. The infrared-vacuum drying, infrared-hot air drying and infrared-heat pump drying, have been investigated and applied in the argo-processing such as seeds, vegetables and fruits [2-8]. Many results have showed that the infrared radiation drying could improve the drying efficiency, reduce the shrinkage of dried materials and maintain the nutrient and functional components when compared to the traditional hot-air drying method. Whereas, there is little work on the infrared radiation heat transfer in the current tobacco industry, especially in the tobacco primary processing. Considering this, in the present work, two kinds of infrared radiation dryer were designed to explore the tobacco infrared radiation drying characteristics, including the fixed bed dryer and cylinder dryer. The effect of radiation heat transfer conditions and vacuum on the drying kinetics and temperature of tobacco leaves was investigated.

2. Materials and Methods

2.1 Materials

The flue cured tobacco C2F from Luoyang of China were chosen as experimental materials. Tobacco leaves were pretreated into cut tobacco by a cutter. The raw material is pretreated as follows: by adding a calculated amount of distilled water to cut tobacco, and moisture content of cut tobacco was adjusted to the desired level of moisture content. In this work, moisture content of the testing cut tobacco was set as 30% (on the wet basis). After adjusting the moisture content, cut tobacco was bagged and put into isothermal and equal humidity equipment to balance moisture for 48h.

2.2 Experimental apparatus

The structure of infrared-vacuum drying apparatus was shown in Fig.1. The drying chamber size is 45*45*45 cm. 4 pieces of ceramic radiant panel with the size of 12*12 cm were arranged in the rectangular on the top of drying chamber. A temperature sensor is installed on ceramic radiant panel and connected to the temperature controller unit, which could control the radiation temperature with the precision of ±1 ℃. A vacuum pump with the swept volume of 4 L/s (S.T.P.) is connected to the drying chamber through exhaust line. The pressure of drying chamber is adjusted and controlled by the flow meter and vacuum

meter in exhaust line. A weighing sensor with the precision of 0.1g is set at the bottom of drying chamber. During the drying experiments, the radiation heat transfer conditions and vacuum degree can be flexibly adjusted according to requirements.
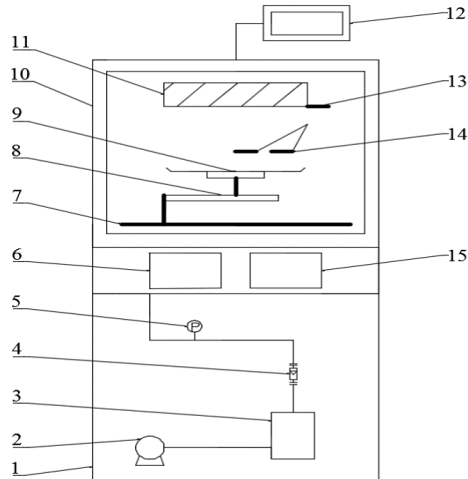
Fig.1 Infrared-vacuum drying apparatus. 1 The bottom of cabinet; 2 Vacuum pump; 3 Buffer vessel; 4 gas flow meter; 5 Vacuum meter; 6 Temperature display panel; 7 Bracket; 8 weighing sensor; 9 Material plate; 10 the upper of cabinet; 11radiant panel; 12 weight display panel; 13 radiation temperature sensor; 14 material temperature sensor; 15 temperature controller

2.3 Experiment methods

Before drying, the radiation temperature and distance are set as the desired levels. Then the apparatus is preheated for 30 min until the stable radiation temperature is reached. The sample of 35g cut tobacco is put into a thin layer on the material plate and then placed on the bracket of weighing sensor. The vacuum pump is started and pressure of drying chamber is adjusted to the desired level. During drying of cut tobacco, the mass and temperature data of sample are collected at the frequency of 30s until the constant weight of sample is reached. Four levels of radiation temperature are investigated, and they are 353 K, 368 K, 383 K and 398 K. The pressure of drying chamber is investigated at the levels of 30 kPa, 45 kPa, 60 kPa and 75 kPa (absolute pressure).

3. Results and discussion

3.1 Infrared-vacuum drying curves of cut tobacco

The moisture and temperature evolution of cut tobacco were investigated at different levels of radiation temperatures, as shown in Fig.2. It can be seen that, when radiation temperature changed from 353 K to 398 K, the drying times of samples were reduced by 50% (when cut

tobacco was dehydrated to the moisture content of 12%). The temperature of cut tobacco during drying also has an increasing trend at higher radiation temperature, and the final temperature of sample has a slight increasing.
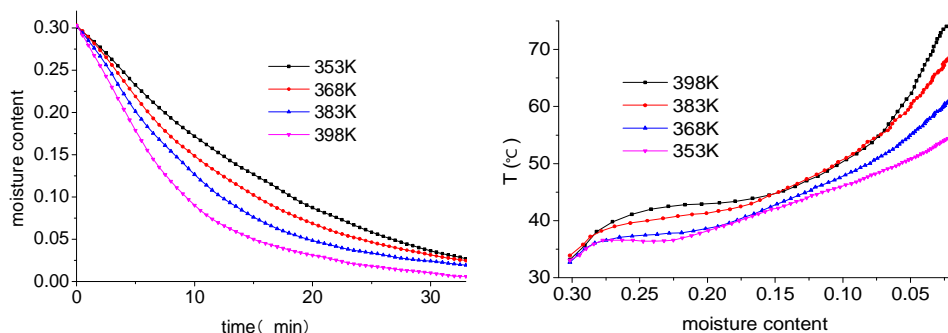
Fig. 2 Effect of radiant temperature on cut tobacco moisture content and temperature

The moisture and temperature evolution of cut tobacco were investigated at different levels of vacuum degrees, as were shown in Fig.3. As can be seen, the vacuum degree has opposite influence on the drying rate and temperature of cut tobacco. Low pressure, namely high vacuum degree, resulted in the increasing of drying rate and the decreasing of final sample temperature. The effect of vacuum degree was associated with its impact on the following two aspects. On the one hand, high vacuum degree could increase the difference of vapor partial pressure between the internal and external of wet materials. At the same time, high vacuum degree also leads to the low boiling point of water, which reduces the evaporation temperature of water during drying. The synthetic effect of the above two aspects caused that drying rate increased and final sample temperature decreased when vacuum degree is increased.
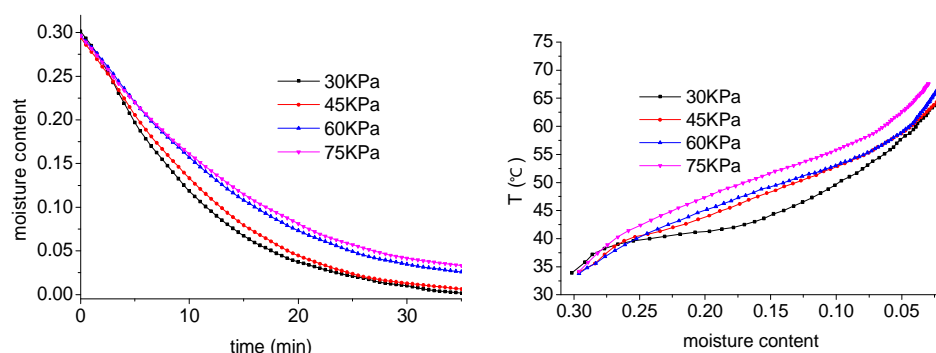
Fig. 3 Effect of vacuum level on cut tobacco moisture content and temperature

3.2 Moisture diffusion coefficient of cut tobacco

According to the Fick's second law[9], the following diffusion equation was used to describe the variation of cut tobacco moisture.

$$\frac{M - M_e}{M_0 - M_e} = \frac{8}{\pi} \sum_{n=0}^{\infty} \frac{1}{(2n + 1)^2} \exp\left[- \frac{(2n + 1)^2 \pi^2 D_e t}{4L^2} \right] \qquad (1)$$

Where, M_0, M and M_e are the moisture content of cut tobacco at t=0, t=t and t=∞, respectively. The D_e is the effective diffusion coefficient of cut tobacco. The t is drying time. L is half of cut tobacco width. In the above equation, the M_e, as equilibrium moisture content of cut tobacco at the drying condition, could be neglected. The L is 0.5mm. The first three terms were taken into account to calculate the effective diffusion coefficient[10]. The calculated values of D_e for two kinds of tobacco were shown in Table 1. It can be seen that the diffusion coefficient of tobacco during infrared-vacuum drying increased with the increasing of radiation temperature and vacuum degree. The radiation temperature has more significant influence on diffusion coefficient than vacuum degree. The diffusion coefficient of middle tobacco leaves C2F is between 0.848×10^{-10} ~ 1.597×10^{-10} m²/s.

Table 1. The D_e experimental values of cut tobacco

Radiation temperature / K	Vacuum degree / kPa	D_e ($\times 10^{-10}$) / m²·s⁻¹
353	30	0.8409
368	30	1.0317
383	30	1.2657
398	30	1.5529
383	45	1.1049
383	60	0.9645
383	75	0.8419

3.3 Pore structure in dried cut tobacco by different drying methods

The microstructure of dired cut tobacco was analyzed by SEM. Different drying methods were compared, including infrared-vacuum drying, infrared drying and triditional hot air drying at 55ºC. The results were shown in the Fig.4. It can be seen that both the infrared-vacuum drying and infrared drying resulted in the porous microstruture in the cross section of cut tobacco. This indicated that the infrared radiation heat transfer decreased the pore drying shrinkage of pore structure compared to the triditional hot air drying, as could be related to the penetrating heating characteristics of infrared radiation.

(a)   (b)   (c)
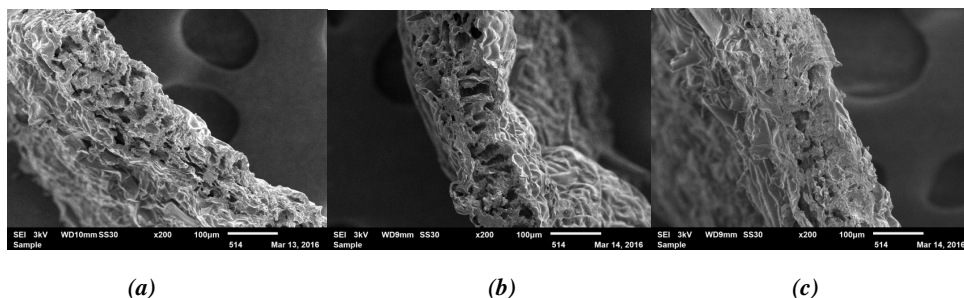
Fig. 4 Pore structure of cut tobacco C2F by different drying methods: （a）dried by infrared radiation and vacuum, （b）dried by infrared radiation, （c）dried by hot air

3.4 Petroleum ether tobacco extracts in dried tobacco

The petroleum ether tobacco extraction mainly consists of volatile oil, resins, fatty acids, waxes, lipids, sterols, and pigments. Its content is often considered as an important index in estimating the quality of tobacco aroma. The petroleum ether tobacco extraction in dried cut tobacco by different drying methods was analyzed, as shown in the Table 2. It can been seen that the infrared radiation heat transfer improved the content of petroleum ether tobacco extraction compared to the triditional hot air drying. The tobacco aroma change during drying mainly could be realted to two factors. The one is the Maillard reaction in tobacco during drying, which leaded to the increase of aroma components. The other one is the evaporative loss of volatile flavor components. The infrared radiation heat transfer may be more beneficial to the Maillard reaction than the hot air drying. However, the the vaccum would cause the increasing loss of volatile flavor components. The effect of two aspects resulted in that the petroleum ether tobacco extraction content for infrared-vacuum drying is higher than that of hot air drying, while lower than that of infrared drying.

Table 2. The petroleum ether extract content

Drying methods	petroleum ether extract content / %
Before drying	3.95
Hot air drying	4.01
Infrared-vacuum drying	4.23
Infrared drying	4.67

4. Conclusions

The infrared-vacuum drying characteristics of flue-cured tobacco leaf were investigated. Drying quality of tobacco was analyzed by comparing to the traditional hot air drying. The results showed that the average drying rate and final temperature of cut tobacco increased

with the increasing of radiation temperature. The vacuum degree has opposite influence on the drying rate and temperature of cut tobacco. Low pressure, namely high vacuum degree, resulted in the increasing of drying rate and the decreasing of final sample temperature. Diffusion coefficient of middle tobacco leaves C2F is between $0.848 \times 10^{-10} \sim 1.597 \times 10^{-10}$ m^2/s. The infrared radiation heat transfer decreased the pore drying shrinkage of pore structure compared to the triditional hot air drying. The infrared drying resulted in the higher petroleum ether tobacco extraction content than infrared-vacuum drying and hot air drying.

5. References

[1] Huang Jianai, Xie Jiangping. 2000. Cigarette Technology (2 nd ed.)[M]. Beijing: Beijing Public House (in Chinese).

[2] Hasan T.Simple modeling of infrared drying of fresh apple slices [J].Journal of Food Engineering, 2006,71(3):311-323.

[3] Zuiliechem DJ, van Riet, Stolp W. An overview of new infrared radiation processes for agriculgural products [C]//Maguer LM,Jelens P, et al. Food Engineering and Processes Applications, Transport Phenomens. New York: Elsevier Applied Science, 1985:595-610.

[4] Fasina O, Tyler RT, Pockard MD. Modeling the infrared radiative heating of agriculture crops [J]. Drying Technology, 1998, 16(9~10):2065-2082.

[5] Sakai N, Hanzawa T. Application and advances in far infrared heating in Japan [J]. Trends in Food Science and Technology, 1994, 5(11):357-362.

[6] Zhang LL, Wang XY, Yu L, Zhang HP. Drying characteristics and color changes of inftared drying eggplant.[J]. Agricultural Engineering, 2012,28: 291-296.

[7] Nathakaranakule A, Jaiboon P, Soponronnarit S. Far-infrared radiation assisted drying of longan fruit[J]. Journal of Food Engineering, 2010,100(4): 662-668.

[8] Jiang Gan, He Shunqiu, Liu Shuzhen. Effect of different drying methods on the quality of Smilax glabra Roxb[J], Journal of Guangdong Pharmaceutical University. 2013，29: 258-261(in Chinese).

[9] Crank J. Mathematics of diffusion (2 nd ed.) [M]. London: Oxford University Press, 1975.

[10] Liu Ze, Li Bin and Yu Chuanfang, Dynamics Analysis of Multiple Heat Transfer Impacts on Intensive Mass Transfer[J]. Tobacco Science & Technology, 2009, 11: 5-10. (in Chinese).

Moisture sorption isotherms and isosteric heat sorption of habanero pepper (*Capsicum chínense*) dehydrated powder

Luna-Flores, Mª*, Peña-Juarez M.Gª, Bello-Ramírez A.Mª, Telis-Romero Jᵇ, Luna-Solano Gª

ª *División de estudios de posgrado e investigación, Instituto Tecnológico de Orizaba, Av. Oriente 9 No 852, C.P 94320, Orizaba Veracruz., México.*

ᵇ Food *engineering and technology department, State University of Sao Paulo, São José do Rio Preto, 15054-000 São Paulo, Brazil*

*E-mail of the corresponding author: moonluna2009@live.com

Abstract

Moisture sorption isotherms of the habanero pepper powder were determined using the Dynamic Vapor Sorption (DVS) method at 20, 25, 35, 45 and 55 °C in a range of water activity from 0.10 to 0.90 at which the processes of drying, packing and storage of habanero pepper are developed. The sorption capacity decreased with increasing temperature at a given water activity and the sorption isotherms showed a sigmoid form (Type II). The hysteresis phenomenon was observed in the sorption isotherms at all temperatures studied and it was more pronounced at temperatures high. The experimental sorption curves were fitting to the GAB, BET and Oswin models. It was concluded that the models that best describe the adsorption and desorption data for habanero pepper dehydrated powder were the GAB and Oswin models. The isosteric heat of water sorption was calculated with the moisture content data in equilibrium. The desorption isotherms present a higher isosteric heat in relation to the adsorption isotherms. In both, the isosteric heat decreased as the moisture content increased.

Keywords: Habanero pepper dehydrated powder; Convective drying; Moisture sorption isotherms; Mathematic models

1. Introduction

Habanero pepper is a variety of red pepper most popular in the Mexican territory, it has a high moisture content (> 80 % wet base) and the main characteristics of the habanero are color (carotenoids), aroma and mainly the pungencia due to the capsaicinoids [1,2]. Therefore, the export and conservation of fresh fruit have several disadvantages because habanero pepper is very perishable and has a limited shelf life. Convective drying is one of the most popular and efficient heat and mass transfer process that allows to prolong and preserve the useful life of foods by reducing water activity (a_w) and decreasing moisture content [3]. The state of water plays an important role in the preservation of food. The degree of sorption of water from a food system depends on the vapor pressure of the water present in the food sample and in the surroundings. The equilibrium moisture content (EMC) is obtained when the vapor pressure of water present in food is equal to the vapor pressure of the surroundings. The water activity (a_w) of a food is an equilibrium property of the water and its constituents present, which defines as the ratio of the partial pressure of the water vapor in the food (p) and the partial pressure pure water vapor (p_0) at the same temperature, as shown in equation 1:

$$a_w = \frac{p}{p_0} = \frac{HR}{100} \tag{1}$$

The relationship between EMC and aw in a range of values at a constant temperature generates an evaluation tool very useful called ``Moisture sorption isotherm´´, which relates the amount of water adsorbed or desorbed in equilibrium. An adsorption isotherm refers to the behavior of dehydrated foods, which tend to adsorb water against the surrounding relative humidity to have equilibrium pressures. While a desorption isotherm refers to the behavior of hydrated foods, which tend to eliminate water to have equilibrium conditions at a given temperature. These behaviors depend on the interaction between water and food components. Sorption isotherms provide information for a variety of processing applications and product stability, such as prediction of moisture transfer, determination of product stability and shelf life, storage conditions, selection of packaging systems [3, 4, 5]. Therefore, the aim of this study was to analyze the isotherms (adsorption and desorption) of the habanero pepper dehydrated powder.

2. Materials and Methods

1.1. Raw material and convective drying of habanero pepper

Habanero pepper was obtained from the city of Orizaba, Veracruz, Mexico. The selected fruits showed an orange color and similar size (4-7 cm length, 3-5 cm width). Samples of habanero pepper were cut into slices 0.6 cm wide and placed on metal trays of a convective

dryer (Polinox SEM-2). The convective drying process was performed at a temperature of 60°C and at an air velocity of 1.5 m/s for 360 min until moisture ≥0.05 g water/g dry solids is constant. The data obtained from drying at 60 °C was plotted as moisture ratio (MR) according to the equation 2:

$$MR = \frac{X - X_e}{X_0 - X_e}$$
(2)

Where X is the moisture content at any time t, X_e is the equilibrium moisture and X_0 is the initial moisture. These experimental sets (MR, t) were fitted to different empirical models from literature applicable to agricultural products: Page, Newton, Henderson & Pabis, Logarithmic and Wang & Sing. These equations for drying kinetics are indicated below (equations 3 to 7), respectively.

$$MR = e^{-kt}$$
(3)

$$MR = e^{-kt^n}$$
(4)

$$MR = a \cdot e^{-kt}$$
(5)

$$MR = c + a \cdot e^{-kt}$$
(6)

$$MR = 1 + a \cdot t + b \cdot t^2$$
(7)

Where n, a, b and c are constants of the models, and *t* is any time in the drying kinetics.

1.2. Physicochemical analysis

During the convective drying process of dehydrated habanero pepper, the evolution curves of water activity and color difference were performed. The water activity was determined at 25 ± 1 °C using a water activity meter (AQUALAB series 3 model TE). The moisture content (g water/ g dry solids) of habanero pepper was measured with a halogen thermobalance (OHAUS, model MB35).

1.3. Moisture sorption isotherms

Habanero peppers were milled in a manual pulverizer of blades at laboratory scale, model GRT-20B of 3000 Watts and 25000 rpm for 3 min to obtain samples of habanero pepper powder to analyze moisture sorption isotherms. The sorption isotherms (adsorption and desorption) were determined by a vapor sorption analyzer (AquaLab VSA), which consists of an equipment that automatically generates moisture sorption isotherms in foods,

allowing the determination of the complex relationship between aw at each reading and the EMC of the sample at a constant temperature. The isotherms were determined at 20, 25, 35, 45 and 55 °C. The VSA equipment generates the static isotherms in equilibrium by the Dynamic Vapor Sorption (DVS) method, which consists of monitoring the weight change of the sample as it is exposed to different controlled relative humidities. The sample is maintained at each humidity for a period of time until the sample reaches a steady state weight change, where the objective is to achieve the equilibrium between the aw and the controlled humidity inside the generator chamber. The experimental sorption isotherms of the habanero chili powder were performed in duplicate.

1.4. Prediction of mathematical models

The mathematical models GAB (Guggenheim & Anderson de Boer), BET (Branauer, Emmett & Teller) and Oswin represented by equations 8, 9 and 10 were used to adjust and predict the experimental values of sorption isotherms (adsorption and desorption).

$$EMC = \frac{CKX_m a_w}{(1 - Ka_w)(1 - Ka_w + CKa_w)} \tag{8}$$

$$EMC = \frac{CX_m a_w}{(1 - a_w)(1 - a_w + Ca_w)} \tag{9}$$

$$EMC = A\left[\frac{a_w}{(1 - a_w)}\right]^B \tag{10}$$

Where: A, B, C and K are constants of the models, a_w is the water activity, EMC is the equilibrium moisture content (g water/g dry solids) and X_m is the moisture content in the monolayer (g water/g dry solids).

1.5. Net isosteric heat of sorption

The net isosteric heat of sorption was determined from moisture sorption using the equation 11, derived from the Clausius Clapeyron equation:

$$\ln(a_w) = -\left(\frac{q_{st}}{R}\right)\frac{1}{T} + C_1 \tag{11}$$

Where a_w is the water activity, T is the absolute temperature (K), q_{st} is the net isosteric heat of sorption (J mol^{-1}), R is the gas constant (J mol^{-1} K^{-1}).

1.6. Results and discussion

Luna-Flores, M.; Peña-Juarez, M..G.; Bello-Ramírez, A. M.; Telis-Romero, J.; Luna-Solano, G.

Figure 1 and 2 show the adjustment of the mathematical models of the drying kinetics and the evolution curves of a_w of habanero pepper during drying as a function of time, observing that the a_w and moisture content of the fresh fruit is relatively high. However, when the drying process is performed, the values of moisture content and a_w decreased significatly. A food with an a_w less than 0.60 and moisture content low is considered safe and stable during storage in relation to microbial growth [6]. The a_w is considered a parameter for the conservation and stability of food as well, it has been used as an important variable to evaluate and reduce the rate of microbial growth, chemical reactions, lipid oxidation and enzymatic activity in the food [5].
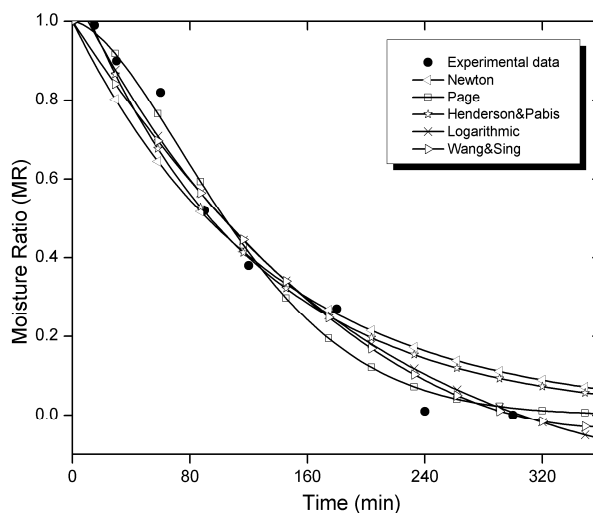
Figure 1. Fitting of the experimental data with the different models tested

Figure 1 shows the experimental data points obtained from temperature 60 °C of the drying process together with the plots corresponding to the fittings obtained for all the models tested. It is observed that the Page and Newton curves are better describing the habanero pepper drying process. On the other hand the models of Henderson & Pabis and Logarithmic do not represent the initial state (t=0 min), while the Wang & Singh model does not exemplify the final state (t=360 min). However, the best model to describe this drying kinetics process is the Page model because it shows a sigmoidal shape in the curve. In Figure 2(a), it is possible to observe how the moisture behavior follows a sigmoidal shape, which is characteristic of the drying process. The initial moisture content was 83.59% and the final content 1.56%. Regarding water activity in Figure 2(b), shows also a sigmoidal shape and it is possible to reach a safe range (below 0.6) at time 180 min.

a)   *b)*
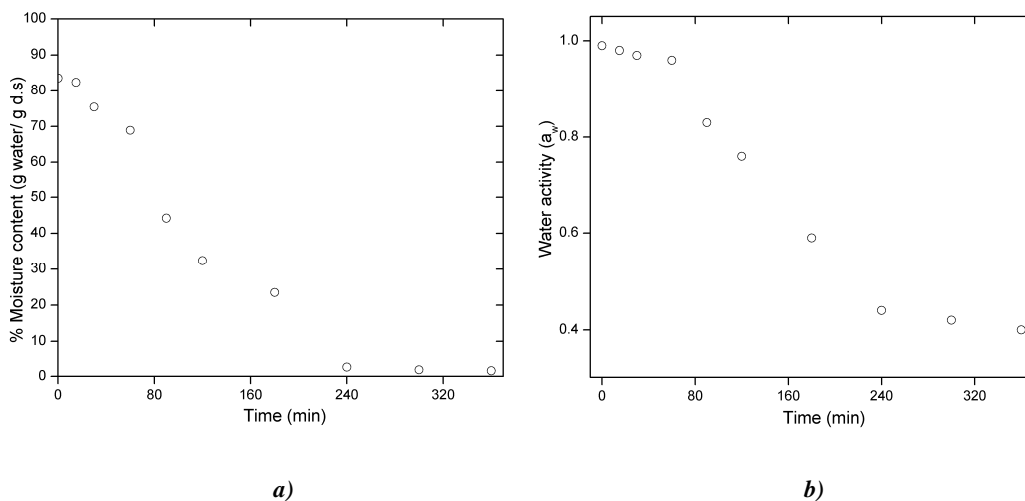
Figure 2. Drying curves for physicochemical parameters of habanero pepper: a) moisture content and b)water activity

The shapes of the adsorption and desorption curves of habanero pepper dehydrated powder showed a behavior similar to the five temperatures (20, 25, 35, 45 and 55 °C) studied and presented a non-linear trend type II (sigmoid) typical shape for most foods [7], which is shown in Figure 3. As the temperature increases, the EMC decreased to a constant water activity, this change generates that the water molecules are activated due to a change in the increase in the pressure of the water vapor inside the particles of habanero pepper powder through a state of excitation, becoming less stable and consequently accelerating the moisture transfer of the food around it [8]. In addition, it was observed a simultaneous increase of the EMC because the food particles are saturated by water molecules according to an incremented in the values of water activity at a constant temperature. This is due to the decrease in the degree or capacity of sorption of water in habanero pepper powder when the temperature increases. In the process of desorption, it was observed that the high and intermediate values of the water activities in the desorption curves of habanero pepper powder present a remarkable decrease of the EMC due to the dissipation of the water molecules present in the surfaces towards the surroundings. This indicates the influence of temperature on the desorption isotherms. However, it is also shown that the desorption curves between low values of a_w (0.3-0.1) and the EMC are very close to each other. This means that the water molecules bind more firmly and the enthalpy of vaporization is greater due to the transition of the water that is strongly attached to the capillaries of habanero pepper powder.
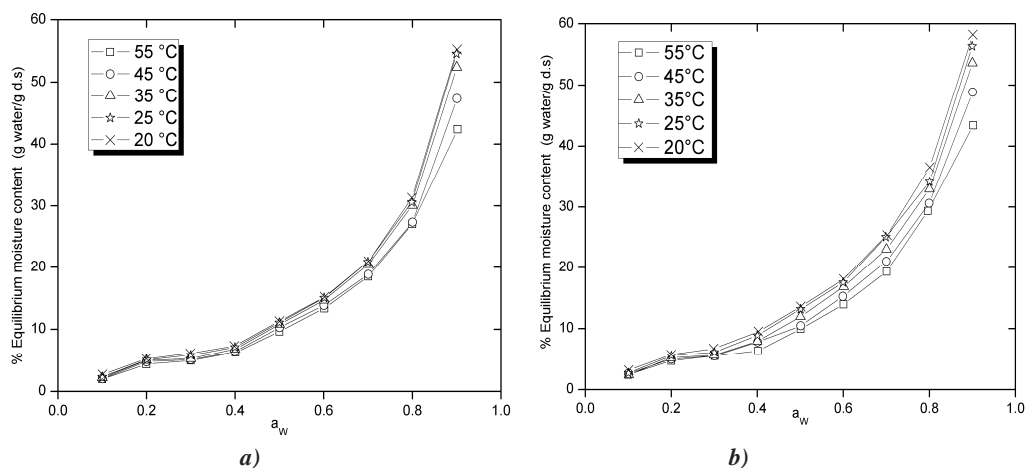
Figure 3. Isotherms of habanero pepper: a) adsorption and b) desorption

The GAB, BET and Oswin models were fitted to evaluate the behavior of moisture sorption isotherms and the goodness of fit for each model was evaluated according to the coefficient of determination (R2), sum of the square error (SSE) and the residual mean square error (RMSE). The results of the non-linear regression analysis are presented in Table 1. The best fits were obtained with the GAB and Oswin models with a R2> 0.995 and R2> 0.987, SSE<7.705 and 19.91, for RMSE<1.133 and 1.687 respectively for the sorption isotherms of habanero pepper dehydrated powder. However, the GAB model presents an advantage due to it presents theoretical bases and the value of moisture content in the monolayer (Xm) whereby it is best model that empirical model of Oswin. The net isosteric heat of sorption (qst) decreased with increasing moisture content. The higher values of qst were found at low moisture contents, this can be explained by the fact that the water molecules are tightly bound to the monolayer structure and food components; and therefore, the quantity of energy needed to adsorb or desorb these water molecules is very high. However, a rapid decrease in sorption isosteric heat was observed when the moisture content began to increase due to the sorption of water molecules in the multilayer. The isosteric sorption heat of habanero pepper powder, which was determined using the Clausius-Clapeyron equation, decrease with an increase of moisture content, ranging from 4.86 KJ mol-1 to 1,07 KJ mol-1 and 7.59 KJ mol-1 to 1,43 KJ mol-1.for adsorption and for desorption witn an equilibrium moisture content ranging from 5 to 45% (g water/g dry solids).

2.   Conclusions

The isotherms of adsorption and desorption of habanero pepper dehydrated powder presented a sigmoid shape (Type II) at five different temperatures: 20, 25, 35, 45 and 55 ° C. According to the results of this study, the GAB model presents a better fit of the

experimental results of the sorption isotherms of the habanero pepper powder with a $R^2>$ 0.995, SSE<7.705 and RMSE<1.133. Habanero pepper powder was less hygroscopic as the temperature decreased. This behavior of sorption can be attributed to the low solubility nature of carbohydrates and bioactive compounds present in habanero pepper powder with water molecules. Water activity values from 0.3 to 0.4 represent the optimum moisture content at which most dehydrated foods will have maximum shelf life. Therefore, considering 0.35 as the average water activity, among these values, the safest for dehydrated habanero pepper powder, the limit equilibrium moisture content for this product should be 7.38%, 7.13%, 6.79%, 6.50% and 6.04% at temperatures of 20 °C, 25 °C, 35 °C, 45 °C and 55 °C respectively, since above this moisture content, enzymatic oxidation, chemical instability and/or oxidation will begin proliferation of microorganisms. Regarding drying kinetics, according to the obtained results, it was concluded that the empirical models that best describe the dehydration kinetics for habanero orange bell pepper are Page and Newton.

3. References

[1] Rhim J. and Hong S. (2011). Effect of water activity and temperature on the color change of red pepper (Capsicum annuum L.) powder. Food Science and Biotechnology, 20, 215–222.

[2] Sganzerla M., Pereira C. J., Tavares de Melo A. M., and Texeira G. H. (2014). Fast method for capsaicinoids analysis from Capsicum chinense fruits. Volumen 64, October 2014, 718–725.

[3] Schmidt S. J. and Won L. J. (2012) Comparison Between Water Vapor Sorption Isotherms Obtained Using the New Dynamic Dewpoint Isotherm Method and those Obtained Using The Standard Saturated Salt Slurry Method, International Journal of Food Properties, 15:2, 236-248.

[4] Basu S., Shivhare U.S. and Mujumdar A.S. (2006). Models for Sorption Isotherms for Foods: A Review. Drying Technology. 24: 917–930.

[5] Tsotsas E. and Mujumdar A. S. (2014). Industrial Moisture and Humidity Measurement. Wiley-VCH Verlag GmbH and Co.

[6] Villegas Santiago J., Calderón S. M., Ragazzo S. A., Salgado C. M. A. and Luna S. G. (2011). Fluidized bed and tray drying of thinly sliced mango (Mangiferaindica) pretreated with ascorbic and citric acid. Journal of Food Science and Technology 46, 1296-1302.

[7] Brunauer, S., Deming, L.S., Deming, W.E. y Troller, E. 1940. On the theory of Van der Waals adsorption of gases. Journal of American Society, 62, 1723-1732.

[8] Kaleemullah S. y Kailapan R. 2004. Moisture Sorption Isotherms of Red Chillies. Biosystems Engineering 88 (1); 95-104.

Observation of microstructure change during freeze-drying by in-situ X-ray Computed Tomography

Nakagawa, K.[a]*; Tamiya, S.[a]; Sakamoto, S.[a]; Do, G.[b]; Kono, S.[c]; Ochiai, T.[d]

[a] Division of Food Science and Biotechnology, Graduate School of Agriculture, Kyoto University, Sakyo-ku Kitashirakawa Oiwakecho, Kyoto 606-8502, Japan

[b] College of Bioresource Science, Nihon University, Japan

[c] Research and Development Center, Mayekawa MFG. Co., Ltd., Japan

[d] Research and Development Headquarters, Asahi Group Foods Ltd., Japan

*E-mail of the corresponding author: kyuya@kais.kyoto-u.ac.jp

Abstract

X-ray computed tomography technique was used to observe microstructure formation during freeze-drying. A specially designed vacuum freeze-drying stage was equipped at the X-ray CT stage, and the frozen and dried microstructures of dextrin solutions were successfully observed. It was confirmed that the many parts of the pore microstructures formed as a replica of the original ice microstructures, whereas some parts formed as a consequence of the dehydration dependent on the relaxation level of the glassy phases, suggesting that the post-freezing annealing is advantageous for avoiding quality loss that relates to the structural deformation of glassy matters.

Keywords: freeze-drying; X-ray CT; ice microstructure; glassy state

1. Introduction

Freeze-drying is known as one of the best drying methods in terms of preservation of product qualities. Due to its higher processing cost than the other drying method, quality assurance is a critical issue to meet requirements of industries. Detailed knowledge on the phenomena occurring in a freeze-drying system plays an important role in further improvement of process design. Freeze-drying process consists of freezing and drying steps. When an aqueous solution is subjected to freezing, an ice crystal phase coincidently forms with the freeze-concentrated phase. In most cases of freeze-dried formulations, the freeze-concentrated phase transforms into a glassy phase, and the water content in the glassy phase can be related to the temperature. The glass transition temperature (T_g) of the maximally freeze-concentrated glassy phase is commonly denoted as T'_g, and this temperature has a critical importance in terms of carrying out an appropriate freeze-drying run. During drying step, water is mainly removed from the ice crystal phase by sublimation (i.e. primary drying). The removal of water coincidently forms dried layer, and the subsequently sublimated water vapor must transfer through the dried cake layer with porous microstructures. The mass transfer resistance in the cake layer is thus controlled by modifying the ice crystal morphologies.[1-3] Water is also removed from the freeze-concentrated glassy phase by vaporization (i.e. secondary drying) at above T'_g. The viscous flow of the glassy phase may cause the loss of the dried layer structure that is called as collapse. The occurrence of collapse is thus provoked by the excessive increase of the product temperature and/or decrease of the evaporation rate. [4-8] Furthermore, it must be noted that the glassy phase in a rapidly frozen solution is not perfectly freeze-concentrated because of the formation of the non-crystalized water (i.e. vitrified water).[9-11] Annealing over T_g reduces the fraction of the amorphous phase toward the completion of the freeze-concentration; this is called as relaxation (glassy phase relaxation). The degree of the relaxation relates to the T_g and viscosity of the glassy state, and it would affect the dehydration rate from the glassy phase and consequently the strength of the dried layer. Therefore, the freeze-dried microstructure forms not only in the freezing step but also in the drying step. The formation of freeze-dried microstructure in the sufficiently freeze-concentrated frozen solution would be different from the one in the immature frozen solution. Our interest in this study was thus to investigate the influence of the glassy state relaxation on the microstructure formation during freeze-drying.

X-ray computed tomography (CT) is a powerful tool to visualize microstructure of a material without sample destruction. In this study, X-ray CT was used to observe microstructure formation during freeze-drying. Our interests in this study is to investigate the primary and secondary drying behavior by using in-situ CT technique with monochromatized X-ray from the synchrotron radiation. A freeze-drying system was set-up at the X-ray CT

stage, and the microstructure change during vacuum freeze-drying of dextrin solution was observed.

2. Materials and Methods

2.1. Materials

Millipore-purified water was used for the sample preparation. Sucrose was purchased from Wako Pure Chemical Industries (Osaka, Japan). Dextrin was donated by Matsutani Chemical industry Co., Ltd. (Hyogo, Japan). Dextrin of which dextrose equivalent (DE) equal to 11 was used in this study. Glass transition temperatures of the maximally freeze-concentrated aqueous dextrin solution (T'_g) measured by DSC was around –11ºC.

2.2. Frozen sample preparation

Aqueous dextrin solution with a concentration of 20 %(w/w) was prepared and filled in a sample stage. Sample stage was composed of a metal base (made by stainless steel) and a plastic tube (diameter 6 mm, height 10 mm). The tube was attached on the metal base to make a space for putting a solution. The bottom of a solution contacts to the metal part. The sample stage with a sample solution was placed on a cupper block pre-cooled in liquid nitrogen so as to freeze inner solution rapidly with keeping its direction of freezing from the bottom to the top. Frozen solutions were subsequently annealed at –5ºC in an electric cooling devise for selected duration (0–12 h). Frozen samples were then stored in a refrigerator at–90ºC until measurement.

2.3. Synchrotron X-ray computed micro tomography

X-ray computed tomography was carried out at synchrotron facility SPring-8 (BL19B2, Hyogo, Japan). Monochromatized X-ray was used for this measurement in order to obtain X-ray attenuation linear coefficient from the tomograms. The X-ray energy was adjusted to 12.4 KeV by a double Si-crystal monochromator (net plane: (111)). As schematized in Fig. 1, the measurement stage was equipped with a turntable with a cold finger of which temperature was controllable by an external air blowing device in the range of –80 to –10ºC. The sample stage with a frozen sample was rapidly fixed on the sample stage pre-cooled at around –15ºC. The sample stage on the turntable was then fully covered with a housing case, and the inner space was evacuated by connecting a vacuum pump in order to start freeze-drying. The top of this housing component was made by acrylic resin with a thickness of 0.5 mm. The X-ray passed through this acrylic window and the sample, and then exposed to X-ray camera that was set 100 mm behind the housing component. An X-ray imaging unit (AA40, Hamamatsu Photonics K.K., Japan) and CCD camera (C4880-41S, Hamamatsu Photonics K.K., Japan)

were used for image acquisition. 256 transmission images were acquired for one set of measurement by rotating the turntable from 0 deg to 180 deg at a speed of 1.2 deg/s. The exposure time of X-ray was set to 0.12 s for taking an image, and the pixel size in the image was 2.92 µm square. A horizontal cross-sectional image (i.e. tomogram) was reconstructed from the transmission image by the filtered back projection method. Freeze-drying run was carried out with the sample stage temperature at around –14ºC, inner pressure around 12 Pa.
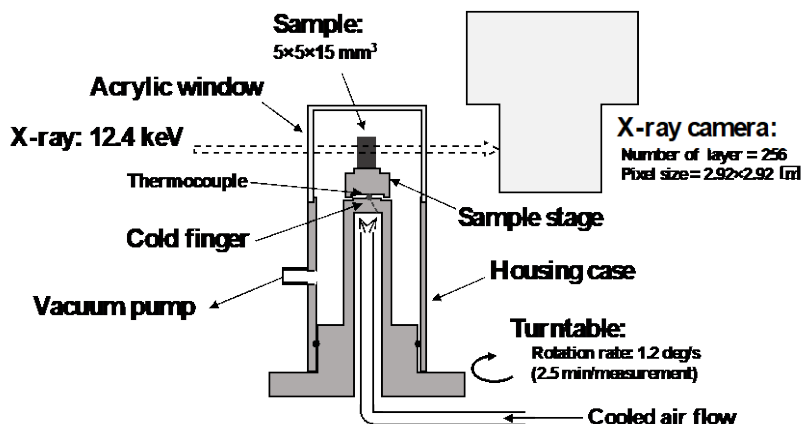
Fig. 1 X-ray CT measurement set-up equipped with freeze-drying stage.

3. Results and Discussions

3.1. CT images during freeze-drying

The freeze-drying runs were carried out and CT images were successfully captured by the present system. First of all, CT images taken from the frozen zones were compared in Fig. 2. The boundary between the ice and freeze-concentrated phases was obviously formed in the sample prepared via longer annealing. One reason is due to the ice crystal size increase by Ostwald ripening mechanism. Another reason is the progress of the freeze-concentration due to the glassy state relaxation. The details of these kinetics during annealing were investigated in a former study of the authors [12], suggesting that both the glassy phase relaxation and Ostwald ripening jointly control the ice crystal growth/ripening kinetics, and the dominant mechanism was depending on the stage of annealing. Furthermore, the progress of freeze-concentration increases the density of the phase, this contribute to increase the attenuation level in the CT image and make clear contrast with the ice phase. It was also suggested that the dextrin-water system required more than 20 hours of annealing time for the completion of the glassy phase relaxation.
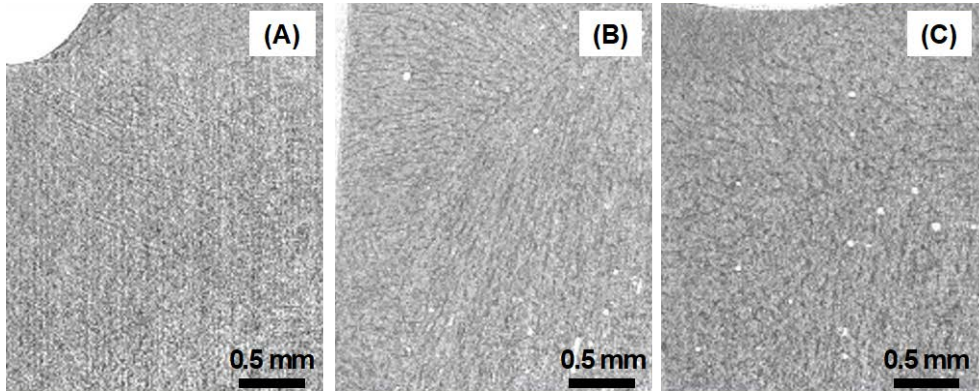
Fig. 2 X-ray CT images of frozen specimens (vertical cross sections); (A) Annealed for 0h, (B) Annealed for 12 h, (C) Annealed for 30 h.
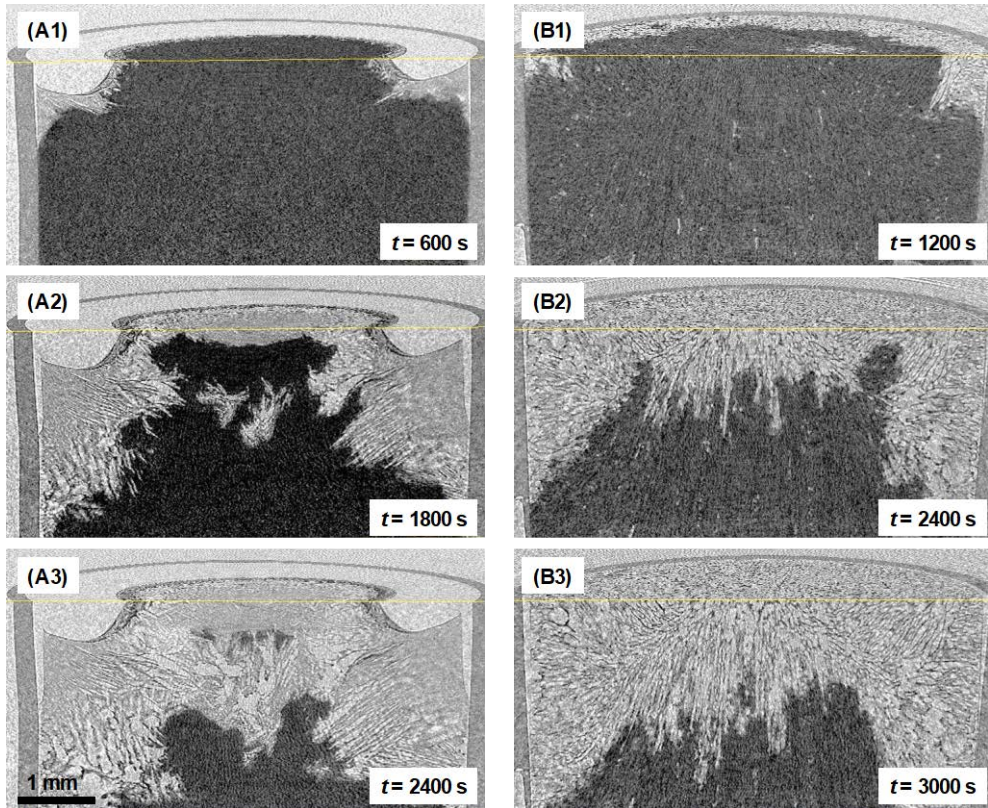
Fig. 3 X-ray CT images of freeze-drying specimens (the duration under vacuum was stamped in the images); (A1–3) Annealed for 0 h, (B1–3) Annealed for 12 h .

3D reconstructed images of the samples during freeze-drying were shown in Fig. 3. It was visibly confirmed from the images of the sample via 12 h of annealing that the ice crystals were removed from the system by maintaining the original architectures made by the freeze-concentrated phase (Fig. 3A). This observation agrees with conventional explanation of a freeze-drying mechanism where a microstructure in a freeze-dried matrix is a replica of the frozen microstructure. On the other hand, this was hardly observed in the images of the sample prepared without annealing (Fig. 3B). Although extremely fine porous structures were formed at the top part, the formations of specific large pores were obvious in this drying system. These large pores were not visible in the frozen zone, and randomly distributed in the sample geometry. Considering that the glassy phase in the non-annealed solution was not perfectly freeze-concentrated, the apparent vapor pressure of this phase is higher than the perfectly freeze-concentrated phase. The apparent water vapor pressure, this is not equilibrium thermodynamic pressure, of the glassy phase is observed lower as the value of $(T-T_g)$ become smaller. This is because the properties of glassy phase is kinetically controlled.[7] Therefore, in the drying of non-annealed solution, water removal from this phase would be accelerated and easily lost its original microstructure.

3.2. Fractal dimension and lacunarity

The previous section discussed about the microstructure formation that occurred simultaneously with dehydration. In order to evaluate the differences in microstructures, the fractal dimension and the lacunarity of the porous microstructures were calculated from the images. Fractal dimension is a measure of structural roughness, whereas lacunarity is a measure of inhomogeneity or texture. In other words, lacunarity is the ratio of void space filled in a fractal structure. Cross sectional images were selected from the dried zone, and converted into binary images (Fig. 3). Image analysis was carried out on the binary images by a software *FracLac version 2015 for ImageJ*. The fractal dimension values for the non-annealed and annealed samples were both calculated as 1.8. The lacunarity values, on the other hand, for the non-annealed and annealed samples were 0.14 and 0.12, respectively. These values suggested that the structural difference between the non-annealed and annealed freeze-dried matrix was mainly due to the formation of the void space. The difference in the lacunarity values implies that the obvious void spaces seen in the non-annealed sample were not casted by ice crystals. Annealing in freeze-drying process has been recognized as a technique to reduce primary drying time and also to alter crystallinity and/or aggregation degree of the components[9, 10, 13-15] The result of this study suggested that these advantages of annealing are realized by avoiding the structural deformation as seen in the freeze-drying of the non-annealed sample, and largely relate to the degree of the glassy phase relaxation.
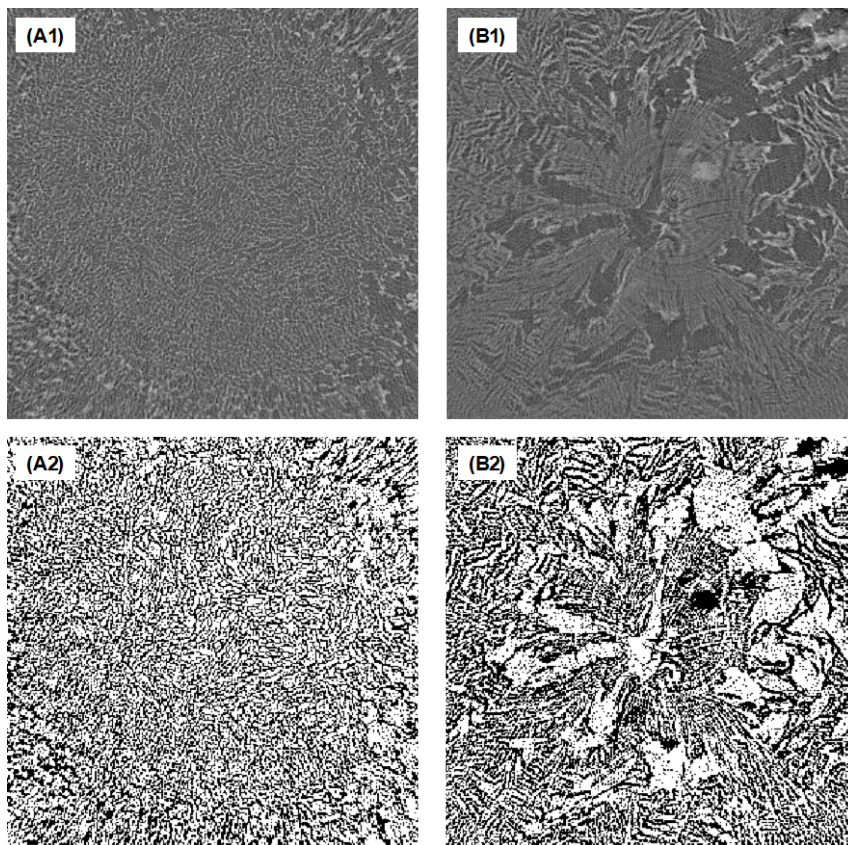
Fig. 4 X-ray CT images of freeze-dried specimens (horizontal cross sections); (A) Annealed for 0h, (B) Annealed for 12 h. Binary images converted from A1 and B1 are shown at the bottom.

4. Conclusions

In-situ computed tomography technique with X-ray from the synchrotron radiation was used to observe microstructure formation during freeze-drying to investigate the primary and secondary drying behavior. A specially designed vacuum freeze-drying stage was equipped at the X-ray CT stage, and the frozen and dried microstructures of dextrin solutions were successfully observed. It was confirmed that the many parts of the pore microstructures formed as a replica of the original ice microstructures, whereas some parts formed as a consequence of the dehydration. This would relate to the relaxation level of the glassy phases. When rapidly frozen and non-annealed solution was subjected to freeze-drying, obvious deformation of the original ice microstructures could be provoked by the water removal from both ice and freeze-concentrated phases. Considering that the glassy phase in the non-annealed solution was not perfectly freeze-concentrated, water was rapidly removed from this phase and lost its original microstructure. It was suggested that the advantages of

annealing are not only to reduce primary drying time due to the modification of ice crystal morphologies but also to avoid quality loss that relate to the structural deformation of the glassy matters.

5. References

[1] Searles, J.A.; Carpenter, J.F.; Randolph, T.W. Annealing to optimize the primary drying rate, reduce freezing-induced drying rate heterogeneity, and determine Tg′ in pharmaceutical lyophilization. Journal of Pharmaceutical Sciences 2001, 90, 872-887.

[2] Nakagawa, K.; Hottot, A.; Vessot, S.; Andrieu, J. Influence of controlled nucleation by ultrasounds on ice morphology of frozen formulations for pharmaceutical proteins freeze-drying. Chemical Engineering and Processing: Process Intensification 2006, 45, 783-791.

[3] Nakagawa, K.; Hottot, A.; Vessot, S.; Andrieu, J. Modeling of freezing step during freeze-drying of drugs in vials. AIChE Journal 2007, 53, 1362-1372.

[4] Slade, L.; Levine, H.; Ievolella, J.; Wang, M. The glassy state phenomenon in applications for the food industry: Application of the food polymer science approach to structure–function relationships of sucrose in cookie and cracker systems. Journal of the Science of Food and Agriculture 1993, 63, 133-176.

[5] To, E.C.; Flink, J.M. 'Collapse', a structural transition in freeze dried carbohydrates. International Journal of Food Science & Technology 1978, 13, 583-594.

[6] Pikal, M.J.; Shah, S. The collapse temperature in freeze drying: Dependence on measurement methodology and rate of water removal from the glassy phase. International Journal of Pharmaceutics 1990, 62, 165-186.

[7] Slade, L.; Levine, H.; Reid, D.S. Beyond water activity: Recent advances based on an alternative approach to the assessment of food quality and safety. Critical Reviews in Food Science and Nutrition 1991, 30, 115-360.

[8] Levi, G.; Karel, M. Volumetric shrinkage (collapse) in freeze-dried carbohydrates above their glass transition temperature. Food Research International 1995, 28, 145-151.

[9] Sahagian, M.E.; Goff, H.D. Effect of freezing rate on the thermal, mechanical and physical aging properties of the glassy state in frozen sucrose solutions. Thermochimica Acta 1994, 246, 271-283.

[10] Ablett, S.; Izzard, M.J.; Lillford, P.J. Differential scanning calorimetric study of frozen sucrose and glycerol solutions. Journal of the Chemical Society, Faraday Transactions 1992, 88, 789-794.

[11] Levine, H.; Slade, L. Principles of "cryostabilization" technology from structure/property relationships of carbohydrate/water systems—a review. Cryo-letters 1988, 9, 21-63.

[12] Nakagawa, K.; Tamiya, S.; Do, G.; Kono, S.; Ochiai, T. Observation of glassy state relaxation during annealing of frozen sugar solutions by X-ray computed tomography. Eur J Pharm Biopharm 2018, 127, 279–287.

[13] Kasper, J.C.; Friess, W. The freezing step in lyophilization: physico-chemical fundamentals, freezing methods and consequences on process performance and quality attributes of biopharmaceuticals. European Journal of Pharmaceutics and Biopharmaceutics 2011, 78, 248-263.

[14] Milton, N.; Pikal, M.J.; Roy, M.L.; Nail, S.L. Evaluation of Manometric Temperature Measurement as a Method of Monitoring Product Temperature During Lyophilization. PDA Journal of Pharmaceutical Science and Technology 1997, 51, 7-16.

[15] Goshima, H.; Do, G.; Nakagawa, K. Impact of Ice Morphology on Design Space of Pharmaceutical Freeze-Drying. Journal of Pharmaceutical Sciences 2016, 105, 1920–1933.

A green coffee based product and its comparasion to commercial products regarding the antioxidant capacity

Sousa, F.C.A.[a]; Souza, E.F[b]; Pontes, S.M.[b]; Leal Junior, W.F.[b]; Freitas-Silva, O.[b] Nogueira, R.I.[b]*

[a] Programa de Pós-graduação em Alimentos e Nutrição (PPGAN) – Universidade Federal do Estado do Rio de Janeiro (UNIRIO), Brazil.
[b] Embrapa Agroindústria de Alimentos, Rio de Janeiro, R.J., Brazil.

*E-mail of the corresponding author: **regina.nogueira@embrapa.br**

Abstract

Green Coffee Products (GCP) consumption have been increased recently and is justified due its benefits to human health, as the antioxidant activity and thermogenic properties and ant mutagenic and ant carcinogenic capacity and also present alleged weight loss control. The aim this work was to elaborate a GCP with Coffea canephora by spray drying and compare its antioxidant capacity to commercial GCP samples by ORAC methodology. The results presented a range of 33.02 – 2,408.05 µmol Trolox/g for commercial products and 1,861.91 µmol Trolox/g for the product obtained in this work.

Keywords: Antioxidant Activity;Green Coffee;Spray Drying;ORAC.

1. Introduction

In recent years, the studies on the biological activity of green bean coffee and their beverages has been more encouraged and explored [1]. Green coffee beans differ in chemical composition according to species and origin. Coffee beans are composed of polysaccharides, lipids and proteins and as secondary compounds caffeine, trigonellin, chlorogenic acids, free sugars (mainly sucrose), free amino acids, diterpenes, melanoidines, among others [2]. However, during the coffee roasting process, several chemical reactions occur at the same time, from which some compounds are degraded, such as proteins, polysaccharides, and chlorogenic acids [3].

A cup of the roasted coffee drink is rich in different and complex bioactive substances, which can present antioxidant activity, being the beverage an important source of the consumption of natural antioxidants [4].

The process and formulation to obtaining food supplements from green coffee may be the differential, as the commercial products of dietary supplements based on green coffee has different formulations which uses various food materials sources of bioactive compounds. Besides the formulation and choice of raw material, since it is known that the robusta coffee beans (*Coffea canephora*) contains more acids chlorogenic than *C. arabica*, which plays an important role in the antioxidant capacity [5]. The product obtained in this work was composed only by green coffee extract from *C. canephora* and maltodextrin.

In addition to the consumption of the traditional coffee beverage made by infusion of roasted and ground coffee, green coffee extract (GCE), commercialized in different forms, such as capsules, flours or liquid extract, has gained a market share by the appeal of antioxidant activity and for the help in the weight loss process [6], since it contains 6 to 12% of chlorogenic acids, of which during the roasting process of the grain for the preparation of the traditional coffee beverage undergoes degradation [7]. In this way the aim of our study was elaborate a GCP with *C. canephora* by spray drying and compare its antioxidant capacity to commercial GCP samples.

2. Materials and Methods

2.1 Green Coffee Products

It was evaluated nine different products of commercial dietary supplements based on green coffee, purchased directly from Rio de Janeiro trade, in the form of capsules or flours and one GCP imported from USA, Figure 1A. A GCP 10 was elaborated under our laboratory conditions, Figure 1B.
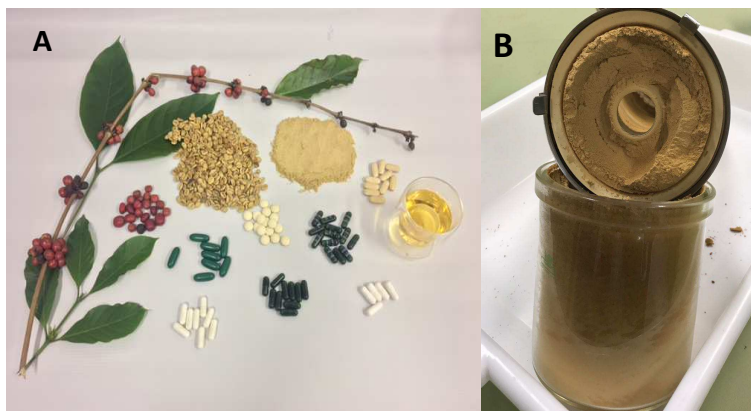
Fig. 1. Market GCP analysed (A), GCP produced by spray drying

2.2 Extraction of bioactives compounds and production of green coffe dietary supplement by spray drying

For extraction of bioactives compounds of robusta coffee (C. canephora) the grains were grounded in an IKA grinder (A11) and sieved (480-680 μm). Then, the aqueous extract was according to a methodology adapted from Liu et al., (2010) [8], using a ratio of 0.11 g/mL (mass/volume) between green coffee and distilled water for the extraction of bioactive compounds in Hielscher model tip ultrasound with 200 watts power for 10 minutes with a sample immersed in an ice bath. After extraction, the samples were taken to the refrigerated centrifuge ROUTINE 38 at 7000 rpm for 14 minutes at 25ºC to separate the solid phase.

In spray drying a first step is to evaluate if it is necessary use of carrier's agents. Priors tests indicating it is indispensable for protection from heat and facilitate its flow into the tower to prevente adherence of product to the equipment walls. The most commonly carrier used is the maltodextrin, a hydrolyzed starch widely that has a property of aiding the dispersion of a product and preventing its agglomeration pipelines. Maltodextrin DE10 (10% equivalent dextrose) was mixed with GCP extract (7 oBrix) using an ultra turrex forming an emulsion to be atomized in a spray dryer. The percentage of maltodextrin was established according to the solids content of extract in this case 70 grams per liter of extract. The spray-drying process was performed using a laboratory-scale Mini Spray Dryer Buchi B-290 (Buchi Labortechnik AG). The emulsion was fed at a flow rate of 0.96 L/h, co-current air flow rate of 25 kg/h and air inlet and outlet with temperatures of 170 °C and 90 °C, respectively, C, using a nozzle of 0.7 mm diameter. The powder product was stored into sealed metallic packaging and conserved at 25 oC until the moment of analyses.

2.3 Extraction of bioactives compounds of commercial products

The extraction of bioactives compounds of the commercial products analyzed in this work followed the same procedures described in the section 2.2 only modifying the ratio mass/volum to (0.067 g/mL).

2.4 Determination of antioxidant capacity by ORAC

The determination of antioxidant capacity by the Oxygen Radical Antioxidant Capacity, equation 1, was done according to Zulueta and colaborators [9] that consisted on the transfer of hydrogen from the antioxidant material (samples or trolox) to the AAPH radical [2,2'-azobis amidinopropane)], avoiding attacking the fluorescein present in the reactional medium. Samples were diluted in sodium phosphate buffer pH 7.4 and transferred to a 96-well microplate 80 μL. It was built a calibration curve, in triplicate, as well as the same amount of the samples besides the blank of the reaction, where 80 μL of phosphate buffer was applied. The plate was taken to the Infinite 200 model Tecan Fluorimeter spectrum at 37 °C programmed with excitation wavelength of 485 nm and emission wavelength of 535 nm. It was dispensed 80 μL of fluorescein solution and performed the excitation e emition reading. After initial reading, it was dispensed 40 μL of the AAPH radical solution and read excitation e emition of all wells at every 5 minutes for 90 cycles. The area under the curve (AUC) was calculated by software (Prism), using the fluorescence reading over the 90 cycles of the analysis. A trolox AUC values were subtracted from the blank AUC and the differences used for the construction of the Trolox calibration curve. The linear and angular coefficients obtained in the calibration curve were used to quantify the samples.

$$Orac \ (\mu mol \ Trolox \cdot g^{-1}) = \frac{\frac{[(AUC \ sample - AUC \ blank) - b]}{a}}{CA} \tag{1}$$

AUC sample = Area Under the Curve of the sample

AUC blank = Area Under the Curve of the blank

b = linear coefficient

a = angular coefficient

CA = Concentration of the sample in solution given in mg/L

2.5 Determination of caffeine nd chlorogenic acid contents in GCP

The determination of caffeine and chlorogenic acid were conducted in triplicates by HPLC Aliance 2695 with PDA detector 2996, with 280 nm and software Empower® (Waters,

Massachusetts, EUA). The cromatographic column used was a BDS Hypersil C18 (5cm x 4,6mm e 3μm – Thermo Scientifc, Massachusetts, EUA), according Rosa and colaborators [10]. The quantification of both analytes were performed by external standardization base on calibration curves made with commercaial analitycal standards.

3. Results and Discussion

The results of antioxidant capacity determined by the ORAC methodology ranged from 33.02 μmol trolox/g to 2,408.05 μmol trolox/g, which shows the heterogeneity of the products (Figure 2). The range of antioxidant capacity of the GCE likely to be due to variation in the formulation of products containing other sources of compounds that exert antioxidant function [11]. The products 2, 3 and 5 showed low range of antioxidant capacity. The GCE supplement elaborated in this study (sample 10) showed an excellent antioxidant potential when compared to commercial green coffee products, besides presenting only coffee and maltodextrin in its formulation. Compared to 9 products analyzed, the product obtained in this work (Sample 10) presented third best antioxidant activity against commercial products.

Liang and colaborators [12] analyzed the antioxidant capacity of green arabic coffee beans from the Dominican Republic, Peru, Sumatra, Papua New Guinea and Ethiopia and obtained values of 410; 450; 420; 380 and 410 μg trolox equivalent/gram.

A great variation in the values of antioxidant capacity from GCP samples were observed, probably due to the different raw material, formulation and ways of processing to obtain each GCE. This information is emphatized through caffeine and chlorogenic acid results obtained by HPLC in our green coffee product. Since our GCP, sample 10, presented greated values for caffeine and clororogenic acid (Figure 3).

The antioxidant capacity of dietary supplements based on green coffee plays an important role which refer to quality of this products since the marketing of this products is around the antioxidant capacity.
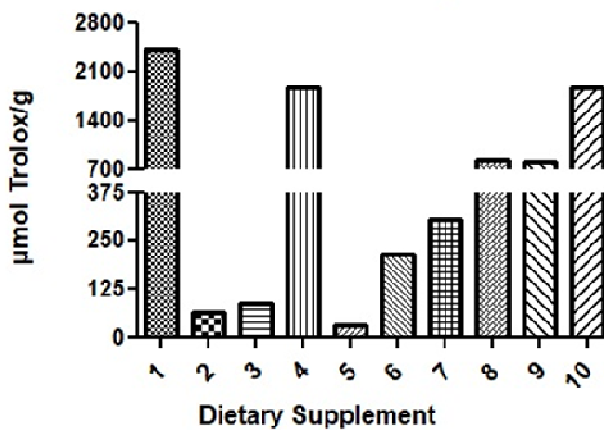
Figure 2. Antioxidant capacity of green coffee products

Dietary supplement

Figure 3. Caffeine (A) and chlorogenic acid (B) contents in green coffee products

4. Conclusions

A product of green coffee extract was elaborated in this work (Sample 10) with great antioxidant capacity .

A great variation in the values of antioxidant capacity from GCP samples were observed, probably due to the different raw material, formulations and ways of processing to obtain each GCP.

The antioxidant capacity of dietary supplements based on green coffee plays an important role which refer to quality of this products since the marketing of this products is basen on their antioxidant activity.

5. References

[1]. Lima, A.R. et al. Compostos bioativos do café: atividade antioxidante in vitro do café verde e torrado antes e após a descafeinação. **Química Nova**, [s.l.], v. 33, n. 1, p.20-24, 2010. http://dx.doi.org/10.1590/s0100-40422010000100004.

[2]. Farah, A.; Santos, T.F. The Coffee Plant and Beans. **Coffee In Health And Disease Prevention**, [s.l.], p.5-10, 2015.. http://dx.doi.org/10.1016/b978-0-12-409517-5.00001-2.

[3]. Alves, R.C.; Casal, S.; Oliveira, B. Benefícios do café na saúde: mito ou realidade?. **Química Nova**, [s.l.], v. 32, n. 8, p.2169-2180, 2009. http://dx.doi.org/10.1590/s0100-40422009000800031.

[4]. Gaascht, F.; Dicato, M.; Diederich, M. Coffee provides a natural multitarget pharmacopeia against the hallmarks of cancer. **Genes & Nutrition**, [s.l.], v. 10, n. 6, p.1403-1409, nov. 2015. http://dx.doi.org/10.1007/s12263-015-0501-3.

[5]. Hendre, P.S & Coffee (Coffea canephora Pierre Ex A. Froehner). **Plos One**, [s.l.], v. 9, n. 12, p.1-34, 2 dez. 2014. http://dx.doi.org/10.1371/journal.pone.0113661.

[6]. Dellalibera, O.; Lemaire, B.; Lafay, S. Svetol ® , green coffee extract , induces weight loss and increases the lean to fat mass ratio in volunteers with overweight problem. **Phytoterapy**, v. 4, n. 4, p. 194–197, 2006.

[7]. Farah, A. et al. Effect of Roasting on the Formation of Chlorogenic Acid Lactones in Coffee. **Journal Of Agricultural And Food Chemistry**, [s.l.], v. 53, n. 5, p.1505-1513, 2005. http://dx.doi.org/10.1021/jf048701t.

[8]. Liu, Q. M. et al. Optimization of ultrasonic-assisted extraction of chlorogenic acid from Folium eucommiae and evaluation of its antioxidant activity. **Journal of Medicinal Plants Research**, v. 4, n. 23, p. 2503–2511, 2010.

[9]. Zulueta, A.; Esteve, M. J.; Frígola, A. ORAC and TEAC assays comparison to measure the antioxidant capacity of food products. **Food Chemistry**, v. 114, n. 1, p. 310–316, 2009.

[10]. Rosa J., Freitas-Silva O., Pacheco S., Godoy R., Rezende, C. LC-MS Based Screening and Targeted Profiling Methods for Complex Plant: Coffee a Case Study. **Current Drug and Metabolisms.** v. 13, p.1244-1250, 2012.

[11]. Costa, A.S.G. et al. Teas, dietary supplements and fruit juices: A comparative study regarding antioxidant activity and bioactive compounds. **LWT - Food Science and Technology**, v. 49, n. 2, p. 324–328, 2012.

[12]. Liang, N. et al. Interactions between major chlorogenic acid isomers and chemical changes in coffee brew that affect antioxidant activities. **Food Chemistry**, v. 213, p. 251–259, 2016.

6. Acknowledgments

Nutritional potential of dehydrated residues from rice milk production

Silva, L. R.[a*]; Casari, A. C. A. B.[a]; Velasco, J. I.[b]; Fakhouri, F. M.[ab]

[a]Faculty of Engineering, Federal University of Grande Dourados. Dourados, MS, Brazil.
[b]Centre Català del Plàstic, Universitat Politècnica de Catalunya, Barcelona, Spain.

*E-mail of the corresponding author: luanramosea@gmail.com

Abstract

The aim of this work was to verify the influence of drying on physical and chemical characteristics of residues from rice milk production. Residues were from the production of white, red and black rice. They were dehydrated in an oven with air circulation at 60ºC for 8h. Characterization of them were carried out by physical and chemical analyses. Residues have presented statistical difference for all parameters measured. Its characterization is necessary to justify its use in other process or application on new products.The residues from rice milk production have high content of nutrients and phenolic compounds, even after dehydration.

Keywords: Nutrients; Oryza sativa; waste.

1. Introduction

Rice is one of the most consumed cereal in the world, mainly in Asian countries[1]. Its sucess is related not only on its nutritional quality or its practicality and applicability on food industry, but also on some characteristics that this grain present, like absence of allergenic substances and gluten[2]. In addition, rice has presented in its composition a high amount of proteins, mineral salts and B vitamins, and a low percentage of lipids, which confer a great nutritional value to the grain and make it a source of energy[3,4].

There are many variety of rices, and some of them, like red or black rice, are source of compounds important for human nutrition. Red and black rice can be considered a source of important compounds for human nutrition and health, such as phenolic compounds, anthocyanins, catechins, and fibers[5,6,7].

Vegetable milk is considered an option for dairy products. It is defined as an aquous extact made by vegetable raw materials[8]. Comparing with cow milk it stand out based on its composition, that presents low fat, cholesterol free, and high percentage of proteins and energy[9]. In addition it is lactose free[10] and made by vegetables, so lactose intolerants and vegans can drink it.

Although vegetable milk is an important food product for consumers, its process generate some residues. Those residues produced still has important compounds which can be used in human diet. An alternative is the dehydration of this material and its application in many other food products. Thus, food industries could reduce its waste of resources on the environment.

The dehydration of residues from food industries is a way to preserve this material by loss of water, however processing and storage conditions have to be studied with the aim of preserving nutrients and bioactive compounds. So, it can be inserted in formulations of many kinds of foods, such as cereal bars, cakes, biscuits, among others.

Thereby, the aim of this work was to verify the influence of drying on physical and chemical characteristics of residues from the production of rice milk.

2. Materials and Methods

Residues were from the production of vegetable milk based on white, red and black rice. They were dehydrated in an oven with air circulation at 60ºC for 8 hours. The characterization of them were carried out by analyses of moisture, ash, lipids, proteins, carbohydrates, total caloric value, Aw, pH, titratable acidity and phenolic compounds.

Moisture content was quantified according to AOAC[11]. Samples were submitted to an oven with air circulation (70ºC for 24 hours) and results expressed in percentage of moisture in wet basis. Ash was carried out by incineration in muffle oven at 550ºC[11], and results expressed in percentage of ash. Lipid was carried out by cold extraction[12] and expressed as percentage of lipids. The determination of protein was done by micro Kjeldahl method and results calculated by conversion factor for rice (5.95) and expressed as percentage of proteins. Carbohydrate was calculated by difference (Nifext fraction). Total caloric value was calculated by multiplicated values of lipid, protein and carbohydrate by Atwater constants and expressed in kcal/100 grams. Water activity (Aw) was carried out by direct measurement in digital hygrometer (Aqualab, Decagon, 3.0 Serie). pH was measured directly with potenciometer, by diluation of 10 g of sample in 100 mL of distillated water. Titratable acidity was determined by titulation with sodium hydroxid[11] and expressed in percentage.

For determination of phenolic compounds, extracts were made according to Rufino et al.[13]. The phenolic compounds were determined by Folin and Ciocalteau method[14], developed by Singleton and Rossi[15], with gallic acid as standart. Results were expressed as mgEAG/g.

All analyses were carried out in triplicate and datas were submitted to variance analyse and compared by Tukey test, with 5% of significance.

3. Results and Discussion

Residues from vegetable milk based on white, red and black rice (Fig. 1) have presented statistical difference (p≤0.05) for all parameters measured (Table 1 and 2).

(a)   *(b)*   *(c)*

Fig. 1 Dehydrated residues from processing of vegetable milk based on white (a), red (b) and black (c) rice.

Table 1. Characterization of residues from processing of vegetable milk based on white, red and black rice (part I).

Rice	Moisture (%)	Ash (%)	Lipid (%)	Protein (%)	Carbohydrate (%)
White	4.11±0.10[b]	0.45±0.01[c]	0.45±0.07[b]	7.56±0.32[c]	87.43±0.49[a]
Red	7.85±0.56[a]	0.99±0.04[b]	2.05±0.13[a]	12.39±0.08[a]	76.73±0.64[c]
Black	2.13±0.04[c]	1.19±0.07[a]	1.81±0.16[a]	10.75±0.02[b]	84.12±0.06[b]

Values in the same column followed by the same letter do not differ by Tukey test at 5% of probability.

According to the composition of residues, protein value is an important parameter that can be observed. Residue from red rice milk presented 12.39% of protein, and make it as a great source of this macronutrient.

Table 2. Characterization of residues from processing of vegetable milk based on white, red and black rice (part II).

Rice	Total caloric value*	Aw	pH	Titratable acidity (%)	Phenolic compounds**
White	384.05±0.10[b]	0.248±0.005[b]	5.93±0.07[b]	1.65±0.07[c]	19.30±0.60[c]
Red	374.01±0.70[c]	0.527±0.002[a]	6.11±0.07[a]	374.01±0.70[c]	110.26±0.01[b]
Black	395.13±0.63[a]	0.195±0.000[c]	6.20±0.02[a]	3.98±0.09[a]	123.41±0.50[a]

*kcal/100 grams; **mg EAG/100 g. Values in the same column followed by the same letter do not differ by Tukey test at 5% of probability.

The characterization of residues from food industry is necessary to justify its use in other process or application on the development of new food products, such as cereal bars, cookies, breads, biscuits, cakes, and others. Using up all nutrients and reducing the waste of them and the environmental impact.

Dehydration process do not degraded the content of phenolic compounds present on the samples. Residue from black rice milk presented highest phenolic compounds content

(123.41 mg EAG/100 g), due to the difference on the variety of rices (white: 19.30 mg EAG/100 g; red: 110.26 mg EAG/100 g).

Even after dehydration, residues still presented a great content of nutrients and bioactive compounds. Many researchers use the dehydration of residues to make flours and use it in new food products. So all important nutrients and compounds is used and consumed by people.

4. Conclusions

In conclusion, residues from rice milk production have high content of nutrients and phenolic compounds, even after dehydrated. Also they can be used on others process to improve the nutritional quality of new food products and reduce the waste of nutrients. Dehydration, at the studied conditions, of the residues from rice milk production is an indicated process for preservation of nutrients and bioactive compounds.

5. Acknowledgment

6. References

[1] Folorunso, A. A.; Omoniyi, S. A.; Habeeb, A. S. Proximate composition and sensory acceptability of snacks produced from broken rice (*Oryza sativa*) flour. American Journal of Food & Nutrition 2016, 6 (2), 39-43.

[2] Silva, R. F.; Ascheri, J. L. R. Extrusão de quirera de arroz para uso como ingrediente alimentar. Brazilian Journal of Food Technology 2009, 12, 190-199.

[3] Carvalho, A. V.; Bassinello, P. Z.; Mattietto, R. A.; Carvalho, R. N.; Rios, A. O.; Seccadio, L. L. Processamento e caracterização de snack extrusado a partir de farinhas de quirera de arroz e de bandinha de feijão. Brazilian Journal of Food Technology 2012, 15 (1), 72-83.

[4] Walter, M.; Marchezan, E.; Avila, L. A. Arroz: composição e características nutricionais. Ciência Rural 2008, 38 (4), 1184-1192.

[5] Hayashi, S.; Yanase, E. A study on the color deepening in red rice during storage. Food Chemistry 2016, 199, 457-462.

[6] 21. Hu, Z.; Tang, X.; Liu, J.; Zhu, Z.; Shao, Y. Effect of parboiling on phytochemical content, antioxidant activity and physicochemical properties of germinated red rice. Food Chemistry 2017, 214, 285-292.

[7] Mau, J. L.; Lee, C. C.; Chen, Y. P.; Lin, S. D. Physicochemical, antioxidant and sensory characteristics of chiffon cake prepared with black rice as replacement for wheat flour. LWT – Food Science & Technology 2017, 75, 434-439

[8] Izadi, T.; Izadi, Z.; Tehrani, M. M.; Pour, M. A.; Moghadam, M. Z.; Shariaty, M. A. Investigation of Optimized Methods for Improvement of Organoleptical and Physical Properties of Soymilk. International Journal of Farming and Allied Sciences 2013, 2 (10), 245–250.

[9] Rehman, S.; Nawaz, H.; Ahmad, M. M.; Hussain, S.; Murtaza, A.; Shahid, S. H. Physico-chemical and sensory evaluation of ready to drink soy-cow milk based. Pakistan Journal of Nutrition 2007, 6 (3), 283-285.

[10] Ikya, J. K.; Gernah, D. I.; Ojobo, H. E.; Oni, O. K. Effect of Cooking Temperature on Some Quality Characteristics of Soy Milk. Advanced Journal of Food Science & Technology 2013, 5 (5), 543–546.

[11] ASSOCIATION OF OFFICIAL AGRICULTURE CHEMISTS. Official methods of analysis of the Association of Official Agriculture Chemists. 18 ed. Mayland: AOAC, 2005.

[12] Bligh, E. G.; Dyer, W. J. A rapid method of total lipid extraction and purification. Canadian Journal of Biochemistry and Physiology 1959, 37 (9), 911-917.

[13] Rufino, M. S. M.; Alves, R. E.; Brito, E. S.; Morais, S. M.; Sampaio, C. G.; Pérez-Jiménez, J.; Saura-Calixto, F. D. Metodologia Científica: Determinação da atividade antioxidante total em frutas pela captura do radical livre DPPH. Comunicado técnico EMBRAPA 2007, 127, 1-4.

[14] Folin, O.; Ciocalteau, V. On tyrosine and tryptophane determinations in pronteins. The Journal of Biological Chemistry 1927, 73, 627-650.

[15] Singleton, V. L.; Rossi Junior, J. A. Colorimetric of total phenolics with phosphomolybdic phosphotungstic acid reagents. American Journal of Enology and Viticulture 1965, 16, 144-158.

Healthy apple snack developed using microwaves

Fartdinov, D.ª; Comaposada, J.ª; Muñoz, I.ª; De Wit, N.ᵇ; Gou, P.ª; Guàrdia, M. D.ª*

[a] IRTA-Food Technology. E-17121 Monells, Girona, Spain.
[b] Faculty of Life Sciences. University of Wageningen, Wageningen, The Netherlands.

*E-mail of the corresponding author: mariadolors.guardia@irta.cat

Abstract

The *MW heating at early or at final stage of drying process to obtain a crispy apple snack was studied. The effect of MW power and time of application was also evaluated on colour, texture, physico-chemical and sensory properties. Apple snack obtained with the MW heating (7.5 min at 3.000 W) at early stage after an osmotic pre-treatment resulted in apple slices more porous and with better sensory attributes than if it is applied at later stage of drying.*

Keywords: *apple; snack; drying; microwaves*

1. Introduction

One of the main barriers for fruit consumption is convenience. The application of new preservation technologies allows developing new food concepts, such as snacks, which can fulfil the consumer demand of convenience and, as a result, increase fruit consumption.

Apple drying has been studied extensively during the few past decades [1-4] by means of processes which combine an osmotic treatment and a conventional convective drying. Results were acceptable and a stable shelf-life over 6 months [5] has been reached. However, these processes are very time consuming (4.5 h). Microwave drying (MW) combined with other drying conventional methods could decrease the processing time [6]. Therefore, including MW in the drying process, could be useful in order to save time and energy and, in addition, improve the snack quality. It is still not clear which is the best time to apply MW to obtain a crispy snack. Some authors [7] assert that MW heating applied at the earlier stage of drying leads to more porous product, whereas others [8,9] indicate that this parameter is enhanced when the MW heating is carried out at the final stage of drying process.

The present work aimed to compare the effect of the MW heating at early or at final stages of drying on the colour, texture, physico-chemical and sensory properties of an apple snack.

2. Materials and Methods

2.1 Sample preparation

Golden Delicious apples and apple juice from local suppliers were stored at 4°C. Quality of the raw material was relatively stable since all the experiments were completed in 1-2 weeks. Apples were washed and manualy sliced at 4±0.3 mm-thickness with a calibrated cork borer. Sugar content of the apple juice was 12.2±0.2° Brix.

2.2 Apple snack processes

The preparation of the apple snack consisted in a three stage process. The stage was an osmotic pre-treatment (O) followed by a combined treatment of MW/Convective drying (C) or C/MW. Different MW power ratios were applied to the product (Table 1).

Table 1. Treatments used to develop the apple snack

Process	Drying Stage 1	Drying Stage 2	MW power ratio (W/g)	MW power (kW)	MW time (s)
1	MW	C	2.98	3.0	452
2	MW	C	5.56	6.0	226
3	C	MW	18.77	3.0	452
4	C	MW	40.76	6.0	226

Osmotic pre-treatment (O)

Apple slices were dipped in apple juice at 4ºC in a solution ratio 1:2 (w/w) for 60 min. Then, moisture content (MC) and water activity (a_w) were measured. After the osmotic treatment and before starting the drying process, samples were blotted by gravity to remove the excess of water.

Microwave drying (MW)

MW heating was carried out in an industrial MW continuous tunnel (F00003801A, MES Technologies, France; see Fig.1). Apple slices were placed onto the conveyor belt (single layer) at 0.45 m/min at 25 ºC. Table 1 shows the MW power ratio applied.

Convective drying (C)

Convective drying (C) was carried out in a conventional dryier placing the apple slices in a single layer onto a grid. Samples were dried at 107±3ºC, RH < 3% and 1.5 m/s air velocity for 60 min. Between drying stages 1 and 2 and at the end of the process, samples were cooled down during 5 min at 15±3ºC.

2.3. Parameters recorded or analysed

Temperature (T)

Temperature was measured with optic fiber probes (FOT-L-NS-484B,FISO Technologies, Canada). The probe was placed inside the apple slice, 15 mm from the surface and connected to a data logger (TMI, FISO Technologies, Canada).

Water activity (a_w)

Water activity (a_w) was measured at 25 °C with an AquaLab Series 3 instrument (Lab-Ferrer, Cervera, Spain). Three replicates per treatment were carried out.

Moisture content (MC)

Moisture content (MC) of the samples was determined by drying until reaching constant weight (Association of Official Analytical Chemists [AOAC], 1990). Three replicates per treatment were carried out.

Density and porosity

True density of dried apple slices was measured by means of a pycnometer using the volumetric displacement method [10]. The apparent density was measured using the solid displacement method [11] and a graduated burette of 100±0.5 ml. Porosity (ε), was calculated according to Eq.1:

$$\varepsilon = 1 - \frac{\rho_b}{\rho_s} \qquad (1)$$

where ρ_b and ρ_s are the bulk density and solid density expressed in g/cm^3. Three replicates per treatment were carried out.

Instrumental Colour measurements

Instrumental colour measurements were carried out with the colorimeter Konica Minolta Chroma Meter CR-400 (AQUATEKNICA, S.A.,Valencia,Spain) with illuminant D65 (2º standard observer ans specular component included) in the CIE-Lab space: L* (lightness), a* (redness) and b* (yellowness) (Commission Internationale de l´Éclairage [CIE], 1976). Colour measurements were performed on 8 samples per treatment and averaging 3 readings.

Instrumental Texture measurements

Texture was measured using a TA.XT plus Texture Analyzer (Stable Micro System Ltd.,Godalming, UK) for force/displacement with a 5 kg load cell, using a spherical probe (P/0.25). Samples were placed onto the HDP/CFS (Crisp Fracture Support Rig and corresponding platform, SMS). Test settings were: speed 7 mm/s, trigger force 0.049 N, probe travel distance 5 mm. A force-time curve was recorded and maximum peak Force (N) was measured. Ten measurements per treatment were carried out.

Sensory analysis

Six trained assessors [12] undertook the sensory analysis on dried apple slices. The generation and selection of the descriptors was previously carried out by 2 open discussion sessions. Product was evaluated for appearance, odour, flavour/taste, texture and overall sensory quality. A non-structured scoring scale [13] was used, where 0 means absence of the descriptor and 10 means very high intensity of the descriptor. Two tasting sessions were carried out. Samples were coded with three random numbers and were presented to the assessors balancing the first-order and carry-over effects.

Statistical analysis

The analyses of variance were performed with the General Linear Model (GLM) procedure of the SAS statistical package (Statistical Analysis System [SAS], 9.4). The model for the physicochemical, instrumental colour, instrumental texture parameters and sensory attributes included the treatment as fixed effect. Differences among means were tested with the Tukey test ($p<0.05$).

3. Results and discussion

Apples used in the present study had 83.3±0.3% moisture content and 5.7±0.8 N firmness.The osmotic pre-treatment was studied only in terms of moisture gain; samples absorved apple juice up to a moisture of 85.1 ±0.04%.

Moisture content (MC), water activity (a_w) and porosity (ε)

Table 2 shows that the application of MW treatment at the 1st drying stage (processes 1 and 2) reduced the MC by about 5 %, while the convective drying (2nd drying stage) reduced the MC by about 70 %. No significant differences were observed in MC and a_w between processes 1 and 2, therefore, the power ratio applied did not affect them. Slice porosity (ε) in process 2 was lower than in process 1. This could be explained by the temperature reached by the slices through the MW heating. In process 2, slices reached up to 68 ºC, while in process 1, up to 55 ºC. Some studies reported that high temperature causes damage in the porous structure and, as a consequence, porosity decreases [14].

Table 2. Moisture content (MC), Water activity (a_w) and porosity (ε) of the apple snack samples

Sampling time	Variable	RMSE	Process			
			1	2	3	4
After stage 1	MC [%]	0.897	79.15[a]	80.32[a]	9.44[b]	8.77[b]
	a_w [-]	0.0091	0.980[a]	0.979[a]	0.191[b]	0.198[b]
After Stage 2	MC [%]	0.796	7.31[b]	7.40[b]	9.91[a]	9.05[a]
	a_w [-]	0.0022	0.165[b]	0.167[b]	0.221[a]	0.201[a]
	ε [-]	0.0084	0.545[a]	0.423[b]	0.494[ab]	0.520[a]

[a] [b] Means without a common superscript in a row are significantly different (p<0.05); RMSE: Root mean standard error; Process 1: MW (7.5 min at 3000 W)+C; Process 2: MW(3.75 min at 6000 W)+C; Process 3: C + MW (7.5 min at 3000 W); Process 4: C + MW (3.75 min at 6000W).

When convective drying was applied at the 1st drying stage (processes 3 and 4), the MC was reduced by about 76 % whereas the MW application at the 2nd stage of drying could not reduce it. The power ratio applied did not significantly affect the MC and a_w. No significant differences in porosity (ε) were observed between processes 3 and 4.

Treatments with the MW application at the 1st stage resulted in a significant reduction of both MC and a_w at the end of the process. Therefore, the MW application at earlier drying stage is more efficient than the MW application at later drying stage under the experimental conditions of the present trial.

Colour and instrumental texture parameters

The driest samples (process 1 and 2) showed the lowest lightness (L*) and the highest redness (a*) (Table 3). This is attributed to the lower MC of these apple slices, although some studies reported that higher a* is also related with the Maillard reaction, caramelization or pigment degradation [5].

These samples also showed the lowest Max. Force, which can be related to their lower MC. The lowest values were observed in samples from process 2, which also have the lowest porosity.

Several studies reported that the higher porosity requires greater compressive strength to fracture samples [15].

Table 3. Instrumental colour and instrumental texture parameters of the apple snack samples

Colour parameter	RMSE	Process			
		1	2	3	4
L*	3.044	74.75[b]	74.52[b]	80.47[a]	76.62[ab]
a*	1.494	6.23[a]	4.37[a]	2.16[b]	2.16[b]
b*	2.180	33.47	32.71	32.41	34.07
Max.Force(N)	1.909	5.40[ab]	3.52[b]	7.43[a]	6.74[a]

[a b] Means without a common superscript in a row are significantly different (p<0.05); RMSE: Root mean standard error; Process 1: MW(7.5 min at 3000 W)+C; Process 2: MW(3.75 min at 6000 W)+C; Process 3: C + MW (7.5 min at 3000 W); Process 4: C + MW (3.75 min at 6000W).

Sensory Analysis

Regarding appearance attributes, no significant differences were observed (results not shown). This fact indicates that, in spite of the differences observed in L* and a* parameters, these were not noticeable by the panelists. Similarly, no significant differences regarding taste/flavour attributes were observed (results not shown). However, samples obtained by process 1 showed a tendency to be scored with a high intensity of apple flavour, which is a desirable attribute.

Processing (MW/C or C/MW) significantly affected dried grass odour, crispiness and easiness to chew of the apple slices (Table 4). Samples obtained in process 1 (MW at the 1st drying stage and low power ratio), tended to be more crispy and more easy to chew. Differences are attributed to its lower MC and higher porosity. Samples of process 2 had lower porosity and these of processes 3 and 4 had higher MC. Other authors reported the effect of MC and porosity on crispiness and chewiness in the same direction [16,17].

Regarding dried grass odour, results showed that samples obtained with processes with higher power (2 and 4) were scored with higher intensity. This effect should be taken into account because this is an attribute not desirable for an apple snack.

Overall sensory quality showed a tendency to be higher in samples of process 1. This result could be explained by the fact that these samples were scored with higher intensity of apple flavour, crispiness and easiness to chew and with lower intensity of dried grass odour.

Table 4. Sensory attributes

Attribute	RMSE	Process			
		1	2	3	4
Dried grass odour	1.10	1.3[b]	2.8[ab]	1.1[b]	3.3[a]
Crispiness	1.81	7.0[a]	4.8[ab]	3.5[b]	4.8[ab]
Easiness to chew	1.49	6.3[a]	3.8[b]	3.5[b]	3.5[b]
Overall sensory quality	1.60	6.8	4.3	4.8	4.8

[a b] Means without a common superscript in a row are significantly different ($p<0.05$); RMSE: Root mean standard error; Process 1: MW(7.5 min at 3000 W)+C; Process 2: MW(3.75 min at 6000 W)+C; Process 3: C + MW (7.5 min at 3000 W); Process 4: C + MW (3.75 min at 6000W).

4. Conclusion

The application time of MW treatment in the apple snack process affects their physico-chemical parameters and sensory attributes. The MW treatment (7.5 mint at 3000 W) applied at the 1st stage of drying followed by convenctive drying results in more porous apple slices and with better sensory attributes.

5. References

[1] Timoumi,S.;Mihoubi,D;Zagrouba,F. Shrinkage,vitamin C degradation and aroma losses during infra-red drying of apple slices. LWT-Food Science and Technology 2007,40(9),1648-1654.

[2] Bi,J.;Wang,X.;Chen,Q.;Liu,X.;Wang,Q.;Lv,J.;Yang,A. Evaluation indicators of puffing Fuji apple chips quality from diffent Chinese origins. LWT-Food Science and Technology 2015,60(2),1129-1135.

[3] Contreras,C.;Martin,M.E.;Martinez-Navarrete,N.;Chiralt,A. Effect of vacuum impregnation and microwave application on structural changes which occurred during air-drying of apple. LWT-Food Science and Technology2005,38(5),471-477.

[4] Schulze,B.;Hubbermann,E.M.;Schwarz,K. Stability of quercetin derivatives in vacuum impregnated apple after drying(microwave vacuum drying,air drying,freeze drying) and storage. LWT-Food Science and Technology 2014,57(1),426-433.

[5] Velickova,E.;Winkelhausen,E.;Kuzmanova,S. Physical and sensory properties of ready to eat apple chips produced by osmo-convective drying. Journal of Food Science and Technology 2014,51(12),3691-3701.

[6] Chandrasekaran,S.;Ramanathan,S.;Basak,T. Microwave food processing-A review.

Food Research International 52 (2013),243-261.

[7] Zhang,M.;Tang,J.;Mujumdar,A.S.;Wang,S. Trends in microwave-related drying of fruits and vegetables. Trends Food Sci Technol 2006,17(10):524-534.

[8] Askari,GR.;Emam-Djomeh,Z.;Mousavi,S.M. Effects of combined coating and microwave assisted hot-air drying on the texture, microstructure and rehydration characteristics of apple slices. Food Sci Technol Int 2006,23(1):39-46.

[9] Argyropoulos,D.;Heindl,A.;Müller,J. Assessment of convection, hot-air combined with microwave-vacuum and freeze-drying methods for mushrooms with regard to product quality. Int J Food Sci Technol 2011,46(2),333-342.

[10] Qiu,J.;, Khalloufi,S.; Martynenko,A.; Van Dalen,G.; Schutyser,M.; Rivera,C.A. Porosity, Bulk Density, and Volume Reduction During Drying: Review of Measurement Methods and Coefficient Determinations, Drying Technology 2015, 33:14, 1681-1699.

[11] Joardder,M.U.H.;Kumar,C.;Brown,R.J.;Karim,M.A. A micro-level investigation of the solid displacement method for porosity determination of dried food.Journal of Food Engineering 166(2015) 156-164.

[12] American Society for Testing and Materials (1981) Guidelines for the selection and training of sensor and panel members. In STP 758 Philadelphia: ASTM

[13] Amerine M, Pangborn R, Roessler E (1965) Principles of sensory evaluation of food. Academic Press, New York.

[14] Rahman,M.S.,Al-Zakwani,I.,Guizani,N. Pore formation in Apple during air-drying as a function of temperatura: Porosity and pore-size distribution. Journal of the Science and Agriculture, 2005, 6(85), 979-989.

[15] Anton A.A.; Luciano F.B.; Instrumental texture evaluation of extruded snack foods: A review Evaluacion instrumental de textura en alimentos extruidos:Una revision. Journal of food, 2007,5:4,245-251.

[16] Zbigniew, Ranachowski & Marzec, Agata.Acoustic properties of foods,2008.

[17] Tsukakoshi,Y, Naito,S., and Ishida,N. Fracture intermittency during a puncture test of cereal snacks and its relation to porous structure. Food Res. Int, 2008, 1, 909-917.

Solar convective drying kinetics and sorption isotherms of *Citrus aurantium* flowers

El Ferouali, H.; Zoukit, A.; Doubabi, S.; Abdenouri, N.*

LSET, Cadi Ayyad University, Marrakech, Morocco.
Cadi Ayyad University, Marrakech, Morocco.

*E-mail of the corresponding author: n.abdenouri@uca.ma

Abstract

Citrus aurantium flowers are high value aromatic and medicinal plants. The storage conditions and quality of dried Citrus aurantium flowers depends on their hygroscopic stability. The equilibrium moisture content was determined at temperatures (from 30 to 60 °C), and the sorption phenomenon is well described by Peleg model. The optimal water activity for the storage of the product was estimated at $a_{wop}=0.373$. Afterwards, the net isosteric heat was evaluated in the range of 88 kJ.mol^{-1} for small values of the moisture content ($X_{eq}=0.14$kg water/kg d.b), and it decreased along with the increase of X_{eq}. The experimental drying curves showed only a falling rate period. Finally, Midilli-Kucuk model was found to be the more suitable to describe the drying kinetic of Citrus aurantium flowers.

Keywords: Drying kinetics; Solar energy; Modeling; Citrus aurantium; Sorption isotherms; Conservation process.

1. Introduction

Medicinal and aromatic plants have a crucial value in the pharmaceutical industry and traditional medicine. Drying is the most used preservation operation in the storage of medicinal and aromatic plants and it is a part of the extraction process of high value substances. The indirect solar drying is more adapted to developing countries; it is economic, fast and leads to a homogeneous and edible product [1].

Citrus aurantium flowers are known for their benefits on nervous balance and digestion [2]. They are often used for the extraction of the main assets. These flowers are very rich in essential oil that can be used in the composition of some perfumes. For the natural medicine, the leaf is used for its sedative and soothing properties. Indeed its essential oil, associated with other bitter principles gives him soothing and relaxing properties. Furthermore, they are usually prescribed to regulate mild sleep disorders and to treat nervousness. In this case, the preservation of this material by drying and the establishment of desorption isotherms are very useful for its conservation [3].

The sorption isotherms are a good way to describe how active water is bound to a wet product [4]. They are also an extremely valuable tool because it provides precious information about the hygroscopic equilibrium [5]. In other words, it is necessary to determine the optimum moisture content and the water activity that must be achieved during drying for better preservation of the dried product.

Only experimental studies allow determining the drying kinetics of products. Therefore, it is interesting to study variations of moisture content for different controllable aerothermal parameters. The mechanisms of these transfers are very complex and they lead to large physical, chemical and biological changes. Hence, the evolution of these parameters must be controlled in order to achieve the best quality [6,7].

The main objectives of this study are:

- To determine the effect of temperature on the moisture desorption and adsorption isotherms of *Citrus aurantium* flowers, and to find the appropriate model that describes its sorption curves.
- To determine the optimal storage condition of the product and the isosteric heat of sorption.
- To investigate the drying kinetics of *Citrus aurantium* flowers.

2. Materials and Methods

2.1. Sorption isotherms

The hygroscopic equilibrium was achieved by the static gravimetric technique [8]. The samples that were used for desorption were fresh and weighed around 1±0.1g. The ones that were used for adsorption had been dried for 24h in an oven at 105°C before putting them on the glass jars; their weight was around 0.1±0.01g. This process was performed at three different temperatures (30, 40 and 50 °C).

2.2. Description of the solar drying

The experimental apparatus consists of an indirect forced convection solar dryer. The solar dryer was described in detail in [9]. The same mass of fresh *Citrus aurantium* flowers (20±1g) was used for each drying experiment. Drying experiments were performed for three temperatures (40, 50 and 60 °C) with the air flow rate of 0.083m^3.s^{-1}.

3. Results

3.1. Desorption and adsorption isotherms

Figs. 1 and 2 show the effect of temperature on desorption and adsorption of *Citrus aurantium* flowers. *Xeq* increases by decreasing temperature at constant water activity. This result may be explained by the higher excitation state of water molecules at higher temperature thus decreasing the attractive forces between them [10]. The sorption isotherms are type II of the IUPAC classification and exhibit a sigmoidal shape; this is consistent with the behavior of other medicinal and aromatic plants [11]. In the present study, the relationship between *Xeq* and a_w at 30, 40 and 50 °C was predicted by applying mathematical models. The used models' equations (GAB, Modified Henderson, Modified Halsey, Modified Oswin , Enderby and Peleg) are given in [12]. The best model, describing sorption isotherms of the product, has the highest value of the correlation coefficient *r* and smallest values of *SEM* and *MRE*. These statistical errors are defined respectively by Eqs. (1) and (2):

$$SEM = \sqrt{\frac{\sum_{i=1}^{N}\left(Xeq_{i,pre} - Xeq_{i,exp}\right)^2}{d_f}}$$

(1)

$$MRE = \frac{100}{N}\sum_{i=1}^{N}\left|\frac{Xeq_{i,pre} - Xeq_{i,exp}}{Xeq_{i,exp}}\right|$$

(2)

Where $Xeq_{i,exp}$ is the *ith* experimental moisture content, $Xeq_{i,pre}$ is the *ith* predicted moisture content, and d_f is the freedom degree of the regression model. The Peleg model gives the best fitting to the experimental data with a correlation coefficient *r* of 0.9847 and 0.9920, SEM of 1.0856 and 1.0562, and MRE of 9.3654% and 10.1268% respectively for desorption and adsorption isotherms.
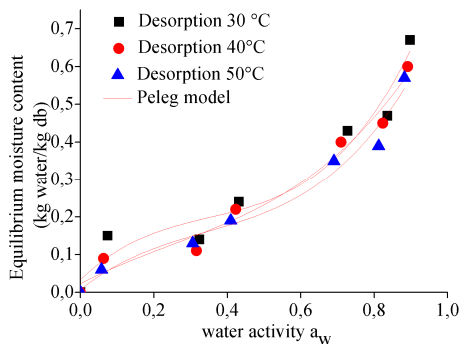
Fig. 1 Desorption isotherms of Citrus aurantium flowers at 30, 40 and 50 °C.
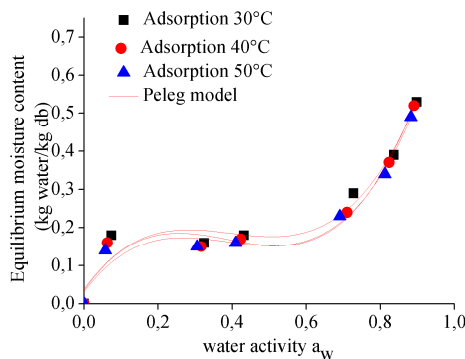
Fig. 2 Adsorption isotherms of Citrus aurantium flowers at 30, 40 and 50 °C.

3.2. Determination of the optimum conditions for the storage

All experimental data of desorption and adsorption at 30, 40 and 50°C were gathered on the same graph (Fig. 3). This curve allowed to determine the value at which the second derivative of *Xeq* equals to zero and consequently the optimum value of water activity for storage. The found value for *Citrus aurantium* flowers (a_{wop}=0.373) is in agreement with the general stability domain of biological products that is between 0.2 and 0.4 [13].
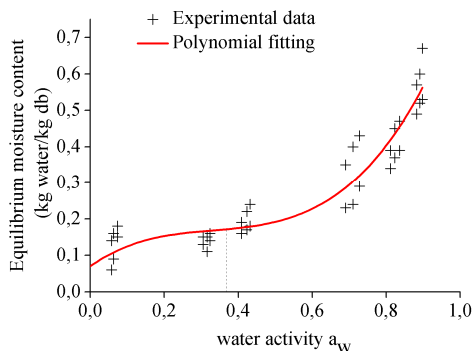
Fig. 3. Determination of the optimal water activity for storage of Citrus aurantium flowers.

3.3. Net isosteric heat

The net isosteric heat of sorption was calculated from the experimental data using the Clausius Clapeyron equation given by Eq. (3):

$$\left[\frac{d(ln a_w)}{d(1/T)}\right]_{X_{eq}} = \frac{-\Delta h_d}{R}$$

(3)

Fig. 4 presents the isosteric heat of sorption of *Citrus aurantium* flowers at temperatures ranging between 30 °C and 50 °C. This curves show that the isosteric heat is higher for small values of the moisture content (88 kJ.mol^{-1} for X_{eq}=0.14kg water/kg d.b) indicating the highest binding energy for water removal, and it decreased along with the increase of the *Xeq* [14].
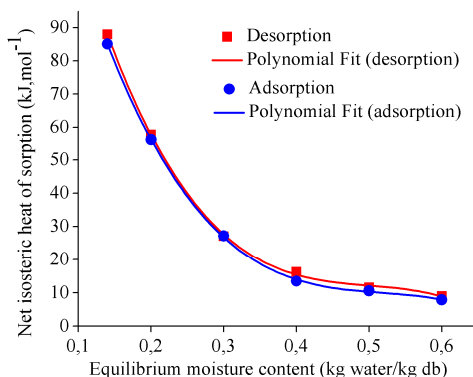
Fig. 4. Net isosteric heat of desorption and adsorption of Citrus aurantium flowers versus equilibrium moisture content.

3.4. Drying kinetics of *Citrus aurantium* flowers

An increase in the drying air temperature had led to a significant reduction in the drying time; from 340 min for a temperature of 40 °C to 220 min for a temperature of 60 °C (Fig. 5). It can be noticed the presence of only the falling drying rate period (phase 2) which is governed by the water diffusion in the material [15].

Several mathematical models are used to describe the macroscopic behavior of the products. In this work, the most models describing drying kinetics were used: Newton, Page, Henderson and Pabis, Logarithmic, Two term, Two term exponential, Wang and Singh, Diffusion approach, Verma et al. and Midilli-Kucuk. The models' expressions are given in literature [16]. The moisture ratio of *Citrus aurantium* flowers during the thin layer drying experiments was calculated by using Eq. (4):

$$X^* = \frac{X - X_{eq}}{X_0 - X_{eq}}$$

(4)

The appropriate model was selected according to the highest correlation coefficient (*r*), the lowest *MBE* (Eq. (5))and the lowest χ^2.

$$MBE = \frac{1}{N} \sum_{i=1}^{N} (X^*_{pre,i} - X^*_{exp,i})$$

(5)

Where *X*exp,i* stands for the experimental moisture ratio found in the measurements; *X*pre,i* is the predicted moisture ratio for this measurement.

Midilli-Kucuk model was selected as the most convenient model to represent the drying behavior of *Citrus aurantium* flowers with R, χ^2 and *MBE* respectively of 0.9991, 0.00037 and 0.00017. These result highlighted the ability of this model to better simulate the change in water content in the solar drying *Citrus aurantium* flowers. Hence, this product presents a weak external resistance to heat and mass transfer [17].
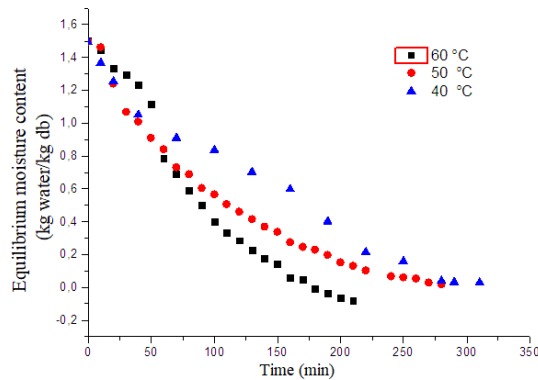
Fig. 5. Variation of moisture content as a function of time.

4. Conclusions

The storage conditions and the quality of dried *Citrus aurantium* flowers depend to a great extent on their hygroscopic stability. Hence, the equilibrium moisture content was investigated at three temperatures in the most convenient range for plants (from 30 to 60 °C). The sorption phenomenon is well described by the semi-empirical Peleg model. The optimal water activity for the storage of the product was estimated at a_{wop}=0.373. Then, the net isosteric heat of sorption of the samples was computed from the predicted sorption data. It was evaluated in the range of 88kJ.mol^{-1} for small values of the moisture content (*Xeq*=0.14 kg water/kg db), and it decreased along with the increase of the *Xeq*; this thermodynamic quantity estimates the required energy for dehydration processes. Drying experiences were conducted in Marrakech (Morocco) by using an indirect forced convection solar dryer at three temperatures (40, 50 and 60°C). The experimental drying curves showed only a falling rate period. Finally, Midilli-Kucuk model was found to be the more suitable to describe the drying kinetic of *Citrus aurantium* flowers.

5. Nomenclature

M_d	Mass of dry matter	kg
M_{eq}	Mass at the hygroscopic equilibrium	kg
X	Moisture content at any time during drying	(kg water/kg db)
X_0	Initial moisture content	(kg water/kg db)
X_{eq}	Equilibrium moisture content	(kg water/kg db)
X^*	Moisture ratio	
a_w	Water activity	
r	Correlation coefficient	
SEM	Standard Error of Moisture	
MRE	Mean Relative Error	%
MBE	Mean bias error	
Δh_d	Net isosteric heat of sorption	$kJ.mol^{-1}$
ΔH_{vap}	Heat of vaporization of pure water at 35 °C	43.53 $kJ.mol^{-1}$
R	Universal gas constant	8.3145 $J.mol^{-1}.K^{-1}$

Greek letters

χ^2	Reduced chi-square	

6. Acknowledgements

7. References

[1] Doymaz, I. Drying behaviour of green beans. Journal of Food Engineering 2005, 69, 161–165.

[2] www.alchimiste.fr , 2008.

[3] Aït Mohamed, L. Etude Physico-chimique de la Qualité et de la Conservation Avant et Après Séchage Convectif Solaire du Gelidium sesquipedale (Algue Rouge) et du Citrus aurantium (Orange Amer)', Thèse de Doctorat, Université Cadi Ayyad, Marrakech, Maroc, 2006.

[4] Abdenouri, N; Idlimam, A.;Kouhila, M. Sorption Isotherms and Thermodynamic Properties of Powdered Milk. Chemical Engineering Communications 2010., 197(8), 1109–1125.

[5] Zhao, P.; Zhong, L.; Zhao, Y.; Luo, Z.. Comparative studies on the effect of mineral matter on physico-chemical properties, inherent moisture and drying kinetics of Chinese lignite. Energy Conversion and Management 2015, 93, 197–204.

[6] El Ferouali, H. ; Zehhar, N. ; et al. EFFECT OF DRYING TECHNIQUES PROCESS ON NUTRITIONAL AND BIOCHEMICAL QUALITY OF GREEN BEANS.In Second Nordic Baltic Drying Conference. Hamburg, Germany, 2017.

[7] El Ferouali, H., Zehhar, N., et al. STUDY OF THE EFFECT OF DIFFFRENT DRYING TECHNIQUES ON NUTRITIONAL QUALITY OF TOMATO SOLANUM LYCOPERSICUM L.. In 6th European drying conference Eurodrying. Liege, Belgium, 2017.

[8] Greenspan, L. Humidity fixed points of binary saturated aqueous solutions, Journal of research of the national bureau of standards 1977, 81(1), 89–96.

[9] El Ferouali, H. et al. CFD study of a designed forced convection solar dryer. application to the drying of punica granatum legrelliae's flowers, in The 20th International Drying Symposium, Gifu, JAPAN, 2016.

[10] Goneli, A. L. D.; Corrêa, P. C.; Oliveira, G. D.; Júnior, P. A. Water sorption properties of coffee fruits, pulped and green coffee. LWT-Food Science and Technology 2013, 50(2), 386-391.

[11] Mujumdar, A. S. Handbook of Industrial Drying. New York: Ed. Marcel Dekker Inc., 2006.

[12] Basu, S.; Shivhare, U. S.; Mujumdar, A. S. Models for Sorption Isotherms for Foods: A Review, Drying technology 2006, 24(8), 917–930.

[13] LE MESTE, M.; ROUDAUT, G. ; CHIOTELLI, E. ; SIMATOS, D. ; COLAS, B. Propriétés fonctionnelles de l'eau dans les aliments: Dossier eau. Industries alimentaires et agricoles 2001, 118(5), 21–28.

[14] Brunauer, S.; Deming, L. S.; Teller, E. On a Theory of the van der Waals Adsorption of Gases, Journal of the American Chemical Society 1940. 62(7),1723–1732.

[15] Al hodali, R.; Bougard, J. Numerical simulation of an agricultural foodstuffs drying unit using solar energy and adsorption process. Université Libre de Bruxelles, Belgium, 1977.

[16] Menges, H. O.; Ertekin, C. Mathematical modeling of thin layer drying of Golden apples. Journal of Food Engineering 2006, 77(1), 119–125.

[17] Midilli, A.; Kucuk, H.; Yapar, Z. A new model for single-layer drying. Drying technology 2002, 20(7), 1503–1513.

Organic apples (cv. Elstar) quality evaluation during hot-air drying using Vis/NIR hyperspectral imaging

Shrestha, L.[a]*; Moscetti, R.[b]; Crichton, S. O. J; Hensel, O.[a]; Sturm, B[a, c]

[a]Department of Agricultural and Biosystems Engineering, University of Kassel, Witzenhausen, Germany

[b]Department for Innovation in Biological, Agro-food and Forest systems DIBAF - University of Tuscia, Italy

[c]School of Natural and Environmental Science, Newcastle University, Newcastle upon Tyne, UK

*E-mail of the corresponding author: sthaluna@gmail.com

Abstract

Organic dried apples are common snacks fulfilling functional as well as nutritional aspects. However, appearance of dried slices does not always satisfy consumer requirements, thus, improvements are needed. In this study, partial least squares (PLS) regression models were successfully developed to monitor changes in colour and moisture content in apple slices during the drying process over the Vis/NIR spectral range. The regression vector analysis results suggested that features at 580, 750 and 970 nm are better for predicting moisture content, while 580 and 680 nm allow to measure the (a*/b*) colour ratio.

Keywords: Drying; Dried apple slices; Moisture content; Colour; PLSR modelling

1. Introduction

The demand for organic dried agricultural products is increasing globally due to their health promoting aspects, ecological protection and biodiversity maintenance. [1,2] Organically grown fruits and vegetables contain a higher polyphenol content compared to conventionally grown ones, having anti-carcinogenic, anti-inflammatory, antimicrobial, antioxidant, antihypertensive, immune modulating, cardio protective, vasodilatory and analgesic proprieties. [3] The majority of people prefer fresh produce; however, it is difficult to preserve perishable foods owing to their high moisture content and high metabolic activity. Thus, drying is one of most important techniques to produce foods with an improved shelf-life, organoleptic quality, and nutritional value and to widen product availability and diversify the market throughout the years. Amongst food commodities, apple is the most common commercial fruit consumed globally [4] due to its nutritional properties. Dried apples be used as raw material in the production of snacks, integral breakfast foods, flour, chips and more, thus increasing in the global market. [5] However, maintaining a proper structure and appearance of dried organic products has been challenging.

Convective hot-air drying is one of the most common and energy intensive drying methods in the food industry. This leads to a dried product with a reduced weight making it suitable for transportation and a prolonged shelf-life with minimal nutrient deterioration during storage. However, the potential negative outcomes of this process are several physical and biochemical changes which might occur leading to quality degradation such as changes in colour, texture, size and shape as well as the organoleptic, nutritional and functional properties during the drying process. This will impact on the consumer acceptability. [6] Most of the quality parameters are highly temperature dependent. [5]

Moisture content measurement is a labour intensive and time consuming during the drying process. Therefore, a non-invasive and non-destructive method is both more useful and favourable to detect quality metrics in a production line setting. The presented method is based on models that were developed from measured data and hyperspectral data relating the products and quality parameters. Many studies have been carried out estimating dried apple quality characteristics. [7-10] However, very few studies have been carried out in the organic sector. Thus, the aim of this study was to determine the impact of the drying temperature on the drying behaviour and colour parameters of organic apple slices, as well as to investigate quality metrics predictions such as moisture content and chromaticity using the visible/near-infrared (Vis/NIR) spectroscopy during the drying process.

2. Materials and Methods

Apples (cv. *Elstar*) were purchased from the Hessische Staatsdomäne Frankenhausen, (Grebenstein, Germany) on the evening before each trial, where they had been stored at 8 ± 1 °C. Fruits of uniform size and colour were used and stored at room temperature overnight until the experiments were conducted. Apples were cored using an apple stainless steel corer of 2.5 cm (lurch, Schineklstrasse 6, Germany) and sliced to 4-mm thickness using an electrical slicer (Graef, Allesschneider Vivo V 20, Arnsberg, Germany). Apple slices were cut into equal diameter using a cookies dicer of 62-mm diameter (Flammable, Germany).

During drying experiments, the samples were dried at 60 ± 2 °C and 70 ± 2 °C for 6 and 4 h, respectively, in a tray dryer (HT mini, Innotech Ingenieursgesellschaft mbH, Germany). The dryer was pre-heated until set temperature was reached before being loaded with the sample. Four replications were performed for each assessment. Batch sampling was performed at 0, 15, 30, 60, 90, 120, 180, 240, 300 and 360 min for 60-°C drying temperature, while at 0, 15, 30, 60, 90, 120, 150, 180, 210 and 240 min for 70-°C drying temperature. In each drying interval, sample weighting, chromaticity and hyperspectral scans were performed and analysed following the procedure mentioned by Crinchton et al., 2017. In addition, the a*/b* ratio was calculated in this experiment.

The spectral data were analysed using Partial least squares regression (PLSR) in relation to the moisture content (gw/gDB) and the CIELab coordinates. PLSR is a regression technique used to find linear relationships between the reflectance spectra and specific qualitative measurement values. The train-test (calibration-prediction) split for the complete dataset was on a 70:30 basis. The classification performance of each PLS model was determined in terms of regression vector (RV).

One-way analysis of variance (ANOVA) was performed to evaluate statistical differences among the drying times. The Tukey's pairwise comparison method was performed, and the Honestly Significant Difference (HSD) was calculated for an appropriate level of interaction ($P < 0.05$). Results were reported as the mean and standard error of the mean.

3. Results and Discussion

3.1. Drying Behaviour

Fig 1. shows the moisture content of the organic apple slices as a function of drying time at 60-°C and 70-°C drying temperatures. As expected, the moisture content decreases gradually with drying time and the drying rate is higher at the highest temperature. [8- 10] The drying time to reach the final moisture content of 0.11 g H_2O/ g D.M were 360 min and 240 min at the drying air temperatures of 60 and 70 °C, respectively. ANOVA indicates

significant effect of drying time on moisture content. The free water content reduced significantly at higher temperature causing higher internal moisture diffusion resistance during the drying process. [4-6]
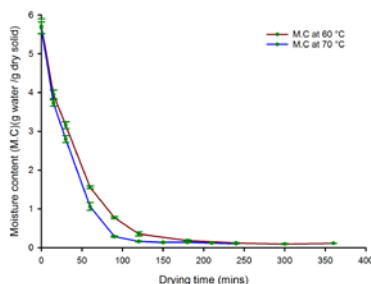
Fig 1. Effect of drying air temperature on moisture content of slices over drying time

3.2. Colour changes

Table 1 depicts the a*/b* ratio of slices at two different drying temperatures. Tukey's test of comparison revealed significant differences at different stages of the drying process for a*/b* value. The greatest change loss occurred at 210 min which was significantly different to that at 0-, 15-, 30- and 60-min drying times. At 210 min, Maillard reaction might occur causing the slices to brown faster (Table.1). Moreover, the enzymatic reaction due to polyphenol oxidase (PPO) is first very likely to occur and afterwards non-enzymatic browning that contributing to changes in colour. The browning reactions occurring during drying can have a significant impact on the final colour of the product. [6]

Table 1. Effect of drying time on a*/b* ratio of organic apple slices. Mean values with no common letters are statistically different according to HSD of (p ≤ 0.05).

Drying at 60- °C and 70- °C	
Drying time (min)	**a*/b ratio**
0	-0.23[d] ± 0.007
15	-0.14[c] ± 0.006
30	-0.13[bc] ± 0.006
60	-0.12[bc] ± 0.005
90	-0.11[abc] ± 0.006
120	-0.10[abc] ± 0.009
150	-0.09[abc] ± 0.011
180	-0.09[abc] ± 0.006
210	-0.07[a] ± 0.010
240	-0.08[ab] ± 0.007
300	-0.09[ab] ± 0.010
360	-0.09[abc] ± 0.006

3.3. Spectral Analysis

PLS regression models with excellent predictability were obtained to monitor changes in moisture content and colour parameters of apple slices during drying process. The model performances for moisture content and a*/b* ratio are presented in Table 2. The prediction model on the test (prediction) set achieved good moisture content predictions with highest R^2 (0.98) and lower RMSEP (0.27 g Water/g D.M) and for a*/b* ratio with R^2 (0.82) and lower RMSEP (0.23). The selection of optimal wavebands was performed using Regression vector (RV) to find the most vital information for moisture content distribution (Fig 2b) and a*/b* ratio (Fig 2c). For moisture content prediction, the highest peak was observed at wavelengths 580 nm and two downward peaks at 750 nm and 970 nm. At 970 nm, there might be the non-bonded O-H stretching second overtone vibration in water and free water molecules in the apple slices. [11,12] In case of the a*/b* ratio, 580 nm and 680 nm were found to be important wavelengths using RV analysis (Fig 2c). Specifically, 680 nm is related to change in chlorophyll content. [9] Moreover, as moisture evaporates during drying, different pigments such as anthocyanins concentration might increase leading to a

change in colour. Noteworthy, moisture content in the product and changes in colour seem to be correlated to each other which have to be optimised during the drying processes to produce acceptable dried slices.

Table 2. Calibration models based on quality metrics using PLSR method

Parameter	Spectral pretreatment (P_t)			LV[a]	RMSE[b]		R^2	
	P_t-1	P_t-2	P_t-3		C[m]	P[n]	C	P
Moisture content	MSC (Mean)	2nd Der	Mean Center	4	0.24	0.27	0.98	0.98
a*/b*	MSC (Mean)	2nd Der	Mean Center	3	0.021	0.023	0.81	0.82

[a] Latent Variables

[b] Root Mean Squared Error

[m] Calibration

[n] Prediction
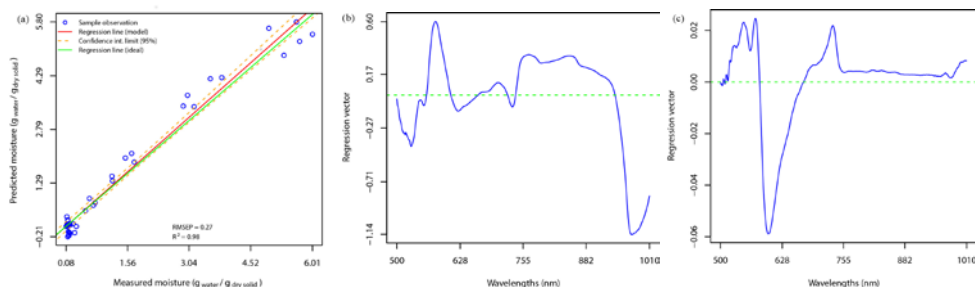
Fig 2. PLS model at full –wavelength range in the spectral range of 500 – 1010 nm . (a) Plot of predicted versus measured moisture content (b) Plot of regression vector for moisture content (c) Plot of regression vector for a/b* ratio*

4. Conclusions

Drying temperature, time and product quality are the important considerations for drying processes. Lowering the drying temperature reduces the drying potential and increases drying time. Colour (a*/b* ratio) parameter changed periodically as the onset of drying. RV of moisture content showed the importance of three wavelengths (i.e. 580, 750, 970 nm) and for colour change (a*/b*) ratio at 580 and 680 nm. RV had a higher prediction accuracy indicating that wavelengths selected are more powerful in predicting the MC and a*/b* colour of organic apple slices. Thus, using this Vis/NIR based technique, can provide an efficient means of quality metric estimation such as moisture content and a*/b* colour prediction information of organic apple slices.

5. Nomenclature

Vis/NIR	Visible to near infrared
PLS	Partial Least Squares regression
HSI	Hyperspectral imaging
RMSE	Root mean squared errors
RV	Regression vector

6. Acknowledgements

7. References

[1] Wier M, Calverley C. Market potential for organic foods in Europe. British Food Journal. 2002 Feb 1;104(1):45-62.

[2] Denver S, Jensen JD. Consumer preferences for organically and locally produced apples. Food Quality and Preference. 2014 Jan 1;31:129-34.Faller AL, Fialho E. The antioxidant capacity and polyphenol content of organic and conventional retail vegetables after domestic cooking. Food Research International. 2009 Jan 1;42(1):210-5.

[3] FAOSTAT, http://faostat3.fao.org/home/E (Accessed 28.03.2018).

[4] Velić D, Planinić M, Tomas S, Bilić M. Influence of airflow velocity on kinetics of convection apple drying. Journal of Food Engineering. 2004 Sep 1;64(1):97-102.

[5] Vega-Gálvez A, Ah-Hen K, Chacana M, Vergara J, Martínez-Monzó J, García-Segovia P, Lemus-Mondaca R, Di Scala K. Effect of temperature and air velocity on drying kinetics, antioxidant capacity, total phenolic content, colour, texture and microstructure of apple (var. Granny Smith) slices. Food Chemistry. 2012 May 1;132(1):51-9.

[6] Sacilik K, Elicin AK. The thin layer drying characteristics of organic apple slices. Journal of food engineering. 2006 Apr 1;73(3):281-9.

[7] Qing Z, Ji B, Zude M. Non-destructive analyses of apple quality parameters by means of laser-induced light backscattering imaging. Postharvest Biology and Technology. 2008 May 1; 48(2):215-22. http://doi.org/10.1016/j.postharvbio.2007.10.004

[8] Crichton, S.; Sturm, B.; Hurlbert, A. Moisture content measurement in dried apple produce through visible wavelength hyperspectral imaging. Paper ID 152186400, *2015 ASABE Annual International Meeting*, Neworleans, LA, USA.

[9] Crichton S, Shrestha L, Hurlbert A, Sturm B. Use of hyperspectral imaging for the prediction of moisture content and chromaticity of raw and pretreated apple slices during convection drying. Drying Technology. 2017 Oct 11:1-3.

[10] Moscetti R, Raponi F, Ferri S, Colantoni A, Monarca D, Massantini R. Real-time monitoring of organic apple (var. Gala) during hot-air drying using near-infrared spectroscopy. Journal of Food Engineering. 2018 Apr 1;222:139-50.

[11] Pu, Y.-Y.; Feng, Y.-Z.; Sun, D.-W. Recent Progress of Hyperspectral Imaging on Quality and Safety Inspection of Fruits and Vegetables: A Review. Comprehensive Reviews in Food Science and Food Safety 2015, 14, 176-188 http://doi.org/10.1111/1541-4337.12123

[12] Romano, G.; Nagle, M.; Argyropoulos, D.; Müller, J. Laser light backscattering to monitor moisture content, soluble solid content and hardness of apple tissue during drying. Journal of Food Engineering 2011, 104(4), 657–662. http://doi.org/10.1016/j.jfoodeng.2011.01.026

Physicochemical parameters and consumer acceptance in espresso and american coffee pods

Parrado, L.X. [a]*; Bahamón, A.F.[a]; Gutierrez, N [a].

[a] South colombian coffee research center-CESURCAFÉ. Universidad Surcolombiana, Neiva, Colombia.

*Corresponding author: u20142131808@usco.edu.co

Abstract

This study presents the consumer acceptance of coffee beverages made from espresso coffee pods (CCE) and american coffee pods (CCA), six quality attributes were evaluated by a sensory panel conformed to judges of different experience level. A physicochemical characterization was made for the coffee powder in CCA and CCE. The beverage preparation via different machines was made for to observe the influence on the consumers acceptance. The coffee powder in CCA showed high aw and high moisture content, this factors should affect the consumer perception; in general, a low acceptance level of coffee beverages made from CCE and CCA was observed, maybe because of the strong habit of consuming filtered coffees.

Keywords: Coffee; Espresso; American; sensory; physiochemical.

1. Introduction

During the preparation of a coffee cup there is a solid-liquid extraction process in which the following steps occur: 1. the water absorption of the ground coffee; 2. the massive transfer of soluble from coffee grinds to hot water; and 3. the separation of the beverage extract and the spent coffee solids. [1]

Among the various processing techniques, filter coffee (drip filter) is the most used coffee obtained by the infusion method, while espresso coffee is the most appreciated coffee produced by the pressure method. In drip filtration methods, water at 92-96 ° C flows through a bed of hardly compressed ground coffee and the extract drips vertically. The turbulence generated in the processing prevents the water from saturated [2]. The sensory properties of coffee prepared by dripping hot water through the ground grain on a filter are affected by particle size, solid / water ratio, contact time and temperature [3]. While an espresso coffee is obtained by the pressure method, water at approximately 9 bar and 88-92 ° C is forced to pass through the compacted coffee beans in a small preparation chamber [2], a fast preparation time and a fine particle size is necessary [4] since the result is strongly affected by the physical condition that controls the filtration process (grinding degree, temperature and water pressure and time) of percolation. The espresso is produced by professional machines and after specific operations carried out by expert hands that define the quality and quantity, the degree of grinding and compression of the coffee to obtain a cup of espresso with specific sensory properties. [5]

The Coffee pods, prepared in single-use (single-use) for coffee machines, have gained considerable popularity due to their end-use convenience and longer shelf life than conventional coffee [1]. The key point of this success is to allow any person, expert or non-expert, to prepare it at any time and in all places (home, car, office and plane) where the limited quantities consumed do not justify or allow the use of professional machines [5]. The pods compatible with Keurig® are composed of a thermoformed multilayer high-barrier capsule, in which a paper or other filtering medium is attached to the side wall near the top of the capsule, forming a filter that separates the capsule into the pods. upper and lower compartments. The roasted and ground coffee beans are introduced into the upper compartment, and then sealed with an aluminum foil lid to form the final product of the PODS [1]. The preparation time in individual coffee is considerably shorter than conventional coffee (30-60 seconds versus 8-12 minutes), and as a result, the contact time with water is relatively shorter. In addition, since the preparation time, the water temperature, the pouring volume and the flow parameters are controlled by the microprocessor and controller of the coffee machine, and the coffee grinds are of portion size in the capsule, the intervention of the user is largely eliminated during the preparation process [1]. The pods compatible with Nespreso used by a simple technology that includes pre-packaged individual doses containing pre-measured and pre-stamped ground coffee.

The ground coffee is hermetically sealed between two thin layers of filter paper, in aluminum or plastic pods [5]. Despite the considerable popularity, the information on the elaboration of coffee pods, the preparation of the drink and the acceptance by consumers is not available in the literature. The objective of this study is to investigate the influence of physicochemical parameters on the encapsulation and acceptance by coffee consumers.

2. Materials and Methods

Five commercial espresso coffee pods (CCE) and five commercial american coffee pods (CCA) were characterized in powder coffee and the beverages made from CCE in single-dose machines C50-US-CW-NE coffee machine (Nespresso®, Switzerland) and CCA extracted in the K50 CLASSIC SERIES coffee machine (Keurig®, United States) were characterized too. For CCE beverages the double-distilled water temperature was 70±2 °C and for CCA beverages it was 80±2 °C. The extraction volume for espresso coffee was 40 ml (35 ml of prepared coffee and 5 ml of foam) and for american coffee it was 177±2 ml (6 oz). the extraction time for espresso coffee was 14±2 seconds and for american coffee it was 25±2 seconds. The water-coffee ratio was 20 g/100 ml for espresso and 7 g/100 ml for american coffee.

The physicochemical parameters evaluated in powder coffee and in the beverages included moisture content from wet basis (%) in infrared balance OHAUS-MB45 (Parsippany, USA) (105 °C for 5 min) according to Zanin et al. [6]; water activity using the AQUALAB VSA (Vapor Sorption Analyzer) equipment from Decagon Devices, Inc.; color (L) in powder coffee and color (L) of the beverages, using the digital colorimeter CR-410 (Konica Minolta Sensing Inc., Japan). Refractive indexes (expressed in ° Brix) were measured with the Atago PR-201α digital refractometer, the titratable acidity (expressed as chlorogenic acid) was determined by titration and pH with the digital potentiometer BP- 3001 (Trans Instruments, Singapore). Measures was made in triplicate.

The sensory attributes of the beverages were evaluated using a QDA quantitative descriptive analysis, a sensory panel conformed to judges of different experience level: Colombian experts in tasting by SCAA methodology (p1), Colombian inexperienced coffee consumers (p2) and Colombian habitual specialty coffee consumers (p3) . The acceptance scale of 6 discrete values in which "I dislike extremely" was evaluated with 0 and "I like extremely" corresponded to 5.

Anova tests were performed ($p < 0.05$) to observe the statistically significant differences in the physicochemical parameters and on the quality attributes evaluated in the sensory panel for espresso coffee and american coffee. The statistical package StatGraphics Plus 5.1 for Windows (Manugistics, Inc., Rockville MD) was used.

3. Results and discussion

Physicochemical characterization

Table 1 presents the results of the comparison of the powder coffee contained in CCE and CCA, in addition the comparison of the parameters obtained in the CCE and CCA beverages. The moisture content, aw, color, in powder coffee from CCE presented statistically significant differences (P<0.05) compared to CCA; likewise, in the analysis of the beverages, pH, oBrix and color presented statistically significant differences (P<0.05) in the two types of drinks.

Table 1. Physicochemical parameters in powder coffee and beverages coffee extracted for espresso and american pods.

Samples	Parameters	CCE	CCA
Powder coffee	Moisture content (%)	2.71±0.62[a]	4.51±1.52[b]
	Water activity (a_w)	0.25±0.11[a]	0.38±0.11[b]
	Roasting degree (L)	23.20±0.53[a]	24.79±1.5[b]
	Titratable acidity	1.68±0.4[a]	1.85±0.36[a]
Beverages	pH	5.21±0.13[a]	4.92±0.11[b]
	Refractive index (°Brix)	3.92±053[a]	1.66±0.45[b]
	Color (L)	32.04±2.89[a]	29.80±1.15[b]

(n = 3) mean ± SD. Different letters, in the same row indicate significant difference (P<0.05).

The moisture content (%) and aw in CCA is significantly higher than in CCE, this result may be influenced by the storage process that depends mainly on factors related to environmental coditions and technological factors such as the availability of oxygen and moisture, the exposed surface area, temperature and packing material [7] ; the CCE moisture content (2.71±0.62%) is similar to that found by Lee et al. [8] for roasted and ground coffee. Apparently the result indicates that the CCE allow less water vapor exchange between the inside of the pods and the surrounding environment. Additionally, taking into account that Cardelly and Labuza [9] reported aw of 0.106% for roasted and ground coffee, the values of aw found for CCA (0.38±0.11%) were much higher, unlike the values of aw for CCE (0.25±0.11%) that were closer to that found by the same author.

The color of roasting in the powder coffee of CCE and the CCA, showed significant differences (p< 0.05), the magnitudes of the coordinate L obtained (23.1±0.5 and 24.1±1.7 respectively) correspond to the degree of dark roasting according to the classification proposed by Franca et al. [10], this result is linked to the generalized concept for the preparation of espressos and American coffee; although L in CCA is significantly higher than in CCE, indicating less roasting degree and higher moisture content.

The refractive index in the beverages, result higher in espresso than in american coffee as shown in Table 1, similar results were obtained by Gloess et al. [11] who determined that espresso coffee has a refractive index closer to 4.0%, the author evaluated this parameters in different machines: a semi-automatic espresso machine, an automatic machine and a Nespresso brand single-use machine. In the american coffee, the same author determined refractive index slightly higher than 1.0%; finding for the filtered coffee extract a refractive index of 1.03±0.01% and for the French press 1.43±0.01%, these results are similar to those found for the CCA.

The pH in beverages is a characteristic that could suggest sensory acidity, according to the results shown in table 1, the pH for the CCE is 5.2±0.1 and for CCA of 4.9±0.1, these results are similar to those found by Ludwig et al [2] who presented for the filtered coffee extract (water-coffee ratio of 6.0% and time extraction time of 75 seconds) a pH of 5.12±0.01 and for espresso (15% water-coffee ratio and 16 seconds of extraction) a pH of 4.9±0.01. Other results such as those obtained by Fujioka et al. [12] showed that the pH in extracted coffee is related to the presence of chlorogenic acids; this author found that the pH in seven types of commercial coffees (with a water-coffee ratio of 3% and filtered) varies from 4.95±0.01 to 5.99±0.01 results very similar to those shown in table 1.

Sensorial analysis in espresso beverages and american coffee beverages.

Table 2 shows the sensory acceptance of coffee beverages made from CCE and CCA, the crema (foam) was evaluated only in espresso coffee since american coffee does not generate it; statistically significative differences ($P < 0.05$) between CCA and CCE was obtained only in Color (L), expressed by P2; while statistically significative differences by panelist type was obtained in all quality attributes, indicating higher strictness in the evalution expressed by P1 and P3, maybe because they have most experience and knowledge in coffee quality.

In the cream evaluation in CCE, the panelists criticized because this is disperse and not homogeneous. According to Gloess et al. [11] that compared several methods of preparation of espresso coffee, found that the crema of the espresso coffee pods was noticeably bigger and of a more intense color compared with other espressos coffees and that the espresso of the semiautomatic machine had the best foam.

Table 2. Sensory Evaluation in beverages made from CCE and CCA

Quality atributes	Panelists	Type	
		CCE	CCA
Color	P1-P3	3.1 ± 0.8^a	3.1 ± 1.0^a
	P2	3.8 ± 0.9^b	3.6 ± 0.8^a
Aroma	P1-P3	2.2 ± 1.2^a	1.6 ± 0.9^a
	P2	3.4 ± 1.0^b	2.7 ± 0.8^b
Flavor	P1-P3	1.9 ± 0.9^a	1.6 ± 0.9^a
	P2	3.0 ± 1.3^b	3.0 ± 1.2^b
Balance	P1-P3	1.9 ± 0.9^a	1.8 ± 0.8^a
	P2	3.2 ± 1.3^b	2.6 ± 1.2^b
Aftertaste	P1-P3	1.7 ± 1.1^a	1.2 ± 1.2^a
	P2	3.1 ± 1.8^b	2.9 ± 1.1^b
Score global	P1-P3	1.8 ± 0.9^a	1.4 ± 0.9^a
	P2	2.8 ± 1.3^b	2.8 ± 1.3^b
crema	P1-P3	2.9 ± 1.2^a	------------
	P2	4.6 ± 0.5^b	------------

n = 3 mean ± SD. Different letters, in the same row for each treatment, indicate significant difference (P≤0.05). Different letters, in the colum for each quality attribute indicate significant difference (P≤0.05).

According to the observations expressed by panelists in the sensory questionnaire, they described greater sensory acidity in espresso coffee, while the results in table 1, the highest titratable acidity and pH concentration occurs in american coffee, which would lead to thinking that it is possible to relate it to sensory acidity. To demonstrate this, it is necessary to do in-depth research of titratable acidity, pH and sensory acidity in an expert panel. The objective of this research was not to evaluate only expert tasters for this reason, we can not assure that the acidity in American coffee is directly due to the sensory acidity perceived by the panel .

4. Conclusions

A high moisture content and aw was found in powder coffee in commercial pods of CCA type, this can significantly affect sensory acceptance since high moisture contents can be indicators of product interaction with the environment given the high degree of hygroscopicity of the coffee. Likewise, the physicochemical parameters studied did not allow demonstrating the correlation between pH and acidity titratable versus sensory acidity, is recommended to deepen the subject by evaluating the acidity content through chemical analysis, titratable acidity, pH and sensory acidity.

In all cases, it was found that the panelists evaluated separately the attributes of color and foam in relation to the other attributes associated with the senses of smell and taste.

In general, the american coffee and espresso coffee pods had low acceptance, perhaps due to the accentuated custom of consumption of filtered coffee in Colombia

5. References

[1] Wang, X., Willian, J., Fu, Y. y Lim, L.-T. (2016) "Effects of capsule parameters on coffee extraction in single-server brewer", Food Research International, 89 (1), pp. 797-805.

[2] Ludwig, I.A., Sanchez L., Caemmerer, B., Kroh, L.W., de Peña, M.P. y Cid, C. (2012) "Extraction of coffee antioxidants: Impact of brewing time and method", Food Research International, 48 (1), pp. 57-64.

[3] Corrochano, B.R., Melrose, J.R., Bentley, A.C., Fryer, P.J. y Bakalis, S. (2014) "A new methodology to estimate the steady-state permeability of roast and ground coffee in packed beds", Journal of Food Engineering, 150, pp. 106-116.

[4] Lingle, T.R (1996) "The coffe brewing handbook", Spelciality Coffe Association, Long Beach, California.

[5] Albanese, D., Di Mateo, M., Poiana, M. y Spagnamusso, S. (2009) "Espresso coffee (EC) by POD: Study of thermal profile during extraction process and influence of water temperature on chemical–physical and sensorial properties", Food Research International, 42 (5-6). Pp. 727-732.

[6] Zanin, R.C., Corso, M.P., Kitzberger, C.S.G., Scholz, M.B.D.S y Benassi, M.D.T (2016) "Good cup quality roasted coffes show wide variation in chlorogenic acids content", LWT-Food Science and Technology, 74, pp. 480-483

[7] Manzocco, L. y Lagazio, C. (2009) "Coffee brew shelf life modelling by integration of acceptability and quality data", Food Quality and Preference, 1 (20), pp. 24-29.

[8] Lee, S.J., Kim, M.K. y Lee, K.-G. (2017) "Effect of reversed coffee grinding and roasting process on physicochemical properties including volatile compound profiles", Innovative Food Science & Emerging Technologies, 44, pp. 97-102.

[9] Cardelli, C. y Labuza, T.P. (2001) "Application of Weibull Hazard analysis to the determination of the shelf life of roasted and ground coffee", LWT-Food Science and Technology, 34 (5), pp. 273-278.

[10] Franca, A.S., Oliveira, L.S., Oliveira, R.C.S., Agresti, P.C.M. y Augusti, R. (2009) "A preliminary evaluation of the effect of processing temperatura on coffee roasting degree assessment", Journal of Food Engineering, 92 (3), pp. 345-352.

[11] Gloess, A.N., Schonbachler, B., Klopprogge, B., D'Ambrosio, L., Chatelain, K., Bongartz, A., Strittmatter, A., Rast, M. y Yeretzian, C. (2013) "Comparision of nine common coffee extraction methods: instrumental and sensory analysis", Eur Food Res Technol, 236 (4), pp. 607-627.

[12] Fujioka, K. y Shibamoto, T. (2008) "Chlorogenic acid and caffeine contents in various commercial brewed coffees", Food Chemistry,106 (1), pp. 217-221.

Physicochemical characterization of mesquite flours.

Sandoval Torres, S.ª*; Reyes López, L.ᵇ; Méndez Lagunas L.ᶜ ; Rodríguez Ramírez J.; Barriada Bernal, G. ᵈ

ᵃ ˒ ᵇ ˒ ᶜ ˒ ᵈ Instituto Politécnico Nacional, CIIDIR Unidad Oaxaca. Hornos No. 103, Col. Noche Buena, Santa Cruz Xoxocotlán, Oaxaca, Mexico.

*E-mail of the corresponding author: **ssandovalt@ipn.mx**

Abstract

Ethnic foods are healthy products interesting for the new societies. Mesquite flour offers another option for making gluten-free recipes as part of a diet for people with celiac disease. The physicochemical properties of mesquite flours (Prosopis laevigata) were characterized. The mesquite pods were dried at 60°C, 15% RH and 2 m/s airflow; then a grinding and sieving process were applied. The nutritional composition and the sorption isotherms were obtained at 30, 35, 40 and 45°C for water activities of 0.07-0.9. The particle-size distribution, morphology and thermal stability of the flours were determined by different methods.

Keywords: Mesquite Flours; drying; isotherms; chemical properties; morphology.

1. Introduction

Mesquite (*Prosopis spp*) are extremophile trees, comprising 44 species around the world [1]. In Mexico, mesquite trees are distributed in northern, central and southern states of the country. In ancient times, the indigenous peoples of Mexico used mesquite pods as food, to produce flour, sirups and bread [2]. The pods having a high protein content in addition to the sucrose content offers a wide potential for the development of new ethnic products [3]. For example, flours of *Prosopis pallida* and *Prosopis juliflora* were obtained from the fractions of different grinds, then a bread was elaborated with 25% wheat flour [4]. In the last years, different studies have analysed the properties of flours of *P. alba, P. chilensis and P. flexuosa* for the elaboration of bakery products. Nevertheless, mesquite flours must satisfy the culinary requirements and the storage condiètions must be well stablished [5]. In this work we determine the physicochemical properties of Mexican mesquite flours (*Prosopis laevigata*) in order to characterize the flour and to identify the storage conditions.

2. Materials and Methods

2.1. Mesquite flours

Prosopis laevigata pods were harvested between April and August 2016 in the community of Santiago Suchilquitongo, In Oaxaca (Mexico). The pods in stage three of maturity were used. Pods were dried in a tunnel dryer at 60°C, relative humidity of 10% and air velocity of 2.6 m/s. The pods were milled by two methods: a) in an Osterizer blender model 465-15 for 20 seconds, and b) in a mill pulverizer for legumes Model HC-2000Y, during intervals of 5 seconds until 20 seconds. The milled material was sieved through #40 (0.420mm) and #60 (0.250mm) sieves. After the sieving process the powder was stored in a vacuum desiccator for 24 hours.

2.2. Physicochemical characterization

The moisture content of pods was determined by the oven-dry method (105°C, during 24 hours). The total raw protein content was determined by the Kjeldahl method (AOAC 960.52, 1997). For the determination of reducing and direct sugars, the Lane-Eynon volumetric method was followed. Total fat extraction was carried out by the Soxhlet method (AOAC 920.3, 1990). Raw fiber (NMX-F-090-S-1978) was obtained by using the flour residues, which were dried at 130 °C in an electric oven for 2 hours. The ash content was obtained by calcining in crucibles at 550°C for 30 min in a muffle oven model KLS 03/10.

The particle size distribution of mesquite flour obtained from the pulverizer was analyzed using the principle of blue laser light diffraction measurement (ISO13320, 2009) by the Microtrac Blueray M3551-1W-BU00 in a humid medium, with a measuring range of 10 nm up to 2000 microns. An ultrasound was applied for 30 seconds with a power of 30 watts to

800 grams of flour, then it was divided in three samples to facilitate the dispersion of the particles.

The mesquite flours were analyzed by Scanning Electron Microscope (SEM) in a JEOL brand microscope, model JIB-4601F, with a spatial resolution of 1.2 nm. Secondary electron detector E-T (Everhart-Thornley) and a range of magnification were taken from 50x to 2500x.

The sorption isotherms of mesquite flour were determined by the gravimetric static method with water activities ranging from 0.07 to 0.97 and temperatures of 30, 35 ,40 and 45°C. The used salts were the following: N_aCl, $MgCl_2$ * 6 H_2O, KOH, KCl, Kl, K_2SO_6, $M_g(NO_3)_2$ * $6H_2O$ [9]. For high water activities, vials were prepared with an antifungal agent, which were introduced into the equilibrium systems. The samples were weighed every 2 days until constant weight was observed. The experimental data was fitted to the GAB (Guggenheim-Anderson-Deboer) model (Equation 1). The parameters of this model were estimated by using the solver tool in excel [6].

$$Xeq = \frac{Xm \bullet C \bullet K \bullet a_w}{(1 - K \bullet a_w) \bullet (1 - K \bullet a_w + C \bullet K \bullet a_w)} \qquad (1)$$

The isosteric heat of sorption (Qst) was determined by solving the equation derived from the Clausius Clapeyron formulation [6] (Equation 2):

$$\left[\frac{\partial \ln(a_w)}{\partial (1/T)} \right]_{CHE} = -\frac{Q_{st} - \lambda}{R} = -\frac{q_{st}}{R} \qquad (2)$$

Samples of mesquite flours conditioned at relative humidity of 7%, 32%, 51% and 67% at 45°C were prepared for a DSC analysis (TA Instruments, model Q2000). The samples started at an initial temperature of 0°C, followed by a heating rate of 2°C /min up to a final temperature of 250°C. The thermogram was obtained by using the TA Instruments Universal Analysis DSC software.

3. Results and Discussion

The nutritional compositions of flours presents a high content of sugars, fiber and protein. It was observed that the carbohydrates increased according to the type of milling, which increases the flour hygroscopicity (Table 1).

Table 1. Nutritional composition of mesquite flours obtained by the two grindings.

Components	Blender		Mill pulverizer	
	Average (g / 100 g)	Standard deviation	Average (g / 100 g)	Standard deviation
Energy content (kcal / 100 g)	170.97	0.07	198.72	0.50
Carbohydrates (g)	24.27	0.09	26.18	0.08
Sugars (g)	7.48	0.03	10.18	0.02
Proteins (g)	12.4	0.08	11.77	0.12
Fats (Lipids) (g)	2.16	0.03	2.90	0.06
Fiber (g)	16.9	0.2	17.25	0.11
Ashes (g)	3.12	0.01	3.45	0.05
Humidity (g H20 / g dry matter)	0.1	0.01	0.10	0.01

The particle size distribution (Fig. 1) showed a smooth and Gaussian distribution. The flour presented a homogeneous distribution with an average particle size of 148 microns, which is adequate to be considered as flour for bakery and confectionery products.
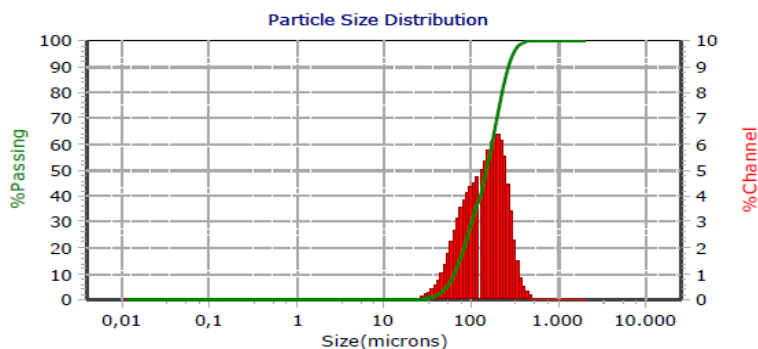
Fig. 1 Particle size distribution.

The SEM images show the morphological characteristics of flours. Figure 2 reveals a surface rounded particle, without rocky parts, or forced cuts. Figure 3 shows a particle organized with smaller particles, forming a tortuous, irregular form, porous, and rocky agglomerate; a strong attraction was observed between the particles with different sizes.
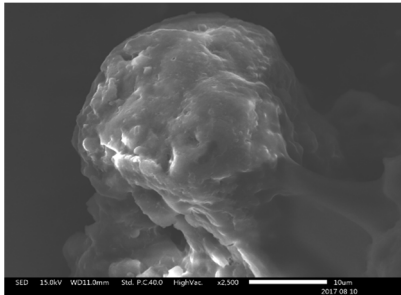
Fig. 2 Micrograph of mesquite flour (Mill pulverizer), 2500x.
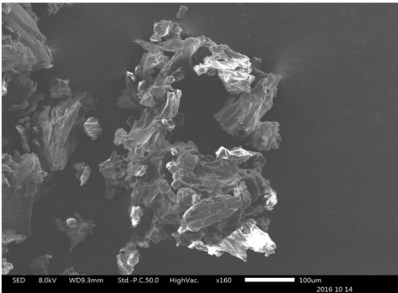
Fig. 3 Micrographs of mesquite flour (Blender), 160x.

The experimental and simulated sorption isotherms at 30, 35, 40 and 45°C are shown in Figure 4, which display a type II form. The shape of the curve indicates a probable small adsorption force in the monolayer [7]. An increase in Xeq was identified when aw is near from 0.65, at this water activity a degradation of flour was observed. This type of isotherm has been obtained in materials containing fibers (wheat, rice, potato, soybean, corn) [8]. Also an interlacing of the curves was observed, indicating a non-dependence on temperature. The GAB model correctly describes the experimental data.
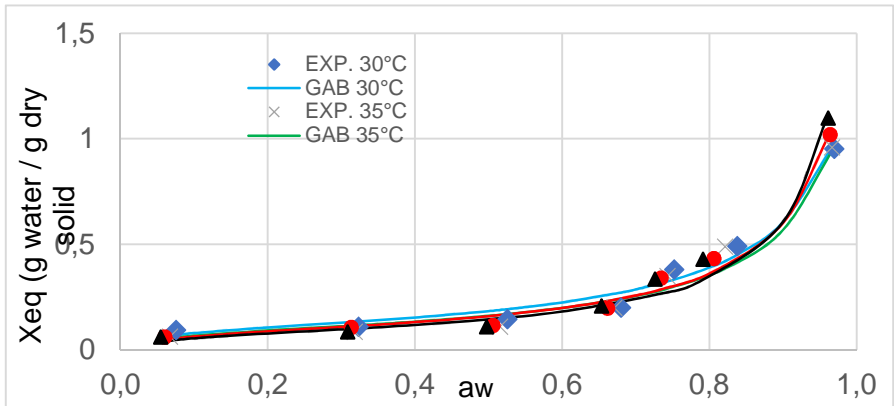
Fig. 4 Adsorption isotherm of mesquite flour (Prosopis laevigata) at the four working temperatures.

Table 2. Parameters obtained from the GAB model

Model	Parameters	30°C	35°C	40°C	45°C
	Xwa				
	(g H20 /g dry matter)	0.1039	0.0905	0.0894	0.0824
	C	22.1997	19.9075	16.6142	15.2432
GAB	k	0.9219	0.9355	0.9475	0.9656
	r^2	0.9898	0.9772	0.9817	0.9773
	s	0.0555	0.0741	0.0592	0.0703

Xwa = Monolayer value; C and k = constants for the model; r^2 = correlation coefficient; s = standard error

Figure 5 shows the isosteric heat (Qst). Qst increases as Xw decreases; At Xw=0.25 the value of Qst is 47.69 kJ/mol and at Xw=0.05 Qst=81 kJ/mol. This fact indicates a low availability of active sites and liaison forces on the surface of the flour [9]. Qst indicates a requirement of 81 kJ/mol in order to remove 0.05 g water/g dry solid, without affecting the stability of the flour.
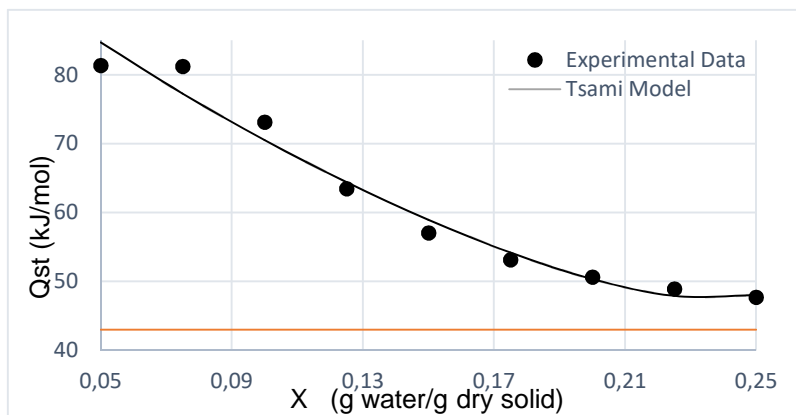
Fig. 5 Isosteric heat of sorption as a function of the moisture content of mesquite flours subjected to constant temperatures of 30, 35, 40 and 45°C.

Figure 6 shows the DSC curves for mesquite flours. A glass transition (Tg) of the mesquite flour was not observed, due to a probable flexibility and mobility of the glucose and fructose chains, as well as the presence and increase in the water content of the sample [10]. The flours displayed a wide thermal stability (0-130°C). The phase transition observed in all the flours were melting points from 148°C to 158°C and crystallizations at 170°C due to the presence of simple sugars, such as fructose.
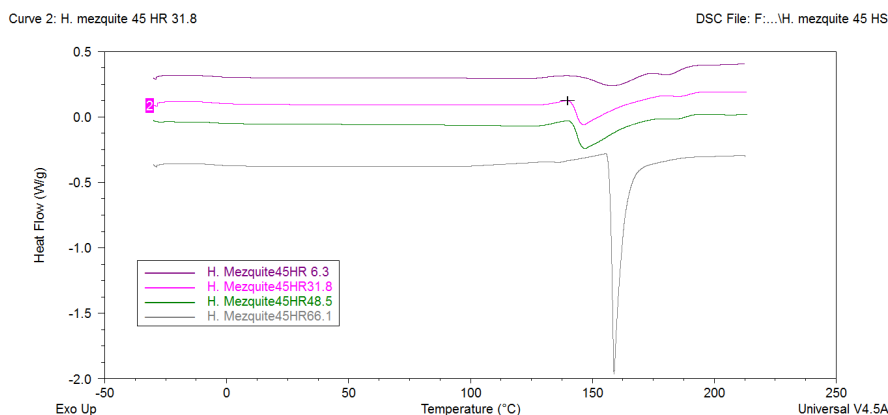
Fig. 6 DSC curves. Flours conditioned at different aw, at 45°C.

4. Conclusions

The nutritional content of the powders reveals important properties for the mesquite flours. Flours have a high content of sugars and fiber, and an important content in protein. Flours are highly hygroscopic, and this fact can be explained by the sugar content. Microscopic images reveal irregular, agglomerated and porous structures. Flour displays a type II isotherm, a water activity higher than 0.6 provoques a degradation of the powders. According to the isosteric heat, 81 kJ/mol are required in order to remove 0.05 g water/g dry solid, without affecting the stability of the flour. The calorimetric data showed a wide thermal stability (0-130ºC) of this material. The flour reveals a potential use for the food industry.

5. Acknowledgements

6. Nomenclature

Subscripts

Xeq	Equilibrium moisture content.
Xm	Monolayer moisture content.
C	Heat-related constant of the monolayer.
K	Heat-related constant of the multilayer.
qst	Net isosteric heat of sorption.

Qst	Total isosteric heat of sorption.
R	Universal constant of the gases.
aw	Activity of water.
T	Temperature.

7. References

[1] Felker, P.; Takeoka, G.; Dao, L.. Pod mesocarp flour of North and South American species of leguminous tree prosopis (mesquite): Composition and food applications. Food Reviews International 2013, 29(4), 49-66.

[2] Figueiredo, A. A. Mesquite: history, composition, and food uses. Food technology 1990, 44, 118-128.

[3] Meyer, D. Processing, utilization and economics of mesquite pods as a raw material for the food industry (Doctoral dissertation, Diss. Techn. Wiss. ETH Zürich, Nr. 7688, 1984. Ref.: H. Neukom; Korref.: F. Escher), 1984.

[4] Grados, N.; Cruz, G. New Approaches to Industrialization of Algarrobo (Prosopis pallida) Pods in Peru. Prosopis: Semiarid fuelwood and forage tree, 1996, 3-25.

[5] Prokopiuk, D.; Cruz, G.; Grados, N.; Garro, O.; Chiralt, A. Estudio comparativo entre frutos de Prosopis Alba y Prosopis pallida. Multequina, 2000, 4, 35-45.

[6] Quirijns, E. J.; Van Boxtel, A. J. B.; Van Loon, W. K. P.; Van Traten, G. Sorption isotherms, GAB parameters and isosteric heat of sorption. Journal of the Science of Food and Agriculture 2005, 85, 1805-1814.

[7] Anderson, R.B. Modification of the BET equation. J. Am. Chem. Soc 1946, 68, 686-691.

[8] Navia, D.; Ayala, A.; Villada, H. Isotermas de adsorción de bioplásticos de harina de yuca moldeados por compresión. Biotecnología en el Sector Agropecuario y Agroindustrial, 2011, 9, 77-87.

[9] Tsami, E. Net isosteric heat of sorption in dried fruits. Journal of Food Engineering 1991, 14, 327–335.

[10] García, E.E. Optimización del secado por aspersión del mucílago de pitahaya en función de sus propiedades reológicas. Instituto Politécnico Nacional: Oaxaca, México. 2011, 93-94.

Thermal stability of amorphous sugar matrix, dried from methanol, as an amorphous solid dispersion carrier

Imamura, K.[*]; Takeda, K.; Yamamoto, K.; Imanaka, H.; Ishida, N.

Division of Chemistry and Biochemistry, Graduate School of Natural Science and Technology, Okayama University, 3-1-1 Tsushima-naka, Kita-ku, Okayama 700-8530, Japan

*E-mail of the corresponding author: kore@cc.okayama-u.ac.jp

Abstract

Developing a technique to disperse hydrophobic ingredients homogeneously in a water-soluble solid matrix (solid dispersion) is one of the topics that have been extensively investigated in the pharmaceutical and food industries. Recently, we have devised a novel solid dispersion technique (surfactant-free solid dispersion), in which a preliminarily amorphized sugar was dissolved in an organic media containing hydrophobic component, without using any surface active substances, and then vacuum dried into the amorphous solid mixture [Food Chem., 197 (2016) 1136; Mol. Pharm., 14 (2017) 791]. In this study, the physicochemical properties, especially thermal stability of the surfactant-free amorphous solid dispersion, were investigated.

Keywords: solid dispersion; amorphous sugar; surfactant-free; vacuum drying; glass transition temperature

1. Introduction

To date, many attempts have been made to improve the solubility of hydrophobic drugs in physiological fluids [1,2]. One promising approach for improving the water solubility of a hydrophobic drug is the use of an "amorphous solid dispersion (ASD)"[3-5], in which hydrophobic drug molecules are dispersed at the molecular level in the carrier matrix comprised of water-soluble substance. When a medicine in the ASD is taken into a human body, the dissolution of the carrier matrix is accompanied by the release of hydrophobic drug molecules [6]. The concentration of the dissolved drug temporarily increases much above the equilibrium solubility (over-dissolution), possibly resulting in the improvement of the bioavailability of the hydrophobic drug [6]. In the solid dispersion of hydrophobic drugs, an amphiphilic polymer such as polyvinylpyrrolidone and hydroxypropyl methylcellulose is frequently used as the carrier matrix [6,7], and a combination of a surfactant with an amorphous carbohydrate matrix has also been reported to be effective for the stable dispersion of drugs [8,9]. On the other hand, we recently developed a new ASD technique that does not involve the use of a surface active agent [10]. In this method, (i) sugar is amorphized and (ii) added to an organic solvent containing a hydrophobic substance, followed by homogenization. (iii) The homogenized solution is then dried to a solid (surfactant-free solid dispersion). The amorphized sugar can be dissolved in an organic solvent such as methanol to a greater extent than a crystalline one. Hydrophobic drugs (Indomethacin, ibuprofen, gliclazide, nifedipine) can be stably embedded in the surfactant-free solid dispersion without any detectable segregation and exhibited marked over-dissolution at the initial stage of the dissolution in water [11].

The stability of the dispersion state of drug molecules in an amorphous carrier matrix is also an important quality aspect of the ASD besides the drug dissolution behavior in water: When hydrophobic drug molecules segregate from the amorphous carrier matrix, the over-dissolution of the drug is mostly precluded. The segregation of hydrophobic drug molecules is caused by the glass-to-rubber transition of the carrier matrix, and the glass transition temperature (T_g) of amorphous carrier matrix therefore is considered to correspond to the drug dispersion stability. In this study, first the T_g values of the surfactant-free solid dispersion were measured and compared to those for authentic freeze-dried ones. As a result, the T_g value of amorphous sugar matrix obtained from an organic solvent (methanol) was found to be significantly lower than that from an aqueous solution and furthermore indicated to be increased, as the result of a heat treatment, to as high as that for the water-originated one. Hence, at the next step, the methanol-originated amorphous sugars were heated under different conditions, including temperature and period, and analyzed for the T_g value and the drug dissolution behavior in water. The mechanism of the markedly low T_g for the methanol-originated amorphous sugars as well as what happens in the heat-treatment were investigated.

2. Materials and Methods

2.1. Materials

α-Maltose, maltitol, palatinose, and trehalose were purchased from Wako Pure Chemical Industries, Ltd., (Osaka, Japan). Indomethacin (γ-form of the crystal) and ibuprofen (Wako Pure Chemical Industries) were used as hydrophobic drugs. Methanol was obtained from Wako Pure Chemical Industry.

2.2. Methods

Vacuum Foam Drying and Heat Treatment The amorphous sugar cake that had been freeze-dried from an aqueous solution [12] was added to a methanol solution, containing a model hydrophobic drug, at the concentration of 100 mg/mL. Immediately thereafter, a 100 µL aliquot of the mixture solution was transferred to a 1.5 mL-polypropylene tube and the resulting solution was then dried under a reduced pressure of around ca. 1 Torr and centrifugation at 30±1˚C for 60 min (methanol-originated sample), using a TOMY Micro Vac MV-100 centrifugal concentrator (TOMY SEIKO Co., ltd., Tokyo, Japan). At this initial drying stage, foaming was minimal. After a 60 min period of initial drying, the residue was punctured with a steel needle, followed by the secondary vacuum drying for an additional 30 min [11]. The subsequent vacuum drying reliably resulted in foaming [11]. These series of procedures had preliminarily been indicated to be indispensable for drying the sample sufficiently (< 0.01 g-MeOH/g-dry matter) within a convenient drying period [11].

The obtained dried sample was alternatively transferred in a glass vial and then heated in a drying oven. The sample vials were sealed with heat-resistant caps to avoid the water sorption in the drying oven. The heating temperature and period were varied from 30 to 120˚C and from 0 to 120 min.

Differential Scanning Calorimetry Differential scanning calorimetry (DSC) analyses of amorphous sugar matrices, obtained from methanol as well as water, were carried out, using a TA Q2000 calorimeter (TA instruments Co., New Castle, DE) equipped with RCS90 cooling system (TA instruments Co.) in the same procedures as was used in our previous study [11]. From the obtained DSC curves, the T_g of the sample was determined as the onset of the corresponding thermal event.

Fourier Transform Infrared Ray Spectroscopy IR spectra for amorphous sugar samples were measured by means of a diffuse diffraction method using an FTIR in the same ways as was used in our previous study [13]. In order to semi-quantitatively estimate the degree of formation of hydrogen bonding in an amorphous sugar matrix, the peak wavenumbers of sugar O-H stretching vibration bands of amorphous sugar samples were analyzed. The IR

band due to sugar O-H stretching vibration (3200~3500 cm^{-1}) was smoothed at 80 points to determine the peak wavenumber.

Specific Molar Volume Analysis A ten mL of methanol or water was put in a 20 mL graduated cylinder, and 0.1~2 g (0.3~6 mmol) of amorphous sugar cake that had been freeze-dried from water and then thoroughly dehydrated over P$_2$O$_5$ [12] was then added to the methanol. α-Maltose was used as a sugar since it can be highly dissolved in methanol from amorphous state compared to the other sugars [10]. The freeze-dried amorphous α-maltose was absolutely dissolved by gently inverting the graduated cylinder several times. After removing bubbles on the cylinder wall, the change in the volume (*dV*) was determined and converted into the apparent partial mole volume of sugar (v_{sugar}) by being divided by the amount of the added sugar (*n g*) (Eq. (1)).

$$v_{sugar} = dV/n \qquad (1)$$

Dissolution Behavior of Hydrophobic Drugs from Solid Dispersion Samples The prepared surfactant-free solid dispersions of model hydrophobic drugs were added to a known amount of water (final drug conc.: 50 µg/mL for indomethacin, 500 µg/mL for ibuprofen) and the suspension was stirred at 200 rpm with a 1.5-cm magnetic stirring bar at 37±1˚C. A 200~1,000 µL aliquot of the suspension was withdrawn and then filtered with 0.2 µm pore size filter (Nihon Millipore K.K., Tokyo, Japan). The concentration of the dissolved model drug was typically measured by UV-vis absorption at specific wavelengths (indomethacin: 318 nm; ibuprofen: 233 nm).

3. Results and Discussion

The DSC thermograms for the surfactant-free solid dispersion sample, obtained by vacuum foam drying from methanol solution, showed single heat capacity shift due to glass-to-rubber transition but no endothermic peak. This demonstrates that the surfactant-free solid dispersion sample was fully amorphous and methanol was fully removed during the vacuum foam drying.

Table 1. Glass Transition Temperatures (T_g) for amorphous sugar matrices, dried from methanol, as well as for Freeze-Dried from water

sugar	T_g (°C)	
	from water	*from methanol*
α-maltose	90±1	36±1 (1st scan)
		72±2 (2nd scan)
palatinose	62±2	21±1
trehalose	102±3	37±3
maltitol	46±2	9±2

Table 1 compares the T_g values of differently dried matrices of sugars. The T_g values for the sugar matrices dried from methanol are ~50˚C lower than those for the samples dried from
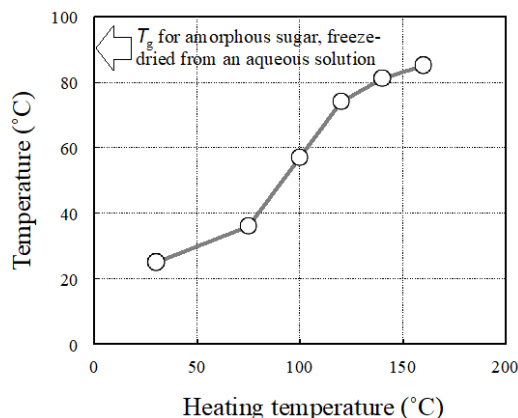
Fig. 1. Influences of heating temperature on T_g values for surfactant-free solid dispersion, obtained from methanol. α-Maltose and indomethacin (1% v/v) were used as sugar and hydrophobic drug, respectively.

aqueous solutions. Considering the fact that the methanol-originated samples had been thoroughly dried, as described above, the T_g value for an amorphous sugar matrix can be deduced to strongly varied, depending on the original solvent type.

As shown in Table 1, when the methanol-originated sugar matrix was scanned twice, the T_g value is markedly increased, suggesting that the thermal treatment may improve the physical stability of the sugar matrix dried from methanol. Hence, the influences of temperature and duration of heating on the methanol-originated sample were investigated.

Figure 1 shows the T_g values for different heating temperatures. As the heating temperature (Fig. 1) and period (data not shown) increase, the T_g increases and appears to reach the value for the water-originated sample.

The dissolution of hydrophobic drugs in water from the heat-treated solid dispersion sample as well as from the unheated ones were measured (Fig. 2). Both the heated and unheated solid dispersion samples show typical "spring and parachute" dissolution curves [14]. Namely, the concentration of dissolved drug jumps up to much above the equilibrium solubility at the early stage ("spring") and then decreases to reach the equilibrium value ("parachute"),
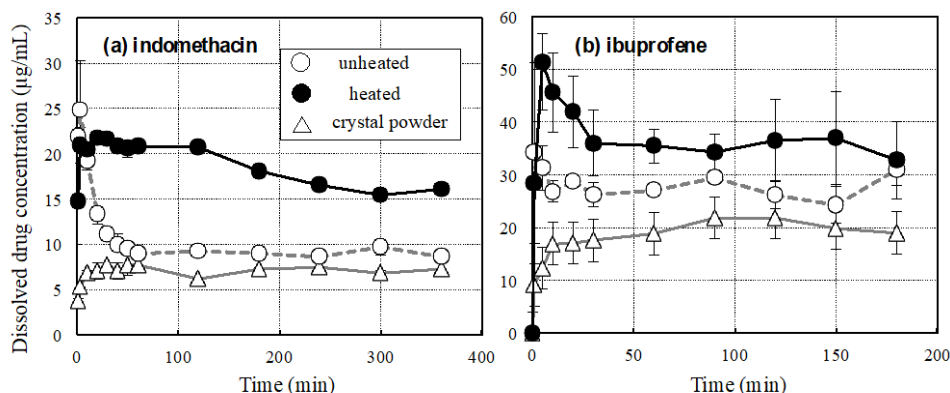
Fig. 2. Dissolution profiles of (a) indomethacin and (b) ibuprofene in water from unheated and heated surfactant-free solid dispersion as well as crystalline powders of model drugs. α-Maltose was used as sugar, and the drug content in the solid dispersion sample was 1% w/w. The amounts of model drug added to the water were 50 μg/mL for (a) indomethacin and 500 μg/mL for (b) ibuprofene. The heat-treatment was conducted at 120°C for 60 min.

whereas the crystalline drug exhibits gradual increase toward the saturation concentration. When compared between the heated and unheated solid dispersions of indomethacin, the decrease in the dissolved indomethacin concentration after the over-dissolution is markedly slowed down as the result of the heat-treatment although the attained maximum dissolved concentration of indomethacin is slightly lowered. On the other hand, in the case for ibuprofen, the attained maximum dissolved concentration is slightly increased as the result of the heat-treatment while the slowing down of the "parachute" process is less significant than in the case for indomethacin. Considering these, the heat-treatment of the surfactant-free solid dispersion, originated from methanol, can be deduced to serve to improve the aqueous dissolution of hydrophobic drug, the effect and extent of which vary depending on the drug type.

At present stage, the mechanism for the improvement of aqueous dissolution of hydrophobic drugs by heating is obscure. However, this study indicates that the heat-treatment can overcome the low T_g of amorphous sugar (carrier) matrix, dried from methanol, and possibly the instability of over-dissolution of hydrophobic drugs. Hence, the possible mechanism for the markedly low T_g for the methanol-originated amorphous sugars and what happened in the heat-treatment were further investigated.

The IR spectra for the amorphous sugar matrices dried from methanol and water were compared (Fig. 3), indicating that the peak position of the absorption due to O-H stretching vibration for the methanol-originated sample (3350 cm^{-1}) was much lower than that for the water-originated one (3388 cm^{-1}). Accordingly, more sugar-sugar hydrogen bondings may be formed in the amorphous sugar matrix dried from methanol than in that from water. On the other hand, when the methanol-originated sample was heated (at 120˚C for 60 min), the peak frequency of O-H stretching vibration was positively shifted toward the value for the water-originated sample (Fig. 3).
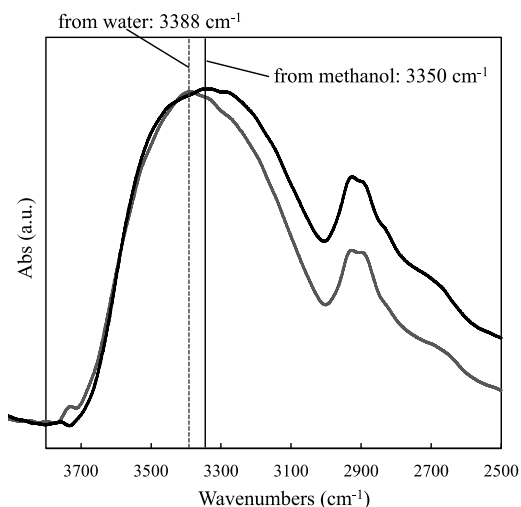
Fig. 3. IR bands for sugar O-H stretching vibration for amorphous matrices, dried from methanol and water. The peak wavenumbers of the IR bands are shown in the figures.

From the volumetric measurements of the methanol and aqueous solution containing different amount of amorphous sugar (α-maltose), the occupied volume of sugar molecule in methanol and water were calculated to be 133 mL/mol and 188 mL/mol, respectively. This

indicates that a sugar molecule may have considerably compact conformation in methanol relative to in water.

Sugar molecule in a poor solvent may change its conformation so as to decrease the solvent-contacting surface area. The lower permittivity of methanol than that of water may allow intramolecular hydrogen bonding in the disaccharide molecule, which would also reduce the occupied volume of a sugar molecule. Consequently, the partial molar volume of α-maltose in methanol is considered to be markedly smaller than in water, as shown above.

When assumed that the sugar molecules in the matrix dried from methanol, more or less, maintain their compact conformation before being drying, the methanol-originated matrix is considered to have smaller mean intermolecular distance and thus greater extent of hydrogen bondings, as indicated by the lower frequency of sugar O-H stretching vibration. It would also follow that the smaller volume assigned to each sugar molecule provides the lower T_g where the free volume of sugar molecule reaches a critical value (Table 1). Furthermore, the markedly small occupied volume of sugar molecule in the matrix obtained from methanol may be accompanied by the distortion of the sugar molecule. The relaxation of sugar molecule to less awkward conformation is thus considered to be time-dependent and accelerated with increasing temperature, as shown in Fig. 1.

4. Conclusion

Amorphous sugar can be temporarily dissolved in methanol and dried into amorphous powders from methanol, which was applied to the surfactant-free solid dispersion of hydrophobic drugs (surfactant-free solid dispersion). However, the T_g of the methanol-originated sample was much lower than that of amorphous sugar dried from water. More hydrogen bonds are formed in the amorphous matrix dried from methanol than in the matrix dried from water. The specific characteristics of the methanol-originated sample were reduced as the result of heating: The T_g and degree of hydrogen bonding for the surfactant-free solid dispersion sample were respectively increased and reduced close to those for amorphous sugar dried from water by heating under appropriate conditions. The heat treatment was indicated to improve aqueous dissolution of hydrophobic drugs (indomethacin and ibuprofen) from the surfactant-free solid dispersion. The comparison of the apparent sugar molar volumes in methanol and water suggested that the occupied volume of sugar molecules in methanol was ~30% smaller than that in water. The markedly lower T_g and higher extent of hydrogen bonding for the methanol-originated amorphous sugar matrix were deduced to closely relate to the highly compact and possibly awkward conformation of sugar molecules in methanol.

5. References

[1] Lipinski, C. A. Poor aqueous solubility-an industry wide problem in drug discovery. *Am. Pharm. Rev*. 2002, *5*, 82-85.

[2] Amidon, G. L. Drug derivatization as a means of solubilizations: Physical and biochemical strategies. In *Techniques of Solubilization of Drug*; Yalkowsky SH, Eds.; Marcel Dekker: New York, 1991, pp 183-211.

[3] Leuner, C.; Dressman, J. Improving drug solubility for oral delivery using solid dispersions. *Eur. J. Pharm. Biopharm.* 2000, *50*, 47-60.

[4] Ilevbare, G. A.; Liu, H.; Edgar, K. J.; Taylor, L. S. Maintaining supersaturation in aqueous drug solutions: impact of different polymers on induction times. *Cryst. Growth Design* 2013, *13*, 740-751.

[5] Li, B.; Konecke, S.; Harich, K.; Wegiel, L.; Taylor, L. S.; Edgar, K. J. Solid dispersion of quercetin in cellulose derivative matrices influences both solubility and stability. *Carbohydr. Polym*. 2013, *92*, 2033–2040.

[6] Huang, Y.; Dai, W-G. Fundamental aspects of solid dispersion technology for poorly soluble drugs. *Acta. Pharm. Sinica B* 2014, *4*, 18-25.

[7] Chadha, R.; Kapoor, V. K.; Kumar, A. Analytical techniques used to characterize drug-polyvinylpyrrolidone systems in solid and liquid states - An overview. *J. Sci. Ind. Res*. 2006, *65*, 459-469.

[8] Jie, L.; Jianming, C.; Yi, L.; Jing, S.; Fuqiang, H.; Zongning, Y.; Wei, W. Glyceryl monooleate/Poloxamer 407 cubic nanoparticles as oral drug delivery Systems: I. In vitro evaluation and enhanced oral bioavailability of the poorly water-soluble drug simvastatin. *AAPS PharmSciTech* 2009, *10*, 960-966.

[9] Yadav, B. V.; Yadav, A. V. Pharmaceutical application of supercritical fluid technique: an overview. *J. Pharm. Res.* 2009, *29*, 31-44.

[10] Satoh, T.; Hidaka, F.; Miyake, K.; Yoshiyama, N.; Takeda, K.; Matsuura, T.; Imanaka, H.; Ishida, N.; Imamura, K. Surfactant-free solid dispersion of fat-soluble flavour in an amorphous sugar matrix, *Food Chem.* 2016, *197*, 1136–1142.

[11] Takeda, K.; Gotoda, Y.; Hirota, D.; Hidaka, F.; Sato, T.; Matsuura, T., Imanaka, H.; Ishida, N.; Imamura, K. Surfactant-free solid dispersions of hydrophobic drugs in an amorphous sugar matrix dried from an organic solvent. *Mol. Pharm.* 2017, *14*, 791–798.

[12] Imamura, K.; Maruyama, Y.; Tanaka, K.; Yokoyama, T.; Imanaka, H.; Nakanishi, K. True density analysis of a freeze-dried amorphous sugar matrix. *J. Pharm. Sci.* 2008, *97*, 2789–2797.

[13] Imamura, K.; Ogawa, T. ; Sakiyama, T. ; Nakanishi, K. Effect of types of sugar on the stabilization of protein in the dried state. *J. Pharm. Sci.* 2003, *92*, 266-274.

[14] Brouwers, J.; Brewster, M. E.; Augustijns, P. Supersaturating drug delivery systems: the answer to solubility-limited oral bioavailability? *J. Pharm. Sci*. 2009, *98*, 2549–2572.

Effect of tray dryer's independent variables (drying temperature and air velocity) on the quality of olive pomace and system's energy efficiency

Baysan, U.[a,b]; Koç, M.[b]; Güngör, A.[c]; Kaymak-Ertekin, F.[a]

[a] Ege University, Faculty of Engineering, Food Engineering Department, 35100, Bornova Izmir, Turkey
[b] Adnan Menderes University, Faculty of Engineering, Food Engineering Department, 09010, Aydın, Turkey
[c] Ege University, Faculty of Engineering, Mechanical Engineering Department, 35100, Bornova Izmir, Turkey

*E-mail of the corresponding author: mehmetkoc@adu.edu.tr

Abstract

In this study, the effects of drying temperature (70, 80, 90°C) and air velocity (0.5, 1.8 m/s) of hot air drying (tray drying) on quality of dried 2-phase olive pomace and system's energy efficiency were investigated. The drying experiments were carried out in a tray dryer. The effects of drying conditions were evaluated with analyzing drying time, the primary and secondary oxidation and calculating specific moisture extraction rate (SMER), moisture extraction rate (MER) and specific energy consumption (SEC). The results showed that increase in drying temperature and decrease in air velocity led to decrease in quality of dried olive pomace.

Keywords: Waste valorization, 2-phase olive pomace, Tray dryer, Energy efficiency, oxidation stability

1. Introduction

The differences in olive oil production methods in terms of 2-phase and 3-phase extraction result in varies wastes in terms of property and quantity [1]. The olive mill waste water and olive pomace (35-40 % moisture) are obtained as wastes in 3-phase extraction, while 2-phase extraction only consists of olive pomace with higher moisture content (60-70 %) as waste. The pollution degree with respect to COD (chemical oxygen demand) and BOD (biological oxygen demand) of olive pomace in 3-phase system are considerably high compared to 2-phase system [2]. Although olive pomace is presented as a waste, it can be used as an ingredient in animal feed additives, fertilizer and source of alternative fuel [3].Moreover, lipase enzyme by fermentation, activated carbon by hydrolysis and biodiesel are also obtained from olive pomace [3]. It is necessary to dry the olive pomace in order to be evaluated as a high-value-added by-product. The drying process improves the processability and durability of the olive pomace. Drying of olive pomace is generally carried out in rotary dryer at a range of 400 to 800°C in the industry [4]. Unfortunately, 2-phase olive pomace (2-POP) cannot be easily dried in rotary dryer at this temperature range due to high moisture content and low thermal stability [5]. For these reasons, 2-POP is mixed with different amounts of 3-phase olive pomace to regulate the moisture content and to avoid the adhesion on dryer wall [4]. However, the quality of 2-POP decreases due to high drying temperature and long drying time. New drying methods should be taken into consideration to overcome this issue.

The aim of this study was to determine the effects of drying temperature and air velocity of tray drying as an alternative drying method on the quality of dried 2-POP and the system's energy efficiency.

2. Materials and Methods

2.1. Materials

2-phase olive pomace (2-POP) was purchased from a factory where 2-phase olive oil is produced by 2-phase extraction system in Aydın, Turkey. Then, it was stored at -25°C until drying experiments. Prior to drying, the samples were thawed at 4°C in a refrigerator. The moisture content of 2-POP was determined as 66.4 % (wb.).

2.2. Drying Procedure

Due to high moisture content, 2-POP was pre-dried in a drum dryer whose conditions were selected as vapor pressure~3 bar (133.52°C), drum rotational speed:~6 rpm, drums gap:~3 mm in order to decrease the moisture content from 66.4% to 50% (wb.). After pre-drying, 1 kg of pre-dried 2-POP having 50% moisture content was dried in a tray dryer (Eksis makine,

Isparta, Turkey) until 8% moisture content at different conditions. Drying temperature (70, 80, 90°C) and air velocity (0.5, 1.8 m/s) were selected as independent variables of tray dryer. Drying experiments of 2-POP were performed at each drying temperature and air velocity, while the sample thickness (0.5 cm) and drying area (25x25 cm) were kept constant for all experiments. All drying experiments were done in duplicate for each drying condition and all analysis was applied triplicate.

2.3. Analysis

2.3.1. Moisture Content

Moisture content of raw, pre-dried and dried olive pomace was determined by vacuum oven at 65°C and 0.25 bar [6]. Moisture content of samples was identified as wet basis.

2.3.2. Oxidation Level

For determination of oxidation level of dried samples, the oil was extracted from 2-POP by cold extraction with chloroform/methanol as solvent. After that, this mixture was evaporated at 50°C by a rotary evaporator (Heidolph, Germany). Peroxide value, free fatty acid and ultraviolet (UV) absorbance (K_{232} and K_{270}) were analyzed to determine oxidation level. *Peroxide value* of samples was analyzed by titration method given in AOAC (1990) [7]. *Free Fatty Acid* analysis was performed by titration used KOH according to Sun-Waterhouse et al. (2011) [8]. *Ultraviolet (UV) Absorbance (K_{232}, K_{270}) value of* oil obtained from samples was measured by spectrophotometer after that oil was diluted in iso-octane (2,2,4-trimethylpentane).

2.3.3. Drying system efficiency

Criteria of Specific Moisture Extraction Rate (SMER), Moisture Extraction Rate (MER) and Specific Energy Consumption (SEC) were calculated to determine drying efficiency of system. *Specific moisture extraction rate (SMER)* (kg water/kWh) shows that the mass of water removed from the product to be dried for consuming per unit the energy kWh. According to Hawlader ve Jahangeer (2006), SMER values were calculated [10]. *Moisture Extraction Rate (MER)* (kg water/h) is defined as the mass of moisture removed from the dryer at the unit time. This proportion is calculated according to Gürlek et al. (2015)[9]. *Specific Energy Consumption (SEC)* (kJ/kg water) is described as the amount of energy required to remove per unit moisture (kg) from the samples during drying. According to Sadi et al. (2015), these values were calculated [10].

2.3.4. Statistical analysis

ANOVA test was conducted to determine the effect of drying temperature and air velocity on dried 2-POP. The statistical analyses were performed using SPSS (Statistical Package for the Social Sciences, SPSS Chicago, Illinois, USA) software version 15.0.

3. Results and Discussion

As a result of drying experiments at different temperatures and air velocities, drying time changed between 74 and 170 min. Drying at high temperature and air velocity (90°C and 1.8 m/s) had a short drying time (74±1.4 min), while drying time (170.0±2.1 min) at low temperature and air velocity (70°C, 0.5 m/s) was longer than other experiments (Table 1). Increase in drying temperature and air velocity caused a decrease in drying time due to the increase heat transfer rate. Increase in air velocity gave rise to accelerate the mass transfer from the surface of samples. Thus, drying time also decreased at high air velocity. Moreover, the process conditions of tray dryer in terms of temperature and air velocity had significant effect on the drying time as given in Table 2 ($p<0.05$).

Olive pomace, which is rich in poly unsaturated fatty acids, is easily exposed to oxidative degradation. Oxidative degradation is one of the important factors for limiting the shelf life of products and causing quality losses [11]. Hence, it is necessary to examine oxidation mechanism during drying of 2-POP.

The drying temperature and air velocity were considerably effective variables on dried olive pomace's peroxide value, free fatty acid, K_{232} and K_{270} values (Table 1). Increase in drying temperature and decrease in air velocity caused an increase in peroxide value, free fatty acid, K_{232} and K_{270} values showing the quality loss of product. Long drying time caused an increase in oxidation level of samples [12]. Although drying at high temperature resulted in a decrease in drying time, the oxidation level of samples dried at high temperature were higher compared to those dried at low temperature (Table 1). According to the literature, oxidation mechanism accelerates with heat treatment. Application of heat treatments at high process time and temperature causes an increase in quality loss of samples [13]. The peroxide, K_{232} and K_{270} values of samples were significantly affected by temperature and air velocity. Although free fatty acid values of samples were affected by drying temperature and velocity, free fatty acid values only changed with drying temperature at significant level (Table 2; $p <0.05$).

Energy consumption of drying process constitutes 10-25 % percentage of industrial energy consumption [14]. Thus, drying processes and systems which are provided to use efficient energy are necessary to develop [4]. SMER, MER and SEC values were calculated and compared to determine tray dryer's system efficiency at different conditions in this study.

Table 1. Results of dried 2-POP's drying time (min), peroxide value (meq O_2 /kg oil), free fatty acid (% Oleic Acid) and specific absorption value at UV light (K_{232}, K_{270}) and results of drying system efficiency definitions at different process conditions

T (°C)	V (m/s)	Drying time (min)	PV	FFA	K_{232}	K_{270}	SMER	MER	SEC
90	**1.8**	74.0 ±1.4	10.55 ±0.38	0.481 ±0.010	0.680 ±0.002	0.328 ± 0.001	0.2820 ± 0.0245	0.314 ± 0.009	3.56 ±0.31
80	**1.8**	82.5 ±3.5	9.57 ±0.02	0.472 ±0.021	0.545 ±0.004	0.301 ± 0.002	0.2746 ± 0.1017	0.247 ± 0.049	3.91 ±0.45
70	**1.8**	102.5 ±3.5	8.64 ±0.64	0.458 ±0.004	0.511 ±0.002	0.284 ± 0.001	0.2493 ± 0.0347	0.170 ± 0.010	4.05 ±0.26
90	**0.5**	117.0 ±4.9	14.38 ±0.01	0.573 ±0.012	0.869 ±0.004	0.373 ± 0.002	0.2072 ± 0.0133	0.126 ± 0.027	4.84 ±0.31
80	**0.5**	132.5 ±3.5	13.35 ±0.74	0.570 ±0.019	0.851 ±0.002	0.367 ± 0.001	0.1833 ± 0.0013	0.096 ± 0.002	5.46 ±0.04
70	**0.5**	170.0 ±2.1	12.91 ±0.33	0.555 ±0.015	0.806 ±0.001	0.359 ± 0.003	0.1820 ± 0.0085	0.063 ± 0.013	5.50 ±0.26

T:Drying Temperature; V: Air Velocity; PV: Peroxide value; FFA: Free fatty acid

Table 2. ANOVA evaluation for each response variable for 2-POP (β_1 : Temperature; β_2 :Air Velocity).

Variation Source	df	*p*-value							
		Drying time (min)	PV	FFA	K_{232}	K_{270}	SMER	MER	SEC
Corrected Model	5	<0.0001	<0.0001	<0.0001	<0.0001	<0.0001	<0.0001	<0.0001	<0.0001
Intercept	1	<0.0001	<0.0001	<0.0001	<0.0001	<0.0001	<0.0001	<0.0001	<0.0001
β_1	2	<0.0001	<0.0001	0.082	<0.0001	<0.0001	0.063	<0.0001	0.12
β_2	1	<0.0001	<0.0001	<0.0001	<0.0001	<0.0001	<0.0001	<0.0001	<0.0001
$\beta_1 \beta_2$	2	<0.0001	0.596	0.931	<0.0001	<0.0001	0.550	0.040*	0.735
R^2		0.993	0.970	0.943	1.000	0.998	0.875	0.951	0.907
Adj-R^2		0.990	0.958	0.919	1.000	0.997	0.823	0.931	0.868

PV: Peroxide value; FFA: Free fatty acid

Results of SMER (kg water/kWh), MER (kg water/h) and SEC (kJ/kg water) values are given Table 1 while their ANOVA results are shown in Table 2. It is necessary to reach maximum SMER and MER value and minimum SEC value in order to operate the dryer with high drying performance and energy efficiency. Motevali et al. (2011) investigated the effect of drying temperature on drying system efficiency. They found that drying system efficiency in tray dryer decreased with increasing temperature at constant air velocity [16]. Increasing drying temperature resulted in increase in SMER and MER values; a decrease in SEC values (Table 1). Although high-energy consumption needed to reach high temperature in tray dryer, energy efficiency of dryer system was increased at high temperature due to shorter drying

time. With increasing air velocity, SMER and MER values had an upward tendency whereas SEC values had a downward tendency. An increase in air velocity caused a decrease in drying time so dryer system's performance was increased. It was determined that SMER and SEC values were significantly affected by temperature (Table 2; $p<0.05$) in contrast to air velocity (Table 2; $p>0.05$). Moreover, temperature and air velocity were effective variables on MER values (Table 2; $p<0.05$).

4. Conclusion

In this study, the effects of temperature and air velocity on quality of dried 2-POP and the system's energy efficiency were determined. Increase in temperature and decrease in air velocity caused an increase in the peroxide value, free fatty acid and specific absorption value at UV light (K_{232}, K_{270}) of 2-POP whereas decrease in the drying time. It was determined that drying at low temperature and high air velocity led to increase in oxidation stability of olive pomace dried in a tray dryer. Maximum SMER, MER and minimum SEC values were expected to determine for high performance and energy efficient dryer system. The effective conditions of tray dryer were specified at high drying temperature and air velocity (90°C and 1.8 m/s). As a conclusion, this study showed that it was necessary to examine the quality of product and energy efficiency of dryer systems together in drying applications.

5. Nomenclature

2-POP	2 phase olive pomace	
FFA	free fatty acid	% Oleic Acid
MER	moisture extraction rate	(kg water/h)
PV	peroxide value	meq O^2/kg oil)
SEC	specific energy consumption	(kJ/kg water)
SMER	specific moisture extraction rate	(kg water/kWh)
T	drying temperature	°C
V	Air velocity	m/s
w.b	wet basis	

6. References

[1]   A. Ranalli and N. Martinelli, "Integral centrifuges for olive oil extraction, at the third millenium threshold. Transformation yields," *Grasas Aceites*, vol. 46, no. 4–5, pp. 255–263, 1995.

[2]   M. D. Liebanes, J. M. Aragon, M. C. Palancar, G. Arevalo, and D. Jimenez, "Fluidized bed drying of 2-phase olive oil mill by-products," *Dry. Technol.*, vol. 24, no. 12, pp. 1609–1618, 2006.

[3]   V. Hernández, J. M. Romero-García, J. A. Dávila, E. Castro, and C. A. Cardona, "Techno-economic and environmental assessment of an olive stone based biorefinery," *Resour. Conserv. Recycl.*, vol. 92, pp. 145–150, 2014.

[4]   R. Arjona, P. Ollero, and others, "Automation of an olive waste industrial rotary dryer," *J. Food Eng.*, vol. 68, no. 2, pp. 239–247, 2005.

[5]   J. S. Torrecilla, J. M. Aragón, and M. C. Palancar, "Modeling the drying of a high-moisture solid with an artificial neural network," *Ind. Eng. Chem. Res.*, vol. 44, no. 21, pp. 8057–8066, 2005.

[6]   Association of Official Analytical Chemists (AOAC), *Official Methods of Analysis*, 13th ed. Arlington, VA: Official Method, 1980.

[7]   Association of Official Analytical Chemists (AOAC), *Official Methods for Analysis*, 15th ed., 2 vols. Arlington, VA: Official Method, 1990.

[8]   D. Sun-Waterhouse, J. Zhou, G. M. Miskelly, R. Wibisono, and S. S. Wadhwa, "Stability of encapsulated olive oil in the presence of caffeic acid," *Food Chem.*, vol. 126, no. 3, pp. 1049–1056, 2011.

[9]   G. Gürlek, Ö. Akdemir, and A. Güngör, "Gıda Kurutulmasında Isı Pompalı Kurutucuların Kullanımı ve Elma Kurutmada Uygulanması," *Pamukkale Üniversitesi Mühendis. Bilim. Derg.*, vol. 21, no. 9, pp. 398–403, 2015.

[10]   T. Sadi, S. Meziane, and others, "Mathematical modelling, moisture diffusion and specific energy consumption of thin layer microwave drying of olive pomace," *Int Food Res J*, vol. 22, no. 2, pp. 494–501, 2015.

[11]   Ö. E. Çoban and B. Patır, "Antioksidan etkili bazı bitki ve baharatların gıdalarda kullanımı," *Gıda Teknol. Elektron. Derg.*, vol. 5, no. 2, pp. 7–19, 2010.

[12]   N. K. Andrikopoulos, N. Kalogeropoulos, A. Falirea, and M. N. Barbagianni, "Performance of virgin olive oil and vegetable shortening during domestic deep-frying and pan-frying of potatoes," *Int. J. Food Sci. Technol.*, vol. 37, no. 2, pp. 177–190, 2002.

[13]   A. Zungur, M. Koç, B. Yalçın, F. Kaymak-Ertekin, and S. Ötleş, "Storage stability of microencapsulated extra virgin olive oil powder," in *9th Baltic Conference on Food Science and Technology "Food for Consumer Well-Being,"* 2014, p. 257.

[14]   E. Eroğlu and H. Yıldız, "Gıdaların ozmotik kurutulmasında uygulanan yeni tekniklerin enerji verimliliği bakımından değerlendirilmesi," *Gıda Teknol. Elektron. Derg.*, vol. 6, no. 2, pp. 41–48, 2011.

[15]   K. J. Chua, S. K. Chou, J. C. Ho, and M. N. A. Hawlader, "Heat pump drying: recent developments and future trends," *Dry. Technol.*, vol. 20, no. 8, pp. 1579–1610, 2002.

[16] A. Motevali, S. Minaei, M. H. Khoshtaghaza, and H. Amirnejat, "Comparison of energy consumption and specific energy requirements of different methods for drying mushroom slices," *Energy*, vol. 36, no. 11, pp. 6433–6441, 2011.

Identification of key factors determining the surface oil concentration of encapsulated lipid particles produced by spray drying

Linke, A. [a*]; Balke, T. [a] ; Kohlus, R.[a]

[a] Department of Food Powders and Process Engineering. University of Hohenheim, Stuttgart, Germany

*E-mail of the corresponding author: annika.linke@uni-hohenheim.de

Abstract

Potential factors leading to surface oil were investigated by analyzing the impact of emulsion properties, atomization and drying conditions separately. An increased oil load, droplet size and in particular the size of droplet aggregates led to significant more surface oil. Increasing the viscosity, inlet temperature and relative humidity resulted in larger particles with a higher encapsulation efficiency. The results indicate that the probability of oil droplets being in contact with the particle surface determines the amount of surface oil. Oil diffusion towards the surface was excluded due to the short residence times and high viscosities.

Keywords: microencapsulation; encapsulation efficiency; emulsion properties; atomization; drying conditions

1. Introduction

Polyunsaturated fatty acids are susceptible to oxidation. Microencapsulation is a strategy to protect lipids against environmental oxygen by embedding oil droplets in a solid matrix acting as an oxygen diffusion barrier. Some droplets are not fully covered and are in contact with the particle surface. This so-called surface oil is not protected and directly exposed to environmental oxygen.

In literature several hypotheses about surface oil creation during spray drying are stated. Apart from emulsion stability, oil droplet disruption during atomization and oil diffusion towards the particle surface are believed to be the main factors leading to surface oil [1]–[3]. Experimental confirmation is partly lacking due to the high number of potential factors interacting with each other and influencing the encapsulation efficiency (EE).

In this study it is hypothesized that the probability of oil droplets being in contact with the particle surface determines the surface oil concentration. The aim of this study is to identify key factors determining the EE by investigating the impact of emulsion properties, feed atomization and drying rate separately.

2. Materials and Methods

High quality fish oil (Omega Oil 1812 TG Gold) was kindly provided by BASF Personal Care and Nutrition GmbH (Illertissen, Germany). Rapeseed oil, maltodextrin DE21 (AGENABON) and Soy Protein Isolate (Vegacon 90) were obtained from Herny Lamotte Oils GmbH (Bremen, Germany), Agrana GmbH (Frankfurt am Main, Germany) and Eurosoy GmbH (Hamburg, Germany), respectively.

2.1. Emulsion and Powder Preparation

Soy protein and maltodextrin DE21 were hydrated in distilled water for 12 h. Oil was dispersed by operating an IKA SPP25 (Staufen, Germany) for 10 min. The emulsion was homogenized in four passes using the homogenizer HL 1.3-400KX (HST Maschinenbau GmbH, Dassow, Germany). Emulsions were spray dried using a pilot plant dryer (type FSD 4.0, GEA-Niro, Copenhagen, Denmark) with a maximum water evaporation capacity of 30 kg/h operated at an airflow of 200 kg/h in the closed loop mode. The feed was atomized using a two fluid nozzle set to 1 bar (ex GEA-Niro). Inlet and outlet temperature were set to 180°C and 85 °C, respectively.

2.2. Analysis

2.2.1. Oil droplet size

Static light scattering: A Mastersizer 2000 (Malvern Instruments Ltd, UK) was used to analyze the oil droplet size according to Mie-Theory. Three samples of each emulsion were measured in triplicate.

Pulsed field gradient: A Bruker minispec mq 20 NMR Analyzer (Bruker, Rheinstetten, Germany), operating at 20 MHz and equipped with a controlled pulsed gradient unit with a probe head H20-10-25-AVXG (Bruker, Rheinstetten, Germany) was operated at 20 °C. The oil droplet size of emulsions and within the powder was determined according to the procedure described by Linke et al. (2017) [4].

2.2.2. Particle Size Distribution

A Mastersizer 2000 (Malvern Instruments Ltd, UK) was used to determine the particle size by dispersing the powder in ethanol. Data were analyzed according to Fraunhofer theory. Three samples of each powder were measured six times.

2.2.3. Oil Load, Surface Oil and Encapsulation Efficiency

The surface oil was removed applying a procedure described by Bae and Lee (2008) with some modifications [5]. Approximately 1 g powder and 10 mL n-Hexane (ROTISOLV® HPLC) were shaken for 2 min. The powder was separated by filtration and washed three times with 10 mL n-Hexane. The oil load of the untreated and washed powder was determined according to a method described by Linke et al (2017). Briefly, a Bruker Minispec MQ20 NMR Analyzer (Bruker, Rheinstetten, Germany) with an absolute probe head H20-18-25-A1 was operated at 40 °C with a resonance frequency of 19.95 MHz. The powder was weighed into tubes and tempered at 40°C for 45 min. The instrument was calibrated with standards consisting of 0.07 and 0.9 g fish oil. The surface oil was calculated by subtracting the remaining oil from the total oil. The encapsulation efficiency was determined by dividing the amount of encapsulated oil by the total oil times 100.

3. Results

3.1. Impact of emulsion properties on the encpasualtion efficiency

In order to vary the emulsion properties in terms of viscosity, oil content and oil droplet size the homogenization pressure, oil load, dextrose equivalent (DE) of the maltodextrin and the soy protein concentration were modified (Figure 1). With increasing ratio of soy protein to oil the $d_{3,2}$ of oil droplets decreased (Figure 1A). Additionally, the diameter measured by static light scattering (SLS) and nuclear magnetic resonance (NMR) differed at concentrations below 0.07 g (w/w) protein per oil. Due to different measurement principles, the latter method measures the size of individual droplets, whereas SLS determines the average diameter of droplet clusters [6], [7]. Insufficient concentrations of soy protein lead to droplet flocculation, which was confirmed by light microscopy (data not shown). Using maltodextrin with a higher DE led to a significant reduction of viscosity, due to shorter glucose chains (Figure 1B). Homogenizing emulsions at higher pressure decreased the oil droplet size, whereas the viscosity remained constant (Figure 1C). In case of an higher oil content the droplet size and viscosity slightly increased (Figure 1 D).
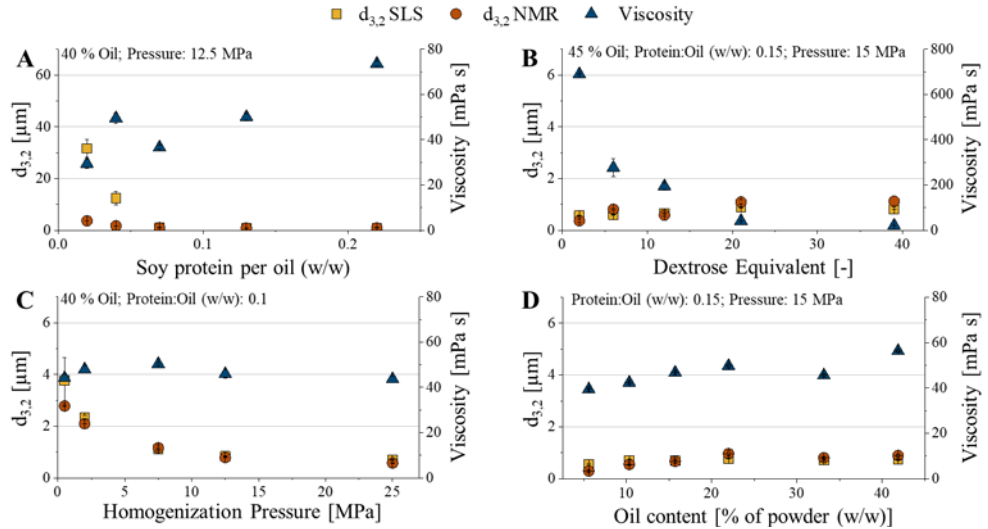
Figure 1: Emulsion viscosity and Sauter mean diameter $d_{3,2}$ of oil droplets determined by static light scattering (SLS) and nuclear magnetic resonance (NMR) as a function of the soy protein concentration (A), dextrose equivalent of maltodextrin (B) homogenization pressure (C) and oil content (D); default settings were set to a solid content of 45% and maltodextrin DE21

3.1.1. Impact of the droplet size on the EE

Modifying the emulsifier concentrations and homogenization pressure resulted in a change in the Sauter mean diameter of oil droplets (Figure 1). Plotting the $d_{3,2}$ as a function of the EE shows that larger droplets lead to a less efficient encapsulation (Figure 2).
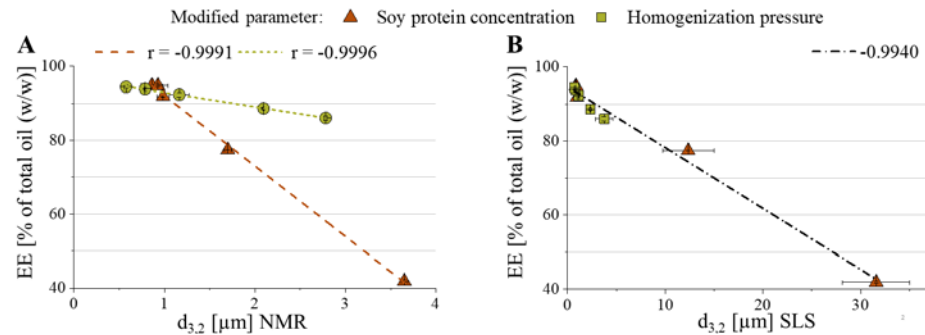
Figure 2: EE [% of total oil] as a function of the Sauter mean diameter $d_{3,2}$ of oil droplets [µm], determined by nuclear magnetic resonance (NMR) (A) and static light scattering (SLS) (B)

In case of the $d_{3,2}$ determined by NMR, the droplet size modified by the homogenization pressure affects the EE less compared to the protein concentration (A), whereas the impact of the diameter measured by SLS is aligned for both samples sets (B). As SLS measures the

size of droplet clusters it is concluded that apart from the individual size, oil aggregates lead to more surface oil. As droplet clusters are larger compared to individual droplets, it is more likely for them being in contact with the powder particle surface and contributing to surface oil.

3.1.2. Impact of the oil load on the EE

The EE and the amount of surface oil is plotted as a function of the oil concentration in the emulsion (Figure 3, A). A higher oil load leads to more surface oil supporting the hypothesis, as the likelihood for droplets being in contact with the particle surface is higher if more oil is present. However, the EE increases up to oil loads of 15 % and decreases at higher concentrations. Even though less oil is located at the particle surface, the ratio to the amount of encapsulated oil fraction is smaller leading to a decreased encapsulation efficiency.
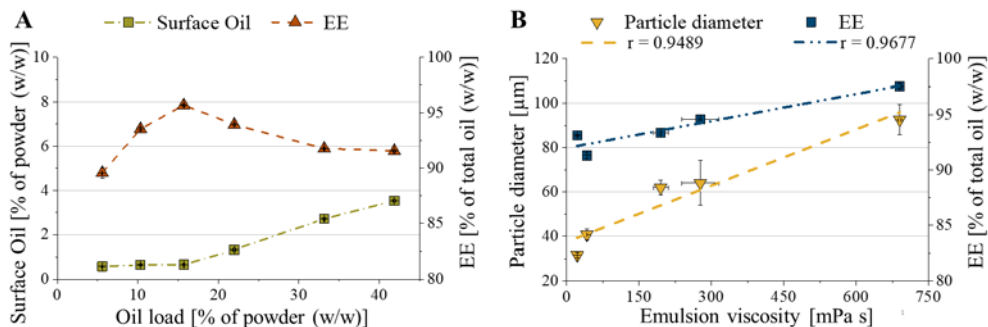
Figure 3: EE [% of total oil] and surface oil as a function of the oil concentration in the emulsion (A); EE and particle diameter $d_{50,3}$ as a function of the viscosity for samples containing maltodextrin with a different dextrose equivalent (B)

3.1.3. Impact of the viscosity

Modifying the dextrose equivalent of the maltodextrin resulted in a change in the emulsion viscosity (Figure 1). With increasing viscosity larger particles and a more efficient encapsulation is obtained (Figure 3, B). It is assumed, that larger particles increase the EE due to a lower ratio of particle surface to particle volume. Thus, the viscosity is affecting the EE indirectly by changing the size of encapsulated lipid particles.

3.2. Impact of drying conditions and particle properties

Figure 4 shows the particle diameter and the EE as a function of the solid content, inlet temperature and relative humidity of the drying medium. A higher solid content and inlet temperature resulted in larger particles, due to a higher viscosity and faster crust formation preventing shrinkage, respectively. A higher humidity in the drying air resulted in slightly

larger particles. This is unexpected, as the drying rate is supposed to decelerate enabling particle shrinkage.
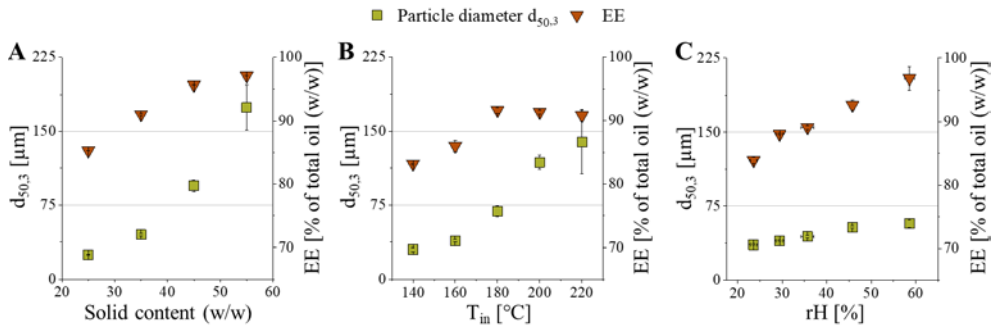
Figure 4: Particle diameter $d_{50,3}$ [μm] and EE [% of total oil] as a function of the solid content, inlet temperature and relative humidity for samples differing in oil concentration and solid content, the default settings were set to a solid content and oil load of 35% and 30%, respectively.

Plotting the EE as a function of the particle diameter shows an increase until a plateau is reached (Figure 5). Apart from the modified drying conditions, particles containing different dextrose equivalent are following the same trend. Larger particles have a lower particle surface to volume ratio. Thus, it is more likely for oil droplets being embedded in the particle center and not being in contact with the particle surface. Particles above approximately 100 µm are powder aggregates. The EE might reach a plateau as aggergates consist of a number of individual particles, which determine the particle surface. Hence, the surface is not decreasing further with increasing aggregate size.
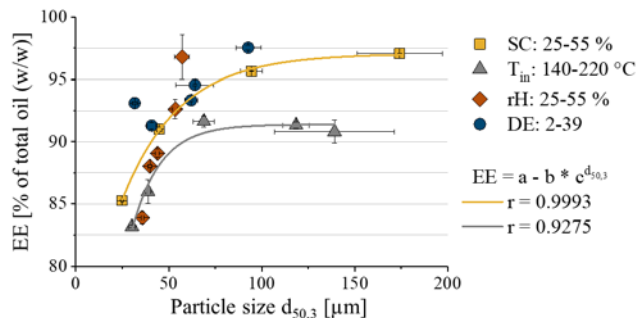
Figure 5: EE [% of total oil] as a function of the particle diameter $d_{50,3}$ [μm]; Samples contain different solid content (SC) and maltodextrin dextrose equivalent (DE) and are spray dried at different inlet temperatures (T_{in}) and relative humidity (rH).

4. Discussion

In this study the impact of potential factors on the encapsulation efficiency during the production of encapsulated lipid particles was investigated. In order to do so, the influence of emulsion properties and spray drying conditions on the surface oil creation was analyzed separately. Due to the number of potential factors and their interaction with each other it is challenging to identify the main contributors causing surface oil.

Smaller particles, oil droplets and in particular oil droplet clusters decreased the encapsulation efficiency significantly. This supports the hypothesis, that the probability of oil droplets being in contact with the particle surface determines the amount of surface oil. This might explain that encapsulated lipid particles produced by a benchtop spray dryer generally have a lower encapsulation efficiency compared to powders obtained on pilot plant scale as the obtained particles are smaller.

Larger particles were obtained at a higher solid content and inlet temperatures. Due to the increased viscosity and the fast drying the mobility of oil droplets was reduced, so that the likelihood of oil diffusing towards the particle surface is decreased. In terms of the increased humidity, the drying medium is more polar, which might prevent oil diffusion additionally. However, due to the short residence times and high viscosity it is suggested that oil droplet diffusion has no significant impact on the encapsulation efficiency.

Increasing the oil load up to 15% resulted in a higher efficiency even though the amount of surface oil was raising. Maximizing the concentration of lipids being fully embedded in the matrix increases the efficiency, but does not necessarily enhance the shelf life, as the absolute amount of surface oil being exposed to environmental oxygen may also increase. Additionally, to the investigated properties the volume of vacuoles in the particles should be considered, as it decreases the ratio of outer particle surface to the effective matrix volume. This might reduce the encapsulation efficiency, due to a higher likelihood of being in contact with the particle surface.

5. Conclusions

In this study the impact of the emulsion properties and spray drying conditions on the encapsulation efficiency was investigated. An increased oil load, smaller particles and larger oil droplets and droplet aggregates led to more surface oil. It supports the hypothesis, that the probability of oil droplets being in contact with the particle surface determines the success of the encapsulation.

6. Nomenclature

$d_{3,2}$	Sauter mean diameter	µm
EE	Encapsualtion Efficiency	%
DE	Dextrose Equivalent	-

7. Acknowledgements

8. References

[1] S. M. Jafari, E. Assadpoor, Y. He, and B. Bhandari, "Encapsulation efficiency of food flavours and oils during spray drying," *Dry. Technol.*, vol. 26, no. 7, pp. 816–835, 2008.

[2] Y. Minemoto, K. Hakamata, S. Adachi, and R. Matsuno, "Oxidation of linoleic acid encapsulated with gum arabic or maltodextrin by spray-drying," *J. Microencapsul.*, vol. 19, no. 2, pp. 181–189, 2002.

[3] R. V. Tonon, C. R. F. Grosso, and M. D. Hubinger, "Influence of emulsion composition and inlet air temperature on the microencapsulation of flaxseed oil by spray drying," *Food Res. Int.*, vol. 44, no. 1, pp. 282–289, 2011.

[4] A. Linke, T. Anzmann, J. Weiss, and R. Kohlus, "Advanced characterisation of encapsulated lipid powders regarding microstructure by time domain-nuclear magnetic resonance," *J. Microencapsul.*, vol. 34, no. 2, pp. 140–150, 2017.

[5] E. K. Bae and S. J. Lee, "Microencapsulation of avocado oil by spray drying using whey protein and maltodextrin," *J. Microencapsul.*, vol. 25, no. 8, pp. 549–560, 2008.

[6] G. J. W. Goudappel, J. P. M. Van Duynhoven, and M. M. W. Mooren, "Measurement of oil droplet size distributions in food oil/water emulsions by time domain pulsed field gradient NMR," *J. Colloid Interface Sci.*, vol. 239, no. 2, pp. 535–542, 2001.

[7] H. Todt, W. Burk, G. Guthausen, A. Guthausen, A. Kamlowski, and D. Schmalbein, "Quality control with time-domain NMR," *Eur. J. Lipid Sci. Technol.*, vol. 103, no. 12, pp. 835–840, 2001.

Technological and nutritional aspects of gluten-free pasta based on chickpea flour and tiger nut flour

Martín-Esparza. M. E. [a]*; Bressi. G. B. [a]; Raga. A. [a]; Albors. A. [a]

[a] Institute of Food Engineering for Development. Food Technology Department. Universitat Politècnica de València. Valencia. Spain.

*E-mail of the corresponding author: eesparza@tal.upv.es

Abstract

Gluten-free (GF) dry egg pappardelle was prepared with tigernut flour (50%), chickpea flour (50%) and pregelatinized TNF (0, 5, 10%), and compared to plain pasta (100% durum wheat semolina). The GF pasta may have a significant higher content of insoluble fibre, minerals and fat rich in oleic acid and a similar protein content. It was not found any clear relationship between the flour functional properties and its proximate composition. The use of PG did not imply an improvement on the firmness but did provide some continuity to the pasta structure.

Keywords: Gluten-free pasta, tigernut flour, chickpea flour, texture, cooking properties.

1. Introduction

The celiac disease is one of the most common food induced disorders worldwide with an estimated mean prevalence of 1% of the total population [1]. To date, the only efficacious treatment for celiac disease affected patients is a gluten-free diet. However, many GF products based on cereals exhibit lower nutritional quality [2] and, not less important, higher glycemic index [3] than their gluten containing counterparts. Since pasta is one of the products that is most demanded by people with celiac disease [4], the aim of this study was to evaluate the chemical composition, the cooking characteristics and microstructure of GF pappardelle prepared with tiger nut and chickpea flours. Chickpea flour is a source of proteins, carbohydrates, dietetic fibre and oligosaccharides. Tigernut flour is a rich source of dietary fibre, high-quality fatty acid profile oil, which is similar to olive and hazelnut oil, minerals and vitamins such as phosphorus, potassium, iron and calcium, as well as vitamins E and C. Therefore, the combination of these flours may lead to an improved nutritional value of the resulting pasta, with a high fibre content and a lower glycaemic index. Despite the great efforts made in the last few decades to produce GF pasta with sensory characteristics similar to durumwheat products (good texture, minimum cooking losses, surface resistance to disintegration, without surface stickiness), the GF pasta currently on the market is still far from what the consumer is looking for [4]. The role of gluten could be replaced by choosing suitable formulations to achieve the desirable quality attributes and also making the dough easy to handle under industrial conditions [5]. Frequently, GF products are formulated using sintetic additives to improve the textural characteristics. Nowadays, both industry and consumer preference is to use other additives from natural sources. Previous studies have demonstrated the positive impact that the use of pregelatinized starch from rice [6] or cassava [7] has on the GF pasta texture. Pregelatinized flour can act as a binder [8] that may lead to the development of a viscoelastic and compact dough, which may contribute to obtain suitable palatability and textural characteristics on the pasta products. In this sense, this work assess the feasibility of replacing chickpea flour by tiger nut pregelatinized flour to improve the cooking behavior and final textural characteristics of dry GF pappardelle based on tiger nut and chickpea flours.

2. Materials and Methods

2.1. Raw materials and characterisation

Commercial durum wheat semolina –DWS– (Harinas Villamayor. S.A., Huesca. Spain). tiger nut flour –TNF–(Tigernuts Traders S.L., Valencia. Spain) and chickpea flour (CP) were used. Fresh eggs, CP and mineral water were purchased in a local market. PG was obtained by hot treatment (80ºC, 20 min, 1:7.5 g/mL deionized water) followed by drying (40ºC, 24 h) and grinding. DWS, TNF, CP and PG were analysed for their water, protein,

fat and ash contents according to the American Association of Cereal Chemists´ approved methods [9] and for their total, soluble and insoluble fibre, amylose/amylopectin ratio and damaged starch according to the corresponding Megazyme methods K-TDFR, K-SDAM and K-AMYL (Megazyme Ltd., Ireland). Digestible carbohydrates were determined by difference (100 – percentage of estimated proximate chemical composition). The particle size distribution (PSD) of DWS, TNF, CP, PG and their mixtures (TNFCPPG0, TNFCPPG5, TNFPPG10) was determined by using a MasterSizer® Laser Diffraction Particle Size Analyser (Malvern Instrument Ltd., Malvern, England). equipped with a PS 65 (dry sample). For each sample, 10–20 g of flour mixture was used. Size distribution was quantified as the relative volume of particles in size bands, presented as size distribution curves (Malvern MasterSizer Micro software v 5.40). The PSD parameters recorded included mean particle diameter/volume mean diameter (D[4.3]) and span value (measurement of the width of the size distribution). The functional properties of DWS, TNF, CP, PG and their blends (TNFCPPG0, TNFCPPG5, TNFPPG10). were determined as follows. The water-holding capacity (WHC) was determined by using the modified methods from [10] and [11]. The fat adsorption capacity (FAC) was determined according to [12]. Each analysis was made in triplicate.

2.2. Pasta preparation

The S formulation, used as the control sample, was obtained by mixing durum wheat semolina (72% w/w), fresh egg (13% w/w) and water (15% w/w). For the GF formulations, TNF and CP were used at 50/50 weight (76% w/w) and mixed with fresh egg (13% w/w) and water (11% w/w). Three GF formulations were assessed, considering three levels for chickpea replacement by pregelatinized TNF (0, 5 and 10% w/w, named henceforth as TNFCPPG0, TNFCPPG5 and TNFCPPG10 respectively). All raw materials were mixed and kneaded in an electric cooking device (Thermomix TM-31, Vorwerk Spain M.S.L., S.C., Madrid). The dried (CP/TNF/PG) and liquid (egg/water) components were separately blended and then kneaded together (10 min for S and 20 min each for GF pasta) with a rest period in between. The resulting doughs were rested for 20 min at 4 ℃ inside a plastic bag in order to enable sample relaxation. Afterwards, the fresh pasta sheets (1.0±0.03 mm thick) were formed by using a domestic pasta making machine (Simplex SP150, Imperia, Italy) coupled with a specific motor (A2500, Imperia, Italy). The pappardelle (4.4 cm width) were obtained by using the Duplex reginette 12/44 mm device (Imperia, Italy). Samples of 7 cm ± 0.03 mm length were then dried for 5.5 h (SCC 62, Rationel, Germany) under controlled temperature (55℃) and relative humidity (60%) conditions (until the pasta reached a water content of 10-12% (similar to that of dried commercial pasta). Once dried, the pappardelle were packed in vacuum bags and stored at 4℃ temperature until further analysis.

2.3. Uncooked pasta structure

FESEM (ULTRA 55, Carl Zeiss AG. Oberkochen. Germany) was used in order to observe the microstructure of dry GF pappardelle (TNFCPPG0, TNFCPPG5 and TNFCPPG10). The samples (cross-section) were fixed on copper stubs, platinum coated and observed using an accelerating voltage of 2 kV.

2.4. Pasta cooking

Dried pappardelle (25 g) was cooked in 300 ml deionised water (98ºC) according to the American Association of Cereal Chemists´ approved method 16-50 [9]. To avoid evaporation losses and maintain the 90% of the initial volume, the flask was partially covered and boiling water was added during cooking. Once reached the optimal cooking time (9 min for S and 5 min for the rest), the pappardelle were removed from the flasks and the cooking process was immediately stopped with 50 ml of cold deionised water. Finally, the pappardelle were drained for 2 min and immediately analysed for its firmness and cooking properties. Cooking trial was made in duplicate for each pasta formulation.

2.5. Cooking properties and cooked pasta firmness

The water absorption index –WAI– (g/g) was calculated from the mass gain and the increase in water content after cooking. The water content in dry and cooked pasta was determined according to the AACC 44-40 method [9]. Cooking loss –%CL– (g/100 g) is the amount of solid substance lost to cooking water and it was determined according to the AACC-approved method 16-50 [9]. The swelling index –SI– was expressed as the relative volume changes (cm^3/cm^3) between the uncooked and cooked pasta. The measurements of the pappardelle (thickness, width and length) were determined with a caliper (PCE-DCP 200N, PCE Ibérica S.L., Albacete, Spain). A TA.XT2 Texture Analyser (Stable Micro Systems. Godalming. Surrey. UK) was used to perform the AACC method 16-50 [9] at a rate of 0.17 mm/s until total sample deformation. Each analysis was made in triplicate for each pasta formulation.

2.6. Statistical analysis

Analysis of variance (ANOVA) was carried out by using Statgraphics Centurion XVI software version 16.1.17 (StatPoint Technologies. Inc., Warrenton, VA) The significance level was p = 0.05 in all cases.

3. Results and discussion

3.1. Characterization of raw solid materials

The chemical composition of the solid raw materials (DWS, TNF, CP and PG) are shown in Table 1. As expected, the TNF and CP fibre (specially insoluble) content was much higher than that of DWS. Fat content was also much higher for TNF, while the highest protein

content was obtained for CP. On the other hand. the highest amount of digestible carbohydrates was obtained for DWS, followed by TNF and CP, being the amylose content lower for TNF. Damaged starch was significantly higher for PG.

Table 1. Proximate chemical composition of solid raw materials (g/100 g). Mean values of three replicates (standard deviation).

	DWS	TNF	CP	PG
Water	13.43 (0.13)[b]	12 (0.7)[c]	11.48 (0.95)[c]	16.8 (0.3)[a]
Protein	13.18 (0.7)[b]	3.7 (0.2)[c]	23.7 (0.07)[a]	-
Fat	0.9 (0.05)[d]	21.44 (0.06)[b]	4.31 (0.03)[c]	23.59 (0.04)[a]
Ash	0.27 (0.03)[c]	2.29 (0.07)[b]	3.298 (0.007)[a]	2.32 (0.03)[b]
Fiber				
-Soluble	2.99 (0.13)[b]	3.5 (1.3)[b]	6 (3)[ab]	7.5 (0.8)[a]
-Insoluble	7 (3)[c]	16.6 (0.8)[b]	24 (0.6)[a]	24 (4)[a]
-Total	9.1 (0.4)[c]	20 (2)[b]	30 (3)[a]	32 (3)[a]
DC*	63.3 (0.2)[a]	40 (2)[b]	28 (4)[c]	-
Amilose (%)	27.2 (1.4)[a]	17 (2)[b]	28 (2)[a]	-
Damaged starch	3.31 (0.12)[b]	0.622 (0.109)[c]	0.6717 (0.005)[c]	20 (3)[a]

Means with different letters in the same row indicate significant differences ($p < 0.05$).

* Digestible carbohydrates calculated by difference

Concerning PG, its chemical composition was near to that of TNF, except for the fibre (due to a higher extraction capacity) and the damaged starch (due to gelatinization) contents. These results suggest that the use of TNF and CP at 50% w/w may allow to obtain GF pasta with a similar protein content and a higher presence of fibre, minerals and fat than the DWS formulation. It can be observed in Table 2 that the average particle size (expressed as the mean diameter of the equivalent volume) was significantly lower for CP, followed by TNF and DWS. Fibre hydration and starch gelatinization could be the responsible for the significantly higher particle size of PG. Furthermore, the uniformity in the particle size distribution (span) was higher in DWS (from industrial milling) and PG (obtained after grinding). The greater presence of fibre in TNF (20 (2)%) and CP (30 (3)%) compared to 9.1 (0.4)% in DWS) -with a much higher insoluble/soluble ratio- (16.6/3.5% in TNF and 24/6% in CP compared to 7/2.99% in DWS) could be responsible for the greater heterogeneity in TNF (span 2.39) or CP (span 6.9). Water holding capacity (WHC) reports the ability of a protein matrix to absorb and retain bound, hydrodynamic, capillary and physically entrapped water against gravity. The results show a significant lower value for DWS, which can be attributed to the higher fibre content of TNF and CP and the smaller particle size of TNF and CP, which implies a larger surface area available for water absorption [13]. The highest WHC obtained for PG may be due to the its higher damaged starch content; however, no effect was observed on the mixture when PG was added at 5

and 10%. The fat absorption capacity (FAC) is attributed to the ability of proteins to bind lipids. Only TNF presents a significant higher value of this parameter.

Table 2. Particle size distribution and Functional properties of solid raw materials and their blends. Mean values of three replicates (standard deviation).

Sample	D[4.3](μm)	Span	WHC (g water/g flour)	FAC (g fat/g flour)
DWS	317.9 (1.8)[b]	1.156 (0.012)[f]	0.9 (0.07)[d]	1.2 (0.2)[b]
TNF	221 (4)[d]	2.39 (0.03)[c]	2.1 (0.2)[b]	1.749 (0.104)[a]
CP	141 (12)[f]	6.9 (0.9)[a]	1.98 (0.2)[b]	1.25 (0.04)[b]
PG	632 (8)[a]	1.77 (0.03)[d]	2.9 (0.2)[a]	1.31 (0.06)[b]
TNFCPPG0	225 (2)[d]	2.382 (0.008)[c]	1.591 (0.112)[c]	1.29 (0.02)[b]
TNFCPPG5	191.3 (0.9)[e]	3.07 (0.05)[b]	1.586 (0.012)[c]	1.3 (0.03)[b]
TNFCPPG10	232 (3)[c]	2.22 (0.03)[c]	1.6 (0.4)[c]	1.19 (0.06)[b]

Means with different letters in the same column indicate significant differences ($p < 0.05$).

3.2. Cooking properties and cooked pasta firmness

Cooking loss, a measure of the amount of solids lost in the cooking water, is considered to be an important indicator of pasta quality [14]. As reported by [15], cooking losses for GF pasta can reach 20-25 % values as compared to those of a wheat semolina pasta due to the better weaker gluten network in which swelled starch granules are worse entrapped. Obtained values in this work (Table 3) are similar to those obtained for other GF pasta based on legume flours [16] and quinoa [17]. No significant differences could be observed for WAI and SI with the percentage of PG used, but both parameters were significant higher for control samples.

Table 3. Cooking properties of pasta formulations. Mean values (standard deviation).

Sample	WAI (g/g)	%CL	SI	F (N)
S	1.74 (0.02)[a]	2.9 (0.2)[c]	0.80 (0.02)[a]	20.6 (0.2)[a]
TNFCPPG0	0.82 (0.05)[b]	11.7 (0.2)[a]	0.62 (0.06)[b]	8.8 (0.5)[b]
TNFCPPG5	0.79 (0.03)[b]	8.7 (0.2)[b]	0.58 (0.03)[b]	7.6 (0.3)[c]
TNFCPPG10	0.81 (0.02)[b]	12.0 (0.2)[a]	0.37 (0.02)[c]	6.5 (0.4)[d]

Means with different letters in the same column indicate significant differences ($p < 0.05$).

A good quality pasta product should present certain degrees of firmness and elasticity, absence of stickiness, appearance uniformity and structural integrity. As expected, the firmness of GF formulations was significantly lower than that of control pasta (Table3), decreasing with higher contents of PG (although variations were small for this parameter). Although the use of PG at 5 or 10% did not imply an improvement on the firmness of cooked pasta, it did provide some continuity to the pasta structure (Figure 1).
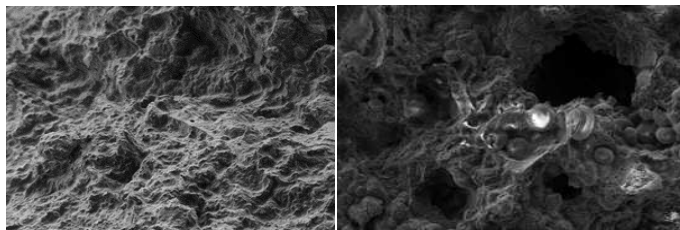
Fig. 1 FESEM dry pasta TNFCPPG0 and TNFCPPG10 (500x).

4. Conclusions

The consumption of gluten free pappardelle formulated with tiger nut and chickpea flours can have positive implications for human health, due to their increased nutritional quality. Cooking losses were acceptable and a certain structural continuity was obtained when pregelatinized tiger nut flour was used, thus further investigations are required.

5. References

[1] Lamacchia, C.; Camarca, A.; Picascia, S.; Di Luccia, A.; Ginafrani, C. Cereal based gluten-free food: How to reconcile nutritional and technological properties of wheat proteins with safety for celiac disease patients. Nutrients 2014, 6, 575-590.

[2] O´Shea, N.; Arendt, E.; Gallagher, E. State of the art of gluten-free research. Journal of Food Science, 2014, 79, 1067-1076.

[3] Foster-Powell, K.; Holt, S.H.A.; Brand-Miller, J.C. International table of glycemic index and glycemic load values: 2002. The American Journal of Clinical Nutrition, 2002, 76, 5-56.

[4] Marti, A.; Pagani, M.A. What can play the role of gluten free pasta? Trends in Food Science & Technology, 2013, 31, 63-71.

[5] Larrosa, V; Lorenzo, G.; Zaritzky, N.; Califano, A. Optimization of rheological properties of gluten-free pasta dough using mixture design. Journal of Cereal Science, 2013, 57(3), 520-526.

[6] Marti, A.; Caramanico, R.; Bottega, G.; Pagani, M.A. Cooking behavior of rice pasta: Effect of thermal treatments and extrusion conditions. Food Science and Technology, 2013, 54, 229-235.

[7] Fiorda, F.A.; Soares Jr. M.S.; da Silva, F.A.; Grosmann, M.V.E.; Souto, L.R.V. Microestructure, texture and colour of gluten-free pasta made with amaranth flour, cassava starch and cassava bagasse. Food Science and Technology, 2013, 54, 132-138.

[8] Fu, B.X. Asian noodles: history, classification, raw materials, and processing. Food Research International, 2008, 41, 888–902.

[9] AACC. Approved methods of the AACC (10th ed). St. Paul, MN, USA: American Association of Cereal Chemists. 2000.

[10] Heywood, A.A., Myers, D.J.; Bailey, T.B., Johnson, L.A. Functional properties of low-fat soy flour produced by an extrusion expelling system. American Oil

Cheminstry Society, 2002, 79, 1249–1253.

[11] Lin C.S; Zayas J.F. Functionality of defatted corn germ proteins in a model system: fat binding capacity and water retention. Food Science, 1987, 52, 1308–1311.

[12] Ahn, H.J.;Kim, J.H., Ng, P.K.W. Functional and thermal properties of wheat, barley, and soy flours and their blends treated with a microbial transglutaminase. Journal Food Science, 2005, 70, 380–386.

[13] Albors, A.; Raigon, M. D.; García-Martinez, M. D.; Martín-Esparza, M. E. 2016. Assessment of techno-functional and sensory attributes of tiger nut fresh egg tagliatelle. LWT-Food Science and Technology, 2016, 74, 183-190.

[14] Gull, A.; Prasad, K.; Kumar, P. Effect of millet flours and carrot pomace on cooking qualities, color and texture of developed pasta. LWT-Food Science and Technology, 2015, 63(1), 470-474.

[15] Mestres, C.; Colonna, P.; Alexandre, M.C.; Matencio, F. Comparison of various processes for making maize pasta. Journal of Cereal Science, 1993, 17, 277–290.

[16] Giuberti, G.; Gallo, A.; Cerioli, C.; Fortunati, P.; Masoero, F. 2015. Cooking quality and starch digestibility of gluten free pasta using new bean flour. Food Chemistry, 175: 43–49

[17] Caperuto, L.C.; Amaya-Farfan, J.; Camargo, C.R.O. Performance of quinoa (Chenopodium quinoa Willd) flour in the manufacture of gluten free spaghetti. Journal of the Science of Food and Agriculture, 2000, 81, 95–101.

Experimental investigation of drying of malt bagasse

Zorzi, B. D.[a]; Machry, K.[a]; Krolow, P.[a] ; Moura, C. M.[b]; Oliveira, E. G.[b]; Rosa, G. S.[a*]

[a] Chemical Engeneering, Federal University of Pampa, Bagé, Brazil

[b] Food Engeneering, Federal University of Pampa, Bagé, Brazil

*E-mail of the corresponding author: gabrielarosa@unipampa.edu.br

Abstract

The aim of this work was to investigate the convective drying process of malt bagasse and to evaluate the influence of this process on the application of this residue as adsorbent in methylene blue removel by adsorption process. The experimental system for drying was a fixed bed dryer with parallel airflow, with operating conditions: air temperature in the range of 40 to 90 ºC and air veocity of 2 m/s. The adsorption experiments were perfomed with solution of methylene blue at 70 ppm concentration. The drying kinetics showed a constant drying rate period followed by a falling drying rate. The results obtained for the dye removal efficiency were 56% for in natura sample and in the range of 81.69% to 93.99% for dried samples.

Keywords: dryin; malt bagasse; adsorption

1. Introduction

Nowadays, environmental problems and energy demands have demanded the search for energies renewable and clean. The use of biomass is part of the concept of sustainable development, besides reducing costs and not harming the environment [1]. Adsorption is a unit operation commonly used to separate solid-liquid, and can be efficient and low cost, using different adsorbents [2]. Solid residues from the agroindustry, such as sugarcane bagasse, coconut mesocarp and wood sawdust, are available in large quantities and can be considered as potential adsorbents due to their low cost due to not receiving any previous treatment and their physical- chemical properties [3].

In the process of brewing many solid wastes are generated, such as malt bagasse. Acording to Ferrari [4], the malt bagasse is the main byproduct resulting from the fermentation process formed by the solid part of the filtration of the fermentation must before boiling. One of the applications of the malt bagasse is the use as low-cost biosorbent in the sorption of dyes. These residues have limitation related to their high moisture content, which has a negative influence on transport, storage and for applications. Thus, the drying of malte bagasse is the first step for the biomass preparation. Piffer et al. [5] studied the adsorption of textile dye on malt bagasse in order to evaluate the efficiency of the process and Zanette et al.[6] reported the adsorption of 5G blue dye using the malt bagasse, verifying the influence of the agitation speed in the process.

The aim of this work was to investigate the convective drying process of malt bagasse and to evaluate the influence of this process on the application of this residue as adsorbent in removal efficiency of methylene blue by adsorption process.

2. Materials and Methods

The raw material was supplied from artisanal beer producers from Bagé, Rio Grande do Sul, Brazil, and was packed in plastic bags at -18 °C until analysis. The moisture content was determined by the oven method at 105 ºC for 24 h.

Figure 1 illustrates the experimental system used in the drying experiments. The experimental system involved a fixed bed dryer. The air flow coming from the blower [a] was monitored by psychrometer [b] and was heated by an electrical heater (c). Measurements of air velocity were performed by an anemometer [f]. In order to monitor mass of samples during the drying experiments a digital balance [e] was used, connected with a tray in the drying chamber.

Fig. 1 Experimental system.

The malt bagasse samples were distributed uniformly as a thin layer onto the stainless steel tray of size 12x0.5 cm and dried. The ranges of operating conditions were defined in preliminary tests. The inlet air temperature (T_{air}) were 40, 60, 75 and 90 °C and air velocity (v_{air}) was 2 m/s. Drying curves (($M-M_e$)/(M_0-M_e) as a function of time) were obtained and the equilibrium moisture content was assumed as the final moisture content, when the drying rate was practically null, for each drying condition.

The calibration curve of methylene blue dye was obtained from different concentrations and their respective absorbances in UV-VIS spectrophotometer at the wavelength of 664 nm. The calibration curve obtained for methylene blue is presented in Equation 1.

$$ABS = 0,1175\,[MB] \qquad (1)$$

where [MB] corresponds to the concentration of the dye in ppm and abs the absorbance.

The adsorption process was performed in a batch system. 2 g of the malt bagasse in natura and dried were first placed in a Erlenmeyer flask. 50 mL of methyle blue solution at a concentration of 70 ppm was added to the flask. The mixture were stirred continuously using a shaker at speed of 150 rpm for 60 min in a constant temperature at 25 °C. After adsorption, each sample containing the solution and adsorbent was subjected to centrifugation at 3000 rmp for 10 min. Then, the concentration of methylene blue were measured using UV-VIS spectrophotometer. The removal efficiency of methylene blue (% Rem) was determined using the Equation 2.

$$\%Rem = \frac{C_0 - C_{eq}}{C_o} \times 100 \qquad (2)$$

where Co is the initial concentration of the dye, C_{eq} is the final concentration.

Experimental data were analyzed by Statistica 7.1 software. Mean comparasions were carried out by Tukey test ($p < 0.05$ was considered as significant).

3. Results and discussion

Figure 2 shows the typical drying curves obtained for malt bagasse.
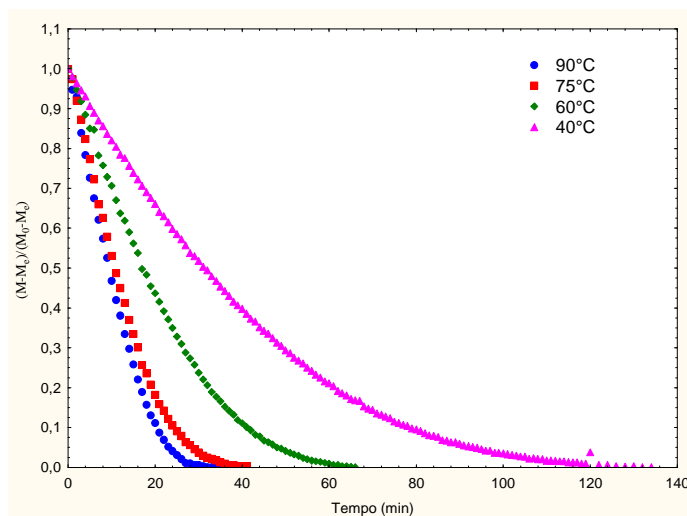
Fig. 2 Drying kinetics at different operation conditions.

In all experiments, the drying kinetics showed a constant drying rate period followed by a falling drying rate period. As expected, an increase in air temperature also significantly increased the drying kinetics and resulted in lower final moisture contents. The moisture content for *in natura* malt was 74.25% ± 0.43 (% w.b.) and after the drying process the results were in the range of 2.6 to 6.9%, similar with results showed by Gonçalves et al. [7]. According to Lopes et al. [8] the final moisture content of the material is directly related to the drying time and temperature. According to Wang and Chen [9] the temperature and moisture content of the material play a very important role in the heat and mass transfers during the drying. At lower temperatures it was necessary a longer time for the removal of water from the material because, according to Vilela and Silva [10], drying requires gradients that help as the driving force for the mass flow of water into the air drying.

Table 1 shows the results to the removal efficiency of the methylene blue dye using malt bagasse samples before and after drying.

Table 1. Removal efficiency of methylene blue.

	in natura	Dried samples			
		40 °C	60 °C	75 °C	90 °C
Rem (%)	56.00±0.87[a]	93.60±0.25[b]	93.71±0.26[b]	93.48±0.13[b]	93.99±0.32[b]

Average±deviation (n=3)
Different letters indicate significant differences between samples ($p < 0.05$)

It can be observed that drying of the adsorbent material favored the adsorption process because it allowed the reduction of moisture content of the adsorbent material, and, consequently, the increase of the intraparticle porosity and adsorption sites as mentioned by Geankoplis [11] and Arim et al. [12]. There were no significant difference (p<0.05) between the removal efficiency using dried samples at differents conditions. Then, the results indicated that the adequate drying condition for malt bagasse is at 90 ºC, since the drying can be faster with lower cost of energy.

4. Conclusion

The malt bagasse drying showed a constant drying rate period followed by falling drying rate period, wich is typical of materials with high moisture content. The dried malt bagasse showed to be efficient in the removal efficiency of methylene blue, with no significant difference between samples dried at differents temperatures. The results showed promising results, and it was possible to affirm that malt bagasse can be used as adsorbent for adsorption of dye, reducing the environmental impact and showing a new application for this residue.

5. References

[1] Cordeiro, L.G. Caracterização e Viabilidade Econômica do Bagaço de Malte Oriundo Cervejarias Para Fins Energéticos. Dissertação de Mestrado. Universidade Federal da Paraíba. 2011.

[2] Oliveira, L.H.; Arraes, D.D.; Gomes, G.E.; Lima, A.E.O.; Ramos, P.H. Estudo Da Adsorção Do Corante Rodamina B Em Argila Natural. 10°Encontro Brasileiro Deadsorção. Guarujá –Sp, 2014.

[3] Matos, T.T.S.; Jesus, A.M.D.; Araújo, B.R.; Romão, L.P.C.; Santos, L.O.; Santosa, J.M. Aplicação De Subprodutos Industriais Na Remoção De Corantes Reativos Têxteis. Revista Virtual Química, V.5, Pp. 840-852, 2013.

[4] Ferrari, V. O Mercado De Cerveja No Brasil. Dissertação De Mestrado. Univerdidade Católica Do Rio Grande Sul, 2008. XII Congresso Brasileiro de Engenharia Química Em Iniciação Científica Ufscar – São Carlos – SP 16 a 19 de Julho de 2017.

[5] Piffer, H.H.; Juchen, P.T.; Veit, M.T.; Fagundes-Klen, M.R.; Palácio, S.M.; Gonçalves, G.C. Estudo Da Dessorção Do Corante Têxtil Reativo Azul 5g Adsorvido Em Bagaço De Malte. In: Anais Do Xi Congresso Brasileiro De Engenharia Química Em Iniciação Científica. São Paulo: Blucher, 2015.

[6] Zanette, J.C.; Piffer, H.H.; Veit, M.T. Biossorção Do Corante Têxtil Azul 5g Utilizando O Bagaço De Malte. In: Anais Do I Encontro Anual De Iniciação Científica, Tecnológica E Inovação. Santa Catarina, 2015.

[7] Gonçalves, C. ; Echevarria, E.R. ; Rosa, G.S. ;Oliveira, E.G.; Biossorção De Corante Catiônico Utilizando O Bagaço De Malte. Anais Do Xxi Congresso Brasileiro De Engenharia Química, Fortaleza, 2016

[8] Lopes, C.R.; Queiroz, A. M.; Silva, K. C.; Mendes, E. C. S.; Silvério, B.C.; Ferreira,M. M. P.; Estudo Cinético De Desidratação E Caracterização Do Bagaço De Malte Resíduo Da Indústria, P. 2697-2702. In: Anais Do Xi Congresso Brasileiro De Engenharia Química Em Iniciação Científica. São Paulo: Blucher, 2015.

[9] Wang, Z.H.; Chen, G. Heat And Mass Transfer In "Xed-Bed Drying. Chemical Engineering Science 54 (1999) 4233}4243, Kowloon, Hong Kong, 1999

[10] Vilela, F.A.; Silva, W. R. Efeitos Da Secagem Intermitente Sobre A Qualidade De Sementes De Miho.P. 185-209. In: Anais Esalq. Piracicaba, 1991.

[11] Geankoplis, C.J. Procesos De Transporte Y Operaciones Unitarias. 3° Edição, México: Cecsa, 1998

[12] Arim, A.L.; Mesquita, V.R.; Echevarria, E.R.; Lima, D.R.; Morais, M.M.; Rosseto,V.; Almeida, A.R.F.; Rodrigues, L.M. Investigação Do Bagaço De Butiá Quaraimana Comomaterial Adsorvente Alternativo Para O Tratamento De Efluentes. In: Anais Do 10° Encontro Brasileirosobre Adsorção. São Paulo, 2014.

[13] Barbosa, R.M. Contribuição Do Mercado De Carbono Para A Viabilidade De Projetos De Eficiência Energética Térmica E De Troca De Combustíveis Em Cervejarias. Dissertação De Mestrado. Universidade De São Paulo, 2010.

[14] Brasil. Ministério Da Agricultura, Pecuária E Abastecimento. Portaria N° 166 De 12 De Abril De 1977. Padronização, Classificação E Comercialização Do Malte Cervejeiro Ou Cevada Malteada Para Fins Cervejeiros.

[15] Foust, A.S.; Wenzel, L.A.; Clump, C.W.; Maus, L.; Andersen, L.B. Princípios Das Operações Unitárias. Rio De Janeiro, Guanabara Dois, 1982. 670 p.

Vitamin C content of freeze dried pequi (*Caryocar brasiliense* Camb.) pulp

Soares, C.T. [a*]; Nogueira, G.F.[a]; Santana, A. A.[b]; Oliveira, R. A.[a]

[a] School of Agricultural Engineering, University of Campinas, Campinas - SP, Brazil.
[b] School of Chemical Engineering, Federal University of Maranhão, SãoLuís - MA, Brazil.

*E-mail of the corresponding author: augustus@feagri.unicamp.br

Abstract

Vitamin C is one of the constituents of pequi pulp. It is a natural antioxidant, capable of sequestering free radicals. The present study aimed to freeze dry a pequi pulp encapsulated with maltodextrin and whey protein and analyze vitamin C content. Vitamin C loss was lower in the experimental run that did not use encapsulating agent. Whereas, the run that used 15% of whey protein concentrate as encapsulant agent in relation to pequi solids presented the highest value (220.74 mg vitamin C / g pequi solids). Freeze drying of pequi pulp is a technique for vitamin C conservation independently of the variation in maltodextrin and whey protein proportion.

Keywords: drying; encapsulating agent; ascorbic acid.

1. Introduction

The pulp of pequi (*Caryocar brasiliense* Camb.) is rich in vitamin C, which present antioxidant capacity [n1]. This fruit is produced in the regions that compose the Brazilian Cerrado biome and because of this, it is an extractive product. The lack of adequate methods of conservation and perishability of the fruit result in great loss [n1]. New technologies allow the aggregation of value to the product and among them is freeze drying. This technique minimizes losses of nutrient compounds during the drying process based on the dehydration by sublimation of a frozen product resulting in a dry material [n2, n3]. Microencapsulation is a technique that maintains product properties as stable as possible and extends its shelf-life. Encapsulating agents protect the core material from interaction with environmental factors such as light, oxygen, temperature and humidity, and among them are maltodextrin and whey protein concentrate (WPC). Maltodextrin is a partially hydrolyzed starch widely used in the food industry as it has a mild and long-lasting flavor [n4]. WPC is an excellent protein isolate in the edible coating, as well as in food enrichment and edible film production [n5]. The objective of this work was to dry the pequi pulp encapsulated with maltodextrin and WPC and to analyze the composition of vitamin C after freeze drying process.

2. Materials and Methods

2.1 Materials

Pequi fruits from a single batch production of the state of Minas Gerais, Brazil, were purchased at the Campinas Supply Center (Ceasa-Campinas) and used on all the experiments. After processing, the samples were stored in a freezer at -60 ± 3 °C and dried by a laboratory freeze dryer (Edwards High Vacuum, Super Modulyo model, Great Britain). Maltodextrin (MOR-REX® 1910, Ingredion, Mogi-Guaçu, Brazil) and whey protein concentrate (WPC 80, Alibra, Campinas, Brazil) were used as encapsulating agents.

2.2 Methods

2.2.1 Preparation of pequi pulp

The fruits were stored in a Biochemical Oxygen Demand (B.O.D.) chamber at 5 °C until their processing stage. The pequi pulp processing followed the subsequent steps: selection, washing, sanitization, peeling, second sanitization, pulping, packaging, homogenization. Homogenization was carried out by a domestic mixer, adding distilled water in the

proportion 1: 1 (pulp:water, m/m) to the pequi pulp and different encapsulants in different concentrations, according to Table 1.

A central composite experimental design with two independent variables and three central points, totalling 11 experimental runs, was performed. The independent variables were the maltodextrin/whey protein concentrate proportion and total concentration of encapsulating in relation to total solids content of pequi pulp.

Vitamin C content after freeze drying were considered the dependent variable (response). Table 1 presents the encoded and real values of independent variables of the experimental design. In Table 1, C_{total}: total concentration of encapsulants in relation to the total solids of pequi pulp. C_{WPS}: whey protein concentrate concentration. C_M: maltodextrin concentration.

Table 1. Experimental design

Run	Independent variables				
	Encoded		**Real**		
	CM %	Ctotal [%]	CM %	CW %	Ctotal [%]
1	-1	-1	14,6	86,4	4,4
2	-1	1	14,6	86,4	25,6
3	1	-1	85,4	14,6	4,4
4	1	1	85,4	14,6	25,6
5	-1,41	0	0,0	100,0	15,0
6	1,41	0	100,0	0,0	15,0
7	0	-1,41	50,0	50,0	0,0
8	0	1,41	50,0	50,0	30,0
9	0	0	50,0	50,0	15,0
10	0	0	50,0	50,0	15,0
11	0	0	50,0	50,0	15,0

Variation of the parameters encapsulant concentration, maltodextrin / WPC (C_{enc}%) and relation between the encapsulant and ST of the pulp ($Total_{ratio}$%).

2.2.2 Freeze drying

The samples were previously prepared with the addition of the encapsulants according to the planning design, forming distinct treatments and, later, placed in stainless steel trays of the freeze-dryer with capacity of 200 g each one and submitted to freezing in a freezer at -

60ºC before starting the freeze-drying process. After freezing, the samples were taken to the freeze dryer, which consists of a vacuum chamber, condenser, refrigeration unit, and vacuum pump. The average time for freeze drying of the samples was about 72 hours. Then, the porous plates obtained in this process were broken using a porcelain mortar and pestle and, after that, homogenized.

2.2.3 Vitamin C

For the analysis of vitamin C, absorbance readings were performed in a spectrophotometer at 760 nm using trichloroacetic acid and Folin-Ciocalteu Phenol 2.0N as reagents, described by Jagota and Dani [n6]. Vitamin C was quantified based on a standard curve fitted from various dilutions of vitamin C (5 to 70 μg). The values were expressed as mg of vitamin C in 100g of pequi pulp.

2.2.4 Statistical analysis

Significant differences between average results were evaluated by analysis of variance (ANOVA) and Tukey test at 5% of level of significance, using SAS software (Cary, NC, USA).

3. Results and discussion

The vitamin C results of the pequi pulp encapsulated with maltodextrin and whey protein are shown in Table 2. Vitamin C for fresh pequi pulp was 311.72 ± 1.25 mg of ascorbic acid g^{-1} solids of pequi. The vitamin C values of the experimental runs ranged from 99.03 to 220.74 mg of ascorbic acid g^{-1} solids of pequi being within the values found by [n7] for spray dried pequi pulp. Run 7, with no encapsulating agent, presented lower vitamin C content compared to the other runs. It is believed that the use of encapsulating agent had a significant effect on the conservation of vitamin C, especially when the percentage of whey protein in the total solids of the pulp was used (run 5). The pequi pulp encapsulated with maltodextrin and whey protein concentrate, after freeze drying process, suffered losses of vitamin C when compared to the fresh pulp. However, when compared to the non-encapsulating agent run, the losses were not pronounced, showing that the technique of encapsulation has protected the oxidation of ascorbic acid from a number of biochemical mechanisms, which are responsible for the loss of vitamin C activity.

Even the lowest content of vitamin C found in experimental runs is superior to that of raw avocado fruit, 'Maçã' banana, 'Nanica' banana, cupuassu, jackfruit, 'Red Delicious' apple,

'Fuji' apple, watermelon, 'Williams' pear, 'Aurora' peach, pomegranate, tamarind, umbu and 'Ruby' grape [n8].

Table 2. Vitamin C for freeze dried pequi pulp using maltodextrin and WPC as encapsulant agent.

Run	C_M (%)	C_{WPS} (%)	C_{total} (%)	Vitamin C (mg / g solids of pequi)
1	14.6	85.4	4.4	183.48±2.77g
2	14.6	85.4	25.6	191.06±0.98ef
3	85.4	14.6	4.4	186.59±1.07gf
4	85.4	14.6	25.6	213.14±2.25bc
5	0.0	100.0	15.0	220.74±2.54a
6	100.0	0.0	15.0	196.62±0.41ed
7	50.0	50.0	0.0	99.03±2.73h
8	50.0	50.0	30.0	202.33±1.47d
9	50.0	50.0	15.0	210.76±3.14c
10	50.0	50.0	15.0	196.06±2.16ed
11	50.0	50.0	15.0	219.41±2.14ba

*Same letters in the column show no statistical difference (p > 0.05).

Experimental data of vitamin C for freeze dried pequi pulp using maltodextrin and WPC as encapsulant agent are shown in Table 2. The experimental values of vitamin C oscillated from 99.03 to 220.74 mg vitamin C/ g solids of pequi.

The determination coefficient (R^2) for the fitted model was 0.75. The model was tested for adequacy and fitness by the analysis of variance (ANOVA) without considering the non-significant terms (p>0.05). The coded second-order polynomial model (Equation 1) was considered significant and predictive.

$$Vit.C \left[\frac{mg}{g_{solids\ of\ pequi}} \right] = 211.98 + 22.53 C_{total} - 26.57 C_{total}^2$$

(1)

Fig. 1 shows the contour plot generated by the proposed model. It is observed that there is no influence of maltodextrin/WPC proportion on Vitamin C values.
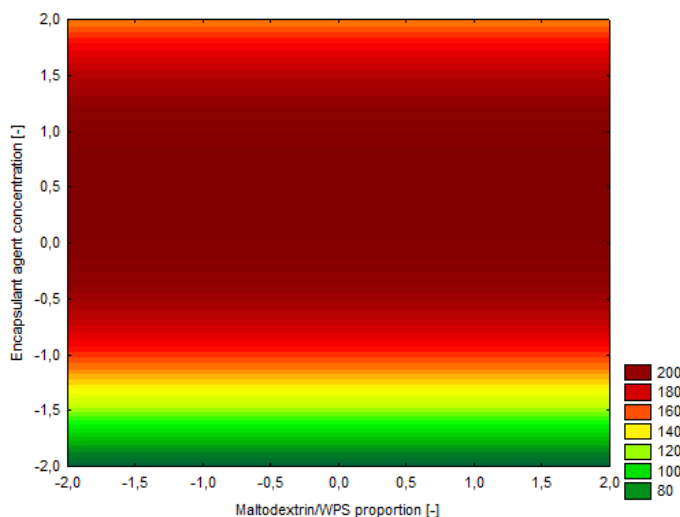
Fig. 1 Response surface for vitamin C content of microencapsulated pequi powder.

4. Conclusions

The experimental run using no encapsulant agent on freeze drying process has a lower vitamin C value because of the absence of protection against ascorbic acid oxidation. The runs that showed the best protection against oxidation of ascorbic acid were those encapsulated with 15% independent of the encapsulant used. Drying of pequi pulp by freeze drying is an excellent technique for the protection of ascorbic acid, regardless of variation (proportion) in the use of maltodextrin and/or whey protein concentrate (WPC).

5. References

[1] Carrazza, L.; Ávila, J. C. C. Manual Tecnológico de Aproveitamento Integral do Fruto do Pequi. Brasília – DF. Instituto Sociedade, População e Natureza (ISPN). Brasil, 2010, p. 7-11.

[2] Ordóñez, J. A. Tecnologia de alimentos: Componentes dos alimentos e processos. Porto Alegre: Artmed, v.1, 2005, p. 220-225.

[3] Fellows, P. J. Tecnologia do Processamento de Alimentos: Princípios e prática. Tradução: Florencia Cladera Oliveira, Jane Maria Rubensan, Julio Alberto Nitzkee Roberta Cruz Silveira Thys – 2° edição – Porto Alegre: Artmed, 2006.

[4] Gibbs, B.F.; Kermasha, S.; Alli, I.; Mulligan, C.N. Encapsulation in food industry: A review. International Journal of Food Science and Food Nutrition, v.50, 1999, p. 213–234.

[5] Yoshida, C. M. P. & Antunes, A. J. Aplicação de filmes proteicos à base de soro de leite. Ciência e Tecnologia de Alimentos, Campinas, v. 29, n. 2, 2009, p. 420-430.

[6] Jagota, S. K. & Dani, H. M. A new colorimetric technique for the estimation of vitamin C using folin phenol reagent. Analytical biochemistry. Panjab University, India, 1982.

[7] Santana, A.; Kurozawa, L.; Oliveira, R.; Park, K.. Spray Drying of Pequi Pulp: Process Performance and Physicochemical and Nutritional Properties of the Powdered Pulp. Brazilian Archives of Biology and Technology, v. 59, 2016, p.1-11.

[8] Nepa – Núcleo de Estudos e Pesquisas em Alimentação (Unicamp). Tabela Brasileira de Composição de Alimentos. 2 ed. Campinas: NEPA-UNICAMP, 2006, 102-104.

Effect of spray drying on volatile compounds of acerola pulp

Nogueira, P. M.[a]; Leite Neta M. T.[a]; Araujo, H. C. S.[a]; Jesus, M. S.[a]; Shanmugam, S.[b]; Narain, N.[a]

[a]Laboratory of Flavor and Chromatographic Analysis, Federal University of Sergipe, Av. Marechal Rondon, s/n, Jardim Rosa Elze, 49100-000, São Cristóvão, SE, Brazil

[b]Department of Pharmacy, Federal University of Sergipe, Av. Marechal Rondon, Jardim Rosa Elze, CEP: 4910 0-000 São Cristóvão, Sergipe, Brazil

*E-mail of the corresponding author: narendra.narain@gmail.com

Abstract

The objective of this work was to optimize the drying conditions in order to obtain acerola powder and to focus on the product aroma quality. Acerola fruits were selected, washed and sanitized before extracting the pulp. An emulsion was obtained by adding maltodextrin in the pulp. The dehydrated powders were obtained in spray dryer by drying at inlet temperatures of 128 and 152 ºC. Twenty five volatile compounds were identified in fresh acerola pulp and in the dehydrated powder. These results prove that use of maltodextrin in spray drying of acerola pulp helps in retention of key aroma compounds in acerola powder.

Keywords: Acerola, Spray drying, dehydration, volatiles, aroma, GC-MS.

1. Introduction

The aceroleira is a fruit tree native to the Antilles, North of South and Central America, that showed good adaptation in several countries being mainly cultivated in Brazil.[1] Its potential as a natural source and capacity for industrial use has attracted the interest of fruit growers and it has attained economic importance in several regions of Brazil.[2] The acerola (*Malpighia glabra*) is a fruit species widely accepted by consumers, which has been prominent in Brazil and the world, mainly because it is one of the main natural sources of vitamin C and carotenoids and it is widely industrialized in the form of frozen pulp, characterizing as functional foods, since it confers benefits in reducing the risk of some non-transmissible chronic diseases such as cancer.[1]

The transformation of acerola fruit into an industrial product will allow its preservation for a prolonged period, but it is also required that the beneficial properties and the fruit´s sensorial characteristics will be maintained to its maximum.[3] Among the techniques used to maintain post-harvest quality of fruit, dehydration, besides being used as a conservation method, prevents deterioration and losses of commercial value and adds value to the product giving rise to a new option in the market.[4]

The spray drying consists of the transformation of the product from the fluid state to dry particles in the form of powder. The dried powder should retain maximum initial characteristics of the fruit pulp and protect it from the adverse conditions of the external environment. For this purpose wall materials or microencapsulants are incorporated into the pulp before drying.[5] Thus, the present work had as objective to optimize the drying conditions of the parameters for atomization of the acerola pulp in spray dryer and evaluate its effect on the volatile compounds of acerola pulp.

2. Materials and Methods

2.1. Fruits purchase

The ripe fruits of acerola were acquired from the Central Market of Supply (CEASA) in the city of Aracaju/SE. The fruits were then taken to the Laboratory of Processing of Vegetable Origin (LPOV), located in the Department of Food Technology (DFT) at the Federal University of Sergipe (UFS).

2.2. Sanitation and pulp extraction

The selected fruits were submitted to selection, sanitization in a solution of 200 ppm of residual chlorine (Sumaveg®) for 10 minutes to eliminate possible microorganisms that

withstood the previous step. The rinse was carried out in solution at 3ppm of active chlorine for 10 minutes. After the rinsing the fruits were washed in water for 10 minutes to remove all chlorine and pulped in a stainless-steel pulp (ITAMETAL), using a 1.5mm diameter screen. The pulp was weighed and packed in polyethylene packages. The packages with the pulps were stored in a freezer at freezing temperature (-21 ° C).

2.3. Spray Drying Process

For the Spray dryer atomization process, tests were carried out by varying the drying air temperature and the carrier agent concentrations, as detailed in Table 1.

Table 1. Formulations and Temperatures used in spray drying process in obtaining dried powder from acerola pulp.

Sample code	Pulp (%)	Maltodextrin (%)	Input Temperature (ºC)	Output Temperature (ºC)
AC 1	86	14	128	65
AC 2	86	14	152	78
AC 3	74	26	128	65
AC 4	74	26	152	78

The spray drying was performed in a spray dryer (LABMAQ, model MSDi 1.0, Riberão Preto-SP, Brazil) with injector nozzle having the orifice of 1.2 mm diameter, air flow of 4.00 m³ / min and air pressure of 4 kgf/cm². The dryer was fed through a peristaltic pump, with rotation speed adjusted as a function of the maximum speed; the flow was 0,44 L/h. Samples were produced with 14 and 26% of maltodextrin and the two inlet temperatures used were 128 and 152 °C (Table 1).

2.4. Determination of Volatile Compounds

The volatile composition of the acerola fresh pulp and dried powder was determined using the purge and trap (P&T) technique by varying 3 different dilutions of the pulp with water (4g:10mL, 4g:20mL and 4g:30mL). The volatiles were captured and concentrated in the P&T system (Tekmar, Model ATOMX, Mason-45040, USA) under the following conditions: 4 g of pulp were diluted with 10 mL of distilled water and taken to the purge and trap system, operating with helium gas flow of 40 mL/min, purging time of 11 min, desorption time of 5 min in a trap containing Tenax/silica gel/charcoal.

2.5. Separation and Identification of Volatile Compounds

The P&T system used the Vocarb3000 trap and analyzed in the gas chromatography system coupled to a mass spectrometer (GC-MS QQQ Agilent 7000). The compounds were separated on carbowax capillary column (30 m x 0.25 mm x 0.25 µm) using helium as the carrier gas (1.0 mL/min). The temperature of the injector was 220°C and the column temperature programming was: 35°C for 2 min, increase at 10°C/min to 100°C, maintaining for 1 min followed by an increase of 3°C/min to 250 °C, totaling 59 min of analysis.

The identification of the volatile compounds was performed by comparing the mass spectra of the sample compounds with those in the NIST (National Institute of Standards & Technology), containing approximately 150,000 reference spectra and by comparing the linear retention index (LRI) of the compounds with those of publications in the literature and LRI calculated on the basis of the retention times of a series of n-alkanes mixtures of C8-C30, C8-C40 and C8-C17, injected at identical analytical conditions.

The linear retention index (LRI) was calculated based on the retention time of the authentic alkane standards versus the number of carbon atoms of the respective alkane standards, multiplied by 100.

The quantification of volatile compounds was related to the percentage area of the peak of each compound and to the total area of all peaks normalized in the chromatogram.

3. Results and Discussion

3.1. Volatile compounds in the fresh pulp and dehydrated powder of acerola.

Aroma is one of the most important attributes in food and it is used to mainly relate the sensory quality of fruit and fruit products. In the determination of volatile compounds of acerola pulp, 25 compounds were found from the sample containing 4g:10mL (Pulp:Water) and the main compounds identified were: ethanol (10.96%), ethyl acetate (9.61%), pent-4-en-1- yl propyl carbonate (8.20%), ethyl hexanoate (6.88%), ethyl butanoate (6.36%), 4-pentenyl butanoate (3.57%), (*E*)-2-hexenal (2.82%) and 4-pentenol (2.32%). For the dilution (4g:20mL) of the pulp, the number of identified compounds decreased, being only the compounds found in the first dilution consisting of ethyl acetate (5.73%), ethanol (11.32%), ethyl butanoate (5.52 %). However, in the third dilution (4g:30mL) only ethyl acetate (11.23%) and ethyl butanoate (2.34%) were identified. The P&T technique generally provides a higher extraction yield, which may be associated with a larger surface of the adsorbent trap in relation to other techniques such as SPME.[6]

In the dried acerola powder, 20 compounds were found in the samples dried at the two temperatures of 128 and 152°C while using a maltodextrin concentration of 26%. This concentration of maltodextrin showed a retention of 80% of aroma in the dried powder. The powder obtained using 14% concentration of maltodextrin did not show a better retention of volatile compounds and only 12 compounds were retained. The main compounds identified in the dried powder were ethyl hexanoate (2.01%), (*E*)-2-hexenal (1.95%), methyl hexanoate (1.2%) and methyl acetate (0.8%). These volatile compounds were reported previously in other studies on acerola aroma.[7,8,9,10,11] Ethyl hexanoate was the main contributor to acerola aroma and its odor quality resembled that of apple peel, being fruity and sweet.[12,13,14]

The concentration of ethyl hexanoate decreased from 6.88% in the fresh pulp to 2.01% in the dried powder as showed in the Figure 1. Nunes et al.[15],studying the effect of drying temperatures in the volatile compounds of guava, reported in spray drying the volatile compounds could be affected by solubility in pulp of fruit lipids and/or residual water, which is probably the major factor contributing to volatiles retention.[16] Therefore, compounds with high vapour pressure and/or low liposolubility tend to be loose the components during drying, whereas compounds with low vapour pressure and/or high liposolubility tend to concentrate in dried powders.
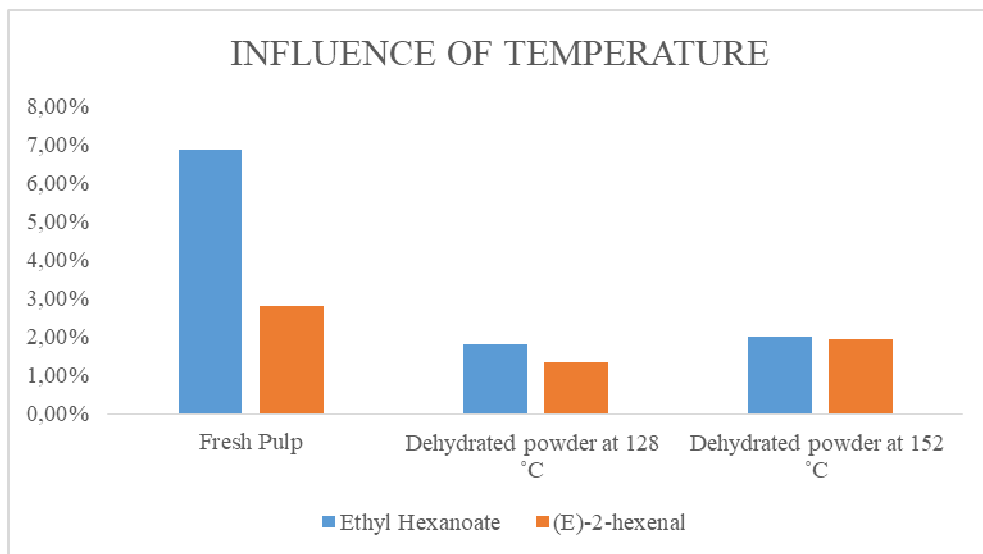
Figure 1: Influence of temperature on the key aroma compounds from acerola pulp

Tong Chin et al.[17] studied the influence of temperature on the retention capacity of the volatile compounds of the dried Durian pulp by atomization process and monitored the key aroma compounds, propanethiol and ethyl propanoate, at two temperatures (170°C and 130°C), noting that at a temperature of 170°C a reduction in the number of volatile compounds occurs.

Other compound that showed reduction was (*E*)-2-hexenal that are reported that together with hexanal it is strongly related to the flavour of fresh guava fruit, providing an herbaceous and fresh aroma note.[18]

The retention f volatile compounds can be influenced by maltodextrin. Maltodextrins with higher DE are more hydrolyzed, and these provide more hydroxyl groups for the interactions with volatile compounds.[19] This interpretation is in accordance with one proposed by Reineccius[20], who found that more volatile compounds were retained in the system containing maltodextrins of higher DE values.

4. Conclusions

The various combinations used for spray drying od acerola pulp by varying drying air temperature and maltodextrin concentrations had influence on volatile compounds. The concentration of 26% of maltodextrin preserved more volatile compounds than the concentration of 14% maltodextrin. Compounds classified as key aroma compounds such as ethyl hexanoate and (*E*)-2-hexenal in fresh acerola pulp were retained in the acerola dried powder. These results prove that use of maltodextrin in spray drying of acerola pulp helps in retention of key aroma compounds in dried acerola powder.

5. References

[1]   Silva, M.L.S.; Menezes, C.C.; Portela, J.V.F.; Alencar, P.E.B.S.; Carneiro, T.B. Teor de carotenoides em polpas de acerola congeladas. Revista Verde de Agroecologia e Desenvolvimento Sustentável, 2013, 8 (1), 170-173.

[2]   Maia, G. A., Sousa, P. H. M.; Santos, G. M.; Silva, D. S.; Fernandes, A. G.; Prado, G. M. Efeito do processamento sobre os componentes do suco de acerola. Ciência e Tecnologia Alimentar, Campinas, 2007.

[3]   Maciel, M.I.S., Melo, E.A.; De Lima, V.L.A.G.; Da Silva, W.S.; Maranhão, C.M.C.; De Souza, K.A. Características sensoriais e físico-químicas de geléias mistas de manga e acerola. Boletim do Centro de Pesquisa de Processamento de alimentos, 2011, 27 (2), 13.

[4] Silva, R.N.G.; Figueiredo, R.M.F.; Queiroz, A.J.M.; Galdino, P.O. Armazenamento de umbu-cajá em pó. Cienc. Rural [online]. 2005, 35 (5), 1179-1184.

[5] Mata, M.E.R.M.C; Medeiros, S.S.A.; Duarte, M.E.M. Microencapsulamento do umbu em pó com diferentes formulações de maltodextrina: estudo do tamanho das partículas por microscopia eletrônica. Revista Brasileira de Produtos Agroindustriais, 2005, 7 (1), 59-70.

[6] Povolo, M.; Contarini, G. Comparison of solid-phase microextraxtion and purge and trap methods for the analysis of the volatile fraction butter. Journal of Chromatography A, 2003, *985*, 117–125.

[7] Boulanger, R.; Crouzet, J. Identification of the aroma components of acerola (*Malphigia glabra* L.): free and bound flavour compounds. Food Chemistry, 2001, *74*(2), 209–216.

[8] Carasek, E., & Pawliszyn, J. Screening of tropical fruit volatile compounds using solid-phase microextraction (SPME) fibers and internally cooled SPME fiber. Journal of Agricultural and Food Chemistry, 2006, 54 (23), 8688–8696.

[9] Pino, J. A.; Marbot, R. Volatile flavor constituents of acerola (*Malpighia emarginata* DC.) fruit. Journal of Agricultural and Food Chemistry, 2001, 49 (12), 5880–5882.

[10] Schippa, C.S.; George, G.; Fellous, R. Constituans volatils de l'acerola. Parfums Cosmet. Aromes, 1993, 113, 81–84.

[11] Vendramini, A. L.; Trugo, L. C. Chemical composition of acerola fruit (*Malpighia punicifolia* L.) at three stages of maturity. Food Chemistry, 2000, 71 (2), 195–198.

[12] Acree, T. E., & Arn, H. (2004). Flavornet and human odor space. Available from: http://www.flavornet.org/flavornet.html. Accessed 20 October 2017.

[13] Garruti, D. S.; Franco, M.R.B.; da Silva, M.A.A.P., Janzantti, N.S.; Alves, G.L. Assessment of aroma impact compounds in a cashew apple-based alcoholic beverage by GC-MS and GC-olfactometry. LWT - Food Science and Technology, 2006, 39 (4), 373–378.

[14] MacLeod, A.J.; Pieris, N.M. Volatile flavor components of soursop (*Annona muricata*). Journal of Agricultural and Food Chemistry, 1981, 29 (3), 488–490.

[15] Nunes, J.C.; Lago, M.G.; Castelo-Branco, V.N.; Oliveira, F.R.; Torres, A.G.; Perrone, D.; Monteiro, M. Effect of drying method on volatile compounds, phenolic profile and antioxidant capacity of guava powders. Food Chemistry, 2016, 197, 881-890.

[16] Taylor, A. J. Physical chemistry of flavor. International Journal of Food Science & Technology, 1998, 33, 53–62.

[17] Tong Chin, S.; Nazimah, S.A.H.; Quek, S.Y.; Man, Y.B.C.; Rahman, R.A.; Hashim, D.M. Changes of volatiles' attribute in durian pulp during freeze- and spray-drying process, 2008, 41, 1899-1905.

[18] Pino, J. A.; Bent, L. Odour-active compounds in guava (Psidium guajava L. cv. Red Suprema). Journal of the Science of Food and Agriculture, 2013, 93, 3114–3120.

[19] Mao, L.; Ross, Y.H.; Miao, S. Effect of maltodextrins on the stability and release of volatile compounds of oil-in-water emulsions subjected to freezeethaw treatment. Food Hydrocolloids, 2015, 50, 219-227.

[20] Reineccius, G. A. Controlled release techniques in the food industry. In S. J. Rich, & G. A. Reineccius (Eds.), Encapsulation and controlled release of food ingredients. Washington: American Chemical Society. 1995, 8-25.

Aroma retention during drying of caja-umbu fruit pulp

Fontes, A. S.ª; Leite-Neta, M. T. S.ª; Matos, P. N.ª; Araujo, H. C. S.ª; Jesus, S. M.ª; Rajkumar, G.ª; Narain, N.ª*

ªLaboratory of Flavor and Chromatographic Analysis, Federal University of Sergipe, Av. Marechal Rondon, s/n, Jardim Rosa Elze, 49100-000, São Cristóvão, SE, Brazil

*E-mail of the corresponding author: narendra.narain@gmail.com

Abstract

This study was aimed to obtain and characterize the dried powder of cajá-umbu (Spondias spp) fruit pulp obtained by spray-drying and lyophilization. Spray-drying of the pulp was done at different temperatures. Analysis of bioactive compounds and volatile compounds was performed. The total phenolic compounds content was high in the dried powder obtained at the temperature of 140 °C. The volatiles analysis of dried powders revealed that the powder dried at 140°C contained a larger number of compounds. The cajá-umbu powder showed that it is a better alternative for storage and conservation since it retained the majority of volatile compounds.

Keywords: *Cajá-umbu, volatile compounds, gas chromatography, mass spectrometry.*

1. Introduction

Aroma is an important characteristic in exotic tropical fruits, which has increasingly attracted consumers due to their peculiar sensorial attributes. Brazil is one of the countries that have a large variety of these fruits, which are usually produced widely and are mostly consumed in fresh form or in the form of juices, ice cream, jams and jellies. Among the large variety of tropical fruits grown mainly in the Brazilian northeast region, fruits belonging to the genus *Spondias,* involving umbu (*Spondias tuberosa* Arruda Camara), yellow mombin (*Spondias mombin* L.), cajá-umbu (*Spondias spp)*, purple mombin (*Spondias purpurea* L.) and amberella (*Spondias dulcis* L. syn. *Spondias cytherea* Sonn.) are prominent. The volatile composition of these fruits pertain to several chemical classes, such as tannins, terpenoids (sesquiterpenes and monoterpenes), flavonoids, etc.[1,2]

The cajá-umbu (*Spondias* spp.) owing to its particular sensorial characteristics, such as aroma and flavor, is a fruit which is very much appreciated in the northeastern region of Brazil. It is native to the semi-arid regions and is cultivated between the states of Rio Grande do Norte, Ceará, Piauí, Pernambuco and Bahia. Its sensorial characteristics possessing strong acidic exotic aroma and attractive color, make this fruit to be highly demanding in the regions of the country where it is found.[3,4,5]

Being a climacteric fruit, the shelf life of cajá-umbu fruit is low and thus it is commercialized in the near by places where it is produced. It is therefore a great challenge to transport and commercialize this fruit to places far from its cultivation. In order to preserve this fruit and to develop new products with increased commercial value, dehydration techniques such as freeze drying and spray drying can be used.

To the best of the author´s knowledge no studies have been performed until the present moment on drying of cajá-umbu fruit and also to identify volatile and bioactive compounds in cajá-umbu dehydrated by these two techniques of drying. Thus the objective of this study was to evaluate the effect of two drying processes - freeze-drying and spray-drying of cajá-umbu pulp (*Spondias* spp) on the retention of volatile and bioactive compounds.

2. Materials and Methods

2.1. Fruit purchase and pulp extraction

The ripe mature fruits of cajá-umbu were acquired from the Center of Supply (CEASA) of the city of Aracaju/SE. These were then taken to the Laboratory of Processing of Vegetable Origin, located in the Department of Food Technology at the Federal University of Sergipe (UFS). The selected fruits were submitted to selection, sanitization pulping and packaging in polyethylene packages.

2.2. Spray Drying

For the Spray dryer process, experiments were performed by varying the drying air temperature (100, 120, 140 and 160°C) while maltodextrin concentration was maintained at 15%. The atomization was performed in a spray dryer with a nozzle atomization system of the brand LABMAQ (model MSDi 1.0, Brazil) with injector nozzle having 1.2 mm diameter orifice, air flow of 4.00 m³/min and pressure of air of 4 kgf/cm². The spray dryer was fed through a peristaltic pump, with rotation speed adjusted as a function of the maximum speed; this flow being 0.52 L/h. The dried powder was stored in glass containers with a screw cap, then sealed and stored in a desiccator at room temperature ($25 \pm 2\ ^0C$).

2.3. Lyophilization

The drying of pulp was also performed in a Christ Freeze Dryer, (model Alpha 1-4 LSC, Germany). The pressure used was 0.42 mbar, at a sublimation temperature within the chamber was - 58°C.

2.4. Separation and Identification of Volatile Compounds

The volatile compounds were captured through the purge and trap system (Tekmar Mark, Model ATOMX), using the Vocarb3000 trap and analyzed in the gas chromatography system coupled to a mass spectrometer (GC- QqQ MS, Agilent 7000) according to the method with adaptations reported by Narain et al.[5] The volatile compounds were analyzed in GC-MS system using a Carbowax column (30 m x 0.25 mm x 0.25 μm). The oven temperature was programmed: initiation at 35°C (held for 2 min) then raised at a rate of 10°C to 100°C (held for 1 min) and finally increased at 3°C/min to 250°C. Volatile compounds were tentatively or positively identified by comparing their mass spectra with the compounds from NIST (National Institute of Standards & Technology) database and comparing the linear retention index (LRI) of the standards and compounds with those of literature publications and other databases (Flavornet, PubChem, Pherobase).

3. Results and Discussion

3.1. Volatile compounds of dehydrated powder

Dehydration reduces the moisture content and therefore can result in the loss of volatile compounds in the final product at the end of the process.[6] Studies on the influence of temperature are very important to guarantee the quality of the final dehydrated product.[7] When developing a powder obtained by spray drying or lyophilization it is necessary to always standardize the best temperature where a powder can be obtained with the aroma very close to that of the fresh fruit. Thus, it is important to study the volatile composition of the product obtained by dehydration at various temperatures in order to define the best condition for obtaining an aromatic product at the end of the process.

In the Table 1 presents the data on number of peaks obtained on the analysis of dried powders obtained at different temperatures used for spray drying and by lyophilization. The volatiles analysis of dried powders revealed that the spray dried product at 140°C contained higher number (29) of compounds, compared to lyophilization which had only 26 compounds.

Table 1: Number of volatile compounds found in various dried powders obtained by spray and freeze drying of cajá-umbu pulp.

Dehydration type	Temperature	Number of peaks
Spray-drying	100°C	18
Spray-drying	120°C	20
Spray-drying	140°C	29
Spray-drying	160°C	19
Lyophilization	-58°C	26

The most representative class of compounds for the dried powders obtained by atomization were the terpenes, and the compound with the highest concentration was limonene at all the operating temperatures of the Spray-dryer (Table 2). Other terpenes identified were α-pinene, cis-α-bisabolene, 3-carene, β-pinene, *m*-xylene. Narain et al.[5] reported the presence of these compounds in ripe cajá-umbu (*Spondias* sp) fruit pulp when the extraction was performed by the Purge & Trap extraction technique and compounds were separated by using Carbo-WAX column and identified in a GC-MS system.

Tong Chin et al.[8] studied the influence of the temperature on the retention capacity of the volatile compounds markers of the atomized durian pulp and monitored the propanethiol and ethyl propanoate compounds at two temperatures of 170°C and 130°C, and reported that at a temperature of 170°C a reduction in the number of volatile compounds occurred. In the present work as seen in Table 1, the temperature at which a higher number of peaks was obtained and also a higher intensity was observed was at 140°C. At this temperature it is also possible to detect the appearance of compounds which at other temperatures were not found, for example, 3-carene, *m*-xylene while there was an increase in the concentration of the esters such as ethyl acetate, ethyl butanoate and ethyl lactate.

The use of high temperatures can also lead to the formation of new compounds in dehydrated products. Gozales-Palomare et al.[9] working with dehydrated powder of *Hibiscus sabdariffa* at temperatures of 150, 160, 170, 180, 190, 200 and 210°C reported the formation of furfuraldehyde in the dehydrated product at temperatures of 180-210°C. Similar results were found for dehydrated cajá-umbu powders at temperatures of 140 and 160°C, being higher in 160°C. According to Nunes et al.[10], the presence of furfural in ODG is probably expected as heating increases ascorbic acid degradation. Therefore, furfural analysis could be used to monitor product quality during guava drying processes as it may be considered as a marker of heating.

Fontes, A. S.; Leite Neta, M. T. S.; Matos, P. N.; Araujo, H.C. S.; Jesus, M. S.; Rajkumar, G.; Narain, N.

Table 2: Volatile compounds present in dried powder of cajá-umbu pulp

Compound	LRI$_{Lit}$	Dried powder-Spray drying				FDP
		100°C	160°C	140°C	120°C	
Ethanal	724	0.322	3.007		2.188	
Pentanal	935		0.544	0.674		
Verbenone				1.837		
Furfural	1455		2.64	0.415		
Acetone		1.966	1.727	2.396	2.524	
3-Methyl-4-propenyl-oxetan-2-one			0.21		0.129	
Ethyl acetate	907	1.841	1.104	2.181	2.007	
Ethyl lactate						16.964
Ethyl butanoate	1037	1.92		0.695	0.431	
Prenylacetate		0.696		0.586	0.38	
Propyl butanoate						8.432
Ethyl isovalerate	1100					1.039
Ethyl octanoate	1436					0.265
Pyrrole	915					6.248
m-xylene	1150			0.461		
3,4-Dimethyl styrene		0.145		0.606	0.129	
Ethanol	932	4.212	3.95	9.914	3.919	
δ-Octalactone						2.054
δ-Nonalactone						1.239
3-Aminobutanoic acid						4.627
α-Pinene	1030	0.644	0.577	3.934	0.604	
1R-α-Pinene	1055					6.22
(*Z*) Hydrated sabinene	1123					0.354
3-Carene	1148			0.116		0.237
1,3,8-*p*-Menthatriene	1158		0.082	1.606		
β-Pinene	1138	0.129	0.114	0.843	0.519	
α-Terpinene	1178					5.001
Limonene	1177	18.92	16.759	15.797	19.37	
(+)-Limonene	1201					18.714
Cyclofenchene						4.628
cis-β-Ocimene	1234			0.463		
Ocimene	1225					4.852
o-Cymene	1261	0.322	0.49	1.277	0.355	
(*E*)-β-Ocimene	1242					1.557
Copaene	1488					0.68
Alloaromadendrene	1599	17.35	18.704	10.537	16.67	
Isocaryophyllene	1570					2.588
cis-α-bisabolene	1543	1.317	1.789	0.824	1.319	
(3*Z*)-2,7-Dimethyl-3-octen-5-yne		0.309	0.207	0.955	0.27	

* LRI - Linear Retention Index; FDP - Freezed dried powder

An interesting factor to be emphasized is the higher presence of esters in the cajá-umbu pulp powder obtained by freeze-drying than in powder obtained by spray-drying. Compounds such as ethyl lactate (16.96%), which possesses a mild odor and propyl butanoate (8.432%) characterized by a fruity odor, were found in significant concentrations. Tietel et al.[11] studying the changes in concentrations of volatile compounds of tangerine reported that a slight increase in temperature caused a decrease in the concentration of esters such as ethyl acetate, ethyl butanoate, ethyl hexanoate. Similar behavior was observed in this study when compared to the lyophilization technique that uses low temperatures, when compared with the spray-drying technique that uses high temperatures.

Another aspect that probably influenced a lower retention of esters in the spray-drying was the retention capacity of the wall material in relation to these compounds. Rosenberg et al.[12] studying the factors that affect ester retention in the spray-drying technique observed that these compounds are not readily retained in the carrier material with a concentration of less than 30%. For the dehydrated cajá-umbu pulp, a similar behavior was observed to that reported by Rosenberg et. al.[12] since the carrier material (maltodextrin) concentration was 15%, thus not resulting in a better retention of the esters.

4. Conclusions

The pulp dehydration in the spray dryer maintained the nutritional and organoleptic characteristics of the fresh pulp resulting in a promising product for marketing purposes. In the identification of the volatile composition of the dried powders, 29 compounds were identified in the spray-drying process at 140°C and 26 compounds in the dehydrated powder by lyophilization. However, the major compound identified was limonene in both dehydration techniques. At all temperatures (100, 120, 140 and 160°C) of dehydration tested by spray drying, the highest number of volatile compounds were identified in the dried powder at a temperature of 140°C. Thus, it is concluded that the optimum dehydration temperature of the cajá-umbu pulp by the spray-drying process is 140°C.

5. References

[1] Lima, E.Q.; Ferreira, C.F.S.L.; Oliveira, E.; Costa, V.C.O.; Dantas M.K.L. Phytochemical characterization of *Spondias sp* and *Spondias tuberosa* Arruda Câmera extracts of occurrence in Paraiba semiarid. Journal of Experimental Biology and Agricultural Sciences, 2017, 5 (5), 713-717.

[2] Galvão, M.S.; Narain, N.; Santos, M.S.P.; Nunes, M.L. Volatile compounds and descriptive odor attributes in umbu (*Spondias tuberosa*) fruits during maturation. Food Research International, 2011, 44, 1919-1926.

[3] Lima, E.D.P.A.; Lima, C.A.A; Aldrigue, M.L.; Gondim, P.S. Caracterização física e química dos frutos da umbu-cajazeira (*Spondias spp*.) em cinco estádios de maturação,

da polpa e néctar. Revista Brasileira de Fruticultura. Jaboticabal, 2002, 24 (2), 338-343.

[4]   Santos, D.C.; Rocha, A.P.T.; Gomes, J.P.; Oliveira, E.N.A.; Albuquerque, E.M.B.; Araujo, G.T. Storage of 'umbu-cajá' pulp powder produced by lyophilization. Revista Brasileira de Engenharia Agrícola e Ambiental, 2016, 20 (12), 1118-1123.

[5]   Narain, N.; Galvão, M.S.; Madruga, S.M. Volatile compounds captured through purge and trap technique in cajá-umbu (*Spondias spp.*) fruits during maturation. Food Chemistry, 2007, 102, 726-731.

[6]   Phoungchandang, S.; Saentaweesuk, S. Effect of two stage, tray and heat pump assisted dehumidified drying on drying characteristics and qualities of dried ginger. Food and Bioproducts Processing, 2010, 89, 429-437.

[7]   Gogus, F.; Ozel, M.Z.; Lewis, A.C. The effect of various drying techniques on apricot volatiles analysed using direct thermal desorption-GC–TOF/MS. Talanta, 2007, 73, 321–325.

[8]   Tong Chin, S.; Nazimah, S.A.H.; Quek, S.Y.; Man, Y.B.C.; Rahman, R.A.; Hashim, D.M. Changes of volatiles' attribute in durian pulp during freeze- and spray-drying process, 2008, 41, 1899-1905.

[9]   Gonzalez-Palomares, S.; Estarrón-Espinosa, M.; Gómez-Leyva, J.F.; Andrade-González, I. Effect of the temperature on the spray drying of Roselle extracts (*Hibiscus sabdariffa* L.) Plant Foods for Human Nutrition, 2009, 64 (1), 62-67.

[10] Nunes, J.C.; Lago, M.G.; Castelo-Branco, V.N.; Oliveira, F.R.; Torres, A.G.; Perrone, D.; Monteiro, M. Effect of drying method on volatile compounds, phenolic profile and antioxidant capacity of guava powders. Food Chemistry, 2016, 197, 881-890.

[11] Tietel, Z.; Lewinsohn, E.; Fallik, E.; Porat, R. Importance of storage temperatures in maintaining flavor and quality of mandarins. Postharvest Biology and Technology, 2012, 64, 175–182.

[12] Rosenberg, M.; Kopelman, J.; Talmon, Y. Factors affecting retention in spray-drying microencapsulation of volatile materials. Journal of Agricultural and Food Chemistry, 1990, 38, 1288-1294.

Blackberry pulp microencapsulation with arrowroot starch and gum arabic mixture by spray drying and freeze drying

Nogueira, G. F.[a]; Fakhouri, F. M.[bc]; Oliveira, R. A.[a*]

[a] School of Agricultural Engineering, University of Campinas, Campinas, SP, Brazil

[b] School of Chemical Engineering, University of Campinas, Campinas, SP, Brazil

[c] School of Food Engineering, Federal University of Grande Dourados, Dourados, MS, Brazil

*E-mail of the corresponding author: augustus@feagri.unicamp.br

Abstract

The objective of this research work was to obtain blackberry pulp powder (BL, without encapsulating agent) and microencapsulated blackberry pulp (ML, with encapsulating agent :mixture of starch arrowroot and gum arabic (1:1)) obtained by freeze drying and spray drying and evaluate their physico-chemical properties. The yield of blackberry freeze drying process was higher than the value found for spray drying process. The presence of encapsulating agent and drying method used for producing the powders influenced the average particle size, diameter, hygroscopicity, solubility, wettability and anthocyanin content of the powders.

Keywords: *process yield; average size; hygroscopicity; solubility; anthocyanin; antioxidant property.*

1. Introduction

Blackberry (*Rubus fruticosus*) cv. Tupy is a fruit rich in anthocyanins and phenolic compounds, which has high antioxidant activity.[1] However, its short shelf life, due to their fragility and high postharvest respiration rate, consists of an enormous challenge for agri-food industries. Application of microencapsulation by spray drying and freeze drying is a technique to maintain or increase the stability of blackberry pulp bioactive compounds and to prolong its shelf life.[2] More specifically, spray drying is a technological process in which a fluid product is transformed into powder by atomizing it into a hot gas stream.[3] Freeze drying is based on dehydration by sublimation of a frozen product resulting in a dry material.[4] Both processes can be used as encapsulation method when it incorporates 'active' material within a protective matrix, which is essentially inert to the material being encapsulated.[5] The arrowroot (*Maranta arundinaceae* L.) starch presents good digestibility [6] and gelling ability [7]. Gum arabic is widely used in food industry. It is nontoxic, odorless and tasteless. It interacts with water and has a wide range of applications, such as emulsification, texture control and flavor encapsulation.[8] Until now, no study used arrowroot starch and gum arabic mixture as encapsulating agent during spray drying or freeze drying. The objective of this research work was to obtain pulp blackberry in powder microencapsulated with mixture of starch arrowroot and gum arabic (1:1) by spray drying and freeze drying processes in order to evaluate the influence of different drying methods and presence of encapsulating agent on the physico-chemical properties of blackberry powders.

2. Materials and Methods

2.1. Materials

Frozen fruits of blackberry (*Rubus fruticosus*), cv Tupy, were acquired from "Agro Monte Verde Eirelli", Cambuí – MG, Brazil, and used in this research work. Pulp was obtained by grinding of blackberry fruit in a blender, previously thawed in the refrigerator (8 °C) for 24 h. Then, pulp was sieved to remove the seeds, homogenized and packed in polypropylene bottles and coated with aluminium foil to protect against photodegradation. The samples were stored in freezer at -40 ± 3 °C until drying process. Blackberry soluble solids content was 9 °Brix, determined with a benchtop refractometer (Reichert, Model AR200, USA). The pulp presented total solids content of 10.3 g/100g of pulp.

The following encapsulating agents were used: arrowroot starch containing 15.24 ± 0.19% of water, 0.40 ± 0.03% of protein, 0.12 ± 0.01 % of fat, 0.33 ± 0.01% of ash and 83.91 ± 0.00% of carbohydrates [9]; and gum arabic (Instantgum®, Colloides Naturels, São Paulo, Brazil) containing 14.00 ± 0.10% of water, 1.38 ± 0.16% of proteins, 0.37 ± 0.02% of

lipids, $3.70 \pm 0.10\%$ of ash and $80.46 \pm 0.00\%$ of carbohydrates.[9] All other reagents used for the analyses presented analytical grade.

2.2 Preparation of blackberry pulp microparticles

Blackberry microparticles were produced from homogenization of blackberry pulp with encapsulating agent, consisting of arrowroot starch and gum arabic mixture (1: 1 mass / mass) in ratio of 1:1.78 (mass / mass, blackberry pulp solids and encapsulating agent). Solution of encapsulating agent and blackberry pulp was performed in a mixer type homogenizer at room temperature for 5 minutes. Spray drying and freeze drying techniques were used to prepare blackberry pulp microparticles.

2.2.1 Spray drying

The freshly prepared solution of blackberry pulp and encapsulating agent (item 2.2) was diluted in water in proportion of 1:2 (w / w) to enable its spraying. A benchtop spray dryer (Model B191, Büchi, Flawil, Switzerland) with feed mass flow rate of 0.2 kg / h was used in the process. Atomization was accomplished using a 0.5 mm double-flow atomizer nozzle. Compressed air was used as atomizing media and the inlet and outlet air temperatures were 143 °C and 105.43 ± 3.13 °C, respectively. Compressed air flow rate was 0.6 m^3 / h and its pressure was maintained at 8 bar. Powders were collected at cyclone and finally transferred for polyethylene packages. These spray dried blackberry microparticles were stored in desiccator containing dried allochroic silica gel at 25 °C.

2.2.2 Vacuum freeze drying

A portion of frozen blackberry pulp with and without encapsulating agent (item 2.2) was freeze dried (Mod. 501, Edwards Pirani, Crawley, West Sussex, UK), with initial temperature of -40 °C, pressure of 0.1 mmHg and final temperature of 25 °C per 2 h, with total cycle time of 48 h. The product obtained was ground in hammer mill (MR Manesco and Ranieri LTDA, model MR020, Piracicaba- Brazil) and sieved. Freeze dried blackberry microparticles were stored in the same conditions of spray dried samples.

2.3 Powder characterization

2.3.1 Drying process yield, moisture content, water activity, hygroscopicity, solubility, wettability, particle size distribution of the blackberry powders

Drying process yield was determined by ratio between powder solids mass and feeding solids mass of blackberry pulp. The powder moisture content was gravimetrically obtained by vacuum oven at 60 °C until constant weight. [9] Water capacity was determined by direct reading at 25 °C, using AquaLab Lite apparatus (Decagon Devices Inc., Pullman, USA).

Hygroscopicity was determined according to methodology proposed by Cai and Corke [10], with some modifications. About 1 g of each powder sample was placed in desiccators containing saturated sodium chloride (NaCl) solution, equivalent to 75.7% relative humidity at 25 °C. After one week, the samples were weighed in triplicate and hygroscopicity was expressed in grams of water absorbed per 100 g of solids dry mass of the sample (g / 100g).

Solubility was determined according to the method of Eastman and Moore (1984), cited by Cano-Chauca et al. [11]. The method consisted of adding 1 g of sample to a vessel containing 100 mL of distilled water, operating with high-speed magnetic stirring - level 4 of magnetic stirrer for 5 minutes, followed by centrifugation at 3000 G for 5 minutes. Aliquot of 25 mL of supernatant was removed and brought to the oven at 105 °C until constant weight. The solubility was calculated by weight difference.

Wettability time was evaluated according to the method described by Hla and Hogekamp [12]. The method consisted in dropping of 1 g of powder over 400 g of distilled water at 25 °C in 600 mL beaker and visual measurement using a stopwatch to determine the time required for presence of powdered material on the water surface.

The particle size distribution was determined by a particle size analyzer based on laser diffraction (Mastersizer 2000, Malvern Instruments, UK). The mean diameter was determined based on the diameter of a sphere with equivalent volume (De Brouckere Mean Diameter, D[4.3]). Samples were analyzed in triplicate with dispersion in 99.5% ethanol.

2.3.2 Anthocyanins content

Anthocyanins in powders were determined according to the method employed by Sims and Gamon [13] with adaptations. Samples were weighed in triplicate and homogenized with 3 mL of cold solution of acetone/Tris-HCl (80:20, volume/volume, pH 7.8 0.2M) for 1 minute. The samples remained at repose for 1 hour, protected from light. Then, they were centrifuged for 15 minutes at 3500 rpm and the supernatants were immediately taken to be read in spectrophotometer (B422 model, Micronal) in visible region at 537 nanometers (anthocyanins). The acetone/tris-HCl solution was used as blank sample. The absorbance values were converted to mg/100g of blackberry pulp solids.

2.3.3 Statistical analysis

Significant differences between average results were evaluated by analysis of variance (ANOVA) and Tukey test at 5% of level of significance, using SAS software (Cary, NC, USA).

3. Results and discussion

Microencapsulated blackberry pulp were successfully obtained by spray drying and freeze drying techniques, using a mixture of arrowroot starch and gum arabic as encapsulating agents. However, spray drying of blackberry pulp without encapsulating agent was not possible. There is great difficulty in drying fruit pulps by spray drying method without addition of encapsulating agent, since fruits are rich in low molecular weight sugars, which have low glass transition temperatures and influence transition temperature of dried particles, hindering drying process by this method. With addition of encapsulating agent, the end glass transition temperature of the pulp and agents mixture tends to increase, reducing stickiness of pulp by microencapsulation and, consequently, decreasing its adhesion in drying chamber, making possible to collect the powder. [14]

The powders presented blackberry characteristic sweet aroma and reddish color. The results of characterization of freeze dried blackberry pulp (BL), microencapsulated freeze dried blackberry pulp (ML) and microencapsulated spray dried blackberry pulp (MS) powders are shown in **Table 1**. The yield of freeze drying process was significantly ($p < 0.05$) higher than value found by spray drying. In spray drying method, losses are due to the material adhered to drying chamber and cyclone, which is generally not suitable for use. Blackberry powders with encapsulating agent (ML and MS) presented significant water contents ($p < 0.05$), lower than the non-encapsulating blackberry (BL) powder. The water activity values for all powders was below 0.3, indicating their microbiological stability (Aw < 0.3).

Particles of ML and ML powders were significantly ($p < 0.05$) higher than MS powder particles and, although BL and ML powders were produced by the same method, ML powder particles were significantly ($p < 0, 05$) smaller than BL powder particles, without encapsulant. The presence of encapsulating agent and the type of method used to produce the powders influenced the average particle diameter of powders. The size of spray particles is directly influenced by the size of spray droplets. Size of these droplets is dependent on type of atomizer and physical properties such as atomizer rotation, atomizer pressure and solution solids concentration.[15] The size of particles produced by freeze drying is a consequence of type of milling and its operating conditions.

Table 1. Characterization of freeze dried blackberry pulp (BL), microencapsulated freeze dried blackberry pulp (ML) and spray dried microencapsulated blackberry pulp (MS) powders.

Analysis	Powder of freeze dried blackberry pulp (BL)	Freeze dried microencapsulated blackberry pulp (ML)	Spray dried microencapsulated blackberry pulp (MS)
Process yield (%)	89.24 ± 2.81A*	95.86 ± 0.89A	57.69 ± 8.97B
Moisture content (%)	10.72 ± 2.81A	4.50 ± 0.31B	1.30 ± 0.10B
Aw (decimal)	0.13 ± 0.01B	0.11 ± 0.01B	0.16 ± 0.02A
Mean diameter D [4.3] (µm)	149.50 ± 2.92A	95.96 ± 5.87B	9.82 ± 0.12C
Hygroscopicity (g of adsorbed water / 100g solids)	21.28 ± 0.45A	12.86 ± 0.14C	17.04 ± 0.30B
Solubility in water (%)	61.26 ± 0.49A	53.84± 0.76B	60.16± 0.60A
Wettability (min)	0.99 ± 0.53B	1.66 ± 0.01B	9.77 ± 0.22A
Total Anthocyanins (mg / 100 g of blackberry solids)	125.27 ± 9.77A	125.99 ± 5.25A	86.35 ± 3.37B

*Same letters in the same line show no statistical difference ($p > 0.05$).

BL powder was shown to be more hygroscopic and more water soluble than powders produced with encapsulating agent. Arrowroot starch and gum arabic used as encapsulants have low hygroscopicity. Accordingly, microencapsulation of blackberry pulp tends to reduce the hygroscopicity of resulting powder. Moreover, although gum arabic is highly soluble in water [16], arrowroot starch in its native form has low solubility in water at room temperature, which probably contributed to decrease the solubility of the blackberry powders. This behavior indicates that the blackberry pulp was actually microencapsulated by the arrowroot starch and gum arabic mixture and by both methods.

The wettability of freeze drying powders (BL and ML) were significantly ($p <0.05$) lower than the value found for spray dried powder. This occurred because powders obtained by freeze drying presented larger particle size (Table 1). Particles of larger sizes have more spaces between them, being more easily penetrated by water.[2] On the other hand, powder particles obtained by spray drying were much smaller and less porous. This led to a larger formation of lumps when they came into contact with water. The low wettability of very

fine powders is due to their high surface tension and the viscous layer formed on the surface of the liquid that prevents capillary flow between the intergranular pores.[17]

Concerning the anthocyanin content, freeze dried blackberry powders (BL and ML) presented values significantly ($p < 0.05$) higher than spray drying (MS) powder. The bioactive compounds losses in spray drying process are related to the large air exposed surface [18] and high temperatures, whereas the loss during freeze drying is associated with the grinding of the material after lyophilization.[19]

4. Conclusions

Freeze drying and spray drying methods were successfully used for powder microencapsulation of blackberry pulp (ML and MS) and only freeze drying method was able to dry blackberry pulp (BL) without encapsulant. The yield of the freeze dried blackberry drying process powders was significantly ($p < 0.05$) higher than the value found for spray drying process. Blackberry powders was microbiological stability. The presence of encapsulating agent and the type of method used to produce the powders influenced in physical chemical characteristics of the powders.

5. References

[1] Machado, A.P.F.; Pasquel-Reátegui, J.L.; Barbero, G.F., Martínez, J. Pressurized liquid extraction of bioactive compounds from blackberry (*Rubus fruticosus* L.) residues: a comparison with conventional methods. Food Research International 2015, 77, 675–683.

[2] Ferrari, C.C.; Ribeiro, C.P.; Aguirre, J.M. Spray drying of blackberry pulp using maltodextrin as carrier agent. Brazilian Journal of Food Technology 2012, 15, 157-165.

[3] Gharsallaoui, A.; Roudaut, G.; Chambin, O.; Voilley, A.; Saurel, R. Applications of spray-drying in microencapsulation of food ingredients: An overview, Food Research International 2007, 40, 1107–1121.

[4] Yamashita, C.; Chung, M.M.S.; dos Santos, C.; Mayer, C.R.M.; Moraes, I.C.F.; Branco, I.G. Microencapsulation of an anthocyanin-rich blackberry (spp.) by-product extract by freeze-drying. LWT - Food Science and Technology 2017, 84, 256-262.

[5] Ré, M.I. Microencapsulation by spray drying. Drying Technology 1998, 16, 1195-1236.

[6] Villas-Boas, F.; Franco, C.M.L. Effect of bacterial β-amylase and fungal α-amylase on the digestibility and structural characteristics of potato and arrowroot starches. Food Hydrocolloids 2016, 52, 795- 803.

[7] Charles, A.L.; Cato, K.; Huang, T-C., Chang, Y-H.; Ciou, J-Y.; Chang, J-S; Lin, H-H. Functional properties of arrowroot starch in cassava and sweet potato composite starches. Food Hydrocolloids 2016, 53, 187-191.

[8] Mothé, C.G.; Rao, M.A. Thermal behavior of gum arabic in comparison with cashew gum. Thermochimica Acta 2000, 357-358, 9-13.

[9] A.O.A.C. Official Methods of Analysis. 18th ed. Association of Official Analytical Chemists, Gaithersburg, Maryland, 2006.

[10] Cai, Y.Z.; Corke, H. Production and properties of spray-dried Amaranthus betacyanin pigments. Journal of Food Science 2000, 65, 1248-1252.

[11] Cano-Chauca, M.; Stringheta, P.C.; Ramos, A.M.; Cal-Vidal, J. Effect of the carriers on the microstructure of mango powder obtained by spray drying and its functional characterization. Innovative Food Science and Emerging Technologies 2005, 5, 420–428.

[12] Hla, P.K., Hogekamp, S. Wetting behaviour of instanized cocoa beverage powders. International Journal of Food Science and Technology 1999, 34, 4, 335-342.

[13] Sims, D.A., & Gamon, J.A. (2002). Relationships between leaf pigment content and spectral reflectance across a wide range of species, leaf structures and developmental stages. Remote Sensing of environment, 81, 337-354.

[14] Santana, A.; Cano-Higuita, D.M.; de Oliveira, R.A.; Telis, V.R.N. Influence of different combinations of wall materials on the microencapsulation of jussara pulp (*Euterpe edulis*) by spray drying. Food Chemistry 2016, 212, 1–9.

[15] Goula, A.M., Adamopoulos, K.G. Retention of ascorbic acid during drying of tomato halves and tomato pulp. Drying Technology 2006, 24, 57-64.

[16] Daza, L.D.; Fujita, A.; Fávaro-Trindade, C.S.; Rodrigues-Ract, J. N.; Granato, D.; Genovese, M. I. Effect of spray drying conditions on the physical properties of Cagaita (*Eugenia dysenterica* DC.) fruit extracts. Food and Bioproducts Processing 2016, 97, 20-29

[17] Schubert, H. Instantization of powdered food products. International Chemical Engineering 1993, 33, 1, 28-45.

[18] Oberoi, D.P.S.; Sogi, D.S. Effect of drying methods and maltodextrin concentration on pigment content of watermelon juice powder. Journal of Food Engineering 2015, 165, 172-78.

[19] Kuck, L.S.; Noreña, C.P.Z. Microencapsulation of grape (*Vitilabrusca* var. Bordo) skin phenol extract using gum arabic, polydextrose, and partially hydrolyzed guar gum as encapsulating agents. Food Chemistry 2016, 194, 569-576.

Drying conditions and analysis of physicochemical characteristics of *Capsicum pubescens*

Sánchez-García, C.[a]; Del Ángel-Coronel, O.A.[a]; Paniagua-Martínez, I.[b]; Luna-Solano, G.[c]; Ramírez-Martínez, A.[a]*

[a] Department of Food Engineering. Tecnológico Nacional de México-Instituto Tecnológico Superior de Huatusco, Huatusco, México.

[b] Faculty of Bioanalysis Campus Veracruz. University of Veracruz, Veracruz, México

[c] Department of Chemistry. Tecnológico Nacional de México-Instituto Tecnológico de Orizaba, Orizaba, México.

*E-mail of the corresponding author: alejandrarm@itshuatusco.edu.mx

Abstract

Capsicum pubescens, a chili specie present in south Mexico (Veracruz state) registers upon 30% loss due to the constraints of the market. Therefore, the objective of this project was to determine the physical and chemical parameters of Capsicum pubescens as well as to evaluate the kinetics of drying of this species. Color tests revealed that the samples were the color was less affected by drying conditions (p>0.05) correspond to those dried at 60ºC (0.5 cm thickness), and 50ºC (0.5 and 1 cm thickness) which coincides with the preference of surveyed population. Thus, Capsicum pubescens may be dried under these conditions.

Keywords: Capsicum pusbescens; drying; sensorial analysis; food loss.

1. Introduction

Most chile belongs to the species *Capsicum annuum* while four other lesser known species have also been domesticated. One of this species, the pepper tree (*C. pubescens*), also known as rocoto and locoto in South America, manzano or peron in Mexico, originated in the Andean highlands with extensions in Central America and Mexico [1] [2]. The varieties of this species of chile vary in shape, and the color changes from green (in its immature state) to yellow, orange or red (mature state) [3]. This species is of recent introduction to Mexico where it is cultivated in states with high elevations (1200 to 3000 m) including the High Mountain regions in the state of Veracruz [4]. *C. pubescens* is mainly cultivated in the months from August to December [5]. Despite this fact, it is highly appreciated in several Mexican states and European markets [5][6] because it is more resistant than other common chile species (*C. annuum*) to aphids and its particular flavor. Even though there is scarce information on its sensory qualities, it has been reported that it contains a relatively greater number of individual capsaicinoids and show more diversity in capsaicinoid profiles than other *Capsicum* species [2]. Moreover, its capsaicin:dihydrocapsaicin ratio is different from *C. annuum* which supports and sustain its particular flavor.

Even though *C. pubescens* seems to possess particular properties and its appreciated in international markets, there is scarce information regarding its conservation. Moreover, local producers from the High Mountains region in the state of Veracruz register up to 30% loss of manzano chile due to the constraints of the market. Convective drying is an excellent option to diminish *C. pubescens* loss as well as to provide national and international markets with product throughout the year. Therefore, the objective of this project was to evaluate the kinetics of drying of this species and to determine the physical and chemical parameters of *Capsicum pubescens* during drying. Also, a sensorial analysis of manzano chili powder obtained after drying of fresh fruit was performed.

2. Materials and methods

2.1 Selection and characterization of the raw material

Samples of *Capsicum pubescens* were collected in their mature state (established by the presence of intense yellow color) in a rural area called Ateopa in the municipality of Alpatlahuac, Veracruz (Mexico, 1860 m altitude) between August 2017 and January 2018. After collecting the samples they were transported to Orizaba, Veracruz to be dried. The samples were cut into slices of 0.5 and 1 cm thickness.

2.2 Drying process

Tests were conducted in a pilot plant scale vertical tray dryer (MOD-SEM-2 Polinox, MX). Drying tests were carried out at temperatures of 50, 60 and 70ºC and the air velocity was imposed at 1.2 m/s. In each test, the drying kinetics were evaluated by recording the

moisture content change as function of time. During the drying process, samples were taken to analyze the main physical-chemical parameters (a_w, moisture content and color) every 15 minutes during the first hour, 30 minutes in the following hour, and finally every 60 min until the water activity of the samples reached 0.6.

2.2.1 Effective diffusion

The effective diffusivity of food products can be estimated by Fick's second law of diffusion. Considering the geometry of the pepper tree samples, diffusion is better estimated through the solution of Fick's equation for slab geometry. For long drying periods, this solution can be simplified to only the first term of the series as:

$$\ln M_R = ln \frac{8}{\pi^2} - \left(\frac{\pi^2 D_{eff} t}{4L^2}\right) \tag{1}$$

Where the moisture content was expressed as the moisture ratio (M_R), D_{eff} corresponds to water diffusivity in m^2/s, t is the time in s and L is the thickness in m. Moisture content ratio was calculated by means of eq. (2):

$$M_R = \frac{X}{X_0} \tag{2}$$

Where X corresponds to the moisture content at any time in g water/g of dry solid and X_0 is the initial moisture content in g water/g of dry solid. Tests were conducted in duplicate.

Drying kinetic data was adjusted to a single exponential as shown in equation 3:

$$M_R = \frac{X}{X_0} = e^{-kt} \tag{3}$$

 where k is a model parameter. The goodness of fit of the data to the model was evaluated by means of the R^2 parameter.

2.3 Sensorial analysis test

Manzano chili samples were subjected to a sensorial analysis by means of an hedonic verbal test of 7 points with untrained panelists (N= 150). The samples were presented simultaneously and later, each panelist evaluated each sample only once accompanied by Mexican yam bean (jicama) (*Pachyrizus erosus*). Each participant was asked to indicate how much they liked each sample, assigning an attribute according to the category reported on a scale which ranged from "I disliked it a lot" to "I really liked it a lot". The samples were coded to identify the condition in wich it was dried. After concluding each test, panelists were asked to drink water as a neutralizer to avoid interference with the next treatment.

2.4 Statistical analysis

Differences between drying kinetics and physicochemical parameters of *C. pubescens* samples regarding the drying parameters as well as the significance in the preference of samples were analyzed through an ANOVA test (MiniTab, 2016).

3. Results and discussion

3.1 Air drying kinetics

Fig. 1 and 2 shows the drying kinetics of *C. pubescens* dried at two thickness (0.5 and 1 cm) and three temperatures (50, 60 and 70ºC) and Table 1 shows the values of the rate constants for the first order kinetic parameter as well as the diffusion coefficient for each drying condition proposed.
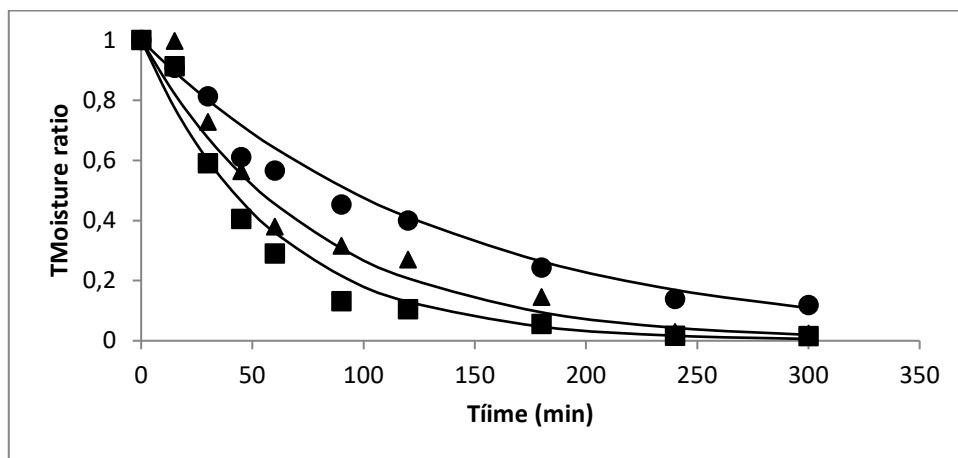
Fig. 1 Drying kinetics of C. pubescens samples of 1 cm thickness (▲=70ºC, ●=60ºC, ♦=50ºC)

Table 1 reveals that the diffusion coefficient is in the range of 10^{-9}-10^{-10} m^2/s which is similar to the diffusion value reported by Lucio-Juárez et al (2012) for habanero chili (*C. chinense*) (5.9470 x10^{-10} m^2/s) which has similar structure to *C. pubescens*. In accordance with the findings of Nguyen and Price [7], the diffusion coefficients for the thicker slices (1 cm) are greater than those for thiner slices (0.5 cm) which are not observed in all foodstuffs. As exposed in this last study, the rate constant from a first order kinectic drying model encompasses several mass transfer mechanisms including the diffusion of water in the falling drying rate.
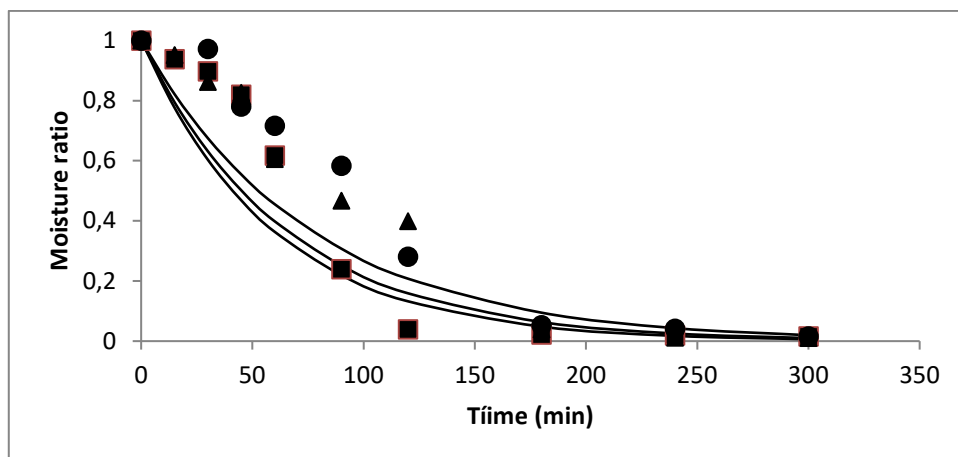
Fig. 2 Drying kinetics of C. pubescens samples of 0.5 cm thickness (▲=70ºC, ●=60ºC, ♦=50ºC)

Table 1. Rate constant and diffusion coefficient for the drying kinetics of C. pubescens

Drying condition	Rate constant (min^{-1})	Diffusion coefficient (m^2/s)
50ºC, 0.5 cm	0.0152	6.4516x10^{-10}
50ºC, 1 cm	0.0075	1.2706x10^{-9}
60ºC, 0.5 cm	0.0168	7.1135 x10^{-10}
60ºC, 1 cm	0.0129	2.1909 x10^{-9}
70ºC, 0.5 cm	0.0177	7.4706x10^{-10}
70ºC, 1 cm	0.0149	2.5267 x10^{-9}

In the present case, the rate constant parameter for the single exponential equation (which is generally related with the diffusion coefficient) effectively represents the drying rates for the samples of 1 cm thickness but is less accurate for samples of 0.5 cm thickness (Fig. 2). Moreover, statistical analysis revealed that the water content difference beetwen samples of chili of 0.5 and 1 cm thickness dried at the same temperature was not significant ($p>0.05$). This may be explained by the internal structure of *C. pubescens* which may play a role in the similarity of loss water at both sample thickness.

3.2 Physicochemical parameters of samples of manazano chili (*C. pubescens*) during the drying process

The color change of the different samples of manzano chili was recorded during the drying process. Table 2 shows the average value of ΔE after 300 min at each drying condition tested for C. pubescens. Results showed that color changed significantly depending on the drying conditions at which samples were subjected ($p<0.05$). After 300 min the lesser color change was observed in samples dried at 60ºC and 0.5 cm, and 50ºC for both sample

thickness (1 cm, and 0.5 cm). Color of C. pubescens (and of chili species in general) is given by carotenoids which may be affected by heat (Hernández-Ortega et al., 2015). Thus, the difference in color may also reflect the loss of carotenoids due to drying.

Regarding the water activity, after 300 min of drying all samples of manzano chili were below 0.6. Analysis test revealed that the decrease of the water activity was not significantly different among the drying conditions studied (p>0.05). The lack of difference between the samples suggests that the loss of water is similar regardless the thickness. This supports the idea that there is a concentration of the water content in thiner samples due to natural causes, such as the internal structure.

Table 2. *ΔE* and *a*$_w$ of slices of C. pubescens (after 300 min) at different drying conditions

Drying condition	ΔE	a_w
50ºC, 0.5 cm	12.26±0.12	0.391±0.55
50ºC, 1 cm	9.6±0.22	0.524±0.71
60ºC, 0.5 cm	7.79±0.03	0.378±0.07
60ºC, 1 cm	15.41±0.57	0.367±0.21
70ºC, 0.5 cm	14.24±0.09	0.301±0.02
70ºC, 1 cm	15.34±0.12	0.405±0.10

3.3 Sensorial analysis test

Statistical analysis revealed that 145 out of 150 people manazano chili powder was highly desirable (p<0.05). We counted the type of samples that were highly accepted (I strongly prefer) by panelists, and we found that nearly 70% preferred the samples dried at 60ºC and 0.5 cm thickness and 60% preferred the samples dried at 50ºC and 1 cm thickness. Interestingly, this drying conditions coincide with those in which the samples showed lesser color change (Table 2). As surveyed population was invited to chose the sample as a function of its flavor, this last result suggests that population relates a good flavor with reddish color.

4. Conclusions

Capsicum pubescens slices dried at different drying conditions showed values of water activity lesser than 0.6 after 300 min process. The diffusion coefficient of thicker samples (0.5 cm) was higher than the values observed in thicker samples (1 cm) similarly with what was observed in bananas. This behavior suggests that there is a concentration of the water content in thiner samples due to natural causes, such as the internal structure. A sensorial analysis test revealed that panelists prefered the samples with lesser color change. As this conditions coincide with those in which the carotenoid content is less damaged C. pubescens may be dried in slices at 60ºC and 0.5 cm or 50ºC and 1 cm.

5. Acknowledgements

6. References

[1] McLeod, M.J.; Guttman, I.; Eshbaugh. H. Early evolution of chili peppers (Capsicum). Economic Botany 1982, 36(4), 361-368.

[2] Zewdie, Y.; Bosland, P. Combining ability and heterosis for capsaicinoids in *Capsicum pubescens*. HortScience 2001, 36(7), 1315-1317.

[3] Oboh, G.; Rocha, J. Distribution and antioxidant activity of polyphenols in ripe and unripe tree pepper (*Capsicum pubescens*). Journal of Food Biochemistry 2007, 31(4), 456-473.

[4] Laborde, J.O.; Pozo C. Presente y Pasado del Chile en Mexico; INIA-SARH. Mexico, 1984

[5] Espinosa-Torres, L.E.; Ramírez-Abarca, O. Rentabilidad de chile manzano (*Capsicum pubescens* RYP) producido en invernadero en Texcoco, Estado de México. Revista Mexicana de Ciencias Agrícolas 2016, 7(2), 325-335.

[6] Rodríguez-Burruezo, A.; Prohens, J.; Raigón, M.D.; Nuez, F. Variation for bioactive compounds in ají (*Capsicum baccatum* L.) and rocoto (*C. pubescens* R. & P.) and implications for breeding. Euphytica 2009, 170(1-2), 169-181.

[7] Nguyen, M.; Price, W. Air-drying of banana: influence of experimental parameters, slab thickness, banana maturity and harvesting season. Journal of food engineering 2007, 79(1), 200-207.

[8] Hernández-Ortega, M., et al. Antioxidant, antinociceptive, and anti-inflammatory effects of carotenoids extracted from dried pepper (*Capsicum annuum* L.). BioMed Research International 2012, 2012, 1-10.

Functional properties of dried tarragon affected by drying method

Koç, B.*; Çağlar, N.; Atar, G.

ªGaziantep University, Faculty of Fine Arts, Dep. of Gastronomy and Culinary Arts, Gaziantep, Turkey

*kocbanu@gmail.com

Abstract

Tarragon is a small shrubby perennial herb in the Asteraceae family. It is cultivated for the use of its aromatic leaves in seasoning, salads, sauces, vinegars, mustard and spices. In this study, tarragon was dried in two different drying equipment (infrared (ID) and microwave dryers (MD)) to compare the drying and final product properties (moisture content, water activity and colour change). Three different output power levels of 125, 250 and 500 W were used for MD, whereas the ID treatment involved three drying temperature levels that were 60, 70 and 80°C. A comparison of the drying kinetics, MD was more effective in shortening drying time when compared with ID.

Keywords: Tarragon, microwave drying, infrared drying, color change

1. Introduction

Herbs and spices are used to season foods throughout the world. These are the aromatic substances that enhance savoury character as flavouring agents and as appetite stimulants. The use of spices has increased significantly over the past years, partly due to renewed interest in dishes that use a wide variety of spices. Tarragon (*Artemisia dracunculus* L.) is a medicinal and aromatic plant that extends all over Eurasia. Tarragon is an herbaceous plant of the Asteraceae family. It is a strong aromatic plant and is also considered as a medicinal plant [1]. Two varieties of tarragon can be distinguished [2; 3]: French Tarragon and Russian Tarragon. French Tarragon of the South European origin is mainly used as a culinary herb in oils, sauces, vinegars, mustard and spices [4; 5]. Tarragon can be consumed as fresh, dried and frozen product. Drying is the main step in the preparation of tarragon for marketing. Not enough data is available in the literature about drying and storage of tarragon.

Correct drying of aromatic plants is necessary for high quality and stable products. The final moisture content (MC) must reach 5-10%. Colour is an important component of quality throughout agriculture and food industry, because colour is closely associated with factors such as freshness, ripeness, desirability and food safety. It is often the primary consideration of consumers when making purchasing decisions. A limited amount of information was found about the stability of dried tarragon and the colour change after drying. Some of tarragon's aspects are lost when it is dehydrated, though, and its colour deteriorates. There has been much research into microwave drying techniques, examining a broad spectrum of fruits and vegetables [6] and others, however, more data are still needed on the effect of microwave drying on the potential role of medicinal plants.

Mathematical modelling of drying processes and kinetics is a tool for process control and can be used to choose suitable method of drying a specific product. The developed models can be used to design new drying systems, determine optimum drying conditions and to accurately predict simultaneous heat and mass transfer phenomena during the drying process. Taking into account the above-mentioned considerations, this study was designed with the objectives to (1) determine the drying characteristics and quality degradation in terms of colour, moisture content and water activity of tarragon subjected to the two drying methods; and (2) examine and compare the applicability of eleven different thin-layer models to the simulation of moisture loss in tarragon during drying.

2. Materials and Methods

2.1. Material

Fresh tarragon leaves of uniform maturity were purchased from the local market at Gaziantep. They were handpicked and cleaned, washed in sufficient tap water twice to remove mud and

other foreign matter and drained completely. The roots and mature stems were removed prior to washing.

2.2. Drying

Drying trials were carried out at three microwave generation power levels: 125, 275, and 625W by using a microwave dryer (Arçelik ARMD580, Turkey). The tarragon leaves (25 g) selected from uniform and healthy plants. Three drying trials were conducted at each power level. The values obtained from these trials were averaged and the drying parameters determined. The rotating glass plate was removed from the oven every 30 s during the drying period and moisture loss determined by weighing the plate using a digital balance (Mettler Toledo PM30, Germany) with 0.01 g precision.

A laboratory scale infrared dryer was used for infrared dehydration of the samples (OHAUS MB200, USA). Approximately 5 g of tarragon leaves were uniformly spread on a dish (12 cm diameter 3 cm height) The drying experiments were conducted at infrared temperatures levels of 60, 70 and 80°C. This drier is equipped with a temperature controller and an electronic balance with an accuracy of ±1°C and ±0.001 g, respectively.

Three drying trials were conducted at each drying temperatures and power levels. Drying process continued until they reached equilibrium state, i.e. constant weight.

2.3. Colour measurement

The colour of fresh and dried leaves was determined by using colorimeter (Hunterlab Colorflex, USA). The results were expressed in accordance with the CIE Lab system. The total colour change (ΔE) of dried tarragon leaves with respect to fresh tarragon was calculated by Eq. (1).

$$\Delta E = \sqrt{\Delta L^2 + \Delta a^2 + \Delta b^2} \tag{1}$$

2.4. Moisture content

Moisture content was determined by drying a sample in an air oven at 105°C until constant mass was obtained.

2.5. Water activity

Water activity was measured with a water activity measurement device (Rotronic, HP23-AW-A, New York) with a 0.0001 sensitivity.

2.6. Mathematical modelling of drying curves

A few theoretical, semi-theoretical and empirical drying models have been reported in the literature. The most frequently used type of model for thin layer drying is the lumped

parameter type, such as the Newton equation [9-11]. The moisture ratio during drying is determined using equation (2):

$$MR = \frac{M_t - M_e}{M_0 - M_e} \qquad (2)$$

where, M_t is the moisture content of the product at any time, M_e is the equilibrium moisture content, M_0 is the initial moisture content all in kg water/kg dry matter.

In this analysis, it was assumed that the moisture gradient driving force during drying is a liquid concentration gradient; meanwhile the effect of heat transfer was neglected as a simplifying assumption. For all experimental conditions, the value of $(M_t-M_e)/(M_0-M_e)$, a dimensionless moisture content was obtained. Because samples were not exposed to uniform relative humidity and temperature continuously during drying, the moisture ratio was simplified as recommended by [7] expressed as follow:

$$MR = \frac{M_t}{M_0} \qquad (3)$$

For mathematical modelling, the equations in Table 1 were tested to select the best model for describing the drying curve equation of the tarragon. The moisture ratio of the tarragon leaves during drying was calculated using equation (3). The goodness of fit of the tested mathematical models on the experimental data was evaluated using coefficient of determination (R^2), mean relative percentage deviation (P) value and the percentage root mean squares error (RMSE) value with higher R^2 values and lower RMSE and P values indicating a better fit [8] as follow:

$$P = \frac{100}{N} \sum_{i=1}^{N} \frac{|Mexp - Mcal|}{Mexp} \qquad (15)$$

$$RMSE = \sqrt{100 \frac{\sum (Mexp - Mcal)^2 / Mexp}{N}} \qquad (16)$$

where M_{exp} and M_{cal} are experimental and predicted moisture content values, respectively, and N is the number of experimental data. A model was considered acceptable if the P values and RMSE values were below 10% and R^2 values were higher than 0.90.

3. Result and Discussion

Microwave drying trials were conducted at output power levels of 125, 275 and 625 W and the influence of each microwave power level on moisture ratio over drying time presented in Fig. 1a. The drying time decreased as microwave power level was increased. The times required for the moisture content of tarragon leaves to decrease from 7.897 to 0.097 % (d.b) were 188, 60 and 40 min at microwave output power levels of 125, 275 and 625W, respectively. The effect of microwave power level of decreasing drying time was observed by [23, 24]. The results indicate that mass transfer is more rapid at higher microwave power

levels because more heat is generated within the sample, creating a larger vapor pressure differential between the interior and the surface of the product [25].

Table 1. Mathematically models used for modelling of drying curves

Model Name	Model Equation		Reference
Lewis-Newton	$MR=\exp(-k*t)$	(4)	[9]
Page	$MR=\exp(-k*t^n)$	(5)	[10]
Modified Page	$MR=\exp(-(k*t)^n)$	(6)	[11]
Henderson and Pabis	$MR=a*\exp(-k*t)$	(7)	[12]
Logarithmic	$MR=a*\exp(-k*t)+c$	(8)	[13]
Two-Term	$MR=a*\exp(-k_0*t)+b*\exp(-k_1*t)$	(9)	[14]
Two-Term Exponential	$MR= a*\exp(-k*t)+(1-a)*\exp(-k*a*t)$	(10)	[15]
Diffusion Approach	$MR= a*\exp(-k*t)+(1-a)*\exp(-k*b*t)$	(11)	[16]
Modified Henderson and Pabis	$MR= a*\exp(-k*t)+b*\exp(-g*t)+ c*\exp(-h*t)$	(12)	[17]
Verma	$MR=a*\exp(-k*t)+(1-a)*\exp(-g*t)$	(13)	[18]
Midilli and Küçük	$MR=a*\exp(-k*t^n)+b*t$	(14)	[19]

MR moisture ratio; a,b,c,g,h coefficients; n drying exponent specific to each equation; k specific to each coefficients equation;t time

Infrared drying trials were conducted at radiation temperature levels of 60, 70 and 80°C. A graph of moisture ratio versus drying time during the infrared drying of tarragon leaves at different temperature levels is presented in Fig. 1b. From the data, moisture ratio decreased over drying time. Furthermore, infrared radiation temperature level influenced the change in moisture ratio of tarragon leaves. The results also showed that when infrared radiation temperature level increases, the time taken to dry tarragon leaves greatly decreased. Accordingly, the drying times required to reduce the moisture content of tarragon leaves to approximately 0.115 % (w.b) were 126, 88 and 66 min when infrared temperature levels of 60, 70 and 80°C, respectively, were applied. A decrease in drying time with increased infrared temperature level has also been reported by other researcher [20].

From these findings it could be stated that drying time for tarragon leaves at 80°C was 2 times shorter than that of 60°C. The experiments data showed that drying time for tarragon leaves at 625 W was 4 times shorter than that of 125W.

The eleven different MR models used to predict the moisture content as a function of drying time are presented in Table 1. The coefficient of determination (R^2), the RMSE and P value were used to assess how well the models characterized the drying curves. The statistical analysis of the models for a given set of drying conditions are shown in Table 2. An analysis of variance indicated that the microwave power and infrared temperature levels significantly affected the drying parameters. Higher microwave power and infrared temperature levels are associated with significant decrease in drying time and moisture ratio which was much more noticeable in microwave than infrared drying. This has been demonstrated in the studies of Azzouz et al. [21]. On the other hand, among the eleven models, the Midilli and Küçük,

model provided the best fit to the microwave and infrared radiation drying data as indicated by a higher R^2 and lower RMSE and P value than those of the other models.

(a)   (b)
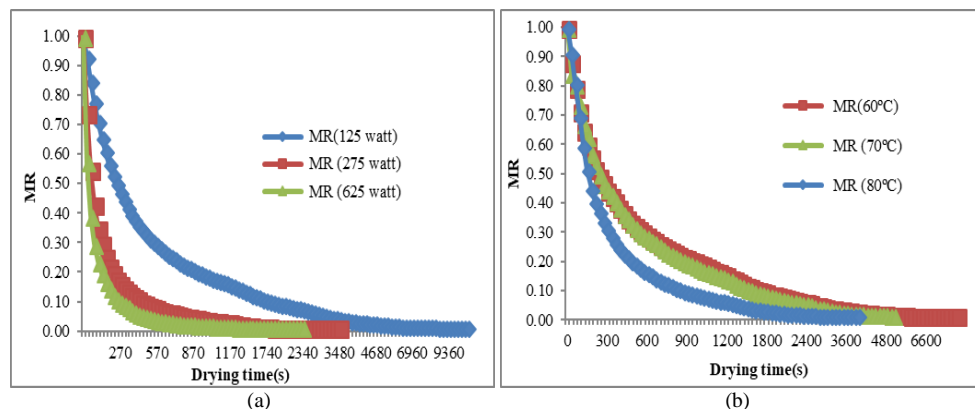
Fig. 1 Variations of moisture ratio as a function of time for different a) infrared drying temperatures, b) microwave drying power

Table 2. Statistical analysis of drying models at various infrared temperatures and microwave powers

		Equation No
		4	5	6	7	8	9	10	11	12	13	14
60 ⁰C	R^2	0.92	1.00	1.00	0.96	0.98	1.00	0.96	1.00	1.00	1.00	1.00
	%RMSE	1.32	0.14	0.14	0.79	0.38	0.23	0.88	0.24	0.23	0.24	0.02
	P	60.2	15.5	15.5	49.7	40.6	18.0	52.1	18.9	18.0	18.9	0.82
70 ⁰C	R^2	0.93	1.00	1.00	0.97	0.98	1.00	0.97	1.00	1.00	1.00	1.00
	%RMSE	1.17	0.06	0.06	0.67	0.46	0.06	0.69	0.09	0.06	0.09	0.02
	P	52.2	13.1	13.1	40.5	33.1	11.4	41.0	12.3	11.4	12.3	2.15
80 ⁰C	R^2	0.97	0.99	0.99	0.97	0.99	1.00	0.99	1.00	1.00	1.00	0.99
	%RMSE	1.03	0.33	0.33	0.86	0.39	0.11	0.63	0.10	0.11	0.10	0.08
	P	54.7	26.6	26.6	50.3	37.2	9.57	43.5	7.80	9.57	7.80	13.8
125 Watt	R^2	0.94	0.99	0.99	0.96	0.98	1.00	0.97	1.00	1.00	1.00	1.00
	%RMSE	1.33	0.34	0.34	1.00	0.46	0.17	0.90	0.17	0.17	0.17	0.08
	P	56.4	26.5	26.5	50.4	47.3	13.6	48.8	13.9	13.6	13.9	14.5
275 Watt	R^2	0.94	0.99	0.99	0.95	0.98	1.00	0.96	1.00	1.00	1.00	0.99
	%RMSE	1.31	0.27	0.27	1.11	0.72	0.13	0.95	0.13	0.13	0.13	0.19
	P	78.0	40.6	40.6	73.6	73.9	29.9	71.4	29.9	29.9	29.9	19.6
625 Watt	R^2	0.93	1.00	1.00	0.94	0.97	1.00	0.96	1.00	1.00	1.00	1.00
	%RMSE	1.21	0.21	0.21	1.07	0.89	0.22	0.95	0.22	0.22	0.22	0.10
	P	85.2	45.5	45.5	83.3	80.6	43.4	80.6	43.4	43.4	43.4	3.93

Water activity of the dried tarragon leaves at different infrared temperatures and microwave power are given in Table 3. Water activity decreased as temperature increased in the infrared dryers. In addition, water activity decreased as microwave power increased in the microwave dryers.

The impact of various drying techniques upon the colour parameters of the dried tarragon leaves was exhibited in Table 3. The *L* value of all the dried tarragon declined considerably

when compared with the fresh tarragon. Additionally, temperature and/or microwave power rise significantly prompted the decline of *L* values and surge of a values which may be by reason of non-enzymatic browning reaction. Among the used microwave drying, the highest *a* value was obtained by the microwave drying at 125 W, while the lowest *a* value loss was obtained by the microwave drying at 625 W. ΔE is a function of a, b and L values, and it was reliant on drying techniques. Microwave drying technique at 275 W resulted in the highest ΔE while lowest ΔE value was attained from the infrared drying technique at 80°C.

Table 3-Comparison between infrared temperatures and microwave power for colour parameters and a_w values

	a_w	L	a	b	ΔE
Fresh	-	35.15[a]±2.18	-8.02[b]±0.20	12.17[ab]±0.19	-
60°C	0.565±0.004	31.07[b]±0.18	-5.96[e]±0.04	11.77[b]±0.19	4,68
70°C	0.336±0.003	31.91[ab]±1.02	-5.56[e]±0.05	12.10[ab]±0.08	4.07
80°C	0.332±0.013	32.68[c]±1.02	-6.11[d]±0.57	12.57[a]±0.63	3.15
125 Watt	0.364±0.001	31.02[b]±0.10	-4.87[a]±0.13	11.84[b]±0.11	5.20
275 Watt	0.154±0.002	30.58[b]±0.64	-5.46[e]±0.43	12.17[ab]±0.56	5.23
625 Watt	0.095±0.002	31.48[ab]±1.07	-6.57[c]±0.23	12.56[a]±0.19	3.96

a-e Means superscript with different alphabets in the same column differ significantly

4. Conclusions

This study characterized the influence of drying conditions on the drying behaviour of tarragon leaves using infrared radiation and microwave drying. It was found that the drying rate increases substantially with the microwave power level or infrared temperature level used. The Midilli model was found to be more suitable for predicting the drying behaviour of tarragon leaves, with the values for R^2 above 0.99 and with the lowest values of RMSE and P values for both drying methods. A comparison of microwave and infrared drying times indicate that irrespective of the power or radiation temperature applied, microwaving is an effective method of shortening the time required for drying to the desired moisture content without charring the samples. Moreover, microwave drying had less influence on the colour and rehydration ratio of the finished product than infrared drying.

5. References

[1] Simon, J.E.; Chadwick, A.F.; Craker, L.E..Herbs: an indexed bibliography, 1971 - 1980: the scientific literature on selected herbs and aromatic and medicinal plants of the temperate zone. Amsterdam, Elsevier; 1984.

[2] Vienne, M.; Braemer, R.; Paris, M.; Couderc H. Chemotaxonomic study of two cultivars of *Artemisia dracunculus* L.: ("French" and "Russian" Tarragon). Biochemical Systematics and Ecology 1989,17(5):373-374

[3] Yaichibe, T.; Masanori, K.; Kenichi, A. Morphological characters and essential oil in Artemisia dracunculus (French Tarragon) and Artemisia dracuncloides (Russian Tarragon). Tokyo Nogyo Daigaku Nogaku Shuho 1997, 41(4):229-238.

[4] Deans, S.G.; Simpson, E.J.M. Artemisia dracunculus- Industrial profiles. Medicinal and Aromatic Plants 2002, (18):91-97.

[5] Ribnicky, D.M.; Poulev, A.; O'Neal, J.; Wnorowski, G.; Malek, D.E.; Jager, R.; et al. Toxicological evaluation of the ethanolic extract of Artemisia dracunculus L. for use as a dietary supplement and in functional foods. Food and Chemical Toxicology 2004, 42(4):585-598.

[6] Bouraout, M., Richard, P. and Durance, T. Microwave and convective drying of potato slices. Journal of Food Process Engineering 1994, 17, 353–363.

[7] Akgun, N.A.; Doymaz, I. Modelling of olive cake thin-layer drying process. Journal of Food Engineering 2005, 68: 455-461.

[8] Goyal, R.K.; Kingsly, A.R.P.; Manikantan, M.R.; Ilyas S.M. Mathematical modelling of thin layer drying kinetics of plum in a tunnel dryer. Journal of Food Engineering 2007, 79(1): 176–180.

[9] Ayensu, A. Dehydration of food crops using a solar dryer with convective heat flow. Solar Energy 1997, 59: 121-126.

[10] Page, G.E. Factors Influencing the Maximum Rates of Air Drying Shelled Corn in Thin Layers M.S. Thesis 1949, Department of Mechanical Engineering, Purdue University, Purdue, USA.

[11] Wang, C.Y.; Singh, R.P. A single layer drying equation for rough rice. ASAE Paper 1978, 78-3001, ASAE, St. Joseph, MI.

[12] Henderson, S.M.; Pabis, S.Grain drying theory. II. Temperature effects on drying coefficients. J. Agr. Eng. Res. 1961, 6:169–174.

[13] Toğrul, I.T.; Pehlivan, D. Mathematical modelling of solar drying of apricots in thin layers. J. Food Eng. 2002, 55:209–216.

[14] Henderson, S.M. Progress in developing the thin layer drying equation. Trans. ASAC 1974, 17:1167–1172.

[15] Sharaf-Eldeen, Y.I.; Blaisdell, J.L.; Hamdy, M.Y. A model for ear corn drying. Trans. ASAE 1980, 23(5): 1261–1265.

[16] Kassem, A.S. Comparative studies on thin layer drying models for wheat. In: Proceedings of the 13th International Congress on Agricultural Engineering 1996., vol. 6, 2–6 February, Morocco.

[17] Karathanos, V.T. Determination of water content of dried fruits by drying kinetics. J. Food Eng. 1999, 39: 337–344.

[18] Verma, L.R.; Bucklin, R.A.; Endan, J.B.; Wratten, F.T. Drying effects of drying air parameters on rice drying models. Trans. ASAE 1995, 85: 296–301.

[19] Akpinar, E.; Midilli, A. Bicer, Y. Single layer drying behaviour of potato slices in a convective cyclone dryer and mathematical modeling. Energy Convers Manage 2003, 44:1689–1705

[20] Sorour, H.; El-Mesery, H. Effect of microwave and infrared radiation on drying of onion slices. International Journal of Research in Applied 2014, 2(5):2347-4580.

[21] Azzouz, S.; Guizani, A.; Jomaa, W.; Belghith, A. Moisture diffusivity and drying kinetic equation of convective drying of grape. J. Food Eng 2002, 55: 323-330.

Effect of the solar dehydration on the antioxidant capacity and the content of flavonoids of the blackberry pulp (rubus spp)

Norman, A. S.[a*]; Ortiz, A. L.[2,3]; Valladares, O. G[2]; Figueroa, I. P.[2]; Ramírez, J. R.[4]

[a] Posgrado en Ciencias de la Sostenibilidad. Universidad Nacional Autónoma de México

[b] Instituto de Energías Renovables. Universidad Nacional Autónoma de México, Morelos, México

[c] Consejo Nacional de Ciencia y Tecnología. Ciudad de México

[d] Instituto Politécnico Nacional, Centro Interdisciplinario de Investigación para el Desarrollo Integral Regional (CIIDIR) Unidad Oaxaca

* E-mail of the corresponding author: azucenanorman@gmail.com

Abstract

Technical performance of two solar drying technologies was evaluated: Solar Greenhouse Drying (SGD) with auxiliary heating system, and Direct Solar Drying (DSD) in order to evaluate its effect on antioxidant activity (AA) and total flavonoids of blackberry (rubus spp) waste destined. The SDG and DSD results were compared with those of the dehydrated samples in an electric stove (ES). The fresh and dried fruits were evaluated; the blackberry seedless pulp was used. The AA and flavonoids showed degradation of 70% and 20% compared to the fresh sample. For both compounds, SGD is the one that offers the greatest conservation.

Keywords: solar drying; antioxidant capacity; flavonoids; blackberry pulp (rubus spp); solar energy

1. Introduction

México was the leader in the production of blackberry in recent years, with 248 thousand 500 tons per year and 13 thousand hectares had been planted for the year 2016 and 96% of the total production corresponds to the state of Michoacán [1,2]. Generally, the largest consumption of blackberries is fresh, but they can be processed and sold in different presentations such as: frozen in bulk or in individual containers, with or without seeds, lyophilized or in juices, in dietary supplements, jelly and jams [3].

The consumption of blackberry has received considerable commercial attention due to its content of phenolic compounds that contribute to its high antioxidant capacity whose health benefits have been well described [3]. Flavonoids have a wide range of biological effects, including antioxidant, anti-inflammatory, antiallergic, anti-ulcer, antibiotic and anticancer properties [3,4]. However, the blackberry is one of the most sensitive and perishable fruit products that exist. It is estimated that 50% of blackberry production is wasted from production to the end of the value chain (both cold and fresh), due to causes associated with the sensitivity of fruits and lack of conservation methods [5].

Solar dehydration technology offers an alternative for food preservation that is economical, needs low maintenance, environmentally friendly and preserves nutrients [6]. The objective of this study was to perform the solar dehydration of the blackberry pulp without seed and in form of a film with a thickness of 0.5 mm, determining the characteristics of the drying using a greenhouse solar dryer and a direct solar dryer. The direct solar dryer was with natural convection and the greenhouse solar dryer with forced convection at 0.5 ms-1 (equipped with three solar air heaters). Additionally, the antioxidant capacity and the flavonoid content were determined as a measure of the quality deterioration of the product.

2. Materials and Methods

2.1. Samples and pretreatment

The samples of fresh blackberry were supplied by a local farmers from Los Reyes Michoacán Valley, the samples were considered "production process", that is, they did not meet export standards. They were frozen and transported to the Renewable Energy Institute, in Temixco Morelos where the tests were carried out. Before carrying out the drying tests, the blackberries were disinfected, pureed in a blender and the seeds were separated from the pulp with a strainer. They were placed in plastic trays of 33x47x1 cm, the pulp formed a homogeneous film with thickness 0.5±0.1 cm and then dehydrated by each of the following methods.

2.2. Drying methods

The experimental study was carried out in Temixco, Morelos with a latitude of 18˚ 50'N and a length of 99˚ 14'W situated at elevation 1299 meters above sea level. The tests were carried out on July 16-17 (first drying), June 21-22 (second drying) and July 5-6 (third drying), of 2017. The samples were dehydrated between 9:30 am and 5:00 pm (solar time) continuously. The DSD and SGD prototypes are described in López, V. et al, [7] and Tamayo [8] and developed in the Renewable Energy Institute, (IER-UNAM).

2.2.1.   *Direct Solar Drying (DSD).*

Two trays with blackberry pulp were placed in the direct dryer prototype (Fig. 1a), with an area of 0.48 m^2 and exposed to direct sunlight until reaching a water loss equilibrium measured with a balace with an accuracy of 0.1 g. The monitoring of the moisture loss of the product during drying was carried out by successive records every 20 minutes (first two hours of drying) and then every 30 minutes (up to constant weight).

2.2.2.   *Solar Greenhouse Drying (SGD).*

Twenty six trays were placed with blackberry pulp (thirteen in each table) extended all along the table (Fig. 1b), inside the drying chamber of the greenhouse which operated with auxiliary solar heating up to constant weight. The recording and monitoring of weight loss was performed in the same way as that described for DSD.

2.2.3.   *Electric Stove (ES).*

Two trays with blackberry pulp were placed inside the electric stove drying chamber at 60±1 ˚C with forced convection at 1 ms^{-1} for seven hours (time required to reach a constant weight loss). The recording and monitoring of weight loss was performed in the same way as that described for DSD and SGD.

a)   b)
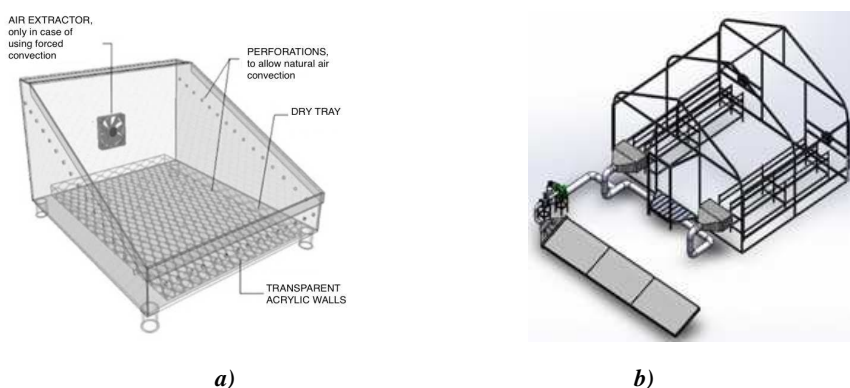
Fig. 1a. Direct Solar Drying (DSD) scheme; 1b. Solar Greenhouse Drying (SGD).

2.3. Extraction of organic compounds

It was weighed 0.5 g of fresh and dried sample of blackberry pulp. Two secuencial extractions of organic compounds was carry out usin 5 ml of methanol at 80%, sonicated in an ultrasound bath for 30 min, centrifuged at 1820 rpm for 10 min. The supernatant was recovered. The total organic extract was filtered with a Pasteur pipette packed and stored in an amber vial at 4°C until analysis.

2.4. Antioxidant activity (AA)

It was used the method developed by Blois, 1958 [9] and described by Brand-Williams et al. in 1995 [10] to determine antioxidant activity by the use of a stable free radical 1,1-diphenyl-2-picrylhydrazyl (DPPH). In total darkness is added 100 μL of the organic extract to a spectrophotometric cell followed by 2.9 ml of DPPH reagent. After reaction for 30 min at 25 °C the absorbance versus prepared blank was read at 517 nm. The results of antioxidant activity of the blackberry pulp (fresh and dried) were expressed as mg of equivalent ascorbic acid per gram of dry matter (mg AAE/g d.m) through the calibration curve with ascorbic acid (all samples were performed in triplicates). The calibration curve range was 0, 5, 9, 12.5, 17, 21 and 25 mg/100ml ($R^2 = 0.98$).

2.5. Total Flavonoid

The total flavonoid content was determined by the aluminum chloride colorimetric assay [11, 12]. An aliquot (1 ml) of extracts or standard solution of quercentine was added to 10 ml amber vial containing 4 ml distilled water and vortexed for 30 seconds. Was added 300 μl $NaNO_2$ at 5%, vortexed for 30 seconds, and incubate at room temperature for 6 minutes. After the time, 300 μl of $AlCl_3$ at 10% was added and keep it for 5 minutes at room temperature. Subsequently, 2 ml of NaOH (1M) was added, and finally the volume of each dilution was completed with 2.4 ml of distilled water. The absorbance versus prepared blank was read at 510 nm after 30 min of reaction at 25 °C . The results of total flavonoid content of the blackberry pulp (three replicates per treatment) are expressed as mg of equivalent quercetin per gram of dry matter (mg QE/g d.m). The calibration curve range was 20, 40, 60, 80 and 100 mg/l ($R^2 = 0.99$).

3.   Results and discussion

3.1. Comparison of drying kinetics

Fig. 2 shows the relationship of the average drying time (n=3) and the final moisture content (less than 32% dry matter) by the different drying methods of the blackberry pulp. The reference of the kinetics is given by drying in electric stove (ES) were the drying time was 480 min at 60°C and 1ms^{-1}, the final moisture content was 0.31 kg of water per kilogram of dry matter. The DSD tests are carried out by natural convection and the SGD with forced convection at 0.5 ms^{-1}. The average drying times for SGD and DSD

corresponded to 960 min respectively, with a moisture content of 0.33 and 0.35 kg_w/kg_{dm}. The drying times for solar technologies do not show significant differences.
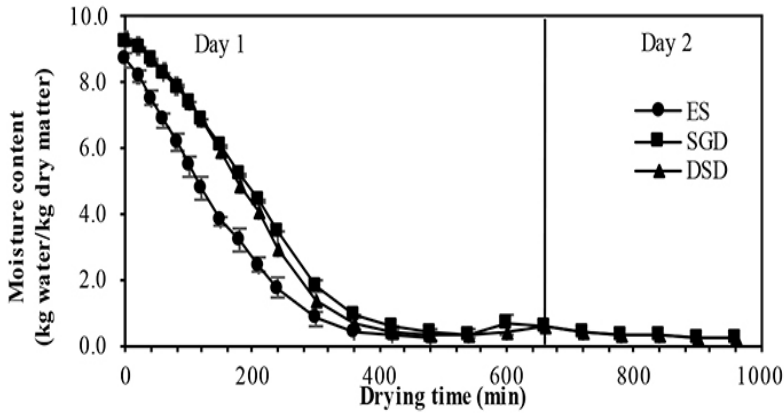
Fig. 2 Comparison of drying kinetics (n=3) by different methods: Solar Greenhouse Drying (SGD), Direct Solar Drying (DSD) and reference in electric stove (ES).

3.2. Antioxidant Activity in blackberry pulp

In Fig.3 the antioxidant activity in the blackberry pulp of the fresh and dehydrated samples by the different technologies are presented. The fresh sample contains 20.22±2.94 mg AAE/g d.m, and on average dehydrated samples loss 70% of their antioxidant capacity compared to fresh samples. The antioxidant activity in the blackberry dehydrated by SGD and DSD (5.86±0.51 and 5.80±0.39 mg AAE/g d.m) is barely greater than the method of drying in the electric stove SE (5.28±0.32 mg AAE/g d.m).
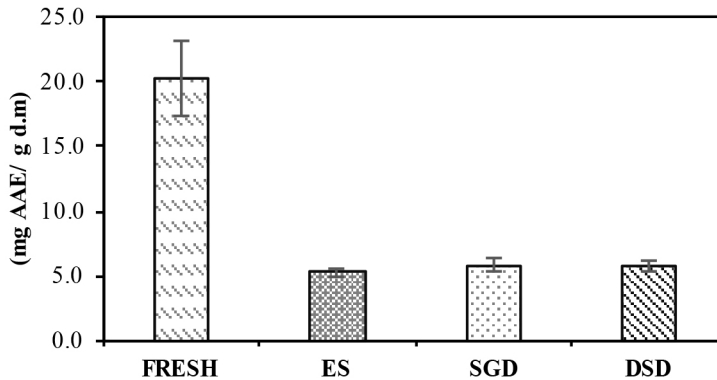
Fig. 3 Antioxidant activity of the blackberry pulp, fresh and dehydrated by different technologies

The concentration of the antioxidant activity is shown in Fig.4a for each of the three tests and for ecah drying technologies. The influence of the average irradiance of the day on the total antioxidant capacity of the samples is shown. For SGD and DSD samples 1 and 3 are

affected by the influence of irradiance, with an inversely proportional correlation, a higher irradiance lower antioxidant activity, a lower irradiance greater antioxidant activity. However, sample 2 of SGD and DSD, seems not to follow this trend.

The Fig. 4b shows the influence of temperature on antioxidant activity, for each of the tests dried by different technologies. The effect is shown by the influence of temperature giving an inversely proportional correlation. That is, the samples subjected to a higher average drying temperature correspond to the lower concentrations of the antioxidant activity. The samples dehydrated in the electric stove at 60 ˚C, are those that have a lower antioxidant activity.
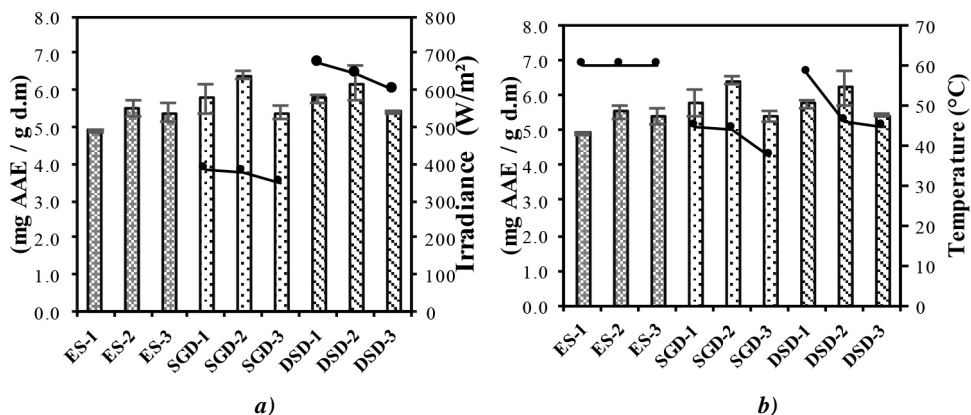
Fig. 4a Antioxidant activity in blackberry pulp and its effect by irradiance; 4b antioxidant activity in blackberry pulp and its effect by temperature.

3.3. Total flavonoid content in blackberry pulp

Fig.5 shows the content of total flavonoids in the blackberry pulp of the fresh and dehydrated sample. The fresh sample contains 12.17 ± 0.79 mg of QE/g d.m. The samples dehydrated by SGD, DSD and ES technologies contain 10.53 ± 0.46, 9.94 ± 0.21 and 8.89 ± 0.24 mg of QE/g d.m. On average the total flavonoids in dehydrated samples are degraded 20% compared to fresh samples.

Fig.6a shows the influence of average irradiance on the total flavonoid content. A correlation of the concentrations was observed for the samples that subjected it to a higher average irradiance, resulting in lower concentration of total flavonoids. In the same way, Fig. 6b shows the influence of the average temperature of the day on the concentration of total flavonoids present. A greater effect due to the temperature is observed, since the samples dehydrated in the electric stove at 60˚C, are those that have a lower concentration, even when they are in darkness inside the drying chamber. Inside the drying chambers of SGD and DSD the samples that were subjected to a higher average temperature are those that show lower concentration of flavonoids, and vice versa.
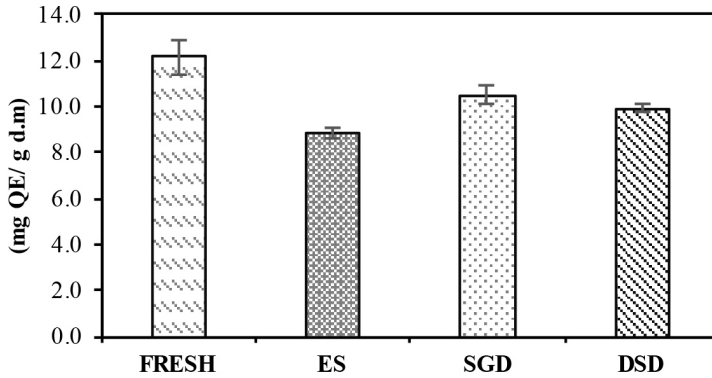
Fig. 5 Total flavonoids in the blackberry pulp, fresh and dehydrated by different technologies

a)   *b)*
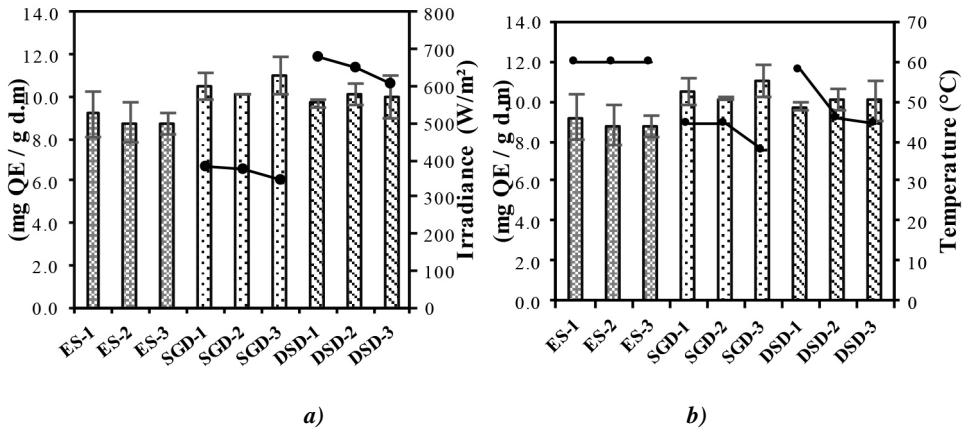
Fig. 6a Total flavonoids in blackberry pulp and its effect by irradiance; 6b total flavonoids in blackberry pulp and its effect by temperature.

4. Conclusions

The samples dehydrated by ES showed an average drying time of 480 min with a final moisture content 0.26 kgw/kgdm. The samples dehydrated by solar technologies do not present significant differences between them, for SGD and DSD the average drying time was 960 min, with final moisture content 0.33 and 0.35 kgw/kgdm.. The antioxidant activity of dehydrated blackberry pulp by different technologies (SGD 5.86 ± 0.51, DSD 5.80 ± 0.39 and 5.28 ± 0.32 mg AAE / gdm) show a decrease of 70% compared to fresh samples (20.22 ± 2.94 mg AAE / gdm). The concentrations of total flavonides in fresh samples corresponding to 12.17 ± 0.79 mg of QE / gdm, and the concentrations measured in the dehydrated samples (SGD 10.53 ± 0.46, DSD 9.94 ± 0.21, 8.89 ± 0.24 mg of QE /

gdm) represent a 20% decrease. In the comparison of solar technologies and electric stove, both solar technologies present a better conservation of flavonoid and antioxidant capacity. In the individual analysis of the tests a relation of temperature and irradiance in the final concentrations was observed, at higher temperature and irradiance, lower concentration of total flavonides and lower antioxidant capacity, having a greater effect on the drying temperature, since the dehydrated samples in the stove at 60°C shows the lowest concentrations.

5. References

[1] SIAP. Sistema de Información Agroalimentaria y Pesquera. Statistical Yearbook of Agricultural Production. 2017. Available: http://nube.siap.gob.mx/cierre_agricola/. [Access:17 September 2017].

[2] Food and Agriculture Organization of the United Nations. FAOSTAT. Available: http://www.fao.org/faostat/. [Access: 15 Febraury 2018].

[3] Kaume, L.; Howard, L. R. and Devareddy, L. The Blackberry Fruit: A Review on Its Composition and Chemistry, Metabolism and Bioavailability, and Health Benefits. J. Agric. Food Chem., 2012, 60 (23) 5716–5727.

[4] Cho, M. J.; Howard, L. R.; Prior, R. L. and Clark, J. R. Flavonoid glycosides and antioxidant capacityof various blackberry, blueberry and red grapegenotypes determined by high-performanceliquid chromatography/mass spectrometry. J. Sci. Food Agric. 2004, 84 (13) 1771–1782.

[5] Sáchez, R. G. La Red de Valor de la Zarzamora. El cluster de Los Reyes, Michoacán un ejemplo de reconversión competitiva. Morelia, 2008.

[6] Orsata, V.; Raghavana, G. S. V. and Soslea, V. Adapting Drying Technologies for Agri-Food Market Development in India. Drying Technol., 2008, 26 (11) 1355 — 1361.

[7] López, V. E., Pilatowsky, F.I and Navarro, O. Drying of Strawberry in a Direct and Indirect Solar Dryer (Effects of Drying Methods on Total Phenolic Content). IJAAEE, 2015, 2 (2) 61-63, 2015.

[8] Tamayo, H. D. Diseño, construcción, intrumentación y evaluación de un secador solar tipo invernadero. México, 2017.

[9] Blois, M. S.. Antioxidant Determinations by the Use of a Stable Free Radical. Nature, 1958, 181, 1199 – 1200.

[10] Brand, W. W.; Cuvelier, M. and Berset, C. Use of a free radical method to evaluate antioxidant activity. LWT-Food Sci. Technol., 1995, 28 (1) 25-30.

[11] Mabry, T.; Markham, K. R. and Thomas, M. B. The systematic identification of flavonoids, Nueva York: Springer, 1970, p. 354.

[12] Zhishen, J.; Mengcheng, T. and Jianming, W. The determination of flavonoid contents in mulberry and their scavenging effects on superoxide radicals. Food Chem., 1999, 64, (4) 555-559, 1999.

Long-term maintenance of dried acellular matrices

Zambon, A.[a,b]; Giobbe, G. G.[a,c]; Vetralla, M.[a,b]; Michelino, F.[a]; Urbani, L.[c,d,e]; Pantano, M. F.[f]; Pugno, N. M.[f,g,h]; De Coppi, P[c]; Elvassore, N.[a,b,c]; Spilimbergo, S.[a]*

[a]Department of Industrial Engineering, University of Padova, via Marzolo 9, 35131 Padova, Italy
[b]Venetian Institute of Molecular Medicine, Via Orus Giuseppe 2, 35129 Padova, Italy
[c]Stem Cells and Regenerative Medicine, Great Ormond Street Institute of Child Health, University College London, 30 Guilford Street, WC1N 1EH London, United Kingdom
[d]Institute of Hepatology London, Foundation for Liver Research, 111 Coldharbour Lane, London, SE5 9NT
[e]Faculty of Life Sciences & Medicine, King's College London
[f]Laboratory of Bio-inspired & Graphene Nanomechanics, Department of Civil, Environmental and Mechanical Engineering, University of Trento, Via Mesiano 77, I-38123 Trento, Italy
[g]Ket Lab, Edoardo Amaldi Foundation, Italian Space Agency, Via del Politecnico snc, 00133 Rome, Italy.
[h]School of Engineering and Materials Science, Queen Mary University of London, Mile End Road, London E1 4NS, UK.

*E-mail of the corresponding author: sara.spilimbergo@unipd.it

Abstract

Dried and sterile acellular esophageal matrix was obtained within a new drying process based on the use of supercritical carbon dioxide (SC-CO₂). Experiments were performed coupling a conventional detergent enzymatic treatment with two different drying methods: (i) SC-CO₂ drying alone; (ii) dehydration in ethanol and a subsequent SC-CO₂ drying. Long term preservation was achieved for several months after drying, demonstrating the maintenance of extracellular matrix (ECM) structure, mechanical properties and biocompatibility within cell repopulation studies in vitro. Overall, the results highlighted the potential of this novel technology to obtain a dry and sterile acellular matrix that can be easily stored for oesophageal regeneration in patients with emergency need.

Keywords: decellularized tissue; supercritical drying; carbon dioxide; tissue engineering; long term storage

1. Introduction

Congenital and acquired diseases may involve surgical esophagus substitution. In adult population, esophageal cancer is the eighth most common cancer in the world [1] while esophageal atresia is a congenital anomaly in children that occurs in 1/2500 to 1/4000 live births [2,3]. Esophageal tissue engineering is an emergent alternative for the development of esophageal substitute as repairing technology [4]. Several esophageal engineered substitutes have been explored using synthetic and natural derived scaffolds and materials [5], however, at present, tissue engineering applications to esophageal replacement are limited to enlargement plasties with absorbable non-cellular matrices [6]. Therefore the development and reinforcement of alternative approach are needed to improve the current state of the art. The use of natural matrices in tissue engineering has become extremely promising as tissue substitute for organ reconstruction. Natural acellular matrices are derived from animal or human organs/tissues within a decellularization process which is able to remove cells and immunogenic material [7]. The result is a natural derives scaffold that retains the architecture of the original tissue and also the molecular components of the native extracellular matrix (ECM). Organ decellularization for tissue engineering has become more and more promising for the organ/tissue replacement with preliminary promising clinical experience [8]. Organ decellularization can be successfully applied to esophagus, resulting in a scaffold that maintains ultrastructure and composition of the native extracellular matrix (ECM) [9]. In a clinical scenario, long term preservation and banking of sterile decellularized organs ready for transplantation would be desirable for patients with emergency needs. However, once produced, decellularized scaffolds can't be stored for long time because sterilization and preservation technologies are still lacking. Improvement of the current state of art could be obtained within supercritical carbon dioxide (SC-CO_2) drying. SC-CO_2 drying has been already used in for the production of biomaterials such as 3D porous scaffolds [10] and hydrogel [11]. Within SC-CO_2 drying the vapor-liquid interface can be avoided with a minor capillary stress for the product that maintains the original structure. SC-CO_2 has a low critical temperature that doesn't degrade thermo sensitive components. SC-CO_2 has also bactericidal properties and it has been deeply investigated as alternative pasteurization and sterilization methods [12,13].

In this scenario the aim of this work is the development of a novel method for the sterilization and long maintenance of decellularized tissue using SC-CO_2 drying.

2. Materials and Methods

Porcine esophagus was chosen as test sample. Esophagi were collected from white domestic piglets (*Sus scrofa domesticus*) from 25 to 40 kg in weight. All surgical procedures and animal handling were carried out in accordance with UK Home Office guidelines under the Animals (Scientific Procedures) Act 1986 and the local ethics

committee. Esophageal decellularization was achieved by using a detergent enzymatic treatment (DET) as previously reported [9]. Two different experimental procedures have been explored for the drying: a single step SC-CO_2 drying at 35°C and 10 MPa up to 360 min, and a combined double step with ethanol (EtOH) for 80 min followed by SC-CO_2 drying (EtOH+SC-CO_2) at 35°C and 10 MPa up to 90 min. A high pressure sapphire window cell (Separex S.A.S.) was used to carry out the experiments. The internal temperature and pressure were set with a thermostatic bath and an HPLC pump (Gilson 25SC). CO_2 (purity 99.990%, Messer) was flowed into the reactor at a constant flow rate of 23 ml/min until 10 MPa; then the pressure was maintained constant by tuning on a micrometric valve. The vessel was depressurized opening the valve at the end of the drying. Samples were packaged for long-term storage in sterile plastic bag at 4°C up to 6 months. Samples were weighted after the treatment assuming that all weight loss was due to the moisture removal from the ECM. Weight reduction was expressed as the ratio of % W_{end}/W_{start}, with W_{end} and W_{start} expressing respectively the weight of the sample after and before the treatment. Microbiological analysis were performed by means of the standard plate count techniques as previously reported [14] for mesophilic bacterial, mesophilic bacterial spores and yeasts and molds. The enumeration was referred to the weight of initial product and expressed in colony forming units CFU/g. The degree of inactivation was calculated considering the $\log(N/N_0)$, where N_0 (CFU/g) and N (CFU/g) is the number of CFU per gram in the untreated and treated sample, respectively. Mechanical characterization was performed with tensile tests with a Midi 10 electromechanical testing machine (Messphysik Materials Testing) at a speed of 0.1 mm/s on regular rectangular peaces fixed at the loading frame. Before testing, the dried samples were rehydrated for 24 h in Phosphate Buffer Saline (PBS-Sigma). Histological analysis were performed on tissue's slice for Haematoxylin and Eosin (H&E), Masson's trichrome (MT) and Alcian blue (all from Bio-Optica). Cytochemistry analyses on tissue's slices were performed using Alexa Fluor 488 Phalloidin (Thermo Fisher) 1:200 and Hoechst (Sigma Aldrich) 10 µM diluted in PBS with 0.1% Triton X-100 (Sigma Aldrich). Color and fluorescence images were obtained using a color camera mounted on fluorescence inverted microscope (Leica DMI4000). Human bone marrow mesenchymal stem cells (hBMMSCs) were provided by the Cell factory of Policlinico Hospital (Milan, IT) and they were used for scaffold repopulation *in vitro*. Cell repopulation experiments were performed up to 8 days of culture in customized microwell evaluating the cell adhesion and viability. Cultured samples were analyzed with Live/Dead viability/cytotoxicity kit for mammalian cells (Thermo Fisher) according to manufacturer's instructions

3. Results and Discussion

Two methods were investigated for the obtainment of a dried acellular esophagus. A successful dried matrix was reached in a shorter time using the combined ethanol and SC-

CO2 treatment. The addition of EtOH as co-solvent during the process positively influenced the solubility of polar solvent in SC-CO2 [15] and therefore reduced the time of drying. In Fig 1 is represented a cylindrical portion of decellularized esophagus before and after the supercritical drying, and after the rehydration in PBS.
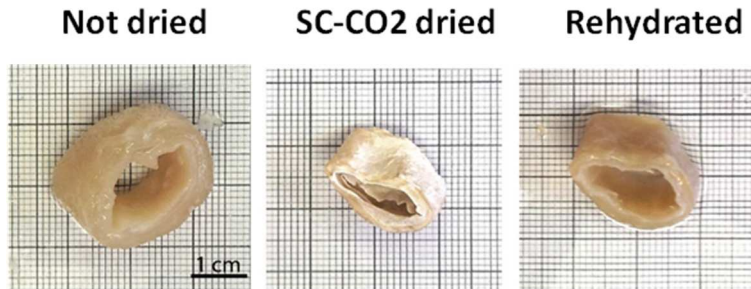
Fig. 1. Picture of cylindrical section of esophagus before (not dried) and after the supercritical drying and the subsequent rehydration in PBS.

Certain shrinkage was observed after the rehydration; mechanical tests didn't show significant differences between the two processes (data not shown) and also a good maintenance of mechanical properties during time (data not shown). The preservation of the esophageal architecture was demonstrated with the presence of the three layers with histological analyses: mucosa, submucosa and muscular layers in all the analyzed samples for H&E (data not shown). MT staining pointed out the maintenance of the collagen in the *lamina propria*, *submucosa* and *intermuscular septa* of the *muscularis externa*. AB staining did not show a further decrease of glycosaminoglycan (GAG) after the drying (data not shown). The preservation of the architecture were obtained till 6 months for the H&E (Fig 2 Top) and confirmed with MT and AB (data not shown). Live and Dead analysis demonstrated good biocompatibility in vitro up to 8 days of culture for the samples dried with the combined process, meaning that $SC-CO_2$ alone was not able to remove some toxic component from decellularization (data not shown). Repopulation tests demonstrated the presence of live cells on the surface; the repopulation was possible also after 3 and 6 months of storage. Fig 2 (centre and bottom) shows the live and dead analysis at the surface for the total nuclei (Hoechst) in blue and for the dead cells in red (Ethidium). Cells shown high viability *in vitro* and therefore good biocompatibility even after 8 days of culture in the samples stored for 6 months. The initial load of natural flora population is shown in Table 1. A complete inactivation of the microorganisms was obtained after the $EtOH-SC-CO_2$ process, while $SC-CO_2$ drying alone was not able to inactivate completely mesophilic bacterial and spores (data not shown).

Zambon, A.; Giobbe, G. G.; Vetralla, M.; Michelino, F.; Urbani, L.; Pantano, M. F.; Pugno, N. M.;
De Coppi, P; Elvassore, N.; Spilimbergo, S.
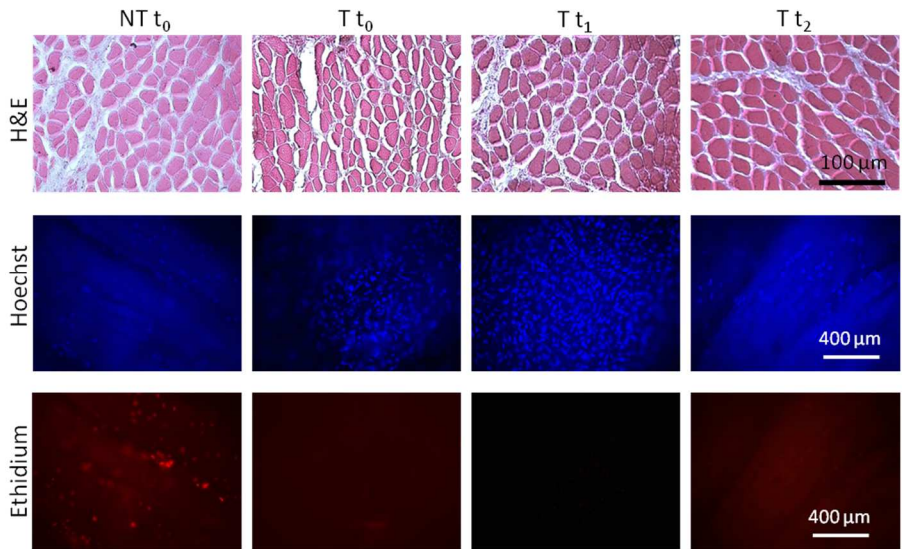
Fig. 2. H&E staining (Top), live and dead analysis for nuclei with Hoechst (centre) and with Ethidium (bottom) at different storage time.

Table 1. Initial microbiological load of the decellularized esophagus before the treatment

Microorganism	Log N_0 [CFU/g]
Mesophilic bacteria	8.22 ± 0.89
Mesophilic spores.	0.57 ± 0.12
Yeast and molds	8.27 ± 0.66

4. Conclusions

Overall the results highlighted the potential of this novel method to obtain a dry acellular matrix that can be stored for long term without substantial change of properties from the native tissue. SC-CO_2 drying represents a promising alternative for the long term maintenance of decellularized tissue.

5. Acknowledgements

6. References

[1] Ferlay, J., et al. "GLOBOCAN 2012 v1. 0, Cancer Incidence and Mortality Worldwide: IARC CancerBase No. 11. Lyon, France: International Agency for Research on Cancer; 2013." Last accessed April (2014).

[2] Spitz L, Kiely E, Pierro A. Gastric transposition in children—a 21-yearexperience. J Pediatr Surg. 2004; 39:276–281.

[3] Sfeir, R., Michaud, L., Salleron, J., & Gottrand, F. (2013). Epidemiology of esophageal atresia. Diseases of the Esophagus, 26(4), 354-355.

[4] Jensen, Todd, Wael Sayej, and Christine Finck. "Esophageal Tissue Engineering." Frontiers in Stem Cell and Regenerative Medicine Research: Volume: 3 3 (2017): 216.

[5] Maghsoudlou P., BSc (Hons.),Eaton S., De Coppi P. Tissue engineering of the esophagus. Seminars in Pediatric Surgery 2014; 23:127–134.

[6] Poghosyan, T., et al. "Esophageal tissue engineering: Current status and perspectives." Journal of visceral surgery 153.1 (2016): 21-29.

[7] Gilbert, Thomas W., Tiffany L. Sellaro, and Stephen F. Badylak. "Decellularization of tissues and organs." Biomaterials 27.19 (2006): 3675-3683.

[8] Elliott, Martin J., et al. "Stem-cell-based, tissue engineered tracheal replacement in a child: a 2-year follow-up study." The Lancet 380.9846 (2012): 994-1000.

[9] Totonelli G, Maghsoudlou P, Georgiades F, Garriboli M, Koshy K, Turmaine M, Ashworth M, Sebire NJ, Pierro A, Eaton S, De Coppi P. Detergent enzymatic treatment for the development of a natural acellular matrix for oesophageal re generation. Pediatric Surgery International, 2013, 29, 87-95.

[10] Pisanti, P., Yeatts, A. B., Cardea, S., Fisher, J. P., & Reverchon, E. (2012). Tubular perfusion system culture of human mesenchymal stem cells on poly-L-lactic acid scaffolds produced using a supercritical carbon dioxide-assisted process. Journal of Biomedical Materials Research Part A, 100(10), 2563-2572.

[11] Baldino, L., Cardea, S., De Marco, I., & Reverchon, E. (2015). Complete glutaraldehyde elimination during chitosan hydrogel drying by SC-CO2 processing. The Journal of Supercritical Fluids, 103, 70-76.

[12] Spilimbergo, S., Matthews, M. A., & Zambon, A. (2018). Supercritical Fluid Pasteurization and Food Safety. In Alternatives to Conventional Food Processing (pp. 153-195).

[13] Qiu, Q. Q., Leamy, P., Brittingham, J., Pomerleau, J., Kabaria, N., & Connor, J. (2009). Inactivation of bacterial spores and viruses in biological material using supercritical carbon dioxide with sterilant. Journal of Biomedical Materials Research Part B: Applied Biomaterials, 91(2), 572-578.

[14] Ferrentino G, Balzan S, Spilimbergo S. Optimization of supercritical carbon dioxide treatment for the inactivation of the natural microbial flora in cubed cooked ham. Int J Food Microbiol. 2013 Feb 15;161(3):189-96

Zambon, A.; Giobbe, G. G.; Vetralla, M.; Michelino, F.; Urbani, L.; Pantano, M. F.; Pugno, N. M.; De Coppi, P; Elvassore, N.; Spilimbergo, S.

[15] Ekart, M. P., Bennett, K. L., Ekart, S. M., Gurdial, G. S., Liotta, C. L., & Eckert, C. A. (1993). Cosolvent interactions in supercritical fluid solutions. AIChE Journal, 39(2), 235–248.

Spray dried proliposomes of *Rosmarinus officinalis* polyphenols: a quality by design approach

Bankole, V. O. [a,b]; Souza, C. R. F.[a]; Oliveira, W. P. [a*]

[a] LAPROFAR group, Faculty of Pharmaceutical Sciences of Ribeirão Preto, University of São Paulo, Ribeirão Preto, Brasil.
[b] Department of Pharmaceutics, Faculty of Pharmacy, Obafemi Awolowo University, Ile-Ife, Nigeria.

*E-mail of the corresponding author: wpoliv@fcfrp.usp.br

Abstract

Harnessing the benefits of rosemary polyphenols is limited by variability in their physicochemical properties. These limitations may be overcome by encapsulation in systems possessing hydro-lipophilic centers thereby accommodating molecules of different polarities. Proliposomes offer a viable option in this regards, being particles which form liposomal suspension in water. Lyophilized extracts of rosemary was encapsulated in hydrogenatedsoyphosphatidylcholine/cholesterol by solvent replacement method. Spray dried proliposomes were obtained with lactose as carrier. Using Central Composite Design, the effects of lipid, extract and carrier concentrations on response variables including bioactive content and retention, moisture content characteristics, recuperation and redispersibility were evaluated by statistical analysis.

Keywords: Polyphenols; antioxidant; proliposomes; spray drying.

1. Introduction

Plant polyphenols have indeed proven to be very worthy antioxidants with evidence of protection of cell constituents against oxidative damage, therefore, limiting the risk of various degenerative diseases associated to oxidative stress.[1] This efficacy together with their safety profile, biocompatibility, multifunctionality, relative affordability and ready availability may have favoured their choice as additives in foods and nutraceticals.[2] Research into polyphenol has garnered much momentum over the years.[3] One important vegetable source of these polyphenol compounds is *Rosmarinus officinalis* L. (Lamiaceae) commonly called rosemary. Extracts of rosemary have been evaluated for antioxidant and various other effects, and its efficacy correlated to high amounts of phenolic acids e.g. rosmarinic acid and caffeic acid; phenolic diterpenes being chiefly carnosic acid and carnosol; and flavonoids.[4] The performance of obtained extract is influenced by processing and environmental conditions to which it is exposed as well as its physicochemical properties. [5] Thus, employment of strategies that ensure incorporation of the multiple bioactive polyphenol components of these extracts for synergistic activity while desirable physicochemical properties are kept intact is evidently desirable. The aim of this study, therefore, is to use Design of Experiments (DoE) in evaluating the effects of composition factors critical to desirable response attributes and system performance during spray drying of proliposomes of rosemary polyphenols.

2. Materials and Methods

2.1 Preparation of rosemary extract
Polyphenol-rich powder extracts of rosemary was obtained by freeze drying. Concentrated liquid extract was congealed at -20 and -80 ºC then lyophilized using VLP 195 FD-115, Thermo Fischer Scientific Lyophilizer at -40 ºC. Dry rosemary powder particles obtained was collected in airtight amber bottles and stored at -20 ºC.

2.2 Quantification of marker compounds in lyophilized extract by HPLC
Polyphenol markers, namely caffeic acid (CA), rosmarinic acid (RA), carnosol (CAR), and carnosic acid (CNA) in the powdered extract were quantified by HPLC. The chromatographic method used was previously developed and validated by our group.[6]

2.3 DoE for evaluation of effect of composition variables in proliposome formulations
Control parameters critical to physicochemical characteristics of proliposome powders were selected using Quality by Design (QbD) approach,with a focus on composition variables. Critical independent variables evaluated were concentration of lipid, extract and drying carrier (relative to liposomal solid content). The effects of these factors on quality attributes of proliposomes such as biomarker retention, biomarker content, water activity and moisture content were investigated. The individual and combined effects of these factors were evaluated at three levels using a completely randomized 2^3 Box-Wilson Central

Composite Design (CCD),[7] with three replicates in the central point. Tables 1 and 2 show the uncoded and coded variables studied, respectively.

Table 1: Uncoded variables and their respective values

Coded variable	Uncoded variables	-1	0	1
A	Lipid concentration (%)	4	7	10
B	Extract concentration (%)	1.5	3	4.5
C	Carrier concentration (%) i.e. Carrier:(Lipid+extract)	1	1.2	1.4

Table 2: CCD for proliposomes of rosemary (coded variables)

Formulation	Coded variables		
	A	B	C
F2	1.000	-1.000	-1.000
F9	-1.682	0.000	0.000
F4	1.000	1.000	-1.000
F3	-1.000	1.000	-1.000
F11	0.000	-1.682	0.000
F13	0.000	0.000	-1.682
F10	1.682	0.000	0.000
F16	0.000	0.000	0.000
F1	-1.000	-1.000	-1.000
F12	0.000	1.682	0.000
F15	0.000	0.000	0.000
F7	-1.000	1.000	1.000
F17	0.000	0.000	0.000
F5	-1.000	-1.000	1.000
F6	1.000	-1.000	1.000
F8	1.000	1.000	1.000
F14	0.000	0.000	1.682

The process model has the following form (Eq. 1):

$$Yi = a_0 + a_1.X_1 + a_2.X_2 + a_3.X_3 + a_{11}.X_1^2 + a_{22}.X_2^2 + a_{33}.X_3^2 + a_{12}.X_1.X_2 + a_{13}.X_1.X_3 + a_{23}.X_2.X_3 + \varepsilon$$

(1)

where: a_0 to a_{33} are the regression coefficients, X_1 to X_3 denotes the factors, Y_i is the relative average or expected response associated with the combination factors and ε represents the experimental error. Statistical significance of linear, quadratic and interaction effects of the investigated variables on evaluated proliposomes properties was assessed through variance analysis (ANOVA) and regression analysis using Statistica® 10 (StatSoft Inc, USA).

2.4 Preparing proliposomes of polyphenol-rich rosemary extract

2.4.1 Incorporation of rosemary polyphenols

Liposomal preparations incorporating polyphenols of rosemary were prepared by solvent replacement method.[8,9] The lipid phase comprised predetermined quantities (by DoE) of hydrogenated soy phosphatidyl choline (Phospolipon 90H - LIPOID GMBH, Ludwigshafen, Germany) and cholesterol (Sigma-Aldrich, St Louis, USA). The aqueous phase consists of a dispersion of lyophilized rosemary extract in purified water. The two phases were brought to the same temperature before the lipid phase was injected into the aqueous phase under agitation. Residual solvent was removed by rotary evaporation at 48 ºC/600 mmHg. Liposomal formulation obtained was dried with lactose (Natural Pharma, SP, Brasil) as the drying carrier (quantity determined by CCD).

2.4.2 Spray drying

Spray dried proliposomes (SDP) were generated from the liquid liposomal formulation (LLF) in a laboratory scale bench top SD-05 spray dryer (Lab-Plant UK Ltd, Huddersfield, UK) with a concurrent flow regime. Spray drying conditions were maintained as follows: atomizer, 1 mm; inlet drying gas temperature, 100 ºC; feed flow rate of liquid formulation, 4 g/min; atomizing air pressure, 1.5 KgF/cm^2; feed flow rate of atomizing air, 17 Lpm; and feed flow rate of spray drying air, 60 m^3/h.

2.5 Proliposome characterization

Proliposome powders were characterized as follows:

2.5.1 Water activity (Aw) and moisture content (Xp)

Moisture content of the spray dried product was determined in a moisture analyzer Sartorius MA35 (Goettingen, Germany). Water activity was measured in an AquaLab 4TEV (Decagon Devices Inc., Pullman, WA) at 25 ºC, using dew point sensor.

2.5.2 Retention and content of biomarker compounds in proliposomes

Total retention and concentration of bioactive markers in proliposomes was evaluated by the HPLC quantification method described. [6] Retention was determined as % biomarker compound quantified in a sample of proliposome powder relative to amount in lyophilized extract contained in the proliposome sample. Total content of biomarker in bulk quantity was determined relative to proliposome powder (w/w). Concentrations were determined by comparison to those of standards.

3. Results and Discussion

3.1 Proliposome characterization

Experimental data of proliposome properties evaluated were subjected to regression analysis to detect the statistically significant effects of composition variables on proliposomes properties. In this way, the linear, quadratic and interaction regression

coefficients and their statistical significance were derived (Table 3). ANOVA and effect estimates assume normal and independent residuals distribution, with mean zero and constant variance.

3.1.1 Water activity (Aw) and Moisture content (Xp)

Water activity (A_w), a measure of the energy state of water present in a system, is a qualitative property independent of sample quantity. It is usually considered as indicative of microbiological stability with values less than 0.5 recommended as enough to guarantee product stability. Results showed that besides the interaction effects between lipid/extract concentration and extract/carrier concentration, only the quadratic effect of carrier concentration also had significant effect on water activity (Table 3). The negative value attributed to the effect may be that water activity is related to the form in which the lactose exists, among other factors. Lactose has been previously used in drying of lipid systems encapsulating polyphenols.[10] Lactose monohydrate has been shown to lose its water of hydration at 100 °C, the drying temperature in this study.[11] Thus, increasing the carrier concentration leads to a higher percentage bound-water loss and lower A_w. While Xp and A_w are mainly related to the drying conditions, formulation composition also plays an important role as drying could promote changes in water binding and dissociation, with effect product properties. On the other hand, carrier concentration showed no level of significance on Xp of SDP while lipid and extract concentrations became significant only at $p \leq 0.1$. Values of A_w and Xp were < 0.5 and 5%, respectively, for SDP (data not shown). This suggests that proliposomes obtained are potentially stable to microbial proliferation.

3.1.2 Retention of selected biomarkers

Retention of RA and CAR in SDP showed significant dependence on similar factors. Linear effects of % extract was observed as highly significant ($p \leq 0.01$) for retention of both compounds. However, while the effect on RA was positive, it was negative for CAR, implying that as the quantity of extract incorporated increases, retention of the former increases while that of the latter decreases. The degradation pattern of CAR in this system appears to be concentration dependent thus giving rise to decreased % retention on increasing concentration,[12] typical of first order degradation. Its higher lipophilicity also suggests favored partitioning into lipidic wall of the proliposomes rather than aqueous core.

Hence, higher extract/lipid ratio favourably retained hydrophilic compounds protected in the aqueous vesicle core against lipophilic components which are no longer efficiently encapsulated and therefore exposed to degradation at the vesicle periphery.[13] The linear effect of % lipid incorporated further demonstrates this relationship, although quasi significant ($p \leq 0.10$) to both RA and CAR retention with respective negative and positive effects. It may be that the negative effect of % lipid on RA retention is related to solubility of the compound. Increasing lipid concentration is suggested to favor retention of lipophilic material such as CAR (positive value for same factor) as against less lipophilic ones such as RA. Evaluated lone factors ranged from being significant ($p \leq 0.05$) to highly significant ($p \leq 0.01$) for CNA retention. Lipid and carrier concentrations showed positive effects on

CAN, similar to CAR and in line with their lipophilicity. Increasing % extract, however, significantly ($p < 0.05$) reduces relative retention of CAN. Since the degradation of CAR is concentration dependent, the reaction is skewed away from buildup of its concentration hence, further degradation of CNA. The significant ($p < 0.05$) positive effect of carrier concentration on CNA retention may be due to protective effect offered by lactose molecules to prevent or slow down it`s degradation.[10,14] Evaluated factors showed no interactive effect on retention properties of bioactive compounds in SDP. In any case, the integrity of the bioactive compounds was largely preserved with proliposome products exhibiting 60.0% – 104.6 % retention. It is noted that these retention extremes is in accordance with the lipophilicity of each compound i.e. more lipophilic compounds such as CAR and CNA have the highest retention values at F11 with the highest lipid ratio whereas the less hydrophobic compound, RA is more concentrated at F9 with least lipid ratio, and vice versa (Table 4). Response surface plots (not shown) for visual effects of relationship between studied variables and biomarker retention response revealed that retention pattern of marker compounds at 0.0 (mean) level of Carrier/C_{Solid} is similar to that at -1.682 (low), and 1.682 (high) levels. While RA retention is facilitated at high level of % extract, both CAR and CNA are favourably retained at high levels of % lipid.

Table 3: Linear, quadratic and interaction regression coefficients and statistical significance for SDP

Formulation	Regression Coefficients for Selected Responses							
	Biomarker Retention (%)			Total Biomarker content (mg/100g)			A_w (-)	Xp (%)
	RA	CAR	CNA	RA	CAR	CNA		
a_0 - Mean/Interc.	97.342*	88.284*	80.157*	116.776*	88.472*	73.005*	0.402*	1.837*
a_1 - $A_{(L)}$	-3.587***	4.827***	4.741*	-45.242*	-22.403*	-19.385*	-0.001	0.239***
a_{11} - $A_{(Q)}$	1.268	-4.116	-1.192	15.738*	3.249	5.187*	0.009	0.290***
a_2 - $B_{(L)}$	7.058*	-12.941*	-3.383*	47.765*	24.194*	23.725*	-0.008	-0.193
a_{22} - $B_{(Q)}$	-4.261**	6.494***	-0.715	-7.387***	-5.343**	-5.788*	0.004	0.260***
a_3 - $C_{(L)}$)	0.013	-0.292	2.175**	-11.404*	-8.819*	-5.249*	0.000	-0.101
a_{33} - $C_{(Q)}$	0.983	-1.050	1.994**	0.136	1.418	2.513**	-0.023**	0.161
a_{12} - $A_{(L)}$* $B_{(L)}$	1.061	0.162	0.674	-8.809***	-2.817	-1.958***	0.023**	0.296***
a_{13} - $A_{(L)}$ * $C_{(L)}$	0.710	-1.565	0.965	4.220	1.963	1.748***	-0.015	-0.216
a_{23} - $B_{(L)}$ * $C_{(L)}$	-0.832	-2.424	-0.740	-5.070	-5.643***	-1.801***	-0.025**	-0.192
R^2adj	0.744	0.720	0.853	0.967	0.951	0.992	0.824	0.751

* Effect significant at $\alpha \leq 0.01$; ** Effect significant at $\alpha \leq 0.05$; *** Effect significant at $\alpha \leq 0.1$

3.1.3 Biomarker composition of proliposomes

Linear effects of lipid and extract concentrations were most significant ($p \leq 0.001$) of factors evaluated. This being that the overall content of polyphenols components of proliposome product is directly proportional to the amount of extract incorporated and inversely to the lipid concentration and is consistent with results obtained for other extracts incorporated in lipid systems. Regression coefficients presented (Table 3) showed that whereas % extract has positive values for all compounds, those of % lipid are negative. R^2 values indicate the adequacy of adjustment of results obtained by the statistical model proposed. Carrier concentration was also highly significant ($p \leq 0.01$) to concentrating all marker compounds in the proliposome. Lone effects of all factors evaluated showed

different levels of significance. Whereas interactions between % lipid and % extract, and % extract and carrier concentration showed quasi significance ($p \leq 0.1$) on the total content of RA and CNA, the same level of significance was observed on CNA content following interaction between % lipid and carrier concentration. These results reveal that polyphenols accumulation is highly dependent on the % extract present and independent of the levels of concentration of carrier. Surface plots (not shown) show effects of the most significant variables (%extract and % lipid) remained visibly constant at all Carrier/C_{Solid} levels.

Table 4: Retention and total concentration of biomarkers in spray dried SDP

Formulation	Biomarker retention in SDP (%)			Total biomarker content of SDP (mg/100g)		
	RA	CAR	CNA	RA	CAR	CNA
F1	97.2±2.8	88.1±1.8	77.4±1.7	579.9±16.6	443.7±9.0	355.7±8.0
F2	86.1±0.8	101.3±2.4	82.0±0.9	245.9±2.2	244.2±5.8	180.2±2.0
F3	102.9±2.2	83.2±2.0	71.1±0.5	1191.6±25.8	814.1±19.5	634.4±4.2
F4	97.8±1.0	83.7±1.0	77.8±0.5	664.2±6.8	479.9±6.0	406.7±2.6
F5	96.9±0.7	103.0±1,6	84.0±0.9	481.9±3.4	432.6±6.5	321.8±3.3
F6	90.5±1.9	96.6±2.4	91.9±3.5	215.1±4.6	193.9±4.9	168.3±6.4
F7	101.0±1.2	75.1±0.9	74.2±0.3	975.1±11.3	611.8±7.0	551.5±2.0
F8	97.1±0.7	82.7±1.7	85.3±1.5	549.3±3.9	395.1±8.3	371.8±6.6
F9	106.4±1.5	62.0±0.4	66.2±1.1	1281.9±18.1	630.8±3.9	614.1±9.9
F10	93.0±0.8	92.4±1.3	86.8±0.5	369.0±3.1	309.3±4.5	265.0±1.5
F11	63.8±2.6	104.6±0.9	83.6±2.2	80.9.0±3.3	150.7±0.9	81.7±2.2
F12	104.4±1.8	73.8±0.5	72.1±0.8	916.0±16.0	546.3±3.9	487.0±5.2
F13	99.3±0.1	87.4±0.1	84.7±1.0	699.6±5.1	519.5±4.8	459.6±5.5
F14	98.5±2.3	84.4±1.1	86.3±1.8	510.1±12.0	368.7±4.8	343.8±7.3
F15	98.1±1.1	88.5±1.4	79.2±1.5	585.4±6.5	425.9±.3	364.1±7.0
F16	97.3±1.2	88.4±1.2	80.4±0.6	580.9±7.2	465.6±6.2	369.3±2.6
F17	97.0±1.0	87.7±0.7	81.0±0.5	578.8±6.0	441.8±3.3	381.3±2.5

4. Conclusions

Proliposome is a viable system for the retention of polyphenols of rosemary. Careful choice of carriers and their appropriate concentration may, however, be necessary towards obtaining these desirable properties. These many factors and possibilities underscore the importance of Design of Experiments, a systematic approach to determine the relationship between factors involved in a process and the effects of those factors on the output of that process. The Central Composite Design is demonstrated as an efficient approach in which the effects of several factors can be assessed within a workable number of experiments.

5. References

[1] Scalbert, A.; Manach, C.; Morand, C.; Rémésy, C.; Jiménez, L. Dietary polyphenols and the prevention of diseases. Critical Reviews in Food Science and Nutrition 2005, 45 (4), 287–306.

[2] Ozsoy, N.; Yilmaz-ozden, T.; Serbetci, T.; Kultur, S.; Akalin, E. Antioxidant, anti-inflammatory, acetylcholinesterase and thioredoxin reductase inhibitory activities of

nine selected Turkish medicinal plants. Indian Journal of Traditional Knowledge 2017, 16 (4), 553–561.

[3] Cortés-Rojas, D.F.; Souza, C.R.F.; Oliveira, W.P. Assessment of stability of a spray dried extract from the medicinal plant *Bidens pilosa* L. Journal of King Saud University - Engineering Science 2016, 28 (2), 141-146.

[4] Tavassoli, S.K.; Mousavi, S.M.; Emam-Djomeh, Z.; Razavi, S.H. Chemical composition and evaluation of antimicrobial properties of *Rosmarinus officinalis* L. essential oil. African Journal of Biotechnology 2011, 10 (63), 13895–13899.

[5] Taghvaei, M.; Jafari, S.M. Application and stability of natural antioxidants in edible oils in order to substitute synthetic additives. Journal of Food Science and Technology 2015, 52 (3), 1272-1282.

[6] Souza, C.R.F. Production of standardized dried extracts of Brazilian medicinal plants: study of the technical and economic feasibility of the process in spout bed (PhD Thesis) 2007, 1-32.

[7] NIST/SEMATECH e-Handbook of Statistical Methods, http://www.itl.nist.gov/div898/handbook/, 2017.

[8] Wagner, A.; Vorauer-Uhl, K. Liposome Technology for Industrial Purposes. Journal of Drug Delivery 2011, 1–9.

[9] Hasan, M.; Hasan, M.; Mondal, J.C.; Hasan, M.Al., Talukder, S.; Rashid, H.A. Liposomes: An advance tools for novel drug delivery system. The Pharma Innovation Journal 2017, 6 (11), 304–311.

[10] Secolin, V.A.; Souza, C.R.F.; Oliveira, W.P. Spray drying of lipid-based systems loaded with Camellia sinensis polyphenols. Journal of Liposome Research 2017; 27 (1), 11–20.

[11] Raut, D.M.; Allada, R.; Pavan, K.V. ; Deshpande, G.; Patil, D.; Patil, A.; Deshmukh, A.; Sakharkar, D. M.; Bodke, P.S.; Mahajan, D.T. Dehydration of Lactose monohydrate: Analytical and physical characterization. Der Pharmacia Lettre 2011, 3 (5), 202–212.

[12] Zhang, Y.; Smuts, J.P.; Dodbiba, E.; Rangarajan, R.; Lang, J.C.; Armstrong, D.W. Degradation study of carnosic acid, carnosol, rosmarinic acid, and rosemary extract (*Rosmarinus officinalis* L.) assessed using HPLC. Journal of Agricultural and Food Chemistry 2012, 60 (36), 9305–9314.

[13] Nakayama, T.; Hashimoto, T.; Kajiya, K.; Kumazawa, S. Affinity of polyphenols for lipid bilayers. Biofactors 2000, 13, 147–151.

[14] Lo, Y.L.; Tsai, J.C.; Kuo, J.H. Liposomes and disaccharides as carriers in spray-dried powder formulations of superoxide dismutase. Journal of Controlled Release 2004, 94 (2-3), 259–272.

[15] Chu, C.; Tong, S.; Xu, Y.; Wang, L.; Fu, M.; Ge, Y.; Y, J.; Xu, X. Proliposomes for oral delivery of dehydrosilymarin: preparation and evaluation in vitro and in vivo. Acta Pharmacologica Sinica 2011, 32 (7), 973–980.

The drying and rehydration process of chayote (*Sechium edule*)

Álvarez-Morales, A. [a]*; Luna-Solano, G.[b]; Ramírez-Martínez, A[a]

[a] Department of Food Engineering. Tecnológico Nacional de México-Instituto Tecnológico Superior de Huatusco, Huatusco, México.

[b] Department of Chemistry. Tecnológico Nacional de México-Instituto Tecnológico de Orizaba, Orizaba, México.

*E-mail of the corresponding author: alejandrarm@itshuatusco.edu.mx

Abstract

Chayote (Sechium edule) is a fruit that is said to be a nutritional and have healing properties. 90% of its weight is made up of water which makes this fruit highly perishable. Convective drying is an excellent option to reduce the loss of this product as well as prolong its shelf life. Thus, the main objective of this work was to assess the physicochemical characteristics of different chayote samples (slices, cubes and strips) during its drying and rehydration process. Results suggest that cubes represent an alternative for commercial use as an additive in foodstuffs due to their size.

Keywords: chayote; convective drying; rehydration process; physiochemical properties.

1. Introduction

The chayote (*Sechium edule*) is native to Mesoamerica where the greatest genetic diversity is found, however, it can also be found in other parts of the world. Mexico is one of the leading producers of this fruit which losses up to 25% of the harvest due to bad practices during the postharvest, particularly during the storage and refrigeration of the product as estimated by local producers. These bad practices lead to physical damages that generate darkening in the pericarp, formation of depressions, incomplete maturation, susceptibility to microbial attack, formation of shoots and weight loss [1].

Resarchers have studied methods for the preservation of the fruit due to its good nutritional and healing properties as well as for its accessibility to low-income groups [2] [3] [4] [5]. Chayote has a low content of lipids, proteins and calories, and is an important source of minerals, aminoacids and vitamins. At the same time, this fruit is highly perishable because about 95% of its fresh weight is water [6]. The reported properties of chayote include diuretic (leaves and seeds), as well as cardiovascular and anti-inflammatory properties (leaves and flesh). Also, the consumption of chayote was associated with the reduction of the retention of urine and burning when urinating when kidney stones are dissolved [7].

The drying process allows prolonging the shelf life of foods with high moisture content. Convective drying may particularly constitute a good option for the conservation of chayote due to the ease of the operation of convective driers as well as the relative simplicity in the handling of the samples to be treated. On the other hand, the analysis of the rehydration of dried food is necessary since it allows to evaluate indirectly the damage that occurred in the food due to the drying process. Moreover, it is fundamental to evaluate the physicochemical properties of rehydrated foods to ensure the conservation of their flavor and sensorial properties. To date, there are few studies where the physiochemical characteristics of the chayote during its drying and rehydration process are evaluated. On that basis, the aim of this work was to, determine the drying characteristics of samples of chayote cut in three different geometric shapes (cubes, slices and strips) dried in a convective dryer at temperature of 60ºC; to study the drying process parameters on the physical and chemical properties of this fruit (water, moisture and color activity); and to study the rehydration process of the samples obtained in the drying process.

2. Materials and Methods

2.1 Selection and characterization of the raw material

Export-quality chayote samples (*Sechium edule v.* virens levis) from the city of Campo Grande located in the municipality of Ixtacxoquitlan, Veracruz were used in the present study. Chayote samples fruits were completely smooth and without spines. They weighted

between 200-300 g, had an average moisture content of 92.8% and water activity (a_w) of 0.994, in average.

After the selection of the samples, they were washed and cut with a manual cutter in three different geometric shapes: slices (5 cm diameter and 0.5 cm thickness), cubes (1 cm length); and strips (7cm height, 1cm length and 0.5cm thickness).

2.2 Drying process

Tests were conducted in a pilot plant scale vertical tray dryer (MOD-SEM-2 Polinox, MX). Drying tests were carried out at a temperature of 60ºC and the air velocity was imposed at 1.2 m/s. In each test, the drying kinetics were evaluated by recording the moisture content change as function of time. During the drying process, samples were taken to analyze the main physical-chemical parameters (a_w, moisture content and color) every 15 minutes during the first hour, 30 minutes in the following hour, and finally every 60 min until the water activity of samples reached 0.6. Tests were conducted in duplicate.

Drying kinetic data was adjusted to three common models employed in the drying process to model data: Page model, Newton model and Henderson-Pabis model (Table 1) where M_R corresponds to the adimensional moisture content and k, k_1, k_2, k_3, a and n are model paramters. For this purpose, the moisture moisture content (M_R) was expressed as the moisture ratio (M_R) by means of eq. (1):

$$M_R = \frac{X}{X_0} \qquad\qquad (1)$$

Where *X* corresponds to the moisture content at any time in g water/g of dry solid and *X_0* is the initial moisture content in g water/g of dry solid. The goodness-of-fit of the data to the proposed models was evaluated by means of the R^2 parameter.

2.2.1 Physicochemical characterization of the chayote

Water activity was determined using the AquaLab equipment (AquaLab Series 3 TE model, USA) in conditions of 25 ± 1°C. Moisture content (X) was determined by means of an Infrared moisure analyzer (Sartorius MA35, USA). In order to obtain more realisitc moisture content values, the moisture analyzer was warmed up for 30 minutes prior the determination of the moisture content. After this, the samples used for the determination of X (1 g) were returned to the dryer chamber where they were previously taken.. The color was determined by using a MiniScan XE plus colorimeter (HunterLab, USA). The color measurement was carried out by placing the sample inside the equipment, thus, acquiring the color parameters corresponding to the luminosity: L *, and chromaticity: a * and b *. The color data was captured in a computer integrated to the colorimeter and processed by a software application (Universal software 4.10, USA) to obtain the total difference of color (ΔE). Tests were conducted in duplicate.

2.3 Rehydration of convective dried chayote samples

The adsorption capacity of the samples was determined by weighing 0.5 g of the dried chayote samples on an electronic analytical balance (Santorius TE14S, USA). Then, the samples were submerged in 150 mL of water at 3 different temperatures: 20, 50 and 85 ° C, respectively. The samples were removed at different times (2, 4, 6, 10, 15, 20, 25, 30, 35, 40, 50 and 60 min). The final weight of the samples was recorded after removing the excess of water from the surface with absorbent paper. The rehydration ratio was calculated as the maximum amount of water absorbed (g) per g of dehydrated material for each experiment at the different times as proposed by Domaz [8]. Tests were conducted in duplicate.

3. Results and discussion

3.1 Air drying kinetics

During the drying process the moisture content of the samples was monitored at different times. The coefficients of drying models and the goodness of fit for chayote samples are given in Table 1. In general, the Page model sufficiently described the drying kinetics for strips and cubes (Fig. 1 and Table 1). All samples showed a slight losss of wáter at the beginning of the process but in the case of slices this slight loss was also observed at the gap of time between 120 and 180 min (Fig. 1). The best model fit for slices was observed with a polinomial model (Fig. 1).

Table 1. Coefficients of convective drying models and goodness of fit for chayote samples

Model	Equation	Sample	Parameter	R^2
Newton	$M_R=\exp(-kt)$	Strips	k= 0.0155	0.9476
		Cubes	k=0.0129	0.8257
		Slices	k=0.0083	0.6167
Henderson-Pabis	$M_R=a*\exp(-k_2t)$	Strips	k_2=0.0153; a=1.1810	0.9315
		Cubes	k_2=0.0129; a=1.4783	0.8237
		Slices	k_2=0.0097; a=1.4264	0.6128
Page	$M_R=(-k_3t^n)$	Strips	k_3=0.0051; n=1.2	0.9521
		Cubes	k_3=4.2868x10^{-7}; n=2.9	0.9866
		Slices	k_3=4.2868x10^{-7}; n=2.9	0.9167

The drying kinetics for sliced samples of chayote previously reported showed a typical first-order kinetic shape. The structure of the seed of chayote is shown in Fig. 2. In general, the seed is composed by three structures: the endocarp, the endosperm, and the cotiledons and it differentiates from other seeds in that its moisture content remains high during maturity. Moreover, the seed remains intact within the fleshy fruit [9]. In the light of the structure of the seed, it seems that the shape of the drying kinetics of the chayote slices

determined in the present work corresponds to a first period into which water loss of flesh occurs and a second period corresponding to the subsequent drying of the seed. Akonor and Tortoe [10] worked with the drying of slices of chayote of thickness of 4±1 mm. Eventhough they did not report neither the exact variety nor the state of maturity of the samples used in the tests a photograph included in their study suggests that the internal structure of the seed of the variety used in their study differs from the structure of the seed used in the present study. As for Huerta-Mora et al. [11], they worked with the drying of slices of chayote of thickness of 2 cm. This fact may diminish the wáter diffusivity of the wáter in the flesh of the fruit, thus, led to a drying kinetic of first order.
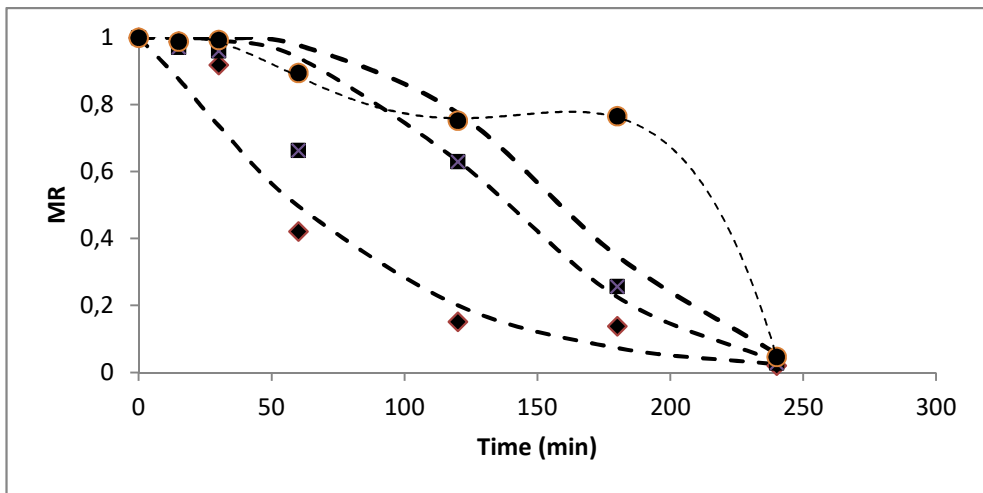
Fig. 1 Drying kinetics of chayote samples (T = 60 ° C). Circles correspond to sliced samples, squares to cubes and the diamonds to strips.

Fig. 2 Chayote slices.

There are few reports in the literature regarding the drying kinetics of cubes and strips of chayote. The calculated values for the coefficients of the Newton model (Table 1) for cubes and strips samples are three times greater in average than those calculated by Ruíz-López [5] for slices. These may indicate that the water loss is facilitated by the shape and the smaller volume of the samples submitted to a drying process which may also be reflected in the rehydration of the samples as it will be discussed below.

3.1.1 Color change of samples of chayote during the drying process

The color change of the different samples of chayote was followed during the drying process. In general, results showed that in general samples after 240 min of drying are slightly darker, less greener and yellower than samples before drying. ΔE determination revealed that the samples that registered less color change correspond to the ones cut into slices followed by cubes.

3.2 Rehydration process of different shapes of dried chayote samples

The rehydration process of the samples of chayote is shown in Fig. 3. In general, the degree of rehydration increased in the first minutes and diminished with time in accordance with the reported previously [11]. The time in which the degree of rehydration began to stabilize corresponds to 20 min for strips, 30 min for slices and 25 min for cubes. The samples that showed a higher capacity of rehydration were the ones cut into cubes in contrast with the chayote slices which showed the lesser rehydration ratio among all samples. Also, higher rehydration ratios were observed when higher water temperatures were employed as reported by Kumar et al [12] for chayote samples (Fig. 3). In order to better explain the higher water gain in cubes, we performed an image analysis with the software ImageJ© to assess the differences of the samples' sizes before and after rehydration. We also calculated the surface area of the dehydrated samples. Tests revealed that the samples that showed the higher ratio surface area and volume corresponds to the cubes followed by the strips and slices. In fact, both, chayote strips and cubes showed a moderate deformation on its length and thickness and length after drying, respectively. However, the samples in cubes recovered its original shape more easily than strips possible due to less mechanical stress present in cubes compared to strips. Despite this fact, all samples presented good rehydration ratios (Fig. 3). Interestingly, Kumar et al [12] reported lesser rehydration ratios for chayote cubes with the same size of our samples (L= 1 cm) compared with the ones found in the present work. According to Lewicki [13], pre-drying and drying may limit the water absorption of plant tissue and at the same time both procedures may intensify the leakage of solubles. Thus, the difference on the rehydration ratios of the samples observed by Kumar et al [12] and us may be due to the pre-drying treatment used by Kumar et al [12] which could led to the leakage of solubles of the samples.
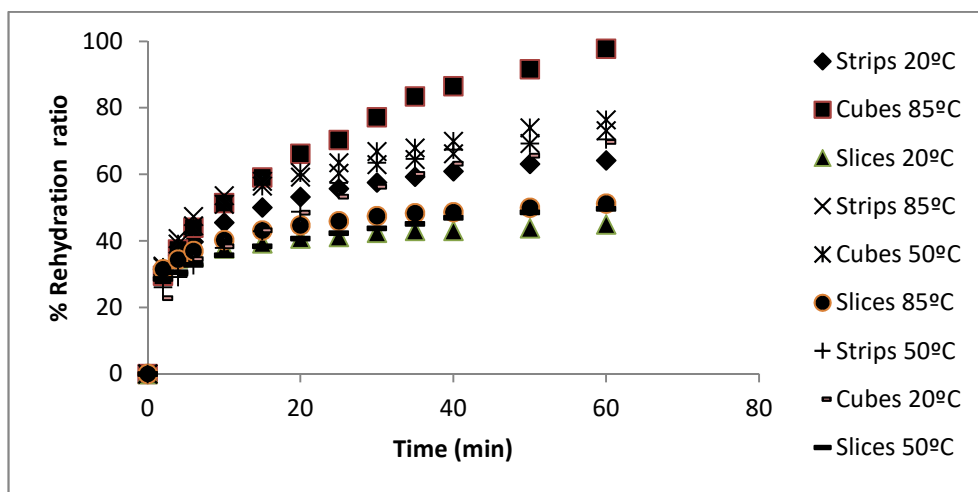
Fig. 3. Rehydration ratios at 20, 50 and 85ºC of chayote samples.

4. Conclusions

The moisture content of chayote samples was reduced by more than 85% through convective drying at 60ºC showing a slight color change at this temperature. Samples in slices showed a second water loss period unlike the other shapes studied which could be attributed to the presence of the seed in these tests. As for the rehydration process, after 60 minutes at three different temperatures (20, 50 and 85ºC), the samples showed a rehydration capacity between 53-98% which confirmed that the internal structure of the samples did not suffer significant structural damage due to convective drying. Also, the rehydration capacity tend to increase as the temperature of the fluid increases as previously reported [12]. According to the results obtained, dried chayote may represent an alternative as complement of food products and, particularly, samples in cubes represent an alternative for commercial use as an additive in instant soups due to their size.

5. References

[1] Kader, A.; Rolle, R. The role of post-harvest management in assuring the quality and safety of horticultural produce; FAO: Rome, 2004.

[2] Alvarenga-Venutolo, S.; Abdelnour-Esquivel, A.; Villalobos-Aránbula, V. Conservación in vitro de chayote (Sechium edule). Agronomía Mesoamericana 2007, 18 (1), 65-73.

[3] Castillo-Reyes, J.; Luna-Solano, G.; Cantú-Lozano, D. Rheological Characterization of Vegetal Pear (Sechium edule). In AIP Conference Proceedings. AIP, 2008. p. 1253-1255.

[4] Pérez-Francisco, J.M.; Cerecero-Enríquez, R.; Andrade-González; Ragazzo-Sánchez, J.A.; Luna-Solano, G. Optimization of vegetal pear drying using response surface methodology. Drying Technology 2008, 26: 1401–1405.

[5] Ruiz-López, I.I.; Huerta-Mora, I. R.; Vivar-Vera, M. A.; Martínez-Sánchez, C. E.; Herman-Lara, E. Effect of osmotic dehydration on air-drying characteristics of chayote. Drying Technology 2010, 28(10), 1201-1212.

[6] Avendaño-Arrazate, C. H.; Cadena-Iñiguez, J.; Arévalo-Galarza, M.; Campos-Rojas, E.; Cisneros-Solano, V.; Aguirre-Medina, J. Las variedades del chayote mexicano, recurso ancestral con potencial de comercialización. México: Grupo Interdisciplinario de Investigación en Sechium edule en México, AC, 2010.

[7] COVECA. 2005. Perfil del chayote, Boletín de la Comisión Veracruzana de Comercialización. Mexican Journal 41–44.

[8] Doymaz, I. Influence of Blanching and Slice Tthickness on Drying Characteristics of Leek Slices. Chemical Engineering and Processing 2008, 47, 41-47.

[9] Aung, L.; Harris, C.; Jenner, J. Chemical growth regulators on postharvest sprout development of Sechium edule Swartz. Phyton (Buenos Aires) 2004, 73, 155-164.

[10] Akonor, P.; Tortoe, C. Effect of blanching and osmotic pre-treatment on drying kinetics, shrinkage and rehydration of chayote (Sechium edule) during convective drying. British Journal of Applied Science and Technology 2014, 4(8), 1215-1229.

[11] Muñoz-López, C.; Urrea-Garcia, G.; Jiménez-Fernandez, M.; Rodríguez-Jiménes, G.; Luna-Solano, G. Effect of drying methods on the physicochemical and thermal properties of Mexican plum (Spondias purpurea L.). CyTA-Journal of Food 2018, 16(1), 127-134.

[12] Kumar , A.; Islam, S.; Kumar, K.; Sarkar, S. Optimization of process parameters for osmotic dehydration of chayote cubes by response surface methodology. International Journal of Agriculture, Environment and Biotechnology 2017, 10(6), 725-737.

[13] Lewicki, P. Effect of pre-drying treatment, drying and rehydration on plant tissue properties: A review. International Journal of Food Properties 1998, 1(1), 1-22.

Drying parameters influence on 'Ameclyae' Opuntia ficus prickly pear oil quality

Hassini, L. [a]*; Desmorieux, H. [b]

[a] University of Tunis El Manar, Faculté des Sciences de Tunis. Laboratoire d'Energétique et des Transferts Thermique et Massique (LETTM), El Manar, 2092, Tunis, Tunisia.
[b] Université Claude Bernard Lyon 1, Laboratoire d'Automatique et de Génie des Procédés (LAGEP), UMR CNRS 5007, 69622 Villeurbanne, France.

*E-mail of the corresponding author: helene.desmorieux2@univ-lyon1.fr

Abstract

The aim of this work is to study the effects of drying conditions on the quality of extracted pricly pear seed oil, specifically α-tocopherol content. Drying experiments were carried on following a full 2^3 factorial design using a vertical drying tunnel. The temperature range was 45 to 70°C, relative humidity range was 15 - 30% and air velocity was 1 and 2 m/s. The Midilli-Kucuk model was found with satisfaction describing the seed air drying curves with a correlation coefficient of 0.999 and a standard error of 0.01. For each drying condition, the extraction of fixed oil seeds was performed at cold using mechanical pressing method. The oil quality was evaluated on the basis of the α-tocopherol content. The α-tocopherol was identified and quantified by high-performance liquid chromatography (HPLC-UV). According to the experimental results, it was found that convective drying of thin layer of seeds at soft air conditions, drying temperature of 45°C, relative humidity of 15% and air velocity of 1m/s give the optimal quality of extracted oil in terms of α-tocopherol content.

Keywords: prickly pear seeds; convective drying; semi-empirical modeling; α-tocopherol seed oil; optimization.

1. Introduction

The constantly research of new essential oil sources should be performed in order to meet the new needs of industry. Prickly pear cactus (*Opuntia ficus-indica*) is extensively cultivated in Tunisia. The current production is estimated at more than 1 200 000 tons of fruits per year.

Seeds constitute about 10-15% of the edible pulp and are usually discarded as waste after extraction of the pulp. According to Stintzing et al.[1], oil processed from the seeds constitutes 7-15% of whole seed weight and is characterized by a high degree of instauration wherein linoleic acid is the major fatty acid (56.1-77%). According to Hasani et al.[2], the most active form of vitamin E in the oils seed is α-tocopherol which is believed to protect the body against degenerative malfunction, particularly cancer and cardiovascular disease.

Fresh prickly pear seeds, by-products from prickly pear fruit processing, are highly perishable and their drying at equilibrium moisture content is recommended for the storage, standardization and the biochemical stability of the product before extraction[3]. According to the literature, convective drying affected the quantity and the quality of the extracted essential oil and volatile compounds from various medicinal and aromatic plants.

Therefore, this work aims (i) to investigate the effect of the hot-air convective drying conditions on the drying kinetics of a thin layer of prickly pear seeds, (ii) to select the best mathematical model predicting the drying curves (iii) to study, according to full 2^3 factorial design approach, the effect of convective drying air conditions on the quality of fixed oil extracted from seeds, on the basis of the α tocopherol content, at temperature ranging from 45 to 70°C, relative humidity between 15 and 30% and air velocity of 1 and 2 m/s.

2. Materials and Methods

Fruit samples of the 'Ameclyae' variety in the ripe stage (Fig.1) were harvested in August from Knais, region of Sousse (Tunisia). They were taken to the laboratory the same day, where they were carefully selected and washed with tap water to remove glochids and impurities. Then the fruits were air-dried during few minutes and manually peeled. Seeds were separated by pressing the whole edible pulp and rinsing the residue, several times abundantly with distilled water.

A laboratory scale convective dryer (designed and constructed in the LETTM laboratory) was used for realising drying tests of thin-layer of seeds. For each experiment, a mass of $500 \pm (1)$ g of fresh prickly pear seeds was distributed on a stainless perforated tray as a thin layer of about 0.5 cm thickness. The tray was suspended to a digital balance, the balance being placed outside the drying chamber. The dryer worked in closed loop and was equipped with an industrial programmable controller to adjust air temperature, air relative humidity and air velocity to a given set point. The mass of the product was continuously measured and recorded by a microcomputer until constant weight. At the end of each

drying test, the essential oil of the seeds was extracted and submitted to qualitative analyses. The dry mass of the product was determined by vacuum oven drying method at $105 \pm 1°C$ for 4 hours. The change in moisture of prickly pear seeds during drying was expressed as a moisture ratio MR defined by the expression of Eq. (1).

$$MR = \frac{X - X_{eq}}{X_o - X_{eq}} \qquad (1)$$

where X, X_o, and X_{eq} are moisture content at any drying time, initial and equilibrium moisture content (kg water/kg dry matter), respectively. This last parameter X_{eq} was experimentally determined at different climatic conditions (desorption isotherms)[4].

Fig. 1 Prickly pear fruit of the 'Ameclyae' variety.

The extraction of oil from dried seeds was performed at cold temperature using liquid/solid separation method. Before the extraction process, the dried seeds were reduced into a fine powder using electronic grinder, at a temperature around 23°C. This mechanical separation processing is the most recommended in agricultural industry for its low cost and it preserves nutrients. There are four tocopherols and four tocotrienols in the seeds oil. α-tocopherol was chosen because it is the most active molecule and represents a good reagent against oxidation parameters. Besides, the α-tocopherol plays a vital role in the human body as antioxidant to neutralize free radicals and protect the cell tissues. The α-tocopherol was identified and quantified by using an analytical HPLC system Agilent Series 1100, equipped with a quaternary pump and a UV-visible detector (diode array detector). Identification of compound was achieved by comparing their retention time values with those of standard curve (concentration versus peak area).

3. Results and discussion

3.1. Chromatograms of α-tocopherol in prickly pear oil

Typical chromatograms of α-tocopherol in seeds oil corresponding to two different drying conditions are presented on Fig. 2.

(a)

(b)
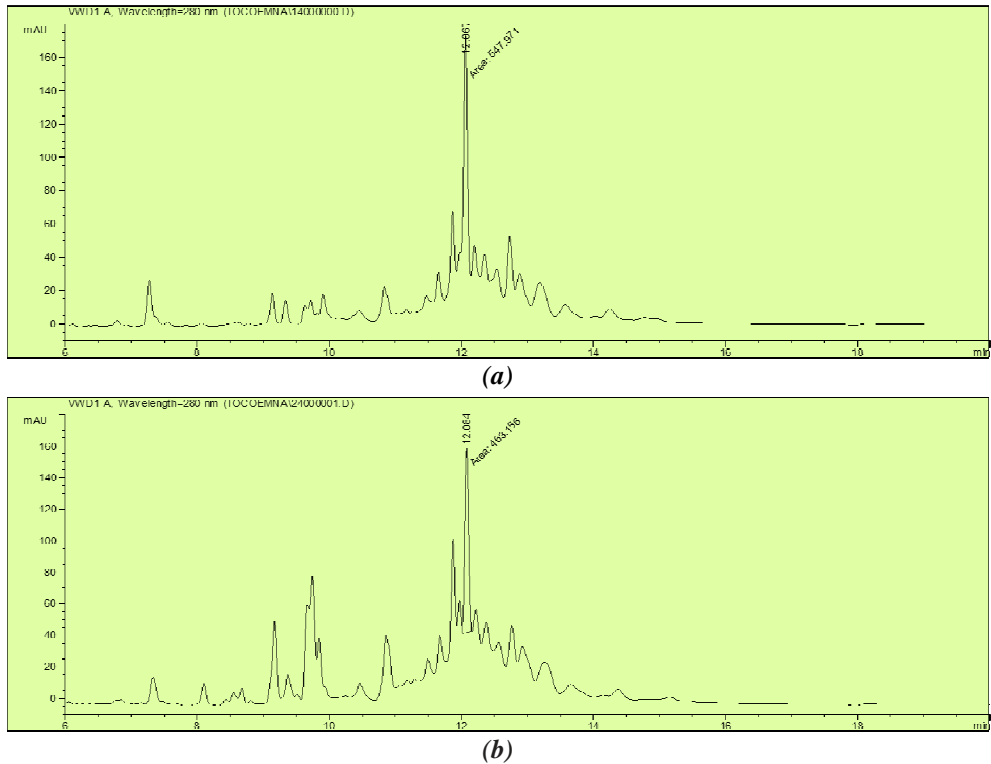
**Fig. 2 Chromatograms of α-tocopherol in prickly pear oil (a) at (T_a = 70°C, HR = 15%, u_a = 2m/s)
and (b) at (T_a = 45°C, HR = 15%, u_a = 2m/s)**

3.2. Experimental drying curves

The drying kinetics curves of thin layer prickly pear seeds at different drying conditions are given on Figs. 3 and 4. As it can be observed, the constant rate-drying period do not appear clearly in drying curves which is similar with those reported in literature: orange seeds by Rosa et al.[5] and grapefruit seeds by Cantu-Lozano et al.[6]. The absence of a clearly constant rate period is due to the difficulty of the capillary migration of water from the wet heart to the rigid surfaces of prickly pear seeds. The heating up period is attributed to the warming of the seeds from the ambient temperature to the over temperature of 45 or 70°C, and shorter by 45°C drying temperature. Otherwise, the air temperature is the operating parameter which affect significantly the drying kinetics of thin layer of seeds as reported by several investigators, e.g. Tang and Sokhansang[7] for lentils and Desmorieux and Decaen[8] for *Spirulina*. Although, the drying process is controlled by the water internal diffusion inside the seeds, the less important effect of air velocity on the drying kinetics can be explained by the dependence of the convective exchange coefficients with the air velocity. This suggests that the moisture content depends on the effective diffusion and can be simply modelled by the Fick's second law and the semi-empirical models derived from it.
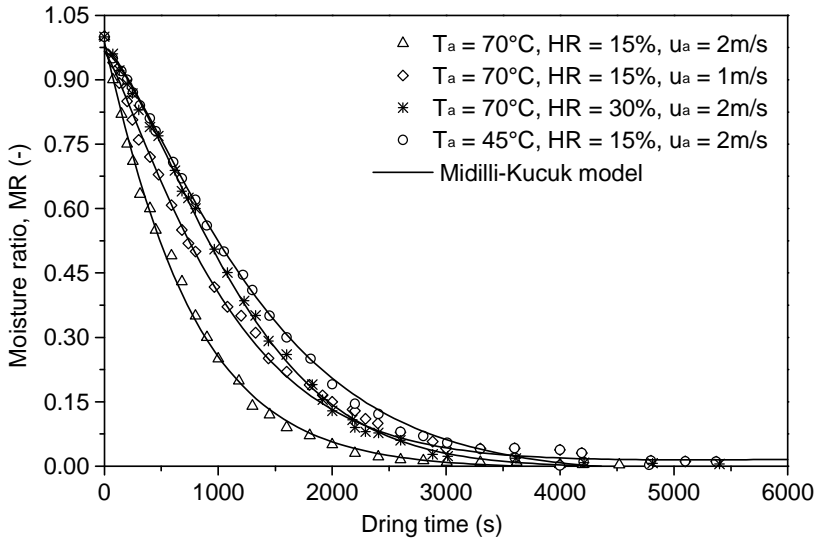
*Fig. 3 Experimental prickly pear seeds moisture ratio versus
drying time at different drying conditions*
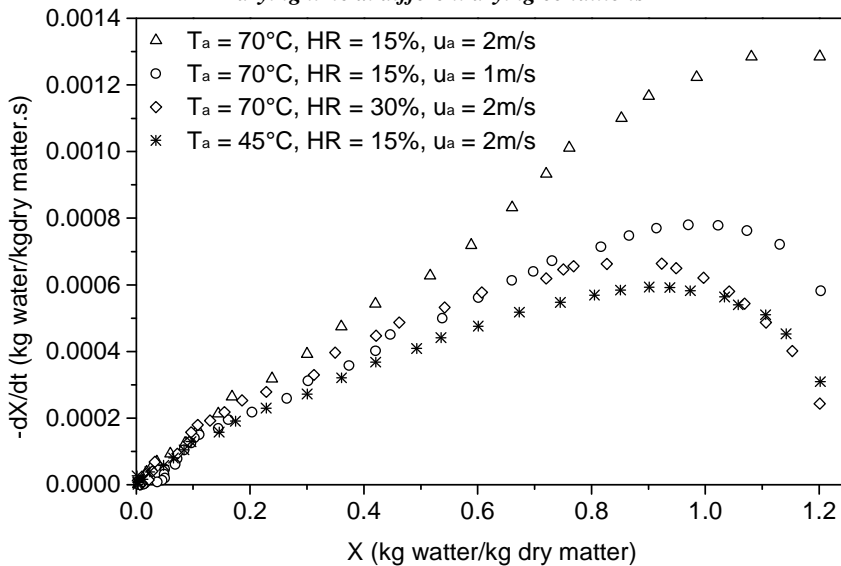
*Fig. 4 Experimental drying rate versus moisture content at
different drying conditions*

3.3. Smoothing of the experimental drying curves

The experimental data obtained were fitted by eight semi-empirical models proposed in the litterature (Newton, Modified Page, Henderson and Babis, Modified Henderson and Pabis, Two-Term, Logarithmic and Midilli-Kucuk). All the models gave high coefficient of determination (r) values in the range 0.9697-0.9998 at 45 °C, 0.9615-0.9998 at 50 °C and

0.9474-0.998 at 70 °C. This indicates that all the models could satisfactorily describe the convetive drying of the prickly pear seeds from 45 to 70°C. According to our results, the Midilli-Kucuk model obtained the highest r value of 0.9992, and the lowest (s) value of 0.0143, averaged over the range of the drying conditions. This selected Midili-Kucuk model is expressed as:

$$MR = n_1 \exp(kt^{n_2}) + n_3 t \qquad (2)$$

3.4. Effect of drying conditions on the extracted oil quality

According to our results, reported in Table 1, α-tocopherol was found in variable concentrations (0.249-0.970 mg/kg). These values are arithmetic mean of at least three separate determinations. They are lower than those reported by Ramadan and Morsel[9] for prickly pear seed oils (56 mg/kg) obtained by solvent extraction and analyzed by HPLC technique. This difference in the α-tocopherol concentration can be explained essentially by the fruit variety, the stage of fruit ripeness, the drying mode prior extraction and also the extraction process. Indeed, according to Tuberoso et al.[10], tocopherol contents were significantly higher ($p < 0.05$) in oils obtained by solvent extraction than by pressing. Furthermore, the amount of α-tocopherol in grape seeds oil was 124,5 mg/kg[11] and in Chia seed oil ranging from 0.4 to 9.9 mg/kg[12].

Table 1. α-tocopherol concentrations corresponding to 2^3 factorial design

Test number	T_a(°C)	HR(%)	u_a (m/s)	Y (mg/kg)
1	45	15	1	0.970
2	70	15	1	0.830
3	45	30	1	0.482
4	70	30	1	0.491
5	45	15	2	0.249
6	70	15	2	0.463
7	45	30	2	0.725
8	70	30	2	0.311

The effect of increasing the air velocity from 1 to 2 m/s, averaged over all levels of air temperature and air humidity, decreases the α-tocopherol concentration from 0.693 to 0.437 mg/kg. Also, the effect of increasing the air humidity from 15 to 30% decreases the α-tocopherol concentration from 0.628 to 0.502 mg/kg. Temperature is a factor of lesser

importance. Indeed, the effect of increasing air temperature from 45 to 70°C decreases the α-tocopherol concentration from 0.606 to 0.523 mg/kg. That mean that α-tocopherol molecule is more stable at heat treatments. Stability of α-tocopherol is explained by the role of phenolic compounds that protect the α-tocopherol from oxidation during the heating. Indeed, Ramadan and Morsel[9] reported that, the amount of phenolic compounds in prickly pear seeds was found to be 403 mg/kg of seeds. According to Rocha et al.[13], drying temperatures is the most important parameter to preserve the active ingredients of volatile oil in gland cells, which are very sensitive to temperature increase. Likewise, Miranda et al.[14] observed an increase in tocopherol content with drying air temperature in quinoa seeds within temperature range of 40-80°C. Our results show that α-tocopherol is more sensitive to increase velocity, which can be linked to oxygen, than to the temperature. These results are consistent with those found by Park et al.[15] who reported that more than 20% α-tocopherol degradation were observed in conditions of 21% oxygen.

4. Conclusions

- The experimental drying kinetics of a thin layer of prickly peer seeds exhibits a heating-up, constant rate and falling rate periods. The drying air temperature was the main factor influencing the drying kinetics.
- The Midilli-Kucuk model was the best for fitting the drying kinetics of prickly pear seeds.
- The relative humidity and the velocity of air were the factors that influence the prickly pear seed oil quality, qualified by α-tocopherol contents after extraction. The convective drying of thin layer fresh seeds at air drying temperature of 45°C, air relative humidity of 15% and air velocity of 1m/s involves the highest quality of extracted oil in terms of α-tocopherol compound concentration. This optimum scenario for best oil quality can be used in photochemical industries.

5. Nomenclature

HR	Air relative humidity	(%)
MR	Moisture ratio	
T_a	Air temperature	(°C)
u_a	Air velocity (m/s)	$(m.s^{-1})$
X	Moisture content on dry basis	$(kg.kg^{-1})$
Y	α-tocopherol concentration	$(mg.kg^{-1})$

6. References

[1] Stintzing, F.C.; Schieber, A.; Carle, R. Cactus pear, a promising component of functional food. Obst, Gemuse und Kartoffelverarbeitung 2000, 85(1), 40-47.

[2] Hasani, N.A.; Yussof, P.A.; Khalid, B.A.K.; Ghapor, M.T.A.; Ngah, W.Z.W. The possible mechanism of action of palm oil gamma-tocotrienol and alpha-tocopherol on

the cervical carcinoma caski cell apoptosis. BioMed Research International 2008, 19, 194-200.

[3] Diaz-Maroto, M.C.; Pérez-Coello, M.S.; Gonzalez Vinas, M.A.; Cabezudo, M.D. Influence of drying on the flavor quality of spearmint (Mentha spicata L.). Journal of Agricultural and Food Chemistry 2003, 51, 1265-1269.

[4] Hassini, L.; Bettaieb, E.; Desmorieux, H.; Sandoval-Torres, S.; Touil, A. Desorption isotherms and thermodynamic properties of prickly pear seeds. Industrial Crops and Products 2015, 67, 457-465.

[5] Rosa, D.P.; Cantu-Lozano, D.; Luna-Solano, G.; Polachini, T.C.; Telis-Romero, J. Mathematical modeling of orange seeds drying kinetics. Ciênc Agrotec Lavras 2015, 39(3), 291-300.

[6] Cantu-Lozano, D.; Vigano, J.; Lassman, A.A.; Cantu, N.A.V.; Telis-Romero, J. Sorption isotherms and drying kinetics of grapefruit seeds. Acta Scientiarum 2013, 35(4), 717-723.

[7] Tang, J.; Sokhansanj, S. A model for thin-layer drying of lentils. Drying Technology 1994 12(4), 849-86.

[8] Desmorieux, H.; Decaen, N. Convective drying of spirulina in thin layer. Journal of Food Engineering 2015, 66, 497-503.

[9] Ramadan, M. F.; Môrsel, J-T. Oil cactus pear (Opuntia ficus-indica). Food Chemistry 2003, 82, 339-345.

[10] Tuberoso, I.G.C.; Kowalczyk, A.; Sarritzu, E.; Cabras, P. Determination of antioxidant compounds and antioxidant activity in commercial oilseeds for food use. Food Chemistry 2007, 103, 1494-1501.

[11] Bele, C.T.; Matea, C.; Raducu, C.; Miresan, V.; Negrea, O. Tocopherol Content in Vegetable. Oils Using a Rapid HPLC Fluorescence Detection Method. Notulae Botanicae Horti Agrobotanici Cluj-Napoca 2013, 41(1), 93-96.

[12] Bruscatto, M.H.; Zambiazi, R.C.; Sganzerla, M.; Pestana, V.R.; Otero, D.; Lima, R.; Paiva, F. Degradation of tocopherols in rice bran oil submitted to heating at different temperatures. Journal of Chromatographic Science 2009, 47, 762-765.

[13] Rocha, R.P.; Melo, E.C.; Radünz, L.L. Influence of drying process on the quality of medicinal plants: A review. Journal of Medicinal Plants Research 2011, 5(33), 7076-7084.

[14] Miranda, M.; Vega-Gálvez, A.; López, J.; Parada, G.; Sanders, M.; Aranda, M. Impact of air-drying temperature on nutritional properties, total phenolic content and antioxidant capacity of quinoa seeds (Chenopodium quinoa Willd.). Industrial Crops and Products 2010, 32, 258-263.

[15] Park, S. R.; Kim, Y. H.; Park, H. J.; Lee, Y. S. Stability of tocopherols and tocotrienols extracted from unsaponifiable fraction of rice bran under various temperature and oxygen condition. Proceedings of the 4th International Crop Science Congress, Brisbane, Australia, 2004.

Generation of high drug loading amorphous solid dispersions by Spray Drying

Costa, B. L. A.*; Sauceau, M. ; Sescousse, R.; Ré, M. I.

Université de Toulouse; Ecole des Mines d'Albi; UMR CNRS 5302; Centre RAPSODEE, F-81013 Albi, France

*E-mail of the corresponding author: bhianca.lins_de_azevedo_costa@mines-albi.fr

Abstract

Amorphous solid dispersions (ASDs) refers to drug - carrier systems, where the drug is dispersed in the carrier at a molecular level. In this work, ASDs were formulated by spray drying. The aim was to achieve high drug loads of an amorphous hydrophobic drug (Efavirenz - EFV) in the carrier Soluplus®. Solid state characterizations (mDSC, XRPD, DVS, Raman, SEM, stability and solubility studies) were done. EFV amorphisation in ASDs (20 to 85% EFV loads) resulted in improved drug solubility compared to unprocessed EFV crystals and tendency of properties evolution over time for ASDs with EFV loads higher than 70 wt%.

Keywords: amorphous solid dispersion, spray drying, high drug loading, soluplus, efavirenz.

1. Introduction

Poorly water-soluble drugs have steadily grown on the global pharmaceutical industry. The technological approach focused on rendering the drug amorphous to improve apparent solubility remains a challenge since amorphous state is metastable in nature with a potential to undergo recrystallization [1]. In order to prevent this conversion, amorphous materials have been stabilized as solid dispersions using generally hydrophilic carriers for stabilization [2].

An amorphous solid dispersion (ASD) refers to drug–carrier systems in which the mechanism of drug dispersion is the key to understand its behavior. Such formulations impart an antiplasticizing effect on the amorphous compound yielding an increase in the glass transition temperature thereby reducing molecular mobility [3]. However, in order to achieve adequate stabilization, solid dispersions are often produced with a relatively low drug load (<30 wt%) dispersed in the carrier at molecular level. The problem is that a low drug-loaded ASD requires a large dose to ensure therapeutic efficacy.

The insertion of high drug load formulations on the market is expected to meet patients demand for fixed, unique and smaller dosage combinations products. Furthermore, the supersaturated combinations may reduce dosage amounts as well as decrease the production in the pharmaceutical industries to supply cost savings. The aim of the current work was to generate, by spray drying, ASDs comprising a hydrophobic drug class II BCS (low solubility, good permeability for oral administration) in a hydrophilic carrier (Soluplus®-SOL) expecting to achieve drug loads higher than 40% w/w in the binary mixtures. The physical stability will be the critical control point. The drug of choice is Efavirenz (EFV). EFV is a non-nucleoside reverse transcriptase inhibitor used in the first-line treatment of HIV with low solubility (3-9 µg/mL) and high permeability [4].

2. Materials and Methods

EFV was kindly supplied by Cristalia Ltd (Itapira, Brazil), SOL (polyvinyl caprolactam-polyvynil acetate-polyethylene glycol) was obtained from BASF corporation (Ludwigshafen, Germany) and Ethanol (Carlo Erba, Italy) was used as organic solvent.

The feeding solution was prepared by dissolving EFV in a 10 wt% solution of Soluplus in ethanol. Binary mixtures EFV-SOL containing from 20 to 85 wt% of EFV were formulated as spray-dried powders. The individual constituents (drug and polymer) were also spray-dried from ethanol solutions and used for comparison purposes.

A Buchi B-290 minispray dryer (Buchi Labortechnik AG, Flawil, Switzerland) equipped with Inert Loop B-295 and an integrated two-fluid 0.7 mm nozzle was used to produce the ASD samples. Compressed nitrogen was used as the drying/carrying gas with a flow rate of 600 L/h. The solution feed rate was typically 3 g/min, the inlet temperature was set to 80±2 °C and the outlet temperature was maintained at 59±2 °C.

X-ray diffraction (XRD), modulated differential scanning calorimetry (mDSC), Raman spectroscopy, Scanning electron microscopy (SEM) and Infrared Spectroscopy (IR) were used to characterize the solid state of the spray-dried samples.

Water sorption isotherms were determined gravimetrically using an automated dynamic water sorption analyzer (DVS). Samples were subjected to 0–95 % relative humidity (RH) sorption-desorption cycle, over 10 % RH increments. For stability studies, samples were analyzed using DVS and exposed to stress conditions at 40 °C and 75 % RH during 15 days. Every 3 days, the samples were quickly analyzed by DSC to monitor changes in the physical state.

Solubility studies of unprocessed EFV crystals and ASDs were carried out in duplicate. For that purpose, an excess amount of samples was added into 30 mL of a dissolution medium containing purified water plus 0.25 wt% of sodium lauryl sulfate (SLS) under agitation at 37±0.5 °C in a water bath. The withdraws were collected from 5 min until 48 h.

3. Results and discussion

3.1. X-ray diffraction (XRD)

The absence of Bragg peaks in X-ray diffractograms (Fig. 1) of all spray-dried solids indicates the complete loss of the crystalline structure of EFV, which becomes amorphous during the spray-drying process.

3.2. Thermal analysis (mDSC)

Thermal analysis was performed to investigate the apparent EFV-Soluplus® miscibility. Fig. 2 shows the single experimental glass transition temperature (T^g) identified for pure contituents and for each binary mixture EFV- SOL loaded with 40, 60 and 85 wt% EFV. The T^g of mixtures (T^g_{mix}) are placed as an intermediary between the pure drug and polymer values and are close to the theoretical values of T^g calculated by Gordon-Taylor (GT) equation (Equation 1). This equation relates the individual contributions of each component in an ideal mixture (with no interactions between the components).

$$T^g_{mix} = \frac{W_{PA}.T^g_{PA} + K.(1 - W_{PA}).T^g_{PO}}{W_{PA} + K.(1 - W_{PA})} \quad (1)$$

T^g_{PA} and T^g_{PO} are the drug and polymer glass transition temperatures (K), respectively. W_{PA} is the drug mass fraction in the mixture. K is defined as fitting parameter characterizing the curvature of the evolution and is defined by equation 2 [5].

$$K = \frac{T^g_{PA} \cdot \rho_{PA}}{T^g_{PO} \cdot \rho_{PO}} \quad (2)$$

Densities (g/cm³), determined by helium picnometry, ρ_{PA} and ρ_{PO}, are 1.39 and 1.18, respectively.

According to XRD and DSC results, an amorphous solid dispersions of EFV- SOL seems to be formed during the spray-drying process.
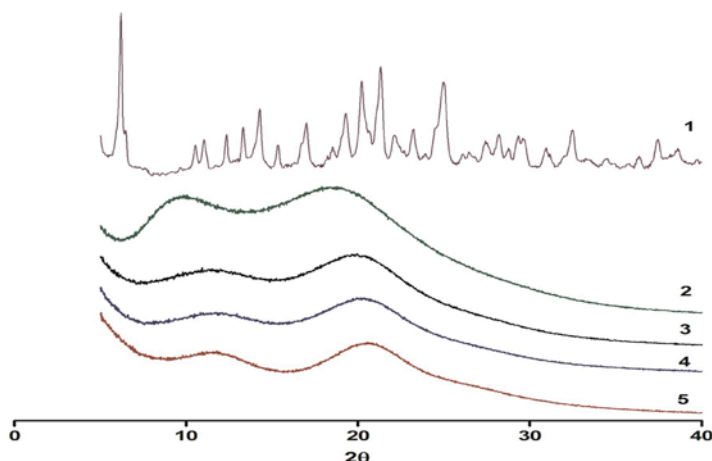
Fig. 1 XRD diffractograms of: (1) pure EFV; (2) pure SOL; (3) 40 % EFV; (4) 60 % EFV and (5) 85 % EFV.
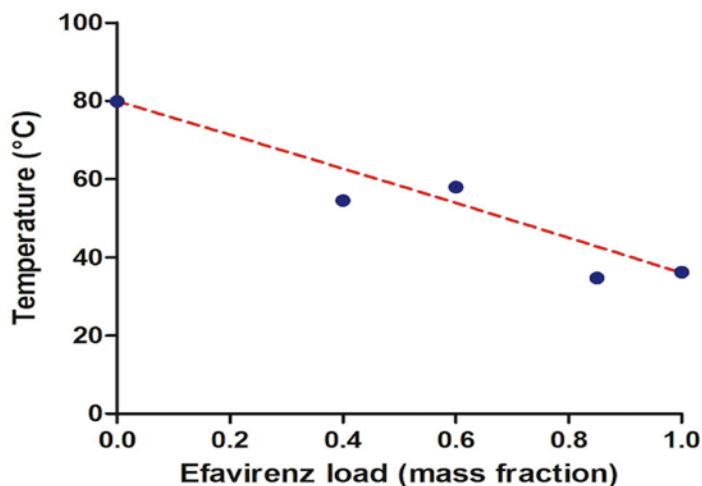
Fig. 2 Glass transition temperature (T^g_{mix}): measured (blue circles) and theoretical values by GT equation (dotted red line).

3.3. Raman microscopy

Raman microscopy was also performed for three EFV-SOL ASD (Fig. 3). They were evaluated by observing the characteristic peaks of pure drug (peak at 2250 cm^{-1}) and pure polymer (peak at 2900 cm^{-1}). As expected, the increase of the drug load in the mixture corresponded to a more

intense characteristic EFV peak. The presence of characteristic peaks of pure components in all ASD Raman spectra shows the absence of specific interactions between the two components and confirms the ideal mixing suggested by the evolution of the mixtures T^g and SOL for all studied drug loads.
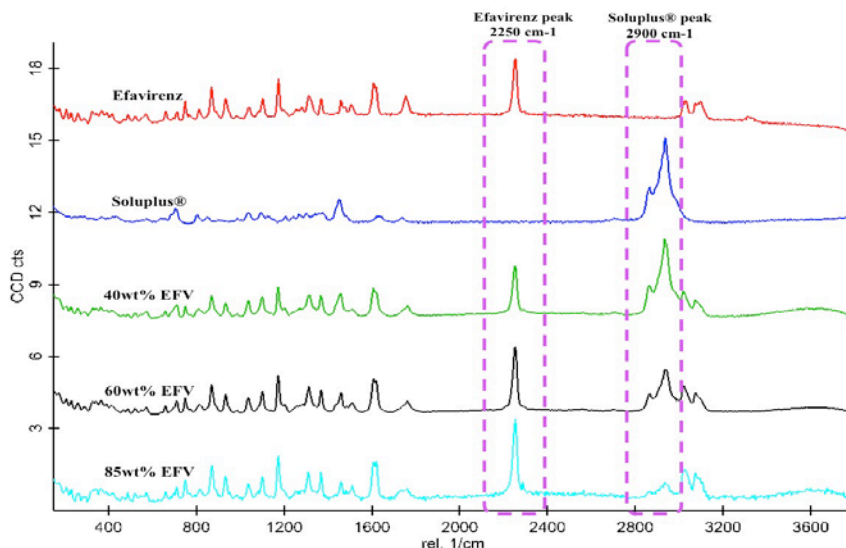
Fig. 3 Raman spectra for the EFV-SOL ASD with different drug loads: 40%; 60%; 85% EFV.

3.4. Scanning electron microscopy (SEM)

SEM images of the spray-dried powders are shown in Fig. 4. ASD EFV-SOL particles are predominantly spherical and different in shape from both original constituants that are the unprocessed EFV crystals (Fig. 4B - long rods with regular and organized multi-face geometry) and the spray-dried polymer (Fig. 4A - wrinkled particles). A good mixing between both compounds could led to these apparently homogeneous solid particles.

3.5. Stability studies

Fig. 5 displays the DVS isotherm plots for the studied samples, showing the change in mass percentage as a function of changing relative humidity. The reversibility of the water uptake was clearly seen in all cases. Taking as example the curves at 75 % RH (Fig. 5B), the tendency of increasing the hydrophobic character of EFV-SOL ASD by increasing the EFV load is demonstrated. The decreased affinity to water with increased drug load could be an interesting attribute for the physical stability of the amorphous drug phase in high drug load ASDs.
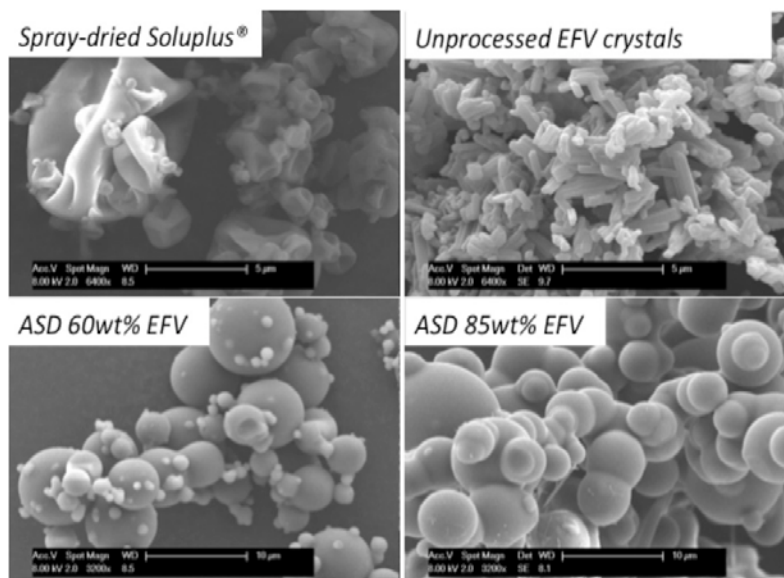
Fig. 4 SEM images of spray-dried ASD constituted by a EFV-SOL binary mixture.
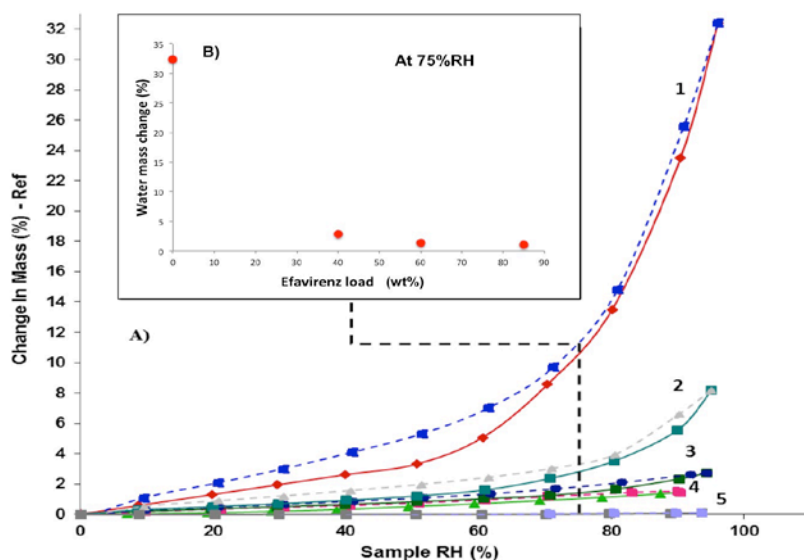
Fig. 5 A) DVS isotherms for 1- pure SOL; 2- 40% EFV; 3- 60% EFV; 4- 85% EFV; 5- pure EFV.
B) Water mass change (%) at 75%RH for the ASD.

The stability results under stress conditions are presented in Table 1. It is noticeable that the samples have evolved over time since T^g_{mix} increases in both cases, suggesting a variation in the amorphous mixture composition. However, we did not observe any particular signs of

amorphous phase separation or drug recrystallisation for the sample loaded with 40 % EFV. Contrarily, 70 % EFV-SOL ASD revealed an evolution of crystallization enthalpy (ΔH) over time, corresponding to a partial EFV recrystallization. This tendance for recrystallization can be attributed to the high drug load of the ASD, probably corresponding to a supersaturated (and instable) amorphous state of the drug. Considering ΔH=52.83 J/g for the unprocessed EFV crystals, it was possible to estimate the percentage of drug recrystallizing in this ASD during storage. Table 1 also shows that, after 15 days of storage, approximately 6.6 % of the amorphous EFV dispersed in Soluplus recrystallized.

3.6. Solubility studies

In Figure 6, the results showed that spray-dried EFV- SOL ASDs produced with 20, 40 and 60 wt% EFV presented a good solubility enhancement in comparison with the unprocessed EFV crystals. EFV- SOL ASDs solubility decreases gradually with drug load increasing in the spray-dried powders. Indeed, EFV- SOL ASD with 20wt% EFV exhibited the maximum apparent EFV solubility over approximately 36h in simulated intestinal fluid.

Table 1. Stability results under stress conditions (40 °C/75 % RH)
for EFV-SOL ASD with drug loads of 40 % and 70 %

t (days)	40 % EFV-SOL T^g_{mix} (°C)	70 % EFV-SOL T^g_{mix} (°C)	Crystallization enthalpy ΔH (J/g)	Crystallization (%)
3	59.8	51.4	1.3	2.4
6	64.9	53.4	2.6	4.9
9	64.1	55.9	2.8	5.3
15	67.2	57.7	3.5	6.6

4. Conclusions

A robust formulation with optimal drug load and excipients is one of the key factors of successfully developing an ASD system. In this work, amorphous solid dispersions of the poorly water soluble compound Efavirenz were prepared with drug loads in the range 20 to 85 wt% EFV, using Soluplus® as hydrophilic carrier and spray drying as the production process. Solubility tests revealed a good solubility enhancement for all ASD compared with crystalline drug solubility. To the best of our knowledge, it is the first study reporting such high levels of drug loading (up to 85 wt%) in supersaturated amorphous solid dispersions of

EFV. However, our results also showed that the physical stability should be a monitoring critical point for EFV-SOL ASDs with EFV loads higher thanv 70 wt% EFV.
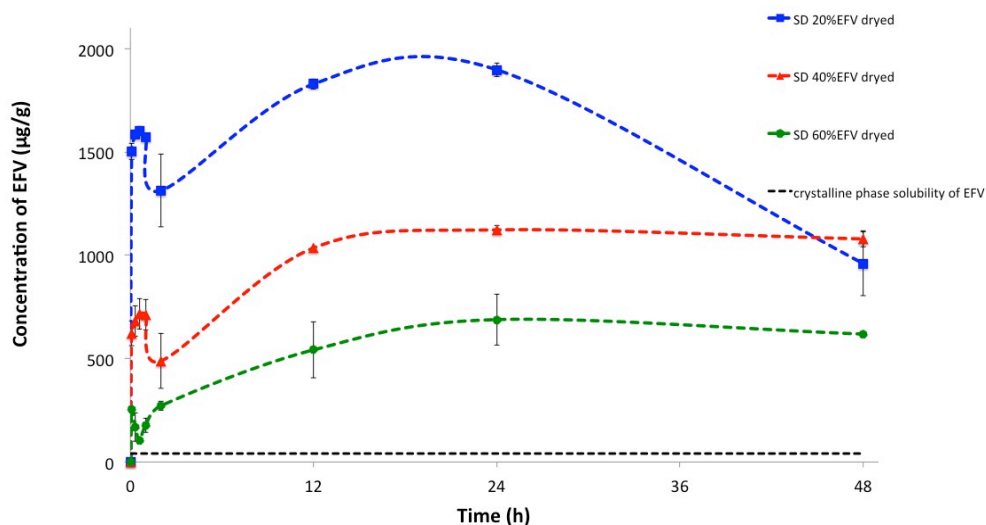
Fig. 6 Kinetic solubility of spray-dried EFV-SOL ASD.

5. References

[1] K. Wlodarski, W. Sawicki, A. Kozyra, and L. Tajber, 'Physical stability of solid dispersions with respect to thermodynamic solubility of tadalafil in PVP-VA', Eur. J. Pharm. Biopharm. Off. J. Arbeitsgemeinschaft Pharm. Verfahrenstechnik EV, vol. 96, pp. 237–246, Oct. 2015.

[2] Z. Lu et al., 'Supersaturated controlled release matrix using amorphous dispersions of glipizide', Int. J. Pharm., vol. 511, no. 2, pp. 957–968, Sep. 2016.

[3] B. B. Patel, J. K. Patel, S. Chakraborty, and D. Shukla, 'Revealing facts behind spray dried solid dispersion technology used for solubility enhancement', Saudi Pharm. J., vol. 23, no. 4, pp. 352–365, Sep. 2015.

[4] C. R. D. Hoffmeister et al., 'Efavirenz dissolution enhancement III: Colloid milling, pharmacokinetics and electronic tongue evaluation', Eur. J. Pharm. Sci. Off. J. Eur. Fed. Pharm. Sci., vol. 99, pp. 310–317, Mar. 2017.

[5] J. A. Baird and L. S. Taylor, 'Evaluation of amorphous solid dispersion properties using thermal analysis techniques', Adv. Drug Deliv. Rev., vol. 64, no. 5, pp. 396–421, Apr. 2012.

Effect of particle size of blueberry pomace powder on its properties

Calabuig- Jiménez, L.[a]; Barrera, C.[a]; Seguí, L.[a]; Betoret, N.[a] *

[a] Institute of Food Engineering for Development. Universitat Politècnica de València. Camino de Vera s/n, 46022, Valencia, Spain.

*E-mail of the corresponding author: noebeval@tal.upv.es

Abstract

Producing dried powders from blueberry pomace allows to reduce its environmental impact and gives value to this waste material. This work aims to evaluate the effect of particle size (fine or coarse) of blueberry pomace dried at 70 ºC on its fibre content and main physicochemical properties, including antiradical capacity, total phenols and anthocyanins content, hydration and emulsifying properties. The effect of storage on antioxidant properties was also evaluated. Results showed a significant effect of particle size on fibre content and consequently, on water retention, holding and emulsifying capacity of the powder. Neither phenols nor anthocyanins were affected by particle size or storage time.

Keywords: blueberry pomace, powders, fibre, antioxidant properties.

1. Introduction

Fruit and vegetables industrialization produces a huge amount of waste with negative impact on the environment and expensive management [1]. Most of this waste is used as animal feed or as fertilizers, both having low economic value. In an environmentally friendly way, it would be very interesting to use agro-food industry waste and by-products as a source of edible ingredients, thus increasing added value of the waste materials. Fruit powders have become an emerging way of consuming fruit and vegetables and it has attracted a growing interest in recent years [2], according to their broad applications in food formulation as colorant, flavoring ingredient or as natural preservatives. Fruit by-products also contain high amounst of health-promoting compounds such as, fibre, proteins, vitamins and minerals [1]. Blueberries has anti-inflammatory properties and has been reported to prevent several diseases. This health benefits have been attributed to their content in various phenolic compounds such as anthocyanins and other flavonoids [3]. Due to the fruit seasonal availability and a recent increase in the production, industrialization of the blueberries into juice, dried fruit and powders has increased in the last years. Fiber and phenolic constituents have higher concentration in blueberry pomace, a by-product of juice processing, than in the fruit itself [1]; in addition, beneficial effects of these by-products on metabolomic alterations have been reported [4]. Fiber content of blueberry pomace may offer functional properties associated with water retention and emulsifiying capacity. Among the processing methods that could be applied to estabilized bluberry pomace, drying an further powdering could be a good way to increase the shelf life of the product [5]. The aim of this research was to evaluate physicochemical properties, including antioxidant properties and other technological properties, of a blueberry pomace powder obtained by air driying at 70 ºC and grinding at two different intensities. Changes on antioxidant properties after 20 weeks of storage were also determined.

2. Materials and Methods

2.1. Blueberry pomace

Frozen blueberries (*V. corymbosum* var. *duke*) were supplied by Samanes S.L (Navarra, Spain) and processed as [7]. Separated blueberry pomace (P) was air dried at 70 ºC (POL-EKO, Controltecnica, S.L., Madrid) until reaching a water activity below 0.3. Dried pomace (DP) was grinded at 10,000 rpm (Thermomix®, Vorwerk, Spain) for 10 s to obtain a coarse powder (CP) and for 2 min at 30 s intervals to obtain a fine powder (FP). Powders were stored in opaque glass jars under controlled relative humidity of 24% at 25±1 ºC until analysis. Antioxidants stability of powders during 20 weeks of storage were evaluated.

2.2. Physicochemical properties

Water activity was measured with a dewpoint hygrometer (Aqualab 4TE; Decagon devices Inc., Pullman WA, USA). **Moisture** was obtained by method described by [7]. **Total soluble solids** content of samples (x_{ss}) were determined by refractometry, measuring Brix degrees of a solution 1:10 (w/v), and transformed into x_{ss} as appropriate. **Specific volume** of powders was obtained by measuring the volume of a sample in a 10 mL test tube. All determinations were performed in triplicate.

Particle size distribution of the powders was determined by diffraction laser (Mastersizer 2000, Malvern Instruments, UK) with air as dispersant at 2.5 bar (dry method) or water (wet method); refraction indexes were 1.52 for the sample and 1.33 for the dispersed phase. Characterization was made in terms of D [4,3], D [3,2], and d_{10}, d_{50} and d_{90}. Provided results are the average of five replicates. **CIEL*a*b* coordinates, hue and chrome** were measured with a spectrocolorimeter (MINOLTA model CM-1000R). Values provided are the average of triplicates. **Fibre content,** Neutral Detergent Fibre (NDF), Acid Detergent Fibre (ADF), and Lignin Detergent Fibre (LDF) were obtained as [8]; these allowed obtaining the amount of hemicellulose (soluble fibre), cellulose, lignin (non-soluble fibre) and total fibre. Fiber determinations were performed in duplicate and results were given in percentage of dry basis (db).

An 80% methanol:water solution was used to extract the **antioxidant compounds** of the fresh pomace (1:20 w/v solution) and the dried powders (1:100 w/v solution). After 1 h of stirring, the mixture was centrifuged at 10,000 rpm for 5 min. Total phenol content of samples was obtained following the Folin-Ciocalteu method slightly modified [9]. Results were given in mg of Gallic Acid Equivalents (GAE) per 100 g of sample (db). Monomeric anthocyanin content was obtained by the pH differential spectrophotometric method as in [10]. Absorbance (Helios Zeta UV/Vis, Thermo scientific, UK) was measured at 510 nm and 700 nm at pH 1.0 and 4.5. In order to obtain the monomeric anthocyanin content equations (1) and (2) were applied, where: Abs_{510} is the absorbance at 510 nm Abs_{700} is the absorbance at 700 nm, Mw: molecular weight of glucosid-3-cyanidin (449.2 g/mol), f: dilution factor, ε: molar extinction coefficient (26,9 L/mol·cm). Results were given as mg of cyanidin-3-O-glucoside equivalents per 100 g of sample (db). The **antioxidant activity** (AA) was measured with DPPH and ABTS methods described in [9]. Presented results were expressed in mg of Equivalent Trolox (ET) per g of sample sample (db). All antioxidant determinations were performed in triplicate.

$$ABS=(Abs_{510}-Abs_{700})_{pH\ 1.0}- (Abs_{510}-Abs_{700})_{pH\ 4.5} \tag{1}$$

$$\text{Total monomeric anthocyanin}= \frac{ABS \cdot Mw \cdot f \cdot 1000}{\varepsilon \cdot l} \tag{2}$$

Hygroscopicity was measured according as the water gained by the powders in a hermetic container with a saturated solution of Na_2SO_4 (81% RH) during one week(g/100 g dry solids). Solubility was determined as the ratio of soluble solids:total solids. **Wettability** was determined as a result of the time in which 2 g of samples takes to get completely wet in water. The **swelling capaci**ty (SC) was obtained from the ratio between the volume of the sample after 18 h at 25 ºC and the initial weight. Results are given in mL/g as the average and standard deviation of thee replicates.

Water holding capacity (WHC) was obtained as the water contained in the hydrated residue per unit of dry matter. It was obtained by means of equation 3, where HR is the weight of the hydrated powder (~1 g of powder hydrated during 18 hours at 25 ºC), and DR the weight of the freeze dried sample (DR). **Water retention capacity** (WRC) was obtained as follows: sample was weighed in a conical tube and hydrated with water during 18 h at 25 ºC. Then,

the tube was centrifuged at 514 x g during 30 min and sample weighed (R+W). After, ther residue was freeze dried and weighed (R). WRC was calculated as the ratio between the W and the R. Results correspond to the average of three replicates.

$$WHC = \frac{HR\text{-}DR}{DR} \qquad (3)$$

Oil holding capacity (OHC, in g of oil per g of powder) was obtained following the method described by [11]. Powdered samples were mixed with sunflower oil and kept overnight at room temperature. Samples were then centrifuged at 1,500 x g during 5 min, the supernatant was discarded and weight of pellet obtained. Results are the average of three replicates. **Emulsifying activity** (EA) was obtained as described by [12]. Samples were diluted in water (2% w/v) and mixed with sunflower oil in a vortex at 2,400 rpm for 5 min. Then, the mixture was centrifuged at 12,857 x g for 5 min and the emulsion volume was obtained according to equation 6, in which VEL refers to the volume of the emulsified layer (mL) and V to the total volume of fluid (mL). **Emulsion stability** (ES) was evaluated using the method described by [12]. The emulstion prepared to obtain EA, was heated up to 80 ºC during 30 min. When tempered again at room temperature, it was centrifuged at 514 x g during 5 min. ES was obtained as equation 7, where V_{REL} is the volume of the emulsion layer (mL) and V is the total volume of fluid (mL).

$$\%EA = \frac{VEL}{V} \cdot 100 \qquad (6)$$

$$\% ES = \frac{V_{REL}}{V} \cdot 100 \qquad (7)$$

3. Results and discussion

Water activity (a_w), moisture content (x_w) and total soluble solids (x_{ss}) of fresh pomace (P), dried pomace (DP) and grinded dried pomace to a coarse powder (CP) or to a fine powder (FP) are shown in table 1.

Table 1. Water activity, moisture (g_w/g) and x_{ss} ($g_{soluble\ solids}$/g) of fresh and dried blueberry pomace. Mean ± standard deviation of three replicates.

	a_w	x_w	x_{ss}
P	0.989±0.003[c]	0.722±0.003[b]	0.079±0.002[a]
DP	0.189±0.004[a]	0.0173±0.0015[a]	0.28±0.011[b]
CP	0.236±0.004[b]	0.0170±0.0019[a]	0.35± 0.011[b]
FP	0.20±0.06[a,b]	0.019±0.0006[a]	0.46±0.012[c]

Values with different superscript letters in the same column are significantly different ($p < 0.05$).

As expected, dried pomace resulted in a much more stable and rich in soluble solids product than wet pomace. After grinding, both the water activity and the soluble solids content increased significantly, thus indicating that the reduction in the particle size promotes the water ability to conduct deterioration reactions and the solutes ability to dissolve. Indeed, the

finer the powder, the greater the breakdown of long polysaccharides chains and the release of shorter and more soluble ones. As a result, not only the soluble solids content of FP was higher than that of CP, but also the fiber content of FP was significantly lower than that of CP (table 2). It is worth noting that the fiber content of any of the powders is over 30% and that insoluble fiber represents around 68% of total fiber, since other properties such as the hydration and emulsifying properties of the powders will depend on them [13].

Table 2. Content (%) of cellulose, hemicellulose, lignin, insoluble fibre and total fibre of coarse (CP) and fine (FP) powders. Mean ± standard deviation of two replicates.

	Cellulose	Hemicellulose	Lignin	Insoluble fiber	Total fiber
CP	18.0 ± 0.4^b	12.847 ± 0.018^b	7.6 ± 0.2^b	25.6 ± 0.8^b	38.5 ± 0.8^b
FP	16.69 ± 0.14^a	10.444 ± 0.003^a	6.6 ± 0.2^a	23.24 ± 0.06^a	33.69 ± 0.06^a

Values with different superscript letters in the same column are significantly different ($p < 0.05$).

Grinding intensity of the powders, for the powder and for the powder in solution, the average size of particles in FP was significantly lower than that in CP (table 3). This will affect hydration related properties of the powders.

Table 3. Results of D [4,3], D [3,2], and d_{10}, d_{50} and d_{90} of particle size distribution of coarse (CP) and fine powder (FP). Mean ± standard deviation of six replicates.

		D[4,3]	D[3,2]	d_{10}	d_{50}	d_{90}
Dry method	CP	659 ± 10^d	239 ± 8^d	129 ± 5^d	606 ± 10^c	1247 ± 17^d
	FP	211 ± 2^a	81 ± 4^a	36 ± 1^a	$170,1 \pm 0,7^a$	446 ± 7^a
Wet method	CP	437 ± 106^c	177 ± 32^c	71 ± 13^c	398 ± 79^b	873 ± 236^c
	FP	293 ± 66^b	100 ± 48^b	52 ± 6^b	209 ± 51^a	680 ± 206^b

Values with different superscript letters in the same column are significantly different ($p < 0.05$).

Specific volume, solubility, hydration and water retention and emulsifying properties of coarse and fine powders are collected in table 4.

Table 4. Results of specific volume, solubility, hydration and water retention properties and emulsifying properties for the powders. Mean ± standard deviation of three replicates.

	CP	FP
Specific volume (mL/g)	9.60 ± 0.12^b	7.57 ± 0.06^a
Solubility (%)	31.6 ± 1.5^a	33.1 ± 0.7^a
Higroscopicity (%)	61 ± 3^a	62.7 ± 1.8^a
Wettability (s)	175 ± 21^b	77 ± 6^a
Swelling capacity (SC, mL/g)	2.88 ± 0.13^b	2.56 ± 0.06^a
Water holding capacity (WHC) (g/g)	5.1 ± 0.2^b	4.63 ± 0.16^a
Water retention capacity (WRC) (g/g)	3.4 ± 0.3^a	3.08 ± 0.18^a
Oil holding capacity (OHC) (g/g)	2.7 ± 0.6^a	2.9 ± 0.5^a
Emulsifying activity (EA, %)	0.4 ± 0.1^a	0.53 ± 0.12^a
Emulsion stability (ES, %)	3 ± 2^b	1.5 ± 0.7^a

Values with different superscript letters in the same row are significantly different ($p < 0.05$).

Regardless of the particle size, solubility of blueberry pomace powders was quite low, but similar to that reported for asparagus fiber [14]. The high fiber content, especially of the insoluble type, would be the main cause of this. In the same way, hygroscopicity was of the order of that obtained by [15]. Among the properties here analyzed, only the specific volume, the wettability, the SC, the WHC and the ES were significantly affected by the particle size of the powder, with higher values in CP samples than in FP ones. This could be due to the higher porosity of the powders of bigger size particles and, consequently, to the higher amount of air retained in their structure [16]. As for wettability, the lower density of CP involved that this sample remained more time on the water surface, thus increasing the time to get completely wet. Although emulsifying properties are reported to be affected by the type, the size, the shape the superficial area and the chemical composition of different fiber particles [17], these took very similar values in the two powders analyzed. OHC, EA and ES of blueberry pomace powders were similar to that of peach, and apple fibers [18]. Color of powders (table 5) were affected by both the drying and the grinding steps. Drying significantly increased all the color coordinates, including chrome and hue. Grinding effect on color was only evident for FP, that resulted slightly less red and yellow than the CP. In any case, differences in the color of the samples were imperceptible to the human eye.

Table 5. CIEL*a*b* coordinate, chroma and hue of fresh pomace (P), dried pomace (DP), coarse (CP) and fine (FP) powder. Mean ± standard deviation of two replicates.

	L*	a*	b*	C	h
P	26.50±1.0[a]	3.0±0.3[a]	0.19±0.3[a]	3.0±0.3[a]	3.7±0.7[a]
DP	37.5±0.3[b]	3.80±0.10[c]	0.65±0.09[b]	3.86±0.08[c]	9.8±1.5[b]
CP	37.52±0.2[b]	3.8±0.08[c]	0.68±0.08[b]	3.9±0.07[c]	10.1±1.3[b]
FP	37.08±0.10[b]	3.37±0.05[b]	0.12±0.05[a]	3.37±0.5[b]	2.0±0.9[a]

Values with different superscript letters in the same column are significantly different ($p < 0.05$).

Antioxidant properties of different samples are shown in table 6. As it can be observed, total phenols content (TP) reached higher values in P and DP than in grinded samples. Within the powders, the higher values obtained for FP could be due to a greater extractability of such compunds as the particle size decreased [13]. As regards the monomeric anthocyanidins content (MA), their content decreased significantly after the drying step because they are sensitive to both temperature and oxidation [19]. Grinding only affected MA content of FP due to its higher surface/volume ratio and its subsequent higher exposure to oxygen. In agreement with these results, the antioxidant activity (AA) of blueberry pomace measured by both DPPH and ABTS methods was significantly reduced due to drying and further grinding.

Table 6. TP content (mg GAE/100 g db), MA (mg glucosid-3-cyanidin/100 g db), AA with DPPH and ABTS methods (mg TE/g db). Mean ± standard deviation of three replicates.

	TP	MA	AA- DPPH	AA- ABTS
P	4.4±0.2[c]	74.5±0.4[c]	145.7±0.6[c]	87.3±0.4[c]
DP	4.48±0.12[c]	48.9±0.7[b]	101.1±0.7[b]	60.0±1.6[b]
CP	3.02±0.12[a]	49.0±0.9[b]	100.8±0.7[b]	55±3[a]
FP	3.36±0.10[b]	31±4[a]	83.8±1.5[a]	57±2[a,b]

Values with different superscript letters in the same column are significantly different ($p < 0.05$).

Antioxidant properties of the powders were measured again after 20 weeks of storage under controlled conditions. Differences between initial and final values of all compounds are shown in table 7. In general terms, the antioxidant properties of the powders remained quite stable during storage, regardless of the powder particle size. Only the antioxidant activity of the coarse powder measured by DPPH was significantly lower after storage.

Table 7. TP (mg GAE/100 g db), MA (mg glucosid-3-cyanidin/100 g db)content and AA with DPPH and ABTS methods (mg TE/g db) reduction after 20 weeks of storage. Mean ± standard deviation of three replicates.

	TP	MA	AA- DPPH	AA- ABTS
CP	-0.18±0.13[a]	0±3[a]	18.4±1.1[b]	-1±2[a]
FP	0.35±0.18[a]	-4±2[a]	8.2±1.1[a]	0.1±1.1[a]

Values with different superscript letters in the same column are significantly different ($p < 0.05$).

4. Conclusions

Thermal treatment associated with drying reduces antiradical capability of blueberry pomace, mainly by reducing total phenol and anthocyanin content. Mechanical damage induced by grinding operation of dried pomace reduces total fiber content determining water and oil interaction properties. This effect results in a lower wettability, swelling capacity, water holding and water retention capacity of fine powder. Although emulsifying activity is not affected by particle size, the emulsion stability is significantly higher in coarse powder.

5. Acknowledgements

6. References

[1] Mirabella, N.; Castellani, V.; Sala, S. Current options for the valorization of food manufacturing waste: a review. Journal of Clean Production 2014, 65: 28-41.

[2] Neacsu, M.; Vaughan, N.; Raikos, V.; Multari, S.; Duncan, G.J.; Duthie, G.G.; Russell, W.R. Phytochemical profile of commercially available food plant powders: their potential role in healthier food reformulations. Food Chemistry 2015, 179: 159-169.

[3] Cho, M.J.; Howard, L.R.; Prior, R.L.; Clark, J.R. Flavonoid glycosides and antioxidant capacity of various blackberry, blueberry and red grape genotypes determined by high-performance liquid chromatography/mass spectrometry. Journal of the Scienceof Food and Agriculture 2004, 84(13): 1771-1782.

[4] Amaya-Cruz, D.M.; Rodríguez-González, S.; Pérez-Ramírez, I.F.; Loarca-Piña, G.; Amaya-Llano, S.; Gallegos-Corona, M.A.; Reynoso-Camacho, R. Juice by-products as a source of dietary fibre and antioxidants and their effect on hepatic steatosis. Journal of Functional Foods 2015, 17: 93-102.

[5] Quek, S.Y.; Chok, N.K.; Swedlund, P. The physicochemical properties of spray-dried watermelon powders. Chemical Engineering and Processing: Process Intensification 2007, 46(5): 386-392.

[6] Castagnini, J.M.; Betoret, N.; Betoret, E.; Fito, P. Vacuum impregnation and air drying temperature effect on individual anthocyanins and antiradical capacity of blueberry juice included

into an apple matrix. LWT-Food Science and Technology 2015, 64(2): 1289-1296.

[7] AOAC Official Method 934.06 Moisture in Dried Fruits.

[8] Mertens, D.R. Gravimetric determination of amylase-treated neutral detergent fibre in feeds with refluxing beakers or crucibles: collaborative study. Journal of AOAC International 2002, 85: 1217-1240.

[9] Seguí, L.; Calabuig-Jiménez, L.; Betoret, N.; Fito, P. Physicochemical and antioxidant properties of non- refined sugarcane alternatives to white sugar. International Journal of Food Science and Technology 2015, 50(12): 2579-2588.

[10] Lee, J.; Durst, R.W; Wrolstad, R.E. Determination of total monomeric anthocyanin pigment content of fruit juices, beverages, natural colorants, and wines by the pH differential method: collaborative study. Journal of AOAC International 2005, 88(5): 1269-1278.

[11] Garau, M. C.; Simal, S.; Rosselló, C.; Femenia, A. Effect of air-drying temperature on physico-chemical properties of dietary fibre and antioxidant capacity of orange (Citrus aurantium v. Canoneta) by-products. Food Chemistry 2007, 104(3): 1014-1024.

[12] Yasumatsu, K.; Sawada, K.; Maritaka, S.; Mikasi, M.; Toda, J.; Wada, T.; Ishi, K. Whipping and emulsifying properties of soybean products. Agricultural and Biological Chemistry 1972, 36(5): 719-727.

[13] Elleuch, M.; Bedigian, D.; Roiseux, O.; Besbes, S.; Blecker, C.; Attia, H. Dietary fibre and fibre-rich by-products of food processing: Characterisation, technological functionality and commercial applications: A review. Food Chemistry 2011, 124(2): 411-421.

[14] Fuentes-Alventosa, J.M.; Rodríguez-Gutiérrez, G.; Jaramillo-Carmona, S.; Espejo-Calvo, J.A.; Rodríguez-Arcos, R.; Fernández-Bolaños, J.; Guillén-Bejarano, R.; Jiménez-Araujo, A. Effect of extraction method on chemical composition and functional characteristics of high dietary fibre powders obtained from asparagus by-products. Food Chemistry 2009, 113(2): 665-671.

[15] Wu-Ng, Y.; Benlloch-Tinoco, M.; García-Martínez, E.; Martínez-Navarrete, N. Impacto de la adición de carboximetilcelulosa en la calidad de kiwi en polvo obtenido por liofilización y atomización. Trabajo de final del Máster en Ciencia e Ingeniería de los Alimentos de la Universitat Politècnica de València 2013.

[16] Forny, L.; Marabi, A.; Palzer, S. Wetting, disintegration and dissolution of agglomerated water soluble powders. Powder Technology 2011, 206(1): 72-78.

[17] López, G.; Ros, G.; Rincón, F.; Periago, M.J.; Martínez, M.C.; Ortuno, J. Relationship between physical and hydration properties of soluble and insoluble fiber of artichoke. Journal of Agriculture and Food Chemistry 1996, 44: 2773-2778.

[18] Martínez-Las Heras, R.; Landines, E.F.; Heredia, A.; Castelló, M.L.; Andrés, A. Influence of drying process and particle size of persimmon fibre on its physicochemical, antioxidant, hydration and emulsifying properties. Journal of Food Science and Technology 2017, 54(9): 2902-2912.

[19] Zoric, Z.; Dragovic-Uzelac, V.; Pedisic, S.; Kurtanjek, Z.; Garofulic, I.E. Kinetics of the degradation of anthocyanins, phenolic acids and flavonols during heat treatments of freeze-dried sour cherry Marasca paste. Food Technology and Biotechnology 2014, 52(1): 101-108.

Changes in antioxidant and probiotic properties of a freeze-dried apple snack during storage

Burca, C.ª; Seguí, L.ª; Betoret, N.ª; Barrera, C.[a]

Functional Foods group. Institute of Food Engineering for Development. Universitat Politècnica de València, Valencia, Spain

*E-mail of the corresponding author: noebeva@tal.upv.es

Abstract

This research developed an apple snack with potential probiotic effect (> 10^7 CFU/g) by combining vacuum impregnation with Lactobacillus salivarius spp. salivarius (CECT 4063) and freeze-drying. Throughout storage (30 days), both the lactobacillus viability and the total flavonoids content decreased. Trehalose adition (10% by weight) to the impregnation liquid and/or its homogenization at 100 MPa accelerated the loss of cell viability but delayed flavonoids degradation and promoted an increase in the amount of phenols and total antioxidants.

Keywords: L. salivarius spp. salivarius; homogenization; trehalose; freeze-drying; antioxidants.

1. Introduction

Helicobacter pylori is a pathogenic bacterium that causes severe gastric problems to a large part of the world's population, especially in less developed countries [1]. Traditional treatments based on antibiotics have side effects and are not 100% effective [2]. Recent studies show that some strains of the *Lactobacillus* genus are effective in the treatment against *Helicobacter pylori*, reducing the colonization of this pathogen, what has promoted the incorporation of *Lactobacillus* in the formulation of certain foods [3]. However, the survival of these microorganisms in food is rather limited, especially in not dairy products. Some food engineering techniques, such as the formulation with certain ingredients (e.g. probiotics) or the modification of the structures conferring protection to the microorganism (e.g. encapsulation) can be applied in order to alter probiotics functionality and/or increase their survival against adverse conditions. Specifically, in this study the effect of trehalose addition (10%, w/w) to the impregnation liquid and/or its homogenization at 100 MPa on *Lactobacillus salivarius* spp. *salivarius* (CECT 4063) survival during the manufacture and storage of a freeze-dried apple snack was evaluated. Given the high content in antioxidant compunds of the raw materials, also changes in this bioactive substances were analyzed.

2. Materials and Methods

2.1. Solid matrix

Apples (var. Granny Smith) cut into 5 mm thick rings (20 and 65 mm of internal and external diameter, respectively) were used as solid matrix for the snack preparation.

2.2. Impregnation liquids

The impregnation liquid was prepared from commercial clementine juice (Hacendado brand). Following the procedure described by Betoret et al. [4], yeast extract (5 g/L) and sodium bicarbonate (9,8 g/L) were added for the optimal microbial growth. When required, 100 g/kg of food grade trehalose (TREHA^{TM}, Cargill, Barcelona, Sapin) were also added to the juice formulation. Once all the ingredients were dissolved, the liquids were inoculated (10^9 CFU/L) with strain CECT 4063 of *Lactobacillus salivarius* spp. *salivarius* (Colección Española de Cultivos Tipo, Universitat de València, Burjassot, Spain) that had been previously grown on MRS Broth agar. After 24 h of incubation at 37 ºC, part of the liquids were homogenized at 100 MPa on a laboratory scale high pressure homogenizer (Panda Plus 2000, GEA-Niro Soavi, Parma, Italy) before their use as impregnation liquids. Four different impregnation liquids were prepared in total (Table 1).

Table 1. Different impregnation liquids employed in the present study.

Impregation liquid	Trehalose (g/kg)	Pressure (MPa)
0%_0MPa	0	0
0%_100MPa	0	100
10%_0MPa	100	0
10%_100MPa	100	100

2.3. Experimental procedure

This section describes the unit operations involved in the manufacture of apple snacks enriched with *Lactobacillus salivarius* spp. *salivarius* (CECT 4063).

First, vacuum impregnation was performed in a vacuum chamber (HERAEUS Vacuun Oven, THERMO SCIENTIFIC) connected to a vacuum pump (ILMVAC, Germany). A vacuum pressure of 50 mbar was applied for 10 min to the apple rings immersed in the corresponding liquid. Then, the atmospheric pressure was restored and maintained for another 10 min.

Vacuum impregnated apple rings were deep-frozen and kept at -40 °C for 24 h (Matek model CVN-40/105). Then, they were placed in a pilot scale freeze-drier (TELSTAR LIOALFA 6-80) at -45 °C and a vacuum pressure of 0.1 mbar for 24 h more.

In the end, freeze-dried apple slices were stored in hermetic and opaque bags and kept under controlled conditions of humidity and temperature for 30 days.

2.4. Analytical determinations

All the analytical determinations were carried out at least in triplicate on liquid and/or solid samples at different stages throughout the snack manufacture process.

2.4.1. Water content and water activity

The apple samples moisture content was determined by drying a known amount of sample in a vacumm oven at 60 ℃ and 200 mbar until it reached a constant weight.

The water activity of apple samples was measured at 25 °C in a properly calibrated dew poin hygrometer (Decagon Aqualab model CX-2, with an accuracy of ± 0.003).

2.4.2. Antioxidant properties

Extracts from solid samples were obtained by mixing 2 g of fresh and impregnated apple or 0.35 g of freeze-dried apple with 10 mL of a 80:20 (v/v) methanol-water solution.

Total phenols content was measured at 760 nm in a Helios Zeta UV/Vis Thermo Scientific spectrophotometer by the Folin-Ciocalteu reagent method [5]. Results were expressed in milligrams of gallic acid equivalents per gram of sample (mg GAE/g).

Total flavonoids content was measured at 368 nm in a Helios Zeta UV/Vis Thermo Scientific spectrophotometer by the colorimetric method of aluminum chloride [6]. Results were expressed in milligrams of quercetin equivalents per gram of sample (mg QE/g).

Antioxidant activity was determined at 515 nm in a Helios Zeta UV/Vis Thermo Scientific spectrophotometer by the DPPH method [7]. Results were expressed in milligrams of trolox equivalents per gram of sample (mg TE/g).

2.4.3. Viable counts

The *Lactobacillus salivarius* spp. *salivarius* (CECT 4063) concentration was analyzed both in the growing medium, the impregnation liquids and the apple samples by the serial dilution and plating method. MRS seeded plates were incubated in anaerobiosis at 37 °C for 3 days. In the case of solid apple samples, the first dilution was carried out in a stomacher bag in which 5 g of sample were crushed with 45 mL of sterile peptone water.

2.5. Statistical analysis

The effect that the different variables considered exert on the obtained results was evaluated with the Statgraphics Centurion XVI program by simple analysis (simple ANOVA) with a 95% confidence level.

3. Results and discussion

3.1. Changes in *Lactobacillus salivarius* spp. *salivarius* (CECT 4063) content

As it is shown in Fig. 1, *Lactobacillus salivarius* spp. *salivarius* (CECT 4063) content in the impregnation liquid (VI liquid) increased significantly by adding 10% of trehalose by weight to its formulation or by its homogenization at 100 MPa. However, the combination of both factors did not notably improve the viable counts.

Similar trends were observed in vacuum impregnated apples (VI apple), whose microbial content was significantly lower than that of any of the impregnation liquids. This is logical considering that only 20% of fresh apple volume is filled with the impregnation liquid during the vacuum impregnation step [8].

Finally, freeze-dried apple samples (FD apple) potential probiotic effect was higher than that of vacuum impregnated ones, but not as high as expected from the decrease in their water content (from 85.3 ± 1.2% in VI apple to 4.97 ± 1.02% in FD apple). Regarding the composition of the impregnation liquid, the addition of trehalose to its composition slightly reduced the adverse effect of freeze-drying on the microbial population. On the contrary, the subsequent homogenization of trehalose enriched juice increased *L. salivarius* spp. *salivarius* vulnerability to the freeze-drying step.
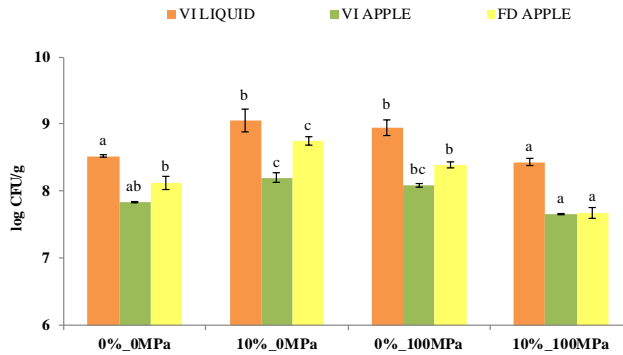
Fig. 1. Microbial counts in the impregnation liquids and both in vacuum impregnated (VI) and freeze-dried (FD) apple samples. Different letters within a single series indicate statistical significant differences at 95% confidence level.

Throughout storage (Fig. 2), *L. salivarius* spp. *salivarius* (CECT 4063) content in freeze-dried apple samples suffered a notable decline, in spite of the low water activity reached by the snack (0.27 ± 0.02). This fact was particularly evident when trehalose and/or pressure were applied to the impregnating liquid, thus suggesting that the stress caused by the osmotic and/or the pressure gradient favored the loss of vialbility and the shortening of the snack self life. Just to mention that for a food to be considered probiotic it must contain at least 10^7 CFU/g when consumed [9]. Only snacks impregnated with liquids 0%_0MPa and 10%_0MPa met this condition at the end of the storage.
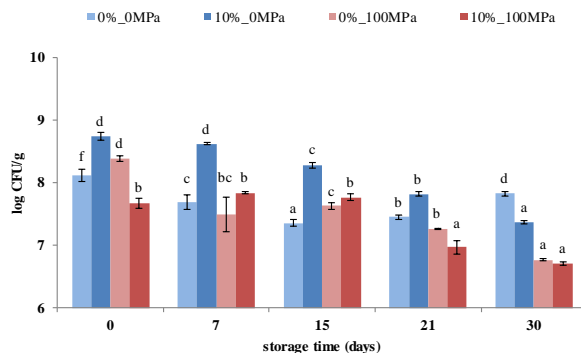
Fig. 2. Changes in microbial counts troughout storage of freeze-dried apple snacks. Different letters within a single series indicate statistical significant differences at 95% confidence level.

3.2. Changes in antioxidant properties

Despite the notable differences observed in their total phenols and flavonoids content, antioxidant capacity assessed by DPPH method both in the impregnation liquids and the vacuum impregnated apple samples were of the same order (Table 2). As expected, all the antioxidants increased their concentration significantly after the freeze-drying step. As for the composition of the vaccum impregnation liquid, neither the addition of trehalose nor the homogenization resulted in a final snack with improved antioxidant properties.

Table 2. Antioxidant properties of the impregnation liquids and both the VI and FD apple samples.

Food matrix	Impregation liquid	total phenols (mg GAE/g)	total flavonoids (mg QE/g)	DPPH (mg TE/g)
VI liquid	**0%_0MPa**	0.78(0.07)[a]	1.01(0.07)[c]	0.70(0.04)[a]
	10%_0MPa	0.79(0.08)[a]	0.904(0.004)[c]	0.78(0.06)[a]
	0%_100 MPa	0.7235(0.0007)[a]	0.954(0.014)[c]	0.7(0.2)[a]
	10%_100 MPa	0.82(0.03)[a]	0.93(0.03)[c]	0.73(0.05)[a]
VI apple	**0%_0MPa**	0.441(0.015)[a]	0.291(0.002)[b]	0.89(0.12)[a]
	10%_0MPa	0.34(0.06)[a]	0.175(0.003)[a]	0.61(0.03)[a]
	0%_100 MPa	0.82(0.11)[a]	0.217(0.002)[ab]	0.92(0.07)[a]
	10%_100 MPa	0.64(0.03)[a]	0.132(0.002)[a]	0.77(0.04)[a]
FD apple	**0%_0MPa**	11.4(0.6)[e]	8.70(0.07)[f]	7.84(0.07)[d]
	10%_0MPa	3.025(0.012)[b]	1.186(0.012)[d]	5.5(0.2)[c]
	0%_100 MPa	6.0(0.3)[d]	2.01(0.14)[e]	5.0(0.3)[c]
	10%_100 MPa	4.8(0.4)[c]	1.19(0.02)[d]	2.3(0.8)[b]

Mean values and standard deviation in brackets. Different superscripts in the same column indicate statistical significant differences at 95% confidence level.

Regarding the stability of the antioxidant compounds throughout the snack storage, it is shown in Fig. 3 the change in each component concentration from the beginning to the end of the storage referred to the initial concentration (Δx^i):

$$\Delta x^i (\%) = \frac{x^i_{t=0} - x^i_{t=30}}{x^i_{t=0}} \cdot 100 \tag{1}$$

where $x^i_{t=0}$ and $x^i_{t=30}$ indicate the component i concentration in freshly made and 30 days stored FD apples, respectively (g of component i/total g).

Generally speaking, the total phenols gain was significantly higher and the total flavonoids loss was significantly lower (p-value < 0.05) in apple snacks that were impregnated with any of the liquids that included trehalose in its composition, but especially in those impregnated with the liquid that was additionally homogenized (10% _100MPa). As a result, these samples also showed a significantly higher increase in the total antioxidant content measured by the DPPH method.
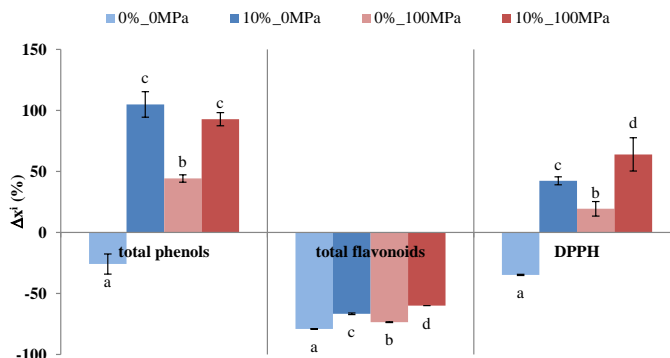
***Fig. 3. Changes in antioxidant properties after 30 days of storage of freeze-dried apple snacks.
Different letters within a single compound indicate statistical significant differences at 95%
confidence level.***

Given the ability of trehalose to protect biological structures [10], apple tissue would have
been less damaged during the freeze-drying step. As a result, antioxidant compounds would
have been less accessible to adverse conditions that promote their degradation. Trehalose
protective effect could be promoted by the reduction in the particle size that implies the
application of a homogenization step [11], thus favouring the inflow of a greater amount of
liquid (and trehalose) into the apple porous structure during the vacuum impregnation.

4. Conclussions

Vacuum impregnation allows to incorporate lactobacillus into the apple porous structure to
a greater or lesser extent, depending on the viable counts in the impregnation liquid. The
subsequent freeze-drying increases apples stability without negatively affecting the microbial
content or the antioxidants content. *Lactobacillus salivarius* spp. *salivarius* survival during
the further storage was negatively affected by the addition of trehalose to the impregnation
liquid and/or its homogenization. On the contrary, the addition of trehalose to the
impregnation liquid and/or its homogenization delayed flavonoids degradation and promoted
an increase in the amount of both phenols and total antioxidants.

5. References

[1] Taylor, D.E.; Blaser, M. The epidemiology of *Helicobacter pylori* infection.
Epidemiologic Reviews 1991, 13: 42-59.

[2] Lopes, D.; Nunes, C.; Martins, M.C.; Sarmento, B.; Reis, S. Eradication of *Helicobacter
pylori*: past, present and future. Journal of Controlled Release 2014, 189: 169-186.

[3] Hamilton-Miller, J.M. The role of probiotics in the treatment and prevention of
Helicobacter pylori infection. International Journal of Antimicrobial Agents 2003, 22:

360-366.

[4] Betoret, E.; Betoret, N.; Arilla, A.; Bennár, M.; Barrera, C.; Codoñer, P.; Fito, P. No invasive methodology to produce a probiotic low humid apple snack with potential effect against *Helicobacter pylori*. Journal of Food Engineering 2012, 110 (2), 289-293.

[5] Singleton, V.L.; Rossi, J.A. Colorimetry of total phenolics with phosphomolybdic-phosphotungstic acid reagents. American Journal of Enology and Viticulture 1965, 16, 144-158.

[6] Luximon-Ramma, A.; Bahorun, T.; Crozier, A.; Zbarsky, V.; Datla, K.; Dexter, D.; Aruoma, O. Characterization of the antioxidant functions of flavonoids and proanthocyanicins in Muritian black teas. Food Research International 2005, 38, 357-367.

[7] Brand-Williams, W.; Cuvelier, M.; Berset, C. Use of a free radical method to evaluate antioxidant activity. LWT-Food Science Technology 1995, 28 (1): 25-30.

[8] Fito, P.; Chiralt, A.; Barat, J.M.; Andrés, A.; Martínez-Monzó, J.; Martínez-Navarrete, N. Vacuum impregnation for development of new dehydrated products. Journal of Food Engineering 2001, 49 (4): 297-302.

[9] Ranadheera, R.D.C.S.; Baines, S.K.; Adams, M.C. Importance of food in probiotic efficacy. Food Research International 2010, 43:1-7.

[10] Conrad, P.B.; Miller, D.P.; Cielenski, P.R.; De Pablo, J.J. Stabilization and preservation of *Lactobacillus acidophilus* in saccharide matrices. Cryobiology 2000, 41 (1): 17-24.

[11] Betoret, E.; Betoret, N.; Carbonell, J.V.; Fito, P. Effects of pressure homogenization on particle size and the functional properties of citrus juices. Journal of Food Engineering 2009, 92 (1): 18-23.

Preliminary study of superheated steam spray drying: A case study with maltodextrin

Fuengfoo, M.[a]*; Devahastin, S.[a]; Niamnuy, C.[b]; Soponronnarit, S.[c]

[a] Advanced Food Processing Research Laboratory, Department of Food Engineering, Faculty of Engineering, King Mongkut's University of Technology Thonburi, 126 Pracha u-tid Road, Tungkru, Bangkok 10140, Thailand

[b] Center of Advanced Studies in Industrial Technology, Department of Chemical Engineering, Faculty of Engineering, Kasetsart University, 50 Ngam Wong Wan Road, Chatuchak, Bangkok 10900, Thailand

[c] Division of Energy Technology, School of Energy, Environment and Materials, King Mongkut's University of Technology Thonburi, 126 Pracha u-tid Road, Tungkru, Bangkok 10140, Thailand

*E-mail of the corresponding author: fengmdf@ku.ac.th

Abstract

A spray dryer was modified and tested with superheated steam as the drying medium. The effect of the inlet temperature on the recovery and morphology of the dried powder was then investigated. The results were compared with those obtained from hot-air spray drying. The results showed that the use of superheated steam and an increase in the inlet temperature led to an increase in the product recovery. The morphological results correlated with those of the product recovery in that superheated steam powder exhibited more inflated skin, leading to less adhesion of the sprayed droplets to the dryer wall.

Keywords: morphology; product recovery; spray drying; superheated steam drying.

1. Introduction

Superheated steam drying is considered to be well established, with many ongoing studies showing that this drying process generally results in products with higher quality, either in terms of physical, chemical or organoleptic properties.[1,2] However, most superheated steam drying studies involved the use of solid samples although in reality many liquid materials also need to be dried. Only a few works are so far available on the use of superheated steam as the medium for drying liquid products, which require the use of, for example, a spray dryer.

The idea of superheated-steam spray drying has been verified mainly only via theoretical analysis or numerical modeling. Frydman et al.[3] and Ducept et al.[4] employed commercial software to simulate the most important features of both superheated steam and hot air spray dryers, including the fields of gas temperature and velocity inside the chamber, droplet trajectories and deposits on the chamber wall. The simulations were experimentally validated by comparing the experimental and simulated residence time distribution of water and KCl solution droplets in the study of Frydman et al.[3] and Ducept et al.[4], respectively. However, these investigators did not make any attempt to investigate the characteristics of the resulting powder.

Among the limited attempts to study superheated steam spray drying, the works of Islam et al.[5,6,7] exist on the use of vacuum superheated steam spray drying to dry orange juice and orange juice with pulp with maltodextrin as the drying aid. Selected characteristics and properties of powder, i.e., moisture content, hygroscopicity, water activity, particle size, particle morphology, color, rehydration behavior and ascorbic acid retention, produced from the solutions of four different combinations of juice:maltodextrin were studied. Nevertheless, no attempt was made to compare the results with those obtained from a hot air spray dryer at equivalent conditions.

More recently, Lum et al.[8] studied the effect of superheated steam drying on the component migration during the formation of multicomponent droplets. The study was conducted by drying fresh milk droplets in the so-called single droplet drying apparatus; the results were then compared with those belonging to hot-air drying conducted in the same apparatus. The results revealed the possibility of controlling component relocation in a multicomponent droplet based on the improved hydrophilicity of the droplet surface as a result of the use of superheated steam, which is hydrophilic in nature, as the drying medium. By appreciating the potential of superheated steam as the medium for spray drying, engineered multicomponent particles with specific features can be produced.

Despite its potential benefits, no attempt has so far been made to experimentally investigate the effect of superheated steam as the drying medium in a typical (multiple-droplet) atmospheric-pressure spray dryer. No comparison also exists with the results belonging to

hot-air spray drying at equivalent conditions in terms of the dryer performance and the characteristics of the dried powder.

In the present study, modification was made to an atmospheric-pressure hot-air spray dryer, so it can be used for superheated steam spray drying. Preliminary study was then conducted to investigate the effect of inlet drying temperature on the product recovery; for simplicity, maltodextrin was used as the test material. Morphology of the powder was also observed to support and explain the measured product recovery. The results were compared with those obtained in the case of hot-air spray drying in the same dryer set-up at the same inlet temperatures.

2. Materials and Methods

2.1. Materials

An aqueous solution (30% w/v) of maltodextrin (DE 10), which was supplied by Chemipan Corporation Co., Ltd. (Thailand), was prepared by dissolving maltodextrin in distilled water and stirring using a magnetic stirrer at 300 rpm for 30 min.

2.2. Spray-dryer set-up

A schematic diagram of the atmospheric-pressure superheated steam spray dryer setup is shown in Fig. 1. A water-tube boiler (Takuma, model TWA-500, Tokyo, Japan), which is able to generate a maximum saturated steam mass flow rate of 500 kg/h at a steam pressure of 7 bar (gauge), was used to supply steam to the system. To remove excess moisture from the steam, a steam pocket (1 inch in diameter), steam header (4 inches in diameter) and steam separator were used. Thermodynamic steam traps were used to drain excess water from the above three components. The steam pressure was adjusted via the use of a pressure reducing valve (Yoshitake, model GD-30, Tokyo, Japan), which was used to control the steam pressure at near-atmospheric pressure of 20 kPa (gauge). An electric heater rated at 9 kW, which was controlled by a proportional-integral-differential (PID) controller (Omron, model E5CN-RMTC-500, Tokyo, Japan) with an accuracy of $\pm 1^o$ C, was used to convert saturated steam into superheated steam. A blower was used to deliver the saturated steam to the heater. The steam velocity was adjusted to 14-15 m/s by the use of two globe valves; the steam velocity was measured using a pitot tube (Testo, model 445, Lenzkirch, Germany) at point A with an accuracy of ± 0.2 m/s. The inlet steam temperature was varied at 160, 170 and 180° C. The inlet steam temperature as well as the outlet steam temperature were measured at points B and C, respectively, and were continuously recorded by type T thermocouples connected to a data logger (Yokogawa, model µR100, Tokyo, Japan).

The drying chamber consists of a stainless steel cylindrical chamber, which is 25 cm in diameter and 50 cm in height, connected to a bottom conical section of 30 cm in height.
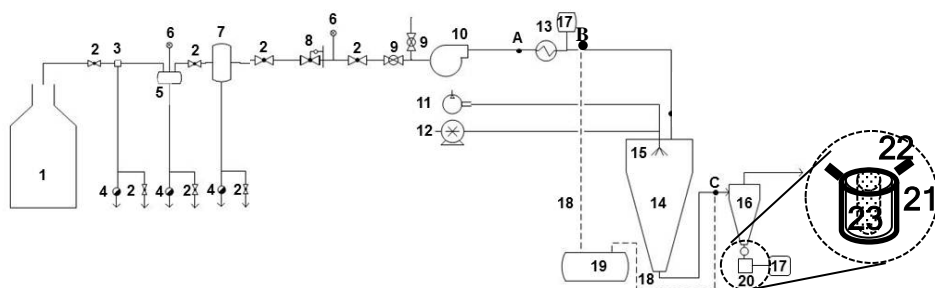
Fig. 1 Schematic diagram of atmospheric-pressure superheated steam spray dryer and associated units: (1) water-tube boiler; (2) globe valves; (3) steam pocket; (4) steam traps; (5) steam header; (6) pressure gauges; (7) steam separator; (8) pressure reducing valve; (9) ball valves; (10) blower; (11) air compressor; (12) liquid feed pump; (13) electrical heater; (14) spray drying chamber; (15) atomizer; (16) cyclone; (17) PID controllers; (18) thermocouples; (19) temperature data logger; (20) powder collector; (21) auxillary heater; (22) steam outlet; (23) cylindrical filter

A two-fluid nozzle with an orifice internal diameter of 1.0 mm was installed at the top of the drying chamber. The nozzle pressure was maintained at around 2 bar (gauge) during all the spray drying experiments. A glass cyclone, which is 10 cm in diameter and 20 cm in height and has the bottom conical section of 30 cm in height, was used to separate dried powder from the exhaust steam. The dryer can also be operated as a hot-air spray dryer with the use of hot air, which can be supplied to the drying chamber via the use of the blower, as the drying medium.

Maltodextrin solution was fed into the drying chamber via a peristaltic pump (Watson-Marlow, Model 505S, Cornwall, UK) at a feed flow rate of 5 mL/min. The obtained powder sample was collected and sealed in an aluminum bag until further analysis.

Since the superheated steam spray drying experiments were conducted at atmospheric pressure, there was inevitable steam condensation in the powder collector. To prevent the condensation of steam within the powder collector, an auxillary heater was used to maintain the temperature within the powder collector at around 105° C; this value is higher than the saturation temperature of the exhaust steam. Moreover, a steam outlet was provided to drain out the exhaust steam. A cylindrical filter made of stainless steel screen of 500 openings per square inch was used to trap dried powder (see an inset in Fig. 1).

2.3. Analytical methods

2.3.1. Product recovery

The percentage product recovery was calculated by the following equation:

$$\frac{W_p}{W_F} \times 100\% \tag{1}$$

where W_p is the amount of solid mass of the collected powder (g) and W_F is the amount of solid mass of the liquid feed (g).

2.3.2. *Scanning electron microscopy*

The morphology of a spray-dried powder sample was observed via the use of a scanning electron microscope (JEOL, JSM-6400LV, Tokyo, Japan) at an accelerating voltage of 10 kV. Each sample was coated with a gold layer and photographed at 300× magnification level.

2.3.3. *Statistical analysis*

The effects of the type of the drying medium and inlet drying temperature as well as their interactions on the product recovery were determined by the univariate full-factorial analysis of variance (ANOVA). Each experiment was carried out in duplicate. All the experimental data were analyzed using SPSS 16.0 for Windows® (SPSS Inc., Chicago, IL) and are presented as mean values with standard deviations. Differences between mean values were established using Duncan's new multiple range tests at a confidence level of 95%.

3. Results and Discussion

3.1. Product recovery

The effects of the type of the drying medium and inlet temperature on the product recovery were investigated and are shown in Table 1. The type of the drying medium and inlet drying temperature had a significant effect on the product recovery ($p < 0.05$). However, there were no interactions between the two parameters ($p > 0.05$).

Use of superheated steam as the spray drying medium led to an increase in the product recovery when compared with the use of hot air. This is probably because superheated steam, which has higher heat transfer coefficient and specific heat capacity, could increase the gas-droplet heat transfer rate. The solid surface was more rapidly formed around a droplet during drying, leading subsequently to less adhesion of the sprayed droplets to the drying chamber wall.[9]

Table 1. Effect of drying medium and inlet temperature on product recovery

Drying medium	Inlet temperature		
	160° C	**170° C**	**180° C**
Superheated steam	38.0 ± 2.82^b	45.0 ± 1.41^a	48.5 ± 2.12^a
Hot air	32.5 ± 2.12^c	34.5 ± 2.12^{bc}	37.0 ± 2.82^b

Values with different superscripts are significantly different ($p < 0.05$).

An increase in the inlet temperature led to an increase in the percentage product recovery. This is because an increase in the drying temperature led to a larger driving force for heat and mass transfer to/from the droplets during drying.[10] This in turn resulted in faster drying and more rapid solid surface formation, leading again to less adhesion of the sprayed droplets to the dryer wall.

3.2. Particle morphology

Microstructural characteristics of the powder were investigated, so that the results can be used to support and explain the measured product recovery. Fig. 2 illustrates the effects of the type of the drying medium and inlet drying temperature on the morphology of the maltodextrin powder.

Superheated steam spray-dried maltodextrin powder exhibited overall morphology as larger spherical particles with inflated skin. This indicated that during superheated steam drying, water vaporization took place rapidly and the solid surface was rapidly formed. Besides, it was found that the process conducted at higher temperatures (170º C, 180º C) resulted in a combination of non-broken particles, fractured spheres and broken shells. Broken shells were due to excessive vaporization of water within the particles during superheated steam drying; such vaporization led to significant volume expansion due to rapid pressure build-up in superheated steam drying and as a result the broken structure if the generated vapor could not move out of the particles fast enough.[2] On the other hand, hot air spray-dried maltodextrin powder exhibited overall morphology as spherical particles with shrivel skin. This is probably due to the results of the slower water evaporation. The skin of the particles remained moist for a longer period of the time, so the particles deflated when vapor condensed within the vacuole as particles were moved into the cooler region of the dryer.

In both the cases of superheated steam and hot air drying, it was found that an increase in the inlet temperature led to a larger size of the dried particles. This is because an increase in the inlet temperature led to a larger driving force for drying to/form the droplets as mentioned earlier.[10] However, it was found that larger particles were obtained in the case of hot air drying than in the case of superheated steam drying at an inlet drying temperature of 160º C. This is probably due to the fact that the drying temperature of   160º C was below the so-called inversion temperature where the drying rate during superheated steam drying was lower than that during hot air drying, leading to the solid surface of particles drying hot air spray drying more rapidly formed than during superheated steam spray drying.
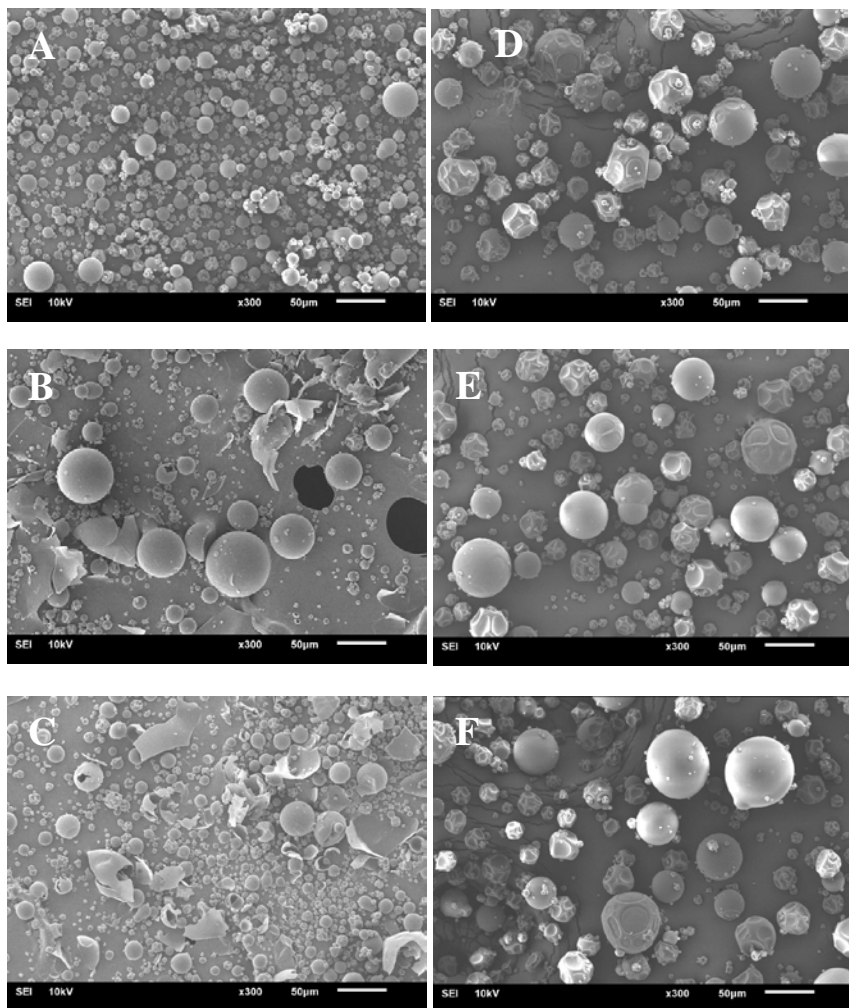
Fig. 2 Morphology of maltodextrin powder dried by superheated steam at (A) 160°C, (B) 170°C and (C) 180°C; dried by hot air at (D) 160°C, (E) 170°C and (F) 180°C

4. Conclusions

Modification was made to an atmospheric-pressure hot air spray dryer to allow the use of superheated steam as the drying medium. Preliminary study was then conducted to investigate the effects of the type of the drying medium and inlet drying temperature on the powdery product recovery. Particle morphology was also evaluated. The use of superheated steam as the drying medium as well as an increase in the inlet temperature could improve the product recovery. The morphological results correlated with the results of the measured product recovery in that superheated steam spray-dried powder was noted as larger spherical

particles with inflated skin, leading subsequently to less adhesion of sprayed droplets to the dryer wall.

5. Acknowledgements

6. References

[1] Alfy, A.; Kiran, B.V.; Jeevitha, G.C.; Hebbar, H.U. Recent developments in superheated steam processing of foods-A Review Critical. Reviews in Food Science and Nutrition 2016, 56, 2191–2208.

[2] Devahastin, S.; Mujumdar, A.S. Superheated steam drying of foods and biomaterials. In Modern Drying Technology, Volume 5; Tsotsas, E.; Mujumdar, A.S., Eds.; Wiley-VCH, Weinheim, Germany, 2014; 57–84.

[3] Frydman, A.; Vasseur, J.; Ducept, F.; Sinneau, M.; Moureh, J. Simulation of spray drying in superheated steam using computational fluid dynamics. Drying Technology 1999, 17, 1313–1326.

[4] Ducept, F.; Sionneau, M.; Vasseur, J. Superheated steam dryer: simulations and experiments on product drying. Chemical Engineering Journal 2002, 86, 75–83.

[5] Islam, M.Z.; Kitamura Y.; Yamano, Y; Kitamura, M. Effect of vacuum spray drying on the physicochemical properties, water sorption and glass transition phenomenon of orange juice powder. Journal of Food Engineering 2016, 169, 131–140.

[6] Islam, M.Z.; Kitamura Y.; Kokawa, M.; Monalisa, K. Degradation kinetics and storage stability of vacuum spray-dried micro wet-milled orange juice (*Citrus unshiu*) powder. Food Bioprocess Technology 2017, 1002–1014.

[7] Islam, M.Z.; Kitamura Y.; Kokawa, M.; Monalisa, K.; Tsai, F.; Miyamura, S. Effects of micro wet milling and vacuum spray drying on the physicochemical and antioxidant properties of orange (*Citrus unshiu*) juice with pulp powder. Food and Bioproducts Processing 2017, 101, 132–144.

[8] Lum, A.; Mansouri, S.; Hapgood, K.; Woo, M.W. Single droplet drying of milk in air and superheated steam: Particle formation and wettability. Drying Technology 2018, https://doi.org/10.1080/07373937.2017.1416626.

[9] Chegini, G.R.; Ghobadian, B. Effect of spray-drying conditions on physical properties of orange juice powder. Drying Technology 2005, 23, 657–668.

[10] Nijdam, J.J.; Langrish, T.A.G. An investigation of milk powders produced by a laboratory-scale spray dryer. Drying Technology 2005, 23, 1043–1056.

Influence of drying temperature and ultrasound application in some quality properties of apple skin.

Martins, M. [a]*; Cortés, E.[b]; Simal, S[c]; Mulet, A.[d]; Pérez-Muelas, N. [d]; Cárcel, J. A.[d]

[a] Department of Food Engenieering. Faculty of Animal Science and Food Engineering, University of Sao Paulo, São Paulo, Brazil.

[b] Technological Institute of Veracruz, Veracruz, México

[c] Department of Chemistry. University of the Balearic Islands, Palma, Spain.

[d] ASPA group. Department of Food Technology. Universitat Politècnica de València, Valencia, Spain

*E-mail of the corresponding author: matheuspmartinss@gmail.com

Abstract

The great amount of waste produced by the food industry can be an interesting source of bioactive compounds. To this end, convective drying is one of the most extended method to stabilize the industrial by-products. However, drying conditions can affect not only drying kinetics but also the bioactivy of some compounds. Apple skin constitutes one of the main by-product generated in apple juice or cider production. It contains important amounts of functional compounds such as polyphenols or vitamin C whose extraction can be interesting. The main aim of this work was to determine the influence of drying conditions, temperature and application of ultrasound, in some quality parameters of dried apple skin. For this purpose, apple skin samples were dried at different temperatures (-10, 30, 50 and 70 ºC) and with (20.5 kW/m³) or without application of ultrasound. Color, total phenolic content, antioxidant activity and vitamin C was measured in fresh and dried samples. The increase of drying temperature and the ultrasound sligthly reduced the antioxidant properties of samples while no influence in sample color was observed.

Keywords: by-product; antioxidant; polyphenol; vitamin C; color.

1. Introduction

The high volume of waste produced in the actual food industries has a great environmental impact. However, in many cases, the waste can be considered as a by-product that constitute a source of interesting bioactive compounds.[1]

Apple is one of the most popular fruits in the world being consumed such as fresh fruit, jam, baby food, juices or snacks. In this sense, apple skin constitutes one of the main by-products generated in the apple industrialization. Apple skin contains great amounts of compounds with high antioxidant capacity, even greater than those present in the flesh.[2, 3, 4] In fact, apple skin can be directly used as a functional ingredient of other food products. [5, 6]. To facilitate the storage and the manage, apple skin must be stabilized and for this purpose convective hot air drying is one of the most applied.[7] However, the temperatures and the long time of processing can damage flavor, nutritional composition or look of dried product.[2, 8]. In fact, the influence about drying process on antioxidant activity of apples and been previously studied not ontly in apple flesh [9, 10, 11] but also in apple skin.[2] Taking into account the final quality of the product, the drying processes at low temperatures emerges as an excellent alternative. However, the low drying rate at this contidions makes necessary the search of methos to intensify the process [22, 23]. In this sense, ultrasound application constitutes an efficient way to intensify mass transport which can shorten the processing time.[12] Moreover, the effects of ultrasound are mainly mechanical which dn't produce a significant heating of the samples.[13]

The main aim of this work was to assess the influence of the drying temperature and ultrasound application on the color and the antioxidant properties of apple skin.

2. Materials and Methods

2.1. Sample preparation
Apples (Royal Gala var.) of similar ripness state were choosen in a local market (Valencia, Spain). The fruits were washed with tap water and peeled using a household peeler. After that, the samples of apple skin were blanched for 30 s in boiling water in order to inactivate the enzyme polyphenol oxidase.[14] Initial moisture content was determined after maintaining apple samples in a vaccumm oven at 60 ºC until constant weight [15].

2.2. Drying
Experiemntal drying processes was carried out at atmospheric freeze-drying and at hot air drying conditions.

2.2.1. Atmospheric freeze-drying experiments

Apple skin samples were placed in a holder with regular distribution that assure the homogeneity of air flow and ultrasound treatment during drying process. After, the set was introduced in a blast freezer (HIBER, mod. ABB BF051, Italy) where samples were frozen at -35 ± 1ºC. Later, the frozen samples were placed in an ultrasonically-assisted convective drier [22] where drying experiments were carried out at -10ºC and 2 m/s, without (AIR-10) and with (US-10; 50 W; 21.9 kHz) ultrasound application. Experiments ended when samples lost 85 % of initial weight.

2.2.2. Hot air drying experiments

Fresh apple skin samples where placed in a similar holder than the used for atmospheric-freeze drying experiments, and placed in a dryer assisted with ultrasound [16]. Drying experiments (2 m/s) were conducte at 30, 50 and 70ºC, without (AIR30, AIR50 and AIR70) and with (US30, US50, US70; 50 W; 21.7 kHz). All the conditions tested were carried out by triplicate.

2.3. Quality parameters

2.3.1. Color

Apple skin sample color was assesd by measuring the CIELab parameters L* (lightness/darkness), a* (redness/greenness) and b* (yellowness/blueness) with the help of a colorimeter CM-2500d (Konica Minolta, Japan). All readings were done in triplicate using a D65 illuminant reference system. Chroma was estimated from Eq. 1.

$$C^* = \sqrt{(a^{*2} + b^{*2})}$$

(1)

2.3.2. Antioxidant properties

An extract of dried apple skin was obtained for measuring antioxidant properties. For this purpose 3 g of sieved powder of apple peel were placed in 25 mL of an ethanol (96 % v/v). (3,5 g of apple's peel powder in 10 mL of ethanol (96 % v/v) in the cas of acorbic acid measurements). The mix was introduced in an ultrasonic cleaner bath (VMR mod. USC-T, USA) forg 15 min. After that, the samples were filtered using nonsterile hydrophobic PTFZ syringe filters of 4.5 μm (VMR, USA).

2.3.3. Antioxidant capacity

Antioxidant Capacity (AC) of the apple skin was determined by the Ferric-Reducing Ability Power (FRAP) method, which was described by Benzie and Strain.[17] The results were expressed as mmol Trolox equivalent per g of dry mass of apple skin.

2.3.4. Total Phenolic Content

The Total Phenolic Content (TPC) of the apple's peel extracts was determined following the Folin-Ciocalteau method.[18] In this case, the results were expressed as mg of Gallic acid equivalent (GAE) per g of dry mass of apple skin.

2.3.5. Ascorbic Acid content

The Ascorbic Acid content (AA) was determined adapting the method proposed by Jagota y Dani [19], and expressed as mg of ascorbic acid content per g of dry mass of apple skin. Every measurements were done in triplicate.

The percentage of retention of the different antioxidant parameters was estimated (Eq. 2)

$$Retention = \frac{P_f}{P_0} \cdot 100$$

(Eq. 2)

where P_0 is the value of the parameter obtained (AC, TPC and AA) from fresh apple skin and P_f from the different dried apple skin samples.

3. Results and Discussion

3.1. Color measurements

The measuerements of apple skin sample color showed that in the AIR experiments, samples dried at the greater drying temperature presented higher luminosity but lower redness and yelowness (Fig. 1). The results obtained at the lower temperature tested were the opposite, being samples less luminous, but with higher values of redness and yellowness attributes being these last characteristics more appreciated for the apple skin of the Royal Gala apple variety.

As for the ultrasound influence on the color, the parameters obtained in US-10 experiments were similar than the obtained at AIR50. The mechanical stress produced by ultrasound over the frozen samples during the long drying period may be the reason for this result. In the case of US30, US50 and US70, the relationship between color parameters and temperature was similar than for AIR experiments.

Regarding the chroma, in the case of AIR experiments, the highest value was obtained at the lowest drying temperature tested, decrasing its value with the increase temperature. (Fig. 1). In the case of US experiments, the US-10 experiments showed significant ($p < 0.05$) lower chroma value than those found at AIR-10. However, at temperatures above freezing point, the application of ultrasound increased the chroma value. In fact, the value obtained in US30 experiments was not significantly different that the obtained in AIR-10, showing

that is possible to achieve the same saturation color in this condition that at atmospheric freeze-drying condition but in a shorter process time.
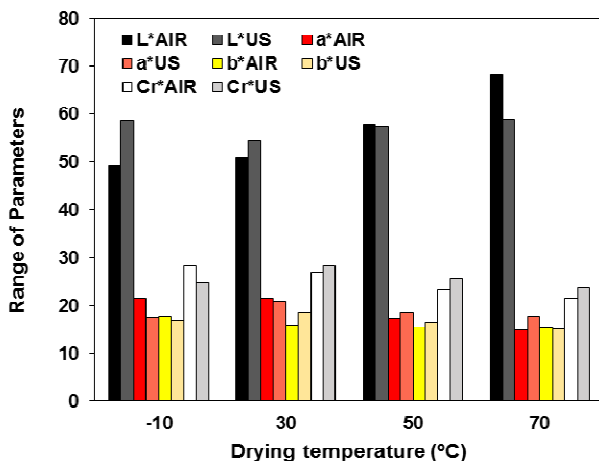
Figure 1. CieLAB Color parameters and chroma of apple skin dried at different temperatures without or with (50 W) ultrasound application.

3.2. Antioxidant Capacity (AC)

The antioxidant capacity (AC) of the fresh apple peel was 42±1 mg Trolox/g d.m, being this value higher than those obtained for other authors in apple's flesh.[10, 11, 12] On the contrary, the retention of AC after drying was in the range.[10, 11, 12]

No seignificant difference wer found about AC retention among the samples dried at different conditions except for AIR30 ones (Table. 1). In this conditions, samples showed a significant ($p < 0.05$) higher percentage of AC retention. In general, the application of ultrasound dind't signficaly affect the AC retention. Therefore, the use of ultrasound can be interesting to reduce drying temperature without significantly affect the AC retention.

3.3. Total Phenolic Compounds (TPC)

The TPC content of dried apple skins was 16.6±0.9 mg de GAE/ g d.m, being in the range found for fresh apple skin by Lata [20], and slightly lower than those found by Henriquez et al. [2]. As expected, the drying process reduced significantly the TPC (Table. 1). Above freezing point, the higher the temperature the lower the TPC retention showing the termo-sensibility of TPC.[2] Regarding the atmospheric-freeze dried samples, TPC of AIR-10 samples was not significantly different than the TPC of AIR50 ones. The previous freezing of AIR-10 samples could contribute to the rupture of some cells increasing the phenolic compounds degradation. The long time spent in this type of drying process could also increase the TPC degradation.

The ultrasound application generated a slightly decrease of the TPC retention. The mechanical stress induced by ultrasound can be responsible of this slight degradation of phenolic compound being this effect more significant when other adverse effects such as high temperature or freein were less important. Santacatalina et al. [9] also found similar effects of ultrasound application in dried apple flesh.

3.4. Ascorbic Acid content

The ascorbic acid (AA) content obtained of fresh apple peel was 1.6±0.2 mg of ascorbic acid/g d.m. As was already expected, the drying produced a partial degradation of this propertie, being the percentage of retention in the range than those found by Moreno et al.[11] In AIR processes above freezing point, the lower the temperature the greater the percentage of AA retention (Table. 1). At -10ºC, the long dying time and the previous freezing of sample can explain the greater AA degradation. Therefore, regarding the antioxidant properties of dried apple skin, the atomospheric-freeze drying is not the more adequate drying method.

As for ultrasound application, no significant ($p < 0.05$) effect on AA retention was observed except when drying took place at 70ºC. In this case, the retention in US70 experiment was significantly ($p < 0.05$) higher than AIR70 process, although these differences were small.

Table 1. Percentage of retention of total phenolic content, antioxidant capacity and ascorbic acid of apple peel after been dried at different temperature with and without ultrasound application.

Treatment	% retention		
	AC	TPC	AA
AIR-10	61.8	64.0	59.8
AIR30	78.9	84.9	88.7
AIR50	59.4	73.4	61.3
AIR70	62.0	59.0	55.0
US-10	60.5	61.1	60.8
US30	69.2	62.3	88.9
US50	58.9	66.3	58.9
US70	67.2	50.8	68.5

4. Conclusion

Drying temperature and ultrasound application affected the apple skin quality. The results obtained showed that the atmospheric freeze-drying was not an interesting drying method for both the long processing time and the no-significant influence on qualtity attributes tested, color and antioxidant properties. General speaking, the influence of ultrasound application during drying on quality attributes was negligible. Then, it constitutes an interesting way to intensify drying process and could permit the reduction of drying

temperature, which can means a energy needs reduction. However ,this last fact must be deeply studied.

5. Acknowledgements

6. References

[1] Martins, N.; Ferreira, I. C.F.R. Wastes and by-products: Upcoming sources of carotenoids for biotechnological purposes and health-related applications. Trends in Food Science & Technology. **2017**, 62, 33-48.

[2] Henríquez, C.; Córdova, A.; Almonacid, S.; Saavedra, J. Kinetic modeling of phenolic compound degradation during drum-drying of apple peel by-products. Journal of Food Engineering. **2014**, 143, 146-153.

[3] Karaman, S.; Tütem, E.; Baskan, K. S.; Apakb, R. Comparison of antioxidant capacity and phenolic composition of peel and flesh of some apple varieties. Journal of the Science of Food and Agriculture. **2013**, 93: 867-875

[4] Escarpa, A.; Gonzalez, M.C. High-performance liquid chromatography with diode-array detection for the determination of phenolic compounds in peel and pulp from different apple varieties. Journal Chromatography. **1998**, vol. 823, no. 1-2, p. 331-337.

[5] Rupasinghe, H.P.V.; Wang, L.; Huber, G.M.; Pitts, N.L.. Effect of baking on dietary fibre and phenolics of muffins incorporated with apple peel poder. Food Chemistry. **2008**, 107, 1217-1224

[6] O'Shea, N.; Arendt, E.K.; Gallagher, E. Dietary fibre and phytochemical characteristics of fruit and vegetable by-products and their recent applications as novel ingredients in food products. Innovative Food Science and Emerging Technologies. **2012**, 16, 1-10

[7] Moses, J.A.; Norton, T.; Alagusundaram, K.; Tiwari, B.K. Novel Drying Techniques for the Food Industry. Food Engineering Reviews. **2014**, 6, 43-55

[8] Lewicki, P. P.; Jakubczyk, E. Effect of hot air temperature on mechanical properties of dried apples. Journal of Food Engineering. **2004,** 64, 307-314.

[9] Santacatalina, J.V.; Rodríguez, O.; Simal, S.; Cárcel, J.A.; Mulet, A.; García-Pérez J.V. Ultrasonically enhanced low-temperature drying of apple: Influence on drying kinetics and antioxidant potential. Journal of Food Engineering. **2014**, 138, 35-44

[10] Rodríguez, O.; Santacatalina, J.V.; Simal, S.; Garcia-Perez, J.V.; Femenia, A.; Rosselló, C. Influence of power ultrasound application on drying kinetics of apple and its antioxidant and microstructural properties. Journal of Food Engineering. **2014**, 129, 21-29.

[11] Moreno, C.; Brines, C.; Mulet, A.; Rosselló, C.; Cárcel, J. A. Antioxidant potential of atmospheric freeze-dried apples as affected by ultrasound application and sample surface. Drying Technology. **2017**, 35(8), 957-968

[12] Musielak, G.; Mierzwa, D.; Kroehnke, J. Food drying enhancement by ultrasound – A review. Trends in Food Science & Technology. **2016**, 56, 126-141.

[13] Cárcel, J.A.; García-Pérez, J.V.; Riera, E.; Rosselló, C.; Mulet, A. Ultrasonically assisted drying. In Ultrasound in Food Processing; Villamiel, M., García-Pérez, J.V., Montilla, A., Cárcel, J.A., Benedito, J., Eds.; John Wiley & Sons Ltd.: United Kingdom, 2017; pp 371-391.

[14] Wolfe, K.L.; Liu, R.H. Apple Peels as a Value-Added Food Ingredient. Journal of Agricultural and Food Chemistry. **2003**, 51, 1676-1683

[15] AOAC, Association of Official Analytical Chemist. Official methods of analysis; Arlington: EEUU, 1997.

[16] Riera, E.; García-Pérez, J.V.; Acosta, V.M.; Cárcel, J.A.; Gallego-Juárez, J.A. A computational study of ultrasound-assisted drying of food materials. In: Knoerzer, K., Juliano, P., Roupas, P., Versteeg, C. (Eds.), Multiphysics Simulation of Emerging Food Processing Technologies. IFT Press, Chicago, USA, 2011; pp. 265-302.

[17] Benzie, I.F.; Strain, J.J. The ferric reducing ability of plasma (FRAP) as a measure of "antioxidant power": the FRAP assay. Anal. Biochem. **1996**, 239, 70-76.

[18] Gao, X.; Bjork, L.; Trajkovski, V.; Uggla, M. Evaluation of antioxidant activities of rosehip ethanol extracts in different test systems. J. Sci. Food Agric. **2000**, 80, 2021-2027.

[19] Jagota, S.K.; Dani, H.M. A new colorimetric technique for the estimation of vitamin C using Folin phenol reagent. Analytical Biochemistry. **1982**, 127(1), 178-182.

[20] Lata, B. Relationship between Apple Peel and the Whole Fruit Antioxidant Content: Year and Cultivar Variation. Journal of Agricutlrual and Food Chemistry. **2007**, 55, 663-671.

Radio frequency-vacuum drying of kiwifruits: kinetics, uniformity and product quality

Wang, S.[ab*]; Zhou, X.[a]

[a] College of Mechanical and Electronic Engineering, Northwest A&F University, Yangling, Shaanxi 712100, China
[b] Department of Biological Systems Engineering, Washington State University, 213 L.J. Smith Hall, Pullman, WA 99164-6120, USA

*E-mail of the corresponding author: shaojinwang@nwsuaf.edu.cn

Abstract

A radio frequency (RF) vacuum technology is proposed for drying kiwifruit slices using a 27.12 MHz, 3 kW RF-vacuum drying system. The results demonstrated that electrode gap, vacuum pressure and sample thickness had major effects on the RF-vacuum drying. The RF-vacuum drying was associated with internal heating and rapid drying, resulting in 65% reduction of hot air (60ºC) drying time. Moreover, kiwifruits dehydrated by RF-vacuum drying were associated with better color stability, higher vitamin C retention and higher rehydration capacity (P<0.05). Overall, the RF-vacuum drying process may provide a more effective and practical method for high-quality dehydration of kiwifruits.

Keywords: radio frequency-vacuum drying; hot air; moisture content distribution; moisture effective diffusivity; quality

1. Introduction

Kiwifruit (*Actinidia deliciosa*) is recognized as "the king of fruits" due to its remarkably high amounts of vitamin C and bioactive compounds with antioxidant activity. The global production of kiwifruit was around 4.27 million metric tons (Mt) in 2016 mainly contributed by China (2.39 Mt), Italy (0.52 Mt), New Zealand (0.43 Mt) and Chile (0.23 Mt). [1] However, kiwifruit is a seasonal fruit being harvested during August-October in China. Owing to high moisture content, fresh kiwifruit is highly perishable after harvest, even under refrigerated storage conditions. Thus, developing a proper postharvest drying technique is an important consideration to overcome the problems of seasonality and extend kiwifruit shelf-life to protect farmers' income and local economy.

The most conventional drying methods for kiwifruits, such as osmotic dehydration and hot air drying, have low technical barriers in developing/undeveloped countries and are preferred in industry, but with intensive labor cost, high energy consumption and long drying time.[2] Microwave (MW) and radio frequency (RF) drying methods also known as dielectric heating generate heat within the food material by molecular friction as a result of dipolar rotation and ionic conduction.[3, 4] RF heating has received increasing attention over the past decade due to its longer wavelength and deeper wave penetration as compared with MW and is thereby technologically more feasible for industrial applications.[5] Furthermore, the use of vacuum in RF heating, resulting in RF-vacuum drying, may further raise drying rate and ensure high quality in the final product because of the reduced drying temperatures as well as oxygen potential and considerably higher vapor pressure gradients between the interior and the surface of materials.

Therefore, the objectives of this study were (1) to determine the effect of RF process variables and sample thickness on the RF-vacuum drying characteristics of kiwifruit slices, (2) to study the drying kinetics and effective moisture diffusivity of hot air and RF-vacuum drying, and (3) to evaluate the quality of dried kiwifruit samples in terms of moisture content uniformity, color, vitamin C content and rehydration capacity.

2. Materials and Methods

2.1. Materials and RF-vacuum drying system

Freshly harvested kiwifruits (*Actinidia deliciosa* cultivar "Hayward") observed visually for similar ripeness and size were obtained from Shaanxi, China. The fruits were then hand peeled and cut into slices with diameter 45.5 ± 5.4 mm and three thicknesses: 6.1 ± 0.2, 8.0 ± 0.2 and 10.0 ± 0.3 mm.

A 3 kW, 27.12 MHz free-running oscillator RF-vacuum drying system (GJ-3-27-JY, Jiyuan High Frequency Electric, Shijiazhuang, China) was used for RF-vacuum drying experiments (Fig. 1). The RF electrode gaps between the two parallel plates (400 mm × 400 mm) could be adjusted from 20 mm to 300 mm to deliver desired RF energy for specific applications. The system pressure (vacuum) in the RF chamber, and sample temperature and mass were continuously recorded by a pressure sensor (APC500, Sensor Way Technologies Inc., Beijing, China) located in the vacuum cavity, four-channel fiber-optic sensor system (HQ-FTS-D120, Heqi Technologies Inc., Xian, China), an electronic scale (AT8106, Pengheng Electronic Inc., Shanghai, China) with a precision of 0.1 g mounted underneath the bottom electrode, respectively, during the entire drying process.
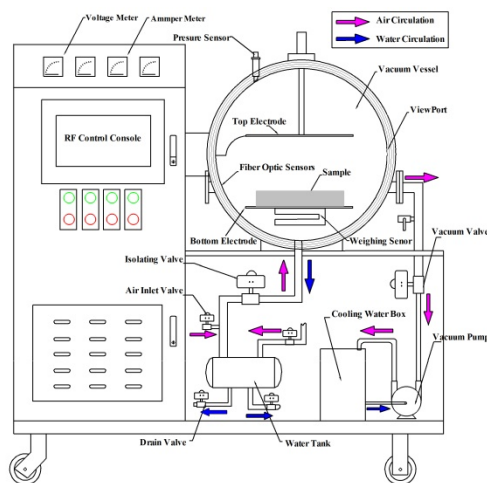
Fig. 1 Schematic view of the 3 kW, 27.12 MHz RF-vacuum drying system

2.2 Moisture content determination and drying procedures

The moisture content of kiwifruit slices was determined following the AOAC Official Method 925.40 and expressed as g[water]/g[solid] through the drying process.

RF-vacuum drying: Twenty-four freshly prepared kiwifruit slices (523.4 ± 18.0 g) were placed uniformly in a single layer inside a container (400 mm *L*× 270 mm *W*× 20 mm *H*) made of polypropylene (PP) with its side and bottom walls perforated with 10 mm diameter holes. Three electrode gaps (50, 60 and 70 mm) with three vacuum pressure levels (0.01, 0.02 and 0.03 MPa) and three sample thicknesses (6, 8 and 10 mm) were selected as process/product variables for determining RF-vacuum drying characteristics. The sample temperature and mass were continuously recorded by the fiber-optic temperature sensors and the electronic scale without having to turn off RF power or taking out samples. The RF-

vacuum drying process was continued until the moisture content of kiwifruit samples reached 0.18 kg/kg (d.b.)

2.3 Mathematical modeling of drying curves

The transient changes in moisture content of kiwifruit samples during drying was expressed as moisture ratio (*MR*) defined as:

$$MR = \frac{M_i - M_e}{M_o - M_e} \qquad (1)$$

where *MR* is the dimensionless moisture ratio, M_i or M_{i-1} (kg/kg, d.b.) is the moisture content at any time *i* or *i-1*, Δt is the drying time interval between time *i* and *i-1* (min), M_0 is the initial moisture content (kg/kg, d.b.) and *Me* is the equilibrium moisture content (kg/kg, d.b.).

2.4 Evaluation of product quality

2.4.1 Moisture content uniformity

Moisture content uniformity was moisture distribution among dried kiwifruit slices in the container. The moisture contents of kiwifruit slices located at 10 representative container locations were measured after drying.

2.4.2 Color

The color (L^*, a^*, b^*) of fresh (control) and dried kiwifruit slice samples was measured using a computer vision system. The total value of color difference (ΔE) was calculated as follows:

$$\Delta E = \sqrt{(L^* - L_o^*)^2 + (a^* - a_o^*)^2 + (b^* - b_o^*)^2} \qquad (2)$$

2.4.3 Vitamin C (ascorbic acid) content

Ascorbic acid content was determined by the standard 2,6-dichloroindophenol titration method.

2.4.4 Rehydration capacity

Rehydration capacity of dried kiwifruit slices was measured according to the method of Maskan (2001) [6]

$$Rehydration\ capacity = \frac{W - W_o}{W_o} \times 100\% \qquad (3)$$

where W_0 and W are the sample weight values (g) before and after rehydration, respectively.

3. Results and Discussion

3.1. RF-vacuum drying and heating characteristics
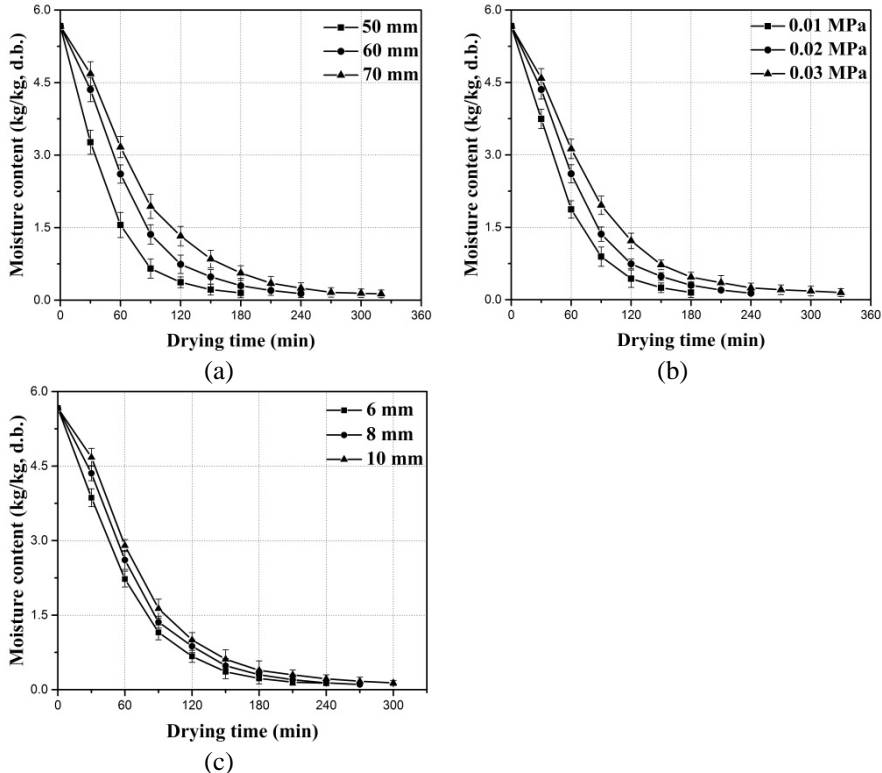
Fig. 2 RF-vacuum drying characteristics of kiwifruits influenced by electrode gap (a), vacuum pressure (b) and sample thickness (c)

The electrode gap, vacuum pressure and sample thickness had significant effects on RF-vacuum heating and drying characteristics of kiwifruit slices (Fig. 2). The RF-vacuum drying profile involved three stages regardless of various operating parameters: Stage I in which RF energy was transformed into thermal one within the materials and sample temperature rapidly increased. Once the moisture vapor pressure in the samples exceeded that of environment, the moisture expulsion process got and the drying rate gradually increased. Stage II began when the product temperature reached the highest value (wet bulb temperature), the drying process entered into a rapid drying period (constant drying rate period) and the sample temperature remained at a fairly constant level. As the drying progressed into Stage III, the loss of water in the samples reduced the associated dielectric properties, resulting in reduced

absorption of RF energy, and led to a gradually decreasing rate of drying toward the final stage of drying. Additionally, the thermal energy required for breaking away bound water is higher than that required for free water. Consequently, the RF-vacuum drying rate gradually decreased and the drying process was dominated by the falling drying rate period (Stage III). In general, the RF-vacuum drying process may limit the temperature raise in the samples and reduce severe thermal deterioration of product quality.

Fig. 3 shows a typical drying temperature-time profile at the core and sub-surface of kiwifruit slices subjected to RF-vacuum and hot air drying, indicating that the RF-vacuum dried materials were heated throughout the sample whereas surface higher temperatures were found in hot air drying.
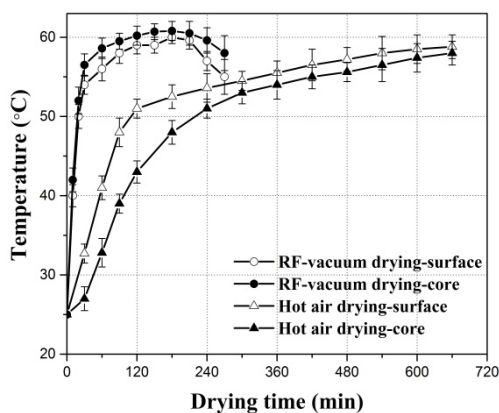
Fig. 3 Typical temperature-time history for sub-surface (2 mm) and core (20 mm) of kiwifruit slices when subjected to hot air and RF-vacuum drying

3.2 Drying kinetics and moisture effective diffusivity

The curves for *MR* versus drying time with the best drying models under hot air and RF-vacuum drying are shown in Fig. 4. The Page model (R^2 of 0.9998 and *RMSE* of 0.0056) was the best fit to describe hot air drying while the logarithmic model (R^2 of 0.9977 and *RMSE* of 0.0145) provided the best fit for RF-vacuum drying. Generally, the drying time for kiwifruit slices was reduced by about 65% when using RF-vacuum drying technology as compared to hot air drying, highlighting the advantage associated with RF-vacuum drying technology.
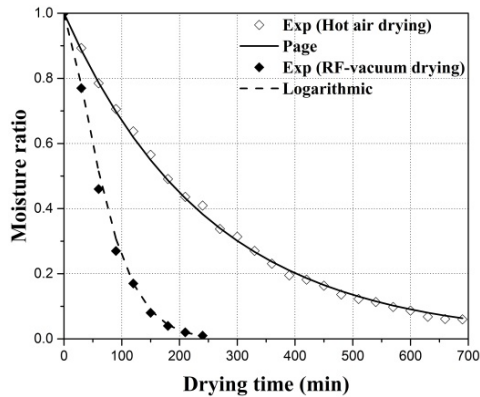
Fig. 4 Drying kinetics of kiwifruit slices when subjected to hot air and RF-vacuum drying

3.3 Quality of dried kiwifruit slices

Table 1 quality characteristics of kiwifruits before and after drying

	L^*	a^*	b^*	ΔE	Vc content (mg/100 g)	RC (%)
Fresh	42.2±1.0a#	-8.9±0.1c	24.7±0.4a	-	115.3±6.5a	-
AD	29.7±3.9c	-0.8±0.8a	20.4±0.6c	15.5±1.4a	45.8±5.6c	115.8±4.5b
RF	36.4±2.2b	-5.4±0.4b	22.2±0.4b	7.1±0.8b	62.5±4.7b	148.4±6.8a

Table 1 summarizes the results for kiwifruit product quality after hot air and RF-vacuum drying. The total color change (ΔE) of RF-vacuum dried kiwifruits was significantly smaller (P<0.05) possibly due to the shorter drying time, lower temperatures and reduced oxygen concentration. The retention ratio of vitamin C was less than 60% or lower (54% and 40% for RF-vacuum and hot air dehydrated samples, respectively. Because vitamin C is oxygen and heat sensitive, and can be degraded through oxidation even under low oxygen conditions during drying. The rehydration capacity of RF-vacuum dried kiwifruits was significantly higher (P<0.05) than that in hot air dried samples. The positive vapor pressure pushed from within foods leads to the creation of a porous, loose and fragile texture for the RF dried kiwifruits and therefore results in better water absorption capacity.

Fig. 5 shows the measured moisture distribution in the samples spread over 10 different compartments after the RF-vacuum and hot air drying. For hot air drying, the sample moisture removal was in line with the direction of air flow and resulted in reduced moisture loss as the tray numbers increased from 1 to 10. But the moisture contents of RF-vacuum dehydrated samples were more random and uniform, thereby demonstrating relatively more uniform moisture distribution in kiwifruit slices with RF-vacuum drying.
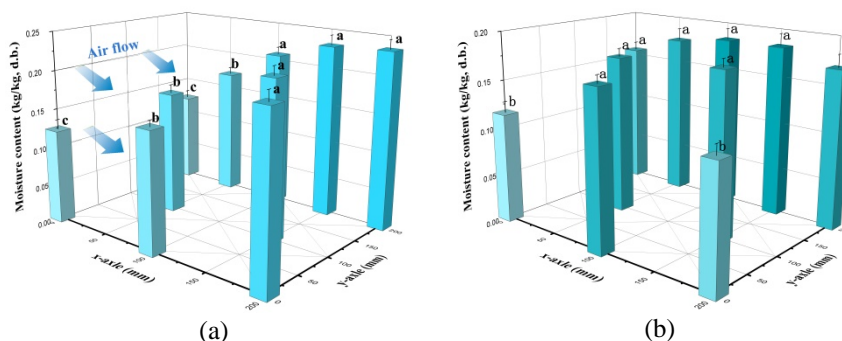
Fig. 5 Moisture distribution of hot air (a) and RF-vacuum (b) dried kiwifruit samples at 10 compartments in the container with x-axis parallel to the hot air flow

4. Conclusion

The RF-vacuum drying protocol of RF-vacuum of kiwifruits is electrode gap of 60 mm, vacuum pressure of 0.02 MPa and kiwifruit slice thickness of 8 mm, reducing more than 65% drying time as compared to AD. Further, the RF-vacuum drying process ensured better quality retention in the dehydrated kiwifruit slices in terms of color, vitamin C content and rehydration capacity due to fast heating/drying rates and low vacuum pressure. Better uniform moisture distribution was achieved when subjected to the RF-vacuum drying than possible with hot air drying. Overall, RF-vacuum drying technology may provide a more effective and practical dehydration method for kiwifruits with acceptable quality attributes.

References

[1] FAOSTAT. Food and agriculture organization of the united states **2018** http://www.fao.org/faostat/en/#data

[2] Mujumdar, A. S. Handbook of industrial drying. Philadelphia, Taylor & Francis **2007**

[3] Ramaswamy, H.; Tang, J. Microwave and radio frequency heating. Food Science and Technology International **2008**, 14*(5)*, 423-427.

[4] Zhou, X.; Gao, H.; Mitcham, E. J.; Wang, S. Comparative analyses of three dehydration methods on drying characteristics and oil quality of in-shell walnuts. Drying Technology **2018**, 36*(4)*, 477-490.

[5] Huang, Z.; Zhu, H.; Yan, R.; Wang, S. Simulation and prediction of radio frequency heating in dry soybeans. Biosystems Engineering **2015**, 129, 34-47.

[6] Maskan, M. Drying, shrinkage and rehydration characteristics of kiwifruits during hot air and microwave drying. Journal of Food Engineering **2001**, 48*(2)*, 177-182.

Characteristics of oven-dried Jerusalem artichoke powder and its applications in phosphate-free emulsified chicken meatballs

Öztürk, B.[*]; Serdaroğlu, M.

Food Engineering Department, Engineering Faculty, Ege University, Bornova, Izmir, Turkey.

*E-mail of the corresponding author: burcu.ozturk@ege.edu.tr

Abstract

In this study, we aimed to investigate chemical and technological characteristics of oven-dried Jerusalem artichoke powder (JAP) to be further incorporated into emulsified chicken meatballs (with/without sodium carbonate) as sodium tripolyphosphate (STPP) replacers. The dietary fiber content of JAP was quite high to improve the health profile of the meat system. JAP samples showed equivalent technological quality to industrial inulin in terms of water-holding, oil-binding, emulsification and gelling abilities. Phosphate-free meatballs formulated with JAP and sodium carbonate had better health impacts compared with phosphate containing meatballs while cooking characteristics were similar. The results showed that oven-dried JAP presented a good health profile and high technological quality to be evaluated as inorganic phosphate replacers in formulation of emulsified poultry products.

Keywords: Jerusalem artichoke, oven-drying, emulsified chicken meatball, sodium tripolyphosphate, phosphate-free

1. Introduction

Jerusalem artichoke (*Helianthus tuberosus* L.) is a natural raw material which highly contains fiber, minerals and vitamins. The tubers are known to be a health-promoting food source that contains inulin, a soluble dietary fiber, instead of starch as a carbohydrate reserve [1, 2]. Today utilization of natural ingredients in the formulation of meat products as phosphate replacers has come into prominence as a novel topic due to health concerns about chemical additives. Phosphates have a common use to improve quality of various meat products by shifting the pH away from isoelectric point, thereby increasing protein functionality and water-holding capacity and enhancing overall quality attributes, however, due to the emerging and newly identified health risks associated with phosphates, there has been a tendency to decrease the amount of their levels in meat product formulations [3-5]. Therefore, Jerusalem artichoke is a promising ingredient that could be used as an economic source of functional components in phosphate-free meat product formulations. In this study, we aimed to investigate chemical and technological characteristics of oven-dried Jerusalem artichoke powder (JAP) to be further incorporated into emulsified chicken meatballs (with/without sodium carbonate) as a clean-label sodium tripolyphosphate (STPP) replacer.

2. Materials and Methods

1.1. Production of Jerusalem artichoke powder (JAP) and emulsified chicken meatballs

Jerusalem artichoke powder (JAP) was produced from fresh and non-damaged tubers. The tubers were obtained from a local producer in Izmir region, washed with tap water, peeled and immediately immersed in citric acid (%1) solution to avoid enzymatic color changes. The tubers were then sliced into 0.2 mm thickness (Berkel Slicers, Italy). Slices were then air-dried in an industrial drying oven (Defne Spices Co., Izmir) at 60±5°C for 8 h. The dried slices were finally ground through a hammer mill (Brook Crompton, UK) and sieved through 0.5 mm. JAP was stored in glass jars prior to meatball production.

Chicken meatballs were formulated either with STPP (control) or JAP and/or sodium carbonate (SC) as STPP replacers. 70% of the chicken breast muscle was minced through 8 mm plate. The rest of the breast muscles (30%) and chicken skin were minced through 3 mm plate and then emulsified with NaCl, STPP, rosemary extract and ice at 4400 rpm for 5 min (control) in a bowl cutter (K+G Wetter, Germany). Other treatments were prepared using 3.8%, 5.7% or 7.6% JAP, with or without 0.2% SC as STPP replacers. After the emulsification procedure, the emulsions were mixed with 8 mm minced breast muscle and the doughs were cold-set at 0°C for 1 h. After that, the doughs were portioned with molds

and cold-set again at -18°C for 20 min. Meatballs were then deep-fat fried with canola oil in an electric fryer (Inoksan, Turkey) at 180±2°C for 3 min. The samples were cooled at 4°C prior to analysis.

1.2. Methods

1.2.1. Characteristics of JAP

Proximate analysis was performed in order to determine total moisture [6], lipid [6], ash [6] and protein [7] content. The water-soluble dietary fiber content of JAP samples was analyzed by Megazyme dietary fiber assay kit (Megazyme International Ireland Ltd., Wicklow, Ireland) according to AOAC [8]. Sucrose, D-glucose and D-fructose concentrations in JAP samples were determined by enzymatic assay (Boehringer Mannheim, R-Biopharm, Germany). In order to evaluate technological quality of JAP samples; water-holding capacity (WHC) [9], oil-binding capacity (OBC) [10], emulsifying capacity (EC) [11] and volumetric gel index (VGI) [12] were analyzed.

1.2.2. Characteristics of emulsified chicken meatballs

The dietary fiber content of meatball samples was calculated from the dietary fiber content and incorporation amount of JAP in meatball formulations. The salt content of the samples was determined according to Mohr method [6]. Cook yield (CY) of the samples were calculated from the weight of pre-cooked and cooked samples according to Murphy et al. [13]. Data was statistically analysed by SPSS software with one-way ANOVA and Duncan Post-hoc tests.

3. Results and Discussions

3.1. Characteristics of JAP

The initial moisture content of fresh Jerusalem artichoke tubers was 82.9%, while the final moisture content of JAP was 5.31%, which indicated that approximately 93% of the water in the raw material could be removed by drying operation. Some images from dried samples could be seen in Fig. 1. Sucrose, D-glucose and D-fructose content of JAP samples were 18.11 g/100 g, 2.6 g/100 g, and 5.8 g/100 g, respectively. Other than that, JAP samples had 11.96% protein, 5.81% ash, and 2.09% lipid. Similar results were previously reported by Praznik et al. [14]. The dietary fiber content of JAP samples was recorded as 58.76%, which is more than half of the chemical composition. This result indicated that dried Jerusalem artichoke tubers represent considerable potential for increasing dietary fiber content and so improving health-promoting effects of meat products as a natural and nutritious ingredient. Our findings were in accordance with Khuenpet et al. [15], who found that inulin content of JAP was 54.86/100 g. The composition of the tubers could differ

depending on varieties, harvesting maturity, storage time, growing conditions and processing technique [14, 15].

Fig. 1 Some images of dried Jerusalem artichoke tubers and the final product

Technological characteristics of JAP samples were as follows: WHC, OBC, and EC of the samples were 3.03±0.60 ml water/g, 3.63±0.45 ml oil/g and 150.0±7.0 ml oil/g, respectively. Afoakwah et al. [16] reported that oven-dried JAP had 4.30±0.10 g water/g WHC and 2.06±0.03 g oil/g OBC, and they stated that OBC of JAP are higher than many other fibers. In their study, freeze-dried JAP samples had higher OBC (3.02±0.14 g oil/g) compared to oven-dried samples, but the values were not as high as our results, probably due to the different origin of the raw materials. Rodríguez-Furlán et al. [9] reported that chicory inulin had 100±5 mL oil/g product EC. This result showed that JAP had a better emulsification ability compared to industrial inulin.

VGI values of JAP samples were recorded as 10.1±1.2%, 53.3±4.8% and 100.0±0.0% in 5%, 10% and 25% (w/v) water solutions, respectively. This result showed that an initial partial gel formation was observed in 5% water solution, whilst JAP samples were able to form a total gel structure in 25% water solution. Gel formation ability of JAP is a considerable quality attribute since the composite gel structure formed after hydrating and swelling of the samples could easily be distributed when used in the meat matrix. Kim et al. [12] reported that 30 and 35% inulin suspensions made 100% gel structure. Thus, JAP

samples could form a gel structure in lower concentrations compared to inulin, in other words gel formation ability was higher in JAP samples than in inulin samples.

3.2. Characteristics of emulsified chicken meatballs

The dietary fiber and salt content of emulsified chicken meatballs are presented in Table 1. Since the dietary fiber content of the meatballs was calculated based on the dietary fiber content of JAP samples, expectedly the values were increased with added JAP. According to this, the samples formulated with 3.8% JAP had 2.23% dietary fiber, while the samples formulated with 7.6% JAP had 4.46% dietary fiber. This result showed that in phosphate-free meat product formulations, utilization of JAP would lead to increase dietary fiber content and thus improve the health profile of the product, besides to provide technological advantages. The salt content of the samples was between 0.77-0.97%, which was significantly affected by formulation ($P<0.05$). The highest salt content was recorded in samples containing STPP (P group), while the lowest salt content was recorded in samples containing 7.6% JAP (J3 and JC3 groups) ($P<0.05$). The relatively higher salt contents of P and C samples among treatments could be arised from the sodium content of these samples. It was noted that increased concentrations of JAP were effective to reduce salt content regardless of sodium carbonate incorporation. This result could be due to the increase in the dietary fiber content with added JAP, which might dilute the sodium chloride used in the formulation.

Table 1. The dietary fiber and salt content of emulsified chicken meatballs

Treatments*	Dietary fiber content (%)	Salt content (%)**
P	0.00	$0.97^a \pm 0.01$
C	0.00	$0.95^b \pm 0.02$
J1	2.23	$0.88^c \pm 0.01$
JC1	2.23	$0.87^c \pm 0.03$
J2	3.35	$0.82^d \pm 0.01$
JC2	3.35	$0.82^d \pm 0.01$
J3	4.46	$0.78^e \pm 0.01$
JC3	4.46	$0.77^e \pm 0.01$

* The meatballs were formulated with **P:** 0.5% STPP, **C:** 0.2% Na_2CO_3, **J1:** 3.8% JAP, **JC1:** 3.8% JAP+0.2% Na_2CO_3, **J2:** 5.7% JAP, **JC2:** 5.7% JAP+0.2% Na_2CO_3, **J3:** 7.6% JAP, **JC3:** 7.6% JAP+0.2% Na_2CO_3.
** Data are presented as the mean values of replications ± standard deviation of the mean. abcd: Means with the different letter in the same column are significantly different ($P<0.05$).

Cook yield (CY) of the treatments are shown in Fig. 2. The values were between 77.19-90.96% and significant changes among treatments were recorded ($P<0.05$). Samples with JAP and sodium carbonate (JC1, JC2, and JC3) showed similar CY to each other, but JC2 samples had higher CY than samples with STPP (P). This data indicated that JC2 samples

showed a better performance than P samples to reduce fluid losses upon cooking. It was concluded that fiber-sourced ingredients have an important effect to meet the behaviors of phosphates by their water-holding ability in case of appropriate pH values. Our results were in agreement with Prabhu and Husak [17], who reported that utilization of native potato starch and sodium carbonate was effective to increase CY of phosphate-free pork loins.
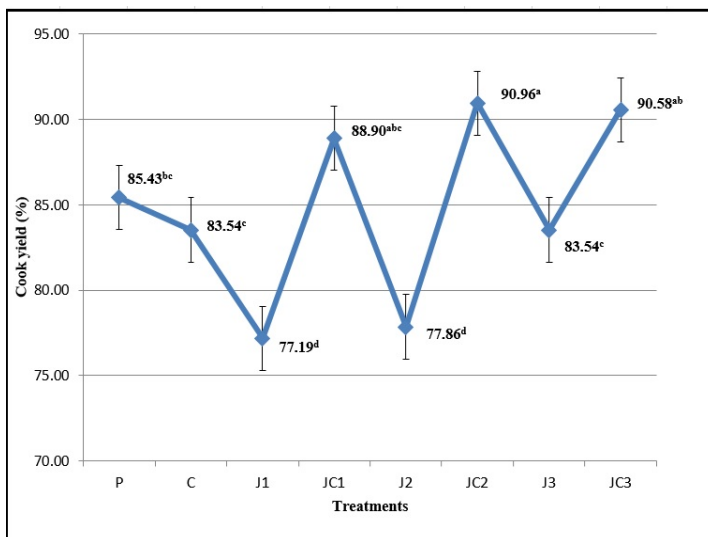
Fig. 2 Cook yield of emulsified chicken meatballs. The meatballs were formulated with P: 0.5% STPP, C: 0.2% Na₂CO₃, J1: 3.8% JAP, JC1: 3.8% JAP+0.2% Na₂CO₃, J2: 5.7% JAP, JC2: 5.7% JAP+0.2% Na₂CO₃, J3: 7.6% JAP, JC3: 7.6% JAP+0.2% Na₂CO₃. The standard deviation of the means ranged between 1.93-4.49. a, b, c: different letters indicate significant difference among means (P<0.05).

4. Conclusions

The results of the present research showed that oven-dried JAP is a health-promoting ingredient in terms of high dietary fiber content and also it has technological advantages over industrial inulin. Utilization of JAP in combination with sodium carbonate in emulsified chicken meatballs have a good potential to enhance the dietary fiber content and reduce the salt content of the product, simultaneously to increase cook yield. Overall, it was concluded that oven-dried JAP presented a good health profile and high technological quality with the aid of SC to be evaluated as inorganic phosphate replacers in formulation of emulsified poultry products.

5. Acknowledgement

6. References

[1] Yang, L.; He, Q.S.; Corscadden, K.; Udenigwe, C.C. The prospects of Jerusalem artichoke in functional food ingredients and bioenergy production. Biotechnology Reports 2015, 5, 77-88.

[2] Kays, S.J.; Nottingham, S.F. Biology and Chemistry of Jerusalem Artichoke: *Helianthus tuberosus* L.; Taylor & Francis Group, New York, 2007.

[3] Sebranek, J. Basic curing ingredients. In Ingredients in meat products: properties, functionality and applications; Tarté, R., Ed.; Springer Publishing: USA, 2008; 1-23.

[4] Petracci, M.; Bianchi, M.; Mudalal, S; Cavani, C. Functional ingredients for poultry meat products. Trends in Food Science and Technology 2013, 33 (1), 27-39.

[5] Lampila, L.E. Applications and functions of food-grade phosphates. Annals of New York Academy of Sciences 2013, 1301, 37-44.

[6] AOAC. Offical Methods of Analysis; 19th Ed.; Association of Offical Analytical Chemists; Gaithersburg, MD, USA, 2012.

[7] AOCS. American Oil Chemists' Society Official Methods and Recommended Practices of the AOCS; 5th Ed.; American Oil Chemists' Society, Champaign, USA, 2004.

[8] AOAC. Offical Methods of Analysis; 16th Ed.; Association of Offical Analytical Chemists; Gaithersburg, MD, USA, 1995.

[9] Rodríguez-Furlán, L.T; Padilla, A.P.; Campderrós, M.E. Development of reduced fat minced meats using inulin and bovine plasma proteins as fat replacers. Meat Science 2014, 96 (2A), 762-768.

[10] Chakraborty, P. Coconut protein isolate by ultrafiltration. In Food engineering and process applications; Meguer, M.L.; Jelen, P., Eds.; Elsevier Applied Science Publishers, New York, USA, 1986; 308-315.

[11] Rodríguez-Furlán, L.T.; Padilla, A.P.; Campderrós, M.E. Inulin like lyoprotectant of bovine plasma proteins concentrated by ultrafiltration. Food Research International 2010, 43 (3), 788-796.

[12] Kim, Y.; Faqih, M.N.; Wang, S.S. Factors affecting gel formation of inulin. Carbohydrate Polymers 2001, 46 (2), 135-145.

[13] Murphy, E.W.; Criner, P.E.; Grey, B.C. Comparisons of methods for calculating retention in cooked foods. Journal of Agricultural and Food Chemistry 1975, 23 (6), 1153-1157.

[14] Praznik, W.; Cieślik, E.; Filipiak-Florkiewicz, A. Soluble dietary fibers in Jerusalem artichoke powders: Composition and application in bread. Nahrung 2002, 46 (3), 151-157.

[15] Khuenpet, K.; Fukuoka, M.; Jittanit, W.; Sirisansaneeyakul, S. Spray drying of inulin component extracted from Jerusalem artichoke tuber powder using conventional and ohmic-ultrasonic heating for extraction process. Journal of Food Engineering 2017, 194, 67-78.

[16] Afoakwah, N.A.; Dong, Y.; Zhao, Y.; Xiong, Z.; Owusu, J.; Wang, Y.; Zhang, J. Characterization of Jerusalem artichoke (Helianthus tuberosus L.) powder and its application in emulsion-type sausage. LWT - Food Science and Technology 2015, 64 (1), 74-81.

[17] Prabhu, G.; Husak, R. Use of sodium carbonate and native potato starch blends as phosphate replacer in natural enhanced pork loins. Meat Science 2014, 96 (1), 454-455.

Quality changes of sucuks produced with turkey meat and olive oil during fermentation and ripening

Zungur-Bastıoğlu, A.[1]; Serdaroğlu, M.[2]; Öztürk, B.[2*]; Nacak, B.[3]

[1]Food Engineering Department, Engineering Faculty, Adnan Menderes University, Aydın, Turkey.
[2]Food Engineering Department, Engineering Faculty, Ege University, Bornova, Izmir, Turkey.
[3]Food Engineering Department, Engineering Faculty, Usak University, Usak, Turkey.

*E-mail of the corresponding author: burcu.ozturk@ege.edu.tr

Abstract

In this study, it was aimed to determine the effects of partial replacement of beef fat with olive oil on quality changes of fermented turkey sausages (sucuk) during processing. Three formulations were prepared by using the lipid phase as 100% beef fat (control), 85% beef fat+15% olive oil and 70% beef fat+30% olive oil. Total moisture, pH, acidity, water activity (aw) and peroxide values were analyzed in sausage dough, at the end of the fermentation and at the end of ripening. The production steps significantly affected moisture decrease in samples, pH and aw values were decreased and acidity was increased in all samples during production. Peroxide value of the samples increased during processing steps and the samples with olive oil had higher peroxide values compared to control. The results showed that during processing steps of fermented turkey sausages, considerable changes could occur depending on lipid type.

Keywords: sucuk, fermented sausage, dry fermentation, fat replacement, olive oil, turkey meat

1. Introduction

Sucuk, one of the most popular Turkish fermented meat sausages, is typically produced from beef, beef backfat and/or tail fat, salt, sugar, garlic, nitrite/nitrates, various spices and other ingredients [1, 2]. However, poultry meat could also be utilized as the raw material of sucuk especially in industrial production to increase product variability and minimize costs. Fermented meat products are known to contain high contents of fat. Although fat plays a key role in most of the quality attributes like color, texture, flavor and nutritional value of meat products [3, 4], today saturated fat reduction and lipid modification approaches for developing healthier meat products are highly encouraged [5]. Olive oil is a well-known health promoting vegetable oil that contains mostly monounsaturated and polyunsaturated fatty acids, tocopherols and phenolic substances [6, 7]. The objective of the present study was to investigate the quality changes during processing of fermented turkey sausages (sucuk) formulated with olive oil as partial beef fat replacers.

2. Materials and Methods

2.1. Production of turkey sucuks

Fresh post-rigor turkey breast muscles were supplied from a local butcher in Izmir. Other ingredients were purchased from local market. Breast muscles were trimmed of visible fat and connective tissues. Turkey meat and beef fat were then minced through a 3 mm plate grinder. Each treatment was formulated to contain 20% total fat. Control (C) group was formulated with 100% beef fat. Olive oil was added to the formulations by replacing 15% (O15) or 30% (O30) of beef fat. The other ingredients added to treatments were salt, saccharose, ascorbic acid, sodium nitrite, garlic powder and spice mix. After mixing all the ingredients homogenously, the sausage doughs were then stuffed into casings using a filling machine (Alpina, Switzerland). Samples were allowed to stand at 22.5°C and 60% relative humidity (RH) for 3 hours before fermentation in a fermentation chamber (Wisd, South Korea). After that, samples were fermented at 23°C and 88% RH until the pH reached 5.4. After fermentation, sausages were ripened at 21°C and 83% RH for 3 days and at 19°C and 73% RH, respectively to drop the moisture under 40%. During the production, sampling was performed in sucuk dough, at the end of fermentation (pH=5.4) and at the end of ripening (final product).

2.2. Methods

The total moisture content of the samples was determined according to AOAC [8]. pH was measured from three different points by using a pH-meter (WTW pH 330i/SET, Germany) with a penetration probe. Acidity was determined by a titrimetric method and expressed as lactic acid % [8]. Water activity (aw) was measured with a water activity measurement

device (Testo AG 400, Lenzkirch, Germany), with a 0.001 sensitivity. For peroxide analyses, fat was extracted with chloroform and methanol according to the method of Flynn and Bramblett [9] and the peroxide value was analyzed according to AOAC [8]. The data were analyzed by one way ANOVA using the SPSS software version 21. Differences among the means were compared using Duncan's Multiple Range Test. A significance level of 0.05 was used for all evaluations.

3. Results and Discussions

The change in total moisture content of the fermented sausages is presented in Fig. 1. The moisture content of sausage doughs was between 61.31-64.33%, while the values were between 40.21-41.40% in final products. The production steps significantly affected moisture decrease in samples due to the removal of free water by drying operation. In final products, O15 samples had lower moisture content compared to other groups ($P<0.05$). While C and O15 had similar moisture contents, moisture increased with higher olive oil levels in the formulation. Formation of an olive oil film between casing and sucuk mixture resulted in an incomplete drying of the product. According to Bloukas et al. [10], the granulated animal fat in sausage mixture helps to loosen up the structure, which aids the continuous release of moisture from the inner layer of the product.
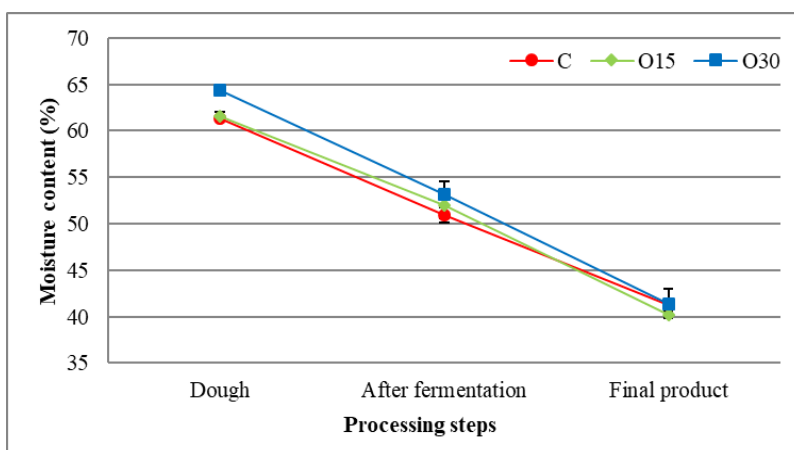
Fig. 1 Moisture content of fermented turkey sausages during processing. The lipid phase of the samples was formulated with C: 100% beef fat, O15: 85% beef fat+15% olive oil, O30: 70% beef fat+30% olive oil

pH values, acidity, and water activity (aw) of sucuk samples recorded during processing are given in Table 1. In sucuk dough, pH values were between 5.80-5.85, no significant

differences were recorded among samples. pH values were significantly decreased and acidity was significantly increased in all samples during production (*P*<0.05) with the effect of lactic acid fermentation. In final products pH values were between 5.23-5.31, pH values of O15 and O30 samples were higher than C samples (*P*<0.05). Geçgel et al. [11] reported that utilization of various vegetable oils in fermented beef sausages resulted in an increment in pH values. Despite the increase in pH values of olive oil treatments, the addition of olive oil had an increasing effect on the acidity of the final products (*P*<0.05). That is probably due to free fatty acids naturally present in olive oil. In sucuk doughs, aw values were recorded between 0.939-0.947, all the samples had similar values. aw values of all the samples were significantly decreased during production (*P*<0.05) due to the decrease in free water content by the drying process. Although no significant differences in aw of the samples were recorded after fermentation, in final products, the samples formulated with olive oil had higher aw values compared to control (*P*<0.05). This result could be arisen from different interactions of various lipids with meat protein matrix affecting drying behavior. The aw values recorded during processing were in accordance with Ensoy [12].

Table 1. The change in pH, acidity and water activity of fermented turkey sausages during production

		Treatments*		
		C	*O15*	*O30*
pH	*Dough*	5.80[a, A]±0.02	5.82[a, A]±0.13	5.85[a, A]±0.29
	After fermentation	5.41[b, A]±0.13	5.43[b, A]±0.21	5.42[b, A]±0.11
	Final product	5.23[c, B]±0.04	5.31[c, A]±0.02	5.29[c, A]±0.03
Acidity	*Dough*	0.54[c, B]±0.01	0.52[c, B]±0.02	0.65[c, A]±0.01
	After fermentation	0.98[b, AB]±0.02	0.94[b, B]±0.01	1.03[b, A]±0.03
	Final product	1.13[a, B]±0.02	1.23[a, A]±0.01	1.29[a, A]±0.04
Water activity (aw)	*Dough*	0.939[a, A]±0.03	0.947[a, A]±0.02	0.939[a, A]±0.00
	After fermentation	0.927[b, A]±0.05	0.934[b, A]±0.04	0.922[b, A]±0.01
	Final product	0.906[c, B]±0.01	0.913[c, A]±0.04	0.917[c, A]±0.00

* The lipid phase of the samples were formulated with **C:** 100% beef fat, **O15**: 85% beef fat+15% olive oil, **O30**: 70% beef fat+30% olive oil

Data are presented as the mean values of replications ± standard deviation of the mean. For different analysis; abcd: Means with the different letter in the same column are significantly different (*P*<0.05). ABC: Means with the different letter in the same row are significantly different (*P*<0.05).

Peroxide values of the treatments are shown in Fig. 2. The values of the dough samples showed that autoxidation reactions had already started before stuffing. Processes of mixing

and stuffing were not carried out under vacuum conditions; therefore the presence of high concentration of oxygen in dough could lead the early development of autoxidation reactions. The processing steps were recorded to increase lipid oxidation of all the samples in terms of peroxide value ($P<0.05$). However, in all cases, peroxide value was lower than 25 meq O2/kg of fat which is the limit of acceptability for fatty foods [13, 14]. Peroxide values of the final products formulated with olive oil were higher compared to control ($P<0.05$), probably due to the high unsaturated fatty acid content of olive oil. Similarly, Geçgel et al. [11] reported that incorporation of different vegetable oils to the formulation of fermented beef sausages caused increments in peroxide values.
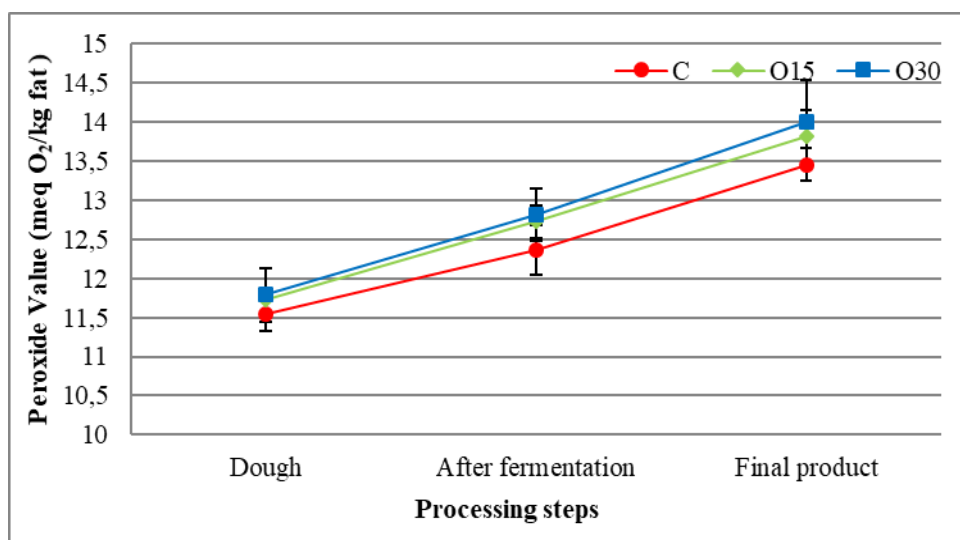
Fig. 2 Peroxide values of fermented turkey sausages during processing. The lipid phase of the samples was formulated with C: 100% beef fat, O15: 85% beef fat+15% olive oil, O30: 70% beef fat+30% olive oil

3. Conclusions

The results showed that during processing steps of fermented turkey sausages (sucuk), considerable changes could occur depending on lipid type. Since olive oil treatments had different pH, acidity and water activity values from control treatments with beef fat, these features could change sensory characteristics and shelf life of the product. Thus, free water content and thereby water activity should be considered during the production of fermented sausages formulated with vegetable oils. In addition, since olive oil is highly susceptible to lipid oxidation and thereby incorporation of it resulted in an increment in peroxide values, utilization of antioxidants or encapsulation of the added oil could be suggested to improve the oxidative stability of the product.

4. Acknowledgment

5. References

[1] Gökalp, H.Y.; Ockerman, H. W. Turkish style fermented sausage (soudjouk) manufactured by adding different starter cultures and using different ripening temperatures. Fleischwirtschaft 1986, 65, 1235-1240.

[2] Gökalp, H.Y. Sucuk üretim teknolojisi, Standard Geleneksel Türk Et Ürünleri Özel Sayısı 1995, 8, 48-55.

[3] Bloukas, J.G.; Paneras, E.D.; Fournitzis, G.C. Effect of replacing pork backfat with olive oil on processing and quality characteristics of fermented sausages. Meat Science 1997, 45 (2), 133-144.

[4] Gandemer, G. Lipids in muscles and adipose tissues, changes during processing and sensory properties of meat products. Meat Science 2002, 62, 309-321.

[5] Jiménez-Colmenero, F.; Salcedo-Sandoval, L.; Bou, R.; Cofrades, S.; Herrero, A.M.; Ruiz-Capillas, C. Novel applications of oil-structuring methods as a strategy to improve the fat content of meat products. Trends in Food Science and Technology 2015, 44, 177-188.

[6] Jiménez-Colmenero, F.; Pintado, T.; Cofrades, S.; Ruiz-Capillas, C.; Bastida, S. Production variations of nutritional composition of commercial meat products. Food Research International 2010, 43, 2378-2384.

[7] Lurueña-Martínez, M.A.; Vivar-Quintana, A.M.; Revilla, I. Effect of locust bean/xanthan gum addition and replacement of pork fat with olive oil on the quality characteristics of low-fat frankfurters. Meat Science 2004, 68, 383-389.

[8] AOAC. Offical Methods of Analysis; 19th Ed.; Association of Offical Analytical Chemists; Gaithersburg, MD, USA, 2012.

[9] Flynn, A.W.; Bramblett, V.D. Effects of frozen storage cooking method and muscle quality and attributes of pork loins. Journal of Food Science 1975, 40, 631-633.

[10] Bloukas, J. G.; Paneras, E. D.; Fournitzis, G. C. Effect of replacing pork backfat with olive oil on processing and quality characteristics of fermented sausages. Meat Science 1997, 45(2), 133-144.

[11] Geçgel, Ü.; Yılmaz, Y.; Ay, A.; Apaydın, D.; Dülger, G.Ç. Soğuk pres yağlar ilave edilerek üretilen fermente sucukların fizikokimyasal özelliklerinin belirlenmesi. Tekirdağ Ziraat Fakültesi Dergisi 2016, 13 (4), 1-11.

[12] Ensoy, Ü. Hindi sucuğu üretiminde starter kültür kullanımı ve ısıl işlem uygulanmasının ürün karakteristikleri üzerine etkisi, PhD Thesis 2004, Ankara University, Ankara, Turkey.

[13] Ergezer, H.; Serdaroğlu, M. Antioxidant potential of artichoke (Cynara scolymus L.) byproducts extracts in raw beef patties during refrigerated storage. Journal of Food Measurement and Characterization 2017, 1–10.

[14] Evranuz, E. Ö. The effects of temperature and moisture content on lipid peroxidation during storage of unblanched salted roasted peanuts: shelf life studies for unblanched salted roasted peanuts. International Journal of Food Science & Technology 2007, 28(2), 193–199.

Impacts of air drying and DIC pretreatments on textural properties of frozen/thawed apple fruits.

Ben Haj Said, L.[a]; Bellagha, S.[a*]; Allaf, K.[b]

[a] Laboratory of valorization of natural heritage and Tunisian food through innovation, National Institute of Agronomy of Tunisia, University of Carthage, 43, Avenue Charles Nicolle, 1082, Tunis Mahrajene, Tunisia

[b] Laboratory of Engineering Science for Environment (LaSIE), UMR 7356 CNRS. Faculty of Science and Technology, University of La Rochelle, avenue Michel Crepeau, 17042 La Rochelle cedex 01, France.

*E-mail of the corresponding author: bellagha.sihemb@gmail.com

Abstract

This research work is about dehydrofreezing assisted by DIC treatment as an innovative conservation process of apple fruits. Samples previously dehydrated and DIC treated were frozen at -30 °C and at two different practical freezing rates. The effects of sample water content (W) and practical freezing rate (PFR) on freezing characteristics and apple texture were examined. Thaw exudate water (TEW) of 200% and 100% db samples was approximately 3 g/100 g water. Whereas, it was lower than 0.5 g/100 g water for samples with 30% db W during thawing at 4 °C. Moreover, the impact of PFR on TEW was significant and very important only for high W samples. For samples whose water content was lower than 100% db, firmness was as higher as the W was lower, without any significant impact of PFR.

Keywords: Dehydrofreezing; Instant controlled pressure drop; Water content; Practical freezing rate; Texture.

1. Introduction

Freezing is a common fruit and vegetable conservation process that preserves the sensorial quality and nutritional compounds [1]. However, in the case of high-water-content perishable fruits and vegetables, the treatment is usually accompanied by irreversible damage of cell structures and possible deterioration of textural quality of the frozen products after thawing due to large ice crystals formed in the tissue during freezing process [2]. Dehydrofreezing which is a preservation process that involves partial dehydration before freezing can be used in order to diminish tissue damage [3-5].

The reduction in the product water content before freezing improves both freezing performance and product quality in the case of *Golden delicious* apples [6]. Process performance is revealed through an improvement of freezing rate and a decrease of freezing time [7] as well as lower energy consumption, lower cost of packaging, distribution, and storage. Whereas, quality improvement includes better preservation of structural and textural characteristics and decrease of thaw exudate water rich on soluble nutrients.

In the other hand, since the partially dried products are not yet microbiologically stabilized, subsequent treatment is necessary, before freezing, for product decontamination.

Likewise, to remove the impact of possible shrinkage of partially dried products instant controlled pressure drop (DIC) process is also required [8].

However, no work has been reported in the literature about mechanical properties after the combined process ''air drying + DIC + freezing''. Hence, the main objectives of this study were to (i) establish a new freezing method, namely, DIC-assisted dehydrofreezing, and to (iii) assess and compare the impacts of water content and practical freezing rate on thaw exudate water and textural characteristics of dehydrofrozen products previously DIC treated.

2. Materials and Methods

2.1. Process treatments

Initial water content (W) of apple fruits (var. *Golden delicious*) was determined according to AOAC official method 934.06 [9]. It was of 700±10% dry basis (db). Discs of 10.0±0.2 mm thick were prepared for process treatments and texture analysis.

2.2. Partial drying

Partially drying experiments were carried out in a airflow dryer under constant conditions: air temperature, air velocity, and air relative humidity of 45 °C, 2 m/s, and 12%, respectively. Drying experiment was stopped once desired water content (W) levels were attained (200, 100, and 30% db).

2.3. DIC treatment

Partially dried apple samples with different water contents (200, 100, and 30% db) were DIC treated by an adequate equipment (ABCAR-DIC Process, La Rochelle, France).

2.4. Freezing

Partially dried and DIC treated apple samples at different water content levels were frozen in a freezer (Whirlpool Model AFG 363/G, Italy) with air temperature of -30 °C at two different practical freezing rates;high practical freezing rate (PFR+) and low practical freezing rate (PFR−) depending on the thermal resistance established between the freezing airflow and the sample surface [7].

2.5. Thawing process

Completely frozen apple samples previously DIC treated were thawed in a refrigerator (FAR Model RT 140, Romania) at 4 °C overnight just before starting the textural measurements [6].

2.6. Quality assessments

2.6.1. Determination of thaw exudate water

Dehydrofrozen DIC treated-apple samples were used to measure thaw exudate water (TEW) expressed in g/100 g water, during the thawing phase [7,10].

2.6.2. Texture measurement

Textural firmness of DIC treated-dehydrofrozen/thawed apple slices was evaluated by measuring the maximum puncture force through a puncture test with a cylindrical puncture probe of 2 mm in diameter at a constant speed of 5 mm/s using Instron Universal Testing machine (Model 5543, USA) [6].

2.7. Statistical analysis

Bifactorial analysis of variance and SNK test were carried out using the Statistical Package for the Social Sciences (SPSS) version 20.

3. Results and discussions

3.1. Thaw exudate water

The impacts of water content (W) of apple samples and practical freezing rate (PFR) on thaw exudate water (TEW) during thawing of DIC treated-dehydrofrozen apple samples were investigated and experimental results are illustrated in Figure 1.
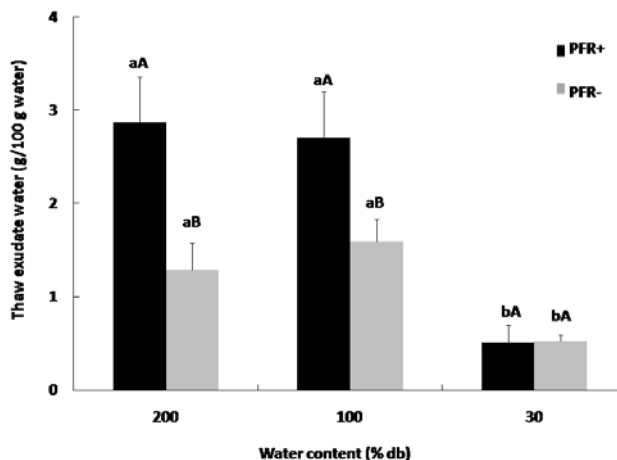
Figure 1. Impacts of water content and practical freezing rate on thaw exudate water (TEW) of DIC treated-dehydrofrozen apples. (Data are expressed as the mean ± standard deviation. Values for the same practical freezing rate having the same letter (a, b and c) for thaw exudate water (TEW) are not significantly different at a confidence level of 95%. Values for the same water content level having the same letter (A, B and C) for thaw exudate water (TEW) are not significantly different at a confidence level of 95%).

Figure 1 shows the impact of the two different practical freezing rates on the thaw exudate water (TEW) of dehydrofrozen DIC treated-apple samples with different water contents (200, 100, and 30% db) during thawing process. Thaw exudate water (TEW) of 200% and 100% db apple samples frozen at -30 °C was approximately 3 g exudate water /100 g water in the product at high practical freezing rate (PFR$^+$) after thawing at a temperature of 4 °C. Indeed, it was lower than 0.5 g/100 g water for apple samples with 30% db water content and frozen at the same practical freezing rate (PFR$^+$).

Previous researches have equally demonstrated that dehydration by hot air causes a diminution in drip loss during the thawing process in the case of dehydrofrozen strawberry and pineapple fruits [11,12]. These authors reported that air drying prior to freezing presents the advantage of decreasing the drip loss and the water exudate volume after thawing process as compared to osmotic dehydration [11,12].

As it is shown in Fig. 1, the higher the initial water content of dehydrofrozen apples, the higher the amount of TEW. Same results were obtained for several dehydrofrozen fruits such as strawberry, kiwi fruits, and pears [13,14]. The TEW decrease during thawing of DIC treated-dehydrofrozen samples may also be explained by a preservation of the structural and textural properties of apple samples as a consequence of the partial removal of water before freezing.

In the other hand, the impact of practical freezing rate on thaw exudate water (TEW) was significant and very important for high water content samples (200% and 100% db). It had less significantly detrimental effect on TEW for lower water content samples (30% db).

3.2. Texture variation

The maximum puncture forces (firmness) after thawing of DIC treated-dehydrofrozen apple samples, which were frozen at two different practical freezing rates (PFR$^+$ and PFR$^-$) are shown in Figure 2.
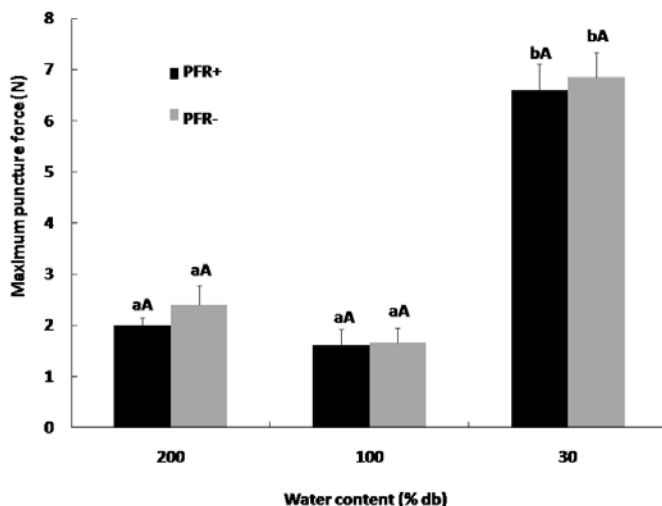
Figure 2. Impacts of water content and practical freezing rate on firmness of DIC treated-dehydrofrozen apples. (Data are expressed as the mean ± standard deviation. Values for the same practical freezing rate having the same letter (a, b and c) for maximum puncture force are not significantly different at a confidence level of 95%. Values for the same water content level having the same letter (A, B and C) for maximum puncture force are not significantly different at a confidence level of 95%).

As it is shown in Figure 2, firmness (maximum puncture force) of DIC treated-dehydrofrozen apple samples was constant (about 2 N) for high water content levels of 200% and 100% db, for both practical freezing rates. It increased for lower water content to reach 6.5 N for 30%-db samples, while no effect due to practical freezing rate was evidenced. ANOVA and LSD tests carried out for the firmness values statistically confirmed these differences. DIC-dehydrofreezing/thawing processes induced a significant ($p<0.05$) increase of firmness with the decrease of sample humidity. Moreover, according to the result of the simple range test (SNK test), two homogeneous groups were identified.

The first group includes 200% and 100%-db apples. The second group only included samples with water content of 30% db.

These results confirmed that the significant impacts of water content on firmness obtained in the case of dehydrofrozen apples without DIC pretreatment, with also an insignificant effect of practical freezing rate. Firmness values of dehydrofrozen/thawed and non DIC pretreated apples were about 2, 4.5, 7, and 12 N for samples with water contents of 700, 200, 100, and 30% db, respectively [7]. Firmness of dehydrofrozen apples was found to be higher for samples non-DIC treated. This difference on firmness is explained by textural modifications caused by DIC treatment applied before freezing as texturing process [6].

Similar results, concerning the impact of air drying performed as freezing pretreatment on textural properties, were obtained for dehydrofrozen/thawed strawberry and kiwi fruits [11]. Airflow drying as freezing pretreatment resulted in dehydrofrozen/thawed products with improved textural properties and higher firmness. Indeed, the low water content of dried samples prevents the cell wall damage and preserve the product structure during freezing and thawing processes [2,6].

4. Conclusions

Fruits and vegetables present a category of food products which is characterized by high water content generally higher than 500% db. This category of agriculture products can also be characterized by initial microbial contamination. Partial drying coupled to instant controlled pressure drop (DIC) as adequate pretreatment should present an intensification way for fruit and vegetable freezing process. The coupling of these operations presents several advantages concerning the product stability through a partial removal of water and a decontaminating pretreatment.

Thaw exudate water for DIC treated-dehydrofrozen apples during the thawing was approximately 3 g/100 g water for high water content samples (200 and 100% db). Whereas, it was lower than 0.5 g/100 g water for samples with 30% db water content. The impact of practical freezing rate on thaw exudate water was significant only for high water contents. For low water content level (30% db), practical freezing rate became a less important parameter for freezing process.

Water content had a significant effect on the textural properties of apple fruits after DIC-dehydrofreezing/thawing processes. In fact, fruit sample firmness increased when water content decreased for both practical freezing rates. Whereas, practical freezing rate had an insignificant impact on apple firmness.

In conclusion, partial removal of water constitutes a promising solution to reduce the negative impacts of freezing on textural quality. This process coupled with a texturizing pretreatment, showing perfect decontamination effects, can be suggested as an innovative fruit and vegetable conservation process. This new method allow obtaining dehydrofrozen

products with high textural quality after thawing and particularly without imposing a severe control of the partial drying step especially for the microbiological quality of products.

5. References

[1] Li, B., & Sun, D.-W. (2002). Novel methods for rapid freezing and thawing of foods – a review. *Journal of Food Engineering*, 54(3), 175-182.

[2] Wu, L., Orikasa, T., Tokuyasu, K., Shiina, T., & Tagawa, A. (2009). Applicability of vacuum-dehydrofreezing technique for the long-term preservation of fresh-cut eggplant: Effects of process conditions on the quality attributes of the samples. *Journal of Food Engineering*, 91(4), 560-565.

[3] James, C., Purnell, G., & James, S. (2014). A Critical Review of Dehydrofreezing of Fruits and Vegetables. *Food and Bioprocess Technology*, 7(5), 1219-1234.

[4] Cheng, L., Sun, D.W., Zhu, Z., & Zhang, Z. (2015). Emerging Techniques for Assisting and Accelerating Food Freezing Processes─A Review of Recent Research Progresses. *Critical Reviews in Food Science and Nutrition*.

[5] Xin, Y., Zhanga, M., Xu, B., Adhikari, B., & Sun, J. (2015). Research trends in selected blanching pretreatments and quick freezing technologies as applied in fruits and vegetables: A review. *International Journal of Refrigeration.*

[6] Ben Haj Said, L., Bellagha, S., & Allaf, K. (2015). Optimization of Instant Controlled Pressure Drop (DIC)-Assisted Dehydrofreezing Using Mechanical Texture Measurements Versus Initial Water Content of Apple. Food and Bioprocess Technology, 1-11.

[7] Ben Haj Said, L., Bellagha, S., & Allaf, K. (2016). Dehydrofreezing of apple fruits: Freezing profiles, freezing characteristics and texture variation. Food and Bioprocess Technology (FABT), Volume 9, Issue 2, 252-261.

[8] Allaf, T., & Allaf, K. (2014). Instant Controlled Pressure Drop (DIC) in Food Processing. Springer.

[9] AOAC. 1990. Association of Official Analytical Chemists (15th edn), Helrich K (ed). Arlington: Virginia 22201, USA.

[10] Maestrelli, A., Lo Scalzo, R., Lupi, D., Bertolo, G., & Torreggiani, D. (2001). Partial removal of water before freezing: cultivar and pre-treatments as quality factors of frozen muskmelon (Cucumis melo, cv reticulatus Naud.). *Journal of Food Engineering*, 49(2–3), 255-260.

[11] Sormani, A., Maffi, D., Bertolo, G., & Torreggiani, D. (1999). Textural and structural changes of dehydrofreeze-thawed strawberry slices: Effects of different dehydration

pretreatments / Cambios texturales y estructurales de rodajas de fresa deshidratadas y descongeladas: Efectos de diferentes pretratamientos de deshidratación. *Food Science and Technology International*, 5(6), 479-485, doi:10.1177/108201329900500605.

[12] Ramallo, L. A., & Mascheroni, R. H. (2010). Dehydrofreezing of pineapple. *Journal of Food Engineering*, 99(3), 269-275.

[13] Moraga, G., MartÍNez-Navarrete, N., & Chiralt, A. (2006). Compositional changes of strawberry due to dehydration, cold storage and freezing-thawing processes. *Journal of Food Processing and Preservation*, 30(4), 458-474.

[14] Marani, C. M., Agnelli, M. E., & Mascheroni, R. H. (2007). Osmo-frozen fruits: mass transfer and quality evaluation. *Journal of Food Engineering*, 79(4), 1122-1130.

Partial drying of apple fruits to improve freeze/thaw quality during long term frozen storage.

Ben Haj Said, L. [a]; Bellagha, S.[a*]; Allaf, K.[b]

[a] Laboratory of valorization of natural heritage and Tunisian food through innovation, National Institute of Agronomy of Tunisia, University of Carthage, 43, Avenue Charles Nicolle, 1082, Tunis Mahrajene, Tunisia

[b] Laboratory of Engineering Science for Environment (LaSIE), UMR 7356 CNRS. Faculty of Science and Technology, University of La Rochelle, avenue Michel Crepeau, 17042 La Rochelle cedex 01, France.

*E-mail of the corresponding author: bellagha.sihemb@gmail.com

Abstract

Apple samples were submitted to partially drying prior to freezing. Then, quality assessments were achieved in order to evaluate the quality of these various frozen samples during frozen-storage. Significant positive effects of water content were observed on thaw exudate water and total color difference of dehydrofrozen/thawed apples. Total polyphenol content and total flavonoid content losses were important for samples without any dehydration pretreatment. They noticeably decreased when water content decreased during the whole period of storage. Thus, a partial removal of water prior to freezing is a relevant way to maintain the stability of fruit quality during long-term frozen-storage.

Keywords: Apple fruits; dehydrofreezing; frozen storage; color; polyphenol.

1. Introduction

Dehydrofreezing is defined as a preservation method for fruits and vegetables characterized by their high water content. It is a process that involves a partial dehydration phase prior to freezing in order to diminish the amount of water and prevents the cell wall damage during freezing and thawing processes due to the increase of water volume during freezing. Previous investigations have demonstrated that dehydrofreezing reduces freezing time and improves freezing rates [1,2]. This combined process improves the textural firmness of frozen/thawed fruits and vegetables [3,4]. Dehydrofreezing reduces the thaw exudate water during thawing stage [3,5,8,10]. Several previous studies were interested on dehydrofreezing impacts on the global quality of fruits and vegetables through the assessment of different parameters such as color [6,7,10], ascorbic acid [3], and bioactive molecules [10]. Frozen fruits and vegetables undergo quality changes throughout the subsequent frozen storage. Moreover, physical changes during storage at negative temperatures may imply ice recrystallization, which results in deleterious textural and nutritional changes. It also would reverse the advantages of fast freezing. By inserting before freezing a pretreatment stage of partial dehydration, the quality loss of fruits and vegetables should be minimized not only during the freezing step but also during frozen storage. As far as we know, little information exists about the impact of the coupling of air drying and freezing processes on the nutritional quality and the bioactive composition of dehydrofrozen/thawed fruits and vegetables during long-period frozen storage. Thus, this study focused on studying the impact of the coupling of air drying and freezing, named dehydrofreezing process on the evolution versus frozen storage time at -18 °C and initial water content of 1/ color, 2/ total polyphenol content, 3/ total flavonoid content, and 4/ the thaw exudate water during thawing of apple fruits.

2. Materials and Methods

2.1. Process treatments

2.1.1. Partial drying

1-cm *Golden delicious* apple disks with initial water content of about 7 ± 0.1 g H_2O/g db (dry basis) were dried in an airflow dryer under constant conditions of airflow temperature (45 °C), velocity (2 m/s), and relative humidity (12%). dehydration was stopped when selected water content levels were reached (2, 1, and 0.3 g H_2O/g db).

2.1.2. Freezing

Samples of fresh and partially airflow dried apple initially containing different water content levels (W); (7 (fresh), and 2, 1, and 0.3 g H_2O/g db (for partially dehydrated

samples)) were frozen in a freezer (Whirlpool Model AFG 363/G, Italy) with an air temperature of -30 °C at forced convection conditions.

2.1.3. Frozen storage

Frozen and dehydrofrozen apple samples were stored at -18 °C for 18 months as Frozen Storage Time FST period. Samples were retrieved each month during the first three months of storage and each 3 months until the end of the storage period for quality assessments.

2.1.4. Thawing

Frozen and dehydrofrozen apple samples were thawed at 4 °C in a refrigerator (FAR Model RT 140, Romania) overnight just before starting the different analyzes.

2.2. Quality assessments

2.2.1. Thaw exudate water

Thaw exudate water (TEW) of frozen or dehydrofrozen apple samples was measured in triplicate for each treatment during the thawing phase [5].

2.2.2. Color measurement

For each sample, parameters L, a, and b were measured three times directly on the product using a colorimeter (Konica Minolta CR-410, Japan). Total color difference (TCD) between fresh and frozen and between dried and dehydrofrozen samples for each initial water content and storage time was calculated.

2.2.3. Total polyphenol content

Total polyphenol contents of fresh, dried, frozen, or dehydrofrozen/thawed apples were assayed during frozen storage [13].

2.3. Statistical analysis

Bifactorial analysis of variance and SNK test were carried out using the Statistical Package for the Social Sciences (SPSS) version 20.

3. Materials and Methods

3.1. Thaw exudate water

Table 1 shows the thaw exudate water (TEW) of apple samples just frozen, dehydrofrozen and during long-term frozen storage at -18 °C for 18 months.

Table 1. Effect of -18°C-storage on thaw exudate water during thawing of dehydrofrozen apple.

FST (months)	TEW (%)			
	W (g H$_2$O/g dry basis db)			
	7	2	1	0.3
0	14.64±0.92[bA]	3.42±0.57[aB]	0.38±0.13[aC]	0.23±0.13[aC]
1	15.03±1.22[bA]	3.47±2.21[aB]	0.75±0.32[aC]	0.25±0.19[aC]
2	16.70±2.05[abA]	3.89±1.38[aB]	0.63±0.10[aC]	0.33±0.08[aD]
3	17.60±1.77[abA]	2.88±1.81[aB]	0.88±0.18[aC]	0.23±0.05[aD]
6	17.18±1.48[abA]	3.68±1.87[aB]	0.75±0.18[aC]	0.27±0.24[aC]
9	17.13±1.49[abA]	3.81±1.26[aB]	0.31±0.31[aC]	0.21±0.16[aC]
12	20.18±0.63[aA]	3.46±1.58[aB]	0.64±0.20[aC]	0.32±0.34[aC]
15	19.08±1.32[abA]	3.53±1.78[aB]	0.33±0.32[aC]	0.22±0.13[aC]
18	19.77±1.05[abA]	4.96±1.11[aB]	0. 83±0.26[aC]	0.38±0.06[aD]

W: Initial water content g H$_2$O/g dry basis db), TEW: Thaw exudate water (g/100 g initial water); FST: Frozen storage time (months). Data are expressed as the mean ± standard deviation. Different letters (A-D) within a same row differ significantly (P < 0.05). Different letters (a-b) within a same column differ significantly (P < 0.05).

As previously indicated, since apple samples have initially before freezing different water contents, the thaw exudate water (TEW) was expressed as gram of water exudate/100 g initial water of concerned product before freezing. The impacts of initial water content (W) of apple samples and frozen storage time (SFT) on thaw exudate water (TEW) were investigated.

During thawing at a temperature of 4 °C, TEW of fresh apple samples without previous dehydration (samples with 7 g H$_2$O/g db as initial water content) was approximately of 15 g/100 g initial water. Fresh apple samples had significantly higher value of TEW than all partially air dried samples. This amount of TEW was important and significantly increased although slightly during the frozen storage time period of 18 months at -18 °C. According to Goncalves et al. [14], during frozen storage, recrystallization of ice crystals may cause more loss of cell turgor causing a leakage of fruit cell content and decrease of cell water holding capacity, resulting in increasing of thaw exudate water versus storage time.

Thaw exudate water was about 4 g/100 g initial water for apple samples with initial water content of 2 g H$_2$O/g db, and about 0.5 g/100 g initial water for samples of 1 and 0.3 g H$_2$O/g db initial water content. This low thaw exudate water level reveals high preservation of structural and textural quality issued from a better preservation of cell walls. This contributes to the slowing down of water loss from the internal cells [11].

From our point of view, the most important point, which is worth to be highlighted here is that, for previously dehydrated apple samples, TEW remained constant and negligible during the whole storage period. Partial removal of water before fruit freezing appeared as a

relevant way to preserve the structural and maintain the textural properties of frozen/thawed fruits. This improves its stability during storage.

3.2. Color

Table 2 shows the total color difference (TCD) induced by freezing/dehydrofreezing and thawing of apple samples during storage at -18 °C for 18 months and after thawing.

Table 2. Effect of -18•C-storage during 18 month-freezing on total color difference of dehydrofrozen apple.

FST (months)	TCD (-)			
	W (g H₂O/g db)			
	7	2	1	0.3
0	33.56±5.94[aA]	31.66±2.06[aA]	21.88±7.71[aA]	15.59±6.15[aB]
1	29.28±3.49[aA]	30.47±6.91[aA]	25.14±5.76[aA]	15.61±4.53[aB]
2	28.20±5.19[aA]	30.15±6.84[aA]	25.72±2.86[aA]	14.03±6.82[aB]
3	31.44±7.12[aA]	34.62±5.98[aA]	22.57±3.67[aA]	10.91±3.96[aB]
6	32.70±1.93[aA]	32.74±8.09[aA]	26.51±7.45[aA]	12.14±5.66[aB]
9	32.71±2.42[aA]	32.48±5.63[aA]	21.09±2.86[aA]	15.10±7.52[aB]
12	27.74±6.21[aA]	32.80±4.23[aA]	25.20±7.54[aA]	13.95±6.91[aB]
15	30.94±5.88[aA]	30.66±5.19[aA]	20.90±6.39[aA]	11.50±5.79[aB]
18	29.34±5.47[aA]	33.34±4.71[aA]	20.81±5.19[aA]	10.56±5.69[aB]

W: initial water content (g H₂O/g db), FST: Frozen storage time (months), TCD: total color difference (-). Data are expressed as the mean ± standard deviation. For each color parameter, different letters (A-B) within a same row differ significantly (P < 0.05). Different letters (a-b) within a same column differ significantly (P < 0.05).

As it is shown in Table 2, the global effect of freezing and thawing processes on color decreased and became negligible for apple samples with low water content. Indeed, the total color difference (TCD) was 33.5 and 15.5 for samples with initial water contents of 7 and 0.3 g H₂O/g db, respectively (Table 2). The freezing/thawing effect decrease is explained by the lower water activity of samples and consequently lower rate of enzymatic browning reactions [22]. The freezing impact decrease on fruit color is also attributed to the air-drying step, which caused the reduction of phenolase activity and enzymatic browning [23]. On the other hand, partial removal of water from fruit cells could protect product color due to lower structural damage as a result of freezing decreasing the enzymatic browning in damaged tissue [4].

In contrast, total color difference was almost constant during the whole storage period of 18 months at -18 °C. According to Forni *et al.* [23], the air-drying step reduced the phenolase activity and thus increased color stability of dehydrofrozen/thawed apricot during storage.

To conclude, the coupling of air drying and freezing processes induced lesser color changes at lower water content levels. These color losses are almost stable during the whole frozen

storage period. Thus, the combination of these two conventional food unit operations is very useful for the color stability of frozen/thawed fruit during storage.

3.3. Total polyphenol content

The results of total polyphenol contents (TPC) in frozen and dehydrofrozen apples with different water contents during frozen storage at -18 °C and after thawing are given in Table 3.

Table 3. Effect of -18•C-storage on total polyphenol content of dehydrofrozen apples.

FST (months)	TPC (g AGE/100 g DW)			
	W (g H$_2$O/g db)			
	7	2	1	0.3
0	0.43±0.04[aA]	0.19±0.03[aC]	0.18±0.01[aC]	0.29±0.01[aB]
1	0.44±0.01[aA]	0.21±0.03[aC]	0.19±0.01[aC]	0.28±0.01[aB]
2	0.43±0.05[aA]	0.19±0.01[aC]	0.18±0.01[aC]	0.27±0.01[aB]
3	0.40±0.03[aA]	0.20±0.02[aC]	0.18±0.01[aC]	0.28±0.01[aB]
6	0.37±0.03[aA]	0.21±0.02[aC]	0.18±0.01[aC]	0.28±0.01[aB]
9	0.38±0.02[aA]	0.20±0.01[aC]	0.19±0.01[aC]	0.27±0.01[aB]
12	0.42±0.02[aA]	0.21±0.01[aC]	0.18±0.01[aD]	0.28±0.01[aB]
15	0.40±0.05[aA]	0.20±0.01[aC]	0.19±0.02[aC]	0.28±0.01[aB]
18	0.39±0.02[aA]	0.20±0.01[aC]	0.17±0.01[aD]	0.26±0.01[aB]

W: Initial water content (g H$_2$O/g db); FST: Frozen storage time (months); TPC: total polyphenol content (g AGE/100 g DW).Data are expressed as the mean ± standard deviation. Different letters (A-D) within a same row differ significantly (P < 0.05). Different letters (a-d) within a same column differ significantly (P < 0.05).

Fresh *Golden delicious* apple samples present a total polyphenol content (TPC) of 0.62 g AGE/100 g db. Partial air drying results in significant reduction of TPC. TPC of partially dried apple samples were 0.26, 0.22, and 0.29 g AGE/100 g db for water contents of 2, 1, and 0.3 g H$_2$O/g db, respectively. TPC losses as compared with fresh samples varied from 52 to 64%. According to Korus [26], hot air drying caused phenolic compounds degradation and promoted polyphenols oxidation by the oxygen absorbed from the air of convective drying. Loss in polyphenol content is also ascribed to their use as reactants in the Maillard reaction.

Similarly, freezing caused significant reduction in TPC. TPC losses were important for apple samples without any pre-dehydration stage and decreased for partially dried apples before freezing. Indeed, TPC losses caused by freezing and thawing processes are about 30, 25, 17, and 5% for samples with initial water contents of 7, 2, 1, and 0.3 g H$_2$O/g db, respectively. In fact, freezing results in cell de-compartmentalization allowing reactions between genuine enzyme activities and their corresponding substrates [27,28]. Therefore, phenolic compounds may already be degraded during thawing due to their interaction with

oxidative enzyme activities such as polyphenoloxidases (PPO) which is more active at high water activity fruit samples [29,30].

As it is shown in Table 3, frozen storage time (FST) had insignificant effect on TPC for frozen and dehydrofrozen/thawed apple samples with different water contents. No data was found about the impact of coupling convective air drying and freezing on the polyphenol content of fruits and vegetables during their frozen storage.

4. Conclusions

The dehydrofreezing performed by coupling airflow dehydration, as pretreatment for partial removal of water from apple fruit cells, prior to freezing resulted in higher preservation quality in terms of reduced thaw exudate water reflecting better texture quality, color retention, and ameliorating the bioactive composition. This combined process guarantees the stabilization of frozen product quality accomplished during subsequent long term frozen storage.

To conclude the partial dehydration of fruits before freezing is a pertinent way to minimize the quality alteration caused by freezing and thawing processes and to obtain products with high quality stability during storage. However, the pretreatment used for water removal must be optimized to minimize the quality losses at this step.

5. References

[1]   Ramallo LA and Mascheroni RH, Dehydrofreezing of pineapple. *J Food Eng* 99: 269-275 (2010).

[2]   Ben Haj Said L, Bellagha S and Allaf K, Dehydrofreezing of Apple Fruits: Freezing Profiles, Freezing Characteristics, and Texture Variation. *Food Bioprocess Tech* 9: 252-261 (2016).

[3]   Ben Haj Said L, Bellagha S and Allaf K, Optimization of Instant Controlled Pressure Drop (DIC)-Assisted Dehydrofreezing Using Mechanical Texture Measurements Versus Initial Water Content of Apple. *Food Bioprocess Tech* 8: 1102-1112 (2015).

[4]   Bolin HR and Huxsoll CC, Partial Drying of Cut Pears to Improve Freeze/Thaw Texture. *J Food Sci* 58: 357-360 (1993).

[5]   Robbers M, Singh RP and Cunha LM, Osmotic-Convective Dehydrofreezing Process for Drying Kiwifruit. *J Food Sci* 62: 1039-1042 (1997).

[6]   Sormani A, Maffi D, Bertolo G and Torreggiani D, Textural and structural changes of dehydrofreeze-thawed strawberry slices: Effects of different dehydration pretreatments / Cambiostexturales y estructurales de rodajas de fresadeshidratadas y descongeladas: Efectos de diferentespretratamientos de deshidratación. *Food Sci Tech Inter* 5: 479-485 (1999).

[7]   Chiralt A, Martínez-Navarrete N, Martínez-Monzó J, Talens P, Moraga G, Ayala A, *et al*, Changes in mechanical properties throughout osmotic processes: Cryoprotectant effect. *J Food Eng* 49: 129-135 (2001).

[8] Maestrelli A, Lo Scalzo R, Lupi D, Bertolo G and Torreggiani D, Partial removal of water before freezing: cultivar and pre-treatments as quality factors of frozen muskmelon (Cucumis melo, cv reticulatus Naud.). *J Food Eng* 49: 255-260 (2001).

[9] AOAC, Association of Official Analytical Chemists (15th edn).In 567 K. Helrich (Ed.). Arlington: Virginia 22201, USA (1990).

[10] Ben Haj Said L, Najjaa H, Neffati M and Bellagha S, Color, Phenolic and Antioxidant Characteristic Changes of *Allium Roseum* Leaves during Drying. *J Food Qual* 36: 403-410 (2013).

[11] Gonçalves EM, Abreu M, Brandãǒo TRS and Silva CLM, Degradation kinetics of colour, vitamin C and drip loss in frozen broccoli (Brassica oleracea L. ssp. Italica) during storage at isothermal and non-isothermal conditions. *Inter J Ref* 34: 2136-2144 (2011).

[12] Van Buggenhout S, Lille M, Messagie I, VanLoey A, Autio K and Hendrick M, Impact of pretreatment and freezing conditions on the microstructure of frozen carrots: Quantification and relation to texture loss. *Euro Food Res Tech* 222: 543-553 (2006).

[13] Van Buggenhout S, Messagie I, Maes V, Duvetter T, Van Loey A and Hendrick M, Minimizing texture loss of frozen strawberries: effect of infusion with pectinmethylesterase and calcium combined with different freezing conditions and effect of subsequent storage/thawing conditions. *Euro Food Res Tech* 223: 395–404 (2006).

[14] Lowithun N and Charoenrein S, Influence of osmodehydrofreezing with different sugars on the quality of frozen rambutan. *Inter J Food Sci Tech* 44: 2183-2188 (2009).

[15] Dermesonlouoglou EK, Giannakourou MC and Taoukis P, Stability of dehydrofrozen tomatoes pretreated with alternative osmotic solutes. *J Food Eng* 78: 272-280 (2007).

[16] Dermesonlouoglou EK, Giannakourou MC and Taoukis P, Stability of dehydrofrozen tomatoes pretreated with alternative osmotic solutes. *J Food Eng* 78: 272-280 (2007).

[17] Dermesonlouoglou EK, Pourgouri S and Taoukis PS, Kinetic study of the effect of the osmotic dehydration pre-treatment to the shelf life of frozen cucumber. *Innov Food Sci Emerg Tech* 9: 542-549 (2008).

[18] Rincon A and Kerr WL, Influence of osmotic dehydration, ripeness and frozen storage on physicochemical properties of mango. *J Food Process Preserv* 34: 887-903 (2010).

[19] Tregunno NB and Goff HD, Osmodehydrofreezing of apples: structural and textural effects. *Food Res Inter* 29: 471-479 (1996).

[20] Forni E, Sormani A, Scalise S and Torreggiani D, The influence of sugar composition on the colour stability of osmodehydrofrozen intermediate moisture apricots. *Food Res Inter* 30: 87-94 (1997).

[21] Marani CM, Agnelli ME and Mascheroni RH, Osmo-frozen fruits: mass transfer and quality evaluation. *J Food Eng* 79: 1122-1130 (2007).

[22] Redmond GA, Gormley TR and Butler F, The effect of short- and long-term freeze-chilling on the quality of cooked green beans and carrots. *Innov Food Sci Emerg Tech* 5: 65-72 (2004).

[23] Korus A and Lisiewska Z, Effect of preliminary processing and method of preservation on the content of selected antioxidative compounds in kale (*Brassica oleracea* L. var. acephala) leaves. *Food Chem* 129: 149–154 (2011).

[24] Tomás-Barberán FA and Espín JC, Phenolic compounds and related enzymes as determinants of quality in fruits and vegetables. *J Sci Food Agri* 81: 853-876 (2001).

Combined effects of sodium carbonate pretreatment and hybrid drying methods on the nutritional and antioxidant properties of dried Goji berries

Song, H. H.; Bi, J. F. *; Chen, Q. Q. *; Zhou, M.; Wu, X. Y.; Song, J. X.

Institute of Food Science and Technology, Chinese Academy of Agricultural Science (CAAS)/ Key Laboratory of Agro-Products Processing, Ministry of Agriculture, Beijing, China

*E-mail of the corresponding author: bjfcaas@126.com (Bi J. F.); celerylc@163.com (Chen Q. Q.)

Abstract

Combined effects of sodium carbonate (SC) pretreatment and hybrid drying methods (freeze drying-instant controlled pressure drop drying (FD-ICPDD), hot air drying (HAD-ICPDD) on nutritional and antioxidant properties of Goji berries were investigated. Compared with distilled water pretreatment, SC pretreatment could obtain products with better quality. Goji dried by FD-ICPDD showed better overall quality than that dried by HAD or FD alone. FD-ICPDD products exhibited higher contents of total Lycium barbarum polysaccharide (140 g/kg), total carotenoids (2.4 g/kg) as well as the strongest ABTS.+ radical scavenging activity (57.6 μmol TE/g). FD-ICPDD could be an alternative drying method for processing valuable agro-products.

Keywords: sodium carbonate, instant controlled pressure drop drying, nutritional properties, antioxidant activity

1. Introduction

Goji is in the Solanaceae family that has been used as a functional food and traditional herb in Asian countries [1]. It contains many active compounds including phenols, carotenoids and polysaccharides possessing biological activates such as anti-aging, antioxidant properties and so on [2]. For preservation, drying is still the main processing method to prolong the shelf-life of Goji [3]. Several drying methods, such as sun drying, hot air drying, vacuum drying, and freeze drying, have been conducted on Goji [4,5]. Each drying technique has advantages and restrictions. However, combined drying process can integrate the strengths of different drying methods so as to preserve quality of final products [6]. Instant controlled pressure drop drying (ICPDD), also called explosion puffing drying (EPD) [7], is an emerging drying technology which always in conjunction with other drying methods like hot air and freeze drying and produce the products with better quality [8]. Drying of fresh Goji is difficult owing to the wax layer on the surface which could block moisture transport. Sodium carbonate (SC) was used as a traditional pretreatment to break the wax layer of Goji so as to accelerate the drying rate. But there is little report about the effect of SC pretreatment coupled with combined drying especially on ICPDD of Goji. Hence, to enhance drying efficiency and improve the overall quality, combined effects of sodium carbonate pretreatment and hybrid drying methods (FD-ICPDD and HAD-ICPDD) on the nutritional and antioxidant properties of Goji was evaluated. Freeze drying and hot air drying were used as comparative study.

2. Materials and Methods

2.1 Sample preparation

2.1.1 Raw material

Goji was grown in Yinchuan, Ningxia Hui Autonomous Region, China with initial water content was about 804 ± 2 g/kg dry base (d.b.). Those without mechanical damage and decay were used and the fruit pedicles were removed before experiment.

2.1.2 Pretreatment

Goji fruits were immersed into the SC solution (20 g/kg) for 1 min at room temperature with the liquid to solid ratio of 10:1 (ml:g). Control samples were treated by distilled water (DW) under the same condition. Fresh Goji fruits were used for HAD and HAD-ICPDD. For FD and FD-ICPDD processing, samples were frozen at -80℃ before used.

2.1.3 Equipment and Drying Process

Freeze dryer (Alphal 1-4Lplus, MARIN CHRIST Co. Ltd Osterode, Germany), hot air dryer (HDS-D120B-D, Haiti Sheng Machinery Co. Ltd., Liaoning, China) and instant controlled pressure drop dryer (Tianjin Qin-de New Material Technology Co. Ltd., Tianjin, China) were used. The drying conditions of four different drying methods are exhibited in **Table 1**. The dried products were ground into powder and pass through a 60 mesh sieve, which were then kept at 4ºC for further chemical analysis.

Table 1. Drying conditions of four different drying methods

Drying Methods[a]	Pretreatments[a]	Drying Conditions	Drying Time(h)
Freeze drying	DW	First drying stage: at -55ºC and 0.37 kPa; Second drying stage: at 25ºC	58 h
	SC	The drying conditions was the same as DW	58 h
Freeze drying -instant controlled pressure drop drying	DW	Freeze drying at -55ºC and 0.37 kPa for 14 h; explosion puffing of 90℃ for 15 min, then vacuum drying at -0.1 MPa and 60ºC for 1.5 h.	15.5 h
	SC	The drying conditions was the same as DW	15.5 h
Hot air drying	DW	The drying time and temperature of air drying was 40ºC (2 h)-50ºC (4 h)-60ºC (12 h), air velocity 1.2 m/s, relative humidity 40%	18 h
	SC	The drying time and temperature of air drying was 40ºC (2 h)-50ºC (4 h)-60ºC (8 h), air velocity 1.2 m/s, relative humidity 40%	14 h
Hot air -instant controlled pressure drop drying	DW	Hot air drying: 40ºC (2 h)-50ºC (4 h); explosion puffing at 90℃ for 15 min, then vacuum drying at -0.1 MPa and 60ºC for 1.5 h.	7.5 h
	SC	Hot air drying: 40ºC (2 h)-50ºC (2.5 h); explosion puffing at 90ºC for 15 min, then vacuum drying at -0.1 MPa and 60ºC for 1.5 h	6 h

2.2 Sample extraction

Methanol-water solution was applied for sample extraction in this study. The extraction method was the same as Istrati et al. (2013) [9]. Samples were then filtered pass through a 0.45 μm microporous membrane for the analysis of total phenolic content, total flavonoid content, and antioxidant activity on the UV-visible spectrophotometer (UV1800, Shimadzu Co. Ltd., Kyoto, Japan).

2.3 Nutritional properties

2.3.1 Total carotenoids content

Total carotenoids content (TCC) was measured according to Knockaert et al. (2012) [10]..

2.3.2 Total Lycium barbarum Polysaccharide content

The total *Lycium barbarum* polysaccharide (LBP) content was performed according to the procedure presented by Zhao et al. (2015) [4] with slight modification. Goji powder was extracted by ultrasonic at 40 kHz for 2 h. After centrifugated, the supernatant was condensed to a proper volume and precipitation was dissolved with ethanol until the concentration of ethanol is over 80%. Then the solution was placed at 4ºC for 24 h to make the LBP settled. The settling was dissolved with distilled water and set to 100 mL. Solutions were analyzed for LBP, by the phenol–sulfuric acid method and concentrations determined against a glucose standard.

2.3.3 Total phenolic content

Briefly, 0.4 mL of the extracts was transferred to the volumetric flask (10 mL) followed by 1 mL of Folin-Ciocalteu's reagent (10 times dilution) and after 6 min 2 mL of sodium carbonate solution (75 g/kg) was added. Then the volumetric flask was adjusted to the total volume with the distilled water and mixed thoroughly. The mixture was allowed to stand for 60 min at 30ºC and measured at 765 nm [11]. The TPC was presented as mg/g dry base (d.b.) of gallic acid equivalents (GAE).

2.4 Antioxidant activity (FRAP and ABTS assay) measurement

The FRAP and ABTS assay were measured according to the method of Wang et al. (2012) [13] and Jihyun et al. (2010) [14], respectively.

2.5 Statistical Analysis

All the experimental data was conducted in three replicates and the results were expressed as mean ± standard deviation. The SPSS V21.0 Software (IBM Corporation, Chicago, USA) was used for statistical analysis, applying a one-way analysis of ANOVA test and Duncan's multiple comparison test at $P < 0.05$.

3. Materials and Methods

3.1 Total carotenoids content

The reddish-orange color of Goji fruits comes from a group of carotenoids, which can be easily oxidized by heat, light, and high oxygen tension [15]. The TCC for fresh Goji was 3.6 g/kg extract and the values of dried Goji was shown in **Table 2**. DW-fruits exhibited lower

TCC values than SC-ones and the lowest TCC (1.6 g/kg) was obtained in HAD (DW) samples, owning to the effect of coexistence of high temperature, oxygen and longer drying time. The highest retention of TCC (71.4%) was observed in FD (SC) samples, possibly because of the lower temperature and vacuum conditions during FD dehydration [16]. Similarly, less losses of TCC (36%) in FD-ICPDD (DW) sample than that of HAD-ICPDD (DW) (43%) ones.

Table 2 Dfferent drying methods and pretreatments on nutritional components and antioxidant activities of Lycium Barbarum

Treatments	TCC （g/kg）	LBP （g/kg）	TPC （mg GAE/g）	FRAP （µmol TE/g）	ABTS （µmol TE/g）
Fresh	3.6±0.1a	169±6a	6.7±0.1e	24.5±1.0f	28.1±1.3g
FD(DW)	2.5±0.0c	105±7c	8.1±0.5d	29.7±2.7e	50.1±1.3c
FD(SC)	2.6±0.1b	107±1c	8.4±0.1d	30.2±2.4e	51.8±0.9bc
FD-ICPDD(DW)	2.3±0.1d	135±9b	10.5±0.1bc	39.1±2.0bc	53.3±0.8b
FD-ICPDD(SC)	2.4±0.0cd	140±0b	11.3±0.3a	43.7±1.0a	57.6±0.5a
HAD(DW)	1.6±0.1g	90±3d	8.1±0.3d	34.3±1.2d	40.0±2.3f
HAD(SC)	1.7±0.1f	91±5d	10.1±0.4c	37.9±1.9c	43.4±1.7e
HAD-ICPDD(DW)	2.1±0.1e	95±1d	11.0±0.4ab	40.9±2.5abc	45.1±0.4de
HAD-ICPDD(SC)	2.3±0.1d	110±1c	11.4±0.3a	41.7±1.7ab	45.7±0.8d

Dates are expressed as dry base. Each value is expressed as mean value ± SD (n = 3). Different letters in the same column indicate significant differences at *p* < 0.05, the same below. GAE: gallic acid equivalent; RE: rutin equivalent; TE: trolox equivalent

3.2 Total LBP content

LBP was one of the major active components in charge of biological activities of Goji [17]. There were significant distinctions of the LBP values between different drying processing. As shown in **Table 2**, the highest retention of LBP (82.9%) was observed in the FD-ICPDD (SC) products, possibly because vacuum conditions of most of drying process. The LBP of FD-ICPD-dried Goji was higher than that of the HAD-ICPD-dried ones. The lowest content of LBP (90 g/kg) was found in HAD (DW) because of the longer drying time (12 h) at relatively higher drying temperature (60ºC). The content of LBP had no significant difference under the DW and SC pretreatments of the same drying method except the HAD-ICPDD.

3.3 Total phenolic content (TPC)

The TPC of dried Goji was significantly influenced by the different pretreatments and drying methods ($p < 0.05$). As shown in **Table 2**, TPC for the fresh samples was 6.7 mg GAE/g, which was similar to that had been reported in the article [5]. The SC pretreatment exhibited higher TPC values than that of DW pretreatment in all the drying methods. For example, the TPC of FD-ICPDD dried samples with SC pretreatment were 7.8% higher than that of DW ones. The highest retention of TPC (11.4 mg GAE/g) was found in HAD-ICPDD (SC) method, whereas the FD (DW) samples had the lowest value (8.1 mg GAE/g). It may be attributed to heat treatment that could liberate some phenolics and flavonoids which are mainly found in bound form in plant matrix [18]. On the other hand, the activity of polyphenol oxidase, which is responsible for oxidation of phenolics, tends to deactivation because of exposure to high temperature [19]. During thermal treatment, the liberation of phenolics might occur due to the decomposition of cellular components and covalent bonds [20]. Hence, the released phenolics tend to be more amenable for extraction. Chang et al. (2006) [21] also found that the values of TPC and TFC of tomatoes had a significant increase compared to the fresh ones either through FD or HAD. The TPC content of FD-ICPDD (SC) were higher than that of the FD (SC) samples (25.3%), which indicated that phenolics could be was liberated after ICPDD treatment.

3.4 Antioxidant Activity

Antioxidants like phenolic compounds could inhibit oxidation reaction by acting on hydrogen donors or free radical acceptors [22]. Due to the complex composition of oxidative processes, the antioxidant activity could not be evaluated only using one single method. FRAP and ABTS assay was used in this study. As shown in **Table 2**, the antioxidant activities of all dried samples were enhanced compared to the fresh ones. Chang et al. (2006) [21] also showed similar results. Besides FD dried samples, significant increase of antioxidant activity of dried Goji was observed after SC pretreatment. The strongest ferrous iron chelating capacity (43.69 μmol TE/g) and ABTS.+ radical scavenging activity (57.55 μmol TE/g) were found in FD-ICPDD-dried Goji. The fact that higher TPC were found in dried samples conducive to higher antioxidant activities compared to the fresh ones (**Table 2**). The FRAP values of FD-ICPDD-dried (SC) samples were 44.5% higher than the FD-dried (SC) samples, respectively, which were in good agreement with the increase of TPC contents (25.3%). Therefore, the ICPDD processing also can increase the antioxidant activity of dried Goji.

4. Conclusions

Nutritional and antioxidant properties of dried Goji were significantly affected by different pretreatments and drying conditions. Compared to DW-pretreated samples, the SC pretreatment was more favorable because its improvement in overall qualities of dried Goji

no matter which drying method was used. In detail, the SC pretreatment products exhibited shorter drying time, higher TPC, LBP, TCC and antioxidant activity.

Under SC-pretreatment, the FD-ICPDD was a more beneficial drying method compared with the FD, HAD and HAD-ICPDD because of the highest retentions of TPC, LBP and antioxidant activities (FRAP and ABTS). For obtaining high-quality and valuable Goji-products, FD-ICPDD should be the best choice. But the increased manufacturing cost because of the FD pre-drying should also be taken into account. HAD-ICPDD could be another alternative technique when energy saving was more considered.

5. References

[1] Jeszka-Skowron, M.; Zgoła-Grześkowiak, A.; Stanisz, E. Potential health benefits and quality of dried fruits: goji fruits, cranberries and raisins. Food Chemistry, 2017, 221, 228-236.

[2] Potterat, O. Goji (Lycium barbarum & L. chinense): phytochemistry, pharmacology and safety in the perspective of traditional uses and recent popularity. Planta Medica, 2010, 76, 7-19.

[3] Cuccurullo, G.; Giordano, L.; Albanese, D. Infrared thermography assisted control for apples microwave drying. Journal of Food Engineering, 2012, 112, 319-325.

[4] Zhao, Q.S.; Dong, B.T.; Chen, J.J.; Zhao, B.; Wang, X.D.; Wang, L.W. Effect of drying methods on physicochemical properties and antioxidant activities of wolfberry (*Lycium Barbarum*) polysaccharide. Carbohydrate Polymers, 2015, 127(AUG), 176-181.

[5] Donno, D.; Mellano, M.G.; Raimondo, E. Influence of applied drying methods on phytochemical composition in fresh and dried goji fruits by HPLC fingerprint. European Food Research and Technology, 2016, 242, 1-14.

[6] Huang, L.L.; Zhang, M. Trends in development of dried vegetable products as snacks. Drying Technology, 2012, 30, 448-461.

[7] Lyu, J.; Yi, J.Y.; Bi, J.F. Impacts of explosion puffing drying combined with hot-air and freeze drying on the quality of papaya chips. International Journal of Food Engineering, 2017, 13.

[8] Chen, Q.Q.; Li, Z.L.; Bi, J.F. Effect of hybrid drying methods on physicochemical, nutritional and antioxidant properties of dried black mulberry. LWT - Food Science and Technology, 2017, 80, 178-184.

[9] Istrati, D.; Vizireanu, C.; Iordachescu, G. Physico-chemical characteristics and antioxidant activity of goji fruits jam and jelly during storage. Annals of the University Dunarea de Jos of Galati Fascicle VI - Food Technology, 2013, 37, 100-110.

[10] Knockaert, G.; Lemmens, L.; Van, B.S. Changes in β-carotene bioaccessibility and concentration during processing of carrot puree. Food Chemistry, 2012, 133, 60-67.

[11] Chan, E.; Lim, Y.Y.; Wong, S.K. Effects of different drying methods on the antioxidant properties of leaves and tea of ginger species. Food Chemistry, 2009, 113,

166-172.

[12] Sun, L.J.; Zhang, J.B.; Lu, X.Y. Evaluation to the antioxidant activity of total flavonoids extract from persimmon (Diospyros kaki L.) leaves. Food and Chemical Toxicology, 2011, 49, 2689-2696.

[13] Wang, Y.T.; Liu, F.X.; Cao, X.M. Comparison of high hydrostatic pressure and high temperature short time processing on quality of purple sweet potato nectar. Innovative Food Science and Emerging Technologies, 2012, 16, 326-334.

[14] Jihyun, J.; Hana, J.; Saerom, L. Anti-oxidant, anti-proliferative and anti-inflammatory activities of the extracts from black raspberry fruits and wine. Food Chemistry, 2010, 123, 338-344.

[15] Dias, M.G.; Camões, M.F.; Oliveira, L. Carotenoid stability in fruits, vegetables and working standards - effect of storage temperature and time. Food Chemistry, 2014, 156, 37-41.

[16] Cui, Z.W.; Li, C.Y.; Song, C.F. Combined microwave-vacuum and freeze drying of carrot and apple chips. Drying Technology, 2008, 26, 1517-1523.

[17] Zhang, X.R.; Qi, C.H.; Cheng, J.P. Lycium barbarum polysaccharide LBPF4-OL may be a new Toll-like receptor 4/MD2-MAPK signaling pathway activator and inducer. International Immunopharmacology, 2014, 19, 132-141.

[18] Hayat, K.; Zhang, X.M.; Chen, H.Q. Liberation and separation of phenolic compounds from citrus mandarin peels by microwave heating and its effect on antioxidant activity. Separation and Purification Technology, 2010, 73, 371-376.

[19] Krapfenbauer, G.; Kinner, M.; Gössinger, M. Effect of thermal treatment on the quality of cloudy apple juice. Journal of Agricultural and Food Chemistry, 2006, 54, 5453-5460.

[20] Papoutsis, K.; Pristijono, P.; Golding, J.B. Effect of vacuum-drying, hot air-drying and freeze-drying on polyphenols and antioxidant capacity of lemon (citrus limon) pomace aqueous extracts. International Journal of Food Science and Technology, 2016, 52, 1-8.

[21] Chang, C. H.; Lin, H.Y.; Chang, C.Y. Comparisons on the antioxidant properties of fresh, freeze-dried and hot-air-dried tomatoes. Journal of Food Engineering, 2006, 77, 478-485.

[22] Shahidi, F.; Zhong, Y. Lipid oxidation and improving the oxidative stability. Chemical Society Reviews, 2010, 39, 4067.

[23] Cui, Z.W.; Li, C.Y.; Song, C.F. Combined microwave-vacuum and freeze drying of carrot and apple chips. Drying Technology, 2008, 26, 1517-1523.

DRYING PROCESS

Oral Presentations

Experimental analysis of particle breakage and powder morphology in foam spray drying

Lewandowski, A.[a]; Jaskulski, M.[a*]; Zbiciński, I.[a]

[a] Faculty of Process and Environmental Engineering, Lodz University of Technology, Wolczanska Str 213., 95-924 Lodz, Poland.

*E-mail of the corresponding author: maciej.jaskulski@p.lodz.pl

Abstract

The paper presents results of experiments of gas admixing foam spray drying of maltodextrin in co-current spray tower. Significant effect of feed foaming on particle sphericity, angle of repose, apparent and bulk density, Hausner ratio and porosity was found. Number of broken particles achieved 60 % for high foaming gas rate (GLR) and inlet air temperature due to particle overheating and bubble expansion. Analysis of the experiments results allowed to determine optimal range of operating conditions to reduce number of damaged particles, to around 15 % for the highest GLR and to minimize product degradation.

Keywords: foamed materials, gas admixing, powder properties, powder quality

1. Introduction

Standard spray drying process can be modified by foaming of feed solution. This technique, called "foam spray drying", can be carried out in two ways: by gas desorption or gas admixing method [1]. In gas desorption process, the feed is foamed due to the bubbles nucleation inside supersaturated droplets after atomization. In gas admixing method, foaming gas is directly injected into the slurry before spraying [2]. Powders obtained after foam spray drying are characterized by lower bulk density, higher porosity and particle sizes, better solubility and wettability than from conventional spray drying. Bubbles trapped in the particles during foaming can expand or deflect during drying producing hollow, spherical or damaged particles.

Properties and quality of powders in foam spray drying results from type of dried material, hydrodynamics of continuous and dispersed phase and operating process parameters [3,4]. Concentration of solid, type of solvent and rheological properties of feed effect particle shape and morphology [5]. Hollow particles are produced from "skin-forming" materials whereas porous and irregular particles are developed from suspensions or colloids [6,7]. In co-current flow of phases agglomeration hardly occur as particle collisions are rare. In counter-current or mixed phase flow, due to intensive air recirculation in drying chamber, particles collide frequently and agglomerate which increases average particle size in the final product [8]. Agglomeration can be also stimulated by the configuration of the nozzles or by the returning of the smallest fractions of particles into the atomization zone. Parameters of spray drying process like feed rate, air flow rate and temperature, air humidity effect drying rate and the final powder properties, e.g. improperly selected will result in particle cracking and degradation due to overheating.

The aim of this paper was to determine optimal parameters of foam spray drying process to produce high quality powders.

2. Materials and Methods

2.1. Spray drying measurement system

Co-current foam spray drying experiments were carried out in spray drying tower at Lodz University of Technology [2]. Drying air was filtered and then heated up by the electrical heaters with power 62 kW. To reduce heat losses to the ambient air, the tower was insulated with the 40 mm layer of glass wool. Feed from thermostated tank was pumped to the top of the dryer, foamed and atomized by pressure nozzle. Dry powder was collected from the set of cyclones installed at the dryer bottom.

2.2.   Foaming system

Gas admixing foaming system consisting of a static mixer and capilarry dispensing gas to the solution and high speed homogenizer was installed at the top of the dryer.

Feed, foamed with nitrogen, was atoimzed by pressure nozzle LN-1 (Spraying System Co., USA). The nozzle operates with pressure up to 3.0 MPa with spray angle up to 70° which reduce powder deposition on the column wall. Initial density and mass flow rate of feed were measured using Coriolis flow meter (Micro-Motion 2400S, Emerson, USA). All parameters wereregistered using data acquisition system (National Instruments, USA).

2.3.   Materials

As a particle crust material maltodextrin DE12 (Nowamyl S.A, Poland) was used in all experiments. Uniform bubble diameters distribution in the emulsion was obtained applying Tween®80 produced by Croda International (UK).

2.4.   Experiments conditions

Foam spray drying experiments were carried out for two initial maltodextrin DE12 concentrations 20% and 35%, constant mass flow rate of feed, 14 kg/h, four initial air temperatures 150°C, 175°C, 200°C and 215°C, for mass flow rate of foaming gas from 0.01 to 0.09 kg/h. Additional spray drying test without foaming of feed was carried out as reference case.

3.   Measurements results

Samples of dry powder were collected and analyzed to determine particle size distribution (PSD), sphericity, angle of repose, apparent and bulk density, Hausner ratio and porosity.

PSD and particle shape were found from the analysis of images taken from the optical microscope OE4 (PZO, Poland) connected to Nikon E4500 camera with support of Image-Pro Plus software (Media Cybernetics Inc., USA). At least 1000 particles per sample were analyzed to obtain representative results of powder morphology. Apparent density of the product was found with application of helium pycnometer AccPyc TC Micromeritics (USA). Bulk density of the powder was determined according to polish standard PN-80/C-04532 whereas angle of repose following polish standard PN-89/C-04840. HR - Hausner ratio was calculated from relation bulk/tapped density.

Examples of selected results of particle morphology are presented in Fig. 1 to 3. Average particle sphericity (Ψ_k) for two different initial MDX concentrations (20 % and 35 %) and for different drying gas temperatures as a function of gas-liquid ratio (GLR) are shown in Fig. 1.
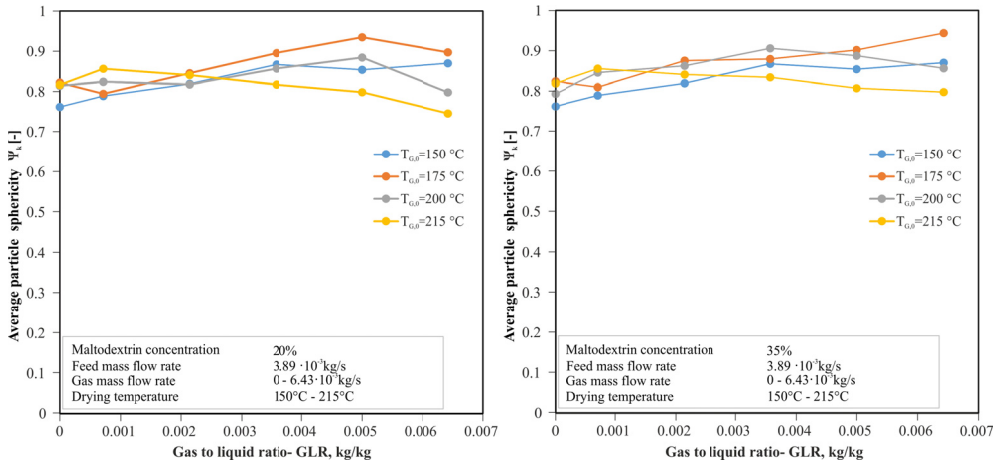
Fig. 1 Average sphericity of particles in collected powders.

Analysis of Fig. 1 shows that number of fully spherical particles increases with increasing of GLR. For the highest GLR and highest inlet air temperature ($T_{G,0} = 215°C$) particles sphericity decreases to 0.7 and 0.8 which is a result of particles breakage due to high thermal expansion of the bubbles.

Table 1 shows average Sauter diameter of particles in the product for different GLR and gas temperatures. We can observe increase of average Sauter diameter with increasing of GLR due to thermal expansion of the gas bubbles. Slight effect of initial gas temperature on average Sauter diameter was found.

For highest GLR and high initial gas temperature increased number of smaller particles was observed as a results of particles breakage in the product.

Table 1. Average Sauter diameter of particles in the product.

Gas to liquid ratio- GLR	Average Sauter diameter, µm			
	$T_{G,0} = 150°C$	$T_{G,0} = 175°C$	$T_{G,0} = 200°C$	$T_{G,0} = 215°C$
$7.14·10^{-4}$	52.96	52.98	51.84	51.91
$2.14·10^{-3}$	55.82	55.05	55.22	51.07
$3.57·10^{-3}$	54.82	58.05	58.00	55.80
$5.00·10^{-3}$	59.82	59.71	55.94	55.07
$6.43·10^{-3}$	57.72	61.91	56.62	57.06

Fig. 2 displays selected morphological properties of the powders: apparent and bulk density, porosity and Hausner ratio and angle of repose as a function of GLR. Analysis of results presented in Fig. 2 shows significant effect of feed foaming on final powder properties.
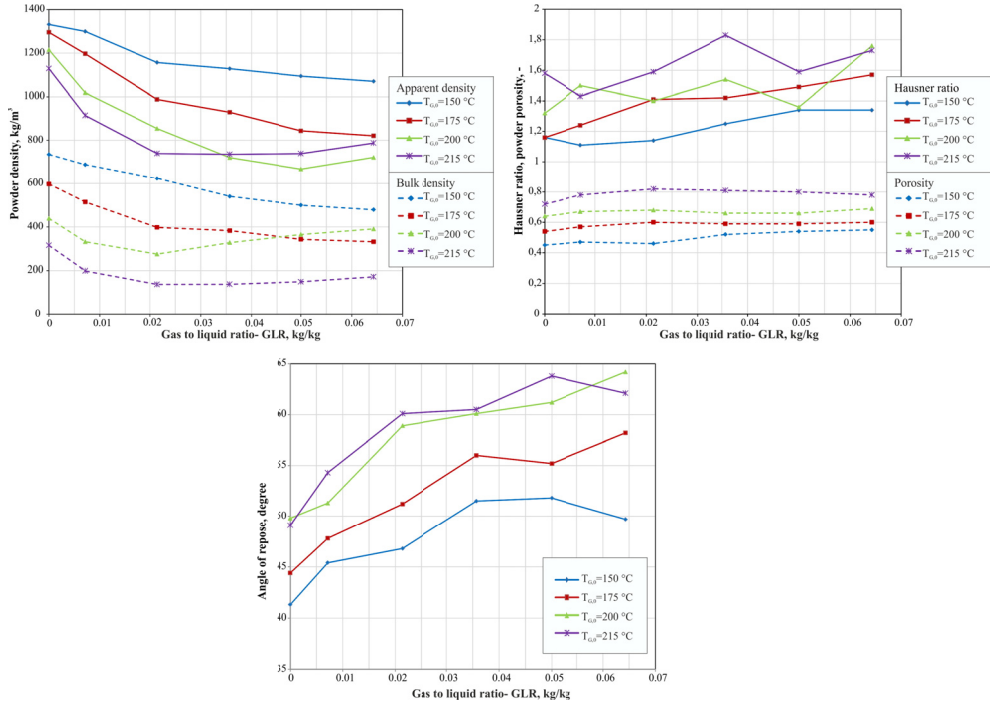
Fig. 2 Morphological properties of the powders.

We observe almost twofold decrease of bulk density of foamed materials in relation to non-foamed feed. Angle of repose and Hausner ratio are growing with increasing of foaming gas flow rate (GLR) and initial temperature of drying air. Flowability of the powder changed from flowable (HR around 1.1) to cohesive (HR above 1.3). For the highest GLR (over $5.00 \cdot 10^{-3}$) and air inlet temperature above 200°C, increase of bulk and apparent density is observed which is a result of filling of free spaces between the particles in the product by fragmented particles. Similar conclusions can be drawn from Fig. 1, where sphericity of particles decreases to $\Psi_k < 0.8$ with increasing of GLR which indicates particle breakage.

Fig. 3 presents experimentally determined ratio between number of broken and undamaged particles as a function of foaming gas flow rate, GLR, for different initial maltodekstrin concentrations.
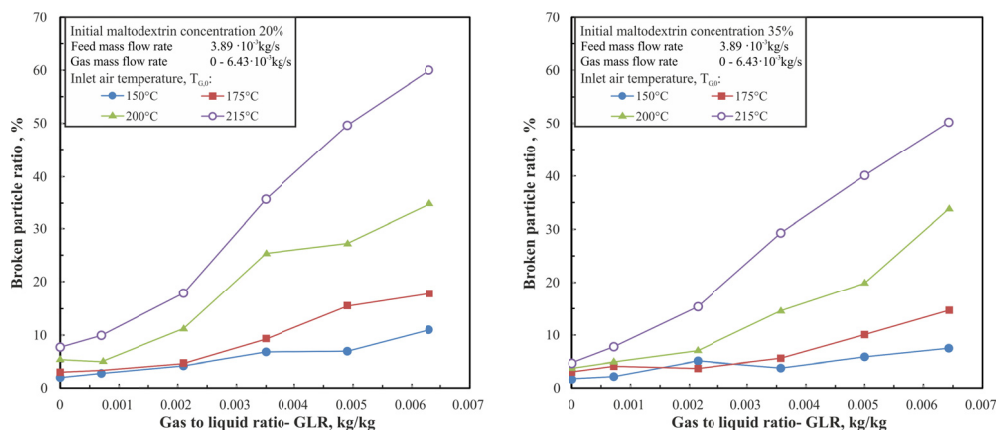
Fig. 3 Broken particle ratio of powder obtained from foamed spray drying experiments for different operating conditions.

Number of broken particles dramatically increases with GLR and inlet air temperature. For GLR above 0.006 kg/kg and the highest drying air temperature, amount of broken particles in the product varies from 5% to 50-60 % due to particle overheating and bubble expansion. Proper selection of foam spray drying process parameters allow to reduce significantly number of damaged particles, to around 15 % even for the highest GLR.

4. Conclusions

Co-current gas admixing foam spray drying tests was carried out in pilot-plant tower to determine physical and morphological properties of maltodextrine powder. Significant effect of feed foaming on sphericity, particle size distribution, angle of repose, apparent and bulk density, Hausner ratio and porosity of the powder was found.

Increase of a number of large and hollow particles with high sphericity and low bulk density, change of Hausner ratio from flowable (HR around 1.1) to cohesive (HR above 1.3) with increase of GLR was found.

For the highest GLR and air inlet temperature above 200°C an increase of bulk and apparent density was observed due to product degradation and fragmentation of particles as a result of high thermal expansion of bubbles.

Number of damaged particles can be significantly reduced, to around 15 % for the highest GLR for properly selected operational foam spray drying process parameters.

5. Nomenclature

GLR	gas/liquid ratio	$kgkg^{-1}$
$\dot{m}$	mass flow rate	kgs^{-1}
T	temperature	°C

Greek letters

Ψ_k	sphericity	-

Subscripts

0	initial
G	gas

6. References

[1]   R. W. Bell, F. P. Hanrahan, and B. H. Webb, "Foam Spray Drying Methods of Making Readily Dispersible Nonfat Dry Milk," J. Dairy Sci., vol. 46, no. 12, pp. 1352–1356, Dec. 1963.

[2]   I. Zbicinski and J. Rabaeva, "Analysis of Gas Admixing Foam Spray–Drying Process," Dry. Technol., vol. 28, no. 1, pp. 103–110, Dec. 2009.

[3]   E. Tsotsas, "Influence of Drying Kinetics on Particle Formation: A Personal Perspective," Dry. Technol., vol. 30, no. 11–12, pp. 1167–1175, 2012.

[4]   D. E. Walton and C. J. Mumford, "Spray Dried Products—Characterization of Particle Morphology," Chem. Eng. Res. Des., vol. 77, no. 1, pp. 21–38, 1999.

[5]   M. Nuzzo, A. Millqvist-Fureby, J. Sloth, and B. Bergenstahl, "Surface Composition and Morphology of Particles Dried Individually and by Spray Drying," Dry. Technol., vol. 33, no. 6, pp. 757–767, Apr. 2015.

[6]   J. Sloth, K. Jørgensen, P. Bach, A. D. Jensen, S. Kiil, and K. Dam-Johansen, "Spray Drying of Suspensions for Pharma and Bio Products: Drying Kinetics and Morphology," Ind. Eng. Chem. Res., vol. 48, no. 7, pp. 3657–3664, Apr. 2009.

[7]   E. Lintingre, F. Lequeux, L. Talini, and N. Tsapis, "Control of particle morphology in the spray drying of colloidal suspensions," Soft Matter, vol. 12, no. 12, pp. 7435–7444, 2016.

[8]   M. Piatkowski and I. Zbicinski, "Analysis of the mechanism of counter-current spray drying," Transp Porous Med, vol. 66, pp. 89–101, 2007.

Spray drying of high viscous food concentrates: Investigations on the applicability of an Air-Core-Liquid-Ring (ACLR) nozzle for liquid atomization

Wittner, M.*; Karbstein, H. P.; Gaukel, V.

Karlsruhe Institute of Technology, Institute of Process Engineering in Life Sciences, Chair I: Food Process Engineering, Kaiserstrasse 12, 76131 Karlsruhe, Germany

*E-mail of the corresponding author: marc.wittner@kit.edu

Abstract

Spray drying is widely used for powder production from liquid concentrates. Often low input temperatures are desired, as many materials, like proteins, are sensitive to heat. However, this demand leads to increased concentrate viscosities. Commonly used pressure swirl atomizers are limited concerning maximum processible viscosity. In this study, a so called Air-Core-Liquid-Ring Atomizer is used for pilot scale spray drying of whey protein concentrate (WPC80) at 40 °C and hence a viscosity of 0.09 Pa s. The produced powder was compared to an industrially produced reference. As a result, no significant differences in particle size distribution and particle morphology were observed.

Keywords: spray drying, atomization, ACLR, high viscous feeds, whey protein concentrate.

1. Introduction

Spray drying is an important and widely used processing technique for powder production form liquid concentrates[1]. The process consists of three main steps: atomization, drying and powder separation. In the atomization step, the bulk concentrate is disintegrated into small droplets, in order to accelerate convective drying. For sufficient drying, all droplets have to be small enough to dry within the given residence time inside the spray dryer[2]. Consequently, mean droplet size and distribution width, generated in the atomization step, are of high importance for the subsequent processing steps. Generally, spray dryers should be operated at the highest possible input dry matter content, in order to insure economic operation[3]. Moreover, low input temperatures are desired, as many spray dried materials are sensitive to heat. Both demands lead to high concentrate viscosities[4] which complicates atomization for all known atomizer techniques[5]. On industrial scale, mainly pressure swirl atomizers are used. In this type of atomizer, high liquid pressures are used to deliver the required atomization energy. This type of atomization is very energy efficient, but the maximum processible viscosity is comparably low[5]. In laboratory or pilot scale spray dryers, often external mixing pneumatic atomizers are used. In this type of atomizer, the kinetic energy of compressed gas is used for droplet disintegration. In contrast to pressure swirl atomizers, the applied disintegration energy can be increased independently of the liquid flow. This allows the production of very small droplet sizes, even at high concentrate viscosity. However, high gas consumption rates of these atomizers do not allow economic operation on larger scales[3].

Internal mixing pneumatic atomizers (IMPA) offer the possibility to atomize high viscous concentrates at low gas consumption rates[6–11]. One specific IMPA, proposed for spray drying purposes, is the so called Air-Core-Liquid-Ring (ACLR)[12] atomizer (see Fig. 1). In this atomizer, liquid concentrate and atomization gas are brought into contact with each other in a mixing chamber, shortly before the exit orifice. The specific gas injection geometry induces a continuous core of compressed gas in the middle of the liquid stream, leading to an enforced annular two phase flow inside the exit orifice. This kind of flow pattern is known to deliver constant spray droplet distributions at high viscosities[12,13].

In the here presented study, a fresh liquid whey protein concentrate WPC 80, delivered by a dairy company, was processed in a pilot scale spray dryer, equipped with an ACLR atomizer. In order to investigate the potential of the ACLR atomizer to process high viscous concentrates, the input temperature before atomization was lowered (40 °C) in comparison to the corresponding industrial process (60 °C) of the supplier, leading to an increase of the viscosity by 50 % up to 0.09 Pa s. The produced powder was compared to the industrially produced reference by means of particle size distribution, water activity, moisture content and particle morphology.

2. Materials and Methods

2.1 Whey protein concentrate WPC 80

For the performed investigation, a fresh whey protein concentrate WPC 80 was used. The concentrate was delivered by Sachsenmilch GmbH, Leppersdorf, Germany. The concentration was executed in a membrane process. The dry matter content was given by the supplier as 36.1 %.

As reference, an industrially spray dried WPC 80 powder of the same supplier was analyzed for comparison to the powder, produced in the pilot scale spray drying process using the ACLR atomizer (See section 2.4).

2.2 Rheological characterization of liquid concentrates

The rheological characterization of the liquid concentrate was performed in a rotary rheometer (MCR 101, Anton Paar GmbH, Graz, Austria), equipped with a coaxial cylinder geometry (CC 27). The measurements were conducted at temperatures of 25, 40 and 60 °C and shear rates between 1 and 1000 s^{-1}.

2.3 Process equipment

2.3.1 ACLR Atomizer

A scheme of the used ACLR atomizer is given in Fig. 1. All parts are produced from stainless steel. The atomization gas is injected into the liquid stream, shortly before the exit orifice. For this purpose, a gas capillary with a diameter of 1.5 mm is used, leading to gas injection area of 1.76 mm^2. The mixing chamber length is 2.4 mm. Diameter and length of the exit orifice are 1.5 mm each.
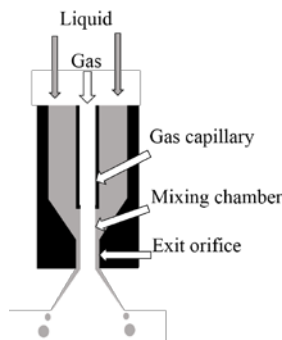
Fig. 1: Scheme of the used ACLR atomizer. ($l_{mixing\ chamber}$ = 2.4 mm, $l_{exit\ orifice}$ = 1.5 mm, $d_{exit\ orifice}$ = 1.5 mm)

2.3.2   Media supplies

The concentrate was supplied by an eccentric screw pump (MD 006-12, seepex GmbH, Bottrop, Germany). The flow rate was adjusted to 15.7 L/h and measured by a flow meter (VSI 044/16, VSE GmbH, Neuenrade, Germany). The concentrate was preheated before atomization to 40 °C in a tube heat exchanger. As atomization gas, compressed air, supplied by a compressor (Renner RSF-Top 7.5, Renner GmbH, Güglingen, Germany), was used. Air pressure was adjusted to 0.55 MPa by a pressure regulator. The gas volume flow through the atomizer's mixing chamber, resulting from gas pressure and liquid flow rate, was measured by a gas flow meter (ifm SD6000, ifm electronic, Essen, Germany) as 3.7 Nm^3/h. The resulting gas to liquid ratio by mass (GLR) was 0.28.

2.3.3   Pilot scale spray drying process

A pilot scale spray dryer (Werco SD20, Hans G. Werner Industrietechnik GmbH, Reutlingen, Germany) with a maximum water evaporation capacity of 20 kg/h was used. The dryer was operated at an inlet temperature of 180 °C, an outlet temperature of 95 °C and a drying air flow of 470 kg/h.

2.4 Powder characterization

The powders were characterized by measurement of particle size distribution, moisture content, water activity and morphology. Particle size distributions where measured by a laser diffraction spectroscope with powder dispersion unit (Horiba LA950, Retsch Technology GmbH, Haan, Germany). Moisture contents were calculated by weight loss after oven drying at 105 °C to constant mass. Water activities were measured by a dedicated measuring instrument (AW Sprint, Novasina, Lachen, Switzerland). Investigations on particle morphology were performed with an environmental scanning electron microscope (FEI Quanta 650 ESEM) at the Laboratory of Electron Microscopy of KIT, Karlsruhe.

3. Results and Discussion

3.1. Rheological characterization of liquid concentrates

In the first step, the shear rate dependent viscosity of the fresh whey protein concentrate WPC 80 was investigated at different temperatures of 25, 40 and 60 °C. All investigations were performed in triplicate. The concentrates showed shear thinning behavior with increasing shear rate at all investigated temperatures. However, the decrease of viscosity between shear rates of 1 and 1000 s^{-1} was pronounced with increasing temperature level. Moreover, the viscosity decreases with decreasing temperature at constant shear rate. (data not shown)

As high shear rates are expected in the atomization process, the viscosity at the highest shear rate, applicable in the used rheometer (1000 s^{-1}) are given in Table 1.

Table 1. Concentrate viscosity at a dry matter content of 36.1 % at a shear rate of 1000 s^{-1} and different temperatures.

Temp. / °C	Viscosity / Pa·s	
	mean	std
25	0.15	0.001
40	0.09	0.001
60	0.06	0.001

In the industrial process the concentrate is preheated to 60 °C before atomization. According to the here presented data, the viscosity in the moment of atomization is 0.6 Pa·s in this case. However, it is reported in literature, that the viscosity of whey protein concentrates might increase in the first hours of storage[14]. As the concentrate had to be transported from the production plant of the supplier to our pilot plant, the viscosities in the industrial process might be lower than the here presented values. In order to observe the viscosity increase over time, rheological measurements were performed directly after receiving the concentrate, as well as one and two days later, though no changes in viscosity were observed (data not shown).

In order to investigate the potential of the used ACLR atomizer to process concentrates at lower preheating temperatures and therefore higher viscosities, the preheating temperature was lowered by 20 K to 40 °C in the performed pilot scale trial. This procedure led to an increase of the viscosity by 50 % up to 0.09 Pa·s in comparison to the industrial process.

3.2. Spray drying process and powder characterization

The spray drying process with an ACLR atomizer was undisturbed during the whole trial time of 83 min. No sticky deposits in consequence of insufficiently dried particles were found inside the drying chamber after the trial. In Fig. 2 cumulative volume distributions of the powder particle sizes produced in the pilot scale spray dryer, as well as of the reference powder, are shown. The particle size measurements were performed fivefold. Both particle size distributions are similar. Small differences were found in fine particles, as well as in particles with sizes lager than 100 µm. The latter can most probably be traced back to agglomeration of primary particles, as the moisture content of the powder, produced in the pilot scale dryer, was significantly higher (9.1 %) than the one of the reference powder (5.4 %). Powders with increased moisture content are known to show increased stickiness an tension to build agglomerates[3]. However, it can be assumed, that the moisture content of powder can be reduced to the value of the reference powder, when the dryer height, and therefore the residence time inside the drying chamber, is increased to industrial level.

Nevertheless, water activity values of 0.20 (ACLR) and 0.12 (reference) show, that microbial stability is insured in both cases.
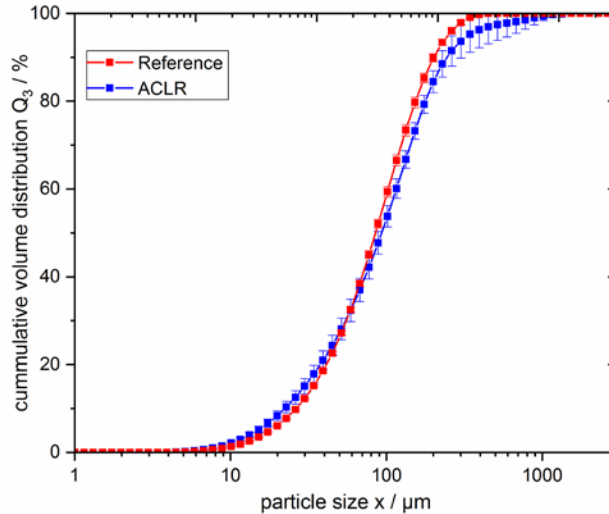
Fig. 2: Cumulative volume distributions Q_3 of powder particles, using ACLR atomization based processes (preheating temperature = 40 °C), as well as of an industrially produced reference powder.

In Fig. 3, overview images of the industrially produced reference powder (left) and of the powder produced in the pilot scale process with ACLR atomizer (right) are shown. Regarding particle morphology, no significant differences between the powder samples were observed. Although, in the reference powder more wrinkled and irregularly shaped particles were found. This fact might be also based on the more progressed drying process, indicated by a lower moisture content.
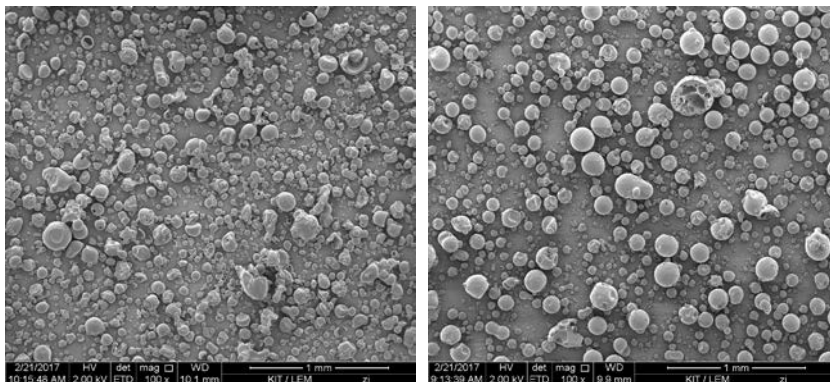
Fig. 3: Scanning electron microscope images of the industrially produced reference powder (left) and of the powder produced in the pilot scale process with ACLR atomizer (right)[15].

4. Conclusions and Outlook

In the presented study, the potential for use of an ACLR atomizer in pilot scale spray drying of a high viscous whey protein concentrate was shown. By decreasing the preheating temperature in comparison to the industrial reference process, the concentrate viscosity was increased by 50 % to a value of 0.09 Pa·s. The produced powder showed similar particle size distribution and particle morphology as the industrially produced reference powder. The moisture content was significantly higher (9.1 %) than the reference value (5.4 %). This is based on the comparably short residence time inside the pilot scale dryer. Increasing the dryer height, and therefore the residence time in the drying chamber, to industrial level, should lead to similar moisture contents. Nevertheless, a microbial stable product was produced in the pilot scale process, according to the water activity value of 0.2.

Further research will be performed in order to use the ability of the ACLR atomizer to atomize high viscous concentrates in spray drying processes. Besides the application of lower preheating temperatures this ability could also be used to atomize concentrates with higher initial dry matter contents, compared to currently used pressure swirl nozzles. Hence, the use of the ACLR atomizer offers the opportunity of energy savings and capacity increases in spray drying processes[16].

References

[1] Mujumdar, A.S., Ed. Handbook of Industrial Drying, 4th ed; CRC Press: Boca Raton, 2015.

[2] Westergaard, V. Milk Powder Technology: Evaporation and Spray Drying; Niro A/S: Kopenhagen, 2004.

[3] Masters, K. Spray Drying in Practice; SprayDryConsult International ApS: Charlottenlund/DK, 2002.

[4] Rao, M.A. Rheology of fluid, semisolid, and solid foods: Principles and applications; Springer: New York, 2014.

[5] Bayvel, L.P.; Orzechowski, Z. Liquid atomization; Taylor & Francis: Washington, DC, 1993.

[6] Stähle, P.; Gaukel, V.; Schuchmann, H.P. Investigation on the Applicability of the Effervescent Atomizer in Spray Drying of Foods: Influence of Liquid Viscosity on Nozzle Internal Two-Phase Flow and Spray Characteristics. *Journal of Food Process Engineering* 2015, 38(5), 474–487.

[7] Schröder, J.; Günther, A.; Wirth, K.-E.; Schuchmann, H.P.; Gaukel, V. Effervescent Atomization of Polyvinylpyrrolidone Solutions: Influence of Liquid Properties and Atomizer Geometry on Liquid Breakup and Spray Characteristics. *Atomization and Sprays* 2013, 23(1), 1–23.

[8] Schröder, J.; Werner, F.; Gaukel, V.; Schuchmann, H.P. Impact of effervescent atomization on oil drop size distribution of atomized oil-in-water emulsions. *Procedia Food Science* 2011, 1, 138–144.

[9] Kleinhans, A.; Georgieva, K.; Wagner, M.; Gaukel, V.; Schuchmann, H.P. On the characterization of spray unsteadiness and its influence on oil drop breakup during effervescent atomization. *Chemical Engineering and Processing: Process Intensification* 2016, 104, 212–218.

[10] Kleinhans, A.; Hornfischer, B.; Gaukel, V.; Schuchmann, H.P. Influence of viscosity ratio and initial oil drop size on the oil drop breakup during effervescent atomization. *Chemical Engineering and Processing: Process Intensification* 2016, 109, 149–157.

[11] Stähle, P.; Gaukel, V.; Schuchmann, H.P. Influence of feed viscosity on the two-phase flow inside the exit orifice of an effervescent atomizer and on resulting spray characteristics. *Food Research International* 2015, 77, 55–62.

[13] Stähle, P.; Gaukel, V.; Schuchmann, H.P. Comparison of an Effervescent Nozzle and a Proposed Air-Core-Liquid-Ring (ACLR) Nozzle for Atomization of Viscous Food Liquids at Low Air Consumption. *Journal of Food Process Engineering* 2017, 40(1).

[13] Kim, J.Y.; Lee, S.Y. Dependence of spraying performance on the internal flow pattern in effervescent atomizers. *Atomization and Sprays* 2001, 11(6), 735–756.

[14] Bylund, G. Dairy processing handbook, 3rd ed; Tetra Pak Processing Systems AB: Lund, 2015.

[15] Wittner, M.O.; Schuchmann, H.P.; Gaukel, V. Energie- und ressourcenschonende Sprühtrocknung von hochviskosen Flüssigkeiten mittels Air-Core-Liquid-Ring (ACLR) Zerstäubung. *FOOD-Lab*, 2017, 1(2).

[16] Fox, M.; Akkerman, C.; Straatsman, H.; Jong, P. de. Energy reduction by high dry matter concentration and drying. *New Food* 2010.

Heat recovery from biomass drying in energy systems

Havlík, J.[a]*; Dlouhý, T.[a]

[a] Department of Energy Engineering, Faculty of Mechanical Engineering, Czech Technical University in Prague, Prague, Czech Republic.

*E-mail of the corresponding author: jan.havlik@fs.cvut.cz

Abstract

This paper deals with energy savings by the heat recovery of waste vapour from moist biomass drying in energy systems. Drying is an energy-intensive process. Energy consumption can be reduced by using indirect drying by recuperating the heat of waste vapour generated in the process; however the vapour is polluted by air and small mechanical particles. Experiments with green wood chips were realized on an indirect dryer with a condensing heat exchanger to experimentally verify the grade and conditions of heat recovery from waste vapour. On the basis of the experimental results, the potential of the heat recovery from waste vapour was evaluated.

Keywords: Indirect drying; Biomass; Waste vapour; Heat recovery.

1. Introduction

Drying is an important process for creating optimal conditions for further material processing in many kind of industrial use. Industrial drying occurs by creating vaporization of the liquid by supplying heat to the wet feedstock. Heat may be supplied by convection (direct dryers) or conduction (contact or indirect dryers) [1]. In direct dryers, the material comes into direct contact with the heating medium, it is often hot air, flue gas or steam. In indirect dryers, the material and the heating medium (steam or hot water) are separated by a heat transfer surface. The heat is fed to the dried material through this surface, which defines the drying space. Generally, indirect dryers are more energy efficient. The typical energy consumption of direct dryers is in the range of 4.0 – 6.0 kJ per kg of evaporated water compared to indirect dryers which consume 2.8 – 3.6 kJ [1]. Additionally, if generated waste vapour is not mixed with drying or penetrating air, it leaves the dryer at a temperature close to 100 °C and its condensing heat can be recovered efficiently.

Drying is an energy-intensive process. The way to reduce the energy intensity of energy systems with drying is through the appropriate integration of contact drying with the use of heat recovery of the released waste vapour from the drying process [2]. The essence of heat recovery is vapour condensation together with gaining the vapour latent heat in an eligible heat exchanger. The main parameters limiting the further usage of this vapour are its purity and sufficient temperature level. The aim of the article is concentrated on an experimental evaluation of the potential and conditions of heat recovery from waste vapour which is generated during the drying of moist biomass in heating and power plants. Examples of heat recovery in the systems with integrated drying are shown in Fig. 1 [2]. The first case is a biomass fired steam power plant with an integrated indirect dryer heated
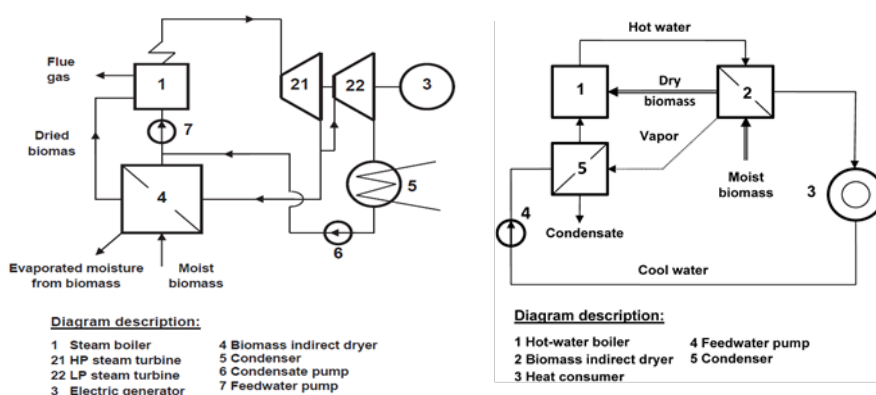
Fig. 1 Energy systems with indirect drying and waste vapour recuperation [2]

by low-pressure steam extracted from the turbine. The integration of the dryer increases the cycle efficiency and power production and allows for further use of the waste vapour for preheating the feed water, external consumption in the heating system or preheating the air for pre-drying the biomass in the convective air dryer. The second system is the integration of an indirect dryer and a waste vapour condenser to a hot-water heating cycle. The indirect dryer is heated by hot water from the boiler while the cooled backwater is preheated in the condenser by the waste vapour from the dryer.

2. Waste vapour recuperation

Waste vapour from biomass drying may contain infiltrated air, aromatics or small mechanical particles released from the biomass during drying, which complicates its energy utilization. A big problem is the infiltrated air contained in the vapour which has a significant influence on the heat transfer during vapour condensation even in small concentrations. Specifically, this negative effect is caused by a reduction in the heat transfer coefficient and at the same time by a decrease in the condensation temperature during the process caused by the decreasing concentration of the condensing water vapour in the mixture [3].

If a mixture of steam with inert gases condenses, non-condensable gases cause a difference in the concentrations of the steam in the bulk gas mixture C_∞ and at the condensation phase interface C_i equally with corresponding steam partial pressures p_∞ resp. p_i and temperatures T_∞ resp. T_i (see Fig. 2). The molecules of steam diffuse through an inert gas towards the vapour-liquid interface and mass transfer occurs [3]. Steam concentrations also decrease along the length. On the other hand, in the case of pure steam condensation, the temperatures T_∞ and T_i are identical and constant during the process.
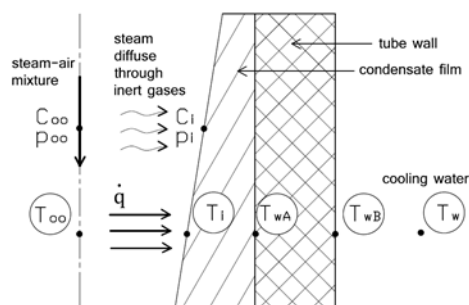
Fig. 2 Heat transfer in a condenser surface

In the examined case, a constant value of the heat flux $\dot{q}$ is considered for calculation of the heat balance (a constant heat flux from condensing steam, through condensate film, through the tube wall and to the cooling water). To determine the condensation temperature at the

phase interface T_i, it is necessary to take into account the mass transfer generated by the different partial pressures at the interface between the gas and the liquid phases p_i, and at the bulk gas mixture p_∞. The process of waste vapour condensation was studied inside the tubes of the vertical tube condenser, and the effect of the operation parameters and a comparison with the pure steam condensation process were analysed in detail in [4].

3. Experimental set-up

The experimental set-up consists of a steam heated indirect dryer and a recovery heat exchanger (Fig. 3).
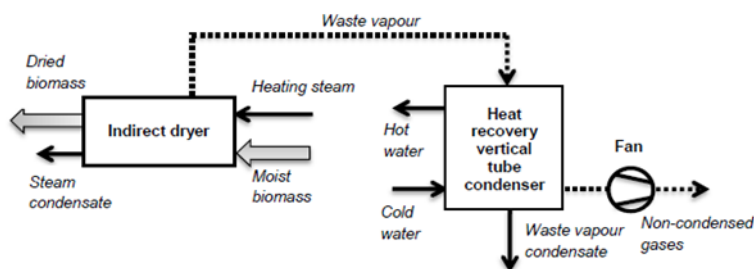
Fig. 3 Scheme of the experimental set-up

The dryer is designed as a rotating drum with a diameter of 600 mm and a length of 2000 mm. The drum walls and wings for material blending consist of heated tubes with condensing steam inside. Dried material is continuously fed inside the drum by a screw conveyer, and leaves it on the opposite side. The drying capacity is about 20 kg of evaporated water per hour. The recovery heat exchanger is designed as a vertical shell-and-tube condenser. The condensing water vapour flows downwards inside vertical tubes and the cooling water flows in a counter current in the outer shell. This configuration is used due to the potential fouling of tubes by small solid particles in the waste vapour from the drying biomass. These particles, which can stick to the tube wall, are spontaneously carried away from the tubes by the condensate blowing out. The heating surface consists of the tube bundle with 49 tubes 854 mm in length and with an internal diameter of 24 mm.

4. Results

Green wood chips with a moisture content from 62 to 66% were used for drying tests with waste vapour utilization (see Fig. 7). In the drying experiments, the moisture reduction in the drying material and the temperature of the outgoing waste vapour during the drying process was investigated. The entire drying process was described by a drying curve, which defines

the decrease in water content in the drying material over time [1]. An example of a drying curve for the dryer filled with material to 24% of the volume is shown in Fig. 4. The initial drop in temperature of the waste vapour is influenced by the heating of the material from the exchange of the inlet temperature to the evaporated temperature and by the air content which is gradually pushed out from the dryer by the generated vapour.
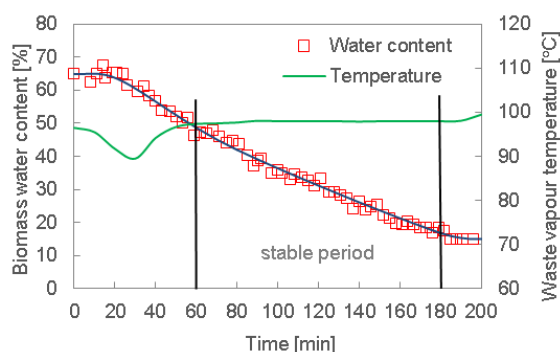
Fig. 4 Drying curve and corresponding waste vapour temperature

The stable temperature and waste vapour generating period between 60 and 180 min of the process in Fig. 4 was chosen for the evaluation of the waste vapour recovery potential. This state would correspond with the continuous operation of a large energy system. The investigated parameters were the amount of gained heat and its temperature level. In Table 1, the measured parameters of the recovery heat exchanger operation and the evaluated results are shown for three repeated experiments. The cooling water flow rate was set to reach its temperature near to a constant level due to better evaluation of a decrease in the condensing vapour temperature along the tube length. The vapour velocity at the inlet of tubes was about 2 m/s.

Table 1. Utilization of waste vapour in the recovery heat exchanger

Measurement	1	2	3
Waste vapour temperature – in / out (°C)	97.6 / 70.4	97.3 / 70.2	97.5 / 70.0
Air concentration in vapour – in / out (%)	8.9 / 77.1	10.1 / 77.4	9,4 / 77.6
Water temperature – in / out (°C)	54.9 / 55.9	54.7 / 55.7	54.6 / 55.6
Results			
Waste vapour utilization – exp. (%)	97.1	96.7	97.0
Waste vapour utilization – teor. (%)	98.8	98.5	98.3

The temperature of the waste vapour leaving the actual biomass dryer was between 99 and 97 °C with an air content of about 8 to 10%. The obtained results were compared with the

theoretically balanced and calculated values based on principles for heat and mass transfer for the case of steam condensation in a binary mixture [3] according to the proposed and experimentally verified model of heat transfer for air-steam condensation in a vertical tube condenser described in [4]. The experimentally determined vapour recovery is in good agreement with the theoretically calculated values for this case. Experimental verification of this process makes it possible to estimate the operation of the device beyond the measured parameters and allows for future optimization.

The bulk gas temperatures T_∞ and the condensation temperature T_i are different and decreasing during condensation. For this reason, some of the waste vapour always flows through the exchanger and does not condense. The temperature courses along the length of the condenser tube for measurement no. 3 are shown in Fig. 5. These courses were theoretically calculated through the use of a model of the heat transfer in a vertical tube condenser [4] regarding the measured temperatures at the inlet and outlet. The growth of the cumulative heat output along the heat transfer area, respective the tube length, was also analysed in Fig 5. An important conclusion for the heat exchanger design and optimization is that the majority (approx. 80%) of the recovered heat was obtained in the first half of the heat transfer surface. When increasing the amount of air to 20%, the surface would be extended by more than 50% to maintain the heat exchanger output. On the contrary, decreasing the air content to 5% would result in a reduction to 72% of the surface.
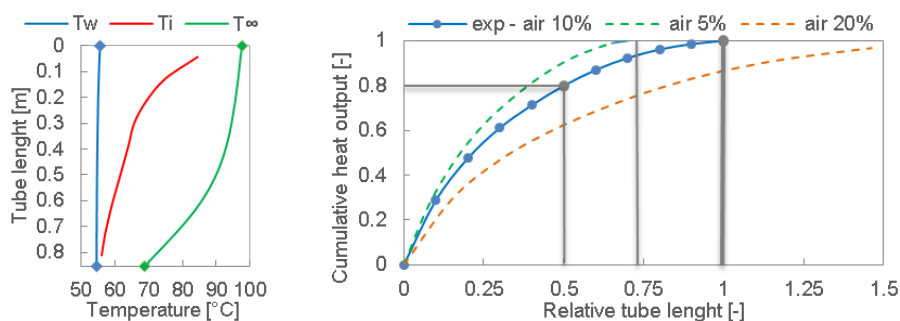
Fig. 5 Parameters change in waste vapour condensation process

In Fig. 6, the dependence of the utilization rate of waste vapour on the amount of infiltrated air (mass concentration) is shown for conditions approaching those of the actual industrial operation. The results are calculated according to the heat transfer model of the vertical tube condenser [4] for inlet temperatures of cooling water at 60 °C, 70 °C and 80 °C. For an appropriate comparison of the heat recovery potential, the geometry of the heat exchanger is

optimized for each case to heat the water by 5 °C, to maintain a vapour velocity at the inlet of 2 m/s and a temperature difference at the vapour outlet and water inlet of 2 °C. This value was chosen as the limit, if we sought to achieve a lower temperature difference, it would be necessary to increase the size of the exchanger with very little impact on increasing the heat output.
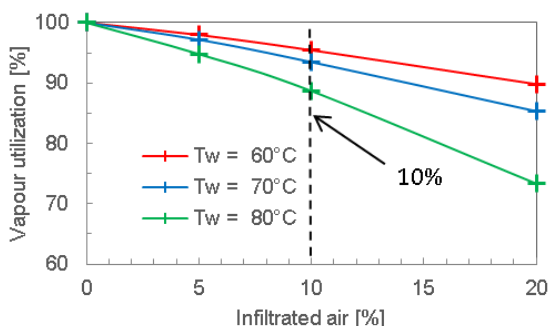
Fig. 6 Potential of waste vapour heat recovery and temperature level of this heat

For the value of infiltrated air of approximately 10% corresponding with the experiments above, the utilization rate would be above 90% for water heating at a temperature of 80 °C, more for water temperatures of 70 °C and 60 °C. However, optimization of the device could result in lower amounts of infiltrated air and a higher level of vapour utilization. On the other hand, a higher level of air penetration significantly decreases the utilization rate.
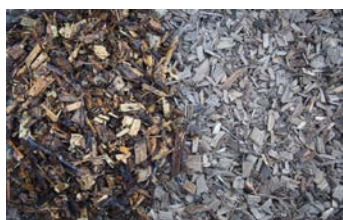
Fig. 7 Tested material – green wood chips before and after drying

Fig. 8 Waste vapour condensate

The obtained condensate from biomass drying contains aromatic and dust particles which were released from the raw fuel during the drying process and carried away by the waste vapour from the dryer. For this reason, the condenser is designed with vertical tubes in which

these particles are spontaneously washed out by the condensate. A comparison of the waste vapour condensate with the pure steam condensate is shown in Fig. 8.

After a series of experiments, a visual inspection of the heat exchanger surface was made and no visible fouling was observed. It can be stated that the proposed heat exchanger configuration is suitable for the condensation of waste vapour from biomass drying.

5. Conclusion

Based on the results of the experiments with the heat recovery from biomass drying, we can conclude that the waste vapour generated in indirect drying systems with limited air penetration has a sufficient potential for further energy utilization. The waste vapour exiting the tested drying device at atmospheric solution reached temperatures ranging from 97 to 99 °C with an air content of about 10%. These conditions correspond with the potential of recovering more than 90% waste vapour condensing heat at the level of gained heat of 80 °C e.g. for water preheat.

The following principles are important in the design of a system with heat recovery of the waste vapour from indirect drying. Even small amounts of air in the waste steam cause a significant decrease in the heat transfer coefficient and the heat output of the recovery heat exchanger. The majority of the heat output is transferred in the first part of the recovery heat exchanger, which allows for economical optimization of its size. Waste vapour from some solid materials can contain small mechanical impurities, which can stick to the heating surface of the recovery heat exchanger, therefore it needs to be customized for cleaning. Condensers with vertical tubes seem to be a good solution in this case.

6. Acknowledgement

7. References

[1] Mujumdar, A. S. Handbook of Industrial Drying; Marcel Dekker: New York, 1990.

[2] Havlík J.; Dlouhý T. Integration of Biomass Indirect Dryers into Energy Systems. Journal of Chemical Engineering of Japan, 2017, 50 (10), 792–798.

[3] Hewitt, G. F.; Shires, G. L; Bott, T. R. Process Heat Transfer. Begell House: New York, 2000.

[4] Havlík, J.; Dlouhý, T. Condensation of the Air-steam Mixture in a Vertical Tube Condenser. EPJ Web of Conferences, 2016, 114, art. no. 02037.

Capillary disconnect during drying in model porous media at different wettability

Rufai, A. K.ª; Crawshaw, J. P.ª, *

ª Qatar Carbonates and Carbon Storage Research Centre, Department of Chemical Engineering, Imperial College London, London, UK. SW7 2AZ.

*E-mail of the corresponding author: j.crawshaw@imperial.ac.uk

Abstract

We carried out drying studies on a 2.5D micromodel based on a thin section of a carbonate rock to investigate the impact of wettability on the capillary disconnect, the moment when liquid films de-pin from the external evaporating surface. While this is coincident with the transition to low evaporation rate (diffusion limited) for deionized-water, our experiments show, the corner wetting films persisted after the transition to low evaporation rate for both water-wet and mixed-wet micromodels for brine, as solid salt continued to build up at the external evaporating surface. Fully oil wet micromodels showed a drying rate transition coincident with de-pinning.

Keywords: Capillary; Liquid films; Micromodel; Wettability; Crystallization.

1. Introduction

Understanding the underlying physics of the drying process in contaminated porous media is central to many of its applications, such as soil remediation, gas injection into geological formations for enhanced oil recovery and CO2 sequestration processes, etc. Although many studies have been done on the kinetics of the drying process in porous media. There are still some knowledge gaps, especially when it comes to adequately predicting the extent of the different stages of evaporation in porous media of varying wettability. Classically, early stages of evaporation from a porous media are characterized by a relatively fast and "almost" constant evaporation rate, known as the constate rate period (CRP). This is followed by a transition period characterized by a large drop in evaporation rate, known as the falling rate period (FRP). The late stage of evaporation is characterized by a very slow evaporation rate limited by vapour diffusion through the porous media, this stage is known as the falling rate period (FRP)Materials and Methods [1-6].

The kinetics of the three periods are controlled by different mechanisms. For de-ionized water in a water-wet porous media, early stage evaporation is by water mass transfer by capillarity through wetting films to the evaporating surface, due to the stronger adhesion of water molecules to the pore walls compared to cohesive between water molecules [2]. Drying here is said to be controlled by external demand such as temperature, the flow rate of drying gas, relative humidity, the surface area of the evaporating surface and so on. During this period, the porous media behaves as though it is fully saturated because the mass transport through capillarity is sufficient to sustain evaporative demand at the surface [3, 5]. Simply, the constant rate period is dominated by capillarity due to hydraulically connected pores [7]. In time, gravity and viscous forces will overcome the capillary driving forces at some depth down the porous media, hydraulic connectivity to the evaporating surface will cease at this point and the drying surface will move to within the porous medium. This marks the end of the constant rate period (stage-1 evaporation) and the beginning of the falling rate and receding front periods (stage-2 evaporation) [4, 5, 7].

There is a very sharp drop in evaporation rate during the falling rate period and , this period can also be called a transition stage as evaporation quickly transitions from a capillarity dominated period to a diffusion dominated period with continued drop in evaporation rate [1, 5, 8] until complete drying (i.e. from CRP to RFP). Hence, internal mass transfers such as vapour diffusion, pore space geometry, thermal and hydraulic conductivities etc. control drying during stage-2 evaporation. Here, the drying rate varies linearly with the square root of time [5, 9]. The drying of brine-containing porous media such as saline aquifers, oil and gas reservoirs, building materials etc. causes the dissolved salt to crystallise within (sub-florescence) and outside (efflorescence) the porous media when the solubility limit of the salt is exceeded [10]. Salt crystallization (crystallisation/dissolution cycles) can cause a

lasting damage to building materials, and these problems are been studied extensively within the civil engineering research community [11-15]. Salt crystallisation can also lead to a significant decrease in porosity and permeability of underground reservoirs like saline aquifers. This decrease in permeability can lead to an increase in injection cost and a reduction of storage potential during CO2 sequestration processes.

A number of phenomena affect drying dynamics and the consequent salt deposition in a porous medium, some of these phenomena have been studied and reported in past literature. For example, the drying rate is strongly influenced by the spatial distribution of the liquid and that, in turn, is controlled by capillary forces at the pore scale. However, the effect of the wetting films and corner menisci on drying kinetics and salt crystallization is still somewhat unclear. In the present study, we aim to shed more light on the effect of porous media wetting conditions on the different stages of evaporative drying. Given that oil reservoirs have a wide range of contact angles (wetting states) and with the fact that capillarity through corner wetting films is strongly dependent on the wetting states of the pore walls. One can assume that the disconnection in capillarity or depinning of the wetting films from the evaporating surface (marking the end of stage-1 evaporation) will be strongly affected by the wetting state of the porous media. Lastly, we have carried out this study with a model porous media, a micromodel based on a thin section image of a carbonate rock. Working with micromodels allow us faster observations (better time resolutions) and direct visual observation of pore-scale processes in a network of pores.

2. Materials and Methods

This study was done using micromodels that are based on a thin-section image of a sucrosic dolomite rock [5, 9]. These micromodels were fabricated with a silicon wafer, covered with a transparent glass, allowing direct real-time visualization of pore-scale processes. The micromodel has a constant etch depth of 25µm, with a matrix dimensions of 2.5 x 1cm². A DSLR (digital single-lens reflex) camera (D800E, Nikon) and an inverted light microscope (AxioObserver A1.m, Zeiss) was used to obtain a wide field of view and high-resolution images respectively. Freshly prepared NaCl solutions were prepared for the different concentrations used in this study, i.e. 0 wt% (deionized water), 18 wt% (3M NaCl solution) and 36 wt% NaCl solution (6M or saturated NaCl solution). Fluorescein (46960-2SG-F, Sigma-Aldrich. 1:700000 v/v) was added to the brine solutions for easier phase differentiation. Brine was injected with a 10 mL syringe (BD Plasipak, BD300013) using s programmable syringe pump (BS-80000, Braintree Scientific Ltd.). After saturating the micromodel with brine, dry air flow-line was attached to one of the inlet ports, while its adjacent port was opened to the atmosphere for continuous flow of dry air through one of the fracture channels in front of the matrix for evaporative drying. As the drying front moves back into the matrix, images of the dry-out evolution were taken at different time intervals and the salt precipitation in its wake was observed in real time. To obtain

quantitative data from the images, ImageJ was used to calculate the dry pore area (equivalent to mass lost by evaporation) of each of the captured images. More explicit details on the micromodels, imaging techniques, experimental procedure and quantitative data acquisition are provided in two recently published papers [5, 9].

2.1 Micromodel Wettability Alteration Technique

The micromodels were originally water-wetting by oxidation of the silicon wafer at high temperature during the manufacturing process. To obtain, mixed-wet and oil-wet conditions, the micromodels were treated with a new wettability alteration technique. Well established techniques based on silane chemistry [16] could not be used because the silane reacts with the water phase (necessary to the generation of mixed wettability) during the treatment. Also, alteration with crude oil [17] could not be used because it renders the micromodel opaque after treatment. The new technique involves a solution of silicone caulk (151 Products Ltd.) (10v/v %) dissolved in Dodecane (≥99%, Sigma-Aldrich) (90v/v %). For mixed-wetting conditions, this solution was injected into the micromodel initially saturated with deionized water and then left to age for about 2 days at ambient conditions. Note that this leaves water wet corners in channels that are otherwise altered to oil wet. The micromodel was then dried by passing dry compressed air through it, before placing it in an oven at 60ºC for 24 hours. For uniformly oil-wetting conditions, the silicone solution was injected straight into a dry micromodel. More details of this new technique are provided in a recently published paper [9].

3. Results and Discussion

We determined the evaporation rates from the experiments by calculating the pore dry area as a function of time. The evaporation rates at ambient conditions and a relative humidity approximately equal to zero for 0 wt% NaCl (deionised water), 18 wt% NaCl brine and 36 wt% NaCl (saturated brine) solution in a water-wet micromodel are plotted in figure 1a. The evaporation rates were initially almost constant before a sharp drop after about 2mins for deionised water, 1min for 18 wt% NaCl and almost immediately for saturated NaCl brine. For deionised water these periods correspond to the classical periods of evaporation expected from earlier experiments and modelling in porous media drying: stage-1 evaporation (or the CRP) in which liquid remains connected to the drying surface through capillary forces, and the stage-2 evaporation (a combination of the FRP and the RFP) at which the hydraulic capillary connection to the evaporating surface is broken and water transport becomes dominated by vapour diffusion.

From figure 1a, the same trend of two stages can be seen for the plots of 18 wt% NaCl brine and saturated NaCl brine albeit with different duration for their stage-1 evaporation. The stage-1 evaporation is almost non-existent for the saturated NaCl brine. However, unlike the deionized case, the transition to stage-2 with brine is not due to capillary

disconnect to the evaporating surface because we continue to see a gradual increase in the amount of salt deposited at the fracture channel, figure 2a and the salt can only be transported in the liquid phase.
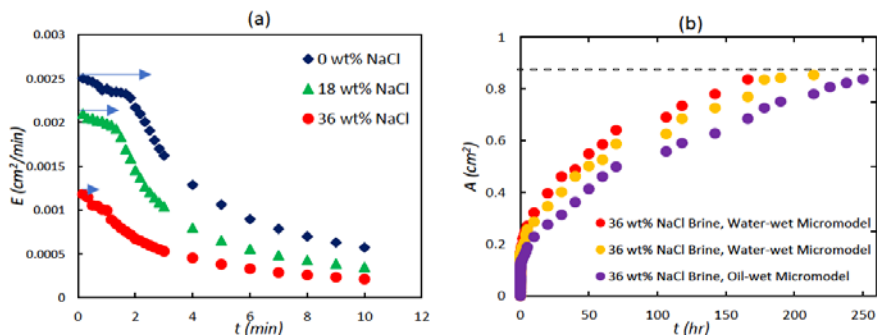
Figure 1. Evolution of drying: (a) Evaporation rate as a function of time for the water-wet micromodel (blue arrows signify the extent of the stage-1 evaporation) and (b) Dry pore area as a function of time for saturated NaCl brine at the three different wetting states ((horizontal black dotted line shows the total pore dry area = 0.7cm²).

The change in slope for the brine solutions is due to the deposited solid salt acting as a physical to mass transfer to the surface, as well as the increase in the viscous resistance due to the relatively higher viscosity of the NaCl brine compared to deionized water.

The same evaporative drying procedure used for the water-wet micromodel was used for the mixed-wet and oil-wet micromodel. Figure 1b shows the plot of the area of the micromodel occupied by air (equivalent to mass lost by evaporation) as a function of time for complete dry-out of saturated NaCl brine in the three wetting states. Although the trends in the plot of the three wetting states are very similar, the duration of complete dry-out increases systematically from the water-wet to oil-wet micromodel. This is as a result of the absence of corner wetting films needed for the high evaporation rate, especially during stage-1 evaporation. Less salt was deposited in the fracture channel of the mixed-wet micromodel compared to the water-wet micromodel as seen in the images in figure 2b.
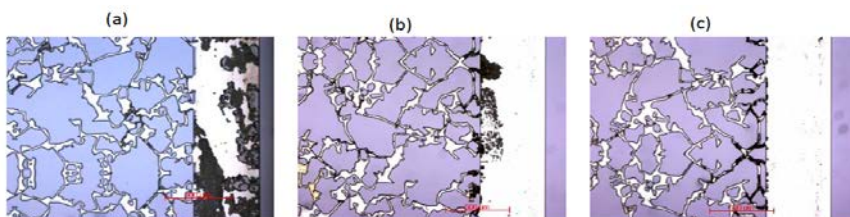
Figure 2. Images showing deposited salt in the evaporating surface and in the matrix below at the end of complete drying (i.e. liquid saturation = 0) for (a) Water-wet micromodel, (b) Mixed-wet micromodel and (c) Oil-wet micromodel.

Further, only a very small amount of salt (probably from the brine solution present in the channel prior to drying) were deposited at the evaporating surface for the oil-wet micromodel, figure 2c. The reason for this is the absence of wetting films needed to maintain hydraulic connectivity to the surface in the fully oil wet case.

Finally, results for the 36 wt% NaCl brine in a water-wet micromodel and oil-wet micromodel are compared directly in figure 3 below. The schematics show liquid films at the corners of the micromodel grains percolating at the onset of drying. The thickness of the films decreases as drying continues until no connected pathway remains to the external evaporating surface. For deionized water, this would mark the onset of slower, stage-2, evaporation. However, from our experiment, the corner wetting films persisted after the transition to low evaporation rate, as sold salt continued to build up at the external evaporating surface.
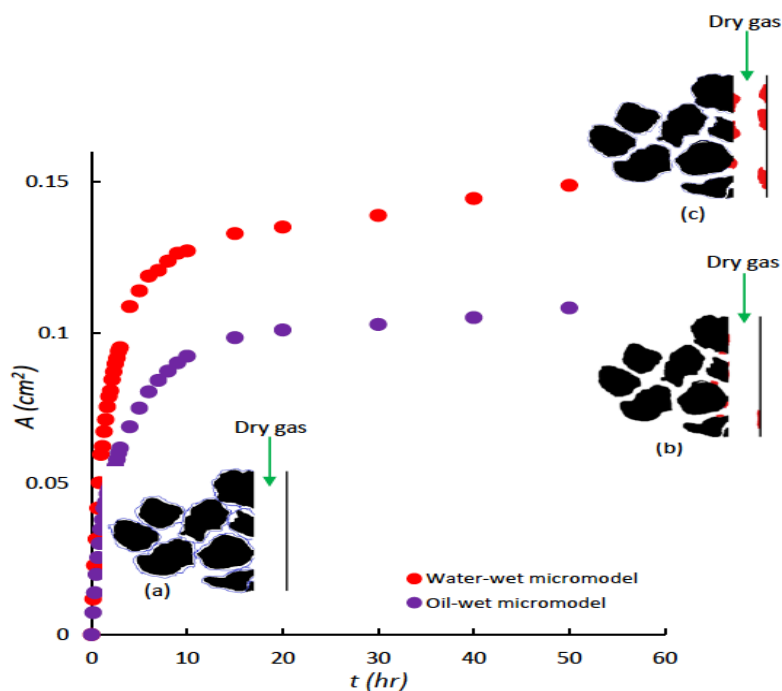
Figure 3. Dry pore area as a function of time for a 36 wt% NaCl brine (saturated) solution in a water-wet micromodel and oil-wet micromodel. The inset images are schematic representations of a section of the micromodel (fracture and matrix) at different times. (a) At the onset of drying with fracture full of gas and thick corner wetting films (t ≈ 10s). (b) During drying in an oil-wet micromodel, with little solid salt in fracture and no corner wetting films (t ≈ 30mins). (c) During drying in a water-wet micromodel, with solid salt in fracture and very thin corner wetting films (t ≈ 30mins). Model grains are represented in black, wetting films are indicated in light blue while deposited solid salt is represented in red.

4. Conclusions

During the CRP (stage-1 evaporation), dry air entering the micromodel to balance the water loss becomes saturated with water vapour, leading to little evaporation occurring at this stage. We studied the effect of capillarity, wetting state and salt precipitation on the duration of the CRP from a model porous media. Evaporation from water-wet and mixed-wet micromodels saturated with deionized water (0 wt% brine) were similar and follow the well-established theory of drying from a porous media: a constant, high evaporation rate maintained by capillary forces through wetting films to the evaporating surface, followed by a transition (break in capillarity to the evaporating surface) to a much lower evaporation rate (stage-2 evaporation) characterized by vapour diffusion. However, for the brine solutions (18 wt% and 36 wt% NaCl brine), capillarity to the evaporating surface was maintained even during stage-2 evaporation, evidenced by the continuous deposition of salt in the fracture of the micromodel well into the FRP (stage-2 evaporation). Hence, the capillary connection can be maintained even during the FRP for the drying of brine contaminated porous media.

The evaporation dynamics for a mixed-wet micromodel and a water-wet micromodel are very similar, the only difference is the slightly earlier transition observed in the mixed-wet micromodel. On the other hand, the oil-wet micromodel emphasized the effect of the wetting state on the evaporation dynamics. The evaporation rate dropped as soon as drying started as a result of the absence of corner wetting films needed to supply evaporative demand at the surface. This leads to very little deposited salt at the fracture as well as an increase in the overall drying time.

5. Acknowledgements

6. References

[1]   N. Shokri, P. Lehmann, and D. Or, "Characteristics of evaporation from partially wettable porous media," *Water Resources Research,* vol. 45, no. 2, p. W02415, 2009.

[2]   F. Chauvet, P. Duru, S. Geoffroy, and M. Prat, "Three periods of drying of a single square capillary tube," *Physical review letters,* vol. 103, no. 12, p. 124502, 2009.

[3]   G. W. Scherer, "Theory of drying," *Journal of the American Ceramic Society,* vol. 73, no. 1, pp. 3-14, 1990.

[4]   P. Lehmann, S. Assouline, and D. Or, "Characteristic lengths affecting evaporative drying of porous media," *Physical Review E,* vol. 77, no. 5, p. 056309, 2008.

[5]   A. Rufai and J. Crawshaw, "Micromodel observations of evaporative drying and salt deposition in porous media," *Physics of Fluids,* vol. 29, no. 12, p. 126603, 2017.

[6]   J. Van Brakel, "Mass transfer in convective drying," 1980.

[7]   N. Shokri, P. Lehmann, and D. Or, "Critical evaluation of enhancement factors for vapor transport through unsaturated porous media," *Water resources research,* vol. 45, no. 10, 2009.

[8]   N. Shokri, P. Lehmann, and D. Or, "Evaporation from layered porous media," *Journal of Geophysical Research: Solid Earth,* vol. 115, no. B6, 2010.

[9]   A. Rufai and J. Crawshaw, "Effect of Wettability Changes on Evaporation Rate and the Permeability Impairment due to Salt Deposition," *ACS Earth and Space Chemistry,* vol. 2, no. 4, pp. 320-329, 2018.

[10]   D. Le, H. Hoang, and J. Mahadevan, "Impact of capillary-driven liquid films on salt crystallization," *Transport in porous media,* vol. 80, no. 2, pp. 229-252, 2009.

[11]   G. W. Scherer, "Crystallization in pores," *Cement and Concrete Research,* vol. 29, no. 8, pp. 1347-1358, 1999.

[12]   A. Goudie and H. A. Viles, *Salt weathering hazard*. Wiley, 1997.

[13]   G. W. Scherer, "Drying, shrinkage, and cracking of cementitious materials," *Transport in Porous Media,* vol. 110, no. 2, pp. 311-331, 2015.

[14]   D. Everett, "The thermodynamics of frost damage to porous solids," *Transactions of the Faraday Society,* vol. 57, pp. 1541-1551, 1961.

[15]   M. Steiger, "Crystal growth in porous materials—I: The crystallization pressure of large crystals," *Journal of crystal growth,* vol. 282, no. 3-4, pp. 455-469, 2005.

[16]   J. W. Grate *et al.*, "Silane modification of glass and silica surfaces to obtain equally oil-wet surfaces in glass-covered silicon micromodel applications," *Water Resources Research,* vol. 49, no. 8, pp. 4724-4729, 2013.

[17]   A. S. Al-Menhali and S. Krevor, "Capillary Trapping of CO2 in Oil Reservoirs: Observations in a Mixed-Wet Carbonate Rock," *Environmental Science & Technology,* vol. 50, no. 5, pp. 2727-2734, 2016/03/01 2016.

Ultrasound assisted low temperature drying of food materials

Sabarez, H.T. [a*]; Keuhbauch, S.[b]; Knoerzer, K.[a]

[a] CSIRO Agriculture & Food, Werribee, Victoria, Australia
[b] Karlsruhe Institute of Technology (KIT), Kaiserstrabe 12, 76131 Karlsruhe, Germany

*E-mail of the corresponding author: henry.sabarez@csiro.au

Abstract

An ultrasonic design based on the indirect transmission of ultrasonic energy from the ultrasound emitter through to the material to be dried was investigated to assist in low temperature drying of food materials. The application of the improved design tested in this work was found to enhance the low temperature drying by shortening the overall drying time of up to 45% (i.e., lower energy consumption and may enable better retention of product quality). This offers a promising approach towards a better applicability of ultrasound in industrial operation, since no direct contact between the sample and the ultrasonic emitter is needed.

Keywords: ultrasound; drying; low temperature; drying intensification.

1. Introduction

Many drying techniques evolved due to the need to produce high quality products that are highly heat-sensitive. Such drying systems include the utilization of low temperatures, but often require a very long drying time, highly energy consuming and detrimental to the product quality. These limitations can be overcome by the combined application of ultrasound, which has been demonstrated in previous studies to intensify the convective drying processes.[1,2] However, the development of ultrasound assisted drying technology at an industrial scale has progressed at a slow pace due to the difficulties in achieving an efficient transmission of ultrasonic energy from the plate transducers to the product while ensuring easy adaptability to conventional drying processes.

The ultrasonic systems reported in the literature for food drying application may be grouped into two main types. The first type is made up of ultrasonic devices that are directly coupled to the food material during drying. The direct contact system can promote an accelerated drying process because this system permits good transfer of ultrasonic energy from the vibrating element to the food material. Nevertheless, the main drawback of this technique may be its difficulty to adapt to traditional airflow drying processes and in operation other than a batch-wise process.

Another type was developed based on the application of airborne ultrasound. The airborne ultrasonic system works without direct contact between the vibrating element and the food material, which seems to offer much better adaptability to conventional air drying processes. However, the main difficulties in this system arise from the inefficient generation of ultrasonic energy in air and the transfer of such ultrasonic energy from air into the product due to the acoustic impedance mismatch and the energy absorption by the air at ultrasonic frequencies.[3]

The aim of this work was to develop and test an improved design concept for an effective application of ultrasound at high frequencies that would allow easy adaption in continuous processing while facilitating efficient ultrasonic energy transmission to intensify low temperature drying of food materials.

2. Materials and Methods

Fresh apples (cv. Granny Smith) obtained from a local market (Werribee, Victoria, Australia) were used as the model test material and were stored at 4°C until further processing. The sample preparation has been described in detail by Sabarez et al.[2] The fresh apple samples were found to have an average initial moisture content of 86.0% (wet basis).

Drying experiments were carried out in a computerised ultrasound-assisted convective drying setup as described elsewhere[2,4], which had been modified to retrofit the improved ultrasound transmission system (Fig. 1). The ultrasonic transmission system consisted of a transmission platform, cooling unit (Model BL-130, Thermoline, Australia) to control the temperature of the transmission platform, and a plate transducer using Blackstone-Ney Ultrasonic Generator (Blackstone-Ney Ultrasonics Inc., Jamestown, New York, USA).
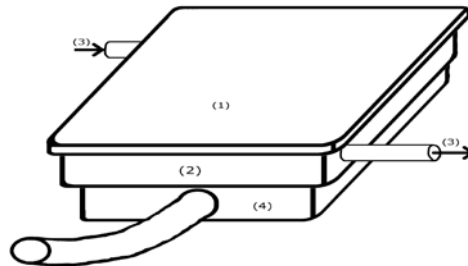
Fig. 1. Ultrasound transmission setup (1=transmission plate; 2=frame for containing the cooling/heating liquid; 3=cooling/heating liquid; 4=transducer).

The advantage of this experimental drying system is that it consists of a number of additional sensors (i.e., thermocouples, infrared noncontact temperature sensors, air velocity sensors, humidity sensors, etc.) that are interfaced to a computer-based data acquisition and control system for continuous online monitoring and recording of the various processing conditions (i.e., drying time, material temperatures, air temperature, air relative humidity, and air velocity).

Two sets of drying experiments were carried out without ultrasound and with ultrasound at a frequency of 40 kHz. In these experiments, the apple ring samples were directly placed on the transmission platform. Four annular apple rings prepared as outlined above were used for each drying experiment. All drying experiments were replicated at least twice. The details of the drying procedure can be found elsewhere.[2,4]

3. Results and Discussion

Figure 2 shows a typical example of the drying kinetics during the convective air drying of 5 mm apple samples (about 100 g) at 40°C temperature (T) without and with ultrasound at 40 kHz frequency with power level of 466 W. These experiments were conducted with drying air velocity (V) and relative humidity (RH) maintained at about 1.2 m/s and 25%, respectively.

It is clear from Figure 2 that the application of ultrasound in combination with convective air drying significantly reduced the overall drying time. To achieve the target moisture content of 25% in wet basis (i.e, typical moisture content of ready-to-eat fruit snacks), analysis of the drying curves revealed that it took about 8.0 hours to dry the apple samples without ultrasound and just 4.4 hours with ultrasound using the improved ultrasonic transmission system. The results indicate a significant reduction in drying time of about 45% with the simultaneous application of ultrasound on the convective drying of apple slices (corresponds to a 32% reduction of energy consumption).
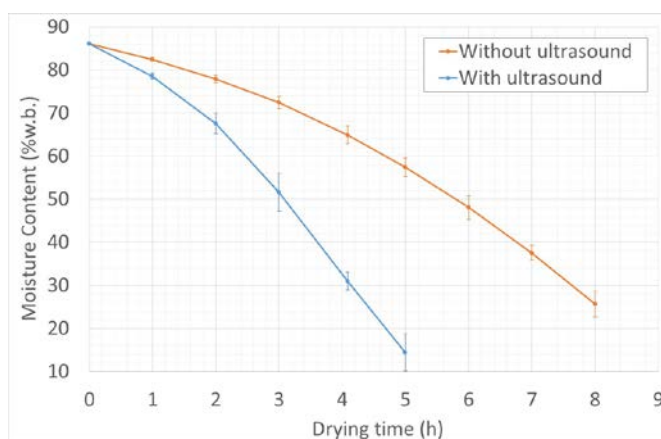
Fig. 2. Effect of ultrasound (40 kHz frequency; 466 W power) on the drying kinetics of apple slices (T=40℃; RH=25%; V=1.2 m/s; 5mm thickness).

The plot clearly shows that the ultrasonic transmission system developed and tested in this work was highly effective in intensifying the convective drying process. It also demonstrates that high frequency ultrasound can assist in enhancing the convective drying process. Although most of the physical mechanisms by which low frequency ultrasound enhanced the drying process are highly suppressed at high frequency, the observed enhancement in drying with high frequency ultrasound may be explained by Stokes' law of attenuation. Higher frequency ultrasound undergoes more attenuation, inducing more microstreaming (a non-thermal effect that occurs due to a pressure gradient generated by aborption of ultrasound during propagation) thereby increasing the diffusivity of water. So far, no studies have been reported on the application of ultrasound at higher frequencies in assisting food drying processes. Most of the studies were carried out at low frequencies (20-26 kHz) with drawbacks of low energy efficiency and high noise levels, with the ultrasonic

energy transmitted either in direct contact between the vibrating plate and the product[5,6] or airborne to the surface of the product.[2,3,4,7,8] These studies have reported significant reductions in drying time with the application of ultrasound, depending on ultrasonic parameters, drying conditions and properties of the materials to be dried.

Sabarez et al.[2] found a significant reduction in drying of up to 57% with the application of airborne ultrasound during drying of 5 mm apple samples. Under these drying conditions, an approximately up to 54% reduction in energy consumption during drying could be achieved with the application of airbone ultrasonic energy. Similarly, Garcia-Perez et al.[7] found a significant reduction in drying time (up to 70% at acoustic power of 90W) with the application of power ultrasound for convective drying of eggplant cylinders. Ortuno et al.[9] observed that the application of ultrasound (power level of 90 W) provided an average reduction in drying time of over 45% for drying of orange peels. They found that the energy saving was close to 30% with ultrasonic application.

The differences in drying time reduction and energy saving between these studies and the present work could be due to the differences in the raw material properties, drying conditions and ultrasonic parameters (i.e., particularly ultrasonic frequency, power and mode of ultrasound transfer). In the present study, high frequency ultrasound is transmitted indirectly through to the transmission platform (liquid and steel) and into the material to be dried. This allows for an efficient transmission of ultrasound to the material to be dried as the mismatch of acoustic impedances of these materials (steel, liquid and food) is minimized, and would enable for operation in conjuction with traditional air drying, along with easy integration in continuous processing as there is no direct contact between the ultrasonic emitter and the food samples to be dried.

4. Conclusions

The application of an improved ultrasound transmission system was found to significantly intensify the low temperature air drying of apple samples by reducing the overall drying time (i.e., lower energy consumption and may enable better retention of product quality). This offers a promising non-thermal means for gentle (i.e., low temperature) drying of food materials to produce premium quality food products, with better applicability at industrial scale as no direct contact between the food material and ultrasonic transducer is needed. In addition, the present study demonstrates that high frequency ultrasound can assist in enhancing convective drying with much reduced noise levels. The results from this work will provide the basis to build upon the development of this technology and justifies further investigations for implementation in industrial drying operations.

5. References

[1] Sabarez, H.T. Airborne ultrasound for convective drying intensification. In Innovative Food Processing Technologies – Extraction, Separation, Component Modification and Process Intensification; Knoerzer, K., Juliano, P., Smithers, G., Eds.; Woodhead Publishing, An Imprint of Elsevier, Elsevier B.V., 2016; 361–386.

[2] Sabarez, H.T.; Gallego-Juarez, J.A.; Riera, E. Ultrasonic-assisted convective drying of apple slices. Drying Technology 2012, 30 (9), 989-997.

[3] Gallego-Juarez, J.A.; Rodriguez-Corral, G.; Galvez-Moraleda, J.C.; Yang, T.S. A new high intensity ultrasonic technology for food dehydration. Drying Technology 1999, 17 (3), 597-608.

[4] Beck, S.M.; Sabarez, H.T.; Gaukel, V.; Knoerzer, K. Enhancement of convective drying by application of airborne ultrasound: a response surface approach. Ultrasonics Sonochemistry 2014, 21, 2144-2150.

[5] Gallego-Juarez, J.A.; Riera, E.; de la Fuente Balanco, S.; Rodriguez-Corral, G.; Acosta-Aparicio, V.M.; Blanco, A. Application of high-power ultrasound for dehydration of vegetables: Processes and Devices. Drying Technology 2007, 25(11), 1893-1901.

[6] Schossler, K.; Jager, H.; Knorr, D. Effect of continuous and intermittent ultrasound on drying time and effective diffusivity during convective drying of apple and red bell pepper. Journal of Food Engineering 2012, 108 (2012), 103-110.

[7] Garcia-Perez, J.V.; Carcel, J.A.; Riera, E.; Mulet, A. Influence of the applied acoustic energy on the drying of carrots and lemon. Drying Technology 2009, 27(2), 281-287.

[8] Kowalski, S.J.; Pawlowski, A. Intensification of apple drying due to ultrasound enhancement. Journal Food Engineering 2015, 156, 1-9.

[9] Ortuno, C.; Perez-Munuera, I.; Puig, A.; Riera, E.; Garcia-Perez, J.V. Influence of power ultrasound application on mass transport and microstructure of orange peel during hot air drying. Physics Procedia 2010, 3, 153-159.

Microwave assisted fluidized bed drying of celery

Kaur, A.[*]; Gariépy, Y.; Orsat, V.; Raghavan, V.

Department of Bioresource Engineering, McGill University, St-Anne-de-Bellevue, Quebec, Canada.

*Email of the corresponding author: amanat.kaur@mail.mcgill.ca

Abstract

The drying kinetics of celery in a microwave assisted fluidized bed dryer was studied at different drying air temperatures (45°C, 55°C and 65°C) and at different initial microwave power densities (0W/g, 1W/g and 2W/g). Dried product quality, product mass, air temperature, air relative humidity, and electric power consumption were used to monitor the performance of the drying process. The results showed that the Midilli-Kucuk model was best in predicting the moisture ratio as a function of drying time. At any given temperature, the utilization of the microwave energy reduced by more than 50% the drying time.

Keywords: drying; celery; MWFBD.

1. Introduction

The ethical implications involved with increasing world food insecurity and food wastage has led researchers to look for methods to reduce food wastage. Drying is one of the oldest and best methods that can be successfully used to reduce food loss and increase shelf-life. Drying results in reduction of spoilage of perishable food, and requirements for product storage and transportation. Various drying methods can be used to achieve the desired dried products; the choice of the dryer depends upon product requirements and process parameters.

Drying using hot air is efficient for falling rate period but takes longer time for constant drying rate period due to high resistance to moisture transfer and reduction in thermal conductivity of the product. Application of microwaves, in addition to hot air, helps in reducing drying times and results in better efficiencies for the constant drying rate period. This increase in efficiency can be attributed to the volumetric heating of the product exposed to microwave energy which leads to evaporation of internal moisture, which creates a pressure gradient for liquid and vapor transfer [1]. In addition, use of hot air with fluidization moves the evaporated moisture away from the surroundings of the product [1].

Celery is a high moisture commodity and it is extremely perishable. Celery is a popular ingredient used in soups and stews to enhance the flavor and aroma [2, 3]. Celery has significant amount of essential oils with different terpenes and limonenes [4], and it is a good source of various vitamins and minerals [2, 4]. It has been used as aphrodisiacs, anthelmintics, antispasmodics, sedatives, stimulants, and tonics. Some authors have reported its beneficial effects to treat against asthma, bronchitis and rheumatism [2-4]. Celery can be used by diabetics or people on low sodium diets due to the presence of an active component similar to insulin [3].

Several studies can be found on drying celery and celery leaves such as microwave drying of celery leaves [5, 6], effect of microwave power on celery leaves in microwave drying [2], and vacuum drying of celery [3]. Zaremba (2007) developed a model and concluded that drying time for sliced celery in fluidized bed was less than fixed bed for same drying temperature [7]. Karathanos (1993) reported on the effects of freeze drying and air drying on the internal structure and final product quality [8].

Drying kinetics is used for the design of drying processes [9]. Drying kinetics behavior helps in the design, optimization and simulation of the drying process [10]. Also, mathematical modeling and simulations are commonly used to optimize the drying process and to improve the final product quality [9]. Optimizing process parameters such as air temperature, microwave power density and air flow rate [11] ensure that the quality attributes such as color, shape, nutritional composition and texture are preserved [12].

The aim of this study was to investigate the drying kinetics of celery in microwave fluidized bed dryer and to assess the effects of drying conditions on the quality of final dried product.

2.   Materials and Methods

2.1 Experimental Procedure

A central composite design was used to study the effects of initial microwave power density (IMPD) and air temperature on the quality of celery in a microwave assisted fluidized bed dryer. The IMPD (W/g) was the applied microwave power at the start of the drying process divided by the initial mass of the product. Both factors had 3 levels each; with initial microwave power density of 0W/g, 1W/g and 2W/g, and drying air temperature of 45°C, 55°C and 65°C. No pretreatments were done in this study. Data acquired was used to determine optimum drying conditions based upon product quality parameters and drying time. Parameters recorded and compared were the drying time, change in color, rehydration ratio, and texture of the rehydrated product. The product mass, air velocity, air and bed temperature were recorded at 10mins intervals. At start, the dryer was run empty to reach steady state conditions. The sliced celery was then added to the drying chambers and the drying cycle was started. A data acquisition system (DAQ) Agilent 34970A was used to record and store process conditions measured by different sensors connected to the dryer. Drying time of the product was the time required to reach final moisture content of 15% wet basis (wb). All trials were performed with 250g of freshly sliced celery pieces. As the drying progressed, the air velocity was adjusted to maintain good fluidization.

2.2 Celery

Fresh celery was bought from local markets and stored in plastic bags in a refrigerator at 4°C. Initial moisture content of celery was determined before each run. It averaged at 94.5± 0.5% wb. Prior to drying, the celery was sliced into pieces using an onion chopper (Starfrit model 093413, Atlantic Promotions Inc., Canada). The chopper blades assembly had opening of 12mm by 12mm.

2.3 Microwave Fluidized Bed Dryer

The schematic diagram of the microwave fluidized bed drying system is presented in Figure 1. An experimental microwave oven (Panasonic Inc., CA) with a maximum output of 700W at 2450 MHz was modified for the drying experiments. Two 2 kW hot-air heaters were used to preheat the air and they were controlled by the same PID controller (CN9500, Temperature Controller, Omega, USA). The fluidization chamber was made of glass with dimensions of 100 mm in diameter by 300 mm in length and it was installed inside the microwave cavity. Perforated plates made of polypropylene were placed at the bottom and top of the fluidizing chamber, and attached to the wall of the microwave cavity. Humidity sensors, temperature probes, and anemometers were installed at different locations inside the air distribution system (Figure 1). Power sensors were used to monitor electrical consumption of heaters, blower and microwave.

RH – Relative Humidity Sensor
T – Temperature probe
1 – Blower
2 – Heaters
3 – Temperature Controller
4 – Gas Distributor
5 – Fluidized bed chamber
6 – Microwave
✕ - Damper
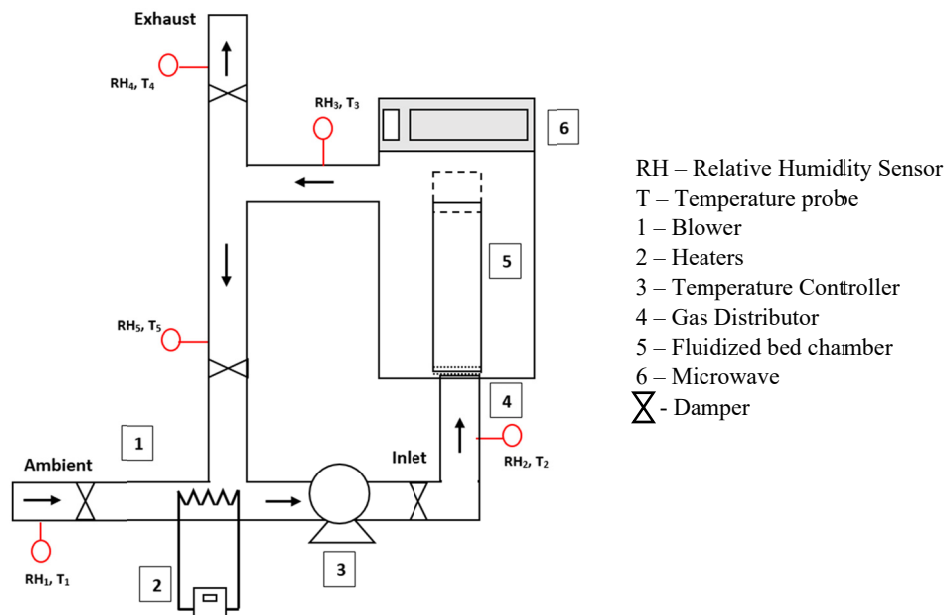
Figure 1. Schematic diagram of the fluidized bed dryer

2.4 Drying Kinetics

Predictive mathematical models found in the literature [13] were used to study the drying kinetics of sliced celery in the microwave assisted fluidized bed dryer. These models express the relationship between the moisture ratio (MR) and the drying time.

MR is dimensionless and it was calculated using the following equation:

$$MR = \frac{M_t - M_e}{M_o - M_e},\qquad(1)$$

where MR is the moisture ratio (dimensionless), M_o is the moisture content dry basis (db) at time t =0, M_t is the moisture content (db) at time t, and M_e is the equilibrium moisture content (db) (=17.647%).

Drying time to reach 15% moisture content (wb) was also calculated and compared to assess the effects of drying conditions.

2.5 Dried Product Properties

The final moisture content of the product was determined by oven drying at 70°C until constant mass was achieved.

Rehydration capacity is an important factor in products that can be used for instant soups [14]. The rehydration capacity of the dried product was determined by immersing 1g of the dried celery in boiling water for 20 mins. It was done in triplicates for all drying conditions.

$$RR = \frac{M_r}{M_d}, \tag{2}$$

where RR is the Rehydration Ratio (dimensionless), M_r is the mass of the rehydrated product (g), and M_d is the mass of the dried product (g).

Visual and textural attributes are important sensory parameters of a food product. Reactions such as pigment degradation (such as carotenoids and chlorophyll), and browning reactions takes place during thermal processing of food products leading to color changes and need to be monitored [5]. A Minolta Chromameter Model CR-300 (Minolta Co. Ltd., Japan) was used to measure the color of the rehydrated samples using the CIE Lab color space. These values were then used to measure the change in color (ΔE) between the fresh and the rehydrated sample. The mechanical properties of the rehydrated samples were measured with an Instron Universal Testing Machine (Instron-4502, Instron Corporation, USA) equipped with a Kramer shear press. The Kramer shear cell was used because it simulates the effect of a single bite. The parameters recorded included the energy required to compress and shear the sample, and the maximum force applied. Texture measurements were made in triplicates.

3. Results and Discussion

3.1 Drying Kinetics

A typical curve representing the changes of moisture content against the drying time is shown in Figure 2.
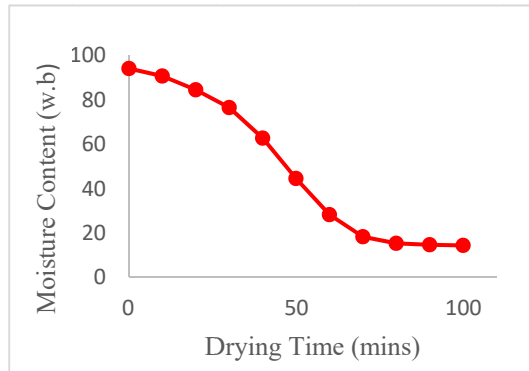
Figure 2. Moisture content vs drying time for drying air temperature 55°C and initial microwave power density (IMPD) 1W/g

Figures 3 and 4 represent typical MR curves for microwave assisted fluidized bed drying of celery at different temperatures and microwave power density. Slope of the drying curves indicate the speed of mass transfer within the sample for the operating conditions used in the drying process. As seen in Figures, the slope of the drying curves increased with increase in temperature and microwave power density.
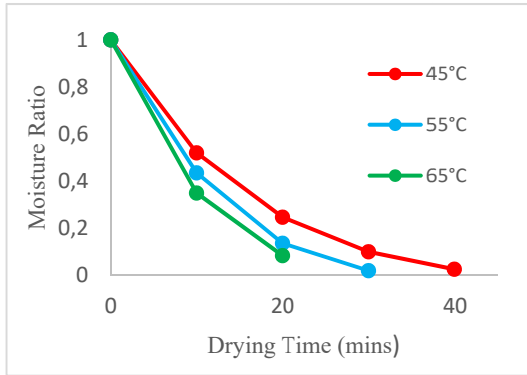
Figure 3. Effect of air temperature at initial microwave power density (IMPD) of 2W/g on moisture ratio during the drying process
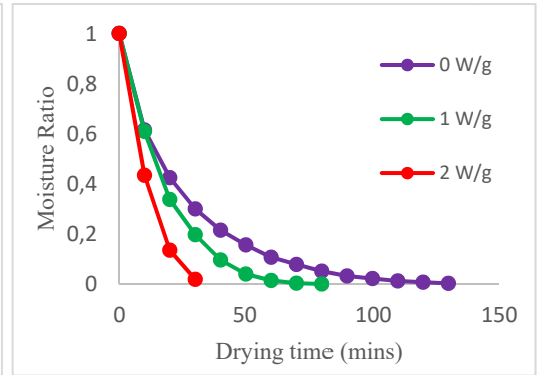
Figure 4. Effect of initial microwave power density at drying air temperature 55°C on moisture ratio during the drying process

3.1.1 Mathematical Model

Out of all the models studied, the Midilli-Kucuk equation was the best model to predict the MR as a function of drying time for drying celery in a microwave assisted fluidized bed dryer at 55°C and 1W/g (Figure 5). The general form of the Midilli-Kucuk equation can be written as:

$$MR = ae^{-k(t)^n} + bt, \qquad (3)$$

where a is a coefficient (dimensionless), b is a coefficient (min^{-1}), t is the dying time (min), k is the drying rate constant (min^{-1}), and n is a dimensionless parameter.

The model had highest R^2 and lowest SSE values amongst 9 drying models used in this study (Table 1) and similar results were reported by Demirhan and Ozbek (2011) for microwave drying of celery leaves [2].
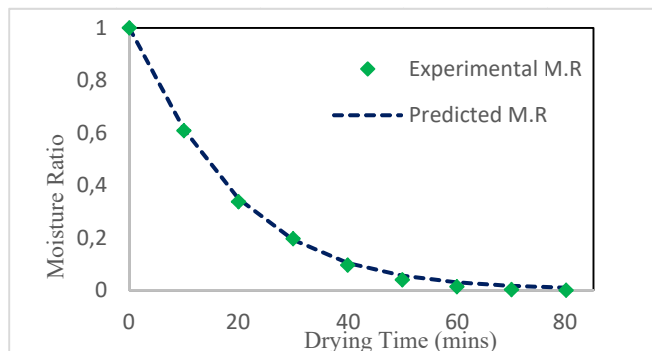
Figure 5 Moisture ratio against drying time for experimental and mathematical model at T = 55°C and IMPD =1W/g (Midilli-Kucuk Equation).

Table 1 Statistical values for different drying conditions

Temp	IMPD	SSE	R^2	a	k	n	b
45	0	2.16E-04	0.9998542	0.999	0.03863	0.9247	-9.29E-08
55	0	2.10E-04	0.9998294	0.9977	0.06697	0.844	4.48E-06
65	0	3.70E-05	0.9999654	1	0.06779	0.9083	3.71E-05
45	1	5.65E-04	0.9994403	0.9984	0.07668	0.854	-1.99E-04
65	1	9.63E-05	0.999881	0.9998	0.05613	1.098	-6.36E-05
55	1	3.03E-04	0.9997072	0.9995	0.03814	1.108	3.12E-05
55	1	4.45E-04	0.9995424	0.9992	0.06708	0.97	6.97E-06
55	1	2.68E-04	0.9997061	0.9994	0.05343	1.044	-4.67E-05
55	1	1.29E-04	0.9998578	0.9984	0.05322	1.045	-4.62E-05
55	1	1.62E-04	0.9998162	0.9993	0.07159	0.9457	-1.03E-04
45	2	1.77E-04	0.9997845	0.9995	0.04842	1.118	-2.46E-04
55	2	1.14E-04	0.9998524	0.9993	0.0433	1.276	2.46E-05
65	2	3.62E-15	1	0.9999	0.07282	1.143	-7.38E-04

3.1.2   Drying Time

The drying time to reach 15% moisture content was calculated for all drying conditions studied and a predictive model was derived (Figure 6). This model can be used to predict drying time as a function of air temperature and IMPD and it is presented below:

$$t = 222.9276 - 1.683 \times T - 50.725 \times IMPD, (R^2 = 0.9187)$$
$$(4)$$

where t is the drying time (mins), T is the Temperature (°C); and IMPD is the initial microwave power density (IMPD) (W/g).

Over the range studied, it was observed that IMPD had more effect on drying time than air temperature. At any given temperature, the drying was reduced by more than 50% when microwave energy was added to the drying process. These results are in agreement with those reported by Alibas [6] on microwave drying of celery leaves. Similar results have been reported by Reyes et al. [15] on microwave drying of potato slices and by Maskan [16] on Kiwifruits. In addition to the positive effect of microwave energy on drying time, fluidization ensured that the product is uniformly dried and it minimized the formation of agglomerates. [17]
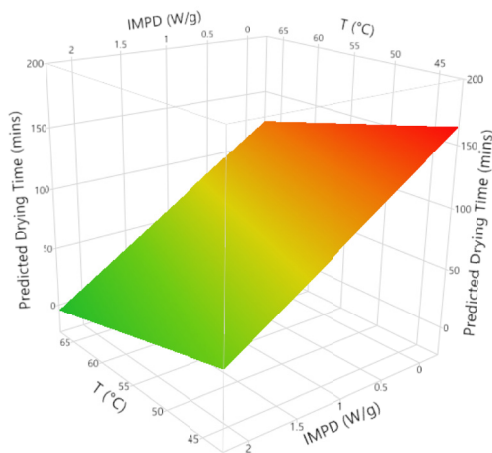
Figure 6. Response surface of the predicted drying time as a function of IMPD (W/g) and air temperature (°C)

3.2 Product Quality Characteristics

3.2.1 Color

Color measurements made on the rehydrated samples indicated that the lowest values of ΔE were obtained at 55°C. The analysis of variance performed on the collected data indicated that the drying air temperature had no significant effect on ΔE and only microwave power had induced changes in color. Changes in color ΔE was therefore modeled as a function of IMPD and yielded the following equation:

$$\Delta E \; = \; 11.712 - 1.5325 \times IMPD - 0.6705 \times IMPD^2, (R^2 = 0.411125) \qquad (5)$$

where IMPD is the initial microwave power density (W/g).

This equation indicates that ΔE was inversely related to IMPD, i.e., color change decreases with increase in microwave power density.

3.2.2 Rehydration Ratio

The analysis performed on the rehydration ratio indicated that only air temperature had a significant effect. It was observed that rehydration ratio decreased with increasing air temperature. The predictive model for the rehydration ratio as a function of drying air temperature is as follows:

$$RR \; = \; 27.90 - 0.781 \times T + 0.00649 \times T^2, (R^2 = 0.6283) \qquad (6)$$

where T is the drying air temperature (°C).

3.2.3 Texture

The effect of process conditions on the mechanical properties of the rehydrated celery pieces was measured and compared. The collected data indicated that mechanical properties

were affected by the drying conditions. Both energy to break and maximum force recorded increased with increasing drying air temperature. Although the IMPD did not have significant effect on the energy to break, it did affect the maximum force recorded. The predictive model describing the effects of temperature and IMPD on the maximum force is as follow:

$$F = -151.120 + 8.330 \times T - 38.016 \times IMPD, (R^2 = 0.5649) \tag{7}$$

where F is the maximum force applied to crush the sample (N), T is the drying air temperature (°C), and IMPD is the initial microwave power density (W/g).

4. Conclusion

In the current study, drying kinetics of celery in microwave fluidized bed drying was investigated. The results showed that the drying time reduced with the addition of microwaves and higher temperatures. Among the different predictive models studied, the Midilli-Kucuk model was found to be the best model for celery in microwave assisted fluidized drying. Rehydration ratios of celery were found to decrease with increasing air temperature and they were not affected by the application of microwave. Amounts of energy to crush the rehydrated samples increased with increasing air temperature but it was not affected by microwave energy. On the other hand, the maximum force required to crush the sample were found to be affected by both temperature and microwave power density.

Bibliography

[1] Feng, H., J. Tang, and R. Cavalieri, Combined microwave and spouted bed drying of diced apples: effect of drying conditions on drying kinetics and product temperature. Drying technology, 1999. **17**(10): p. 1981-1998.

[2] Demirhan, E. and B. Özbek, Thin-layer drying characteristics and modeling of celery leaves undergoing microwave treatment. Chemical Engineering Communications, 2011. **198**(7): p. 957-975.

[3] Madamba, P.S. and F.A. Liboon, Optimization of the vacuum dehydration of celery (Apium graveolens) using the response surface methodology. Drying Technology, 2001. **19**(3-4): p. 611-626.

[4] Ježek, D., et al., Dehydration of celery by infrared drying. Croatica Chemica Acta, 2008. **81**(2): p. 325-331.

[5] Demırhan, E. and B. Özbek, Color change kinetics of celery leaves undergoing microwave heating. Chemical Engineering Communications, 2011. **198**(10): p. 1189-1205.

[6] Alibas, I., Mathematical modeling of microwave dried celery leaves and determination of the effective moisture diffusivities and activation energy. Food Science and Technology (Campinas), 2014. **34**(2): p. 394-401.

[7] Zaremba, R. and M. Jaros, Theoretical model for fluid bed drying of cut celery. Polish Journal of Food and Nutrition Sciences, 2007. **57**(2 [A]): p. 211-214.

[8] Karathanos, V., Collapse of structure during drying of celery. Drying Technology, 1993. **11**(5): p. 1005-1023.

[9] Khoshtaghaza, M.H., H. Darvishi, and S. Minaei, Effects of microwave-fluidized bed drying on quality, energy consumption and drying kinetics of soybean kernels. Journal of food science and technology, 2015. **52**(8): p. 4749-4760.

[10] Senadeera, W., et al., Influence of shapes of selected vegetable materials on drying kinetics during fluidized bed drying. Journal of Food Engineering, 2003. **58**(3): p. 277-283.

[11] Marella, C. and K. Muthukumarappan, Processing Aids for Improving Heat Transfer during Drying of Granular Food Materials. Journal of Food Processing & Technology, 2013. **2013**.

[12] Kompany, E., et al., DEHYDRATION KINETICS AND MODELLING. Drying Technology, 1993. **11**(3): p. 451-470.

[13] Zang, F., Evaluation of Drying Behavior of Broccoli (Brassica oleracea L.) in Hot air and Microwave Drying Systems. 2015, McGill University.

[14] Sanjuán, N., et al., Modelling of broccoli stems rehydration process. Journal of Food Engineering, 1999. **42**(1): p. 27-31.

[15] Reyes, A., et al., A comparative study of microwave-assisted air drying of potato slices. Biosystems Engineering, 2007. **98**(3): p. 310-318.

[16] Maskan, M., Drying, shrinkage and rehydration characteristics of kiwifruits during hot air and microwave drying. Journal of Food Engineering, 2001. **48**(2): p. 177-182.

[17] Goksu, E.I., G. Sumnu, and A. Esin, Effect of microwave on fluidized bed drying of macaroni beads. Journal of Food Engineering, 2005. **66**(4): p. 463-468.

The consumption of exergy for lignite drying with different technologies: a comparative theoretical study

Liu, M. [a]; Wang, S. [a]; Liu, R. [a]; Han, X. [a];Yan, J. [a*]

[a] State Key Laboratory of Multiphase Flow in Power Engineering. Xi'an Jiaotong University, Xi'an, 710049, P. R. of China

*E-mail of the corresponding author: yanjj@mail.xjtu.edu.cn

Abstract

Pre-drying is an effective method to upgrade lignite and broaden its utilization areas. Various drying technologies could be applied to pre-dry lignite. The drying temperature in these drying technologies are different, which means that energy at different grades is used in these dryers. To analyze the irreversibilities of drying process, the exergetic analysis models are developed in this study. The exergy feeding and consumption rates are defined as the indicators. Various lignite drying technologies are calculated and quantitatively compared. Results show that exergy consumption rate for steam fluid-bed dryer is the smallest, which is 432.6 kJ (kg H_2O)$^{-1}$.

Keywords: lignite; drying technologies; exergy analysis; thermodynamics

1. Introduction

Lignite, a kind of low rank coal, is widely used as feeding fuel for power plants. However, power plants directly using raw lignite always have low efficiency and high pollutant emissions. Pre-drying is a proved method to improve the utilization efficiency of lignite[1]. Many types of dryers could be applied to dry lignite. The heat consumption rate is usually used to evaluate the performance of dryers, which is defined as the amount of energy consumed to evaporate 1 kg water with the unit of kJ (kg H_2O)$^{-1}$. However, energies used to dry lignite are in different grades. The heat consumption rate could not perfectly reflect performances of dryers based on the second law of thermodynamics. Exergy is a concept of thermodynamics expressing the maximum useful work possible contained in energy[2]. It is widely used to evaluate energy grades and the performance of energy processes.

Exergetic analyses were conducted on various lignite dryers in this study. Lignite drying technologies were reviewed firstly and thermodynamic analysis models were then developed. The exergy feeding and consumption rates are defined to evaluate the performance of dryers in the viewpoint of exergetic analysis and are compared quantitatively for various lignite dryers.

2. Materials and Methods

2.1. Lignite drying technologies

Drying of lignite could be classified to evaporative drying and mechanical-thermal dewatering. In this paper, we focus on the evaporative drying technologies. The evaporative drying is an energy intensive process, because water in lignite needs to absorb a lot of heat to evaporate. For the evaporative drying technologies, flue-gas or steam could be applied as the drying heat sources. Dryers uses steam as heating source are classified as steam dryers, including rotary-tube dryer and steam fluid-bed dryer. Characteristics and working parameters of steam dryers are listed in Table 1. When flue-gas is used to pre-dry lignite, the dryers are classified as flue-gas dryers. Characteristics and working conditions of flue-gas dryers are listed in Table 2.

Table 1 Operation parameters of steam dryers[3]

Dryer type	Characteristics	Heating medium parameters	
		Inlet	Outlet
Rotary-tube dryers	Using air as carrier as evaporative moisture; consisted of a drum equipped with tubes.	~180°C/0.4~0.5MPa	~Saturated water
Steam fluid-bed dryers	Lignite drying in slightly superheated steam; steam fluid-bed with internal heaters.	~140°C /0.32MPa	~Saturated water

Table 2 Operation parameters of flue-gas dryers[4]

Dryer type	Characteristics	Heating medium temperature /°C	
		Inlet	Outlet
Rotary	Drying along with disintegration; cocurrent mode.	750	120
Pneumatic	Short drying time; Lignite lifted by drying gas during pneumatic transport drying.	600	100
Fluid-bed	Easy to control; High drying intensity due to good mixing and high temperature heating medium.	450	75
moving bed	Possibility of full automation; compact construction and simple design.	175	80

2.2. Thermodynamic analysis models

2.2.1 Dryer model

The dryer model is indicated in Fig.1. As shown in Fig.1, 1 kg raw lignite is fed into the dryer, and λ kg water contained in lignite is dried out. m_a kg air is leaked into or used as carrier gas for drying 1 kg raw lignite. m_h kg heating medium (flue-gas or steam) releases heat in the dryer to dry lignite. In some types of dryers the heating medium directly contacts with lignite and leaves the dryer as dryer exhaust. While in some indirect dryers (rotary-tube dryer, etc.), the heating medium only exchanges heat in the dryer.
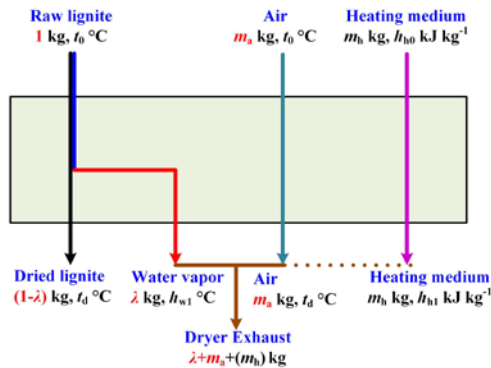
Fig. 1 Schematic diagram of Dryer.

The degree of pre-drying, λ, is defined to express the mass of water removed from per unit mass of raw lignite as

$$\lambda = \frac{M_{raw} - M_{upg}}{1 - M_{upg}} \tag{1}$$

where M_{raw} and M_{upg} are the mass of water contained in per unit mass of raw and dried lignite, respectively.

The minimum energy consumption, which is only absorbed by lignite to increase temperature and water to evaporate, for drying 1 kg lignite could be evaluated with

$$q_{d0} = \lambda \cdot (h_{dw} - h_{w0}) + (1 - \lambda) \cdot (h_{c1} - h_{c0}) \tag{2}$$

where h_{dw} and h_{w0} are enthalpies of the water contained in dryer exhaust and raw lignite respectively, kJ kg^{-1}; h_{c1} and h_{c0} are enthalpies of dried lignite at the outlet and inlet temperatures respectively, kJ kg^{-1}.

The energy absorbed by possible in-leaking or carrier air is

$$q_{da} = m_a \cdot Cp_a (t_d - t_0) \tag{3}$$

where Cp_a is the specific heat capacity of air, kJ kg^{-1} K^{-1}; t_{d1} and t_{a0} are temperatures of dryer exhaust and ambient respectively, °C.

Based on the energy balance in the dryer, the mass of heating medium is

$$m_h = \frac{q_{d0} + q_{da}}{\eta_d \cdot (h_{h0} - h_{h1})} \tag{4}$$

where h_{h0} and h_{h1} are enthalpies of heat medium led into and output from the dryer, kJ kg^{-1}; η_d is the thermal efficiency of dryer, kJ kg^{-1}.

To evaluate the mass flow rate of drying heat source, the rate of drying medium to dry out 1 kg water is defined as

$$K_h = \frac{m_h}{\lambda} \tag{5}$$

2.2.2 Exergetic analysis model

The dead point is the benchmark for the exergetic analysis. When the exergy carried by the dryer exhaust is recovered by cooling, the dryer exhaust could be cooled to the ambient temperature and becomes saturated moist gas. Therefore, the compositions of saturated moist gas is defined as the deadpoint compositions. The deadpoint pressure and temperature for the exergetic analysis are

$$p_0 = 0.1 \text{MPa} \tag{6}$$

$$T_0 = 293.15\text{K} \tag{7}$$

In the drying process, substances include lignite, gas (flue-gas and air), water (liquid and steam) and dryer exhaust. Assumptions of ideal gas mixture for the dryer exhaust are used. The exergy of water component is calculated with

$$E_w = h_w - h_{w0} - T_0(s_w - s_{w0}) + \bar{R}_w T_0 \ln \frac{y_w}{y_{w0}} \tag{8}$$

where h_w and h_{w0} are the enthalpies of water at calculation and deadpoint conditions respectively, kJ kg^{-1}; s_w and s_{w0} and are the entropies at calculation and deadpoint conditions respectively, kJ kg^{-1} K^{-1}; $\bar{R}_W$ is gas constant of water vapor, kJ kg^{-1} K^{-1}; y_w and y_{w0} are volume fractions of water vapor at calculation and deadpoint conditions.

It is assumed that the flue-gas or air component has constant specific heat (average specific heat Cp_g, kJ kg^{-1} K^{-1}). Then the exergy of gas component is

$$E_g = Cp_g(T_g - T_0 - T_0\ln\frac{T_g}{T_0}) + R_g T_0 \ln \frac{y_g}{y_{g0}} \tag{9}$$

where T_g is temperature at calculation condition, K; $\bar{R}_g$ is gas constant of gas, kJ kg^{-1} K^{-1}; y_g and y_{g0} are volume fractions of gas at calculation and deadpoint conditions.

The physic exergy carried by the dried lignite is

$$E_l = Cp_l(T_d - T_0 - T_0\ln\frac{T_d}{T_0}) \tag{10}$$

where Cp_l is the constant specific heat of lignite, kJ kg^{-1} K^{-1}; T_d is the temperature of lignite at the outlet of dryer, K.

To quantitatively compare the thermodynamic performance of various dryers, the exergy feeding rate is defined as

$$e_f = \frac{E_h}{\lambda} \tag{11}$$

where E_h is the exergy fed into the dryer by drying heat source, kJ.

The exergy carried by the dried lignite or dryer exhaust can be recovered by heat recovered, whereas the internal exergy loss (exergy destruction) in the dryer and external exergy loss

along with heat loss of the dryer could not be recovered. The exergy consumption rate is defined as

$$e_c = \frac{E_h - E_l - E_e}{\lambda} \tag{12}$$

The exergy feeding rate e_f (kJ (kg H_2O)$^{-1}$) expresses the exergy feeding amount to dry 1 kg water out from raw lignite, and the exergy consumption rate e_c (kJ (kg H_2O)$^{-1}$) expresses the irreversibilities and heat loss of lignite dryers.

3. Results and discussions

We use Yimin lignite as the reference coal to carry out quantitative analysis[5]. Moisture contents of raw lignite is 39.5% and it is assumed to be dried to 15% in the dried lignite. The constant specific heat of lignite is 1.3 kJ kg^{-1}.

3.1. Heat balance of lignite dryers

The heat balance of lignite dryers listed in Tables 1 and 2 is calculated. The mass flow rate of heat source for drying 1 kg water out from lignite is compared in Fig.2. As shown in Fig.2, the mass flow rate of heat source varies greatly. The heat released by per unit flue-gas is significantly lower than that released by per unit steam. Therefore, K_h for flue-gas dryers is bigger than that for steam dryers. The K_h is above 29 for the moving bed dryer, because the temperature drop of flue-gas for the moving bed dryer is only 95 °C. For the steam fluid-bed dryer and rotary-tube dryer, the rates of drying medium are 1.38 and 1.49, respectively.
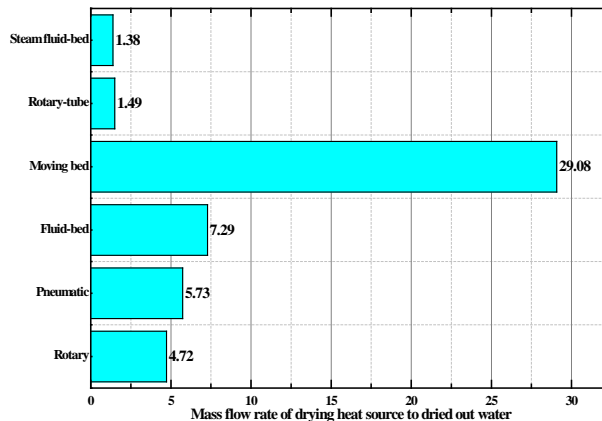
Fig. 1 Schematic diagram of Dryer.

3.2. Comparison of exergy feeding and consumption rates

Based on the heat balance of lignite dryers, exergetic analyses were conducted. The exergy feeding and consumption rates for lignite dryers were compared in Fig.3. As shown in Fig.3, the exergy feeding rate and exergy consumption rate for dryers vary greatly. The flue-gas of 750 °C is used to dry lignite in the rotary dryer, so the exergy feeding rate is as big as 1837.9 kJ (kg H_2O)$^{-1}$. If the exergy contained in dryer exhaust and dried lignite could be recovered, the exergy consumption rate could be decreased to 1424.8 kJ (kg H_2O)$^{-1}$. The low temperature heat source is used to dry lignite for the steam dryers. The exergy feeding rates for rotary-tube dryer and steam fluid-bed dryer are 1131.7 and 955.2 kJ (kg H_2O)$^{-1}$, respectively. In the steam fluid-bed dryer, no air is used as carrier gas, so more exergy could be recovered from dryer exhaust. The exergy consumption rate for steam fluid-bed dryer is only 432.6 kJ (kg H_2O)$^{-1}$.

Air is always used as carrier gas for the rotary-tube dryer. In Fig.3, the mass flow rate of air for drying 1 kg water is assumed as 3 kg. The mass flow rate of carrier gas for rotary-tube dryer will indeedly influence the exergy feeding rate and exergy consumption rate, which is shown in Fig.4. As shown in Fig.4, the exergy feeding rate increases linearly with mass flow rate of carrier air. For more exergy can be recovered in dryer exhaust when less air is used as the carrier gas, the exergy rate reduction of exergy consumption rate compared with exergy feeding rate decreases with the increase of mass flow rate of carrier gas.
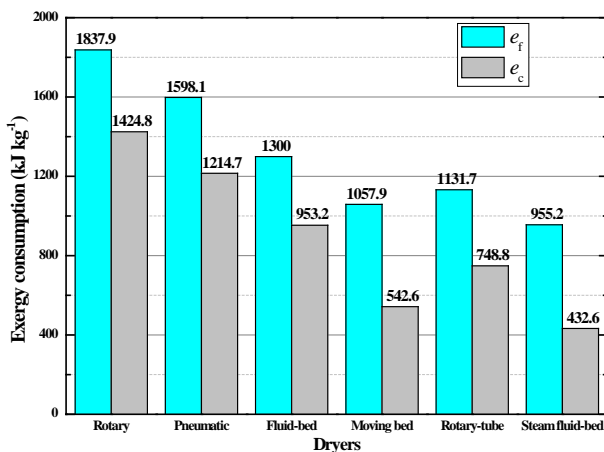
Fig. 3 Comparison of exergy consumption rate.
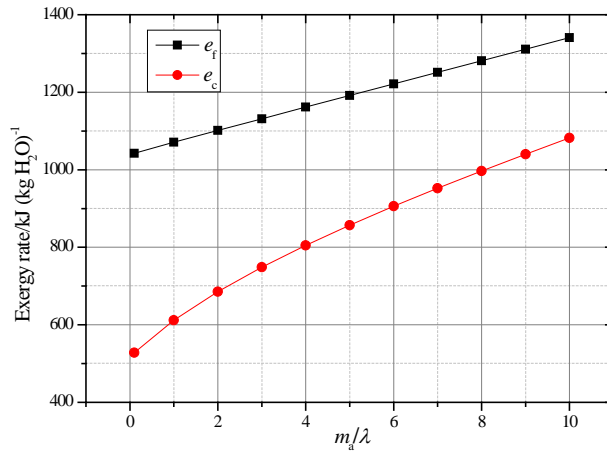
Fig. 4 Influence or carrier air on exergy feeding and consumption rates for rotary-tube dryer.

4. Conclusions

The heat consumption rate for lignite drying is a conventional indicator to evaluate the performance of lignite dryers. However, the drying temperature for various drying technologies are different, which means that energy at different grades is used in these drying technologies. The heat consumption rate could not evaluate the irreversibilities in drying process. Therefore, the exergetic analysis models are developed in this paper, and the exergy feeding rate and exergy consumption rate are defined as indicators for exergy analysis. Quantitative analyses on lignite dryers reveal that irreversitbilities vary greatly for lignite drying technologies. Dryers using low temperature heat as dryer heat source consume less exergy in the drying process. The exergy consumption rate for steam fluid-bed dryer is the smallest, which is 432.6 kJ (kg H_2O)$^{-1}$.The aim of this paper is to provide a guidance for the development and study of lignite drying technologies in the viewpoint of reduction for exergy consumption.

5. References

[1] Liu, M.; Li, G.; Han, X. Q.; Qin, Y. Z.; Zhai, M. X. ;Yan, J. J. Energy and exergy analyses of a lignite-fired power plant integrated with a steam dryer at rated and partial loads. DRYING TECHNOLOGY 2016, 35 (2), 203-217.
[2] Bejan, A. Advanced engineering thermodynamics. John Wiley & Sons: 2016.
[3] Kakaras, E.; Ahladas, P. ;Syrmopoulos, S. Computer simulation studies for the integration of an external dryer into a Greek lignite-fired power plant. Fuel 2002, 81 (5), 583-593.
[4] Mujumdar, A. S.Handbook of industrial drying. CRC press: 2014.
[5] Liu, M.; Yan, J.; Chong, D.; Liu, J. ;Wang, J. Thermodynamic analysis of pre-drying methods for pre-dried lignite-fired power plant. Energy 2013, 49, 107-118.

CT-scanning of the drying process of Eucalyptus nitens

Couceiro, J. [a]*; Hansson, L. [b]; Ahec, A. [c]; Sandberb, D. [a]

[a] Department of Engineering Sciences and Mathematics. Division of Wood Science and Enginering. Luleå University of Technology (LTU), Skellefteå, Sweden.

[b] Department of Ocean Operations and Civil Engineering. Norwegian University of Science and Technology (NTNU), Ålesund, Norway.

[c] Department of Wood Science and Technology. University of Ljubljana Biotechnical Faculty, Ljubljana, Slovenia.

*E-mail of the corresponding author: jose.couceiro@ltu.se

Abstract

The drying of Eucalyptus nitens is a troublesome process as the species is extremely prone to drying defects. This paper reports ongoing research to improve the understanding of surface checking and cell collapse in Chilean grown Eucalyptus nitens during drying. Computed tomography (CT) scanning was used as a powerful tool for studying the internal changes in the wood-material during the drying process. Different levels of temperatures have been tested with the same equilibrium moisture content (EMC) conditions and low air velocity. The results confirm that a low drying temperature and a low air velocity, which results in a slow rate of drying, reduce internal cell collapse and surface checking .

Keywords: Cell collapse; computed tomography; surface checks; wood drying; internal checks

1. Introduction

Eucalyptus is the largest single source of market pulp in the world [1] . In Chile, 35% of the forest plantations are eucalyptus (mainly *Eucalyptus globulus* and *Eucalyptus nitens*) [2]. The production of eucalyptus wood in Chile has been increasing during the last 40 years, but the volume of eucalyptus used as sawn timber has nevertheless decreased during that period.

The desire to increase the use of eucalyptus and to improve its processing has driven research in various fields. Blackburn [3] provides a wide picture of the existing knowledge of eucalyptus wood from different points of view: materials science, genetics, forest management and commercialized products. More recently, Sharma et al. [4] studied a new method to improve the quality of *Eucalyptus nitens* and *Eucalyptus bosistoana* solid wood by eliminating growth stresses. Kong et al. [5] investigated the use of steaming as pre-treatment for *Eucalyptus grandis* and *Eucalyptus urophylla* wood and identified potential ways to improve the drying process.

One of the reasons for the low use of eucalyptus in solid wood products is the difficulties in the drying process, which usually result in an unacceptable level of defects, often due to cell collapse [6-8]. Cell collapse is a process that occurs mainly when there is free water in the wood cells and thin-walled cells cannot withstand the tension forces generated when the liquid water is displaced [9]. The literature reports research that addresses surface and internal checking and cell collapse of different eucalyptus species from various viewpoints, e.g. anatomical [10-12], materials science [6, 13-14] and genetics [15-16].

The topic of collapse in wood drying has been studied extensively. Recently, Yang and Liu [9] provided an extensive review of the literature on the collapse behaviour of different eucalyptus species and, based on these reports, proposed different measures to reduce it, such as pre-heating (both with steam and with microwaves), re-conditioning and several methods to control the drying parameters.

Different scanning technologies have been applied to study the cell collapse: Wentzel-Vietheer et al. [17] tried to identify collapse zones in *Eucalyptus globulus* with near infrared spectroscopy (NIR). Ananías et al. [18] used a Quintek Xray Ring Tree Analyzer to measure the width and density of annual rings while studying how the location of the cell within the stem influences collapse.

The work presented in this article is a part of a larger project where the drying of *Eucalyptus nitens* is studied. To study internal cell collapse, an unique equipment that combines a drying chamber and a medical computed tomography (CT) scanner is used in such a way that the wood specimens can be scanned during drying in controlled conditions.

It is then possible to explore what happens in the interior of a wood piece during the drying process and also to study the changes in dimension and density.

2. Materials and Methods

Eucalyptus nitens was harvested from Chilean plantations, sawn and shipped in the green state to northern Sweden, where the experiments took place. The specimens were sawn in dimensions of 47 x 162 x 600 mm and 27 x 162 x 600 mm with different orientations in the log cross-section (*Fig. 1*). Prior to drying, the cross-sections of the specimens were sealed with a heat-resistant silicone.

A specially designed laboratory drying kiln that fits within the void of a Siemens Somatom Emotion Duo medical CT-scanner was used (*Fig. 2*). With this equipment, it is possible to scan the inside of the kiln without interrupting the drying process, and thus to inspect in real time internal features of the wood specimens as they are drying. The control parameters are the air velocity and the dry and wet bulb temperature (T_d and T_w).
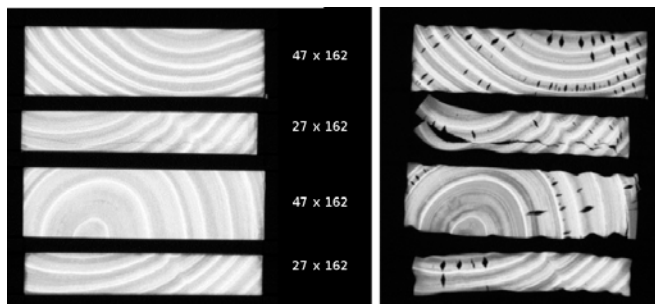
Fig. 1: CT-images of the cross section of the specimens before (Left) and after drying - experiment No. 4 in Table 1 (Right).

Fig. 2: Drying kiln and CT-scanner. The specimen is located in the metal tube that fits within the gantry of the scanner.

2.1. Drying processes

The part of the project presented here consisted of slow drying under stable conditions. The aim was to maintain a constant air velocity just below 1 m/s, and conditions for the same equilibrium moisture content (EMC) 16% (modifying the psychrometric difference in each run) and under these conditions to apply different drying schedules at four different temperatures, with four samples in each run in the chamber (*Table 1*). This was not always possible, as such a low air velocity made it difficult for the control system to hold the climate because the humidity in the chamber is controlled by the psychrometric difference, which requires a higher air velocity. *Fig. 3* shows the actual temperature and humidity trends in each experiment, showing the difficulties of reproducing such schedules in some cases (compared with the set points shown in *Table 1*) and the consequences of several malfunctions of the equipment that had to be dealt with while the tests were running.

Table 1: Temperatures set points for each experiment.

Experiment No.	Dry-bulb T (°C)	Wet-bulb T (°C)
1	90	87.9
2	60	57.3
3	25	22.5
4	40	36.9
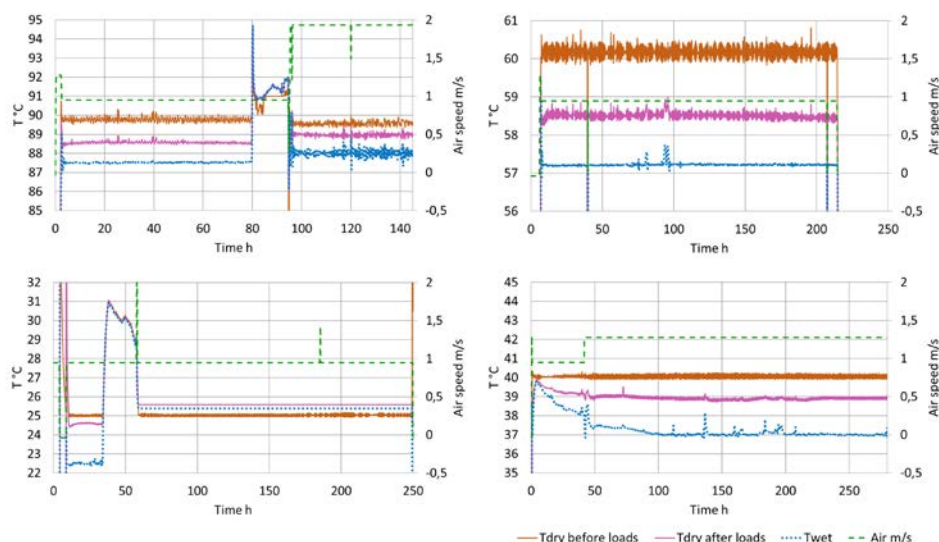
Fig. 3: Actual temperature and air velocity trends in the four experiments using the set points indicated in Table 1: 1 (top left), 2 (top right), 3 (bottom left) and 4 (bottom right).

2.1.1. *Experimental issues*

Several issues arose during the experiment that made it necessary to change some of the parameters so that the drying kiln would continue running. During experiment No. 1, the steam valve broke and it could not be replaced with the chamber in operation. To keep the experiment running and the EMC at a reasonable level, the air velocity was increased to around 1.9 m/s. The chamber also experienced malfunction early on during experiment No. 3, and the data for wet-bulb temperature (T_w) and dry-bulb temperature (T_d) after loads are not reliable after about 60 h. Experiments No. 2 and No. 4 ran reasonably well. During experiment No. 4, the chamber had problems in reaching the working conditions for the test, and the air velocity was therefore incremented after around 40 h.

2.2. Data processing

The data obtained from the CT-scanner are images in DICOM format, which translate into grey-scale images in which a lighter colour represents a high density and a darker colour represents a low density (*Fig. 1*). Each pixel of the image represents a volumetric entity (so called voxel) defined by the pixel size and the thickness of the scanning beam. In these experiments the voxel size was 0.49 x 0.49 x 10 mm^3. Being a grey-scale image, each pixel has one numeric value associated with it (the CT-number), and the images can thus be processed as matrixes in mathematical software like, for example, Matlab, and this is the case with the data here presented. Making use of the density relationship between the CT-number and the density of the scanned material, mass can be inferred and, thus, real time studies of moisture content (MC), defined as the ratio of the weight of the water in the wood to the dry weight of the wood, can be made.

The MC is calculated from the CT-images by dividing the difference between the average mass of the wood pixels in the wet wood image and the average mass of the wood pixels in the dry wood image by the average mass of the wood pixels in the dry wood image. This method is somehow analogous to the gravimetric method, which consist on dividing the difference in weight of a wood specimen at a given MC and in totally dry condition by the weight of the wood specimen in totally dry condition.

3. Results and Discussion

Two main aspects were studied: the drying rate and the evolution of internal cell collapse and surface checking.

3. 1. Drying rate

As shown in *Table 2*, the lowest temperature gave the best drying rate, which is a confirmation of the validity of the traditional drying schedules used in Chile, which are performed at around 28°C with very low air velocity. A dry shell can be seen in experiment No. 3 (25°C T_d), and to a shorter extent in experiment No. 4 (40°C T_d), but not in the

experiments at higher temperatures. Nevertheless, the results show that the drying rate is almost as high at 90°C as it is at 25°C, which was one the hypothesis. Unfortunately, there is a high spread on the results, which suggest that conclusions should be drawn carefully.

Table 2: The drying rate of the different specimens sorted by dimension.

Experiment No.	Temp. °C	27 x 162	27 x 162	47 x 162	47 x 162	Mean
1	90	-0.45	-0.19	-0.25	-0.30	-0.30
2	60	-0.30	-0.18	-0.15	-0.16	-0.20
3	25	-0.39	-0.37	-0.27	-0.29	-0.33
4	40	-0.26	-0.25	-0.25	-0.19	-0.24

3.2. Cell collapse and surface checking

Table 3 shows how the checking and cell collapse varied in each experiment. *Fig. 1* shows, as an example, the checking and collapse occurring during experiment No. 4. If time were the only parameter to evaluate, experiment No. 4 (at 40°C T_d) could be considered to show the best behaviour regarding the appearance of surface checks, while the CT-images showed that collapse took place more slowly in experiment No. 3 (at 25°C T_d).

Table 3: Visibility of the first checks (surface) and cell collapse (internal checks) shown in hours into the drying process.

Experiment No.	First checks after: (h)	Visible collapse After: (h)
1	35	72
2	58.5	68.5
3	56	77
4	71	71

Nevertheless, the comparison between these results must take into account the differences in the processes and in the drying rate in the different experiments.

3.3. Future work

More research will be performed trying to take into account all the factors that may influence the quality of the final product regarding both surface checking and cell collapse. Multivariate statistical studies may be useful in the future. The development of the equipment and the method to replicate these drying schedules also needs more work, as processes with low temperatures and air velocities has shown to be troublesome. Furthermore, research on the implementation of pump-drying is currently being carried out, which shows a potential for energy savings as the fans are intermittently stopped during much of the drying time.

4. Conclusions

The drying of *Eucalyptus nitens* has been shown to differ to some extent with regard to the appearance of checks and cell collapse-related features depending on the temperature, but the drying rate does not seem to be greatly affected by temperature. It can be concluded from these studies that *Eucalyptus nitens* should be dried at a low temperature and a low air velocity, as is done industrially in Chile, to avoid damage. Improving the efficiency of the drying process in terms of time and, thus, energy, does not seem likely as the process must be slow in order to avoid surface checking and cell collapse. The results do not suggest that high temperature drying would give higher drying rate, thus the increase in energy consumption would not be worth it.

5. Acknowledgements

6. References

[1] OECD - Organisation for Economic Cooperation and Development. Consensus Document on the Biology of Eucalyptus spp. Paris, 2014.

[2] Gysling, A. J.; Álvarez, V. C.;Soto, D. A.; Pardo, E. J.; Poblete, P. A.; Bañados, J. C. Chilean Statistical Yearbook of Forestry 2017. Statistical Bulletin N°159. Metropolitan Office, Forestry Institute, Santiago, Chile, 2018.

[3] Blackburn, D. P. Improving Eucalyptus Nitens for Sawn-Board, Veneer and Paper Products. Doctoral thesis, University of Tasmania, 2012.

[4] Sharma, M.; Walker, J. C. F.; Chauhan, S. S. Eliminating Growth-Stresses in Eucalyptus: A Scoping Study with *E. bosistoana* and *E. nitens*. In *Wood is Good*; Springer, Singapore, 2007; pp 47-54.

[5] Kong, L.; Zhao, Z.; He, Z.; Yi, S. Development Of Schedule To Steaming Prior To Drying And Its Effects On *Eucalyptus Grandis × E. Urophylla* Wood. *European Journal of Wood and Wood Products* 2017, 76, 591-600.

[6] McKinley, R.; Shelbourne, C.; Low, C.; Penellum, B.; Kimberley, M. Wood properties of young Eucalyptus nitens, E. globulus, and E. maidenii in northland, New Zealand. *New Zealand Journal of Forestry Science*. 2002, 32(3), 334-356.

[7] Shelbourne, C., Nicholas, I., McKinley, R., Low, C., McConnochie, R., Lausberg, M. Wood density and internal checking of young Eucalyptus nitens in New Zealand as

affected by site and height up the tree. *New Zealand Journal of Forestry Science*. 2002, 32(3), 357-385.

[8] Lausberg, M.; Gilchrist, K.; Skipwith, J. Wood properties of Eucalyptus nitens grown in New Zealand. *New Zealand Journal of Forestry Science*. 1995, 25(2), 147-163.

[9] Yang, L.; Liu, H. A Review of Eucalyptus Wood Collapse and its Control during Drying. *BioResources*. 2018, 13(1), 2171-2181.

[10] Wilkes, J.; Wilkins, A. Anatomy of collapse in eucalyptus species. *IAWA Journal*. 1987, 8(3), 291-295.

[11] Chauhan, S. S.; Walker, J. Relationships between longitudinal growth strain and some wood properties in eucalyptus nitens. *Australian Forestry*. 2004, 67(4), 254-260.

[12] Valenzuela, C.; Bustos, A.; Lasserre, J.; Gacitúa, E. Characterization nanomechanics of wood cell structure and anatomy in Eucalyptus nitens and its relation to the cracking cracking and fractures in round wood. Maderas: Ciencia y Tecnología. 2012, 14(3), 321- 337.

[13] McKenzie, H. M.; Turner, J. C. P.; Shelbourne, C. J. A. Processing young plantation-grown Eucalyptus nitens for solid-wood products. 1: Individual-tree variation in quality and recovery of appearance-grade lumber and veneer. *New Zealand Journal of Forestry Science*. 2003, 33(1), 62-78.

[14] Ilic, J. Shrinkage-related degrade and its association with some physical properties in Eucalyptus regnans F. muell. *Wood Science and Technology*.1999, 33(5), 425- 437.

[15] Hamilton, M. G.; Raymond, C. A.; Harwood, C. E.; Potts, B. M. Genetic variation in Eucalyptus nitens pulpwood and wood shrinkage traits. *Tree Genetics Genomes*. 2009, 5(2), 307-316.

[16] Kube, P. D.; Raymond, C. A. *Breeding to minimize the effects of collapse in Eucalyptus nitens*. CRC for Sustainable Production Forestry: Tasmania, Australia 2002.

[17] Wentzel-Vietheer, M.; Washusen, R.; Downes, G. M.; Harwood, C.; Ebdon, N.; Ozarska, B.; Baker, T. Prediction of non-recoverable collapse in Eucalyptus globulus from near infrared scanning of radial wood samples. *European Journal of Wood and Wood Products*. 2013, 71(6), 755-768. doi:10.1007/s00107-013-0735-y

[18] Ananías, R. A.; Sepúlveda-Villarroel, V.; Pérez-Peña, N.; Leandro-Zuñiga, L.; Salvo-Sepúlveda, L.; Salinas-Lira, C.; Cloutier, A.; Elustondo, D. M. Collapse of Eucalyptus nitens wood after drying depending on the radial location within the stem. *Drying Technology*. 2014, 32(14), 1699-1705.

Effects of different drying methods on the physicochemical properties of powders obtained from high-oleic palm oil nanoemulsions

Hernández-Carrión, M.; Moyano-Molano, M.; Ricaurte, L.; Moreno, F.L.; Quintanilla-Carvajal, M.X.[*]

Faculty of Engineering. Universidad de La Sabana, Bogotá, Colombia

*E-mail of the corresponding author: maria.quintanilla1@unisabana.edu.co

Abstract

Nanoencapsulation is an efficient process to incorporate high nutritional oils, such as high oleic palm oil (HOPO). Several drying technologies can be applied for obtaining HOPO powders. The aim of this work was to study the effect of two different drying methods (spray-drying, SP and freeze-drying, FD) on some physical properties and microstructure of powders obtained from HOPO nanoemulsions. Results showed that FD powders presented lower a_w and bulk density, and higher dissolution rate than SD powders. Results suggest that SD could be a more economical alternative to FD in order to obtain HOPO powders with low moisture and a_w.

Keywords: freeze-drying; high oleic palm oil; nanoemulsion; spray drying.

1. Introduction

Nanoencapsulation is an efficient process to encapsulate bioactive compounds and thus allows the incorporation of high nutritional oils, such as high oleic palm oil (HOPO) [1]. Nanoencapsulation often begins with the production of nanoemulsion [2]. One of the techniques used for obtaining nanoemulsions is microfluidisation; it has been widely used and represents a highly efficient method for producing nanoemulsions containing small-sized droplets (100-500 nm) [3].

Several drying technologies can be applied for obtaining HOPO powders such as freeze-drying and spray-drying. The final product obtained from these methods may differ in physicochemical properties and microstructures [4]. Spray drying is widely used in commercial production of milk powders, fruits and vegetables [5]. This method has several advantages such as rapid drying, large throughput and continuous operation. During the drying process, the feed solution is sprayed in droplets in a stream of hot air [6]. The liquid droplets are dried in seconds as a result of the highly efficient heat and mass transfers [7]. The finished product can be made in the form of powder, granules or agglomerates [8]. Freeze drying, also known as lyophilisation, is a drying process in which the food is first frozen then dried by direct sublimation of the ice under reduced pressure. To carry out a successful freeze drying operation, the pressure in the drying chamber must be maintained at an absolute pressure of at least 620 Pa [7]. Freeze drying is generally considered as the best method for production of high quality dried products [9]. But, it suffers from high production costs, high energy consumptions, and low throughputs [10].

So, the aim of this work was to study the effect of two different drying methods, spray drying and freeze drying on some physical properties and microstructure of powders obtained from nanoemulsions of HOPO.

2. Materials and Methods

2.1. Materials

HOPO (Fedepalma, Bogotá, Colombia); whey powder was bought in a local market (Bogotá, Colombia); soy lecithin (Bellchem International, Medellín, Colombia); and native corn starch (Cimpa SAS, Bogotá, Colombia).

2.2. Nanoemulsion preparation

The coarse emulsions were homogenised in an mixer (Imusa, Bogotá, Colombia), incorporating whey powder (29.76%, w/w), followed by the sequential addition of native corn starch (0.24%, w/w), and HOPO (14%, w/w) to the distilled water over 2 min. Subsequently, such emulsions were processed to obtain the nanoemulsions. The soy lecithin

concentration was held constant at 10% w/w with respect to the HOPO concentration (1.4%, w/w). The nanoemulsions were obtained following the methodology of Quintanilla-Carvajal et al., [11] with some modifications at 20,000 psi pressure for 2 cycles.

2.3. Drying technologies

Two different drying methods were applied: spray-drying (SP), and freeze-drying (FD).

2.3.1. Spray drying

HOPO powders produced by SD (SDP) were obtained in a pilot scale spray dryer (Niro MM-PSR, GEA Process Engineering A/S, Denmark) using two-fluid nozzle as atomisation device at 1 bar of pressure. The nanoemulsions were fed into the atomiser by a peristaltic pump (Watson-Marlow, United Kindom). The inlet and outlet temperatures of the drying air were 190 and 90°C, respectively.

2.3.2. Freeze drying

HOPO powders produced by FD (FDP) were obtained in a pilot scale freeze dryer (Labconco, USA). The nanoemulsion was poured into a stainless pan to form a layer of 10 mm. The samples were frozen at −40 °C with a cooling rate of 0.5°C/min for 16.5 h. Then, the samples were sublimated at a temperature of -20°C for 12 h and a desorption temperature of 20°C for 24 h. The pressure on the chamber was 0.018 mbar. Then, an analytical batch mill (A 11 M Basic, IKA, USA) at 28,000 rpm during 10 s was used for the obtention of the FDP.

2.4. Physical properties of the powders

2.4.1. Moisture

The moisture content of the powders was measured from 0.3 g of sample employing an EM 120-HR moisture analyser (Precisa Gravimetrics AG, Dietikon, Switzerland). Measurements were performed in triplicate.

2.4.2. Water activity (a_w)

The water activity of the powders was measured using an AquaLab Series 4 aw meter (Decagon Devices, Inc., Pullman, WA) after the samples were stabilised at 25 °C for 30 min. The measurements were performed in triplicate.

2.4.3. Dissolution rate (DR)

The dissolution rate was carried out by adding 2 g of the powders into 50 mL of distilled water [12]. The mixture was agitated in a 100 mL low form glass beaker with a magnetic stirrer (Heidolph, Schwabach, Germany) at 900 rpm. The time (s) required for the material to completely dissolve was recorded. The measurements were performed in triplicate.

2.4.4. Bulk density (BD)

The bulk density of the powders was measured by weighing 2 g of sample and placing it in a 10 mL graduated test tube. The test tube was tapped by hand and the bulk density was calculated as the ratio between the mass (g) of powder contained in the test tube and the volume occupied [13]. The measurements were performed in triplicate.

2.5. Microstructure

For the analysis of the structure of the HOPO powders a scanning electron microscope (Phenom Pro, Cecoltec Ltda, Bogotá, Colombia) was used. Samples were placed on the SEM slides with the aid of colloidal silver. An acceleration voltage of 5 kV and two different magnifications of 1000x and 4000x were used.

2.6. Statistical analysis

Data were subjected to variance analysis (ANOVA), using the least significant difference (LSD) test with a 95% ($p < 0.05$) confidence interval to compare the test averages (Statgraphics Plus 5.1, Manugistics, Inc., Rockville, MD, USA).

3. Results and Discussion

3.1. Physical properties

Physical properties of the HOPO powders obtained using two different drying methods, SD and FD are shown in Table 1. Results showed that no significant differences ($p > 0.05$) were obtained between the moisture of FDP compared to that obtained in SDP (Table 1). Although no significant differences in moisture content were found, both methods are totally adequate for emulsion drying because in industrial food, moisture values under 15% prevent microorganism growth, increase structural stability and retards deterioration reactions as sugar crystallization, non enzymatic browning and aroma losses [14].

Table 1. Physicochemical properties of HOPO powders obtained by two different drying methods

Drying method	Moisture (%)	a_w	DR (s)	BD (g/mL)
SD	2.43[a] (0.05)	0.1621[a] (< 0.01)	83.00[a] (9.9)	0.6366[a] (0.01)
FD	2.31[a] (0.01)	0.0701[b] (0.01)	146.00[b] (5.7)	0.5154[b] (< 0.01)

DR: dissolution rate; BD: bulk density.
The values in parenthesis are the standard deviations.
[abc]In the same column, means without the same letter reveal significant differences ($p < 0.05$) according to the LSD multiple range test.

On the other hand, FDP presented lower a_w values ($p < 0.05$) than SDP (Table 1). This may be caused because the high vacuum used. The high vacuum gradient can affect the water transfer rate within the molecular structure, resulting in a lower residual a_w in the final product [15]. In the SD method, increasing the temperature of the inlet air, increases the temperature gradient between the air flow and the emulsion, which results in the increase of heat transfer and, therefore, the rate of evaporated water [16]. In addition, the rapid drying in the SD method produces a homogeneous particle size that helps a faster contraction of the particles after water evaporation, generating a minimum amount of available water [17]. It is known that with an a_w below 0.3, the water present is not enough to behave like a solvent, which decreases the mobility of the products available for degradation reactions and microbial growth [18]. In this sense, both drying technologies allow obtaining stable products from the point of view of water activity.

In relation to bulk densisty (BD), FDP presented lower BD values ($p < 0.05$) than SDP (Table 1). Baeghbali et al, [19] when studying the effect of different drying methods on the physical properties of pomegranate juice obtained that spray dried samples had higher BD compared to refractance window dried samples because of the fine structure of the spray dried sample. It is known that BD is directly related to the moisture content of the powders. With less moisture content, less water will be present in the structure, which allows more empty spaces between the particles and the interior of these. In this way, increasing the porosity, will increase the surface area per unit volume, and finally will decrease the BD [20]. This fact would explain the higher BD obtained in spray dried HOPO powders due to its high moisture content compared to that obtained by FD.

Finally, FDP presented higher DR values ($p < 0.05$) than SDP (Table 1). Similar results were obtained by Caparino et al., [4] when studying the effect of different drying methods on the physical properties and microstructure of mango powder. These authors obtained higher solubility (lower DR) on the spray dried mango powder compared to freeze dried product. They established that the atomization of mango puree during spray drying could contribute to solubility of spray-dried product. This fact would explain the higher solubility obtained in spray dried HOPO powders compared to that obtained by FD.

3.2. Microstructure

Scanning electron micrographs of HOPO powders obtained by different drying processes are shown in Fig.1. Spray-dried HOPO powders (Fig. 1A and 1C) has spherical or oval shape and smooth surface particles due to effect of spray-drying condition, which was maintained at inlet temperature of 190°C during drying. On the other hand, freeze dried HOPO powders (Fig. 1B and 1D) showed a skeletal-like structure. Similar results were obtained by Caparino et al [4] when studying the effect of different drying methods on the

physical properties and microstructure of mango powder. These authors obtained a more spherical shape, and more smooth and porous surface on spray dried mango powder compared to freeze dried product. The smooth spherical-shaped HOPO powder could contributed to its high solubility and BD compared to the freeze drying method.
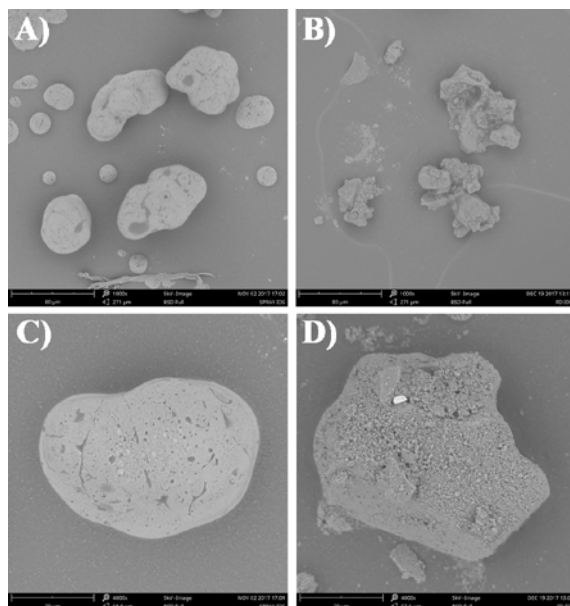
Fig. 1 Scanning electron microscopy micrographs for powders of HOPO nanoemulsions obtained using spray drying (A, C) and freeze drying (B, D). Magnification: 1000x (A,B), 4000x (C, D).

4. Conclusions

Results showed that of the four response variables analysed, three were significantly affected by the drying method applied ($p < 0.05$). No significant differences ($p > 0.05$) were obtained between the moisture of FD powders compared to those obtained by SD. Moreover, FD powders presented lower activity water and BD, and higher DR than SD powders. These important changes in the physicochemical properties of the powders of HOPO could be related to structural modifications observed. So, results suggest that SD could be a more economical alternative to FD in order to obtain HOPO powders with low moisture and activity water and higher solubility.

5. Acknowledgements

6. References

[1] Ricaurte, L., M.d.J. Perea-Flores, A. Martinez, and M.X. Quintanilla-Carvajal. Production of high-oleic palm oil nanoemulsions by high-shear homogenization (microfluidization). Innov. Food Sci. Emerg. Technol., 2016. 35, 75-85.

[2] Pan, H., L. Yu, J. Xu, and D. Sun. Preparation of highly stable concentrated W/O nanoemulsions by PIC method at elevated temperature. Colloids and Surfaces A: Physicochemical and Engineering Aspects, 2014. 447, 97-102.

[3] Lee, L. and I.T. Norton. Comparing droplet breakup for a high-pressure valve homogeniser and a Microfluidizer for the potential production of food-grade nanoemulsions. J. Food Eng., 2013. 114(2), 158-163.

[4] Caparino, O.A., J. Tang, C.I. Nindo, S.S. Sablani, J.R. Powers, and J.K. Fellman. Effect of drying methods on the physical properties and microstructures of mango (Philippine 'Carabao' var.) powder. J. Food Eng., 2012. 111(1), 135-148.

[5] Kha, T.C., M.H. Nguyen, and P.D. Roach. Effects of spray drying conditions on the physicochemical and antioxidant properties of the Gac (Momordica cochinchinensis) fruit aril powder. Journal of Food Engineering, 2010. 98(3), 385-392.

[6] Saravacos, G.D. and A.E. Kostaropoulos. Handbook of Food Processing Equipment; Springer International Publishing: 2002.

[7] Toledo, R.T. Fundamentals of Food Process Engineering; Springer US: 2007.

[8] Nindo, C.I. and J. Tang. Refractance Window Dehydration Technology: A Novel Contact Drying Method. Drying Technology, 2007. 25(1), 37-48.

[9] Ratti, C. Hot air and freeze-drying of high-value foods: a review. Journal of Food Engineering, 2001. 49(4), 311-319.

[10] Caparino, O. Characteristics and quality of freeze-dried mango powder pre-frozen at different temperatures. Philippine Agricultural Scientist Journal, 2000. 83(4), 338-343.

[11] Quintanilla-Carvajal, M.X., H. Hernández-Sánchez, L. Alamilla-Beltrán, G. Zepeda-Vallejo, M.E. Jaramillo-Flores, M. de Jesús Perea-Flores, A. Jimenez-Aparicio, and G.F. Gutiérrez-López. Effects of microfluidisation process on the amounts and distribution of encapsulated and non-encapsulated α-tocopherol microcapsules obtained by spray drying. Food Research International, 2014. 63, Part A, 2-8.

[12] El-Tinay, A.H. and I.A. Ismail. Effects of some additives and processes on the characteristics of agglomerated and granulated spray-dried roselle powder. Acta Alimentaria, 1985. 14(3), 283-295.

[13] Ferrari, C.C., S.P. Marconi Germer, I.D. Alvim, and J.M. de Aguirre. Storage stability of spray-dried blackberry powder produced with maltodextrin or gum arabic. Drying Technology, 2013. 31(4), 470-478.

[14] Tontul, I. and A. Topuz. Effects of different drying methods on the physicochemical properties of pomegranate leather (pestil). LWT - Food Science and Technology, 2017. 80, 294-303.

[15] Moayyedi, M., M.H. Eskandari, A.H.E. Rad, E. Ziaee, M.H.H. Khodaparast, and M.T. Golmakani. Effect of drying methods (electrospraying, freeze drying and spray drying) on survival and viability of microencapsulated Lactobacillus rhamnosus ATCC 7469. Journal of Functional Foods, 2018. 40, 391-399.

[16] Hu, L., J. Zhang, Q. Hu, N. Gao, S. Wang, Y. Sun, and X. Yang. Microencapsulation of brucea javanica oil: Characterization, stability and optimization of spray drying conditions. Journal of Drug Delivery Science and Technology, 2016. 36, 46-54.

[17] Carvalho, A.G.S., V.M. Silva, and M.D. Hubinger. Microencapsulation by spray drying of emulsified green coffee oil with two-layered membranes. Food Research International, 2014. 61, 236-245.

[18] Ortiz-Jerez, M.J., T. Gulati, A.K. Datta, and C.I. Ochoa-Martínez. Quantitative understanding of Refractance Window™ drying. Food Bioprod. Process., 2015. 95, 237-253.

[19] Baeghbali, V., M. Niakousari, and A. Farahnaky. Refractance Window drying of pomegranate juice: Quality retention and energy efficiency. LWT - Food Science and Technology, 2016. 66, 34-40.

[20] Artiga-Artigas, M., A. Acevedo-Fani, and O. Martín-Belloso. Effect of sodium alginate incorporation procedure on the physicochemical properties of nanoemulsions. Food Hydrocolloids, 2017. 70, 191-200.

Multifluid macroscopic approach to drying in papermaking

Durán-Olivencia, F. J.[a*]; Farzad, M.[a]; Tilley, B. S.[b]; Yagoobi, J. S.[a]

[a] Multi-Scale Heat Transfer Laboratory, Mechanical Engineering Department, Worcester Polytechnic Institute, Worcester, MA 01609, USA

[b] Department of Mathematical Sciences, Worcester Polytechnic Institute, Worcester, MA 01609, USA

*E-mail of the corresponding author: fjduranolivencia@wpi.edu

Abstract

Drying process represents one of the main energy-consuming stages for a broad variety of manufacturers. However, despite its significant impact on energy efficiency, most implementations at manufacturing level do not operate within the optimal conditions.

This work investigates the interplay among different parameters involved into the paper-drying process. To do so, we analyze both experimental and numerical results. The theoretical approach couples a non-isothermal flow, along with the heat transfer and transport of different fluids participating. Our results, experimental and numerical, show a good agreement according to the characteristic drying time scale. The results thus enable to estimate the impact of different mechanisms into drying process.

Keywords: paper-drying process; free water; bound water; papermaking.

1. Introduction

Drying porous media is an experience surrounding us every single day. Food, building material, paper pulp, textiles or tissues are some examples of the engineering applications wherein the drying process has a central impact.

Porous media refers to materials presenting a pores network. In most applications, these cavities are filled with different fluids: gases and liquids. The interaction between those fluids and the solid matrix is what ultimately regulates the mass transfer concurring in this complex pores network. Indeed, understanding the complex dynamic of drying rate has been of interest for the past decades. At high saturation level, the water may be described using its bulk properties, that is called free water[1]. Although the latter represents a significant percentage of the water inside the structure (roughly 80% in most cases), drying the remaining water, physical or chemically adsorbed into the solid matrix (bound water), requires a considerable energetic effort.

Unfortunately, an exact description about bound water demands a microscopic approach for the solid-fluid interaction. Such description involves knowing the peculiarities of geometrical irregularities as well as forces at the molecular level between walls and fluid, which turns the problem into a challenge both theoretical and numerical. Nonetheless, in most practical cases, a so accurate insight is unnecessary or leads to an impossible undertaking.

To tackle this multi-scale scenario, we investigate the drying process on paper using the porous media theory. We followed, therefore, a macroscopic approach which provides an intuitive description averaging all minutiae at the microscopic level. We turn in this way the micro-scale effects into volume and surface terms in the governing equations at macro-scale[2]–[4].

This paper analyze a real case in which a non-isothermal flow is addressed to the porous medium, initially wholly saturated. We explore thus the interplay among mass and energy transfer, pressure distribution, or the evolution of evaporation front among other parameters. To do so, we combine a numerical approach with experimental results. Our results enable to clarify the transition between free and bound water, elucidating the role played by the main control parameters during the experiment.

Section 2 presents the problem formulation, discussing the physics and assumptions considered in the macroscopic approximation. Section 3 details the numerical and experimental results. Finally, Section 4 brings together the leading conclusions, highlighting potential mechanisms to investigate in future works to incorporate the bound water effect at low saturation level.

2. Problem formulation

In this section, we motivate the macroscopic formulation of the porous medium and its interaction with the flow passing it through as well as the heat transfer induced. The first paragraph is dedicated to the geometrical setting since that helps to bear in mind an intuitive workflow to formulate the corresponding governing equations later.

2.1. Geometrical setting

Fig. 1 shows a schematic sketch about the geometrical setup modeled in this work. As the
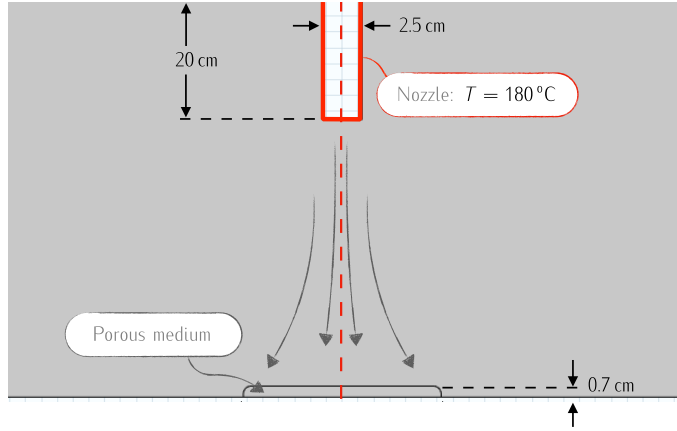
Fig. 1. Schematic sketch of the setting investigated in this work.

figure illustrates, we simulate the problem in a two-dimensional case. For low Reynolds numbers, that is a reasonable assumption that trims the computational effort considerably.

2.2. Governing equations: A miscible fluids formulation

The macroscopic approach comes up averaging over a representative elementary volume[5]. At this high level, there is no trace of surface topology at micro-scale, and the porous medium is then reduced to a continuum view. Solid-fluid interaction is thus modelled via a distributed energy loss induced by the flow going through the solid matrix.

Hence, at such high level, the flow field for the gas phase (dry air and water vapor) is governed by a single Navier-Stokes equation (NSE)[6]. Indeed, inside the porous medium, the energy losses induced by the solid matrix require some additional considerations. Those are, essentially, concerning on the way the solid matrix modulates different contributions in the NSE, turning eventually this into a Brinkman equation (BE)[7]. Thus, outside the porous medium, the gas-phase flow is described by a non-isothermal NSE:

$$\frac{\partial \rho_g}{\partial t} + \nabla \cdot \left[\rho_g \mathbf{u}_g \right] = 0,$$

$$\rho_g \left[\frac{\partial \mathbf{u}_g}{\partial t} + \mathbf{u}_g \cdot \nabla \mathbf{u}_g \right] = \nabla \cdot \left[-p\mathbf{I} + \mu_g \left(\nabla \mathbf{u} + \nabla \mathbf{u}_g^{\mathrm{T}} \right) - \frac{2}{3} \mu_g \left(\nabla \cdot \mathbf{u} \right) \right], \tag{1}$$

where ρ_g and μ_g are air density and dynamic viscosity, respectively. Inside the porous structure, however, Equation (1) must be modified considering the drag induced by the solid matrix, what eventually results in the BE[3]

$$\left(\frac{\rho_g}{\varepsilon} \right) \left[\frac{\partial \mathbf{u}_g}{\partial t} + \mathbf{u}_g \cdot \nabla \mathbf{u}_g \right] = -\nabla p + \mu_g \tau \nabla^2 \mathbf{u}_g - \frac{\mu_g}{k} \mathbf{u}_g - \frac{c}{k^{1/2}} \rho_g \left| \mathbf{u}_g \right| \mathbf{u}_g, \tag{2}$$

where the last two terms of the RHS represent Darcy[8] and Forscheimer[9], [10] resistances, respectively. The coefficients ε, k_g and τ are the porosity, permeability of the gas phase, and tortuosity, respectively. The coefficient c comes from an experimental fitting; we consider the experiments carried out by Hoang et al.[11] which are an example of such empirical relationship between c and k.

Water vapor velocity field may be described in terms of $\mathbf{u}_g$, including the diffusion of vapor into the dry air (binary diffusion, Bird et al.[12])

$$\mathbf{u}_v = \frac{\mathbf{u}_g}{S_g \varepsilon} - \frac{M_a D_e}{M_v \rho_v} \nabla \rho_v, \tag{3}$$

where an effective porosity ($S_g \varepsilon$) and diffusivity (D_e) are considered. The first one according to the saturation level, whereas the effective diffusivity depends on the local temperature, porosity, and tortuosity[13]

$$D_e = D_v \varepsilon^{4/3} S_g^{10/3}, \tag{4}$$

where D_v is the bulk diffusivity of the water vapor in the air.

Liquid phase (water), conversely, not require such a sophisticated formulation to compute its velocity field. Water inside the porous media reaches velocities much smaller than the gas phase. This fact enables to describe the water velocity field using a Darcy's law, depending solely on the pressure gradient induced into the gas phase dynamic

$$\mathbf{u}_l = -\frac{k_l}{\mu_l S_l \varepsilon} \nabla p, \tag{5}$$

where $S_l \varepsilon$ reflects an effective porosity as a function of local saturation level.

The lack of concrete pores, conceptually, leads to the impossibility to track the interaction between two phases concurring within the porous medium. Essentially, because there is no way to define an interface, and consequently the interfacial energy stored. Even though, mechanisms such as capillary or evaporation may be included in the transport of different phases considering their average contribution over the REV. Phases are thus represented as miscible fluids; which is entirely consistent with the mean-field character of REV approximation. Transport of liquid and gas phases are formulated then as a conventional balance equation:

$$\frac{\partial c_l}{\partial t} + \mathbf{u}_l \cdot \nabla c_l - D_{\text{cap}} \nabla^2 c_l = -\dot{m}_{\text{evap}},$$
$$\frac{\partial c_v}{\partial t} + \mathbf{u}_v \cdot \nabla c_v - D_e \left(\frac{M_a}{M_g} \right) \nabla^2 c_v = \dot{m}_{\text{evap}}, \tag{6}$$

where D_{cap} represents the diffussivity induced by the capillary effects[3], and $\dot{m}_{\text{evap}}$ is the mass flux evaporating

$$\dot{m}_{\text{evap}} = \nu_{\text{evap}} \left(a_{\text{w}} c_{\text{sat}} - c_v \right). \tag{7}$$

The coefficient ν_{evap} [s^{-1}] accounts the evaporation rate, whereas a_{w} represents the water activity[4]; c_v is the concentration of water vapor at a given time; and c_{sat} is the saturation

concentration

$$c_{\text{sat}} = \frac{p_{\text{sat}}(T)}{RT},$$ (8)

where p_{sat} is the saturation pressure, and R is the gas constant.

Nonetheless capillary, water activity, or intrinsic porous properties depend overall on the water saturation level[4]. Those levels are, however, closely related to the corresponding concentration via the relationship:

$$S_l = \frac{c_l M_l}{\rho_l \varepsilon},$$ (9)

which, ultimately, means the ratio of mass of a given species in an elementary volume over the total. On the other hand, given that phases are connected each other in an elementary volume via conservation of mass, the gas saturation level turns out to be:

$$S_g = 1 - S_l.$$ (10)

Saturation variables alleviate the heat transfer problem inside the solid structure, reducing it to the general energy balance for a single phase flow;

$$\rho_m C_{p,m} \left[\frac{\partial T}{\partial t} + \mathbf{u}_m \cdot \nabla T \right] = \nabla \cdot (k_m \nabla T) - \mathscr{L}_{\text{evap}} \dot{m}_{\text{evap}},$$ (11)

where the subscript $\dot{m}_{\text{evap}}$ indicates the average thermal properties, which results from a weighted average between the two phases coexisting within the porous structure

$$
\begin{aligned}
\rho_m &= S_g \rho_g + S_l \rho_l, \\
C_{p,m} &= \frac{C_{p,g} S_g \rho_g + C_{p,l} S_l \rho_l}{\rho_m}, \\
k_m &= S_g k_g + S_l k_l, \\
\mathbf{u}_m &= \frac{\mathbf{\Gamma}_g C_{p,g} + \mathbf{\Gamma}_l C_{p,l}}{\rho_m C_{p,m}},
\end{aligned}
$$ (12)

where

$$\mathbf{\Gamma}_{l,g} = \rho_{l,g} \mathbf{u}_{l,g}$$ (13)

is the flux of each phase.

Finally, according to the modeling detailed in this section, the water dynamic inside the porous structure is described as a combination of different mechanisms interconnected with each others. Hence, free and bound water concepts are not considered as discrete states within the continuum approach, but rather as asymptotic modes induced by a combination of mechanisms involve in drying process.

2.3. Implicit assumptions and limitations

The theoretical model above mentioned connects micro- and macro- scales via water activity and solid matrix properties. There are two critical points, however, assumed in such

continuum description:

- *Water activity*. Although the theoretical model is part of a macroscopic framework, water activity (Eq. (7)) brings in the microscopic dynamic of water via sorption isotherms. We followed the IUPAC recommendations[14], which mainly divide the physisorption mechanisms into five classes according to the original classification carried out by Brunaer et al.[15]. In particular, we implemented the type I (Langmuir isotherm), since that is commonly exhibited in micropores.

- *Average properties*. Porous media properties used in this work were chosen from both theoretical and experimental relationships for different porous media including foods[4].

3. Results and discussion

This section itemizes the major findings derived from the theoretical model introduced in the previous section.

3.1. Drying curve

Fig. 2 (left) shows the numerical drying curve. The evolution of moisture content exhibits, mostly, two different areas: a linear region, which is linked in the literature to free water; and another nonlinear region at low saturation levels associated with bound water wherein surface effects become dominant.

As we mentioned above, the theoretical model presented in this work is not aimed at differentiating between free and bound water, at least in the conventional manner. Mainly, because these concepts revolve around discrete states, which is hardly fit with the continuum framework proposed. Water activity and the corresponding sorption isotherm are used then
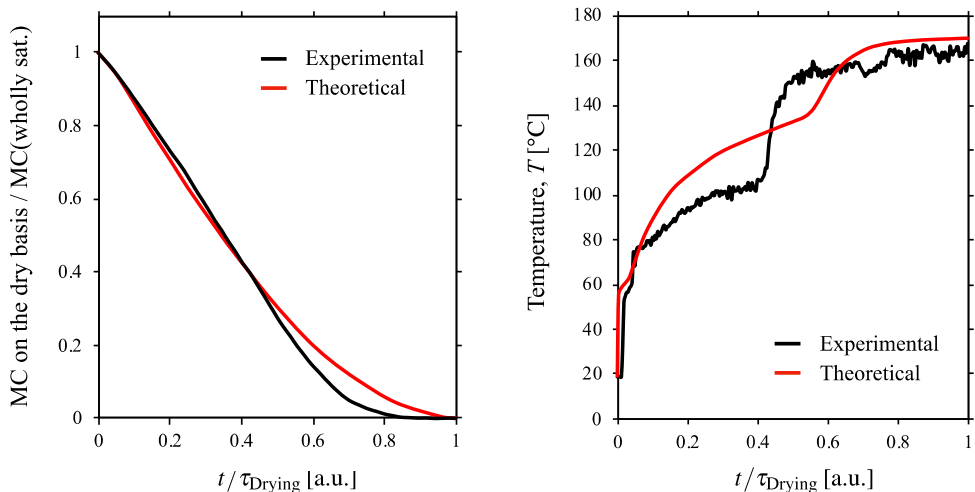
Fig. 2. (Left) Drying curve. (Right) Temperature evolution at surface center. Both graphs are referred to the drying time scale, τ_{Drying}; time required to reach a 0.2% water saturation level. That enables a qualitative comparision between experimental and theoretical results. Experimental curves were obtained according to the setup detailed by Farzad et al. [16].

as the natural way to connect micro- and macro-scales concurring along the transient. Therefore, the nonlinear region appears as a combination of different factors involving not only fluid-wall interaction at micro-scale via water activity, but also the evolution of others macroscopic magnitudes as the pressure and temperature distributions.

The good agreement (qualitatively) between numerical and experimental curves supports the theoretical insight proposed in this work. Such validation enables to explore the role of each macroscopic control parameters in the sorption process, and thereby in the drying dynamic.

3.2. Temperature evolution at surface center

Fig. 2 (right) displays another characteristic response throughout the drying process evolution: temperature evolution at the surface center of the sample.

Surface center is the point at which the flow is addressed (Fig. 1). The flow outside porous structure quickly reaches a steady situation. As the curve details (Fig. 2–right), the two-step profile reveals the dependency with other factors such as the evolution of evaporation front. Otherwise, the combination of convection and conduction mechanisms would lead to a single step curve.

4. Conclusions

Recent work about the drying dynamic inside porous media provides a continuum theoretical framework to deal with multiple scales concurring during the drying process. Free and bound water are posed as asymptotic water modes inside the solid structure rather than two different and discrete states. Our results are in good agreement (qualitatively) with their experimental counterparts. Drying curve exhibits not only the linear part usually assigned to free water, but also nonlinearities associated with bound water at low saturation levels. In its turn, the temperature evolution at the surface center of the sample presents the two-step profile observed experimentally. On the other hand, the pressure and temperature distributions inside the solid structure unveil the way the evaporation front advances through the solid matrix. The nonlinear advancement of the evaporation front through the porous structure pushes the water to the edge of the domain where the heat transfer drops considerably

Nevertheless, these results must be analyzed with extreme care since we assumed two critical points. First, we considered a Langmuir adsorption isotherm as the sorption dynamics modulating the water activity inside the solid structure. While it is true that it is commonly used in micropores, there is no enough experimental evidences to support this assumption in the case we worked with. For instance, capillary condensation is a potential adsorption isotherm to be considered, since it explains the way alternating wide and narrow parts of pores may enhance evaporation or condensation processes. On the other hand, solid matrix properties were considered as an average based on a bunch of theoretical and experimental relationships including different porous media.

Therefore, given that the theoretical framework presented in this work connects the micro- and macro- scales via porous medium properties and the adsorption isotherm, a more complete description of these two factors is required. They do are currently under a more in-depth investigation in our laboratory both experimental and theoretically.

5. Acknowledgements

(CARD), a US National Science Foundation Industry University Cooperative Research Center. CARD is located at Worcester Polytechnic Institute and the University of Illinois at Urbana-Champaign (co-site).

6. References

[1] P. A. Vesilind, "The Role of Water in Sludge Dewatering," *Water Environment Research*, vol. 66, no. 1, pp. 4–11, 1994.

[2] M. C. Asensio, "Transport phenomena during drying of deformable, hygroscopic porous media: Fundamentals and applications," PhD Thesis, 2000.

[3] A. K. Datta, "Porous media approaches to studying simultaneous heat and mass transfer in food processes. I: Problem formulations," *Journal of Food Engineering*, vol. 80, no. 1, pp. 80–95, 2007.

[4] A. K. Datta, "Porous media approaches to studying simultaneous heat and mass transfer in food processes. II: Property data and representative results," *Journal of Food Engineering*, vol. 80, no. 1, pp. 96–110, 2007.

[5] J. Bear, *Dynamics of flow in porous media*. 1972.

[6] G. K. Batchelor, *An Introduction To Fluid Dynamics*, Cambridge University Press. 2002.

[7] H. C. Brinkman, "A calculation of the viscous force exerted by a flowing fluid on a dense swarm of particles," *Flow, Turbulence and Combustion*, vol. 1, no. 1, p. 27, Dec. 1949.

[8] H. Darcy, *Les fontaines publiques de la ville de Dijon: exposition et application ...* Victor Dalmont, 1856.

[9] J. É. J. Dupuit, *Études théoriques et pratiques sur le mouvement des eaux dans les canaux découverts et à travers les terrains perméables: avec des considérations relatives au régime des grandes eaux, au débouché à leur donner, et à la marche des alluvions dans les rivières à fond mobile*. Dunod, 1863.

[10] S. Whitaker, "The Forchheimer equation: A theoretical development," *Transport in Porous Media*, vol. 25, no. 1, pp. 27–61, Oct. 1996.

[11] M. Hoang, P. Verboven, M. Baelmans, and B. Nicolaï, "A continuum model for airflow, heat and mass transfer in bulk of chicory roots," *Transactions of the ASAE*, vol. 46, no. 6, p. 1603, 2003.

[12] R. B. Bird, W. E. Stewart, and E. N. Lightfoot, *Transport Phenomena*, 2nd ed. New York: Wiley, 2002.

[13] R. Millington and J. Quirk, "Permeability of porous solids," *Transactions of the Faraday Society*, vol. 57, pp. 1200–1207, 1961.

[14] M. Thommes *et al.*, "Physisorption of gases, with special reference to the evaluation of surface area and pore size distribution (IUPAC Technical Report)," *Pure and Applied Chemistry*, 2015.

[15] S. Brunauer, L. S. Deming, W. E. Deming, and E. Teller, "On a theory of the van der Waals adsorption of gases," *Journal of the American Chemical society*, vol. 62, no. 7, pp. 1723–1732, 1940.

[16] M. Farzad, M. Yang, J. S. Yagoobi, and B. S. Tilley, "Drying of Moist Food Snacks With Innovative Slot Jet Reattachment Nozzle," in *International Drying Symposium*, Valencia, Spain, 2018.

Freeze dried quince (*Cydonia oblonga*) puree with the addition of different amounts of maltodextrin: physical and powder properties

Unlueroglugil, Ö.[a]; Yuksel, H.[a*]; Koç Calıskan, G.[a]; Dirim, S.N.[a]

[a]Department of Food Engineering, University of Ege, Izmir, Turkey.

*E-mail of the corresponding author: hirayuksel@gmail.com

Abstract

This study aims to determine the drying behavior of quince puree and as an adverse effect powdered sugar added quince puree with the addition of maltodextrin. The addition of powdered sugar increases the drying time and the total amount of energy and the same time slightly decreases the moisture content and water activity values. The color values and the properties on these values changed both with the addition of maltodextrin and powdered sugar. The density values, flow properties and reconstitution properties are significantly affected by the amount of maltodextrin in plain or powdered sugar added samples.

Keywords: quince, freeze-drying, maltodextrin, powder properties.

1. Introduction

Quince which is rich in vitamins A, B and C, sugar, crude fiber and minerals such as potassium, phosphorus and calcium [1]. Fresh fruits and vegetables are easily deteriorated due to their high moisture content, which can be prevented by a variety of preservation methods and one of these methods is the drying process. The drying process was first initiated by drying in the sun, but due to the lack of long processing times and standard product handling, industrial drying methods have been developed such as freeze-drying. The freeze-drying process is based on the principle of free water sublimation in freezing under low pressure, and desorption removal of bound water. Therefore, the water is removed by the vacuum in the solid phase and the loss of the valuable components such as minerals, vitamins and aromas are minimized in the product structure. Freeze dried products are well known with high nutritional value and having a porous structure.

This study aims to determine the drying behavior of quince puree and as an adverse effect powdered sugar added quince puree with the addition of maltodextrin. In addition, the physical, and powder properties of the obtained quince powders and the energy consumption through the freeze drying operation was also determined.

2. Materials and Methods

2.1. Material

The fresh quince fruits were obtained from a local supermarket in Izmir, Turkey. They were washed, peeled, seeds removed, and grounded into puree by using a home type blender (Tefal Smart, MB450141, Turkey). Maltodextrin (MD) with Dextrose Equivalence (DE) value of 10-12 (AS Chemical Industry and Commerce Limited Company, Turkey) was added directly to puree and to the powdered sugar (PS) containing puree in suitable amounts (4-6-8-10% by weight).

2.2. Methods

2.2.1. Freeze Drying

The experiments were performed in a pilot scale freeze dryer (Armfield, FT 33 Vacuum Freeze Drier, England). The ground powders were stored in aluminum polyethylene packaging material (ALPE) in the dark at 20±1°C.

2.2.2. Analysis applied to powders

The moisture content of the quince puree powders was carried out with 0.5-1 g of samples, which were dried in an oven at 105 °C until reaching a constant weight. The water activity values were measured by using a Testo-AG 400, Germany water activity measurement device. The color (L*, a*, and b* values) values of the quince puree powders were

measured with a Minolta CR-400 Colorimeter, Japan and the results were expressed in accordance with the CIE Lab. System. The total color change (ΔE), Chroma, Hue Angle (°), Browning (BI), whiteness (WI) and yellowness (YI) index were calculated according to the method of Pathare and Opara, 2012 [2]. For the determination of bulk density, tapped density, flowability and cohesiveness values in terms of Carr index (CI), and Hausner ratio (HR), the average wettability time (s) and solubility of powder were determined with the method of Jinapong, 2008 [3]. The dispersibility, porosity and hygroscopicity values were determined according to Gong et al., 2008, Jinapong 2008 and Cai and Corke, 2000 respectively [3, 4, 5].

2.2.3. Statistical Analysis

Data were analyzed using statistical software SPSS 16.0 (SPSS Inc., Chicago, IL, USA). The data were also subjected to analysis of variance (ANOVA) and Duncan's multiple range test (α=0.05) to determine the difference between means. The drying experiments were replicated twice and all analyses were triplicated.

3. Results and Discussions

The drying time of samples, the energy consumption of the freeze dryer, the moisture content and water activity values of the dried quince puree powders are given in Table 1.

Table 1. The energy consumption, moisture content, and water activity values of the samples

Samples	Energy Consumption (KWH)	Moisture Content (% Wet Basis, wb)	Water Activity
4% MD	8.47±0.01 [xp]	8.61±0.43 [xp]	0.43±0.01 [yr]
6% MD	8.47±0.01 [xp]	8.40±0.44 [xp]	0.41±0.01 [xr]
8% MD	8.47±0.01 [xp]	7.77±0.42 [xp]	0.41±0.01 [xr]
10% MD	8.47±0.01 [xp]	7.72±0.13 [xp]	0.44±0.01 [zr]
4% PS+4% MD	10.06±0.01 [xr]	7.67±0.21 [xp]	0.43±0.002 [tp]
4% PS+6% MD	10.06±0.01 [xr]	7.32±0.57 [xp]	0.40±0.02 [zp]
4% PS+8% MD	10.06±0.01 [xr]	7.05±0.22 [xp]	0.37±0.008 [yp]
4% PS+10% MD	10.06±0.01 [xr]	6.78±0.11 [xp]	0.37±0.01 [xp]

x-t Different letters in the same column indicate a significant difference between the concentration of MD at *P* < 0.05.
p-r Different letters in the same column indicate a significant difference between the samples with MD or 4%PS+MD at *P* < 0.05.

To determine the energy efficiency of drying the energy consumption and the product quality have been identified as the key factors. The first and second sets of samples were dried for 15 hours and 18 hours, respectively.

Considering the energy consumption per hour of drying (0.559 kWh), the highest energy consumption value (10.06 kWh) was in the sample set where MD was added to quince puree with 4% PS. The moisture content of the samples was not significantly different. Dried foods (with water activity values of 0.20-0.40) were considered as stable for browning, microbial growth and enzymatic reactions [6]. According the Table 1, the water activity (aw) values of the powders are very near or slightly higher the upper limit.

The measured color values of the dried samples are given in Figure 1. The highest L (brightness) value was achieved in the samples added with only 4% maltodextrin, while the highest brightness value was attained by addition of maltodextrin at 6% concentration together with the powdered sugar. Positive values of a* and b* indicate redness, yellowness, respectively. The highest values were observed from quince powder with 10% MD. As the amount of added maltodextrin increased, a decrease in L value was observed.

Fig. 1 The color values of quince puree powders.

The properties of the powders based on the color measurement are given in Table 2. Considering the results of color measurement, the highest total color change (ΔE) was detected in samples of added with 8% MD and PS and a significant increase in the total color change was observed as the amount of MD added to the samples increased. In the Hue angle, a significant decrease was observed with the addition of MD to quince puree but no effect was observed for PS containing puree ($P < 0.05$). sample with 10% maltodextrin, which has the highest Chroma value, was accepted as the sample with the highest color intensity perceived by humans. In food products containing powdered sugar, the highest browning index value, which is one of the most common indicators of browning, has been detected on the level of quince with 8% maltodextrin added. The whiteness index (WI), which indicates the degree of discoloration during the drying process, represents the extreme whiteness of food products [7].

Table 2. The total color change, hue angle, chroma values, browning, whiteness, and yellowness index of the powders.

Samples	ΔE	Hue Angle	Chroma	Browning Index (BI)	Whiteness Index (WI)	Yellowness Index (YI)
4% MD	32.18±1.21 [xp]	1.28±0.17 [tr]	29.31±0.29 [xp]	58.34±1.54 [xp]	58.62±0.35 [xp]	57.10±0.40 [xp]
6% MD	28.58±1.21 [xp]	1.25±0.00 [zr]	28.01±1.52 [xp]	60.54±3.77 [xp]	54.84±0.79 [xp]	59.95±0.69 [xp]
8% MD	24.58±1.33 [xp]	1.12±0.02 [xp]	36.15±2.75 [yr]	107.58±13.82 [yr]	43.87±0.52 [xp]	78.29±1.83 [xp]
10% MD	26.94±2.05 [xp]	1.17±0.00 [yp]	38.04±1.55 [zr]	109.54±2.34 [zr]	43.03±0.64 [xp]	87.69±0.66 [xp]
4% PS+ 4% MD	32.54±0.79 [yp]	1.19±0.00 [xp]	28.01±0.43 [xp]	65.66±2.26 [tp]	53.08±0.39 [xp]	59.47±0.47 [xp]
4% PS+ 6% MD	35.85±0.84 [zr]	1.20±0.01 [yp]	27.54±0.29 [xp]	60.73±2.97 [zr]	53.47±0.58 [xp]	58.90±0.71 [xp]
4% PS+ 8% MD	36.09±3.38 [tp]	1.20±0.01 [yr]	27.79±0.30 [xp]	61.54±1.67 [xp]	55.15±0.72 [xp]	56.89±0.89 [xp]
4% PS+ 10% MD	31.46±4.45 [xr]	1.20±0.04 [yr]	27.69±0.50 [xp]	61.61±3.52 [yp]	56.25±0.99 [xp]	55.84±1.63 [xp]

x-t Different letters in the same column indicate a significant difference between the concentration of MD at $P < 0.05$.
p-r Different letters in the same column indicate a significant difference between the samples with MD or 4%PS+MD at $P < 0.05$.

As shown in Table 2, as the maltodextrin content increases, a decrease in this value is observed. Yellowness value is related to general product degradation by light, chemical exposure and processing. This value is basically used to measure the amount of such degradation with a single value [8]. The results showed that increasing the MD content resulted in a significant increase in the yellowness value whereas increasing the MD and PS cause decrease in these values (P<0.05).

The results of the powder properties of the freeze dried quince powders are given in Table 3 and 4. The powder properties are important for the functional, economical, and commercial consideration of the powder products [10]. The average wettability and solubility times of the freeze-dried quince powders were found to be as 3 seconds and the amount of maltodextrin and the addition of powdered sugar did not affect the wettability and solubility times of the samples (P>0.05, data was not given.). The highly porous structure and similar residue moisture content may be the reason for the low wettability and solubility times.

Table 3. The powder properties of freeze-dried quince powders

Samples	Bulk Density (kg/m³)	Tapped Density (kg/m³)	Flowability (Carr Index)	Cohesiveness (Hausner Ratio)
4%MD	109.88±1.40[xp]	164.03±8.44[yp]	32.95±2.60[zr] (Fair)	1.49±0.06[zr] (High)
6%MD	119.55±15.86[xp]	146.35±18.41[xp]	18.35±0.57[xp] (Good)	1.22±0.01[xp] (Intermediate)
8%MD	153.57±35.36[yp]	203.64±33.43[zp]	25.00±5.05[yp] (Fair)	1.34±0.09[yp] (Intermediate)
10%MD	150.00±28.28[yp]	199.11±18.94 [zp]	25.00±7.07[yp] (Fair)	1.34±0.13[yp] (Intermediate)
4%PS+4%MD	182.62±5.72[yr]	261.00±47.70 [xr]	29.05±5.77[xp] (Fair)	1.42±0.22[xp] (High)
4%PS+6%MD	224.05±4.55[zr]	345.54±46.72 [yr]	34.47±10.18[xr] (Fair)	1.54±0.24[xr] (High)
4%PS+8%MD	157.85±15.92[xp]	248.93±80.08 [xp]	38.30±10.65[xr] (Bad)	1.65±0.28[xr] (High)
4%PS+10%MD	194.89±45.80[yr]	286.80±28.52 [xr]	30.68±8.03[xr] (Fair)	1.45±0.17[xr] (High)

x-t Different letters in the same column indicate a significant difference between the concentration of MD at $P < 0.05$.
p-r Different letters in the same column indicate a significant difference between the samples with MD or 4%PS+MD at $P < 0.5$.

The bulk and tapped density values of freeze-dried quince powders with MD significantly increased depending on the increasing amount of (P<0.05). Comparatively higher bulk and tapped density values were observed for the quince powders with powdered PS and MD (P<0.05). It may be due to the higher solid amount of quince puree with 4%PS+MD compared to the quince puree with MD. Cai and Corke (2000) [5] reported that the increase in solid concentration in the feed which makes the particles heavier resulted in higher bulk density. For this reason, the higher bulk density values were obtained at the higher MD concentrations and the 4%PS addition. The flowability and cohesiveness properties of the quince powders in terms of the CI and HR were evaluated, the higher CI and HR values mean that the powder is more cohesive and less able to flow freely. The higher CI and HR values were observed for the sample with 4%MD and 4%PS+6%MD, 4%PS+8%MD, and 4%PS+10%MD. The CI and HR values significantly decreased according to the addition of the amount of MD (P<0.05). The addition of MD to the quince puree improved the flowability of the powders. Comparatively higher CI and HR values were observed for the quince powders with 4%PS and MD (P<0.05). It may be due to lower glass temperature of

powdered sugar which causes the stickiness.

Table 4. The other powder properties of freeze-dried quince powders

Samples	Particle Density (kg/m³)	Porosity (%)	Dispersibility (%)	Hygroscopicity (%)
4%MD	1690.50±183.14 [tp]	90.24±1.06[yp]	75.83±5.12[xp]	12.93±0.82[yp]
6%MD	1486.34±21.52[zp]	88.96±2.29[yr]	78.66±3.15[xp]	11.09±1.73[xp]
8%MD	941.14±14.52 [yp]	82.57±3.10[xp]	82.41±5.41[xp]	12.06±0.63 [xyp]
10%MD	746.63±19.21[xp]	78.03±2.16[xp]	82.01±2.28 [xp]	11.66±0.55[xp]
4%PS+4%MD	1977.09±65.59[tr]	86.03±4.63[xp]	73.39±6.74[xp]	18.38±0.54[zr]
4%PS+6%MD	1863.39±36.26 [zr]	81.10±3.68[xp]	77.74±1.54 [Xp]	17.69±0.51[yr]
4%PS+8%MD	1622.21±16.59[xr]	84.65±0.13[xp]	81.78±2.41[yp]	18.32±0.52[zr]
4%PS+10%MD	1745.24±49.81[yr]	82.86±4.89[xp]	81.18±3.59[yp]	16.13±0.13[xr]

x-t Different letters in the same column indicate a significant difference between the concentration of MD at $P < 0.05$.
p-r Different letters in the same column indicate a significant difference between the samples with MD or 4%PS+MD at $P < 0.5$.

The particle density of quince powders with MD and 4%PS+MD ranged between 746.63-1690.50 kg/m³ and 1622.21- 1977.09 kg/m³ and the particle density of the powders significantly decreased depending on the increasing MD concentration (P<0.05). The porosity values (%) of the quince powders significantly decreased depending on the increasing MD concentration (P<0.05). The higher porosity values were observed for quince powders with MD compared to the quince powders with 4%PS+MD, however, the differences between the samples generally were not found to be significantly important (P>0.05, except quince powder with 6%MD). No significant differences were observed between the dispersibility values of the quince powders on MD concentration (P>0.05) and the addition of the powdered sugar to the quince pure with MD did not affect the dispersibility values of the quince powder (P>0.05). The hygroscopicity values of quince powders with MD were not found to be statistically different (P>0.05). The higher hygroscopicity values were generally obtained from the samples, which have lower moisture (quince powder with 4%PS+MD) contents.

4. Conclusion

In this study, the physical and the powder properties of the quince powders with maltodextrin and powdered sugar were determined. In a result of the physical analysis, as the amount of added maltodextrin increased, a decrease in L value was observed while a* and b* is the highest value at 10% concentration. Furthermore, quince powder with 10% maltodextrin and powdered sugar has the lowest value of moisture content and water

activity. Besides, the drying process time of the samples with only maltodextrin is shorter than another group. According to analysis of the powder properties, the addition of maltodextrin and powdered sugar did not affect the wettability and solubility times of the samples. The porosity values, CI and HR values decreased depending on the addition of the amount of MD. The hygroscopicity values and dispersibility of quince powders with MD were not found to be statistically different.

5. References

[1] Rop, O.; Balik, J.; Řezníček, V.; Jurikova, T.; Škardová, P.; Salaš, P.; Sochor, J.; Mlček, J.; Kramářová, D. Chemical characteristics of fruits of some selected quince. Czech J. Food Sci. 2011, 29, 65–73.

[2] Pathare P.B.; Opara L.O. Colour Measurement and Analysis in Fresh and Processed Foods: A Review. Food Bioprocess Technology, 2013, 6:36-60.

[3] Jinapong, N.; Suphantharika, M.; Jamnong, P. Production of instant soymilk powders by ultrafiltration, spray drying and fluidized bed agglomeration. Journal of Food Engineering, 2008, 84, 194-205.

[4] Gong, Z.; Zhang, M.; Mujumdar, A. S.; Sun, J. Spray drying and agglomeration of instant bayberry powder, Drying Techonology, 2008, 26, 116-121.

[5] Cai, Y.Z.; Corke, H. Production and properties of spray-dried amaranthus βcyanin pigments. Institute of Food Technologists, 2000, 65, 1248–1252.

[6] Marques, L.G.; Ferreira, M.C.; Freire, J.T. Freeze-drying of acerola (Malpighia glabra L.), Chemical Engineering and Processing, 2007, 46, 451–457.

[7] Hsu, C. L.; Chen, W.; Weng, Y. M.; Tseng, C. Y. Chemicalcomposition, physical properties, and antioxidant activities of yamflours as affected by different drying methods. Food Chemistry, 2003, 83 (1), 85– 92.

[8] Rhim, J.; Wu, Y.; Weller, C.; Schnepf, M. Physical characteristics of a composite film of soy protein isolate and propylene-glycol alginate. Journal of Food Science, 1999, 64(1), 149 –152.

[9] Çalışkan Koç, G.; Dirim, S.N. Spray dried spinach juice: powder properties. Journal of Food Measurement and Characterization. DOI: 10.1007/s11694-018-9781-9 (in press), 2018.

Drying the corn in a farm heat pump dryer with fluidized bed

Rudobashta, S.P.[a]*; Zueva, G.A.[b]; Dmitriev, V.M. [c]; Muravleva, E.A.[d]

[a] Department of Heat Engineering, Hydraulics and Enterprises Energy Supply. Russian State Agrarian University – MAA after K. A. Timiryazev, Moscow, Russia

[b] Department of Higher and Applied Mathematics, Ivanovo State University of Chemistry and Technology, Ivanovo, Russia

[c] Department of Life Safety, Tambov State Technical University, Tambov,   Russia

[d] Department of Heat Engineering, Hydraulics and Enterprises Energy Supply. Russian State Agrarian University – MAA after K. A. Timiryazev, Moscow, Russia

*E-mail of the corresponding author: rudobashta@mail.ru

Abstract

The possibility of using a heat pump as a part of on-farm drying plant is considered taking drying of corn grain as an example. The methodology for kinetic calculations of a drying plant with a batch fluidized bed for granular materials is developed. These calculations are based on the use of an analytical solution for the problem of mass conductivity and taking into account the time-related changes in drying agent parameters over the layer height. To determine the concentration dependence of the mass-conductivity coefficient, a zonal method has been used.

Keywords: heat pump; dryer; kinetic calculation.

1. Introduction

To increase the efficiency of using a heat pump in a farm, it can be used for heating a farmhouse in winter, and for household needs in summer, for example, for drying seed grains. The drying of corn grains in a farm is discussed in the paper.The objectives of this work are: 1) analysis of the efficiency of using a heat pump in grain dryer, 2) developing an engineering method for the kinetic calculations of a periodically operating fluid bed dryer based on the analytical method of kinetic calculations, 3) obtaining the data on the mass conductivity of corn grains.

2. Farm heat pump dryer (HPD)

The moisture content of corn harvested from the field is in many cases higher than that required by storage conditions, so it is removed by thermal drying. For this purpose, a farmer heat pump plant with a fluidized bed of periodic operation can be used in a farm specializing in the production of seed-quality grains. A thermodynamic analysis was performed for the operation of such an installation in which the source of low-potential heat is the ground and the drying agent is atmospheric air heated by a heat pump to a temperature of 60°C. The R600a was taken as the refrigerant and its thermodynamic parameters were taken from literature.[1] As the result of analysis, it was found that 1) the energy conversion coefficient is $\Psi = 2.98$; 2) the energy saving for heating the drying agent is 66.4% due to the use of the heat pump, 3) for a fluidized-bed HPD at drying corn with a mass load of 75 kg, the total electric energy costs for the process (for heat pump and for air purge through the dryer) are ~ 16 kW, which is acceptable for operation of the dryer in the farm. Thus, the performed analysis and calculations show using HPD for drying corn seeds on a farm is fully justified.

3. Kinetic calculation of a batch fluidized bed dryer (FBD)

The level of development the theory of drying, the mathematical modeling methods, the availability of effective computational programs, the widespread distribution of personal computers allow to use successfully the mathematical methods for the kinetic calculations of dryers - analytical[2, 3] and numerical ones.[4, 5] Such methods of kinetic calculations of continuous dryers for disperse materials has been developed. The operation of a batch dryer differs by the nonstationarity of the process, and it must be taken into account in the design calculation. In this paper, we present a method that takes into account the nonstationarity of the process. At the development stage the general kinetic problem was decomposed into two levels: microkinetic and macrokinetic. At the microkinetic level, the drying kinetics of single corn kernels were considered, and the influence of technological factors on the process was taken into account at the macrokinetic level. When formulating the microkinetic model, it was assumed that the grain is isotropic and assumes a shape of a

sphere with a radius R which volume is equal to the grain volume. The zonal method of calculation was used: the entire range of the moisture content of the material during the drying process was divided into a number of concentration zones, for each of which was given the necessary values of the mass conductivity coefficient and of other characteristics of the process. The drying duration in these zones was calculated by the analytical solution of the mass-conductivity problem in a regular mode[6]

$$\tau_i = \frac{R^2}{\mu_i{}^2 \cdot k_i} \cdot \ln \frac{B_i}{\bar{E}_i}, \tag{1}$$

where μ_i is the first positive root of the characteristic equation for the solution of the problem at the i-th zone [6]; $\bar{E}=(\bar{u}(\tau)-u_e)/(\bar{u}_{in}-u_e)$ represents the relative average volume moisture content of the grains; $\bar{u}$ - average moisture content of grain, kgkg^{-1}; B_i is the first preexponential factor of the solution of the mass-conductivity problem[6]. The grain temperature was calculated on the basis of the solution of the heat conduction problem.[6] This solution for the medium-volume temperature of a spherical body has the form[6]

$$\overline{\Theta} = \frac{\bar{t}(\tau) - t_a}{t_{in} - t_a} = \sum_{n=1}^{\infty} B_n \left[\exp(-\mu_n^2 Fo) + \frac{R_V}{R} KoLu \frac{\mu_n^2}{Bi} \times \right.$$

$$\left. \times \sum_{m=1}^{\infty} B_m \frac{\mu_m^2}{\mu_m^2 - Lu \cdot \mu_m^2} \left[\exp(-\mu_m^2 Fo \cdot Lu) - \exp(-\mu_n^2 \cdot Fo) \right] \right], \tag{2}$$

where $\bar{t}$ - average temperature of grain, ºC; B_n are coefficients that depend on the Biot number thermal; R_V is the ratio of the volume of the body to its surface (for a sphere R_V = 3); Fo - Fourier number caloric; Ko - Kossovitch number; Lu - Luikov number.

In describing the process at the macrokinetic level, it was assumed that in the FBD of a batch action, the solid phase is completely mixed, and the gas phase is ideally displaced. The moisture content and temperature of the drying agent in such a dryer vary both over layer height and in time. The kinetic calculation was carried out by the zonal method - based on the average values of the air parameters in the concentration zones ($u_{in.i}\dots u_{f.i}$), which were found from the equations of material and heat balance. To take into account changes in air parameters over time, the successive approximations method was applied: first, the drying time τ_i required to change the moisture content of the material from $u_{in \cdot i}$ to $u_{f.i}$ was set, and then it was determined by calculation using equation (1). At the macrokinetic level, the following basic values were calculated: 1) the rate of fluidization beginning, at which the working air velocity was selected, and then the mass air flow in the

dryer (kgs^{-1}) was determined; 2) the average in time τ_i moisture content of the air at the outlet from the dryer $\overline{d}_{fi}$ and then the average moisture content of the air in the layer on the time interval τ_i: $\overline{d}_{la.i}$; 3) the average in time τ_i temperature of the air at the outlet from the dryer $\overline{t}_{a.f.i}$, and then - the average air temperature in the layer. The average values of the temperature and air moisture content in the layer were used to find the mass coefficient and the equilibrium moisture content of the material in the zones.

4. Experimental research. Materials and Methods

The experiments were performed to determine the equivalent diameter, density, mass conductivity and hygroscopic properties of corn grain of the following three varieties currently cultivated in Russia: Pioneer PR-8521, Pioneer PR-7709 FAO 160, Mysodur Amelior F-70. Equivalent diameter was determined by measuring the volume of a group of grains using a graduated cylinder, density - by measuring the volume and their mass. For the Pioneer PR7709 FAO 160 corn, the following has been determined: $d_{eq} = 8.24$ mm, $\rho = 1065$ kgm^{-3}. The dependence k=f(u,t) was determined by the zonal method with the experimental drying curve taken in the absence of an external diffusion resistance.[6] Drying curves were obtained for 10 corn kernels of the same equivalent diameter $d_{eq} = 2R$ - in a specially designed experimental setup with a triple replication of the tests, at five drying agent temperatures: 40, 50, 60, 70 and 80 °C , at air velocity 5 ms^{-1}. There is no external diffusion resistance at this air flow (its absence was judged by the fact that the change in the air velocity by half did not affect the drying curve). Corn grains were placed between the coils of the spring suspension, which was blown by the air stream in the transverse direction. The weight of the samples during drying was measured using the Techniport torsion balance PRLT with accuracy of 1 mg without removing grains from the drying chamber. The data obtained in the experiment on the coefficient of mass conductivity are shown in Fig. 1 for corn Pioneer PR-8521 (for other varieties the dependencies are similar). The data analysis allowed to draw the following conclusions: 1) the dependence of k on u for different varieties of corn is of the same character, the values of the mass coefficient for different varieties are close in magnitude; 2) the mass conductivity coefficient changes significantly with the moisture content of the material, it requires to take this change into account when drying; 3) the functions k=f(u,t) have the form characteristic for the seeds of other crops - such as canola, wheat, rye, barley, but greater in their values; 4) the rate of drying is limited by internal mass transfer.

***Fig. 1** Dependencies* **k = f(u)** *for corn kernels of Pioneer PR-8521: 1 –* t_a *= 40 ºC; 2 – 50 ºC; 3 – 60 ºC; 4 – 70 ºC; 5 –* t_a *= 80 ºC (points - experiment, lines - calculation).*

5. Verifying the adequacy of the mathematical model

The adequacy of the model describing the microkinetic has been verified by comparing the experimental curve for drying the corn kernels located in a longitudinally blown monolayerat a low air velocity (1.8 ms^{-1}) and the drying curve calculated for these conditions using the obtained data (note that the values of the mass coefficient were found from the drying curves, with an other air velocity ~ 5 ms^{-1}). Figure 2 allowes to compare the experimental and calculated drying curves, and it shows satisfactory match. The adequacy of the mathematical model describing the kinetics of corn grain drying in a batch fluidized bed

***Fig. 2** Comparison of calculated (line) and experimental (points) drying curves for corn kernels of variety Pioneer PR-7709 FAO-16 (*t_a *= 50ºC,* **v** *= 1.8 ms^{-1}).*

dryer has also been verified by comparison of the calculated and experimental drying curves, the latter being obtained under laboratory conditions. The scheme of the laboratory dryer is shown in Fig. 3. In the experiment, a curve was obtained for drying corn grain in a layer (dryer diameter 150 mm, fixed bed height 190 mm), measuring the air velocity, temperature and moisture content of the air at the entrance to the material layer and at the outlet from it. Fig. 4 showes the comparison of the calculated and experimental drying

Fig. 3 Scheme of laboratory installation: 1 - air temperature meter; 2 - drying chamber; 3 - corn; 4, 7 - gas distribution grids; 5 - air heating chamber; 6 - glass balls; 8 - gas blower; 9 - frequency converter, 10 - measuring diaphragm; 11 - pressure transmitter, 12 - secondary device, 13 – motor.

Fig. 4 Drying curves for grain variety PIONEERE PR-7709 FAO-16 in a batch fluidized bed dryer ($t_{a.in}$ = 53°C; v = 2.3 ms^{-1}).

curves whereas Fig. 5 presents the comparison of calculated and experimental air temperatures at the outlet from the layer of drying material. As can be seen, the experimental data compare well with the calculated ones.

Fig. 5 Air temperature at the entrance to the material layer $t_{a.in}$ (1) and at the outlet from the layer $t_{a.f}$:(2 - experiment, 3– calculations).

6. Conclusions

1) The feasibility of using HPD in a farmer dryer for corn seed is shown. 2) A zonal analytical method for engineering calculation of a periodically operating dryers with a fluidized bed of particulate material is developed. 3) Data on corn kernels required for calculations are obtained. 4) There is an internal diffusion kinetic regime when drying corn. 5) The adequacy of the mathematical model for drying kinetics to the real process is shown.

7. Nomenclature

a	thermal diffusivity	m^2s^{-1}
c	mass heat capacity	$Jkg^{-1}K^{-1}$
k	coefficient of mass conductivity	m^2s^{-1}
λ	thermal conductivity coeffcient	$Wm^{-1}K^{-1}$
r	radial coordinate	m
r^*	heat of vaporization	Jkg^{-1}
R	radius of spherical particle	m
t	temperature	^oC
u	moisture content of grain	$kgkg^{-1}$

v	velocity of air	ms^{-1}

Greek letters

α	heat transfer coefficient	$Wm^{-2}K$
ρ	grain density	kgm^{-3}
τ	time	s

Subscripts

a	air
e	equilibrium
f	finite
in	initial
la	layer

Dimensionless numbers

$Bi = \alpha R/\lambda$ - Biot number

$Fo = a\tau/R^2$ - Fourie number

$Lu = k/a$ - Luikov number

$Ko = r^*(u_{in}-u_e)/(c(t_a-t_i))$ - Kossovitch number

8. References

[1] Alves-Filho, O. Heat Pump Drying: Theory, Design and Industrial Application; New Dry Tech: Trondheim, 2013.

[2] Rudobashta, S.; Zueva, G. Drying of seeds through oscillating infrared heating. Drying Technology, 2016, 34. (5), 505-515.

[3] Rudobashta S. P.; Zueva G. A.; Kartashov E. M. Heat and mass transfer when drying a spherical particle in an oscillating electromagnetic field. Theoretical Foundations of Chemical Engineering, 2016, 50 (5), 718-729.

[4] Bon J.; Kudra T. Enthalpy-Driven Optimization of Intermittent Drying. Drying Technology, 2007, 25 (4), 523 – 532.

[5] Vaquiro H. A.; Clemente G.; Garcia-Perez J. V.; Mulet A.; Bonb J. Enthalpy-driven optimization of intermittent drying of Mangifera indica L. Chemical Engineering Research and Design. 2009, 87, 885–898.

[6] Rudobashta, S.P. Mass Transfer in the Solid Phase Systems; Chemistry: Moscow, 1980 (in Russian).

Ultrasonic atomizing-assisted spray drying: Effect on the quality of skimmed milk powders

Wangm, Y.[a*]; Cui, Y. [a]; Wang, B. [b]; Zhang, M. [a]

[a] State Key Laboratory of Food Science and Technology. Jiangnan University, Wuxi, China

[b] School of Food and Biological Engineering, Jiangsu University, Zhenjiang, China

*E-mail of the corresponding author: wyc453@163.com

Abstract

Skimmed milk powders (SMP) were produced by ultrasonic atomizing-assisted spray drying (UASD). It was found that UASD can produce high quality SMP (with < 5% moisture content and < 2% insolubility) at lower inlet temperatures (~130℃). The particle size of the UASD-SMP was 10 times smaller (decreased from ~20 µm to 4 µm) than the tranditionally spray-dried SMP and the color appeal of UASD-SMP was also better (L* value increased by > 6 %). Overall, this research shown that UASD can be used to produce small particle size and high quality SMP.

Keywords: Skimmed milk powder; ultrasonic atomization; spray dryer; particle size distribution; color

1. Introduction

Atomizer is the key component of a spray dryer. It greatly affects the particle size and the quality of the final products. Rotary atomizer and pressure atomizer are the most commonly used atomizers in spray drying. Rotary atomizing produces droplets with a droplet size of 1-600µm whereas pressure atomizing generates droplets that ranged from 10-800µm [1-2]. After water evaporation process, these droplets are generally dried to >20µm dried particles [3]. Therefore, installation of a nano-micro sized automizer in a spray dryer is expected to obtain the dried products with a smaller particle size.

Ultrasonic atomizing possesses many advantages. It produces small droplets. and is easy for absorption in human digestive system. Unlike the traditional atomizing methods that rely on high pressure or high-speed motion to smash liquid samples, ultrasonic atomizing utilized the low ultrasonic vibration energy as the driven force [4]. Besides, by adjustment of the amplitude of the vibration, the atomizing speed can be precisely controlled. Therefore, the droplets produced by ultrasonic atomizing are more regular, uniform and smaller than those droplets generated by traditional atomizing methods [5].

This research used fresh aqueous skimmed milk as the representative raw material. The relationships between the processing parameters (e.g. inlet temperature) and the product quality of ultrasound atomizing-assisted spray drying were systematically studied. The water content, solubility, color profile, protein content, particle size distribution, acidity, bulk density and microstructure of the final dried products were determined. These processing parameters and quality profiles were compared with those particles produced using a rotary atomizer-equipped spray dryer. The findings of this study contribute to the understanding and application of the atomizing-assisted spray drying.

2. Materials and Methods

2.1. Materials

Skimmed milk: Arla skimmed milk (1L, manufactured in Germany) was obtained from a Auchan supermarket in Wuxi. The skimmed milk contains 3.6g/100mL protein, 0g/100mL lipid, 5.1g/100mL carbohydrate, 50mg/100mL sodium and 120 mg/100mL calcium.

2.2. Methods

2.2.1. Experimental design and equipment
The experimental design and related equipment is shown in Table 1 and Table 2, respectively. Regarding the experimental design, different inlet temperatures were used to analyses the effects of drying parameters on the quality of the ultrasound atomizing-assisted spray dried products.

Table 1. Experimental design of this study

Drying Methods	Inlet Temperature (℃)	Quality analyses
UASD	110、130、150、170、190	Water content、color profile、protein
RDSD	130、150、170、190、210	content、acidity、bulk density、

UASD-Ultrasound atomizing-assisted spray drying, RDSD-High-speed rotating dish spray drying

Table 2. Equipment used in this study

Equipment	Product model	Manufacture
High-speed rotating dish	QZR - 5	Linzhou Drying Equipment Co., Ltd,
Color meter	CR - 400	Canon Inc, Japan
Electronic balance	PL 203	Mettlet Toledo Co., Ltd, China
Mastersizer	2000	Malvern Inc, England
Scanning electro microscope	S-4800	Hitachi Co., Ltd, Japan
Lipid meter	SOX-406	Hanon Instruments Co., Ltd, China
Electric drying oven with	GZX-9140MBE	Boxunshiye Co., Ltd, China

2.2.2. Research platform of UASD

In this study, the ultrasonic atomizer was manufactured with 10 ultrasonic vibrators. The size of this ultrasonic atomizer is: 255mm length × 90mm width × 30mm height. The oscillating frequency of the ultrasonic atomizer was 1.7MHz with a maximum atomizing capacity of 0.5kg/h. The droplet size obtained by ultrasonic atomizing process was within the range of 2-10µm. The temperature of the feed solutions was controlled by a combined temperature controller and feed-recycling system. The temperature controller was manufactured by Thermo Electron Co., Ltd (HAAKE DC10-K10, Germany), which works in the temperature range of 10-100ºC. The ultrasonic atomizing system is connected with a high-speed rotating dish spray dryer. The size of this spray dryer is 1600mm length × 2200mm width × 2500mm height. The water evaporation capacity and the electrical heating powder of this spray dryer is 5kg/h and 16KW, respectively. At the working stage, the rotary atomizer that equipped in the spray dryer was removed, and a thermal resistant tube was used to link the spray dryer and the ultrasonic atomizing system. The tube was inserted in the drying chamber with a reveal part of ~200mm.

2.2.3. Determination of the drying parameters of UASD and RDSD

In order to achieve a desirable atomizing effect, skimmed milk have to be diluted and stored at a suitable temperature. A high concentration and low temperature environment results in a low atomizing capacity. However, if the temperature of the skimmed milk exceeds the protection range of the ultrasonic atomizer, the atomizing system will automatically close and stop working. We have done preliminary experiments and optimized the atomizing conditions (data not shown). In this study, the skimmed milk used

for UASD was diluted by adding distill water at a milk to water ration of 1:2.5; The temperature of this diluted solution was controlled at 30-35ºC. The skimmed milk that used for RDSD was directly dried without any treatment.Regarding the atomizing capacity, the centrifuge frequency of high speed rotating dish spray dryer was 300Hz with an atomizing capacity of 900mL/h; the oscillating frequency of the ultrasonic atomizer was 1.7MHz with an atomizing capacity of 100mL/h.

2.2.4. Measurements of the quality profiles of the skimmed milk powders produced by UASD and RDSD

Water content: water content of the SMP produced by the two drying methods was determined by an electric drying oven (Table 2) with forced convection according to a national standard method (GB/5009.3-2016) [6].

Solubility: solubility of the SMP produced by the two drying methods was determined according to a national standard method (GB / 5413.29 – 2010) [7].

Color profiles: color profiles of the SMP were measured by using a CR-400 color meter (Table 2). The L, a and b value represents the extent of white/black, red/green, yellow/blue color of the skimmed milk after drying, respectively.

Acidity: acidity of the SMP produced by the two drying methods was measured according to a national standard method (GB / 5009.239 - 2016) [8].

Particle size: particle size of the dried products was determined by using a master sizer (Table 2) [9]. Each measurement was performed for triplicates and the average data was reported.

Microstructure: Morphological characteristics of the SMP produced by the two drying methods was determined by using S-4800 scanning electro microscope (Table 2). The acceleration voltage was 1.0kv. The dried products were coated by a palladium-gold alloy coating instrument (manufactured by Bal-Tec. Inc). The scanning electro microscope images of SMP samples were captured within a range of 600 – 2400 magnifications.

3. Results and Discussion

3.1. Water content of the dried SMP using UASD and RDSD as a function of different inlet temperatures

As shown in Table 3, inlet temperature significantly affected water content of the SMP ($p<0.05$). Higher inlet temperatures resulted into a lower water content of the UASD-SMP and RDSD-SMP. At an inlet temperature of ≥170ºC, no significant difference was observed for the water content of UASD-SMP and RDSD-SMP samples ($p>0.05$). When inlet temperature was ≤150ºC, the water content of UASD-SMP was lower than that of RDSD-SMP. The water content of the RDSD-SMP was >5% at an inlet temperature of 130ºC.

However, the water content of the UASD-SMP was below this national acceptable moisture content at an inlet temperature of 110ºC. The findings of this section indicate that lower inlet temperature (of spray drying) was required to achieve an acceptable water content of SMP by applying UASD method. This was attributed to the small droplet size of ultrasonic atomizing, which allows the fast evaporation of water.

Table 3. Water content of the skimmed milk powders obtained by UASD and RDSD

Inlet temperature (ºC)	110	130	150	170	190	210
UASD-SMP	4.317	4.091[a]	2.524[a]	2.145[a]	1.601[a]	-
RDSD-SMP	-	5.241[b]	3.105[b]	2.075[a]	1.574[a]	1.445

*The data with different superscript at a same column is significantly different ($p<0.05$).

3.2. Solubility of the dried SMP using UASD and RDSD as a function of different inlet temperature

At a certain extent, changes of solubility of SMP indicates the denaturation of proteins. Thus, low SMP solubility could be resulted by the denaturation of its protein component, negatively affecting its rehydration performance. Furthermore, different particle size of the dried powders also contributes to the varied solubilities of SMP.

As shown in Table 4. Solubility of the UASD-SMP decreased significantly with an increased inlet temperature ($p<0.05$). At an inlet temperature of ≤130ºC, the solubility of UASD-SMP was 98.66-98.97% (meets the national standard of >97%); At an inlet temperature of >130ºC, the solubility of UASD-SMP decreased sharply to 89.72-95.01%. Regarding the RDSD-SMP, the dried powders possessed a solubility of >97% within the whole inlet temperature range of 110ºC – 210ºC. Overall, these findings indicated that solubility of the UASD-SMP was susceptible to inlet temperatures of spray drying. High inlet temperature(>130ºC), small droplets size and tiny dried particles caused the denaturation of proteins component in SMP and significantly reduced its solubility ($p<0.05$).

Table 4. Solubility of the skimmed milk powders obtained by UASD and RDSD.

Inlet temperature(ºC)	110	130	150	170	190	210
UASD-SMP	98.66	98.97[a]	95.01[a]	90.79[a]	89.72[a]	-
RDSD-SMP	-	98.95[a]	97.82[b]	97.83[b]	97.71[b]	97.96

*The data with different superscript at a same column is significantly different ($p<0.05$).

3.3. Color profile of the dried SMP using UASD and RDSD as a function of different inlet temperature

The color profiles of UASD-SMP and RDSD-SMP are provided in Table 5. As shown in Table 5. Inlet temperature of the spray drying processes did not cause significant effects on the lightness color of SMP ($p>0.05$). However, the UASD-SMP was significantly lighter

than RDSD-SMP (p<0.05). Inlet temperature of the spray drying processes significantly affected the a* value of SMP (p<0.05). High inlet temperature decreased the a* value. At the same inlet temperatures, a* value of the UASD-SMP was significantly lower than that of the RDSD-SMP. This means that the UASD-SMP samples were less red than RDSD-SMP. High inlet temperature increased the b* value. At the same inlet temperatures, b* value of the UASD-SMP was significantly higher than that of the RDSD-SMP, indicating a more yellowness color.

Table 5.color value of the skimmed milk powders obtained by UASD and RDSD

Inlet temperature(ºC)	color value	110	130	150	170	190	210
	L*	98.31	97.47[a]	97.81[a]	97.55[a]	97.42[a]	-
UASD-SMP	a*	-2.65[a]	-2.42[a]	-2.53[a]	-2.58[a]	-3.02[a]	-
	b*	11.28	11.61[a]	12.08[a]	13.03[a]	14.66[a]	-
	L*	-	95.25[b]	95.62[b]	96.23[b]	96.55[b]	95.36
RDSD-SMP	a*	-	-2.22[b]	-2.02[b]	-2.38[b]	-2.71[b]	-3.22
	b*	-	10.05[b]	9.68[b]	10.21[b]	10.65[b]	12.51

*The data with different superscript at a same column is significantly different (p<0.05).

3.4. Acidity of the dried SMP using UASD and RDSD as a function of different inlet temperature

Acidity of the UASD-SMP and RDSD-SMP samples is presented in Table 6. The acidity of both UASD-SMP and RDSD-SMP were lower than the national standard value of 18°T. UASD-SMP was more acidic than RDSD-SMP, indicating the less oxidation occurred during the drying process. This might be due to the shorter water evaporation period and lower inlet drying temperature of the UASD process.

Table 6. Acidity of the skimmed milk powders obtained by UASD and RDSD

Drying Methods	Acidity（°T）
UASD (inlet temperature of 130ºC)	15.91[a]
RDSD(inlet temperature of 170ºC)	16.89[b]

*The data with different superscript at a same column is significantly different (p<0.05).

3.5. Particle size of the dried SMP using UASD and RDSD

The average particle size and particle size distribution of the UASD-SMP and RDSD-SMP samples is presented in Fig. 1. The particle size of UASD-SMP was >5 times smaller than that of RDSD-SMP samples. This is due to the differences between the droplets produced by ultrasonic atomizing and high-speed rotary atomizing. The ultrasonic atomized droplet size was in a range of 2-10 µm, and hence the surface area to contact the drying medium was enlarged enormously. This not only resulted into a fast water evaporation period, but also significantly reduced the particle size of SMP (p<0.05).
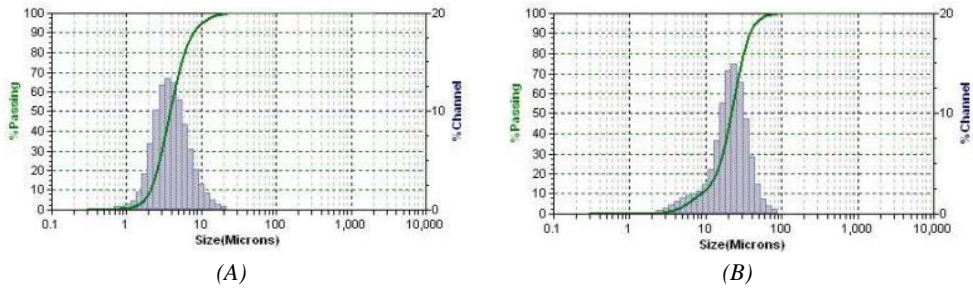
Fig.1 Particle size distribution of (A) UASD-SMP obtained at 130ºC inlet temperature and (B) RDSD-SMP obtained at 150ºC inlet temperature

3.6. Morphological characteristics of the dried SMP using UASD and RDSD

The morphology of SMP samples were monitored by scanning electro microscopy (Fig.2). The particles obtained through UASD were much smaller than those produced by RDSD, which was also confirmed by the laser diffraction measurements as mentioned in section 3.5. The UASD particles were irregular, shrunk and compacted; the microstructure of RDSD particles was spherical, uniformly distributed and loosely organized with a few broken skins. These differences in microstructure of SMP might explain the lower solubility of UASD-SMP, e.g. the uniformity of UASD-SMP was lower than that of RDSD-SMP, the structure of UASD-SMP was more compact than RDSD-SMP.
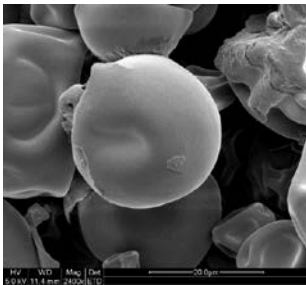
RDSD-SMP (×2400 magnification)   UASD-SMP (×2400 magnification)
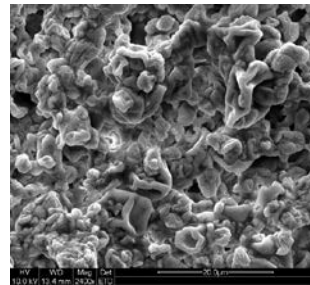
Fig. 2 Scanning electro microscopy images of the dried SMP using UASD and RDSD

4. Conclusions

This research systemically compared and studied the quality aspect of SMP obtained by a novel drying method. The innovative UASD is expected to produce high quality and small particle size SMP. UASD required as low as 110ºC inlet temperature to obtain dried SMP (<5% water content), which was almost 50ºC lower than the inlet temperatures used for the traditional spray drying. Furthermore, the particle size of the UASD-SMP (~4µm) was >5 times smaller than that of the RDSD-SMP. The color appeal of the UASD-SMP was >6% lighter than that of the RDSD-SMP. These findings indicated that UASD is a promising

drying method to produce high quality powders for food and pharmaceutical industries. However, there are still a few scientific issues have not been solved for the UASD method. E.g. the atomizing capacity of high-solid content solutions is relatively low; the final dried products is difficult to collect though the gas-solid separator that designed for the traditional spray drying. Therefore, further research on UASD is recommended to be carried out in the drying field.

5. Acknowledgement

6. References

[1]   Nandiyanto A. B. D., Okuyama K. Progress in developing spray-drying methods for the production of controlled morphology particles: From the nanometer to submicrometer size ranges. Advanced Powder Technology, 2011, 22(1):1-19.

[2]   Mujumdar A. S. Handbook of Industrial Drying, third edition. New York, CRC Press, 2006, 215-254.

[3]   Filkova I., Huang L.X., Mujumdar A.S. Industrial spray drying systems. In Handbook of Industrial Drying; Mujumdar, A.S., Ed.;CRC Press: New York, 2007; 215–254.

[4]   Julianna C. Simon, Oleg A. Sapozhnikov, Vera A. Khokhlova, et al. Ultrasonic atomization of liquids in drop-chain acoustic fountains. Journal of Fluid Mechanics , 2015 , 766 :129-146.

[5]   Huang H., Yao X., Wang M. Q., Wu X. Q. The measurements of atomizing properties of ultrasonic atomizing system. Piezoelectrics & Acoustooptics (in Chinese), 2004, 26(1): 62-64.

[6]   Determination of water content in foods. National Standard of China, GB/T 5009.3-2016; Standardization Administration of the P.R. China: Peking, 2016.

[7]   Determination of solubility in foods for infants and young children, milk and milk products. National Standard of China, GB/T 5413.29-2010; Standardization Administration of the P.R. China: Peking, 2010 .

[8]   Determination of acidity in foods. National Standard of China, GB/T 5009.239-2016; Standardization Administration of the P.R. China: Peking, 2016.

[9]   Wang B., Timilsena Y. P., Blanch E., et al. Characteristics of bovine lactoferrin powders produced through spray and freeze drying processes. International Journal of Biological Macromolecules, 2017, 95:985-994.

Agitated thin-film drying of spinach juice

Qiu, J.*; Boom, R. M.; Schutyser, M.A.I.

Laboratory of Food Process Engineering, Wageningen University, Wageningen, The Netherlands

*E-mail of the corresponding author: jun.qiu@wur.nl

Abstract

Agitated thin film dryers (ATFD) has been considered as an effective technology for drying viscous liquid foods, pastes or pureed foods. In this study, a lab-scale ATFD was developed and applied for drying of juices from spinach leaves at varying temperature (60 – 90 °C), feed rate (0.3 – 0.5 kg/h) and blade rotation speed (300 – 600 RPM) combinations. Juice suspensions were successfully dried into powder with a moisture content ranging from 0.049 to 0.114 kg/kg total. Increasing the wall temperature and feed rate were found to improve the specific evaporation rate and evaporation rate of the ATFD, respectively. The blade rotation speed had limited effect on the water removal rate, while it played a crucial role in powder formation.

Keywords: Food solution; Spinach juice; Thin film drying; Scraped surface; Vacuum conductive drying.

1. Introduction

Drying is a commonly used technology to preserve food products. Various types of dryers have been developed that are tailored to specific feed properties and product requirements [1]. The most commonly applied drying technologies to liquid feeds can be categorized into two types, i.e. convective and conductive drying. Spray drying is one of the most commonly applied convective drying methods, where energy for evaporation is supplied by hot air to the product that is dispersed in micron-sized droplets [2]. Drum and agitated thin film drying are conductive drying methods, where energy for evaporation is supplied by steam condensation and transferred via a wall to the product that is applied at the other side. Whereas drum drying is more readily applied and effective for drying of viscous liquid foods, pastes or pureed foods, agitated thin film drying is not yet widely applied [1, 3]. Comparing to spray drying, drum drying is more efficient as it consumes on average 40% less energy due to a.o. lower energy loss via the exhaust gas [2, 4]. A major drawback of atmospheric drum drying is however that the product is exposed to the boiling temperature (100 °C), which can lead to undesired damage to heat sensitive foods [1, 3]. Operation of drum drying processes under reduced pressure could be an attractive alternative as well, but capital costs of vacuum drum dryers are relatively large. Agitated thin film drying (ATFD) is therefore identified as a promising alternative conductive drying method.

Only very few studies investigated ATFD. Pawar et l. [1, 5] mathematically studied the heat transfer and mass transfer during ATFD and proposed a stage-wised penetration theory model, by assuming ideal mixing between the bow wave and the thin film. However, the model was validated with ATFE instead of ATFD experiments. Because during ATFD the feed will transform from a viscous liquid into a paste and subsequently into a powder, this may be expected to have large influence on the mass and heat transfer during operation [6]. Hitherto, to the best of our knowledge no experimental studies have systematically investigated product transformation during ATFD drying and its consequence on the drying behaviour. It may be expected that the product properties will have large influence on the drying behaviour in an ATFD.

The aim of this study was therefore to obtain better understanding of drying behaviour of foods during ATFD drying and how this is influenced by process. Suspensions prepared from spinach leaves were selected as model system to investigate the influence of drying parameters, i.e. heating temperatures, feeding rates and rotation speeds.

2. Materials and Methods

2.1. Material
Spinach suspensions for ATFD experiments were prepared starting from fresh spinach leaves, which were purchased from the local supermarket. The fresh spinach leaves were

juiced by an Angelia AG-7500 Juicer (Angel Co. Ltd, Republic of Korea). After juicing, the squeezed juice and fibre residues were collected separately. The obtained insoluble fibre residues were dried by a hot air oven (Binder, Tuttlingen, Germany) at 60 ˚C for 20 hours. The dried fibres were milled by the Rotor Mill Pulverisette-14 (FRITSH International, USA) at 6000 RPM with a 0.2 mm sieve. The drying and milling of fibres was necessary because the fibre particles had to be small enough to avoid blockage of the feeding pump. Subsequently, the milled fibres were added back into the squeezed juice to obtain a spinach suspension with approximately again 2% w/w fibers. In addition, around 5 drops of Antifoam B aqueous silicone emulsion (Sigma-Aldrich®, Zwijndrecht, Netherlands) was added into 1 litre juice to prevent excessive foaming.

2.2. Lab-scale Agitated Thin Film Drying

A lab-scale agitated thin film dryer was custom build for the experiments. The ATFD chamber was made from transparent glass to facilitate observation of the used heat exchange area. The ATFD chamber was equipped with a Liebig condenser and a dropping funnel (L.G.S. B.V, Ubbena, Netherlands) to condense and quantify the vapour release. The entire system was operated under reduced pressure (50 mbar) using a vacuum pump (type, country). Experiments were performed to determine the (specific) evaporation rates of the spinach suspensions at different drying conditions. The spinach suspension was preheated to 33 ˚C and then supplied to the system with a flow rate ranging from 0.3 kg/h to 0.5 kg/h. The drying temperatures of the heating chamber ranged from 70 to 90 ˚C. The condenser was operated with cooling water of 2 ˚C. The amount of condensed water was measured and used to obtain the evaporation rate. The specific evaporation rate was calculated by dividing by the evaporation rate by the used heat exchange area.

2.3. Analysis of the moisture content and water activity

Powders were collected at the bottom of the lab-scale ATFD for analysis of the moisture content and water activity. To determine the moisture content, around 1.5 g of the powder was dried in a hot air oven (Binder, Tuttlingen, Germany) at 105 ˚C for 16 hours. The water activity was measured by an AquaLab 4TE dew point water activity meter (METER Food, Munich, Germany). Measurements were carried out in duplicate.

3. Results and discussion

The lab-scale ATFD setup was used to dry the prepared spinach suspensions at different drying conditions, which are reported in Table 1. The effect of the drying temperature on the evaporation rate and the specific evaporation rate was determined, as shown Fig. 1. Fig.

1 (A, B) showed that with the increase of drying temperature, the evaporation rate did not change significantly (p > 0.05), while the specific evaporation rate significantly increased (p < 0.05), based on one-way ANOVA analysis. This is because at higher drying temperature, the surface area used for drying decreased, as shown in Fig. 1 (C). The smaller surface area used for drying in this situation is related to the higher heat flux from the hot wall towards the sample at increased wall temperatures, which results in a higher specific evaporation rate. In this case the maximum feed rate can be increased, which benefits the capacity of the equipment.

A

B

C

60 °C   70 °C   80 °C   90 °C
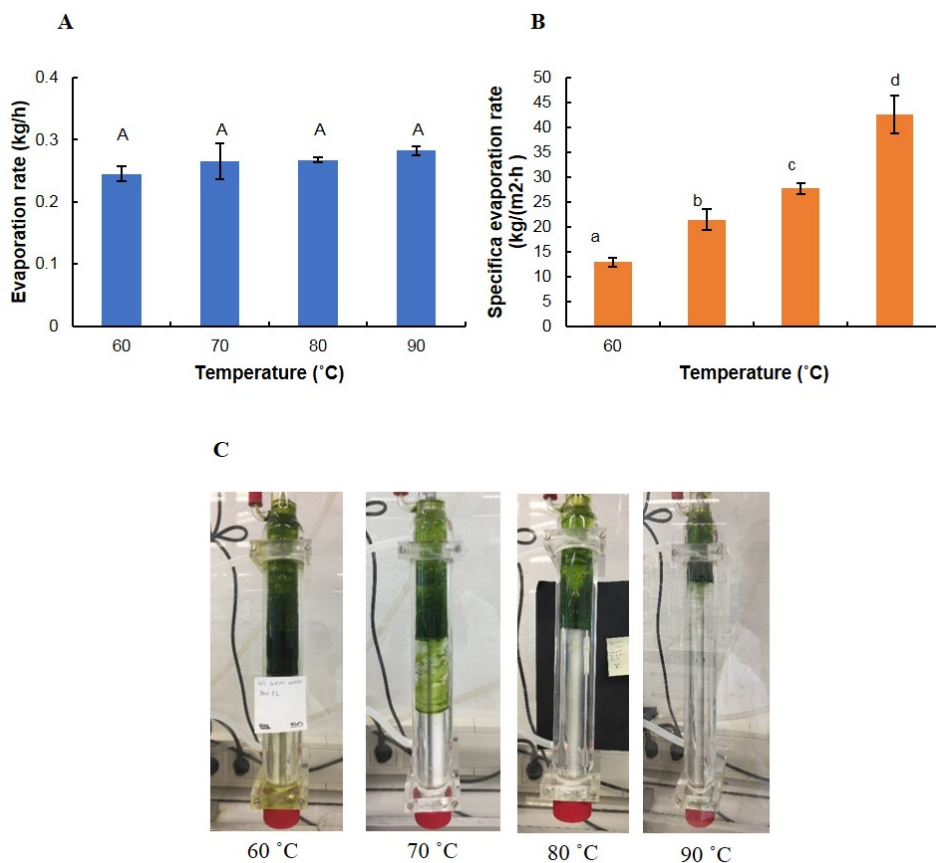
Fig. 1(A) The evaporation rate and (B) the specific evaporation rate in the ATFD for different temperatures (Rotation speed = 600 RPM, Feed rate = 0.3 kg/h). The error bars represent the standard deviation of the experimental data (n = 3). The same letters represent no significant difference at the 95% confidence interval. (C) The visual image of usage the ATFD chamber under different drying temperatures.

Table 1 The fraction of the used heating exchange area, the moisture content and water activity of the powder at different drying conditions

No.	Drying conditions				Fraction of used heating area (-)*	Moisture content (kg/kg total)*	Water activity (a_w)*
	Feed rates (kg/h)	Drying temperature (°C)	Rotation speed (RPM)	Vacuum (mbar)			
1	0.3	60	600	50	0.58[a] ± 0.03	0.096 ± 0.009	0.55 ± 0.02
2	0.3	70	300	50	0.38[b] ± 0.05	NaN**	NaN**
3	0.3	70	400	50	0.42[ab] ± 0.11	0.087 ± 0.002	0.57 ± 0.02
4	0.3	70	500	50	0.39[b] ± 0.04	0.102 ± 0.001	0.58 ± 0.01
5	0.3	70	600	50	0.38[b] ± 0.07	0.114 ± 0.003	0.60 ± 0.01
6	0.3	80	600	50	0.29[bc] ± 0.01	0.078 ± 0.013	0.53 ± 0.03
7	0.3	90	600	50	0.20[cd] ± 0.02	0.049 ± 0.002	0.26 ± 0.07
8	0.4	90	600	50	0.29[bd] ± 0.02	0.071 ± 0.031	0.46 ± 0.19
9	0.5	90	600	50	0.34[bd] ± 0.08	0.098 ± 0.071	0.56 ± 0.20

a-d : The same letters represent no significant difference at the 95% confidence level;

* : Each value is expressed as mean ± SD;

**: Not a number.

Fig. 2 and Fig. 3 shows the influence of the rotation speed and the feed rate on the evaporation rate and the specific evaporation rate. From Fig. 2, we can observe that both the evaporation rate and the specific evaporation rate did not change at different rotation speeds (p > 0.05). This observation is opposite to simulations with the model proposed by Pawar et al. [1]. Pawar et al. [1] proposed that the heat transfer coefficient of the ATFD may be derived from the heat penetration theory and increases with the rotation speed. Therefore, the specific evaporation rate should increase as well. However, Pawar et al. [1] also experimentally observed that the water evaporation rate was independent of the speed of the blades, when they concentrated the 20% w/w ammonium sulphate solution in an ATFE. The differences between the experimental data and the model predictions are discussed later in more detail.

According to Fig. 3, we found that the effect of the feed rate is opposite to that of the temperature. The increased feed rate resulted in an increase in the evaporation rate ($p < 0.05$) while it did not affect the specific evaporation rate ($p > 0.05$), which can be explained by the increased usage of heat exchange area (Table 1).

Table 1 shows the moisture content and water activity (a_w) of the dried spinach powder and the fraction of dissolved powder at different drying conditions. It can be seen that the moisture content of the powder ranges from 0.049 to 0.114 kg/kg total and the water activity of the powder ranges from 0.26 to 0.60. Although foods with $a_w < 0.6$ may be considered as microbiologically stable, further drying in for example a fluidized bed would be recommended for vegetable powders to further decrease the water activity to $a_w < 0.2$ [7]. It should be mentioned that during experiment No. 2, no powder was produced. Probably this was due to the low rotation speed, which did not provide enough shear stress to fracture the material. Therefore, even though the rotation speed does not affect the heat transfer (Fig. 2), it plays a crucial role to induce powder formation.
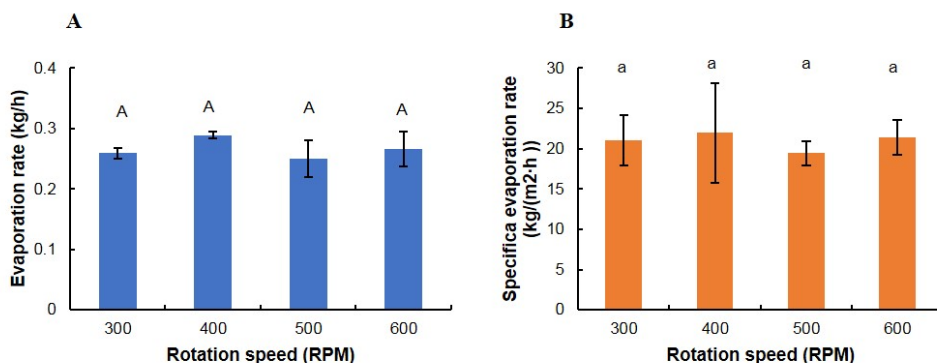
Fig. 2 (A) The evaporation rate and (B) the specific evaporation rate in the ATFD for different rotation speeds (Temperature = 70 °C, Feed rate = 0.3 kg/h). The error bars represent the standard deviation of the experimental data (n = 3). The same letters represent no significant difference at the 95% confidence interval.
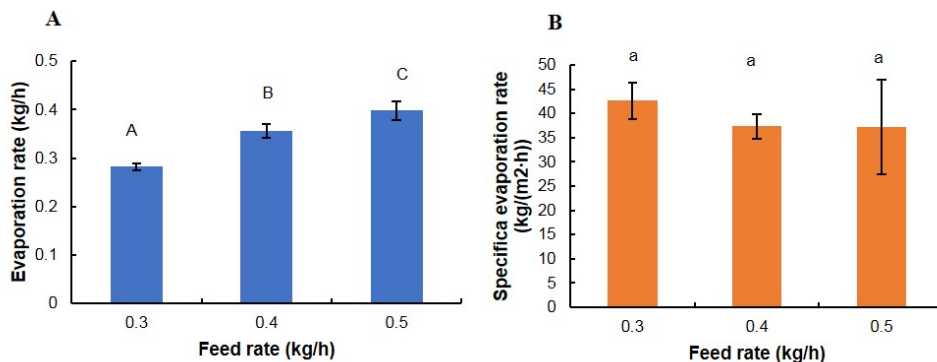
Fig. 3 (A) The evaporation rate and (B) the specific evaporation rate in the ATFD for different feed rates (Temperature = 90 ˚C, Rotation speed = 600 RPM). The error bars represent the standard deviation of the experimental data (n = 3). The same letters represent no significant difference at the 95% confidence interval.

4. Conlusion

In this study suspensions prepared from spinach leaves were dried in a lab-scale agitated film dryer under different conditions. Obtained spinach powders were flowable, although the final moisture contents were relatively high. The drying behaviour was characterised and especially wall temperature appeared to determine the specific evaporation rate, which can benefit the dryer capacity. Surprisingly, blade rotation speed did not affect the drying rate, but appeared crucial to break up the material into small powder particles during the process.

References

[1] Pawar, S.B., et al., Mathematical modeling of agitated thin-film dryer. Drying Technology, 2011. 29(6): p. 719-728.

[2] Devahastin, S. and A.S. Mujumdar, Indirect dryers, in Handbook of Industrial Drying, Fourth Edition. 2006, CRC Press: Boca Raton. p. 137-149.

[3] Daud, W.R.W., Drum Dryers, in Handbook of Industrial Drying, Fourth Edition. 2006, CRC Press: Boca Raton.

[4] Nindo, C. and J. Tang, Refractance window dehydration technology: a novel contact drying method. Drying Technology, 2007. 25(1): p. 37-48.

[5] Pawar, S.B., A. Mujumdar, and B. Thorat, Flow pattern and heat transfer in agitated thin film dryer. Chemical Engineering and Processing: Process Intensification, 2011. 50(7): p. 687-693.

[6] Zeboudj, S., et al., Modelling of flow in a wiped film evaporator. Chemical Engineering Science, 2006. 61(4): p. 1293-1299.

[7] Quek, S.Y., N.K. Chok, and P. Swedlund, The physicochemical properties of spray-dried watermelon powders. Chemical Engineering and Processing: Process Intensification, 2007. 46(5): p. 386-392.

Influence of the low temperature drying process on optical alternations of organic apple slices

Bantle, M. [a]*; Kopp, C. [a]; Claussen, I.C. [a]; Tolstorebrov, I. [b]

[a] SINTEF Energy Research, Department of Energy Processes, NO-7465 Trondheim, Norway
[b] Norwegian University of Science and Technology, Department of Energy and Process Technology, NO 7465 Trondheim, Norway

*E-mail of the corresponding author: Michael.Bantle@sintef.no

Abstract

Drying conditions for convective driers are often based on empirical approaches in which the final product quality is evaluated post processing. Modern sensor technology and data processing enable second-by-second quality analyses but conventional systems do not utilize this possibility. An industrial convective drying chamber was modified with a camera system to investigate the product during the drying process. The obtained data was analyzed on color alternation (CIE-L*a*b* color space and Browning Index), shrinkage and deformation. Both, shrinkage and deformation show minor dependence on drying conditons. The investigation shows the time depending optical parameter at different drying conditions. This might offer new "smart" drying programs with focus on improved product quality.

Keywords: color alternation; shrinkage; deformation; convective drying; smart drying

1. Introduction

Organic products are a growing market for European producers and commonly associated with a sustainable food chain. The production of organic processed food is mostly carried out by small and medium sized enterprises which are facing a double challenge regarding the consumer awareness for high quality products and legal standards. In recent years the organic sector has put significant effort in the development of clear definitions of gentle and quality oriented processing. Drying was identified as a preservation technology which operate inefficient with respect to raw material utilization, resulting product quality as well as energy efficiency. Consumers mostly don't know about the used amount of energy behind a dried food product or its quality standards during the drying process. This is a problem especially for organic foods which are expected to be produced sustainable and with high quality regardless to its magnitude of processing. European Community legislation only has explicit rules for agricultural production and additives used in processed food. There is a clear correlation between product quality and drying conditions and low temperature drying is commonly used for products which require gentle processing.

There has been a vast development of sensor technology in the last decade and several mass-produced optical analyzing tools are available at the market. However, industrial drying systems mostly do not utilize the possibilities which e.g. camera sensors offer. Drying of organic apples is mostly performed as batch processes by SMEs and drying conditions (mainly temperature) are empirically determined. As a result, the product quality is not monitored or controlled during processing and final product quality is first determined at the end of drying.

For the present investigation the potential of low temperature drying of organic apples was evaluated at different relative humidity with respect to color changes and product deformation during processing. A camera sensor was installed in an industrial drier which enabled determination of optical alternations of the product like color alternation, shrinkage and deformation in a continuous way without any interruption of the drying process. The results are used to suggest an improved control strategy.

2. Materials and Methods

2.1 Product preparation

Organic apples of the sort "Red Delicious" with the origin Italia were used for the experiments. The apples were obtained from a local organic supplier in Trondheim, Norway and stored in a refrigerator at 8°C until further processing. The apples were cut in slices of 5 mm thickness by using a cutter machine. The core and the apple skin wasn't removed so that slicing the apples was the only processing. The time between getting the apples out of the fridge, cutting and starting the experiment was always within 5 min.

2.2 Experimental setup

The experiments were executed in a convective drying chamber with a dimension of ca. 3m * 1.5m * 1m with a tray area of 50 m^2. The drying chamber is equipped with an electric heater to set the drying temperature, a ventilator to set the air velocity and a heat pump to set the relative humidity. To avoid any interruptions or influences of the drying process due to measuring, a test rack was built and placed within the drying chamber at a representative point in the middle of the drier trays with all relevant measuring devices attached. The camera system (UI-5240CP-C-HQ Rev.2, company iDS Imaging Development Systems, Germany) contained a built-in heater to avoid influences of the image quality due to the surrounding temperatures in the drying chamber. The illumination was the LED-barlight (LHF300-M12-WHI, company Stemmer Imaging, Germany) with a color temperature of 6500K. The camera system was used to measure color alternations and deformations like shrinkage. To obtain also the sidelong deformation of the apple slices, a mirror was placed in a 45° angle next to the slices. In addition to the optical alternations there was also a pyrometer used for measuring the surface temperature of the apple slices and a scale (SB32000, company Mettler Toledo) to record the weight loss during the drying process. For each test series, four apple slices were analyzed by the camera system. The remaining space on the test rack was filled up with apple slices of the same thickness. The surface temperature of one representative apple slice was measured by the pyrometer. The process parameters of the test series are listed in Table 1 and are based on industrial low temperature drying conditions for organic apple producers. The drying temperature of 40 °C was used as reference case.

Table 1: Overview of the investigated drying conditions for organic apples.

Test series name	Humidity	Temperature	Air velocity
T20_RH25	25 %	20 °C	1,5 m/sec
T20_RH40	40 %	20 °C	1,5 m/sec
T20_RH60	60 %	20 °C	1,5 m/sec
T40_RH25	25 %	40 °C	1,5 m/sec

2.2 Optical analysis

For analyzing the optical alternations, an image was taken by the camera every 5 minutes and analyzed with a special application using the OpenCV libraries for image processing. An example is shown in Figure 1. The deformation of the apple slices was defined by the deviation of the actual slice area and the area of a corresponding circle whose diameter is the maximum width of the actual slice (yellow circle in Figure 1, left image). The ratio between these two areas gives a quantitative value about the deformation. A perfect round shaped apple slice e.g. would have the same area than its calculated minimum circle which results in a deformation of 1, proceeding deformation results in a value less than 1. The same principle was used to determine the deformation of the sidelong view but with using a minimum

rectangle (yellow rectangle in Figure 1, middle image). The shrinkage was defined by the ratio of the area of the actual apple slice and the area of the apple slice at the beginning of the drying process. The color alternation was measured by reading the color information of each pixel within the apple slices and averaging it (Figure 1, right image). The so obtained RGB values were transformed into the CIE-XYZ color space according the ISO Standard 13655 which is the base of the CIE-L*a*b* color space and the Browning Index.
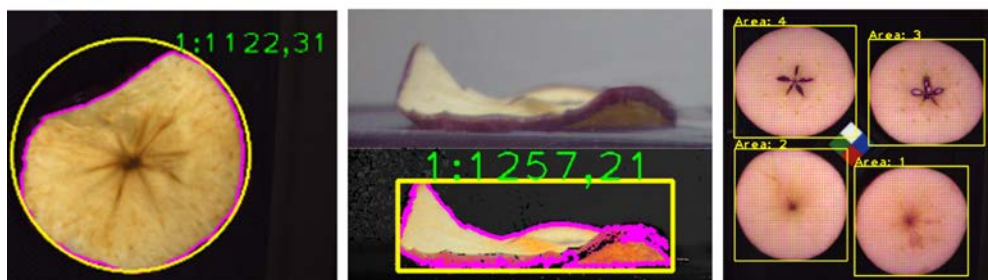
Figure 1:Measuring principle of the deformation top view (left), deformation sidelong (middle), color alternation (right)

The CIE-L*a*b* color model was developed with the aim of linearizing the representation of colors with respect to human color perception and at the same time creating a more intuitive color system [1]. The dimensions in this color space are the luminosity L* and the two-color components a*, b*, which specify the color hue and saturation along the green-red and blue-yellow axes, respectively. The CIE-L*a*b* color space is often used in literature to describe the color of food.

The Browning Index is an indicator of the color change due oxidation of a freshly cut fruit or vegetable surface during storage or drying. The best known and most often quoted Browning Index is a form of excitation purity that follows the suggestion of Buera et al. (1985) [2] and is expressed as follows [3]:

$$BI = \frac{(x_{D65} - 0,32)}{0,162} * 100 \tag{1}$$

(for Illuminant: D65 and Standard Observer 10°)

where *x* is the CIE Chromaticity value and calculated by the CIE-XYZ values

$$x = \frac{X}{(X + Y + Z)} \tag{2}$$

3. Results and discussion

Figure 2 shows the moisture ratio of the different test series over the drying time. The grey areas behind each test series shows the uncertainties of the data. The results shows that the

differences between the T20_RH40 and T20_RH25 test series is much less than compared to the T20_RH60 test series. The same behavior was already measured in other publications for the drying of Temu Putih Herb, coriander leaves, okra and pistachio nuts [4]. The test series T40_RH25 however shows a much quicker drying than the other test series what indicates that the drying temperature has much more influence on the drying kinetics than the relative humidity.
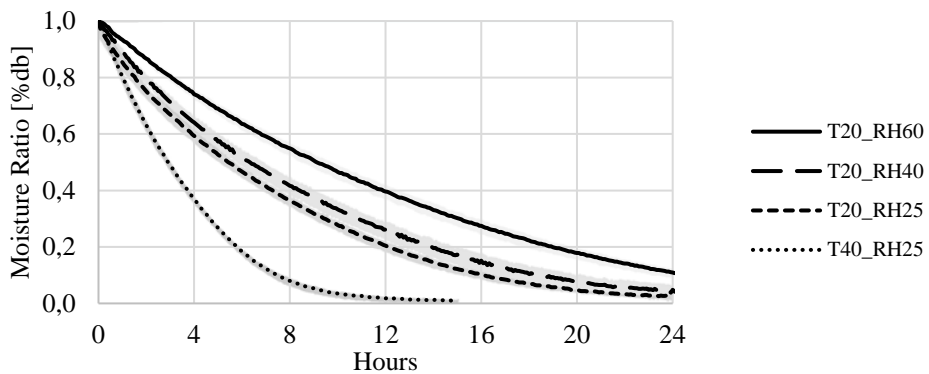
Figure 2: Moisture Ratio of organic apples at different drying conditions

The graph in Figure 3 shows that the CIE-L* value is basically decreasing for all experiments over the whole drying process, what means that the apple slices became darker. Hereby the biggest rate of change happens within the first 2-3 hours, afterwards the change rate becomes insignificant. The values of the T20_RH60 test series shows a continuous decrease of the CIE-L* value whereas the other test series have a minimum after about 2 hours with a followed increase of the CIE-L* value and a continuous decreasing afterwards.

Browning is one of the main quality parameters of dried apple slices and the consumer acceptance drops significant for products with increased brownish appearance. The browning Indices (BI) in Figure 4 shows, that the BI increases for all test series during the drying time. The biggest changing rate is taken place within the first 2-3 hours. All test series have a similar behavior where the browning index decreases after the first 2-3 hours and increases again afterwards. The T40_RH25 test series is much more distinct in its curve progression than the other test series and has a higher browning index than the T20_RH25 test series. This suggests, that a higher drying temperature and a higher relative temperature increases the browning index.
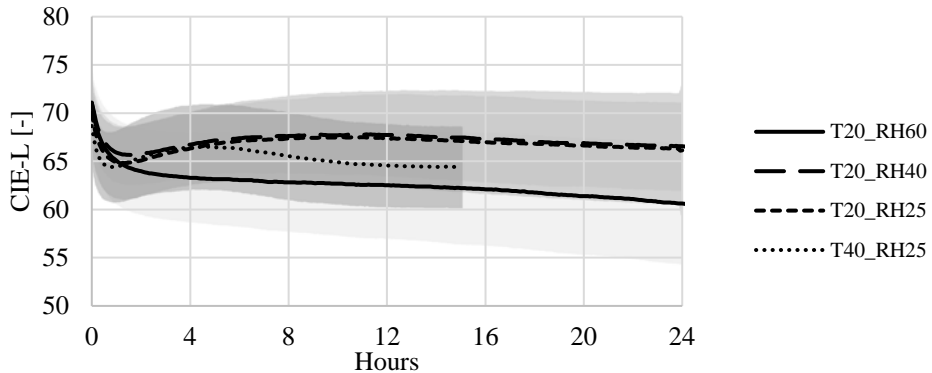
Figure 3: CIE-L* values of organic apples at different drying conditions
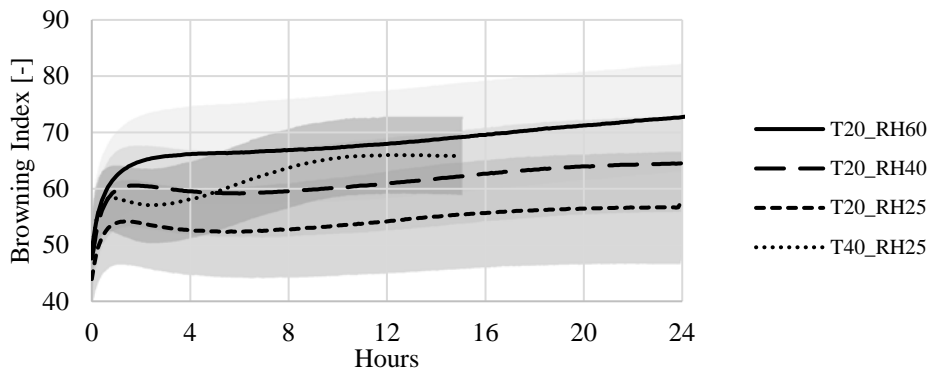
Figure 4: Browning index of organic apples at different drying conditions

Browning is mostly a surface effect and all tests showed clearly that this effect occurs in the beginning of drying when naturally the product surface is dried. This gives an indication that the product quality with respect to browning could be improved by a low temperature and low humidity drying period in the beginning. Once the surface is dried and stabilized the drying temperature could then be increased so that the drying time is reduced. With the current system it is possible to program such a control algorithm in a way that the drying conditions are continuously adapted to the color change and browning of the product.

Figure 5 shows the shrinkage of the apple slices related to the area of the top frontal view over the Moisture Ratio. All test series shows an area shrinkage at the end of the drying process between ca. 25% and 35%. Hereby the shrinkage seems to be nearly linear to the moisture ratio for a certain time and converges then to an end value. The curve progress of all test series is similar what indicates, that the relative humidity has only a minor influence on the area shrinkage process of the apple slices.

The sidelong deformation results in Figure 6 doesn't start at 100% since the apples slices in the beginning of drying are not a perfect rectangle. All test series shows an increasing

deformation over the drying time. Thereby the test series with 20°C drying temperature shows a similar curve progression whereas the curve progression of the T40_RH25 test series is taken place much faster. The magnitude of the deformation at the end of each test series is like all test series about 30% but varied very strong from apple slice to apple slice.
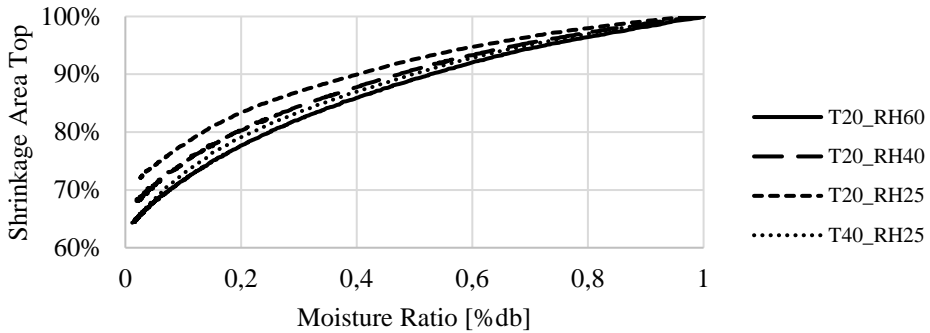
Figure 5: Top view shrinkage of organic apples at different drying conditions.
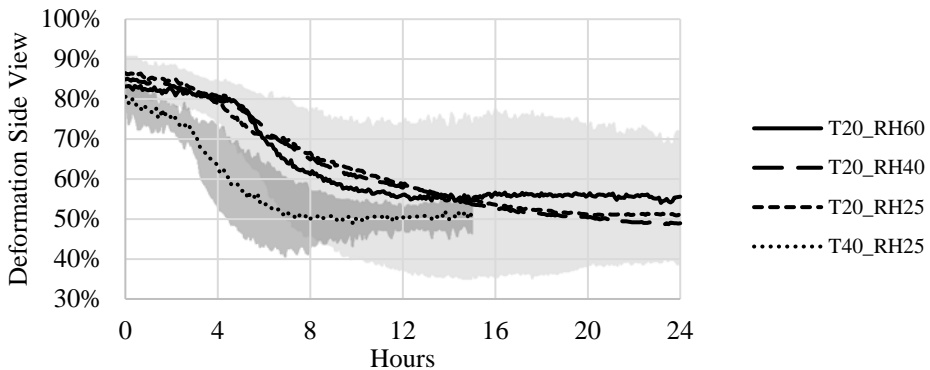
Figure 6: Side view deformation of organic apples at different drying conditions

The observations regarding deformation and shrinkage can be related to a certain mechanical stress in the product once the water is removed. Consequently, the deformation and shrinkage of the final product can most likely not be minimized by improved drying conditions. However, it can be considered to end the drying process with a higher final water content when the product is less shrunk or deformed. This would decrease the drying time and increase the amount market ready product.

4. Conclusion

The application of a sophisticated, robust camera system in combination with image processing algorithm can measure optical alternations of the drying product like shrinkage, deformation and color alternation in very precise and continuous way. The browning of

organic apple slices showed a clear correlation to the humidity of the drying air, while the drying temperature only had secondary influence. The shrinkage and deformation of the product is mostly related to the moisture content of the product and the drying conditions seem not to influence the final shrinkage or deformation rate. Based on the achieved results an optimized control strategy for the industrial batch drier is suggested in which the product is first dried at low temperature and low humidity to reduce the browning effect, followed by short drying period at higher temperatures, which is finalized when the acceptable shrinkage and deformation is reached. This will result in a preservation process in which the drying conditions are continuously adjusted by the measured product changes. Such "Smart-Drying" systems require an advanced control system in which the process parameters like humidity and temperature are controlled by the actual optical conditions to improve the drying process with focus on product quality.

5. Nomenclature

BI	Browning Index	-
CIE-XYZ	color space according the ISO Standard 13655	-
x	Chromaticity value	-

6. Acknowledgement

7. References

[1] Burger, W., Digital image processing : an algorithmic introduction using Java. 2016, New York, NY: Springer Berlin Heidelberg. pages cm.

[2] al., B.e., Definition of colour in the non enzymatic browning process. Die farbe, 1986. 32: p. 318-322.

[3] Hirschler, R., Whiteness, Yellowness and Browning in Food Colorimetry, in Color in Food: Technological and Psychophysical Aspects, M.d.P. Buera, Editor. 2016.

[4] Manalu, L., et al., The thin layer dring of temu Putih Herb, 2009

Synthesis of titanium dioxide precursor by the hydrolysis of titanium oxychloride solution

Le Bideau, P.[a*] ; Richard-Plouet, M.[b] ; Glouannec, P.[a] ; Magueresse, A.[a]; Iya-Sou, D.[b]; Brohan, L.[b]

[a] Univ. Bretagne Sud, IRDL, UMR CNRS 6027, F-56100, Lorient, France
[b] Institut des Matériaux Jean Rouxel (IMN), Université de Nantes, CNRS, F-44322, Nantes, France

*E-mail of the corresponding author: pascal.le-bideau@univ-ubs.fr

Abstract

This communication focuses on the development of an approach to improve the synthesis of [Ti8O12(H2O)24]Cl8.HCl.7H2O crystals which is one of the precursor for titanium dioxide TiO2 particles. This study provides a significant improvement in crystallization kinetics with a production rate increased by a factor nineteen by intensifying heat and mass transfers compared to the process in a close vessel. This enhancement was made possible by the development of a new reactor to control the heat and mass transfers involved. In parallel with the experimental set-up, a numerical model representative of the transfer phenomena was initiated. The first numerical results are encouraging and present a good agreement with the measurements.

Keywords: Heat and mass transfer; Co-desorption, Modelling, Experiment

1.   Introduction

Titanium dioxide TiO_2 particles are widely used in various applications. Thanks to its high refractive index, the industrial production of TiO_2 is mainly dedicated to produce pigments as whitening agent in paints [1]. This transition metal oxide is also well known for its n-type semi-conductivity leading to many applications such as gas sensor [2] or solar cell [3]. Additionnally its bandgap close to 3.2 eV gives interesting properties related to its photoactivity such as photocatalysis, self cleaning, light induced superhydrophilicity, among others. Titanium dioxide can be synthesized from various precursors such as alkoxides or inorganic salts. Depending on the pH, single crystals of $[Ti_8O_{12}(H_2O)_{24}]Cl_8.HCl.7H_2O$ were demonstrated to selectively lead to different varieties of nanostructured titanium dioxide [4]. The crystals can be obtained by the hydrolysis of titanium oxychloride solution $TiOCl_2,xHCl,yH_2O$, called aqueous solution of titanium tetrachloride. Due to the reactivity of the latter with water, it may be difficult to properly ensure the reproductibility of syntheses. Therefore a smart strategy is to use $[Ti_8O_{12}(H_2O)_{24}]Cl_8.HCl.7H_2O$ as reactant because of the known composition of the crystals and their solubility in polar solvents. With the adequate air temperature and air humidity conditions, the aqueous solution of titanium tetrachloride reacts to produce those crystals in releasing water and hydrochloric acid in the surrounding environment [5]. The formation process of $[Ti_8O_{12}(H_2O)_{24}]Cl_8.HCl.7H_2O$ is a complex process involving several species and several reaction kinetics. The aim here is to treat mass and heat problems in a highly reactive and deformable medium in order to get insight in the crystallization mechanisms and further optimize the process in order to accelerate the crystallisation. Figure 1 presents a simplified view of the different phenomena involved during the formation of $[Ti_8O_{12}(H_2O)_{24}]Cl_8.HCl.7H_2O$. The commercial solution is initially composed of 3 species: $TiOCl_2$, H_2O and HCl which react under particular ambient conditions of temperature and humidity to form $[Ti_8O_{12}(H_2O)_{24}]Cl_8.HCl.7H_2O$. During the process, $TiOCl_2$ and H_2O species are consumed while HCl and $[Ti_8O_{12}(H_2O)_{24}]Cl_8.HCl.7H_2O$ species are produced. At the solution/air interface, H_2O and HCl, are transferred to the ambient environment by evaporation. This evaporation causes on the one hand a variation in the volume of the mixture (shrinkage) and on the other hand a modification in the thermal and mass balance leading to temperature and concentration gradients within the mixture.
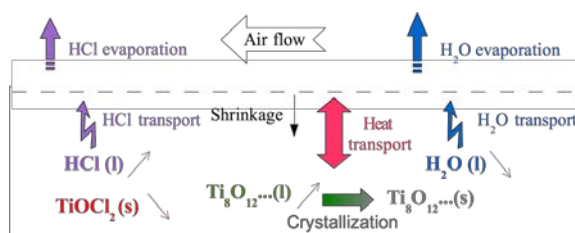
Fig. 1 Schematic description of physical phenomena

After a brief presentation of the titanium oxychloride solution, the static reactor, the laminar air flow reactor and the metrology used are described. A numerical model predicting the mass behavior of the solution during the first stage of process (before the crystallization kinetic) is presented. The experimental results obtained with the static and dynamic configurations are then discussed and show the capabilities to intensify the crystal production. The first numerical results are finally introduced.

2. Materials and Methods

2.1. Product description

At ambient temperature (T = 25°C), titanium oxychloride solution (Cristal) is a viscous, yellow liquid which is highly hygroscopic and very acidic (pH far below 1).The titanium oxychloride solution encloses [$TiOCl_2(H_2O)_2$] species dissolved in aqueous hydrochloric solution with the following composition: $1.375HCl, 5H_2O$. This solution is composed (in percentage by weight) of 54.9 % of the initial species ($TiOCl_2(H_2O)_2$), 16.1 % of HCl and 29 % of water. Based on this composition, the solvent proportion is 64,2 % of water and 35.8 % of HCl. This formulation was validated by placing the commercial solution in an atmosphere containing 36 %wt HCl and verifying the mass balance. In classical conditions (T = 25 °C and HR ≈ 50 %), HCl-H_2O co-desorption leads to the crystallisation of [$Ti_8O_{12}(H_2O)_{24}$]$Cl_8.HCl.7H_2O$. This crystals formation requires a mass loss of 41.6 %wt : 15.2 %wt water and 26.4 %wt HCl.

2.2. Crystallization reactors

2.2.1. Static reactor

The first syntheses were performed in a dessiccator containing a crystallizer filled with 2 mL of titanium oxychloride solution (solution height approx. 2 mm). A H_2SO_4/H_2O mixture is deposited at the dessiccator base in order to set the relative humidity close to 55 % at ambient temperature. Mass variations and crystals formation are monitored by carrying out discontinuous successive *ex situ* measurements.

2.2.2. Laminar air flow reactor

In order to intensify the massive exchanges and thus the production rate of crystals, a new experimental set-up was developed (Fig. 2). It consists in a rectangular PMMA duct (height: 11 cm, width: 17 cm) in which a PMMA crucible (10 cm x 10 cm) is placed. Air flow is blown parallel to the surface of the crucible containing the solution. This crucible which contained 22 mL of titanium oxychloride solution (solution height approx. 2.5 mm) is positioned on a weighing system that allows continuous mass monitoring. A heating system stuck below the crucible allowed us to control the solution temperature. The inlet air

conditions (temperature and relative humidity) are controlled by an upstream system equipped with a heat pump and a humidifier. Temperature sensors placed at upstream, downstream track air temperature variations. Other thermocouples are also stuck on heating element and positioned in the solution. A velocity sensor measures the air speed at the inlet of the duct. All these sensors are connected to a data acquisition system. In the same time, images of the solutions are recorded to track the shrinkage and the crystals formation.
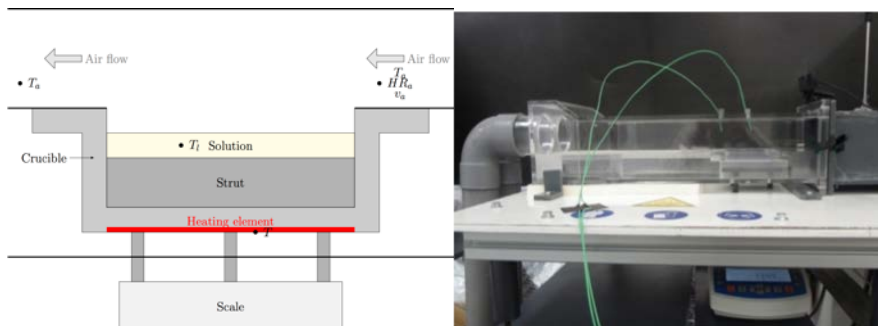
Fig. 2 Laminar air flow reactors description

2.3.   Numerical modeling

First, a numerical approach is initiated to predict the mass loss of the solution during the first step of the process (before the beginning of the crystallization). This model based on the mass conservation equations written for the solvents (HCl and H_2O) and the solute [$TiOCl_2(H_2O)_2$] should predict solvent concentrations as a function of the surrounding air conditions and/or the temperature of solution imposed by the heating system. The solution temperature is not computed but imposed based on experimental measurements.

The model assumptions are as follows: the initial solution (homogeneous) consists of 3 species [$TiOCl_2(H_2O)$]$_2$, H_2O and HCl; the species transport only takes place by diffusion (Fick's diffusion); the species transfer is assumed to be one-dimensional; the shrinkage is assumed to be linear; water reacts with the solute and is consumed to form HCl species.

2.3.1.   Governing equations

The application of mass conservation principle leads to write the following equations:

$$\frac{\partial \rho_s}{\partial t} + \text{div}(\rho_s \overrightarrow{v_s}) = 0 \tag{1}$$

$$\frac{\partial \rho_i}{\partial t} + \text{div}(\rho_i \overrightarrow{v_s}) = -\text{div}(\overrightarrow{J_i}) + S_i \tag{2}$$

With ρ the mass density (kg m^{-3}), J the mass flow (kg m^{-2} s^{-1}), S the mass source (kg m^{-3} s^{-1}) and v the shrinkage velocity (m s^{-1}). The subscript i refers to HCl noted A or water noted W.

2.3.2. Boundaries conditions

At the interface between the solution and the crucible base, no mass transfers occur:

$$-\mathbf{n}\left(\vec{J_l}\right) = 0 \qquad (4)$$

At the interface between the solution and the air flow, mass transfers depend on the difference of vapor densities between the product at the surface (surf) and the surrounding air (a):

$$-\mathbf{n}\left(\vec{J_l}\right) = h_m\left(\rho^v_{i,surf} - \rho^v_{i,a}\right) \qquad (5)$$

With h_m the mass transfer coefficient (m s^{-1}).

Water vapor and hydrochloric acid vapor are assumed to be ideal gas and the previous relation is expressed as a function of the partial pressure at the product surface and the partial vapor pressure of the ambient atmosphere. Considering that the initial complex does not affect the HCl/water mixture, it can be assumed that the partial vapor pressures of HCl/water mixture only depend on the temperature and concentration of HCl [6].

3.   Results and discussion

3.1.   Static syntheses

Various syntheses performed at room temperature and with a relative humidity set at 55 % present similar and repeatable behaviors. In figure 3, a first mass loss is observed during the first hours of drying caused by a significant release of solvents (HCl and water). This first stage goes on until the mass loss reaches about 15 % (≈ 15 h). At this stage, the first crystalline seeds appear and the crystallization kinetic accelerates. Co-desorption is then slowed down as long as the crystals grow and agglomerate. At the end of the process, the mass loss corresponds to about 41 %wt of the initial mass which matches with the predicted value by chemical equations. Under these conditions, about 25 days are required to form the crystals with a production rate per unit surface of about 630 g/(week.m^2).
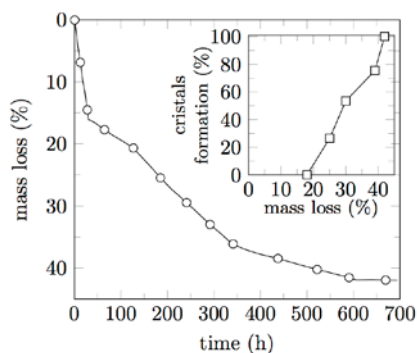
Fig. 3 Mass loss and crystals formation during static syntheses

3.2.   Dynamic syntheses

In a second step, syntheses were performed using the laminar airflow reactor. First experiments are carried out without direct heating (Fig. 4). The air temperature (T_a) is set to 28 °C and relative humidity (HR_a) varies between 45 % and 55 %. The air velocity (v_a) is set to about 0.45 m s^{-1}.
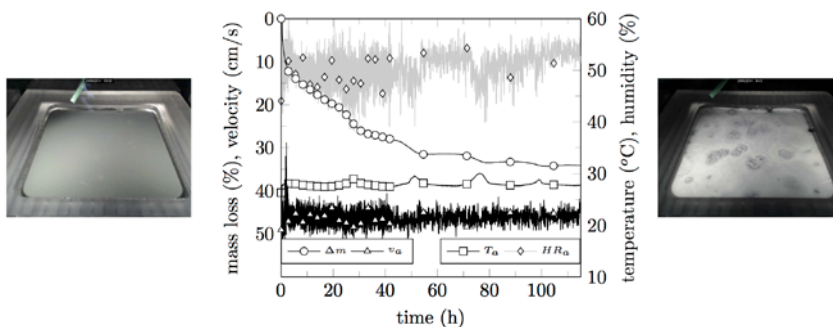
Fig. 4 Dynamic synthesis without direct heating, images of the crucible before (left) and after (right) crystallization, evolution of the mass loss, temperature and relative humidity with time (middle)

In these conditions, the first stage which corresponds to a mass loss (Δm) of 15 % is completed in about 8 h. The stationary phase is reached after 110 h (> 4 days). At the end of process, the mass loss corresponds to about 35 %wt and not 41 % as expected. This result can be explained by a crystallization at the surface which prevents the mass diffusion (HCl and water) from the medium toward the surface. The production rate of crystals is about 2.2 kg/(week.m^2) being more than 3 times the static production rate.

In order to intensify the mass transfer and thus reduce the synthesis time experiments are carried out with a direct heating (Fig. 5). The air temperature (T_a) is set to 27 °C and relative humidity (HR_a) varies between 50 % and 60 %. The air velocity (v_a) is set to 0.45 m s^{-1}.
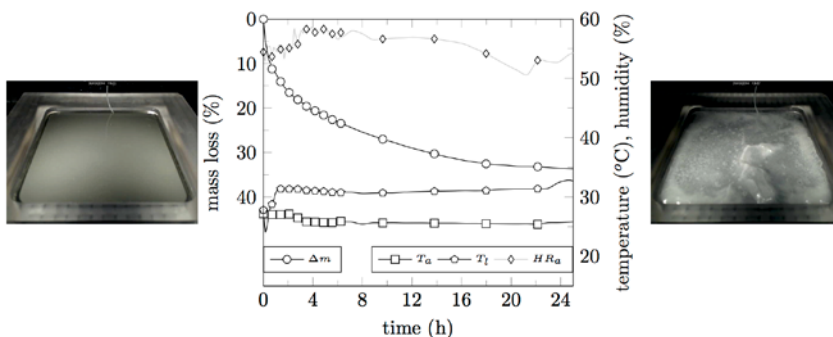
Fig. 5 Dynamic synthesis with direct heating, images of the crucible before (left) and after (right) crystallization, evolution of the mass loss, temperature and relative humidity with time (middle)

The solution temperature (T_l) varies from 27°C to 32°C during the first two hours due to switching on of the heating element (heating element temperature about 42°C). The first stage which corresponds to a mass loss of 15 % is completed within about 2 h. The stationary phase is reached after 24 h. At the end of process, the mass loss corresponds to about 34 %wt which is very similar to the value obtained in the previous case (without heating element). In this condition, the production rate of crystals is about 12 kg/(week.m^2), i.e., 19 times the production rate achieved in static mode.

3.3. Numerical results

The numerical model is tested for the dynamic configuration in the first hours of the synthesis process (before the beginning of the crystallization). The predicted mass losses are compared with the experimental ones for the tests performed without and with direct heating (Fig. 6). For these two configurations, the numerical results present a good agreement with the measurements. Experimentally, the solution density varies from 1.58 at the initial state to 1.5 when the mass loss reaches 20 %.
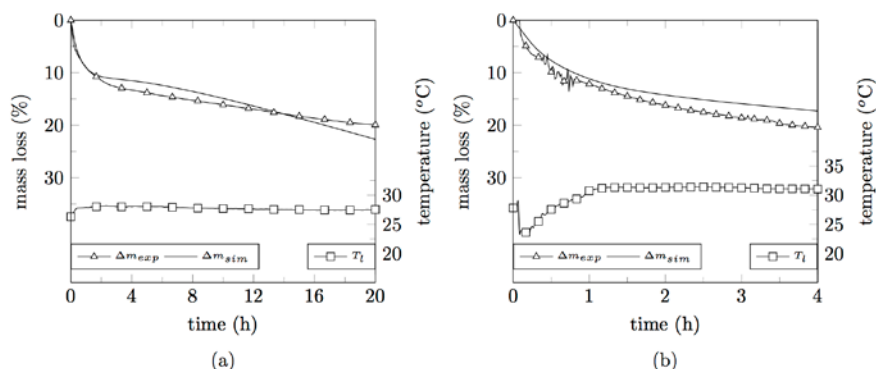
***Fig. 6** Evolution of the temperature (open square), experimental (open triangle) and simulated (line) mass losses without (a) and with (b) direct heating, as a function of time*

4. Conclusions

Under static conditions, the production of $[Ti_8O_{12}(H_2O)_{24}]Cl_8.HCl.7H_2O$ crystals requires several weeks. In order to improve the production rate, a laminar air flow reactor with temperature and humidity controls was developed. With adequate conditions (air and solution temperature and air relative humidity), a significant improvement in the crystals production was obtained from 630 g/(week.m^2) to 12 kg/(week.m^2). These encouraging results could be improved in future by studying more extensively the temperature/humidity pair providing the best yield. In parallel, a numerical model describing mass transfers (before crystallization began) was initiated. The first numerical results correctly reflect experimental observations and encourage further development.

5.   Acknowledgement

6.   References

[1]   Pfaff, G.;Reynders, P. Angle-dependent optical effects deriving from submicron structures of films and pigments. Chemical Reviews 1999, 99(7), 1963-1982.

[2]   Zhu, Y.; Shi, J.; Zhang, Z.; Zhang, C., Zhang, X. Development of a gas sensor utilizing chemiluminescence onf nanosized titatnium dioxide. Analytical Chemistry 2002, 74(1), 120-124.

[3]   Carp, O.; Huisman, C.L.; Reller, A. Photoinduced reactivity of titanium dioxide. Progess in Solid State Chemistry 2004, 32 (1-2), 33-177.

[4]   Liu, C.E.; Rouet, A.; Sutrisno, H.; Puzenat, E.; Terrisse, H.; Brohan, L.; Richard-Plouet, M. Low temperature synthesis of nanocrystallizes titanium oxides with layered of tridimensional frameworks, from $[Ti_8O_{12}(H_2O)_{24}]Cl_8.HCl.7H_2O$. Chemistry of Material 2008, 20, 4739-4748.

[5]   Brohan, L.; Sutrisno, H.; Puzenat, E.; Rouet, A.; Terrisse, H. French CNRS Patent 0305619, May 9, 2003; International Publication WO 2004/101436 A2, Nov 25, 2004; European CNRS patent (EP) 04 742 604.4, Nov 24, 2005; Japan (JP) CNRS Patent 2006-530327, Oct 16, 2006; United States (US) CNRS Patent 018344/0578, Feb 4, 2006.

[6]   Perry, R.H.; Green, D.W. Perry's chemical engineers'handbook, McGraw-Hill: New York, 1999.

Stabilization of *Lactobacillus sp. with enhanced thermal resistance by spray-drying*

Rivera, D.[a*]; Valverde, M.[a]; Valera, A.[a]; Torrejón, A.[a]; Espí, J.[a]; Gómez, E.[a]; Ruiz, B.[a].

[a] AINIA Centro Tecnológico. Valencia, Spain

*E-mail of the corresponding author: jdrivera@ainia.es

Abstract

Combining biotechnology and encapsulation by spray-drying is possible to obtain microorganisms-based products in powder format without losing viability. A methodology based on the improvement of the thermal stress resistance of selected strains of Lactobacillus sp. and subsequent culture stabilization by spray-drying by optimizing the process parameters and using thermal protectant materials has been developed. The results obtained showed that the final product kept the viability of the initial culture in addition to be a solid, powdery and ease-to-handle product.

Keywords: thermal resistance; spray-drying; probiotics; viability; fermentation; encapsulation.

1. Introduction

Sectors such as food and agriculture are looking for products based on microorganisms (i.e. probiotics, biofertilizers) with the aim of conferring a beneficial physiological effect on the host; most of them are available in liquid form. The challenge of these sectors is to offer them in powder formats for decreasing costs and to facilitate their use and applications. Vacuum and freeze drying are two drying technologies used for this end. The main disadvantages of freeze-drying are the high energy input and long processing times [1].Vacuum drying is faster and cheaper because it operates at a temperature above the freezing point. Other dryin technology, convective drying, can cost from 4 to 8 times less than freeze drying. However, the quality of the obtained dried products can be much lower, with a drastic reduction in the volume and colour changes [2].

Spray drying is a widely used technology to dry liquids and it is used in different sectors of food industry ensuring microbiological stability avoiding risks of chemical and/or biological degradations and obtaining product with specific properties like instantaneous solubility [3]. Processing costs are six times lower than freeze drying [2,4], however, the high temperature can lead to cell damage. The enhancement of the thermal resistance of the cell culture can be one alternative [5]. The addition to the medium of ingredients that may induce osmotic shock may strengthen the cell membrane [6]. The preadaptation of cells to heat is another possible strategy. During thermal stress, proteins heat shock is produced. These proteins may help to repair misfolded proteins during spray drying [6]. The use of protectant materials during the spray drying process can also enhance the survival of the microorganisms [7,8] being carbohydrates, such as trehalose, glucose, maltodextrin, inulin, fructo-oligosaccharides or potato starch [5], the most commonly used in food industries [9].

This microencapsulation processes can increase the microorganisms survival, not only during the spraying process, but also providing extra protection against ambient conditions or gastrointestinal conditions, allowing probiotics to reach the gut in an adequate amount [10, 11].

The aim of this study was to obtain microorganisms-based products in a powder format without losing viability by combining biotechnology and spray-drying. For this purpose, this study has been focused on different aspects: process variables, including formulation of the feed (thermal protectants, and encapsulating materials) and different stress methods for the culture.

2. Materials and Methods

2.1. Materials

A probiotic strain of *Lactobacillus sp.* isolated in previous works from cured meat was used in this study. The reference culture medium was MRS Broth, purchased from VWR.

Osmotic stress was induced by bifferent amounts of Sodium Chloride (Scharlau). Different protectant materials were used in the spray drying tests; Maltodextrin from Roquette, Trehalose, from Hayashibara, and modified starch, from Ingredion. All of them were food grade products.

2.2. Methods

2.2.1. Production of Lactobacillus sp. culture

For the screening of the spray drying conditions, a single batch of 20 L of *Lactobacillus sp* was produced using a stirring tank bioreactor (BIOSTAT C plus from Sartorius Stedim, Germany). The operating conditions were: Temperature: 37ºC; Medium: MRS Broth 52 g·L^{-1}. Dissolved Oxygen > 40% (controlled by cascade). When the culture reached the stationary phase, the culture was harvested using a high-speed refrigerated bench centrifuge (Sigma 6K15). After the harvesting, viable count of the product was done in order to know the concentration of the culture, measured in colony-forming units (CFU/mL).

2.2.2. Stabilization of the culture

The cultures of *Lactobacillus* sp. were stabilized by spray drying using a laboratory spray dryer (Büchi B-290, Switzerland). The operating conditions were: feed rate: 3-6 ml·min^{-1}; inlet temperatures: 105-115 ºC. Outlet temperatures between 51 and 71ºC. The tests were performed with different carriers: thermal protectant materials and encapsulating materials (Table 1).

Table 1. Concentration of the thermal protectant materials

Samples	Trehalose (%)(m/m)	Maltodextrin (%) (m/m)	Starch (%) (m/m)
1-3	30,20	---	---
4-7	7,50	23,26	---
8-11	7,50	15,53	7,76
12-42	4,28	9,15	4,57

2.2.3. Preadaptation of Lactobacillus cultures to spray drying to enhance thermal resistance.

Shake flask cultures were performed to study the effect of the culture conditions in the final viability of the spray dried products. Two effects were studied (thermal and osmotic stress) and Surface Response Methodology (SRM) was used for the design of a 3-level factorial experimental design in 9-runs with triplicates. The following variables were selected as response: the concentration of the cultures (CFU/mL), the concentration of the microencapsulated microorganism (CFU/g) and the viability of the product after spray drying was calculated as follow:

$$Viability\ (\%) = \frac{\log(Total\ CFU_{spray\ drying})}{\log(Total\ CFU_{culture})} \qquad (1)$$

The cultures were grown in 500 mL shake flask with 150 mL of MRS broth. The initial optical density of the cultures, measured at 600 nm, was adjusted to 0.1 The cultures were maintained at 37ºC and 150 rpm. Different levels of thermal and osmotic stress were applied to the cultures according to the following experimental design.

To induce osmotic stress, when the cultures reached an optical density of 0,4-0,5, they were centrifugated and resuspended to 150 mL of MRS or MRS broth supplemented with Sodium Chloride (according to Table 2). To induce thermal stress, when the cultures reached an optical density of 0,8-1,0, the flasks were introduced in a water bath at the specified temperature (according to Table 2). The cultures were spray-dried once they reached stationary phase (30 hours of process).

Table 2. Experimental Design.

	Thermal Stress (ºC)	Osmotic Stress (M)
R-1	49	--
R-2	42	0,3
R-3	49	0,6
R-4	--	0,3
R-5	42	0,6
R-6	42	--
R-7	49	0,3
R-8	--	--
R-9	--	0,6

3. Results

3.1. Effect of the inlet temperature

First of all, several tests of *Lactobacillus* sp. culture were carried out with the aim to know the effect of the inlet temperature in the microorganisms viability. In these tests, trehalose was used as material for thermal protection.

Table 3. Effect of the inlet temperature on the microorganisms viability

Sample	Tin (ºC)	Tout (ºC)	Viability (%)
1	105	55	79,6%
2	110	68	75,6%
3	115	71	80,7%

As expected, low inlet temperatures give, in general terms, high viability. Opposite to what it might appear, inlet temperature do not have a direct effect on the survival of microorganisms. The reason is that the viability does not depend only on the initial temperature, but also on the residence time and, in general, the temperature profile of the process, from the feed to the final dried product. In this situation, the outlet temperature has

a remarkable importance. The residence time depends on several variables of the process, feed composition and concentration, and also de design of the spray dryer equipment.

Effect of the feed composition

Table 4 shows the feed composition and the results of viability. Trials 12 to 15 were performed using the same carriers but with a lower concentration, as shown in Table 1.

Fig. 1 shows the effect of the feed composition and the inlet temperature, on the microorganisms viability. It can be seen that the effect of the feed composition, specially its concentration, are the relevant aspects to increase the viability in the final product.

Best results of viability were achieved for an inlet temperature of 115ºC combined with the trehalose/maltodextrin/starch as protectants. As shown in Fig. 2, the feed composition (Carriers) is the most relevant parameter on the microorganisms viability in the final product. The effect of the feed composition is bigger than the temperature due to its high estadistical significance. The selection of the carrier is relevant, but its concentration in the feed is even more relevant. This effect is due to that a lower concentration implies lower outlet temperatures and therefore, higher viability. However, lower carrier concentration in the feed leads to bigger costs, so this parameter needs to be optimized for industrial processes.

Table 4. Effect of the thermal protectants and wall materials on the microorganisms viability

Sample	Feed Composition	Inlet T (ºC) (±2ºC)	Viability (%)
1	Trehalose	105	79,6%
2	Trehalose	110	75,6%
3	Trehalose	115	80,7%
4	Trehalose/maltodextrin	100	81,5%
5	Trehalose/maltodextrin	105	80,3%
6	Trehalose/maltodextrin	110	79,3%
7	Trehalose/maltodextrin	115	77,0%
8	Trehalose/maltodextrin/Starch	100	77,1%
9	Trehalose/maltodextrin/Starch	105	78,8%
10	Trehalose/maltodextrin/Starch	110	81,6%
11	Trehalose/maltodextrin/Starch	115	75,0%
12	Trehalose/maltodextrin/Starch	100	78,3%
13	Trehalose/maltodextrin/Starch	105	82,4%
14	Trehalose/maltodextrin/Starch	110	87,3%
15	Trehalose/maltodextrin/Starch	115	87,9%
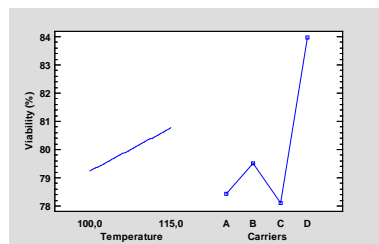
Fig. 1 Principal effects for viability (%)

Fig. 2 Pareto Diagram for CFU/g

A: Trehalose (Sample 1-3)

B:Trehalose/maltodextrin (Sample 4-7)

C: Trehalose/maltodextrin/Starch (sample 8-11)

D: Trehalose/Maltodextrin/Starch (Sample 12-15)

Trehalose with maltodextrin seems to produce slightly better results than the combination of three carriers, but the addition of starch improves the encapsulation effect on the particles. The encapsulation of the microorganisms, lead to improved protection, longer shelf life, and lower damage during gastrointestinal tract in case of probiotics.

3.2. Preadaptation of *Lactobacillus* cultures to spray drying to enhance thermal resistance.

The average results of the response variables selected for the experimental design on Table 2 are shown in Table 5. Taking into consideration the previous results of viability, mass yield, and the effect of the inlet temperature;this last was fixed at 105ºC for the rest of the study. As it can be shown, the variations in the fermentative process did not affect significantly the viable count of the culture. However, they had an effect in the viable count of the microencapsulated product and therefore in the final viabilitiy.

Table 5. Preadaptation of Lactobacillus cultures to spray drying to enhance thermal resistan

	Thermal Stress (ºC) (±2ºC).	Osmotic Stress (M) (±0,01M)	CFU/mL	CFU/g	Viability (%)
R-1	49	--	$2,66 \cdot 10^9$	$2,67 \cdot 10^8$	88,57%
R-2	42	0,3	$4,27 \cdot 10^9$	$2,12 \cdot 10^9$	95,11%
R-3	49	0,6	$2,16 \cdot 10^9$	$1,00 \cdot 10^9$	94,61%
R-4	--	0,3	$3,42 \cdot 10^9$	$2,97 \cdot 10^8$	88,40%
R-5	42	0,6	$2,63 \cdot 10^9$	$1,40 \cdot 10^9$	95,24%
R-6	42	--	$2,23 \cdot 10^9$	$2,75 \cdot 10^8$	89,59%
R-7	49	0,3	$5,85 \cdot 10^9$	$1,25 \cdot 10^8$	84,07%
R-8	--	--	$3,58 \cdot 10^9$	$3,08 \cdot 10^8$	88,63%
R-9	--	0,6	$2,64 \cdot 10^9$	$1,45 \cdot 10^9$	94,89%
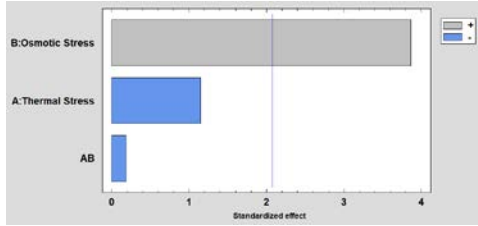
Fig. 3 Pareto chart of standardized effects for sprayed product viable count, Log (CFU/g)
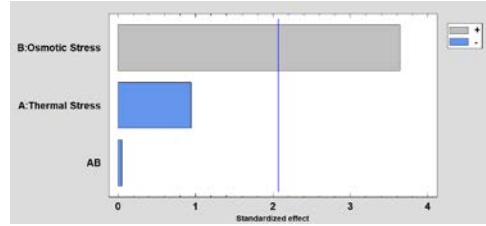
Fig. 4 Pareto chart of standardized effects for sprayed product viability (%)

According to Fig. 3, Osmotic stress has a significative effect in the final viability (%) as well in the final concentration of the microorganisms (CFU/g).The optimal conditions for maximizing the final viable count and viability are shown in Fig. 5, Fig. 6, Fig. 7 and Fig. 8.
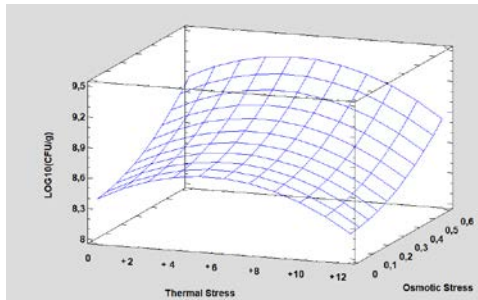
Fig. 5 Estimated surface response for sprayed product viable count, Log (CFU/g)
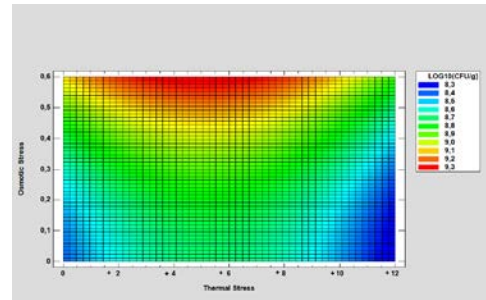
Fig. 6 Contours for estimated response surface for sprayed product viable count, Log (CFU/g)
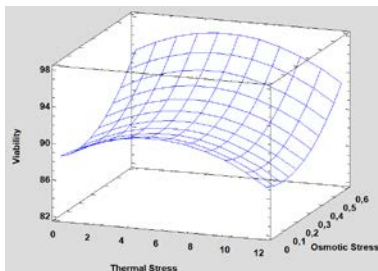
Fig. 7 Estimated surface response for sprayed product viability
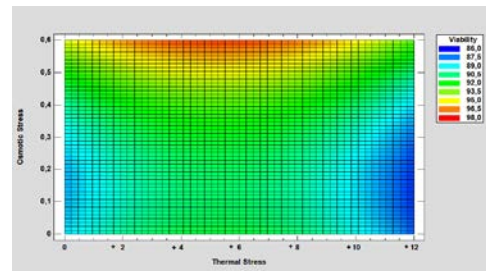
Fig. 8 Contours for estimated response surface for sprayed product viability

For the final viability of the product, the estimated surface response shows that the optimal value for the viability, which can reach 97,264% could be achieved by applying osmotic stress of 0,6M and a thermal shock at 43,28ºC.

4. Conclusions

Thermal processing of microorganisms for their stabilization and encapsulation can be done by Spray drying without loosing viability. Combining biotechnology and encapsulation by spray-drying is possible to obtain microorganisms-based products in powder format keeping their viability.

Feed composition has a highlighted effect on viability. Some carries as trehalose can be included as thermal protectants, improving microorganisns resistance against temperature. Other carriers, can be included with the objective of improving process yields, or giving added valuable properties to the final product, as encapsulating materials.

The concentration of carriers of the feed has also a remarkable effect, because lower concentrations lead to lower temperatures during the process. However, it is directly related to processes costs, so it must be optimized for industrial processes.

In addition, modificantions in the fermentative process of the microorganism, as a preadaptatiton of the cells to spray drying may increase even more the final viability of the product. According to the results of the present study, the final viability of the product may increase from 79,6 % to 82,4% by the apropiate selection of protective materials, and from 82,4% to 95,2% by the preadaptation of the microorganism during its fermentation.

5. References

[1] Nedovic, V.; Kalusevic, A.; Manojlovic, V.; Levic, S.; Bugarski, B. An overview of encapsulation technologies for food applications. Procedia Food Science 2011, 1, 1806-1815.
[2] Barbosa, J.; Borges, S.; Amorinm, M.; Pereira, M.J.; Oliveira, A.; Pintado, M.E.; Teixeira, P. Comparison of spray drying, freeze drying and convective hot air drying for the production of a probiotic orange powder. Journal of Functional Foods 2015, 17, 340-351.
[3] Gharsallaoui, A.; Roudaut, G.; Chambin, O.; Voilley, A.; Saurel, R. Applications of spray-drying in microencapsulation of food ingredients: An overview. Food Research International 2007, 40, 1107-1121.
[4] Knorr, D. Technology aspects related to microorganisms in functional foods. Trends in Food Science & Technology 1998, 9, 295-306.
[5] Huang, S.; Vignolles, M.-L.; Chen, X.D.; Loir, Y.L.; Jan, G.; Schuck, P.; Jeantet, R. Spray drying of probiotics and other food-grade bacteria: A review. Trends in Food Science & Technology 2017, 63, 1-17.
[6] Fu, N; Chen, X. D. Towards a maximal cell survival in convective thermal drying processes. Food Research International 2011, 44, 1127-1149.
[7] Liu, H.; Gong, J.; Chabot, D.; Miller, S.S.; Cui, S.W.; Ma, J.; Zhong, F.; Wang, Q. Protection of heat-sensitive probiotic bacteria during spray-drying by sodium caseinate stabilized fat particles. Food Hydrocolloids 2015, 51, 45-467.
[8] Arslan, S.; Erbas, M.; Tontul, I.; Topuz, A. Microencapsulation of probiotic *Saccharomyces cerevisiae* var. *boulardii* with different wall materials by spray drying. LWT – Food Science and Technology 2015, 63, 685-690.
[9] Santivarangkna, C.; Higl, B.; Foerst, P. Protection mechanisms of sugars during different stages of preparation process of dried lactic acid starter cultures. Food Microbiology 2008, 25, 429-441.
[10] Li XY, Chen XG, Sun ZW, Park HJ, Cha D-S. 2011. Preparation of alginate/chitosan/ carboxymethyl chitosan complex microcapsules and application in Lactobacillus casei ATCC 393. Carbohydr Polym 83:1479e85
[11] Desai KGH, Park HJ. 2005. Recent developments in microencapsulation of food ingredients. Drying Technol 23:1361e94.

CFD study of air flow patterns and droplet trajectories in a vortex chamber spray dryer

Rahman, U.J.U.[*]; Baiazitov, I.; Pozarlik, A.K.; Brem, G.

ThW group, Department of TFE. University of Twente, Enschede, The Netherlands

**E-mail of the corresponding author: u.jamilurrahman@utwente.nl

Abstract

In order to develop an alternative spray drying technology, a high drying rate in a smaller volume must be achieved. In this paper, results of CFD study are presented, carried out to investigate the possibility of spray drying in a novel design vortex chamber. The model is validated against experimental data, that makes a good agreement with an average error of 7% with only air and 24% with water spray. Results of temperature fields and droplet impact positions are discussed. The computations demonstrate that vortex chamber spray dryer can be an attractive solution for drying technology.

Keywords: CFD; spray drying; vortex chamber; atomization.

1. Introduction

Spray drying is a widely used process for converting liquid feed into dry powder [1]. However, the technology has only little improved over time. This comes with an inherent weakness; conventional spray dryers need great volumetric flow rates of air and thus high capital costs [2]. Additionally, low inlet temperatures and small gas-solid slip velocities lead to low drying rates. In order to develop an alternative spray drying technology, high inlet temperatures whilst maintaining a small residence time must be accomplished [3]. Therefore, a new technology for spray drying called vortex chamber spray dryer (VC) is investigated here. Additionally, high-G fluidization in VC, leads to intensification of interfacial heat, mass and momentum transfer [4, 5].

The high temperatures and turbulent multiphase flow in spray drying, make it difficult to design and optimize the dryer. For this purpose, Computational Fluid Dynamics (CFD) modeling has emerged as a vital tool in understanding the flow fields and gas-particle dynamics [6, 7]. In this research, a CFD model is developed to investigate air flow patterns and droplet trajectories for spray drying in a novel multi-zone VC dryer. The predicted results are compared against available experimental data. An overall drying performance is evaluated based on temperature profiles, particle's moisture content, impact positions and product quality obtained at the outlets.

2. Methodology

2.1. CFD methodology

The simulations have been performed in the commercial CFD package FLUENT 16.0. The flow in a spray dryer is a dispersed multiphase flow, therefore, the Eulerian-Langrangian approach was used. A three dimensional steady state model with k-epsilon turbulence model is used to simulate the gas phase. A two way coupling is applied to consider the heat, mass and momentum exchange between the continuous and discrete phase. The discrete phase turbulence is modeled using stochastic tracking model. The details of the CFD methodology and the governing Navier-Stokes, turbulence and discrete phase equations can be found in the literature and FLUENT user guide [8-10]. In order to simply the computations, the droplet-droplet interactions, agglomeration and coalesce is not considered. Also, only the evaporation model is used for droplet drying i.e. droplets are not porous and contains only surface moisture.

2.2. Geometry and boundary conditions

The VC geometry simulated in this study is shown in Figure 1. presenting the inlets and outlets (due to confidentiality reasons the exact dimensions are not presented). Such setup of VC offers two separate temperature zones: axial hot zone in the cylinder and relatively cold zone in VC. Hot air enters the dryer through a honey comb flow distributor hence diminishing

small turbulences in the cylinder. The VC is made up of six wheels, each wheel consisting of 36 inlet slots through which air enters the chamber tangentially, creating a high-G vortex flow. Droplets are injected, counter flow to hot air using a pressure nozzle. The position of the atomizer is depicted in Fig.1.
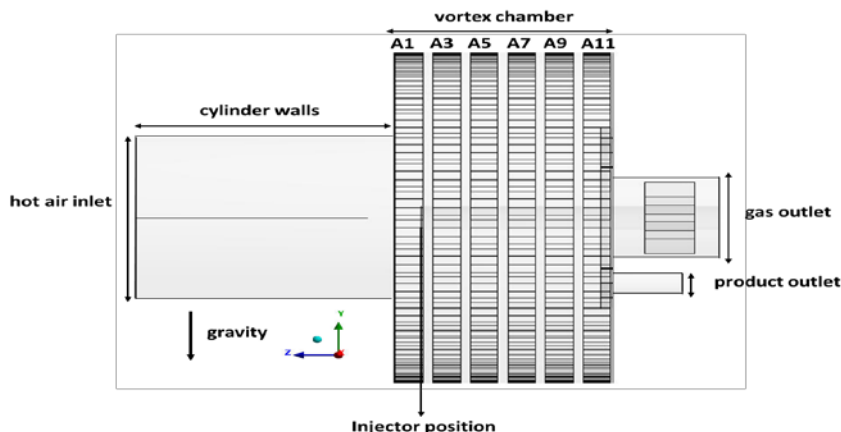
Figure 1. Geometry of vortex chamber spray dryer

The hot air inlet temperature is 350 °C and mass flow rate is 682 kg/hr while cold air average temperature to VC is 132 °C and mass flow rate of 615 kg/hr. The outlets are set to pressure of 5000 Pascal. The chamber walls are treated as adiabatic i.e. no heat loss to the environment is considered. A spray feed rate of 23 kg/hr is sprayed at a temperature of 65 °C with an injection velocity of 70 m/s. Droplet size distribution is modeled using Rosin-Rammler method. A spread parameter of 2.05 as reported by Kievet was used [11]. The maximum and minimum droplet size is set to 90 and 20 microns respectively while the mean droplet size of 52 microns [12] is used. Furthermore, a restitution coefficient of 0.2 is applied on VC walls.

3. Results and discussion

This section presents the predicted results of the CFD model. The model is validated against the available experimental data. Furthermore, an overall drying performance is evaluated based on particle impact positions and product obtained at outlets.

3.1. Grid independency study

For the grid independency study, three grid sizes; 1.5M, 3M and 5.5M elements were used. By comparing temperature profiles at 3 different locations, an average error of less than 1% was found between the coarsest and finest mesh. Since, the difference was not significant, the grid of 1.5M elements is applied for further research.

3.2. Validation of CFD model against experimental data

The experimental data used for the model validation is obtained from the work of Thomas et al. [13]. It should be pointed out that, during experiments, it was not possible to operate the VC in steady-state, due to the clogging of the nozzle. The thermocouples, V1 and V4 are located in the outer region of VC at top and bottom respectively, V6 and V8 are located in the middle transition region of VC at left and right respectively while the thermocouples V12 and V13 are located in the central core of the VC. The thermocouples are positioned on each wheel in the axial direction.
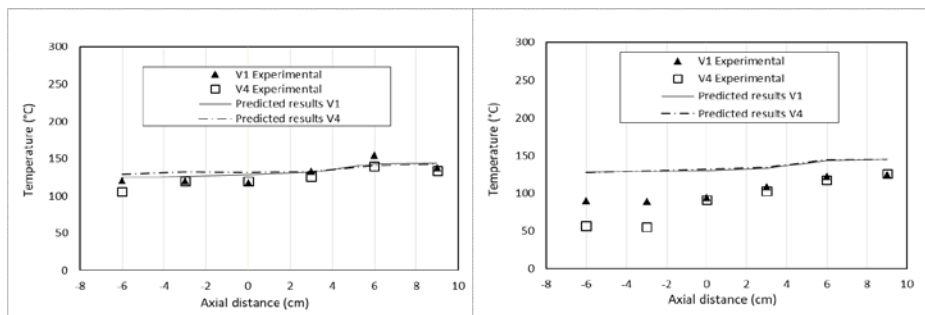
Figure 2. Comparison of results for V1 and V4 probes a) only air (left) b) with water spray (right)

The Figure 2a shows a comparison of predicted temperature profiles against experimental data for probes V1 and V4. The model makes a good agreement with an average error of 2% and 9% for V1 and V4, respectively. It can be seen that model slightly over estimates the temperature. The error can be caused by no heat loss assumption in the model whereas in the experiments heat loss can occur. Figure 2b, gives comparison with water spray. A relatively bigger error; 30% and 60% is seen for V1 and V4 respectively. Much lower temperatures; 50-80 °C for wheels A1 and A3 are observed in the experiments. However, these can be due to water impinging and evaporating on the thermocouple. Another reason could be that in the model spray penetrates into the hot cylinder where major evaporation takes place, and thus predicted results with only air and with spray do not show significant difference.

The Figure 3a shows the comparison of predicted air temperature against experimental data for thermocouples V12 and V13. The predicted results correspond well with the experimental data with an average error 1% and 7% for V12 and V13 respectively. Moreover, low temperature values in experimental measurements suggests, stronger radial mixing of hot air with the rotating cold air. Figure 3b, shows the comparison with spray. The experimental measurements show a strong asymmetry between V12 and V13. The dissymmetry might be induced by the product outlet being, too close to the gas outlets causing the spray to instantly deflect back on one side giving much lower temperatures for V13. The effect is less pronounced in the predicted results. An average error of 6% and 20% is obtained for V12 and V13 probes, respectively.
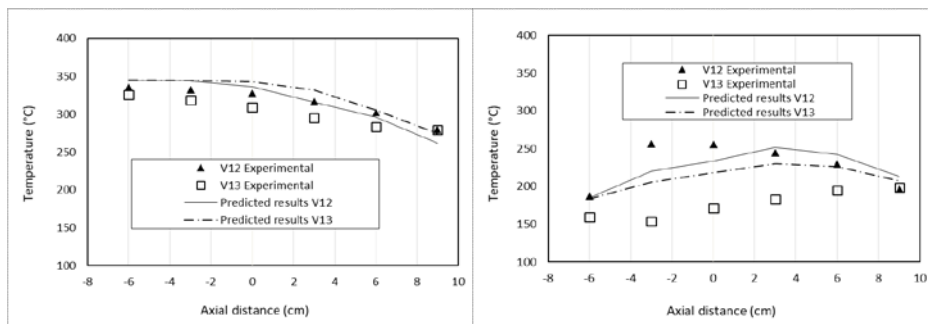
Figure 3. Comparison of results for probes V12 and V13 a) only air (left) b) with water spray (right)

Figure 4a, shows the comparison of predicted results for thermocouples V6 and V8. An opposing trend with an under prediction of temperature is seen for the middle-transition region. An average error of 11% for V6 and 13% for V8 is seen. The results imply a similar trend to that observed for the core region i.e. a stronger radial mixing of hot air with rotating cold air, that gives higher temperatures in the middle region of VC in the experiments.

Figure 4b, shows the predicted results against experimental measurements with water spray. The results shows a good agreement between numerical and experimental data with average error of 12% and 20% for V8 and V6 respectively. Plots show a similar trend of low temperature at the front two wheels where the biggest discrepancies are seen. This can again be explained with water droplets, which in experiments, do not penetrate into the hot cylinder but instead moves to the front of VC (A1 and A3 wheels).
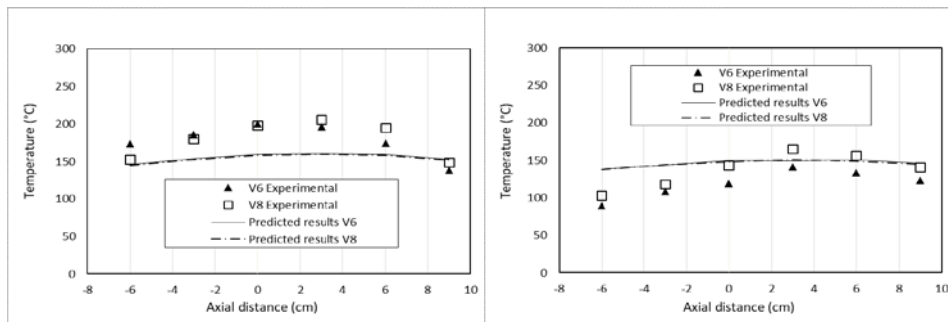
Figure 4. Comparison of results at probes V6 and V8 a) only air (left) b) with water spray (right)

3.3. Influence of multi component spray injection

In this section, the discussion has been extended by using 56 kg/hr of feed with 40% solid content and feed density of 1080 kg/m^3. A performance analysis of VC dryer is drawn based on particles impact positions, separation efficiency and mass of product recovered at the outlets. Figure 5, presents the temperature profiles on two axial planes for air flow only. A small reflux of cold air, from VC to cylinder can be seen on both planes. The reflux is caused

mainly by two reasons; low pressure in the cylinder and the influence of product outlet's back pressure. Such recirculating zones can be problematic, since it can lead to product deposition on cylinder walls. Furthermore, two temperature regions are visible in the dryer: a hot zone in the cylinder and around the nozzle and cold zone on the outer region of the VC.
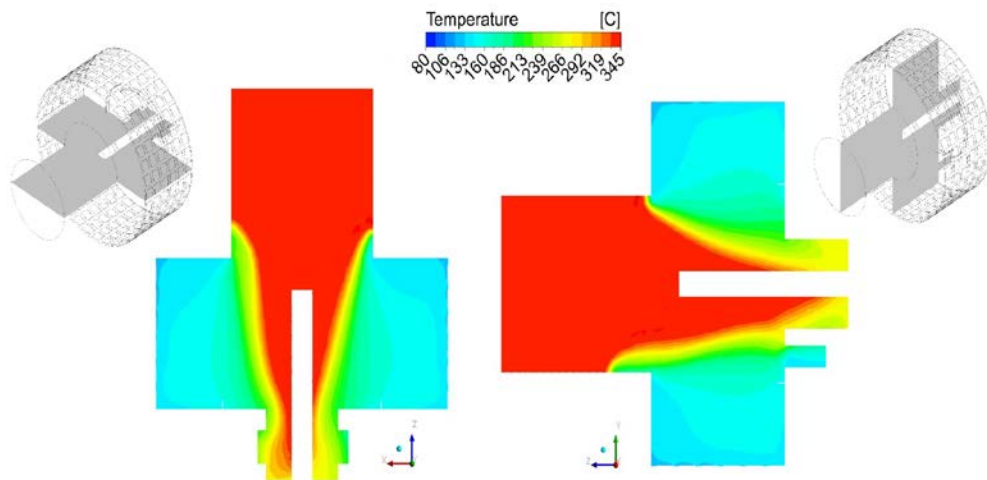
Figure 5. Temperature patterns on two axial planes, only air

Figure 6, illustrates the temperature patterns with spray (40% solid content). It can be seen that temperature profiles are asymmetric. The reason for this is mainly, the strong back pressure caused by the product outlet, forcing the droplets to instantly deflect back. Moreover, it can be seen that significant evaporation takes place in the hot zone while in the VC temperature drop is mostly near wheels-A1 and A3.
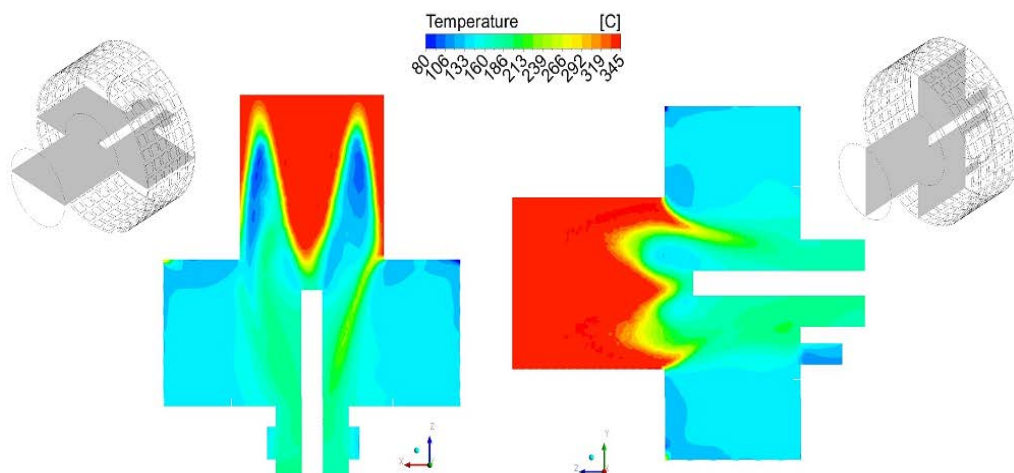
Figure 6. Temperature patterns on two axial planes, with water spray

3.3.1.Particle trajectories

In order to design and optimize a dryer, it is of prime interest to predict the trajectories of different sizes particles. Figure 7, reveals the particle trajectories for different particle size ranges, as a function of water mass fraction. These figures indicate that particles below 45 µm are instantly deflected back and leave via gas outlets. The particle sizes between 45-80 µm, are very uniformly distributed over VC. These particles mostly leave via product outlet. A mean particle size of 30 and 40 µm and a mean residence time of 0.48 and 1 seconds is found at gas and product outlet, respectively. Particles bigger than 80 µm are mostly impinging the honey comb air inlet or cylinder walls and only a few return to VC. Thus, it can be concluded that a maximum of 80 µm particle size, can be successfully dried without any risk of deposition on the walls. Moreover, all particles impinging VC walls are dried with zero moisture content.

Figure 7. Particle trajectories as a function of water mass fraction
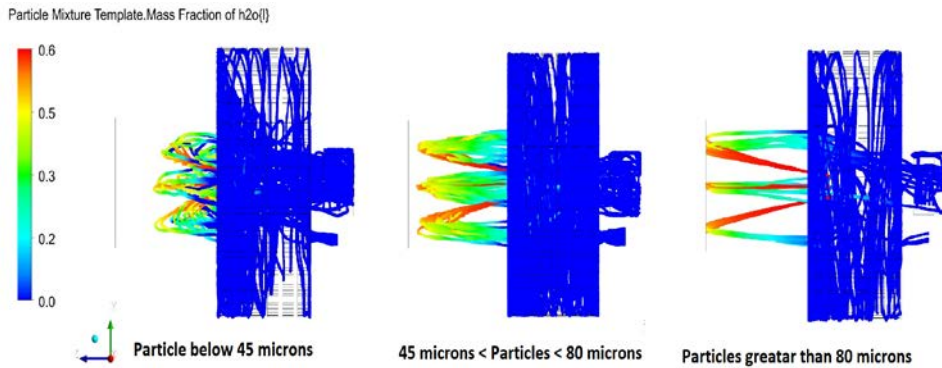
Table 2, shows an overall drying performance as discussed by Huang et al [14]. Some of the particles are trapped in circulating zones and do not escape. These are removed from calculations after 10 seconds.

Table 1. Overall drying performance of vortex chamber spray dryer

	Percentage (%)	Deposit rate (kg/hr)
Gas outlets	56	15
Product outlet	18	4.5
Cylinder walls	3.5	0.7
Hot air inlet	12.5	0.8
Incomplete	10	1.4
Gas outlet temperature (°C)	155	
Energetic Specific Consumption (KJ/Kg.H_2O)	10,000	

4. Conclusions

A three-dimensional CFD model for spray drying in a VC was developed. A good agreement was made with the experimental data, depicting an overall average error; 7% and 24% with only air and with water spray respectively. The results depict small recirculation zones of cold air in cylinder, causing asymmetric spray patterns. It was found that a large proportion of particles leave via the gas outlets. In order to have an efficient VC dryer, separation of smaller particles from air is necessary. Based on the CFD research, it can be concluded that redesign of current VC configuration is necessary in order to harvest its full potential.

5. Acknowledgements

6. References

[1] Masters, K., *Spray drying handbook*. 1991: Longman Scientific & Technical.
[2] Mujumdar, A.S., *Handbook of industrial drying*. 2015.
[3] Kudra, T. and A.S. Mujumdar, *Advanced Drying Technologies*. 2001: Taylor & Francis.
[4] De Wilde, J., *Gas–solid fluidized beds in vortex chambers.* Chemical Engineering and Processing: Process Intensification, 2014. **85**: p. 256-290.
[5] Eliaers, P., et al., *Modeling and simulation of biomass drying in vortex chambers.* Chemical Engineering Science, 2015. **123**: p. 648-664.
[6] Jin, Y. and X.D. Chen, *A Three-Dimensional Numerical Study of the Gas/Particle Interactions in an Industrial-Scale Spray Dryer for Milk Powder Production.* Drying Technology, 2009. **27**(10): p. 1018-1027.
[7] Kuriakose, R. and C. Anandharamakrishnan, *Computational fluid dynamics (CFD) applications in spray drying of food products.* Trends in Food Science & Technology, 2010. **21**(8): p. 383-398.
[8] Fletcher, D., *Computational Fluid Dynamics Simulation of Spray Dryers—An Engineer's Guide.* Drying Technology, 2017. **35**(7): p. 903-903.
[9] Woo M.W., H.L.X., Mujumdar A.S., Daud W.R.W, *CFD simulation of spray dryer.* Spray Drying Technology. Vol. one. 2010.
[10] Frydman, A., et al., *Simulation of Spray Drying in Superheated Steam Using Computational Fluid Dynamics.* Drying Technology, 2007. **17**(7-8): p. 1313-1326.
[11] Kieviet, F.G., *Modeling quality in spray drying.* 1997.
[12] M.Klaassen, *Near filed atomization in pressure swirl nozzle. Experimental investigation regarding inpact of fluid properties and nozzle specifications on spray characteristics,*, in *TFE (Thermal Engineering Group)*. 2016, University of Twente: Enschede.
[13] Tourneur, T., A.d. Broqueville, and J.D. Wilde, *Experimental and CFD study of multi-zone vortex chamber spray dryers*, in *International Symposium on Chemical Reactor Engineering-ISCRE 25*. 2018.
[14] Huang, L.X., K. Kumar, and A.S. Mujumdar, *A comparative study of a spray dryer with rotary disc atomizer and pressure nozzle using computational fluid dynamic simulations.* Chemical Engineering and Processing: Process Intensification, 2006. **45**(6): p. 461-470.

Augmenting natural convection and conduction based solar dryer

Chavan, A.[*]**; Sikarwar, A.; Tidke, V.; Thorat, B.**

Department of Chemical Engineering, Institute of Chemical Technology, Nathalal Parekh Marg, Matunga (East), Mumbai-400019, India, Tel:+91-22-33612023/2001

*E-mail of the corresponding author: thoratbn@gmail.com

Abstract

Solar conduction dryer (SCD) is a unique technology that uses conduction, convection and radiation mechanism of heat transfer making it one of the most efficient drying system. The SCD is one of the most effective piece of equipment's designed indigenously and it has tremendous potential to capitalize in erstwhile nations of tropical and torrid region where there is abundance of solar insolation. SCD, the most cost-effective dryer which runs on no electricity has already made inroads in the global market. In the present study, CFD studies were carried out for a given geometry and the corresponding boundary conditions.

Keywords: Solar Energy; Solar Conduction Dryer; CFD modeling.

1. Introduction

Drying is a complex operation involving transient transfer of heat and mass along with several rate processes, such as physical or chemical transformations, which, in turn, may cause changes in product quality as well as the mechanisms of heat and mass transfer. Physical changes that may occur includes: shrinkage, puffing, crystallization, glass transitions and so on [1]. As it is well known, drying is the most energy intensive operation of the industrial processes [2]. Energy efficiency in drying ranges from a low value of under 5 % for the chemical process industries to 35 % for the papermaking operations [1]. Thus, there is strong contention among the researchers around the globe to develop a simplified and low-cost approach that can minimise or nullify the energy requirement through combination of efficient design and optimized process variables.

Keeping these aspects in mind, several researchers have developed different type of solar dryers in last couple of decades to dry food materials as per the local need and indigenous technology. These dryers were based on the heat transfer mechanism of radiation and natural/ forced convection. They can be categorised in three types, such as, integral (direct), distributed (indirect) and mixed mode. In direct type of solar drying, the sun rays are directly incident on material while in indirect type, the air would absorb the heat and transfer it to the material. In mixed mode, the combinatorial heat transfer mechanism plays a crucial role in drying [3]. Thus, based on the above categorization, the following are some of the popular solar dryers in vogue, i.e. Natural convection cabinet dryer, Forced convection indirect dryer, Green house dryer, Solar tunnel dryer.

As described above, these dryers are working on the principle of one or maximum two heat transfer mechanisms. Solar conduction dryer is the first technology in the world that uses all the three modes of heat transfer, viz., conduction, convection and radiation making it one of the most efficient systems [4]. SCD works without the need for electricity and most importantly at zero operating cost, following the three principles of 'A's, i.e. availability, affordability and accessibility [5]. It costs 3-5 times less than the next competing solar dryer and has payback period of 100 days against cost of electricity saving. SCD is recognized by UNEP-Bayer Ag (Germany) as top four global sustainable technologies and by University of Texas-Austin as global leading social venture. US-AID has included SCD in its Feed the future (FTF) program.

Computational fluid dynamics (CFD) is a highly powerful tool to predict the performance and can help us to optimize the dryer geometry under given operating conditions without actually performing too many experiments. Various solar based designs like (a) solar air heater [6-9]; (b) drying systems such as direct, indirect, mixed [10-12] were simulated using computational fluid dynamics CFD modelling helps us to get the detailed inside look

in the flow field development, temperature distribution [13], humidity profiling and drying time [14].

The objective of the proposed work is not to understand the existing models and compare them, but to make use of these models with certain additional features and incorporate those state equations for all the three modes of heat transfer, which is the major highlight and selling point of the award-winning technology of Solar Conduction Dryer (SCD). Based on the experimental insights and the foregoing literature, CFD model was developed. Here, the results of CFD models based on combinatorial heat transfer mechanism were compared with the experimental findings. Certain alterations to the existing design were possible to be thought about and they were brought fore as an addendum to the design of the existing/ commercial SCD.

2. Materials and Methods

2.1. Drying Equipment

Fig. 1 Solar Conduction Dryer.

The Solar conduction dryer (SCD) is a solar dryer (Figure 1) developed at advanced drying laboratory of Institute of Chemical Technology (formerly UDCT) Mumbai, India. This equipment utilizes solar power in the form of conductive, convective as well as radiation way of heat transfer for drying. The structure of SCD comprises of four drying chambers constructed from hollow sections of stainless steel. The dryer has four drying trays, covering a surface area of 1.04 m² each. Transparent plastic (Polycarbonate Multiwall Sheet) was used to cover the trays. The trays were coated with black colour special food grade coating, where the products to be dried are placed. The trays were insulated properly so as to minimize the heat losses to the surrounding. A low height air vent to create air current is provided at the middle of the dryer in the horizontal direction which also separates the drying chambers in two portions (parts), as shown in Figure 1. Each portion contains two drying trays. Atmospheric air enters from the front of the trays and it carries away the moisture of the sample through the canopy by means of natural convection. The

movement of the tray is by sliding them in and out through a designed channel for loading purpose.

2.2. Model (Governing equations for CFD)

Mass continuity, momentum, energy and radiation equations were solved to simulate the flow and temperature distribution in the unit. The solar load model available in FLUENT consists of a combination of a solar ray tracing algorithm and a radiation model called surface to surface (S2S). The solar ray tracing algorithm works as the source of the solar heat and the S2S radiation model accounts for the internally scattered energy. The sources for this energy are the surfaces exposed to the solar rays and thus soaked with solar heat energy. Equations are not being reproduced here, as the same could be obtained from Ansys.

3.   Results and Discussion

SCD was simulated at measured solar radiation flux of 1000 W/m^2. A full-scale 3D simulation of SCD resulted in a symmetric flow pattern. Experimental data also suggested symmetric profile in thermal measurements across the two parts. Hence, half section of the SCD was simulated under the given conditions. Figure 3 shows the flow pattern of air as predicted by the CFD model. It can be seen that the flow is mostly straight without any lateral components. Small circulation zone was observed at the centre of dryer (region where the flow from both the inlets meet and then flows upwards towards the outlet). Here, the flow is predominantly laminar in nature.

3.1. Flow pattern in solar conduction dryer
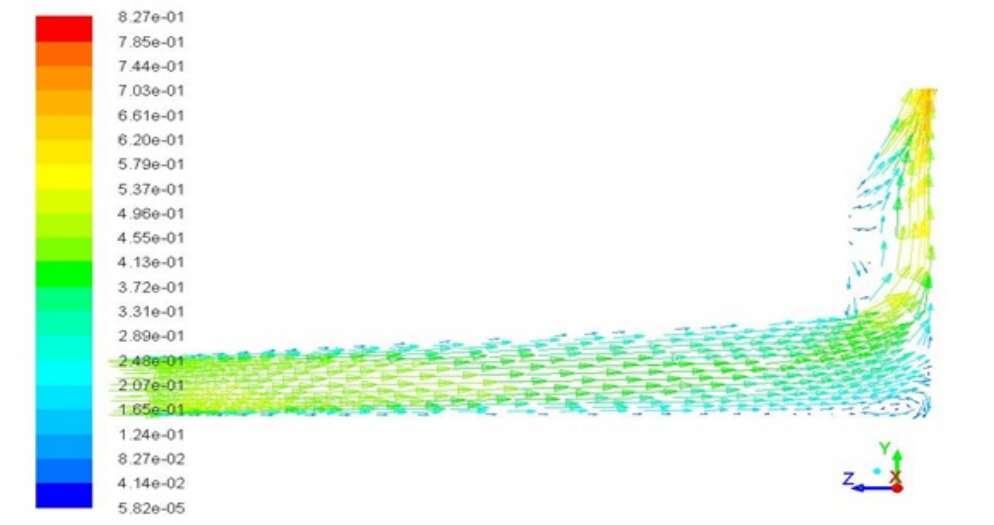
Fig. 2 Flow pattern of air from inlet to centre of dryer.

3.2. Comparison between experimental and simulated temperature of bottom plate and top plate of SCD

The thermal measurement of the bottom plate (Figure 3) indicates sharp rise in the temperature. The temperature remains constant in the dryer section. In the central part, a small dip in the temperature was observed, probably due to the negligible presence of air (hot) adjacent to the bottom plate. As the air gets heated from inlet to dryer section and as soon as it comes at the chimney section, it swirls off through it because of low density. This is very important observation, as it indicates the temperature variation in the dryer in tune with the entry and exit effect of the air. This temperature drop was very well captured in simulation results. Figure 4 compares the predicted temperatures with measured data. It can be deduced that the simulation results are in good agreement with the experimental data.
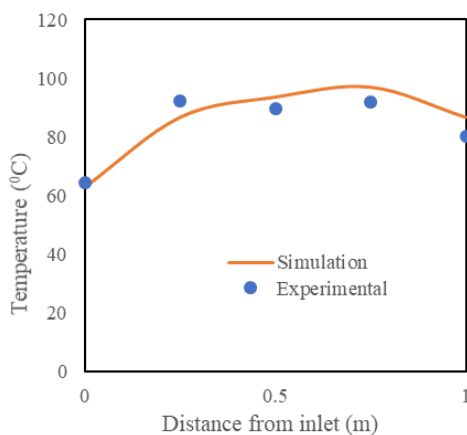
Fig. 3 Comparison of experimental and simulation temperature (Bottom plate).
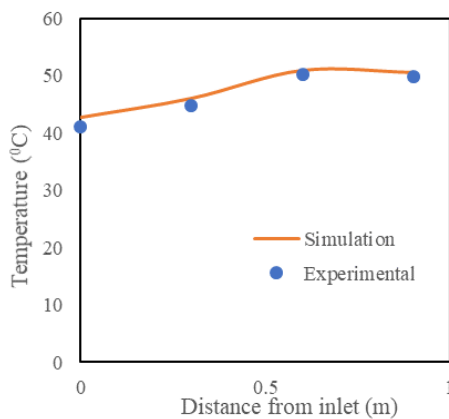
Fig. 4 Comparison of experimental and simulation temperature (Top plate).

3.3. Proposed design of modified solar conduction dryer (Design 1)

As per the patented design of solar conduction dryer, there is a loading space gap between the polycarbonate sheet (top plate) and the black coated aluminium plate (bottom plate). The gap is around more than 10 cm between these two. In order to maximize the utilization of energy and material loading capacity, we can alter the interiors of existing SCD. The modified design (Design 1) will contain an array of plates placed in a staggered manner between the top plate and the bottom plate. The array of plates is designed in such a way that the solar energy reach to the bottom plate. The plates were arranged as shown in Figure 5. Simulations were done described in results and discussion for the staggered plates arrangement. Simulations were performed till the steady results are obtained. These results are as shown in Figures 6-8.
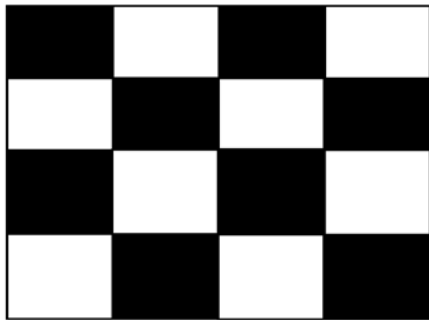
Fig. 5 Intermediate plate structure in modified SCD (Design 1).
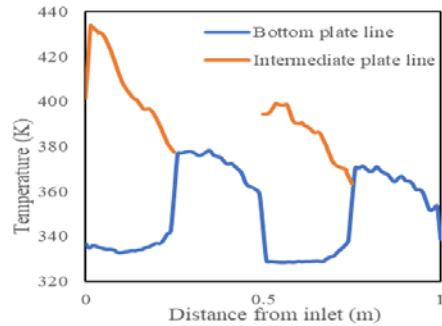
Fig. 6 Temperature profile of intermediate and bottom plate in modified SCD (Design 1).
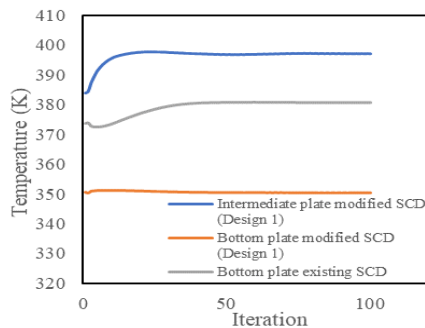
Fig. 7 Area weighted average temperature of bottom plate and intermediate plate in existing and modified SCD (Design 1).
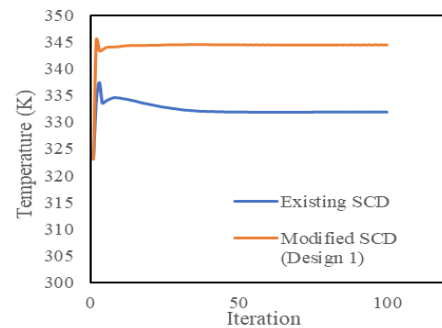
Fig. 8 Area weighted average temperature at outlet in existing and modified SCD (Design 1).

3.4. Comparison between existing and groove bottom plate SCD (Design 2)

It was found in the literature that the grooved or corrugated absorber plate creates maximum heat transfer area. There are so many type of grooved plates. So, the idea was that the use of that concept in our case. From the figures 11 and 12, it was found that, there is considerable difference of area weighted average temperature of bottom plate and the outlet air temperature. The use of groove absorber in the place of flat absorber provides a large surface area for heat transfer to the air stream. The convective heat transfer from bottom plate to air increases in this case but the loss is largely compensated by the increased heat transfer to the flowing air [15].

4. Conclusions

The CFD model has been successfully developed to predict the temperature of top and bottom plate. The model predictions are in good agreement with the measured data in

summer as well as winter environmental conditions. CFD simulations of modified solar conduction dryer was also carried out and it gives higher performance. Modified SCD is superior than the existing SCD in terms of outlet air velocity, outlet air temperature, intermediate plate temperature and material handling capacity. The material handling capacity can be increased by as high as 50 %. SCD contained groove bottom plate simulations were also done and it was found that there was increase in the outlet air temperature compared to existing SCD.

Figure 9: Front view of groove bottom plate (Design 1).
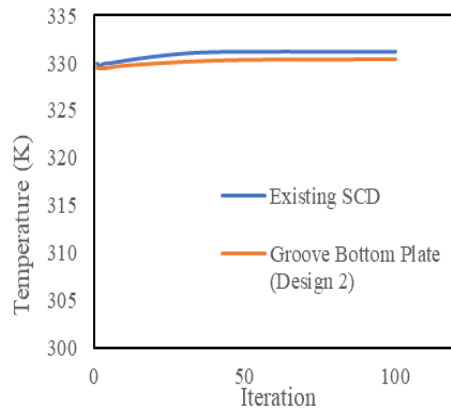
Figure 10: Area weighted average temperature of top plate in existing and groove bottom plate SCD (Design 2).
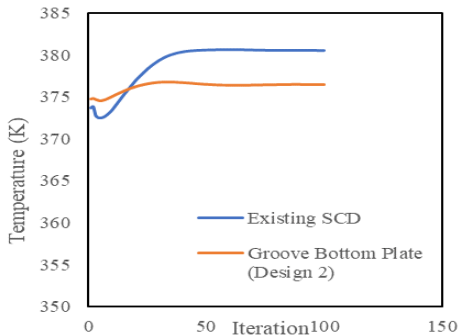
Figure 11: Area weighted average temperature of bottom plate in existing and groove bottom plate SCD (Design 2).
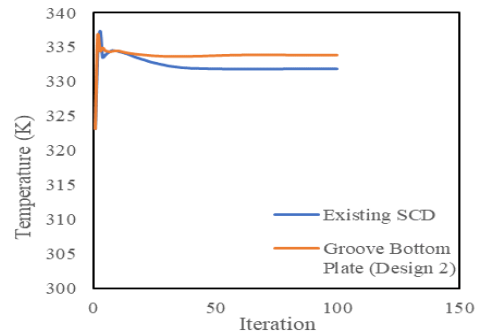
Figure 12: Area weighted average temperature of outlet temperature of air in existing and groove bottom plate SCD (Design 2).

5. References

[1]   Mujumdar, A. S. Handbook of Industrial drying. 3, Ed. U. S. A.: CRC Press 2006.

[2] Bennamoun, L. An Overview on application of exergy and energy for determination of solar drying Efficiency. International Journal of Energy Engineering 2012, 2(5), 184-194.

[3] Bennamoun, L. Reviewing the experience of solar drying in Algeria with presentation of the different design aspects of solar dryers. Renewable and sustainable energy reviews 2011, 15, 3371-3379.

[4] Tidke, V.; Thorat, B.; Kokate, S. Solar Conduction Dryer with Controlled Radiation. PCT/IN/2012/000843 (2014).

[5] Professor Thorat's personal communication with Professor Arun Mujumdar, 2017.

[6] Yadav, A. S.; Bhagoria, J. L. A CFD (Computational Fluid Dynamics) based heat transfer and fluid flow analysis of a solar air heater provided with circular transverse wire rib roughness on the absorber plate. Energy 2012, 15, 1127-1142.

[7] Boulemtafes-Boukadoum, A.; Benzaoui, A. CFD based analysis of heat transfer enhancement in solar air heater provided with transverse rectangular ribs. Energy Procedia 2014, 50, 761-772.

[8] Singh A.; Singh, S. CFD investigation on roughness pitch variation in non-uniform cross-section transverse rib roughness on Nusselt number and friction factor characteristics of solar air heater duct. Energy 2017, 128, 109-127.

[9] Gawande, V. B.; Dhole, A. S.; Zodpe, D. B.; Chamoli, S. A review of CFD methodology used in literature for predicting thermos-hydraulic performance of a roughened solar air heater. Renewable and Sustainable Energy Reviews 2016, 54, 550-605.

[10] Chauhan, P. S.; Kumar, A.; Tekasakul, P. Applications of software in solar drying systems: A review. Renewable and Sustainable Energy Reviews 2015, 51, 1326-1337.

[11] Prakash, O.; Laguri, V.; Pandey, A.; Kumar, A.; Kumar, A. Review on various modelling techniques for the solar dryers. Renewable and Sustainable Energy Reviews 2016, 62, 396-417.

[12] Romero, V. M.; Cerezo, E.; Garcia, M. I.; Sanchez, M. H. Simulation and validation of vanilla drying process in an indirect solar dryer type prototype using CFD Fluent program. Energy Procedia 2014, 57, 1651-1658.

[13] Norton, T.; Sun, D. Computational fluid dynamics (CFD) an effective and efficient design and analysis tool for the food industry: A review. Trends in Food Science and Technology 2006, 7 (11), 600-620.

[14] Carlescu, P.; Arsenoaia, V.; Rosca, R.; Tenu, L. CFD simulation of heat and mass transfer during apricots drying. LWT- Food Science and Technology 2017, 85, 479-486.

[15] Anuradha, A.; Oomen, R. Fabrication and performance evaluation of a V-groove solar air heater. International Journal of Scientific and Engineering Research 2013, 4(6), 2072-2080.

Post-harvest treatment of algerian broad beans using two different solar drying methods

Chouicha, S.; Boubekri, A.*; Berbeuh, M. H.; Mennouche, D.; Frihi, I.; Rzezga, A.

Université Kasdi Merbah Ouargla, Laboratoire de développement des Energies Nouvelles et Renouvelables dans les Zones Arides et sahariennes, Faculté des Sciences Appliquées, Ouargla 30000 Algeria

 *E-mail of the corresponding author: boubekri.abdelghani@univ-ouargla.dz

Abstract

This work was carried up in the objective to valorize the broad beans, largely harvested in Algeria, by solar drying means. In the present research paper, an experimental study was conducted on solar drying of broad beans by two different methods. Experimental trials were performed on a direct and an indirect laboratory scale solar dryers at Ouargla university in the southern of Algeria. Selected samples were dried at 50°C, 55°C, 60°C and 65°C. In both two applied cases, drying curves were obtained and compared. Among twelve consulted drying models the Page model was correlated with satisfaction to describe the solar drying of broad beans using a non linear regression analysis method. Operating and thermal performances of the two used drying systems were checked by the energy effeceincy and economic calculation. Obtained results showed that the direct solar drying ensures good preservation of the final product with a drying time of 5 hours.

Keywords: solar drying ; convective drying ; broad bean ; quality

1. Introduction

Faba bean (Vicia faba L.) is one of the oldest crops and ranks the sixth in production among the different legumes grown in the world after soybean, peanut, beans, peas, and chickpeas. Faba bean is popular legume food with high yield capacity and high nutritional value. It is widely used in the Mediterranean region as source of protein in both human and animal nutrition. It is a popular breakfast food and also used as vegetable green or fresh canned. In Algeria, faba bean is one of the most important pulse crop cultivated due to the richness of seed protein content. Also, The most important organic components of faba bean seeds are proteins 20-41% of seed dry matter, carbohydrates (51-68%), 12% fiber, 1.2-4% lipids vitamins and minerals [1].   Due to its chemical composition, fava bean is a suitable food for diabetics and may help prevent heart disease and reduce levels of blood glucose vitamins and minerals [2]. The major producer countries include China, Indonesia, India, Turkey, Egypt, Spain, France and Algeria. Broad beans is grown on 12,000 ha areas in Algeria, with a production of 60,787 tons in 2013 [3]. Due to their seasonal and perishable nature, broad beans must be subjected to some form of preservation such as canning, freezing, or cold storage in order to make them available for later consumption [4]. Drying is practiced to enhance the storage life, to minimize losses during storage, and to reduce transportation costs of agricultural products [5]. Solar drying of agricultural products is one of the most important potential applications in the Algerian Sahara. Farmers and citizens dry crops particularly menthe, tomato, abricots, and broad beans. Traditional open sun drying is practiced on a large scale in Ouargla regions where the agriculture suffers from high product losses due to inadequate drying, fungal growth, encroachment of insects, birds and rodents, etc. The problems associated with open-air drying can be solved through the use of a solar dryer which can reduce crop losses and improve the quality of dried product significantly compared to traditional drying method. Solar dryers used in agriculture for food and crop drying are used for industrial drying processes. They can be proved to be a very useful device from the energy conservation point of view. Such a process not only saves energy but also saves a lot of time, occupies less area, improves quality of the product, makes the process more efficient, and also protects the environment [6]. A research group in the laboratory of renewable energy in aride zones (LENREZA) at Ouargla University, Algeria, worked in this field of solar drying. Two types of solar dryer: indirect hybrid solar dryer and direct active solar dryer have been constructed and tested in Ouargla climatic conditions. In the direct solar dryer the product to be dried receives energy from both direct exposure to solar radiation; also the product being dried is protected from rain, insects, and dust. They found the product to have high-quality in terms of flavor, color, and texture. In all cases, the use of a direct convective solar dryer considerably reduces drying time in comparison to open-sun drying. The Passive solar dryers have the advantage of cheap, easy construction from locally available materials and

do not require any other energy during operation. Their major drawbacks are the decrease drying rates, important drying time and the very high internal temperature with the likelihood of overheating the product [7, 8]. Various drying techniques are employed to dry different food products. Each technique has its own advantages and limitations. Choosing the right drying techniques is thus important in the process of drying of the perishable products. To reduce its dependence on solar radiation for operation and to improve the quality of drying many studies on drying of fruits and vegetables using solar dryers with different sizes and designs exist in literature [9]. We can refer to some works such as on drying of potato [10], green pepper, green bean and squash[11], apricot [12], pistachio, and other products. However, studies on drying of broad beans are scarce. Therefore, the analyze of chemical composition and improving of production were experimentally investigated [13-16]. No information is available on the drying behavior of broad beans in the open literature. Therefore the main objectives of this study are to investigate the valorization by drying of broad beans for both direct and indirect solar drying conditions, and to study the thin layer drying modeling of broad beans.

2. Materials and Methods

Fresh local broad beans (Faba vicia l) were bought at local market in Ouargla, Algeria. They were singled out one by one using a visual criterion like color, size, absence of physical damage and uniform maturation degree. Dry pods were removed manually by visual inspection. The broad beans pods were then shelled manually.

2.1. Description of the Drying System

Two different solar driers were used in this study (Fig. 1 a, b). They are both laboratory scale prototypes, suitable for the agroalimentary products, designed and assembled by the energy conversion research unit at LENREZA laboratory, University of Ouargla, Algeria. The direct forced convective dryer (fig. 1a) consists mainly of a drying room and a chimney. The indirect forced convective drier system (fig. 1b) is composed of solar collector with simple circulation inclined by 31°C (Ouargla city altitude, Algeria). Air circulation and air exit are aspired by a fan (trade mark KFA-30 A; at a speed of 1400 rotation /mn).

2.2 Moisture Measurements

Moisture was determined with a kern moisture analyzer operating at the following conditions: sample weight (45g), analysis temperature (105°C). The device stops automatically once weight of dehydrated sample is constant. Moisture content is expressed as a percentage value. Three measurements were taken, and the mean value of relative moisture is 2.2 % ± 0.1 in dried base. During the experiments, broad beans were dried to the final moisture content of 0.13 kg water / kg dry matter [17]
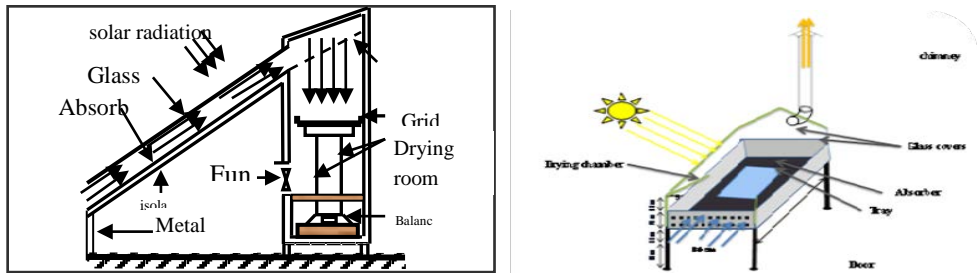
Fig. 1 Schematic diagrams of an indirect active hybrid solar–electrical dryer and a direct solar dryer.

2.3 Experimental Procedure and Measures

Prior to each experiment, the product samples were weighed with a pricision of 0.01 g then reweighed at equal time intervals. So the check in was done each 60 minutes. The desired final moisture content were defined as the standard moisture ensuring a suitable storage of the vegetable product wich is about 0.13 kg water/kg dry matter [4]. The experiment is stopped when the desired final water content is reached.

3. Mathematical Modeling of Drying Kinetics

Experimental results of moisture ratio versus drying time were adapted to the theoretical semi models most significant, largely widespread in the process of drying. The report/ratio of moisture (MR) and the drying rate of broad beans during the experiments of drying were calculated using the following equations:[18,19]

$$MR = \frac{X - X_e}{X_0 - X_e} \qquad (1)$$

$$\frac{dX}{dt} = \frac{X_{t+\Delta t} - X_t}{\Delta t} \qquad (2)$$

3.1. Data Analysis

The coefficient of determination (R^2), reduced chi-square (χ^2), and root mean square error (RMSE) were used in this study to evaluate the goodness of fit. To get the best fit of the experimental data, the coefficient of determination R^2 should be higher and the χ^2 lower.

Table 1. Empirical models of drying

N°	Model equation	Name	References
01	$XR(t)=exp(-kt)$	Newton	O'callghan et al (1971)
02	$XR(t) = exp(-k\ t^n)$	Page	Page (1948)
03	$XR(t) = exp(-k\ t)$	Page modified	Overhults et al (1973)
04	$XR(t) = A\ exp(-k\ t)$	Henderson et Pabis	Hunderson and pabis (1969)
05	$XR(t) = A\ exp(-k\ t) + B$	Logarithmique	Yagciolu et al (1999)
06	$XR(t) = A_1\ exp.(-k_1\ t) + A_2\ exp.(-k_2\ t)$	Two terms	Sharefeldeen et al (1980)
07	$XR(t) = 1 + A_1\ t + A_2 t^2$	Wang et Singh	Wang and singh (1978)
08	$XR(t) = A\ exp.(-k\ t) + (1-A)\ exp.(-kbt)$	Diffusional Approach	Sharef eldeen et al (1979)
09	$XR(t) = A\ exp.(-k_1\ t) + (1-A)\ exp.(-k_2\ t)$	Verma	Verma et al (1979)
10	$XR(t) = A_1\ exp.(-k_1\ t) + A_2\ exp.(-k_2\ t) + A_3\ exp.(-k_3\ t)$	Henderson et Pabis modified	Kara thano (1999)
11	$XR(t) = A\ exp.(-k\ t) + (1-A)\ exp.(-A\ k\ t)$	Two terms exponential	Sharef eldeen et al (1980)
12	$XR(t) = A_1 exp(-kt^n) + A_2\ t$	Midilli et autres	Diamante and murno (1991)

4. Results and Discussion

4.1. Drying behavior as influenced by the dryer type
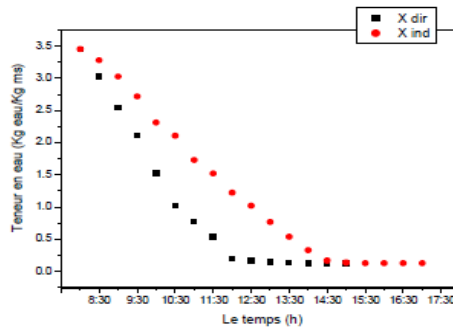
Fig. 2 Moisture content evolution versus time

Figure 2 presents the variation in the moisture content as a function of time in the types of driers direct and indirect, it is clear that the moisture content decrease continuously with drying time, the type of solar dryer affected drying time and product quality. The drying time taken to reduce moisture content from 2.2±0.1 kg water/kg dm to final moisture of 0.13±0.1 kg water/kg dm was 5h for the direct solar dryer and 8h for the indirect one. Obtained experimental results proved the importance of the direct process in the

valorization of the product compared to the indirect one. In reference to available literature, it is also evident that both the two tested methods are more efficient than the sun drying method traditionally adopted by farmers.

4.2 Suitable Model for Describing Drying Process

4.2.1 Models and Statistical Criteria

By using of Curve-Expert software, it was noted that the values of the three used statistical criteria (standard error (S), coeff. Correlation (r), and Chi Square) appear very similar, making it difficult to distinguish between 12 models. According to the calculation results we saw that for the Page model, the minimum value of the standard error S= 0.000819, the correlation coefficient R corresponds to a large value R = 0.999848, with a minimum value of Chi square = 0.010008 so the empirical page model describes solar drying of broad beans

4.2.2 Expression of the Page Model Parameters as a function of Temperature

The following results were obtained by curve fitting using the curve-Expert1.3 software for each parameter. The empirical relation found between the parameters of the equation of page model and temperature are developed and are plotted in Fig3.
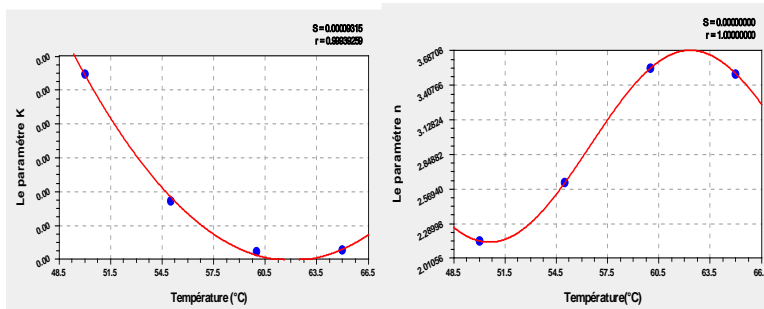
Fig 3. Evolution of K and n parameters with temperature

Finally the expressions adopted for the general equation according to the Page model with the parameters depending from time and temperature of the drying air, are given below.

$$XR\ (t) = exp.\ (-k\ t^n) \tag{6}$$

$$n(T) = 2.916086 + 0.775023*cos(0.267699T - 4.114475) \tag{7}$$

$$K(T) = 0.091139 + 0.002939T + 2.369690e\text{-}005T \tag{8}$$

5. Conclusion

In this study, post harvest treatment of broad beans, by hot air direct and indirect solar drying means, is presented. Based on the experimental results reported herein, the following conclusions can be made. Solar drying has allowed us to minimize post-harvest losses, and preserve the final quality of the dried product, especially when the search aims the

conservation for a long term. Experimental results showed that broad beans dried in direct solar drier had shorter drying time than other dried in indirect convective solar dryer. The semi theoretical models, namely, Page model was used to describe the drying kinetics of broad beans with a satisfactory correlation. An empirical equation, with temperature dependent parameters, was successfully adopted. The most adaptable solar dryer for drying of the broad beans is the direct solar dryer. Although this adaptation depends on techno-economic parameters and social considerations. The criteria for energy consumption and profit on the cost led to place the direct solar dryer as more efficient and more profitable economically.

References

[1] M.H. Hendawey, A.M.A. Younes. Biochemical evaluation of some faba bean cultivars under rainfed conditions at El-Sheikh Zuwayid . Annals of Agricultural Sciences Volume 58, Issue 2, December 2013, Pages 183–193

[2] Cecilia Baginsky, Álvaro Peña-Neira, Alejandro Cáceres, Teresa Hernández, Isabel Estrella, Héctor Morales, Ricardo Pertuzé, Phenolic compound composition in immature seeds of fava bean (*Vicia faba* L.) varieties cultivated in Chile Journal ofFood Composition and Analysis Volume 31, Issue 1, August 2013, Pages 1–6

[3] Food and Agriculture Organization. Agriculture data, 2012. Available at: http://faostat.fao.org/site/567/DesktopDefault.aspx?PageID= 567#ancor (accessed July 23, 2012).

[4] İbrahim Doymaz, Fergun Kocayigit, Drying and Rehydration Behaviors of Convection Drying of Green Peas journal of Drying Technology . Drying Technology, 29: 1273–1282, 2011

[5] Pallav Purohit, Atul Kumar, Tara Chandra Kandpal. Solar drying vs. open sun drying: A framework for financial evaluation Solar Energy 80 (2006) 1568–1579

[6] S. Boughali, H. Benmoussa, B. Bouchekima, D. Mennouche, H. Bouguettaia, D. Bechki, Crop drying by indirect active hybrid solar – Electrical dryer in the eastern Algerian Septentrional Sahara. Solar Energy 83 (2009) 2223–2232

[7] S. VijayaVenkataRamana, S. Iniyanb, Ranko Goicc. A review of solar drying technologies. Renewable and Sustainable Energy Reviews 16 (2012) 2652– 2670

[8] Dilip Jain , Rajeev Kumar Jain. Performance evaluation of an inclined multi-pass solar air heater with in-built thermal storage on deep-bed drying application Journal of Food Engineering 65(2004) 497–509

[9] Tadahmun A. Yassen, Hussain H. Al-Kayiem. Experimental investigation and evaluation of hybrid solar/thermal dryer combined with supplementary recovery dryer. Solar Energy 134 (2016) 284–293

[10] Seyfi Şevik Experimental investigation of a new design solar-heat pump dryer under the different climatic conditions and drying behavior of selected products. Solar Energy Volume 105, July 2014, Pages 190–205

[11]Akpinar, E., Midilli, A., Bicer, Y., 2003. Single layer drying behaviour of potato slices in a convective cyclone dryer and mathematical modelling. Energy Convers. Manage. 44, 1689–1705.

[12]Yaldiz, O., Ertekin, C., 2001. Thin layer solar drying of some vegetables. Drying Technol. 19, 583–596.

[13]Serpil Sahin, Gulum Sumnu, Ferihan Tunaboyu Usage of solar assisted spouted bed drier in drying of pea food and bioproducts processing 91 (2013) 271–278

[14]Guillermo Petzold, Marisa Caro, Jorge Moreno, Influence of blanching, freezing and frozen storage on physicochemical properties of broad beans (*Vicia faba* L) International Journal of Refrigeration Volume 40, April 2014, Pages 429–434

[15] S.K. Sathe Beans: Overview Encyclopedia of Food Grains (Second Edition) 2016, Pages 297–306 Volume 1: The World of food Grains

[16] Marçal Plans, Joan Simó, Francesc Casañas, Roser Romero del Castillo, Luis E. Rodriguez-Saona, José Sabaté, Estimating sensory properties of common beans (*Phaseolus vulgaris* L.) by near infrared spectroscopy, Food Research International, Volume 56, February 2014, Pages 55–62

[17] Lijiao Kan, Shaoping Nie, Jielun Hu, Sunan Wang, Steve W. Cui, Yawen Li, Sifan Xu, Yue Wu, Junqiao Wang, Zhouya Bai, Mingyong Xie, Nutrients, phytochemicals and antioxidant activities of 26 kidney bean cultivars, Food and Chemical Toxicology

DRYING PROCESS

Poster Presentations

Drying the corn in a farm heat pump dryer with fluidized bed

Rudobashta, S.P.[a]*; Zueva, G.A.[b]; Dmitriev, V.M. [c]; Muravleva, E.A.[d]

[a] Department of Heat Engineering, Hydraulics and Enterprises Energy Supply. Russian State Agrarian University – MAA after K. A. Timiryazev, Moscow, Russia

[b] Department of Higher and Applied Mathematics, Ivanovo State University of Chemistry and Technology, Ivanovo, Russia

[c] Department of Life Safety, Tambov State Technical University, Tambov, Russia

[d] Department of Heat Engineering, Hydraulics and Enterprises Energy Supply. Russian State Agrarian University – MAA after K. A. Timiryazev, Moscow, Russia

*E-mail of the corresponding author: rudobashta@mail.ru

Abstract

The possibility of using a heat pump as a part of on-farm drying plant is considered taking drying of corn grain as an example. The methodology for kinetic calculations of a drying plant with a batch fluidized bed for granular materials is developed. These calculations are based on the use of an analytical solution for the problem of mass conductivity and taking into account the time-related changes in drying agent parameters over the layer height. To determine the concentration dependence of the mass-conductivity coefficient, a zonal method has been used.

Keywords: heat pump; dryer; kinetic calculation.

1. Introduction

To increase the efficiency of using a heat pump in a farm, it can be used for heating a farmhouse in winter, and for household needs in summer, for example, for drying seed grains. The drying of corn grains in a farm is discussed in the paper.The objectives of this work are: 1) analysis of the efficiency of using a heat pump in grain dryer, 2) developing an engineering method for the kinetic calculations of a periodically operating fluid bed dryer based on the analytical method of kinetic calculations, 3) obtaining the data on the mass conductivity of corn grains.

2. Farm heat pump dryer (HPD)

The moisture content of corn harvested from the field is in many cases higher than that required by storage conditions, so it is removed by thermal drying. For this purpose, a farmer heat pump plant with a fluidized bed of periodic operation can be used in a farm specializing in the production of seed-quality grains. A thermodynamic analysis was performed for the operation of such an installation in which the source of low-potential heat is the ground and the drying agent is atmospheric air heated by a heat pump to a temperature of 60°C. The R600a was taken as the refrigerant and its thermodynamic parameters were taken from literature.[1] As the result of analysis, it was found that 1) the energy conversion coefficient is $\Psi = 2.98$; 2) the energy saving for heating the drying agent is 66.4% due to the use of the heat pump, 3) for a fluidized-bed HPD at drying corn with a mass load of 75 kg, the total electric energy costs for the process (for heat pump and for air purge through the dryer) are ~ 16 kW, which is acceptable for operation of the dryer in the farm. Thus, the performed analysis and calculations show using HPD for drying corn seeds on a farm is fully justified.

3. Kinetic calculation of a batch fluidized bed dryer (FBD)

The level of development the theory of drying, the mathematical modeling methods, the availability of effective computational programs, the widespread distribution of personal computers allow to use successfully the mathematical methods for the kinetic calculations of dryers - analytical[2, 3] and numerical ones.[4, 5] Such methods of kinetic calculations of continuous dryers for disperse materials has been developed. The operation of a batch dryer differs by the nonstationarity of the process, and it must be taken into account in the design calculation. In this paper, we present a method that takes into account the nonstationarity of the process. At the development stage the general kinetic problem was decomposed into two levels: microkinetic and macrokinetic. At the microkinetic level, the drying kinetics of single corn kernels were considered, and the influence of technological factors on the process was taken into account at the macrokinetic level. When formulating the microkinetic model, it was assumed that the grain is isotropic and assumes a shape of a

sphere with a radius R which volume is equal to the grain volume. The zonal method of calculation was used: the entire range of the moisture content of the material during the drying process was divided into a number of concentration zones, for each of which was given the necessary values of the mass conductivity coefficient and of other characteristics of the process. The drying duration in these zones was calculated by the analytical solution of the mass-conductivity problem in a regular mode[6]

$$\tau_i = \frac{R^2}{\mu_i^2 \cdot k_i} \cdot \ln \frac{B_i}{\overline{E}_i}, \qquad (1)$$

where μ_i is the first positive root of the characteristic equation for the solution of the problem at the i-th zone [6]; $\overline{E} = (\overline{u}(\tau) - u_e)/(\overline{u}_{in} - u_e)$ represents the relative average volume moisture content of the grains; $\overline{u}$ - average moisture content of grain, kgkg^{-1}; B_i is the first preexponential factor of the solution of the mass-conductivity problem[6]. The grain temperature was calculated on the basis of the solution of the heat conduction problem.[6] This solution for the medium-volume temperature of a spherical body has the form[6]

$$\overline{\Theta} = \frac{\overline{t}(\tau) - t_a}{t_{in} - t_a} = \sum_{n=1}^{\infty} B_n \left[\exp(-\mu_n^2 Fo) + \frac{R_V}{R} KoLu \frac{\mu_n^2}{Bi} \times \right.$$

$$\left. \times \sum_{m=1}^{\infty} B_m \frac{\mu_m^2}{\mu_m^2 - Lu \cdot \mu_m^2} \left[\exp(-\mu_m^2 Fo \cdot Lu) - \exp(-\mu_n^2 \cdot Fo) \right] \right], \qquad (2)$$

where $\overline{t}$ - average temperature of grain, ºC; B_n are coefficients that depend on the Biot number thermal; R_V is the ratio of the volume of the body to its surface (for a sphere $R_V = 3$); Fo - Fourier number caloric; Ko - Kossovitch number; Lu - Luikov number.

In describing the process at the macrokinetic level, it was assumed that in the FBD of a batch action, the solid phase is completely mixed, and the gas phase is ideally displaced. The moisture content and temperature of the drying agent in such a dryer vary both over layer height and in time. The kinetic calculation was carried out by the zonal method - based on the average values of the air parameters in the concentration zones ($u_{in.i} \ldots u_{f.i}$), which were found from the equations of material and heat balance. To take into account changes in air parameters over time, the successive approximations method was applied: first, the drying time τ_i required to change the moisture content of the material from $u_{in \cdot i}$ to $u_{f.i}$ was set, and then it was determined by calculation using equation (1). At the macrokinetic level, the following basic values were calculated: 1) the rate of fluidization beginning, at which the working air velocity was selected, and then the mass air flow in the

dryer (kgs^{-1}) was determined; 2) the average in time τ_i moisture content of the air at the outlet from the dryer $\overline{d}_{fi}$ and then the average moisture content of the air in the layer on the time interval τ_i: $\overline{d}_{la.i}$; 3) the average in time τ_i temperature of the air at the outlet from the dryer $\overline{t}_{a.f.i}$, and then - the average air temperature in the layer. The average values of the temperature and air moisture content in the layer were used to find the mass coefficient and the equilibrium moisture content of the material in the zones.

4. Experimental research. Materials and Methods

The experiments were performed to determine the equivalent diameter, density, mass conductivity and hygroscopic properties of corn grain of the following three varieties currently cultivated in Russia: Pioneer PR-8521, Pioneer PR-7709 FAO 160, Mysodur Amelior F-70. Equivalent diameter was determined by measuring the volume of a group of grains using a graduated cylinder, density - by measuring the volume and their mass. For the Pioneer PR7709 FAO 160 corn, the following has been determined: $d_{eq} = 8.24$ mm, $\rho = 1065$ kgm^{-3}. The dependence k=f(u,t) was determined by the zonal method with the experimental drying curve taken in the absence of an external diffusion resistance.[6] Drying curves were obtained for 10 corn kernels of the same equivalent diameter $d_{eq} = 2R$ - in a specially designed experimental setup with a triple replication of the tests, at five drying agent temperatures: 40, 50, 60, 70 and 80 °C , at air velocity 5 ms^{-1}. There is no external diffusion resistance at this air flow (its absence was judged by the fact that the change in the air velocity by half did not affect the drying curve). Corn grains were placed between the coils of the spring suspension, which was blown by the air stream in the transverse direction. The weight of the samples during drying was measured using the Techniport torsion balance PRLT with accuracy of 1 mg without removing grains from the drying chamber. The data obtained in the experiment on the coefficient of mass conductivity are shown in Fig. 1 for corn Pioneer PR-8521 (for other varieties the dependencies are similar). The data analysis allowed to draw the following conclusions: 1) the dependence of k on u for different varieties of corn is of the same character, the values of the mass coefficient for different varieties are close in magnitude; 2) the mass conductivity coefficient changes significantly with the moisture content of the material, it requires to take this change into account when drying; 3) the functions k=f(u,t) have the form characteristic for the seeds of other crops - such as canola, wheat, rye, barley, but greater in their values; 4) the rate of drying is limited by internal mass transfer.

Fig. 1 Dependencies k = f(u) *for corn kernels of Pioneer PR-8521: 1 – t*$_a$* = 40 ºC; 2 – 50 ºC; 3 – 60 ºC; 4 – 70 ºC; 5 – t*$_a$* = 80 ºC (points - experiment, lines - calculation).*

5. Verifying the adequacy of the mathematical model

The adequacy of the model describing the microkinetic has been verified by comparing the experimental curve for drying the corn kernels located in a longitudinally blown monolayerat a low air velocity (1.8 ms^{-1}) and the drying curve calculated for these conditions using the obtained data (note that the values of the mass coefficient were found from the drying curves, with an other air velocity ~ 5 ms^{-1}). Figure 2 allowes to compare the experimental and calculated drying curves, and it shows satisfactory match. The adequacy of the mathematical model describing the kinetics of corn grain drying in a batch fluidized bed

Fig. 2 *Comparison of calculated (line) and experimental (points) drying curves for corn kernels of variety Pioneer PR-7709 FAO-16 (t*$_a$* = 50ºC, v = 1.8 ms*$^{-1}$*).*

dryer has also been verified by comparison of the calculated and experimental drying curves, the latter being obtained under laboratory conditions. The scheme of the laboratory dryer is shown in Fig. 3. In the experiment, a curve was obtained for drying corn grain in a layer (dryer diameter 150 mm, fixed bed height 190 mm), measuring the air velocity, temperature and moisture content of the air at the entrance to the material layer and at the outlet from it. Fig. 4 showes the comparison of the calculated and experimental drying

Fig. 3 Scheme of laboratory installation: 1 - air temperature meter; 2 - drying chamber; 3 - corn; 4, 7 - gas distribution grids; 5 - air heating chamber; 6 - glass balls; 8 - gas blower; 9 - frequency converter, 10 - measuring diaphragm; 11 - pressure transmitter, 12 - secondary device, 13 – motor.

Fig. 4 Drying curves for grain variety PIONEERE PR-7709 FAO-16 in a batch fluidized bed dryer ($t_{a.in} = 53^oC$; $v = 2.3 ms^{-1}$).

curves whereas Fig. 5 presents the comparison of calculated and experimental air temperatures at the outlet from the layer of drying material. As can be seen, the experimental data compare well with the calculated ones.

Fig. 5 Air temperature at the entrance to the material layer $t_{a.in}$ (1) and at the outlet from the layer $t_{a.f}$:(2 - experiment, 3– calculations).

6. Conclusions

1) The feasibility of using HPD in a farmer dryer for corn seed is shown. 2) A zonal analytical method for engineering calculation of a periodically operating dryers with a fluidized bed of particulate material is developed. 3) Data on corn kernels required for calculations are obtained. 4) There is an internal diffusion kinetic regime when drying corn. 5) The adequacy of the mathematical model for drying kinetics to the real process is shown.

7. Nomenclature

a	thermal diffusivity	m^2s^{-1}
c	mass heat capacity	$Jkg^{-1}K^{-1}$
k	coefficient of mass conductivity	m^2s^{-1}
λ	thermal conductivity coeffcient	$Wm^{-1}K^{-1}$
r	radial coordinate	m
r^*	heat of vaporization	Jkg^{-1}
R	radius of spherical particle	m
t	temperature	ºC
u	moisture content of grain	$kgkg^{-1}$
v	velocity of air	ms^{-1}

Greek letters

α	heat transfer coefficient	$Wm^{-2}K$
ρ	grain density	kgm^{-3}
τ	time	s

Subscripts

a	air
e	equilibrium
f	finite
in	initial
la	layer

Dimensionless numbers

$Bi = \alpha R/\lambda$ - Biot number

$Fo = a\tau/R^2$ - Fourie number

$Lu = k/a$ - Luikov number

$Ko = r^*(u_{in}-u_e)/(c(t_a-t_i))$ - Kossovitch number

8. References

[1] Alves-Filho, O. Heat Pump Drying: Theory, Design and Industrial Application; New Dry Tech: Trondheim, 2013.

[2] Rudobashta, S.; Zueva, G. Drying of seeds through oscillating infrared heating. Drying Technology, 2016, 34. (5), 505-515.

[3] Rudobashta S. P.; Zueva G. A.; Kartashov E. M. Heat and mass transfer when drying a spherical particle in an oscillating electromagnetic field. Theoretical Foundations of Chemical Engineering, 2016, 50 (5), 718-729.

[4] Bon J.; Kudra T. Enthalpy-Driven Optimization of Intermittent Drying. Drying Technology, 2007, 25 (4), 523 – 532.

[5] Vaquiro H. A.; Clemente G.; Garcia-Perez J. V.; Mulet A.; Bonb J. Enthalpy-driven optimization of intermittent drying of Mangifera indica L. Chemical Engineering Research and Design. 2009, 87, 885–898.

[6] Rudobashta, S.P. Mass Transfer in the Solid Phase Systems; Chemistry: Moscow, 1980 (in Russian).

Heat and mass transfer modelling of continuous Wurster spray granulation with external product classification

Müller, D. ᵃ*; Bück, A.ᵃ,ᵇ; Tsotsas, E.ᵃ

ᵃ Department of Thermal Process Engineering. Otto von Guericke University, Magdeburg, Germany

ᵇ Institute of Particle Technology. FAU Erlangen-Nuremberg, Erlangen, Germany.

*E-mail of the corresponding author: daniel.mueller@ovgu.de

Abstract

Wurster granulation with external product classification can be used for stable continuous coating or layering processes. It has been ascertained from recent population balance simulations that the ratio of the spray rate to the nuclei feed rate can be used to control the thickness of the sprayed product layer. However, thermal conditions are not considered by population balances regarding the particle size as distributed property. For this reason, heat and mass transfer is investigated in the present contribution by modelling of several subprocesses. The results can be used to discuss the cause of fluidized bed destabilization due to over-wetting.

Keywords: continuous operation; Wurster fluidized bed; spray granulation; spray limits; heat and mass transfer.

1. Introduction

The continuous Wurster spray granulation with external product classification is suitable for particle growth processes such as coating and layering with constant product specifications (size, layer or porosity distribution) and product yields. As ascertained by recent results and from former studies [1], higher spray rates and lower feed rate are needed to achieve larger layer thicknesses. Thereby the spray rate is limited by thermal conditions, fluidization gas saturation, drying kinetic and agglomeration tendency which might lead to process instability due to over-wetting. For this reason it is aimed in this contribution to describe the heat and mass transfer of the Wurster-granulator by diverse models, to determine spray limits and to discuss the cause of process destabilization.

2. Process configuration and modelling

The present contribution bases on a former case study of Hampel [1] describing the here discussed process with a two-zone population balance model whose simulated product size distributions has been validated by lab scale experiments for a certain range of process parameters. The heat and mass transfer of this Wurster granulation process should be investigated with several model approaches such as an ideal two-component particle growth model, steady state particle circulation in Wurster-chamber, pneumatic transport and spray deposition in Wurster-tube (spray zone denoted with α) as well as drying and heating outside the Wurster tube (drying zone denoted with 1-α).

2.1. Reference case – Experimental design and modelling

The experimental design of the continuous Wurster spray granulation in Hampel's investigations [1] consists of a conical fluidized bed apparatus which is interconnected to a straight-duct air classifier as illustrated in Fig. 1a). Particles are raised through the Wurster-tube due to high gas velocities and are sprayed with a solid-containing liquid. Above the Wurster-tube particles fall back into the drying zone. The particle circulation has been described, e.g. by Börner et al. [2]:

$$\tau_{1-\alpha} = \tau_\alpha \frac{1-\alpha}{\alpha},\tag{1}$$

wherein τ_α and $\tau_{1-\alpha}$ represent the residence time (s) of the spray zone and the drying zone, respectively. Further, α is defined as the volume fraction (m³/m³) of spray zone related to the total volume of the disperse system (spray zone and drying zone).

2.2. Heat and mass transfer modelling

The heat and mass model is illustrated in Fig. 1b) and assumes basically the following aspects. Particles circulate through spray and drying zone with constant residence times. The interior of Wurster-tube is seen as spray zone and the drying zone is assumed as a homogeneous fluidized bed describing the outer region of the Wurster-tube. Stationary pneumatic transport and moistening of particles takes place in the spray zone, wherein swarm sinking is also considered. The temperature of the particles leaving the spray zone is assumed to be the wet bulb temperature. Finally, evaporation of sprayed water content (drying period) and particle heating (heating period) occur in the drying zone until the particles re-enter the spray zone.
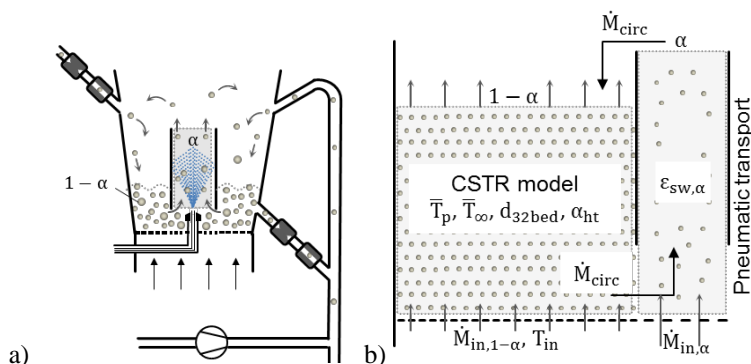
Fig. 1 a) Wurster spray granulation chamber with an interconnected straight-duct air classifier [1], b) Two-zone heat and mass transfer model.

Furthermore, a simplified two-component particle growth model is used in order to approximate the stationary size distribution of fluidized bed particles. This model contains several assumptions such as: mono-sized feed and product, mono-shaped disperse system of solid spheres, constant feed and spray rate, evenly distributed particle growth rate, non-distributed residence time due to permanent classifying with an ideal separation performance and steady state conditions. As a conclusion, a two-component single particle model consisting of a spherical core and a spherical layer with a well-defined core diameter and coating layer thickness can be derived. The number density distribution regarding the size of the fluidized bed particles turns out to be a uniform distribution. Hence, the Sauter diameter $d_{32,bed}$ and an average effective particle density $\bar{\rho}_{p,eff}$ among the population can be obtained analytically which are both needed for the description of heat and mass transfer.

2.2.1. Pneumatic transport in spray zone

The residence time in the spray zone is a parameter which is required for the two-zone population balance of the abovementioned reference case. The spray zone residence time is approached in this contribution based on the assumption of stationary pneumatic transport with constant solid volume fraction:

$$\tau_\alpha = \frac{L_{wt}}{u_{g,\alpha}/\varepsilon_{sw,\alpha} - k_{sw}u_s(d_{32,bed})} \text{ and } k_{sw} = \left(1 - \varepsilon_{sw,\alpha}\right)^{5,5(Ar)^{-0,06}}. \quad \text{(2a) and (2b)}$$

Eq. 2a takes into account the Wurster-tube length L_{wt} (m), the spray zone gas velocity $u_{g,\alpha}$ (m/s) and the solid volume fraction in spray zone $\varepsilon_{sw,\alpha}$ (m³/m³) which can be estimated by CFD-DEM simulations. Further Eq. 2a includes the swarm sinking correction k_{sw} (-) and the terminal sinking velocity u_s (m/s) of a single sphere. The swarm sinking factor k_{sw} can be calculated with Eq. 2b suggested by Richardson and Zaki [3].

2.2.2. Fluidization gas cooling, particle drying and particle heating in drying zone

The fluidization gas cooling is depicted schematically in Fig. 2a). Fig. 2b) shows the drying period and the heating period of a single particle with retention time $t_{1-\alpha}$ (s) in the drying zone.
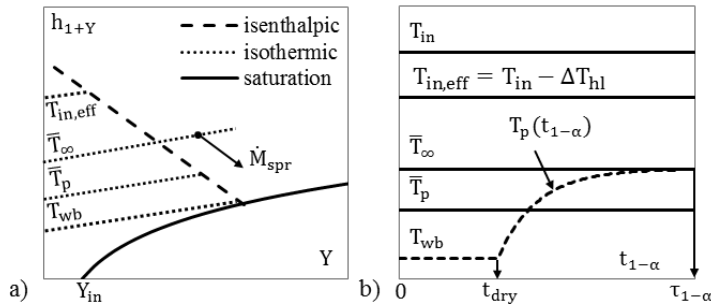
Fig. 2 a) Schematic Mollier-diagram illustrating the temperature range inside the Wurster-granulator, b) Single particle temperature evolution versus retention time in the drying zone.

The average gas temperature $\overline{T}_\infty$ (°C) in the drying zone is calculated with incoming gas temperature T_{in} (°C) below the distributor plate, with the temperature drop ΔT_{hl} (°C) due to heat losses at the gas distributer plate, the solid content of spray solution x_s (kg/kg), with the evaporation energy $\Delta h_{eva}°$ (J/kg) of deposited spray solvent and others:

$$\overline{T}_\infty = T_{in} - \Delta T_{hl} - \frac{\left(\dot{M}_{spr}(1-x_s) - \dot{M}_{in,\alpha}\frac{\varphi_\alpha Y_{sat}(T_{in},Y_{in})}{1+Y_{in}}\right)\Delta h_{eva}°(T_{wb})}{\dot{M}_{in,1-\alpha}c_{p,fl}} \tag{3}$$

Particles, leaving the spray zone and entering the drying zone, have been cooled down to the wet bulb temperature. The particle temperature evolution in the drying zone is divided into two segments: the drying period as first segment and the heating period as second segment. The time interval of 0 to the required drying time t_{dry} defines the drying period. Within the drying period, the particle temperature T_p remains at the wet bulb temperature T_{wb}. The heating period starts directly after complete evaporation of coating humidity where the particle temperature is still at the wet bulb temperature. The particle temperature rises subsequently and approaches the average surrounding temperature of the fluidization gas $\overline{T}_\infty$ with increasing drying zone retention time. Finally the particles enter the spray zone at the total residence time $\tau_{1-\alpha}$ in the drying zone. The particle temperature curve of the heating period is obtained from the energy balance of a single particle:

$$T_p = \overline{T}_\infty - (\overline{T}_\infty - T_{wb})\exp(-St'(t_{1-\alpha} - t_{dry})). \tag{4}$$

The particle heating kinetic is represented by the modified Stanton number St' (1/s) which is defined with $St' = 6\alpha_{ht}/(d_{32,bed}\overline{\rho}_{p,eff}c_p)$ and the heat transfer coefficient α_{ht} (W/m²/K) can be determined with Gnielinski's approach [4]. The drying time is approximated by an energy balance assuming constant drying rate. In order to estimate the average particle temperature $\overline{T}_p$ in the drying zone, the time function of the particle temperature (Eq. 4) has been integrated with retention time $t_{1-\alpha}$ and devided by the total residence time in drying zone $\tau_{1-\alpha}$:

$$\overline{T}_p = T_{wb}\frac{t_{dry}}{\tau_{1-\alpha}} + \overline{T}_\infty\left(1 - \frac{t_{dry}}{\tau_{1-\alpha}}\right) - (\overline{T}_\infty - T_{wb})k_{ht} \tag{5}$$

$$k_{ht} = \frac{1 - e^{-St'(\tau_{1-\alpha} - t_{dry})}}{St'\tau_{1-\alpha}}. \tag{6}$$

Thereby k_{ht} is introduced as a coefficient of heating kinetic including the influence of the modified Stanton number on the average particle temperature.

2.3. Parameter setting

The parameter values of the material properties, mass flow and inlet temperature of the fluidization gas as well as the bed mass are chosen according to the reference case [1] and are listed in Table 1. Therein are also given further parameters which are the swarm solid volume fraction $\varepsilon_{sw,\alpha}$ and the relative air humidity φ_α in the spray zone. Both parameters are adapted to measured fluidized bed temperature. Beside this, a heat loss temperature difference ΔT_{hl} has been determined from measurements determining the temperature below and above the distributor plate.

Table 1. Model parameters

d_f	d_{pr}	$\rho_{f,eff}$	$\rho_{c,eff}$	$\dot{M}_{in}$	x_s	T_{in}	M_{bed}	$\varepsilon_{sw,\alpha}$	φ_α	ΔT_{hl}
mm	mm	$\dfrac{kg}{m^3}$	$\dfrac{kg}{m^3}$	$\dfrac{kg}{h}$	$\dfrac{kg}{kg}$	°C	kg	$\dfrac{m^3}{m^3}$	-	K
0.3	0.4	1380	806	70	0.32	70	1	0.02	0.35	5.7

In the present contribution, model results based on Table 1 and three different spray rates (0.8 kg/h, 1.1 kg/h and 1.3 kg/h) are investigated.

3. Results and Discussion

Several spray rate independent parameters of the Wurster granulation can be obtained from the presented the heat and mass transfer model, see in Table 2. These include the Sauter diameter of the bed particles $d_{32,bed}$, the swarm correction factor k_{sw}, the single particle sinking velocity u_s, the superficial gas velocity in spray zone $u_{g,\alpha}$ as well as the residence time in spray zone τ_α and drying zone $\tau_{1-\alpha}$. It can be seen that the swarm effect can not be neglected with a factor 0.93. The sinking velocity is smaller than the spray zone gas velocity which is a requirement for stable circulation in the Wurster-granulator. The spray zone residene time is much lower than the drying zone residence time.

The drying time t_{dry}, the heat transfer coefficient α_{ht}, the modified Stanton number St′, the heating kinetic factor k_{ht}, the average gas temperature $\overline{T}_\infty$ and the average particle temperature $\overline{T}_p$ are calculated for three different spray rates $\dot{M}_{spr}$, respectively (see Table 3). The drying time increases linearly with spray rate and it is negligibly small compared to the residence time in the drying zone. The low drying time is caused by the high heat and mass transfer conditions of the fluidized bed. The particle heating coefficient is small. Thus the contribution of the particle heating kinetic to the average particle temperature can be neglected. Hence, the average particle temperature hardly differs from the average gas temperature in the drying zone due to the low drying times and the low particle heating kinetic coefficients.

Table 2. Spray rate independent model results

$d_{32,bed}$	k_{sw}	u_s	$u_{g,\alpha}$	τ_α	$\tau_{1-\alpha}$
mm	-	m/s	m/s	s	s
0.35	0.93	1.79	2.02	0.508	27.949

Table 3. Spray rate dependent model results

$\dot{M}_{spr}$ $\dfrac{kg}{h}$	t_{dry} s	α_{ht} $\dfrac{W}{mK}$	St' 1/s	k_{ht} %	$\overline{T}_{\infty}$ °C	$\overline{T}_p$ °C
0.8	0.018	503.6	3.19	1.234	43.30	43.06
1.1	0.027	506.7	3.21	1.226	31.77	31.67
1.3	0.034	509.0	3.22	1.221	24.29	24.08

The model results of the spray rate of 0.8 kg/h are compared with the measured fluidized bed temperature of a Wurster batch granulation process spraying a solution with 32 wt-% sodium bencoate solution on MCC-particles.
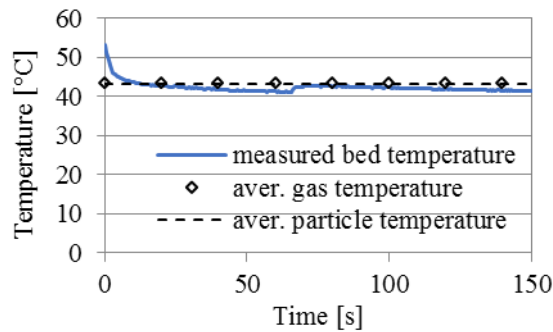
Fig. 3 Model-based average gas and average particle temperature adapted to measured fluidized bed temperature.

Additionally, several batch processes spraying pure water have been conducted for different bed masses (0.5 kg, 1 kg, 1.5 kg, and 2 kg) and different fluidization gas temperatures (70°C, 80°C and 90°C). Thereby the spray rate has been increased until destabilization of the fluidized bed took place.

4. Conclusions

Although the drying kinetic in the drying zone is ascertained as large, process destabilization due to over-wetting takes place far below the point of saturation. For this reason, it is presumed that the enhancement of agglomeration tendency with the larger spray rates cause the destabilization. Agglomerated particles might not be raised through the Wurster-tube for the reason that the sinking velocity is strongly increased. Hence agglomerates accumulate at the bottom of the fluidized bed, block the particle circulation and finally destabilize the fluidization.

5. Nomenclature

Ar	Archimedes number	-
c	heat capacity	$Jkg^{-1}K^{-1}$
$\dot{M}$	mass flow	kgs^{-1}
Y	air moisture load content	$kgkg^{-1}$

Greek letters

φ	relative moist of air	-

Subscripts

c	dried coating material
eff	effective
in	inlet fluidization gas
sat	saturation

6. References

[1] Hampel, N. Bück, A. Peglow, M. Tsotsas, E. Continuous Pellet Coating in a Wurster Fluidized Bed Process, Chemical Engineering Science 2013, 86, 87–98.

[2] Börner, M.; Peglow, M.; Tsotsas, E. Derivation of parameters for a two compartment population balance model of Wurster fluidized bed granulation. Powder Technology 238 (2012), 122-131.

[3] Richardson, J. F., Zaki, W. N. Trans. Inst. Chem. Engrs. 1954, 32, 35-53.

[4] Gnielinski, V. Wärme- und Stoffübertragung in Festbetten, Chem.-Ing.-Tech. 1980, 52, 228-236.

Concept of heat recovery in drying with chemical heat pump

Tylman, M.[a]; Jaskulski, M.[a]; Wawrzyniak, P.[a*]; Czapnik, M.[b]

[a] Faculty of Process and Environmental Engineering, Lodz University of Technology, 213 Wolczanska Str, 90-924 Lodz, Poland.

[b] Chemat, 85A Przemysłowa Str., 62-510 Konin, Poland

*E-mail of the corresponding author: pawel.wawrzyniak@p.lodz.pl

Abstract

Drying is one of the most energy intensive unit operations. It easily accounts for up to 15% of all industrial energy consumption. In the most drying processes heat is required to evaporate moisture which is later removed with a flow of air. The hot, humid air leaving the dryer is often considered as a waste stream, and a large fraction of energy is lost. The aim of the theoretical and experimental concept study presented here was to evaluate a method of reclaiming energy from low temperature waste streams and converting it to useful in industry saturated steam of temperature from 120 to 150 °C. Chemical heat pump concept based on the dilution and concentration of phosphoric acid was used to test the method in the laboratory. Heat of dilution and energy needed for water evaporation from the acid solution were experimentally measured. The cycle of successive processes of dilution and concentration has been experimentally confirmed. Theoretical model of the chemical heat pump was tested and coefficient of performance measured. Energy balance of the drying system and efficiency increase of the dryer supported with chemical heat pump were calculated.

Keywords: *Efficiency of drying; energy recovery; chemical heat pump*

1. Introduction

Drying is very intensive unit operation which, on the global scale, can accounts for up to 15% of all energy used in the industry [1](Chua et al. 2001). In many cases a large fraction of energy applied for drying is wasted with low temperature streams leaving the process [2](Ogura et al. 2005). Any energy recovery system in the drying can reduce significantly process energy consumption. Applications of heat pump technology offers energy saving potential along with temperature and humidity control. Drying assisted with heat pumps exploiting consecutive compression, condensation, expansion and evaporation of working fluid, is an object of research since eighties of last century. Dryers with heat pumps ensure economical process and at the same time product's quality especially agriculture and food products. In the recent years chemical heat pumps have gained more interest as offering higher temperatures and possibility to store energy in chemical substances.

Chemical heat pumps (CHP) are using reversible exothermal and endothermal chemical reactions to transfer energy, increase the temperature of working fluids and sometimes to store energy by chemical substances [3](Kawasaki et al. 1999). Selection of these chemical substances is important to absorb and release heat energy [4](Kato et al. 1996). Numerous chemical substances can be used in CHP to create a cycle of chemical reactions. The following substances have been proposed as working fluids: water systems: hydroxide/oxide, salt hydrate/salt or salt hydrate, ammonia systems: ammoniate/ammoniate or salt, amine complex with salt, sulfur dioxide systems: sulphite/oxide, phyrosulphate, carbon dioxide systems: carbonate/oxide, barium oxide/barium carbonate, hydrogen systems: hydride or metal, hydrogenation/ dehydrogenation [5](Wongsuwan et al. 2001).

Unlike the "classical" vapor compression heat pumps CHP enable to achieve significantly higher temperatures of heated medium which is crucial for the potential application, e.g., for production of saturated steam usually applied as a heating medium in majority of industrial processes. Despite the presented advantages, currently, there are no installations using CHP for low-grade waste heat recovery available on the market.

CHP absorbs energy via endothermic and release energy via exothermic in the form of chemical. CHP systems utilize the reversible chemical reaction to change the temperature level of the thermal energy, which stored by chemical substances [3](Kawasaki et al. 1999). These chemical substances are important in absorb and release heat energy [4](Kato et al. 1996). Various chemical substance can be use in CHP for chemical reaction, for examples, water system (hydroxide/oxide, salt hydrate/salt or salt hydrate), ammonia system (ammoniate/ammoniate or salt, amine complex with salt), sulfur dioxide system (sulphite/oxide, phyrosulphate), carbon dioxide system (carbonate/oxide, barium oxide/barium carbonate), hydrogen system (hydride or metal, hydrogenation/ dehydrogenation), etc. has been proposed as working medium [5](Wongsuwan et al. 2001).

One of promising chemical systems for CHP is water solution of phosphoric acid where waste heat of low temperature level is accumulated in endothermic and released in exothermic dilution of phosphoric acid [6](Ducheyne 2017). The results of dilution heat laboratory measurement will be presented.

The distant aim of the project is to apply CHP system to saturated steam production needed for drying using abundant waste heat available from cooling electricity generator.

2. CHP concept

The basic configuration of CHP is shown on Fig.1. In general CHP consists of a generator, a reactor, condenser and an evaporator. Waste heat, in most cases at the same temperature, is provided to the generator Q_G and the evaporator Q_E while upgraded heat is delivered by reactor Q_R. Part of the heat at low temperature is removed from the condenser Q_C. Usually to increase efficiency of CHP cycle internal heat exchanger transferring heat between solutions is added [7](Horuz and Kurt 2010).
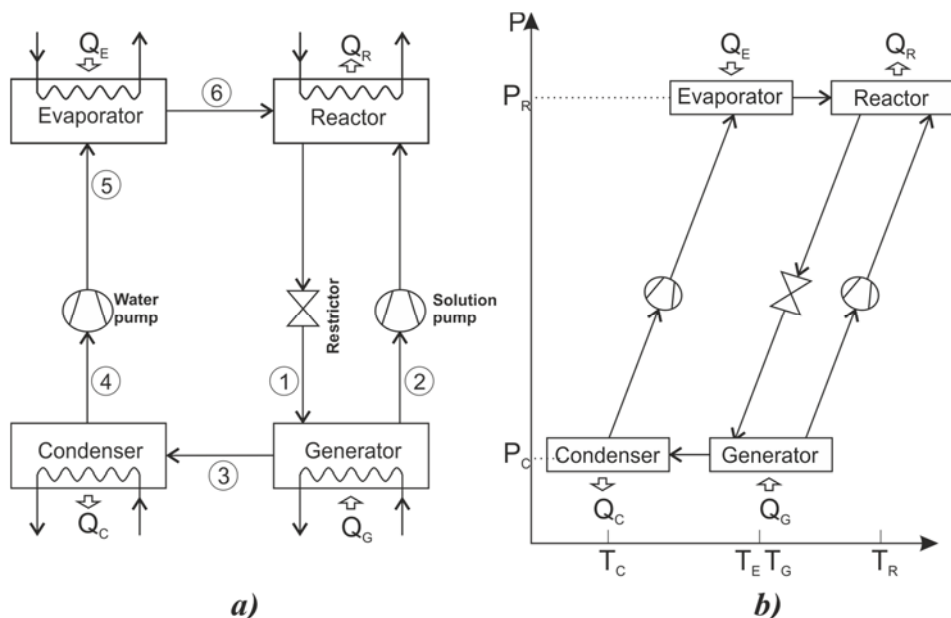
Fig. 1 Chemical heat pump: a) CHP schematic, b) CHP the pressure vs. temperature diagram.

In the presented CHP concept two component working fluid is used. Primary fluid absorbs secondary fluid producing upgraded heat while waste heat is consumed in an endothermic evaporation of secondary fluid. In the study solution of phosphoric acid will be primary while water secondary fluid.

The solution leaving the generator at high concentration will be referred as strong solution, while solution returning from the reactor to generator at lower concentration of phosphoric acid will be referred as a weak solution.

The CHP presented in Fig 1a operate with the cycle depicted in Fig. 1b The weak solution 1 is entering the generator where part of the secondary fluid is evaporated and strong solution 2 is produced. Strong solution is returned to the reactor, while vapour 3 removed from solution is condensed, pumped and heated. Water or water vapour enters the reactor where it is mixed with strong solution 2'. The heat of dilution increase the temperature of cooling water. Weak solution is returned to the generator. The CHP operate at two pressure levels, lower which is saturation pressure at the condenser temperature and upper level which is saturation pressure at the evaporator temperature. As Fig. 1b present there are three temperature levels of CHP: a generator, a condenser and reactor. In most cases the evaporator and generator are using the same heat source so their operation temperatures are the same.

The performance of CHP can be increased with heat exchanger transferring energy from weak solution to strong solution, or modifying path of the stream providing waste heat. Every industrial application is different and CHP system should be well fitted to the real needs. To do so an exact process model, based on validated experimental data of heat consumption and production, should be developed.

3. Materials and Methods

3.1. Materials

The 85% by weight phosphoric acid was purchased from Sigma-Aldrich and used without further purification. Demineralized water was used in all dilution experiments.

3.2. Apparatus and calculation of results

Measurements of the heat of dilution were conducted using a diathermic reaction calorimeter (Fig. 2) equipped with PTFE measuring cell **1** with a capacity of: 50 cm^3 and an automatic injection system **8**. Temperature was measured using a thermocouple type K **5** of diameter of 0.5 mm. The control and acquisition of data from the measurement system was carried out using the LabView sofware.

Heat of dilution of phosphoric acid was calculated using the following heat balance:

$$\Delta H_{dil} = r_u \cdot \Delta T_{cor1} \tag{1}$$

Where: ΔH_{dil} - heat generated during dilution of phosphoric acid, J; r_u - heat capacity of the system ; ΔT_{cor1} - rectified temperature increase determined by graphical method for the process of acid dilution.

Heat capacity of the system was determined by measuring Joule heat provided to the system by heating coil.

$$r_u = \frac{U \cdot i \cdot t}{\Delta T_{cor2}} \qquad (2)$$

Where: U - potential difference applied to the heating coil, V; i - electric current passing through the heating coil, A; t – heating time, sec; ΔT_{cor2} - rectified temperature increase determined by graphical method for the electric heating process of the system.
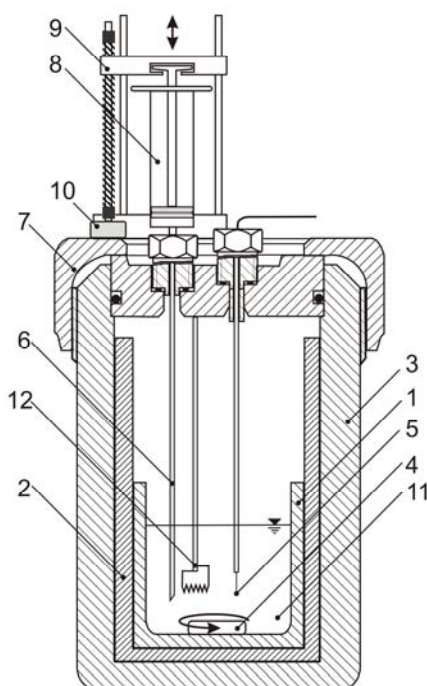
Fig.2 Scheme of the calorimeter

1 – PTFE measuring cell, 2 - insulation inserts, 3 – bomb calorimeter, 4 – magnetic stirrer, 5 – thermocouple, 6 – stainless steel needle, 7 – cover, 8 – syringe, 9 – autosampler controlled by a microprocessor, 10 – stepping motor for autosampler drive, 11 – reaction mixture, 12 - heating coil

3.3. Methodology

A sample of acid was placed in a PTFE measuring cell of the reaction calorimeter. Deionized water was injected with autosampler, and the injection time was 0.2 sec. The mass of the

water used for the dilution of the acid was determined by the difference of the weight of the syringe with water before and after the measurement, with a weighing accuracy of $\Delta m = \pm$ 0.0001g. Temperature measurement with a sampling rate of 0.01/ sec lasted 10 minutes. Then, for the obtained reaction mixture, the thermal capacity of the system was measured using a heating coil. The electrical parameters of the process for all measurements were set at $U = 5V$ and $i = 1.2$ A, the heating time of the system was 15 sec. The obtained dependences $T = f(t)$ were used to determine the values: ΔT_{cor1}, ΔT_{cor2} by graphical method. After taking into account the accuracy of the mass measurement and the characteristics of the instruments used, the method error was determined to be $\pm 3\%$.

4. Results and discussion

The heat of dilution has been determined over the molar concentration range from 57.8 to 11.8 *m* (85%-53% by weight) at ambient pressure. The heat of dilution between molality of initial m_1 and final m_2 molality are given in the Table 1.

Table 1. Experimental data for phosphoric acid heat of dilution measurement

Run	m_1 mol/kg	m_2 mol/kg	ΔT_{cor1} K	n_{H2O}/n_{H3PO4} -	ΔH_{dil} kJ/mol
1	57.827	29.916	12.206	1.855	3.842
	29.916	20.852	5.505	2.662	2.659
	20.852	15.734	2.848	3.528	1.840
	15.734	12.875	1.071	4.311	1.448
2	57.827	28.458	12.823	1.951	3.795
	29.916	19.053	4.889	2.913	2.230
	20.852	13.894	2.249	3.995	1.409
	15.734	11.182	0.931	4.964	1.281
3	57.827	30.627	12.359	1.812	4.101
	30.627	20.087	5.603	2.763	2.303
	20.087	14.990	2.392	3.703	1.675
	14.990	11.826	1.055	4.694	1.320
4	57.827	18.455	16.204	3.008	2.262
5	57.827	36.657	9.925	1.514	5.379
6	57.827	36.076	10.100	1.539	5.225

Plot of heat of dilution versus molar ratio of solvent and solute is given in Fig. 3. The heat of dilution of aqueous phosphoric acid solutions, presented in Fig3, show a large curvature for molar ratio less than 3.

Our results are in a good agreement with the values of dilution heat obtained by other workers for low concentration phosphoric acid. [8, 9](Wakefield 1972, Millero 1978).
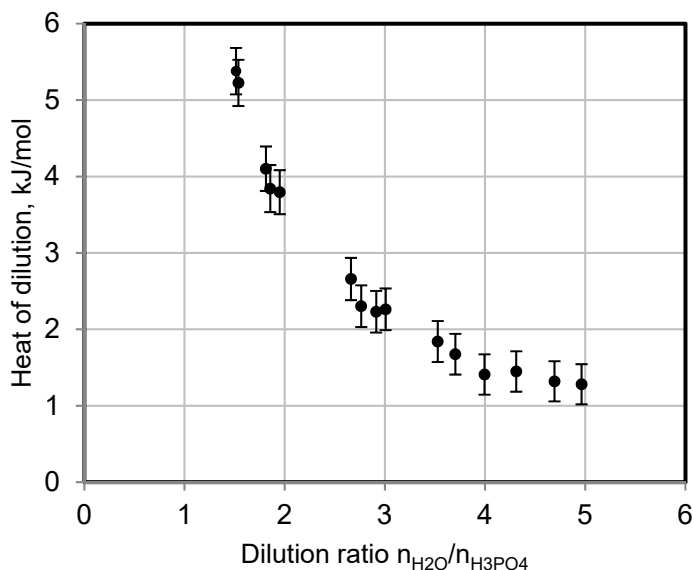
Fig.3 Phosphoric acid heat of dilution vs water /acid molar ratio.

5. Conclusions

Heat pump technology can improve heat efficiency of many drying processes. Low temperature systems are intensively studied and already implemented in the industry. Chemical heat pumps offers prospect to generate heat flux at elevated temperature.

Heat of dilution for phosphoric acid of high concentration was experimentally measured at isobaric conditions. Thermal effect of dilution strongly depends on acid concentration.

Laboratory experiments proved that phosphoric acid and water can be used as a efficient working system in CHP. Heat of dilution important for energy recovery in heat pump reactor, enable to produce technologicaly useful heat flux from waste heat source.

6. Nomenclature

Q	heat flux, J	W
ΔH_{dil}	heat of dilution	J mol^{-1}
r_u	heat capacity	J K^{-1}
ΔT	temperature increase	K
U	potential difference	V
i	electric current	A

Subscripts

R	reactor
E	evaporator
C	condenser
G	generator
cor1	temperature increase of acid dilution
cor2	temperature increase for the electric heating

7. Acknowledgements

8. References

[1] Chua K.J.; Mujumdar A.S.; Hawlader M.N.A; Chou S.K; Ho J.C. Batch drying of banana pieces – effect of stepwise change in drying air temperature on drying kinetics and product color. Food Res Int 2001, 34, 721–731.

[2] Ogura H.; Yamamoto T.; Otsubo Y.; Ishida H.; Kage H.; Mujumdar A.S. A control strategy for chemical heat pump dryer. Drying Technology 2005, 23, 1189–203.

[3] Kawasaki H.; Watanabe T.; Kanzawa A. Proposal of a chemical heat pump with paraldehyde depolymerization for cooling system. Applied Thermal Engineering 1999, 19, 133–143.

[4] Kato Y.; Yamashita N.; Kobayashi K.; Yoshizawa Y. Kinetic study of the hydration of magnesium oxide for a chemical heat pump. Applied Thermal Engineering 1996, 16, 853–862.

[5] Wongsuwan W.; Kumar S.; Neveu P.; Meunier F. A review of chemical heat pump technology and applications. Applied Thermal Engineering 2001, 21, 1489–1519.

[6] Ducheyne w.; Stevens C.; Bonte S.; Rousseau S.; Van der Pol E. New industrial chemical heat pump from Qpinch, IEA Heat Pump Conference, 15-18 May 2017 Rotterdam.

[7] Horuz I.K.; Bener K. Absorption heat transformers and an industrial application. Renewable Energy 2010, 35, 2175-2181,

[8] Wakefield Z.; Luff B.; Reed R. Heat Capacity and Enthalpy of Phosphoric Acid, J. Chem. Eng. Data 1972, 17(4), 420–423.

[9] Millero F.J.; Duer W.C.; Shepard E.; Chetirkin P.V. The enthalpies of dilution of Phosphate solutions at 30°C. Journal of Solution Chemistry 1978, 7(12), 877–889.

Drying characteristics and quality of lemon slices dried undergone Coulomb force assisted heat pump drying

Chin, S. K.[a]*; Lee, Y. H.[b]; Chung, B. K.[c]

[a] Chemical Engineering, Newcastle University in Singapore, 537 Clementi Road #6-01, SIT@Ngee Ann Polytechnic Building , Singapore 599493, Singapore

[b] Department of Chemical Engineering, LKC Faculty of Engineering and Science, Universiti Tunku Abdul Rahman, Jalan Sungai Long, Kajang, 43500, Selangor Darul Ehsan, Malaysia

[c] Department of Electrical and Electronic Engineering, LKC Faculty of Engineering and Science, Universiti Tunku Abdul Rahman, Jalan Sungai Long, Kajang, 43500, Selangor Darul Ehsan, Malaysia

*E-mail of the corresponding author: kent.chin@newcastle.ac.uk

Abstract

In this research, a Coulomb force assisted heat pump (CF-HP) dryer was invented for the purpose of improving the drying characteristics and product quality of biomaterials. As compared to heat pump drying alone, the assistance of Coulomb force in heat pump dryer enhanced the drying rates and effective moisture diffusivity of lemon slices up to 26%, which eventually shortened the total drying time to 40%. This saved the total energy consumption of HP drying by 31.5%. High retention of vitamin C and TPC were also found in CF-HP dried slices due to mild drying temperature and fast drying rate.

Keywords: Coulomb force; Heat pump drying; Drying rate; Vitamin C; Total Phenolic Content (TPC).

1. Introduction

Heat pump (HP) drying is one of the advanced drying methods that have been used for drying of many agriculture products. It is known as an energy efficient drying method which can produce good product quality as drying is conducted at mild temperature and low relative humidity[1,2]. However, mild temperature drying limits the moisture diffusion in the drying materials, which in turn lengthened the total drying time. Hybrid drying involving heat pump combined with other methods such as ultrasound, radio frequency / microwave heating, infrared heating and solar heating also been studied by researchers with the purpose to stimulate the moisture diffusivity and thus drying rate of the drying materials during heat pump drying[3]. Nevertheless, most of the hybrid drying methods like are lack of practical application for drying of heat sensitive biomaterials[4].

In this research, an electricity-assisted (Coulomb force) heat pump (CF-HP) drying is proposed as an alternative drying method for the drying of biomaterials such as lemon slices. In CF-HP drying, a high voltage wire mesh is incorporated in the heat pump dryer in order to enhance the removal rate of bound moisture, which in turn counteracts the long drying time required due to mild temperature drying. Owing to the bipolar property of moisture content inside the lemon slices, a positive net force (Coulomb force) can be induced when the lemon slices are placed near to the high voltage, but low frequency mesh. The generated force stimulates the moisture diffusion in the lemon slices which consequently dried by convective air flow produced by heat pump dryer. As there is no heating involved in drying process, the desired properties of the dried lemon slices can be preserved. Hence, CF-HP drying is envisaged to be a successor of heat pump drying in terms of high drying rate and moisture diffusivity, short total drying time, low energy consumption and good quality of dried products.

2. Materials and Methods

2.1 Sample preparation

Fresh Eureka lemons were sliced crosswise into circular slices. The average thickness of slices was measured as $3.0 \pm 0.5 \times 10^{-3}$ m and the initial weight of each slice was recorded as $8.20 \pm 0.05 \times 10^{-3}$ kg. The average surface area of the slices was calculated as 2.38×10^{-3} m^2. The lemon slices were dried until equilibrium moisture content (EMC) achieved.

2.2 Drying methods

2.2.1 Heat pump drying

A laboratory scale heat pump dryer is designed and fabricated by I-Lab Sdn. Bhd., Selangor, Malaysia. The heat pump (HP) dryer consists of a drying chamber of dimensions

0.8 m × 0.6 m × 0.6 m and a heat pump system. Mild temperature dehumidifier air produced by the heat pump system is used as a drying medium and force circulation of convective air is produced by a blower. The dryer was operated at drying temperature of 22°C and 34% relative humidity (RH) when the auxiliary heater was turned off whereas the drying temperature was 31°C and 24% RH when the auxiliary heater was on. The average air velocity in the chamber was maintained at 1.1 ms^{-1}.

2.2.2 Coulomb force assisted heat pump drying

For Coulomb force assisted heat pump (CF-HP) drying, a high voltage system was incorporated inside the heat pump drying chamber, as shown in Fig. 1. The high voltage source which determined to be 1.5×10^4 V and 50Hz, was generated by using a transformer. The output of transformer was connected to the wire mesh, where the string meshes and lemon slices were being loaded on. The effective distance between the lemon slices and wire mesh was determined to be 3×10^{-3} m. The drying condition of the hybrid heat pump drying was similar to heat pump drying in section 2.2.1. CF-HT-HP drying is the CF-HP drying with auxiliary heater being switched on.
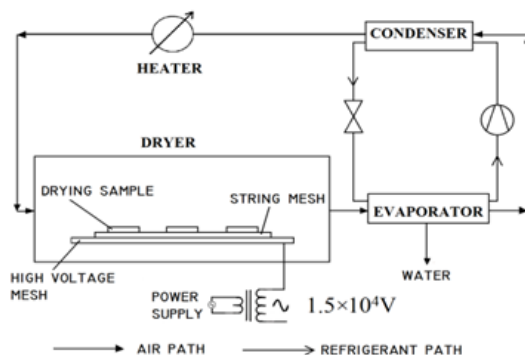
Fig. 1 Simplified diagram of the Coulomb force assisted heat pump (CF-HP) dryer

2.2.3 Oven drying

Lemon slices were dried in a laboratory scale hot air convection oven (Memmert, UFB500) at three different temperatures which were 40°C, 50°C, and 60°C, at the corresponding relative humidity (RH) of 33.4%, 20.2% and 12.6%, respectively. The average air velocity inside the chamber was determined as 0.6 ms^{-1}. Oven dried lemon slices were used as reference samples which meant for the quality comparison with samples dried by heat pump and Coulomb force assisted heat pump drying methods.

2.2.4 Freeze drying

Lemon slices were pre-frozen in a deep freezer (ARDO-CV382 Upright Freezer) at -40°C for 24 hours, before freeze dried in a laboratory scale freeze dryer (Labconco) at -40°C and 13.3 Pa. The total drying time for freeze drying of lemon slices was set at 48 hours to obtain the optimum vitamin C and TPC retention in freeze dried lemon slices[5]. The freeze dried slices were used as control sample for the determination of vitamin C and TPC in the dried slices subjected to different drying methods.

2.3 Energy consumption

Total energy consumption for heat pump and Coulomb force assisted heat pump drying was measured by the power meter (D02A, ± 1W).

2.4 Drying rate and moisture diffusivity

The initial moisture content (M_0), moisture content at a given drying time t (M_t), equilibrium moisture content (M_{eq}), moisture ratio (MR_t) and drying rate (R) of the lemon slices were calculated by equations (1) – (5) whereas the moisture diffusivity (D_{eff}) of the samples was determined using Fick's second model (equation (6)), by assuming the lemon slices to be of the shape of slab.

$$M_0 = \frac{W_0 - W_d}{W_d} \quad (1); \quad M_t = \frac{W_t - W_d}{W_d} \quad (2); \quad M_{eq} = \frac{W_{eq} - W_d}{W_d} \quad (3); \quad MR_t = \frac{M_t - M_{eq}}{M_0 - M_{eq}} \quad (4)$$

$$R = \frac{W_d}{A_s}\left|\frac{F_{t+1} - F_t}{t_{i+1} - t_i}\right| \quad (5); \quad MR = \frac{8}{\pi^2}\left[\sum_{n=0}^{99}\frac{1}{(2n+1)^2}\exp\left(\frac{-(2n+1)^2 \pi^2 D_{eff} t}{l^2}\right)\right] \quad (6)$$

Where W_0, W_t, W_d, and W_{eq}, refer to initial weight of the sample (kg), weight of the sample in the middle of drying process at time t (kg), bone dry weight of the sample (kg), and equilibrium weight of the sample (kg), respectively. A_s is denoted as the surface area of the samples (m²), F_t is the free moisture content of the sample at time t (kg H_2O / kg dry material). l, t and n are the sample's thickness (m), drying time (s) and a positive integer, respectively.

2.5 Quality analysis

2.5.1 Vitamin C

Dried lemon slices were cut into small pieces of equivalent size and subjected to extraction process at 4°C for 24 hours using 0.05 L of metaphosphoric acid-acetic acid (HPO3-CH3COOH) as extracting solvent. After removal of solid slices by vacuum filtration, the supernatants were titrated into 5×10^{-3} L of indophenol standard solution (IS). The amount

of supernatants, Vs used to decolourize the IS solution was recorded. Equation (7) was used to determine the vitamin C (kg Ascorbic acid / kg dry weight) in dried lemon slices which derived based on the standard curve obtained using Ascorbic Acid as standard solution[6].

$$\text{Vitamin C} = \frac{0.31V}{V_s W_d} \qquad (7)$$

Where V is the volume of the extracting solution used (L)

2.5.2 Total phenolic content (TPC)

Similar to vitamin C analysis, dried lemon slices were cut into small pieces of equivalent size and subjected to extraction process at 4°C for 24 hours using 0.05 L of solvent which made up of acetone, distilled water and hydrochloric acid in volume percentage of 75%, 22% and 3%, respectively. After removal of solid slices by vacuum filtration, 1×10^{-3} L of supernatant was titrated into 5×10^{-3} L of 0.2N Folin-Ciocalteau reagent and held for 3 minutes. Then, 4×10^{-3} L of 7.5% sodium carbonate solution (Na2CO3) was added into the mixture and incubated in dark at room temperature for 30 minutes to allow colour development. Subsequently, the extract was adjusted with 0.04 L of distilled water and the absorbance (A) of the extract was measured at 7.65×10^{-7} m in a single beam spectrophotometer (JENWAY 6320D). Equation (8) was used to determine the TPC (kg Gallic acid / kg dry weight) in dried lemon slices which derived based on the standard curve obtained using Gallic acid as standard solution[7].

$$\text{TPC} = \frac{AD_f V}{9.02W_d} \qquad (8)$$

Where D_f is dilution factor.

3. Results and Discussion

3.1 Drying rate, effective moisture diffusivity and total drying time

Table 1. Average drying rate, effective moisture diffusivity and total drying time of heat pump and Coulomb force assisted heat pump dried lemon slices

Drying Method	Average Drying Rate (R) ($\times10^{-5}$ kg H$_2$O / m^2.s)	Average Effective Diffusivity (D$_{eff}$) ($\times10^{-11}$ m^{2}s^{-1})	Reduction of Total Drying Time (%)
HP	5.33	2.95	–
CF-HP	5.83	3.25	31.6
CF-HT-HP	6.67	3.73	39.9

Table 2. Power and total energy consumption of heat pump and Coulomb force assisted heat pump drying methods

Drying Method	Power (W)	Total Energy Consumption ($\times 10^8$J)
HP	1723.07	9.20
CF-HP	1726.62	6.30
CF-HT-HP	3150.11	10.11

As shown in Table 1, the highest average drying rate was found for CF-HT-HP drying, followed by CF-HP and HP drying of lemon slices. As compare to heat pump drying alone, the average drying rate and effective moisture diffusivity of Coulomb force assisted heat pump drying were found to improved up to 25.1% and 26.4%, respectively. The induced Coulomb force in lemon slices during hybrid heat pump drying decreased external mass transfer resistance rendered by the high electric field, which consequently intensified the drying rate and enhanced the moisture diffusivity from core to product surface. This reduced the total drying time of 31.6% and 39.9% for CF-HP and CF-HT-HP drying, respectively. In terms of energy consumption, CF-HP drying is more efficient in energy saving as it required the least energy, which is only 68.5% and 62.3% of the total amount of energy required by HP and CF-HT-HP drying, respectively as indicated in Table 2.

3.5 Vitamin C content of dried lemon slices
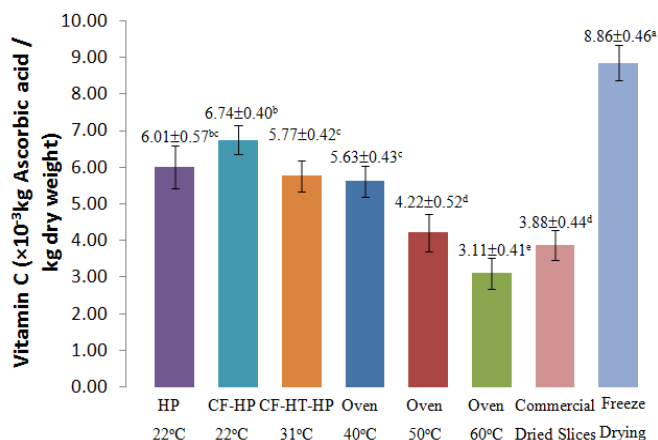
Fig. 2. Comparison of vitamin C in lemon slices for different drying methods. Vitamin C contents with different superscript letters indicate a significant difference at p<0.05.

Based on Fig. 2, except for freeze dried samples, CF-HP dried lemon slices showed the highest amount of vitamin C among all samples. The vitamin C content of CF-HP dried slices is significantly higher than oven dried slices due to mild temperature drying condition

and high drying rate. Similar to this, the amount of vitamin C in heat pump and CF-HT-HP dried samples were found to be 2.5% to 93.2% higher than oven dried samples. This indicates drying of lemon slices at mild temperature could minimize the deterioration of vitamin C during the dying process. In addition, integration of Coulomb force in heat pump drying (CF-HP) enhanced the drying rate and shortened the total drying time required as compared to HP drying which led to a better vitamin C retention in dried lemon slices. Due to increased drying temperature, the used of auxiliary heater in CF-HT-HP drying reduced the vitamin C content in lemon slices as compared to those dried with CF-HP and HP method, resulted in lower vitamin C content similar with those found in lemon slices dried at 40ºC. Lowest amount of vitamin C in 50ºC and 60ºC oven dried lemon slices could be due to combination of thermal and oxidative degradations of vitamin C. However, freeze dried lemon slices preserved the highest vitamin C among of all as drying at high vacuum could mitigate oxidative degradation of vitamin C[6]. Commercial dried products which commonly dried by solar or hot air drying method are found to retain low amount of vitamin C attributed to thermal degradation and oxidative destruction of vitamin C due to prolong drying time[7].

3.6 TPC content of dried lemon slices
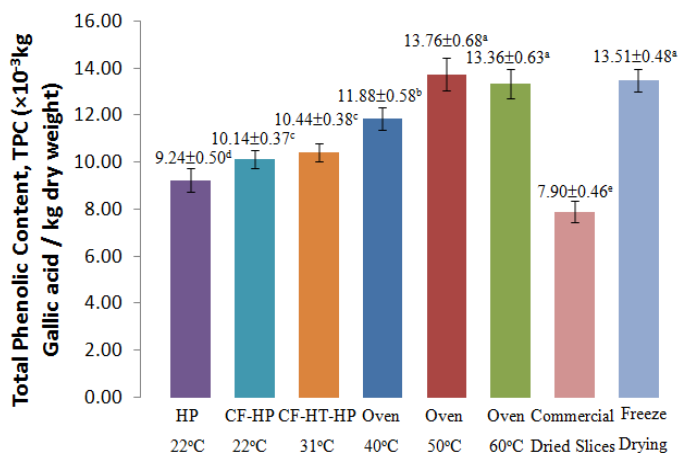
Fig. 3. Comparison of total phenolics content (TPC) in lemon slices for different drying methods. TPC with different superscript letters indicate a significant difference at p<0.05.

In contrast to the retention of vitamin C, oven dried slices at elevated temperature (50ºC and 60ºC) retained the highest amount of TPC as shown in Fig 3. According to Vega-Galvez et al., high retention of TPC in fruits dried at elevated temperature could be due to the conversion of phenolic molecules from other forms of phenolic compounds, which led to greater amount detected[8]. Furthermore, high drying rate and short drying time of the

lemon slices at elevated temperature also prevents the degradation of TPC attributed to volatilization, oxidation and heat destruction process. The effect of drying rate and drying time on the TPC of dried slices was further shown by the heat pump and hybrid heat pump dried slices. Among of them, the TPC in CF-HP and CF-HT-HP dried slices were insignificantly different, but they were significantly higher than the TPC of HP dried slices although drying was conducted at mild temperature. Similar to the results of vitamin C analysis, TPC in commercial dried lemon slices was the lowest among of all due to low drying rate and prolong drying time of open sun drying or solar drying.

4. Conclusion

Coulomb force assisted heat pump drying intensified the drying rates, enhanced the moisture diffusivity and consequently reduced the total energy consumption and drying time of lemon slices as compared to conventional heat pump drying method. In terms of product quality, it appears that CF-HP drying is a highly recommended drying method for the preservation of antioxidants.

5. References

[1] Chua, K.J.; Chou, S.K.; Yang, W.M. Advances in heat pump systems: a review. Applied Energy 2010, 87(12), pp. 3611 - 3624.

[2] Goh, L.J.; Yusof Othman, M.; Mat, S.; Ruslan, H.; Sopian, K. Review of heat pump systems for drying application. Renewable and Sustainable Energy Reviews 2011, 15(9), pp. 4788 - 4796.

[3] Patel, K.K.; Kar, A. Heat pump assisted drying of agricultural produce an overview. Journal of Food Science and Technology 2012, 49(2), pp. 142 - 160.

[4] Barzegar, M.; Zare, D.; Stroshine, R.L. An integrated energy and quality approach to optimization of green peas drying in a hot air infrared-assisted vibratory bed dryer. Journal of Food Engineering 2015, 166, pp. 302 - 315.

[5] Lai, M.W. Vitamin C Retention of freeze dried lemon fruit slices under different freeze drying conditions. Universiti Tunku Abdul Rahman. Kuala Lumpur, 2014.

[6] Burg, P.; Fraile, P. Vitamin C destruction during the cooking of a potato dish. LWT - Food Science and Technology 1995, 28(5), pp. 506 - 514.

[7] Ndawula, J.; Kabasa, J.; Byaruhanga, Y. Alterations in fruit and vegetable β-carotene and vitamin C content caused by open-sun drying, visqueen-covered and polyethylene-covered solar-dryers. African Health Sciences 2004, 4(2), pp. 125 - 130.

[8] Vega-Gálvez, A.; Scala, K.D.; Rodriguez, K.; Lemus-Mondaca, R.; Miranda, R.; Lopez, J.; Perez-Won, M. Effect of air drying temperature on physico-chemical properties, antioxidant capacity, color and total phenolics content of red pepper. Journal of Food Chemistry 2009, 117(4), pp. 647 – 653.

Impact of thin lyer drying on bioactive compounds of jaboticaba (*Plinia cauliflora*) peels

Machry, K. [a*]; Morais, M. M.[b]; Rosa, G. S.[b]

[a] Undergraduated of Chemical Engineering. Federal University of Pampa, Bagé, Brazil.

[b] Professor of Chemical Engineering. Federal University of Pampa, Bagé, Brazil.

*E-mail of the corresponding author: kar.machry@hotmail.com

Abstract

Jaboticaba (Plinia cauliflora) is a Brazilian fruit with a high content of anthocyanins compounds. Peel corresponds to 30 % of the fruit weight and it is considered a residue since just the pulp is used. The aim of this work was to analyze the convective drying process of the jaboticaba peels. Moisture content of dried peels showed a range of 7.17 to 13.26 (% w.b.). The results also reported that jaboticaba peels have high anthocyanins content (fresh: 1162.99 ± 41.35 mg/100g d.b) and it was possible to maintain these compounds even after the drying process (1052 to 1270 mg/100g d.b).

Keywords: jaboticaba; peel; drying; residue; anthocyanins.

1. Introduction

Jaboticaba (*Plinia cauliflora*) is a Brazilian fruit, with color dark blue purple characteristic of the peel[1]. This seasonal fruit grow in the tree trunk and it can be found in Midwest and Southeasts regions of the country at September to February. The peel corresponds about 30 % of the total fruit weight and is rich in anthocyanins and phenolics compounds that are natural antioxidants presented in fruits, vegetables and plants[2]. Anthocyanins provides color to the fruit and can be used as natural colorant in food, cosmetic and pharmaceutical products, however the temperature, light and oxygen influence on stability of this compounds[2]. They are considered natural antioxidants and can to provide health benefits when associated with human diet by reducing cardio vascular risk factors, abdnominal aortic atherosclerosiss[3]. Besides that, the peels are generally discarded as waste and only the pulp of fruit is used.

The high moisture content presents in jaboticaba peel require a treatment to storage. To conserve fruit and vegetables, facilitate the storage and the transportation, drying is an important unit operation that envolvs heat and mass transfer[4], considered one of the oldest methods of food preservation[5]. Whitout water, the microorganisms presents in the dried material can not to multiply[6]. Convection is possibly the most common mode of drying particulate or sheet-form or pasty solids. Heat is supplied by heated air or gas flowing over the surface of the solid. The surface of the material is exposed to air flow and the moisture content is removed by convection[7].

The aim of this work was to analyze the convective drying process of the jaboticaba peel and to determine the influence of air temperature (50 to 80 °C) and the air velocity (1 to 2 m/s) on the anthocyanins compounds.

2. Materials and Methods

Fresh jaboticaba (*Plinia cauliflora*) fruits were collected from a private farm located in São José do Cedro, Santa Catarina, Brazil (26° 27' 18'' S, 53° 29' 39'' W), in late September 2017. The peels were separeted of the pulp and washed with running water. Subsequently, the peels were sanitized in a solution of sodium hypochlorite and stored in sealed opaque bags at - 18 °C until use. The moisture content of the samples was determined in triplicate using an oven at 105 °C for 24 h.

2.1 Extraction procedure and Anthocyanins compounds

The peels were milled using a analytic mixer (GEHAKA, A 11), after 1 g milled peels were added to 50 mL of an acidified ethanol solution (50 % v/v, pH=1) in erlenmeyers. The maceration extraction was performed in duplicate using a shaker (NOVA ÉTICA, 109-1) at 150 rpm for 1 h. After extraction process, the extract was filtered with vaccum pump using filter paper twice to obtain a better separation between the solid and the liquid phase.

To quantify the anthocyanins content presents in jaboticaba peels was used a modify Fuleki and Francis[8] method. The extract absorbances were determined in triplicate using a UV/VIS spectrophotometer (EQUILAM, 755B) at 520 nm and calculated by Equation 1. Results were expressed as milligrams of cyaniding 3-glucoside equivalents per 100 g of sample, majority anthocyanins presents on jaboticaba peel.

$$Ant\ (\frac{mg}{100\ g_{w.b.}}) = \frac{Abs \cdot V_1 \cdot 1000}{w \cdot 982} \tag{1}$$

where *Abs* is the absorbance, V_1 is the volume of total extract in mL, *w* is the weight of the sample in grams, *1000* the correction factor to result be expressed in 100 grams of sample and *982* is the coefficient of extinction (982 to mg of cyaniding 3-glucoside).

2.2 Drying experiments

The drying experiments were carried out in a convective hot-air dryer (EcoEducacional) (Fig. 1). The experimental system involved a fixed bed dryer. The air flow coming from the blower (a) was monitored by an psychrometer (b) and was heated by an electrical heater system (c). Measurements of air velocity were performed by an anemometer (f). In order to monitor the mass of jaboticaba peel samples during the drying experiments a digital balance (± 0.01 g) (e) was used, connected with a tray in the drying chamber. 20 g of jaboticaba peels were distributed uniformly as a thin layer into the stainless steel tray (137 mm in diameter and 7 mm of high) and dried.

Fig. 1 Drying system.

An experimental design was performed, where the independent variables were the inlet air temperature (T_{air}) and air velocity (v_{air}). The anthocyanins content was analyzed as dependents variable. Drying time were fixed in 2 h to observe the anthocyanins degradation with temperature and air velocity. The drying curves (($M-M_e$)/(M_o-M_e) as a function of time)

were obtained. The equilibrium moisture content was assumed as the final moisture content when the drying rate was practically null, at each drying condition.

3. Results and discussion

Fig. 2 shows (A) fresh jaboticaba peels (B) dried jaboticaba peels (80 ℃; 1 m/s). It can be verified the shrinkage of samples due the fast water removal from the intercellular spaces[9] of the peel. Table 1 shows the results of final moisture content and anthocyanins content for dried samples.
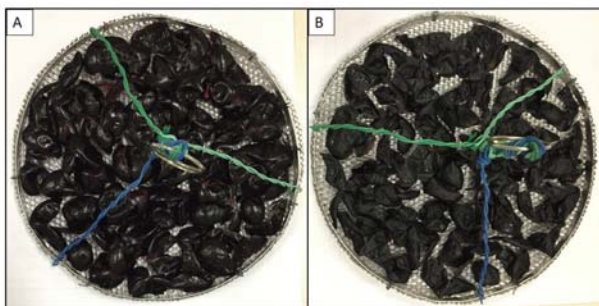
Fig. 2 Fresh jaboticaba peels (A) and dried jaboticaba peels (B).

Table 1. Results of moisture and athocyanins contents.

Runs	T (ºC)	v air (m/s)	Moisture (w.b. %)*	Anthocyanins (mg/100g d.b.)*	Anthocyanins (mg/100g w.b)
1	50	1	11.91 ± 0.26	1095.94 ± 10.82	965.34 ± 9.53
2	80	1	7.17 ± 0.24	1051.94 ± 31.95	975.76 ± 29.66
3	50	2	13.26 ± 0.14	1269.88 ± 22.63	1101.07 ± 19.63
4	80	2	7.20 ± 0.00	1249.46 ± 64.22	1159.47 ± 59.60
5	65	1,5	9.53 ± 0.39	1241.76 ± 30.66	1123.31 ± 27.74
6	65	1,5	10.19 ± 0.89	1253.23 ± 39.19	1125.49 ± 35.20

* avarage ± standard deviation

The fresh sample of jaboticaba peels showed a initial moisture content of 76.74 ± 0.71 % (w.b.). The results for anthocyanins content was 1162.99 ± 41.35 mg/100g (d.b.), which corresponds to 267.71 ± 6.88 mg/100 g (w.b.). Garcia[10] reported results of anthocyanins content in jaboticaba peels between 310 and 315 mg/100g (w.b.).

Regarding the dried samples, the results of moisture content were in range of 7.17 and 13.26 % (w.b.). Flours in general must to have moisture content below 15 %[11] to inhibit the microbial growth, but there isn't a specific resolution to moisture content of jaboticaba peels. The anthocyanins contents were in the range of 1051.94 to 1269.88 mg/100 g (d.b.). Leite-Legatti et al.[12] reported 732.77 mg/100 g (w.b.) and Lima[13] found 1585 mg/100 g (w.b.) in freeze dried jaboticaba peels. Dried peels in present study showed anthocyanins content almost twice higher than Alves[14], that reported in theirs study that the anthocyanins content was 588 mg/100 g (d.b.) to samples dried at 60 ºC. Theses differences could be due plant varieties, cultivation practices, environmental and geographical factors[13]. Higher results to anthocyanins compounds in some dried samples on the present study could be related with the formation of new antioxidants compounds. It was observed by Dewanto[15] for tomatoes. Freitas[16] also reported similar behavior with freeze dried butiá samples (pulp and peel), which showed an increase of anthocyanins compounds. Moreover, the moisture content in fresh samples can hamper the anthocyanins extraction. Also, the differences between anthocyanins for fresh and dried samples could be related with morphological changes in the structure of the cells during the drying process[17].

Typical drying curves obtained are illustrated in Fig. 3. Overall drying kinetic curves obtained for jaboticaba peels under different drying conditions showed the same behavior.
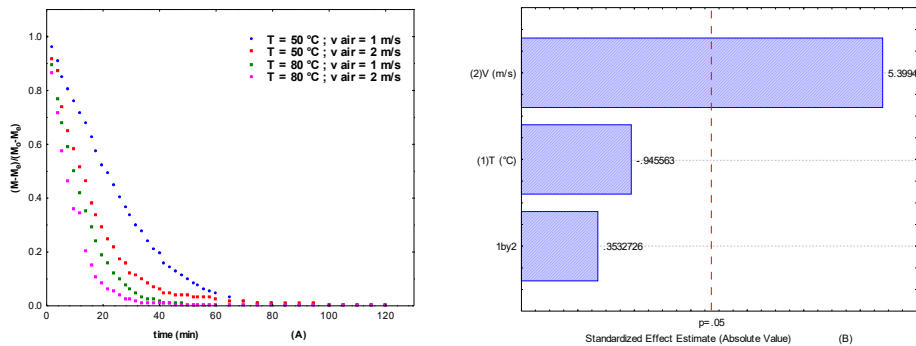
Fig. 3 (A) Drying curves at 50 and 80 ºC; (B) Pareto chart of standardized effecs.

As expected, an increase in air temperature and air velocity also significantly increased the drying kinetics and resulted in lower final moisture content. The presence of a constant-rate drying period to indicates that the moisture content is on the surface and the main heat transfer mechanism in this period is the convection. According to Geankoplis[6], the final moisture content decrese with the increase of the temperature. The difference of vapour pressure between the surface of the material and the hot air increase with the increasing of the temperature, decreasing the exposure time until the equilibrium. Moreover, higher temperatures increase the mass and heat transfer coefficients.

The results for the effects of operating variables on anthocyanins content obtained from statistical analysis are shown in the Pareto diagram (Fig. 3 (B)). It can be verified that only the effect of air velocity was significant for anthocyanins content at a confidence level of 95 % in the ranges studied. The results indicated that anthocyanins content can be maximized by increasing the air velocity from 1 to 2 m/s. It's inferred that in higher velocities there are the presence of vortices which help to increase the mass and heat transfer coefficients. These vortices are accentuated due the concave structure of the jaboticaba peel. The results indicated that the adequate drying condition is at 80 ºC and 2 m/s, since it was the condition that showed lower drying time, and consequently represents a lower cost of the process.

4.   Conclusions

The jaboticaba peel drying was analyzed in this study. The results showed that the samples had an inicial moisture content of 76.71 % (w.b.) and after the drying process the values were in range of 7.17 to 13.26 (% w.b.). Jaboticaba peels showed a high anthocyanins content, even after drying process. The drying process showed that the air temperature and air velocity had an influence on the increase of the drying rate and a reduction of the process time. The statistical analysis of the results showed that the air velocity was significant at a confidence level of 95 % for anthocyanins content. Jaboticaba peels are a residue that can be used as additive of flour in food industry since this material showed a high content of bioactive compounds.

5. References

[1]   Oliveira, A. L.; Brunini, M. A.; Salandini, C. A. R.; Bazzo, F. R. Caracterização tecnolõgica de jabuticabas "sabará" provenientes de diferentes regiões de cultivo. Rev. Bras. Frutic., v. 25, n. 3, p. 397-400. São Paulo, Brasil, 2003.

[2]   Tonon, R. V.; Brabet, C.; Hubinger, M. D. Anthocyanin stability and antioxidant activity of spray-dried acai (Euterpe oleracera Mart.) juice produced with different carrier agents. Food Research International, 2010, 43, 907-914.

[3]   Sant'Anna, V.; Gurak, P. D.; Marczak, L. D. F.; Tessaro, I. C. Tracking bioactive compounds with colour changes in foods – A review. Dyes and Pigments 98 (2013) 601-608.

[4]   Panchariya, P. C.; Popovic, D.; Sharma, A. L. Thin layer modelling of black tea drying process. Journal of Food Engineering. 52 (2002). 349-357.

[5]   Akipinar, E. K.; Bicerm Y.; Yildiz, C. Thin layer drying of red pepper. Journal of Food Engineering v. 59 p. 99-104, 2003.

[6]   Geankoplis, C. J. Procesos de transporte y operaciones unitarias. 3a Edición. Compañía Editorial Continental, S. A . de C. V: México, 1998.

[7]   Mujumdar, A. Handbook of Industrial Drying. 3 ed. Taylor and Francis; 1287 pp, 2006.

[8]   Fuleki, T.; Francis, F. J. Quantitavive Methods for anthocyanins: 1. Extraction and

determination of total anthocyanins in cranberries. Journal of Food Science, v. 33, p. 72-77, 1969.

[9] Mandamba, P. S; Bucle, Driscoll, R. H.; Buckle, K. A. Shrinkage, Density and Porosity of Garlic During Drying. Journal of Food Engineering, v. 23, p. 309-319, 1994.

[10] Garcia, L. G. C. Aplicabilidade Tecnológica da Jabuticaba. Dissertação de mestrado. Goiás, Brazil, 2014.

[11] Agência Nacional de Vigilância Sanitária. Resolução – CNNPA nº 12, de 1978.

[12] Leite-Legatti, A. V.; Batista, Â. G.; Dagrano, N. R. V.; Marques, Castro, A.; Malta, L. G.; Riccio, M. F.; Eberlin, M. N.; Machado, A. R. T.; Carvalho-Silva, L. B.; Ruiz, A. L. T. G.; Carvalho, J. E.; Pastore, G. M.; Júnior, M. R. M. Jaboticaba peel: Antioxidant compounds, antiproliferative and antimutagenic activities. Food Reserch International v. 49 p. 596-603, 2012.

[13] Lima, A. de J. B. Caracterização e Atividade Antioxidante da Jabuticaba [Myrciaria cauliflora (Mart.) O. Berg]. Tese de doutorado. Minas Gerais, Brazil, 2009.

[14] Alves, A. P. de C. Casca de Jabuticaba (*Plinia jaboticaba* (Vell.) Berg): Processo de Secagem e Uso como Aditivo em Iogurte. Dissertação de mestrado. Minas Gerais, Brazil, 2011.

[15] Dewanto, V.; Wu, X.; Adom, K. K.; Laiu, R. H. Thermal Processing Enhances the Nutritional Value of Tomatoes by Increasing Total Antioxidant Activity. J. Agric. Food Chem, v. 50, p. 3010-3014, 2002.

[16] Freitas, V. Rossato, V. Rosa, G. Influência do Processo de Secagem na Casca e Polpa de Butiás no Conteúdo de Antocianinas e Carotenóides. ENEMP, 2013.

[17] Bejar, A. K.; Kechjaou, N.; Mihoubi, B. Effect of Microwave Treatment On Physical and Functional Proprieties of Orange (*Citrus Sinensis*) Peel and Leaves. Food Processing & Technology, v. 2, 2011.

Experimental investigation on pore size distribution and drying kinetics during lyophilization of sugar solutions

Foerst, P.[a]*; Lechner, M.[a], Vorhauer, N.[b]; Schuchmann, H.[c]; Tsotsas, E.[b]

[a] Chair of Process Systems Engineering. Technical University of Munich, Freising, Germany
[b] Chair of Thermal Process Engineering. Otto-von-Guericke University Magdeburg, Germany
[c] Wilhelm Büchner Hochschule, Pfungstadt, Germany

*E-mail of the corresponding author: petra.foerst@tum.de

Abstract

The pore structure is a decisive factor for the process efficiency and product quality of freeze dried products. In this work the two-dimensional ice crystal structure was investigated for maltodextrin solutions with different concentrations by a freeze drying microscope. The resulting drying kinetics was investigated for different pore structures. Additionally the three-dimensional pore structure of the freeze dried samples was measured by μ-computed tomography and the pore size distribution was quantified by image analysis techniques. The two- and three-dimensional pore size distributions were compared and linked to the drying kinetics.

Keywords: pore size distribution; freeze drying; maltodextrin solution; freeze drying microscope

1. Introduction

Lyophilisation or freeze drying is commonly applied to stabilize (bio-)pharmaceutical substances and high value foods for long-term storage. During drying, the thickness of the dried layer is steadily increasing. Therefore, the mass transfer resistance becomes the dominating factor causing very long process times [1]. The mass transfer resistance is directly linked to the pore structure of the frozen solution. The pore structure is also important for the freeze drying of particulate matter as it determines the intra-particle mass transfer resistance and process efficiency. Furthermore, collapse phenomena are directly linked to the pore structure as the pore structure determines the maximum product temperature. The pore structure is determined by the freezing process prior to sublimation and is depending on cooling rate, nucleation temperature and solid content of the solution [2].

The pore structure is the decisive factor for the formation of the drying front of both particulate systems and frozen liquids. Therefore it is the aim of this work to investigate the influence of the process parameters cooling rate, annealing treatment and solid concentration on the pore size distribution of maltodextrin solutions as model systems.

Regarding the quantitative evaluation of pore size distribution it has to be distinguished between the evaluation of the frozen system and the dried system. In most cases it is assumed that no shrinkage occurs during freeze drying and the pore size of the frozen system is not different to the dried system. For frozen systems the ice crystal size distribution is mostly determined from sliced frozen samples by light microscopic techniques or Cryo-SEM [3]. In dried systems, mostly SEM and more recently μ-computed tomography are used for the evaluation of pore structure of freeze dried products [4, 5]. The aim of this work is to compare the two-dimensional ice crystal structure as observed in a freeze drying microscope with the three-dimensional pore structure measured by μ-computed tomography (μ-CT) and to link the pore structure to the drying kinetics.

2. Materials and Methods

Maltodextrin solution (DE 10-14 from medesign I.C. GmbH) was used as model substance. Solutions of maltodextrin were prepared by using bi-distilled water with the following concentrations: 5%, 10% and 20% (w/w).

2.1 Freeze drying microscope

The controlled cooling of the solutions was carried out with the cryostage FDCS196 (Linkam Instruments, Tadworth, UK) coupled to an Olympus BX51 polarized light microscope (Olympus Microscopy, Essex, UK) equipped with a Pixelink PL-A662 camera (Pixelink, Rochester, USA). A quantitiy of 10 μl of the sample was loaded into a 15 mm

diameter quartz glass crucible, which was placed on a silver block in the stage. The controlled temperature ranged between -196°C to 125 °C. The sample was enclosed by a spacer to achieve a uniform thickness of 690 µm. Thus the sample forms a cylindrical disk with a diameter of 4.3 mm and a height of 690 µm. Temperature was measured using a Pt100 temperature sensor from Linkam Instruments (accuracy ± 0.1 °C). By calibrating the 20x magnification lens (LMPlan Fl 20x/0.40) with a scale, the lengths and dimensions of the microscopic images were calculated using Linksys32 software.

2.2 Freezing and drying experiments and microscopic image analysis

After placing the liquid sample onto the quartz crucible, the stage was sealed and all samples were cooled to -50°C at a defined cooling rate. Two different cooling rates were investigated: 0.5 K/min and 20 K/min. Furthermore two annealing treatments were investigated: In Treatment I the sample was heated to -10 °C for 90 min after freezing and cooled back to -50 °C. In treatment II the sample was heated to -5 °C after freezing for 180 min and cooled back to -50 °C. After reaching -50 °C, pictures were taken to evaluate the two-dimensional ice-crystal size distribution of the frozen samples. The subsequent drying step was carried out with a shelf temperature of -18 °C and a pressure of 10 Pa for all freezing protocols. During drying, a picture was taken every 10 s. As soon as primary drying was finished which was determined by the disappearance of the drying front, the silver block was heated to 30 °C and the secondary drying was carried out overnight until a final water content of approx. 2% was achieved. The samples were then taken out of the cryostage and stored in a desiccator until further evaluation of the dry pore structure by µ-CT.

For the evaluation of the ice crystal size, the software Linksys 32 was used. Three pictures of each sample were taken and 100 ice crystals were manually analysed per picture. The ice crystals were analysed by edging the ice crystals. From the ice crystal contour the equivalent diameter x_{pm} of a sphere with equal area of projection was obtained.

2.3 µ-CT measurements and image analysis

The samples that were evaluated for ice crystal size and drying kinetics, were taken for the µ-CT analysis as well. Three-dimensional X-ray µ-CT scans were performed using the XCT1600 system from Nordson Matrix Technologies GmbH (Feldkirchen, Germany). The cylindrical freeze-dried cakes from the freeze drying microscope were cut with a razor knife to prepare cuboid pieces (length and width about 2 mm) out of the center of the dried solids. The imaging system was adjusted to operate at a tube voltage of 60 kV and current intensity of 20 µA. X-ray shadow images were acquired with a pixel resolution of 1 µm and 2000 projections with an exposure time of 4487 ms. The obtained images were reconstructed into a series of 2-D images using the CERA Xplorer software (Siemens

Healthcare GmbH, Erlangen). The resulting 3-D images consisted of more than 2000 slices encoded in 16-bit precision.

Image processing and analysis were done with MAVI Fraunhofer ITWM software (Fraunhofer Institute for Industrial Mathematics, Kaiserslautern). Fig. 2 shows part of the image analysis steps performed with MAVI. First, the original data set was cropped into three cubic sub-volumes of 400x400x400 voxels equivalent to 400x400x400 μm^3 (Fig. 2a). Afterwards, a global threshold was defined to separate pores and solid. The global threshold was adjusted to the water content in the solutions; i.e. 0.8 for the 20% solution, 0.9 for the 10% solution and 0.95 for the 5% solution. After transformation of the greyscale into binary images (Fig. 2b), a Euclidean distance transformation was carried out, which created a distance map by assigning each background voxel a grey value based on the distance to the closest foreground voxel (Fig. 2c). Thereby, local minima were identified. To avoid oversegmentation of pore structure, a h-minima transformation was then performed with a global $h = 10$. This value was chosen by comparison of the results with the two-dimensional ice-crystal structure (see section 3.1). Subsequently, the individual pores were segmented using the watershed segmentation method. All remaining regional minima served as water sources for the flooding. The lines where water from different basins met were identified as the watershed lines. Separated cells were produced from the logical difference between the watershed lines and the initial binary image (Fig. 2d). Finally, the object features tool of MAVI was used to obtain the volume of the individual pores. The equivalent pore diameter values were determined by calculating the diameters of spheres corresponding to the pore volumes. Therefore the equivalent diameter x_v of a sphere with the same volume was determined.
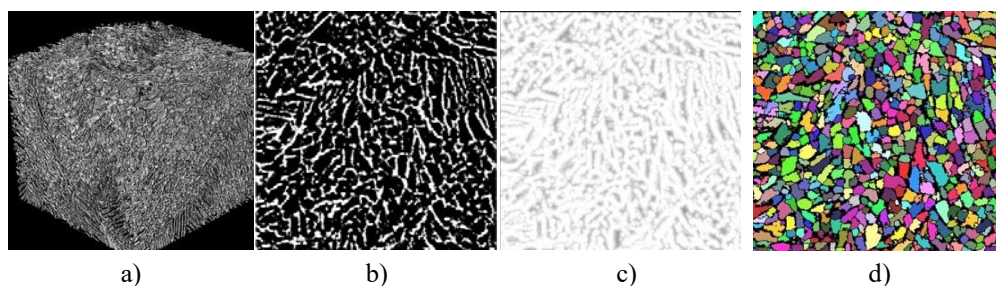
Fig. 2. Illustration of all steps performed for the image analysis with MAVI: 3D image of cubic sub-volumes of 400x400x400 voxels (a), binarized image (c), distance map after Euclidean distance transform (d), watershed image (e)

2.4 Evaluation of drying rate

After keeping the sample at -50°C for 15 min the pressure was decreased by a rotary vane pump to 10 Pa. Then the samples were heated to -18 °C at a rate of 3 K/min. Due to the cylindrical geometry of the sample, the drying proceeded in radial direction. As the dried part of the sample appears much darker than the frozen part, the radial drying front could be

easily visualized. The distance between edge of the sample (R_0) and the drying front over time r(t) was measured at three positions every minute. From the movement of the drying front Δr the drying rate was calculated.

$$\dot{m} = \frac{\rho_{ice}\,2\pi\,r\,h\,\varepsilon\Delta r}{\Delta t} \tag{1}$$

Here, ρ_{ice} is the density of ice at the sublimation temperature, r is the radius of the sublimation front, h the height of the sample (690 µm), ε the porosity and $\Delta r/\Delta t$ the change in sublimation front distance.

3. Results

3.1 2D ice crystal structure

At first, the two-dimensional ice-crystal size distribution was evaluated for the different freezing protocols and solid concentrations. Fig. 3 shows the two-dimensional ice crystal size distribution for three different solid concentrations with and without annealing treatment.
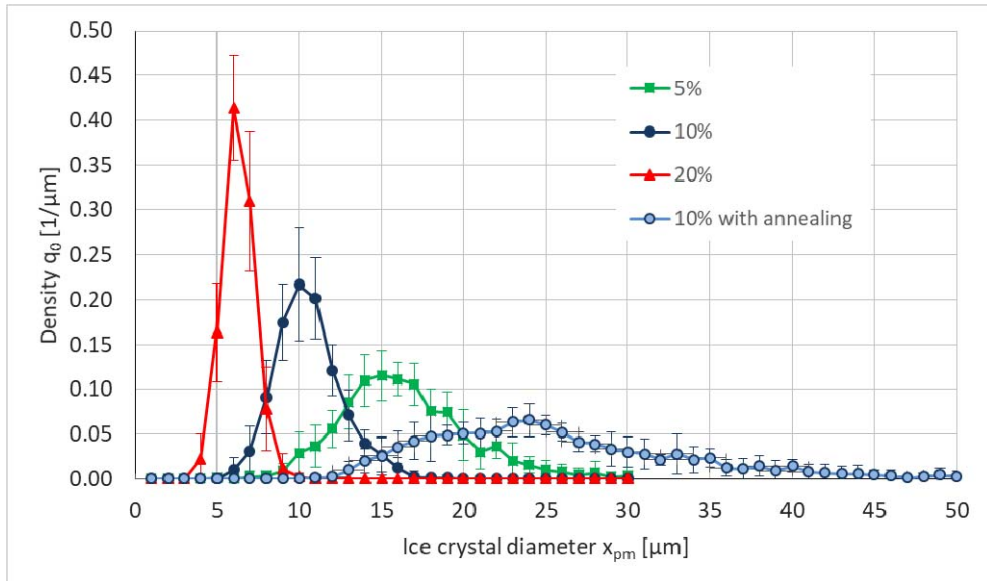
Fig. 3. Ice crystal diameter for frozen maltodextrin solutions at -50°C for different solid contents. Freezing was carried out with a cooling rate of 20 K/min. For the 10% solution, the ice crystal size distribution for annealing treatment II (-5°C/180min) is also shown

It was found that the freezing rate had no significant influence on ice crystal size distribution (data not shown), but an annealing treatment above Tg`(annealing treatment II) led to a much broader and coarser ice crystal size whereas the annealing treatment I had no influence on ice crystal size (data not shown). Next to the annealing treatment, the solid concentration had the largest impact on ice crystal size. Fig. 3 shows that the lowest solid concentration (5%) leads to the largest ice crystal diameters and also to the broadest distribution.

3.2 3D pore structure

The cylindrical disks prepared in the freeze drying microscope were further dried until about a water content of 2%. From the dried samples, a µ-CT image with a resolution of 1 µm was taken in order to evaluate the three-dimensional pore structure. As indicated in section 2.3, a h-minima transformation was performed to avoid oversegmentation. The h value is therefore a free parameter. The parameter h was chosen such that the modes of the 2D and 3D distribution coincide. The comparison between 2D ice crystal diameter x_{pm} and 3D for the different freezing protocols and solid contents is shown in Fig. 4.
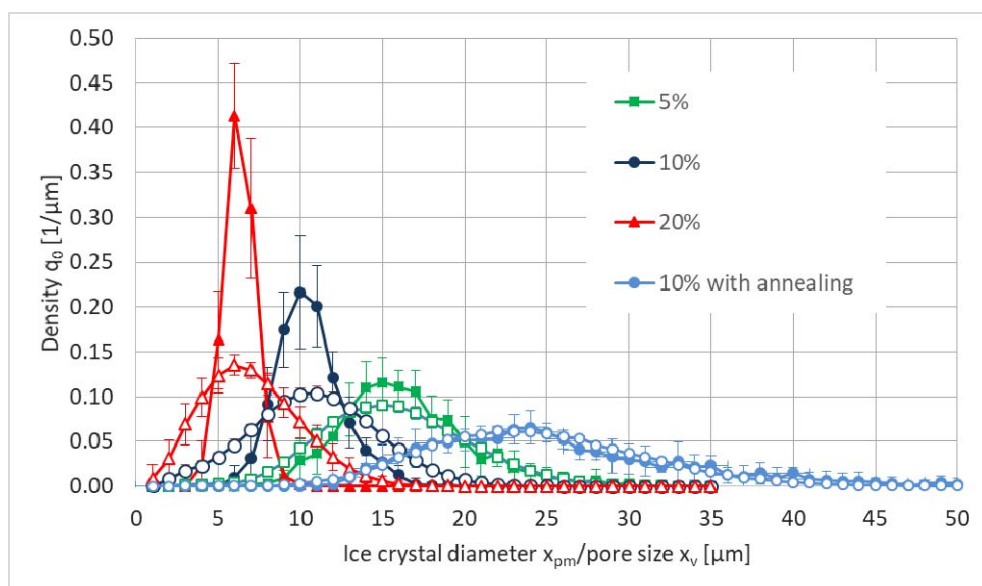
Fig. 4. Comparison between 2D and 3D Structure. Density distribution of ice crystal sizes (filled symbols) in comparison to pore sizes of dried cake (empty symbols) for different solid contents (freezing rate 20 K/min) and annealing treatment

Fig. 4 shows that the discrepancy between 2D ice crystal size and 3D pore size becomes smaller with increasing pore size. The reason could be that the resolution limit in the light microscope is higher than in the µ-CT and therefore the larger sizes match better. As both

measurements refer to different equivalent diameters, another reason could be that the shape of the pores is dependent on size and that small pores are less spherical. This issue has to be investigated in more detail in future. At last we were interested in the effect of pore structure on drying kinetics. For that we investigated the relationship between mean ice crystal size (modal value) and maximum drying rate as well as drying time. This correlation is shown in Fig. 5. An exponential relationship was found showing the high importance of pore size on drying kinetics.
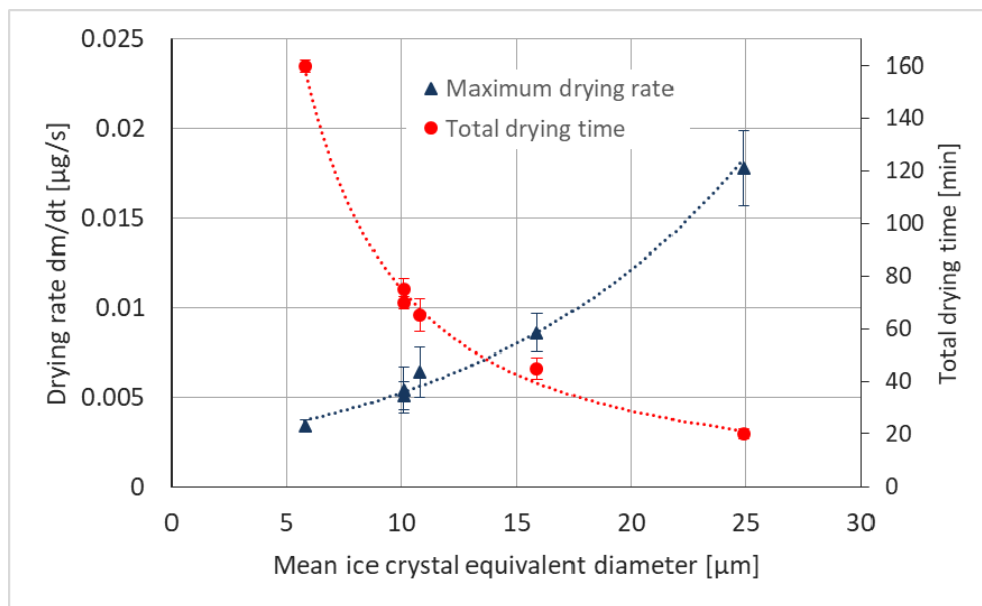
Fig. 5.: Correlation between mean ice crystal diameter and maximum drying rate and total drying time.

4 Conclusions

The work shows the high importance of pore size distribution for the freeze drying process. It was shown that it is possible to evaluate the three-dimensional pore structure with μ-computed tomography and image analysis and that the pore size is strongly dependent on the solid concentration and on an annealing treatment prior to drying. This means that it is possible to design the pore structure to meet the requirements of the freeze drying process. The work shows the applicability of the μ-CT measurement of pore size distribution and shows that for small pore sizes there is a discrepancy between two- and three-dimensional pore size. This relationship has to be investigated further.

5   Nomenclature

x_{pm}	diameter of sphere with same mean area of projection	m
x_v	diameter of sphere with same volumt	m
h	height	m
R	radius of sample	m
r	radius of sublimation front	m
q_0	density distribution	μm^{-1}

Greek letters

ε	porosity	-
ρ	density	kgm^{-3}

Subscripts

ice	ice
0	initial

6   References

[1] Pliske. R.; Müller, U.; Kohlus, R. Untersuchungen zur Steigerung der Trocknungsgeschwindigkeit der Gefriertrocknung. Chemie Ingenieur Technik 2015, 87(7), 1006-1010

[2] Searles, J. A.; Carpenter, J.F.; Randolph, T.W. The ice nucleation temperature determines the primary drying rate of lyophilization for samples frozen on a temperature-controlled shelf. Journal of Pharmaceutical Sciences 2001, 90, 860-871

[3] Hottot, A.; Vessot, S.; Andrieu, J. A direct characterization method of the ice morphology. Relationship between mean crystals size and primary drying times of freeze-drying processes. Drying Technology 2004, 22(8), 2009-2021

[4] Pisano, R.; Barresi, A.A.; Capozzi, L.C: Novajra, G.; Oddone, I.; Vitale-Brovarone, C. Characterisation of the mass transfer of lyophilized products based on X-ray micro-computed images. Drying Technology 2017, 35(8), 933-938

[5] Mousavi, R.; Miri, T.; Cox, P. W.; Fryer, P. J. A Novel Technique for Ice Crystal Visualization in Frozen Solids Using X-Ray Micro-Computed Tomography. Journal of Food Science 2005, 70(7), 437–442.

Microwave-assisted convective drying of kale (*Brassica oleracea* L. var. *sabellica* L.) at stationary and non-stationary conditions

Mierzwa, D.[*]; Szadzińska, J.

Department of Process Engineering, Poznań University of Technology, Poznań, Poland

*E-mail of the corresponding author: dominik.mierzwa@put.poznan.pl

Abstract

This paper concerns hybrid drying of kale. Eight different schedules of drying were tested experimentally to find out the influence of microwave enhancement on the kinetics (drying rate and time), energy consumption of convective drying and quality of products. Different power of microwaves and modes of microwave application were tested. Quality of products was assesed through water activity and colour measurements, as well as retention of ascorbic acid. The results obtained in the studies allowed to state that intermittent application of high-power microwave pulses may lead to a meaningful reduction of drying time and high quality of the dry products.

Keywords: hybrid drying; intermittent drying; kale; ascorbic acid; colour

Microwave-assisted convective drying of kale (Brassica oleracea L. var. sabellica L.) at stationary and non-stationary conditions

1. Introduction

Kale (*Brassica oleracea* L. var. *sabellica* L.) is a common vegetable consumed in many countries, mainly in soups and salads. It may be described as a green headless leafy cabbage with long petioles and large midribbed leaves. Kale is recognized as a valuable source of many vitamins and nutrients. Moreover, kale is an excellent dietary source of natural antioxidants. Beneficial properties of Brassica vegetables have been attributed to the presence of bioactive compounds such as phenolic compounds and ascorbic acid, associated with a reduced risk of cardiovascular diseases and several types of cancer.[1]

Refrigeration and freezing are the easiest methods of food preservation. Regrettably, chilling of the raw material maintains acceptable characteristics only for a few days. On the other hand, freezing may cause significant sensory quality degradation. Besides, both refrigeration and freezing require a lot of energy which may not be accessible, especially in undeveloped countries. Drying is another method of food preservation. It is easier and less demanding in terms of apparatus construction. Ultimately, natural sun drying may be realized without any apparatus just with the use of solar radiation. Usually however, food products are dried by forced convection (with hot air) using various dryer designs (cabinet, tunnel, chamber, drum etc.).[2]

Unluckily, food processing may have both beneficial and detrimental effects on the phytochemicals in vegetables.[3] Drying operation is usually accompanied by physical, biological and chemical changes, which influence the product quality, and finally the consumer choice. The main effect of drying is related with degradation of heat-sensitive phytochemicals, such as vitamins, antioxidants, minerals, pigments and other bioactive compounds.[4] For these reasons, new drying technologies are sought to minimize the detrimental influence of this processing method on the products quality. The aim of this research was to analyse the influence of intermittent application of microwaves during convective drying on process kinetics, energy consumption and quality of products. Different modes of microwave enhancement and a changeable power of radiation were tested experimentally to determine their influence on the analysed parameters.

2. Materials and Methods

Fresh kale (*Brassica oleracea* L. var. *sabellica* L.) was bought on a local market and stored for at least 24 h under refrigeration at 4°C. Before drying, 500 g of raw material was rinsed and cut into smaller pieces. Next, the samples were dried in a hybrid rotary dryer[5] in eight different schedules (Table 1).

No.	Code	Description	T (°C)	v (m/s)	P_{mw} (W)
1	CV	convective drying			0
2	CVMW1				100
3	CVMW2	microwave-assisted conv. drying			200
4	CVMW3		50	2	300
5	CVMW5				500
6	IT1				100-300
7	IT2	hybrid intermittent drying			300-100
8	IT3				1000

All the CVMW programs were realized in stationary conditions – constant application of microwaves during convective drying. For the IT1 and IT2 programs, the microwaves were also applied continuously, but the MW power was reduced (from 300 to 100 W in IT1) or increased (from 100 to 300 W in IT2) by 10 W for every 10 % of the weight loss. In the IT5 program, convection drying was supported periodically (for every 15 minutes) by high-power microwave impulses (1000 W) lasting 5 min each one. The effectiveness of drying schedule was assesed on the basis of its kinetics, energy consumption and product quality. The kinetics of particular process was analysed through comparison of drying curves – the evolution of moisture ratio (MR) in time, and the average values of drying time (DT) and rate (DR). The moisture ratio (MR) was designated by the following equation:

$$MR = \frac{MC_t - MC_{eq}}{MC_i - MC_{eq}} \qquad (1)$$

where MC_i, MC_t, and MC_{eq} are the initial, instantaneous (for a given time of the process) and equilibrium moisture contents.

The initial moisture content (MC_i) of the material was determined with a moisture analyser (XM120; Precisa, Switzerland; precision 0.01%). The equilibrium moisture content (MC_{eq}) was assumed constant during the research and equalled 0.05. The moisture content at a given time of the process (MC_t) was expressed as the ratio of moisture mass to the initial mass of the wet sample. Energy consumption was measured with a standard electricity meter (precision 0.01 kWh) and recalculated to the MJ per gram of evaporated moisture (EC).

The product quality was assessed on the basis of colour, water activity, and ascorbic acid measurements. The colour of the fresh or dry material was measured with the use of colorimeter (CR400; Konica Minolta, Japan; precision 0.01). On the basis of the obtained CIE Lab tristimulus colour coordinates (L^*, a^*, and b^*), a relative colour change parameter (dE) was determined by:

$$dE = \left(dL^{*2} + da^{*2} + db^{*2}\right)^{0.5} \qquad (2)$$

where dL*, da* and db* constitute differences between CIELab coordinates of fresh and dried samples.

Water activity (aw) was measured for both fresh and dried samples by using a laboratory meter (LabMaster-aw; Novasina, Switzerland; precision 0.001) at constant temperature of the chamber (25°C). Ascorbic acid content was determined by the modified method[6], with the use of spectrophotometer (UV 5100; Hitachi, Japan; precision 0.01). The absorbance was measured at the wavelength of 734 nm, and next recalculated with the use of analytical curve. Next, the ascorbic acid loos (AL) was determined as:

$$AL = \left(1 - \frac{AC}{AC_0}\right) \cdot 100\% \qquad (3)$$

where: AC_0 and AC is the ascorbic acid content for fresh and processed sample, respectively.

3. Results and discussion

3.1. Drying kinetics

In Figure 1, the evolution of moisture ratio (MR) and the average drying rate (DR) for particular drying processes are presented.
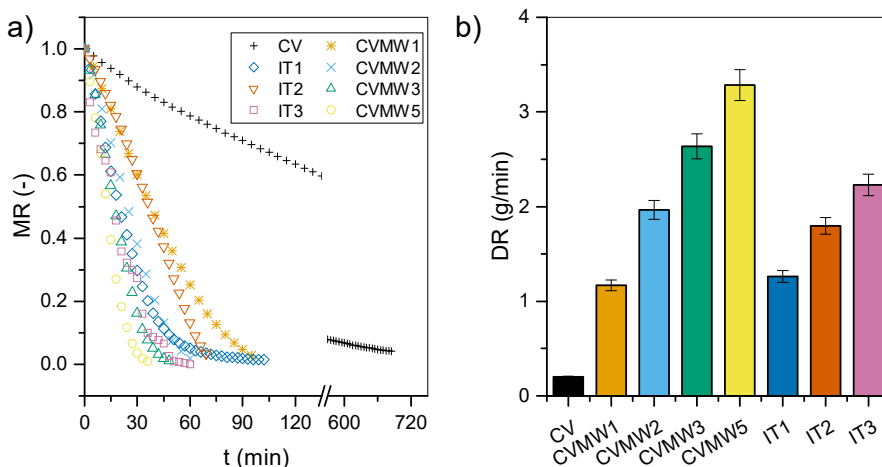
Fig. 1. a) evolution of the moisture ratio (MR) and b) average drying rate (DR) in particular drying processes.

Application of MW during stationary processes (CVMW1-5), visibly affected the kinetics of convective drying (Fig. 1a). The higher MW power the faster drying rate (Fig. 1b) and shorter drying process as a consequence (Fig. 2a). In case of intermittent processes (IT1-3) the DR diminished noticeably, but the drying time was still significantly shorter than for CV. A comparison of IT1 and IT2 allows to state that starting with a higher MW power at the beginning of intermittent drying is more efficient than gradually increasing of MW power. Both drying rate and drying time were better for the IT2 program, where MW power was reduced from 300 to 100 W by 10 W for every 10% of the weight loss. Application of pulsed high-power microwaves during IT3 program positively influenced the kinetics of CV. The drying rate was higher than in other nonstationary schedules and almost all stationary ones (Fig. 1b). It resulted in visibly shorter drying time (Fig. 2a).
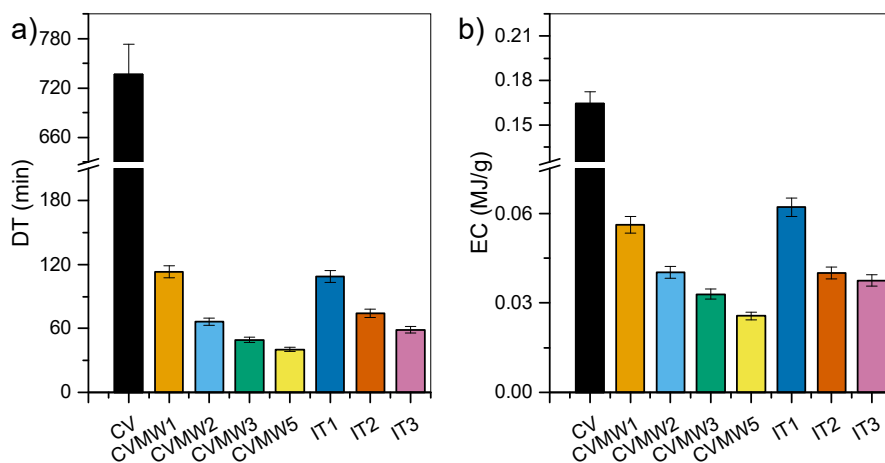
Fig. 2. Average values of a) drying time (DT) and b) energy consumption (EC).

Figure 2b presents the average energy consumption for different drying schedules. One can see that application of microwaves during stationary (CVMW1-5) and nonstationary (IT1-3) processes affected the total energy consumption. The highest values of this parameter was observed for CV, whereas the lowest one for CVMW5. Such results stay in good agreement with other kinetic parameters (DR and DT). It also implies that microwaves effectively improved the drying process of kale. The ineffective interaction of microwaves causes a negligible decrease in drying time, which connected with a larger instantaneous consumption of electricity (than for a purely convective operation), results in an increase in the total energy consumption.

3.2. Quality of products

In Figure 3, the average values of water activity (aw) and ascorbic acid loss (AL) are presented, respectively.
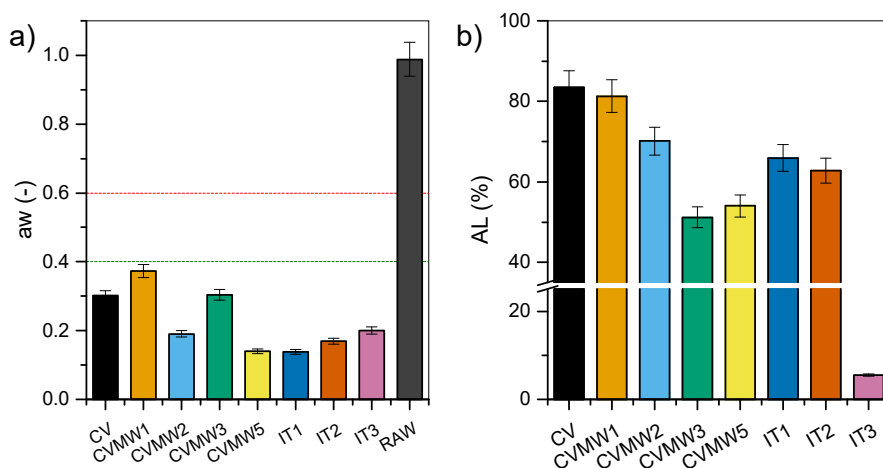
Fig. 3. Average values of the: a) water activity (aw) and b) ascorbic acid loos (AL).

It is generally assumed that if the processed product is characterized by aw below 0.6 it can be acknowledged as stable in terms of microbiological safety.[7] All dry products obtained by different schemes were characterized by the aw below 0.4, which means that there is no microbial proliferation.[8] The analysis of the ascorbic acid loos (Fig. 3b) allows to state that all of the tested processes negatively affected retention of this valuable compound. The smallest leakage of ascorbic acid (below 10%) was observed for IT3, where high-power impulses of MW were applied. It may result from the relatively short duration of drying and a small increase in the sample temperature. During this process, microwaves were applied only for 5 minutes, and then a 15-minutes the so-called *relaxation period* was introduced. The main aim of application of the *relaxation period* was to 'equalize' the material after intensive microwave drying. During this period, the temperature of samples decreased and the humidity distribution becomes more aligned. It surely resulted in milder drying conditions in comparison to severe stationary microwave-assisted convective processes (CVMW). Nevertheless, the ascorbic acid content in products dried by hybrid methods was higher than for solely convective process (CV). A small retention of ascorbic acid surely results from significantly longer drying time. Only in case of CVMW1, where the weakest microwave enhancement was applied (100 W), the amount of ascorbic acid was similar to CV. Such result is quite unexpected and means that six-fold reduction in drying time did not affect the retention of the ascorbic acid present in dried products.
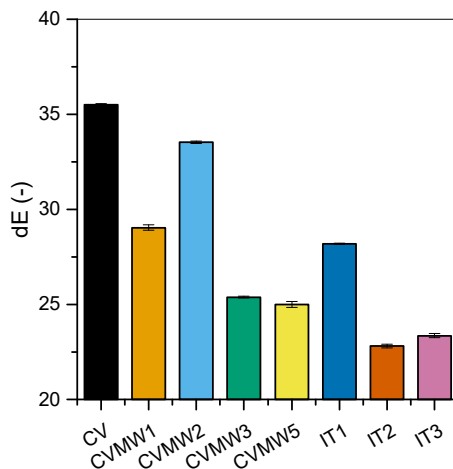
Fig. 4. Average values of the relative colour change (dE).

The last analysed parameter was colour of the dry products. Figure 4, shows the relative colour change (dE). It can be seen, that all drying procedures influenced significantly the colour of the obtained products. Change in colour is mainly attributed to chlorophyll and carotenoids degradation. Chlorophyll is highly susceptible to degradation during processing and storage, and depends on temperature, pH, time, enzyme, oxygen and light. Carotenoids have been proven to be more stable during thermal processing compared with chlorophylls, but may be isomerized and oxidized under the influence of heat, light and oxygen, and others.[9] As expected, the highest value of relative colour change (dE) was observed for CV, whereas the smallest values of this parameter were noticed for nonstationary processes, i.e. IT2 and IT3. It is a very positive effect because the reduction of MW radiation (in terms of both power and time) was aimed at this programs at the increase of the product quality. Interesting results were also observed for stationary schedules CVMW3 and CVMW5. Taking into account the progress of dE for CVMW1 and CVMW2, it was supposed to be higher for CVMW3 and CVMW5. Surprisingly, the value of dE decreased in these schedules which implies that colour of products depends on the drying time.

4. Conclusions

The continuous application of microwave radiation positively influences the kinetics of convective drying. The higher power of microwaves causes faster drying, shorter duration of the process and lower energy consumption. Unfortunately, microwave-assisted convective drying may negatively affect the quality of products. It was found that application of low power microwaves (100 and 200 W) is not favourable in terms of colour and retention of ascorbic acid. The higher power of continuous microwave enhancement (300 and 500 W) allows preserving both colour and ascorbic acid to a greater degree.

Intermittent microwave-assisted drying can be an attractive alternative for both solely convective and stationary microwave-assisted convective processes. All kinetic and quality parameters attained values similar to those observed for stationary hybrid processes (CVMW). Additionally, it was found that the high-power microwave impulses very positively influence the retention of ascorbic acid.

5. Acknowledgement

6. References

[1] Podsędek, A. Natural antioxidants and antioxidant capacity of Brassica vegetables: A review. LWT – Food Science and Technology 2007, 40, 1–11.

[2] Mujumdar, A.S. Handbook of Industrial Drying; CRC Press: Boca Raton, 2015.

[3] Buena, A. et al. Total and individual carotenoids and phenolic acids content in fresh, refrigerated and processed spinach (*Spinacia oleracea* L.). Food Chememistry 2008, 108, 649–656.

[4] Devahastin, S.; Niamnuy, C. Modelling quality changes of fruits and vegetables during drying: A review. International Journal of Food Science & Technology 2010, 45, 1755–1767.

[5] Musielak, G.; Mierzwa, D.; Kroehnke, J. Food drying enhancement by ultrasound – A review. Trends in Food Science & Technology 2016, 56, 126–141.

[6] Rutkowski, M.; Grzegorczyk, K. Modifications of spectrophotometric methods for antioxidative vitamins determination convenient in analytic practice. Acta Scientiarum Polonorum Technologia Alimentaria 2007, 6 (3), 17–28.

[7] Kahveci, K.; Cihan, A. Transport phenomena during drying of food materials. In Focus on Food Engineering Research and Developments; Pletney, V.N., Ed.; Nova Science Publishers Inc.: New York, 2007; 13–163.

[8] Tapia, M.S.; Alzamora, S.M.; Chirife, J. Effects of Water Activity (aw) on Microbial Stability: As a Hurdle in Food Preservation. In Water Activity in Foods: Fundamentals and Applications; Barbosa Cánovas, G.V., Fontana Jr., A.J., Schmidt, S.J., Labuza, T.P., Eds.; Blackwell Publishing Ltd.: Oxford, 2007; 239–271.

[9] Korus, A. Effect of Preliminary and Technological Treatments on the Content of Chlorophylls and Carotenoids in Kale (*Brassica Oleracea* L. var. *Acephala*). Journal of Food Processing and Preservation 2013, 37, 335–344.

Improvement of pea protein isolate powder properties by agglomeration in a fluidized bed: comparison between binder solutions

Nascimento, R. F.[a]; Andreola, K.[a]; Rosa, J. G.[a,b]; Taranto, O. P.[a*]

[a] School of Chemical Engineering, University of Campinas, Campinas, São Paulo, Brazil
[b] Federal Institute of Espírito Santo, Vila Velha, Espírito Santo, Brazil

*E-mail of the corresponding author: val@feq.unicamp.com

Abstract

This study aimed to compare the agglomeration process of pea protein isolate (PPI) using water and aqueous gum Arabic solution as binder liquids. Drying air temperature and binder flow rate were set at 75 °C and 3.1 mL/min, respectively. Moisture content, mean particle size, wetting time and flowability were analyzed. Using water as binder liquid, the responses were (4.0 ± 0.4)%, 316.13 ± 16.73 µm, 10 s and free flow, respectively. Aqueous gum Arabic solution provided (2.9 ± 0.5)%, 462.67 ± 51.23 µm, 3 s and free flow as responses. Gum Arabic solution showed to be a more promising binder.

Keywords: *Agglomeration; Pulsed fluidized bed; Pea protein isolate; Wetting time; Flowability.*

1. Introduction

The food and pharmaceutical industries use fluid bed agglomeration to improve the physicochemical properties of powders, such as wettability, density, flowability and moisture content.[1,2] The improvement of these properties depends on the operating conditions, the properties of the raw material and the binder solution.[2]

Fluid bed agglomeration consists of atomizing a binder liquid in a fluidized bed of particles and is considered as successive humidification and drying operations.[3] First, the liquid is atomized into the particles generating liquid bridges; then hot air removes water by transforming the liquid bridges into solid bridges to form agglomerates.[4] This is a complex process because it depends not only on the characteristics of the particulate solid, but also on the operational parameters and properties of the binder solution.[5]

The pea exhibits high protein content, ranging from 23 to 33% depending on the species. In addition, it has a good nutritional value, being rich in essential amino acids, vitamins and minerals.[6,7] Pea protein isolate (PPI) has great potential as a substitute for soy protein in industrial processes. However, the powder produced by spray drying is cohesive rather than instantaneous, consisting of fine particles, limiting its use in the industrial process.[8]

The main factors to be considered in the fluidized bed agglomeration process are flow and concentration of the binder solution, atomization pressure, temperature and velocity of fluidization air and bed relative humidity.[5]

Thus, the objective of this work was to analyze the influence of binder solutions on the characteristics of agglomerated PPI in pulsed fluidized bed. At the end of the process, the improvement in the wetting time, flowability and particle size distribution of the agglomerated PPI were analyzed.

2. Materials and Methods

2.1. Materials

Samples containing 0.20 kg of a commercial PPI (CA Gramkow®, Brazil) were used as raw material for all the agglomeration experiments. The PPI contains 6.4% of moisture, above 80.0% of protein, 1.12% of fibers, 7.88% of lipids, 0.28% of carbohydrates and about 4.3% of others constituents. The particle size of raw PPI, measured by laser diffraction and represented by percentiles D10, D50 and D90, were 33.30, 81.0 and 181.92 µm, respectively.

The binder solutions were water and aqueous gum Arabic solution, both at room temperature (± 27 °C). The concentration of aqueous gum Arabic solution was 15% w/w; it was prepared by submitting gum Arabic (Nexira Brasil Comercial, Brazil) and distilled

water to magnetic stirring until complete dissolution of the binder, which was verified visually.

2.2. Equipment and process variables

Experiments were performed in a rotating pulsed fluidized bed (RPFB). Details of this equipment are described by Andreola et al.[9]

The following operational conditions were kept fixed: sample mass at 0.2 kg, nozzle height at 300 mm, pulsation frequency at 4 Hz, atomizing air pressure at 7.0 Psi and binder amount at 76 mL. The fluidizing air velocity, fluidizing air temperature and binder flow rate were set at 0,39 m/s, 75 °C and 3.1 mL/min, respectively. The operating conditions were selected based on preliminary experiments (data not shown) that were performed to obtain an agglomerated product in stable fluidization conditions. Experimental responses express the average of three replicates.

2.3. Moisture content, mean particle size and particle size distribution

The moisture content in the samples was determined by an infrared moisture analyzer (MB200, Ohaus Corporation, USA), that was previously calibrated according to the AOAC standard methodology.[10]

The mean particle diameters and particle size distributions of raw and agglomerated PPI were measured by Mastersize S (Malvern Instruments, Malvern, UK).

2.5. Wetting time and flowability

Wetting time was measured as the time required for 3 g of powder to disappear from the surface of water (80 mL at 27 °C) when the slider that separates the powder and liquid sections were removed.[11] The Hausner index (*HR*) was calculated from the bulk (ρ_b) and tapped (ρ_t) densities of the raw and agglomerated powder, as shown in Eq. (1).

$$HR = \frac{\rho_t}{\rho_b} \qquad\qquad (1)$$

Classification of powder flowability based on the *HR* value is given in Table 1.[12]

Table 1. Classification of powder flowability based on the Hausner index (HR)

HR	Flowability
<1.2	Free
1.2-1.4	Intermediate
>1.4	Non-free

3. Results and discussion

3.1. Raw material and binders properties

Commercial PPI shows density and mean diameter of 1.2659 ± 0.0035 g/cm^3 and 81.00 ± 0.61 μm, respectively, and its fluidization behavior could be classified as pertaining to Geldart group A. Wetting time was over 300 s and *HR* was 1.3, classifying the flowability as intermediate. The large particle distribution is the main factor responsible for high wetting time and low flowability, because it provides more compacted bed, decreasing the porosity.[2,9,12]

Density, superficial tension and rheology of both liquid binders must be considered. Water presents density of 1.00 g/cm^3, superficial tension of 7.2 x 10^6 mN/m and Newtonian behavior; while gum Arabic solution presents 1.0522 ± 0.0002; 47.35 ± 0.69 and pseudoplastic behavior, respectively.

3.2. Process responses

3.2.1. Moisture content

In agglomeration using water as liquid binder, moisture content reaches $(4.0 \pm 0.4)\%$, while with the use of gum Arabic solution, moisture content was $(2.9 \pm 0.5)\%$, after 24.5 min of atomization and 10 min of drying. For both cases, this parameter was at least 2% lower, getting at 3.5%, compared to the raw material.

Low moisture contents are important mainly for material storage. Temperature at 75 °C is enough to promote water evaporation of the system, making the product drier. Binder flow rate at 3.1 mL/min also provide this type of product, whereas the binder wets the particles less and, when associated with temperature, its evaporation is more effective.[2,9]

Fig. 1. shows the relative humidity at bed exit. Although the same temperatures and flow rates were used for both conditions presented, the environment inside the bed remained moister, at least 20% higher, when the water was used as a binder. The fact that the gum Arabic solution has 15% solids, can produce this effect, since there is less water available.
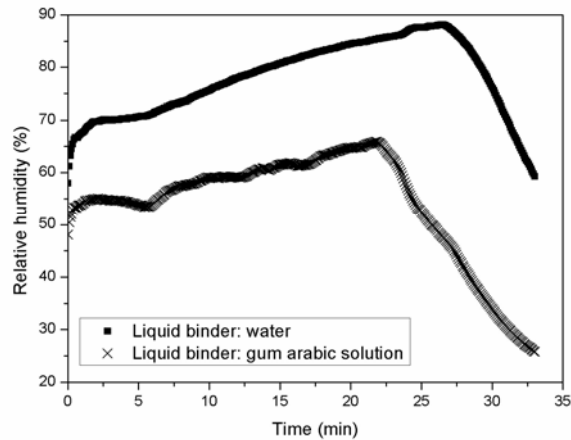
Fig. 1. Relative humidity at bed exit in relation to time.

3.2.2. Mean particle size and particle size distribution

Both liquid binders afforded agglomerated PPI with diameter larger than the initial size of raw PPI. To water as binder, particles increased 3.8 times, reaching 316.1 ± 16.7 µm, and when gum Arabic solution was used, the particle size reached 462.7 ± 51.3 µm, corresponding to a growth of 5.7 times. We also detected several particles with diameter higher than 600 µm. The particle size distribution to raw and agglomerated PPI is presented in Fig. 2.
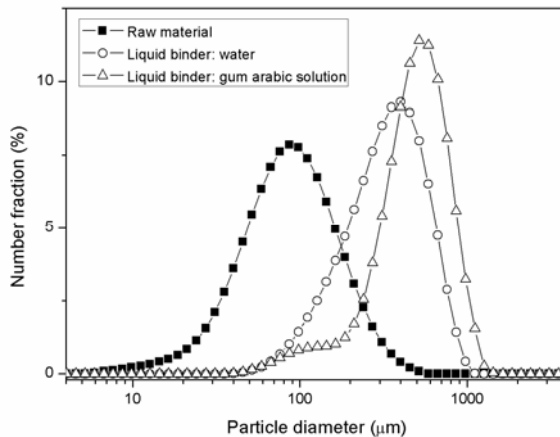
Fig. 2. Particle size distribution of raw and agglomerated PPI.

Agglomerated product also presented fines with diameter of less than 50 µm, which represented approximately 19% and 24% to agglomeration process with water and gum

Arabic solution, respectively. These fines correspond to non-agglomerated particles and may originate from breaking of the agglomerates by friction within the moving bed.

3.3. Wetting time

Compared with raw PPI, agglomerated PPI underwent faster wetting, even though the powders were not completely immersed into water. Agglomerated PPI achieved complete wetting in less than 10 s, to agglomeration with water, and 3 s, to gum Arabic solution which attests to its greater capacity to absorb moisture. It represents a decrease of 97% and 99% in wetting time, respectively.

The presence of fine particles allows for a more compact powder during storage, i. e., the smaller particles can penetrate into the spaces between the larger particles, so the product occupies less space.[11,13]

3.4. Flowability

Agglomeration process with water furnished bed density (ρ_b) of 0.2579 ± 0.0058 g/cm^3, and compact bed density (ρ_t) of 0.2970 ± 0.0070 g/cm^3. Already for agglomeration for gum Arabic solution, $\rho_b = 0.1640 \pm 0.0284$ g/cm^3 and $\rho_t = 0.1939 \pm 0.0284$ g/cm^3. The *HR* values obtained for agglomerated PPI were 1.15 and 1.18, classifying the product as free. Raw PPI consists of fine particles, which may confer the material a strong cohesive behavior, whereas agglomeration improves PPI flowability. Although the flowability of agglomerated PPI is not yet ideal, this product exhibited significantly better handling properties than raw PPI.

4. Conclusions

The particle agglomeration of PPI occurs due to the pulverization of liquid binder on the surfaces of the particles, resulting in a wetted sticky surface and subsequent particle coalescence. On particle drying, the agglomerated structure consolidates, leading to particle enlargement.

Agglomeration of PPI using gum Arabic solution produced larger granules with high flowability and lower cohesiveness when compared to agglomeration with water and spray dried raw material. Additionally, size enlargement also resulted in an improvement of instant properties that was characterized by the higher wettability of the granules.

5. Nomenclature

Greek letters

ρ	density	gcm^{-3}

Subscripts

b	bulk
t	tapped

6. References

[1] Avilés-Avilés, C., Dumoulin, E., Turchiuli C. Fluidized bed agglomeration of particles with different glass transition temperatures. Powder Technology 2015, 270, 445–452.

[2] Machado, V.G., Hirata, T.A.M., Menegalli, F.C. Agglomeration of soy protein isolate in a pulsed fluidized bed: experimental study and process optimization. Powder Technology 2014, 254, 248–255.

[3] Pont, V.; Saleh, K.; Steinmetz, D.; Hémati, M. Influence of the physicochemical properties on the growth of solid particles by granulation in fluidized bed. Powder Technology 2001, 120, 97–104.

[4] Iveson, S.M.; Litster, J.D.; Hapgood, K.; Ennis, B.J. Nucleation, growth and breakage phenomena in agitated wet granulation processes: a review. Powder Technology 2001, 117, 3–39.

[5] Dacanal, G.C., Menegalli, F.C. Selection of operational parameters for the production of instant soy protein isolate by pulsed fluid bed agglomeration. Powder Technology 2010, 203, 565–573.

[6] Lam, A.C.Y., Karaca, A.C., Tyler, R.T., Nickerson, M.T. Pea protein isolate: structure, extraction, and functionality. Food Reviews International 2018, 34, 126–147.

[7] Muneer, F.; Johansson, E.; Hedenqvist, M.S.; Plivelic, T.S.; Markedal, K.E.; Petersen, I.L.; Sørensen, J.C.; Kuktaite, R. The impacte of newly produced protein and dietary fiber rich fractions of yellow pea (*Pisum sativum* L.) on the structure and mechanical properties of pasta-like sheets. Food Research International 2018, 106, 607–618.

[8] Boye, J.I., Aksay, S., Roufik, S., Ribéreau, S., Mondor, M., Farnworth, E., Rajamohamed, S.H. Comparison of the functional properties of pea, chickpea and lentil protein concentrates processed using ultrafiltration and isoelectric precipitation techniques. Food Research International 2010, 43, 537–546.

[9] Andreola, K., Silva, C.A.M., Taranto, O.P. Agglomeration and drying of rice protein concentrate in a rotating pulsed fluidized bed: in-line monitoring of particle size. Paper presented at the International Drying Symposium 2016.

[10] Official Methods of Analysis of the AOAC. Association of Official Analytical Chemists Inc, 1995.

[11] Hogekamp, S., Schubert, H. Rehydration of food powders. Food Science Technology International 2003, 9, 223–235.

[12] Turchiuli, C., Eloualia, Z., El Mansouri, N., Dumoulin, E. Fluidised bed agglomeration: agglomerates shape and end-use properties. Powder Technology 2005, 157, 168-175.

[13] Tonon, R.V., Brabet, C., Hubinger, M.D. Influence of process conditions on the physicochemical properties of acai (*Euterpe oleraceae* Mart.) powder produced by spray drying. Journal of Food Engineering 2008, 88, 411–418.

Influence of drying conditions on the acacia gum particle growth in fluidized bed agglomeration: in-line monitoring of particle size

Rosa, J. G.[a,b*], Nascimento, R. F.[a], Andreola, K.[a] and Taranto, O. P.[a]
[a]School of Chemical Engineering, University of Campinas, Campinas, São Paulo, Brazil
[b]Federal Institute of Espírito Santo, campus Vila Velha, Vila Velha, Espírito Santo, Brazil

*E-mail of the corresponding author: jugrosa@gmail.com

Abstract

Acacia gum is an important food emulsifier that presents poor instant properties which can be improved by fluidized bed agglomeration. This study investigated the influence of drying conditions on particle growth kinetics using an in-line particle size monitoring by spatial filter velocimetry. The drying conditions varied according to the binder flow rate and the fluidizing air temperature. The particle growth kinectis showed drying conditions dependence. At mild drying conditions the growth rate and the process yield were higher. The in-line particle size monitoring was useful to observe the influence of the drying conditions on the growth kinetics.

Keywords: fluidized bed agglomeration; acacia gum; particle growth kinectis; in-line monitoring.

1. Introduction

Acacia gum is a food additive that has several functions and it is mostly used as an emulsifier, for its effectiveness as a long time stabilizer on oil in water emulsions.[1] This gum can be used as a fiber food enricher and as a sucrose replacer, in food formulations, as it causes equivalent sensation in the mouth.[2,3] In addition, it stands out in the food additives market because it is natural, of vegetable origin and does not undergo chemical modifications.[4] The powdered acacia gum is a powder with fine particles, which is difficult to handle, and shows poor dispersion properties. However, the agglomeration process can improve its quality.[5]

The particles agglomeration process is used at the pharmaceutical and food industry to improve the characteristics of its powdered products and is often performed in fluidized beds since this equipment provides high rates of heat transfer.[6] Fluidized bed agglomeration process involves the particles fluidization by hot air flow and liquid binder atomization onto these particles. The hot air flow is also responsible for the binder evaporation, causing the particles drying and granules to consolidate. The fluidized bed agglomeration is a complex process, that can be influenced by several process parameters like the binder kind and flow, the fluidizing air temperature, and the binder atomization pressure.[7,8]

The agglomeration kinetics knowledge is important since the particle size growth is the goal of agglomeration processes. The spatial filter velocimetry (SFV) is an in-line particle size monitoring that provides the granule growth and breakage as a function of granulation time by the measurement of the particle chord lengths. This technique is a new method and has been used successfully in recent studies.[9,10,11] The SFV particle size monitoring can improve the knowledge about what favors particle size increase or its breakage providing important information to the granulation kinetics study.

There are not many experimental studies about food agglomeration kinetics. This work presents a study about powdered acacia gum agglomeration kinetics. The particle growth rate was monitored by in-line particle size monitoring using a spatial filter velocimetry probe for differents drying conditions.

2. Materials and Methods

2.1. Materials

Spray dried acacia gum (Spraygum BB - Nexira Brasil Comercial) was used as raw material for the agglomeration experiments. The acacia gum wet basis moisture content ($X_{w.b.}$) is less than 10.0%. The binder solution was distilled water at room temperature ($\pm$ 27 ºC).

2.2. Characterization of raw and agglomerated acacia gum

Characterization of raw and agglomerated acacia gum were done based on the median particle size (*D50*), powder flow characteristics, wetting time (t_w) and $X_{w.b.}$. The raw material

particle size was measured by *SFV* probe as described above and also by laser diffraction (Mastersizer 3000, MAZ3000 Malvern Instruments, Malvern, UK). Powder flow characteristics were determined by the Carr index (*ICarr*) values, as described by Turchiuli et al.[12] The *tw*, was the time required for the complete wetting and immersion of 3.0 g of the sample in 70 ml of water at room temperature.[13] $X_{w.b.}$ was measured for the raw material, at the end of the bind atomization and at the end of the drying using a halogen moisture analyzer (HR83, Mettler Toledo).

2.3. Equipment and agglomeration process

The agglomeration experiments were run in a lab-scale fluidized bed. The fluidized bed chamber had a conical base constructed from transparent acrylic Plexiglas®. The bed pressure drop, the air temperature, and the air relative humidity were monitored and recorded by a data acquisition system and processed in the LabVIEW 8.6TM software. Details of the equipment and the data acquisition system are described by Andreola et al.[14] However, in this study, the equipment was operated without air pulsation.

Three different agglomeration conditions were performed, in triplicate, to evaluate the influence of drying conditions on growth kinetics and particle growth rate of powered acacia gum. The process parameters that varied were the binder flow rate (*Q*) and fluidizing air temperature (*T_air*) in the following way: condition 1 (E1), 1.5 mL/min and 85 ºC; condition 2 (E2), 2.3 mL/min and 75 ºC and condition 3 (E3), 3.0 and 65 ºC. The sample mass, initial fluidizing air velocity, the volume of binder, atomization air pressure and atomization nozzle height were kept constant at 0.4 kg, 0.28 m/s, 80 mL, 6.7 psi and 0.35 m, respectively. The increase in fluidizing air velocity was necessary to maintain a stable fluidization, it was increased (step 0.03 m/s) every 5 min until 0.43 m/s.

The process time was different once the binder volume was fixed and the process was carried out until the agglomerated moisture content reached a lower or equal value than that one of the raw material. The E1 had not a drying period and E2 and E3 had an 8 minutes drying period time.

2.4. Process yield

The process yield (*Yld, %*) was determined based on the initial sample mass ($m_{initial}$) and the final product (m_{final}) by the Eq. 1. The m_{final} was obtained discounting particles larger than 850 µm, separated by sieving, from the product mass remained at the end of the experiments. The mean process yield, for each experimental condition, was calculated and a statistical analysis was made by Tukey's test, at a confidence level of 90% (p <0.10).

$$Y = \frac{m_f}{m_i}.100 \qquad (1)$$

2.5. In-line particle size measurement and granule growth rate

The in-line particle size was monitored by Parsum IPP70 probe (Chemnitz, Germany) that employes the SFV principle to measure the "chord" (size) of the particles. Details of the equipment, its accessories and methodology were described by Silva and Taranto.[10] For further analysis of the growth rate of the particle time dependence, an appropriate software, Inline Particle Probe 7.14, obtained the particle size data and sent it to LabVIEWTM 8.6 software via OPC server protocol, this procedure was developed by Silva and Taranto.[10] This system record the particle size and size distribution every 5.12 seconds. The ring buffer size used in the Parsum measurements, 5000 particles, was chosen according to preliminary tests performed (not shown). The median particle size in volume (*D50v*) was evaluated and the last ten measurements for each run were used to calculate the mean *D50v* of the agglomerated. The agglomerated *D50v* for the three experimental condition was compared by Tukey's test, at a confidence level of 90% (p < 0.10).

The granule growth rate (*R*) was calculated as defined by (Eq 2.).[15] Its value was calculated for each period of 1.7 minutes, that means that d_i was the D50v at the initial time and d_f was the D50v reported approximately 1.7 minutes after the d_i report.

$$R(\%) = \frac{(d_f - d_i)}{d_i} \cdot 100 \qquad (2)$$

3. Results and discussion

3.1. Characterization of raw and agglomerated acacia gum

The laser diffraction measurements for the raw material were *D10*: 21.9 ± 0.2 μm, *D50*: 65.2 ± 1.0 μm and *D90*: 143.6 ± 2.0 μm. The values of *D50v* measured by *SFV* probe before the spray phase (approximately 111.5 μm) were higher than those obtained by laser diffraction, once the median size obtained by laser diffraction is close to the *SFV* probe measurement limit, i. e., 50 μm. However, the values of *D90v* measured by *SFV* probe (approximately 154.0 μm) were close to the off-line measurement, indicating that the probe measurements are reliable.

The final acacia gum powder *D50v* increased for all experimental conditions (Table 1). The largest increase in particle size occurred at mild drying conditions (E3). At more intense drying conditions the final particle size was smaller and the *D50v* was statistically equal for the conditions E1 and E2. Similar result was observed by Hirata et al.[16] for agglomeration of similar material using water as a binder. At mild drying conditions, the adhesion among particles is favored by the more wet and sticky surface. Milder conditions also favored higher process yield (Table 1). Under drier conditions (E1) the particle size was smaller and the process time is longer which resulted in larger material elutriation. This was also observed

during fluid bed agglomeration of rice protein concentrate, very fine particles, by Andreola et al.[14]

Table 1: Experimental conditions and their results.

Conditions	Q[1]	Tair[2]	D50v[3]	Y[4]	h_{out}[5]	Flowability
Raw material	-	-	65.18±1.0			moderate
E1	1,5	85	270.7±19.6[a]	50.4±6.0[a]	34.9±2.7	moderate
E2	2,3	75	275.3±8.2[a]	61.4±6.0[a,b]	47.0±6.4	moderate
E3	3,0	65	285.7±13.7[b]	64.3±6.0[b]	53.4±8.2	moderate

[1]Binder flow rate (mL/min); [2]Fluidizing air temperature (ºC); [3] Median particle size in volume (μm); [4]Process yield (%) and [5]Mean relative humidity of the warm–moist air flowing out of the bed (%).

The agglomeration process presented different results concerning the handling properties, wetting time and flowability. All agglomeration conditions improved the acacia gum instant properties. The raw material did not get completely wetted even after 600 s, on the other hand the agglomerated were completely wetted in less than 5 s. Regarding to the flowability, agglomerated acacia gum was similar to the raw material (Table1).

3.2. Particle growth rate

The triplicate of the granule growth kinetics for the different experimental conditions is presented in Fig. 1, it shows that there was reproducibility of the particle growth behavior for the process. Although the final particle size was similar for the three experimental condition, the particle growth behavior was different.

At condition E1, with more intense drying condition, the particle growth was almost continuous (Fig. 1(a)). However, the particle size enlargement was slower compared to the other two conditions (Fig. 1 (d)). At that condition, binder availability is smaller and consequently less liquid bridges were formed between the particles.

The particle growth rate (*R*) for the three experimental is presented in Fig. 2. The particle growth rate oscillated during the process showing that the particle size growth results from positive a balance from agglomeration and break.

The R for the E1 condition confirms a slower size enlargement presented since it presents the lowest mean value (Fig. 2). It oscillated around 2% during the process and presented few negative values that indicates an absence of particle breaking by attrition and collision. This is observed because in that condition a constant wetting occurred causing a continuous increasing of the particle size. In that condition, the fluidization was more vigorous which associated with the highest temperature and time of process could have contributed to form stronger and larger granules as observed by Andreola et al.[14]
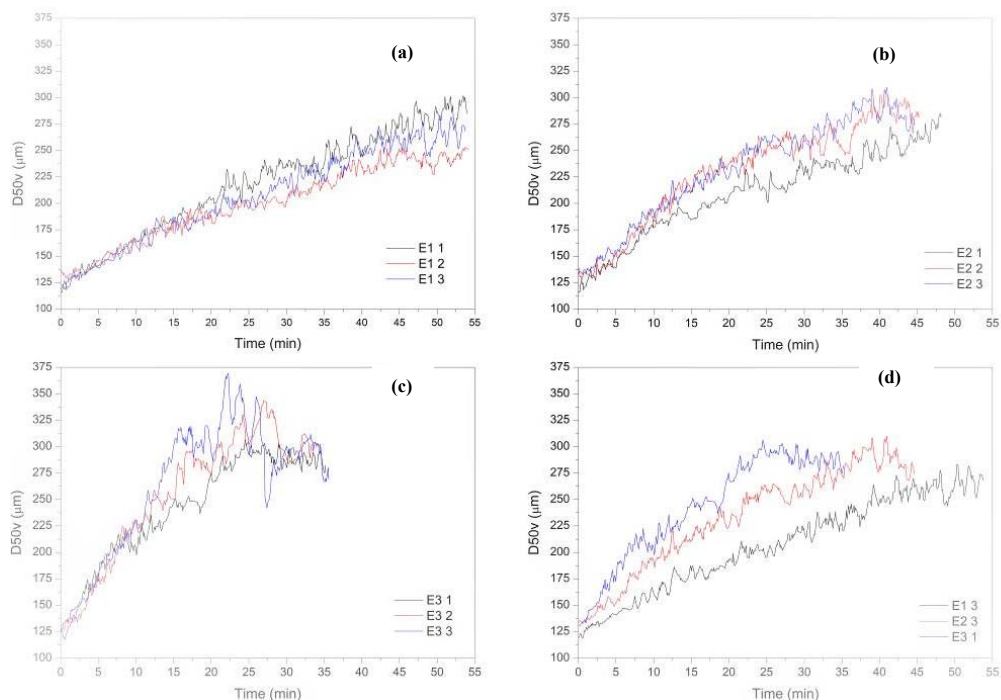
Figure 1: In-line D50v triplicate data for (a) E1, (b) E2, (c) E3. Comparative in-line D50v data for E1, E2 and E3 (d).

The experimental condition E2 presented a larger particle growth at the beginning of the process that decreased with the binder spraying time (Fig. 1(b)). In that condition, the particle growth rate (Fig. 2) presented a smaller oscillation, compared to the other conditions, and a downward trajectory with the progress of the process. The particle growth rate presents some negative values, especially in the drying period, indicating that there were some breaking of particles by attrition and collision.

The milder drying condition E3 presented the higher particle growth at the beginning (R > 10%, Fig. 2) that results in the largest particle size recorded (D50v > 350 µm). However a decreasing at the D50v during the drying period was observed (Fig. 1(c)). The R for condition E3 had a higher oscillation and more expressive negative value in comparison to the condition E2. It is related to the fact that the wetter and larger granules are more susceptible to the broken down by attrition.[17] Under these conditions, the worst fluidization regime was observed due to the formation of large agglomerates, which may also have impaired the consolidation of the granules. In spite of the breaks, the final particle size was the largest of the three conditions.
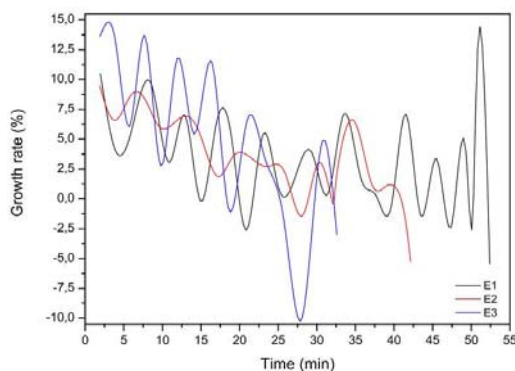
Figure 2: Particle growth rate for the different experimental conditions.

4. Conclusion

The fluidized bed agglomeration process improved the acacia gum powder instant properties. The in-line SFV particle size measurement made it possible to observe the growth rate of the particle. The operating conditions influenced both the particle final D50v and the behavior of the granule growth kinetics. The milder drying condition provided larger granules and higher yield in the process. However, it is interesting to analyze an intermediate condition between E2 and E3 for the production of larger and more stable granules.

5. References

[1] Dror, Y; Cohen, Y; Yerushalmi-Rozen R. Structure of Gum Arabic in Aqueous Solution. Journal of Polymer Science: Part B: Polymer Physics 2006, 44, 3265–3271.

[2] Phillips, G.O.; Ogasawara, T.; Ushida, K. The regulatory and scientific approach to defining gum arabic (Acacia senegal and Acacia seyal) as a dietary fibre. Food Hydrocolloids 2008, 22, 24–35.

[3] Baray, S. Acacia Gum. In: Cho, S. S.; Samuel, P. Fiber Ingredients - Food Applications and Health Benefits. [S.l.]: CRC Press, 2009, 121–134.

[4] Islam, A.M.; Phillips, G.O.; Sljivo, A.; Snowden, M. J.; Williams, M. A. A review of recent developments on the regulatory, structural and functional aspects of gum arabic. Food Hydrocolloids 1997, 11 (4), 493–505.

[5] Fuchs, M.; Turchiuli, C.; Bohin, M.; Cuvelier, M.E.; Ordonnaud, C.; Peyrat-Maillar, M.N.; Dumoulin, E. Encapsulation of oil in powder using spray drying and fluidised bed agglomeration. Journal of Food Engineering 2006, 75, 27–35.

[6] Kunii, D.; Levenspiel, O. Fluidization Engineering. 2.ed. New York: John Wiley, 1991, 489 p.

[7] Hemati, H., Cherif, R., Saleh, K., Pont, V. Fluidized bed coating and granulation: influence of process-related variables and physicochemical properties on the growth kinetics. Powder Technology 2003, 130, 18–34.

[8] Tan, H.S.; Salman, A.D.; Hounslow, M.J. Kinetics of fluidised bed melt granulation I: the effect of process variables. Chemical Engineering Science 2006, 61, 1585–1601.

[9] Wiegel, D.; Eckardt, G.; Priese, F.; Wolf, B. In-line particle size measurement and agglomeration detection of pellet fluidized bed coating by Spatial Filter Velocimetry. Powder Technology 2016, 301, 261–267.

[10] Silva, C.A.M; Taranto, O.P. Real-time monitoring of gas–solid fluidized-bed granulation and coating process: evolution of particle size, fluidization regime transitions, and psychometric parameters, Drying Technology 2015, 33, 1929–1948.

[11] Burggraeve, A.; Kerkhof, V.D.; Hellings, M.; Remon J.P., Vervaet; De Beer, T. Evaluation of in-line spatial filter velocimetry as PAT monitoring tool for particle growth during fluid bed granulation. European Journal of Pharmaceutics and Biopharmaceutics 2010, 76, 138–146.

[12] Turchiuli, C.; Eloualia, Z.; Mansouri, N.; Dumoulin, E. Fluidised bed agglomeration: agglomerates shape and end-use properties. Powder Technology 2005, 157, 168–175.

[13] Hogekamp, S.; Schubert, H. Rehydration of food powders. Food Science and Technology International 2003, 9, 223–235.

[14] Andreola, K.; Silva, C.A.M.; Taranto, O.P. Production of Instant Rice Protein Concentrate by Rotating Pulsed Fluidized Bed Agglomeration using Hydrolyzed Collagen Solution as Binder. Chemival Engineering Transactions 2016, 49, 115–120.

[15] Hu, X.; Cunningham, J.C.; Winstead, D. Study growth kinetics in fluidized bed granulation with at-line FBRM. International Journal of Pharmaceutics 2008, 347, 54–61.

[16] Hirata, T.A.M; Dacanal, G.C.; Menegalli, F.C. Effect of operational conditions on the properties of pectin powder agglomerated in pulsed fluid bed. Powder technology 2013, 245, 174–181.

[17] Reynolds, G.K., Fu, J.S., Cheong, Y.S., Hounslow, M.J., Salman, A.D. Breakage in granulation: a review. Int. J. Pharm. 200, 60, 3969–3992.

Agglomeration of Hydrolyzed Collagen with Blackberry Pulp in a Fluidized Bed

Viegas, T. R. [a*]; Taranto, O. P. [a]

[a] School of Chemical Engineering. University of Campinas, Campinas, Brazil

*E-mail of the corresponding author: thaynaviegas@gmail.com

Abstract

Hydrolyzed collagen (HC) is a fine powder applied in the pharmaceutical and food industries which has shown good results in the treatment of diseases related to bones, skin and joints. In this study, HC particles were agglomerated in order to increase particle size, optimizing its use as a food ingredient, its handling and its storage. Agglomeration is a process that not only enlarge the size of fine particles, but also improves its properties, such as instantanization time and flowability. The aim of this work was the agglomeration of HC in a fluidized bed having blackberry pulp as a liquid binder. A full factorial design 2^2 was used to study the effect of the temperature of the fluidizing air (60, 70, 80ºC) and the flow rate of the liquid binder (0.8, 1.2, 1.6 mL/min) on the process yield, mean particle size, water activity and total anthocyanins content. It was observed that anthocyanins content from the blackberry pulp had higher values with lower temperatures. Water activity had lower values with higher temperatures, but in all conditions, it was lower than 0.6. The enlargement of the granules was observed in all conditions studied, increasing up to 275%. Process yield varied from 67,9 to 80,0%. In all conditions, the instantanization time and flowability improved compared to hydrolyzed collagen before agglomeration.

Keywords: hydrolyzed collagen; agglomeration; granulation; fluidized bed; blackberry pulp

1. Introduction

Chronic non-communicable diseases (NCD) are responsible for almost 60% of the global mortality rate [1] and for 72% of the Brazilian mortality rate [2]. Chronic respiratory diseases, cardiovascular diseases and diabetes are examples of NCD, caused mainly by poor diet and physical inactivity. To change that, it is essential to increase the consumption of vegetables, fruits, cereals and replace foods rich in sodium or simple carbohydrates [2]. To contribute to the reversal of such a scenario, this work presents a feasible production method of agglomerated HC as an instant functional food and protein supplement rich in anthocyanins.

Agglomeration, also known as granulation, increases the size of particles, which then are called granules or agglomerates. This process is applied in the chemical, pharmaceutical and food industries to improve particle handling, storage and transportation, as well as particles' properties, such as flowability and instantanization time [3]. Regarding the food industry in particular, agglomeration enables the granules to achieve specific properties and size intervals [4].

The agglomeration process using a fluidized bed, although complex, shows many advantages, such as good heat and mass exchange and the performing of all steps of a given process in the same equipment [5]. The agglomeration process occurs when the particles are fluidized and dried by the heated air which is admitted through the bottom of the bed, while an atomization nozzle humidifies the particles with a binder.

This work aims to find the most suitable condition (binder flow rate and fluidizing air temperature) for the agglomeration of HC in a fluidized bed, using blackberry pulp as a binder in order to increase the particles' sizes, improve the particles' properties and add the nutritional benefits of blackberry pulp to the agglomerates. Collagen has been studied for over a century and its demand in the market only increases [6], because it is a protein product with amino acids that are essential to the human diet [7], which shows positive results in the treatment of diseases related to the bones, skin and joints [8, 9, 10]. Blackberry pulp, on the other hand, is rich in vitamins, iron and anthocyanins, which helps in the prevention of degenerative diseases such as cancer and diabetes [11].

2. Materials and Methods

2.1 Equipment and process variables

The lab-scale fluid bed (Fig. 1) used to perform the experiments has a cylindrical Plexiglas base and column (11). On top, there is a cyclone (13) to collect the elutriated fine particles. In the entrance of the bed, a perforated plate (10) distributes the air uniformly. The inlet air is supplied by a 7.5 HP WEG (2) air blower, delivered to the system by a 2" internal diameter galvanized steel pipe, and then passes through a bed of silica gel (5). The blower is connected

to a frequency inverter (2a) (WEG CFW 08). The air velocity was determined by a hot wire anemometer (IMPAC, Delta Ohm, HD2903TC2.2) (4).
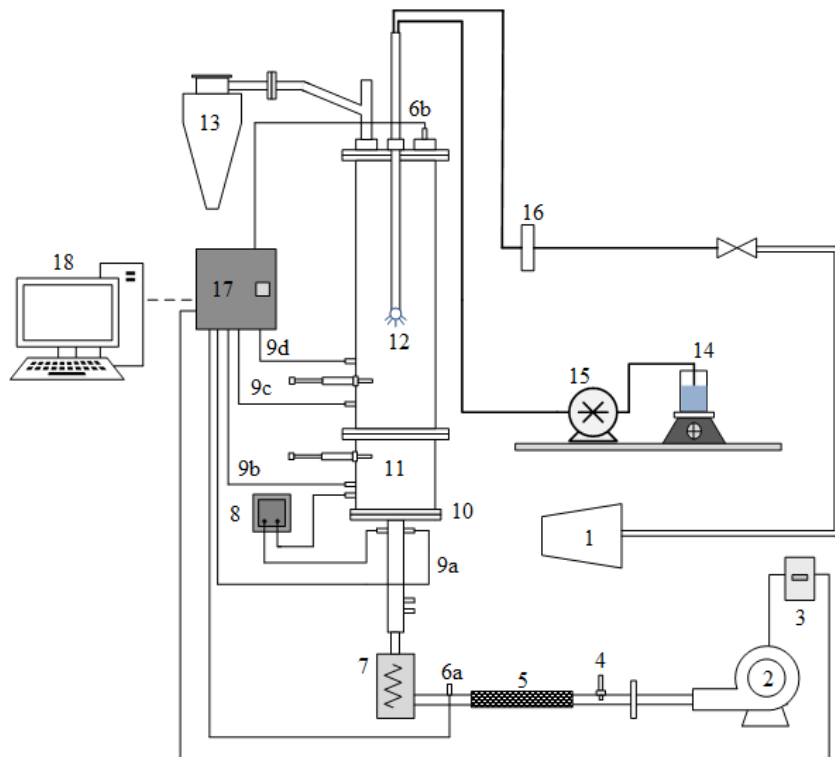
Fig 1. Experimental System

The air temperature in the plenum chamber was adjusted by a set of electrical resistors (7) controlled by a PID regulator (Novus, N1100). Pt-100 Thermoresistances (Novus, Ø 3.0 mm x 100 mm) measure the temperature of the system in the plenum chamber (9a) and the other three points (9b, 9c and 9d) the column. Two sensors (6a and 6b) (RHT-XS, Novus) provide the values of relative humidity and dry bulb temperature at the input (before the resistors) and in the fluid bed output, controlled by a PID regulator (Novus, N1200). The pressure drop in the bed is provided by a differential transducer (Cole Parmer, XLDP) (8).

A peristaltic pump (15) (Cole Parmer, 7780-60, Masterflex L / S) carries blackberry pulp (14) used as a binder in the granulation process. A double fluid type spray nozzle (Spraying Systems, SU12A) produces a cone-shaped spray of droplets. The atomizing pressure for obtaining the droplets is provided by a compressor (MSV 40 Max, 10 horsepower) (1) and

regulated by a Norgren pressure regulator. This compressed air is filtered (16) (Parker, Hannifin Ltd.) before being used in the atomization.

The pressure, temperature and humidity sensors are connected to a computer, by a data acquisition system, which consists of a NI cDAQ-9172 (National Instrument) (17) board that collects the data at a defined sampling rate. LabVIEW 8.6TM (Virtual Instrument Engineering Workbench) software, by means of virtual instruments (VI), makes the interface between the process and the data acquisition board. The program was installed on an Intel® Core i5 computer with 4.0 GB of RAM (18).

2.2 Water Activity

The water activity was measured by AQUALAB S3TE.

2.3 Particle Diameter

The HC particles were observed using a digital microscope (Dino-Lite AM4515ZT) after being dispersed on several glass slides to obtain at least 500 particles. The images were analyzed using the software IMAGE J v1.50i (National Institutes of Health, USA), allowing the calculation of the particles mean diameters[12].

2.4 Anthocyanins Content

The anthocyanins content was determined using the differential pH method [13].

2.5 Process Yield

The process yield was calculated by the ratio of the mass of HC fed per the final mass in the fluid bed.

2.6 Instantanization time

The instantanization time was considered the time required for 3 g of the sample to disappear from the water surface (60 mL at 27 °C), using an apparatus described by [14].

2.7 Flowability

The flowability of raw and granulated HC was obtained using the Carr index (Table 1). The powder is submitted to 500, 750, or 1250 taps in the equipment Autotap Tap Density Analyzer (DAT-4, Quantachrome instruments®), following the standard 616 of the North American Pharmacopeia [15].

Table 1. Classification of powder flowability based on the Carr index

Icarr (%)	Flowability
< 15	Very Good
15-20	Good
20-35	Fair
35-45	Bad
> 45	Very Bad

2.8 Moisture Content

The humidity was determined by a Moisture Analyzer with halogen light heating (HR83, Mettler Toledo).

3. Results and Discussion

The yield was higher with the lowest binder flow rate and with the maximum or minimum temperature (T_f) used, resulting in a surface plot with significant curvature (Fig 2-a). The biggest particles (275% bigger than raw HC) occurred with lower binder flow rate and temperature (Fig. 2-b), since in this condition the moisture content was lower. Partial defluidization was observed using higher values of binder flow rate, reducing the impact between particles and, therefore, their size, as also observed by [16]. As for the moisture content (Fig. 2-c), lower binder flow rate and higher temperature resulted in a minimum value of moisture content, as expected and observed by [16]. However, even at higher temperature, the binder flow rate had more impact in the moisture content, since higher values of Q_{lig} resulted in a moister agglomerated HC. The AT (dry basis) was higher when the temperature was minimum (Fig. 2-d), as the degradation of anthocyanins was minimum in this case.

Water activity was lower than raw HC and higher than Commercial HC (Table 2), and since all the values were aw<0.6, microbial growth will not happen in the powder [17]. The instantanization time of agglomerated HC reduced considerably when compared to raw HC and Commercial HC because of the size and morphological changes in the particles, as observed by [17]. Therefore, the bigger the HC particles, the faster was the IT. Moreover, the flowability of agglomerated HC improved from Fair (raw HC) to Good or Very Good.
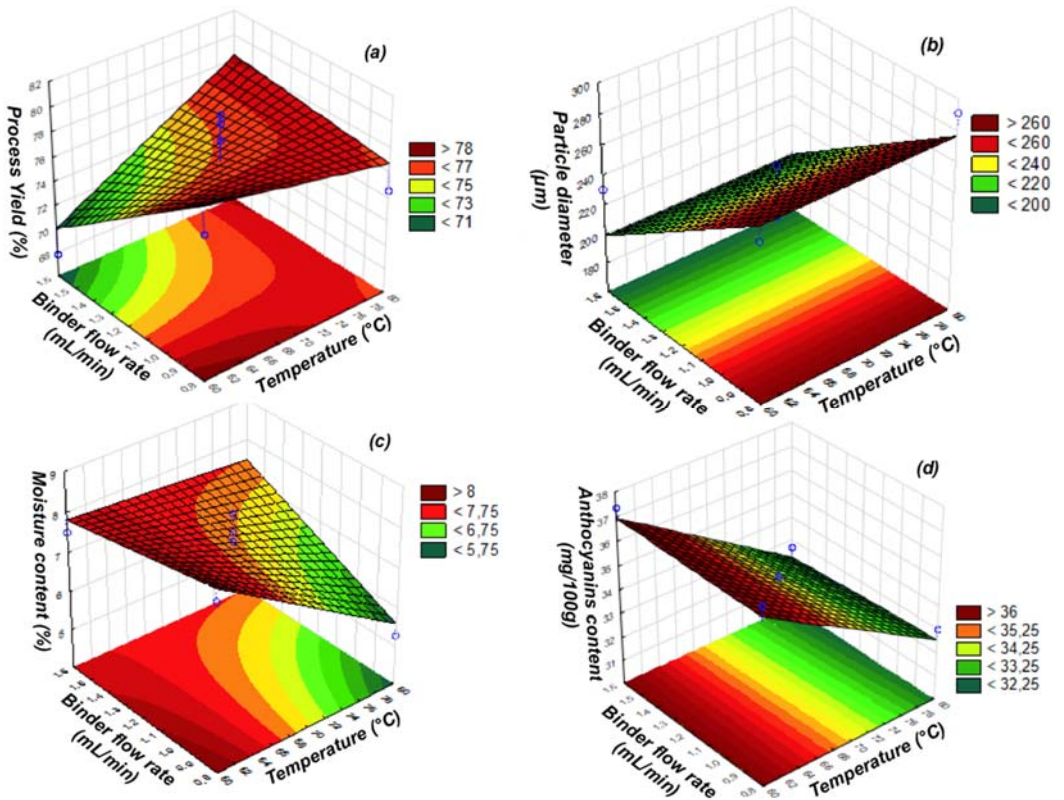
Fig 2. Surface plot of Process Yield, Particle diameter, Moisture content and Anthocyanins content versus Temperature and Binder flow rate.

Table 2. Results of the experimental design (nozzle height: 300 mm, mass of sample: 500g).

Experimental Run	T_f (°C)	Q_{lig} (mL/min)	Yld (%)	Mst (% d.b.)	dp_m (µm)	AT (mg/100g)	IT (s)	aw	Icarr (%)
HC	-	-	-	7.45	96.96	-	170	0.490	22.18
1	80 (1)	1.6 (1)	76.2	7.17	172.03	32.67	2.2	0.396	17.39
2	80 (1)	0.8 (-1)	74.6	5.27	291.23	33.04	1.65	0.386	14.29
3	70 (0)	1.2 (0)	78	7.71	218.46	34.91	2.2	0.425	13.91
4	70 (0)	1.2 (0)	79.3	7.47	251.64	33.55	2.15	0.420	16.67
5	70 (0)	1.2 (0)	80	8.17	233.14	33.66	2.1	0.423	16.95
6	60 (-1)	1.6 (1)	67.9	7.5	230.62	37.39	2.25	0.437	12.39
7	60 (-1)	0.8 (-1)	77.8	8.24	266.64	37.31	1.85	0.430	13.51
Commercial HC[1]	-	-	-	8.15	198.2	-	9	0.404	16.52

[1] Commercial Agglomerated HC already sold in market (Commercial HC - GELITA)

4. Conclusions

The central points (tests 4, 5 and 6) presented the best overall results: they presented bigger particles than the ones of Commercial HC, an increase of more than 200% compared to raw HC. In those tests, the process yield was, in average, 79.1%. The moisture content values had an average of 7.78%, lower than that of the Commercial HC. The AT content values were low in all the tests and further studies are needed to reduce the degradation of anthocyanins by light and high temperature. The water activity values were in a range that assures product safety for all the tests and the instantanization time decreased in relation to raw HC and Commercial HC. Thus, we produced a powder larger in size, with adequate moisture and process yield, which can be commercialized or used as an ingredient rich in anthocyanins.

5. Nomenclature

T_f	Fluidizing temperature	°C
Q_{lig}	length co-ordinate	M
Yld	Yield	%
Mst	Moisture content	% d. b.
dp_m	Particle mean diameter	µm
AT	Anthocyanins content	mg/100g
IT	Instantanization time	*s*
aw	Water activity	-
$Icarr$	Carr Index	*%*

6. References

[1] Unwin N, Alberti KG. Chronic non-communicable diseases. Ann Trop Med Parasitol. 2006;100(5-6):455-64.

[2] Minestério da Saúde. Plano de estratégias de Ações Estratégicas para o Enfrentamento das Doenças Crônicas Não Transmissíveis no Brasil 2011-2022. Ministério da Saúde. Retrieved January 18, 2018, from http://bvsms.saude.gov.br/bvs/publicacoes/plano_acoes_enfrent_dcnt_2011.pdf

[3] Saleh, K. and Guigon, P., 2009a. Mise en oeuvre des poudres – Granulation humide: bases et théorie. Techniques de l'ingénieur, J2253 V1, 1-14.

[4] Smith, P. G. (2007). Applications of fluidisation in food processing. Oxford: Blackwell Science.

[5] Saleh, K. and Guigon, P., 2009b. Mise en oeuvre des poudres – Techniques de granulation: humide et liants. Techniques de l'ingénieur, 1-14.

[6] Vinnars, E.; Wilmore, D. (2003). History of parenteral nutrition. *Journal of Parenteral and Enteral Nutrition*, 27(3), 225-231.

[7] Bilek, S. E.; Bayram, S. K. (2015). Fruit juice drink production containing hydrolyzed collagen. *Journal of Functional* Foods, 14, 562-569.

[8] Moskowitz, R. W. (2000). Role of collagen hydrolysate in bone and joint disease. Seminars in Arthritis and Rheumatism, 30(2), 87-99. doi:10.1053/sarh.2000.9622

[9] Sibilla, S.; Borumand, M. (2015). Effects of a nutritional supplement containing collagen peptides on skin elasticity, hydration and wrinkles. Journal of Medical Nutrition and Nutraceuticals, 4(1), 47.

[10] Proksch, E.; Segger, D.; Degwert, J. et al. Oral supplementation of specific collagen peptides has beneficial effects on human skin physiology: a double-blind, placebo-controlled study. Skin Pharmacol Physiol. 2014;27(1):47-55.

[11] Sancho, R. A., & Pastore, G. M. (2012). Evaluation of the effects of anthocyanins in type 2 diabetes. Food Research International, 46(1), 378-386.

[12] Dacanal G.C., Menegalli F. C., 2010, Selection of operational parameters for the production of instant soy protein isolate by pulsed fluid bed agglomeration, Powder Technology, 203, 565–573,

[13] LEE, Jungmin; DURST, Robert W; WROLSTAD, Ronald E. Determination of Total Monomeric Anthocyanin Pigment Content of Fruit Juices, Beverages, Natural Colorants, and Wines by the pH Differential Method: Collaborative Study. AOAC International, [s.l.], v. 88, n. 5, p.1269-1278, set. 2005.

[14] Hogekamp, S.; Schubert, H. Rehydration of food powders, Food Sci. Technol. Int. 9 (2003) 223–235.

[15] U.S. PHARMACOPEIAL CONVENTION. **616**: Bulk Density and Tapped Density of Powders. United States: 2011 The United States Pharmacopeial Convention, 2011.

[16] Andreola K., Butzge J.J., Silva C.A.M., Kis L.S., Rocha S.C.S, Taranto O.P, 2015, Effect of operating conditions on the agglomeration and drying of hydrolyzed collagen in a fluidized bed, First Nordic Baltic Drying Conference, 17 -19 June, Gdansk, Poland.

[17] Rahman, S. Food Properties Handbook. CRC Press, 2008.

Intermittent–microwave and convective drying of parsley

Szadzińska, J.[*]; Mierzwa, D.

Department of Process Engineering, Poznan University of Technology, Poznan, Poland

*E-mail of the corresponding author: justyna.szadzinska@put.poznan.pl

Abstract

The studies present convective drying of parsley with an intermittent microwave application. Eight different drying programs including convective drying (CV) were carried out in a laboratory-scale hybrid dryer. The influence of intermittent conditions on drying time, drying rate, energy efficiency and product quality was analysed. The results demonstrated that intermittent–microwave convective drying improves the drying kinetics and reduces energy consumption. Moreover, a higher retention of vitamin C, smaller color change and a better ability to rehydration were observed for the parsley samples dried using intermittent drying than for CV.

Keywords: *intermittent drying, microwaves, energy, vitamin C, rehydration.*

1. Introduction

Many experimental investigations have shown that combined drying methods result in higher drying effectiveness from both kinetic and quality aspect. Drying based on the combination of various techniques, i.e., hybrid drying, is still an emerging drying technology in food industry. [1, 2] One of the possibilities to improve the drying kinetics and product quality can be intermittent drying. As one of the recommended methods for wegetable and fruit dehydration, consists of drying at non-stationary conditions, where the process parameters change periodically in time, e.g. varying temperature or varying mode of energy input. [3,4] The main aim of this solution is to prevent the loss of product quality and to enhance the energy efficiency. Intermittent microwave-convective drying has the opportunity to develop, as it is competitive to other more expensive alternative methods, such as, for example lyophilization. Parsley (*Petroselinum crispum*) is a popular plant of celery family (*Apiaceae*). Both its roots and leaves are used for culinary, medical and cosmetic purposes. It is a valuable spice vegetable which owes its aromatic properties to the essential oil. Ingredients found in parsley, e.g., vitamin C and E, polyphenols, carotenoids, have strong antioxidant properties, and their presence in the human diet is considered to be an important factor reducing the risk of civilization diseases. [5]

The aim of the studies was to analyze the effectiveness of hybrid drying in non-stationary conditions with respect to process kinetics, energy consumption and quality of dry parsley. The influence of intermittent microwave application in convective drying on the total drying time, drying rate, energy usage and quality characteristics such as colour change (dE), water activity (aw), retention of vitamin C, radial shrinkage (RS) and rehydration capacity (RC) were investigated in this study, and compared with processes carried out in constant conditions (convective and convective-microwave drying).

2. Materials and Methods

Fresh parsley roots (*Petroselinum crispum*) cultivated in Poland were used as a research material. 50g parsley samples in the form of slices (32 mm diameter, 5 mm thick) were dried in a laboratory-scale hybrid dryer equipped with an air-heating system, microwaves (2.45 GHz, max. power of 500 W) generated by a magnetron, pyrometer (infrared thermometer) and a standard electricity meter. The samples with an average initial moisture content of 0.84 kg·kg^{-1} w.b. were dried to a final moisture content of 0.1 kg·kg^{-1} w.b. using eight drying programs including convective drying as a reference (Table 1). The first four drying procedures were conducted using stationary conditions (i.e., convective drying (CV) and convective-microwave drying (CVMW)), whereas the next four procedures were performed using non-stationary conditions (i.e. intermittent–microwave and convective drying (IT1-4)). The basis for all IT programs was continuous CV with MW (ON/OFF)

cycles applied at the beginning of each drying test. The drying conditions were changed in terms of the air temperature, number of MW cycles or MW power to avoid overheating of the dried material. The drying processes were operated at 30°C or 50°C, or with a variable air temperature T_a (50°C/30°C). The microwave power was constant and set at 100 W, 300 W or 500 W. Irrespective of the type of drying program, the air velocity was constant throughout the entire process, i.e. 0.4 m/s.

Table 1. Description of the drying programs.

No.	Acronym	Description	T_a [°C]	MW [W]	MW cycles duration
1	CV30	Convective drying	30	0	NA
2	CV50	Convective drying	50	0	NA
3	CVMW30	Convective-microwave drying	30	100	CONT
4	CVMW50	Convective-microwave drying	50	100	CONT
5	IT1	Intermittent drying	50/30	100	ON up to T_m=50°C/ 15 min OFF
6	IT2	Intermittent drying	50/30	100	ON up to T_m=50°C/ 30 min OFF
7	IT3	Intermittent drying	30	500	ON up to T_m=50°C/ 15 min OFF
8	IT4	Intermittent drying	30	300	ON up to T_m=50°C/ 15 min OFF

CV – convection, MW – microwaves, IT – intermittent, T_a – air temperature, T_m – material temperature, CONT – continuous, NA – not applicable

2.1. Process kinetics and energy consumption

The drying kinetics was assessed on the basis of the moisture ratio (MR), drying rate (DR), drying time (DT) and the energy consumption (EC). The parameters were determined as follows:

$$MR = \frac{MC_t - MC_{eq}}{MC_i - MC_{eq}}, \qquad (1)$$

$$DR = \frac{dm}{DT},$$ (2)

where: MC_i, MC_t and MC_{eq} are the initial, instantaneous (for a given time of the process) and equilibrium moisture contents, dm is the total weight loss of the sample, and DT is the total drying time, i.e. until the moisture content reaches equilibrium.

The initial moisture content of the raw material was determined using a moisture analyser (XM120 Precisa, Switzerland). Each drying program was repeated in triplicate and the total drying time (DT) was averaged for data interpretation. The energy consumed by the whole apparatus during the drying processes was measured with a standard electricity meter and recalculated to MJ per 1 gram of evaporated moisture. The average EC was determined by:

$$EC = \frac{E_p \cdot 3.6}{dm},$$ (3)

where: E_p is the average energy consumption in kWh measured in drying process, and dm is the total weight loss of the sample.

2.2. Quality assessment

The product quality was assessed in terms of the total colour change (dE), water activity (aw), retention of vitamin C (AA), radial shrinkage (RS) and the rehydration capacity (RC). The total colour change was measured using a colorimeter (CR-400 Konica Minolta, Japan) and indicated using CIELab colour space:

$$dE = \left(dL^{*2} + da^{*2} + db^{*2}\right)^{0.5},$$ (4)

where: L* indicates lightness and a*, and b* are the chromaticity coordinates which indicate color directions from red to green (a*) and from yellow to blue (b*).

Water activity (aw) was measured for fresh and dry product at 25°C using the LabMaster-aw Standard (Novasina AG, Switzerland). The measurement of aw for dry samples was conducted after a 24-hour incubation in a desiccator, since the moisture profile needs to be aligned after drying. Retention of vitamin C (AA) in the parsley root was determined by the spectrophotometric method. [6] The Radial shrinkage (RS) was assessed on the basis of image analysis. Photographs taken on the samples were subjected to basic treatment and used in Fiji software (v. 1.51u) for calculation of shrinkage in accordance with equation:

$$RS = \left(\frac{1 - A_d}{A_0}\right) \cdot 100\%,$$ (5)

where: A_d and A_0 are the surfaces of dry and raw parsley samples, respectively.

Dried samples were rehydrated in boiling distilled water at temperature of 100°C for 5 min, without stirring. The ratio of material to water was 1:50 (w/w). After rehydration the samples were blotted with a filter paper and weighed. The rehydration capacity (RC), described as percentage water gain, was calculated according to Seremet et al., 2016. [7]

3. Results and discussion

3.1. Drying kinetics

The drying kinetics of parsley root was evaluated on the basis of drying and temperature curves. Figure 1 shows the results of moisture ratio, average drying rate and enegy consumption obtained during drying in constant and intermmitent conditions.

a)   b)
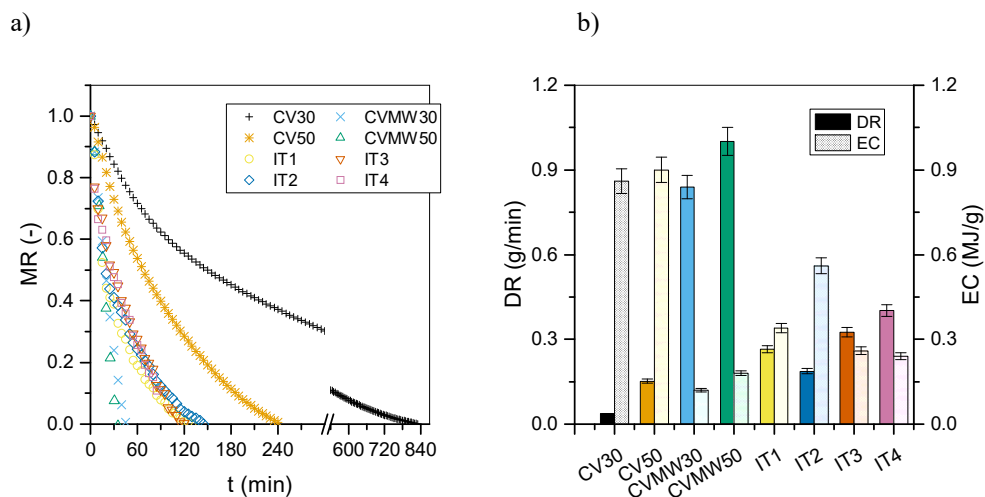
Fig. 1. Moisture ratio MR (a) and average values of drying rate DR, and energy consumtion EC (b) for different drying programs.

The CV drying was found to be the longest process as the parsley samples achieved the final moisture content after about 14 and 4 hours for 50°C (CV50) and 30°C (CV30), respectively. As can be seen in Fig. 1b, also CV the samallest value of the drying rate was obtained. The results of hybrid drying, i.e., CVMW, showed a significant reduction in drying time, namely about 95% as compared to CV. Similarly, the average drying rate for CVMW was the highest amongst all the drying procedures. In turn, intermittent drying (IT) demonstrated shorter drying times, namely by 82-86%, in comparison to CV, but on the other hand a considerable increase in DT and lower values of DR than those of the CVMW. As follows from Fig. 1a, longer OFF cycles during IT2 increased the total drying time and thus decreased noticeably the drying rate, as compared to IT1. However, which is surprising, a lower MW power applied in IT4 increased the drying rate in comparison with IT3. In case of the energy effectiveness (Fig. 1b), the lowest energy efficiency was

observed for CV, as the highest EC was obtained. The average energy consumption was definitely lower for all the IT processes, but the highest energy efficiency was found for CVMW. It was noticed that energy usage is proportional to the total drying time.

3.2. Product quality

The quality of parsley samples was evaluated on the basis of several quality characteristics. Figure 2 presents the results of colour change and water activity between fresh and dry product.

a) b)
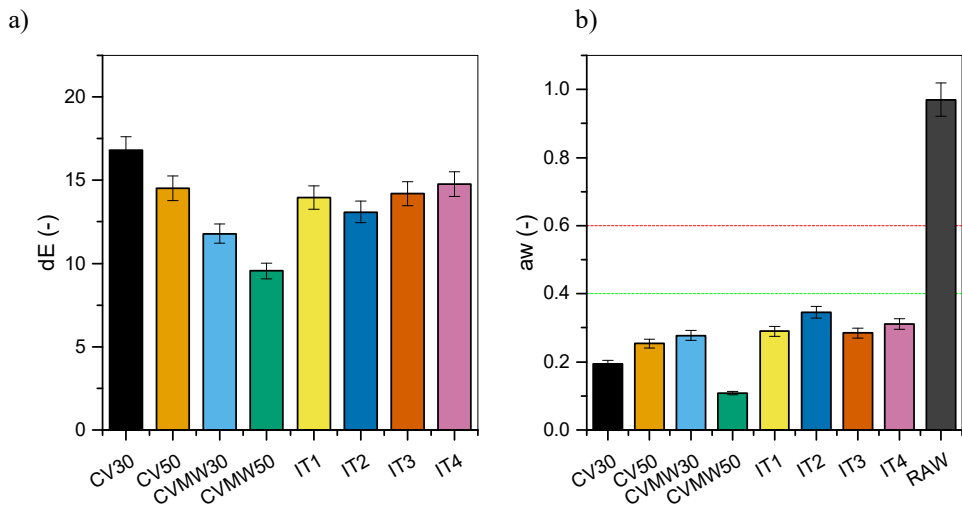
Fig. 2. Total colour change dE (a) and water activity aw (b).

The highest total color change (16.79) was observed for CV30. Thus, the discoloration of parsley was due to continuous and prolonged application of hot air during drying. Astonishingly, despite continuous MW in CVMW, the colour change was visibly lower than for CV as well as for IT. As follows from Fig. 2a, dE after intermittent drying (IT1-4) was found to be similar to that of CV50, i.e. 14, on average. However, the results of colour coordinate (L*) proved that the overall change in colour for CV and IT samples increased due to higher value of lightness after drying. In consequence, it means a positive change in colour, i.e., "brightening" of the samples dried by CV and IT. The next quality factor was water activity aw (Fig. 2b), which allows to verify the microbiological stability of dry product, e.g., development of microflora, product durability. The fresh material was characterized by the water activity of 0.970, on average. After each drying process water activity was less than its critical value, i.e. 0.6, thus the microbial growth (bacteria, yeasts and molds) was inhibited and biologically stable products were obtained. Secondly, aw of dry parsley samples was lower than 0.4, which means that many reactions, e.g. enzymatic, non-enzymatic (Maillard) and oxidation have been blocked. [8]

Figure 3 presents the results of vitamin C retention, radial shrinkage and rehydration capacity. CVMW50 contributed to the lowest vitamin C retention amongst all the analysed drying programs (Fig. 3a). In turn, for CVMW30 the retention was 57%, and was also higher than for CV. In case of IT, the value of AA was in the range of 54-93%. The highest content of AA was obtained for IT3. In general, intermittent application of microwaves in convective drying allowed the parsley to retain more vitamin C then in case of CV or CVMW.
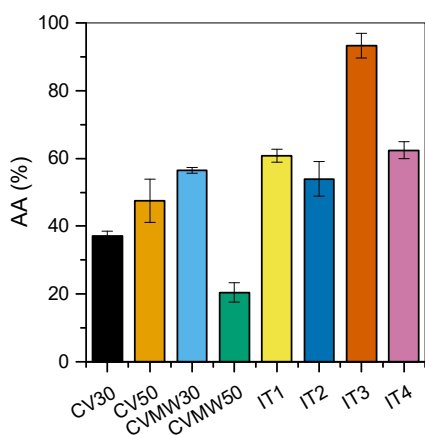
a)   b)
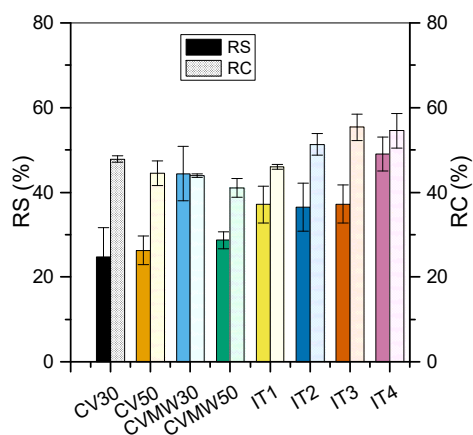
Fig. 3 Retention of ascorbic acid AA (a), radial shrinkage RS and rehydration capacity RC (b).

The results of radial shrinkage (Fig. 3b), showed that type of process may influence the appearance of samples significantly. The products dried in stationary conditions were characterized by a slightly lower RS in comparison to the non-stationary ones. The only exception is CVMW30, where the observed RS was similar as for IT. Nevertheless, the smallest shrinkage was observed for the material dried by CV, regardless of the air temperature.The last quality parameter evaluated in this work was rehydration capacity (RC), which gives information on the ability of the material to absorb water. As follows from Fig. 3b, the rehydration capacity of samples dried by CV and CVMW increased with the decrease of temperature. Therefore, due to the increase in air temperature (i.e., form 30°C to 50°C), a destruction of plant tissue structure must have occured. In case of IT1-4, a higher RC was observed. Moreover, the value of RC incrased with the OFF time and also with MW power applied during intermittent drying.

4. Conclusions

The effect of different methods including non-stationary drying on kinetics and quality characteristics of parsley root was discussed. The results of the drying tests showed that intermittent drying reduces drying time by 86%, increases the drying rate and thus

improves the energy efficiency (up to 80%) as compared to convective drying. Furthermore, it was found that microwaves applied intermittently in convective drying contributes to better product quality from the colour, vitamin C retention and rehydration property point of view.

5. Acknoledgement

6. References

[1] Huang, L.I.; Zhang, M. Trends in development of dried vegetable products as snacks. Drying Technology 2012, 30 (5), 448–461.

[2] Kowalski, S.J.; Mierzwa, D. Hybrid drying of red bell pepper: Energy and quality issues. Drying Technology 2011, 29 (10), 1195–1203.

[3] Łechtańska, J.M.; Szadzińska, J.; Kowalski, S.J. Microwave- and infrared-assisted convective drying of green pepper: Quality and energy considerations. Chemical Engineering and Processing: Process Intensification 2015, 98, 155–164.

[4] Soysal, Y.; Ayhan, Z.; .Eştürk, O.; Arıkan, M.F. Intermittent microwave–convective drying of red pepper: drying kinetics, physical (colour and texture) and sensory quality. Biosystems Engineering 2009, 103 (4), 455–463.

[5] Wójcik-Stopczyńska, B.; Czajka, J.; Kiedos, P. Effect of pre-treatment and freezing on changes of nutrients and nitrates in parsley roots. Bromatologia i Chemia Toksykologiczna 2016, XLIX, 4, 748–755.

[6] Rutkowski, M.; Grzegorczyk, K. Modifications of spectrophotometric methods for antioxidative vitamins determination convenient in analytic practice. ACTA SCIENTIARUM POLONORUM, Technologia Alimentaria 2007, 6(3), 17–28.

[7] Seremet (Ceclu), L.; Botez, E.; Nistor, O.V.; Andronoiu, D.G.; Mocanu, G.D. Effect of different drying methods on moisture ratio and rehydration of pumpkin slices. Food Chemistry 2016, 195, 104–109.

[8] Labuza, T.P.; Tannenbaum, S.R.; Karel, M. Water content and stability of low moisture and intermediate-moisture foods. Food Technology 1970, 24 (5), 35–42.

Influence of process conditions on quality of spouted bed dried okara

Scafi, G.A.O.[a]; Lazarin, R.A.[a]; Kurozawa, L.E.[a*]

[a] School of Food Engineering. University of Campinas, Campinas, Brazil.

*E-mail of the corresponding author: louisek@unicamp.br

Abstract

This study aimed to evaluate the spouted bed drying of okara with inert particles of polypropylene. A central composite rotatable design was carried out to verify the effect of drying air temperature and air flow on moisture content, techno-functional properties and trypsin inhibitors activity of dried product. Higher temperatures decreased emulsifying properties and trypsin inhibitor activity, probably due to thermal protein denaturation. In order to obtain a dried okara with maximum techno-functional properties and minimum moisture content and trypsin inhibitor activity, the optimal drying conditions were suggested: air temperature of 60ºC and air flow of 180 m³/h.

Keywords: soy pulp; spouted bed drying; trypsin inhibitor activity; techno-functional properties; optimization

1. Introduction

During the processing of soymilk and tofu, an insoluble residue, also know as okara or soy pulp, is generated. Since the sales volume of soymilk of worldwide reached 13.5 billion liters in 2015[1], significant quantities of okara are underutilized as animal feed or discarded, resulting in environmental problems. However, okara can be used for human consumption or as ingredient to increase the functional properties of food products due to its considerable high protein content[2].

Soy proteins play an important role in the food industry due to their nutritive value and ability to improve the functional properties. Okara proteins, whose main fractions are the basic 7S globulin and 11S[3], presented better emulsion stability and similar emulsion activity than soy protein[4]. Moreover, unlike other vegetable proteins, okara proteins have all of the essential amino acids necessary for good health[5]. However, okara contains trypsin inhibitor, which have been considered an antinutritional factor of soy consumption by promoting the reduction of protein digestibility[6].

Thus, aiming the use of okara by the food industry, some preservation method must be applied to improve its shelf life, since okara contains high moisture content (75-80%) and is very perishable. Amongst the several methods employed for preservation, drying is a process in which water activity of food is reduced by removal of moisture by vaporization or sublimation. However, okara is a material difficult to dry, since its wet particles are cohesive. Moreover, the diffusion of internal moisture is slow, resulting in long drying time when it is dried in static dryers[7]. These drawbacks can be solved using dynamic dryers, such as spouted bed dryer, and by adding inert particles to the moist and cohesive material.

The objective of the current work is to evaluate the spouted bed drying of okara, analyzing the influence of process parameters on dried product quality.

2. Materials and Methods

2.1. Material

Soybean (*Glycine max* (L.) Merr.) cultivar BRS 257, which is lipoxygenase-free, was acquired from SL Alimentos (Mauá da Serra, Brazil). Polypropylene particles were used as inert material. Trypsin and benzoyl-DL-arginine-4-nitroanilide hydrochloride substrate (BAPNA) (Sigma-Aldrich, St. Louis, USA) were used for analysis of the trypsin inhibitors.

2.2. Preparation of okara

The okara was obtained from soymilk processing according to Baú and Ida[8]. Soybeans were soaked in water at 1:3 ratio (w:w, soybean:water) for 12 h at 8°C, drained and homogenized with distilled water at 1:8 ratio (w:w, soybean:water) using an industrial blender (model LB-25, Skymsen®, Brusque, Brazil) for 5 min. The mixture was filtered, obtaining the insoluble

fraction okara. The moisture content of okara was 75.2±0.1% (wet basis). Ash, lipid and protein contents of okara, obtained by AOAC[9], were in dry basis 3.5±1.0%, 13.9±0.5% and 35.1±1.0%, respectively. Carbohydrate content (dry basis), calculated by difference, was 47.4±1.5%. Samples were stored at -18°C and thawed according to the quantity required for spouted bed drying.

2.3. Spouted bed drying of okara

The drying of okara was carried out in a spouted bed dryer (model FBDG3, O'Hara Technologies, Ontario, Canada). The dryer consists of a conical base with an inferior diameter of 85 mm, superior diameter of 393 mm, height of 400 mm and inlet orifice diameter of 48 mm. The upper part of conical base consists of a cylindrical column.

Previous to drying of okara, the spouted bed dryer was put into operation with 1 kg of inert particles. Heated air was blowed at the inferior part of conical base at different flow rates (Table 1). After the permanent regime was reached, 500 g of moist okara were introduced into the dryer. For all experiments, total drying time was 30 min. The load of inert particles, mass of okara:mass of particle inert ratio and drying time were determined in preliminar tests. At the end of drying, dried okara was separated from the inert particles by sieve with 2 mm opening.

A central composite rotatable design was carried out to verify the effect of drying air temperature (40 to 80ºC) and air flow (140 to 180 m^3/h) on moisture content, techno-functional properties (emulsifying capacity, emulsion stability and water absorption index) and trypsin inhibitors activity of dried product. Experimental data were fitted to Equation (1)[10].

$$y = b_0 + b_1 x_1 + b_2 x_2 + b_{11} x_1^2 + b_{22} x_2^2 + b_{12} x_1 x_2 \qquad (1)$$

Where: y is the response, b_0, b_1 and b_2, b_{11} and b_{22}, and b_{12} are the constant, linear, quadratic and cross-product regression coefficients, respectively, and x_1 and x_2 represent the coded values of the T_{in} and W variables, respectively.

Regression coefficients of the predictive models were obtained by the Protimiza software (http://experimental-design.protimiza.com.br). Coefficients within a confidence level above 90% were considered significant ($p < 0.1$). Non-significant terms were eliminated, and the model was tested for adequacy by analysis of variance (Anova), coefficient of determination (R^2) and F-test.

Table 1. Screening design for spouted bed drying of okara, regression coefficients and Anova

Assay	Independent variables		Dependent variables				
	T_{in}	W	X	WAI	EC	ES	TI
1	46	146	16.9±3.8	5.6±0.5	1953.7±2.7	53.9±0.5	8.5±0.8
2	74	146	9.1±0.8	4.4±0.2	1616.2±1.9	52.9±2.0	10.5±0.4
3	46	174	12.0±0.7	4.9±0.3	1931.3±38.0	55.0±1.0	10.4±0.6
4	74	174	4.3±0.2	4.4±0.4	1593.4±21.0	47.6±0.7	6.2±0.1
5	40	160	17.8±1.4	4.8±0.0	2076.3±37.8	53.9±1.5	10.4±0.5
6	80	160	3.6±0.6	4.0±0.7	1490.1±28.8	51.8±3.5	8.1±0.6
7	60	140	6.6±1.0	4.2±0.2	1558.1±34.3	50.1±2.2	11.2±0.7
8	60	180	5.4±0.2	3.8±0.5	1518.0±0.3	50.7±1.0	6.5±0.5
9	60	160	5.2±0.3	4.4±0.3	1660.2±35.8	53.1±2.7	7.1±0.2
10	60	160	6.6±2.4	4.2±0.3	1680.6±24.3	53.6±1.0	6.2±0.0
11	60	160	5.5±0.2	4.8±0.8	1687.1±5.2	54.5±0.3	7.2±0.1
Regression coefficients							
b_0			6.4	4.5	1637.6	53.5	6.8
b_1			-4.7	-0.3	-188.1	-1.4	-0.7
b_{11}			2.8	NS	93.8	NS	1.2
b_2			-1.4	NS	NS	NS	-1.1
b_{22}			NS	NS	NS	-1.4	1.0
b_{12}			NS	NS	NS	-1.6	-1.5
R^2			0.90	0.39	0.89	0.78	0.91
F_c			21.8	5.7	34.1	8.5	10.7
F_t			3.07	3.36	3.11	5.27	3.45

NS is non-significant ($p > 0.1$)

2.4. Analytical methods

2.4.1. Physicochemical properties of the dried okara

Moisture content was determined gravimetrically in triplicate in an oven at 105°C for 24h[9]. The water absorption index (WAI, g absorbed water/g sample) analyses were carried out according to Seibel and Beléia [11]. The emulsifying capacity (EC, mL oil/g protein) was analyzed by continuous addition of oil to the sample until phase inversion of the emulsion, when the conductivity of the emulsion was below 10 μS[12]. For emulsion stability (ES, %), emulsion was prepared with okara and oil and placed in a 50 ml graduated cylinder and stored at room temperature. The volume of the emulsified layer was observed until no variation was observed[13]. The ES was calculated as the ratio of the emulsified layer and the total volume. The trypsin inhibitor activity (TIU/g solid) was determined according to the AOCS[14], by

extracting of the degreased sample with water for 30 min, followed by buffer Tris (0.05 mol/L, pH 8.2, containing CaCl2 0.02 mol/L). One trypsin unit (TU) was arbitrarily defined as an increase of 0.01 absorbance units at 410 nm for 10 mL of a reactive mixture (2 mL sample aliquot, 2 mL trypsin solution, 5 mL benzoyl-DL-arginine-4-nitroanilide hydrochloride substrate solution and 1 mL acetic acid solution). The trypsin inhibitor unit (TIU) was calculated as the difference in the absorbance between a standard test and the sample test.

3. Results and Discussion

3.1. Spouted bed drying of okara

The experimental data for moisture content (X), water absorption index (WAI), emulsifying capacity (EC), emulsion stability (ES) and trypsin inhibitor activity (TI) were fitted to Equation 1. The regression coefficients, F-values, p-values and R^2 are presented in Table 1. After exclusion of non-significant terms (p>0.1), the predictive models were tested for accuracy of fit by Anova. When the calculated F-value Fc was greater than the tabulated F-value Ft, the variation was explained by the regression and not by the residues. Thus the regression was significant, and the model could be considered predictive. However, for the WAI, the R^2 was low and the model was not predictive. Figure 1 shows the response surfaces generated by the proposed models.

As expected, higher temperature and air flow led to lower moisture content (Fig. 1a). Air flow played a significant role in fluid dynamic of particles. At higher air flow, there is a better contact between sample particles and air drying, improving the heat and mass transfer. Analyzing Figures 1(b) and 1(c), temperature had a significant and negative effect on emulsifying capacacity and emulsion stability, in which higher temperatures led to lower response values. These results were expected, since the okara proteins are thermosensitive, probably occurring their denaturation during the drying process. Several process parameters, such as pH and ionic strength, affect the functionality of proteins, especially temperature. Heat treatment has a great impact on the structure and, as consequence, on the emulsifying functionality of proteins[15]. Similarly to the emulsion properties, lower values of trypsin inhibitor activity were obtained at higher temperature and air flow (Fig.1d). Besides trypsin inhibitor is reversibly denatured by short heating to 80°C and irreversibly denatured by heating to 90°C[16], the highest drying temperature used in the current work (74°C) caused significant loses on its activity.

(a)

(b)

(c)

(d)
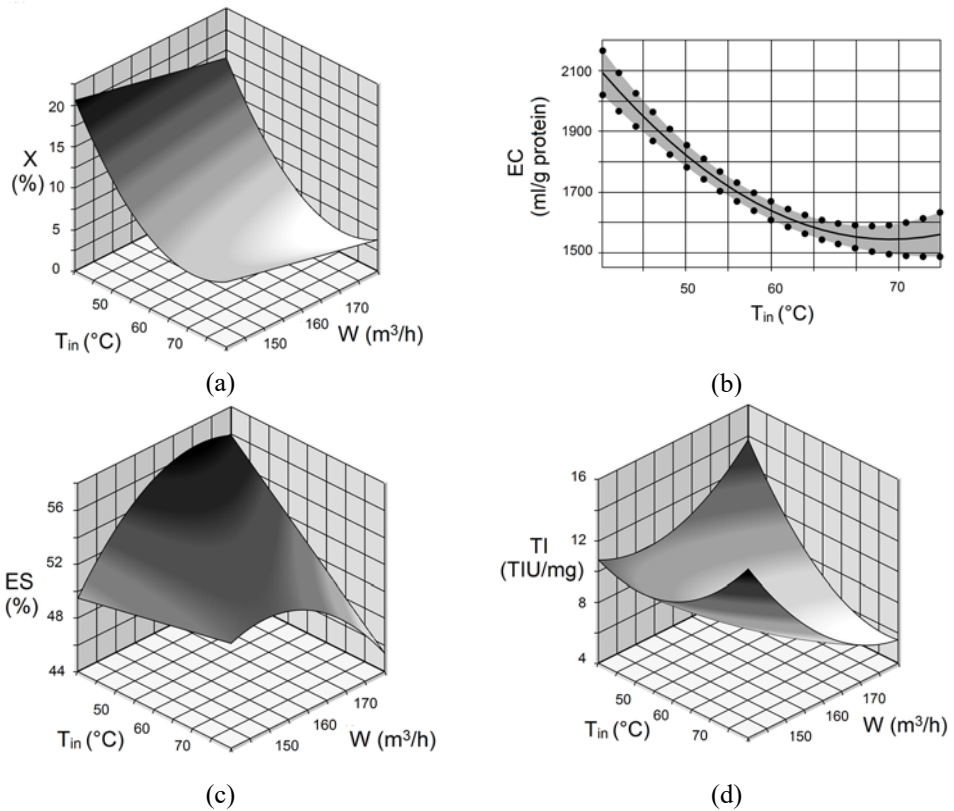
Fig. 1. Influence of independente variables on the responses: (a) moisture content; (b) emulsifying capacity; (c) emulsion stability and (d) trypsin inhibitors activity

3.2. Characterization of the spouted bed dried okara obtained under the optimum condition

Analyzying the responses surfaces (Fig. 1), the spouted bed drying of okara was optimized for maximum techno-functional properties and minimum moisture content and trypsin inhibitor activity. The optimal drying conditions were: 60ºC and 180 m³/h. Under optimal conditions, dried okara had a moisture content of 4.8±0.1% emulsifying capacity of 1754.3±18.0 ml/g protein, emulsion stability of 48.8±0.3%, water absorption index of 4.7±0.52 g/g sample and trypsin inhibitor activity of 6.7±0.1 TUI/mg sample.

In order to verify the influence of spouted bed drying on okara, these quality properties were also determined for freeze dried okara. As results, the emulsifying capacity and emulsion stability of freeze dried okara was respectively 2182.8±30.7 ml/g protein and 51.4.8±0.4%. On the other words, spouted bed drying caused a reduction of 19.6% and 5.1% on emulsion properties. On the other hand, an improvement on nutritional properties was observed, in

which spouted bed drying reduced 27% of trypsin inhibitor activity of product (9.3±0.3 TUI/mg sample).

4. Conclusions

The spouted bed drying showed to be suitable to obtain dried okara with good technofunctional properties, mainly emulsifying capacity. In order to obtain maximum emulsion properties and minimum trypsin inhibitor activity, the optimal condition was proposed: 60°C and 180 m³/h. There was a significant retention of emulsifying capacity and emulsion stability and reduction on trypsin inhibitor activity after spouted bed drying.

5. Nomenclature

EC	emulsifying capacity	ml g^{-1} protein
ES	emulsion stability	%
TI	trypsin inhibitors activity	Trypsin inhibitor unit (TIU) mg^{-1} sample
T_{in}	Inlet air temperature	°C
W	Air flow	$m^3\ h^{-1}$
WAI	water absorption index	$g\ g^{-1}$ sample
X	moisture content	% (wet basis)

6. Acknowledgements

7. References

[1] Statista. The portal for statistic. Sales volume of soymilk worldwide in 2015 and 2018: 2018. https://www.statista.com/statistics/645662/soy-milk-sales-volume-worldwide (accessed Mar 19, 2018).

[2] Sbroggio, M.F.; Montilha, M.S.; Figueiredo, V.R.G.; Georgetti, S.R.; Kurozawa, L.E. Infuence of the degree of hydrolysis and type of enzyme on antioxidant activity of okara protein hydrolysate. Food Science and Technology 2016, 36(2), 375–381.

[3] Stanojevic, S.P.; Barac, M.B.; Pesic, M.B.; Vucelic-Radovic, B.V. Composition of proteins in okara as a byproduct in hydrothermal processing of soy milk. Journal of Agricultural and Food Chemistry 2012, 60(36), 9221–9228.

[4] Puechkamut, Y.; Panyathitipong, W. Characteristics of proteins from fresh and dried residues of soy milk production. Kasetsart Journal - Natural Science 2012, 46(5), 804–811.

[5] Waliszewski, K.N.; Pardio, V.; Carreon, E. Physicochemical and sensory properties of corn tortillas made from nixtamalized corn flour fortified with spent soymilk residue

(okara). Journal of Food Science 2002, 67(8), 3194–3197.

[6] Stanojevic, S.P.; Barac, M.B.; Pesic, M.B.; Zilic, S.M.; Kresovic, M.M.;Vucelic-Radovic, B.V. Mineral elements, lipoxygenase activity, and antioxidant capacity of okara as a byproduct in hydrothermal processing of soy milk. Journal of Agricultural and Food Chemistry 2014, 62(36), 9017–9023.

[7] Muliterno, M.M.; Rodrigues, D.; Lima, F.S.; Ida, E.I.; Kurozawa, L.E. Conversion/degradation of isoflavones and color alteration during drying of okara. LWT – Food Science and Technology 2017, 75, 512–519.

[8] Baú, T.R.; Ida, E.I. Soymilk processing with higher isoflavone aglycone content. Food Chemistry 2015, 183, 161–168.

[9] AOAC. Official Methods of Analysis, 19th ed. Association of Official Analytical Chemists International: Washington, D.C, 1995.

[10] Rodrigues M.I; Iemma, A.F. Experimental design and process optimization; CRC Press: Boca Raton, 2014.

[11] SEIBEL, N.F.; BELÉIA, A.D.P. The chemical characteristics and technological functionality of soybean based ingredients [*Glycine Max* (L.) Merrill]: carbohydrates and proteins. Brazilian Journal of Food Technolgy 2009, 12(2), 113–122.

[12] BARBIN, D.F.; NATSCH, A.; MÜLLER, K. Improvement of functional properties of rapeseed protein concentrates produced via alcoholic processes by thermal and mechanical treatments. Journal of Food Processing and Preservation 2011, 35(3), 369–375.

[13] SURH, J.; DECKER, E.A.; McCLEMENTS D.J. Properties and stability of oil-in-water emulsions stabilized by fish gelatin. Food Hydrocolloids 2006, 20(3), 596–606.

[14] AOCS. American Oil Chemist's Society. Sampling and analysis of oilseed by-products. Trypsin Inhibitor Activity. AOCS Official Method Ba 12-75. Champaign, IL, USA, 2009.

[15] KEERATI-U-RAI, M.; CORREDIG, M. Heat-induced changes in oil-in-water emulsions stabilized with soy protein isolate. Food hydrocolloids 2009, 23(8), 2141–2148.

[16] Steiner, R.F.; Frattali, V. Purification and properties of soybean protein inhibitors of proteolytic enzymes. Journal of Agricultural and Food Chemistry 1969, 17(3), 513–518.

Effect of temperature and mode of drying on bioactive compounds and quality of germinated parboiled rice

Klaykruayat, S.ᵃ ; Mahayothee, B.ᵇ* ; Nagle, M.ᶜ ; Müller, J.ᵃ

[a] Institute of Agricultural Engineering. Tropics and Subtropics Group. Universität Hohenheim, Stuttgart, Germany.

[b] Department of Food Technology. Faculty of Engineering and Industrial Technology. Silpakorn University, Nakhon Pathom, Thailand.

[c] Agricultural Research and Development Program. Central State University, Wilberforce, Ohio, USA.

*E-mail of the corresponding author: mahayothee_b@su.ac.th, busarakornm@yahoo.com

Abstract

Germinated parboiled rice (GPR) is recognized as a functional food because it is rich in bioactive compounds, especially gamma-aminobutyric acid (GABA). GPR was produced by soaking, incubating, steaming, and then drying using a high-precision hot air dryer. The results indicated that air flow mode and drying temperature had significant effects on the quality of GPR. Drying at higher temperatures and shorter times conserved GABA content. Using through-flow mode decreased drying time and prevented color change. However, a slightly lower percentage of head rice yield was observed. Moreover, using through-flow mode negatively affected the hardness loss after cooking.

Keywords: Germinated parboiled rice; Drying mode; Gamma-aminobutyric acid; Head rice yield

1. Introduction

Germinated parboiled rice (GPR) is a product that can be promoted as a functional food. The characteristics of GPR are shorter cooking time, softer texture and higher contents of bioactive compounds than the normal rice. Nowadays, the GPR production in Thailand is performed by soaking paddy rice in water and then incubating until the radicle grows to a length of 0.5 - 1.0 mm. After that, the germinated paddy is steamed until being cooked. Subsequently, the germinated parboiled paddy is sun dried to a final moisture content of 14%.[1] Dried germinated parboiled paddy is dehusked, then the final product is packed.

During the germination, enzymes in paddy rice are activated and bioactive substances greatly increase.[2] Gamma-aminobutyric acid (GABA) is a free amino acid, substantially increased by the germination process.[3] GABA has a beneficial effect on human health, such as decreasing stress-related nerve impulses in the brain and promoting relaxation and sleep.[4] Parboiling is a hydrothermal process, causing certain changes in paddy rice, including taste, texture, starch gelatinization, inactivation of enzymes, easier dehusking and increased head rice yield.[3] Sootjarit et al.[5] reported that germinated rice rapid drying at high temperatures (80ºC - 140ºC) resulted in a significant higher GABA content in comparison to drying at a lower temperature (50ºC). However, high temperature can easily cause overheating and cracking of grains which leads to low milling quality.[6]

Therefore, the suitable drying temperature for GPR production to conserve overall quality considering GABA content, milling and cooking properties is essential. Besides the drying temperature, the effect of air flow mode in the drying chamber is also important for efficient the drying process of a good quality GPR.

"Hom-Nil" is a pigmented Thai rice. It is also known as purple rice, that contains varieties of bioactive compounds such as antioxidants, phenolics, β-carotene and anthocyanins.[7] Nowadays, it is commonly used for producing GPR in Thailand. Thus, the objective of this study was to study the effect of drying temperatures and modes of drying air on the GABA content and quality of germinated parboiled purple rice.

2. Materials and Methods

Thai purple paddy rice variety 'Hom Nil' with a moisture content of $11.28 \pm 0.28\%$ (w.b.) was used in this study. Paddy rice was purchased from the farmer in Nakorn Pathom, Thailand and brought to Stuttgart, Germany by airfreight. It was cleaned to separate foreign matter before conducting the experiments.

2.1. Preparation of germinated parboiled rice (GPR)

Purple paddy rice 'Hom Nil' was soaked in water at 35°C for 24 h before draining then incubated at 35°C for 16 h. Germinated paddy rice was then parboiled by steaming for 30

min. The germinated parboiled paddy was dried under various conditions. Thin layer convective drying was conducted using a high-precision hot air laboratory dryer designed at the Institute of Agricultural Engineering, University of Hohenheim, Germany.[8] Germinated parboiled paddy samples were dried under two different air flow modes, over-flow (OF) and through-flow (TF), in a drying chamber (Fig. 1). Drying temperatures were varied at 40, 50, 60, 70 and 80°C with a constant specific humidity of 25 g/kg dry air and an air velocity of 1.0 m/s. The temperature inside the germinated parboiled paddy was monitored by thermocouples inserted into the middle of rice kernels during the drying process. Drying was carried out until the moisture content of germinated parboiled paddy rice reached 13% (w.b.). Drying experiments were performed in triplicate. Dried germinated parboiled paddy was kept in vacuum-sealed aluminium foil pouches at 23 ± 2°C and humidity of 52 ± 3% for 1 day before dehusking. The husk was removed from kernel using a laboratory de-husker (TR250, Kett, Califonia, USA). One hundred grams of germinated parboiled rice (GPR) was then vacuum packed in aluminium foil pouches and kept at a temperature of 23 ± 2°C and humidity of 52 ± 3% before quality analyses.

Over-flow mode (OF)   **Through-flow mode (TF)**

Fig. 1 Hot air direction in two air flow modes inside drying chamber of the dryer.

2.2. Quality analyses

2.2.1. *Head rice yield (HRY)*

After dehusking, the head rice yield was determined using the following formula:[9]

HRY (%) = (mass of head rice / mass of GPR) × 100   (1)

2.2.2. *Color measurement*

A colorimeter (CR-400, Minolta Co., Ltd., Tokyo, Japan) was used to measure color of a whole kernel of dried GPR. Rice samples were filled in a petri dish with diameter of 100 mm and thickness of 15 mm. Measurements were made with illumination area of 11 mm in five positions of a petri dish. The color values were reported in L*, a*, b* color coordination system with a D65 illuminant and 10° observer.

2.2.3. *Texture analysis*

Hardness of cooked GPR was measured using a texture analyzer (TA-XT2i, Stable Micro systems, Surrey, UK) with slightly modified method of Srisang et al.[10] Before testing, the

samples were prepared by cooking 25 g GPR samples in a 250 mL beaker, with 75 mL distilled water about 30 min. Ten of cooked rice kernels were selected from the center of the beaker after cooled at $23 \pm 2°C$ for 30 min. The cylindrical probe with a size of 50 mm was used for testing cooking characteristics. The peak force of the first compression is represented as hardness. The texture profile analysis was repeated five times per replicate.

2.2.4. *Determination of gamma-aminobutyric acid (GABA) content*

Sample extraction was performed with a modified method of Hayat et al.[11] GPR samples were ground and sieved through 1 mm mesh. Five grams of ground sample were added 20 mL of 80% (v/v) methanol and then homogenized for 3 min. The suspension was centrifuged at 5000 rpm, 4ºC for 10 min and the supernatent was collected. Extraction steps were repeated twice then the whole supernatant was filtered through a 0.45 μm of nylon membrane filter with vacuum pump. Supernatants were evaporated under a vacuum at 60°C using a rotary evaporator and adjusted to 5 mL using 80% methanol. The extracted solution was kept at -18°C until analysis.

The GABA contents were determined by a HPLC (model RF-20A prominence, Shimadzu, Kyoto, Japan). The extracted solution (1 mL) was mixed with 1 mL of derivatizing reagent (0.75% of 2-hydroxynaphthaldehyde) and 0.6 mL of borax buffer (pH 8.0). The reaction was performed at 80ºC for 10 min.[12] After the derivatization, chromatographic separation was done by a C_{18} column (Phenomenex, California, USA) at 30°C using methanol : water (62 : 38 v/v) at a flow rate of 1 mL/min as a mobile phase and detected by a diode array UV detector at 254 nm. Results are expressed in mg GABA per 100 g (d.b.). Authentic GABA (Sigma-Aldrich, Munich, Germany) was used as a standard.

3. Results and Discussion

3.1. Drying time

After germination, samples absorbed water, and therefore, the moisture content increased from 11.28 ± 0.28 to $36.32 \pm 0.19\%$ (w.b.). After steaming, the moisture content of paddy increased to $41.51 \pm 0.71\%$ (w.b.). The drying times required for removing the water in parboiled germinated paddy to the moisture content of 13% (w.b.) at the drying temperatures of 40, 50, 60, 70 and 80°C in an OF mode were 390, 195, 130, 100 and 85 min, respectively, while in TF mode were 180, 110, 75, 55 and 45 min, respectively. As expected, higher drying temperature reduced the drying time in both drying air flow modes. Drying using a TF mode shortened the drying time by about half compared to an OF mode at each temperature. This result could be explained by the more uniform airflow distribution in a drying chamber when using a TF mode compared with an OF mode.[13] Uniformity of drying air velocity is known to improve the heat distribution.[14]

3.2. Quality of dried GPR

3.2.1. Head rice yield

Fig. 2 presents the temperatures of drying air, inside temperatures of GPR kernels during drying and the percentages of HRY after dehusking. For a TF mode, a slightly lower percentage of HRY was observed, as compared with the same drying temperature in an OF mode (Fig. 2 F). This present finding is consistent with other research which found that HRY decreased when drying temperature increased.[9] This result can be explained in part by the kernel temperature of TF samples, which increased faster than those of OF samples at the same drying temperature (Fig. 2 A-E). This phenomena caused the cracking inside GPR kernels and lead to kernel breakage during dehusking. The findings are in agreement with Tirawanichakul et al.[15] where the drying air temperature affected HRY of paddy.
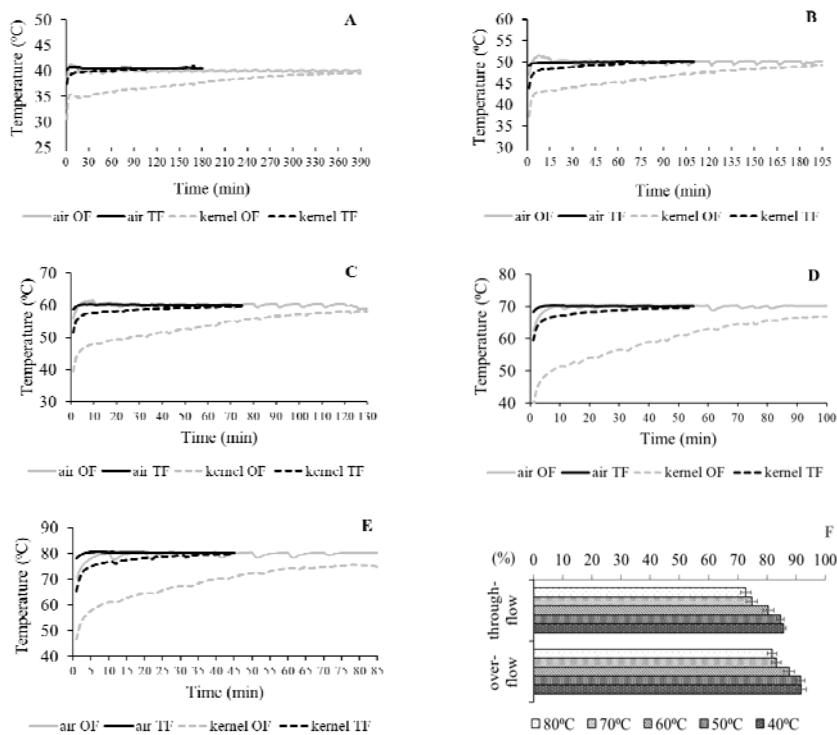
Fig. 2 Hot air and GPR kernel temperature during drying at 40ºC (A), 50ºC (B), 60ºC (C), 70ºC (D), 80ºC (E) and percentage of head rice yield (F) in two airflow modes.

3.2.2. Color of GPR

In this study, airflow mode had a significant effect on color of GPR (Fig. 3). GPR obtained from the drying process with a TF mode had higher lightness (L*) and redness (a*) than

using an OF mode. Comparing between two drying air flow modes, TF mode showed color values closed to the color of raw materials. The purple color of rice kernels is due to the presence of anthocyanin in the bran.[16] Difference in color changes in these two airflow modes might be caused by different contact intensity between hot air and rice bran that affected the degradation of anthocyanin contents. However, the study of an impact of airflow modes on the anthocyanin contents in GPR is currently ongoing. Chen et al.[17] reported that using different drying methods, significantly affects the rice color.
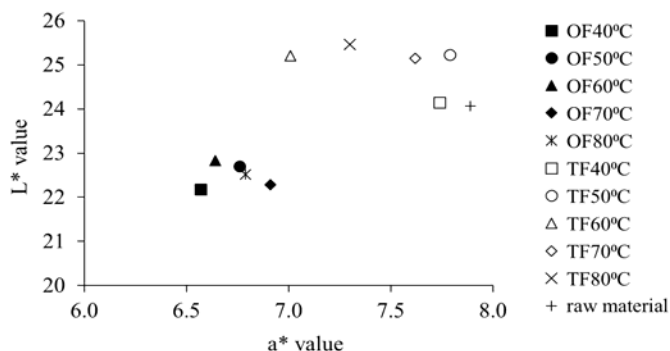
Fig. 3 Color of GPR obtained from drying at various drying temperatures in two airflow modes.

3.2.3. *Hardness of cooked GPR*

Hardness of cooked GPR was different among the difference drying conditions (Table 1). Hardness of dried GPR samples using OF mode was higher than TF mode. This study found a decreasing trend in hardness when increased drying temperature was used under both airflow modes. Drying GPR at 40 and 50°C in OF mode showed higher hardness than brown rice (123 ± 6 N). However, higher drying temperature leads to the reduction of hardness after cooking. Cracking inside grain kernels could result in an increase of water uptake and consequently cause lower hardness in rice. This was confirmed by a percentage of HRY mentioned in previous section of this study.

Table 1. Hardness of cooked dried GPR at various drying temperatures in two airflow modes.

Drying Temperature (°C)	Hardness (N) of cooked GPR	
	over-flow	through-flow
40	140 ± 6 [a]	111 ± 4 [b]
50	133 ± 4 [a]	109 ± 5 [bc]
60	99 ± 5 [d]	73 ± 0 [e]
70	101 ± 8 [cd]	66 ± 1 [ef]
80	94 ± 1 [d]	60 ± 1 [f]

Data are the mean values ± standard deviation and different letters indicate significant difference among mean values in lines and columns (P≤ 0.05 according to Duncan's test).

3.2.4. GABA content

GABA content significantly increased after germination process and elevated again after parboiled process (Fig. 4A). After drying (Fig. 4B), GABA content decreased, especially after prolonged drying at low temperature. Drying at higher temperatures and shorter times prevented GABA degradation, especially at 80ºC. This finding is in agreement with Cheevitsopon and Noomhorm[18] who showed drying temperature and time had significant effects on GABA content in rice. In addition, this study found that airflow modes did not significantly influence the levels of GABA.
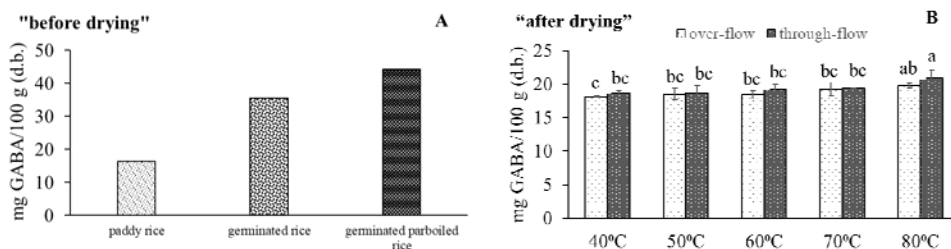
Fig. 4 GABA content of GPR dried at various temperatures in two airflow modes.
Values are the mean and bars indicate standard deviation and different letters indicate significant difference among mean values (P≤ 0.05 according to Duncan's test).

4. Conclusions

The present study was designed to determine the effect of drying conditions on GABA content and quality of GPR. After drying, GABA content of all samples increased compared to the paddy rice due to the germination and steaming process. However, GABA content decreased after drying, especially after prolonged drying at low temperature. Overall, this study showed that GPR drying under the optimal drying conditions, namely using TF mode, significantly conserved color of GPR. However, using an TF mode at high drying temperature leads to low percentage of HRY and reduced hardness after cooking.

5. References

[1] Saerekui, P. Good manufacturing practices for germinated brown rice. Thai Agricultural Standard 2009, TAS 4404-2012, 79–83.

[2] Moongngarm, A.; Saetung, N. Comparison of chemical compositions and bioactive compounds of germinated rough rice and brown rice. Food Chemistry 2010, 122 (3), 782–788.

[3] Cheevitsopon, E.; Noomhorm, A. Effects of parboiling and fluidized bed drying on the physicochemical properties of germinated brown rice. International Journal of Food Science & Technology 2011, 46 (12), 2498–2504.

[4] Dinesh Babu, P.; R. Subhasree, S.; Bhakyaraj, R.; Vidhyalakshmi, R. Brown rice-beyond the color reviving a lost health food - a review. Journal of Agronomy and Crop Science 2009, 2 (2), 67–72.

[5]   Sootjarit, S.; Jittanit,W.; Surojanametakul, V. Effects of drying methods on the nutritional and physical quality of pre-germinated rice. American Society of Agricultural and Biological Engineers 2011, 54 (4), 1423–1430.

[6]   Hashemi, J. Investigation of fissure formation during the drying and post drying of japonica aromatic rice. International Journal of Agriculture and Biology 2008, 6, 179–184.

[7]   Daiponmak, W.; Senakun, C.; Siriamornpun, S. Antiglycation capacity and antioxidant activities of different pigmented Thai rice. International Journal of Food Science & Technology 2014, 49, 1805-1810.

[8]   Argyropoulos, D.; Heindl, A.; Müller, J. Assessment of convection, hot-air combined with microwave-vacuum and freeze-drying methods for mushrooms with regard to product quality. International Journal of Food Science & Technology 2011, 46, 333–342.

[9]   Pruengam, P.; Soponronnarit, S.; Prachayawarakorn, S.; Devahastin, S. Rapid drying of parboiled paddy using hot air impinging stream dryer. Drying Technology 2014, 32 (16), 1949-1955.

[10] Srisang, N.; Prachayawarakorn, S.; Varanyanond, W.; Soponronnarits, S. Germinated brown rice drying by hot air fluidization technique. Drying Technology 2011, 29, 55–63.

[11] Hayat, A.; Jahangir, T. M.; Khuhawar, M. Y.; Alamgir, M.; Siddiqui, A. J.; Musharraf, S. G. Simultaneous HPLC determination of gamma amino butyric acid (GABA) and lysine in selected Pakistani rice varieties by pre-column derivatization with 2-Hydroxynaphthaldehyde. Journal of Cereal Science 2014, 60 (2), 356–360.

[12] Khuhawar, M. Y.; Rajper, A. D. Liquid chromatographic determination of gamma-aminobutyric acid in cerebrospinal fluid using 2-hydroxynaphthaldehyde as derivatizing reagent. Journal of Chromatography B 2003, 788, 413–418.

[13] Udomkun, P.; Argyropoulos, D.; Nagle, M.; Mahayothee, B.; Janjai, S.; Müller, J. Single layer drying kinetics of papaya amidst vertical and horizontal airflow. LWT - Food Science and Technology 2015, 64, 67-73.

[14] Nagle, M.; González Azcárraga, J. C.; Mahayothee, B.; Haewsungcharern, M.; Janjai, S.; Müller, J. Improved quality and energy performance of a fixed-bed longan dryer by thermodynamic modifications. Journal of Food Engineering 2010, 99, 392-399.

[15] Tirawanichakul, S.; Prachayawarakorn, S.; Varanyanond, W.; Tungtrakul, P.; Soponronnarit, S. Effect of fluidized bed drying temperature on various quality attributes of paddy. Drying Technology 2004, 227 (7), 1731–1754.

[16] Hou, Z.; Qin, P.; Zhang, Y.; Cui, S.; Ren, G. Identification of anthocyanins isolated from black rice (Oryza sativa L.) and their degradation kinetics. Food Research International 2013, 50 (2), 691–697.

[17] Chen, X.; Qian, P.; Zhang, X.; Liu, F.; Lu, R. Improving instant rice quality by novel combined drying. Drying Technology 2014, 32,1448–1456.

[18] Cheevitsopon, E.; Noomhorm, A. Effects of superheated steam fluidized bed drying on the quality of parboiled germinated brown rice. Journal of Food Processing and Preservation 2015, 39, 349-356.

Theoretical Study and Case Analysis for a Pre-dried Pyrolysis Coupled Lignite-Fired Power System

Liu, Rongtang[a]; Liu, Ming[a*]; Yan, Junjie[a]

[a]State Key Laboratory of Multiphase Flow in Power Engineering,Xi'an Jiaotong University, Xi'an 71 0049, China

[*]E-mail of the corresponding author: ming.liu@mail.xjtu.edu.cn

Abstract

Lignite, a kind of low rank coal, has the characteristics of high moisture, high volatile, high ash and low heat value. The low-temperature pyrolysis technology is potential to improve the utilization efficiency of lignite. Therefore, a lignite-based energy system integrated with pre-drying and low-temperature pyrolysis was proposed in this paper. To assess the influence of pre-drying process, theoretical models were developed based on thermodynamics, and a case analysis was then performed to get the quantitative effect of pre-drying on efficiency of energy utilization. Results show that pre-drying on PPPS theoretical model can significantly improve the utilization of lignite by 1.46%.

Keywords: Lignite; Pre-drying; Low-temperature pyrolysis; Energy efficiency; Case analysis.

1. Introduction

Lignite is worldwidely considered as inferior fuel with abundant supply.[1] It is mainly used in power plants. However, the conventional lignite-fired power system (CLPS) is costly, not efficient and with high pollutant emissions. Lignite upgrading technologies, including pre-drying and pyrolysis, are effectively to improve lignite utilization efficiency. Therefore, many researches were conducted for the lignite pre-drying[2, 3, 4] and pyrolysis[5, 6] technologies. However, these two technologies are isolatedly used. The integration of the lignite pre-drying and pyrolysis may realize the energy cascade utilization and then increase the utilization of lignite. Therefore, a pre-dried pyrolysis coupled lignite-fired power system (PPPS) was proposed in this paper.

The proposal of PPPS aims to overcome the disadvantages of the pyrolysis process by the integration of pre-drying. However, the research on influences of pre-drying process on pyrolysis system is not deepgoing and unambiguous. In this paper, theoretical models were developed based on thermodynamics, and a case analysis was then performed to get the quantitative effects of pre-drying. Moreover, the energy and exergy analysis were carried out to uncover the energy saving mechanism.

2. System proposal

The schematic of a PPPS is schematically presented in Fig.1 Raw lignite (point 1) is fed into the steam dryer and pre-dried primarily. The primary pre-dried lignite (point 2) is then fed into the drying unit and pre-dried ultimately. Afterwards, the ultimate pre-dried lignite (point 3) is led to the pyrolysis unit, heated by the elevated temperature flue gas, pyrolyzed and separated into char (point 4), tar (point 13), pyrolysis gas (point 21) and water (point 12) in pyrolysis furnace. The tar and pyrolysis gas are recycled as products. Nevertheless, the char is converted by a series of energy forms and transformed into electricity (point 20), eventually. Waste steams (point 5, 6, and 12) generated in the process are exhausted to environments. The heat source of pyrolysis furnace is the elevated temperature flue gas (point 11) extracted from the boiler unit and led to the inlet of the burner. The heat source of the drying unit in the pyrolysis system is the flue gas (point 10) exhausted from the pyrolysis chamber. The flue gas (point 9) is extracted to the boiler unit by the pump after releasing heat in the drying unit, the waste heat of which is recycled by the regenerative air preheaters. The heat source of the steam pre-drying unit is the 5# low-pressure extraction steam (point 7) from the turbine unit. The steam is led to the steam dryer, condensed after releasing heat, and recovered in the de-aerator. The steam dryer makes full use of the low grade energy contained by the extraction steam from regenerative system, and reduces the heat load in the pyrolysis system.
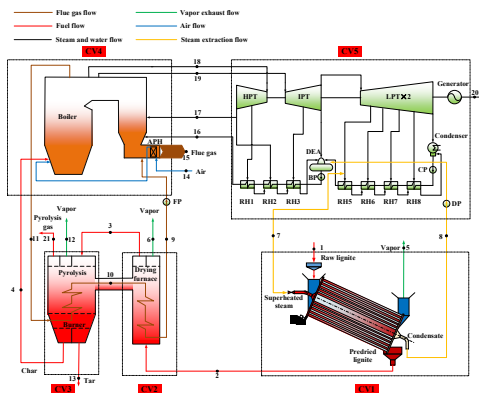
Fig.1 The pre-dried pyrolysis coupled lignite-fired power system. Note: APH, air preheater; HPT, high-pressure turbine; IPT, intermediate-pressure turbine; LPT, low-pressure turbine; DEA, de-aerator; RH, regenerative heater; CP, condensate pump; BP, boiler feed-water pump exchangers; DP, drain water pump; FP, flue gas backflow pump; CV1, steam pre-drying unit; CV2, drying furnace unit; CV3, pyrolysis unit; CV4, boiler unit; CV5, steam turbine unit.

3. Model development

In this paper, the reference pressure and the temperature are given, as follows;

$$p_0 = 0.1013 \text{ MPa} \tag{1}$$

$$T_0 = 298.15 \text{ K} \tag{2}$$

The calculations of enthalpy, higher heating value, and exergy are all based on this condition. In this part, the belt pyrolysis furnace is selected as pyrolysis model. The following pyrolysis reaction occurs when the temperature and pressure of the pyrolysis furnace remains constant.

$$\text{predried lignite(s)} \rightarrow \text{char(s)} + \text{tar(l)} + \text{gas(g)} + \text{water(g)} \tag{3}$$
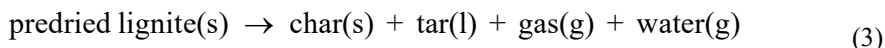
The parameters in pyrolysis process are shown in Table 1, where HHV_* is higher heating value; h_* is the specific enthalpy at $kJ \cdot kg^{-1}$; t_* is the temperature at °C; λ_* is pyrolysis production rate defined as the (*) mass rate produced from unit mass of feed for pyrolysis furnace, $kg \cdot kg^{-1}$. μ (γ) is the degree of pre-drying defined as the moisture mass released from unit mass of raw lignite (primary predried lignite), $kg \cdot kg^{-1}$.

Table 1. The parameters of pyrolysis process.

Predried lignite	Char	Tar	Gas	Water
P_0	P_0	P_0	P_0	P_0
h_{ul}	h_c	h_t	h_g	h_{wa}
HHV_{ul}	HHV_c	HHV_t	HHV_g	−
t_{ul}	t_p	t_p	t_p	t_p
−	λ_c	λ_t	λ_g	λ_{wa}
$B(1\text{-}\mu)(1\text{-}\gamma)$	$\lambda_c \cdot B(1\text{-}\mu)(1\text{-}\gamma)$	$\lambda_t \cdot B(1\text{-}\mu)(1\text{-}\gamma)$	$\lambda_g \cdot B(1\text{-}\mu)(1\text{-}\gamma)$	$\lambda_{wa} \cdot B(1\text{-}\mu)(1\text{-}\gamma)$

By applying an enthalpy balance for the overall pyrolysis, the flue gas mass flow (D'_f) needed in the pyrolysis can be obtained:

$$D'_f = \frac{\lambda_c \left(HHV_c + h_c \right) + \lambda_t \left(HHV_t + h_t \right) + \lambda_g \left(HHV_g + h_g \right) + \lambda_{wa} h_{wa} - \left(HHV_{ul} + h_{ul} \right)}{\left(h_{pin} - h_{fin} \right) \cdot \eta_p}$$

$$\cdot B \left(1 - \mu \right) \left(1 - \gamma \right) \tag{4}$$

where η_p is the thermal utilization efficiency of the pyrolysis furnace; and h_{pin} is the specific enthalpy of flue gas in pyrolysis furnace inlet. Pyrolysis gases products are obtained as mixture, containing CO, H_2, CO_2 and hydrocarbons (CH_4, C_2H_4, C_2H_6, C_3H_6 and C_3H_8). The HHV_g is calculated as follow;

$$HHV_g = \sum w_i \cdot HHV_i \tag{5}$$

where HHV_i is the higher heating value of constituent (i) in pyrolysis gas calculated by CoolProp and w_i is the mass fraction of constituent (i). D_f and D'_f are equal by adjusting t_{fin} in MATLAB. D_f is the flue gas mass flow needed in the drying furnace unit. The energy and exergy flow ratios of each control volume and the power system to the input energy or exergy are defined as follows;

$$\varepsilon_L^{en} = \frac{Q}{B \cdot LHV_{raw}} \times 100\% \tag{6}$$

$$\varepsilon_H^{en} = \frac{Q}{B \cdot HHV_{raw}} \times 100\% \tag{7}$$

$$\varepsilon^{ex} = \frac{E}{B \cdot HHV_{raw}} \times 100\% \tag{8}$$

where LHV is the lower heating value at $kJ \cdot kg^{-1}$; Q is the energy flow based on LHV in equation (6) and based on HHV in equation (7) at kW; E is the exergy flow at kW; and ε is the efficiency.

4. Results and discussion

4.1. Results of calculation

4.1.1 Reference case

The lignite pyrolysis power system (LPPS, only involving CV2, CV3, CV4 and CV5 in Fig.1) is derived from a conventional lignite-fired power system (CLPS)[7] with the pyrolysis system integrated, the parameters of which are set with reference to the CLPS. The parameters of live steam and reheat steam, including temperature, pressure and mass flow rate of LPPS are assumed similar to those of the CLPS. The temperature of boiler flue gas before the air preheater is assumed to be the same as the CLPS. The boiler exhaust temperature decreases to 126°C in the LPPS. The performances of the LPPS are calculated, and the thermodynamic properties of the state points of the LPPS are shown in Table 2.

Table 2. Thermodynamic properties of the state points of LPPS.

Point	Substance	Temperature °C	Pressure MPa	Mass flow rate,kg·s⁻¹	Exergy kJ·kg⁻¹	Exergy flow,kW
2	Raw lignite	25	0.1013	187.9878	13080	2458900
3	Predried lignite	300	0.1013	122.9542	20111	2472700
4	Char	550	0.1013	84.7154	23913	2025800
6	Steam	200	0.1013	65.0336	520.16	33828
9	Flue gas	350	0.1013	526.1187	119.11	62665
10	Flue gas	752.2	0.1013	526.1187	409.53	215460
11	Flue gas	1200	0.1013	526.1187	823.43	433220
12	Steam	550	0.1013	8.6068	927.96	7986.8
13	Tar	550	0.1013	6.4797	34652	224530
14	Air	25	0.1013	799.1080	0	0
15	Flue gas	126	0.1013	863.3152	18.178	15693
16	Water	284	30.400	527.7806	348.08	183710
17	Steam	323.3	4.8310	448.2778	810.70	363420
18	Steam	566	24.200	527.7806	1533.3	809260
19	Steam	566	4.3480	448.2778	1125.3	504460
20	Electricity	–	–	–	–	600000
21	Pyrolysis gas	550	0.1013	19.8079	17956	355670

By calculation, the thermal efficiency of the LPPS is 52.886% based on LHV, and 47.997% based on HHV. The exergy efficiency of the LPPS is approximately 48.00%.

4.1.2 Pre-dried pyrolysis coupled lignite-fired power system

The PPPS is put forward in previous part as shown in Fig.1.The parameters are assumed similar to those of the LPPS. The performances of the PPPS are calculated, and the thermodynamic properties of the state points are shown in Table 3.

Table 3. Thermodynamic properties of the state points of PPPS.

Point	Substance	Temperature °C	Pressure MPa	Mass flow rate,kg·s⁻¹	Exergy kJ·kg⁻¹	Exergy flow,kW
1	Raw lignite	25	0.1013	168.4627	13080	2203492
2	Predried lignite	99.6	0.1013	126.6086	17417	2205200
3	Predried lignite	300	0.1013	110.1837	20111	2215900
4	Char	550	0.1013	75.9166	23913	1815400
5	Steam	99.6	0.1013	41.8541	485.45	20318
6	Steam	200	0.1013	16.4249	545.46	8959.2
7	Steam	258.1	0.4232	53.4036	783.17	41824
8	Water	145.7	0.4232	53.4036	82.178	4388.6
9	Flue gas	420.96	0.1013	356.1046	162.25	57778
10	Flue gas	600	0.1013	356.1046	287.78	102480
11	Flue gas	1200	0.1013	356.1046	823.44	293230
12	Steam	550	0.1013	7.7129	927.96	7157.3
13	Tar	550	0.1013	5.8067	34652	201210
14	Air	25	0.1013	716.1097	0	0
15	Flue gas	126	0.1013	773.6530	18.177	14063
16	Water	284	30.400	527.7806	348.08	183710
17	Steam	323.3	4.8310	448.2778	810.70	363420
18	Steam	566	24.200	527.7806	1533.3	809260
19	Steam	566	4.3480	448.2778	1125.3	504460
20	Electricity	–	–	–	–	569870
21	Pyrolysis gas	550	0.1013	17.7506	17956	318730

By calculation, the thermal efficiency of the PPPS is 54.507% based on LHV, and 49.458% based on HHV. The exergy efficiency of the PPPS is approximately 49.46%. Obviously, due to the steam pre-drying process, the PPPS theoretical model can evidently increase the efficiency of the LPPS by approximately 1.46% based on the HHV, and by 1.62% based on the LHV at the calculation condition.

4.2. Energy and exergy analysis

4.2.1 Energy analysis

The energy flows and losses of the LPPS and PPPS are illustrated in Fig.2a and Fig.2b respectively. The energy input to the system is expressed by the HHV of raw lignite in order to avoid the phenomenon of "Non-conservation of energy"[8]. The energy outputs involve 14.46% in the pyrolysis gas, 9.13% in the tar and 24.40% in electricity. The highest amount of energy loss is from the turbine unit, followed by the drying furnace in the LPPS. 29.63% energy is extracted from the boiler unit and only 56.83% energy is transferred to the steam. Comparatively, the electricity output in the PPPS is improved by 1.46%. However, the pyrolysis gas and tar outputs are invariable because of the constant yield for the pyrolysis unit. Only 22.38% energy is extracted from the boiler unit and 63.42% energy is transferred to the steam. Using the energy analysis, the reason for the improved efficiency of the PPPS can be explained. The energy mostly discharged from the turbine is recycled by pre-drying lignite, and this energy is mainly transferred to the available energy in lignite.

(a)   *(b)*
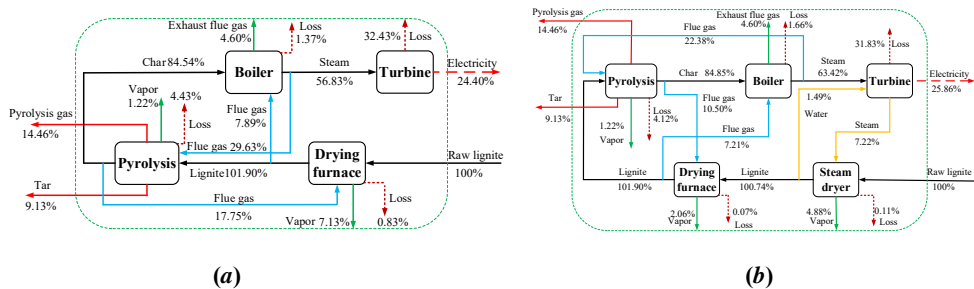
Fig.2 Energy flow and loss charts:(a)LPPS and (b) PPPS.

4.2.2 Exergy analysis

On the basis of the Table 2 and Table 3, the exergy flow, loss and destruction charts between the units of the LPPS and PPPS are illustrated in Fig. 3a and Fig. 3b, the data of which represent the exergy ratio to the input exergy of the system. The maximal loss and destruction in LPPS are the combustion process in the boiler unit, followed by the drying furnace unit. The low grade steam is firstly used to pre-dry the lignite, and then, the flue gas at the low temperature is used as the pre-drying heat source. In the whole drying process, the heat transfer temperature difference of PPPS is much lower than that of LPPS. Therefore, the exergy lost during the pre-drying is decreased significantly. Meanwhile, the lesser exergy extracting from the boiler also decreases the exergy lost in the boiler unit. Because of the exergy extracting, the lost in turbine is increased slightly. The exergy analysis suggests that the low heat transfer temperature difference and low grade energy recycling make the exergy efficiency increased.
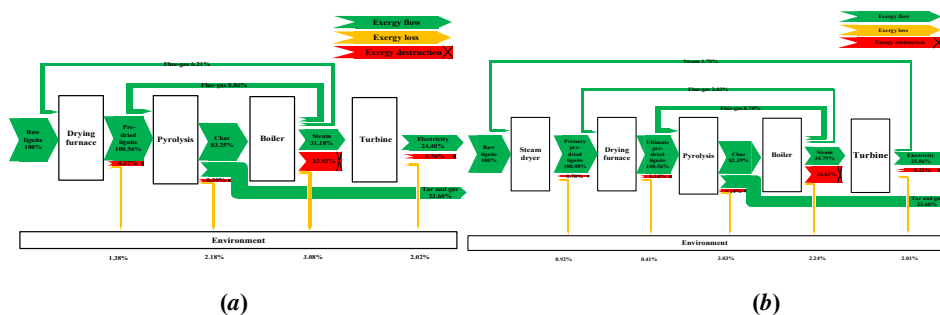
Fig.3 Exergy flow, loss and destruction charts:(a)LPPS and (b) PPPS.

5. Conclusions

A novel lignite-based energy system integrated with PPPS was proposed and thermodynamically analyzed in this paper. The thermal efficiency of the power system could be significantly increased by 1.62% (1.46%) based on the LHV (HHV). The energy mostly discharged from the turbine is recycled by pre-drying lignite, and this energy is mainly transferred to the available energy in lignite. The exergy analysis suggests that the low heat transfer temperature difference and low grade energy recycling make the exergy efficiency increased.

6. References

[1] Thielemann, T.; Schmidt, S.; Peter Gerling, J. Lignite and hard coal: Energy suppliers for world needs until the year 2100-An outlook. International Journal of Coal Geology 2007, 72(1), 1-14.

[2] Karthikeyan, M. Minimization of moisture readsorption in dried coal samples. Drying Technology 2008, 26(7), 948–955.

[3] Liu, M.; Yan, J.; Wang, J.; Chong, D.; Liu, J. Thermodynamic analysis on a lignite-fired power system integrated with a steam dryer: Investigation on energy supply system of the dryer. Drying Technology 2015, 33(12), 1510-1521.

[4] Liu, M.; Wang, J.; Yan, J.; Chong, D.; Liu, J. A combined-type fluid-bed dryer suitable for integration within a lignite-fired power plant: System design and thermodynamic analysis. Drying Technology 2014, 32(8), 902-909.

[5] Yi, Q.; Feng,J.; Lu, B.; Deng, J.; Yu, C.; Li, W. Energy evaluation for lignite pyrolysis by solid heat carrier coupled with gasification. Energy& Fuels 2013, 27(8) 4523-4533.

[6] Zhang, Y.; Wang, Y.; Cai, L.; Yao, C.; Gao, S.; Li, C.; Xu, G. Dual bed pyrolysis gasification of coal: Process analysis and pilot test. Fuel 2013, 112, 624-634.

[7] Liu, M.; Yan, J.; Bai, B.; Chong, D.; Guo, X.; Xiao, F. Theoretical study and case analysis for a predried lignite-fired power system. Drying Technology 2011, 29(10), 1219-1229.

[8] Liu, M.; Li, G.; Han, X.; Qin, Y.; Zhai, M.; Yan, J. Energy and exergy analyses of a lignite-fired power plant integrated with a steam dryer at rated and partial loads. Drying Technology 2017, 35(2), 203-217.

The Effect of Ohmic Heating Pretreatment on Drying of Apple

Kutlu, N.ª; Yilmaz, M. S.ª; Arslan, H.ª; Isci, A.ª*; Sakiyan, O.ª

ª Ankara University, Department of Food Engineering, Golbasi, Ankara, Turkey

*E-mail of the corresponding author: isci@ankara.edu.tr

Abstract

In this study, effects of ohmic pretreatment on the drying rates and color kinetics of apple were investigated. Apple slices were treated at different electric field strengths (20-30 and 40 V/cm) at 60°C for 1 min. Drying process was applied at 60°C-2 m/s by using a tray-dryer. ΔE and moisture content were calculated. These values were fitted to the semi-theoretical thin-layer drying and the zero and first-order kinetic model. The shortest drying time was found samples treated with 30 V/cm. Wang&Singh model gave the superior fit to the experimental data. ΔE fitted well to the zero-order kinetic model.

Keywords: *: Ohmic heating, drying, kinetic models, thin-layer models, apple.*

1. Introduction

The main purpose of drying is to reduce the water activity in order to extend the shelf life. The dried product has the lowest microbiologic deterioration and enzyme activity.[1] Besides, quality attributes like aroma and the nutritional value are protected by reducing the moisture. The other purpose of the drying process is to provide convenience for transportation and storage via reducing the volume of product.[2] The drying process is generally applied to fruits and vegetables.

The apple which belongs to Rosaceae, the rose family, is a mild season fruit. Apple which has rich antioxidant components, carbohydrates, essential minerals and dietary fiber has a great importance in terms of taste and nutritional value [3]. North Anatolia, Black Sea shore region, Central Anatolia, and East Anatolia plateau are the fields in Turkey which are suitable for apple cultivation. In our country, mainly Starking, Golden Delicious, Star Crimson and Granny Smith are cultivated among 30 strains of apples from all over the world.[4]

Pretreatment of foods before drying takes place to reduce the drying time and also increase the quality of the product. There are different types of pretreatment such as hot-water blanching, osmotic dehydration, ultrasonication. Ohmic heating is one of the newest alternative pretreatment methods.[5-7] With ohmic process, the alternative electric current is passed through the food. The process is also called thermal processing method.[8]

Thin layer drying is the drying of food samples by layer. Thin layer drying has been taken part in several studies in recent years. The reason is the convenience of application and less data requirement.[9]

The main purpose of this study is to pretreat the apple samples (Golden Delicious variety) with ohmic heating and to dry using tray dryer. The samples were pretreated at different electric field strengths (20, 30, 40 V/cm) at 60°C for 1 minute. After the pretreatment process, the samples were dried by a tray dryer at 2 m/s air velocity at 60°C. Moisture ratio and changes in color were recorded. These values were fitted to the semi-theoretical thin-layer drying and the zero and first-order kinetic models.

2. Material and Methods

2.1. Material

Apples used in this study were bought from local market in Ankara, Turkey. They were peeled and cut into slices with dimensions of 15×15×5 mm. The initial moisture content of the fresh apple samples was 85±1% (wb) and it was measured by infrared moisture analyzer (MA150, Sartorius, Germany) at 105°C.

2.2. Methods

2.2.1. Ohmic Heating Pre-Treatment

Ohmic heating pretreatment was performed using (CLOH-1000, CLS, Turkey), specially designed and manufactured by Caliskan company. 90 mL of water was added to the 20 g of apple sample. Afterwards, apple slices were exposed to different electric field strengths (20, 30 and 40 V/cm) at 60°C for 1 min. Samples were filtered and weighed at the and of the process. All experiments were done in duplicates.

2.2.2. Hot-air Drying

Hot-air drying was performed in a tray dryer (Eksis, TK-LAB, Turkey). Samples dried without pretreatment was used as a control. The control samples were treated with air at 60ºC and velocity of 2 m/s. For the main drying process, the ohmic pretreated samples were dried at 60ºC and with an air velocity of 2 m/s. The weight of samples was recorded at 5 min intervals and drying was continued until no further variation in their weight were observed. The dried samples were cooled in desiccators and vacuum packed in heat-sealed low-density polyethylene bags.

2.2.3. Thin Layer Modelling

To define drying kinetics of apple samples, dimensionless moisture ratio (MR) values were calculated. MR were determined from moisture content data (kg water/kg db) obtained during drying by using equation 1:

$$MR = \frac{M_t - M_e}{M_0 - M_e}$$

(1)

where, M_t, M_0 and M_e are the moisture content at time t, the initial moisture content and the equilibrium moisture content of the sample (kg water/kg db), respectively.

Four different thin layer drying models (Table 1) were applied to drying curves. Sigma plot was used to predict model parameters. The model with the lowest Root Mean Square Error (RMSE) and the chi-square (χ^2) was defined as the best model describing the thin layer drying behavior of apple.[10] The parameters were calculated using equation 2 and 3.

$$RMSE = \left[\frac{1}{N} \sum_{i=1}^{N} \left(MR_{exp,t} - MR_{pre,t} \right)^2 \right]^{1/2}$$

(2)

$$\chi^2 = \frac{\sum_{i=1}^{N} \left(MR_{exp,t} - MR_{pre,t} \right)^2}{N - n}$$

(3)

where $MR_{exp;i}$ and $MR_{pre;i}$ are the experimental and predicted moisture ratios of data i, respectively. N is the number of experimental data points and n is the number of constants in the model.

Table 1. Thin layer models equations

Model	Model Name	References
$MR=exp(-kt^n)$	Page	[11]
$MR=aexp(-kt)$	Henderson and Pabis	[12]
$MR= aexp(-kt)+c$	Logarithmic	[13]
$MR=1+at+bt^2$	Wang & Singh	[14]

2.2.4. Color Values and Color Kinetics

The color values of dried and fresh apple samples were measured by using Minolta Color Reader (CR-400, Japan) and expressed as the CIE L*, a*, and b* color scale. The average of ten different readings from the same region was reported.

Total color differences were calculated using equation 4:

$$\Delta E = \sqrt{(L^*_0 - L^*_t)^2 + (a^*_0 - a^*_t)^2 + (b^*_0 - b^*_t)^2} \tag{4}$$

where L^*_0, a^*_0, b^*_0 are the initial color measurements of raw apple samples and L^*_t, a^*_t, b^*_t are the color measurements at specified time. ΔE values are applied to zero (equation 5) and first order (equation 6) kinetic models:[15]

$$C = C_0 \pm kt \tag{5}$$

$$C = C_0 exp(\pm kt) \tag{6}$$

where C_0 is the initial value of color, C is the color value at a specified time, k is the kinetic rate constant and t is time.

3. Results and Discussions

The effect of electric field strengths on drying time was depicted in Fig. 1. The results showed that the samples treated with 30 V/cm electric field strength was found to have the shortest drying time. Compared to control group, ohmic heating pretreatment have decreased the drying time by 24, 35 and 29% for the samples treated with 20, 30 and 40 V/cm electrical field strengths, respectively. It was also observed that moisture ratio decreased continuously with drying time.
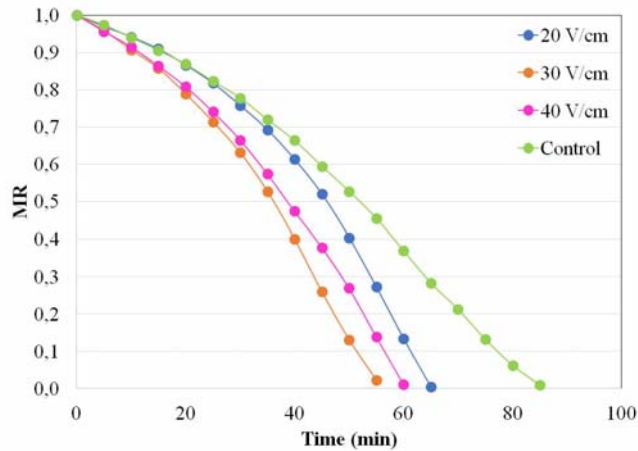
Fig. 1. Effect of electric field strenghts on drying time

The moisture ratio data were fitted to four different thin layer drying models (Table 1). RMSE (Root Mean Square Error), $\varkappa^2$ (chi-square) and R^2 (coefficient of determination) values were used to compare the relative goodness of fit of experimental data. The results showed that Wang & Singh model gave the superior fit to the experimental data compared to other models (Table 2). Similar model results were found in the other papers with different drying methods.[16-20]

Table 2. Statistical parameters and coefficients of models at different electrical field strengths for Wang & Singh model

Process Conditions	RMSE	$\varkappa^2$	R^2	a	b
Control	0.010166735	0.000116283	0.9978	-0.005576	-0.0000773
20 V/cm	0.010646449	0.000132238	0.9983	-0.001900	-0.0002048
30 V/cm	0.001837387	0.000004051	0.9987	-0.006242	-0.0002164
40 V/cm	0.002985566	0.000010534	0.9998	-0.006250	-0.0001698

Final color values and color kinetics of ohmic pretreated dried apples were determined in the study. The color differences (ΔE) were calculated by using the measurable color values (L*, a* and b*) at different electrical field strengths. The ΔE values were fitted to zero and first order kinetic models (Fig. 2 and 3). The results showed that the ΔE values were fitted well to the zero-order kinetic model. Similar results can also be found in the literature.[21-25]
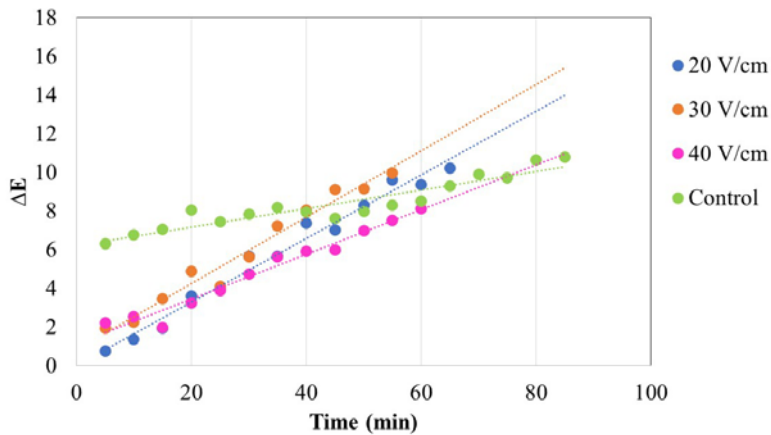
Fig. 2. Zero order kinetic model
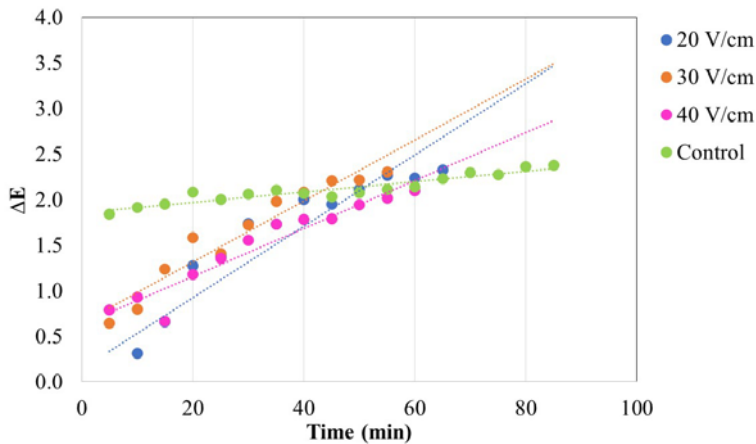
Fig. 3. First order kinetic model

Table 3. Zero and first order kinetic model parameters

Process Conditions	Model	C_0	k	R^2
Control	$C=C_0+kt$	6.304804	0.0490	0.8754
	$C=C_0 \exp(-kt)$	1.841312	0.0057	0.8868
20 V/cm	$C=C_0+kt$	0.750296	0.1643	0.9791
	$C=C_0 \exp(-kt)$	-0.287290	0.0392	0.8602
30 V/cm	$C=C_0+kt$	1.903552	0.1717	0.9710
	$C=C_0 \exp(-kt)$	0.643721	0.0335	0.9291
40 V/cm	$C=C_0+kt$	2.194434	0.1158	0.9682
	$C=C_0 \exp(-kt)$	0.785924	0.0263	0.9209

4. Conclusions

Ohmic heating is an emerging thermal process technology. Ohmic heating can be used successfully as a pretreatment method in the drying process of food materials. As a conclusion in this study, the samples treated with 30 V/cm electric field strength was found to have the shortest drying time. Compared to control group, ohmic heating treatments have decreased the drying time by 24, 35 and 29% for the samples treated with 20, 30 and 40 V/cm electrical field strengths, respectively. Wang & Singh models gave the superior fit to the experimental data compared to other models. In addition, the color values fitted well to the zero-order kinetic model.

5. Nomenclature

wb   Wet basis

db   Dry basis

6. References

[1] Cemeroglu, B.; Özkan, M. 2004. Kurutma teknolojisi, Meyve Sebze İsleme Teknolojisi, 2. Cilt, Cemeroğlu, Bizim Büro Yayınevi, Ankara, Turkey, pp. 479-613.

[2] Ceylan, İ.; Aktaş, M.; Dogan, H. Güneş Enerjili Kurutma Fırınında Elma Kurutulması Journal of Polytechnic, 2006, 9 (4), 289-294.

[3] Coskun, S.; Askın, M.A. Bazı Yerli Elma Çeşitlerinin Pomolojik ve Biyokimyasal Özelliklerinin Belirlenmesi. Süleyman Demirel Üniversitesi Ziraat Fakültesi Dergisi 2016, 11 (1), 120-131.

[4] Mordogan, N.; Ergün, S. Golden ve Starking Elma Çeşitlerinin Şeker İçerikleri ve Bitki Besin Elementleri ile Olan İlişkileri. Ege Üniv. Ziraat Fak. Derg 2002, 39 (1), 103-110.

[5] Salengke, S.; Sastry, S.K. Effect of ohmic pretreatment on the drying rate of grapes and absorption isotherm of raisins. Drying Technology 2005, 23, 551-564.

[6] Icier, F. Ohmic blanching effects on drying of vegetable byproduct. Journal of Food Process Engineering 2010, 33, 661-683.

[7] Jaeger, H.; Roth, A.; Toepfl, S.; Holzhauser, T.; Engel, K.H.; Knorr, D.; Vogel, R.F.; Bandick, N.; Kulling, S.; Heinz, V.; Steinberg, P. Opinion on the use of ohmic heating for the treatment of foods. Trends in Food Science&Technology 2016, 55, 84-97.

[8] Hosainpour, A.; Darvishi, H.; Nargesi, F.; Fadavi, A. Ohmic pre-drying of tomato paste. Food Sci Technol Int. 2014, 20 (3),:193-204.

[9] Kutlu, N.; İşci, A.; Sakiyan, O. Gıdalarda ince tabaka kurutma modelleri. Gıda 2015, 40 (1), 21-27.

[10] Wang, J.; Xi, Y.S. Drying characteristics and drying quality of carrot using a two-

stage microwave process. Journal of Food Engineering 2005, 68, 505-511.

[11] Sarsavadiva, P.; Sawhney, R.; Pangavhane, D.R.; Sing, I. Drying behaviour of brined onion slices. J Food Eng 1999, 40, 219-226.

[12] Henderson, S.M.; Pabis, S. Grain drying theory I: Temperature effect on drying coefficient. Journal of Agriculture Research Engineering 1961, 6, 169-174.

[13] Yaldız, O.; Ertekin, C.; Uzun, H.I. Mathematical modeling of thin layer solar drying of sultana grapes. Energy 2001, 26, 457-465.

[14] Wang, C.Y.; Singh, R.P. A Single Layer Drying Equation for Rough Rice. Am. Soc. Agr. Eng. 1978, 78, pp.3001, St. Joseph, MI.

[15] Dadali, G.; Demirhan, E.; Ozbek, B. Color Cahnge Kinetics of Spinach Undergoing Microwave Drying. Drying Technology 2007, 25, 1713-1723.

[16] Soponronnarit, S.; Pongtornkulpanich, A.; Prachayawarakorn, S. Drying characteristics of corn in fluidized bed dryer. Drying Technology 1997, 15 (5), 1603–1615.

[17] Khawas, P.; Dash, K.K.; Das, A.J.; Deka, S.C. Drying characteristics and assessment of physicochemical and microstructural properties of dried culinary banana slices. International Journal of Food Engineering 2015, 11 (5), 667-678.

[18] Blanco-Cano, L.; Soria-Verdugo, A.; Garcia-Gutierrez, L.M.; Ruiz-Rivas, U. Modeling the thin-layer drying process of Granny Smith apples: Application in an indirect solar dryer. Applied Thermal Engineering 2016, 108, 1086-1094.

[19] Seshachalam, K.; Thottipalayam Velliangiri, A.; Selvaraj, V. Drying of carrot slices in a triple pass solar dryer. Thermal Science 2017, 21 (2), 389-398.

[20] Vijiyan, S.; Thottipalayam Velliangiri, A.; Kumar, A. Thin layer drying characteristics of curry leaves (murraya koenigii) in an indirect solar dryer. Thermal Science 2017, 21 (2), 359-367.

[21] Barreiro, J.A.; Milano, M.; Sandoval, A.J. Kinetics of colour change of double concentrated tomato paste during thermal treatment. Journal of Food Engineering 1997, 33 (3-4), 359-371.

[22] Chutintrasri, B.; Noomhorm, A. Color degradation kinetics of pineapple puree during thermal processing. LWT - Food Science and Technology 2007, 40 (2), 300-306.

[23] Dadali, G.; Demirhan, E.; Özbek, B. Color change kinetics of spinach undergoing microwave drying. Drying Technology 2007, 25, 1713-1723.

[24] Demirhan, E.; Özbek, B. Color change kinetics of microwave-dried basil. Drying Technology 2009, 27, 156-166.

[25] Demirhan, E.; Özbek, B. Color change kinetics of tea leaves during microwave drying. International Journal of Food Engineering 2015, 11 (2), 255-263.

Energy performance of an industrial superheated steam heat pump flash dryer for drying of bio-fuel

Renström, R.[a]*; Johansson-Cider, H.; Brunzell, L. [c]

[a] Karlstad University, Environmental and Energy Systems, 651 88 Karlstad, Sweden,
Tel +46547001000

*E-mail of the corresponding author: roger.renstrom@kau.se

Abstract

Drying is an energy demanding industrial process and methods for reducing the energy consumption of drying is of interest to industry as well as society. This article presents the drying system of a biofuel factory. Steam is used as the refrigerant. Superheated steam is used as drying gas in a flash dryer with 28.8 tons/h dewatering capacity. The system includes an energy recovering water heat pump that receives its heat from the excess drying steam and heats the dryer. The SMER of the drying process ranges between 3 and 4 and the COP of the heat pump process ranges between 4 and 5.5 during one production season of peat drying. Variations in performance can be explained by variations in inlet moisture content and production rate. The example of this drying system shows the feasibility of drying in superheated steam, heat pump drying and water as refrigerant in high-temperature heat pumps.

Keywords: steam drying; heat pump process; peat; sawdust; industrial operation

1. Introduction

Methods for reducing the energy consumption of drying processes are of interest to industry as well as society. There is also a desire to replace fossil fuels with renewable fuels, such as fuel pellets or briquettes made from biomass. Compact biomass in the form of fuel pellets or briquettes has a higher heating value, lower moisture content and higher density than unprocessed biofuel; their properties are also more uniform. Pelletizing or briquetting thus improves transport properties as well as storage and combustion properties [1].

Wet biomass must be dried before briquetting and pelletizing. Various dryer designs can be chosen, depending on the properties of the material being dried and on available sources of energy [2]. Packed moving bed dryers can achieve the desired moisture content of 5-25 % at drying temperatures of 80-150 °C. They are relatively cheap, but require a larger installation area than other dryers. Rotary dryers are common for drying woodchips and sawdust. They operate reliably and enable heat recovery from the exhaust drying medium, which increases the energy efficiency of the system. Pneumatic dryers, also known as flash dryers, are compact and suitable for drying particles or granules [3]. In a flash dryer the particles are mixed with a high temperature drying gas, often air or flue gas, and transported by the drying gas at a high velocity. High flow velocity mixes well and gives high heat and mass transfer rates. The technology is, however, associated with high energy consumption. Typical energy consumption for a flash dryer is 4500-9000 kJ/kg of water [2], but energy efficiency can be improved by heat recovery of the exhaust drying medium [3]. In a flash dryer, steam can be used as drying gas. Steam has many advantages over air and flue gas. The energy advantage of steam as drying gas is that it simplifies heat recovery by enabling dryer integration, which is the factor that determines the energy efficiency of a steam dryer [4]. By recovering energy in a superheated steam drying process, more than 90 % of energy needs can be reduced [5]. As an example, a superheated steam flash dryer at Rockhammar mill, Sweden, uses 0.4-0.7 GJ per ton pulp whereas the same flash dryer with air as drying gas requires 3.0-3.5 GJ per ton pulp, a reduction by 75-90 % [6]. The environmental advantage of steam drying is that the dryer does not result in air pollution, since drying gas is not released into the atmosphere. The excess steam condensate will, on the other hand, need wastewater treatment as it can contain terpenes, fatty acids, formaldehyde and other types of contamination, depending on type of biomass and drying conditions. These organic compounds are released from the biomass as it is heated [7] [8] [9] [10] [4]. A further benefit of steam drying is that since there is no oxygen present in the dryer no oxidation can occur, this in turn leads to a minimal risk of ignition during operation [6].

Heat pump drying is a way of reducing energy consumption even further. It also brings additional benefits such as improved process control, which in its turn is beneficial for the quality of many dried products, such as foodstuffs. Drying of foodstuffs and timber are the two fields in which heat pump drying has so far reached the market [11]. The technology of

heat pump drying has been known for decades, but it is still under-exploited. Heat pump dryers are claimed to be complex systems: a change in one component brings changes to other components as well [11] [12].

This article describes an example of large-scale industrial heat pump drying of biofuel. In the heat pump drying system, steam is used both as drying gas in a flash dryer, and as refrigerant in a vapor compression heat pump cycle. It was designed by GEA Exergy and built by MoDo Chemetics in 1989 for peat drying, but is today also used for sawdust drying. Production data differs between sawdust and peat drying. To enable comparison with dimensioning data this article focuses on peat drying. The system layout is presented, along with its energy performance for one production season of peat drying. Variations in energy performance, deviation from dimensioning data, and experiences from operation are considered. Implications of this drying system for the design of future biomass dryers are finally discussed.

2. Materials and Methods

The dryer is part of a stand-alone biofuel factory with two identical lines for drying, each one with a design capacity of dewatering 28 tons/h. The plan for 2016-2017 is to produce 83,000 tons of wood fuel pellets and 25,000 tons of peat fuel briquettes. This drying system uses steam both as drying gas in a flash dryer, and as refrigerant in a vapor compression heat pump cycle. These two steam cycles are never mixed. In this article, drying steam denotes steam in the drying cycle and refrigerant denotes the water vapor in the vapor compression cycle.

2.1. Dryer

A flash dryer is used in which small particles of peat or sawdust are mixed with drying steam and transported through the dryer. Two fans in series circulate the drying steam. The dryer consists of five vertical shell-and-tube heat exchangers, each 20 meter high, as can be seen in Figure 1.

Refrigerant condenses on the shell side of the heat exchangers, transferring its latent heat to the drying steam. Drying steam and wet biomass flow inside the tubes. Each shell holds 73 or 97 tubes. The number of tubes increases with the direction of the drying process. Wear has caused some tubes to break, and to prevent leakage from the shell side to the tube side, these tubes have been welded shut, which reduces the heat transfer area of the dryer by 12 % in Line 1 and 8 % in Line 2 compared with design. The residence time of the biomass in the flash dryer is approximately 20 seconds.

Fig. 1 The five 20m high heat tube shells.

2.2. Biomass

Inlet moisture content of the grinded peat varies between 55 % and 65 % during a season. Short-term variations in moisture content of incoming raw material can cause fluctuations in the system and need to be avoided, whereas the long-term variations are well known. Lower moisture content is found at the end of the summer and the moisture content then increases during winter due to outdoor storage.

The first step before drying is preheating. Preheating is done at atmospheric pressure with an excess flow of flash steam and venting steam that is in contact with the biomass. Since steam condenses on the biomass in the preheater, it is impossible to determine the temperature and moisture content of the biomass accurately as it enters the flash dryer. The biomass enters the dryer through a mixing chamber where it is mixed with the drying steam; it is then transported through the five heat exchangers of the flash dryer by the flow of drying steam. Dry biomass is separated from the drying steam in a cyclone. Before leaving the system, the material goes into the flash tank where the pressure is reduced to atmospheric pressure. The moisture content at the outlet is 8-10 %.

2.3. Refrigerant

The refrigerant is water and works in a vapor compression heat pump process. After the compressor, the refrigerant pressure is 1.0-1.4 MPa and the temperature is 220-240 °C. At this state the refrigerant enters the flash dryer, where it is cooled down to its saturation temperature, condensates and leaves the dryer as saturated liquid. Its heat is transferred to the

drying steam and enables the water in the biomass to evaporate. In the superheater/subcooler, the liquid refrigerant is subcooled, thereby superheating the drying steam. The expansion valve is included in the steam converter, where the refrigerant pressure is dropped to 0.32 MPa. Liquid refrigerant receives heat from the excess drying steam and vaporizes. It then enters the four-stage turbo compressor as saturated steam at 0.32 MPa. The refrigerant mass flow rate is approximately 8 kg/s and the compressor has a maximum power consumption of 4.0 MW. If required, more refrigerant can be added to the system from a supply water tank included in the steam converter.

2.4. Performance parameters

The Specific Moisture Evaporation Rate (SMER) is defined as

$$SMER = \frac{amount\ of\ water\ evaporated}{energy\ input\ to\ dryer} = \frac{m_{excess\ steam}}{w_{compressor} + w_{fan}}, kg/kWh \tag{1}$$

The reciprocal of SMER is the Specific Energy Consumption (SEC);

$$SEC = \frac{energy\ input\ to\ the\ dryer}{amount\ of\ water\ evaportated} \tag{2}$$

In Equations 1 and 2, the amount of water evaporated is the same as the amount of excess steam condensate. The total energy supplied to the dryer is the electrical energy supplied to the compressor and the fans.

The COP, the coefficient of performance, determines the effectiveness of a heat pump process:

$$COP = \frac{Desired\ output\ (heat)}{Required\ input\ (work)} = \frac{Q_{dryer}}{w_{compressor}} \tag{3}$$

In Equation 3 the desired output is the heat released from the refrigerant as it condenses in the dryer and the required input is the electrical power to the compressor. The desired output (Qdryer), is calculated using Equation 4.

$$Q_{dryer} = \left(h_{in} - h_{sat} + h_{fg}\right) \cdot m_{refridgerant}, kW \tag{4}$$

3. Results

Results are presented for the averages of the selected performance indicators and their variations during the production season. Dimensioning data of the factory are included for comparison. The average values of the performance parameters are reported in Table 1, in which the dimensioning data and operational data during 2014-2015 are compared. The dimensioning data represent the maximum capacity of the drying system under ideal conditions. As can be seen in Table 1, it was not operated at maximum capacity during the

production season of 2014-2015. The dewatering rate was approximately 76 % of the dimensioning value. It should be noted that the total power consumption was larger in the operational data, despite a lower production rate. Contrary to what could be expected based on production rate and power consumption, the value of COP is higher in operational data than in dimensioning data.

Table 1. Average values of performance parameters along with dimensioning data.

	Dimensioning data	Operational data	
		Line 1	Line 2
Production rate {tons/h}	22.2	13.8	15.6
Moisture evaporation rate (MER) {tons/h}	27.8	20.6	21.5
Inlet moisture content (MC) {%}	60.0	63.6	61.9
Total power consumption {kW}	5390	5680	5550
Coefficient of performance (COP)	4	4.32	4.64
Specific energy consumption (SEC) {kWh/ton}	210	276	260
Specific moisture evaporation rate (SMER) {kg/kWh}	5.16	3.63	3.87

4. Discussion

As reported in Table 2, the operational data shows lower values of production rate and moisture evaporation rate than does the dimensioning data. This result is expected; the factory is not operated at its full production capacity. More interesting results from Table 2 is that both the total power consumption and the value of COP is higher during operation than in the dimensioning data. The lower refrigerant condensation temperature that is required to achieve the desired drying rate can explain the higher value of COP. As the temperature difference between condenser and evaporator of the heat pump cycle decreases, COP increases. This also explains the variations in COP that are seen during the season. In order to achieve a higher production rate, the discharge pressure of the compressor is raised, thereby raising the condensing temperature and decreasing COP. The larger value of total power consumption can perhaps be due to deterioration of the components after many years of use, and the decrease in heat transfer are that is seen due to wear. SMER ranges between 3 and 4 with averages of 3.63 and 3.87. As can be seen in Figure 8 and Figure 10, the maximum values of SMER and COP are not coinciding. This shows the importance of specifying both dryer performance, such as SMER or SEC, and heat pump performance,

COP, when reporting the performance of a heat pump dryer. The differences in performance between Line 1 and Line 2 are likely to be due to larger heat transfer area in Line 2.

The factory has supplied all data that are used in calculations of performance parameters. Data on power consumption and production rate are very important for their economic monitoring and should be considered as highly reliable. The only measurement that can be doubted on its quality is the refrigerant flow rate, which is used in the calculation of COP. Its average value is however correct and the average values of COP presented in this article can thereby be considered as reliable.

Heat pump performance and temperature range largely depends on the refrigerant used. Refrigerants today often have negative side effects on environment and human health and represent a fire hazard. Water has none of the negative side effects that are seen in other refrigerants. Using water as refrigerant enables heat pumps to reach higher temperatures; the temperatures needed for many industrial purposes. Water refrigerant heat pumps can thus find application both in upgrading waste heat into useful heat or steam, and in drying systems requiring a higher drying temperature than what can be reached with traditional refrigerants. The compressor is reported by scientific literature to be a challenging component in the water refrigerant heat pump, but in this drying system there have been no compressor problems. In high-temperature heat pump systems, water is the ideal refrigerant.

This heat pump dryer is a complex drying system. The drying cycle and the heat pump cycle are linked together both in the flash dryer and in the steam converter. Fluctuations in inlet moisture content of raw material will cause fluctuations in the amount of excess steam available for vaporizing the refrigerant. Finding and maintaining the energy balances at the right pressures represents a difficulty when operating the system as fluctuations causes variations in outlet moisture content and product quality. But this unique system has proven successful by running continuously with only small modifications from 1989 until today (2017).

5. Conclusion

Knowledge from operation of this dryer is valuable for designing efficient new drying systems. It proves both that complexity does not have to be a problem for heat pump dryers and that water is an excellent refrigerant in high temperature heat pumps.

6. References

[1] Ståhl, M., Wood fuel pellets : sawdust drying in the energy system. Karlstad University studies: 2005:47. 2005: Karlstad : Division for Engineering Sciences, Physics and Mathematics, Department of Environmental and Energy Systems, Karlstads universitet, 2005.

[2] Mujumdar, A.S., Handbook of Industrial Drying. Vol. 2. 1995: Marcel Dekker Inc.

[3] Pang, S. and A.S. Mujumdar, Drying of Woody Biomass for Bioenergy: Drying Technologies and Optimization for an Integrated Bioenergy Plant. Drying Technology, 2010. 28(5): p. 690-701.

[4] Wimmerstedt, R., Steam Drying — History and Future. Drying Technology, 1995. 13(5-7): p. 1059-1076.

[5] Sloth Jensen, A., Drying in superheated steam under pressure, in Fifth Nordic Drying Conference. 2011: Helsinki, Finland.

[6] Romdhana, H., C. Bonazzi, and M. Esteban-Decloux, Superheated Steam Drying: An Overview of Pilot and Industrial Dryers with a Focus on Energy Efficiency. Drying Technology, 2015. 33(10): p. 1255-1274.

[7] Banerjee, S., Mechanisms of terpene release during sawdust and flake drying. Holzforschung, 2000. 55(4): p. 4.

[8] Björk, H. and A. Rasmuson, Formation of organic compounds in superheated steam drying of bark chips. Fuel, 1996. 75(1): p. 81-84.

[9] Spets, J.P. and P. Ahtila, Reduction of organic emissions by using a multistage drying system for wood-based biomasses. Drying Technology, 2004. 22(3): p. 541-561.

[10] Granstrom, K., Emissions of monoterpenes and VOCs during drying of sawdust in a spouted bed. Forest Products Journal, 2003. 53(10): p. 48-55.

[11] Chus, K.J., et al., Heat Pump Drying: Recent Development and Future Trends. Drying Technology, 2002. 20(8): p. 1579-1610.

[12] Minea, V., Heat-Pump-Assisted Drying: Recent Technological Advances and R&D Needs. Drying Technology, 2013. 31(10): p. 1177-1189.

Spray drying of soymilk: evaluation of process yield and product quality

Olmos, B.D.F.[a]; Penha, C.B.[a]; Kurozawa, L.E.[a*]

[a] School of Food Engineering. University of Campinas, Campinas, Brazil.

*E-mail of the corresponding author: louisek@unicamp.br

Abstract

The aim of this work was to evaluate the effect of inlet air temperature and gum Arabic concentration on yield of spray drying of soymilk and powder quality (moisture content, water activity and antioxidant capacity). Since soymilk had a significant lipid content, gum Arabic played a significant role as an emulsion stabilizer, improving process yield and preserving antioxidant capacity. However, temperature did not affect antioxidant capacity. The optimal condition to obtain higher antioxidant capacity was: 30% of gum Arabic and 160°C. The powder obtained under optimized condition was characterized regarding to bulk density, particle size distribution and morphology.

Keywords: soymilk; spray drying; ferric reduction power FRAP; DPPH scavenging ability; scanning electron microscopy.

1. Introduction

Recently, the ready-to-drink soymilk has become popular, in which sales volume of worldwide in 2015 reached 13.5 billion liters[1]. Vegan and helthy diet folowers are one of the major consumers because it is lactose- and gluten-free beverage and contains high-quality proteins, dietary fiber and antioxidant compounds, such as phenolic compounds[2,3]. However, some conservation method is necessary in order to increase its shelf life. Of the several drying methods, spray drying is suitable for heat-sensitive products, such as soymilk, promoting higher retention of nutrients due to the short residence time[4].

When exposed at higher temperature during spray drying, fat present in soymilk (18 g/100 g solids)[5] becomes molten, resulting in particle adhesion on the dryer chamber and low product recovery[6]. Part of this problem can be solved by adding a carrier agent to the feed solution before drying, in order to decrease the fat content[7]. Moreover, since soymilk is an oil-in-water emulsion, the thermodynamic instability of this system can result in larger oil droplets due to coalescence of droplets dispersed in soymilk. The larger the oil droplets are, the higher the breakup during atomization of the emulsion in the spray dryer chamber[8]. This breakup of the emulsion favors the increase in of the surface oil, decreasing the product recovery[9]. Thus, the addition of carrier agent with good emulsifying properties, such as gum Arabic, enhances emulsion stability and, as consequence, product recovery.

The objective of this work was to evaluate the effect of inlet air temperature and gum Arabic concentration on the process yield and powder quality (moisture content, water activity and antioxidant capacity).

2. Materials and Methods

2.1. Material

Soybean (*Glycine max* (L.) Merr.) cultivar BRS 257, which is lipoxygenase-free, was acquired from SL Alimentos (Mauá da Serra, Brazil). Gum Arabic (GA) Instantgum BB (Nexira, São Paulo, Brazil) was used as the wall material. DPPH 2,2-diphenyl-1-picrylhydrazyl and TPTZ 2,4,6-tris(2-pyridyl)-S-triazine were used as reagent for the analysis of antioxidant capacity, and Trolox 6-hydroxy-2,5,7,8-tetramethylchroman-2-carboxylic acid as standard (Sigma-Aldrich, Saint Louis, USA).

2.2. Preparation of soymilk

Soymilk was obtained according to Baú and Ida[2]. About 3 kg of soybeans were soaked in water at 1:3 ratio (w:w, soybean:water) for 12 h at 8°C. The grains were drained and homogenized with distilled water at 1:8 ratio (w:w, soybean:water) using an industrial blender. The slurry was filtered and pasteurized at 90°C for 3 min, obtaining the soymilk. The chemical composition of soymilk, obtained by AOAC[10], was (wet basis): moisture

content of 94.8±0.1%, ash content of 0.2±0.0%, lipid content of 1.3±0.1%, protein content of 2.4±0.0% and carbohydrate content, calculated by difference, of 1.4%. Samples were stored at -18°C and thawed according to the quantity required for spray drying.

2.3. Spray drying of soymilk

Before spray drying, gum Arabic was dissolved in soymilk at different concentrations (Table 1) using a magnetic stirrer. After, the mixture were homogenized at 20,000 rpm for 5 min in order to emulsify the fat soymilk and break up the clots, returning to a fluid consistency. About 400 g of feed solution were fed into the laboratory scale spray dryer (MSD 1.0, Labmaq, Ribeirão Preto, Brazil) by a peristaltic bomb at flow rate of 0.4 L/h. The feed solution was atomized into spray dryer chamber by a two-fluid atomizer spray nozzle with an orifice of 0.7 mm in diameter, using compressed air at flow rate of 40 L/h. Inlet air temperature was used according to Table 1. For each assay, the collected powder was weighed for subsequent calculation of process yield, which was the ratio of total solids mass in the powder to total solids mass in the feed solution.

Spray drying experiments were carried out according to a central composite rotatable design (Table 1) in order to evaluate the effect of inlet air temperature and gum Arabic concentration on the responses process yield, moisture content, water activity and antioxidant capacity. Experimental data were fitted to Equation (1) [11].

$$y = b_0 + b_1 x_1 + b_2 x_2 + b_{11} x_1^2 + b_{22} x_2^2 + b_{12} x_1 x_2 \tag{1}$$

Where: y is the response, b_0, b_1 and b_2, b_{11} and b_{22}, and b_{12} are the constant, linear, quadratic and cross-product regression coefficients, respectively, and x_1 and x_2 represent the coded values of the T_{in} and GA variables, respectively.

Regression coefficients of the predictive models were obtained by the Protimiza software (http://experimental-design.protimiza.com.br). Coefficients within a confidence level above 90% were considered significant ($p < 0.1$). Non-significant terms were eliminated, and the model was tested for adequacy by analysis of variance (Anova), coefficient of determination (R^2) and F-test. For powder moisture content, the analysis of results indicated the model was linear, and the expansion of the screening design to a central composite rotatable design, with the addition of axial points (tests 5 to 8), was not necessary.

Table 1. Screening design for spray drying of soymilk, regression coefficients and Anova

Assay	Independent variables		Dependent variables				
	T_{in}	GA	Y	X	Aw	FRAP	DPPH
1	140	13	45.6	2.6±0.1	0.149±0.006	25.1±2.0	243.3±14.8
2	180	13	54.1	1.1±0.0	0.093±0.010	30.2±0.3	223.6±13.5
3	140	27	59.2	3.5±0.4	0.043±0.002	44.9±3.9	514.3±15.7
4	180	27	60.5	1.4±0.4	0.088±0.005	46.6±0.8	482.4±5.2
5	132	20	64.9	-	0.112±0.009	40.3±2.3	330.3±39.5
6	188	20	57.0	-	0.170±0.004	36.6±0.5	285.3±24.5
7	160	10	40.1	-	0.165±0.012	26.6±0.7	168.3±10.4
8	160	30	60.7	-	0.095±0.008	43.7±1.1	543.3±26.5
9	160	20	69.8	2.2±0.1	0.168±0.012	43.7±1.1	343.6±3.5
10	160	20	64.2	2.0±0.2	0.108±0.016	37.0±0.6	293.2±31.3
11	160	20	66.6	2.4±0.0	0.122±0.006	37.4±0.8	319.3±8.7
Regression coefficients							
b_0			66.9	2.2	0.12	36.9	327.6
b_1			NS	-0.9	NS	NS	-14.4
b_{11}			-3.2	-	NS	NS	NS
b_2			6.1	0.3	-0.03	7.6	132.52
b_{22}			-8.4	-	NS	NS	22.18
b_{12}			NS	NS	NS	NS	NS
R^2			0.88	0.95	0.36	0.90	0.98
Fc			17.2	38.0	5.0	80.3	124.3
Ft			3.07	4.32	3.36	3.36	3.07

NS is non-significant (p>0.1)

2.4. Analytical methods

2.4.1. *Physicochemical properties of the powders*

Moisture content was determined gravimetrically in triplicate in an oven at 105°C for 24h[10]. A thermohygrometer Aqualab (4 TEV, Decagon, Pullman, USA) was used to measure water activity at 25°C. Bulk density was calculated by dividing the mass of powder by the volume occupied in the cylinder after tapped by hand. Particle size distribution and mean diameter particle D_{43} were obtained, in triplicate, using a laser light scattering analyzer (Mastersizer, model 2000, Malvern, UK). Particle microstructures were evaluated by a scanning electron microscope (Leo 440i, LEO Electron Microscopy/Oxford, Cambridge, England).

2.4.2. Antioxidant capacity of the powders

Prior to the analysis, 0.5 g of powder were dissolved in 8 mL of destilled water. Antioxidant capacity by donating hydrogen atoms to the DPPH radical and by ferric reduction power FRAP were determined according to Brand-Williams et al.[12] and Benzie and Strain[13], respectively. For DPPH and FRAP method, after reaction, the sample absorbance was measured at 517 and 595 nm, respectively, using an UV-visible spectrophotometer. Analytical curves with different concentrations of Trolox, ranging from 1,000 to 5,000 µM for DPPH and 50 to 600 µM for FRAP method, were used for the subsequent calculation of the results in µmol Trolox equivalent (TE)/g of soymilk solids. All assays were performed in triplicate.

3. Results and discussion

3.1. Spray drying of soymilk

The regression coefficients for the responses, F-values, p-values and R^2 are presented in Table 1. After exclusion of non-significant terms (p>0.1), the predictive models were tested for accuracy of fit by Anova. When the calculated F-value Fc was greater than the tabulated F-value Ft, the variation was explained by the regression and not by the residues. Thus the regression was significant, and the model could be considered predictive. Figure 1 shows the response surfaces generated by the proposed models.

Analyzing Figure 1(a), GA had greater influence on process yield than T_{in}. As expected, the increase of GA up to 22.5% enhanced powder recovery, since the addition of carrier agent decreased the fat content in the feed solution. This fact reduces the particle adhesion on the dryer chamber, which could occur due to the fat melting during spray drying[7]. However, an opposite behavior could be seen at GA above 22.5%. This result can be related to the high powder moisture content (Fig. 1(b)). Higher carrier agent concentration increases the feed viscosity, resulting in greater droplets atomized during spray drying. Thus, there is a poor heat and mass transfer between the droplets and drying air, resulting in the formation of wetter and sticker particles.

The antioxidant capacity of spray-dried soymilk ranged from 168.3 to 543.3 µmol TE/g for DPPH and 25.1 to 46.6 µmol TE/g solids of soymilk for FRAP method. Since soymilk solution presented 742.6±36.2 and 200.2±6.2 µmol TE/g solids, there was a retention of antioxidant capacity varying from 22.7 to 73.2% and 12.5 to 23.3%, for DPPH and FRAP methods, respectively. Figures 1(c) and 1(d) show the positive effect of gum Arabic concentration on antioxidant capacity for both methods. Since soymilk had a significant lipid content, gum Arabic played a significant role in spray drying as an emulsion stabilizer, encapsulating and preserving the antioxidant substances present in soymilk.
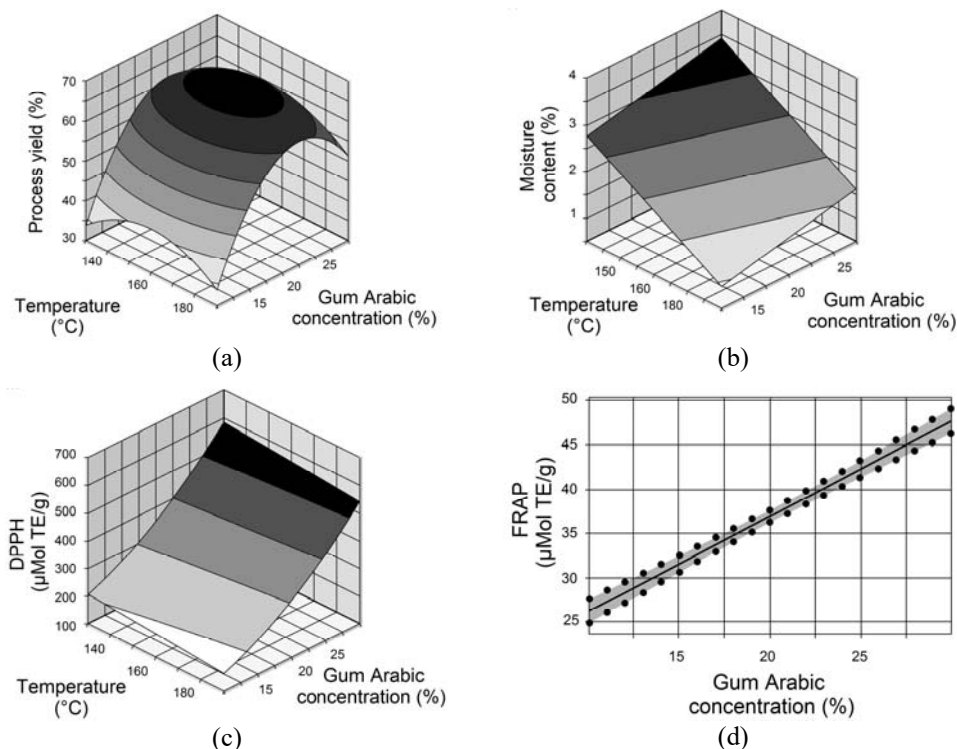
Fig. 1. Influence of independente variables on the responses: (a) process yield, (b) moisture content and (c) antioxidant capacity by DPPH and (d) FRAP methods

3.2. Characterization of the powder obtained under the optimum condition

HIgher process yield and antioxidant capacity were obtained at 160°C and 30% of GA. Under this optimum condition, process yield was 58.7%. The powder presented moisture content of 1.5±0.2%, antioxidant capacities by FRAP and DPPH methods of 38.9±1.6 µmol TE/g and 586.0±0.1 µmol TE/g, respectively; bulk density of 0.40±0.01 mg/ml and mean diameter size of 9.18±0.33 µm. Particle size distribution and the morphology evaluated by scanning electron microscopy were shown in Figure 2. Particles presented a continuous wall without fissures or cracks. Such characteristics is desirable to effectively protect the antioxidant compounds. However, particles had an irregular structure, which adversely affect the flow properties of the powders. This morphology can be result from slow film formation during drying of the atomized droplets, causing their shrinkage during the final stages of drying and cooling[14].

(a)

(b)
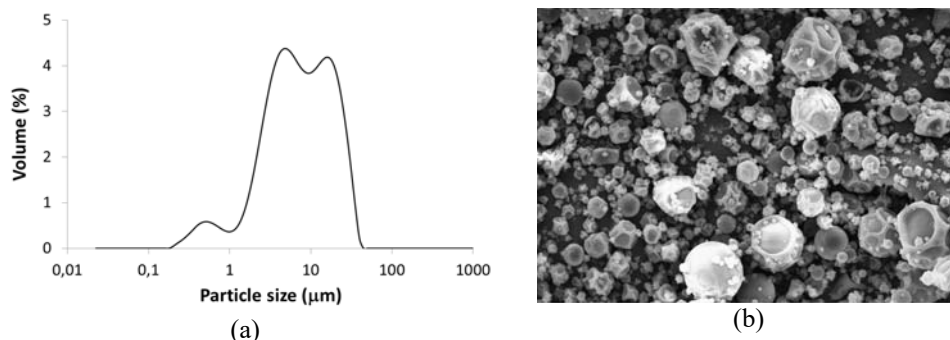
Fig. 2. Particle size distribution (a) and micrograph of the spray-dried soymilk with magnification of ×2000 (b)

4. Conclusions

This work demonstrated the significant role of gum Arabic in spray drying of soymilk as an emulsion stabilizer, since there was an improvement on product recovery and retention of antioxidant capacity. In order to obtain maximum process yield and antioxidant capacity, the optimal condition was proposed: 30% of GA and 160°C, in which process yield was 58.7%. There was a siginificant retention of antioxidant capacity by donating hydrogen atoms to the DPPH radical (78.9%) after spray drying; however only 19.4% of ferric reduction power of soymilk solution was preserved.

5. Nomenclature

Aw	water activity	
DPPH	DPPH scavenging ability	µmol TE/g soymilk solids
FRAP	ferric reduction power	µmol TE/g soymilk solids
GA	gum Arabic concentration	%
T_{in}	Inlet air temperature	°C
X	moisture content	% (wet basis)
Y	process yield	%

6. Acknowledgements

7. References

[1] Statista. The portal for statistic. Sales volume of soymilk worldwide in 2015 and 2018: 2018. https://www.statista.com/statistics/645662/soy-milk-sales-volume-worldwide (accessed Mar 19, 2018).

[2] Baú, T.R.; Ida, E.I. Soymilk processing with higher isoflavone aglycone content. Food Chemistry 2015, 183, 161–168.

[3] Zhao, D.; Shah, N.P. Changes in antioxidant capacity, isoflavone profile, phenolic and vitamin contents in soymilk during extended fermentation. LWT – Food Science and Technology 2014, 58 (2), 454–462.

[4] Masters, K. Spray drying handbook. Longman Scientific and Technical: London, 1991.

[5] TACO. Brazilian Table of Food Composition / NEPA – UNICAMP. 2004. Campinas: NEPA-Unicamp. 42p. (in portuguese).

[6] Foster, K.D.; Bronlund, J.E.; Paterson, A.H.J. The contribution of milk fat towards the caking of dairy powders. International Dairy Journal 2005, 15(1), 85–91.

[7] Santana, A.A.; Martin, L.G.P.; Oliveira, R.A.; Kurozawa, L.E.; Park, K.J. Spray drying of babassu coconut milk using different carrier agents. Drying Technology 2017, 35(1), 76–87.

[8] Munoz-Ibanez, M.; Azagoh, C.; Dubey, B.N.; Dumoulin, E.; Turchiuli, C. Changes in oil-in-water emulsion size distribution during the atomization step in spray-drying encapsulation. Journal of Food Engineering 2015, 167, 122–132.

[9] Soottitantawat, A.; Yoshii, H.; Furuta, T.; Ohkawara, M.; Linko, P. Microencapsulation by spray drying: Influence of emulsion size on the retention of volatile compounds. Journal of Food Science 2003, 68(7), 2256–2262.

[10] AOAC. Official Methods of Analysis, 19th ed. Association of Official Analytical Chemists International: Washington, D.C, 1995.

[11] Rodrigues MI and Iemma AF. Experimental design and process optimization. CRC Press: Boca Raton, 2014.

[12] Brand-Williams, W.; Cuvelier, M.E.; Berset, C. Use of a free radical method to evaluate antioxidant activity. LWT-Food Science and Technology 1995, 28(1), 25–30.

[13] Benzie, I.F.F.;Strain, J.J. The ferric reducing ability of plasma (FRAP) as a measure of "antioxidant power": The FRAP assay. Analytical Biochemistry 1996, 239(1), 70–76.

[14] Arana-Sánchez, A.; Estarrón-Espinosa, M.; Obledo-Vázquez, E.N.; Padilla-Camberos, E.; Silva-Vázquez, R.; Lugo-Cervantes, E. Antimicrobial and antioxidant activities of Mexican oregano essential oils (*Lippia graveolens* H.B.K.) with different composition when microencapsulated in β-cyclodextrin. Letters in Applied Microbiology 2010, 50(6), 585–590.

The prediction model of moisture content's stabilization during tobacco strip drying process

Mingjian Zhang[a], Feng Huang[b], Qing Chen[b], Le Wang[a, *], Haisheng Wang[a], Bin Li[a], Bin Wang[a]

[a] Key Laboratory of Tobacco Processing Technology, Zhengzhou Tobacco Research Institute of CNTC, Zhengzhou, China.

[b] Hua Huan International Tobacco Co., Ltd., Chuzhou, China.

*E-mail of the corresponding author: wangl@ztri.com.cn

Abstract

A mathematical model was established to predict the mean value and variance of tobacco strip during drying processing, based that the physical and chemical properties of tobacco strip as agriculture products show probability distributions. The results show that the model can predict the mean value of moisture content at different times, and there is a certain deviation in predicting the variance of moisture content at initial stage of drying process. However, the prediction value of the variance of tobacco strip is much more accurate while the moisture content is between 8% and 10%, which is the interval of quality requirements.

Keywords: tobacco strip; drying; mean value;variance model.

1. Introduction

The studies on the drying process of tobacco raw materials[1] focused on the dynamic characteristics of water migration, due to its important effect on the physical and sensory quality of tobacco products[2-3]. Moreover, the water stability was an important product quality control target in the drying process. The current researches on the dynamic drying process of tobacco materials mainly involved the prediction of the water migration law under different drying methods, temperatures, humidities and pressures through thin layer models, semi experiences and empirical models[4-6]. However, as a agricultural product, tobacco raw materials did not have the uniform physical and chemical properties, always showing widespread characteristics. Tobacco strip was constantly switched between the humidifying section and the drying section, leading to a non-equilibrium state during the dynamic processing of tobacco strip. Therefore, It is difficult to describe the production stability by the mean moisture content of tobacco strip. In this study, the Newton model was selected as the basic model for describing the drying processing of tobacco strip. Combining the approximate calculation method of the mean value and variance of multidimensional continuous random variable nonlinear function, a prediction model of water stability was finally established to describe the mean value and variance of tobacco strip's moisture content during the drying processing of tobacco strip. Moreover, the model validation was carried out by comparing with the measured experimental data.

2. Materials and Methods

2.1. Materials

The experimental tobacco samples included tobacco strips(C_2F and C_2L, 2015) from Fujian, Jiangxi, Hunan, Sichuan, Anhui, Henan, Jilin, Liaoning and other provinces.

The length and width of tobacco strip samples were about 2cm×2cm, and the tobacco strips were put into a constant temperature and humidity box with 40°C and 80% relative humidity(RH), equilibrated 24 hours, then were sealed in self-sealing bag.

2.2. Measurement of tobacco strip's equilibrium moisture content

The equilibrium moisture contents of tobacco strip samples were measured by an test device for tobacco isothermal adsorption/desorption property. The mass of samples were 1.0g, The gas flow rate was 4800ml/min, the drying temperature was set at 70°C, the relative humidity was set to 30%, and the drying time was 2h. The equilibrium moisture contents were calculated by the final mass and the initial mass of tobacco strip samples.

3. Prediction model of moisture content stability during tobacco strip drying process

Although tobacco strip drying process were carried out under the same temperature and humidity treatment conditions, the initial moisture content, the balance moisture and the drying rate of the tobacco strip samples showed random distribution. Therefore, the drying model shoud be further established base on its probability distribution characteristics.

3.1. The mathematical expectation and approximate variance

When each factor is a continuous random variable, and the influence to the result is a nonlinear function, the expectation and variance of the random variable function can be calculated by an approximate method. The calculation method is to expand the nonlinear function of the random variable at its expected value Taylor series, abandon the high order term and calculate the expectation and variance of the random variable function. For multivariate random variables, the expression of mathematical expectation and variance is as follows:

If x_i（i =1, 2, $\cdots$, n）were the independent random variables，the mathematical expectation $E(x_i) = \mu_i$, the variance $D(x_i) = \sigma_i$, and the random variable function $Z(x_i) = g(x_1, x_2,..., x_n)$ has two order continuous partial derivative at point ($\mu_1, \mu_2,..., \mu_n$), then the mathematical expectation

$$E(Z) \approx g(\mu_1, \mu_2,..., \mu_n) + \frac{1}{2}\sum_{i=1}^{n}\frac{\partial^2 g}{\partial x_i^2}\sigma_i^2 \qquad (1)$$

And the approximate variance

$$D(Z) \approx \frac{1}{2}\sum_{i=1}^{n}\left(\frac{\partial g}{\partial x_i}\right)^2 \sigma_i^2 \qquad (2)$$

3.2. Newton drying model based on multidimensional continuous random variables

The Newton model was used as the basic drying model，and the decision coefficient(R^2) and the chi square(χ^2) were used for the evaluation of the model. For Newton model, the drying rate is proportional to the moisture content.

$$\frac{dx}{dt} = -k\left(x - x_e\right)$$
$$x(0) = x_0 \qquad (3)$$

In the upper formula, x, k, x_e and x_0 respectively indicate the mean value of the moisture content(db.), drying rate constant, equilibrium moisture content(db.) and initial moisture content(db.) of tobacco strips. The relationship between water and time is obtained as follows by solving the above equations.

$$x(t) = (x_0 - x_e)\exp(-kt) + x_e \tag{4}$$

During the actual drying process of tobacco strips, σ_k^2, σ_e^2 and σ_x^2 respectively indicate the variance value of drying rate constant, equilibrium moisture content(db.) and initial moisture content(db.) of tobacco strips. As the drying rate constant, equilibrium moisture content(db.) and initial moisture content(db.) of tobacco strips were independent, The moisture content's mean and variance valuse of tobacco strips at t time could be calculated as follows as a mean and variance of a random variable function.

$$E[x(t)] \approx \left[(x_0 - x_e)\exp(-kt) + x_e\right] + \frac{1}{2}(x_0 - x_e)\exp(-kt)t^2\sigma_k^2 \tag{5}$$

$$D[x(t)] \approx \exp(-2kt)\left[\sigma_x^2 + (x_0 - x_e)^2 t^2\sigma_k^2 + \sigma_e^2\right] - 2\exp(-kt)\sigma_e^2 + \sigma_e^2 \tag{6}$$

From the formula (5) and (6), the mean and variance values of moisture content during the actual drying process could be calculated by mean values of Newton model parameters, and the error decreased with exponential function. Moreover, the variance of moisture content decreased exponentially with the increasing drying time, and finally decreased to the variance of equilibrium moisture content (σ_e^2).

4. Results and discussion

4.1. The drying kinetic curves of tobacco strips

The drying kinetic curves of 83 types of tobacco strips samples from different localities were obtained under the drying temperature of 70°C and 30% RH(Fig. 1). The above results showed that, the initial moisture contents of the sample were distributed in an interval after the same pretreatment, and the moisture contents changed at different drying rates. Moreover, the moisture of the tobacco strips rapidly decreased at the initial stage during a fast drying stage. Then the drying rates reduced gradually leading to a slow drying process, and finally reached the equilibrium moisture contents under the drying condition. The distribution of the equilibrium moisture contents was more concentrated. The moisture content decreased with exponential trend during the whole drying process.
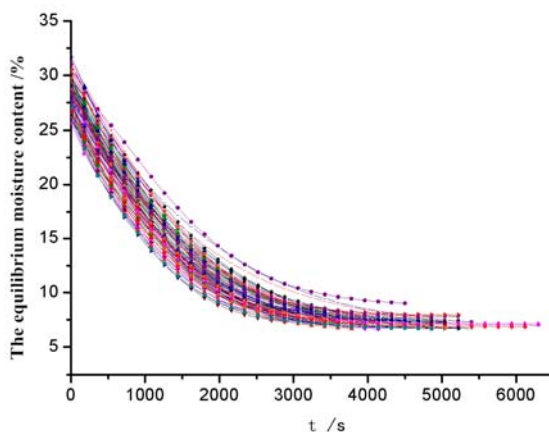
Fig. 1 The drying kinetic curves of tobacco strips.

4.2 Probability statistics

The frequency (H) distribution of the initial moisture content, equilibrium moisture content and drying rate constant (k) of Newton model under the same drying conditions were shown in Fig. 3. The results indicated that the initial moisture content, equilibrium moisture content and drying rate constant had the same normal distribution form and all the decision coefficients(R^2) of Newton model were higher than 0.985, showing that the Newtong model was suitable for calculating these drying process. The correlation analysis of the initial moisture content, equilibrium moisture content and drying rate constant (k) of Newton model was shown in Table 1. The results showed that these above factors had weak positive correlation and negative correlation, according with the model requirements for independent variables.
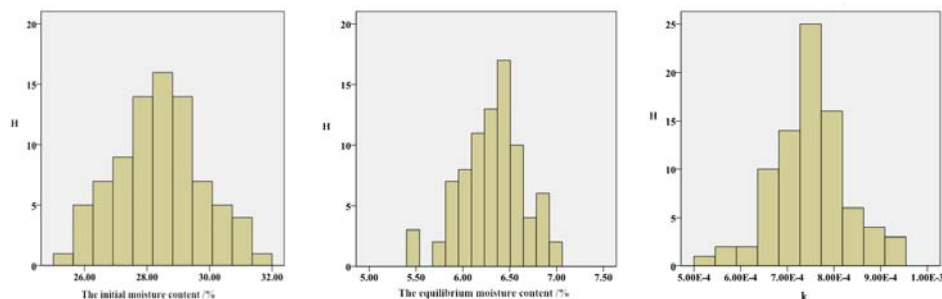
Fig. 2 The frequency (H) distribution of the initial moisture content, equilibrium moisture content and drying rate constant (k) of Newton model under the same drying conditions

Table 1. The correlation analysis

Factor	k	The initial moisture content	The equilibrium moisture content
k	1		
The initial moisture content	-0.296	1	
The equilibrium moisture content	-0.457	0.545	1

4.3 Model validation

The predicted moisture content's mean and variance values during the drying processing of tobacco strips were compared with the measured values in Fig. 3. The results showed that the difference between the predicted and measured mean values of tobacco strips moisture content (db.) was relatively small, which indicated that this model could predict the mean value of the whole drying process. Moreover, the difference between the predicted and measured variance values of tobacco strips moisture content (db.) increased first and then decreased, while the predicted variances obtained by approximate method were a little smaller than the actual statistical value, due to the nonlinearity of Newton model and a certain correlation of these model parametes. It was worth noting that the target moisture (db.) in the typical tobacco strips drying processing were between 8.7% and 11.1%, which was included in the critical area of free water and combined water. In this moisture content interval, the difference between predicted values and measured values became rather small, which indicated that the predicted model was reliable between the moisture content interval of the drying process quality requirement.
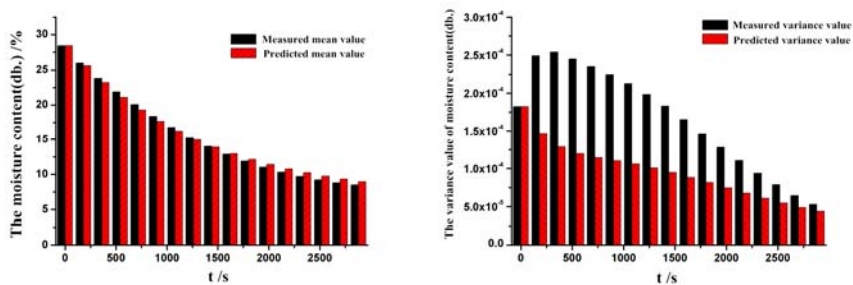
Fig. 3 The measured and predicted moisture content's mean and variance values during the drying processing of tobacco strips.

5. Conclusion

Combining the approximate calculation method of the mean value and variance of multidimensional continuous random variable nonlinear function, a mean and variance prediction model of the tobacco strips' moisture contents during the drying process was established base on Newton model. Moreover, the distribution and linear correlation between the initial moisture content, equilibrium moisture content and drying rate constant were discussed, which was consistent with the application requirements of the model. The predicted model showed good performance on the prediction of mean moisture contents during the whole drying process. The prediction of moisture contents' variance had a certain deviation in the initial drying stage, while the predicted variances were more accurate between the moisture content (db.) interval (8.7%~11.1%) of the drying process quality requirement, which was included in the critical area of free water and combined water.

6. References

[1] Legros, R.; Millington, CA; Clift, R. Drying of tobacco particles in a mobilized bed. Drying Technology 1994, 12 (3), 517–543.

[2] Wang H.; Xin H.; Liao Z.; et al. Study on the effect of cut tobacco drying on the pyrolysis and combustion properties. Drying technology 2014, 32(2): 130-134.

[3] Zhu W. K.; Wang Y.; Chen L. Y.; et al. Effect of two-stage dehydration on retention of characteristic flavor components of flue-cured tobacco in rotary dryer. Drying technology 2016, 34(13): 1621-1629.

[4] Geng F.; Xu D.; Yuan Z.; et al. Numerical simulation on fluidization characteristics of tobacco particles in fluidized bed dryers. Chemical Engineering Journal 2009, 150(2-3): 581-592.

[5] Feng H.; Qing C.; Le Y. U.; et al. Study on the thin layer kinetics models of humidifying and drying of tobacco strips. Acta Tabacaria Sinica 2014, 20(6): 34-40.

[6] Xin Y. N.; Zhang J. W.; Li B. Drying kinetics of tobacco strips at different air temperatures and relative humidities. Journal of Thermal Analysis and Calorimetry 2018, 132(2): 1347-1358.

Influence of intermittent and continuous microwave heating on drying kinetics and wood behavior of Eucalyptus Gomphocephala

Habouria, M.[a]; Ouertani, S.[a]; Azzouz, S.[a]; Jomaa, W.[b]; Elaib, M. T.[c]; Elcafci, M. A.[a]

[a] Laboratoire d'Energétique et des Transferts Thermique et Massique, Département de Physique, Faculté des Sciences de Tunis, University of Tunis El Manar.

[b] Institut de Mécanique et d'Ingénierie de Bordeaux, University of Bordeaux

[c] Laboratoire de Gestion et de Valorisation des Ressources Forestières. INRGREF, University of Carthage

*E-mail of the corresponding author: mariam.habouria@gmail.com

Abstract

The aim of this work was to determine the microwave drying kinetics of Eucalyptus Gomphocephala wood and to investigate the influence of intermittent and continuous heating processes on the end quality of dreid samples. The average moisture content evolution and temperature of wood samples under different microwave powers were analyzed in terms of drying time and internal temperature level. Results show that the increase of microwave power level decreses the drying time and increases the internal wood temperature. Based on qualitative observations on the state of dried samples, the intermittent microwave powers intensity process present the optimal processing parameter in microwave drying of Eucalyptus wood species.

Keywords: microwave drying; power; intermittent; continuous; Eucalyptus wood.

1. Introduction

Drying is an operation process consisting of the removal or reduction of water from a product. This process is often used as a final production step before selling or packaging products, especially wood, to ensure its structural stability, to remove fungal attacks and to improve its mechanical performance... There are different methods of drying wood, and the majority of industrial dried timber is processed with convective drying. This conventional drying of wood is slow and costly process [1]. For that reason, interest is oriented to study the electro heating technology of wood, in particular, microwave energy for specific applications in the wood industry to achieve specific objectives, such as reducing the drying time and energy consumption, accelerate internal transfers of mass and heat and providing good mechanical properties with high strength [2,3].

The principle of microwave heating is based on the concept of internal generation of heat. If wood is exposed to an electromagnetic field with such high frequency as is characteristic for microwave, the water molecules, which are dipoles, begin to rotate at the same frequency as the electromagnetic field. At a frequency of 2.4 GHz the alternating electric field component oscillates very quickly and the strong agitation, provided by cyclic reorientation of molecules, produce friction of water molecules can result in an intense internal heating of wood [3,4]. The interaction between microwave and wood material depends on power and frequency of microwave oven, on geometric and dimensions of the wood sample, on water content and the dielectric properties [4]. During drying, moisture, temperature, and gas pressure gradients involve product shrinkage and then development of strain and stress fields inside the Eucalyptus wood samples. So, the quality of drying of eucalyptus wood vary according to the type of microwave drying. According to our bibliographic research, few published works concerning the impact of microwave heating on qualitative behavior of dried Eucalyptus wood and no information about Gomphocephala wood has been published, and there is a lack of information on the continuous and intermittent microwave heat treatment of Eucalyptus wood. Intermittent drying is based on oscillating of operation conditions such as the temperature, relative humidity, speed of the air flow… This technique should make it possible to relax some of the mechanical stress induced by drying inside the material [5]. Microwave drying under controlling conditions has been the subject of some research works. Lars H. [6] has shown that microwave drying under controlled temperature conditions reduces internal stress and prevents checks of samples. L. Hansson, A.L. Antti (a) [7] showed that controlled microwave drying can improve a better wood resistance in a shorter drying time and the results are comparable to those obtained by conventional drying. In addition, Bruno Monteiro Balboni et al [8] have shown that drying at high microwave power produces reductions of wood strength and more drying defects than low microwave power. The

present work is particularly interested in the microwave drying of Eucalyptus wood (Gomphocephala) from the northeastern region of Tunisia. Kinetics of intermittent and continuous microwave drying of wood sample under different microwave power were analyzed in order to determine the drying temperatures levels and to evaluate the potential of microwave irradiation on the final behavior of dried wood.

2. Materials and Methods

2.1. Eucalyptus wood (Gomphocephala)

Eucalyptus trees are characterized by their ecological plasticity and their rapid growth. It covers 18 million ha in 90 countries in the world. Eucalyptus is mainly used in the wood industry and it is also used as an energy source or in building. Previous studies have shown that Eucalyptus wood has a specific sensitivity during final drying as collapse, cracks and warps [9]. The samples of green Eucalyptus wood used in this work were recommended by the INRGREF. The samples are rectangular (30* 5 * 2 cm3) size boards, sawn in the fibers direction (longitudinal direction) and have an initial average moisture content of 52%, (Fig.1). The mass of dry wood was obtained after keeping the samples in a controlled temperature oven at 103°C until a constant mass was reached. These samples are wrapped with cellophane paper and stored in a refrigerator until the date of the experiments to retain their green state properties. The drying conditions achieved are presented in (Table 1).

Fig.1 Eucalyptus tree (Gomphocephala): region of Oued Ksab, Tunis, Tunisia.

Table 1: Parameters of continuous and intermittent microwave heat treatment for different microwave power.

Drying conditions	Microwave power (Watt)	Continuous drying (min)	Intermittent drying (min)		
			Total drying	Microwave drying	One complete "on -off" cycle
P_{1max}	300	95	1020	780	7
P_{2max}	500	40	736	363	15
P_{3max}	1000	12	445	180	25

2.2. Drying unit: Laboratory Microwave oven

The experimental setup used in this work is a laboratory microwave oven (Fig.2) with a working cavity of 34 x 33 x 20 cm3, a relative humidity ranging from 10 to 90% and a vapor extracting system. This microwave oven operating at 2.45 GHz frequency is able to provide a maximum power of 1000 W. During the drying process, the lumbers were placed at the center of the drying chamber and removed periodically to measure their mass. The wood temperature is also measured during the experiment. The product moisture content in the dry basis (kg of water/ kg of dry matter) is calculated according to the following relationship:

$$M(\%) = \frac{W - W_d}{Wd} \times 100 = \frac{W_{water}}{W_d} \times 100 \qquad (1)$$

The moisture content ratio was given by the following equation:

$$MR = \frac{M}{M_{ini}} \qquad (2)$$

Fig.2: Laboratory microwave oven BP-301.

3. Results and discussion

3.1. Kinetics of continuous and intermittent microwave drying

The effect of microwave power on the evolution of the average moisture content of Eucalyptus wood (Gomphocephala) is shown in (Fig.3). For both kinds of drying an increase of microwave power decreases the drying time and increases both the core temperature and therefore the internal gas pressure of wood sample.

Figure4 shows the simultaneous evolution of the average moisture content and the temperatures of the top surface, the bottom surface and the center of the wood during for a continous microwave drying at a high level of microwave power. The beginning corresponds to a warming phase where temperature evolves quickly and water content drops slightly. The second phase corresponds to a vaporization phase where temperature is mostly constant near 100°C and water content decreases rapidly. The third phase is the

heating one, where the loss of water slows down and the temperature of the wood increases. This behavior is similar to those observed by other researchers [10].

3.2. Influence of continuous and intermittent process on final quality of dried wood

At this section we will focus on qualitative evaluation of the impact of continuous and intermittent heat treatment on the final quality of dried Eucalyptus wood. The adopted approach is based on qualitative observations on the final state of the dried wood in terms of deformations, warping, slits, checks, splits and colorations.
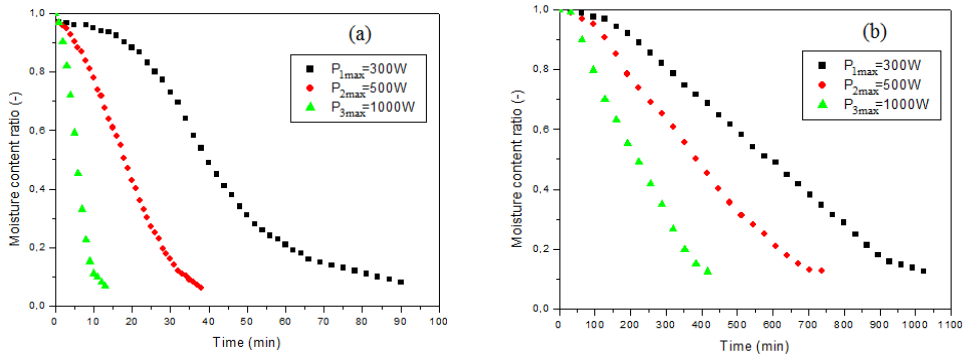
Fig.3: Moisture content versus time for different drying conditions.(a) continuous drying;

(b) intermittent drying.
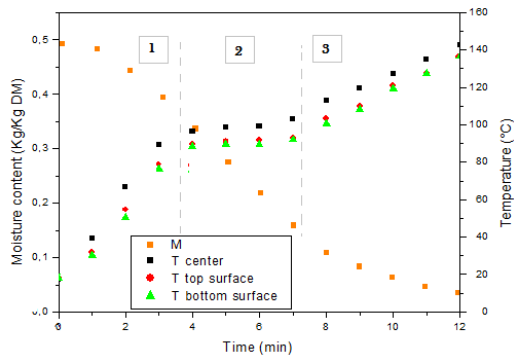
Fig.4: Core and surfaces temperature and moisture content versus time at high microwave power.

These observations are illustrated by photos of the wood samples relating to each type of drying achieved. Figure5 shows the wood sample dried continuously under high microwave power (1000W). After 12 min of drying, the black color appears indicating a carbonization of the ligneous material of the wood.

Fig.5: Effect of continuous microwave drying of wood at a maximum power (1000 W).

In addition, the darkening is located in the center of the plate illustrating the intense internal volumetric heating in the case of microwave heat treatment [11]. In the case of of continous drying process under 500 Watts of microwave power, these defects are observed at the end of drying (Fig.6).

Fig.6: Effect of continuous microwave drying of wood at 500 W; Before and after drying.

During a rapid drying at high microwave power, an over gas pressure is generated under the increasing of internal temperature of wood. The temperature increases continuously (up to 120°C) and passes through the boiling point of water and the resultant intense internal gas pressure pushes the water, so the mixture of water and gas will be forced out from the wood. Indeed, the high microwave power generate the over gas pressure inside the wood, which can break some intercellular bonds and causes internal checks, cracks and fissures in the wood structure. In order to avoid the problems related to the overpressure of the internal gas and the carbonization of wood material due to high temperatures, it is necessary to apply relatively low microwave power. Also, under the low microwave power 300 Watts we abserved the warping of the wood samples at the end of the continuous drying process (Fig.7). Indeed, temperature increases on the board surface. The degradation occurs in wood heated above 100°C, and can affect the chemical constituents of the cell wall or cause major structural damage. This efect was already observed by Eva Hermoso et al.[12].

Fig.7: Effect of continuous microwave drying of wood at 300 W of power; Before and after drying.

The second solution proposed in this study is to apply an intermittent drying process. This process is only considered at the microwave power level, and the conditions of drying are shown in (Table 1). The qualitative observations are illustrated by the photos of dried wood samples, (Fig.8). It is observed that drying defects related to the level of microwave power in the continuous drying are absent in the intermittent drying. The absence of the various defects can be explained by the cooling of wood sample and mechanical stress relaxation during the intermittency phase.

Fig.8: Effect of intermittent microwave drying of wood at 500 W; Before and after drying.

One can notice that oscillation of the microwave power between 0 and P_{max} increases drying time compared to continuous drying (See Figure 3) but allows to reduce average temperature and internal gaz phase. The optimization of the intermittency phases make it possible to optimize drying in terms of drying time and wood quality.

4. Conclusions

The experimental results indicated that increasing the microwave power decreases the drying time and increases both the core temperature and the internal gas pressure of wood samples. The phenomenon of internal heat generation during microwave drying wood was verified by the temporal evolution of temperature curves. A qualitative analysis of dried wood samples proves that the intermittent microwave drying reduces the defects related of drying and improved product quality compared with continuous microwave drying. As an extension of this work, mechanical tests of axial compression and static bending strength will be held. Optimization of intermittency phases will be also carried by the help of modelling heat, mass and mechanical behavior of wood sample on intermittent microwave drying.

5. Nomenclature

P	Microwave power	Watt
T	Temperature	°C
W	Wood sample mass	kg
W_{water}	Water mass	kg
W_d	Wood sample dry mass	kg
M_{ini}	Initial moisture content	kg water/kg DM

6. Acknowledgments

7. References

[1] S. Ouertani, A. Kouba, S. Azzouz, L. Hassini, K. Ben Dhib, A. Belghith, Vacum contact drying kinetics of Jack pine wood and its influence on mechanical properties : industrial applications, Heat Mass Transf.DOI 10.1007/s00231-014-1476-0, 2014.

[2] Turner, I.W.; Puiggali, J.R.; Jomaa, W. A numerical investigation of combined microwave and convective drying of a hygroscopic porous material. A study based on pine wood. Chemical Engineering Research & Design 1998, 76, 193–209.

[3] S. Ouertani, L. Hassini, S. Azzouz, S.S. Torres, A. Belghith, A. Koubaa, Modeling of combined microwave and convective drying of wood: Prediction of mechanical behavior via internal gas pressure, Drying Technology, ID: 1022828 DOI:10.1080/07373937.2015.1022828, 2015.

[4] F. Erchiqui, 3d numerical simulation of thawing frozen wood using microwave energy: frequency effect on the applicability of the beer–lambert law, Drying Technology, Volume 31, Pages 1219-1233, 2013.

[5] Thouraya Salem. Séchage intermittent du bois d'oeuvre : étude expérimentale et numérique. Matériaux. Université de Lorraine, 2016. Français. <NNT : 2016LORR0177>.

[6] Lars Hansson, Microwave Treatment of Wood. University of Technology LTU Skelleftea Division of Wood Physics, 2007.

[7] L. Hansson et A.L. Antti (a). The effect of microwave drying on Norway spruce woods strength: a comparison with conventional drying. Journal of Materials Processing Technology 141 (2003) 41–50

[8] Bruno Monteiro Balboni et al. Microwave treatment of *Eucalyptus macrorhyncha* timber for reducing drying defects and its impact on physical and mechanical wood properties. Eur. J. Wood Prod. DOI 10.1007/s00107-017-1260-1

[9] Ihsane LOULIDI et al. Impact energy on notched and unnotched specimens of wooden Eucalyptus Gomphocephala under variation of moisture. Sciences et Technologie B – N°36, (Décembre 2012), pp 9-14.

[10] G. Du, S. Wang, Z. Cai, Microwave drying of wood strands, Drying Technology, Volume 23, Pages 1-16, 2005.

[11] Lars Hansson, Microwave Treatment of Wood. University of Technology LTU Skelleftea Division of Wood Physics, 2007.

[12] Eva Hermoso, Abel Vega. Effect of microwave treatment on the impregnability and mechanical properties of Eucalyptus globulus wood. Maderas. Ciencia y tecnología 18(1): 55 - 64, 2016

Drying of acerola residues in a roto-aerated dryer assisted by infrared heating

Silva, P. B. [a*]; Nogueira, G. D. R.[a]; Duarte, C. R. [a]; Barrozo, M. A. S. [a*]

[a] Chemical Engineering School. Federal University of Uberlândia, Uberlândia, MG, Brazil,

*E-mail of the corresponding author: masbarrozo@ufu.br; priscilabernardeseq@gmail.com

Abstract

Acerola (Malpighia emarginata D.C.) is a tropical fruit which has attracted recent industrial interest, due to its high levels of bioactive compounds and vitamin C. However, acerola processing generates a substantial amount of wastes, which can represent up to 40% of total processed volume. The drying of acerola residues in a new dryer, developed by our research group, named as roto-aerated dryer, has been investigated. This dryer provides a better fluid-particle contact than the conventional rotary dryer. A pre-drying system with infrared lamps has been installed in the feed of this new dryer. The effect of the pre-treatment of this fruit residues with ethanol was also investigated. The results shown that the roto-aerated dryer assisted by infrared radiation hybrid combined with a pre-treatment with ethanol is a good alternative for processing fruit residues, aiming their reuse. It was possible to identify conditions under which the phenolic, flavonoid, and antioxidant capacity presented high levels after drying. The main phenolic compounds were idenfied by HPLC.

Keywords: Drying; roto-aerated dryer; infrared; acerola

1. Introduction

Byproducts of fruit processing industries, such as seeds, kernels and bagasse, which were previously considered wastes, have high potential to be used as food supplement. This aspect, along with the increasing global interest in environmental friendly technologies, explains the interest in a better utilization of fruit processing industries residues [1].

Acerola (Malpighia emarginata D.C.) is a tropical fruit originates from tropical America. Its pleasant flavor and the high levels of vitamin C have led to its increasing use in the form of juice, jelly and compote. The residues of acerola processing can contain higher amounts of phenolic and other bioactive compounds than the edible fleshy parts. [1]

A challenge faced by drying of this fruit residues is to reduce the exposure time at elevated temperatures, which may cause deterioration of the bioactive compounds present in the material [2]. Rotary dryers are interesting alternatives for drying of fruit residues, because of their flexibility in handling a wider range of materials than other types of dryers. Several studies in the literature [3] have focused on developing modifications on rotary dryers to improve their performance. Thus, another version of the rotary dryer, named as roto-aerated dryer, was designed by our research group. The main characteristic of this non-conventional rotary dryer is the effective contact time between hot air and wet solids and consequently the drying efficacy [3].

In this work, a pre-drying system with infrared lamps has been installed in the infeed conveyor of this new dryer. The effect of a pre-treatment of the acerola residues with ethanol was also analyzed. The drying performance of this novel system was investigated. The quality parameters, such as phenolics and flavonoids contents were also studied.

2. Materials and Methods

2.1. Material

The acerola wastes used in this work came from industrial juice processing (Fruteza Company, from Sao Paulo-Brazil). The material was stored in frozen at approximately -18°C. The Samples were removed from the freezer 12 hours prior to the drying and then placed in the refrigerator at 5ºC to thaw.

2.2. Experimental apparatus and conditions

Figure 1 shows a schematic diagram of the experimental apparatus which consist of a 7.5-HP blower coupled to a duct; an air heating system comprised of electric resistances controlled by a variac and the roto-aerated dryer. The solids feed was performed through a conveyor belt (3) mounted below a reservoir (4), where the wet particulate material was stored. The material was conveyed to another conveyor (5) in order to more effectively adjust the feed rate. On the second conveyor belt was mounted a pre-drying system with

four infrared lamps (6). The power of the lamps was adjusted by a Variac transformer (0 to 1200 W). The drum (7) inclination angle was 3º, and the rotation speed was 2.7 rpm. The drum used in this study was 1.5 m long and 0.29 m wide. The configuration of the roto-aerated dryer had 56 mini-pipes (8): 10 mini-pipes near the solids feed, with 0.004 m diameter; 12 mini-pipes in the middle with 0.006 m diameter, and 34 mini-pipes near the solids discharge with 0.009 m diameter. The mini-pipes had a length of 0.095 m and they were placed at 0.02 m from the particle bed. The solids flow rate was of 0.045 kg min^{-1}. The temperatures of the air and solids were measured using copper–constantan thermocouples calibrated by means of a thermostatic bath and a mercury thermometer with a precision of 0.05 ºC. The relative humidity ranged between 30 and 40%. For the conditions used in the present work,the holdup ranged from 65.6 g to 194.2 g. The residence time (τ) was determined by the ratio between hold up and the solids flow rate. The pre-treatment with ethanol have been performed spraying 93.2∘GL ethanol onto the residues, in the proportion of 2 L of alcohol to 3 kg of solids [4].
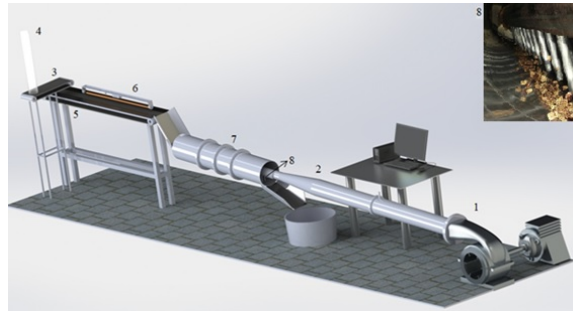
Fig. 1 Experimental apparatus.

The experimental conditions were chosen considering a central composed design [3] with 3 replicates at the center levels (Table 1). The independent variables analyzed were the air velocity (v), air temperature (T) and infrared lamp power (P).

Table 1. Experimental design

Exp.	T (ºC)	v (m/s)	P (W)	Exp.	T (ºC)	v (m/s)	P (W)
1	80.0	1.5	600.0	11	115.0	1.3	850.0
2	80.0	1.5	1100.0	12	115.0	3.3	850.0
3	80.0	3.0	600.0	13	115.0	2.3	511.7
4	80.0	3.0	1100.0	14	115.0	2.3	1188.3
5	150.0	1.5	600.0	15	115.0	2.3	850.0
6	150.0	1.5	1100.0	16	115.0	2.3	850.0
7	150.0	3.0	600.0	17	115.0	2.3	850.0
9	150.0	3.0	1100.0	18	180.0	2.3	1188.3
8	67.6	2.3	850.0	19*	180.0	2.3	1188.3
10	162.4	2.3	850.0				

* With pre-treatment with ethanol

2.3. Quality parameters

The moisture content was determined by the oven method at 105 ± 3 °C for 24 h. The Kjeldahl method was used to determine the protein content, while the crude lipid and total dietary fibers (TDF) were determined using the Soxhelt method and neutral detergent 20% method, respectively, according to AOAC methods [5]. The carbohydrate content was determined by the difference. Minerals were quantified by X-ray fluorescence (FRX) using a Shimadzu device (EDX-720).Total phenolics content (TPC) were determined by the Folin Ciocalteu method [6], using gallic acid monohydrate (99%). Total flavonoids content (TFC) were determined using the colorimetric method described by Zhishen et al. [7]. DPPH analyzes were performed according to Brand-Williams et al. [8] to obtain the amount of antioxidant necessary to decrease the initial DPPH• concentration by 50% (IC_{50}). The phenolic acids was identified through HPLC according to Ribeiro et al. [9]. All analyses of antioxidant compounds were performed in triplicate and the results expressed in mean value $\pm$ SD. The differences between means were analyzed by analysis of variances (ANOVA with $p < 0.05$).

3. Results and Discussion

The characterization of acerola residue showed that this material had a high concentration of total fibers (51.12 ± 0.52 g/100 g d.w.). The Food Nutrition Board (FNB), through the Indicated Daily References (DRI), set the appropriate recommendation for 38 g fibers for men and 25 g for women, both adults. The amount of protein (10.13 ± 0.15 g/100 g d.w.), lipids (5.43 ± 0.37 g /100 g d.w.) and carbohydrates (30.86 ± 0.12 g/100 g d.w.) demonstrate the potential of this material to be used as a food supplement, aiming to add protein and energy values. The results of the X-ray fluorescence spectrometry (FRX) analysis showed the predominance of potassium (3650 mg/100g d.w.), calcium (805 mg/100g d.w.) and phosphorus (420 mg/100g d.w.) in the acerola residue. Magnesium (130 mg/100g d.w.) and molybdenum (30 mg/100g d.w.) were also detected. These compounds participating in metabolic reactions and are also associated with prevention of cardiovascular disease, decreased osteoporosis, diabetes and Alzheimer's [1].

Figure 2 show the results of drying of acerola residues in the roto-aerated dryer assisted by infrared radiation. The initial moisture content of the material was 78.7 ± 0.8 g/100 g w.b., and after the infrared radiation ($M_{infrared}$) reached until 59.1 g/100 g w.b. (Experiment 14 (E14) - 1188 W), a 24.3% of moisture reduction. The exposure time of the material to the infrared lamps was 9 min. For the powers of 600, 850 and 1100 W the average moisture reduction was 1.9 ± 0.1%, 11.4 ± 1.0% and 18.3 ± 1.6%, respectively.

(a)

(b)

(c)

(d)
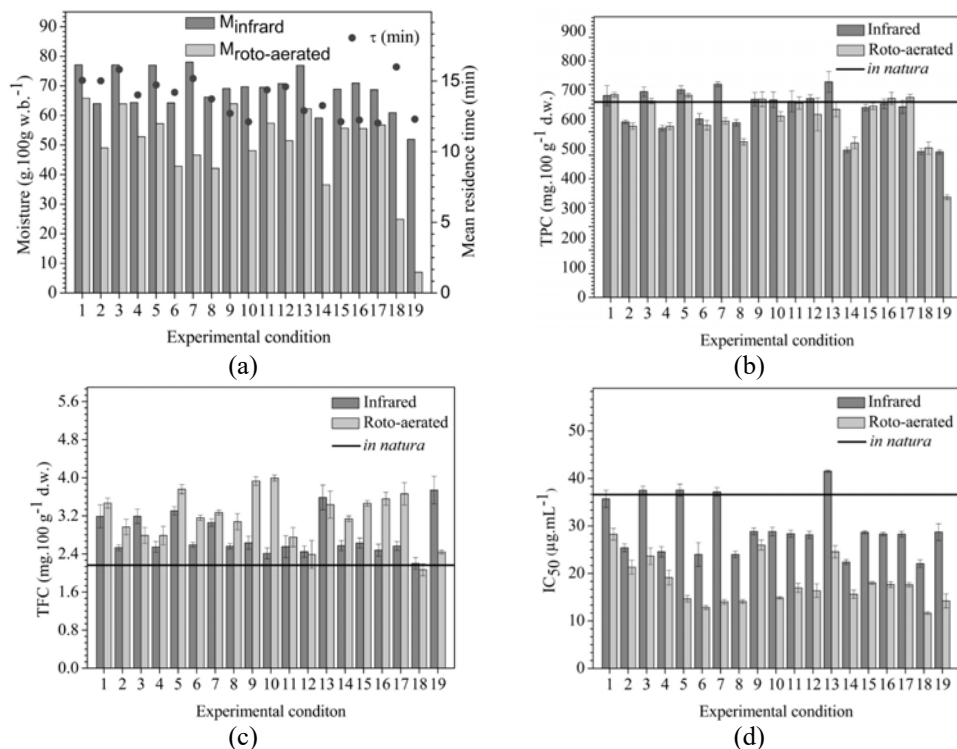
Fig. 2 Results of drying of the acerola residue after infrared and roto-aerated.

The moisture of the material fed to the roto-aerated dryer varied according to the power of the infrared pre-drying, which was 77.3 ± 0.5 (600 W), 69.7 ± 0.9 (850 W) and 64.7 ± 1.0 (1100 W) g/100 g w.b. The average residence time of the material in the dryer ranged from 3.0 min (E17) to 6.8 min (E3). The final moisture of the material after the roto-aerated dryer (M_{roto}) ranged from 65.8 to 36.6 g/100 g w.b. for conditions E1 and E14, respectively. Therefore, it was possible to reduce the initial moisture content of the material by up to 53.5 % in a period of 13.5 min. This is a short time when compared to other drying techniques already used for dehydration of the acerola residue. The tray dryer requires 120 to 220 min [10] and the fixed bed of 25 cm of thickness requires 159.3 to 300.7 min [11]. The reduced time required for drying in a roto-aerated dryer is due to its excellent fluid-particle contact [3]. It is also worth mentioning that prolonged drying times can result in the degradation of bioactive compounds [2].

The last two experiments (E18 and E19) were performed at the same operating conditions (180.0 ºC, 2.3 m/s and 1188.3 W). However, the experiment E19 was performed with pre-treatment with ethanol. The moisture reduction after the infrared was 22.9% and 34.0% and after the roto-aerated was of 59.1% and 91.1%, for the acerola residue with (E19) and without ethanol pre-treatment (E18), respectively.

Considering that a drying process can affect the final quality of the product, it is also important to evaluate the quality indices. The quality of acerola residues has been evaluated by the quantification of total phenolic compounds (TPC), total flavonoids (TFC) and antioxidant activity (IC_{50}).

Figure 2-b shows that TPC was lower in the conditions with higher power of the infrared lamps and/or higher drying air temperature. Phenolic losses may occur due to enzymatic and non-enzymatic oxidative reactions. Similar results were found by Nunes et al. [12] in guava drying. According to Maillard and Berset [13], thermal degradation also may contribute to phenolic losses. The highest reductions were 21.0 % (522.0 ± 20.0 mg/100g d.w.) and 23.6% (504.7 ± 21.0 mg/100g d.w.) for conditions E14 (moisture 36.6 g/100 g w.b.) and E18 (24.9 g/100 g d.w.), respectively. Despite the reductions in TPC, the dried material presents good potential and can be considered as with intermediate concentrations according to Vasco's classification [14].

Fig. 2-c shows that the TFC of the acerola residues after drying, in all operating conditions, have been in higher levels. The highest levels of TFC were obtained in intermediate levels of infrared power and drying air velocity (E9 and E10). This behavior might be explained by the liberation of phenolic compounds due to the breaking of the cellular constituents during the drying process and due to presence of melanoidins and from the Maillard reaction, thereby interfering with the antioxidant properties [12].

The antioxidant activity was evaluated using the DPPH* radical capture method, the results were expressed as IC_{50} (µg sample / mL capable of reacting with 50% of the radical present in the DPPH * solution). Thus, the lower the IC_{50} value, the higher the antioxidant activity of the analyzed material. The lowest IC_{50} values were found in conditions E6, E7, E8, E10, E14 and E18, which had high drying air temperature and/or high infrared power, as can be seen in Figure 2-d. These were experimental conditions with greater moisture removal. However, even under these conditions the antioxidant activity was high. The heating of the material may increase the free flavonoid content and consequently the antioxidant capacity, which may change due to several factors such as the increase of the antioxidant power of the polyphenols in an intermediate state of oxidation, the increase of the reduction of sugars and the formation of products from Mailard reaction [1].

Phenolic acids were determined in HPLC by comparison with the retention time of standards. Four phenolic acids were detected in the HPLC analyzes: gallic (165.3-280.1 mg/100 g d.w.), caffeic (4.12-18.3 mg/100 g d.w.), chlorogenic (0.6-3.5 mg/100 g d.w.) and p-coumaric (2.6-13.2 mg/100 g d.w.) acids. The gallic acid content presented a reduction in relation to the fresh residue (261.0 ± 13.6 mg / 100 g d.w.), this reduction was greater for the conditions with higher drying air temperature and infrared power. Similar behaviors were found for caffeic (16.9 ± 1.2 mg/100 g d.w.) and chlorogenic (7.2 ± 0.5 mg/100 g

d.w.) acids. During drying processes, the activation of oxidative enzymes, such as polyphenoloxidase and peroxidase, in addition to the thermal degradation can lead to the loss of phenolic compounds [15]. Drying also dissociates some phenolic compounds, thereby altering chemical structures, transforming insoluble phenolic compounds into more soluble forms and making phenolic compounds more available for quantification, besides the formation of new compounds with antioxidant properties [15].

4. Conclusions

The results showed that the new dryer system developed by our research group is a good alternative for drying of acerola wastes. It was possible to identify conditions with high moisture removal and short residence times that are suitable conditions to perform an efficient drying process with a preservation of product quality. It was possible to identify conditions under which the phenolic, flavonoid, and antioxidant capacity presented high levels after drying. The main phenolic compounds were idenfied by HPLC.

5. Acknowledgements

6. References

[1] Duzzioni, A.G., Lenton, V.M., Silva, D.I.S. & Barrozo, M.A.S. (2013). Effect of drying kinetics on main bioactive compounds and antioxidant activity of acerola (Malpighia emarginata D.C.) residue. International Journal of Food Science & Technology, 48, 1041–1047.

[2] Arenas, K. S. L.; Victoria, M. T. C. Y.; Vizcarra, M. G.; Vera, C. M.; Sosa, I. A. Effect of agitated bed drying on the retention of phenolic compounds, anthocyanins and antioxidante activity of roselle (*Hibiscus sabdariffa L.*). International Journal of Food Science & Technology, v. 51, p. 1457-1464, 2016.

[3] Silverio, B.C., Arruda, E.B., Duarte, C.R. & Barrozo, M.A.S. (2015). A novel rotary dryer for drying fertilizer: Comparison of performance with conventional configurations. Powder Technology, 270, 135-140.

[4] Braga, A.M.P.; Silva, M.A.; Pedroso, M.P.; Augusto, F.; Barata, L.E.S. Volatile composition changes of pineapple during drying in modified and controlled atmosphere. International Journal of Food Engineering, v.6, p.1556-3758, 2010.

[5] AOAC. (1995). Official methods of analysis. Association of official analytical chemists, Gaithersburg.

[6] Singleton, V.L. & Rossi, J.A. (1965). Colorimetry of total phenolics with phosphomolibidic_phosphotungistic acid reagents. The American Journal of Enology

and Viticulture, 16, 144-158.

[7] Zhishen, J., Mengcheng, T. & Jianming,W. (1999). The determination of flavonoid contents in mulberry and their scavenging effects on superoxide radicals. Food Chemistry, 64, 555–559.

[8] Brand-Wiliams, W., Cuvelier, M.E., Berset, C. Use of a free radical method to evaluate antioxidant activity. Food Science and Technology, v. 28, p.25-30, 1995.

[9] Ribeiro, L. F.; Ribani, R. H.; Francisco, T. M. G.; Soares, A. A.; Pontarolo, R., Haminiuk, C. W. I. Profile of bioactive compounds from grape pomace (Vitis vinifera and Vitis labrusca) by spectrophotometric, chromatographic and spectral analyses. Journal of Chromatography B, v. 1007, p. 72-80, 2015.

[10] Nóbrega, E. M. M. A. (2012) Secagem de resíduo de acerola (*Malphigia emarginata DC.*): estudo do processo e avaliação do impacto sobre o produto final. Master's thesis. Federal University of Rio Grande do Norte, Brazil, 102 p..

[11] Silva, D. I. S. (2015). Study of heat and mass transfer in fixed bed drying targeting the use of acerola residue (*Malpighia emarginata DC*). PhD Thesis, Federal University of Uberlândia, Brazil, 252 p.

[12] Nunes, J. C.; Lago, M. G.; Castelo-Branco, V. N.; Oliveira, F. R.; Torres, A. G.; Perrone, D.; Monteiro, M. Effect of drying method on volatile compounds, phenolic profile and antioxidant capacity of guava powders. Food Chemistry, v. 197, p.881-890, 2016.

[13] Maillard, M. N.; Berset, C. Evolution of antioxidant activity during kilning: Role of insoluble bound phenolic acids of barley and malt. Journal of Agricultural and Food Chemistry, Vol. 43, n. 7, p. 1789-1793, 1995.

[14] Vasco, C.; Ruales, J.; Kamal-Eldin, A. Total phenolic compounds and antioxidant capacities of major fruits from Ecuador. Food Chemistry, v. 111, n. 4, p. 816-823, 2008.

[15] Tomaino, A.; Cimino, F.; Zimbalatti, V.; Venuti, V.; Sulfaro, V.; De Pasquale, A.; Saija, A. Influence of heating on antioxidant activity and the chemical composition of some spice essential oils. Food Chemistry, v. 89, p. 549−554, 2005.

Drying of microalga *Spirulina platensis* in a rotary dryer with inert bed

Silva, N. C.; Silva, T. C.; Santos, A. O.; Graton, I. S.; Duarte, C. R.; Barrozo, M. A. S.[*]

School of Chemical Engineering, Federal University of Uberlandia, Uberlandia, Minas Gerais, Brazil.

*E-mail of the corresponding author: masbarrozo@ufu.br

Abstract

The aim of this work is investigate the use of a rotary dryer with inert bed for drying of microalga Spirulina platensis. The influence of air temperature, feed rate, rotation speed and inerts filling degree was quantified. The contents of main bioactive compounds were also analyzed. The results shown that the used drying system proved to be an interesting alternative for a possible use of this microalga, if performed under adequate conditions. It was identified conditions with high drying performance and with the preservation of product quality.

Keywords: Spirulina platensis; rotary dryer; inert bed; bioactive compounds.

1. Introduction

Spirulina platensis is one of the species of cyanobacterium microalgae that has gaining recent attention because of its nutritional and medicinal properties. Several studies reported the potential use of Spirulina biomass due the high presence of proteins, vitamins, minerals, antioxidant and anti-inflammatory compounds as the phycocyanin[1, 2, 3]. Despite this, the Spirulina is very perishable due its high moisture content that contributes to degradation, hamper transport and storage, and reduce the shelf life. Thus, it is necessary apply a drying technique that allows use properly this material in food or pharmaceutical industries.

The most traditional methods used to drying microalgae are spray drying, freeze-drying, solar drying and convective hot air drying[4, 5]. However, the rotary dryers appears as an interesting alternative because their flexibility and high processing capacity. Conventional rotary dryers have flights, which lift solids and make them cascade across the dryer section. Most of the drying occurs during the free fall of solids from the flights, because of the large gas-solids surface contact area[6]. However, conventional rotary dryers are typically used for granular materials and are not suitable for pastes. Thus, the use of an inert bed (as metal or ceramic spheres, for example) is an interesting alternative for paste drying in rotary drums, since the inert increase the contact surface between hot air and material, and prevents the loss of material on the walls and dryer structures[7, 8].

In the present work, the drying of *Spirulina platensis* in a rotary dryer with inert bed was investigated. The effects of process variables on the drying yield was quantified and the impacts of these variables on the main bioactive compounds contents (total phenolics, total flavonoids, citric acid and phycocyanin) were also analyzed.

2. Materials and Methods

2.1. Raw material

The microalga *Spirulina platensis* used in this study was provided by the company Brasil Vital, located in the state of Goias, midwest Brazil. The material was previously filtered in vacuum, stored in small portions and frozen in a freezer.

2.2. Experimental apparatus

The experimental apparatus, shown in Fig. 1, consists of: a radial blower (Kepler-Weber, 112M), an electric heater connected to a voltage variator to adjust the air temperature, the rotary drum coupled a rotation system composed by a motor and frequency inverter (WEG, CF08) to control the rotation speed, and a Stairmand cyclone separator (diameter 10 cm) with a flask in its underflow to collect the dried material. The Spirulina *in natura* were fed in the system with a peristaltic pump (Masterflex, 7553-70) connected to a velocity variator.

The rotary drum used in this study was a stainless steel cylinder with 12 cm of inner diameter and 36 cm of length. Three stainless flights with 2.5 cm are also placed into the drum for uniform axial distribution of inerts during the drying. The inerts particles used were porcelain spheres with diameter of 1.9 cm and density of 2.32 g/cm^3.

1 – Blower	
2 – Electric Heater	
3 – Voltage Variator	
4 – Rotary Drum	
5 – Motor	
6 – Frequence Inverter	
8 – Cyclone Separator	
9 – Collect flask	
10 – Feed Tank	
11 – Peristaltic Pump	
12 – Velocity Variator	
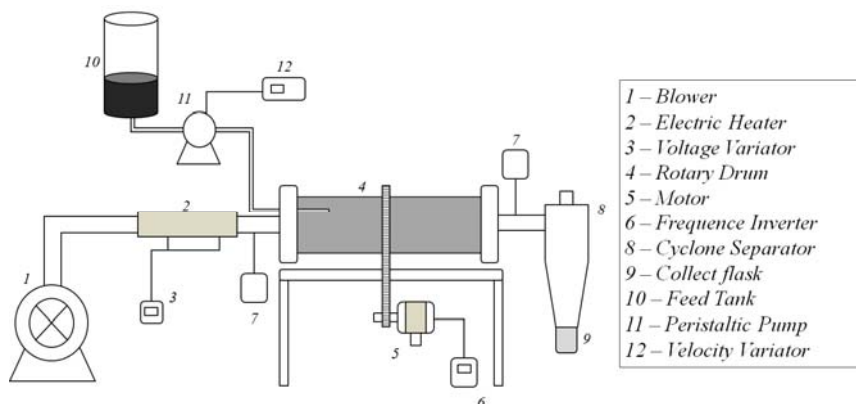
Fig. 1 Experimental apparatus.

2.3. Experimental design

The experiments were conducted following a orthogonal central composed design with four independent variables and two replicates at the center level, totaling 26 experiments. The independent variables analyzed were: the air temperature (T), feed intermittence (FI), inert filling degree (FD) and rotation speed (RS). In each experiment were used about 100g of Spirulina microalga. The coded and real variable values are shown in Table 1.

Table 1. Coded and real variable values

Design Factors	-1.483	-1	0	+1	+1.483
Air temperature (ºC)	40.3	50.0	70.0	90.0	99.7
Feed Rate (min)	2.6	5.0	10.0	15.0	17.4
Filling Degree (%)	12.1	15.0	21.0	27.0	29.9
Rotation Speed (RPM)	35.2	40.0	50.0	60.0	64.8

The *Air Temperature (T)* was measured at the inlet of the drum. The wet Spirulina was fed in cycles, in an intermittent system of feed of 10 g of material and a rest for a determined

time (defined as the variable *Feed Intermittence*). The *Filling Degree (FD)* was calculated based in the cylinder geometry and the properties of inert bed, as density and porosity, and the rotation speed (RS) were measured using a digital tachometer. The response studied was the Drying Yield (DY), that is the percentage ratio of the quantity of material (dry base) collected in the cyclone underflow to the quantity of microalga fed into the dryer (in dry base).

2.4. Analysis of bioactive compounds

The experiments with the highest values of Drying Yield (DY) had their bioactive compounds analyzed to evaluate the impact of the operational conditions on the quality of the final product. The total phenolics content (TPC) was determined by the *Folin-Ciocalteau* method [9]. The total flavonoids content (TFC) was determined using the method described by Zhishen *et al.*[10]. The acidity (CA), expressed in the presence of citric acid in the samples, was determined by AOAC[11] method. The phycocyanin content (PC). was performed based on the methodology of Costa *et al.*[2].

3. Results and Discussion

3.1. Analysis of dehydration yield (DY)

The most significant operating variables can be observed in Equation 1, through the parameters obtained by the multifactor ANOVA (R^2= 0.9048 and α = 0.10). The effect of the studied variables on the drying yield can be visualized in Figure 2.

$$DY = 60.46 + 3.14.FD - 2.05.FD^2 + 1.51.RS - 1.99.RS^2 - 2.04.FI^2 - 0.83.T.FI$$
$$- 2.08.T.RS - 1.51.FI.FD - 1.49.FI.RS$$

$$(1)$$
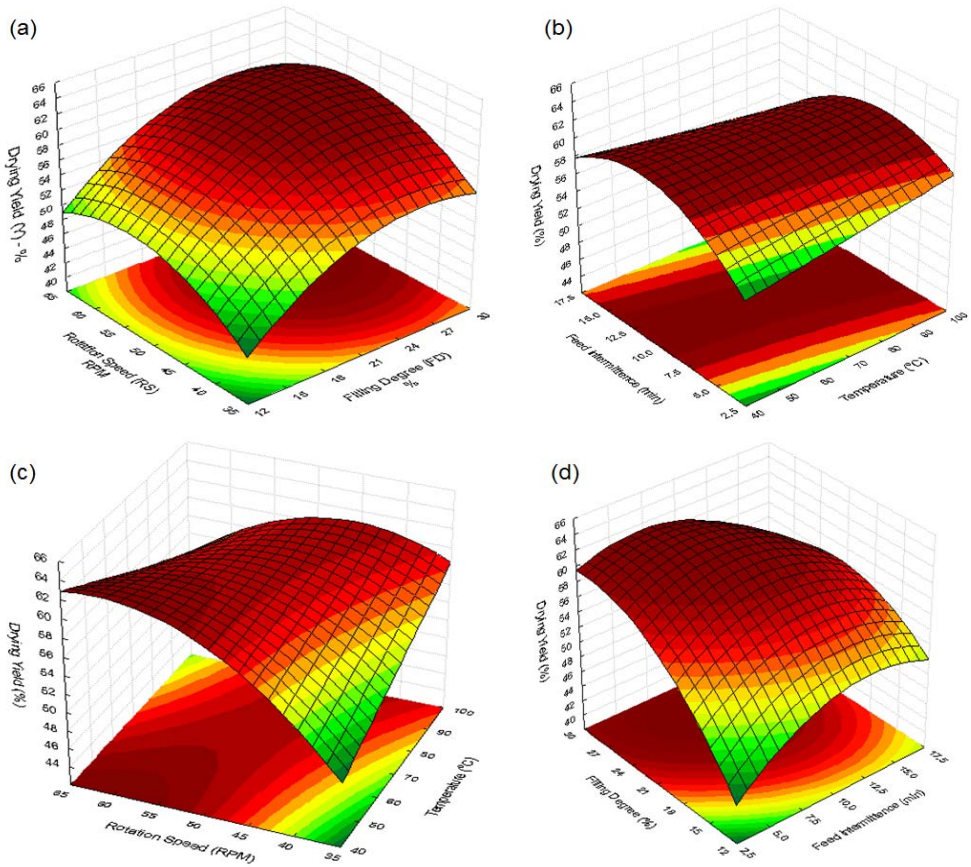
Fig. 2 Drying Yield (DY) response surfaces.

The variables: filling degree (FD) and rotation speed (RS) presented non linear effects on the DY (Equation 1 and Figure 2a). In general, the experiments performed at higher values of these variables produced a great quantity of dried material, hence the best results of DY. The effect of the temperature on DY was present by means of the interation with intermittence (FI) and rotation speed (RS). The best results were obtained with the association of low temperatures and high levels of RS or with intermediate levels of RI, as can be seen in Figure 2b and Figure 2c.

The analysis of the results showed that the higher drying yields can be obtained in experimental conditions of high Filling Degree (FD) and Rotation Speed (RS), combined with Intermediate Feed Intermittences (FI) and low process Temperatures (T). For the

conditions of the experimental design, the highest values of DY were obtained in the Experiments expressed in the Table 2.

Table 2. Experiments with the highest Drying Yields (DY)

Experiments	T (ºC)	FR (min)	FD (%)	RS (RPM)	DY (%)
4	50.0	5.0	27.0	60.0	63.28%
8	50.0	15.0	27.0	60.0	60.12%
17	40.3	10.0	21.0	50.0	61.88%
24	70.0	10.0	21.0	64.8	60.42%

3.2. Analysis of Bioactive Compounds
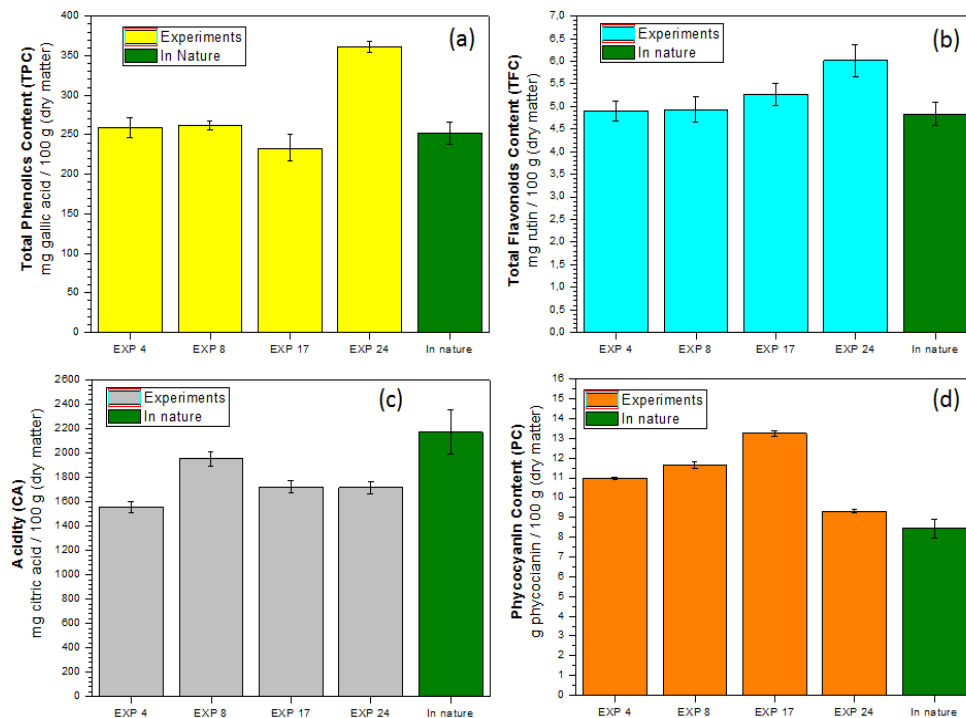
Fig. 3 Bioacitve compounds content in the experiments with the highest Drying Yield (DY).

The bioactive compounds content obtained in the four experiments showed in Table 2 are presented in Figure 3. It can be observed that for the experiments performed in the

conditions that led the greatest yields, the main bioactive compounds were preserved, indicating that this drying methodology has good effect on the quality of final dried Spirulina. This bioactive content behavior was also also related by Chism & Haard[12] that observed the liberation of these compounds accumulated in vegetal cell organelles as vacuoles, due to rupture in the internal structure of the material during the moisture removal. Dorta *et al.*[13] also claimed that inactivation of certain enzymes responsible for the degradation of bioactive compounds can occur during the drying process, resulting in their preservation.

4. Conclusions

The drying of microalga *Spirulina platensis* using a rotary dryer proved to be an interesting alternative for use of this material. All the variables analised showed statistical significance in the results of yield. The combination of low temperatures, high filling degree, high rotation speed and intermediate feed intermittence allowed obtain the highest drying yields. It was also possible obtain bioactive compounds content near than present in fresh biomass in the experiments analyzed, indicating a positive effect of this process of moisture removal on the final quality of dried product.

5. References

[1] Agustini, T.W.; Suzery, M.; Sutrisnanto, D.; Ma'ruf, W.F.; Hadyanto. Comparative Study of Bioactive Substances Extracted from Fresh and Dried *Spirulina sp*. Procedia Enviromental Sciences 2015, 23, 282-289.

[2] Costa, B.R.; Rodrigues, M.C.K.; Rocha, S.F.; Pohndorf, R.S.; Larrosa, A.P.Q., Pinto, L.A.A. Optimization of *Spirulina Sp*. Drying in Heat Pump: Effects on the Physicochemical Properties and Color Parameter. Journal of Food Processing and Preservation 2016, 40, 934-942.

[3] Dissa, A.O.; Desmorieux, H.; Savadogo, P.W.; Segda, B.G.; Koulidiati, J. Shrinkage, porosity and density behavior during convective drying of spirulina. Journal of Food Engineering 2010, 97, 410-418.

[4] Oliveira, E.G.; Rosa, G.S.; Moraes, M.A.; Pinto, L.A.A. Characterization of thin layer drying of *Spirulina platensis* utilizing perpendicular air flow. Bioresource Technology 2009, 100, 1297-1303.

[5] Show, K.Y.; Lee, D.J.; Chang, J.S. Algal biomass dehydration. Bioresource Technology 2013, 135. 720-729.

[6] Silva, P.B., Duarte, C.R., Barrozo, M.A.S. Dehydration of acerola (*Malpighia emarginata D.C.*) residue in a new designed rotary dryer: Effect of process variables on main bioactive compounds. Food and Bioproducts Processing 2016, 98, 62–70.

[7] Honorato, G.C. Design of a Rotary Dryer for Shrimp Cephalothorax Drying. Federal University of Rio Grande do Norte, Brazil, 185p., 2006 (Doctoral Thesis).

[8] Moura, B.D. Study of Drying Dynamics in a Rotary Dryer with Intermittent Feeding.

Federal University of Rio Grande do Norte, Brazil, 123p., 2016 (Doctoral Thesis).

[9] Singleton V.L.; Rossi J.A. Colorimetry of total phenolics with phosphomolibidic–phosphotungistic acid reagents. American Journal of Enology and Viticulture 1965, 16, 144–158.

[10] Zhishen J.; Mengcheng, T.; Jianming, W. The determination of flavonoid contents in mulberry and their scavenging effects on superoxide radicals. Food Chemistry 1999, 64, 555–559.

[11] AOAC, Association of Official Analytical Chemists. Official methods of analysis. Gaithersburg, MD: AOAC 1995.

[12] Chism, G.W.; Haard, N.F. Characteristics of edible plant tissues. In: O.R., Fennema, Food Chemistry 1996, 943-1011, New York, Marcel Dekker, Inc.

[13] Dorta, E.; Lobo, M.G.; Gonzalez, M. Using drying treatments to stabilise mango peel and seed: effect on antioxidant activity. LWT - Food Science and Technology 2012, 45, 261–268.

The intermittent drying of wheat by microwave and fluidized bed drying

Turkoglu, T.ª; Baykal, H.ª; Yuksel, H.ª*; Caliskan Koc, G.ª; Dirim, S.N.ª

ª Department of Food Engineering, University of Ege, Izmir, Turkey.

*E-mail of the corresponding author: hirayuksel@gmail.com

Abstract

The objective of the study is to investigate the effects of different drying processes (convective hot air, microwave, and fluidized bed drying) and combined drying methods on the drying characteristics and physical properties of the dried wheat and the power consumption of the dryers. The lowest moisture content and water activity values were observed for the 25min of drying in fluidized bed dryer (60°C) and following 16min in microwave dryer (540W). The lowest power consumption was observed in the 60°C-180W fluidized bed-microwave combination (0.77kWh) compared to the other combined trials.

Keywords: wheat; convective drying; microwave drying; fluidized bed drying intermittent drying.

1. Introduction

The ready to us products that are precooked and dried are called as "parboiled"[1]. The main objective of parboiling on wheat is a versatile that can be used in bread, salads, casseroles, stew, desserts, and served as side dish.

Drying is applied to decrease the moisture content and water activity in the product, to inhibit the growth of the microorganisms and prolonging the shelf life of the final product. One of most common drying methods is convective hot air drying. However, this method has many disadvantages such as lengthy drying time, darkening in color [2], the high temperature damaging the product quality and high power consumption [3]. The microwave drying provided an alternative way since it is an advantageous method due to its short drying time, ease of process control, power saving and drying homogenization. In fluidized bed dryer, the products in the granular structure are fluidized and excess moisture in the product structure is removed by a drying air. In addition, fluid bed drying process provides such as a good solids mix, high-speed heat-mass transfer and easy transport of substances advantages [4]. Therefore, fluid bed dryers are preferred due to their high heat transfer rates [5]. The drying industry utilizes large quantities of energy and for this reason one of the most important challenges of the drying industry is to reduce the power cost of obtaining good quality dried products. For this reason, drying operations can be applied intermittently in order not to damage the structure of the food, to adversely affect the quality and to save power [5].

The objective of this work is to investigate the effects of different drying processes (convective hot air, microwave, and fluidized bed drying) and combined drying methods on the drying characteristics and physical properties of parboiled wheat. In addition, the power consumption of the dryers was measured to use in the comparison.

2. Materials and Methods

2.1. Material

Wheat (*Triticum aestivum*) was supplied from a local market in İzmir/TURKEY. Wheat samples were soaked in the water (1:10 wheat:water ratio (weight:weight), (w:w)) at the room temperature (25°C) overnight and was parboiled at 100°C for half an hour in the water (1:2 wheat:water ratio, (w:w)) and drained. The initial moisture content of the samples was 60.48±0.63 %.

2.2. Methods

2.2.1 Drying Processes

Pre-processed wheat samples were dried by using different drying methods and their combinations. The weight loss of the samples was measured by using an electronic balance

(Ohaus AR2140, USA) until constant weight was reached. The drying conditions are given in the following Table 1.

Table 1. Drying methods and conditions

Convective hot air drying	Fluidized bed drying	Microwave drying
Armfield Lim., Ringwood, Hampshire, UK	Sherwood Scientific, UK	Arçelik MD595, Turkey
70°C and 1.6 m/s air velocity	60, 70, 80°C and 1.6 m/s air velocity	180W, 360W, 540W, 720W, and 900W
every 5 min. of weight measurement	every 5 min. of weight measurement	every 1 min. of weight measurement

Intermittent fluidized bed-microwave drying		Intermittent microwave- fluidized bed drying
60-70-80°C temperatures, 1.6m/s air flow for 25 min + microwave dryer (180-360-540W)		180-360-540W for 14 min + 60-70-80°C, 1.6m/s air flow

2.2.2 Analysis

The power consumptions of the dryers were measured by power measurement device (Makel M310.2218, Turkey). The moisture content of the dried wheat samples were determined according to AOAC (2000). The water activity and color (L*, a*, and b*) values of the samples were measured by using a water activity measurement device (Testo-AG 400, Germany) and a colorimeter (Minolta CR-400, Japan), respectively. The results were expressed in accordance with the CIE Lab. System and the Chroma and Hue Angle (°) values were calculated according to Maskan et al. (2000) [6].

2.2.3 Determination of the drying behavior of the parboiled wheat samples

The moisture content versus time and drying rate versus moisture content plots were prepared according to Maskan et al. (2000) [6].

2.2.4 Statistical Analysis

Data were analyzed using statistical software SPSS 16.0 (SPSS Inc., Chicago, IL, USA). The data were also subjected to analysis of variance (ANOVA) and Duncan's multiple range test (α=0.05) to determine the difference between means. The drying experiments were replicated twice and all analyses were triplicated.

3. Results and Discussions

The power consumption of the dryers, and the moisture content and water activity values of the dried wheat samples are given in Table 2. The highest power consumption value

(18.63kWh) was observed for convective dryer because of long drying time (145min, data was not given). Considering the power consumption in the fluidized bed dryer (heating and blowing the air), the higher drying air temperatures caused a shorter drying time, and a shorter drying time caused significantly less power consumption (P<0.05). Toğrul (2006) and Chen et al., (2001) [7,8] reported that the convective and fluidized drying methods have some disadvantages such as high power consumption due to long drying time. The lowest power consumption values were observed for microwave drying because of the low drying time (Figure 1). In addition, Alibas (2006) [9] reported that the microwave drying is a widely used method due to low drying time and power consumption. The power consumption significantly increased from 0.07 to 0.39kWh as microwave power increased from 180 to 900W (P<0.05) and the power values 720 and 900W were eliminated from intermittent drying trials because of the higher power consumption and lower quality properties than other microwave drying powers. According to Table 1, it can be said that the power consumption of fluidized bed dryer can be decreased by combining it with microwave dryer and even the lower power consumption values were observed for fluidized bed-microwave combination compared to the microwave-fluidized bed-combination. Demiray et al. (2017) [10] reported that under convective drying conditions at the beginning of the drying the moisture removal rate is high, however, at the low moisture content values convective drying was not advantageous due to slow diffusion rate. For this reason, it can be stated that the fluidized bed-microwave combination is more advantageous with the higher evaporation rate, and lower power consumption compared to the microwave-fluidized bed-combination.

As can be seen from Table 1, the moisture content and water activity values of samples are generally lower than the limits (10% and in the range of 0.1 to 0.4, respectively (Quek et al., (2007), [11], (except convective dried samples) indicating their microbial safety for long terms of storage. The moisture content and water activity values significantly affected by the drying techniques (P<0.05). Significantly higher moisture content values were observed for the samples which were dried at the convective dryer and fluidized bed dryer (P<0.05). The moisture content values of samples increased depending on the increase of the drying air temperature in the fluidized bed dryer might be due to the crust formation which prevents the removal of moisture. Microwave dried samples have the significantly lower moisture content values compared to convectively dried samples (P<0.05). The lowest water activity values were observed for the fluidized bed-microwave dried samples and the water activity values significantly decreased depending on the increasing drying air temperatures (P<0.05). The moisture content and water activity values for the fluidized bed-microwave dried samples were found to be significantly lower compared to the convectively and microwave-fluidized bed dried samples (P<0.05).

Table 2. The power consumption, moisture content, and water activity values of the dried wheat

Drying methods and the conditions		Power Consumption (kWh)	Moisture Content (% wet basis, wb)	Water Activity
Convective Hot Air	70°C, 1.6m/s	18.63±0.01[f]	7.37±0.22[bc]	0.45±0.00[i]
Fluidized Bed	60°C, 1.6 m/s	2.03±0.02[e]	8.58±0.92[c]	0.26±0.03[f]
	70°C, 1.6m/s	1.38±0.01[cd]	8.59±0.74[c]	0.25±0.01[e]
	80°C, 1.6 m/s	1.16±0.03[c]	10.80±0.54[e]	0.22±0.01[d]
Microwave	180W	0.07±0.01[a]	1.53±0.32[a]	0.20±0.02[d]
	360W	0.22±0.01[a]	3.96±0.26[b]	0.21±0.03[d]
	540W	0.29±0.02[a]	2.05±0.28[b]	0.21±0.05[d]
	720W	0.36±0.01[b]	1.21±0.10[a]	0.31±0.02[g]
	900W	0.39±0.03[b]	1.68±0.18[a]	0.36±0.04[f]
Microwave- Fluidized Bed	180W-60°C, 1.6 m/s	1.60±0.02[cd]	8.04±0.91[d]	0.24±0.01[e]
	360W-60°C, 1.6 m/s	1.26±0.01[cd]	8.26±0.22[a]	0.31±0.02[g]
	540W-60°C, 1.6 m/s	0.91±0.02	6.23±0.46[a]	0.43±0.01[h]
Fluidized Bed- Microwave	60°C-180W1.6 m/s	0.77±0.01[bc]	3.81±0.34[b]	0.10±0.02[c]
	60°C-360W, 1.6 m/s	0.88±0.01[bc]	1.18±0.25[a]	0.06±0.04[a]
	60°C-540W, 1.6 m/s	0.94±0.01[c]	1.09±0.29[a]	0.08±0.02[b]

a– I show the significant difference between the same column in the samples according to the moisture content, water activity, and power consumption (P<0.05).

The total color change, Hue angle, and chroma values of the samples are given in Table 3. The L*, a* and b*values of the parboiled wheat are measured 63.43±0.63, -0.57±0.38 and 15.13±0.12 respectively. The total color change (ΔE) of dried samples with respect to parboiled wheat was calculated and the significantly higher total color change values were observed for microwave dried samples (P<0.05). It was clearly seen that the total color change was dramatically decreased in the intermittent drying methods especially in the fluidized bed- microwave drying method. The color change may be due to the degradation of the pigments, browning reactions or burning. The higher hue angle values were measured for microwave dried samples indicating higher redness values in this drying method. The chroma value indicates the degree of saturation of color and is proportional to the strength of the color [6]. The lowest chroma values were observed for fluidized bed-microwave dried wheat samples.

The drying rates were calculated and plotted against the moisture content as shown in Fig. 1. The drying generally occurred in falling rate period in the all drying methods due to the high evaporation rate of moisture.

Table 3. The total color change, hue angle and chroma values of the dried wheat

Drying method and the condition		Colour		
		ΔE	Hue Angle	Chroma
Convective Hot Air	70°C, 1.6m/s	7.58±0.51[a]	1.51±0.00[d]	21.67±0.57[ab]
Fluidized Bed	60°C, 1.6 m/s	10.86±0.29[bcd]	1.49±0.0[ab]	20.13±0.39[ab]
	70°C , 1.6m/s	16.88±0.26[d]	1.38±0.01[ab]	25.35±0.39[ab]
	80°C, 1.6 m/s	10.78±0.03[c]	1.49±0.01[a]	21.49±0.40[ab]
Microwave	180W	35.24±2.75[a]	1.15±0.06[d]	19.96±3.46[ab]
	360W	30.12±1.09[bcd]	1.16±0.02[bc]	24.05±0.90[ab]
	540W	30.03±0.50[d]	1.07±0.01[abc]	20.25±0.70[ab]
	720W	29.81±0.63[bcd]	1.15±0.02[ab]	21.55±0.25[b]
	900W	33.80±0.50[bcd]	1.15±0.01[ab]	22.80±0.67[ab]
Microwave-Fluidized Bed	180W-60°C	11.37±1.09[bcd]	1.51±0.03[bc]	21.00±3.44[b]
	360W-60°C	15.05±0.87[ab]	1.45±0.02[ac]	25.54±0.80[ab]
	540W-60°C	13.17±2.23[d]	1.46±0.03[ab]	21.13±2.08[a]
Fluidized Bed-Microwave	60°C-180W	6.25±3.75[d]	0.51±1.47[ab]	16.56±2.75[ab]
	60°C-360W	6.79±1.47[cd]	1.53±0.02[abc]	18.18±2.4[ab]
	60°C-540W	8.98±1.96[ab]	1.47±0.02[cd]	22.81±1.99[ab]

a–d shows the significant difference between the same column in the samples according to the total color change, hue angle and chroma (P<0.05).

Since almost all of the drying of biological products take place in the falling rate period [6] the drying rate of samples increased depending on increasing in drying air temperature and/or microwave power and the required drying time and the power consumption generally significantly decreased (P<0.05). In the all drying techniques, initially higher drying rates were observed and the samples tended to dry slowly at the last stages of drying.

It may be due to shrinkage or crust formation resulting in low transport rate of water and prolonged drying time. The highest drying rate values were observed for the microwave dried wheat grains where the lowest values were observed for the fluidized bed-microwave dried samples. The microwave drying supplies a higher drying rate compared to convective drying methods because of the heat generation inside food material which causes a rapid moisture evaporation in microwave drying [12].

The drying characteristics of wheat samples during drying were determined from the mass loss in the samples of the known initial moisture content (66.48±0.63%, wb) and are given in Figure 2. as expected, high amounts of moisture were removed at the early stages of drying due to the higher moisture diffusion and at the later stages, the removal of moisture decreased gradually.

(a)

(b)

(c)

(d)
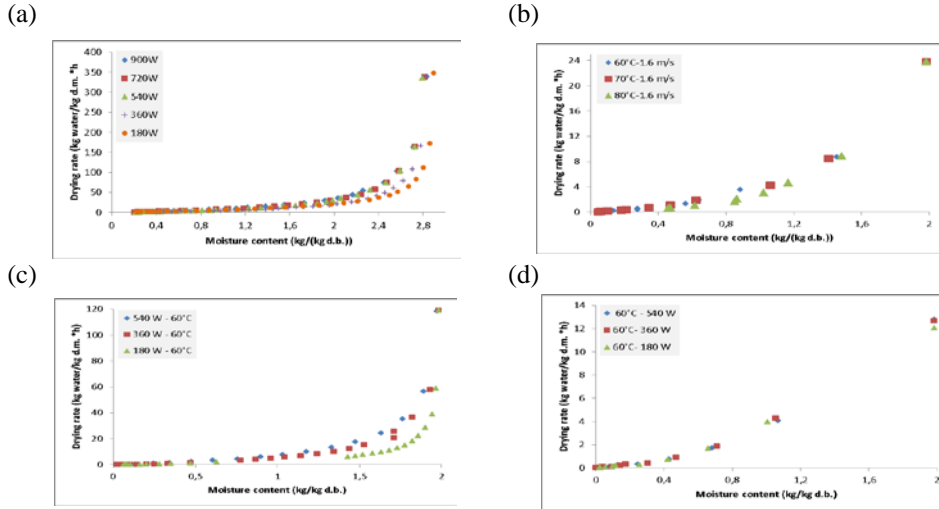
Fig. 1 The drying rate versus moisture content for (a)Microwave drying, (b)Fluidized bed drying (c) Microwave-fluidized bed combination, (d) Fluidized bed-microwave drying combination.

As expected, drying time of samples decreased with increasing microwave power and/or drying air temperature. Drying behavior of the wheat samples showed similar trend for the all the drying methods.

(a)

(b)

(c)

(d)
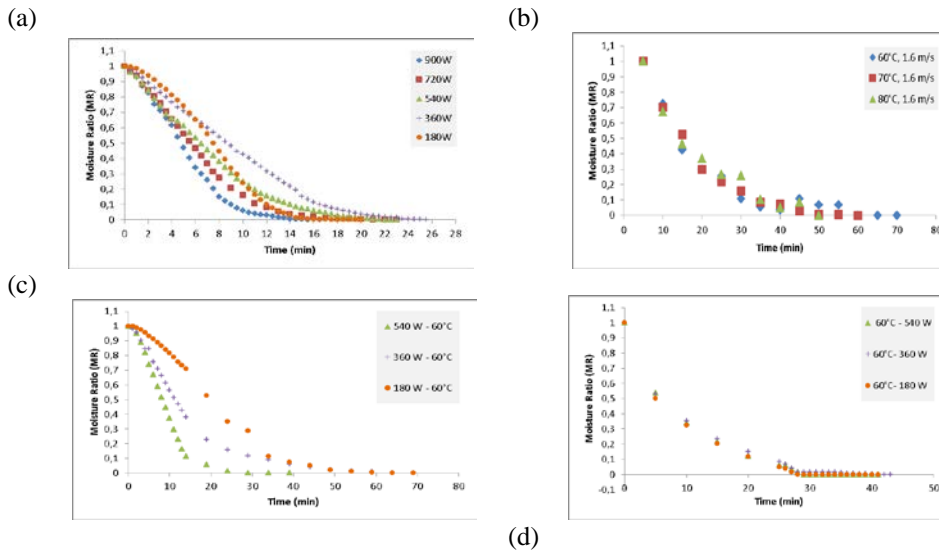
Fig. 2 The drying Characteristics for (a) Microwave drying, (b) Fluidized bed drying (c) Microwave-fluidized bed combination, (d) Fluidized bed-microwave drying combination.

4. Conclusions

In this study, the drying characteristics (moisture ratio vs. time graphs) and the physical analysis (moisture content, water activity, and color determination) of the single dried and combined dried wheat samples were determined. The power consumption for each drying method was also evaluated. Although, the lowest power consumption (0.07kWh) was observed for 180W microwave drying condition, considering the quality of the dried wheat especially the highest total color change was determined by this drying condition. The lowest moisture content (1.09%) and the water activity (0.06) values were observed at 60°C-540W fluidized bed-microwave dried and 60°C-360W fluidized bed- microwave dried wheat. The lowest total color change values were observed in fluidized bed-microwave dried wheat samples in the range between 6.28-8.98. The results showed that the fluidized bed-microwave drying methods were better for the physical properties and the low power consumption when they are compared to the microwave-fluidized bed combinations.

5. References

[1] Mohapatra, D.; Rao, P.S. A thin layer drying model of parboiled wheat. Journal of Food Engineering 2005, 513-518.

[2] Politowicz, J.; Lech, K.; Sanchez-Rodríguez, L.; Figiel, A., Szumny, A., Grubor, M., Barrachina, A. Volatile composition and sensory profile of oyster mushroom as affected by drying method. Drying Technology 2017.

[3] Kotwaliwale, N.; Bakane, P.; Verma, A. Changes in textural and optical properties of oyster mushroom during hot air drying. Journal of Food Engineering 2007, 78, 1207-1211.

[4] Mujumdar, A.S. Handbook of Industrial Drying, Third Edition, Taylor & Francis Group, LLC, 2006.

[5] Milota, M. R. Engineering Study on the Drying of Wood Particles in a Fluidized Bed, A Thesis Submitted to Oregon State University, 1984. USA.

[6] Maskan M.Microwave/air and microwave finish drying of banana Journal of Food Engineering 2000, (44) 71-78.

[7]Toğrul, H. Suitable drying model for infrared drying of carrot, Journal of Food Engineering 2006, 77: 610-619.

[8] Chen, G.; Wang, W.; Mujumdar, A.S. Theoretical study of microwave heating patterns on batch fluidized bed drying of porous material, Chemical Engineering Science 2001, 56, 6823–6835.

[9] Alibas, I. Characteristics of chard leaves during microwave, convective, and combined microwave convective drying. Drying Technology 2006, 24(1):1425- 1435.

[10] Demiray, E.; Seker, A.; Tulek, Y.; Drying kinetics of onion (Allium cepa L.) slices with convective and microwave drying Heat and Mass Transfer, 2017, 53, (5)1817–1827.

[11] Quek, S.Y.; C, N.K. ; S, P.J. The physicochemical Properties of Spray Dried Watermelon Powders, Chemical Engineering and Processing 2007, 46 (5), 386-392.

[12] Reyes, A.; Cero_n, S.; Zu_n~iga, R.; Moyano, P.A comparative study of microwave-assisted air-drying of potato slices. Biosystem Engineering 2007, 98, 310–318.

Mechanistic Modeling Expedites the Development of Spray Dried Biologics

Carrigy, N.B.[a]; Liang, L.[b]; Wang, H.[a]; Kariuki, S.[c]; Nagel T.E.[d]; Connerton, I.F.[b]; Vehring, R.[a*]

[a] Department of Mechanical Engineering. University of Alberta, Edmonton, Canada.

[b] School of Biosciences. University of Nottingham, Nottingham, UK.

[c] Centre for Microbiology Research. Kenya Medical Research Institute, Nairobi, Kenya.

[d] Phages for Global Health. Oakland, USA.

*E-mail of the corresponding author: reinhard.vehring@ualberta.ca

Abstract

Spray drying can be used to extend the shelf life of biologics stored at ambient temperature. Empirical and statistical design of experiments approaches typically require a relatively large number of experiments to determine suitable formulation and spray drying process parameters. An alternative approach, which may require fewer experiments, is to use mechanistic models to select these parameters. In this paper, mechanistic models are applied to develop a bacteriophage powder expected to have long-term physical stability at ambient temperature. The developed powder may be useful for decreasing incidences of foodborne illness in Kenya.

Keywords: bacteriophage powder; glass transition temperature; supplemented phase diagram; spray drying; stability.

1. Introduction

Empirical and statistical design of experiments approaches are commonly used for selecting formulation and process parameters during the development of spray dried biologic products. An alternative approach is to use mechanistic models developed based on an understanding of fundamental underlying principles. That is the approach undertaken in this work wherein a dry powder bacteriophage (phage) dosage form is designed to have target characteristics without requiring a substantial number of spray drying experiments. The powder is intended for use in broiler chicken feed to decrease *Campylobacter jejuni* in the chicken gut, with the end goal of decreasing the prevalence of foodborne illness in Kenya, which is abnormally high.[1,2] The development process can be divided into the following steps, discussed individually in this paper: 1) formulation; 2) atomization; 3) solvent evaporation and particle formation; 4) particle collection and analysis; 5) storage and transport.

2. Materials and Methods

A modified Büchi B-191 laboratory-scale spray dryer (Büchi Labortechnik AG; Flawil, Switzerland), schematically shown in Figure 1, was used to spray dry different *myoviridae* phages that can infect *Campylobacter jejuni*: CP30A, CP20, and CP8. These phages were isolated from chicken excreta and are present in chicken gut.[3] A transmission electron micrograph (TEM) of phage CP20 is given in Figure 2.
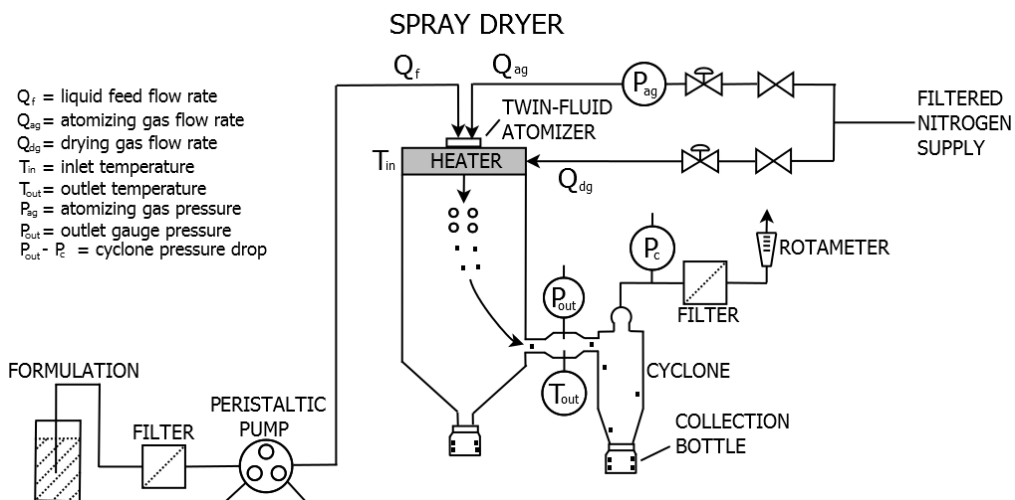
Fig. 1 Schematic of the modified laboratory-scale Büchi B-191 spray dryer.
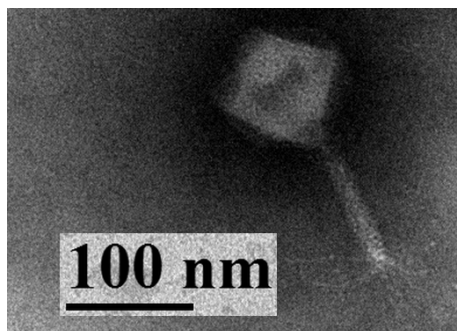
Fig. 2 TEM of phage CP20.

2.1 Formulation

The formulations were chosen to consist of L-leucine (Fisher Scientific, Cat. No. AC125121000; NH, USA) and D-(+)-trehalose dihydrate (Fisher BioReagents, Cat. No. BP2687; NH, USA) as dissolved solids in aqueous solution with phage (pH ~6.5). Trehalose is thought to stabilize biologics on drying by forming an amorphous glass that allows hydrogen bonds lost on desiccation of the biologic to be replaced.[4] Leucine forms a shell that decreases particle cohesiveness.[5]

For spray drying experiments, stock phage lysates were filtered and centrifuged to reduce the impurity content to < 0.5 mg mL^{-1}, and then diluted 1:100 into two aqueous formulations: (F1) 7.5 mg mL^{-1} leucine, 22.5 mg mL^{-1} trehalose; (F2) 12 mg mL^{-1} leucine, 18 mg mL^{-1} trehalose. In the literature similar formulations have been successfully used to stabilize spray dried phage.[6-9] Further details regarding the choice of these formulations are given in the following sections. Plaque assay was used to measure the presence and extent of titer reduction due to dilution of phage into the above formulations. The results are presented in Section 3.1.

2.2 Atomization

The spray dryer uses a twin-fluid atomizer to generate droplets. An atomizing gas flow rate of 1.5×10^{-4} kg s^{-1} and a spray rate of 1.7×10^{-5} kg s^{-1} were used. A characteristic shear rate on the order of 1×10^5 s^{-1} was expected according to a model presented by Ghandi *et al.*[10] In the literature,[7] phage have remained active after atomization at similar shear rates. To verify minimal titer reduction, filtered phage CP30A lysate in formulation F1 was atomized onto a filter, from which liquid was drawn for assay. The results are presented in Section 3.2.

The air-to-liquid ratio (ALR), defined as the ratio of the mass flow rates of atomizing gas and liquid feed, was 8.8. From the ALR and data for the present atomizer given by Hoe *et al.*,[11] an initial droplet diameter of ~9 μm was predicted. Using a model presented by

Boraey *et al.*,[12] and the formulation compositions given in Section 2.1, the aerodynamic diameter at the time of shell formation was predicted to be ~2 μm, which can be collected with the cyclone.

2.3 Solvent Evaporation and Particle Formation

Solvent from the liquid droplets generated by atomization quickly evaporates into the drying chamber of the spray dryer. The surface temperature of the droplets is typically assumed to remain near the wet bulb temperature for most of the evaporation process due to evaporative cooling;[13] therefore, thermal deactivation of the phage is not expected during initial stages of solvent evaporation. The dissolved solid that reaches critical supersaturation at the surface first may nucleate and form a crystalline shell. This is the particle formation stage, which has been described by Vehring *et al.*[14] The formulation compositions in Section 2.1 were designed using mechanistic models such that leucine would reach supersaturation much earlier than trehalose, allowing for enough time to nucleate and crystallize leucine at the surface (11.5 milliseconds for F1 and 15.8 milliseconds for F2). Since previous work has demonstrated that conditions similar to F1 may not be sufficient for obtaining a fully crystalline leucine structure when phage lysate is present in the formulation, F2 was also tested with the expectation that it would form a fully crystalline leucine structure.[9]

A spray dryer process model, developed based on similar models in the literature,[15,16] was used to predict the outlet temperature and the outlet relative humidity. The outlet temperature was predicted to be ~50°C and the outlet relative humidity ~3% for an inlet temperature of 70°C, a spray rate of 1.7×10^{-5} kg s^{-1}, and a drying gas flow rate of 8.5×10^{-3} kg s^{-1}.

2.4 Particle Collection and Analysis

A cyclone was used to collect the powder in a glass collection bottle. The collection efficiency is defined as the percent of the mass of dissolved solids in the feed solution recovered in the collection bottle. The collected powder containing phage was analyzed for solid state using Raman spectroscopy (using a custom device developed by Wang *et al.*[17]) and for particle morphology using scanning electron microscopy (SEM) (Zeiss Sigma FESEM, Oberkochen, Germany). Results are presented in Section 3.4.

2.5 Storage and Transport

Moisture uptake during storage and transport can result in crystallization of trehalose, which is known to deactivate phage.[18] Therefore, it is crucial that the packaging material is moisture-equilibrated. In this study, a Steady State / Stability Test Chamber (910W-4, Lunaire Environmental, Williamsport, PA, USA) was used to equilibrate the powder and packaging to 4% relative humidity, with subsequent packaging occurring in the chamber.

Carrigy, N.B.; Liang, L.; Wang, H.; Kariuki, S.; Nagel, T.E.; Connerton, I.F.; Vehring, R.

The relative humidity was chosen according to moisture uptake data and the information contained in Figure 3, described below. The packaging consisted of the powder in a vial, which was packaged in a double heat-sealed aluminum foil bag along with a satchel of silica gel desiccant (McMaster Carr, 2189K16; Elmhurst, USA), all of which were further packaged in another double heat-sealed aluminum foil bag along with another satchel of silica gel desiccant. The packaged spray dried powder, along with liquid controls, were shipped from Edmonton, Canada, to Nottingham, UK, in a Styrofoam box to minimize temperature variations. The titer after the complete development and shipping process will be determined by resuspension of the powder and plaque assay.

Throughout long-term stability studies, the powder should remain at a near-constant moisture content as, over time, moisture can lead to glass transition and crystallization. This tendency is demonstrated in a supplemented phase diagram that was developed for a trehalose-water system and is shown in Figure 3. With this diagram, the physical stability of the amorphous solid phase can be predicted *a priori* for a designed storage temperature, moisture content, and hence relative humidity. Use of this diagram is crucial for achieving long-term physical stability. The curve of the well-mixed glass transition temperature was developed using the Gordon-Taylor equation with a k-value of 5.9 and respective glass transition temperatures of 387 K for dry trehalose and 138 K for water.[19] As a rule of thumb, long-term storage should be performed for conditions at least 50°C below the glass transition temperature.[20]
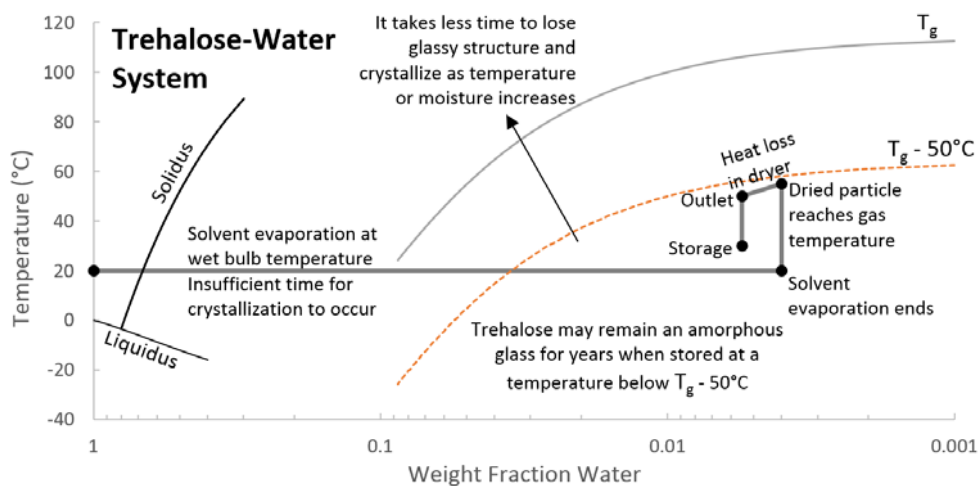
Fig. 3 Supplemented phase diagram developed for a trehalose-water system. Modified from Hoe et al.[21] with the present process parameters and material properties.

3. Results and Discussion

3.1 Formulation

Filtered phage CP30A lysate had no titer reduction over a period of 20 days when stored at 30°C in water, buffer, or formulation F1. A storage temperature of 40°C led to no titer reduction in buffer after 1 day but to > 1 log(pfu/mL) titer reduction after 10 days. A storage temperature of 50°C led to no titer reduction in buffer for at least 6 hours. No titer reduction was observed shipping CP30A in F1 within a vial in a Styrofoam box without temperature control from Nottingham, UK, to Edmonton, Canada, and back. This stability indicated that it is feasible to perform liquid control measurements with each experiment.

3.2 Atomization

The atomization titer reduction of phage CP30A in F1 was ~0.25 log(pfu/mL), which is less than the value of ~0.75 log(pfu/mL) reported in the literature for phages PEV2 and PEV40,[7] where similar predicted shear rates were used.

3.3 Solvent Evaporation and Particle Formation

The outlet temperature matched predictions from the process model within 2°C.

3.4 Particle Collection and Analysis

The collection efficiency was 54% for both formulations, which is typical for nominal batch sizes of ~1.5 grams. Raman spectroscopy confirmed trehalose was amorphous while leucine was mostly crystalline for both formulations. SEM (Figure 4) indicated that the phage lysate affected the particle morphology. It is possible that residual components in the phage lysate concentrated on the surface and interfered with the sensitive shell deformation and crystallization processes. This morphology was also present for other phage spray dried with leucine and trehalose in the literature, for which good powder flowability and long-term biological stability at 20°C were still achieved.[9]
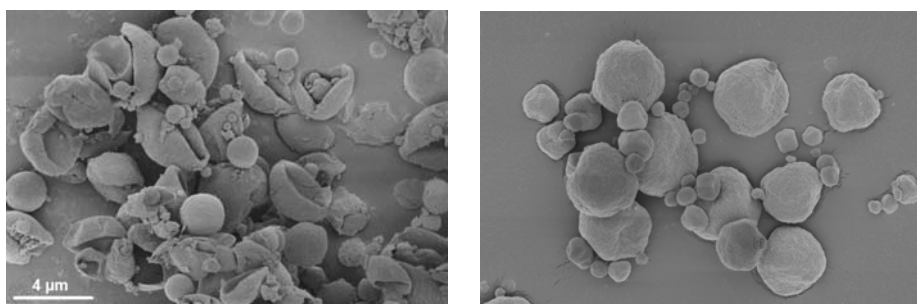
***Fig. 4** SEM of spray dried F1 without (left) and with (right) phage CP20. The same scale bar applies to both images.*

3.5 Storage and Transport

The supplemented phase diagram in Figure 3 suggests that the developed powder will have long-term physical stability without the need for refrigeration when a low relative humidity is maintained in the packaging. The biological stability of the phage in the powder during storage and transport will be determined.

4. Conclusions

Mechanistic models were used to select formulation and spray drying process parameters for stabilizing phage. Further results will be presented at the conference.

5. References

[1] O'Reilly, C.E.; Jaron, P.; Ochieng, B.; Nyaguara, A.; Tate, J.E.; Parsons, M.B.; Bopp, C.A.; Williams, K.A.; Vinjé, J.; Blanton, E.; Wannemuehler, K.A.; Vulule, J.; Laserson, K.F.; Breiman, R.F.; Feikin, D.R.; Widdowson, M.A.; Mintz, E. Risk factors for death among children less than 5 years old hospitalized with diarrhea in rural western Kenya, 2005-2007: a cohert study. PLoS Medicine 2012, 9 (7), e1001256.

[2] World Health Organization, Food and Agricultural Organization of the United Nations & World Organisation for Animal Health. The global view of campylobacteriosis: report of an expert consultation, Ultrecht, Netherlands, 9-11 July 2012. World Health Organization. http://www.who.int/iris/handle/10665/80751.

[3] Loc Carrillo, C.; Atterbury, R.J.; El-Shibiny, A..; Connerton, P.L.; Dillon, E.; Scott, A.; Connerton, I.F. Bacteriophage therapy to reduce *Campylobacter jejuni* colonization of broiler chickens. Applied and Environmental Microbiology 2005, 71 (11), 6554-6563.

[4] Crowe, J.H.; Carpenter, J.F.; Crowe, L.M. The role of vitrification in anhydrobiosis. Annual Review of Physiology 1998, 60, 73-103.

[5] Feng, A.L.; Boraey, M.A.; Gwin, M.A.; Finlay, P.R.; Kuehl, P.J.; Vehring, R. Mechanistic models facilitate efficient development of leucine containing microparticles for pulmonary drug delivery. International Journal of Pharmaceutics 2011, 409 (1-2), 156-163.

[6] Matinkhoo, S.; Lynch, K.H.; Dennis, J.J.; Finlay, W.H.; Vehring, R. Spray-dried respirable powders containing bacteriophage for the treatment of pulmonary infections. Journal of Pharmaceutical Sciences 2011, 100 (12), 5197-5205.

[7] Leung, S.S.Y.; Parumasivam, T.; Gao, F.G.; Carrigy, N.B.; Vehring, R.; Finlay, W.H.; Morales, S.; Britton, W.J.; Kutter, E.; Chan, H.K. Production of inhalation phage powders using spray freeze drying and spray drying techniques for treatment of respiratory infections. Pharmaceutical Research 2016, 33 (6), 1486-1496.

[8] Leung, S.S.Y.; Parumasivam, T.; Gao, F.G.; Carter, E.A.; Carrigy, N.B.; Vehring, R.; Finlay, W.H.; Morales, S.; Britton, W.J.; Kutter, E.; Chan, H.K. Effect of storage conditions on the stability of spray dried, inhalable bacteriophage powders. International Journal of Pharmaceutics. 2017, 521 (1-2), 141-149.

[9] Leung, S.S.Y.; Parumasivam, T.; Nguyen, A.; Gengenbach, T.; Carter, E.A.; Carrigy, N.B.; Wang, H.; Vehring, R.; Finlay, W.H.; Morales, S.; Britton, W.J.; Kutter, E.; Chan, H.K. Effect of storage temperature on the stability of spray dried bacteriophage powders. European Journal of Pharmaceutics and Biopharmaceutics. 2018, 127, 213-222.

[10] Ghandi, A.; Powell, I.B.; Howes, T.; Chen, X.D.; Adhikari, B. Effect of shear rate and oxygen stresses on the survival of *Lactococcus lactis* during the atomization and drying stages of spray drying: A laboratory and pilot scale study. Journal of Food Engineering 2012, 113 (2), 194-200.

[11] Hoe, S.; Ivey, J.W.; Boraey, M.A.; Shamsaddini-Shahrbabek, A.; Javaheri, E.; Matinkhoo, S.; Finlay, W.H.; Vehring, R. Use of a fundamental approach to spray-drying formulation design to facilitate the development of multi-component dry powder aerosols for respiratory drug delivery. Pharmaceutical Research. 2014, 31 (2), 449-465.

[12] Boraey, M.A.; Vehring, R. Diffusion controlled formation of microparticles. Journal of Aerosol Science. 2014, 67, 131-143.

[13] Masters, K. Spray Drying: An Introduction to Principles, Operational Practice and Applications; Leonard Hill: London, 1972.

[14] Vehring, R.; Foss, W.R.; Lechuga-Ballesteros, D. Particle formation in spray drying. Journal of Aerosol Science 2007, 38 (7), 728-746.

[15] Dobry, D.E.; Settell, D.M.; Baumann, J.M.; Ray, R.J.; Graham, L.J.; Beyerinck, R.A. A model-based methodology for spray-drying process development. Journal of Pharmaceutical Innovation 2009, 4 (3), 133-142.

[16] Ivey, J.W.; Vehring, R. The use of modeling in spray drying of emulsions and suspensions accelerates formulation and process development. Computers & Chemical Engineering 2010, 34 (7), 1036-1040.

[17] Wang, H.; Boraey, M.A.; Williams, L.; Lechuga-Ballesteros, D.; Vehring, R. Low-frequency shift dispersive Raman spectroscopy for the analysis of respirable dosage forms. International Journal of Pharmaceutics. 2014, 469 (1), 197-205.

[18] Vandenheuvel, D.; Meeus, J.; Lavigne, R.; Van den Mooter, G. Instability of bacteriophages in spray-dried trehalose powders is caused by crystallization of the matrix. International Journal of Pharmaceutics 2014, 472 (1-2), 202-205.

[19] Chen, T.; Fowler, A.; Toner, M. Literature review: supplemented phase diagram of the trehalose-water binary mixture. Cryobiology 2000, 40 (3), 277-282.

[20] Hancock, B.C.; Shamblin, S.L.; Zografi, G. Molecular mobility of amorphous pharmaceutical solids below their glass transition temperatures. Pharmaceutical Research 1995, 12 (6), 799-806.

[21] Hoe, S.; Boraey, M.A.; Ivey, J.W.; Finlay, W.H.; Vehring, R. Manufacturing and device options for the delivery of biotherapeutics. Journal of Aerosol Medicine and Pulmonary Drug Delivery 2014, 27 (5), 315-328.

Drying of moist food snacks with innovative slot jet reattachment nozzle

Farzad, M.[a]*; Yang, M.[a]; Yagoobi, J.[a]; Tilley, B.[b]

Center for Advanced Research in Drying (CARD)

[a] Department of Mechanical Engineering. Worcester Polytechnic Institute (WPI), Worcester, USA

[b] Department of Mathematical Sciences. Worcester Polytechnic Institute (WPI), Worcester, USA.

*E-mail of the corresponding author: mfarzad@wpi.edu

Abstract

Drying of moist porous media such as paper, pulp and food products is one of the most energy intensive processes in industry. Impinging jet nozzles are commonly used in various drying processes. There have been many efforts to improve the transport characteristics of impinging jet nozzles. Utilizing innovative Slot Jet Reattachment (SJR) nozzle is an approach to make the drying process more efficient. This is mainly because these nozzles overcome the high flow rate constraint associated with the traditional Slot Jet (SJ) nozzle.

In this paper, the drying characteristics of the SJR nozzle with exit angles of +20˚ and +45˚ are experimentally investigated. The samples used are snack cookies. The results are compared with those of SJ nozzle under the same mass flowrate. The results indicate that significant enhancements in drying rates are achievable with both SJR nozzles compared to SJ nozzle.

Keywords: Drying; Porous Food Snack; Slot Jet Reattachment Nozzle; Slot Jet Nozzle

1. Introduction

Energy is one of the grand challenges for manufacturers in the 21st century. In traditional industrial processes, the energy required for drying can take up to 25% of the corresponding total energy use [1]. Energy efficient and uniform drying of food products such as fruits, chips, and cookies is of critical importance to the product quality. Slot Impinging Jet (SJ) nozzles are widely used to dry food in traditional food industry, providing the principal heat and mass transfer mechanism in the drying process. To design a proper impinging jet nozzle with sufficient efficiency, many factors need to be considered: nozzle geometry and size, nozzle configuration, nozzle-to-surface separation, jet-to-jet separation, cross flow, jet exit velocity and surface motion [2].

Among such various factors, an innovative Slot Jet Reattachment (SJR) nozzle, has been developed by Page and Seyed-Yagoobi [3] and Seyed-Yagoobi et al. [4]. Compared to the conventional SJ nozzle, the innovative SJR nozzle can alter the direction of impinging air flow to an outward radial direction, with a flow reattaching on a ring away from the centerline, where the stagnation point occurs (see Fig. 1). Heat and mass transfer is maximized along the reattachment ring. Due to the nature of turbulent viscous mixing along the boundary layers of the impinging air, a secondary flow is introduced through mass entrainment, which means part of the air steam directs inward radially to form a circulation region underneath the bottom plate of the nozzle. A relatively low-pressure distribution is maintained. The intense turbulent flow is the principal reason for the high mass and heat transfer rate. These flow characteristics of the SJR nozzles provides significant advantages over the conventional SJ nozzles. By using SJR nozzles, the average heat transfer over the surface as well as local heat transfer rate can be greatly enhanced, and a controllable exerted force minimizes the mechanical impact to fragile food products.

2. SJR Nozzle

SJR nozzle is a modified version of SJ nozzle. The schematic of SJR nozzle with exit angle of 45˚ is shown in Fig. 1 [5]. This innovative nozzle can be fabricated in different exit angles. Based on the application, exit angle can be toward the surface (positive angle) and outward the surface (negative angle). Explicitly, net force exerted on the impingement surface can be controlled by the exit angle of the nozzle. The flow exits the nozzle in two directions, First is in direction of minor axis which is in oval shape and second is in direction of major axis which is radial [4] [5] (Fig. 2).

In SJ nozzle, stagnation point is right under the center line and maximum heat transfer happens at the center of impingement surface but in SJR nozzle reattachment point is observed in an oval shape away from the center line of the nozzle. Therefore, reattachment area in SJR nozzle covers a larger space than that of SJ nozzle and moves outward and inward direction which leads to a higher average heat and mass transfer coefficient.
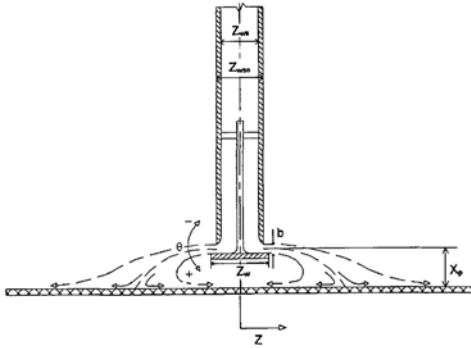
Fig. 1 Schematic of SJR nozzle
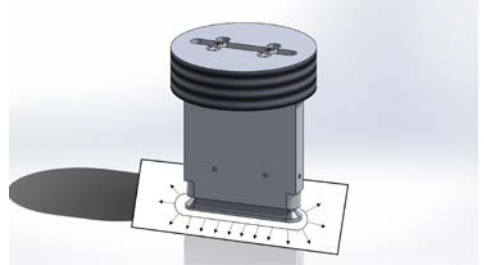
Fig. 2 Flow direction on impingement surface under SJR nozzle

In this study, all the tests were conducted with two SJR nozzles with exit angles of +20˚ and +45˚. The geometrical parameters of these nozzles and SJ nozzle are listed in Table 1.

Table 1. Geometrical parameters of SJ and SJR nozzles

Parameters (mm)	SJ Nozzle	SJR 20˚	SJR 45˚
L	73	73	73
b	-	4	4
X_p	80	14	16
Z_w	-	18	14
Z_{ws}	9.25	10	9.25

3. Experimental Set Up and Procedure

The experiments were conducted at the optimum distance between the exit opening of nozzle and the impingement surface. Drying test with SJ nozzle was run based on optimal height of nozzle to surface spacing of 80 mm [4]. X_p for SJR+20˚ and SJR+45˚ was fixed at 14 mm and 16 mm, respectively, to accommodate for swelling of the samples during the early stage of drying [5]. In this paper, the samples used are raw cookie doughs. Each experiment consisted of two cookies. The drying characteristics with SJR and SJ nozzles are experimentally obtained and compared to illustrate the resultant enhancements in drying rates with the use of SJR nozzle. The comparisons are made under identical air mass flowrates.

The schematic of the apparatus used for this study is shown in Fig. 3. Air was conducted to the apparatus through 0.5 in diameter plastic hose from an upstream air supply. A threaded on/off valve was used to control the air mass flowrate. A rotameter was utilized to measure the air mass flow rate. For heating the air, an 8.5 kW torch electrical heater was utilized which was connected to a PID unit controller to regulate the power required to reach the desired temperature. Following the electrical heater, a solenoid valve activated with a timer was used to redirect the incoming air away from the sample during the sample weight recording. Threaded nozzle was connected interchangeably to the solenoid valve. A scale with an accuracy of 0.001 g was used to capture the sample weight during the drying process. Adjustable stand was used to hold the digital scale and adjust the distance between the nozzle and impingement surface. J-type thermocouples were used to measure the temperatures in different locations such as at the exit of electrical heater, nozzles exit, and impingement surface. Surface pressure was measured by a pressure transducer. The apparatus was well insulated to minimize the heat loss to ambient.
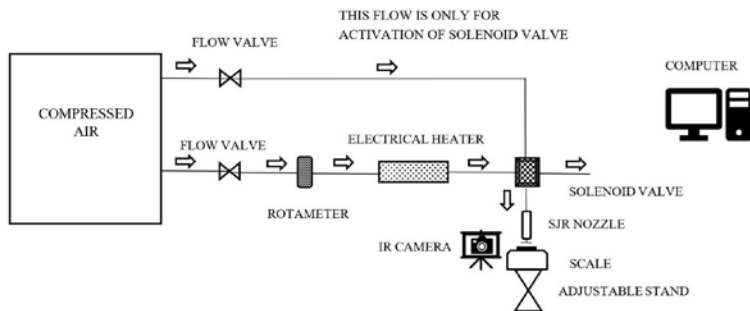
Fig. 3 Simplified schematic of apparatus used for this study

4. Experimental Results

All the tests were conducted under the same air exit temperature of 260 ˚C and two different mass flow rates. Operating conditions for mass flowrates of 0.005 kg/s (i.e. case 1) and 0.01 kg/s (i.e. case 2) are listed in Table 2 and Table 3.

Figure 4 shows the percent dry basis moisture content (DBMC) as a function of drying time. The corresponding operating conditions are shown in Table 2. The results indicate that the drying times to reach a specific DBMC with SJR nozzles are much shorter than those of SJ nozzle. For example, it took 31 minutes with SJ nozzle to reach a 10 percent DBMC level while with SJR+20˚ and SJR+45˚ the DBMC of 10 percent was reached in 18 and 15 minutes, respectively, corresponding to 42 and 52 percent decrease in drying time. To reach a lower DBMC of 4.5 percent, the SJ, SJR+20º, and SJR45º required 76, 40, and 38 minutes,

respectively, corresponding to 47 and 50 percent reduction in drying times. Figure 4 also shows that the performance of the two SJR nozzles are almost similar with air flowrate of 0.005 kg/s.
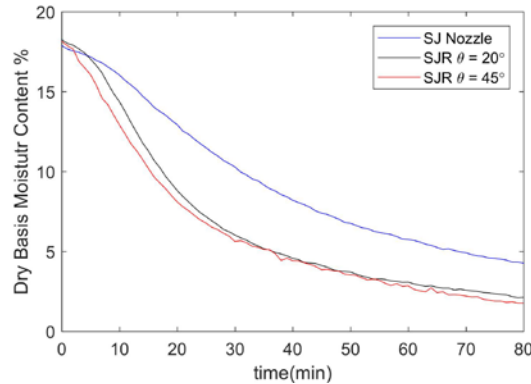
Fig. 4 Dry basis moisture content with air flowrate of 0.005 kg/s

Figure 5 shows similar results to those of Fig. 4 but under a higher air mass flowrate of 0.01 kg/s. The corresponding operating conditions for Fig. 5 are listed in Table 3. According to Fig. 5, the drying rates are higher with SJR nozzles compared to SJ nozzle at this higher air flowrate as well. However, the percent enhancements are lower than those of lower air flowrate of 0.005 kg/s. This is expected because as the air flowrate increases the drying rate increases as well regardless of the type of nozzle used making it more difficult to enhance the drying rate with SJR nozzles. However, the main reason for the SJR nozzles superior performance compared to SJ nozzle performance under the same exit air flowrate is mainly due to the differences in their flow fields. Specifically, the reattachment zone associated with an SJR nozzle is by far larger than the stagnation zone of the SJ nozzle resulting in a higher averaged heat transfer coefficient with SJR nozzles.
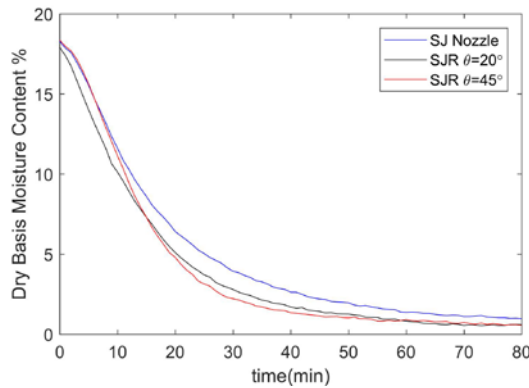
Fig. 5 Dry basis moisture content with air flowrate of 0.01 kg/s

Another appropriate way of evaluating the performance of three nozzles is to compare their drying rates as a function of percent DBMC as illustrated in Fig. 6. According to this figure, the drying rates of innovative nozzles are substantially higher than those of conventional nozzle over the whole range of sample moisture content. For instance, at DBMC of 15%, the drying rates for SJ, SJR+20˚, and SJR+45˚ nozzles are 0.07, 0.141, and 0.146 g/s, respectively.
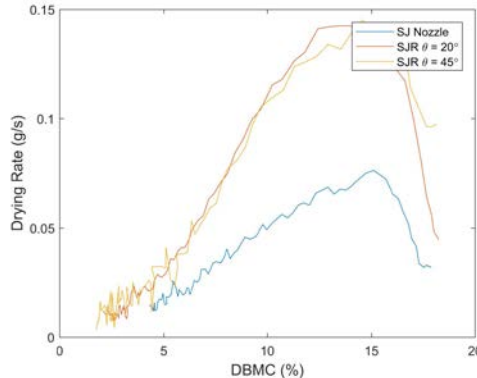
Fig. 6 Comparison of drying rate between SJ and SJR nozzles

To confirm repeatability of the data, drying experiments with SJR+20˚ under the mass flowrate of 0.01 kg/s and temperature of 260˚C were carried out three times. The minimum and maximum percent standard deviations of dry basis moisture content were 0.04 and 1.52. Additionally, the same repeatability tests were performed for SJ nozzle under the same operating conditions. The minimum and maximum percent standard deviations of dry basis moisture content were 0.05 and 0.92.

5. Conclusions

The convective air drying characteristics of two SJR nozzles with exit angles of +20º and +45º were compared to a conventional impinging SJ nozzle drying characteristics. The results confirmed that both SJR nozzles provide superior drying performance compared to that of SJ nozzle under the equivalent air mass flowrate. SJR nozzles are especially suitable for drying applications where it is crucial to protect fragile samples from being damaged by direct airflow impingement.

6. Acknowledgement

7. Nomenclature

b	Exit width of the SJR nozzle	mm
D_h	Cross sectional hydraulic diameter of SJ nozzle	mm
$D_{h,exit}$	Exit hydraulic diameter of SJR nozzle (2b)	mm
DBMC	Dry basis moisture content	
DR	Drying rate	g/s
$\dot{m}$	Mass flowrate	kg/s
Re	Reynolds number:	
	$Re_{SJ} = (V.D_h)/\nu$	
	$Re_{SJR} = (V.D_{h,exit})/\nu$	
SJR	Slot Jet Reattachment	
L	Length of nozzle	mm
T	Temperature	˚C
V	Exit velocity	m/s
$V_{s/c}$	Slot channel velocity	m/s
X_p	Distance between nozzle exit and impingement surface	mm
Z_{ws}	Inside width of slot jet	mm

Z_w	Bottom plate width of SJR nozzle	Mm

Greek letters

θ	Exit angle of SJR nozzle	degrees

8. References

[1] U.S. Department of Energy, "Quadrennial Technology Review 2015," Washington, DC, 2015.

[2] P. Suna, "Heat and Mass Transfer in Impingement Drying," *Drying Technology,* vol. 11, no. 6, pp. 1147-1176, 1993.

[3] R. Page and J. Seyed-Yagoobi, "A New Concept for Air or Vapor Impingement Drying," *Tappi Journal,* vol. 73, no. 9, pp. 229-234, 1990.

[4] J. Seyed-Yagoobi, V. Narayanan and R. Page, "Comparison of Heat Transfer Characteristics of Radial Jet Reattachment Nozzle to In-Line Imping Jet Nozzle," *Journal of Heat Transfer,* vol. 120, pp. 335-341, 1998.

[5] V. Narayanan, J. Seyed-Yagoobi, R. Page and S. Alam, "Effect of Exit Angle on the Heat Transfer Characteristics of Jet Reattachment Nozzle and its Comparison to a Slot Jet Nozzle," in *ASME National Heat Transfer*, Baltimore, Maryland, 1997.

[6] V. Narayanan, J. Seyed-Yagoobi and R. Page, "Heat Transfer Characteristics of Slot Jet Reattachment Nozzle," *Journal of Heat Transfer,* vol. 120, no. 2, pp. 348-356, 1998.

Changing spray-dried lactose-whey protein isolate particle structure with drying conditions

De Souza Lima, R. [a*]; Guttierez, G.[a]; Arlabosse, P.[a] ; Ré, M.-I.[a]

[a]Université de Toulouse, IMT Mines Albi-Carmaux, CNRS UMR 5302, Centre RAPSODEE, Campus Jarlard, 81013 Albi cedex 09, France

*E-mail of the corresponding author: rogerlima.w@gmail.com

Abstract

Spray drying has become not merely a drying process, but also an important tool for engineering solid structures, specially for multi-component feeds. In that way, it is important to know how the drying conditions and liquid formulations affect the particle final solid structure. In the present study, we investigated the changes on the solid structure of a spray-dried binary mixture of lactose and whey protein isolate under different process and formulation conditions. Particle morphology, diameter, porosity and occluded air were analyzed. Total solid content in the feed was the parameter of highest impact on the spray-dried particle's occluded air volume.

Keywords: spray drying; solid structure; porosity; hollow particless.

1. Introduction

The first significant industrial use of spray drying concerned the dairy industry in the 1920s. This operation first attracted attention for its capacity of quickly producing particulate material with controllable size distribution, bulk density, moisture content and the possibility of drying heat-sensitive substances [1]. For many years, spray drying had been mainly seen as solely a drying operation to produce large amounts of powder, remove most of the feed's solvent and enhance product storage and stability.

However, this perception changed over the years driven by the increasing demand for particles with engineered end-use properties, that is to say particles with improved properties like dissolution rate, controlled release, flowability, wettability, compactibility and coating [2, 3]. Therefore, spray drying has become nowadays a tool for designing solid structures, specially from multi-component feeds.

The aforementioned particle properties are affected by the drying parameters, such as air temperature, air humidity and initial droplet size, as well as the feed liquid state (solution, emulsion, suspension), nature of the substances to be dried and their concentration [4]. To accurately design solid particles, it is important to understand how the particle solid structure is influenced by the drying conditions and feed composition.

The aim of the present work was to investigate the effect of some drying and formulation parameters on the solid structure of particles produced by spray drying. An aqueous solution of lactose and whey protein isolate (model solution in the food industry) was dried under different air inlet temperatures, nozzle diameters and initial solid loads. The variation of particle morphology, diameter, porosity and occluded air were analyzed.

2. Materials and Methods

2.1. Materials

α-lactose monohydrate and whey protein isolate (WPI) were kindly provided by Pierre-Fabre Laboratory (France) and Lactalis (France), respectively, and used as received.

2.2. Methods

2.2.1. Solution preparation

The sample solutions were prepared by mixing lactose and WPI powders in distilled water at a constant protein-to-sugar mass ratio of 50:50. The total dissolved solid content in the liquid feed varied from 10, 20 to 26 % w/w. In order to completely dissolve the solutes and to avoid protein denaturation, the samples were heated at 30 °C and gently agitated with a magnetic stirrer for 8 hours.

2.2.2. Spray drying

A laboratory-scale spray dryer (B-290 Advanced, Büchi, Switzerland) was used to spray dry the sample solutions. The air inlet temperature was fixed at 103 °C or 120 °C. Two different nozzle diameters were used, 0.5 mm and 2.0 mm. The experiments were carried out with an aspiration rate of 95 % with a corresponding air flow rate of 33.25 m^3/h and a feed rate of 4.27 mL/min. The powder collected after drying was stored at room temperature in a flask. Table 1 represents the experimental conditions employed in the present work.

Table 1. Sample solutions parameters and drying conditions

Sample	Lactose percentage (% w/w)	WPI percentage (% w/w)	Total solid content (% w/w)	Nozzle diameter (mm)	Air inlet temperature (°C)
S1	5.0	5.0	10.0	2.0	103.0
S2	9.9	9.9	19.8	2.0	103.0
S3	13.0	13.0	26.0	2.0	103.0
S4	10.0	10.0	20.0	0.5	120.0

2.2.3. Spray-dried particles characterization

The particle diameter was evaluated by laser diffraction (Malvern Mastersize 3000, Malvern Instruments) after dispersing the powder in 2-propanol. The particle size distribution was calculated with the Mie theory using the refractive index values of n = 1.378 for 2-propanol and n = 1.57 for the spray-dried particles.

To assess the particle morphology, the spray-dried samples were examined with scanning electron microscopy (SEM) (ESEM FEG Philips). The acceleration voltage was 8 kV. The particles were placed on an adhesive carbon tape and sputter-coated with platinum.

Liquid pycnometry was employed in order to evaluate the apparent density of the spray-dried powder. The apparent density was calculated by knowing exactly the mass of powder and 2-isopropanol inserted into the pycnometer. The measurements were done in triplicate.

Helium pycnometry (Accupyc 1340, Micromeritics) was used to determine the particle true density. Two grams of powder were dried under vacuum in an oven at 70 °C, to evaporate any remaining moisture, and added to the pycnometer's measuring cell. The true density was obtained after 25 cycles of filling-draining helium in the measurement cell.

3. Results and discussion

Lactose is a compound frequently present in spray drying of dairy produts, since it is the main carbohydrate in bovine milk. This sugar is also employed as protective agent when stress-sensitive substances are spray dried, like whey protein [5].

The different drying conditions presented in Table 1 did not cause any change in the particle morphology. The spray dried powders presented a hollow core with a wrinkled surface, as can be seen from the SEM micrographs in Figure 1. A wrinkled morphology was also observed in previous studies with protein-to-sugar mass ratios of 70:30 [6] and 80:20 [5]. Spray-dried skim milk [7] also presented the same surface roughness.

The laser diffraction results in Table 2 are given in volume fractions. The particle size distribution is represented by three percentages of particles having at most the indicated diameters. The Span number displays the distribution width. From these measurements, it is possible to observe as expected an increase in the mean spray-dried particle size with more concentrated feed formulations.. The solid crust appears sooner on more concentrated liquid droplets in comparison to more diluted ones, due to the proximity to saturation. Therefore, the resulting external diameter remains bigger.

Table 2. Laser diffraction measurements for the mixture 50 % lactose – 50 % whey protein isolate (w/w, on dry basis) on the different samples

Sample	Total solid content (% w/w)	Volume mean diameter d-4,3 (µm)	d-10 (µm)	d-50 (µm)	d-90 (µm)	Span
S1	10.0	9.1 ± 0.0	2.6 ± 0.0	8.9 ± 0.0	15.4 ± 0.1	1.4 ± 0.0
S2	19.8	10.5 ± 0.1	2.8 ± 0.0	10.3 ± 0.0	17.9 ± 0.1	1.5 ± 0.0
S3	26.0	12.3 ± 0.1	2.6 ± 0.0	12.1 ± 0.1	21.8 ± 0.1	1.6 ± 0.0
S4	20.0	5.4 ± 0.0	1.6 ± 0.0	5.2 ± 0.0	9.5 ± 0.0	1.5 ± 0.1

The measure of apparent density from the liquid pycnometry includes open and closed pores in the particles. The helium pycnometry gives the particle true density from the adsorption of helium to the solid's surface through the open pores. Due to the low-porous nature of the present spray-dried samples, the presence of closed pores can be neglected for the sake of density and porosity calculations. These density values are presented in Table 3. It is important to note that the particles (micrographs in Figure 1) show a densely packed crust region, so one can suggest that the porosity estimations take into account mainly the air fraction presented in the particle hollow core.
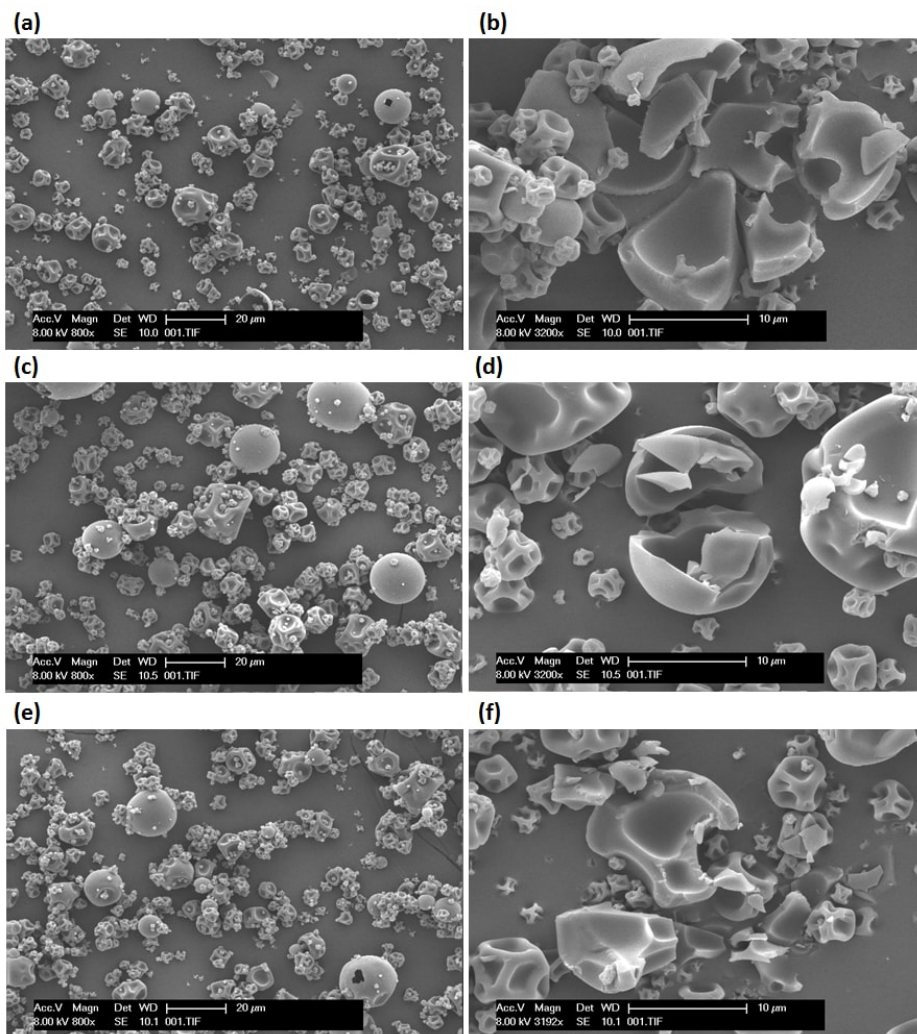
Figure 1. SEM micrographs of spray-dried lactose-whey protein isolate particles illustrating the same trend of wrinkled surface produced from droplets of different total solid content. 10 % w/w (a – b), 20 % w/w (c – d), 30 % w/w (e – f)

For the purpose of visualization, the density results were written in terms of particle porosity, and thus occluded air, so that a modification of the particle crust can be examined. To calculate the porosity, the mass of air contained in the particle's pores was neglected. In that way, the apparent and true densities were used to evaluate the porosity, as indicated in Equation 1.

Table 3. Evolution of occluded air measured from the spray-dried particle's porosity and apparent density

Sample	Total solid content (% w/w)	Apparent density (g/cm³)	True density (g/cm³)	Porosity	Occluded air (cm³/g)
S1	10.0	0.81 ± 0.0	1.37 ± 0.0	0.41	0.50
S2	19.8	0.88 ± 0.0	1.30 ± 0.0	0.32	0.36
S3	26.0	0.92 ± 0.0	1.25 ± 0.0	0.26	0.28
S4	20.0	0.86 ± 0.0	1.37 ± 0.0	0.37	0.43

$$\varphi = \frac{\rho_{true} - \rho_{apparent}}{\rho_{true}} \qquad (1)$$

Where φ is the particle porosity. The volume of occluded air in the particle per gram of powder can be calculated from the porosity as follows,

$$V_{occluded\ air\ /\ g\ powder} = \varphi \frac{1}{\rho_{apparent}} \qquad (2)$$

It is interesting to note from Table 3 that an increase of approximately 40 % on the particle occluded air was accomplished by reducing the total solid content from 26 % w/w to 10 % w/w, for the same air inlet temperature and nozzle diameter. However, an increase of only 10 % on the particle occluded air was obtained by modifying the air inlet temperature and the nozzle size from [103 °C, 2 mm] to [120 °C, 0.5 mm], for the same total solid fraction.

The displayed occluded air results along with the mean particle diameters (d-4.3) from Table 2 give an indirect qualitative information about the particle crust width. When comparing the samples S1 and S3, the mean particle diameter is relatively close, but the particle occluded air difference is more important, as mentioned in the previous paragraph. Consequently, one can suggest that the lower solid content on the particles from sample S1 generated a thinner crust compared to that of the particles from S3.

The amount of occluded air in the particle is an important issue in cases when there are oxidation-sensitive compounds present in the particle solid structure. In that way, to avoid a particle inner oxidation, a reduction of the occluded air should be considered [8].

4. Conclusions

In the present study, particles containing an equal mixture of lactose and whey protein isolate were obtained through spray drying. In order to observe changes in the particle solid structures, the sample solutions were spray dried under different total solid contents, air inlet temperatures and nozzle diameters. The resulting particles were analyzed through scanning electron microscopy, laser diffraction, liquid pycnometry and helium pycnometry. In that way, the particle morphology, diameter, porosity and occluded air could be assessed.

It was observed that a hollow and wrinkled particle morphology was obtained from all the spray dried samples. A slight increase in the mean particle diameter was observed with higher solid contents. A change in the total solid content had a higher impact on the particle's occluded air than the coupled air inlet temperature and nozzle diameter. It is important to note that the porosity and occluded air estimations were related to the quantity of air present in the particle hollow core, due to the low-porous nature of the particle's crust obtained. A higher occluded air amount can lead to oxidation issues if there are sensitive substances in the particle solid structure. A possible solution would then be the use of higher solid contents in the liquid feed, to generate particles with a lower occluded air volume.

5. References

[1]   Masters, K. Spray Drying Handbook. 5th edition. Longman Scientific & Technical, 1991, p. 725.

[2]   Ré, M.-I. Formulating Drug Delivery Systems by Spray Drying. Drying Technology 2006, 24.4; 433–446.

[3]   Munoz-Ibanez, M. et al. The microstructure and component distribution in spray-dried emulsion particles. Food Structure 2016, 8; 16–24.

[4]   Nandiyanto, A. B. D.; Okuyama, K. Progress in developing spray-drying methods for the production of controlled morphology particles: from the nanometer to submeter size ranges. Advanced Powder Technology 2011, 22.1 ; 287–296.

[5]   Haque, M. A.; Adhikari, B.; Putranto, A. Predictions of drying kinetics of aqueous droplets containing WPI-lactose and WPI –trehalose by application of composite reaction engineering approach (REA). Journal of Food Engineering 2016, 189; 29–36.

[6]   Haque, M. A.; Chen, J.; Aldred, P.; Adkikari, B. Drying and denaturation characteristics of whey protein isolate in the presence of lactose and trehalose. Food Chemistry 2015, 177; 8–16.

[7]   Kim, E. H. –J.; Chen, X. D.; Pearce, D. On the mechanisms of surface formation and the surface compositions of industrial milk powders. Drying Technology 2003, 21; 265–278.

[8]   Keogh, M. K.; O'Kennedy, B.T.; Kelly, J.; Auty, M. A.; Kelly, P. M.; Fureby, A.;

Haahr, A. –M.Stability to oxidation of spray-dried fish oil powder microencapsulated using milk ingredients.Food Chemistry and Toxicology 2001, 66; 217–224.

Pulsed Electric Fields (PEF) as pre-treatment for freeze-drying of plant tissues

Al-Sayed, L. [a]; Boy, V. [b*]; Madieta, E. [c]; Mehinagic, E. [c]; Lanoisellé, J.-L. [b]

[a] Societal Transition and Agriculture (430 b), Institute of Social Sciences in Agriculture, University of Hohenheim, 70599 Stuttgart, Germany

[b] Univ. Bretagne Sud, UMR CNRS 6027, IRDL, F-56300 Pontivy, France

[c] Unité GRAPPE, Ecole Superieure d'Agricultures Angers Loire (ESA), INRA, 55, rue Rabelais BP 30748, 49007 Angers Cedex 01, France

*E-mail of the corresponding author: virginie.boy@univ-ubs.fr

Abstract

The influence of pulsed electric fields (PEF) treatment on freeze-drying for potato and strawberry tissues was investigated. Samples were pre-treated by PEF ($E = 400 \ V \ cm^{-1}$) for different treatment times. Freeze-drying was carried out at -17°C and 18.4 Pa or 30 Pa for potato and strawberry tissues, respectively. The effects of PEF pre-treatment was compared with intact samples. The drying time was reduced by 35% for potato and 30% for strawberry. The sample rehydration capacity and the electrolytes released during the rehydration were higher for pre-treated samples. Strawberries texture was characterized by the hardness, the cohesiveness and the springiness.

Keywords: Pulsed Electric fields; Freeze-drying; Potato; Strawberry; Textural Properties.

1   Introduction

Freeze-drying process is well-known to produce high quality products. However, the use of this process is limited because of the long drying time and the high energy consumption. For this reason, scientists keep searching for new pre-treatments to improve heat and mass transfers during the freeze-drying process without affecting the quality of the final products.

The relevance of using the pulsed electric fields (PEF) to enhance the performances for various modes of drying was pointed out.[1] It was reported that, exposing a biological tissue to an external electric field for few microseconds cause a transcient increase in the transmembrane potential. This alters the organization of the cytoplasmic membrane by forming pores which increases the cell membrane permeabilization.[2]

A few studies have shown the ability of the PEF treatment on fruits and vegetables to accelerate the freeze-drying process by increasing the drying rate and/or reducing the drying time.[3-6]

While these results are promising, researches are still needed to confirm these findings for different plant tissues and to examine the efficiency of the PEF assisted freeze-drying process on the quality of the final products. The objective of this work was to investigate the influence of coupling PEF treatment and freeze-drying on the dehydration kinetics of potato and strawberry tissues, and to investigate the effect of using this innovative process on the rehydration and textural properties of freeze-dried products.

2   Materials and Methods

2.1   Sample preparation

Potatoes (Agata) and strawberries (Charlotte and unknown variety from Spain) were bought from a local market (Pontivy, France) and stored in a refrigerator (4°C). Initial moisture contents were (85.2 ± 1.0) % and (91.7 ± 0.4) % in wet basis (w/w), respectively. Cylindrical potato (18 mm diameter and 25 mm height) and strawberry samples (20 mm diameter and 27 mm height) were prepared.

2.2   Pulsed Electric Field (PEF) pre-treatment

The electric field treatment was carried out using a PEF generator (2.5 kV/24 mA, Effitech, Pau, France). The generator supplies near-rectangular monopolar pulses. N series of pulses (-) were imposed during the treatment. Each series was composed of n pulses (-) with pulse duration t_i (μs) and pulse repetition time Δt (s). Two consecutive series were separated by an intertrain time Δt_t (min). This time between series was fixed at 5 min in

order to control the increase in the product temperature (10°C in our case). The total PEF treatment time (s) was defined as $t_t = n \cdot N \cdot t_i$.

For potato samples, the PEF treatement was realized according to the following protocol: $E = 400$ V cm^{-1}, $N = 12.5$, $n = 240$, $t_i = 100$ μs, $t_t = 0.3$ s.

For strawberry samples, the same electric field strength, pulse duration and pulse number in each series were applied ($E = 400$ V cm^{-1}, $n = 240$, $t_i = 100$ μs). For the study of the disintegration kinetics during the PEF treatment, $N = 16$ series were required to reach the totally disintegrated tissue which corresponds to a PEF treatment time $t_t = 0.384$ s. For the studies of the dehydration kinetics and the effect of PEF treatement on the freeze-dried strawberries, different number of series were applied ($N = 0.5$, 1, 2, 3, 4 series) correspondent to various PEF treatment times ($t_t = 0.012$ s, 0.024 s, 0.036 s, 0.048 s and 0.096 s). After the PEF pre-treatment, the samples were frozen and stored in a freezer (Fryka Kältetechnic, Esslingen am Neckar, Germany) at -80°C until needed.

The degree of tissues damage was assessed from the conductivity disintegration index Z (-), calculated as $Z = \sigma - \sigma_i / \sigma_d - \sigma_i$.[7] σ is the electrical conductivity measured at time t (S cm^{-1}), σ_i the conductivity of the intact sample (S cm^{-1}) and σ_d the conductivity of the totally damaged sample (S cm^{-1}). σ_d was determined from the measurements of the electrical conductivity of a tissue after a freeze-thaw cycle.

2.3 Freeze-drying experiments

The freeze-drying experiments were carried out using a VirTis Advantage XL-70 freeze-dryer (Sp Scientific, Warminster, USA). The frozen samples (-80°C) were introduced in the freeze-dryer on a pre-cooled heating shelf fixed at -50°C. For both products investigated, the temperature inside the freeze-dryer chamber was set at -17°C. The pressure inside the freeze-dryer chamber was kept at 18.4 Pa and 30 Pa for potato and strawberry tissues respectively. During the secondary drying, the plate temperature was risen to 45°C. Triplicate samples were weighted using a precision balance (Acculab ALC-110.4, accuracy 10^{-4} g, Sartorius, Goettingen, Germany). The relative mass, (m/m_i) was calculated by dividing m, which is the measured mass at time t (g) by m_i, the initial mass (g).

2.4 Quality analysis

2.4.1 Rehydration ratio

The rehydration ratio was determined by weighing a sample before and after soaking it in distilled water at room temperature (24 ± 1) °C for one minute. These measurements were done for triplicate samples.

2.4.2 Electrolyte release during rehydration

The amount of electrolytes released during rehydration was determined by measuring the changes in electrical conductivity of the rehydration solution. These experiments were carried out with intact and PEF pre-treated samples with different treatment times ($t_t = 0.012$ s, 0.024 s, 0.048 s, 0.072 s and 0.096 s). The electric resistance of the solution was measured using an impedance meter (Agilent U1733C, Keysight Technologies, USA) at 100 KHz frequency. The samples were first weighted and placed inside a small beaker filled with distilled water (conductivity of 0.001 S m^{-1}). The liquid-solid ratio was fixed at 80. A magnetic stirrer was used to carefully agitate the mixture (100 tr min^{-1}). A small quantity of the solution (800 μL) was taken at different times during 2 h and was placed inside a cuvette electrodes (Eppendorf 800 μL), then it was connected to the impedance meter. The electrolyte release during rehydration was determined at room temperature (24 ± 1) °C. These measurements were done for triplicate samples.

2.4.3 Texture analysis

The textural properties were determined through a Texture Analyser (MTS Synergie 200 H, Helmut Singer Elektronik, Aachen, Germany). Texture profile analysis TPA was carried out for freeze-dried slices of strawberry of 20 mm diameter. These textural measurements were performed with intact and PEF pre-treated samples with different treatment times (0.024 s, 0.048 s, 0.072 s and 0.096 s). For each condition, twenty five replicates were analysed. The trials were done using a cylindrical probe of 25 mm diameter. Two compressions were realized with an interval of 5 s between cycles. The samples were compressed to 50% of their original height, using a load cell 1 kN and the compression rate was 30 mm min^{-1}. From the force-time curves, the hardness, the cohesiveness and the springiness were determined.[8]

3   Results and discussion

Fig. 1 presents the electrical conductivity disintegration index, Z, versus the total PEF treatment time for potato and strawberry tissues.
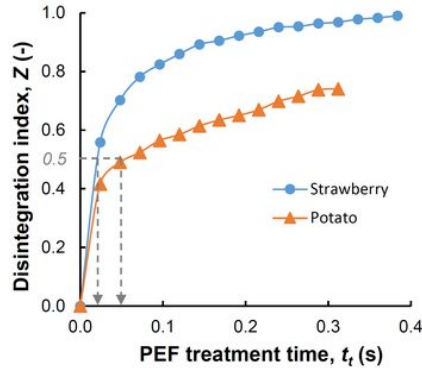
Fig. 1 Electrical conductivity disintegration index, Z **, versus the total PEF treatment time for potato and strawberry tissues.**

The disintegration index, Z, increases continuously during the PEF treatment. However, the evolution is not identical for potato and strawberry tissues. From Fig. 1, the half-permeabilization, defined as the time for which the disintegration degree $Z = 0.5$ is reached, was determined.

Strawberry is more sensitive to PEF treatment with a half-permeabilization happened after less than 0.024 s of treatment time compared to potato tissue which required a two-fold treatment time (0.05 s).

In order to investigate the benefits of PEF pre-treatement on the freeze-drying process, potato and strawberry were prepared, frozen at -80°C and freeze-dried.

Fig. 2 depicts the relative mass of the sample, m/m_i, as a function of the freeze-drying time for strawberry samples.
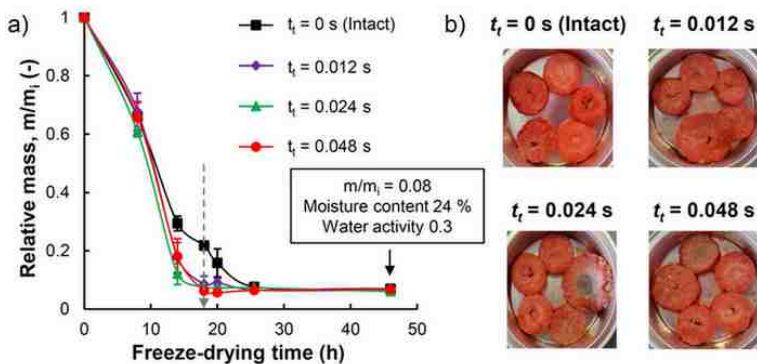
Fig. 2 a) Relative mass of the sample, m/m_i **, as a function of the freeze-drying time for intact and PEF pre-treated strawberry samples with different treatment times; b) Photographies of samples.**

PEF pre-treatment accelerates the freeze-drying process and no difference is observable between the pre-treated samples with different treatment times (Fig. 2a). Eighteen hours are sufficient to dry the pre-treated samples, against 46 h for intact ones. Thus, the PEF pre-treatment is able to reduce the drying time of strawberry by 30%. Visually, the appearance of PEF pre-treated samples after freeze-drying is slightly damaged compared with intact ones (Fig. 2b). For potato samples, the positive effect of the PEF pre-treatment on the freeze-drying rate is also obtained and the drying time is shortenend by 35% (not shown).

The rehydration ratio is almost doubled for PEF pre-treated freeze-dried strawberries compared with intact ones. Moreover, the electrolyte release during the rehydration process increases with the PEF treatment time (Fig. 3).
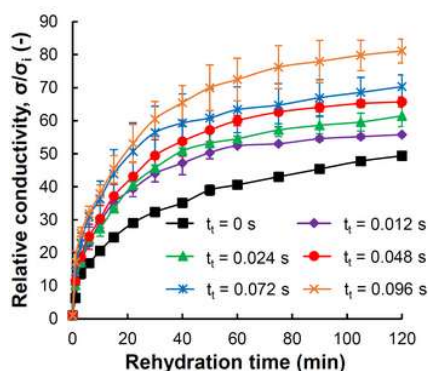
Fig. 3 Relative conductivity, σ/σ_i as a function of time during the rehydratation of freeze-dried strawberries at different PEF treatment times.

These results come from the fact that PEF pre-treatment causes breaks in the cell membrane which facilitates the release of the cell components towards the extracellular medium.[9,3] The concentration of the ionic components increases with the PEF treatment time as a consequence of a greater damage in the cell membrane. The statistical analysis indicated that PEF pre-treatment has a significant effect on the rehydration ratio (p-value < 0.05).

Fig. 4 shows the average values of the hardness and the springiness for intact and pre-treated freeze-dried strawberry slices for different PEF treatement times.
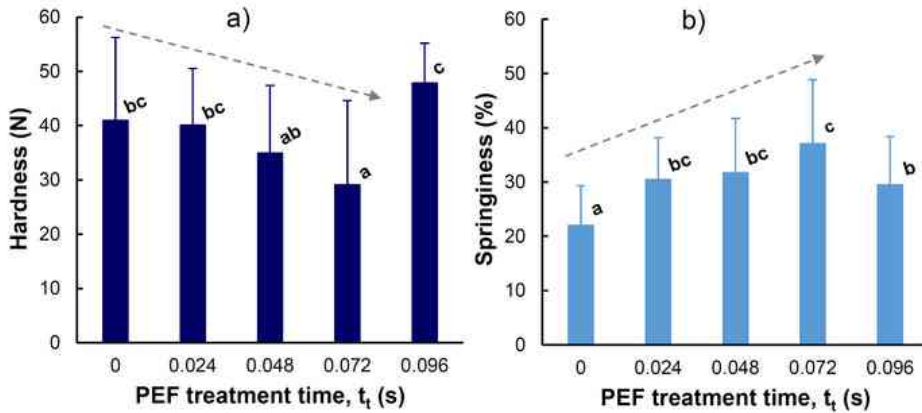
Fig. 4 Hardness and springiness for intact and pre-treated freeze-dried strawberry slices for different PEF treatment times.

The hardness represents the maximal force required to deform the sample in mastication during the first compression and the springiness characterizes the product elasticity. After the PEF pre-treatment, the strawberry tissues have lost a part of their initial strength. Thus, the hardness values decrease for increasing PEF treatment times until the time reaches 0.096 s (Fig. 4a). Both springiness and cohesiveness of pre-treated samples increase compared with the intact ones and this increase becomes all the more important as the PEF treatment time is high (springiness: Fig. 4b and cohesiveness: not shown). All these results can be explained by the irreversible damage in the cell membrane caused by the PEF pre-treatment.[10] However, after an intensive PEF pre-treatement (0.096 s) the cells have lost their cellular turgor components and we assume that all the residues from the cells aggregate and forme a tougher structure.

4   Conclusions

The influence of coupling PEF treatment and freeze-drying process for potato and strawberry tissues was investigated. PEF pre-treatment was able to reduce the drying time of 35% and 30% for potato and strawberry, respectively. A significant rehydration capacity was found for pre-treated and freeze-dried strawberries. Strawberries texture was characterized by the hardness, the cohesiveness and the springiness.

5   Acknowledgements

6   References

[1]   Barba, F.J.; Parniakov, O.; Pereira, S.A.; Wiktor, A.; Grimi, N.; Boussetta, N.; Saraiva, J.A.; Raso, J.; Martin-Belloso, O.; Witrawa-Rajchert, D.; Lebovka, N.; Vorobiev, E. Current applications and new opportunities for the use of pulsed electric fields in food science and industry. Food Research International 2015, 77 (4), 773-798.

[2]   Vorobiev, E.; Lebovka, N. Electrotechnologies for extraction from food plants and biomaterials; Springer: New York, 2008.

[3]   Jalté, M.; Lanoisellé, J.-L.; Lebovka, N.I. ; Vorobiev, E. Freezing of potato tissue pre-treated by pulsed electric fields. LWT – Food Science and Technology 2009, 42 (2), 576-580.

[4]   Ben Ammar, J.; Lanoisellé, J.-L. ; Lebovka, N.I. ; Van Hecke, E. ; Vorobiev, E. Effect of a pulsed electric field and osmotic treatment on freezing of potato tissue. Food Biophysics 2010, 5 (3), 247-254.

[5]   Wu, Y.; Guo, Y.; Zhang, D. Study of the effect of high-pulsed electric field treatment on vaccum freeze-drying of apples. Drying Technology 2011, 29 (14), 1714-1720.

[6]   Parniakov, O.; Bals, O.; Lebovka, N.; Vorobiev, E. Pulsed electric fields assisted vacuum freeze-drying of apple tissue. Innovative Food Science and Emerging Technologies 2016, 35, 52-57.

[7]   Lebovka, N.I.; Bazhal, M.I.; Vorobiev, E. Estimation of characteristic damage time of food materials in pulsed-electric fields. Journal of Food Engineering 2002, 54 (4), 337-346.

[8]   Szczesniak, A. S. Texture is a sensory property. Food Quality and Preference 2002, 13 (4), 215-225.

[9]   Taiwo, K.A.; Angersbach, A.; Knorr, D. Influence of high intensity electric field pulses and osmotic dehydration on the rehydration characteristics of apple slices at different temperatures. Journal of Food Engineering 2002, 52 (2), 185-192.

[10] Lebovka, N.I.; Praporscic, I.; Vorobiev, E. Effect of moderate thermal and pulsed electric field treatments on textural properties of carrots, potatoes and apples. Innovative Food Science & Emerging Technologies 2004, 5 (1), 9-16.

Hot air drying characteristics and nutrients of apricot *armeniaca vulgaris lam* pretreated with Radio Frequency(RF)

Peng, M.C.[a]; Liu, J.X.[a]; Lei, Y.[a]; Yang, X.J.[a]; Wu, Z.H.[b]; Huang, X.L.[a]

[a] College of Food Engineering and Nutritional Science, Shaanxi Normal University, Shaanxi xi'an, 710119, China

[b] College of Mechanical Engineering, Tianjin University of Science and Technology, 1038 Dagu South Rd., Hexi, Tianjin, 300222, China

*E-mail of the corresponding author: cauxlhuang@hotmail.com

Abstract

Apricot pretreated with RF and then dried with convective hot air at 65℃, 3.0m/s in this research. RF pretreatment time of 20, 30, 40 and 50min were chosen. Results showed that, there is only falling rate period during apricot hot air drying, and the drying rate of apricot is improved significantly; Herdenson and Pabis model is suitable for apricot hot air drying; retentions of flavonoids, polyphenols and Vc in dried apricot were higher than those of fresh apricot; when RF treating time was chosen 30mins, nutrients retentions of Vc, flavonoid and polyphenols were 0.9543mg/100g, 5.4089mg/100g and 7.3382mg/100g, separately.

Keywords: apricot fruit, hot air drying, drying rate, nutrients, radio frequency

1. Introduction

Apricot originated in China. It has a wide distribution, high yield, good quality and unique flavor. However, fresh apricot fruit with high moisture content above 80% is easy to corrupt at normal temperature even cold storage[1]. Drying is an effective method to extent selft life of apricot. Half dried preserved apricot fruits are popular to Chinese. So, there are several literals about drying of apricot fruits. Wang studied on thin layer drying of apricot at low temperature and different air velocities, and temperature is the main factor affecting drying rate [2]. Natural air drying of apricot is time consuming and induces serious browning which affects the quality of dried apricot[3]. In order to prevent browning, blanching before drying or sulphur treated during drying is usual applied. And these treatments either high temperature, nutrients loss[4] or unsafe for health. New type of heating method, RF receives more and more attentions in recent years for lots of advantages such as selective heating, self-balancing effect of moisture content, large energy penetration depth and fast heating rate[5], etc. There are several literatures on RF used in drying of agricultural products, deinsectization, sterilization[6,8]. Zhang and others [9] investigated RF conbimed with hot air drying red jujube, drying time was shortened by 2/3. In roder to reduce drying time and improve the quality of dried apricot, RF technique was applied in this paper, and then convective hot air drying at 65°C was conducted.

2. Materials and Methods

2.1. Samples preparation

Apricot *armeniaca vulgaris lam* was provided by the institute of plum and apricot, Xi'an, in May to July,2017. Fresh apricots were stored at 3-4°Cand must be used within one week. The initial moisture of fresh apricot ranged from 85% to 86% wet basis which was determination by oven drying at 103°C. Samples were cut in half and the cores were removed, and then immersed in 2% sodium bisulfite solution for 1 hour to restrain browning.

2.2. RF pretreatment of apricot

Apricot fruits were moved into the RF equipment and the plate distance was set 60.0mm. The power of the radio frequency equipment is 6.0KW and the frequency is 27.1Hz. RF treated time was chosen for 20, 30, 40, and 50min.

2.3. Hot air drying experiment of apricot

After RF pretreatment, apricot was dried with convective hot air at 65°C and air velocity of 3.0m/s. During the drying period water content of apricot was declined from nearly 84% to about 20%. In order to analyze the drying characteristics of apricot pretreated with RF, the weights of samples were obtained by electronic balance with an accuracy of 0.001g every 60 minutes.

2.4. Nutrients assay

The flavonoid content of apricot fruit pulp was analyzed according the method described by Liang[10] with slight amendent. 1.0ml of filtrate was placed in a 25ml volumetric flask, and then 6ml of distilled water and 1.0ml of sodium nitrite (1:20) were added in turn and shaked well. After 6 minutes, 1.0ml of aluminium nitrate (1:10) was added and shaked well, and 6minutes later, 10.0ml of sodium hydroxide (1:10) was added and shake well. After 15 minutes' standing, the final volume was made up to 25ml with distilled water and shade well. And the sample was placed in colorimetric tube and the absorbance was measured at 510nm.

Phenolic content in apricot was determined by the Folin-Ciocalteau method[11]. 2,6-dichlorophenol indophenol method[12] was applied to assay vitamin C content of apricot in this study.

All measurements were conducted in triplicate.

3. Results and discussion

3.1. Drying characteristics of apricot preteated with RF

After RF pretreatment, the apricot fruit was dried with hot air at 65℃ and on the velocity of 3.0m/s. There is only falling rate period during apriod hot air drying, shown in Figure 1. The drying rate of apricot pretreated with RF was obviously higher than that of control sample, because RF treatment can improve the permeation of apricot, that would induce moisture migrate quickly. In the range of 20-50minutes RF treated, the drying rate of apricot fruit increased with the increase of RF treated time. And the drying rate of apricot fruit with 50 minutes' RF pretreatment was the highest, while that of apricot with 20minutes' RF treatment was the lowest. May be the longer RF treated time, the permeation of apricot tissue was better, which makes it easier for moisture migrate in subsequent drying process.
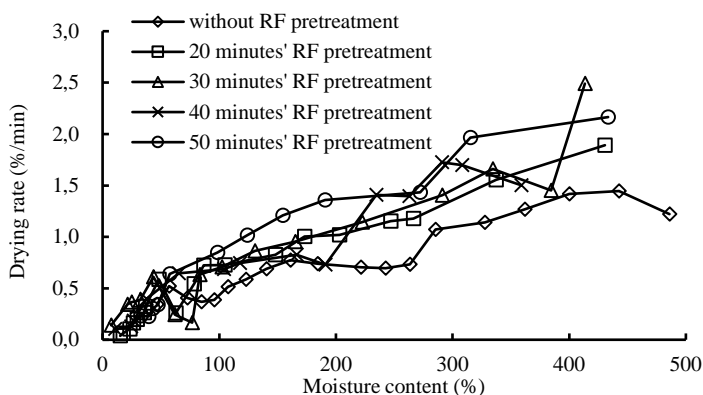
Fig.1 Drying rate curves of apricot during hot air drying after different RF pretreatments

In this paper, moisture ratio was applied to analyze the drying characteristics, shown in equation (1)[13,14].

$$MR = \frac{M_t - M_e}{M_0 - M_e} \qquad (1)$$

Where, M_0, M_e and M_t stand for initial moisture content, equation moisture content and moisture content at any time, sepretively, dry basis, %. As M_e was difficult to determinte at laboratory, it was neglected in this paper. So, equation(1) was simplified as equation(2).

$$MR = \frac{M_t}{M_0} \qquad (2)$$

From the curves of moisture content of apricot preteated with RF during hot air drying, as showed in figure 2, moisture content of apricot pretreated with RF delined more fast than that of control samples. And the drying time was shorten by 10% to 34%. That means RF ptretreatment could save drying time and energy.
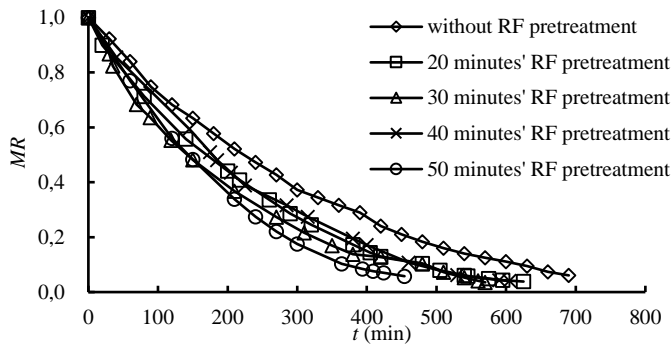
Fig.2 Curves of moisture ratio of apricot changing with drying time during hot air drying

3.2. Hot air drying model of apricot pretreated with RF

There are many mathematics models to describe drying characteristics of fruits and vegetables[15-19]. Through analyse of experiment data, it was found that, Herdenson and Pabis model, Page model and Lemus model, showed in table 1, were better consistent with experiment data. R^2, χ^2, and RMSE of evey model, as equations from (3) to (5), were used as indications to evaluate drying model. Henderson and Pabis model has the highest R2 ranging from 0.9715 to 0.9955, and has lower χ^2 and RMSE. So Henderson and Pabis model was better fit for experiment data.

$$R^2 = 1 - \frac{\sum_{i=1}^{N}(MR_{exp,i} - MR_{pre,i})^2}{\sum_{i=1}^{N}(\overline{MR}_{exp} - MR_{pre,i})^2} \qquad (3)$$

$$\chi^2 = \frac{\sum_{i=1}^{N}(MR_{exp,i} - MR_{pre,i})^2}{N - n} \qquad (4)$$

$$RMSE = \sqrt{\frac{\sum_{i=1}^{N}(MR_{exp,i} - MR_{pre,i})^2}{N}} \qquad (5)$$

Table 1 R^2, RMSE, χ^2 of hot air drying models for apricot pretreated with RF

RF treatment time/min	Model name	Model equation	Model parameters		R^2	RMSE	χ^2
			a	k			
20	Henderson and Pabis	$MR=a\exp(-kt)$	1.0432	-8.7×10^{-5}	0.9900	0.0386	0.0016
30			0.9867	-9.8×10^{-5}	0.9715	0.0525	0.0031
40			1.1035	-9.5×10^{-5}	0.9879	0.0703	0.0057
50			1.0839	-10.8×10^{-5}	0.9927	0.0505	0.0030
			k	n			
20	Page	$MR=\exp(-kt^n)$	6.6177×10^{-5}	1.0237	0.9895	0.0279	0.0009
30			2.4486×10^{-3}	0.6724	0.9255	0.0593	0.0039
40			3.9567×10^{-5}	1.0796	0.9929	0.0394	0.0018
50			0.5086×10^{-5}	1.3344	0.9871	0.0607	0.0043
			a_1	a_2			
20	Lemus	$MR=a_1+a_2t^{1/2}$	0.9070	-4.6×10^{-3}	0.9644	0.0460	0.0027
30			0.8862	-4.8×10^{-3}	0.9872	0.0403	0.0018
40			0.8856	-4.6×10^{-3}	0.9751	0.0460	0.0024
50			0.9826	-5.8×10^{-3}	0.9820	0.0349	0.0014

3.3. Analyze of nutrients in dried apricot

3.3.1. Flavonoids in apricot pretreated with RF

At the bigining of drying, total flavonoid content was the one of fresh apricot. From figure 3(a), it was known that, as moisture descrease, total flavonoid contents of apricots pretreated with RF were increased firstly and then declined, but higher than that of fresh apricot. The reason might be RF treatment induce fruits tissue collapsed that would favorable for testing nutrients. It also can be found that, when RF treatment time was chosen 40min, flavonoid contents of apricot maitaned highest level during the hole drying process, those of apricots pretreated with 30min and 50min were flowed by, and the last was 20minutes' RF pretreatment. The main reason might be tissue permeation of apricot would improve as the RF treteated time but there exists a limit level for permeation; and prolong RF pretreated time, nutrients were degraded or decomposed.

When dying was finished, flavonoid content in dried apricots also maintaned higher than of fresh apricot (0.9075mg/100g). The main reason would be that RF destroyed internal structures of apricots, and flavones in tissue were easy to dissolve out.

3.3.2. Polyphenol content in apricot pretreated with RF

It was obvious showed that, after 30 and 40 minutes' RF pretreatment, polyphenol contents of apricot during hot air drying maitaned the highest level, and those of samples with 20 munites' RF pretreatment were follow by, and those of samples with 50 munites' RF

pretreatment were the lowest, showed in figure 3(b). The reason for this phenonena as the above. But, longer time RF pretreatment may destroy polyphenol tissue and induced oxidation. The result from this study were consistent with that from Zhao et al[20]. During the hot air drying process, polyphenol contents maintain stable level and did not decline with the descrease of moisture content of apricot.
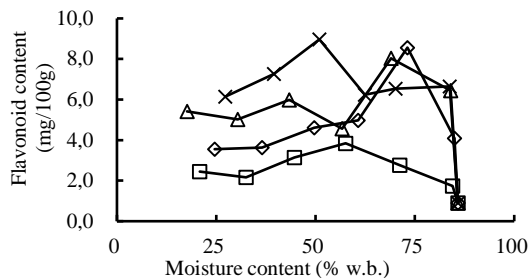
(a) Flavonoid contents
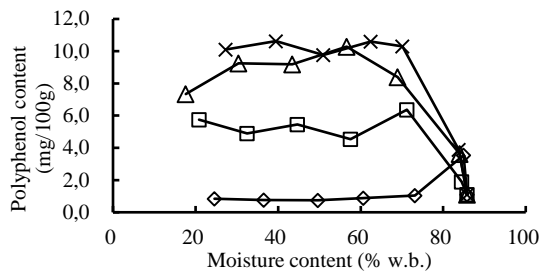
(b) Polyphenol Content
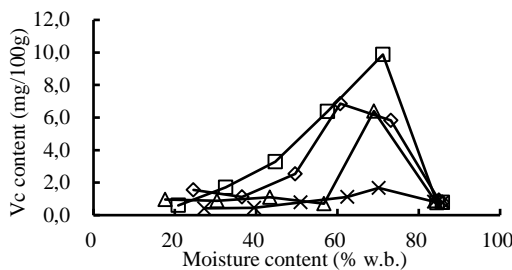
(c) Vc content

—□— 20 minutes' RF pretreatment   —△— 30 minutes' RF pretreatment
—✕— 40 minutes' RF pretreatment   —◇— 50 minutes' RF pretreatment

Fig.3 Nutrients of apricot pretreated with RF changing with moisture content in hot air drying

3.3.3. Vitamin C in apricot pretreated with RF

As soon as RF pretreated, Vc content in apricot were sharply increased compared to that of fresh sample, showed in figure 3(c). However, Vc is heat sensitive material, as drying

processing, it was decreased as the descrease of moisture content of apricot. And the 40 minutes' RF pretreatment could induce the better permeation of apricot tissue analzed above, so more Vc in apricot was exposed on the surface of wet matial, that meant more Vc would degrade wthen exposed in high temperature condiction. When hot air drying was finished, Vc contents of dried apricot with different RF pretreated were slightly higher than that of fresh fruit (0.7817mg/100g).

From the above nutrients analyze, when RF treating time was chosen 30 minutes, nutrients retentions of flavonoid, polyphenols and Vc were 5.4089mg/100g, 7.3382mg/100g, and 0.9543mg/100g, separately.

4. Conclusions

RF treatment could improve the hot air drying rate of apricot, and saving time and energy. After RF pretreatment, nutrients of flavonoids and polyphenol in apricot were improved and maintain higher levels during hot air drying, although vitamin C was higher just after RF pretreatment, it was degraded during hot air drying. Overall, RF would be a new pretreatment technique for fruit and vegetables drying.

Acknowledgements

5. References

[1] Oluranti, E.; Campbell, I.A.; Merwin.; Olga, I. Characterization and the effect of maturity at harvest on the phenolic and carotenoid content of northeast USA apricot(Prunus armeniaca) varieties. Journal of Agricultural and Food Chemistry 2013, 61, 12700-12710.

[2] Wang, N.; Liu, W.X.; Li, F.C.; Du. Z.L. Thin layer drying model of apricot at low temperature. Transactions of the Chinese Society for Agricultural Machinery 2011, 42(1), 140-144.

[3] Zhang, Z.N.; Wang, J.; Zhang, X.Y.; Shi, Q.L. Effects of radio frequency assisted blanching on polyphenol oxidase, weight loss, texture, color and microstructure of potato. Food Chemistry 2018, 248,173-182.

[4] Cabras, P.; Angioni, A.; Vincenzo, L. Pesticide residues on field-sprayed apricots and in apricot drying processes. Journal of Agricultural and Food Chemistry 1998, 46, 2306-2308.

[5] Liu, Y.H.; Wang, S.J.; Mao, Z.H.; Tang, J.M.; Tiwari, G. Heating patterns of white bread loaf in combined radio frequency and hot air treatment. Journal of Food Engineering 2013, 116, 472-477.

[6] Zhang, S.; Zhou, L.Y.; Ling, B.; Wang, S.J. Dielectric properties of peanut kernels, ssociated with microwave and radio frequency drying. Biosystems engineering 2016, 145, 108-117.

[7] Tiwari, G.; Wang, S.; Tang, J.; Birla, S.L. Analysis of radio frequency (RF) power

distribution in dry food materials. Journal of Food Engineering 2011,104, 548-556.

[8] Hansen, J.D.; Drake, S.R.; Heidt, M.L.; Watkins, M.A.; Tang, J.; Wang, S. Radio frequency-hot water dips for postharvest codling moth control in apples. Journal of Food Processing and Preservation 2006, 30(6), 631-642.

[9] Wang, J.; Olsen, R.G.; Tang, J.; Tang, z. Influence of mashed potato dielectric properties and circulating water electric conductivity on radio frequency heating at 27 MHz. Journal of Microwave Power & Electromagnetic Energy 2008, 42(2), 31-46.

[10] Liang, X.F. et.al. Extraction technology of flavonoids from ginkgo biloba L. Shells Medicinal Plant 2012, (10), 64-69.

[11] Oluranti, E.; Campbell, I.A.; Merwin.; Olga, I. Padilla-Zakour characterization and the effect of maturity at harvest on the phenolic and carotenoid content of northeast USA apricot (Prunus armeniaca) varieties. Journal of Agricultural and Food Chemistry 2013, 61, 12700−12710.

[12] O'Callaghan, J.R.; Menzies, D.J.; Bailey, P.H. Digital simulation of agricultural dryer performance. Journal of Agricultural Engineering Research 1971, 16(3), 223-244.

[13] Xiao, H.W.; Pang, C.L.; Wang, L.H.; Bai, J.W.; Yang, W.X.; Gao, Z.J. Drying kinetics and quality of Mounkka seedless grapes dried in an air-impingement jet dryer. Biosystems Engineering 2010, 105, 233-240.

[14] Danae, D.K.; Tzia, V.; Gekas. A knowledge base for the apparent mass diffusion coefficient (D_{EFF}) of foods. International Journal of Food Properties 2000, 3(1), 1-14.

[15] Arslan, D.; Özcan, M. M. Drying of tomato slices: changes in drying kinetics, mineral contents, antioxidant activity and color parameters Secado de rodajas de tomate: cambios en cinéticos del secado, contenido en minerales, actividad antioxidante y parámetros de color CyTA. Journal of Food 2011, 9(3), 229-236.

[16] Silva, W.P.; Silva, C.M.D.P.S.; Gama, F.J.A.; Gomes, J.P. Mathematical models to describe thin-layer drying and to determine drying rate of whole bananas. Journal of the Saudi Society of Agricultural Sciences 2014, 13, 67-74.

[17] Baini, R.; Langrish, T.A.G. Choosing an appropriate drying model for intermittent and continuous drying of bananas. Journal of Food Engineering 2007, 79; 330-343.

[18] Yu, H.M.; Zuo, C.C.; Xie, Q.J.; Makinde, O.D. Drying characteristics and model of chinese hawthorn using microwave coupled with hot air. Mathematical Problems in Engineering 2015, 1-15.

[19] Bi, J.F.; Yang, A.J.; Liu, X.; Wu, X.Y.; Chen, Q.Q.; Wang, Q.; Lv, J.; Wang, X. Effects of pretreatments on explosion puffing drying kinetics of apple. LWT-Food Science and Technology 2015, 60, 1136-1142.

[20] Zhao, E.L.; Wang, M.H.; Zhan, J.L.; Yang, J.Study on microwave-assisted extraction of polyphenol from corn bract based on response surface methodology and its antioxidant activity. Molecular Plant Breeding 2018, online first (in Chinese with English abstract)

Quality analysis of fresh and dried mangoes

S. Arendt[a, b], K. Jödicke[a*], W. Hofacker[a], W. Speckle[b]

[a] Institute of Applied Thermo- and Fluiddynamics, HTWG Konstanz University of Applied Sciences.
[b] Environmental Analysis Laboratory, University of Applied Sciences Ravensburg-Weingarten

*E-mail of the corresponding author: katrin.joedicke@htwg-konstanz.de

Abstract

Organic acids, sugar and colour define the quality and the taste of mangoes. The quality deteriorates during drying on a single-layer-dryer. Quality losses can be reduced by using drying parameters that influence the quality less. In this research, the contents of ascorbic acid, organic acids and sugar as well as colour changes and shrinkage are analysed. Analyses are carried out at different temperatures, dew point temperatures and air velocities using HPLC, IC and UV/Vis- spectrometry. The quality criteria showed the lowest changes at a temperature of 60°C, dew point temperature of 20°C and an air velocity of 0.9 m/s.

Keywords: organic acids; sugars; colour; shrinkage; thin-layer-dryer.

1. Introduction

The world's population is projected to reach nine billion by 2050. It is expected that the number of people suffering from chronic undernourishment (1 billion in 2010) will therefore increase significantly by 2050. Due to this fact, it is vital to make the food available more useful during production. In developing and transition countries, the main focus should be on reducing post-harvest losses [1]. These losses can be avoided if the shelf life of the products is extended. In order to extend the shelf life of the investigated products, it is necessary to influence the microbial population by changing the conditions in the products; so microorganisms cannot grow and reproduce. One method to make agricultural products more durable is drying [2]. During drying, the agricultural products lose water and the living conditions for microorganisms become increasingly harsher. But during drying, the products undergo a loss of quality, e.g. changes in taste, degradation of vitamins and temperature sensitive acids and change in colour. Optimal drying parameters can reduce such quality losses and preserve the essential quality criteria of the investigated agricultural products. In this study, the content of ascorbic-, citric- and malic acid as well as the sugar content of fresh and dried mangoes are analysed. Analyses are carried out on mangoes dried with an experimental single-layer-dryer described by ARENDT using HPLC, IC and UV/Vis instruments [3].

2. Materials and Methods

The mango plant originates from the tropics of India and Burma. Its edible pulp is yellow tor orange-red and is protected by a leathery shell, which in ripe state has a green to orange-red colour, depending on the variety. [4]

2.1. Quality Criteria of Mangoes

Because humans and animals have lost their ability to synthesize ascorbic acid out of carbohydrates, it is essential to ingest ascorbic acid within their diet. Ascorbic acid is an important compound in all living organisms and maintains metabolic functions. The best way to reach the daily necessity of 250 to 300 mg is by consuming fruits and vegetables. Ascorbic acid acts like an antioxidant against free radicals and can reduce cancer risks and risk for arteriosclerosis [5, 6, 7]. Environmental conditions like light, temperature, oxygen, cations, trace elements and the pH-value can influence the ascorbic acid content in fruits [5, 7]. Therefore the content of ascorbic acid in mangoes can vary from one fruit to another. The stability of ascorbic acid in food products or an aqueous medium depends on different ambient conditions. Factors lowering the content of ascorbic acid include light, oxygen, high temperature, alkaline pH-values, enzymatic reactions and catalytically active metal ions [7, 8]. Citric acid is found in every living cell because it is produced as an intermediate in the citric acid cycle and is required for energy generation. Like other antioxidants, it is able to conserve fat, colours, flavors and vitamins in food. Furthermore, it is able to

complex heavy metals and acts like an important inhibitor against uroliths [9, 10, 11]. Together with malic acid, citric acid contributes significantly to the flavor of fruits and vegetables [12]. The riper the fruit is, the lower its content of malic acid [12]. Malic acid also has a supportive effect on antioxidants and therefore inhibits enzymatic browning in truncated or injured fruits and vegetables [13]. Malic acid occurs in L- and D-form, but only L-malic acid is present in nature. Malic acid is found in all living cells because it also appears as an intermediate in the citric acid cycle and is required for energy generation [13]. The primary sugars available in mangoes are sucrose, glucose and fructose. Together with polyphenols and the organic acid content, the sugar content defines the taste of fruits and vegetables [14, 15]. The carbohydrates are the energy providers for the human body and also serve as construction material of cells. [7, 16]

2.2. Sample Preparation and Experimental Set-up

Mangoes were purchased at a local supplier in Konstanz, Germany. For analysis fresh and dried mangoes were frozen in liquid nitrogen and pulverized in a Moulinex mill. In each series of experiments, the mangoes were dried in a laboratory single-layer-dryer. For the drying process, the through flow principle was applied with air temperatures of 40°C, 60°C, 80°C and 94°C, dew point temperatures of 5°C, 10°C, 20°C, 30°C and 37°C and air velocities of 0.6 m/s, 0.9 m/s, 1.2 m/s and 1.4 m/s. The homogenized samples were extracted for measuring quality criteria.

2.2.1. Ascorbic Acid Extraction

The fresh and dried mangoes were prepared according to the European Standard EN 14130 [18]; diluted meta-phosphoric acid was used to extract the samples. This suspension was then filtered. A certain amount of the filtrate was diluted with an L-cysteine solution, and adjusted to a pH-value between 7.0 and 7.2. The solution was then stirred for a defined time and set to a value between 2.5 and 2.8 on the pH-scale. Prior to injection to the HPLC ultrapure water was added to the solution until a defined volume was reached. Furthermore, the samples were filtered with a 0.45 µm filter to prevent pollution of the RP- (reversed phase-) column [18] before the injection to the HPLC.

2.2.2. Organic Acid Extraction

The fresh and dried mangoes were diluted in ultrapure water and extracted for 30 minutes in an ultrasonic bath. Then the samples were filtered and subsequently injected to the IC-system. Prior to IC analysis the filtrates were filtered through a 0.45 µm filter to prevent the organic acid column (ion-exclusion chromatography (IEC)) from pollution.

2.2.3. Sugar Extraction

For sugar extraction, fresh and dried mango samples were diluted with ultrapure water. The samples were extracted for 10 minutes on a magnetic stirrer. Then the diluted samples were

filtered and processed like described in the manual of the enzymatic test of R-BIOPHARM AG. Following this enzyme kit, the content of sucrose, D-glucose and D-fructose were measured using an UV/Vis-spectrometer. Samples were prepared in a way that enables the determination of D-glucose content before and after the enzymatic hydrolysis of sucrose. Subsequently, the content of D-fructose was determined. [19]

2.2.4. Experimental

The ascorbic acid extracts of fresh and dried mango samples were analysed by an HPLC System (1260 Infinity, AGILENT TECHNOLOGIES, INC.). The used column was a LiChrosher (5 µ C18 100A; 4.0 x 250 mm). The ascorbic acid (L(+)-ascorbic acid) was analysed by isocratic elution using an eluent consisting of ultrapure water with KH_2PO_4 and methanol with N-cetyl-N,N,N-trimethyl-ammonium bromide according to the European Standard EN 14130. Detection of the ascorbic acid was carried out with a diode-array-detector at a wavelength of 254 nm. [18] The extracts of the organic acids were analysed using the METROHM ion chromatograph 883 Basic IC plus. The sample components were separated on a chromatographic ion-exclusion chromatography (IEC) column, Organic Acid 6.1005.200 from METROHM GmbH & Co. KG (particle size of 9 µm, length of 250 mm, diameter of 7.8 mm). As mobile phase acetone diluted with 0.5 mmol/L H_2SO_4 was used (standard eluent) [20]. A suppressor cell was placed prior to the conductivity detector. Sugar content analysis of the extracted and prepared mangoes was done using an UV/Vis spectrometer at a fixed wavelength of 340 nm [19].

3. Results and Discussion

The drying process was carried out using an experimental approach, which was developed by a Design of Experiment (DoE) software. A response surface plan with central composite design was created. Air temperatures (40°C, 60°C, 80°C, 94°C), dew point tempera-tures (5°C, 10°C, 20°C, 30°C, 37°C) and air velocities (0.6 m/s, 0.9 m/s, 1.2 m/s, 1.4 m/s) were used as variable parameters. The aim was to determine the influence of these factors on the quality of the dried samples (mango slices with an initial thickness of 0.4 cm). For fresh mangoes, almost constant ascorbic acid contents were detected. Small variations in the contents would be due to natural variations of the fresh product. Fig. 1 shows the retention of ascorbic acid in dried mangoes plotted against the drying temperature.
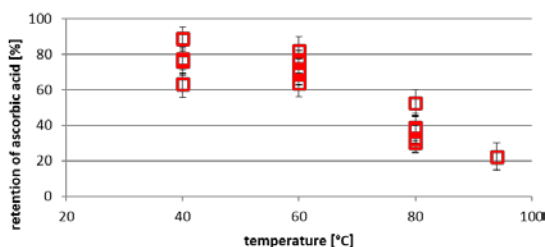
Fig. 1 Retention of ascorbic acid in mangoes

As shown in fig. 1, the content of ascorbic acid decreases due to drying (retention < 100%). The degradation level increases with increasing drying temperatures. This was expected because the ascorbic acid decomposes during drying at high temperatures and in the presence of oxygen [8]. The concentration of citric acid in dried mangoes (fig. 2) shows nearly the same tendency as the concentration of ascorbic acid. It decreases as the drying temperature increases, and thus, during shorter periods of drying times.
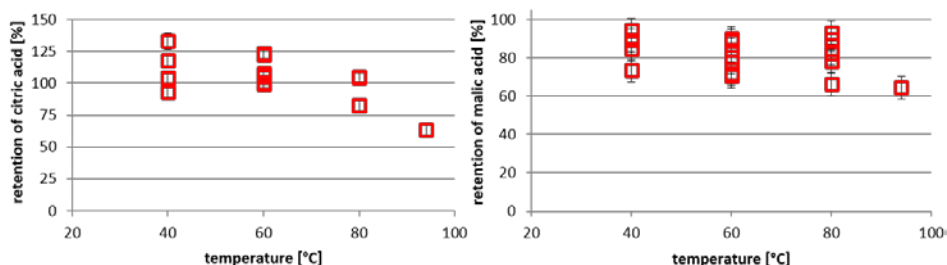
Fig. 2 Retention of organic acids in mangoes

In the case of the malic acid (fig. 2) in dried mangoes, the results showed some variations when compared to those of ascorbic and citric acid. The trend of degradation with increasing drying temperatures can only be slightly noticed. It can be concluded that malic acid is reduced during drying, but remains nearly independent of the drying temperature. Fig. 3 shows the content of the three main sugars (glucose, fructose, sucrose) in mangoes. As shown in fig. 3 (left), the content of glucose increases during drying.
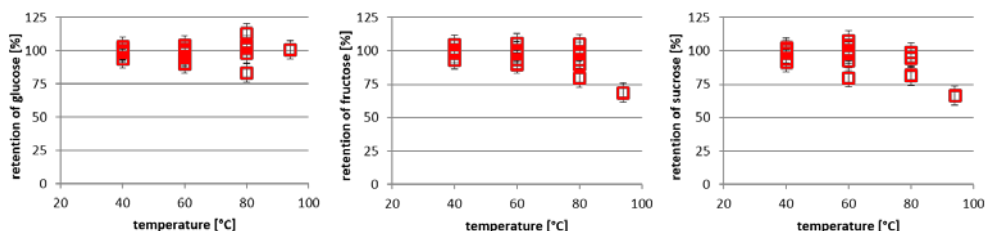
Fig. 3 Retention of sugar in mangoes

The contents of fructose (fig. 3, center) and sucrose (fig. 3, right) decrease as the drying temperatures increase. The content of glucose seems to be nearly independent of the drying temperature or increases slightly. This increase of glucose and at the same time degradation of sucrose is due to the fact that sucrose is a disaccharide consisting of two molecules: one fructose and one glucose [21]. During drying, it seems that sucrose divides back into its two constituting molecules. The rate at which the sucrose molecules split is higher at high drying temperatures, which in turn means that the contents of fructose and glucose increase. As shown in fig. 3, the content of glucose rises slightly with increasing drying temperature compared to fructose which decreases, because fructose and glucose are also degraded

during drying. Nevertheless, the degradation especially for glucose seems to be muffled because of the continuous splitting of sucrose [16, 21].

The colour of the dried samples was also compared with the colour of the fresh fruit. For an easy comparison, the *CIE L*, a*, b** colour space is used. a^* represents the colour space from green to red; b^* from blue to yellow and L^* represents the brightness (white to black). The total colour difference *TCD* is calculated out of these values using equation (1):

$$TCD = \sqrt{(\Delta L^*)^2 * (\Delta a^*)^2 * (\Delta b^*)^2} \tag{1}$$
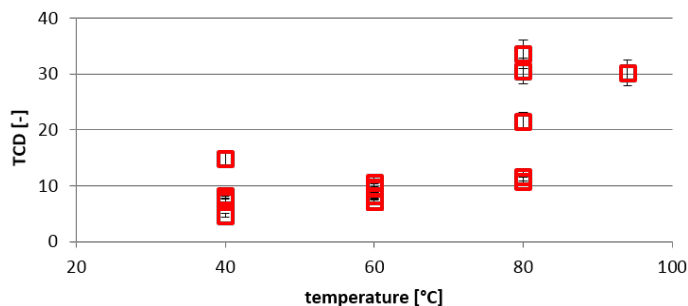
Fig. 4 Colour changes in mangoes

As it can be seen in fig. 4, the *TCD* increases as the drying temperatures increase. This is not only recognizable from fig. 4, but also from fig. 5, which shows, that the mango powder gets darker as the temperature increases.
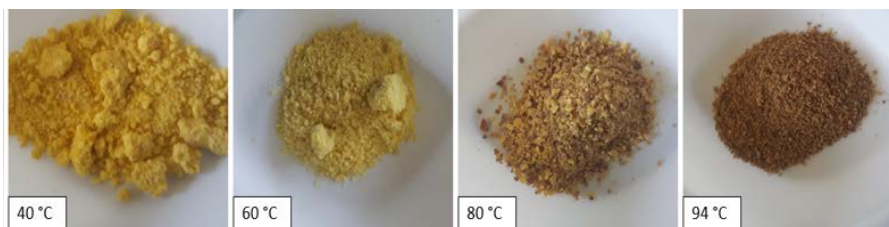
Fig. 5 Colour changes in mangoes (photo)

At last the retention of the surface area (shrinkage *S*) of mango samples before and after drying was compared. The retention of surface is calculated using equation (2), where P_0 and P represent the amount of pixels before and after drying, respectively.

$$S = 100 - \left(\frac{P}{P_0} * 100\right) \tag{2}$$

As it can be seen in fig. 6, the retention of the surface decreases as the drying temperatures increase. This is due to the fact that mangoes loose water during drying and become smaller.
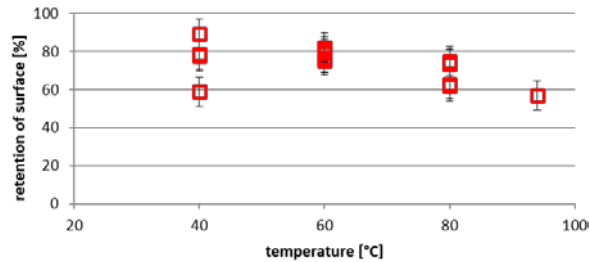
Fig. 6 Surface retention of mangoes

4. Conclusions

It can be concluded that the drying temperature has the largest influence on changing the quality criteria during the drying process of mangoes. The evaluation according to DoE revealed that dew point temperature as well as air velocity have a slight effect on the changing of the quality criteria. Furthermore, it was found that dew point temperature should be kept at 20°C and air velocity at 0.9 m/s. It could be shown that concentrations of ascorbic and citric acid in dried mangoes decrease with increasing drying temperatures. The content of malic acid as well as that of glucose seem to be nearly independent of the drying temperature. The contents of sucrose and fructose decreased during drying. The degradation of sucrose can be explained with the splitting of this molecule into fructose and glucose. Fructose seems to be more instable towards heat so it decreases more than glucose. This is due to the fact that sucrose consists of molecules of fructose and glucose and is divided into these two substances during drying [16, 21]. An optimal air temperature for the drying of mangoes could be found at around 60°C, because all of the mentioned components show a low or the lowest change/degradation values. The changes in the mentioned quality criteria should be kept as low as possible because organic acids as well as the different sugars are responsible for the taste of the mangoes and possesses health promoting qualities.

5. Acknowledgements

6. References

[1] Priefer, C., Jörissen, J, *Frisch auf den Müll – Verringerung der Lebensmittelverluste als Ansatz zur Verbesserung der Welternährung*, Karlsruhe KIT, (2012)
[2] Maskan, M., *Kinetics of colour change of kiwifruits during hot air and microwave drying,* Journal of Food Engineering, 48, (2001), 169-175
[3] Arendt, S., *Qualitätsuntersuchung an getrockneten Agrarprodukten*, (2013), 55-57
[4] Franke, W., *Nutzpflanzenkunde - Nutzbare Gewächse der gemäßigten Breiten, Subtropen und Tropen,* Georg Thieme Verlag Stuttgart, New York, (1997)

[5] Isler, O., Brubacher, G., Ghisla, S., Kräutler, B., *Vitamine II, Wasserlösliche Vitamine*, Georg Thieme Verlag Stuttgart, New York, (1988)

[6] Zeitler, S., *Ascorbinsäure (Vitamin C)*, Available: http://daten.didaktikchemie.uni-bayreuth.de/umat/vitamin-c_1/vitamin-c.htm, [10.06.2013], (2003)

[7] Biesalski, H. K., Grimm, P., *Taschenatlas Ernährung*, Georg Thieme Verlag Stuttgart, New York, (2007)

[8] Santos, P. H. S., Silva, M. A., *Retention of Vitamin C in Drying Processes of Fruits and Vegetables—A Review*, Drying Technology, **26**, (2008) 1421-1437

[9] Die Verbraucher Initiative e.V., *zusatzstoffe-online.de - Informationen zu Lebensmittelzusatzstoffen,* Available: http://www.zusatzstoffe-online.de/zusatzstoffe/113.e330_citronens%E4ure.html [18.04.2017], (2006)

[10] Verein für unabhängige Gesundheitsberatung Europa (UGB), *UGB – Gesundheitsberatung unabhängig - kompetent – nachhaltig,* Available: www.ugb.de/exklusiv/fragen-service/ist-zitronensaeure-als-zusatzstoff-schaedlich/?zusatzstoff-zitronensaure, [05.08.2013], (2014)

[11] Onmeda - Für meine Gesundheit, Available: medikamente.onmeda.de/Wirkstoffe/Natriumcitrat/wirkung-medikamente-10.html, [18.04.2017], (2007)

[12] Gaffron, F. Available: https://energy-drink-magazin.de/2013/03/apfelsaure-e296-10549, [18.04.2016], (2013)

[13] Die Verbraucher Initiative e.V., *zusatzstoffe-online.de - Informationen zu Lebensmittelzusatzstoffen,* Available: http://www.zusatzstoffe-online.de/zusatzstoffe/92.e296_apfels%E4ure.html, [18.04.2017], (2013)

[14] Internationale Normung von Obst und, Gemüse, *Leitfaden zu objektiven Testmethoden zur Bestimmung der Qualität von Obst und Gemüse sowie Trocken- und getrockneten Erzeugnissen*, Organisation for Economic Co-Operation and Development, (2005)

[15] Senser, F., Scherz, H., Kirchhoff, E., *Lebensmitteltabelle für die Praxis, Der kleine Souci-Fachmann-Kraut*, Deutsche Forschungsanstalt für Lebensmittelchemie: Wissenschaftliche Verlagsgesellschaft mbH Stuttgart, (2004)

[16] Ebermann, R., Elmadfa, I., *Lehrbuch Lebensmittelchemie und Ernährung*, Springer, Wien, (2011)

[17] Ramallo, L., Mascheroni, R., *Quality evaluation of pineapple fruit during drying process,*" Food and Bioproducts Processing, **90**, (2012), 275–283

[18] EUROPEAN STANDARD EN 14130, *Lebensmittel - Bestimmung von Vitamin C mit HPLC*, Brüssel, (2003)

[19] R-BIOPHARM AG (Roche), *Sucrose/D-Glucose/D-Fructose UV method for the determination of sucrose, D-glucose and D-fructose in foodstuffs and other material*, Darmstadt

[20] Metrohm AG, Das Säulenprogramm - Die ganze Welt der Ionenchromatographie, Herisau, (2011)

[21] Schwedt, G., Schreiber, J., Taschenatlas der Lebensmittelchemie, 2nd edition, Wiley-VCH, Weinheim, (2005)

Salting kinetics, salt diffusivities and proximate composition in osmotically dehydrated Pirarucu muscle

Barretto, T.L.[a,b]; Betiol, L.F.L.[a]; Bellucci, E.R.B.[a]; Telis-Romero, J.[a]; Barretto, A.C.[a*]

[a] Department of Food Technology and Engineering, Institute of Biosciences, Humanities and Exact Sciences, São Paulo State University (UNESP), Rua Cristóvão Colombo, 2265, 15.054-000, São José do Rio Preto, SP, Brazil

[b] Federal Institute of São Paulo – IFSP, Campus Barretos, C-1 Avenue 250, Zip Code 14781-502 Barretos, São Paulo, Brazil

*E-mail of the corresponding author: andreasb@ibilce.unesp.br

Abstract

Pirarucu (Arapaima gigas Schinz) farming has been encouraged and, among meat preservation techniques, the salting process is a relatively simple and low-cost method. The objective of this work was to study the sodium chloride diffusion kinetics in Pirarucu during wet salting. Limited volumes of brine (20% w/w) were employed with wet salting assays carried at 3, 4 and 5 brine/muscle ratios, and brine temperatures of 10, 15 and 20 ᵒC. The analytical solution of Fick's second law considering one-dimensional diffusion through an infinite slab in contact with a well-stirred solution of limited volume was used to calculate the effective salt diffusion coefficients. Salt diffusivities in muscle were found to be in the range of 2.07 and 8.80 × 10⁻¹⁰ m²/s. The wet salting of Pirarucu is greatly influenced by temperature and by the brine/muscle ratio by volume.

Keywords: Pirarucu; Arapaima gigas Schinz; salt diffusion coefficients; brine.

1. Introduction

The pirarucu (*Arapaima gigas Schinz*) is one of the largest freshwater fish in the world, reaching approximately 2 to 3 meters in length and up to 200kg in weight in its natural habitat. The fish inhabits the Amazon River basin in South America and is one of the five most widely cultivated and marketed species in the region [1, 2, 3, 4]. It is economically and ecologically important to the riverside population due to its high commercial and nutritional value [3, 5]. Due to its great adaptability, high market value, good sensory characteristics, expressive size and rapid development, the pirarucu has been a focus of several studies, mainly in relation to its captive breeding [6].

The increase in the pirarucu farming in aquaculture production systems has highlighted the economic significance of this species in recent years, mainly due to its nutritional quality. However, its marketing and consumption throughout the year faces some barriers due to the many changes occurring in the product because of enzyme and microbiological activities, which can affect the flavor, odor, color and texture and lead to rapid deterioration, resulting in fish of lower quality [7, 8].

Studies on shelf-life of food products depend on the knowledge of internal and external characteristics that can affect the speed of deterioration, such as packaging technologies, storage conditions, formulation and conservationamong others [8]. Salting is one of the oldest food conservation processes [9, 10]. The concentration of sodium chloride influences the technological properties of the food, such as water retention capacity, viscosity, texture, emulsification, influences the properties of proteins and promotes sensory acceptance [11, 12].

Salting is a good alternative for producing processed food because it is a relatively simple, low-cost technique and can be carried out in places with little infrastructure. Brining is a specific process of osmotic dehydration that is conducted by immersing the product in concentrated saline solution [13]. In this operation, two main mass transfer processes occur. The water migrates from the meat to the brine and solutes from the brine transfer to the meat. Consequently, changes in the composition of solids produce a decrease in the amount of water available for degradation reactions by enzymes and microorganisms [14, 15].

The diffusion of salt in meats and meat products has been the objective of some studies [16]. Diffusion is an important mass transfer phenomenon, responsible for the transport of sodium and chloride [17]. The mass transfer between the brine and the product is usually controlled by the diffusion rate of the solutes. Diffusion rates are calculated using solution diffusion coefficients for solids [18]. Food and foodstuffs present irregular shapes and have regions of different compositions that make the mathematical modeling difficult and some alternatives should be considered to deal with the heterogeneity of materials [16, 19, 20].

Water loss and absorption of solids during osmotic dehydration have been modeled using Fick´s second law. Some studies use analytical solutions for transfer of one-dimensional mass based on laboratory studies carried out with a great excess of agitated solution, in order to ensure a variation in the composition of the solution and simplify the calculations involved [21]. To determine the effective diffusivity of salt in caiman meat, Romanelli & Felício [22] used the same approach. However, the management of large volumes of solution is an obstacle to the process at an industrial scale, leading to an increase in production costs.

The knowledge of the diffusion rates is important, as it allows the correct determination of the necessary processing time, having control over the exact final concentration of salt and its distribution in the product. Several articles have been published on mass transfer and diffusion of salt in meat and fish products [23, 24]. So, the aim of this study was to evaluate the proximate composition of the pirarucu raw material and investigate the sodium chloride diffusion kinetics in pirarucu muscle during wet salting.

2. Materials and Methods

This study focused on the sodium chloride diffusion in pirarucu muscle during the wet salting process using a limited volume of brine (20% w/w). The experiments were developed and done in the meat and meat products laboratory of the Department of Engineering and Food Technology of the Sao Paulo State University – UNESP-IBILCE.

The material used in this study consisted of a frozen Pirarucu fillets (*Arapaima gigas Schinz*) purchased from a single supplier, in a local supermarket in the city of Manaus (Brazil). The fillets were transported to UNESP-IBILCE (São José do Rio Preto, Brazil), stored under freezing and thawed under refrigeration temperature for 24 hours for evaluation of its physical characteristics, such as size and weight, and also the proximate composition, before salting. Moisture, ash and protein contents were determined according to the AOAC [25] method. The lipid content was determined, following the method described by Bligh & Dyer [26].

Sodium chloride solution was used as the osmotic agent. The sodium chloride used was of food grade, the other chemical compounds used for the determinations of sodium chloride, proteins and lipids were of analytical grade.

Experiments were carried out with a brine concentration of 20% (w/w), at temperatures of 10, 15 and 20 ºC and volume ratios of brine/muscle (V^L / V^S) of 3, 4 and 5.

Fillet densities before salting and at different periods after salting were measured according to the liquid displacement method [13]. Brine densities were measured by means of a pycnometer at 25 °C.

Fillets were weighed and placed inside flasks of 500 ml containing brine at a pre-determined volume, temperature and salt concentration. The flasks were then maintained in a refrigerated orbital agitator, being removed at different time intervals, when the brine was drained and weighed and the fillets were dried with absorbent paper, weighed and ground. Two aliquots for salt content, estimated as the ash contents in a muffle furnace at 550 °C. Two aliquots of brine were taken to measurethe salt content. The salt content was obtained according to the Mohr method [27].

The governing equation for the unsteady-state one-dimensional diffusion in a plane slab was given by Fick's second law, also called the diffusion equation, and the analytical solution of the stated problem was given by Crank [28] as:

$$\frac{M_t}{M_\infty} = 1 - \sum_{n=1}^{\infty} \frac{2\alpha(1+\alpha)}{1+\alpha+\alpha^2 q_n^2} \exp\left(\frac{-D_{eff} q_n^2 t}{L^2}\right) \tag{1}$$

where M_t is the total amount of solute in the solid at time t, M_∞ is the corresponding quantity at equilibrium, L is half of the slab thickness and q_n are the non zero positive roots of the equation

$$\tan q_n = -\alpha q_n \tag{2}$$

In order to adjust equation (1) to the experimental data and obtain the effective diffusivity values, parameters m, α, and qn were determined according to Telis et al. [13].

The effective diffusivities were obtained by a non-linear adjustment of the first six terms of the series corresponding to equation (1), which was performed using the Statistica software (StatSoft Inc., V.7.0).

3. Results and discussion

The proximate composition of Pirarucu muscle is shown in Table 1. Similar results were found by Martins et al. [29], when analyzing the proximal composition of pirarucu muscle.

Table 1. Proximal composition of the Pirarucu muscle (n=3).

	Proximate composition (%) (mean ± standard deviation)
Moisture	78.99 ± 0.07
Protein	20.30 ± 0.21
Lipid	0.41 ± 0.17
Ash	1.08 ± 0.07

The results for the effective diffusivity of salt at each temperature studied in the three brine/muscle ratios are shown in Table 2.

Table 2. Effective diffusivity at different brine/muscle ratios and temperatures during wet salting of Pirarucu.

Brine/muscle ratio	Temperature (ºC)	Effective diffusivity x 10^{10} (m^2/s)
3	20	8,79
	15	5,30
	10	2,07
4	20	8,67
	15	5,62
	10	2,77
5	20	8,80
	15	5,71
	10	3,17

Table 2 shows that the brine/muscle ratio has a low effect, since effective diffusivities were very similar for the different ratiosat the same temperatures. Similar behavior was observed by Medina-Vivanco et al. [30] when they studied tilapia muscle.

Effective diffusivities increased with increasing temperatures (Table 2) for all brine/muscle ratios. Similar results were observed by Telis et al. [13] who studied salting diffusivities in caiman muscle. Low temperatures are recommended because fish is a very perishable food. Brás & Costa [31] used salting temperatures from 12 ºC to 18 ºC for salting different fishes. According to Chiralt et al. [32], higher temperatures not only affect the rate of diffusion

phenomenon but also may affect the viscoelastic properties of the solid matrix, with a softening of the structure accompanying the temperature increase. An additional effect in salt gain rates could arise from the reduction in brine viscosity at higher temperatures.

Salted fish products have a long shelf life due to their low water activity and the flora selection that a high salt content media implies [31].

4. Conclusions

Salt effective diffusion coefficients are in the range from 2.07 to 8.80×10^{-10} m^2/s.

The wet salting process of pirarucu is great influenced by temperature: the higher the temperature in the wet salting process, the higher the effective diffusion coefficients; and, to a lesser extent, by the brine/muscle volume ratio though lower temperatures are better because fish is a perishable food.

5.   References

[1] Torres, F. F., Troncoso, O. P., Nakamatsu, J., Grande, C. J., & Gomez, C. M. (2008). Characterization of the nanocomposite laminate structure occurring in fish scales from Arapaima gigas. Materials Science and Engineering, 28(8), 1276-1283.

[2] Currey, J. D. (2010). Mechanical properties and adaptations of some less familiar bony tissues. Journal of the Mechanical Behavior of Biomedical Materials, 3(5), 357-372.

[3] Castello, L. (2008). Nesting habitat of pirarucu Arapaima gigas in floodplains of the Amazon. Journal of Fish Biology, 72, 1520-1528.

[4] Watson, L. C., Stewart, D. J., & Teece, M. A. (2013) Trophic ecology of Arapaima in Guyana: giant omnivores in Neotropical floodplains. Neotrop Ichthyol, 11, 341–349.

[5] Castello, L., Stewart, D. J., & Arantes, C. C. (2011). Modeling population dynamics and conservation of arapaima in the Amazon. Reviews in Fish Biology and Fisheries, 21(3), 621-640.

[6] Cavero, B. A. S., Pereira-filho, M., Roubach, R., Ituassú, D.R., Gandra, A.L., & Crescêncio, R. (2003). Efeito da densidade de estocagem na eficiência alimentar de juvenis de pirarucu (Arapaima gigas) em ambiente confinado, Acta Amazonica, 33 (4), 631-636.

[7] Baslar, M., Kılıc-lı M., & Yalınkılıc, B. (2015). Dehydration kinetics of salmon and trout fillets using ultrasonic vacuum drying as a novel technique. Ultrason Sonochemistrym, 27, 495–502.

[8] Teodoro, A. J., De Andrade, E. C. B., & Mano, S. B. (2007). Avaliação da utilização de embalagem em atmosfera modificada sobre a conservação de sardinhas (Sardinella brasiliensis), Ciência e Tecnologia de Alimentos, 27 (1), 158-161.

[9] Albarracín W., Sánchez, I. C., Grau, R. & Barat, J. M. (2011). Salt in food processing;

usage and reduction: a review, International Journal of Food Science and Technology, 46 (7), 1329-1336.

[10] Nguyen. M. V., Thorarinsdottir, K. A., Gudmundsdottir, A., Thorkelsson, G., & Arason, S. (2011). The effects of salt concentration on conformational changes in cod (Gadus morhua) proteins during brine salting, Journal of Food Chemistry, 125(3), 1013-1019.

[11] Costa-Corredor, A., Muñoz, I., Arnau, J., & GouIon, P. (2010). Uptakes and diffusivities in pork meat brine-salted with NaCl and K-lactate, LWT - Food Science and Technology, 43 (8), 1226-1233.

[12] Nguyen, M. V., Arason, S., Thorarinsdottir, K. A., & Thorkelsson, G. A. (2010). Influence of salt concentration on the salting kinetics of cod loin (Gadus morhua) during brine salting, Journal of Food Engineering, 100(2), 225-231.

[13] Telis, V. R. N., Romanelli, P. F., Gabas, A. L., & Telis-Romero, J. (2003). Salting kinetics and salt diffusivities in farmed Pantanal caiman muscle, Pesquisa Agropecuária Brasileira, 38(4), 529-535.

[14] Sabadini, E., Carvalho, B. C., Sobral, P., & Hubinger, M. D. (1998). Mass transfer and diffusion coefficient determination in the wet and dry salting of meat, Drying Technology, 16 (9/10), 2095-2115.

[15] Barat, J. M., Grau, R., Ibáñez, J. B., Pagan-Moreno, M. J., Flores, M., & Toldrá, F. (2006). Accelerated processing of dry-cured ham. Part I. Viability of the use of brine thawing/salting operation Meat Science, 72 (4), 757-765.

[16] Graiver, N., Pinotti, A., Califano, A., & Zaritzky, N. (2009). Mathematical modeling of the uptake of curing salts in pork meat, Journal of Food Engineering, 95(4), 533-540.

[17] Barat, J. M., Rodríguez-Barona, S., Andrés, A., & Fito, P. (2003). Cod salting manufacturing analysis, Food Research International, 36(5), 447-453.

[18] Floury J., Rouaud, O., Le Poullennec, M., & Famelart, M. H. (2009). Reducing salt level in food: Part 2. Modelling salt diffusion in model cheese systems with regards to their composition, LWT Food Science and Technology, 42(10),1621-1628.

[19] Alizadeh, E., Chapleau, N., de-Lamballerie, M., & Le-Bail, A. (2009). Impact of freezing process on salt diffusivity of seafood: application to salmon (Salmo salar) using conventional and pressure shift freezing, Food Bioproccess Technology, 2(3), 257-262.

[20] Aursand, I.G., Veliyulin, E., Böcker, U., Ofstad, R., Rustad, T., & Erikson, U. (2008). Water and salt distribution in Atlantic Salmon (Salmo salar) studied by low-field 1H NMR, 1H and 23Na MRI and light microscopy: effects of raw material quality and brine salting J.Agric. Food Chem., 57(1), 46-54.

[21] Raoult-wack, A. L. (1994). Recent advances in the osmotic dehydration of foods. Trends in Food Science and Technology, Oxford, 5, 255-260.

[22] Romanelli, P. F., & Felício, P. E. (1995). Estudo da salga da carne de jacaré do Pantanal Caiman crocodilus yacare (Daudin, 1802) (Reptilia-Crocodilia). Ciência e Tecnologia de Alimentos, 15(3), 251-254.

[23] Martins, M. G., Martins, D. E. G., & Pena, R. S. (2015). Drying kinetics and hygroscopic behavior of pirarucu (Arapaima gigas) fillet with different salt contents, LWT Food science and Technology, 62(1), 144-151.

[24] Andreeta-Gorelkina, I. V., Gorelkin, I. V., & Rustad, T. (2016). Determination of apparent diffusion coefficient in balls made from haddock mince during brining, Journal of Food Engineering, 175, 8-14.

[25] Association of Official Analytical Chemists. (2007). Official Methods of Analysis. 18ed. Horwitz, W. (Ed.) Washington, DC, Revisão 2.

[26] Bligh, E. G.; Dyer, W. J. (1959). A rapid method for total lipid extraction and purification. Canadian Journal of Biochemistry and Physiology, 37, 911-917.

[27] James, C.S. (1995). Analytical chemistry of foods. Glasgow: Blackie Academic & Professional, 177 p.

[28] Crank, J. (1975). The mathematics of diffusion. 2nd ed. Oxford: Clarendon, 414p.

[29] Martins, M. G., Martins, D. E. G., Pena, R. S. (2017). Chemical composition of different muscle zones in pirarucu (Arapaima gigas). Food Science and Technology, 37(4), 651-656.

[30] Medina-Vivanco, M.; Sobral, P.J.A.; Hubinger, M.D. Mass transfer during dewatering and salting of tilapia for different volume brine to fillets ratios. In: International Drying Symposium, 11., 1998, Halkidiki, Proceedings of the 11th International Drying Symposium, Thessaloniki: Mujumdar, A.S. (Ziti Publishing Company), 1998. v.A, p.852-859.

[31] Brás, A.; Costa, R. (2010). Influence of brine salting prior to pickle salting in the manufacturing of various salted-dried fish species. Journal of Food Engineering, 100, 490-495.

[32] Chiralt, A.; Fito, P.; Barat, J.M.; Andrés, A.; González-Martínez, C.; Escriche, I.; Camacho, M.M. (2001). Use of vacuum impregnation in food salting process. Journal of Food Engineering, 49, 141-151.

Influence of fat level reduction in the drying of Italian salami

Bis-Souza, C. V.[a]; Pollonio, M.A.R.[b], Penna, A.L.P.[a], Barretto, A. C. S.[a*]

[a] Department of Food Technology and Enginneering. UNESP- São Paulo State University, São José do Rio Preto, SP, Brazil.
B Department of Food technology, UNICAMP – University of Campinas, Campinas, SP, Brazil.

*E-mail of the corresponding author: andreasb@ibilce.unesp.br

Abstract

The aim of this study was to evaluate the influence of fat reduction in the drying process of Italian salami. Two Italian salami formulations: HFS (High Fat Sausage) with 20g/100g of pork back fat and LFS (Low Fat Sausage) with 11.2g/100g of pork back fat were analyzed as water activity, weight loss, proximate composition and pH. The evaluation times were 0, 3, 7, 10 and 13 days of drying.The reduction of more than 25% in the fat content of Italian salami affected the weight loss in the drying process, but did not affect the moisture, pH and water activity.

Keywords: Low-fat; fermented sausage; weight loss; healthier meat products; ripening time.

1. Introduction

Currently, there is an increase in consumer demand for healthier food products that have low calorie and low fat content. Because of this trend, the meat product manufacturers are seeking to develop new formulations of tradicional products, reducing fat content and using fat substitut on the aim of producing healthier meat products [1].

The high fat content in fermented sausages contributes to the sensory characteristics, such as taste, texture, juiciness, mouthfeel, lubricity and appearance, and its reduction can directly affect the acceptability of the product [2, 3]. However, there is an association between excessive consumption of saturated fat and increased risk of heart disease and some cancers [4, 5].

The drying stage of the fermented sausage represents an important factor for determining the physicochemical and sensorial properties of the final product. The duration of the drying step of the sausage is related to the diameter. This stage of the process should always be performed at temperatures, between 12°C and 15°C. The sausage can lose up to 40% of its weight during the drying and this loss must be gradual to avoid deformation of the final product [6].

Fat reduction in dry fermented sausages is one of the most difficult because the excessive reduction of fat can leads to harder products and can increase the weight loss. But according to Olivares et al [2], those defects can be avoided if appropriate processing and climatic conditions of the drying process are applied correctly. So, the aim of this study was to evaluate the influence of fat reduction level on the drying process of Italian type salami.

2. Materials and Methods

2.1. Italian type Salami drying process

The samples were manufactured in the Laboratory of Meat and Derivatives at the Faculty of Food Engineering, University of Campinas (São Paulo, Brazil). Two levels of pork back fat were added in the Italian type salami formulation: HFS (High Fat Sausage) with 20g/100g of pork back fat added and 80g/100g of lean pork / LFC (Low Fat Sausage) with 11.2g/100g of pork back fat added and 88g/100g of lean pork. The other ingredients of the formulation were: sucrose (2g/100g), sodium chloride (2.5g/100g), sodium erythorbate (0.5g/100g), sodium nitrite (0.015g/100g), sodium nitrate (0.015g/100g), white pepper (0.5g/100g), garlic (0.2g/100g), nutmeg (0.2g/100g) and a starter culture (0.25 g/kg; SPX Floracarn, Chr Hansen).

All ingredients were mixed with the raw material using a blender for approximately 5 minutes. After, the treatments were stuffed in cellulose cases (diameter of 50 mm) and they were cut into pieces 15 cm in length. For each treatment 25 pieces (approximately 250 g

each) were made and each sample was soaked in a solution of potassium sorbate (20%). The temperature ad relative humidity parameters (T ºC/RH %) were: 25 ºC/95% (first day), 24 ºC/93% (second day), 23 ºC/91% (third day), 22 ºC/89% (fourth day), 21 ºC/87% (fifth day), 20 ºC/85% (sixth day), 18 ºC/85% (seventh day), 15 ºC/75% (until the end of ripening process). The air velocity during all the process was 0.5 m/s. The processing was performed twice.

2.2. Ripening analysis

Water activity was measured in triplicate using Aqualab Decagon equipment (Decagon Devices Inc., Pullman, USA).

The moisture, ash and protein content quantification was performed according to AOAC [7]. Fat content was measured using the Bligh & Dyer method [8]. This analysis was performed in triplicate.

The pH was measured using a digital pH meter with penetration probe, in triplicate, in the same piece of salami.

To calculate the weight loss, the same samples were weighed throughout the drying process and the loss was determined by the difference calculation between the initial weight and the final weight (n=5).

2.3. Statistical analysis

The data obtained were analyzed by analysis of variance (ANOVA), and the differences between the means of the results were evaluated by the Fisher test ($P \leq 0.05$) at a significance level of 5%. The software used was MiniTab 16.

3. Results and discussion

3.1. Proximate composition

The moisture content of Italian type salami was different between batches only after the drying process (Table 1).

Table 1. Proximate composition of Italian type salami high fat content (HFS) and low fat content (LFS) after 0 and 13 days of dry process.

Analysis	Days of drying	HFS	LFS	SEM[1]	*p value*
Moisture (%)	*0*	65.17[A]	64.13[A]	0.245	*0.066*
	13	32.20[B]	39.10[A]	0.770	*0.012**
Fat (%)	*0*	13.5[A]	10.21[B]	0.488	*0.02**
	13	30.44[A]	22.80[B]	0.772	*0.01**
Ash (%)	*0*	3.61[A]	3.47[A]	0.071	0.182
	13	5.35[A]	5.85[A]	0.412	0.349
Protein (%)	*0*	15.56[B]	18.60[A]	0.352	*0.013**
	13	26.14[A]	28.94[A]	0.956	0.075

[AB]Different letters in the same line differ significantly ($P < 0.05$) by the Fisher's test. *Significant.
[1]SEM: Standart error of the mean.

LFS had higher moisture content because of the fat reduction. Similar results were reported by Olivares et al [2] that manufacture dry sausage using different pork back fat content and the lowest (13.2%) had the highest moisture at the end of the dryng process.

The results for ash and protein did not show differences at the end of the drying process. The reduction of fat level achieved was approximately 25%. So, it is possible to classify this product as an Italian type Salami with reduced saturated fat content (light), according to the corresponding legislation [9].

2.2. Ripening analysis

The results for the water acttivity, pH and weight loss during the drying proceso of salami type Italian are presented in Figure 1.
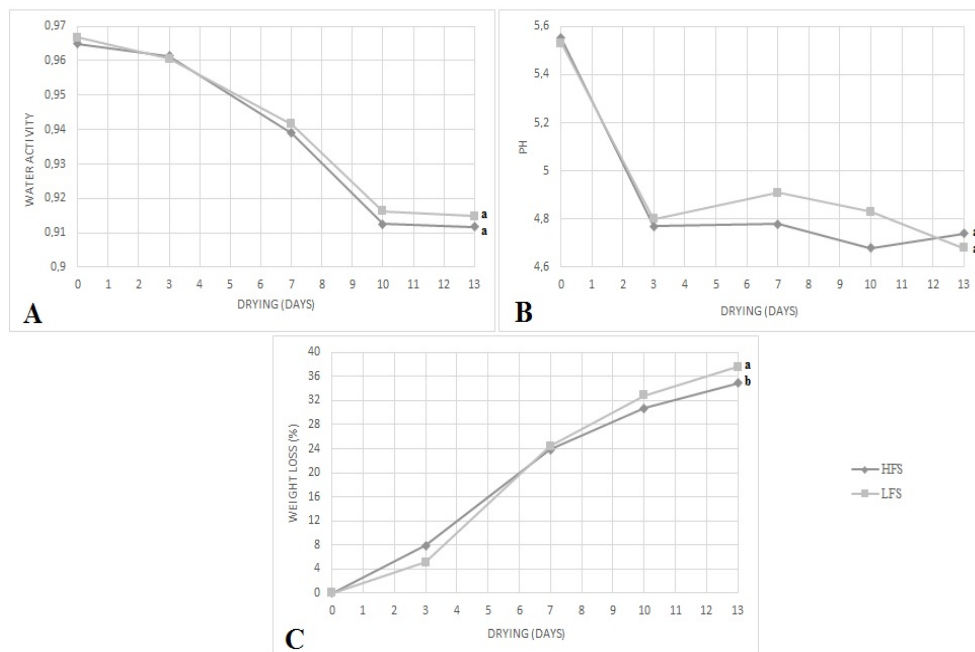
Fig. 1. Evolution of water actitvy (A), pH (B) and weight loss (C) during the drying process of Italian type salami.

[a,b]Different letters in the graphic differ significantly ($P < 0.05$) by the Fisher's test

The water activity (Fig.1A) of the treatments was reduced during processing (13 days), starting at 0.96 and reducing to 0.9. The high fat sausage (HFS) didn't show difference wáter activity from the low fat sausage (LFS) at the end of the drying processing. So the reduction in the pork fat of Italian type salami did not affect this technological parameter. This result is in agreement with Fonseca et al [10] that reported that the reduction in fat content (10%, 20% and 30% fat) in fermented dry salsichon had no significant effect on the water activity of the final product.

The initial pH (Fig.1B) of the batch was 5.6. After 3 days of processing, the pH value was near 4.6 for all treatments, indicating that micro-organisms present in the fermenting starter culture produced lactic acid from the sugars present in the formulation, reducing the pH. Othes authors also reported a significant reduction of pH from day 0 to day 3 in the production of fermented sausage [11, 12].

To ensure the loss of water during the drying process, the pH should reach values close to the isoelectric point of the meat (pH 5.0). According to Price and Schiweigert [13] acidification contributes to the texture of the product, as well as in the formation of

aromatic compounds and the typical salami flavor. This rapid drop in pH value, close to 4.6 ensures product stability and provides microbiological protection against gram negative bacteria. The reduction in the pork fat content did not affect the pH value during the drying of the fermented sausage.

HFS showed the lowest (p>0.05) weight loss (Fig.1.C) (%) compared to the other treatments (LFS), showing that fat level may influence yield. This result is in agreement with the results presented by Ham et al [14], who observed that the fermented salami with fat reduction had the lowest yield when compared to the control treatment (with no reduction in fat content).

4. Conclusions

The reduction of 25% in the fat content of Italian type salami can be used to produce a healthier dry fermented meat product without affected the technological parametrs such as moisture, pH and water activity durind the drying process.

5. References

[1] Menegas, L. Z.; Pimentel, T. C.; Garcia, S.; Prudencio, S. H. Dry-fermented chicken sausage produced with inulin and corn oil: Physicochemical, microbiological, and textural characteristics and acceptability during storage. Meat Science 2014, 93 (3), 501-506.

[2] Olivares, A.; Nnavarro, J. L.; Salvados, A.; Flores, M. Sensory acceptability of slow fermented sausages based on fat content and ripening time. Meat Science 2010, 86 (2), 251-257.

[3] Lorenzo, J. M.; Franco, D. Fat effect on physico-chemical, microbial and textural changes trough the manufactured of dry-cured foal sausages Lipolysis, proteolysis and sensory properties. Meat science, 2012, 92 (4), 704-714.

[4] Afshari, R.; Hosseini, H.; Mousavi Khaneghah, A.; Khaksar, R. Physico-chemical properties of functional low-fat beef burgers: Fatty acid profile modification. LWT - Food Science and Technology 2017, 78(1), 325–331

[5] Han, M.; Bertram, H. C. Designing healthier comminuted meat products: Effect of dietary fibers on water distribution and texture of a fat-reduced meat model system. Meat Science 2017, 133(1), 159-165.

[6] Rech, R. A. Produção de salame tipo italiano com teor de sódio reduzido. Masters dissertation, Federal University of Santa Maria, 2010.

[7] AOAC. Official Methods of Analysis of AOAC International. Association of Official Analysis Chemists International, 2007.

[8] Bligh, E. G.; Dyer, W. J. A rapid method of total lipid extraction and purification. Canadian Journal of Biochemistry and Physiology 1959, 37(8), 911–917.

[9] BRASIL, Ministry of Health. National Health Surveillance Agency (ANVISA) Resolution - RDC No. 54 of November 12, 2012. Technical Regulation on complementary Nutrition Information. http://portal.anvisa.gov.br/documents/%2033880/2568070/rdc0054_12_11_2012.pdf/c5ac23fd-974e-4f2c-9fbc-48f7e0a31864 (accessed Nov 08, 2017).

[10] Fonseca, S.; Gómez, M.; Dominguez, R.; Lorenzo, J. M. Physicochemical and sensory properties of Celta dry-ripened " salchichón" as affected by fat content. Grasas Y Aceites 2015, 66(1), e059.

[11] Bagdatli, A.; Kundakci, A. Optimization of compositional and structural properties in probiotic sausage production. Journal of Food Science and Technology 2016, 53(3), 1679-1689.

[12] Park, W.; Kim, J. H.; Ju, M. G.; Hong, G. E.; Yeon, S. J. Enhancing quality characteristics of salami sausages formulated with whole buckheat flour during storage. Journal of Food Science and Technology 2017, 54 (2), 326, 332.

[13] Price, J. F.; Schweigert, B. S. Ciencia de la Carne y de los Productos Carnicos. 2. ed., Zaragoza: Acribia, 1994. 581 p.

[14] Ham, Y. K.; Hwang, K. E.; Kim, H. W.; Song, D. H.; Kim, Y. J.; Choi, Y. S.; Kim, C. J. Effects of fat replacement with a mixture of collagen and dietary fibre on small calibre fermented sausages. International Journal of Food Science and Technology 2016, 51(1), 96–104.

Process of parboiling rice by microwave-assisted hot air fluidized bed technique

Prachayawarakorn, S.[a*]; Saniso, E.[b]; Swasdisewi, T.[c]; Soponronnarit, S.[d.]

[a]Department of Chemical Engineering. Faculty of Engineering. King Mongkut's University of Technology Thonburi, 126 Pracha-Uthid Road, Bang Mod, Thung khru, Bangkok 10140, Thailand.

[b]Division of Physics, Faculty of Science Technology and Agriculture, Yala Rajabhat University, 133 Tesaban Road 3, Amphur Muang, Yala 95000, Thailand.

[c]Division of Thermal Technology, School of Energy, Environment and Materials, King Mongkut's University of Technology Thonburi, 126 Pracha-Uthid Road, Bang Mod, Thung khru, Bangkok 10140, Thailand.

[d]Division of Energy Technology, School of Energy, Environment and Materials, King Mongkut's University of Technology Thonburi, 126 Pracha-Uthid Road, Bang Mod, Thung khru, Bangkok 10140, Thailand.

*E-mail of the corresponding author: somkiat.pra@kmutt.ac.th

Abstract

In this work the new process of producing parboiled rice (PB) by combinatintion of microwave and hot air fluidized bed (MWFB) was proposed and investigated. Results showed that the drying time was shorter with smaller bed depth, higher drying temperature and higher microwave power. The initial grain temperature, drying temperature, bed depth and microwave power strongly affected the gelatinization of rice starch. The PB produced by MWFB caused a very small broken kernel (1-2%). The whiteness was decreased with increase in drying time, initial grain temperature, drying temperature and microwave power. The specific energy consumption was increased with increasing such operating parameters.

Keywords: Drying; Parboiled rice; Fluidized bed; Microwave.

1. Introduction

PB producion in the industrial scale around the world can normally be done by wet-heat process. This process mainly consists of soaking, steaming and drying step. In the steaming step, the saturated steam, normally produced by high pressure boiler, is used to gelatinize the rice starch [1]. After steming, the rice starch appears translucance. In addition to the wet heat process, the dry heat process is also used in a small scale factory. By the dry-heat process, hot air or roasting with or without sand is practicall utilized. The later process involves conduction heating of moisten paddy at a higher temperature with shorter drying duration. The starch gelatinization with no retrogradation is specifically found, unlike to the wet heat process, because of the simultaneous rapid loss of water from the paddy during conduction heating was studied by Mahanta and Bhattachaya [2]. Pillaiyar et al. [3] reported that the roasting sand at temperature of 125°C could get the fully PB but with mild effect. The parboiling became severe at high temperatures. Roasting the soaked paddy at 250°C could reduce the cooking time of the PB. A sand temperature of 125-150°C is considered as suitable condition for producing PB by this technique

The wet-heat PB production requires many components such as the boiler, steam pipe and auxiliary devices, while the dry-heat PB process using sand roasting [4] needs to separate the paddy-sand mixture after parboiling. To eliminate the restrictions on the steaming and sand separation in PB production, the MWFB was proposed and investigated. The microwave (MW) drying has been studied by many researchers and applied with many products. But, the work involing with parboiling rice is still limited in the literature. It appears only work reported by Kahyaoglu et al. [5] for parboiling wheat using MW-assisted spouted bed drying. They found that the MW-assisted spouted bed drying at the MW power of 3.5 and 7.5 W/g reduced drying time by at least 60% and 85%, respectively compared to spouted bed drying. As mentioned above, in this work, the new process of producing PB by MWFB was proposed and investigated. In the experiment, the drying kinetics and quality of head rice yield (HRY), the degree of starch gelatinization (DSG), morphology, whiteness value and specific energy consumption (SEC) were investigated.

2. Materials and Methods

2.1. Materials

The Suphanburi 1 paddy variety was stored at ambient air temperature for 6 months. Paddy was soaked at the temperature of 69±1°C for 5 h (47±1% d.b.) and different initial grain temperatures of 32, 55 and 65°C was dried by MWFB and FB dryers.

2.2. MWFB dryer

Fig. 1 shows the MWFB dryer. The system consists of a stainless steel cylindrical drying chamber with an inner diameter of 21 cm and height of 80 cm, a 19 kW electric heaters, a backward-curved blade centrifugal fan driven by a 2.2 kW (3 HP) motor and 5 MW magnetrons with each rated at 800 W (2.45 GHz). The magnetrons were installed at 5.5, 11.5, 17.5, 23.5 and 30.0 cm above distributor plate of the drying chamber.
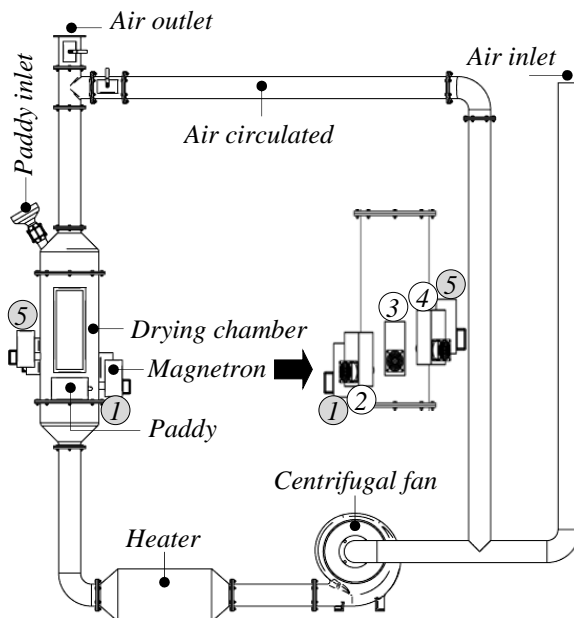
Fig. 1 A schematic diagram of a MWFB dryer.

2.3. Experimental design

The soaked paddy was dried by MWFB and FB at temperatures of 130, 150 and 170°C with a MW power of 1.6, 2.4 and 4.0 kW. Bed depth of 5 and 10 cm, as well as an inlet superficial air velocity of 4.6 m/s and recycled exhaust air fraction of 0.8 were used. After reaching predetermined drying time, the paddy was taken out from the dryer and the samples were gently dried in shade to obtain a final moisture content of 15±1% d.b. The experiment was performed in duplication. The MC of paddy was determined acording to AACC 1995 [6] method at a temperature of 103±2°C for 72 h. It was done in triplicate and the mean value was reported.

The dried paddy sample (150±1 g) was dehusked using a rubber roll hulling machine (Ngeksenghuat, model P-1, Thailand) and milled rice to remove bran using a miller (Ngeksenghuat, model K-1, Thailand). Whole and broken grains were graded automatically using a cylindrical rice separator (Ngeksenghuat, model I-1, Thailand). The milling test was performed in duplicate and the HRY was calculated by the following equation.

$$\%HRY \quad = \quad \frac{W_{hr}}{W_p} \times 100 \qquad (1)$$

where W_{hr} is mass of head rice sample (g) and W_p is mass of paddy sample (g).

The DSG of the rice samples was characterized by the Differential Scanning Calorimeter (DSC) (Perkin Elmer, model DSC-7, USA). A sample was ground into powder and 3 mg rice flour sample was put into an aluminium pan and mixed with 10 mL distilled water. The pan was sealed and kept to equilibrate at room temperature for 1 h. After that, the sample was heated from 40 to 110°C at a scanning rate of 10°C/min. The determinations were done duplication and the DSG was calculated by the following equation.

$$\%DSG = \left[1 - \frac{\Delta H}{\Delta H_C}\right] \times 100 \tag{2}$$

where ΔH is the enthalpy change of starch in dried rice (J/g dry matter) and ΔH_c is the enthalpy change of reference rice starch (J/g dry matter).

The scanning electron microscope (SEM) (JEOL, model JSM-6610LV, Japan) with accelerating voltage 5 kV was used to examine the starch granules morphology. Before test, the sample was attached to an SEM stub and coated by sputter coater (Cressington, model 108 Auto, UK) with a pure copper 99.99% layer. While, the whiteness of rice samples was determined by a Kett digital whiteness meter (model C-300, Japan). Before measuring, the whiteness meter was calibrated with a white colored reference that has a standard value of 86.3. Each measurement was performed in 10 replicates and the mean value was reported.

3. Results and Discussion

3.1 Drying characteristics

The experimental results showed that the bed depth of 5 cm, the grain temperature was significantly higher than that at the bed depth of 10 cm approximated by 5-15°C. With the MWFB drying, it could reduce MC faster than the FB drying by approximately 2-5% d.b. When the grain gets the MW, the water molecules are rapidly rotated by MW frequencies (2.45 GHz). The heat is rapidly generated, especially in the middle of the paddy grain. As a result, the grain temperature in the MWFB was significantly higher than that of FB about 5-10°C. The higher grain temperature in the MWFB can accelerate the travel of moisture from the inside to the external, resulting in higher rate of drying [8].

At the same time, the drying time to reach an intermediate MC of 20±2% d.b. was shorter with smaller bed depth, higher drying temperature and higher MW power, as shown in Fig. 2(a). Considering the effect of initial grain temperature as shown in Fig. 2(b), the drying rate for the grain temperature of the paddy sample that had higher initial grain temperature was insignificantly different from that of the sample with lower initial grain temperature although the grain temperature at higher intial grain temperature was higher during drying. This is possibly due to the fact that the moisture movement during drying might be in the liquid form and controlled by liquid diffusion. In the liquid diffusion, the variation of temperature between 32 and 65°C does not provide a big difference of effective diffusion coefficient of water (only 1-2% d.b. moisture difference).
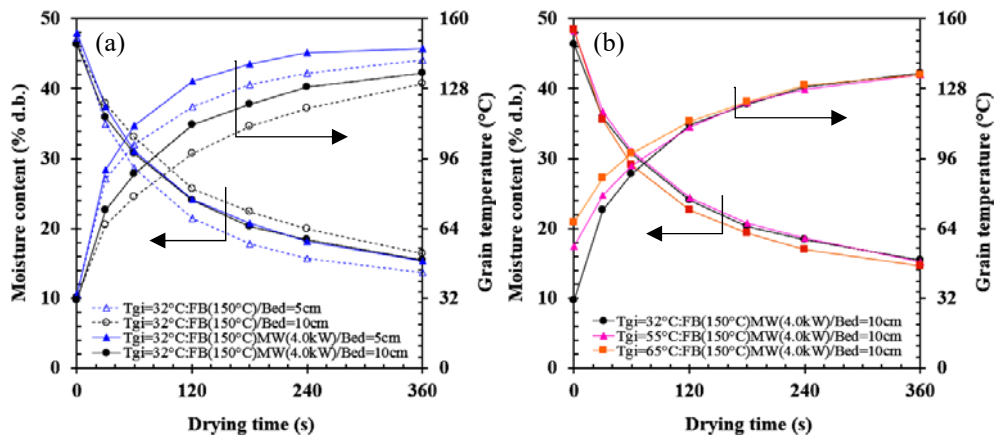
Fig. 2   Evalution of MC and grain temperature of soaked paddy dried by FB and MWFB.

Tgi=32°C/FB(150°C)/DSG=56%

Tgi=32°C/FB(150°C)MW(4.0kW)/DSG=85%

Tgi=32°C/FB(170°C)MW(2.4kW)/DSG=70%

Tgi=55°C/FB(170°C)MW(2.4kW)/DSG=96%
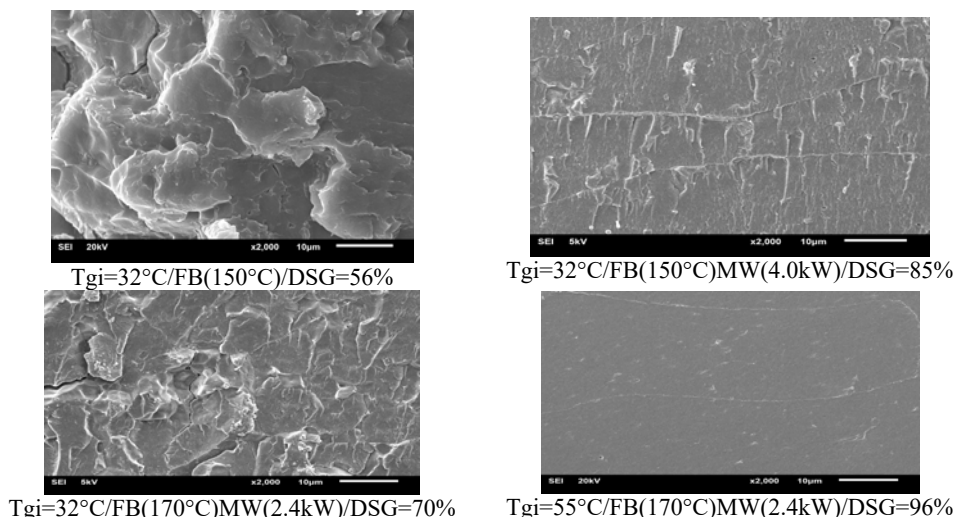
Fig. 3   SEM images at the interior area of soaked paddy dried by FB and MWFB (Bed=10 cm)

3.2   Degree of starch gelatinization

The use of FB drying at the temperature of 130-170°C allowed starch to be gelatinized in a range of 41-65% for initial grain temperatures of 32°C and 10 cm bed depth. At this DSG range, the PB is classified as the mildly PB [8] and the kernel that appeared white belly was not found although the starch gelatinization was incomplete. As the soaked paddy was dried at the bed depth of 5 cm, the rice starch was gelatinized in a range of 48-100%, depending on the drying temperature. The FB drying at 170°C could produce the severely PB.

As the MW(4.0kW) was combined with FB, the PB dried at the temperature of 150°C or higher was designated as severely PB. The complete gelatinization of rice starch was found

with the soaked paddy dried by FB(170°C)MW(4.0kW), FB(150°C)MW(4.0kW), FB(170°C)MW(2.4kW) when the initial grain temperatures of 32, 65 and 65°C, respectively, was employed at the bed depth of 10 cm. Also the soaked paddy dried by FB(170°C) and FB(170°C)MW(4.0kW) at initial grain temperature of 32°C and bed depth of 5 cm had complete gelatinization of rice starch as shown in Table 1.

3.3 Morphology

Fig. 3 show the starch granules of the soaked paddy dried by FB(150°C) and MW(4.0 kW)FB(150°C) with initial grain temperature of 32°C, it seem that some starch granules still appeared at the interior of the rice kernel when the soaked paddy dried by FB only whereas the starch granules of the soaked paddy dried by MWFB were smooth with the complete loss of granular morphology of the rice.

In case of soaked paddy at the initial grain temperatures of 32 and 55°C dried by MW(2.4 kW)FB(170°C), some starch granules still appeared at the at the interior of the rice kernel when the soaked paddy dried at initial grain temperature of 32°C whereas the starch granules of the soaked paddy dried at initial grain temperature of 55°C were smoothest with the complete loss of granular morphology of the rice, indicating the complete starch gelatinization. This is consistent with the result of degree of starch gelatinization.

3.4 Head rice yield

Table 1 shows the HRY of PB produced by MWFB yielded a very small broken kernel (1-2%) after drying with including tempering at the drying temperature above 130°C for MW powers of 2.4 and 4.0 kW. The small broken kernel can be attributed to the higher DSG. Hiowever, considering the initial grain temperature effect, this parameter did not much effect on the HRY, the value laying between 68 and 70%. However, the operation of MW(4.0 kW)FB(170°C) must be avoided although the starch gelatinization was completed. This is because the grain temperature dried at this condition was raised to 150°C causing the grains to be puffed and resulting lower HRY.

3.5 Colour

The whiteness value of PB was decreased with increase in initial grain temperature, drying temperature and MW power and with decreasing bed depth as shown in Table 1 for both tempering and no tempering. The whiteness value of MWFB drying was significantly lower than that of FB drying at the same initial grain temperature, drying temperature and MW power because the paddy grain temperature in the MWFB drying is higher than that of FB drying. The higher grain temperature time more accelerates a higher rate of Maillard reaction [9]. The PB samples that falled in the severely PB category (DSG>70) had yellowish brown colour (Gold parboiled rice), which corresponded to the whitness value of 22-24. When the soaked paddy was dried by at 170°C, MW power of 4.0 kW and at a bed depth of 5 cm, the product colour was reddish, which was unacceptable in the market.

3.6 Specific energy consumption

Considering in Table 1, it was found that drying the soaked paddy at the initial grain temperature 32°C at 170°C and at bed depth of 5 cm spent the SEC of 4.6 MJ/kg$_{water\ evap.}$

Table 1. DSG, HRY, SEC and whiteness of soaked paddy dryied by FB and MWFB.

Drying conditions		DSG (%)	HRY (%)		Whiteness		SEC (MJ/kg$_{water}$ evap.)
			T	NT	T	NT	
Bed = 10 cm	*Initial grain temperature of 32°C*						
	FB(130°C)	41.1	68.8	64.3	27.3	31.6	-
	FB(150°C)	55.6	69.4	65.4	25.1	29.5	-
	FB(170°C)	65.5	71.3	70.0	25.8	31.0	-
	FB(130°C)MW(4.0kW)	60.5	69.7	65.6	25.2	28.5	-
	FB(150°C)MW(4.0kW)	85.2	69.2	67.3	21.9	25.7	10.1
	FB(170°C)MW(2.4kW)	69.7	70.1	68.1	23.3	21.5	-
	FB(170°C)MW(4.0kW)	100.0	71.9	70.5	23.3	26.4	7.6
	Initial grain temperature of 55°C						
	FB(150°C)MW(4.0kW)	94.3	69.9	67.8	21.1	25.6	10.1
	FB(170°C)MW(1.6kW)	85.9	69.8	67.9	23.9	25.2	-
	FB(170°C)MW(2.4kW)	95.8	70.6	68.8	21.0	26.5	5.1
	Initial grain temperature of 65°C						
	FB(170°C)	83.9	69.5	66.5	24.4	29.2	-
	FB(130°C)MW(4.0kW)	70.6	68.5	65.6	24.3	27.3	-
	FB(150°C)MW(2.4kW)	72.8	69.8	67.3	20.3	24.9	-
	FB(150°C)MW(4.0kW)	100.0	70.4	67.5	21.0	23.1	10.0
	FB(170°C)MW(1.6kW)	92.9	69.6	67.7	21.3	23.5	-
	FB(170°C)MW(2.4kW)	100.0	70.5	68.9	20.3	22.8	5.1
Bed = 5 cm	*Initial grain temperature of 32°C*						
	FB(130°C)	48.6	69.7	65.5	24.0	25.6	-
	FB(150°C)	80.4	71.5	69.7	21.1	24.3	-
	FB(170°C)	100.0	69.2	68.4	16.4	22.9	4.6
	FB(130°C)MW(4.0kW)	70.2	68.9	65.5	18.7	23.2	-
	FB(150°C)MW(4.0kW)	91.2	70.6	69.8	17.8	23.5	-
	FB(170°C)MW(4.0kW)	100.0	65.6	59.4	12.5	17.8	10.8
Traditional method		100.0	70.0-71.5		21.5-26.2		6.4-7.5
Raw rice		0.0	-	50.3	-	45.2	-
Soaked rice		7.8	-	52.8	-	37.0	-

Bed = Bed depth, T = Tempering, NT = No tempering

This SEC was significantly lower than that dried by FB(170°C)MW(4.0kW) by 57% and less than the SEC from the traditional PB production by 32%. The use of higher initial grain

temperature (65ºC) could reduce the MW power to 2.4 kW and the SEC was reduced by 27% as compared to the traditional method

4. Conclusions

The MWFB could produce PB with a complete degree of starch gelatinization without the need of steam for parboiling rice. This makes it easier to produce PB and reduces the complexity and size of the plant. The production of PB with FB(170ºC) alone at initial grain temperature of 32ºC and bed depth of 5 cm have lower SEC than the traditional PB production by 32%. The increasing initial grain temperature up to 55 and 65°C for soaked paddy dried by FB(170ºC)MW(2.4kW) at the bed depth of 10 cm could reduce the SEC in the production of PB by 27% as compared to the traditional method.

5. Acknowledgements

5. References

[1] Bhattachaya, S. Kinetics on colour changes in rice due to parboiling. Journal of Food Engineering 1996, 29(1), 99-106.

[2] Mahanta, C.L.; Bhattacharya, K.R. Relationship of starch changes to puffing expansion of parboiled rice. J Food Sci Technol 2010, 47(2), 182-187.

[3] Pillaiyar, P.; Singaravadivel, K.; Desikachar, H.S.R. Quality changes in HTST processing of rice parboiling. J Sci Food Agric 1994, 65, 229-231.

[4] Ali, S.Z.; Bhawacharya, K.R. High-temperature drying-cum. Parboiling of paddy. Journal of Food Process Engineering 1980, 4, 123-136.

[5] Kahyaoglu, L.N.; Sahin, S.; Sumnu, G. Spouted bed and microwave-assisted spouted bed drying of parboiled wheat. Food and bioproducts processing 2012, 90(2), 301-308.

[6] AACC. Approved method of the American association of cereal chemists (9th ed.). MN: American Association of Cereal Chemists: St. Paul, 1995.

[7] Rattanadecho, P.; Makul, N. Microwave-assisted drying: a review of the state of the art. Drying Technology: An International Journal 2016, 34(1), 1-38.

[8] Lamberts, L.; De Bie, E.; Derycke, V.; Veraverbeke, W.S.; De Man, W.; Delcour, J.A. Effect of Processing Conditions on color change of brown and milled parboiled rice. Cereal Chemistry 2006, 83(1), 80-85.

[9] Lamberts, L.; Rombouts, I.; Brijs, K.; Gebruers, K.; Delcour, J. A. Impact of parboiling conditions on maillard precursors and indicators in long-grain rice cultivars. Food Chemistry 2008, 110(4), 916-922.

Modelling batch drying of fine sand in a fountain confined conical spouted bed

Pablos, A.[a]; Tellabide, M.[a*]; Estiati, I.[a]; Vicente, J.[b]; Aguado, R.[a]; Olazar, M.[a]
[a] University of the Basque Country UPV/EHU, Spain
[b] Novattia Desarrollos Ltd., Spain

*E-mail of the corresponding author: mikel.tellabide@ehu.eus

Abstract

A rigorous model based on hydrodynamic considerations and mass and energy balances has been proposed for batch drying of fine sand in a fountain confined conical spouted bed. The results show that the proposed model predicts acceptably the evolution with time of moisture content in the solid and the final moisture content for the different operating conditions, with the mass transfer coefficient being the only adjustable parameter.

Keywords: Fine sand; spouted bed; batch drying; modelling.

1. Introduction

Although numerous studies on drying have been reported in the literature concerning spouted beds, there are few ones approaching process modelling, which is due to the complexity involving the mathematical description of the phenomena occurring in the drying chamber, i.e., aspects involving thermodynamics, hydrodynamics, and heat and mass transfer. Therefore, the most common procedure is to perform approximations, which, depending on the rigor of the model, simplify the system behaviour in any of the mentioned aspects.

Most of the studies published are based on developing a macroscopic bed model that considers the mass and energy balances and the dynamics of the drying process. The drying mechanisms for the spout and annular zones are considered in these models. Becker and Sallans [1] made the first rigorous analysis of the continuous drying process of wheat in a conventional spouted bed, based on the assumption that bed height is enough to reach thermal equilibrium between exiting gas and the upper surface of the bed. In this way, diffusion of water from the solid inside to the surface limits the drying process. Later, Becker and Isaacson [2] and Viswanathan et al. [3] applied the same model to discontinuous drying, assuming an effective surface moisture content calculated from the dynamic equilibrium moisture content. The latter is obtained experimentally and, unfortunately, there is no data published in the literature. Chu and Hustrulid [4] demonstrated that even being convenient to assume that moisture content at the surface takes a constant value to facilitate calculation, computer problems are generated [2].

For discontinuous operation, Zuritz and Singh [5] proposed to calculate the moisture content on the surface by means of the variation of outlet air temperature and relative humidity. The authors tested an empirical equation that describes the desorption isotherms of equilibrium moisture. Later, Zahed and Epstein [6] deepened in this question using an empirical equation that relates the diffusion coefficient with temperature and solid moisture content. In addition, these authors propose that for continuous operation residence time distribution can be applied to the solids that make up the bed. With these two contributions, thermal equilibrium model with internal diffusion control has demonstrated its capacity to provide a good representation of wheat drying both for discontinuous and continuous operation.

Furthermore, Jumah et al. [7] developed a model for discontinuous corn drying using a novel jet spouted bed under constant and intermittent drying conditions. Unlike previous works, they do not assume thermal equilibrium at the end of the bed and also take into account temperature gradient within the bed. Kalwar and Raghavan [8] worked on drying of husked corn under minimum spouting velocity and found that there is no constant drying period. However, Wetchacama et al. [9] and Nguyen [10,11] found that moisture reduction rate remains constant.

Madhiyanon et al. [12] proposed a batch drying model for vegetable grains. They assumed the process was neither in thermal equilibrium nor in isothermal regime, and it was validated with the experimental results for corn discontinuous drying in a two dimension spouted bed dryer. Unlike the previous studies, the modelling of spout and annular zones was made separately for a better description of drying thermodynamics. The model results agree with those predicted by grain circulation model, empirically formulated by Kalwar and Raghavan [8].

Recently, Markowski et al. [13] published a study of drying dynamics of barley in a spouted bed and determined the influence of grain shape, which is considered in the model by the value of the effective diffusivity of moisture. Significant differences were observed when starting from an ellipsoidal or spherical geometry, so these results show that the proper definition of the solid geometry is essential for moisture diffusivity determination. They also demonstrated that assumption of spherical geometry is not a correct assumption when a great accuracy is desired in the predictions.

Although there is a relatively large amount of studies on drying in spouted beds, very few use conical spouted beds for drying solids [14-17]. Olazar et al. [18] proposed a model to predict the evolution of sand moisture in a conical spouted bed with nonporous draft tube. In this model, three regions (spout, annular zone and fountain) were considered and mass balances were described for water in solid and gaseous phases. The model was validated with experimental results. Based on these studies, this paper proposes a rigorous model for the batch drying in conical spouted beds, which is based on mass and energy balances and has only one adjustable parameter.

2. Materials and Methods

Drying of solids was carried out in a pilot plant consisting of a stainless steel conical vessel (1.62 m height, D_c=0.36 m column diameter, D_0=0.05 m inlet diameter and γ=32º base angle) provided with an open-sided draft tube (A_0/A_T ratio of 60%) and a new fountain confinement device, which consists of a stainless steel pipe with the upper end closed. This device is under patent, and its dimensions are therefore confidential. Experiments were carried out at four temperatures (30, 50, 100 and 150 ºC), three air velocities (u/u_0= 1.2, 2 and 3) and four wet sand pulses (0.5, 1, 1.5 and 2 kg).

Modelling of drying is based on the assumption that the spouted bed behaves like a perfect mixing ideal vessel. Therefore, it is considered that all particles have the same moisture content and temperature at any time, and also that air humidity and temperature is the same at the drying chamber and the outlet. In addition, the model considers the humidity content of the gas at the inlet and exit, and the fact that the solid remains in the bed during the run.

The procedure for the simulation is similar to that followed in the experimentation. A bed of dry sand is being spouted at a temperature corresponding to the outlet gas and a given mass of wet sand (x_{so}=15% w/w) is added at t=0 as a pulse injection.

Based on these assumptions, the following mass and energy balances are considered: 1) Water mass balance for the wet sand added, 2) water mass balance for the gas phase, 3) energy balance for the wet sand added, 4) energy balance for dry sand (initial bed) and 5) energy balance for the gas phase, which should take into account heat losses from the drying chamber to the atmosphere.

Given that the experimental study showed that both gas and solid temperatures do not remain constant during the process, air, liquid water and steam properties are calculated at the corresponding temperature at each time and position. This includes air viscosity and density (μ and ρ_g, respectively), water vapor pressure (P_{vw}), diffusivity of water into air (D_{AB}), volumetric gas flow and velocity (u), mass transfer coefficient (K), heat capacity of water, steam and air (C_{pw}, C_{pv} and C_{pg}, respectively), thermal conductivity of the air (k_g), heat transfer coefficient of the gas (h) and latent heat of water vaporization (λ).

Drying rate, R_w, is defined as:

$$R_W = Ka(y_{sat} - y_g)|\rho_g|_{T_g} \qquad (1)$$

where K is the mass transfer coefficient, a the gas-solid interface area or wet area, y_{sat} the equilibrium moisture at the gas-liquid interface (or saturation humidity), y_g the gas moisture in the drying chamber (and at the exit) and $|\rho_g|_{T_o}$ the density of the gas at the inlet temperature.

The gas-liquid interface area or wet area, a, depends on the moisture content of the particle. When moisture content of sand is high, the water covers the entire surface of the particle and, as explained above, R_w is constant. When humidity drops to the value corresponding to the critical humidity, $x_{s,c}$, the water cannot cover the entire surface of the particle, and therefore the interface area causes a gradual decrease in the drying rate. These two stages are described by Eq. 2 and 3:

$$x_s > x_{s,c} \rightarrow a = A \qquad (2)$$

$$x_s \leq x_{s,c} \rightarrow a = A\frac{x_s}{x_{s,c}} \qquad (3)$$

In addition, runs have been carried out assuming a time depending exchange area, even during the drying step at constant rate. This assumption is based on the fact that sand agglomerates are formed at the beginning, but their diameter decrease during the drying process, and therefore the mass transfer surface increases. Accordingly, in addition to Eqs. 2 and 3, various mathematical functions have been tested to monitor this surface change over time (straight line, vertical parabola, hyperbolic tangent and exponential).

The critical humidity point, $x_{s,c}$, is determined based on the experimental results. The equilibrium moisture at the gas-liquid interface, y_{sat}, expressed as a percentage by weight on a dry basis, is calculated from the vapour pressure of the water at the temperature of the solid.

3. Results and discussion

Once the value of best fit has been determined for the single adjustable parameter (mass transfer coefficient, K) the model suitably predicts the reduction in sand moisture content, as shown in the parity plot in Fig. 1, in which the experimental values of x_c have been plotted versus the calculated ones. As observed, the model underestimates the drying rate in the first half of the drying period (for high values of x_s), whereas in the second half (low values of x_s) the model predicts a faster drying than that measured experimentally.
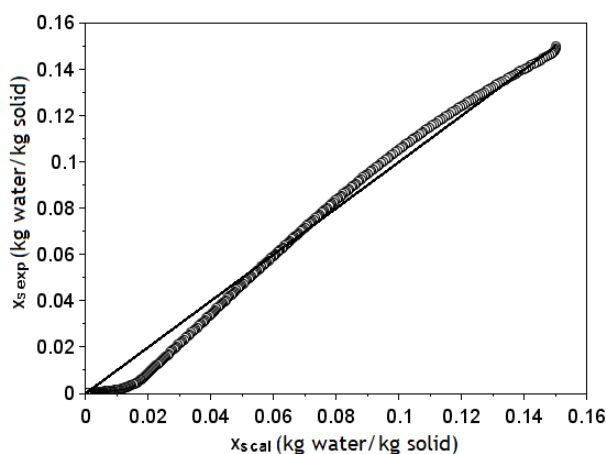
Fig. 1 Experimental and calculated values of water content in the added sand.

Fig. 2 shows the evolution with time of the experimental and calculated values of bed moisture content, x_s, and the absolute humidity of the air at the outlet gas, y_g. It is observed that calculated values of x_s are very close to the experimental ones, but there is a considerable difference between calculated and experimental values of y_g. The model is not able to predict the typical curve in drying processes, in which humidity peaks at a very short time, it then decreases smoothly until a constant value is reached, and finally undergoes a sharp decrease to reach the critical moisture content. The calculated values show an evolution without the initial peak, and the absolute humidity of the air remains approximately constant with a higher value than the experimental one.
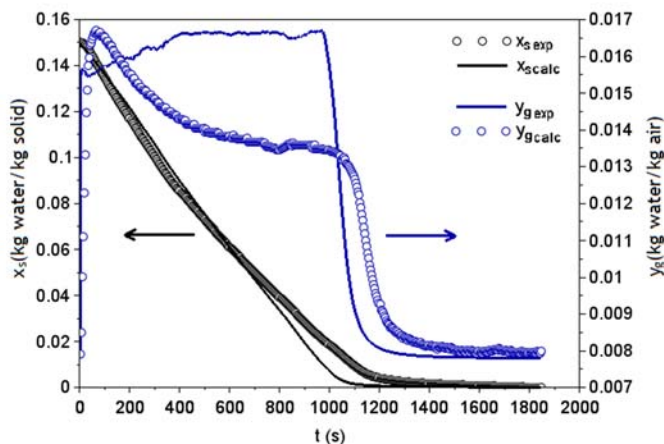
Fig. 2 Evolution with time of the solid moisture content and the air absolute humidity. Points, experimental values, lines, calculated with the proposed model.

To correct these differences, the heat transfer estimation should be improved in the model, since the predictions of the outlet gas temperature by the model do not match the experimental results, and this fact has a great impact on the value of y_g. Accordingly, we are at present involved in the analysis of several options for the estimation of the parameters involving heat transfer, such as the heat transfer coefficients in the bed and those related to heat losses.

4. Conclusions

The proposed model predicts acceptably the evolution with time of moisture content in the solid and the final moisture for the different operating conditions, with the mass transfer coefficient being the only adjustable parameter.

The model underestimates the drying rate in the first half of the process, whereas overestimates in the second half. In order to overcome these shortcomings, heat transfer description should be improved by means of a more detailed definition of convective coefficients and global transfer coefficients for heat loss.

5. Nomenclature

a	Gas-liquid interface area	m^2kg^{-1}
A	Surface area of the solid	m^2kg^{-1}
x_s	Moisture content by solid mass unit	

x_{s0}	Initial moisture content by solid mass unit	-
$x_{s,c}$	Critical moisture content by solid mass unit	-
y_g	Moisture content by air mass unit	-

6. Acknowledgements

7. References

[1]   H. A. Becker y H. R. Sallans, «Drying wheat in a spouted bed. On the continuous, moisture diffusion controlled drying of solid particles in a well-mixed, isothermal bed», *Chemical Engineering Science*, vol. 13, n.º 3, pp. 97-112, 1961.

[2]   H. A. Becker y R. A. Isaacson, «Wheat drying in well-stirred-batch and continuous-moving-bed dryers», *Can. J. Chem. Eng.*, vol. 48, n.º 5, pp. 560-567, oct. 1970.

[3]   K. Viswanathan, M. S. Lyall, K. S. Negi, y B. C. Raychaudhury, «Experimental and theoretical study of batch drying of whaeat in spouted beds.», 1984, pp. 552-558, pn.

[4]   Shu-Tung Chu and Andrew Hustrulid, «General Characteristics of Variable Diffusivity Process and the Dynamic Equilibrium Moisture Content», vol. 11, n.º 5, 1968.

[5]   C. A. Zuritz y R. P. Singh, «Simulation of rough rice drying in a spouted bed», *Paper - American Society of Agricultural Engineers*, 1980.

[6]   A. H. Zahed y N. Epstein, «Batch and continuous spouted bed drying of cereal grains: The thermal equilibrium model», *Can. J. Chem. Eng.*, vol. 70, n.º 5, pp. 945-953, oct. 1992.

[7]   R. Y. Jumah, A. S. Mujumdar, y G. S. V. Raghavan, «Batch Drying Kinetics of Cornin a Novel Rotating Jet Spouted bed», *Canadian Journal of Chemical Engineering*, vol. 74, pp. 479-486, 1996.

[8]   M. I. Kalwar y G. S. V. Raghavan, «Batch Drying of Shelled Corn in Two-Dimensional Spouted Beds with Draft Plates», *Drying Technology*, vol. 11, n.º 2, pp. 339-354, ene. 1993.

[9]   S. Wetchacama, S. Soponronnarit, T. Swasdisevi, J. Panich-ich-orn, y S. Suthicharoenpanich, «Drying of High Moisture Paddy by Two-Dimensional Spouted Bed Technique», en *Proceedings of the First Asian-Australian Drying Conference (ADC'99)*, Bali, Indonesia, 1999, pp. 300-307.

[10] L. H. Nguyen, «Evaluation of a Modified Spouted Bed Dryer for High Moisture Grain Drying. Tesis para la University of New South Wales.», PhD Tesis, University of New South Wales, Australia, 2000.

[11] L. Hung-Nguyen, R. H. Driscoll, y G. Srzednicki, «Modeling the drying process of paddy in a triangular spouted bed», en *Proceedings of the 12th International Drying Symposium, IDS2000*, Amsterdam, 2000, vol. 269.

[12] T. Madhiyanon, S. Soponronnarit, y W. Tia, «Industrial-Scale Prototype of Continuous Spouted Bed Paddy Dryer», *Drying Technology*, vol. 19, n.º 1, pp. 207-216, ene. 2001.

[13] M. Markowski, I. Białobrzewski, y A. Modrzewska, «Kinetics of spouted-bed drying of barley: Diffusivities for sphere and ellipsoid», *Journal of Food Engineering*, vol. 96, n.º 3, pp. 380-387, feb. 2010.

[14] J. Costa, F. B. Freire, J. T. Freire, y M. L. Passos, «Spouted beds of inert particles for drying suspension», *Drying Technology*, vol. 24, n.º 3, pp. 315-325, 2006.

[15] M. L. Passos, G. Massarani, J. T. Freire, y A. S. Mujumdar, «Drying of pastes in spouted beds of inert particles: Design criteria and modeling», *Drying Technology*, vol. 15, n.º 2, pp. 605-624, 1997.

[16] H. Altzibar, G. Lopez, S. Alvarez, M. J. San Jose, A. Barona, y M. Olazar, «A draft-tube conical spouted bed for drying fine particles», *Drying Technology*, vol. 26, n.º 3, pp. 308-314, 2008.

[17] L. Spreutels, B. Haut, J. Chaouki, F. Bertrand, y R. Legros, «Conical spouted bed drying of Baker's yeast: Experimentation and multi-modeling», *Food Research International*, vol. 62, pp. 137-150, abuztua 2014.

[18] M. Olazar, G. Lopez, H. Altzibar, A. Barona, y J. Bilbao, «One-dimensional modelling of conical spouted beds», *Chemical Engineering and Processing*, vol. 48, n.º 7, pp. 1264-1269, jul. 2009.

[19] B. Thorley, K. B. Mathur, J. Klassen, y P. E. Gishler, «Effect of Design Variables on Flow Characteristics in a Spouted Bed», *National Research Council of Canada*, 1958.

[20] W. Du, W. Wei, J. Xu, Y. Fan, y X. Bao, «Computational fluid dynamics (CFD) modeling of fine particle spouting», *International Journal of Chemical Reactor Engineering*, vol. 4, sep. 2006.

[21] C. J. Lim y K. B. Mathur, «Modeling of particle movement in spouted beds», en *Fluidization*, J. F. Davidson y D. L. Keairns, Eds. Cambridge: Cambridge University press, 1978, pp. 104-109.

[22] N. Epstein y J. R. Grace, «Spouting of Particulate Solids», en *Handbook of Powder Science & Technology*, M. E. Fayed y L. Otten, Eds. New York: Van Nostrand Reinhold, 1984, pp. 507-536.

[23] G. A. Lefroy, «The Mechanics of Spouted Beds. Tesis para la University of Cambridge», PhD Tesis, University of Cambridge, Cambridge, 1966.

[24] G. A. Lefroy y J. F. Davidson, «Mechanics of the spouted beds», *Trans Inst Chem Eng*, vol. 47, n.º 5, pp. t120-t128, 1969.

[25] R. G. Szafran y A. Kmiec, «CFD Modeling of Heat and Mass Transfer in a Spouted Bed Dryer», *Ind. Eng. Chem. Res.*, vol. 43, n.º 4, pp. 1113-1124, feb. 2004.

Study of the behavior of a multistage dryer provided with downcomer

Verduzco Mora, L.A.ª; Martínez Vera C.ª; Vizcarra Mendoza, M.G. ª*
ªUniversidad Autónoma Metropolitana – Iztapalapa, CDMX, México.

*E-mail of the corresponding author: mgvm@xanum.uam.mx

Abstract

We study the behavior of a multi-stage fluidized bed dryer operated continuously with dowcomers. With the kinetics of silica gel drying depending on the mass of solids in the dryer and the gas feeding temperature, E = 14.5 KJ/mol, and the distribution of residence times of solids through the dryer, modeling by N tanks agitated in series, the experimental moisture content of the solids coming out of the dryer is compared with the predicted by the Vanecek model.

Keywords: fluidization; gel of sílice; continuous multistage dryer.

1. Introduction

Drying is one of the most important operations in the chemical, metallurgical, pharmaceutical and food industry, among others, being the drying in fluidised beds, one of the most successful techniques in the drying of solids such as seeds, fertilizers, polymers, minerals and other important chemicals [1, 2, 3].

In general, fluidised solids can be considered perfectly mixed, therefore, in a batch-operated dryer, a uniform treatment of the solids being dried is guaranteed; However, when the equipment is operated continuously, the solids that come out of the dryer present distribution of residence times and therefore different degrees of drying [4]. An option to overcome these disadvantages is the use of multi-stage fluidized bed columns [5]. By passing the solids through several stages connected in series, either in vertical or horizontal arrangement tends to reach a piston flow pattern, which is tantamount to narrowing the distribution of residence times. It can be stated therefore that as long as the flow of solids deviate from the perfect mixing and tent to the piston flow, the particle population coming out of the dryer will have a more uniform moisture content. In the operation of multi-stage fluidized bed columns with downcomers, one of the difficulties presented is to keep the flow of solids from stage to stage stable [4,6,7,8] It has been established that the zone of stable operation of these equipment is function of the fluxes of solid and gas through the column, as well as of the employment or not of a reduction in the inferior cross-section of the downcomer. This considerably decreases the treatment capacity of the solids, which may represent a limitation for the application of this technology.

This research evaluates the influence of the number of stages, the relatiom between the length of the downcomer to diameter of the dryer (L/D) and the air supply temperature on the final moisture content in silica gel particles. The continuous operation is modelled through an integral type model derived from the equation proposed by Vanecek[9].

1.1. Mathematical model of continuous dryer

The performance of a continuous fluidized bed dryer can be evaluated from the drying kinetics obtained experimentally in a batch dryer and by the use of the corresponding function of the residence time distribution of solids (E(t)) in the continuous operation of the dryer. This is expressed mathematically by Eq. (1) [9].

$$X_e = \int_0^\infty X(t)E(t)d\tau \qquad (1)$$

1.1.1. Drying kinetics

Considering that the drying kinetics of silica gel can be represented by an exponential model similar to Newton's second law of cooling, the following expression is proposed, Eq. (2):

$$-\frac{dX}{dt} = kX \qquad (2)$$

This expression is integrated, considering that at t = 0, $X = X_0$, thus obtaining Eq. (3)

$$X = X_0 \times EXP(-kt) \qquad (3)$$

where k, is a coefficient that considers the effects of the air supply temperature, according to an Arrhenius type equation and that is represented by the following relationship:

$$k = A \times EXP\left(-\frac{E}{RT}\right) \qquad (4)$$

Where, A is the preexponential factor, E the activation energy and R the universal constant of the gases. Substituting Eq. (4) in Eq. (3), the drying kinetics is obtained as a function of temperature and time, Eq. (5):

$$X = X_o \times EXP\left[-A \times EXP(-{^E/_{RT}})t\right] \qquad (5)$$

1.1.2. Resident Time Distribution (RTD)

To establish the residence time distribution function of the solids (E (t)) that go through the multi-stage dryer, the series of stirred tanks model[10] was used.

Thus the DTR as a function of time is given by Eq. (6), for N geometrically identical stages[2]

$$E(t) = \frac{1}{\tau_i}\left(\frac{t}{\tau_i}\right)^{N-1} \times \frac{1}{(N-1)!} * e^{-t/\tau_i} \qquad (6)$$

Where τ_i is the residence time of the solids in stage i.

1.1.3. Moisture content of the solids at the exit of the multi-stage dryer.

Finally, substituting the equations (5) and (6) in (1), we obtain the equation for the calculation of the moisture content of the solids at the exit of the multistage dryer as a function of the temperature and the number of stages:

$$X_e = \int_0^\infty \left\{ \left[X_o * EXP\left[-A \times EXP(-{^E/_{RT}})t\right]\right] \times \left[\frac{1}{\tau_i}\left(\frac{t}{\tau_i}\right)^{N-1} \times \frac{exp\left(-\frac{t}{\tau_i}\right)}{(N-1)!}\right]\right\} dt \qquad (7)$$

2. Materials and Methods

2.1. Materials

Silica gel was used: $d_p = 1.8 \times 10\text{-}3$ m, $\rho_p = 2.1 \times 10^3$ Kg / m³, $\varepsilon_{mf} = 0.67$, $\varphi = 1$, $U_{mf} = 1.4$ m/s, solid type D of the Geldart classification.

2.2. Methods

2.2.1. Experimental Dryer

Fig. 1 shows the equipment used in this study and that served to perform the hydrodynamic study of the column, stable operation and distribution of residence times of the solids, the kinetics of drying of the silica gel and the continuous operation of the multistage dryer.
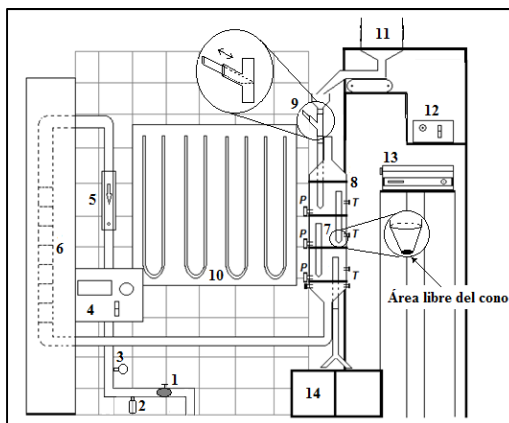
Fig. 1. Multi-stage dryer. 1.- Valve, 2.- Humidity trap, 3.- Pressure regulator, 4.- Feed air temperature control, 5.-Rotameter, 6.- Electric resistance heater, 7.- Downcomers, 8 .- Multi-stage Column (0.095 m ID × 0.25 m height, each stage), 9.-Valve for tracer injection, 10.- Manometers in U, 11.- Feeder of solids, 12.- Control of the feeder of solids, 13.- Temperature recorder, 14.- Collector of solids P.- Points to measure pressure drops, T.- Ports for temperature measurement.

2.2.2. Drying Kinetics

The fluid bed dryer operated in batch with a single stage, is thermally stabilized at one of the previously established temperatures (T), 50, 60 or 70 °C and one of the loads of solids in the dryer (W_i), 0.360, 0.720 or 1.080 Kg of gel of silica, corresponding to the height (L) to bed diameter (D) ratio of 0.5, 1.0 and 1.5, respectively. The air velocity remained constant at 2.24 m / s (1.6 Umf). During each experimental run, samples of approximately 2.0×10^{-3} Kg are taken and stored hermetically to later determine their moisture content. At the same time the temperatures in the bed are monitored. This routine is repeated for all temperatures and solids loads contemplated in the experimental domain.

2.2.3. Residence Time Distribution of solids

The "pulse" type of stimulus-response technique was used. Once the dryer operates continuously and in a steady state, an amount of tracer (silica gel with blue indicator) is "injected" into the feed stream (approximately 0.025 Kg), once this is done the valve is opened again so that the fresh solid continues to feed continuously. When the tracer enters the bed, the time starts to be taken and from this point samples of the concentration of tracer

are taken at the exit of the column in 30 seconds lapses. The function of RTD is obtained from the methodology reported by Levenspiel[2]. The tracer injection is done quickly enough to avoid that the downcomer is left without solids and thus avoid a possible destabilization in the column.

3. Results and discussion

From a previous study, the stable operation area of the multistage column was determined by operating the downcomers with a conical reduction, in its lower part equivalent to 45% of free area [1]. In this way, the solid and air fluxes were fixed respectively, in 5.3 x 10-4 Kg$_{ds}$ / s and 5.2 x 10-3 Kg$_{dg}$ / s, which remain constant during the experiments.

3.1. Drying Kinetics

In Fig. 2 are shown the moisture profiles in the solid as it dries for the different air feed temperatures to the dryer. It can be seen that the constant drying period ranges from X_o = 0.37 KgH$_2$O / Kg$_{ds}$ to a critical point that oscillates between 0.15 and 0.20 KgH$_2$O / Kg$_{ds}$. It is observed that all the curves present period of constant drying speed and that as the load of solids in the dryer increases, the temperature of the bed takes longer to reach the air inlet temperature. In the same way, the higher the load of solids in the bed, the drying is slower, because there is more moisture to remove for a constant flow of air.
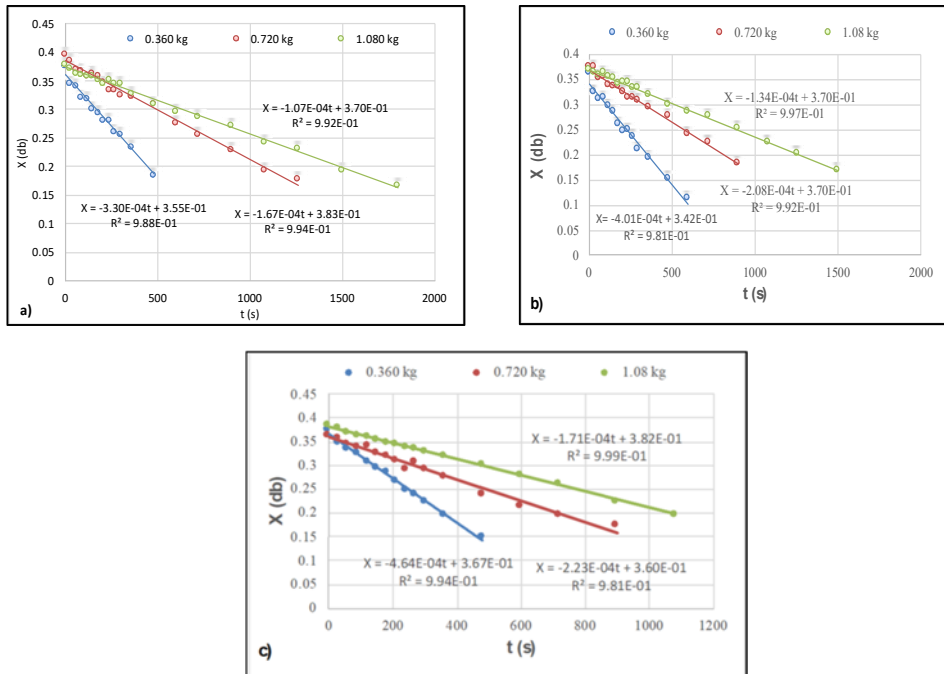
Fig. 2.- Drying kinetics of the silica gel in the period of constant drying as a function of the charge of solids in the dryer. a) 50ºC; b) 60ºC; c) 70 ºC

When plotting the linearized form of Eq. 3, applied to the constant drying period, we obtain the value of the constant k, which is presented in table 1 for the different experimental conditions.

Table 1.- Values of the silica gel drying constant

T (°K)	W (kg)	k x 10³ (s⁻¹)	E (KJ/mol)	A (s⁻¹)
323	0.36	1.330		
333	0.36	1.720	14.78	0.337
343	0.36	1.830		
323	0.72	0.622		
333	0.72	0.758	14.42	0.135
343	0.72	0.850		
323	1.08	0.434		
333	1.08	0.500	14.51	0.096
343	1.08	0.595		

It can be seen that practically the loading of solids in the dryer does not appreciably affect the value of the activation energy, however this parameter affects the value of the pre-exponential factor, as can be seen in Fig. 3.
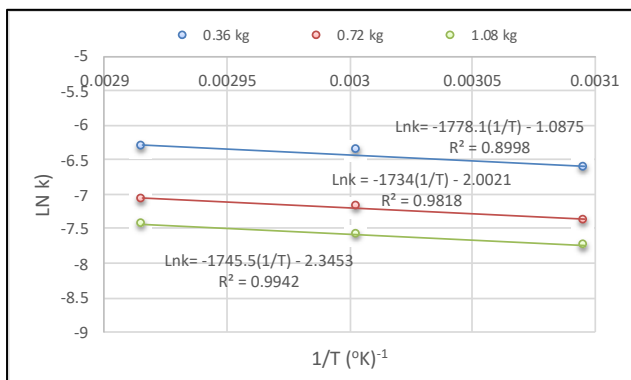
Figure 3.- Activation Energy and Pre-exponential Factor.

3.2. Residence Time Distribution

The table 2 shows the values corresponding to the residence time that the solids remain in a stage at the different L / D ratios.

<div align="center">***Table 2. RTD of the solids in the multi-stage fluidized bed dryer***</div>

L/D	W (kg)	τ (s)
0.5	0.120	226
1.0	0.240	453
1.5	0.360	680

3.3. Continuous operation of the multistage dryer.

For $N = 3$, $\tau_i = 680$ s, $(L/D)_i = 1.5$ (0.360 Kg), Eq. (7) left:

$$X_e = \frac{X_o}{2\tau_i^3} \int_0^\infty \left[t^2 EXP - \left((0.096 * EXP(-\frac{1750}{T}) + \frac{1}{\tau_i}) t \right] dt \qquad (8)$$

The results obtained by comparing the experimental humidity of the output of the dryer solids with those calculated with the Eq. (7) are presented in Fig. 4
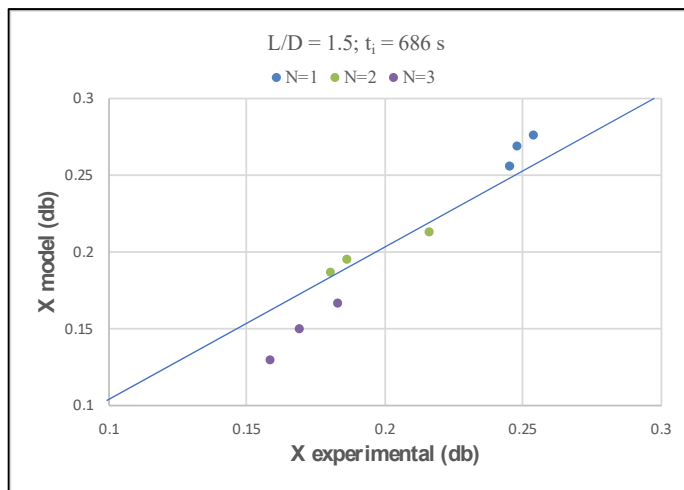
Fig. 4 Prediction of moisture content at the dryer outlet at different temperaturas

4. Conclusion

In this paper we show that the equation proposed by Vanecek, 1966, reasonably well predicts the humidity of the solids that come out of a multistage dryer.

It was found that the activation energy related to the drying process is independent of the load of solids in the dryer, but not for the pre-exponential factor.

Finally, it was found that the drying kinetics can be reasonably well represented by a first order power law model

5. References

[1] Srinivasa C., Thomas P. P., Varma Y. B. G., Drying of Solids in Fluidized Beds. Ind. Eng. Chem. Res. 1995, 34, 3068-3077.

[2] Kunii D., Levenspiel O. Fluidization Engineering; Ed. Butterworth-Heinemann1991.

[3] Zahed A. H., Epstein N., Batch and Continuous Spouted Bed Drying of Cereal Grains. The Thermal Equilibrium Model. The Canadian J. of Chem. Eng. 1992, 70, 945-953.

[4] Martín I. G., Marcilla A., Font R. y Asensio M. Stable Operating Velocity Range for Multistage Fluidized Bed Reactor with Downcomers, Powder Techn.1995, 85,193-201.

[5] Srinivasa C., Subramanian N. B. Some Drying Aspects of Multistage Fluidized. Beds, Chem. Eng. Tecnol. 1998, 21, 961-966.

[6] Mohanty C. R., Rajmohan B., Meikap B. C. Identification of stable operating ranges of a counter current multistage fluidized bed reactor with downcomer. Chemical Engineering and Processing: Process Intensification 2010, 49, 104-112.

[7] Mohanty C.R., Adapala S., Meikap B.C. Hold-up Characteristics of a Novel gas-solid Multistage Fluidized Bed Reactor for Control of Hazardous Gaseous Effluents. Chem. Eng. Journal 2009, 148, 115-121.

[8] Santiago T., Anaya I., Alamilla L., Chanona J. J., Gutierrrez G. F., Vizcarra M.G., Hydrodynamics and Operational Parameters of a Continuous Multistage Vertical Fluidized Bed System, Revista Mexicana de Ingeniería Química 2007, 6 59-63.

[9] Vanecek V., Markvart M., Drbohlav R., Fluidized Bed Drying; Leonard Hill, London, 1966.

[10] Verduzco-Mora, L.A., Martínez-Vera, C., Vizcarra-Mendoza, M.G. Hidrodinámica de un secador multietapas de lecho fluidizado continuo con vertederos. Revista Mexicana de Ingeniería Química 2015, 14(2), 467-479

Strawberries hybrid drying combining airflow, dic technology and intermittent microwaves

Amami, E.[a,b,c]*; Besombes, C.[c]; Kechaou, N.[d]; Allaf, K.[c]

[a]Université de Manouba. Laboratoire de recherche « Physiopathologies, Alimentations et Biomolécules (PAB) ». Institut Supérieur de Biotechnologie Sidi Thabet 2020, Ariana, Tunisie.
[b]Université de Tunis El Manar. Institut Supérieur des Sciences Biologiques Appliquées de Tunis, Unité de recherche « Chimie des matériaux et de l'Environnement », 9, rue Zouhair Essafi Tunis 1006 Tunisia.
[c]University of La Rochelle, Laboratory of Engineering Science for Environment (LaSIE UMR 7356 CNRS), Avenue Michel Crépeau, 17042 La Rochelle, France.
[d]Université de Sfax. Groupe de recherche en Génie des Procédés Agroalimentaires. Ecole Nationale d'Ingénieurs de Sfax (ENIS), Sfax, Tunisia.

*E-mail of the corresponding author: ezzeddineamami@yahoo.fr

Abstract

1-cm strawberry slices were partially airflow-dried at 50 °C, to reach 0.25 g H2O/g db. Optimized DIC treatment was performed at 350 kPa for 10 s. The final drying stage of these DIC-expanded slices was achieved from 0.25 to 0.1 g H2O/g db (dry basis) using intermittent Pulsed Micro-Wave Drying PMWD to prevent from the paradoxical step of coupled conduction heat transfer with deep generation and transfer of vapor. PMWD was defined at constant 100 W for 3.25±0.05 g with constant active time ton maintained at 2 s, and tempering time toff ranged between 2 and 10 s, or with a continuous way. By decreasing both energy consumption and total drying time of DIC-expanded slices using intermittent microwave, the whole cost significantly decreased to be much lower than the conventional MWD drying, with a great increasing of the quality.

Keywords: Airflow Drying; Instant Controlled Pressure-Drop DIC; Swell-Drying; Pulsed Micro-Wave Drying; Physical and Chemical Characteristics..

1. Introduction

Dehydration of strawberry aims at extending product availability while preserving nutritional components, and gains a noticeable increase [1]. Major disadvantages of airflow drying of strawberry are lengthy drying time and low energy efficiency [2, 3]. The three most crucial aspects of airflow drying resides in 1/ a first stage of superficial evaporation of water allowing the material core to have low temperature (Wet-bulb temperature), which implies ample preservation of nutritional contents (color, antioxidants…), 2/ a shrinkage of the low-temperature glass-transition polymers; this leads to a weaker effective diffusivity of water, and 3/ a final paradoxical stage of coupled heat conduction and Fick vapor diffusion transfer. This last generates a high-temperature/long-time stage source of the most part of degradation of the active molecules. The quality of the final dried product and its cost mainly depend on the final stage of drying [4].

The swell-drying of strawberry for crispy, high nutritional quality was defined by Alonzo-Macias et al. (2012) [5] as an Instant Controlled Pressure Drop DIC texturing treatment following a first stage of airflow drying. DIC targets at remedying the product shrinkage via a controlled expansion improving process kinetics and final quality of dried products. This operation doesn't reduce the famous final paradoxical stage of airflow drying, which occurs when the main evaporation process occures within the matrix. Al Haddad et al. 2008 [4] were the first researchers to propose to remedy such a paradoxical stage drying through a distinct final stage of drying using Darcy process issued from Micro-Wave drying, overheated steam drying, or Multi-Flash Autovaporization MFA drying.

Thus Al Haddad et al. 2008 [4] were the only researchers who experimentally defined for green apple strips and sweet potato slices an efficient and economic three-stage drying process of hot air drying combined to a DIC texturing stage, and finally using microwave assisted ambient temperature airflow dehydration. In their study, each drying kinetic was carried out through 720 W power and different number of cycles. Each cycle consisted in subjecting the products to microwave assisted by ambient temperature air for 30 seconds and then sweeping the products with only air at ambient temperature for one minute. The use of MW may ensures a deep and almost uniform heating way implying the same required orientation of the both gradients of temperature ($T_i > T_s$ for heating) and vapor pressure ($p_{vi} > p_{vs}$) between the core and the superficial zone of the product. It should be an effective manner to overcome the paradoxical stage improving thus the drying kinetics.

Microwaves are an attractive source of thermal energy, generate volumetric internal heating within the product, increasing the internal total pressure (air+vapor) [6]. Microwave drying using continuous microwave energy is rapid and energy-efficient compared to conventional airflow drying [7]. However, the too rapid mass transport caused by MW power and uneven temperature and moisture distribution may cause overheat in the sample, provoking deep dark-point tissue damage, and/or undesirable changes in the food texture [8]. Some of the limitations of single MW drying can be overcome by combining MW energy with conventional heating or by using microwave energy in a pulsed manner in order to maximize drying efficiency possibly improving the product quality [7].

Moreover, intermittent Pulsed Microwave Drying PMWD operation has proven itself a good method to avoid uneven over-heating by allowing redistribution of temperature and water to diffuse through

the sample during power-off time [9]. PMWD has to be defined and performed in order to improve both drying process performance (kinetics, etc.) and preserve swell-dried strawberry quality attributes (color, antioxidant content, etc.). This study would be a basis to extend this operation to other fragil fruits, and technically support the industrial scale of final products for various applications (baby foods, nutraceutics…) to make them commercially available.

To define an efficient and economic hybrid drying process, this work compiled 1/ a first conventional stage airflow drying AFD, 2/ a second stage of well-controlled texturing process of Instant Controlled Pressure-Drop DIC, and 3/ a microwave dehydration (MWD) whose driving force is the gradient of the total pressure of Darcy's permeability, which advantageously replaces Fick's diffusion mass-transfer. Two features prevent thermal MW energy from accumulating in the material through the removal of the generated vapor, by 1/ replacing the too compact AFD structure by porous swell-dried materials; the high porosity induces a high permeability of the vapor, and 2/ using a pulsed PMWD.

Therefore, using the intermittet microwave drying after SD, this current work aimed to 1/ examine the effectiveness and optimize the PMWD applied in early stage of drying from the point of view of overall final quality of dried slices of strawberry, a heat sensitive fruit, and 2/ evaluate the effectiveness of intermittent PMWD drying at optimized conditions (t_{on}; t_{off}) compared with continuous microwave, airflow drying and freeze-drying (FD) in terms of drying kinetics and visual attributes of dried rehydrated SD strawberries.

2. Materials and Methods

2.1 Fresh materials

Fresh strawberries camarosa cultivar were purchased from a local market in La Rochelle (France). The strawberries were manually cut parallel to the main axis into halves (for FD) or 1cm slices (AFD and CMWD) of average 37±2 mm length, 18±1 mm width and 15±1 mm thickness with a stainless steel knife and weighted. The fresh samples had a moisture content of 11.66±1.42 g H_2O/g db (dry basis).

2.1.1 *Drying of the fresh strawberry*

30.5±0.5 g strawberry slices were spread out evenly and subjected to three different drying methods based either on single continuous drying, namely (i) microwave drying "(CMWD)" at 20 °C; (ii) airflow drying "(AFD) at 50°C" and (iii) freeze drying [5]. In this cases the pulse ratio (PR)=(t_{on}+t_{off})/t_{on}=1.

- Airflow drying (AFD)

Strawberry slices were dried in a airflow dryer (Memmert: Universal Oven UNB Model 800) at 50 °C with an air flux of 1.2 m s^{-1}. They were dried until attaining 0.10 g H_2O/g db (dry basis). These samples were recorded as AFD 50°C.

- Microwave drying (MWD)

A domestic combined microwave oven with convection (Samsung, Model CE107F-S. Korea) with maximum output 900 W at 2450 MHz. In each experiment, strawberry slices of 30±0.5 g were placed in petri dish putting at the center of a glass turntable disc in the microwave chamber. Drying

experiments were carried out with 100 W microwave power level at 20 °C. The average value of effective MW power is about 62 W.

- Freeze Drying (FD)

A freeze-drying equipment (RP2V model, Serail, France) was used for drying the strawberry halves. Three steps were used : external freezing (2 h at -20°C), sublimation (-20 °C, 0.66 Pa/12 h) and desorption (25 °C, 0.66 Pa/12 h) [5].

2.2 Pulsed Microwave drying (PMWD) of the rehydrated Swell dried SD strawberries

The batch of 1-cm sliced strawberries was partially airflow dried (Memmert: Universal Oven UNB Model 800) at 50 °C and an air flux of 1.2 m/s until 0.25 g H_2O/g db. Afterwards, the partially airflow dried strawberries were textured by an optimized DIC treatment (0.35 MPa as saturated steam pressure for 10 s) [5]. Finally, after DIC treatment, a traditional airflow drying at 50 °C was performed to get 0.08 g H_2O/g db as final water content. These samples were analyzed and recorded as control or SD.

50 g of swell-dried slices of strawberries (Fragaria ananassa) placed in zipped airtight bags were rehydrated from 0.08 to 0.25 g H_2O/g db and stored in a cold chamber at 5 ºC by 24 h to homogenize their water content. Approximately, 3.25±0.05 g of rehydrated SD expanded strawberry slices were spread out evenly and subjected to three different drying methods achieved from W= 0.25 to 0.1 g H_2O/g db based either on hybrid three stage drying process, namely (vi) airflow drying at 50 °C; (v) Pulsed microwave drying "(PMWD)" at 20 °C ambient temperature with active time t_{on} maintained at 2 s at constant 100 W, and three values of tempering time t_{off} at 2, 5, and 10 s, and (vi) a continuous operation of microwave was also performed (10 s t_{on} and 20 s t_{off} is the proper intermittent cycle of continuous use of domestic microwave oven at 100 W).

From literature, initial know-how of LaSIE's research team, and preliminary experiments, two independent processing factors of PMWD process and their own respective ranges were selested; they were t_{on} (2 s), and t_{off} (2-10 s). The petri dish was removed from the oven and weighted at regular intervals at the end of power-off times during the drying period. By recording the successive times of t_{on} and t_{off}, we determined the moisture loss and drying rate during the pulsed microwave drying.

The measurements of moisture loss were performed by a gravimetric method at 60°C until weight stabilization, according to AOAC 930.04 [10], and expressed in g H_2O/g db. After drying, each sample was photographed for assessing the sample visual quality. Drying Rate (DR) (g H_2O/(g db min)) was calculated from the water contents dry basis values (g H_2O/g db) W_t and W_{t+dt} at time values of t and t+dt, respectively. t was the apparent drying time ($t_{on}+t_{off}$) (s) :

$$DR = \frac{W_{t+dt} - W_t}{dt} \tag{1}$$

2.3 Estimation of pressure within the superficial zone of the product during the first cycles

By assuming that the holes of initial sample were full of water without any presence of air, the pressure inside the material matrix, expressed in Pa, can be estimated versus the mass of generated vapor/pulsed cycle (g/cycle) and the initial volume of water in the product (m^3), as follow:

$$\text{Internal vapor pressure} = \frac{m_v RT}{M_{H_2O} V_w} = \frac{\rho_v RT}{M_{H_2O}} \tag{2}$$

Where, M_{H2O} is the molar mass of water (18 g/mol), T is the product temperature (K), R is the universal gas constant, and V_w is the water volume (m³). The amount of water transformed into vapor per cycle should be correlated with the evaporation enthalpy Δh_{vap}:

$$m_v = \frac{0.62 * t_{on} * P}{\Delta h_{vap}} \tag{3}$$

3. Results and Discussion

3.1 Effect of PR on drying kinetics
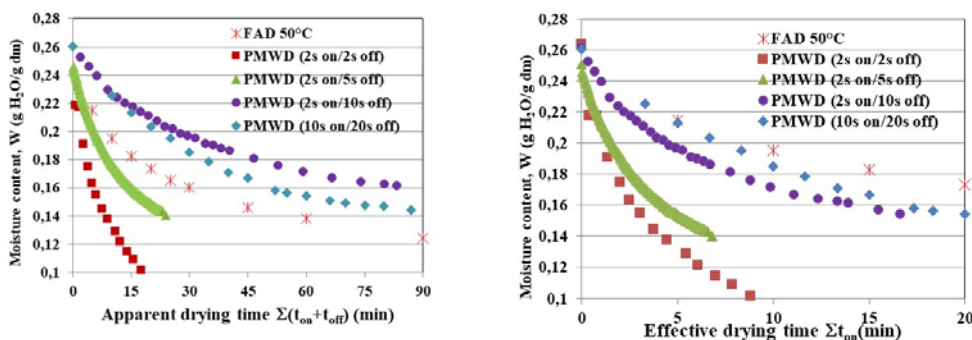
Fig. 1 The moisture content versus time curves for the AFD 50°C, PMWD (100 W) of rehydrated SD strawberries (load of 3.25 g) for apparent drying time $\Sigma(t_{on}+t_{off})$ and effective drying time Σt_{on}.

As shown in Figure 1, moisture content (W) continuously decreased vs drying time. To reach W=0.1 g H_2O/g db, PMWD (2 s t_{on}/ 2-5 s t_{off}) had a crucial acceleration of the drying process compared with AFD 50 °C. At PMWD (2s t_{on}/2s t_{off}), W of about 0.1 g H_2O/g db was reached in 19.6 min, which means only 9.8 min effective drying time. PMWD (10 s t_{on}/20 s t_{off}) was lesser effective and resulted in poor product quality. This trend can be explained by a too high value of t_{on}= 10 s, which would result in increasing the internal heat with a generation of a dispersed deep case-hardening in different place within the volum. Higher tempering period results in an easier water balance within the sample, although without any modification of such a dispersed deep case hardening. By coupling an adequate low values of the active time t_{on}, and high tempering period t_{off}, greater availability of Darcy's transfer of vapor can occur. Nevertheless, an excess of t_{off} normally results in negative impact in terms of kinetic.

3.2 Effect of PR on drying rate versus apparent drying times

For PMWD, a zigzag pattern of successive cycles of high peak/falling rate period was observed. This could be attributed to the redistribution of moisture and temperature during the tempering time provided by the thermal diffusion resulting in better water homogeneity and, thus, rapid moisture removal during the subsequent active microwave [11]. Thus, PMWD increase the pore pressure and a total pressure gradient between the internal and external media is established due to phase transitions and the thermodiffusion effect, thus leading to a highly effective Darcy-type vapor transfer.
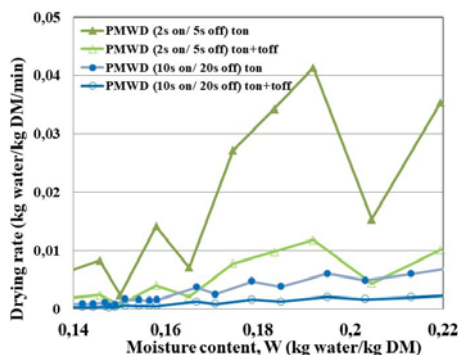
Fig. 2 Drying rate of PMWD operating parameters (effective drying time Σt_{on} or apparent drying time $\Sigma(t_{on}+t_{off})$) versus moisture content of rehydrated SD strawberries.

The drying rate of different pulsed microwave drying conditions was affected by tempering time t_{off} (Fig 2). Generally, total drying rate has been as faster as t_{off} decreased (shorter tempering time). This resulted in higher temperature and, thus, higher vapor pressure with, normally higher Darcy's vapor mass-transfer. The drying rate value calculated versus the effective drying time, was much higher. This result is crucial for industrial application and can be revealed through an adequate time and/or space intermittent repartition. Moreover, these phenomena did not strictly depend on PR. Thus, for approximatively the same PR=3, PMWD (2 s t_{on}/5 s t_{off}) were 5 times more accelerated than (10 s t_{on}/20 s t_{off}).

3.3 Quality attributes

3.3.1 Surface pressure during the first cycles

Table 1 shows for t_{on}=2s aninput heating energy substantially increasing with tempering time t_{off}. Moreover, PMWD conducted at lower t_{off} resulted in lower total effective drying time (t_{on}) and specific energy consumption compared to other intermittent combinations. This is because the higher the tempering time t_{off}, the colder the surface because of superficial convection.

Table 1. Values of the total drying time, total ON drying time, specific consumed energy and estimated surface pressure for PMWD rehydrated swell-dried strawberries at different PR.

t_{on} (s)	t_{off} (s)	PR=($t_{on}+t_{off}$)/t_{on}	T (°C)	$\Sigma(t_{on}+t_{off})$ (s)	Σt_{on} (s)	P (bar)
2	2	2	20	1176	588	1.915
2	**5**	**3.5**	20	3185	910	1.919
2	10	6	20	5988	998	1.888
10	**20**	**3**	20	10800	3600	5.203
-	-	1 (AFD)	50	16200	16200	-

3.3.2 Visual Attributes

The first step of airflow drying AFD at 50 °C gave good visual attributes of the strawberry slices. Just after DIC-texturing, SD strawberry slices maintained the good natural visual color. On the other hand,

it is wee-known that the freeze-dried strawberries lose their natural redness initial color. With SD slices as control samples, only PMWD (2 s t_{on}/5 s t_{off}) gave no black/brown spots within the slice.
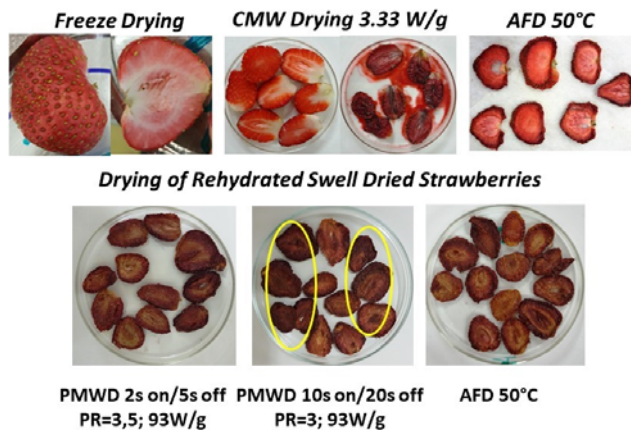
Fig. 2 Appearance of exemplary strawberries slices after continuous and PMWD modes.

Nevertheless, as soon as the PMWD active time is above a certain level ($t_{on} > 10$ s), many black spots emerged with less efficient drying kinetics. This can be attributed to deep "case hardening" delimiting areas with high internal tissue damage.

4. Conclusions

Based on both final product quality and operation performance, a multi-criteria optimization of Pulsed Microwave Drying PMWD was achieved. Microwave active time ton and tempering time toff were defined and optimized at 2 s and 2 to 5 s, respectively. Although the microwave power was kept at 100 W for 3.25 g of strawberry slices, this MW distribution has prevented heat accumulation and put in equilibrium the internal water distribution, thus well generating vapor and its effective transfer towards the surrounding medium. These well-defined strawberries dried by AFD/DIC swell-drying and those of PMWD at t_{on}=2 s and t_{off}=2 s exhibited the highest antioxidant activity and total phenol content.

Hence, the present three stage-intensified drying of AFD/DIC swell-drying/PMWD allowed the strawberry to effectively get the advantage of low internal temperature, thus acting against the paradoxical situation and remove the residual water from the porous matrix (after DIC) following Darcy's permeability as transfer way of residual vapor. With low energy consumption of DIC-expansion and intermittent microwave, and since the drying kinetics was greatly increased, the total cost should become significantly lower than the simple Continuous MicroWave Drying.

5. Nomenclature

MWD	Conventional Micro-Wave Drying	-
CMWD	Continuous Microwave Drying	-
PMWD	Pulsed Micro-Wave Drying	-
AFD	Airflow Drying	-
DIC		-

SD	Instant Controlled Pressure-Drop, which is a second stage well-controlled texturing process	-
(PR)	Swell-Drying, which combines a conventional (airflow) drying with DIC-texturing.	
	pulse ratio=$(t_{on}+t_{off})/t_{on}=1$	

Subscripts

t_{on}	Active time, where both input MW heating energy and vapor mass-transfer occure together	s
t_{off}	Tempering time, where there is no input MW heating energy, and vapor mass-transfer mainly following Darcy's law, is assumed to be negligible.	s
T_i and T_s	Temperature values at the core and the superficial zones, respectively	°C
p_{vi} and p_{vs}	Absolute vapor pressures at the core and the superficial zones, respectively	Pa

6. References

[1] 1. Giampieri, F.; Tulipani, S.; Alvarez-Suarez, J. M.; Quiles, J. L.; Mezzetti, B.; Battin, M. The strawberry: Composition, nutritional quality and impact on human health. Nutrition 2012, 28, 9-19.

[2] Doymaz, I. Airflow drying kinetics of strawberry. Chemical Engineering and Processing 2008, 47, 914–919.

[3] Amami, E.; Khezami, W.; Mezrigui, S.; Badwaik, L. S.; Bejar, A. K.; Perez C. T.; Kechaou, N. Effect of ultrasound-assisted osmotic dehydration pretreatment on the airflow drying of strawberry. Ultrasonics Sonochemistry 2017, 36, 286–300.

[4]   Al Haddad, M.; Mounir, S.; Sobolik, V.; Allaf, K. Fruits & Vegetables Drying Combining Hot Air, DIC Technology and Microwaves," International Journal of Food Engineering 2008, 4 (6), Article 9. DOI: 10.2202/1556-3758.1491.

[5] Maritza, A.M.; Sabah, M.; Anaberta, C.M.; Montejano-Gaitán, J.G.; Allaf, K..Comparative Study of Various Drying Processes at Physical and Chemical Properties of Strawberries (Fragariavarcamarosa). Procedia Engineering 2012, 42, 267–282.

[6] Tang, J.; Feng, H.; Lau, M. Microwave heating in food processing. Advances in Bioprocessing Engineering 2002, 1-43.

[7] . Zhang, M.; Tang, J.; Mujumdar, A.S.; Wang, S. Trends in microwave-related drying of fruits and vegetables. Trends in Food Science & Technology 2006, 17, 524-534.

[8] Venkatachalapathy K.; Raghavan, G. S. V. Microwave drying of whole, sliced and pureed strawberries. Agricultural Engineering Journal 2000, 9, (1), 29-39.

[9] Gunasekaran, S. Grain drying using continuous and pulsed microwave energy.Drying Technology1990, 8 (5), 1039-1047.

[10] AOAC Official methods of analysis of the association of official analytical chemists. Moisture in dried fruits. (No. 930.04), Washington 1990.

[11] Gunasekaran, S. Pulsed microwave-vacuum drying of food materials. Drying Technology1999, 17(3), 395–412.

Bubble behavior of fructooligosaccharides syrup during the belt drying process

Zhao, L.[a,c]; Wang, D.[a]; Du, T.[a]; Yang, J.[c]; Li, J.[a,b]; Wu, Z.[a,b*]

[a]College of Mechanical Engineering, Tianjin University of Science & Technology, Tianjin, China 300222.

[b]Tianjin Key Laboratory of Integrated Design and On-line Monitoring for Light Industry & Food Machinery and Equipment Tianjin, China 300222.

[c]Key Laboratory of Efficient Utilization of Low and Medium Grade Energy, MOE, School of Mechanical Engineering, Tianjin University, Tianjin, China, 300072.

*E-mail of the corresponding author: wuzhonghua@tust.edu.cn

Abstract

This paper is aiming to study experimentally the bubbling and drying characteristic of fructooligosaccharides syrup in the belt drying process. A series of bubble images were acquired by a high-speed image acquisition system during the drying process. By analyzing the characteristics of bubble and drying, the drying process of fructooligosaccharides was divided into three periods: boiling transfer, natural convection and conduction and diffusion period. The drying rate in different transfer stage was: boiling transfer > natural convection > heat conduction and diffusion. The results of the study are of reference value to belt drying.

Keywords: fructooligosaccharides; belt drying; digital image processing; heat and mass transfer

1. Introduction

Fructooligosaccharides (FOS), also known as fructo oligosaccharides or oligosaccharides, is a kind of functional food additive which is widely used in food, health care products, dairy products, daily chemicals and feed. FOS is not digested and absorbed into the human body, but goes directly into the large intestine. It achieves the purpose of health care by selectively stimulating the proliferation of Bifidobacterium. Japan, Europe, Australia, New Zealand, the United States, China and other countries have approved the FOS as a functional food additive to add in food, health care products, even infant, diabetic food [1,2].

FOS syrup is made from sucrose and inulin by enzymatic method. Dehydrated FOS powder is easier to store and further utilized. There are three main drying technologies in industry to drying FOS syrup: spray drying, freeze drying and belt drying. In spray drying process: the viscosity of FOS syrup is too high to be atomized; the product's powder collecting rate is only about 45%, most of the dried products stick in the pipeline because its lower melting point [3]. Although vacuum freeze-drying can guarantee product quality, higher equipment investment and operating costs and longer drying cycle make this drying method difficult to industrialize [4]. In belt drying, the heat efficiency and product's powder collecting rate is far higher than spray drying. Many researchers thought that the heat transfer way in belt drying is only thermal conduction [5]. It was observed that the liquid material would boiling if the temperature of the conveyor belt was higher than the boiling point of the liquid material, so the heat transfer mode of the belt drying is not only thermal conduction but also boiling transfer and natural convection. The purpose of this study is to determine boiling heat transfer period, natural convection and thermal conduction period.

2. Materials and Methods

2.1. Materials and equipments

FOS powder: its purity was 95%; Distilled water; conveyor belt with a specification 80mm x 80mm; High speed image acquisition system; Digital display temperature controlled electric heating plate; Electronic balance.

2.2. Experimental method

Figure 1 showed the schematic diagram of the experimental system. The FOS syrup was dropped on the conveyor belt with a 1.5ml dropper, and then put it on the heating plate at a set temperature. The mass of the material was weighed in a certain time interval. Then the drying curve under different drying conditions was obtained. In this experiment, the temperatures were set at 120°C, 130°C, and 140°C, respectively.

During the drying process, the camera was placed above the material and the bubble image was taken and recorded at regular intervals. Placed the CCD high-speed camera horizontally, recorded the image of material's thickness at regular intervals.
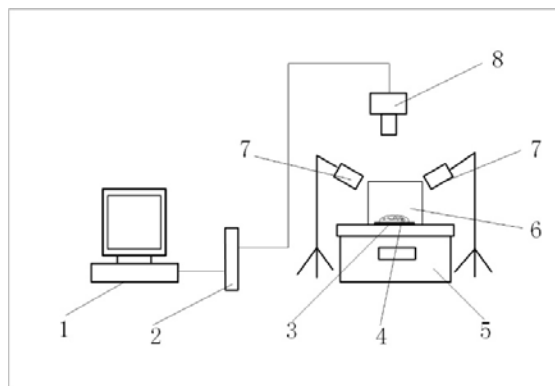
Fig. 1 Schematic diagram of an experimental device. 1. Computer, 2. acquisition card, 3. conveyor belt, 4. FOS syrup, 5. digital display temperature control heating plate, 6. transparent plexiglass cover, 7. LED lamps, 8. CCD high-speed camera.

2.3. Image processing

The captured bubble images were imported to in the imageJ software to mark the bubble boundary, gray scale transformation, edge extraction, binaryzation, hole filling and watershed segmentation, and then the binary image of the bubble was obtained. By photographing the steel ruler and marking the pixel size of 1cm length, the conversion relation between the actual length and pixel could be obtained. In addition, The pixel area of bubbles was obtained by using the particle analysis tool in imageJ software, and then convert it to the actual area. In the same way, the total area of the material could be measured by marking the material boundary.

3. Results and discussion

3.1. Drying characteristic

Figure.2 showed the drying curves and drying rate curves of FOS syrup with a concentration of 60% at different heating temperature conditions. Overall, the higher the heating temperature, the greater the drying rate, and the lower the final moisture content of the dried product. The drying rate had a distinct rising stage at 130°C, 140°C; while decreased from the beginning of drying at 120°C. The boiling point of the 60% FOS syrup was determined to be 105°C. When the heating temperature was 120°C, the degree of superheat, the difference between the heat plate temperature and the material saturation temperature, was too low to keep the material boiling. The boiling period lasted too short to

show on the drying rate curve, and the transfer mode in liquid material turned from boiling transfer to natural convection mode along with the evaporating of the moisture. As the drying process proceeds further, the material concentration was greater and greater, the corresponding viscosity and boiling point increased, which made the material more and more difficult to flow, the transfer process was mainly heat conduction and diffusion, so the drying rate in the whole drying process was getting lower and lower.

（a）*Drying curves (60%)*   （b）*Drying rate curves (60%)*
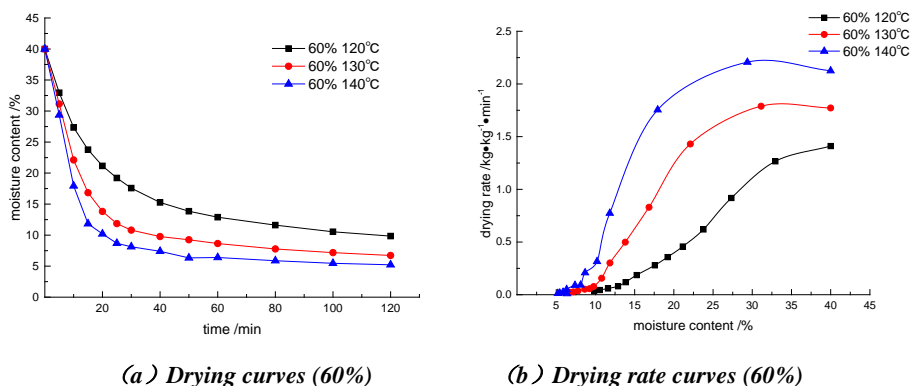
Fig. 2 Drying characteristic curves at different drying temperature

At 130°C, 140°C heating temperature, the degree of superheat was great enough to keep the material boiling for a while. At the beginning of drying process (the preheating section was too short to be ignored), the transfer mode inside the FOS syrup was mainly boiling transfer mode, so there was a distinct raising stage in the drying rate curves at 130°C, 140°C. With the further development of the drying process, the transfer mode in the material changed into natural convection, heat conduction and diffusion in turn, this was the same like at 120°C.

（a）*Drying curves (140℃)*   （b）*Drying rate curves (140℃)*
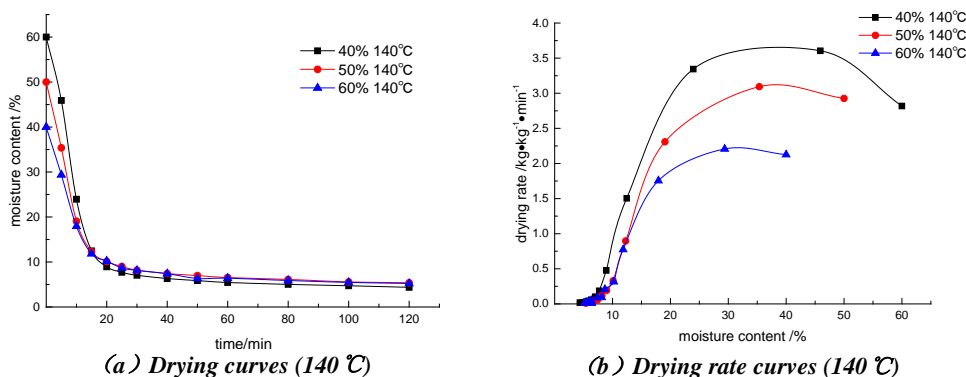
Fig. 3 Drying characteristic curves (initial concentration comparison)

21ST INTERNATIONAL DRYING SYMPOSIUM
EDITORIAL UNIVERSITAT POLITÈCNICA DE VALÈNCIA

Figure 3 showed the drying curves and drying rate curves of FOS syrup with different concentrations at the same drying temperature 140℃. There was a distinct rising stage in drying rate curves under these three concentrations which indicated that there must be boiling transfer period during the drying processes. The lower the concentration, the greater the drying rate. As everyone knows: the boiling point of the solution decreased with the decreased of concentration. At the same heating temperature 140℃, the temperature difference between the heating plate and the lower concentration material was greater than that of the higher concentration material, so the boiling process was more intense which induced a greater drying rate.

3.2. Bubble behavior and transfer mode
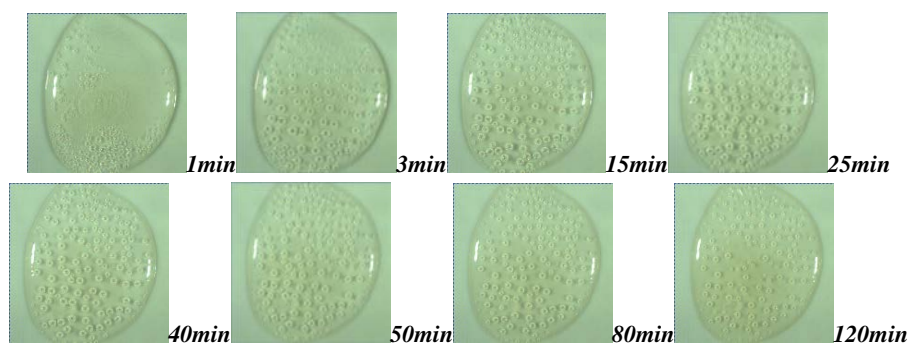
Fig. 4 Bubble images of different time (60% 120℃)

Figure4 showed the bubble behaviors inside FOS syrup with the concentration of 60% under 120℃ temperature. When the drying process was carried out for 1 minute, there were small bubbles formed on the heating plate. This indicated that the material had entered the boiling transfer period. The bubbles grew rapidly in 1-3 minutes because the material temperature was higher than that of the saturated vapor in bubbles. As the drying process proceeded, the degree of superheat decreased along with the increased of the liquid concentration, the bubbles grew up a little within 3-25 minutes. This indicated that the material temperature was a little higher than the saturated vapor temperature in the bubbles, the material concentration increased a little in this period, which meant that the drying rate was slower than the boiling transfer period. The transfer mode would be natural convection because the material fluidity was better in this period. After 25 minutes, the size of the bubble shrunk more and more slowly until the end of the drying. It was observed that the material had no fluidity in this period, so the transfer mode was heat conduction and diffusion.

Figure5 showed the bubble behaviors during drying process of 60% FOS syrup at 140℃. When the drying process was carried out for 5 minute, there were small bubbles formed on the heating plate. This indicated that the material had entered the boiling transfer period.

The bubbles grew rapidly in 5-7 minutes and joint together. In 7-10 minutes the bubbles interacted with each other, some formed larger bubbles, some ruptured. All of these bubble behaviors were because the material temperature was higher than that of the saturated vapor in bubbles. As the drying process proceeded, the degree of superheat decreased along with the increased of the liquid concentration, and the bubbles' behavior had a little change within 10-23 minutes. This indicated that the material temperature was a little higher than the saturated vapor temperature in the bubbles. The material concentration increased a little in this period, which meant that the drying rate was slower than the boiling transfer period. The transfer mode would be natural convection because the material fluidity was better in this period. After 23 minutes, the size of the bubble shrunk more and more slowly until the end of the drying. It was observed that the material had no fluidity in this period, so the transfer mode was heat conduction and diffusion. Table 1 showed the transfer modes during drying process under different drying conditions.
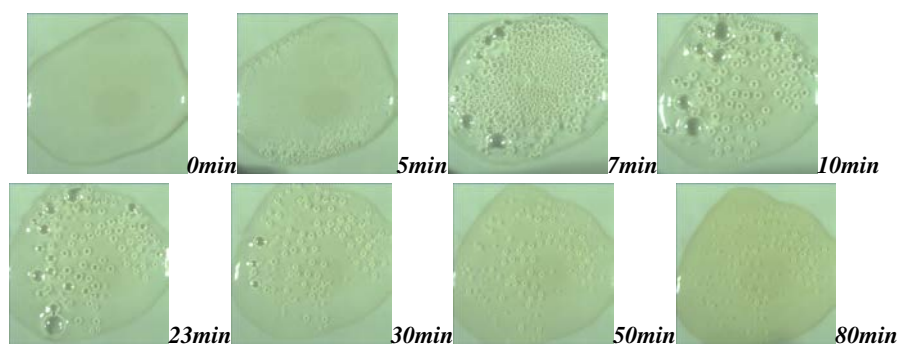
Fig. 5 Bubble images of different time (60% 140℃)

Table 1. The time of different stages (140℃)

FOS syrup concentration	boiling transfer	natural convection	heat conduction and diffusion
40%	0-13min	13-25min	>25 min
50%	0-12min	12-24min	>24 min
60%	0-10min	10-23min	>23 min

3.3. Drying rate

From the above analysis, it could be concluded: most of the moisture in the FOS syrup was removed in boiling and natural convection transfer period. Table 2 showed the average drying rate in different drying period at 140℃.

The calculation formula was as follows:

$$U = -\frac{mdX}{Adt} \qquad （1）$$

Where: U: the drying rate, kg/m^{2}h;

m: the weight of the dry material, kg;

X: moisture content (d.b.);

A: transfer area, m^2.

For boiling and natural convection transfer period, A was the area of the material projected on the heating plate, A$_j$.

For heat conduction and diffusion period, $A = A_j - A_b$

A_b :the bubbles projected area on the heating plate;

t: the drying time, min.

Table 2. The drying rate of different stages (140°C)

concentration	The drying rate of different stages/kg*m^{-2}*h^{-1}		
	boiling	natural convection	conduction and diffusion
40%	5.221	0.404	0.020
50%	4.408	0.381	0.030
60%	3.343	0.687	0.034

From Table 2 it could be concluded: the drying rate in boiling transfer period was 1 order of magnitude of that in natural convection period, and 2 orders of that in heat conduction and diffusion period.

4. Conclusion

(1) According to the bubble behaviors, the transfer mode in fructooligosaccharides syrup was divided into boiling transfer, natural convection and heat conduction and diffusion stage at higher heating temperature (130℃, 140℃, 150℃ for 60% syrup); at lower heating temperature (120℃), the boiling transfer was too short to be ignored and the transfer mode in material was mainly natural convection and heat conduction and diffusion.

(2)The drying rate in different transfer stage was: boiling transfer > natural convection > heat conduction and diffusion. At the same temperature, the lower the material concentration, the greater the drying rate; for the same material concentration, the higher the heating temperature, the greater the drying rate.

(3) In the boiling transfer period, there was distinct rising stage in drying rate curves, while decreased from the beginning without boiling transfer period.

5. Reference

[1] You Xin. Function and prospect on oligosaccharide. China Food Additives 2008(3):45-49.

[2] Yasmin, A.; Butt, M.S.; Yasin, M. et al. Compositional analysis of developed whey based fructooligosaccharides supplemented low- calorie drink. Journal of Food Science & Technology 2015, 52(3):1849-1856.

[3] MI Yun-hong. Preparation of G- FOS Powder by Spray Drying and Study on Characteristics of Powder. Drying Technology & Equipment2008, 6(2):82-85.

[4] LV Xiaoling.; Ding Jicheng.; MA Shuqing. Study on the Processing of High-purity Fructooligosaccharide by Vacuum Freeze-drying. Food and Fermentation Industries2008, 34(12):72-74.

[5] Liu Xuesong.; Qiu Zhifang.; Wang Longhu. et al. Mathematical modeling for thin layer vacuum belt drying of Panaxnotoginsengextracct. Energy Conversion and Management2009, 50(4):928-932.

Production of dry-cured pork loin using water vapour permeable bags

Fuentes, A., Verdú, S., Fuentes, C., Grau, R., Barat, J.M.

CUINA group. Department of Food Technology. Universitat Politècnica de València, Valencia, Spain

*E-mail of the corresponding author: anfuelo@upvnet.upv.es

Abstract

The aim of the present study was to develop an alternative method to the traditional curing process using water vapour permeable bags to obtain a dry-cured pork loin product. The dry-cured pork loins obtained by this mew process showed an adequate hygienic quality and good sensory acceptance. The salting-curing process using water permeable bags requires less manipulation, reduces waste generation and allows greater control during processing. This technique could be an interesting alternative to the traditional processes, improving the hygienic quality of the products and minimizing the environmental impact.

Keywords: Dry-cured loin; Salting; Water vapour permeable bags; Physicochemical properties; Sensory.

1. Introduction

The meat industry innovations are focus on improving the traditional curing processes. Producers seek new methods to reduce processing times, minimise salt waste, reduce overall weight loss and/or improve the hygienic quality. In this line, a new salting process in which the exact amount of salt to be absorbed by the product is directly dosed was proposed by Fuentes et al.[1]. This controlled procedure has been applied to different fish products reducing waste and product variability. The combination of this controlled salting process and vacuum packaging was able to accelerate NaCl absorption and dehydration, and can therefore cut the total processing time without affecting physicochemical parameters and sensory traits as compared with traditional fish products. Recently, materials with high water vapour transmission rates have been investigated. The use of highly water vapour-permeable bags (WP) facilitates the control of product dehydration by managing the temperature and humidity conditions, as with the traditional methods (unpacked) and minimising the risk of microbial contamination[2]. The combination of controlled salting process with WP bags has been studied to obtain smoke-flavoured fish with similar sensory traits to smoke products obtained by traditional methods and would optimise yields, reduce waste, speed up processes, maintain the hygienic quality during processes, and facilitate transportation and distribution at the same time[3,4]. For this reason, we considered that this promising technique could be implemented in the meat sector; making necessary adjusmtents.

The aim of the present study was to develop an alternative method to the traditional curing process using water vapour permeable bags to obtain a dry-cured pork loin product with physicochemical, microbiological and sensory characteristics similar to traditional products.

2. Materials and Methods

2.1. Experimental design

Pork loin processing was carried out using a controlled salting process where the exact amount of salt, necessary for the product to reach a targeted salt concentration, was dosed. The amount of salt added to each sample was individually calculated from the initial pork loin weight and the initial meat moisture. Pork loins were covered with a thin and homogeneous layer of salt, and then, vacuum-packed in the water vapour permeable bags. Initially, the salting-drying process was carried out at 85% relative humidity (RH) and 4 °C, and these conditions were modified during the process until reaching 65% RH and 10 ºC. The loins were kept in the drying chamber until a weight loss of 40% was reached. At the end of the process, the loins were analysed to determine their physicochemical parameters (moisture, salt, aw, pH, total nitrogen and non-protein nitrogen), texture, colour, microbial

counts (mesophilic bacteria, lactic acid bacteria and *Enterobacteriaceae*), and sensory profile.

2.2. Analitical determinations

2.2.1. *Physicochemical analyses*

During processing, weight changes in pork loin (ΔM_t) were calculated considerinf the sample weight at each time and the initial sample weight.

Moisture and lipid content were determined according to the AOAC methods[5]. The pH measurements were taken by a micropH 2001 digital pH-meter (Crison Instruments, S.A., Barcelona, Spain) with a puncture electrode (Crison 5231) at five different locations on pork loin sample. Chloride content was determined after sample homogenisation in distilled water using an automatic Sherwood Chloride Analyser Model 926 (Sherwood Scientific Ltd., Cambridge, UK). Water activity (a_w) was measured with an Aqualab dew point hygrometer model 4TE (Decagon Devices, Inc., Washington, USA). Total nitrogen (TN) and non-protein nitrogen (NPN) was measured following the method described by Standnik and Dolatowski[6].

Colour determination was directly performed on the pork loin slices. A Minolta CM-700-d photocolorimeter (Minolta, Osaka, Japan) was used, with a 10° observer and illuminant D65. Using the CIE L*a*b* coordinates (where L* is lightness, a* deviation towards red or green, and b* deviation towards yellow or blue), the psychophysical magnitudes of hue (hab*) and chroma (Cab*) were calculated.

A texture profile analysis (TPA) was performed on the prok loin samples with a Texture Analyser TA.XT2® 174 (Stable Micro Systems, Surrey, UK) equipped with a load cell of 250 N. For this measurement, a flat-ended cylindrical plunger (7.5mm diameter) was employed. This plunger was pressed into the sample at a constant speed of 1 mm/s until it reached 50% of sample height. Samples for this analysis were obtained from middle part of each loin, which were sliced and cut to obtain parallelepiped pieces (1x1x3 cm). Force-distance curves were processed to obtain hardness, chewiness, adhesiveness, springiness, cohesiveness and resilience parameters.

2.2.2. *Microbiological analyses*

Mesophilic bacteria, *Enterobacteriaceae* and lactic acid bacteria were determined according to the methods given by the following ISO standards [7,8,9]. The results were expressed as log cfu/g.

2.2.3. *Sensory nalysis*

A trained panel undertook the sensory evaluation using quantitative descriptive analaysis (QDA). Tests were done with the semi-structured scales (from 0 (very low) to 10 (very

high) by which attributes such red colour intensity, color homogeneity, brightness, hardness, adhesiveness, odour and cured flavor were evaluated.

2.3. Estatistical analysis

One-way analysis of variance (ANOVA) was conducted to establish significant differences between samples.The least significant difference (LSD) procedure was used to test for differences between averages at the 5% significance level. Statistical treatment was performed using Statgraphics Centurion XVI (Manugistics Inc., Rockville, MD, USA).

3. Results and discussion

3.1. Changes in phisicochemical parameters

During the elaboration of the dry-cured pork loin, the loins were weighed periodically with the aim of determining the product weight loss at each sampling time and estimating the end of the drying period (Fig. 1). The salting-curing process lasted for 75 days. In this sense, considering that cured loins have usually a curing period of about 3 months, it could be established that this new process would allow to slightly reduce processing time.
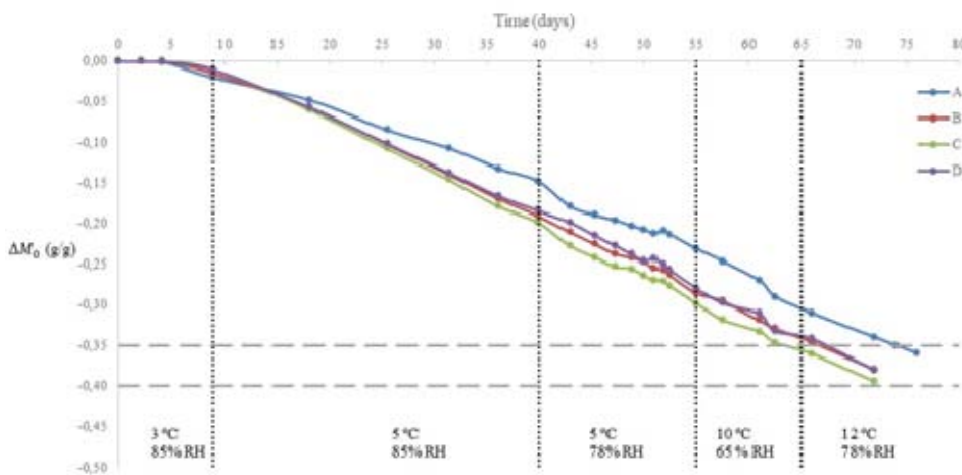
Fig. 1 Total weight changes during the salting process in pork loins obtained by using water permeable bags (average value ± standard deviation of each batch).

After processing, moisture of the dry-cured pork loin samples was determined. Moisture was separately measured in the central and in the outer part of the slices in order to detect crust formation during the process. Significant differences were observed between the moisture values of the central and outer parts of the loins (p<0.001), being these differences lower than 2% which evidences the absence of crusting in the pieces obtained by the

procedure developed in this work. Average moisture values were within the range established for commercial products.
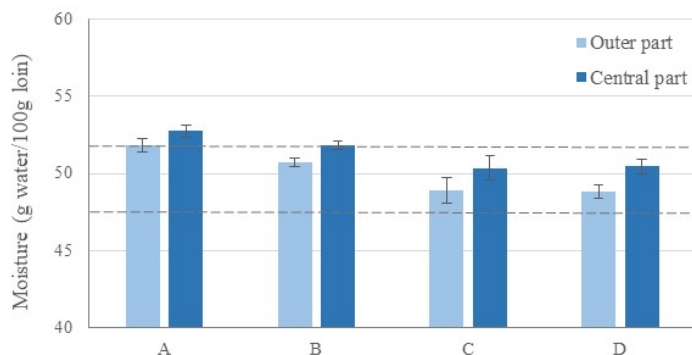
Fig. 2. Moisture values of dry-cured pork loins (mean values ± standard deviation, n=3). The dashed lines represent reference values.

Values of pH, salt content, and a_w in the different batches processed by the new procedure are shown in table 1.

Table 1. Physicochemical parameters in pork loins (average value ± standard deviation, n=3).

Parameter	A	B	C	D
pH	5.66 ± 0.02	5.78 ± 0.02	5.79 ± 0.05	5.87 ± 0.06
NaCl	4.43 ± 0.12	4.7 ± 0.2	4.59 ± 0.16	4.69 ± 0.14
a_w	0.9263 ± 0.0004	0.9196 ± 0.0001	0.9171 ± 0.0053	0.9198 ± 0.0015
TN	5.3 ± 0.6	5.3 ± 0.32	5.1 ± 0.5	4.7 ± 0.8
NPN	153 ± 15	199 ± 1.9	158 ± 30	196 ± 33

NaCl: salt content (g NaCl/100 g); TN: total nitrogen (mg/100 g dry matter), NPN: non-protein nitrogen (mg/100 g dry matter)

Salt content in the dry-cured products obtained in this study was similar than those reported by other authors[10,11]. The water content reduction and NaCl incorporation in the meat product as a consequence of the salting-curing process led to a aw values reduction. No significant differences were observed regarding to total nitrogen and non-protein nitrogen among samples. During curing period, the proteolytic breakdown of meat proteins increases nonprotein nitrogen concentration in the product. These changes in proteins are an important source of flavour compounds through the involvement of amino acids and small peptides[12]. The lower NNP content could be attributed to the shorter ageing period in the present study compared with the traditional processes

Mecanical and colour parameters were similar than those reported in other studies for this type of product (data not shown). These results indicate that the new procedure do not modify texture and appearance of the dry-cured loin compared to the traditional products.

3.2. Microbial analyses

The counts for mesophilic, lactic acid bacteria and *Enterobacteriaceae* are shown in Table 2. Dry-cured pork loin samples, showed low levels of mesophilic bacteria and *Enterobateriaceae* counts were below the detection limit ($<10^2$ CFU/g).

Table 2. Counts of mesophilic, lactic acid bacteria and Enterobacteriaceae (average values ± standard deviation, n=3)

Parameter	A	B	C	D
Mesophilic bateria	3.9 ± 0.2	3.7 ± 0.3	4.1 ± 0.5	3.16 ± 0.12
Lactic acid bacteria	3.1 ± 0.2	3.2 ± 0.3	3.6 ± 0.5	3.05 ± 0.13
Enterobacteriaceae	nd	nd	nd	nd

These results indicate that the hygienic conditions employed during processing were correct, wich allow to obtained a dry-cured product with a high hygenic quality. As it can be observed, the new procedure does not affect the growth of lactic acid, whose development is considered necessary to control the proliferation of certain altering microorganisms such as coliform bacteria[13].

A sensory analysis was carried out to check the acceptability of the new dry-cured pork loin. The tested samples were those obtained by the new technology (WP) and the commercial ones. The overall scores marked by the assessors for the sensory attributes of the samples are depicted in Fig. 3. No significant differences were recorded between samples for colour homogeneity, brightness and adhesiveness ($p>0.05$). However, commercial samples had a higher intnesity regarding the colour, hardness, and cured flavour. The lower intensity of those attributes in the new products could be correlated with dry-curing time. The increase on taste active components during processins of dry-cured meat products has been reported[14], therefore length of curing exibit a strong correlation with the typical flavour of these type of products.
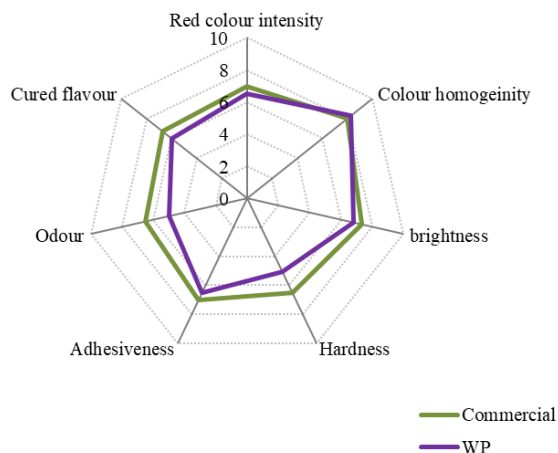
Fig. 3. Score average for the different attributes evaluated in samples of commercial dry-cured prok loin and the new product (WP).

4. Conclusions

The processing conditions used and the exact dosage of the salt have been adequate to obtain a dry-cured pork loin with moisture, salt and a_w values similar to the commercial products. These conditions have allowed to obtain a product with an adequate hygienic quality and a sensory profile similar to the traditional product. This new salting-curing process using water vapor permeable bags present several advantages compared to the traditional processes such as the lower handling of the product, waste reduction and higher control of the process.

5. References

[1] Fuentes, A.; Barat, J.M.; Fernández-Segovia, I.; Serra, J.A. Study of sea bass (*Dicentrarchus labrax* L.) salting process: kinetic and thermodynamic control. Food Control 2008, 19 (8), 757–763.

[2] Rizo, A.; Mañes, V.; Fuentes, A.; Fernández-Segovia, I.; Barat, J.M. Physicochemical and microbial changes during storage of smoke-flavoured salmon obtained by a new method. Food Control 2015, 56, 195-201.

[3] Rizo, A.; Mañes, V.; Fuentes, A.; Fernández-Segovia, I.; Barat, J.M. A novel process for obtaining smoke-flavoured salmon using water vapour permeable bags. Journal of Food Engineering 2015, 149, 44-50.

[4] Rizo, A., Fuentes, A., Fernández-Segovia, I., Barat, J.M. Smoke-flavoured cod obtained by a new method using water vapour permeable bags. Journal of Food Engineering 2016, 179, 19-27.

[5] Official Methods of Analysis, Association of Official Analytical Chemists, Washington 1997

[6] Stadnik, J.; Dolatowski, Z.J. Changes in selected parameters related to proteolysis during ageing of dry-cured pork loins inoculated with probiotics. Food Chemsitry 2013, 139, 67-71.

[7] ISO 15214. (1998). Horizontal method for the enumeration of mesophilic lactic acid bacteria e Colony-count technique at 30 ºC. Geneva, Switzerland: International Organization for Standardization.

[8] ISO 21528-2. (2004). Horizontal methods for the detection and enumeration of Enterobacteriaceae Part 2: Colony-count method. Geneva, Switzerland: International Organization for Standardization.

[9] ISO 4833. (2003). Horizontal method for the enumeration of microorganisms. Colony-count technique at 30 ºC. Geneva, Switzerland: International Organization for Standardization.

[10] Ventanas, J., (2006). El jamón ibérico. Madrid: Ediciones Mundi-Prensa.

[11] Aliño, M.; Grau, R.; Toldrá, F.; Blesa, E.; Pagán, M.J.; Barat,J.M. Influence of sodium replacement on physicochemical properties of dry-cured loin, Meat Science 2010, 83(3), 423─430

[12] Morales, R.; Serra, X.; Guerrero, L.; Gou, P. Softness in dry-cured porcine biceps femoris muscles in relation to meat quality characteristics and processing conditions. Meat Science 2007, 77(4), 662–669.

[13] Yamanaka, H.; Akimoto, M.; Sameshima, T.; Arihara, K. Itoh, M. Effects of bacterial strains on the development of the ripening flavor of cured pork loins. Journal of Animal Science 2005, 76: 499-506.

[14] Flores, M.; Aristoy, M.C.; Spanier, A.M.; Toldrá, F. Non-Volatile Components Effects on Quality of "Serrano" Dry-cured Ham as Related to Processing Time. Journal of Food Science 1997, 62, 1235-1239.

Reducing sodium content in dry-cured pork loin. A novel process using water vapour permeable bags

Fuentes, A., Verdú, S., Fuentes, C., Grau, R., Barat, J.M.

CUINA group. Department of Food Technology. Universitat Politècnica de València, Valencia, Spain

*E-mail of the corresponding author: anfuelo@upvnet.upv.es

Abstract

The objective of the present study was to test the feasibility of a new salting-curing process using water vapour permeable bags to obtain a reduced sodium dry-cured loin. The process was applied with and without partial substitution of sodium chloride by potassium chloride. The developed methodology allows to obtain a dry-cured pork loin with partial sodium substitution similar to the product without reduced sodium content, regarding to their physicochemical parameters, texture and colour. The results indicated that the new process allowed to obtain a cured meat product with 50% less sodium and similar characteristics than the traditional products.

Keywords: sodium replacement; water vapour permeable bags; dry-cured loin; salt content; physicochemical parameters .

1. Introduction

Numerous studies have demonstrated that the dietary intake of sodium significantly influences blood pressure levels and contributes to an increased risk of coronary heart disease and strokes[1,2]. In industrialized countries, the sodium intake exceeds the nutritional recommendations; for these reasons, health national and international authorities have set targets for a reduction in the sodium consumed in the diet[3]. Studies reveal that the principle sources of sodium in the diet are processed foods. A common EU framework for salt reduction has been developed to reduce the salt intake at population level. In this sense, the EU framework will focus on a limited number of food categories, but which contribute largely to salt intake in the diet in many Member States. Certain food categories such as bread, meat products, cheeses and ready meals have been identified as being among the major contributors across the EU, and are therefore targets for salt reduction at EU level[4]. Manufacturers of dry-cured meat products are facing the challenge to lower the sodium content in their products [5,6]. In dry-cured meat products, sodium chloride is an essential ingredient which contributes to the water holding capacity, protein binding, colour, flavour and texture. Moreover, salt decreases water activity (a_w), and this significantly affects the shelf-life of foodstuffs[7]. In addition to an overall bacteriostatic effect of salt, it can also cause a slight shift in the microbial flora toward slower growing, gram positive bacteria species that are less detrimental to product quality and require more time to reach spoilage levels. The partial replacement of sodium chloride by potassium chloride has been proposed as a possible strategy to reduce the sodium content of this type of products [8-11]. KCl is less expensive than other salt replacers, has similar properties as NaCl, and also exhibits possible health benefits[12,13]. However, the addition of KCl is limited by its bitter and astringent taste demanding a careful choice of the level of substitution[12]. Gou et al. [14] found that NaCl can be replaced by KCl up to 40 % with only slightly affecting sensory properties in fermented sausages and dry-cured loin. In this sense, Armenteros et al.[12] further reported that substitutions of up to 50 % by KCl are possible affecting neither sensory properties nor proteolysis and lipolysis phenomena in dry-cured loin. However, during processing the water transport is influenced if KCl is present leading to a decreased weight loss during salting.

The objective of the present study was to test the feasibility of a new salting-curing process using water vapour permeable bags to obtain a reduced sodium dry-cured loin. A novel salting-curing process using water vapour permeable bags was applied with and without partial substitution of sodium chloride by potassium chloride.

2. Materials and Methods

2.1. Experimental design

The salting process was carried out with a thermodynamic control by placing a known amount of salt on the product surface and allowing it to dissolve and penetrate[16]. The amount of salt to be added to the loin was calculated considering a moisture and salt content in the final product similar to the comemercial dry-cured loin (X_{obj}^{Cl} = 0.06 g Cl/g dry material and x^w_f = 0.47 g/g (w/w)). Chloride amount, M_{Cl} (g of chloride), added to each loin was individualy calculated according to Eq. (1) considering the initial weight of the loins, M_0 (g):

$$M_{Cl} = X_{obj}^{Cl} \cdot M_{Cl} \cdot (1 - x_0^w)$$

(1)

Finally, salt amount, M_{salt} (g), was calculated according to the salt composition (100% NaCl and 50% NaCl:50% KCl). Pork loins were covered with a layer of salt, and then, samples were vacuum-packed in the water vapour permeable bags. Initially, the salting-drying process was carried out at 90% relative humidity (RH) and 3 °C, and these conditions were modified during the process until reaching 65% RH and 20 ºC. Pork loins were kept in the drying chamber and periodically weighted until reaching a weight loss of 50%.

2.2. Analitical determinations

2.2.1. *Physico-chemical analyses*

Moisture content was determined in accordance with AOAC methods 950.46[16]. Chloride content was determined after sample homogenisation in distilled water using an automatic chloride analyser (Sherwood Scientific Ltd., Cambridge, UK). The same extract was used to determine sodium and potassium contents by absorption spectrophotometry.The pH measurements were taken by a digital pH-meter (Crison Instruments, S.A., Barcelona, Spain) with a puncture electrode at five different locations on pork loin sample. Water activity (a_w) was measured with a dew point hygrometer (Decagon Devices, Inc., Washington, USA). Texture profile analysis (TPA) was performed by use of a Texture Analyser TA.XT2® (Stable Micro Systems, Surrey, UK) equipped with a load cell of 250 N. Samples were obtained by cutting out parallelepiped pieces of 1 x 1 x 2,5 cm from the central part of each loin silce. For TPA analysis a flat-ended cylindrical plunger (7.5cm diameter) was pressed into the sample at a constant speed of 1mm/s until it reached 50% of the sample height. Force-distance curves were processed in order to obtain the texture parameters: hardness, cohesiveness, elasticity, chewiness and resilience. Colour determination was performed using a photocolorimeter (Minolta, Osaka, Japan) with a 10° observer and illuminant D65. The colour system employed was CIE L*a*b*.

2.2.2. Sensory analysis

Nine selected and trained assessors evaluated the dry-cured products using quantitative descriptive analaysis (QDA). Sensory attributes were grouped in visual appearance of the slice (color intensity and colour homogeneity), texture (hardness, adhesiveness and chewiness) and flavor (saltiness and cured flavour). Attributes were scored using an unstructured scale from 0 (very low) to 10 (very high).

2.3. Statistical analysis

One-way analysis of variance (ANOVA) was conducted for each physicochemical parameter and sensory attribute to establish significant differences between the typer of salt employed. The least significant difference (LSD) procedure was used to test for differences between averages at the 5% significance level. Statistical treatment was performed using Statgraphics Centurion XVI (Manugistics Inc., Rockville, MD, USA).

3. Results and discussion

The average values of moisture, aw, and chloride, sodium and potassium content in pork loin samples salted with both type of salt are shown in Figure 1. As expected, the salting-drying process significantly lowered the moisture and aw values, and chloride concentration increased compared with fresh meat. The procedure combining a controlled salting with the permeable bags was applied to reduce the impact of the different cations diffusivities duirng the salt uptake. In this procedure, the exact amount of salt to be absorbed by the loin is directly dosed and then packing forces the salt uptake, minimizing the differences in the Na and K transport. In order to determine mass transfer differences between salts, after processing pork loins were analyzed differentiating between the outer part and central part and the edges of said sections. This differentiation would also allow to detect crust formation. The crust formation poses serious problems for the certification of Serrano ham as a Guaranteed Traditional Speciality (ETG). According to ETG Serrano specifications, the moisture gradient between the outer part and the centre of the ham should not be higher than 12%[17].

Average moisture values of outer and central parts of the slices were 50.2% and 59.9% (w/w) for loins salted with 100% NaCl and 60.3% and 51.1% (w/w) for loins salted with 50% KCl-50% NaCl. No significant differences were observed depending on the type of salt used. It should be noted that the moisture values in the center of the loins were higher than what would be desirable for this type of product. According to the quality standard of meat products, dry-cured loin ("embuchado lomo") should have a maximum moisture content of 55.0%[18]. Taking into account the physico-chemical characteristics defined in this standard, it would be interesting to optimize the curing conditions with the aim of reducing the moisture content in the final product.
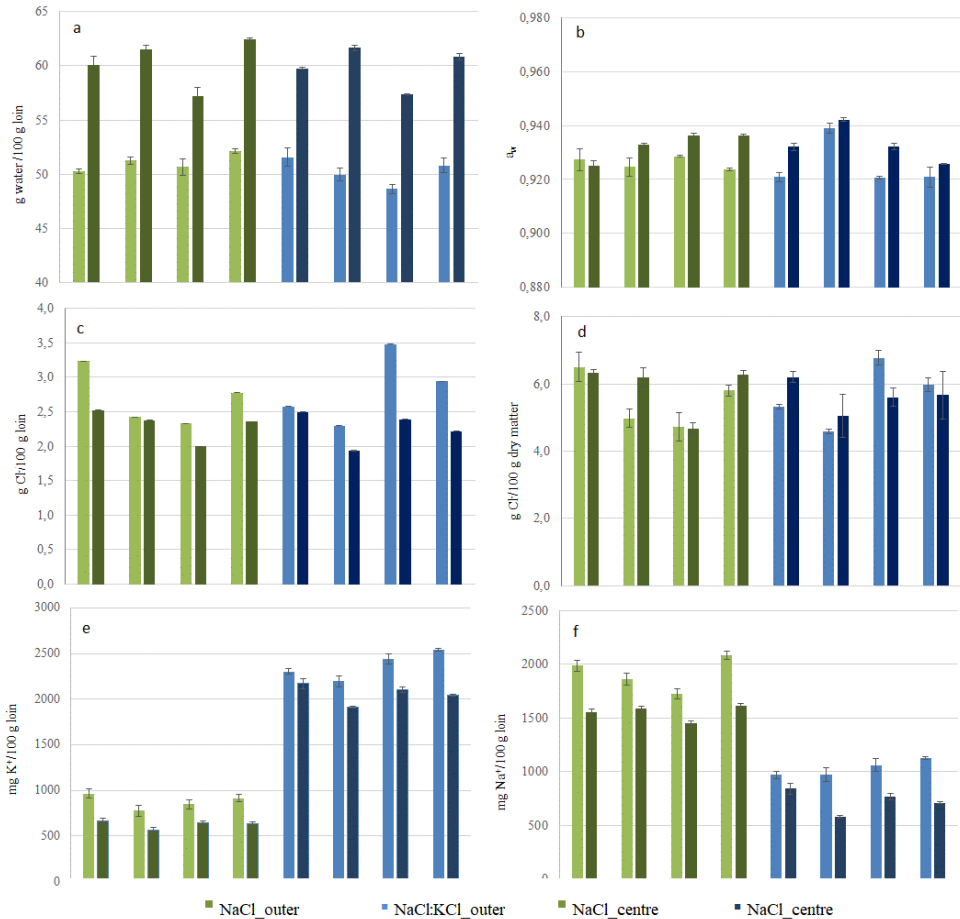
Figure 1. Moisture (a), a_w (b), chloride content expressed in wet basis (c), chloride content expressed in dry basis (d), sodium content (e), potassium content (f) of the dry-cured loin samples obtained by using 100% NaCl and 50%NaCl-50%KCl. Mean values ± standard deviation (n = 3).

Similar differences between slice areas were observed in chloride, potassium, and sodium content (Fig. 1). Solute concentration in the central part of the slice was significantly lower than in the outer part of the slice (p<0.001). The application of the new salting-curing process has made it possible to achieve a 50% reduction in sodium in the final product, as it had been established as a target. These results are especially interesting when compared with the alternatives salts in traditional processes, where it is not guaranteed that the final product will maintain this Na: K ratio, due to the differences in diffusivity of both salts. This ratio in the product with low sodium content was close to 1 (Na: K), being a nutritional advantage.

Different studies have shown that sodium substitution by potassium could affect the mass transfer phenomena that occurs during the salting process. In this sense, different authors have reported that partial sodium replacement by potassium decreased water loss during processing[13,19]. This could be explained by the larger size of the K^+ ion, which would have more difficulty in penetrating inside the muscle. The salt uptake and water outflow occurs simultaneously, for this reason when replacement strategies are applied using traditional techniques final products had higher moisture values, longer curing processes are required or higher amounts of salt should be dosed to achieve an adequate a_w value.

Dry-cured pork loin exhitited pH values ranged from 5.8 to 6.2 (data not shown) During processing, the pH values show a tendency to increase slightly, both in the surface and in the interior, throughout the process[20]. The type of salt did not affect any of the texture parameters evaluated (data not shown). These results agreed with those obtained in other studies where the effect of the partial sodium replacement by other salts in dry-cured meat products has been evaluated[5,13,12,15]. Aliño et al [15] concluded that the partial substitution of NaCl by KCl in dry-cured pork loin did not affect texture of the product, except for a slight reduction of the elasticity when sodium substitution by potassium was higher than 50%. Colour of samples was affected by the type of salt employed. In this sense, pork loins salted with 100% NaCl showed values of a and b coordinates higher than samples salted with 50% KCl-50% NaCl. Differences in lightness were not statistically significant (data not shown).

The overall scores marked by the assessors for the sensory attributes of the different evaluated samples are depicted in Fig. 4. No significant differences were recorded between samples for colour and texture attribute ($p > 0.05$), although the scores for taste and odour were slightly higher for pork loins salted with 100% NaCl.
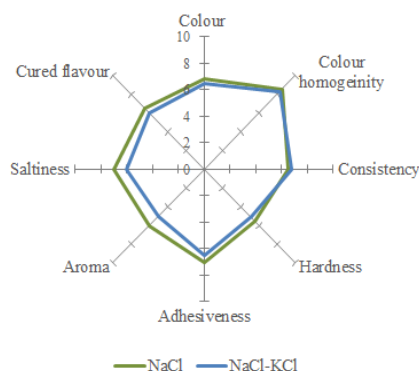
Fig. 2. Sensorial analysis of pork loin salted with 100% NaCl and 50%NaCl:50% KCl

4. Conclusions

The developed methodology allows to obtain dry-cured products with partial replacement of sodium by potassium chloride with similar characteristics than products without reduced sodium content. The conditions of relative humidity and temperature used in this study have not been adequate to avoid the crusting of the pieces during the processing of cured loin. The replacement of 50% of NaCl by KCl had significant effect on some of the sensory atributes. The new process of controlled salting-curing using water vapor permeable bags allows to reduce the handling operations of the product and the use of salt, which is an advantage to help improve the hygienic quality of the product and reduce the environmental impact the generation of brine waste that is produced in these industries

5. References

[1] Inguglia, E.S.; Zhang, Z.; Tiwaria, B.K..; Kerry, J.P.; Burgess, C.M.. Salt reduction strategies in processed meat products – A review. Trends in Food Science & Technology 2017, 59, 70─78.

[2] Ruusunen, M., Puolanne, E., 2005. Reducing sodium intake from meat products. Meat Science 70, 531–541.

[3] WHO/FAO, Diet, nutrition and the prevention of chronic diseases. WHO Technical Report Series 916, World Health Organization, Geneva, 2003.

[4] European Commision. Food and Health in Europe. Survey on Members States' Implemeentation of EU Salt Reduction Framework 2003. http://www.euro.who.int/document/E82161.pdf.

[5] Aliño, M.; Grau, R.; Fuentes, A.; Barat, J.M. Influence of low-sodium mixtures of salts on the post-salting stage of dy-cured ham process. Journal of Food Engineering 2010, 99, 198─203.

[6] Toldra, F., Reig, M. Innovations for healthier processed meats. Trends in Food Science & Technology 2011, 22(9), 517-522.

[7] Toldrá, Fidel, and M. Barat. "Recent patents for sodium reduction in foods." Recent patents on food, nutrition & agriculture 1.1 (2009): 80-86.

[8] Gelabert, J.; Gou, P.; Gerrero, L; Arnau, J. Effect of sodium chloride replacement on some characteristics of fermented sausages. Meat Science 2003, 65, 833─839.

[9] Ibañez, C.; Quitanilla, C.; Irigoyen, A.; Cid,C.; Astiasarán, I.; Bello, J. (1996). Dry fermented sausages elaborated with Lactobacillus plantarum- Staphylococcus carnosus. Part I: Effect of partial replacement of NaCl with KCl on the stability and the nitrosation process. Meat Science, 44:227─234

[10] Wu, H.; Zhang, Y.; Long, M.; Tang, J.; Yu, W.; Wang, J.; Zhang, J. Proteolysis and sensoray properties of dry-cured bacon as affected by partial substitution of sodium chloride with potassium chloride. Meat Sciecne 2014, 96, 1325─1331.

[11] Aliño, M.; Grau, R.; Toldrá, F.; Blesa, E.; Pagán, M.J.; Barat,J.M. Influence of sodium replacement on physicochemical properties of dry-cured loin, Meat Science 2010, 83(3), 423─430

[12] Armenteros, M.; Aristoy, M. C.; Barat, J.M.; Toldrá, F. Biochemical changes in dry-cured loins salted with partial replacements of NaCl by KCl. Food Chemistry 2009, 117(4), 627─633.

[13] Aliño, M.; Grau, R.; Toldrá, F.; Blesa, E.; Pagán, M. J.; Barat, J. M. Influence of sodium replacement on physicochemical properties of dry-cured loin. Meat Science 2009, 83, 423─430.

[14] Gou, P.; Guerrero,L.; Gelabert, J.; Arnau, J. Potassium chloride, potassium lactate and glycine as sodium chloride substitutes in fermented sausages and in dry-cured pork loin. Meat Science 1996, , 42:37-48.

[15] Fuentes, A; Barat, J.M.; Fernández-Segovia, I.; Serra J.A. Study of sea bass (*Dicentrarchus labrax* L.) salting process: kinetic and thermodynamic control Food Control 2008, 19 (8), 757-763

[16] Official Methods of Analysis (16th ed.), Association of Official Analytical Chemists, Washington (1997)

[17] Fundación Jamón Serrano (1998). Pliego de condiciones para elaboración del Jamón Serrano.

[18] BOE, Boletín Oficial del Estado (2014). Real Decreto 474/2014, de 13 de junio, por el que se aprueba la norma de calidad de derivados cárnicos.

[19] Comaposada, J. Arnau, P. Gou, Sorption isotherms of salted minced pork and of lean surface of dry-cured hams at the end of the resting period using KCl as substitute for NaCl. Meat Science 2007, 77(4), 643─648

[20] Arnau, J.; Serra, X.; Comaposada, J.; Gou, P. & Garriga, M.Technologies to shorten the drying period of dry-cured meat products. Meat Science 2007, 77, 81–89.

Study on the general dynamic model of biomass drying processes

Wang L.[a]*; Li X.[a]; Li Q.L.[b]*; Lu D.F.[a]; Li B.[a]; Zhu W.K.[a]; Zhang M.J.[a]; Zhang K.[a]; Deng N.[a]

[a]Zhengzhou Tobacco Research Institute of CNTC, Zengzhou 450001, China
[b]China Tobacco Sichuan Industrial Co., Ltd., Fujian 361022, China

*E-mail of the corresponding author: 181368810@qq.com

Abstract

Nowadays most studies of drying processes dynamics are established on empirical models without clear physical meanings, which could not predict the drying characteristic on different dryers. In order to describe the change of temperature and water content in the cut tobacco in different dryers, a mathematical model based on heat and mass transfer phenomena was developed, and the model employed the relationship of equilibrium moisture content and air humidity as basis, the difference of moisture between biomass and wet air as mass transfer driver, and the difference of temperature between biomass and wet air as heat transfer driver. The drying experiments under different air temperature and humidity are carried out on the batch rotary dryer, and the variance of temperature and moisture content in the biomass is obtained by using infrared thermometer and oven. The model is validated by two parameters with experiment data under each condition of air temperature and humidity. The results show that the drying dynamic model is well on accuracy and universality, and it could be applied on different drying device to predict the characteristic of kinds of drying processes.

Keywords: cut tobacco; drying dynamics; equilibrium moisture content; heat transfer; mass transfer.

1. Introduction

Drying is an important operation to manufacture many products that benefit mankind being drying technology more widely used in biomass, such as drying of grains, seeds, fruits, vegetables, fodder, woody particles, tobacco, and so on.

Measuring the drying process of each individual particle or fiber is almost impossible, but many researchers prefer to gain understanding of the processes in the most comprehensive way as possible. Mohammad et al. (2016) applied the eXtended Discrete Element Method (XDEM) to simulate the temperature, moisture content and drying rate of woody particles during drying in a circulating cylinder. Koji et al. (2014) investigated a simplified quantitative model that simulates changes in the water content and the temperature of the tobacco midrib, and the validity of the model is examined. Zhu et al. (2015) introduced a two-stage convective drying strategy for cut tobacco drying, and the temperature and moisture evolution of cut tobacco were simulated by developed heat and mass transfer models. The above results indicate that obtaining the material's temperature and water content changes in detail under different operating conditions and fitting of measured data with an appropriate drying model can help us to set the optimum operation condition, as well as improve the quality of material in drying process.

Drying process of biomass using the rotary dryer is the one of important process in cigarette factory. Rotary dryers are designed so as to force the drying material to circulate along the unit while in contact with the air, in such way the best mass and heat exchange is attained. Good control scheme may further help improve the intrinsic quality and external quality of tobacco production. Thus a comprehensive understanding of the process characteristics of tobacco water content and surface temperature in the rotary dryer are useful information for setting up suitable control schemes. So the present work has been undertaken to study the drying characteristics of cut tobacco by using a specially designed rotary dryer. A dynamic model has been implemented and found to be satisfactory. The temperature and water content evolution of the cut tobacco as biomass at different drying temperatures were calculated and compared with the results of the experimental investigation.

2. Materials and methods

Cut tobacco was used in this study，which was produced in the Fujian Province of China. Before each experiment, water contents of the cut tobacco samples were adjusted to 22.5±0.1 % by adding calculated amounts of water to the cut tobacco samples respectively.

In order to obtain real time drying characteristics of the material in the dryer, a laboratory rotary dryer was purposely designed in the principle shown in Fig 1.
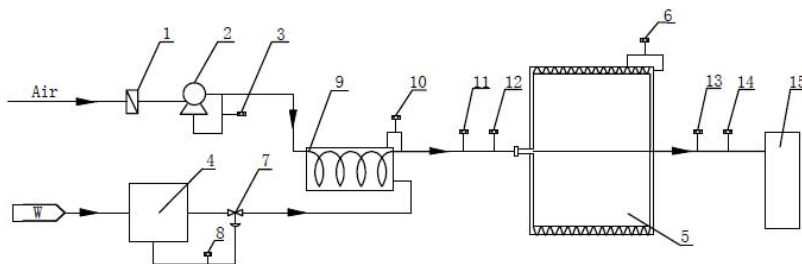
Fig. 1. Schematic diagram of the laboratory scale rotary dryer: (1)air filter, (2)blower, (3)air flow meter, (4)steam generator, (5)drying chamber, (6)chamber temperature controller, (7)electrical valve, (8)vapor flow meter, (9)mixing chamber with electrical heater, (10) air temperature controller, (11)inlet air temperature and humidity recorder, (12)inlet air flow meter, (13)outlet air temperature recorder, (14)outlet air humid recorder, (15)drain

The length of the laboratory dryer is just 1.0 meter, and its diameter has maintained the same diameter as industrial rotary dryer about 1.9 meters. During the experiments, the, inlet humidity and temperature can be controlled to any practical value as the inducstrial dryer by mixing air with the superheated steam, while the average velocity of the flow was also set at a prescribed value. By detecting the water contents and temperatures of the cut tobacco sample at different drying moments, we can simulate the whole drying process with this laboratory rotary dryer.

The drying experiments were carried out in the laboratory drying chamber. The inlet temperature was respectively set to 338, 358, 378, 398 and 418 K, while the average velocity of the flow was kept to 0.067 ms^{-1}, and only the compressed air from atmospheric environment (28 ℃ and RH 0.77) was used without inducing the steam in the current study.

During the drying process, the sampling interval was set to 30 seconds, and the sampling groove was quickly pulled out from the chamber. The temperature of the cut tobacco samples in the groove was quickly measured by an infrared thermal imaging device within 2 seconds, and simultaneously cut tobacco samples were taken to offline to measure the water contents separately by weight loss method. The each sample amount taken away for weight analysis was 10 g approximately, which is 0.5 % of the total 2 kg.

3. Mathematical model

In order to simulate the mass transfer process, we assume that on the surface of biomass, there exists a film of wet air, which is equilibrium with water content in the biomass. The relationship of equilibrium can be written as

$$RH_e = 1 - \exp\left(-ATX^B\right) \tag{1}$$

where RH_e represents the relative humidity of the film, T denotes the temperature of biomass, the parameter A and B indicate the drying characteristic of biomass.

According to the Antoine equation, the vapor pressure of the film can be expressed as the product of saturated vapor pressure and relative humidity, which is

$$p_e = 1.1939 \times 10^{10} \exp\left(-\frac{3826.36}{T - 45.47}\right) RH_e \tag{2}$$

where p_e is the vapor pressure of the film with Pa.

Using the state equation of ideal gas, we can get the concentration of vapor in the film as

$$C_e = \frac{1.1939 \times 10^{10} \exp\left(-\dfrac{3826.36}{T - 45.47}\right)\left(1 - \exp\left(-ATX^B\right)\right)}{RT} \tag{3}$$

where C_e represents the concentration of vapor in the film with unit mol.m^{-3}.

Meanwhile, the vapor concentration in the bulk surrouding the biomass, which indicates dry air, can be express as

$$C_b = \frac{1.1939 \times 10^{10} \exp\left(-\dfrac{3826.36}{T_b - 45.47}\right) RH}{RT_b} \tag{4}$$

where C_b represents the vapor concentration in the bulk with unit mol.m^{-3}, and T_b is the temperature in the bulk, which is equal to the temperature of the rotary dryer wall.

In order to obtain the mass transfer equation of drying process, we assume that only the convective mass transfer occurs but the diffusion is ignored, so the rate of mass transfer can be written as the product of the convective mass transfer coefficient and driver of mass transfer, which is expressed as the difference of vapor concentration in common. The above statement can be translated as the following formula

$$N = h_m A_m \Delta C \tag{5}$$

where $h_m A_m$ is convective mass transfer coefficient including the mass transfer surface area.

So the drying process of biomass per kilogram can be gotten as the following differential equation

$$\frac{1}{M_{H_2O}}\frac{dX}{dt} = N \tag{6}$$

where X is the dry base moisture content of biomass with unit kg.kg^{-1}, M_{H_2O} is molecular mass of water, and its unit is kg.mol^{-1}.

On the other hand, the heat transfer equation of drying process is not difficult to describe. Since the change of temperature of biomass can be contributed to two facts, the one is convective heat transfer from the hot air, the other is endothermic vaporization during the drying of cut tobacco. So the heat transfer equation can be written as

$$\left(XC_{p,w} + C_{p,t} \right)\frac{dT}{dt} = hA_m(T_b - T) + \Delta H_w \frac{dX}{dt}$$

where hA_m denotes the convective heat transfer coefficient combined with inseparable heat transfer area, ΔH_w is the latent heat of vaporization of water, $C_{p,w}$ is the specific heat capacity of the water with unit J·m^{-3}·K^{-1} and $C_{p,t}$ is the specific heat capacity of cut tobacco with unit J·m^{-3}·K^{-1}.

For the integrity of the heat transfer equation, the latent heat of vaporization and the specific heat equation of water are functions of bulk temperature, and they can be expressed as

$$\Delta H_w = 2891833\left(1 - \frac{T_b}{647.13}\right)^{0.321}$$

$$C_{p,w} = 1.459\times10^{-6}T_b^4 - 1.971\times10^{-3}T_b^3 + 1.005\times T_b^2 - 228.7T + 23750$$

But the specific heat capacity of cut tobacco is remained constant for simplication of the mathematical model, which is obtained as the following value as

$$C_{p,t} = 1.4286\times10^3$$

In summary, the mass transfer equation and the heat transfer equation are clearly shown, which is the govering equations of the drying process. In the mathematical model, the two parameters A and B is related to the properties of biomass, and the convective mass and heat transfer coefficients are the key factors of the model, which are determined by the operation conditions such as inlet velocity of hot air. The two coefficients can not be accuraly obtained before the drying experiments or by other independent experiments, but they could be fitted by the temperature and moisture curves of biomass during drying process.

4. Results and discussion

The mathematical model was fitted by using the functions ode45 and lsqnonlin on MATLAB® 2017a to get the heat transfer and mass transfer coefficients, where the function ode45 is used for solving the ordinary differential equations by 4 order Runge-Kutta methods, and the function lsqnonlin is used for exploring the optical parameters by nonlinear least squares method. Through the experiment data at different dryer temperature, the heat transfer coeffiecient is 31.2245 with unit $W \cdot m^{-3} \cdot K^{-1}$ and the mass transfer coeffiecient is 0.0651 with unit $kg \cdot m^{-3} \cdot K^{-1}$. It is obvious that the two most important parameters keep constant for all the drying conditions at different inlet temperature.

Figure 2 shows the temperature and moisture content of cut tobacco in the rotary dryer at different inlet temperature range from 338K to 418K. It can be seen that the simulated curves of water content and temperature are well consistent with the experiment data at each time. It is mean that the mathematical model with only two coefficients can reveal the main mechanism of the drying processing in the labarotary rotary dryer.

It is easy to see that the moisture content of cut tobacco decreases with time and the temperature of cut tobacco increases with time. Moreover, the variance of both moisture content and temperature can be separated into three stages. At the initial stage, the temperature rises up fastly but the moisture content goes down slowly, then the temperature remains stable and the moisture content falls down with constant drying rate at the medium stage, finaly at the last stage the temperature of cut tobacco grows up distinctly but the sample moisture content slightly decreases for a long time. We also can find that when the inlet temperature increases, the first stage almostly keeps unchanged, and the medium stage continues a short time period, but the last stage occupies a long time.
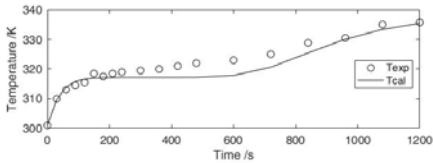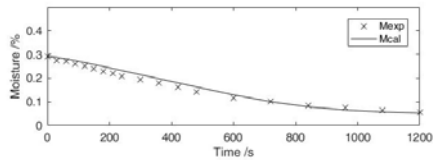
(a) 338K
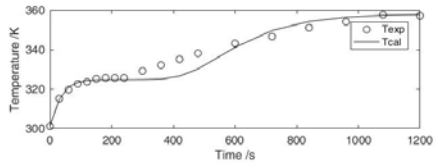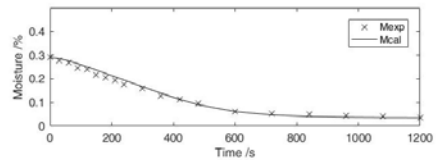
(b)358K
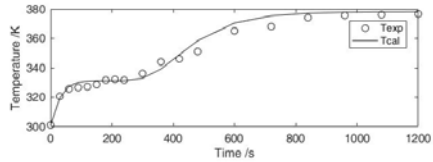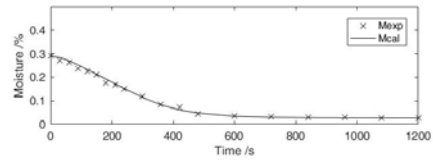
(c) 378K
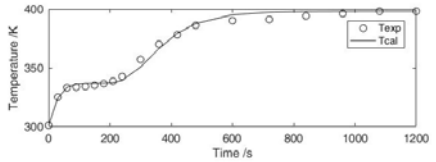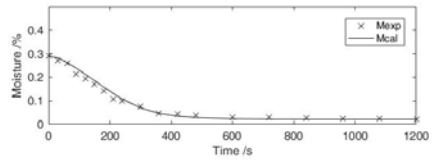
(d) 398K
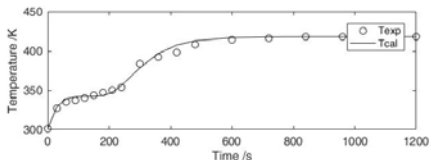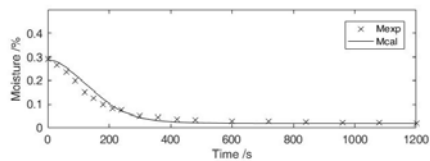
(e) 418K

Fig. 2. the Comparsion of experiment data and simulated data of moisture content and temperature with inlet temperature range from 338K to 418K

5. Conclusions

A laboratory rotary dryer was designed to simulate the drying process of biomass. The evolutions of the water content and surface temperature of cut tobacco at different drying temperatures were investigated. The determination of heat and mass transfer coefficients by calculating from the experimental data of temperature and water content appears as a more convenient method. The mathematical model with equilibrium relationship of moisture content could represent the drying characteristics of cut tobacco accurately. Moreover, the current work provides the essential basis for the future computational fluid-dynamic (CFD) simulation of tobacco drying in industry production line.

6. References

[1] Mohammad, M.; Bernhard, P. Effect of particle size distribution on drying characteristics in a drum by XDEM: A case study. Chemical Engineering Science., 2016, 152, 689-698.

[2] Koji, S.A.; Kazuyuki, T.S.; Takahisa, K.A.; A drying model of tobacco midrib expanding in air flow. Japan Journal of Food Engineering, 2010, 11, 91- 96.

[3] Zhu, W.K.; Wang, L.; Duan, K.; Chen, L. Y.; Li, B. Experimental and numerical investigation of the heat and mass transfer for cut tobacco during two-stage convective drying. Drying Technology, 2015, 33, 907-914.

Evaluation of Izmir Tulum cheese pieces by drying with tray dryer at different air flow rates and temperatures

Kizilalp, G.; Polat, I.; Urgu, M.; Koca, N.[*]

Ege University, Engineering Faculty, Food Engineering Department, Izmir, Turkey

*E-mail of the corresponding author: nurcan.koca@ege.edu.tr

Abstract

Izmir tulum cheese pieces were dried using a tray dryer at different air flow rates (1.0 and 1.8 m/s) and temperatures (45°C, 55°C and 65°C). The increase in temperature and air flow rate increased bulk and tapped bulk densityand decreased the water holding capacity. The lowest lightness and highest redness were obtained in samples dried at 65°C. The samples dried at 55°C and 1 m/s had the highest flavor and overall impression scores. As a result, a dried cheese product to benefit from left-over pieces obtained during packaging was developed, having advantages such as easy to transport, store and package.

Keywords: Izmir Tulum cheese; tray dryer; physical, chemical and sensory properties.

1. Introduction

Drying is one of the oldest method and has recently been applied to various food products to gain different functions. Cheese is exposed to drying process to increase its shelf life, decrease the transport and storage costs and improve some functional properties. Dehydrated cheese is generally used as a food ingredient to improve the flavor and mouthfeel of cheese [1, 2, 3].

Izmir Tulum cheese is a Turkish traditional cheese produced mostly by small or medium scale dairies. It is one of most consumed cheese type in Turkey, characterized with a white or cream color, high fat content, a crumbly and semi-hard texture. During the production of Izmir Tulum cheese, cheese pieces are left-over in large quantities during packaging of the cheese in the industrial production. The goal of the research is to evaluate these cheese pieces by drying with tray dryer which is the easiest drying method of producing dehydrated cheese in small scale dairies. The final quality of the dried cheese can be significantly affected by drying conditions. Therefore, it is necessary to evaluate the drying conditions to obtain a dehydrated food with a high quality. With this research, a new dehydrated cheese product was developed as an ingredient for different purposes in foods such as using in pasta, salad and pizza, etc. and the new product gives an advantages to consumer to use easily at home.

2. Materials and Methods

2.1. Material

Izmir tulum cheese purchased from the local market in Izmir. Samples were transported under cold conditions to the laboratory. Cheeses were grinded to obtain homogenous sample and dry easily. Samples were processed within a day.

2.2. Drying process

The preliminary tests were carried out to determine the duration of drying. The water activity value was considered to be below 0.8. For drying of cheese, 100 grams of grated cheese samples were put on a tray and dried in a pilot-scale tray drier (TK Lab5, Turkey) at different air flow rates (1 m/s and 1.8 m/s) and temperatures (45°C, 55°C, 65°C) for two hours. Dried cheese samples were grinded by food processor (Tefal Masterbland). Grinded dried cheese pieces were kept in glass jars during the analyses. Production procedure was replicated twice.

2.3. Compositional analysis

Moisture and ash contents of cheese and dried cheese samples were determined by gravimetric method [4, 5]. Kjeldahl method was used for protein content of the samples [5]. Fat contents of cheese and dried cheese samples were determined by Van Gulik [6] and Gerber [7] methods, respectively. pH values of cheese and dried cheese samples were measured with a digital pH meter (pH 320, WTW, 82362 Weilheim, Germany), and titratable acidity was expressed as percent lactic acid [5].

2.4. Water activity

Water activity of dried cheese samples were measured by using a water activity measurement device (Testo, Freiburg, Germany).

2.5. Bulk, tapped densities and Carr Index value

Bulk density of the dried samples was measured by pouring the samples to the 100-ml measuring cylinder and recorded the weight [8]. The measuring cylinder was tapped 200 times and the volume was recorded to calculated the tapped density [8]. Carr Index values of dried cheese samples were also evaluated according to Equation 1 [9].

$$CI = \frac{(\rho_{tapped} - \rho_{bulk})}{\rho_{tapped}} x\ 100$$

(1)

2.6. Water holding capacity

Water holding capacity (WHC) of dried cheese samples were measured according to Heywood et al. [10] and Traynham et al. [11] with some modifications. 2.5 g of dried samples was weighed to 50 ml centrifuge tube. Then, for each sample 10 mL of distilled water were added and well mixed with the sample. Samples stood at room temperature for 3 hours. The mixture was centrifuged at 2680 rpm for 30 min. Just after centrifugation, the supernatant was carefully decanted and the new mass of the sample was recorded. WHC (%) was calculated as Equation 2 :

$$WHC\ (\%) = \frac{Total\ water\ mass}{Dry\ matter\ mass}$$

(2)

2.7. Color evaluation

Color values of cheese and dried cheese samples were measured in terms of L (lightness), a (redness and greenness), and b (yellowness and blueness) using a Hunter ColorFlex colorimeter (HunterLabColorFlex CFLX 45-2 colorimeter). Then, color differences (ΔE) and chroma values (color intesity) of the samples were calculated using Equations 3 and 4,

respectively [12]. Color values of Izmir tulum cheese was taken as reference for the calculation of color differences.

$$\Delta E = \sqrt{(L_0 - L)^2 + (a_0 - a)^2 + (b_0 - b)^2} \tag{3}$$

$$Kroma = \sqrt{a^2 + b^2} \tag{4}$$

2.8. Sensory evaluation

Desirability of dried cheese samples scales in terms of color, appearance, texture, taste and overall acceptability using unipolar scales were determined by 40 panelists. . Unipolar scale ratings between 1 and 5 referring from not like at all to like very much.

2.9. Statistical analysis

Statistical data analyses was performed by using SPSS version 21.0. Data was analyzed by analysis of variance (ANOVA) and Duncan's multiple range test at 95% confidence interval.

3. Results and Discussion

3.1. Chemical composition

The moisture, ash, protein fat, titratable acidity values varied from 13.02 to 16.74%, from 8.79 to 9.53%, from 36.55 to 40.10%, from 36.28 to 37.71% and from 1.494 to 1.674%, respectively (Table 1). Different drying conditions did not have any significant effect on moisture and water activity values of samples. The higher fat values were obtained in samples dried at 45°C for both flow rates. Increasing temperature at the same air flow rate resulted in a decrease in acidity values.

Table 1. Composition of Izmir Tulum cheese and dried cheese samples

Analysis	Cheese	1 m/s – 45°C	1 m/s - 55°C	1m/s- 65°C	1,8 m/s-45°C	1,8 m/s- 55°C	1,8 m/s-65°C
Moisture (%)	44,19±0,08	16,74±2,11[a]	16,60±1,31[a]	13,02±0,27[a]	14,24±1,72[a]	15,52±1,52[a]	14,28±2,20[a]
Ash (%)	5,87±0,03	8,79±0,05[a]	9,25±0,11[ab]	9,53±0,13[b]	9,46±0,37[b]	9,42±0,32[b]	9,41±0,15[b]
Protein (%)	23,94±0,72	36,55±0,38[a]	36,95±0,08[a]	39,31±0,12[b]	37,10±0,15[a]	39,50±0,06[b]	40,10±0,32[b]
Fat (%)	46,58±0,71	37,69±0,74[b]	36,28±0,16[a]	36,63±0,09[ab]	37,71±0,23[b]	36,83±0,89[ab]	36,99±0,08[ab]
Acidity (% lactic acid)	0,981±0,04	1,674±0,05[b]	1,592±0,01[ab]	1,567±0,10[ab]	1,611±0,06[ab]	1,521±0,01[a]	1,494±0,05[a]
aw	0,985	0,709±0,64[ab]	0,716±0,43[b]	0,700±0,68[a]	0,701±0,00[a]	0,705±0,29[ab]	0,705±0,00[ab]

[a–b]Means within a row with different superscripts differ for dried cheese samples ($P < 0.05$).

3.2. Bulk and tapped densities, Carr Index value and water holding capacity

Densities and flowability of the dried samples is important for the manufacturer and the end user for packaging, handling, storage, transportation, etc. The bulk densities of samples were found between 0,512 and 0,555 g/cm³ (Table 2). The increase in drying temperature resulted in an increase in bulk densities of the samples. However, tapped density values of

the samples did not significantly change with different drying conditions. The classification of the flowability based on Carr Index are very good (<15), good (15–20), moderate (20–35), bad (35–45), and very bad (>45). In this study, flowability of the samples was found to be moderate level. WHC of the samples varied from 33,0 to 35,6%. The lowest WHC were obtained in samples dried at 1,8 m/s air flow rate and 65°C. This sample was found as harder in mouth by the panelists. The WHC of the samples dried at 1 m/s were high when compared to the samples dried at 1,8 m/s flow rate.

Table 2. Bulk and tapped densities, Carr Index and water holding capacity values of dried cheese samples

Analysis	1 m/s - 45°C	1 m/s -55°C	1m/s- 65°C	1,8 m/s-45°C	1,8 m/s-55°C	1,8 m/s-65°C
BD (g/cm³)	0,512±0,00[a]	0,533±0,00[ab]	0,555±0,00[b]	0,549±0,02[b]	0,552±0,01[b]	0,552±0,00[b]
TD (g/cm³)	0,713±0,05[a]	0,728±0,07[a]	0,731±0,04[a]	0,741±0,05[a]	0,726±0,06[a]	0,729±0,06[a]
CI	28,1	26,7	24,0	25,9	23,3	24,3
WHC (%)	35,6±0,14[c]	34,3±0,21[bc]	33,4±0,35[ab]	34,8±0,21[c]	33,3±0,14[ab]	33,0±0,07[a]

[a–b]Means within a row with different superscripts differ for dried cheese samples ($P < 0.05$). BD:bulk density, TD: tapped density, CI: Carr Index value, WHC: water holding capacity.

3.3. Color evaluation

Color of the dried foods is an important quality attribute for customer satisfaction and selection. The color values of dried samples were shown in Table 3. The lowest lightness and highest redness were found in samples dried at 65°C even at different air flow rates. Also, no significant changes were found in yellowness of the samples with the changes in air flow rates or temperature. ΔE values of the samples calculated with reference sample-Izmir Tulum cheese. When ΔE value is greater than 3, it can be distinguished by eyes easily [13]. All samples have ΔE value higher than 3. Therefore, their differences were distinguished by eyes. However, increase in air flow rate at same temperature resulted in a decrease in ΔE value.

Table 3. Color values of dried cheese samples

	L	A	B	ΔE	Chroma
Drying Conditions	85,29±0,41	2,18±0,00	25,19±0,06	-	-
1 m/s - 45°C	83,58±0,91[ab]	3,36±0,06[a]	36,41±0,13[b]	11,4±0,27[bc]	36,57±0,14[b]
1 m/s - 55°C	84,38±0,61[b]	3,23±0,04[a]	35,38±0,35[ab]	10,3±0,28[ab]	35,53±0,34[ab]
1 m/s - 65°C	82,18±0,97[a]	5,01±0,11[c]	36,13±0,74[b]	11,7±0,97[c]	36,48±0,74[b]
1,8 m/s-45°C	83,25±0,00[ab]	3,37±0,23[a]	35,76±0,23[ab]	10,8±0,24[ab]	35,92±0,24[ab]
1,8 m/s-55°C	84,03±0,41[b]	3,30±0,12[a]	35,03±0,57[a]	10,00±0,60[a]	35,19±0,56[a]
1,8 m/s-65°C	82,88±0,23[ab]	4,17±0,37[b]	35,58±0,01[ab]	10,8±0,03[ab]	35,83±0,06[ab]

[a–c]Means within a row with different superscripts differ for dried cheese samples ($P < 0.05$).

3.4. Sensory evaluation

The sensory evaluation results were shown in Table 4. The samples that were dried at 1 m/s - 55°C had the highest score in terms of taste and overall acceptability, whereas lowest scores were found in samples dried at 65°C. However, the samples that exposed to drying at 1.8 m/s - 65°C has the highest score in terms of color and appearance.

Table 4. Sensory evaluation results for dried cheese samples

Drying Conditions	Color	Appearance	Texture	Flavor	Overall acceptability
1 m/s - 45°C	3,37±0,25[a]	3,42±0,33[ab]	3,66±0,13[c]	3,51±0,05[ab]	3,76±0,13[ab]
1 m/s - 55°C	3,51±0,26[ab]	3,44±0,08[ab]	3,48±0,12[bc]	3,92±0,11[b]	3,89±0,35[b]
1 m/s - 65°C	3,49±0,43[ab]	3,20±0,49[a]	2,58±0,12[a]	3,21±0,28[ab]	3,12±0,00[a]
1,8 m/s-45°C	3,56±0,26[ab]	3,42±0,56[ab]	3,00±0,21[ab]	3,20±0,48[ab]	3,45±0,64[ab]
1,8 m/s-55°C	3,52±0,61[ab]	3,42±0,53[ab]	3,08±0,45[ab]	3,25±0,35[ab]	3,32±0,39[ab]
1,8 m/s-65°C	3,68±0,37[b]	3,59±0,15[b]	2,98±0,31[a]	3,03±0,45[a]	3,17±0,25[ab]

[a–c]Means within a row with different superscripts differ for dried cheese samples ($P < 0.05$).

4. Conclusions

Higher water activity of foods tends to support the growth of microorganisms, especially molds which causes quality depletion and economical losses. Molds require a water activity level at least 0.80. In this study, the water activity of the dried Izmir Tulum cheese samples did not change with different drying conditions, and samples had water activity values that were below 0.72. Although the densities and water holding capacity of samples changed by the drying parameters, these differences were not very important from the practical point of view. On the other hand, increasing air flow rate and temperature resulted in harder surface of samples, which was not preferred by panelists. The highest flavor and overall impression scores were found in samples dried at 1 m/s and 55°C. In conclusion, a dried cheese using a tray drier has several advantages such as easy to transport, store and packaging. However, there is a need a further study to evaluate the storage stability of the product.

5. Acknowledgements

6. References

[1] Fox, P.F.; Cogan, T.M.; Guinee, T.P.; McSweeney, P.L.H. Fundamentals of Cheese Science; Aspen Publications: Gaithersburg, 2000.

[2] Guinee, T.P.; Kilcawley, K.N. Cheese: Cheese as an ingredient. In Cheese Chemistry, Physics and Microbiology; Fox, P.F., McSweeney, P.L.H., Cogan, T.M., Guinee, T.P.,

Eds.; Elsevier/Academic Press: London, 2004; 395–428.

[3] Guinee, T.P. Cheese as a food ingredient. In Encyclopedia of Dairy Sciences; Fuquay, J.W., Fox, P.F., McSweeney, P.L.H., Eds.; Elsevier/Academic Press: London, 2011; 822–833.

[4] International Dairy Federation. Determination of the total solid content (cheese and processed cheese). IDF Standard 4A. International Dairy Federation (IDF): Brussels, 1982.

[5] AOAC. Official methods of analysis of AOAC International. 18th ed. AOAC International: Gaithersburg, 2007.

[6] International Dairy Federation. Cheese, determination of fat content - Van Gulik butyrometers method. IDF Standard 5B, International Dairy Federation (IDF): Brussels, 1986.

[7] International Dairy Federation. Milk-Determination of fat content–Gerber butyrometers. IDF Standard 105. International Dairy Federation (IDF): Brussels, 1981.

[8] Jinapong, N.; Suphantharika, M.; Jamnong, P. Production of instant soymilk powders by ultrafiltration, spray drying and fluidized bed agglomeration. Journal of Food Engineering 2008, 84, 194–205.

[9] Carr, R.L. Evaluating flow properties of solids. Chemical Engineering 1965, 72, 163–168.

[10] Heywood, A.A.; Myers, D.J.; Bailey, T.B.; Johnson, L.A. Functional properties of low-fat soy flour produced by an extrusion-expelling system. Journal of the American Oil Chemists' Society 2002, 79(12), 1249-1253.

[11] Traynham, T.L.; Myers, D.J.; Carriquiry, A.L.; Johnson, L.A. Evaluation of water-holding capacity for wheat–soy flour blends. Journal of the American Oil Chemists' Society 2007, 84(2), 151-155.

[12] Askari, G.R.; Emam-Djomeh, Z.; Mousavi, S.M. Investigation of microwave treatment on the optical properties of apple slices during drying. Drying Technology 2008, 26, 1362–1368.

[13] Francis, F.J.; Clydesdale, F.M. Food colorimetry: Theory and applications. Molecular Nutrition and Food Research 1977, 21(1), 90-91.

LNT microwave-multiphase transport model for the microwave drying of lignite thin layer

Fu, B. A.[a,b]*; Chen, M. Q.[a,b]; Li, Q. H.[c]*

[a]Institute of Thermal Engineering, School of Mechanical, Electronic and Control Engineering, Beijing Jiaotong University, Beijing 100044, China
[b]Beijing Key Laboratory of Flow and Heat Transfer of Phase Changing in Micro and Small Scale, Beijing 100044, China
[c]Key Laboratory for Thermal Science and Power Engineering of Ministry of Education, Department of Thermal Engineering, Tsinghua University, Beijng, 100084, P. R. China

*E-mail of the corresponding author: 13116340@bjtu.edu.cn

Abstract

The LNT microwave-multiphase transport model has been applied to the microwave drying of lignite thin layer. Microwave energy, temperature and moisture distribution were obtained to gain a comprehensive understanding on the heat and mass transfer mechanism of the drying process. The required drying time of experiments decreased by 50, 63, 67, and 83%, respectively, with the power level rising from 119 to 700 W, while that decreased by 60, 72, 76 and 86%, respectively, for simulation results. The temperature values of the corner and edge of the lignite thin layer were higher than that of the center region, which corresponded to the microwave energy distribution. The moisture ratio profiles, temperature profiles and temperature distribution indicated good agreement between the experimental and simulation results, providing confidence in the modeling approach, which made it possible to obtain the moisture distribution successfully via simulation method

Keywords: microwave; lignite; thin layer.

1. Introduction

Lignite is considered as the main energy source for electricity generation and industry feedstocks because of its abundant reservation and cheap price. The high moisture content in lignite leads to low calorific value, low energy utilization efficiency and high transportation cost. Drying prior to pyrolysis, gasification and combustion can improve the utilization efficiencies of the downstream devices. Microwave drying is an efficient method for lignite pre-treatment due to its high drying rate, volumetric heating and precise process control. Apart from experimental studies, numerical modelling is another way to further understand the physics of microwave heating of food. In order to take every possible transport phenomenon for each phase into consideration, and describe the coupled transport mechanisms in a numerical manner, some efforts have been devoted to the modeling of the microwave drying process. With the advancement of computational power and efficient numerical methods, some researchers employed commercial software to provide an exact solution for the Maxwell's equations. Based on the conservation equations elaborated by Whitaker, some researchers derived mechanistic models to highlight the heat and mass transfer characteristics during microwave drying [1]. A coupled electromagnetic, heat and mass transfer model without accounting for pressure driven flow was established by Law et al. [3] to examine the temperature and moisture content distribution in oil palm kernels during microwave drying. They noted that the calculated results fitted the experimental ones, and the cracks of oil palm kernels was prone to occur at the core of the kernel. According to the pumping phenomenon noted by some researchers experimentally, Zhu et al. [4] modified the above model by taking the vapor pressure into account, which would cause moisture diffusion both in liquid and vapor phase. In the case of the microwave drying of potato spheres, good agreement was found between the experimental data and predicted values. In spite of the complete and predictable model developed or modified by the above researchers, the available models still need to be amended with newly discovered physical phenomenon and theory. Swiss scientist Charles Soret discovered that the concentration difference can be built under temperature gradient and the thermo-diffusion phenomenon was referred to as Soret effect [5]. Reversely, the temperature gradient also could be generated by concentration difference, and the diffusion-thermal phenomenon was known as Dufour effect [6]. As a matter of fact, samples can be heated with microwave radiation due to the dipoles orientation [7], and the temperature gradient would be built for the non-uniform microwave energy distribution and energy decay. Corresponding to the dipoles orientation caused by the oscillating electric and magnetic field, Stewart et al. and Lehmann found that liquid crystals showed a uniform rotation under temperature gradient. The thermal polarization phenomenon was also confirmed by Muscatello et al. [8] and Bresme et al. [9] in subsequent numerical calculations, and they found that the water molecules rotation in the direction of temperature gradient would lead to electrostatic field, whose magnitude would scale linearly with the increasing temperature gradient. Based on the complex coupling effects involving the heat and mass transfer and the molecular polarization, the non-equilibrium thermodynamic theory was applied to modify the available models, which can provide more accurate prediction for the coupled heat and mass transfer in porous media during microwave drying.

In the present study, the LNT microwave- multiphase transport model was employed to thin-layer lignite, which is the typical loose structure, to validate the experimental results in terms of moisture ratio and temperature profiles and distribution. The proposed model will

also be compared with the mechanistic ones with respect to deviation and calculation time. In addition, light is shed on the diffusion-thermal and electric-thermal effect and the microwave-induced coupling transmission mechanism for loose structures during drying process.

2. Materials and Methods

2.1. Problem formulation

The heat and mass transfer in the lignite thin-layer under microwave irradiation is simplified in Fig. 1. The lignite thin-layer is exposed to the environment where intense microwave energy is introduced from the right side of the oven. The driving force for the liquid water and water vapor diffusion in the thin-layer is the concentration and temperature gradient. The thermal diffusion is caused by the coupling effects of the temperature gradient, the molecular polarization and the liquid water and water vapor diffusion. The molecular polarization is produced by the alternating electromagnetic field and temperature gradient. The heat and mass transfer between the lignite thin-layer and the surroundings only occurs at the top surface.

2.2. Major hypotheses

In order to clarify the heat and mass transfer characteristics within the loose structures, the following hypotheses are taken into consideration for the model simplification: (1) local thermodynamic equilibrium exists; (2) the thermodynamic flows scale linearly with the thermodynamic forces; (3) the coupling ratio between the molecular polarization and heat flow presents linear correlation with the average temperature of the sample; (4) all phases are continuous; (5) initial moisture content and temperature within the material are assumed to be uniform; (6) non shrinkage or deformation during drying process; (7) water vapor pressure is shared by all fluid phases; (8) Both the lateral and bottom sides of the lignite thin-layer are insulated; (9) the moisture migration into the surroundings only occurs at the top side of the lignite thin-layer in vapor phase; (10) gravity effect are neglected.

2.3. Governing equations

The heat and mass transfer characteristics within the lignite thin-layer during microwave drying can be modelled by the Maxwell equation and the modified mass and energy conservation equations based on the non-equilibrium thermodynamics.

The Maxwell equation is given by [4]：

$$\nabla \times E = -j\omega\mu_0 H \tag{1}$$

$$\nabla \times H = j\varepsilon_0\varepsilon E \tag{2}$$

$$\nabla \times \varepsilon E = 0 \tag{3}$$

$$\nabla \times H = 0 \tag{4}$$

where, E is the electric field intensity, V m^{-1}; H the magnetic field intensity, T; ε the complex relative permittivity of lignite thin-layer, which is determined by dielectric constant ε' and dielectric loss factor ε'', ε_0 permittivity of free space, 8.85×10^{-12} F m^{-1}.

Based on the non-equilibrium thermodynamics, the established mass and energy conservation equations from the former publication [4] can be derived as below and the details can be found in the previous research [10].

The mass conservation equation can be modified as:

$$\rho_s \frac{\partial M}{\partial t} = \left\{ \left(\lambda_{gq} + \lambda_{lq} \right) \nabla T \right\} + \nabla \left(K_g \nabla p_g \right) + \nabla \left(K_l \nabla p_l \right) \qquad (5)$$

where ρ_s is the density of the lignite thin-layer, kg m^{-3}; M the moisture content (water vapor and liquid water) on dry basis; λ_{gq} and λ_{lq} the Soret coefficient for vapor and liquid phase, respectively; K_g and K_l the permeability for vapor and liquid phase, respectively; p_g and p_l the water vapor and liquid water pressure, respectively, Pa.

The energy conservation equation can be derived as:

$$\frac{\partial \rho_{eff} C_{eff} T}{\partial t} = \nabla \left(\lambda \nabla T \right) + \nabla \left\{ \frac{a}{\tau} \left(\varepsilon_0 \chi E_{eq} - P \right) \right\} + h_g \nabla \left(K_g \nabla p_g \right) + h_l \nabla \left(K_l \nabla p_l \right) - \gamma I + Q_{mic} \qquad (6)$$

where ρ_{eff} is the effective value of sample denstiy, kg m^{-3}; $C_{p,eff}$ the effective value of sample specific heat capicity, J kg^{-1} K^{-1} [11]; a the coupling ratio, V; τ the polarization relaxation time, s; h_g and h_l the molar enthalpy of water vapor and liquid water, respectively, kJ mol^{-1}; γ the latent heat of evporation, kJ kg^{-1}; I the evaporation rate, kg m^{-3} s^{-1}; Q_{mic} the rate of microwave energy absroption, W m^{-3}. λ the thermal conductivity involving the pure heat conduction and substance diffusion, W m^{-1} K^{-1}. The details are reported by the previous research.

2.4 Geometry model

According to the physical dimensions and shapes of the microwave oven, the geometry model is established with a 460×360×290 mm cube and three square frustum metal bumps, which can be applied to improve the uniformity of the microwave energy distribution and obtain accurate simulation results. The dimensional details of the metal bumps can be seen in Fig.2. The microwave energy is generated by a coaxial antenna (10.5 mm in radius and 12 mm in height) and introduced into the oven via a rectangular waveguide.

(a) Geometric model.   (b) Meshed geometric model.
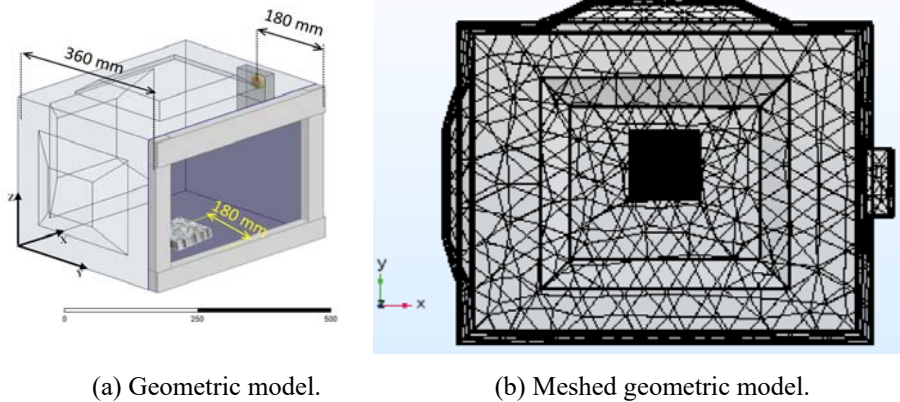
Fig.1 Geometric model for the microwave dryer setup.

2.6 Physical model and Initial and boundary conditions

The physical model, initial and boundary conditions and parameters in the simulation are listed in ref [10], the mathematic and physical models related to coupling mechanism between the heat and mass transfer, and the molecular polarization in a lignite thin layer were developed as above. The governing equations and boundary conditions would be solved by the finite element commercial software COMSOL Multiphysics.

3. Results and discussion

3.1 Drying rates profiles

The drying and drying rates profiles of experiments and simulations were shown in Fig. 2. From Fig. 2, the microwave power levels had a significant effect on drying time. Time required for microwave drying was shortened with the increase in power level. As shown in Fig. 2 (a), the simulation data fitted the experimental data well with average deviation of 5% for 119 and 700 W, while 10% for 231-539 W.

3.2 Temperature profiles

The temperature profiles of three points (L, C and R) were shown in Fig. 3. Three periods, detected in the temperature profiles for lignite sample with power level of 119 to 700 W, were the rapid heating period (corresponding to the warm-up and constant rate periods in Fig. 2 (a)), the cooling period (corresponding to the falling rate periods in Fig. 2 (a)) and the final isothermal period, respectively, while only rapid heating period (corresponding to the warm-up, constant rate period and the falling rate period in Fig. 2 (a)) and final isothermal period were detected in the simulation results.
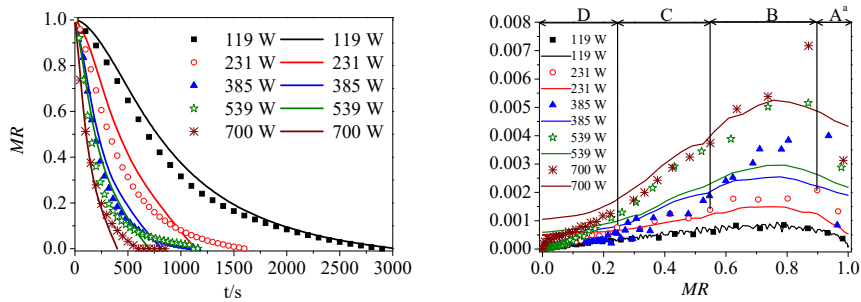
(a) Drying profiles of lignite thin layer   (b) Drying rates of lignite thin layer.

Fig.2. Drying and drying rates of lignite thin layer between 119-700 W. Dots and solid line indicates experimental and simulation data, respectively. Aᵃ–D represents the warm-up period, the constant rate period, the first falling rate period and the second falling rate period, respectively.

The comparison of temperature between the experimental and simulation data for five power levels was illustrated in Fig. 3. The simulation data fitted the experimental data well with average deviation of 5% for 119 W and about 10% for 231-539 W, 15% for 700 W.
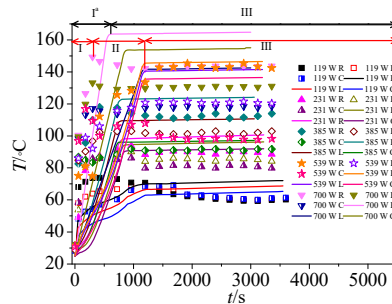
Fig.3. Temperature profiles of lignite thin layer between 119-700 W. Dots and solid line indicates experimental and simulation data, respectively. Iᵃ: the heating up period; II: the cooling down period; III: the isothermal period.

3.3 Microwave energy and temperature distribution

The temperature distribution of experiments and simulations at 385 W were shown in Fig. 4. As illustrated in Fig. 4, the non-uniform temperature distribution of sample surface was evidenced by experiments and simulation results with the moisture ratio of 0.8 and 0.2 at 385 W. The temperature distribution obtained by simulation method possessed similar trend with experimental results, which verified the calculation results of temperature distribution based on numerical simulation.
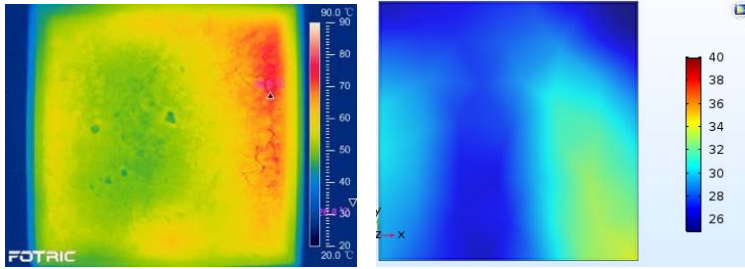
(a) Experimental results. (b) Simulation results.

MR=0.8
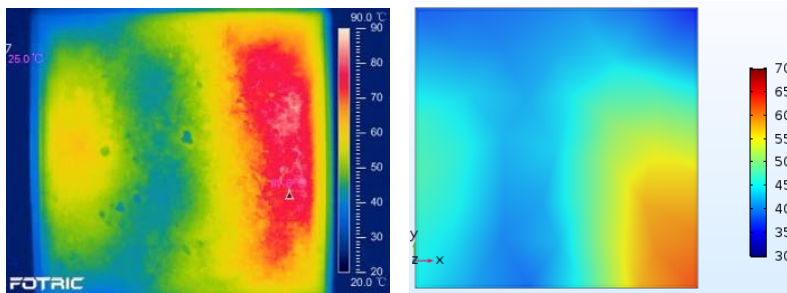
(a) Experimental results. (b) Simulation results.

MR=0.2

Fig.4. Temperature distribution of experiments and simulation.

3.4 Moisture distribution

Moisture distribution in lignite thin layer at 385 W was illustrated in Fig. 5. As shown in Fig. 5, the moisture content was lower at the right and left regions in the lignite thin layer, which corresponded to the temperature distribution.
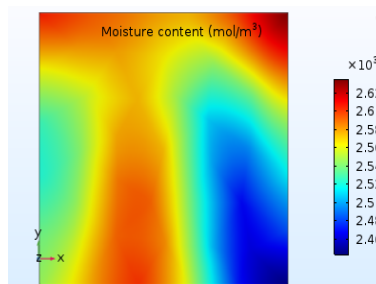
Fig.5. Moisture content distribution in sample at 385 W (MR=0.8).

4. Conclusions

The LNT microwave-multiphase transport model has been applied to simulate the microwave drying behavior of lignite thin layer successfully. Microwave energy, temperature and moisture distribution were obtained to gain a comprehensive understanding on the heat and mass transfer mechanism of the drying process. The simulation data of the moisture ratio fitted the experimental data well with average deviation of 5% for 119 and 700 W, while 10% for 231-539 W. The average deviation of temperature between the simulation and experimental data were 5% for 119 W and about 10% for 231-539 W, while 15% for 700 W. The coupled electromagnetics and multiphase porous media made it possible to obtain the moisture distribution via simulation method. Further investigation on the moisture distribution will be carried out via MRI experiments to verify the simulation result.

5. Referrence

[1] A.K. Datta, Porous media approaches to studying simultaneous heat and mass transfer in food processes. I: Problem formulations, J. Food Eng. 80 (1) (2007) 80-95.

[2] K. Pitchai, S.L. Birla, J. Subbiah, D. Jones, H. Thippareddi, Coupled electromagnetic and heat transfer model for microwave heating in domestic ovens, Journal of Food Engineering 112 (1) (2012) 100-111.

[3] M.C. Law, E.L. Liew, S.L. Chang, Y.S. Chan, C.P. Leo, Modelling microwave heating of discrete samples of oil palm kernels, Applied Thermal Engineering 98 (2016) 702-726.

[4] H. Zhu, T. Gulati, A.K. Datta, K. Huang, Microwave drying of spheres: Coupled electromagnetics-multiphase transport modeling with experimentation. Part I: Model development and experimental methodology, Food and Bioproducts Processing 96 (2015) 314-325.

[5] M.A. Rahman, M.Z. Saghir, Thermodiffusion or Soret effect: Historical review, Int. J. Heat Mass Transfer 73 (2014) 693-705.

[6] D. Pal, H. Mondal, Influence of chemical reaction and thermal radiation on mixed convection heat and mass transfer over a stretching sheet in Darcian porous medium with Soret and Dufour effects, Energy Convers. Manage. 62 (2012) 102-108.

[7] B.A. Fu, M.Q. Chen, Y.W. Huang, H.F. Luo, Combined effects of additives and power levels on microwave drying performance of lignite thin layer, Drying Technology 35 (2) (2017) 227-239.

[8] J. Muscatello, F. Romer, J. Sala, F. Bresme, Water under temperature gradients: polarization effects and microscopic mechanisms of heat transfer, PCCP 13 (44) (2011) 19970-19978.

[9] F. Bresme, A. Lervik, D. Bedeaux, S. Kjelstrup, Water Polarization under Thermal Gradients, Phys. Rev. Lett. 101 (2) (2008) 020602.

[10] B.A. Fu, M.Q. Chen, Q.H. Li, J.J. Song, Non-equilibrium thermodynamics approach for the coupled heat and mass transfer in microwave drying of compressed lignite sphere, Appl. Therm. Eng. 133 (2018) 237-247.

[11] A.K. Datta, Porous media approaches to studying simultaneous heat and mass transfer in food processes. II: Property data and representative results, J. Food Eng. 80 (1) (2007) 96-110.

Description of atmospheric freeze-drying of brown seaweeds (Saccherina Latissima) with respect to thermal properties and phase transitions

Tolstorebrov, I.ᵃ*; Eikevik, T. M.ᵃ; Petrova, I.ᵃ; Bantle, M.ᵇ

[a] Department of Energy and Process Engineering, Norwegian University of Science and Technology, NO-7049 Trondheim, Norway, Tel.: +47 73593742,
[b] Sintef Energy Research, Trondheim Norway

*E-mail of the corresponding author: ignat.tolstorebrov@ntnu.no

Abstract

Thermal properties of brown seaweeds (Saccharina latissima) were determined using DSC technique in the temperature range between -150.0 and 50.0 °C. The following phase transitions were detected: glass transitions, incipient point of ice melting and freezing point. The ice content and amount of unfrozen water was detected by analysis of the melting peak. The ice content reduction in the product was predicted for different moisture contents and temperatures for atmospheric freeze-drying process.

Keywords: brown seaweeds, ice fraction, freeze-drying, glass transition

1.   Introduction

Most of the seaweeds, which are used for food purpose in Norway belong to aquaculture products, when hatching, growth and harvesting is controlled continuously. The harvesting season occupies approximately 2 weeks to provide the best quality of the seaweed's blades. The processing technology requires immediate processing of raw seaweeds to ensure production of sustainable and high quality product. Due to high quantities of raw seaweeds during harvesting the immediate freezing is applied to prevent deterioration. However, drying is the common way to preserve food products like seaweed and most of the seaweeds are sold in a dried form [1]. Solar and natural drying of seaweeds is a cost-effective method. At the same time climate conditions can result in a high final moisture content in dried product[2] due to high moisture absorption ability [3], aslo, the process 5 or 7 days [4]. Due to this, the producers of Saccharina Latissima consider the atmospheric freeze-drying process as the most reliable for the given processing condition. Design of equipment and adjustment of the processing parameters is complicated without knowledge of thermal phase transitions at freezing temperatures. The study discusses the thermal properties of seaweeds and seaweed's mucus and their influence on the atmospheric freeze-drying process. The investigation of seaweeds mucus was introduced due to high amount this substance on the blades, which provide stickness of the particles (blades) during atmospheric freeze-drying.

2.   Materials and Methods

2.1 Characterization of raw material

The brown algae *Saccharina latissima*, which is commonly referred as kelp (Sugar kelp or kombu) was used for the experiments. The seaweeds was cultivated for one year in an aquaculture farm, which is situated in Sør-Trøndelag (Norway). Harvesting season was 15 days in May 2017 to maintain the best quality of the seaweeds and avoid high amount of biofouling. The seaweed was harvested into nets (75-150 kg). The nets were buffered in the seawater at the farm where they were kept in refrigerated seawater (-1.0 °C) for 1 week before freezing. Then the seaweed was weighed out and packed inside vacuum bags with high barrier properties (2.0 kg each). Freezing was at –46 °C until temperature in the center of the bag reached -18.0 °C. After freezing the bags were packed in cardboard boxes, put on pallets and placed in freeze storage at -18 °C. The kelp was delivered in a frozen state by the supplier (June 2017). Chemical composition of the aquaculture seaweeds is given in the Table 1. Protein content of the seaweeds was determined at 11.2 % d.b., which was in a common range for brown seaweeds between 3.0 and 15.0 % [5]. The aquaculture seaweeds form Damariscotta bay (USA) had a protein content of 6.87 % d.b. [6], which was in the range (between 9.9 and 7.6 % d.b.) of the previously obtained results for wild sugar kelp form Scotland, Isle of Seil [7].

Table 1. Chemical composition of Saccharina latissima at harvesting season (analysis performed by accredited analytical laboratory Kystlab preBIO, Frøya, Norway).

Chemical composition	%, d.b.	Minerals , mg/kg d.b.	
Proteins	11.2	Potassium	84000
Fats	2.9	Sodium	52000
Carbohydrates	55.3	Calcium	10000
Incl. Dietary fiber	46.6	Magnesium	7500
Ash	37.9	Sulfur	7300
Incl. Salt (NaCl)	14.6	Iodine	3670
Water	900.0	Phosphrus	1700

2.2 DSC analysis

The DSC analysis was done with a DSC Q 2000 (TA instruments, USA) equipped with a Liquid Nitrogen Cooling System. The heat capacity was calibrated with a sapphire in the range between –150.0 and 180.0 °C. Helium was chosen as a purge gas at 25 mL/min, according to TA's instrument recommendations. The reference sample was an empty hermetically sealed aluminum pan.

In this study, the small particles of seaweed blades were used for DSC. The samples with masses between 13.0 mg and 20.0 mg were placed into aluminum pans with hermetic lids. The pans were sealed with a Tzero® DSC Sample Encapsulation Press (TA Instruments, USA). The pans were placed by an autosampler into the DSC cell. Samples were cooled and equilibrated for 5 minutes at –150.0 °C; the cooling rate was 10.0 °C/min. The annealing procedure was applied at –50.0 °C. This was done to avoid cold crystallization during scanning. Then the samples were heated up to 50.0 °C (application of higher temperatures was not effective due to evaporation of moisture) with the heating rate of 10.0 °C/min.

2.3 Determination of glass transition

The glass transition was determined with TA Universal Analysis 2000 version 4.5A software (TA instruments, USA). The glass transition is characterized with the following parameters: the onset, end and inflection points. It should be noted, that the glass transition in seaweeds with high moisture content is relatively weak. Thus, the inflection point was determined as a negative peak of the derived heat flow curve [8].

2.4 Determination of end of freezing and initial freezing point

The onset of ice melting (or end of freezing point), was determined by analyzing the DSC heating curve. The freezing point was estimated as a minimum value of the ice melting endothermic peak on the DSC heat flow curve.

2.5 Determination of ice fraction and unfreezable water

The amount of unfreezable water and ice fraction was detected by the DSC melting curve analysis. The DSC melting peaks were integrated with the sigmoidal tangent baseline function from the onset of ice melting point. The ice fraction was determined as a ratio of melting energy to latent heat of fusion of pure ice. As soon as melting energy of ice is a function of temperature, the empirical equation suggested by Riedel[9] was used for correction of obtained values. The amount of unfreezable water was obtained as the difference between the total water fraction in the product and the ice fraction.

2.6 Statistical analysis

The analysis of variance (ANOVA: single test and two-factor test with replication) was applied to analyze the obtained data. The difference was considered significant at $p<0.05$. All the experimental points were done in six parallels, except of desorption isotherm determination, where each point represents a single experiment.

A regression analysis was done with a software DataFit 8.1 program (Oakdale Engineering). The quality of the regression was evaluated with the following parameters: F-Ratio, Prob(F) and R^2. F-Ratio is the ratio of the mean regression sum of the squares divided by the mean error sum of the squares. Prob(F) is the probability that the null hypothesis is true. R^2 is the coefficient of multiple determinations. The standard deviation is introduced in the brackets after the values given in the text.

3. Results and Discussion

3.1 Glass transition phenomena in raw seaweeds and seaweed mucus

Two type of material were investigated: seaweed's blades and seaweeds mucus. The DSC investigation revealed two glass transitions at the ultra-low temperature region at -84.77(1.35) and -62.14(0.46) °C for seaweed's blades and at -74.44(2.15) and -55.02(0.48) °C for mucus. It should be noted, that the glass transition phenomena was weak due to high amount of water fraction in the product, however, the negative peak was clearly observed on the derived heat flow curve. In previous study of Sappati et. al., [6] only one glass transition event was determined.

The occurrence of two glass transition refer to different fractions of unfreezable water, which forms independent maximal freeze concentrated solutions. Each of the solution has unique point of glass transition. The presence of more than one glass transition for low-moisture foods, which contain carbohydrates and proteins, was reported before [10]. It is explained by transitions of blends and thermal history of the sample. Also, immiscible compounds which forms individual maximal-freeze concentrations can cause the several

glass transitions, however, it is not a strict rule [11]. As a conclusion, one can state that the second order phase transition will not influence on the

3.2 End of freezing and melting peaks of raw seaweeds and seaweed mucus

The so-called "end of freezing" is an equivalent of the incipient point of ice melting on DSC heat flow curve considering equilibrium freezing process. This point can be found on heat flow curve derived by time. The detailed information of the method available in Tolstorebrov et., al. [12]. Seaweeds blades and mucus showed different end of freezing point -52.23(1.61) and -42.1(0.65) °C. This information was used for derivation of melting peak for obtaining melting energy.

The melting endotherm consisted of two peaks for both seaweed blades and mucus, (Fig, 1). The low temperature narrow melting peak reflects crystallization of salts (mostly *NaCL*), the peak was integrated in the melting peak of ice, which occupied the temperature diapason between end of freezing and initial freezing point. Initial freezing point was determined as extremum of the ice melting peak -1.31(0.06) and -1.31(0.24) °C for seaweed blades and mucus respectively.
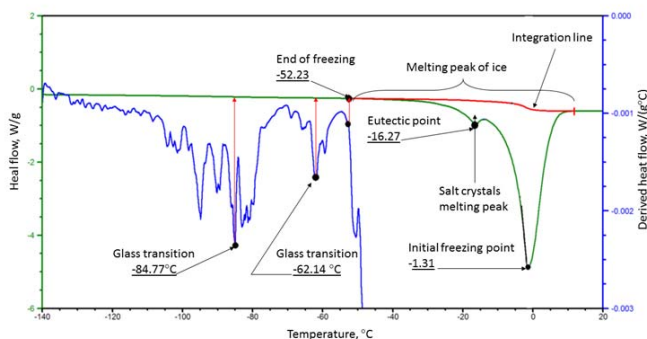
Fig. 1. Thermal transitions in seaweed's blade: heat flow curve and derived by temperature heat flow curve.

Analysis of the melting peak revealed that significant part of moisture was in a crystalline form at freezing temperatures. The value of melting energy was found at 271.2(5.0) and 259.35(0.95) for seaweeds blades and mucus respectively. It is remarkable, that the highest amount of ice was formed in seaweed's blades while the highest moisture content was determined for mucus 91.97(0.6) vs. 88.67(0.6) % w.b. Relatively high initial freezing point and ice content create good conditions for atmospheric freeze-drying process.

3.3 Ice content and unfreezable water in seaweed's blades and mucus

Seaweed blades showed 10.39(0.59)% w.b. of unfreezable water, while the value of 17.02(1.35) % w.b. was determined for mucus. The value of unfreezable water in mucus is

relatively high when compares with other foods. This will result in a low content of solids in the maximal freeze concentration solution, which is formed during transition of water into ice. At the end point of freezing the freeze consternation was at 52.13(0.45) and 31.14(1.05) % w.b. for seaweed's blades and mucus respectively.

Both types of samples showed a significant increasing of ice content in vicinity of initial freezing point, (Fig. 2), which is typical for seafood products of a high moisture content. The concentration of ice reached 63.9 and 66.2% w.b. at -10.0 °C and 33.39 (0.42) and 34.04(0.9) at -5.0 °C for seaweed blades and mucus respectively. These temperature diapason is considered to be the most common for atmospheric freeze-drying process application[13]. The model of Schwartzberg [14] was used to describe the process of ice formation.

The model accuracy were weak for seaweed blades due to the influence of mucus, while the quality of the model for mucus was relatively good (R^2>0.98, F(Ration)>500, Prob(F)=0).
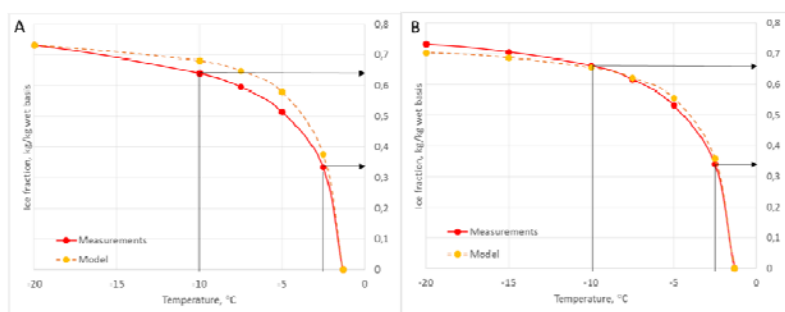
Fig.2. Ice fraction in seaweeds (left) and mucus(right) with respect to temperature. The diagrams introduces experimental data and models.

One can notice that the values of ice content are not so different in the seaweed blade and mucus (for the same temperature intervals). At the same time, the concentration of solids (kg/kg w.b.) is low and varies significantly between the samples, which influence on the ice development during the atmospheric freeze-drying process. The data, obtained in this chapter is essential for prediction of ice content during the freez-drying process.

3.4 Development of ice content with respect to total moisture content

The ice content in a product is in equilibrium with freeze concentrated solution and temperature: decreasing of the temperature results in the increasing of ice content, while increasing of solids in a freeze concentrated solution provoke the ice melting. Classical explanation of atmospheric freeze-drying process includes sublimation of ice and formation of dry front in the product. However, this situation will not occur in the case of seaweeds,

as soon as ice crystals will be covered by the layer of unfrozen brine, which include dissolved salt ion, carbohydrates (mannitol) and proteins. Obviously, evaporation of unfrozen brine will be predominant. This will increase the concentration of solids in the concentrated solution and the ice crystals will melt.

Fig. 3 introduces the decreasing of ice content with respect to totl moisture content. The ice melting ocuurs much more rapidly for mucus. Thus, the surface of the product will show the different drying behavior when compared with the whole blades. The application of temperatures below the initial freezing point is suitable only at a high moisture content in the product, when the moisture content (kg/kg w.b.) decreases, for example, to 76.0 % (seaweeds) and 84.0 % mucus at -5.0 °C the application of freezing temperatures is not required, as soon as the process can not be considered as a freeze-drying.
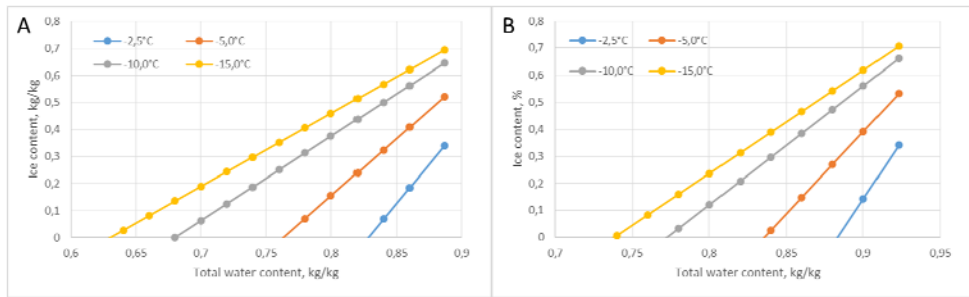
Fig. 3. Equilibrium ice fraction in seaweeds(left) and mucus(right) for different atmospheric-freeze drying temperatures (with respect to total water content)

Diagram on the figure 3 can be used for determination the desired freeze-drying temperatures. It should be noted, that the real content of ice will be a function of weight ratio: blade weight to mucus weigt.

4. Conclusions

The two glass transition phenomena was detected at the ultra-low temperature region at -84.77(1.35) and -62.14(0.46) °C for seaweed's blades and at -74.44(2.15) and -55.02(0.48) for mucus. Seaweeds blades and mucus showed different end of freezing point -52.23(1.61) and -42.1(0.65) °C. The unfreezable water content in seaweed blades was at 10.39(0.59)% w.b., while the value of 17.02(1.35) % w.b. was determined for mucus. Due to this the maximal freeze concentration was at 52.13(0.45) and 31.14(1.05) % solids w.b. for seaweed's blades and mucus respectively. The aplucation of atmospheric freeze-drying process is limited by theses values: full ice melting when the total moisture content is still high (during drying process).

5. Acknowledgement

6. References

[1] Forster, J.; Radulovich, R.; Chapter 11 - Seaweed and food security. In Seaweed Sustainability; D.J. Troy, Eds., Academic Press: San Diego, 2015; 289-313

[2] Phang, H.-K.; Chu, C.-M.; Kumaresan, S.; Rahman, M.M.; Yasir, S.M. Preliminary study of seaweed drying under a shade and in a natural draft solar dryer. International Journal of Science and Engineering 2015, 8(1), 10-14.

[3] Lemus, R.A.; Pérez, M.; Andrés, A.; Roco, T.; Tello, C.M.; Vega, A. Kinetic study of dehydration and desorption isotherms of red alga Gracilaria. LWT - Food Science and Technology 2008, 41(9), 1592-1599.

[4] Fudholi, A.; Othman, M.Y.; Ruslan, M.H.; Yahya, M.; Zaharim, A.; Sopian, K. Design and testing of solar dryer for drying kinetics of seaweed in Malaysia. In Proceedings of the 4th WSEAS international conference on Energy and Development, Environment and Biomedicine, Corfu Island, Greece, August 24-26, 2011; 119-124.

[5] Fleurence, J. Seaweed proteins. Trends in Food Science & Technology 1999, 10(1), 25-28.

[6] Sappati, P.K.; Nayak, B.; van Walsum, G.P. Effect of glass transition on the shrinkage of sugar kelp (Saccharina latissima) during hot air convective drying. Journal of Food Engineering 2017, 210, 50-61.

[7] Schiener, P.; Black, K.D.; Stanley, M.S.; Green, D.H. The seasonal variation in the chemical composition of the kelp species Laminaria digitata, Laminaria hyperborea, Saccharina latissima and Alaria esculenta. Journal of Applied Phycology 2015, 27(1), 363-373.

[8] Tolstorebrov, I.; Eikevik, T.M.; Bantle, M. Thermal Phase Transitions and Mechanical Characterization of Atlantic Cod Muscles at Low and Ultra-low Temperatures. Journal of Food Engineering 2014, 128, 111-118.

[9] Riedel, L. Eine formel zur berechnung der enthalpie fettarmer lebensmittel in abha˚ngigkeit von wassergehalt und temperatur. Bureau of Standards Journal of Research 1978, 5, 129-133.

[10] Figueroa, Y.; Guevara, M.; Perez, A.; Cova, A.; Sandoval, A.J.; Muller, A.J. Effect of sugar addition on glass transition temperatures of cassava starch with low to intermediate moisture contents. Carbohydrate Polymers 2016, 146, 231-237.

[11] Gaikwad, A.N.; Wood, E.R.; Ngai, T.; Lodge, T.P. Two Calorimetric Glass Transitions in Miscible Blends Containing Poly(ethylene oxide). Macromolecules 2008, 41(7), 2502-2508.

[12] Tolstorebrov, I.; Eikevik, T.M.; Bantle, M. A DSC study of phase transition in muscle and oil of the main commercial fish species from the North-Atlantic. Food Research International 2014, 55, 303-310.

[13] Claussen, I.C.; Ustad, T.S.; Strømmen, I.; Walde, P.M. Atmospheric Freeze Drying— A Review. Drying Technology 2007, 25(6), 947-957.

[14] Schwartzberg, H.G. Effective heat capacities for the freezing and thawing of food. Journal of Food Science 1976, 41(1), 152-156.

Description of atmospheric freeze-drying process of organic apples using thermo-physical properties

Tolstorebrov, I.[a]*; Eikevik, T. M.[a]; Petrova, I.[a]; Shokina, Y.[b]; Bantle, M.[c]

[a] Department of Energy and Process Engineering, Norwegian University of Science and Technology, NO-7049 Trondheim, Norway, Tel.: +47 73593742

[b] Department of Food Production Technology, Murmansk State Technical University, Murmansk Russian Federation

[c] Sintef Energy Research, Trondheim Norway

*E-mail of the corresponding author: ignat.tolstorebrov@ntnu.no

Abstract

This study discusses the influence of temperature and total moisture content on ice fraction in organic apples during atmospheric freeze-drying process. The ice formation of glass transition events were described by Clausius-Clapeyron and Gordon Taylor equations. The obtained data is essential for design the drying process and for understanding the limiting factors.

Keywords: ice fraction, organic apples, atmospheric freeze/drying, glass transition

1. Introduction

Atmospheric freeze drying (AFD) of apples results in improved quality of the product which is reflected in better appearance, high porosity and better color, when compared with conventional drying [1, 2]. However, the properties of the foods with high moisture content can vary significantly when dehumidifying at the selected freezing temperatures. Extensive research was previously conducted to model and explain physical phenomena of AFD of apples [3-5]. The studies revealed high amount of unfrozen moisture when drying at -5.0 and -10.0 °C. However, ice development in apples during AFD process is still unclear. Thus, it is of a great importance to gain a deeper understanding of the thermal properties of apples during drying to further decrease undesired changes of product properties. The aim of current study was the investigation of the development of thermal properties and ice content at different freeze-drying temperatures. Such comparisons will give the essential information to understand factors, which influence the process and limits the AFD process. The same principle can be applied to design the drying regimes of other organic foods, which contain significant amount of sugars (fruits and berries).

2. Materials and Methods

2.1 DSC analysis

Raw and vacuum-freezed dried salmpes were used for experiments. The desired moisture content of vacuum freeze-dried samples was obtained by equilibration in climate camera at defined conditions. The DSC analysis was done wit DSC Q 2000 (TA instruments, USA) equipped with a Liquid Nitrogen Cooling System. Helium was chosen as a purge gas at 25 mL/min, according to TA's instrument recommendations. The reference sample was an empty hermetically sealed aluminum pan. The samples with masses between 13.0 mg and 20.0 mg were placed into aluminum pans with hermetic lids. Samples were cooled and equilibrated for 5 minutes at –150.0 °C; the cooling rate was 10.0 °C/min. The annealing procedure was applied at –50.0 °C. This was done to avoid cold crystallization during scanning. Then the samples were heated up to 150.0 °C with the heating rate of 10.0 °C/min.

2.2 Determination of glass transition

The glass transition was determined with TA Universal Analysis 2000 version 4.5A software (TA instruments, USA). The glass transition is characterized with the following parameters: the onset, end and inflection points. It should be noted, that the glass transition in seaweeds with high moisture content is relatively weak. Thus, the inflection point was determined as a negative peak of the derived heat flow curve [6].

2.3 Determination of end of freezing and initial freezing point

The onset of ice melting (or end of freezing point), was determined by analyzing the DSC heating curve. The freezing point was estimated as a minimum value of the ice melting endothermic peak on the DSC heat flow curve.

2.4 Determination of ice fraction and unfreezable water

The amount of unfreezable water and ice fraction was detected by the DSC melting curve analysis. The DSC melting peaks were integrated with the sigmoidal tangent baseline function from the onset of ice melting point. The ice fraction was determined as a ratio of melting energy to latent heat of fusion of pure ice. As soon as melting energy of ice is a function of temperature, the empirical equation suggested by Riedel[7] was used for correction of obtained values. The amount of unfreezable water was obtained as the difference between the total water fraction in the product and the ice fraction.

2.5 State diagram

The thermal transitions can be introduces using the state diagram. A typical state diagram consists of two curves: the freezing curve and the glass transition curve. The freezing curve represents the influence of a solid matter content on the reduction of the freezing point. In this investigation it was obtained from the data of the freezing point of semi-dried apples with different moisture contents. The decrease of the freezing point δ (°C) was modeled with the Clausius-Clapeyron equation modified for food by Schwartzberg [8], equation (1):

$$\delta = -\frac{\beta}{M_w}\ln\left(\frac{1-x_s-Bx_s}{1-x_s-Bx_s+Rx_s}\right) \tag{1}$$

where β – molar freezing point constant, 1860 (kg K)/(kg mol); M – molecular mass, kg/kmol; B – ratio of unfreezable water to the total solids content, kg/kg; R – molecular mass ratio of water and solids, kDa/kDa; x_s – solid fraction kg/kg w.b.

The glass transition curve shows the influence of the solid content on the glass transition temperature ($T_{g,i}$). It was modeled with the Gordon-Taylor equation [9], equation (2):

$$T_{gt} = \frac{x_s T_{gt,s} + k x_w T_{gt,w}}{x_s + k x_w} \tag{2}$$

where, x_s – solid fraction kg/kg w.b.; k – system's constant in Gordon-Taylor equation; $T_{gi,s}$ – galss transition of pure solids; $T_{gi,w}$ – glass transition of pure water.

2.6 Statistical analysis

A regression analysis was done with a software DataFit 8.1 program (Oakdale Engineering). The quality of the regression was evaluated with the following parameters: F-Ratio, Prob(F) and R^2. F-Ratio is the ratio of the mean regression sum of the squares

divided by the mean error sum of the squares. Prob(F) is the probability that the null hypothesis is true. R^2 is the coefficient of multiple determinations. The standard deviation is introduced in the brackets after the values given in the text.

3. Results and Discussion

3.1 Thermo-physical properties of apples

The DSC heat flow curve for fresh apples revealed the following endothermic processes: glass transition of unfreezable solution, and melting of freezable water. The unfreezable solution consists of solids and unfreezable water. It is also referred to as maximal freeze concentrated solution [10]. One of the remarkable properties of this solution is its high viscosity. The ice formation is usually not detected when the solids concentration exceeds the value of the maximal freeze concentrated solution. The example of the thermal transitions in apples is introduced on Figure 1a,b.
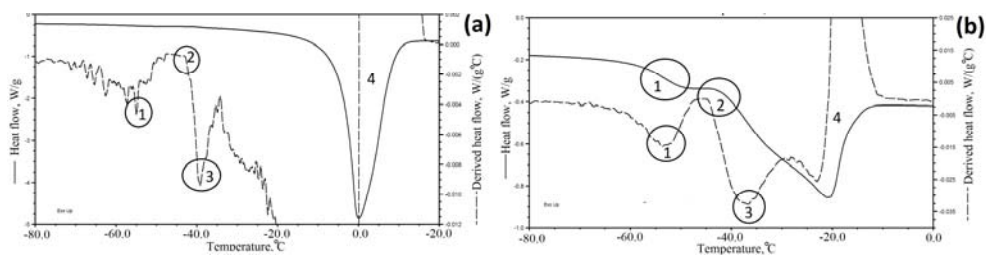
Fig. 1 Example of thremal transitions in apples: raw (left) and dried (right): 1- inflection point of glass transition, 2- end of freezing (insipient point of ice melting); 3- eutectic point; 4- ice melting peak.

Glass transition of fresh apples was relatively weak due to a high content of freezable water, but it was easily detected on the derived heat flow curve ($T_{g,i}$ = -55.08 °C, Figure 1a, left, dashed line). At the same time, decreasing of amount of freezable water by drying (semi-dried blanched apples, Figure 1b) made the glass transition shift visible on the heat flow curve, $T_{g,i}$ = -53.42 °C. All the apple samples, which showed an ice melting peak, formed the same maximal freeze concentration of 79.0 % solids w.b. irrespective of the moisture content. Thus, the glass transition shift was detected in the same temperature range ($T_{g,i}$ between -55.5 and -53.0 °C) as for fresh blanched apples. As soon as the temperature of glass transition is a function of average molecular weight of the system. Such a dependence was determined before for other types of foods [6].

At the same time, the samples, which did not show an ice melting peak (the concentration of solids ≥79.0 % w.b.), showed a different trend. The glass transition strongly depended on the moisture content: it increased within decreasing of the moisture in the sample.This study determined the inflection point of glass transition of dried apples (0.5 (0.3) % d.b.) in

the range between 38.0 and 46.0 °C. Such a deviation can be explained by accumulation of moisture during sample preparation for DSC. Water molecules work as plasticizers and even a small amount of moisture can decrease glass transition temperature significantly [10]. A recent study revealed the glass transition for dried apples in the range between 33.0 and 84.0 °C [11], when the glass transition was affected by drying temperature from 30.0 to 60.0 °C. However, this study did not show such a dependence for AFD conditions.

The melting peak (solid line, Figure 1a,b) of the freezable water occurred in very narrow temperature range, which indicated the high amount of free water in the product. However, the incipient point of melting (end of equilibrium freezing) was detected at a temperature of -44.2(1.2) °C. The eutectic point was detected on the DSC heat flow curve in the temperature range between -39.2 and 37.4 °C. It was introduced as a weak bend of the melting peak line and as a negative peak on the derived heat flow curve (in the range between -39.11 and -37.40 °C), see Figure 1a,b.

Integration of the melting peak from the incipient point of melting with respect to Riedel's equation [12] allowed to calculate the amount of frozen matter vs. temperature, Figure 2a. The amount of unfreezable water, which was calculated as a difference between total water content and the ice fraction, was found at 3.7 (0.3) % w.b. Thus, apples include solid fraction, freezable and unfreezable water. Most of the freezable water was in crystalline form in the temperature range between -3.0 and -10.0 °C, Figure 2a. Such temperatures is a typical range for the AFD process [3, 13]. At the same time, the moisture content of unfrozen solution at these temperatures was also very high and varies in the range between 60.0 and 43.0% w.b., Figure 2b. This significantly influenced the drying process. The retreating of the ice front from the surface to the inner parts of the product with the formation of a porous zone, which phenomena is widely used for modelling of AFD process, [13] will not occur in such a case. The process of evaporation of the unfrozen moisture and ice melting due to depression of freezing point is much more likely to occur.
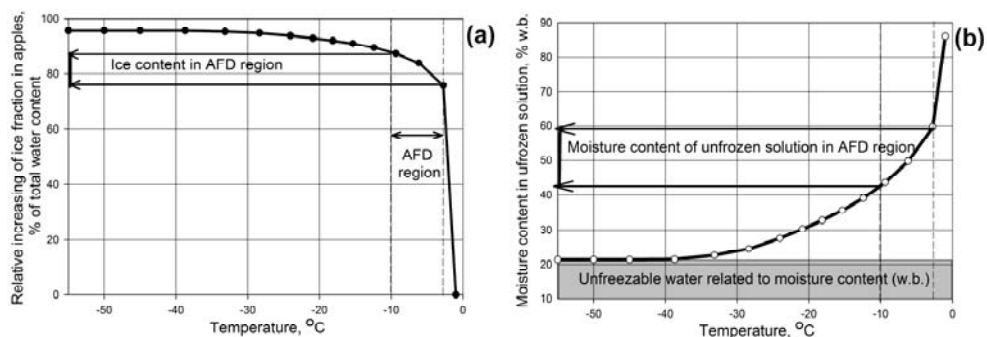
Fig. 2 Ice content increasing in apples (left), Moisture content in unfrozen solituion(right)

3.2 The state diagram for organic apples

The state diagram, which is constructed on the basis of equations (1) and (2), is introduced in Figure 3. The inflection point of glass transition was used for the modeling. These two lines split the diagram area into four regions with respect to solid content and temperature. The amorphous region appears above the freezing point depression line (Clausius-Clapeyron's equation: R=5.48*10^-5; B=12.78*10^-2); this region is common for atmospheric convection drying of foods. The region of ice and amorphous unfrozen solution is situated between the freezing point depression line and glass transition line. The region of the glassy state can be found below the glass transition line (Gordon-Taylor equation: k=4.19; $T_{gi.s}$=42.09 °C).
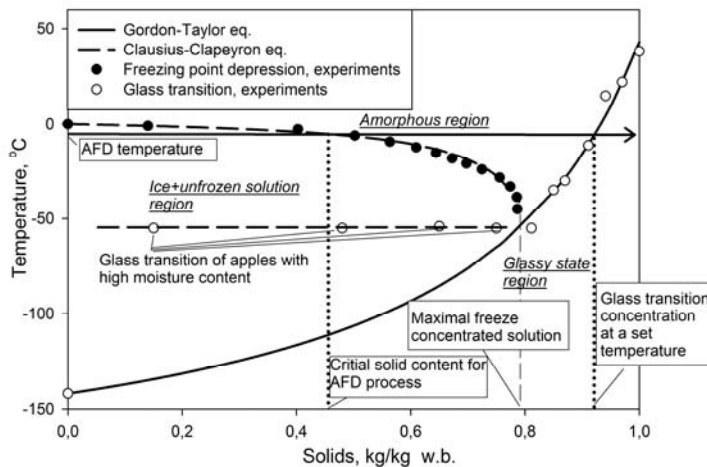
Fig. 3 State diagram for apples: experimental results and modelling (F(Ratio)>600;Prob(F)=0)

The application of the state diagram, Figure 3, allows to predict indirectly the amount of ice during drying at different processing temperatures with respect to the moisture content. Further, the natural limitation of the AFD process can be determined. The minimum AFD temperature is influenced by the formation of maximal freeze concentration, when further decreasing of the temperature does not influence on ice content in the product. The overall amount of ice at any time of the drying process can be easily determined knowing the actual moisture content and the critical solid content, which is a function of the drying temperature, equation (3):

$$x_{Ice,T} = x_{W,T} - (1 - x_{s,crtt,T}) \tag{3}$$

where, $x_{ice,\tau}$ – ice content at any time of the AFD process (kg/kg w.b.); $x_{w,\tau}$ – water content at any time of AFD process (kg/kg w.b.); $x_{s,crit,T}$ – critical solid content at the AFD drying temperature (kg/kg w.b.).

Critical solid content is the maximum available concentration of solids in unfrozen solution at freezing temperature. It can be determined using equation (1) or Figure 3. Due to this, it is possible to control AFD process using the weight reduction as a reference. For example, Duang et al., [14] suggested to decrease the temperature of the drying air from -5.0 to -10.0 °C to avoid ice melting during atmospheric freeze-drying.

The full melting of ice will occur when the concentration of the solid fraction reaches the critical solids content at a given freezing temperature, Figure 3 (dotted line). At such conditions, the process became the typical low temperature convection drying. Another important issue is glass transition of the samples, when the amorphous solution will solidify. Such a phenomenon depends on the solid fraction and temperature (Gordon-Taylor equation). The subsequent increase of temperature before reaching the glass transition concentration at a given temperature is essential to decrease the drying time. The viscosity of an amorphous solution in the vicinity of the glass transition reaches 10^{12} Pa*s [15]. This can decrease the drying rate significantly. At the same time, crossing the glass transition line will make the product crispy and brittle, as soon as the viscous-elastic characteristics of the product disappear in the region [6].

4. Conclusions

The temperature of glass transition of fresh and dried apples was determined at -55.08 and -53.42 °C respectiveely. The inflection point of glass transition of dried apples was detected in the range between 38.0 and 46.0 °C. Both fresh and dried apple samples showed the same maximal freeze concentration of 79.0 % solids w.b. irrespective of the moisture content. The incipient point of melting was found at -44.2(1.2) °C. The eutectic point was detected in the temperature range between -39.2 and 37.4 °C. The amount of unfreezable water was determined at 3.7 (0.3) % w.b. The moisture content of unfrozen solution varied in the range between 60.0 and 43.0% w.b. at -3.0 and -10.0 respectively. The process of AFD should be held in the temperature range below the melting temperature with respect ot moisture content, but the temperature should be increased after the ice melting. The region of glass transition should be avoided for rapid and efficient drying.

5. Acknowledgement

6. References

[1] Stawczyk, J.; Li, S.; Witrowa-Rajchert, D.; Fabisiak, A. Kinetics of Atmospheric Freeze-drying of Apple. Transport in Porous Media 2007, 66(1), 159-172.

[2] Reyes, A.; Mahn, A.; Huenulaf, P. Drying of Apple Slices in Atmospheric and Vacuum Freeze Dryer. Drying Technology 2011, 29(9), 1076-1089.

[3] Claussen, I.C.; Strømmen, I.; Hemmingsen, A.K.T.; Rustad, T. Relationship of Product Structure, Sorption Characteristics, and Freezing Point of Atmospheric Freeze-Dried Foods. Drying Technology 2007, 25(5), 853-865.

[4] Claussen, I.C.; Andresen, T.; Eikevik, T.M.; Strømmen, I. Atmospheric Freeze Drying—Modeling and Simulation of a Tunnel Dryer. Drying Technology 2007, 25(12), 1959-1965.

[5] Lourenço, S.O.; Barbarino, E.; De-Paula, J.C.; Pereira, L.O.D.S.; Marquez, U.M.L. Amino Acid Composition, Protein Content and Calculation of Nitrogen-to-protein Conversion Factors for 19 Tropical Seaweeds. Phycological Research 2002, 50(3), 233-241.

[6] Tolstorebrov, I.; Eikevik, T.M.; Bantle, M. Thermal Phase Transitions and Mechanical Characterization of Atlantic Cod Muscles at Low and Ultra-low Temperatures. Journal of Food Engineering 2014, 128, 111-118.

[7] Riedel, L. Eine formel zur berechnung der enthalpie fettarmer lebensmittel in abha˚ngigkeit von wassergehalt und temperatur. Bureau of Standards Journal of Research 1978, 5, 129-133.

[8] Schwartzberg, H.G. Effective heat capacities for the freezing and thawing of food. Journal of Food Science 1976, 41(1), 152-156.

[9] Gordon, M.; Taylor, J., S. Ideal Copolymers and the Second-order Transitions of Synthetic Rubbers in Non-crystalline Copolymers. Journal of Applied Chemistry 1952, 2(9), 493-500.

[10] Rahman, M.S. Food Stability Beyond Water Activity and Glass Transtion: Macro-Micro Region Concept in the State Diagram. International Journal of Food Properties 2009, 12(4), 726-740.

[11] Mrad, N.D.; Bonazzi, C.; Boudhrioua, N.; Kechaou, N.; Courtois, F. Moisture Sorption Isotherms, Thermodynamic Properties, and Glass Transition of Pears and Apples. Drying Technology 2012, 30(13), 1397-1406.

[12] Riedel, L. Kalorimetrische untersuchungen über das gefrieren von seefischen. Kaltetechnik 1956, 8, 374-377.

[13] Claussen, I.C.; Ustad, T.S.; Strømmen, I.; Walde, P.M. Atmospheric Freeze Drying—A Review. Drying Technology 2007, 25(6), 947-957.

[14] Duan, X.; Ding, L.; Ren, G.-y.; Liu, L.-l.; Kong, Q.-z. The Drying Strategy of Atmospheric Freeze Drying Apple Cubes Based on Glass Transition. Food and Bioproducts Processing 2013, 91(4), 534-538.

[15] Champion, D.; Le Meste, M.; Simatos, D. Towards an Improved Understanding of Glass Transition and Relaxations in Foods: Molecular Mobility in the Glass Transition Range. Trends in Food Science and Technology 2000, 11(2), 41-55.

Exploring drying conditions for Mexican mesquite pods (*Prosopis laevigata*)

Sandoval, S.; López, D.; Rodríguez, J.; Méndez, L.; Aquino, L. V.

Instituto Politécnico Nacional, CIIDIR Unidad Oaxaca. Hornos No. 1003, Col. Noche Buena, Santa Cruz Xoxocotlán, CP. 71230. Oaxaca, México.

*E-mail of the corresponding author: ssandovalt@ipn.mx

Abstract

Mesquite pods contain a high nutritional content, then a protein rich flour can be obtained. Prosopis Laevigata pods were collected from Oaxaca and Durango. Three stages of maturity were identified. The internal structure of the pods was analyzed by scanning electron microscopy (SEM). The pods were dried at 40°C, 50°C and 60°C, 10% relative humidity and air velocity of 2.6 m/s. From experimental data, the characteristic curve was obtained. SEM Images showed a heterogeneous and tortuous structure. The internal structure of the material is a limiting factor for mass transfer. The effective coefficient diffusion for each drying experiment was determinated.

Keywords: Drying; mesquite; pods.

1. Introduction

The mesquite is an extremophile tree that grows in arid and semi-arid zones around the world. In Mexico, mesquite is found in northern, central and southern states of the country and in the past was used as a bread, flour, and syrup [1]. The pods having a high content of protein, sugar, calcium, iron and fiber present a wide potential in the development of food products [2]. In order to process the pods a specific drying process is mandatory. Mesquite pods are a highly hygroscopic material due to the high sugar content [3]. The pods have a low moisture content (0.14 g water / g dry mater); however they tend to absorb moisture quickly in humid environments. After drying pods should at least reach a moisture content of 0.06 g water / g dry matter, otherwise they cannot be efficiently milled [4].

2. Materials and Methods

Prosopis laevigata pods were harvested between April and August 2017 in Oaxaca and Durango (Mexico). The color was measured with a HunterLab Model E-Z spectrophotometer using the CIELab color scale. In the CIELab color scale, the parameter L* represents the luminosity of the material; the parameter a* represents changes of coloration from red to green, and the parameter b* indicates a coloration that goes from yellow to blue. The sugars were quantified following the method NMX-F-312-1978. The mesquite pods were analyzed by electron microscopy, using a JEOL brand electronic scanning microscope (SEM), model JIB-4601F, with a spatial resolution of 1.2 nm. Pods without deterioration were selected for drying. The moisture content of the pods was measured by the oven-dry method (NMX-F-083-1986).

The pods were dried in a tunnel dryer (patent 304462). The temperature, relative humidity, and air velocity were controlled and logged. A National Instrument FP-1000 system was used, in order to log the data. The temperature of the material was measured using J-type thermocouples (Vaisala Veriteq SP 1700). A steam generator model TV / G2F Anghinetti SRL was used for the humidification of the air. Only pods from Oaxaca in stage 3 were dried at three different temperatures (40 °, 50 ° C and 60 ° C) and the Durango pods in stage 3 were dried only at 60 °C. Drying experiments were conducted at constant relative humidity (10%) and air velocity of 2.6 m/s.

2.2. The characteristic drying curve.
The experimental kinetics were normalized and the characteristic drying curve was obtained. The reduced moisture content was computed as follows:

$$W_r = \frac{W_t - W_{eq}}{W_i - W_{eq}} \qquad (1)$$

A polynomial equation of order 6 was used to depict the experimental drying kinetics, after that the drying rate was computed. The reduced drying rate (dWr) was calculated by using dWref:

$$dWr = \frac{dW}{dW_r} = \left[-\frac{dW}{dt}\right]_r = f(W_r) \qquad (2)$$

According to Equation 2, the reduced drying rate dWr is a function of the reduced moisture content Wr, so an equation is derived to describe the complete kinetics using the following conditions:

$$f(W_r) = 0 \; if \; W_r = 0 \qquad (3)$$

$$0 < f(W_r) =< 1 \; if \; 0 < W_r < 1 \qquad (4)$$

$$f(W_r) = 1 \; if \; W_r = 1 \qquad (5)$$

The graphs of reduced moisture content versus reduced drying rate can be described with a straight line for both Oaxaca and Durango pods ranging from reduced moisture content of 1 to 0.01. The initial phase of the of drying rate curves are discarded since it happens very fast and the final period is not taken into account by the model because it represents very low moisture contents [5]. The deduction of the linear model is presented below:

$$W = C + \left(W_{r0} - W_{eq}\right)\left[\left(1 + \frac{d}{c}\right) e^{\frac{-C*dWref*t}{W_{r0} - W_{eq}}} - \frac{d}{c}\right] \qquad (6)$$

3. Results and Discussion

According the Cielab scale, three stages of maturity were defined (Table 1). In Stage 1 pods show a green coloration, in stage 2 the pods are brighter with a reddish coloration. In stage 3 the pods increase in brightness compared to the previous stages, reddish and yellow coloration is still observed, but in a lower intensity compared to stage 2.

Table 1. CIElab color parameters of mesquite pods at different stages of maturity

Stage 1	Stage 2	Stage 3
L*70.75 +/- 0.6632	L*71.46 +/- 0.8423	L*73.87(2017) +/- 0.5754
a*-45.84 +/- 0.1567	a*8.68 +/- 0.3214	a*3.66 (2017) +/- 0.1345
b*64.78 +/- 0.4892	b*71.13 +/- 0.5919	b*26.4 (2017) +/- 0.2598

The content of sugars (Table 2) in the three stages of maturity has significant differences; the green pods have a bitter taste, while the mature pods have a sweeter taste. Stage 1 pods have less sugar than other stages of maturity also a bitter taste which isn't good for further processing, stage 2 pods have a higher sugar content however their moisture content (3.08 g.

water/g. dry matter) makes them difficult to dry and a high moisture content after drying makes them unusable for further processing; pods in stage 3 have a sugar content that makes them sweet and a moisture content of 0.22 g. water/g. dry matter. Pods from Durango in stage 3 have a significantly higher sugar content than pods from Oaxaca which prolongs the drying time due the hygroscopic behavior of the sugars on the mesocarp.

Table 2. Sugar content in the different states mesquite pods

100 g of Pods.	Stage 1 (Oaxaca)	Stage 2 (Oaxaca)	Stage 3 (Oaxaca)	Stage 3 (Durango)
Sugars.	6.55 g +/- 0.0680	8.15 g +/- 0.3552	7.42 g +/- 0.1305	14.42 g +/- 0.1178

The seeds (Fig. 1) are covered by the endocarp; they have a semi-spherical, brown, smooth and shiny texture. In Fig. 2 a) we observe a cross section of the seed where the tegument constituting the outermost layer of the seed, the endosperm is divided into different sections each with similar structure, finally the embryo is observed in the central and inner part of the seed. The seed measures 2.5 mm thick. In Fig. 2 b) we observe the surface of the tegument presenting a homogeneous conformation with no pores. In Fig. 2 c) the image shows the back part of the tegument as well as the plumule. In Fig. 2 d) we can observe the space between and the endocarp where the seed is contained.
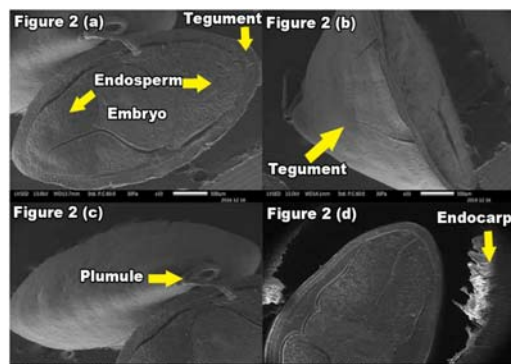
Fig. 1 Longitudinal image of the seed.   **Fig. 2 Transverse images of the seed obtained by SEM.**

The mesocarp thickness varies from each pod. This domain is rich in carbohydrates and has a highly hygroscopic nature [6]. It presents a tortuous, rubbery structure and cavernous sections. It is strongly attached to the endocarp and epicarp.

Figure 3 a) shows a section of the mesocarp, which has a heterogeneous, tortuous and rubbery conformation; these characteristics together with the hygroscopic capacity represent a further difficulty in the removal of moisture during drying. Figure 3 b) presents a section of the mesocarp attached to the inner layer of the epicarp, showing an irregular, tortuous, heterogeneous and rubbery structure; strongly adhered to the epicarp. Figures 3 c) and 3 d)

show a cross section of the pod focusing on the mesocarp, again showing an irregular,
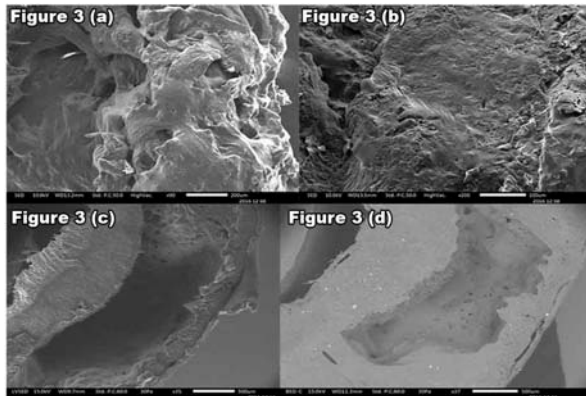
Fig. 3 Transverse images of the mesocarp obtained by SEM.

heterogeneous and tortuous conformation; presenting cavernous portions that present a further difficulty when predicting how moisture diffuses towards the surface.

In Fig. 4, we show the kinetics for the drying condition at 40°C and 50°C. The pods reached the equilibrium moisture content (W) at different times.. An inconvenience of drying at 40 and 50°C is the high moisture content at the end of drying, since a milling process requires pods with a very low moisture content.
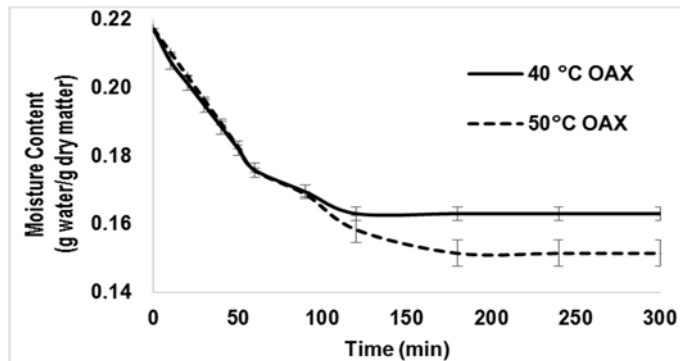
Fig. 4 Drying kinetics of mesquite pods stage 3 at 40 ° and 50 ° C (Oaxaca).

In Fig. 5 we observe the drying kinetics for drying at 60°C for pods from Oaxaca and Durango. The pods from Oaxaca had an initial moisture content of 0.2234 g water/g dry matter, meanwhile the Durango pods an initial moisture content of 0.1815 g water/g dry matter. In spite of a fast heating period, pods offer an important resistance to moisture

migration due to its microstructure. During the heating period of drying where the evaporation rate increases, the free water diffuses more easily.
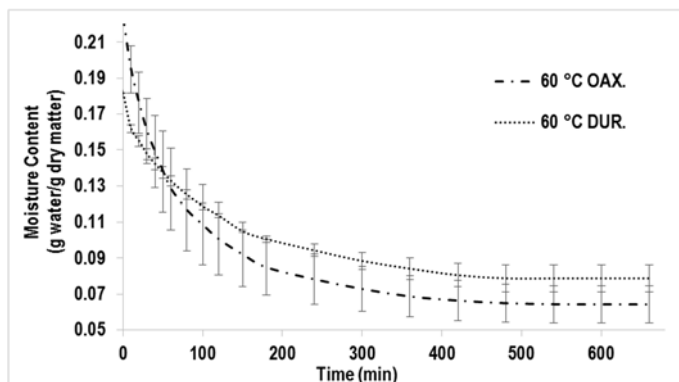
Fig. 5 Drying kinetics of mesquite pods stage 3 at 60 ° C (Oaxaca and Durango).

Table 3 shows the parameters obtained by the characteristic curve model. Figures 6 and 7 show the experimental drying kinetics of Oaxaca and Durango at 60 °C and the characteristic curve.

Table 3. Calculated parameters of the characteristic drying curve model.

Temperature °C	dWref	c	d
Oaxaca 60 °C	0.0022	1.0488	0.0014
Durango 60 °C	0.0011	0.9036	0.0067

The characteristic curve (Fig. 6 and 7) shows a good agreement with the experimental data for drying at 60°C (Oaxaca) and 60°C (Durango). This empirical model has the advantage of predicting how pods are dried without the need to know all their properties.
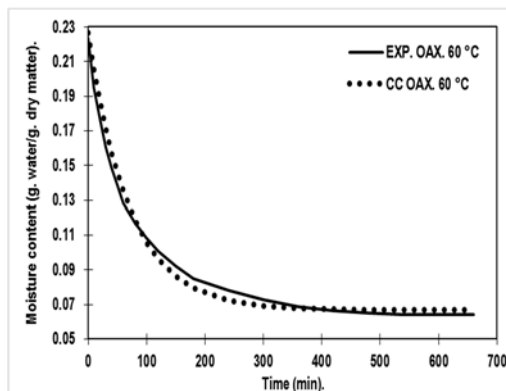
Fig. 6 Comparison of experimental data and the characteristic curve model (Oaxaca 60 °C).
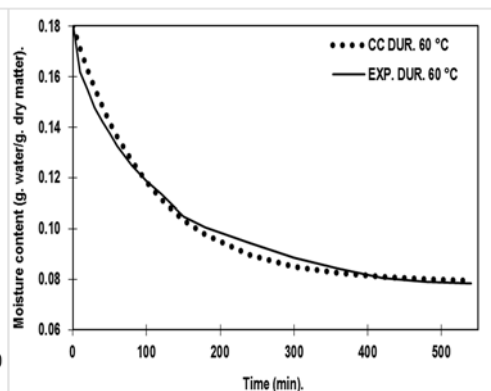
Fig. 7 Comparison of experimental data and the characteristic curve model (Durango 60 °C).

4. Conclusions

The drying process of mesquite pods (*Prosopis laevigata*) was studied. Three stages of maturity were identified and the internal structure of the pod which plays a very important role in drying. The periods of maturity are followed by physical changes such as color and chemical changes such as the sugar and moisture content. The pods in stage 3 of maturity have a sweet flavor and a lower moisture content which is apropiate for drying. Mesquite pods have a heterogeneous and tortuous structure, which is a barrier that hinders the diffusion of moisture. This fact must be considered due to the increase in economic and energy costs when this drying process is carried out on a larger scale. The pods from Oaxaca and Durango must be dried at a minimum temperature of 60°C to obtain a quality dry product. The characteristic drying curve was deduced and it shows a good representation of drying kinetics. The mesquite pods are a multidomain food then the diffusion in a multidomain food must be studied.

5. Acknowledgments

6. Nomenclature

Subscripts

c	Characteristic drying curve coefficient.
C	C Constant.
d	Characteristic drying curve coefficient.
dWr	Reduced drying rate.
dWref	Reference drying rate.
t	Time
W	Moisture content.
Weq	Equilibrium moisture content.
Wr	Reduced moisture content.

7. References

[1] De La Rosa, A.P.; Hernández, J. T. F.; Portugal, V. O.; Castañeda, J. G. Processing, nutritional evaluation, and utilization of whole mesquite flour (Prosopis laevigata). Journal of food science 2006, 71(4), 315-320.

[2] Choge, S. K.; Pasiecznik, N. M.; Wright, J.; Awan, S.Z.; Harris, P.J.C. Prosopis pods as human food, with special reference to Kenya. Water SA. 2007,33(3).

[3] Grados, N.; Ruiz, W.; Cruz, G.; Díaz, C.; Puicón, J. Productos industrializables de la algarroba peruana (Prosopis pallida): Algarrobina y Harina de Algarroba. Multequina, 2000, 9(2), 119-132.

[4] Felker, P.; Grados, N.; Cruz, G.; Prokopiuk, D. Economic assessment of production of flour from Prosopis alba and P. pallida pods for human food applications. Journal of Arid Environments, 2003. 53(4), 517-528.

[5] Jannot, Y.; Talla, A.; Nganhou, J.; Puiggali, J. R. Modeling of banana convective drying by the drying characteristic curve (DCC) method. Drying technology, 2004. 22(8), 1949-1968.

[6] Meyer, D. Processing, utilization and economics of mesquite pods as a raw material for the food industry PhD Thesis. Techn. Wiss. ETH Zürich, 1984.

Effects of thermal intermittence on fruit characteristics and drying time in convective drying of mango (*Mangifera indica* L.)

Amado, L. R.[a]; Silva, K. S.[b]; Mauro, M. A.[a*]

[a] UNESP - São Paulo State University, Institute of Biosciences, Humanities and Exact Sciences (IBILCE), São José do Rio Preto, SP, Brazil

[b] UEM - State University of Maringá, Umuarama, PR, Brazil

*Corresponding author: cidam@ibilce.unesp.br

Abstract

This study investigated the influence of the intermittent drying conditions on drying kinetics and on color and carotenoid retention of mangoes. The drying conditions were 95°C (40 min) and 80°C (40 min) in the first stage combined with 70°C and 60°C in the second stage, and continuous drying (70°C and 60°C) as control. Drying time was reduced by thermal intermittence and carotenoid retention was more affected by temperature than drying time. The results also highlighted the carotenoid sensitivity to 70°C temperature, showing the importance of limiting the temperature of the mango to 60°C during the two drying stages.

Keywords: *Intermittent drying; thermal intermittence; carotenoid; color.*

1. Introduction

Convective drying process provides many advantages over the shelf life extension of the food products. However, the drying of fruits in its most conventional way, can affect the nutritional quality of the dried products, due to prolonged exposure to oxygen and high temperatures. A possible way to reduce the negative effects of convective drying and still reduce energy consumption is to apply it under conditions of thermal intermittence, in which the conditions of time and temperature are modified during the same operation [1]. The drying of fruits with application of the thermal intermittence is based on their high moisture content at the beginning of the drying, whose surface temperature remains lower than the air because of water evaporation. This allows a higher temperature to be initially used and, consequently, reduces the drying time without causing significant damage to the product [2].

Regarding thermal intermittence, it is noted that this process is widely used in drying of grains and seeds, where tempering periods are used to reduce moisture gradients and avoid cracks [3,4]. However, there is a gap in the literature with regard to drying with thermal intermittence applied to high moisture food products. Among the existing works, most of them focus on the economy that the intermittence provides to the drying process, without evaluating the quality of the product, which can be considered a problem with respect to the nutritional aspects of food. Several authors have shown that intermittent drying conditions can lead to significant reductions in drying time and energy demand. For example, Váquiro et al. (2009) [5] dehydrated mango slices applying intermittence and obtained increased drying rates and reduced overall operating time, indicating a decrease in energy consumption. However, as foods with high water content are susceptible to many changes due to chemical and biochemical reactions, it is important to evaluate quality through parameters such as color and nutrient retention [2,3].

The mango (*Mangifera indica* L.) is one of the most consumed fruits in the world, which is associated with their sensory properties and its high nutritional value, especially because of the antioxidant substances such as carotenoids, related to the prevention of several chronic-degenerative diseases and responsible for the mango color [6,7]. However, it is known that the mango is a seasonal fruit and presents considerable post-harvest losses, therefore, the use of preservation techniques like of convective drying is very important for these fruit, aiming to increase their shelf life.

The objective of this study was to evaluate the influence of the intermittent drying conditions on drying kinetics of mangoes as well as on their color and retention of carotenoids during process, aiming to reduce the time of operation and improve the sensory and nutritional quality of the dry mango.

2. Materials and Methods

2.1. Sample preparation

The mangoes (*Mangifera indica* L.) cv. Palmer with an average soluble solids content of 11.0 ± 1.4 °Brix and a moisture content between 81.8 and 86.0 % on wet basis (w.b.) were acquired from nearby farms the region of São José do Rio Preto - São Paulo. In order to have a similar degree of maturity in all drying trials, the fruits were selected visually and based on manual contact. In each drying trial, nine mangoes (4.5 kg) randomly selected from a total of approximately 100 fruits were used. The mangoes were sanitized, sliced (0.54 ± 0.03 cm thick) with an electrical slicer (ECO, Brazil) and then, cut in circles (3.5 cm diameter) with a manual cutter.

2.2. Drying trials

The drying trials were performed using two identical fixed bed dryers with forced heated air convection according to Filippin (2018) [2]. A hot wire anemometer (Delta OHM, Italy) was used to determine the average velocity of the air in the drying chamber, which was approximately 1 m·s⁻¹.

Six drying conditions were performed in duplicate, four of which were intermittent (I) in two stages, with the first stage at 95 °C (H=higher temperature) or 80 °C (L=lower temperature), held for 40 minutes, and the second stage at 60 °C (L) or 70 °C (H). The other two conditions corresponded to continuous (C) dryings at 60 °C and 70 °C (controls) (Table 1). The time range of the first stage was determined by monitoring the surface temperature of mango slices at the beginning of drying, considering as stop criterion the period that corresponds, approximately, to the time to reach the second stage temperature. All dryings were stopped when the samples reached moisture of approximately 8.7 % (± 1.1). To establish the total drying time, the initial moisture of the samples was previously determined and the stopping point was based on the weight of the trays with the samples, which was previously calculated so that the samples reached the desired final moisture. The samples were weighed successively during drying using a semi-analytical balance (Gehaka, BK 4000, Brazil). The equilibrium moisture was determined in samples left in the dryer until reaching constant weight. Temperature and time values of the drying stages, as well as abbreviations used in the following tables of this work are shown in Table 1.

Table 1. Temperature and time conditions for Intermittent and Continuous dryings

Trial	Abbreviation	Temperature (°C)		Time (min)	
		1th Stage	2nd Stage	1th Stage	2ndStage
Intermittent drying					
Intermittent (80 °C / 60 °C)	I-LL	80	60	40	230
Intermittent (95 °C / 60 °C)	I-HL	95	60	40	200
Intermittent (80 °C / 70 °C)	I-LH	80	70	40	200
Intermittent (95 °C / 70 °C)	I-HH	95	70	40	170
Continuous drying					
Continuous (60 °C)	C-L	60		360	
Continuous (70 °C)	C-H	70		300	

2.3. Drying kinetics

The effective diffusion coefficients of water were determined according to the Fick's second law, applied to an infinite flat plate. The analytical solution of the diffusion equation in its modified form, in terms of the mass fractions (dry basis, d.b.) and integrated on distance, is presented by Eq. (1) [8]:

$$X = \frac{\overline{X}_w(t) - X_w^{eq}}{X_w^0 - X_w^{eq}} = \frac{8}{\pi^2} \sum_{n=1}^{\infty} \frac{1}{(2n-1)^2} \exp\left[-(2n-1)^2 \frac{\pi^2 D_{eff} t}{e^2} \right] \tag{1}$$

where X is the residual moisture content, dimensionless; $\overline{X}_w$ represents the mean mass fraction of the water on a dry weight basis (kg · kg^{-1}) at the drying time t (s); X_w^0 and X_w^{eq} represents the water mass fraction on a dry weight basis (kg · kg^{-1}) at the initial moment ($t = 0$) and at equilibrium (eq); D_{eff} represents the effective diffusion coefficient (m^2·s^{-1}); e is the thickness of the samples (m); n is the number of terms in the series.

The shrinkage of the sample was considered by applying a simplified procedure that incorporates the volumetric contraction in an approximate way in Eq. (1) through the characteristic dimension (e) as a function of the water content. From the fruit volume variation during drying, the final thicknesses of the samples were estimated considering that shrinkage occurred in the same proportion, in each dimension of the solid [9], as follows:

$$\frac{e}{e_0} = \left(\frac{V}{V_0} \right)^{1/3} \tag{2}$$

where e (m) is the thickness at time t (s) and V (m^3) is the volume at time t (s); sub index 0 represents initial time ($t = 0$).

The volumes were calculated based on the thickness and diameter measurements performed on the mango samples, before and after each drying experiment. The thickness was then described as a linear function of the water content, on a dry basis, and incorporated into the Eq (1), to fit the model to the experimental results.

Water diffusion coefficients were determined according to Eq. (1), for each stage, separately, as described by Filippin (2018) [2]. The fitting method used in the estimation of the nonlinear parameters was based on the Levenberg–Marquardt algorithm [10].

2.4. Analytical methods

Thickness, total solids, total carotenoid, and color parameters were analyzed before and after drying, besides diameter after drying. The thickness was measured using a digital micrometer (MDC-25SB, Mitutoyo, Japan) and the diameter using a pachymeter (Stainless Hardened, 806178, USA), both used to calculate the volumetric variation of the samples during drying. Total solids content was determined gravimetrically, in a vacuum oven (TE-395, Tecnal, Brazil) at 60 °C until constant weight. Total carotenoid content was determined by spectrophotometric reading (Thermo Scientific, GENESYS 10S UV-VIS, EUA) (absorbance at 450 nm) as β-carotene, according to Rodriguez-Amaya and Kimura (2004) [11] and its retention during drying was analyzed as Eq. (3):

$$Ret(\%) = 100 \frac{(\mu g \text{ carotenoid/kg dried mango}) \times kg \text{ dried mango after drying}}{(\mu g \text{ carotenoid/kg raw mango}) \times kg \text{ raw mango before drying}} \qquad (3)$$

Color parameters based on the CIELAB system (L*, a*, b*) were obtained using a Colorflex spectrophotometer (HunterLab, Resto, USA). All color parameters (P*) measured after drying (t) were evaluated in relation to their corresponding values before drying (t=0). The process conditions that presented the ratios P*(t)/P*(t=0) tending to unity were considered effective in reducing the color changes.

2.5. Statistical methods

The fitting efficiency of the diffusion coefficient was evaluated by the correlation coefficient R^2 and the mean relative error (P %), according to Eq. (4):

$$P\ (\%) = \frac{100}{n} \sum_{1}^{n} \frac{\left| y^{\exp} - y^{cal} \right|}{y^{\exp}} \qquad (4)$$

where y^{calc} represents the water content on a dry basis, $y^{\exp}$ is the experimental value, and n is the number of observations or residuals.

3. Results and discussion

3.1. Drying kinetics

Table 2 shows the values for diffusivity (D_{eff}) and the determination coefficients (R^2) and relative errors (P(%)) for the drying trials. In relation to the diffusion coefficients, in general, the higher temperatures lead to higher diffusion coefficients.

Evaluating the fit of the model, high P (%) values were observed for the second stage of intermittent drying and for continuous drying (above 10%), as the error measurement makes the relative deviations very high when the water content is very small. However, the coefficients of variation (R^2) were all higher than 0.986, indicating satisfactory fit.

From the determination of the diffusivity, the moisture (dry basis) graphs were plotted as a function of time (Fig. 1) of the predicted values, which were compared with the experimental data. From the graphs, it can be observed that the predicted values are close to those observed for both intermittent drying stages and for continuous drying (Fig. 1).

Table 2. Effective diffusion coefficients ($D_{eff} \times 10^{10}$ ($m^2 \cdot s^{-1}$)) for the Intermittent (1th and 2nd Stage) and Continuous dryings, number of repetitions (Rep), total drying time, R^2 and P(%)

Trial	Rep	Total time (min)	D_{eff}	R^2	P (%)	Mean D_{eff}	D_{eff}	R^2	P (%)	Mean D_{eff}
			1th Stage				2nd Stage			
Intermittent drying										
I-LL	1	270	4.08	0.997	1.0	3.88±0.27	2.35	0.992	14.0	2.10±0.36
	2		3.69	0.997	1.2		1.84	0.998	14.0	
I-HL	1	240	4.54	0.997	1.7	4.91±0.52	2.42	0.992	12.9	2.38±0.06
	2		5.28	0.999	0.8		2.33	0.987	13.4	
I-LH	1	240	3.91	0.995	1.4	3.78±0.19	2.93	0.991	16.9	2.86±0.11
	2		3.65	0.997	0.9		2.78	0.992	25.7	
I-HH	1	210	5.61	0.998	1.2	5.16±0.63	3.28	0.986	29.2	2.99±0.42
	2		4.72	0.997	1.2		2.69	0.986	23.1	
Continuous drying										
C-L	1	360	-	-	-	-	2.36	0.998	17.8	2.17±0.28
	2		-	-	-		1.97	0.997	13.9	
C-H	1	300	-	-	-	-	2.89	0.998	14.3	2.83±0.09
	2		-	-	-		2.76	0.997	13.3	
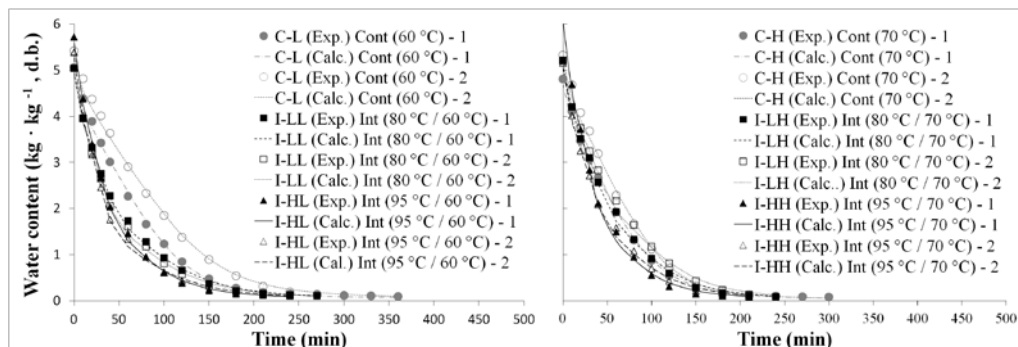
Fig. 1 *Experimental* (**Exp.**) *and predicted* (**Calc.**) *values for the water content (d.b.) as a function of drying time, for intermittent* (**I-**) *and continuous* (**C-**) *trials.*

3.2 Color and carotenoid retention

The carotenoid retention and normalized color parameter values of the dried mango are presented in Table 3. Drying at 95 °C/60 °C (I-HL) was the condition that provided the best preservation of carotenoid, followed by 80 °C/60 °C (I-LL), and also the continuous drying at 60 °C (C-L), which highlighted the carotenoid sensitivity to 70°C.

The color parameters did not show relevant changes in the different operating conditions. However, it was possible to verify that the greatest variations in the normalized a* parameters were related to the continuous dryings (C-L and C-H), and also with those intermittent dryings in which the second stage temperature was 70 °C (I-LH and I-HH). This suggests therefore, that long drying times and 70°C temperature could affect them more intensively.

Table 3. *Carotenoid retention* **Ret (%)** *and normalized color parameters* **P*(t)/P*(t=0)** *for each repetition* (**Rep**) *of intermittent* (**I-**) *and continuous* (**C-**) *trials.*

Trial	Rep.	Ret (%)	Mean Ret (%)	L*$_{dried}$/L*$_{fresh}$	a*$_{dried}$/ a*$_{fresh}$	b*$_{dried}$/ b*$_{fresh}$
I-LL	1 2	70.27 65.46	67.86±3.40	0.95±0.03	1.21±0.33	0.91±0.06
I-HL	1 2	67.08 69.36	68.22±1.61	1.03±0.03	1.13±0.01	1.02±0.00
I-LH	1 2	57.09 60.09	58.59±2.12	0.95±0.04	1.55±0.48	0.98±0.03
I-HH	1 2	54.65 54.81	54.73±0.11	0.96±0.06	1.54±0.64	0.93±0.05
C-L	1 2	67.71 61.13	64.42±4.65	0.92±0.11	1.70±0.32	0.95±0.10
C-H	1 2	59.51 62.03	60.77±1.78	0.93±0.05	1.90±1.04	1.05±0.25

4. Conclusions

Despite the drying conditions causing only small changes in the color parameters, they seemed to be more affected by the long drying times. More noticeably, the total drying time was reduced by thermal intermittence, by the increase of the first stage temperature of all intermittent dryings, and also when the second stage was 70 °C. Temperature affected carotenoid retention more than drying time, and their sensitivity to 70 °C confirmed the importance of limiting the sample temperature to 60 °C during the two drying stages.

5. References

[1] Kumar, C.; Karin, M. A.; Joardder, M. Intermittent Drying of Food Products: A Critical Review. Journal of Food Engineering, 2014, 121, 48–57.

[2] Filippin, A. P.; Molina Filho, L.; Fadel, V.; Mauro, M. A. Thermal intermittent drying of apples and its effects on energy consumption. Drying Technology, 2018. https://doi.org/10.1080/07373937.2017.1421549

[3] Kowalski, S. J.; Szadzinska, J.; Lechtanska. Non-stationary drying of carrot: Effect on product quality. Journal of Food Engineering, 2013, 118, 393-399.

[4] Shei, H.J.; Chen, Y.L. Computer simulation on intermittent drying of rough rice. Drying Technology. 2002, 20, 615–636.

[5] Vaquiro, H. A.; Clemente, G.; Garcia-Perez, J. V.; Mulet, A., Bon, J. Enthalpy-Driven Optimization of Intermittent Drying of *Mangifera indica L.* Chemical Engineering Research and Design. 2009, 87(7), 885–898.

[6] Dorta, E.; González, M.; Lobo, M. G.; Sánchez-Moreno, C.; Ancos, B. Screening of phenolic compounds in by-product extracts from mangoes (*Mangifera indica* L.) by HPLC-ESI-QTOF-MS and multivariate analysis for use as a food ingredient. Food Research International. 2014, 57, 51–60.

[7] Faria, A. F.; Hasegawa, P. N.; Chagas, E. A.; Pio, R.; Purgatto, E.; Mercadante, A. Z. Cultivar influence on carotenoid composition of loquats from Brazil. Journal of Food Composition and Analysis. 2009, 22, 196-203.

[8] Crank, J. The mathematics of Diffusion. 2nd ed . Oxford: Claredon Press, 1975.

[9] Molina Filho, L.; Frascareli, E. C.; Mauro, M. A. Effect of an Edible Pectin Coating and Blanching Pretreatments on the Air-Drying Kinetics of Pumpkin (*Cucurbita moschata*). Food and Bioprocess Technology. 2016, 9(5), 859–871.

[10] Marquart, D. W. An Algorithm for Least-Squares Estimation of Nonlinear Parameters. Journal of the Society for Industrial and Applied Mathematics. 1963, 11(2), 431–441.

[11] Rodriguez-Amaya, D. B.; Kimura, M. Screening method for sweetpotato and cassava. In: HarvestPlus Handbook for Carotenoid Analysis, International Food Policy Research Institute (IFPRI), Washington, D. C., 2004, 58.

Development of cost-effective protocol for preparation of dehydrated paneer (Indian cottage cheese) using freeze drying

Sharma, S.[a*]; Nema, P. H.[a]; Emanuel, N.[a]; Singha, S.[b]

[a] National Institute of Food Technology Entrepreneurship and Management, Haryana, 131028, India
[b] Centre for Rural Technology, Indian Institute of Technology, Guwahati, Assam 781039, India

*E-mail of the corresponding author: sadhana.foodtech@gmail.com

Abstract

Nowadays, there is high consumer demand in the market for simple to prepare, convenient, healthy and natural foods. Paneer or Indian cottage cheese is an acid and heat coagulated milk product which serves as a rich source of animal proteins for the vegetarians. Due to high moisture content (58-60 %), it is highly perishable in nature. Drying of paneer would undoubtedly extend the shelf life of paneer and also help in value-addition of paneer. Dehydrated paneer would find numerous ways to be use. Drying of paneer by conventional methods poses threats including case-hardening and non-uniform incomplete drying, poor rehydration characteristics, longer drying time, yellow discoloration and oiling off during drying. Freeze drying remains the best in retaining the quality of dried food products. Though it is highly expensive due to high processing and operation costs. The present study focuses on developing cost-effective protocol for freeze-drying of paneer. Efforts have been made by use of pre-treatments prior subjecting to freeze drying. The dehydrated product would be shelf-stable and can be rehydrated to its original state having flavor and texture comparable to the fresh form. Moreover, the final product after rehydration would be more fresh and softer than its frozen counterparts. The developed product would be easily kept well for few years at room temperature without any addition of preservatives.

Keywords: Paneer; freeze-drying; color; rehydration ratio; pre-treatment

1. Introduction

Paneer is an important indigenous product which is obtained by heat treating the milk followed by acid coagulation using suitable acid viz. citric acid, lactic acid, tartaric acid, alum, sour whey. Traditionally, India has been a paneer consuming nation with about 5% of milk produced being converted into paneer [1]. As per a conservative estimate, Indian paneer market is expected to grow at Compound annual growth rate of 18% till 2020. Paneer is quite popularly being used in a number of traditional Indian recipes. It is highly perishable with about 58% moisture content (wb). Various attempts have been made to improve the shelf life of paneer by employing different physical and chemical methods. These include low temperature treatment (refrigeration and freezing), chemical treatment, heat treatment, drying, hurdle technology and packaging. However drying remains the best preservation method in achieving a shelf stable product while retaining the quality attributes, it alters the physicochemical characteristics in the dried product. Vishweshwariah (1987) achieved a shelf-life of up to 2 months dehydrated paneer (5-9 % moisture) dried using hot air drying at 75°C for 4 hrs. Rehydration characteristics of were poor and lacked cohesiveness due to irreversible denaturation of proteins and rehydrated paneer was tough and rubbery [2]. Srivastava et al. (2013) reported that time required for drying paneer is 33% higher in VD as compared to low pressure superheated steam drying (LPSSD). Moreover, the effective diffusivity decreased with increase in pressure during vacuum drying of paneer [3]. Singh et al. (2004) conducted hot and cold diffusion of paneer cubes with sodium chloride and potassium sorbate solution and subsequent microwave drying was done. Maximum rehydration ratio was achieved in cold (1.03) and hot (1.09) diffused microwave dried paneer cubes at 30°C for 10 minutes [4]. Undoubtedly, Freeze drying is a standard processing technique for drying of heat sensitive food materials. However, due to its high cost of operation the technology the cost of FD may be as much as 200–500% higher than that of hot air drying, which greatly reduced economic competitiveness of FD products. Hence to widen its application, various approaches have been studied to modify the freeze-drying process. Pre-treatment prior to drying is a good approach to improve the drying kinetics while retaining the product quality. Blanching is known to enhance mass transport in the tissue and affect the drying behavior. Similarly, osmotic pre-treatment with calcium chloride affects the rigidity of the cell membrane and thus assist in removal of water from the tissues during drying. In an effort to reduce drying time, and indirectly the energy consumption, the present research aims to study the effect of pre-treatments viz blanching and calcium choride treatment on the drying characteristics and product qualities of paneer dried with freeze drying. Dried paneer offers numerous culinary applications. It can be used in curry preparation similar to paneer-in-curry, a delicacy in Indian cuisine. It may be added to granola/ trail mix, soup mix, yielding a high energy snack. If grounded to a powder, it may be use as a cheesy spice mix, or used as

popcorn seasoning. Dried paneer powder may be added to pizza dough or added to a white sauce to turn it into a paneer sauce.

2. Materials and Methods

2.1 Material

Paneer was kept at 4°C in a refrigerator until use. The initial moisture content of paneer was about 55% (wb). It was diced in to a cube of two size 1×1×1cm3 with stainless steel knife.

2.2 Pre-treatments

Paneer cubes were pretreated with two different ways (i) blanching and (ii) dipping in salt solution. Hot Water blanching was carried out by immersing paneer cubes into 100°C for 1 min distilled water in a stainless steel pan heated by an induction cooking plate. The weight ratio of paneer cubes and distilled water was 1:2. After the pretreatment, the samples were cooled using a fan until there was no visible water on the surface of the material. The blanching pretreatment was carried out in triplicate. Salt treatment was done by dipping paneer cubes in solution containing 0.5% calcium chloride for 10 min. Paneer cubes and salt solution was in the ratio of 1:10. After pretreatment cubes were then removed, and drained using stainless steel mesh. Before drying, samples were blotted to remove the surface moisture and put in the drying chamber.

2.3 Drying Equipment and Procedure

Freeze drying (FD) was performed in a laboratory-scale FDL-10N-50-8M freeze-dryer (MRC, Beijing, China) for 12 hrs and 18 hrs to evaluate the difference in moisture content reduction and quality achieved at the two time intervals. The paneer cubes (200 g) were frozen at −20°C in a freezing chamber and freeze-dried to a moisture content of 5–6% (w.b.) at an absolute pressure of 0.100 mbar with a chamber temperature of 20°C and a condenser temperature -50°C. The dehydrated paneer samples were packaged into polyethylene bags with silica gel.

2.4 Moisture Content

Moisture content was determined by the hot air oven method. At regular time intervals during the drying process, samples were taken out and dried for 8 h at 105°C until constant weight. The initial moisture content of the paneer was found to be 54.52 % (w.b.). The tests were performed in triplicate.

2.5 Measuring of Energy Consumption

Industrial freeze drying processes is complicated and quite expensive. For making it feasible for a sumptuous food such as paneer, a lower cost approach to this process needs to

be researched. However, the energy consumption of a drying process is measured by energy cost checker, but for the present study emphasis is given to predict which pre-treatment is the best in maximally reducing the moisture content in given time duration, 12hrs and 18 hrs. This will assist to indirectly reduce the overall energy consumption of the drying.

2.6 Color

The color is one of the most important appearance attribute of food materials since it influences consumer acceptability [5]. The color measurements can be used in an indirect way to estimate color change of foods since it is simpler and faster than chemical analysis. Hunter color parameters (L, a, b) have previously proved valuable in describing visual color deterioration. The color of raw and dried samples Colour measurement was done by using Colorimeter (Model: Chroma Meter CR-400, Konica Minolta). The location of any color in the CIELAB color space is determined by its color coordinates, CIEL* (L*=0(black) and L*=100 (white)), CIEa* (-a*=greenness and +a*= redness), and CIEb*(-b*=blueness and +b*=yellowness). The paneer cubes were scanned at three different locations to determine the average L*, a*and b* values as the average of the five measurements. The paneer cubes were cut into small portion with knife and put into adapter for color measuring. The total color differences (TCD) were estimated from the coordinates of the color by applying the following equation (1):

$$TCD = \sqrt{(L_0^* - L)^2 + (a_0^* - a)^2 + (b_0^* - b)^2} \qquad (1)$$

where, L_0^* is the degree of lightness of control sample, a_0^* is the degree of redness and greenness at control sample and b_0^* is the degree of yellowness and blueness at control sample.

2.7 Rehydration Process

Dried food products are usually rehydrated before consumption. Rehydration can be in general defined as a complex process involving different physical processes such as capillary flow, convection or diffusion [6]. Rehydration capacity indicates degree of damage (cell or structure disruptions) to foodstuff caused during drying. It involves imbibition of water, swelling and finally leaching out of soluble solids from dried food stuffs [7]. Rehydration capacity is studied by reconstituting the dried product in distilled water and amount of equilibrium moisture absorbed within a stipulate time is determined.. Treatments such as drying and rehydration produce changes in the structure and composition of product tissues [8]. The dried paneer cubes were soaked in controlled temperature of 100°C distilled water and were analysed for weight gain after every 1 min by first removing surplus water from the surface using blotting paper. The weight used in each experiment was 1 ± 0.1 g of dehydrated paneer samples. The weighing was performed on a digital balance. A dried paneer cube was added to 150 mL of distilled water. The

sample weighing was performed in triplicate. The rehydration ratio (RR) was evaluated from equation (2) below:

$$RR = \frac{M_r}{M_d} \tag{2}$$

where M_r is the weight of paneer cubes after rehydration (g) and M_d is the weight of paneer cubes after drying (g)

2.8 Statistical Analysis

Data analyses were determined and analyses of variance (ANOVA) were conducted by ANOVA procedure. Mean values were considered significantly different when $P < 0.05$.

3. Results and Discussion

In order to assess the advantage of the pre-treatment prior to freeze drying, the reduction in moisture content, color, and rehydration between the pre-treated dried products were compared. The freeze dried (FD) sample with no pre-treatment was used as a control.

3.1 Amount of moisture removed

There has been more reduction in the moisture content when the sample was pre-treated. Blanching for 2 minutes significantly increased the amount of water removed up to 57% and 22.6 % as compared to the control sample for both 12hrs and 18hrs drying duration respectively(Table 1). This was because blanching causes disruption of cell membranes and a concomitant faster and more complete drying [7]. This implies that with use of blanching, the time of drying can be reduced, and therefore the overall energy consumption.

Table 1. Effect of Pre-Treatment and drying time on Moisture Content of Dehydrated Paneer

Pre-treatment	Drying time (hrs)	Final moisture content (%, w.b.)	% Reduction in final moisture content in control sample
Control sample (No pre-treatment)	12	15.207	-
	18	7.522	-
Blanching (1 min)	12	11.345	25.4
	18	6.445	14.3
Blanching (2 min)	12	6.522	57
	18	5.825	22.6
CaCl$_2$	12	8.155	46.4
	18	6.275	16.6

Initial moisture content = 54.52 % wb

3.2 Color of paneer cubes associated with different pre-treatments

The drying causes many changes in color of paneer cubes irrespective of any pre-treatments done. TCD for all drying treatments with respect to the control (FD) is reported in Table 2. It was observed that the color of pre-treated paneer cubes was significantly darker (L value) in comparison with fresh paneer cubes. Out of the pre-treated samples, the lowest value for color change was observed in blanching (2 mins) for 18 hrs dried paneer cubes.

Table 2. Colour Difference of dried paneer cubes after pre-treatments

Pre-treatment	Drying time (hrs)	Color parameters			
		L	a	b	TCD
Control sample (No pre-treatment)	12	56.53	2.31	17.28	40.62
	18	61.28	3.61	18.64	36.78
Blanching (1 min)	12	60.24	2.9	16.84	39.56
	18	61.2	3.08	17.18	36.24
Blanching (2 min)	12	62.53	3.04	16.75	35.67
	18	63.86	3.15	17.19	33.80
CaCl2	12	59.08	3.28	17.85	38.49
	18	60.23	3.2	15.52	36.61
Fresh paneer	-	80.20	1.65	11.01	16.29

3.3 Effect of different pre-treatments on RR and moisture content of dried paneer cubes

The values of the RR for the different drying methods dried paneer sample are detailed in Table 3. In all the rehydration trials, there was an initial reduction in the weight of the sample followed by a constant increase. This loss in weight may be due to the fat oozing out in the water during rehydration. This fat loss process might opens pathway and creates space, surface micro-holes and capillaries for more water imbibitions resulting in an increase in the weight. This consolidated, rigid structure leads to the absence of pathways for water access. The RR was slightly higher, affected by $CaCl_2$ treatment, showing a 3.6% and 9% increase in 12 hrs and 18 hrs dried sample respectively as compared to the control.

Table 3. Rehydration ratio of Freeze dried paneer for different pre-treatments

Pre-treatment	Drying time (hrs)	Maximum Rehydration Ratio (RR)	% Increase in RR
Control sample (No pre-treatment)	12	1.12 (after 8 mins)	-
	18	1.11 (after 9.5 mins)	-
Blanching (1 min)	12	1.06 (after 6.5 mins)	-
	18	1.1 (after 10 mins)	-
Blanching (2 min)	12	1.1 (after 10 mins)	-
	18	1.06 (after 3.5 mins)	-
CaCl$_2$	12	1.16 (after 5.5 mins)	3.6
	18	1.21 (after 14.5 mins)	9

*(-) implies no increase in the RR value, either it remains same or decreases.

.
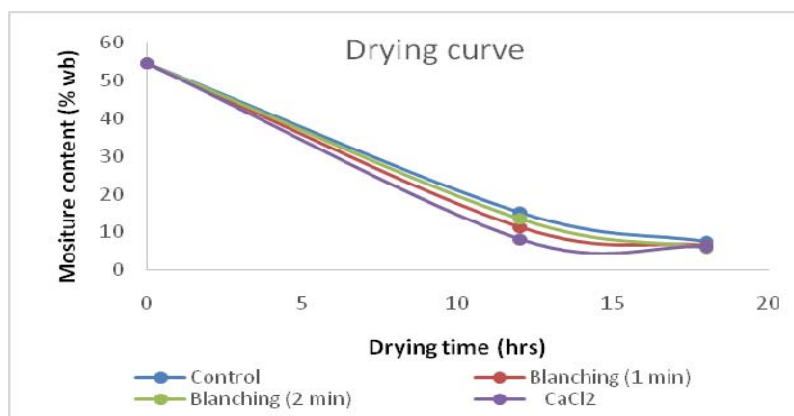
Fig. 1 Moisture content after 12 hrs and 18 hrs freeze drying

From the figure 1, it can be clearly observed that like CaCl$_2$ can reduce the drying time by 30% as compared to the control sample. This was followed by blanched (1 min) and then by blanched (2min).

4. Conclusions

By comparing the two pre-treatments i.e. blanching for 1 min. 2 min and CaCl$_2$ dipping for 10 min, it can be concluded that blanching promises to increase more amount of water removal from the paneer cubes. Also, the color loss was least in the blanched dried sample. But for a good rehydration ratio, CaCl$_2$ proves to be a good pre-treatment as compared to blanching. Moreover, it is more probable that by combining air drying and freeze drying better quality can be achieved in reduced time and energy consumption.

5. Acknowledgement

6. References

[1] Chandan RC. Manufacture of paneer. In: Gupta S, Gupta S, editors. Dairy India 2007. 6. New Delhi: Dairy India Yearbook, A Dairy India publication; 2007a. pp. 411–412.

[2] Vishweshwariah, L. (1987). Studies on dehydration and deep freezing of paneer. J. of Food Sci. & Tech. 24(2): 95-96.

[3] Srivastava, S. and Kumbhar, B. K. (2013). A Comparative study of low pressure superheated steam (LPSS) and vacuum drying (VD) of paneer. Agricultural Engineering Today, 37(2): 7-13.

[4] Singh, S., Rai, T. (2004). Process optimization for diffusion process and microwave drying of paneer. J Food Sci Technol 41(5):487–491.

[5] Maskan, M. 2001. Kinetics of color change of kiwifruits during hot air and microwave drying. J. Food Eng. 48, 169–175.

[6] Vreeker, R., Li, L. and Fang, Y. (2008). Drying and Rehydration of Calcium Alginate Gels. Food Biophysics, 3:361–369.

[7] Jamradloedluk, J., Nathakaranakule, A., Soponronnarit, S., and Prachayawarakorn, S. (2007). Influences of drying medium and temperature on drying kinetics and quality attributes of durian chip. Journal of Food Engineering, 78: 198–205.

[8] Cox, S., Gupta, S. and Abu-Ghannam, N. 2012. Effect of different rehydration temperatures on the moisture, content of phenolic compounds, antioxidant capacity and textural properties of edible Irish brown seaweed. LWT – Food Sci. Technol. 47, 300–307.

[9] Acevedo, N.C., Briones, V., Buera, P. and Aguilera, J.M. 2008. Microstructure affects the rate of chemical, physical and color changes during storage of dried apple discs. J. Food Eng. 85, 222–231.

The effect of different wall materials on the production of suppressed-pungent capsaicin microparticles

Varhan, E.ª; Kasimoglu, Z.ᵇ; Koç, M.ª*; Sahin-Nadeem, H.ª

ªAdnan Menderes University, Engineering Faculty, Department of Food Engineering, 09010, Aydın, Turkey
ᵇAkdeniz University, Engineering Faculty, Department of Food Engineering, 07058, Antalya, Turkey

*E-mail of the corresponding author: mehmetkoc@adu.edu.tr

Abstract

The aim of this study was to investigate the effects of wall materials types on the production of double-layered and suppressed-pungent capsaicin microparticles via spray chilling method. For this purpose, palm oil and different proteins (gelatin, sodium caseinate and whey protein) were used as wall materials, while soy lecithin was selected as stabilizer. Sample encapsulated only with palm oil (single-layered) was used as control. Centrifuge stability and kinetic stability were analyzed on the prepared emulsions. Total and surface capsaicin, microencapsulation efficiency, melting point temperature and fusion enthalpy analysis were carried out on the capsaicin microparticles obtained by spray chilling.

Keywords: Capsaicin; Spray chilling method; Pungency; Double-layered microparticles

1. Introduction

Red hot chili peppers from plants of the Capsicum genus in the Solanaceae family are the pungent and carmine fruits generally used as spice to give pungent or hot sensation to many dishes. Capsaicinoids, the group of secondary metabolites, are responsible for the pungency of chili peppers. The main compound of the capsaicinioids is capsaicin (8-methyl-N-vanillyl-6-nonenamide) and it has a high bioavailability with a lot of benefits on human health especially on the cancerous cells. In addition, it can relieve neuropathic pains and is used in symptomatic therapy of arthritis, muscle and join pains. Conversely to its advantages, capsaicin can cause irritation on the human digestive system based on overconsumption. It can induce burning sensation on the mouth, alimentary canal and stomach of people who are more sensitive to pungency. Therefore, microencapsulation of capsaicin with an appropriate method and suppressing of its pungency via the relevant microencapsulation method is important for taking advantages of capsaicin and reducing its negative effects on the human health [1]. Spray chilling method is an alternative technique for microencapsulation of functional components because it serves rapid, easy-to-use and relatively cheap process [2]. Spray chilling technology, which uses oil-based substances as wall materials, has been used increasingly day by day in different industries such as pharmaceutical and food. The objective of the present study was to produce suppressed-pungent capsaicin microparticles by spray chilling method and to investigate the effects of wall materials type on the emulsion stability, physical properties and microencapsulation efficiency of capsaicin microparticles.

2. Materials and Methods

2.1. Materials

Capsaicin (66.7%) (Xian Sobeo Biotech, China) was used as core material. Ethanol (Sigma-Aldrich, Germany) used for dispersing capsaicin. Hydrogenated palm oil was supplied by Felda Iffco (Izmir, Turkey), while refined sunflower seed oil, whey protein isolate, gelatin, sodium caseinate and soy lecithin were obtained by a local market.

2.2. Emulsion preparation

Capsaicin was dissolved in ethanol (1:1) using ultrasonic bath for 10 min. Then, the capsaicin solution was mixed with palm oil containing soy lecithin as a stabilizer. . This oily capsaicin mixture was transferred into aqueous protein solution drop by drop under Ultra Turrax homogenizer, worked at 10000 rpm for 3 min. The final mixture was then added into molten palm oil (in circulation water bath at 65°C) and homogenized again at 10000 rpm for 3 min. For control samples, with or without stabilizer, molten palm oil was mixed with ethanolic capsaicin solution and homogenized at the same conditions. Palm oil, gelatin, Na-Caseinate and whey protein isolate were used as wall materials while soy lecithin was used as stabilizer.

The composition of emulsions was given in Table 1, where the concentrations are given as ratios of components in total 200 g final mixture.

Table 1. The percent composition of emulsions

Exp. No	Palm oil	WPI	Na-Cas	Gelatin	Soy Lecithin	Sunflower oil	Ethanol	Water	Capsaicin
1	90.5	-	-	1.50	0.50	0.90	0.30	6	0.30
2	90.5	-	1.50	-	0.50	0.90	0.30	6	0.30
3	90.5	1.50	-	-	0.50	0.90	0.30	6	0.30
4	90.5	-	0.75	0.75	0.50	0.90	0.30	6	0.30
5	90.5	0.75	-	0.75	0.50	0.90	0.30	6	0.30
6	90.5	0.75	0.75	-	0.50	0.90	0.30	6	0.30
7	90.5	0.50	0.50	0.50	0.50	0.90	0.30	6	0.30
8	98.9	-	-	-	0.50	-	0.30	0	0.30
9	99.4	-	-	-	-	-	0.30	0	0.30

2.3. Emulsion stability

Emulsion stability of capsaicin emulsions was evaluated with kinetic and centrifuge stability analysis. In order to analyze the kinetic stability of obtained emulsions, 10 ml of each emulsion was transferred to a test tube and kept in water bath at 65°C for 4 hours. The volume of lower phase measured after 2 hours. The kinetic stability of the emulsions was calculated as sedimentation index via following equation (1):

$$SI = (H_{l@t}/H_i) \times 100 \tag{1}$$

where SI, $H_{l@t}$ and H_i indicate sedimentation index, lower phase height at *t* time and initial height of emulsion, respectively [3].

The centrifuge stability of samples was measured as follow; 10 mL of emulsion was immediately poured into graduated centrifuge tube and centrifuged at 10000 rpm for 10 minutes. Then the centrifuge stability of the emulsion was calculated by equation (2):

$$CS = (H_l/H_i) \times 100 \tag{2}$$

where CS, H_l and H_i indicate centrifuge stability, height of lower phase and initial height of emulsion, respectively [4].

2.4. Spray chilling

Capsaicin emulsions fed into the spray chilling system in order to obtain solid lipid capsaicin microparticles. Spray chilling process was carried out by using Bakon-B15 (Izmir, Turkey).

The inlet temperature of cooling air (10°C), the temperature of nozzle (60°C), the feeding temperature (65°C) and air flow rate (10L/min) were kept constant during spray chilling.

2.4. Melting point temperature (T_m) and fusion enthalpy (ΔH)

T_m and ΔH of capsaicin microparticles were determined by using DSC (Perkin-Elmer DSC 6000, Turkey). For this purpose, 10 mg of capsaicin microparticles was weighed directly into the DSC aluminum sample pan and sealed with a lid. The purge gas was nitrogen (50mL/min) and the temperature ranged from 25 to 90°C with a heating rate of 15°C/min. The data were then processed using Pyris Manager Software (Perkin-Elmer).

2.5. Powder yield

The powder yield was defined as the ratio between the total collected powder and theoretical powder quantity from the sprayed solution and calculated as shown in equation (3).

$$Powder\ yield\ (\%) = \frac{Powdered\ capsaicin\ microparticles(g)}{Feeding\ emulsion\ (g)} \times 100 \qquad (3)$$

2.6. Total and surface capsaicin content and microencapsulation efficiency (ME)

The total and surface capsaicin contents of the microparticles were determined using high performance liquid chromatography (Shimadzu Corporation, Kyoto, Japan) according to Consoli et al. [3] with some modifications. The chromatography conditions were: 60°C column temperature, 5 µl sample volume, 1.5 ml/min flow rate, acetonitrile:water (50:50) mobile phase and 222 nm with UV-detector. Microencapsulation efficiency was calculated by the following equation (4).

$$ME\ (\%) = (TC - SC/EC) \times 100 \qquad (4)$$

where ME, TC, SC and EC indicate microencapsulation efficiency, total capsaicin amount of microparticles, surface capsaicin amount of microparticles and total capsaicin amount in emulsion, respectively.

2.7. Statistical analysis

All measurements were performed in triplicate. Results are expressed as mean ± standard deviations. All results were analyzed using SPSS version 15.0 Windows program (SPSS Inc., Chicago, IL). To observe significant differences between the samples, paired t-test was used at a 5% significance level.

3. Results and Discussions
3.1. Emulsion stability

The emulsions are thermodynamically unstable systems. Therefore, protein based emulsifiers are mostly used to improve the stability of emulsions. These emulsifiers vary widely in their ability to form and stabilize emulsions depending on their molecular and physicochemical

characteristics [5]. The emulsion stabilities of capsaicin emulsions (emulsion number 1-7) prepared with different wall materials were evaluated as kinetic and centrifuge stability. The stability analysis for control samples (emulsion number 8 and 9) were not performed due to being a dispersion not an emulsion.
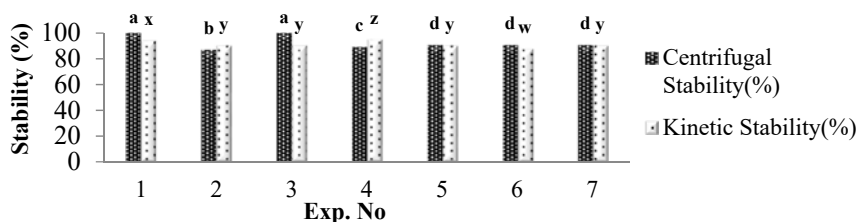
Fig. 1 Kinetic stability and centrifugal stability results of capsaicin loaded emulsions

The emulsion stability study revealed that most of the emulsions were kinetically (87.5-100%) and centrifugally (86.75-100%) stable as shown in Fig 1. Consoli et al. [5] also found similar stability results for gallic acid encapsulation with spray chilling method. The emulsion prepared with gelatin was found to be the most stable kinetically while adding Na-Caseinate and whey protein isolate to emulsions resulted in a decrease in kinetic stability. Gelatin has good water holding capacity because the small pore size of the gel network tightly holds water molecules by capillary forces [5]. Therefore, the separation of aqueous phase was prevented in capsaicin emulsions. The results of centrifugal stability of emulsions showed that emulsions prepared with whey protein and gelatin had the highest stability values. Whey proteins are much more rigid as compared to caseins [6]. Therefore, high concentrations of sodium caseinate resulted in low stabilities of emulsions as reported previously [7].

3.2. T_m and ΔH

The melting point temperature (T_m) and fusion enthalpy (ΔH) of encapsulated capsaicin microparticles were given in Table 2. Adding whey protein into emulsions as wall material resulted in an increase T_m of the capsaicin particles, while gelatin-containing microparticles had a lower melting point temperature. On the other hand, Na-caseinate did not have a significant effect on the melting point of the microparticles, but it caused higher melting point than that of gelatin-containing microcapsules. As shown in Table 2, melting points of double-layered samples (except 3th sample) were calculated lower than that of the single layered sample. It was probably due to the creation of the less ordered structure of the inner structure of the lipid matrix and/or the small size effect which could be explained by Gibbs-Thomson equations [8]. Wang et al. [9] reported that microencapsulation of capsaicin decreased the melting temperature. The capsaicin, nanocapsulated with single coacervation in that study [10], melted at 75°C (T_m) and absorbed 160.7 J/g energy. In our study, capsaicin was encapsulated with gelatin (single layered) and melting point temperature and absorbing

energy were calculated as 100°C and 199.9 J/g, respectively. Differences between T_m and ΔH values of the previous and the present study can be resulted from the encapsulation form (single or double layered) and encapsulation technique.

3.3. Product yield

The high product yield is one of the advantages of the spray chilling. The product yield values of the samples obtained from spray chilling were reported as over 75% [11]. Product yield of the capsaicin microparticles obtained from spray chilling method in the present study agreed with the data in the literature. Encapsulation form (single or double layered) did not significantly affect the product yield results and the results were in the range of 77-87%. The samples obtained from the emulsions added by whey protein and gelatin had the higher product yields as compared to that of containing Na-caseinate. The lower product yield value of the samples added by Na-caseinate could be resulted from viscoelastic properties and high gelling power of the Na-caseinate. Therefore, caseinate containing emulsions could stick to drying chamber in spray chilling equipment due to its adhesive structure [12].

3.4. Total and surface capsaicin contents and microencapsulation efficiency (ME)

Total and surface capsaicin contents and microencapsulation efficiency results of the capsaicin microparticles were shown in Table 2. The results showed that capsaicin could be effectively encapsulated with the oil-based wall materials and the amount of surface capsaicin could be reduced. In terms of surface capsaicin content, the microparticles had relatively less amounts of capsaicin on their surfaces. Maximum surface capsaicin content was calculated as 2.08 ppm for single layered (only palm oil) encapsulated sample. On the other hand, double layered (palm oil-soy lecithin-whey protein) encapsulated sample showed the best encapsulation efficiency with the surface capsaicin content of 2.04 ppm. Microencapsulation efficiency of the emulsions increased with an increase in whey protein concentration in the emulsions. In addition, microencapsulation efficiency of the emulsions containing gelatin was higher than that of containing Na-Caseinate. This could be attributed to the viscoelastic properties and gelling power of casein. The maximum microencapsulation efficiency of 99.73% was determined for double-layered (palm oil-whey protein) encapsulated sample, while the minimum result was calculated as 80.48% for the samples produced by single-layered (only palm oil) encapsulation. The results showed that the melting point temperatures significantly affected the microencapsulation efficiency of the samples. The microencapsulation efficiency increased with the increasing melting point. In the previous study with ascorbic acid encapsulation by spray chilling [13], palm and palm seed oil (43°C melting point) were used as wall material while soya lecithin was used as stabilizer. The encapsulation efficiency values of the samples varied from 68.2 to 72.5%. Differences in the encapsulation efficiency results of the previous study and the present study can be resulted from the double-layered microencapsulation used in our study.

Table 2. Total and surface capsaicin, microencapsulation efficiency and thermal characteristics of the capsaicin microcapsules

Exp. No	TC (ppm)	SC (ppm)	ME (%)	T_m (°C)	ΔH (J/g)
1	39.87±0.27[c,d]	2.04±0.15[c]	94.57±0.30[c,d]	48.81±0.09[a]	85.13±0.48[c,d]
2	35.76±2.62[a,b]	1.92±0.01[b,c]	84.61±6.52[a,b]	49.40±1.01[a]	85.17±2.91[b,c]
3	41.93±0.62[d]	2.04±0.06[c]	99.73±1.68[d]	50.05±0.16[a]	83.48±3.75[a,b,c]
4	38.65±0.02[b,c,d]	1.71±0.02[a,b]	92.36±0.08[b,c,d]	49.06±0.34[a]	79.13±4.44[a]
5	40.75±0.34[d]	2.04±0.08[c]	96.78±1.04[c,d]	48.88±0.32[a]	83.67±2.47[b,c,d]
6	41.53±0.27[d]	1.93±0.02[b,c]	99.01±0.72[d]	48.80±1.08[a]	92.54±4.21[d]
7	40.23±0.09[c,d]	2.05±0.08[c]	95.44±0.41[c,d]	48.65±0.10[a]	80.25±4.28[a,b]
8	37.31±0.76[a,b,c]	1.53±0.05[a]	89.45±1.77[b,c]	48.53±0.02[a]	85.95±2.90[a,b,c]
9	34.27±0.07[a]	2.08±0.07[c]	80.48±0.02[a]	49.54±0.85[a]	84.76±2.77[b,c]

Different letters (a, b, c or d) above the columns indicate significant difference between the emulsion formulation

4. Conclusions

Capsaicin has a high bioavailability with a lot of benefits on human health. However, it is inconsumable for some people because of irritating effect. Therefore, it can be microencapsulated to suppress its pungency. In the present study, capsaicin is effectively microencapsulated by spray chilling technique by using palm oil and whey protein (as wall materials) and soy lecithin (as stabilizer). The encapsulation efficiencies of the whey protein based emulsions were higher than that of the other emulsions. Furthermore, the sensible pungency of capsaicin can be reduced from 40 ppm to 1.71 ppm (the minimum surface capsaicin content) with double-layered microencapsulation by spray chilling. By this way, capsaicin was converted to a suppressed-pungent component that can be consumed by sensitive people.

5. Nomenclature

DSC	differential scanning calorimeter
min	minutes
μm	micrometer
rpm	revolutions per minute

6. Acknowledgments

7. References

[1] Topuz. A. The Effects of different gamma irradiation doses and storage on some chemical microbiological and sensory qualities of paprika (Capsicum annuum L.). Doctoral thesis. Akdeniz University. Institute of Science and Technology. Food En

[2] Okuro. P.K.; de Matos Jr. F.E.; Favaro-Trindade. C.S. Technological challenges for spray chilling encapsulation of functional food ingredients. Food Technology and Biotechnology 2013. 51 (2). 171-182.

[3] Consoli. L.; Grimaldi. R.; Sartori. T.; Menegalli. F.C.; Hubinger. M.D. Gallic acid microparticles produced by spray chilling technique: Production and characterization. *LWT*-Food Science and Technology. 2016. 65. 79-87.

[4] Sciarini. L.S.; Maldonado. F.; Ribotta. P.D.; Perez. G.T.; Leon. A.E. Chemical composition and functional properties of Gleditsia triacanthos gum. Food Hydrocolloids. 2009. 23 (2). 306-313.

[5] McClements. D.J. (2016). Food emulsions: principles, practices and techniques. Florida. USA. CRC press

[6] Kinsella. J. E.. & Morr. C. V. (1984). Milk proteins: physicochemical and functional properties. Critical Reviews in Food Science & Nutrition. 21(3). 197-262

[7] Srinivasan. M.. Singh. H.. & Munro. P. A. (2000). The effect of sodium chloride on the formation and stability of sodium caseinate emulsions. Food Hydrocolloids. 14(5). 497-507

[8] Teeranachaideekul. V.. Chantaburanan T.. Junyaprasert. V.B. Influence of state and crystallinity of lipid matrix on physicochemical properties and permeation of capsaicin-loaded lipid nanoparticles for topical delivery. Journal of Drug Delivery Science and Technology. 2017. 39. 300-307.

[9] Wang. J.C.. Chen. S.H.. Xu. Z.C. Synthesis and Properties Research on the Nanocapsulated Capsaicin by Simple Coacervation Method. Journal of Dispersion Science and Technology. 2008. 29. 687–695.

[10] Ilic. I.. Dreua. R.. Burjakb. M.. Homarb. M.. Kerca. J.. Srcica. S. Microparticle size control and glimepiride microencapsulation using spray and processing conditions. Advanced Powder Technology. 2009. 25. 1. 292–300.

[11] Maschke. A.. Becker. C.. Eyrich. D.. Kiermaier. J.. Blunk. T.. Gopferich. A. Development of a spray congealing process for the preparation of insulin-loaded lipid microparticles and characterization thereof. European Journal of Pharmaceutics and Biopharmaceutics. 2007. 65. 175–187.

[12] Chen, J., Dickinson, E. On the temperature reversibility of the viscoelasticity of acid-induced sodium caseinate emulsion gels. International Dairy Journal. 2000. 10. 541-549.

[13] Matos-Jr. F.E.. Comunian. T.A.. Thomazini. M.. Favaro-Trindade. C.S. Effect of feed preparation on the properties and stability of ascorbic acid microparticles produced by spray chilling. LWT - Food Science and Technology. 2017. 75. 251-260.

Microbial load reduction using modified Solar Conduction Dryer with composite filters

Jadhav, P.; Ashokkumar, S.; Nagwekar, N.*

Department of Chemical Engineering, Institute of Chemical Technology (formerly UDCT),

N. Parekh Road, Matunga (E), Mumbai India-400019

*E-mail of the corresponding author: nupurnagwekar@gmail.com

Abstract

The present work studies the microbial load reduction in sapota and beet root by three different drying methods i.e. Open Sun Drying (OSD), Solar Conduction Drying (SCD) and a modified SCD with filters (SCDF). Parameters analyzed were water activity, moisture content, drying kinetics, Total Viable Counts, Total Fungal Counts and ash content. It was found that the samples dried in SCDF showed least microbial counts, faster drying times and lower ash content as comparison to OSD. This study shows that SCD and its modification provide a better alternative for low cost drying of fruits and vegetables for quality retention.

Keywords: Microbial reduction; SCD Filters; Sapota; Beetroot.

1. Introduction

The global dehydrated food market is being driven by lifestyle changes and dietary choices. An increase in nutritional awareness among the consumers is pushing the industries and researchers to develop novel technologies which will increase the shelf-life of the product without compromising the nutrition and quality. As per APEDA [1], India exported 87,279.99 MT of dried and preserved vegetables worth USD 162.88 Million during 2016-17. Though large in volume, there is plenty of scope of improvement in the value.

Small and medium scale producers require low cost dryers which are easily adaptable to a variety of agri-produce.[2] In rural India, where agricultural losses are predominant and there is lack of cold storage facilities, Open Sun Drying (OSD) is followed extensively. The advantages of OSD are simplicity and zero equipment cost. The disadvantages are longer duration of drying, microbial contamination, insect infestation and overall quality degradation.[3] To overcome these disadvantages, many models of solar dryers have been developed.[4] Solar Conduction Dryer (SCD), an indigenously developed Indian technology, is being used by 1500 farmers at household level and micro food processing centers. SCD uses all three modes of heat transfer i.e. conduction, natural convection and radiation. It is electricity-free and completely dependent on solar energy.

Sapota (*Achrassapota* L.) (Family Sapotaceae) commonly known as chiku in India, is an energy rich fruit with high total soluble solids (20-22%), digestible sugars, protein, fat, fiber and minerals.[5] It is perishable and easily susceptible to microbial contamination due to high moisture content (69.05 - 75.7%), and sugar content (11.14 - 20.43%).[6] The fruits are also easily bruised, which leads to wastage.[7] Beetroot (*Beta vulgaris*) is a root vegetable that belongs to the family of Chenopodiaceae. Beetroot is also characterized by high moisture content, an abundance of nutrients and proximity to soil due to which it forms a favorable habitat for microbial contaminants.

The objective of this study is to analyze effect of different drying methods on the microbial quality of sapota and beet root samples. The three drying methods under study are Open Sun Drying (OSD), Solar Conduction Drying (SCD) and SCD with filters at the air inlet (SCDF). The drying kinetics, moisture content, water activity and ash content of the samples are also analyzed.

2. Materials and Methods

2.1. Sample collection

3 Kg of both Sapota and Beetroot each were procured from a local market in Mumbai. After washing and air drying, fresh samples were sliced into pieces of 4-5 mm thickness. A part of it was analyzed directly as fresh sample and the rest was dried using OSD, SCD and

SCDF. The fresh and dried samples were analyzed for Moisture Content (MC), water activity (a_w), Total Viable Count (TVC), Total Fungal Count (TFC) and ash content.

2.2. Open Sun Drying (OSD)

Open sun drying was carried out by placing the slices on sheets made up of 12 micron PET (polyethylene terephthalate) + 50 micron LDPE (low density polyethylene). The arrangement was covered by a steel mesh to prevent loss of samples to animals and birds.

2.3. Solar Conduction Dryer (SCD)

(a)   (b)
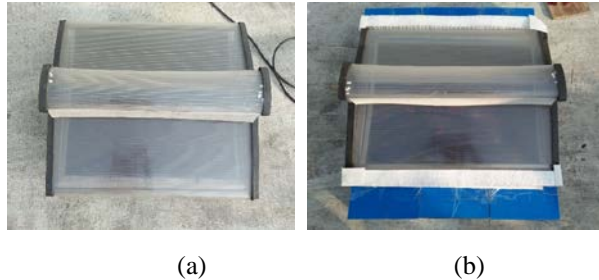
Fig. 1 (a) Solar Conduction Dryer; (b) Solar Conduction Dryer with Filters

SCD, as shown in Figure 1 (a) (top view) consists of 1mx1m tray on which sapota and beetroot slices were loaded and allowed to dry. The surface of the tray provides a temperature of 50-60°C with air velocity in the range of 0.1-0.2 m/s generated due to natural convection (PCT/IN2012/000843). During the experimental days, the relative humidity of surrounding air was recorded to be 52-60 % at 25-30°C (ambient temperature).

2.4. Solar Conduction Dryer with Filters (SCDF)

Filter material (Khosla Profil Pvt.Ltd.), is made up of polypropylene with a thickness of 1.35-1.47 mm (+/-8%) and pore size of 0.1μ with maximum temperature resistance of 80°C. Filters were placed at both the air inlets of the SCD, as shown in Figure 1 (b) (white coloured filter cloth visible at both open ends of the dryer).

Moisture Content was measured using Shimadzu MOC-120H electronic moisture balance. Water activity (a_w) was measured using a LabSwift Novasina water activity meter. Drying kinetics was studied by measuring the weight of the samples at fixed intervals throughout the drying time to determine the drying rate.

The novel part of SCDF is the use of composite filter attached in such a way so as to provide minimal pressure drop. This is ensured by following ergun type equation.[8]

$$\frac{\Delta P}{\frac{1}{2}\rho V^2} = \frac{A}{NRe} \approx 1 \qquad (1)$$

The design of filter is in such a way that there is no kinetic head loss and discharge coefficient (C) derived from the equation 1 takes the following form.

$$V = C \frac{\sqrt{2\Delta P}}{\rho} \qquad (2)$$

Where C is close to 1.

2.5. Microbiological Analysis

The fresh and dried samples of Sapota and Beetroot were subjected to Total Viable Count (TVC) analysis performed by Conventional Plate Count method as recommended by USFDA BAM.[9] Total Fungal Count (TFC) was performed by Pour Plate method as recommended by FSSAI (2012) [10]. The ash analysis was performed as per the method recommended by FSSAI.[11]

3. Result and discussion

3.1. Drying Kinetics

(a)   (b)
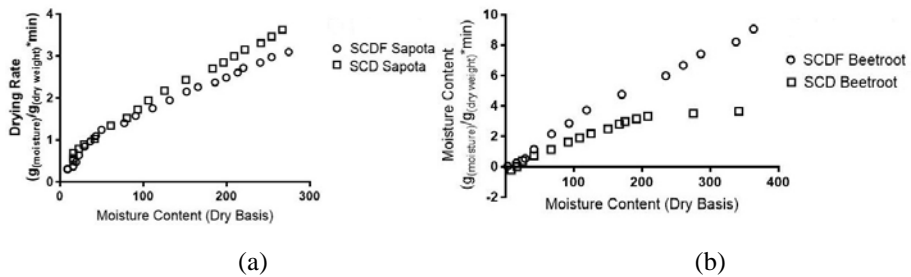
Fig. 2 (a) Drying Curve for SCD and SCDF Sapota (b) Drying Curve for SCD and SCDF Beetroot
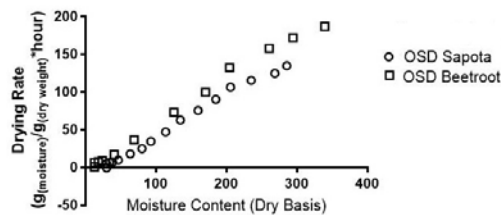
Fig. 3 Drying Curve for OSD Sapota and Beetroot

From Figure 2 and 3 it can be seen that the drying rate of OSD is higher than SCD and SCDF. The time required for drying by SCD and SCDF of Sapota and Beetroot were found to be comparable. Sapota drying required 510 minutes in OSD whereas SCD and SCDF

required 200 and 240 minutes respectively. For beetroot, the drying times for OSD, SCD and SCDF were 456, 180 and 210 minutes respectively. These values indicate that the drying times in SCD and SCDF are almost half as that of OSD. The drying curves showed a falling-rate period and constant rate period was not observed.[12]

3.2. Water activity and Moisture Content

As seen in Table 1, the a_w of fresh samples of both Sapota and Beetroot was found to be above 0.9. The a_w of the OSD was found to be marginally higher than 0.6, whereas that of SCD and SCDF was found to be well below 0.6. An ANOVA: Single Factor Test revealed significant difference in the means of a_w [F(3,8) = 2569.5 , p = 1.59E-09] and MC [F(3,8) = 181.5, p = 4.29E-06] of OSD, SCD and SCDF sapota samples at 5% level of significance. Significant difference was observed in the means of a_w [F(3,8) = 27289.3 , p = 1.33E-12] and MC [F(3,8) = 10.21, p = 0.012] of OSD, SCD and SCDF beetroot samples. OSD samples showed higher a_w and MC values as compared to SCD and SCDF. This is due to the temperature difference the food product experiences i.e. 28-30°C for OSD and 50-60°C for SCD and SCDF leading to higher equilibrium moisture content in OSD samples.

Table 1. Mean ± SD of Sapota and Beetroot water activity (a_w) and % Moisture (on wet basis)

Sample (Sapota)	Water activity (a_w)	% Moisture (wb)	Sample (Beetroot)	Water activity (a_w)	% Moisture (wb)
Fresh	0.936+0.003	69.6+1.34	Fresh	0.951+0.001	88.4+2.61
OSD	0.702+0.009	5.4+0.35	OSD	0.625+0.002	12+2.89
SCD	0.341+0.002	1.2+0.49	SCD	0.407+0.002	5.4+0.98
SCDF	0.391+0.0007	4.8+0.28	SCDF	0.301+0.001	6.2+1.55

3.3. Effect of Drying methods on Total Viable Counts (TVC) and Total Fungal Counts (TFC)
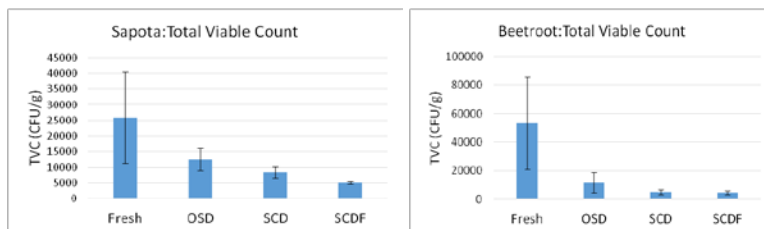
Fig. 4 Total Viable Count of Sapota and Beetroot fresh and dried samples

The results for TVC and TFC of Sapota and Beetroot are shown in Figure 4 and 5. The comparison of the log reduction in TVC and TFC is given in Table 2. The highest log reduction is found in TVC for SCD and SCDF in beetroot followed by sapota. SCDF performs better in terms of higher log reduction in both sapota and beetroot samples as compared to SCD. Both SCD and SCDF show close to 1 log reduction for TVC counts in beetroot. Previous studies have reported reduction in food microbial counts due to use of thermal drying techniques. Rahman et al. (2000) reported decimal reduction time (time required for 1 log reduction) of 12.66 hrs for drying of Tuna mince at 60°C which decreased up to 2.63 hrs as the drying temperature was increased to 100°C. [13]
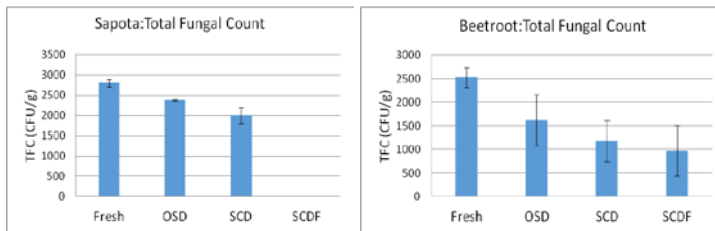
Fig. 5 Total Fungal Count of Sapota and Beetroot fresh and dried samples

Table 2. Comparison of log reduction in the TVC and TFC values of OSD, SCD and SCDF

Sample	Drying Method	TVC Log reduction	TFC Log reduction
Sapota	OSD	0.378	0.072
	SCD	0.514	0.146
	SCDF	0.705	ND
Beetroot	OSD	0.685	0.180
	SCD	1.041	0.308
	SCDF	1.092	0.407

3.4. Ash Content
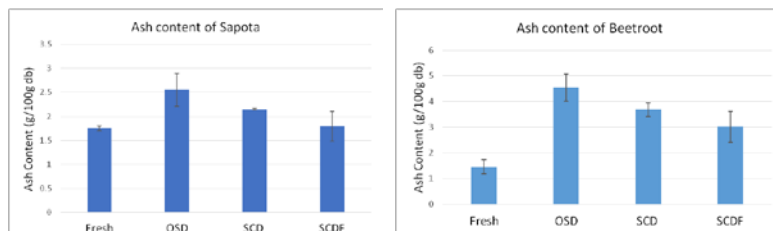
Fig. 6 Ash content (g/100g) (dry basis) in Fresh, OSD, SCD and SCDF samples

Ash content of a food sample represents the inorganic residue which remains after complete oxidation of the organic matter.[14] All the three drying processes are solar-based, hence ash content helps to measure the inorganic content added in the sample during drying either due to settling of dust, sand or extraneous matter from the environment. As seen in Figure. 6, ash content is highest in OSD samples (completely exposed), followed by SCD (partially covered) and the least in SCDF (filter protected) samples.

3. Conclusions

SCD and SCDF showed better product quality with respect to drying time, microbial load reduction and lower ash content as compared to OSD. SCD and SCDF could attain 1 log reduction with a decimal reduction time of 180 mins and 200 mins respectively. The addition of filters to the current design of SCD showed lowered microbial counts as compared to SCD. OSD is currently extensively used by low-income farmers and producer groups. SCD and its modification with filter has the potential to replace open sun drying as a cheap and efficient process without compromising the product safety and quality.

4. Nomenclature

OSC	open sun drying	
SCD	solar conduction drying	
SCDF	solar conduction drying with filter	
TVC	total viable count	
TFC	total fungal count	
a_w	water activity	
MC	moisture content	Pascals
P	pressure drop	m/s
V	velocity of air	
NR_e	air flow Reynolds number	
A	constant in laminal flow	

Greek letters

ρ	Density	Kg/m^3

5. References

[1] APEDA: Ministry of Commerce & Industry, Government Of India http://apeda.gov.in/apedawebsite/SubHead_Products/Dried_and_Preserved_Vegetables.htm

[2] Tiwari, A. A Review on Solar Drying of Agricultural Produce. In Journal Food Process Technology 2016, 7: 623.

[3] Aravindh, M.A.; Sreekumar, A. Solar Drying—A Sustainable Way of Food Processing. In Energy Sustainability Through Green Energy; Green Energy and Technology; Sharma, A., and Kar, S.K. Ed.; Springer India, 2015; 27-46.

[4] Visavale, G.L. Principles, Classification and Selection of Solar Dryers. Solar drying: Fundamentals, Applications and Innovations; Hii, C.L., Ong, S.P., Jangam, S.V. and Mujumdar, A.S. Eds.; TPR Group.: Singapore, 2012, 1-50.

[5] Suhasini. J.; Kanamadi, V.C.; Swamy, G.S.K.; Shirol, A. M.; Chavan, M. Performance of sapota (*Achrassapota* L.) varieties and hybrids under Ghataprabha command area. Karnataka Journal of Agricultural Sciences 2011, 25, 548-551.

[6] Morton, J. Sapodilla. Fruits of warm climates; Curtis F. Dowling Ed.; Miami, FL, 1987; 393–398.

[7] Ganjyal G.M.; Hanna M.A.; Devadattam D.S.K. Processing of Sapota (Sapodilla). Powdering. Journal of Food Technolgy 2005, 3(3), 326-330.

[8] Thorat, B. N.; Kataria, K.; Kulkarni, A.V.; Joshi, B. J. Pressure drop studies in bubble column. Journal of the American Chemical Society 2001, 40 (16), 3675–3688.

[9] Maturin, L.; Peeler, J.T.; Aerobic Plate Count. Microbiological Methods & Bacteriological Analytical Manual (BAM), 8th edition, Revision A. U.S. Food and Drug Administration: Maryland, 1998.

[10] FSSAI; Estimation of Yeast and Mold in Food and Beverages. In Manual of Methods of Analysis of   Foods: Microbiological Testing; Food Safety and Standards Authority of India, Ministry of Health and Family Welfare, Government of India [online]: New Delhi, 2012, 45-46.

[11] FSSAI; Estimation of Yeast and Mold in Food and Beverages. In Manual of Methods of Analysis of   Foods: Microbiological Testing; Food Safety and Standards Authority of India, Ministry of Health and Family Welfare, Government of India [online]: New Delhi, 2012, 45-46.

[12] Nagwekar, N.; Tidke, V.; Thorat, B.N. Microbial and biochemical analysis of dried fish and comparative study using different drying methods. In Handbook of Drying Technology 2017, 35 (12), 1481-1491.

[13] Rahman, M.S.; Guizani, N.; Al-Ruzeiki, M.; Al Khalasi, A.S. Microflora Changes in Tuna Mince during Convection Air drying. Drying Technology 2000, 18 (10), 2369-2379.

[14] Marshall, M.R. Ash Analysis. Food Analysis; Heldman.D.R. Ed.; Springer: Boston, MA, 2010; 105-115.

Pressure drop characteristics of adjustable slotted distributor in fluidized bed

Tong, Z. [a]; Chaoran, L. [b]; Qing, X. [a, b]; Zhanyong, L. [a, b]*; Juan W. [a, b]

[a] International Joint Research Center of Low-Carbon Green Process Equipment; College of Mechanical Engineering, Tianjin University of Science & Technology, Tianjin 300222, China
[b] Tianjin Key Laboratory of Integrated Design and On-line Monitoring for Light Industry & Food Machinery and Equipment, Tianjin 300222, China

*E-mail of the corresponding author: zyli@tust.edu.cn

Abstract

In this paper, a fluidized bed with a adjustable slotted gas distributor was used to study fluidization in a 230 mm×200 mm rectangular fluidized bed by adjusting the spacing between the two slotted gas distributors. The pressure drop of the distributor at different inlet gas velocities was obtained and the change law between pressure drop and distance between distributors was summarized. This study provides a theoretical basis for the application of adjustable slotted gas distributor fluidized bed.

Keywords: Geldart D; Adjustable slotted gas distributor; Pressure drop

1. Introduction

Fluidized bed was used in various chemical units, which was common in the production processes of agricultural products, food, pharmacy, biochemistry and so on. It can strengthen the contact and transfer between the fluid and the particles [1-3], which was characterized by good gas-solid mixing, high mass transfer and heat transfer rate, uniform bed layer and strong controllability.

Among them, the most widely used gas-solid fluidized bed was mainly composed of bed, gas distribution device and gas-solid separation device (mostly a cyclone separator). In these parts, the most important part of the whole fluidization operation was the gas distribution device, that is, the gas distributor. The study found that there were many differences between the area near the distributor and the main body of the bed, and more and more attentions had been paid to the distributor [4]. The distributor should have a certain pressure drop so that the gas can be evenly distributed. Usually, the pressure drop of the distributor is greater than 1/10 to 3/10 of the total bed pressure drop. But in practical operation, the pressure drop of the distributor is as small as possible to reduce the energy consumption, and sometimes it is designed around 5% of the total bed pressure drop of [5]. A gas distributor that can perform well fluidization operation should be able to achieve uniform distribution of gas, low energy consumption, no leakage and clogging, convenient operation and long service life.

The distributor used in various applications were various. The original gas distributor was porous distributor, that is, the holes with the same diameter were distributed on the distributor. With the development of fluidization technology, more and more distributors were applied in the actual operation. Zhao et al. [6] used a tubular gas distributor to study the fluid dynamic behavior in an internal circulating fluidized bed. Chen et al. [7] used tilted gas distributor to investigate the depth of the distributor jets in a gas-solid fluidized bed. Hassan et al. [8] used porous gas distributor and tubular gas distributor to numerically study the solids circulation flux in an internal circulating fluidized bed.

At present, the distributor design was mainly composed of a single-layer distributor, and was often applied only to one type of material in the operation processes or the applicable materials had a narrow range of particle size distribution, it cannot be automatically adjusted according to operation requirements, without adequate consideration of the pressure drop of the distributor, the energy consumption was large.

The purpose of this study was to use a self-developed adjustable slotted gas distributor[9] for empty bed fluidization experiments. The pressure drop of the distributor at different inlet gas velocities were obtained, and the change law between pressure drop and distance

between distributors was summarized. It provided a theoretical basis for the application of adjustable slotted gas distributor fluidized bed.

2. Experimental

2.1. Experimental process and equipment

The experimental process is shown in Fig. 1. The gas generated by the blower was regulated by the bypass valve. The flow rate was shown by the gas flowmeter (VA300 type, flow rate 2~600 m^3/h, German CS Instruments). After that, it entered a rectangular fluidized bed (homemade, 230 mm×200 mm) equipped with an adjustable slotted gas distributor (opening rate 6%). There were two pressure measuring points on the bed, all along the axial direction of the fluidized bed, respectively 30 mm below the distributor and 30 mm above the distributor. Differential pressure transmitter (TRD-150205A, measuring range 0~1500 Pa, Tianjin Run Da Zhong Ke Instrument Co., Ltd.) was connected to two pressure measuring points through the trachea to measure the pressure drop of the distributor. The data recorded by the paperless recorder (TRD-21R, Tianjin Run Da Zhong Ke Instrument Co., Ltd.).
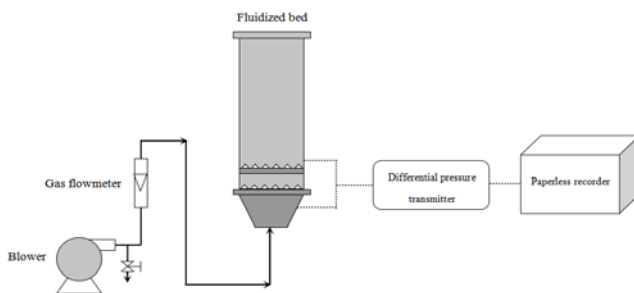
Fig. 1 Experimental flow chart.

A self-designed fluidized bed with a adjustable slotted gas distributor was used in the experiment. The distributor was made up of two slotted gas distributors. As shown in Fig. 2, the upper distributor size was 340 mm×220 mm, the slit area size was 220 mm×190 mm, the distributor opening rate was 6%, the number of the angle steel was 6, the side length of the angle steel was 23 mm, the distance between the angle steel was 2 mm and the height of the angle steel was 16 mm. As shown in Fig. 3, the lower distributor size was 220 mm×190 mm, the distributor opening rate was 6%, the number of the angle steel was 6, the side length of the angle steel was 23 mm, the distance between the angle steel was 2 mm and the height of the angle steel was 16 mm. Two distributors were connected by two guide components. The upper distributor was bolted to the bed. The lower distributor can move up and down under the guidance of the guide rail, so as to achieve the effect of adjusting the distance between distributors.
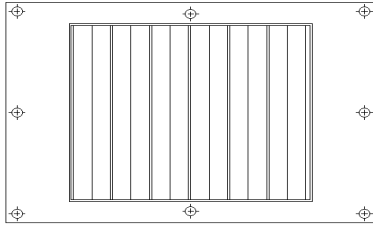
Fig. 2 Upper distributor.
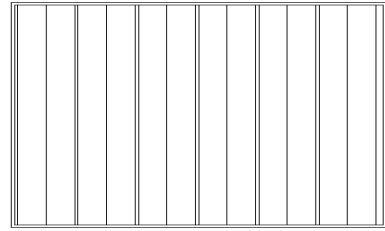
Fig. 3 Lower distributor.

2.2. Experimental method

The adjustable double-layer slotted gas distributor was connected to the fluidized bed with different distance between distributors (d) (0 mm, 10 mm, 20 mm, 30 mm and 40 mm). The pressure transmitter was connected to the bed through the trachea and the pressure transmitter was connected to the paperless recorder. Open the blower, open to maximum and gradually reduce the opening, control the gas flow from the maximum 310 m^3 / h to become smaller and keep the open interval of 10 m^3/h. The recording interval of the paperless recorder was 1s, each interval recorded for 60 s. The average value was the pressure drop ($\triangle$P) of the empty bed under the corresponding gas velocities (v). Each group of experiments was repeated 3 times and the average value of the data was taken.

3. Result and discussion

3.1. Influence of distance between distributors on pressure drop

The pressure drop of the distributor was the pressure loss caused by the gas passing through the distributor. Fig. 5 showed the relationship between pressure drop and gas velocity of an adjustable slotted gas distributor under different distance between distributors. It can be seen from the figure that the pressure drop of the distributor increased with the increase of gas velocity, while the pressure drop of the distributor was different at different distance between distributors. When the spacing between the distributors was 0 mm, that was, when the two distributors were almost close, the pressure drop produced by gas passing through the distributor was large and the pressure drop value was close to the 20 mm spacing. It was considered that when the distance between distributors was too small, the flow area between the plates was too small, so the pressure drop was larger. When the distance between the distributors gradually increased from 10 mm to 40 mm, the pressure drop of the distributor increased with the increase of the distance between the distributors at different gas velocities. This was because when there was a certain space between two distributors. The gas needed to consume more energy when it flowed through the space area, so it produced a certain pressure drop.
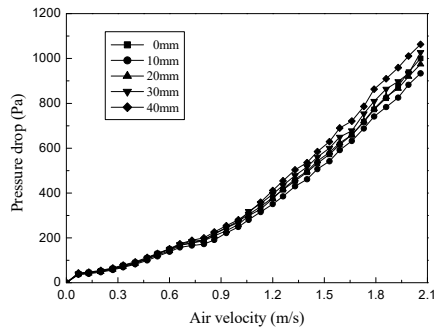
Fig. 4 Variations in pressure drop at different distance between distributors

3.2. Influence of gas velocity on pressure drop.

Fig. 5 showed the relationship between pressure drop and distance between distributors when the gas velocity was 1.59~2.06 m/s, that was, when the gas velocity was large. It can be seen from the figure that when the distance between distributors was the same, the difference between the pressure drops of the distributors corresponding to the adjacent gas velocity were not differ much as the gas velocity decreased, and the difference was approximately 50 Pa. Fig. 6 showed the relationship between pressure drop and distance between distributors when the gas velocity was 0.07 to 0.53 m/s, that was, when the gas velocity was small. It was clearly showed in the figure that when the distance between the distributors was the same, the difference between the pressure drop of the distributor corresponding to the adjacent gas velocity was also decreasing with the decrease of the gas velocity and the difference reduced from 20 Pa to 5 Pa. This was because when the gas velocity was small, the gas flow was relatively stable, so when the gas velocity changed, the pressure drop had a smaller change.
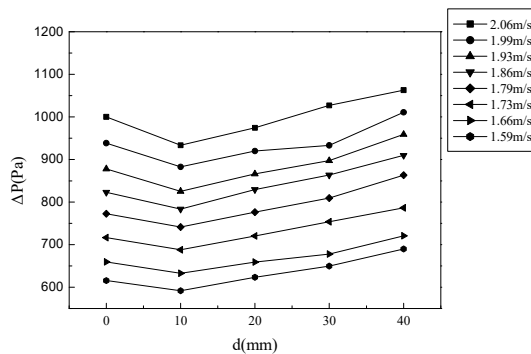
Fig. 5 Influence of pressure drop on distributor when gas velocity was 1.59~2.06 m/s
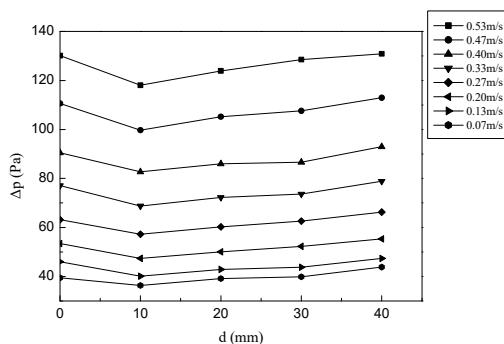
Fig. 6 Influence of pressure drop on distributor when gas velocity was 0.07~0.53 m/s

3.3 Experimental design analysis

It can be seen from Fig. 5 and Fig. 6 that except for the distance between distributors was 0 mm, at the same gas velocity, when the distance between the distributors increased from 10 mm to 40 mm, the change of the pressure drop of distributor showed a trend of linear function. Furthermore, under different gas velocities, the gradient of the pressure drop was approximately the same. This showed that the influence of the spacing between the distributors on the pressure drop was regular.In this paper, the results of orthogonal test were analyzed by Minitab software.

3.3.1. Intuitionistic analysis

Fig. 7 showed the mean main effects plot. It can be seen from the figure that the gas velocity had a significant effect on the pressure drop of distributor and the shape of the image was roughly a parabola. This showed that when the gas velocity was small, the gas velocity had little effect on the pressure drop, but as the gas velocity increased, the impact became greater. This further proved the previous conclusion.
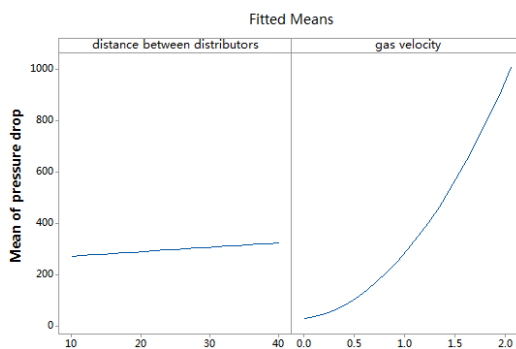
Fig. 7 Main effects plot.

3.3.2. Regression analysis

Table.1 Regression analysis

Term	Coef	SE Coef	T-Value	P-Value	VIF
Constant	42.85	5.75	7.46	0.000	
v	-5.79	8.08	-0.72	0.475	20.16
d	-0.559	0.193	-2.90	0.004	3.82
v*v	206.25	3.29	62.71	0.000	15.16
d*v	2.230	0.161	13.85	0.000	8.82

Use Minitab statistical software to perform linear regression analysis on this orthogonal test. The results of the analysis were shown in Table. 1. By analyzing the above data, it can be seen that the self-interaction item of gas velocity had the most significant effect on the pressure drop, followed by the interaction term of the gas velocity and distance between distributors. In the regression analysis, the P value corresponding to the gas velocity was 0.475, which was significantly greater than 0.05. Therefore, the impact of gas velocity on the distributor was not significant. Through the regression analysis, the regression equation of the distributor pressure drop was also obtained:

$$\Delta p = 42.85 - 0.559d - 5.79v + 206.25v^2 + 2.230d \cdot v \qquad (1)$$

4. Conclusions

A self-designed adjustable slotted gas distributor was used to carry out fluidization experiment. The results showed that when the distance between distributors was 0 mm, pressure drop generated by the gas through the distributor was large. When gas velocity was 2.09 m/s, pressure drop can reach 1040 Pa and pressure drop value was similar to when the spacing was 20 mm. When distance between distributors gradually increased from 10 mm to 40 mm, pressure drop of the distributor increased with increase of spacing at different gas velocities. However, when gas velocity was low, the difference between pressure drop corresponding to the adjacent gas velocity decreased with the decrease of the gas velocity. Through the experimental design analysis, it was concluded that the self-interaction of gas velocity had the most significant effect on the pressure drop, and the fitting relationship between pressure drop, gas velocity and distance between distributors was obtained: $\Delta P = 42.85 - 0.559 \ d - 5.79 \ v + 206.25 \ v^2 + 2.230 \ d \cdot v$.

5. References

[1] Chongdian, S.; Jianjun, Wu. Fluidized bed technology in low rank coal drying engineering. China Powder Science and Technology 2015, 21(1): 91-95.

[2] Jianguo, Y. Optimization of gas distribution in a fixed fluidized bed reactor. Chemical Engineering 2017, 45(3): 64-68.

[3] Qin, L.; Yinfeng, Z.; Mao, Y.; Zhongmin, L. Application of electrical capacitance tomography for gas-solid fluidized bed measurement. CIESC Journal 2014, 65(07): 2504-2512.

[4] Zigang, Y.; Jianzhong, Y. Shallow fluidization. Chemical Industry and Engineering Progress 1983, (02): 6-9.

[5] Yong, J. Fluidized Engineering Principle. Tsinghua University Press 2002.

[6] Wenli, Z.; Tiefeng, W.; Chenjing, W.; et al. Hydrodynamic behavior of an internally circulating fluidized bed with tubular gas distributors. PARTICUOLOGY 2013, 11(6): 664-672.

[7] Weibo, C.; Junguo, L.; Zhonghu, C.; et al. Study on jet depth on slanted distribution plate in gas-solid fluidized bed. Chemical Reaction Engineering and Technology 2014, 30(01): 10-14.

[8] Hassan, M.; Schwarz, M.P.; Feng, Y.; et al. Numerical investigation of solid circulation flux in an internally circulating fluidized bed with different gas distributor designs. Powder Technology 2016, 301: 1103-1111.

[9] Zhanyong, L.; Tong, Z.; Qing, X. An adjustable fluidized bed uniform air distribution system and its control system. Tianjin: CN107202320A, 2017-09-26.

Coating effect of micro-sized droplets impacting on low temperature spherical particles

Wu, X.[a]; Ma, X.[b]; Xu, Q.[a]; Li, Z.[a*]; Wang, R.[a]

[a]International Joint Research Center of Low-Carbon Green Process Equipment; College of Mechanical Engineering, Tianjin University of Science & Technology, Tianjin 300222, China.
[b]Tianjin Key Laboratory of Integrated Design and On-line Monitoring for Light Industry & Food Machinery and Equipment, Tianjin 300222, China.

*E-mail of the corresponding author:zyli@tust.edu.cn (Z. Li).

Abstract

In this paper, the effect of spray droplets on the coating of cold spherical particles was studied.The microcapsule granulator produces micron-sized droplets to coat the spherical particles in cold storage, and the high-definition camera and precision balance are used to photograph and weigh the particles before and after the spraying. The droplets are obtained by using the image and data processing technology coating area and coating quality, the droplet coating effect was evaluated by a number of dimensionless parameters such as coating ratio and mass ratio.By orthogonal design experiment and uncertainty analysis, the effects of droplet size and flow rate, spherical particle temperature and diameter on coating effect were studied, and the effect of droplet group coating on low temperature spherical particles was obtained.

Keywords: Spray freeze drying; Droplets; coating; Spherical particles.

1. Introduction

Since 1948, when Benson et al. first used the technique of spray freezing to study the surface area of protein particles [1], this technology has been developing for more than 60 years and has obtained some representative research results. For example, in 1964 Werly used spray-frozen technology to obtain submicron powder products, marking that the spray freezing technology has been developed to the stage of producing products [3]; in 1989, Chen Zuyao and others first prepared Ba-Y by means of SFD method. Cu-O system composite oxide ultrafine powder [2]; 1994, the technology applied for a European patent; in 1998, Maa et al. proposed the preparation of protein microspheres using SFD technology for the first time [5]; in 2006, it achieved regular freezing. Dry alternative to vacuum freeze-drying reduces the energy consumption of SFD technology [6]. After more than half a century of development, SFD technology is gradually maturing, and it has been applied in the fields of medicine, food, chemical products, and biological products [7].

In order to solve the phenomena of agglomeration of powders, non-uniform powder particle size and other phenomena, to further improve the application of spray freeze-drying technology in engineering practice and achieve mass production, Li Zhanyong et al [4]proposed an inert particle fluidized bed spray freeze-drying Equipment. In order to deeply study the freezing mechanism of atomized droplets impacting the carrier particles, this paper studied the coating area of cryogenic spherical particles by droplets in experiments.

2. Materials and Methods

2.1. Experimental Materials

Since the coated particles were image-collected after the coating experiment, in order to facilitate the image processing, the material used in this experiment was ink. The inert carrier particles use different diameters of organic glass spheres. The effects of different experimental conditions on the droplet coating process were experimentally studied. By setting different flow rates of 6 and 8 mL/min, atomized droplets of diameter 0.2 mm were obtained. The diameters of the glass spheres were taken as 3, 4 and 5 mm, respectively. Each set of experiments was performed 3 times.

2.2. Experimental device

The droplets are generated by a Droplets generator, which uses laminar liquid jets and vibrates at high frequencies to produce extremely uniform round microcapsule particles as shown in Figure.1. Applied to the protection and storage of drugs, microorganisms,

enzymes or cells, the purpose of microencapsulation is to use a polymer mechanism to protect or stabilize the active ingredient, and it can also be used to produce uniform atomized droplets. The device can generate highly reproducible uniform drop particles whose particle size can be pre-set to 0.2 mm depending on the choice of nozzle, with a narrow particle size distribution (<5% standard deviation).
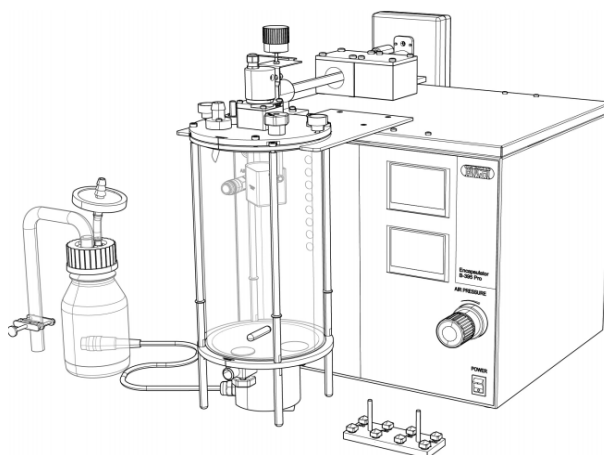
Fig.1 Droplets generator

For this study, the collision process of atomized droplets impinging on a solid surface at a temperature of -25 °C was studied. Such a low degree of subcooling metal particles at room temperature, the water vapor in the air quickly frozen on the metal surface to form ice, change the structure of the particle surface structure impact on the droplet collision process. In this experiment, a freezer (Haier Company) was used as a cooling space. Its cooling range was as low as -50 °C. The internal dimensions of the refrigerator were 100 cm in length, 70 cm in width, and 60 cm in height. The top has a 12 cm diameter feed hole.

2.3 Experimental parameters

The experimental data image was processed by Image J software, and the projected area of the coating liquid film was calculated by converting the image into a grayscale image and pixel scanning to obtain the ink coating area. As shown in Figure. 2.
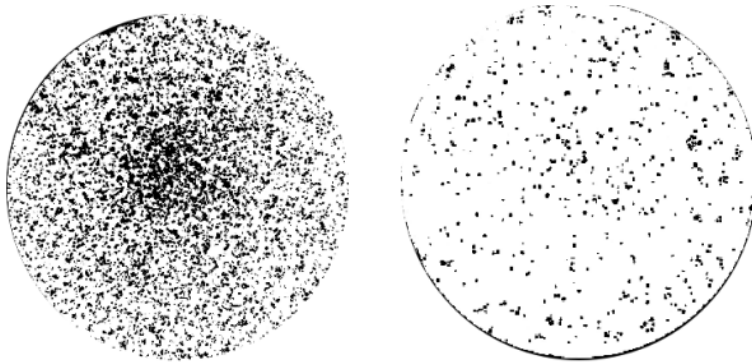
(a)Total area of coated projection S₁   *(b) After coating area removed S₂*

Fig.2 Coated image after processing

Coating area:

$$S = S_1 - S_2 \tag{1}$$

The S_1 refers to the total area of the projection of the projection, and the S_2 refers to the projection area after the removal of the particles.

Coating ratio:

$$c = \frac{S}{n \times \pi r^2} \times 100\% \tag{2}$$

The n refers to the number of particles, and R refers to the radius of the particles.

Coating amount:

$$M = (M_1 - M_2) - (m_1 - m_2) \tag{3}$$

In the formula, M_1 refers to the total mass after coating, M_2 refers to the total mass before coating, m_1 refers to the mass of the empty disk after coating, and m_2 refers to the mass of the empty disk before coating.

3. Results and Discussion

3.1 Effect of Particle Diameter Change on Coating

The background of the experimental study in this paper is the collision and coating of atomized droplets with fluidized, undercooled carrier particles. For this reason, it is of great significance to investigate the influence of particle diameter on the coating area of droplets.

In this experiment, 0.5, 1, 2, and 3 g of ink were coated on glass balls with diameters of 3, 4, and 5 mm at a flow rate of 6 mL/min and 8 mL/min, respectively, of droplets with an average diameter of 0.2 mm. Study the change in coated area with ball diameter.
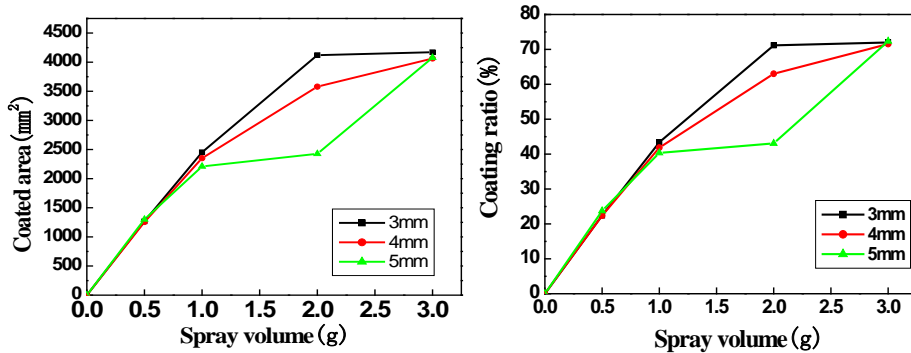
(a) flow rate of 6mL / min
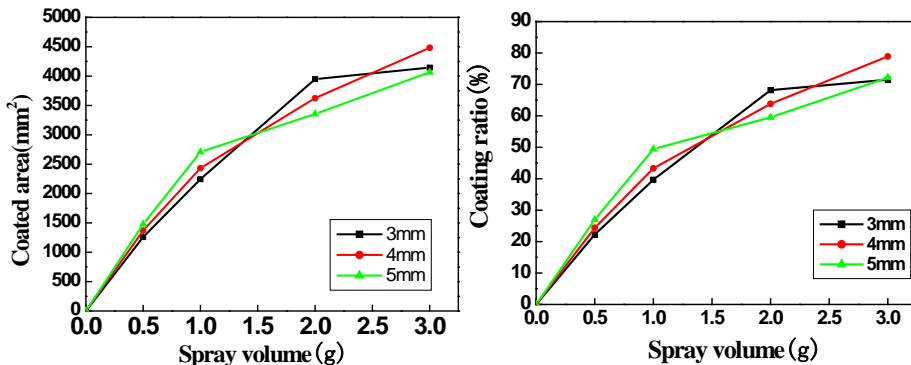
(b) flow rate of 8mL / min

Fig. 3 Variation of coating area and coating ratio with spray amount for different particle sizes under two flow rates

As shown in Fig. 3(a), at a spray flow rate of 6 mL/min, from the start of spraying to when the spray amount reaches 1g, the coating rate hardly varies with the diameter of the particles, the coated area of the particles is basically the same, and the coating ratio is about 40 %, when the spray amount is 1-2 g, the particle diameter increases, the coating rate decreases, from 2-3 g, the particle diameter increases, the coating rate increases, but when the spray amount is 3 g, three kinds The coated area of the particles is substantially the same, and the coating ratio reaches 70 %. As shown in Fig. 3(b), at a flow rate of 8 mL/min, from the start of spraying to when the spray amount reaches 1 g, the particle diameter increases, the coating rate gradually increases, and the particle diameter increases from 1-3 g. Increasing, the coating rate decreases. However, when the spray amount was 1.5 g, the

coating area of the three particle sizes was substantially the same, and the coating ratio was about 55 %.

(a) flow rate of 6mL / min　　　　　*(b)flow rate of 8mL / min*
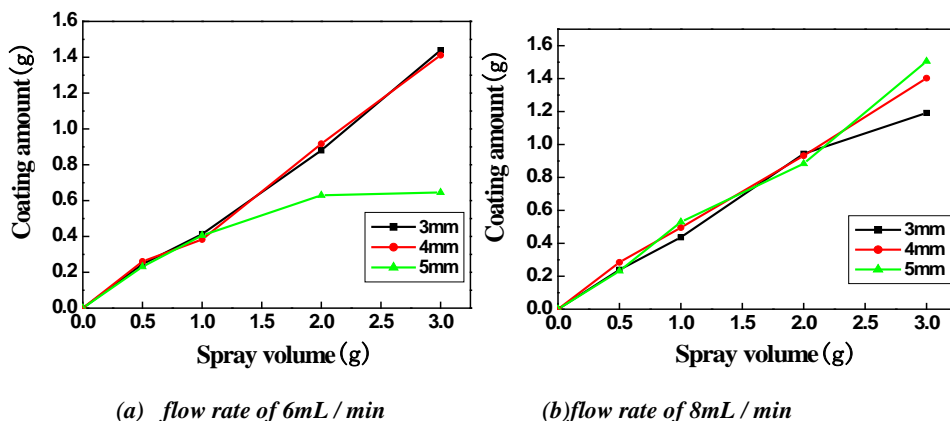
Fig. 4 Change of coating amount with spray amount under different flow rate and different particle size

As shown in Fig. 4(a), at a spray flow rate of 6 mL/min, the coating amount increases as the amount of spray increases, coating of 3, 4 mm particles is almost the same, but the coating amount of 5 mm particles is apparently seen. It is much smaller than other diameter particles. As shown in Fig. 4(b), at the spray flow rate of 8 mL/min, the spraying amount of the three kinds of particle granules was basically the same from the beginning of the spraying to 2 g, and after 2 g, the particle diameter increased, and the coating was applied. The amount increases.

3.2 Influence of Change in Atomization Flow Rate on Coating

(a)　　　　　　　　　*(b)*
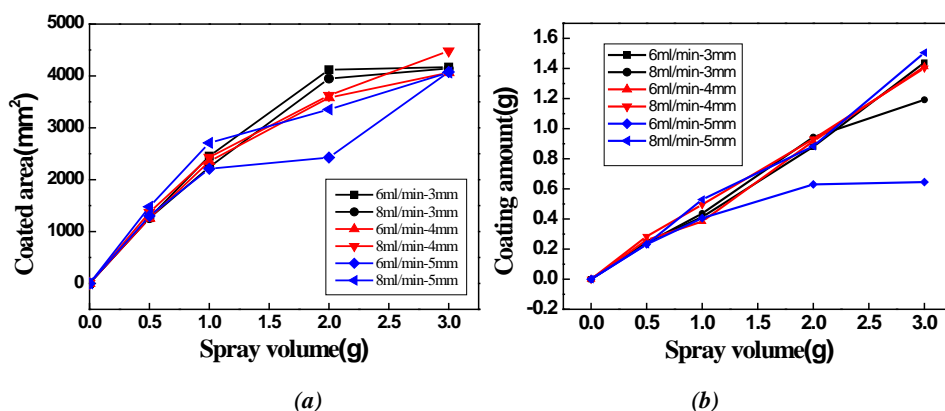
Fig. 5 Change in Coating Area with Spray Volume

As shown in Fig. 5(a), when the particle diameter is 3 mm, the coated area under the two flow rates shows almost the same change trend; when the particle diameter is 4mm, the coated area at 8 mL/min is slightly larger than 6 mL/min when the same spray amount is applied; When the particle diameter is 5mm, the coating area under 8 mL/min conditions is much higher than 6 mL/min under the same spray amount condition, but when the spray amount reaches 3 g, the coated area is the same. It can be seen that when the particle diameter is small, the flow has little influence on the coating. As the particle diameter increases, the influence of the flow on the coating increases, and the larger the flow, the larger the coated area. As shown in Fig. 5(b), when the particle diameter is 3 or 4 mm, the coating amount is basically the same with the variation of the spray amount at different flow rates; with a particle diameter of 5 mm, the coating flow rate of 6 mL/min is much lower than the flow rate of 8 mL/min.

From the above two figures, it can be seen that the particle diameter has a significant effect on the coating. When the particle diameter increases, the curvature of the particle surface decreases, so that the droplets are likely to accumulate on the surface of the particles, so that the coating area is reduced; when the flow rate increases At that time, the influence of the curvature of the particles on the coating is reduced, because the kinetic energy of the spray droplets increases, so that the droplets spread more, so that the influence of the curvature of the particles is reduced.

4. Conclusions

When the spray flow rate is 6 mL/min, the particle diameter has little effect on the coating when the spraying starts to 1 g. With the progress of the coating, the larger the particle diameter, the smaller the coating rate; when the spray flow rate is 8 mL /min, the larger the particle diameter before the coating ratio is 55%, the larger the coated area, and the larger the particle diameter and the smaller the coated area after the 55% coating ratio.

With the same amount of spray, as the particle diameter increases, the flow rate increases and the coating area increases, but when the spray amount reaches 3 g, the coated area is almost the same; when the particle size becomes larger, the spray flow increases. The coating amount increases.

5. References

[1] Rogers, S.; Wu, W. D.; Saunders, J. Characteristics of milk powders produced by spray freeze drying. Drying Technology 2008, 26 (4), 404-412.

[2] Leuenberger, H.; Plitzko, M.; Puchkov, M. Spray-freeze-drying in a fluidized bed at normal and low pressure. Drying Technology 2006, 24 (6), 711-719.

[3] Yeom, G. S.; Song, C. S. Experimental and numerical investigation of the characteristics of spray-freeze drying for various parameters: effects of product height, heating plate temperature, and wall temperature. Drying Technology 2010, 28 (2), 165-179.

[4] Zhanyong Li et al. An inert particle spray freeze-drying equipment and method. Chinese patent. 201110103036.9, 2011.

[5] Hans Leuenberger. Process of drying a particulate material and apparatus for implementing the process. US Patent, 4608764, 1986.

[6] Worthington, A. M. T. he splash of a drop and allied phenomena. Smithsonian Report 79, 972-982.

[7] Gangtao Liang, S. S. et al. Experimental observations of special phenomena of liquid droplets striking a slanted surface liquid film. Acta Physica Sinica, 2013, 62 (8), 084707-1-7.

Hybrid and intermittent drying of carrot (*Daucus carota* var. Nantes)

Szadzińska, J.; Mierzwa, D.[*]; Bukowski, K.

Department of Process Engineering, Poznań University of Technology, Poznań, Poland

*E-mail of the corresponding author: dominik.mierzwa@put.poznan.pl

Abstract

A combination of high power airborne ultrasound and microwaves in hot air drying was developed to investigate the effect of intermittent mode on process effectiveness and quality of carrot. The drying experiments were carried out in an innovative hybrid dryer. The course of moisture ratio, drying rate, specific energy and water consumption, colour, water activity and shrinkage were discussed. The results showed that intermittent ultrasound and microwaves in convective drying accelerate the heat and mass transfer, leading to shorter drying time and faster drying rate. It was found that hybrid-intermittent drying can improve the energy efficiency and product quality.

Keywords: intermittent drying; ultrasound; microwaves; energy; shrinkage.

1. Introduction

Current trends in industrial equipment design or engineering in general place emphasis on the ecological aspect of production. Drying as a food processing method is particularly a good field for engineers and scientists to implement new or improve existing designs. Its most widely used method, hot air drying, is notorious for its bad energy efficiency (a result of constant drying agent replacement, necessary to finish the process) and long drying time.[1] What is more, consumers' dietary knowledge is on the rise, which means that product quality should be taken into consideration as well. In that matter, convective drying also has its drawbacks, as it has a substantial impact on the dried foodstuffs' appearance, flavor and nutrients content.[2] In latest years some ideas how to improve drying and driers have been reported. Among others, they include hybrid techniques and drying at non-stationary (intermittent) conditions. Former's principle of operation is a simultaneous use of two or more drying methods (heat sources), such as hot air and microwaves. In such a way, different mechanisms of energy transfer are employed, what makes the drying process faster and more energy-efficient. Latter, is based on providing a variable amount of heat during the process, so there are periods of intensive evaporation and so called *relaxation*, when moisture and temperature gradients inside the dried material are reduced. That results in reduction of thermal energy and better product quality, however it may also increase the drying time.[3, 4]

In this research, carrot was selected to be an example of a foodstuff. Its distinctive orange color and shape, good nutritious value (content of dietary fiber, vitamins A, K, B6, carotenoids, lutein, zeaxantin) allowed it to take a place in various cuisines.[5, 6] Carrots are consumed in various forms, for example raw, boiled, soups, juices or even a cake. Furthermore, when dried, it can be used as an ingredient for dried vegetable mixes. In this paper, a novel drying technique involving hybrid methods in intermittent conditions is investigated. Both of those concepts examined alone proved to improve all three of crucial properties of drying: kinetics, energy consumption and product quality.

2. Materials and Methods

Carrot roots (*Daucus carota*, var. Nantes) used for the drying experiments were purchased from a local market and stored for at least 24 h at 4°C. Before drying, the carrots were rinsed, peeled and cut into cubes (1.5 cm side). Next, 50 g carrot samples were dried in a hybrid dryer[7], using eight different drying programs (Fig. 1).
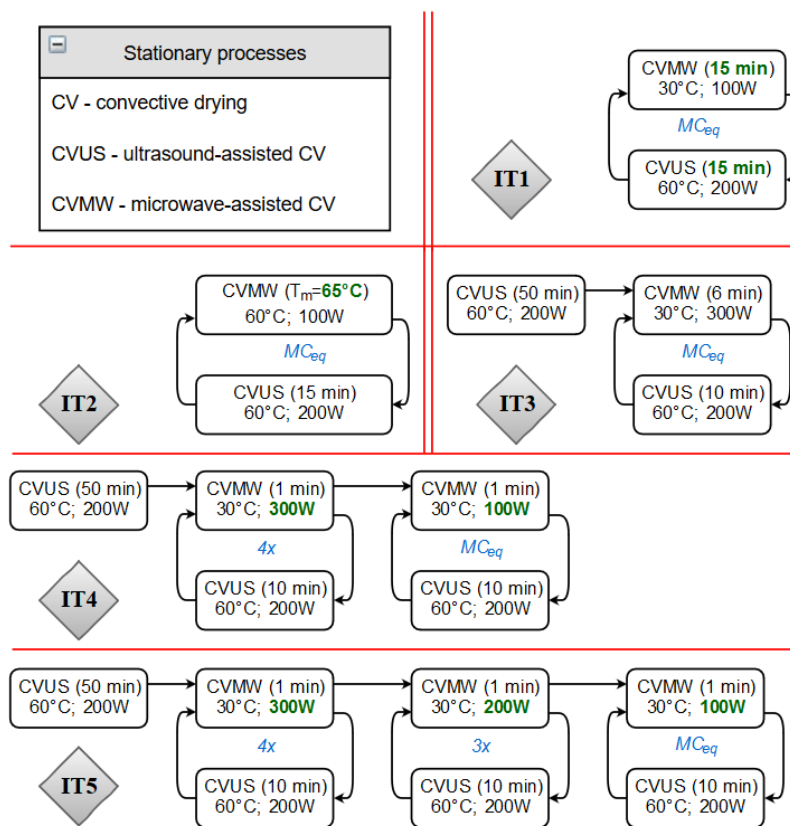
Fig. 1. Schematic illustration of the course drying programs used in the studies:
T_m – material temperature, MC_{eq} – equilibrium moisture content, 4x – number of loop repetitions.

The drying processes were realized in stationary and non-stationary conditions. The stationary ones (CV, CVMW, CVUS) were conducted at the same air temperature (T_a=60°C) with a constant air velocity (v_a=2 m/s), and with a changeless microwave or ultrasound power (P_{mw}=100 W – CVMW; P_{us}=200W – CVUS). The intermittent processes (IT1-5) were carried out in variable drying conditions (Fig. 1).

2.1. Process kinetics and energy consumption

The drying kinetics was assessed on the basis of the moisture ratio (MR), drying rate (DR), drying time (DT) and the specific energy consumption (SEC). The moisture ratio (MR) was determined from the following equation:

$$MR = \frac{MC_t - MC_{eq}}{MC_i - MC_{eq}} \qquad (1)$$

where: MC_i, MC_t and MC_{eq} are the initial, instantaneous (for a given time of the process) and equilibrium moisture content.

The initial moisture content (MC_i) of the carrot was determined with the moisture analyzer (XM120; Precisa, Switzerland; precision 0.01%). The equilibrium moisture content (MC_{eq}) was constant during the research and equaled 0.05 kg·kg^{-1} db. The moisture content at a given time of the process (MC_t) was expressed as the ratio of moisture mass to the initial mass of wet sample. The energy consumption was measured with a standard electricity meter (precision 0.01 kWh) and recalculated to MJ per kg of evaporated moisture (SEC). Because some devices in the drying system require tap water as a coolant, the specific water consumption (SWC), that is dm^3 of water per kg of evaporated moisture, was also measured.

2.2. Quality assessment

The product quality was assessed on the basis of water activity, color, volumetric shrinkage and apparent density. The color of the fresh/dry carrot was measured with the use of colorimeter (CR400; Konica Minolta, Japan; precision 0.01). For this purpose, several randomly chosen (fresh/dried) samples were ground in a laboratory mill (A11; IKA; Germany). On the basis of the obtained CIE Lab tristimulus color coordinates (L*, a*, and b*), the relative color change (dE) was determined:

$$dE = \left(dL^{*2} + da^{*2} + db^{*2}\right)^{0.5} \qquad (2)$$

where: dL^*, da^* and db^* are the differences between particular color coordinates (L*, a*, b*), obtained for the raw and dry material, respectively.

The water activity (aw) was measured for fresh/dried samples with the use of laboratory aw meter (LabMaster-aw; Novasina, Switzerland; precision 0.001) at constant temperature of the chamber (25°C). The volumetric shrinkage of the carrot samples (VS) was determined with the use of modified toluene method developed by Mazza.[8] The volumetric shrinkage was calculated with the following equation:

$$VS = \left(1 - \frac{V_d}{V_0}\right) \cdot 100\% \; , \qquad (3)$$

where: V_d and V_0 are the volumes of dry and fresh sample, respectively.

3. Results and discussion

3.1. Drying kinetics, energy and water consumption

In Figure 1, the evolution of moisture ratio (MR) and the average drying rate (DR) for different drying processes were presented.
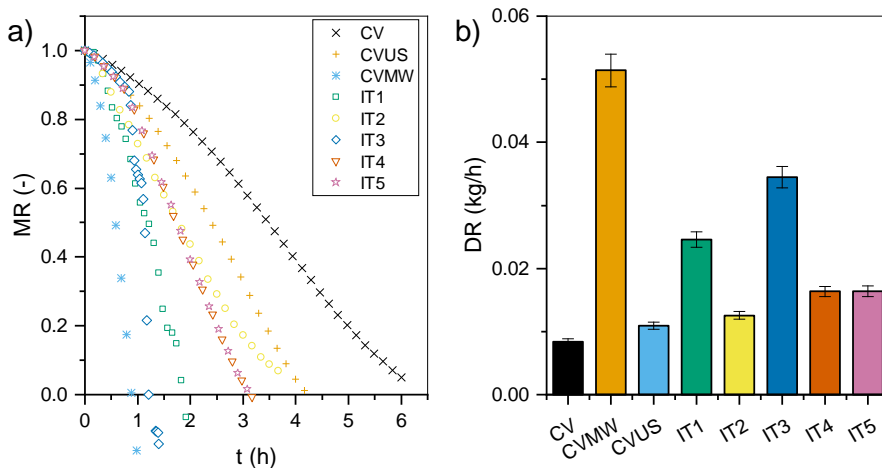
Fig. 1. Evolution of moisture ratio MR (a) and the average values of drying rate DR (b).

As follows from figure 1, the convective drying (CV) was the slowest drying procedure and lasted about six hours. The application of microwave radiation during convective drying reduced the overall drying time by 85%, as compared to CV. In turn, the ultrasound assistance in convective drying (CVUS) improved the drying kinetics, shortened the drying time by 32%, and increased the drying rate by about 30% in comparison to CV. The total drying time for the samples dried by IT processes was in the range of 1-4 hours. Therefore, hybrid drying with intermittent MW and US application enabled to achieve the desired effect, i.e. increase in process efficiency.

Figure 2 shows the specific energy (SEC) and water consumption (SWC) for different drying strategies. The highest electric energy consumption was observed for CVUS, and the lowest for CVMW (Fig. 2a). Satisfactory results were obtained for intermittent drying. But the differences between the total energy consumed in the IT1-5 procedures were dependent on both durations of MW and US application. In turn, as follows from figure 2b, the longer MW radiation time the more water consumed in the drying process. The IT2-5 methods are characterized by much smaller and similar values of SWC than CVMW and IT1, which is a very positive effect. It means also, that modification of convective-microwave drying into intermittent mode ensures less water consumption.
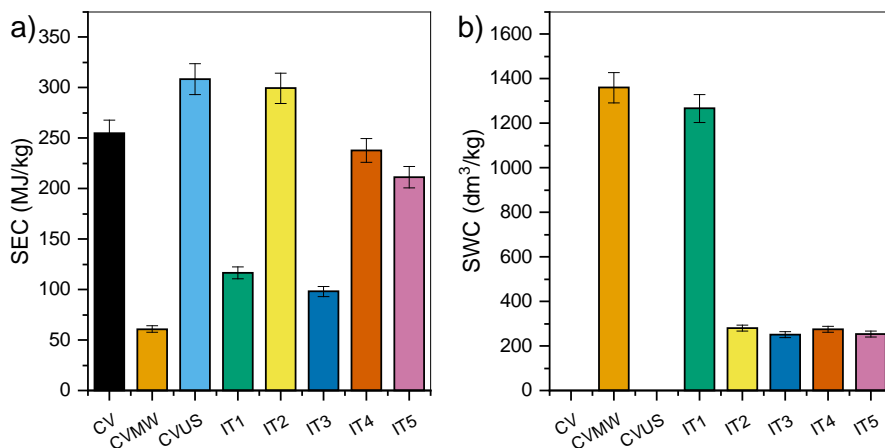
Fig. 2. Specific energy consumption SEC (a) and water consumption SWC (b).

3.2. Quality characteristics

After drying the carrot samples were assessed in terms of water activity (aw), color change (dE), volumetric shrinkage (VS) and apparent density (ρ_a). Figure 3a presents the water activity of raw and dry material. As follows from this graph the aw value was reduced from about 0.989 (for fresh carrot root) to on average 0.333 for dry products.
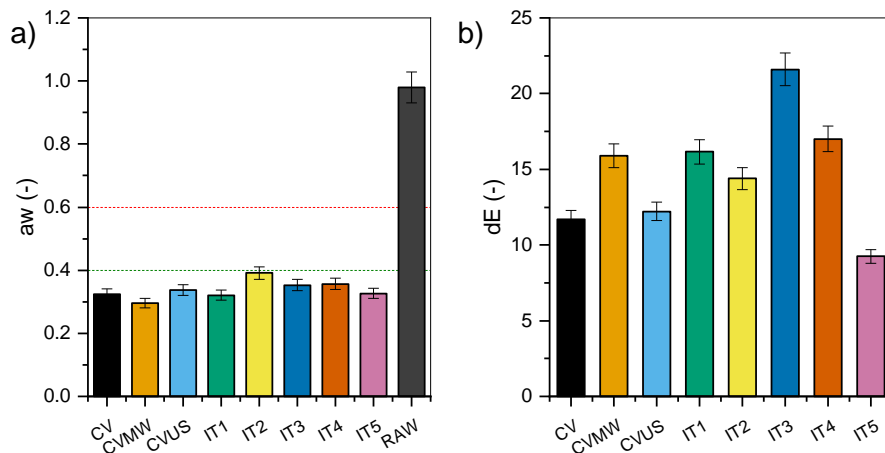
Fig. 3. Water activity aw (a) and relative color change dE (b).

According to Labuza et al.[9], when the water activity is below 0.4 the dried products are stable in terms of the growth of bacteria, yeast and molds, and natural decay processes (e.g. non-enzymatic browning).

As follows from the data presented in figure 3b, the highest and the lowest relative color change was obtained for the samples dried by intermittent methods (IT3 and IT5 respectively). However, the other samples did not differ significantly, among specific drying programs, i.e. stationary and non-stationary. The exception is CVMW, for which the color change was close to those of IT.

The next quality factor assessed in the studies was volumetric shrinkage (Fig. 4a). On the basis of the results, it was found that the carrot samples dried by CV and CVUS shrank by 85%, on average. In turn, the rest of the samples dried by CV combined with MW, were characterized by a lower shrinkage. This effect results from the so-called "puffing". The best shape retention was observed for the IT3 samples, but the value of VS is also fairly high. These results were confirmed by calculation of additional value, i.e. apparent density ρ_a (Fig. 4b).
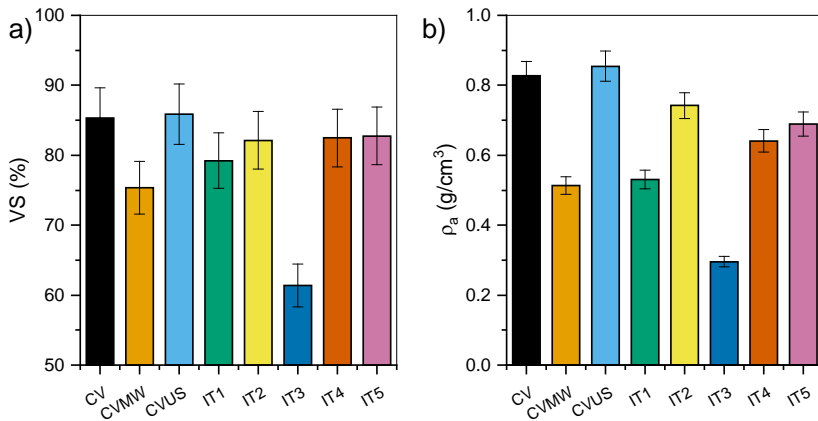
Fig. 4. Volumetric shrinkage VS (a) and apparent density ρ_a (b).

The highest value of ρ_a was observed for the CVUS drying whereas the lowest value of ρ_a was observed for the IT3 drying. Lower values of ρ_a means higher total volume of the sample, and thus a lower shrinkage after drying. Furthermore, a lower value of the apparent density means that dry sample is characterized by higher porosity (assuming same mass of samples). Therefore, the results of volumetric shrinkage and apparent density demonstrated, that the final physical and microstructural properties of the carrot samples depend on the drying technique and are better for simultaneous MW and US application in convective drying.

4. Conclusions

The results showed that intermittent ultrasound and microwaves in hot air drying improve significantly the process efficiency as compared to the CV drying. Furthermore, it was demonstrated that intermittent drying can reduce both energy and water consumption as well as improves the quality of dry carrots. Adequate choice of process parameters positively affects the product color and its physical properties such as lower shrinkage (shape retention) and higher porosity.

5. Acknowledgement

6. References

[1] Musielak, G. Advanced drying techniques; Poznań University of Technology: Poznań, 2013 (in Polish).

[2] Nowacka, M.; Śledź, M.; Wiktor, A.; Witrowa-Rajchert, D. Physical and chemical properties of microwave dried food products. ŻYWNOŚĆ. Nauka. Technologia. Jakość 2012, 6 (85), 5–20 (in Polish).

[3] Chua, K.J.; Mujumdar, A.S.; Chou, S.K. Intermittent drying of bioproducts—an overview. Bioresource Technology 2003, 90 (3), 285–295.

[4] Kowalski, S.J.; Szadzińska, J.; Łechtańska, J. Non-stationary drying of carrot: Effect on product quality. Journal of Food Engineering 2013, 118 (4), 393–399.

[5] U. S. D. o. Agriculture, „National Nutrient Database for Standard Reference," [Online]. Available: https://ndb.nal.usda.gov/ndb/search/list?qlookup=11124&format=Full.

[6] Alasalvar, C.; Grigor, J.M.; Zhang, D.; Quantick, P.C.; Shahidi, F. Comparison of volatiles, phenolics, sugars, antioxidant vitamins, and sensory quality of different colored carrot varieties. Journal of Agricultural and Food Chemistry 2001, 49 (3), 14101416.

[7] Kowalski, S.J.; Mierzwa, D. US-assisted convective drying of biological materials. Drying Technology 2015, 33 (13), 1601–1613.

[8] Mazza, G. Dehydration of carrots: Effect of pre-drying treatments on moisture transport and product quality. Journal of Food Technology 1983, 18, 112–123.

[9] Labuza, T.; Tannenbaum, S.; Karel, M. Water content and stability of low moisture and intermediate-moisture foods. Food Technology 1970, 24 (5), 543–550.

Determination and modelling of the particle size dependent residence time distribution in a pilot plant spray dryer

Ruprecht, N. [a*]; Kohlus, R.[a]

[a] Department of Process Engineering and Food Powders, University of Hohenheim, Stuttgart, Germany

*E-mail of the corresponding author: nora.ruprecht@uni-hohenheim.de.

Abstract

The residence time distribution (RTD) in a pilot plant spray dryer was characterised for two kinds of air distributors (centrifugal and parallel flow) and for different atomizing air pressures. To determine the RTD - and the RTD of different particle size fractions - the particle concentration and size at the dryer outlet was measured continuously using a particle counter. Results were modelled using the Bodenstein number and the CSTR in series model. An increasing nozzle pressure leads to a decrease in mean residence time and a more narrow distribution. The influence of nozzle pressure is more pronounced than of air distributor and particle size fraction.

Keywords: Residence time distribution; Particle size; Bodenstein number modelling; Nozzle influence; Mechanism of air distribution

1. Introduction

The drying behaviour in a classical spray dryer is determined by the nozzle zone, where the first contact between the hot gas and the product occurs, as well as by the main drying within the drying chamber. In order to describe the drying process, knowledge of the residence time distribution is needed. In addition to the mechanism of air distribution, this is dependent on the nozzle flow and the geometry of the spray dryer. One hypothesis for describing the flow pattern in the drying chamber is based on relatively large vortices leading to different trajectories and residence times depending on the particle inertia or particle size, respectively [1].The residence time of the particles should be sufficient to ensure the desired moisture reduction of the feed but not too long in order to avoid thermal damage like degradation or loss of volatiles. Large deviations in the residence time of different particles, as indicated by a broad residence time distribution (RTD), lead to an inhomogeneous product.

In general, the RTD is determined by tracer injection at the dryer inlet and measuring the response at the outlet by taking samples in predefined time steps and analysing them with respect to their tracer concentration. This tracer can for example be an optically visible [2,3] or conductive [4,5] substance. Especially for fast processes like spray drying this discontinuity of the measurement leads to a too low resolution.

The most common approach for modelling the RTD is using a number of continuous stirred tank reactors (CSTR) in series [6],where the distribution of residence times E(t) [-] over time t [s] is described by the mean residence time τ [s] and the number of CSTR in series N [-].

$$E(t) = \frac{N}{(N-1)!} \cdot e^{-N\frac{t}{\tau}} \cdot \left(\frac{Nt}{\tau}\right)^{N-1} \tag{1}$$

Various CSTR in series with different tank numbers and residence times can also be set in serial or parallel connection which might account for different flow regimes within the system [4,5].

Another approach for modelling the RTD is the dispersion model, which is based on the Fokker-Planck differential equation, describing the change of concentration c [1/m³] over time t [s] and space z [m].

$$\frac{\delta c}{\delta t} = -w \cdot \frac{\delta c}{\delta z} + M_{ax} \cdot \frac{\delta^2 c}{\delta z^2} \tag{2}$$

w [m/s] is the average particle velocity and M_{ax} [m²/s] the axial mixing coefficient describing the derivation from radial flow pattern due to axial dispersion. In dependene of the boundary conditions M_{ax} can be calculated directly from the dimensionless variance of the measured RTD. A better way is to fit M_{ax} directly to the measured data[7] instead of using these simplifications, although it requires solving the differential equation multiple times. From M_{ax} the dimensionless Bodenstein number, which indicates the ratio of convective to dispersive transport, can be calculated.

$$Bo = \frac{w \cdot L}{M_{ax}} \tag{3}$$

Here, L [m] is the characteristic length. A low Bodenstein number indicates a broad distribution, a high number a narrow distribution.

Residence time distributions can also be modelled by linking CFD with particle tracing and observing the particle number over time at the outlet [8]. Thus, measurements of the RTD can be used to prove theoretical models.

In the present study, the particle RTD was determined using a particle counter. A pulse of maltodextrin was injected into a continuous water stream. When water is sprayed, the droplets evaporate and no particles are recognised by the detector at the dryer outlet. When maltodextrin particles pass the detector, it recognises the particle concentration as well as their size. This set-up allows a continuous measurement of the particle residence time.

2. Materials and Methods

2.1 Experimental set up

For the spray drying trials a pilot plat spray dryer (GEA Niro, Søborg, Denmark) with the dimensions 3.1 m x 1.2 m was used. As an injection signal, a 30 s pulse of 20 % (w/w) maltodextrin DE 21 (Agrana, Vienna, Austria) solution was injected into a continuous water stream by changing the position of a three-way valve.
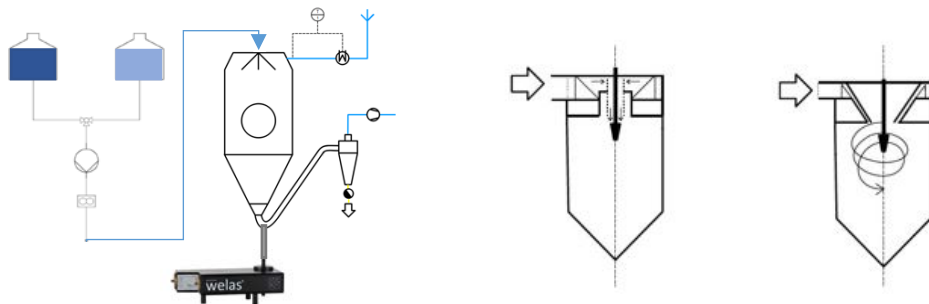
Fig. 1: Experimental set up, parallel and centrifugal air distributor (left to right)

A hollow metal tube with 2 mm inner diameter, connected to a scattered light detector (Aerolossensor welas 2300, Palas, Karlsruhe, Germany), was inserted in the tower at the outlet of the drying chamber (see Fig. 1). The scattered light detector allows measuring the particle concentration and size within the air stream. From the particle concentration over time the RTD can be calculated.

In order to investigate the effect of the air distributor and nozzle pressure on the RTD the following settings were chosen:

Table 1: Drying parameters

Air rate	Feed rate	Inlet temperature air	Outlet temperature air
230 kg/h	9 kg/h	180 °C	90 °C

Table 2: Air distributor and nozzle pressure

Air distributor	Parallel		Centrifugal
Nozzle	2 fluid nozzle, 2 mm orifice diameter		
Nozzle pressure (rel.) [bar]	1	2	3
Atomizing air rate [kg/h]	12	18	25

Trials with a nozzle pressure of 1 bar were performed 9 times, with 2 and 3 bar 5 times each.

2.2 Modelling of the residence time distribution

The output signal E_{out} (t), measured by the scattered light detector, results from the convolution of the injection signal E_{in} (t) with the RTD of the spray dryer.

$$E_{out}(t) = E_{in}(t) * RTD \tag{4}$$

Here, * indicates the convolution product. Consequently, the RTD can be calculated from deconvolution of the measured output signal with the input signal. Convolution and deconvolution were performed by applying the convolution theorem, whereat numerical Fourier transformation and inverse transformation of discrete data was performed by using the commands implemented in MATLAB®. The obtained RTD were fitted to the CSTR in series model (equation 1) and the dispersion model (equation 2) using the method of least squares. The mean residence time τ was determined from the measured RTD. The mean flow velocity w for the dispersion model was calculated from τ and the tower length. Equation 2 was solved numerically using the *pdepe* solver in MATLAB®.

The particle size distribution q_0 [1/m] for each time step was obtained by the Palas measuring device. The characteristic diameters $d_{10,0}$ and $d_{90,0}$ were calculated from the total q_0 distribution. For three classes ($d < d_{10,0}$, $d_{10,0} < d < d_{90,0}$, $d > d_{90,0}$) the residence time distribution was calculated from the number of particles within a class at each time step.

3. Results and Discussion

3.1 Residence time distribution

With increasing nozzle pressure the measured particle RTD becomes more narrow, as shown in the exemplary curves in Fig. 2.

Centrifugal

Parallel

| $\Delta p = 1$ bar | $\Delta p = 2$ bar | $\Delta p = 3$ bar |
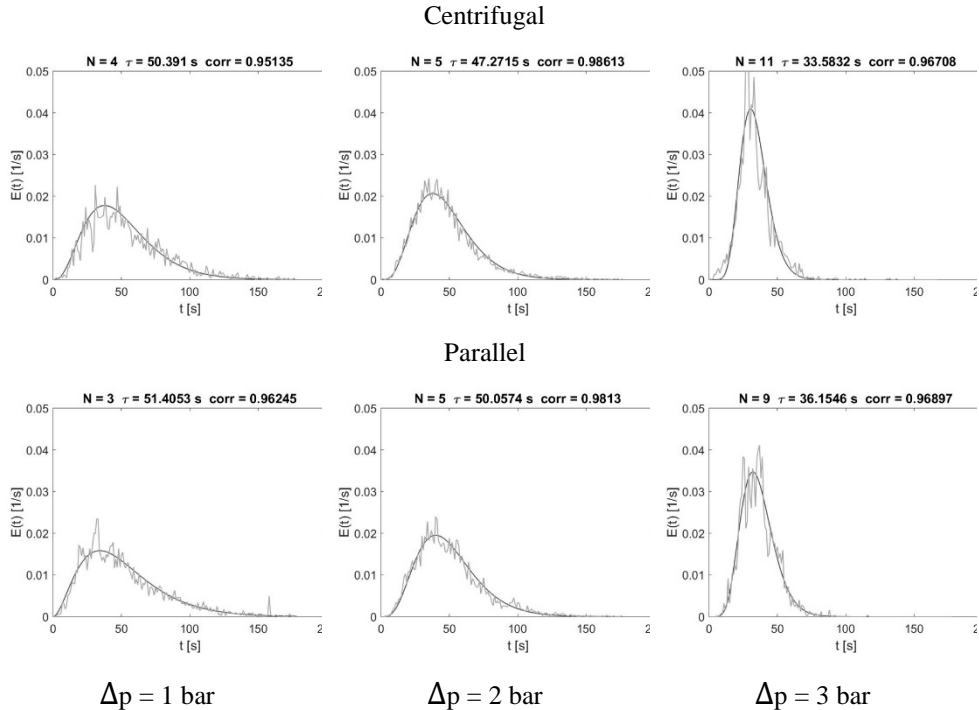
Fig. 2: Influence of nozzle pressure on RTD for centrifugal and parallel air distributor

In the CSTR in series model, this can be seen in an increasing N (For centrifugal: N = 4.5–4.4 – 10.8, for parallel 3.4 – 7.0 – 8.4). Furthermore there is a decrease in mean residence time τ with increasing nozzle pressure (For centrifugal: 47.67 s – 45.84 s – 35.58 s, for parallel 53.75 s – 44.48 s – 37.05 s). The latter effect can be seen for both air distributors, whereas no significant difference between the centrifugal (●) and the parallel air distributor (♦) can be observed. It was expected that the centrifugal air distributor would lead to an increase in mean residence time.
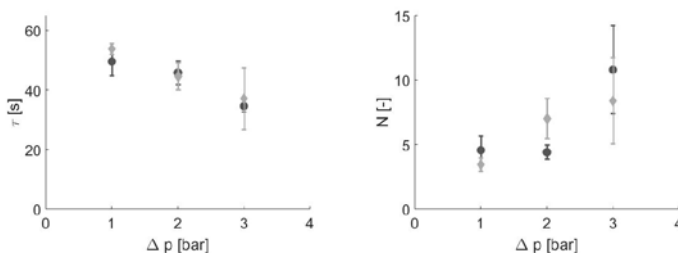
Fig. 3: Mean residence time τ (left) and number of ideal stirred tank reactors in series N (right) for centrifugal (●) and parallel (♦) air distributor at different nozzle pressures

The mean particle residence time is larger than the mean air residence time, which was calculated as 29 s at the given process conditions. The flow within a spray chamber can be described by different flow regimes with a fast main central gas jet and a slower flow close to the wall [9]. Due to an increasing nozzle pressure there is a higher acceleration of the feed by the pressurized gas and a decrease in spray cone angle. Therefore the amount of particles staying in the faster core jet is increased, which leads to the effects seen in Fig. 2 and Fig. 3. Modelling the flow pattern by using an only one- parametric model is possible, which indicates only little formation of different flow regimes at the tested process conditions.
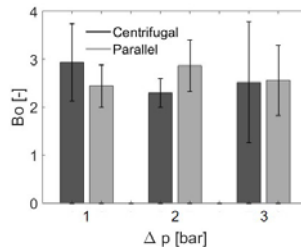
Fig. 4: Bodenstein number for centrifugal and parallel air distributor at different nozzle pressures

The Bodenstein number Bo shows no clear dependency of the nozzle pressure and the air distributor and is approximately constant. The value of the Bodenstein number of 2 - 4 is in accordance with literature data [10].

If the measuring system and injection signal are both constant, variations in the RTD are due to variations in the process, e.g. spontaneous formation of vortices. The RTDs, fitted to the CSTR in series model, are shown in Fig. 5 for all 9 trials at 1 bar nozzle pressure.
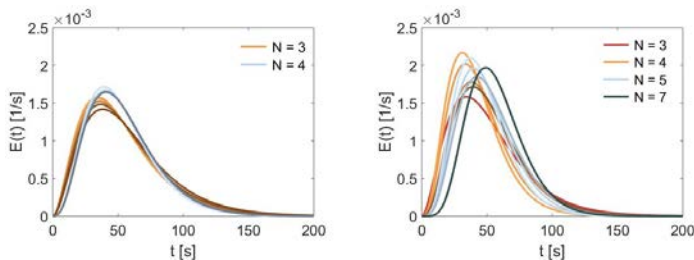
Fig. 5: Variations in RTD for parallel (left) and centrifugal (right) air distributor at 1 bar nozzle pressure.

The RTDs measured with the parallel air distributor can be modelled by using N = 3 and N = 4. The mean residence time τ is in the range of 51.4 s to 57.4 s. The RTDs measured with the centrifugal air distributor show a larger variance with a N of 3, 4, 5 and 7 and τ from 41.4 s to 57.1 s. The flow within the spray drying chamber caused by the centrifugal air distributor seems to be less stable and more susceptible to fluctuations as indicated by this larger variance.

3.2 Particle size dependent residence time distribution

In Fig. 6 the RTDs from Fig. 2 are shown for different size fractions.

Centrifugal

d$_{10,0}$ = 3.4 µm   d$_{90,0}$ = 8.1 µm   d$_{10,0}$ = 2.5 µm   d$_{90,0}$ = 7.0 µm   d$_{10,0}$ = 1.5 µm   d$_{90,0}$ = 3.9 µm

Parallel

d$_{10,0}$ = 2.5 µm   d$_{90,0}$ = 7.5 µm   d$_{10,0}$ = 1.5 µm   d$_{90,0}$ = 4.9 µm   d$_{10,0}$ = 1.4 µm   d$_{90,0}$ = 4.2 µm

Δp = 1 bar Δp = 2 bar Δp = 3 bar
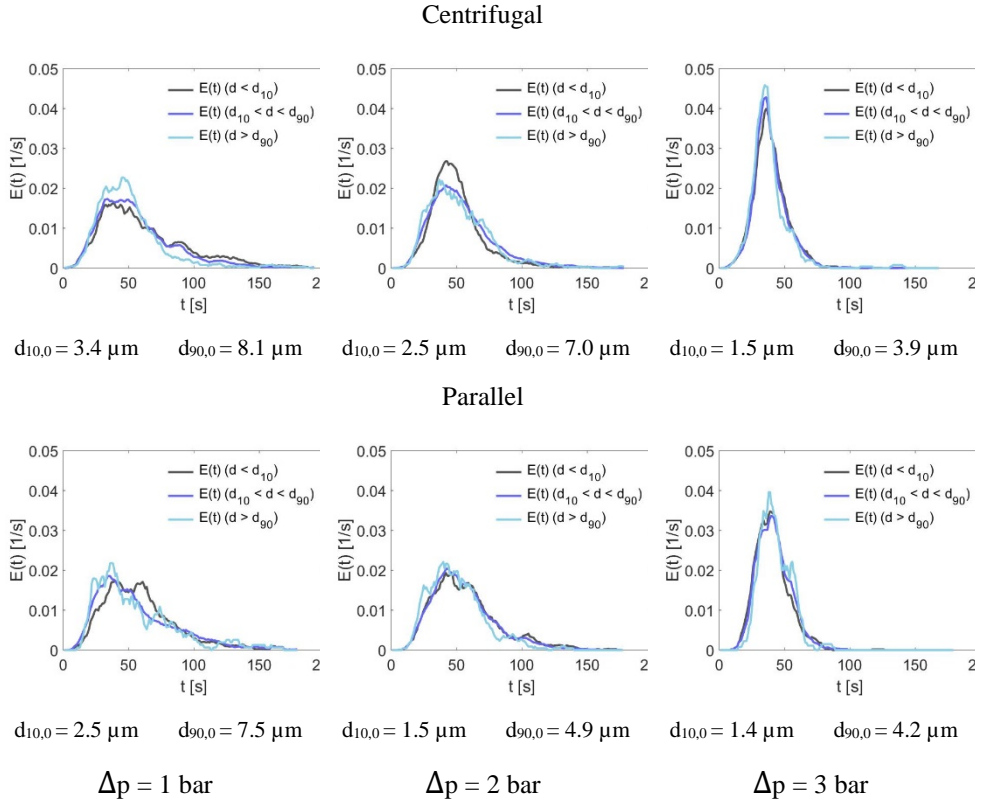
Fig. 6: Influence of nozzle pressure on RTD for different particle size fractions for centrifugal and parallel air distributor

The mean particle size decreases with increasing nozzle pressure due to the reduction of initial droplet size. No significant difference between the RTDs of the different size fractions can be observed. Thus, the effects of an increasing nozzle pressure on RTD (see Fig. 3) are not caused by the decreased particle size.

It was expected that different particle sizes will lead to different trajectories and therefore to different residence times [1]. As indicated by the small difference in between d$_{10,0}$ and d$_{90,0}$, the particle size distribution is narrow which might lead to no size fraction effects in the RTD being visible.

4.   Conclusions

The residence time distribution in a pilot plant spray dryer was characterised for different kinds of air distributors (centrifugal and parallel flow) as well as for different atomizing air pressures (1, 2 and 3 bar relative pressure). The measurement is based on a quasi-continuous acquisition of the particle concentration and size at the dryer outlet using a scattered light detector. The measured RTDs can be described by models with only one parameter, like the CSTR in series model, which indicates only little formation of different flow regimes at the tested process conditions.

An increasing nozzle pressure leads to a decrease in mean residence time and a more narrow distribution but the mean particle residence time is larger than the mean air residence time. The influence of nozzle pressure is more pronounced than of air distributor and particle size fraction.

In further studies the effect of a broader particle size distribution will be investigated.

5.   References

[1] Rähse, W.; Dicoi, O. Produktdesign disperser Stoffe: Industrielle Sprühtrocknung. *Chemie Ingenieur Technik* 2009, 81(6), 699–716.

[2] Kieviet, F.; Kerkhof, P.J. Measurements of Particle Residence Time Distributions in A Co-Current Spray Dryer. *Drying Technology* 1995, 13(5-7), 1241–1248.

[3] Bachmann, P.; Bück, A.; Tsotsas, E. Investigation of the residence time behavior of particulate products and correlation for the Bodenstein number in horizontal fluidized beds. *Powder Technology* 2016, 301, 1067–1076.

[4] Tylor, T. Powder and Air Residence Time Distributions in Countercurrent Spray Dryers. *Proceedings of 9th International Drying Symposium* 1994, Vol. A, 463–470.

[5] Jeantet, R.; Ducept, F.; Dolivet, A.; Méjean, S.; Schuck, P. Residence time distribution: A tool to improve spray-drying control. *Dairy Science and Technology* 2008, 88(1), 31–43.

[6] Levenspiel, O. Chemical reaction engineering, 2nd ed; Wiley: New York, 1972.

[7] Bachmann, P.; Tsotsas, E. Analysis of Residence Time Distribution Data in Horizontal Fluidized Beds. *Procedia Engineering* 2015, 102, 790–798.

[8] Kieviet, F.G. Modelling quality in spray drying, 1997.

[9] Blei, S.; Sommerfeld, M. CFD in Drying Technology- Spray-Dryer Simulation. In Modern Drying Technology: Comutational Tools at Different Scales; Tsotsas, E., Mujumbar, A.S., Eds.; Wiley, 2007; 155–204.

[10] Fitzer, E.; Fritz, W. Technische Chemie: Eine Einführung in die chemische Reaktionstechnik ; mit 36 Tabellen und 31 Rechenbeispielen, 2nd ed; Springer: Berlin, 1982.

Application of microwaves in the convective drying of ceramic

Rajewska, K. ; Pawłowski, A.

Institute of Technology and Chemical Engineering, Poznań University of Technology,
ul. Berdychowo 4, 60-965 Poznań, Poland

*E-mail of the corresponding author: kinga.rajewska@put.poznan.pl

Abstract

The paper demonstrates microwave and convective drying processes in different combinations of kaolin cylindrical samples in laboratory scale. Analysis of the kinetics and sample temperature evolution show that the moment of application and electromagnetic field duration have the biggest influence on characteristics of the drying curve and quality of dried material. Dried samples were subjected to strength tests using the Brazilian method in order to determine the relation between its quality and different drying programs.

Keywords: ceramic, convective drying, microwave drying, strength test.

1. Introduction

The use of microwave technology in industrial chemical processing has been developed since the 1970s. This is related to the general tendency to reduce production costs and care for the environment. One of the industrial processes using microwaves as a source of heat is drying. Microwave energy, alone or in combination with conventional energy sources (hybrid methods) enables precise control of the drying process in order to achieve higher efficiency and better product quality in the shortest possible time. In conventional drying, heat is transported to the surface of the material by conduction, convection or radiation and into the material through heat conduction. Moisture is initially evaporated from the surface, and the remaining water diffuses to the surface. This is often a slow process and the diffusion rate is limited. Process time is determined by the heat flow rate in the material from the surface, which depends on its specific heat, thermal conductivity, density and viscosity. Microwaves as a form of thermal energy, manifest themselves through their interaction with materials. The electromagnetic field initially interacts with the outer layers of the material. The inner part of the material is heated when the heat moves from the outer layers to the inside. Most of the moisture evaporates before leaving the material. If the material is very wet and the pressure inside is rapidly increasing, the fluid will be removed from the material due to the pressure difference. This creates a kind of pumping action that ejects the liquid to the surface, often in the form of steam. This results in very fast drying without the need to overheat the atmosphere and emit greenhouse gases from the heat source. The energy is transferred by the material to the electromagnetic way, not as a heat flux. Therefore, the heating rate is not limited, and the uniformity of heat distribution is significantly improved.

In general terms, according to literature data, the group of materials processed using microwave energy includes: food, plants, textiles, wood, soils and other biological materials [n1]. Among the works concerning the use of microwaves in drying, one can find a group of publications regarding the use of dielectric heating in industrial processes [n2, n3, n4]. Another group of publications are purely experimental works concerning both kinetics and material quality [n5, n6]. The next set of works are articles binding theoretical modeling of the drying process with experiments [n7, n8, n9, n10]. In the works that take into account the issue of the quality of the dried material, the emphasis is mainly on the effect of reducing the mechanical properties. The papers [n11, n3, n5] mainly concern the theoretical analysis of volumetric, intermittent drying, which is to reduce the gradients of moisture distribution, and hence the smaller deformations of the dried products. The theoretical part concerns analysis of stresses generated during drying. In turn theoretical work [n12] contains a very detailed and advanced model of the dielectric drying process.

The presented work concerns the investigation of the influence of microwaves on drying kinetics and mechanical strength of kaolin after drying, as the estimation of the quality of microwave dried products only by surface examination may not be sufficient

2. Materials and Methods

The material used in the research was ceramic kaolin. A slurry was prepared with a moisture content of 0.4 kg/kg$_{db}$. Then a sample was formed with cylindrical geometry (diameter - 60 mm, height - 60 mm). In the dryer it is possible to control the speed and temperature of the air entering the chamber and the microwave power. Temperature measurements were made using optical fibers in two places: in the axis, half the height of the cylinder (T_{in}) and at a distance of 0.5 cm from the upper surface of the cylinder (T_{out}).The strategy of combining the above-mentioned drying methods used in this work was partly based on Schiffmann's proposal [n13].

As part of the work, seven different drying programs were carried out. The speed and temperature of the air entering the drying chamber were changed, as well as the stage in which the microwave energy process was supported (Table 1). The criterion of the end of the process was to obtain a sample moisture of 0.06 kg/kg$_{db}$. Regardless of the drying strategy, the critical moisture content corresponding to the theoretical boundary between the constant and decreasing drying rate, was on average 0.23 kg/kg$_{db}$. Additionally, the mechanical strength of the samples was analyzed using the Brazilian method.

Table 1. Process data

	v [m/s]	T [°C]	application of MW – 100 W
Exp.1	3	80	-
Exp.2	3	80	the whole process
Exp.3	3	80	constant rate period
Exp.4	3	80	falling rate period
Exp.5	3	26	the whole process
Exp.6	3	26	constant rate period
Exp.7	2	26	the whole process

1.1. Results and discussion

As a graphical presentation of the process, the drying curves, the drying rate and the temperature of the material were presented, because these parameters show sufficiently the kinetics of the process. The first was to perform convection drying without microwave energy support (Fig. 1).
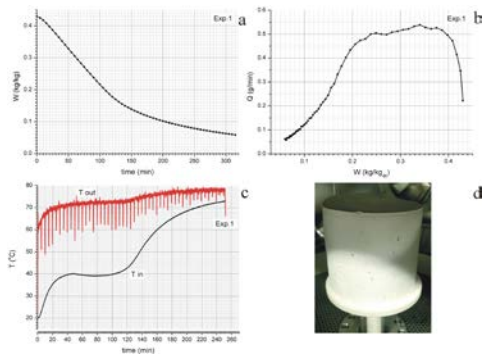
Fig. 1 Experiment 1.
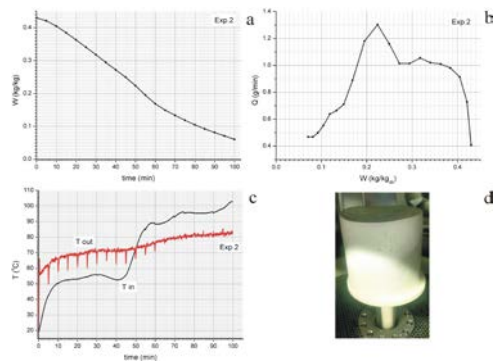
Fig. 2 Experiment 2.
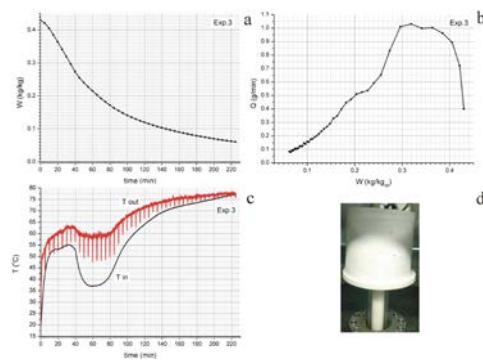
Fig. 3 Experiment 3.
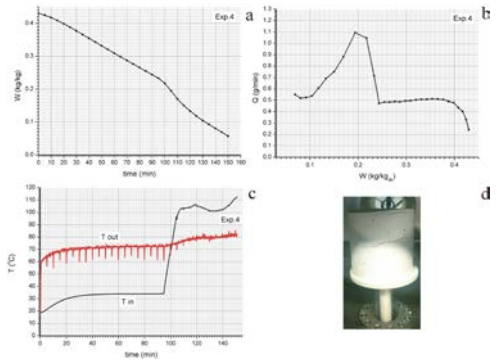
Fig. 4 Experiment 4.
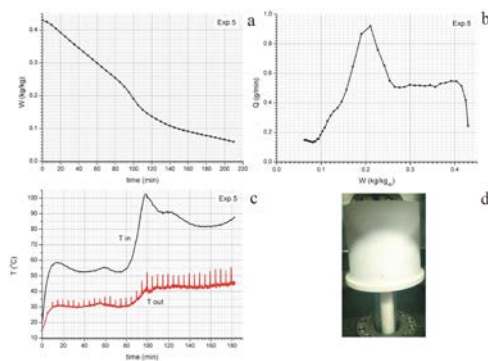
Fig. 5 Experiment 5.
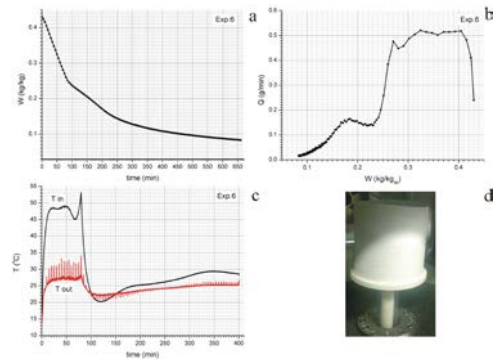
Fig. 6 Experiment 6.

The heating period is clearly visible, a period of constant drying rate at which the material temperature and the drying rate are constant and amount to 0.5 g/min. Then the process enters the second phase, the drying rate decreases and the temperature of the material increases. The final drying criterion is reached after five hours, the material temperature reaches 73°C. In the sample photograph taken after the end of the process (Fig. 1d), a surface crack running circumferentially about 0.5 cm under the edge of the upper surface of the cylinder can be seen. Fig. 2 illustrates the course of the process with continuous exposure of the material to the microwaves. The total drying time is three times shorter and the drying speed in the first phase is twice as high as in Exp. 1. Also, the temperature of the material being subjected to microwave treatment is higher and amounts to 52°C during a constant drying rate. At the end of this phase, the drying rate increases rapidly, and after reaching critical moisture content, it decreases to the end of the process. The material temperature reaches 103ºC. Small circumferential cracks can be seen on the side of the sample. A further drying strategy is shown in Fig. 3. Microwave energy enhances convective drying during heating and constant drying rates. After turning off the microwave generator, the drying rate and material temperature decreases accordingly, however, because the average moisture content in the material has not yet reached the critical value, the phase of the constant drying rate is continued, but under conditions with Exp. 1. At the end of the process, the material temperature reaches about 77ºC. In the upper part of the cylinder, a distinctive characteristic circumferential crack was again created without a net of smaller cracks.

In Experiment 4, microwaves were used during the decreasing drying rate of the period (Fig.4). Initially, the drying rate was 0.5 g/min (according to data from Exp.1), after turning on the microwave generator the drying rate increased sharply with the increase of the material temperature. Then, with the decrease of the moisture content, the drying rate decreased and the material temperature reached 120 ºC at the end of the process. The dried sample according to this strategy has been destroyed. In addition to the crack located circumferentially in the upper part, a deep circumferential fracture in the middle of the heights dividing the sample into two parts appeared.

The next three processes were carried out with the heater turned off. In Exp. 5 (Fig.5), the

energy of the electromagnetic field enhances the entire process. The total drying time increased in relation to a similar process, but with the heater turned on (Exp.2). The material temperature during the constant drying rate was 55 °C. As in the case of Experiment 2, the mass flux doubled in the final stage of the constant drying rate and then the temperature of the material reached a maximum value of 102 °C. The dried sample was free of any defects visible to the naked eye.

In Experiment 6 (Fig.6), the microwaves were turned on during the heating period and the

constant drying rate. The drying rate was maintained at 0.5 g/min. After switching off the microwaves, it decreased to 0.15 g/min and was maintained until critical humidity was reached and then decreased. The temperature of the material was maintained at about 50 °C in the first drying period, then it dropped after switching off the microwaves to the temperature of the drying medium, i.e. around 25 °C. The sample, similarly to the previous process, has no scratches or cracks potentially weakening the material.

In the last process the air velocity was reduced from 3 m/s to 2 m/s. Reducing the speed of the drying medium caused the temperature of the wet thermometer to increase by 5 °C compared to a similar process with higher airflow (Exp. 5). However, the remaining process parameters such as the total drying time and the mass flux rate remained unchanged. A few small scratches are visible on the surface of the dried sample.

Analyzing the temperature curves of the dried sample (Fig. 1c-6c), some characteristic steps can be observed. They illustrate how to use the energy delivered to the material by convection, with microwaves or in combination. During the heating period, the temperature of the material and water contained in it increases (sensible heat). At the same time, in the final phase of the heating period volatile substances start to evaporate (latent heat). The start of the evaporation process therefore slows down the temperature increase. Next comes the equilibrium stage - constant temperature of the material. Latent heat of evaporation absorbs most of the energy. The process is in the constant phase of the drying rate. The next stage of the temperature rise occurs due to evaporation of most volatile components. Sensible heat absorbs most of the energy supplied. A phase of decreasing drying rate follows. The drying process from the point of view of mass transport is best illustrated by the drying rate curves (Fig. 1b-6b). In strategies with continuous microwave assist (Exp. 2, 5, 7), a sudden increase in mass flux was noted at the final stage of the constant drying rate period when the evaporation surface moves back into the material. The temperature and pressure in the pores increase, which results in a temporary acceleration of the rate of moisture removal from the deeper layers of the material. This effect is not observed in a conventional process. After a sudden increase, the temperature stabilizes and the process enters the final stage of decreasing speed. Then the water remains are removed from the deeper layers of the material. The moisture diffusion path in the pores lengthens and the capillary processes play a greater role in mass transport.

In the visual assessment of the dried samples, a characteristic circumferential crack is always observed near the upper surface of the cylinder in the case of drying with hot air. This is the result of the greatest drying stresses occurring there. The destructive power determined in the Brazilian test is also lower in these processes: 350 N (Exp.1), 280 N (Exp. 2), 320 N (Exp. 3), than in processes without convection heating: 530 N (Exp 5) and 450 N (Exp 7).

2. Conclusions

The use of microwaves during drying results in undoubtedly shortening the drying time, but also an increase in temperature, which is not always beneficial. The application of microwave energy in the phase of decreasing drying rate (one of Schiffmann's proposals) does not work in the case of brittle materials with the geometry used in this work.

The drying strategies used in this work have a significant impact on both the drying time and the final quality of the product.It turns out that the best strategy due to the drying time and the quality of the material is the use of microwave support throughout the process, but without convection heating. The drying time has been shortened and the quality improved compared to conventional drying. These tests do not provide enough information when and how long to turn on microwaves to achieve optimal results. They only indicate that it is possible to shorten the process time and even improve the quality of the material.

3. Nomenclature

T	temperature	°C
W	moisture content	$kgkg_{db}^{-1}$
Q	drying rate	$gmin^{-1}$

Subscripts

in	inside
out	outside
db	dry body

4. References

[1] Mujumdar, A.S. ed., Handbook of industrial drying, fourth edition, Taylor & Francis Group, 2015.

[2] Tinga, W.R.; Nelson, S.O. Dielectric properties of materials for microwave processing – tabulated, Journal of Microwave Power 1973, 8(1), 23-65.

[3] Schiffmann, R.F. Microwave and Dielectric Drying in A.S. Mujumdar (Ed.): Handbook of Industrial Drying, Marcel Dekker, New York, USA, 1987.

[4] Metaxas, A.C. Microwave heating, Power Engineering Journal, 1991.

[5] Itaya, Y.; Uchiyama, S.; Hatano, S.; Mori, S. Drying enhancement of clay slab by microwave heating. In proceedings of IDS, Brazylia, 2004.

[6] Lei, L.Y.; Zhang, Y.L.; Peng, J.; Li, C. Microwave dryling characteristics and kinetics of ilmenite. Transactions Nonferrous Metals Society of China 2011, 21, 202-207.

[7] Wei, Ch.K.; Davis, H.T.; Davis, E.A.; Gordon, J. Heat and mass transfer in water-laden sandstone: microwave heating. AICHE Journal 1985, 31(5), 842-848.

[8] Zielonka, P.; Gierlik, E.; Matejak, M.; Dolowy, K. The comparison of experimental and theoretical temperature distribution during microwave wood heating. Holtz als Roh- and Werkstoff 1997, 55, 395-398.

[9] Ratanadecho, P.; Aoki, K.; Akahoriu, M. Experimental and numerical study of microwave drying in unsaturated porous material. Int. Comm. Heat Mass Transfer 2001, 28(5), 605-616.

[10] Ratanadecho, P.; Aoki, K.; Akahoriu, M. Influence of irradiation time, particle sizes and initial moisture content during microwave drying of multi-layered capillary porous materials. J. Heat Transfer 2002, 124(2), 1-11.

[11] Zhang, D.; Mujumdar, A.S. Deformation and stress analysis of porous capillary bodies during intermittent volumetric thermal drying. Drying Technology 1992, 10(2), 421-443.

[12] Rajagopal, K.R.; Tao, L. Modeling of the microwave drying process of aqueous dielectrics. Z. Angew. Math. Phys. 2002, 53, 923-948.

[13] Schiffmann, R.F. Microwave and dielectric drying. In A.S. Mujumdar (Ed.), Handbook of Industrial drying-1, New York: Marcel Dekker Inc. 1995, 345-372.

Drying of algae by various drying methods

Bheda, B.ª; Shinde, M.ᵇ; Ghadge, R.ᵇ; Thorat, B N.ª*

[a] Advanced Drying Laboratory, Department of Chemical Engineering, Institute of Chemical Technology (formerly UDCT), Mumbai, India

[b] Reliance Industries Limited, India

*E-mail of the corresponding author: bn.thorat@ictmumbai.edu.in

Abstract

Algae drying was carried out using Vacuum Tray Dryer and an Innovative Solar Conduction Dryer. Algae was dried in a Vacuum Tray Dryer at 60°C under varied pressure conditions and makes use of specially designed double condenser system. The open sun drying and solar conduction dryer (SCD) was also used for algae drying. Comparison between open sun drying and solar conduction dryer were done and it was found that the solar conduction dryer gives high performance than the open sun drying. It was also found that, the conductive heat transfer mode plays a crucial role in the solar conduction dryer.

Keywords: Vaccum Dryer; Solar Conduction Dryer; Algal Drying.

1. Introduction

Algae is a potential source of high-value products such as pigments, nutraceuticals, and protein-rich biomass as food supplements. Microalgae have the following advantages over terrestrial plants:

1. Microalgae has less growth in fresh water than saline or contaminated water.

2. Microalgae has less competition with food for arable lands but can be cultured in seas or in ponds or barrain lands [1].

3. Microalgae can grow faster and also accumulate oil more efficiently than higher plants and oilseed crops [2,3].

4. Microalgae can also produce valuable raw materials which are its coproducts (e.g., proteins, pigments, unsaturated fatty acids, carotenoids, and vitamin) [4], used in the animal feed, food, cosmetics, and pharmaceutical industries.

5. Microalgae can convert CO_2 into biomass with a high efficiency of CO_2 utilization [5,6]. In general, 1.83 kg CO2 consumed gives 1kg of dry biomass of CO_2.[3]

Production of these high-value products from algae requires dry algal biomass with moisture less than 10 % [7]. Drying of algae is also essential for storage since harvested algae slurry is perishable and can spoil within a short time. However, microalgae in cultivated medium has low biomass concentration (0.1-1% w/w) and mechanical dewatering of algae in the cultivated medium can produce algae slurry having 20-30% w/w algal biomass [8,9].

In this paper we shall be going through the various drying methods that have been attempted and the drying kinetics comparison study being carried out.

2. Materials and Methods

The harvested and dewatered algal biomass was obtained from Reliance Industries Limited. The centrifuged algae was collected in a can and transported to Institute of Chemical Technology, Mumbai, India and stored in the refrigerator at 4°C until the drying experiments to prevent putrefaction. Before experiments, the slurry was brought back to ambient conditions. Trials were conducted in a Teflon coated plate of dimensions 21 cm x 27 cm x 5 cm. Trials conducted in Vacuum Tray Dryer and Solar Conduction Dryer.

2.1. Vacuum Tray Dryer

It is a conventional vacuum tray dryer manufactured by Salvis Lab, which originally had a single condenser for condensing the vapours generated in the dryer. The operating temperature was 60°C, hence the single condenser was inefficient in condensing and therefore a second condenser was added to it. The condensers were attached to a chiller whose temperature was maintained at 4°C. The condenser was attached to a measuring cylinder, where the volume collected is measured. A flask containing silica gel was placed between the vacuum pump and cylinder, which acted a water trap, to prevent the uncondensed water from entering into the vacuum pump. The sample was dried over a pressure range of 30-50 mbar.

The samples were weighed and taken in the Teflon coated plate and kept for drying. The tray dryer and chiller were first allowed to attain the desired temperature of 60°C and 4°C respectively. The sample was then loaded to the dryer and a vacuum pressure applied. The water collected in the measuring cylinder was noted at a regular interval of 10 minutes. However, the rate of drying drastically reduces after 8 hours, and the water collected in the measuring cylinder barely increases by a milliliter even after 30 minutes.

2.2. Solar Conduction Dryer

An innovative Solar Conduction Dryer (WO2014097307A1) [10] was used for drying the sample. "The dryer comprises a radiation absorbing heat conducting surface, and a convection channel formed by a radiation controlling cover over the conducting surface" [10]. The solar drying experiment took place in Mumbai (19.0239° N, 72.8575° E), India. The sample was loaded in a Teflon coated plate, weighed and kept inside the dryer, whose loss in weight was measured at a regular interval of 30 minutes. The other parameters that were measured and noted included the surface temperature of algae, surface temperature of the conduction plate and the atmospheric temperature using an infrared thermometer gun. Experiments were carried out between 09:00 hours and 16:00 hours on sunny days in the month of December 2017. At the end of the day (16:00 hours), the partially dried sample was covered with an aluminum foil and kept inside a drawer, for continuing the drying study the subsequent days. The drying experiment was continued till no change in weight was observed.

3. Mathematical Models

3.1. Thin-layer Drying Model

The thin-layer model is usually represented by the equation in terms of drying parameters to characterize the changes of the mean moisture content of food product during drying.

The parameters that account for the combined effect of various transport phenomena in the drying process can be determined from the graphical method [11-12]. It can be expressed as:

$$\phi = k_0 \exp(-kt) \tag{1}$$

where k_0 and k represent the lag factor and drying constant of food product, respectively. The moisture diffusion coefficient, D_{eff} can be obtained from the following expression:

$$D_{eff} = k \frac{L_d^2}{\mu_1^2} \tag{2}$$

Where L_d is the moisture diffusion path and μ_1 is the characteristic parameter which can be obtained from the equation:

$$\mu_1^2 = \left(\mu_1\right)_\infty^2 \frac{1}{1+\dfrac{A_1}{Bi_m^{\ p}}} \tag{3}$$

where Bi_m represents the Biot number for mass transfer. The $(\mu_1)_\infty$ is the value of μ_1 at $Bi_m = \infty$. The values of the constants $(\mu_1)_\infty = 1.5708$; $A_1 = 2.24$; $p = 1.02$, considering the algae to be a slice inside the plate. The Biot number can be obtained in terms of lag factor, k_0 of drying characteristic curve using following relation [13]:

$$Bi_m = \frac{5.132 \ln k_0}{1 - 3.948 \ln k_0} \tag{4}$$

Knowing the value of D_{eff}, the convective mass transfer coefficient, h_m can be calculated from the standard relation

$$h_m = Bi_m \frac{D_{eff}}{L_d} \tag{5}$$

The characteristic parameters μ_1 and Biot number Bi_m computed from respective Eqs. (3) and (4) are used in D_{eff} and h_m estimation.

4.   Results and Discussion

Figure 1 shows the dimensionless moisture content against drying time for the repeated experiments under a varied vacuum pressure of 30 millibar and 50 millibar in the vacuum tray dryer having an initial weight of 200 gm at 60 °C.
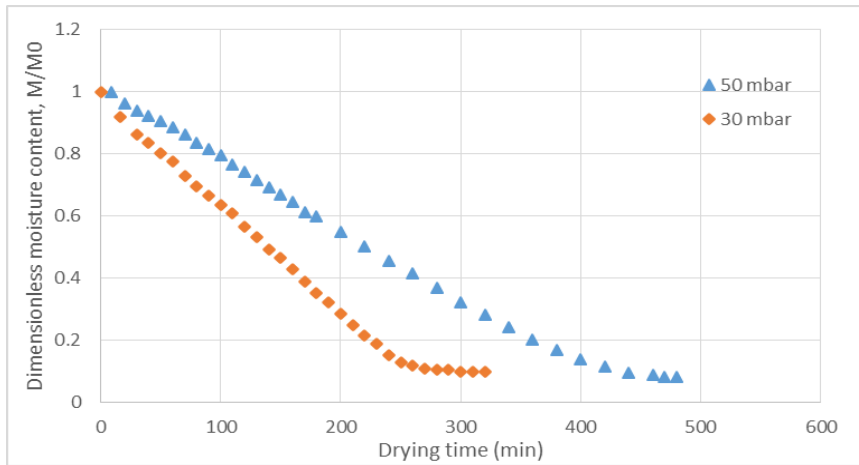
Figure 1. Variation in drying time with the change in vacuum applied

Table 1. Results of mass transfer co-efficients (D_{eff} and h_m) & Biot number (Bi_m) for the 30 mbar and 50 mbar pressure.

	30 mbar	50 mbar
Biot Number	1.435×10^{-4}	8.951×10^{-5}
D_{eff} (m²/s)	9.451×10^{-8}	8.043×10^{-8}
h_m (m/s)	2.296×10^{-4}	1.074×10^{-4}

As it can be seen that by reducing the vacuum pressure from 50 millibar to 30 millibar, the drying time reduces and hence there is an increase in the drying rate. This fact is quantitatively reflected in the values obtained in Table 1.

Figure 2 shows the dimensionless moisture content against drying time for the open sun and solar conduction dryer for 200 gm algae slurry. As expected, solar conduction dryer gives higher performance than the solar conduction dryer. Solar conduction dryer takes less time than the open sun drying to achieve the required moisture content. Effective diffusivity (D_{eff}), mass transfer coefficient (h_m) and mass transfer Biot number (Bi_m) values are depicted in Table 2. These values suggests that the solar conduction dryer gives higher performance than the open sun drying.
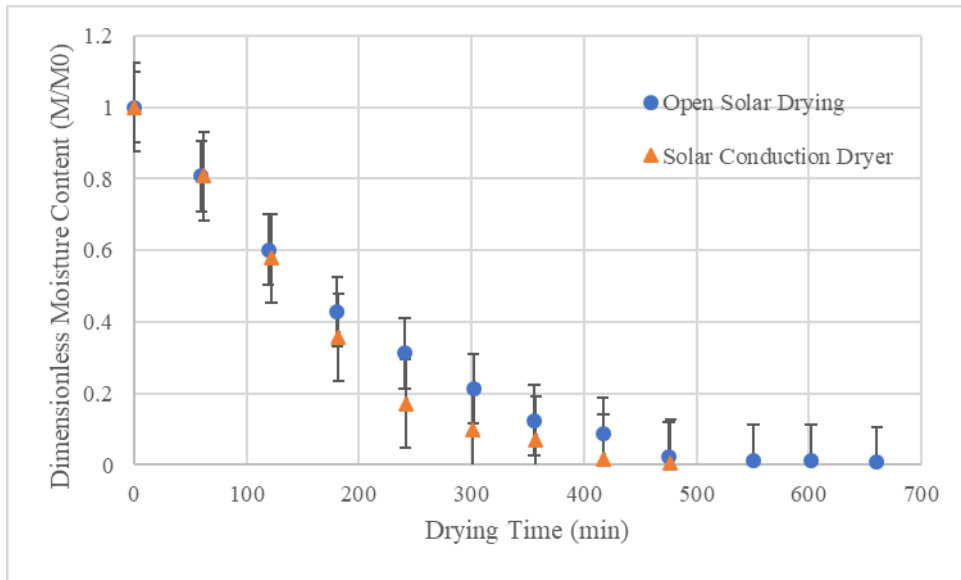
Figure 2. Comparison between the performance between open sun drying and solar conduction dryer for algae drying

Table 2. Results of mass transfer co-efficients (D_{eff} and h_m) & Biot number (Bi_m) for open sun drying and Solar Conduction Drying.

	Solar Conduction Dryer	**Open sun drying**
Biot Number	5.517×10^{-5}	6.56×10^{-5}
D_{eff} (m²/s)	1.355×10^{-7}	1.24×10^{-7}
h_m (m/s)	8.826×10^{-5}	8.04×10^{-5}

5. Conclusions

Algae drying was done by using various methods such as vacuum, open sun drying and solar conduction dryer. Vacuum drying suggests that, by reducing the pressure there was reduction in the drying time. At low pressure, the value of effective diffusivity and mass transfer coefficient were higher. Comparison between open sun drying and solar conduction dryer was done. It was found that, the performance for solar conduction dryer was higher than the open sun drying. The performance was checked on the basisi of effective diffusivity and mass transfer coefficient. Comparison between the solar conduction dryer and vaccum dryer suggests that the time required for Solar Conduction Drying is longer than Vacuum Tray Drying, however the operation cost for Solar Conduction Drying is negligible.

6. References

[1] Rubin, E. S.; Mantripragada, H.; Marks, A.; Versteeg, P.; Kitchin, J.; The outlook for improved carbon capture technology, Progress in Energy and Combustion Science, 38(5), 630–671 (2012).

[2] Spolaore, P.; Joannis-Cassan, C.; Duran, E.; Isambert, A.; Commercial applications of microalgae, Journal of Bioscience and Bioengineering, 101(2), 87–96 (2006).

[3] Yusuf, C.; Biodiesel from microalgae, Biotechnology Advances, 25(3), 294–306 (2007).

[4] Scott, S. A.; Davey, M. P.; Dennis, J. S; Horst, I.; Lea-Smith, D. J.; Smith, A. G.; Biodiesel from algae: Challenges and prospects, Current Opinion in Biotechnology. 21(3), 277–286 (2010).

[5] Shelef, G.; Sukenik, A.; Green, M. Microalgae harvesting and processing: a literature review, (0), (1984).

[6] Khan, S. A.; Rashmi.; Hussain, M. Z.; Prasad, S.; Banerjee, U. S.; Prospects of biodiesel production from microalgae in India, Renewable and Sustainable Energy Reviews, 13(9), 2361–2372 (2009).

[7] Brennan, L.; Owende, P.; Biofuels from microalgae—A review of technologies for production, processing, and extractions of biofuels and co-products. Renewable and Sustainable Energy Reviews 14, 557-577 (2010)

[8] Hannon, M.; Gimpel, J.; Tran, M.; Rasala, B.; Mayfield, S.; Biofuels from algae: challenges and potential, Biofuels, 1(5), 763–784 (2010).

[9] Bhujade, R.; Chidambaram, M.; Kumar, A.; Sapre, A; Algae to Economically Viable Low-Carbon-Footprint Oil, Annual Review of Chemical and Biomolecular Engineering, 8(1), 335–357 (2017).

[10] Michael, H.; Javier, G.; Miller, T.; Beth, R.; Stephen, M.; Biofuels from algae: challenges and potential. Biofuels 1(5), 763–784 (2010).

[11] Tidke, V.; Thorat, B.N.; Kokate, S.; Solar Dryer, WO2014097307A1, (2012).

[12] Dincer, I.; Dost, S; A modelling study for moisture diffusivities and moisture transfer coefficients in drying of solid objects. International journal of energy research 20, 531-539 (1996).

[13] Tripathy, P.P.; Kumar, S; A methodology for determination of temperature dependent mass transfer coefficients from drying kinetics: Application to solar drying. Journal of Food Engineering 90, 212-218 (2009).

[14] Pflug, L.J; Blaisdell, J. L; Methods of analysis of precooling data. ASHRAE journal 5, 33-40 (1963).

The influence of ethanol on the convective drying and on the nutritional quality of dekopon slices

Mello-Junior, R. E.[a*]; Resende, N. S.[a]; Corrêa, J. L. G.[a]; Pio, L. A. S.[b]; Carvalho, E. E. N.[a]

[a] Department of Food Science. Federal University of Lavras, Minas Gerais, Brazil.
[b] Department of Agricultural. Federal University of Lavras, Minas Gerais, Brazil.
*E-mail of the corresponding author: ronaldo_uba@hotmail.com

Abstract

Dekopon or Hallabong (Citrus reticulate "Shiranui") is a hybrid fruit that belongs to the citrus fruits. The scientific and commercial interests in dekopon is due to its nutritional composition. The objective of the study was to verify the influence of ethanol as a pretreatment in reducing drying time as well as maintaining nutritional quality (vitamin C, total phenolic compounds, and antioxidant activity) of dekopon slices. The drying with ethanol at 70 °C promoted the greatest reduction in drying time, but the processed pretreated samples at 50 °C presented the highest level of nutritional quality parameters.

Keywords: drying time; vitamin C; phenolic compounds; antioxidant activity.

1. Introduction

The vitamin C, consisting of ascorbic and dehydroascorbic acid, is widely found in fruits and foods, being characterized by its instability to technological processes [1, 2]. There are also other health-promoting substances, such as phenolic compounds, which are secondary metabolism in plants that have been identified as major antioxidants in fruits [3]. Those compounds are present in the fresh form of fruits and vegetables, especially in citrus fruits. Dekopon (*Citrus reticulata* "Shinarui") is among the citrus fruits. It is a cross between Kiyomi (*Citrus uses Marcov*. x *Citrus sinensis Osbeck*) and Ponkan (*Citrus reticulata Blanco*). The commercial value of dekopon is due to its sweet taste and pleasant aroma [4, 5].

Generally, fruits and vegetables in their fresh form show high moisture content and water activity, providing high degradation rates which may cause significant postharvest losses. To minimize these effects, various processing techniques can be used, as drying. Convective drying is a simple but time consumer process with consequent high energy demand. High temperatures reduce the drying time, but could carry out to food quality and nutritional composition reduction [6]. In order to minimize the negative effects of drying, some pretreatments such as ultrasound [7], osmotic dehydration [8] and ethanol application in the environment and on the surface of the samples are commonly used [9, 10].

The aims of this work were to (i) investigate the effects of the immersion of the samples in ethanol on drying time, (ii) examine the influence of ethanol and drying temperature on phenolic compounds content, vitamin C and antioxidant activity.

2. Materials and Methods

2.1. Sample preparation

Dekopon (*Citrus reticulata "Shinarui"*) were selected based on uniform maturation characteristic with peel color. The fruits were washed and sanitized with sodium hypochlorite solution [11] and stored at 7 °C (±2 °C) until the beginning of each experiment. The moisture content of the fresh dekopon (method 934.06, AOAC (2005)) was 5.92±0.01 kg H_2O kg^{-1} d.b.

For the experiments, the samples were peeled manually, eliminating the edges of the fruit. Samples were sliced with the aid of a stainless steel knife and a cutter so as to standardize the size of the slices. After cutting, the dekopon slices presented standardized dimensions 3.27±0.32 mm x 60.54±1.12 mm (thickness x diameter) and were measured using a digital caliper (Western, DC-60 model, Zhejiang, China).

2.2. Convective drying

The convective drying was performed in a tunnel dryer (Eco Engenharia Educacional, MD018 model, Brazil) The mass variation of samples during the drying was monitored using a digital balance (Marte Científica, AD33000 model, Brazil) (accuracy± 0.01 g) coupled to the sample holder allowing to obtain the kinetics of drying. In each experiment, 145.113±5.862 g of fresh fruits (totaling five slices) were dried. The process was performed until an average final moisture content of 0.235±0.054 kg H_2O kg^{-1} d.b.

The drying process followed a 2x2 factorial design to study the effects of air temperature variation (50 and 70 °C) [11] and the immersion or not of the samples in ethanol, as a pretreatment. Air velocity was keep at 2.00 m s^{-1} [12]. Pretreatment samples were completely immersed in 95% ethanol in a petri dish for 10 s [13] in a ratio sample/ethanol of 1:1 (weight/weight) approximately. The moisture content of the dried dekopon was determined according to the AOAC (2005). The water activity (a_w) determination was performed in a hygrometer (Aqualab, 3-TE model, Decagon Devices, Inc., Pullman, WA, USA).

2.3. Quality analysis

The total phenolic compounds were quantified using an adaptation of the method of Folin-Ciocalteau. Quantification was performed by spectrophotometer reading at 750 nm and the results expressed in mg of gallic acid.100 g^{-1} dry matter [14].

The ascorbic acid (vitamin C) determination was performed by the colorimetric method, 2,4 dinitrofenilhidrazina [15] and the results expressed as % retention of ascorbic acid in the dry product, according to Eq. 1

$$\% \, retetntion = \left(\frac{\text{g ascorbic ácid in the dehydrated sample}}{\text{g ascorbic ácid in the fresh sample}} \right) * 100 \tag{1}$$

The total antioxidant activity (AAT) by DPPH (2,2-diphenyl-1-picrylhydrazyl) [16]. The results are expressed as % sequestration. The percentage of sequestration expresses the ability of the food to inhibit the action of the reactive species present in the DPPH radical.

2.4. Statistical analysis

All analytical determinations were performed in triplicate. Parameter values are expressed as the means±standard deviation. The results were analyzed using analysis of variance

(ANOVA) and the Tukey test at 5% significance to compare the mean values using Statistic (Statsoft, Tulsa, USA).

3. Materials and Methods

3.1. Convective drying

The Fig. 1 shows the evolution of drying of dekopon slices treated and unpretreated with ethanol, at 50 and 70 °C. The drying time for the pretreated fruits to reach a final moisture content of 0.235 ± 0.051 kg H_2O kg^{-1} d.b was 300.33 ± 0.95 and 1193.33 ± 0.64 min for 70 and 50 °C respectively. For the untreated samples the total drying time was 343.33 ± 0.91 and 1540.00 ± 0.83 min for 70 and 50 °C respectively.
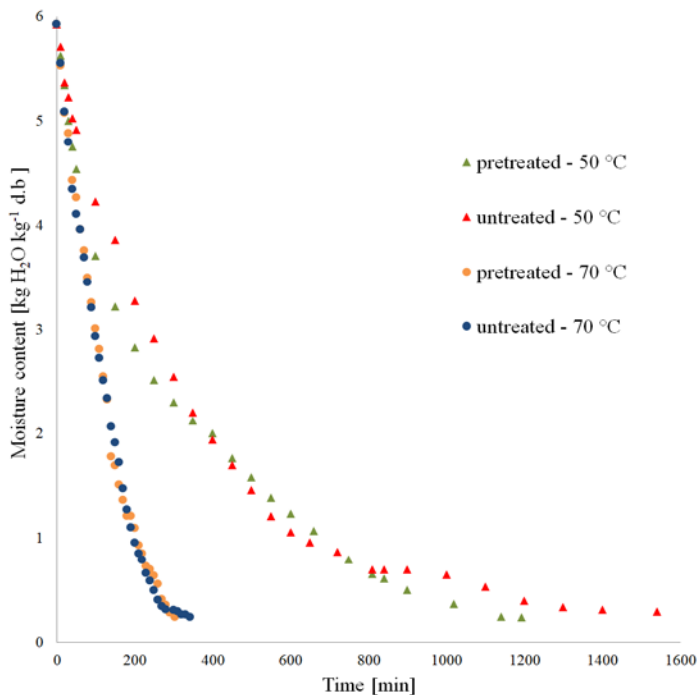
Fig. 1 Evolution of moisture content of treated ethanol immersion and untreated dekopon at 50 e 70 °C.

The experiments at 70 °C with pretreatment and without pretreatment did not obtain a significant difference between them ($p>0.05$), presenting times of 303.33 ± 2.49^{a} min and

343.33±2.65ª min, respectively. However, these experiments differed statistically from the others ($p<0.05$), in addition, the experiments at 50 °C with pretreatment and without pretreatment showed a statistical difference between them ($p<0.05$), reaching a final processing time of 1193.33±3.46[b] min and 1540.00±1.73[c] min. These data demonstrate the effectiveness of the application of ethanol to the samples of dekopon slices as well as the increase of the drying air temperature with respect to the reduction of the total process time, which can bring benefits mainly in the energy economy. The use of ethanol in direct contact with the sample, as pretreatment to convective drying, was studied by [10] during the drying of banana having the same effect in relation to the increase of the diffusivity allowing the pretreated experiments to present a lower drying time. With the application of the ethanol under the sample, a homogeneous mixture is formed (ethanol has hydroxyl that binds with water by hydrogen bond) and this mixture presents a higher vapor pressure when compared to the solution without ethanol, justifying the reduction of the drying process [10, 11, 17]. As the temperature of the air increases, a higher rate of drying occurs due to the greater mobility that the water reaches inside the pores, reducing the internal resistance to the transport of moisture [7], and similar results are found in the literature [18, 19].

The a_w is an important parameter in food preservation and the results have proved the efficiency of the drying process in reduced the values. The fresh samples presented a_w of 0.97±0.02ª, differing from the others ($p<0.05$). The experiments at 50 °C with pretreatment, and without pretreatment, as well as those of 70 °C with pretreatment and without pretreatment, presented a_w of 0.36±0.05[b], 0.37±0.03[b], 0.38±0.05[b], and 0.360±0.021[b] ($p>0.05$), respectively, according to literature [20].

3.2. Quality analysis

The effect of air temperature drying and ethanol immersion on the phenolic content, vitamin C retention and total antioxidant activity of dekopon slices dehydrated are showed in Table 1.

Table 1. Phenolic content, vitamin C retention and total antioxidant activity in dekopon slices dehydrated

Conditions	Phenolic [mg 100 g⁻¹]	AAT [%sequestration]	Vitamin C [%retention]
50 °C, pretreated	766.67±10.25ª	74.80±0.12ª	39.09±0.91ª
50 °C, untreated	642.89±6.14[b]	59.06±1.14[b]	32.45±0.04[b]
70 °C, pretreated	622.16±6.06[bc]	51.71±0.59[c]	30.71±0.03[c]
70 °C, untreated	609.75±4.77[c]	49.54±0.80[d]	28.85±0.09[d]

Different letters mean significant difference ($p<0.05$).

The reduction of bioactive compounds in foods and the degradation of phenolic are usually pointed as drying disadvantages. The lowest phenolic compounds, percentage of retention of vitamin C and total antioxidant activity were found in the experiments at 70 °C. By the drying, the polyphenols could have interactions with other compounds or have their chemical structure changed [3]. Temperature have a negative effect on phenolic [21]. The increase in temperature also brings reductions in the vitamin C, a thermosensitive compound [22]. In addition, the effect of the use of ethanol was clearly evidenced. The higher retention and antioxidant activity were found with the use of ethanol. Moreover, one can see that those indexes were more relevant at lower temperatures. For example, the antioxidant activity was 26.7% higher by the use of ethanol at 50 ℃ whereas it was 4.4 % higher by the same use at 70 ℃. The alcohol causes a more intense evaporation of water, reducing the time of exposure of the sample to the drying process, minimizing the effects of temperature under the quality parameters analyzed [23].

4. Conclusions

The immersion in ethanol and the use of higher temperatures lead to shorter drying time. In addition, the quality compounds analyzed had greater preservation in the experiment at 50 °C and with application of ethanol, evidencing the importance of the use pretreatment as well as the choice of the range temperature process.

5. Acknowledgment

6. References

[1] Herbig, A.; Renard, C. M. G. C. Factors that impact the stability of vitamin C at intermediate temperatures in a food matrix. Food Chemistry 2017, 220 (1), 444–451

[2] Rodrígues-Roque, M. J., Ancos , B.; Sánches-Moreno, C.; Cano, M. P.; Elez-Martínez, P.; Martín-Belloso, O. Impact of food matrix and processing on the in vitro bioaccessibility of vitamin C, phenolic compounds, and hydrophilic antioxidant activity from fruit juice-based beverages. Journal. Functional Foods 2015, 14, 33–43.

[3] Méndez-Lagunas, L.; Rodríguez-Ramírez, J.; Cruz-Gracida, M.; Sandoval-Torres, S.; Barrida-Bernal, G. Convective drying kinetics of strawberry (Fragaria ananassa):

effects on anti-oxidant activity, anthocyanins and total phenolic content. Food Chemistry 2017, 230 (1), 174–181.

[4] Choi, H. Impact odorants of Citrus Hallabong [(C. unshiu Marcov × C. sinensis Osbeck) × C. reticulata Blanco] cold-pressed peel oil. Journal Agricultural Food Chemistry 2003, 51 (9), 2687–2692.

[5] Song, H. S.; Phi, N. T. L.; Park, Y.; Sawamura, M. Volatile profiles in cold-pressed peel oil from Korean and Japanese Shiranui. Biosci. Biotechnol. Biochem., 2006, 70 (3), 737–739.

[6] Kumar, C.; Joardder, M. U. H.; Farrell, T. W.; Millar, G. J.; Karim, M. A. Mathematical model for intermittent microwave convective drying of food materials. Drying. Technology 2016, 34 (8), 962–973.

[7] Corrêa, J. L. G.; Rasia, M. C.; Mulet A.; Cárcel, J. A. Influence of ultrasound application on both the osmotic pretreatment and subsequent convective drying of pineapple (Ananas comosus). Innovative Food Science and Emerging Technologies 2017, 41, 284–291.

[8] Mendonça, K. S.; Corrêa, J. L. G.; Junqueira, J. R. J.; Cirillo, M. A.; Figueira, F. V.; Carvalho, E. E. N. Influences of convective and vacuum drying on the quality attributes of osmo-dried pequi (Caryocar brasiliense Camb .) slices. Food Chemistry 2017, 224 (1), 212–218.

[9] Santos, P. H. S.; Silva, M. A. Kinetics of L-Ascorbic acid degradation in pineapple drying under ethanolic atmosphere. Drying Technology 2009, 27 (9), 37–41.

[10] Corrêa, J. L. G.; Braga, A. M. P.; Hochheim, M.; Silva, M. A. The influence of ethanol on the convective drying of unripe, ripe, and overripe bananas. Drying Technology 2012, 30 (8), 817–826.

[11] Silva, D. M.; Pires, C. R. F.; Lima, J. P.; Pereira, A. S.; Silva, C. A. Desidratação osmótica para obtenção de cagaita passa. Journal bionergy food Science 2015, 2 (4), 226–233.

[12] Garau, M. C.; Simal, S.; Femenia, A.; Rosselló, C. Drying of orange skin: drying kinetics modelling and functional properties. Journal Food Engineering 2006, 75 (2) 288–295.

[13] Lurie, S.; Pesis, E.; Gadiyeva, O.; Feygenberg, O.; Ben-Arie, R.; Kaplunov, T.; Zutahy, Y.; Lichter, A. Modified ethanol atmosphere to control decay of table grapes during storage. Postharvest Biol. Technology 2006, 42 (3), 222–227.

[14] Waterhouse, A. L. Polyphenolics: determination of total phenolics. In Current protocols in food analytical chemistry; Wrolstad, R. E., Eds.; John Wiley & Sons Org.: New York, 2002.

[15] Strohecker, R.; Henning, H. Analisis de vitaminas: métodos comprovados; Paz Montalvo: Madrid, 1967.

[16] Rufino, F. D. S.; Alves, M. S. M.; Brito, R. E.; Morais, E. S.; Sampaio, S. M.; Jiménez, C. G.; Calixto, J. P. Metodologia científica: determinação da atividade

antioxidante total em frutas pela captura do Radical livre ABTS; Empresa Brasileira de Pesquisa Agropecuária: Fortaleza, 2007.

[17] Alavi, S.; Ohmura, R.; Ripmeester, J. A. A molecular dynamics study of ethanol-water hydrogen bonding in binary structure I clathrate hydrate with CO_2. Journal Chemistry Physical 2011, 134, 54702-54702.

[18] Wojdylo, A.; Figiel, A.; Lech, K.; Nowicka , P.; Oszmianski, J. Effect of convective and vacuum – microwave drying on the bioactive compounds , color , and antioxidant capacity of sour cherries. Journal Bioprocess Technology 2014, 7 (3), 829–841.

[19] Nascimento, E. M. G. C.; Mulet, A.; Ascheri, J. L. R.; Wanderlei, P. C.; Cárcel, J. A. Effects of high-intensity ultrasound on drying kinetics and antioxidant properties of passion fruit peel. Journal Food Engineering 2015, 170, 108–118.

[20] Junqueira, J. R. J.; Corrêa, J. L. G.; Oliveira, H. M.; Avelar, R. I. S.; Pio, L. A. S., Convective drying of cape gooseberry fruits : Effect of pretreatments on kinetics and quality parameters. Food Science Technology 2017, 82, 404–410.

[21] Acosta-Estrada, B. A.; Gutiérrez-Uribe, J. A.; Serna-Saldívar, S. O. Bound phenolics in foods , a review. Food Chemistry 2014, 152, 46–55.

[22] Saini, R. K.; Shetty, N. P.; Prakash, M. Giridhar, P. Effect of dehydration methods on retention of carotenoids, tocopherols, ascorbic acid and antioxidant activity in Moringa oleifera leaves and preparation of a RTE product. Journal Food Science Technology 2014, 51 (9) 2176–2182.

[23] Junqueira, J. R. J.; Resende, N. S.; Mendonça, K. S.; Pereira, M. C. A.; Vilas Boas, E. V. B.; Corrêa, J. L. G. Secagem a vácuo de hortaliças não convencionais pretratadas com etanol. In Proceedings Brazilian Congress of Chemical Engineering, Fortaleza, Brazil, September 25-29, 2016;1- 8.

Osmotic dehydration of eggplant, carrot and beetroot slices: Effect of vacuum on phenolic acid composition

Junqueira, J. R. J.[a]*; Corrêa, J. L. G.[a]; Mendonça, K. S.[b]; Mello-Júnior, R. E.[a]; Carvalho, L. B.[a]

[a] Department of Food Science. Federal University of Lavras, Lavras, Brazil.
[b] Department of Agrarian Science. Federal Institute of Education, Science and Technology of Minas Gerais, Bambuí, Brazil.

*E-mail of the corresponding author: jrenatojesus@hotmail.com

Abstract

The aim of this work was to evaluate the influence of vacuum application on the phenolic acid content of osmodehydrated eggplant, carrot and beetroot samples. The contents of catechins and chlorogenic acid were determined by HPLC analysis. Changes in the contents of phenolic acids after the osmotic processes were observed. It was found a reduction in catechins and chlorogenic acids, probable due to the migration and degradation losses. In a general way, the vacuum reduced the catechin and chlorogenic acid contents, compared to the osmotic dehydration at atmospheric pressure.

Keywords: Pulsed vacuum osmotic dehydration; chlorogenic acid; catechins.

1. Introduction

The osmotic dehydration (OD) is a technique that provides partial water removal from a food product, with low energy consumption by been carried out at room or moderate temperatures [1]. It is based on the immersion of pieces of fresh fruits or vegetables in a hypertonic solution. The process involves simultaneous counter-current water diffusion from the food to the solution and solute diffusion into the food, under the influence of osmotic pressure gradient [2,3]. It is considered a pretreatment to many processes and preserves physical, chemical and sensorial characteristics of food with few changes on its integrity [4,5].

A mass transfer rate increase can be achieved with the vacuum application in the beggining of the OD, in a process presented as pulsed vacuum osmotic dehydration (PVOD) [6]. The reduction in the pressure causes liberation of the ocluded gases in the pores of the fruit and vegetables making them expelled, due to the action of hydrodynamic mechanisms (HDM) enhanced by pressure difference, increasing the surface area for mass transfer [7–9].

The PVOD process is related to the intensification of water loss and solid uptake, compared with OD. Besides this two mass fluxes, the lixiviation of some nutrients affect qualitatively the nutritional and functional properties of the food subjected to this process [6–8].

As the water is removed, some water soluble constituints, as vitamins and phenolic acids are lixiviated, implying in significative nutritional losses [10]. The vegetables are source of bioactive compounds, among them, the phenolic acids. They confer antioxidant properties and are therefore indicated for the treatment and prevention of cancer, cardiovascular disease and other diseases [11]. This work aimed to evaluate the effect of different vacuum pressures applied in the OD of eggplant, carrot and beetroot slices in the phenolic acid content.

2. Materials and Methods

2.1 Sample and osmotic solution preparation

Fresh eggplants (*Solanum melongena* L.), carrots (*Daucus carota* L.) and beetroots (*Beta vulgaricus* L.) were purchased in a local market (Lavras, MG, Brazil) and stored in a refrigerator at 8 ± 1 ºC before the experiments.

All of the vegetables were washed with tap water, peeled and sliced (2.00 cm length x 2.00 cm width x 0.40 ± 0.03 cm thickness) using a stainless steel mold. The ternary osmotic solution was prepared with distilled water, sucrose (40 kg 100 kg^{-1} (w/w)) and sodium chloride (10 kg 100 kg^{-1} (w/w)).

2.2 Osmotic processes

The osmotic processes were performed in an osmotic dehydrator with temperature and inner pressure control (Fig 1) [8]
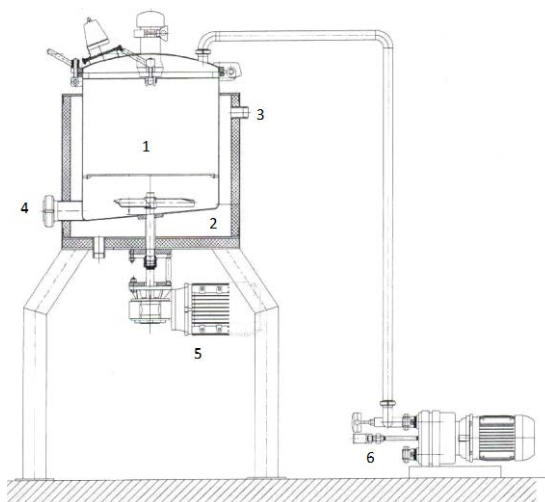
Fig. 1 Vacuum pulse osmotic dehydration device. 1 - inside osmotic dehydrator, 2 – thermal jack; 3 - outlet of thermal jacked section 4 - output to remove osmotic solution, 5 - motor coupled to the blade inside dehydrator to promote agitation; 6 - vacuum pump.

The experiments were conducted in three different conditions and the total time of the osmotic process was 300 min. Part of this time, in the beginning of the process (10 min), could involve vacuum pulse application, followed by atmospheric pressure restoration (755 mmHg). The treatments are presented in the Table 1.

Table 1. Experimental conditions

Treatment	Conditions
1	OD (absolute pressure = 755 mmHg)
2	PVOD (absolute pressure = 455 mmHg)
3	PVOD (absolute pressure = 155 mmHg)

The processes temperature was set at 35 ± 1 ºC and the ratio of solution to vegetable was 1:10 (w/w). After the osmotic processes, the samples were removed from the solution and immersed in a bath of cold distilled water during 10 s to stop the osmosis and to remove

solution excess. The surface of the samples was gently wiped with absorbent paper, and they were weighed and submitted to moisture content determination [12] and cromatography analyzes. All the experiments were performed in four replicates.

2.3 Chromatography analyses

The polyphenols for high performance liquid efficiency chromatography (HPLC) were extracted using 2.5 g of pulp and 20 mL solution containing 70% methanol in water (v/v) [13]. Briefly, the samples were homogenized and placed in an ultrasonic bath at 20 ºC for 60 min. The extracts were centrifuged at 1400 g for 15 min at 4 ºC and filtered through Whatman nº 2 filter paper. The extracts were again filtered with regenerated cellulose filters 0.45 μm (Millipore, Bedford, MA, USA) and stored at −18 °C until the analyses.

The chromatographic analyses were performed using an Ascentis C18 5-lm (250 mm x 4 mm) column. The mobile phase consisted of 2% (v/v) acetic acid in water (mobile phase A) and 70:28:2 methanol/water/acetic acid (mobile phase B), set to a flow rate of 1.0 mL min-1 and conducted using a gradient elution programme and a 65 min run time. The injection volume was 20 μL. Analyses were performed at 15 ºC. The phenolic compounds generated a UV–Vis spectral result in the HPLC chromatogram at 280 nm. Quantitative determination of compounds was conducted by comparison with dose–response curves based on *m/z* data from authentic standards of individual polyphenols [14]. The results of three replicates were expressed as mg 100 g^{-1} (d. b.).

2.4 Statistical analyses

The results were subjected to analysis of variance (ANOVA) using software STATISTICA 8.0® (Statsoft, Tulsa, USA). Tukey's test was used to compare means at the 5% significance level ($p < 0.05$).

3. Results and discussion

For the identified phenolic acids, significant differences after the osmotic processes ($p \leq 0.05$) have been found (Table 2) for all the vegetables.

According to the Table 2, catechin was identified in all the different vegetables, with higher concentration in beetroot samples, followed by carrot and eggplant. The chlorogenic acid (5-O-caffeoyl-quinic acid; CQA) was observed only in the eggplant samples.

A reduction in the catechin content was observed for all osmodehydrated vegetables (Table 2). This occurred probable due to the migration and lixiviation losses, that are related with

the mass transfer during the osmotic dehydration. It is well known that as the water is removed from the products (due to the osmotic pressure gradient between the material and the osmotic solution), some water soluble compounds also migrate from the cell tissue to the liquid media [15–17]. For the beetroot samples, the catechins were lightly preserved in the treatment 2 (PVOD with absolute pressure of 455 mmHg) (Table 2).

Table 2. Phenolic acid content of fresh and osmodehydrated vegetables [mg 100 g⁻¹] (d.b.)

Treatments	Fresh	1	2	3
Catechin				
Eggplant	21.26 ± 1.66^a	12.22 ± 1.24^b	13.42 ± 0.61^b	2.40 ± 0.15^c
Carrot	36.89 ± 2.89^a	28.72 ± 1.44^b	31.42 ± 2.06^b	21.09 ± 0.10^c
Beetroot	215.48 ± 4.31^a	90.17 ± 3.93^c	116.67 ± 4.20^b	75.17 ± 2.88^d
Chlorogenic acid				
Eggplant	367.71 ± 11.43^a	219.07 ± 11.42^b	183.17 ± 8.29^c	82.92 ± 3.62^d

Average value ± standard deviation. Mean followed by different letters in the row differs significantly ($p < 0.05$), according to Tukey's test.

Comparing the catechin content in fresh and osmodehydrated blueberries [18] also observed significant reduction in its retention. They concluded that the vacuum application reduced the catechin content, compared with OD treatment.

Studies indicate that the main phenolic compound in the eggplant is the chlorogenic acid [19]. Its content was reduced in PVOD treatments by 50-75 % (Table 2). This phenolic compound is a hydroxycinnamic acid derivative, and such a reduction occured probable due to the mass transfer intensification when the vacuum was applied [20-22]. Nevertheless, the losses of this polyphenol acid was also observed in OD treatment. This indicates that besides the losses by lixiviation, some oxidative and hydrolytic modifications were observed.

According to the Table 2, the vacuum application implied in a pronounced phenolic reduction, compared to the OD. The retention in phenolic compounds are desirable, once they present a wide range of biological activities, related to the risk decrease of heart and neurodegenerative diseases, and certain forms of cancers [23].

4. Conclusions

The osmotic dehydration of vegetables (eggplant, carrot and beetroot) was achieved in different conditions. It was observed changes in the phenolic acid contents after the osmotic processes. It was found a reduction in catechins and chlorogenic acids, probable due to the migration and degradation losses. In a general way, the vacuum reduced the catechin and chlorogenic acid contents, compared to the OD. It was concluded that the osmotic process (under vacuum or atmospheric pressure) reduces the analyzed phenolic acid content.

5. Acknowledgements

6. References

[1]   Mendonça, K.S.D.; Corrêa, J.L.G.; Junqueira, J.R.J.; de Angelis Pereira, M.C.; Cirillo, M.A. Mass transfer kinetics of the osmotic dehydration of yacon slices with polyols. Journal of Food Processing and Preservation 2017, 41, 1–8.

[2]   Akbarian, M.; Moayedi, F.; Ghasemkhani, N.; Ghaseminezhad, A. Impact of antioxidant edible coatings and osmotic dehydration on shrinkage and colour of " Quince " dried by hot air. International Journal of Bioscience 2014, 4(1), 27–33.

[3]   Vieira, G.S.; Pereira, L.M.; Hubinger, M.D. Optimisation of osmotic dehydration process of guavas by response surface methodology and desirability function. International Journal of Food Science and Technology 2012, 47(1), 132–140.

[4]   Abbasi Souraki, B.; Ghaffari, A.; Bayat, Y. Mathematical modeling of moisture and solute diffusion in the cylindrical green bean during osmotic dehydration in salt solution. Food and Bioproducts Processing 2012, 90(1), 64–71.

[5]   Corrêa, J.L.G.; Ernesto, D.B.; Alves, J.G.L.F.; Andrade, R.S. Optimisation of vacuum pulse osmotic dehydration of blanched pumpkin. International Journal of Food Science and Technology 2014, 49, 2008–2014.

[6]   Fante, C.; Corrêa, J.; Natividade, M.; Lima, J.; Lima, L. Drying of plums (*Prunus sp*, c.v Gulfblaze) treated with KCl in the field and subjected to pulsed vacuum osmotic dehydration. International Journal of Food Science and Technology 2011, 46, 1080–1085.

[7]   Fito, P. Modelling of vacuum osmotic dehydration of food. Journal of Food Engineering 1994, 22(1–4), 313–328.

[8]   Viana, A.D.; Corrêa, J.L.G.; Justus, A. Optimisation of the pulsed vacuum osmotic

dehydration of cladodes of fodder palm. International Journal of Food Science and Technology 2014, 49, 726–732.

[9] Oliveira, L.F.; Mendonça, K.S.; Corrêa, J.L.G.; Junqueira, J.R.J.; Justus, A. Efeito de ondas ultrassônicas e de pulso de vácuo nos parâmetros de qualidade peras osmoticamente desidratadas. Caderno de Ciências Agrárias 2016, 8(1), 38–48.

[10] Bera, D.; Roy, L. Osmotic dehydration of litchi using sucrose solution : Effect of mass transfer. Journal of Food Processing and Technology 2015, 6(7), 1-7.

[11] Soares, S.E. Ácidos Fenólicos Como Antioxidantes. Revista da Nutrição 2002, 15(1),71–81.

[12] AOAC. Official methods of analysis of the association of official analytical chemist 2010, 17th edition, Washington, DC.

[13] Ramaiya, S.D.; Bujang, J.S.; Zakaria, M.H.; King, W.S.; Shaffiq Sahrir, M.A. Sugars, ascorbic acid, total phenolic content and total antioxidant activity in passion fruit (Passiflora) cultivars. Journal of the Science and Food Agricultural 2013, 93(5), 1198–1205.

[14] Gonçalves, G.A.S.; Resende, N.S.; Carvalho, E.E.N.; Resende, J.V.; Vilas Boas, E.V.B. Effect of pasteurisation and freezing method on bioactive compounds and antioxidant activity of strawberry pulp. International Journal of Food Science and Nutrition 2017, 68(6),682–694.

[15] Corrêa, J.L.G.; Rasia, M.C.; Garcia-Perez, J.V.; Mulet, A, Jesus Junqueira, J.R.; Cárcel, J.A. Use of ultrasound in the distilled water pretreament and convective drying of pineapple. Drying and Energy Technologies 2015.

[16] Corrêa, J.L.G.; Justus, A.; Oliveira, L.F.; Alves, G.E. Osmotic dehydration of tomato assisted by ultrasound: evaluation of the liquid media on mass transfer and product quality. International Journal of Food Engineering 2015, 11(4), 505–516.

[17] Ahmed, I.; Qazi, I.M.; Jamal, S. Developments in osmotic dehydration technique for the preservation of fruits and vegetables. Innovative Food Science and Emerging Technologies 2016, 34, 29–43.

[18] Moreno, J.; Gonzales, M.; Zúñiga, P.; Petzold, G.; Mella, K.; Muñoz, O. Ohmic heating and pulsed vacuum effect on dehydration processes and polyphenol component retention of osmodehydrated blueberries (cv. Tifblue). Innovative Food Science and Emerging Technologies 2016, 36, 112–119.

[19] Singh, A.P.; Luthria, D.; Wilson, T.; Vorsa, N.; Singh, V.; Banuelos, G.S. Chlorogenic acid retention in white and purple eggplant after processing and cooking. Food Chemistry 2015, 64(3), 802–808.

[20] Moraga, M.J.; Moraga, G.; Fito, P.J.; Martínez-Navarrete, N. Effect of vacuum impregnation with calcium lactate on the osmotic dehydration kinetics and quality of osmodehydrated grapefruit. Journal of Food Engineering 2009, 90 (3), 372–379.

[21] Corrêa, J.L.G.; Ernesto, D.B.; Mendonça, K.S. Pulsed vacuum osmotic dehydration of tomatoes: Sodium incorporation reduction and kinetics modeling. LWT - Food

Science and Technology 2016, 71, 17–24.

[22] Oliveira, L.F.; Corrêa, J.L.G.; Angelis Pereira, M.C.; Ramos, A.L.A.; Vilela, M.B. Osmotic dehydration of yacon (*Smallanthus sonchifolius*): Optimization for fructan retention. LWT - Food Science and Technology 2016, 71, 77–87.

[23] Luthria, D.; Singh, A.P.; Wilson, T.; Vorsa, N.; Banuelos, G.S.; Vinyard, B.T. Influence of conventional and organic agricultural practices on the phenolic content in eggplant pulp: Plant-to-plant variation. Food Chemistry 2010, 121(2),406–411.

Drying characteristics of wastewater sludge according to outside air inflow conditions

Oh, S. H. [a*]; Park, K. H.[a]; Yu, B. H. [a]; Kim, S. I.[a]

[a] Energy Saving Technologies Laboratory. Korea Institute of Energy Research, Daejeon, Korea

*E-mail of the corresponding author: Sanghyun.Oh@kier.re.kr

Abstract

The purpose of this study is to analyze the changes of drying efficiency according to the inflow conditions of outside air into the drying equipment during the drying process in order to reduce the energy used in the drying process of sludge. We conducted the experiment using a vertical thin film dryer. Materials used for the experiment are sewage sludge. As a result of the study, higher drying efficiency was obtained in the case of outside air inflow than in the case of no outside air inflow. In addition, optimum condition of outside air inflow was derived.

Keywords: Drying; Sludge; Drying efficiency; Air inflow condition

1. Introduction

The disposal of waste such as sludge on land is a social problem in response to the prohibition of marine discharges of waste. Most of the wastes such as sludge have a very high water content and it is necessary to dry them in order to treat them on the land. Various studies have been conducted on drying for wastewater sludge treatment.

It is very important to analyze the characteristics of sewage sludge for the treatment of sewage sludge because the characteristics of sewage sludge vary according to the area and temperature. Wang et al.[1] has studied the properties and toxicity of sewage sludge in more than six regions of China. Krzeminski et al.[2] studied the relationship between the properties of the sludge and the seasonal temperature. This study suggests that the sludge varies according to the season.

In recent years, research on sewage sludge has been focused on the treatment of sewage sludge. Especially, the sewage sludge has a high water content, and therefore, a drying process is essential for the treatment. Drying process for sewage sludge treatment has been using hot air or steam. Recently, various pretreatment processes and new heat sources have been studied to improve energy efficiency. Na et al.[3] studied the improvement of dewatering performance by applying ultrasonic treatment to sludge. In this study, it was mentioned that ultrasonic pretreatment had a positive effect on sludge dewatering and also helped to reduce volume and mass of sludge.

Recently, various methods of utilizing various heat sources have been researched to reduce the energy cost for the sewage sludge treatment process. Lye Bennamoun[4] reviewed various studies on sludge drying using solar energy. There are many reasons to utilize ocean heat energy for sludge drying, but most of all to reduce the energy cost of the drying process.

This study was also conducted to reduce the energy input to the sludge drying process. In particular, the efficiency of the drying process is the most energy involves higher costs is necessary in order to take advantage of the waste.This study analyzed the characteristics of the energy efficiency change of the system by introducing outside air into the existing sludge drying process and conducted an experimental study on a method for obtaining higher system efficiency.

2. Materials and methods

In this study, we used a vertical thin film dryer. The vertical thin film dryer is a device for drying various sludge and waste material using. Vertical thin film dryer is using non-continuous indirect heat drying method, drying the sludge and waste products. Figure 1 shows the vertical thin film dryer used for this study.
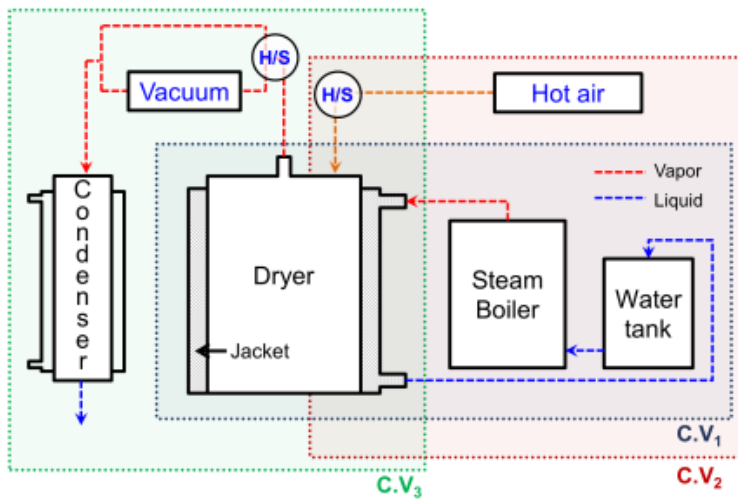
Fig. 1 The image and schematic of experimental facility.

The sludge with an initial moisture content of 80% or more can be dried to a final moisture content of 10 to 20% by using this experimental facility. The experimental facility includes a main body(dryer), a water tank, a steam boiler, an exhaust gas blower, a cooling tower, an exhaust gas condensing heat exchanger, and a platinum catalyst deodorizer. A stirrer blade is installed in the main body(dryer) so that the wastewater sludge is agitated during drying

and the heat transfer between the material and the jacket is performed well. The material used in the experiment is sewage sludge from urban areas.

Table 1. Experimetal test cases

Cases	Detail
Inflow X	No outside air inflow
Inflow 1	Inflow of air from 10 minutes after operation
Inflow 2	Inflow of air from 20 minutes after operation
Inflow 3	Inflow of air from 30 minutes after operation
Inflow 4	Inflow of air from 40 minutes after operation
Inflow 5	Inflow of air from 50 minutes after operation

The initial moisture content is about 80%. In this study, the drying was carried out until the final moisture content was 10% or less. The pressure of the steam supplied to the system is 2 kg / cm 2, and the temperature inside the chamber is 155 ° C on average. The supply of steam was on / off controlled based on the pressure. The pressure and temperature were measured at intervals of 5 seconds using a data logger. In order to improve the accuracy of the experiment, only the initial water content and the final water content were measured without extracting the sample during the experiment.

As mentioned above, this study evaluated the drying performance by introducing outside air into the conventional vertical thin film drying apparatus. For the study, the experiment was carried out under the condition that no external air was introduced and the external atmosphere was introduced. The total experiment time was 60 minutes, and the detailed experimental conditions are shown in Table 1.

The purpose of this study is to improve the energy efficiency of the drying system by changing the outside air inflow operating conditions of the vertical thin film drying system. The initial moisture content and moisture content after sludge drying were measured. In order to confirm the energy input during each drying experiment, a strategic meter was installed to add the total power of all systems. The pressure inside the chamber and the relative humidity were measured so that the inside of the chamber can be confirmed. Based on this, the energy efficiency of the system is calculated and the system drying energy efficiency calculation formula is as follows.

$$Drying\ efficiency = \frac{Amount\ of\ water\ evaporation}{Input\ energy\ amount} \times 100\% \quad (1)$$

3. Result

Table 2. shows the results of the experiments conducted through this study. The initial sample weight was 10 kg. The initial and final moisture contents were measured as described above. The calculated drying efficiency is shown in Figure 2.

Table 2. Experimetal test cases

Cases	Material (kg/s)	Initial moisture contents(%)	Final moisture contents(%)
Inflow X	10.08	80.39	8.7
Inflow 1	10.08	83.64	7.36
Inflow 2	10.82	83.64	6.7
Inflow 3	10.17	83.92	5.17
Inflow 4	9.99	78.43	3.31
Inflow 5	10.17	82.83	11.82

As shown in Figure 2., the drying efficiency in the condition with outside air inflow is higher than the drying efficiency in the the condition without outside air inflow. As drying proceeds in conventional drying systems, the humidity inside the dryer is kept close to 100%. This means that the drying resistance is increased. However, by introducing outside air inflow, the humidity inside the chamber can be lowered during the drying process. This means a decrease in drying resistance and is directly related to improvement in drying efficiency.

Experiments were carried out by varying the outside air inflow conditions in order to check the influence of the outside air inflow in detail. In this study, the experiment was conducted for the case where the outside air was introduced after a certain period of time after the device was operated. Figure 2 shows that the drying efficiency increases as the initial operating time is kept longer and the outside air inflows to the latter part.

Generally, in the case of drying system, the drying rate is kept constant after the initial operation, so that the drying efficiency is maintained above a certain level irrespective of the inflow of outside air. However, as the drying progresses, the drying rate is reduced and the drying efficiency is reduced.

That is, if the outside air inflow is carried out at the latter stage of the experimental test, the drying efficiency of the system can be increased because the reduction in the internal drying resistance can be prevented in the drying system entering the reduced drying section.
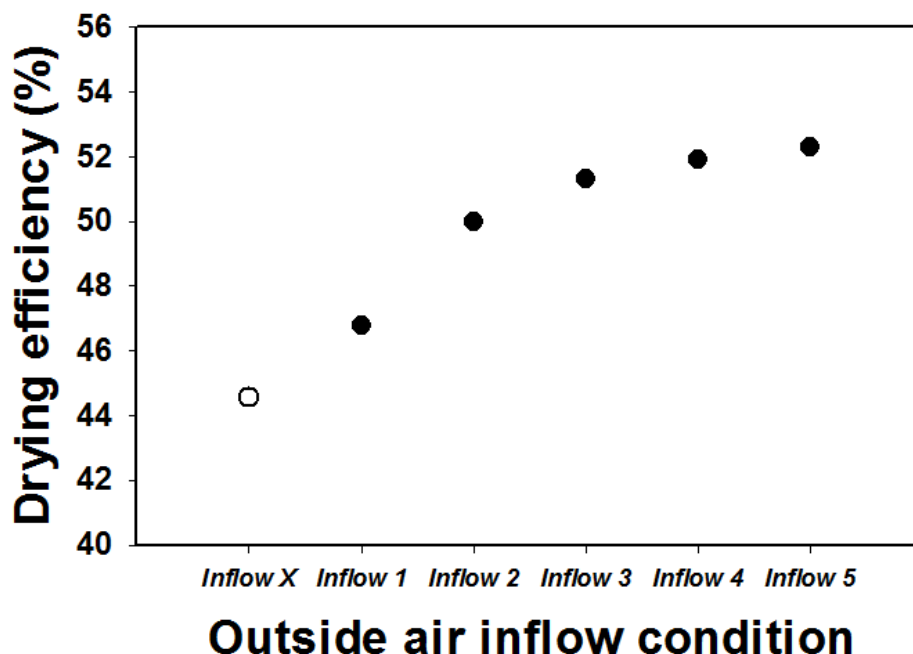
Fig. 2 Drying efficiency depending on outside air inflow conditions.

The final water content is the lowest in *Inflow 4*. As a result, it can be seen that there is an optimum point in the inflow condition of the outside air. Considering both final water content and drying efficiency, *Inflow 4* is the optimal driving test in this study.

4. Conclusions

In this study, we studied about drying characteristics of wastewater sludge according to outside air inflow conditions. We conducted the experiment using a vertical thin film dryer. And experimental studies were conducted with and without outside air inflow and with various outside air inflow conditions. Materials used for the experiment are sewage sludge.

As a result of the study, higher drying efficiency was obtained in the case of outside air inflow than in the case of no outside air inflow. In addition, optimum condition of outside air inflow was derived. This is because the drying resistance inside the drying device is reduced through the inflow of outside air. Also, it was confirmed that higher drying efficiency can be obtained by progressing the inflow of air outside the rate reducing drying zone.

5. Acknowledgements

6. References

[1] Wang, C.; Hu, X.; Chen, M.L.; Wu, Y.H., Total concentrations and fractions of Cd, Cr, Pb, Cu, Ni and Zn in sewage sludge from municipal and industrial wastewater treatment plants. Journal of Hazardous Materials, 2005, B119, 245–249.

[2] Krzeminski, P.; Iglesias-Obelleiro, A.; Madebo, G.; Garrido, J.M.; van der Graaf, J.H.J.M.; van Lier, J.B., Impact of temperature on raw wastewater composition and activated sludge filter ability in full-scale MBR systems for municipal sewage treatment. Journal of Membrane Science, 2012, 423-424, 348-361.

[3] Na, S.; Kim, Y.U.; Khim, J., Physiochemical properties of digested sewage sludge with ultrasonic treatment. Ultrasonics Sonochemistry, 2007, 14, 281–285.

[4] Bennanoun, L., Solar drying of wasterwater sludge: A review. Renewable and Sustainable Energy Reviews, 2012, 16, 1061–1073.

Impact of processing temperature on drying behavior and quality changes in organic beef

Von Gersdorff, G. J. E.[*]**; Shrestha, L.; Raut, S.; Retz, S. K.; Hensel, O.; Sturm, B.**

[a] Department of Agricultural & Biosystems Engineering, University of Kassel, Witzenhauen, Germany

*E-mail of the corresponding author: g.gersdorff@uni-kassel.de

Abstract

The drying of beef has gained an increasing interest and the organic market shows an increasing demand for dried beef products. In this study, organic beef meat slices were dried at 50 °C, 60 °C and 70 °C. Moisture content and color was measured throughout the drying process alongside Vis/VNIR hyperspectral images of the slices. The results of the total color difference (ΔE) showed the biggest change for samples dried at 50 °C (ΔE = 25.6). The a_w value was the lowest for slices dried at 50 °C (0.744). The hyperspectral data gave promising results regarding non-invasive prediction of moisture content and color.

Keywords: beef drying; drying behavior;color; hyperspectral imaging; quality.

1. Introduction

The dehydration of meat has a long tradition as a preservation method and is still an option in areas where no refrigeration is available. Meat is a valuable protein source. However, a high protein and water content is exactly the reason why meat is also very perishable product and meat is often linked to foodborne disease [1–4]. There are various options for dehydration, e.g. whole muscles or parts of the muscles, which are very common as intermediate meat products such as ham or are known as *biltong* in South Africa and need to be sliced into bite-sized pieces after drying. Further examples for dried meat products are *jerky* from the USA and *charqui* from countries of South America which are cut to thin slices even before drying. While charqi is usually an important ingredient for daily meals and is rehydrated by cooking, jerky is a typical ready-to-eat snack food. There are neither restrictions regarding the meat variety (beef, pork, chicken etc.), nor regarding the varieties of spices that are added before drying (salt, pepper, honey, etc.). Further, smoking can present a post-drying processing step, but have been shown to influence the drying behavior, while the final product color is not influenced [5,6].

In organic processing, the food additives are highly restricted and the processing itself is the main factor to gain high quality products. In this paper, beef was dried at 50, 60 and 70 °C to a jerky style product to investigate the influence on the final product quality. Drying behavior and development of color were investigated The reflectance of the samples was detected by hyperspectral imaging to investigate the option of implementation of non-invasive control systems into beef drying.

2. Materials and Methods

2.1. Meat type

For the experiment the roast beef (*longissimus dorsi*) of 4 26 months old heifers carcass weight 320 kg) of Uckermarker breed was used which led to four repetitions for each drying temperature. The beef was shock frozen 2 days after slaughter and stored at -18 °C until use. 24 h before each drying experiment, the beef was thawed at 4 °C for 24 h.

2.2. Sample preparation

The thawed beef was sliced with an electrical slicer (Graef, Allesschneider Vivo V 20, Arnsberg, Germany) with the fiber to slices of five mm thickness and cut to 50 x 50 mm samples with a knife. The initial weight was determined with a lab balance (lab scales, E2000D, Sartorius, Göttingen, Germany), further the color was determined with a Chroma Meter CR-400 (Minolta, Osaka, Japan) measured on three spots per sample and expressed using the CIELAB color space. Eight slices were used per repetition, four were dried in an oven (SLE 500, Memmert GmbH, Germany) at 105 °C for 24 hours after the drying

process to calculate the initial and final moisture content, the remaining samples were analysed with a water activity meter (LabSwift. Novasina, Lachen, Switzerland) to determine their a_w-values.

2.3. Drying process

The samples were dried at 50, 60 and 70 °C in a hot air tray dryer (HT mini, Innotech Ingenieursgesellschaft mbH, Germany). The samples were weight and the color was determined invasively by taking the samples out of the dryer every 20 minutes for the first hour of drying, in a 30 min interval for the second hour and hourly afterwards. Based on an estimated initial moisture content of 73 %, the drying process was stopped after 420 min for the drying temperature of 70 °C, after 480 min at 60 °C and after 600 min at 50 °C.

2.4. Calculations

Based on the weighing during drying and after oven drying for 24 hours, the moisture content (MC) on the dry basis was calculated and the moisture ratio (MR) was determined with the following equation (simplified by Rayaguru and Routray (2012) [7]):

$$MR = \frac{M}{M_i} \qquad (1)$$

With M_t and $M_{t+\Delta t}$ as moisture content in gH_2O/gDM at time t and $t+\Delta t$ and the time in hours. The color change ΔE at every time of measurement compared to the initial color was calculated by:

$$\Delta E = \sqrt{(L_i - L_t)^2 + (a^*_i - a^*_t)^2 + (b^*_i - b^*_t)^2} \qquad (2)$$

with i representening the initial L-, a*- and b*-values and t the values for color at every time.

2.5. Hyperspectral imaging

The samples were also imaged with an hyperspectral camera before and during drying in the intervals mentioned above. The visible near-infrared (VNIR) hyperspectral imaging systems consists of an ImSpector V10E PFD camera coupled to a linear translation stage (SPECIM Spectral Imaging Ltd., Finland). 27 cm above the belt conveyor tray (working speed 8mm/s) a 35 mm lnes (Xenoplan 1.9/35, Schneider Optische Werke GmbH, Germany) was positioned, which resulted in a spatial area of 0.03 mm^2 per pixel. This setting allowed to capture spectral data of 400-1010 nm in 1.5 nm increments. More details, including the image processing with Matlab software package (Matlab R2013a) are described by Crichton et al. (2017 a,b) [8,9], Retz et al. (2017) [10] and von Gersdorff et al. (2018) [6].

3. Results and Discussion

3.1. Drying behavior and water activity

The drying curves of beef dried at 50, 60 and 70°C are illustrated in Figure 1 a), further Figure 1 b) represents the drying rate (DR). As compared to Başlar et al. (2014) [6], who investigated the drying of beef with three different drying methods at 55, 65 and 75°C, the beef dried the fastest at the highest temperature due to a higher heat and mass transfer at higher temperatures [7]. The MR decreases exponentially, with is in accordance with other raw materials e.g. pumpkin [8], diverse vegetables [9] and apples [10], only to mention a few, and can be explained by a high heat and mass transfer coefficient during surface evaporation [7] in the initial stage of drying. During drying, the flux of moisture from the inside to the surface decreases and is smaller than the evaporation on the surface [11]
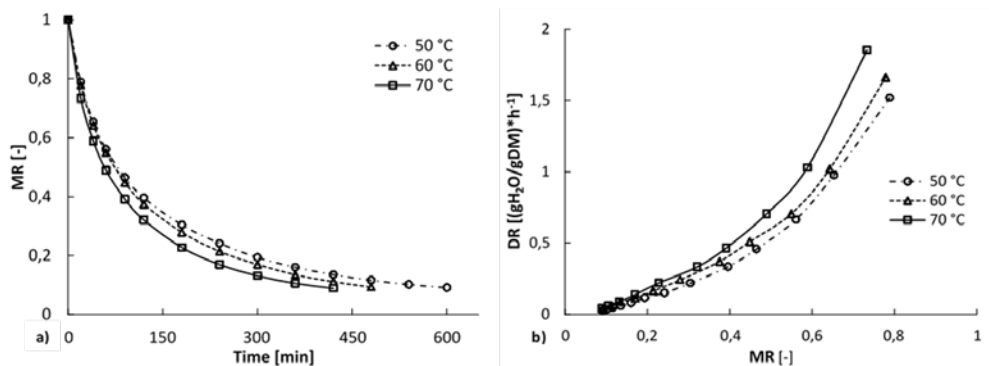
Figure 1: Drying curves of beef dried at 50, 60 and 70 °C a) and related drying rates (DR) Figure 1b)

However, the distance between the drying curves of 70 and 60 °C is obviously bigger than between 60 and 50 °C. This can be explained by a significantly higher drying rate of beef during drying at 70 °C, which becomes clearer by illustrating the drying rate (DR) as a function of moisture ratio (MR) (Figure 1 b). With 1.85 (g H_2O/g DM)*h^{-1} beef dried at 70 °C shows the highest DR after 20 min of drying and a MR of 0.73, but decreases rapidly with the decreasing MR during drying. The distance between the three DR curves decreases during drying and at low MRs the DR is nearly the same regardless of the temperature applied. This might be an effect of the decreasing heat and mass transfer mentioned above, but also struchtural changes (e.g. protein denaturation) might occur during protein and collagen denaturation[12,13] which effects the transfearability of water.

The water activity was 0.753 ($\pm$ 0.047) for beef dried at 50 °C, 0.762 ($\pm$ 0.034) for 60 °C and 0.763 ($\pm$ 0.038) for 70 °C. Therefore, all the samples are safe from growth of the most

bacteria and from mycotoxin production of mold and yeasts ($a_w \leq 0.85$) [4], and although the 50 °C samples showed the lowest water activity, the highest standard deviation indicate not a significant influence between the drying temnperatures.

3.2 Development of color

The development of L a* and b* values and the related change of color during drying is illustrated in Figure 2 a)-d). The graphs show that meat is not a homogenous product which is expressed in different values for CIELAB data before any heat treatment was applied at point 0. The development for L values for beef dried at 60 and 70 °C is very similar, the lightness of beef dried at 50 °C decreases more during the whole drying process compared to the dehydration at 70 °C. The development of the lightness seems to be linked directly to the moisture content, while the redness (Figure 2b) develops unequal for different dehydration temperatures until a certain moisture content is reached. Those investigations are not in line compared to drying of ostrich jerky, where the drying air temperature was found to have an influence and not the moisture content [14] and needs further investigations. An air temperature of 50 °C seem to retain the red color better, expressed in a slight increase in redness
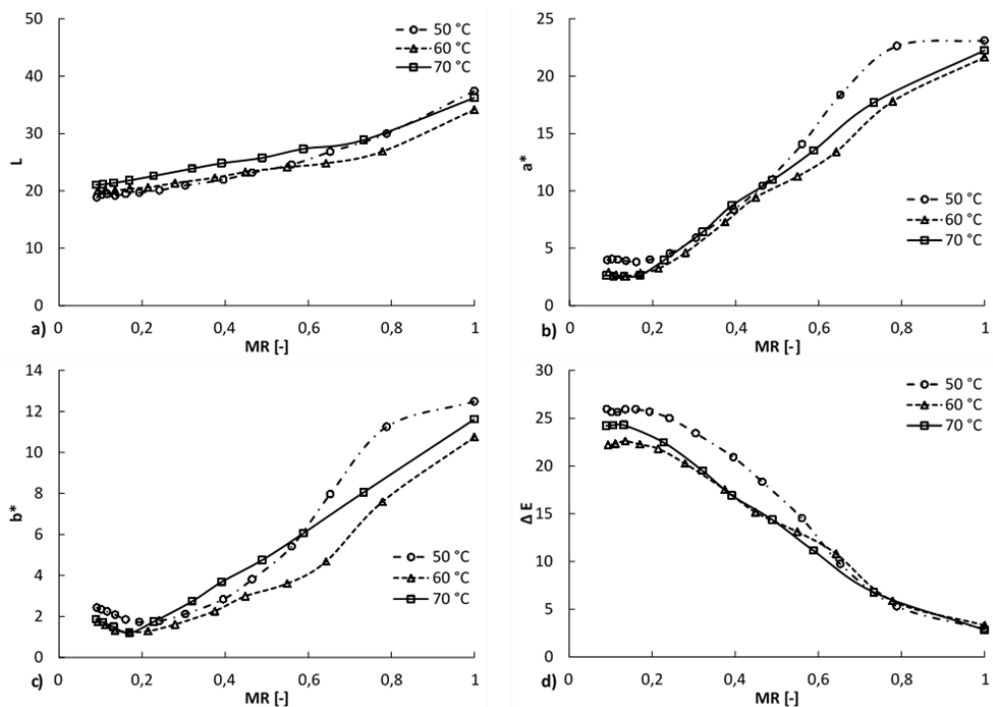
Figure 2: Development of L- a- and b*-values during drying og beef a 50, 60 and 70 °C (a-c) and corresponding color change ΔE as functions of MR.*

compared to the 60 and 70 °C, however, the initial a-value might be the influencing factor for the final redness. The yellowness is not an indicator of moisture content at higher moisture contents, as it develops very different throughout the three drying temperatures until a low moisture content is reached and the b*-value develops nearly the same from a certain point on for all three drying temperatures. Regarding the the total color change (ΔE), beef samples dried at 50 °C changes the most in color, while samples dried at 60 °C showed the lowest change related to the initial color. For all samples the color stops changing at a low moisture content. However, usually the drying should be as short as possible, as long drying periods may influence both the energy efficiency and the quality parameters negatively [15], which might explain the higher ΔE for the 50°C processing. The second highest ΔE for samples dried at 70 °C might be explained by the denaturation of proteins due to heat treatment [12,16]. However, the non-invasive measurements might also have an influence on the color development due to the differences in temperature (cooling during measurements, heating up in the drying intervals).

3.3 Hyperspectral imging

The relative reflectance of raw beef, dried for 120 min at 50, 60 and 70°C and beef dried to the final moisture content is shown in Figure 3. The reflectance of beef is at the highes level in the visible spectral region in the red range due to the red color of the beef, mwhich was documented by Wu et al. (2013) [17] before.
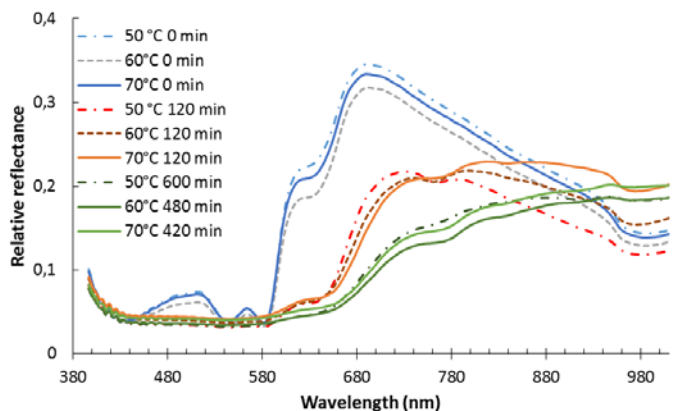
Figure 3: Relative reflectance of beef dried at 50, 60 and 70 °C air temperature after 0 and 120 minutes of dehydration and at final moisture content.

The reflectance is decreasing over time which is reasoned by the decreasing moisture content during dehydration. Further, both, the visible and the NIR region of the spectrum affects the relative reflectance. The drying temperature affects the reflectance during drying (120 minutes) in particular in the NIR region, samples dried to the final moisture content show nearly the same reflectance, regardless of the drying air temperature, which might be

due to different moisture contents after the same time after drying at different temperatures. However, differences in reflectance spectra do not necessarily affect the successful implementation of color and moisture content prediction models like shown for apple drying [8].

4. Conclusion

The present investigations show the shortest drying time for the highest drying time, but there are indications, that drying a lower air temperature might save quality attributes better, while too low temperatures again might influence the quality negatively. As quality indicator, final color shows minor changes for beef dried at 60 °C compared to 50 °C and 70 °C. However, the difference in color was not visible with the bare eye and might further be negatively influenced by the invasive measurements which needs further research. The spectral results will be further investigated and used to build prediction models to test the useful implementation of simplified non-invasive sensors.

5. Acknowledgements

6. References

[1]   Nemser, S.M.; Doran, T.; Grabenstein, M.; McConnell, T.; McGrath, T.; Pamboukian, R.; Smith, A.C.; Achen, M.; Danzeisen, G.; Kim, S.; Liu, Y.; Robeson, S.; Rosario, G.; Wilson, K.M.; Reimschuessel, R. Investigation of Listeria, Salmonella, and Toxigenic Escherichia coli in Various Pet Foods. *Foodborne pathogens and disease* [Internet]. **2014**, *0*(9), 1–4.

[2]   Calicioglu, M.; Sofos, J.N.; Kendall, P.A. Influence of marinades on survival during storage of acid-adapted and nonadapted Listeria monocytogenes inoculated post-drying on beef jerky. *International Journal of Food Microbiology*. **2003**, *86*(3), 283–292.

[3]   Zhou, G.H.; Xu, X.L.; Liu, Y. Preservation technologies for fresh meat – A review. *Meat Science* [Internet]. **2010**, *86*(1), 119–128.

[4]   Beuchat, L.R.; Komitopoulou, E.; Beckers, H.; Betts, R.P.; Bourdichon, F.; Fanning, S.; Joosten, H.M.; Ter Kuile, B.H. Low–Water Activity Foods: Increased Concern as Vehicles of Foodborne Pathogens. *Journal of Food Protection* [Internet]. **2013**, *76*(1), 150–172.

[5] Von Gersdorff, G.J.E.; Crichton, S.O.J.C.; Retz, S.K.; Hensel, O.; Sturm, B. Drying of fresh organic beef with different pretreatments. In: The 20th International Drying Symposium (IDS 2016), Gifu, Japan. 2016.

[6] von Gersdorff, G.J.E.; Porley, V.E.; Retz, S.K.; Hensel, O.; Crichton, S.O.J.; Sturm, B. Drying behavior and quality parameters of dried beef (biltong) subjected to different pre-treatments and maturation stages. *Drying Technology*. **2018**, *36*(1), 21–32.

[7] Rayaguru, K.; Routray, W. Mathematical modeling of thin layer drying kinetics of stone apple slices. *International Food Research Journal*. **2012**, *19*(4).

[8] Crichton, S.; Shrestha, L.; Hurlbert, A.; Sturm, B. Use of hyperspectral imaging for the prediction of moisture content and chromaticity of raw and pretreated apple slices during convection drying. *Drying Technology*. **2017**, *0*(0), 1–13.

[9] Crichton, S.O.J.; Kirchner, S.M.; Porley, V.; Retz, S.; von Gersdorff, G.; Hensel, O.; Sturm, B. High pH thresholding of beef with VNIR hyperspectral imaging. *Meat Science*. **2017**, *134*, 14–17.

[10] Retz, S.; Porley, V.E.; von Gersdorff, G.; Hensel, O.; Crichton, S.; Sturm, B. Effect of maturation and freezing on quality and drying kinetics of beef. *Drying Technology*. **2017**, *35*(16), 2002–2014.

[11] Traffano-Schiffo, M.V.; Castro-Giráldez, M.; Fito, P.J.; Balaguer, N. Thermodynamic model of meat drying by infrared thermography. *Journal of Food Engineering* [Internet]. **2014** [cited 2016 Jan 25], *128*, 103–110.

[12] Martens, H.; Stabursvik, E.; Martens, M. Texture and Colour Changes in Meat during Cooking Related to Thermal Denaturation of Muscle Proteins. *Journal of Texture Studies*. **1982**, *13*(3), 291–309.

[13] Tornberg, E. Effects of heat on meat proteins - Implications on structure and quality of meat products. *Meat science* [Internet]. **2005** [cited 2016 Feb 22], *70*(3), 493–508.

[14] Lee, S.W.; Kang, C.S. Effects of moisture content and drying temperature on the physicochemical properties of ostrich jerky. *Nahrung - Food*. **2003**, *47*(5), 330–333.

[15] Chou, S.K.; Chua, K.J. On the study of the drying behavior of a heat-sensitive biomaterial undergoing stepwise-varying temperature schemes. *Industrial & engineering chemistry research*. **2003**, *42*(20), 4939–4952.

[16] King, N.; Whyte, R. Does it look cooked? A review of factors that influence cooked meat color. *Journal of Food Science*. **2006**, *71*(4), R31–R40.

[17] Wu, D.; Wang, S.; Wang, N.; Nie, P.; He, Y.; Sun, D.W.; Yao, J. Application of Time Series Hyperspectral Imaging (TS-HSI) for Determining Water Distribution Within Beef and Spectral Kinetic Analysis During Dehydration. *Food and Bioprocess Technology*. **2013**, *6*(11), 2943–2958.

Thermal - Vacuum dehydration and dispergation of dispersed materials

V. Kutovyi[a,b] V. Tkachenko[a,b], A. Nikolaenko[a]

[a] *National Science Center "Kharkov Institute of Physics and Technology"1, Akademicheskaya Str., Kharkov, 61108, Ukraine*
[b] *V. N. Karazin Kharkiv National University, 4, Area of Liberty, Kharkov, 61077, Ukraine, Tel.: +38 057 349 10 82,*

E-mail:kutovoy@kipt.kharkov.ua

Abstract

Scientific and technical studies on the intensification of removal moisture from dispersed materials and their simultaneous dispergation in the hollow heating element of a thermo-vacuum apparatus is researched. Continuous thermo-vacuum dehydration and dispergation process of zirconium hydroxide, brown coal, graphite, sawdust, biological materials is considered. Based on conducted studies was made conclusions about perspective to use this technology. Thermo-vacuum technology is different from the other by low-temperature heating, low time processing, humidity indicators controlling and nano-dispersion grinding.

Keywords: dehydration, dispergation, energy saving

1. Introduction

Intensification of production processes as well as solution the problems of energy and resource saving at dehydration of dispersed materials has become increasingly important in recent times.

There are drying installations in which the mechanical process of dispersion and dehydration of dispersed material are used in parallel; it leads to intensification of the process and reduction in capital expenditures [1]. In this case, preheated air is used as a drying agent.

In the paper [2] it is shown, that a significant amount of heat is released at fine grinding of materials in impact-reflective mills. This phenomenon is associated with impact and friction of material particles on working surfaces of the mill, emergence of new surfaces during destruction and also due to turbulence of the dust-gas mixture in the working zone of the mill.

Thus, heat occurrence in the process of fine grinding in impact-reflective mills ensures in parallel the processes of dehydration and dispersion of various materials.

However, due to lack of a rational technology for performing dehydration and dispersion in parallel, such processes have not became widely used in practice, especially in chemical technology.

There are various methods and devices designed for dehydration of agricultural dispersed materials [3, 4]. However, they require considerable energy consumption and do not ensure obtaining a product with specified characteristics, in particular, dispersion and humidity which largely affect its quality.

2. Materials and methods

Thermal-vacuum energy-efficient pulse-impact method for continuous dehydration and dispersion of wet materials has been developed on the basis of the performed theoretical and experimental studies. The proposed method is based on the principle of combining the rapid evacuation and thermal heating upon direct contact of a wet material with a heated surface of the spiral heater, which provides instantaneous heating of wet material particles in vacuum to a specified temperature. The contact of the wet material with the heated wall of the heater causes heat transfer from the heater wall to the surface layer of the material, and the reduced pressure inside the heating element allows moisture to be removed from the material at a temperature substantially below the vaporization temperature at atmospheric pressure. The rate of destruction of the surface layer of the wet material depends on the heating temperature and its internal state.

The thermal-vacuum installation for continuous dehydration and dispersion is presented in Fig. 1 [5].

The installation consists of a feed hopper (1), hollow heater (2), vacuum pump (3), pipelines (4, 11), cyclone (5), receiver of dried raw materials (6) and rotary valve (7). It has thermocouples (8, 13), control panel (9), conveyor (10), filter (12), level sensor for dried raw material (14), vacuum gauge (15).

This installation design provides simultaneously both high-performance continuous dehydration and dispersion of material in heat insulated space.
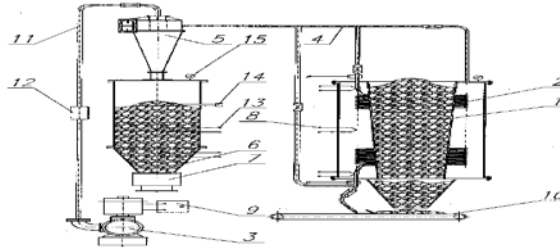
Fig. 1. Diagram of the thermal-vacuum installation

3. Results

3.1. Dehydration and dispersion of zirconium hydroxide

Let us consider a continuous process of production of zirconium dioxide fine-dispersed powder from zirconium hydroxide in a thermal-vacuum installation. The initial humidity of zirconium hydroxide is 80%, the diameter is 6mm, the length is within the range of 10 - 15 mm. Zirconium hydroxide together with an air enter the lower cavity of the heating element. The rate of a two-phase flow in the thermal-vacuum installation is determined from the expression:

$$\upsilon = \frac{\pi \cdot r^2 \cdot d^2 \cdot P \cdot \rho \cdot v_1}{2 \cdot \beta \cdot l \cdot \eta}, \quad (1)$$

where, υ - rate of a two-phase flow in the heating element, m/s;

r – internal radius of the heating element, m; d –diameter of the particle to be dried, m;,

P – average pressure in the heating element, Pa;

ρ – medium density kg/m³; v_1 – hovering rate, m/s;

β – friction coefficient, kg / s; l – the heater length, m; η – coefficient of air dynamic viscosity, Pa s.

Moving inside the heating element of the thermal-vacuum installation (Fig. 1) the zirconium hydroxide granules (Fig. 2, a) come into contact with heated walls of the heater.

Fig. 2, a. Zirconium hydroxide
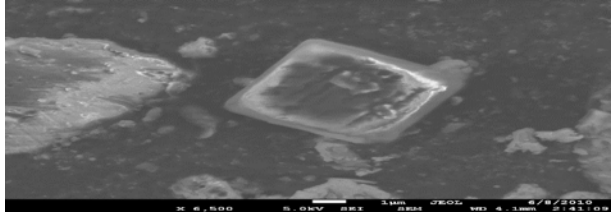
Fig. 2, b. Zirconium dioxide

An instantaneous heating of zirconium hydroxide to a temperature T_1, which is above the evaporation temperature T2 (T1> T2), occurs. Local intensive vapor emission occurs inside the body of zirconium hydroxide granules under reduced ambient pressure. An instantaneous pressure gradient occurs as a result of vapor emission and zirconium hydroxide granule falls into small particles, which increases liquid removal from the material to be dried. Zirconium hydroxide with an initial humidity of 80%, diameter of 6 mm and length of 10 ... 15 mm turns into a fine-dispersed powder of zirconium dioxide with moisture of 1%, fraction of 0.1 - 10 μm. There are no conglomerates in this powder. (Fig.2, b). The process of zirconium dioxide obtaining from zirconium hydroxide in thermal-vacuum installation takes 15 seconds.

The moisture ($m_{вл}$) removed from the material to be dried in the thermal-vacuum installation is directly proportional to the heater power (P_H), the heating temperature of the material to be dried (T), the coefficient of heat exchange between the heating element and the material to be dried (a), the evaporation area (S). It is inversely proportional to the environment pressure (P_c), the vapor kinematic viscosity (v), the impact elasticity of the material to be dried (W), the volume of the material to be dried (V) [6].

$$m_{вл} = \frac{2 \cdot (m_{общ} - m_c) \cdot P_H \cdot T \cdot a \cdot S}{P_{c.} \cdot v \cdot W \cdot V} \text{ , (2)}$$

where, m_{total} – total mass of the wet material, kg; m_c – mass of the material during dehydration, kg.

3.2. Dehydration and dispersion of brown coal

Dehydration and dispersion of brown coal (Fig. 3, a) in thermal-vacuum installation reduces the content of sulfur and nitrogen in coal, which leads to decreasing the amount of harmful emissions into the atmosphere during its combustion. The minimum particle size of the dried coal was 40 nm (Fig. 3, b), the moisture content was less than 2%. The moisture of the initial stock was 40%, the size - 6 mm. Drying the brown coal took 14 s, its color varied from brown to black. The temperature of the dried brown coal at the heating element output did not exceed 76 ° C. At the same time, the quantity of energy expended for dehydration and dispersion of brown coal does not exceed 600 MJ

Fig. 3, a. Initial brown coal
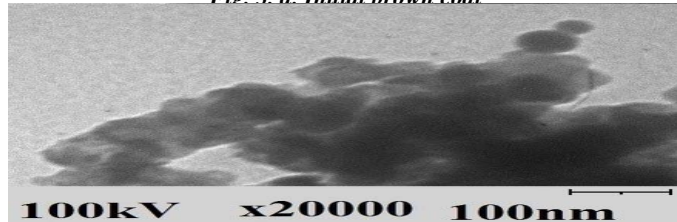
Fig. 3, b. Electron microscopy of dried brown coal

3.3. Dehydration and dispersion of graphite

Nano-dispersed graphite of size 10 - 40 nm was obtained from fine-dispersed graphite in the thermal-vacuum installation (Fig. 4 a, b). The processing time was 15 s. The process was continuous. The quantity of energy expended for dehydration and dispersion of graphite was 320 MJ / t.

Fig. 4, a. Initial graphite
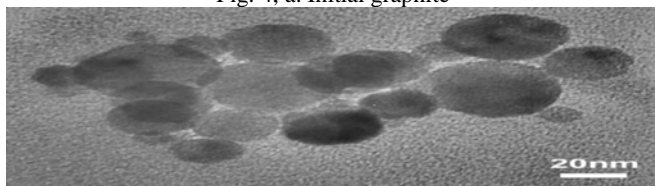
Fig. 4, b. Graphite processed in thermal-vacuum installation

3.4. Dehydration and dispersion of sawdust

An energy-saving, highly effective thermal-vacuum technique of continuous dehydration of wood-working industry wastes was developed. Dehydration of wet sawdust depending on the temperature of the heating element was studied. The quantity of thermal energy expended for dehydration did not exceed 360 MJ / t. Dried pine-tree sawdust and its

moisture content depending on the temperature of the heating element in the thermal-vacuum installation is presented in
Fig. 5 (b, d, g). The sawdust initial humidity is 70%. (Fig. 5, a).

Fig. 5, a. Initial sawdust Humidity 70%

Fig. 5, b. Heater temperature 150^0C, Humidity 20%
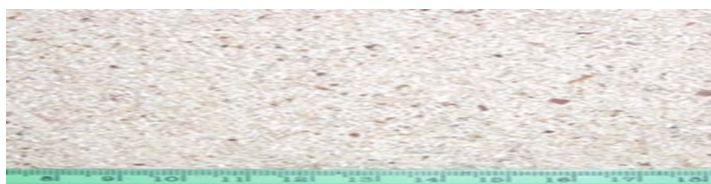
Fig. 5, d. Heater temperature 200^0C, Humidity 5%
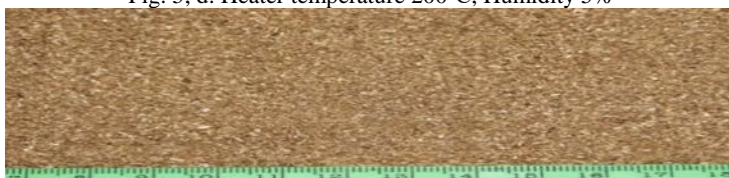
Fig. 5, g. Heater temperature 250^0C, Humidity 1%

Sawdust dehydration in the thermal-vacuum installation lasts for 20 s, the process is continuous.

3.5. Dehydration and dispersion of agricultural products

Dehydration of sugar production waste was carried out in the thermal-vacuum installation. The initial humidity was 65%. Fig. 6, a. The temperature of the dried beet pulp did not exceed $50^°$C. Humidity - 5%. Fig. 6, b. Dehydration time was 20 c. The process was continuous. Nutritive substances are kept. The quantity of thermal energy expended for dehydration was equal to 720 MJ / t.

Fig. 6, a. Initial pulp

Fig. 6, a. Dried pulp

Thermal-vacuum drying of alfalfa with humidity of 48% is presented in Fig. 7, a. After drying the alfalfa moisture was 12%. See Fig. 7, b. Drying time was 20s. Nutritive substances were kept. Heat energy consumption was 580 MJ / t

Fig. 7. a. Initial alfalfa

Fig. 7. b. Dried alfalfa

The results of study on moisture removal from dispersed materials depending on mode parameters of the thermal-vacuum installation made it possible to create an industrial science and technology base for developing energy-efficient thermal-vacuum installations, to define requirements for optimizing the technological processes of dispersed materials dehydration taking into account their physicochemical and structural compositions, to reduce energy cost per unit of the dried product, to speed up the dehydration process, to develop a highly efficient termal-vacuum technology of production of fine-dispersed

materials of high purity, to keep quality and ecological purity of the products obtained. This method allows simultaneously to remove moisture from the dispersed material and to disperse it.

The development results are of current interest for updating the existing and creation of new thermal-vacuum drying installations.

4. Conclusions

1. Scientific and technical studies on the intensification of removal moisture from dispersed materials: zirconium hydroxide, brown coal, graphite, sawdust, biological materials are researched. The regularities of heat exchange processes between heating element and wet dispersed material in the hollow spiral-heating element of the thermo-vacuum apparatus are established. Demonstrated that in thermo-vacuum apparatus by 15 seconds it possible to obtain dried nano-dispersed materials.

2. A low-temperature thermo-vacuum dehydration technology of biological materials was developed. Conducted studies demonstrated that most optimal, from the point of view of preserving biological material quality, is dehydration mode at temperatures up to 50 °C.

3. Conducted scientific and technical studies are relevant to improve existing equipment and creation of new heat-technological equipment.

5. References

[1] Shishkov, N.I.; Oparin, S.A.; Soroka; P.I.; Zrazhevskij, V.I; Issledovanie sovmeshhennyx processov izmelcheniya i sushki v melnice udarnootrazhatelnogo dejstviya. Materiali V Mizhnarodnoï naukovo-praktichnoï konferenciï "Nauka i osvita, 2002 (19), Dnipropetrovsk – Doneck, 2002, 49-50.

[2] Pat. №88108 Ukraïna, MPK S 01 V31/36. Sposib oderzhannya karbidu kremniyu / Soroka P. I., Bila A. O. ta in.; zayavnik ta patentovlasnik DVNZ «UDXTU».-№ a 200802934; zayavl.06.03.08; opubl.10.09.09, Byul.№ 17, 6.

[3] Oparin, S.; Leshhenko, V.; Soroka, P. Raschet texnologicheskix parametrov processa izmelcheniya v melnice udarno-otrazhatelnogo dejstviya, Naukovi praci ONAXT., 2010, (37), 118-122.

[4] Pat. №96082 Ukraïna MPK V02S13/14 Vidcentrovij mlin udarnoï diï / Soroka P. I., Oparin S. O.; zayavnik ta patentovlasnik DVNZ «UDXTU». – № a 2001096302. Zayavl. 25.05.2010. – Opubl. - 27.12.2010. - Byul. №18.

[5] International Patent, a20507488 27.07.2005 UA, MПK F26B5/04; F26B23/06; F26B23/00. Apparatus for Drying of Wet Dispersed Raw Materials. / V.O. Kutovyi. – #PCT/UA2005/000051; Filling. 15.01.2005; Pudlic. 01.02.2007; Publication number W0/2007/013866. – 6p.

[6] Kutovyi, V.; Lutsenko, A.; Skoromnaya, S.; Tkachenko, V. Physical model of simultaneous disparaging and dehydration of fine porous material in thermal vacuum installation, Energy, Energy Saving and Rational Nature Use, 1-2 (7, 8), 2017, 5-16.

Development of polyphenols-enriched maple sugars by freeze- and vacuum drum drying technologies

Bhatta, S.[a,b]*; Stevanovic, T.[a,b]; Ratti, C.[a,c]

[a] Institute of Nutrition and Functional Foods (INAF), Laval University, QC G1V0A6 Canada.

[b] Renewable Materials Research Center (CRMR), Laval University, QC G1V0A6, Canada.

[c] Department of Soil and Agri-Food Engineering, Laval University, QC G1V0A6, Canada

*E-mail of the corresponding author: sagar.bhatta.1@ulaval.ca

Abstract

Hot water extract of sugar and red maple bark was added to maple syrup and dried by freeze (FD) and vacuum drum drying (VD) techniques. Addition of maple bark extracts to syrup helped to develop polyphenols-enriched maple sugar. X-ray diffraction revealed that sugar obtained from FD was amorphous in nature, while crystalline when dried by VD. Furthermore, the observation of maple sugar samples under scanning electron microscopy showed smooth and porous surface for FD sugar, while rough and grainy surface for VD sugar. Hausner ratio indicated that sugar produced by VD showed better flow characteristics than FD sugar.

Keywords: drying techniques; maple syrup; phenolics; microstructure

1. Introduction

Drying of foods, solid (fruit and vegetables) or liquid (juices and syrups), increase their shelf life along with ease in handling and transportation. However, drying of foods cause the modifications of its physicochemical properties. In general, drying involving high temperatures effect thermo-labile compounds. Freeze drying (FD) is well-known technique for drying foods containing heat-sensitive and oxidative compounds such as polyphenols, because of the use of very low temperature and high vacuum. However, drying time and operation costs are major drawbacks of freeze drying [1]. Vacuum drum drying (VD) is another technique that operates at high temperature under vacuum, making it possible to dry food faster in comparison to freeze drying. Similar to FD, it may also preserve oxidative compounds due to the use of vacuum. Physical properties of powder such as moisture, flowability, morphology, etc depends on the type of drying method used [2, 3]. Therefore, drying techniques ought to be selected carefully, depending on the desired quality of the final product.

Canada accounts for approximately 71% of maple syrup production in the world (Statistics Canada, 2016). Maple syrup is a natural sweetener with high nutritional value based mainly on its sucrose, minerals, proteins and polyphenols [4]. Depending on the percentage of light transmission (at 560nm), maple syrups are classified into four grades: golden, amber, dark and very dark (Canadian Food Inspection Agency). A class of "very dark" maple syrup, which has light transmission less than 25%, is considered as substandard. Therefore, drying of such substandard maple syrup to produce a maple sugar can add value to a natural sweetener containing minerals, polyphenols, etc. However, the polyphenols are present at a very low concentration in maple syrup. When dried, the concentration of polyphenols may further diminish. Therefore, the main objective of this work was to produce polyphenol-enriched maple sugar by adding, red and sugar maple bark extracts to maple syrup, and subsequently drying the mixture.

For this study, freeze drying and vacuum drum drying technologies were explored. Thus obtained maple sugars were examined for total phenol content, moisture content, flow characteristics, crystallinity and morphology in order to study the effect of drying methods on developing the polyphenol-enriched sugars.

2. Materials and Methods

2.1. Hot water bark extraction and addition of extracts to maple syrup

Maple barks (sugar and red maple) were extracted using hot water following the method previously described by Geoffroy et al. [5]. Hot water extracts of maple barks were then added (at 0.01 % w/v) to maple syrup (very dark, 66 °Brix) and subsequently dried. Maple

syrup without any extract was considered as control. Hereafter, dried maple syrup (without extract, control) will be denoted as MS, while maple syrup with sugar and red maple bark extract are identified as MS-SX and MS-RX, respectively.

2.2. Drying experiments

Freeze drying (FD) was done by using a laboratory freeze dryer (Freeze Mobile 24, Virtis Company Inc., Gardiner, NY). Sample was frozen at -40 °C overnight and freeze-dried for 25h. The heating plate temperature was initially set at -36 °C, vacuum level was below 30 mtorr and the condenser at -90 °C.

For this study, a laboratory-scale vacuum drum dryer (Buflovak, Buffalo, USA) was used. Sample was fed between the nips of two rotating drums, where drum temperature increased up to 110 °C. The dried maple sugar powder were scraped off using in-built scrapers.

The obtained FD and VD samples were vaccum packed and stored in 4 ℃ for further analyses.

2.3. Analyses of maple sugar powder

2.3.1. Total phenolic content

Total phenolic content (TPC) in maple sugar powder was determined using the Folin-Ciocalteu method using microplate spectrophotometer (X Mark™, BIO-RAD) following the method used by Zhang et. al [6]. The results were expressed in milligram gallic acid equivalent per gram of oven dry sample (mg GAE/100g sample, db). TPC was measured in triplicates.

2.3.2. Moisture content

Moisture content of maple sugar powder was measured by vacuum-oven method at 70 °C and -22 in.Hg vacuum for 24h. Analyses were done in triplicates.

2.3.3. Flow properties

Hausner ratio (HR) was used to obtain the indication on flow characteristic of maple sugar powders. HR was calculated using the measured bulk and tapped density of the sample. Bulk density was measured by pouring the known mass of sample (m) to a cylindrical glass tube and volume occupied (V_b) was noted. For the tapped density, the glass tube was tapped from the vertical distance of 12±2 cm until no successive differences in volume (V_t) was recorded. Bulk and tapped densities were calculated using the following formula; m/V_b and m/V_t, respectively. Measurements were done in triplicates.

2.3.4. *X-ray powder diffraction*

The crystallinities of freeze and vacuum dried maple sugars were analyzed by powder X-ray diffractometer (SIEMENS/Bruker, Germany). Samples were measured at a diffraction angle (2θ) between 0 to 50° under operational conditions of 40 kV and 40 mA using Co ($K\alpha_{1+2}$) radiation.

2.3.5. *Microstructural analysis by environmental scanning electron microscopy (ESEM)*

Freeze and vacuum dried maple sugar samples were analyzed by environmental scanning electron microscopy (ESEM). The samples were scanned at 500X magnification at 20 kV.

3. Results and Discussion

3.1 Effect of drying on total phenolics of maple sugar powder

Regardless of the type of drying techniques used, TPC of sugars containing maple bark extracts showed higher values than the control. Sugar containing red maple bark extract presented higher TPC value than other sugar samples. This can be explained by the higher phenolic content of the red maple bark extract [7]. MS-RX obtained from VD had around 8% higher TPC than the control (MS). In general, FD method is preferred to dry a food containing a thermo-labile compound such as phenolics. On contrary, we observed that VD maple sugars had relatively higher TPC than those of FD sugars. This could be due to high temperature in VD that could have caused the breaking of the phenolic-glycoside bonds. Resulting in more phenolics becoming readily available to form complex with Folin's reagent while determining TPC by Folin-Ciocalteu method. However, it has yet to be validated by identifying the phenolic profile in maple sugar powders using techniques of chromatography and mass spectrophotometry.

3.2 Moisture content

Moisture content of freeze-and vacuum dried maple sugars are presented in Fig. 1. The moisture content in VD maple sugar (0.6-0.7%, on dry basis) was signigicantly lower than that of FD (4 to 5 %, dry basis). The drying temperature in VD was higher (110 °C) than in FD. Therefore, it was obvious that VD produced sugars had lower moisture content than that of FD. Similar tendency was also observed for the production of mango powder by freeze and drum drying [8].
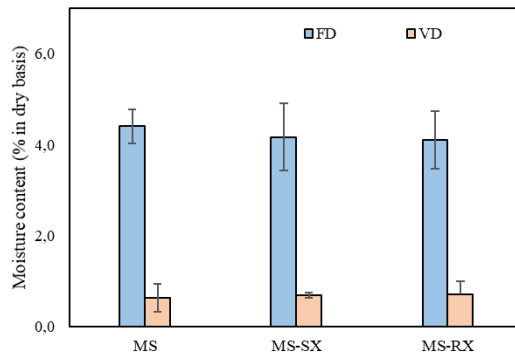
Fig. 1 Moisture content of freeze-and vacuum drum dried maple sugars. MS: maple sugar, MS-SX: maple sugar with sugar maple bark extract, MS-RX: maple sugar with red maple bark extract, FD: freeze-drying, VD: vacuum drum drying.

3.3 Flow characteristics of maple sugar

The calculated Hausner ratio of FD and VD maple sugars are presented in Table 1. Lower the Hausner ratio, the better is the flow properties [3]. The Hausner ratio was signigicantly higher ($P<0.05$) for the FD maple sugars (1.45 to 1.48, poor to very poor) than that for VD sugars (1.14 to 1.20, good to fair flow). Therefore, VD maple sugars showed better flow characteristic than that of FD.

Table 1. Flow characteristics of freeze-and vacuum dried maple sugars.

Drying techniques	Sample	Hausner ratio
	MS	1.45 ± 0.03^{a}
FD	MS-SX	1.48 ± 0.07^{a}
	MS-RX	1.47 ± 0.06^{a}
	MS	1.14 ± 0.02^{b}
VD	MS-SX	1.20 ± 0.04^{b}
	MS-RX	1.20 ± 0.05^{b}

Values represent Mean±S.D. [a,b] different superscript letters in the same column are significantly different ($P<0.05$) by Tukey's test.

3.4 Effect of drying on crystallinity of maple sugar

Fig. 2 depicts the profile of X-ray diffractogram of maple sugars produced by FD and VD techniques. Amorphous material shows large and disperse peaks due to disorderly arraged molecules in amorphous state. On the other hand, crystalline material shows sharp and defined peaks since the molecules are present in a highly ordered state. From Fig. 2, it can be observed that freeze dried maple sugar (FD_MS) is in amorphous state, whereas vacuum dried maple sugar (VD_MS), in crystalline state. However, the degree of crystallinity has yet to be identified. Crystalline state is important for the stability of food powders. Considering this results, VD sugars seemed to have an advantage of stability.
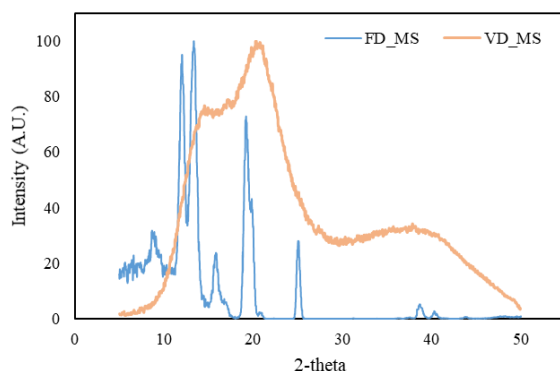
Fig. 2 X-ray powder diffractogram of maple sugars produced by different drying methods. FD_MS, freeze dried maple sugar, VD_MS: vacuum dried maple sugar.

3.5 Microstructural analysis

Microstructural analysis of maple sugar obtained from FD and VD techniques are shown in Fig. 3. FD maple sugar showed irregular and porous structure (Fig. 3a). Freeze-dried food normally shows porous structure due to the fact that ice removal by sublimation during drying prevents shrinkage and volume reduction [1]. Vacuum-dried maple sugar resulted in rough and grainy surface (Fig. 3b). The difference in microstructure of FD and VD maple sugars can also be related to the the difference in their crystallinity (shown in Fig. 2).
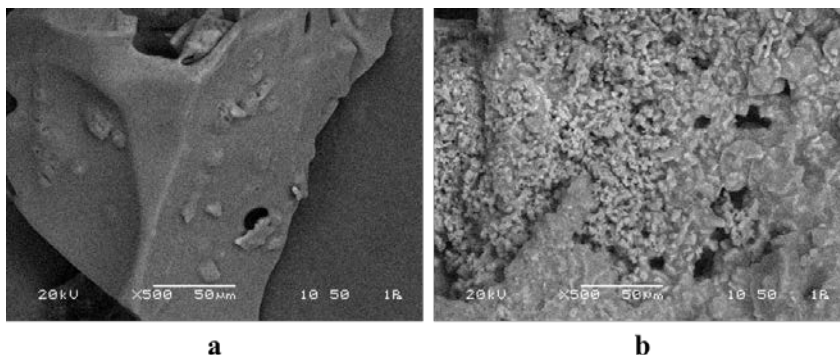
Fig. 3 Enviromental scanning electron micrograph (ESEM) of freeze-dried (a) and vacuum dried (b) maple sugar.

4. Conclusions

Considering the overall results, polyphenol-enriched maple sugar obtained either by FD or VD have potential applications in foods, particularly as sweetener for natural food products. For instance, FD maple sugar could be used in instant-drinks owing to its amorphous (powder) nature and VD sugar as functional food ingredient due to its high phenolic content as well as its better flow characteristics.

5. References

[1]   Ratti, C. Hot air and freeze-drying of high-value foods: A review. Journal of Food Engineering 2001, 49 (4), 311–319.

[2]   Jaya, S.; Das, H. A vacuum drying model for mango pulp. Drying Technology 2003, 21 (7), 1215–1234.

[3]   Seerangurayar, T.; Manickavasagan A.; Al-ismaili, A. M.; Al-mulla, Y. A. Effect of carrier agents on flowability and microstructural properties of foam-mat freeze dried date powder. Journal of Food Engineering 2017, 215, 33–43.

[4]   Ball, D. W. The Chemical Composition of Maple Syrup. Journal of Chemical Education 2007, 84 (10), 1647.

[5]   Geoffroy, T. R.; Fortin, Y.; Stevanovic, T. Hot-water extraction optimization of sugar maple (Acer saccharum marsh.) and red maple (Acer rubrum l.) bark applying principal component analysis. Journal of Wood Chemistry & Technology Feb. 2017, 1–12.

[6]   Zhang, Q.; Zhang, J.; Shen, J.; Silva, A.; Dennis, D. A.; Barrow, C. J. A simple 96-well microplate method for estimation of total polyphenol content in seaweeds.

Journal of Applied Phycology 2006, 18 (3–5), 445–450.

[7]   Bhatta, S.; Ratti, C.; Poubelle, P. E.; Stevanovic, T. Nutrients, Antioxidant Capacity and Safety of Hot Water Extract from Sugar Maple (Acer saccharum M .) and Red Maple (Acer rubrum L .) Bark. Plant Foods for Human Nutrition 2018, 73 (1), 25-33.

[8]   Caparino, O. A.; Tang, J.; Nindo, C. I.; Sablani, S. S.; Powers, J. R.; Fellman, J. K. Effect of drying methods on the physical properties and microstructures of mango (Philippine ' Carabao ' var .) powder. Journal of Food Engineering 2012, 111 (1), 135–148.

Effect of incorporation of blackberry particles obtained by freeze drying on physicochemical properties of edible films

Nogueira, G. F.[a]; Fakhouri, F. M.[bc]; Oliveira, R. A.[a*]

[a] School of Agricultural Engineering, University of Campinas, Campinas, SP, Brazil

[b] School of Chemical Engineering, University of Campinas, Campinas, SP, Brazil

[c] School of Food Engineering, Federal University of Grande Dourados, Dourados, MS, Brazil

*E-mail of the corresponding author: augustus@feagri.unicamp.br

Abstract

This research work aimed to evaluate the physicochemical properties of arrowroot starch films plasticized with glycerol and incorporated in film-forming solution directly (D) and by sprinkling (S) with 0%, 20%, 30%, 40% (mass blackberry solids / biopolymer mass) of blackberry pulp (BL) powder and freeze dried microencapsulated blackberry pulp (ML) using mixture of gum arabic and arrowroot starch (1: 1, mass / mass). Thickness, water solubility and water vapour permeability of the films significantly increased with increasing concentration of blackberry powder. Compared to arrowroot starch film (0%), the surface of films with BL and ML powder became irregular and rough.

Keywords: Lyophilization; microstructure; water solubility; water vapor permeability; packing.

1. Introduction

Fruit pulp has great potential to be incorporated in the film-forming solution in order to produce edible films with functional compounds such as preservation agents (antimicrobial or antioxidant compounds), innovative colours and flavours, as well as suitable mechanical and barrier properties of the biopolymer.[1] Thus, blackberry is a fruit that has great potential to supply these requirements and be used in combination with arrowroot starch to form a biopolymer matrix to create edible films. Blackberry (*Rubus fruticosus*) cv. Tupy is a fruit rich in anthocyanins and phenolic compounds, which has high antioxidant activity.[2] However, using its beneficial effects is limited because its bioactive compounds exhibit instability when exposed to high temperature, light, oxygen, among other conditions, changing their functional and antioxidative properties.[3] This situation can be mitigated by applying microencapsulation technologies in order to protect it from unfavourable environments. Freeze drying is a technological process based on dehydration by sublimation of a frozen product resulting in a dry material.[4] These processes can be used as encapsulation method when it incorporates 'active' material within a protective matrix, which is essentially inert to the encapsulated material.[5] Recently, the incorporation of micro and nano particles in film-forming solution to produce starch films with modified structure and properties have shown promise.[6] Therefore, the objective of this work was to incorporate directly and by sprinkling, blackberry pulp powder and microencapsulated blackberry pulp powder in arrowroot starch film-forming solution.The influence of type of incorporation and variation of concentration of blackberry powders on physicochemical properties of edible films were investigated.

2. Materials and Methods

2.1. Materials

In this work, frozen fruits of blackberry (*Rubus fruticosus*), cv Tupy, were acquired from "Agro Monte Verde Eirelli", Cambuí – MG, Brazil. Blackberry soluble solids content was 9°Brix, determined with digital refractometer with 0–90 °Brix range and 0.2 °Brix resolution (Reichert, Model AR200, USA). Blackberry pulp presented total solids content of 10.3 g/100g of pulp. For microencapsulation of blackberry pulp, arrowroot starch and Instantgum® gum arabic (Colloides Naturels, São Paulo, Brazil) were used as encapsulating agents. In elaboration of edible biodegradable films, arrowroot starch containing $15.24 \pm 0.19\%$ of water, $0.40 \pm 0.03\%$ of protein, $0.12 \pm 0.01\%$ of fat, $0.33 \pm 0.01\%$ of ash and $83.91 \pm 0.00\%$ of carbohydrates [7] and amylose content of $35.20 \pm 1.63\%$, determined according to the methodology described by Martinez and Cuevas (1989), with adaptations [8], was used as film-forming matrix and glycerol P.A. (Reagen, Quimibrás Indústrias Químicas S.A.- Rio de Janeiro, Brazil) as plasticizing agent.

2.2 Microencapsulation of blackberry pulp by freeze drying

Blackberry pulp was obtained by grinding the fruits in a blender, filtered through a sieve to remove the seeds, and homogenized. Blackberry pulp was added to the encapsulating agent, arrowroot starch and gum arabic mixture (1: 1 mass / mass) in a ratio of 1:1.78 (mass / mass, blackberry pulp solids for encapsulating agent). Solution of encapsulating agent and blackberry pulp was performed in a mixer type homogenizer at room temperature for 5 minutes. Portions of frozen blackberry pulp with and without encapsulating agent was lyophilized (Mod. 501, Edwards Pirani, Crawley, West Sussex, UK), with an initial temperature of -40 °C, pressure of 0.1 mmHg, and final temperature of 25 °C per 2 h, with total cycle time of 48 h. The resulting product was ground in a hammer mill (MR Manesco and Ranieri LTDA, model MR020, Piracicaba- Brazil), sieved and stored in polyethylene packages in desiccators, for further analysis.

2.3 Incorporation of blackberry into film-forming suspension

2.3.1. Preparation of film-forming suspension.

Film-forming suspension was obtained by dispersing arrowroot starch in distilled water (4%, mass / mass, as optimized by Nogueira, Fakhouri & Oliveira, [9]). This suspension was heated to 85 ± 2 °C in a thermostatic bath (TECNAL, Brazil), with constant agitation, for about 5 minutes. The freeze dried blackberry pulp (BL) and the freeze dried microencapsulated blackberry pulp (ML) were added to film-forming suspension in different concentrations, 0%, 20%, 30% and 40% (mass/mass of dry starch) in two different ways. The first one consisted of direct incorporation in film-forming suspension and the second one was by sprinkling into film-forming suspension. Glycerol was added to the solution at concentration of 17% (mass/mass of total solids, [9]).

2.3.2. Direct incorporation of blackberry powder into film-forming suspension (D.

Freeze dried blackberry pulp (BL) and freeze dried microencapsulated blackberry pulp (ML) were added directly into film-forming suspension and homogenized in previously mentioned proportions. Aliquots of 25 mL of resulting suspensions were distributed on support plates (12 cm diameter). Films were dried at room temperature (25 ± 5 °C), until they could be easily removed from the plates, approximately for 24 h. Films were conditioned at 25 °C and 55 ± 3% of relative humidity for 48 h, before their characterization.

2.3.3. Incorporation of blackberry powder by sprinkling into film-forming suspension (S).

Aliquots of 25 mL of resulting film-forming suspension were distributed on support plates (12 cm diameter). Freeze dried blackberry pulp (BL) and freeze dried microencapsulated blackberry pulp (ML) were dispersed through a stainless steel sieve (53 mesh), homogeneously in all the surface area of film-forming suspension already disposed on the plates. Then, films were dried for 24 h at room temperature (25 ± 5 °C). After drying, films were removed from the support plates and conditioned at 25 °C and 55 ± 3% relative humidity for 48 h, before their characterization.

2.4 Films characterization

2.4.1 Microstructure

Electronic Scanning Electron Microscope with X-ray Dispersive Energy Detector (SEM) bench (model of MEV: Leo 440i, model of EDS: 6070, Leo 440i - LEO Electron Microscopy/Oxford- Cambridge, England) was used to observe morphological characteristics of surface and cross section developed for sample of the films formulations.

2.4.2 Film Thickness and solubility in water

Films thicknesses were measured with accuracy of ± 0.001 mm, at ten different regions of the film, using a micrometer (Mitutoyo brand, model MDC 25M, MFG / Japan).
Water solubility of films was determined according to the method proposed by Gontard, Guilbert, and Cuq. [10] and expressed according to Equation (1).

$$\text{Solubilized material}(\%) = \frac{m_{si} - m_{sf}}{m_{si}} \times 100 \qquad (1)$$

In which 'msi' is the initial dry mass of the films (g), 'msf' is the final dry mass of the non-solubilized films (g).

2.4.3 Water vapor permeability

Water vapor permeability rate of the films was determined gravimetrically based on ASTM E96-80 method [11], using an acrylic cell, with a central opening (diameter of 4.3 cm), in which the film was fixed. The bottom of the cell was filled with dried calcium chloride, creating a dry environment inside (0% relative humidity at 25 ° C). This cell was placed in desiccator containing saturated sodium chloride (75 ± 3% RH), equalized for 48 h previously to analysis. Water vapor transferred through the film was determined by mass gain of calcium chloride. The cell weight was recorded daily for, at least, 7 days. The film thickness consisted on the average of 5 random measurements made on different parts of

the samples. The water vapor permeation rate (PVA) was performed in triplicate and calculated by Equation (2).

$$PVA = \frac{e}{A \, x \, \Delta p} \, x \dot{M} \tag{2}$$

In which 'PVA' is permeability to water vapor (g.mm / m^2.day.kPa), 'e' is mean film thickness, 'A' is permeation area (m^2), 'Δp' is partial vapor pressure difference between two sides of films (kPa, at 25 ºC), '$\dot{M}$' is absorbed moisture rate, calculated by linear regression of weight gain and time, in steady state (g/day).

2.4.4 Statistical analysis

Significant differences between average results were evaluated by analysis of variance (ANOVA) and Tukey test at 5% level of significance, using SAS software (Cary, NC, USA).

3. Results and discussion

Differences in microstructure of the films can be visualized in Figure 1, by scanning electron microscopy (SEM). Control film (0%) presented organized and continuous polymer matrix and regular surface (Figure 1 A-C). Films developed with 40% of blackberry presented rougher and irregular surfaces and exhibited structural characteristics directly related to those observed for BL and ML powders, which consequently hampered its solubilization. The cross-section images of 40% BLD and MLD films (Figure 2 D-F and J-L, respectively), showed continuous regions and disorganized regions due to the presence of BL and ML particle within arrowroot starch matrix formed during the films drying. BL and ML particles were integrated in arrowroot starch matrix, showing good compatibility between materials. Using sieve to sprinkle BL and ML powder over the film-forming suspension allowed falling homogenously over the entire surface area of films. It can be seen in Figure 2 G-I, in which, when 40% ML were sprayed under the film-forming suspension. Some regions with BL and ML agglomerations could also be observed in films for both types of incorporation. This may be due to poor dispersion of powders in high concentrations in the film-forming solution, given its high viscosity.
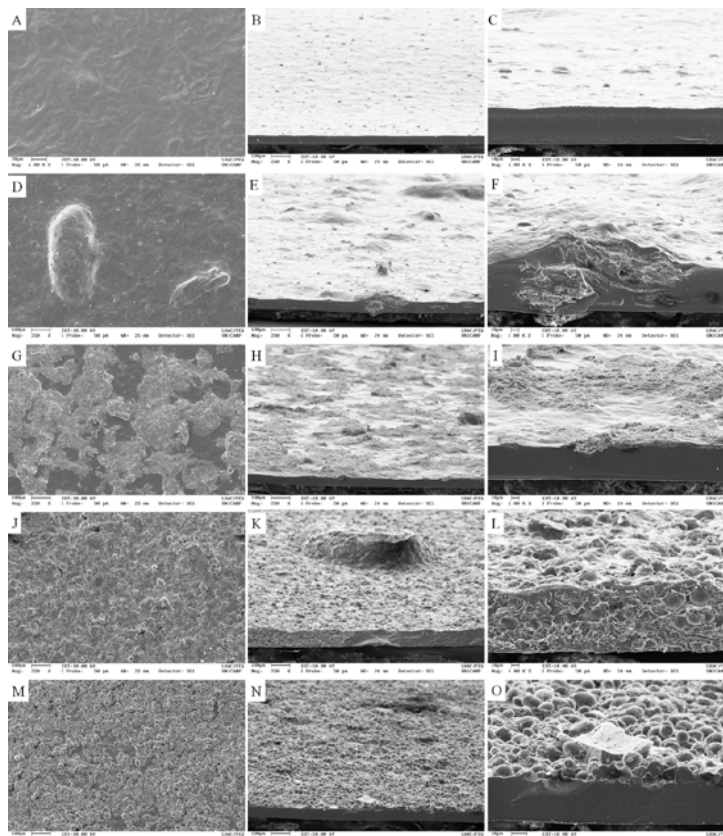
Figure 1. SEM images of the films with 0% and 40% of freeze dried blackberry pulp (BL) and freeze dried microencapsulated blackberry pulp (ML) incorporated directly (D) and by sprinkling (S): (A, B and C) surface and cross section of control film; (D, E and F) surface and cross section of 40% BLD film; (G, H and I) surface and cross section of 40% BLS film; (J, K and L) surface and cross section of 40% MLD film; (J, K and L) surface and cross section of 40% MLS film. Images A, C, F, I, L and O with 250x magnification and images B, D, E, G, H, J, K, M and N with 1000x magnification.

Thickness of films significantly increased ($p<0.05$) with increasing concentration of BL and ML powder incorporated directly (D) and by sprinkling (S) as compared to control film (0%) (Table 1), although, in all cases, the film-forming suspension volume by plate area remained constant. The increased solid content and possible agglomeration of BL and ML in polymer matrix, evidenced by prominences on the surface of films by SEM (Figure 1), could explain this result.

Table 1. Thickness, solubility in water and permeability to water vapor of films with 0%, 20%, 30% and 40% of freeze dried blackberry pulp (BL) and freeze dried microencapsulated blackberry pulp (ML) directly incorporated (D) and by sprinkling (S).

Films	Thickness (mm)	Solubility in water (%)	Permeability to water vapor (g.mm/m^2.day.kPa)
0%	0.065 ± 0.005 [d]	14.18 ± 0.26 [g]	3.62 ± 0.27 [hdfge]
20% BLD	0.092 ± 0.005 [dc]	21.64 ± 0.93 [fe]	3.03 ± 0.10 [hfge]
30% BLD	0.121 ± 0.014 [bdaac]	22.76 ± 1.13 [dfe]	6.63 ± 0.39 [bc]
40% BLD	0.154 ± 0.054 [bac]	26.14 ± 1.16 [dce]	5.40 ± 0.47 [dce]
20% BLS	0.082 ± 0.006 [d]	19.26 ± 1.68 [fe]	1.67 ± 0.12 [h]
30% BLS	0.098 ± 0.013 [bdc]	24.65 ± 1.95 [dce]	2.38 ± 0.45 [hg]
40% BLS	0.113 ± 0.016 [bdac]	27.98 ± 2.69 [bc]	3.47 ± 0.14 [hfge]
20% MLD	0.150 ± 0.024 [bac]	21.74 ± 1.70 [fe]	2.43 ± 0.36 [hg]
30% MLD	0.146 ± 0.022 [bac]	22.18 ± 0.36 [dfe]	7.80 ± 0.07 [ba]
40% MLD	0.154 ± 0.010 [ba]	23.69 ± 0.77 [dfce]	9.23 ± 0.47 [a]
20% MLS	0.147 ± 0.017 [bac]	27.14 ± 2.45 [dc]	4.42 ± 0.17 [dfge]
30% MLS	0.153 ± 0.005 [bac]	33.89 ± 2.50 [a]	5.08 ± 1.87 [dfce]
40% MLS	0.173 ± 0.011 [a]	32.33 ± 1.39 [ba]	5.57 ± 1.05 [dc]

*Same letters in the same column show no statistical difference (p > 0.05).

Incorporated films with BL and ML by sprinkling were more water soluble than films with blackberry powder incorporated directly. Differently to direct incorporation, the incorporation by sprinkling allowed particles of powder stayed only in the surface of the films. As blackberry powders were porous and showed a high hydrophilicity, it is believed that, when the films were immersed in water, the particles rehydrated rapidly leading to their solubilization. Solubilization of the particles probably created holes in the surface of the films, which allowed the acess of water molecules into the starch matrix facilitating their solubilization.

Films with only 20% BL and ML presented lower water vapor permeability rates than the 0% film. This behavior was attributed to a better dispersion of blackberry powder at low concentrations in the film-forming solution increasing compactness of the films, which may have hindered the passage of water molecules. It is also possible that presence of blackberry powder particles within the starch matrix, as well as on the surface, has introduced a tortuous path for the passage of water molecules, which may have led to a decreasing behavior in water vapor permeability. At concentrations above 30%, there was an increase in water vapor permeability due to the presence of agglomerated blackberry dust particles.

4. Conclusions

The type of incorporation and concentration of the blackberry into filmogenic solution (directly or by sprinkling) influenced the structure, thickness, water solubility and permeability to water vapor of resulting films.

5. References

[1] Espitia, P.J.P.; Du, W.-X.; Avena-Bustillos, R.D.J.; Soares, N.D.F.F.; McHugh, T. H. Edible films from pectin: Physical–mechanical and antimicrobial properties – A review. Food Hydrocolloids 2014, 35, 287–296.

[2] Machado, A.P.F.; Pasquel-Reátegui, J.L.; Barbero, G.F., Martínez, J. Pressurized liquid extraction of bioactive compounds from blackberry (*Rubus fruticosus* L.) residues: a comparison with conventional methods. Food Research International 2015, 77, 675–683.

[3] Ferrari, C.C.; Ribeiro, C.P.; Aguirre, J.M. Spray drying of blackberry pulp using maltodextrin as carrier agent. Brazilian Journal of Food Technology 2012, 15, 157-165.

[4] Yamashita, C.; Chung, M.M.S.; dos Santos, C.; Mayer, C.R.M.; Moraes, I.C.F.; Branco, I.G. Microencapsulation of an anthocyanin-rich blackberry (spp.) by-product extract by freeze-drying. LWT - Food Science and Technology 2017, 84, 256-262.

[5] Ré, M.I. Microencapsulation by spray drying. Drying Technology 1998, 16, 1195-1236.

[6] Shi, A.-M.; Wang, L.-J.; Li, D.; Adhikari, B. Characterization of starch filmscontaining starch nanoparticles: part 1: Physical and mechanical properties. Carbohydrate Polymers 2013, 96, 593–601.

[7] A.O.A.C. Official Methods of Analysis. 18th ed. Association of Official Analytical Chemists, Gaithersburg, Maryland, 2006.

[8] Zavareze, E. da R.; El Halal, S.L.M.; Pereira, J.M.; Radünz, A.L.; Elias, M.C.; Dias, A.R.G. Chemical characterization and extraction yield of rice starch with different amylose contents. Brazilian Journal of Food Technology 2009, II SSA, janeiro.

[9] Nogueira, G.F.; Fakhouri, F.M.; de Oliveira, R.A. Extraction and characterization of arrowroot (Maranta arundinaceae L.) starch and its application in edible films. Carbohydrate Polymers 2018, https://doi.org/10.1016/j.carbpol.2018.01.024

[10] Gontard, N.; Guilbert, S.; Cuq, J.L. Edible wheat gluten films: influence of the main process variables on film properties using response surface methodology. Journal of Food Science 1992, 57, 190-199.

[11] ASTM. Standard test methods for water vapor transmission of materials. Method E96-80. In: Annual book of American Standard Testing Methods. Philadelphia: ASTM, 1989.

Investigation of spray agglomeration process in continuously operated horizontal fluidized bed

Du, J. [a*]; Bück, A.[a,b]; Tsotsas, E.[a]

[a] NaWiTec, Thermal Process Engineering, Otto von Guericke University Magdeburg.

[b] Institute of Particle Technology, FAU Erlangen-Nuremberg, Cauerstraße 4, D-91058 Erlangen, Germany.

*E-mail of the corresponding author: jiajie.du@ovgu.de

Abstract

Spray fluidized bed agglomeration is an important process in particle formation and is widely used in the chemical, pharmaceutical and food industry. In this study a continuously operated horizontal fluidized bed is employed to obtain a continuous agglomeration process. It is conducted with glass beads (d_{st}=200 μm) and water-based binder hydroxy-propyl-methyl-cellulose (HPMC) sprayed by three top nozzles. The steady state is reached and samples are taken periodically and analyzed. The influence of fluidization air temperature and configurations of internal weirs are studied.

Keywords: horizontal fluidized bed, spray agglomeration, continuous process

1. Introduction

Size enlargement processes have the purpose of changing the physical properties of powders in order to meet desired product specifications such as size, shape, flowability, density, solubility or porosity [1]. Among various heavily used apparatuses, spray fluidized bed agglomerator is an important one and widely used in the chemical, pharmaceutical and food industry. The most significant advantage of this apparatus is that it allows the combination of binder dispersion and drying in a single process [2]. In the agglomeration process, fluidized particles are wetted by spraying a liquid; agglomeration occurs when a wet particle collides with another particle forming initially a liquid bridge which solidifies by drying. A lot of attention has been paid on the study of this process but most of them are batch operated process. Among them the effect of process parameters such as binder addition rate, binder viscosity, fluidization velocity, air temperature, the morphology of agglomerates as well as the simulation based on population balance equation and Monte Carlo method have been studied [3,4,5,6]. However, many producers look for a continuous process for economic reasons instead of a batch process with high labor and dead-time. In this study, a horizontal fluidized bed is employed because it has serval advantages such as the possibility to control different processes in separated chambers and possibility to control particle residence time distribution.

2. Materials and Methods

2.1. Plant and materials

In this paper, the agglomeration process was performed in a continuously operated horizontal fluidized bed (GF/Procell 20, Glatt GmbH, Weimar, Germany). A schematic flow diagram of the experimental fluidized bed is shown in Fig. 1. The dimensions of the horizontal fluidized bed are 1m in length and 0.2m in width. By installation of internal weirs, the bed can be separated into four chambers. With different settings of internal weirs, underflow and overflow can be achieved. To control the bed height, different heights of outlet weirs can be applied. The particles inlet speed was controlled by a twin screw feeder together with a rotary valve at the end of the feeding pipe which was used to isolate the bed from the atmosphere. The outlet was controlled by a rotary valve with constant rotation speed. The pulse injection of the tracer used in the residence time distribution measurement is enabled by an additional sewer port in the steady state of the system. The fluidization air was provided by two fans; one was at inlet and one at outlet. By adjusting the power of the two fans, the pressure inside the bed can be controlled. The fluidization air was heated by an electrical heater being separated into four pipes and entering the bed. The air speed and temperature in each pipes can be controlled by the open ratio of the two valves separately. Process parameters such as the fluidization air speed, the heater temperature, the open ratio

of valves, the spraying rate and etc. were controlled Distributed Control System station. The cross section of the upper side of the process chamber was expanded to reduce gas velocity and, thus, enforce the return of entrained particles in the fluidized bed. For the spraying system, maximum three top spray nozzles provided by Düsen-Schlick GmbH, Untersiemau, Germany, model 940/3 with orifice diameter 0.8 mm, two-fluid nozzle, could be used. The nozzles are placed at a height of 320 mm from the distributor. The spray rate was controlled by a piston pump and the atomizing air pressure was controlled by an adjustable valve.
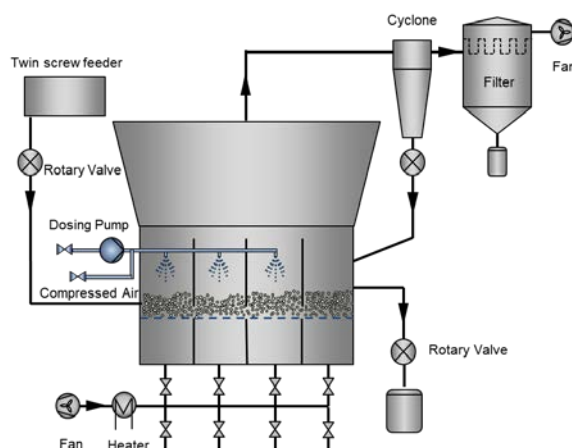
Fig. 1 Schematic representation of the plant GF/Procell 20 (Glatt GmbH).

The particles used for the experiments were glass beads (Sigmund Lindner GmbH, Germany), had a high sphericity of 0.89 and density 2500 kg/m^3, and were nearly mono-disperse. Measurements by Camsizer (Retsch Technologies GmbH, Haan, Germany) resulted in a very narrow range size distribution of the primary particles, with diameters between 150 µm to 320 µm and the Sauter diameter of 200 µm. The binder used was hydroxy-propyl-methyl-cellulose (HPMC, trade name Pharmacoat 606, from Shin-Etsus, Japan) water solution.

2.2. Experimental parameters

To study the influence of process parameters, seven experiments were carried out, denoted by No. 1-7 (Table 1). Reference Exp. NO. 2 was defined and then only one of the process variables was changed at a time. For all experiment, the feed rate was controlled at 400

g/min and fluidization air speed at 1.1 m/s. The binder used was 4wt% and relative air pressure in the nozzle was 1 bar. The influence of fluidization air temperature was studied by running experiments with different air temperature at 100, 80, 70 and 60°C. To study the influence of the configuration of internal wires, three internal weirs were employed and the gap height between the weirs and the air distribution plate were 10 and 5 mm. For all experiment, the outlet weir height was 200 mm.

To start the experiments, the plant was heated to the needed temperature then the feeder was started for the feeding. Apart from this metered feed, an initial feed of 6 kg of glass beads was fed instantly to promote the growth of the bed. The steady state was reached when the inlet and outlet mass flow rate of the particles were equal. After this stage, the binder pump was started. Samples were collected at the outlet periodically and used for analysis. The process time in each experiment was 130 -150 min.

Table 1. Main experimental parameters

Exp. NO.	Inlet Air Temperature T_a [°C]	Spray rate $\dot{m}_b$ [g/min]	Number of internal Weirs	Gap height in underflow [mm]
1	100	72	-	-
2 (Ref.)	80	71	-	-
3	70	73	-	-
4	60	71	-	-
5	80	72	3	10
6	80	71	3	5

2.3. Experimental result analysis

In the first set of experiments the fluidization air temperature has been varied. As Fig. 2 displays, the largest Sauter diameters of agglomerates were obtained at the lowest air temperature experiment NO.4 at air temperature 60°C. Agglomeration rate decreased with the increase of air temperature. At lower temperature, the process took a longer time to reach the steady and the lower temperature also introduced more fluctuations because more particles stuck to the wall due to the higher moisture inside the bed. A decrease in agglomeration rate with increasing gas inlet temperature was also reported in batch operated agglomeration process [4,5]. At higher temperature binder droplets evaporate and shrink faster after having been sprayed from the nozzle, which decreases the height of sessile droplets. Some spray droplets may not even find a chance to hit the particle surface. In both cases, the number of particle collisions leading to agglomeration decreases [7]. From what showed in SEM pictures, at higher temperature despite using the same amount

of binder, there are more dried droplets layering on the outer surface of particles, meaning that the process tends to move from agglomeration towards coating.
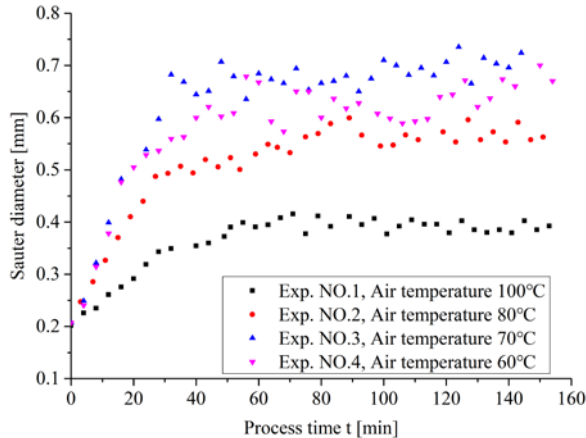
Fig. 2 Sauter diameter versus time at different air temperatures.

Fig. 3 shows the Characteristic diameters $X_{10,3}$, $X_{50,3}$, $X_{90,3}$ and bed mass change during the process. Compared to the Sauter diameter the same trend was observed that at a lower temperature a higher agglomeration rate and bigger agglomerates are achieved, combined with a wider size distribution of agglomerates at the end of the experiment. With bigger agglomerates the process needs longer time to reach the steady state. There was a fast increasing of bed mass in the first 20 min of spraying. Bigger agglomerates also lead to a higher bed mass. When the air temperature was 70 and 60°C, a continuous increasing of bed mass was seen after 100-120 min which means that there is a high risk of defluidization in these two experiments.

In the second set of experiments, the internal weirs were used and the gap height was changed to see the influence of internals weirs on particle size distribution. The internal weirs are commonly used in such horizontal fluidized bed to control the flow behavior of particles. As Fig. 4 displays, the smallest Sauter diameter was achieved from the experiment with internal weirs which have the smallest gap height. During the present experiments, a slower rate of size increase was observed when the internal weirs were installed. The particle size distribution shows the internal weirs influence the flow behavior of the particles which could be shown more clearly in the residence time distribution measurement. By the installation of the weirs, more accessories were installed inside the bed which means more particles could stick. During the process, a hammer was used to knock the wall to clean the sticking particles on the walls and nozzles to prevent the formation of big lumps or the blocking of nozzles.
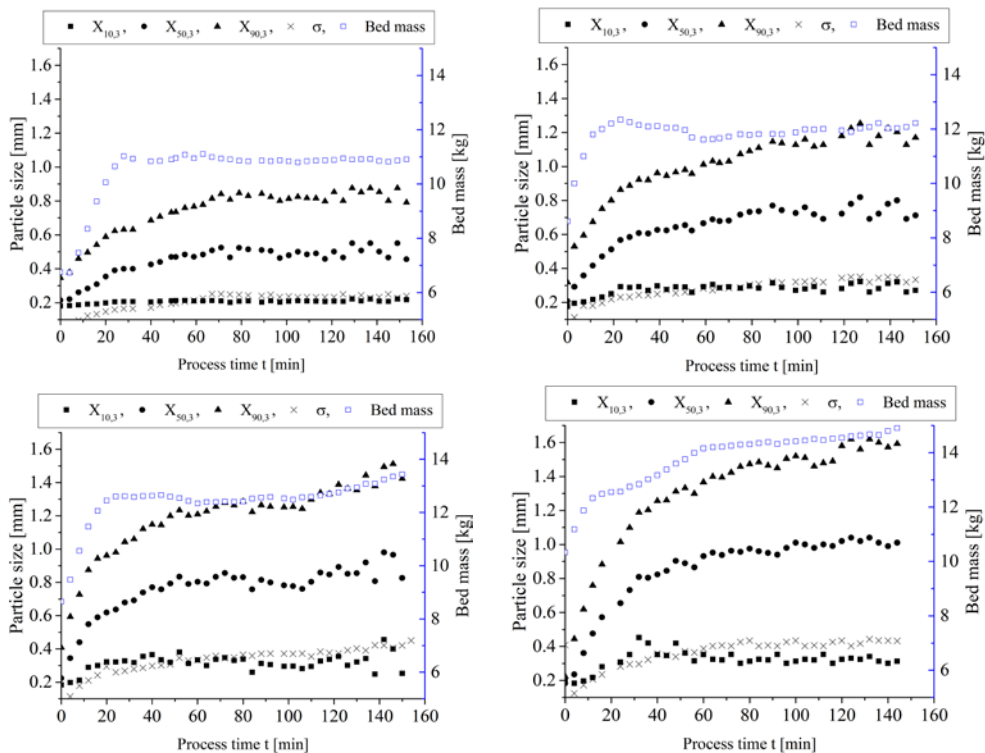
Fig. 3 Characteristic diameter $X_{10,3}$, $X_{50,3}$, and $X_{90,3}$, the standard deviation σ and bed mass of experiments at temperature 100 (left, top), 80 (right, top), 70 (left, bottom) and 60°C (right, bottom).
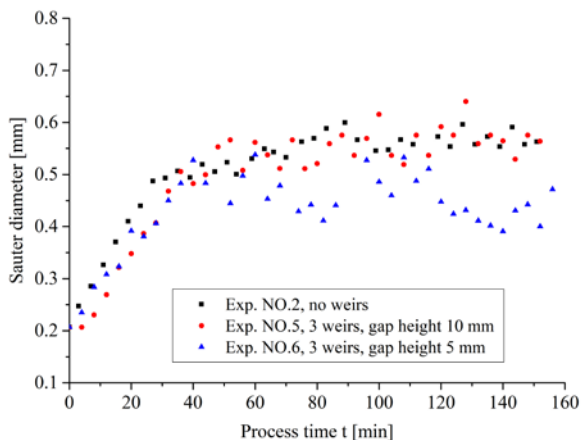
Fig. 4 Sauter diameter versus time with different internal weirs configurations.
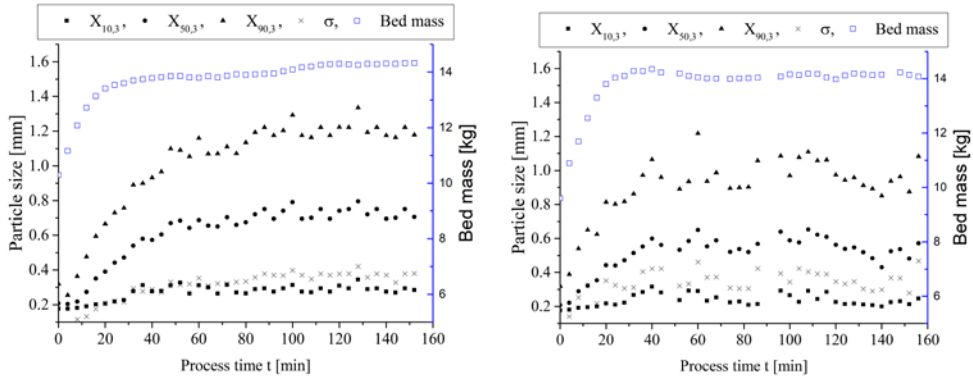
Fig. 5 Characteristic diameter $X_{10,3}$, $X_{50,3}$, and $X_{90,3}$, the standard deviation σ and bed mass of experiments with internal weirs gap height 10 mm (left) and gap height 5 mm (right).

In Fig. 5, when compared to the reference experiment, it was observed that with internal weirs the starting bed mass of experiment is higher than without internal weirs because by separating process chambers, the spray has less influence on the fluidization of particles in last chamber. The internal weirs with gap height 10 mm have little influence on the size of agglomerates as well as on the width of size distribution. When the gap height was decreased to 5 mm, they decreased the size of agglomerates and a higher standard deviation of particle size distribution was observed which means a wider size distribution was achieved.

3. Conclusions

In this work, a continuously operated horizontal fluidized bed was used to conduct a spray agglomeration. The influence fluidization air temperature and configuration of internal weirs is presented. It was observed that an increase of air temperature results in decrease of agglomerate size and the width of size distribution combine with more fluctuations during the process. The internal weirs with gap height 10 mm have little influence on the size distribution of products, but when the height is decreased to 5 mm, they will decrease the size of products while increasing the width of size distribution. In future work, more parameters will be changed to study the influence the parameters such as particle feed rate, binder concentration and spray rate. To describe the continuous spray agglomeration, process a stochastic modelling approach based on a Monte Carlo method will be developed and compared with the experimental results.

4. Acknowledgements

5. Nomenclature

T	temperature	℃
$\dot{m}$	mass flow rate	g/min
$X_{10,3}$	particle size Q3(x_{10})=0.1	mm
$X_{50,3}$	particle size Q3(x_{50})=0.5	mm
$X_{90,3}$	particle size Q3(x_{90})=0.9	mm

Greek letters

σ	standard deviation	mm

Subscripts

a	air
b	binder

6. References

[1] Ennis, B. Agglomeration and size enlargement session summary paper. Powder Technology 1996, 88, 203–225.

[2] Litster, J.; Ennis, B. The Science and Engineering of Granulation Processes; Kluwer Academic Publishers, 2004.

[3] Thielmann, F.; Naderi, M.; Ansari, M.; Stepanek, F. The effect of primary particle surface energy on agglomeration rate in fluidized bed wet granulation. Powder Technol 2008, 181, 160–168.

[4] Terrazas-Velarde, K.; Peglow, M.; Tsotsas, E. Kinetics of fluidized bed spray agglomeration for compact and porous particles. Chemical Engineering Science 2011, 66(9), 1866–1878.

[5] Dadkhah, M.; Tsotsas, E. Influence of process variables on internal particle structure in spray fluidized bed agglomeration. Powder Technology 2014, 258, 165–173.

[6] Hussain, M.; Kumar, J.; Tsotsas, E. Modeling aggregation kinetics of fluidized bed spray agglomeration for porous particles. Powder Technology 2015, 270, 584–591.

[7] Tsotsas, E. Influence of drying kinetics on particle formation: A personal perspective, Drying Technology 2012, 30:11-12, 1167-1175.

Finish drying and surface sterilization of bay leaves by microwaves

Kapoor, A.; Sutar, P. P. [*]

[a] Department of Food Process Engineering, National Institute of Technology Rourkela, Odisha, India

*E-mail of the corresponding author: sutarp@nitrkl.ac.in

Abstract

Bay leaves (Laurus nobilis L.) refers to aromatic leaves which are native to minor regions of Asia. In order to extend the shelf life of the bay leaves its water activity and the surface micro-organisms were reduced using microwave heating at different power densities in the range 32.14 to 142.85 Wg^{-1}. Treatment time at each power level was maintained constant at 150 s. The maximum reduction in water activity and moisture content occurred at highest power density. The heating time-temperature profile was obtained at all power levels. TPC, color change and browning index (BI) of bay leaves were measured in order to determine the effect of microwave treatment on microbial reduction and quality. The highest reduction in TPC was found in leaves heated at 142.85 Wg^{-1} power density along with acceptable quality parameters of the treated bay leaves.

Keywords: Bay leaves; Microwave heating; TPC; Colour change.

1. Introduction

Bay leaves hail from the bay tree and originally belongs to the family Lauraceae which is scientifically known as Laurus nobilis. It is believed to have been originated in Asia minor region, from where it is distributed to all over Mediterranean region and other parts of Asia. Bay leaves began to find its medicinal use during the European Middle Ages. Bay leaves belonging to various different origins were studied by different researchers for its chemical composition. In almost all the cases, 1,8-cineole was found to be the major component with percentages ranging between 31.4% and 56% [1,2]. Other compounds that are also present in appreciable amount include trans-sabinene hydrate, linalool, a-terpinyl-acetate, sabinene, methyl eugenol and eugenol [3]. The various benzene compounds like eugenol, methyl eugenol and elemicin, present in bay leaves with percentages ranging between 1% and 12%. These compounds are responsible for the sensory qualities of bay leaves [4]. The essential oil content of bay leaves varies with the source of origin of the bay leaves and it is different for bay leaves obtained from different resources. Generally, the essential oil content of bay leaves ranges from 1% to 3% on a fresh weight basis. Bay leaves have a strong aroma but are also quite bitter. The bitterness of bay leaves can be reduced to an acceptable extent by drying. Thus the essential oils in dried bay leaves contribute to a strong, spicy aroma and are widely used throughout the world as a flavor enhancer in varieties of foods. Being one of the best-known flavoring leaves all over the world, they find their use in soups, sauce, sausages, stews, pickles and also act as an essential ingredient of the herb mixes. As a medicinal plant, bay leaves have been used as a cure for rheumatism, earaches and skin rashes. In addition, it has been also employed as a stomatic, carminative, astringent, stimulatory, emetic, emmenagogic, diaphoretic, abortifacient agent, and as an insect repellent. Essential oil obtained from bay leaves has also found its use in the cosmetic industry. Micro-organisms exist in the dried bay leaves which affects the shelf life. In order to extend the shelf life of the bay leaves its water activity must be decreased and the microbes present in the surface must be inactivated. Thus, it requires finished drying and surface sterilization. Recently, microwave heating has gained popularity due to its various advantages like quick and uniform heating, high-temperature short time treatment, inactivation of microbes without much damage to food quality [5]. Considering all the above reviews, this study aims to carry out microwave finish drying and surface sterilization of bay leaves.

2. Materials and Methods

2.1. Raw materials

The bay leaves were collected from the local market of Rourkela, Odisha, India. The samples collected were stored in a refrigerator (4°C) until usage to prevent any type of quality deterioration in the product.

2.2. Determination of moisture and water activity

Moisture content and the water activity were determined for both the control untreated samples and the microwave treated samples. For determination of the moisture content, vacuum oven method was used. The water activity of the conditioned sample was measured using water activity meter (Rotronic, HC2-AW, Rotronic measurement solution, Switzerland) at initial temperature 20.02 °C and relative humidity 53%.

2.3. Microwave finish drying

2.3.1. Experimental Setup

Finished drying and surface sterilization of the bay leaves were carried out in a microwave oven. A programmable domestic microwave oven (Samsung, Model-CE73JD) with a maximum output of 800 W at 2450MHz was used for the experiments. The dimensions of the microwave cavity were 310 mm width, 290 mm height, and 220 mm depth. The oven was fitted with a fan, a glass turntable (30 cm diameter) and a digital controller to adjust the pulsation of microwave power and total heating time. Schematic diagram of the microwave heating system is shown in Fig. 1. The efficiency of the microwave oven was calculated according to USFDA (United State Food and Drug Administration) procedure at different power levels and the average efficiency was determined. The heat absorbed by water (220 g) was equated to the input energy[6]. During the drying process, the microwave oven was operated at five different power densities 32.14, 53.57, 80.35, 107.14 and 142.85 Wg^{-1} and a constant treatment time was maintained at 150 s. The surface temperature of the bay leaves was regularly measured at an interval of 10 s using infrared sensor (IRL380-KUSAM MECO, India) up to 150 seconds at each power density. For accuracy in results, the temperature was measured at three different points each time and its average was taken as the final temperature.
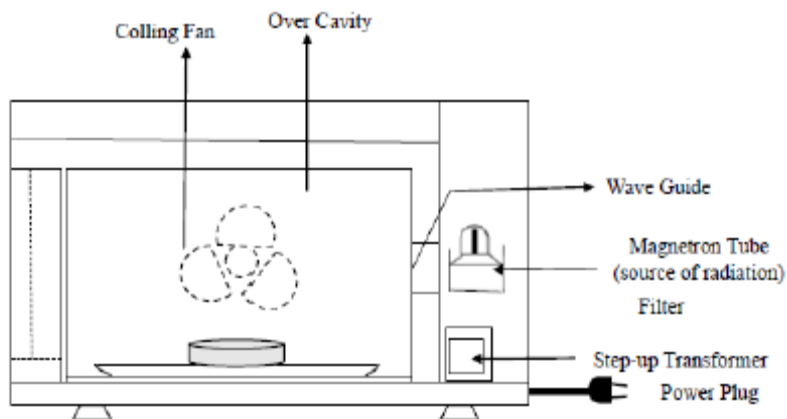
Figure 1. Schematic diagram of the microwave heating system

2.4. Microbial analysis

Microbial analysis was performed on the bay leaves in order to find the effect of microwave treatment on the reduction of microbial contamination. In this regard, the Total Plate Count (TPC) per gram was done both for the control sample and the final samples treated at different microwave power densities.

2.4.1. Culture Preparation

Firstly, the culture media was prepared by mixing 28g of nutrient agar with 1000 mL of distilled water. It was then properly mixed with help of a stirrer and heated up to 60°C for proper dissolution of the nutrient agar in the distilled water. Media was then transferred to the glass bottles leaving some headspace at the top. Glass bottles were autoclaved at 15 psi at 121°C for 15 minutes. After completion of the autoclave heating, the media was allowed to cool below 50°C. The media was then poured into pre-sterilized Petri dishes such that a uniform layer of culture (2-3 mm) was obtained. The whole pouring process of the culture media was carried out under laminar flow hood in order to prevent any kind of contamination.

2.5. Color analysis

The color of the fresh and treated bay leaves was measured by scanning them with help of HP scanner. The scanned samples were then analyzed with help of Adobe Photoshop software. The color value of samples was measured at three different points for accuracy and expressed as L (whiteness or brightness/darkness), a (redness/ greenness) and b (yellowness/ blueness) at any time, respectively. The total color change (ΔE) indicates the overall color change and quantification was done using the equation given below [7]:

$$\Delta E = [(L-L^*)^2 + (a-a^*)^2 + (b-b^*)^2]^{0.5} \qquad (1)$$

where L, a, and b are respective values measured during high power short time microwave finish drying. The L^*, a^*, and b^* are values of the fresh sample (before microwave finish drying).The browning index (BI) were calculated from L, a, b values and used to describe the brown color produced due to heat accumulation during the decontamination process. The equation to calculate BI is given below:

$$BI = [100(x - 0.31)]/0.17 \qquad (2)$$

Where

$$x = (a + 1.75\ L)/(5.645L + a - 3.012b) \qquad (3)$$

3. Results and Discussion

3.1. Effect of power density on moisture content and water activity

The moisture content and the water activity was measured for both the control and treated samples. The results obtained showed that the average initial moisture content of bay leaves was 10.68% (wb) which was reduced up to safe moisture content. The maximum reduction in the moisture level occurred when bay leaves were treated at the power density of 142.85Wg^{-1}. In this case, final moisture content obtained was 1.24% (wb). Similar trends were obtained for the water activity of bay leaves; initial average water activity of bay leaves was measured to be 0.89. The maximum reduction in the water activity occurred at 142.85 Wg^{-1} and reached to 0.18. Table 1 gives the moisture content and the water activity for bay leaves treated at different power densities.

Table 1. Final moisture content, water activity and TPC log reduction in the microwave treated bay leaves

Power Density (W g^{-1})	Final Moisture Content (%, wb)	Water activity	Log Reduction	ΔE	BI
32.14	2.23	0.41	0.115	0.58	49.90
53.57	1.87	0.35	0.291	0.65	55.78
80.35	1.75	0.27	0.532	1.20	58.92
107.14	1.66	0.23	0.780	1.39	63.59
142.85	1.24	0.18	1.069	1.62	69.92

3.2. Effect of microwave power density on product temperature and microorganisms

Bay leaves samples were treated for 150 seconds at each of the five microwave power densities. The surface temperature of the bay leaves was measured regularly during the microwave treatment of bay leaves. The time-temperature profile obtained at different power densities showed that maximum surface temperature reached was 101.6°C in the case when bay leaves were treated at 142.85Wg^{-1} for 150 s. While minimum surface temperature reached was 75.85°C when bay leaves were treated at 32.14 Wg^{-1} for 150 s. Total plate count (TPC) was done for both control and microwave treated samples of bay leaves. Results showed that plate count was minimum for the sample treated at 142.85Wg^{-1}. While the treatment at 32.14Wg^{-1} obtained a maximum number of plate counts. Total log reduction was also calculated for samples treated at different power densities and it ranged from 0.115 to 1.069. The log reduction at different power densities is given in Table 1.

3.3. Effect of microwave power density on color change and browning index

Color analysis was performed to determine the color change (ΔE) which was encountered during the microwave treatment of the bay leaves. Browning Index (BI) was also calculated for both initial and the microwave treated samples. Results obtained showed that maximum color change of 1.62 was obtained when the sample was treated at 142.85 Wg^{-1}. Similar results were obtained for Browning Index (BI) that is a maximum BI value of 69.92 was obtained for microwave treatment at 142.85 Wg^{-1}.

4. Conclusions

Maximum water activity reduction from 0.89 to 0.18 occurred at 142.85 Wg^{-1} power density. Microbial analysis was performed in order to determine the effect of microwave treatment on microbial reduction of bay leaves. TPC was obtained for fresh as well as microwave treated samples. Maximum log reduction (1.069) was achieved in the sample treated at 142.85 Wg^{-1} power density for 150 seconds. The color change was also quantified and the Browning Index (BI) was measured which indicated the less effect of microwave treatment on the color of the product. It can be concluded from the results that high power density short time microwave finish drying turns out to be an effective alternative for drying and surface sterilization of bay leaves with acceptable quality parameters.

5. Acknowledgements

6. References

[1] Doymaz, I; Pala, M. Hot-air drying characteristics of red pepper. Journal of Food Engineering 2002, 55, 331–335.

[2] Drouzas, A.E; Tsami E; Saravacos, G.D. Microwave/ vacuum drying of model fruit gels. Journal of Food Engineering 1999, 39, 117–122.

[3] Demir, V; Gunhan, T; Yagcioglu, A.K; Degirmencioglu, A. Mathematical modelling and the determination of some quality parameters of air-dried bay leaves. Biosystems Engineering 2004, 88, 325–335.

[4] Feng, H. Analysis of microwave assisted fluidized-bed drying of particulate product with a simplified heat and mass transfer model. International Communications in Heat and Mass Transfer 2002, 29, 1021–1028.

[5] Shirkole S. S. and Sutar P.P. High power short time microwave finish drying of paprika (*Capsicum annuum* L.): development of models for moisture diffusion and color degradation. Drying Technology 2018, DOI:10.1080/07373937.2018.1454941

[6] USFDA. United State Food and Drug Administration. HEW publication (FDA), Rockville, Maryland, Montgomerypp, Procedure for field testing microwave oven, 1977, pp 13

[7] Behera G, Sutar PP, Aditya S. Development of novel high power-short time (HPST) microwave assisted commercial decontamination process for dried turmeric powder (Curcuma Longa L.). Journal of Food Science and Technology. 2017 Nov 1;54(12):4078-91.

Moisture sorption characteristics of pistachio

Koç, B. [a*]; Atar, G.; Çaglar, N.

[a] Gaziantep University, Faculty of Fine Arts, Department of Gastronomy and Culinary Arts, Gaziantep, Turkey

* kocbanu@gmail.com

Abstract

In this study, the moisture adsorption isotherm of pistachio was determined at 25°C and relative humidity (10-90%), using the standard static, gravimetric method. Eleven sorption models were tested to fit the experimental data. A non-linear regression analysis method was used to evaluate the constants of the sorption equations. The GAB equation gave the best fit to the experimental data for a wide range of water activity, while BET gave the best fit for a water activity range of 0.1-0.5. The agreement between experimental and predicted values of these models was found to be satisfactory.

Keywords: Moisture adsorption isotherm; Sorption model; Pistachio

1. Introduction

Pistachios are one of the oldest edible nuts known to mankind, which are originated from Asia Minor, and are cultivated from Pakistan to Greece and even Italy and U.S.A. But pistachios originated from Gaziantep Region of Turkey, are worldwide known with its high quality and rich distinctive flavor. Pistachios are subjected to various processes after they are harvested. Proper harvesting and postharvest handling are two key activities in achieving maximum yield of good quality pistachio nuts, which effect marketability and profit. Process steps may vary with respect to desired product. For consuption as snack, processing of the nuts includes dehulling, washing, drying to 60–80 g/kg moisture (related to whole kernel) in dryers at 65°C for 6 to 7 h or by sun-drying for 3 to 4 d, salting by immersion in 100 g/kg sodium chloride solution for 15 min, roasting at 150 to 180°C for 30 min and packaging [2]. In this operation, water absorption and water vapor adsorption and desorption processes are very important, the air-watersolid equilibrium relations in the pistachio nuts determine the optimal conditions of post-harvest physical treatments and storage [3]. The water activity (a_w) of food describes the energy state of water in the food, and hence, its potential to act as a solvent and participate in chemical/ biochemical reactions and growth of microorganisms. It is an important property that is used to predict the stability and safety of food with respect to microbial growth, rates of deteriorative reactions and chemical/physical properties [4]. Sorption isotherms can also be used to design their suitable packaging and storage conditions, and to select proper ingredients for preparation of a formulated intermediate moisture food. However, very limited data are available on sorption isotherms of different pistachio varieties [1]. It is well known that sorption isotherms of foodstuffs are very important for design, modelling and optimization of many processes. Hossain et al. [5] pointed out the importance of those data in drying, aeration, predicting of stability and quality during packaging and storage of food. Moisture sorption isotherms of foods provide critical information that can be used in predicting shelf-life by theoretical calculation. Moisture sorption isotherms can also be used to investigate structural features such as specific surface area, pore volume, pore size distribution, and crystallinity of food products. Many research studies on the sorption isotherms of certain foods, temperature dependence of isotherms, determination of heat of sorption, and mathematical models to represent sorption isotherms have been reported in the literature [6]. Many theoretical, semi-theoretical and empirical sorption models to describe the sorption behavior of foods other substrates have been proposed in the literature [7]. The objectives of this study were to determine the water sorption behavior of the pistachios originated from Gaziantep Region of Turkey at 25°C and relative humidities ranging from 10 % to 90% to propose a mathematical model for prediction of its sorption behaviour as a function of temperature, to evaluate the constants of sorption isotherm models.

2. Materials and Methods

2.1. Materials

Roasted pistachio sample was obtained from a local market at Gaziantep. All chemicals used in the preparation of saturated salt solutions were reagent grade (Merck) and water used was deionized distilled water.

2.2. Determination of Sorption Characteristics of Roasted Pistachio

A static gravimetric method was used to determine the sorption isotherms at 25 ºC of the roasted pistachio nuts. 10 saturated salt solutions with an average water activity of between 0.10 and 0.90 were prepared for the glass jars which can be closed to prevent air ingress. 0.3g pistachio samples were weighed and placed together with two witness samples to each jar. A small amount of toluene was placed in jars with saturated salt solutions with high water activity to prevent microbial spoilage. After the jars were closed tightly, they were placed to an oven set at a constant temperature of 25 ºC. Samples were weighed at 1-week intervals. The weighing continued until no difference more than 0.001 g it was found. The equilibrium moisture content of the samples was determined by drying at 105 ºC for 4 hours. The equilibrium moisture content was plotted against the water activities to form the moisture sorption isotherms. The water activity values of the saturated salt solutions at 25°C are given in Table 1.

Table 1. Water activity values of the saturated salt solutions at 25ºC used in the experiment

SALT	aw (25 ºC)
LiCl	0,1130
CH_3COOK	0,2251
$MgCl_2$	0,3278
K_2CO_3	0,4316
$Mg(NO_3)_2$	0,5289
NaBr	0,5757
$SrCl_2$	0,7085
NaCl	0,7529
NH_3SO_4	0,8099
KCl	0,8430

The experimental sorption data of all samples at three different temperatures was fitted to sorption equations (with six two-parameters, five three–parameters and one four parameter) shown in Table 2. The parameters of the sorption models were estimated from the experimental results using nonlinear regression analysis (SPSS 13.0 for Windows), which

minimizes the residual sum of squares. Best-fitting equations were evaluated with the mean relative percentage deviation (P) value and the percentage root mean squares error (RMSE) value. P value and RMSE value are defined as

$$P = \frac{100}{N} \sum_{i=1}^{N} \frac{|Mexp - Mcal|}{Mexp} \qquad (6)$$

$$RMSE = 100 \sqrt{\frac{\sum (Mcal - Mexp)^2 / Mexp}{N}} \qquad (7)$$

where Mexp and Mcal are experimental and predicted moisture content values, respectively, and N is the number of experimental data. A model was considered acceptable if the P values and RMSE values were below 10% and R^2 values were higher than 0.90.

Table 2. Equations describing the sorption equilibrium isotherms

Name of the Equation	Equation	
BET (Brunauer, Emmet and Teller) [8]	$M = \dfrac{M_0 c a_w}{[(1 - a_w) + (c - 1)(1 - a_w)a_w]}$	(1)
GAB (Guggenheim-Andersen-de Boer) [9]	$M = \dfrac{M_0 C K a_w}{[(1 - K a_w)(1 - K a_w + C K a_w)]}$	(2)
Halsey [10]	$a_w = \exp[-k/M^n]$	(3)
Henderson [11]	$1 - a_w = \exp(-kTM^n)$	(4)
Oswin [12]	$M = k \left(\dfrac{a_w}{1 - a_w} \right)^n$	(5)

3. Results and Discussion

Sorption isotherms are graphs that provide very useful information about the state of the food, determined by plotting the water content of the food at constant temperature versus the water activity of the food. These isotherm graphs are basically as follows; adsorption or desorption isotherms obtained by demonstrating the increased water content of the dry food at constant temperature or the decreasing water content of the wet food against the changing water activity [7]. The sorption data of whole pistachio nuts shows remarkable hysteresis in the multimolecular range and in the cappilary condensation range (between R = 0.10- 0.80). Above this region the difference between adsorption and desorption tends to disappear [3]. Several sorption equations (GAB, BET, Simit, Halsey, Henderson, Iglesias-Chirife, Chung-Pfost, Oswin, Caurie, and Langmuir et al.) that considered the relationship between water activity, moisture content of food and water binding energy, were developed to represent the sorption isotherms of the foods. However, these equations do not adequately represent all the food. The reason for this is the high heterogeneity of foods in structure and composition. The

BET equation, which is one of the first sorption equations and widespread employed, can successfully represent the isotherm when the water activity is less than 0.50 [7]. GAB model is about monolayer moisture concept and provides the value of monolayer moisture content of the material, as most other models not have this parameter. The monolayer moisture content (M_0) indicates the amount of water that is strongly adsorbed to specific sites on the surface of food and is regarded as the moisture content affording the longest time with minimum quality loss at a given temperature [13].

The adsorption isotherm of pistachio at 25˚C is shown in Fig. 1. The equilibrium moisture content at each a_w represents the mean value of three replications. The standard deviation of each experimental point (kg/kg dry solids) was within the range of 0.003 to 0.05.
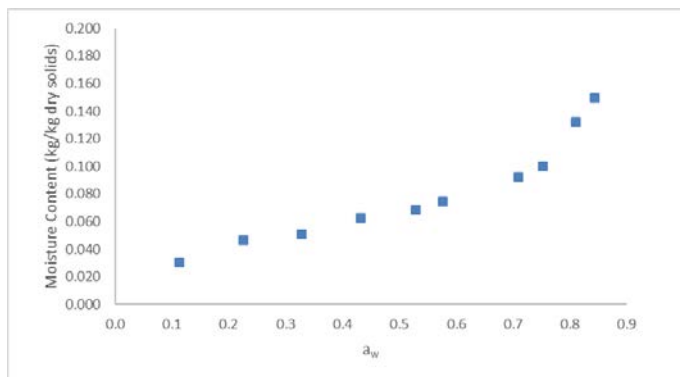
Fig.1 Adsorption isotherms of roasted pistachio 25ºC.

The adsorption isotherms of pistachio showed type II behaviour according to the BET classification, typical of the many sorption isotherms of food [14]. The equilibrium moisture content increases with increasing a_w, at constant temperature. Similar results have been reported in literature for the sorption curve of pistachio [14].

The results of non-linear regression analysis of fitting the sorption equations to the experimental data are presented in Tables 3. The mean relative percentage deviation (P), the percentage root mean squares error (RMSE) and correlation coefficient (R^2) values are also given in Tables 3.

The GAB equation (Table 3) gave the best fit to the experimental adsorption data of pistachio for a wide range of water activity (0.10-0.9). This observation is consistent with the results obtained by Maskan [14]. Constant K value for pistachio in the GAB equation was 0.821. The value of K provides a measure of the interactions between the molecules in multilayers with the adsorbent and tends to fall between energy value of the molecules in the monolayer and that of liquid water. The monolayer moisture content (M_0) helps to define physical and chemical stability of foods since it has a direct influence on lipid oxidation, enzyme activity,

non-enzymatic browning, flavour preservation and product structure. The BET and GAB monolayer moisture contents for pistachio were 0.038 kg/kg dry solid and 0.046 kg/kg dry solid, respectively (Tables 3). M_0 value obtained by the GAB equation was higher than those obtained by the BET model. Moreover, the Oswin, Halsey and Henderson equations (Table 3) gave a satisfactory prediction of the adsorption equilibrium moisture content of pistachio.

Table 3. Estimated parameters and P (%), RMSE (%), R² values of the sorption equations

Model	Parameters	Temperature 25 (˚C)
BET[a]	M_0	0.038
	C	22.79
	P (%)	4.439
	RMSE (%)	0.028
	R^2	0.961
GAB	M_0	0.046
	C	8.457
	K	0.821
	P (%)	5.924
	RMSE (%)	0.456
	R^2	0.984
Halsey	k	0.005
	n	1.834
	P (%)	9.333
	RMSE (%)	2.853
	R^2	0.986
Henderson	k	0.208
	n	1.685
	P (%)	10.99
	RMSE (%)	4.616
	R^2	0.963
Oswin	k	0.068
	n	0.441
	P (%)	6.714
	RMSE (%)	0.573
	R^2	0.975

[a] a_w range for BET equation was 0.11-0.5, only the first four data points were used.

As seen in Table 3, the BET equation gives the lowest P % and RMSE % value in the water activity range 0.11-0.5. Furthermore, the GAB equation representing multi-layer adsorption gave the best fit to the experimental data for pistachio. The experimental adsorption data and the predicted values obtained from different sorption models at 25°C are shown in Fig. 2.

It should be noted that, the goodness of fit of any sorption model to the experimental data shows only a mathematical quality and not the nature of the sorption process [15].
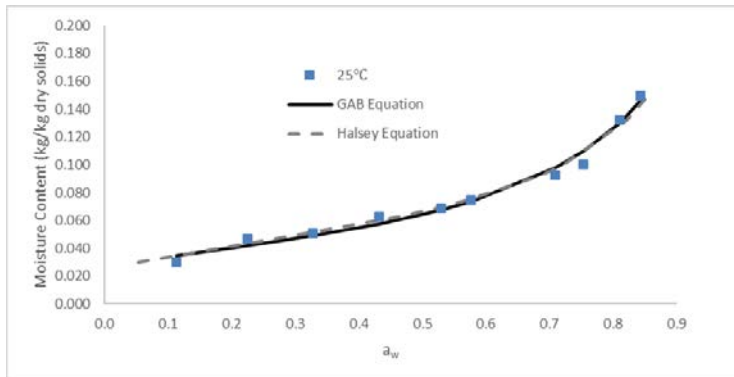
Figure 2. Comparison of experimental and predicted adsorption equilibrium moisture contents of pistachio at 25˚C.

4. Conclusions

The equilibrium moisture content of pistachio increased with increasing water activity at constant temperature. Among the sorption models tested, the GAB equation was recommended for characterising the adsorption behaviour of pistachio in the water activity range of 0.11-0.87. The adsorption data were also expressed by the Halsey equations in the wide range of water activity and by the BET equation in the range of water activity 0.1-0.5.

5. References

[1] Tavakolipour, H. Postharvest Operations Of Pistachio Nuts; Journal Food Science Technology India, 2015, 52(2) ,1124-1130.

[2] Yanniotis, S.; Zarmboutis, I. Water Sorption Isotherms Of Pistachio Nuts; Lebensmittel-Wissenschaft Und-Technologie 1996, 29, 372–375.

[3] Maskan, M.; Karatas, S. Sorption Characteristics Of Whole Pistachio Nuts; Drying Technology 1997, 15 (3&4), 1119-1139 .

[4] Aktas, T.; Polat, R. Changes In The Drying Characteristics And Water Activity Values Of Selected Pistachio Cultivars During Hot Air Drying Journal of Food Process Engineering 2007, 30, 607–624.

[5] Furmaniak, S.; Terzyk, A. P.; Gauden, P.A.; Gerhard, R.; Applicability Of The Generalised D'Arcy And Watt Model To Description Of Water Sorption On Pineapple And Other Foodstuffs; Journal of Food Engineering 2007, 79, 718–723.

[6] Koc, B.; Yilmazer, S. M.; Balkir, P.; Ertekin, K. F.; Moisture Sorption Isotherms And Storage Stability Of Spray-Dried Yogurt Powder; Drying Technology 2010, 28, 816–822.

[7] Erbas, M.; Candal, C.; Kılıc, O.; Mutlu, C.; Determination And Solution Of Moisture Sorption Isotherms Of Foods; Resarch Gate- GIDA 2016, 41 (3),171-178.

[8] Brunauer, S.; Emmett, P.H.; Teller, E. Adsorption of gases in multimolecular layer. Journal of American Chemists Society 1938, 60: 309-319.

[9] Van den Berg, C. Development of B.E.T. like models for sorption of water of foods; theory and relevance. In Properties of Water in Foods. Eds. D. Simatos and J. L. Multon. Martinus Nijhoft, Dordrecht, p. 119, 1985.

[10] Halsey, G. Physical adsorption on non-uniform surfaces. Journal of Chemistry and Physics 1948, 16: 931-937.

[11] Henderson, S.M. A basic concept of equilibrium moisture. Agricultural Engineering 1952, 33: 29-32.

[12] Oswin, C.R. The kinetics of packing life. III. The isotherm. Journal of Chemical Industry 1946, 65: 419-423.

[13] Wani, S. A.;Kumar, P.; Moisture Sorption Isotherms And Evaluation Of Quality Changes In Extruded Snacks During Storage; LWT - Food Science and Technology 2016,74, 448-455

[14] Maskan, M.; Gogus, F.; The Fitting Of Varios Models to Water Sorption Isotherms Of Oistachio Nut Paste; Journal Of Food Engineering 1997, 33, 227-237.

[15] Kaymak-Ertekin, F.; Gedik, A. Sorption isotherms and isosteric heat of sorption for rapes, apricots, apples and potatoes. Lebensmittel- Wissenschaft und Technologie 2004, 37: 429-438.

Influence of ultrasound assist during combined drying on ceramic materials quality and drying kinetics

Pawłowski, A. [*]; Trawińska, W.

Institute of Technology and Chemical Engineering, Department of Process Engineering, Poznań University of Technology, Poznań, Poland.

*E-mail of the corresponding author: Andrzej.Pawlowski@put.poznan.pl

Abstract

Presented in this article studies show the investigation of ultrasound application as a new method for improvement of ceramic materials processing and their influence on mechanical properties of dried samples. Ultrasound were applied during convective and convective-microwave processes carried out in two different temperatures. Obtained results indicate increase of drying rate due to sonification and what's more interesting they affect the material strength parameter. The experiments indicate that the effectiveness of ultrasound assist depends on the drying temperature and such dependency is observed mainy when considering dry product quality parameter.

Keywords: ceramics; hybrid drying; material strength

1. Introduction

Drying of clay like materials is a very important industrial process which allow to achieve ceramics with very useful, specific properties like, e.g. high durability, electrical and thermal resistance and other. It is the first step after molding or casting which lead to reduction of the moisture content and gives a possibility to further calcination of such products. Dry product before calcination needs to have not only very limited moisture content but also can not have fractures. Thus why drying process is so important as it contributes into final product quality or possibility for postprocessing of such product.

To achieve a good quality of dried products the drying process needs to be carred out in the way which allow to reduce internal drying stresses, the main cause of material destruction[1-4]. Tension which appears in dried products are mainly the result of highly nonuniform distribution in temperature and moisture content throught the material, thus why using several drying techniques simultaneously or using nonstationary drying is presented as a method to diminish unwanted effects[5-7]. Application of such drying programs not only allow to achieve better quality of dry products but also if appropriately determined lead to reduction in energy consumption, which is one of the most important parameter considered when presenting new drying solution affecting their economical effectiveness.

In the mentioned hybrid drying processes in last years ultrasound were applied as one of the method to enhance the drying process, however they were considered mainly for thermal sensitive products like fruits and vegetables[8]. Nevertheless, described in the literature interaction with the material in the form of, e.g. heating or vibrating effect[9] could affect positively also other than biological products like for example ceramics[10]. The processes proposed in this work present modern drying technique in which high power ultrasound are used to affect drying kinetics and processed material propertiess.

2. Materials and Methods

The investigated material was kaolin KOC clay produced by Polish company Surmin Kaolin S.A. The material before preparing a moulding mass was dried for 24h in 120ºC. Next, a dry powder was mixed with a specific amount of demineralized water which allows to achieve an initial moisture content of 40% $_{d.b.}$. Wet material was closed in a sealed box and left for 48h, so the moisture distribution in the mass became uniform. After that time the mass was portioned into 200g batch and stored separately in a sealed containers at temperature of 5ºC. For each experiment from single 200g batch 7 samples in the form of cylinders with a diameter of 21mm and a height of 26mm were molded and placed in a dryer trace. The experiment were performed in a hybrid dryer according to 6 drying

schedules presented in Table 1. The apparatus allowed to control and collect all important process parameters and is described in detail in other author work[9].

Table 1. Drying processes and parameters

Drying program	Convection	Microwaves	Ultrasound
CV_{80}	80°C air flow 4m/s	-	-
$CVUS_{80}$	80°C air flow 4m/s	-	200W
$CVMWUS_{80}$	80°C air flow 4m/s	100W in 2 cycles	200W
CV_{50}	50°C air flow 4m/s	-	-
$CVUS_{50}$	50°C air flow 4m/s	-	200W
$CVMWUS_{50}$	50°C air flow 4m/s	100W in 3 cycles	200W

Application of microwaves was performed periodically in a given number of cycles which last 5 minutes with the following 30 minutes relaxation periods. Such procedure allows not to destroy ceramics samples during processing with microwave appication.

As drying processes were carried out till the material reach $2\%_{d.b.}$ moisture content, before mechanical tests the samples were placed for 48h in exsiccator, so all examined cylinders would had exactly the same parameters. Compression tests were carried out axialy on Cometech strength machine with 20mm/min compression speed.

3. Results and discussion

The first series of experiments was carried out for higher drying temperature both as a single convective process as also with application of ultrasound and microwaves. The kinetics of such processes is presented in figure 1 and was evaluated on the basis of MR(time) curves where MR is defined as follows:

$$MR = \frac{X_t - X_{eq}}{X_0 - X_{eq}} \qquad (1)$$

In the above equation X value indicates the material moisture content (kg/kg d.b.) and subscripts specify the time at which they were determined, that is: t - given time of the process, eq is the end of process (equilibrium moisture content) and 0 is at the beginning of the process (initial value).
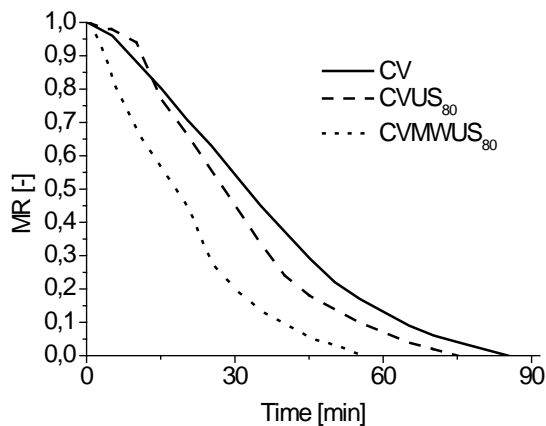
Fig. 1 Kinetics of processes carried out at 80ºC

In Figure 1, one can see the characteristic behaviour of material dried only with ultrasound assist at the beginning of the process. In the heating period the water loss is visibly lower as compared to the CV process, however in the next period the drying rate increases significantly and leads to reduction of the overall drying time up to 11 minutes. This characteristic kinetics was observed in number of repeats thus why it can be stated that for such processes ultrasound application could be applied after heating period what allows to additional improvement of drying kinetics. In the second process assisted with ultrasound (CVMWUS$_{80}$) the kinetics showes the influence of short application of microwaves which allows to reduce the drying time significantly. Longer application of microwaves was not justified as earlier work of autor[10] indicates their negative effect on the material structure as also its strength.

The next series of experiments was performed in a lower drying air temperature to verify if ultrasound assist in other conditions transfer onto the drying kinetics and material properties differently. Figure 2 presents the drying curves achieved for processes carried out in 50ºC. In opposite to process carried out in higher temperature, the CVUS$_{50}$ process do not show very slow drying tendency during heating period but from the beginning offer higher drying rates than pure convection. This reflects in higher reduction in drying time even up to 85 minutes. So high reduction in drying time could results also from the fact that a lower temperature of processing affects the air density which influence greately the reduction of acoustic wave attenuation.
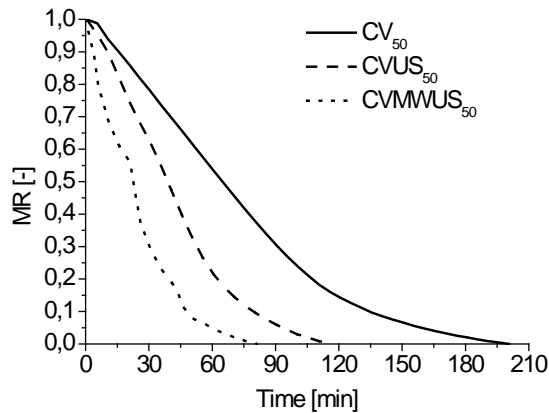
Fig. 2 Kinetics of processes carried out at 50°C

Additional periodical application of microwaves in the CVMWUS$_{50}$ process allows to increase the average drying rate and in total reduces the drying time to the level achieved during CVUS$_{80}$. Similar drying time for those processes affects also similar appearanece of the sample surface with small number of narrow cracks. The samples achieved after drying are presented in Figure 3.
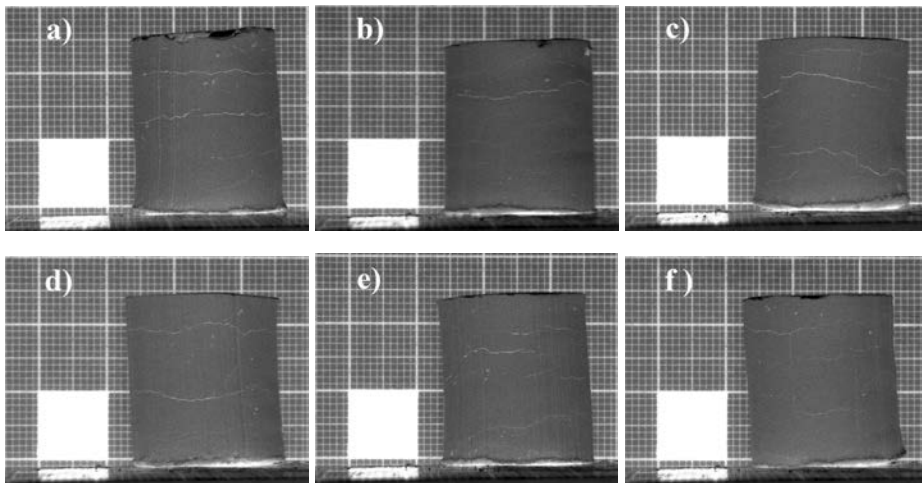
**Fig. 3 Dry samples structure achieverd after different dryingprocesses; a) CV$_{80}$, b) CVUS$_{80}$,
c) CVMWUS$_{80}$, d) CV$_{50}$, e) CVUS$_{50}$, f) CVMWUS$_{50}$**

The presented above pictures show that ultrasound application affects positively the sample quality, however beter results were observed at higher drying air temperature, especially without microwave application. Slightly other influence of ultrasound was observed at

lower air temperatures where the best quality was observed in case the samples dried by $CVMWUS_{50}$. In this temperature application of ultrasound itself do not cause visible improvement of product structure. The above investigation of samples appearance does not however investigate their mechanical properties, thus why the results of strength tests for the dried samples are tabulated in Table 2.

Table 2. Material strength and energy consumption in different drying processes

Drying program	Strength [N]	Standard deviation [N]	Energy consumption [kWh]	Standard deviation [kWh]
CV_{80}	180,38	23,78	2,28	0,01
$CVUS_{80}$	199,77	13,51	2,44	0,08
$CVMWUS_{80}$	196,27	22,61	1,87	0,18
CV_{50}	260,06	15,57	1,95	0,04
$CVUS_{50}$	203,38	23,42	2,07	0,17
$CVMWUS_{50}$	206,15	17,96	1,63	0,28

The results of compression test correlates fully with a sample appearance for processes carried out at temperature of 80ºC. In those processes ultrasound assitst reflects in the increase of material strength both for pure convective dryng and also for the process enhanced with microwaves. However the mechanical properties determined during strength tests do not cover with visual quality determination for samples dried at a lower temperature. It is observed that application of ultrasound as also microwaves during convective drying in 50ºC affects significantly reduction of material strength, nevertheless without negative influence on product appearance. The reason of such specific behaviour could be tracked back into varied acoustic wave propagation and attenuation in different air temperatures, however it exact explanation is very difficult. From one side the vibration carried by mechanical wave could affect the clay particles arrangement and its strength, but from the other side it do not explain why the improvement of drying rate at lower temperature is greater. Nevertheless, when considering the material strength and drying time for particular processes it can be stated that $CVUS_{80}$ and $CVMWUS_{50}$ give almost identical, very good results. Thus why to indicate the most effective process in which ultrasound are applied it is necessary to consider the energy needed to remove a specific amount of water from the material. As all samples have the same volume and initial moisture content the overall energy consumed during specific process can be compared directly. The energy consumption presented in Table 2 showes that the most similar processes from quality and kinetic point of view ($CVUS_{80}$ and $CVMWUS_{50}$) differ

significantly by the energy consumption. The process carried out at a lower temperature consumes more than one third less energy what shows its great advantage. Also other processes carried out at a lower temperature are more effective from energy point of view comparing with the ones carried out at 80ºC, where the only expception is the CVMWUS$_{80}$ process which offers similar energy consumption.

4. Conclusions

The application of ultrasound shows different influence on both drying kinetics and material strength depends from temperature in which they were applied. Application of acoustic waves in all cases affects in reduction of processing time, however at a lower air temperature their influence on drying rate is greater probably due to a lower wave attenuation. Ultrasound affect also the material strength, however their influence is ambiguous and depends on drying air temperature. At a lower temperature sonification affects negatively on the material resistance, whereas at a higher temperature it improves product strength. However, for both temperatures ultrasound improve the product appearance as the sonificated samples had a better surface quality with a lower amount of narrow cracks.

Considering all of the processes and material parameters the CVMWUS$_{50}$ program can be pointed as the best drying process due to a quite short drying time and also a lower energy consumptionless energy, and a reasonable material strength and product appearanece. Nevertheless, the ultrasound enhancement during all drying schemes brings some advantages in the process, but sonification should be applied with a grate care and determination of the most important parameters onto which we would like to affect using ultrasound.

5. Acknowledgements

6. References

[1] Musielak, G.; Mierzwa, D. Permanent strains in clay-like material during drying. Drying Technology 2009, 27 (7), 894-902

[2] Itaya, Y.; Okouchi, K.; Mori, S. Effect of heating modes on internal strain-stress formation during drying of molded ceramics. Drying Technology 2001, 19 (7), 1491-1504

[3] Mihoubi, D.; Bellagi, A. Stress generated during drying of saturated porous media. Transport in Porous Media 2009, 80 (3), 519-536

[4] Heydari, M.; Khalili, K. Investigation on the effect of Young's modulus variation on

drying – induced stresses. Transport in Porous Media 2016, 112(2), 519-540

[5]   Mierzwa, D.; Kowalski, S.J.; Kroehnke, J. Hybrid drying of carrot preliminary processed with ultrasonically assisted osmotic dehydration. Food Technology and Biotechnology 2017, 55 (2), 197-205

[6]   Kouchakzedeh, A. The hybrid drying of pistachios by solar energy and high electric field. Agricultural Engineering International: CIGR Journal 2016, 18 (1), 129-137

[7]   Xu, F.; Chen, Z.; Huang, M.; Li, C.; Zhou, W. Effect of intermittent microwave drying on biophysica characterisics of rice. Journal of Food Process Engineering 2017, 40 (6), Article number e12590

[8]   Charoux, C.M.G.; Ojha, K.S.; O'Donnell, C.P.; Cardoni, A.; Tiwari, B.K. Applications of airborne ultrasonic technology in the food industry. Journal of Food Engineering 2017, 208, 28-36

[9]   Kowalski, S.J.; Pawłowski, A. Intensification of apple drying due to ultrasound enhancement. Journal of Food Engineering 2015, 156, 1-9

[10] Pawłowski, A.; Mierzwa, D. Hybrid drying of ceramic materials – kinetics, quality and energy issues. In proceedings of International Drying Symposium, Gifu, Japan, August 7-10, 2016; P2-48

Microencapsulation of passion fruit extract (*Passiflora biflora*) by spray drying

Aguilar, D.ª; Rodríguez, O.ª; Luna, G.ᵇ; Zarate G.ª; Bello L.ª*

[a] Technological University Center Veracruz, Av. Universidad Federal Highway 350. No Cuitláhuac La Tinaja. Location Two roads CP 94910, Cuitlahuac, Veracruz, Mexico.
[b] Department of Graduate Studies and Research, Technological Institute of Orizaba Oriente, Av. 9 No. 852, Col. Emiliano Zapata, CP 94320, Orizaba, Veracruz, Mexico.

* E-mail of the corresponding author: licet.bello@utcv.edu.mx

Abstract

Anthocyanins pulp and peel passionfruit extracted by leaching using water as a solvent where the operating conditions of spray drying were evaluated for a microencapsulated. The variables were temperature input (180,200 and 220 ° C), MD (6,8y10%), AP (1,3y5%) and outlet temperature 80 ° C, was achieved noted that during the drying process moisture decreased to 85% due to this high in MD and AP, this also increases the content of ST. Color significantly was not affected by spray drying..

Keywords: *Passionfruit, abstract, encapsulants, spray microencapsulation.*

1. Introduction

Passionfruit (*Passiflora biflora*) is a wild fruit ovoid neotropical as shown in (Fig 1) and belongs to the Passifloraceae family, is a liana with smooth variable leaves are generally wider than long, with two lobes that occur with the cut end, rounded or slightly stippled. [n1] In recent years it has sought ways to replace artificial pigments thus has opted for extraction of certain natural pigments from different plants and fruits, is why in the present research, the extraction process is evaluated own compounds of passion fruit by microencapsulation technique by spray drying.

Fig. 1 Passiflora biflora

Microencapsulation by spray drying corresponds to the transformation of a fluid into a solid material, shaped by atomizing minute droplets into a hot drying medium. One of the great advantages of this process, besides its simplicity, is suitable for heat sensitive materials because the exposure time at elevated temperatures is very short ranging between 5 and 30 seconds [n3, n5]. Anthocyanins belong to the flavonoid family, composed of two aromatic rings, a and β joined by a chain of 3 carbons [n2], these pigments are widely distributed in fruits and flowers, offering attractive colors such as orange, red and blue [n6]. One of the most important and studied food characteristics is the color,the Interest in anthocyanin pigments in scientific research have increased in recent years, due not only to the color that give products that contain them but its likely role in reducing heart disease, cancer, diabetes, anti-inflammatory, improvement of visual acuity and cognitive performance; these preventive and therapeutic effects are mainly associated with its antioxidant properties [n4] The objective of this research was microencapsulated anthocyanins pulp and peel passion fruit by spray drying with maltodextrin and potato starch, evaluating the influence of the conditions drying.

2. Materials and Methods

2.1 Raw material

Passionfruit (Passiflora Biflora) was harvested and collected in the high mountains, Cordoba, Veracruz, Mexico

2.2 Fruit packaging.

The fruit was placed at room temperature (25 ° C) for 2 hours to return to its initial state, the subsequent detachment of the peduncle performed and seed making a homogenization between the pulp and peel of the fruit into a sterile glass papillary.

2.3 Extraction of anthocyanins.

Once homogeneous mixture extraction was performed by placing the fruit in water at 30 ° C for 2 hours, to obtain the anthocyanins in the solvent, filtration was performed on Whatman paper to remove solids from the extract.

2.4 Experimental design.

The amounts used were determined by an Box-Behnken experiment design have three variables to consider: Inlet temperature, % maltodextrin and potato starch %. □

Box-Behnken desingns always have 3 levels per factor, is a type of design response surface that does not have an embedded fractional factorial designt, where the design points are in combinations of high and low levels of factors and their midpoints [n8].

2.5 Determination of moisture.

Moisture determination of passion fruit extract was performed in a thermobalance of Sartorius, Model MA35 brand. At a temperature of 121 ° C.

2.6 Determination of Total Solids.

It was determined by weight difference according to the result of % moisture.

2.7 Determination of color.

The color measurement was performed to extract Colorquest XE colorimeter for liquids where "L", "a" and "b" values were obtained. Determining color for dry passionfruit was performed with a colorimeter MiniScan XE plus the mark Hunterlab obtaining values "L", "a" and "b".

2.8 Determination of water activity (aw).

The water activity (aw) was measured with an Aqualab, model series 3 computer.

3.Results and discussions

3.1 Fruit Yield

In (Table 1). integral yield mature fruit, which is formed by 8% shell, 80% pulp and 10% seed and the other 2% is the organic waste [n1] is shown.

Table 1. Performance passionfruit (Passiflora biflora)

Sample	Total weight (g)	Pulp weight (g)	Seed weight (g)	Shell weight (g)	Shell yield (%)	Seed yield (%)	Pulp yield (%)
A	104.5698	83.5903	9.8471	7.7998	7.4589	9.4167	79.9377
B	108.6584	86.6302	9.2321	8.5462	7.8651	8.4964	79.7271
C	112.9454	87.5682	10.9358	8.5821	7.5984	9.6823	77.5314

Source: [n1]

Table 2. Results obtained from the extract in different concentrations

Sample	Temperature (ºC)	Maltodextrin (% m/v)	Potato Starch (% m/v)	Humidity (%)	ST (%)
1	180	6	3	92.11	7.89
2	180	10	3	87.81	12.19
3	220	6	3	91.71	8.29
4	220	10	3	85.83	14.17
5	180	8	1	87.64	13.36
6	180	8	5	90.30	9.70
7	220	8	1	90.81	9.19
8	220	8	5	87.81	12.19
9	200	6	1	89.05	10.95
10	200	6	5	86.85	13.15
11	200	10	1	91.82	8.18
12	200	10	5	82.12	17.88
13	200	8	3	86.23	13.77
14	200	8	3	89.22	10.78
15	200	8	3	89.56	10.44

In (Table 2). Results show the humidity and ST obtained extract at different concentrations which shows that the amount of maltodextrin and starch added potato is directly proportional to the % obtained, showing that the higher the added amount increases occurs in solids and a decrease moisture.

In (Fig. 2) is observed that a high level of MD and an average level of AP the highest content of total solids in the samples are present, this may be due to the degree of solubility of potato starch samples, since increasing this concentration could suffer saturation in the solution, affecting the homogeneity of the sample.
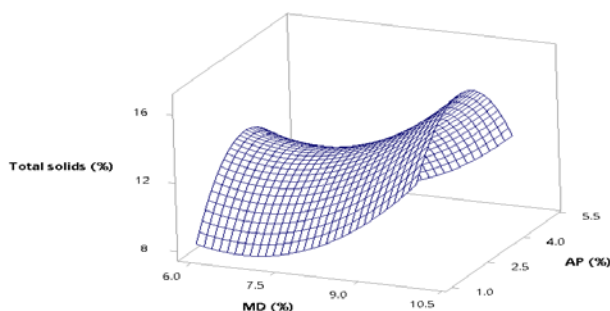
Fig. 2. Correlation of TS content

In (Fig. 3) the graphical response surface moisture, it is clear that its content decreases until 85% with a content of, high MD and low AP, as the one that is shown to microencapsulated ascorbic acid by spray drying with two matrices maltodextrin and soluble potato starch, the moisture value reported is $0.038 \pm 1.5\%$, which is low by these drying conditions.[n9]
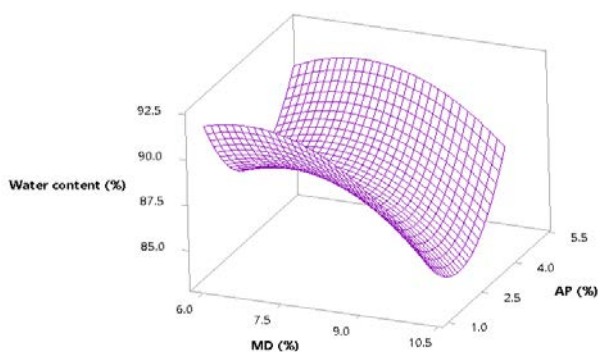
Fig 3. Correlation of moisture content

In (Table 3) results according to the color parameters are shown, the luminosity (L), chromaticity (a*, b*) in the extract, the changes (L) clearly observed were diminished as

was increased the number of solids, however parameters (a * b *) had a trend toward red and blue, which notes the presence of anthocyanins which are responsible for the red, orange, blue and purple colors fruits, flowers and other plant products.

Table 3.- Results of chromaticity in different concentrations extract

Sample	Chromatic parameters		
	L	a*	b*
1	1.71	-0.05	-0.35
2	1.46	-0.43	-0.17
3	1.26	-0.34	-0.07
4	1.21	-0.39	-0.43
5	1.39	-0.29	-0.05
6	1.45	-0.90	0.20
7	1.34	-0.66	-0.74
8	1.38	-0.17	-0.29
9	1.47	-0.52	-0.30
10	1.31	-0.25	0.13
11	1.69	-0.91	0.13
12	1.43	-0.28	-0.14
13	1.57	-0.80	0.06
14	1.31	-0.40	-0.31
15	0.83	-0.90	-0.71

Table 4. Results obtained after performing spray drying

Sample	H (%) ± DS	ST (%) ± DS	aw ± DS
1	5.04 ± 0.06	94.97 ± 0.06	0.308 ± 0.03
2	7.07 ± 0.64	92.94 ± 0.64	0.411 ± 0.01
3	5.06 ± 0.18	94.94 ± 0.18	0.308 ± 0.03
4	5.15 ± 0.12	94.86 ± 0.12	0.345 ± 0.01
5	8.28 ± 0.49	91.72 ± 0.49	0.380 ± 0.01
6	6.87 ± 0.19	93.14 ± 0.19	0.327 ± 0.01

In (Table 4) the results obtained are shown after performing spray drying which shows that in runs 3 and 4 there is a lower moisture content 5.06% and 5.15% respectively, resulting in

a greater amount of ST, is therefore it is considered that in a matter of performance is optimal to use an amount of maltodextrin 10% because this presents better results.

In (Table 5) color results obtained in the pigment are shown, where the parameters (L, a*, b *) had a color trend toward red and blue resulting in the run, number 2 and 6 have a higher intensity is the color, which results show the presence of anthocyanins, demonstrating that the spray drying does not alter the anthocyanins present in the fruit.

Table 5. Results of chromaticity obtained after performing spray drying

Sample	Chromatic parameters		
	Luminosity L ± DS	Chromaticity a ± DS	Chromaticity b ± DS
1	46.87 ± 0.21	6.65 ± 0.13	-5.16 ± 0.05
2	42.50 ± 0.18	8.36 ± 0.04	-3.14 ± 0.19
3	39.95 ± 0.21	5.45 ± 0.49	-3.06 ± 0.08
4	45.42 ± 0.49	5.18 ± 0.04	-2.35 ± 0.21
5	46.06 ± 0.44	7.37 ± 0.21	-1.60 ± 0.47
6	44.22 ± 0.30	8.26 ± 0.10	-1.73 ± 0.49

4. Conclusions

From the extract obtained color leached from fruit of the passion fruit one microoencapsulado product was achieved maltodextrin by spray drying, where according to the experiment performed and the results obtained it is established that the optimum conditions for the pigment are the runs 3 and 4 with an inlet temperature of 180 ° C, MD 10% D10, 5.1% of AP and a temperature of 80 ° C outlet, because in these higher performances are obtained and although They do not exhibit the greatest color intensity but they present a good one, which represents the existence of anthocyanins, which makes them be suitable for obtaining the pigment by spray drying.

5. Nomenclature

L	Luminosity	
a* y b*	Chromaticity	
H	Humidity	%
ST	Total solids	%
MD	Maltodextrin	%
AP	Potato starch	%
aw	Water activity	%

6. References

[1] Aguilar, Daniela, and others. "Morphology and physicochemical characterization of the passion fruit (Passiflora biflora)." Mexico Research Center (2017).

[2] Arrazola, Guillermo, Irina Herazo, and Armando Alvis. "Microencapsulation of anthocyanins Eggplant (Solanum melongena L.) by spray drying and Evaluation of color stability and antioxidant capacity." Research Group Process and Plant Agro-Industry (2014): 31-42. □

[3] Hernández, Oreste Dario Lopez. " Oily substances microencapsulation by spray drying.» Cuban Journal of Pharmacy (2010): 381-389.

[4] Pastrana, Karla Guadalupe Lopez, et al. "Microencapsulation of natural pigments obtained from the peel and pulp of fruits of Opuntia spp.» Newsletter ICAP Agricultural Sciences (2017). □

[5] Poveda, Maria Jose Tapia. Ascorbic Acid microencapsulation by spray drying with starch and maltodextrin. Ecuador, 2017.

[6] Prieto, Gerardo Avendano and Buitrago Baudilio Acevedo. "Microencapsulation process of natural dyes in strawberry (Fragaria vesca)." Ontare (2014): 7-34.

[7] Yepez, José Luis Villacrez. Development of microencapsulated by spray drying from blackberry fruits (Rubus glaucus Benth). Colombia, 2013.

[8] Montgomery, Douglas C. Design, and analysis of experiments. Mexico DF: Limusa SA de CV, 2005.

[9] Palma Rodriguez, Hugo Miguel, and others. "Ascorbic acid microencapsulation by spray-drying in native and acid-modified starches from different botanical sources." (2013) 65, 584-592.

Microwave drying in fluidized bed to dehydrate microencapsulated *Saccharomyces cerevisiae* cells. Temperature control strategies

Mardaras, J.ª; Lombraña, J.I.ª*;Villarán, M.C.[b]

ª Department of Chemical Engineering. Faculty of Science and Technology, University of the Basque Country,P.O Box 644. 48080 Bilbao (Spain)

[b] Health & Food Area.Health Division, TECNALIA Research & Innovation. 01510 Miñano, Alava (Spain)

*E-mail of the corresponding author: ji.lombrana@ehu.es

Abstract

Alginate microcapsules containing cell yeasts of the species Saccharomyces cerivisae, used as a reference microorganism, were studied here to improve the protection of cell activity during food processing. Here a novel drying process was proposed to optimize processing conditions.

The dehydration of microcapsules by microwaves and under near fluidizing conditions (NFMD), allows performing dehydration employing lower temperatures to maintain high viability levels and a high quality end product. Thus, strategies based on the combination of different thermal gradients and processing temperatures were analysed through a series of NFMD experiments.

Keywords: microwave drying, fluidization, probiotics, cell viability.

1. Introduction

In this work, the novel Near Fluidizing Microwave Drying (NFMD) process is studied to avoid some of the problems with lyophilization and spray drying. Microwave heating adequately controlled is specially recommended for drying. Through this process, the heat is generated inside the microcapsules, causing a thermal gradient from inside out, which favours the elimination of the moisture [1]. Microwave drying is a technology that is being developed widely in the food industry [2]. Drying of the microcapsules through the application of microwaves presents as primary characteristic, the inverse temperature gradient, favouring the drying of the microcapsules from inside out, as opposed to conventional drying methods. The application of this inverse temperature gradient involves much lower temperatures and operating times [3]; [4]. Based on previous kinetic studies of the microwave drying operation, three perfectly differentiated phases during the dehydration of microcapsules have been found [5].

As an extension of the study, here the effect of control variables in the applied energy for the drying process of microcapsules were studied. Several operating conditions were analysed combining different values of thermal levels of control variables: air and product temperature. Finally, the viability of each thermal level applied by microwaves was compared with the results obtained by freeze-drying.

2. Materials and Methods

2.1. Preparation of microcapsules and viability analysis

Microcapsules were prepared following a variant to that indicated in the bibliography [6]. In this work, dry yeast extract (*Saccharomyces cerevisiae*, ZYMAFLORE®) supplied by LAFFORT (France), containing an active cell concentration higher than $2 \cdot 10^{10}$/g, was used as cell culture material. Capsules were extracted from the solution by filtration and, once eliminated the superficial water, they were conveniently packaged and stored for 18 h in covered traysduring18 h in a freezer at 4 ºC until the start of the drying experiment. This leads to initial moisture content between 7.1 and 7.3 g water/g d.s. in all the cases.

The evaluation of viable encapsulated yeast was carried out by homogenizing 0.1 g of filtered microsphere slurry in 10 mL of sodium citrate 0.1 M for 10 min and stirred. The plates were incubated for 2 days at 37 °C and the encapsulated yeast enumerated as cfu/g d.s.

2.2. Drying experiments

The experiments were carried out according to the procedure NFMD, consisting of dry cell capsules, under fluidizing conditions, through the supply of heat by microwaves. Microwave power was regulated during the drying process in order to achieve certain values of temperature in the microcapsules and the temperature of the air being introduced into the bed of particles.

Nine thermal strategies were tested in this study combining three levels for the air temperature with other three levels for the product surface temperature through temperature T_f (Table 1). The inlet air temperature levels considered were: 5ºC, room temperature (20ºC) and 40ºC. The different experiments were defined on the basis of combining these three air temperature levels with three different target surface temperatures of the microcapsules. Since it was difficult to measure the temperature of the microcapsules directly, T_f was controlled instead, measuring the temperature of the air film in contact by a fiber optic probe placed inside the microcapsules bed.

Table 1   Definition of the thermal levels in the NFMD experiments.

	Phase I			Phase II			Phase III	Code
Exp.	T_{in}^*	T_f^*	T_s^*	T_{in}^*	T_f^*	T_s^*		
1	5	10	15	5	17.5	30		Ll/Ml
2	5	17.5	30	20	25	30	5 ºC/h decreasing	Ml/Mm
3	5	10	15	40	27.5	15		Ll/Lm
4	20	25	30	5	17.5	30	rate of T_{in}	Mm/Hl
5	20	17.5	15	20	25	30		Lm/Ml
6	20	17.5	15	40	42.5	45	(from 40 ºC)	Lm/Hm
7	20	17.5	15	20	32.5	45		Lm/Hh
8	40	27.5	15	40	42.5	45		Lh/Hh
9	40	35.5	30	20	32.5	45		Mh/Hm

The code used in Table 1 refers to the thermal conditions employed in Phases I and II. The first two letters correspond to Phase I and the other two, separated by a slash, to Phase II. At each phase, the first capital letter refers to the target temperature for the surface (T_s^*): L=15°C (Low), M = 30 °C (Medium), and H = 45 °C (High). The second letter refers to the inlet air temperature T_{in}^* using the same but in small letters: l = 5 °C, m = 20 °C and h = 40 °C. Thus, in Experiment 3 (Ll/Lm), low thermal level was applied either for Phase I or II, except for the thermal gradient in Phase II, where a 40 ºC inlet air temperature was applied.

3. Results and discussion

The air velocity was used as indicator variable to define the phase boundaries, rather than the water content, which would have been much less accessible for following the process.

3.1. Variation of the minimum fluidization velocity

The microcapsules obtained as described in the previous section had an initial moisture content of around 85% (X=0.85±0.03) at the beginning of the drying. Under these conditions, microcapsules have a high adherence so that, initially, the experimental minimum fluidization velocity u^*_{mf} of the bed was considerably higher than that obtained theoretically.

Initially, the experimental minimum fluidization velocity, u^*_{mf}, was 1.39 m/s, about 3 times higher than the theoretical minimum fluidization velocity, u_{mf}, obtained in accordance to the previous equations. Velocity decreases rapidly as drying progresses, while the theoretical value u_{mf} decreases slowly only affected by the decrement in density and particle size d_p along the drying. When the humidity of the particles reaches a value around X = 0.5, the microcapsules lose the adherence shown at the beginning of the process so that the experimental minimum fluidization velocity becomes equal to the theoretical. In such a situation: $u^*_{mf} = u_{mf} = 0.29$ m/s (see Table 2) and it was set in this study as a reference for the definition of the end of Phase II or beginning of Phase III. From this moment, the residual moisture of the particles is removed exclusively by convective heating (microwave is off).

Table 2. Data of X, u_{mf}, d_p and time in the transitionPhase II-III, in the different NFMD strategies

Heatings trategy	Phase II				Phase III		
	t(min)	$X^{(1}$	d_P(m)	$u_{mf}^*/u_{mf}^{(2}$	t(min)	$X^{(1}$	d_P(m)
Ll/Ml	35	0.44	1.69E-03	0.30/0.32	275	0.045	1.13E-03
Ml/Mm	30	0.49	1.76E-03	0.30/0.30	195	0.070	1.16E-03
Ll/Lm	18	0.55	1.86E-03	0.38/0.28	240	0.072	1.16E-03
Mm/Hl	25	0.49	1.76E-03	0.30/0.30	240	0.070	1.16E-03
Lm/Ml	25	0.57	1.88E-03	0.40/0.30	235	0.070	1.16E-03
Lm/Hm	20	0.39	1.63E-03	0.30/0.30	210	0.071	1.16E-03
Lm/Hh	23	0.48	1.75E-03	0.28/0.32	240	0.078	1.17E-03
Lh/Hh	15	0.54	1.84E-03	0.28/0.36	240	0.081	1.18E-03
Mh/Hm	20	0.5	1.78E-03	0.32/0.30	240	0.072	1.16E-03

[1]Units of X_{in} and X: g water/g w.b. [2]Units of u_{mf}^* and u_{mf}: m/s

An acceptable correspondence of the moisture content X with the minimum fluidization velocity values used in each phase can be seen in Table 2. Thus, the average values of X corresponding to the end of Phase I and II, for all the experimental conditions tested, were 0.75 and 0.49 with a standard deviation of 0.040 and 0.051, respectively.

3.2. Drying kinetics analysis

In Figure 1, the mass loss profiles of NFMD Experiments 1 and 2, in terms of *MR* (moisture ratio dry basis), are compared with spray-drying and freeze-drying of product with similar water content. The drying time spent in the NFMD is clearly lower than freeze-drying and only a few minutes longer than the time observed in spray drying (about 100 min) but the thermal levels applied are considerable. Consequently, NFMD presents very favourable characteristics for the drying of thermosensible materials with similar efficiencies to those obtained by spray-drying, taking into account the duration of cycles and power consumption [7].
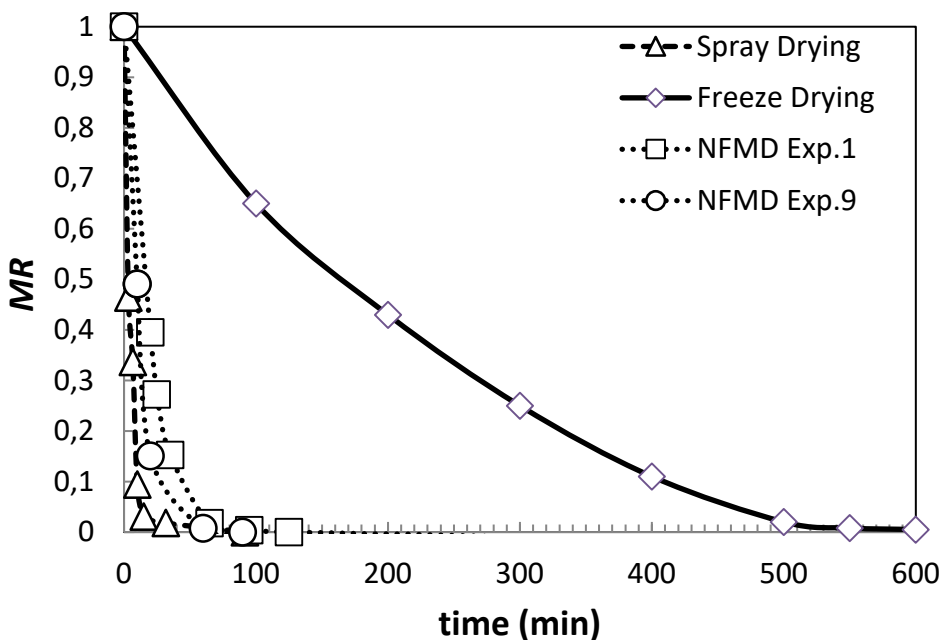
Figure 1. Drying kinetics of NFMD compared to freeze-drying (Rudy et al., 2015) and spray-drying.

When analyzing the thermal profiles, it is necessary to take into account the strong reduction of mass during Phases I and II that directly affects the thickness of the bed through a reduction of the particle size, as shown in Table 2 above. An idea of the reduction of the size associated with the water loss is shown in Figure 2 for Experiment 7 (Lm/Hm). Thus, Figure 2a and 2b correspond to the start and end of Phase I, where one can see the important size difference with respect to the rest of the drying (Figure 2c and 2d). As a result, an important reduction

in the thickness of the bed, up to a 25% of the initial value, was observed at the end of Phase II.
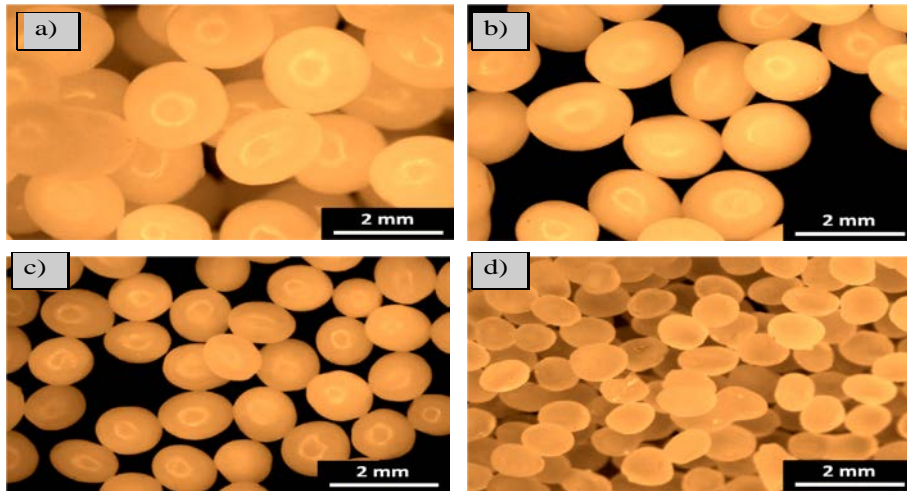
Fig. 2   *Micrograph of the microcapsules at different drying times for Experiment 7 (Lm/Hm): a) Xin=0.80, dp=2.12 mm; b) X=0.51, dp=1.8 mm; c) X=0.24, dp=1.4 mm; d) X=0.05, dp=1.1 mm.*

3.3. Quality of the dehydrated product

The lower the water activity, the better the stability of the dry food product, but in very low water activities, the oxidisation of membrane lipids can also reduce viability [8].

The moisture content was determined by the Karl-Fischer method. Results were obtained on wet basis, expressed as percent (*KF*) that permits to determine the dry solid fraction taking into account the mass loss during drying. The results of *KF* from each experiment were used to confirm the dry solid fraction of capsules.

The probiotic viability or survival ratio (in %) of the microorganisms in each experiment is defined accorindg to Chávarri *et al*.[6]. It is based on a count of colony forming units (cfu), taking the log values in the initial sample (*cfu$_0$*) and after drying (*cfu$_{fin}$*). According to Table 3, the average data of drying rate for each experiment, the time of processing, water activity, *KF*, and the survival % of the overall process are shown at the end of each drying conditions**.** The NFMD experiments were made by triplicate in order to analyse the effect of possible process variability on the viability results. In Table 3, one can see that the standard error of the survival values were in all cases lower than 1.6%.This proves a good process control with the used operating variables and the subsequent reproducibility of experiments.

Table 3   *Quality parameters obtained for all experiments.*

Exp.	r_{I-II}	$M_{fin\,II}$	r_{global}	time (min)	KF	Survival (%)	Code
1	0,114	0,783	0,017	275	6,726	74.42±1.01	Ll/Ml
2	0,126	0,946	0,024	195	7,522	96.00±1.37	Ml/Mm
3	0,219	1,245	0,021	240	7,706	93.83±0.28	Ll/Lm
4	0,184	0,945	0,023	240	7,577	88.65±0.04	Mm/Hl
5	0,163	1,309	0,023	235	7,458	91.78±0.03	Lm/Ml
6	0,198	0,646	0,022	210	7,599	87.69±0.15	Lm/Hm
7	0,159	0,907	0,019	240	8,414	77.62±0.54	Lm/Hh
8	0,349	1,184	0,026	240	8,830	74.44±1.13	Lh/Hh
9	0,254	0,992	0,025	240	7,726	55.00±0.98	Mh/Hm
Lyo.			0,007	720	8,855	91.18±1.44	-

[*]Units:$r_{I,\,II}$ and r_{global}: g H_2O/g d.s. min, $M_{fin\,II}$: g H_2O/g d.s.

4. Conclusions

The NFMD process has proved to be a feasible technology for microencapsulated microorganisms dehydration.The global value of drying rate was in all NFMD cases around 0.02 g water/g d.s., spite of the significant differences when referring Phases I and II. The long duration of Phase III dilutes somehow the differences of preceding phases.

The operating conditions applied and the temperature gradient from product to air or viceversa generate a convective heat flow that leads to an extra heat contribution (medium air temperature; i.e. Experiment 1) or heat loss (low air temperature; i.e. Experiment 9). Despite the negative effect on energy consumption that occurs when the air temperature is low or medium, this circumstance seems to favour the quality of the dehydrated product as in Experiment 2, showing high survival values of 96%.

5. References

[1] Lombraña, J.I., Rodriguez. R., Ruiz. U. Moisture Microwave-Drying of Sliced Mushroom.Analysis of Temperature Control and Pressure. Innovative Food Science & Emerging Technologies 2010, 11, 652-660

[2] Kudra, T. Mujumdar, A,S. Advanced Drying Technologies. Marcel Dekker, Basel, Switzerland, 2009.

[3] Feng, H., Yin, Y.and Tang, J. Microwave Drying of Food and Agricultural Materials:

Basics and Heat and Mass Transfer Modelling. Food Engineering Reviews 2012, 4, 89-106.

[4]   Li, Z., Raghavan, G.S.V., Wang, N., Vigneault, C. Drying rate control in the middle stage of microwave drying. Journal of Food Engineering 2011, 104, 234-238.

[5]   Ruiz, U., Lombraña, J.I. (). Effects of the inverse temperature gradient in microwave drying kinetics of pasta.17th International Drying Symposium, Magdeburg, Germany, 2010, 2098-2104.

[6]   Chávarri, M., Marañón, I., Ares, R., Ibáñez, F. C., Marzo, F., Villarán, M. d. C. Microencapsulation of a probiotic and prebiotic in alginate-chitosan capsules improves survival in simulated gastro-intestinal conditions. International Journal of Food Microbiology 2010, 142(1–2), 185-189.

[7]   Schmitz-Schug, I., Kulozik, U., Foerst, P. Modeling spray drying of dairy products – Impact of drying kinetics, reaction kinetics and spray drying conditions on lysine loss. Chemical Engineering Science 2016, 141, 315-329.

[8]   Viernstein, H., Raffalt, J., Polheim, D. Stabilisation of probiotic microorganisms. In: Nedovic, V., Willaert, R. (Eds.), Applications of Cell Immobilisation Biotechnology. Springer, Dordrecht, The Netherlands, 2005, 439–455.

Influence of the temperature and ultrasound application in drying kinetics of apple skin

Martins, M. [a*]; Cortés, E.[b]; Rosselló, C[c]; Peña, R.[d]; Cárcel, J. A.[d]

[a] Department of Food Engenieering. Faculty of Animal Science and Food Engineering, University of Sao Paulo, São Paulo, Brazil.

[b] Technological Institute of Veracruz, Veracruz, México

[c] Department of Chemistry. University of the Balearic Islands, Palma, Spain.

[d] ASPA group. Department of Food Technology. Universitat Politècnica de València, Valencia, Spain

*E-mail of the corresponding author: matheuspmartinss@gmail.com

Abstract

The great amount of waste produced by food industry contains interesting bioactive compounds. The extraction of these compounds requires the by-products previous stabilization being the convective drying one of most used techniques to this end. Drying conditions can affect both drying kinetics and final quality of products. The apple skin, byproduct of apple juice or cider industries, is rich in functional compounds such as polyphenols or vitamin C. The main goal of this contribution was to quantify the influence of temperature and ultrasound application in drying kinetics of apple skin. For this purpose, drying experiments at different temperatures (-10, 30, 50 and 70 ºC) and with (20.5 kW/m³) and without application of ultrasound were carried out. Drying kinetics were modelled by using a diffusion based model. As can be expected, the higher the temperature the faster the drying. Ultrasound application accelerated the process at every temperature tested being the influence slightly lower than found from the literature for other products. This can be attributed at the physical structure of the apple skin, less porous than the pulp. In any case, the application of ultrasound significantly reduced the drying time.

Keywords: by-products; dehydration;diffusivity; mass transfer.

1. Introduction

The food industry generates a great amount of waste that produces an important environmental impact. However, these by-products could be considered as a source of interesting bioactive compounds.[1] Apple is one of the most consumed fruits in the world.[2, 3, 4] The main by-product generated by juices and cider industries is the apple skin. This by-product presents a very important antioxidant activity [5] containing flavonoids such as cyanidin glycosides and quercetin glycosides which are not present in the pulp.[6, 7] Therefore, it can be used as a source of these compounds or directly as a functional ingredient.[7, 8]

Convective hot air drying is one of the most applied methods to estabilize products and by-products [9] facilitating their management, storage and transport. However, drying can induce significant changes in product quality.[4, 9, 10] Thus, the influence of drying process on antioxidant capacity of apples [11, 12, 13] and apple skin [4] has been already studied. The drying processes at low temperature emerges as an excellent way to preserve the thermal-sensitive compounds.[14] However, at these conditions, the low rate of drying must be intensified to avoid log processing times. [15] In this sense, ultrasound application comes up as an efficient alternative to intensify drying process.[16]

The aim of this work was to assess the influence of the drying temperature and ultrasound application on drying kinetics of apple skin.

2. Materials and Methods

2.1 Sample preparation

Apple fruits (Royal Gala var.) were selected with a similar maturation degree, washed and peeled. Apple skin was blanched in boiling water for 30 s to inactivate the enzyme polyphenol oxidase.[17] Moisture content was determined by differential weighing between fresh and dried samples in an vacuum oven at 60ºC.[18]

2.2 Drying

The drying processes were carried out by an atmospheric freeze-drying and a hot air drying process.

2.2.1 Atmospheric freeze-drying experiments

Samples were placed in a sample-holder, frozen in a blast freezer (HIBER, mod. ABB BF051, Italy) at -35 ± 1ºC and placed in an ultrasonically-assisted convective drier.[15] Drying process was carried out at -10ºC, 2 m/s, without (AIR-10) and with (US-10) ultrasound application (electrical input of 50 W) by triplicate. The process finished when samples lost 85% of its initial weight.

2.2.2 Hot air drying experiments

These experiments were carried out at 30, 50 and 70ºC with (US30, US50, US70) and without (AIR30, AIR50, AIR70) the ultrasound application (electrical input of 50 W).[19] All the runs were performed by triplicate at 2 m/s and until samples lost 85% of initial weight.

2.3 Modelling

An unidimensional diffusion-based model was considered for modelling the experimental drying kinetics (Eq. 1).

$$\frac{\partial W(x,t)}{\partial t} = D_e \frac{\partial^2 W(x,t)}{\partial x^2}$$

(1)

Where W is the local moisture content of sample (kg water/kg dry matter, d.m.); D_e is the effective moisture diffusivity (m^2/s); x is the direction of the moisture transport (m); t is the drying time (s). Effective moisture diffusivity was considered constant during the process and it was assumed isotropic and uniform samples. Although, at atmospheric freeze-drying conditions, this fact is far from the reality, the model allowed to quantify the influce of the estudied process variables and to compare the drying kinetics.[11] The external layer of apple peel was considered a waterproof surface. The external resistance to mass transport was included in the model by means of Eq. 2.

$$-D_e \rho_{ss} \frac{\partial W_p(L,t)}{\partial x} = k(a_w(L,t) - \varphi_{air})$$

(2)

where a_w is the water activity of samples, ρ_{ss} is the density of the dry solid (kg d.m./m^3), L is the experimental average thickness of the apple peel samples, φ_{air} is the relative humidity of the drying air and k is the mass transfer coefficient (kg water/m^{2}s). An implicit finite difference method was chosen to estimate the model parameters, D_e and k, using Matlab 2011B® (The Mathworks, Inc, Natick, USA).

The percentage of explained was used to measure the goodness of the model fitting.

$$\% VAR = \left(1 - \frac{S_{xy}^2}{S_y^2}\right) \cdot 100$$

(3)

S_{xy}^2 and S_y^2 are the calculated moisture content of apple peel the variance of the experimental, respectively.

3. Results and Discussion

3.1 Experimental drying kinetics

The initial moisture content of apple skin was 4.99 ± 0.07 (kg water/kg d.m.). Only the falling rate of moisture content was considered in drying kinetics.

As expected, temperature significantly affected the process kinetics; the higher the temperature the faster the drying (Table 1). Thus, the average time needed to reach a moisture content of 1 kg of water/ kg of dry matter at 30ºC was 4.6 times greater than those needed at 70 ºC. The atmospheric freeze-drying experiments were the slowest processes due to the low level of energy available for moisture transport at these conditions.

Ultrasound application significantly shorten the drying processes (Fig. 1). The influence in time process reduction was higher as lower the drying temperature. Thus, the drying at atmospheric freeze-drying conditions (-10 ºC) assisted by ultrasound was 3.2 times faster than without ultrasound. At 30 º C, ultrasound application produced a 2.4 times shortening of drying process.

Table 1. Drying time needed to achieve a moisture content of 1 kg water/kg dry matter during drying of apple peel at different temperatures without ultrasound application.

Treatment	Drying time (h)
AIR-10	68.1 ± 23.4
AIR30	$4.1 \pm 0,92$
AIR50	$1.3 \pm 0,29$
AIR70	$0.9 \pm 0,10$

3.2 Drying kinetics modeling

Taking into account the limitation of the model used, the modelling permitted to quantify the influence of the process variables on drying kinetics. The figure of the explained variance obtained showed the goodness of the model fit to the experimental data (Table 2).

Temperature significantly affected the values of D_e identified. Thus, the higher the temperature the greater the D_e figure. It can be highlithed the fact that the value of D_e found at atmospheric freeze-drying conditions (-10 ºC) was one order of magnitude smaller than those identified at temperatures above freezing point (Table 2). As a general rule, the identified D_e were in the range than those found by others authors drying apple flesh at similar temperatures.[11, 12, 13]
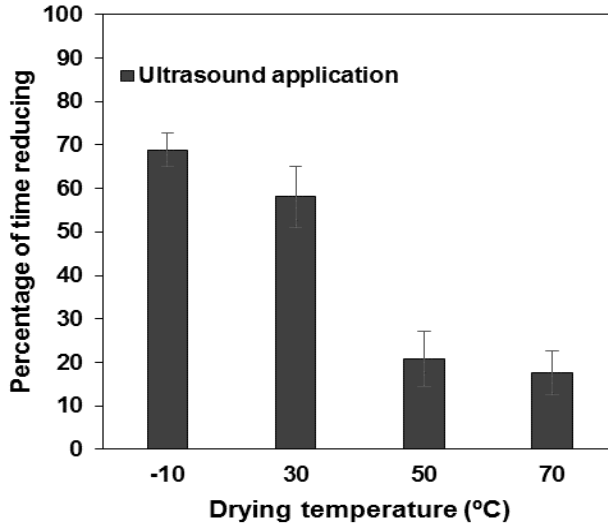
Figure 1. Percentage of time reduction by the application of ultrasound (50 W) during apple skin drying at different temperatures.

The relationship between D_e and temperature was modeled using an Arrhenius type equation (Eq. 4).

$$D_e = D_0 exp\left(\frac{E_a}{RT}\right)$$

(6)

Where D_0 is a pre-exponential factor (m^2/s), E_a is the activation energy (kJ/mol), R is the universal gas constant (kJ/mol K) and T the absolute temperature (K). The fit for AIR experiments was adequate (r^2>0.99) and the E_a obtained, 32.51 kJ/mol, was in the range of products such as passion fruit peel [20].

Ultrasound application increased the identified D_e value being this increase higher as lower was the drying temperature. Thus, at -10 ºC, ultrasound application increased 74% the D_e while this increase was only 10 % at 70 ºC. This fact has been preoviously observed in other products such as apple flesh [12] or passion fruit peel [20]. The D_e observed in the US experiments at at -10, 30 and 50 ºC also followed an Arrhenius type relationship (r2>0.99). The E_a obtained for these experiments was lightly lower than those found for AIR experiments (25.86 kJ/mol for US vs 32.51 kJ/mol for AIR) that would indicate that the US assisted drying will could be a less temperature dependent process than the AIR experiments. This fact means that the ultrasound application can make possible the

lowering of the drying temperature. The pre-exponential factor was also lower for US ($1.6 \cdot 10^{-5}$ m^2/s) than for AIR experiments ($8.6 \cdot 10^{-5}$ m^2/s).

As for the mass transfer coefficient (k) neither temperature nor ultrasound application significantly affected the figures identified (Table 2). However other authors have found significant influence of these variables on k [11, 12]. This fact could indicate that, at the drying conditions tested, the influence of external resistanced compared with the internal one was negligible. Therefore, the effect of studied variables on internal resistence could mask the effect on external one and then, the model can not identify any influence on k.

Table 2. Effective diffusivity and mass transfer coefficient identified by using a diffusion model. Percentage of variance explained by the model. Letters in the same column show homogenous groups determined for Least Significance Difference (p<0.05) intervals.

Treatment	D_e (x 10^{-10} m^2/s)	k (x 10^{-3} kg water/m^{2}s)	% var
AIR-10	0.3 ± 0.1^a	1.9 ± 0.4^a	98.7
AIR30	1.7 ± 0.6^b	0.8 ± 0.2^b	99.1
AIR50	5 ± 3^c	1.9 ± 0.5^a	99.6
AIR70	9 ± 2^d	2.3 ± 0.2^a	99.9
US-10	1.16 ± 0.02^b	2.0 ± 0.4^a	98.4
US30	5.49 ± 0.02^c	1.8 ± 0.3^a	99.4
US50	10 ± 2^d	2.0 ± 0.3^a	99.8
US70	10 ± 1^d	2.4 ± 0.7^a	99.8

In view of the results obtained, the ultrasound application can be considered as an interesting means of intensify drying processes at moderate temperatures.

4. Conclusion

Temperature and ultrasound application are able to significantly affect the apple skin drying. The higher the temperature the faster the process. The ultrasound application can also reduce the drying process time being this reduction more significant as lower the temperature. The atmospheric freeze-drying of apple peel was a very time consuming process even when was intensified by an ultrasound application.

5. Acknowledgements

6. References

[1] Martins, N.; Ferreira, I. C.F.R. Wastes and by-products: Upcoming sources of carotenoids for biotechnological purposes and health-related applications. Trends in Food Science & Technology. **2017**, 62, 33-48.

[2] Lamperi, L.; Chiuminatto, U.; Cincinelli, A.; Galvan, P.; Giordani, E.; Lepri, L.; Del Bubba, M. Polyphenol levels and free radical scavenging activities of four apple cultivars from integrated and organic farming in different Italian areas. Journal of Agriculture and Food Chemistry. **2008**, 56, 6536-6546.

[3] Henríquez, C.; Córdova, A.; Almonacid, S.; Saavedra, J. Kinetic modeling of phenolic compound degradation during drum-drying of apple peel by-products. Journal of Food Engineering. **2014**, 143, 146-153

[4] Boyer, J.; Liu R. H. Apple phytochemicals and their health benefits. Nutr J. **2004**, 3:1-15.

[5] Karaman, S.; Tütem, E.; Baskan, K. S.; Apakb, R. Comparison of antioxidant capacity and phenolic composition of peel and flesh of some apple varieties. Journal of the Science of Food and Agriculture. **2013**, 93: 867-875

[6] Escarpa, A.; Gonzalez, M.C. High-performance liquid chromatography with diode-array detection for the determination of phenolic compounds in peel and pulp from different apple varieties. Journal Chromatography. **1998**, vol. 823, no. 1-2, p. 331-337.

[7] Rupasinghe, H.P.V.; Wang, L.; Huber, G.M.; Pitts, N.L.. Effect of baking on dietary fibre and phenolics of muffins incorporated with apple peel poder. Food Chemistry. **2008**, 107, 1217-1224

[8] O'Shea, N.; Arendt, E.K.; Gallagher, E. Dietary fibre and phytochemical characteristics of fruit and vegetable by-products and their recent applications as novel ingredients in food products. Innovative Food Science and Emerging Technologies. **2012**, 16, 1-10

[9] Moses, J.A.; Norton, T.; Alagusundaram, K.; Tiwari, B.K. Novel Drying Techniques for the Food Industry. Food Engineering Reviews. **2014**, 6, 43-55.

[10] Lewicki, P. P.; & Jakubczyk, E. Effect of hot air temperature on mechanical properties of dried apples. Journal of Food Engineering. **2004,** 64, 307-314.

[11] Santacatalina, J.V.; Rodríguez, O.; Simal, S.; Cárcel, J.A.; Mulet, A.; García-Pérez J.V. Ultrasonically enhanced low-temperature drying of apple: Influence on drying kinetics and antioxidant potential. Journal of Food Engineering. **2014**, 138, 35-44

[12] Rodríguez, O.; Santacatalina, J.V.; Simal, S.; Garcia-Perez, J.V.; Femenia, A.; Rosselló, C. Influence of power ultrasound application on drying kinetics of apple and its antioxidant and microstructural properties. Journal of Food Engineering. **2014**, 129, 21-29.

[13] Moreno, C.; Brines, C.; Mulet, A.; Rosselló, C.; Cárcel, J. A. Antioxidant potential of atmospheric freeze-dried apples as affected by ultrasound application and sample surface. Drying Technology. **2017**, 35(8), 957-968

[14] Claussen, I.C.; Ustad, T.S.; Strommen, I.; Walde, P.M. Atmospheric freeze-drying – A review. Drying Technology. **2007**, 25, 947-957.

[15] Cárcel, J.A.; García-Pérez, J.V.; Riera, E.; Rosselló, C.; Mulet, A. Ultrasonically assisted drying. In Ultrasound in Food Processing; Villamiel, M., García-Pérez, J.V., Montilla, A., Cárcel, J.A., Benedito, J., Eds.; John Wiley & Sons Ltd.: United Kingdom, 2017; pp 371-391.

[16] Musielak, G.; Mierzwa, D.; Kroehnke, J. Food drying enhancement by ultrasound – A review. Trends in Food Science & Technology. **2016**, 56, 126-141.

[17] Wolfe, K.L.; Liu, R.H. Apple Peels as a Value-Added Food Ingredient. Journal of Agricultural and Food Chemistry. **2003**, 51, 1676-1683

[18] AOAC, Association of Official Analytical Chemist. Official methods of analysis; Arlington: EEUU, 1997.

[19] Riera, E.; García-Pérez, J.V.; Acosta, V.M.; Cárcel, J.A.; Gallego-Juárez, J.A. A computational study of ultrasound-assisted drying of food materials. In: Knoerzer, K., Juliano, P., Roupas, P., Versteeg, C. (Eds.), Multiphysics Simulation of Emerging Food Processing Technologies. IFT Press, Chicago, USA, 2011; pp. 265-302.

[20] Do Nascimento, E.M.G.C; Mulet, A.; Ramírez-Ascherí, J.L.; Piler De Carvalho, C.W.; Cárcel, J.A. Effects of high-intensity ultrasound on drying kinetics and antioxidant properties of passion fruit peel. Journal of Food Engineering. **2016**, 170, 108-11

Drying intensification by vibration: fundamental study of liquid water inside a pore

Chen, W.ª; Colin, J.ª*; Casalinho, J.ª; Ben Amara, M.E.A.ᵇ; Stambouli, M.ª; Perré, P.ª

ª LGPM. CentraleSupélec. Université Paris-Saclay, Gif-sur-Yvette, France
ᵇ LESTE. École Nationale d'Ingénieurs de Monastir. Université de Monastir, Tunisie.

*E-mail of the corresponding author: julien.colin@centralesupelec.fr

Abstract

Vibration is a promising way to intensify the drying process through heating-up due to viscous dissipation, activation of internal liquid transfer and increase of external transfer. To better assess the possible contribution of these effects, we choose a multiscale approach.

This paper is focused on the pore scale, simulated by a capillary tube partially filled with water subjected to sinusoidal vibrations. We studied the displacement of water inside this tube through image analysis. This configuration mimics the moisture transfer inside the pores of a porous media during drying.

The experimental device developed in this study is applicable to a wide range of configurations, such as symmetrical or asymmetrical vibrations.

Keywords: drying intensification, acoustic vibration, pore scale, symmetrical and asymmetrical signals, image processing.

1. Introduction

Vibration is a promising way for the intensification of drying [1], especially for porous media. The present work is focused on the study of the effect of vibration to assist moisture migration inside these materials. Several phenomena may be involved [2,3] such as internal heat generation by viscous dissipation, intensification of transfer at the exchange surfaces, activation of vapor diffusion by oscillating bulk velocity, change of wetting angle, etc. In this paper, we focus on the liquid water behavior inside a unique pore during vibration.

2. Materials and Methods

The experimental set consists of a capillary glass tube partially filled with water, a vibration chain and an optical bench controlled by a PC.
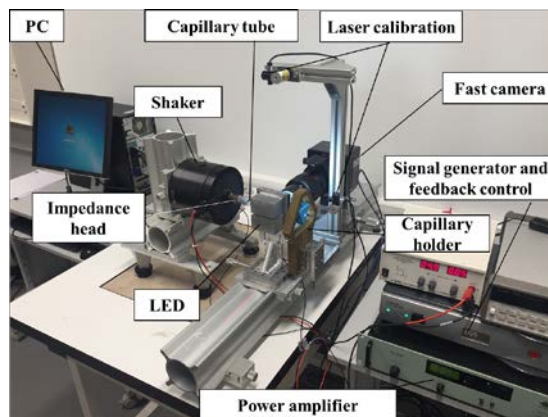
Fig. 1 A general view of the experimental device.

2.2 Capillary tube and water index

Capillary tubes – inner diameter (*ID*) = 0.6 or 2.2 mm, length = 15 cm, carefully cleaned with Mucasol solution (3 %, ROTH) – are used for simulating a unique pore. Considering the difficulty of tracking the position of a smooth tube, a notch is machined on the top external wall as a mark to observe its movement. An index of distilled water is placed in this tube. In the present work, a constant index length was used, in the range 10.1 to 10.2 mm.

2.3 Vibration chain

A Brüel & Kjær vibration chain (Fig. 1) vibrates the capillary tube horizontally. A power supply (type 2718) amplifies the signal from the generator (LDS LASER$_{USB}$, 64 bits) to the vibration exciter (type 4809, maximum 8 mm peak-to-peak displacement, from 10 Hz to 20 kHz). An impedance head (type 8001, with a piezoelectric accelerometer and force gauge sharing the same housing, operating frequency range up to 10 kHz) – fastened between the

exciter and the tube, and connected to the signal generator – allows a feedback control. At the other end of the tube, a 3D-printed holder reduces the vertical oscillations due to the gravity and possible resonances. Series of tests were performed with sinusoidal vibrations:

$$x_{cap}(t) = A sin(\omega t) \qquad\qquad (1)$$

where A is the amplitude, ω the angular frequency and f the frequency ($\omega = 2\pi f$).

2.4 Image acquisition system

The tube and liquid movement are monitored thanks to an optical bench, comprising a high-speed camera (FASTCAM Mini AX100, by Photron: up to 4000 fps at full resolution of 1024×1024 with a grey level coded on 12 bits), controlled by a PC, and a backside illumination. The perpendicularity of the tube and the optical bench axis is calibrated using two line lasers.
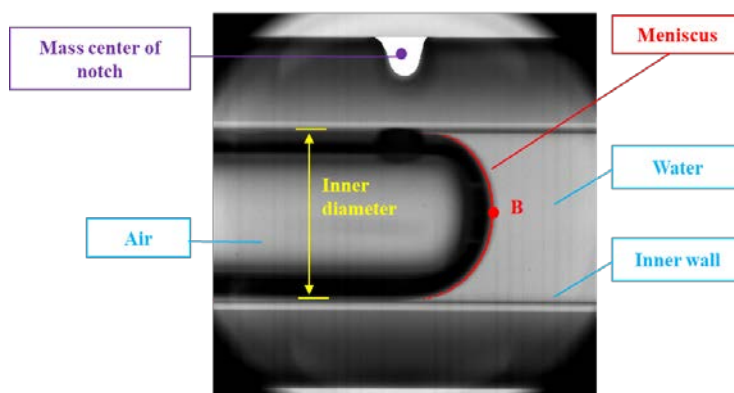
Fig. 2 Water index meniscus inside a capillary tube.

2.5 Image processing

The behavior of the water index is studied by image processing through the displacement of the meniscus (Fig. 2), *i.e.* the interface between water and air. Obtained images are analyzed using a custom Matlab program. The core of the program consists in the recognition of the inner wall, the meniscus and the notch. The boundaries between phases are characterized by a transition from light to dark. Point B is the intersection of the tube axis and the meniscus. The coordinate of the mass center of the notch (white area in Fig. 2) is used to follow the position of the capillary tube.

3. Raw data

For each test, we register 50 pictures per period over a total of 7 periods. Fig. 3 presents images obtained for $ID = 2.2$ mm, $f = 30$ Hz and $A = 2$ mm. Red arrow depicts the tube direction and the blue one shows the water direction compared with the previous position.

For this test, we notice that the menisci are not perfectly symmetrical to the horizontal plane: gravity is not negligible anymore for the 2.2mm-inner diameter tube.

t_0 $t_0+6.67$ ms $t_0+13.33$ ms
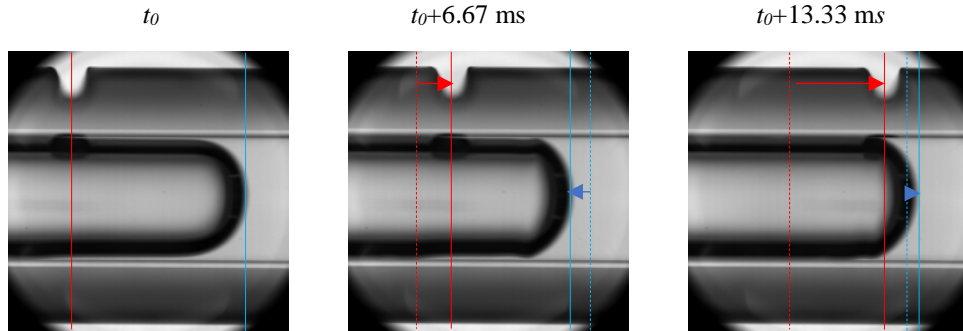
Fig. 3 Displacement of the water index during half period (ID = 2.2 mm, f = 30 Hz, A = 2 mm)
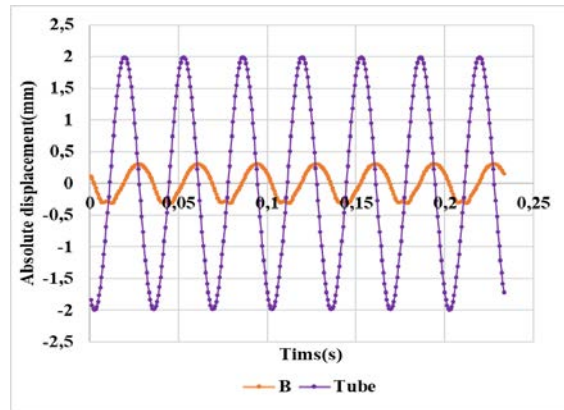
Fig. 4 Absolute displacements of water and tube vs. time (ID = 2.2 mm, f = 30 Hz, A = 2 mm)

We can also notice that the absolute displacement amplitude of the water index is lower than the one of the capillary tube. At this high frequency, inertia dominates the forces acting on the system (viscous and capillary forces). This observation is confirmed by all positions determined by image processing. In this case, as the absolute movement of water (Fig. 4) is much smaller than the tube movement, the relative movement of water inside the tube has almost the same amplitude as the imposed movement. For these parameters, the phase change of water movement is about $\pi/2$.

4. Results

In order to study a wide range of contrasted situations, the values of three parameters were systematically tested: inner diameter (0.6 and 2.2 mm), frequency (10, 20 and 30 Hz) and amplitude (0.5, 1, and 2 mm). Thus, we obtained a dataset of 18 experiments. The images

analysis for all tests depicts a high diversity of water index behavior, especially for menisci shape and displacement amplitude. To explain this variability, it is mandatory to quantify the relative importance of three parameters: surface tension, viscosity and inertia. For this purpose, we introduce two dimensionless numbers:

4.1. The capillary effect

N_c is the ratio of capillary force F_c over inertia F_i:

$$F_c = 2\pi R\sigma \quad (2)$$

$$F_i = ma = \pi R^2 l\rho A\omega^2 \quad (3)$$

hence
$$N_c = \frac{2\sigma}{Rl\rho A\omega^2} \quad (4)$$

where R is inner radius of capillary, σ the surface tension, l the length of the index, and ρ the water density.
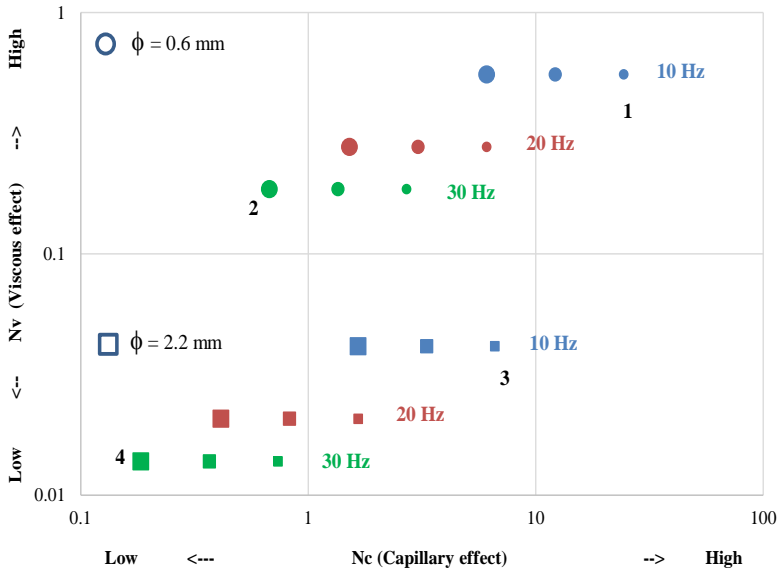
Fig. 5 Representation of all tests performed in the present study according to their respective effects of capillary forces and viscosity; One marker size per signal amplitude, (small = 0.5 mm, medium = 1 mm and large = 2 mm)

4.2. The viscous effect

N_v is the ratio of the characteristic time of the signal (half-period) over the characteristic diffusion time:

$$N_v = \frac{\mu}{2f\rho R^2} = \frac{\delta^2}{R^2} \qquad (5)$$

where μ is the dynamic viscosity of water and δ the thickness of the Stokes boundary layer.

All tests performed in this study can therefore be represented by one marker in the plane defined by the values of N_c and N_v (Fig. 5). From all these tests, four contrasted situations are selected for an in-depth study.
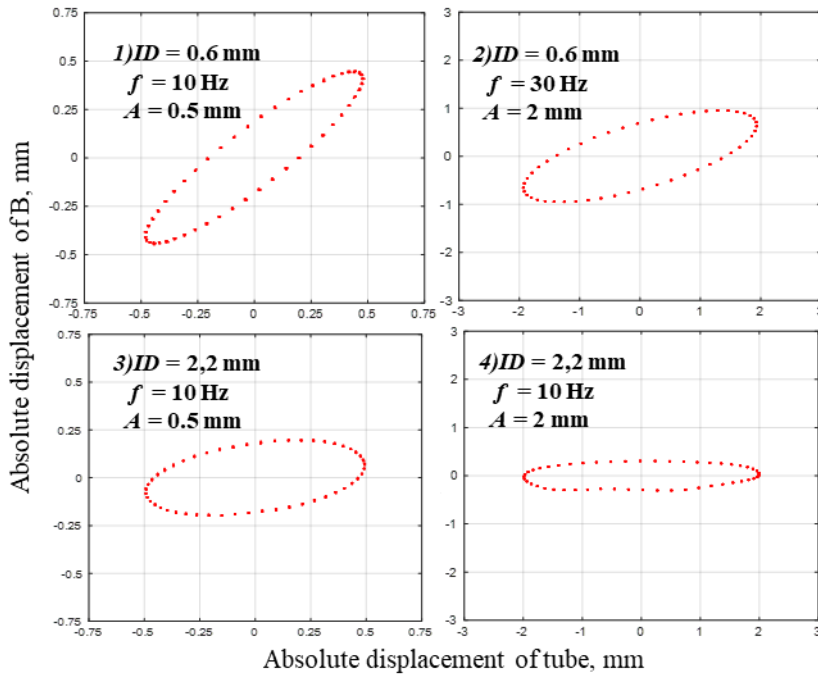
Fig. 6 Lissajous curves (absolute displacement of point B plotted versus tube displacement) for the four configurations selected for the in-depth analysis (points in Fig. 5)

4.3. Focus on contrasted situations

In order to provide a more in-depth analysis of the relative effects of the physical phenomena (viscosity, surface tension, inertia), Lissajous curves were plotted for each selected test (Fig. 6). These curves consist in plotting the absolute displacements of the water index (point B) as a function the tube displacement. On these closed curves, we can easily observe the ratio between the tube and water amplitude (respectively width and height of the ellipse according x and y) and the phase change between the signal (twice the angle between the first bisector and the main axis of the ellipse)

For test 1, the capillary effect dominates inertia and the viscous effect is not negligible (see the position of point 1 in Fig. 5). As a result, the water index flows the tube movement with a slight hysteresis. This explains why the curve is long and narrow along the direction 45°: almost same amplitudes and same phase. For the same tube diameter (0.6 mm) but a larger frequency and a larger amplitude (test 2), N_c is smaller than the unit. Consequently, the water index is not able anymore to follow the tube movement: the water index amplitude is ca. half the signal amplitude and the phase change increases. For test 3, as seen in Fig. 5, the capillary effects are quite important, but the viscous effects are now negligible, due to the larger tube diameter. Finally, test 4 lies at the very bottom-left of Fig. 5, which means very weak viscous and capillary forces. Accordingly, the water index is almost at rest in spite of the tube movement.

5. Conclusions and perspectives

In this work, we highlighted on the effect of vibrations on the movement of a water index in a capillary tube.

Then, various parameters were tested: tube diameter, frequency and amplitude of the tube movement. In order to quantify the effects of the parameters, two dimensionless numbers were introduced to see the effect of viscous and capillary forces compared to the index inertia. All data collected in four contrasted selected tests are perfectly explained by these dimensionless numbers.
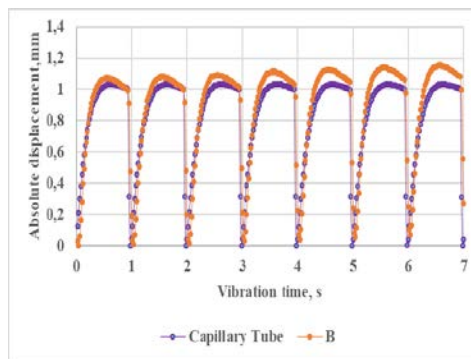
Fig. 7 Absolute displacements of B and tube (ID = 2.2 mm, f = 1 Hz, A = 1.03 mm)

Finally, by using an asymmetrical signal, we prove that the index movement can be forced in a chosen direction. In this sense, Fig. 7 depicts a preliminary, but promising test. Using a

saw-tooth wave at low frequency, we obtained an obvious global movement of the index to the right along the successive periods. This trend was inverted when changing the phase of the signal, which proves that the water movement is really due to the asymmetric signal.

Additional tests as well as modeling approaches are in progress in our team to further investigate the effect of vibrations on liquid movement, and the numerical validation of some experimental results has also been done.

6. Nomenclature

a	acceleration	ms^{-2}		m	mass	kg
A	sine	m		N_c	capillary effect	
f	frequency	Hz		N_v	viscous effect	
F	force	N		R	inner radius	m
ID	inner diameter	m		t	time	s
l	length	m		x	coordinate along the	mm

Greek letters

δ	Stokes boundary layer	mm
μ	dynamic viscosity	Pa×s
ρ	density	kgm^{-3}
σ	surface tension	Nm^{-1}
ω	angular frequency	rads^{-1}

Subscripts

c	capillary
cap	capillary tube
i	inertia

7. References

[1] Kroehnke J.; Radziejewska-Kubzdela E.; Musielak G., Stasiak M.; Bieganska-Marecik R. Ultrasonic-assisted and microwave-assisted convective drying of carrot-drying kinetics and quality analysis. In Proceedings of 5th European Drying Conference, Budapest, Hungray, October 21-23, 2015, 171-178.

[2] Lebovka, N.; Eugene V.; Farid C. Enhancing extraction processes in the food industry. CRC Press, 2011.

[3] Suzuki K.; Hosaka H.; Yamazaki R. Drying characteristics of particles in a constant drying rate period in vibro-fluidized bed. Journal of Chemical Engineering of Japan, 1980, 13(2): 117-122.

Wall deposition experiments in a new spray dryer

Huang, X.; Zhong, C.; Langrish, T. A. G.[*]

Drying and Process Technology Research Group, School of Chemical and Biomolecular Engineering, University of Sydney, Sydney, Australia

*E-mail of the corresponding author: timothy.langrish@sydney.edu.au

Abstract

Wall deposition tests have been conducted on a new spray-drying sytem. Solutions of salt and skim milk powder have been dried with different inlet temperatures (170 °C and 230 °C) and solid contents (8.8 wt% and 30 wt%). The experiment showed that increasing the temperature caused an decrease in the amount of deposition for salt solution, but an increase for skim milk. The experiments also showed that a higher solid content caused an increase in deposition. The trends agreed with the studies using a conventional spray dryer, but the amount of deposition appeared to be lower in the new spray dryer at the same operating conditions

Keywords: Spray drying; wall deposition

1. Introduction

Spray-drying techniques have been applied in a wide range of industries. One of the key issues that occurs when using spray dryers for food materials is wall deposition. During the drying process, the particles, especially if they contain sugar-rich and fat-rich food materials, may stick on the wall of the drying chamber [1]. Many workers have focused on the effects of operating conditions on the degree of wall deposition, such as the temperatures and the solid content. At a certain moisture content, the sticky point is the critical temperature at which particles transform into a sticky state due to the increase in the molecular mobility and the formation of solid bridges between particles. Studies by Roos & Karel [2] showed a close relationship between the sticky point and the glass-transition temperature Tg of the dried materials. Solid content is another important factor affecting the formation of deposits. Goula & Adamopoulos [3] have suggested that, for food products with higher hygroscopicity (e.g. skim milk, sucrose, tomato pulp), increasing the feed concentration increases the moisture adsorption rate on the surface of particles. Another possible effect of increasing the feed concentration is to change the particle moisture content. The moisture content within each droplets may vary with feed concentration, depending on the droplet sizes [4].

A new spray-drying system has been established in the School of Chemical and Biomolecular Engineering in the University of Sydney. The preliminary studies on the flow pattern of the spray dryer have shown that the design improved the stability of the flow field near the chamber wall, which may help to reduce wall deposition. The aim of the project is to evaluate the wall deposition performance of the new spray dryer using different feed materials and operating conditions, including inlet temperatures and feed concentrations. The experiment also compared results with previous studies using spray dryers of conventional designs.

2. Materials and Methods

A schematic diagram of the system is shown in Figure 1. The stainless steel chamber is insulated using glass wool insulation blankets. The drying chamber consists of two drying columns of 30 cm in diameter. Chamber one is 2.2 m, and chamber two is 1.6 m in height. The columns comprise seven detachable sections in total, with the actual drying process starting from section 2. The chamber is fitted with a two-fluid nozzle atomizer (Buchi B-290, Switzerland). Feed solutions of all the tested materials have been introduced through the atomiser using a liquid flowrate of 27 ml/min and an atomising air flowrate of 10 L/min, which were selected according to previous experimental studies using a conventional spray dryer [5], [6]. The operating conditions for different materials have been shown in Table 1. Multiple stainless steel plates have been placed at the side wall of each section of the chamber as well as the bottoms of both columns, in order to measure the deposition fluxes. After removing the plates from all the sections, each section has been washed with water to

dissolve all the remaining deposits. Portions of the wash solutions have been dried at 80 °C for 24 h, in order to calculate the total mass of deposits based on the weight of the collected solutions. The total mass of deposits has been used to calculate the deposition rate, which is the total mass of deposits divided by the total sprayed solids.

Table 1 Operating conditions for different feed materials applied in the experiment.

Feed material	Inlet temperature (°C)	Feed concentration (wt%)
Salt	170/230	8.8
Skim milk	170/230	8.8/30
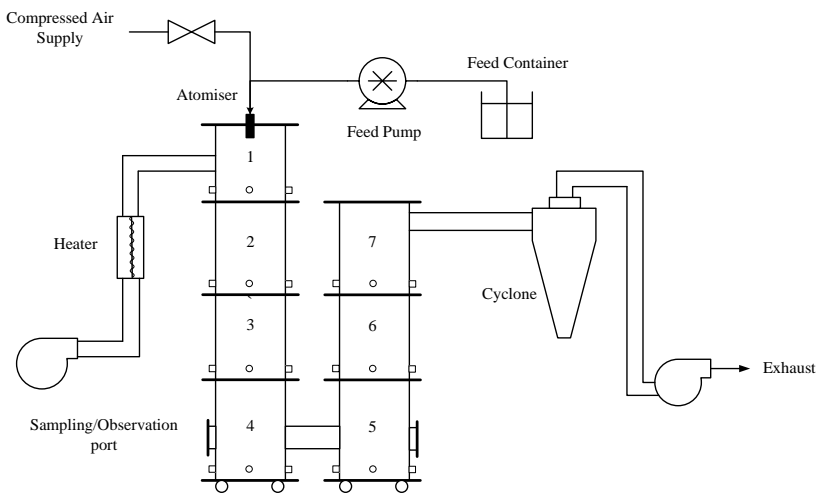
Figure 1 Schematic diagram of the new spray-drying system.

3. Results and Discussion

3.1. Investigation of the influence of inlet temperature using salt and skim milk

The inlet temperature was chosen to be the first parameter to be investigated, because it was noticed that the design features and the insulation of the new spray-drying system provided a relatively low heat loss to the environment (around 20 W/K). The difference in temperature profile could lead to different wall deposition behaviour compared with conventional spray-dryer designs. The qualitative observations of the deposition patterns at different sections of the drying chamber have been shown in Table 5. The measurements of deposition fluxes and deposition rates have been shown in Table 2.

For the salt solutions, it can be first observed from Table 5 that there appeared to be no severe formation of wall deposits on the chamber wall, with only a thin, dusty layer observed in sections 3, 4 and 5. Increasing the inlet temperature from 170 °C to 230 °C has shown no

significant effect on the deposition pattern. It should be noted that, at the bottom of section 4, the deposition tended to form an evenly distributed layer, whilst at the bottom of section 5, the deposition pattern changed into spotted deposits. Such differences between indicated two different processes of forming wall deposits in the drying chamber. Kota & Langrish [6] suggested that deposition could be formed by two mechanisms: inertial deposition, caused by the inertia of particles, and turbulent deposition, caused by the random movement of particles due to turbulence in the air flow. In chamber one (section 4), the particles from the atomiser travelled directly towards the chamber wall/bottom, then formed an evenly-distributed deposit, mainly due to particle inertia. As the particles proceeded to chamber two (section 5), the recirculation flow caused the particles to agglomerate into large particles and formed spotted deposits. From Table 2, it can also be observed that the the deposition fluxes were higher on the bottom of sections 4 and 5, which indicated that the inertial deposition may be the dominant mechanism casuing deposition. At a higher temperature of 230 °C, the measurements have shown slight reductions on both the side walls and the chamber bottoms. Such reductions could be caused by a lower moisture content, thus less adhesive forces caused by liquid bridges [7].

Table 2 Wall deposition fluxes and deposition rates of 8.8 wt% salt and skim milk feed solutions at different sections of the drying chamber.

		Salt (170 °C)	Salt (230 °C)	Skim milk (170 °C)	Skim milk (230 °C)
Side wall Deposition Fluxes ($g·m^{-2}·h^{-1}$)	**Section 2**	0.5	0	0.3	0.5
	Section 3	2.0	0.7	2.7	3.0
	Section 4	1.5	0.3	1.0	1.0
	Section 5	2.0	1.6	5.5	3.5
	Section 6	1	0	1.3	0.7
	Section 7	0	0	0	0
Bottom Deposition Fluxes ($g·m^{-2}·h^{-1}$)	**Section 4**	10	11	7.0	9.5
	Section 5	22	15	12	14
Overall average ($g·m^{-2}·h^{-1}$)		4.9	3.6	4.0	4.0
Side wall average ($g·m^{-2}·h^{-1}$)		1.2	0.4	2.0	1.4
Bottom average ($g·m^{-2}·h^{-1}$)		16	13	9.3	12
Chamber 1 deposition rate (%)		2.0	1.8	2.8	3.2
Chamber 2 deposition rate (%)		3.4	1.3	3.3	4.4
Cyclone deposition rate (%)		2.3	1.5	1.4	2.9
Total deposition rate (%)		7.7	4.6	7.6	10.5

In comparison with salt solutions, skim milk showed some differences in response to the increase in the inlet temperature. From Table 5, it can be seen that the deposition produced by the skim milk at 170 °C appeared to be similar to that produced by salt. As the temperature

increased to 230 °C, however, colour changes could be observed in the deposition. The brownness of the deposition indicated that Maillard reactions and possibly caramalisation may have occured at the higher temperature. Previous studies using a conventiaonl spray dryer [5] reported a deposition flux of around 16 $g·m^{-2}·h^{-2}$ at the inlet temperature of 170 °C, which was higher than the values measured in this work (maximum of 12 $g·m^{-2}·h^{-2}$). The lower deposition in the new spray dryer could be caused by a more stable flow pattern and relatively smaller heat loss of the new system. However, as the inlet temperature increased to 230 °C, the deposition flux in the conventional spray dryer was reported to be 8 $g·m^{-2}·h^{-2}$, lower than the values measured at the bottoms of the new system. Maillard reactions and caramelisation could cause such higher deposition flux in the new dryer, as the reactions produced complex compounds [8], thus led to changes in the particle compositions and the glass transition temperature.

3.2 Investigation of the influence of feed concentration using skim milk

From the comparison of the wall deposits obtained at different inlet temperatures, it was strongly suggested that the higher drying temperature of 230 °C could lead to changes in the particle compositions. To avoid introducing additional variables, the investigation of the effect of feed concentration was conducted at the inlet temperature of 170 °C. The qualitative observations of the deposition pattern have still been shown in Table 5, and the measurement of deposition fluxes and deposition rates have been shown in Table 3.

From Table 5, it can be observed that the bias in the deposition became more obvious at the higher feed concentration in sections 3 and 4 than that in section 5. Four plates were placed in each of section 3, 4 and 5 in order to better interpret the distribution of the wall deposition, and the percent deviations for each section have been shown in the brackets of Table 3. It can be seen that for the feed concentration of 8.8 wt%, the percent deviation was found to be the highest in section 3 (96%), and sections 4 and 5 showed a similar degree of deviation (57% and 54%). At the higher feed concentration, no apparent change was observed in the percent deviation in section 3 and 4 (90% and 52%), but a reduction was seen in section 5 from 54% to 17%. Such changes in section 5 suggested that the formation in section 5 underwent a different process from that in sections 3 and 4. The inertial deposition due to the direct impact of the spray appeared to be the main cause of the deposition, as well as the biased deposition pattern in sections 3 and 4, regardless of the feed concentration. By contrast, with a higher feed concentration, particle of larger sizes may be less influenced by the turbulent flow, thus forming the deposition around section 5.

The deposition fluxes measured in this experiment were again compared with the results using a conventional spray dryer [5], [6]. As shown in Table 4, the new spray dryer showed lower deposition fluxes at the same operating conditions, with the average deposition fluxes reported to be 16 $g·m^{-2}·h^{-1}$ compared with 4 $g·m^{-2}·h^{-1}$ at a concentration of 8.8 wt%, and 130

g·m^{-2}·h^{-1} compared with 50 g·m^{-2}·h^{-1} with a 30 wt% feed solution. Despite the overall lower deposition flux, the new drying system showed the increasing trend similar to the previous studies, as shown in Table 4. There are several reasons that could lead to the increaing wall deposition fluxes: 1) higher the specific moisture content due to larger droplet sizes; 2) the hygroscopicity of skim milk increases with the solid content, which could hinder the drying process; 3) particles with higher solid content tended to form crust of higher thickness, which could reduce the evaporation of moisture within the crust.

Table 3 Wall deposition fluxes and deposition rates of 8.8 wt% and 30 wt% skim milk feed solutions at different sections of the drying chamber. Inlet temperature = 170 °C.
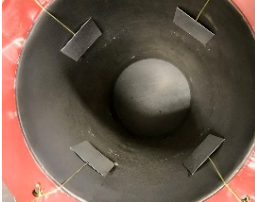
		Skim milk (8.8 wt %)	Skim milk (30 wt%)
Side wall Deposition Fluxes (g·m^{-2}·h^{-1})	**Section 2**	0.3	6
	Section 3	2.7 (96%)	63 (90%)
	Section 4	1.0 (57%)	17 (52%)
	Section 5	5.5 (54%)	98 (17%)
	Section 6	1.3	13
	Section 7	0	5
Bottom Deposition Fluxes (g·m^{-2}·h^{-1})	**Section 4**	7.0	121
	Section 5	12	74
Overall average (g·m^{-2}·h^{-1})		4.0	50
Side wall average (g·m^{-2}·h^{-1})		2.0	33
Bottom average (g·m^{-2}·h^{-1})		9.3	98
Overall average w.r.t solid flowrate (g·m^{-2})		0.026	0.10
Side wall average w.r.t solid flowrate (g·m^{-2})		0.013	0.069
Bottom average w.r.t solid flowrate (g·m^{-2})		0.065	0.20
Chamber 1 deposition rate (%)		2.8	3.2
Chamber 2 deposition rate (%)		3.3	4.4
Cyclone deposition rate (%)		1.4	2.9
Total deposition rate (%)		7.6	10.5

Note: values in the brackets show percentages of the deviation with respect to the average deposition fluxes of the plates in the same chamber.

Table 4 Average deposition fluxes of skim milk solutions dried at inlet temperature of 170 °C using a conventional spray dryer and the new spray-drying system in this work.

	Feed concentration (%)	Average deposition flux (g·m^{-2}·h^{-1})
Ozmen & Langrish [5]	8.8	16
Kota & Langrish [6]	30	130
This work using the new spray dryer	8.8	4.0
	30	50

Table 5 Qualitative observations of wall depositions formed at different sections of the drying chamber.

	Section 3 (1 m from atomiser)	Section 4 (1.5 m from atomiser)	Section 5
Salt 8.8 wt% 170 °C			
Salt 8.8 wt% 230 °C			
Skim milk 8.8 wt% 170 ° C			
Skim milk 8.8 wt% 230 °C			
Skim milk 30 wt% 170 °C			

4. Conclusion

Wall deposition tests have been conducted on a a new spray dryer in order to investigate its performance at different operating conditions, and compare it with a conventional design. The increase in the inlet temperature from 170 °C to 230 °C has caused a slight reduction in wall deposition rate for salt solutions, but an increase in the value for skim milk solutions. Such a difference could be caused by the change in the composition of skim milk deposits as a result of Maillard reactions. The experiments with different feed concentrations showed an

increase in wall deposition when the solid content increased from 8.8 wt% to 30 wt%. Such an increasing trend agreed with the previou studies using a conventional spray dryer, although the actual amount of wall deposition appeared to be lower in the new spray dryer. Overall, the experiments provided some valuable information to improve the design of the new system.

5. References

[1] B. R. Bhandari and T. Howes, "Relating the Stickiness Property of Foods Undergoing Drying and Dried Products to their Surface Energetics," Dry. Technol., vol. 23, no. 4, pp. 781–797, 2005.

[2] Y. Roos and M. Karel, "Applying state diagrams to food processing and development.," Food Technol., vol. 45, no. 12, pp. 66, 68–71, 1991.

[3] A. M. Goula and K. G. Adamopoulos, "Spray drying of tomato pulp: Effect of feed concentration," Dry. Technol., vol. 22, no. 10, pp. 2309–2330, 2004.

[4] L. Tajber, O. I. Corrigan, and A. M. Healy, "Spray drying of budesonide, formoterol fumarate and their composites-II. Statistical factorial design and in vitro deposition properties," Int. J. Pharm., vol. 367, no. 1–2, pp. 86–96, 2009.

[5] L. Ozmen and T. A. G. Langrish, "An Experimental Investigation of the Wall Deposition of Milk Powder in a Pilot-Scale Spray Dryer," Dry. Technol., vol. 21, no. 7, pp. 1253–1272, 2003.

[6] K. Kota and T. A. G. Langrish, "Fluxes and Patterns of Wall Deposits for Skim Milk in a Pilot-Scale Spray Dryer," Dry. Technol., vol. 24, no. 8, pp. 993–1001, 2006.

[7] M. J. Hanus and T. A. G. Langrish, "Re-entrainment of wall deposits from a laboratory-scale spray dryer," Asia-Pacific J. Chem. Eng., vol. 2, no. 2, pp. 90–107, 2007.

[8] S. Martins, S. I. F. S. Martins, and W. M. F. Jongen, "A review of Maillard reaction in food and implications to kinetic modelling A review of Maillard reaction in food and implications to kinetic modelling," Trends Food Sci. Technol., vol. 11, pp. 364–373, 2001.

Drying kinetics and selected physico - chemical properties of fresh cranberries preserved with microwave - vacuum process

Piecko J*, Konopacka D., Mieszczakowska-Frąc M., Kruczyńska D, Celejewska K.

Research Institute of Horticulture, Konstytucji 3 Maja 1/3 Str., 96-100 Skierniewice, Poland.

*E-mail of the corresponding author: jan.piecko@inhort.pl, phone +48 46 8345427

Abstract

A one stage drying process for dried cranberry production, employing a vacuum microwave technique, is proposed. The process consists of a specific sequence of microwave energy dosage at a given vacuum level. During the 60 minute process, three sub-stages can be identified: osmotic dehydration, intensive water evaporation and stabilization. Mass transfer, as well as quality changes during the process, has been described, and the final product quality compared to purchased control. The proposed method of dried cranberry production resulted in a microbiologically stable product (a_w=0.62) of a decent sensory quality, with an antioxidant potential three times higher than traditional products.

Keywords: Vaccinium macrocarpon; microwave-vacuum drying; ready-to-eat snack

1. Introduction

The cranberry (*Vaccinium macrocarpon*) fruit is recognized worldwide as a rich source of numerous phytonutrients with confirmed pharmacological and antioxidant properties [1]. Due to a high acid content, as well as an astringent taste, the fresh fruits are unacceptable for direct consumption. In an effort to make cranberries more appealing to consumers, one idea is to dry them, which unfortunately also means adding sugar. The traditional method of dried cranberry production is a time and energy-consuming process, which is realized in three stages: skin pre-treatment, sugar infusion by osmotic dehydration and final drying. Cranberry fruits, like many other fruits are covered by a cutin layer consisting of fatty acid polymers which exist to protect the fruit from losing water. Although the wax layer is beneficial in plant biology, it restricts processing by inhibiting osmotic dehydration and further drying processes. Cutting the fruits into halves allows the interior fruit tissue to be exposed to osmotic solution as well as increasing the evaporation surface during final hot air drying. Sadly, cutting the fruit also leads to several negative consequences, such as a higher leakage of sap or an increase in nutrient oxidation during the final drying. Available literature documents numerous attempts to intensify the osmotic dehydration of cranberries through various pre-treatments [2–3], as well as attempts to accelerate the drying process by applying new drying techniques [4–6]. Among the new techniques, a hybrid technique including microwave technology has been intensively investigated [7]. According to the latest reports the drying time can be reduced to less than 100 min [3]. The other problem associated with dried sweetened cranberry production is the time needed to infuse sugar, which can take up to 24 hours [8]. Despite the introduction of some new ideas to reduce the osmotic dehydration process [3,5], the waste sucrose syrup collected after the process, remains a serious technological and environmental problem.

The aim of this paper is to present an idea combining sugar infusion and final drying of freshly cut cranberry fruit, which can be realized within 60 min in the same reaction chamber by using a vacuum microwave technique.

2. Materials and Methods

Cranberry fruits (`Ben Lear` cv) taken out of cold storage (2°C) were thoroughly washed with tap water and cut in half. The osmo-dried cranberry production was realized using a laboratory vacuum-microwave dryer (PromisTech, Wrocław, Poland). The standard polypropylene reaction chamber was replaced with a glass drum, which allowed the management of liquid medium. Just before drying, a batch of 100 g freshly cut cranberry fruit halves were placed into a 2 L capacity glass drum and mixed with 80g of 40% sucrose solution. When the system reached the ambient temperature (20.0 ± 2.0°C), the process was started. The drying procedure was developed using a specific sequence of microwave energy

dosage at a given vacuum level. The drying period lasted 60 min, within which, three sub-stages can be identified, as is presented in Table 1 (PL, Patent Pending, 2018).

Table 1. The technical parameters of the vacuum microwave drying of halved fresh cranberries

Stage	Duration [min]	Operation	Preasure [hPa]	Max sample temperature [°C]	Microwave power [Watt/g]
1	15	Osmotic dehydration	30 ± 2	34.0 ± 0.8	1.00
2	30	Evaporation	30 ± 2	57.0 ± 3.0	3.25
3	15	Stabilization	6 ± 2	30.0 ± 1.0	0

The density of microwave power introduced into the drying chamber ensured that the material temperature was kept below 60°C. The mass transfer, and the quality changes of the material, was monitored in 7 mid-points, after 5, 10, 15, 20, 30, 35, 45 min and after process completion. To follow real drying dynamics, the process was terminated after a given time, and the material collected for analyses, after which a new procedure with a new batch of raw material was begun. For each mid-point of the process water removal rate was determined as the difference between the total weight of material at the given point. The material temperature was measured by a manual pyrometer, and then the material was checked for moisture content, density, anthocyanin content and antioxidant capacity. The appearance of the material was captured by a camera. The fruit samples taken between 5-30 min of the process, prior to measurement, were gently rinsed with water to remove residual syrup and blotted with paper towels. A fresh portion of fruit was used to obtain each sample taken for each time interval. The final product quality was also evaluated by a sensory panel, and the experimental dried fruit were compared to dried cranberries purchased in the market (one bulk product and one commercially packed). The experiment was carried out in two technological repetitions.

2.1. Physical, chemical and sensory analyses

The dry matter content was determined using the gravimetric method by drying the sample to a constant weight at 70°C under vacuum conditions (3 kPa) according to PN-90/A-75101/03 [9]. The density of the dried berries was determined using hydrostatic scales (Radwag) and calculated using the following formula:

$$\rho_s = \frac{ms_1}{ms_1 - ms_2} * \rho_t$$

where, ρ_s indicated sample density (g/cm^3), ms_1 sample mass in the air (g), ms_2 sample mass in toluene (g), and ρ_t density of toluene (g/cm^3). For each experimental point the measurements were repeated for 6 individual fruit halves.

Water activity was measured 24 h after drying, using HC2-AW-USB station probes connected to a PC running HW4-P-QUICK-V3 software (Rotronic, B&L, Poland).

Antioxidant activity was determined according to the method described by Re et al. [10]. Measurements were recalculated to micromoles of Trolox equivalents per gram of dry weight (µmol Trolox/g DW).

Total anthocyanin content was quantified using the pH differential method [11]. The results were calculated as cyanidin-3-glucoside, and expressed in mg/100 g DW of the analyzed sample. For each mid-point of particular technological repetition, two independent analytical replicates were carried out.

Sensory analysis. Both experimentally dried fruit and the commercially purchased products were assessed by a well-trained panel using a profiling method. The samples were evaluated in individual sensory booths under white light (6500 K). All samples, marked with 3-digit codes, were served in duplicate in random order. Panelists were asked to evaluate fifteen sensory attributes: three aroma attributes (fruity, untypical, overall), two textural attributes (hardness and overall), five flavour/taste attributes (fruity, sweet, sour, astringent, bitter, and off-flavour) and overall flavour, as well as overall quality. The results were finally expressed in 10-point scale.

2.2. Statistical analysis

The data was processed using the STATISTICA 13.0 software package (StatSoft Inc., Tulsa, USA). To determine the difference between experimental and commercial products the analysis of variance (ANOVA) and a Duncan´s multiple range test at p = 0.05 was used.

3.   Results and Discussion

The dehydration kinetics of the fresh cranberry halves subjected to the one stage process realized in a vacuum- microwave reactor is illustrated in Fig. 1. Along with the parameters outlining the mass transfer intensity, the sample temperature is also given (Fig 1A). As the drying process proceeded simultaneously with osmotic dehydration, the obtained drying kinetics presents an untypical shape. In the first 15 min of the process, the drying rate gradually decreased (Fig. 1B), probably due to the effect of the increase of the syrup viscosity surrounding the surface of the fruit. During this stage the soluble solids of the fruit increased from 8.9 ± 0.1 to $15.1 \pm 1.1°$Brix, which was also reflected by the increase of the sample dry matter (Fig. 1A), caused mainly by the infusion of sugar into the fruit. The predominant effect of the osmosis mechanism at this stage, is indicated by the very low WRR (Water Removal Rate), which after 15 min of the process reached the minimum.

When the residue of syrup liquid had run out, the second stage of drying was initiated by a microwave power increase up to 3.25 Watt/g of the initial sample weight. Immediately, the
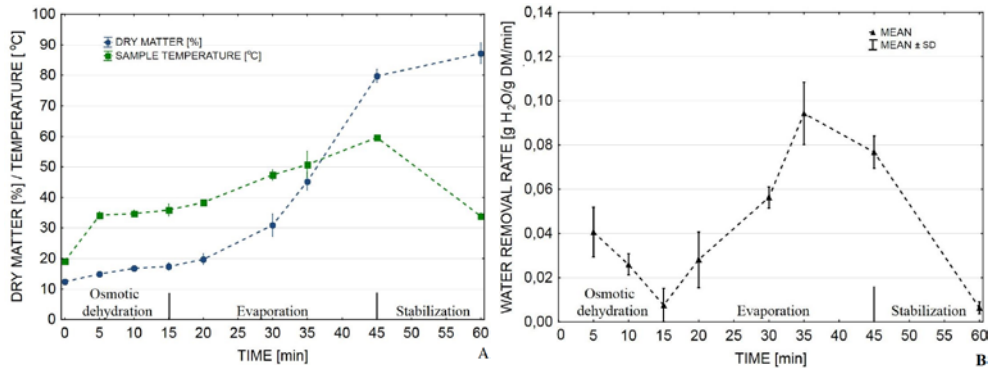
Fig. 1 Diagram of changes monitored for osmo-dehydrated cranberries during drying process (A) material temperature and dry matter contents (B) water removal rate, MEAN ± SD (n=2)

WRR accelerated, and the water evaporation intensity increased for about 20 min, until it gained a maximum value of 0.094 g H_2O/g DM/min, after which the WRR started to decline, and despite the still relatively high water content (2g H_2O/g DM) in the dried material, the sample temperature continued to rise. When the temperature was approaching 60°C, the MW power was automatically reduced to avoid overheating. The temperature limit was set on the basis of other authors work [12], where 60°C is reported as crucial in polyphenol degradation in sour cherries subjected to microwave-vacuum drying. After 45 min of the process the microwave power was switched off, but water evaporation still occurred, with a steadily decreasing WRR, which can also be attributed to the low water content in the sample. These observations follow the typical pattern of sample temperatures when fruits are subjected to microwave drying [8,13].

In Fig. 2 the quality changes of the dried material during the dehydration process are presented. During the first twenty min the sample density rose from the initial value of 0.87
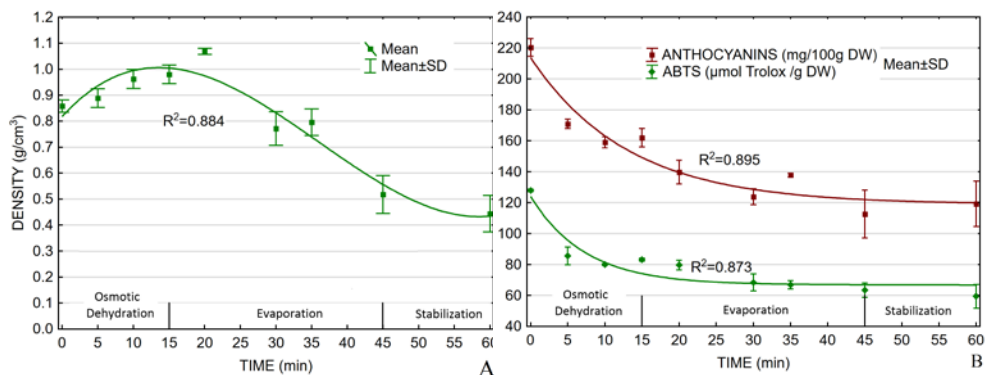
Fig. 2 Trends in the quality changes of osmo-dehydrated cranberry fruit during the drying process: (A) fruit density; (B) anthocyanin content and antioxidant activity (ABTS•+), MEAN ± SD (n=2).

± 0.02 to over 1 g/cm^3 (Fig. 2A), which indicates slight material shrinkage, as is illustrated in Photo 1 (B).
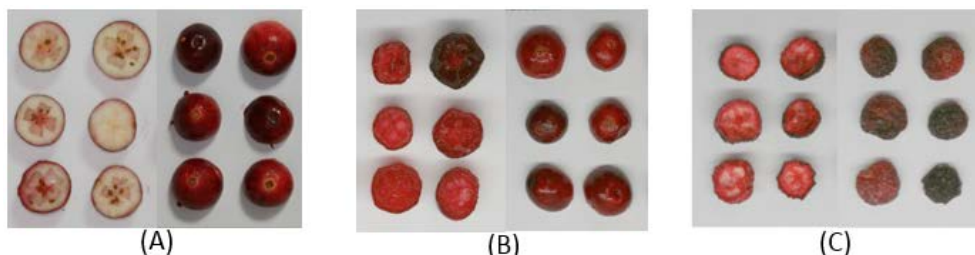
Photo 1. Cross-section and outside appearance of raw material (A), osmotically infused fruits after 15 min (B) and final product (C).

To some extent, the increase in the density of the material can be explained by the fact that the intercellular spaces were replaced by the infused sugar syrup. In the next 40 min the fruit density decreased steadily, by up to 0.48 ± 0.02 g/cm^3, which represents almost half the initial density of the fresh material. This phenomena is typical for vacuum drying, where rapid mass transfer is accompanied by a typical expansion in a so-called "puff up" effect [14]. In Fig 2B, the effect of process time on the bioactive component content is presented. The raw material used in the study contained on average 220 ± 4 mg/100 g DW of total anthocyanins, which means that cranberries grown in Poland are able to accumulate as much anthocyanin as the Canadian clones [15]. Although the drying process lasted only 60 min, and the sample temperature did not exeed 60ºC, the evident negative effect on both anthocyanin content and antioxidant activity (ABTS$^{\bullet+}$) was observed. When compared to fresh fruit, the loss of anthocyanins reached almost 50%, and its final content in dried product amounted to 119 ± 10 mg/100g DW. A similar pattern was found for antioxidant activity, which decreased from 127 ± 0.2 to 57 ± 1.3 μmol Trolox/g DW (Fig. 2B). According to data in literature, anthocyanin degradation in halved cranberries is higher than for sour cherries dried in similar microwave-vacuum conditions [15]. As is clearly presented in Fig. 2B, the antioxidant activity of dried cranberries expressed by ABTS$^{\bullet+}$, corresponds with the gradual decrease in anthocyanins. Similar findings have been reported by other authors [13,16] who indicated the anthocyanin content as having a major impact on the total antioxidant capacity of the cranberry fruits.

To be able to identify the advantages of our product, the experimental material (Photo 1, C) was compared to commercially available product. The comparison comprised sensory attributes, antioxidant properties and water activity. The results are gathered in Table 2. Sensory evaluation of the product showed that, when compared to commercial products, the experimental cranberry (MW-V) was characterized by a more intensive fruity aroma, but unfortunately, despite higher water activity, also by an inferior texture. It was also perceived

as less sweet, which resulted in a rating of only 4.8 (out of 10) in the overall quality assessment.

Table 2. The comparison of chosen quality characteristics of dried cranberries available in the market and the experimental product (MW-V).

| Product type | Sensory attributes (0-10 points) | | | | | | ABTS [µmol Trolox/g fresh weight] | Water activity |
	Fruity aroma	Fruity flavour	Sourness	Overall texture	Sweetness	Overall quality		
Bulk product	2.8[b*]	4.8[b]	3.3[a]	7.4[b]	6.2[b]	6.8[b]	15.0[b]	0.55[a]
Commercially packed	1.5[a]	3.7[a]	2.7[a]	7.1[b]	6.2[b]	4.9[a]	9.9[a]	0.54[a]
MW-V	3.1[b]	4.9[b]	5.8[b]	4.9[a]	4.4[a]	4.8[a]	51.8[c]	0.62[b]

Means in columns marked with the same letter do not differ significantly according to Duncan MRT at p = 0.05.

Surprisingly, the highest overall quality was indicated for commercial, unpacked cranberries, which were expected to be of lower quality than the packed ones, which were assessed as having an untypical aroma and being off-flavour, which can be attributed to the flavor of oxidized oil, resulting in a low sample acceptance. Despite a slightly lower sensory appreciation than the commercial product, the dried cranberry produced using our method was characterized by three times more antioxidant potential. The ABTS$^{\bullet+}$ values seen in the experimental product were on average 51.9 ± 5.5 (Table 2), whereas for cranberries purchased in the market the values were as low as 15.02 ± 0.2 and 9.88 ± 0.2 µmol Trolox/g fresh weight for the bulk product and commercially packed, respectively.

4. Conclusions

The proposed method of sweetened dried cranberry production resulted in a microbiologically stable product ($a_w = 0.62$) after a 60 min process. Sensory evaluation of the product showed that compared to commercial products, the experimental cranberry was characterized by a richer fruit aroma, but unfortunately, also by an inferior texture and lower sweetness sensation, which resulted in a rating of only 4.8 (out of 10) in the overall quality assessment. Despite a unfavourable sensory appreciation, the dried cranberry produced using our method was characterized by three times more antioxidant potential, thus further process optimization seems advisable.

We can summarize, that the presented idea of production sweetened ready-to-eat dried cranberries using a one stage process combining osmotic treatment with a vacuum microwave dehydration technique can be considered as an alternative to traditional dried cranberry production.

5. Acknowledgements

6. References

[1] Menghini, L.; Leporini, L.; Scanu, N.; Pintore, G., La Rovere, R.; Di Filippo, E.S.; Pietrangelo, T.; Fulle S. Effect of phytochemical concentrations on biological activities of cranberry extracts. Journal of Biological Regulators Homeostatic Agents 2011,25(1), 27-35.

[2] George, S.D.St.; Cenkowski, S.; Muir,W.E. A review of drying technologies for the preservation of nutritional compounds in waxy skinned fruit. North Central ASAE/CSAE Conference, Manitoba, Canada, September 24-25, 2004; 04-104.

[3] Zielinska, M.; Zielinska, D.; Markowski, M. The Effect of Microwave-Vacuum Pretreatment on the Drying Kinetics, Color and the Content of Bioactive Compounds in Osmo-Microwave-Vacuum Dried Cranberries (*Vaccinium macrocarpon*). Food and Bioprocess Technology 2018, 11(3), 585–602.

[4] Zielinska, M.; Markowski, M. Effect of microwave-vacuum, ultrasonication, and freezing on mass transfer kinetics and diffusivity during osmotic dehydration of cranberries. Drying Technology 2017, 14(5), 1–12.

[5] Wray, D.; Ramaswamy, H.S. Microwave-Osmotic/Microwave-Vacuum Drying of Whole Cranberries: Comparison with Other Methods. Journal of Food Science 2015, 80(12), E2792-802.

[6] Grabowski, S.; Marcotte, M.; Poirier, M.; Kudra, T. Drying characteristics of osmotically pretreated cranberries - energy and quality aspects. Drying Technology 2007, 20(10), 1989–2004.

[7] Beaudry, C.; Raghavan, G.S.V.; Rennie, T.J. Microwave Finish Drying of Osmotically Dehydrated Cranberries. Drying Technology 2003, 21(9), 1797–1810.

[8] Beaudry, C.; Raghavan, G.S.V.; Ratti, C.; Rennie, T.J. Effect of Four Drying Methods on the Quality of Osmotically Dehydrated Cranberries. Drying Technology 2004, 22(3), 521–539.

[9] PN-90/A-75101/03. Fruit and vegetable preserves. Preparation of samples and methods of physicochemical tests. Determination of dry matter content by gravimetric method.

[10] Re, R.; Pellegrini, N.; Proteggente, A.; Pannala A.; Yang M.; Rice-Evans, C. Antioxidant activity applying an improved ABTS radical cation decolorization assay. Free Radical Biology and Medicine 1999, 26(9-10), 1231-1237.

[11] Giusti, M.; Wrolstad, E.R. Characterization and Measurement of Anthocyanins by UV-Visible Spectroscopy. Current Protocols in Food Analytical Chemistry. John Wiley & Sons, Inc. Hoboken, 2001.

[12] Wojdyło, A.; Figiel, A.; Lech, K.; Nowicka, P.; Oszmiański, J. Effect of Convective and Vacuum–Microwave Drying on the Bioactive Compounds, Color, and Antioxidant Capacity of Sour Cherries. Food and Bioprocess Technology 2014, 7(3), 829–841.

[13] Leusink, G.J.; Kitts, D.D.; Yaghmaee, P.; Durance, T. Retention of antioxidant capacity of vacuum microwave dried cranberry. Journal of Food Science 2010, 75(3), C311-6.

[14] Zhang, M.; Tang, J.; Mujumdar, A.S.; Wang, S. Trends in microwave-related drying of fruits and vegetables. Trends in Food Science & Technology 2006, 17(10), 524–534.

[15] Abeywickrama, G.; Debnath, S.C.; Ambigaipalan, P.; Shahidi, F. Phenolics of Selected Cranberry Genotypes (Vaccinium macrocarpon Ait.) and Their Antioxidant Efficacy. Journal of Agricultural and Food Chemistry 2016, 64(49), 9342–9351.

[16] Zheng, W.; Wang, S.Y. Oxygen radical absorbing capacity of phenolics in blueberries, cranberries, chokeberries, and lingonberries. Journal of Agricultural and Food Chemistry 2003, 51(2), 502–509.

Influence of drying technique on physicochemical properties of bimodal meso-macropore structure of silica support

Panchan, N.[a]; Niamnuy, C.[b,c*]; Chukeaw, T.[b]; Seubsai, A.[b,c]; Devahastin, S.[d]; Chareonpanich, M.[b,c]

[a] Department of Chemical Engineering, Faculty of Engineering, Mahanakorn University of Technology, Bangkok, Thailand

[b] Department of Chemical Engineering, Faculty of Engineering, Kasetsart university, Bangkok, Thailand

[c] NANOTEC Center for Nanoscale Materials Design for Green Nanotechnology and Center for Advanced Studies in Nanotechnology for Chemical, Food and Agricultural Industries, Kasetsart University, Bangkok, Thailand

[d] Advanced Food Processing Research Laboratory, Department of Food Engineering, Faculty of Engineering, King Mongkut's University of Technology Thonburi, Bangkok, Thailand

*E-mail of the corresponding author: fengcdni@ku.ac.th

Abstract

Drying process directly affect in structure of the silica support for catalysts . Therefore, we herein prepared bimodal meso-macropore structure of silica by sol-gel method and investigated the silica support obtained from various drying techniques, namely, hot air drying (HA), microwave drying(MW)and freeze drying (FD)by means of BET and BJH N_2-sorption, and SEM. The results showed a significant effect of drying technique on the textural properties of the dried bimodal porous silica support. In addition, it was found that freeze drying could enhance surface area of silica support with higher than 500 m^2/g.

Keywords: bimodal meso-macropore structure silica support: drying technology: freeze drying: hot air drying: microwave drying

Influence of drying technique on physicochemical properties of bimodal meso-macropore structure of silica support

1. Introduction

Silica supports are widely used in field of catalysis. High surface area, large pore size and large pore volume of silica are often desired for catalyst supports in many reactions. Bimodal meso-macropore structure of silica is suitable for use as support in aspect of high dispersion of metal catalyst and good mass and heat transfer [1]. Generally, akyl orthosilicates are used as a silica source for the preparation of silica support. Moreover, organic surfactant are also used as the pore structure-directing agent (template) of silica support. However, they are not appropriate in term of commercial, safety and green approach production due to their high cost, flammability, difficulties in handling or storage, and toxic to environment [2-3]. Therefore, sodium silicate is an interesting as silica source and chitosan is an alternative bio-template, in aspect of lower cost and cleaner production of silica support. In order to modify the textural properties of silica support, especially in preparing the meso-macro struacture of silica, is always conducted by chemical techniques. For example, Li et al. [4] had prepared meso-macroporous structure of silica by using tetrametoxysilane (TMOS) as silica source and polyethylene glycol (PEG) as template, Blin et al. [5] proposed the usage of decane as an effective expander to enlarge the pore size of mesoporous silica. It is found that these techniques are not only use more expensive chemicals but also impractical in green processing which effected to the environment. Besides, it is found that the preparation methods are more complicated for industrial scale [6].

However, many previous researches have been suggested that drying is a physical process that directly affects on structure of the prepared silica support [7-9]. The hot air drying is the process that thermal energy is transferred to the interior of the wet-gel silica via conduction, depends on the thermal conductivity of the wet-gel silica [2]. While, in the microwave drying, water, presented in the wet-gel silica, absorbs the microwave throughout the entire mass, causing molecular vibration with respect to the oscillating electric field of the microwave and the generated heat is transferred homogenously to a molecular scale throughout the bulk [2,10]. Whereas, freeze drying, moisture is removed by sequentially freezing the water/solvent and subliming it at low pressure [10]. As per the abovementioned, we interested and attempt to apply the drying techniques in term of physical techniques to modify textural properties of silica support instead of those chemical techniques. Due to the drying is easier and effective method with lower cost [6].

Therefore, we herein prepared bimodal meso-macropore structure of silica supports by sol-gel method using sodium silicate as a silica source and chitosan as a template, and investigated comprehensively the properties of silica support obtained from various drying techniques, namely, hot air drying (HA), microwave drying (MW) and freeze drying (FD).

2. Materials and Methods

The silica supports were prepared using sol-gel method. Firstly 0.4 g of chitosan was dissolved in 100 mL of 2% v/v acetic acid in deionized water under continuously stirred at 300 rpm and control temperature using water bath at 40 °C for 30 min. Then, 5.4 g of sodium silicate solution (based on 1 g of SiO_2) were primarily diluted with 10 mL of deionized water and added to the chitosan solution. The solution was adjusted to pH of 6 by dropwise addition of 2 M hydrochloric solution. After that, the hydrolysis-condensation reaction was carried out at 40 °C with continuously stirred for 3 h, and then the resulting mixture was aged in the Teflon-lined autoclave at 100 °C for 24 h. The precipitated wet-gel silica products were filtered, washed several times with distilled water. Then, the washed wet-gel silica cake was dried using different drying techniques (hot air drying, microwave drying and freeze drying). Dried-gel silica were finally ground and calcined at 600 °C with the heating rate of 2°Cmin⁻¹ for 4 h in order to remove chitosan template. The obtained white silica powder was kept in vacuum container. Hot air drying was carried out in a hot air dryer (Binder GmbH, RedLine RF115, Tuttlingen, Germany) at the operating temperature of 80, 100 and 120 °C for 120, 90 and 60 min, respectively. Microwave drying was carried out in a microwave oven (Samsung, MS28H5125BK, Seoul, Korea). The oven was operated at a frequency of 2.45 GHz and a power of 600, 850 and 1000 W for 40, 30 and 20 min, respectively. Freeze drying was carried out in a freeze dryer (Thermo Fisher Scientific, Supermodulyo-230, Waltham, MA) with vacuum pressure for 24 h. Pior to use the freeze dryer, the wet-gel silica cake was freeze in the freezer at -20°C for 24 h. The prepared silica support obtained from various drying techniques were characterized by means of Brunauer, Emmett and Teller (BET) and BJH N_2-sorption (Quantachrome Instruments, Autosorb-1C, Boynton Beach, FL) and Scanning electron microscopy (SEM) (FEI, Quanta 450, Hillsboro, OR).

3. Results and discussion

The results of textural properties (BET specific surface area, average pore diameter and cumulative pore volume) of silica supports prepared by various drying techniques were summarized in Table 1. It was clearly noticed that the largest BET specific surface area was obtained for dried silica support by using freeze dryer. Whereas, silica supports, dried by using hot air and microwave dryer, were relative lower BET surface area. In addition, the average pore diameter and cumulative pore volume for freeze dried silica support were much grater than those of hot air and microwave dried silica support.

Table 1. Textural properties for silica supported dried by using microwave, hot air and freeze drying

Sample	Surface area[a] (m^{2}g^{-1})	Pore diameter (nm)		Pore volume (cm^{3}g^{-1})
		Mesoporous[b]	Macroporous[c]	
HA80	376	13.1	~400	1.23
HA100	401	12.6	~250	1.24
HA120	406	12.4	~150	1.28
MW600	414	12.6	~150	1.30
MW850	390	13.3	~350	1.30
MW1000	413	12.5	~250	1.30
FD	700	17.0	171.6, 500<	2.18, 4.05

[a] Specific surface area calculated by BET method.
[b] Pore diameter (mesopore) measured by BJH desorption method.
[c] Pore diameter (macropore) estimated from SEM.

The N_2-sorption isotherm results for silica supports dried by using MW, HA and FD were given in Fig.1. It was found that HA and MW dried silica sample showed similar isotherm although differences in surface area, pore volume and pore size were observed. These isotherms exhibited hysteresis loop which correspond to the type IV isotherms at high relative pressure range of 0.75-0.9. It was due to the capillary condensation of N_2 gas occurring in the mesopores. Therefore, the type IV isotherm was considered as the characteristic of mesoporous materials [2,11]. In addition, it was clearly noticed that the isotherm for freeze dried silica support exhibited significant difference hysteresis loop, which corresponded to the composite isotherm type IV-II. The sharp increase of N_2, at relative pressure range of 0.8 to above 0.9, indicated the presence of large meso-macropores or interparticle adsorption and condensation [3,12].

Pore size distribution of silica supports dried by using various drying methods were presented in Fig.2. It was found that the pore size distribution for silica supports corresponded to the results of pore size of silica listed in Table 1. It can be seen that hot air and microwave dried silica supports also showed similar and uniform pore size distribution with mesopores diameter of around 12 nm. While freeze dried silica support showed broader pore size distribution with mesopores diameter of 17 nm and clearly showed macropores diameter of 171.6 nm. The SEM image for silica support obtained by different drying techniques were

presented in Fig.3. It was clearly observed that the texture of HA dried silica support are closely packed particles when drying temperature increased from 80 to 120°C. It was due to the water molecules were constantly eliminated during the drying process. It led to the increasing of sol concentration, increasing in the capillary force and also created fluid drag which caused the particles to come closer to each other and forms aggregate to achieve greater stability [2,6,13]. In comparison with MW drying found that, the MW dried silica support had the higher porous of structure with larger pore size and pore volume. This could be due to fusion of some of the smaller particles during microwave drying [10]. The freeze dried silica support exhibited the lossely packed, highly porous and sponge-like particles with the macropore of interparticle voids. In the FD process, the effect of capillary force was avoided due to it involves solid-gas transition. The volume expansion occurred during the liquid water transformation to solid in the freezing process also could contribute to the loose packing [13]. In addition, the macropore diameter estimated by SEM images (Fig.3) for all of silica samples listed in Table 1.
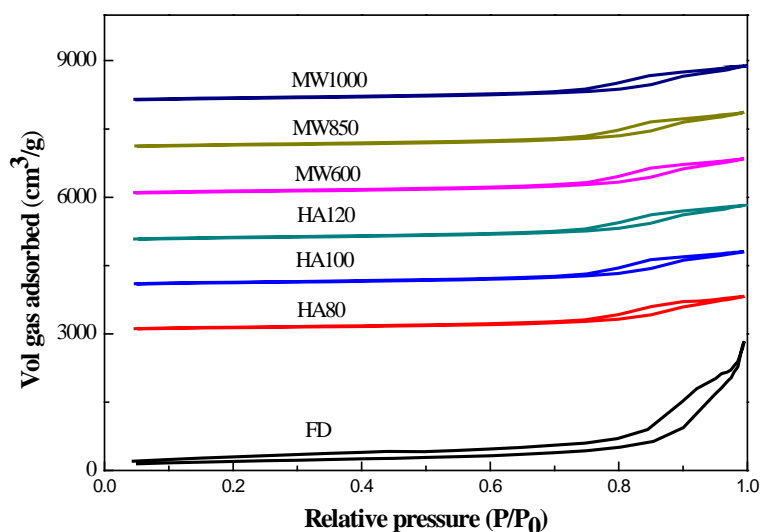
***Fig. 1** N2-sorption isotherm for silica supports dried by using microwave, hot air and freeze drying.*
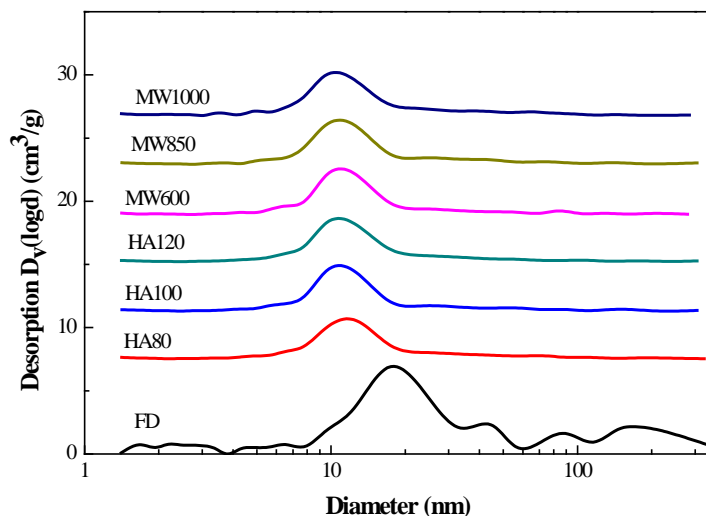
Fig. 2 Pore size distribution for silica supports dried by using microwave, hot air and freeze drying.

4. Conclusion

The bimodal meso-macropore structure of silica supports were successfully prepared by sol-gel method using sodium silicate as a silica source and chitosan as a template. The textural properties of the prepared silica supports obtained from various drying techniques were investigated comprehensively. The freeze drying technique led to the highest surface area, largest pore size and pore volume of silica support among the hot air and microwave drying techniques. In addition, the application of the prepared bimodal porous silica support in catalysis field is based on kind of reaction, that should be further studied.
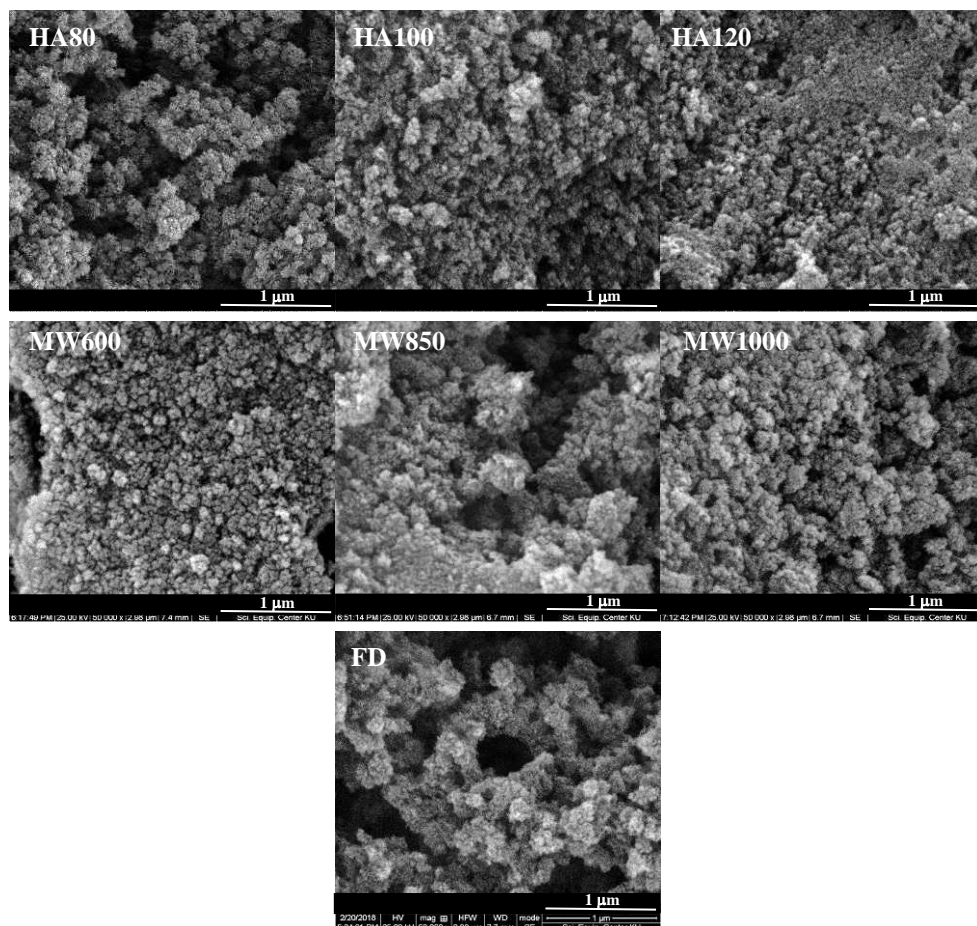
Fig. 3 SEM images for silica support dried by using microwave, hot air and freeze drying.

5. Acknowledgements

6. References

[1] Tanggarnjanavalukul, C.; Donphai, W.; Witoon, T.; Chareonpanich, M; Limtrakul, J. Deactivation of nickel catalysts in methane cracking reaction: effect of bimodal meso-macropore structure of silica support. Chemical Engineering Journal 2015, 262, 364-

371.

[2] Sarawade, P.; Kim, J. K.; Hilonga, A.; Quang, D. V.; Kim, H. T. Effect of drying technique on the physicochemical properties of sodium silicate-based mesoporous precipitated silica. Appiled Surface Science 2011, 955-961.

[3] Witoon, T.; Chareonpanich, M.; Limtrakul, J. Synthesis of bimodal porous silica from rice husk ash via sol-gel process using chitosan as template. Materials Letter 2008, 62, 1476-1479.

[4] Li, H.; Hou, B.; Wang, J.; Huang, X.; Chen, C.; Ma, Z.; Cui, J.; Jia, L.; Sun, D.; Li, D. Effect of hierarchical meso-macroporous structures on the catalytic performance of silica supported cobalt catalysts for Fischer-Tropsch synthesis. Catalysis Science and Technology 2017, 7, 3812-3822.

[5] Blin, J. L.; Otjacques, C.; Herrier, G.; Su, B. L. Pore size engineering of mesoporous silicas using decane as expander. Langmuir 2000, 16, 4229-4236.

[6] Pan, Y.; He, S.; Gong, L.; Cheng, X.; Li, C.; Li, Z.; Liu, Z.; Zhang, H. Low thermal-conductivity and high thermal stable silica aerogel based on MTMS/Water-glass co-precursor prepared by freeze drying. Materials and Design 2017, 113, 246-253.

[7] Shahzamani, M.; Bagheri, R.; Masoomi, M.; Haghgoo, M.; Dourani, A. Effect of drying method on the structural and porous texture of silica-polybutadiene hybide gels: supercritical vs. ambient pressure drying. Journal of Non-Crystalline Solids 2017, 460, 119-124.

[8] Duraes, L.; Ochoa, M.; Rocha, N.; Patricio, R.; Duarte, N.; Redondo, V.; Portugal, A. Effect of drying conditions on the microstructure of silica based xerogels and aerogels. Journal of Nanoscience and Nanotechnology 2012, 12, 1-7.

[9] Lekhal, A.; Glasser, B. J.; Khinast, J. G. Drying of support catalysts. In Catalyst Preparation: Science and Engineering; Regalbuto, J., Ed.; CRC Press: Boca Raton, 2007; 375-400.

[10] Annie, D.; Chandramouli, V.; Anthonysamy, S.; Ghosh, C.; Divakar, R. Freeze drying vs microwave drying-methods for synthesis of sinterative thoria powder. Journal of Nuclear Materails 2017, 484, 51-58.

[11] Bhagat, S. D.; Kim, Y. H.; Yi, G.; Ahn, Y. S.; Yeo, J. G.; Choi, Y. T. Mesoporous SiO_2 powders with high specific surface area by microwave drying of hydrogels: A facile synthesis. Microporous and Mesoporous Materials 2008, 108, 333-339.

[12] Baďurová, E.; Raabová, K.; Bulánek, R. One-pot synthesis of iron doped mesoporous silica catalyst for propane ammoxidation. Dalton Transactions 2014, 43, 3897-3905.

[13] Rahman, I. A.; Vejayakumaran, P; Sipaut, C. S.; Ismail, J.; Chee, C. K. Effect of the drying techniques on the morphology of silica nanoparticles synthesized via sol-gel process. Ceramics International 2008, 34, 2059-2066.

Superheated Steam Dryer application for drying of sticky and pasty materials – particular referents to distillers wet grain and soluble (DWGS)

Verma, P.[a*]; Sune, H.[b]; Aaron, W.[c]

[a] Managing Director, Swedish Exergy AB, Gothenburg, Sweden

[b] Senior Process Advisor, Swedish Exergy AB, Gothenburg, Sweden and former lecturer, Chalmers University of Technology, Gothenburg, Sweden.

[c] Process Department Head, Swedish Exergy AB, Gothenburg, Sweden

*E-mail of the corresponding author: prem.verma@swedishexergy.com

Abstract

Swedish Exergy AB commercialised superheated steam drying technology – an invention from Chalmers University of Technology. New application for drying and valorisation of DWGS has been successfully developed and deployed at one of the sites in Europe. The technology has been adapted to this application. Key development includes novel and innovative concept of back-mixing in pressurised loop.

Keywords: Super-heated steam drying; PSSD, DWGS, DDGS, Back-mixing.

1. Introduction

Pressurised Super-heated steam drying (PSSD) technology was re-invented by Claes Svensson Münter at Chalmers University of Technology, Gothenburg, Sweden. This novel and innovative technology found commercial application from research laboratory. In 1979, first full scale commercial plant was built and commissioned for drying of CTMP at a small paper mill in Sweden. Many other premier institutions have done research work on use of steam for drying and modification of product properties. TNO in Holland has done notable work on modification of product properties using steam at different pressures and conditions. NUS under leadership of Dr Mujumdar [1] has done extensive research work in the field of superheated steam drying and product quality modifications. All the research shows tremendous benefits for the technology. With net heat consumption 150 kWh/ton water evaporation; PSSD is world's most energy efficient drying process. Swedish Exergy AB since inception has been working on commercializing this technology with mixed success. High capital expenditure is biggest hinder. However, Swedish Exergy has successfully applied PSSD in one of the most difficult applications. Purpose of this paper to present this application and highlight results achieved.

2. Materials and Methods

2.1. Application Industry and Process Description

The application industry is grain based distillery plant. Process of ethanol from grain based distillery is briefly described below.

Grain from storage silos is milled either as dry milling or wet milling. Fig.1 shows process with wet milling. Slurry after wet milling is cooked in jet cookers before fermentation process. Sugar are converted into alcohol in fermentation and separated in distillation process. Remains from bottom of distillation process containing solids rich in protein is de-cantered. Separated solids are mixed with thin phase concentrated in an evaporator plant. This mix (DWGS) with 75% moisture content is dried in PSSD. Heat energy to PSSD is supplied from high pressure steam, thermal oil, natural gas or bio-gas. For every ton evaporated water, 750 kW thermal energy is put into the PSSD indirectly. Out of this 600 kW is recovered as low pressure (2-4 barg) steam and used for jet cooking, distillation and evaporation. Dried product (DDGS) with 10% moisture content is cooled after the dryer and sold as animal feed.
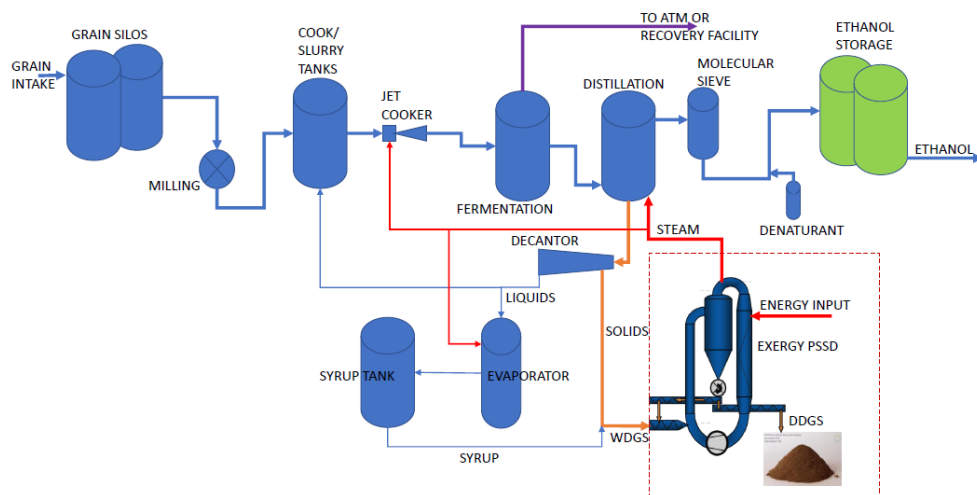
Fig. 1: Grain based distillery integrated with PSSD.

PSSD technology is closed loop system consisting of a circulation fan, heat exchanger, drying conduits, cyclone, feeding rotary valve and discharge rotary valve. Drying media is kept in closed loop circulation and drying energy is added indirectly through the heat exchanger. We product is fed through feeding rotary valve to the closed loop system. Drying takes place in drying conduits in very short time of less than 10 seconds. Product is separated in a cyclone from circulating drying media and discharged through bottom of the cyclone via discharge rotary valve. Separated drying media is circulated back to the heat exchanger for addition of drying energy. The process continues in this manner. As more and more moisture is evaporated in the closed loop, pressure increases inside the closed loop. Some of the evaporated moisture is bled-off through a control valve keeping constant pressure inside the closed loop. See fig. 2 for PSSD components.

Sticky and pasty material is handled in the dryer by back-mixing system. Fig 3 is picture of commercial plant installed in an ethanol plant in Italy.

SUPERHEATED STEAM DRYER WITH BACKMIXING

1. Evaporated moisture
2. Super heater
3. Cyclone
4. Drying conduits
5. Dried product
6/7/8. Back-mixing equipment
9. Discharge Rotary Valve
10. Wet feed
11. Circulation Fan
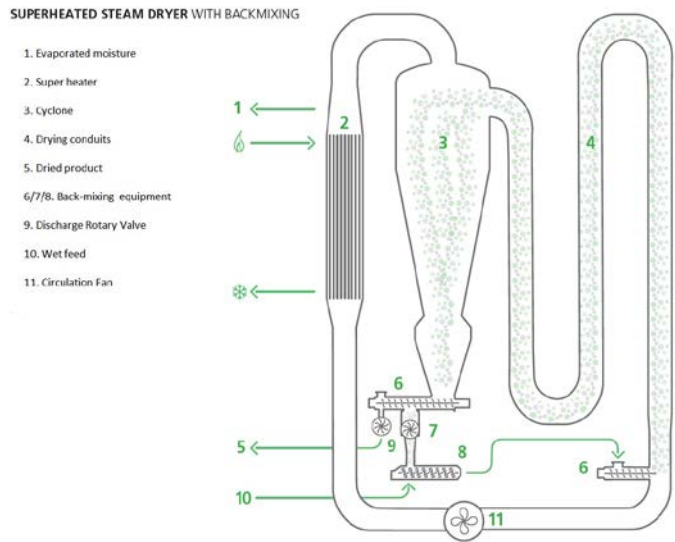
Fig. 2: Schematic of PSSD used for DDGS production

Fig. 3: Picture of PSSD commercial plant

21ST INTERNATIONAL DRYING SYMPOSIUM
EDITORIAL UNIVERSITAT POLITÈCNICA DE VALÈNCIA

2.2. Process Integration and energy efficiency

PSSD energy recovery potential makes it best candidate to integrate with other processes in the distillery. Steam generated from DWGS moisture is used for jet-cooking, distillation and evaporation processes in the plant. A typical energy and mass balance for a 10 ton/h DWGS plant is shown in table 1.

Table 1: Heat and Mass Balance for 10 ton/h DWGS plant

Input to PSSD				
Media	**Pressure, MPa**	**Temperature, °C**	**Mass, kg/h**	**Heat, kW**
DWGS – 75% moisture	-	70	10 000	685
Net heat input	-	-	-	4 911
Heat from electricity used for rotating machinery	-	-	-	150
Total	-	-	10 000	5 746
Output from PSSD				
DDGS – 10% moisture content	-	100	2 777	136
Steam generated in the dryer and recovered as low pressure steam	0,3	145	7 000	5 341
Flash off and leakages	0	100	223	169
Thermal losses	-	-	-	100
Total	-	-	10 000	5 746

2.3. Product Quality Improvements

2.3.1. Sterilization

Closed loop PSSD works as continuous autoclave and product is 100% sterilized at the end of the PSSD process. Live tests with salmonella has been done to demonstrate this. This means product can be sold with guarantees which means higher value product.

2.3.2. Protein digestibility and by-pass protein

Product when used as animal feed for animals with multiple stomachs like cows, DDSG produced with PSSD process offers additional product quality benefits of improved protein digestibility and by-pass protein [2]. Product gets cooked during drying process.

2.3.3. No oxidation

Closed loop PSSD does not allow ingress of atmospheric air inside the PSSD which provides oxygen free process medium ensuring that product is not oxidized. O2 measurements conducted using sensitive O2 measuring probes have confirmed oxygen free media inside the PSSD. Product maintains excellent uniform color and texture. See product picture shown in fig 4.

Fig. 4: Picture of DDGS produced from PSSD process

2.4. Novel and innovative back mixing system

Swedish Exergy has developed and implemented at commercial stage a novel and innovative back mixing system operating at same pressure as PSSD operating pressure (fig 5.0). This unique back-mixing method offers many benefits over traditional back-mixing methods.

1. Very short mixing time.
2. Excellent mix production
3. Smaller equipment
4. Very uniform product dryness
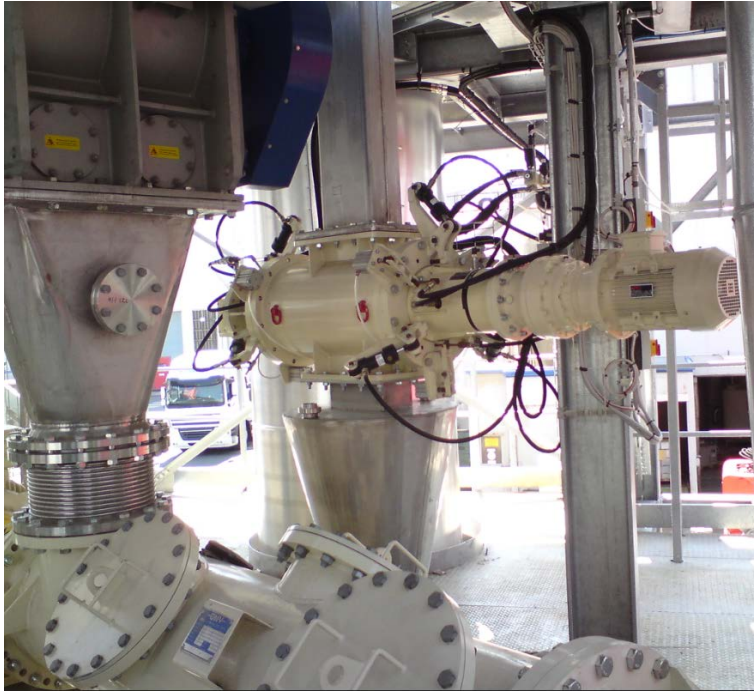
Fig. 5: Picture of novel and innovative back-mixing system as part of PSSD process

3. Conclusions

Commercialization of PSSD has been a challenge and still is. Swedish Exergy has successfully commercialized PSSD for production of animal feed from waste stream in ethanol production process. Valorization of waste streams or by-products is big focus for the industry. PSSD has big potential to help industry to valorize the waste and by-products.

Example illustrated in this paper is concrete evidence. Other potential industries who can benefit from PSSD technology are breweries, food and feed industry, oil seeds industry etc.

4. Nomenclature

CTMP Chemical Thermo Mechanical Pulp

SHSD Super-heated steam drying

DWGS Distiller Wet Grain and soluble

DDGS Distillers Dry Grain and Soluble

PSSD Pressurised Super-heated steam dryer

5. References

[1] Dr Mujumdar; Handbook of Industrial Drying, Fourth Edition, July 2014.

[2] Claes Münter; Josef Dalen; Lars Lind; Method for reducing degradability of animal feed protein, 1996

[3] SLU, Fodder Book, 2010

[4] SLU, Nutritional Digestibility of wheat wet and dry distiller grain in growing pigs, 2011

DRYING & ENVIRONMENT

Oral Presentations

Biodrying process: A sustainable technology for treatment of municipal solid wastes organic fraction

Kechaou, N.[a]* ; Ammar E[b].

[a] Groupe de Recherche en Génie des Procédés Agro-alimentaires, Laboratoire de Mécanique des Fluides Appliquée, Génie des Procédés et Environnement, Ecole Nationale d'Ingénieurs de Sfax, Université de Sfax, BP 1173, 3038, Sfax, Tunisia.

[b] Laboratoire Gestion des Environnements côtiers et urbains, Université de Sfax, BP 1173, 3038, Sfax, Tunisia.

*E-mail of the corresponding author: nabil.kechaou@enis.tn

Abstract

The Municipal Solid Waste of Agareb (Sfax –Tunisia), characterized by high organic fraction and moisture contents is the most worrying pollution source that must be managed by innovative treatment and recycling technologies. Bio-drying, as a waste to energy conversion technology, aims at reducing moisture content of this organic matter. This concept, similar to composting, is accomplished by using the heat generated from the microbial degradation of the waste matrix, while forced aeration is used. The purpose of this work was to reduce the moisture content of the waste, by maximizing drying and minimizing organic matter biodegradation, in order to produce a solid recovered fuel with high calorific value.

Keywords: Municipal solid wastes; organic matter; biodrying; composting; energy recovery.

1. Introduction

The accumulation of municipal solid waste (MSW) is a matter of concern for the developing countries in the present time. The rapid urbanization followed by the industrial development and construction activities is supposed to be the major reason for MSW accumulation [1]. Waste to energy (WTE) technology has the potential to reduce the volume of the original waste by 90%, depending on the composition by recovering the energy [2, 3]. But the net energy yield from waste to energy conversion processes depend upon the density, composition and relative percentage of moisture of the waste [4]. Here comes the importance of biodrying process for the treatment of municipal solid waste with high moisture content. The biodrying process can be promising for treating mixed municipal solid waste containing large proportion of organic compounds, since high moisture content of the organic materials will increase the wetness of the entire MSW matrix. Biodrying is a suitable method to treat very humid waste, which would release high quantity of leachate if waste is directly burned without any pre-treatment [5].

Biodrying is an aerobic convective evaporation process which reduces the moisture content of the waste, with minimum aerobic degradation. The major difference of biodrying from composting is that the major objective is not to maximise the degradation process of organic material, but only to degrade the waste enough to generate biological heat to dry the waste [6]. The biodrying process is distinct from composting in that the output of composting process is stabilized organic matter, but the output of biodrying is only partially stabilized. Also biodrying process is of short duration one and hence the emission factors are also short lasting. Process of biodrying utilizes the auto thermal heat genera- tion due to microbial action on waste material instead of thermal treatments in conventional drying process. Hence this is an energy saving process when compared to drying since it effectively utilizes the biological heat energy [7, 8].

Biodrying reactor aims to pre-treat the waste at the lowest pos- sible detention time in order to produce a high quality refuse derived fuel (RDF). Biodrying process increases the energy content of solid waste by maximising removal of moisture present in the waste matrix and preserving most of the gross calorific value of the organic chemical compounds through minimal biodegradation [9]. The solid derived fuel from biodrying process is the best renewable fuel [9, 10, 11, 12, 13]. The strategy based on temperature feedback control will be more promising for biodrying technology and the issue of homogeneity of the output of the biodrying process is a subject need to be improved and hence to be investigated in future ([14]. In biological stabilization processes the temperature parameter is more qualitative than quantitative [15]. The biodrying process is critical for control of physical and mechanical properties [6].

In Tunisia, environmental preoccupations are among the priorities of the Government. Since 1990, Tunisia has triggered an environmental assessment process targeting the definition and implementation of a proactive national strategy and safeguarding the environment. This strategy dealing with the environment preservation was established and strengthened with the implementation of sustainable development. The municipal solid waste (MSW) management, an important task to protect human health, the environment and to preserve national resources was taken into account by the Government. Indeed, the Tunisian Government allocates a huge budget for MSW management and treatment. According to National Agency of Solid Waste Management (ANGed), 2.2 M of tons of household waste are annually generated (0.5 kg/inhabitant/day). These wastes are dumped in the landfields (9 in the country). Such strategy is cost and inefficient solution considering the large dumping land needed and the loss of available resources (68% organic matter in MSW) that could be recycled based on circular economy. Consequently, the ANGed started implementing a strategy where recycled waste is reconsidered, allowing waste reduction and incomes. Also, to boost the waste reduction and the materials recycling, political programs were set in the five-year program of the development plan (2016-2020). Moreover, the Ministry of Environment and Sustainable Development was engaged to improve the solid waste valorization all over the country, based on a partnership between public and private sectors. The Government announced its investment for waste valorization by giving financial support to encourage such strategy, reducing the landfilling of biodegradable waste. The recovery of MSW will reduce greenhouse gas emissions and increases the use of renewable fuels in energy production.

The objective of this work was to conceive a laboratory prototype for the treatment and the recovery of the organic fraction from MSW by an innovative bio-drying process, in order to produce a solid fuel recycling (CSR). In this new bio-drying technology, the exothermic reactions were recycled for the evaporation of the highest part of the waste humidity, with the lowest bioconversion of organic carbon to produce a dry high-calorific fraction. This is usually shredded and can be used either in densified or bulk form as fuel in industrial boilers or in furnaces such as those in the cement plant.

2. Materials and Methods

2.1. Raw material

The studied waste was collected from the municipality of Agareb (region situated at 20 km in the West of Sfax city (Tunisia). After removing glass and metal debris from this municipal solid waste the organic fraction and the moisture content were 59% (w/w, in wet weight) and 70% of total solids (w/w) respectively.

2.2. Experimental setup and operation

The conceived prototype (figure 1) is a bed plexiglass reactor of internal dimensions (1 m x 0.5 m x 0.6 m) with a support made of a stainless steel grid to support a capacity of about 60 kg of solid waste.

The drying air is blown by a centrifugal fan of 0.75 kW power, controlled by a timer allowing the automatic operation fuction and shutdown of the system in order to maintain a defined air flow rate. The air flow crosses upward the waste from the bottom, activating the biological reactions and goes out of the biological reactor from the upper side. Finally, the process-air is discharged into the atmosphere after progressin through the bed. The experimental study evaluated and compared different tests according to the air flow rate and the stirring frequency, in order to choose the best working conditions.

Fig.1 The prototype of bio-drying

Each trial lasted approximately 10 days. After adequate waste mixing, the reactor was fed by 45 kg of the selected and homogeeized MSW organic matter fraction, having a density of 450 kg/m^3. The airflow was set at 0.7 m^3 per kg of wet waste per hour for the first test and 0.4 m^3 per kg of wet waste per hour for the second and third trials. The temperature was measured by thermometers set inside the bed reactor, at 5 points scanning all the bed. The ventilation was set on a mode working at a frequency ventilation of 10 min on/20 min off. The waste was manually agitated every 2 days for the first 2 tests (tests 1 & 2) and then

every 4 days for the last test (test 3). The waste was sampled every two days. The humidity rate and the organic matter degradation were determined gravimetrically after drying at 105 °C.

2.3. Sampling methods

Waste samples were collected from the bed reactor for analysis 2 days during the biodrying process. The moisture content was determined as quickly as possible to limit evaporative losses. The organic matter, total organic carbon, kjeldahl nitrigen and metals are measured later in the laboratory. All these analyzes are carried out in duplicate. Leachte and condensate water were collected every day and analysed for volume, ph, total organic carbon (TOC) and ammonia concentration.

2.4. Analytical methods

- The moisture content of solid samples was determined by gravimetric method.

- According to the standard (JIS K0102.14.4, 1995), the same crucible used for dry matter determination is placed in a muffle furnace at 550°C for two hours for calcination. The residual mass is weighed and the organic matter and the ASH will be calculated.

- The nitrogen content was measured with Kjeldahl nitrogen analyser.

- The TOC concentration was measured by a total carbon/total nitrogen (TC/TN) analyser.

- In order to get an idea of the lower heating value (LHV), we have chosen to estimate this value by using the CHANNIWALA correlation [16]. and which requires knowledge of the composition of the product in carbon, nitrogen and other compounds:

    LHV (MJ/kg) = 0.3491 C + 1.1783 H + 0.1005 S - 0.1034 O - 0.0151 N - 0.0211 ASH

    with C, H, O, N, S, ASH: product composition of carbon, hydrogen, oxygen, nitrogen, sulfur and ASH in %.

3. Results and discussion

Three tests were carried out in this work: the first has an air flow of 0.7 m^3/h kg $_{MSW}$ under a capacity of 46 kg of waste with a manual turning every 2 days. The second and third tests were carried out at a rate of 0.4 m^3/h kg $_{MSW}$ under a 50 kg daily turning load every 2 and 4 days respectively for the second and the third test. The three tests were carried out at a ventilation frequency of 10 minutes "on" / 30 minutes "off", that is to say, the fan runs for a period of 10 minutes and stops for 30 minutes before to start the cycle again.

3.1. Temperature evolution

Figure 2 illustrate the evolution of the inlet and outlet air temerature as well as the mean temperature of waste for three tests.

(a)

(b)

(c)
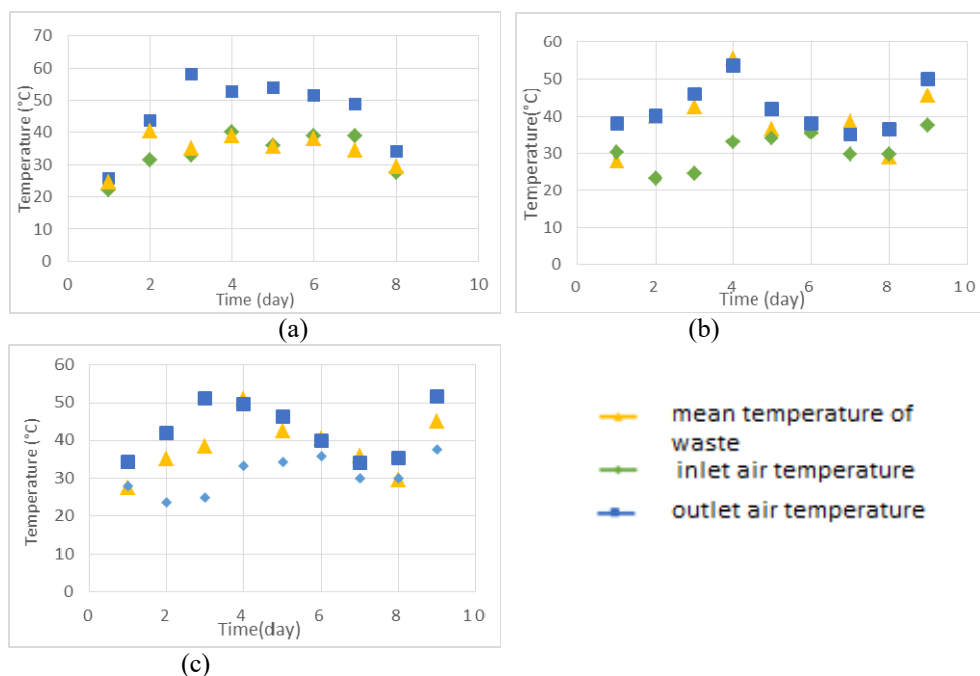
Fig.2 Temperature evolution versus time
a (trial 1) - b (trial 2) – c (trial 3)

For the first (Figure 2-a) test with the highest air flow rate (0.7 m³/h kg $_{MSW}$), the waste temperature is practically equal to the temperature of Air at the inlet and does not exceed 40°C, the air is cooling the waste and the phenomenon of bio-drying didn't take place.

For the second (Figure 2-b) and the third test (Figure 2-c) the temperature changes are quite similar. At the end of the 4th day, the waste temperature reached 51°C and 55.5°C respectively in the 2nd and 3rd tests due to the fermentation of waste.

By comparing test 1 and test 2, we find that for an air flow equal to 0.4 m³/h kg $_{MSW}$ the waste temperature is quite simlar to the outlet air during the first days of the experiment. From the 4th day The fermentation phenomenon is reduced and the temperature of waThese results show that the fermentation effect is more figured when using a low air flow rate.

3.2. Degradation of organic matter

Degradation of organic matter is well sought in the case of the composting process, but it has an undesirable effect in the bio-drying process. So we must minimize this degradation. Analyzes were carried out every 2 days to monitor the mass fractions of dry matter, organic matter and mineral matter (ASH content) of the solid waste in Figure 3 illustrates the evolution of degraded organic matter per kilogram of waste. The highest air flow gives the highest degradation of organic matter. Tests 2 and 3 have the same air flow rate but a

different frequency of agitation, the one having the high frequency, undergoes the slight degradation. These results are similar to other research (Zhao et al., 2011).
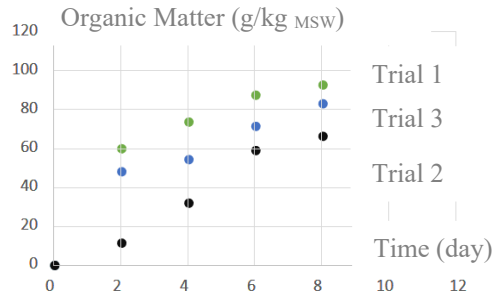
Fig. 3 The evolution of degraded organic matter versus time

4. Conclusions

During the biodrying process, the temperature evolution showed an increase in the second and third trials, and reached 51.0°C and 55.5°C respectively in these experiments, because of the fermentation held. Consequently, the water content was reduced from 70% to 9.0 and 9.1% and 21.4 % (respectively for the three trials. A significant decrease in water was noticed during the 2 first-days, the water evaporation rate begins to decrease from the third day and that with low agitation frequency. The final product 'CSR' has the best water content compared to that of higher agitation. The assessed calorific value of the three trials were 17.1, 19.66 and 19.16 MJ/kg respectively for the three experimented air-flow rate and agitation frequency.

5. References

[1] Chattopadhyay, S., Dutta, A., Ray, S., 2007. Existing municipal solid waste management of Kolkata – deficiencies and solutions. J. IAEM 34 (3), 161–167.

[2] Wang, L., Gang, H., Gong, X., Bao, L., 2009. Emission reductions potential for energy. from municipal solid waste incineration in Chongqing. Renewable Energy 34, 2074–2079.

[3] Kathiravale, S., Abu, M.P., Yunus, M.M., Abd-Kadir, K.Z., 2003. Predicting the quality of the refuse derived fuel from the characteristics of the municipal solid waste. In: 2nd Conference on Energy Technology towards a Clean Environment, 12–14

[4] Fobil, J.N., Carboo, D., Armah, N.A., 2005. Evaluation of municipal solid waste (MSW) for utilisation in energy production in developing countries. Int. J. Environ. Technol. Manage. 5, 76–87.

[5] Zhang, D.Q., He, P.J., Jin, T.F., Shao, L.M., 2008. Bio-drying of municipal solid waste with high water content by aeration procedures regulation and inoculation. Bioresour. Technol. 99, 8796–8802.

[6] Velis, C., Longhurst, P., Drew, G.H., Smith, R., Pollard, S.J.T., 2009. Biodrying for mechanical–biological treatment of wastes: a review of process science and engineering. Bioresour. Technol. 100, 2747–2761.

[7] Rada, E.C., Franzinelli, A., Taiss, M., Ragazzi, M., Panaitescu, V., Apostol, T., 2007. Lower heating value dynamics during municipal solid waste bio-drying. Environ. Technol. 28, 463–469.

[8] Rada, E.C., Venturi, M., Ragazzi, M., Apostol, T., Stan, C., Marculescu, C., 2010. Bio-drying role in changeable scenarios of Romanian MSW management. "Waste. Biomass Valor' 01, 271–279.

[9] Adani, F., Baido, D., Calaterra, E., Genevini, P., 2002. The influence of biomass temperature on biostabilization–biodrying of municipal solid waste. Bioresour. Technol. 83, 173–179.

[10] Rada, E.C., Ragazzi, M., Panaitescu, V., Apostol, T., 2005. An example of collaboration for a technology transfer: municipal solid waste biodrying. In: Maragherita di Pula, S. (Ed.), Proceedings Sardinia 2005. Tenth International Waste Management and Landfill Symposium. Cagliari, Italy, 3–7 October 2005, Paper 044.

[11] Sugni, M., Calcaterra, E., Adani, F., 2005. Biostabilization–biodrying of municipal solid waste by inverting air-flow. Bioresour. Technol. 96, 1331–1337.

[12] Wiemer, K., Kern, M., 1994. Mechanical–Biological Treatment of Residual Waste based on the Dry Stabilate Method. M.I.C. Baeza-Verlag, Witzenhausen, Germany.

[13] Staber, W., Flamme, S., Fellner, J., 2008. Methods for determining the biomass content of waste. Waste Manage. Res. 26, 78–87.

[14] Zhang, D.Q., He, P.J., Shao, L.M., 2009. Sorting efficiency and combustion properties of municipal solid waste during biodrying. Waste Manage. 29 (11), 2816–2823.

[15] Adani, F., Tambone, F., Gotti, A., 2004. Biostabilization of municipal solid waste. Waste Manage. 24, 775–783.

[16] Channiwala S A et Parikh P P., (2002). A unified correlation for calculating HHV from proximate analysis of solid fuels. Fuel, 81, 1051-1063.

[17] Zhao, L., Gu, W.M., He, P.J., Shao, L.M.: Biodegradation potential of bulking agents used in sludge biodrying and their contribution to bio-generated heat. Water Res 45 (6), 2322-2330 (2011).

Fluidized bed drying of petals of *Echium amoenum Fisch.* and *C.A. Mey*: energy analysis and carbon footprint

Nadi, F. [a*]; Atuonwu, J.C. [b]

[a] Department of Agricultural Machinery Mechanics, Azadshahr Branch, Islamic Azad University, Azadshahr, Iran

[b] Centre for Sustainable Energy use in Food Chains, Brunel University London, Uxbridge, Middlesex, UB8 3PH, the United Kingdom.

*E-mail of the corresponding author: f.nadi@iauaz.ac.ir

Abstract

The energy performance and carbon footprint associated with the fluidized bed drying of petals of Echium amoenum Fisch. and C.A. Mey are experimentally evaluated at three temperatures (40,50,60°C) and air velocities (0.50,0.75,1.00m/s). The maximum and minimum specific energy consumption are observed to occur at 40°C and 1ms⁻¹ (79.18MJ/kg) and 60°C and 0.5m/s (22.60MJ/kg), respectively. The greenhouse gas emission is in the range, 0.10-8.40kgCO₂eq, varying with drying conditions in the same manner as energy consumption, with natural gas-fired systems performing better than oil-fired systems. High-temperature, low-air velocity drying is thus, favourable for energy-efficient and sustainable fluidized bed drying of the petals.

Keywords: fluidized bed dryer; greenhouse gas; specific energy consumption; Iran.

1. Introduction

Echium amoenum Fisch. and C.A. Mey grows in a narrow region of northern Iran and the Caucasus [1]. Its dried violet-blue petals have medicinal (demulcent, anti-inflammatory, analgesic, sedative tonic, tranquillizing and diaphoretic) properties, and are useful as remedies for cough, sore throat and pneumonia [2, 3]. Hence, it is important for the drying of these petals to be energy-efficient and sustainable, while yielding high-quality products.

From ancient times, solar energy has been used to dry agricultural products. However, sun drying has several disadvantages such as poor food quality, insufficient control over the drying process, long drying times and contamination, all of which, could be avoided using industrial dryers [4]. The control of thermal treatment conditions is important during industrial drying of medicinal plants as the final product quality largely depends on the treatment conditions. In general, the drying temperature of medicinal plants should not exceed a certain level, to retain active compounds [5]. In this regard, drying in the fluid bed is attractive due to the homogeneous heat treatment of products, which allows better control of the conditions even at temperatures higher than those that cause thermal degradation of the product [6, 7].

Fluidization also has several other benefits such as increasing moisture uniformity, facilitating the use of higher drying temperatures and hence, increasing drying capacity, allowing for better mass and heat transfer, smaller-size dryer chambers, lower costs and higher-quality products [8].

As drying is an energy-intensive process, accounting for about 10-25% of the national industrial energy of the developed world [9, 10], it is very important that drying processes are energy-efficient. It is therefore not surprising that energy efficiency has over the years been a key driver of research and development in drying technology [10]. Preserving limited fossil fuels, reducing carbon footprint to combat climate change and improving the economics of drying-related processes are clear motivations for reducing energy consumption in drying [11]. The first step in identifying opportunities to save energy in drying processes, is an in-depth analysis of energy use. The evaporation load to remove water from the product under different drying conditions indicates energy consumption [11].

Energy consumption affects global warming, which in turn, affects humans and ecosystems in different ways: rising temperatures, changes in rainfall and rainfall rates, changes in the rate of melting of snow and ice, rising sea levels, changes in the geographical population distribution and even the extinction of some animals and plants [12].

Actions aimed at reducing energy usage must therefore be taken urgently in all processing activities. For drying in particular, using renewable energy sources, optimizing every part of

the process and using control devices to detect and minimize GHG injection into the atmosphere are some of the possible actions.

Singh *et al.* [13] studied CO_2 production during potato slice drying. They compared the CO_2 emissions of the sun, fossil fuels (coal, diesel fuel, natural gas) and electricity. Results showed that replacing coal with solar energy significantly reduced carbon emissions.

Kumar and Kandpal [14] analyzed the carbon emission potentials of drying various products using solar energy and other fuels in India. It was reported that increasing the proportion of solar energy, relative to the other fuels (coal, natural gas, wood) during agricultural product drying could lead to significant reductions in carbon emissions.

Piacentini and Mujumdar [12] studied climate change due to the drying of agricultural products. Given the high energy-demand of the drying operation, the authors proposed the use of renewable sources, optimizing the drying process and adopting energy efficient practices to reduce GHG emissions.

Motevali and Tabatabaei [15] studied SO_2, CO_2 and NO_X emissions during the drying of dog-rose using hot-air, infrared, hybrid hot air-infrared, microwave, hot air-microwave, vacuum, and hybrid photovoltaic-thermal solar dryers. The results showed that GHG emissions increased with temperature and air velocity in the hot air dryer, and reduced when infrared and hybrid hot air-infrared energy are used instead of hot air. The GHG emissions of hybrid photovoltaic-thermal solar dryers were less than the emissions of the hot air dryer.

The literature review shows little research on the GHG emissions of dryers. The aim of this research is to explore the energy consumption and effects of different drying conditions on greenhouse gas emissions for petals of *Echium amoenum Fisch. and C.A. Mey.*

2. Materials and Methods

2.1. Experimental procedure and energy analysis

A laboratory-scale fluidized bed dryer (details can be found in [16]) constructed at the Department of Agricultural Machinery Engineering of Azadshahr University, Iran, was used to conduct the drying experiments. It consisted of an air-heating device, chamber, and control systems for air and temperature. The fluidized bed chamber, made of stainless steel with inside dimensions of 250 mm×250 mm×300 mm, is connected with a fan, a duct made of stainless steel to supply air, while the distributor plate, with thickness of 1 mm and holes of 3 mm in diameter, was tightly fixed to the bottom of the chamber. The fluidizing air is supplied by a 1.5-kW blower, while an anemometer is used to regulate the air velocity manually. The heating unit consists of three fin heaters each of 800 W power, using thermostat-type temperature controls in order to adjust the desired drying temperature.
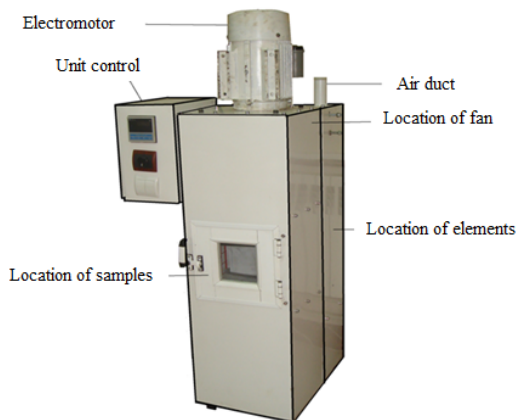
Fig. 1 Fluidized bed dryer

The total energy consumed during the experimental drying operation was estimated from the sum of the thermal and mechanical energies. Equation (1) was used to calculate the thermal energy for different temperatures.

$$E_{th} = \left(A.v.\rho_a.C_a.\Delta T \right).t \tag{1}$$

where, A, v, ΔT, t, ρ_a and C_a are the cross-sectional area of the distributor plate, the air flow rate, temperature difference between the dryer inlet and ambient air, drying time, density and specific heat capacity of the inlet air, respectively. The density and specific heat capacity of the air were respectively calculated [17] as:

$$\rho_a = \frac{353.049}{T_a} \tag{2}$$

$$C_a = 1.04841 - \frac{3.83719T}{10^4} + \frac{9.45378T^2}{10^7} - \frac{5.49031T^3}{10^{10}} + \frac{7.92981T^4}{10^{14}} \tag{3}$$

The mechanical energy used to move the air by the blower was determined by [18]:

$$E_{mec} = \Delta PvAt \tag{4}$$

where $\Delta P = 0.5f$h v^2 ρ, with ΔP as the pressure drop, h, product thickness, and f, the resistance to airflow.

Specific energy consumption SEC (kJ/kg) is the total energy required to remove 1kg of water from the product during the drying process and is expressed by the following equation.

$$SEC = \frac{E_{th} + E_{mec}}{m_w} \qquad (5)$$

where, m_w is the mass of removed water from the product during the drying operation. It is obtained from equation (6).

$$m_w = \frac{W_0 \left(M_0 - M_f \right)}{100 - M_f} \qquad (6)$$

where W_0 is initial weight,, M_0 is initial moisture content and M_f is final moisture content.

2.2. GHG emissions

The main source of power in many dryers is electricity [15]. Hence, the GHG emissions from the driving power plant indicates the amount of energy consumed during the drying process. The conventional power generation system in Azadshahr city, courtesy of Neka Power Plant, is a combined-cycle and steam system, and this study analyzes GHG emissions of this power plant. The mean GHG emissions (CO_2) from the Neka Power Plant (steam and combined-cycle) using primary fuels (natural gas and heavy oil) for generating 1 kW energy are shown in Table 1. As the fluidized bed dryer used in this experiment is driven by electricity from this power plant, the total CO_2 emissions due to the drying process is evaluated under the different power house/fuel type scenarios in Table 1. In each case, the total CO_2 emissions is the product of the conversion factor and the corresponding total energy consumption ($E_{th} + E_{mech}$), in kWh, with allowances made for power plant, transmission line and distribution losses (a total of 16.45%).

Table 1. CO_2 emissions and pollutants from power plant of Neka

Power House Type	Fuel type	CO_2 Conversion Factor (g/kWh)
Combine-cycle	Natural Gas	450
	Gas oil	622
Steam	Natural Gas	63
	Heavy Oil	1025

3. Result and discussion

3.1. The effect of drying conditions on specific energy consumption

The specific energy consumption and the total energy required under the different conditions of fluidize bed drying *E. amoenum* petals are presented in Fig. 2. An analysis of the results shows that the minimum specific energy consumption of 22.56 MJ/Kg occurs at 60°C air temperature and 0.5 m/s air velocity, while the maximum specific energy consumption of

79.18 MJ/Kg occurs at 40°C air temperature and 1 m/s air velocity. This implies that, the maximum specific energy consumption is approximately 3.5 times the minimum specific energy consumption. The energy required for fluidized bed drying of *E. amoenum* petals is observed to decrease with temperature, and increase with air velocity. This is partly attributable to the reduction in drying time with increasing air temperature, Also, at any given temperature, the specific energy consumption and the total energy required were higher at higher fluidization velocity, because higher air velocity did not reduce the drying time considerably due to the fact that the moisture transfer inside the material was controlled by the diffusion process. Similar findings have also been reported by other researchers. A higher air velocity reduces the proportion of the input energy utilized by the dryer, thus, increasing the heat losses in the dryer exhausts. This implies increased energy consumption.
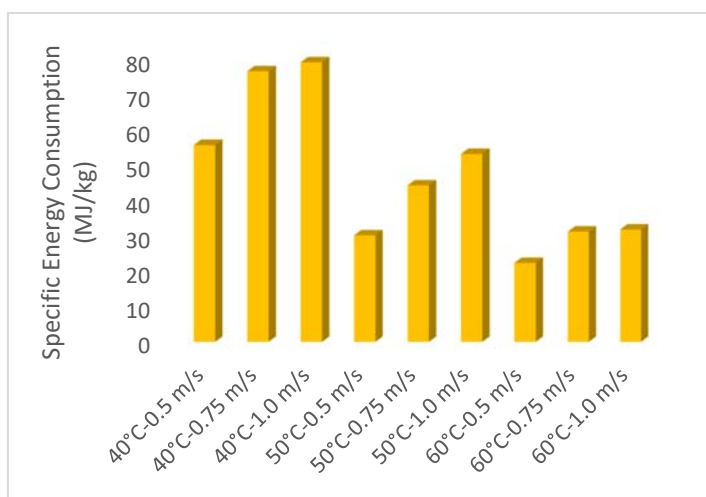
Fig. 2 The effects of different drying conditions on the specific energy consumption

3.2. The effects of drying conditions on CO_2 emissions

Fig. 3 shows the CO_2 emissions by the Neka Power Plant, which is a combined-cycle and steam plant, using different fuels for drying 1 kg of *E. amoenum* petals. This figure shows the variations in temperature and air velocity in a fluid bed dryer and the corresponding CO_2 emissions. Increasing the air flow leads to increased CO_2 emissions due to the corresponding increased energy consumption. The emissions however, decrease with temperature as a result of the corresponding drop in the energy consumption. The least CO_2 emissions occur at 60°C and 0.5m/s, while the maximum occurs at 40°C and 1m/s. As Fig. 2 shows, the maximum CO_2 production for all the studied drying conditions occurs for the combined-cycle-gas oil power plant, while the minimum occurs for the steam-natural gas plant. The maximum CO_2

emissions recorded for the combined-cycle-gas oil power plant at 40°C and 1m/s was approximately 80.3 times, its level at the steam-natural gas plant at 60°C and 0.5m/s.
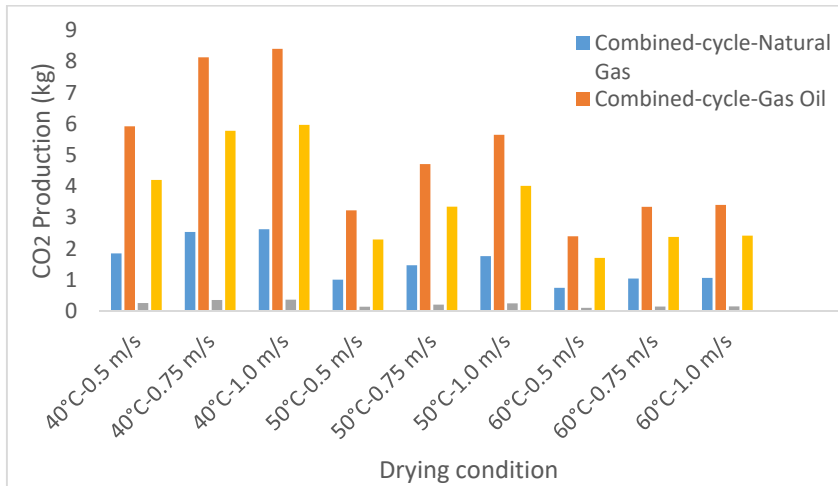
Fig. 3 The effect of in temperature and air velocity variations in a fluid bed dryer on carbon emissions of power plants

4. Conclusion

In this study, the effect of drying air velocity and temperature on energy consumption and greenhouse gas (CO_2) emissions from a fluidized bed dryer was evaluated. From the results, the total energy consumption increased with air velocity for each drying temperature, and decreased with temperature for each air velocity. The GHG (CO_2) emission levels also varied with drying air temperature and velocity in the same manner. The lowest carbon footprint occurs when the natural gas-fired steam plant is used, while the highest corresponds to the use of oil-fired combined-cycle power plant. High-temperature, low-air velocity drying is thus, advantageous for the fluidized bed drying of *Echium amoenum Fisch. and C.A. Mey* petals, from a sustainability viewpoint.

5. References

[1]   Rechinger, K.H. Flora Iranica; Akademische Druck- Und Verlagsanstalt: Graz, 1967.

[2]   Hooper, D. Useful Plants and Drugs of Iran and Iraq; Field Museum of Natural History: Chicago, 1937.

[3]   Amin, Gh.R. Popular Medicinal Plants of Iran. Press; Iranian Research Institute of Medicinal Plants: Tehran, 1991.

[4]   Motevali, A.; Amiri Chayjan, R. Effect of various drying bed on thermodynamic characteristics. Case Studies in Thermal Engineering 2017, 10, 399-406.

[5] Nadi, F. Bioactive compound retention in Echium amoenum Fisch. & C. A. Mey. petals: Effect of fluidized bed drying conditions. International Journal of Food Properties 2017, 20(10), 2249-2260.

[6] Hoebink, J.H.B.J.; Rietema, K. Drying granular solids in fluidized bed. Chemical Engineering Science 1980, 35, 2135-2140.

[7] Giner, S.A.; Michelis, A. D.E. Evaluation of the thermal efficiency of wheat drying in fluidized beds: influence of air temperature and heat recovery Journal of Agricultural Engineering Research 1988, 41, 11-23.

[8] Peglow, M.; Cunäus, U.; Tsotsas, E. An analytical solution of population balance equations for continuous fluidized bed drying. Chemical Engineering Science 2011, 66(9), 1916-1922.

[9] Atuonwu, J.C.; van Boxtel, A.J.B.; van Deventer,H.C.; van Straten. G. On the controllability and energy sensitivity of heat-integrated desiccant adsorption dryers. Chemical Engineering Science 2012, 80(1), 134-147.

[10] Mujumdar, A.S. Principles, classification and selection of dryers. In Handbook of Industrial Drying; Mujumdar A.S., Eds.; CRC Press: Florida, 2007.

[11] Kemp, I.I.C. Fundamentals of Energy Analysis of Dryers. In Modern Drying Technology; Tsotsas E.; Mujumdar, A.S. Eds.; Wiley-VCH: Weinheim, 2014.

[12] Piacentini, R.P.; Mujumdar, A.S. Climate Change and Drying of Agricultural Products. Drying Technology 27, 2009 27(5), 629–635.

[13] Singh, S.; Kumar, S. Solar drying for different test conditions: Proposed framework for estimation of specific energy consumption and CO2 emissions mitigation. Energy 2013. 51, 27-36.

[14] Kumar, A.; Kandpal, T.C. Solar drying and CO2 emissions mitigation: potential for selected cash crops in India. Solar Energy 2005, 78, 321-329.

[15] Motevali, A.; Tabatabaee Koloor, R. A comparison between pollutants and greenhouse gas emissions from operation of different dryers based on energy consumption of power plants. Journal of Cleaner Production 2017, 154, 445-461.

[16] Nadi, F., Development of a New Model for Mass Transfer Kinetic of Petals of Echium Amoenum Fisch & Mey under Fluidized Bed Conditions. Food Tevhnology and Biotechnology, 2016. 54(2): p. 217-227.

[17] Perry, H. Chemical engineer's handbook; McGraw Hill: New York, 1984.

DRYING & ENVIRONMENT

Poster Presentations

Preservation of mesophilic mixed culture for anaerobic palm oil mill effluent treatment by convective drying methods

Chin, S. K.[a]*, Tan, D. T.[b], Tan, H. M.[b], Poh, P. E.[b]

[a] Chemical Engineering, Newcastle University in Singapore, 537 Clementi Road #6-01, SIT@Ngee Ann Polytechnic Building , Singapore 599493, Singapore

[b] Chemical Engineering Discipline, School of Engineering, Monash University Malaysia, Jalan Lagoon Selatan, 47500, Selangor Darul Ehsan, Malaysia

*E-mail of the corresponding author: kent.chin@newcastle.ac.uk

Abstract

While anaerobic digestion is a reliable method that treats the waste and produces renewable biomethane fuel, the necessary sludge in liquid form is difficult to handle due to the constant biogas generation. Therefore, this study investigates the possibility of convective air drying, namely heat pump and hot air circulation oven as preservation methods for anaerobic microbial sludge. Drying was conducted at various temperatures, ranging from 22℃ to 70℃. The study found that heat pump drying at 22℃ resulted in highest COD removal of 55.3% as well as the least log reduction in methanogens and anaerobes at 1.4 and 2.4, respectively.

Keywords: *Chemical Oxygen Demand (COD); Heat pump drying; Hot air drying; Log reduction; Methane yield*

1. Introduction

Palm oil mill effluent (POME) is liquid waste containing oil, plant debris, and nutrients produced from palm oil milling process. In Malaysia, the most widely used effluent treatment scheme is the anaerobic/facultative ponds. Anaerobic digestion is the decomposition of organic material whereby the end products are biogas and sludge. This process is desirable due to low costs and low energy demand involved besides producing a biologically stable final product with good fertilizing properties as well high nutrient content. However, Difficulty in supplying the solid-liquid mixture of microbial seed sludge for anaerobic treatment of POME has raised several issues that must be overcome in order to promote the practicality of this treatment option. Main concerns include limitations in storage and transportation due to constant biogas generation from the anaerobic digestion [1]. Drying of the seed sludge allows easier storage of additional sludge as the mass and volume are greatly reduced due to majority of water content evaporated[2]. In addition to space conservation, the dried product can be more easily transported in its inactive form, where biodegradation and biogas production is halted in its dormant form which prevents fire hazard and risk of over-pressurisation[3]. There have been many studies conducted for the preservation of microorganisms. Numerous studies have shown that high cell viability of pure cultures can be achieved using freeze drying technique[4.] Despite its wide applicability, this method is cost intensive and requires long drying time which could be harmful to several delicate microorganisms[5]. Thus, relatively inexpensive convective air drying has been considered as promising alternative to address problems encountered in freeze drying.

To date, research on the application of convective air drying for microorganism preservation, or more specifically for mixed culture preservation, is rather scarce and largely limited to agricultural and dairy industry. Hence, this study aims to develop dried mesophilic mixed culture from economical convective air drying methods, namely heat pump and hot air circulation oven. Various drying conditions were also investigated to achieve the highest possible cell survival, methane yield, and treatment performance during treatment of POME.

2. Materials and Methods

2.1 Sample preparation

Seed sludge and palm oil mill effluent (POME) were obtained from the palm oil mill at Seri Ulu Langat in Dengkil, Malaysia. During cultivation, intermittent feeding of POME as substrate was done in order to maintain the microbial population in the seed sludge.

2.2 Cultivation of mixed culture in UASB batch reactor

An up-flow anaerobic sludge blanket (UASB) reactor with an effective volume of 2.5 L as shown in Fig.1 (separate attachment) was used to cultivate mesophilic sludge. To start-up, 625 mL of seed sludge which represents 25% of the working volume is fed to the tank, while the remaining 75% consists of diluted POME. pH of the system was maintained in the range of 6.8-7.2 through the addition of 2 mol/L $NaHCO_3$ to ensure satisfactory methanogenic activity[6]. Treated effluent was collected by letting the mixture in the bioreactor to settle for 30 minutes. After which the top portion of the mixture was collected as supernatant and sent for qualitative and quantitative analysis. COD removal is used as criteria for increasing load in the feed to maintain the effectiveness of the system, especially when COD removal is higher than 80% or when there is less than 5% increase for 3 consecutive readings. The then matured mixed culture seed sludge was extracted from the batch reactor for drying procedure.

2.3 Drying methods

25 g of the mesophilic mixed culture sludge was extract from the bioreactor and used to perform drying experiment in three replicates. The sludge was dried until equilibrium moisture content (EMC) by using different drying methods as described in the following sections.

2.2.1 Heat pump drying

A laboratory scale heat pump dryer fabricated by I-Lab Sdn. Bhd., Selangor, Malaysia was used in this research. The heat pump dryer consists of a drying chamber of dimensions 0.8 m × 0.6 m × 0.6 m and a heat pump system. Mild temperature dehumidifier air produced by the heat pump system was used as a drying medium to dry the sludge in the chamber. The dryer operated at temperature of 22℃ and relative humidity (RH) of 38.1%. In addition, the dryer is equipped with an auxiliary heater which can be switched on to give drying temperature of 32℃ and RH of 29.5%. The average air velocity in the drying chamber was recorded at 2 m/s across the two drying conditions.

2.2.2 Hot air circulation oven drying

Hot air circulation oven (Memmert UFB500) was used to conduct drying of sludge at average temperature and relative humidity of 40.0℃, 50.0℃, 60.0℃, 70.0℃ and 19.9%, 16.1%, 7.4%, 4.7%, respectively. The drying chamber has a dimension of 53 cm × 47 cm × 39 cm where air is circulated by an air turbine with measured average velocity of 1.9 m/s for all drying temperatures.

2.4 Drying rate and moisture diffusivity

The initial moisture content (M_0), moisture content at a given drying time t (M_t), equilibrium moisture content (M_{eq}), moisture ratio (MR_t) and drying rate (R) of the mesophilic mixed culture sludge were calculated by equations (1) – (5) whereas the moisture diffusivity (D_{eff}) of the samples was determined using Fick's second model (equation (6)).

$$M_0 = \frac{W_0 - W_d}{W_d} \quad (1); \quad M_t = \frac{W_t - W_d}{W_d} \quad (2); \quad M_{eq} = \frac{W_{eq} - W_d}{W_d} \quad (3); \quad MR_t = \frac{M_t - M_{eq}}{M_0 - M_{eq}} \quad (4)$$

$$R = \frac{W_d}{A_s} \left| \frac{F_{t+1} - F_t}{t_{t+1} - t_i} \right| \quad (5); \quad MR = \frac{8}{\pi^2} \left[\sum_{n=0}^{99} \frac{1}{(2n+1)^2} \exp\left(\frac{-(2n+1)^2 \pi^2 D_{eff} t}{l^2} \right) \right] \quad (6)$$

Where W_0, W_t, W_d, and W_{eq}, refer to initial weight of the sample (kg), weight of the sample in the middle of drying process at time t (kg), bone dry weight of the sample (kg), and equilibrium weight of the sample (kg), respectively. A_s is denoted as the surface area of the samples (m^2), F_t is the free moisture content of the sample at time t (kg H$_2$O / kg dry material). l, t and n are the sample's thickness (m), drying time (s) and a positive integer, respectively.

2.5 Quality analysis

The quality of dried mixed culture mesophilic sludge was evaluated by assessing the viability of microorganisms after drying. To do that, the dried mixed culture was first rehydrated before it can be evaluated for cell survival, COD removal, and methane yield.

2.5.1 Rehydration of mixed culture

Rehydration was performed by adding distilled water in the amount equivalent to that lost during drying process and agitated in incubator shaker at 37°C and 250 rpm for 18 hours. The resultant rehydrated mixed cultures were then evaluated for cell survival by obtaining the most probable number (MPN) of microorganisms contained in the sample. The rehydrated sludge was also evaluated for its performance in treating POME through assessment of the COD removal and methane yield.

2.5.2 Cell survival

MPN enumeration was conducted to obtain the cell count of microorganisms following drying process. Culture medium was prepared by dissolving 30 grams of tryptic soy broth (TSB) in 1 L of distilled water. Next, serial dilutions of seed sludge were prepared by adding 1 mL of sample into 9 mL of sterile distilled water until a 10^{12} times dilution is

obtained. Subsequently, 1 mL from each dilution number was then inoculated into vials containing TSB. This was done in triplicates for each dilution to enable comparison with 3-tubes most probable number (MPN) table. The vials were then incubated under anaerobic condition for 8 days at 55°C. To obtain the MPN of total anaerobes, each vial was first determined to be either positive if the mixture was cloudy or negative if the mixture was clear after incubation. The combination of positive and negative tubes was then compared against MPN table to obtain a corresponding MPN value[7]. In contrast, MPN for methanogens was obtained by detecting the presence of methane using biogas analyser (Binder Combimass Ga-m). Vials were marked as positive if methane is detected and negative otherwise. The combination of positive and negative tubes was compared against the same table as for total anaerobes. The cell survival of microbes was subsequently determined by equation (7).

$$Log\ Reduction = \log\left(\frac{MPN_{before\ drying}}{MPN_{after\ drying}}\right) \qquad (7)$$

2.5.3 COD removal

A 250 mL Schott Duran Bottle was set-up as bioreactor where 50 mL of rehydrated mixed culture was used to treat 150 mL of POME after pH adjustment by adding 1 mol/L sodium bicarbonate. Supernatant was collected regularly for a period of 12 days from the bioreactor after allowing 30 minutes settling time. It was then analysed for COD level by following HACH Method 8000 which is USEPA approved for wastewater analyses (Standard Method 5220 D). The COD removal of the rehydrated sample was calculated using Equation (8).

$$COD\ Removal = \frac{(COD_{initial} - COD_{final})}{COD_{initial}} \times 100\% \qquad (8)$$

2.5.4 Methane yield

Daily monitoring of bioreactor was conducted over 12 days period to obtain both biogas volume (mL) and methane composition (%). Biogas volume was measured by capturing the produced gas in an inverted measuring cylinder while its composition was obtained using biogas analyser Binder COMBIMASS® Ga-m.

3. Results and Discussion

3.1 Drying rate, effective moisture diffusivity, total drying time and EMC

Tables 1 shows that low temperature drying using heat pump took longer time compared to high temperature drying using hot air circulation oven drying as heat pump was operated at drying temperature that is equal to- or below ambient temperature and thus relies on low relative humidity as the main driving force. Generally, higher temperature of drying air enables greater transfer of heat from air to water molecules in the mixed culture. This gives

rise to higher rate of evaporation (i.e. drying rate) and hence shorter total drying time required for the sludge to achieve EMC. Air at higher temperature also has greater capacity to hold moisture and thus hotter air is able to remove more water molecules than colder air of the same flow rate. In terms of effective moisture diffusivity, the values of D_{eff} increased notably with increasing drying temperatures for both heat pump drying and hot air circulation oven drying. Lower relative humidity at high drying temperature promoted moisture concentration gradient between the surface of drying sample and its inner interstices, which stimulates the moisture diffusion from the interior of the sample to the surface and thus produced dried sludge with low EMC. Nevertheless, better survival of microorganism is achieved by drying at low temperature and relatively short drying time due to minimisation of heat and osmotic stresses[8]. Therefore, it is important to weigh over the importance of achieving high cell survivability over short drying time resulted from elevated drying temperature. Moreover, the performance of mixed culture in treating POME after subjected to drying process must also be considered.

Table 1. Average drying rate, effective moisture diffusivity, total drying time and EMC of heat pump and hot air circulation oven dried mesophilic mixed culture

Drying Method	Average Drying Rate (R) (g H₂O / m².s)	Average Effective Diffusivity (D_{eff}) ($\times 10^{-8} m^2 s^{-1}$)	Total Drying Time (h)	EMC (g H₂O/ g dry solid)
Heat pump (22ºC)	4.67	0.85	26.6	0.148
Heat pump (32ºC)	5.78	0.97	23.0	0.046
Oven (40ºC)	8.57	3.39	7.5	0.034
Oven (50ºC)	12.87	3.88	5.8	0.026
Oven (60ºC)	19.41	4.25	4.5	0.017
Oven (70ºC)	21.55	4.62	3.5	0.012

3.2 Cell survival, COD removal and methane yield

According to Table 2, the lowest log reduction for methanogens and anaerobes were obtained from 22°C-drying for heat pump drying with 1.4 & 2.4 and from 50°C for hot air circulation oven with 1.5 & 5.6, respectively. Generally, higher log reductions indicate that more cell deaths occur during the drying process. Higher cell survivability was found towards milder drying temperature was likely due to the nature of mesophilic mixed culture which thrives at 20-35°C combined with reduced thermal inactivation when drying was conducted at relatively lower temperatures[9]. As such, the mesophiles within mixed culture suffer from higher cell inactivation at higher temperature drying in a hot air circulation oven. As compared with mesophilic seed sludge, mesophilic mixed culture dried at the

various drying temperatures still gives comparable average COD removals in the range of 46.8% to 55.3%, with fairly similar trend with the preceding cell viability, where more favourable results were obtained with decreasing drying temperature. This is indicated in Table 3 where mixed culture dried at 22°C gave rise to higher COD removal as compared to other drying temperatures. In terms of methane yield, mesophilic mixed culture that was dried at 50°C in a hot air circulation oven produces highest yield at 37.6 mL CH$_4$/g COD when compared with other drying temperatures. It is most likely that a balance between drying temperature and drying duration was reached at 50°C-drying, producing dried sludge with moisture content that favours the survival of methanogens, eventually resulting in second highest values for both N_M (after HP 22°C) and N_M/N_A (after 60°C) as illustrated in Table 2. Optimum moisture content as well as drying time are both directly affected by drying temperature and could influence the cell viability in mixed culture after drying[4].

Table 2. Most probable number (MPN) and log reduction of mesophilic mixed culture following drying process

Drying Technique	Most Probable Number (ml^{-1})			Log Reduction	
	Methanogens, N_M	Anaerobes, N_A	N_M/N_A (%)	Methanogens	Anaerobes
Mesophilic seed sludge	$9.30 \cdot 10^1$	$1.99 \cdot 10^{12}$	$4.67 \cdot 10^{-9}$	n/a	n/a
Heat Pump (22°C)	$0.36 \cdot 10^1$	$7.50 \cdot 10^9$	$4.80 \cdot 10^{-8}$	1.4	2.4
Heat Pump (32°C)	$0.24 \cdot 10^1$	$1.15 \cdot 10^9$	$2.08 \cdot 10^{-7}$	1.6	3.2
Oven (40°C)	$0.16 \cdot 10^1$	$2.90 \cdot 10^6$	$5.52 \cdot 10^{-5}$	1.8	5.8
Oven (50°C)	$0.29 \cdot 10^1$	$4.60 \cdot 10^6$	$6.30 \cdot 10^{-5}$	1.5	5.6
Oven (60°C)	$0.21 \cdot 10^1$	$2.30 \cdot 10^6$	$9.13 \cdot 10^{-5}$	1.6	5.9
Oven (70°C)	$0.20 \cdot 10^1$	$3.60 \cdot 10^6$	$5.56 \cdot 10^{-5}$	1.7	5.7

Table 3. COD removal and methane yield of mesophilic mixed culture before and after drying under heat pump and hot air circulation oven

Drying Technique	COD Removal (%)	Methane Yield (mL CH$_4$/g COD)
Mesophilic Seed Sludge	67.4 ± 9.8	44.1 ± 10.5
Heat Pump (22°C)	55.3 ± 8.9	17.9 ± 1.74
Heat Pump (32°C)	52.8 ± 5.6	14.1 ± 1.66
Oven (40°C)	52.9 ± 2.7	13.9 ± 1.55
Oven (50°C)	53.5 ± 3.4	37.6 ± 2.89
Oven (60°C)	50.2 ± 4.5	22.3 ± 3.61
Oven (70°C)	46.8 ± 7.0	37.2 ± 2.90

4. Conclusion

Heat pump drying of mixed culture mesophilic sludge takes considerably longer time to reach EMC as compared to hot air circulation oven drying at elevated temperature. Nevertheless, in term of quality analysis, heat pump dried mesophilic mixed culture at mild temperature (22ºC) gave rise to the best methanogenic survival, anaerobic survival, and COD removal among of all. The highest methane yield was produced by hot air circulation oven dried mesophilic mixed culture at 50ºC. It might appear that either one of these two drying conditions could be considered as the most suitable drying condition for mixed culture mesophilic sludge depending on the desired outcome. However, hot air circulation oven drying at 50°C could be more practical in industrial setting as drying duration is shorter.

5. References

[1] Choi, W.H.; Shin, C.H.; Son, S.M.; Ghorpade, P.A.; Kim, J.J.; Park, J.Y. Anaerobic treatment of palm oil mill effluent using combined high-rate anaerobic reactors. Bioresource technology 2013, 141, 138–44.

[2] Li, J.; Fraikin, L.; Salmon, T.; Plougonven, E.; Toye, D.; Léonard, A.; Convective drying behavior of sawdust-sludge mixtures in a fixed bed. Drying Technology 2016, 34 (4), 395–402.

[3] Chávez, B.E.; Ledeboer, A.M. Drying of Probiotics: Optimization of Formulation and Process to Enhance Storage Survival. Drying Technology 2007, 25 (7–8), 1193–1201.

[4] Zayed, G.; Roos, Y.H. Influence of trehalose and moisture content on survival of Lactobacillus salivarius subjected to freeze-drying and storage. Process Biochemistry 2004, 39 (9), 1081–1086.

[5] Tambunan, A.H. Freeze Drying Characteristics of Medicinal Herbs. Drying Technology 2001, 19 (2), 325–331.

[6] Kasali, G.B.; Senior, E.; Watson-Craik, I.A. Preliminary investigation of the influence of pH on the solid-state refuse methanogenic fermentation. Journal of Applied Bacteriology 1988, 65 (3), 231–239.

[7] Man, J.C. MPN tables, corrected. European Journal of Applied Microbiology and Biotechnology 1983, 17 (5), 301–305.

[8] Morgan, C.A.; Herman, N.; White, P.A.; Vesey, G. Preservation of micro-organisms by drying; a review. Journal of Microbiological Methods 2006, 66 (2), 183–93.

[9] Perdana, J.; Bereschenko, L.; Fox, M.B.; Kuperus, J.H.; Kleerebezem, M.; Boom, R.M.; Schutyser, M.A.I. Dehydration and thermal inactivation of Lactobacillus plantarum WCFS1: Comparing single droplet drying to spray and freeze drying. Food Research International 2013, 54 (2), 1351–1359.

Assessment of the conditions of the thermoplastic extrusion process in the bioactive and mechanical properties of flexible films based on starch and Brazilian pepper

Fakhouri, F.M. [a,b]∗ ; Freitas de Lima, F.[a,d]; Cardoso, C.A.L.[c]; Martelli. S.M.[a]; Antunes, M.[b]; Mei, L.H. I.[d]; Yamashita, F.[e]; Velasco, J.I. [b]

[a]Faculty of Engineering, Federal University of Grande Dourados. Dourados, MS, Brazil.
[b]Centre Català del Plàstic, Universitat Politècnica de Catalunya, Barcelona, Spain.
[c] Research Center in Biodiversity, State University of Mato Grosso do Sul, MS, Brazil.
[d] Faculty of Chemical Engineering, State Univeristy of Campinas, SP, Brasil.
[e]Faculty of Food Engineering, State University of Londrina, PR, Brazil.

*E-mail of the corresponding author: farayde@gmail.com

Abstract

The objective of this work was to produce, through the thermoplastic extrusion process followed by blowing, manioc starch-based flexible films added with Brazilian pepper oil as an antioxidant and plasticizer agent, and verify if the bioactive compounds contained in the fresh pepper oil are present after the drying step of the thermoplastic extrusion. After analysis by gas chromatography-mass spectrometry volatiles compounds were identified in the films. Pepper oil also influenced the mechanichal properties of the films.These results suggest that the temperatures used in the process, kept some of the existing compounds in the Brazilian pepper essential oil adhered to the packages.

Keywords: Termoplastic extrusion, temperature, bioactivs compounds.

1. Introduction

Plastic films of petrochemical origin are currently used on a large scale in food packaging, and their use is contingent upon their mechanical and barrier properties. Although chemically stable, they are not biodegradable and cause environmental impact. One of the alternatives to this problem would be the development of edible and/or biodegradable films using raw materials from renewable sources.

The bioplastics industry is still in beginning, looking to identify and exploit market niches not only for the biodegradability, recycling and / or replacement of plastics of petrochemical origin by plastics from renewable sources, also concerned about the carbon cycle and sustainability. Bioplastics are defined as materials which, containing variable percentage biopolymers, can be molded by heat and pressure. They are potential alternatives to conventional thermoplastic polymers of petrochemical origin, such as polyolefins and polyesters [1].

Starch is a polysaccharide of plant origin, widely found in the international market, capable of forming films both by the casting technique and by the thermoplastic extrusion process. Films made with starch can also introduce additives into the packaging, such as natural antioxidant and antimicrobial agents.

The Brazilian pepper (*Schinus terebinthifolius Raddi*) is originally from Peru and is widely distributed throughout the Americas, including the Northeast, Southeast, South and Midwest of Brazil[2].   The fruit has healing properties attributed to the different volatile compounds that are distributed in its various organs, such as bark, leaves, flowers, fruits and seeds[3]. It is used in the food industries, as well as its essential oil in the development of pharmaceuticals and cosmetics[4]. The species has increasing pharmacological use, and is considered by popular medicine as an anti-inflammatory, antimicrobial and strong antioxidant agent[4,5,6].

The process of extrusion allows the thermoplastification of a solid material by the application of heat and mechanical work, being the main process to obtain the bioplastics. It is a highly versatile process in which the extruder can behave as a heat exchanger due to the thermal changes occurring between the material to be extruded and the equipment [7].

In this context, the objective of this work was to produce, through the thermoplastic extrusion process followed by blowing, manioc starch-based flexible films added with Brazilian pepper oil as an antioxidant and plasticizer agent, and verify if the bioactive compounds contained in the fresh pepper oil are present after the drying step of the thermoplastic extrusion process to obtain the biodegradable film. In parallel, we analyzed

Fakhouri, F. M.;Freitas de Lima, F.; Cardoso, C. A. L.; Martelli. S. M., Antunes, M.; Innocentini
Mei, L. H.; Yamashita, F.; Velasco, J. I.

the mechanical properties of the films to verify the effect of the pepper oil concentration on tensile strength, elongation and elasticity of the films.

2. Materials and Methods

Materials: manioc starch, glycerol and brazilian pepper essential oil.

The films were produced by thermoplastic extrusion following buy blowing in single screw extruder. The range of temperature was 90 to 130oC and the velocitiy 35 rpm, the same condictions proposed by Fakhouri [8]. Three formulations were produced: i) manioc starch with glycerol (25%), ii) manioc starch, glycerol (25%) and brazilian pepper essential oil (2%) and iii) manioc starch, glycerol (25%) and brazilian pepper essential oil (3%).

Chemical characterization by Gas Chromatography : The analyzes were performed using a gas chromatograph equipped with a mass spectrometer detector (GCMS-QP2010 Ultra, Shimadzu, Kyoto, Japan). employing a fused silica DB-5 capillary column (J & W, 5% de phenyl-dimethylpolysiloxane) with 30 m in length x 0.25 mm i.d., 0.25 μm film thickness, under the following conditions: carrier gas helium (99.999% and flow rate 1.0 mL min-1); 1 μL injection volume, split ratio (1:20), with initial oven temperature of 50ºC and heating from 50º to 280ºC at 3ºC min-1. The injector temperature, transfer line and detector temperatures were 250ºC. The MS scan parameters included electron impact ionization voltage at 70 eV, a mass range of 45 to 600 m/z and a scan interval of 0.3 s. Temperature-programmed retention indices were calculated using a mixture of alkanes (C8-C30) as external references and compared with Adams[9]. The identifications were completed by comparing the mass spectra obtained in the NIST21 and WILEY229 databases and literature data [8].

Total flavonoids quantification by Spectrophotometry: The flavonoids content was determined in the acetonic extracts of extruded S. terebinthifolius using the colorimetric method involving the reaction with aluminum chloride by Chang [10] with adaptations for extrudates. Extracts were prepared with 100 g of sample added in 500 mL of acetone (50% w/v), and they were kept under constant agitation (150 rpm) for five hours. The sample was filtered, and the filtrate was considered the flavonoid extract for analysis.

The extract was reacted with aluminum chloride and the readings were performed in a spectrophotometer (Biochrom – Libra S60) adjusted at 415 nm. Quercetin solutions at nine concentrations (0.01 to 0.2 µg.µL-1) were reacted with sodium aluminum chloride in order to construct a standard curve. The results were expressed as milligrams of quercetin equivalent (QE mg.100g-1 sample) using the quercetin standard curve.

Elastic modulus, tensile strength and elongation at rupture will be determined using a texturometer (Universal testing machine Galdabini SUN 2500, TA-HDi Texture Analyser (Stable Microsystem, Surrey, England), the condictions were perfomed by ASTM methods[11].

3. Results and Discussion

After analysis by gas chromatography-mass spectrometry, fourteen volatile compounds were found in the essential oil of S. terebinthifolius (Table 1). Among these compounds, we highlight the iso-sylvestrene (34.12%), α-thujene (17.13%), myrcene (8.25%), α-phellandrene (6.68%), β-longipinene (5.90%) and sylvestrene (5.87%). After the thermoplastic extrusion process at temperatures ranging from 90 to 130°, 5 volatile compounds were identified, knowingly: α-pinene, sabinene, β-pinene, limonene and α-copaene.

Table 1. Monoterpene and sesquiterpene chemical characterization by gas-chromatography and total flavonoids quantification by spectrophotometry of Schinus terebinthifolius Raddi oil and extruded.

Compounds	RIᵃ	RIᵇ	Essential oil	Extruded (2%)	Extruded (3%)
α-thujene	923	924	17.13	-	-
α-pinene	939	939	1.03	17.43	18.68
α-fenchene	953	953	3.83	-	-
Sabinene	975	976	-	9.54	10.13
β-pinene	980	980	1.19	8.79	8.67
Myrcene	988	988	8.25	-	-
α-phellandrene	1002	1002	6.68	-	-
Iso-sylvestrene	1007	1007	34.12	-	-
Sylvestrene	1025	1025	5.87	-	-
Limonene	1030	1029	-	15.24	15.41
Fenchone	1083	1083	3.69	-	-
α-copaene	1377	1377	-	9.91	10.12
β-longipinene	1400	1400	5.90	-	-
Aromadendrene	1465	1465	4.63	-	-
Biciclogermacrene	1517	1517	3.21	-	-
δ-cadinene	1519	1519	2.29	-	-
Sphatulenol	1619	1619	1.34	-	-
Total flavonoids (mg.100g QE)	-	-	-	60.77	63.49

ᵃRetention índex calculated; ᵇRetention índex literature. The values of gas chromatography are expressed in % and the total flavonoids are expressed in mg.100g of quercetin equivalent.

Fakhouri, F. M.;Freitas de Lima, F.; Cardoso, C. A. L.; Martelli. S. M., Antunes, M.; Innocentini
Mei, L. H.; Yamashita, F.; Velasco, J. I.

Higher concentrations of pepper oil influenced the mechanical properties of the films, causing a significant increase in the elongation of the films and decrease of the tensile strength and elasticity (Figure 1).

a

b

c
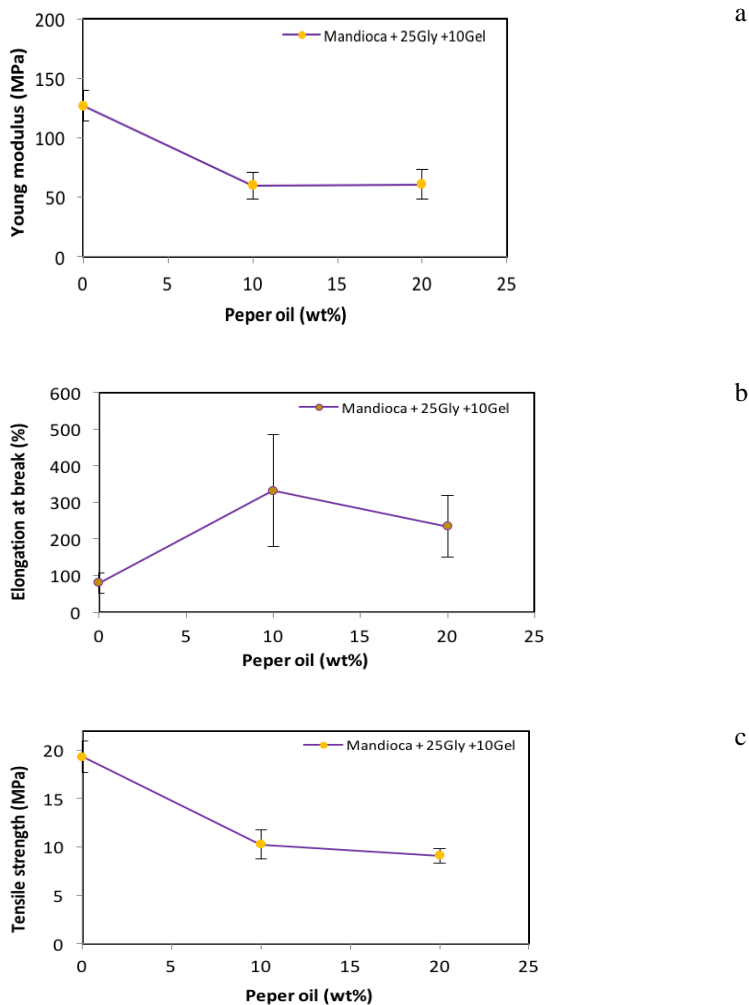
Figure 1. (a) Yong modulus (MPa), (b) Elogation at break (%) and (c) Tensile Strenght (MPa) of flexible films from starch and Brazilian pepper.

4. Conclusions

It was possible to obtain flexible films by manioc starch, glycerol and brazilian pepper essential oil by thermoplastic extrusion following buy blowing. After the thermoplastic extrusion process, five volatile compounds were identified, knowingly: α-pinene, sabinene, β-pinene, limonene and α-copaene in the flexible films. The brazilian pepper essential oil aso influenced the mechanical properties of the films.

These results suggest that the temperatures used in the thermoplastic extrusion process, although high, kept some of the existing compounds in the Brazilian pepper essential oil adhered to the packages.

5. Acknowledgment

6. References

[1] Queiroz, A. U. B., Collares-Queiroz, F. P., Innnovation and industrial trends in bioplastics. Polymer Reviwes, 2009, 49 (2) , 65-78.

[2] Barbosa, L. C. A., Demuner, A. J., Clemente, A. D., Paula, V. F. D., & Ismail, F. Seasonal variation in the composition of volatile oils from Schinus terebinthifolius Raddi. Química Nova, 2007, 30(8), 1959-1965.

[3] Santos, A. C. A. D., Rossato, M., Agostini, F., Serafini, L. A., Santos, P. L. D., Molon, R. & Moyna, P. (2009). Chemical composition of the essential oils from leaves and fruits of Schinus molle L. and Schinus terebinthifolius Raddi from Southern Brazil. Journal of Essential Oil Bearing Plants, 2009, 12(1), 16-25.

[4] Bendaoud, H., Romdhane, M., Souchard, J. P., Cazaux, S., & Bouajila, J. Chemical composition and anticancer and antioxidant activities of Schinus molle L. and Schinus terebinthifolius Raddi berries essential oils. Journal of food science, 2010, 75, 6.

[5] Medeiros, K. C., Monteiro, J. C., Diniz, M. F., Medeiros, I. A., Silva, B. A., & Piuvezam, M. R. Effect of the activity of the Brazilian polyherbal formulation: Eucalyptus globulus Labill, Peltodon radicans Pohl and Schinus terebinthifolius Radd in inflammatory models. Revista Brasileira de Farmacognosia, 2007, 17(1), 23-28.

[6] Formagio, A. N., Iriguchi, E. K., Roveda, L. M., Vieira, M. D. C., Cardoso, C. L.,

Zarate, N. H., ... & Kassuya, C. L. Chemical composition and anti-inflammatory activity of the essential oil of Schinus terebinthifolius Raddi (Anacardiaceae) fruits. Latin American Journal of Pharmacy, 2011, 30(8), 1555-1559.

[7]   Olku, J., Linko, P. Effects of thermal processing on cereal based food systems. Food-Quality and nutricion research priorities for thermal processing, Dawney, W.K., eds London, Applied Science Publishers, 1997, 352 p.

[8]   Fakhouri, F.M., Costa, D.L.M, Yamashita, F., Martelli, S. M., Jesus, R. Alganer, K., Innocentini Mei, L. H., Collares Queiroz, F.P. Comparative study of processing methods for starch/gelatin films. Carbohydrate polymers, 2013, 95, 681.

[9]   Adams, R.P., Identification of essential oil components by gas chromatography/mass spectrometry. 4°ed. Illinois USA: Allured Publishing Corporation, Carol Stream, 2007, 804 p.

[10] Chang C. C., Yang M. H., Wen H. M., & Chern J. C. Estimation of total flavonoid content in propolis by two complementary colorimetric methods. Journal of Food and Drug Analysis, 2002,10, 178-182.

[11] Method D 882-83: Standard test methods for tensile properties of thin plastic sheeting, 1980.

Bread preservation with use of edible packaging

Silva, V.S. [a*]; Fakhouri, F. M.[b]; Arias, L. V. A.[a]; Aguiar, R. H.[a]; Oliveira, R.A. [a]
[a]Faculty of Agricultural Engineering .University of Campinas, Campinas, Brazil.
[b] Faculty of Food Engineering. University of Grande Dourados, Dourados, Brazil.

*E-mail of the corresponding author: vinutry@yahoo.com.br

Abstract

We live in a world that usually use plastic bags either to go shopping or to pack the snack for a short trip. However, packaging makes life easier and serves as protection for products such as food. Bread is a common food product that needs packaging in order to be protected at storage and transportation. Therefore, with aim of reducing petroleum derived packagin g consumption it was developed an edible film from potato starch to packeg bread and some quality characteristics like water content, firmness and weight loss were evaluated, showing that edible film can be used as a packaging

Keywords: *biopolymers; edible coatings; packaging materials; starch; storage.*

1. Introduction

Bread is the product obtained by the cooking dough at pan, showing elastic and homogeneous crumb, fine pores, thin and soft crust, produced from a mixture of flour, water, yeast and salt [n1]. This is a perishable product because of its high water activity so, its marketing period is short.

One of the shelf life limiting factors is the aging that occurs because of regress and favours to increase crumb firmness, giving a sensation of drying product by the ingestion   [n2] this added to the necessary of decrease operational costs and expand the market let the bakers to require new technologies and the development of new methods of dough production [n3].

In this manner, the edible film technology has been implemented recently, there are applied indirectly to the product in the way of a thin layer that acts like a modified atmosphere, being a barrier for gas exchanges and loss of water vapor that can improve handling and the visual appearance of the protected food product [n4; n5].

On the other hand, the use of packaging to increase shelf life is not to recently, however several researches have studied the use of non-conventional packaging. Production of edible films from biopolymers is na alternative technology that has been highlighting because of its ability of increase the conservation time and allows higher handling and marketing flexibility of the product [n6]. Films can be obtained by different types of materials, being more used the polysaccharides, proteins and lipids [n5].

Starch is a polysaccharide that besides being the main source of carbohydrates for human nutrition, also has technological relevance for food, pharmaceutical, paper, textile, materials and oil drilling industries. According to the industry it can be used like a thickener, colloidal stabilizer, gelling agent, paste former and adhesive [n7]. Do to the above, its lower cost and high availability [n8], this polysaccharide stood out to be used at the productive chain. Starch can be obtained from plants and depending on each plant the reserves source of energy can be found in higher quantities at different regions of the plant like such as grains, roots, rhizomes, seeds and stems. The main commercial sources of this carbohydrate are corn, potato and cassava [n9].

In productive chain of bread the packaging is the last stage in which special care must be taken to guarantee longer shelf life. Success in Market depends on product intrinsic quality and packaging effectiveness to preserve and keep quality. Convectional procedure to packaging applied in bakery industry use atmospheric air and coverage materials approved for food. Several researches shown the effectiveness of the packing keeping bread quality characteristics, delaying loss of water content and fungi growth [n10, n 11].

2. Materials and Methods

2.1. Elaboration of filmogenic solution

To produce edible coatings was used methodology proposed by Fakhouri [n12]. Macromolecule used was commercial potato starch (3% for 100 mL of distilled water). The starch and water were deposited in glass beakers and homogenized. This solution was brought to the thermostatic bath (Quimis, Q334 M-14, SP, Brazil) heated to 80 ° C. After obtaining the filmogenic solution of potato starch the glycerol is added in a gentle manner to avoid blistering in sample. The film-forming solution was dispersed in petri dishes and dried in an air circulating oven (45 °C) for 6 hours. After drying, films were utilization for packing bread in sealing machine, and stored at room temperature by 3 days.
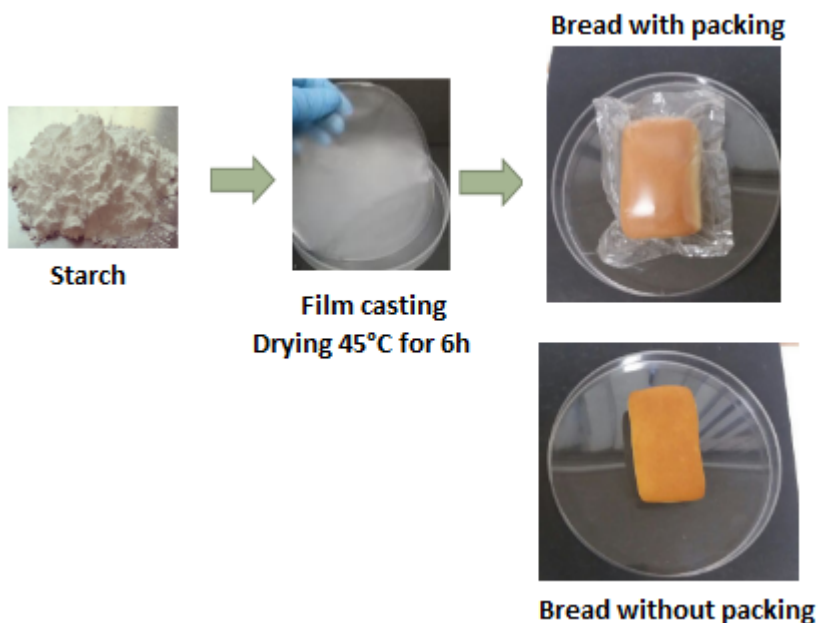
Fig. 1 Production and application of edible packaging of starch potato

It was used small breads (Bisnaguito, Pullman), with weight $\cong$ 23 g for unit, obtained local commerce from Campinas city, Brazil. Ingredients contained in small breads: wheat flour fortified with iron and folic acid, sugar, sunflower oil, invert sugar, salt, fatty acid monoglyceride emulsifier, sodium stearoyl-2-lactyl lactate, conservative calcium propionate.

2.2. Determination of Water content of bread

Water content of bread was determined by oven drying at 105 °C until constant weight. Three slices obtained of bread center (10 ± 1 mm thickness) for each of two repetitions were used.

2.3. Firmness of bread

Firmness was measured using the texture analyzer (TA.XT Plus, Stable Micro Systems Co. Ltd., UK) equipped with a 30 kg load cell and connected with a Warner Bratzler blade set with a speed of 1 mm.s^{-1} . Three measurements were collected for each treatment and day (0 and 3). Firmness was measured as the maximum shear strength values and expressed as maximum force (N).

2.4. Weight loss of bread

Weight loss of bread was determined by weighing the sample in initial day and three days after, in three repetitions were made.

2.5. Statistical analysis

Data were submitted analysis of comparison of means by the Tukey test (p< 0.05) through the statistical package Statistics 9.0.

3. Results and Discussion

The changes in moisture content, firmness and weight loss of bread are shown at Table 1. The initial crumb moisture content of bread tended to decrease during storage, similar to the observed by Licciardello et al [n13] and others studies [n14, n15] in differently packed durum wheat bread samples. One of the objectives of a packaging system is to reduce water loss, and this can be achieved by materials with suitable barrier to water vapor. The observed results were therefore undesirable to low moisture content value of samples.

Texture is an important characteristic in consumer's perception of food and influences the purchasing decisions. Firming of bread is one of the quality factors in bread ageing and one of the most common parameters used to evaluate staling. A significant increase in firmness was observed for all samples during storage. This result agreed with the water content measures that evidenced likely of starch retrogradation in samples (Table 1), result too observed in other studies [n13, n14, n15].

The products packaged when compared to unpacked showed similar weight loss, however when texture values were observed, sample with packaging showed a lower value than sample without packaging. Indicating that the first one lost less mass than the second, which presented increase of firmness, probable dryness of product. The results showed that

the packaging did not adversely affect the product, since there was no significant difference between the treatments.

Table 1. Moisture content, firmness and weight loss of bread

Storage time (days)	Bread unp	Bread WP
Moisture content (%)		
0	26,54±0,15	26,54±0,15
3	16,94±0,65[a]	16,44±0,08[a]
Firmness (N)		
0	0,2±0,06	0,2±0,06
3	1,9±0,15[a]	1,89±0,37[a]
Weight loss (g)		
0	23,36±0,41	25,99±0,57
3	20,21±0,04 (3,15±0,45)[a]	22,65±0,31 (3,34±0,48)[a]

unP=unpacked; WP= with packing

Values are the average ± standard deviation (n=3). Demonstrated lower case letters that in the same parameter not different from each other ($p < 0.05$).

At the research led by Cioban et al. [n16] showed that the signs of bread degradation begin to appear after the third day in agreement with what was shown in this work, the smooth and rigid crust becomes wrinkled, elastic and soft, compressing core turns into brittles and becomes less compressing and rigid when stored.

5. Conclusions

Based on results analysis, when comparison product with and without packaging , bread characteristics in initial phase of storage exhibit allowing only slight changes, with respect weight loss, compared to packed product.. However, in storage time the moisture content and firmness not extended the standard shelf life.

These packaging could be used to keep the product separation by form unitary as primary packaging, for product that would be consumed on same day. Resulting in the decrease of packaging consumption derivate of the petroleum used for same purpose and which has high degradation time. In this context, developing of packaging with potato starch can promote reduction environmental damage.

Another application for such packaging derived from renewable material would be in products which are desirable maintaining the breath, such as some fruits. But, with they were not significant differences between the treatments it is necessary to develop other

analysis with more days in different environments to better conclude the packing functionality.

6. **References**

[1] Tweed, A.R. A look at French "French Bread". Cereal Fooods world, v.28, n.27, p.397-399, 1983.

[2] Stauffer, C.E. Frozen bakery products. IN: MALLETT, C.P. (ed) . Frozen Food Technology Cambridge: Chapman & Hall, 1994.

[3] Báguena, R.; Soriano, M. D.; Martinezanaya, M. A; De Barber, C. B. Viability and performance of pure yeast strains in frozen wheat dough. , Journal of food science v.56, n.6, p.1690-1694, 1991

[4] Fakhouri, F.M.; Fontes, L. C. B.; Gonçalves, P. V. M.; Milanez, C. R.; Steel, C. J.; Collares-Queiroz, F. P. Filmes e coberturas comestíveis compostas à base de amidos nativos e gelatina na conservação e aceitação sensorial de uvas *Crimson*. Ciência e Tecnologia de Alimentos, v.27, n.2, p. 369-375, 2007.

[5] Falguera, V.; Quintero, J.P.; Jiménez,A.; Muñoz,J.A.; Ibarz, A. Edible films and coatings: Structures, active functions and trends in their use. Trends in Food Science & Technology, v. 22, p. 292-303, 2011.

[6] Li, J.M; Nie, S. P. The functional and nutritional aspects of hydrocolloids in foods. Food Hydrocolloids, v. 53, p.46-61, 2016.

[7] Singh, N.; Singh,J.; Kaur, L.; Sodhi, N.S.; Gill, B.S. Morphological, thermal and rheological properties of starches from different botanical sources. Food Chemistry, 81, 219–231, 2003.

[8] Souza, A.C.; Benze, R.; Ferrão, E. S. ; Ditchfield, C.; Coelho, A. C. V. ; Tadini, C. C. Cassava starch biodegradable films: Influence of glycerol and clay nanoparticles content on tensile and barrier properties and glass transition temperature. LWT - Food Science and Technology, v. 46, p. 110-117, 2012.

[9] Ferrari, T. B; Leonel, M.; Sarmento, S. B.S. Características dos rizomas e do amido de araruta (*Maranta arundinacea*) em diferentes estádios de desenvolvimento da planta. Brazilian Journal of Food Technology, v.8, n.2, p. 93-98, 2005.

[10] Licciardello, F.; Capri, L.; Muratore, G. Influence of packaging on the quality maintenance of industrial bread by comparative shelf life testing. Food Packaging and Shelf Life, 1 , 19-24, 2014.

[11] Pagani, M.; Lucisano, M.; Mariotti, M.; Limbo, S..Influence of packaging material on bread characteristics during ageing Packaging Technology and Science, 19, 295-302, 2006.

[12] Fakhouri, F.M. Bioplásticos flexíveis e biodegradáveis à base de amido e gelatina. Tese (Doutorado em Tecnologia de Alimentos) – Faculdade de Engenharia de Alimentos, Universidade Estadual de Campinas. Campinas, SP, 271 p., 2009.

[13] Licciardello, F.; Giannone, V.; Del Nobile, M. A.; Muratore, G.; Summo, C. Giarnetti ,M.; Caponio, F.; Paradiso, V. M.; Pasqualone, A.. Shelf life assessment of industrial durum wheat bread as a function of packaging system. Food Chemistry, 224, 181–190, 2017.

[14] Licciardello, F.; Cipri, L.; Muratore, G. Influence of packaging on the quality maintenance of industrial bread by comparative shelf life testing. Food Packaging and Shelf Life,1, (1), 19-24, 2014.

[15] Pagani, M.; Lucisano, M. ;Mariotti, M.; Limbo, S. Influence of packaging material on bread characteristics during ageing. Packaging Technology and Science, 19 (5) (2006), pp. 295-302

[16] Cioban, C.; Milin, A.; Cozma, A.; Aurel, A. Impact of packaging on bread quality and conservation. Lucrări Ştiinţifice, 52, 241-246, 2009.

INDUSTRIAL DRYING

Current needs of the pharmaceutical industry: opportunities and challenges for implementing novel drying technologies

Langford, A. [a]; Luy, B. [b]; Ohtake, S. [a]*

[a] Pfizer, Inc. BioTherapeutics Pharmaceutical Sciences, Chesterfield, MO, USA.
[b] Meridion Technologies GmbH, Müllheim, Germany.

*E-mail of the corresponding author: Satoshi.ohtake@pfizer.com

Abstract

Commercial drying methods are limited either by high production costs or significant quality loss due to process-related stresses. The near-ubiquitous use of freeze-drying in the pharmaceutical industry makes it the standard to which other drying technologies are compared. However, the shortcomings of lyophilization warrant evaluation of new techniques and the benefits they offer, such as compatibility with continuous manufacturing. Novel drying technologies must also overcome barriers to commercial implementation including, but not limited to, scalability and integration into a GMP environment. There remain several opportunities for further research which direct focus and investment strategy for the next generation pharmaceutical drying technologies.

Keywords: pharmaceuticals; manufacturing technology; implementation; lyophilization; scalability

1. Introduction

The dehydration of wet material can enable convenient storage options, decrease transportation costs, and improve the ease of sample handling. The specific mechanism of water removal plays a significant role in whether these benefits are achieved since the drying process impacts the material's physical and chemical properties. A combination of consumer demands for improved functional properties (e.g., rapid dissolution, longer shelf life) and manufacturers' concerns with the financial and operational aspects of a drying process are major drivers for implementing novel drying technologies in industrial applications (Fig. 1). In the food industry, J. A. Moses and coauthors rightly point out that "with technology and market-driven demands, new dryers will continually be developed."[1]

Efficiency
- Shorter drying times
- Increased capacity

Quality
- Enhanced product attributes
- Benefits of hybrid-drying

Operation
- Improved safety
- Better process controls

Finance
- Lower cost
- Reduced environmental impact

Fig. 1 Drivers for novel drying technologies. Figure adapted from Moses et al. [1]

It is critical for the pharmaceutical industry to have a similar mindset regarding drying technologies, especially since pharmaceuticals employ considerably fewer number of drying techniques during manufacture compared to foodstuffs. Additional drivers for the evaluation of new drying technologies include, but are not limited to, improved energy efficiency, reduced environmental impact (e.g., use of renewable energy sources), and compatibility with continuous manufacturing process. For these reasons, having a strategy for evaluating and implementing new manufacturing technologies is critical to meet the demands for reducing manufacturing costs and delivering next generation therapeutics.

2. Challenges and opportunities for new technology implementation

While we remain optimistic that the best scientific ideas will be appropriately nurtured, there are many obstacles to their growth, development, and future implementation. In simple terms, humans are often innately resistance to change. As we explore unknown areas, we move away from safety and comfort and into risk and potential frustration. Therefore, it is critical to keep an open mind when new technologies are being assessed. Management (in industry) should be wary to stifle an idea simply because it may not be

easily implemented or scalable. Pushing through the initial resistance associated with developing a new manufacturing technology may lead to long-term benefits. Consumers (i.e., HCP and patients) may need to be re-educated to utilize products with 'atypical' features since novel drying technologies may produce products possessing unique physical properties (e.g., density, color), which may differ from those being produced by currently-accepted technology.

A biopharmaceutical technology management strategy outlined by Thakur et al. describes a four-phased approach to improving capabilities which involves observation, alignment, decision, and action.[2] Observation requires detailed collection of information and data from both internal and external sources. A market assessment conducted by Janssen summarized seven key technology themes that may impact the manufacturing process.[2] These technology themes include; process innovation, single use/modularity, continuous, automation/robotics, data analysis, disruptive, and customer facing. Technology trends impacting all aspects of biopharmaceutical processing, including upstream and downstream bioprocessing, formulation and fill, and packaging/devices, can be easily sorted into these overarching themes.[2]

In some ways, regulators are playing a leading role in the conversation on the implementation of new manufacturing technologies. A statement released in September 2017 describes the FDA's commitment to pharmaceutical innovation, not only in regards to novel therapeutics, but also in the manufacturing technologies used to produce them. [3] CDER's Office of Pharmaceutical Quality created an Emerging Technology program to "promote the adoption of innovative approaches to pharmaceutical manufacturing… and [provide] a route for companies to engage with the FDA prior to regulatory submission".[3] In spite of these support structures in place, Munk [4] has summarized a number of challenges being encountered for implementation, including: 1) need for precedence, 2) need for a defined regulatory path, robust single-use technology, and robust process analytical technology (PAT) tools, 3) lack of comfort level and control tools, 4) lack of easy fit for continuous manufacture into existing infrastructure, facilities, and quality systems, 5) need for economic justification and adaptation of current quality or regulatory programs, and 6) need for unit operations to be fully developed for continuous processing.

While some of these concerns are specific to continuous manufacture, the core principles apply to the resistance shown and felt by the industry to accept the implementation of any new technology. There are further pharma-specific aspects for consideration. For legacy products, new technologies are not easily implemented; tremendous amounts of effort have been invested to fulfill the regulatory requirements of product approval and maintain the validated status. Often, the introduction of a new technology would represent a 'Major Change' that requires a very costly repetition of validation and requalification work, in addition to the risk that may be associated with the use of new technology.

Alternatively, a new technology may be introduced in conjunction with a new compound. This, however, narrows the range of potential users to introduce a new technology to the Rx-based industry. Furthermore, very significant risk is linked to the development of new compounds, which can fail in late development stages or even after market approval. To invest in a cGMP manufacturing site with a new technology that is not available in other sites of the company, or industry, for a new compound further increases the risk.

3.   Challenges/limitations with lyophilization

Lyophilization is the industry standard for drying of biopharmaceutical products and a significant fraction of pharmaceutical industry's knowledge is devoted specifically to freeze-drying.[5] Even though it is common-practice, there are several drawbacks to the lyophilization process, such as 1) high energy consumption, 2) long processing times, 3) significant production and maintenance cost, and 4) limited manufacturing and container closure flexibility.

The energy efficiency of a fully loaded production-scale lyophilizer was reported by Alina Alexeenko to be as low as 1.5 to 2%.[6] In general, drying processes are one of the most energy intensive unit operations.[7] The long drying process times during freeze-drying, which can vary from several hours to days, may also limit the number of batches that can be produced at manufacturing site. In some cases, the lyophilizer capacity may be the limiting factor to overall manufacturing production rate. This is one of the main reasons that significant effort is focused on optimizing the primary and secondary drying times during the freeze-drying cycle.[8] Since lyophilization is a batch process, it will also be challenging to adapt the technology into a continuous manufacturing process. From a container closure perspective, as previously mentioned, the primary packaging is limited to containers that are suitable for lyophilization (e.g. vial or bottles).

Despite these limitations, freeze-drying is a robust and scalable process that is widely applied in the pharmaceutical industry. In all likelihood, freeze-drying will remain the predominant method for drying pharmaceuticals; however, the drawbacks highlighted here demonstrate the potential benefit of evaluating next generation drying technologies that may overcome these challenges.

4.   Potential solution to limitations associated with lyophilization

In alignment with the technology management strategy, spray-freeze drying is a unique drying technology that is being evaluated for biopharmaceuticals due to the plethora of its offerings, which among them include manufacturing process innovation and new packaging options for customers [9-11]. Spray freeze-drying technology can be aimed at two major focus areas: product innovation and increased manufacturing flexibility. With respect to manufacturing flexibility, a major aspect is the production of homogeneous, free flowing and sterile microspheres as bulk that can be filled into vials, or any other container closure systems, at any time, with flexible (vial) dosing and batch quantities (e.g. even personalized medication). In contrast to conventional vial lyophilization, the general sequence of operation is reversed by having the lyophilization process prior to the filling process. With this technology, a long and rigid supply chain can be made flexible and cold chain logistics can be facilitated.

Since the product is already freeze-dried, the primary packaging does not need to be suitable for lyophilization; this allows for direct filling into syringes or any other application devices that would not be suitable for conventional shelf freeze-drying.

With respect to product innovation, the availability of free flowing bulk that can be dosed and filled allows to formulate combination products by compounding on the filling line. Furthermore, the availability of the increased product surface not only facilitates the drying due to increased heat and mass transfer, but also reduces reconstitution time. This specifically applies when high protein concentration products (up to 200 mg/ml) are processed. Spray freeze-drying is a good example of a technology that has successfully progressed through the technology management process and will continue to mature as more applications are investigated.

As described above, the introduction of new, disruptive technologies in pharmaceutical applications has its challenges, which has an impact on the overall product development timeline that needs to be taken into account (i.e., from first process development studies to cGMP operations). This can easily cover a period of 10+ years. This time span is a challenge even for an established technology provider, as the return on investment for the development does not occur prior to broader implementation in the industry, and the profitability is not in the range of new pharmaceutical compounds. The risks and challenges are greater for start-up companies that need to survive economically in that long development period.

Nevertheless, there are possibilities to balance these risks. It is advisable to team up with a major Big Pharma partner that, besides the economical strength and possible application, brings regulatory competence and IP strengths to the development process. At a certain level of maturation, it may be possible to look for additional companies, which could then form a User Group, or a consortium, in order to address the development needs that are associated with the implementation of a new technology as well as regulatory considerations. In regard to the latter, it may be preferable to solicit participation of regulatory bodies that can comment on their evaluation criteria, which will reduce the risk of surprises regarding the acceptability of the technology.

Alternatively, it may be possible to look for applications outside of pharma that do not carry the intrinsic risks and other time-consuming formal evaluation as in pharma applications. In these sectors, faster development and evaluation can be accomplished. Even with this approach, the challenge still remains to progress developments that are specific to the pharmaceutical application in parallel to reduce the time associated with implementation.

5. Conclusions

While the pharmaceutical industry continues to demonstrate its creativity associated with novel compounds in development (now venturing into the realms of gene and cell therapy, while a decade ago, it was solely focused on monoclonal antibodies), the processing technology has not kept its pace. This is not a reflection of the paucity of innovation associated with processing technology. Regulatory aspects, in which conventional testing or validation procedures and routines that are well accepted may no longer be applicable, pose another challenge that pharma companies face when considering the introduction of new processes. The introduction of a disruptive new technology is often only possible if a promising new compound strongly requires the benefits of that new technology, and if the

business case allows for the additional costs that are linked to its introduction. These concerns can broadly be classified as economic, logistical, technical, and psychological and all elements need to be overcome in order for successful implementation of a new technology.

6. References

[1] Moses, J. A.; Norton, Tomás; Alagusundaram, K.; Tiwari, B. K. Novel drying techniques for the food industry. *Food Engineering Reviews* **2014**. 6 (3):43-55.

[2] Thakur, R.; Simmen, T.; Merkle, S.; Venkataraman, R.; Handor, C.; Van den Heuvel, R. Evaluating technology and innovation in biopharmaceutical manufacturing. *Pharmaceutical Technology* **2016**. 40 (8):22-27.

[3] FDA in Brief: FDA issues guidance to help advance novel technology to improve the reliability and safety and help lower the cost of pharmaceutical manufacturing. 2017.

[4] Munk, M. 2017. "The industry's hesitation to adopt continuous bioprocessing: recommendations for deciding what, where, and when to implement." BioProcess International.

[5] Pikal, Michael J. Freeze Drying. In *Encyclopedia of Pharmaceutical Technology*; Swarbrick, James, Eds.; Informa Healthcare USA, Inc., 2006; pp 1807-1833.

[6] Alexeenko, A. 2011. "Controlling the freeze-drying process: Simulations and modeling." World Lyophilization Summit, Boston, Massachusetts.

[7] Raghavan, G. S. V.; Rennie, T. J.; Sunjka, P. S.; Orsat, V.; Phaphuangwittayakul, W.; Terdtoon, P. Overview of new techniques for drying biological materials with emphasis on energy aspects. *Brazilian Journal of Chemical Engineering* **2005**. 22 (2):195-201.

[8] Tchessalov, S.; Dixon, D.; Warne, N. 2018. Lyophilization above collapse. US9884019B2.

[9] Luy, B.; Plitzko, M.; Struschka, M. 2016. Process line for the production of freeze-dried particles. EP2764309.

[10] Struschka, M.; Plitzko, M.; Gebhard, T.; Luy, B. 2016. Rotary drum for use in a vacuum freeze-dryer. EP2764310.

[11] Plitzko, M.; Struschka, M.; Gebhard, T.; Luy, B. 2015. A process line for the production of freeze-dried particles. EP2764311.

Dryer performance – Reducing energy consumption, improving the product and sharing information

Whaley, M.[a]*; Poandl, F.[b]

[a] Principle Process Engineer, Buhler Aeroglide
[b] Associate Chief Engineer, Buhler Aeroglide.

*E-mail of the corresponding author: michael.whaley@buhlergroup.com

Abstract

The evaporation of water is a major energy consumer around the world where the evaporation of water from agricultural products, natural resources, processed foods and feeds, and petrochemical products is required for long term storage, subsequent processing or other desired attributes.

The control of product attributes associated with drying can also be challenging in terms of measurement and modelling which may lead to inefficiencies in the operation of a dryer.

This discussion below will address solutions to improve the thermal efficiency of dryers and to control the critical properties of the product being dried. In addition, the benefits of haring information between the dryer supplier and the dryer operator will be discussed through the use of the Industrial Internet of Thing

Keywords: *heat recover; design; control.*

1. Heat Recovery for Conveyor Dryers

In a well-balanced conveyor dryer, the energy associated with evaporation of water represents approximately 65% of the thermal energy input. The remaining energy is consumed by the hot exhaust air stream, the temperature increase in the product, and ambient losses to the environment. Much of this energy may be recovered by cooling the product after the drying step and using this air within the dryer, recovering the sensible and latent heat in the exhaust to pre-heat make-air, recovering energy for steam condensate, and improving the insulation of the dryer construction.

In order to reduce operating costs, energy conservation and heat recovery should be paramount to the configuration of any unit operation, specifically thermal drying. Numerous drying technologies benefit from energy recovery; however, the platform of this study focuses on reducing utility consumption in regards to conveyor drying. Gel drying applications are used as examples for recovering energy and recycling heat within the dryer. Drying the gel yields effluent streams with sufficient internal energy to justify modifying the process design of the dryer for heat recovery. Opportunities for heat recovery include cascading airflow, heat recovery from the exhaust air, and condensateflashing to maximize the energy from the steam supply.

Drying wet material requires a large amount of energy/mass transfer to obtain the desired final moisture content of the product. The physical properties of the gel have an inlet moisture typically around 50-60% wwb, while the desired outlet moisture range is 3-5% wwb. Depending upon the nature of the gel, the product is first tested in a laboratory dryer to establish optimal drying conditions for air temperature, velocity, and bed depth. Many cellulous or protein derived gel polymers are sensitive to air temperature, unlike refined gel polymers from petroleum based reactions. The latter is considered for the purpose of this analysis. Dryer components (fans, heat source, etc.) are designed for high process air temperatures (T range 165-180°C) and flow rates through the stacked bed of product (V range of 1.6-2 m/s) in order to facilitate a high rate of evaporation. A typical gel conveyor dryer configuration can be seen in Figure 1.

Buhler Aeroglide has a proprietary heat and mass balance spreadsheet, in which the process is broken down to identify areas where energy can either be reduced or reused. Figure 2 shows an approximate energy consumption profile for a conveyor dryer, without heat recovery, producing dried gel at five tons per hour. As seen in the bar chart, water evaporation requires the most amount of energy due to the phase change. The second largest contribution to the thermal load is from heating a supply of cool dry make-up air in exchange for hot wet exhaust air. For this example, the most beneficial savings can be achieved by recovering the thermal energy used to evaporate the water and heat the make-up air. These dryers also have a cooling zone; therefore, heat from the product can be recovered by

recycling air from the cooling exhaust. Improving the dryer design to limit ambient heat losses will also improve the energy efficiency.
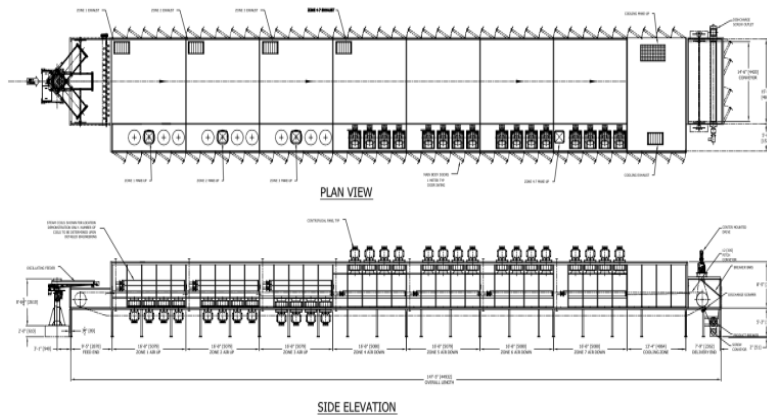
Figure 1 - Gel dryer configuration
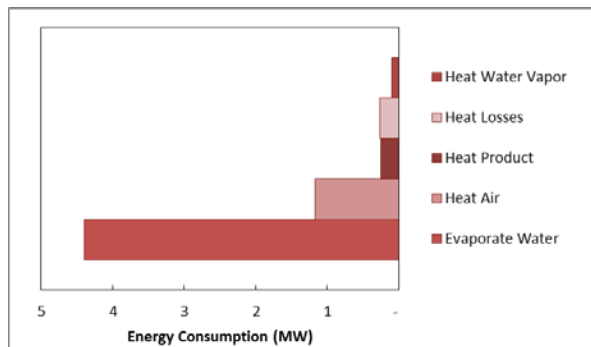

Figure 2 - Gel energy breakdown

For dryers without heat recovery, over six mega-watts of energy is required to produce five tons per hour of dried gel. These values do not include the electrical load to operate the mechanical equipment (conveyors, fans, etc.). Gel drying application are ideal for heat recovery because the production and evaporation rates are substantial for systems producing more than four tons per hour. Thermally processing gel incurs high energy consumption and utility costs. As mentioned previously, the gel enters the dryer with an average moisture content between 50-60% wwb and exits at 3-5%. Operating expenses, for a dryer demanding 6 MW of thermal energy for evaporation, are considerable.

The operating costs associated with the dryer can be reduced based on the energy recovery options. However, there were parameters that were constant throughout the simulations. The quality of the air entering the dryer was defined at ambient conditions (TDB=20°C) and sea level. Also, the general dryer configuration and process parameters were standardized while

modeling the energy options. The defined process operating conditions and assumed rheological properties are in noted in Table 1. As mentioned, the overall configuration of the dryer in regards to airflow direction, drying/cooling area, and general arrangement were consistent. In terms of design, the conveyor dryer is a single pass, single plenum machine. Each simulation had six drying zones with an extended cooling zone. The direction of airflow in the first three zones were upflow, proceeded by downflow air in the later sections of the dryer.

Table 1 - Dryer process parameters

Parameter	Value
Production Rate (kg/hr)	5.000
Inlet Moisture (% wwb)	60
Outlet Moisture (% wwb)	5
Wet Density (kg/m^3)	460
Product Depth (mm)	100
Retention Time (min)	30
Air Temperature (°C)	160
Air Velocity (m/s)	1,65

(a)   (b)   (c)
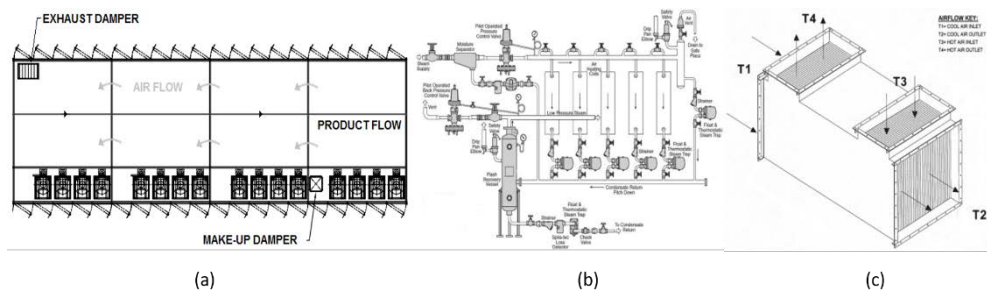
Figure 3 - (a) Buhler aeroglide cascading air flow, (b) Flash steam system (c) Air to heat exchanger

The simulations share many design features in common; however, the energy recovery features were unique to each. This study focused primarily on cascading airflow, air-to-air heat recovery from exhaust to make-up, and condensate flashing to preheat make-up air. Figures 3a, 3b (Spirax Sarco Inc., "Design of Fluid Systems - Hook-Ups" 2012. pg. 97), and 3c (Munters Corporation, "Counterflow Plate Type Air-to-Air Heat Exchangers" 2013) provide illustrations of the equipment.

2.1 Base Design

The first scenario that was modeled had no heat recovery in addition to the recirculated air. The results of the energy and mass balance for Case 1 can be seen in Table 2. The dryer's

exhaust and makeup air flow were set to provide absolute humidity levels in the exhaust of 0.15 kg_{H2O}/kg_{DA}.

Table 2 - Case 1: Results

Dryer Performance	Value
Energy Usage (kW)	6.045
Steam Usage (kg/hr)	11.442
Spec. Energy Consumption (kJ/kg$_{Evp}$)	3.166
Spec. Steam Consumption (kg$_{Steam}$/kg$_{Evp}$)	1,66
Spec. Moisture Extraction Rate (kg$_{Evp}$/kWh)	1,14
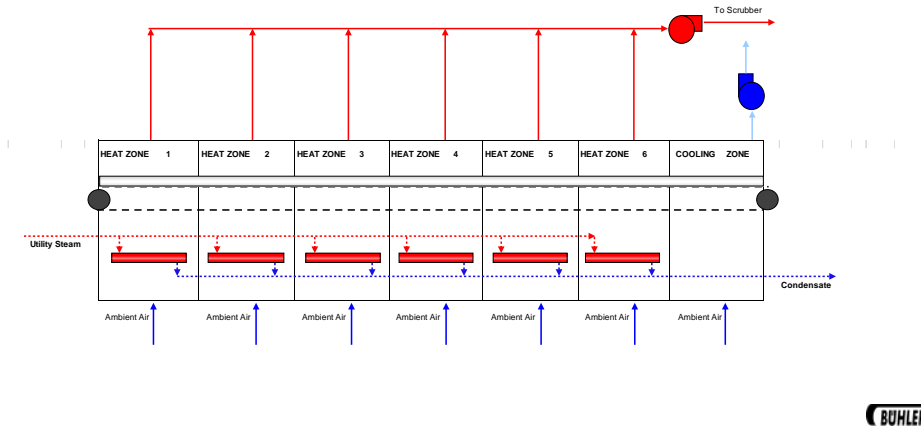
Figure 4 - Case 1: Process flow diagram

Case 1 represents the most energy intensive and least cost effective option from an operating perspective. This scenario is a reference point for the following simulations and it is identical to the energy breakdown shown in Figure 2. Table 2 shows the specific energy and steam consumption along with the specific moisture extraction rate. These values are frequently used to compare similar drying applications but at varying sizes and production rates. They will be used as a baseline for the following energy Cases.

1.2 Cooler exhaust air used as dryer make-up air

The second scenario focused on heat recovery from the cooling exhaust. In this design, the air being exhausted from the cooling section was ducted to the makeup air dampers entering each heat zone. The makeup air to each zone was no longer at ambient conditions; rather, it was preheated (T_{DB}=30°C). The cooling exhaust air flow rate was set based on the required makeup air mass flow rate. Similarly to Case 1, it was assumed that the quality of the air entering the cooler was at ambient conditions (T_{DB}=20°C) and sea level.

Table 3 shows the calculated energy and mass balance results for Case 2. When compared to Case 1, there was a 2% savings in energy usage. As expected, the specific energy and steam consumption are less because the same about water was evaporated using less energy. Similarly, the specific moisture extraction rate increased because it is inversely proportional.

Table 3 - Case 2: Cooling exchaust make-up air results

Dryer Performance	Value
Energy Usage (kW)	5.908
Steam Usage (kg/hr)	11.183
Energy Savings (%)	2%
Spec. Energy Consumption (kJ/kg$_{Evp}$)	3.094
Spec. Steam Consumption (kg$_{Steam}$/kg$_{Evp}$)	1,63
Spec. Moisture Extraction Rate (kg$_{Evp}$/kWh)	1,16
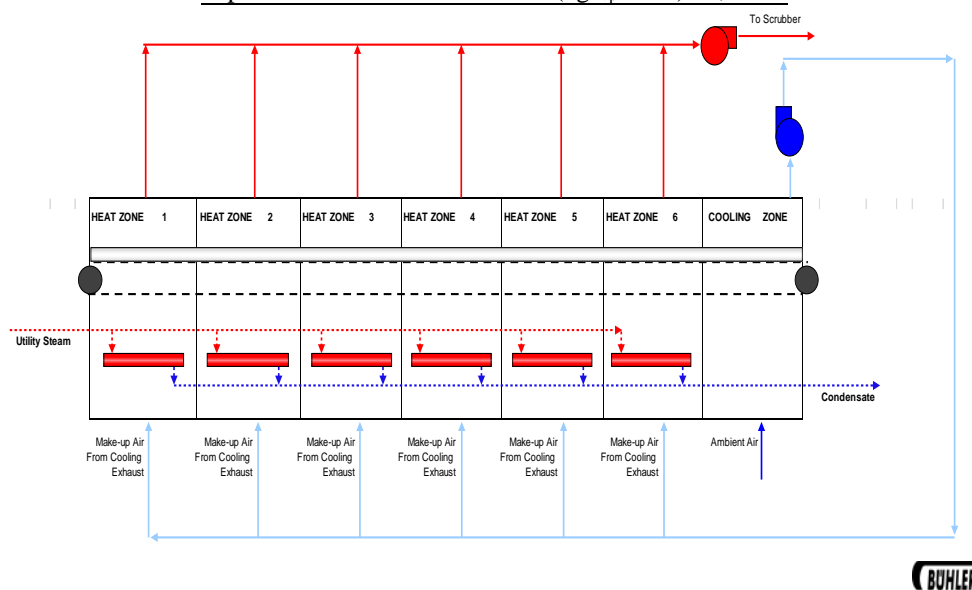
Figure 5 - Case 2: Process flow diagram

1.3 Cascading airflow

Cascading airflow was simulated in Case 3. Similarly to Case 2, the cooling exhaust is utilized as make-up air; however, it only enters the dryer in heat zones 1, 2, and 6. The make-up air is introduced in zone 6. The exhaust from zone 6 internally "cascades" as the make-up air to zone 5. This design is continued to zone 3, where it is finally exhausted from the dryer. The cascading design conserves energy by reusing relatively dry preheated air.

Table 4 - Case 3: Cascading air flow results

Dryer Performance	Value
Energy Usage (kW)	5.803

Steam Usage (kg/hr)	10.983
Energy Savings (%)	4%
Spec. Energy Consumption (kJ/kg$_{Evp}$)	3.039
Spec. Steam Consumption (kg$_{Steam}$/kg$_{Evp}$)	1,60
Spec. Moisture Extraction Rate (kg$_{Evp}$/kWh)	1,18

Depending upon the drying characteristics of the product and the configuration of the dryer, some applications permit cascading airflow through all the heat zones. A prime example of cascading airflow would be a rubber dryer. Consequently for gel drying, there is a high evaporation load in the first two heat zones in addition to the change in airflow direction from zones 2 to 3. Therefore, it is mechanically and thermodynamically impractical to cascade airflow from zone 6 to zone 1 for gel drying applications.

Table 4 depicts the results of the energy analysis for cascading airflow. In comparison to Case 1, there is a 4% reduction in energy consumption.

1.4 Flash steam

Table 5 - Case 4: Flash steam result

Dryer Performance	Value
Energy Usage (kW)	5.456
Steam Usage (kg/hr)	10.328
Energy Savings (%)	10%
Spec. Energy Consumption (kJ/kg$_{Evp}$)	2.857
Spec. Steam Consumption (kg$_{Steam}$/kg$_{Evp}$)	1,50
Spec. Moisture Extraction Rate (kg$_{Evp}$/kWh)	1,26

Flash steam is generated when high pressure condensate, from the internal steam coils, is released to low pressure. The excess latent heat allows some of the condensate to re-evaporate into steam (Spirax Sarco Inc., "Design of Fluid Systems – Steam Utilization" 2012). The design for the flash steam systems requires that the low pressure flash steam be a minimum of 520 kPa below the high pressure condensate.

In the drying simulation, the low pressure flash steam is utilized via an external steam coil. The exhaust air from the cooling section is ducted to the low pressure steam coil. After the air is preheated by the flash steam, it is then distributed to each heat zone.

In the simulator, the condensate was leaving the dryer at 1765 kPa and the flash tank was operating at 690 kPa. Based on the energy balance, the dryer produced condensate at a rate of 10,330 kg/hr. The flash steam system was able to recover nearly 500 kW of power from the high pressure condensate in the form of lower pressure steam. Table 5 lists the values from the flash steam energy balance. The flash steam modifications yielded energy savings of 10% when compared to the base case scenario.
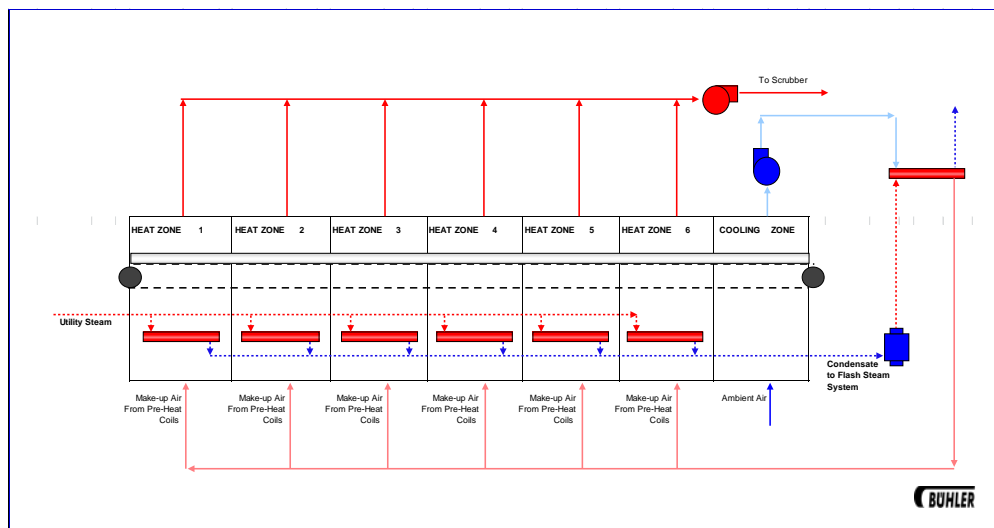
Figure 6 - Case 4: Process flow diagram

1.5 Air-to-air heat exchanger

The air-to-air heat exchanger recovers heat from the exhaust streams that would have otherwise been released to the environment. Once again, the make-up air is supplied from the cooling exhaust/transfer fan. An illustration of the dryer configuration can be seen Figure 8.

A counter-current parallel plate and frame heat exchanger is used to reduce pressure drop and achieve improved approach temperatures between the hot exhaust air and cooler make-up air. Pressure drop becomes a concern while sizing transfer and exhaust fans. Typically, the pressure drop across the heat exchanger is between 620-750 Pa; thus, significantly increasing the fans' motor sizing. There are also design considerations in regards to the approach temperatures of the make-up air. For petroleum based gel polymers, the efficiency of the heat exchanger is limited by the formation of condensation in the exhaust stream. The humid exhaust air contains gel particulate, which will foul the heat exchanger if water condenses along the heat transfer surface area. Therefore, the exhaust temperature must maintain at least an 11°C buffer above the dew point temperature. ($T_{EX} \geq T_{DEW}+11$°C). This exhaust temperature set point is used as a design parameter for the heat exchanger.

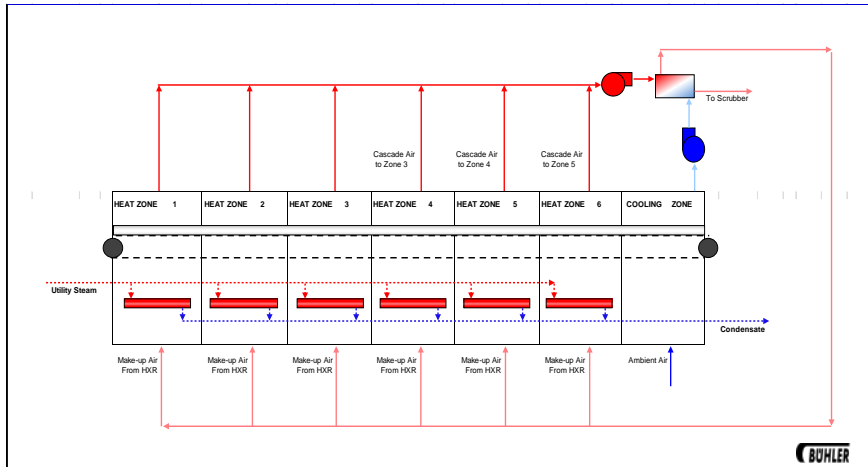*Figure 7 - Case 5: Process flow diagram*

Table 6 - Case 5: Heat exchanger results

Dryer Performance	Value
Energy Usage (kW)	5.396
Steam Usage (kg/hr)	10.213
Energy Savings (%)	11%
Spec. Energy Consumption (kJ/kg$_{Evp}$)	2.826
Spec. Steam Consumption (kg$_{Steam}$/kg$_{Evp}$)	1,49
Spec. Moisture Extraction Rate (kg$_{Evp}$/kWh)	1,27

Despite these design considerations, counter-current air-to-air heat exchangers improve the energy efficiency of system. Table 6 shows the benefits of recovering energy from the exhaust air stream to preheat the make-up air.   There were 11% energy savings; however, case studies show potential energy savings up to 16% (Mujumdar A. "Handbook of Industrial Drying" CRC Press. November 2006).

1.6 Combined energy conservation measures

Table 7 - Case 6: Cambined energy conservation results

Dryer Performance	Value
Energy Usage (kW)	4.917
Steam Usage (kg/hr)	9.306
Energy Savings (%)	19%
Spec. Energy Consumption (kJ/kg$_{Evp}$)	2.575
Spec. Steam Consumption (kg$_{Steam}$/kg$_{Evp}$)	1,35
Spec. Moisture Extraction Rate (kg$_{Evp}$/kWh)	1,40

Case 6 combined the energy features described in Cases 2-5. First, the exhaust air from the cooling section was passed through an air-to-air heat exchanger. Hot exhaust air from zones

1, 2, and 3 ran counter-current to the preheated make-up air. The second feature involved further heating the make-up air using flash steam coils. Then, the hot make-up air was ducted to zones 1, 2, and 6. Finally, the air was cascaded from zone 6 to 3, where it was exhausted from the dryer.
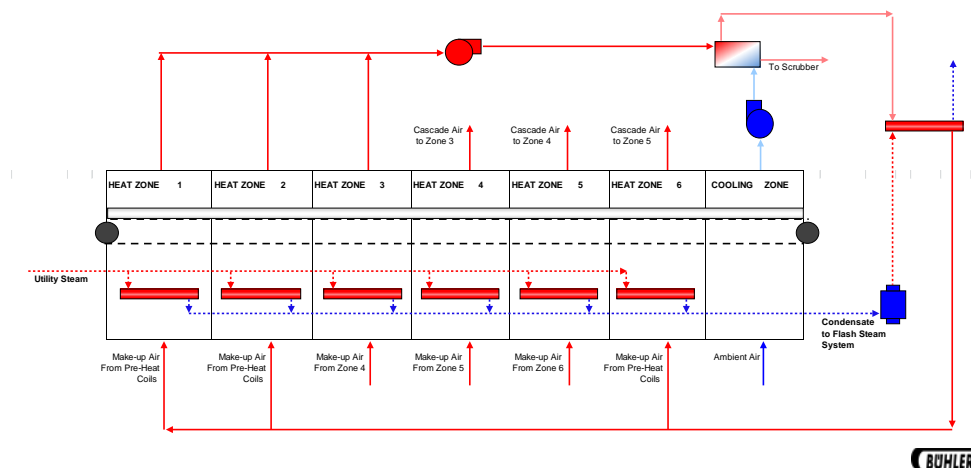
Figure 8 - Case 6: Process flow diagram

The combined energy savings from the heat recovery features was 19% when compared to Case 1. The specific steam consumption was determined to be 1.35 kg_{Steam}/kg_{Evp}.

2.7 Energy Savings Results

The energy savings were calculated using a mass and energy balance at the design conditions. A nominal throughput of five tons per hour was selected as the production rate for the gel dryer. Operating parameters were consistent with the industry's standard. The theoretical savings are summarized in Table 8.

The heat recovery options were compared separately to the base case scenario, which had no energy saving features. Each energy case was not added incrementally to the same simulation. Since each energy saving option was evaluated and optimized independently, there are overlapping savings between each option. Therefore, the "Combined" savings are not cumulative and will not equal the sum of the individual options.

Table 8 - Energy conservatioin measure results summary

Dryer Production Rate 5000 kg/hr	Steam Usage (kg/hr)	Energy Usage (kW)	Spec. Steam Consumption (kgSteam/kgEvp)	Spec. Energy Consumption (kJ/kgEvp)	Spec. Moisture Extraction Rate (kgEvp/kWh)	Energy Saving (%)
Base Case	11.442	6.045	1,66	3.166	1,14	-
Cooling Exhaust MUA	11.183	5.908	1,63	3.094	1,16	2%
Cascading	10.983	5.803	1,60	3.039	1,18	4%
Flash Steam	10.328	5.456	1,50	2.857	1,26	10%
Heat Exchanger	10.213	5.396	1,49	2.826	1,27	11%
Combined	9.306	4.917	1,35	2.575	1,40	19%

2. Product Quality Control

During drying, the control of product quality attributes is critical to successful production. Parameters such as moisture content, color, and specifically for nut roasting the reduction in pathogens should be measured and controlled within the process. Methods for modelling and/or measuring these key product quality parameters will be discussed as well as how the dryer process parameters may be manipulated to maintain the values within the users' specifications.

3.1 Increased dryer yield

Even small percentage gains can mean significant increases in yield and profitability over time. A product moisture control will automate the dryer operation to optimize performance, bringing more product closer to target moisture. This increases overall yield by preventing over drying. It also eliminates the risks associated with under drying. Continuous monitoring, constant control uses suitable sensor technology for the specific product to be dried. Typically larger extruded products, the moisture content can be determined via their dielectric properties using microwave or capacitive sensors. While fine materials or surface drying applications near infrared based sensors are successful. These types of sensors coupled with controls that use algorithms built on decades of technical drying experience allow dryer manufacturers to provide benefits to their customers. The resulting

comprehensive closed loop system delivers full time automated control of the dryer. The moisture content at the dryer's output is sampled continuously and the necessary adjustments to the dryer are made immediately, eliminating the need for manual sampling and the associated time gaps between sampling, testing, and making dryer adjustments. This fully automated method significantly increases the frequency of sampling and moves more of the product closer to the target moisture content. Consistent, reliable dryer management improves energy efficiency by making the correct dryer control decisions quickly and reliably. Moisture content targets can be input by operator or by recipe control, and the dryer will automatically establish and maintain the optimal drying environment for the remaining production run. This eliminates the wasted energy and product that can result from manually attempting to reach a moisture target.

3.2 Ensuring safe thermally processed food.

In the USA alone, the annual cost of foodborne outbreaks caused by harmful bacteria, is $17B USD. Each recall can cost a single company up to $30M USD per incident. The number of recalls have doubled over the last 10 years. As a consequence of these incidents, there are new legal requirements (FSMA - Food Safety Modernization Act) in the USA that put much more pressure on food manufacturers in the form of increased government oversight and greater customer scrutiny. One recall due to food safety failings can be disastrous to a company or a brand.

Beyond the financial considerations, there are far greater consequences from food safety incidents. The Centers for Disease Control and Prevention (CDC) estimates that each year roughly 1 in 6 Americans (or 48 million people) get sick, 128,000 are hospitalized, and 3,000 die of foodborne diseases. As part of the food supply chain, we all bear a moral obligation to ensure we are producing the safest food possible for consumption by the public.

3.2.1 Regulatory requirements

In 2011, the Food Safety Modernization Act became law. It is the most sweeping reform of US food safety laws in more than 70 years. With it came many new legal requirements for food processors. Among these new requirements is the need to guard against bacterial hazards in the food production process. Processors must now:

- Analyze potential hazards in the food being processed
- Put preventive controls in place
- Validate the process to show the controls work
- Record process data to show the controls are met
- Be able to recall data quickly upon request

For many foods where bacteria presence is known or expected, a kill step is the typical control. This step separates unsafe raw material from a safe-to-eat consumer product. The

kill step is usually a high temperature process, meaning processors can use existing processes originally designed for operations such as roasting of nuts, as a kill step for bacteria. Gaining insights to a process to ensure that it is capable of delivering the required kill, and then monitoring and recording processing conditions, is currently done using tedious methods that are time consuming, costly, manual, and vulnerable to human errors and adulteration. Many times there are also conflicts between food safety and quality needs.

3.2.2 Ensuring the Kill Step

With enhanced processing monitoring, food manufacturers can now take full advantage of their dryer manufacturer's food safety expertise and food technology knowledge to meet these new challenges. A system that can provide a continuous real time view into the thermal process, enables operators to react faster to process changes, reducing product losses and increasing production time, while its digital data recording, storage, and reporting capabilities help to reduce the vulnerabilities associated with manual and paper-based methods.

3. Sharing Success – A Partnership between Dryer Users and Dryer Manufacturers

Having this process instrumentation and controls isolated at the plant level does not benefit the corporation as a whole. Utilizing the Industrial IoT and data analytics allows this information to be shared throughout the plant, multiple corporate facilities and the process equipment vendor. Some of the benefits of this partnership are listed below.

1. It will be possible for the drying process to be monitored in real-time from any location. This will allow the management to respond to unexpected upsets, eliminate wasted idle time, and reduce inventory ready to ship to customers. Data from multiple sites will allow comparison of plant efficiencies and methodologies to improve each production line.

2. Connected dryers can be monitored and managed remotely. The dryer operator does not need to directly in front of a control panel in order to adjust the process. Smart sensors and algorithms can be used to better understand what is happening within the drying process which can improve the final product, conserve energy costs and improve overall profitability.

3. The dryer information from multiple sites can be monitored and modelled to form a predictive maintenance algorithm. This will allow dryer operators to reduce downtime and achieve a greater return on their capital investment.

4. Information may be used to study cause and effects that may result in material not meeting specifications. Data affecting quality can be sent to the right people in real time so that they may make informed decisions and work to identify problems, find the root cause and implement solutions. This data can then be used to confirm the solution.

5. This information can help the management team make decisions in a competitive environment in real time by seeing what is happening on their plant floors throughout

the company. This will allow them to better manage overall operating costs and efficiencies.

6. Conclusions

A partnership between an equipment supplier and the user of the equipment can have many benefits as described above that can lead to the optimal use of energy (minimize energy input into the drying step) to lower operating costs. Communications and data sharing through the Internet of Things will allow the partnership to succeed through multiple plant locations to result in the optimal use of resources, plant process lines and increased production quality.